

THE
PHILOSOPHICAL MAGAZINE

EDITOR

PROFESSOR N. F. MOTT, M.A., D.Sc., F.R.S.

EDITORIAL BOARD

SIR LAWRENCE BRAGG, O.B.E., M.C., M.A., D.Sc., F.R.S.

ALLAN FERGUSON, M.A., D.Sc.

SIR GEORGE THOMSON, M.A., D.Sc., F.R.S.

PROFESSOR A. M. TYNDALL, C.B.E., D.Sc., F.R.S.

VOL. XLII.—SEVENTH SERIES

JANUARY—DECEMBER 1951

Reprinted by

WM. DAWSON & SONS LTD.,

with the permission of

TAYLOR & FRANCIS LTD.

“ Meditationis est perscrutari occulta ; contemplationis est admirari
perspicua . . . Admiratio generat quæstionem, quæstio investigationem,
investigatio inventionem.”—*Hugo de S. Victore.*

—“ Cur spirent venti, cur terra dehiscat,
Cur mare turgescat, pelago cur tantus amaror,
Cur caput obscura Phœbus furrugine condât,
Quid toties diros cogat flagrare cometas,
Quid pariat nubes, veniant cur fulmina cœlo,
Quo micet igne Iris, superos quis conciat orbes
Tam vario motu.”

J. B. Pinelli ad Mazonium.



CONTENTS OF VOL. XLII. (Nos. 324-335)

(SEVENTH SERIES)

NUMBER 324—JANUARY

	Page
I. The Propagation of a Radio-Atmospheric. By K. G. BUDDEN, Cavendish Laboratory, Cambridge	1
II. Total Cross-Sections of Hydrogen and Carbon for High Energy Neutrons. By A. E. TAYLOR, T. G. PICKAVANCE, J. M. CASSELS and T. C. RANDLE, Atomic Energy Research Establishment, Harwell.	20
III. The Interaction between an Oblique Shock-wave and a Turbulent Boundary-layer. By O. BARDSLEY and W. A. MAIR, Fluid Motion Laboratory, University of Manchester. (Plates I.-IV.)	29
IV. Collision broadening at Microwave Frequencies. By D. C. M. LESLIE, M.A., Clarendon Laboratory, Oxford	37
V. Anisotropy of Electrical Resistivity of Cold-Rolled Cubic Metals and Alloys. By T. BROOM, Division of Tribophysics, C.S.I.R.O., Melbourne, Australia	56
VI. The Origin of Cosmic Ray Stars. By J. B. HARDING, Imperial College, London	63
VII. On the Velocity of Second Sound in Liquid Helium II. By H. N. V. TEMPERLEY, King's College Cambridge	74
VIII. The Disintegration of Lead Nuclei by Cosmic Rays. By P. E. HODGSON, Imperial College of Science and Technology, London. (Plate V.) ..	82
IX. Landau Diamagnetism and Meissner Effect. By A. PAPAPETROU, Physics Department, University of Manchester	95
X. Correspondence :—	
Calculation of the Density of States Curve for the 3d Electrons in Nickel. By G. C. FLETCHER and E. P. WOHLFARTH, Department of Mathematics, Imperial College, London	106
Stars produced in Nuclear Emulsions by 150 MeV. Neutrons. By E. W. TITTERTON, Atomic Energy Research Establishment, Harwell	109
Hammer Tracks in Neutron and Proton Induced Stars. By E. W. TITTERTON, Atomic Energy Research Establishment, Harwell ..	113
XI. Notices of New Books and Periodicals received :—	
J. A. V. BUTLER and J. J. RANDALL's Progress in Biophysics	118
H. ALFVÉN's Cosmical Electrodynamics	118
WILLIAM WILSON's A Hundred Years of Physics	119
R. A. FISHER's Contributions to Mathematical Statistics	119
H. and B. S. JEFFREYS's Methods of Mathematical Physics	119

NUMBER 325—FEBRUARY

XII. The Waveforms of Atmospherics and the Propagation of very Low Frequency Radio Waves. By P. W. A. BOWE, Cavendish Laboratory, Cambridge. (Plate VI.)	121
XIII. A Calculation of the Elastic Constants of Aluminium. By R. S. LEIGH, Mathematics Department, Imperial College, London	139

ME424

75

3 new

	Page
XLII. The Use of Plasticine Models to Simulate the Plastic Flow of Metals. By A. P. GREEN, B.A., British Iron and Steel Research Association, Sheffield, Mechanical Working Division. (Plates XV. & XVI.)	365
XLIII. Collective Electron Ferromagnetism: Rectangular Energy Bands. By E. P. WOHLFARTH, Ph.D., Department of Mathematics, Imperial College, London	374
XLIV. The Virial Theorem in Quantum Mechanics. By T. L. COTTRELL and S. PATERSON, I.C.I. Ltd., Nobel Division, Research Department, Stevenston, Ayrshire	391
XLV. The Processing of Thick Photographic Emulsions. By A. D. DANTON, A. R. GATTIKER and W. O. LOCK, H. H. Wills Physical Laboratory, University of Bristol. (Plate XVII.)	396
XLVI. A Theory of the Plastic Distortion of a Polycrystalline Aggregate under Combined Stresses. By J. F. W. BISHOP and R. HILL, H. H. Wills Physical Laboratory, University of Bristol	414
XLVII. Abstract :—	
The Capacitance of a Parallel-Plate Condenser with an Anisotropic Dielectric Cylinder in Torsion between its Plates. By C. MACK, The British Cotton Industry Research Association, Shirley Institute, Manchester	428
XLVIII. Correspondence :—	
The Resistance-Minimum in Gold. By D. K. C. MACDONALD and I. M. TEMPLETON, The Clarendon Laboratory, Oxford	432
The Range-Energy Relation for Slow Alpha-Particles in Air. By JOAN M. FREEMAN and W. E. BURCHAM, Cavendish Laboratory, Cambridge	434
XLIX. Notices of New Books and Periodicals received :—	
K. JELLINEK's <i>Weltsystem, Weltäther, und die Relativitätstheorie, and Verständliche Elemente der Wellenmechanik.</i>	438
P. VIGOUREUX's <i>Ultrasonics.</i>	439
R. HILL's <i>The Mathematical Theory of Plasticity.</i>	439
Prof. HUGO STEINHAUS's <i>Mathematical Snapshots.</i>	439
OLIVER HEAVISIDE's <i>Electromagnetic Theory.</i>	440

NUMBER 328—MAY

L. Hyperfine Structure in Paramagnetic Salts and Nuclear Alignment. By B. BLEANEY, F.R.S., Clarendon Laboratory, Oxford	441
LI. The Communal Entropy of Dense Systems. By J. A. POPLÉ, Department of Theoretical Chemistry, University of Cambridge	459
LII. Grain Boundary Diffusion in Metals. By A. D. LE CLAIRE, Atomic Energy Research Establishment, Harwell	468
LIII. The Rectification and Observation of Signals in the Presence of Noise. By R. E. BURGESS, B.Sc., National Physical Laboratory	475
LIV. A Radio Echo Apparatus for the Delineation of Meteor Radiants. By A. ASPINALL, J. A. CLEGG, Ph.D., and G. S. HAWKINS, Jodrell Bank Experimental Station, University of Manchester. (Plates XVIII. & XIX.)	504

	Page
LV. Transit-time Phenomena in Electron Streams.—III. The Electron-Ion Plasma and Beam Fluctuations. By D. K. C. MACDONALD, Clarendon Laboratory, Oxford.....	515
LVI. The Production of Mesons in Proton-Proton Collisions. By J. C. GUNN, E. A. POWER and B. F. TOUSCHEK, Department of Natural Philosophy, University of Glasgow.....	523
LVII. The Energy Loss of Slow Deuterons in D ₂ O. By A. P. FRENCH, Cavendish Laboratory, Cambridge and G. F. P. SEIDL, Brookhaven National Laboratory, Upton, Long Island, U.S.A.....	537
LVIII. The Photodisintegration of the Deuteron. By W. M. GIBSON, H. H. WILLS Physical Laboratory, University of Bristol and T. GROTDAL, J. J. ORLIN and B. TRUMPY, Fysik Institut, University of Bergen.....	555
LIX. Correspondence :—	
Alpha-particles from the Proton Bombardment of Oxygen-18. By J. SEED, Cavendish Laboratory, Cambridge.....	566
The Isomeric State of RaE. By N. FEATHER, F.R.S., The University, Edinburgh.....	568
An Example of the ($n, p; \pi^-$) Reaction in the Photographic Emulsion. By S. J. GOLDSACK and N. PAGE, University of Manchester. (Plate XX.).....	570

NUMBER 329—JUNE

LX. A Mechanism for the Growth of Deformation Twins in Crystals. By A. H. COTTRELL and B. A. BILBY, Department of Metallurgy, University of Birmingham.....	573
LXI. On Virial Coefficients and the Born-Green Theory of Fluids. By G. S. RUSHBROOKE and H. I. SCOINS, Clarendon Laboratory, Oxford..	582
LXII. The Critical Magnetic Fields of Aluminium, Cadmium, Gallium and Zinc. By B. B. GOODMAN and E. MENDOZA, Royal Society Mond Laboratory, Cambridge.....	594
LXIII. A Mechanical Kick-sorter (Pulse Size Analyser). By S. G. F. FRANK, O. R. FRISCH and G. G. SCARROTT, Cavendish Laboratory, Cambridge.....	603
LXIV. A Localizing Geiger Counter. By S. G. F. FRANK, Cavendish Laboratory, Cambridge.....	612
LXV. The Development of Deformation Textures in Metals.—Part II. Body-Centred Cubic Metals. By E. A. CALNAN and C. J. B. CLEWS, National Physical Laboratory.....	616
LXVI. Highly Forbidden Transitions in Decay of Na ²⁴ . By J. F. TURNER and P. E. CAVANAGH, Atomic Energy Research Establishment, Harwell.....	636
LXVII. The Thermal Conductivity of Some Alloys at Low Temperatures. By R. BERMAN, Clarendon Laboratory, Oxford.....	642
LXVIII. Observation of Cosmic Ray Events in Nuclear Emulsions Exposed in a Glacier at 3550 m. By J. B. HARDING, Imperial College, London.....	651

	Page
LXIX. Correspondence :—	
Meson Production in the Atmosphere. By J. D. PULLAR and E. G. DYMOND, Department of Natural Philosophy, University of Edinburgh.....	663
Cross-section of the Reaction ${}^9\text{Be}(p, p2n){}^7\text{Be}$ at 156 MeV. By T. C. RANDLE, J. M. DICKSON and J. M. CASSELS, Atomic Research Establishment, Harwell.....	665
The Reactions ${}^{11}\text{Be}(\gamma\alpha){}^7\text{Li}$ and ${}^{11}\text{B}(\gamma\text{T}){}^8\text{Be}$. By MARGARET E. CALCRAFT and E. W. TITTERTON, Atomic Energy Research Establishment, Harwell.....	666
Observation of Growth of Cadmium Iodine from Aqueous Solution. By A. J. FORTY, H.H. Wills Physical Laboratory, University of Bristol. (Plate XXI.).....	670

NUMBER 330—JULY

LXX. Anelastic Measurements of Diffusion Coefficients in F.C.C. Substitutional Solid Solutions. By A. D. LE CLAIRE, Atomic Energy Research Establishment, Harwell.....	673
LXXI. The Distribution of Energy in Randomly Modulated Waves. By DAVID MIDDLETON, Cruft Laboratory, Harvard University, U.S.A.....	689
LXXII. Observations on the Multiple Scattering of Ionizing Particles in Photographic Emulsions.—Part I. The Value of the Scattering Constant. By K. GOTSTEIN, M. G. K. MENON, J. H. MULVEY, C. O'CEALLAIGH and O. ROCHAT, H. H. Wills Physical Laboratory, University of Bristol..	708
LXXIII. On Combined Bending and Twisting of Thin Tubes in the Plastic Range. By D. HILL and M. P. L. SIEBEL, University of Bristol...	722
LXXIV. Internal Barriers in Semi-Conductors. By H. K. HENISCH, Ph.D., A.Inst. P., Department of Physics, The University, Reading.....	734
LXXV. The Moving Griffith Crack. By ELIZABETH H. YOFFE, Ph.D.	739
LXXVI. Total Cross-Sections of the Elements for 156 MeV. Neutrons. By A. E. TAYLOR, T. G. PICKAVANCE, J. M. CASSELS and T. C. RANDLE, Atomic Energy Research Establishment, Harwell.....	751
LXXVII. Metallic Conduction—The "Internal Size-Effect". By D. K. C. MACDONALD, Clarendon Laboratory, Oxford.....	756
LXXVIII. The Radiations of ${}^{203}\text{Hg}$ as Observed by a New Method. By H. W. WILSON and S. C. CURRAN, Department of Natural Philosophy, The University, Glasgow.....	762
LXXIX. Microscopic Studies on Beryl Crystals.—I. Observation of Uni-Molecular Steps. By L. J. GRIFFIN, H. H. Wills Physical Laboratory, University of Bristol. (Plates XXII. & XXIII.)	775
LXXX. A Design of an Ultrasonic Delay-Line. By T. GOLD, Cavendish Laboratory, Cambridge.....	787
LXXXI. A High Precision Pulse Height Analyser of Moderately High Speed. By G. W. HUTCHINSON, M.A., and G. G. SCARROTT, Cavendish Laboratory, Cambridge.....	792
LXXXII. Correspondence :—	
On a Generalization of Wilson's Hypothesis. By GEORGE LUCHAK, Defence Research Board Experimental Station, Ralston, Alberta.....	807

NUMBER 331—AUGUST

	Page
LXXXIII. Crystal Dislocations—Elementary Concepts and Definitions. By F. C. FRANK, H. H. Wills Physical Laboratory, University of Bristol . .	809
LXXXIV. The Axis of Distortion of a Twisted Elastic Prism. By D. G. ASHWELL, Engineering Laboratory, Cambridge	820
LXXXV. The Reflection of very Low Frequency Radio Waves at the Surface of a Sharply Bounded Ionosphere with Superimposed Magnetic Field. By K. G. BUDDEN, Cavendish Laboratory, Cambridge	833
LXXXVI. Note on the Analytic Continuation of the S-Matrix. By N. G. VAN KAMPEN, Institute for Theoretical Physics, Copenhagen, Denmark	851
LXXXVII. The Attenuation of Nucleon Cascades in Lead. By W. G. V. ROSSER and M. W. SWIFT, The University, Manchester	856
LXXXVIII. On the State of Stress in a Plastic-Rigid Body at the Yield Point. By R. HILL, H. H. Wills Physical Laboratory, University of Bristol	868
LXXXIX. A Theory of the α , α' Phases in the Al-Zn System. By R. S. LEIGH, Mathematics Department, Imperial College, London	876
XC. Time and Frequency Uncertainty in Waveform Analysis. By P. M. WOODWARD, B.A., T.R.E., Ministry of Supply	883
XCI. The Beta Spectrum of Tritium. By G. M. INSCH and S. C. CURRAN, Department of Natural Philosophy, Glasgow University	892
XCII. A Theoretical Investigation of the Compression of a Ductile Material between Smooth Flat Dies. By A. P. GREEN, British Iron and Steel Research Association, Sheffield, Mechanical Working Division. (Plate XXIV.)	900
XCIII. The Development of Deformation Features in Metals.— Part III. Hexagonal Structures. By E. A. CALNAN, B.Sc., and C. J. B. CLEWS, Ph.D., National Physical Laboratory	919
XCIV. Observations on the Multiple Scattering of Ionizing Particles in Photographic Emulsions.—Part II. The Scattering of Positrons at 105 and 185 MeV. By M. G. K. MENON, C. O'CEALLAIGH, and O. ROCHAT, H. H. Wills Physical Laboratory, University of Bristol	932
XCv. Correspondence :—	
The Reaction $^{10}\text{B}(\gamma, d) 2^4\text{He}$. By M. J. BRINKWORTH and E. W. TITERTON, A.E.R.E., Harwell, Didcot, Berks.	952
The Disintegration of Light Nuclei by Cosmic Rays. By P. E. HODGSON, Imperial College of Science and Technology, London	955
ERRATUM to G. W. HUTCHINSON and G. G. SCARROTT's Paper (July 1951)	957
XCvi. Notices of New Books and Periodicals received :—	
J. CORNER's Theory of the Interior Ballistics of Guns	958
J. BOUMAN's Selected Topics in X-Ray Crystallography	958
FRITZ LONDON's Superfluids—Macroscopic Theory of Super- conductivity	958
R. W. B. PEARSE and A. C. TAYLOR's The Identification of Molecular Spectra	959
F. D. ROSSINI's Chemical Thermodynamics	959
E. HOWARD SMART's Advanced Dynamics	960
OLIVER HEAVISIDE's Electromagnetic Theory	960

NUMBER 332—SEPTEMBER

	Page
XCVII. An Unbranched Laminar Model of the Intermediate State of Superconductors. By C. G. KUPER, Royal Society Mond Laboratory, Cambridge	961
XCVIII. The Cascade Production of Cosmic Ray Stars and the Relative Number of Charged and Uncharged Particles. By Sir GEORGE THOMSON and P. E. HODGSON, Imperial College of Science and Technology, London	978
XCIX. The Deflection of a Cable due to a Single Point Load. By E. MARKLAND, The University of Nottingham	990
C. The State of Ionization in Lithium Hydride. By M. S. AHMED, University College, London	997
CI. Observations on Carborundum of Growth Spirals Originating from Screw Dislocations. By AJIT RAM VERMA, Royal Holloway College, University of London. (Plates XXV.—XXVIII.)	1005
CII. The Growth of Carborundum: Dislocations and Polytypism. By F. C. FRANK, H. H. Wills Physical Laboratory, University of Bristol.	1014
CIH. The Correlation Function in the Analysis of Directive Wave Propagation. By HENRIK NODTVEDT, Cavendish Laboratory, Cambridge.	1022
CIV. Masses and Modes of Decay of Heavy Mesons.—Part I. κ -Particles. By C. O'CEALLAIGH, H. H. Wills Physical Laboratory, University of Bristol. (Plates XXIX. & XXX.)	1032
CV. Masses and Modes of Decay of Heavy Mesons.—Part II. τ -Particles. By P. H. FOWLER, M. G. K. MENON, C. F. POWELL and O. ROCHAT, H. H. Wills Physical Laboratory, University of Bristol. (Plates XXXI. & XXXII.)	1040
CVI. Observations on the Multiple Scattering of Ionizing Particles in Photographic Emulsions.—Part III. Statistics of the Sampling Distributions of Second Differences and the Technique of Overlapping Cells. By C. O'CEALLAIGH and O. ROCHAT, H. H. Wills Physical Laboratory, University of Bristol.	1050
CVII. Correspondence :—	
The τ -Meson. By P. E. HODGSON, Imperial College of Science and Technology, London	1060
Paramagnetic Resonance in Gadolinium Ethylsulphate. By B. BLEANEY, R. J. ELLIOTT, H. E. D. SCOVIL and R. S. TRENAM, The Clarendon Laboratory, Oxford	1062
CVIII. Notices of New Books and Periodicals received :—	
Reports on Progress in Physics, Vol. XIV, 1951.	1064

NUMBER 333—OCTOBER

CIX. Theory of Barium Titanate.—Part II. By A. F. DEVONSHIRE, H. H. Wills Physical Laboratory, University of Bristol.	1065
CX. Remarks on the Two-Fluid Model of Helium II. By R. B. DINGLE, Royal Society Mond Laboratory, Cambridge.	1080
CXI. Observations on the Multiple Scattering of Ionizing Particles in Photographic Emulsions.—Part IV. Protons of 336 MeV. from the Berkeley Cyclotron. Cosmic Ray Protons and Mesons of 5 to 50 MeV. By K. GOTSTEIN and J. H. MULVEY, H. H. Wills Physical Laboratory, University of Bristol.	1089

	Page
CXII. Electron and Gamma Ray Spectroscopy with Scintillation Detectors. By R. C. BANNERMAN, G. M. LEWIS and S. C. CURBAN, Department of Natural Philosophy, The University of Glasgow.....	1097
CXIII. The Properties of Neutral V-Particles. By R. ARMENTEROS, K. H. BARKER, C. C. BUTLER and A. CACHON, The Physical Laboratories, University of Manchester. (Plates XXXIII.-XL.).....	1113
CXIV. The Nuclear Scattering of Electrons and Positrons in Argon. By A. F. HOWATSON and J. R. ATKINSON, Natural Philosophy Department, Glasgow University	1136
CXV. Micro-slip in Metal Crystals. By A. F. BROWN and R. W. K. HONEYCOMBE, Cavendish Laboratory, Cambridge. (Plate XLI.).....	1146
CXVI. Some General Theorems for Non-Linear Systems Possessing Resistance. By WILLIAM MILLAR, Atomic Energy Research Establishment, Harwell	1150
CXVII. Some General Theorems for Non-Linear Systems Possessing Reactance. By COLIN CHERRY, Imperial College, London	1161
CXVIII. A Perturbation Treatment of Closed States in Quantized Field Theories. By B. TOUSCHEK, Department of Natural Philosophy, The University, Glasgow.....	1178
CXIX. Correspondence :—	
On Loading Nuclear Emulsions with Wires. By M. DANYSZ and G. YEKUTIELI, H. H. Wills Physical Laboratory, University of Bristol.....	1185
Neutron Emission from Nuclei Excited by High Energy Protons. By D. M. SKYRME, Atomic Energy Establishment, Harwell, and W. S. C. WILLIAMS, University College, London	1187
The Photodisintegration of ^{10}B into Neutron, Proton and two α -Particles. By M. J. BRINKWORTH and E. W. TITTERTON, Atomic Energy Research Establishment, Harwell	1191

NUMBER 334—NOVEMBER

CXX. The Interaction in the Theory of Beta Decay. By D. L. PURSEY, Department of Natural Philosophy, Glasgow University.....	1193
CXXI. Ultrasonic Propagation in Liquid Helium near the Lambda-Point. By A. B. PIPPARD, The Royal Society Mond Laboratory, Cambridge.....	1209
CXXII. The Synthesis of Elastic Dislocation Fields. By F. R. N. NABARRO, Department of Metallurgy, The University of Birmingham....	1224
CXXIII. Observations on the Multiple Scattering of Ionizing Particles in Photographic Emulsions.—Part V. Scattering Measurements on Tracks of Slow Protons. By M. G. K. MENON and O. ROCHAT, H. H. Wills Physical Laboratory, University of Bristol.....	1232
CXXIV. Nuclear Transmutations Produced by Cosmic-Ray Particles of Great Energy.—Part VI. Experimental Results on Meson Production. By U. CAMERINI, J. H. DAVIES, P. H. FOWLER, C. FRANZINETTI, H. MUIRHEAD, W. O. LOCK, D. H. PERKINS and G. YEKUTIELI, H. H. Wills Physical Laboratory, University of Bristol. (Plates XLII.-XLIV.).....	1241

	Page
CXXV. Nuclear Transmutations Produced by Cosmic Ray Particles of Great Energy.—Part VII. Interpretation of the Experimental Results. By U. CAMERINI, J. H. DAVIES, C. FRANZINETTI, W. O. LOCK, D. H. PERKINS and G. YEKUTIELI, H. H. Wills Physical Laboratory, University of Bristol.....	1261
CXXVI. Associated Penetrating Particles of Cosmic Rays Underground. By H. J. J. BRADDICK, W. F. NASH and A. W. WOLFENDALE, The Physical Laboratories, University of Manchester.....	1277
CXXVII. On Field Theories with Non-localized Interaction. By JERZY RAYSKI, Nicolas Copernicus University, Torun, Poland.....	1289
CXXVIII. A Theoretical Derivation of the Plastic Properties of a Polycrystalline Face-Centred Metal. By J. F. W. BISHOP and R. HILL, H. H. Wills Physical Laboratory, University of Bristol.....	1298
CXXIX. Note on the Boundary Layer on a Rotating Sphere. By L. HOWARTH, F.R.S., Department of Mathematics, University of Bristol..	1308
CXXX. The Melting Curve at High Pressures. By C. DOMB, Clarendon Laboratory, Oxford.....	1316
CXXXI. Correspondence :—	
The Influence of Exchange Energy on the Specific Heat of Free Electrons in Metals. By A. B. LIDIARD, King's College, London.....	1325
A Dislocation Reaction in the Face-Centred Cubic Lattice. By W. M. LOMER, Cavendish Laboratory, Cambridge... ..	1327
Lattice Defects in Silver Bromide at Room Temperature. By H. D. KEITH and J. W. MITCHELL, University of Bristol.....	1331
A Note on the Trace of the Product of Dirac's Matrices. By L. M. YANG, The University, Edinburgh.....	1333
Three-Photon Decay of Positronium. By J. M. RADCLIFFE, University of Birmingham.....	1334
CXXXII. Notices of New Books and Periodicals received :—	
L. P. WHEELER's Josiah Willard Gibbs.....	1335
R. H. MACMILLAN's An Introduction to the Theory of Control in Mechanical Engineering; and G. H. FARRINGTON's Fundamentals of Automatic Control....	1335
Errata	1336

NUMBER 335—DECEMBER

CXXXIII. Microscopic Studies on Beryl Crystals.—II. Dislocations and the Growth of {1010} Prism Faces. By L. J. GRIFFIN, H. H. Wills Physical Laboratory, University of Bristol. (Plates XLV.—LII.)	1337
CXXXIV. The Photo-electric Disintegration of Three- and Four-Particle Nuclei. By J. C. GUNN and J. IRVING, Department of Natural Philosophy, University of Glasgow.....	1353
CXXXV. The Recrystallization Texture of Drawn Aluminium Wire. By J. SAWKILL and N. THORLEY, Physics Department, King's College, Newcastle-upon-Tyne. (Plate LIII.).....	1369
CXXXVI. On the Quantum Mechanics of Helium II. By O. PENROSE, Royal Society Mond Laboratory, Cambridge.....	1373

	Page
CXXXVII. On the Tomonaga Method for Intermediate Coupling in Meson Field Theory. By R. H. DALITZ and D. G. RAVENHALL, Department of Mathematical Physics, University of Birmingham.....	1378
CXXXVIII. Application of Dislocation Theory to the Polytypism of Silicon Carbide. By V. VAND, Chemistry Department, The University, Glasgow	1384
CXXXIX. The Fitting of Polynomials to Unequally-Spaced Data. By J. G. HAYES and T. VICKERS, National Physical Laboratory, Middlesex.	1387
CXL. Dislocations in Thin Plates. By J. D. ESHELBY and A. N. STROH, H. H. Wills Physical Laboratory, University of Bristol.....	1401
CXLI. The Influence of Deviations from the Debye Spectrum on the Electrical Conductivity of Metals. By F. H. J. CORNISH and D. K. C. MACDONALD, Clarendon Laboratory, Oxford.	1406
CXLII. Effects of the Recoil on Allowed β -Transitions. By O. KOFOED-HANSEN, Institute for Theoretical Physics, University of Copenhagen	1411
CXLIII. Thermal Convection in a Magnetic Field. By W. B. THOMPSON, University of Toronto	1417
CXLIV. The Boundary Layer in Three Dimensional Flow.—Part II. The Flow near a Stagnation Point. By L. HOWARTH, F.R.S., Department of Mathematics, University of Bristol	1433
CXLV. Correspondence :—	
On the Calculation of Characteristic Temperatures from the Elastic Constants. By M. BLACKMAN, Physics Department, Imperial College, London	1441
Inelastic Scattering of Deuterons. By R. HUBY and H. C. NEWNS, Department of Theoretical Physics, The University of Liverpool.....	1442
Experiments on the Unsaturated Helium II Film. By R. BOWERS, D. F. BREWER and K. MENDELSSOHN, F.R.S., Clarendon Laboratory, Oxford	1445
The Upper Limit for the Neutrino Rest Mass. By O. KOFOED-HANSEN, Institute for Theoretical Physics, University of Copenhagen.....	1448
Errata	1450
Obituary—Dr. ALLAN FERGUSON.....	1451
Index to Volume.....	1452

PLATES

- I.-IV. Illustrative of O. BARDSLEY and W. A. MAIR's Paper on the Interaction between an Oblique Shock-wave and a Turbulent Boundary-layer.
- V. Illustrative of P. E. HODGSON's Paper on the Disintegration of Lead Nuclei by Cosmic Rays.
- VI. Illustrative of P. W. A. BOWE's Paper on the Wave-forms of Atmospherics and the Propagation of very Low Frequency Radio Waves.
- VII. & VIII. Illustrative of S. O. C. SØRENSEN's Paper on Emission of Energetic Helium and Lithium Fragments in Nuclear Explosions.
- IX.-XII. Illustrative of O. BARDSLEY's Paper on the Conditions at a Sharp Leading Edge in Supersonic Flow.
- XIII. Illustrative of J. E. HOOPER, D. T. KING and A. H. MORRISH's Paper on Pair Production by Fast Electrons.
- XIV. Illustrative of S. AMELINCKX's Paper on An Interferometric Study of Cleavage Surfaces of Artificially Grown Crystals of Sodium Chloride.
- XV. & XVI. Illustrative of A. P. GREEN's Paper on the Use of Plasticine Models to Simulate the Plastic Flow of Metals.
- XVII. Illustrative of A. D. DAINTON, A. R. GATTIKER and W. O. LOCK's Paper on the Processing of Thick Photographic Emulsions.
- XVIII. & XIX. Illustrative of A. ASPINALL, J. A. CLEGG and G. S. HAWKIN's Paper on a Radio Echo Apparatus for the Delineation of Meteor Radiants.
- XX. Illustrative of S. J. GOLDSACK and N. PAGE's Correspondence on an Example of the $(n, p; \pi^-)$ Reaction in the Photographic Emulsion.
- XXI. Illustrative of A. J. FORTY's Correspondence on Observation of Growth of Cadmium Iodine from Aqueous Solution.
- XXII. & XXIII. Illustrative of L. J. GRIFFIN's Paper on Microscopic Studies on Beryl Crystals.—Part I. Observation of Uni-Molecular Steps.
- XXIV. Illustrative of A. P. GREEN's Paper on a Theoretical Investigation of the Compression of a Ductile Material between Smooth Flat Dies.
- XXV.-XXVIII. Illustrative of AJIT RAM VERMA's Paper on Observations on Carborundum of Growth Spirals Originating from Screw Dislocations.
- XXIX. & XXX. Illustrative of C. O'CEALLAIGH's Paper on Masses and Modes of Decay of Heavy Mesons.—Part I. κ -Particles.

- XXXI. & XXXII. Illustrative of P. H. FOWLER, M. G. K. MENON, C. F. POWELL and O. ROCHAT's Paper on Masses and Modes of Decay of Heavy Mesons.—Part II. τ -Particles.
- XXXIII.—XL. Illustrative of R. ARMENTEROS, K. H. BARKER, C. C. BUTLER and A. CACHON's Paper on the Properties of Neutral V-Particles.
- XLI. Illustrative of A. F. BROWN and R. W. K. HONEYCOMBE's Paper on Micro-slip in Metal Crystals.
- XLII.—XLIV. Illustrative of U. CAMERINI, J. H. DAVIES, P. H. FOWLER, C. FRANZINETTI, H. MUIRHEAD, W. O. LOCK, D. H. PERKINS and G. YEKUTIELI's Paper on Nuclear Transmutations Produced by Cosmic-Ray Particles of Great Energy.—Part VI. Experimental Results on Meson Production.
- XLV.—LII. Illustrative of L. J. GRIFFIN's Paper on Microscopic Studies on Beryl Crystals.—Part II. Dislocations and the Growth of {1010} Prism Faces.
- LIII. Illustrative of J. SAWKILL and N. THORLEY's Paper on the Recrystallization Texture of Drawn Aluminium Wire.
-
-

THE PHILOSOPHICAL MAGAZINE

A JOURNAL OF THEORETICAL EXPERIMENTAL
AND APPLIED PHYSICS

First published in 1798

[SEVENTH SERIES—VOL. 42]

I *The Propagation of a Radio-Atmospheric.*

By K. G. BUDDEN,
Cavendish Laboratory, Cambridge*.

[Received October 5, 1950.]

SUMMARY.

Previous authors have discussed the propagation of radio-atmospherics by assuming that the space between the earth's surface and the ionosphere behaves like a wave-guide. If the surfaces of such a guide are treated as perfect conductors, then there is one mode of propagation, the "zero-order" mode, which is unattenuated at all frequencies. In such a guide the wave-form of the received e.m.f. due to one mode at a great distance from a lightning flash can be calculated, and for modes of non-zero order it would be of an oscillatory type similar to that observed in many atmospherics from distant sources. But it would also include a large undistorted impulse due to the energy propagated in the zero-order mode, and this is not observed in practice. Moreover, recent measurements of the amplitudes of the component frequencies of atmospherics have shown that frequencies below about 7.5 kc./s. are heavily attenuated during propagation from the source to the receiver, and this is inconsistent with the presence of a zero-order mode which is unattenuated at all frequencies.

This paper shows that if one surface of the wave-guide is an imperfect conductor, then all the modes, including the zero-order mode, are heavily attenuated below a certain critical frequency. There are two modes whose amplitudes are much greater than those of all other modes, and these both give an oscillatory response to a lightning flash at a great distance. There is no longer any mode of propagation which would give an undistorted impulse at a great distance from the source.

* Communicated by J. A. Ratcliffe.

The critical frequency depends most markedly on the height of the ionosphere, and to a smaller extent on the characteristics of the ionized medium. The changes in the measured curves of attenuation versus frequency from day to night, and during sudden ionospheric disturbances are consistent with the changes in the height of reflection of very long waves which are known to occur at these times.

The relation between the treatment of propagation in terms of wave-guide modes, and in terms of successively reflected "rays" is discussed.

§ 1. INTRODUCTION.

THE nature of the radio-atmospherics observed with a receiver at a given point depends on: (a) the nature of the sources; (b) the length and characteristics of the propagation paths. Some recent experiments (Gardner 1951, Bowe 1951) have been concerned with the characteristics of the propagation path for different frequency components in the spectrum of the atmospherics. They have shown that frequencies below about 7.5 kc./s. are heavily attenuated. The amount of attenuation, and the exact frequency below which it occurs, depends upon whether it is day or night, and changes also during a sudden ionospheric disturbance. The object of this paper is to suggest a possible mechanism to explain these results. The mechanism suggested will also account for the oscillatory nature of the wave-form of atmospherics coming from great distances.

In § 3, § 4 and § 5, it is assumed that the atmospheric travels in a "wave-guide" formed between a perfectly conducting earth and an imperfectly conducting, sharply bounded ionosphere. Previous authors have discussed the propagation of waves in this type of wave-guide, but their discussions have been inadequate for our present purpose for various reasons. Thus Hales (1948) has discussed the propagation of an atmospheric in a wave-guide with perfectly conducting walls. We shall show that, although this model at first seems attractive, the "zero-order" mode is unattenuated at all frequencies, and hence the experimental results cannot be satisfactorily explained. Eckersley (1932), in a mathematical paper designed primarily to illustrate the nature of his "phase-integral" method of calculation, arrived at expressions like those which we derive here, but he did not apply them to our problem.

Most observers are agreed that the wave-forms of atmospherics can be divided roughly into two main types (Schonland *et al.* 1940, Laby *et al.* 1940, Rivault 1945). In one type the wave-form is short and irregular in shape, but the irregularities are repeated roughly at intervals which correspond to the repeated reflection of a pulse from the ionosphere. This type of atmospheric appears to be fairly well explained by the mechanism of successive reflection. The other type is oscillatory and the wave-form is much smoother than for the first type. It has been vaguely suggested (*e.g.* Schonland *et al.* 1940, p. 184) that it could be produced

by the smooth merging together of the separate reflections of the first type, but no detailed explanation has been given of how this could occur, and, indeed, the two types of wave-form are so different that it is difficult to see how one could be converted into the other.

Hales (1948) came near to explaining the wave-form of an atmospheric from a distant source. He first discussed the explanation of the oscillatory type of atmospheric in terms of a wave-guide with perfectly conducting walls, and concluded that its wave-form could be explained with this model. We show in § 6 that we do not agree with this explanation which again neglected the zero-order mode. Hales next considered the case where one boundary had a finite conductivity, and showed that, with this model, he could explain the existence of the "slow tail" of the atmospheric, but he did not reconsider the production of the oscillatory type of atmospheric by this model.

In § 6 it is shown how the oscillatory type of atmospheric would be produced by transmission in a wave-guide system of the type discussed in this paper, and in § 7 it is indicated how the transition from the first to the second type of wave-form can come about.

§ 2. THE NATURE OF THE SOURCES.

The results of Gardner and Bowe were analysed in such a way that the characteristics of the source were eliminated. In discussing the frequency dependence of the characteristics of the propagation path, therefore, it is unnecessary to consider the exact nature of the source of an atmospheric. The wave-form of a single atmospheric, however, does depend upon the disturbance producing it, and some assumption about the source must therefore be made. It will be assumed in what follows that the atmospheric is the result of the instantaneous destruction of a short vertical electric dipole situated at the surface of the earth, so that the dipole moment of the source varies with time as shown in fig. 1 (*a*). The signal that would be received at a distance in free space from such a source would be a double impulse, as shown in fig. 1 (*b*). In the continuous spectrum of this source the amplitude is proportional to the frequency.

§ 3. RAYS AND WAVE-GUIDE MODES.

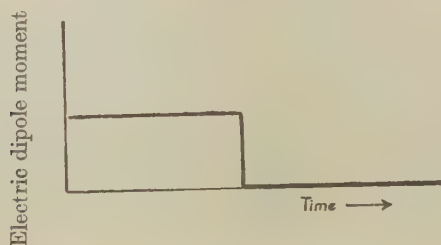
The propagation of an atmospheric from the initial lightning flash to the receiver may be discussed by either of two methods; these will be called (*a*) the method of successive reflections, (*b*) the method of wave-guide modes. In (*a*) the received e.m.f. is regarded as a succession of impulses arriving at the receiver, the first after propagation direct from the source, and the succeeding ones after one, two, etc. reflections at the ionosphere.

In method (*b*) the space between the surface of the earth and the ionosphere is treated as a wave-guide. In this guide the propagation of certain modes is possible. The characteristics of each of these modes

must be found, and also the amplitude excited in each mode by a given source. The received e.m.f. is then found by adding the contributions from all the modes.

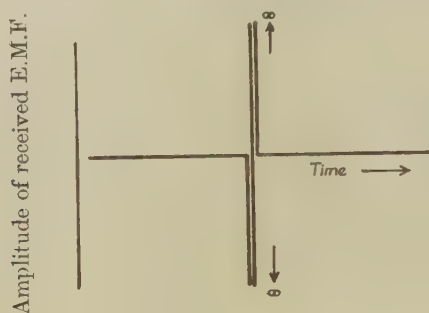
If the ionosphere is an imperfect reflector, method (a) is the simplest when the receiver is close to the source, say within a few hundred kilometres, since then the amplitude of the direct wave and the first and possibly second reflected waves are large compared with the reflected waves of higher order, and these can therefore be neglected. At larger

Fig. 1 (a).



Idealized lightning flash. Variation of dipole moment of source with time.

Fig. 1 (b).



Signal received in free space from idealized lightning flash.

distances the incidence of the waves on the ionosphere is more oblique, so that the reflection coefficient is higher, and consequently the received e.m.f. is composed of a large number of reflections of comparable amplitude. In this case method (b) is simpler, since it is normally found that there is a marked difference between the attenuation coefficients of the various wave-guide modes, and at large distances the least attenuated mode is much greater than all the others. At short distances, the amplitudes in a large number of modes are comparable, and calculation of the received e.m.f. by the "mode" method is therefore complicated.

§ 4. EARTH AND IONOSPHERE CONSIDERED AS A WAVE-GUIDE.

Let us first consider the over simplified case where the earth and the ionosphere are both perfect conductors. A wave-guide of rectangular cross-section has four surfaces. We consider the limiting case where two of these surfaces are separated to an infinite distance, and we shall say that the guide has infinite horizontal width, but a finite vertical width, h . We consider only signals in which the electric vector is in the plane of propagation.

The elementary theory of wave-guides shows that waves can be propagated in a series of different modes. When both surfaces of the guide are perfect conductors, there is one mode in which the electric field is constant across the guide and perpendicular to its surfaces. This mode suffers no attenuation at any frequency. It will be called the mode of order zero. Higher-order modes are propagated without attenuation if the frequency is greater than the "cut-off" frequency, which is different for each mode, but for frequencies below the "cut-off" there is heavy attenuation. The "cut-off" frequency depends on the width of the guide, and the order of the mode.

It is tempting to suggest that this "cut-off" accounts for the great attenuation observed on the lowest frequencies, but it can readily be seen that this simplified model is not in accord with observation. Thus, if we assume a distance of 50 km. between the two boundaries, the first-order mode would cut-off at a wavelength of 100 km., *i. e.* 3 kc./s., the second-order would cut-off at 6 kc./s., and so on. The e.m.f. received at a great distance from a lightning flash, on a receiver tuned to 10 kc./s. would be comprised predominantly of four modes of orders 0, 1, 2, 3, while the e.m.f. from the same atmospheric at 5 kc./s. would include two modes of orders 0 and 1. The resulting e.m.f. at either frequency would depend on the relative phases of the e.m.f.s in the various modes, but the ratio of the resultant amplitudes received at these two frequencies would clearly be of the order of 2 : 1. The zero-order mode is propagated without attenuation, so that it is present at all frequencies, and this model therefore predicts that the signal should have appreciable amplitude, however low the frequency to which the receiver is tuned. But the observed amplitude at 10 kc./s. is very much greater than twice the amplitude at 5 kc./s., and at still lower frequencies the e.m.f.s from distant atmospherics are almost imperceptible, showing that there can be no unattenuated zero-order mode. Moreover, on this model a curve showing the variation of amplitude with frequency should have a series of approximately equal steps at, say, 3 kc./s., 6 kc./s., 9 kc./s., corresponding to the cut-off frequencies of the various modes. The curve plotted from the observations (Gardner 1950, fig. 4) shows a single steep increase at about 6 kc./s. There are no similar increases at 12 kc./s., 18 kc./s., etc.

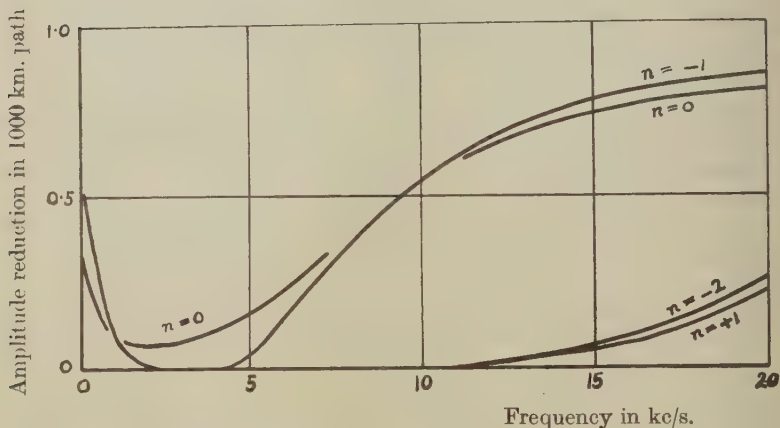
We can therefore reject the model using a wave-guide with perfectly reflecting surfaces for two reasons :—

surfaces were perfectly conducting. Fig. 4 shows that for frequencies up to about 16 kc./s. the signal amplitudes at 1000 km. from the source, in the modes of orders -2 and $+1$, are much smaller than in the modes of order 0 and -1 . It is readily verified that the amplitudes in modes of still higher orders are much smaller still. Hence, for an explanation of the experimental results, it is sufficient, as a first approximation, to consider modes of orders 0 and -1 only.

§ 6. THE WAVE-FORM OF AN ATMOSPHERIC.

In the introduction we mentioned two methods of studying the characteristics of the propagation path of an atmospheric. These were (a) a determination of the frequency response characteristic of the path (Gardner 1950, Bowe 1951); (b) the study of the wave-form of

Fig. 4.



Fractional reduction in received e.m.f. for 1000 km. path in modes of various order (n). $h=50$ km. $p_r=6 \times 10^4$ sec. $^{-1}$

an atmospheric from a distant source. These two methods may at first appear to be unrelated, but in fact they depend on the same properties of the path. For, if the curve showing variation of amplitude with frequency is given for the path, the response of the system to an impulse can be calculated*. Hence, any model which is inadequate to explain the variation of amplitude with frequency is also inadequate to explain the oscillatory wave-form of an atmospheric from a distant source.

* It would seem that we should also need to know how the phase varies with frequency, but in fact the amplitude and phase characteristics of any system are interrelated, and if the amplitude curve is given, it is possible, subject to certain restrictions which do not apply here, to find both the phase characteristic and the impulse response. See, for example, Murakami and Corrington (1948).

Hales (1948) has attempted to explain the oscillatory type of atmospheric wave-form by considering the distortion of an impulse as it travelled through a wave-guide with perfectly conducting walls, but he took no account of the zero-order mode. The zero-order mode must be present, and since it would be unattenuated at all frequencies, it would not produce any distortion, and so there should be a large undistorted impulse at the beginning of an atmospheric of the oscillatory type. This is not observed, and so we cannot accept Hales' explanation without modification. We have now also shown that the observed variation of amplitude with frequency cannot be explained if the guide has perfectly conducting walls, since the zero-order mode is not attenuated. It is therefore necessary to assume that one surface of the wave-guide has finite conductivity.

We shall now examine the wave-form which we should expect to receive after an atmospheric has travelled for a considerable distance (1000 km.) through such a guide. The calculation has been made for the modes of order 0 and -1 , and for a source of the type described by fig. 1. For this purpose, we have to evaluate the integral

$$I(t) = \int_{-\infty}^{\infty} p \sin i \cdot e^{ipt} \text{Hi}_1(k\rho \sin i) \cdot j \cdot dp$$

(see Appendix B), where i is given by equation (3), ρ is the distance travelled, and $k \doteq p/c$. It is sufficiently accurate to use the first term of the asymptotic expression for the Bessel function Hi , and with this approximation the integral reduces (omitting a constant factor) to

$$\int_{-\infty}^{\infty} (p \sin i)^{\frac{1}{2}} e^{i\pi/4} \exp \{j(pt - k\rho \sin i)\} \cdot dp.$$

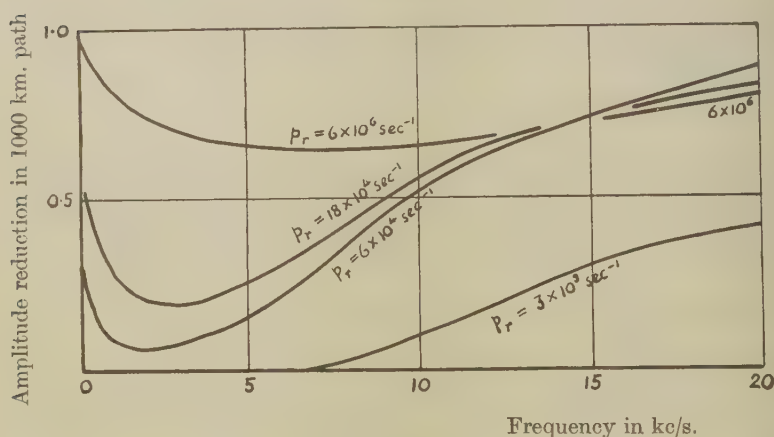
The integrals were evaluated numerically with the help of Be Lipson strips (Beevers and Lipson 1936). The results for the modes of order 0 and -1 were found to be identical within about 10 per cent. This was not unexpected in view of the similarity of the two curves for these modes in fig. 4. Modes of higher orders have much smaller amplitudes (see fig. 4) and therefore are not included. Fig. 5 shows the result for either mode, and this is also the form of the e.m.f. which results when the two modes are added together. It is seen that the wave-form is oscillatory, and that the instantaneous frequency and amplitude both decrease with time. This behaviour is typical of many atmospheric wave-forms observed in practice. This calculation extends and completes that of Hales (1948), in which both walls of the wave-guide were assumed to be perfect conductors.

Hales has suggested that the characteristics of the zero-order mode at very low frequencies in a wave-guide with imperfectly conducting walls may explain the "slow tail" which is often observed to follow the main part of an atmospheric wave-form. He has shown that the observed delay between the beginning of an atmospheric and the peak of the

the attenuation coefficient as a function of frequency. Equation (3) does not give a convenient explicit expression for $\cos i$, and a method of successive approximation was therefore used. The results for the zero-order mode are shown in fig. 2 for $h = 50$ km. The curves show the fractional reduction of signal amplitude for a path of 1000 km. in the wave-guide. (A similar curve has been given by Hales (1948), *loc. cit.*, fig. 4, curve, 5, but it refers to a mode of non-zero order, and no curves are given for the zero-order mode.)

The parameter p_r determines the nature of the upper boundary. When $p_r \rightarrow \infty$, the upper boundary becomes a perfect conductor, and the zero-order mode should be unattenuated at all frequencies. It will be seen that, for large values of p_r , there is very little attenuation at any frequency. For smaller values of p_r , the medium is an imperfect conductor, and there is then some attenuation which is most marked at frequencies between

Fig. 2.



Fractional reduction in received e.m.f. for 1000 km. path in the zero-order mode, as a function of frequency. $h = 50$ km.

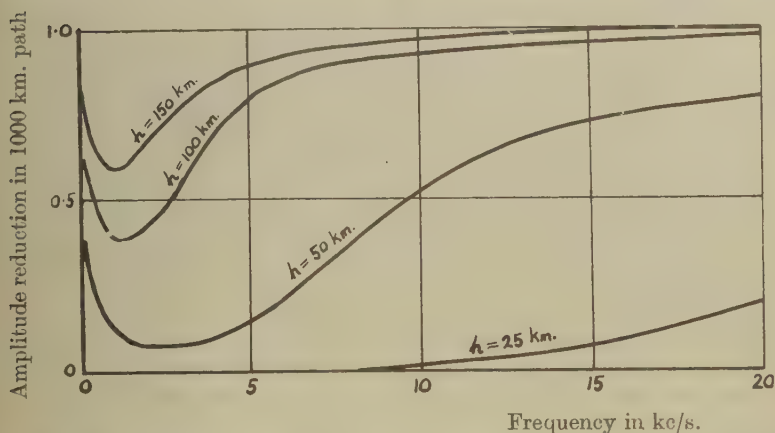
2 and 8 kc./s. The increase in the attenuation as the frequency decreases from about 10 to about 5 kc./s. is very similar to that observed in the experiments mentioned in §1. The frequency near which this decrease of amplitude occurs is seen to be fairly independent of the characteristics of the upper surface. It does, however, depend markedly on the width of the guide (height of the ionosphere), as is illustrated in fig. 3 in which the various curves all relate to the same value of p_r , but different values of the height h .

When p_r is zero, the upper medium is a "dielectric" with dielectric constant unity. The reflection coefficient is zero, so that all the energy incident on the upper boundary is propagated into the medium. If p_r is very small, a large proportion of the energy is propagated into the medium

and all the modes are heavily attenuated, and are "leaky". (For a full discussion of "leaky" modes, see Booker and Walkinshaw (1946)). It would be necessary to add the effects of a very large number of modes to calculate the received signal in this case. However, the order of magnitude of N and ν for the ionosphere are known, and these show that it is unlikely that we shall be concerned with very small values of p_r .

The form of the curves of figs. 2 and 3 depend only on the two parameters p_r and h . A small change of p_r would not result in any marked change in the frequency where the attenuation curve has greatest slope. A change of 10 km. in h would have an appreciable effect on this frequency. It has been shown (Gardner 1950, Bowe 1951) that the curve relating attenuation to frequency changes from night to day and during a Sudden Ionospheric Disturbance, in such a way that the cut-off frequency

Fig. 3.



Fractional reduction in received e.m.f. for 1000 km. path in the zero-order mode, as a function of frequency. $p_r = 6 \times 10^4 \text{ sec.}^{-1}$

becomes greater. It is also known (Best, Ratcliffe and Wilkes 1936; Budden, Ratcliffe and Wilkes 1939; Bracewell and Straker 1949) that the height of reflection of very long waves falls in the passage from night to day, and during a Sudden Ionospheric Disturbance. It therefore seems probable that the changes in the attenuation curves are produced mainly by the changes in height of reflection.

For a given value of p_r , it is necessary to find how many modes must be used to calculate the received e.m.f. at a given distance from the source. The results of calculations for the modes of order -2 , -1 , 0 , $+1$, and for a distance of 1000 km., are shown in fig. 4 for the case of $p_r = 6 \times 10^4 \text{ sec.}^{-1}$ and $h = 50$ km. These modes would have "cut-off" frequencies of 6 kc./s., 3 kc./s., 0 kc./s., 3 kc./s. respectively, if both guide

- (a) Observations show that at very low frequencies the signal amplitudes from distant atmospherics are much smaller than they would be if an unattenuated zero-order mode were present.
- (b) The observed variation of signal amplitude with frequency is of the wrong form.

As the next approximation we therefore assume that the ionosphere is a homogeneous medium, whose plane lower boundary forms the upper surface of the wave-guide which has a plane, perfectly conducting earth as its lower surface. The effect of the earth's magnetic field is neglected. The medium is assumed to contain N electrons per c.c., and these are assumed to make an average of ν collisions per second. Let p be the angular frequency of a component of the signal. At the level where very long waves are reflected ν is of the order 10^7 sec.^{-1} . We shall, therefore, assume that $\nu \gg p$. Then, if μ is the refractive index of the medium, we have

$$\mu^2 = 1 - jp_r/p, \quad . \quad . \quad . \quad . \quad . \quad . \quad . \quad . \quad (1)$$

where

$$p_r = 4\pi N e^2 / m \nu,$$

e = charge of electron,

m = mass of electron.

We shall now investigate the modes which can be propagated in this guide. We consider only waves in which the magnetic vector is horizontal. Any one mode can be considered as composed of two component plane waves* equally inclined to the boundaries of the guide. Either of these may be considered as being continuously produced by the reflection of the other at a bounding surface. After a part of a wave-front has undergone two reflections, it is parallel to its original direction, and the phases and amplitudes of the original and of the twice reflected wave must agree. This means that only certain discrete values of the angle of inclination of the wave normal are possible. The excess path travelled by the wave-front of the twice reflected wave is $2h \cos i$. The difference of phase of the original and of the twice reflected wave is therefore $2(\cos i)h \cdot p/c$ (this is, in general, complex), and the (complex) ratio of the amplitudes resulting from this excess path is $\exp \{-j(2 \cos i \cdot h \cdot p/c)\}$. There is also a change of phase and of amplitude due to the reflection of the component plane wave at the upper boundary, and if the (complex) reflection coefficient is R , then for a self-consistent mode, we shall have

$$R \cdot \exp \{-j(2 \cos i \cdot h \cdot p/c)\} = 1 = e^{2\pi j n},$$

where n is an integer and is the phase difference, measured in cycles, between the original and the twice reflected wave.

* The two component plane waves which form a single mode are not, of course, to be confused with the direct and reflected rays of different order which are considered in the ray picture.

Now R is the Fresnel reflection coefficient of the upper surface for angle of incidence i . It is given by

$$R = \{\mu^2 \cos i - \sqrt{(\mu^2 - \sin^2 i)}\} / \{\mu^2 \cos i + \sqrt{(\mu^2 - \sin^2 i)}\}, \quad . . . \quad (2)$$

so that we obtain

$$\begin{aligned} & \{\mu^2 \cos i - \sqrt{(\mu^2 - \sin^2 i)}\} / \{\mu^2 \cos i + \sqrt{(\mu^2 - \sin^2 i)}\} \\ & = \exp \{j(2 \cos i h p/c + 2\pi n)\}, \quad . . . \quad (3) \end{aligned}$$

where h is the width of the wave-guide (height of the ionosphere), c is the velocity of electromagnetic waves in free space, and n is a positive or negative integer which is the "order" of the mode.

This formula, in slightly different form, was given by Eckersley (1932, equation 3.21). From it the angle of incidence i can be found for each value of n , and in general i is complex. The attenuation coefficient of the mode is then easily found, and is equal to

$$|\mathcal{I}(\sin i)| \cdot p/c. \quad \quad (4)$$

(" \mathcal{I} " means "imaginary part").

It is still necessary to find the amplitude which is excited by a given source in each of the modes. For a vertical electric dipole, the amplitude radiated along a ray at an angle i to the vertical is proportional to $\sin i$. This means that in a mode in which one component wave has its wave normal at an angle i to the vertical, the amplitude excited by a vertical electric dipole is proportional to $\sin i$.

The amplitude also depends upon the frequency spectrum of the source. For a source of the type described in fig. 1, the amplitude is proportional to the frequency. On general physical grounds, therefore, we should expect the amplitude excited by a vertical electric dipole in any one mode to be proportional to

$$p \cdot \sin i, \quad \quad (5)$$

where i is given by equation (3). A more mathematical proof of this is given in Appendix A.

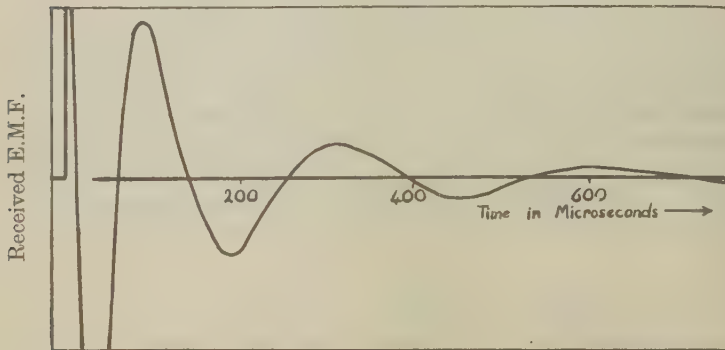
If $R=1$ (perfect reflector), $\sin i$ has the same value for modes of order n and $-n$. The n th mode is then really a degenerate case, where the two modes of orders n and $-n$ are superimposed. The degeneracy is removed when $R \neq 1$. The use of a negative order to describe a mode is merely a matter of convenience. All modes, whether of positive, negative, or zero order, have the same general form. It is, however, important to stress that, by inserting values of n of equal magnitude but opposite sign in equation (3), we derive the properties of different modes.

§ 5. ATTENUATION CURVES.

Our main reason for considering the finite conductivity of the upper boundary was to see whether it alters the attenuation of the zero-order mode. The formulæ (3) and (4) have therefore been used to calculate

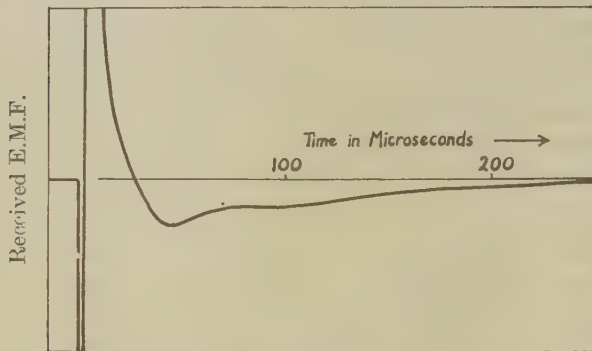
"slow tail" is consistent with a reasonable value of the width of the guide. (Hales' discussion of the main part of the atmospheric appears to refer only to modes of non-zero order, and his discussion of the "slow tail" only to the zero-order mode.)

Fig. 5.



Received e.m.f. in mode of order 0 or -1 at 1000 km. from idealized lightning flash. $h=50$ km. $p_r=6 \times 10^4 \text{ sec.}^{-1}$

Fig. 6.



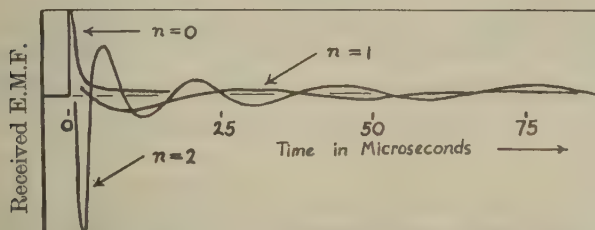
Received e.m.f. in plane wave resulting from the reflection of impulsive plane wave at the surface of an ionized medium. Angle of incidence 60° .

§ 7. EQUIVALENCE OF "RAY" PICTURE AND "MODE" PICTURE.

The calculations of the received signal, treated either by the ray method or by the mode method, can both be made exact, and must therefore give the same result. It is, however, interesting to discuss the interrelation of the two methods. It would seem at first sight that the ray method would result in the arrival at the receiver of a series of sharp impulses resulting from varying numbers of reflections of the origina

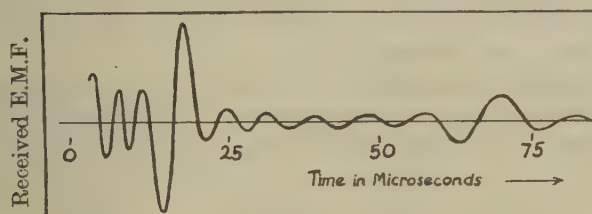
impulse at the earth's surface and at the ionosphere, and it is difficult to see how a series of sharp impulses can combine to give a smooth curve like that of fig. 5. It must be remembered, however, that the Fresnel reflection coefficient (equation 2) is a function of frequency, and a single reflection therefore results in distortion of the incident signal. Fig. 6

Fig. 7 (a).



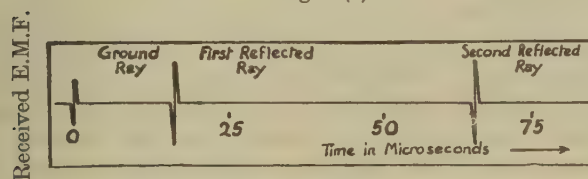
Received e.m.f. in first three modes at 1000 km. from "lightning flash".
Wave-guide with perfectly conducting walls. $h=50$ km.

Fig. 7 (b).



Sum of received e.m.f.s in first seven modes ($n=0$ to 6, inclusive).

Fig. 7 (c).



Impulses received according to "ray" theory.

shows the form of this distortion for reflection at an angle of incidence of 60° from the plane surface of an ionized medium of the type already discussed, with $p_r = 6 \times 10^4 \text{ sec.}^{-1}$. Hence it is clear that the successive reflected waves are no longer sharp impulses, but have comparatively smooth wave-forms, which, when added together, would give a smooth curve, such as that of fig. 5.

If both surfaces of the wave-guide are perfect conductors, there is no distortion of the signal at reflection, and the received e.m.f. must then be a succession of sharp impulses. But this succession of impulses must also result from the addition of a large number of modes. The way in which this occurs is illustrated in fig. 7. Here the curves are plotted assuming that both guide surfaces are perfect conductors, that the source and receiver are both at the earth's surface, and that $h=50$ km. The source is assumed to be an impulse of the type described by fig. 1. There is an analytic expression for the impulse response for one mode of order n for this case, at a distance from the source. If $\rho \gg h$ and $ct - \rho \ll \rho$, this can be shown (see Appendix B) to be approximately proportional to *

$$\{\cos(\pi X n/h) + (\pi X n/h) \sin(\pi X n/h)\} / X^3, \quad \dots \quad (6)$$

where $X^2 = c^2 t^2 - \rho^2$.

In fig. 7(a) the values of this function for the first three modes are plotted; fig. 7(b) shows the result of adding together the first seven modes ($n=0$ to 6 inclusive). Fig. 7(c) shows the succession of double impulses that would be received on a ray picture. With only seven modes, the first and second reflected impulses are already becoming accentuated, and it is clear that, by including a sufficient number of modes, the mode picture and the ray picture would give the same result. In this case the high-order modes are not attenuated, and therefore the mode method is not the best for calculating the received e.m.f.

We have thus shown that, when the number of modes contributing to the received e.m.f. is large, the resulting signal is a succession of impulses, so that the wave-forms are of the first type mentioned in the introduction. If the number of contributing modes is small, the received e.m.f. is oscillatory and therefore of the second type. The transition from the first to the second type could occur as the number of contributing modes decreased. Thus we might expect that atmospherics from nearby sources would be of the first type, while those from more distant sources would be of the second type.

§ 8. POSSIBLE EXTENSIONS OF THE THEORY.

Since we are concerned with very long waves, it is probable that the ion density and collision frequency in the ionosphere vary greatly in a distance small compared with one wavelength, and therefore, in the theory of propagation of very long waves, many authors have treated the ionosphere as a sharply bounded, homogeneous medium, as a first approximation. In discussing the propagation of very long radio waves to great distances, Rydbeck (1944) has used the method of Watson (1919), which is essentially a treatment in terms of wave-guide modes. Both these authors allow for the curvature of the earth's surface. Rydbeck

* A series of terms like (6) is not uniformly convergent but can be shown to be "summable (C2)" (see Whittaker and Watson 1935, *Modern Analysis*, para. 8.43). If the electric dipole at the source were destroyed in a small but finite time, the resulting series would be uniformly convergent.

has discussed the cases where the ionosphere is assumed to be (a) a sharply bounded, homogeneous medium, (b) a medium in which the ion density has a maximum and varies parabolically with height, (c) a medium in which the ion density varies as the square of the height above its lower edge. He concludes that, for the modes of lowest order, there is not much difference in the behaviour for the three cases. Rydbeck gives numerical results for only a few single frequencies. His formulæ could be used for calculating curves showing attenuation as a function of frequency, but the calculation would be laborious because of the complexity of the formulæ.

No allowance has been made for the effect of the earth's magnetic field. If this effect is included, the ionized medium becomes doubly refracting. It is still possible to consider propagation in terms of wave-guide modes. When a plane wave is incident from below on the boundary of the medium, the state of polarization of the reflected wave is in general different from that of the incident wave. For a given mode, it is necessary to ensure that a component wave, after two reflections at the wave-guide surfaces, has not only the same amplitude and phase as the original component wave, but also the same polarization. The result is that the number of possible modes of a given order is doubled, and the electric field of the wave is no longer wholly in the plane of propagation.

ACKNOWLEDGMENTS.

This work was carried out at the Cavendish Laboratory as part of a programme of Radio Research supported by the Department of Scientific and Industrial Research. I am indebted to Mr. J. A. Ratcliffe for helpful discussions throughout the course of the work.

REFERENCES.

- BEEVERS C. A., and LIPSON, H., 1936, *Proc. Phys. Soc.*, **48**, 772.
 BEST, J. E., RATCLIFFE, J. A., and WILKES, M. V., 1936, *Proc. Roy. Soc. A*, **156**, 614.
 BOOKER, H. G., and WALKINSHAW, W., 1946, *Phys. Soc. Report on Meteorological Factors in Radio-wave Propagation*, p. 80.
 BOWE, P. W. A., 1951 (*to be communicated to the Philosophical Magazine*).
 BRACEWELL, R. N., and STRAKER, T. W., 1949, *Mon. Not. Roy. Ast. Soc.*, **109**, 28.
 BUDDEN, K. G., RATCLIFFE, J. A., and WILKES, M. V., 1939, *Proc. Roy. Soc. A*, **171**, 188.
 ECKERSLEY, T. L., 1932, *Proc. Roy. Soc. A*, **136**, 499.
 GARDNER, F. F., 1950, *Phil. Mag.*, **41**, 1259.
 HALES, A. L., 1948, *Proc. Roy. Soc. A*, **193**, 60.
 LABY, T. H., McNEILL, J. J., NICHOLLS, F. G., and NICKSON, A. F. B., 1940, *Proc. Roy. Soc. A*, **174**, 145.
 MURAKAMI, T., and CORRINGTON, M. S., 1948, *R.C.A. Review*, **9**, 602.
 RIVAULT, R., 1945, *Comptes Rendus, Acad. Sci. Paris*, **221**, 540, or *Notes Préliminaires du Laboratoire National de Radioélectricité*, No. 65.
 RYDBECK, O., 1944, *On the Propagation of Radio Waves*; *Trans. Chalmers Univ., Gothenberg, Sweden*, Nr. 34.
 SCHONLAND, B. F. J., ELDER, J. S., HODGES, D. B., PHILLIPS, W. E., and VAN WYK, J. W., 1940, *Proc. Roy. Soc. A*, **176**, 180.
 WATSON, G. N., 1949, *Proc. Roy. Soc. A*, **95**, 546.

APPENDIX A.

WAVE-GUIDE MODES EXCITED BY A VERTICAL DIPOLE.

In this appendix, we deduce an expression for the horizontal magnetic field produced in a wave-guide of the type discussed in the paper, by a vertical electric dipole of constant angular frequency p at the surface of the earth. In Appendix B, we shall use the result to deduce the field when the source is a lightning flash of the type shown in fig. 1, and when both surfaces of the wave-guide are perfect conductors.

Suppose the source is a vertical electric dipole of moment $P = \exp(jpt)$. Then we shall show that the horizontal magnetic field \mathcal{H} , at a horizontal distance ρ from the source and at height z , is proportional to

$$\sum_{n=-\infty}^{+\infty} p^2 \cdot \sigma_n \text{Hi}_1(k \cdot \sigma_n \rho) \cdot \cos \{(jq_n - 2\pi n)z/2h\} \exp(jpt). \quad (7)$$

Each term of this series is the field in one mode. σ_n is the value of $\sin i$, for the n th mode when n is zero or positive, and the complex conjugate of $\sin i$ when n is negative. We have written $R = e^{-q}$ and q_n is the value of q when i has the value appropriate to the n th mode. The angle i is given by equation (3). Hi is Jeffreys' notation for a Bessel function of the third kind (Jeffreys and Jeffreys 1946, *Mathematical Physics* (Cambridge), p. 544).

The expression (7) can be predicted on general physical grounds. Thus the factor $p^2 \sigma_n$ when multiplied by $1/p$ (which is proportional to the amplitude of the frequency p in the dipole moment of the ideal lightning flash) gives $p \sin i$ which is simply the expression (5) of § 4. The cosine term is a "standing wave" term which arises through the combination of the upgoing and downgoing component waves of each mode. The Bessel function represents a wave propagated outwards from the source with cylindrical symmetry. For large values of ρ , it is proportional to $\{\exp(-jk\sigma_n\rho)\}/\sqrt{(k\sigma_n\rho)}$.

The mathematical derivation of (7) is given below in outline. The method used is similar to that developed by Watson (1919).

We use spherical polar coordinates r, θ, ϕ , with the dipole source at the origin. We also use z for distance measured vertically upwards, and $\rho = \sqrt{(x^2 + y^2)}$ for the horizontal distance measured radially from the origin. Then the field of the dipole in free space is given by the Hertz vector $\Pi_0 = \exp(jpt) \cdot \{\exp(-jkr)\}/r$. This may be written

$$\Pi_0 = (jk/2\pi) \cdot \exp(jpt) \int_{\pi/2-j\infty}^{\pi/2+j\infty} d\phi \cdot \int_{-\infty}^{\infty} (S/C) dS \cdot \exp\{-jk(x \cos \phi \sin \theta + y \sin \phi \sin \theta + z \cos \theta)\},$$

where $S = \sin \theta$, $C = \cos \theta$.

The integrand represents a plane wave whose wave normal has the direction (θ, ϕ) . The radiated field is thus expressed as the sum of an infinite number of such waves. Note that it is necessary to include complex values of ϕ and θ .

Each plane wave undergoes successive reflections at the earth and the ionosphere. To get the complete resultant Hertz vector, Π , we must add to the original Hertz vector the expressions for the various reflected waves. It is permissible first to perform the integration with respect to ϕ , since the reflection coefficient, R , of the ionosphere is independent of ϕ . Then we have

$$\Pi_0 = \frac{1}{2} j k \exp(jpt) \cdot \int_{-\infty}^{\infty} \text{Hi}_0(kS\rho) \cdot \exp(-jkCz) \cdot (S/C) \cdot dS.$$

The phases of the successive reflected waves are easily seen to contain factors $\exp(\pm j \cdot 2hkC)$, $\exp(\pm j \cdot 4hkC)$, etc., since they originate at image sources at heights $\pm 2h$, $\pm 4h$, etc. Hence the complete field is given by

$$\begin{aligned} \Pi = & \frac{1}{2} j k \exp(jpt) \int_{-\infty}^{\infty} S/C \cdot dS \text{Hi}_0(kS\rho) \\ & \times \left[\sum_{r=0}^{\infty} R^r \cdot \exp(-j \cdot 2v h k C) + \sum_{v=1}^{\infty} R^v \exp(+j 2v h k C) \right]. \end{aligned}$$

By suitable manipulation of the contours, this series may be transformed into another series, corresponding to the "residue" series of Watson. The result is

$$\begin{aligned} \Pi = & (j\pi/2h) \exp(jpt) \left[\sum_{n=-\infty}^{-1} \text{Hi}_0(kS_{-n}^*) \cos\{(jq_n - 2\pi n)z/2h\} \right. \\ & \left. + \sum_{n=0}^{+\infty} \text{Hi}_0(kS_n\rho) \cdot \cos\{(jq_n - 2\pi n)z/2h\} \right]. \quad \dots \quad (8) \end{aligned}$$

Here we have written $R = e^{-q}$. An asterisk * denotes a complex conjugate. The terms of the last series are the various wave-guide modes. The values S_n are the poles of the integrand, and are given by

$$2hkC_n = jq_n + 2\pi n, \quad \dots \quad (9)$$

where $C_n^2 = 1 - S_n^2$.

Equation (8) is derived by an application of the "residue theorem" of complex variable theory. We note at this stage how the full mathematical treatment gives two results:—

- (a) the characteristics of each mode; these arise from equation (9), which leads directly to equation (3) and gives the *positions* of the poles of the integrand in the complex S -plane;
- (b) the amplitudes excited in each mode by the source; these are the terms of equation (8) and are the residues of the integrand at the poles.

If the ionosphere is a perfect reflector, $q=0$, and the S_n 's are all real or purely imaginary. Then (8) becomes

$$\Pi = (j\pi/2h) \cdot \exp(jpt) \left[\text{Hi}_0(k\rho) + \sum_{n=1, 2, \dots} 2 \cos(\pi n z/h) \cdot \text{Hi}_0(k S_n \rho) \right]. \quad (10)$$

The summation includes all values of n for which S_n is real. Terms for which S_n is imaginary refer to heavily attenuated (evanescent) modes, and may be neglected when ρ is large.

The horizontal magnetic field \mathcal{H} of the signal is derived from the Hertz vector thus

$$\mathcal{H} = \partial^2 \Pi / \partial t \cdot \partial \rho.$$

Then for the mode of order n , we have, from (8) (imperfectly reflecting ionosphere),

$$\mathcal{H}_n = \left\{ \frac{S_n}{S_n^*} \right\} (\pi p^2 / 2hc) \text{Hi}_1 \left\{ k \rho \frac{S_n}{S_n^*} \right\} \cos \{ i q_n - 2\pi n z / 2h \} \exp(jpt) \dots \begin{matrix} n \geq 0 \\ n < 0 \end{matrix}.$$

This leads to equation (7).

For a perfectly reflecting ionosphere, we have, from (10),

$$\mathcal{H}_n = (\pi p^2 S_n / hc) \cdot \text{Hi}_1(k S_n \rho) \cdot \cos(\pi n z / h) \exp(jpt).$$

APPENDIX B.

IMPULSE RESPONSE OF ONE MODE.

Equations (8) and (10) give the Hertz vector of the signal when the source is a vertical electric dipole at the earth's surface, oscillating with constant angular frequency, p , and constant amplitude.

If the source is a lightning flash as illustrated in fig. 1, the dipole moment of the source (fig. 1(a)) can be expressed as the Fourier integral

$$P(t) = \int_{-\infty}^{\infty} \{ \exp(jpt) \} / jp \cdot dp.$$

Each component frequency in the Fourier spectrum initiates a series of modes such as that of equation (8) or (10).

We consider only one mode, the n th, for the case where both earth and ionosphere are perfect conductors (equation 10). We assume that the receiver is at the earth's surface, so that $z=0$. We use the value of S_n given by (9) when $q=0$. The Fourier component of angular frequency p then gives, for the n th mode only,

$$\Pi = (j\pi/2h) \exp(jpt) \cdot 2\text{Hi}_0 \{ k\rho \sqrt{(1 - \pi^2 n^2 / h^2 k^2)} \}.$$

The complete impulse response for the n th mode is therefore

$$\Pi_{in} = (\pi/h) \int_{-\infty}^{\infty} \{\exp(jpt)\} / jp \cdot dp \cdot \text{Hi}_0\{k\rho\sqrt{(1-\pi^2 n^2/h^2 k^2)}\}.$$

Hence

$$\partial \Pi_{in} / \partial t = (\pi/h) \int_{-\infty}^{\infty} \exp(jpt) \cdot jdp \cdot \text{Hi}_0\{\sqrt{(p^2 - \pi^2 n^2 c^2/h^2)} \cdot \rho/c\}.$$

This integral can be reduced to a standard form (see, for example, McLachlan and Humbert 1941, *Mémoires des Sciences Mathématiques*, Fascicule 100, p. 34). Its value is

$$\partial \Pi_{in} / \partial t = (\pi c/hX) [\cos(\pi nX/h) - (2/\pi) \sin(\pi nX/h) \log_e \{(ct+X)/\rho\}],$$

where $X^2 = c^2 t^2 - \rho^2$.

To find the horizontal magnetic field which the n th mode contributes to the received signal, this expression must be differentiated again with respect to ρ . We are interested in values of X which are small compared with ct and ρ . We also assume $\rho \gg h$. Then it is readily shown that the log. term is negligible, and we have

$$\mathcal{H}_{in} = \partial^2 \Pi_{in} / \partial t \partial \rho = (\pi c p / h X^3) \{\cos(\pi nX/h) + (\pi nX/h) \sin(\pi nX/h)\}.$$

This leads to equation (6).

II. Total Cross-Sections of Hydrogen and Carbon for High Energy Neutrons.

By A. E. TAYLOR, T. G. PICKAVANCE, J. M. CASSELS and T. C. RANDLE,
Atomic Energy Research Establishment, Harwell*.

[Received October 6, 1950.]

ABSTRACT.

Measurements of the attenuation of a beam of high energy neutrons in carbon and polythene have been made in good geometry. The total cross-sections of hydrogen and carbon have been found to be $0.0464 \pm 0.0012 \times 10^{-24} \text{ cm.}^2$ and $0.330 \pm 0.003 \times 10^{-24} \text{ cm.}^2$ respectively, at an effective neutron energy of $156 \pm 3 \text{ MeV.}$

INTRODUCTION.

THE present work has been the first of a series of experiments on high energy neutrons produced by the 110-inch frequency-modulated cyclotron (Pickavance, Adams and Snowden (1950)) at the Atomic Energy Research Establishment, Harwell. In the course of the measurement of the neutron-proton cross-section, the total cross-section of carbon was also measured and this result is included. The experiments have already been reported briefly (Taylor, Pickavance, Cassels and Randle (1950)), and the purpose of the present paper is to describe the work in more detail.

The total neutron cross-section of hydrogen has been measured at 40 MeV. and 90 MeV. by Hadley, Kelly, Leith, Segrè, Wiegand and York (1949), at 95 MeV. by De Juren and Knable (1950), and at 260 MeV. by Kelly, Leith, Segrè and Wiegand (1950); recent measurements by Moyer and de Juren (1950) at energies between 90 MeV. and 270 MeV. were published almost simultaneously with our preliminary report. The experimental results so far obtained are in mutual agreement within experimental error.

The method of observation in the work described here was similar to that used at Berkeley by Hadley *et al.* (1949) and by Kelly *et al.* (1950). Measurements of the attenuation of a neutron beam in carbon and polythene were made in good geometry. The neutron detector was a triple coincidence counter telescope, into which protons were scattered from a polythene disc placed in the neutron beam.

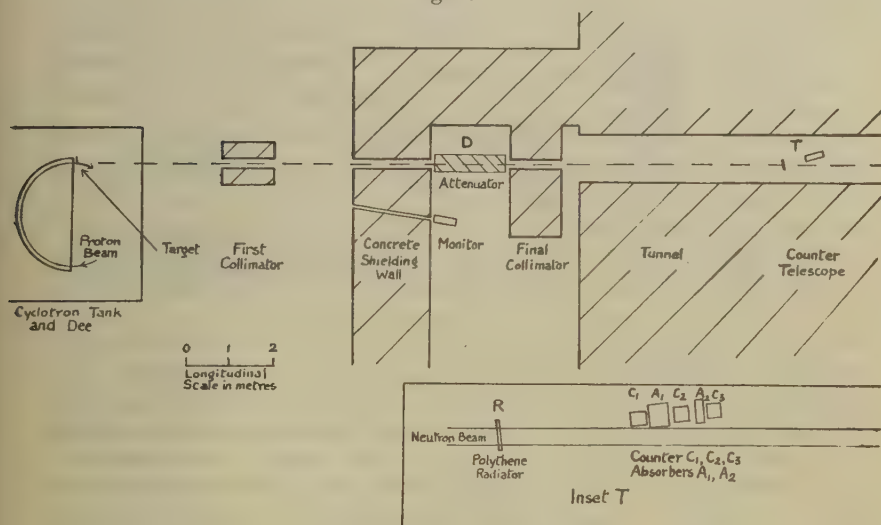
* Communicated by the Authors.

APPARATUS.

Collimation of the Neutron Beam.

A beryllium target, 8.9 mm. thick, was mounted in the cyclotron vacuum chamber near the edge of the dee at a radius of $48\frac{1}{2}$ inches, where it intercepted a beam of about 1 microampere mean current of 171 MeV. protons. Neutrons emerging near the forward direction (fig. 1) passed through a thin aluminium window in the vacuum chamber wall, and were then collimated by a series of 5 cm. diameter holes in concrete blocks and shielding walls. The shielding, which was divided into three parts, had a total thickness of 4.3 metres. The neutron attenuators were placed between the second and third walls and the neutron detector was in a long tunnel beyond the third wall. The collimating holes, the polythene radiator and the neutron attenuator holder were aligned with the target with the help of a theodolite.

Fig. 1.



Geometrical layout.

Neutron Detector.

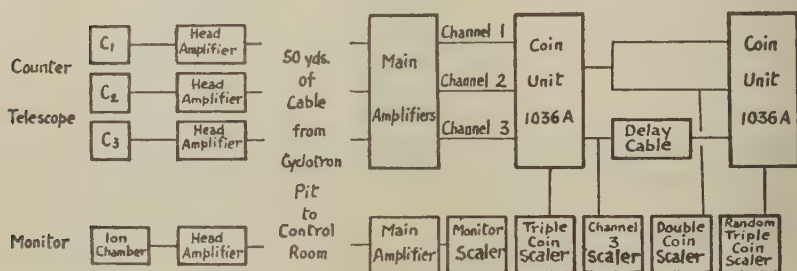
The proton radiator (R, fig. 1) was a polythene disk 19 mm. thick and 6.3 cm. in diameter, placed at a distance of 16 metres from the target. Protons ejected from the disc at an angle of 10° to the forward direction were detected by a telescope consisting of three proportional counters C_1, C_2, C_3 separated by carbon absorbers A_1, A_2 . All the counters were clear of the main neutron beam. Each counter was cylindrical in shape, 5 cm. in diameter and 5 cm. long, with a 46 mg./cm.² copper window at each end and a 0.02 cm. tungsten wire stretched across the diameter.

The gas filling was a mixture of argon (96 per cent) and carbon dioxide (4 per cent) at a total pressure of 52 cm. of Hg and the operating voltage was about 2 kilovolts.

Each of the counters was connected to a linear amplifier channel (fig. 2) with a high frequency response up to 1.5 Mc/s., consisting of a head amplifier feeding through about 50 yards of correctly terminated coaxial cable to a main amplifier in a remote counting room. A differentiation time constant of 0.6 microseconds was used and all coupling time constants in the later stages of the amplifier were kept short to reduce the dead time following a large background pulse. With the actual neutron background encountered there was no difficulty from dead time effects.

The output pulses of the main amplifiers were mixed in a standard triple coincidence unit Type 1036A. The "tuning" of this coincidence unit was carried out in the usual way, by adjusting gate-open times and delay times in the individual channels until all real coincidences were

Fig. 2.



Block diagram of counting apparatus.

counted; the gate-open times finally used were 0.5 microseconds. The amplifier and discriminator were adjusted to register a count on the arrival of 10,000 electron charges in a pulse. Standard scaling units type 1009A were used to register the mixed pulses and the counts in each channel.

A second triple coincidence unit enabled the accidental coincidences to be measured during the normal counting runs. Double coincidences between channels 1 and 2 were fed into the final mixer stage of the second coincidence unit, and mixed with the single pulses from channel 3. The pulses from channel 3 were delayed by $2\frac{1}{2}$ microseconds in a coiled inner coaxial line, so that no genuine coincidences could be recorded. There was a considerable counting rate of genuine double coincidences caused by recoil protons which had sufficient energy to pass through the first two counters, but were brought to rest in the absorber A₂ between the second and third counters. Thus the background consisted of accidental coincidences between the mixed channel 1 and 2 pulses and the random counts of channel 3 caused by relatively slow neutrons emerging from the shielding walls.

All three counter voltages were adjusted to be on a plateau of triple coincidence counting rate against voltage in any arrangement used, thus ensuring that the fastest protons were being counted and that any slight drifts of voltage had a negligible effect on the counting rate.

The Neutron Attenuators.

A revolving drum (D, fig. 1), carrying four tubes 1.6 metres long and 6.3 cm. inside diameter, was slung between the second and third shielding walls, about 8 metres in front of the neutron detector. A carbon attenuator, 120.23 gm./cm.², was mounted in one tube and a polythene ((CH₂)_n) attenuator containing 136.93 gm./cm.² of polythene in another. One tube was left empty, and a copper bar, sufficiently long to remove virtually all the neutrons from the beam, was fixed in a fourth position. The drum could be driven by remote control from the counting room, so that measurements in the various positions could be made in rapid succession. Impurities in the carbon and polythene were such as to have a negligible effect on the attenuation. A second pair of attenuators, containing 70.76 gm./cm.² of carbon and 82.41 gm./cm.² of polythene respectively, was also used.

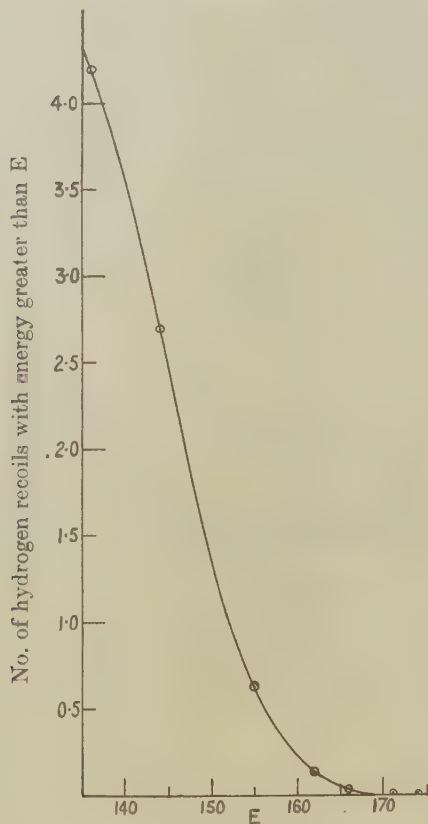
THE EFFECTIVE NEUTRON ENERGY.

The triple coincidence telescope detected neutrons in two distinct ways, since protons were ejected from both the hydrogen and the carbon content of the polythene radiator. A test with a graphite radiator showed that during the total cross-section measurements 93 per cent of the counts arose from hydrogen recoils and 7 per cent from nuclear reactions in carbon. The hydrogen recoils were elastic so that neutron energies could be inferred directly from the energies of the protons actually detected. On the other hand, only a lower limit could be placed on the energy of the neutrons detected through nuclear reactions in the carbon. This lower limit was fortunately rather high, because of the ¹²C(*n*, *p*)¹²B threshold of 13.2 MeV.

Throughout the total cross-section measurements the absorbers A₁ and A₂ were kept equal to 11.26 and 3.35 gm./cm.² respectively. The carbon equivalent of all the copper windows of the counters, together with the air separating them, was 0.21 gm./cm.². A further 1.00 gm./cm.² of carbon equivalent was added because the protons, on the average, traversed half the thickness of the polythene radiator. With the help of the range-energy relation in carbon (Taylor 1950) the minimum mean proton energy detected was found to be 145 MeV. Since the telescope was set at an angle of 10° to the neutron beam the minimum neutron energy detected was, on the average, 149 MeV. Now, the energy of the primary protons in the cyclotron was 171 MeV., so that there were no neutrons of energy greater than 169 MeV. The effective energy of the experiment was thus quite closely defined from the outset.

If the total cross-sections measured are assumed not to vary rapidly with energy, then the effective energy can be fixed still more accurately. First, the effective energy $E_{\text{eff}}^{\text{H}}$ of the neutrons detected through hydrogen recoils was found by means of the following subsidiary experiment. The absorber A_2 in the telescope was increased in steps to a maximum of 9.15 gm./cm.^2 and the triple coincidence rate determined at each setting,

Fig. 3.



Hydrogen recoil energy in MeV.
Integral spectrum of hydrogen recoils.

first with a polythene radiator and then with a carbon radiator. The integral spectrum of the hydrogen recoils (fig. 3) was then found from the difference between these two sets of results. Small corrections of the order of 2 per cent had to be applied to allow for the increased nuclear absorption of the protons in the extra absorber. After translating hydrogen recoil energies into neutron energies, $E_{\text{eff}}^{\text{H}}$ was found to be $155 \pm 3 \text{ MeV}$.

The effective energy E_{eff}^C of the neutrons detected through nuclear reactions in carbon could not be found experimentally. This did not matter greatly because only 7 per cent of the protons came from this source.

The high n, p threshold in carbon restricted the corresponding neutron energies to the comparatively narrow range from 162 to 169 MeV. The value of E_{eff}^C was guessed to be 165 ± 2 MeV.

Giving E_{eff}^H 93/7 times the weight of E_{eff}^C , the overall effective energy of the experiment was found to be 156 ± 3 MeV. This value has been slightly revised from that given in our earlier report.

The estimated error of the effective energy includes some allowance for possible inaccuracies in the range-energy relation. The results displayed in fig. 3 show clearly that this source of error was small. The maximum neutron energy was 169 MeV., so that the maximum possible hydrogen recoil energy was 164 MeV. The curve of fig. 3 should therefore reach the energy axis at 169 MeV., remembering that half the radiator thickness has been added in arriving at the energy scale. In fact, the experimental intersection is at 169 ± 2 MeV.

THE BEAM MONITOR.

The neutron output of the cyclotron was monitored by counting the pulses in an ionization chamber placed in a standard position behind the second shielding wall (fig. 1), where it was not affected by changing the neutron attenuator. Tests showed that the monitor counting rate was proportional to the cyclotron beam current.

EXPERIMENTAL PROCEDURE.

A complete cycle consisted of three successive measurements of the ratio of triple coincidence counts to the monitor counts with a polythene attenuator, a carbon attenuator and finally with no attenuator. The duration of counting was so arranged that about 300 triple coincidences were recorded in each run, and with a proton beam of 1 microampere mean current a complete cycle could be completed in about half an hour. Occasionally, between cycles, a blank run was performed with the long copper attenuator. In all, 19 cycles of readings were taken with the longer carbon and polythene attenuators, and 6 cycles with the shorter ones as a test for "hardening" and other effects which might have introduced errors.

Accidental triple coincidences represented a background which had to be subtracted from the counts observed during the experiment: they were measured by the method described above. Although the single channel counting rates were all far greater than the real triple coincidence counting rate, the background was only about 1 per cent with an attenuator in position. The background represented by the counting rate behind the long copper attenuator was negligibly small, showing that there were no serious leaks in the shielding.

RESULTS.

The measure of the incident neutron beam upon the counter telescope has been taken as the number of real triple coincidences divided by the monitor counts.

Calling the ratio T_0 , T_c , T_p where the subscripts refer to the beam unattenuated, and attenuated by carbon and polythene respectively, then :

$$\ln T_0/T_c = (N\sigma)_c$$

and

$$\ln T_0/T_p = (N\sigma)_p,$$

where N is the number of atoms per cm^2 of attenuator and σ their cross-section. Hence

$$\ln T_c/T_p = (N\sigma)_p - (N\sigma)_c.$$

If $(\Delta N\sigma)_c$ represents the excess of carbon in the polythene over that in the carbon attenuator, then :

$$(N\sigma)_H = \ln T_c/T_p - (\Delta N\sigma)_c,$$

where the subscript H refers to the hydrogen content of the polythene. The results are presented as the ratios of T_0/T_c and T_c/T_p for each cycle of the experiment. The mean value of these ratios then is used and the standard deviation quoted is that determined from the deviations from this mean. The values of the standard deviations so found differ little from the values expected from the total number of counts in the whole experiment.

TABLE I.

Short Attenuator.

Cycle	T_c/T_p	T_0/T_c
A	1.360	3.780
B	1.436	2.981
C	1.320	2.919
D	1.413	3.598
E	1.312	3.373
F	1.412	2.890

From the results in Table I, the values of T_c/T_p and T_0/T_p are 1.376 ± 0.025 and 3.257 ± 0.182 respectively; the standard deviations expected from the total number of counts are 0.044 and 0.104 respectively. With these values the total cross-sections σ_c , σ_H for carbon and hydrogen are :

$$\sigma_c = 0.333 \pm 0.016 \times 10^{-24} \text{ cm}^2$$

$$\sigma_H = 0.0454 \pm 0.0025 \times 10^{-24} \text{ cm}^2$$

From the results in Table II. the mean values of T_c/T_p and T_0/T_c are 1.649 ± 0.0242 and 7.310 ± 0.127 respectively, the standard deviations expected from the total number of counts being 0.0271 and 0.098 respectively. The total cross-sections with these values are :

$$\sigma_C = 0.330 \pm 0.003 \times 10^{-24} \text{ cm.}^2$$

$$\sigma_H = 0.0467 \pm 0.0014 \times 10^{-24} \text{ cm.}^2$$

The weighted means of these results are :

$$\sigma_C = 0.330 \pm 0.003 \times 10^{-24} \text{ cm.}^2$$

$$\sigma_H = 0.0464 \pm 0.0012 \times 10^{-24} \text{ cm.}^2$$

TABLE II.

Long Attenuator.

Cycle	T_c/T_p	T_0/T_c
A	1.714	7.810
B	1.596	7.364
C	1.913	7.139
D	1.779	7.682
E	1.402	8.406
F	1.845	6.747
G	1.547	6.915
H	1.625	7.674
I	1.750	6.765
J	1.640	6.807
K	1.622	6.724
L	1.672	7.235
M	1.675	6.808
N	1.600	7.431
O	1.629	6.866
P	1.558	7.812
Q	1.515	7.739
R	1.650	7.955
S	1.493	7.004
T	1.683	
U	1.715	

CONCLUSION.

This value of the hydrogen cross-section is in line with the results of experiments at Berkeley (Hadley *et al.* 1949, Kelly *et al.* 1949, De Juren and Moyer 1950, De Juren and Knable 1950). However, it is too low to be compatible with the theoretical total cross-sections calculated with the interactions suggested by present meson theories (Burhop and Yadav 1949, Christian and Hart 1950).

ACKNOWLEDGMENT.

We wish to thank the cyclotron operating crew for their cooperation throughout these experiments. This paper is published by permission of the Director of the Atomic Energy Research Establishment, Harwell.

REFERENCES.

- BURHOP, E. H. S., and YADAV, H. N., 1949, *Proc. Roy. Soc. A*, **197**, 505.
CHRISTIAN, R. S., and HART, E. W., 1950, *Phys. Rev.*, **77**, 441.
DE JUREN, J., and KNABLE, N., 1950, *Phys. Rev.*, **77**, 606.
DE JUREN, J., and MOYER, B. J., 1950, *Bull. Am. Phys. Soc.*, **25**, 4, J. 8.
HADLEY, J., KELLY, E., LEITH, C., SEGRÈ, E., WIEGAND, C., and YORK, H., 1949, *Phys. Rev.*, **75**, 351.
KELLY, E., LEITH, C., SEGRÈ, E., and WIEGAND, C., 1950, *Phys. Rev.*, **79**, 96.
PICKAVANCE, T. G., ADAMS, J. B., and SNOWDEN, M., 1950, *Nature*, **165**, 90.
TAYLOR, A. E., PICKAVANCE, T. G., CASSELS, J. M., and RANDLE, T. C., 1950, *Nature*, **165**, 967.
TAYLOR, A. E., 1950, *Phil. Mag.*, **41**, 966.

III. *The Interaction between an Oblique Shock-wave and a Turbulent Boundary-layer.*

By O. BARDSLEY and W. A. MAIR,
Fluid Motion Laboratory, University of Manchester *.

[Received October 10, 1950.]

[Plates I. to IV.]

SUMMARY.

Schlieren photographs have been taken to show the reflection of oblique shock-waves of different strengths at the turbulent boundary-layer on the wall of a supersonic wind-tunnel. A weak shock-wave is reflected as a compression followed by an expansion; this is in agreement with Lighthill's theory in which the boundary-layer is replaced by a non-turbulent inviscid layer with the same velocity distribution as a turbulent boundary-layer. For stronger incident shock-waves the reflected wave moves upstream of the incident one to a point where the boundary-layer starts to thicken. Thus the incident and reflected shock-waves cross outside the boundary-layer. Near the point where the incident shock-wave meets the boundary-layer, the rate of growth of the boundary-layer suddenly decreases and an expansion occurs. For very strong shock-waves a Mach type of interaction occurs, with a short normal shock-wave between two intersections.

The supersonic wind-tunnel and optical system used for these experiments are briefly described.

§ 1. INTRODUCTION.

THE experiments were made in a small intermittent supersonic wind-tunnel at a Mach number of 1.965, using a wedge to produce an oblique shock-wave. The strength of the shock-wave was varied by changing the angle of incidence of the wedge. The interaction between the shock-wave and the turbulent boundary-layer on the tunnel wall was investigated by schlieren photography.

§ 2. NOTATION.

p_1 = static pressure before incident shock-wave.

p_2 = static pressure after incident shock-wave.

$\chi = \frac{p_2 - p_1}{p_1}$ = strength of incident shock-wave.

δ = stream deflection produced by incident shock-wave.

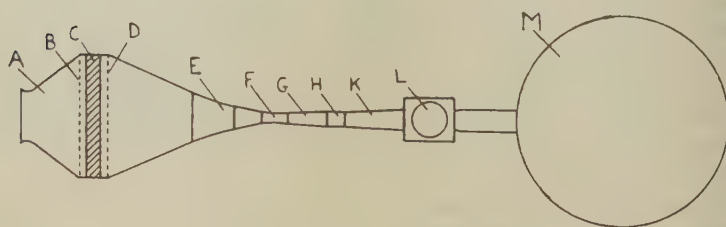
* Communicated by the Authors.

- α_0 = theoretical angle between undisturbed stream and incident shock-wave, calculated from a given value of δ .
 α_1 = angle between undisturbed stream and incident shock-wave, measured at upstream edge of "fan" in photograph.
 α_2 = angle between undisturbed stream and incident shock-wave, measured at downstream edge of "fan" in photograph.

§ 3. DESCRIPTION OF WIND-TUNNEL.

The arrangement of the wind-tunnel is shown in fig. 1. The large reservoir M consists of three modified Lancashire boilers having a total capacity of about 130 cu.m. This reservoir is connected to the other parts of the wind-tunnel by the quick-operating valve L. Before starting the wind-tunnel the reservoir is evacuated to an absolute pressure of about 0.1 atmosphere. The valve L is then opened and air enters the intake A from the atmosphere, is dried by the silica gel C and passes

Fig. 1.



Intermittent supersonic wind tunnel.

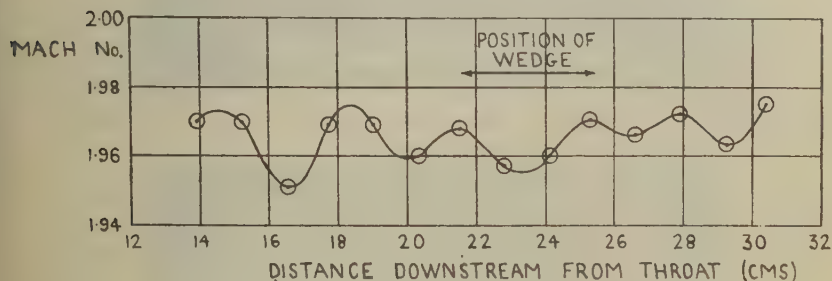
through the contraction E to the working section F. The working section is rectangular, with a height of 12.7 cm. and a width of 10.2 cm., the shaped nozzle blocks being at the top and bottom, with parallel glass plates at the sides. Downstream of the working section there is a gradually expanding passage G, in which the supports for the models are fixed. This is followed by a transition to a section H and a subsonic diffuser K leading to the valve L.

In the drier the silica gel bed C is 19 cm. thick and has a frontal area of 2.65 sq. m. With a Mach number of 1.965 in the working section (area 129 sq. cm.) the mean velocity of the air passing through the silica gel is only 0.58 m. per sec. This small velocity makes it possible to use a cotton-wool filter B to clean the incoming air and so prevent contamination of the silica gel by dirt from the atmosphere. A wire gauze D is placed after the silica gel to reduce the turbulence caused by the structure supporting the silica gel compartment. The total pressure drop caused by the cotton-wool, silica gel, and wire gauze is about 15 cm. of water.

A small centrifugal fan and a 12 Kw. electric heater are provided for regenerating the silica gel as required by blowing hot air through it. The maximum duration of each run of the wind-tunnel is about 45 seconds. For many purposes a much shorter time is sufficient, and several runs can then be made with one evacuation of the reservoir. At a Mach number of 1.965 the pressure in the reservoir when the normal shock-wave begins to move upstream into the working section is 0.665 times the stagnation pressure upstream of the throat. The diffuser efficiency may be defined as the work done in isentropic compression, between the condition before and the pressure after the diffuser, divided by the decrease of kinetic energy in the diffuser. Using this definition the efficiency is 0.75, a value consistent with the results obtained by Neumann and Lustwerk (1949) for a similar type of diffuser.

The distribution of static pressure along the centre line of one side of the working section was measured, using a brass side-plate fitted with pressure holes instead of the usual glass window. From these static pressures the corresponding Mach numbers were calculated, assuming

Fig. 2.



Distribution of Mach No. along centre line.

that the stagnation pressure was equal to the static pressure in the drier immediately after the gauze D. (Measurements with a pitot tube at high subsonic speeds have shown that this assumption is correct, outside the boundary-layer, within 0.2 per cent of the dynamic pressure.) The distribution of Mach number obtained in this way is shown in fig. 2; for the purpose of the present experiments the mean Mach number is assumed to be 1.965.

§ 4. HUMIDITY MEASUREMENTS.

The humidity of the air passing through the wind-tunnel cannot be measured in the limited time available while the tunnel is running, and an indirect method is therefore necessary. The tunnel is run about three times, starting with an absolute pressure of about 0.1 atmosphere in the reservoir and continuing each run until the pressure in the reservoir is

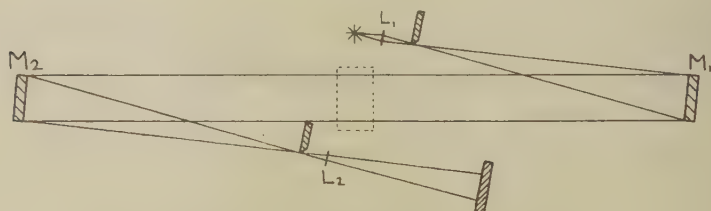
atmospheric. When this has been done nearly all the air in the reservoir has passed through the drier, and a sample of air from the reservoir is therefore representative of the air passing through the wind-tunnel. A compressor is then used to pump air from the atmosphere through the silica gel drier into the reservoir, so that the pressure is slightly greater than atmospheric. A steady stream of air from the reservoir is then passed through a frost-point hygrometer of the type described by Brewer, Cwilog and Dobson (1948).

When the silica gel has just been regenerated the water vapour content of the dried air passing through the wind-tunnel is always less than 1 part in 5000 by weight, and is sometimes very much lower. Normally, the silica gel is regenerated when the water content of the dried air has risen to about 1 part in 2500 by weight.

§ 5. OPTICAL SYSTEM.

The optical apparatus used for the schlieren photographs was a conventional two-mirror system as shown in fig. 3. The two spherical

Fig. 3.



Schlieren optical system.

concave mirrors M_1 and M_2 have a focal length of 152 cm. and a diameter of 12.7 cm. L_1 is a condenser lens and L_2 is a long-focus achromatic object lens. For setting up and adjusting the apparatus, and for visual observation of the schlieren image on a screen, a "compact source" mercury vapour lamp is used. The very high brightness of this lamp gives good illumination on the screen, even when the second knife-edge is very close to the position giving complete cut-off. This facilitates exact adjustment of the knife-edges and mirrors.

§ 6. PHOTOGRAPHS OF OBLIQUE SHOCK-WAVES.

The wedge used to produce the shock-waves was 3.8 cm. long in the direction of the stream, had an apex angle of 10.1° , and was made of hardened high-carbon steel. It was ground and lapped to give a constant angle with as sharp an edge as possible; the thickness of the leading edge was measured and found to be between 2.5 and 12μ . The wedge extended across the whole width of the working section and was supported by two arms on the downstream side.

FIG. 4.

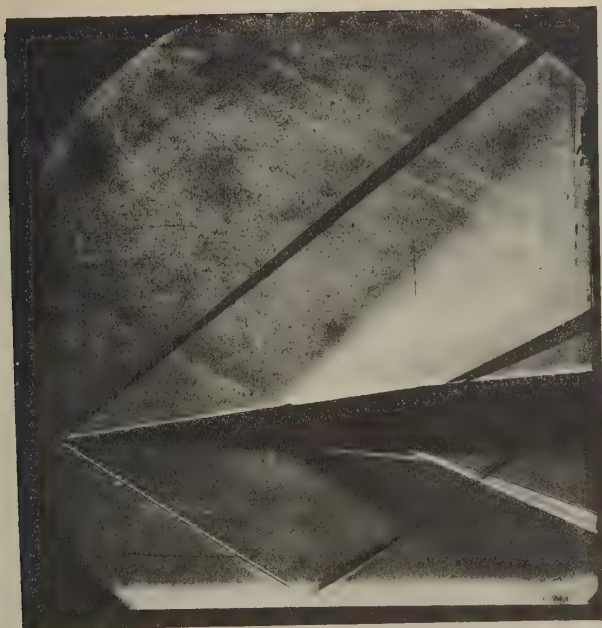
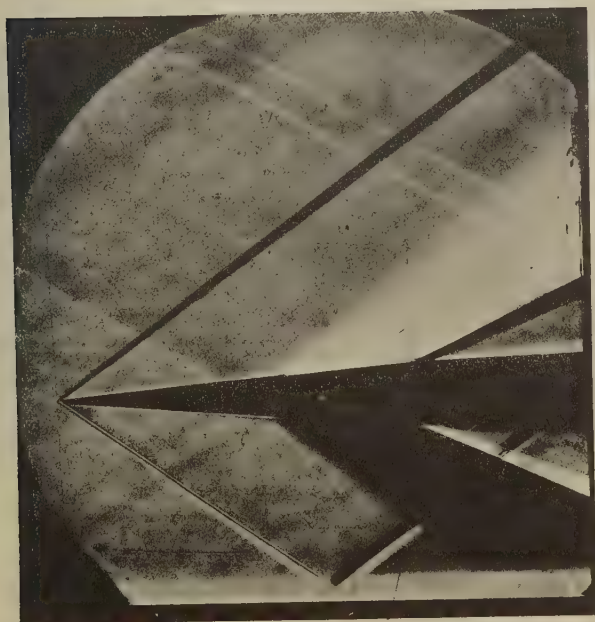


FIG. 5.



To face page 32

FIG. 6.

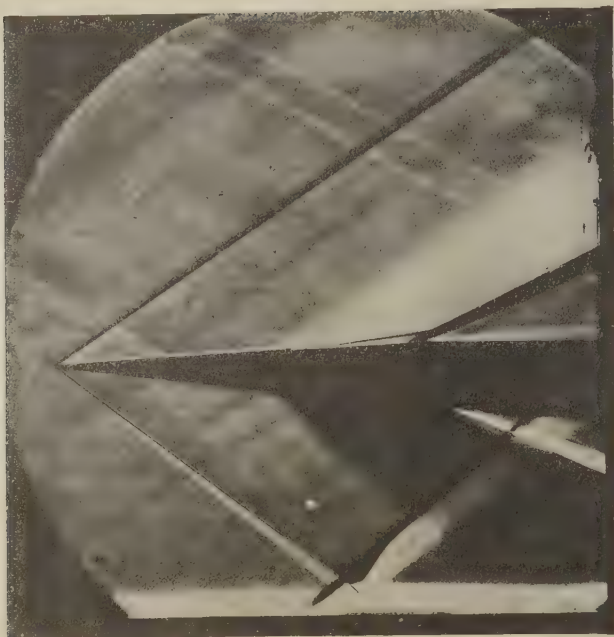


FIG. 7.



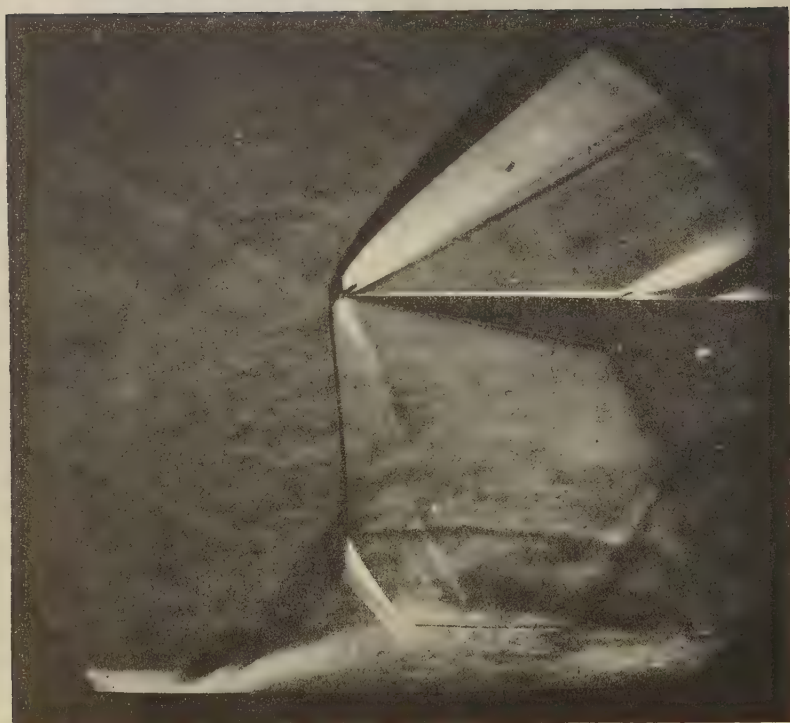
FIG. 8.



FIG. 9.



FIG. 10.



The schlieren system was arranged with horizontal knife-edges so that increasing air density in an upward direction corresponded to a light region in the photograph.

Preliminary visual observations showed that the flow was steady, so that a relatively long exposure ($\frac{1}{20}$ th second) could be used for the photographs. The mercury vapour lamp gave considerably more light than was necessary for photography, and a slow "process" film was used, with a yellow filter to reduce its effective speed. This arrangement was convenient, as it enabled a single light source to be used for visual observation and photography. Figs. 4 to 9 (Pls. I. to IV.) are photographs of the flow for positions of the wedge giving deflection angles (δ) of 2.9° , 5.0° , 7.3° , 9.8° , 12.1° and 15.2° . In each case the flow is from left to right. Table I. gives the strengths (χ) of the incident shock-waves, calculated from the values of δ .

§ 7. DISCUSSION OF PHOTOGRAPHS.

The arms supporting the wedge continue downstream beyond the edge of the field of view. The position of the back of the wedge is revealed by the two large expansion regions. The joints in the supporting arms produce two shock-waves at the right-hand side of each photograph. In addition, several wavelets from the liners are visible and a scratch on one of the glass walls may be seen in the bottom left-hand corner of each photograph. In fig. 7 the vertical black line across the middle of the photograph is a reference mark to show the position of the wedge in the tunnel.

The thickness of the light region representing the boundary-layer on the tunnel wall is about 4 mm. at a point 24 cm. downstream of the throat. This indicates that the boundary-layer was turbulent, as would be expected at such a high Reynolds number (1.34×10^5 per cm. in the working section). In all cases the tunnel wall was flat at the point of incidence of the shock-wave.

In each photograph the thickness of the line representing the incident shock-wave increases with distance from the leading edge of the wedge. This is probably because the flow is not two-dimensional, so that the shock-wave is not plane over the whole section of the tunnel. The reduced velocity in the outer part of the turbulent boundary-layer on each glass wall increases the shock-wave angle in that region and hence explains this fan-shaped appearance. Thus the downstream side of the "fan" represents the true position of the shock-wave outside the boundary-layer. This explanation is supported by fig. 4, showing the weakest incident shock-wave, in which the fan-shaped region is very faint except at the downstream edge. Similarly, in figs. 4 to 7, the same effect can be seen in the fan-shaped region representing the shock-wave on the upper surface.

In Table I. the stream deflections and shock-wave angles are considered. For a given stream deflection angle (δ) the theoretical value of the

shock-wave angle (α_0) has been calculated and compared with the measured angles at the upstream and downstream edges of the fan (α_1 and α_2). It can be seen that α_0 agrees much better with α_2 than with α_1 , again showing that the downstream edge of the fan corresponds to the position of the shock-wave outside the boundary-layer. Part of the difference between the values of α_0 and α_2 may be explained by the growth of the boundary-layer on the wedge, causing an increase in the effective value of δ .

In the light fan-shaped region representing the incident shock-wave in figs. 4 to 7, there is a dark line near the downstream edge. The reason for this is not understood but further work is being done to investigate the flow at the sharp leading edge of a wedge.

TABLE I.

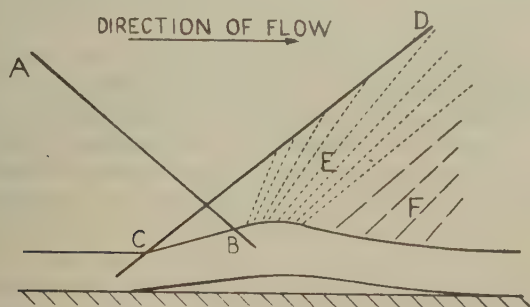
Fig. no.	δ	χ	α_0	α_1	α_2
4	2.9°	0.17	33.0°	—	33.6°
5	5.0°	0.31	34.9°	37.4°	35.6°
6	7.3°	0.48	37.2°	39.5°	37.8°
7	9.8°	0.68	39.8°	42.1°	40.1°
8	12.1°	0.90	42.6°	45.9°	43.4°
9	15.2°	1.20	46.6°	49.4°	47.1°

Figs. 4 and 5 show that a weak shock-wave is reflected as a compression followed by an expansion, *i. e.* as a pressure *ridge*. The dark region after the expansion indicates that there is a further compression there, with a smaller density gradient than in the first compression. The expansion appears to get weaker with increasing distance from the boundary; this would be expected as a result of interaction with the compression waves. At a sufficient distance from the boundary the expansion probably disappears completely, and the reflection of a weak shock-wave is then simply another shock-wave. These conclusions are in agreement with Lighthill's theory (1950) in which the boundary-layer is replaced by a non-turbulent inviscid layer with the same velocity distribution as a turbulent boundary-layer.

The above description applies to incident shock-waves with strengths (χ) up to about 0.4. For these strengths there is no appreciable thickening of the boundary-layer upstream of the shock-wave and no separation. When the strength of the shock-wave is more than about 0.4, however (figs. 6 to 9, Pls. II. & III.), the boundary-layer begins to thicken and separate on the upstream side of the incident wave and the reflected shock-wave moves up to this point. Thus the incident and reflected shock-waves cross at a point outside the boundary-layer. As the incident shock-wave becomes stronger the foot of the reflected wave moves further upstream and the point of intersection moves further away

from the boundary. An expansion still occurs after the reflected shock-wave, but this remains near the point where the incident shock-wave meets the boundary-layer. In this region the rate of growth of the boundary-layer suddenly decreases, and there is a corresponding deflection of the stream due to the expansion. In figs. 6 and 7 there is a dark region after the expansion, indicating a further gradual compression similar to that occurring with the weaker shock-waves. The concave shape of the outer edge of the boundary-layer in this region can be seen clearly in fig. 7. The boundary-layer must always have a concave shape where there is a compression region, but it is not easily seen in the other photographs. The second compression would be expected to occur also for the stronger shock-waves in figs. 8 and 9 but in these photographs it is almost outside the field of view. (The dark region representing the compression after the expansion in figs. 6 and 7 should not be confused with the dark expansion region caused by the back of the wedge.)

Fig. 11.



Reflection of oblique shock-wave of medium strength ($0.5 < \chi < 0.9$).

The dark region near the tunnel wall in figs. 7 to 9 shows that the boundary-layer has separated near the foot of the reflected shock-wave. This dark region is just visible in fig. 6 ($\chi = 0.48$), suggesting that separation of the boundary-layer occurs if χ is more than about 0.45. Figs. 6 and 7 show a re-attachment of the boundary-layer further downstream. This probably occurs in all cases, but in figs. 8 and 9 the point of re-attachment is outside the field of view.

Fig. 11 is a diagram showing the typical configuration for incident shock-waves of strength (χ) between 0.5 and 0.9. AB is the incident shock-wave entering the boundary-layer at B. The boundary-layer separates and begins to thicken at C, and the reflected shock-wave CD passes through this point. At a short distance downstream of B there is an expansion region E where the rate of growth of the boundary-layer decreases rapidly through zero. After the expansion the outer edge of the boundary-layer becomes concave and this causes a gradual compression in the region F.

In fig. 9 the strength of the incident shock-wave is so great that its interaction with the reflected wave is of Mach type, with a short normal shock wave between two intersections. Experiments by Fage and Sargent (1947) have shown that a strong normal shock-wave has a bifurcated foot where it enters a turbulent boundary-layer. It is suggested that the bifurcation at the foot of the Mach shock-wave in fig. 9 is similar to that of any normal shock-wave interacting with a turbulent boundary-layer at this Mach number, since the conditions at the upper end of the Mach shock-wave should not have much effect on the bifurcation at the lower end. For example, a similar configuration was observed with the wedge set at an incidence so high that the tunnel was choked and the normal starting shock-wave remained in the working section (fig. 10). (For this photograph a short-duration flash was used, as the flow was not quite steady.) The bifurcation of the normal shock-wave in this case is similar to that shown at the foot of the Mach shock-wave in fig. 9.

This means that for any oblique shock-wave with $\chi > 1.2$ the bifurcated foot of the Mach shock-wave and the separating boundary-layer would be generally similar to figs. 9 and 10.

It is perhaps of interest to point out the vortex sheets that arise at the intersections of the shock-waves in figs. 8, 9 and 10.

At lower Mach numbers than in these experiments (*i. e.* $M < 1.965$) Mach reflection would occur for weaker incident shock-waves. Thus the upper limit of shock-wave strength giving a cross formation similar to fig. 11 (without a Mach shock-wave) would decrease with Mach number. At the same time the lower limit of shock-wave strength giving this configuration would probably not change much with Mach number, since it depends on the separation or thickening of the boundary-layer caused by the shock-wave. Thus the range of shock-wave strengths giving a cross formation, without a Mach shock-wave, would become more restricted with decreasing Mach number. This means that for sufficiently low Mach numbers this formation would not occur for a shock-wave of any strength. Weak shock-waves would give reflections like figs. 4 and 5 and stronger ones would give Mach reflection, either with or without a bifurcated foot. This probably explains why Fage and Sargent (1947) did not find configurations like figs. 6, 7 and 8.

REFERENCES.

- BREWER, A. W., CWILONG, B., and DOBSON, G. M. B., 1948, *Proc. Phys. Soc.*, **60**, 52-70.
 FAGE, A., and SARGENT, R. F., 1947, *Proc. Roy. Soc. A*, **190**, 1-20.
 LIGHTHILL, M. J., 1950, *Quart. Journ. Mech. App. Math.* (in press).
 NEUMANN, E. P., and LUSTWERK, F., 1949, *Journ. App. Mech.*, **16**, 195-202.

IV. Collision broadening at Microwave Frequencies.

By D. C. M. LESLIE, M.A.,
Clarendon Laboratory, Oxford *.

[Received September 14, 1950.]

SUMMARY.

A theoretical formula is deduced for the broadening and shift of spectral lines due to collisions; this formula is valid in the microwave region, for gases at low pressures. It is assumed that the partial collision amplitudes f for the bimolecular collision problem are known, and using these, the equation of motion of the two-molecule density matrix is found. A formula for the line broadening and shift follows from this.

Using the equation of motion of the density matrix, it is also shown that a Boltzmann distribution is the only equilibrium one.

§1. INTRODUCTION.

THERE are three causes of the broadening of the spectral lines emitted by a gaseous radiator, namely, radiation damping, Doppler broadening, and effects due to intermolecular interactions. These effects are very complicated, and it is only at low pressures, where bimolecular collisions are the dominant interaction mechanism, that a detailed theoretical treatment is feasible. The low-pressure effect is called collision broadening.

Reducing the gas pressure naturally reduces the pressure broadening, and in the optical region, this effect is obscured by Doppler broadening. However, Doppler broadening is proportional to the radiated frequency ω , while collision broadening is independent of ω ; hence, at sufficiently low frequencies, collision broadening must predominate. It turns out that this is the case in the microwave region ($\lambda \sim 1$ cm.).

Since the war, a number of accurate experiments have been done on collision broadening in the microwave region—notably those of Bleaney and Penrose (1947) on the inversion spectrum of NH_3 —and this has stimulated theoretical work on the subject.

Karplus and Schwinger (1948) have taken the important step of transcribing the classical theories of Van Vleck and Weisskopf (1945) and Fröhlich (1946) into quantum form; they are then able to account for saturation. They show that the correct tool for this type of calculation is von Neumann's density matrix; its equation of motion may be written

$$\frac{\partial \mathbf{U}}{\partial t} = \frac{1}{i\hbar} (\mathbf{H}^0 \mathbf{U} - \mathbf{U} \mathbf{H}^0) + \frac{\partial_e \mathbf{U}}{\partial t}, \quad (1.1)$$

* Communicated by Professor M. H. L. Pryce.

where H^0 is the internal Hamiltonian of one molecule, and $\partial_e/\partial t$ denotes the rate of change of an operator due to collisions. Their assumption is equivalent to setting

$$\frac{\partial_e U}{\partial t} = -\sigma(U - U_e), \quad (1.2)$$

where U_e is the equilibrium statistical matrix (we use the terms "density" or "statistical" matrix indifferently). The original collision-broadening theory of Lorentz was equivalent to setting

$$U_e = \text{const. exp } (-H^0/kT).$$

Van Vleck and Weisskopf (1945) pointed out that in the microwave region, the oscillating electric field applied to the gas (such measurements are always made in absorption) was essentially "slow," *i.e.*, that the collisions would attempt to maintain an instantaneous Boltzmann distribution.

$$U_e = \text{const. exp } \{-(H^0 - \mu \cdot \mathbf{F} \cos \nu t)/kT\}$$

ν being the frequency of the applied field. Owing to the rapid variation of this field, the actual statistical matrix will be different from U_e . This assumption gives a line shape in agreement with experiment.

However, this phenomenological approach does not give any theoretical connection between the line width σ and the intermolecular potential $V(\mathbf{r})$. A theory due to Anderson (1949) has had considerable success in this direction, but it contains a number of assumptions which can be avoided. The theory presented below is restricted only by fundamental physical assumptions, namely that the gas pressure is small, and the applied field slow, in the sense explained above: this is believed to be true in the microwave region.

§ 2. CALCULATION OF $\partial_e U/\partial t$.

Karplus and Schwinger's equation (1.2) is certainly too restrictive, but for a U not far removed from equilibrium, the equation

$$\left\langle a \left| \frac{\partial_e U}{\partial t} \right| b \right\rangle = \sum_{cd} L(ab, cd) \langle c | U - U_e | d \rangle, \quad . . . (2.1)$$

must hold, since the definition of equilibrium is

$$\frac{\partial_e U_e}{\partial t} = 0.$$

The object of this section is to calculate the coefficients $L(ab, cd)$ in terms of known quantities.

We have explained that we are taking bimolecular collisions to be the only mechanism producing broadening, and we therefore want to investigate the effect of bimolecular collisions on S , the statistical matrix of an individual molecule (U is an averaged statistical matrix). We shall

have to use a generalized statistical matrix D describing the external, as well as the internal, motions of the molecule. The external coordinates are continuous, and hence, in a coordinate representation, D will be a matrix in the internal coordinates, with each element a function of two external vector variables \mathbf{r} and \mathbf{r}' (such a representation was first discussed by Born and Green, 1947).

S is very simply related to D , being its external trace ;

$$S = \iint D(\mathbf{r}, \mathbf{r}') \cdot \delta(\mathbf{r} - \mathbf{r}') \cdot d^3\mathbf{r} \cdot d^3\mathbf{r}' = \int D(\mathbf{r}, \mathbf{r}) \cdot d^3\mathbf{r}, \quad \dots \quad (2.2)$$

the integral being taken over unit volume. As a simple example, the matrix

$$D = S \exp [i\mathbf{k} \cdot (\mathbf{r} - \mathbf{r}')] ,$$

describes a plane wave in a specified internal condition S .

To discuss bimolecular collisions, we must work in a 2-molecule Hilbert space, which is the direct product of two one-molecule spaces.

$$\mathcal{H}_2 = \mathcal{H}_1^{(1)} \times \mathcal{H}_1^{(2)} .$$

As long as there is no correlation between molecules about to collide, which is certainly true in dilute gases, D_2 the density matrix in \mathcal{H}_2 , is given before collision, by

$$D_2 = D_1^{(1)} \wedge D_1^{(2)} ,$$

where the symbol \wedge denotes the Kronecker product of two matrices. D_2 has to describe the external motion of two molecules, and will therefore be a function of four vector variables, $D_2(\mathbf{r}_1, \mathbf{r}_2; \mathbf{r}'_1, \mathbf{r}'_2)$. S_2 , the two-molecule internal density matrix, is obtained from D_2 by a process analogous to (2.2)

$$S_2 = \iint D_2(\mathbf{r}_1, \mathbf{r}_2; \mathbf{r}_1, \mathbf{r}_2) \cdot d^3\mathbf{r}_1 \cdot d^3\mathbf{r}_2, \quad \dots \quad (2.2 a)$$

S_1 , the one-molecule internal density matrix, is then found from

$$S_1^{(1)} = \text{Tr}_2(S_2). \quad \dots \quad (2.2 b)$$

Tr_2 denoting the operation of taking the trace over the internal coordinates of molecule 2.

We shall suppose that we have, as a basis for \mathcal{H}_1 , a complete normal orthogonal sequence (c.n.o.s.) $\{|y\rangle\}$ of eigenvectors of H^0 , the internal Hamiltonian of one molecule, corresponding to energies $\{E_y\}$. A suitable basis for \mathcal{H}_2 is then the c.n.o.s.

$$\{|a\rangle\} = \{|y\rangle|z\rangle\} ,$$

whose energies are $\{E_a\}$, $E_a = E_y + E_z$.

The Hamiltonian of a system of two interacting molecules is

$$H_2 = H^0(1) + H^0(2) + \frac{1}{2m} (p_1^2 + p_2^2) + V ,$$

where $H^0(1)$ and $H^0(2)$ are the internal Hamiltonians of the molecules (1) and (2), \mathbf{p}_1 and \mathbf{p}_2 their momenta, and V the interaction potential between them. Since we are assuming the electric field to be slow, we do not need to consider it while discussing collisions. We set

$$H^0(1) + H^0(2) = H_2^0,$$

the two-molecule internal Hamiltonian, which satisfies

$$H_2^0 |a\rangle = E_a |a\rangle.$$

We also set

$$\mathbf{r} = \mathbf{r}_1 - \mathbf{r}_2, \quad \mathbf{R} = \frac{1}{2}(\mathbf{r}_1 + \mathbf{r}_2),$$

and similarly with \mathbf{r}' , \mathbf{r}'_2 ; then

$$H_2 = H_2^0 - \frac{\hbar^2}{m} (\nabla_r^2 + \frac{1}{4} \nabla_R^2) + V(\mathbf{r}). \quad (2.3)$$

The equation of motion of D_2 is

$$i\hbar \frac{\partial D_2}{\partial t} = H_2 D_2 - D_2 H_2,$$

and with H_2 in the form (2.3), this can be separated. We write

$$H_2 = H'_2 - \frac{\hbar^2}{4m} \nabla_R^2, \quad \text{where } H'_2 = H_2^0 - \frac{\hbar^2}{m} \nabla_r^2 + V(\mathbf{r})$$

and

$$D(\mathbf{r}, \mathbf{R}; \mathbf{r}', \mathbf{R}') = \rho(\mathbf{r}, \mathbf{r}') \cdot \mathbf{J}(\mathbf{R}, \mathbf{R}'),$$

ρ and \mathbf{J} must then satisfy

$$i\hbar \frac{\partial \rho}{\partial t} = H'_2 \rho - \rho H'_2 \quad (2.4 a)$$

and

$$i\hbar \frac{\partial \mathbf{J}}{\partial t} = -\frac{\hbar^2}{4m} (\nabla_R^2 - \nabla_R'^2) \mathbf{J}(\mathbf{R}, \mathbf{R}'), \quad (2.4 b)$$

ρ is therefore a matrix in the internal variables, but \mathbf{J} is a function of \mathbf{R} and \mathbf{R}' only. A particular solution of (2.4 b) is

$$\mathbf{J}(\mathbf{R}, \mathbf{R}') = \exp \{i\boldsymbol{\kappa} \cdot (\mathbf{R} - \mathbf{R}')\},$$

representing uniform motion of the centre of gravity of the two-molecule system. A more general solution of this type is

$$\mathbf{J}(\mathbf{R}, \mathbf{R}') = \int f(\boldsymbol{\kappa}) \exp \{i\boldsymbol{\kappa} \cdot (\mathbf{R} - \mathbf{R}')\} d^3\boldsymbol{\kappa},$$

where $f(\boldsymbol{\kappa})$ is a normalized function giving the distribution of velocities of the centres of gravity of the two-molecule systems. At equilibrium, $f(\boldsymbol{\kappa})$ will be a Maxwellian distribution, since the oscillating electric field will not influence the external motion of the molecules.

We cannot solve (2.4 *a*) in the same way, since as we shall explain shortly, $V(\mathbf{r})$ must be taken to be time-dependent. S_2 is then given by

$$S_2 = \iint \rho(\mathbf{r}, \mathbf{r}) J(\mathbf{R}, \mathbf{R}) \cdot d^3\mathbf{r} d^3\mathbf{R},$$

$$(\text{since } d^3\mathbf{r}_1 \cdot d^3\mathbf{r}_2 = d^3\mathbf{r} \cdot d^3\mathbf{R})$$

$$= \iint \rho(\mathbf{r}, \mathbf{r}) f(\boldsymbol{\kappa}) \cdot d^3\mathbf{r} \cdot d^3\boldsymbol{\kappa} = \iint \rho(\mathbf{r}, \mathbf{r}) \cdot d^3\mathbf{r}.$$

The coordinate \mathbf{R} does not, therefore, enter into the problem, and we have only to find a suitable solution of (2.4 *a*).

Now if we were to solve the ordinary static collision problem, we should only find the effect of one collision on a molecule. To attempt to find the effect of repeated collisions using a time-independent V would mean solving a many-body dynamical problem.

This can be avoided by solving a two-molecule time-dependent problem (it is our assumption that binary collisions are the only important interaction mechanism that makes this simplification possible). We take the potential to be given by

$$V(\mathbf{r}, t) = V(\mathbf{r}) \text{ if } T - \tau \leq t \leq T \quad (T > 0), \\ = 0 \text{ otherwise,}$$

$V(\mathbf{r})$ being the given time-independent interaction potential. The initial condition is that at time $t=0$

$$\rho(\mathbf{r}, \mathbf{r}') = \int S_2 g(\mathbf{k}) \exp \{i\mathbf{k} \cdot (\mathbf{r} - \mathbf{r}')\} \cdot d^3\mathbf{k},$$

corresponding to a superposition of plane waves; $g(\mathbf{k})$ is a velocity distribution function which we shall later be able to show to be Maxwellian. We shall show how the solution of this problem can be used when we have obtained it.

We shall assume that the asymptotic solution of the time-independent two-molecule collision problem is known in wavefunction form. In detail, we shall know that if the incident wave is given by

$$\langle a, \mathbf{r} | \mathbf{I} \rangle = [\exp(i\mathbf{k} \cdot \mathbf{r})] \delta_{am}, \quad \dots \quad (2.5 \ a)$$

(representing a wave with momentum $\hbar\mathbf{k}$ incident on a scatterer in state $|m\rangle$), then the asymptotic scattered wave will be given by

$$\langle a, \mathbf{r} | \mathbf{S} \rangle = \frac{\exp(ik_{ma}r)}{r} \langle a | f(\mathbf{k}, \mathbf{k}_{ma}) | m \rangle, \quad \dots \quad (2.5 \ b)$$

where

$$k_{ma}^2 = k^2 + \frac{m}{\hbar^2} (E_m - E_a). \quad \dots \quad (2.6)$$

The coefficients f all being known. The complete asymptotic solution of the collision problem is then

$$| \mathbf{C} \rangle = | \mathbf{I} \rangle + | \mathbf{S} \rangle. \quad \dots \quad (2.5 \ c)$$

All states occurring in formula (2.5) are two-molecule states. The ket $|C\rangle$ is usually thought of as being given by Schrödinger's equation—a differential equation—but it can equally well be regarded as being determined by the integral equation

$$\langle a, \mathbf{r} | S \rangle = - \frac{m}{4\pi\hbar^2} \sum_b \int \frac{\exp(i\mathbf{k}_{ma}\sigma)}{\sigma} \langle a | V(\mathbf{s}) | b \rangle \langle b, \mathbf{s} | C \rangle d^3\mathbf{s}, \quad (2.7)$$

where $\sigma = \mathbf{r} - \mathbf{s}$.

The determination of the f 's in the case of inelastic scattering is always very difficult, and it is made doubly so in these collision-broadening problems by the fact that we are usually dealing with non-central potentials. The Born approximation is not satisfactory, since the thermal motions with which we are concerned are quasi-classical (see Anderson, 1949). This problem is quite distinct from the statistical problem now under discussion, but it is hoped to take it up in a later paper.

The scattered wave (2.5 *b*) has the form of a spherical wave in free space; this form can therefore only be valid at large distances from the scattering centre, where the interaction potential is inappreciable (this is what we mean when we call it an asymptotic solution). A solution of this kind will only tell us about that part of the line broadening due to "permanent" changes in the molecules produced by collisions; this type is referred to as "impact" broadening, and will plainly depend on the intermolecular velocity.

The other type, called "statistical" broadening, is due to transient changes in the molecules, which disappear as they move apart. Statistical broadening may be pictured as being due to changes in the energy levels of molecule (1) due to the influence of molecule (2). This will alter the radiated frequency, and the aggregate effect is to broaden the lines of the spectrum. These two types of broadening have been carefully discussed by Margenau and Watson (1936).

The actual broadening will be due to a mixture of the two types, but it is generally thought that the collision broadening of microwave lines is mainly of the impact type: this is because collisions only last for a fraction of a cycle of the applied electric field. Recently, Howard and Smith (1950) have measured the temperature dependence of a prominent line in the inversion spectrum of NH_3 ; their measurements support this view.

We must now consider the solution of (2.4 *a*). It may be written in the form

$$\rho(t) = R(t)\rho(0)R^*(t),$$

where the unitary operator R satisfies

$$i\hbar \frac{\partial R}{\partial t} = H_2 R. \quad \dots \dots \dots (2.8)$$

Because of the form of $\rho(o)$, the equation for $\rho(t)$ is equivalent to

$$\langle a, \mathbf{r} | \rho(t) | b, \mathbf{s} \rangle = \sum_{cd} \int g(\mathbf{k}) \cdot d^3\mathbf{k} \cdot \langle a | \phi(\mathbf{r}, t) | c \rangle \langle c | S_2(0) | d \rangle \langle d | \phi^*(\mathbf{s}, t) | b \rangle, \quad (2.9)$$

where ϕ is defined by

$$\langle a | \phi(\mathbf{r}, t) | b \rangle = \int \langle a, \mathbf{r} | R(t) | b, \mathbf{s} \rangle \exp(i\mathbf{k} \cdot \mathbf{s}) \cdot d^3\mathbf{s}.$$

We shall now show that ϕ can be simply expressed in terms of the f 's.

We write

$$H'_2 = H_0 + V(\mathbf{r}, t),$$

where H_0 , the "non-interaction" part of H'_2 , is defined by

$$H_0 = H_2^0 + \frac{1}{m} p^2.$$

Later, we shall need the symbol H_0 to denote $H^0 - \boldsymbol{\mu} \cdot \mathbf{F} \cos \nu t$: this sort of duplication is inevitable if we wish to use "H" for all the Hamiltonians occurring in the problem.

(2.8) is equivalent to the integral equation

$$R = \exp(H_0 t / i\hbar) + \frac{1}{i\hbar} \int_{T-\tau}^T \exp\{H_0(t-t')/i\hbar\} V \cdot R(t') dt'.$$

From this, we deduce that ϕ satisfies

$$\begin{aligned} \langle a | \phi(\mathbf{r}) | m \rangle &= [\exp(i\mathbf{k} \cdot \mathbf{r})] \cdot \delta_{am} \cdot \exp \frac{(E_m + \hbar^2 k^2 / m)t}{i\hbar} \\ &+ \frac{1}{i\hbar} \sum_{b'} \int_{T-\tau}^T \int \langle a, \mathbf{r} | \exp\{H_0(t-t')/i\hbar\} | b, \mathbf{s} \rangle d^3\mathbf{s} \\ &\times \langle b | V(\mathbf{s}) | c \rangle \langle c | \phi(\mathbf{s}) | m \rangle dt'. \end{aligned}$$

The interpretation of the representative

$$\langle a, \mathbf{r} | \exp\{H_0(t-t')/i\hbar\} | b, \mathbf{s} \rangle$$

is not immediately obvious, but, by transforming from a momentum representation, we find that it is equal to

$$\frac{\delta_{ab}}{(2\pi\hbar)^3} \left(\frac{\pi}{ix}\right)^{3/2} \exp\left\{i\left(\frac{\sigma^2}{4x\hbar^2} - mE_a x\right)\right\},$$

where $x = (t-t')/m\hbar$ and $\sigma = \mathbf{r} - \mathbf{s}$. Now for $t < T - \tau$, $\phi|m\rangle$ varies with t according to

$$\exp \frac{(E_m + \hbar^2 k^2 / m)t}{i\hbar}.$$

showing that it is a ket-vector corresponding to a state of energy $(E_m + \hbar^2 k^2 / m)$. Now the system we are considering is conservative, so that its energy will be the same for $t > T - \tau$. Hence, if we define ψ by

$$\langle a | \phi(\mathbf{r}, t) | m \rangle = \langle a' | \psi(\mathbf{r}, t) | m \rangle \exp \frac{(E_m + \hbar^2 k^2 / m)t}{i\hbar},$$

ψ will not have any oscillatory dependence on t . It will satisfy the integral equation

$$\langle a | \psi(\mathbf{r}) | m \rangle = \delta_{am} \exp(i\mathbf{k} \cdot \mathbf{r}) + \frac{m}{i(2\pi\hbar)^3} \Sigma_b \int \langle a | V(\mathbf{s}) | b \rangle d^3\mathbf{s} \\ \times \int_{x_1}^{x_2} \left(\frac{\pi}{ix}\right)^{3/2} \left\{ \exp i \left(\frac{\sigma^2}{4x\hbar^2} + \hbar^2 k_{ma}^2 x \right) \right\} \cdot \langle b | \psi(\mathbf{s}) | m \rangle dx,$$

where
$$x_1 = \frac{t-T}{m\hbar} \quad \text{and} \quad x_2 = \frac{t-T+\tau}{m\hbar}.$$

The x -integral may be evaluated by the method of stationary phases (see Jeffreys and Jeffreys, 1946, p. 474). The asymptotic form of the equation turns out to be

$$\langle a | \psi(\mathbf{r}) | m \rangle = \delta_{am} \exp(i\mathbf{k} \cdot \mathbf{r}) - \frac{m}{4\pi\hbar^2} Q(r) \Sigma_b \int \frac{\exp(ik_{ma}\sigma)}{\sigma} \\ \times \langle a | V(\mathbf{s}) | b \rangle \langle b | \psi(\mathbf{s}) | m \rangle d^3\mathbf{s},$$

where
$$Q(r) = 1 \quad \psi \quad \frac{2\hbar k_{ma}(t-T)}{m} \leq r \leq \frac{2\hbar k_{ma}(t-T+\tau)}{m} \\ = 0 \quad \text{otherwise}$$

Hence, by comparison with (2.7), we infer that

$$\langle a | \psi(\mathbf{r}) | m \rangle = \delta_{am} \cdot \exp(i\mathbf{k} \cdot \mathbf{r}) + Q(r) \frac{\exp(ik_{ma}r)}{r} \langle a | f(\mathbf{k}, \mathbf{k}_{ma}) | m \rangle.$$

Hence in this problem, the "scattered wave" (represented by the second term) is the same as in the time-independent problem inside a shell of radii

$$\frac{2\hbar k_{ma}(t-T)}{m} \quad \frac{2\hbar k_{ma}(t-T+\tau)}{m}$$

and zero outside this shell. This shell is just the region which is classically accessible to the molecules, so that this equation is what we would expect on classical grounds. Using it, we can calculate $\rho(t)$, and hence $S_2(t)$ by integration over the external coordinates. We find, asymptotically, that

$$\langle a | S_2(t) | b \rangle = \exp(-i\omega_{ab}t) \{ \langle a | S_2(0) | b \rangle + \tau \Sigma_{c,d} K(ab, cd) \langle c | S_2(0) | d \rangle \}, \quad \dots \quad (2.10)$$

where $\hbar\omega_{ab} = E_a - E_b$, and

$$K(ab, cd) = \int g(\mathbf{k}) d^3\mathbf{k} \left\{ \frac{2\hbar k_{ca}}{m} \int \langle a | f(\mathbf{k}, k_{ca}\mathbf{n}) | c \rangle \langle b | f(\mathbf{k}, k_{ca}\mathbf{n}) | d \rangle d\mathbf{n} \right. \\ \left. + \frac{4\pi\hbar}{im} [\langle a | f(\mathbf{k}, \mathbf{k}) | c \rangle \delta_{bd} - \overline{\langle b | f(\mathbf{k}, \mathbf{k}) | d \rangle} \delta_{ac}] \right\}, \quad \dots \quad (2.11)$$

\mathbf{n} is the unit vector in the direction of \mathbf{r} , and $d\mathbf{n}$ denotes integration over solid angle, *i. e.*, over all directions of scattering; $g(\mathbf{k})$ is the velocity distribution function. There are energy restrictions on the states occurring in the various terms of $K(ab, cd)$; these are

$$\begin{aligned}\omega_{ab} &= \omega_{cd} \text{ for the first term} \\ \omega_{ac} &= 0 \quad \text{,,} \quad \text{second ,,} \\ \omega_{bd} &= 0 \quad \text{,,} \quad \text{third ,,}\end{aligned}$$

The first term represents the true scattered wave, while the second and third terms represent "shadow scattering" or loss from the incident wave due to the scattering process (we shall later justify this identification by classical analogy).

In the absence of the interaction V , the time development of the density matrix is given by

$$\langle a | Z_2(t) | b \rangle = \exp(-i\omega_{ab}t) \langle a | S_2(0) | b \rangle$$

(the symbol Z will always be used in this sense in future). Equation (2.10) can then be written

$$\langle a | S_2(t) | b \rangle = \langle a | Z_2(t) | b \rangle + \tau \sum_{cd} K(ab, cd) \langle c | Z_2(t) | d \rangle, \quad (2.10 a)$$

which represents the effect of the interaction as a term proportional to τ , the time during which it is effective.

In future, the symbols $|a\rangle, |b\rangle, |c\rangle$, and $|d\rangle$ will be reserved for two-molecule states, and all other symbols will refer to one-molecule states. The quantity we are really interested in is not S_2 , but S_1 : now $S_2 = S_1^{(1)} \wedge S_1^{(2)}$, or, in representative form

$$\langle a | S_2 | b \rangle = \langle g | S_1^{(1)} | h \rangle \langle v | S_1^{(2)} | Z \rangle.$$

Taking the trace of (2.10 a) over the coordinates of molecule (2), we get

$$\begin{aligned}\langle g | S_1^{(1)}(t) | h \rangle &= \langle g | Z_1^{(1)}(t) | h \rangle \\ &+ \tau \sum_{ij, wx, y} K(gy, hy; ij, wx) \langle i | Z_1^{(1)}(t) | w \rangle \langle j | Z_1^{(2)}(t) | x \rangle.\end{aligned} \quad (2.12)$$

From a quantum-mechanical view-point, the molecule (1) must be regarded as interacting with all the $(N-1)$ other molecules in unit volume. Thus equation (2.12) is incomplete, and should actually read

$$\begin{aligned}\langle g | S_1^{(1)}(t) | h \rangle &= \langle g | Z_1^{(1)}(t) | h \rangle \\ &+ \tau \sum_{r=2}^N \sum_{ij, wx, y} K(gy, hy; ij, wx) \langle i | Z_1^{(1)}(t) | w \rangle \langle j | Z_1^{(r)}(t) | x \rangle.\end{aligned}$$

The matrix U of §1 is defined by

$$NU = \sum_{r=1}^N S_1^{(r)},$$

and similarly we may define

$$NW = \sum_{r=1}^N Z_1^{(r)}.$$

Since N is very large, (2.12) can be written, with negligible error,

$$\begin{aligned}\langle g | S_1^{(1)}(t) | h \rangle &= \langle g | Z_1^{(1)}(t) | h \rangle \\ &+ N\tau \sum_{ij, wx, y} K(gy, hy; ij, wx) \langle i | Z_1^{(1)}(t) | w \rangle \langle j | W(t) | x \rangle.\end{aligned}$$

The same equation holds for any other molecule in the gas, *i. e.*

$$\begin{aligned}\langle g | S_1^{(r)}(t) | h \rangle &= \langle g | Z_1^{(r)}(t) | h \rangle \\ &+ N\tau \sum_{ij, wx, y} K(gy, hy; ij, wx) \langle i | Z_1^{(r)}(t) | w \rangle \langle j | W(t) | x \rangle.\end{aligned}$$

Summing this over all r , we have finally

$$\begin{aligned}\langle g | U(t) | h \rangle &= \langle g | W(t) | h \rangle \\ &+ N\tau \sum_{ij, wx, y} K(gy, hy; ij, wx) \langle i | W(t) | w \rangle \langle j | W(t) | x \rangle,\end{aligned}$$

and in particular

$$\begin{aligned}\langle g | U(T) | h \rangle &= \langle g | W(T) | h \rangle \\ &+ N\tau \sum_{ij, wx, y} K(gy, hy; ij, wx) \langle i | W(T) | w \rangle \langle j | W(T) | x \rangle.\end{aligned}\tag{2.13}$$

This formula is only true as long as the interval $(T - \tau, T)$ is short, since it does not allow for the possibility of a molecule making more than one collision. But we are interested in the behaviour of $U(t)$ over relatively long intervals of time; since we are assuming the applied field to be slow even one period is, for our purpose, a long time.

The second term on the right-hand side of (2.13) represents the redistribution of molecules among the various states by the collision process: this rearrangement is going on continually. In the problem we have, as it were, "frozen" the gas in the distribution $U(0)$ up to time $t = T - \tau$, and have then found the effect of single collisions on this distribution.

Now up to the time $t = T - \tau$, when the interaction is switched on, $U(t) = W(t)$, so that we can subtract $U(T - \tau) = W(T - \tau)$ from both sides of (2.13), to give

$$\begin{aligned}\langle g | U(T) - U(T - \tau) | h \rangle &= \langle g | W(T) - W(T - \tau) | h \rangle \\ &+ N\tau \sum_{ij, wx, y} K(gy, hy; ij, wx) \langle i | W(T) | w \rangle \langle j | W(T) | x \rangle.\end{aligned}$$

This shows clearly that (2.13) represents an infinitesimal portion of the redistribution process, and must be regarded as a differential equation

$$\left\langle g \left| \frac{\partial U}{\partial t} \right| h \right\rangle = \left\langle g \left| \frac{\partial W}{\partial t} \right| h \right\rangle + N \sum_{ij, wx, y} K(gy, hy; ij, wx) \langle i | W | w \rangle \langle j | W | x \rangle,$$

since it is only true for every short time-intervals. Now from the definition of V

$$\frac{\partial W}{\partial t} = \frac{1}{i\hbar} (H^0 W - W H^0),$$

so that

$$\begin{aligned} \left\langle g \left| \frac{\partial U}{\partial t} \right| h \right\rangle &= \frac{1}{i\hbar} \langle g | H^0 W - W H^0 | h \rangle \\ &+ N \sum_{ij, wx, y} K(gy, hy; ij, wx) \langle i | W | w \rangle \langle j | W | x \rangle. \end{aligned}$$

Since the interval τ is so small, the difference between U and V on the right-hand side of this equation may be neglected, and it may finally be written

$$\begin{aligned} \left\langle g \left| \frac{\partial U}{\partial t} \right| h \right\rangle &= \frac{1}{i\hbar} \langle g | H^0 U - U H^0 | h \rangle \\ &+ N \sum_{ij, wx, y} K(gy, hy; ij, wx) \langle i | U | w \rangle \langle j | U | x \rangle. \end{aligned}$$

This interpretation of (2.13) as a differential equation is most easily grasped by thinking of the redistribution process as occurring in successive "rounds." If the initial density matrix is $V = U_0$, this will be reduced to U_1 by the first round of collisions. For the second round, we must then write $V = U_1$, and obtain as a solution $U = U_2$, and so on. Plainly, these rounds must be of infinitesimal length since, in a finite interval, there is always a finite possibility of a molecule making more than one collision. By comparison with (1.1), we see that

$$\left\langle g \left| \frac{\partial_e U}{\partial t} \right| h \right\rangle = N \sum_{ij, wx, y} K(gy, hy; ij, wx) \langle i | U | w \rangle \langle j | U | x \rangle. \quad (2.14)$$

The equilibrium statistical matrix U_e is defined by $\partial_e U_e / \partial t = 0$, i. e.

$$\sum_{ij, wx, y} K(gy, hy; ij, wx) \langle i | U_e | w \rangle \langle j | U_e | x \rangle = 0.$$

We are interested in the value of $\partial_e U / \partial t$ when U is fairly near equilibrium, i. e., when

$$Y = U - U_e$$

is small compared to U_e . Substituting this into (2.14) and neglecting the term of order Y^2 , we get

$$\begin{aligned} \left\langle g \left| \frac{\partial_e U}{\partial t} \right| h \right\rangle &= N \sum_{ij, wx, y} K(gy, hy; ij, wx) [\langle i | U_e | w \rangle \langle j | Y | x \rangle \\ &+ \langle i | Y | w \rangle \langle j | U_e | x \rangle] \\ &= N \sum_{ij, wx, y} [K(gy, hy; ij, wx) + K(gy, hy; ji, wx)] \\ &\times \langle i | U_e | w \rangle \langle j | Y | x \rangle, \end{aligned}$$

on rearranging the dummy indices on the second term. Comparing this last formula with (2.1), we see that

$$L(gh, wx) = N \sum_{i,j,y} [K(gy, hy; iw, jx) + K(gy, hy; wi, xj)] \times \langle i | U_e | j \rangle, \quad (2.15)$$

the specific formula for the coefficients L which we wanted to find.

§3. THE DERIVATION OF U_e .

We should expect U_e to be a Boltzmann distribution

$$\langle i | U_e | j \rangle = \frac{\exp(-E_i/kT)}{\sum_i \exp(-E_i/kT)} \delta_{ij}. \quad (3.1)$$

but we have to show that this matrix satisfies the equation $\partial_c U_e / \partial t = 0$. We shall do this by showing that the solution of

$$\sum_{c,d} K(ab, cd) \langle c | S_2 | d \rangle = 0$$

is

$$\langle c | S_2 | d \rangle = \frac{\exp(-E_c/kT)}{\sum_c \exp(-E_c/kT)} \delta_{cd},$$

for the validity of (3.1) then follows by taking the trace of this equation with respect to the coordinates of molecule (2).

To justify this last equation, we need to prove a reciprocity theorem, analogous to the Lorentz theorem of electrodynamics, which states

$$\langle b | f(k\alpha, -k_{ba}\beta) | a \rangle = \langle a | f(k_{ba}\beta, -k\alpha) | b \rangle. \quad (3.2)$$

This is easy enough to prove for elastic scattering, but for inelastic scattering it becomes somewhat complicated, owing to the large number of coordinates involved. In order to keep the writing to a minimum, we shall only prove the theorem for the simplest possible case, that of the scattering of electrons by a hydrogen atom. The generalization of this to more complex cases is obvious enough, if rather tedious.

We take the proton as the centre of coordinates (assuming it to be so massive compared to the electrons that it does not move), and let the coordinates of the bound and free electrons be \mathbf{r}_1 and \mathbf{r}_2 respectively. We expand the overall wavefunction $\psi_1(\mathbf{r}_1, \mathbf{r}_2, t)$ in terms of the eigenfunctions $\{\phi_m(\mathbf{r}_1)\}$ of the scatterer

$$\psi_1(t) = \sum_n \phi_n(\mathbf{r}_1, t) F_n(\mathbf{r}_2, t)$$

We also take another solution $\psi_2(t)$ of the equation of motion, and expand it in the form

$$\psi_2(-t) = \sum_m \phi_m^*(\mathbf{r}_1, t) G_m(\mathbf{r}_2, -t)$$

[since $\phi_m^*(t)$ and $\phi_m(-t)$ have the same dependence on t]. We can thus show that F and G must satisfy the equation.

$$\sum_n \sum_n \phi_m^*(t) \phi_n(t) \left\{ i\hbar \frac{\partial}{\partial t} [G_m(-t) F_n(t)] - \frac{\hbar^2}{2m} [G_m \nabla^2 F_n - F_n \nabla^2 G_m] \right\} = 0,$$

the argument being much the same as that used to deduce the wave-mechanical current vector. We now integrate this over $d^3\mathbf{r}_1$, and since the $\{\phi_n\}$ form a c.n.o.s., we get

$$\sum_n \left\{ i\hbar \frac{\partial}{\partial t} [G_n(-t) F_n(t)] - \frac{\hbar^2}{2m} [G_n \nabla^2 F_n - F_n \nabla^2 G_n] \right\} = 0,$$

If ψ_1 and ψ_2 correspond to states of the same energy, the time-variations of F_n and G_n are equal and opposite, so that the first term is zero; also the time factors cancel in the second term, giving

$$\sum_n (G_n \nabla^2 F_n - F_n \nabla^2 G_n) = 0$$

or, by Green's theorem

$$\sum_n \int_S (F_n \nabla G_n - G_n \nabla F_n) \cdot d\mathbf{s} = 0, \quad . \quad . \quad . \quad . \quad (3.3)$$

S being any closed surface. This equation is true for any inelastic scattering process.

In agreement with (2.5), we take F_n and G_n to be given asymptotically by

$$F_n(\mathbf{r}) = [\exp(i\mathbf{k}r\mathbf{n} \cdot \boldsymbol{\alpha})] \delta_{na} + \frac{\exp(ik_{na}r)}{r} \langle n | f(k\boldsymbol{\alpha}, k_{na}\mathbf{n}) | a \rangle$$

$$G_n(\mathbf{r}) = [\exp(ik_{ba}\mathbf{n} \cdot \boldsymbol{\beta})] \delta_{nb} + \frac{\exp(ik_{nb}r)}{r} \langle n | f(k_{ba}\boldsymbol{\beta}, k_{na}\mathbf{n}) | b \rangle.$$

These refer to states of the same energy; F represents a wave incident in direction $\boldsymbol{\alpha}$ on the scatterer in state $|a\rangle$, while G represents the scatterer in state $|b\rangle$ and the incident wave coming in direction $\boldsymbol{\beta}$. Substituting these into (3.3), and performing the integrations, the theorem (3.2) follows at once.

Another result which we need follows from the fact that the operator R introduced in equation (2.8) is unitary. This gives us the equation

$$\sum_c \int \langle a | \phi^*(\mathbf{r}) | c \rangle d^3\mathbf{r} \langle c | \phi(\mathbf{r}) | b \rangle = \delta_{ab}$$

and using our equation for ϕ , this reduces to

$$\sum_{ac} k_{ac} \int \langle c | f(\mathbf{k}, k_{ac}\mathbf{n}) | a \rangle \langle c | f(\mathbf{k}, k_{ac}\mathbf{n}) | b \rangle \cdot d\mathbf{n} = -4\pi \text{Im} \{ \langle a | f(\mathbf{k}, \mathbf{k}) | b \rangle \},$$

. . . (3.4)

(subject to the restriction $w_{ab}=0$). (3.2) and (3.4) represent basic restrictions on any set of f 's for a collision problem. (3.2) tells us that the cross-section for any given process is the same as the cross-section

for the inverse process, while (3.4) is a consequence of the conservation of mass; any particles scattered must be compensated by losses from the incident "beam."

By repeated use of the reciprocity theorem, we can show that (3.4) is equivalent to

$$\Sigma \int k_{ca} g(\mathbf{k}_{ca}) d^3 \mathbf{k} \cdot \int \langle a | f(\mathbf{k}, k_{ca} \mathbf{n}) | c \rangle \overline{\langle b | f(\mathbf{k}, k_{ca} \mathbf{n}) | c \rangle} \cdot d\mathbf{n} \\ = -4\pi I m \{ \int g(\mathbf{k}) d^3 \mathbf{k} \langle a | f(\mathbf{k}, \mathbf{k}) | b \rangle \}, \quad . \quad . \quad . \quad (3.4 a)$$

$g(\mathbf{k})$ being the velocity distribution function.

Our object is to find a value of S_2 which makes

$$\langle a | C | b \rangle \Sigma_{cd} K(ab, cd) \langle c | S_2 | d \rangle$$

zero, C being proportional to the two-molecule scattered wave. Now we know, on general statistical-mechanical grounds, that S_2 must be diagonal in an energy representation, so that we need only consider the diagonal elements $K(aa, cc)$ of the array $K(cd, ab)$ (this can be proved directly, using the reciprocity theorem). We then have

$$\langle a | C | a \rangle = \Sigma_c K(aa, cc) \langle c | S_2 | c \rangle \\ = \Sigma_c \int \int \frac{2\hbar k_{ca}}{m} | \langle a | f(\mathbf{k}, k_{ca} \mathbf{n}) | c \rangle |^2 d\mathbf{n} \cdot d^3 \mathbf{k} \\ \times \{ g(\mathbf{k}) \langle c | S_2 | c \rangle - g(\mathbf{k}_{ca}) \langle a | S_2 | a \rangle \} \quad . \quad . \quad . \quad (3.5)$$

from (3.4 a). (3.5) can be compared with the corresponding classical equation, for $\langle c | S_2 | c \rangle$ can be identified with ρ_c , the fraction of molecules in the state $|c\rangle$, while

$$\frac{k_{ca}}{k} | \langle a | f(\mathbf{k}, k_{ca} \mathbf{n}) | c \rangle |^2$$

is $\sigma_{ca}(\mathbf{n})$, the differential cross-section for a collision in which the scatterer goes from state $|c\rangle$ to state $|a\rangle$, the scattered particle going off in direction \mathbf{n} . Remembering that $2\hbar k/m$ is just v , the relative molecular velocity before collision, (3.5) may be written

$$\langle a | c | a \rangle = \Sigma_c \int \int v \cdot \sigma_{ca}(\mathbf{n}) \{ g(\mathbf{k}) \rho_c - g(\mathbf{k}_{ca}) \rho_a \} d^3 \mathbf{k} \cdot d\mathbf{n}.$$

This is identical with the classical expression obtained by direct physical arguments, which confirms the accuracy of our analysis. The first term represents the increase in the population of state $|a\rangle$ due to molecules being knocked into this state from other states; the second term represents losses in this population due to molecules being knocked out of this state. This argument identifies the terms of (2.11).

Now an argument, due originally to Boltzmann shows that $\langle a|C|a\rangle$ is zero if, and only if,

$$g(\mathbf{k}) = \left(\frac{\hbar^2}{\pi m k T} \right)^{3/2} \exp(-\hbar^2 \mathbf{k}^2 / m k T),$$

and

$$S_2 = A \exp(-H_2^0 / kT)$$

(A being a normalizing constant); i. e., if $g(\mathbf{k})$ is a Maxwellian velocity distribution, and S_2 is a Boltzmann density matrix. Hence we have shown that

$$\langle i|U_e|j\rangle = \langle i|\rho_B|i\rangle \delta_{ij}$$

where

$$\langle i|\rho_B|i\rangle = \frac{\exp(-E_i/kT)}{\sum_i \exp(-E_i/kT)},$$

(ρ_B thus being properly normalized). The formula (2.15) for $L(gh, wx)$ thus becomes

$$L(gh, wx) = -N \sum_{i,u} [K(gy, hy; i\omega, ix) + K(gy, hy; \omega i, xi)] \langle i|\rho_B|i\rangle. \quad (3.6)$$

§4. DEDUCTION OF A CLOSED FORMULA FOR σ .

In future, we shall use the symbol σ_{gh} to denote the "complex breadth" of the spectral line corresponding to the transition $g \rightarrow h$. By this, we mean that σ_{gh} is a complex number whose real and imaginary parts give the line breadth and shift respectively. We want to obtain an expression for σ in terms of the $L(gh, wx)$.

The equation of motion of S , including the effect of the applied electric field, is

$$\left\langle g \left| \frac{\partial S}{\partial t} \right| h \right\rangle = \frac{1}{i\hbar} \langle g|H_0 S - S H_0|h\rangle + \sum_{wx} L(gh, wx) \langle w|S - S_e|x\rangle,$$

where

$$H_0 = H^0 - \boldsymbol{\mu} \cdot \mathbf{F} \cos \nu t.$$

We solve this by making the weak-field approximation, putting

$$S = S_e + \mathbf{D} \cdot \mathbf{F}$$

and ignoring terms in F^2 . In the microwave region, all energy differences are $\ll kT$, so that

$$S_e \sim 1 - \frac{H_0}{kT} + \frac{\boldsymbol{\mu} \cdot \mathbf{F}}{kT} \cos \nu t.$$

This gives us the equation of motion

$$\left\langle g \left| \frac{\partial \mathbf{D}}{\partial t} \right| h \right\rangle = \frac{\nu \sin \nu t}{kT} \langle g|\boldsymbol{\mu}|h\rangle - i\omega_{gh} \langle g|\mathbf{D}|h\rangle + \sum_{wx} L(gh, wx) \langle w|\mathbf{D}|x\rangle. \quad (4.1)$$

Now rotational degeneracy must always be present. This is a consequence of the fact that, in an infinitesimal applied field such as we are considering here, all permitted orientations of the molecule have the same energy. We shall assume that there is no other form of degeneracy present; this is usually so, and when it is not the theory given below can easily be extended.

Hence any state must be labelled

$$|g, m_g\rangle,$$

where m_g is the magnetic quantum number; E_g is, of course, independent of m_g . We shall assume that there is no accidental degeneracy, that is that ω_{jk} cannot equal ω_{gh} unless $|j\rangle \equiv |g\rangle$ and $|k\rangle \equiv |h\rangle$. It seems likely that this assumption is correct for all actual atomic systems.

Suppose now that the applied field is in the z -direction; we shall then want to know D_z , and taking account of the orientational degeneracy, (4.1) may be written

$$\begin{aligned} \langle g, m_1 | \left(\frac{\partial}{\partial t} + i\omega_{gh} \right) D_z | h, m_2 \rangle &= \frac{\nu \sin \nu t}{kT} \langle g, m_1 | \mu_z | h, m_2 \rangle \\ &+ \sum_{w, m_3; x, m_4} L(g, m_1; h, m_2; w, m_3; x, m_4) \langle w, m_3 | D_z | x, m_4 \rangle. \end{aligned}$$

Now since $\mathbf{D} \cdot \mathbf{F}$ is a scalar, \mathbf{D} must transform like a vector; that is to say that \mathbf{D} and $\boldsymbol{\mu}$ transform in the same way under a rotation, so that

$$\langle g, m_1 | D_z | h, m_2 \rangle = \langle g | \lambda | h \rangle \langle g, m_1 | \mu_z | h, m_2 \rangle,$$

where the representatives $\langle g | \lambda | h \rangle$ are independent of the indices m . Then λ is given by

$$\begin{aligned} \langle g, m_1 | \mu_z | h, m_2 \rangle &\left\{ \langle g | \left(\frac{\partial}{\partial t} + i\omega_{gh} \right) \lambda | h \rangle - \frac{\nu \sin \nu t}{kT} \right\} \\ &= \sum_{w, x} \langle w | \lambda | x \rangle \sum_{m_3, m_4} L(g, m_1; h, m_2; w, m_3; x, m_4) \langle w, m_3 | \mu_z | x, m_4 \rangle. \end{aligned} \quad (4.2)$$

The general solution of this equation is extremely complicated. However, in the case where the breadth of the lines is much less than their separation, we can derive a simple formula for σ . This is obviously the case of practical importance, since when the lines begin to overlap seriously, it will not be possible to measure their breadths.

The case not covered by this assumption is that of a very wide variation in the spacing of the lines. Thus, if two spectral lines were very close together, they might be merged while the spectrum was apparently well resolved. However, this line would probably have an anomalous shape, and if such an effect were found experimentally, it would be quite easy to check the above explanation.

In mathematical form, this assumption is equivalent to

$$\omega_{jk} - \omega_{mn} \gg L(gh, wx),$$

for any set of indices. We now suppose that ν , the frequency of the applied field, is near ω_{gh} , in the sense that $\omega_{gh} - \nu = \Delta$ is of the same order of magnitude as L . It is quite easy to show that, under these assumptions,

$$\langle j | \lambda | k \rangle \text{ is of magnitude } \frac{1}{kT} \frac{\nu}{\omega_{jk} - \omega_{gh}} \quad (j, k \neq g, h),$$

while

$$\langle g | \lambda | h \rangle \text{ is of magnitude } \frac{1}{kT} \frac{\nu}{\Delta}.$$

Hence $\langle g | \lambda | h \rangle$ is much larger than the other representatives of λ , and therefore in the sum on the right-hand side of (4.2), only the terms containing $\langle g | \lambda | h \rangle$ need be retained. [This assumes that $L(g, m_1; h, m_2; g, m_3; h, m_4)$ is not much smaller than the other coefficients L ; but this would give rise to a very narrow line, which would plainly be anomalous]. (4.2) then becomes a simple equation for $\langle g | \lambda | h \rangle$

$$\begin{aligned} & \left\{ \left(\frac{\partial}{\partial t} + i\omega_{gh} \right) \langle g, m_1 | \mu_z | h, m_2 \rangle \right. \\ & \quad \left. - \sum_{m_3, m_4} L(g, m_1; h, m_2; g, m_3; h, m_4) \langle g, m_3 | \mu_z | h, m_4 \rangle \right\} \\ & \quad \times \langle g | \lambda | h \rangle = \frac{\nu \sin \nu t}{kT} \langle g, m_1 | \mu_z | h, m_2 \rangle. \quad \dots \quad (4.3) \end{aligned}$$

Since we know that $\langle g | \lambda | h \rangle$ is independent of the indices m , we clear them out, and at the same time convert (4.3) from a vector to a scalar equation, by multiplying both sides by

$$\langle h, m_2 | \mu_z | g, m_1 \rangle = \overline{\langle g, m_1 | \mu_z | h, m_2 \rangle},$$

and summing over m_1 and m_2 . This gives us

$$\left(\frac{\partial}{\partial t} + i\omega_{gh} - \sigma_{gh} \right) \langle g | \lambda | h \rangle = \frac{\nu \sin \nu t}{kT}, \quad \dots \quad (4.4)$$

where

$$\sigma_{gh} =$$

$$\frac{\sum_{m_1 m_2 m_3 m_4} L(g, m_1; h, m_2; g, m_3; h, m_4) \langle g, m_3 | \mu_z | h, m_4 \rangle \langle h, m_2 | \mu_z | g, m_1 \rangle}{\sum_{m_1 m_2} |\langle g, m_1 | \mu_z | h, m_2 \rangle|^2} \quad \dots \quad (4.5)$$

By comparison with the calculations of Karplus and Schwinger, we see that this corresponds to a line of Van Vleck-Weisskopf shape, with a complex breadth σ_{gh} . An equation substantially equivalent to (4.5) has already been deduced by Anderson (1949), by a different method.

We have equations giving $L(gh, wx)$ in terms of $K(ab, cd)$ and $K(ab, cd)$ in terms of the f 's, so that we can obtain a formula for σ_{gh} in terms of the f 's. The details of the substitution are quite trivial, though rather tedious; the result is

$$\sigma_{gh} = \frac{N \int \Omega_{gh}(\mathbf{k}) g(\mathbf{k}) d^3\mathbf{k}}{\sum_{m_1, m_2} |\langle g, m_1 | \mu_z | h, m_2 \rangle|^2}, \quad (4.6)$$

where $g(\mathbf{k})$ is the Maxwellian velocity distribution, and

$$\begin{aligned} \Omega_{gh} = & \frac{2\hbar}{m} \left[\sum_{i, m_i; y, m_y; m_1, m_3} \langle i | \rho_B | i \rangle \langle g, m_1 | \mu_z | h, m_1 \rangle \langle h, m_3 | \mu_z | g, m_3 \rangle \right. \\ & \times \{ \overline{\langle h, m_3; y, m_y | f(\mathbf{k}, k_{iy}\mathbf{n}) | h, m_1; i, m_i \rangle} \\ & \times \langle g, m_3; y, m_y | f(\mathbf{k}, k_{iy}\mathbf{n}) | g, m_1; i, m_i \rangle \\ & + \overline{\langle h, m_3; y, m_y | f(\mathbf{k}, k_{iy}\mathbf{n}) | i, m_i; h, m_1 \rangle} \\ & \times \langle g, m_3; y, m_y | f(\mathbf{k}, k_{iy}\mathbf{n}) | i, m_i; g, m_1 \rangle \} d\mathbf{n} \Big] \\ & + \frac{4\pi\hbar}{im} \left\{ \left[\sum_{i, m_i; m_1} \langle i | \rho_B | i \rangle |\langle g, m_1 | \mu_z | h, m_1 \rangle|^2 \right. \right. \\ & \times \overline{\langle h, m_1; i, m_i | f(\mathbf{k}, \mathbf{k}) | h, m_1; i, m_i \rangle} \\ & \left. \left. - \langle g, m_1; i, m_i | f(\mathbf{k}, \mathbf{k}) | g, m_1; i, m_i \rangle \right] \right. \\ & + \left[\sum_{m_1, m_3} \langle g, m_1 | \mu_z | h, m_1 \rangle \langle h, m_3 | \mu_z | g, m_3 \rangle \right. \\ & \times \overline{\langle g | \rho_B | g \rangle \langle h, m_3; g, m_1 | f(\mathbf{k}, \mathbf{k}) | g, m_3; h, m_1 \rangle} \\ & \left. \left. - \langle h | \rho_B | h \rangle \langle g, m_3; h, m_1 | f(\mathbf{k}, \mathbf{k}) | h, m_3; g, m_1 \rangle \right] \right\}, \quad (4.6a) \end{aligned}$$

(the last two f terms are not necessarily equal, since f need not be Hermitian). This will, in general, be a complex quantity, so that we would expect collisions to shift lines as well as to broaden them. It is quite easy to show that if $E_i \ll kT$

$$\frac{\text{shift}}{\text{breadth}} = O\left(\frac{E_i}{kT}\right).$$

Hence in the microwave region, the shift will be a relatively small effect, and it is not surprising that it has not yet been detected.

The equation (4.6) is believed to be more accurate than that used by Anderson. However, using Anderson's equation, it is quite easy to calculate σ_{gh} from a known $V(\mathbf{r})$, while using this equation, it is very difficult because of the difficulty of determining the f 's. It is therefore hoped to show, in a later paper, that Anderson's equation is a first

approximation to our (4.6), and to estimate the error of this approximation (which will presumably be mainly due to neglect of inelastic collisions).

I am much indebted to Professor M. H. L. Pryce for the advice and encouragement he has given me during the course of this work, and to the D.S.I.R. for a maintenance grant.

REFERENCES.

- ANDERSON, 1949, *Phys. Rev.*, **76**, 647.
BLEANEY and PENROSE, 1947, *Proc. Roy. Soc. A*, **189**, 358.
BORN and GREEN, 1947, *Proc. Roy. Soc. A*, **191**, 168.
FRÖHLICH, 1946, *Nature, Lond.*, **157**, 478.
HOWARD and SMITH, 1950, *Phys. Rev.*, **77**, 840.
JEFFREYS and JEFFREYS, 1946, *Methods of Mathematical Physics* (Cambridge: University Press).
KARPLUS and SCHWINGER, 1948, *Phys. Rev.*, **74**, 1020.
LORENTZ, 1906, *Proc. Amst. Acad. Sci.*, **8**, 59.
MARGENAU and WATSON, 1936, *Rev. Mod. Phys.*, **8**, 22.
VAN VLECK and WEISSKOPF, 1945, *Rev. Mod. Phys.*, **17**, 227.

V. *Anisotropy of Electrical Resistivity of Cold-Rolled Cubic Metals and Alloys.*

By T. BROOM,

Division of Tribophysics, C.S.I.R.O., Melbourne, Australia*.

[Received September 11, 1950.]

ABSTRACT

The electrical resistivity of cold-rolled copper, low carbon steel, brass and sterling silver has been found to vary with direction of measurement. The magnitude of the anisotropy may be qualitatively accounted for by considering the effect of oriented dislocations. The temperature coefficients of resistivity of these rolled metals are isotropic to within 0.5 per cent. These results indicate that deviations from Matthiessen's rule are to be expected.

§1. INTRODUCTION.

THE effect of cold work on the electrical resistivity of cubic metals and alloys has been studied mainly after wire-drawing (Boas 1947). However, the possibility of development of anisotropy of electrical resistivity by cold-work has generally been overlooked. Matsuda (1925), in a general investigation of the effect of cold-rolling on the physical properties of copper and aluminium and their alloys, found small but not systematic differences between the resistivities of longitudinal and transverse specimens. Becker and Born (1925) showed that anisotropy of electrical resistivity in cold-rolled tungsten could not be greater than 5 per cent.

In the present paper experimental evidence is given for the existence of anisotropy in cold-rolled cubic metals, and an explanation of this effect is put forward.

§2. EXPERIMENTAL.

(i) *Materials.*

The six cubic metals selected for study were aluminium of commercial purity, tough-pitch copper, fine silver, low carbon (0.07 per cent) steel, $\alpha + \beta$ brass, and sterling silver; their analyses are given in Table I.

Annealed strips of each metal, about 60 mm. wide and 2.5 mm. thick, were reduced 95 per cent in thickness (to 0.125 mm.) by cold-rolling. Specimens of about 60×2 mm. were cut from the strip at 0° , 45° and 90° to the rolling direction. Some of these specimens were then recrystallized by vacuum annealing.

* Communicated by Dr. W. Boas.

(ii) *Determination of Resistivity.*

A Kelvin Double Bridge was used for all measurements of electrical resistance and the conventional current and potential contacts were made using a system of four needle points on each specimen in turn. The resistance of the 20 mm. length between the potential needle contacts was measured while the specimens were immersed in a bath maintained at $1.0 \pm 0.3^\circ \text{C}$. The usual precautions were taken to eliminate errors due to parasitic E.M.F.s. Some resistance measurements were also made at 0°C . in melting ice and at -183°C . in boiling oxygen in order to determine whether the temperature coefficients of resistivity were isotropic.

For the calculation of resistivities the average cross-section of each specimen was found by determining its weight and length and by assuming a value for the density*. As the thickness of the strips from which the specimens were cut was not uniform across the width, the average cross-section found for specimens cut at 45° and 90° to the direction of rolling was not that of the central 20 mm. over which the resistance measurements were made.

The difficulty in measuring the actual thickness of the central portion of specimens was avoided by remeasuring the resistance of the specimens of each orientation after they had received a suitable vacuum annealing treatment. The resistivity of annealed cubic metals is isotropic, so that differences in the results obtained from the annealed specimens of different orientations were attributed to the effect of non-uniformity of thickness. The value of resistivity found for specimens at 0° to the rolling direction was assumed to be free from this error. The test of anisotropy was whether the fractional change of resistivity on annealing varied with orientation. For this, a statistical treatment was developed.

(iii) *Statistical Treatment.*

In each of the three orientations, 10 specimens were taken and the resistivities x_{ij} ($i=1, 2, 3$; $j=1, 2, \dots, 10$) were measured. After annealing the specimens were found to have resistivities x'_{ij} ($i=1, 2, 3$; $j=1, 2, \dots, 10$). Let $x_{i\bullet}, x'_{i\bullet}$ ($i=1, 2, 3$) denote the mean resistivity for each set of ten specimens. We require to test whether the change in mean resistivity on annealing is dependent on orientation.

Assuming that the variation within each set of 10 measurements is due solely to random fluctuations, we have, as a pooled estimate, S^2 , of the error variance,

$$S^2 = \frac{\sum_{i=1}^3 \sum_{j=1}^{10} (x_{ij} - x_{i\bullet})^2 + \sum_{i=1}^3 \sum_{j=1}^{10} (x'_{ij} - x'_{i\bullet})^2}{60 - 6},$$

* The assumed densities in evaluation of resistivity were: aluminium, 2.70; copper, 8.94; silver, 10.60; 0.07 per cent carbon steel, 7.80; 64/36 brass, 8.50; sterling silver, 10.31 gm./cm.³.

The estimated error variance of the mean of 10 specimens is $S^2/10$ and as the variance of the difference of two variates is the sum of the variances of both variates, the difference $(x_{i\bullet} - x'_{i\bullet})$ is seen to have an estimated error variance of $S^2/5$. To compare the resistivity differences for any two orientations we therefore employ the standard error, $\sqrt{\frac{2}{5}}S$. In the present case, referring to the t -table, we have $t=2.01$ for 54 degrees of freedom and probability $P=0.05$. Hence, if the resistivity differences at two orientations differ by greater than 2.01 times the standard error, the effect of orientation is significant.

It was found convenient to express the difference between means of cold-worked and annealed specimens of any one orientation as a fraction of the "annealed" resistivity in that direction and accordingly, the standard errors were calculated as fractions of the annealed resistivity.

TABLE I.

Analyses of Materials Used.

Aluminium	0.5% Fe; 0.2% Si; traces of Mn, Mg, Cr and Cu.
Copper	0.12% O_2 (1.06% Cu_2O); traces of Ag, Ni and Fe.
Fine Silver	Traces of Mg and Cd.
Mild Steel	0.07% C; 0.21% Mn.
Brass	63.5% Cu; 36.5% Zn; traces of Ag, Mn and Fe.
Sterling Silver	92.8% Ag; 7.2% Cu; traces of Mg and Cd.

§3. RESULTS.

No changes in resistivity of the fine silver specimens were found after a "high" temperature annealing treatment, and it was assumed that the cold-rolled strip had previously recrystallized at room temperature. No results for silver are therefore reported.

The resistivities of the annealed metals used, determined at 1°C . on specimens at 0° to the rolling direction, are given in the second column of Table II. The fractional changes in resistivity, $\Delta\rho/\rho$, on annealing (and their standard errors) relative to the resistivities of the annealed specimens are also given in Table II. for each orientation. The last column gives the anisotropy of resistivity of the 95 per cent cold-rolled metals used, calculated as

$$\frac{1+(\Delta\rho/\rho)_0}{1+(\Delta\rho/\rho)_{90}} = \frac{(\rho_D/\rho_A)_0}{(\rho_D/\rho_A)_{90}},$$

where ρ_D, ρ_A are the resistivities of deformed and annealed specimens, respectively.

Table III. gives the values of the ratios of the resistances of specimens at -183°C . to those of the same specimens at 0°C . The ratios must be independent of orientation for the annealed specimens and the variation found gives an estimate of the experimental error. It will be seen that the ratios for the rolled materials are also independent of orientation within this error (~ 0.5 per cent).

§ 4. DISCUSSION.

The average values for the increase of resistivity accord well with published results, except in the case of copper. Table III. shows that for steel, brass and sterling silver, the transverse resistivity was significantly less than that in the direction of rolling. The reverse was found for copper.

TABLE II.

Fractional Increase of Resistivity on Cold-Rolling (95 per cent Reduction in Thickness).

Metal	Resistivity at 1° C. ohm. cm × 10 ⁻⁶	$\Delta\rho/\rho \times 10^2$ (at 1° C.)			Anisotropy of resistivity
		Orientation to rolling direction			
		0°	45°	90°	
Aluminum	2.63	1.58 ± 0.41	2.07 ± 0.41	1.86 ± 0.41	0.998 ± 0.008
Copper	1.74	4.03 ± 0.46	3.93 ± 0.46	5.04 ± 0.47	0.990 ± 0.009
Steel	9.86	3.63 ± 0.40	2.32 ± 0.40	2.65 ± 0.40	1.010 ± 0.008
Brass	6.42	25.13 ± 0.31	23.46 ± 0.31	23.07 ± 0.32	1.018 ± 0.006
Sterling Silver	1.76	20.19 ± 0.45	19.34 ± 0.44	17.88 ± 0.44	1.020 ± 0.008

TABLE III.

Change of Resistance with Temperature.

Metal	Condition	R_{-183}/R_0		
		Orientation to rolling direction		
		0°	45°	90°
Aluminium	Annealed	0.198	0.201	0.202
	Rolled	0.214	0.217	0.215
Copper	Annealed	0.268	0.268	0.269
	Rolled	0.299	0.299	0.299
Steel	Annealed	0.187	0.187	0.185
	Rolled	0.205	0.206	0.204
Brass	Annealed	0.695	0.694	0.696
	Rolled	0.758	0.758	0.758
Sterling Silver . .	Annealed	0.327	0.328	0.329
	Rolled	0.437	0.438	0.434

This anomalous behaviour of copper may be attributed to the high oxide content, which may also be the cause of the high value of the increase in resistivity. The resistivities at 45° to the rolling direction were intermediate

within experimental error, between the longitudinal and transverse resistivities. No significant effect of orientation was found for aluminium, but it should be noted that the error was high, relative to the increase of resistivity, and an effect of the magnitude found for the other metals would have been undetected.

The isotropy of the temperature coefficients of resistivity (Table III.) is, at first, surprising. However, Grüneisen and Goens (1924) found that the temperature coefficients of zinc and cadmium single crystals were isotropic, despite the pronounced anisotropy of resistivity.

The present results indicate that deviations from Matthiessen's Rule can be expected for a worked cubic metal in which the resistivity is anisotropic. Rutter and Reekie (1950) have recently found deviations which they interpreted in terms of an increase, due to cold-work, in the thermal component of resistivity. It is suggested that a part, at least, of the deviations found by them was due to the dependence of resistivity on the direction of measurement. From considerations given below it will be seen that anisotropy of resistivity is likely to be more marked in drawn wires (as used by Rutter and Reekie) than in rolled metals.

Three possible causes of the anisotropy of resistivity can be considered ; the effect of (i) a second phase, (ii) general lattice strains, and (iii) oriented dislocations.

(i) The effect of a second phase.

None of the metals used was single phase. However the anisotropy found appears to be independent of the estimated quantity of second phase (compare *e.g.* aluminium and steel). Again, the anisotropy developed in brass and sterling silver was similar, although in the case of brass, the second phase has higher hardness and lower resistivity than the matrix and in the case of sterling silver these properties are very similar for both phases. From this indirect evidence it is probable that the presence of second phases had little influence on the anisotropy of the metals used*.

(ii) The effect of general lattice strains.

Bridgman (1925) has studied the effect of tension, within the elastic range, on the transverse and longitudinal resistivities of annealed, flat specimens of several metals. The development of anisotropy was shown and found to vary approximately linearly with the applied load.

This behaviour was presumably due to deformation of the cubic lattice under the externally applied stress. In cold-rolled strip the sum of the internal stresses must be zero, and any effect depending linearly on the stress is therefore also zero. This condition holds approximately in the strip with a high degree of preferred orientation of the crystals. However, if the distribution of crystal orientations is such that the sum of the strains is not zero, owing to the anisotropy of elastic constants, an effect on the electrical resistivity may be expected.

* These considerations apply only when no cracks develop between the second phase and the matrix. It is tentatively suggested that in the present experiments the copper, which contained 1.1 per cent Cu_2O , had a higher transverse resistivity than longitudinal owing to the formation of longitudinal cracks.

A gross overestimate of the magnitude of this effect may be set by considering the application of a stress equal to the yield stress of the material used. For iron, Bridgman gives the values of $+1.42 \times 10^{-6}$ for the longitudinal and $+0.54 \times 10^{-6}$ for the transverse fractional changes of resistivity per kilogram per sq. cm. If we assume a value of 8000 kg./cm.^2 for the yield stress, we have 1.007 for the maximum value of the anisotropy. For copper, assuming a value of 4000 kg./cm.^2 for the yield stress, and using Bridgman's values of $+1.75 \times 10^{-6}$ and -2.4×10^{-6} per kg./cm.^2 for the longitudinal and transverse coefficients respectively, we find the maximum anisotropy to be 1.015.

These values are comparable with those found in the present experiments, but it should be emphasized that the effect of internal stresses will be very much less than that of a uniaxial stress equal to the yield value. The effect of long-range internal stresses can therefore be regarded as unimportant.

(iii) The effect of oriented dislocations.

Recent calculations of Mackenzie and Sondheimer (1950) on the increase of resistivity produced by cold work lead to a prediction of anisotropy. They consider the scattering of conduction electrons by dislocations and show that the increase in resistance parallel to a dislocation axis is zero while the increase in the slip direction exceeds that normal to the slip plane by a factor of about 2, depending on Poisson's ratio.

During the rolling of polycrystalline metals, the dislocations introduced will not be oriented at random as slip will occur preferentially along favourably oriented slip directions. When cold-rolling has produced a preferred orientation, a complete calculation of the anisotropy would require an estimate of the relative abundance of dislocations perpendicular to each slip direction in each of the slip planes in the ideal preferred orientation produced by cold-rolling. Such a calculation is very sensitive to the distribution of dislocations among the various slip planes and of crystal orientations so that an estimate is not given here. However, it is clear that the present results for anisotropy of increase of resistivity $(\Delta\rho/\rho)_0/(\Delta\rho/\rho)_{90}$ (brass 1.195, silver 1.130, steel 1.370) can be explained by the above considerations if appropriate assumptions (suggested by the mode of deformation) are made.

Recent developments of dislocation theory by Cottrell and Bilby (1949) have led Bhatia (1949) to predict anisotropy of resistance change during strain ageing in iron single crystals. Interstitial solute atoms are assumed to form "atmospheres" around non-randomly oriented dislocations owing to the presence of local lattice strains. In such a case, the effect of dislocations alone, as considered above, would be enhanced. It is interesting to note that in the present experiments the highest value of anisotropy of resistivity increase (1.370), was found for steel. This suggests that the diffusion of carbon atoms to dislocations, as considered by Bhatia, had occurred and accentuated the purely dislocation effects.

From the above considerations it is concluded that the major cause of anisotropy of resistivity of cold-rolled cubic metals is the presence of oriented dislocations,

ACKNOWLEDGMENTS.

The author is indebted to the Goldsmiths' Company for a Dominions (Travelling) Scholarship and to the Division of Tribophysics, C.S.I.R.O., for laboratory facilities. The assistance given by Dr. W. Boas in many helpful discussions is gratefully acknowledged. Thanks are also due to the staff of the Defence Research Laboratories, Maribyrnong, for the analyses; to Mr. E. J. Williams of the Section of Mathematical Statistics, C.S.I.R.O., for suggesting the statistical procedure; and to Mr. E. D. Hondros for assistance in the experimental work.

REFERENCES.

- BECKER, R., and BORN, F., 1925, *Zeit. f. Tech. Physik*, **6**, 356.
BHATIA, A. B., 1949, *Proc. Phys. Soc. B*, **62**, 229.
BOAS, W., 1947, *Introduction to the Physics of Metals*, Melbourne University Press, p. 124.
BRIDGMAN, P. W., 1925, *Proc. Amer. Acad. Arts Sci.*, **60** (8), 423.
COTTRELL, A. H., and BILBY, B. A., 1949, *Proc. Phys. Soc. A*, **62**, 49.
GRÜNEISEN, E., and GOENS, E., 1924, *Zeit. f. Physik*, **26**, 250.
MACKENZIE, J. K., and SONDHEIMER, E. H., 1950, *Phys. Rev.*, **77**, 264.
MATSUDA, T., 1925, *Sci. Rep. Tohoku Imp. Univ.*, **14**, 343.
RUTTER, J. W., and REEKIE, J., 1950, *Phys. Rev.*, **78**, 70.

VI. *The Origin of Cosmic Ray Stars.*

By J. B. HARDING.

Imperial College, London, S.W.7 *†.

[Received October 13, 1950.]

ABSTRACT.

Estimates for the energy and momentum lost by particles which produce stars when passing through the nuclei in a photographic emulsion support the conclusions reached in a previous paper that the majority of disintegrations are not produced by neutrons which are captured in a single nuclear encounter. The ratio of these two quantities, which have been obtained from the detailed statistical analysis of the various particles produced in nuclear disintegrations, suggests that nuclei are partially transparent to high energy neutrons which at 3600 m. have sufficient energy to produce a small number of stars.

INTRODUCTION.

IN a previous paper (Harding 1949 a) the nature of the radiation responsible for the production of cosmic ray stars has been discussed by considering the momentum and energy transfer from the incident particle to the excited nucleus. An estimate for the transfer of momentum was obtained from the angular distribution of the residual nuclei, or recoil fragments, which are left when the original nuclei have cooled down by particle emission. However, this analysis was carried out for stars formed in C2 "Nuclear Research" emulsion which is not capable of recording tracks left by protons of more than 50 MeV. It is therefore necessary to re-examine the former experimental data and to include further results obtained with electron sensitive plates in order to investigate the validity of the previous conclusion, viz., that the majority of nuclear disintegrations at 3600 m. are produced by nucleons, but that these are not absorbed catastrophically in a single encounter.

EXPERIMENTAL RESULTS.

(a) The angular and range distributions of recoil fragments are given in the previous paper, as is the size distribution of stars examined. In this paper the size of a star is denoted by the number of evaporation (black) tracks.

* Communicated by Sir George Thomson. F.R.S.

† Present address: Atomic Energy Research Establishment, Harwell.

(b) The variation of the α/p ratio with star size has been given by Perkins (1950) and Page (1950). The ratios assumed in this paper for stars in heavy elements (Ag, Br) are :

Star-size	2, 3 and 4	5-14	15
α/p ratio	0.4	0.5	0.45

(c) The particles responsible for the "grey" tracks in these stars are mainly protons of energies 30-350 MeV. (Harding 1950). In plates exposed at high altitudes, Amerini *et al.* (1950) have shown that about 5 per cent of such tracks are produced by mesons. In the following we assume that all "grey" tracks are produced by protons. (It would be easier to maintain our original conclusions were we to assume a certain percentage to be produced by mesons, as for a given momentum transfer the energy transfer would be greater than for protons.)

From an analysis of these "grey" tracks (see Appendix) we obtain the following :

Average energy (including binding energy) per particle = 90 MeV.

Average downward momentum per particle = 110 ± 20 MeV./c.

(d) It is intended to apply momentum and energy consideration to the heavy nuclei, but in the previous paper a certain number of stars arising through the disintegration of the light elements (C, O, N) were also observed. In order to allow for such stars we recall an experiment (Harding 1949 b) designed to give information on these light stars, *i. e.* on stars formed in layers of gelatin.

Having now observed 38 such stars, we estimate that 35 ± 6 per cent of a random sample of stars in C-2 emulsion arise through the disintegration of the light elements.

Assuming a cross-section for star production proportional to $A^{2/3}$ (which is approximately correct), we estimate that from these 38 stars we should expect a charge of 260e to be emitted. We have seen

62 protons (deuterons or tritons) : charge 62e,

54 α -particles (some may be due to heavier fragments but identification uncertain) : charge $\geq 108e$,

3 particles identified as having $Z \geq 3$: charge $\sim 10e$.

Estimated charge due to tracks of length *greater* than 10μ , these tracks remaining in gelatin layers, *i. e.* "lost", charge $\sim 10e$. In the Appendix we show that in a random sample of small stars there are three-quarters "grey" proton per star. We interpret these as "knock-on" protons, and they should therefore be produced in light nuclei, from which they should stand more chance of escaping than from heavy nuclei. We are therefore justified in assuming that at least three-quarters "grey" proton are produced per light star, *i. e.* emitted charge $\geq \frac{3}{4} \cdot 38e = 29e$.

Therefore total emitted charge is $\geq 219e$.

Therefore missing charge per star is $< 41e$ 38,

This must all go into tracks of $<10\mu$, and these must remain in the gelatin layer. It seems unreasonable, and is certainly not expected from evaporation theory, to suppose that we get one short proton per light star. Rather we *assume* that one-third of these stars have a "recoil" of average charge $3e$. As will become apparent later on, it will be easier to maintain the original conclusions, viz., stars are not produced by neutrons which are captured at the first nuclear collision, if we were to assume one-quarter or one-fifth of the light stars to have "recoils" of 4 or $5e$.

In the previous paper a random sample of 411 stars were examined, and hence 144 ± 25 are estimated to arise from light elements. A further 202 stars with six or more prongs, *i. e.* stars arising from heavy elements, were also included in the previous statistics. 279 recoils were observed, of which we assume $(144 \pm 25)/3 = 48 \pm 8$ are fragments from light nuclei.

FORMULATION OF THE SCHEME FOR STAR PRODUCTION.

We consider a star-producing particle ("primary" for shortness) of initial energy and momentum E_1, \bar{P}_1 respectively travelling at an angle γ to the downward vertical. It emerges from the nucleus with energy and momentum E_2, \bar{P}_2 in the laboratory system, and is accompanied by a small number of "knock-on" (grey) protons and neutrons which carry away energy and momentum E_3 and \bar{P}_3 . In escaping from the nucleus, the knock-on particles will undergo further collisions which leave the nucleus, now of mass m , in an excited state and moving with a small velocity. Let V_1 be the downward component of this velocity. We can now apply the laws of conservation of energy and momentum:

$$\left. \begin{aligned} E_1 - E_2 &= E_3 + \mathcal{E} & (=E, \text{ say}), \\ (\bar{P}_1 - \bar{P}_2) \cdot \bar{n} &= \bar{P}_3 \cdot \bar{n} + mV_1 & (=P, \text{ say}). \end{aligned} \right\} \quad \dots \quad (1)$$

where \mathcal{E} is the excitation energy of the nucleus—its kinetic energy is negligible—and \bar{n} is unit vector in the downward direction.

While moving, this excited nucleus will evaporate α -particles, protons and neutrons. We assume that this process is isotropic in the centre of mass system of the excited nucleus. In general this excited nucleus does not possess sufficient energy to break up completely, and a residual nucleus, or recoil fragment, will be left. If this possesses sufficient energy it will be recorded as a short track. In fact we define a recoil track as one of less than 10μ , and it is now necessary to estimate the distribution in mass of recoil fragments by considering the numbers of "knock-on" and evaporated particles.

From the 613 stars analysed, 469 are estimated to arise through the disintegration of silver and bromine. We assume that the size distribution of the 144 light stars is similar to that of silver stars of two to five tracks. This is suggested by the size distribution of the gelatin stars. We have

assumed silver and bromine stars to have similar size distribution. (The final result is very insensitive to the exact assumptions made about these size distributions.)

It can then be shown that for the heavy stars 1.6 "grey" protons are knocked on per star. Since a heavy nucleus contains about $1\frac{1}{2}$ neutrons per proton we assume that $1\frac{1}{2} \times 1.6$ neutrons are also directly knocked on by the primary particle. Therefore $3\frac{1}{2}$ fast nucleons are knocked on per star. (From the recent Berkeley results it would seem that the $n-n$ scattering cross-section is smaller than the $n-p$ cross-section, in which case we might expect fewer knock-on neutrons. As will become apparent later on, such an assumption would make it easier for us to maintain our original conclusions.)

Since we observe a β -ray in less than 5 per cent of the stars, we conclude that the recoils are generally stable fragments. As the average α/p ratio of ejected particles is ~ 0.5 while the original neutron/proton ratio in a heavy nucleus is 1.25, it follows that 1.5 neutrons must be evaporated for each proton.

If we now assume that the ratio of silver to bromine stars depends on the ratio of their geometric cross-sections and their relative abundance in the emulsion, we can now estimate the distribution in mass of the heavy recoil fragments. Two peaks are observed in this distribution since we start with two groups of nuclei. From the point of view of further calculations it will be sufficiently accurate to consider two "average" recoil groups, one of mass 93, charge 41e, and the other of mass 67, charge 30e. These average recoils occur with relative frequencies 216 and 253 respectively. Range velocity curves for such fragments were obtained by the method discussed in the previous paper.

ESTIMATION OF THE ENERGY TRANSFER, E.

We have on average $3\frac{1}{2}$ nucleons knocked-on by the primary. Therefore from the experimental results our best estimate for E_3 is $90 \times 3\frac{1}{2} = 315$ MeV. It has here been necessary to assume that the angular and energy distribution of particles producing "grey" tracks is the same in light and heavy nuclei, for we use the distribution which was obtained for a random sample ($\sim \frac{1}{3}$ light stars) to estimate E_3 , and later P_3 (see Appendix). For stars of medium size (~ 6 tracks) the distribution of energy of protons evaporated from an excited nucleus can be represented by

$$P(E) dE = \frac{E - V}{T^2} \exp \{-(E - V)/T\} dE,$$

where $V = 5$ MeV. and $T = 4$ MeV. For neutrons we assume the same distribution, but with $V = 0$ MeV. A similar distribution can be fitted to the α -particle spectrum with $V = 7$ MeV.

Allowing 4 MeV. as binding energy of an α -particle and 8 MeV. for protons and neutrons, we estimate that, for the heavy stars examined, the average energy per star taken by α -particles, neutrons and protons is 40, 100 and 90 MeV. respectively. Thus $\mathcal{E} = 230$ MeV.

Therefore our best estimate for E is $315 + 230 = 545$ MeV.

ESTIMATION OF THE DOWNWARD MOMENTUM TRANSFER, P.

For the three and a half knocked-on nucleons our best estimate of P_3 is $3\frac{1}{2} \times 110 = 385 \text{ MeV./c.}$

We have now to estimate the downward velocity V_1 of the excited nucleus, and for this we will use the angular distribution of the recoil fragments as given in paper I.

Assume that we can observe all recoils of range greater than 3μ . This assumption is justified below. Our previous results gave 77 recoils observed to travel upwards and 133 downwards. We now believe that 48 of these could be produced from light elements, but unfortunately we have no information about their angular distribution. The greater the downward excess of recoils the greater the downward velocity of the excited nucleus. It is unreasonable to suppose that the light recoils are collimated upward. Therefore if we wish to determine the downward velocity of the heavy nuclei by subtracting from the observed angular distribution of recoils those due to light nuclei, we will obviously obtain the greatest downward excess of heavy recoils (and hence greatest velocity) by assuming that the light recoils are isotropic, *i. e.* if

$$R = \frac{\text{No. of heavy recoils travelling upwards}}{\text{No. of heavy recoils travelling downwards}},$$

$$R_{(\text{max})} = \frac{(77 \pm \sqrt{77}) - (24 \pm \sqrt{24})}{(133 \pm \sqrt{133}) - (24 \pm \sqrt{24})} = 0.49 \pm 0.1.$$

(This, then, is the most unfavourable case to take if we are trying to confirm our original conclusion.)

In any given star the velocity of a recoil in the laboratory system will be the vector sum of the downward velocity component V_1 and a velocity V_2 , where

$$m_{\mathbf{R}} \mathbf{V}_2 = -\mathbf{P}_{\mathbf{R}}, \quad . \quad . \quad . \quad . \quad . \quad . \quad . \quad . \quad . \quad . \quad (2)$$

m_r being the mass of the recoil fragment and P_E being the resultant momentum of the evaporated particles in the centre of mass system of the excited nucleus. In practice there is a distribution of P_E which can be calculated according to "Random Walk" theory. Let M_X be the number of stars with N prongs. If all particles carried off equal momentum P then the differential distribution $\rho_1(P_E) dP_E$ is given by (Lindhard (1943)) :

$$\rho_1(P_E) dP_E = K P_E^2 \left\{ \sum_N \frac{\exp(-3P_E^2/2NP'^2)}{(2\pi NP'^2/3)^{3/2}} M_N \right\} dP_E.$$

In practice there is also a distribution in the momentum carried off by the individual particles, *i. e.* a distribution $\rho_2(P') dP'$ which is calculated from the energy spectra of the particles. Therefore we obtain

$$\rho_1(P_E) = K' P_E^2 \int_{P_E=0}^{\infty} \left\{ \sum_N \frac{\exp(-3P_E^2/2NP'^2)}{(2\pi NP'^2/3)^{3/2}} M_N \right\} \rho_2(P') dP'.$$

From this distribution we can therefore obtain the velocity distribution $\rho(V_2) dV_2$ of the two groups of recoils in the centre of mass system of the excited nucleus by using equation (2).

If a recoil is observed to travel upwards with velocity V it must have been ejected upward in the centre of mass system with a velocity greater than V . Averaging over all recoils observed with velocity V in the top hemisphere we have that the average velocity $(\bar{V}_2)_{up} = Vf_1(V_1/V)$. Similarly, in the lower hemisphere, recoils with velocity V in the laboratory system must be ejected with velocities V_2 in the centre of mass system smaller than V . On the average $(\bar{V}_2)_{down} = Vf_2(V_1/V)$. The functions f_1 and f_2 can be obtained in an analytical form and their numerical values obtained for any given value V_1/V . It can now be shown that if V_A, V_B are recoil velocities in the laboratory system corresponding to ranges of 3 and 10 μ , then

$$\frac{\text{No. of recoils up}}{\text{No. of recoils down}} = R = \frac{\int_{V_A f_1}^{V_B f_1} (1 - V_1/V_2) \rho(V_2) dV_2}{\int_{V_A f_1}^{V_B f_1} (1 + V_1/V_2) \rho(V_2) dV_2}.$$

We assume a value for V_1 , calculate the limits to the integrals and hence determine R by numerical integration. We can therefore plot a graph against V_1 and hence determine the value of V_1 for the experimental value of $R=0.49$. The value so obtained is 0.9×10^8 cm./sec.

Averaged over the silver and bromine we obtain $mV_1 = 270$ MeV./c.

Hence our best estimate for the downward momentum transfer P (for the assumption regarding the light recoils) is $270 + 385 = 655$ MeV./c. (Were we to assume that the light recoils were collimated downwards to the same extent as the heavy recoils, this analysis would give $V_1 = 0.7 \times 10^8$ cm. sec., giving an estimate of 595 MeV./c. for P . Taking the other limiting hypothesis, in which all the light recoils are collimated downwards, our estimate for P would be 425 MeV./c.

ESTIMATION OF RANGE DISTRIBUTION OF RECOIL FRAGMENTS.

We have assumed that we can observe all recoil fragments of range greater than 3 μ . To test this we calculate the expected range distributions of recoil fragments and compare them with the observed distributions in the upper and lower hemisphere.

It can be shown (see paper I.) that the differential velocity distributions $N(V) dV$ for recoils in the laboratory system are given by

$$(a) \text{ (Upper hemisphere)} \quad N(V) = -\frac{V}{2V_1} \int_{\sqrt{V^2 + V_1^2}}^{V+V_1} \frac{\rho(V_2)}{V_2} dV_2,$$

(b) (Lower hemisphere)

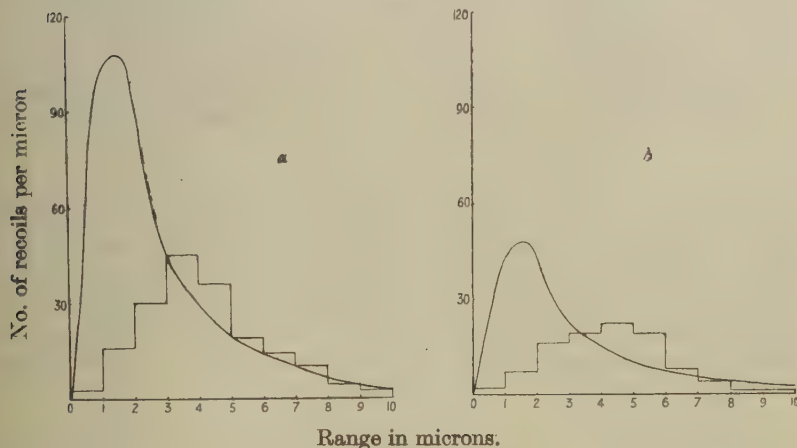
$$N(V) = -\frac{V}{2V_1} \int_{V-V_1}^{\sqrt{V^2 + V_1^2}} \frac{\rho(V_2)}{V_2} dV_2.$$

These distributions have been worked out (taking $V_1 = 0.9 \times 10^8$ cm./sec.) for the two groups ($A = 93, Z = 41$, and $A = 67, Z = 30$) of fragments. Using theoretical range-velocity curves, calculated according to the method given in the previous paper, the range distributions were obtained and are shown in fig. 1.

DISCUSSION OF ERRORS IN P AND E.

It is here convenient to discuss the errors arising from statistical consideration. We assume first that all energy measurements are correct, but because of the uncertainty of the angular distribution of the "grey" tracks, the estimated momentum of 110 MeV/c is only correct to ± 20 MeV/c (standard deviation—see Appendix). Due to the finite number of stars examined, there is an uncertainty in R (for any given assumption about light recoils). For $R = 0.49 \pm 0.1$ we obtain limits for the downward momentum of the excited nucleus of 205 and 330 MeV/c.

Fig. 1.



Assuming these uncertainties in momentum can be represented by error distributions, it can be shown that the uncertainty in P can also be represented by an error distribution with a standard deviation of 75 MeV/c. i. e., $P = 655 \pm 75$ MeV/c.

Due to uncertainties in the grain-counting technique, there must be an uncertainty in our estimate of E of the order of 10 per cent. However, if we overestimate E, we overestimate P and *vice versa*, and thus the error in the ratio P/E is not so important. Therefore, if in the further analysis we assume the 10 per cent error in E, the resultant error in the ratio will be slightly overestimated. Thus

$$P/E = \frac{655 \pm 75}{545 \pm 55} = 1.20 \pm 0.18.$$

(In these system of units $c = \text{unity}$.)

EFFECT OF AN ANGULAR DISTRIBUTION OF THE PRIMARIES.

So far we have estimated the downward momentum transfer. The true momentum transfer will be greater. We must now take an angular distribution of the primaries, $P(\gamma)d\gamma$, in order to estimate the true average magnitude of $\bar{P}_1 - \bar{P}_2$.

Assume $P(\gamma) = \cos^2 \gamma \sin \gamma$, where γ is the angle with the downward vertical. This distribution has been found for the hard component of cosmic rays by counter technique, and seems to hold for the angular distribution of the ionizing primaries of stars formed in electron sensitive emulsions (Coates 1949, Page 1950).

We will now investigate the hypothesis that the star primary is captured by the nucleus. In this case the resultant momentum transfer will be along the direction of the primary particle. Assuming that the energy distribution of the primaries is independent of their direction, it may be shown that for the above angular distribution, the downward component of the average momentum is three-quarters of the magnitude of the true momentum transfer.

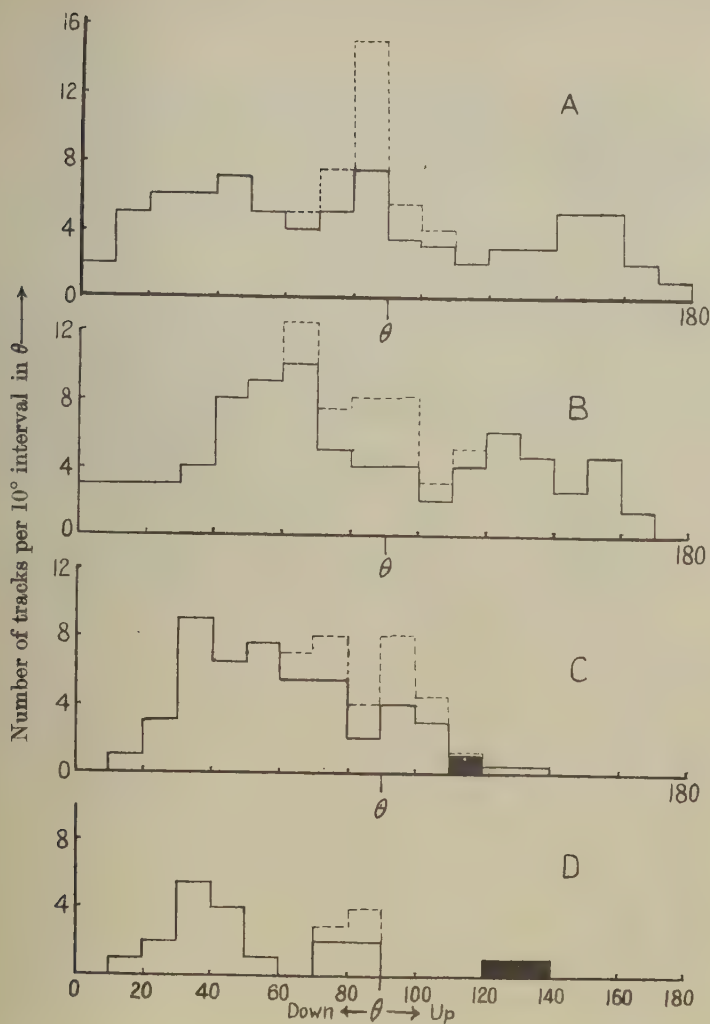
Hence, if the primaries are captured, the ratio of the momentum to energy transfer is $4/3 \times (1.20 \pm 0.18) = 1.6 \pm 0.2_4$, and it is on the basis of this ratio that we test assumptions about the primary particles.

DISCUSSION OF RESULTS.

80 per cent of the stars at 3600 m. are formed by non-ionizing radiation (Brown *et al.* 1949). We will therefore assume neutrons of average energy 545 MeV. produce one star. In this case the momentum transfer will be 1150 MeV./c, and thus $P/E = 2.1$. The probability of experimental results being consistent with this value is 0.015, and we therefore see that, even with the most unfavourable assumptions about the angular distribution of recoil fragments from light elements, the hypothesis that neutrons are captured in a single encounter with a heavy nucleus is untenable. Taking $P/E = 1.6$ for a neutron defines its energy as 1200 MeV. The results are therefore consistent with neutrons producing a small number, $\sim 1200/545 \doteq 2$, of stars.

In 9 per cent of the stars we observe one fast particle (if a proton its energy is above 350 MeV.) to be emitted in a downward direction. It is reasonable to suppose that this is the primary particle escaping from the nucleus, possibly after change of charge. A further 5 per cent of stars show showers of fast particles, the majority of which are known to be mesons (Camerini *et al.* 1950). From the point of view of the above momentum and energy considerations the ejection of fast mesons could take place as an alternative to the re-emission of the primary particle. Thus in 14 per cent of stars fast particles are observed to leave, and hence it is necessary to assume that in about $50 - (9 + 5) = 36$ per cent of stars fast neutrons capable of further star production must be emitted. Hence we should expect the absorption cross-section for the primaries to be less than the collision cross-section. Taking the latter quantity

Fig. 2.



Distribution of the values of θ , zenith angle for "grey" tracks assumed to be produced by protons of energy

- (a) 30-50 MeV.
- (b) 50-100 MeV.
- (c) 100-200 MeV.
- (d) 200-350 MeV.

The shaded portions represent tracks which are likely to have been produced by the star primary rather than by a particle ejected in the disintegration. The dotted lines represent corrections which have been applied for loss of steeply dipping tracks.

as determined by the geometrical nuclear cross-section we do in fact obtain a smaller value for the absorption cross-section for lead, aluminium, carbon, air and water (see Bernadini, 1950).

ACKNOWLEDGMENTS.

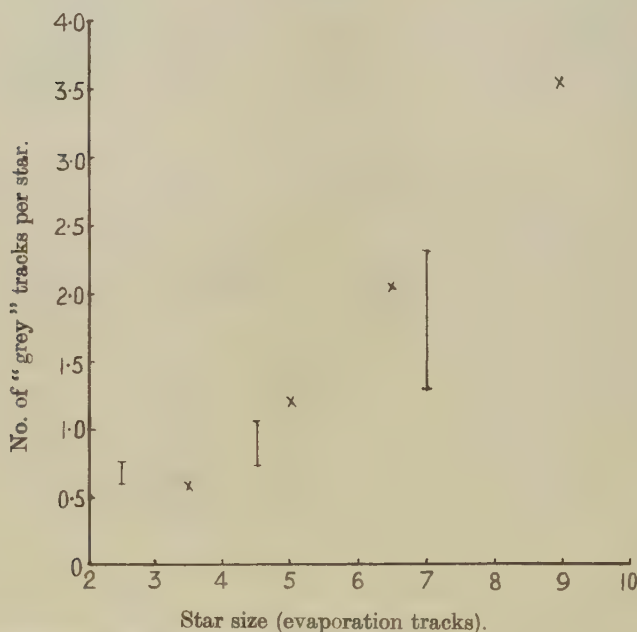
I wish to express my thanks to Professor Sir George Thomson for his helpful discussions on this problem.

APPENDIX.

A. *The Angular Distribution of the "Grey" Tracks.*

A random sample of 295 stars formed in electron sensitive emulsion exposed at 3600 m. have been analysed with the co-operation of Messrs. P. E. Hodgson and T. T. Li. The plates were calibrated by grain-counting on ρ -meson tracks and then the energies of the particles, assumed

Fig. 3.



Average number of "grey" tracks as a function of the number of evaporation tracks. For comparison, \times indicates results of Brown *et al.* 1949.

to be protons, which produce the "grey" tracks were obtained from grain-density measurements. In figs. 2 *a*, *b*, *c*, *d* we show the distribution in zenith angle of the tracks produced by protons 30–50, 50–100, 100–200,

200–350 MeV. The variation in the number of such “grey” tracks with star size is shown in fig. 3. Good agreement is obtained with the results of Brown *et al.* (1949).

The statistics for the angular distributions are somewhat poor, and thus, if we take the energy measurements as correct, we estimate

(a) Average energy (K.E. + binding energy) per “grey” proton = 90 MeV.

(b) Average downward momentum per “grey” proton = 110 ± 20 MeV./c.

REFERENCES.

- BERNADINI, G., CORTINI, C., and MANFREDINI, A., *Phys. Rev.*, **76**, 1792.
 BROWN, R. H., *et al.*, 19—, *Phil. Mag.*, **40**, 862.
 CAMERINI, U., *et al.*, 1950, *Phil. Mag.*, **41**, 413.
 CHANDRASEKHAR, S., 1943, *Rev. Mod. Phys.*, **15**, 1.
 COATES, A. C., and HERZ, R. H., 1949, *Phil. Mag.*, **40**, 1088.
 HARDING, J. B., 1949 a, *Phil. Mag.*, **40**, 530; 1949 b, *Nature, Lond.*, **163**, 440; 1950, *Nature, Lond.*, **165**, 273.
 PAGE, N., 1950, *Proc. Phys. Soc. A*, **63**, 250.
 PERKINS, D. H., 1950, *Phil. Mag.*, **41**, 138.

VII. *On the Velocity of Second Sound in Liquid Helium II.*

By H. N. V. TEMPERLEY,
King's College Cambridge *.

[Received October 25, 1950.]

ABSTRACT.

Some recent experiments by Atkins and Osborne (1950) in the Mond Laboratory give values for the velocity of second sound at very low temperatures in close agreement with Landau's (1941) predictions. It is shown that such results cannot be obtained from any theory of Tisza-London type, unless it is postulated that other states besides the very lowest one contribute to ρ_s , the density of superfluid. Landau's (1941) method of calculating ρ_s can be applied to any model and does imply such a postulate.

It is concluded that the experimental results only throw light on the correct method of calculating ρ_s and cannot be regarded as evidence in favour of Landau's quantum hydrodynamics. On the other hand, the fact that liquid He^3 does not show superfluid properties can no longer be regarded as evidence against Landau's theory, as the predictions of the Landau and Tisza-London types of theory are identical for both the perfect Bose-Einstein and the perfect Fermi-Dirac gases.

§1. INTRODUCTION.

RECENT measurements, Pellam and Scott (1950), have confirmed that the velocity of "second sound" passes through a minimum value at about 1°K. and begins to rise rapidly at lower temperatures. Recent work by Atkins and Osborne in the Mond Laboratory (1950) confirms the existence of this rapid rise, and shows further that, at very low temperatures, the velocity approaches a value of the order of 150 metres/sec. This is in agreement with Landau's (1941) prediction that the ratio of the velocities of propagation of first and second sound should at very low temperatures tend to the value $\sqrt{3}$. In this paper, we shall show that such a result cannot be obtained from any theory which treats liquid helium II as a condensed Bose-Einstein assembly, the lowest state constituting the superfluid, but that this must not be taken to mean that the hypothesis of the essential connection between Bose-Einstein condensation and the properties of liquid helium II will have to be abandoned; nor can it be regarded as evidence for the soundness or otherwise of Landau's quantum hydrodynamics (the theoretical validity of which has been questioned by some workers). We shall also show that the difference

* Communicated by the Author.

between the two types of theory is not nearly as great as is usually thought, because both theories give precisely the same result when applied to the perfect gas model, and the absence of superfluidity in pure liquid He^3 can be understood on the basis of either theory.

§ 2. THE TWO-FLUID CONCEPTION.

The velocity of "second sound" can be shown; see, for example, Landau (1941) to be given by the expression

$$c_2^2 = \frac{\rho_s S^2}{\rho_n (\partial S / \partial T)},$$

where S is the entropy per unit mass.

This result follows according to either theory and can be derived independently of any physical model, making the assumptions that helium II consists of a solution or intimate mixture of two fluids, each having its own density and velocity field, the normal fluid with density ρ_n resembling an ordinary liquid, the superfluid with density ρ_s being unable to transport any entropy. This set of assumptions has been found to be capable of accounting for a large number of the experimental facts, and it is usually referred to collectively as the two-fluid theory. Now $\partial S / \partial T$ can be found directly from specific heat measurements, and S can be obtained from them by numerical integration following a reasonable extrapolation to absolute zero, so that a measurement of c_2 may also be regarded as a measurement of ρ_s / ρ_n . A quite independent measurement of this ratio can be made, Andronikashvili (1948), by measuring the angular momentum of a pile of disks on a common axis, oscillating in liquid helium II, and identifying the relative density of the superfluid with that fraction of the liquid not "carried round" by the disks. Agreement between these two methods is satisfactory down to 1.3°K .

§ 3. THE DIFFERENCE BETWEEN THE TWO THEORIES.

There seem to be two main differences between the two theories. The first difference, which is not a fundamental one, consists of the use by Landau (1941) of the Debye model, in which attention is fixed, not on the atoms themselves, but on the quantized sound waves that represent their relative motion. Tisza (1950), on the other hand, assumes that a satisfactory model of liquid helium can be obtained by modifying the energy spectrum appropriate to a gas of non-interacting helium atoms in a vessel. Evidently the true state of affairs in a liquid involves some compromise between these two models, one of which we may describe as "solid-like" while the other is "gas-like". They appear to have quite different statistical mechanical consequences, because the total number of material particles is fixed, while the total number of sound quanta may vary, but this difference is only apparent. Either type of model may be specified by the density of energy-levels as a function of energy, or, which amounts to the same thing, by the relationship between the energy and total momentum of an elementary excitation. Given a particular model of one

kind, it seems to be almost always possible to devise a distribution of energy-levels so that a model of the other kind may give the same partition function, and the two types of model may, in a sense, be regarded as two different approximate descriptions of an assembly, rather than as embodying different physical assumptions.

The really important difference arises from the methods of calculating ρ_s/ρ . The most natural assumption to make in a theory of Tisza-London type is simply to put this ratio equal to the fraction of atoms occupying the very lowest state of the assembly, so that this method is obviously not directly applicable to a model of Debye type. Landau's (1941) method, which consists of imagining the assembly to be in statistical equilibrium with a body moving with a very small velocity and then calculating its mean momentum statistically, is applicable to a model of either type (irrespective of whether his quantum hydrodynamics is sound or not) so that a direct comparison of the two methods is possible. They give the same result for the perfect Bose-Einstein gas, and for the perfect Fermi-Dirac gas both methods predict that ρ_s should be zero, but, in general, the two methods give quite different results, and the experimental evidence thus indicates that Landau's method of calculating ρ_s/ρ is more correct than that suggested above for the Tisza-London type of theory, which is tantamount to saying, that if liquid helium II can be represented as a condensed Bose-Einstein assembly other states of the material particles besides the very lowest one contribute to ρ_s . Landau (1941) also considers, but does not actually use, an alternative method of calculating ρ_s/ρ by imagining the assembly set into rotation with a small angular velocity, calculating the mean angular momentum, and comparing it with the "rigid body" value. He assumes tacitly that the two methods give the same result. By considering the perfect gas model by both methods, we shall show that they are likely to give substantially the same results, though the "rotation" method is, logically, slightly preferable. There is a possibility that, at extremely low temperatures, the two methods might not agree for all models.

§4. THE CALCULATION OF c_2 ACCORDING TO THE LONDON-TISZA TYPE OF THEORY.

We shall consider only the behaviour of ρ_s/ρ_n and c_2 at very low temperatures (as it is already clear that there is no significant difference between the predictions of the two types of theory above 1°K.) for which purpose we need only specify the low-energy end of the spectrum relating energy and momentum of excitations. We assume for this region the following relation between the energy E and the length of the momentum vector p . $E = Ap^n$ where A and n are constants. Now an integration over phase space involves an integration over the three components of momentum, and the volume element in momentum space is $p^2 dp \sin \theta d\theta d\phi$. If we change the variable from p to E , we see that the model is equivalent to assuming a density of energy-levels $4\pi A' E^t$ where $t = \frac{(3-n)}{n}$. We make

the calculation, first by calculating the occupation number of the lowest state, then by Landau's method. For the assembly to be capable of a Bose-Einstein condensation, we must have $t > 0$, i. e. $n < 3$. In practice, since the energy of a particle obeying Schrödinger's equation will always contain a term $p^2/2m$, we probably have $n \leq 2$.

For the total occupation of all the states but the lowest

$$N - N_0 = 4\pi A' \int_0^\infty dE E^t [\exp(E/kT) - 1] \text{ per unit volume.} \quad (1)$$

For sufficiently low temperatures, we may neglect the difference between ρ_n/ρ_s and ρ_n/ρ , so that

$$\frac{\rho_n}{\rho_s} \approx \frac{N - N_0}{N} = \frac{4\pi A'}{N} \Gamma(t+1) \zeta(t+1) (kT)^{t+1}, \quad (2)$$

by expanding the denominator of the integrand in powers of $\exp(-E/kT)$ and integrating term by term. ζ is the Riemann zeta-function. The free energy per unit volume is given by

$$F = 4\pi A' kT \int_0^\infty dE E^t \log [1 - \exp(-E/kT)], \quad (3)$$

from which we obtain for the entropy the expression

$$S = - \frac{\partial F}{\partial T} = 4\pi A' k (kT)^{t+1} (t+2) \Gamma(t+1) \zeta(t+2). \quad (4)$$

Substituting for S and $\partial S/\partial T$ in the expression for c_2 we get

$$c_2^2 = \frac{NkT}{\rho} \frac{(t+2)\zeta(t+2)}{(t+1)\zeta(t+1)}. \quad (5)$$

It is interesting that this expression is independent of A' , and only varies quite slowly with t or n . Inserting for N/ρ the value 1.6×10^{23} appropriate to liquid helium, we deduce that at very low temperatures $c_2 \approx 45T^{1/2}$ metres/sec. Thus, if the above method of calculating ρ_s/ρ_n is correct, we should expect the behaviour of c_2 at very low temperatures to be practically independent of the distribution of energy-levels. Now it is known, Pellam and Scott (1950), that the curve for c_2 begins to turn upwards at a temperature just above 1° K. and they report a value of 33.9 m./sec. at some unknown temperature below this. This is not a high enough value to exclude the possibility that the law just mentioned is obeyed at very low temperatures but very recent work in the Mond Laboratory by Atkins and Osborne (1950), in which velocities up to 150 m./sec. have been observed, seems to rule out this possibility quite definitely.

§5. CALCULATIONS OF c_2 ACCORDING TO LANDAU.

We now give the calculation for the same set of models according to Landau's method (1941). We shall apply it first of all to the general assembly obeying Bose-Einstein statistics, the Debye model and the perfect gas then appearing as particular cases. (There is, however, no difficulty in applying it to assemblies obeying Fermi-Dirac statistics for which the

complete energy-spectrum is known, knowledge of the low energy end of the spectrum being no longer sufficient.) The method is as follows :— We suppose the whole assembly in statistical equilibrium with a body moving with a very small velocity, v , along the z -axis and then calculate the mean value of the momentum, the energy-levels of the assembly first being modified to the values that would be measured by an observer moving with the velocity v . Now there will be no change in the potential-energy if the whole assembly is referred to moving axes, while the change in kinetic energy associated with the r th state will be $vp_z^{(r)}$, where $p_z^{(r)}$ is the z component of momentum referred to fixed ones.

The justification of this process is as follows : Schrödinger's equation for non-interacting particles in a potential field V is

$$\frac{\hbar^2}{8\pi^2m} \nabla^2 \psi - \frac{i\hbar}{2\pi} \frac{\partial \psi}{\partial t} - V\psi = 0.$$

Taking axes moving relative to the original ones with a velocity v in the z -direction, we have

$$z = z' + vt', \quad t' = t,$$

and the equation becomes

$$\frac{\hbar^2}{8\pi^2m} \nabla'^2 \psi - \frac{i\hbar}{2\pi} \frac{\partial \psi}{\partial t'} + \frac{i\hbar}{2\pi} v \frac{\partial \psi}{\partial z'} - V\psi = 0,$$

which shows, from the definition of the momentum operator, that the energy is changed by vp_z by the change of axes.

A slight logical difficulty arises for the "particles in a box" model, because the Schrödinger equation cannot be solved in a compact form using the set of axes moving relative to the end wall of the box. It is necessary therefore, either to assume that the assembly is "infinite" in the z direction, or else that the z -ends of the "box" are joined up to make a torus, in which case the model becomes a limiting case of the "rotation" model considered below. In a true "box" model, the introduction of the term vp_z can have no effect on the distribution of momentum in the positive and negative z directions (in spite of the difference in energies) because the amplitudes of the forward and backward travelling waves are constrained by walls perpendicular to the z direction to be the same. With an "infinite" or toroidal "box" this difficulty does not arise. Landau is therefore calculating the modifications in the occupation numbers of the wave-functions referred to the fixed axes that has to occur in order that the assembly may be in equilibrium relative to an observer moving with the new axes. The method can quite easily be generalized to a model requiring the many-body wave-equation.

Thus, for the assembly in equilibrium with a moving body, we must replace E_r , the energy of the r th level, by $E_r - vp_z^{(r)}$. The mean value of the momentum in the z -direction is then

$$\int_0^{2\pi} \int_0^\pi \int_0^\infty \frac{p_z \cdot p^2 dp \sin \theta d\theta d\phi}{\lambda \exp(E - vp_z)/kT - 1}, \quad \dots \dots \dots (6)$$

which, to the first order in v , may be written

$$-\int_0^{2\pi} \int_0^\pi \int_0^\infty p \cos \theta \cdot p v \cos \theta \cdot \frac{\partial}{\partial E} \left(\frac{1}{\lambda \exp(E/kT) - 1} \right) p^2 dp \sin \theta d\theta d\phi. \quad (7)$$

Since $E = A p^n$ we have $\partial/\partial E \equiv (1/n A p^{n-1})(\partial/\partial p)$ and we may now integrate by parts with respect to p , the integrated term vanishing at both limits (provided $n < 5$). The integration over the angular coordinates in momentum space leads to the factor $4\pi/3$ so that the total momentum of the assembly is then

$$\frac{4\pi}{3} \frac{5-n}{nA} v \int_0^\infty \frac{p^{4-n} dp}{\lambda \exp(E(p)/kT) - 1} \text{ per unit volume,} \quad (8)$$

and the effective mass, identified by Landau with the "mass of the normal fluid" is obtained simply by dividing this by v . For an assembly such as the Debye model, where the number of quanta present is not fixed, we have $\lambda = 1$, while for a degenerate Bose-Einstein assembly λ is very nearly unity and we have

$$N = \frac{1}{\lambda - 1} + 4\pi \int_0^\infty \frac{p^2 dp}{\exp(E(p)/kT) - 1}, \quad (9)$$

the energy of the lowest level being taken as zero. For the perfect gas $E = p^2/2m$ so that $n = 2$ and $A = 1/2m$, in which case expression (8) is exactly equal to the integral in equation (9) multiplied by mv , which means that the atoms in the very lowest state do not participate in the motion, this state contributing to equation (9) but not contributing to expression (8) because the momentum of the very lowest state, referred to the fixed axes, is zero for a large assembly. Thus, for the perfect gas, both methods of calculation give the same result for ρ_s/ρ and therefore for c_2 also whereas, if the energy is any other function of the momentum, as will occur if there are interactions between the atoms, the results of the two methods of calculation may be quite different. For example, if n equals unity, we conclude that c_2 tends to the constant value $A/\sqrt{3}$ at low temperatures, just as was found by Landau for phonons for which $A = c_1$, the velocity of ordinary sound, whereas equation (5), with $t = \frac{1}{2}$, gives the result to be expected using the London-Tisza type of approach, plus the assumption that the superfluid is identical with the lowest state of the assembly.

Equations (6)-(9) can easily be modified to suit the Fermi-Dirac assembly and, for the perfect gas, we conclude that the "effective" mass of the assembly is precisely the same as its actual mass, so that nothing of the nature of a "superfluid component" is to be expected according to Landau's method of calculation. The non-appearance of superfluidity in liquid He^3 cannot therefore be regarded as evidence against Landau's theory,

§6. ARE LANDAU'S TWO METHODS OF CALCULATING ρ'_s/ρ_n EQUIVALENT?

We return to the perfect Bose-Einstein gas, but we suppose it to be contained in a cylinder of radius a and length d . The possible wave-functions and energy-levels are

$$\left. \begin{aligned} \psi_{l,n,\nu} &= \sin \frac{l\pi z}{d} J_\nu \left(\frac{j_{n,\nu} r}{a} \right) \exp(\pm i\nu\theta), \\ E_{l,n,\nu} &= \frac{\hbar^2}{8\pi^2 m} \left[\frac{l^2 \pi^2}{d^2} + \frac{(j_{n,\nu})^2}{a^2} \right], \end{aligned} \right\} \quad \dots \quad (10)$$

where $j_{n,\nu}$ is the n th zero of $J_\nu(x)$ which is given by the asymptotic expression $j_{n,\nu} \sim (n + \frac{1}{2}\nu - \frac{1}{4})\pi$ which is, in fact, fairly accurate even for small values of n and ν . By forming the partition function, replacing the sums by integrals in the usual way, and changing the variables of integration from n and ν to $n + \frac{1}{2}\nu$ and $n - \frac{1}{2}\nu$, we can easily show that, as we should expect, the partition function is in the limit, the same for a cylindrical enclosure as for a rectangular one and that the assembly shows the phenomenon of "condensation" into the lowest level in exactly the same way. It is possible to deal with a toroidal box by introducing Y_ν as well as J_ν . However, if we imagine the whole assembly in equilibrium with a body rotating with a small angular velocity and make a calculation analogous to that of equations (6) to (9) we reach a similar conclusion, with the difference that *all* the states with ν equal to zero are devoid of angular momentum, and can therefore contribute nothing to the mean angular momentum of the assembly. The "number of superfluid atoms" therefore now comprises not only the number in the very lowest state, but *all* those with $\nu=0$. The number N_1 of atoms in such states, apart from the very lowest, can be obtained by summing the ordinary expression for the occupation number over all possible values of l and n , which gives, if the sums are replaced by integrals:

$$N_1 = \int_0^\infty \int_0^\infty \frac{dl \, dn}{\lambda \exp[(\hbar^2/8mkT)(l^2/d^2 + n^2/a^2)] - 1} \quad \dots \quad (11)$$

This integral diverges if λ is precisely equal to unity, but, since $N_0 = 1/(\lambda - 1)$ expression (11) implies

$$N_s - N_0 + N_1 = N \left[1 - \left(\frac{T}{T_0} \right)^{3/2} \right] + \frac{T}{T_0} O(N^{2/3} \log N_0), \quad \dots \quad (12)$$

where T_0 is the transition temperature. Thus the difference between the two methods is actually negligible for the perfect gas model for a very large assembly unless the temperature is extremely low, but this calculation does at least show the possibility of the "linear" and "rotational" definitions of ρ_s/ρ_n giving differing results for some models.

§7. CONCLUSIONS.

(a) The assumption that Helium II is a condensed Bose-Einstein assembly and that ρ_s/ρ is proportional to the occupation of the lowest state is disproved by extending measurements of c_2 to lower temperatures.

(b) This experimental decision does not necessarily mean that liquid helium does not show Bose-Einstein condensation or something similar. It is possible to retain this assumption, provided that one admits that other states besides the very lowest one contribute to ρ_s in all cases except the perfect gas, which seems to be an "accidental" exception.

(c) The fact that He^3 does not show superfluidity does not, by itself, mean that Landau's ideas are wrong. As we have seen, Landau's (1941) method predicts no superfluidity for the perfect Fermi gas. No reasonable analogue of the Debye model is known that will represent the excitations of a degenerate Fermi assembly, so a calculation using such a model cannot be made.

ACKNOWLEDGMENTS.

I should like to thank Dr. K. R. Atkins and Mr. D. V. Osborne for showing me their results before publication, and for helpful discussions.

REFERENCES.

- ANDRONIKASHVILI, E. L., 1948, *J. Exp. & Th. Phys. U.S.S.R.*, **18**, 429.
 ATKINS, K. R., and OSBORNE, D. V., 1950, *Phil. Mag.*, **41**, 1078.
 LANDAU, L., 1941, *Jour. Phys. U.S.S.R.*, **5**, 71.
 PELLAM, J. R., and SCOTT, R. B., 1949, *Phys. Rev.*, **76**, 869.
 TISZA, L., 1950, Report on Conference on Low Temperature Physics at Massachusetts Institute of Technology.

VIII *The Disintegration of Lead Nuclei by Cosmic Rays.*

By P. E. HODGSON,
Imperial College of Science and Technology, London*.

[Received October 25, 1950.]

[Plate V.]

SUMMARY.

Cosmic-ray stars in lead have been investigated by means of photographic plates in close contact with lead foil. The energy distributions of protons and alpha-particles from lead stars have been determined and are compared with the prediction of the evaporation theory. The mean ratio of doubly to singly charged particles is estimated, and an approximate value of the rate of star production in lead deduced.

§ 1. INTRODUCTION.

THE photographic plate method has already been used (Harding, Lattimore and Perkins 1949) to investigate nuclear disintegrations in the emulsion caused by high energy cosmic-ray particles. Unfortunately, however, the disintegrations cannot be ascribed to any particular element, apart from specific nuclear reactions in the light elements of the emulsion, which can be identified in exceptional cases. Also, although stars from which more than eight charged particles are emitted must be due to the disintegrations of one of the heavy elements of the emulsion, there still remains the ambiguity between silver and bromine.

In order to overcome this difficulty, Harding (1949) has used sandwich emulsions composed of alternate layers of emulsion and pure gelatine. Any star observed to start in the gelatine layer must be due to the disintegration of one of the constituents of gelatine, viz. carbon, oxygen or nitrogen. Attempts have also been made in this laboratory to study disintegrations of lead nuclei by incorporating layers of lead phosphate in the emulsion. However, the amount of lead which can be incorporated in this way without impairing the transparency of the emulsion is so small that to obtain a reasonable number of stars a prohibitively large plate area would have to be scanned.

In the experiment described in this paper we have exposed plates with the emulsion in contact with lead foil, and analysed the stars originating in it.

§ 2. EXPERIMENTAL PROCEDURE.

Lead foil was rolled on to the emulsion of Ilford C2 100 micron nuclear research plates. It adhered well but, in order to ensure that there was no gap between the foil and the emulsion, the plates were tightly clamped together.

* Communicated by Sir George Thomson, F.R.S.

After exposure to cosmic rays on the Jungfraujoch, the lead was peeled off the emulsion, which was then developed in the usual manner. The plates were scanned twice, at magnifications of 130 and 270, to reduce the possibility of missing stars originating in the lead.

C2 emulsion was used instead of the more sensitive G5, firstly because the large number of tracks crossing the latter emulsion makes searching difficult and also increases the number of apparent two-track stars in the lead due to the chance concurrence of unrelated tracks; secondly, C2 emulsion gives good discrimination between proton and alpha-particle tracks, permitting the (α/p) ratio to be found; thirdly, since only evaporated particles are recorded in C2 emulsion, it may be assumed that the particles observed were isotropically emitted from the lead nuclei, an assumption which greatly simplifies the calculation of their probabilities of observation.

Each lead star was examined and the numbers of protons and alpha-particles from it which ended in or passed through the emulsion were recorded. The distance of the centre of the star from the emulsion surface was found by a simple geometrical method. The projected range of each track and the difference in depth between the two ends of its emulsion path was measured and hence, assuming the thickness of the emulsion to be exactly 100μ , the range in emulsion of each particle was found. A geometrical calculation gave the range of the particle in the lead before it reached the emulsion. Any deviation of the emulsion thickness from the assumed value of 100μ produces a proportional error in all measurements perpendicular to the plane of the emulsion. Measurements on the undeveloped emulsion of similar plates led to the conclusion that such deviation can be of the order of 5 per cent.

Grain counts were made on all tracks of protons which passed through the emulsion except those making an angle of more than 56° with the plane of the emulsion. The latter were rejected, as grain counts on such steep tracks are unreliable. The energy-grain-density curve for the emulsion was constructed in the usual manner, using the tracks of protons and mesons which ended in the emulsion.

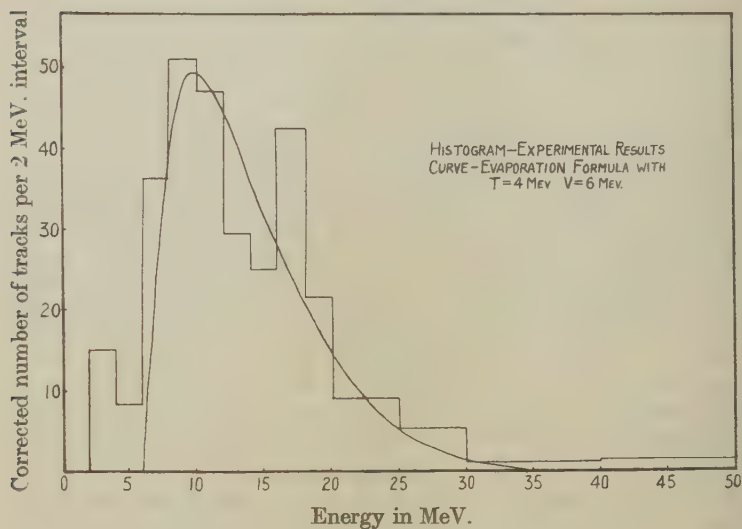
§ 3. SUMMARY OF RESULTS AND METHOD OF ANALYSIS.

The range and grain density measurements were used to determine the energy distributions of the protons and alpha-particles in the way described in §4. The results are shown in figs. 1 and 2. The mean energy of emission of the protons was 14.2 MeV., and that of the alpha-particles 27.7 MeV.

The apparent proton size distributions of the stars observed in the first and second fifty micron layers of lead from the emulsion surface are shown in Table I. The term "proton size distribution" means the distribution of star sizes obtained by counting only the protons associated with the stars. The constants of the best exponential curves to fit these distributions were found by the method of least squares. The

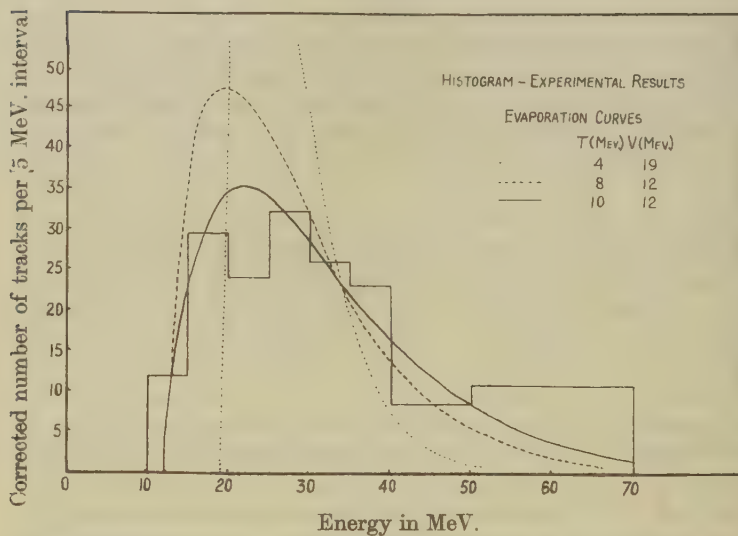
justification for assuming that the size distribution is of exponential form is discussed in § 7. Then, using the size distribution conversion

Fig. 1.



Corrected proton energy distribution for stars in lead based on 95 tracks.

Fig. 2.



Corrected alpha-particle energy distribution for stars in lead based on 28 tracks.

functions derived in § 8, the proton size distribution of the stars in lead was deduced. Hence, using the value of the (α/p) ratio obtained in § 6, the total size distribution of the lead stars was found by an analogous use of the conversion functions. From the time of exposure and the area of plate scanned the rate of production of lead stars at the Jungfraujoch was deduced. These calculations are summarized in Table II.

A lead star, from which four protons and two alpha-particles reach the emulsion, is shown in Pl. V.

§ 4. DETERMINATION OF THE PROTON AND ALPHA-PARTICLE ENERGY DISTRIBUTIONS.

All the tracks due to particles from stars in the lead from which at least three particles reached the emulsion were examined. "Stars" having only two apparent tracks were excluded since many of these are due to the chance concurrence of unrelated single tracks (see § 10).

The energies of emission of particles which ended in the emulsion were evaluated directly from their ranges in emulsion and lead using the respective range-energy curves (H. Bradner *et al.* 1950, Montgomery 1949).

The energies at the mid-points of their emulsion paths of those particles passing through the emulsion were evaluated from the grain densities of their tracks. Then, as before, the energies of emission of the particles were calculated.

Each track was weighted by the reciprocal of the probability that a particle of that energy, emitted from a nucleus at that distance from the emulsion surface, should enter the emulsion or pass through it, whichever is applicable. Allowance was made for the tracks rejected on account of their steepness.

The proton and alpha-particle energy distribution histograms obtained are shown in figs. 1 and 2 together with evaporation curves calculated as follows:

Assume that

(a) The nucleus evaporates down the Heisenberg valley with $\partial N/\partial Z=2.3$.

(b) The binding energies of the emitted particles are $Q_p=Q_n=7.7$ MeV., $Q_\alpha=2.6$ MeV.

(c) Only protons, alpha-particles and neutrons are emitted in the evaporation process.

In addition we have, from the experimental results:

(d) The energy distributions correspond to stars from which on the average about eight protons are emitted. This value was calculated from the true and observed proton size distributions and the distribution in depth of the stars in the lead.

(e) From the energy distributions the mean energies of emission are $\bar{E}_p=14.2$ MeV., $\bar{E}_\alpha=27.7$ MeV.

(f) The (α/p) ratio for lead stars is 0.34 ± 0.07 (§ 6). Thus about three alpha particles are associated with a star from which eight protons are emitted. Also, to satisfy assumption (a), twenty-six neutrons must be emitted.

Let the mean nuclear temperature be T . Then

Energy removed by protons is $(14.2 + 7.7) \times 8$ MeV.

Energy removed by alpha particles is $(27.7 + 2.6) \times 3$ MeV.

Energy removed by neutrons is $(2T + 7.7) \times 26$ MeV.,

i. e. mean excitation energy $\bar{U} = 52T + 466$ MeV.

It has been shown by Le Couteur (1950) that

$$3T/2 = T_{\max} = \frac{2}{A} \sqrt{\bar{U}}.$$

Also, for silver plus bromine, $A = \sqrt{\left(\frac{A}{3.1}\right)}$, where A = atomic weight.

$$\therefore \bar{U} = \frac{9T^2 A^2}{16} = 37.5T^2, \quad \text{whence } T \sim 4.3 \text{ MeV.}$$

From the evaporation formula (Harding, Lattimore and Perkins 1949)

$$P(E) dE = \frac{E - V}{T^2} \exp\left(-\frac{E - V}{T}\right) dE,$$

where V is the height of the nuclear potential barrier, it can be shown that the mean energy of emission $\bar{E} = 2T + V$.

$$\therefore V_p = \bar{E}_p - 2T = 14.2 - 8.6 \sim 6 \text{ MeV.}$$

and

$$V_\alpha = \bar{E}_\alpha - 2T = 27.7 - 8.6 \sim 19 \text{ MeV.}$$

where the suffixes p and α refer to the values of V , T and \bar{E} appropriate to the proton and alpha-particle energy distributions respectively.

The evaporation curve with $T = 4$, $V = 6$ fits the experimental proton results quite well, which shows that the energy-temperature relationship in lead is consistent with that in silver plus bromine, within the accuracy of the experimental results.

The value of the potential barrier height for protons is considerably less than the 9.6 MeV. obtained by interpolation from the results given by Bethe (1937), which, however, were determined from low energy scattering. This difference may be ascribed to (i) violent oscillations of the nucleus due to the high excitation causing local lowering of the potential barrier, (ii) quantum mechanical penetration of the barrier, and (iii) broadening of the energy distribution by experimental error. For emulsion stars in silver plus bromine of a similar size to the lead stars examined, Harding, Lattimore and Perkins obtained a value $V \sim 4$ MeV., which is less than the value for lead, as expected. The number of nucleonic collisions made by the primary in the target nucleus increases with A , but the resulting temperature for the same initial excitation decreases as A increases.

The temperature of 4 MeV. found for the lead disintegrations is less than the $5\frac{1}{2}$ MeV. found by Harding, Lattimore and Perkins for silver plus bromine, which indicates that the latter effect outweighs the former, although the experimental errors make comparison uncertain.

Considering the alpha-particle energy distribution, we should have

$$V_{\alpha}=2V_p. \quad \therefore V'_{\alpha}=12 \text{ MeV.}; \quad \therefore T'_{\alpha}=\frac{1}{2}(27.7-12)\sim 8 \text{ MeV.}$$

The experimental results agree better with $V'_{\alpha}=12$, $T'_{\alpha}=8$ than with $V_{\alpha}=19$, $T_{\alpha}=4$. This indicates that the alpha-particles cannot all be considered as sharing in the normal evaporation, a conclusion also reached by Harding, Lattimore and Perkins from the examination of silver plus bromine stars. They suggested that the alpha-particles are evaporated off in an initial process of higher excitation and, therefore, higher nuclear temperature. Another explanation, which does not exclude this process, is that some of the alpha-particles are not evaporated at all, but come from the disintegration of highly excited nuclear splinters (Perkins 1950, Hodgson 1950).

In these calculations no account has been taken of the deuterons and tritons which, since they form about 15 per cent of the particles from silver plus bromine stars, are probably emitted also from lead stars. There is little advantage in increasing the accuracy of theory and experiment until the proportion of such particles has been evaluated. This can only be done by a series of grain counts on long tracks parallel to the surface of the emulsion. From the very nature of this experiment such tracks are not available.

§ 5. DETERMINATION OF P_p AND P_{α} .

Let P_p and P_{α} be respectively the probabilities that a proton or an alpha-particle from a star in the lead is observed in the emulsion. Both are functions of f , the distance from the star to the emulsion surface. Since C2 emulsion, in which only low energy particles are recorded, was used, it may be assumed that the particles were isotropically emitted from the lead nuclei.

Particles whose directions of emission make a small angle with the emulsion surface have less chance of being observed than those making a large angle, both because of their limited range and the increasing likelihood of their being missed due to the limited field of view of the microscope objective. Therefore

$$P = \int_0^{\pi/2} \frac{\sin \theta}{2} R(f, \theta) D(f, \theta) d\theta,$$

where θ is the angle the track makes with the perpendicular to the emulsion surface, and $R(f, \theta)$ is the probability that a track has range greater than $f \sec \theta$, *i. e.*

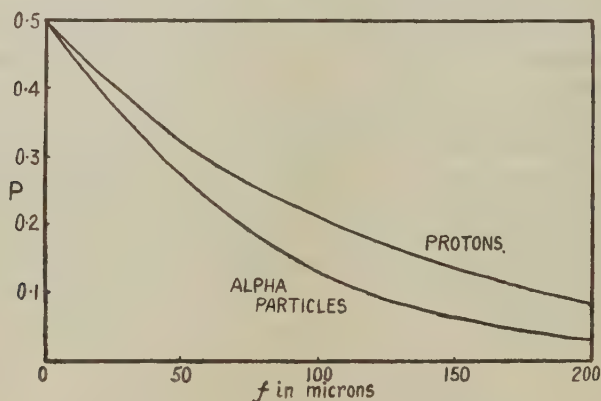
$$R(f, \theta) = \int_{E_1}^{\infty} \frac{E-V}{T^2} \exp\left(-\frac{E-V}{T}\right) dE,$$

where T and V are the constants of the energy distribution and E_1 is the energy of a particle of range $f \sec \theta$ in lead (Montgomery 1949). $D(f, \theta)$ is the probability that a track of inclination θ passing right through the emulsion from a star f microns in the lead is found. Since it depends on the distance from where the particle enters the emulsion to the foot of the perpendicular from the star to the emulsion, it may be written

$$D(f, \theta) \sim D(f \tan \theta).$$

$D(f \tan \theta)$ is unity for values of $f \tan \theta$ from 0 to about 100 microns, after which it drops quite steeply to zero. It depends, of course, on the care with which the plates are scanned, and on the field of view of the objective used.

Fig. 3.

Variation of P with f for protons and alpha-particles.

The distribution in θ of the proton tracks from stars from which at least three particles entered the emulsion was measured for several ranges of f and compared with the curve of $\frac{1}{2} \sin \theta R(f, \theta)$. This curve represents the distribution expected if $D(f, \theta) \equiv 1$, that is, no tracks missed, and it was calculated from the appropriate energy distribution (see § 4). From the amounts by which the experimental results fell short of those expected, $D(f \tan \theta)$ was calculated for several values of $f \tan \theta$. The mean value of $D(f \tan \theta)$ was used to find P_p and P_α as functions of f by graphical evaluation of the above integral. The results are shown in fig. 3.

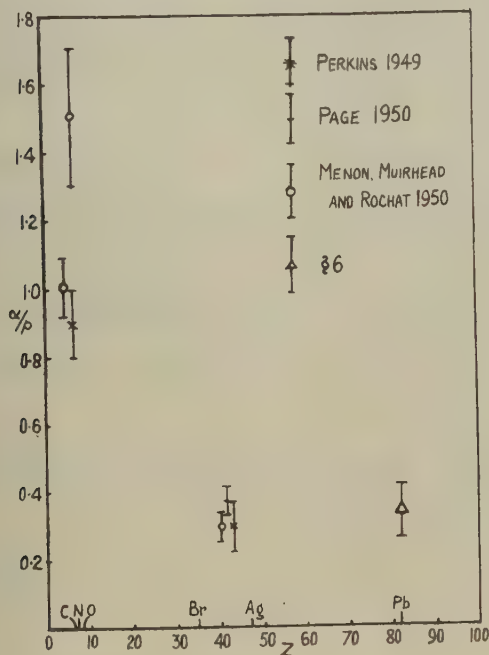
These curves show that it is best to ignore all stars for which $f > 100 \mu$, as the probability of particles from them being detected is small.

§ 6. THE α/p RATIO FOR LEAD STARS.

The numbers of alpha-particles and protons from stars in various ranges of f were counted and divided by the corresponding P . This gave a mean value for the α/p ratio, averaged over all star sizes, of 0.34 ± 0.07 .

Here, as elsewhere, the α/p ratio means, more strictly, the ratio of the number of doubly charged to the number of singly charged particles. Fig. 4 shows the variation of mean α/p ratio with nuclear charge, based on the results of several authors.

Fig. 4.

Variation of mean α/p ratio with nuclear charge.

§ 7. THE SIZE DISTRIBUTION ASSUMPTION.

Several authors (George and Jason (1949), Page (1950) and unpublished work at Imperial College) have shown that the size distribution of stars formed by cosmic rays in C2 emulsion at 3500 m. may be represented by the formula

$$N_n = N_0 \exp(-\xi n),$$

where N_n is the number of stars of n tracks, N_0 is a constant and

$$\xi \sim 0.5 \quad \text{for} \quad 3 \leq n \leq 8$$

$$\text{and } \xi \sim 0.33 \quad \text{for} \quad n > 8.$$

These figures for the differential size distribution have been calculated from those given by George and Jason for the integral size distribution.

Emulsion stars can be formed either in the light elements carbon, oxygen and nitrogen, or in the heavy elements silver and bromine. The largest star that can be produced in the light elements is one of eight tracks in oxygen, but, since the stars in light elements have about the same numbers of alpha-particles as protons, very few light element stars have more than five tracks.

These observations strongly suggest that the emulsion size distribution is composed of the superposition of two exponential curves, one of the form $\exp(-0.33n)$ for the heavy elements, and another, of greater slope, for the light. The slope of the light element curve may be calculated from the figures given above, and is found to be ~ 0.6 .

It therefore seems reasonable to assume that the size distribution for lead stars has exponential form also.

The assumption is only approximate, since it gives a finite number of stars with $n > Z$, whereas the true number is zero.

§ 8. SIZE DISTRIBUTION CONVERSION.

Suppose the stars produced in the lead have a proton size distribution given by

$$N_n^p = N_0 \exp(-\xi_p n) \quad (n \geq 2),$$

where n = number of protons evaporated from the nucleus,

N_n^p = number of stars with n evaporated protons,

N_0 and ξ_p are constants.

N_0 depends on the intensity of the star-producing radiation, the number of lead nuclei and the time of exposure, and ξ_p on the material in which the stars are produced and on the energy distribution of the star-producing radiation.

Then an n -track star in a layer distant between f and $f+df$ from the emulsion surface will have a probability of being observed as an m -track star in the emulsion given by

$$\frac{n!}{(n-m)! m!} P_p^m (1-P_p)^{n-m},$$

where P_p is a function of f .

The total number of m -track stars from the layer df observed in the emulsion will therefore be

$$M_m df = \sum_{n=m}^{n=N} \frac{n!}{(n-m)! m!} P_p^m (1-P_p)^{n-m} N_0 \exp(-\xi_p n) df.$$

N is the number of tracks in the largest possible star in lead. Since the number of stars with $n > N$ predicted on an exponential law is extremely

small for lead (less than 1×10^{-4} per cent), N may, without appreciable error, be replaced by infinity in the above sum.

$$\begin{aligned} \therefore M_m &= \sum_{n=m}^{n=\infty} \frac{n!}{(n-m)! m!} P_p^m (1-P_p)^{n-m} N_0 \exp(-\xi_p n) \\ &= N_0 P_p^m \exp(-\xi_p m) \{1 - (1-P_p) \exp(-\xi_p)\}^{-(m+1)} \\ &= \frac{N_0}{1 - (1-P_p) \exp(-\xi_p)} \left\{ \frac{P_p \exp(-\xi_p)}{1 - (1-P_p) \exp(-\xi_p)} \right\}^m \\ &= M_f \exp(-\xi_f m), \end{aligned}$$

where

$$M_f = \frac{N_0}{1 - (1-P_p) \exp(-\xi_p)} \quad \text{and} \quad \exp(\xi_f) = \frac{\exp(\xi_p) - (1-P_p)}{P_p}.$$

This is the observed proton size distribution of the stars produced in the layer df . Thus, provided P_p is known, the actual proton size distribution of the stars in lead at any particular depth f can be calculated from the observed proton size distribution.

§ 9. THE TOTAL SIZE DISTRIBUTION.

The method of determining the proton size distribution has been outlined in § 8, and that for the (α/p) ratio in § 6. It has also been shown (unpublished work at Imperial College) that the distribution of alpha-particles and protons among the stars is nearly random in the sense that the emission of one particle gives no information on the probability of emission of another similar particle. Recent work (Perkins 1950, Hodgson 1950) has shown that close pairs or triplets of particles from the disintegration of unstable nuclear fragments are sometimes emitted from stars, but the frequency of such events is so small that their effect on the randomness of emission can be neglected.

The total size distribution of the lead stars was deduced from the proton size distribution in exactly the same way as the latter was found from the observed proton size distribution. The formulae of § 8 were used with ξ_p replaced by ξ , ξ_f by ξ_p , N_0 by N , and M_f by N_0 . P was replaced by the probability that a given track from a star is a proton,—that is, $p/(\alpha+p) = [(\alpha/p)+1]^{-1}$.

The total size distribution of the stars in lead is then given by

$$N_n = N_T \exp(-\xi n),$$

where

n = number of charged particles in a star,

N_n = number of stars with n charged particles,

N_T , ξ constants as before.

§10. EXPERIMENTAL RESULTS FOR THE RATE OF STAR PRODUCTION.

The proton size distributions of the stars observed in the lead are shown in Table I. The numbers of apparent two-track stars have been

TABLE I.

Numbers of Lead Stars with Different Numbers of Protons, with Two-track Stars corrected for Chance Coincidences of Single Tracks.

Range of f	Number of protons								
	2	3	4	5	6	7	8	9	10
$0 < f < 50 \mu$	11.7	7	3	3	1	—	—	1	1
$50 < f < 100 \mu$	12.1	7	2	2	—	—	1	—	—

corrected for those due to the chance coincidence of unrelated single tracks. These are quite a serious source of error, being as numerous as the real two-track stars on the plates used, and hence the final number of two-track stars is subject to considerable uncertainty. The number of spurious three- or more-track stars is negligible.

The best values of ξ_f and M_f to fit these distributions, together with the proton and total size distributions calculated from the observed proton size distribution, are shown in Table II. The close agreement between the

TABLE II.

Results of Calculation of Total Size Distribution. To convert to stars per nucleus per day at the Jungfraujoch, multiply the numbers of stars obtained by substituting the above values in the exponential formula by 5×10^{-24} .

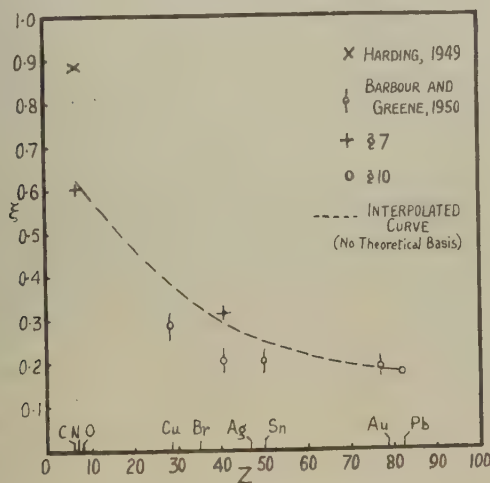
Range of f	Apparent proton size distribution		P_p	Real proton size distribution		$[(\alpha/p)+1]^{-1}$	Total size distribution	
	ξ_f	M_f		ξ_p	N_0		ξ	N_T
$0 < f < 50 \mu$	0.45	22.8	0.42	0.21	12.1	0.75	0.17	9.5
$50 < f < 100 \mu$	0.71	52.5	0.26	0.24	21.4	0.75	0.18	16.8

final values of ξ is probably fortuitous in view of the poor statistics. However, the slope of the lead size distribution is certainly less than that for silver plus bromine, which is expected from the considerations of § 7.

The variation of slope of size distribution with nuclear charge is shown in fig. 5 together with the results of other authors. Those of Barbour and Greene were obtained with G5 plates, and so are rather lower than the other values of ξ , which refer to stars in G2 plates. The result of Harding, obtained by the gelatine sandwich method, is based on a rather small number of stars, and therefore has less accuracy than the value obtained in § 7.

The final values of N_T , which should be equal, are only considered reliable to within about a factor of two.

Fig. 5.



Variation of slope of size distribution with nuclear charge.

§ 11. CONCLUSIONS.

The method outlined here for investigating cosmic-ray stars is only suitable for materials of high nuclear charge. This is due to the relatively small probability (~ 0.3 on the average for stars with $0 < f < 100 \mu$) that a track from a star outside the emulsion will be observed, and to the variation of size distribution slope with nuclear charge. This results in stars in light elements appearing in most cases as two-track stars, if at all. It is very difficult to correct accurately for spurious two-track stars: indeed, it is probably best to neglect them altogether. Therefore only a very small fraction of the stars from a light element will be analysed, and thus a prohibitively large plate area would have to be scanned to find a sufficient number.

For light elements the sandwich method of Harding is therefore superior. But for heavy elements, which cannot be incorporated in a sandwich in satisfactory quantities, the method described here is preferable.

Recently, Barbour and Greene (1950) have exposed metal foils with emulsion on either side. This doubles the value of P , and so the above objections do not apply to this method providing the foil is thin and is in good contact with both emulsions. These conditions are, however, very difficult to fulfil in practice.

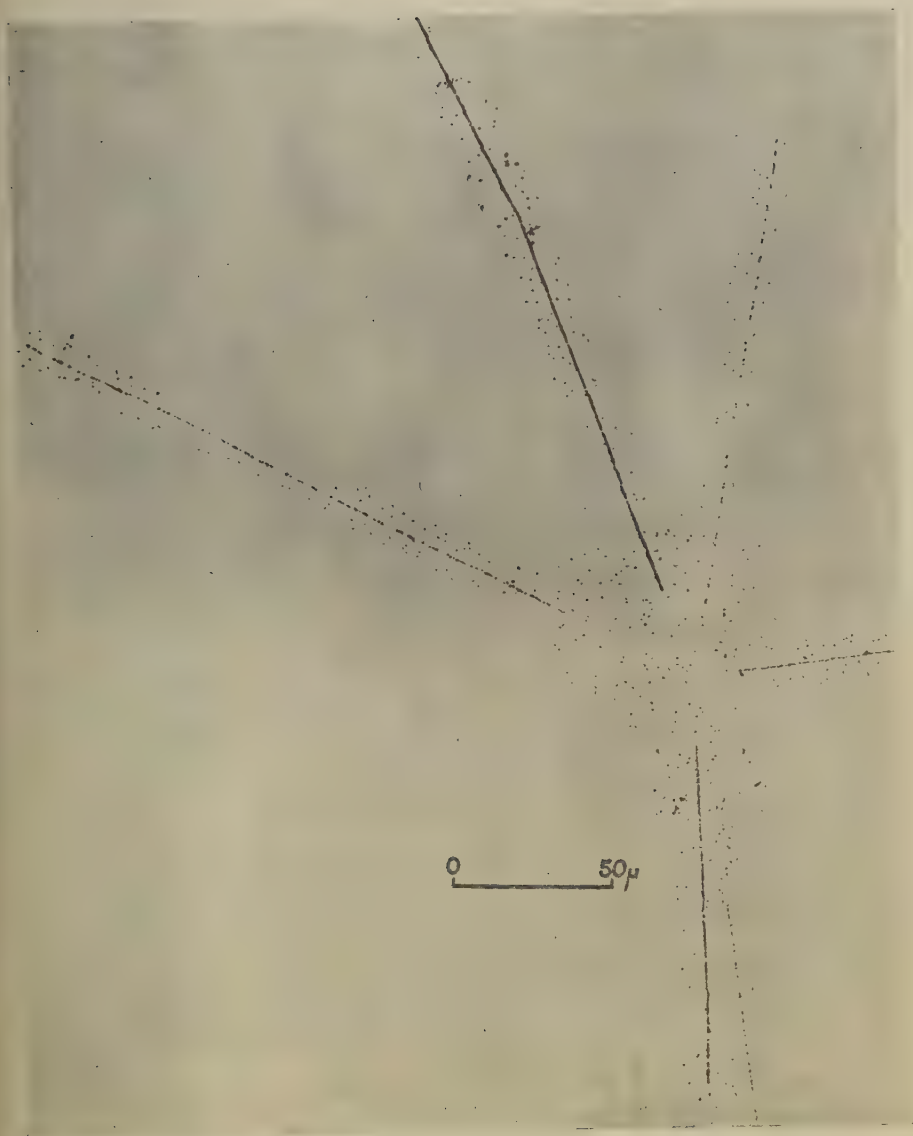
All methods will tend to give a low value for the relative cross-section, because stars outside the emulsion are very much more difficult to find than those in it.

ACKNOWLEDGMENTS.

I should like to express my gratitude to Professor Sir George Thomson, Mr. N. C. Barford and Mr. J. B. Harding for many valuable discussions, and to Dr. K. J. Le Couteur for suggesting the calculations of § 4. I am also indebted to Mr. S. Lattimore who initiated the experiment, carried out the preliminary exposures, and has been a constant source of assistance and advice.

REFERENCES.

- BARBOUR, I., and GREENE, L., 1950, *Phys. Rev.*, **79**, 406.
 BETHE, H. A., 1937, *Rev. Mod. Phys.*, **9**, 172.
 BRADNER, H., SMITH, F. M., BARKAS, W. H. and BISHOP, A. S., 1950, *Phys. Rev.*, **77**, 462.
 GEORGE, E. P., and JASON, A. C., 1949, *Proc. Phys. Soc. A*, **62**, 243.
 HARDING, J. B., LATTIMORE, S. and PERKINS, D. H., 1949, *Proc. Roy. Soc. A*, **196**, 325.
 HARDING, J. B., 1949, *Nature, Lond.*, **163**, 440 (and private communication).
 HODGSON, P. E., 1950, *Nature, Lond.*, **165**, 355.
 LE COUTEUR, K. J., 1950, *Proc. Phys. Soc.*, **63**, 259 (and private communication).
 MENON, M. G. K., MUIRHEAD, H., and ROCHAT, O., 1950, *Phil. Mag.*, **41**, 583.
 MONTGOMERY, D. J. X., 1949, *Cosmic Ray Physics*, p. 350 (Princeton University Press).
 PAGE, N., 1950, *Proc. Phys. Soc. A*, **63**, 250.
 PERKINS, D. H., 1949, *Phil. Mag.*, **40**, 601; 1950, *Proc. Roy. Soc. A*, **203**, 339.



Disintegration of a lead nucleus from which four protons and two alpha particles reach the emulsion.

IX. *Landau Diamagnetism and Meissner Effect.*

By A. PAPAPETROU,

Physics Department, University of Manchester*.

[Received October 26, 1950.]

SUMMARY.

A magnetic field of the form

$$H_z = 2\pi H_0 \cdot \cos\left(2\pi \frac{y}{\lambda}\right), \quad H_x = H_y = 0,$$

is considered, and its influence on free electrons is discussed to the first approximation. A field of the form

$$H_z = 2\pi H_0 \cdot \cos\left(2\pi \frac{x}{\lambda}\right) \cdot \cos\left(2\pi \frac{y}{\lambda}\right)$$

has been considered too. It is shown that, if in a superconductor the distribution of the electrons in momentum space differs a little from the spherical one, an internal field of the second type will be formed inside the superconductor; the Meissner effect then follows for not too strong external fields.

§1. INTRODUCTION.

LANDAU'S first investigation of the influence of a magnetic field on the orbital motion of free electrons has been followed by a number of similar calculations, for free electrons as well as for real metal-electrons. All these calculations refer to a homogeneous magnetic field, this being justified by the very small magnetic susceptibility of the metals under ordinary conditions.

An entirely different situation presents itself in the case of a superconductor, in which an external magnetic field penetrates only to a very small depth (order of magnitude 10^{-5} cm.). Instead of considering a homogeneous field now it is more reasonable to split the magnetic field into its Fourier components. In the simplest case of a superconductor in the form of an infinite plane slab (of constant thickness) we get the one-dimensional Fourier components

$$H_z = 2\pi H_0 \cos\left(2\pi \frac{y}{\lambda}\right), \quad H_x = H_y = 0. \quad (1)$$

(Oy-axis normal to the slab, Oz-axis in the direction of the field.) The most important components will have wavelengths of the order of magnitude

* Communicated by the Author.

of the penetration depth, *i. e.* $\lambda \approx 10^{-5}$ cm. For a superconductor of prismatic form the Fourier components will be two-dimensional. The most important components will be

$$H_z = 2\pi H_0 \cos\left(2\pi \frac{x}{\lambda}\right) \cos\left(2\pi \frac{y}{\lambda}\right), \quad . \quad . \quad . \quad . \quad (2)$$

again with $\lambda \approx 10^{-5}$ cm.

In the present paper we shall investigate the behaviour of the metal-electrons in a magnetic field firstly of the form (1), and then of the form (2), in both cases to the first approximation only. As we shall see later, the results of this investigation show us a possible explanation of the Meissner effect.

Strictly speaking we ought to base our calculations on the properties of the real metal-electrons, *i. e.* to consider not only the magnetic field (1) or (2), but also the periodic electrostatic field of the lattice. However, such a calculation would be extremely complicated, if possible at all. Hence, we shall restrict ourselves to the case of free electrons. The results will, in any case, have only qualitative significance.

In the first section we shall consider the one-dimensional magnetic field (1): in the second section the two-dimensional field (2). In the third section we shall discuss the results of those calculations in connection with the Meissner effect.

§ 2. THE ONE-DIMENSIONAL FIELD.

We assume that the electron-gas occupies the whole space and we impose on the wave-functions the usual periodicity condition with a period-length a . The unperturbed wave-functions are then

$$\psi_{\xi, \eta, \zeta} = a^{-3/2} \cdot \exp\left\{\frac{2\pi i}{a}(\xi x + \eta y + \zeta z)\right\}, \quad . \quad . \quad . \quad (3)$$

ξ, η, ζ being integer numbers (positive or negative). The unperturbed energy is

$$E_0 = \epsilon_1(\xi^2 + \eta^2 + \zeta^2), \quad . \quad . \quad . \quad . \quad (4)$$

with

$$\epsilon_1 = \frac{\hbar^2}{2ma^2} \cdot \quad . \quad . \quad . \quad . \quad (4a)$$

The vector-potential of the field (1) is

$$A_x = -H_0 \lambda \sin\left(2\pi \frac{y}{\lambda}\right), \quad A_y = A_z = 0, \quad . \quad . \quad . \quad (5)$$

In the general formula for the perturbing potential

$$V = \frac{ieh}{2\pi mc} (\mathbf{A} \text{ grad}) + \frac{e^2}{2mc^2} \mathbf{A}^2$$

we shall omit the second term, since we restrict ourselves to the first approximation. We find then immediately

$$V\psi_{\xi, \eta, \zeta} = \frac{e\hbar H_0 \xi}{2imcn_0} (\psi_{\xi, \eta+n_0, \zeta} - \psi_{\xi, \eta-n_0, \zeta}), \quad \dots \quad (6)$$

where $n_0 = \frac{a}{\lambda} = \text{positive integer.} \quad \dots \quad (7)$

The perturbation method gives then for the perturbed wave-function

$$\Psi_{\xi, \eta, \zeta} = \psi_{\xi, \eta, \zeta} + \frac{ieH_0 \xi \lambda^2}{\hbar c} \left(\frac{1}{2\eta+n_0} \psi_{\xi, \eta+n_0, \zeta} + \frac{1}{2\eta-n_0} \psi_{\xi, \eta-n_0, \zeta} \right) \dots \quad (8)$$

This formula shows that we shall have single states only if we assume

$$n_0 = \text{odd integer,} \quad \dots \quad (7a)$$

since in this case there will be no vanishing denominators in (8). The final results of the calculations are the same for $n_0 = \text{even}$ or odd. We can, therefore, introduce the assumption (7a)—which simplifies the summation over the occupied electron states—without imposing any unnecessary restriction. The magnetic energy will then be zero for all states,

$$\delta E = 0, \quad \dots \quad (9)$$

i. e. in this approximation the energy of the electron state reduces to (4).

The state described by the wave function Ψ is associated with a current density \mathbf{s} given by the general formula

$$\mathbf{s} = \frac{\hbar e}{i \cdot 4\pi m c} (\Psi^* \text{grad } \Psi - \Psi \text{grad } \Psi^*) - \frac{e^2}{mc^2} \Psi \Psi^* \mathbf{A}.$$

Introducing in this formula the expression (8) we find

$$s_x = \frac{e^2 H_0}{mc^2 a^2 n_0} \cdot \sin\left(2\pi \frac{y}{\lambda}\right) \cdot \left[1 + \frac{2\xi^2}{n_0} \left(\frac{1}{2\eta-n_0} - \frac{1}{2\eta+n_0} \right) \right] + \frac{\hbar e \xi}{mca^4}. \quad (10)$$

The last term, which does not contain H_0 , can be disregarded because it gives a vanishing contribution when we sum over all occupied states. The components s_y, s_z contain only the term corresponding to the last one in (10), and consequently we may put

$$s_y = s_z = 0.$$

Taking into account (5) we may write (10) in the form

$$s_x = -\frac{e^2 A_x}{mc^2 a^3} \left[1 + \frac{2\xi^2}{n_0} \left(\frac{1}{2\eta-n_0} - \frac{1}{2\eta+n_0} \right) \right] \dots \quad (10a)$$

Before going further it is worth seeing up to what values of H_0 our formulæ will be valid. The condition for the validity of the perturbation method is that the coefficients of $\psi_{\xi, \eta \pm n_0, \zeta}$ in (8) be small compared with 1. For the large majority of occupied states we have $|\xi| \approx \xi_{\max}$ and $|2\eta \pm n_0| \approx \eta_{\max} = \xi_{\max}$. Therefore, the condition for the validity of our formulæ will be

$$\frac{eH_0 \lambda^2}{\hbar c} < 1;$$

with $\lambda \approx 10^{-5}$ cm. this gives $H_0 < 1000$ gauss. In the most unfavourable cases the quantity $2\eta \pm n_0$ will apparently take a value of the order of magnitude 1. But this is not true, as one can see by assuming $n_0 =$ even integer and calculating in detail the case $\eta = \pm n_0/2$; it turns out that the smallest values of the denominators $2\eta \pm n_0$ are of the order of magnitude n_0 . Thus in the most unfavourable cases the ratio $\xi/2\eta \pm n_0$ will be $\xi_{\max}/n_0 \approx 100$, and therefore our formulæ will be valid for $H_0 < 10$ gauss. These maximum fields are of the order of magnitude of the critical fields in superconductivity. We thus see that the perturbation method is the appropriate one for the discussion of the behaviour of a superconductor in a magnetic field.

The total current-density S_x will be the sum of s_x over all occupied states. Thus from (10 a)

$$S_x = -\frac{e^2 A_x}{mc^2 a^3} \left[N + \sum_{\xi\eta\zeta} f \cdot \frac{2\xi^2}{n_0} \left(\frac{1}{2\eta - n_0} - \frac{1}{2\eta + n_0} \right) \right]. \quad (11)$$

N is the total number of electrons contained in the volume $V = a^3$ and f is the Fermi distribution function,

$$f = \frac{2}{1 + \exp(\epsilon - \epsilon_0/kT)}.$$

We have to calculate the sum appearing in the bracket of (11).

We introduce the functions

$$\omega_\mu(\eta) = \int_0^\infty \lambda^\mu f(\lambda, \eta) d\lambda, \quad (12)$$

where

$$f(\lambda, \eta) = \frac{2}{1 + \exp(\lambda + \epsilon_1 \eta^2 - \epsilon_0/kT)}.$$

We find then, if we denote by $\sum_{\xi\zeta}$ summation for $\eta = \text{const.}$,

$$\left. \begin{aligned} \sum_{\xi\zeta} f &= \frac{\pi}{\epsilon_1} \cdot \omega_0(\eta), \\ \sum_{\xi\zeta} f \xi^2 &= \frac{\pi}{2\epsilon_1^2} \cdot \omega_1(\eta). \end{aligned} \right\} \quad (13)$$

Hence

$$\sum_{\xi\eta\zeta} f \cdot \frac{2\xi^2}{n_0} \left(\frac{1}{2\eta - n_0} - \frac{1}{2\eta + n_0} \right) = \frac{\pi}{\epsilon_1^2 n_0} \sum_{\eta} \omega_1(\eta) \cdot \left(\frac{1}{2\eta - n_0} - \frac{1}{2\eta + n_0} \right).$$

This formula can be written also in the form *

$$\sum_{\xi\eta\zeta} f \frac{2\xi^2}{n_0} \left(\frac{1}{2\eta - n_0} - \frac{1}{2\eta + n_0} \right) = \frac{\pi}{2\epsilon_1^2 n_0} \sum_{\eta} \frac{1}{\eta} \left[\omega_1 \left(\eta + \frac{n_0}{2} \right) - \omega_1 \left(\eta - \frac{n_0}{2} \right) \right].$$

We are interested in the case

$$n_0 \ll \eta_{\max},$$

* If we put $2\eta \pm n_0 = 2\eta'$ and then write η instead of η' . In the new summation η will take the values $\pm \frac{1}{2}, \pm \frac{3}{2}, \dots$

in which the function $\omega_1(\eta)$ changes very little when η changes by $n_0/2$. Hence, we can develop $\omega_1(\eta \pm n_0/2)$ in a Taylor series :

$$\omega_1\left(\eta \pm \frac{n_0}{2}\right) = \omega_1(\eta) \pm \frac{n_0}{2} \omega_1'(\eta) + \frac{n_0^2}{2 \cdot 4} \omega_1''(\eta) \pm \frac{n_0^3}{6 \cdot 8} \omega_1'''(\eta) + \dots,$$

the dashes meaning derivatives with respect to η . It follows then

$$\omega_1\left(\eta + \frac{n_0}{2}\right) - \omega_1\left(\eta - \frac{n_0}{2}\right) = n_0 \omega_1'(\eta) + \frac{n_0^3}{24} \omega_1'''(\eta) + \dots,$$

and consequently

$$\sum_{\xi \eta \zeta} f \frac{2\xi^2 \zeta^2}{n_0} \left(\frac{1}{2\eta - n_0} - \frac{1}{2\eta + n_0} \right) = \frac{\pi}{2\epsilon_1^2} \sum_{\eta} \frac{1}{\eta} \left[\omega_1'(\eta) + \frac{n_0^2}{24} \omega_1'''(\eta) + \dots \right]. \quad (14)$$

From the definition (12) we find the general formula

$$\omega_{\mu}'(\eta) = -2\mu\epsilon_1\eta\omega_{\mu-1}(\eta). \quad . \quad . \quad . \quad . \quad . \quad (15)$$

Hence

$$\omega_1'(\eta) = -2\epsilon_1\eta\omega_0(\eta),$$

and after repeated differentiation

$$\omega_1'''(\eta) = -4\epsilon_1\omega_0'(\eta) - 2\epsilon_1\eta\omega_0''(\eta).$$

The right-hand side of (14) then takes the form

$$\frac{\pi}{\epsilon_1} \sum_{\eta} \left\{ -\omega_0(\eta) - \frac{n_0^2}{12} \cdot \frac{1}{\eta} \omega_0'(\eta) - \frac{n_0^2}{24} \omega_0''(\eta) \right\}. \quad . \quad . \quad . \quad (14a)$$

The first term of this sum will cancel the term N in the bracket of (11) since, according to the first of equations (13),

$$N = \sum_{\xi \eta \zeta} f = \frac{\pi}{\epsilon_1} \sum_{\eta} \omega_0(\eta).$$

The last term of (14a) can be written in the form of an integral,

$$\sum_{\eta} \omega_0''(\eta) = \int_{-\infty}^{+\infty} \omega_0''(\eta) \cdot d\eta;$$

this is zero because for $\mu \geq 0$ the functions $\omega_{\mu}(\eta)$ and their derivatives vanish when $\eta \rightarrow \pm \infty$. It follows then

$$S_x = \frac{e^2 A_x}{mc^2 a^3} \cdot \frac{\pi n_0^2}{12 \epsilon_1} \sum_{\eta} \frac{1}{\eta} \omega_0'(\eta). \quad . \quad . \quad . \quad . \quad . \quad (15)$$

We still have to calculate the sum in (15). We first notice that for $\mu=0$ the integral in (12) can be evaluated exactly and gives

$$\omega_0(\eta) = 2kT \lg \{1 + \exp(\epsilon_0 - \epsilon_1 \eta^2 / kT)\}.$$

It follows then

$$\omega_0'(\eta) = -4\epsilon_1\eta \frac{1}{1 + \exp(\epsilon_1 \eta^2 - \epsilon_0 / kT)}.$$

Now we see that the quantity $1/\eta(\omega'_0(\eta))$ changes slowly even in the neighbourhood of $\eta=0$, and consequently we can evaluate the sum appearing in (15) by integration :

$$\sum_{\eta} \frac{1}{\eta} \omega'_0(\eta) = -4\epsilon_1 \int_{-\infty}^{+\infty} \frac{dy}{1 + \exp(\epsilon_1 \eta^2 - \epsilon_0/kT)}.$$

We are interested in the case

$$\epsilon_0 \gg kT,$$

in which this integral can be evaluated by a well-known method*. The result is

$$\sum_{\eta} \frac{1}{\eta} \omega'_0(\eta) = -8\epsilon_1^{1/2} \epsilon_0^{1/2} \left[1 - \frac{\pi^2}{24} \left(\frac{kT}{\epsilon_0} \right)^2 \right].$$

Introducing this in (15) we get

$$S_x = -\frac{2\pi}{3} \frac{e^2 n_0^2 A_x}{mc^2 a^3} \sqrt{\left(\frac{\epsilon_0}{\epsilon_1} \right)} \cdot \left[1 - \frac{\pi^2}{24} \left(\frac{kT}{\epsilon_0} \right)^2 \right]. \quad (15a)$$

The dependence of S_x on the temperature is not shown directly in (15a) because ϵ_0 itself is dependent on T . The dependence of ϵ_0 on T can be determined by calculating the number N of electrons in terms of ϵ_0 and T . The result is

$$N = \frac{8\pi}{3} \left(\frac{\epsilon_0}{\epsilon_1} \right)^{3/2} \cdot \left[1 + \frac{\pi^2}{8} \left(\frac{kT}{\epsilon_0} \right)^2 \right] = \frac{8\pi}{3} \left(\frac{\epsilon_{00}}{\epsilon_1} \right)^{3/2},$$

if we denote by ϵ_{00} the value of ϵ_0 for $T=0$. Introducing ϵ_{00} in (15a) and taking into account (4a) we finally find

$$S_x = -\frac{2\pi}{3} \frac{e^2 A_x}{mc^2 \lambda^2 \hbar} \sqrt{(2m\epsilon_{00})} \cdot \left[1 - \frac{\pi^2}{12} \left(\frac{kT}{\epsilon_{00}} \right)^2 \right]. \quad (16)$$

This result can be brought to a more familiar form. Let us calculate a distribution of magnetic moment \mathbf{m} equivalent to the distribution of current \mathbf{S} by means of the general formula

$$\mathbf{S} = \text{curl } \mathbf{m}.$$

If then we introduce the magnetic susceptibility χ ,

$$\mathbf{m} = \chi \mathbf{H},$$

we find (provided that χ is independent of x, y, z)

$$\mathbf{S} = \chi \cdot \text{curl } \mathbf{H}. \quad (17)$$

Hence in our case

$$\chi = S_x / \frac{\partial H_z}{\partial y}.$$

Considering (16) we find

$$\chi = -\frac{e^2 \sqrt{(2m\epsilon_{00})}}{6\pi mc^2 \hbar} \cdot \left[1 - \frac{\pi^2}{12} \left(\frac{kT}{\epsilon_{00}} \right)^2 \right], \quad (18)$$

* See e. g. Fröhlich, *Elektronentheorie der Metalle* (Springer 1936), p. 357.

which is identical with the Landau susceptibility of free electrons in a homogeneous field. This is not surprising at all, since *e.g.* for $\lambda \approx 1$ cm. we should have demanded that our calculations lead to the Landau susceptibility (18); our conclusion is now that this is generally true, if only $n_0 \ll \eta_{\max}^*$.

Coming back to equation (10 a) we stress an important feature of it. The current s_x produced by the magnetic field (1) acting on any given electron state is *not of the order of S_x/N , but very much larger*. The smallness of S_x (or of χ) is the consequence of a very complete cancellation of much larger terms, this cancellation being due to the spherically symmetric distribution of the electrons in momentum space†. If we disregard the states with $\xi^2 \lesssim n_0^2$ —which are relatively few because of the assumption $n_0 \ll \eta_{\max} = \xi_{\max}$ —, the second term in the bracket of (10 a) will be predominant. We see then that we shall have a strong *paramagnetic*‡ current if $|\eta| < n_0/2$, or a strong *diamagnetic* current if $|\eta| > n_0/2$. We shall make use of this fact in the last section of the present paper.

Instead of the metal extending infinitely in all three dimensions we may equally well consider a slab of finite thickness in the Oy -direction, *e.g.* the one filling the space $0 < y < a$. The calculations are very similar to those given above. But there is one characteristic difference in so far that we cannot now start with the field H_z given by (1). The reason is that, as can be seen immediately, the quantity $V\psi$ cannot in this case be developed in a series of the unperturbed wave functions ψ . The difficulty disappears if we consider the field

$$H_x = 2\pi H_0 \sin\left(2\pi \frac{y}{\lambda}\right),$$

i. e. a field *vanishing on the surface of the metal*. The perturbation method gives then for s_x a formula very similar to (10 a); for S_x and χ we get again equations (16) and (18).

§3. THE TWO-DIMENSIONAL FIELD.

The calculations are similar to those for the one-dimensional field. Therefore, it will be sufficient if we just indicate the main points and give the final results.

Since we wish to arrive again at a relation of the form $s \propto \mathbf{A}$, we must impose on \mathbf{A} the condition

$$\operatorname{div} \mathbf{A} = 0.$$

* In the case $n_0 \approx \eta_{\max}$ or $n_0 \gg \eta_{\max}$ the evaluation of the sum in (11) would have lead to a final result different from (16); but these cases are of no physical importance, and, therefore, we do not discuss them here.

† The same is true also in the case of a weak homogeneous field; compare Papapetrou (1937).

‡ It is well known that the first term in the bracket of (10 a) by itself would lead to a diamagnetic current as strong as that which is necessary for the explanation of the Meissner effect.

We find, then, that the vector-potential of the field (2) is

$$\left. \begin{aligned} A_x &= -\frac{1}{2}H_0\lambda \cos\left(2\pi\frac{x}{\lambda}\right) \sin\left(2\pi\frac{y}{\lambda}\right), \\ A_y &= \frac{1}{2}H_0\lambda \sin\left(2\pi\frac{x}{\lambda}\right) \cos\left(2\pi\frac{y}{\lambda}\right), \\ A_z &= 0. \end{aligned} \right\} \dots \dots (19)$$

We shall consider the case of an infinitely large piece of metal, in which the unperturbed wave functions will be given by (3). The perturbation method leads, then, to the following expression for the perturbed wave functions :

$$\begin{aligned} \Psi_{\xi, \eta, \zeta} &= \psi_{\xi, \eta, \zeta} \\ &+ \frac{ieH_0\lambda^2}{8\hbar c} \left\{ (\xi - \eta) \left(\frac{1}{\xi + \eta + n_0} \psi_{\xi + n_0, \eta + n_0, \zeta} + \frac{1}{\xi + \eta - n_0} \psi_{\xi - n_0, \eta - n_0, \zeta} \right) \right. \\ &\left. - (\xi + \eta) \left(\frac{1}{\xi - \eta + n_0} \psi_{\xi + n_0, \eta - n_0, \zeta} + \frac{1}{\xi - \eta - n_0} \psi_{\xi - n_0, \eta + n_0, \zeta} \right) \right\} \quad (20) \end{aligned}$$

where again $n_0 = a/\lambda$. This formula shows that we shall have degenerate states when $\xi \pm \eta = \pm n_0$. These degenerate states, for which a separate calculation would be necessary, cannot be avoided by an assumption like (7a). But again we could avoid them if we replaced the field (2) by a field of the form

$$H_z = 2\pi H_0 \cos\left(2\pi\xi_0\frac{x}{a}\right) \cdot \cos\left(2\pi\eta_0\frac{y}{a}\right)$$

with *e. g.* $\xi_0 - \eta_0 = 1$; if $\xi_0, \eta_0 \gg 1$, this field is physically equivalent to the field (2). The degenerate states occurring in the case $\xi_0 = \eta_0 = n_0$ have only the effect of making the calculation of the total current **S** (by summation of **s** over the occupied states) essentially more complicated. But the final results are exactly the same in both cases, *i. e.* with and without degenerate states. Hence, it will be sufficient if we consider here the non-degenerate states described by (20).

The current **s** associated with the state described by (20) is found to be

$$\mathbf{s} = -\frac{e^2\mathbf{A}}{mc^2a^3} \left[1 + \frac{1}{2} \left\{ \frac{(\xi - \eta)^2}{(\xi + \eta)^2 - n_0^2} + \frac{(\xi + \eta)^2}{(\xi - \eta)^2 - n_0^2} \right\} \right] \dots (21)$$

The calculation of the total current **S** from **s** can be made in much the same way as in the one-dimensional case. The final result is

$$\mathbf{S} = -\frac{4\pi}{3} \frac{e^2\mathbf{A}}{mc^2\lambda^2\hbar} \sqrt{2m\epsilon_{00}} \cdot \left[1 - \frac{\pi^2}{12} \left(\frac{kT}{\epsilon_{00}} \right)^2 \right], \dots (22)$$

differing from the corresponding one-dimensional formula (16) by a factor 2. If we calculate the equivalent susceptibility from (17), we find again the Landau value (18).

As in the one-dimensional case, here also the small value of \mathbf{S} or χ is due to a cancellation of much larger contributions of the individual states, again because of the spherical distribution of the electrons in momentum space. If we disregard the (relatively few) states for which $\xi^2, \eta^2 \lesssim n_0^2$, we see from (21) that the states for which either $(\xi - \eta)^2 < n_0^2$ or $(\xi + \eta)^2 < n_0^2$ are strongly paramagnetic; those are the states which in momentum space occupy positions inside the two layers of thickness $n_0\sqrt{2}$ along the planes $\xi \pm \eta = 0$. The states situated outside those two layers are strongly diamagnetic.

Instead of the metal extending infinitely in all three dimensions we could consider a prismatic piece of the metal, *e. g.* one filling the space $0 < x, y < a$. When we try to solve the perturbation problem, we see again, as in the one-dimensional case, that this cannot be done with the field (2); instead we must take the field

$$H_z = 2\pi H_0 \sin\left(2\pi \frac{x}{\lambda}\right) \sin\left(2\pi \frac{y}{\lambda}\right),$$

which vanishes on the surface of the metal. The calculation leads, then, to a formula for \mathbf{s} which is essentially the same as equation (21). We notice for the subsequent discussion that the paramagnetic states have momentum vectors whose projections on the ξ, η -plane are directed at 45° to the normal on the surface of the metal.

§ 4. DISCUSSION. THE MEISSNER EFFECT.

Equation (11) can be written in the form

$$\mathbf{S} = -\frac{e^2 \mathbf{A}}{mc^2 a^3} N_{\text{eff}}, \quad \quad (23)$$

$$\text{with} \quad N_{\text{eff}} = N + \sum_{\xi\eta} \int \frac{2\xi^2}{n_0} \left(\frac{1}{2\eta - n_0} - \frac{1}{2\eta + n_0} \right). \quad \quad (24)$$

A similar relation holds in the two-dimensional case. It has been stressed by London a long time ago that the Meissner effect demands for N_{eff} a value of $N_{\text{eff}} \approx N$.

The results of the previous calculations suggest a very simple way for increasing N_{eff} to a value of $N_{\text{eff}} \approx N$. This will be the case if the effect giving rise to superconductivity produces a certain deformation of the otherwise spherically symmetric distribution of the electrons in momentum space, without influencing appreciably the wave functions and the currents \mathbf{s} of the individual states; *i. e.* if we assume that in the superconductor the distribution of the occupied states in momentum space is not exactly spherical, but that there are certain *prominences* on top of the Fermi sphere. The alternative independent explanation would be by assuming that in the superconductor the distribution of the electrons remains essentially spherical, but the wave functions and the currents \mathbf{s} of the electron states are changed as much as is needed in order to account for the necessary increase of N_{eff} . Though both these

factors most probably contribute to the actual increase of N_{eff} , we shall restrict ourselves to the discussion of the first one, for the simple reason that even a qualitative discussion of the second factor would be extremely difficult. After all, it is almost certain that the first will be present in any case; and its effects will, most probably, be there even in the presence of the second factor.

By closer examination one sees that it is not possible to explain the Meissner effect by simply assuming that the prominences will be oriented in such a way as to contain strongly diamagnetic states. The reason is obvious. There are other orientations in which the prominences would contain paramagnetic states. And since diamagnetism corresponds to an increase of energy, while paramagnetism leads to a decrease of energy, the prominences will actually take the orientations corresponding to the strongest possible paramagnetism.

If the prominences are not too small, this tendency towards paramagnetism may lead to the formation of a self-consistent *internal magnetic field*. By this we mean a field \mathbf{H} either of the form (1) or (2), which gives rise to a current \mathbf{S} so large that, in its turn, this current produces just the field \mathbf{H} . It is possible to determine the order of magnitude of the size of the prominences required for this purpose. From the general relation

$$\Delta \mathbf{A} = -4\pi \mathbf{S}$$

we find
$$N_{\text{eff}} \approx -\frac{mc^2 V}{e^2 \lambda^2} \quad (V=a^3).$$

On the other hand, it follows from (10 a) or (21), if we denote by N' the number of electrons contained in the prominences*,

$$N_{\text{eff}} \approx -N' \frac{\xi_{\text{max}}^2}{n_0^2} = -N' \frac{\xi_{\text{max}}^2 \lambda^2}{a^2}.$$

Combining the last two relations, and taking in account that $\xi_{\text{max}}^2 \approx N$, we find

$$\frac{1}{\lambda^4} \approx n' n^{2/3} \frac{e^2}{mc^2}, \quad \dots \dots \dots (25)$$

with $n=N/V$, $n'=N'/V$. Introducing the values $\lambda \approx 10^{-5}$ cm. and $n \approx 10^{22}$ cm $^{-3}$ we get from (25) $n' \approx 10^{-4} n$.

It seems to-day certain that the effect leading to superconductivity is the interaction of the metal-electrons with the thermal vibrations of the lattice, as suggested recently by Fröhlich (1950). It is significant that in Fröhlich's theory prominences of the size required above are

* If there were one prominence only, we should have to consider the last term in the expression of \mathbf{s} given by (10): a state with one prominence only is associated with a permanent current independent of the magnetic field. We avoid such a state—which, according to the general theorem of Bloch, cannot be the state of lowest energy—by assuming that prominences occur in pairs directed in opposite directions.

energetically possible. We, therefore, introduce the following *postulate*: The superconducting state is associated with an internal magnetic field of the form (2)*. In view of the very peculiar magnetic properties of the superconducting state the assumption that this state has an intrinsic magnetic structure is quite plausible. The only general restriction which we might, at present, impose on this structure is that it must be of a *microscopic* nature, since in the absence of an external field the superconductor shows no macroscopic field at all. This condition is fulfilled by the field (2).

The explanation of the Meissner effect is now straightforward. According to the remark at the end of §3 the prominent directions will be at right angles to the Oz-axis and at 45° to the normal on the surface of the metal. As regards the external magnetic field, which declines exponentially inside the superconductor, it is to be expected that the prominences will act on it in the same way as on the one-dimensional field (1) (with the axis Oy along the normal to the surface). Since $n_0 \ll \eta_{\max}$, the states contained in the prominences will have $|\eta| > n_0/2$ and, therefore, we shall have diamagnetism for the external field. Of course, this will be true only for not too strong external fields \mathbf{H}' : Because of the diamagnetism of the superconductor as regards external fields, the field \mathbf{H}' will increase the energies of the electron states inside the prominences. Hence, it will tend to decrease the size of the prominences: and when \mathbf{H}' reaches a certain critical value, the prominences will disappear, *i. e.* the superconducting state will be destroyed.

The present considerations leave the value H_0 of the internal field entirely undetermined; we might only guess that this value should be of the same order of magnitude as the critical magnetic field of the superconductor. For a theoretical determination of H_0 it will be necessary to pursue the calculations to a higher approximation.

REFERENCES

- FRÖHLICH, H., 1950, *Phys. Rev.*, **79**, 845.
 PAFAPETROU, A., 1937, *Z. Phys.*, **107**, 387.

* A field of the form (1) could exist only in an infinite layer or, alternatively, in a thin closed cylindrical ring.

X. CORRESPONDENCE.

Calculation of the Density of States Curve for the 3d Electrons in Nickel.

By G. C. FLETCHER† and E. P. WOHLFARTH,
Department of Mathematics, Imperial College, London‡.

[Received November 23, 1950.]

IT is the purpose of this letter to present some preliminary results of calculations of the density of states, $N(E)$, for the 3d electrons in a face-centred cubic lattice, using the approximation of tight binding. The calculations are applied in the main to nickel. The final results have an important bearing on the physical properties of transition metals, such as magnetic, electrical and thermal properties. Comparison may be made with the results of analogous calculations by Krutter (1935) and Slater (1936), who employed the cellular approximation.

The details of the tight binding approximation are well known (see, for example, Mott and Jones 1936). The atomic wave functions which have been used, and which correspond to the fivefold degenerate 3d level of the isolated atom, are

$$\begin{aligned}\phi_1 &= a_1 x y f(r)/r^2, & \phi_2 &= a_2 y z f(r)/r^2, & \phi_3 &= a_3 z x f(r)/r^2, \\ \phi_4 &= a_4 (x^2 - y^2) f(r)/r^2, & \phi_5 &= a_5 (3z^2 - r^2) f(r)/r^2, \quad . \quad (1)\end{aligned}$$

where $f(r)$ is the normalized radial function of the isolated atom and the a_i are normalizing constants for the angular functions. Using (1) Bloch type functions may be constructed and the energy calculated from the determinantal equation

$$|H_{mn} - E\delta_{mn}| = 0, \quad m=1 \dots 5, \quad n=1 \dots 5. \quad . \quad . \quad . \quad (2)$$

The elements H_{mn} may be expressed in the general form

$$H_{mn} = \sum_{l=1}^3 A_{mn}^{(l)} \eta_{mn}^{(l)}(\mathbf{k}). \quad . \quad . \quad . \quad . \quad . \quad (3)$$

Here the $\eta_{mn}^{(l)}$ are functions of the three Cartesian components of the reduced wave vector \mathbf{k} , expressible in terms of circular functions of $\frac{1}{2}ak_x$, $\frac{1}{2}ak_y$, $\frac{1}{2}ak_z$, where a is the lattice constant. The coefficients $A_{mn}^{(l)}$ have the general form

$$A_{mn}^{(l)} = \int \phi_i^*(\mathbf{r} - \mathbf{R}) \Delta V \phi_j(\mathbf{r} - \mathbf{R}') d\tau, \quad . \quad . \quad . \quad . \quad (4)$$

† Now at Department of Mathematics, University College, Exeter.

‡ Communicated by Professor H. Jones.

where \mathbf{R} , \mathbf{R}' refer to the position of a central atom and one of its nearest neighbours, and where ΔV is the difference in the potential due to an atom when isolated and when in interaction with its nearest neighbours in the metal. Owing to the symmetry properties of the angular functions in (1) some of the coefficients vanish and the others are interdependent, such that only six independent coefficients had to be calculated. For this purpose the most suitable available values of $f(r)$ in (1) and of $V(r)$, the potential due to an isolated atom, were taken to be those of Hartree and Hartree (1936) for Cu^+ with exchange. These could be approximated to closely by simple algebraical expressions, involving exponentials. The atomic polyhedron was taken to be spherical and the assumption made that $\Delta V=0$ inside the central polyhedron and that outside it $\Delta V=V(|\mathbf{r}-\mathbf{R}'|)$. The integrations in (4) were carried out using prolate spheroidal coordinates. The resulting algebraical expressions for the coefficients were evaluated using the appropriate value of the interatomic distance. The values of the six independent coefficients range from 0.033 eV. to 0.260 eV., and these values, as that for the total width of the 3d band, are of such an order of magnitude as to justify the use of the tight binding approximation in this case.

With the H_{mn} known at all points in the Brillouin zone the energy may be calculated by solving (2). The functions $\eta_{mn}^{(l)}$ are, however, quite complicated, and hence it was decided, *in the first place*, to neglect arbitrarily certain of the non-diagonal elements such that the quintic equation (2) breaks into a cubic (arising from the atomic functions ϕ_1 , ϕ_2 and ϕ_3) and a quadratic (arising from ϕ_4 and ϕ_5). This approximation also underlies the calculations of Jones and Mott (1937) on the body-centred cubic lattice and is implicit in much of the work of Brooks (1940) on ferromagnetic anisotropy. Calculations are now proceeding which aim at solving the complete quintic in the energy range of interest for nickel, near the top of the band. Certain results may, however, be obtained at once, and, in addition, such comparison as may be made gives very close agreement with experiment using the curve which has been calculated so far. It is believed that although inclusion of the remaining H_{mn} may distort the energy surfaces derived from the two independent equations, the effect on the final $N(E)$ curve is less serious. The highest energies are found, in any case, to correspond to regions of the zone where the neglected H_{mn} are small. Finally the energy values which have already been computed may, in many cases, be used as first approximations to the roots of the complete quintic.

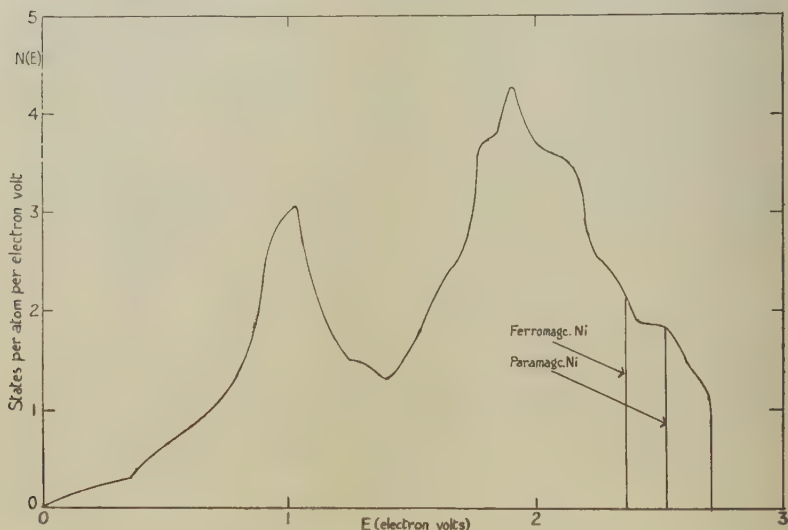
The two resulting determinantal equations were solved in the range $k_x, k_y, k_z > 0$ at all points of a lattice formed by taking intervals of $\pi/6a$, Cardan's method being used to solve some 500 cubics. (In the cellular approximation it was possible to calculate the energies at only very much fewer points in the zone). Constant energy contours were constructed in the planes $k_z = \nu\pi/6a$ ($\nu=0 \dots 12$) for each of the five solutions. Finally $N(E)$ curves were calculated by graphical integration.

A check on this stage of the calculation is provided by the fact that the area under each of the five curves corresponds to one electronic state per atom. The resulting provisional $N(E)$ curve, the sum of the five constituent curves, is shown in the figure.

The following deductions of particular interest may be made :

(1) The total width of the $3d$ band is 2.70 eV. This result is independent of the neglect of the non-diagonal elements mentioned. The value is about half that given by Slater (1936), with whose $N(E)$ curve the present curve may be compared.

(2) The value of the degeneracy temperature for nickel calculated for 0.3 vacant states per atom, corresponding to the right-hand vertical line in the figure, is 2.04×10^3 deg. K., in very close agreement with the value deduced by Wohlfarth (1949) from the magnetic and thermal properties.



Provisional density of states curve for nickel.

E , electronic energy in eV., measured from zero at the bottom of the band.

$N(E)$, density of states, such that the total area under the curve corresponds to five states per atom of either spin. Fermi limits for paramagnetic, ferromagnetic nickel as shown.

(3) The linear low temperature electronic heat coefficient, γ , for ferromagnetic nickel (left-hand vertical line) is deduced to be $1.15 \times 10^{-3} \text{ cal mol.}^{-1} \text{ deg.}^{-2}$. The observed value is 1.74×10^{-3} , but as this includes a contribution due to the conduction electrons, the significant value for comparison is somewhat lower, possibly 1.5×10^{-3} .

(4) A completely general result concerning the degeneracy character at the centre of the zone, $\mathbf{k}=0$, states that here the five energy levels split into a threefold and a twofold degenerate level, separated, in general,

by a finite gap. This result is completely verified in the present case, the gap being found to be 0.88 eV., again independently of the neglect of the non-diagonal elements mentioned. In calculations using the cellular method, on the other hand, the degeneracy at $\mathbf{k}=0$ is found to be almost invariably fivefold—a result of the approximations used in the method.

It is hoped to publish fuller details when the effect of the approximation indicated above has been more completely investigated. The necessary calculations are, however, so troublesome that it was felt that a preliminary account of work already completed may be of interest.

We are indebted to Professor H. Jones for his most helpful advice, and one of us (G. C. F.) to London University for a postgraduate studentship.

REFERENCES.

- BROOKS, H., 1940, *Phys. Rev.*, **58**, 909.
 HARTREE, D. R., and HARTREE, W., 1936, *Proc. Roy. Soc. A*, **157**, 490.
 JONES, H., and MOTT, N. F., 1937, *Proc. Roy. Soc. A*, **162**, 49.
 KRUTTER, H. M., 1935, *Phys. Rev.*, **48**, 664.
 MOTT, N. F., and JONES, H., 1936, *Theory of the Properties of Metals and Alloys* (Oxford: University Press).
 SLATER, J. C., 1936, *Phys. Rev.*, **49**, 537.
 WOHLFARTH, E. P., 1949, *Proc. Roy. Soc. A*, **195**, 434.

Stars produced in Nuclear Emulsions by 150 MeV. Neutrons.

By E. W. TITTERTON*,

Atomic Energy Research Establishment, Harwell†.

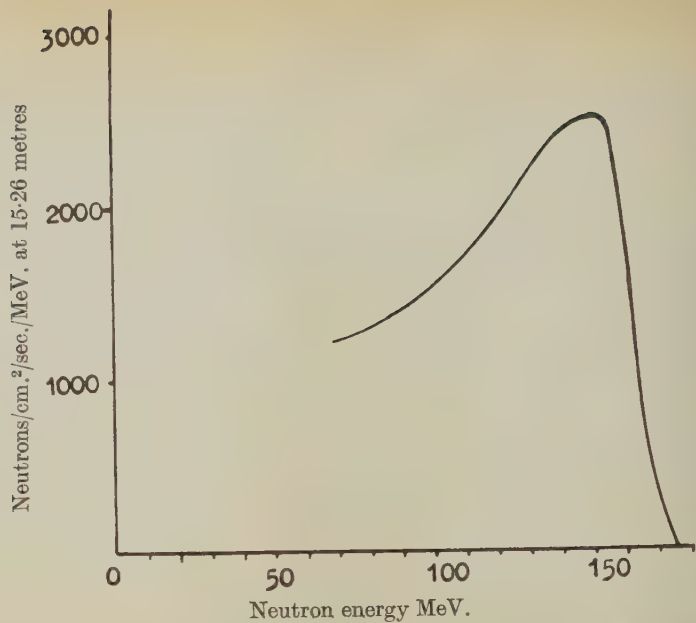
[Received November 6, 1950.]

GARDNER AND PETERSON (1949) and Gardner (1949) have used the Berkeley cyclotron to carry out an investigation of stars induced in nuclear emulsions under deuteron and α -particle bombardment. Several authors, notably Harding *et al.* (1948) and Page (1950) have investigated cosmic ray induced stars and recently there have been several papers describing stars induced by π^- meson capture both for cosmic-ray mesons (Menon *et al.* 1950) and artificially created mesons (Chester and Goldfarb, Adelman and Jones 1950).

In the present experiments a fast neutron beam, obtained from the Harwell Cyclotron by bombarding a beryllium target with 170 MeV. protons, has been used to irradiate C_2 , G_5 and NT_4 plates and the neutron induced stars have been studied. The neutron spectrum (Cassels *et al.* 1950) is indicated in fig. 1 and gives a maximum yield at 150 MeV. The neutron flux was determined by integration and includes neutrons from 60 MeV. to the maximum of the spectrum. At the plate location the flux was 2×10^5 n/cm.²/sec.

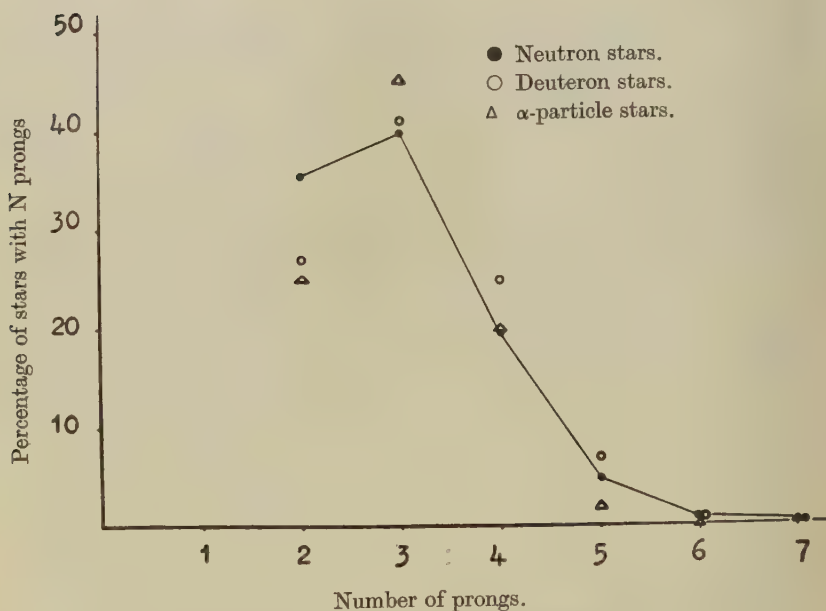
* Communicated by the Author.

† Now on the staff of the Australian National University, Canberra.



Fast neutron spectrum from Beryllium target bombarded by 170 MeV protons.

Fig. 2.



Percentage of stars having N prongs plotted against prong number.

Full circles : Present neutron induced stars.

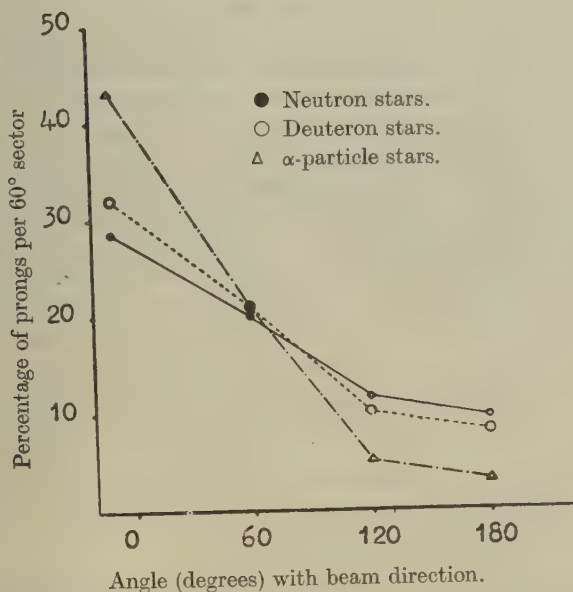
Open circles : Deuteron stars (Berkeley).

Triangles : α -particle stars (Berkeley).

Five thousand stars have been examined to date and preliminary results were reported at the Harwell Conference (Titterton 1950). The stars can be classified into three main groups :—

1. Those having a single energetic proton in addition to other low energy prongs. The proton is apparently knocked-on by the incoming neutron and the remaining excited nucleus breaks up to give further fragments. The spectrum of the knocked-on protons has been examined and extends to 55 MeV.
2. Stars in which the prongs are collimated in the forward direction but contain low energy tracks. These stars are presumably caused by disintegration of the light elements O, C, N present in the emulsion.

Fig. 3.



Angular distribution of star prongs measured in the plane of the emulsion.

Full circles : Neutron induced stars.
 Open circles : Deuteron induced stars.
 Triangles : α-particle induced stars.

3. Stars in which the prongs are distributed more or less isotropically about the incoming neutron direction. These probably result from the Ag and Br atoms in the emulsion and are true evaporation stars. Evaporation stars are well known in plates exposed to the cosmic radiation and have been treated theoretically by Le Couteur (1950).

The prong spectrum of the stars is plotted in fig. 2 where it is compared with spectra obtained in Berkeley for deuteron and α-particle induced stars. The distributions are similar except that more two-prong stars are

found in the present experiments. This difference is probably due to the fact that the emulsions employed were more sensitive than those used in the Berkeley experiments where protons of energy greater than 17 MeV. were not recorded. The angular distribution of the star prongs about the beam direction in the focal plane of the objective is shown in fig. 3 where the fraction of prongs falling in 60° sectors is given as a function of the angular position of the sector. Comparison with Berkeley results shows good agreement with the deuteron distribution which might be expected, since in this case, many of the stars are probably formed by the capture of a proton or neutron in a stripping process. The greater predominance of tracks in the forward direction in the α -particle bombardment is compatible with the greater momentum transfer in this case.

As the relative contributions to the star population by the heavy and light constituents of the emulsion are unknown the cross-section for star production is averaged over all the elements in the emulsion, excluding hydrogen which cannot give rise to a multiparticle star. The value obtained is 54 mB which is considerably smaller than the 210 mB found for 170 MeV. α -particles by Gardner (1949).

If it is assumed, as seems reasonable, that in this energy range the cross-sections are in the ratio of the geometric cross-sections then the cross-section for star production in the light elements (C, N and O) is 25 mB and in the heavy elements (Ag and Br) is 95 mB. Because of uncertainties in the measurement of the neutron flux these values are not accurate to better than ± 30 per cent.

The plates were searched by Miss E. M. Chellingworth, Miss M. Hart, Miss K. B. Treacy and Mrs. B. Naish. The help of Mr. M. M. Cheshire, of the Cyclotron Group, in operating the machine is gratefully acknowledged.

REFERENCES.

- ADELMAN and JONES, 1950, *Science*, **111**, 226.
GARDNER, 1949, *Phys. Rev.*, **75**, 379.
GARDNER and PETERSON, 1949, *Phys. Rev.*, **75**, 364.
CASSELS, RANDLE, PICKAVANCE and TAYLOR, 1950, *Harwell Conference Report*.
A.E.R.E., G.M 68, p. 24.
MENON, MUIRHEAD and ROCHAT, 1950, *Phil. Mag.*, **41**, 583.
PAGE, 1950, *Proc. Phys. Soc. A*, **63**, 250.
HARDING, LATTIMORE and PERKINS, 1949, *Proc. Roy. Soc. A*, **196**, 325.
LE COUTEUR, 1950, *Proc. Phys. A*, **63**, 259.
CHESTER and GOLDFARB, 1950, *Phys. Rev.*, **78**, 683.
TITTERTON, 1950, *Harwell Conference Report*, A.E.R.E. G.M 68, p. 25.

Hammer Tracks in Neutron and Proton Induced Stars.

By E. W. TITTERTON †,

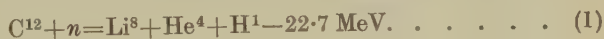
Atomic Energy Research Establishment, Harwell ‡.

[Received November 6, 1950.]

IN the course of the experiments described in the preceding letter, 21 of the 5000 neutron stars were observed to be characterized by "hammer" tracks. Of these stars 18 were found in ($\frac{1}{2}$ and 3 in G₅ emulsions. Such events are common in emulsions exposed to the cosmic radiation (Franzinetti and Payne 1948) but were not reported by Gardner and Peterson (1949) or by Gardner (1949) in the work with deuterons and α -particles. The events are usually attributed to ^8Li nuclei which, after coming to rest in the emulsion, undergo decay according to the scheme $^8\text{Li} \xrightarrow{\beta^-} ^8\text{Be}^*, ^8\text{Be}^* \rightarrow 2^4\text{He}$. An alternative possibility has been suggested by Alvarez (1950) following his discovery of the nucleus ^8B which undergoes a similar decay scheme $^8\text{B} \xrightarrow{\beta^+} ^8\text{Be}^*, ^8\text{Be}^* \rightarrow 2^4\text{He}$.

The hammer tracks observed in the present experiment, whether they are due to ^8Li or ^8B , almost certainly result from the break-up of light elements since the emission of such fragments from Ag or Br nuclei at these excitation energies would be an improbable process due to the impenetrability of the Coulomb barrier. The prong spectrum and angular distribution for the 21 stars are compared with the equivalent distributions obtained in the case of neutron induced stars without hammer tracks in fig. 1 (a) and fig. 1 (b). The comparison is compatible with the view that the events are due to the disintegration of the light elements in the emulsion.

Accepting this view application of the principles of charge and, to a lesser degree, momentum conservation, then allows conclusions to be drawn about the reactions responsible for these stars. Thus of the three-particle stars the majority (7) appear to result from the reaction

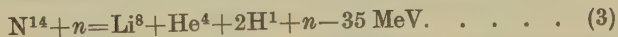


and three from the reaction



the proton being knocked-on with high velocity as indicated in the micrograph of fig. 2.

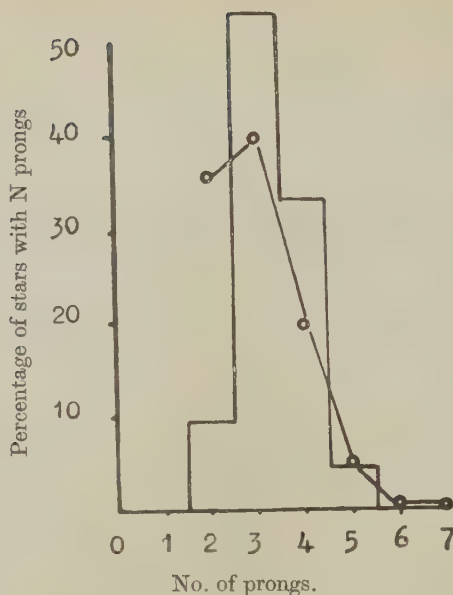
Of the seven four-particle stars only one can be due to carbon as all others have, in addition to the hammer track, at least one other prong of charge two. Four appear to be described by the reaction



† Communicated by the Author.

‡ Now on the staff of the Australian National University, Canberra.

Fig. 1(a).

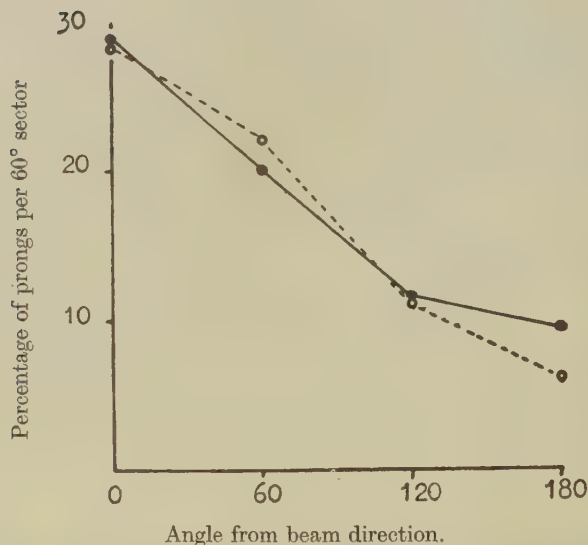


Per cent of stars with N prongs plotted against the prong number N.

Histogram : Stars with hammer tracks.

Circles : All other stars.

Fig. 1(b)

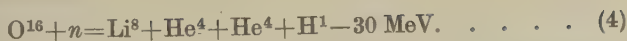


Per cent of prongs per 60° sector as a function of angle between centre of sector and the beam direction.

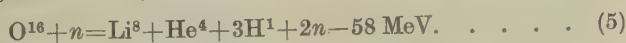
Open circles : Stars with hammer tracks.

Closed circles : Stars without hammer tracks.

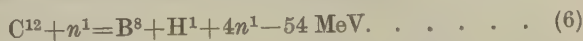
and two by the reaction



The five-prong star can only be due to oxygen and may be described by

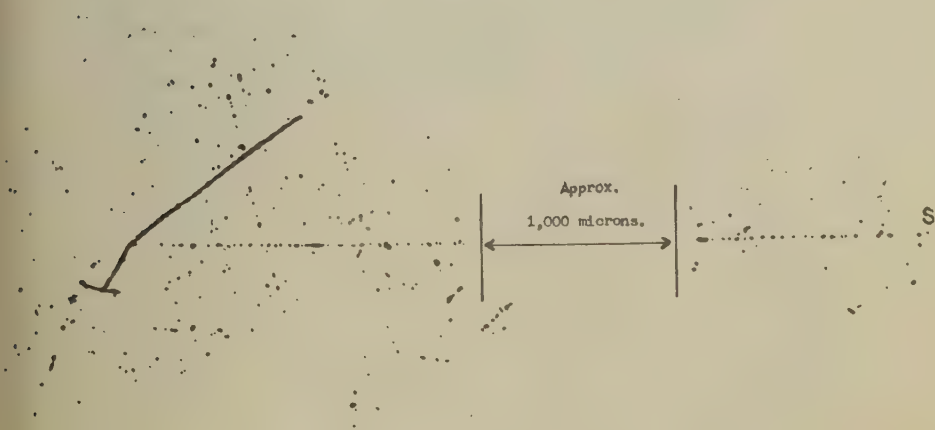


Of the 21 events only the two-particle stars could reasonably involve the nucleus B^8 . One of these comprises the hammer track plus a fast proton and on charge conservation grounds is therefore



the other shows a gross momentum unbalance about the incoming neutron direction and has a second track of $Z \geq 2$. It could be either Li^8 or B^8 .

Fig. 2.



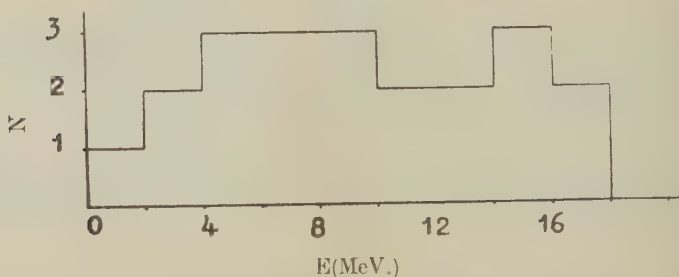
Micrograph of star assigned to reaction (2).

These results suggest that Li^8 is a much more likely residual nucleus than B^8 and, accepting the above assignments, the cross-section for Li^8 production, averaged over C, N and O atoms in emulsion is found to be $0.6 \pm 0.2 \text{ mB}$. The energy spectrum of the Li^8 nuclei is indicated in fig. 3 (a) and the energy release in the break-up of the resulting Be^8 nuclei is given in fig. 3 (b). The latter histogram is in agreement, within the statistics, with that found for Be^8 resulting from the reaction $\text{Be}^9 \gamma p \text{Li}^8$ (Titterton 1950).

Experiments are now in progress to study stars produced by 170 MeV. protons and the preliminary results show a similar percentage of stars with hammer tracks. This agrees with Wright (1950) who finds that ^8Li is formed when a variety of elements are bombarded with 340 MeV. protons and also with 190 MeV. deuterons. Furthermore, in a study of 3000 π^- meson induced stars Adelman and Jones found 11 cases of hammer

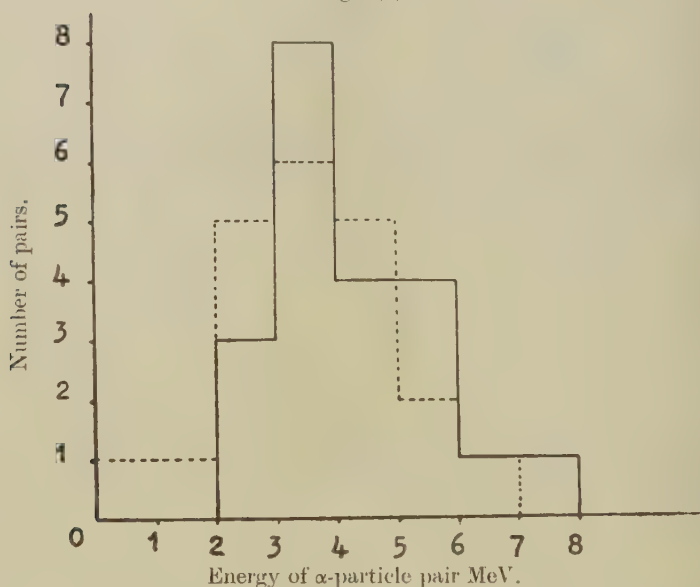
track emission. This frequency compares well with that observed in the present experiments with neutrons and protons as might be expected since the nuclear excitation in this case would be about the same value

Fig. 3(a)



Energy spectrum of ^8Li nuclei emitted from the stars.

Fig. 3(b)



Energy release in the break-up of the ^8Be nucleus forming the head of the hammer.

Full lines, present 21 events.

Dotted lines, events resulting from the reaction $\text{Be}^8 \rightarrow \gamma p \text{Li}^8$.

(142 MeV.). Combination of these results suggests that ^8Li should be found as a residual nucleus in the break-up of highly excited light nuclei and it should therefore have been found in the high energy α -particle bombardments.

The mechanism proposed by Wright (1950) to explain Li^8 production from light elements requires the incoming particle to be captured and the compound nucleus to boil off the necessary number of neutrons and protons leaving a residue consisting of ^8Li . This is not in general agreement with the present observations. As shown above an excited nucleus is formed by inelastic scattering or by capture of the neutron and then breaks up into charged particles of which a large proportion are α -particles. In general very few neutrons are emitted.

Thanks are due to Miss M. Hopkins for microscope work and Mr. T. A. Brinkley for the photomicrograph.

REFERENCES.

- ADELMAN and JONES, 1950, *Phys. Rev.*, **111**, 226 ; *Science*, **111**, 226.
ALVAREZ, 1950, *Harwell Conference Report*, A.E.R.E. G/M 68, p. 43.
FRANZINETTI and PAYNE, 1948, *Nature, Lond.*, **161**, 735.
GARDNER, 1949, *Phys. Rev.*, **75**, 379.
GARDNER and PETERSON, 1949, *Phys. Rev.*, **75**, 364.
TITTERTON, 1950, *Nature, Lond.*, **165**, 721.
WRIGHT, 1950, *Phys. Rev.*, **79**, 838.

XI. *Notices of New Books and Periodicals received.*

Progress in Biophysics. Edited by J. A. V. BUTLER and J. J. RANDALL, F.R.S. (Butterworths.) Price 50s.

THE boundaries of biophysics have never been easy to define, but this well-produced volume helps both to indicate the fringe of recent advances and to consolidate the ground already won. As the editors point out, biochemistry and physiology have their own domains and mere application of a physical or chemical technique to a biological problem does not necessarily constitute a passport to this mandated territory. Perhaps the main justification for a subdivision of science such as biophysics is that it provides opportunities for cross-fertilization which may generate offspring more bold and vigorous than the parents.

Throughout the volume, with separate chapters by a number of experts, there is noticeable a healthy tendency to stress what may be called the dynamic aspects of the various subjects.

There is a good author index but the subject index is rather brief for a volume covering so wide a field. For most readers too, it would be more convenient if the separate bibliographies were arranged in alphabetical order. It would also be helpful if in future editions all the contributors could be induced to provide summaries of their material and personal views.

Dr. Butler and Professor Randall have performed a valuable service in producing a work in which there is so much information, some wisdom and no little wit.

W. G. W.

Cosmical Electrodynamics. By H. ALFVÉN. (Oxford.) Price 25s.

THE subject of which this book treats is a new one. It deals with the electromagnetic behaviour of an ionized compressible gas in hydrodynamic motion, and with the applications of this study to problems in astrophysics.

At present we are very far from having a complete solution of the electrodynamic-hydrodynamic problem in its most general form. Unfortunately a proper investigation of the astrophysical effects requires nothing short of such a complete solution. So we are forced to makeshift methods. These have mostly followed one or other of two lines. There is the cautious school of thought that accepts only those electromagnetic effects that seem unavoidable. The second school of thought, on the other hand, accepts every electromagnetic effect whose existence cannot be disproved. For example, this school will regard an electric field as being present in a particular problem so long as its existence cannot be disproved, whereas the first school will not accept the existence of the electric field unless its absence can be disproved. Dr. Alfvén belongs to the second school of thought, and to the reader of his book this carries an important advantage. For Dr. Alfvén's applications of electromagnetism to astrophysics are so extensive that many of the ideas set forth in his book are reasonably certain to have permanent value. Which these are, however, the reader must discover by his own efforts.

One of the most important current issues concerns the relation between the electric current density in an extremely diffuse ionized gas, the electromagnetic field, and the motion of the gas. This affects not only the structure of the solar atmosphere, but also whether or not there can be a galactic magnetic field of appreciable magnitude. Alfvén quotes a formula due to Cowling without apparently noticing that Cowling's result depends on the assumption that the gas is not being appreciably accelerated. This places an important restriction on the use of Cowling's formula which may be stated briefly as follows:—To an observer moving with a particular element of gas the electric and magnetic fields at the position of the element are substantially parallel. Without this result it seems impossible to attempt, as Alfvén does, the investigation of very diffuse gases.

Another question that is now open to doubt is whether under normal conditions the general solar magnetic field can extend much above the photosphere. Certainly the observed variations of angular velocity from one part of the Sun's atmosphere to another are inconsistent with the simple dipole field assumed by Alfvén. This has serious repercussions on the sections dealing with the structure of the chromosphere and corona.

In reading this book one can hardly fail to notice the author's tendency to claim a displacement of a problem as its solution. For instance, it would not be reckoned a complete answer to a question such as: "Why did you arrive at work so early this morning?" to say: "Because I left home an hour before my usual time." Yet this is what Alfvén does on numerous occasions; for example, in the problem of the reversal of the magnetic polarities of sunspots, in that of the darkening of sunspots, and in postulating the electric field necessary to accelerate the auroral particles.

But in spite of all criticism, and the author can hardly expect some of his ideas to escape criticism, this book cannot fail to be most useful to all who are interested in the problems of solar physics and of cosmic rays. It should be on the book-shelves of every astrophysicist. F. HOYLE.

A Hundred Years of Physics. By WILLIAM WILSON. [Pp. 519.] (Duckworth and Co., London, 1950.) Price 21s.

THOSE who hope to find in this volume a history of the revolutionary changes in physical ideas which have taken place during the period covered (1850-1950) may be somewhat disappointed. The book is rather a kind of supplementary text, suitable for revision purposes, in which rather more than the usual emphasis is laid on the chronology of the various topics considered. An honours graduate in Physics—actual or potential—could read it with pleasure and profit; but the author's claim in his preface that the reader needs very little previous knowledge of physics and very slight mathematical equipment must be taken *cum grano salis*. For the rest, the book is well written, well produced, with many references to the original publications and a satisfactory index. N.T.

Contributions to Mathematical Statistics. By R. A. FISHER. Wiley (Chapman and Hall.) Price 60s. net.

THIS volume is a collection of reprints of 43 papers by an eminent statistician selected by him as the more important of his published papers. They cover a wide variety of subjects and are accompanied in many cases by author's notes added for the purpose of the volume. Though photographically reproduced from the original journals, the volume is attractively prepared on good paper. Many will find in it a useful work of reference and study.

Methods of Mathematical Physics. By H. and B. S. JEFFREYS. Second Edition. [Pp. 708.] (Cambridge University Press.) Price £4 4s. 0d. net.

THE value of this important work is shown by the appearance of a second edition only four years after the original. The first edition was reviewed in this journal (Vol. 38, p. 226, 1947). It has now been considerably revised, in some cases by the addition of new material or the expansion of old, as in the account of matrices and the treatment of relaxation methods. In other cases the subject-matter has been mainly re-written, as in the chapter on multiple integrals. Where possible the proofs have been either replaced by shorter ones or generalized.

An extraordinarily wide range of topics is covered, as indeed must be the case in achieving the authors' aim to give an account of those parts of pure mathematics that are most frequently needed in physics.

[The Editors do not hold themselves responsible for the views expressed by their correspondents.]

NOTICE TO CONTRIBUTORS

UNIT OF HEAT

The Council of the Royal Society, having considered a memorandum entitled "The Unit of Heat", recommends that quantities of heat and all other dependent concepts such as specific heat, latent heat, entropy etc., should in future be expressed both in joules and in calories.

The Editors express the hope that, in submitting papers for publication in the *Philosophical Magazine*, contributors will also adopt this procedure.

ERRATA.

An Interferometric Study of some Optical Properties of Evaporated Silver Films, by R. C. FAUST, *Phil. Mag.*, 1950, **41**, 1238.

P.1241, line 5, read "glass substrate" for "glass substitute".

P.1243, line 30, read "rate of evaporation" for "rate of absorption".

P.1254, Insert the reference

BROSSEL, J., 1947, *Proc. Phys. Soc. Lond.*, **59**, 224.

XII. *The Waveforms of Atmospherics and the Propagation of very Low Frequency Radio Waves.*

By P. W. A. BOWE,
Cavendish Laboratory, Cambridge*.

[Received November 28, 1950.]

[Plate VI.]

SUMMARY.

The responses of narrow-band receivers to individual radio atmospherics have been observed in order to describe the propagation of radio waves of frequency 2 kc./s. to 10 kc./s. over the surface of the earth. It has been found that the atmospherics from a fixed distance are sufficiently uniform to enable the relative attenuations of different frequencies to be deduced. The study reveals that waves of frequency below about 8 kc./s. are heavily attenuated during the daytime but are propagated freely at night. The attenuation is greater during a sudden ionospheric disturbance.

These results confirm and extend those obtained recently by Gardner. They can be explained in outline on a theory recently proposed by Budden.

§1. INTRODUCTION.

SEVERAL workers have shown that the waveforms of some atmospherics can be interpreted in terms of irregularly shaped radio impulses reflected one, two and more times from the ionosphere (Laby, McNeill, Nicholls, Nickson, 1940; Schonland, Elder, Hodges, Philips and van Wyk, 1940). Under good conditions it is often possible to deduce the height of reflection of these impulses, and heights of about 85 km. have been deduced.

Other workers (Bracewell, Budden, Ratcliffe, Straker and Weekes 1951) have investigated the propagation of very long radio waves emitted by commercial senders, and a considerable body of knowledge now exists concerning the height from which these waves are reflected by the ionosphere, and their intensity.

It is clearly of interest to compare the results of the two types of experiment. Unfortunately, when this comparison is attempted, a serious difficulty arises because in the atmospherics observed the shape of the impulse which is successively reflected from the ionosphere is usually irregular, and varies from sample to sample, so that it is impossible to specify with any accuracy the radio frequency to which it corresponds.

* Communicated by Mr. J. A. Ratcliffe.

In the work to be described in this paper radio atmospherics are used in a different way to investigate the propagation of very long radio waves. A single atmospheric is applied simultaneously to four narrow-band receivers tuned to different very low frequencies between 2 kc./s. and 10 kc./s., and the responses are compared. The relative responses on the different frequencies (which might be called the spectrum at the receiver) will depend on (a) the relative intensities excited in the different frequencies by the particular lightning flash being measured (which might be called the spectrum at the source), and (b) the characteristics of the transmission path between the flash and the receiver. In order to separate these two factors, the atmospherics received from flashes at different distances have been compared.

The assumption is made that, statistically, all flashes excite the same spectrum at the source, at least in the region of very low frequencies here considered, and a search is made for some significant change produced in the received spectrum as the distance of the flash changes. For one of the two classes of atmospherics received, described in more detail below, it has been found possible to establish a change of this kind accompanying a change of distance. This provides confirmation of the original assumption that there is some statistical constancy in the spectrum produced at the source by different lightning flashes. That change in the spectrum which accompanies increase of distance is attributed to the propagation conditions. It is also found that the propagation conditions, deduced in this way, change from day to night and during a sudden ionospheric disturbance. The results are summarized and discussed in § 5.

The recorded atmospherics fell into two easily distinguishable classes as follows.

Class I. had a fairly smooth "waveform" with marked low frequency periodicity of a more or less regular nature. The narrow-band amplifiers tuned to frequencies below 10 kc./s. gave a large response with atmospherics of this class. An example is shown in Pl. VI. (i.).

Class II. had a highly irregular "waveform" which showed an erratic variation with many short period fluctuations. When the overall amplitude of this type of atmospheric, as recorded on the wide-band receiver, was of the same order as that of an atmospheric of Class I., the response of the narrow-band amplifiers was much smaller for frequencies below 10 kc./s. An example of Class II. is shown in Pl. VI. (ii.) and can be compared with the atmospheric of Class I. shown in Pl. VI. (i.).

It appears that these two classes of atmospheric are different at the source, and in this paper only those of Class I., which gave an appreciable response on the narrow-band receivers, are considered. They formed about 75 per cent of the atmospherics recorded. The two different classes have been noticed by most workers in the subject, and Appleton and Chapman (1937) have ascribed them to the leader (Class II.) and return (Class I.) strokes of the lightning flash. For the purposes of the

present paper, it is sufficient to distinguish between them by the nature of the recorded waveforms.

It will be shown in §4 that, when atmospherics of Class I. are selected in this way, their spectrum at the source is, within limits, the same for all atmospherics, so that changes in the spectrum due to propagation conditions can be shown up. Since atmospherics of Class II. produce only small radiation at the frequencies here considered, we assume that they do not radiate appreciably at these frequencies and therefore have a different spectrum at the source. Both classes of atmospheric have been received from distances up to 1700 kilometres.

The sources of atmospherics which were received and analysed in the way here described were simultaneously located by radio direction finding methods by the "Sferic" section of the Meteorological Office. This provided the measure of distance to the source of the atmospheric.

In the work described here each atmospheric was received on four narrow-band receivers tuned to four different very low frequencies, and for the sake of comparison, the waveform of the atmospheric as received on an aperiodic amplifier was simultaneously recorded. The responses at the four spot frequencies represent four points on the spectrum of the received atmospheric and could be deduced if that spectrum were known. In several cases the spectrum of the received atmospheric has therefore been deduced from the waveform by numerical Fourier analysis and it has been shown that the responses on the four tuned receivers correctly represented the four points on the spectrum. It was at one time thought that the method of numerical Fourier analysis of the waveform would be simpler than the method of reception on four narrow-band receivers, but it has proved that the latter method is in fact simpler and quicker. Since a large number of results are required for making a statistical analysis, the method of observation with the four receivers has therefore been used.

The results described in this paper confirm and extend those recently obtained by Gardner (1950). He recorded the integrated "level" of atmospherics received on four narrow-band receivers tuned to four different very low frequencies and observed how these levels altered with time of day and with the distance of a storm centre. He deduced information about the propagation conditions on the different frequencies.

While he was working in Cambridge, Gardner also constructed the equipment, described in outline in this paper, for recording the response of narrow-band receivers to individual atmospherics, and obtained some preliminary results with it before the present author took over the work from him. It is hoped that the equipment will be described in detail in a paper by Gardner.

The results given in this paper, and the corresponding results of Gardner, have been explained, at least in outline, by Budden (1951). A preliminary comparison of his theory with the present results is made in §5.

§ 2. EXPERIMENTAL METHOD.

The atmospherics were received on a vertical aerial and passed through a cathode follower to an aperiodic receiver and four tuned receivers all in parallel, as shown in fig. 1. The output of each receiver was applied to a separate cathode ray tube and when an atmospheric arrived all five tubes were photographed. Thus the waveform of the transient was recorded together with the response of four tuned receivers to it.

Fig. 1.

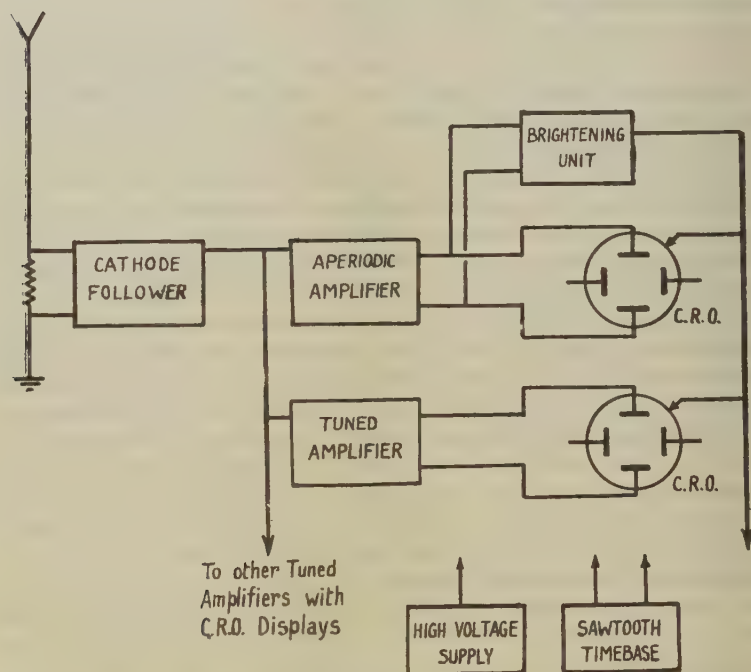


Diagram showing the experimental arrangement for recording atmospherics on an aperiodic and several narrow-band receivers.

2.1. Receiving Unit.

The vertical aerial, which was erected on a site near Cambridge relatively free from noise, had a length of 9 metres and a capacity to ground of $120 \mu\text{F}$. The voltage in the aerial was applied to the grid of a cathode follower across a grid resistor of 10^6 ohms, situated at the bottom of the aerial. A long cable connected the low impedance output of the cathode follower to a pre-amplifier with a step attenuator, the output of which was applied to the five receivers in parallel.

The aperiodic receiver had a gain which was constant to within 1 db. for frequencies between 800 c./s. and 50 kc./s. and gave an output which

was proportional to the electric field at the aerial. It had two stages of amplification followed by cathode and anode followers to give a push-pull output to the cathode ray tube.

Each tuned receiver had a bandwidth of about 180 c./s. between half-power points, and each was tuned to a different frequency somewhere between 2 kc./s. and 10 kc./s. Each receiver consisted of an amplifier with a tuned-grid stage followed by a second amplifier, from which positive and negative feedback were applied to the first amplifier in order to narrow the bandwidth. Each receiver was followed by anode and cathode followers to give push-pull output for the cathode ray tube.

2.2. Display Unit.

The output from each of the four receivers was applied to the Y deflection plates of four 3-in. cathode ray tubes. The same sawtooth time-base voltage was applied to the X plates of each tube; the time of sweep was about 2 milliseconds and the time of fly-back was less than 5 microseconds. This time-base was freely running so that the atmospheric appeared at a random place on the trace.

The grids of the cathode ray tubes were normally maintained at a negative potential so that no trace appeared. The output of the aperiodic receiver was connected to a brightening unit which, when an atmospheric above a certain small amplitude arrived, applied a positive pulse to the grids so as to brighten the tubes for the duration of one time-base sweep, and this trace was automatically photographed. The film was moved on manually and, to avoid double exposure, a delay was provided in the brightening unit so that, after brightening once, the circuit was inoperative for about half a second.

A typical record obtained in this way is shown in Pt. VI. (i.). The waveform as received by the aperiodic amplifier is shown on the centre trace and the responses of the four narrow-band receivers on the other traces. Each trace brightened at a point (*a*) and continued bright to (*b*), whence the fly-back returned the spot to (*c*) and the rest of the time-base was completed.

2.3. Measurement of Distance.

The distance to the source of the atmospherics was determined by taking advantage of the "Sferic" direction finding organization of the Air Ministry Meteorological Office (Ockenden 1947), and the grateful thanks of the author are due to the Director and staff for helpful co-operation.

Use was made of the routine service by which the sources of individual atmospherics are located by the intersections of radio bearings taken simultaneously at four widely-spaced observing stations. The use of telephone connection during an experiment enabled individual atmospherics recorded at Cambridge to be identified with sources located by the "Sferic" organization.

The distance to the source was then measured directly. There was a small chance of mis-identification, but this was not serious enough to affect the results. The sources could generally be located to an accuracy of about 10 per cent up to 1000 km. and less accurately beyond, but this was quite sufficient for the present purpose.

§ 3. THE SPECTRUM OF THE RECEIVED ATMOSPHERICS.

We shall here discuss the spectrum of the received atmospheric as deduced from Fourier analysis of the recorded waveform and relate it to the observed responses from the narrow-band receivers.

3.1. *The Output from the Tuned Receivers.*

It is interesting to notice the way in which the narrow-band receivers respond to the input transient depicted at (2), Pl. VI. (i.). If we look, for example, at the recorded response of the receiver tuned to 7.5 kc./s. we see that, while the original transient is arriving, the amplitude is building up so that, when the transient is over, the circuit is left performing a decaying oscillation with a decay time determined by the band-width of the amplifier. The amplitude of this oscillation represents the amplitude of the appropriate Fourier component in the analysis of the transient. The amplitude of the final decaying oscillation cannot, of course, be decided until the transient is over, so that the response during the building-up period need not bear any relation to the final amplitude when the transient is over. The record of the response on 3.5 kc./s. shows this well: during the "build-up" period there is quite a large response, but when the transient is over, the circuit has settled down to give a negligibly small decaying oscillation, corresponding to the fact that the Fourier component of frequency 3.5 kc./s. is too small to record.

The four narrow-band receivers were calibrated by observing their responses to a test signal which consisted of a rectangular pulse of voltage of known amplitude and of duration 14 μ sec. This pulse was repeated fifty times per second but, of course, only occasional ones were recorded. Each of these pulses had an effectively uniform spectrum over the relevant range of frequencies 2 kc./s. to 10 kc./s. Although it is considered that the absolute response of the different receivers could be made equal by this method of calibration, it will become apparent, in what follows, that the conclusions to be reached in this paper do not depend on this adjustment for equality. All the measurements were made in terms of the ratio of the responses at two frequencies, and the way in which that ratio changes from time to time. It is only necessary, then, that the ratio of the responses should be determined, and this was done by the method of calibration described.

A similar argument helps us to avoid a difficulty in the measurement of the responses on the narrow-band receivers. There might be some doubt as to whether the amplitude of the decaying oscillation should be

measured at the time when the transient is finished, or whether the decay should be allowed for, and the amplitude be estimated at the time when the transient started. Since, however, we are only concerned with the ratio of amplitudes on the different frequencies, it does not matter which measurement is taken, provided it is kept the same for all frequencies.

Records of the type illustrated in Pl. VI. were made on photographic film and were measured by projecting and comparing with a scale.

3.2. Direct Fourier Analysis of the Transient.

The method described in the previous section could be thought of as giving four points on the frequency spectrum of the received atmospheric. It was at one time thought that this information could be more easily obtained by performing a Fourier analysis of the transient recorded on the wide-band amplifier, and, moreover, it appeared that if the analysis were performed in this way, attention need not be restricted to four frequencies. Some of the records of transient responses were therefore analysed by ordinary methods of Fourier analysis, as described below. It soon became apparent, however, that the labour of performing a full Fourier analysis was considerable, and, since the aim of the work was to record numerous atmospherics from which statistical deductions could be made, this method was not continued. It proved to be much simpler and quicker to use the apparently more complicated method of the four tuned receivers to obtain the Fourier components at the four chosen frequencies.

It is, however, of interest to see how far the Fourier analysis of the recorded wave-form agreed with the magnitudes of the Fourier components deduced from the responses of the four narrow-band amplifiers. For this purpose the transient waveform was redrawn on as large a scale as possible and three standard methods of Fourier analysis were used. These were :—

- (1) An electro-mechanical analyser developed by the Admiralty Research Laboratory (Barber, Ursell, Darbyshire and Tucker 1946).
- (2) Beevers Lipson Strips (Ross 1943).
- (3) Hollerith Computing Machine (Hodgson, Clews and Cochran 1949).

Fig. 2 (a) gives the results of applying methods (1) and (2) to the waveform shown and fig. 2 (b) shows the results of applying methods (2) and (3) to another waveform. It will be seen that in each case the deductions made by the two different methods agree quite well. The points marked by crosses show the relative magnitudes of the Fourier components as determined by measurement of the responses on the narrow band receiver. These magnitudes have been adjusted so that the point for 7.5 kc./s. falls on the computed curve. It will be seen that they agree well with the results calculated by direct Fourier analysis of the transients, and we are satisfied that the method of using the four tuned receivers gives reliable results for the ratio of Fourier components at the relevant frequencies.

Fig. 2 (a).

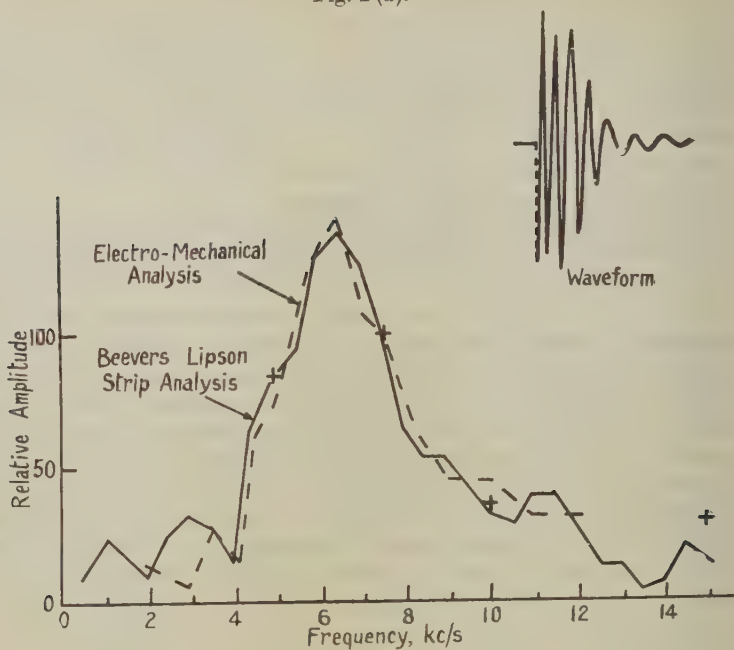
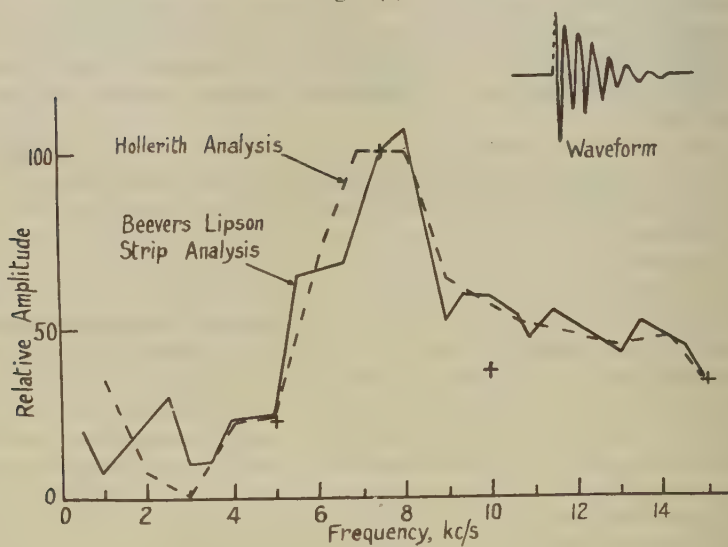


Fig. 2 (b).



The received spectra of two atmospherics as deduced by the methods indicated. The four points deduced from the responses of the tuned receivers are indicated by crosses. The waveform analysed is also shown.

It might be thought that an important part of the atmospheric waveform might fail to be recorded on the wide-band receiver because of the time lost before the cathode-ray trace was brightened by the atmospheric. The good agreement between the spectra computed from the recorded waveform and the responses of the four narrow-band receivers shows that there is no difficulty of this kind in the range of frequencies here considered.

§ 4. ANALYSIS OF RESULTS.

4.1. *Method of Analysis.*

In order to clarify the method of analysis, it is convenient to define some attenuation factors. Consider a lightning flash which has a radiation field $A\phi(f)$ at the source, where A depends on the strength of the source and $\phi(f)$ represents the way in which the field varies with the frequency f . Then in free space the field received at a distance r would be given by $A\phi(f)/r$. Suppose now that this atmospheric were transmitted a distance r over the surface of the earth and that as a result each component frequency f suffered an attenuation $\rho(f, r)$; so that the received field would be given by

$$E(f, r) = \frac{A}{r} \phi(f) \rho(f, r).$$

Now let the field produced by a source at a distance r be measured at a series of different frequencies $f_0, f_1, f_2 \dots f_n$, and let the result be expressed as a ratio between the field at the frequency f_n and the field at a reference frequency f_0 so that we obtain the quantity

$$E(f_n, r)/E(f_0, r) = \{\phi(f_n)/\phi(f_0)\} \{\rho(f_n, r)/\rho(f_0, r)\}.$$

Next, suppose that these measurements are made for several atmospherics at a series of different distances, and that the ratio $E(f_n, r)/E(f_0, r)$ is plotted as a function of r . The resulting curve will show how the ratio $\rho(f_n, r)/\rho(f_0, r)$ of the attenuation factors at the two frequencies f_n and f_0 varies with distance. Since the attenuation factor $\rho(f, r)$ is unity for all frequencies when the distance is small, the intercept on the axis at $r=0$ will give the magnitude of $\phi(f_n)/\phi(f_0)$, which depends on the spectrum of the atmospheric at the source.

It is of course most unlikely that the spectrum $\phi(f)$ of the atmospheric at the source is the same for all atmospherics. If, however, they do not differ too much among themselves then, by taking enough observations on atmospherics originating at all distances, it may be possible to draw a smooth curve through the set of observed points so as to show, with some real significance, how the ratio $\rho(f_n, r)/\rho(f_0, r)$ of the attenuation factors varies with distance. We shall show that, in fact, the spectra $\phi(f)$ are sufficiently nearly the same for frequencies between 2 and 10 kc./s. for this procedure to be of use.

4.2. Measurements under Normal Conditions.

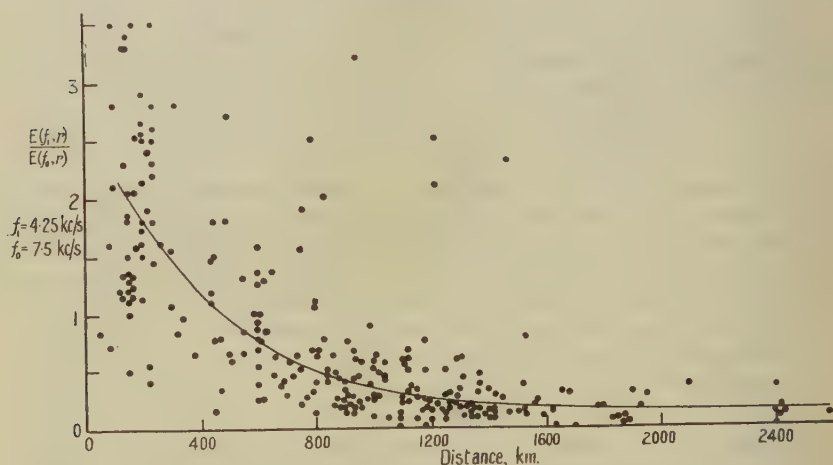
In order to examine seasonal changes the observations are grouped in four sets as summarized in Table I. which lists the frequencies used, the number of experimental runs, the number of atmospherics recorded, and the distances between which the sources were located.

TABLE I.

Set	Occasion	Frequencies kc./s.	No. of runs	No. of atmospherics	Distance of sources, km.
A	Winter day	(3.5), 5, 7.5, 10	11	70	600-3600
B	Night	3.5, 5, 7.5, 10	10	55	1000-3000
C	Summer day	3.5, 5, 7.5, 10	11	195	300-2000
D	Summer day	2.25, 4.25, 6.25, 7.5	21	255	0-3000

In order to analyse the results the frequency 7.5 kc./s. was taken as the standard frequency f_0 , and for each atmospheric observed the ratio $E(f_n, r)/E(f_0, r)$ was deduced and plotted against the measured distance

Fig. 3 (a).



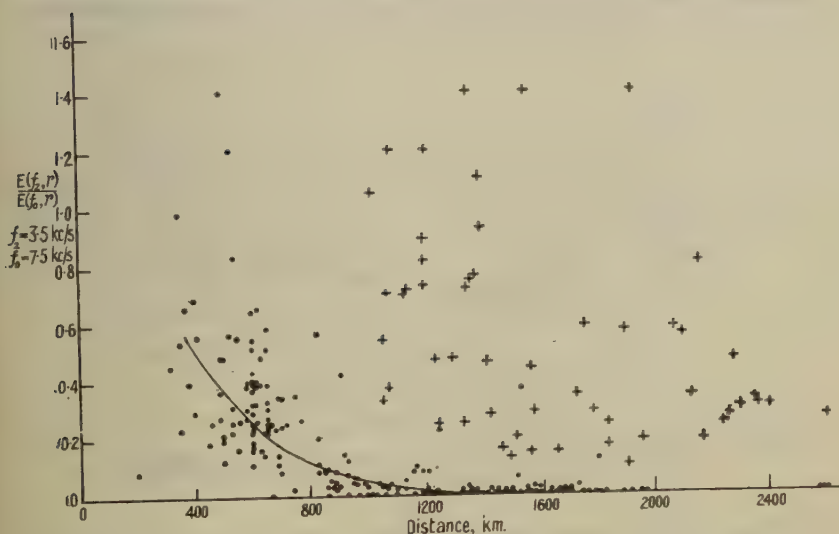
To show how the ratio $E(f_1, r)/E(f_0, r)$ of field strengths at 4.25 kc./s. ($=f_1$) and 7.5 kc./s. ($=f_0$) for atmospherics at different distances, varies with distance. All observations were made in daytime.

r of the source. A series of plots of this kind was made for each of the frequencies observed. Fig. 3 (a) shows the results obtained on summer days for $f_1 = 4.25$ kc./s. and $f_0 = 7.5$ kc./s.

It will be seen that although there is a considerable spread in the observed points, of the order of about 10:1 at all distances, it is nevertheless possible to draw a smooth curve through them which clearly has some significance and which shows that the ratio decreases as the distance increases. We deduce from this curve that the intensity of waves of frequency 4.25 kc./s. decreases more rapidly with distance than that of waves of frequency 7.5 kc./s.

There is, of course, a very considerable spread amongst the observed points plotted in the figure. This is caused largely by the differences in the ratio $\phi(f_1)/\phi(f_0)$ from one atmospheric to another, but some of it

Fig. 3 (b).



To show how the ratio $E(f_2, r)/E(f_0, r)$ of field strengths at 3.5 kc./s. ($=f_2$) and 7.5 kc./s. ($=f_0$) for atmospherics at different distances, varies with distance.

- + Observations at night.
- Observations during the day.

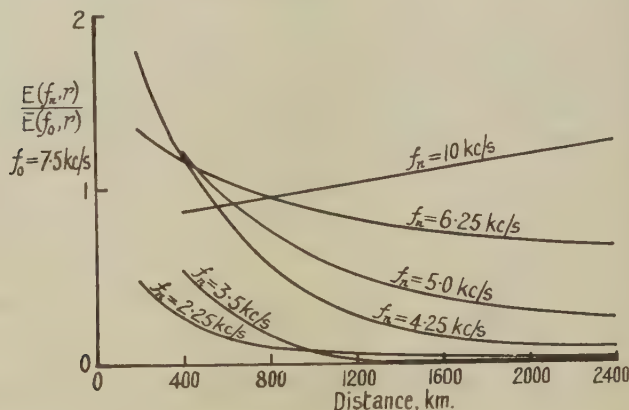
is also probably due to inaccuracies in the measurements of the distance of the source, and to wrong identifications between some of the atmospherics whose distance was measured and those whose spectral response was determined. Examination of the results on all frequencies and at all times has led us to think that the ratio $\phi(f_1)/\phi(f_0)$ varies by a factor of about 10:1 from atmospheric to atmospheric.

Fig. 3 (b) in which the ratio $E(f_2, r)/E(f_0, r)$ is plotted against r for $f_2=3.5$ kc./s. and $f_0=7.5$ kc./s., shows similar results. Observations obtained by day are shown as dots, and a smooth curve has been drawn to lie evenly amongst them. Observations taken by night are shown

by crosses. It will be seen that, during the day, for distances greater than about 1200 km. the response on 3.5 kc./s. is in nearly all cases so small as to be negligible and is less than 1/100th of the response on a frequency of 7.5 kc./s.* It is clear that, whereas waves of frequency 7.5 kc./s. can be transmitted over these distances during the day with comparative ease, those of frequency 3.5 kc./s. are heavily attenuated. This result, shown clearly by these observations alone, is the most striking feature of the transmission characteristic which we shall summarize in the next section.

The other important point which arises from fig. 3(b) is concerned with the marked difference between the results for day and night. It is clear that although waves of frequency 3.5 kc./s. cannot be transmitted over distances greater than 1200 km. by day they are transmitted almost as easily as those on 7.5 kc./s. by night.

Fig. 4.



Curves showing how the average ratio of field strength $E(f_n, r)/E(f_0, r)$ varies with distance for $f_0 = 7.5$ kc./s. and f_n as indicated.

Results obtained with the other frequencies have been plotted in the same way and smooth curves have been drawn through the points. The complete plots are not reproduced, but the smooth curves are shown in fig. 4 for the summer day observations. These observations were nearly all made within two hours of local noon, and most of the atmospherics came from directions between 030° and 135° E. of N. The analysis was based on those recorded atmospherics for which a definite location was obtained by the Sferics organization.

The night and winter-day observations did not include a sufficient number of atmospherics to enable similar curves to be drawn, and they

* The different response on the two frequencies of 7.5 and 3.5 kc./s. for a distant atmospheric in the daytime is well illustrated by the example shown in Pl. VI. (i).

are not presented here in detail. However, the observations on 3.5 kc./s. already mentioned do establish the important fact that the received amplitude $E(f_2, r)/E(f_0, r)$ for $f_2=3.5$ kc./s., $f_0=7.5$ kc./s., $r=1000$ km. is at night about ten times what it is during the day. This means that the attenuation factor $\rho(f_2, r)/\rho(f_0, r)$ is at night ten times what it is during the day.

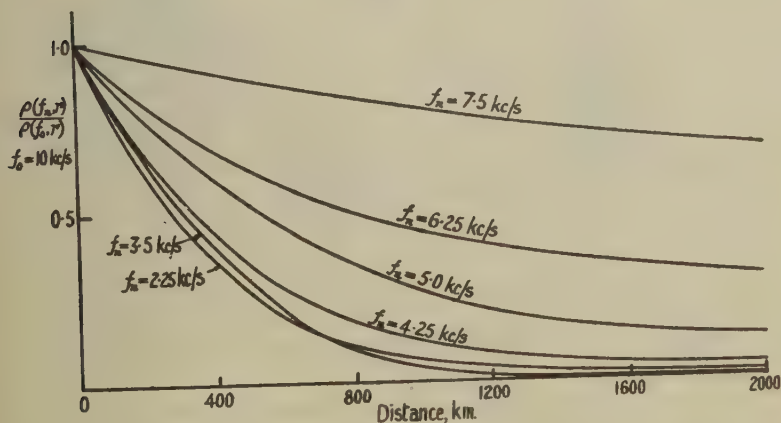
4.3. Deduction of Attenuation Curves.

The curves of figs. 3 and 4 show how the quantities

$$\{\phi(f_n)/\phi(f_0)\}\{\rho(f_n, r)/\rho(f_0, r)\}$$

vary with distance when f_0 is taken as 7.5 kc./s. It is now desirable to normalize these curves so that they pass through the value unity for small distances; they then give information about the attenuation

Fig. 5.



Curves showing how the ratio of attenuation coefficients $\rho(f_n, r)/\rho(f_0, r)$ varies with distance for $f_0=7.5$ kc./s. and f_n as indicated.

coefficients alone, but not about the ratios $\phi(f_n)/\phi(f_0)$. The normalizing factor was obtained by extrapolating the curves to zero distance. It is also convenient to take a new frequency, 10 kc./s., for f_0^* , and we then obtain, for summer daytime, the series of curves shown in fig. 5 in which $\rho(f_n, r)/\rho(f_0, r)$ is plotted against distance with $f_0=10$ kc./s.

It is convenient to present the same results in still another way, as shown in fig. 6, in which the ratios $\rho(f, r)/\rho(f_0, r)$ are plotted against frequency f for three different distances $r=500, 1000$ and 2000 km. In these curves f_0 was taken as 10 kc./s. and if there were no attenuation at this frequency, the curves would represent attenuation as a function

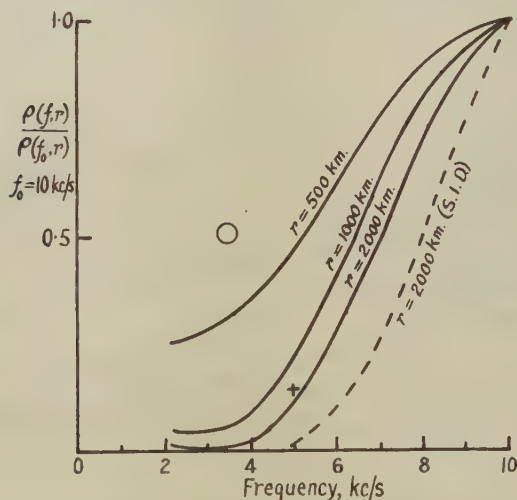
* In the preliminary calculations it was more convenient to take $f_0=7.5$ kc./s. because one of the receivers was working on this frequency in every experiment, but there was not always a receiver tuned to 10 kc./s.

of frequency at the three distances; if there be some attenuation on 10 kc./s., the curves showing total attenuation as a function of frequency would have their scales altered by different amounts so that they would no longer all pass through the same point at 10 kc./s.

By a different experimental method Gardner (1950) has plotted similar curves, and the cross at 5 kc./s. (fig. 6) represents his results for atmospherics originating from a distance of about 1500 km. It agrees well with the present results.

Neither the winter nor the night observations are sufficient to enable similar attenuation curves to be drawn. The night observations on 3.5 kc./s. shown in fig. 3(b) do, however, indicate, as has been mentioned before, that the attenuation factor $\rho(f_2, r)/\rho(f_0, r)$ for $f_2=3.5$ kc./s.,

Fig. 6.



Summary of attenuation coefficients for different conditions.

- Variation of ratio of attenuation coefficients $\rho(f, r)/\rho(f_0, r)$ with frequency f for $f_0=10$ kc./s. and r as indicated. Normal day conditions.
- - - Similar curve for $r=2000$ km. during an S.I.D.
- + Value obtained by Gardner for atmospherics from about 1500 km.
- Night attenuation on 3.5 kc./s. for atmospherics from 1000 km.

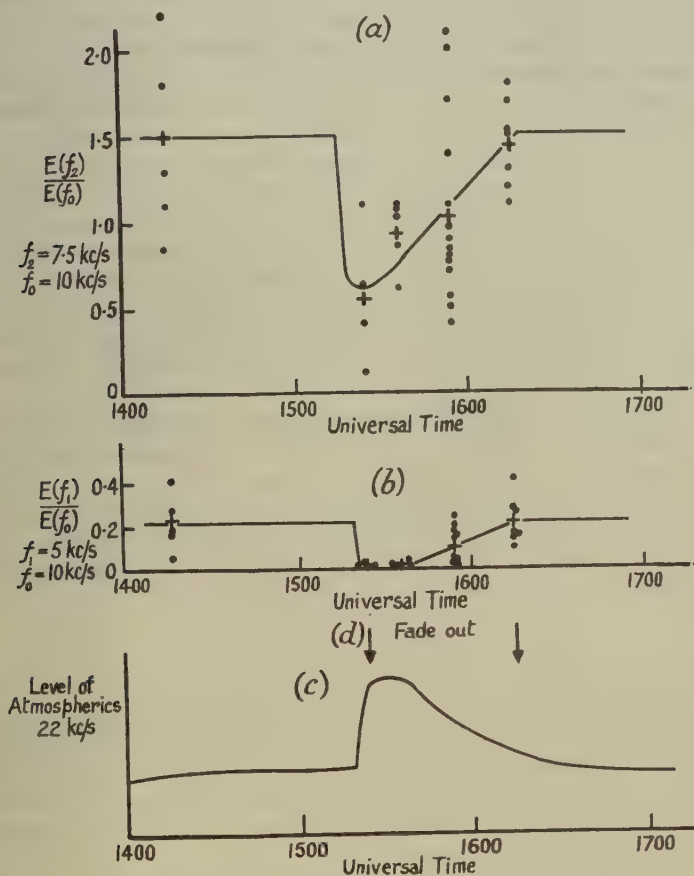
$f_0=7.5$ kc./s., $r=1000$ km. during the night is about ten times what it is during the day. Since the day attenuation is about 0.05, this gives a value of 0.5 for the attenuation at 3.5 kc./s. This value is shown by the open circle on fig. 6.

4.4. Measurements during a Sudden Ionospheric Disturbance.

It has been noted by Gardner (1950) that, during a Sudden Ionospheric Disturbance (S.I.D.), the integrated level of atmospherics decreases on frequencies below 7 kc./s., so that the spectrum of an individual atmospheric

might be expected to show a similar change. Fortunately it was possible to make observations during a large S.I.D. on 20th February 1950. Atmospherics were recorded at five separate times before, during and after the S.I.D., as indicated in fig. 7. The set of observations at 1550 G.M.T. was made while the "Sferic" organization was operating.

Fig. 7.



Effect of S.I.D. on 20th February 1950, on atmospherics from 2400 km.

- (a) Change in ratio of received field strength of atmospherics, $E(f_2, r)/E(f_0, r)$ when S.I.D. occurs.
- (b) Change in ratio of received field strength of atmospherics $E(f_1, r)/E(f_0, r)$ when S.I.D. occurs.
- (c) Sudden enhancement of integrated level of atmospherics on 22 kc/s.
- (d) Beginning and end of fadeout reported by B.B.C.

Crosses indicate mean values for sets of points.

so that definite distances were available for the atmospherics recorded. In addition the routine "Sferic" charts of the Meteorological Office indicated that there was a strong source of atmospherics at a distance of 2400 km. throughout the whole day and very little activity elsewhere. From this it can be stated, with some certainty, that the recorded atmospherics originated in this distant storm.

The results are shown in fig. 7. In (b) the quantity $E(f_1)/E(f_0)$ is plotted for $f_1=5$ kc./s. and $f_0=10$ kc./s., in (a) the same ratio is plotted for $f_1=7.5$ kc./s. and $f_0=10$ kc./s., in (c) the integrated "level" of atmospherics as recorded on 22 kc./s. is shown, and (d) shows the extent of the "fade out" as reported by the B.B.C. In (a) and (b) each recorded atmospheric is indicated by a dot, and the mean values for the set of dots in each series is shown by a cross. The curves are drawn through the crosses. The most striking effect is seen in curve (b) which shows that, near the peak of the S.I.D., the component of frequency 5 kc./s. decreased about ten times compared with the component of frequency 10 kc./s. This is in good agreement with Gardner's observation that the integrated "level" of atmospherics as received at 5 kc./s. may often become too low to observe during an S.I.D. Although the corresponding decrease on 7.5kc./s., shown in curve (a), is also noticeable, it is not so marked.

It is possible to apply the results shown in fig. 7 to the daytime attenuation curve of fig. 6 so as to derive an attenuation curve which would represent the conditions during an intense S.I.D. Since fig. 7 applies to a distance of about 2400 km., we use it to modify the attenuation curve of fig. 6 drawn for the approximate distance of 2000 km., and we arrive at the dashed curve in fig. 6 to represent the conditions during the S.I.D.

§ 5. CONCLUSIONS.

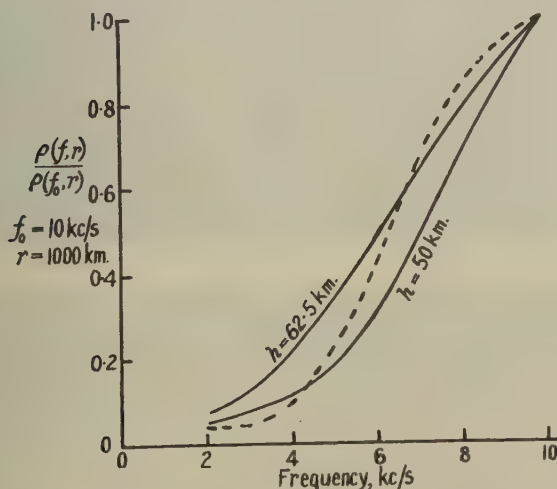
The final conclusions of this work are represented by the attenuation curves of fig. 6. These curves show how the attenuation factor $\rho(f, r)$ at different distances varies with frequency relative to the attenuation $\rho(f_0, r)$ at a standard frequency f_0 . The three full curves are for normal daytime conditions, the dotted curve for abnormal daytime conditions during a sudden ionospheric disturbance and the open circle indicates the result for 3.5 kc./s. during the night.

From the nature of the results it cannot be claimed that the curves are accurate to more than about 50 per cent. It can be seen, however, that an accuracy of this order is adequate to establish the general nature of the propagation characteristics of the space between the earth and the ionosphere in the frequency range 2 kc./s. to 10 kc./s.

A first attempt at a theoretical explanation of these results has been made by Budden (1951). From consideration of the waveguide formed by the earth and ionosphere, he has deduced theoretical curves similar to those of fig. 6. Budden proceeds on the assumption that the

ionosphere has a sharp lower boundary at high h , with appropriate values of electron density and collision frequency. From an extension of his theory, attenuation curves for 1000 km. path for heights of 62.5 km. and 50 km. have been obtained. These are shown in fig. 8, together with the experimental curve for the attenuation 1000 km. from the source. It can be seen that there is semi-quantitative agreement between the theory and the experimental results. According to Budden's theory, the curve will be moved to the right for decrease in reflection height and to the left for increase. It is probable that movements of this kind explain the different experimental curves obtained during an S.I.D. and during the night.

Fig. 8.



Comparison of experimental attenuation curve with curves deduced from theory of Budden.

- — — — Experimental curve for $r = 1000 \text{ km.}$
- Theoretical curves for 1000 km. path and height of reflecting layer h as indicated.

ACKNOWLEDGMENTS.

This work was done as part of a programme of radio research supported by the Department of Scientific and Industrial Research at the Cavendish Laboratory, Cambridge. The author wishes to acknowledge the debt due to F. F. Gardner for his part in the construction of the equipment. The author is a Scientific Trainee of the Australian Department of Supply and wishes to thank the Department for enabling him to work at the Cavendish Laboratory.

REFERENCES.

- APPLETON, E. V., and CHAPMAN, F. W., 1937, *Proc. Roy. Soc.*, **158**, 1.
 BARBER, N. F., URSELL, F., DARBYSHIRE, J., and TUCKER, M. J., 1946, *Nature, Lond.*, **158**, 329.
 BRACEWELL, R. N., BUDDEN, K. G., RATCLIFFE, J. A., STRAKER, T. W., and WEEKES, K., 1951. Submitted for publication to Institution of Electr. Eng's.
 BUDDEN, K. G., 1951, *Phil. Mag.*, **42**, 1.
 GARDNER, F. F., 1950, *Phil. Mag.*, **41**, 1259.
 HODGSON, M. L., CLEWS, C. J. B., and COCHRAN, W., 1949, *Acta Crystallographica*, **2**, 113.
 LABY, T. H., McNEILL, J. J., NICHOLLS, F. G., NICKSON, A. S. B., 1940, *Proc. Roy. Soc.*, **174**, 145.
 OCKENDEN, C. V., 1947, *Meteorological Magazine*, **76**, 1.
 ROSS, M. A. S., 1943, *Nature, Lond.*, **152**, 302.
 SCHONLAND, B. F. J., ELDER, J. S., HODGES, D. B., PHILLIPS, W. E., and VAN WYK, J. W., 1940, *Proc. Roy. Soc.*, **176**, 180.
-

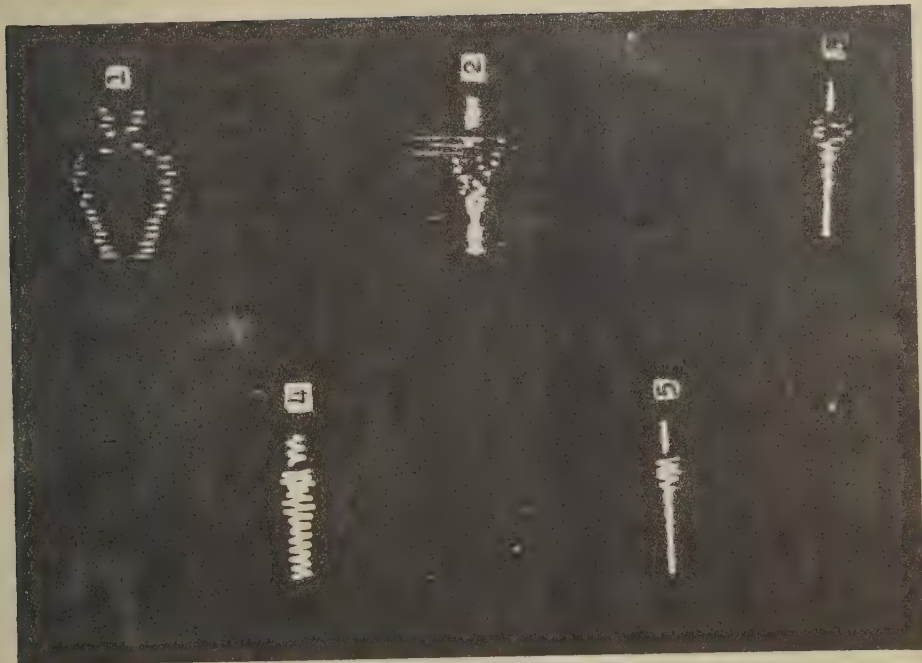
CAPTION FOR PLATE VI.

Two examples of the record made on individual atmospherics. For both examples (i.) and (ii.) the traces are the responses of different amplifiers as follows :—

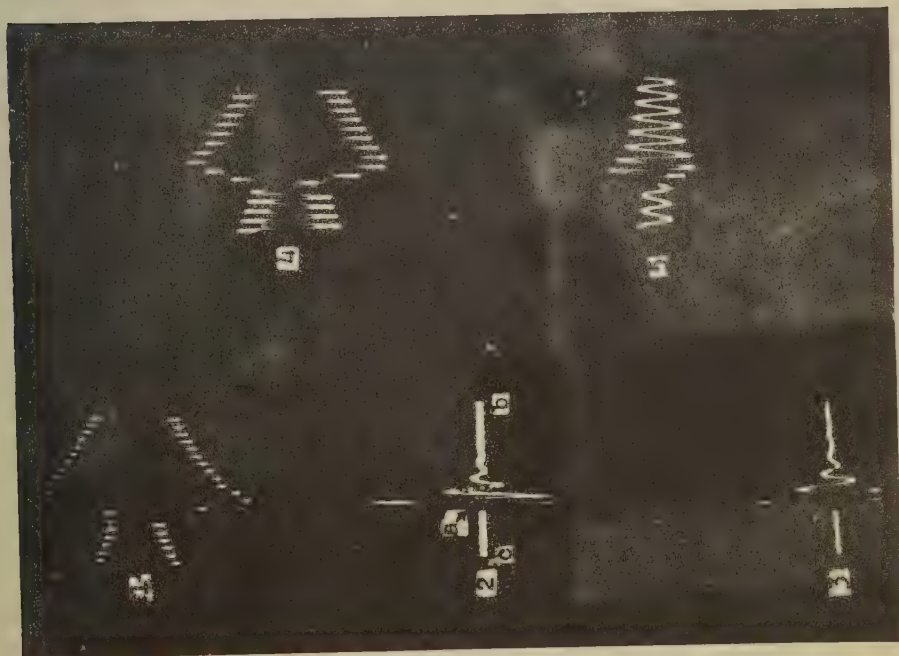
1. Tuned to 10 kc./s.
2. Wide-band.
3. Tuned to 3.5 kc./s.
4. Tuned to 7.5 kc./s.
5. Tuned to 5 kc./s.

In example (i.), trace 2, (*a*) indicates the beginning of the atmospheric when the trace is brightened, and (*b*) is when the time-base starts the fast return to (*c*). The trace is bright for the duration of one timebase stroke so that the trace finishes just before (*a*). All traces in both (i.) and (ii.) are obtained in the same way.

Example (i.) is typical of Class I. mentioned in the text and example (ii.) of Class II.



(ii)



(i)

XIII. *A Calculation of the Elastic Constants of Aluminium.*

By R. S. LEIGH,

Mathematics Department, Imperial College, London*.

[Received November 21, 1950]

SUMMARY.

A calculation is made of the elastic constants of aluminium which correspond to pure shears without change of volume, and an explanation is given for the fact that aluminium crystals are almost elastically isotropic. Conclusions are drawn about the nature of the density of states near the Fermi surface, and it is shown how the elastic constants may be expected to depend on electron concentration in aluminium solid solutions.

§1. INTRODUCTION.

It is well known that the total energy of a metal may be expressed approximately as a sum of separate terms. If we can calculate how these terms change as the metal is sheared, we can obtain the elastic constants of the metal as a corresponding sum of separate contributions.

Calculations of the shear constants (*i. e.* the elastic constants which relate to homogeneous strains without change of volume) of single crystals of metals have hitherto only been carried out for monovalent metals, namely the alkali metals and copper (Fuchs 1936). In these metals two important contributions appear, which arise respectively from (i.) the purely electrostatic correction term which has to be added to the potential energy obtained by using the sphere approximation of Wigner and Seitz, and (ii.) the term in the energy which is due to the non-Coulomb forces between the ion-cores. The first of these contributions is very anisotropic, the anisotropy ratio $\{C_{44}/\frac{1}{2}(C_{11}-C_{12})\}_{\text{el. st.}}$ being 8.9 for a face-centred cubic, and 7.4 for a body-centred cubic structure. For these monovalent metals the Fermi surface is approximately a sphere lying wholly inside the first Brillouin zone. The effect on the Fermi energy of movements of the bounding planes of the zone as the metal is sheared is therefore small, and the corresponding contribution to the elastic constants is negligible. In the case of metals of higher valency, however, this is no longer the case. In this paper we make an estimate of the contribution to the elastic constants from the Fermi energy in the case of aluminium, this metal being chosen for the following reason. Jones (1949) has pointed out that in the case of aluminium the contribution to the elastic constants from the non-Coulomb interaction between the ions must be negligible because of the large clearance between the ion-cores. The experimental values of the constants for aluminium, however, which are almost isotropic, are not consistent with their arising solely from the very anisotropic electrostatic contribution.

* Communicated by Professor H. Jones.

We are therefore led to look for another important contribution. The room temperature values for aluminium, as given by Lazarus (1949), are

$$\frac{1}{2}(C_{11}-C_{12})=2.085 \cdot 10^{11} \text{ dynes cm.}^{-2} \text{ and } C_{44}=2.853 \cdot 10^{11} \text{ dynes cm.}^{-2}.$$

It is shown in this paper that it is in fact possible to account for each of these observed values as a sum of contributions from the Fermi energy and from purely electrostatic energy terms. The large positive contribution to C_{44} from the electrostatic terms is balanced, apparently accidentally, by a correspondingly large negative contribution from the Fermi energy. In order to obtain agreement with the observed values of both C_{44} and $\frac{1}{2}(C_{11}-C_{12})$, it is necessary to assume that there are some overlapping electrons over the square faces of the Brillouin zone as well as over the hexagonal faces.

Following on these calculations it is also possible to see how the elastic constants would be expected to change with electron concentration as metals of higher or lower valency are dissolved in aluminium. There does not appear to be any experimental data relating to this.

§ 2. THE TOTAL ENERGY IN THE HARTREE APPROXIMATION.

In metals with more than one valence electron per atom, the approximate form for the wave functions of the higher states used by Wigner and Seitz for monovalent metals, viz., $\psi_0(\mathbf{r}) \exp(i\mathbf{k} \cdot \mathbf{r})$, where $\psi_0(\mathbf{r})$ is the wave function of the lowest state, can no longer be used. It follows that the Fermi energy now contains a potential as well as a kinetic part, and the valence electron density is no longer given by $-e|\psi_0|^2$. In view of this, it is necessary to reconsider the theory of the division of the total energy into separate terms.

In what follows we shall, as a first approximation, neglect valence electron exchange and correlation effects, and use the simple Hartree approximation. We do this because of the extreme difficulty of making any estimate of the contribution to the elastic constants from the correlation energy, which in metals of valency higher than one must depend on the zone structure. It would in principle be possible to make an estimate of the contribution from the exchange energy, which must also depend on the zone structure, but as these two terms are so closely related to each other it would be difficult to interpret the significance of the results.

In the Hartree approximation, the total energy W per atom, referred to a system of separated ion-cores and valence electrons, is given by the equation

$$NW = 2 \sum_{\mathbf{k}} \epsilon_{\mathbf{k}} - \frac{e^2}{2} \iint \frac{\rho(\mathbf{r})\rho(\mathbf{s})}{|\mathbf{r}-\mathbf{s}|} d\mathbf{r} d\mathbf{s} + \frac{1}{2} \sum_l \sum_{l'} U_l(|\mathbf{R}_l - \mathbf{R}_{l'}|), \quad (l \neq l'), \quad (1)$$

where the summation over \mathbf{k} extends over all occupied states, the integrations, and summations over l and l' , are taken over the space occupied by N atoms, and the $\epsilon_{\mathbf{k}}$ are the one-electron energy parameters in the Hartree equations

$$\left[-\frac{\hbar^2}{8\pi^2 m} \nabla^2 + V(\mathbf{r}) \right] \psi_{\mathbf{k}} = \epsilon_{\mathbf{k}} \psi_{\mathbf{k}}. \quad (2)$$

Here $V(\mathbf{r})$ is the self-consistent field given by the equation

$$V(\mathbf{r}) = \phi(\mathbf{r}) + e^2 \int \frac{\rho(\mathbf{s})}{|\mathbf{r} - \mathbf{s}|} d\mathbf{s},$$

where $\phi(\mathbf{r})$ is the potential energy of an electron in the field of all the ions in a given volume, $\rho(\mathbf{r})$ is the number density of valence electrons given by the relation $\rho(\mathbf{r}) = 2 \sum_{\mathbf{k}} |\psi_{\mathbf{k}}(\mathbf{r})|^2$, and the integration is taken over the same volume. The $\psi_{\mathbf{k}}$ are supposed normalised over the volume occupied by the N atoms. \mathbf{R}_i denotes the position vector of an ion, and $U_i(R)$ is the energy of interaction between two ions at a distance R apart.

Let us now define an energy $E(\mathbf{k})$ for every state by the relation $\epsilon_{\mathbf{k}} = \epsilon_0 + E(\mathbf{k})$, and let us introduce the wave function of the lowest state normalized over a single atomic cell, viz., $u_0(\mathbf{r})$, where $u_0(\mathbf{r}) = \sqrt{N} \psi_0(\mathbf{r})$. If we then use equation (2) for $\mathbf{k} = 0$, and let Z denote the number of valence electrons per atom, we find that NW is equal to the sum of the following four terms :

$$(i.) \quad -NZ \frac{\hbar^2}{8\pi^2 m} \int_{\text{cell}} u_0 \nabla^2 u_0 d\mathbf{r},$$

the kinetic energy of the lowest state multiplied by the number of electrons ;

$$(ii.) \quad 2 \sum_{\mathbf{k}} E(\mathbf{k}),$$

the Fermi energy ;

$$(iii.) \quad \frac{1}{2} \sum_i \sum_{i'} U_i(\mathbf{R}_i - \mathbf{R}_{i'}) + Z \int \phi(\mathbf{r}) u_0^2(\mathbf{r}) d\mathbf{r} \\ + \frac{Z^2 e^2}{2} \iint \frac{u_0^2(\mathbf{r}) u_0^2(\mathbf{s})}{|\mathbf{r} - \mathbf{s}|} d\mathbf{r} d\mathbf{s}, \quad (\mathbf{l} \neq \mathbf{l}'),$$

which is the potential energy of a system consisting of the ion-cores and a charge distribution of density $-Ze u_0^2(\mathbf{r})$; and

$$(iv.) \quad -\frac{e^2}{2} \iint \frac{[Zu_0^2(\mathbf{r}) - \rho(\mathbf{r})][Zu_0^2(\mathbf{s}) - \rho(\mathbf{s})]}{|\mathbf{r} - \mathbf{s}|} d\mathbf{r} d\mathbf{s},$$

which is the negative of the self potential energy of the charge distribution $-e[Zu_0^2(\mathbf{r}) - \rho(\mathbf{r})]$ which vanishes identically in the case when the approximation $\psi_{\mathbf{k}} = \psi_0 \exp(i\mathbf{k} \cdot \mathbf{r})$ is valid.

We have now to consider the contributions made by these terms to the elastic constants.

Calculations by Raimes (1950) of u_0 in magnesium, using the sphere approximation of Wigner and Seitz, indicate that in divalent as well as monovalent metals the wave function of the lowest state is very flat near to the boundary of the atomic cell. The first stages of a similar calculation for aluminium indicate that the same is true in this case. It follows, as has been shown in the case of monovalent metals, that there is no appreciable contribution to the elastic constants from the kinetic energy of the lowest state.

The term in (iii.) which represents the ion-ion interaction may be separated into a Coulomb term, and non-Coulomb terms arising from polarization effects and exchange repulsion between closed shells. An estimate of the clearance between ion-cores, as given by Jones (1949), shows that in the case of aluminium contributions to the elastic constants from these non-Coulomb terms are negligible.

§ 3. THE COULOMB TERMS.

Let us now consider the contributions to the elastic constants from the term (iv.) above and the Coulomb part of (iii.). With regard to the latter, there is nothing different from the case of a monovalent metal. We assume that the distribution $u_0^2(\mathbf{r})$ around each lattice point moves, effectively unchanged, with that lattice point as the metal is sheared. Then the contributions to the elastic constants are approximately the same as those from a set of positive charges $Ze\Omega u_0^2(r_s)$ in a uniform sea of negative charge of density $-Ze u_0^2(r_s)$, where Ω is the atomic volume in the metal and $u_0^2(r_s)$ is the value of $u_0^2(\mathbf{r})$ at the boundary of an atomic cell.

We now consider whether it is possible to estimate the contributions from the term (iv.) in a similar way. As the boundary conditions of those wave functions which correspond to states on the bounding planes of the Brillouin zone require that they vanish over certain planes of the atomic polyhedron, we should expect that the value of $\rho(\mathbf{r})$ at a point on the boundary of the atomic polyhedron would be less than $Zu_0^2(r_s)$. The distribution $-e[Zu_0^2(\mathbf{r}) - \rho(\mathbf{r})]$, which is electrostatically neutral as a whole, has thus a resultant positive charge in a region about a lattice point, and is negative outside this region. Let us now consider what happens as the metal is sheared. Since both the self-consistent field and the shape of the atomic polyhedron change, it follows that the wave functions, and so $\rho(\mathbf{r})$, will change in a very complex way. $\rho(\mathbf{r})$ has, however, two general properties, apart from its periodicity, which depend only on the symmetry of the metal lattice; its normal gradient over the boundary of an atomic polyhedron is zero, and it has in the equilibrium position, in common with $V(\mathbf{r})$ and $\psi_0(\mathbf{r})$, the full cubic symmetry of the lattice. It is thus, like $u_0^2(\mathbf{r})$, very nearly spherically symmetrical near the centre of an atomic cell. It is reasonable to assume that this nearly spherically symmetrical part moves almost unchanged with the lattice point. It also seems reasonable, as a first approximation, to average over the surface of the atomic cell and neglect actual details of what happens near to and over the different parts of the boundary. The contributions to the elastic constants are then approximately the same as those from a set of point charges $e\Omega[Zu_0^2(r_s) - \rho(r_s)]$ in a uniform sea of negative charge of density $-e[Zu_0^2(r_s) - \rho(r_s)]$, where $\rho(r_s)$ is the mean value of $\rho(\mathbf{r})$ over the boundary of an atomic cell.

The contributions to the elastic constants from a face-centred cubic lattice of point charges $+e$ set in a uniform sea of negative charge of density $-e\Omega$ have been evaluated by Fuchs (1936), and are

$$\frac{1}{2}(C_{11} - C_{12}) = 0.1058(e^2/2a) \quad \text{and} \quad C_{44} = 0.9479(e^2/2a) \quad \text{per atom,}$$

where a is the lattice constant in A.U. From our discussion above it follows that we have to multiply these values by a factor Z_{eff}^2 given by the relation

$$Z_{\text{eff}}^2 = \Omega^2 \{ [Zu_0^2(r_s)]^2 - [Zu_0^2(r_s) - \rho(r_s)]^2 \}.$$

In aluminium, $u_0^2(r_s)$ is almost equal to the average value of $u_0^2(\mathbf{r})$, so that putting $Z=3$ we have

$$Z_{\text{eff}}^2 = 9 - [3 - \Omega \rho(r_s)]^2. \quad (3)$$

Finally, inserting the value of the lattice constant for aluminium ($a=4.041$ A.U. at room temperature), we have for an estimate of the contributions to the shear constants from Coulomb terms:

$$\frac{1}{2}(C_{11} - C_{12}) = Z_{\text{eff}}^2 \cdot 0.183 \cdot 10^{11} \text{ dynes cm.}^{-2},$$

and $C_{44} = Z_{\text{eff}}^2 \cdot 1.639 \cdot 10^{11} \text{ dynes cm.}^{-2}$, where Z_{eff}^2 is given by (3).

We see at once that this contribution to C_{44} is already by itself much greater than the observed value. It is difficult to see how the value of $\Omega \rho(r_s)$ could be less than say 1.5, and this gives a minimum value for Z_{eff}^2 of 6.75, and corresponding contributions to the elastic constants of $\frac{1}{2}(C_{11} - C_{12}) = 1.2 \cdot 10^{11} \text{ dynes cm.}^{-2}$ and $C_{44} = 11.1 \cdot 10^{11} \text{ dynes cm.}^{-2}$, to be compared with the observed values of 2.1 and $2.9 \cdot 10^{11} \text{ dynes cm.}^{-2}$ respectively.

§ 4. THE FERMI ENERGY.

Since we have no exact knowledge of the energy surfaces in momentum space, and moreover no idea of how they change as the metal is sheared, we can only proceed by making simple assumptions consistent with known general properties of these surfaces.

Aluminium has a face-centred cubic structure and therefore a body-centred reciprocal lattice, and the Brillouin zone is the well known truncated octahedron. The energy surfaces cut the bounding planes of the zone normally; they are also generally considered to be approximately spherical near to the origin, and spheroidal in the second zone near to the centres of the faces. There are three valency electrons per atom, the first zone containing sufficient states for exactly two of these with each state doubly occupied. The remaining electrons occupy states overlapping the hexagonal faces, which are the nearest to the origin, with possibly a few overlapping the square faces. There is also the possibility that the first zone may be not quite full.

Let us consider how the reciprocal lattice, and so the Brillouin zone, changes as the metal undergoes a shear. The strain energy W of a cubic lattice is given in terms of the three independent elastic constants, C_{11} , C_{12} and C_{44} , by the equation

$$W = W_0 + \frac{1}{2}C_{11}(e_x^2 + e_y^2 + e_z^2) + C_{12}(e_y e_z + e_z e_x + e_x e_y) + \frac{1}{2}C_{44}(\gamma_{yz}^2 + \gamma_{zx}^2 + \gamma_{xy}^2), \quad (4)$$

where e_x , e_y and e_z are the diagonal components of the strain tensor \mathbf{e} , and $\frac{1}{2}\gamma_{yz}$, $\frac{1}{2}\gamma_{zx}$ and $\frac{1}{2}\gamma_{xy}$ are the shear components. We shall choose two pure shears which correspond respectively to $\frac{1}{2}(C_{11} - C_{12})$ and C_{44} .

A shear corresponding to $\frac{1}{2}(C_{11}-C_{12})$. Consider a strain consisting of compression or extension in the (001) direction accompanied by that uniform expansion or contraction in the perpendicular plane necessary to keep the volume constant. We can express the sheared face-centred cubic lattice as follows :

$$\mathbf{a}_1 = \frac{a}{2} \frac{1}{A} \left(0, 1, \frac{1}{\xi} \right), \quad \mathbf{a}_2 = \frac{a}{2} \frac{1}{A} \left(1, 0, \frac{1}{\xi} \right), \quad \mathbf{a}_3 = \frac{a}{2} \frac{1}{A} (1, 1, 0),$$

where in the equilibrium position $A = \xi = 1$, and to keep the volume constant during a finite strain we must take $A^3 = 1/\xi$. Remembering that the displacement $\boldsymbol{\tau}$ at \mathbf{r} is given by $\boldsymbol{\tau} = \mathbf{r} \cdot \mathbf{e}$, it follows that the components of \mathbf{e} in this case are as follows :

$$e_x = e_y = 1/A - 1, \quad e_z = 1/\xi A - 1, \quad \text{and} \quad \gamma_{yz} = \gamma_{zx} = \gamma_{xy} = 0.$$

Inserting these values into (4) we find that

$$\frac{1}{2}(C_{11} - C_{12}) = \frac{3}{4} \left(\frac{d^2 W}{d\xi^2} \right)_0, \quad \dots \dots \dots (5)$$

where the suffix zero implies the value at the equilibrium position. The sheared reciprocal lattice, defined by the relations $\mathbf{a}_i \cdot \mathbf{b}_j = 2\pi \delta_{ij}$, where δ_{ij} is the Kronecker delta, is given by the vectors \mathbf{b}_j as follows :

$$\mathbf{b}_1 = \frac{2\pi}{a} A(-1, 1, \xi), \quad \mathbf{b}_2 = \frac{2\pi}{a} A(1, -1, \xi), \quad \mathbf{b}_3 = \frac{2\pi}{a} A(1, 1, -\xi).$$

A shear corresponding to C_{44} . Consider a strain which is the same as the previous one except that the (001) is replaced by the (111) direction. The metal lattice in this case may be expressed in the form :

$$\mathbf{a}_1 = \frac{a}{2} \frac{\delta}{B} (\eta - 1, 1, 1), \quad \mathbf{a}_2 = \frac{a}{2} \frac{\delta}{B} (1, \eta - 1, 1), \quad \mathbf{a}_3 = \frac{a}{2} \frac{\delta}{B} (1, 1, \eta - 1),$$

where $\delta = 2[(1+\eta)(2-\eta)]^{-1}$, and in the equilibrium position $B = \delta = \eta = 1$. For constant volume we must take $B^3 = 4[(1+\eta)^2(2-\eta)]^{-1}$. In this case we have $e_x = e_y = e_z = \frac{1}{2}(\delta/B)(3-\eta) - 1$, $\gamma_{yz} = \gamma_{zx} = \gamma_{xy} = (\delta/B)(\eta - 1)$, and

$$C_{44} = \frac{1}{3} \left(\frac{d^2 W}{d\eta^2} \right)_0 \dots \dots \dots (6)$$

The reciprocal lattice is given by the vectors

$$\mathbf{b}_1 = \frac{2\pi}{a} B(-\eta, 1, 1), \quad \mathbf{b}_2 = \frac{2\pi}{a} B(1, -\eta, 1), \quad \mathbf{b}_3 = \frac{2\pi}{a} B(1, 1, -\eta).$$

In each case of course the first derivatives of the energy vanish at the equilibrium position.

The faces of the Brillouin zone are formed by the planes which bisect perpendicularly the lines joining the origin of the reciprocal lattice to its nearest and next nearest neighbours. We can thus determine in each of the two strains the altered positions of these planes and of the corner points where they meet.

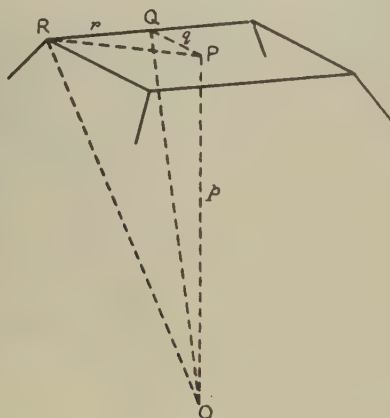
We shall consider separately the contributions to the elastic constants from a completely filled first zone and from overlapping electrons. We shall also consider what the effect of holes in the first zone would be if they were present.

Contributions from a completely filled first zone. The following treatment is suggested by regarding the actual energy surfaces as the spherical surfaces given by the relation

$$E(\mathbf{k}) = \alpha_0 \frac{\hbar^2 k^2}{8\pi^2 m} \quad . \quad . \quad . \quad . \quad . \quad . \quad (7)$$

so modified as to cut the faces of the zone normally. We find that when we approximate to these modifications in a simple empirical way the resulting contributions to the elastic constants differ only slightly from the

Fig. 1.



A typical tetrahedron, in this case at a square face.

values we would obtain by considering simply the change in the energy of a zone in which the surfaces are given by (7). We conclude that this is true whatever the exact nature of the surfaces near to the faces.

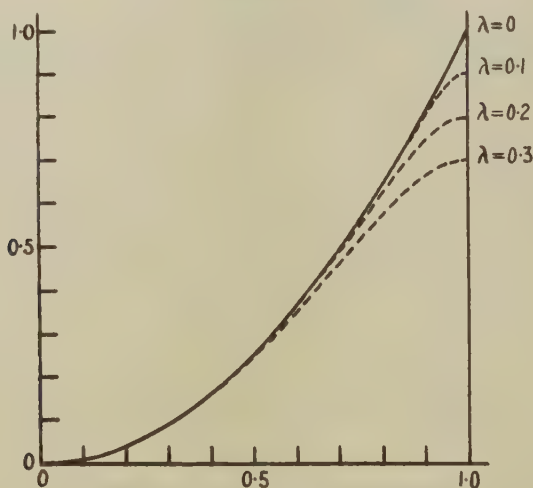
Let us suppose that the first zone energies at the centres of all the faces and at the corner points are the same fraction $(1-\lambda)$ of the energies at these points given by (7). Let us also suppose that α_0 and λ remain constant during a shear, so that the energies at these points vary as the squares of the distances from the origin. Let us then divide the zone into tetrahedra (fig. 1) whose vertices are the origin O, the symmetrical centre P of a face (which even in the strained zone is the point at which it is met by the perpendicular from the origin), a corner point R of that face, and the foot Q of the perpendicular from P to an edge of the face adjacent to R. There are 144 of these tetrahedra, 12 to each hexagonal face and 8 to each square face.

We have now to find an empirical relation which expresses $E(\mathbf{k})$ as a function of \mathbf{k} within a single tetrahedron and satisfies the following conditions. If taken in all the tetrahedra with the appropriate dimensions in each one, it must fill the whole zone with energy surfaces which are continuous and continuously differentiable. We require it to satisfy the assumptions we have made, and it must possess the general features we have already described. Such a relation is

$$E(\mathbf{k}) = \alpha_0 \frac{h^2}{8\pi^2 m} \left\{ k^2 - \lambda \left[p^2 \left(\frac{k'_z}{p} \right)^{2/\lambda} + q^2 \left(\frac{k'_y}{q} \right)^{2/\lambda} + r^2 \left(\frac{k'_x}{r} \right)^{2/\lambda} \right] \right\}, \quad (8)$$

where k'_z , k'_y and k'_x are measured in each tetrahedron in the directions of OP, PQ and QR respectively, and p , q and r are the appropriate lengths of these edges. Fig. 2 shows how the parameter λ modifies the surfaces so that they cut the faces normally. $E(\mathbf{k})/(\alpha_0 h^2 p^2/8\pi^2 m)$ is shown as a function of k'_z/p along OP for different values of λ .

Fig. 2.



The effect of the parameter λ in expression (8). $E(\mathbf{k})/(\alpha_0 h^2 p^2/8\pi^2 m)$ is shown as a function of k'_z/p along OP.

We have now to use these surfaces to calculate the first zone part W_F^I of the Fermi energy. The contribution from a single tetrahedron is

$$\frac{2}{8\pi^3} \alpha_0 \frac{h^2}{8\pi^2 m} pqr [Fp^2 + Gq^2 + Hr^2],$$

where

$$F = \frac{1}{10} - \frac{\lambda^2}{2(2+3\lambda)}, \quad G = \frac{1}{20} - \frac{\lambda^3}{2(2+3\lambda)(1+\lambda)},$$

$$H = \frac{1}{60} - \frac{\lambda^4}{2(2+3\lambda)(1+\lambda)(2+\lambda)}.$$

For each tetrahedron p , q , and r are functions of the strain parameter, ξ or η . We find that because of the high symmetry of the distortions we have chosen there are only six different tetrahedra in the first shear, and five in the second. Summing over all the tetrahedra we obtain W_F^I as a function of the strain parameter in each case. For the shear corresponding to $\frac{1}{2}(C_{11}-C_{12})$ we find for the contribution to the energy per unit volume

$$W_F^I = \frac{\alpha_0 h^2}{2ma^5} \xi^{-5/3} [F(16\xi + 36\xi^3 - 16\xi^5 + 3\xi^7) + G(16\xi - 12\xi^3 + 16\xi^5 - 5\xi^7) + H(16\xi - 20\xi^3 + 8\xi^5 + 2\xi^7)],$$

and for the shear corresponding to C_{44}

$$W_F^I = \frac{3\alpha_0 h^2}{2ma^5} \left[\frac{4}{(1+\eta)^2(2-\eta)} \right]^{5/3} \frac{1}{(1+\eta)^2} [F(16 - 128\eta + 406\eta^2 - 341\eta^3 + 96\eta^4 + 10\eta^5 - 6\eta^6 - \eta^7) - G(40 - 300\eta + 578\eta^2 - 499\eta^3 + 184\eta^4 - 22\eta^5 - 2\eta^6 + \eta^7) + H(64 - 152\eta + 158\eta^2 - 121\eta^3 + 96\eta^4 - 46\eta^5 + 10\eta^6 - \eta^7)].$$

From these expressions we find that

$$\left(\frac{dW_F^I}{d\xi} \right)_0 = \left(\frac{dW_F^I}{d\eta} \right)_0 = 0,$$

and, using relations (5) and (6), that the contributions to the elastic constants from a completely filled first zone are

$$\frac{1}{2}(C_{11}-C_{12}) = \frac{\alpha_0 h^2}{3ma^5} \left[1 + \frac{6\lambda^2(4+2\lambda-11\lambda^2)}{(2+3\lambda)(1+\lambda)(2+\lambda)} \right],$$

and

$$C_{44} = \frac{\alpha_0 h^2}{ma^5} \left[1 - \frac{2\lambda^3(8+7\lambda)}{(2+3\lambda)(1+\lambda)(2+\lambda)} \right].$$

We see that the effect of taking a value of λ different from zero is very small. Even with a value of λ as large as 0.3 the variation in the elastic constants is only of the order of 0.3×10^{11} dynes cm.⁻². We shall therefore take as our estimates of the contributions to the elastic constants from a filled first zone the values corresponding to $\lambda=0$. These are

$$\frac{1}{2}(C_{11}-C_{12}) = 1.5\alpha_0 \cdot 10^{11} \text{ dynes cm.}^{-2} \quad \text{and} \quad C_{44} = 4.5\alpha_0 \cdot 10^{11} \text{ dynes cm.}^{-2}$$

at room temperature. We do not know the value of α_0 in aluminium, but we are unlikely to be involved in serious error by taking it to be unity.

Contributions from overlapping electrons. We shall make here the simple assumption that during shear the energy surfaces over a face in the second zone move with that face without change relative to it. We shall also neglect the small effect of finite temperature on the Fermi distribution, and suppose that the states are completely filled with two electrons each up to an energy ζ .

It is easy to see what happens as the metal is sheared, if we remember that the number of electrons per atom remains exactly three, and the energy ζ , while changing its value, is the same for different parts of the Fermi surface. As the distances of the faces from the origin vary, electrons will transfer from those faces receding from the origin to those approaching it. The change in the Fermi energy has thus two causes: the shift of the energy surfaces as a whole with the faces, and the relaxation effect of the electron transfer. Let us examine this in detail.

It follows from the symmetry of the reciprocal lattice that the perpendicular distances from the origin of opposite faces of the zone are always equal, so that we may take these faces together in pairs. Since faces of one kind, hexagonal or square, do not in general remain at equal distances from the origin during shear, we shall refer to the pairs of faces by two suffices, i denoting the kind of face, and j the different pairs of that kind. Let us define the density of states $N(E)$ as the number of electrons per atom per unit energy range, allowing for two electrons being in each state, and denote by $N_i(E - E_{ij})$ the contribution to $N(E)$ from the pair of faces with energy E_{ij} at the centre of a face. Then the total number of electrons per atom, n_{ij} , occupying states over this pair of faces in the sheared state is given by

$$n_{ij} = \int_0^{\zeta - E_{ij}} N_i(\epsilon) d\epsilon. \quad \dots \dots \dots (9)$$

If we denote by W_F^H the total contribution to the Fermi energy from overlapping electrons, we have that

$$W_F^H = \sum_{i,j} W_{ij},$$

where

$$\begin{aligned} W_{ij} &= \int_{E_{ij}}^{\zeta} N_i(E - E_{ij}) E dE \\ &= n_{ij} E_{ij} + \int_0^{\zeta - E_{ij}} N_i(\epsilon) \epsilon d\epsilon. \quad \dots \dots \dots (10) \end{aligned}$$

If we let x stand for either strain parameter, ξ or η , and differentiate equation (9) with respect to x , we have

$$\frac{dn_{ij}}{dx} = N_i(\zeta - E_{ij}) \left(\frac{d\zeta}{dx} - \frac{dE_{ij}}{dx} \right). \quad \dots \dots \dots (11)$$

Since the number of electrons per atom does not depend on x , we have

$$\sum_{i,j} \frac{dn_{ij}}{dx} = 0. \quad \dots \dots \dots (12)$$

If we assume that during shear the energies at the centres of all faces of one kind, hexagonal or square, are the same function of the perpendicular distance of the face from the origin, it follows that dE_{ij}/dx is proportional to dp_{ij}/dx , where the constant of proportionality depends only on i , and so $\sum_j dE_{ij}/dx$ is proportional to $\sum_j dp_{ij}/dx$. We find below that the vanishing of $\sum_j (dp_{ij}/dx)_0$ for all i follows as a geometrical consequence of the volume remaining constant. We have then

$$\sum_j \left(\frac{dE_{ij}}{dx} \right)_0 = 0. \quad \dots \dots \dots (13)$$

Taking together equations (11) and (12) in the equilibrium position, and using equation (13), we find that

$$\left(\frac{d\zeta}{dx}\right)_0 = 0. \quad . \quad . \quad . \quad . \quad . \quad . \quad (14)$$

If we now differentiate equation (10) twice with respect to x , use equations (11), (12), (13) and (14), and sum over i and j , we find that $(dW_F^{II}/dx)_0 = 0$, and

$$\left(\frac{d^2 W_F^{II}}{dx^2}\right)_0 = \sum_i \left[n_i \sum_j \left(\frac{d^2 E_{ij}}{dx^2} \right)_0 - N_i (\zeta_0 - E_i) \sum_j \left(\frac{dE_{ij}}{dx} \right)_0^2 \right], \quad (15)$$

where n_i , ζ_0 and E_i are the equilibrium position values of n_{ij} , ζ and E_{ij} respectively.

We can obtain estimates of the values of the summations over j in equation (15) by assuming that the energies E_{ij} vary as the squares of the distances from the origin of the points they refer to. Equation (15) then has the form

$$\left(\frac{d^2 W_F^{II}}{dx^2}\right)_0 = \sum_i [\lambda_i n_i E_i - \mu_i N_i (\zeta_0 - E_i) E_i^2], \quad . \quad . \quad . \quad (16)$$

where the λ_i and μ_i are numerical coefficients.

The squared distances of the faces from the origin in each shear are as follows. In the shear corresponding to $\frac{1}{2}(C_{11} - C_{12})$, the four pairs of hexagonal faces are at the same distance $(\pi/a)A(2 + \xi^2)^{1/2}$ from the origin, the pair of square faces in the (001) direction are at a distance $(2\pi/a)A\xi$, and the other two pairs are at a distance $(2\pi/a)A$. In the shear corresponding to C_{44} , the pair of hexagonal faces in the (111) direction are at a distance $(\pi/a)\sqrt{3}B(2 - \eta)$ from the origin, the other three pairs are at a distance $(\pi/a)B(2 + \eta^2)^{1/2}$, and the three pairs of square faces are at a distance $(\pi/a)\sqrt{2}B(3 - 2\eta + \eta^2)^{1/2}$. From a knowledge of these distances it is easy to evaluate the coefficients λ_i and μ_i for each shear, and to verify the result $\sum_j (dp_{ij}/dx)_0 = 0$ in each case. The following table shows the contributions to the elastic constants per atom from overlapping electrons over hexagonal and square faces, obtained from equation (16) using relations (5) and (6).

	Hexagonal faces	Square faces
$\frac{1}{2}(C_{11} - C_{12})$	$\frac{8}{3}n_a E_a$	$2n_b E_b - 2N_b E_b^2$
C_{44}	$\frac{8}{3}n_a E_a - \frac{16}{9}N_a E_a^2$	$2n_b E_b$

n_a and n_b are the numbers of electrons per atom in the equilibrium position over one pair of hexagonal and square faces respectively, N_a and N_b the corresponding contributions to the density of states per atom at the Fermi surface, and E_a and E_b the equilibrium position energies at the centres of the faces. In each case the positive term involving the λ coefficient may be regarded as arising directly from the shift of the energy surfaces as a

whole with the faces, and the negative term involving the μ coefficient as arising from electron transfer between the faces. This electron transfer term only arises of course when some of the faces in question approach the origin and others recede from it. Thus it does not appear in the contributions from hexagonal faces to $\frac{1}{2}(C_{11}-C_{12})$ or from square faces to C_{44} , as in these cases the faces remain at an equal distance from the origin.

We can further reduce the number of parameters involved by approximating to the energy surfaces with spheroids. For the surfaces over the face given by the suffices i and j , we have

$$E = E_{ij} + \frac{\hbar^2}{8\pi^2 m} [k_x'^2 + k_y'^2 + \alpha_i(k_z' - p_{ij})^2],$$

where k_z' is measured perpendicular to the face, and α_i remains constant during shear. We then have

$$n_i = \frac{\Omega}{4\pi^3} \frac{4\pi}{3} \frac{1}{\sqrt{\alpha_i}} \left[\frac{8\pi^2 m}{\hbar^2} (\zeta_0 - E_i) \right]^{3/2},$$

and

$$N_i = \frac{3}{2} \frac{n_i}{\zeta_0 - E_i} \quad \dots \dots \dots (17)$$

The effect of the presence of holes in the first zone. We can proceed exactly as with overlapping electrons, the only differences being changes of sign. The following table shows contributions to the elastic constants corresponding to two ways in which holes could occur, viz. (i.) at the corner points, and (ii.) in approximately plane regions over the square faces, as suggested by Matyas (1948).

	Holes at the corner points	Holes over the square faces
$\frac{1}{2}(C_{11}-C_{12})$	$-\frac{44}{5}n_c E_c - \frac{4}{25}N_c E_c^2$	$-2n_d E_d - 2N_d E_d^2$
C_{44}	$-\frac{28}{5}n_c E_c$	$-2n_d E_d$

n_c is the number of holes per atom in one closed region, formed by the holes at four corner points (there are six closed regions in all), and n_d is the number over one pair of square faces; N_c and N_d are the corresponding contributions to the density of states per atom at the Fermi surface; and E_c and E_d are the first zone energies at the corner points and the centres of the square faces respectively. It will be noticed that the terms arising from the shift of the energy surfaces are negative for holes.

§ 5. DISCUSSION.

As we do not know the values of any of the parameters which appear in our results, viz. $\rho(r_s)$, α_a and α_b , E_a and E_b etc., we cannot make a direct calculation of the elastic constants. We can however see whether it is possible, by assuming reasonable values for these parameters, to account for the observed values of the constants as the sum of the three contributions which enter into the present theory. In doing this we can make use of

two observed quantities which depend on the band structure. These are: (i.) the width of the soft X-ray emission spectrum, given by Skinner (1940) as 11.8 eV., which corresponds to ζ_0 ; and (ii.) the electronic specific heat, given by Kok and Keesom (1937) as $3.484 \times 10^{-4} \text{ T cal. deg.}^{-1} \text{ mol.}^{-1}$, which is given in terms of the density of states per atom at the Fermi surface by the expression $(\pi^2/3)kN(\zeta_0)RT$, giving $N(\zeta_0)=0.614$ per eV. per atom.

Let us leave aside for the moment the possibility of holes in the first zone. If there is only overlap over the hexagonal faces, then we have $4n_a=1$ and $4N_a=N(\zeta_0)$, and the contributions from overlapping electrons to $\frac{1}{2}(C_{11}-C_{12})$ and C_{44} are $\frac{2}{3}E_a$ and $\frac{2}{3}E_a-\frac{4}{9}N(\zeta_0)E_a^2$ respectively. Using relation (17) we find $\zeta_0-E_a=2.4$ eV., and therefore $E_a=9.4$ eV. These contributions to the elastic constants are then $\frac{1}{2}(C_{11}-C_{12})=6.3$ eV. per atom $=6.1 \times 10^{11}$ dynes cm.⁻², and $C_{44}=-17.8$ eV. per atom $=-17.3 \times 10^{11}$ dynes cm.⁻². The very large negative contribution to C_{44} , due to electron transfer between the hexagonal faces, is just what we are looking for to balance the large positive Coulomb and first zone contributions. The contribution to $\frac{1}{2}(C_{11}-C_{12})$ however is even by itself much greater than the observed value of this constant, viz., 2.1×10^{11} dynes cm.⁻². This value can only be reduced by supposing that there is some overlap over the square faces as well as the hexagonal faces. We then have a negative contribution to $\frac{1}{2}(C_{11}-C_{12})$ from electron transfer between them. We now have five parameters, viz. $\rho(r_s)$, E_a , E_b , α_a and α_b , to relate to four observed quantities, viz. ζ_0 , $N(\zeta_0)$, and the two elastic constants. Since the number of overlapping electrons over the square faces is small, it is reasonable to use the approximate expression for α_b derived from the theory of nearly free electrons, viz. $\alpha_b=1+2E_b^{(0)}/(E_b-E_b^{(0)})$, where $E_b^{(0)}$ is the free electron energy at the centre of a square face, i. e. $(\hbar^2/8\pi^2m)(2\pi/a)^2=9.2$ eV. We then find that the values we have to assign to the parameters, in order to reproduce the observed values of the elastic constants, are as follows: $Z_{\text{eff}}^2=6.9_7$, and therefore $\Omega\rho(r_s)=1.5_8$; $E_a=9.0_8$ eV. and $\alpha_a=1.9_4$; $E_b=11.2_1$ eV. and $\alpha_a=10.2_1$. The corresponding values of n_a and n_b are 0.24_2 and 0.01_1 per atom respectively, and those of N_a and N_b are 0.133_4 per eV. per atom and 0.027_0 per eV. per atom respectively. The following table shows the constitution of the observed elastic constants as explained by this model. The units are 10^{11} dynes cm.⁻².

Contributions	$\frac{1}{2}(C_{11}-C_{12})$	C_{44}
Coulomb	1.3	11.4
First zone	1.5	4.5
Overlapping electrons	-0.7	-13.0 ₅
Total (observed)	2.1	2.8 ₅

It will be noticed that the value we have to assume for α_a is much lower than would be given by an expression corresponding to the one we have used for α_b . This is not a serious objection, however, as the region of

occupied states over the hexagonal faces goes well beyond the range of validity of such an expression. On the other hand it still seems reasonable to approximate, as we have done, to the general shape of the energy surfaces with spheroids, while leaving α_a unspecified.

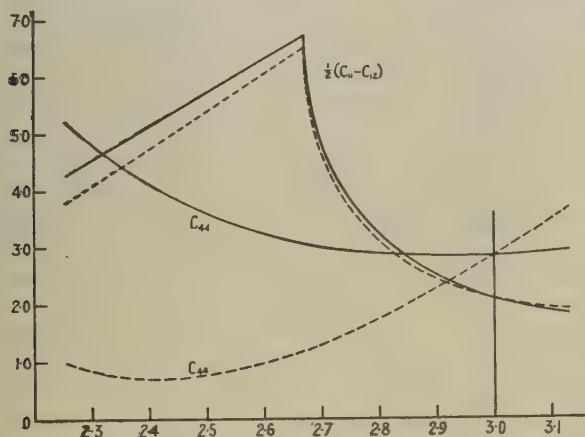
It is of interest to enquire whether the observed constants could be explained by assuming the existence of holes in the first zone instead of overlap over the square faces. We see however that in the case of holes at the corner points the coefficient of the term in $\frac{1}{2}(C_{11}-C_{12})$ arising from electron transfer is very small. In fact, if we assume spherical energy surfaces about the corner points, we find that in order to account for the observed values of both elastic constants consistently with known values of ζ_0 and $N(\zeta_0)$, and with a value of $\Omega\rho(r_s)$ not less than 1.5, it is necessary to assume that there are at least 0.3 holes per atom (*i. e.* 0.05 in a single closed region), and that the corner point energy E_c is at least as high as 16.5 eV. This is 5 eV. above the free-electron energy of $(\hbar^2/8\pi^2m) 5(\pi/a)^2 = 11.5$ eV. In the case of holes over the square faces, the coefficients of the terms are of course the same as for overlapping electrons there, the only difference being the sign of the term arising directly from the shift of the energy surfaces, and this is very small as long as the number of electrons or holes is small. It is thus possible to explain the elastic constants in the same way. We should however have to assume a value of E_d a little greater than ζ_0 , *i. e.* about 3 eV. above the free-electron energy of 9.2 eV. These high first zone energies would imply energy surfaces which are very different from those of the simple model we have been using, and the present theory is not really adequate for their discussion. It is clear, however, that the elastic constants cannot be explained by assuming a small number of holes at the corner points in the same way as they can be by assuming a small number of overlapping electrons over the square faces. This is because in the shear corresponding to $\frac{1}{2}(C_{11}-C_{12})$ the corner points do not move as much as the centres of the square faces, so that the resulting amount of electron transfer is smaller, and the corresponding negative contribution to the elastic constant is not large enough to balance the large positive contribution from the hexagonal faces. There still remains the possibility that there are a small number of holes at the corner points, as well as overlapping electrons over the square faces, but this would have only a very small effect on the elastic constants.

§ 6. VARIATION OF THE ELASTIC CONSTANTS WITH ELECTRON CONCENTRATION.

When metals of valency higher or lower than three are dissolved substitutionally in aluminium, and the valency electrons of the soluble atoms are shared with the whole metal, there is a change in the number of occupied states in the band scheme. The consequent change in the height of the filled region leads to a change in the contributions to the elastic constants from overlapping electrons. The full curves in fig. 3 show the effect on the total elastic constants of the variation of these contributions

with the electron concentration per atom. The large rise in $\frac{1}{2}(C_{11}-C_{12})$ with falling electron concentration is due to the decrease in magnitude of the negative term arising from electron transfer between the square faces in the corresponding shear. This term is proportional to the contribution from these faces to the density of states at the Fermi surface, and so is proportional to the cube root of the number of overlapping electrons there. There is thus a very sharp change in $\frac{1}{2}(C_{11}-C_{12})$ at an electron concentration of approximately 2.67 per atom, which is the point at which there is just no overlap over the square faces. Similarly, as the electron concentration falls still further, and the number of overlapping electrons over the hexagonal faces becomes small, C_{44} begins to rise rapidly. There are also changes in the details of the energy surfaces in momentum space, and so in

Fig. 3.



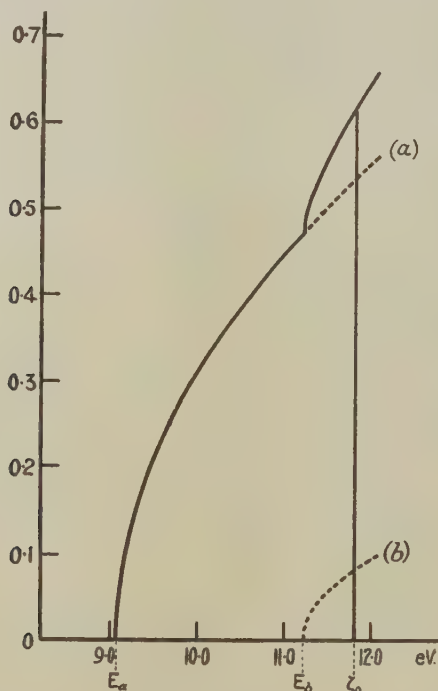
Variation of the elastic constants with electron concentration (units 10^{11} dynes cm.^{-2}). The full curves show the effect of the variation of the contributions from overlapping electrons alone. In the broken curves an allowance has been made for the change in the Coulomb contribution.

the density of states curve, but we should expect the effect of these changes on the elastic constants to be relatively small.

At some point as the electron concentration decreases, holes will appear in the first zone. From the results we have obtained in §4 for the contributions to the elastic constants from holes, we should expect that this would have little effect on C_{44} but would lead to a sharp fall in the value of $\frac{1}{2}(C_{11}-C_{12})$. The magnitude of this would depend on the curvature of the energy surfaces near the point of highest energy in the first zone. If there were no overlap over the square faces in pure aluminium, but instead holes in the first zone, then the variation of the elastic constants with electron concentration would be different from that shown in fig. 3, and would depend on the position of the point of highest energy in the

first zone. If the holes were at the corner points there would be a rather large decrease in both $\frac{1}{2}(C_{11}-C_{12})$ and C_{44} with decreasing electron concentration. If they were over the square faces the effect for small changes of electron concentration would be similar to that shown in fig. 3; it is not possible to say what would happen at lower electron concentrations, except that we should not expect a sharp change in $\frac{1}{2}(C_{11}-C_{12})$ of the kind that arises from the disappearance of overlap over the square faces.

Fig. 4.



The contributions to the density of states, $N(E)$ per eV. per atom from overlapping electrons over (a) hexagonal faces, and (b) square faces. The full curve is the sum of curves (a) and (b).

As well as changes in the Fermi energy contributions to the elastic constants, there are also changes in the Coulomb contributions arising from the changes in electron density in the metal. This effect is probably small in the case of $\frac{1}{2}(C_{11}-C_{12})$ because of the small Coulomb contribution, but it is important in the case of C_{44} . In order to obtain an estimate of the size of this effect in the case, for example, of a divalent solute, let us consider a crystal of the pure solute in a hypothetical face-centred cubic phase with the same lattice constant as aluminium. We should expect the value of $\Omega\rho(r_s)$ in this crystal to lie between say 1.0 and 2.0, and so Z_{eff}^2 between 3.0 and 4.0. As the concentration of this solute in aluminium

varies from zero to unity, the Coulomb contributions to the elastic constants change from the values for pure aluminium to those for this hypothetical crystal. The values between these two limits will depend on the exact nature of the changes in the electron density. The broken curves in fig. 3 have been obtained by supposing that Z_{eff}^2 varies linearly with solute concentration between the values of 6.9, for pure aluminium and 3.5 for an electron concentration of 2.0 per atom. It is difficult to see how the net effect on the elastic constants can be such as to give rise to values which are very different from these.

There does not appear to be any experimental data available relating to the change in the single crystal elastic constants with electron concentration. One difficulty is that only very small quantities of other metals are soluble in aluminium at room temperature without a phase change occurring. The most soluble are magnesium and zinc, which dissolve to the extent of about 2 atomic per cent, corresponding to a fall in electron concentration of 0.02 per atom. This should give, according to the broken curves in fig. 3, an increase in $\frac{1}{2}(C_{11}-C_{12})$ of approximately $0.05 \cdot 10^{11}$ dynes cm^{-2} and a decrease in C_{44} of approximately $0.12 \cdot 10^{11}$ dynes cm^{-2} . This corresponds to a change in the ratio $C_{44}/\frac{1}{2}(C_{11}-C_{12})$ from 1.37 to 1.28, a decrease of 6.4 per cent. The only way to measure the effect of larger changes of electron concentration would be to make observations either at higher temperatures or on quenched solutions. The most favourable case for this is that of zinc, which has a maximum solubility of 66.5 atomic per cent at 382°C . This corresponds to an electron concentration of 2.335 per atom. Other possibilities are magnesium, with a maximum solubility of 16 atomic per cent at 450°C ., and silver, with a maximum solubility of 18 atomic per cent at 538°C . These correspond to electron concentrations of 2.84 and 2.64 per atom respectively. Copper has a maximum solubility of 2.5 atomic per cent at 548°C , corresponding to an electron concentration of 2.95 per atom. Silicon appears to be the only element with more than three valency electrons per atom which is appreciably soluble even at high temperatures, the maximum solubility in this case being approximately 2 atomic per cent at 577°C . This corresponds to an electron concentration of 3.02 per atom.

ACKNOWLEDGMENTS.

The author is indebted to Professor H. Jones, who suggested the problem, for his continual help and advice, and to the Senate of the University of London for the award of a Postgraduate Studentship.

REFERENCES.

- FUCHS, K., 1936, *Proc. Roy. Soc. A*, **153**, 622 and **157**, 444.
 JONES, H., 1949, *Physica*, **15**, 13.
 KOK, J. A., and KEESOM, W. H., 1937, *Physica*, **4**, 835.
 LAZARUS, D., 1949, *Phys. Rev.* [2], **76**, 544.
 MATYAS, Z., 1948, *Phil. Mag.* [7], **39**, 429.
 RAIMES, S., 1950, *Phil. Mag.* [7], **41**, 568.
 SKINNER, H. W. B., 1940, *Phil. Trans. Roy. Soc. A*, **239**, 95.

XIV. *The Condensation of a Perfect Bose-Einstein Gas.—I.*

By A. R. FRASER,
 Royal Society Mond Laboratory, Cambridge*.

[Received October 24, 1950.]

ABSTRACT.

Schubert (1946) and others have drawn attention to the fact that the standard derivations of the formulæ for the behaviour of a perfect Bose-Einstein gas are invalid in the region where condensation should occur. In this paper a new and rigorous derivation is given of formulæ for the macroscopic behaviour of such a gas.

§1. INTRODUCTION.

SCHUBERT (1946) and Dingle (1949) have pointed out that discussions of the phenomenon of condensation in a perfect Bose-Einstein gas by London (1938) and Fowler and Jones (1938) are invalid because of the divergence of some of the series used. Temperley (1949) has considered the behaviour of a model with equally spaced energy levels and has concluded that the usually accepted formulæ are incorrect in this case.

In this paper formulæ for the macroscopic behaviour of a perfect Bose-Einstein gas will be found by a method similar to one used by Kahn and Uhlenbeck (1938) in considering the condensation of an imperfect gas. We shall have in mind the particular case of a perfect gas in a cubic box, but the results will be expressed in a more general form so that they may be applied to a perturbed system such as a perfect gas in an external field.

In a second paper (Fraser 1951) formulæ for the occupation numbers of the energy levels will be obtained.

All the thermodynamic functions for a perfect gas of N particles can be found from the partition function†

$$Z_N = \Sigma' \exp \{ -\mu \sum_i n_i \epsilon_i \}, \quad \dots \dots \dots (1)$$

where $\mu = 1/kT$, Σ' means the sum over all values of the set of positive integers n_0, n_1, n_2, \dots such that $\sum_i n_i = N$, and $\epsilon_0, \epsilon_1, \epsilon_2, \dots$ are the energy levels for the individual particles. In particular, the free energy of the gas is given by the relation

$$F = -kT \log Z_N, \quad \dots \dots \dots (2)$$

* Communicated by the Author.

† See, for instance, Schroedinger, E. *Statistical Thermodynamics* (Cambridge, 1945).

and all other thermodynamic functions can be derived from this by well known relations.

For a Bose-Einstein gas it is easily seen that Z_N is the coefficient of ζ^N in

$$\prod_i [1 + \zeta \exp(-\mu\epsilon_i) + \zeta^2 \exp(-2\mu\epsilon_i) + \dots]^{\omega_i} = \prod_i [1 - \zeta \exp(-\mu\epsilon_i)]^{-\omega_i}, \quad (3)$$

where ω_i is the weight of the level with energy ϵ_i . We can therefore write

$$Z_N = \frac{1}{2\pi i} \oint_{\zeta} \zeta^{-(N+1)} \prod_i [1 - \zeta \exp(-\mu\epsilon_i)]^{-\omega_i} d\zeta, \quad (4)$$

where the contour includes the origin, but excludes the poles $\zeta = \exp(\mu\epsilon_i)$ on the real axis. In the method used by Fowler (1936) this integral is evaluated by the method of steepest descents, but this has been shown by Schubert to be invalid in the neighbourhood of the condensation point.

In this paper we shall find an expression for the free energy per particle as the volume and the number of particles tend to infinity in such a way that the number per unit volume remains constant.

§2. THE ASYMPTOTIC FORM OF THE PARTITION FUNCTION.

The energy levels ϵ_i will depend on the volume of the gas and we must first impose some restrictions on this dependence. We write

$$\frac{1}{s} \sum_i \omega_i \exp(-s\mu\epsilon_i) = a_s(V), \quad (5)$$

where $a_s(V)$ is a function of the volume only, and require that there exists a set of functions $b_s(\rho)$, depending only on the density $\rho = N/V$, such that, for $N > M$, where M is any integer,

$$\left. \begin{aligned} & \text{(i) } a_s(V) < (1 + \delta_M) N b_s(\rho) \quad \text{for all } s, \\ & \text{(ii) } a_s(V) > (1 - \delta_M) N b_s(\rho) \quad \text{for all } s < s_M, \\ & \text{(iii) the radius of convergence of } \sum_{s=1}^{\infty} b_s(\rho) x^s \text{ is unity,} \\ & \text{and (iv) } \sum_{s=1}^{\infty} s b_s(\rho) \text{ is finite,} \end{aligned} \right\} \quad (6)$$

where δ_M tends to zero and s_M tends to infinity as M tends to infinity. We will in future write merely b_s for $b_s(\rho)$. A discussion of these restrictions will be relegated to the appendix where it will be shown that they are satisfied by the energy levels for a perfect gas in a cubic box. We see from the definitions that the b_s 's are always positive.

Rewriting (3), we find that Z_N is the coefficient of ζ^N in $\exp \sum_i \zeta^{\omega_i} \zeta^{\epsilon_i}$, and hence that Z_N may be considered as a monotonically increasing

function of the a_r 's. It follows that if we define functions $Z'_{N,M}$ and $Z''_{N,M}$ such that

$$\left. \begin{aligned} Z'_{N,M} &= \frac{1}{2\pi i} \oint \zeta^{-(N+1)} \exp \left\{ N(1+\delta_M) \sum_{s=1}^{\infty} b_s \zeta^s \right\} d\zeta, \\ Z''_{N,M} &= \frac{1}{2\pi i} \oint \zeta^{-(N+1)} \exp \left\{ N(1-\delta_M) \sum_{s=1}^{\infty} b_s \zeta^s \right\} d\zeta, \end{aligned} \right\} \quad (7)$$

then $Z'_{N,M} > Z_N > Z''_{N,M}$ for all $N > M$.

The contours are to be taken round the origin but inside the radius of convergence of $\sum b_s \zeta^s$. $Z'_{N,M}$ and $Z''_{N,M}$ are always positive since the b_s 's are.

We can now find

$$\log R' = - \lim_{N \rightarrow \infty} \left(\frac{1}{N} \log Z'_{N,M} \right) \quad \text{and} \quad \log R'' = - \lim_{N \rightarrow \infty} \left(\frac{1}{N} \log Z''_{N,M} \right)$$

by observing, following Kahn and Uhlenbeck (1938), that R' and R'' are the radii of convergence of the series $\sum_N Z'_{N,M} x^N$ and $\sum_N Z''_{N,M} x^N$. In these two series, $Z'_{N,M}$ and $Z''_{N,M}$ refer to the same density for all N , while in generating series of the type (3) the Z_N refer to a fixed set of energy levels and therefore to a fixed volume.

We can now transform the functions $\sum_N Z'_{N,M} x^N$ and $\sum_N Z''_{N,M} x^N$ in a manner which is precisely the same as that of Kahn and Uhlenbeck (1938) and which we shall consequently only outline here.

Using (7) we may write

$$\begin{aligned} \sum_N Z'_{N,M} x^N &= \frac{1}{2\pi i} \oint \zeta^{-(N+1)} \exp \left\{ N(1+\delta_M) \sum_{s=1}^{\infty} b_s \zeta^s \right\} d\zeta \\ &= \frac{1}{2\pi i} \oint \frac{d\zeta}{\zeta - x \exp \left\{ (1+\delta_M) \sum_{s=1}^{\infty} b_s \zeta^s \right\}}, \end{aligned} \quad (8)$$

so long as we choose the contour so that

$$\left| x \frac{\exp \left\{ (1+\delta_M) \sum_{s=1}^{\infty} b_s \zeta^s \right\}}{\zeta} \right| < 1 - \epsilon, \quad \epsilon > 0,$$

everywhere on the contour. This condition is sufficient for the validity of the interchange of the sum and integral operations, and can always be satisfied for small enough x .

For sufficiently small x it may be shown that

$$\zeta - x \exp \left\{ (1+\delta_M) \sum_{s=1}^{\infty} b_s \zeta^s \right\}$$

has only one root, ζ'_M , say, inside the contour. This is the only pole which contributes to the integral (8). We can therefore write

$$\Sigma Z'_{N,M} x^N = \frac{1}{1 - x f_{1,M}(\zeta'_M)} = \frac{1}{1 - g_{1,M}(\zeta'_M)}, \quad . . . (9)$$

where
$$f_{1,M}(\zeta) = \frac{d}{d\zeta} \exp \left\{ (1 + \delta_M) \sum_{s=1}^{\infty} b_s \zeta^s \right\}, \quad (10)$$

$$g_{1,M}(\zeta) = (1 + \delta_M) \sum_{s=1}^{\infty} s b_s \zeta^{s-1}, \quad (11)$$

$$\frac{1}{x} = \frac{\exp \left\{ (1 + \delta_M) \sum_{s=1}^{\infty} b_s \zeta'^s_M \right\}}{\zeta'_M}, \quad (12)$$

and
$$\frac{dx}{x} = \frac{d\zeta'_M}{\zeta'_M} \{1 - g_{1,M}(\zeta'_M)\}. \quad (13)$$

Since we have shown that (9) is true for small x , it follows that, if the series in (10), (11) and (12) are replaced by their analytical continuations, (9) will be the analytical continuation of $\Sigma Z'_{N,M} x^N$.

Since all the $Z'_{N,M}$ are positive, the radius of convergence R' is such that $x=R'$ is the first singularity of $\Sigma Z'_{N,M} x^N$ as x increases along the positive real axis.

$\Sigma Z'_{N,M} x^N$ and its analytical continuation will be regular in that region of the x -plane which is mapped by the region of the ζ'_M -plane in which

$$\left. \begin{array}{l} (a) \ g_{1,M}(\zeta'_M) \neq 1 \\ \text{and } (b) \ g_{1,M}(\zeta'_M) \text{ is regular.} \end{array} \right\} (14)$$

Conversely, at points corresponding to those at which (a) or (b) is violated, $\Sigma Z'_{N,M} x^N$ and its analytical continuation will have a singularity.

We see from (13) that ζ'_M is a monotonically increasing function of x as x moves along the positive real axis until (a) is violated. Hence $x=R'$ corresponds to the smallest real positive value of ζ'_M for which (a) or (b) is violated. Because of postulate (6, iii), the first singularity of $g_{1,M}(\zeta)$ is at $\zeta=1$, and it follows that (a) will be violated before (b) if and only if $g_{1,M}(\zeta)=1$ has a real positive root less than 1.

Hence, if $(1 + \delta_M) \sum_{s=1}^{\infty} s b_s \zeta^s = 1$ has a real positive root $\zeta'_{0,M} < 1$,

$$\frac{1}{R'} = \frac{\exp \left\{ (1 + \delta_M) \sum_{s=1}^{\infty} b_s \zeta'^s_{0,M} \right\}}{\zeta'_{0,M}},$$

while, if no such root exists,

$$\frac{1}{R'} = \exp \left\{ (1 + \delta_M) \sum_{s=1}^{\infty} b_s \right\}.$$

Since $\text{Lt}_{N \rightarrow \infty} (Z'_{N,M})^{1/N} = 1/R'$ and $Z_N < Z'_{N,M}$ for all M , we can write

$$\text{Lt}_{N \rightarrow \infty} \left(\frac{1}{N} \log Z_N \right) \leq \text{Lt}_{M \rightarrow \infty} \text{Lt}_{N \rightarrow \infty} \left(\frac{1}{N} \log Z'_{N,M} \right) = \sum_{s=1}^{\infty} b_s \zeta_0''^s - \log \zeta_0', \quad (15a)$$

when $\sum b_s \zeta_0''^s = 1$ has a real positive root $\zeta_0' < 1$, and

$$\text{Lt}_{N \rightarrow \infty} \left(\frac{1}{N} \log Z_N \right) \leq \text{Lt}_{M \rightarrow \infty} \text{Lt}_{N \rightarrow \infty} \left(\frac{1}{N} \log Z'_{N,M} \right) = \sum_{s=1}^{\infty} b_s \quad (15b)$$

if no such root exists.

In a precisely similar manner we find that

$$\Sigma Z''_{N,M} = \frac{1}{1 - g_{2,M}(\zeta_M'')},$$

where

$$g_{2,M}(\zeta) = (1 - \delta_M) \sum_{s=1}^{s_M} b_s \zeta^s$$

and

$$\frac{1}{x} = \frac{\exp \left\{ (1 - \delta_M) \sum_{s=1}^{s_M} b_s \zeta_M''^s \right\}}{\zeta_M''}.$$

In this case, since $g_{2,M}(\zeta)$ is a finite series, $\Sigma Z''_{N,M} x_N$ can only become singular if $g_{2,M}(\zeta_M'') = 1$. Hence

$$\left. \begin{aligned} \text{Lt}_{N \rightarrow \infty} \left(\frac{1}{N} \log Z''_{N,M} \right) &= (1 - \delta_M) \sum_{s=1}^{s_M} b_s \zeta_{0,M}''^s - \log \zeta_{0,M}'' \\ \text{where } (1 - \delta_M) \sum_{s=1}^{s_M} b_s \zeta_{0,M}''^s &= 1. \end{aligned} \right\} \quad (16)$$

Since $Z_N > Z''_{N,M}$ for all M ,

$$\text{Lt}_{N \rightarrow \infty} \left(\frac{1}{N} \log Z_N \right) \geq \text{Lt}_{M \rightarrow \infty} \text{Lt}_{N \rightarrow \infty} \left(\frac{1}{N} \log Z''_{N,M} \right),$$

and therefore we can deduce from equation (16) that, if $\sum_{s=1}^{\infty} b_s \zeta_0''^s = 1$ has a real positive root $\zeta_0'' < 1$,

$$\text{Lt}_{N \rightarrow \infty} \left(\frac{1}{N} \log Z_N \right) \geq \sum_{s=1}^{\infty} b_s \zeta_0''^s - \log \zeta_0''. \quad (17)$$

If, however, $\sum_{s=1}^{\infty} b_s \zeta_0''^s = 1$ has no solution less than one, the solution of $(1 - \delta_M) \sum_{s=1}^{s_M} b_s \zeta^s = 1$ will tend to one from above as M tends to infinity, since $\sum_{s=1}^{\infty} b_s \zeta^s$ diverges for $\zeta > 1$. In order to find the value of the limit of the right-hand side of (16) as M tends to infinity, we must evaluate

$$\text{Lt}_{M \rightarrow \infty} \left\{ (1 - \delta_M) \sum_{s=1}^{s_M} b_s \zeta_{0,M}''^s \right\},$$

where

$$(1 - \delta_M) \sum_{s=1}^{s_M} b_s \zeta_{0,M}''^s = 1.$$

We write $\zeta''_{0,M} = 1 + \epsilon_M$. Since $\sum_{s=1}^{\infty} s b_s \zeta^s$ diverges for $\zeta > 1$, ϵ_M tends to zero through positive values as M tends to infinity. Now

$$\begin{aligned} (1 - \delta_M) \sum_{s=1}^{\theta_M} b_s \zeta''_{0,M} &= (1 - \delta_M) \sum_{s=1}^{\theta_M} b_s (1 + \epsilon_M)^s \\ &= (1 - \delta_M) \left\{ \sum_{s=1}^{\theta_M} b_s + \epsilon_M \sum_{s=1}^{\theta_M} s b_s (1 + \theta \epsilon_M)^{s-1} \right\}, \quad (0 < \theta < 1) \\ &< (1 - \delta_M) \sum_{s=1}^{\theta_M} b_s + \epsilon_M. \end{aligned}$$

We also have the inequality

$$(1 - \delta_M) \sum_{s=1}^{\theta_M} b_s \zeta''_{0,M} > (1 - \delta_M) \sum_{s=1}^{\theta_M} b_s.$$

$$\text{Therefore } \lim_{M \rightarrow \infty} \left\{ (1 - \delta_M) \sum_{s=1}^{\theta_M} b_s \zeta''_{0,M} \right\} = \lim_{M \rightarrow \infty} \left\{ (1 - \delta_M) \sum_{s=1}^{\theta_M} b_s \right\} = \sum_{s=1}^{\infty} b_s.$$

Hence, if $\sum_{s=1}^{\infty} s b_s \zeta^s = 1$ has no solution less than one, equation (16) yields, in the limit of M tending to infinity,

$$\lim_{N \rightarrow \infty} \left(\frac{1}{N} \log Z_N \right) \geq \sum_{s=1}^{\infty} b_s. \quad \dots \dots \dots (18)$$

§ 3. ASYMPTOTIC FORM OF THE FREE ENERGY.

By combining the inequalities (15), (17) and (18) we obtain an equality which, combined with equation (2), may be written

$$f = \lim_{N \rightarrow \infty} \frac{F}{N} = -kT \lim_{N \rightarrow \infty} \left(\frac{1}{N} \log Z_N \right) = -kT \left\{ \sum_{s=1}^{\infty} b_s \zeta_0^s - \log \zeta_0 \right\}, \quad (19 a)$$

if $\sum_{s=1}^{\infty} s b_s \zeta^s = 1$ has a real positive solution $\zeta_0 < 1$; if, on the other hand,

there is no such solution,

$$f = -kT \lim_{N \rightarrow \infty} \left(\frac{1}{N} \log Z_N \right) = -kT \sum_{s=1}^{\infty} b_s, \quad \dots \dots (19 b)$$

where f is the free energy per particle.

The change in the form of the free energy which occurs when $\zeta_0 = 1$ corresponds to "condensation". We shall show, in the appendix, that for a perfect gas in a cubic box

$$b_s = \frac{(2\pi m k T)^{3/2}}{\rho \hbar^3 s^{5/2}}.$$

Therefore, for such a gas, the free energy per particle is

$$f = - \frac{(2\pi m)^{3/2}}{\rho \hbar^3} (kT)^{5/2} \sum_{s=1}^{\infty} \frac{\zeta_0^s}{s^{5/2}} + kT \log \zeta_0, \quad (T > T_0)$$

$$f = - \frac{(2\pi m)^{3/2}}{\rho \hbar^3} (kT)^{5/2} \sum_{s=1}^{\infty} \frac{1}{s^{5/2}}, \quad (T < T_0)$$

where

$$\frac{(2\pi m kT)^{3/2}}{\rho \hbar^3} \sum_{s=1}^{\infty} \frac{\zeta_0^s}{s^{3/2}} = 1,$$

and T_0 is defined by the equation

$$\frac{(2\pi m kT_0)^{3/2}}{\rho \hbar^3} \sum_{s=1}^{\infty} \frac{1}{s^{3/2}} = 1.$$

These expressions are equivalent to those derived by London (1938) and Fowler and Jones (1938), and all the macroscopic characteristics of the condensation phenomenon can be derived from them.

The expressions (19 a) and (19 b) can be written in a more familiar way by observing that

$$sb_s = \text{Lt}_{N \rightarrow \infty} \left\{ \frac{1}{N} \sum_i \omega_i \exp(-s\mu\epsilon_i) \right\},$$

the limit to be taken with the density kept constant. If all the series are uniformly convergent, we can write

$$\begin{aligned} \sum_{s=1}^{\infty} b_s \zeta_0^s &= \text{Lt}_{N \rightarrow \infty} \left\{ \frac{1}{N} \sum_i \omega_i \sum_{s=1}^{\infty} \frac{\{\zeta_0 \exp(-\mu\epsilon_i)\}^s}{s} \right\} \\ &= \text{Lt}_{N \rightarrow \infty} \left\{ \frac{1}{N} \sum_i \omega_i \log [1 - \zeta_0 \exp(-\mu\epsilon_i)] \right\}. \end{aligned}$$

Similarly

$$\sum_{s=1}^{\infty} sb_s \zeta_0^s = \text{Lt}_{N \rightarrow \infty} \left\{ \frac{1}{N} \sum_i \frac{\omega_i}{\zeta_0^{-1} \exp(\mu\epsilon_i) - 1} \right\}.$$

Thus, we can write the free energy per particle, in the limit as N tends to infinity, in the form

$$f = - \text{Lt}_{N \rightarrow \infty} \left[\frac{kT}{N} \left\{ \sum_i \omega_i \log [1 - \zeta_0 \exp(-\mu\epsilon_i)] - N \log \zeta_0 \right\} \right],$$

where

$$\text{Lt}_{N \rightarrow \infty} \frac{1}{N} \sum_i \frac{\omega_i}{\zeta_0^{-1} \exp(\mu\epsilon_i) - 1} = 1,$$

or, if there is no solution ζ_0 to this equation, $\zeta_0 = 1$. This expression for the free energy is identical with that which is obtained by the method of steepest descents.

APPENDIX.

It remains to discuss the validity of the postulates (6).

In order that postulates (i.) and (ii.) should be justified, we require that the number of energy levels for each particle between E and $E+dE$ should be of the form $V\{g(E)+h(E, V)\} dE$ where $h(E, V)$ tends to zero as V tends to infinity. An assumption of this nature is necessary if the free energy per particle is to tend to a definite value as V tends to infinity. If the density of energy levels has the form assumed, then

$$\begin{aligned}\sum_i \omega_i \exp(-s\mu\epsilon_i) &= V \int_0^\infty \{g(E)+h(E, V)\} \exp(-s\mu E) dE \\ &= \frac{V}{s\mu} \left\{ \int_0^\infty g\left(\frac{x}{s\mu}\right) e^{-x} dx + \int_0^\infty h\left(\frac{x}{s\mu}, V\right) e^{-x} dx \right\} \\ &\sim \frac{N}{\rho s\mu} \int_0^\infty g\left(\frac{x}{s\mu}\right) e^{-x} dx = \frac{N}{s} b_s \quad \text{as } V \rightarrow \infty.\end{aligned}$$

The validity of the inequalities (i.) and (ii.) depends on the form of the functions $g(E)$ and $h(E, V)$, and a general discussion is impracticable. Husimi (1939) has given expressions for $g(E)$ and $h(E, V)$ for a perfect gas in a cubic box, but it is more convenient, in this case, to evaluate the b_s by the following method. If the gas is in a cubic box of side a , the energy levels are

$$\epsilon_{l,m,n} = \alpha kT(l^2 + m^2 + n^2),$$

where $\alpha = \hbar^2/8mkTa^2$ and l, m, n are positive integers. Therefore

$$\sum_i \omega_i \exp(-s\mu\epsilon_i) = \left[\sum_{l=1}^\infty \exp(-s\alpha l^2) \right]^3.$$

$$\text{Now} \quad \sum_{l=1}^\infty \exp(-s\alpha l^2) < \int_0^\infty \exp(-s\alpha x^2) dx < \sum_{l=0}^\infty \exp(-s\alpha l^2),$$

$$\text{and therefore} \quad \frac{1}{2} \left(\frac{\pi}{s\alpha} \right)^{1/2} - 1 < \sum_{l=1}^\infty \exp(-s\alpha l^2) < \frac{1}{2} \left(\frac{\pi}{s\alpha} \right)^{1/2}.$$

$$\text{Hence} \quad \sum_i \omega_i \exp(-s\mu\epsilon_i) < \frac{N}{\rho \hbar^3} \left(\frac{2\pi mkT}{s} \right)^{3/2} \quad \text{for all } s,$$

and

$$\sum_i \omega_i \exp(-s\mu\epsilon_i) > \frac{N}{\rho \hbar^3} \left(\frac{2\pi mkT}{s} \right)^{3/2} (1 - \delta_M) \quad \text{for } N > M \text{ and } s < s_M,$$

where

$$s_M = \frac{2\pi mkT}{9\hbar^3} \left(\frac{M}{\rho} \right)^{2/3} \delta_M^2.$$

Thus, we see that postulates (i) and (ii) are justified in this case with

$$b_s = \left(\frac{2\pi mkT}{s} \right)^{3/2} \frac{1}{\rho s \hbar^3}.$$

Postulate (iii.), that $\sum_s b_s x^s$ has radius of convergence unity, is not essential and has been made for simplicity only. If we assume, more generally, that the radius of convergence is r , the condition for (19a) to hold becomes $\zeta_0 < r$ and (19b) becomes

$$f = -kT \sum_{s=1}^{\infty} b_s r^s.$$

Since $\exp(-s\mu\epsilon_i)$ is a decreasing function of s , we see from (5) and (6, i. and ii.) that r cannot be less than one. r will be greater than one only if b_s contains a factor $\exp(-s\beta)$, and this can only happen if $g(E)$ is zero for $0 < E < \beta/\mu$. This case, however, can be reduced to the case of $r=1$ by a change of the zero of energy.

Postulate (iv.) has also been made for simplicity only. If $\sum_s b_s$ is divergent, condition (a) of (14) will always be violated before condition (b). This means that the gas will not condense, since equation (19b) will never apply. An example of this behaviour is to be found in the two-dimensional Bose-Einstein gas, for which $b_s = 2\pi mkT/\rho s^2 h^2$.

REFERENCES.

- DINGLE, R. B., 1949, *Proc. Cam. Phil. Soc.*, **45**, 275.
 FOWLER, R. H., 1936, *Statistical Mechanics* (Cambridge: University Press).
 FOWLER, R. H., and JONES, H., 1938, *Proc. Cam. Phil. Soc.*, **34**, 573.
 FRASER, A. R., 1951, *Phil. Mag.*, **42**, 165.
 HUSIMI, K., 1939, *Proc. Phys.-Math. Soc. Japan* (3rd series), **21**, 759.
 KAHN, B., and UHLENBECK, G. E., 1938, *Physica*, **5**, 399.
 LONDON, F., 1938, *Phys. Rev.*, **54**, 947.
 SCHUBERT, G., 1946 and 1947, *Z. Naturforsch.*, **1**, 113 and **2 a**, 250.
 TEMPERLEY, H. N. V., 1949, *Proc. Roy. Soc., A*, **199**, 361.

XV. *The Condensation of a Perfect Bose-Einstein Gas.—II*

By A. R. FRASER,
Royal Society Mond Laboratory, Cambridge*.

[Received October 24, 1950.]

ABSTRACT.

In an earlier paper formulæ were given for the macroscopic behaviour of a perfect Bose-Einstein gas. In this paper formulæ are given for the mean occupation numbers of the energy levels and for the fluctuations in these numbers. These formulæ are in agreement with those obtained by earlier (invalid) methods.

§1. INTRODUCTION.

As in the earlier paper (Fraser 1951), we shall consider a perfect Bose-Einstein gas of N particles in which the energy levels of the individual particles are $\epsilon_0, \epsilon_1, \epsilon_2, \dots$ with weights $\omega_0, \omega_1, \omega_2, \dots$. We shall find asymptotic expressions for \bar{n}_i , the mean occupation number of the i th level, in the limit as N tends to infinity.

Schubert (1946) and Dingle (1949) have pointed out that the derivation of the mean occupation numbers by the method of steepest descents is invalid at low temperatures. Expressions for the occupation numbers in the *most probable* configuration of the system may be obtained by other methods, but these are also open to criticism (see, for example, Dingle 1949.) It is well known that expressions for the occupation numbers which are obtained by the "mean value" and "maximum probability" methods are, in general, identical, and it is of particular interest to verify this equivalence of a Bose-Einstein gas, since the fluctuations in the occupation numbers are unusually large. The formula usually given for the fluctuation is

$$\overline{(\bar{n}_i - n_i)^2} = \bar{n}_i + (\bar{n}_i)^2, \quad \dots \dots \dots (1)$$

which may be compared with

$$\overline{(\bar{n}_i - n_i)^2} = \bar{n}_i$$

and

$$\overline{(\bar{n}_i - n_i)^2} = \bar{n}_i - (\bar{n}_i)^2,$$

for a Boltzmann and a Fermi-Dirac gas respectively. The validity of equation (1) will be discussed in § 6.

* Communicated by the Author.

§2. EXACT EXPRESSIONS FOR THE MEAN OCCUPATION NUMBERS.

We start from the partition function Z_N , defined by the equation

$$Z_N = \sum' \exp \left(-\mu \sum_{i=0}^{\infty} n_i \epsilon_i \right),$$

in which $\mu = 1/kT$, and \sum' means the sum over all values of the set of positive integers n_0, n_1, n_2, \dots such that $\sum_i n_i = N$. Z_N may be considered as the coefficient of ζ^N in

$$\sum_N \zeta^N = \prod_{j=0}^{\infty} [1 - \zeta \exp(-\mu \epsilon_j)]^{-\omega_j}. \quad (2)$$

Expressions for the mean values of the occupation numbers and their products can then be expressed as functions of Z_N (Schrodinger 1945).

$$\bar{n}_i = -\frac{1}{\mu Z_N} \frac{\partial Z_N}{\partial \epsilon_i}, \quad (3)$$

$$\overline{n_i n_j} = \frac{1}{\mu^2 Z_N} \frac{\partial^2 Z_N}{\partial \epsilon_i \partial \epsilon_j}. \quad (4)$$

If we differentiate equation (2) with respect to ϵ_i and pick out the coefficient of ζ^N , we see that (3) takes the form

$$\bar{n}_i(N) = \omega_i \sum_{r=1}^N \frac{Z_{N-r}}{Z_N} \exp(-r\mu \epsilon_i). \quad (5)$$

Here $\bar{n}_i(N)$ has been written instead of \bar{n}_i , since we will consider the behaviour of \bar{n}_i as a function of the total number of particles N .

Since $\sum_i \bar{n}_i(N) = N$, equation (5) leads to

$$NZ_N = \sum_{r=1}^N Z_{N-r} \sum_i \omega_i \exp(-r\mu \epsilon_i). \quad (6)$$

Setting $N=1, 2, 3, \dots$ in turn in equation (6), we have, in principle, a method of finding Z_N . Thus equations (5) and (6) are sufficient to determine $\bar{n}_i(N)$.

From (5) we can also obtain the important relation

$$\bar{n}_i(N+1) = \frac{Z_N}{Z_{N+1}} (\omega_i + n_i(N)) \exp(-\mu \epsilon_i). \quad (7)$$

This relation has been obtained by Ansbacher and Ehrenberg (1949) who point out that, if we assume that $\bar{n}_i(N+1) = (1+\delta)\bar{n}_i(N)$ and neglect δ , we immediately obtain

$$\bar{n}_i(N) = \frac{\omega_i}{(Z_{N+1}/Z_N) \exp(\mu \epsilon_i) - 1}. \quad (8)$$

However, this procedure is only justified if δ is small compared with $1 - \exp(-\mu \epsilon_i) Z_N / Z_{N+1}$. In fact, if $i=0$ and the gas is condensed, both these quantities are of order $1/N$ and δ cannot be neglected. For $i \neq 0$ it seems that the neglect of δ is usually justified, but we shall make no assumption of this nature.

§ 3. PROPERTIES OF THE PARTITION FUNCTION.

We shall define a quantity $\lambda_i(N)$ by the relation

$$\bar{n}_i(N) = \frac{\omega_i}{\lambda_i^{-1}(N) \exp(\mu \epsilon_i) - 1}, \quad \dots \quad (9)$$

$\lambda_i(N)$ will, in general, be a function of the temperature as well as of i and N , but we shall only be concerned with its variation with N at constant temperature.

Substituting (9) into equation (7), we find

$$\bar{n}_i(N+1) = \frac{Z_N}{Z_{N+1}} \lambda_i^{-1}(N) \bar{n}_i(N) \quad \dots \quad (10)$$

and
$$\lambda_i^{-1}(N+1) = \frac{Z_{N+1}}{Z_N} + \exp(-\mu \epsilon_i) \left(1 - \lambda_i(N) \frac{Z_{N+1}}{Z_N} \right) \quad \dots \quad (11)$$

Summing equation (10) over all i , we obtain

$$N+1 = \frac{Z_N}{Z_{N+1}} \sum \lambda_i^{-1}(N) \bar{n}_i(N). \quad \dots \quad (12)$$

We can now prove that

$$\frac{Z_N}{Z_{N+1}} < \exp(\mu \epsilon_0) \quad \text{for all } N. \quad \dots \quad (13)$$

Let M be the lowest value of N for which (13) is untrue, so that

$$\frac{Z_M}{Z_{M+1}} \geq \exp(\mu \epsilon_0) \quad \dots \quad (14)$$

(equation (6) shows that M is greater than zero). The inequality (13) is true for all $N < M$ and hence, by (5) and (9), $\lambda_i(N) < \exp(\mu \epsilon_0)$ for $N \leq M$. Therefore, from (10) and (14), $\bar{n}_i(M+1) > \bar{n}_i(M)$ for all i and, from (7) and (14), $\bar{n}_0(M+1) > 1 + \bar{n}_0(M)$. Thus $\sum_i \bar{n}_i(M+1) > 1 + \sum_i \bar{n}_i(M)$, which is impossible.

Therefore there is no value M for which (14) is true and hence (13) is true for all N .

If we use the inequality (13) in the equation (5), we find

$$\begin{aligned} n_i(N) &< \omega_i \sum_{r=1}^N \exp[-r\mu(\epsilon_i - \epsilon_0)], \\ &< \frac{\omega_i}{\exp[\mu(\epsilon_i - \epsilon_0)] - 1}. \quad \dots \quad (15) \end{aligned}$$

Therefore, if
$$N_c = \sum_{i \neq 0} \frac{\omega_i}{\exp[\mu(\epsilon_i - \epsilon_0)] - 1}, \quad \dots \quad (16)$$

is finite, we must have $\bar{n}_0(N) > N - N_c$ whenever $N > N_c$. Thus condensation must occur whenever the energy levels are such that the series defining N_c converges, since, when the total number of particles exceeds N_c , a finite proportion of the particles must be in the lowest state.

Since (16) can be considered as defining a characteristic temperature T_c , associated with a given number of particles, we can say that a gas containing a fixed number of particles must be condensed at temperatures less than T_c . It should be emphasized that this result, in common with all those obtained in this section, is true for a general set of energy levels (provided only that the series in (16) converges) and for a finite number of particles. In order to show that the gas is not condensed at temperatures above T_c and to find the exact distribution of particles among the energy levels, we must consider the limiting case of large numbers of particles, but finite densities.

We shall first prove some other useful inequalities which are always true. From equations (10) and (11) we obtain the relation

$$\begin{aligned} n_i(N+2) &= \frac{Z_{N+1}}{Z_{N+2}} \left\{ \frac{Z_{N+1}}{Z_N} + \exp(-\mu\epsilon_i) \left(1 - \lambda_i(N) \frac{Z_{N+1}}{Z_N} \right) \right\} \bar{n}_i(N+1) \quad (17a) \\ &= \frac{Z_{N+1}}{Z_{N+2}} \left\{ \lambda_i^{-1}(N) + \frac{Z_N}{Z_{N+1}} \exp(-\mu\epsilon_i) \left(\lambda_i^{-1}(N) - \frac{Z_{N+1}}{Z_N} \right) \right\} \bar{n}_i(N). \end{aligned} \quad (17b)$$

We can now prove, by induction, that

$$\frac{Z_N}{Z_{N+1}} \lambda_i^{-1}(N) > 1 \quad \text{for all } N \text{ and } i. \quad (18)$$

We assume (18) to be true for all i when $N=M$. Therefore the inner bracket expressions on the right-hand sides of (17a) and (17b) are positive for $N=M$. If we also use the inequality (13) we can write

$$\frac{Z_{M+1}}{Z_{M+2}} \cdot \frac{Z_{M+1}}{Z_M} \bar{n}_i(M+1) < \bar{n}_i(M+2) < \frac{Z_{M+1}}{Z_{M+2}} \left\{ 2\lambda_i^{-1}(M) - \frac{Z_{M+1}}{Z_M} \right\} \bar{n}_i(M).$$

Hence, summing over all i and using (12), we find

$$\frac{Z_{M+1}}{Z_{M+2}} \cdot \frac{Z_{M+1}}{Z_M} (M+1) < M+2 < \frac{Z_{M+1}}{Z_{M+2}} \cdot \frac{Z_{M+1}}{Z_M} (M+2). \quad (19)$$

From equation (11) and the right-hand side of the inequality (19) we obtain

$$\frac{Z_{M+1}}{Z_{M+2}} \lambda_i^{-1}(M+1) > \frac{Z_{M+1}}{Z_{M+2}} \cdot \frac{Z_{M+1}}{Z_M} > 1.$$

Therefore (18) is true for $N=M+1$. It is true for $N=0$ and hence is always true. Consequently (19) is true for all M and can be rewritten in the form

$$\frac{Z_{N+1}}{Z_{N+2}} \frac{N+1}{N+2} < \frac{Z_N}{Z_{N+1}} < \frac{Z_{N+1}}{Z_{N+2}}. \quad (20)$$

This relation, expressing the fact that Z_N/Z_{N+1} is a slowly increasing function of N , is of great importance in evaluating the asymptotic values of the mean occupation numbers.

§ 4. THE MEAN OCCUPATION NUMBERS ABOVE THE CONDENSATION TEMPERATURE.

In this and the following sections we shall be concerned with the asymptotic behaviour of quantities such as $\bar{n}_i(N)$ when the number of particles N and the volume V tend to infinity in such a way that the density $\rho = N/V$ remains finite and constant. The volume enters into the expressions implicitly, since the distribution of the energy levels depends on it.

$$\text{Since} \quad \frac{Z_{N-r}}{Z_N} = \frac{Z_{N-r}}{Z_{N-r+1}} \cdot \frac{Z_{N-r+1}}{Z_{N-r+2}} \cdots \frac{Z_{N-1}}{Z_N},$$

the inequality (20) shows that

$$\left. \begin{aligned} \left(\frac{Z_{N-1}}{Z_N} \right)^r &> \frac{Z_{N-r}}{Z_N} > a_r \left(\frac{Z_{N-1}}{Z_N} \right)^r, \\ a_r &= \frac{N(N-1) \cdots (N-r+1)}{N^r - 1} \end{aligned} \right\} \cdots \cdots \cdots (21)$$

By the use of Stirling's expansion for $\log(N!)$, we find that

$$a_r = 1 - \frac{r^2}{2N} + \frac{r}{2N} + O\left(\frac{r^4}{N^2}\right).$$

From equation (5), we see that if M is any integer less than N ,

$$\bar{n}_i(N) = \omega_i \sum_{r=1}^M \frac{Z_{N-r}}{Z_N} \exp(-r\mu\epsilon_i) + \omega_i \sum_{r=M+1}^N \frac{Z_{N-r}}{Z_N} \exp(-r\mu\epsilon_i),$$

and, by (21),

$$\sum_{r=1}^M \left(\frac{Z_{N-1}}{Z_N} \right)^r \exp(-r\mu\epsilon_i) > \sum_{r=1}^M \frac{Z_{N-r}}{Z_N} \exp(-r\mu\epsilon_i) > \sum_{r=1}^M a_r \left(\frac{Z_{N-1}}{Z_N} \right)^r \exp(-r\mu\epsilon_i).$$

Let $M = N^\alpha$, where α is less than $\frac{1}{2}$; then $a_r \sim 1$ as N tends to infinity, as long as r is not greater than M . Hence

$$\sum_{r=1}^{N^\alpha} \frac{Z_{N-r}}{Z_N} \exp(-r\mu\epsilon_i) \sim \sum_{r=1}^{N^\alpha} \left(\frac{Z_{N-1}}{Z_N} \right)^r \exp(-r\mu\epsilon_i).$$

Therefore

$$\begin{aligned} \bar{n}_i(N) &\sim \omega_i \sum_{r=1}^{N^\alpha} \left(\frac{Z_{N-1}}{Z_N} \right)^r \exp(-r\mu\epsilon_i) + \omega_i \sum_{r=N^\alpha+1}^N \frac{Z_{N-r}}{Z_N} \exp(-r\mu\epsilon_i) \\ &= \omega_i \sum_{r=1}^{\infty} \left(\frac{Z_{N-1}}{Z_N} \right)^r \exp(-r\mu\epsilon_i) \\ &\quad - \omega_i \left\{ \sum_{r=N^\alpha+1}^{\infty} \left(\frac{Z_{N-1}}{Z_N} \right)^r \exp(-r\mu\epsilon_i) - \sum_{r=N^\alpha+1}^N \frac{Z_{N-r}}{Z_N} \exp(-r\mu\epsilon_i) \right\}. \end{aligned}$$

$$\text{Hence} \quad \bar{n}_i(N) \sim \frac{\omega_i}{(Z_N/Z_{N-1}) \exp(\mu\epsilon_i) - 1} - \omega_i R(N, \alpha),$$

where, by (21),

$$O < R(N, \alpha) < \sum_{r=N^{\alpha}+1}^{\infty} \left(\frac{Z_{N-1}}{Z_N} \right)^r \exp(-r\mu\epsilon_i).$$

Thus

$$\bar{n}_i(N) \sim \frac{\omega_i}{(Z_N/Z_{N-1}) \exp(\mu\epsilon_i) - 1} \left\{ 1 - \theta \left[\frac{Z_{N-1}}{Z_N} \exp(-\mu\epsilon_i) \right]^{N^{\alpha}} \right\}, \quad (22)$$

where $0 < \theta < 1$, and α is any positive number less than $\frac{1}{2}$. Since, by (13), $Z_{N-1}/Z_N < \exp(\mu\epsilon_0)$, $1 - (Z_{N-1}/Z_N) \exp(-\mu\epsilon_0)$ is positive and less than 1. Thus if we write $x = 1 - (Z_{N-1}/Z_N) \exp(-\mu\epsilon_0)$,

$$\begin{aligned} \lim_{N \rightarrow \infty} \left(\frac{Z_{N-1}}{Z_N} \exp(-\mu\epsilon_i) \right)^{N^{\alpha}} &= \lim_{N \rightarrow \infty} \{ \exp[-\mu N^{\alpha}(\epsilon_i - \epsilon_0)] (1-x)^{N^{\alpha}x} \} \\ &< \lim_{N \rightarrow \infty} \{ \exp[-\mu N^{\alpha}(\epsilon_i - \epsilon_0)] \exp[-N^{\alpha}x] \}. \end{aligned}$$

Hence, if either $(\epsilon_i - \epsilon_0)$ or x is of order greater than $N^{-\alpha}$, the coefficient of θ in (22) tends to zero as N tends to infinity.

$$\text{Thus} \quad \bar{n}_i(N) \sim \frac{\omega_i}{(Z_N/Z_{N-1}) \exp(\mu\epsilon_i) - 1}, \quad \dots \dots \dots (23)$$

(a) at all temperatures if $(\epsilon_i - \epsilon_0)^{-1} = o(N^{\alpha})$,

or (b) for all i if $[1 - (Z_{N-1}/Z_N) \exp(-\mu\epsilon_0)]^{-1} = o(N^{\alpha})$, (24)

where α is any number less than $\frac{1}{2}$.

(23) is, of course, the well-known formula for the occupation numbers, and (24a) shows that it is always true except for some levels with energy very close to that of the lowest level.

We will show, however, that the condition (b) under which (23) is valid is satisfied for all temperatures except those in the immediate neighbourhood of or below the condensation temperature. This conclusion is to be expected from the fact that (b) demands only that the number of particles in the lowest state should be of order less than $N^{\frac{1}{2}}$.

For convenience we write $\lambda = Z_{N-1}/Z_N$, so that (23) takes the form

$$\bar{n}_i(N) = \frac{\omega_i}{\lambda^{-1} \exp(\mu\epsilon_i) - 1}.$$

So long as the condition (24b) is obeyed, the identity $\sum_i \bar{n}_i(N) = N$ takes the limiting form $F(\lambda, T) = \rho$, where

$$F(\lambda, T) = \lim_{N \rightarrow \infty} \left\{ \frac{1}{V} \sum_{i \neq 0} \frac{\omega_i}{\lambda^{-1} \exp(\mu\epsilon_i) - 1} \right\}.$$

The omission of the term corresponding to $i=0$ makes no difference for large N , since $\bar{n}_0(N)$ is of order less than $N^{\frac{1}{2}}$. The equation $F(\lambda, T) = \rho$ may be used to define λ as a function of T (for given ρ) and the condensation temperature may be defined as the value of T , T_c say, for which $\lambda = \exp(\mu\epsilon_0)$.

This value of λ is clearly outside the range of validity of (24b) and this definition may be considered at present as purely conventional, although it should be observed that it corresponds to the definition of the condensation point given, for finite N , in equation (16). Any temperature $T' > T_c$, such that $(T' - T_c)$ is some finite temperature difference, however small, will correspond to a value of λ , λ' say, which differs from the limiting value $\exp(\mu\epsilon_0)$ by some finite amount. It is clear that, for large enough N , (24b) will be satisfied if Z_{N-1}/Z_N is equal to λ' and hence (23) will be true at the temperature T' . It follows that (23) is true, in the limit of large N , for all temperatures greater than T_c .

§ 5. THE MEAN OCCUPATION NUMBERS BELOW THE CONDENSATION TEMPERATURE.

In the last section we defined a temperature T_c by the equation

$$\lim_{V \rightarrow \infty} \frac{1}{V} \sum_{i \neq 0} \frac{\omega_i}{\exp[\mu_c(\epsilon_i - \epsilon_0)] - 1} = \rho = \lim_{N, V \rightarrow \infty} (N/V), \quad \dots \quad (25)$$

where $\mu_c = 1/kT_c$; we have already remarked that this is equivalent to the limiting form of equation (16) in which we considered the temperature as fixed and the number of particles as our independent variable. It is now convenient to return to that view-point and to define the critical number of particles at a temperature T by the equation

$$N_c = \sum_{i \neq 0} \frac{\omega_i}{\exp[\mu(\epsilon_i - \epsilon_0)] - 1}, \quad \mu = 1/kT.$$

From inequality (15) we see that $\bar{n}_0(N) > N - N_c$, and from equation (5) and inequality (21) we see that

$$\bar{n}_0(N) < \frac{\omega_0}{(Z_N/Z_{N-1}) \exp(\mu\epsilon_0) - 1},$$

and hence

$$\frac{\omega_0}{(Z_N/Z_{N-1}) \exp(\mu\epsilon_0) - 1} > N - N_c.$$

We thus obtain the inequality

$$1 < \frac{Z_N}{Z_{N-1}} \exp(\mu\epsilon_0) < 1 + \frac{\omega_0}{N - N_c} \quad \text{if } N > N_c, \quad \dots \quad (26)$$

where the left-hand side is a restatement of (13).

Let us consider the number of particles, N , to be such that $N - N_c = rN$, where r is some positive number. Then (26) becomes

$$1 < \frac{Z_N}{Z_{N-1}} \exp(\mu\epsilon_0) < 1 + \frac{\omega_0}{rN},$$

similarly

$$1 < \frac{Z_{N-M}}{Z_{N-M-1}} \exp(\mu\epsilon_0) < 1 + \frac{\omega_0}{rN - M},$$

where $M < rN$. By forming the product of these inequalities with M running from zero to N^β , where β is some number less than 1 (so that $N^\beta \ll rN$ for large N), we obtain, after some rearrangement

$$\exp(\mu \epsilon_0 N^\beta) > \frac{Z_{N-N^\beta}}{Z_N} > \left(1 + \frac{\omega_0}{rN - N^\beta}\right)^{-N^\beta} \exp(\mu \epsilon_0 N^\beta), \quad (N^\beta < rN).$$

If we now use this inequality for Z_{N-N^β}/Z_N in equation (5) and proceed in a manner similar to that used in the derivation of (22), we find

$$\bar{n}_i(N) \sim \frac{\omega_i}{\exp[\mu(\epsilon_i - \epsilon_0)] - 1} \{1 - \theta \exp[-N^\beta \mu(\epsilon_i - \epsilon_0)]\},$$

where $0 < \theta < 1$.

If $(\epsilon_i - \epsilon_0)$ is of order $N^{-\gamma}$ where $\gamma < 1$, β can be chosen so that $\gamma < \beta < 1$ and the coefficient of θ is exponentially small for $i \neq 0$. For a perfect three-dimensional gas, for instance, $\gamma = 2/3$, so that this condition is met. Thus

$$\left. \begin{aligned} \bar{n}_i(N) &\sim \frac{\omega_i}{\exp[\mu(\epsilon_i - \epsilon_0)] - 1}, \quad i \neq 0, \\ \text{and hence } \bar{n}_0(N) &\sim N - \sum_{i \neq 0} \frac{\omega_i}{\exp[\mu(\epsilon_i - \epsilon_0)] - 1}. \end{aligned} \right\} \dots \dots (27)$$

(27) has been proved for $N - N_c = rN$, where r is any positive number, however small, so long as it remains finite as N tends to infinity.

If the particle density ρ is such that the condensation temperature, defined by (25) is T_c , then any temperature $T'' < T_c$ will correspond to a critical density ρ'' , where

$$\lim_{V \rightarrow \infty} \left\{ \frac{1}{V} \sum_{i \neq 0} \frac{\omega_i}{\exp[\mu''(\epsilon_i - \epsilon_0)] - 1} \right\} = \rho'',$$

and $\mu'' = 1/kT''$. ρ'' will be less than ρ by some finite difference, $r\rho$ say. Therefore at the temperature T'' , $N - N_c = rN$ and the argument used above is valid. Hence equation (27) is valid at all temperatures $T < T_c$.

Thus we may sum up the results of this and the preceding section as follows.

If T_c is defined by the equation

$$\lim_{V \rightarrow \infty} \left\{ \frac{1}{V} \sum_{i \neq 0} \frac{\omega_i}{\exp[\mu_c(\epsilon_i - \epsilon_0)] - 1} \right\} = \rho = \lim_{V, N \rightarrow \infty} N/V,$$

where $\mu_c = 1/kT_c$, then

$$\bar{n}_i(N) \sim \frac{\omega_i}{(Z_N/Z_{N-1}) \exp(\mu \epsilon_i) - 1} \quad \text{for } T > T_c,$$

and

$$\left. \begin{aligned} \bar{n}_i(N) &\sim \frac{\omega_i}{\exp[\mu(\epsilon_i - \epsilon_0)] - 1}, \quad i \neq 0, \\ \bar{n}_0(N) &= N - \sum_{i \neq 0} \bar{n}_i(N), \end{aligned} \right\} \quad \text{for } T < T_c.$$

In obtaining these expressions we have assumed that the limit used in defining T_c exists and that $(\epsilon_1 - \epsilon_0)$ is of order greater than $N^{-\gamma}$, $\gamma < 1$.

§ 6. FLUCTUATIONS.

We have seen in equation (4) that

$$\overline{n_i n_j} = \frac{1}{\mu^2 Z_N} \frac{\partial^2 Z_N}{\partial \epsilon_i \partial \epsilon_j}.$$

By differentiating (2) twice we find

$$\begin{aligned} \overline{n_i n_j} &= \omega_i \omega_j \sum_{r=2}^N \frac{Z_{N-r}}{Z_N} \frac{\exp [-(r-1)\mu\epsilon_i] - \exp [-(r-1)\mu\epsilon_j]}{\exp (-\mu\epsilon_i) - \exp (-\mu\epsilon_j)} \exp [-\mu(\epsilon_i + \epsilon_j)] \\ &= \frac{1}{\exp (-\mu\epsilon_i) - \exp (-\mu\epsilon_j)} \{ \omega_j \exp (-\mu\epsilon_j) \overline{n_i} - \omega_i \exp (-\mu\epsilon_i) \overline{n_j} \} \quad \text{if } i \neq j, \\ &\quad \dots \dots \dots (28) \end{aligned}$$

and when $i=j$, we find

$$\overline{n_i^2} = \overline{n_i} + \omega_i (\omega_i + 1) \sum_{r=2}^N \frac{Z_{N-r}}{Z_N} (r-1) \exp (-r\mu\epsilon_i), \quad \dots \dots (29)$$

(28) and (29) are exact formulæ.

By arguments similar to those which lead to equations (23) and (27), we obtain from (29)

$$\overline{(n_i - \overline{n_i})^2} \sim \frac{(\overline{n_i})^2}{\omega_i} + \overline{n_i}$$

for all i when $T > T_c$ and for $i \neq 0$ when $T < T_c$.

To find the value of $\overline{n_0^2}$ for $T < T_c$, we observe that

$$N \overline{n_0} = \overline{n_0^2} + \sum \overline{n_0 n_i},$$

hence

$$\overline{(n_0 - \overline{n_0})^2} = \overline{n_0^2} - \sum_{i \neq 0} \overline{n_i} - \sum_{i \neq 0} \overline{n_0 n_i}$$

and using (28) with $j=0$, we obtain

$$\overline{(n_0 - \overline{n_0})^2} = \overline{n_0} \left\{ \sum_{i \neq 0} \overline{n_i} - \sum_{i \neq 0} \frac{\omega_i}{\exp [\mu(\epsilon_i - \epsilon_0)] - 1} \right\} + \sum_{i \neq 0} \frac{\omega_0 \exp [\mu(\epsilon_i - \epsilon_0)] \overline{n_i}}{\exp [\mu(\epsilon_i - \epsilon_0)] - 1}. \quad \dots \dots (30)$$

Although $\overline{n_i}$ is given asymptotically by (27) for $T < T_c$, we cannot necessarily neglect the first term in (30), since

$$\overline{n_0} \sum_{i \neq 0} \left(\overline{n_i} - \frac{\omega_i}{\exp [\mu(\epsilon_i - \epsilon_0)] - 1} \right),$$

while negligible compared with $\overline{n_0} \sum_{i \neq 0} \overline{n_i}$ need not be negligible in comparison with the second term in (30). Since, by (5) and (13),

$$\overline{n_i} < \frac{\omega_i}{\exp [\mu(\epsilon_i - \epsilon_0)] - 1},$$

we can deduce from (30) that

$$\overline{(n_0 - n_0)^2} < \sum_{i \neq 0} \frac{\omega_0 \exp [\mu(\epsilon_i - \epsilon_0)] \bar{n}_i}{\exp [\mu(\epsilon_i - \epsilon_0)] - 1} \sim \frac{\omega_0}{\exp (\mu \epsilon_0)} \sum_{i \neq 0} \frac{(\bar{n}_i)^2 \exp (\mu \epsilon_i)}{\omega_i}.$$

Thus we have shown that

$$\left. \begin{aligned} \overline{(n_i - n_i)^2} &\sim \frac{(\bar{n}_i)^2}{\omega_i} + n_i, & \text{for all } i \text{ if } T > T_c, \\ \overline{(n_i - n_i)^2} &\sim \frac{(\bar{n}_i)^2}{\omega_i} + n_i, & \text{for all } i \neq 0, \\ \overline{(n_0 - n_0)^2} &\leq \frac{\omega_0}{\exp (\mu \epsilon_0)} \sum_{i \neq 0} \frac{(\bar{n}_i)^2 \exp (\mu \epsilon_i)}{\omega_i}, & \left. \begin{aligned} &\text{if } T < T_c. \end{aligned} \right\} \end{aligned} \right\}$$

The expressions for these fluctuations which are obtained by the method of steepest descents differ from these only in that the "less than or equals" sign in the expression for $\overline{(n_0 - n_0)^2}$ when $T < T_c$ is replaced by an "equals" sign. The expressions for $i \neq 0$ are sometimes quoted as holding generally, even for $i = 0$ in the condensed state. That this cannot be so can easily be seen, for if

$$\overline{(n_0 - n_0)^2} = (n_0)^2 + \bar{n}_0$$

(we have taken $\omega_0 = 1$ for simplicity), then

$$\bar{n}_0^2 = 2(\bar{n}_0)^2 + \bar{n}_0.$$

At a sufficiently low temperature more than $1/\sqrt{2}$ of the total number of particles will be in the lowest state. Therefore $2(\bar{n}_0)^2$ will be greater than N^2 and hence \bar{n}_0^2 will be greater than N^2 . This is impossible, since $n_0 < N$. The formulæ which Fowler (1936) obtains by the method of steepest descents are not open to this criticism and reduce to the formulæ given above with the inequality replaced by an equality.

§ 7. CONCLUSIONS.

The formulæ obtained in this paper show that the expressions obtained by the method of steepest descents are correct, except possibly for a very small range of temperature near the condensation temperature which decreases to zero as the number of particles and the volume increase to infinity. The only new assumption which we have made is that the separation between the lowest pair of energy levels, $(\epsilon_1 - \epsilon_0)$, is of order greater than $N^{-\gamma}$, where $\gamma < 1$. If this assumption were not made, complications would arise in the condensation phenomenon even if the orthodox formulæ were valid everywhere, since condensation would take place into more than one level. If, for instance, $\epsilon_1 - \epsilon_0 = \epsilon/N$, then if

$$\bar{n}_i = \frac{1}{\lambda^{-1} \exp (\mu \epsilon_i) - 1}$$

and $\bar{n}_0 = \alpha N$, λ would have the value

$$\lambda = \frac{\exp(\mu\epsilon_0)}{1 + 1/\alpha N}$$

and \bar{n}_1 the value

$$\bar{n}_1 = \frac{N}{\mu\epsilon + 1/\alpha}.$$

In other words, a comparable number of particles would have condensed into the level above the lowest.

From the results obtained in §§4 and 5 we can deduce that the macroscopic behaviour of a perfect Bose-Einstein gas is identical with that found by London (1938) and Fowler and Jones (1938). This is in agreement with the conclusions reached in paper I. (Fraser 1951).

The only work which appears to be in positive disagreement with the results obtained by the method of steepest descents is that of Temperley (1949). Since this work deals essentially with a finite (although large) number of particles, it is difficult to compare with the conclusions of §§4 and 5 of this paper. Temperley's conclusion that, in his particular model, condensation only takes place at a temperature much lower than that predicted by the method of steepest descents is, however, in disagreement with the consequences of equations (15) and (16). This disagreement arises from the choice of a criterion for condensation. Temperley has required that, when the gas is condensed, all particles added to the gas should go into the lowest state. This, however, can never occur for a gas consisting of a finite number of particles. In fact equations (10) and (18) of this paper show that the addition of a single particle leads to an increase of all the occupation numbers. It is only in the limit of infinite volume that we can speak of the occupation numbers of the excited states being independent of the total number of particles when the gas is condensed. Relations deduced by Temperley for his model can be used to prove that, when the temperature is below the orthodox condensation temperature, almost all particles added to the system condense into the lowest state.

ACKNOWLEDGMENTS.

I wish to thank Mr. H. N. V. Temperley and Mr. O. Penrose for helpful discussions. I am also indebted to the Department of Scientific and Industrial Research for a maintenance grant.

REFERENCES.

- ANSBACHER, F., and EHRENBERG, W., 1949, *Phil. Mag.*, **40**, 626.
 DINGLE, R. B., 1949, *Proc. Cam. Phil. Soc.*, **45**, 275.
 FOWLER, R. H., 1936, *Statistical Mechanics* (Cambridge: University Press).
 FOWLER, R. H., and JONES, H., 1938, *Proc. Cam. Phil. Soc.*, **34**, 573.
 FRASER, A. R., 1951, *Phil. Mag.*, **42**, 156.
 LONDON, F., 1938, *Phys. Rev.*, **54**, 947.
 SCHROEDINGER, E., 1945, *Statistical Thermodynamics* (Cambridge: University Press).
 SCHUBERT, G., 1946 and 1947, *Z. Naturforsch.*, **1**, 113, and **2a**, 250.
 TEMPERLEY, H. N. V., 1949, *Proc. Roy. Soc. A*, **199**, 361.

XVI. *The Unsteady Flow of Viscous Incompressible Fluid Inside an Infinite Channel.*

By L. SOWERBY,

Department of Applied Mathematics, University of Liverpool†.

[Received November 22, 1950.]

SUMMARY.

The problem considered is the motion of viscous incompressible fluid inside an infinite wedge-shaped channel of angle π/n , the channel being started suddenly from rest with uniform velocity in the direction of its length. The solution is obtained by considering a suitable Green's function for the heat conduction equation. The velocity is found to be expressible either in terms of error functions or in the form of integrals which are suitable for computation, depending on the value of n . In all cases the skin friction appears as a simple expression involving well known functions.

Particular reference is made to the right angled channel ($n=2$), the results being extended, by Rayleigh's hypothesis, to include some discussion of the steady flow inside a right angled channel having leading edges normal to the incident stream. From this, also, an approximation is derived for the frictional force on the interior of a finite rectangular channel of suitable dimensions.

1. *Statement of Problem.* Choosing cylindrical coordinates (r, θ, z) , two semi-infinite plates coinciding with the planes $\theta=0$, $\theta=\pi/n$, respectively, form an infinite wedge-shaped channel of angle π/n (n is an integer ≥ 1). The region inside the channel is filled with viscous incompressible fluid, and initially the channel and the fluid are at rest. At $t=0$ the channel is set in motion impulsively with uniform velocity W parallel to Oz ; the problem is to determine the subsequent motion of the fluid.

2. *The Equation of Motion and Boundary Conditions.* Let (u, v, w) be the components of velocity of the fluid in the given coordinate system; in particular, w is the component parallel to the axis $r=0$. Then it is clear that there is a solution of the hydrodynamical equations, and the solution of the above problem, in which $u=v=0$, provided $w(r, \theta, t)$ can be determined to satisfy

$$\frac{\partial w}{\partial t} = \nu \left(\frac{\partial^2 w}{\partial r^2} + \frac{1}{r} \frac{\partial w}{\partial r} + \frac{1}{r^2} \frac{\partial^2 w}{\partial \theta^2} \right), \quad \dots \dots \dots (2.1)$$

† Communicated by Dr. A. Fletcher.

and the boundary conditions

$$\left. \begin{aligned} w &= 0 \quad \text{when } t=0, \\ w &= W \quad \text{if } \theta=0, \theta=\pi/n, \\ w &\longrightarrow 0 \quad \text{as } r \longrightarrow \infty (\theta \neq 0, \pi/n), \end{aligned} \right\} \text{when } t > 0 \quad . \quad . \quad . \quad (2.2)$$

(ν is the coefficient of kinematic viscosity.)

3. *The Solution of (2.1)* It is convenient to write

$$w^* = W - w \quad . \quad . \quad . \quad (3.1)$$

so that w^* must also satisfy the equation (2.1) and the boundary conditions

$$\left. \begin{aligned} w^* &= W \quad \text{when } t=0, \\ w^* &= 0 \quad \text{if } \theta=0, \theta=\pi/n \\ w^* &\longrightarrow W \quad \text{as } r \longrightarrow \infty (\theta \neq 0, \pi/n), \end{aligned} \right\} \text{when } t > 0. \quad . \quad . \quad (3.2)$$

The expression for w^* can be obtained directly by considering a Green's function relating to the equation (2.1) and appropriate to the boundary considered (Carslaw and Jaeger 1947). An expression is obtained for $w^*(r, \theta, t)$ at the point (r', θ') , say, and the required Green's function, u , is of the form

$$u = F(r, \theta, r', \theta', t - \tau) \quad . \quad . \quad . \quad (i.)$$

(in this, and in all that follows, we take $t > \tau$.)

We require u to satisfy the equation

$$\frac{\partial u}{\partial t} = \nu \left(\frac{\partial^2 u}{\partial r^2} + \frac{1}{r} \frac{\partial u}{\partial r} + \frac{1}{r^2} \frac{\partial^2 u}{\partial \theta^2} \right) \quad . \quad . \quad . \quad (ii.)$$

and the following conditions

$$\lim_{t \rightarrow \tau + 0} u = 0. \quad . \quad . \quad . \quad (iii.)$$

everywhere in the region $S(0 \leq \theta \leq \pi/n)$, except at the point (r', θ') where

$$u \longrightarrow \frac{1}{4\pi\nu(t-\tau)} \exp \left[-\frac{1}{4\nu(t-\tau)} (r^2 + r'^2 - 2rr' \cos(\theta - \theta')) \right], \quad . \quad . \quad (iv.)$$

and also

$$u = 0 \quad \text{if } \theta = 0, \theta = \pi/n. \quad . \quad . \quad . \quad (v.)$$

In addition, we shall require u and $\partial u / \partial \theta$ to tend to zero in a suitable manner as $r \longrightarrow \infty$, to ensure the vanishing of a certain line integral. The function u which we shall choose will certainly satisfy this last condition. Finally, under these conditions, and the conditions imposed on w^* , the required expression for w^* is

$$w^*(r', \theta', t) = W \int_{\theta=0}^{\pi/n} \int_{r=0}^{\infty} u_{\tau=0} r \, dr \, d\theta. \quad . \quad . \quad . \quad (3.3)$$

It remains, therefore to select the appropriate function u .

Consider

$$u(r, \theta, r', \theta', t - \tau) = \frac{1}{4\pi\nu(t - \tau)} \times \sum_{m=0}^{n-1} \left[\begin{aligned} &\exp - \frac{1}{4\nu(t - \tau)} \left\{ r^2 + r'^2 - 2rr' \cos \left(\theta' - \left\{ \theta + \frac{2m\pi}{n} \right\} \right) \right\} \\ &- \exp - \frac{1}{4\nu(t - \tau)} \left\{ r^2 + r'^2 - 2rr' \cos \left(\theta' - \left\{ 2(m+1)\frac{\pi}{n} - \theta \right\} \right) \right\} \right] \end{aligned} \quad (3.4)$$

Then u satisfies (ii.), since each term is a solution of (ii.), and clearly all the remaining conditions (iii.)–(v.) are also satisfied. Moreover, u and $\partial u / \partial \theta \rightarrow 0$ suitably as $r \rightarrow \infty$, so that

$$w^*(r', \theta', r) = W \int_{\theta=0}^{\pi/n} \int_{r=0}^{\infty} u(r, \theta, r', \theta', t) r dr d\theta,$$

or, reverting to the usual notation,

$$w^*(r, \theta, t) = W \int_{\alpha=0}^{\pi/n} \int_{z=0}^{\infty} u(z, \alpha, r, \theta, t) z dz d\alpha, \quad \dots \quad (3.5)$$

where

$$u(z, \alpha, r, \theta, t) = \frac{1}{4\pi\nu t} \times \sum_{m=0}^{n-1} \left[\begin{aligned} &\exp - \frac{1}{4\nu t} \left\{ z^2 + r^2 - 2rz \cos \left(\theta - \left\{ \alpha + \frac{2m\pi}{n} \right\} \right) \right\} \\ &- \exp - \frac{1}{4\nu t} \left\{ z^2 + r^2 - 2rz \cos \left(\theta - \left\{ 2(m+1)\frac{\pi}{n} - \alpha \right\} \right) \right\} \right] \end{aligned} \quad (3.6)$$

It is at once evident that the expression (3.5) satisfies the boundary conditions on $\theta=0$, $\theta=\pi/n$, since the integrand u is zero for these values of θ . The expression can be reduced further by carrying out the integration with respect to z , and, indeed, except for a certain group of the integers n , the integration with respect to α can also be performed, the expression then reducing to a (finite) sum of tabulated functions.

Writing $p^2 = 1/4\nu t$, $c = \cos(\theta - \beta)$, $s = \sin(\theta - \beta)$, we have

$$\begin{aligned} &\frac{1}{4\nu t} \int_{z=0}^{\infty} \exp \left\{ -\frac{1}{4\nu t} (z^2 + r^2 - 2rz \cos \{\theta - \beta\}) \right\} z dz \\ &= p^2 \exp(-p^2 r^2 s^2) \int_{z=0}^{\infty} \exp \{-p^2 (z - rc)^2\} z dz \\ &= p^2 \exp(-p^2 r^2 s^2) \int_{-rc}^{\infty} \exp(-p^2 x^2) \cdot (x + rc) dx \\ &= \frac{1}{2} \exp(-\eta^2) + \eta c \cdot \exp(-\eta^2 s^2) \frac{\pi^{\frac{1}{2}}}{2} \{1 + \operatorname{erf}(\eta c)\}, \end{aligned}$$

where

$$\eta = \frac{r}{2(\nu t)^{\frac{1}{2}}}, \text{ and } \operatorname{erf}(y) = \frac{2}{\pi^{\frac{1}{2}}} \int_0^y \exp(-x^2) dx.$$

Hence, placing $\gamma_m = \theta - 2m\pi/n$

$$w^* = \frac{W}{2\pi^{\frac{1}{2}}} \int_{\alpha=0}^{\pi/n} \eta \sum_{m=0}^{n-1} \left[\begin{array}{l} \cos(\gamma_m - \alpha) \cdot \exp(-\eta^2 \sin^2 \{\gamma_m - \alpha\}) \{1 + \operatorname{erf}(\eta \cos \{\gamma_m - \alpha\})\} \\ - \cos(\gamma_{m+1} + \alpha) \cdot \exp(-\eta^2 \sin^2 \{\gamma_{m+1} + \alpha\}) \{1 + \operatorname{erf}(\eta \cos \{\gamma_{m+1} + \alpha\})\} \end{array} \right] dx \quad (3.7)$$

or, writing $f(\eta, \phi) = \cos \phi \cdot \exp(-\eta^2 \sin^2 \phi) \{1 + \operatorname{erf}(\eta \cos \phi)\}$, . . . (3.8)

$$\begin{aligned} w^* &= \frac{W}{2\pi^{\frac{1}{2}}} \sum_{m=0}^{n-1} \left[\int_{2m\frac{\pi}{n}-\theta}^{(2m+1)\frac{\pi}{n}-\theta} \eta f(\eta, \phi) d\phi - \int_{\theta-2(m+1)\frac{\pi}{n}}^{\theta-(2m+1)\frac{\pi}{n}} \eta f(\eta, \phi) d\phi \right] \\ &= \frac{W}{2\pi^{\frac{1}{2}}} \sum_{m=0}^{n-1} \left[\int_{2m\frac{\pi}{n}-\theta}^{(2m+1)\frac{\pi}{n}-\theta} \eta f(\eta, \phi) d\phi - \int_{(2m+1)\frac{\pi}{n}-\theta}^{2(m+1)\frac{\pi}{n}-\theta} \eta f(\eta, \phi) d\phi \right] \\ &\quad \text{(since } f(\eta, \phi) \text{ is an even function of } \phi) \\ &= \frac{W}{2\pi^{\frac{1}{2}}} \sum_{m=0}^{2n-1} (-1)^m \int_{m\frac{\pi}{n}-\theta}^{(m+1)\frac{\pi}{n}-\theta} \eta f(\eta, \phi) d\phi. \end{aligned}$$

$$\text{Thus } \frac{w^*}{W} = \frac{1}{2\pi^{\frac{1}{2}}} \sum_{m=0}^{2n-1} (-1)^m \int_{m\frac{\pi}{n}-\theta}^{(m+1)\frac{\pi}{n}-\theta} \eta f(\eta, \phi) d\phi \quad . . . \quad (3.9)$$

$$= \frac{1}{2\pi^{\frac{1}{2}}} \sum_{m=0}^{2n-1} (-1)^m \int_0^{\pi/n} \eta f\left(\eta, \phi + \frac{m\pi}{n} - \theta\right) d\phi. \quad (3.10)$$

From these last results it can easily be verified that w^* does, in fact, satisfy the remaining boundary conditions (3.2), the first and third of these now being included in the single condition $w^* \rightarrow W$ as $\eta \rightarrow \infty$ ($0 < \theta < \pi/n$). For convenience, take $n \geq 2$, and consider

$$I_m = \int_{\phi_m}^{\phi_m + \frac{\pi}{n}} \eta f(\eta, \phi) d\phi,$$

where $\phi_m = m\pi/n - \theta$.

Then, since $0 < \theta < \pi/n$, the range $\phi_m \leq \phi \leq \phi_m + \pi/n$ excludes the points $\phi = 0, \phi = \pi$ except when $m = 0, n$ respectively. Thus, if $m \neq 0, n$

$$\begin{aligned} I_m &= \int_{\phi_m}^{\phi_m + \frac{\pi}{n}} \eta \cos \phi \cdot \exp(-\eta^2 \sin^2 \phi) \cdot \{1 + \operatorname{erf}(\eta \cos \phi)\} d\phi \\ &= \exp(-\eta^2 \sin^2 \xi) \eta \cos \xi \int_{\phi_m}^{\phi_m + \frac{\pi}{n}} \{1 + \operatorname{erf}(\eta \cos \phi)\} d\phi, \end{aligned}$$

where $\phi_m < \xi < \phi_m + \pi/n$.

Hence, since $\sin \xi \neq 0$, and $|\operatorname{erf} x| < 1$,

$$I_m \rightarrow 0 \quad \text{as } \eta \rightarrow \infty.$$

In the cases $m=0$ and n , $\cos \phi$ does not change sign in the range of integration, so that

$$I_m = \{1 + \operatorname{erf}(\eta \cos \xi)\} \int_{\phi_m}^{\phi_m + \frac{\pi}{n}} \eta \cos \phi \cdot \exp(-\eta^2 \sin^2 \phi) d\phi \\ = \frac{\pi^{\frac{1}{2}}}{2} \{1 + \operatorname{erf}(\eta \cos \xi)\} \left[\operatorname{erf}\left(\eta \sin\left(\phi_m + \frac{\pi}{n}\right)\right) - \operatorname{erf}(\eta \sin \phi_m) \right].$$

Now, if $m=n$, $\cos \xi < 0$, so that $\operatorname{erf}(\eta \cos \xi) \rightarrow -1$ as $\eta \rightarrow \infty$, and therefore $I_n \rightarrow 0$. But if $m=0$, $\cos \xi > 0$, and $\phi_0 < 0 < \phi_0 + \pi/n$, and therefore $I_0 \rightarrow 2\pi^{\frac{1}{2}}$ as $\eta \rightarrow \infty$. This establishes the required result.

Thus, finally, the expression for w is given by

$$\frac{w}{W} = 1 - \frac{1}{2\pi^{\frac{1}{2}}} \sum_{m=0}^{2n-1} (-1)^m \int_{\frac{m\pi}{n} - \theta}^{(m+1)\frac{\pi}{n} - \theta} \eta f(\eta, \phi) d\phi, \quad \dots \quad (3.11)$$

Henceforward we shall consider the simplification of this result when n takes certain values. Accordingly, it is convenient to introduce the suffix n , w now being replaced by w_n , and so on for other quantities we shall consider. In particular w_1 and τ_1 will refer to the velocity and skin friction respectively for the standard flat plate problem of Rayleigh (1911).

$$\text{Writing} \quad g(\eta, \phi) = \cos \phi \cdot \exp(-\eta^2 \sin^2 \phi) \quad \dots \quad (3.12)$$

$$\text{and} \quad h(\eta, \phi) = \cos \phi \cdot \exp(-\eta^2 \sin^2 \phi) \operatorname{erf}(\eta \cos \phi), \quad \dots \quad (3.13)$$

$$\text{then} \quad f(\eta, \phi) = g(\eta, \phi) + h(\eta, \phi),$$

$$\text{and} \quad g(\eta, \phi + \pi) = -g(\eta, \phi),$$

$$h(\eta, \phi + \pi) = h(\eta, \phi).$$

The expression (3.11) now simplifies as follows:—

(i.) $\underline{n=2p+1}$ (p an integer ≥ 0). The terms involving h in (3.11) vanish, and hence

$$\frac{w_n}{W} = 1 - \frac{1}{\pi^{\frac{1}{2}}} \sum_{m=0}^{2p} (-1)^m \int_{\frac{m\pi}{n} - \theta}^{(m+1)\frac{\pi}{n} - \theta} \eta \cos \phi \cdot \exp(-\eta^2 \sin^2 \phi) d\phi \\ = 1 - \frac{1}{2} \sum_{m=0}^{2p} (-1)^m \left[\operatorname{erf}\left(\eta \sin\left\{(m+1)\frac{\pi}{n} - \theta\right\}\right) - \operatorname{erf}\left(\eta \sin\left\{\frac{m\pi}{n} - \theta\right\}\right) \right],$$

$$i. e. \quad \frac{w_n}{W} = 1 + \sum_{m=0}^{2p} (-1)^m \operatorname{erf}\left(\eta \sin\left\{\frac{m\pi}{n} - \theta\right\}\right). \quad \dots \quad (3.14)$$

(ii.) $\underline{n=2p}$ (p an integer ≥ 1). In this case the terms in g in (3.11) vanish, and we have

$$\frac{w_n}{W} = 1 - \frac{1}{\pi^{\frac{1}{2}}} \sum_{m=0}^{2p-1} (-1)^m \int_{\frac{m\pi}{n} - \theta}^{(m+1)\frac{\pi}{n} - \theta} \eta \cos \phi \cdot \exp(-\eta^2 \sin^2 \phi) \cdot \operatorname{erf}(\eta \cos \phi) d\phi, \quad \dots \quad (3.15)$$

(ii.a) There is a further simplification of (3.15) if $n=4p+2$ (p an integer ≥ 0).

For, writing

$$I_m = (-1)^m \int_{\frac{m\pi}{n} - \theta}^{\frac{(m+1)\pi}{n} - \theta} \eta \cos \phi \cdot \exp(-\eta^2 \sin^2 \phi) \cdot \operatorname{erf}(\eta \cos \phi) d\phi,$$

then

$$\begin{aligned} I_{2p+1+m} &= (-1)^{m+1} \int_{\frac{\pi}{2} + \frac{m\pi}{n} - \theta}^{\frac{\pi}{2} + \frac{(m+1)\pi}{n} - \theta} \eta \cos \phi \cdot \exp(-\eta^2 \sin^2 \phi) \cdot \operatorname{erf}(\eta \cos \phi) d\phi \\ &= (-1)^{m+1} \int_{\frac{m\pi}{n} - \theta}^{\frac{(m+1)\pi}{n} - \theta} \eta \sin \phi \cdot \exp(-\eta^2 \cos^2 \phi) \cdot \operatorname{erf}(\eta \sin \phi) d\phi, \end{aligned}$$

and therefore

$$\begin{aligned} I_m + I_{2p+1+m} &= (-1)^m \int_{\frac{m\pi}{n} - \theta}^{\frac{(m+1)\pi}{n} - \theta} \left[\eta \cos \phi \cdot \exp(-\eta^2 \sin^2 \phi) \cdot \operatorname{erf}(\eta \cos \phi) \right. \\ &\quad \left. - \eta \sin \phi \cdot \exp(-\eta^2 \cos^2 \phi) \cdot \operatorname{erf}(\eta \sin \phi) \right] d\phi \\ &= (-1)^m \frac{\pi}{2} \left[\operatorname{erf}(\eta \cos \phi) \cdot \operatorname{erf}(\eta \sin \phi) \right]_{\frac{m\pi}{n} - \theta}^{\frac{(m+1)\pi}{n} - \theta}. \end{aligned}$$

Thus, finally

$$\frac{w_n}{W} = 1 + \sum_{m=0}^{2p} (-1)^m \operatorname{erf} \left(\eta \cos \left\{ \frac{m\pi}{n} - \theta \right\} \right) \cdot \operatorname{erf} \left(\eta \sin \left\{ \frac{m\pi}{n} - \theta \right\} \right). \quad (3.16)$$

The results (3.14) and (3.16) give simple expressions for w_n in terms of error functions, and deal with all cases of n with the exception of the group $n=4p$ (p an integer). In this case w_n may be computed from (3.15). The first three examples of w_n are

$$\left. \begin{aligned} w_1 &= W[1 - \operatorname{erf}(\eta \sin \theta)] \quad (\text{Rayleigh's case}), \\ w_2 &= W[1 - \operatorname{erf}(\eta \cos \theta) \cdot \operatorname{erf}(\eta \sin \theta)], \\ w_3 &= W \left[1 - \operatorname{erf}(\eta \sin \theta) - \operatorname{erf}(\eta \sin \{\pi/3 - \theta\}) \right. \\ &\quad \left. + \operatorname{erf}(\eta \sin \{2\pi/3 - \theta\}) \right] \end{aligned} \right\} \quad (3.17)$$

In all cases the velocity distribution must be symmetrical about the plane $\theta = \theta_n = \pi/2n$. Fig. 1 shows $1 - w_n/W$ plotted against $\theta_n - \theta$ for $\eta=1, 2, 3$ respectively in the cases $n=2$ and $n=3$.

4. *The Skin Friction.* Since the motion is symmetrical about $\theta = \theta_n$ it is clearly sufficient to consider the skin friction τ_n on one plate only. Selecting the plate $\theta=0$, then for $t>0$

$$\begin{aligned} \tau_n &= -\frac{\mu}{r} \cdot \frac{\partial w_n}{\partial \theta} = -\frac{\mu}{2(\nu t)^{1/2}} \cdot \frac{\partial w_n}{\partial \theta} \quad (\text{evaluated for } \theta=0) \\ &= \frac{\mu W}{4(\nu t)^{1/2}} \sum_{m=1}^{2n-1} (-1)^m \left[f\left(\eta, \frac{m\pi}{n}\right) - f\left(\eta, \left\{m+1\right\} \frac{\pi}{n}\right) \right] \\ \text{or} \quad \tau_n &= \frac{\mu W}{2(\nu t)^{1/2}} \sum_{m=1}^{2n-1} (-1)^m f\left(\eta, \frac{m\pi}{n}\right), \quad (4.1) \end{aligned}$$

(4.1) gives an expression for τ_n for all values of n , and it follows immediately that

$$\tau_n \rightarrow \tau_1 \text{ as } \eta \rightarrow \infty. \quad (4.2)$$

That is, sufficiently far from the corner, the skin friction approximates to Rayleigh's value for the flat plate problem.

For, if $m \neq 0, n$, then $\sin m\pi/n \neq 0$, and $f(\eta, m\pi/n) \rightarrow 0$ as $\eta \rightarrow \infty$

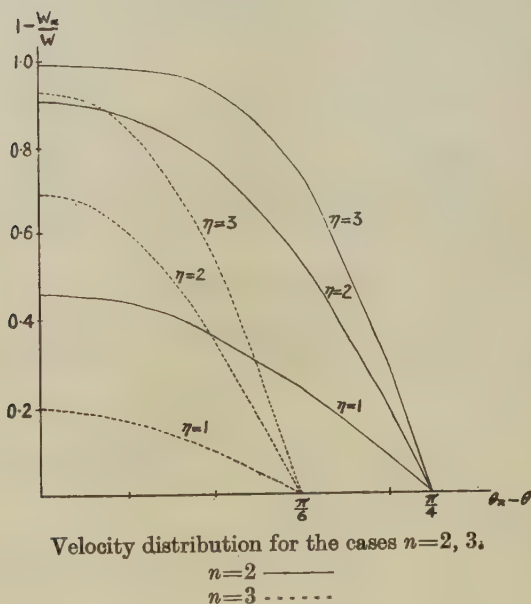
while if $m = n, f(n, m\pi/\eta) = -(1 - \operatorname{erf}(\eta)) \rightarrow 0$ as $\eta \rightarrow \infty$

and if $m = 0, f(\eta, m\pi/n) = 1 + \operatorname{erf}(\eta) \rightarrow 2$ as $\eta \rightarrow \infty$.

If $n > 1$, then $\tau_n = 0$ when $\eta = 0$, (4.3)

$$\text{since } \tau_n(0) = \frac{\mu W}{2(\pi \nu t)^{\frac{1}{2}}} \sum_{m=0}^{2n-1} (-1)^m \cos \frac{m\pi}{n} = \begin{cases} \frac{\mu W}{(\pi \nu t)^{\frac{1}{2}}} & (n=1) \\ 0 & (n>1) \end{cases}$$

Fig. 1.



Further, if $n > 1$, it follows that

$$\tau_1 - \tau_n > 0. \quad (4.4)$$

To establish this, consider the following simplified expressions for $\tau_1 - \tau_n$

(i.) $n = 2p + 1$ ($p \geq 1$)

$$\tau_1 - \tau_n = \frac{2\mu W}{(\pi \nu t)^{\frac{1}{2}}} \sum_{m=0}^p (-1)^{m+1} \cos \frac{m\pi}{n} \cdot \exp \left(-\eta^2 \sin^2 \frac{m\pi}{n} \right). \quad (4.5)$$

(ii.) $n=2p$

$$\tau_1 - \tau_n = \left\{ \begin{array}{ll} \frac{\mu W}{(\pi \nu t)^{\frac{1}{2}}} \left[1 - \operatorname{erf} \eta + 2 \sum_{m=1}^{p-1} (-1)^{m+1} \cos \frac{m\pi}{n} \right. \\ \quad \times \exp \left(-\eta^2 \sin^2 \frac{m\pi}{n} \right) \operatorname{erf} \left(\eta \cos \frac{m\pi}{n} \right) \Big] & (p > 1), \\ \frac{\mu W}{(\pi \nu t)^{\frac{1}{2}}} [1 - \operatorname{erf} \eta] & (p = 1). \end{array} \right\} \quad (4.6)$$

Now $1 - \operatorname{erf}(\eta) > 0$, and the terms in the series (4.5) and (4.6) are alternately positive and negative and decreasing, each series beginning with a positive term. This establishes (4.4).

Since $\tau_1 - \tau_n \rightarrow 0$ as $\eta \rightarrow \infty$, it is possible to determine α_n such that τ_n is within 1 per cent (say) of τ_1 when $\eta > \alpha_n$.

Using (4.5) and (4.6) the following approximate values are easily obtained

$$\alpha_2 = 1.9,$$

$$\alpha_3 = 2.5,$$

$$\alpha_4 = 3.2,$$

$$\alpha_5 = 3.8.$$

As one would expect, α_n increases with n , that is, with the sharpness of the corner.

Thus in all the cases $n > 1$, the skin friction vanishes at the corner itself, but increases away from the corner until it attains the value τ_1 ; this occurs (to within 1 per cent) when η exceeds α_n .

Frictional Force parallel to Oz. The frictional force F_n per unit length on the section $0 \leq r \leq b$ is $\int_0^b \tau_n dr$, so that

$$F_1 - F_n = \int_0^b (\tau_1 - \tau_n) dr = 2(\nu t)^{\frac{1}{2}} \int_0^{b'} (\tau_1 - \tau_n) d\eta, \quad (4.7)$$

where $b' = \frac{b}{2(\nu t)^{\frac{1}{2}}}$.

Assuming for the moment the convergence of the infinite integrals, (4.7) may be written

$$F_1 - F_n = E_n - 2(\nu t)^{\frac{1}{2}} \int_{b'}^{\infty} (\tau_1 - \tau_n) d\eta, \quad (4.8)$$

where

$$E_n = 2(\nu t)^{\frac{1}{2}} \int_0^{\infty} (\tau_1 - \tau_n) d\eta, \quad (4.9)$$

(so that $E_n > 0$ if $n > 1$).

The convergence of the infinite integrals follows from (4.5) and (4.6) since, in the first place,

$$\int_{x_1}^x (1 - \operatorname{erf} \eta) d\eta = x(1 - \operatorname{erf} x) - x_1(1 - \operatorname{erf} x_1) + \frac{1}{\pi^{\frac{1}{2}}} [\exp(-x_1^2) - \exp(-x^2)],$$

and as $x \rightarrow \infty$, $x(1 - \operatorname{erf} x) \rightarrow 0$, so that

$$\int_{x_1}^{\infty} (1 - \operatorname{erf} \eta) d\eta = \frac{1}{\pi^{\frac{1}{2}}} \exp(-x_1^2) - x_1(1 - \operatorname{erf} x_1), \quad \dots \quad (4.10)$$

while the integrals arising from the terms of the series converge, since $\sin m\pi/n \neq 0$.

Writing $E_n = \mu W \lambda_n$, F_{2n+1} and λ_{2n+1} can be found directly, and in certain special cases so can F_{2n} and λ_{2n} . From (4.1) and (4.9) it follows that λ_n is a function of n only.

The terms on the right-hand side of (4.8), and subsequent approximations to them, can be calculated by considering $Q_n(X)$, where

$$Q_n(X) = \frac{2(vt)^{\frac{1}{2}}}{\mu W} \int_X^{\infty} (\tau_1 - \tau_n) d\eta,$$

$$i. e. \quad Q_n(X) = \frac{1}{\pi^{\frac{1}{2}}} \int_X^{\infty} \left[2 + \sum_{m=0}^{2n-1} (-1)^{m+1} f\left(\eta, \frac{m\pi}{n}\right) \right] d\eta. \quad \dots \quad (4.11)$$

Thus

$$\lambda_n = Q_n(0). \quad \dots \quad (4.12)$$

$Q_n(X)$ decreases as X increases (since $\tau_1 - \tau_n > 0$), and it is clear from (4.5), (4.6) and (4.10) that $Q_n(X) \rightarrow 0$ as $X \rightarrow \infty$.

From (4.5), for $n = 2p + 1$, we have

$$Q_n(X) = 2 \sum_{m=1}^p (-1)^{m+1} \cot\left(\frac{m\pi}{n}\right) \left[1 - \operatorname{erf}\left(X \sin \frac{m\pi}{n}\right) \right], \quad \dots \quad (4.13)$$

and therefore

$$\lambda_n = 2 \sum_{m=1}^p (-1)^{m+1} \cot\left(\frac{m\pi}{n}\right). \quad \dots \quad (4.14)$$

$Q_n(X)$ can also be evaluated in the special cases $n = 2$ and $n = 4$. Using (4.6) and (4.10)

$$Q_2(X) = \frac{2}{\pi^{\frac{1}{2}}} \left[\frac{1}{\pi^{\frac{1}{2}}} \exp(-X^2) - X(1 - \operatorname{erf} X) \right] \quad \dots \quad (4.15)$$

and

$$\begin{aligned} Q_4(X) = & \frac{2}{\pi^{\frac{1}{2}}} \left[\frac{1}{\pi^{\frac{1}{2}}} \exp(-X^2) - X(1 - \operatorname{erf} X) \right] \\ & + \frac{2\sqrt{2}}{\pi^{\frac{1}{2}}} \int_X^{\infty} \exp(-\tfrac{1}{2}\eta^2) \cdot \operatorname{erf}\left(\frac{1}{\sqrt{2}}\eta\right) d\eta \\ & : \frac{2}{\pi^{\frac{1}{2}}} \left[\frac{1}{\pi^{\frac{1}{2}}} \exp(-X^2) - X(1 - \operatorname{erf} X) \right] + 1 - \operatorname{erf}^2\left(\frac{1}{\sqrt{2}}X\right), \quad \dots \quad (4.16) \end{aligned}$$

from which $\lambda_2 = 2/\pi$, $\lambda_4 = (2/\pi) + 1$.

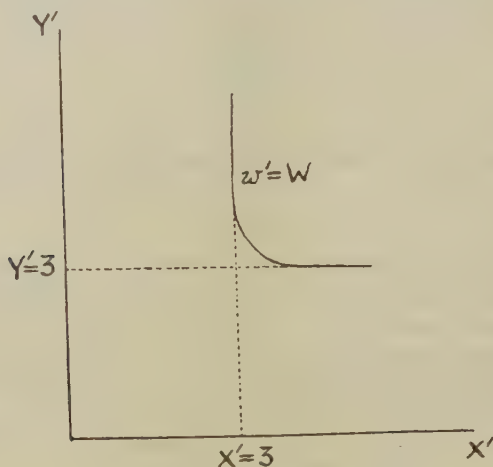
Rayleigh's hypothesis would give, for the steady flow problem, a velocity pattern of the form

$$\frac{w'}{W} = \text{erf}(X') \cdot \text{erf}(Y'), \quad \dots \quad (5.3)$$

where
$$X' = \frac{1}{2}x \left(\frac{W}{\nu z} \right)^{\frac{1}{2}}, \quad Y' = \frac{1}{2}y \left(\frac{W}{\nu z} \right)^{\frac{1}{2}}.$$

From the point of view of boundary layer theory, therefore, we should expect some thickening of the boundary layer in the vicinity of the corner, as indicated in fig. 2, while away from the corner the divergence from the flat plate flow will be negligible. Now the exact solution of the boundary layer equations for the steady flow past a flat plate (Blasius 1908)

Fig. 2.



Boundary layer in right angled corner.

shows that the mainstream velocity is attained when $Y' = 3$, and not $Y' = 2$ as indicated by Rayleigh's hypothesis. Accordingly, in this problem, it is probable that the influence of the corner on the boundary layer is effectively confined to the region $0 \leq X' \leq 3$, $0 \leq Y' \leq 3$. Failing an analytical solution of this problem, a numerical approach would require an assumption such as this. Carrier, in his solution (Carrier 1946) makes this assumption, though Howarth has pointed out that certain of the equations of motion have been disregarded, and the solution is therefore open to objection.

Referring back to the unsteady problem, we have for the frictional force F per unit length of a section of width b the approximate result (using 4.18))

$$F = \mu W \left[\frac{b}{(\pi \nu t)^{\frac{1}{2}}} - \frac{2}{\pi} \right], \quad \dots \quad (5.4)$$

provided $b/2(vt)^{\frac{1}{2}} > 1.6$. From this we can deduce an approximation to the frictional force when a rectangular channel of sides a and b is set in motion in the same way as the original boundary. Bearing in mind the requirements of the velocity distribution (5.2) then, provided

$$a, b > 8(vt)^{\frac{1}{2}}, \quad (5.5)$$

the frictional force per unit length on the channel would be given by

$$F = 2\mu W \left[\frac{a+b}{(\pi vt)^{\frac{1}{2}}} - \frac{8}{\pi} \right], \quad (5.6)$$

taking into account all four interior faces of the channel.

If we now extend this result, by Rayleigh's hypothesis, to the problem of steady flow through the interior of a rectangular channel of finite length l , then if

$$a, b > 8 \left(\frac{\nu l}{W} \right)^{\frac{1}{2}}, \quad (5.7)$$

the force per unit length at distance z would be

$$2\mu W \left[(a+b) \left(\frac{W}{\pi \nu z} \right)^{\frac{1}{2}} - \frac{8}{\pi} \right], \quad (5.8)$$

and the skin friction coefficient C_f for the interior of the channel would be given by

$$\begin{aligned} C_f &= \frac{1}{\rho W^2 l (a+b)} \int_0^l 2\mu W \left[(a+b) \left(\frac{W}{\pi \nu z} \right)^{\frac{1}{2}} - \frac{8}{\pi} \right] dz \\ &= 4 \left(\frac{\nu}{\pi W l} \right)^{\frac{1}{2}} \left[1 - \frac{4l}{a+b} \left(\frac{\nu}{\pi W l} \right)^{\frac{1}{2}} \right]. \quad (5.9) \end{aligned}$$

The result (5.9) would be of greater interest if corresponding results were available for the flow on the outside of the channel. That is, it would be useful to extend the investigation to wedge-shaped channels of any angle β . For this, a solution of (2.1) as a Fourier series in θ would be available, but it should also prove fruitful to investigate a solution of period 2β in θ given by Carslaw (1910) for use as a suitable Green's function. In this latter case it may not be possible to reduce the expression for w to single integrals, but nevertheless the method may yield an expression for τ in terms of an integral, and this would be more useful than the infinite series in any discussion of the limiting value of τ remote from the corner.

I should like to thank Professor Howarth and Mr. K. Stewartson of Bristol University for their kind assistance to me in the preparation of this paper.

REFERENCES.

- BLASIUS, H., 1908, *Zeitschr. für Mathematik und Physik*, Bd. 56, p. 1—.
 CARRIER, G. F., 1946, *American Quarterly of Applied Maths.* (Brown University).
 4, 367–370.
 CARSLAW, H. S., 1910, *Proc. Lond. Math. Soc.*, [2] 8, 365–374.
 CARSLAW, H. S., and JAEGER, J. C., 1947, *Conduction of heat in solids* (Chap. XIII).
 (Oxford University Press).
 HOWARTH, L., 1950, *Proc. Camb. Phil. Soc.*, 46, pt. 1, 127–140.
 RAYLEIGH, LORD., 1911, *Phil. Mag.*, [6] 21, 697–711.

XVII. *Emission of Energetic Helium and Lithium Fragments in Nuclear Explosions.*

By S. O. C. SÖRENSEN*.

The H.H. Wills Physical Laboratory, University of Bristol †.

[Plates VII. & VIII.]

SUMMARY.

A phenomenological description is given of the processes which lead to the emission of energetic heavy particles from cosmic ray stars. The frequency, angular distributions and energy spectra of the particles have been determined. These, and an analysis of the associated stars, indicate that the particles cannot be generated by an evaporation process. On the other hand, direct knocking on of the heavy particle by the primary can be excluded. The fragments must therefore result from interactions which are intermediate between these two extreme possibilities. No connection has been found between the ejection of energetic heavy particles and meson showers.

INTRODUCTION.

As a result of experiments with photographic plates exposed to cosmic radiation, several reports have been given within the last few years of observations on energetic heavy nuclear "fragments" ejected during the explosive disintegration of nuclei. A striking feature of these phenomena is that the heavy particles are frequently emitted with energies much greater than that which can be accounted for in terms of the electrostatic repulsion of the residual nucleus. The problem therefore arises as to the physical mechanism through which it is possible to endow these particles with kinetic energies greatly in excess of their binding energy without disrupting them in the process. The emission of the particles is rare, and it appears likely that an extensive investigation will be necessary to explain their production in detail. It therefore appears appropriate to give a preliminary report on the material already available. As the expulsion of heavy charged particles presents similar problems to that of the ejection of α -particles, which occur much more frequently, a closer study of the latter has also been included in this investigation.

The plates used in the investigation were coated with Ilford G5 emulsion, 400 μ thick, and were exposed by means of free balloons at geomagnetic latitude 54° N. In order to have well-defined conditions for the experiment only material exposed at approximately the same altitude has been employed. This was obtained in two level flights of which details are given in Table I.

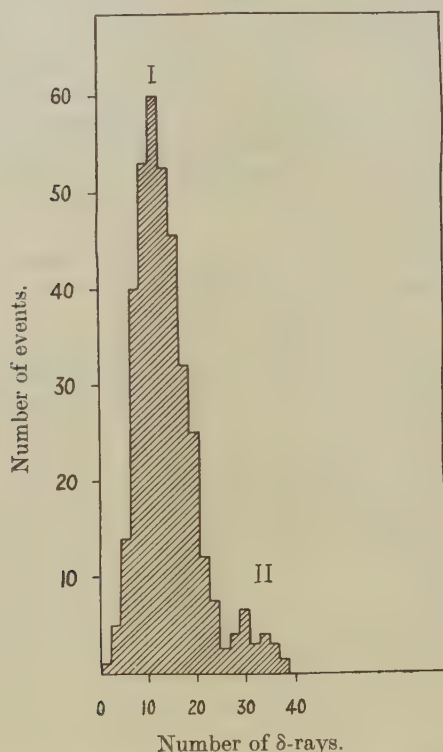
* Communicated by Professor C. F. Powell, F.R.S.

† On leave from the Physical Institute, University of Oslo.

It is reasonable to assume that the given ratio represents an upper limit only, since some helium tracks of unusually low δ -ray density may have been missed in scanning the plates. This "loss" may account for the slight asymmetry in the distribution I.

That the great majority of the particles are stable or long-lived isotopes of the corresponding elements is proved by the fact that no secondary particles, such as electrons, are observed to be emitted at the point where the particles come to rest. None of the lithium fragments showed the characteristic "hammer" tracks due to Li^8 .

Fig. 1.



Histogram showing the distribution of the total number of δ -rays (≥ 3 grains) in the last 700μ of the track of the fragment.

In neither of the two flights have any long tracks of heavier particles been found although a great number of heavier "low energy fragments" and "taper tracks" have been observed with a range less than 700μ .

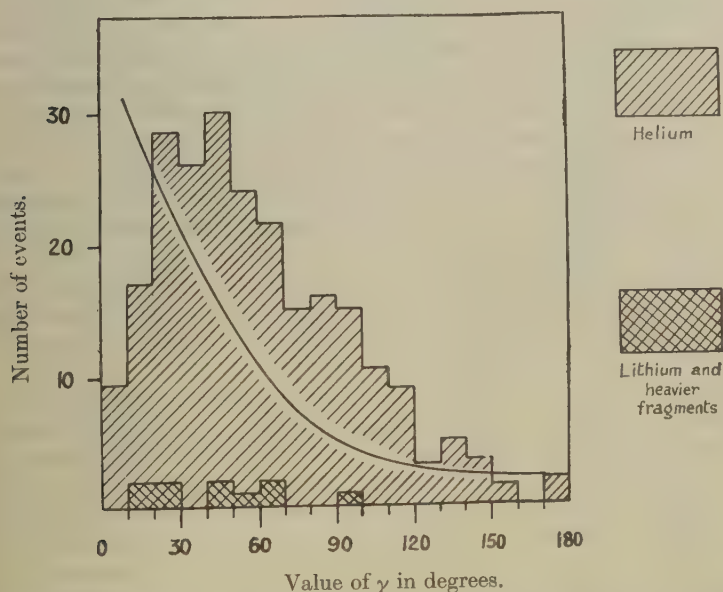
ANGULAR DISTRIBUTIONS.

In those cases in which the heavy particle has been emitted from a nuclear explosion of which the incident particle can be distinguished, the angle, γ , between its track and the line of motion of the "primary"

particle has been determined. It has been assumed as a sufficient criterion that a track is that of a particle producing a particular nuclear explosion if its specific ionization is near the minimum value for charge $|e|$; and if it is the only such track in the "upper hemisphere" of the star. Camerini *et al.* (1949) have shown that the great majority of tracks so defined are due to particles which approached the nucleus and caused its disintegration.

Histograms showing the distribution of the observed values of γ , for helium particles and heavier fragments respectively, are shown in fig. 2. The curve gives the angular distribution of the particles with charge $2e$ in number per unit solid angle. In making these observations the spatial

Fig. 2.



Histogram showing the distribution of the angle between the direction of motion of the primary and the heavy particle. The full curve shows the results transformed to correspond to the intensity per unit solid angle.

orientation of each track, taking into account the angle of dip in the emulsion has been determined. It will be seen that the difference in direction is usually less than 90° , but that much larger values are sometimes found.

The number of heavier fragments is very small, but it appears that there is a collimation in the direction of the primary, a result in agreement with the observations made by Perkins on energetic heavy fragments.

With the criterion for the definition of a primary particle employed above, "stars" produced by particles with charge $2e$ are automatically eliminated. A large fraction of the "stars" from which heavy fragments

are emitted (~ 20 per cent) are produced however, by fast α -particles at the altitude of the exposure and a special investigation of the angular distributions in these cases would be of interest. The difficulty in identifying the α -particle primaries except in those favourable cases in which the tracks are longer than 3 mm., has made the available material too small to allow any significant conclusions to be drawn.

THE DISTRIBUTION IN ENERGY OF THE HELIUM PARTICLES.

A number of recent papers have dealt with the energy spectrum of the various charged particles emitted in the disintegration of nuclei with very high excitation energy (Harding *et al.* 1949, Perkins 1950 b, Page 1950). The main purpose of these investigations has been to check the "evaporation theory" of highly excited nuclei (Weisskopf 1937, Bagge 1944, Le Couteur 1950) and satisfactory agreement has been obtained between theory and experiment. The particles considered in these investigations have energies up to ~ 50 MeV., but all the authors report the existence of a high energy "tail" due to processes which are probably totally different from that of evaporation. The new method of combining "multiple scattering" and "grain density" (Fowler 1950) has made it possible to investigate this high energy "tail", and energy spectra of the ejected mesons, protons, and deuterons have been determined (Camerini *et al.* 1950). It is reasonable to assume that most of the particles considered in the present investigation are the corresponding particles with charge $\geq 2e$, and it is of interest to compare the spectra for the different groups of particles.

Owing to the high grain-density in the tracks of non-relativistic particles, with charge $\geq 2e$ in the new electronsensitive plates, the energy cannot be measured by grain counting. One way of overcoming this difficulty is to measure the ranges of the particles and to extrapolate range-energy relations, a method which is necessarily confined to particles arrested in the emulsion. However, an ambiguity exists in the application of range-energy curves, for the particles of charge $2e$ and $3e$ because of the presence of different isotopes. It has been shown, for example, by applying scattering methods to the longest tracks in the group, that both isotopes He^3 , He^4 contribute to the main group I. of fig. 1. It has not yet been possible, however, to determine the ratio of the two types.

Assuming all the particles in fig. 1 with less than 25 δ -rays in the last 700μ of the track to be α -particles, and applying geometrical corrections for loss, we obtain the differential spectrum, fig. 3, which shows the kinetic energy, E , of the helium nuclei at their points of creation. Isotropic angular distribution with respect to the vertical was assumed.

The longest observed track of a particle with charge $2e$, ending in emulsion, has a range ~ 1 cm., a value which corresponds to an α -particle with an energy of about ~ 200 MeV. No helium particles with relativistic energies have been observed ejected from stars as secondaries,

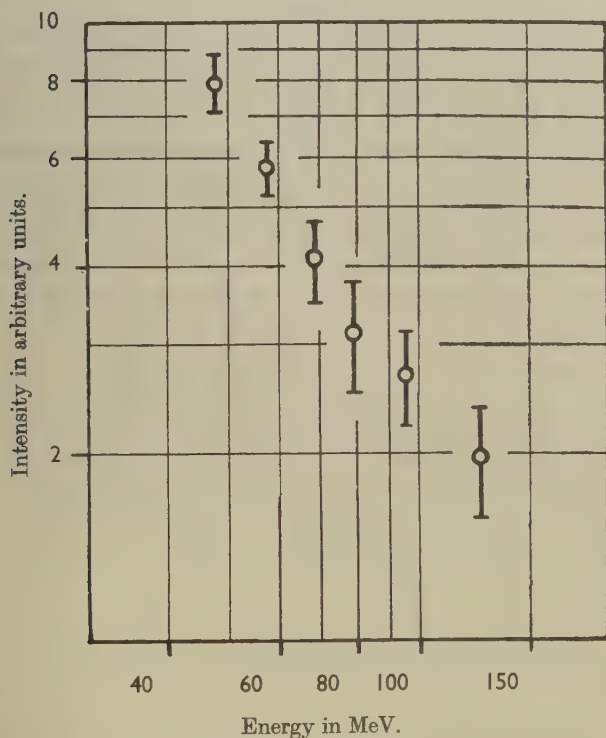
except in the nuclear collisions produced by heavy primaries in which they occur as fragments in the "break-up" of heavier nuclei. (Bradt and Peters 1950, Dainton and Kent 1950).

A comparison of the energy spectrum in fig. 3 with the corresponding results for protons, and deuterons and tritons as determined by the scattering method, suggests that they are rather similar in form. The spectrum may be approximately represented by a power law of the form

$$N(E) dE = \frac{\text{const}}{E^K} dE \quad (2),$$

where K is of the order of 1.6.

Fig. 3.



Differential distribution in the kinetic energy of α -particles ejected from stars..

The lithium fragments are too few to deduce the form of their energy spectrum, but all the fragments which have been found to end in the emulsion have a range less than 1600μ . This value corresponds to an energy of 145 MeV. for Li_7^+ .

CHARACTERISTICS OF THE "STARS" ASSOCIATED WITH THE EMISSION OF HEAVY "FRAGMENTS".

As a second mode of attack on the problem, a statistical analysis of the disintegrations from which heavy particles are emitted has been made, and a determination of their frequency of occurrence. Out of a total number of 15,000 stars in the HA. 21 plates, 189 stars of 3 or more prongs have been found from which emerge particles with charge $\geq 2e$, and of range $> 700 \mu$. The total number of stars giving rise to the events described in the present paper is 400. In this analysis we have included stars leading to ejection of heavy particles, which although leaving the emulsion before being brought to rest, have such a track-length and δ -ray density as to indicate that their total range in the emulsion would be greater than 700μ . Stars caused by heavy primaries have been excluded, since the mechanism of disintegration in these cases may be different. Stars of the latter type commonly show a marked asymmetry due to collimation of the secondary fragments with regard to the line of motion of the primary. Pl. VII. shows a photomicrograph of an example of this type, in which a heavy primary with charge $Z=12 \pm 1e$ collides with a nucleus of silver or bromine in the emulsion and produces an energetic disintegration with 38 heavily ionizing secondary particles. Several examples of this type of event have been found in the two flights. The most striking feature of the event shown in Pl. VII. is the expulsion of a very heavy non-relativistic fragment of range 550μ . A comparison of this track with others due to particles which have been identified indicates that its charge was $Z=5 \pm 1e$.

(a) The distribution in N_h .

Using the terminology introduced by Brown *et al.* (1949), we may divide the tracks of particles emitted from stars into three groups according to their grain density g , as compared with g_{\min} the grain density of a relativistic particle of charge $|e|$:

- (1) "Thin" tracks $g_{\min} \leq g < 1.4g_{\min}$ (shower particles).
- (2) "Grey" tracks $1.4g_{\min} < g < 5g_{\min}$.
- (3) "Black" tracks $g > 5g_{\min}$.

The sum of the "grey" and "black" tracks from a star is represented by the symbol N_h , and the number of shower particles by n_s .

Fig. 4 gives the distribution in N_h for all the stars which emit energetic helium particles: the observations have been confined to stars with $n_s \geq 1$ or with a singly charged relativistic primary. The corresponding values of the total release of energy are indicated in the figure.

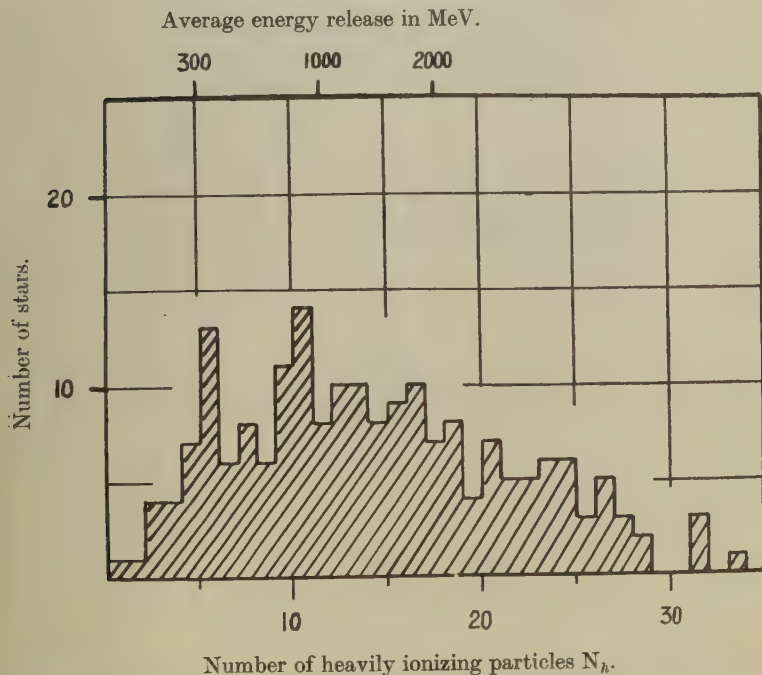
The distribution is seen to extend up to $N_h \sim 35$, with a broad maximum for $N_h \sim 11-17$.

The probability, P , that a star with a given N_h has an associated energetic helium particle is given by a comparison of the distribution shown in fig. 4 with the curve showing the frequency of occurrence of all

stars of this class. This is known for the HA. 21 plates (Table I.), and fig. 5 gives the result plotted in logarithmic scale. The figure shows that there is an extremely rapid rise in the probability of emission of energetic heavy particles with increase in N_h . If, for a given N_h , the number of stars which emit energetic helium particles is represented by N_{He} , and the total number of stars by N_{total} , the results of fig. 5 may be represented approximately by the relation

$$P = \frac{N_{He}}{N_{total}} = \text{const. } e^{2N_h} \quad (3)$$

Fig. 4.



Histogram showing the distribution in N_h of stars emitting a single energetic helium particle.

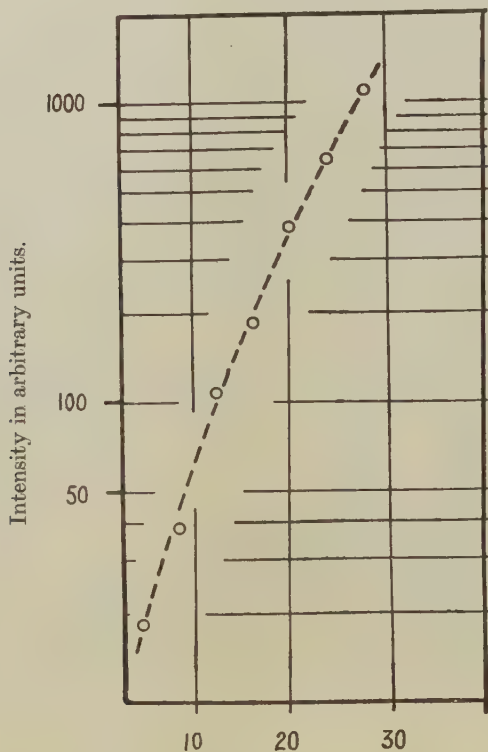
The size distributions of stars emitting energetic helium particles or heavier nuclei is given in fig. 6.

Fig. 6 *b* shows the distribution in N_h of all the stars which simultaneously emit two or more fast heavy particles ($R > 700 \mu$) *e. g.* two α -particles, or one α -particle and a lithium fragment. The displacement of the whole distribution towards higher N_h is immediately apparent. No star of this type has been observed in the lighter elements (C, N, O) in the

emulsion. Pl. VIII. shows a photomicrograph of a star in which a helium particle and a lithium fragment are ejected, simultaneously with range respectively $1200\ \mu$ and $1000\ \mu$.

In order to see if the distribution in N_h varies appreciably when particles of different energy are considered, the observations on particles with charge $2e$ were divided into two groups according to whether the range

Fig. 5.



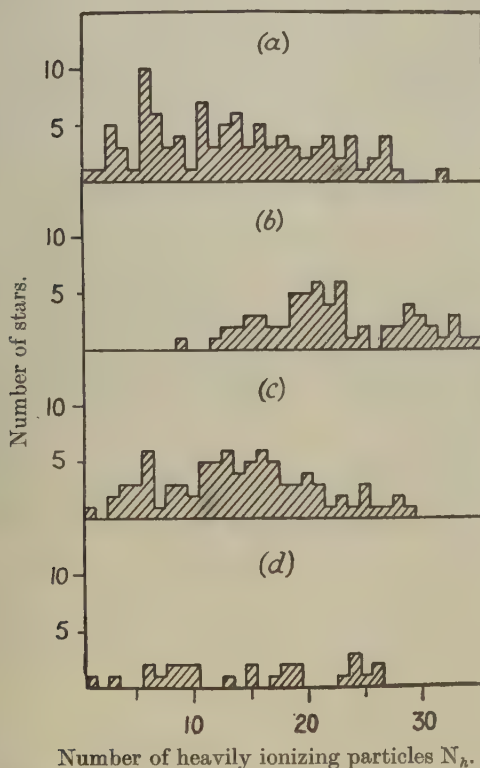
Number of heavily ionizing particles N_h .

The probability of the ejection of an energetic helium particle as a function of N_h .

of the particle was in the interval from $700\ \mu$ to $1500\ \mu$ or greater than $1500\ \mu$. The corresponding values of the kinetic energy for α -particles are $45\text{ MeV.} < E < 70\text{ MeV.}$ and $E > 70\text{ MeV.}$ respectively. The resulting distributions in N_h for the associated stars are shown in fig. 6 *a* and *c*. It is found that, within the statistical fluctuations, the two distributions are similar in form. It appears therefore that no very strong correlation exists between the particular energy with which a helium particle is

emitted and the energy release in the associated star. In this connection, it may be remarked that the longest α -particle observed (~ 1 cm.) was emitted from a star with N_h only 4. Further, a number of heavy particles have been found with energies up to ~ 140 MeV. which are not associated with any other heavily ionizing particles—a point which will be discussed later.

Fig. 6.



Histograms showing the distribution in N_h of stars emitting :—

- (a) A single helium particle with range between 700μ and 1500μ .
- (b) Simultaneously two heavy particles.
- (c) A single helium particle with range greater than 1500μ .
- (d) Energetic fragments with charge $Z \geq 3$.

The distribution in N_h of stars which emit energetic heavy fragments with charge $> 2e$ is shown in fig. 6 d. We have here included a few stars which emit particles heavier than lithium fragments and which are found in other exposures.

(b) *Heavy particles and shower production.*

Heisenberg (1949) suggests that a state analogous to "turbulence" exists as a result of creation of mesons during the impact of a particle on a nucleus. This would result in an increase of the "viscosity" of nuclear matter by which a higher probability should exist for dragging out "lumps" of nucleons from the parent nucleus.

In order to determine if there is any correlation between the production of energetic heavy particles and meson showers, the stars have been divided into different groups according to the values of N_h and number of shower particles n_s . For each group the ratio between the number of stars with energetic helium particles N_{He} and the total number of stars in the HA. 21 plates N_{total} has been computed. The result is shown in Table II. (The absolute values in the Table are in arbitrary units.)

TABLE II.

The ratio $\frac{N_{He}}{N_{total}}$.

$\begin{matrix} N_h \\ n_s \end{matrix}$	3-9	10-16	17-23	≥ 24
1	1.2 ± 0.8	5.8 ± 3.6	21 ± 4	30 ± 11
2-3	0.8 ± 0.3	4.4 ± 1.1	21 ± 5	50 ± 17
≥ 4	1.2 ± 0.7	4.6 ± 1.7	11 ± 3	42 ± 12

There is thus no significant difference in the ratios for groups of stars with the same N_h and various number of shower particles which indicates that no very strong connection exists between the ejection of energetic heavy particles and meson showers. The majority of heavy particles considered are helium nuclei, but the same conclusions appear to be valid for heavier fragments, in accordance with previous results (Perkins 1950 a).

(c) *Single energetic helium particles.*

A striking feature of the present investigation is the observation of single energetic helium particles, starting and ending in the emulsion without any associated star. One example has been found with a range of 2200μ corresponding to an energy ~ 85 MeV., and four with ranges $\sim 1500 \mu$ corresponding to energies ~ 70 MeV. Further single heavy tracks are observed to start in the emulsion and pass out of the surfaces.

Two-prong stars have been observed consisting of an energetic helium particle and a short track representing the recoil nucleus of range $\sim 5-10 \mu$, or with a "thin" track due to a singly charged particle with ionization near the minimum value. The latter is presumably the primary, and in most cases makes a very small angle with the direction of the heavy particle.

The single tracks may be either true one-prong stars, or stars in which the remaining particles emitted are neutrons.

Note added in proof.—Recently a two prong star has been found consisting of a “grey” track and the track of a helium particle of range $12,370 \mu$; this corresponds to an α -particle energy of 236 MeV. The grain density and scattering of the “grey” track is consistent with that of a relativistic α -particle, presumably the primary. The angle between the direction of motion of the two particles is 16° .

DISCUSSION.

Firstly it seems safe to exclude any explanation of the heavy fragments based on the nuclear evaporation processes. We are here observing particles of kinetic energy far in excess of that due to electrostatic repulsion. Further, the angular distributions suggest a process, quite different from that of evaporation, where the particles are emitted almost isotropically with respect to the primary.

At first sight the phenomena are very suggestive of a direct “knocking on” effect of the heavy particle by the primary or by one of the nucleons itself recoiling from the primary. Thus the fragment would leave the nucleus before energy had been statistically shared among the nucleons, that is in a time very short compared with the “cooling down” time.

We select out of the present material all the stars with one or more shower particles. In general primary particles in these stars will have energies E_p in excess of 1000 MeV. Fig. 7 shows a plot of the kinetic energy E_α of the helium nuclei against γ , the angle which they make with respect to the primary. The curves A and B represent the function

$$E_\alpha = \frac{4m_p m_\alpha}{(m_p + m_\alpha)^2} \cdot E_p \cos^2 \gamma \quad . \quad . \quad . \quad . \quad . \quad (4)$$

calculated from the conservation laws for a free non-relativistic collision between the two particles where m_α is the mass of an α -particle and m_p that of a proton. The curves A and B refer to $E_p = 200$ MeV. and 500 MeV. respectively. It is clear that the vast majority of the α -particles cannot have been ejected as a result of a direct collision with the primary, even supposing that both the α -particles and the primary have suffered some energy loss in their passage through the nucleus. Thus we conclude that most of the helium fragments have been ejected by encounters with secondary nucleons. This conclusion is supported by the observation of α -particles at angles greater than 90° to the primary, which must necessarily result from secondary effects.

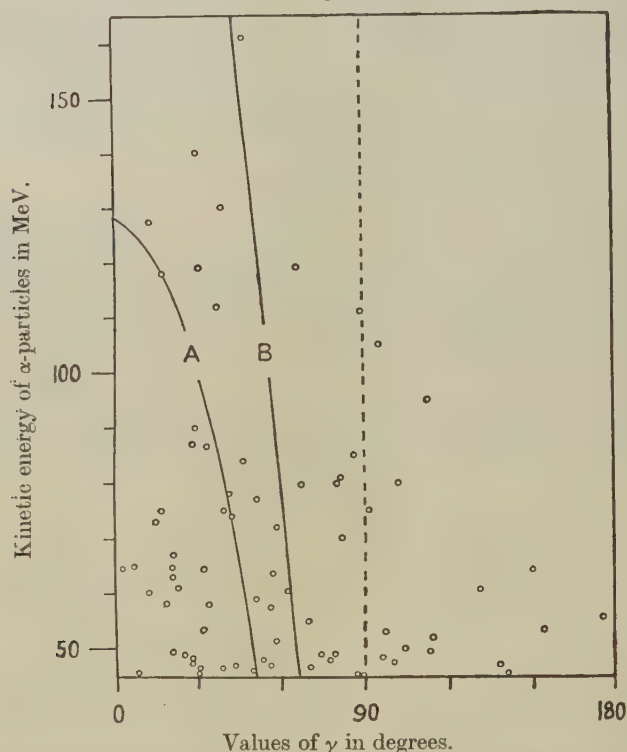
A similar analysis applied to the lithium fragments gives the same result.

The energy which an energetic secondary can transfer to the fragment would depend mainly on the relative impact parameter for the collision. This is in agreement with the absence of correlation between the energy of the heavy particle and the size of the associated star.

The close correspondence between the energy spectra for helium particles, protons and deuterons might imply a similarity in their respective ejection mechanisms. The process by which one nucleon can eject an energetic aggregate of nucleons from the parent nucleus remains to be explained. This phenomenon could perhaps be interpreted in terms of long range nuclear forces.

A point worth mentioning concerns the masses of the heavy particles in the present investigation. It may well be that a large proportion of the helium particles are of mass 3, since a surprisingly large number of

Fig. 7.



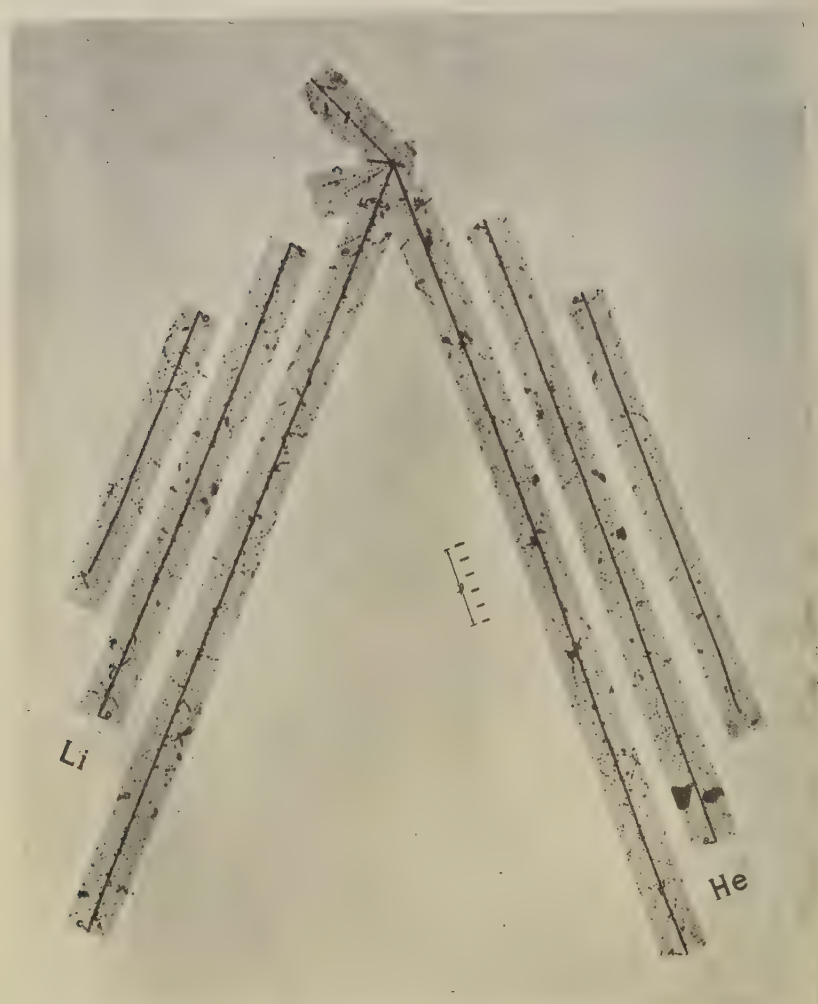
A plot of the kinetic energy against angle with primary of α -particles from stars with $n_s \geq 1$. (For explanation of curves, see text).

energetic tritons are observed to be ejected from stars (Camerini and Fowler, private communication). Measurements are now being made to determine the He^3/He^4 -ratio by the scattering method.

The present observations imply the existence of aggregates of nucleons as temporary sub-units of the nucleus. More detailed investigations may possibly throw light on the much discussed problem of the α -particle clustering in nuclei (von Weizsäcker 1938, Wergeland 1941, Wheeler 1941).



A nucleus of Magnesium ($Z=12\pm1$) strikes a silver or bromine nucleus in the emulsion. From the disintegration emerges a slow particle of charge $Z=5\pm1$.



Simultaneous ejection of an energetic helium particle and a lithium fragment from a nuclear explosion.

ACKNOWLEDGMENTS.

I should like to express my gratitude to Professor C. F. Powell, F.R.S., for offering the facilities to carry out this work, and for his continued interest and help; and I take this opportunity of thanking the research workers of this laboratory, in particular Dr. D. H. Perkins, for many discussions and suggestions. A few plates used in the present investigation were supplied by Fysisk Institutt A, University of Oslo for which I wish to thank Professor J. Holtsmark. I am indebted to the Royal Norwegian Industry Department and Norges Teknisk Naturvitenskapelige Forskningsraad for a scholarship for studying nuclear physics in England.

REFERENCES.

- BAGGE, 1944, *Phys. Z.*, **39**, 461.
BRADT and PETERS, 1950, *Phys. Rev.*, **77**, 54.
BROWN, CAMERINI, FOWLER, HETTLER, KING and POWELL, 1949, *Phil. Mag.*, [7], **40**, 862.
CAMERINI, COOR, DAVIES, FOWLER, LOCK, MUIRHEAD and TOBIN, 1949, *Phil. Mag.*, [7], **40**, 1073.
CAMERINI, FOWLER, LOCK and MUIRHEAD, 1950, *Phil. Mag.*, [7], **41**, 413.
DAINTON and KENT, 1950, *Phil. Mag.*, [7], **41**, 963.
FOWLER, 1950, *Phil. Mag.*, [7], **41**, 963.
FRANZINETTI and PAYNE, 1948, *Nature, Lond.*, **161**, 735.
HARDING, LATTIMORE and PERKINS, 1949, *Proc. Roy. Soc. A*, **196**, 325.
HEISENBERG, 1949, *Z. Phys.*, **126**, 569.
LE COUTEUR, 1950, *Proc. Phys. Soc. A*, **63**, 259.
PAGE, 1950, *Proc. Phys. Soc. A*, **63**, 250.
PERKINS, 1950 a, *Proc. Roy. Soc. A*, **203**, 399; 1950 b, *Phil. Mag.* [7], **41**, 138.
SÖRENSEN, 1949, *Phil. Mag.* [7], **40**, 947.
VON WEIZÄCKER, 1938, *Naturwiss.*, **26**, 209, 225.
WERGELAND, 1941, *Norske Vidensk. Selsk. Skrifter*, No. 1.
WEISSKOPF, 1937, *Phys. Rev.*, **52**, 295.
WHEELER, 1941, *Phys. Rev.*, **59**, 27.

XVIII. A Note on Hildebrand's Approximation for Thermal Pressures in Solids.

By KUN HUANG,

Department of Theoretical Physics, University of Liverpool*.

[Received November 28, 1950.]

ABSTRACT.

The validity of a widely used approximation for thermal pressures due originally to Hildebrand is discussed. The distinction between the "vibrational" pressure and the thermal pressure is stressed; Hildebrand's expression is shown to lie intermediate between the two for all temperatures. Since the percentage difference between the two pressures diminishes monotonically with increasing temperature, the accuracy of the approximate expression improves with increasing temperature. But at temperatures comparable with the Debye temperature, Hildebrand's expression is much closer to the vibrational (10 per cent error) than the thermal pressure (40 per cent error). It follows further from the discussion that the linearly extrapolated volume from any temperature to the absolute zero lies intermediate between the real volume at absolute zero of temperature and the volume corresponding to *static* equilibrium.

It is the purpose of the present note to discuss the validity of an approximation, which was first introduced by Hildebrand (1931) and has since been widely used in connection with the accurate calculations of cohesive energies and interatomic forces of solids (Born and Mayer 1932, Mayer and Helmholtz 1932, Huggins and Mayer 1933, Fowler 1936, Huggins 1937, 1947). It is based on the assumption that the energy of a solid can be approximately considered as consisting of a purely volume-dependent and a purely temperature-dependent part. Hildebrand's procedure is the following: Let us write the internal energy of a solid as

$$E = U + E_{\text{vib}}, \quad \dots \dots \dots (1)$$

where E_{vib} and U refer respectively to the vibrational energy and the remaining, purely volume-dependent static energy. It is assumed that one can approximately write

$$\frac{dU}{dV} \cong \left(\frac{\partial E}{\partial V} \right)_T = \left(\frac{\partial F}{\partial V} \right)_T + T \left(\frac{\partial S}{\partial V} \right)_T \quad \dots \dots \dots (2)$$

F , S being respectively the Helmholtz free energy and the entropy; or, since for normal pressures one can put $p = -(\partial F / \partial V)_T = 0$,

$$\frac{dU}{dV} \cong T \left(\frac{\partial S}{\partial V} \right)_T \quad \dots \dots \dots (3)$$

$T(\partial S / \partial V)_T$ is thus used approximately as the "thermal pressure".

* Communicated by Professor H. Fröhlich.

Despite the wide usage of the approximation, no pertinent discussions of its validity have, however, been offered. Hildebrand (1931) has attempted a partial justification empirically, by trying to show that alternative determinations of the interatomic forces using the above relation at different temperatures, yield the same result; the results thus obtained in fact show a distinct drift with the corresponding temperatures used. Sometimes it has been implied that (3) is valid owing to the small magnitude of the vibrational energy E_{vib} . This has led to the suggestion that (3) is a good approximation at not too high temperatures (Fowler 1936); the reverse is in fact the case (see below).

The Mie-Grüneisen equation (Grüneisen 1926):

$$p + \frac{dU}{dV} = \frac{\gamma E_{\text{vib}}}{V} \quad . \quad . \quad . \quad . \quad . \quad . \quad (4)$$

which may, for instance, be deduced by following either the Einstein or Debye treatment of vibrations, is ideally suited to a discussion of the above approximation. Differentiating (4) with respect to T , we obtain

$$\left(\frac{\partial p}{\partial T}\right)_V = \frac{\gamma C_v}{V} \quad . \quad . \quad . \quad . \quad . \quad . \quad (5)$$

Moreover, for normal pressures, we can put $p=0$ in (4):

$$\frac{dU}{dV} = \frac{\gamma E_{\text{vib}}}{V} \quad . \quad . \quad . \quad . \quad . \quad . \quad (6)$$

Remembering that

$$\left(\frac{\partial S}{\partial V}\right)_T = \left(\frac{\partial p}{\partial T}\right)_V$$

and comparing (3) and (5), we see that the Hildebrand approximation for the thermal pressure is given by $\gamma TC_V/V$, whereas it follows from (6) that $\gamma E_{\text{vib}}/V$ represents the true value; the ratio of the approximate to the true value is thus

$$R = \frac{TC_V}{E_{\text{vib}}} \quad . \quad . \quad . \quad . \quad . \quad . \quad (7)$$

which, we remark, is equal to unity only for temperatures high enough for the classical energy partition law to hold.

One notes that, owing to the fact that the energy of zero-point vibrations depends only on the volume, the "thermal pressure" can in fact be defined in two different senses:

(i.) One can include the zero-point energy as part of U . All the above formulæ remain correct as they stand, if E_{vib} refers only to the thermal vibrations. The thermal pressure defined in this way vanishes at $T=0^\circ \text{K.}$ (see (6)).

(ii.) Alternatively, one may, as we have already assumed above, take U as the purely static energy. Then the zero-point energy has to be included in E_{vib} . It follows that E_{vib} approaches a finite value for $T=0^\circ\text{K}$. in this case, and the corresponding "thermal pressure" does not vanish; we shall thus refer to it as the *vibrational pressure*.

Hildebrand's approximation is ambiguous on this point, i. e. whether $T(\partial S/\partial V)_T$ should refer to the thermal or vibrational pressure; it is probably understood differently by different authors using it. To be consistent with the idea of dividing the energy into a volume-dependent and temperature-dependent part it would indeed appear the more appropriate to identify Hildebrand's expression $T(\partial S/\partial V)_T$ with the *thermal* pressure rather than the *vibrational* pressure. For one would attempt to include all the purely volume-dependent terms in U , hence also the zero-point energy; moreover, as the approximate expression $T(\partial S/\partial V)_T$ vanishes at $T=0^\circ\text{K}$., it points once more to (i.) as the more fitting interpretation.

Using the Debye theory, one finds that the ratio ρ defined in (7) is only a function of T/Θ (Θ the Debye temperature), whether E_{vib} refers to the total vibrational energy or only the thermal part. The curves ρ versus T/Θ for both of these alternatives are given in the adjoining figure. Curve (i.) corresponds to the case that E_{vib} refers only to the thermal vibrations, and curve (ii.) refers to the alternative case, where E_{vib} is the total vibrational energy. If we interpret Hildebrand's expression as referring to the thermal pressure (see (i.)), curve (i.) gives the ratio of the approximate to the true value; if, on the other hand, we interpret Hildebrand's expression as referring to the vibrational pressure (see (ii.)), then curve (ii.) represents the proper ratio. Both curves are seen to approach the line of unity towards high temperatures; however, for the temperature range of practical interest, the Hildebrand's expression is much more accurate, if interpreted as the vibrational pressure (curve (ii.)) rather than the purely thermal pressure (curve (i.)). *This is exactly the reverse of the more naive anticipation explained earlier.* For all the alkali-halides except LiF and NaF, Hildebrand's expression used at room-temperatures will be within 10 per cent of the actual vibrational pressure.

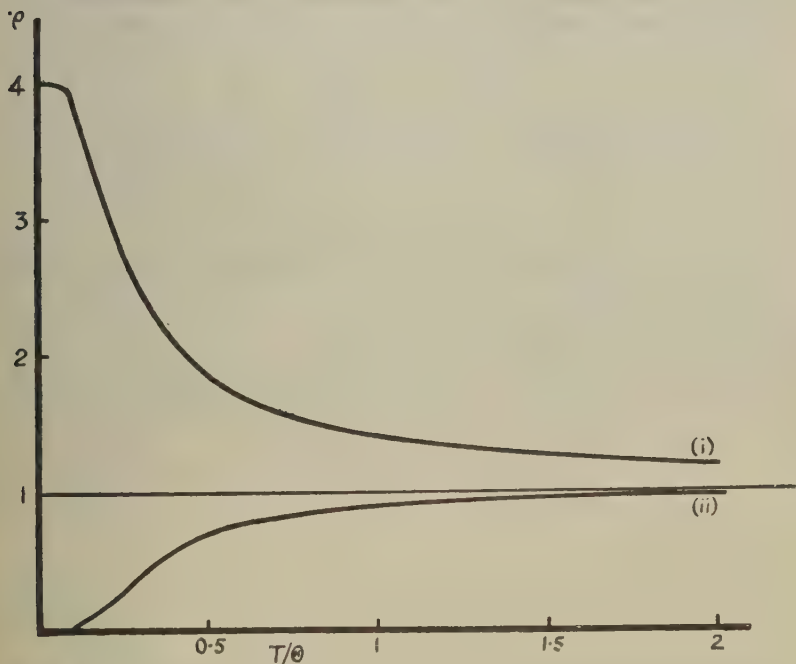
An interesting conclusion can be drawn from considering the equilibrium V_0 defined by the equation

$$\left(\frac{dU}{dV}\right)_{V_0} = 0 \quad . \quad . \quad . \quad . \quad . \quad . \quad (8)$$

with the approximate equation (3). By expanding dU/dV in (3) with respect to $V-V_0$ about the above equilibrium position and neglecting second and higher order terms, we find readily that

$$V_0 \approx V - \frac{T(\partial S/\partial V)_T}{(d^2U/dV^2)_0} \quad . \quad . \quad . \quad . \quad . \quad . \quad (9)$$

The interpretation of V_0 from the point of view of this approximation is as ambiguous as the interpretation of Hildebrand's expression itself: if the latter is taken as the thermal pressure (i.), then U should include the zero point energy and the corresponding V_0 is the volume of the solid at $T=0^\circ \text{K}$; but if it is taken as the vibrational pressure (ii.), U is the static energy and V_0 is the static equilibrium volume corresponding to the hypothetical case that the atoms were at rest. The fact that the curves (i.) and (ii.) lie respectively above and below the line of unity shows that Hildebrand's expression has a value intermediate between the true thermal pressure and the true vibrational pressure, whatever the temperature. It follows, as a moment's consideration will show, that



Ratio of Hildebrand's pressure to the thermal (i.) and vibrational pressure (ii.).

the value of V_0 as given by (9) lies in fact between the equilibrium volume of the static case and the actual volume at the absolute zero of temperature. Moreover, if the relation (9) is used at room temperatures, V_0 should be much nearer to the static equilibrium value than the value at $T=0^\circ \text{K}$, for we have seen that the approximate expression should be much nearer to the vibrational than the thermal pressure.

Now if we write on the right-hand side of (9)

$$\left(\frac{\partial S}{\partial V}\right)_T = \left(\frac{\partial p}{\partial T}\right)_V = \frac{-(\partial V/\partial T)_p}{(\partial V/\partial p)_T} = -\left(\frac{\partial V}{\partial T}\right)_p \left(\frac{\partial p}{\partial V}\right)_T$$

and put approximately

$$\left(\frac{\partial p}{\partial V}\right)_T \cong -\left(\frac{\partial^2 U}{\partial V^2}\right)_0, \quad (\text{difference } \sim 10 \text{ per cent})$$

(9) becomes simply

$$V_0 \cong V - T \left(\frac{\partial V}{\partial T}\right)_p \quad . \quad . \quad . \quad . \quad . \quad . \quad . \quad . \quad (10)$$

This means that the equilibrium volume V_0 deduced from Hildebrand's approximation is practically identical with that obtained by a simple linear extrapolation to the absolute zero of temperature. Hence we can express the conclusion of the last paragraph in the rather interesting form: *the linearly extrapolated value for the volume of a solid from any temperature to the absolute zero lies in between the static equilibrium volume and the actual volume at absolute zero of temperature.* Moreover, if it is extrapolated from a temperature comparable or higher than the Debye temperature of the solid, the result is expected to lie much nearer to the static equilibrium value.

REFERENCES.

- BORN, M., and MAYER, J. E., 1932, *Zeit. f. Phys.*, **75**, 1.
 FOWLER, R. H., 1936, *Statistical Mechanics* (Cambridge: University Press), 2nd Ed., p. 324.
 GRÜNEISEN, E., 1926, *Handb. d. Phys.*, **10**, 1.
 HILDEBRAND, J. H., 1931, *Zeit. f. Phys.*, **67**, 127.
 HUGGINS, M. L., and MAYER, J. E., 1933, *J. Chem. Phys.*, **1**, 643.
 HUGGINS, M. L., 1937, *J. Chem. Phys.*, **5**, 143; 1947, *J. Chem. Phys.*, **15**, 212.
 MAYER, J. E., and HELMHOLTZ, L., 1932, *Zeit. f. Phys.*, **75**, 19.

XIX. *The Emission of Li^8 from Cosmic Ray induced Nuclear Disintegrations.*

By P. E. HODGSON,
Imperial College of Science and Technology, London*.

[Received November 18th, 1950.]

SUMMARY.

Lithium 8 nuclei ejected from cosmic-ray induced disintegrations have been investigated using the photographic plate method. Earlier work has been confirmed, and the frequency and energy distribution of the Li^8 nuclei determined and compared with the predictions of the evaporation theory. Some nuclear reactions involving the production of Li^8 have been identified.

§ 1. INTRODUCTION.

IN 1947, Occhialini and Powell observed a T-shaped track caused by a particle emitted from a nuclear disintegration in a photographic plate exposed to cosmic rays. These events are also known as "hammer" tracks.

Franzinetti and Payne (1948) analysed thirty examples and confirmed Occhialini and Powell's conclusion that they are due to the emission of lithium 8 nuclei which decay into two alpha-particles and an electron, although the electron track was not observed in their less sensitive plates. This was later observed by Occhialini and by Pickup and Voyvodic (1949) in emulsions sensitive to particles of minimum ionization.

This work has been confirmed, and, in addition, the frequency and energy distributions of the Li^8 particles determined.

§ 2. EXPERIMENTAL PROCEDURE AND SUMMARY OF RESULTS.

Several batches of Ilford Nuclear research plates, coated with C2 and G5 emulsions, and exposed to the cosmic rays on the Jungfraujoch, have been examined for hammer tracks associated with stars.

The energy distribution of the secondary alpha-particles was found from their ranges in the emulsion and it agreed with the results of Franzinetti and Payne (1948) for hammer tracks associated with cosmic ray stars and those of Baxter, Burcham and Paul (1950) and Rumbaugh, Roberts and Hafstad (1937) for Li^8 nuclei produced artificially.

Electron tracks were found associated with most of the hammer tracks in electron-sensitive emulsions.

The angular distribution of the ejected particles was measured and is discussed in § 4.

The angular distribution of the hammer tracks was found to be consistent with isotropic emission of the Li^8 nuclei.

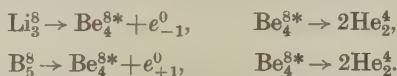
* Communicated by Sir George Thomson.

The frequency of emission of particles forming hammer tracks is given in § 5 and compared with the predictions of the evaporation theory for lithium 8 nuclei of zero spin.

§ 3. NATURE OF THE PARTICLE CAUSING THE HAMMER TRACKS.

Tracks of decay electrons were found associated with most of the hammer tracks occurring in electron-sensitive emulsions. The electron is energetic enough to be at or near minimum ionization and yet slow enough to be quite considerably scattered. The electron tracks are therefore difficult to see and are in general only found if the emulsion is developed to its fullest sensitivity.

Hammer tracks associated with a decay electron may be due either to Li_3^8 or, as recently suggested by Alvarez (1950), B_5^8 :—



Because of the higher charge of B_5^8 its emission probability will be less than that of Li_3^8 .

The experimental results are not incompatible with some of the hammer tracks being without a decay electron, and attributable to Be_4^8 . In this case the excited state of Be_4^8 must be a metastable one of long life since the life-time of the broad state at 3 MeV. is far too short to allow the nucleus to come to rest in the emulsion before disintegrating.

Since Li_3^8 and B_5^8 decay via the same excited state of Be_4^8 (Alvarez 1950) no distinction can be made between them from the energy distribution of the secondary alpha-particles.

It seems likely that the majority of the particles producing hammer tracks are Li_3^8 and in what follows it will be assumed that they are all attributable to this nucleus.

§ 4. THE ENERGY DISTRIBUTION OF THE Li^8 NUCLEI.

The energies of the lithium nuclei were determined from their ranges and a range-energy curve derived from that of Bradner, Smith, Barkas and Bishop (1950) for protons by the relation

$$E = mf \left(\frac{R\epsilon^2}{m} \right)$$

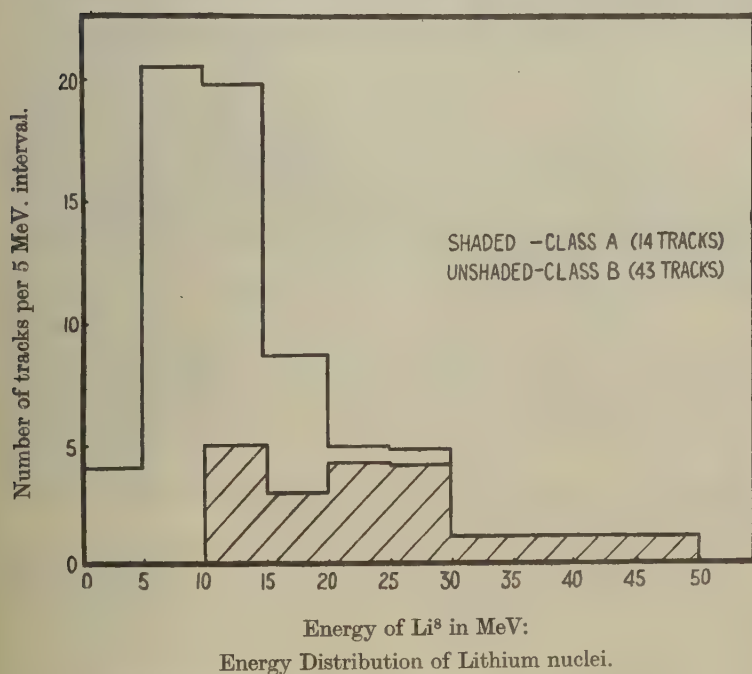
where E , R , ϵ and m are the energy, residual range, charge and mass of the particle. At very low energies the lithium nucleus picks up electrons and reduces its effective charge. The above formula cannot be used in this region with accuracy. But, since this lowering of effective charge takes place, for lithium nuclei, only over the last two or three microns, its effect is small and has been neglected.

It was found that the average energy of the lithium nuclei from large stars was appreciably greater than that of those from small stars.

This may be explained by assuming that the lithium nuclei from large stars are ejected from energetic disintegrations of silver or bromine, while the lithium nuclei from small stars are the residues after the ejection of protons and alpha-particles in the disintegration of carbon, oxygen or nitrogen. This interpretation has also been advanced recently by Courtenay Wright (1950) after examination of Li₃⁸ nuclei associated with stars produced in various gases by the cyclotron beam.

In order to test this hypothesis, all stars associated with hammer tracks were separated into two classes, namely those with more than four tracks (including the hammer track), and those with less. The additional

Fig. 1.



condition was applied that stars with a recoil, a short heavily ionizing track characteristic of the disintegration of a heavy nucleus, were included in the former class, irrespective of their numbers of tracks. These classes are called A and B. In addition, it is possible for a lithium nucleus to be the residue after the complete disintegration of a silver or bromine nucleus. Only one example has been found, in a star of 27 tracks, and it was included in class B.

The energy distribution of the lithium nuclei is shown in fig. 1, the two classes being distinguished by shading. The observed distribution was

corrected for those long tracks which were lost because they passed out of the emulsion. The disparity between the energy distributions of lithium nuclei in the two classes is strong support for the above hypothesis on the mechanism of their production.

§ 5. FREQUENCY OF EMISSION.

In all, it was found that 74 hammer tracks were associated with stars in emulsion containing 23,700 stars of more than two tracks. Hammer tracks associated with stars caused by π^- -mesons are omitted from these figures and will be considered later (§ 7). The total emission frequencies, for C2 and G5 emulsions, are shown in Table I. The value for G5 emulsion is less than that for C2 on account of the greater number of stars with more than two tracks.

The fraction of hammer tracks in class A is also given in Table I.

TABLE I.

	Observed	Corrected
Hammer tracks \div No. of stars >2 tracks in C2 emulsion	0.0032 ± 0.0007	0.0052 ± 0.0012
Hammer tracks \div No. of stars >2 tracks in G5 emulsion	0.0023 ± 0.0005	0.0034 ± 0.0006
Fraction of hammer tracks of class A	0.27 ± 0.07	0.33 ± 0.08

The frequency of emission of particles causing hammer tracks is plotted in fig. 2 as a function of star size and compared with the calculations on the evaporation theory by Le Couteur for the emission of lithium 8 of zero spin from nuclear disintegrations of various sizes. Comparison of the observed and calculated frequencies, which should only be made for hammer tracks of class A, shows good agreement.

Hammer tracks are lost if they pass out of the emulsion (see § 4) and also if the angle between the projected directions of the lithium and the two alpha-particles is too small to be resolved. The frequencies of emission have been corrected for tracks lost in both these ways.

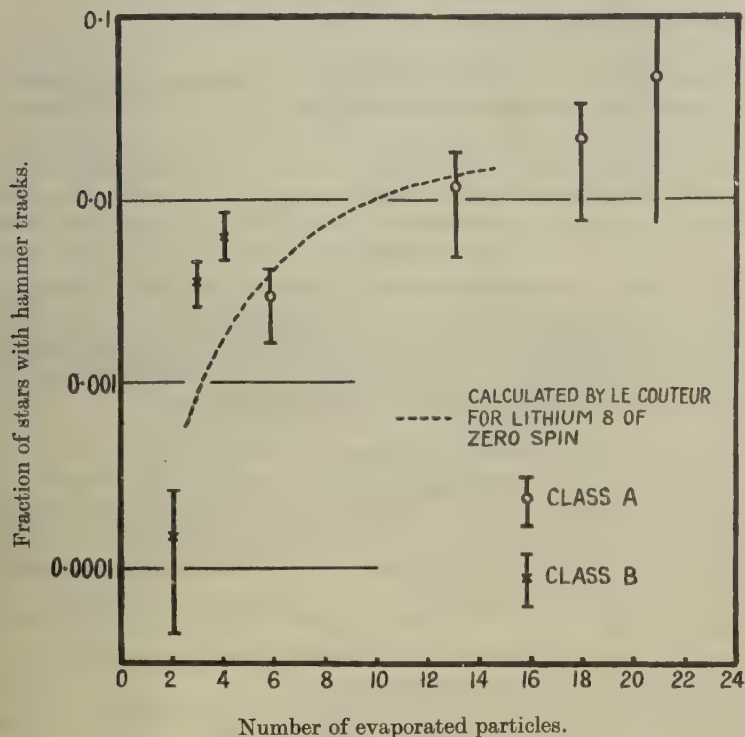
From the frequencies of emission given above, and assuming an approximate value of the intensity of star-producing radiation at the Jungfrauoch, values of the cross-section for production of Li^8 from light nuclei can be deduced which are of the same order of magnitude as those given by Courtenay Wright (1950) and Titterton (1950).

§ 6. NUCLEAR REACTIONS IN THE LIGHT ELEMENTS.

On the assumption that the hammer tracks of class B come from the disintegration of light nuclei it is often possible, when the event occurs in C2 emulsion, to identify the nuclear reaction concerned. The identification is subject to some uncertainty because lightly ionizing particles

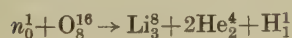
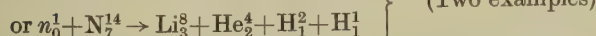
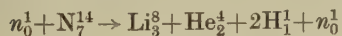
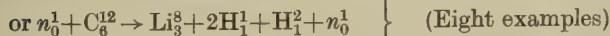
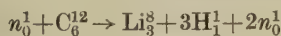
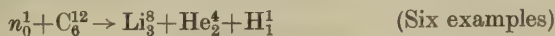
are not visible in C2 emulsion, and protons, deuterons and tritons are not always separable. Analysis of events in G5 emulsion was not attempted because of the difficulty of distinguishing between protons and alpha-particles. It is possible to confirm the reactions by measurement of energy and momentum balance, providing no neutrons are emitted.

Fig. 2.



Fraction of stars with hammer tracks as a function of star size.

The following reactions have been identified

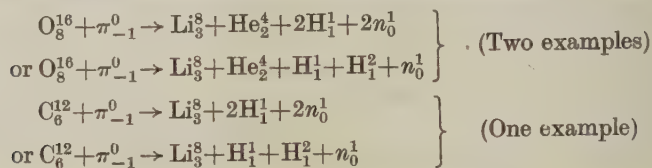


(One example)

§ 7. LITHIUM NUCLEI EMITTED FROM STARS INITIATED BY π^- -MESONS.

In addition to the hammer tracks analysed above, six have been observed associated with stars produced by π^- -mesons. The total number of such mesons in the emulsion examined was 1160. The fraction of meson-produced stars with hammer tracks is therefor 0.005 ± 0.003 , a value which agrees with the 0.003 given by Bradner (1950) and the $11/3000$ or 0.004 ± 0.001 found by Adelman and Jones (1949).

The following nuclear reactions have been identified :—



ACKNOWLEDGMENTS.

I should like to express my thanks to Professor Sir George Thomson and Mr. N. C. Barford for many valuable discussions, to Dr. K. J. Le Couteur for communicating the results of his calculations on the emission probability of Li⁸, and to Dr. E. P. George and Mr. J. Evans for permitting me to examine a number of hammer tracks in their plates.

REFERENCES.

- ADELMAN, F., and JONES, S. B., 1949, *Phys. Rev.*, **75**, 1468.
 ALVEREZ, L. W., 1950, Harwell Conference on Nuclear Physics, *Phys. Rev.*, **80**, 519.
 BAXTER, A. S., BURCHAM, W. E., and PAUL, E. B., 1950, *Phil. Mag.*, **41**, 937.
 BRADNER, H., 1949, *U. C. R. L.*, 486, 38.
 BRADNER, H., SMITH, F. M., BARKAS, W. H., and BISHOP, A. S., 1950, *Phys. Rev.*, **77**, 462.
 FRANZINETTI, C., and PAYNE, R. M., 1948, *Nature, Lond.*, **161**, 735.
 LE COUTEUR, K. J. (Private Communication.)
 OCCHIALINI, G. P. S., and POWELL, C. F., 1947, *Nature, Lond.*, **159**, 93.
 PICKUP, E., and VOYVODIC, L., 1949, *Phys. Rev.*, **76**, 1534.
 RUMBAUGH, L. H., ROBERTS, R. B., and HAFSTAD, L. R., 1938, *Phys. Rev.*, **54**, 1103.
 TITTERTON, E. W., 1950, Harwell Conference on Nuclear Physics; 1951, *Phil. Mag.*, **42**, 109, 113.
 WRIGHT, S. COURTENAY, 1950, *Phys. Rev.*, **79**, 838.

XX. The Law of Constant Resolved Shear Stress in Crystal Plasticity.

By F. R. N. NABARRO.

Department of Metallurgy, The University of Birmingham*,

[Received December 27, 1950.]

ABSTRACT.

The formula of Peach and Koehler for the total force acting on a dislocation in a stressed crystal is derived by the use of a theorem due to Colonnetti. The same method distinguishes conservative motions of the dislocation, which do not alter the volume, from other motions. The component of the total force which produces conservative motions acts in the glide plane, and is proportional to the same component of the total stress as appears in the law of resolved shear stress discovered experimentally by Schmid.

THE forces acting on dislocations are most conveniently derived by the use of a theorem due to Colonnetti (1915). Consider a body containing a closed loop of dislocation with Burgers vector \mathbf{b} , and cover this loop with a cap. Let an element of this cap have area $d\Sigma$, and let the body be subject to external stresses as a result of which the force acting across this element $d\Sigma$ of the cap is $\mathbf{X} d\Sigma$. The signs of the vectors \mathbf{b} , $d\Sigma$ and $d\sigma$ must be determined conventionally. The convention used here is that of Peach and Koehler (1950). Colonnetti's theorem then states that the work W_e done by the external forces when the dislocation is formed is given by

$$W_e = - \iint \mathbf{b} \mathbf{X} d\Sigma. \quad (1)$$

If the stress produced by the external forces is \mathbf{p} , \mathbf{X} is given by

$$\mathbf{X} d\Sigma = - \mathbf{p} d\Sigma, \quad (2)$$

and

$$W_e = \iint \mathbf{b} \mathbf{p} d\Sigma. \quad (3)$$

Suppose now that an element $d\sigma$ of the dislocation moves a distance $d\mathbf{x}$. The area of the dislocation loop is increased by

$$\delta\Sigma = d\mathbf{x} \wedge d\sigma, \quad (4)$$

and the external forces do work

$$\begin{aligned} \delta W_e &= \mathbf{b} \mathbf{p} \cdot (d\mathbf{x} \wedge d\sigma) \\ &= [(\mathbf{b} \mathbf{p}) \wedge d\sigma] \cdot d\mathbf{x}. \end{aligned} \quad (5)$$

The force $d\mathbf{F}$ on the element $d\sigma$ is thus given by

$$d\mathbf{F} = (\mathbf{b} \mathbf{p}) \wedge d\sigma. \quad (6)$$

This is the result of Peach and Koehler.

* Communicated by the Author.

It is now necessary to distinguish between those motions of the dislocation which conserve the volume of the crystal (conservative motions) and those motions which produce interstitial ions or vacancies (non-conservative motions). Only conservative motions can lead to steady slip, though non-conservative motions may be important in work hardening and especially in thermal recovery. The necessary and sufficient condition that a motion should be conservative is that a uniform hydrostatic pressure p should do no work when the motion occurs. For such a pressure, $\mathbf{b}\mathbf{p}$ is given by $\mathbf{b}\mathbf{p}=\mathbf{b}p$, and it follows from (5) that the motion is conservative if

$$(\mathbf{b} \wedge d\boldsymbol{\sigma}) \cdot d\mathbf{x} = 0. \quad \dots \dots \dots (7)$$

Thus the motion is always conservative if $\mathbf{b} \wedge d\boldsymbol{\sigma} = 0$, that is to say, if the element of dislocation is of pure screw type. If \mathbf{b} and $d\boldsymbol{\sigma}$ are not parallel, they define a plane, the *glide plane*, and the motion is conservative only if $d\mathbf{x}$ lies in this plane. The normal to the glide plane is the unit vector \mathbf{n} defined by

$$\mathbf{n} = (\mathbf{b} \wedge d\boldsymbol{\sigma}) / |\mathbf{b} \wedge d\boldsymbol{\sigma}|. \quad \dots \dots \dots (8)$$

The component $d\mathbf{f}$ of the force $d\mathbf{F}$ which is effective in producing slip is the component lying in the glide plane, given by

$$\begin{aligned} d\mathbf{f} &= d\mathbf{F} - \mathbf{n}(\mathbf{n} \cdot d\mathbf{F}) \\ &= -\mathbf{n} \wedge (\mathbf{n} \wedge d\mathbf{F}). \quad \dots \dots \dots (9) \end{aligned}$$

Now

$$\begin{aligned} \mathbf{n} \wedge d\mathbf{F} &= \mathbf{n} \wedge [(\mathbf{b}\mathbf{p}) \wedge d\boldsymbol{\sigma}] \\ &= (\mathbf{b}\mathbf{p})(\mathbf{n} \cdot d\boldsymbol{\sigma}) - d\boldsymbol{\sigma}[\mathbf{n}(\mathbf{b}\mathbf{p})] \\ &= -d\boldsymbol{\sigma}(\mathbf{b}\mathbf{p}\mathbf{n}), \end{aligned}$$

and so

$$d\mathbf{f} = (\mathbf{n} \wedge d\boldsymbol{\sigma})(\mathbf{b}\mathbf{p}\mathbf{n}). \quad \dots \dots \dots (10)$$

Since $\mathbf{p}\mathbf{n}$ is the force acting across unit area of the glide plane, the force per unit length tending to produce glide is b times the component in the glide direction of the force acting across unit area of the glide plane, and acts in the glide plane normal to the line of the dislocation. If a loop of dislocation lies entirely in the glide plane, its conservative motions are confined to this plane (except for those elements which are of pure screw type), and its whole length is subjected to the same normal force tending to increase the area of the loop. This is in accordance with the experimental result (Schmid 1924) that slip begins when the "resolved shear stress" $\mathbf{b}\mathbf{p}\mathbf{n}/b$ reaches a value which is characteristic of the crystal, but independent of the other components of the applied stress.

REFERENCES.

- COLONNETTI, G., 1915, *R.C. Accad. Lincei* [5], **24**, 404.
 PEACH, M., and KOEHLER, J. S., 1950, *Phys. Rev.* [2], **80**, 436.
 SCHMID, E., 1924, *Proc. Internat. Cong. Appl. Mech.*, Delft, p. 342.

XXI. CORRESPONDENCE

The Production of Neutrons by High Energy Protons.

By J. M. CASSELS, T. C. RANDLE, T. G. PICKAVANCE and A. E. TAYLOR*,
Atomic Energy Research Establishment, Harwell.

[Received December 8, 1950.]

THE production of neutrons by high energy protons has been investigated with the help of a differential detector. The third counter in the triple coincidence telescope used previously for total cross-section work (Taylor, Pickavance, Cassels and Randle 1950) was replaced by a gridded ionization chamber sensitive only to comparatively slow protons. It followed that protons ejected from the polythene radiator were counted only if they possessed energies lying between certain limits set by a carbon absorber placed immediately in front of the chamber. The counts resulting from n, p collisions in the hydrogen content of the polythene were separated out by background runs with a carbon radiator. After correcting for protons lost while slowing down in the absorber, absolute neutron fluxes in the range 50–200 MeV. could be found with the help of the Berkeley experiments on the n, p interaction (Hadley, Kelly, Leith, Segrè, Wiegand and York 1949, Brueckner, Hartsough, Hayward and Powell 1949, Kelly, Leith, Segrè, and Wiegand 1950).

The correct operation of the telescope was checked by using it to determine the total cross sections of carbon and hydrogen at 156 and 110 MeV. The results were consistent with those of other work at Berkeley and at Harwell, showing that neutrons of the intended energy were being detected.

The energy spectra of the neutrons produced by bombarding beryllium, carbon, aluminium and uranium targets were then investigated (figs. 1–4). These targets had thicknesses of 1.67, 1.09, 1.19 and 1.82 grms.-cm.⁻² respectively. The resolution diagrams in fig. 1 show the "smearing" effect of the neutron detector only. There is additional lack of resolution caused by the slowing down in the target of the primary protons, whose energy was initially 171 MeV. The magnitude of this can be gauged from the mean proton energies set out in the Table, column 2. No corrections for "smearing" have been applied to the results given. The fluxes shown in the diagrams refer to a point 15.3 metres from the target at an angle of $2\frac{1}{2}^\circ$ from the forward direction. They are normalized to an actual current of 1 microampere being accelerated by the cyclotron, but the effective current was greater than this because protons could traverse the target several times before being lost. It was found to be 3.4 microamperes in the carbon target by measurement of the rate of production of ¹¹C, a process

* Communicated by the Authors.

Fig. 1.

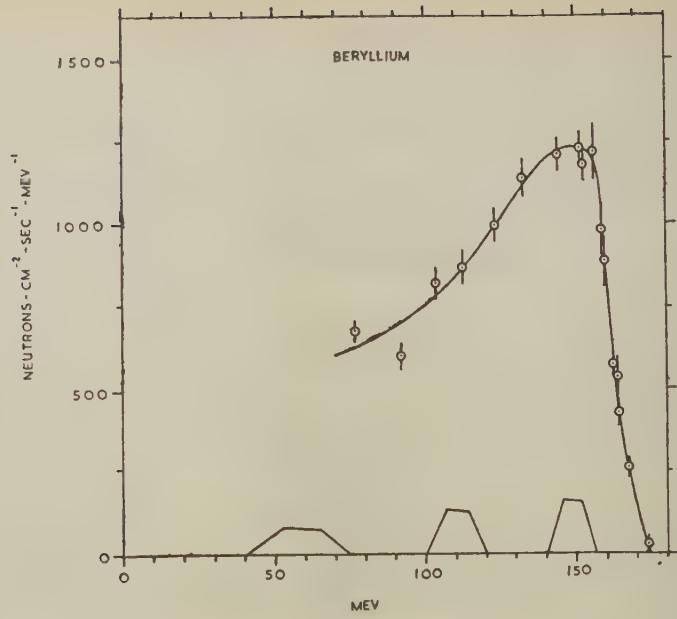
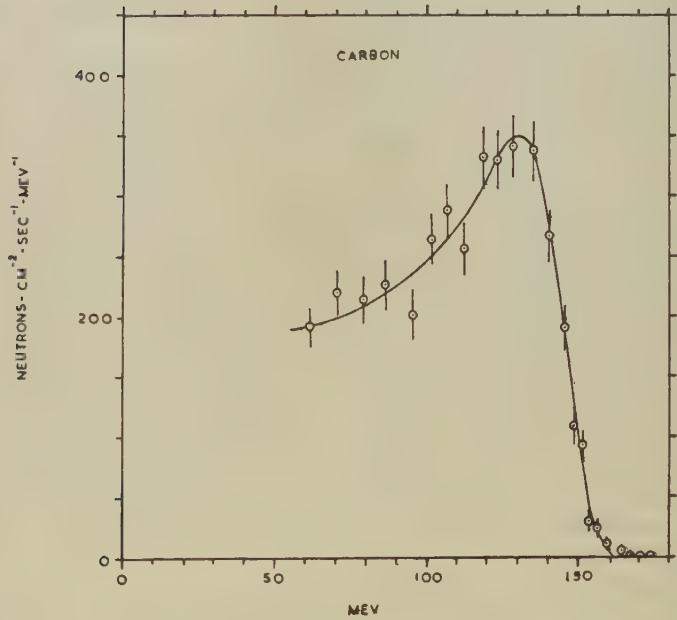


Fig. 2.



Figs. 1-2. Neutron spectra obtained from beryllium, carbon, aluminium and uranium by bombardment with 171 MeV. protons.

Fig. 3.

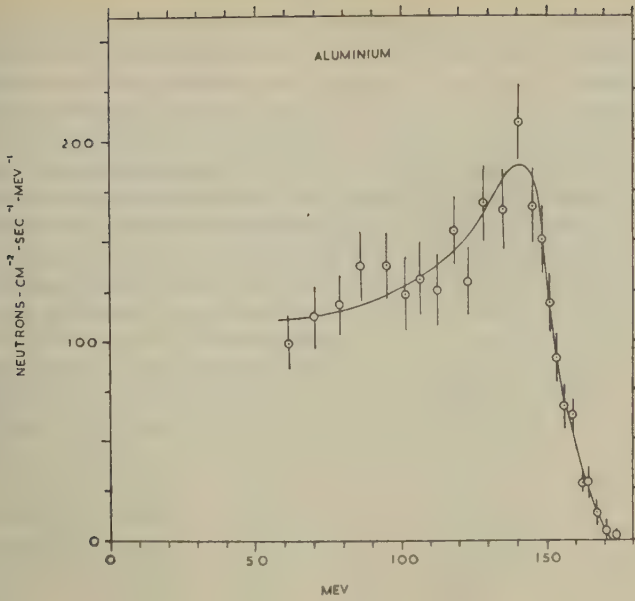


Fig. 4.

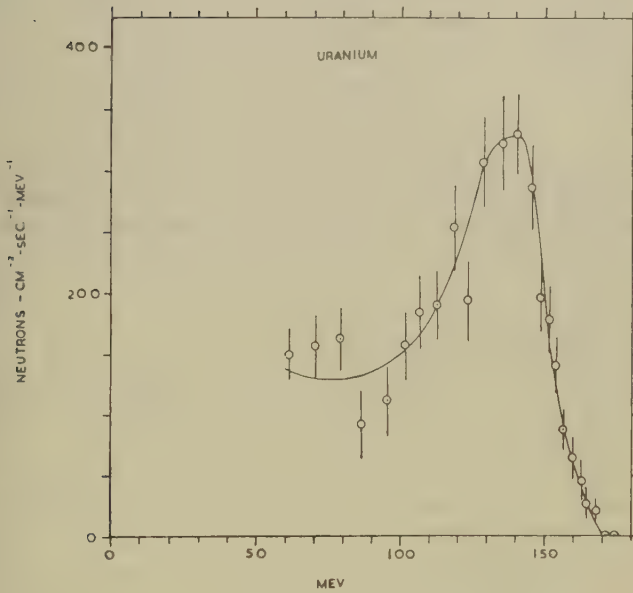


Fig. 3-4. Neutron spectra obtained from beryllium, carbon, aluminium and uranium by bombardment with 171 MeV. protons.

for which the cross-section is known from work at Berkeley (Aamodt, Peterson and Phillips, private communication, 27th February, 1950). Knowing this effective current, it was possible to calculate the differential cross-section, at an angle of $2\frac{1}{2}^\circ$ from the forward direction, for the production in carbon of neutrons with energy greater than 60 MeV. (see Table, column 3). If a constant fraction of the cyclotron beam was lost at each traversal of the target, then the mean energy of the primary protons was 155 MeV.

The loss of protons in the target is determined by multiple Coulomb scattering (Moyer, private communication), and it has been found for the Harwell cyclotron that the number of times the proton beam passes through a target at a given orbit radius is such as to bring the r.m.s. angle of multiple scattering up to a constant value, provided that the target is thin enough to make several traversals necessary. Using this principle, the neutron production cross-sections in beryllium and aluminium were obtained. The mean proton energies in these two targets were 156

Target element	Mean proton energy (MeV.)	Production cross-sections $\times 10^{27}$ (cm ²)	
		$2\frac{1}{2}^\circ$	5°
Beryllium	156	91 + 45 — 30	99 \pm 19
Carbon	155	47 + 23 — 16	72 \pm 15
Aluminium	166	122 + 61 — 41	—
Uranium	166	1520 + 760 — 507	—

and 166 MeV respectively. The uranium target was thick enough to suggest that the beam went through it only once, and the cross-section and mean proton energy given were calculated on this basis. These four cross-sections may be in error by a factor of 1.5 either way because systematic errors could have been introduced in estimating the cyclotron beam current during the various runs.

The neutron production cross-sections in beryllium and carbon targets at an angle of 5° to the forward direction were also measured, in another and more direct way (see Table, column 4). The gridded chamber in the telescope was replaced by a counter sensitive to high energy protons and the carbon absorber adjusted so that all neutrons over 60 MeV. were counted. The beryllium target for this experiment consisted of two thick sheets of beryllium interleaved with three thin sheets of carbon. After two short runs in which neutrons produced were counted for each target in turn, the targets were removed from the cyclotron and the ^{11}C content of each measured with a calibrated counter. The background measurements required to find the fraction of counts in the telescope due to hydrogen

recoils had been done on the previous day, so that effectively no ^{11}C counts remained from those runs at the time of the calibration run. With the help of the known $^{12}\text{C}(\text{p}, \text{pn})^{11}\text{C}$ cross-section, the neutron production cross-sections could be found. The stated standard error is intended to include all systematic errors.

The shape of the beryllium spectrum reported here seems quite consistent with the results of other experiments using protons of 110 MeV. (Bodansky 1950) and 340 MeV. (Fox, Leith, Wouters and MacKenzie 1950).

We hope to improve and extend these results and publish them, with a more detailed account, at some future time.

REFERENCES.

- BODANSKY, D., 1950, *Phys. Rev.*, **80**, 481.
 BRUECKNER, K., HARTSOUGH, W., HAYWARD, E., and POWELL, W. M., 1949, *Phys. Rev.*, **75**, 555.
 FOX, R., LEITH, C., WOUTERS, L., and MACKENZIE, K. R., 1950, *Phys. Rev.*, **80**, 23.
 HADLEY, J., KELLY, E., LEITH, C., SEGRÈ, E., WIEGAND, C., and YORK, H., 1949, *Phys. Rev.*, **75**, 351.
 KELLY, E., LEITH, C., SEGRÈ, E., and WIEGAND, C., 1950, *Phys. Rev.*, **79**, 96.
 TAYLOR, A. E., PICKAVANCE, T. G., CASSELS, J. M., and RANDLE, T. C., 1950 a, *Nature, Lond.*, **165**, 967; 1950 b, *Phil. Mag.* (in the press).

The Velocity Brownian Movement.

By D. K. C. MACDONALD *,
 Clarendon Laboratory, Oxford.

[Received December 14, 1950.]

DR. FÜRTH'S amplifying and detailed discussion (Fürth 1950) of the example I appended to illustrate the main argument of my paper (MacDonald 1950) is welcome, but does not, of course, alter any of the fundamental conclusions. Nevertheless, may I make the following brief comments:—

(1) The purpose of my example, which it appears Dr. Fürth may have misunderstood, was to show that the available statistical data on the observed *velocity* of a Brownian particle *would* indeed be already sufficient to determine D (and hence $k=6\pi\eta aD/T$), at least in order of magnitude, if a reasonable value for the discrimination-period of human vision were assumed. Since I was in fact only concerned with demonstrating the underlying principle I deliberately chose for simplicity the familiar one-dimensional Brownian movement equation.

(2) The use of the standard deviation to approximate the mean absolute velocity is clearly a good approximation for a "stationary" system in thermal equilibrium as for the Brownian particle (or in the general

* Communicated by the Author.

kinetic theory of gases) but, of course, for a system with an externally superposed mean velocity (as in a current-carrying medium) the two need have no connection with one another.

(3) The thesis underlying Dr. Fürth's first two sections is not entirely clear to me. However, no physical variable can have a frequency-spectrum extending without limit and consequently, of course, can never be *perfectly* random (and therefore non-differentiable). It is nevertheless quite customary to refer to a quantity as varying stochastically if within the frequency-range of observation the "power" spectrum is effectively flat as, for example, in the case of thermal noise from a resistor at all accessible radio frequencies and normal temperatures.

REFERENCES.

FÜRTH, R., 1950, *Phil. Mag.*, **41**, 1255.

MACDONALD, D. K. C., 1950, *Phil. Mag.*, **41**, 814.

XXII. Notices of New Books and Periodicals received.

Structural Chemistry of Inorganic Compounds, Vol. I. By W. HÜCKEL.
(Elsevier Publishing Co. Inc.) Price \$9. (£3 10s. 0d.)

THIS is essentially a book for use in the latter stages of a University degree course. About one-eighth of the book is taken up by an excellent historical survey. The remainder is about equally divided between a presentation of the coordination theory which is the basis of the author's systematization, and a discussion of atomic structure and physical methods for investigating molecular structure. This order is a little unusual, and emphasizes the importance attached to stereo-chemistry and the coordination approach.

The author can be congratulated on the large amount of recent information which he has included, though no mention is made of the optical resolution of the dodecammine-hexol-tetracobaltic salts, the first resolution of a purely inorganic compound. An incorrect structure is assigned to this group of salts. The correct structure has in fact been determined by X-ray analysis, contrary to the statement on p. 166.

[The Editors do not hold themselves responsible for the views
expressed by their correspondents.]

XXIII. *Renormalization of the Meson-Photon-Nucleon Interaction.*

By P. T. MATTHEWS †,
Clare College, Cambridge, England ‡.

[Received October 27, 1950.]

ABSTRACT

It is shown by direct calculation to fourth order in the coupling constants that all divergences, except those arising from the scattering of mesons by mesons, can be removed from the combined interaction of charged spinless mesons, nucleons (scalar interaction) and the electromagnetic field by mass and 'charge' renormalization. The remaining divergence can be cancelled to this order by assuming a direct interaction between mesons with a suitably chosen coupling constant.

§ 1. INTRODUCTION.

DYSON (1949) has put Feynman's (1949) graphical technique for calculating the S-matrix elements in electrodynamics into the Schwinger (1948) Tomonaga (1946) form and has shown that the consistent application of mass and charge renormalization yields a finite theory to any order in the coupling constant. The analogous treatment of the scalar interaction of spinless mesons with nucleons has been given by the author (Matthews 1950 a) and also a summary of the graphical method as applied to charged spinless mesons in the electromagnetic field (1950 b). This latter interaction has been treated independently and in much greater detail by Rohrlich (1950). Here the extent to which renormalization is effective in removing the divergences from the combined interaction of neutrons, protons, charged spinless mesons (scalar interaction) and the electromagnetic field is considered by direct calculation to fourth order in the coupling constants e and f . It is shown that for the removal of all divergencies, except those from the scattering of mesons by mesons, by mass and "charge" renormalization certain conditions between the infinite constants, which determine the renormalized charge, have to be satisfied. It is checked that these conditions are satisfied to second order. The remaining divergencies from the scattering of mesons by mesons can certainly be removed, to this order, by the introduction of a direct interaction between mesons with a suitably chosen constant thus leading to a finite S-matrix. (A brief report of these results has been published elsewhere (Matthews 1950 c).)

One of the conditions referred to above occurs in the interaction of spinless mesons with the electromagnetic field. Since the completion of these calculations, more general proofs of it have been given by Dyson (1950) and

† Communicated by the Author.

‡ Now at the Institute for Advanced Study, Princeton, N.J., U.S.A.

by Rohrlich (1950), based on gauge invariance. A similarly general solution has since been given by Salam (1950) of the present problem by a development of the work of Ward (1950). The problem in its complete generality is much complicated by the overlapping of divergent parts similar in principle to the "a" and "b" divergencies in self energy parts discussed by Dyson (1949, § VII) and no proof has yet been given, though there seems little doubt that this scheme does in fact lead to a finite S-matrix up to any order.

§ 2 PRIMITIVE DIVERGENTS.

The Hamiltonian in the interaction representation of the combined interaction for pseudo-scalar mesons is

$$H = \sum H_i, \quad (i=1, 2, 3) \quad (1)$$

where

$$H_1 = \left(\frac{ie}{\hbar c} \right) A_\mu \left(\phi^* \frac{\partial \phi}{\partial x_\mu} - \frac{\partial \phi^*}{\partial x_\mu} \phi \right) - \left(\frac{ie}{\hbar c} \right)^2 A_\mu A_\nu \phi^* \phi \delta_{\mu\nu}, \quad . . . (2)$$

$$H_2 = i \bar{\psi} \gamma_5 (\tau_- \phi^* + \tau_+ \phi) \psi + \delta \lambda \phi^{*2} \phi^2, \quad (3)$$

$$H_3 = ie \bar{\psi} \gamma_\mu \tau_P \psi A_\mu. \quad (4)$$

τ_+ operating on a neutron gives a proton and on a proton gives zero. τ_- is the same operator with the neutron and proton reversed. τ_P gives a proton when operating on a proton and zero when operating on a neutron. The terms required for mass renormalization have not been included. A term in H_1 explicitly dependent on the surface direction has also been omitted. This can be ignored without error if the corresponding term in the P-bracket of two derivatives of ϕ is also ignored (Matthews 1949.) Any scattering effect in which both the real and virtual processes are specified can be represented by a graph. Dotted lines denote photons, wavy lines with double arrow denote mesons, full lines with double arrows denote protons and full lines with single arrows denote neutrons. Thus double arrows signify the movement of charge and for charge to be conserved the double arrowed lines (either full or wavy) must form continuous loops (open or closed). Single arrows determine the motion of neutrons (as opposed to anti-neutrons) and for consistency the nucleon lines must form continuous loops of either single or double arrows. At any vertex with a photon line entering the other two lines must be double arrowed. At a meson-nucleon vertex the nucleon lines must be one double and one single arrow. If these rules are observed the τ -factors can be neglected. The rules for obtaining the corresponding S-matrix element can be summarized as follows (see Dyson (1949), Rohrlich (1950) and Matthews (1950 a and b)):

- (i.) Each internal photon line give a factor

$$\hbar c \delta_{\mu\nu} (2\pi)^{-3} \int D_F(p) d^4 p.$$

- (ii.) Each integral meson line gives a factor

$$\hbar c (2\pi)^{-3} \int \Delta_F(p) d^4 p.$$

(iii.) Each internal nucleon line gives a factor

$$(2\pi)^{-3} \int S_F(p) d^4p.$$

(iv.) Each meson-photon 3-vertex gives a factor

$$ie(\hbar c)^{-2}(2\pi)^4(p_\mu + p'_\mu)\delta(p - p' + q),$$

where p and p' are the four-vectors of the meson lines entering and leaving the vertex, respectively. (The factor $(p_\mu + p'_\mu)$ arises from the derivatives in H_2 .)

(v.) Each meson-photon 4-vertex gives a factor

$$-ie^2(\hbar c)^3(2\pi)^4\delta_{\mu\nu}\delta(p - p' + q - q').$$

(vi.) Each proton-photon vertex gives a factor

$$e(\hbar c)^{-1}(2\pi)^4\gamma_\mu.$$

(vii.) Each meson-nucleon vertex gives a factor

$$f(\hbar c)^{-1}(2\pi)^4\gamma_5.$$

(viii.) Each external photon line gives $A_\mu(k)$, each external meson line entering or leaving the graph gives $\phi(k)$ or $\phi^*(k)$, respectively. Each external nucleon line entering or leaving the graph gives $\bar{\psi}(k)$ or $\psi(k)$, respectively.

(ix.) There is a further numerical factor of $(-1)^{n-l-1}$, where n is the number of nucleon vertices and l is the number of closed nucleon loops. Finally, the whole integral is multiplied by the number of ways the operators can be paired off by interchanging the roles of the two photon operators at the 4-vertices.

The condition for primitive divergent graphs can be derived by Dyson's method (1949) and is

$$(3/2)E_n + E_m + E_p < 5, \quad \dots \quad (5)$$

where E_n , E_m , and E_p are the numbers of external nucleon, meson and photon lines, respectively. Since the nucleon factors appear in H in pairs, E_n in (5) must be either two or zero. If E_n is two then for (5) to be satisfied, either E_m or E_p must be zero. Since the charge bearing lines in any graph form continuous loops, the number of external charge bearing (double arrowed) lines in any part must be even †. These considerations together show that the primitive divergents for the three field mixture, in terms of their external lines, are the same as for the separate pairs of interacting fields. They may, however, have different internal structure. Some of the new graphs are illustrated in fig. 1. (It should be noted that these all satisfy the charge conservation and consistency conditions given above).

† In the author's treatment of the meson-nucleon interaction⁵ (1950 a), it was wrongly stated that for neutral mesons the divergences from parts with three external meson lines cancel by a type of Furry theorem (Furry 1937). Genuine divergences may arise from this type of graph for neutral mesons, but are definitely excluded for charged mesons by the charge conservation rule.

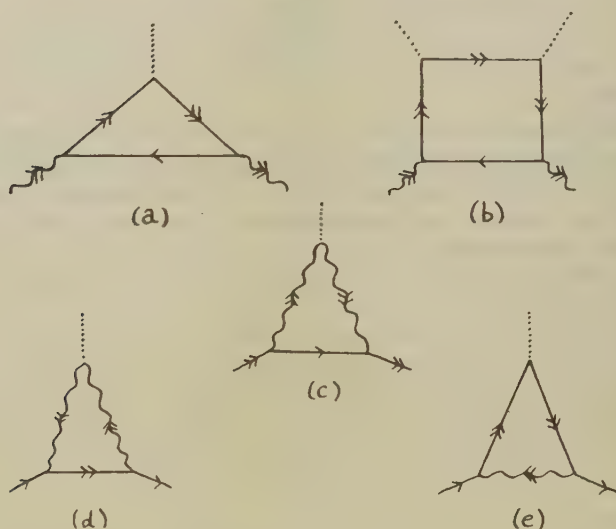
§3. RENORMALIZATION CONDITIONS.

Considerations are now restricted to fourth order in the coupling constants e and f . To calculate the probability of any process one draws all the irreducible graphs of the process to this order. It should be remembered that C-parts (with two external meson and two external photon lines) are divergent. Any such part (except that with a single internal meson line; fig. 2 (a)) is replaceable by a 4-vertex and counted as reducible. To obtain the corrections, after mass renormalization, due to the insertions of self-energy, vertex and C-parts, D_F and Δ_F must be replaced by D'_F and Δ'_F defined as

$$D'_F(p) = \left(1 + \frac{\alpha}{2\pi} A\right) D_F(p) + D_{F1}^{(2)}(p), \quad \dots \quad (6)$$

$$\Delta'_F(p) = \left(1 + \frac{\alpha}{2\pi} C + \frac{\beta}{2\pi} C'\right) \Delta_F(p) + \Delta_{F1}^{(2)}(p), \quad \dots \quad (7)$$

Fig. 1.



where $\alpha = e^2/4\pi\hbar c$ and $\beta = f^2/4\pi\hbar c$. A , C and C' are infinite constants defined analogously to those occurring in Dyson's treatment of electrodynamics. $D_{F1}^{(2)}$ and $\Delta_{F1}^{(2)}(p)$ are finite and of second order in the coupling constants. The $S_F(p)$ factors for proton and neutron lines must be replaced, respectively, by

$$S_F^P(p) = \left(1 + \frac{\alpha}{2\pi} B + \frac{\beta}{2\pi} B'\right) S_F(p) + S_{F1}^{P(2)}(p), \quad \dots \quad (8)$$

$$S_F^N(p) = \left(1 + \frac{\beta}{2\pi} B'\right) S_F(p) + S_{F1}^{N(2)}(p). \quad \dots \quad (9)$$

Also the vertex factors $\gamma_5, \gamma_\mu, (p_\mu + p'_\mu)$ and $\delta_{\mu\nu}$ must be replaced

$$\Gamma_5(p, p') = \left(1 + \frac{\alpha}{2\pi} P + \frac{\beta}{2\pi} P'\right) \gamma_5 + A_{51}^{(2)}(p, p'), \quad . \quad . \quad . \quad . \quad (10)$$

$$\Gamma_\mu(p, p') = \left(1 + \frac{\alpha}{2\pi} L + \frac{\beta}{2\pi} L'\right) \gamma_\mu + A_{11}^{(2)}(p, p'), \quad . \quad . \quad . \quad . \quad (11)$$

$$\Phi_\mu(p, p') = \left(1 + \frac{\alpha}{2\pi} N + \frac{\beta}{2\pi} N'\right) (p_\mu + p'_\mu) + \Phi_{\mu 1}^{(2)}(p, p'), \quad . \quad . \quad (12)$$

$$\Theta_{\mu\nu}(p, p', q) = \left(1 + \frac{\alpha}{2\pi} R + \frac{\beta}{2\pi} R'\right) \delta_{\mu\nu} + \Theta_{\mu\nu 1}^{(2)}(p, p', q), \quad . \quad . \quad . \quad (13)$$

P, P', L, L' , etc. are infinite constants and the final terms in these equations are all finite. The constants B and L have been calculated explicitly by Karplus and Kroll (1950). The "infinite parts" of the constants C, N and R have been calculated independently by Rohrlich (1950). Also external line factors must be replaced by $(1 + \alpha/4\pi A)A_\mu(k)$, for a photon, $(1 + \alpha/4\pi C + \beta/4\pi C')\phi(k)$ for a meson, $(1 + \alpha/4\pi B + \beta/4\pi B')\psi$ for a proton and $(1 + \beta/4\pi B')\psi$ for a neutron.

Fig. 2.



The idea of charge renormalization is to express any infinite term occurring in the calculation of a matrix element as a constant infinite multiple of a finite term of lower order and then to show that these infinite multiples can be absorbed by defining the observed coupling constants e_1 and f_1 as double power series in e and f . To see whether this can be done consistently in this case, consider the scattering of photons by mesons. The only irreducible graphs are shown in fig. 2. For renormalization to be effective, the infinite multiples of these graphs arising from the substitutions (7) and (12) into fig. 2 (a) and (13) into fig. 2 (b) must be the same, since each graph is of order e^2 . There are also infinite multiples arising from substitutions in external lines, but since these are the same for both graphs they need not be considered. The required conditions are

$$2N + C = R, \quad . \quad . \quad . \quad . \quad . \quad . \quad (14)$$

$$2N' + C' = R'. \quad . \quad . \quad . \quad . \quad . \quad . \quad (15)$$

Condition (14) allows for insertions involving mesons and photons only and has been checked by Rohrlich (1950) and by the author (1950 b). Condition (15) arises from the additional parts due to virtual nucleons. (The term $2N'$ comes from the insertion of fig. 1 (a) in the two vertices of fig 2 (a),

C' from a meson self energy part due to virtual nucleons in the internal line of fig. 2 (a), and R' from the insertion of fig. 1 (b) in the 4-vertex of fig. 2 (b). This condition has also been checked. The required charge renormalization is

$$e_1 = e \left[1 + \frac{\alpha}{2\pi} \left(N + C + \frac{A}{2} \right) + \frac{\beta}{2\pi} (N' + C') \right], \quad . . . \quad (16)$$

since each factor e is associated with a 3-vertex a meson line and half a photon line. As has just been verified, this same renormalization absorbs the factors R and R' from the C -parts.

If processes involving real protons and photons are now considered, other infinities will arise from the substitutions (6), (8) and (11). These are removed by the charge renormalization

$$e_1 = e \left[1 + \frac{\alpha}{2\pi} \left(B + L + \frac{A}{2} \right) + \frac{\beta}{2\pi} (B' + L') \right]. \quad . . . \quad (17)$$

For consistency this must be identical with (16). That is, it is required that

$$B + L = N + C, \quad \quad (18)$$

$$B' + L' = N' + C'. \quad \quad (19)$$

In fact it is found that

$$B = -L, \quad B' = -L', \quad N = -C = R, \quad N' = -C' = R'. \quad . . \quad (20)$$

This means that the whole effective charge renormalization comes from photon self energy parts which are the same for both meson-photon and proton-photon effects, thus leading to the same charge renormalization for both.

For meson-nucleon effects the infinities arising from the substitutions (7), (8), (9) and (10) can be removed by the renormalization

$$f_1 = f \left[1 + \frac{\alpha}{2\pi} \left(\frac{B}{2} + \frac{C}{2} + P \right) + \frac{\beta}{2\pi} \left(B' + \frac{C'}{2} + P' \right) \right]. \quad . . \quad (21)$$

This can be made independently of (16).

A further possible source of divergence is from graphs with one photon and two neutron external lines (fig. 1 (d) and (e)). Since no (finite) single vertex of this type exists no renormalization is possible.

However, though each graph diverges separately, the total is finite and no difficulty arises. These graphs lead to the finite neutron magnetic moment which has been discussed in this framework by Case (1949)).

The only remaining divergencies are those from the scattering of mesons by mesons (M -parts), with four external meson lines. This can occur either through virtual nucleons, (f^4), or virtual photons, (e^4), and in each case gives a genuine divergence. To this order these divergences can be cancelled by a suitable choice of the constant in the direct interaction $\delta\lambda\phi^{*2}\phi^2$. This device has been considered more generally by the author (1950a) for the meson-nucleon interaction and by Rohrlich (1950) for the meson-photon interaction. The former treatment was very incomplete because secondary infinities from parts such as fig. 3 were not considered.

Rohrlich's development is more thorough but there are difficulties when such parts appear inside self energy parts which are not dealt with in detail. This point will be discussed further in a forthcoming paper by Mr. A. Salam.

The whole of the discussion is also applicable to scalar mesons. (It is only necessary to replace $(\gamma_5)_{\alpha\beta}$ by $-i\delta_{\alpha\beta}$.)

Fig. 3.



ACKNOWLEDGMENTS.

The author would like to thank Professor W. Pauli for suggesting this problem and for his continued interest, also Dr. N. Kemmer and Mr. A. Salam for stimulating discussions and Drs. F. Rohrlich and D. Feldman for helpful criticism.

APPENDIX.

The calculation of the infinite constants was performed by the methods due to Feynman (1949) as employed by Karplus and Kroll (1950). The "infinite parts" of all the constants can be expressed in terms of

$$I = \frac{1}{i\pi^2} \int \frac{d^4k}{k^2 + \mu^2}$$

and are

$$\begin{aligned} A &= -\frac{3}{2}I, & P &= \frac{1}{2}I, & P' &= 0, \\ N &= -C = R = -I, & B &= -L = \frac{1}{2}I, \\ N' &= -C' = R' = I, & B' &= -L' = \frac{1}{2}I. \end{aligned}$$

(It is readily seen that the single and double arrows cannot be inserted consistently in the graph of this order corresponding to P' . This is not true for higher orders.)

REFERENCES.

- CASE, K. M., 1949, *Phys. Rev.*, **76**, 1.
 DYSON, F. J., 1949, *Phys. Rev.*, **75**, 486, 1736; 1950, Private communication.
 FEYNMAN, R. P., 1949, *Phys. Rev.*, **76**, 749, 769.
 FURRY, W., 1937, *Phys. Rev.*, **51**, 125.
 KARPLUS, R., and KROLL, N. M., 1950, *Phys. Rev.*, **77**, 536.
 MATTHEWS, P. T., 1949, *Phys. Rev.*, **76**, 1254; 1950 a, *Phil. Mag.*, **41**, 185;
 1950 b, *Phys. Rev.*, **80**, 292; 1950 c, *Ibid.*, **80**, 292.
 ROHRlich, F., 1950, *Phys. Rev.*, **80**, 666.
 SALAM, A., 1950, *Phys. Rev.*, **79**, 910.
 SCHWINGER, J., 1948, *Phys. Rev.*, **74**, 1439; **75**, 651.
 TOMONAGA, S., 1946, *Prog. Theor. Phys.*, **1**, 27.
 WARD, J. C., 1950, *Phys. Rev.*, **77**, 293; **78**, 182.

XXIV. *A Generalization of Reversion Formulæ with their Application to Non-linear Differential Equations.*

By A. C. SIM,
Standard Telecommunication Laboratories Ltd.*

[Received January 11, 1951.]

SUMMARY.

The formulæ for algebraic reversion are extended to revert a class of non-integral power series, and also generalized to revert series in which the coefficients contain operators. These formulæ are shown to have a simple and powerful application to non-linear differential equations; which they expand into an infinite sequence of linear equations.

§1. INTRODUCTION.

THE studies of semiconductors and saturable iron-cored coils are two of many important fields in modern physics and engineering which lead to non-linear problems of practical importance. Such problems occur also, for example, in aerodynamic and navigational theories, in the analysis of electronic circuits, and in nuclear physics. A comprehensive survey of the theory of non-linear mechanics has been published by Minorsky (1947), from which it is clear that the number of methods which are not restricted to one type of problem is very small, and most of the remainder are concerned with non-linear oscillatory equations. The method of reversion described herein is applicable to a wide variety of equations, of which some appear otherwise intractable, provided the equations are expansible in powers of the unknown quantity.

The existing reversion formulæ are applicable only to algebraic equations, and are used extensively for the calculation of roots. The problem may be defined as follows. Given the series

$$\lambda = \sum_{r=1}^{\infty} a_r \cdot y^r, \quad \dots \dots \dots (1)$$

the coefficients A_r in the reverted series expansion

$$y = \sum_{r=1}^{\infty} A_r \cdot \lambda^r \quad \dots \dots \dots (2)$$

have to be found. Van Orstrand (1910) has published a very full account of such formulæ and their applications. In addition, a special type of series occurring in the theory of Bessel functions and having the form

$$\{y^{-1} + a_1 y + a_3 y^3 + \dots\} = \lambda \quad \dots \dots \dots (3)$$

has been reverted by Bickley and Miller (1943).

* Communicated by Professor D. Gabor.

If the series (1) and (2) converge * it is clear that (2) is a solution of the equation (1), but not necessarily the only solution. In fact it is the solution which vanishes as λ approaches zero, and is, in general, the smallest real solution. If equation (1) possesses no real solution (2) will diverge.

The reversion formulæ may be obtained in two ways, of which the most obvious is the substitution of (2) into (1). The quantities A_r are then found by equating the coefficients of λ^r on each side of the equation. A more elegant approach, due to Harkness and Morley (1898), involves differentiating (2) with respect to y and multiplying each side by λ^{-r} . This gives

$$\lambda^{-r} = d\lambda/dy \{A_1 \lambda^{-r} + \dots + r A_r \lambda^{-1} + \dots\}. \quad (4)$$

It is then argued that the relation $\lambda^n \cdot d\lambda/dy = (n+1)^{-1} \cdot d\lambda^{n+1}/dy$ is true for all n except $n=-1$; and since λ^{n+1} is a power series in y , its derivative cannot contain a term proportional to $\lambda^{-1} \cdot d\lambda/dy$, because this can only arise from the differentiation of $\log \lambda$. It follows therefore, from (4), that the coefficient of y^{-1} in the power series expansion of λ^{-r} is $r A_r$, and hence

$$r A_r = \text{coefficient of } y^{-1} \text{ in } \{a_1 y + a_2 y^2 + \dots\}^{-r}. \quad (5)$$

It is clear that the evaluation of (5) will assume that the coefficients a_r commute, and this method therefore fails in general when operators are involved.

§2. REVERSION.

The series (1) and (3) described above are special cases of the non-integral power series

$$\{a_0 y^{(1+n\alpha)} + a_1 y^{(1+n+1\alpha)} + \dots + a_r y^{(1+n+r\alpha)} + \dots\} = \lambda \phi(x). \quad (6)$$

This series is the most general one that can be reverted. The coefficients a_r may be any functions of x , d/dx , or any other operator, but they must be independent of y . The real quantity α is quite arbitrary; n is an integer—positive, negative, or zero, and λ is a constant.

In the reversion of (6) it is most convenient to consider $y^{(1+n\alpha)}$ as the unknown quantity. Inspection shows that the reverted series will be in powers of y^m where $m = \alpha/(1+n\alpha)$, so that the solution may be assumed to have the form

$$y^{(1+n\alpha)} = \sum_{r=0}^{\infty} A_r \cdot \lambda^{mr}. \quad (7)$$

In determining A_r the extended multinomial theorem is required. This may be written in the form

$$\{u_1 k + u_2 k^2 + \dots + u_r k^r + \dots\}^v = \sum_{r=0}^{\infty} \sum_p \frac{\Gamma(1+v)}{\Gamma(1+q)} \cdot \frac{u_2^{p_2} \dots u_r^{p_r}}{p_2! \dots p_r!} \cdot u_1^q k^{(v+r)}, \quad (8)$$

* Harkness and Morley (1893) have shown that the reverted series (2) converges in the same domain as the original series (1).

where the exponents q and p_r assume all values which satisfy the two relations

$$(p_2 + p_3 + \dots + p_r) = (\nu - q),$$

$$(p_2 + 2p_3 + \dots + (r-1)p_r) = r.$$

It should be noted that p_r and $(\nu - q)$ are positive integers, and when ν is negative, the ratio $\Gamma(1+\nu)/\Gamma(1+q)$ in (8) should be replaced by

$$(-1)^{(\nu-q)} \cdot \Gamma(-q)/\Gamma(-\nu).$$

By direct substitution of (7) into (6) using (8), the reversion coefficients are found to be given by

$$a_0 \cdot A_0 = \phi(x),$$

$$a_0 \cdot A_1 = -a_1 \cdot A_0^{(1+m)},$$

$$a_0 \cdot A_2 = -\{a_1 \cdot (1+m)A_0^m A_1 + a_2 \cdot A_0^{(1+2m)}\},$$

$$a_0 \cdot A_3 = -\{a_1 \cdot (1+m)[mA_0^{(m-1)}A_1^2/2! + A_0^m A_2] \\ + a_2 \cdot (1+2m)A_0^{2m} A_1 + a_3 \cdot A_0^{(1+3m)}\},$$

$$a_0 \cdot A_4 = -\{a_1 \cdot (1+m)[m(m-1)A_0^{(m-2)}A_1^3/3! + mA_0^{(m-1)}A_1 A_2 + A_0^m A_3] \\ + a_2 \cdot (1+2m)[2mA_0^{(2m-1)}A_1^2/2! + A_0^{2m} A_2] \\ + a_3 \cdot (1+3m)A_0^{3m} A_1 + a_4 \cdot A_0^{(1+4m)}\},$$

and the general term

$$a_0 \cdot A_r = - \left. \begin{aligned} &\sum_{s=1}^r a_s \cdot \sum_p \frac{\Gamma(2+ms)}{\Gamma(1+p_0)} \cdot A_0^{p_0} \cdot \frac{A_1^{p_1} \dots A_{r-s}^{p_{r-s}}}{p_1! \dots p_{r-s}!}, \end{aligned} \right\} \dots \quad (9)$$

where $(p_1 + p_2 + \dots + p_{r-s}) = (1 + ms - p_0)$

and $(p_1 + 2p_2 + \dots + (r-s)p_{r-s}) = (r-s).$

Note that $(1 + ms - p_0)$ is always a positive integer.

In the general term of (9) when $(1 + ms)$ is negative the ratio

$$\Gamma(2+ms)/\Gamma(1+p_0)$$

should be replaced by $(-1)^{(1+ms+p_0)} \cdot \Gamma(-p_0)/\Gamma(-1-ms).$

In general, the formulæ given by (9) represent a sequence of linear ordinary differential, or integro-differential equations determining the functions A_r . The equation $a_0 \cdot A_0 = \phi(x)$ is referred to as the *generating equation* and its solution A_0 is termed the *generating function* since the complete solution is expressed in terms of it. The generating function is a first approximation to the true solution and the generating equation is a linear approximation of the original non-linear equation.

It may be noted that if the coefficients a_r commute a simplified formula can be obtained by the method of Harkness and Morley. It is then convenient to change the notation, writing the series in the form

$$z^\beta \{a_0 + a_1 z + \dots + a_r z^r + \dots\} = \lambda, \quad \dots \quad (10)$$

in which β has replaced $(n+\alpha^{-1})$ and z is written for y^α . The function $\phi(x)$ is now included in λ . Any arbitrary power of z may be found in this case so that a solution may be assumed in the form

$$z^s = (\lambda/a_0)^{sm} \sum_{r=0}^{\infty} B_r \lambda^{rm}, \quad \dots \quad (11)$$

where s is quite arbitrary but real, and m now represents β^{-1} . The coefficients A_r for this series are found to be

$$\begin{aligned} B_0 &= 1, \quad B_1 = -sm \cdot a_0^{-(1+m)} a_1, \\ B_2 &= sm \{ (1 + \overline{2+s \cdot m}) a_0^{-2(1+m)} a_1^2 / 2! - a_0^{-(1+2m)} a_2 \}, \\ B_3 &= -sm \{ (1 + \overline{3+s \cdot m}) (2 + \overline{3+s \cdot m}) a_0^{-3(1+m)} a_1^3 / 3! \\ &\quad - (1 + \overline{3+s \cdot m}) a_0^{-(2+3m)} a_1 a_2 + a_0^{-(1+3m)} a_3 \}, \\ B_4 &= sm \{ (1 + \overline{4+s \cdot m}) (2 + \overline{4+s \cdot m}) (3 + \overline{4+s \cdot m}) a_0^{-4(1+m)} a_1^4 / 4! \\ &\quad - (1 + \overline{4+s \cdot m}) (2 + \overline{4+s \cdot m}) a_0^{-(3+4m)} a_1^2 a_2 / 2! \\ &\quad + (1 + \overline{4+s \cdot m}) a_0^{-2(1+2m)} (a_1 a_3 + a_2^2 / 2!) - a_0^{-(1+4m)} a_4 \}, \end{aligned}$$

and the general term

$$\left. \begin{aligned} B_r &= s/(s+r) \sum_p \frac{(-1)^{(p_0-rm)} \cdot \Gamma(p_0+sm)}{\Gamma(s+r \cdot m)} \cdot a_0^{-p_0} \cdot \frac{a_1^{p_1} \dots a_r^{p_r}}{p_1! \dots p_r!}, \\ \text{where} \quad (p_1 + p_2 + \dots + p_r) &= (p_0 - rm, \\ (p_1 + 2p_2 + \dots + rp_r) &= r. \end{aligned} \right\} \dots \quad (12)$$

In this case when $(s+r)m$ becomes negative the quantity

$$(-1)^{(p_0-rm)} \cdot \Gamma(p_0+sm) / \Gamma(s+r \cdot m)$$

must be replaced by the ratio $\Gamma(1-\overline{s+r \cdot m}) / \Gamma(1-p_0-sm)$.

Whilst Van Orstrand has dealt adequately with the application of reversion formulæ to equations not involving operators, it may be noted that the extended form of equation given by (10) offers alternative forms of solution, and will also yield results when applied to some equations containing fractional powers. For example, the equation

$$(x^3 + c_2 x^2 + c_1 x) = c_0$$

reverts to a series in powers of c_0 . It may be, however, that c_0 is very large and c_1 is the smallest coefficient. Division of the equation by x gives $(x^2 + c_2 x - c_0 x^{-1}) = -c_1$ which may also be reverted, producing a more convergent series. It is also possible, using (12) to revert the equation $(c_a x^a + c_b x^b) = c_0$ for any values of a and b provided they are real.

§3. NON-LINEAR EQUATIONS.

To apply the general reversion formulæ (9) to a non-linear differential equation, the equation must first be expanded in an ascending or descending power series of the unknown function y —the coefficients being expressed in terms of x and $D=d/dx$, and arranged so that they contain no negative powers of D . If a general solution is required, the *generating coefficient* a_0 , which is the first one in the series, must be of the highest degree in D so that the generating equation has the same order as the equation to be solved.

The set of equations given by the reversion formulæ (9) are all similar in form to the generating equation, although the functions of x on the right-hand side become progressively more complicated as r increases. Each equation, therefore, will give rise to the same number of arbitrary constants. For a complete solution of the equation to be reverted, a *general* solution of the generating equation must be found, whilst only *particular* solutions of the remaining equations for A_r are required. The choice of these particular solutions affects not only the form of the series obtained, but also the ease with which the arbitrary constants are determined from the boundary conditions of the problem, and the convergence and complexity of the reverted series.

If the reverted solution of an equation does not contain sufficient arbitrary constants, or does not converge in a convenient range, the form of solution may frequently be improved by a change of variable. In all applications, therefore, every conceivable form of the expanded equation should be considered, to decide which one is most advantageous. Convergence of the reverted solution must be examined in each individual case, since a general discussion does not appear to be possible. Because of the complexity in deriving a large number of terms of the reverted series, it is usually easiest to check its accuracy and convergence by substituting the few terms obtained into the equation, and examining the remainder which results. Even this procedure can be very formidable, in which case a numerical substitution into the equation affords the only practical verification.

§4. EQUATIONS WITH INITIAL BOUNDARY CONDITIONS.

It is generally the case that the arbitrary constants in the solution of a non-linear equation are so woven within it that their determination becomes a difficult task. In this section it will be shown that when the generating equation is linear with constant coefficients, as is frequently the case in practise, a form of solution can always be found by reversion which makes the calculation of arbitrary constants from initial conditions as easy as in the case of a linear equation. This is achieved by choosing the particular solutions for the functions A_r so that they all vanish (and also their first $n-1$ derivatives where n is the order of the equation), when the independent variable is zero. The constants can then be rigorously calculated by regarding the generating function as the complete solution for the

purpose. The particular form of the generating function thus obtained can then be used for the derivation of the subsequent terms in the series until sufficient accuracy is obtained from them.

It is now assumed that the generating coefficient a_0 is a polynomial in powers of $D=d/dx$ with constant coefficients. If the degree of this polynomial (equal to the order of the non-linear equation), is n , the inverse of a_0 may be expanded into partial fractions. Let these partial fractions have the form

$$a_0^{-1} = \left\{ \sum_{q=1}^{n-R} \frac{\gamma_q}{(D+\alpha_q)} + \sum_{s=1}^t \sum_{q=1}^{r_s} \frac{\delta_{q,s}}{(D+\beta_s)^q} \right\}, \quad \dots \quad (13)$$

in which $-\alpha_1, -\alpha_2, \dots$, are the non-repeating zeros of a_0 , and $-\beta_1, -\beta_2, \dots$, are t roots which are repeated r_1, r_2, \dots, t , times. The coefficients γ_q and $\delta_{q,s}$ are constants depending on the polynomial coefficients which are not defined here. The quantity R is the difference between the degree of the polynomial and the number of non-repeating roots, i.e. $R = \sum r_s$.

The reversion functions A_r are all defined by the operation of the collection of operators given by (13) on a function of x which is known or can be explicitly determined. Let $f(x)$ represent this function for a particular A_r . It is desired to find a particular solution to this operation which will vanish with its first $n-1$ derivatives when x is zero, then $D^u \cdot a_0^{-1} \cdot f(x)$ is required for $u=0, 1, \dots, n-1$.

With the aid of the contracting notation

$$\delta_s(\beta_s - \delta_s)^u \equiv \sum_{q=1}^u \frac{(-1)^{q-1} \cdot u!}{(u-q)! q!} \cdot \beta_s^{(1+u-q)} \cdot \delta_{q,s}, \quad \dots \quad (14)$$

it can be found by means of simple algebraic manoeuvres that

$$\sum_{q=1}^r \frac{D^u \delta_{q,s}}{(D+\beta_s)^q} = \delta_s \sum_{q=1}^u (\delta_s - \beta_s)^{q-1} \cdot D^{u-q} + (\delta_s - \beta_s)^u \sum_{q=1}^r \left\{ \frac{\delta_s}{D+\beta_s} \right\}^q \quad \dots \quad (15)$$

Thus in the determination of A_r the only operations that need to be considered are $D^q \cdot f(x)$ and $(D+\beta_s)^{-q} \cdot f(x)$. The first of these is simply a repeated differentiation, whilst the second is readily interpreted using the operator shifting theorem. A solution which vanishes when x is zero can thus be written

$$(D+\beta_s)^{-q} \cdot f(x) = e^{-\beta_s x} \int_0^x dx \int_0^x dx \dots (q \text{ times}) \int_0^x e^{\beta_s x} \cdot f(x) \cdot dx. \quad \dots \quad (16)$$

Since a_0 is defined to be a polynomial of degree n in D , if a_0^{-1} is expanded in powers of D^{-1} the series obtained will commence with a term in D^{-n} . But, by expanding the right-hand side of (13) in powers of D^{-1} some terms containing lower powers are obtained. By equating the two expansions it follows that the coefficients of D^{-k} in the expansion of (13) for $k=1, \dots, n-1$, are zero. In the notation of (14) this result can be found to be

$$\left\{ \sum_{q=1}^{n-R} \alpha_q^k \gamma_q + \sum_{s=1}^t (-1)^k \delta_s (\delta_s - \beta_s)^k \right\} = 0 \quad k=0, 1, \dots, (n-2). \quad (17)$$

It now follows from (13) and (15) that

$$[D^u \cdot A_r]_{x=0} = \left\{ \sum_{k=0}^{n-1} \sum_{q=1}^{n-R} (-1)^k \alpha_q^k \gamma_q D^{(u-1-k)} \cdot f(x) \right. \\ \left. + \sum_{s=1}^t \delta_s \sum_{k=0}^{u-1} (\delta_s - \beta_s)^k D^{(u-1-k)} \cdot f(x) \right\}_{x=0} \\ u=0, 1, \dots, (n-1) \quad r \neq 0. \quad (18)$$

Finally, from (17) and (18) it is seen that if a solution for A_r is obtained in this special case that vanishes when $x=0$, then its first $(n-1)$ derivatives will also vanish when $x=0$, i. e.

If $A_r=0$ when $x=0$, then

$$(d^u A_r / dx^u)_{(x=0)} = 0 \text{ for } u=1, 2, \dots, (n-1), \quad (19)$$

when a_0 is a polynomial of n th degree in D with constant coefficients.

§ 5. A SPECIAL EQUATION.

Apart from the general power series (6), it is possible to revert the equation

$$P \cdot y = \{\phi(x) + f(y)\} \quad (20)$$

when $f(y)$ is any function of x and y , but $\phi(x)$ is independent of y as before. P is any operator. Note that it is not possible to extract a common factor λ in this case. This form of reversion may be useful when the equation is not expansible in powers of y , since the procedure does not demand this. To solve the equation a solution may be assumed to exist in the form

$$y = \{P^{-1} \cdot \phi(x) + F(x)\} \quad (21)$$

and this may be substituted into (20). A power series in $F(x)$ is then obtained by expanding $f(y)$ using Taylor's theorem. The resulting series can then be reverted by means of the formulæ already derived in § 2 of this paper. The final reverted solution is then

$$y = \sum_{r=0}^{\infty} C_r \quad (22)$$

in which

$$P \cdot C_0 = \phi(x), \\ (P - f') \cdot C_1 = f(C_0), \\ (P - f') \cdot C_2 = f'' \cdot C_1^2 / 2!, \\ (P - f') \cdot C_3 = \{f'' \cdot C_1 C_2 + f''' \cdot C_1^3 / 3!\} \text{ etc.} \quad (23)$$

with the abbreviation $f^r \equiv \left[\frac{\partial^r}{\partial x^r} \cdot f(y) \right]_{y=C_0}$

A similar set of formulæ may be derived for the case when (20) is without operators, and it is easy to verify that the result is equivalent to that obtained by Lagrangian expansion (Whittaker and Watson 1950).

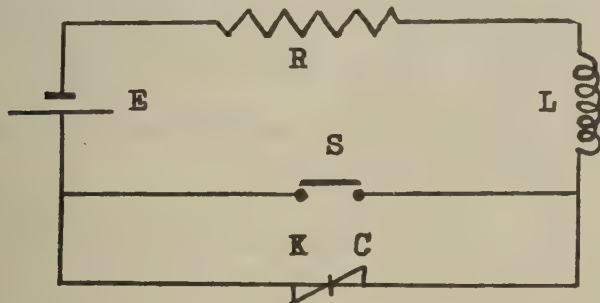
§ 6. ILLUSTRATIONS.

(1) Semiconducting materials are sometimes used for shunting switches to reduce transients in the breaking of inductive circuits. In the circuit of fig. 1, an inductive coil is represented by resistance R and inductance L in series, and it is supplied from a battery of voltage E . The switch S is shunted by a non-linear resistor possessing the characteristic $V=KI^c$, where V is the voltage across it, I the current through it, and K and c are constants. The equation satisfied by the current may be written

$$I_0 = \{D \cdot I + I + aI^c\}, \quad \dots \dots \dots (24)$$

where the constant a represents the ratio K/R , and the operator D is equivalent to $L/R \cdot d/dt$. I_0 is the initial value of I , equal to E/R .

Fig. 1.



This equation has the special form discussed in § 4. The generating equation is $(D+1) \cdot I = I_0$ so that the generating function is

$$I_0(1 - \exp[-Rt/L]) + A \exp[-Rt/L],$$

where A is a constant. Regarding this as the complete solution for the purpose of determining A , it is found that the exponential terms vanish, so that in this case the generating function is simply I_0 . From this and equation (9), the next term in the reverted series is $-(D+1)^{-1} \cdot aI_0^c$, and the series is found to be

$$I = \{I_0 - aI_0^c(1 - \exp[-Rt/L]) + ca^2I_0^{(2c-1)}(1 - \exp[-Rt/L])(1 + Rt/L) \dots\}. \quad \dots \dots (25)$$

As in the case of algebraic reversion, if the unknown quantity I is replaced by a known approximate solution plus a new dependent variable, the reverted series will then converge more rapidly. In this problem it is known that the initial value of I is I_0 , so that the substitution of $(I' + I_0)$ for I should improve convergence. This transforms the equation to

$$\{(D+1) \cdot I' + a(I' + I_0)^c\} = 0. \quad \dots \dots \dots (26)$$

Defining parameters p and q by

$$p = [1 + acI_0^{c-1}] \quad q = ac(c-1)I_0^{c-2}/2$$

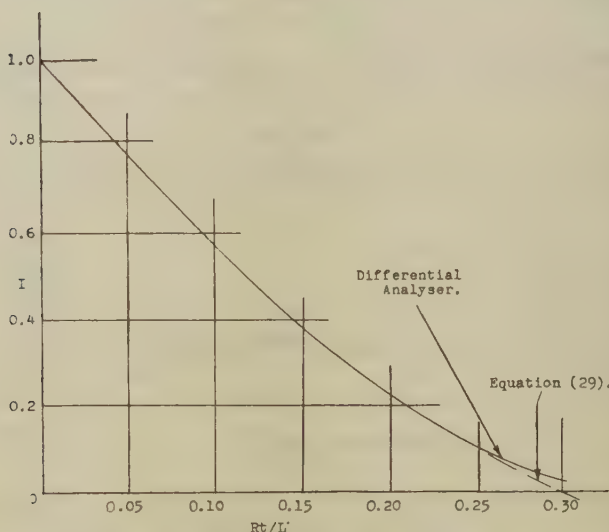
and expanding the second term in (26) by the binomial theorem puts the equation in a suitable form for reversion

$$\{(D+p)I' + qI'^2 + \dots\} = -aI_0^c \quad \dots \quad (27)$$

Reversion of this series produces a series more rapidly convergent when a and c are large, and no less convergent when they are small

$$I = \{I_0 - ap^{-1}I_0^c(1 - \exp[-pRt/L]) - a^2p^{-3}qI_0^c(1 - \exp[-2pRt/L] - 2Rt/L \cdot \exp[-pRt/L]) \dots\}. \quad (28)$$

Fig. 2.



This problem has been analysed by Fairweather and Ingham (1941) using a differential analyser, and it is interesting to compare equation (28) with their results. As a particular numerical case, let $c=0.2$, $K=240$, $R=50$ and $E=50$. Then $I_0=1$, $a=4.8$, $p=1.96$, and $q=-0.384$. Equation (28) then assumes the form

$$I = \{1 - 2.45(1 - \exp[-1.96Rt/L]) - 1.182(1 - 3.92 \exp[-1.96Rt/L] - \exp[-3.92Rt/L]) \dots\}. \quad (29)$$

In fig. 2 a plot of this expression is compared with the curve obtained on the differential analyser.

(2) The functional equation* $f(x+1)=e^{f(x)}$ may be written in the form $e^{(1)} \cdot f(x)=e^{f(x)}$, and with $y=f(x)$ this may be expanded into the series

$$\{(e^{(1)} - 1) \cdot y - y^2/2! - y^3/3! \dots\} = 1. \quad \dots \quad (30)$$

* This problem was communicated by Professor K. W. Miller of the Armour Research Foundation, Chicago, Ill.

A solution of this equation is required that vanishes when $x=0$. Using the expansion

$$(e^D - 1)^{-1} = D^{-1} \{1 - D/2 + D^2/12 \dots - (-1)^n D^{2n} \cdot B_n / (2n)!\},$$

where B_n is the n th Bernoulli number, the generating function is seen to be $A_0 = (e^D - 1)^{-1} \cdot 1 = (x+a)$ where a is a constant, and in this case $a=0$. Proceeding with the reversion leads to

$$y=f(x) = \{x + x(1-x)[(1-2x)/12 + (2-13x+17x^2-8x^3)/240 \dots]\}. \quad (31)$$

(3) The performance of an anharmonic oscillator satisfies the equation

$$\{(D^2 + a^2) \cdot y + by^2\} = 0. \quad (32)$$

For a general solution the generating function is $A \cos(ax+c)$ where A and c are constants. Reversion then produces the series

$$y = \{A \cos(ax+c) - bA^2/2a^2[1 - \cos(ax) + \cos(ax+2c)/3 - \cos 2(ax+c)/3 - \sin(2c) \cdot \sin(ax)] \dots\}. \quad (33)$$

(4) The Thomas-Fermi equation of atomic theory is, in dimensionless form,

$$\frac{d^2\phi}{dx^2} = x^{-1/2} \cdot \phi^{3/2} \quad \text{with} \quad \phi(0)=1, \quad \phi(\infty)=0. \quad (34)$$

Referring to the general expression (6), it is seen that for this case

$$a_0 = D^2, \quad \alpha = \frac{1}{2}, \quad n=0, \quad m = \frac{1}{2}, \quad a_1 = -x^{-1/2}$$

and all the remaining a_r are zero. ($\phi(x)$ in (6) is zero.)

The generating function is clearly of the form $(b+ax)$. If b is put equal to 1 to satisfy the first boundary condition, the subsequent functions A_r must be chosen so that they vanish when x is zero. Thus

$$\begin{aligned} A_1 &= \int_0^x \int_0^x x^{-1/2} \cdot (1+ax)^{3/2} \cdot dx \, dx \\ &= a^{-3/2} \{z(1+z^2)^{1/2} [z^4/6 + 2z^2/3 - 1/8] \\ &\quad + (1+6z^2)/8 \cdot \log [z + (1+z^2)^{1/2}]\} \quad (35) \end{aligned}$$

in which $z^2=ax$.

This function is cumbersome to handle in the evaluation of A_2 , and it is convenient to approximate by assuming that z is small. (35) may then be shown to yield the power series

$$A_1 \approx a^{-3/2} \{4z^3/3 + 2z^5/5 + 3z^7/70 + \dots\}. \quad (36)$$

This approximation may be used to extend the solution until further terms are small compared with z^7 . Proceeding in this way a power series is obtained for $\phi(x)$

$$\begin{aligned} \phi(x) &= \{1 + ax + 4x^{3/2}/3 + 2ax^{5/2}/5 \\ &\quad + x^3/3 + 3a^2x^{7/2}/70 + 2ax^4/15 \dots\}. \quad (37) \end{aligned}$$

This series is identical with that obtained by Baker (1930) by a method of successive approximations. If the full form for A_1 given by (35) is retained, and an approximate form of A_2 is used a series will be found that converges more rapidly than (37).

It is interesting to note that an alternative solution can be found by solving (34) for $\phi^{3/2}$ instead of ϕ . In this case the parameters are

$$a_0 = D^2, \quad \alpha = 5/2, \quad n = -1, \quad m = -5/3, \quad a_1 = -x^{-1/2}.$$

§7. CONCLUSION.

It has been shown that it is possible to revert series involving certain fractional powers of the unknown variable, and that the coefficients in these series need not be algebraic. The application of reversion to non-linear differential equations has been found to be simple, and applicable to a wide variety of problems. It is particularly suited to problems with initial boundary conditions. It suffers from the presence of "secular terms" in common with other series methods (Minorsky 1947), and is not usually suitable when the non-linear terms are large.

The author is grateful for permission to publish this work, from Standard Telecommunication Laboratories Ltd., and also from the British Thomson-Houston Company Ltd. where the work was commenced.

REFERENCES.

- BAKER, E. B., 1930, "The Application of the Fermi-Thomas Statistical Model to the Calculation of Potential Distributions in Positive Ions", *Phys. Rev.*, **36**, 630.
- BICKLEY, W. G., and MILLER, J. C. P., 1943, "Notes on the Reversion of a Series", *Phil. Mag.* [7], **34**, 35.
- FAIRWEATHER, A., and INGHAM, T., 1941, "Subsidence Transients in Circuits Containing a Non-linear Resistor, with Reference to the Problem of Spark-quenching", *J. Instn. Elect. Engrs.*, **88**, Pt. I, 330.
- HARKNESS, J., and MORLEY, F., 1893, *Treatise on the Theory of Functions* (London: Macmillan and Co.), p. 116; 1898, *Introduction to Analytic Functions* (London: Macmillan and Co.), p. 144.
- MINORSKY, N., 1947, *An Introduction to Non-linear Mechanics* (Ann Arbor: J. W. Edwards and Co.).
- VAN ORSTRAND, C. E., 1910, "Reversion of Power Series", *Phil. Mag.*, [6] **19**, 366.
- WHITTAKER, E. T., and WATSON, G. N., 1950, *A Course of Modern Analysis* (Cambridge: University Press), p. 133.

XXV. *The Boundary Layer in Three Dimensional Flow.—Part I.*
Derivation of the Equations for Flow along a General Curved Surface.

By Professor L. HOWARTH, F.R.S.,
 Department of Mathematics, University of Bristol*.

[Received January 9, 1951.]

SUMMARY.

The general equations of boundary layer flow along a curved surface S are set up in an appropriate system of orthogonal coordinates and the importance of the curvatures in the general case is made evident.

It is shown that, for a general flow, the necessary and sufficient condition for the curvatures to disappear from the equations of flow is that the boundary layer should be along the surface of a cylinder or a plane.

The form assumed by the equations when S is a surface of revolution is derived.

In Part II. there will be a discussion of the flow in the vicinity of a stagnation point on a general surface.

THE COORDINATE SYSTEM.

LET us denote the equation of the given surface S by

$$\chi(x, y, z) = 0. \quad (1)$$

This surface together with all parallel† surfaces constitutes a Lamé family of surfaces‡

$$\zeta(x, y, z) = \text{const.} \quad (2)$$

It follows that two families of surfaces

$$\xi(x, y, z) = \text{const.} \quad \text{and} \quad \eta(x, y, z) = \text{const.} \quad (3)$$

exist such that the three families ξ, η, ζ form a triply orthogonal family. The intersections of the original surface with the members of ξ and η are the lines of curvature of S § and the surfaces $\xi = \text{const.}$, $\eta = \text{const.}$ are, in fact, the developables formed by the normals along the lines of curvature on S ||.

* Communicated by the Author.

† See Weatherburn 'Differential Geometry', p. 158, "A surface which is at a constant distance along the normal from another surface S is said to be parallel to S ".

‡ *Op. cit.*, p. 207 or p. 218. Ex. 2.

§ Weatherburn, *op. cit.*, p. 211. Dupin's Theorem.

|| *Op. cit.*, p. 207.

If h_1, h_2, h_3 are the length elements in our coordinate system then, by definition h_3 is a function of ζ only. We can, without loss of generality, take it to be unity, ζ then representing distance measured normal to S.

THE EQUATIONS OF MOTION.

In terms of these coordinates, denoting by u, v, w the corresponding velocity components,

$$\text{div } \mathbf{V} = \frac{1}{h_1 h_2} \left[\frac{\partial}{\partial \xi} (h_2 u) + \frac{\partial}{\partial \eta} (h_1 v) + \frac{\partial}{\partial \zeta} (h_1 h_2 w) \right], \quad \dots \dots \dots (4)$$

$$\text{curl } \mathbf{V} = \frac{1}{h_2} \left[\frac{\partial w}{\partial \eta} - \frac{\partial}{\partial \zeta} (h_2 v) \right], \frac{1}{h_1} \left[\frac{\partial}{\partial \zeta} (h_1 u) - \frac{\partial w}{\partial \xi} \right], \frac{1}{h_1 h_2} \left[\frac{\partial}{\partial \xi} (h_2 v) - \frac{\partial}{\partial \eta} (h_1 u) \right] \quad \dots \dots \dots (5)$$

The components of acceleration are

$$\left. \begin{aligned} \frac{\partial u}{\partial t} + \frac{u}{h_1} \frac{\partial u}{\partial \xi} + \frac{v}{h_2} \frac{\partial u}{\partial \eta} + w \frac{\partial u}{\partial \zeta} + \frac{uv}{h_1 h_2} \frac{\partial h_1}{\partial \eta} - \frac{v^2}{h_1 h_2} \frac{\partial h_2}{\partial \xi} + \frac{wu}{h_1} \frac{\partial h_1}{\partial \zeta}, \\ \frac{\partial v}{\partial t} + \frac{u}{h_1} \frac{\partial v}{\partial \xi} + \frac{v}{h_2} \frac{\partial v}{\partial \eta} + w \frac{\partial v}{\partial \zeta} - \frac{u^2}{h_1 h_2} \frac{\partial h_1}{\partial \eta} + \frac{uv}{h_1 h_2} \frac{\partial h_2}{\partial \xi} + \frac{wv}{h_2} \frac{\partial h_2}{\partial \zeta}, \\ \frac{\partial w}{\partial t} + \frac{u}{h_1} \frac{\partial w}{\partial \xi} + \frac{v}{h_2} \frac{\partial w}{\partial \eta} + w \frac{\partial w}{\partial \zeta} - \frac{u^2}{h_1} \frac{\partial h_1}{\partial \zeta} - \frac{v^2}{h_2} \frac{\partial h_2}{\partial \zeta}. \end{aligned} \right\} \quad \dots \dots \dots (6)$$

On making the usual boundary layer assumptions, with the additional assumption that h_1, h_2 and all their first derivatives are $O(1)$, we have the following equations of motion

$$\frac{\partial u}{\partial t} + \frac{u}{h_1} \frac{\partial u}{\partial \xi} + \frac{v}{h_2} \frac{\partial u}{\partial \eta} + w \frac{\partial u}{\partial \zeta} + \frac{uv}{h_1 h_2} \frac{\partial h_1}{\partial \eta} - \frac{v^2}{h_1 h_2} \frac{\partial h_2}{\partial \xi} = -\frac{1}{\rho h_1} \frac{\partial p}{\partial \xi} + \nu \frac{\partial^2 u}{\partial \zeta^2}, \quad (7)$$

$$\frac{\partial v}{\partial t} + \frac{u}{h_1} \frac{\partial v}{\partial \xi} + \frac{v}{h_2} \frac{\partial v}{\partial \eta} + w \frac{\partial v}{\partial \zeta} + \frac{uv}{h_1 h_2} \frac{\partial h_2}{\partial \xi} - \frac{u^2}{h_1 h_2} \frac{\partial h_1}{\partial \eta} = -\frac{1}{\rho h_2} \frac{\partial p}{\partial \eta} + \nu \frac{\partial^2 v}{\partial \zeta^2}, \quad (8)$$

$$\frac{\partial p}{\partial \zeta} = O(1) \quad \dots \dots \dots (9)$$

and the equation of continuity is

$$\frac{1}{h_1 h_2} \left[\frac{\partial}{\partial \xi} (h_2 u) + \frac{\partial}{\partial \eta} (h_1 v) \right] + \frac{\partial w}{\partial \zeta} = 0. \quad \dots \dots \dots (10)$$

The length elements h_1, h_2 are not completely arbitrary; the Lamé relations, in our case, lead to the following results:—

- (i.) $\frac{1}{h_2} \frac{\partial h_1}{\partial \eta}$ and $\frac{1}{h_1} \frac{\partial h_2}{\partial \xi}$ are each functions of ξ and η only,
- (ii.) h_1 and h_2 are each of the form $F(\xi, \eta) + \zeta G(\xi, \eta)$,
- (iii.) $\frac{\partial}{\partial \xi} \left(\frac{1}{h_1} \frac{\partial h_2}{\partial \xi} \right) + \frac{\partial}{\partial \eta} \left(\frac{1}{h_2} \frac{\partial h_1}{\partial \eta} \right) + \frac{\partial h_1}{\partial \zeta} \frac{\partial h_2}{\partial \zeta} = 0. \quad \dots \dots \dots (11)$

Furthermore, if K_1 is the principal curvature on the surface $\xi = \text{const.}$ in the direction of the parameter η (the curve $\zeta = \text{const.}$ on this surface) and K_2 is similarly the principal curvature on the surface $\eta = \text{const.}$ in the direction of the parameter ξ .

$$K_1 = -\frac{1}{h_1 h_2} \frac{\partial h_2}{\partial \xi} \quad \text{and} \quad K_2 = -\frac{1}{h_1 h_2} \frac{\partial h_1}{\partial \eta}. \quad (12)$$

The surfaces $\xi = \text{const.}$ and $\eta = \text{const.}$ being developables, their other principal curvatures are zero, of course.

Also if K_a and K_b are the principal curvatures of the surface $\zeta = \text{const.}$ in the directions ξ and η increasing

$$K_a = -\frac{1}{h_1} \frac{\partial h_1}{\partial \xi}, \quad K_b = -\frac{1}{h_2} \frac{\partial h_2}{\partial \xi}. \quad (13)$$

Therefore, in terms of the curvatures K_1 , K_2 , the equations of motion (7), (8), and (10) may be written

$$\frac{\partial u}{\partial t} + \frac{u}{h_1} \frac{\partial u}{\partial \xi} + \frac{v}{h_2} \frac{\partial u}{\partial \eta} + w \frac{\partial u}{\partial \zeta} - K_2 uv + K_1 v^2 = -\frac{1}{\rho h_1} \frac{\partial p}{\partial \xi} + \nu \frac{\partial^2 u}{\partial \xi^2}, \quad (14)$$

$$\frac{\partial v}{\partial t} + \frac{u}{h_1} \frac{\partial v}{\partial \xi} + \frac{v}{h_2} \frac{\partial v}{\partial \eta} + w \frac{\partial v}{\partial \zeta} + K_2 u^2 - K_1 uv = -\frac{1}{\rho h_2} \frac{\partial p}{\partial \eta} + \nu \frac{\partial^2 v}{\partial \eta^2}, \quad (15)$$

$$\frac{1}{h_1} \frac{\partial u}{\partial \xi} + \frac{1}{h_2} \frac{\partial v}{\partial \eta} + \frac{\partial w}{\partial \zeta} - K_1 u - K_2 v = 0, \quad (16)$$

where the values of h_1 , h_2 , K_1 and K_2 may, to the orders of approximation involved, be taken in the surface S . As in two dimensional theory, we must suppose p prescribed, in virtue of (9), by the flow outside and then equations (14)–(16) are the equations which serve to determine u , v , w .

UNIQUENESS.

Considering the field of flow as a whole, the system of orthogonal coordinates we have set up is clearly not unique. For example, for an ellipsoid the confocal system is an obvious alternative. Nevertheless, since by Dupin's theorem the curves of intersection of a triply orthogonal family are lines of curvature on each it follows that, however we set up the orthogonal coordinate system, the surfaces $\xi = \text{const.}$ and $\eta = \text{const.}$ must intersect the surface S in its lines of curvatures. Hence, no matter how we choose our triply orthogonal family to contain S , the various possibilities for the families $\xi = \text{const.}$ and $\eta = \text{const.}$ must all touch the families we have chosen along the lines of curvature of S . Since we are concerned in boundary layer theory only with the immediate vicinity of S our equations represent the unique form for an orthogonal coordinate system, apart that is, from the choice of scales for ξ and η .

The general flow along the surface of a right circular cone of semi-angle α makes an instructive illustration. The coordinate system we have developed consists of

- (i.) cones parallel to the given cone ;
- (ii.) cones orthogonal to the given cone ;
- (iii.) meridian planes.

In cylindrical polar coordinates r, ϕ, z we may express these families as

$$\xi = \phi, \quad \eta = z \cos \alpha + r \sin \alpha, \quad \zeta = z \sin \alpha - r \cos \alpha, \quad \dots \quad (17)$$

so that
$$h_1 = \eta \sin \alpha - \zeta \cos \alpha = r, \quad h_2 = h_3 = 1, \quad \dots \quad (18)$$

$$K_1 = 0, \quad K_2 = -\frac{1}{h_1} \sin \alpha. \quad \dots \quad (19)$$

Spherical polar coordinates R, θ, ϕ with corresponding velocity components U, V, W would be an obvious alternative system. In the comparing the two we should have

$$u = W, \quad v = U \cos (\theta - \alpha) - V \sin (\theta - \alpha), \quad w = U \sin (\theta - \alpha) + V \cos (\theta - \alpha)^* \quad \dots \quad (20)$$

and at the surface of the cone

$$\frac{1}{h_1} \frac{\partial}{\partial \xi} = \frac{1}{R \sin \alpha} \frac{\partial}{\partial \phi}, \quad \frac{\partial}{\partial \eta} = \frac{\partial}{\partial R}, \quad \frac{\partial}{\partial \zeta} = \frac{1}{R} \frac{\partial}{\partial \theta}, \quad \dots \quad (21)$$

It can then be verified that the two sets of equations are identical.

DISCUSSION.

The presence of the terms K_1 and K_2 in eqns. (14)–(16) makes manifest the importance of curvature in the general problem, though it should be noted that the significant curvatures are not the principal curvatures of S but the non-zero principal curvatures of the two orthogonal families ξ and η . In this respect, the theory differs from the two dimensional theory where curvature effects, so long as the curvatures are not very large or change very rapidly, disappear from the equations. We may, in consequence, in three dimensional boundary layer flow expect effects additional to those we might reasonably associate with the addition of an extra dimension.

When K_1 and K_2 both vanish we have what is clearly an exceptional case in this respect and it is of some interest to determine the surfaces so defined. Although the vanishing of K_1 and K_2 refers only to values at the surface S , it can readily be established that they must in consequence vanish everywhere on the developables. Hence the developables $\xi = \text{const.}$ and $\eta = \text{const.}$ are planes.

Furthermore, we may now establish that one of these families consists of parallel planes. For, suppose, if possible, that two members of $\xi = \text{const.}$ are non-parallel planes. Any member of $\eta = \text{const.}$ must then, since it is orthogonal to both the chosen planes, meet them and must have

* Since differentiations have to be carried out it is obviously insufficient to consider surface values of u, v, w only.

a normal whose direction cosines are uniquely defined by the direction cosines of their normals. In other words, the family $\eta = \text{const.}$ must consist of parallel planes. Hence we infer that at least one of the families $\xi = \text{const.}$ and $\eta = \text{const.}$ must consist of parallel planes. Suppose it is $\eta = \text{const.}$ We can then without loss of generality express the equations of the two systems in the forms.

$$z = \eta, \quad \dots \dots \dots (22)$$

$$y = x f(\xi) + g(\xi), \quad \dots \dots \dots (23)$$

Suppose the third family is expressed by

$$F(x, y, z) = \zeta, \quad \dots \dots \dots (24)$$

Then, considering the three surfaces with parameters ξ_1, η_1, ζ_1 , which pass through the point x_1, y_1, z_1 we must have

$$z_1 = \eta_1, \quad y_1 = x_1 f(\xi_1) + g(\xi_1), \quad F(x_1, y_1, z_1) = \zeta_1, \quad \dots \dots (25)$$

and, since the surfaces are orthogonal

$$\frac{\left(\frac{\partial F}{\partial x}\right)_{x=x_1}}{1} = \frac{\left(\frac{\partial F}{\partial y}\right)_{y=y_1}}{f(\xi_1)} = \frac{\left(\frac{\partial F}{\partial z}\right)_{z=z_1}}{0}, \quad \dots \dots \dots (26)$$

Hence the surfaces $\zeta = \text{const.}$ are, in general, cylinders with generators parallel to the z axis; they include as a special case (when $f(\xi) = 0$) planes.

We may conclude therefore that it is only for boundary layers attached to cylinders and planes that the curvature effects vanish from the equations of motion. Moreover, in these cases, the boundary layer equations may be taken in Cartesian form. This is obvious for the case of the plane. For the cylinder it follows from eqn. (12) that h_1 is independent of η and h_2 is independent of ξ and therefore by condition (ii.) of p. 240 that in the surface S the length elements h_1, h_2 can each without loss of generality be transformed into unity. Thus in the case of the cylinder the equations may be written in Cartesian form with ξ as distance measured around a right section, η as distance measured along the generators and ζ as distance measured normal to S . We thereby recover the standard result in two dimensional flow and obtain the result already justified in particular by previous investigators that the equations in this form are valid for three dimensional flow past a yawed cylinder.

Finally we may obtain the forms taken by K_1 and K_2 when the surface S is one of revolution. The lines of curvature of S are then the meridian curves m and the "parallels" p . Thus the surfaces $\xi = \text{const.}$ are the meridian planes and hence

$$K_1 = 0.$$

The surfaces $\eta = \text{const.}$ are the right circular cones generated by the normals to S along the curves p . Let us consider a particular surface $\eta = \text{const.}$ generated by the normals to S along a particular parallel p_1 . Then if R is the length of the normal to this cone intercepted between p_1 and the axis of rotation

$$|K_2| = \dots$$

XXVI. *A Covariant Formulation of the Bloch-Nordsieck Method.*

By W. THIRRING and B. TOUSCHEK,

Department of Natural Philosophy, The University, Glasgow*.

[Received November 29, 1950.]

SUMMARY.

The results of the Bloch-Nordsieck method are derived in a covariant manner, based on a covariant form of the commutation-relations in momentum space.

§ 1.

IN this paper we shall give a covariant derivation of the well known Bloch-Nordsieck (1937) results on the multiple production of low energy quanta. A full proof will be based on the interpretation of the field theoretical set of equations recently given by Yang and Feldman 1950. In § 3 a derivation of the same result from the Dyson-Feynman form of the S-matrix will be outlined.

Though the results obtained here are not new, and have in fact been discussed by several authors, the importance of the Bloch-Nordsieck problem as the only problem in the theory of fields which admits an accurate solution seems to justify a general reformulation of the procedure. The simplification which enables one to find an accurate solution rests on the neglect of the recoil of the source particles, the motion of which is assumed to be given. The theory of fields contains a second problem of this kind in which the rôles of Fermi- and Bose-particles are interchanged. Though this problem can be solved in principle, no manageable form of solution has been found so far. If the solutions of both problems could be handled with equal ease they could be made the basis of a new approximation method. An approximation of this type would have the advantage that the trivial effects of higher powers of the interaction constant (unitarity of the S-matrix) would be considered in every step of the procedure, and only the genuine higher order effects expressing the intrinsic non-linearity of the system would be subjected to gradual approximation. It seems essential for such a programme that the Bloch-Nordsieck result should be given in a covariant form, though its immediate practical applications are of course non-relativistic.

§ 2.

We consider a system of coupled fields. The Bose field will be described by a wave operator $\phi(x)$, and we shall restrict the first part of this discussion to scalar particles. The extension to more general Bose fields is

* Communicated by the Authors.

straight-forward. The source particles are summarily described by a source density $\rho(x)$; x denotes a point in space-time. The field equations are written in the Yang-Feldman form :

$$\begin{aligned}\phi(x) &= \phi^{\text{in}}(x) + \int dx' \rho(x') D_r(x-x') \\ &= \phi^{\text{out}}(x) + \int dx' \rho(x') D_a(x-x'),\end{aligned}$$

where the functions $D_r(x)$ and $D_a(x)$ are the retarded and advanced solutions of the Poisson equation

$$(\square^2 - \mu^2) D_{r,a}(x) = \delta(x). \quad . \quad . \quad . \quad . \quad . \quad (1)$$

Since both ϕ^{in} and ϕ^{out} are solutions of the homogeneous wave equation $(\square^2 - \mu^2)\phi^{\text{in}} = 0$ and, therefore, satisfy identical commutation relations of the form

$$[\phi^{\text{in}}(x), \phi^{\text{in}}(x')] = -iD(x-x') \quad . \quad . \quad . \quad . \quad . \quad (2)$$

they must be connected by a unitary transformation

$$\phi^{\text{out}}(x) = \phi^{\text{in}}(x) + \int (D_r - D_a) \rho(x') dx' = S^{-1} \phi^{\text{in}}(x) S, \quad . \quad . \quad . \quad . \quad (3)$$

and it has been shown by Yang and Feldman that the unitary matrix S thus defined is identical with the Feynman-Dyson S -matrix.

Since ϕ is a c -number—the motion of the source particles is fixed— ϕ^{out} differs from ϕ^{in} only by a multiple of the unit matrix. $D_a - D_r$ is an odd invariant solution of the homogeneous wave equation, and actually

$$D_a(x) - D_r(x) = D(x).$$

The further calculation is considerably facilitated by transforming to k -space. This gives

$$\begin{aligned}\phi^{\text{out}}(x) &= \frac{1}{(2\pi)^3} \int dk \delta(k^2 - \mu^2) \phi^{\text{out}}(k) e^{ikx} \\ &= \frac{1}{(2\pi)^3} \int dk \delta(k^2 - \mu^2) [\phi^{\text{in}}(k) - \rho(k) \epsilon(k)] e^{ikx}, \quad . \quad . \quad . \quad . \quad (4)\end{aligned}$$

where the first equation is a definition of the Fourier transform $\phi^{\text{out}}(k)$. Use has been made of the Fourier representation

$$D(x) = -\frac{i}{(2\pi)^3} \int dk \delta(k^2 - \mu^2) \epsilon(k) e^{ikx}$$

of the D -function; $\epsilon(k)$ is ± 1 according to $k_0 \gtrless 0$ and $\rho(k)$ is defined by

$$\rho(x) = \frac{1}{(2\pi)^4} \int dk \rho(k) e^{ikx}. \quad . \quad . \quad . \quad . \quad . \quad (5)$$

In the following the abbreviation $\delta\phi(k) = -\rho(k)\epsilon(k)$ will be used.

The energy momentum 4-vector for the incoming wave is given by

$$P_v^{\text{in}} = \frac{1}{(2\pi)^3} \int_{k_0 > 0} dk \delta(k^2 - \mu^2) k_v \phi^{\text{in}}(k)^+ \phi^{\text{in}}(k),$$

and a similar expression holds for the outgoing wave. The number of quanta in the incoming wave is

$$N^{\text{in}} = \frac{1}{(2\pi)^3} \int_{k_0 > 0} dk \delta(k^2 - \mu^2) \phi^{\text{in}}(k)^+ \phi^{\text{in}}(k). \quad . \quad . \quad (6)$$

In the present case we want to consider an experiment in which quanta are only observed over a limited range of frequency. We shall therefore introduce an interval Δ in k -space which contains only this range of frequencies. It is then easily seen that N_Δ —resulting from equation (6) by integrating only over the interval Δ —is still an integral positive number. This follows from the commutation relations

$$\delta(k'^2 - \mu^2) \delta(k^2 - \mu^2) [\phi^+(k) \phi(k')] = -(2\pi)^3 \delta(k - k') \epsilon(k) \delta(k'^2 - \mu^2) \quad . \quad (7)$$

for the free fields, which can be derived from equation (2). Using (7), one obtains

$$\delta(k^2 - \mu^2) [N_\Delta \phi(k)] = -\phi(k) \delta(k^2 - \mu^2)$$

$$\delta(k^2 - \mu^2) [N_\Delta \phi^+(k)] = +\phi^+(k) \delta(k^2 - \mu^2)$$

for any $k \in \Delta$.

Since we want to determine the probability for the production of a certain number n of quanta in Δ , we shall assume that the incoming wave does not carry any quanta at all in Δ . Then if χ_0 is the eigenvector ($|\chi_0|^2 = 1$) describing such a state, we have

$$\delta(k^2 - \mu^2) \phi^{\text{in}}(k) \chi_0 = 0 \quad . \quad . \quad . \quad (8)$$

for every $k \in \Delta$. For the outgoing wave χ'_0 is the corresponding vacuum state and the basis-vectors for the 1, 2, . . . n particle states are

$$\chi'_1(k_1) = \frac{1}{\sqrt{1!}} \phi^{\text{out}}(k_1)^+ \chi'_0 \delta(k_1^2 - \mu^2),$$

$$\chi'_2(k_1 k_2) = \frac{1}{\sqrt{2!}} \phi^{\text{out}}(k_1)^+ \phi^{\text{out}}(k_2)^+ \chi'_0 \delta(k_1^2 - \mu^2) \delta(k_2^2 - \mu^2),$$

$$\chi'_n(k_1 \dots k_n) = \frac{1}{\sqrt{n!}} \phi^{\text{out}}(k_1)^+ \dots \phi^{\text{out}}(k_n)^+ \chi'_0 \prod_i \delta(k_i^2 - \mu^2).$$

The most general n -particle state can then be described by a Hilbert vector,

$$F_n^r = \frac{1}{(2\pi)^{3n}} \int_\Delta dk_1 \dots \int_\Delta dk_n u_n^r(k_1 \dots k_n) \chi_n(k_1 \dots k_n), \quad . \quad . \quad (9)$$

where $u_n^r(k_1, \dots, k_n)$ is a symmetric "Schrödinger-function" and the index r indicates one particular distribution of the quanta over the element Δ of k -space. To normalize F_n^r such that $F_n^r N_\Delta F_n^r = n$ we have to make

$$\frac{1}{(2\pi)^{3n}} \int_\Delta dk_1 \dots \int_\Delta dk_n \prod_i \delta(k_i^2 - \mu^2) |u_n^r|^2 = 1.$$

The proof of this is analogous to that for the well known case of oscillator eigenfunctions and can be carried out simply by using the method developed by Becker and Leibfried (1946). We shall use a complete set of orthogonal functions u_n^r , *i.e.* such a set that every symmetric function $f_n(k_1, \dots, k_n)$ defined in Δ can be expanded in terms of the u_n^r . The u 's will then satisfy the completeness relation

$$\frac{1}{(2\pi)^{3n}} \sum_r \int_{\Delta} \delta(k_i^2 - \mu^2) u_n^{r*}(k_1 \dots k_n) u_n^r(k'_1 \dots k'_n) = \frac{1}{n!} \sum_P \int_{\Delta} \delta(k_i - k'_i). \quad (10)$$

The symmetrized δ -function on the right-hand side of this equation can be replaced by the ordinary δ -function whenever it occurs multiplied by a function symmetric in the k_1, \dots, k_n .

The probability amplitude for the creation of n particles in a state r is now given by

$$(F_n^r \chi_0) = \frac{1}{(2\pi)^{3n}} \times \frac{1}{\sqrt{n!}} \int_{\Delta} dk_1 \dots \int_{\Delta} dk_n \Pi \delta(k_i^2 - \mu^2) \times u_n^{r*}(k_1 \dots k_n) (\chi_0'(\phi(k_1) + \delta\phi(k_1)) \dots (\phi(k_n) + \delta\phi(k_n)) \chi_0).$$

On account of equation (8) only the product term $\delta\phi(k_1)\delta\phi(k_2) \dots \delta\phi(k_n)$ gives a non-vanishing contribution. Since we are not interested in the particular distribution of the quanta inside the interval Δ we have to sum the squared amplitude over all the distributions defined by u_n^r . Thus, by using the completeness relation (10),

$$\sum_r |F_n^r \chi_0|^2 = \frac{1}{n!} \bar{n}^n |\chi_0' \chi_0|^2 = \omega_n(\Delta), \quad \dots \quad (11)$$

where

$$\bar{n} = \frac{1}{(2\pi)^3} \int_{\Delta} dk \delta(k^2 - \mu^2) |\delta\phi(k)|^2. \quad \dots \quad (12)$$

Since the total probability must be one we have

$$|\chi_0' \chi_0|^2 = e^{-\bar{n}}. \quad \dots \quad (13)$$

\bar{n} is the average number of quanta produced: $\bar{n} = \sum_n n \omega_n(\Delta)$. It can also be found by considering the vacuum expectation value $\chi_0 N^{\text{out}} \chi_0$ of N^{out} .

Since the interval Δ is arbitrary, this—in a sense—is a generalization of the Bloch-Nordsieck result. It shows how redundant information, *e.g.* the distribution of energy and momentum over the quanta in Δ , can be eliminated by the use of the completeness relation. Another link with the case of infinitesimal intervals considered by Bloch and Nordsieck lies in the addition theorem of Poisson distributions: Let the interval Δ be divided into two subintervals, Δ_1 and Δ_2 . Then $\bar{n} = \bar{n}_1 + \bar{n}_2$ and

$$\omega_n(\Delta) = \frac{(\bar{n}_1 + \bar{n}_2)^n}{n!} \exp\{-(\bar{n}_1 + \bar{n}_2)\} = \sum_{m=0}^n \omega_m(\Delta_1) \omega_{n-m}(\Delta_2).$$

The validity of the Poisson distribution in two subintervals therefore insures the validity of a Poisson distribution for the whole interval, and the proof can be easily extended to cover the case of an arbitrary number of subintervals.

It remains to define the source function $\rho(k)$ for the particular case where a source particle is scattered at $x=0$. Transcribing the above argument to a Maxwell field, we replace $\rho(x)$ by a vector source function $j_\mu(x)$ of a point electron, viz.,

$$j_\mu(x) = e \int_{-\infty}^{+\infty} p_\mu(\tau) \delta(x - \tau p(\tau)) d\tau$$

where, e.g., $p_\mu(\tau) = p_\mu$ for $\tau < 0$ and $p_\mu(\tau) = p'_\mu$ for $\tau > 0$. The sudden change in momentum imposes the restriction that in applying the result to a real scattering process one should limit the admissible frequency range to frequencies $\ll 1/\tau$, where τ is the effective time of collision. Otherwise a sudden change of momentum would be too rough an approximation. According to equation (5) we have for the Fourier transform of $j_\mu(x)$

$$j_\mu(k) = e \left(\frac{p_\mu}{(pk)} - \frac{p'_\mu}{(p'k)} \right),$$

The average number of quanta can be determined from equation (12):

$$\bar{n} = \frac{e^2}{(2\pi)^3} \int_{\Delta} dk \delta(k^2 - \mu^2) \left[\frac{(pe)}{(pk)} - \frac{(p'e)}{(p'k)} \right]^2,$$

where e is a polarization vector.

In the case of mesons $\rho(x)$ will be of the form

$$\rho(x) = g \int_{-\infty}^{+\infty} \sigma(\tau) \delta(x - \tau p(\tau)) d\tau,$$

where $\sigma(\tau)$ is a function describing an internal degree of freedom of the source particles, as e.g. their spin or isotopic spin. Both p and σ can change at $\tau=0$. In this case the Fourier transform of the source density is given by

$$\rho(k) = g \left\{ \frac{\sigma(-)}{(pk)} - \frac{\sigma(+)}{(p'k)} \right\}.$$

n can be easily determined from equation (12).

§ 3.

We shall now briefly indicate the derivation of the above results with Dyson's S-matrix

$$S = 1 - i \int \phi(1) \rho(1) + \frac{(-i)^2}{2!} \int P \phi(1) \rho(1) \phi(2) \rho(2) + \dots \quad (14)$$

Here $\phi(1)$ means $\phi(x)$ at the point x_1 , P is the operator arranging the factors in the product in order of time, and the integrations are to be extended over the whole x_1, \dots, x_n space. The problem consists in finding the matrix elements of S which lead from the vacuum state to a state where n particles are present. To this matrix element we shall get contributions from the $n+1$ st, $n+3$ rd, \dots terms in the expansion (14). A typical term of $n+2l$ th order will contain n factors $\phi(1)$ which create the final particles, l factors

which create l virtual particles, which are finally annihilated by the remaining l factors. In calculating the matrix element one has to keep in mind that one gets a factor

$$\binom{n+2l}{n}$$

corresponding to the number of possibilities of picking n ϕ 's out of the total $n+2l$ ϕ 's. A further factor $n!$ arises from the permutations of the n created particles among the n creation operators $\phi(1)$. The matrix element will therefore be of the form

$$\langle 0|S|n\rangle = (-i)^n [P\{\langle 0|\phi|k_1\rangle \dots \langle 0|\phi|k_n\rangle \rho(1) \dots \rho(n) \\ \times \left[1 + \frac{(-i)^2}{2!} \langle 0|\phi(n+1)\phi(n+2)|0\rangle + \dots \right], \dots] \quad (15)$$

where Dirac's notation for the matrix elements has been used. It should be noted that the expression in the square brackets is independent of n . The relative probabilities for the production of a given number of particles are thus given by the first non-vanishing approximation. Integrating the squared matrix element over all energy momentum vectors of the quanta, we obtain

$$|\langle 0|S|n\rangle|^2 = \frac{1}{(2\pi)^{3n}} \times \frac{1}{n!} \int_{\Delta_1 \dots \Delta_n} dk_1 \dots dk_n |\rho(k_1)|^2 \dots |\rho(k_n)|^2 \\ \times \prod_i \delta(k_i^2 - \mu^2) []^2.$$

The $1/n!$ arises from the fact that one wants to integrate all the k 's over the same interval. Since the particles are not distinguishable, one has to divide by $n!$. $[]^2$, which is the square of the bracket in equation (15), can be determined as before with the aid of the unitarity of the S-matrix. It gives only a normalization of the probability. The result is again

$$|\langle 0|S|n\rangle|^2 = \frac{\bar{n}^n}{n!} e^{-\bar{n}},$$

with n , as before, defined by equation (12).

One of us (W. T.) is indebted to the Nuffield Foundation for the award of a Fellowship during the tenure of which this work was carried out.

REFERENCES.

- BLOCH, F., and NORDSIECK, A., 1937, *Phys. Rev.*, **52**, 54.
 YAND, C. N., and FELDMAN, D., 1950, *Phys. Rev.*, **79**, 972.
 BECKER, R., and LEIBFRIED, G., 1946, *Phys. Rev.*, **69**, 34.

XXVII. *Absorption of Penetrating Shower Secondaries.*

By D. M. RITSON*,
 Dublin Institute for Advanced Studies†.

[Received November 23, 1950.]

ABSTRACT.

Measurements with a penetrating shower set at sea level showed an apparent mean free path for absorption of the secondaries of penetrating showers of 405 ± 1 gr./cm.² for lead and 350 ± 40 gr./cm.² for iron.

INTRODUCTION.

MEASUREMENTS for the absorption of penetrating shower secondaries have been made previously for lead for thicknesses of 100 gm./cm.²—200 gm./cm.² (Walker 1950). A comparison of the differential absorption for lead and iron under a large thickness of lead (150 gm./cm.²) has been made by (Piccioni 1950).

The measurements reported below give results for the absorption of the secondaries in the range 60 gm./cm.²—450 gm./cm.² for lead and 60 gm./cm.²—260 gm./cm.² for iron.

These investigations were started at a time when it was considered that the penetrating particles of a shower were predominantly π mesons. Later results have shown that the particles capable of transversing 20 centimetres of lead will be composed almost equally of protons and π mesons (Camerini *et al.* 1950). Thus such an investigation does not throw direct light on the π mesons interaction.

However, the background data provided by such an investigation of the effect of lead absorber thickness on the counting rate of a "penetrating shower" set and the further data obtained on the penetration of the shower secondaries of an "extensive shower", appeared to make the publication of a brief report of my investigation worth while.

EXPERIMENTAL.

Measurements were made on penetrating showers at sea level with the apparatus shown in fig. 1.

The top six counters (marked either A, B, or C) and the lower ten counters marked either D or E were of active area 3.5 cm. \times 50 cm. Each counter in the top tray was separated from its neighbour by 2.5 cm. of lead. The tray was covered by 15 cm. of lead, the side shielding consisted of 10 cm. of lead, and there was a thickness of 2.5 cm. of lead immediately beneath the tray.

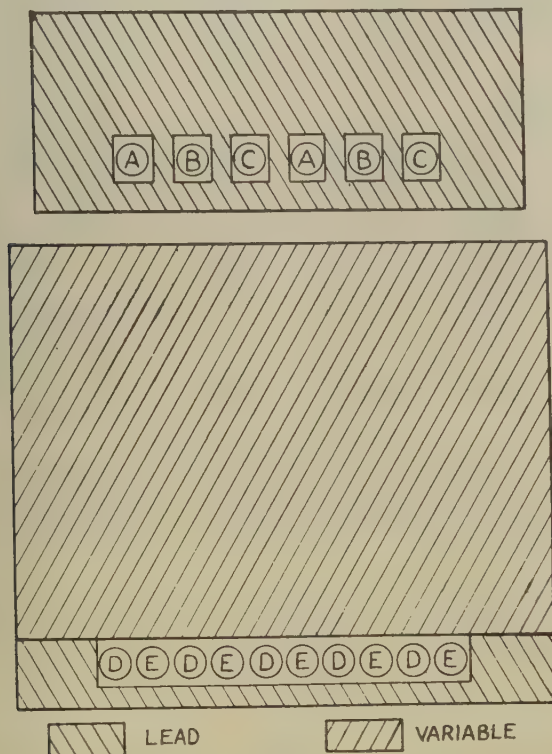
* Communicated by Professor C. B. A. McCusker.

† Now at Department of Physics, University of Rochester.

The absorber S_1 over the lower ten counters was variable. The side shielding again consisted of 10 cm. of lead.

Coincidences (A B C D E) were recorded. In order to record penetrating showers simultaneously accompanied by air showers, the pulse X_3 was taken from coincidences between three extended trays, and coincidences A B C X_3 , A B C D E X_3 were recorded throughout the experiment. (The three extended trays each of area 750 cm.^2 were simultaneously used in another experiment, in which they were covered with thicknesses of lead, water, carbon, iron, up to one cascade unit, thick.)

Fig. 1.



RESULTS.

Fig. 2. plots the logarithm of the rate A B C D E against thickness of the absorber S_1 in g./cm.^2 of lead. It will be seen that the results can be represented by an exponential absorption for lead with mean free path $405 \pm 30 \text{ gm./cm.}^2$. (The results were corrected for barometric variations to a pressure of 1015 millibars using a barometer coefficient of -1 per cent per millibar.) A measurement was made with an absorber thickness S_1

composed of 7.5 cm. of lead directly over the counters, and 48 gm./cm.² of carbon above the lead. The observed rate was 0.87 ± 0.05 per hr. Comparison with the lead absorption curve shows that this rate corresponds to a lead absorber thickness of 90 ± 40 gm./cm.².

Measurements made with absorber S_1 composed of 260 gm./cm.² of iron gave an observed rate corrected to 1015 mbs atmospheric pressure, of 0.52×0.03 c.p.h.r. corresponding to a lead absorber thickness of 300 gm./cm.² thus giving the stopping power of iron relative to lead as 1.15 ± 0.15 .

Fig. 2.

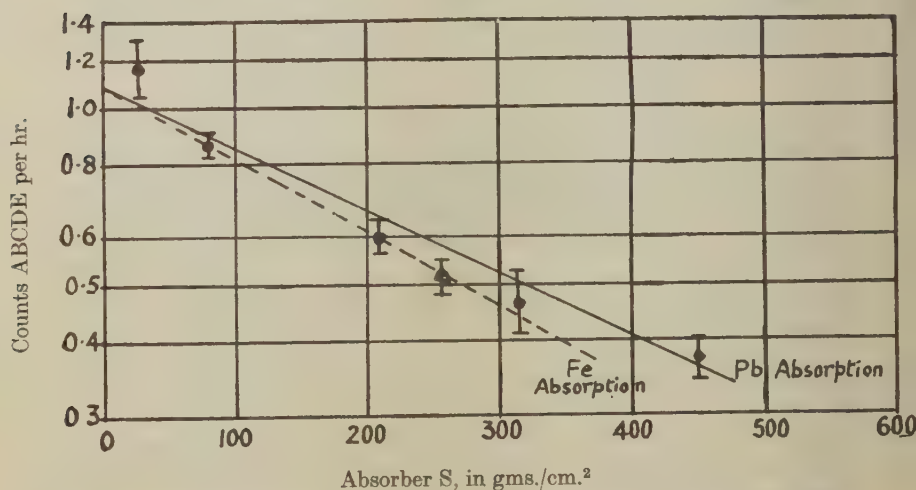


Fig. 2 shows the counting rate $ABCDE$ plotted against absorber thickness in gm./cm.². The triangular point at 260 gm./cm.² refers to iron absorber. The full line is the best curve for lead absorber, and the dotted line is the best for iron absorber.

Table I. gives the rate of accompanied showers. As the absorber over the extended trays was varied during the course of the experiment we compare the ratios

$$\frac{ABCDE X_3}{ABC X_3}.$$

Including all results for small absorber thicknesses we obtained a value of

$$\frac{ABCDE X_3}{ABC X_3}$$

of 0.71 ± 0.10 . If the absorption of the accompanied showers was the same as for non-accompanied showers we should expect a ratio of 0.31 ± 0.04 for 450 gm./cm.² of lead absorber. The observed value of 0.55 ± 0.10 gives an indication that the accompanied penetrating showers are more penetrating than the non-accompanied, though the statistical weight is poor,

Discussion and Comparison with other Experiments.

Similar penetrating shower measurements have been made by Piccioni (1950), Walker (1950). The number of penetrating secondaries, however, necessary to cause a count varied in the two experiments. The data of Walker (1950), also Piccioni (1950) show that the repartition of shower size under various thicknesses of absorber does not appear to alter. Accordingly the absorption curves obtained in the different experiments should be similar.

The values obtained for the apparent mean free paths in Lead by Piccioni and Walker, are respectively, 360 ± 40 gm./cm.² and 405 ± 110 gm./cm.². Our value of 405 ± 30 gm./cm.² is in good agreement. Further Piccioni obtained a ratio for the stopping powers of Iron and Lead of 1.02 ± 0.13 in agreement with our value of 1.15 ± 0.15 .

TABLE I.

Data on Penetrating Showers Accompanied by Extensive Air Showers.

Thickness of S ₁ Absorber	Time (hrs.)	Number of Counts A B C X ₃	Number of Counts A B C D E X ₃
26 gm./cm. ² of lead	97	3	3
78 gm./cm. ² of lead	140	9	7
105 gm./cm. ² of lead	128	11	5
78 gm./cm. ² of lead plus 50 gm./cm. ² of carbon	339	18	14
210 gm./cm. ² of lead	284	21	12
315 gm./cm. ² of lead	137	8	3
450 gm./cm. ² of lead	500	31	17
260 gm./cm. ² of iron	444	29	18

The interpretation of these results is not straightforward, but it is now clear from the results with both cloud chambers and photographic plates, (Brown and McKay 1950, Camerini *et al.* 1950) that the high energy secondaries of penetrating showers are a mixture of protons, neutrons and π -mesons.

At any level in the absorber there will be simultaneous absorption and production of ionizing particles, the measured absorption thus being only indirectly related to the actual absorption processes taking place in the material.

Stress has been laid (Piccioni 1950, *cf.* Greisen 1950 for discussion of Piccioni's results) on the fact that if nuclear processes predominate for absorption and production the stopping powers of iron and lead should be in the ratios of the geometric cross sections *i. e.* 1.55 : 1, and not in the ratios of the stopping powers for ionization losses of 1.1 : 1. This, however,

is too simple an approach to the problem. In the presence of some degree of transparency such as would be expected for nucleons with energies of the order of 1 Bev, and for π -mesons in the 100 Mev—1 Bev range, the ratio of the cross sections for nuclear interactions would be considerably lower. In addition ionization loss processes will play some role and a ratio of the order of 1.2—1.4 would not therefore be in contradiction with present views as to the relatively strong interactions of π -mesons and nucleons.

It is to be expected that the nucleons forming part of the extensive showers will have a harder energy spectrum than those nucleons not accompanied by extensive showers, and thus those nucleons should give rise to higher energy events with greater penetrating power.

ACKNOWLEDGMENTS.

The author is indebted for helpful discussion throughout this work with Profs. Janossy and McCusker and to very considerable assistance by Mr. Millar in running the experiment.

REFERENCES.

- BROWN and MCKAY, 1950, *Phys. Rev.*, **77**, 342.
CAMERINI, FOWLER, LOCK and MUIRHEAD, 1950, *Phil. Mag.*, **41**, 413.
GREISEN, 1950, *Phys. Rev.*, **77**, 713.
PICCIONI, 1950, *Phys. Rev.*, **77**, 6.
WALKER, 1950, *Phys. Rev.*, **77**, 686.

XXVIII. *The Conditions at a Sharp Leading Edge in Supersonic Flow.*

By O. BARDSLEY,

Fluid Motion Laboratory, University of Manchester*.

[Received January 10, 1951.]

[Plates IX.—XII.]

SUMMARY.

Schlieren photographs have been taken to show the supersonic flow past a sharp wedge placed at an incidence large enough to give an expansion region on one side. In addition to the flow phenomena predicted by inviscid theory, the photographs show a weak shock wave immediately upstream of the expansion region. Various possible explanations of this are considered and it is shown that the shock wave is caused by the slight bluntness of the leading edge, although the thickness of the leading edge is only about 8μ . It cannot be explained by considering the growth of the boundary layer, neither is there any evidence of boundary-layer separation.

§ 1. INTRODUCTION.

ACCORDING to inviscid theory, the supersonic flow past a perfectly sharp wedge consists of two independent regions separated by the wedge. If the angle of incidence of the wedge is sufficiently large there is a centred expansion on one side and a shock wave on the other. It was expected that this theoretical flow pattern might not be found in practice, either because of viscous effects or because of bluntness of the leading edge. Some experiments were therefore made to investigate the supersonic flow past a wedge at a high incidence.

§ 2. NOTATION.

M, Mach number.

 p , pressure before shock wave. Δp , rise of pressure in shock wave.

R, Reynolds number.

 $s = \Delta p/p$, shock-wave strength.

T, absolute temperature.

 t , thickness of body near leading edge. u_1 , velocity outside boundary layer. x , distance from leading edge.

* Communicated by W. A. Mair.

- y , distance from axis.
 δ_1 , displacement thickness of boundary layer in compressible flow.
 δ_1^* , displacement thickness of boundary layer in incompressible flow.
 γ , ratio of specific heats.
 θ^* , momentum thickness of boundary layer in incompressible flow.
 μ , coefficient of viscosity.
 ν , coefficient of kinematic viscosity.
 σ , Prandtl number.

§ 3. EXPERIMENTAL DETAILS.

The intermittent supersonic wind tunnel, the two-mirror schlieren system, and the technique for measurement of humidity have already been described by Bardsley and Mair (1951). The mean Mach number in the working section during the present experiments was 1.965. An alternative optical system which produced a magnified image was used for figs. 6-8 (Pls. XI. & XII.). In this system the object lens was removed and the second mirror arranged to give an enlarged image of a selected area of the working section on the screen. Measurements of the humidity of the air passing through the tunnel showed that the water-vapour content was always less than 1 part in 2000 by weight.

The wedge used was 1.27 cm. long in the direction of the stream, had an apex angle of 10.0° and extended across the whole width of the tunnel. It was made of high-carbon steel, ground and lapped to make the leading edge as nearly perfect as possible, with a constant apex angle. An estimate of the thickness of the leading edge was obtained using a shadowgraph technique. The profile of the wedge was illuminated and a short-focus convex lens was used to form an image magnified 25 times on a screen. Several typical parts of this image were photographed before and after the experiments. Before the experiments about 90 per cent of the span had a profile similar to that shown in fig. 1 (Pl. IX.); the remaining 10 per cent was similar to that shown in fig. 2 (Pl. IX.). After the experiments about 50 per cent of the span had deteriorated to the condition shown in fig. 2, the remainder being unaltered. The deterioration was probably caused by dust in the air stream, although the total running time of the tunnel was only about 2 minutes.

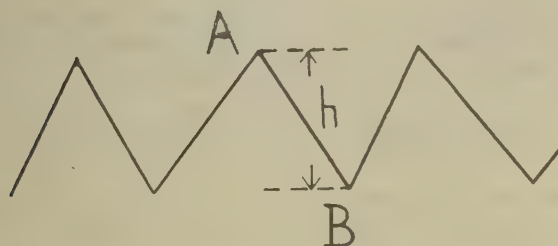
Fig. 9 is a diagrammatic representation of the indentations shown in figs. 1 and 2. The average depth of the indentations (h) was measured on the photographs. Assuming that the wedge angle was constant and that the thickness at a point A was very small (2μ), the thickness at a point B was calculated. This thickness was found to be 5μ for the parts of the edge in better condition (fig. 1) and 12μ for the deteriorated parts (fig. 2). The same method and assumptions were used previously on a similar wedge and gave good agreement with the thickness as measured by a calibrated microscope.

The wedge was supported in the wind tunnel by two arms on the downstream side. The position of these arms was altered, as required, to change the angle of incidence of the wedge.

The knife edges in the schlieren system were horizontal and were arranged so that in all the photographs increasing density in an upward direction was represented by a dark region.

Preliminary visual observations, using a mercury-vapour lamp, showed that the flow on the lower side of the wedge was rather unsteady when the deflection angle at the upper surface was greater than about 7° . This unsteadiness appeared to be due to the interaction between the shock wave on the lower side of the wedge and the boundary layer on the bottom wall of the tunnel. Because of this unsteadiness a short-duration flash (effective exposure about 5 microseconds) was used as the light source for photography. Photographs of the flow are shown in figs. 3-5 (Pls. X. & XI.) for positions of the wedge giving stream deflection angles (on the expansion

Fig. 9.



Indentations in leading edge.

side) of 0° , 5° , and 10° . (The possible error in these angles is $\pm 1^\circ$.) At the Mach number of these experiments (1.965) the maximum deflection at an attached shock wave is 22.3° , so that with this wedge (10° apex angle) the deflection at the expansion could not exceed 12.3° .

§ 4. DISCUSSION OF THE PHOTOGRAPHS.

The arms supporting the wedge continue downstream beyond the field of view; the position of the back of the wedge is revealed by the expansion region on the lower side. The wake is clearly visible in figs. 4 and 5, and shock waves can be seen where the direction of flow changes to that of the wake. The bump that appears about two-thirds of the way along the upper surface of the wedge is a small piece of rubber sealing-material at one of the glass side plates. In figs. 3-5 the region representing the shock wave on the high-pressure side of the wedge is fan-shaped in appearance. This is caused by curvature of the shock wave as it enters the turbulent boundary layers on the glass side-walls of the tunnel.

In each photograph the flow past the wedge is similar to that predicted by inviscid theory, but in addition there is a shock wave immediately upstream of the expansion region. This must be caused either by viscosity or by the slight bluntness of the leading edge. Three alternative explanations are considered below.

Firstly, consider the rate of growth of the boundary layer. In the experiments the shock wave occurs for a stream deflection angle (measured at the surface of the wedge) as large as 10° . The boundary layer is therefore considered at the point where its rate of growth is equal to 10° . Blasius' solution (1908) of the laminar boundary-layer equations for incompressible flow past a flat plate shows that the displacement thickness is

$$\delta_1^* = 1.72(\nu x/u_1)^{\frac{1}{2}},$$

and the momentum thickness θ^* is given by

$$\theta^*/\delta_1^* = 0.386,$$

where ν is the kinematic viscosity, u_1 is the velocity outside the boundary layer and x is the distance from the leading edge of the plate. It follows from Howarth's solution (1948) for a flat plate (assuming $\sigma=1$ and $\mu \propto T$) that for compressible flow the displacement thickness is

$$\delta_1 = \delta_1^* \left[1 + \frac{\gamma-1}{2} \left(1 + \frac{\theta^*}{\delta_1^*} \right) M^2 \right].$$

Hence in our case an approximate value of the displacement thickness of the boundary layer on the surface of the wedge is given by

$$\delta_1 = 4(\nu x/u_1)^{\frac{1}{2}}.$$

The rate of growth of the boundary layer is then

$$\frac{d\delta_1}{dx} = 2 \left(\frac{\nu}{u_1 x} \right)^{\frac{1}{2}} = 2R^{-\frac{1}{2}},$$

where $R = u_1 x/\nu$, the Reynolds number at the station x .

At the point where the rate of growth is equal to 10° (≈ 0.2 radians),

$$\frac{d\delta_1}{dx} = 0.2 = 2R^{-\frac{1}{2}},$$

therefore $R=100$.

The boundary-layer theory is not strictly applicable for such a small Reynolds number. However, since the theory would make $d\delta_1/dx \rightarrow \infty$ as $x \rightarrow 0$ it follows that the actual rate of growth near the leading edge must be smaller than that given by the theory. Hence at the point where the rate of growth of the boundary layer is 10° , x is not greater than the value given by $R=100$. The stagnation conditions are atmospheric, so

that the Reynolds number in the test section can be expressed as 1.34×10^5 per cm. Therefore when $R=100$,

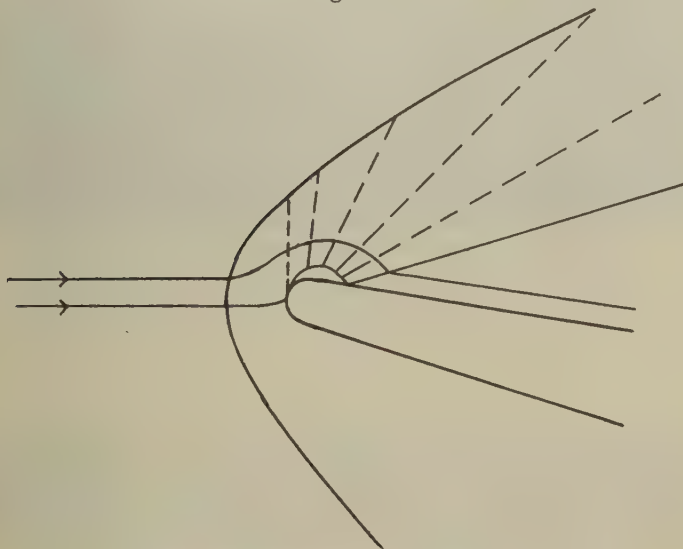
$$x = \frac{100}{1.34 \times 10^5} \approx 8 \times 10^{-4} \text{ cm.},$$

and at this point

$$\delta_1 = 4R^{-1/2}x \approx 3 \times 10^{-4} \text{ cm.}$$

Thus if there were a point at which the boundary layer grew so rapidly that the sign of the stream deflection was consistent with the presence of a shock wave, the values of x and δ_1 at this point would be of the same order

Fig. 10.



Flow with separation of boundary layer.

of magnitude as the thickness of the leading edge itself. This suggests that the effect of the boundary layer on the formation of the shock wave in front of the expansion is small compared with the effect of the bluntness of the leading edge.

Secondly, consider the possibility of boundary-layer separation. This is a well known phenomenon in the case of flow past blunt-nosed bodies and has been observed, for example, by Liepmann (1950) and by Holder, Tomlinson and Rogers (1949). In their experiments the bodies were at zero incidence and it was found that for sufficiently blunt noses there was a separation of the boundary layer near the nose, followed by re-attachment with an oblique shock wave at the point of re-attachment. If this type of flow occurred on the expansion side in the present experiments the pattern observed would be similar to that shown in fig. 10. In particular, a shock

EXPLANATION OF THE PLATES.

PLATE IX.

Fig. 1.

Leading edge in good condition.

Fig. 2.

Leading edge in deteriorated condition.

PLATE X.

Fig. 3.

Stream deflection angle 0° .

Fig. 4.

Stream deflection angle 5° .

PLATE XI.

Fig. 5.

Stream deflection angle 10° .

Fig. 6.

Stream deflection angle 0° .

PLATE XII.

Fig. 7.

Stream deflection angle 5° .

Fig. 8.

Stream deflection angle 10° .



Fig. 1.

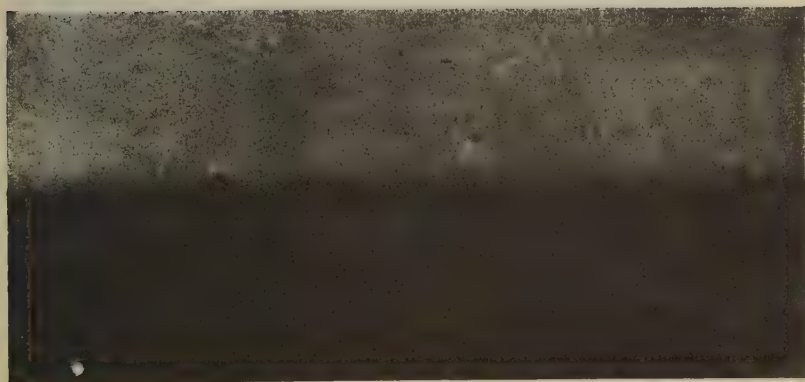


Fig. 2.

Fig. 3.

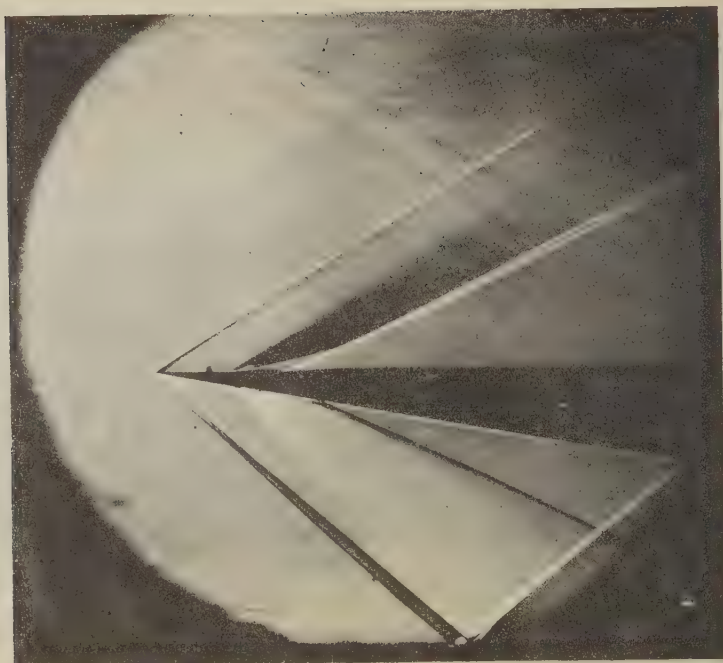
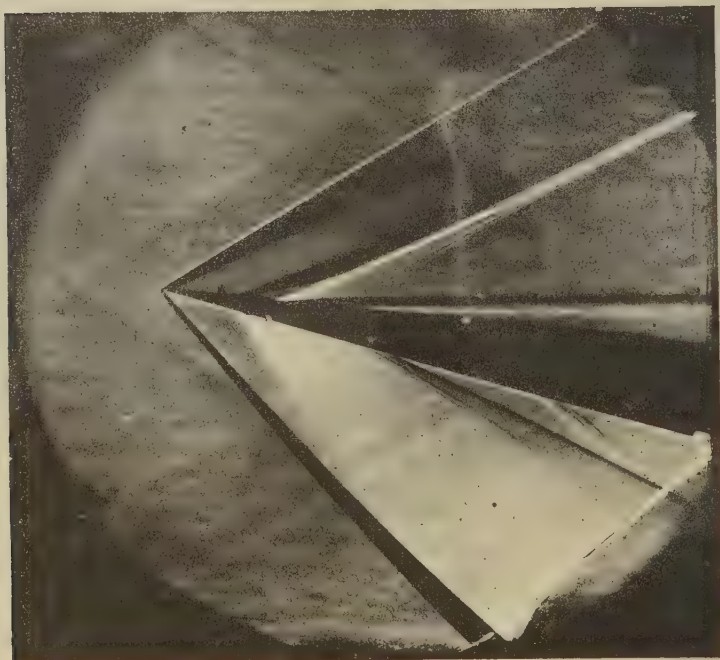


Fig. 4.



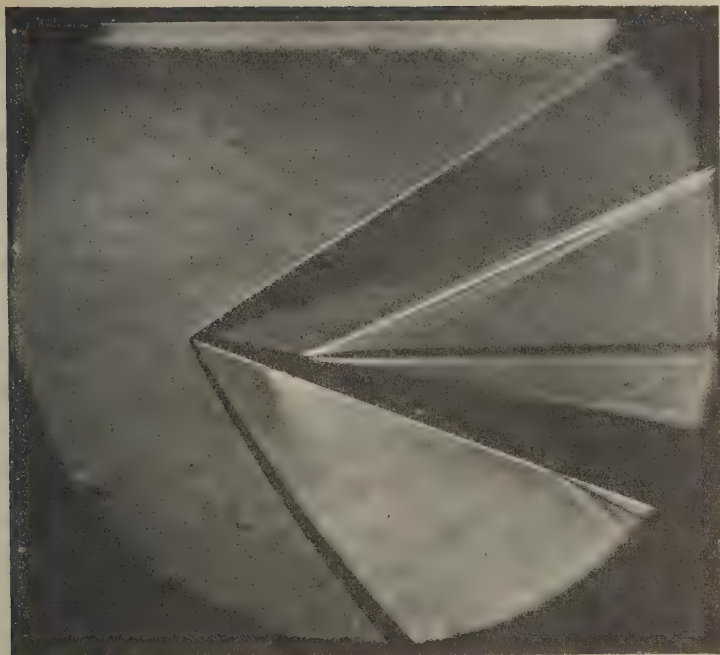


Fig. 5.

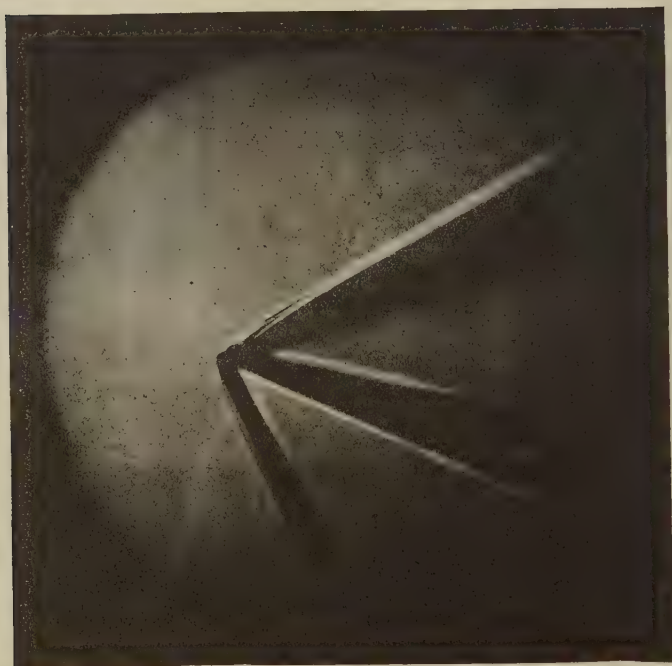


Fig. 6.

Fig. 7.



Fig. 8.



wave would be visible on the downstream side of the expansion. No shock wave can be seen in this position in figs. 3-5, but to investigate this further the schlieren system was modified, as described earlier, to give an enlarged image. Photographs produced by this system are shown in figs. 6-8; the scale of these is such that the wedge chord is approximately three-quarters of the diameter of the field of view. These show the flow for stream deflection angles of 0, 5, and 10° , and correspond to figs. 3, 4, and 5 respectively. Again, there is no sign of a second shock wave that would indicate boundary-layer separation. Moreover, a theoretical investigation by Mair (not yet published) has shown that a shock wave having a strength ($s = \Delta p/p$) as small as about 0.01 should be detectable with this schlieren apparatus. The deflection of the stream at a shock wave of this strength is only about 0.2° .

Lastly, consider the effect of the finite thickness of the leading edge. The inclination of the shock wave at a large distance from the leading edge was measured and found to be about 31.7° in all the photographs. This corresponds to a shock-wave strength (s) of 0.08. Since the possible error in measuring the shock-wave angle is about $\pm \frac{1}{2}^\circ$, the corresponding error in s is ± 0.035 , so that only the order of magnitude of the shock-wave strength can be found by this method. As already mentioned, a shock wave having a strength of this order should be easily visible in the photographs.

Now consider the theoretical relation between the shock-wave strength and the thickness of the leading edge of the wedge. For inviscid flow, Friedrichs (1948) has shown that the strength of the shock wave from the leading edge of a thin two-dimensional body with a rounded nose is inversely proportional to the square root of the distance from the axis, for large values of this distance. This can be written in the dimensionless form

$$s = k(t/y)^{\frac{1}{2}},$$

where k is a constant (for geometrically similar bodies), y is the distance from the axis, and t is a length defining the size of the body, taken as the thickness near the leading edge. Applying this result to the photographs of the flow past a flat plate with a blunt nose, obtained by Holder, Tomlinson and Rogers (1949), the constant k is found (by measuring the shock-wave angles) to be about 3. If it is assumed that the irregularly shaped edge of the wedge (figs. 1 and 2) gives a flow at large distances similar to that produced by a two-dimensional blunt nose of thickness t , the equation $s = 3(t/y)^{\frac{1}{2}}$ can be applied to the present experiments.

Putting $t = 8 \times 10^{-4}$ cm. (an average value) and $y = 6$ cm., we get $s = 0.035$. Since the value of y at the upper boundary of figs. 3-5 is only about 5 or 6 cm., this calculation shows that a shock wave having a strength of the same order of magnitude as that observed can be explained by the known slight bluntness of the leading edge, without any consideration of viscosity.

§ 5. CONCLUSIONS.

It has been shown that the difference between the observed flow past a wedge (as sharp as possible) and that predicted by the idealized theory can be explained by the bluntness of the leading edge. There is evidence that viscosity has no significant effect on the formation of the shock wave upstream of the expansion region.

If experiments of this kind were made with a leading edge of greater thickness, the strength of the shock wave for a given value of y would be greater. The effect of the growth of the boundary layer would then be even less important, and only if the boundary layer separated could viscosity have any significant effect.

It may be noted that in these experiments the Reynolds number, based on the thickness of the leading edge, was very small compared with that in most other experiments on flow past blunt-nosed bodies. It is suggested that this difference in Reynolds number is important and may explain the absence of boundary-layer separation in the present experiments.

ACKNOWLEDGMENTS.

The author wishes to thank Professor M. J. Lighthill and Mr. W. A. Mair for their suggestions, and for the interest they have taken in the work. During the course of the research the author was assisted by a grant from the Aeronautical Research Council.

REFERENCES.

- BARDSLEY, O., and MAIR, W. A., 1951, *Phil. Mag.*, **52**, 1.
 BLASIUS, H., 1908, *Zeit. Math. Phys.*, **56**, 4-13.
 FRIEDRICHS, K. O., 1948, *Communications on Applied Mathematics*, Vol. 1, pp. 211-245.
 HOLDER, D. W., TOMLINSON, R. C., and ROGERS, E. W. E., 1949, A.R.C. 12418 (to be published).
 HOWARTH, L., 1948, *Proc. Roy. Soc. A*, **194**, 16.
 LIEPMANN, H. W., 1950, U.S. Naval Ordnance Laboratory Report 1133.

XXIX. *Matrix Elements for Octupole Radiative Transitions.*

By A. P. FRENCH,
Cavendish Laboratory, Cambridge *.

[Received December 11, 1950.]

DURING the analysis of some recent experiments on the angular correlation between alpha particles and gamma rays (Barnes, French and Devons 1950) it was necessary to find values of the matrix elements for certain octupole transitions. These were derivable from general formulæ obtained by Fierz (1949) by group-theoretical methods. Although Fierz deals with multipole radiation of any order, his formulæ do not cover all possible transitions. If j represents the total angular momentum of the initial state, which goes over to a state of angular momentum $j + \Delta j$ with the emission of radiation of multipole order 2^l , then the cases treated by Fierz are limited to $\Delta j = \pm l$ or $\pm(l-1)$. It was thought to be of interest to extend calculations to all possible values of Δj for the particular case of octupole radiation, since radiation of this order (or even higher) seems to appear rather frequently in nuclear problems.

The method used was a simple extension of that applied by Condon and Shortley (1935) to the problem of quadrupole transitions. We assume that the initial state is characterized by j , by its component m along some specified axis (which we shall take as the polar axis Oz in spherical polar coordinates, and by other observables α , with which we are not immediately concerned. The final state is characterized in a similar way by (j', m', α') . The matrix element of electric octupole moment for a transition between the states may then be written as follows:

$$\begin{aligned}
 (\alpha j m | \mathbf{r} \mathbf{r} \mathbf{r} | \alpha' j' m') \\
 = \sum_{\alpha'' j'', \alpha''' j'''} \sum_{m'', m'''} (\alpha j m | \mathbf{r} | \alpha'' j'' m'') (\alpha'' j'' m'' | \mathbf{r} | \alpha''' j''' m''') \\
 \times (\alpha''' j''' m''' | \mathbf{r} | \alpha' j' m').
 \end{aligned}$$

For given values of (α'', j'') and (α''', j''') this summation has for all (m'', m''') a common factor $G(j'', j''')$ given (in the Condon and Shortley notation) by

$$G(j'', j''') = (\alpha j \vdots r \vdots \alpha'' j'') (\alpha'' j'' \vdots r \vdots \alpha''' j''') (\alpha''' j''' \vdots r \vdots \alpha' j').$$

In order to perform a final summation over the (j'', j''') and so obtain the octupole matrix element in manageable form, it is necessary to relate the various $G(j'', j''')$. This can be done through the requirement that $\mathbf{r} \times \mathbf{r}$ shall be zero. If we put

$$\mathbf{r} = ix + jy + kz,$$

$$\mathbf{R} = x - iy,$$

then one must have

$$z\mathbf{R} - \mathbf{R}z = 0.$$

* Communicated by Professor D. R. Hartree.

This equation can be multiplied through from the left or from the right with z or R , and one can then demand that matrix elements such as $(\alpha jm | zzR - zRz | \alpha' j' m')$ shall be zero. The matrix elements of R and z in the (j, m) scheme are tabulated (Condon and Shortley, p. 62), so it is an easy matter to obtain a set of equations connecting the $G(j'', j''')$. Once this is done, a matrix element of octupole moment can be expressed in the form

$$(\alpha jm | \mathbf{r} \mathbf{r} \mathbf{r} | \alpha' j' m') = g(j, m, j', m') \times G,$$

where G is the same for all transitions $m \rightarrow m'$ having (α, j) and (α', j') the same. g is then a definite function of the j 's and m 's and can be found.

The radiation field is obtained from the electric moment by writing

$$\mathbf{E}(\theta, \phi) = \text{const} \times (\theta_0 \theta_0 + \varphi_0 \varphi_0) \cdot (\alpha jm | \mathbf{r} \mathbf{r} \mathbf{r} | \alpha' j' m') : \mathbf{r}_0 \mathbf{r}_0,$$

where $\mathbf{r}_0, \theta_0, \varphi_0$ are the unit vectors of a spherical polar system. The double dot product here denotes a scalar product of \mathbf{r}_0 with each of the two right-hand members of every triad of vectors appearing in the octupole moment. The form of the field depends, of course, only on Δm . The possibilities are listed below for convenience, normalized to an outgoing intensity of $4\pi/7$.

$$\mathbf{E}(0) = \frac{\sqrt{3}}{4} \theta_0 \sin \theta (5 \cos^2 \theta - 1) = \frac{\sqrt{3}}{4} \mathbf{L}(0) \quad \text{say,}$$

$$\mathbf{E}(\pm 1) = \frac{1}{8} [\theta_0 \cos \theta (15 \cos^2 \theta - 11) \pm i \varphi_0 (5 \cos^2 \theta - 1)] e^{\pm i \varphi} = \frac{1}{8} \mathbf{L}(\pm 1) \quad ,,$$

$$\mathbf{E}(\pm 2) = \frac{\sqrt{10}}{8} [\theta_0 \sin \theta (3 \cos^2 \theta - 1) \pm i \varphi_0 \sin 2\theta] e^{\pm 2i \varphi} = \frac{\sqrt{10}}{8} \mathbf{L}(\pm 2) \quad ,,$$

$$\mathbf{E}(\pm 3) = \frac{\sqrt{15}}{8} [\theta_0 \sin^2 \theta \cos \theta \pm i \varphi_0 \sin^2 \theta] e^{\pm 3i \varphi} = \frac{\sqrt{15}}{8} \mathbf{L}(\pm 3) \quad ,,$$

The matrix elements for all possible types of electric octupole transition are set out below. The corresponding formulae for magnetic transitions are obtained by rotating \mathbf{E} through 90° about \mathbf{r}_0 in the usual way. The matrices are, of course, Hermitian, but for convenience in use a complete tabulation is given. The coefficients A, B, C , etc., are the quantities G mentioned above.

$$\Delta j = +3$$

$$(j, m | \mathbf{E} | j+3, m \pm 3) = \mp \frac{1}{4} A \sqrt{\{(j \pm m + 1)(j \pm m + 2)(j \pm m + 3)(j \pm m + 4) \\ \times (j \pm m + 5)(j \pm m + 6)\}} \mathbf{L}(\pm 3),$$

$$(j, m | \mathbf{E} | j+3, m \pm 2) = \frac{1}{2} A \sqrt{\{(j + m + 1)(j - m + 1)(j \pm m + 2)(j \pm m + 3) \\ \times (j \pm m + 4)(j \pm m + 5)\}} \mathbf{L}(\pm 2),$$

$$(j, m | \mathbf{E} | j+3, m \pm 1) = \mp \frac{1}{4} A \sqrt{\{(j + m + 1)(j - m + 1)(j + m + 2)(j - m + 2) \\ \times (j \pm m + 3)(j \pm m + 4)\}} \mathbf{L}(\pm 1),$$

$$(j, m | \mathbf{E} | j+3, m) = -A \sqrt{\{(j + m + 1)(j - m + 1)(j + m + 2)(j - m + 2) \\ \times (j + m + 3)(j - m + 3)\}} \mathbf{L}(0).$$

$$\Delta j = +2$$

$$\begin{aligned}(j, m | \mathbf{E} | j+2, m \pm 3) &= \frac{3}{4} B \sqrt{\{(j \mp m)(j \pm m + 1)(j \pm m + 2)(j \pm m + 3) \\ &\quad \times (j \pm m + 4)(j \pm m + 5)\} \mathbf{L}(\pm 3)}, \\ (j, m | \mathbf{E} | j+2, m \pm 2) &= \mp \frac{1}{2} B (2j \mp 3m) \sqrt{\{(j \pm m + 1)(j \pm m + 2)(j \pm m + 3) \\ &\quad \times (j \pm m + 4)\} \mathbf{L}(\pm 2)}, \\ (j, m | \mathbf{E} | j+2, m \pm 1) &= \frac{1}{4} B (j - 3m) \sqrt{\{(j + m + 1)(j - m + 1)(j \pm m + 2) \\ &\quad \times (j \pm m + 3)\} \mathbf{L}(\pm 1)}, \\ (j, m | \mathbf{E} | j+2, m) &= -3Bm \sqrt{\{(j + m + 1)(j - m + 1)(j + m + 2) \\ &\quad \times (j - m + 2)\} \mathbf{L}(0)}.\end{aligned}$$

$$\Delta j = +1$$

$$\begin{aligned}(j, m | \mathbf{E} | j+1, m \pm 3) &= \pm \frac{1}{4} C \sqrt{\{(j \mp m - 1)(j \mp m)(j \pm m + 1)(j \pm m + 2) \\ &\quad \times (j \pm m + 3)(j \pm m + 4)\} \mathbf{L}(\pm 3)}, \\ (j, m | \mathbf{E} | j+1, m \pm 2) &= -\frac{1}{6} C (j \mp 3m - 2) \sqrt{\{(j \mp m)(j \pm m + 1)(j \pm m + 2) \\ &\quad \times (j \pm m + 3)\} \mathbf{L}(\pm 2)}, \\ (j, m | \mathbf{E} | j+1, m \pm 1) &= \mp \frac{1}{4} C \left[\frac{j(j+7)}{15} \pm \frac{m(2j-1)}{3} - m^2 \right] \sqrt{\{(j \pm m + 1) \\ &\quad \times (j \pm m + 2)\} \mathbf{L}(\pm 1)}, \\ (j, m | \mathbf{E} | j+1, m) &= -C \left[\frac{j(j+2)}{5} - m^2 \right] \sqrt{\{(j - m + 1)(j + m + 1)\} \mathbf{L}(0)}\end{aligned}$$

$$\Delta j = 0$$

$$\begin{aligned}(j, m | \mathbf{E} | j, m \pm 3) &= -\frac{1}{4} D \sqrt{\{(j \mp m - 2)(j \mp m - 1)(j \mp m)(j \pm m + 1) \\ &\quad \times (j \pm m + 2)(j \pm m + 3)\} \mathbf{L}(\pm 3)}, \\ (j, m | \mathbf{E} | j, m \pm 2) &= \mp \frac{1}{2} D (1 \pm m) \sqrt{\{(j \mp m - 1)(j \mp m)(j \pm m + 1)(j \pm m + 2)\} \\ &\quad \times \mathbf{L}(\pm 2)}, \\ (j, m | \mathbf{E} | j, m \pm 1) &= \frac{1}{4} D \left[\frac{(j-1)(j+2)}{5} \mp m - m^2 \right] \sqrt{\{(j \mp m)(j \pm m + 1)\} \\ &\quad \times \mathbf{L}(\pm 1)}, \\ (j, m | \mathbf{E} | j, m) &= -Dm \left[\frac{(3j^2 + 3j - 1)}{5} - m^2 \right] \mathbf{L}(0).\end{aligned}$$

$$\Delta j = -1$$

$$\begin{aligned}(j, m | \mathbf{E} | j-1, m \pm 3) &= \mp \frac{1}{4} E \sqrt{\{(j \pm m + 1)(j \pm m + 2)(j \mp m)(j \mp m - 1) \\ &\quad \times (j \mp m - 2)(j \mp m - 3)\} \mathbf{L}(\pm 3)}, \\ (j, m | \mathbf{E} | j-1, m \pm 2) &= -\frac{1}{6} E (j \pm 3m + 3) \sqrt{\{(j \pm m + 1)(j \mp m)(j \mp m - 1) \\ &\quad \times (j \mp m - 2)\} \mathbf{L}(\pm 2)}, \\ (j, m | \mathbf{E} | j-1, m \pm 1) &= \pm \frac{1}{4} E \left[\frac{(j+1)(j-6)}{15} \mp \frac{m(2j+3)}{3} - m^2 \right] \\ &\quad \times \sqrt{\{(j \mp m)(j \mp m - 1)\} \mathbf{L}(\pm 1)}, \\ (j, m | \mathbf{E} | j-1, m) &= -E \left[\frac{(j-1)(j+1)}{5} - m^2 \right] \sqrt{\{(j - m)(j + m)\} \mathbf{L}(0)}.\end{aligned}$$

$$\underline{\Delta j = -2}$$

$$(j, m | \mathbf{E} | j-2, m \pm 3) = \frac{3}{4} F \sqrt{\{(j \pm m + 1)(j \mp m)(j \mp m - 1)(j \mp m - 2) \\ \times (j \mp m - 3)(j \mp m - 4)\} \mathbf{L}(\pm 3)},$$

$$(j, m | \mathbf{E} | j-2, m \pm 2) = \pm \frac{1}{2} F (2j \pm 3m + 2) \sqrt{\{(j \mp m)(j \mp m - 1)(j \mp m - 2) \\ \times (j \mp m - 3)\} \mathbf{L}(\pm 2)},$$

$$(j, m | \mathbf{E} | j-2, m \pm 1) = \frac{1}{4} F (j \pm 3m + 1) \sqrt{\{(j + m)(j - m)(j \mp m - 1) \\ \times (j \mp m - 2)\} \mathbf{L}(\pm 1)},$$

$$(j, m | \mathbf{E} | j-2, m) = -3 F m \sqrt{\{(j + m)(j - m)(j + m - 1)(j - m - 1)\} \mathbf{L}(0)}.$$

$$\underline{\Delta j = -3}$$

$$(j, m | \mathbf{E} | j-3, m \pm 3) = \pm \frac{1}{4} G \sqrt{\{(j \mp m)(j \mp m - 1)(j \mp m - 2)(j \mp m - 3) \\ \times (j \mp m - 4)(j \mp m - 5)\} \mathbf{L}(\pm 3)},$$

$$(j, m | \mathbf{E} | j-3, m \pm 2) = \frac{1}{2} G \sqrt{\{(j + m)(j - m)(j \mp m - 1)(j \mp m - 2)(j \mp m - 3) \\ \times (j \mp m - 4)\} \mathbf{L}(\pm 2)},$$

$$(j, m | \mathbf{E} | j-3, m \pm 1) = \pm \frac{1}{4} G \sqrt{\{(j + m)(j - m)(j + m - 1)(j - m - 1) \\ \times (j \mp m - 2)(j \mp m - 3)\} \mathbf{L}(\pm 1)},$$

$$(j, m | \mathbf{E} | j-3, m) = -G \sqrt{\{(j + m)(j - m)(j + m - 1)(j - m - 1) \\ \times (j + m - 2)(j - m - 2)\} \mathbf{L}(0)}.$$

REFERENCES.

- BARNES, C. A., FRENCH, A. P., and DEVONS, S., 1950, *Nature, Lond.*, **166**, 145.
 CONDON, E. U., and SHORTLEY, G. H., 1935, *The Theory of Atomic Spectra*
 (Cambridge: University Press).
 FIERZ, M., 1949, *Helv. Phys. Acta.*, **22**, 489.

XXX. *Fluctuations in the Intensity of Radio Waves from Galactic Sources.*

By C. G. LITTLE and A. MAXWELL,
Jodrell Bank Experimental Station, University of Manchester*.

[Received January 18, 1951.]

SUMMARY.

It has been shown previously that the fluctuations in the intensity of radio energy from the galactic sources have a local terrestrial origin. This paper describes further observations of the two most intense sources, in the constellations of Cygnus and Cassiopeia, taken over a wide range of angles of elevation. At high angles of elevation the radio fluctuations are shown to be correlated with the occurrence of "spread" ionospheric echoes from the F region. When the sources are low on the northern horizon fluctuations are always observed; these are probably introduced by the passage of radio waves through the continuously disturbed ionospheric regions at high magnetic latitudes. Spaced receiver observations taken over base lines of 0.1, 4 and 11 km. enable the scale of the radio energy diffraction pattern across the ground to be determined.

§ 1. INTRODUCTION.

FLUCTUATIONS in the galactic radio emissions from the region of Cygnus were first observed by Hey, Parsons and Phillips (1946). They concluded that these fluctuations originated in a high intensity variable source of small angular diameter. Subsequently Bolton and Stanley (1948), using an interference technique, discovered a localized source of angular width $< 8'$ in the Cygnus region, from which they recorded a variable component of radiation at 100 Mc./s. At this time it was generally assumed that the variable component was due to true variations in the source emission. Recent combined work by Smith (1950), Little and Lovell (1950), has shown, however, that the fluctuations in the radio emission from a galactic source are not inherent in the source itself, but are impressed on the incoming radiation as it passes through the earth's ionosphere.

The occurrence of fluctuations at night when the electron density of the lower ionospheric layers is small suggests that the F region is the most probable origin of the fluctuations. (The existence of fluctuations when a source is high in elevation indicates that tropospheric refraction is not the cause of the phenomenon.) It was suggested by Little and Lovell that diffraction of the incident radiation by irregularities in the F region

* Communicated by Dr. A. C. B. Lovell.

would suffice to account for the observed fluctuations. An analysis of the occurrence of fluctuations and of "spread" F echoes which are believed to be associated with such irregularities has now been completed and is given in § 4.

The spaced receiver observations referred to above were made at transit of the two most intense galactic sources, in Cygnus (Declination approximately $+40^{\circ} 30'$, Right Ascension $19^h 57^m$) and in Cassiopeia (Declination approximately $+58^{\circ}$, Right Ascension $23^h 21^m$). This work has now been extended to all angles of elevation by using aerials movable in azimuth and elevation. In this way it has been possible to investigate in more detail the effect of the ionosphere on the radiation.

§ 2. APPARATUS.

The apparatus consisted of two equipments working on a frequency of 81.5 Mc./s., each using a directional aerial, movable in azimuth and elevation, a sensitive, high gain receiver and a recording meter. One receiver was sited permanently at the Jodrell Bank Experimental Station, Cheshire (Lat. $53^{\circ} 14' N.$, Long. $2^{\circ} 18' W.$), and was connected to a 30 ft. aperture, focal plane paraboloid aerial (free space beam width $\pm 11^{\circ}$, $\pm 15^{\circ}$ to half power). A mobile equipment with an array of two Yagi aerials (beam width $\pm 11^{\circ} \pm 21^{\circ}$) was used at spacings up to 11 km. from Jodrell Bank.

The receivers used were of the conventional superheterodyne type, modified to include two preamplification stages of low noise factor, and two stages of post detection amplification for recording weak signals. The characteristics of the receivers were: Frequency 81.5 Mc./s., bandwidth 0.6 Mc./s., output time constant 0.2 seconds, noise factor 4, overall gain 10^8 . All receiver power supplies were carefully stabilized. Pen recording milliammeters were used as recording instruments, with chart speeds ranging from 12 inches per minute to 3 inches per hour.

In this paper, when it is stated that galactic noise fluctuations were "not observed" it is implied that the fluctuations were less than the ripple in the receiver noise output. For the apparatus used, the minimum detectable level was of the order of $1/500$ of the total receiver noise, corresponding to a 5–10 per cent modulation of the source intensity. Strong galactic noise fluctuations showed peak intensities up to 40 times the minimum detectable fluctuation level.

§ 3. METHOD OF OBSERVATION.

The experiments were carried out over the period May 1949–December 1950, and may be divided into 3 sections: (i.) Transit observations to investigate the correlation between the fluctuations and local ionospheric phenomena. (ii.) Continuous observations to investigate the changes in amplitude and period of the fluctuations with elevation of the source. (iii.) Spaced receiver observations to determine the linear dimensions of the ionospheric irregularities responsible for the fluctuations,

§ 4. OBSERVATIONS AT TRANSIT —CORRELATION WITH SPREAD F.

The experiments of Smith, Little and Lovell, referred to in §1, showed that the fluctuations must originate in a local medium. An analysis of a series of transit observations, taken over the period May 1949–December 1950, has now been made to establish the extent of the correlation of the fluctuations with the ionospheric discontinuities which give rise to a “spread” in the critical frequency and height of F region echoes.

Table I. compares the occurrence of galactic noise fluctuations and spread F conditions during the transit of the Cygnus and Cassiopeia sources. The galactic noise observations, made at Jodrell Bank, refer to the period ± 1 hour from transit, whilst the ionospheric observations were made at Slough, some 230 km. to the South, and refer to the period transit ± 2 hours.

TABLE I.

Correlation of galactic noise fluctuations with spread F.

Radio source	No. of occasions when spread F and galactic noise observations were made	No. of occasions when spread F and noise fluctuations were		Spread F observed but no galactic noise fluctuations	Galactic noise fluctuations observed but no Spread F
		(i.) Both observed	(ii.) Both absent		
Cygnus	205	53 (26%)	106 (52%)	16 (8%)	30 (14%)
Cassiopeia	195	69 (35%)	74 (38%)	36 (19%)	16 (8%)

Transit observations May 1949 to December 1950.

It is seen that the galactic noise fluctuations and spread F were simultaneously present, or absent, for 75 per cent of the observations, *i. e.* only 25 per cent of the runs indicate the presence of the one without the other. (Smith, Little and Lovell have shown that there is a 10 per cent chance that fluctuations will be observed at only one of two sites 210 km. apart and hence a correlation figure higher than 90 per cent cannot be expected.)

§ 5. SPACED RECEIVER EXPERIMENTS.

Previous work with spaced receivers showed that there was no correlation between (transit) fluctuations observed on two receivers separated by a distance of 210 km. but that a fairly good correlation existed for a spacing of 4 km. These experiments have been continued and extended to all angles of elevation to discover where correlation ceases. The results may be summarized as follows:

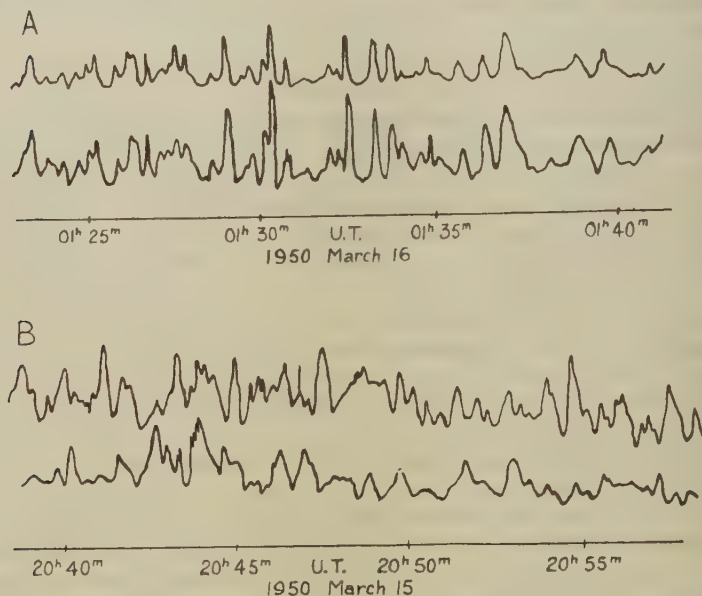
(i.) Two receivers located at the same site, observing the same source, record identical fluctuations.

(ii.) For a separation of 110 m., the correlation coefficient is still extremely high ($> .98$). The deviation from unity is within the range of the experimental limitations.

(iii.) As already reported (Little and Lovell 1950), at 4 km. the correlation between the fluctuations is not complete, but remains high with a correlation factor varying between 0.5 and 0.95.

(iv.) Over an 11.2 km. North-South base line there is no correlation between transit fluctuations. However, when a source is near lower culmination the "effective" base line (*i.e.* the projection of the actual base line on a plane normal to the line of sight) becomes small,

Fig. 1.



Cassiopeia fluctuation records taken simultaneously by two receivers 11 km. apart on a North-South base line.

Records A: Correlation 0.9 (effective base line 4.1 km.).

Records B: No correlation (effective base line 7.7 km.).

and the correlation factor may rise to as much as 0.95. This is illustrated in fig. 1, in which correlations between fluctuations for different effective base lines are compared, and in Table II., which shows the change in the correlation as the Cassiopeia source nears lower culmination. (The base line used was actually 10° E. of North so that the effective base line is given by $11.2 \sin [\cos^{-1} (\cos \alpha \cos \beta - 10)]$, where α is the angle of elevation and β the azimuth angle.)

(v.) At 210 km., between Cambridge and Jodrell Bank, there is no correlation between transit fluctuations.

TABLE II.

Change of cross-correlation coefficient between fluctuation records
with change of effective base line.

Hours after transit	Elevation degrees	Azimuth degrees	Effective base line Kilometres	Correlation between fluctuation records
0-9	85-23		11.2-6.4	correlation not significant
10	23	344	6.4	0.4
11	22	352	5.3	0.6
12	21	0	4.4	0.7
13	22	8	4.1	0.9
14	23	16	4.6	0.8
15	27	24	5.6	0.5
16	31	32	6.8	correlation not significant
17-24	31-85		6.7-11.2	correlation not significant

§ 6. CONTINUOUS OBSERVATIONS.

During the year November 1949–November 1950 some 3000 hours of observations were made on the Cygnus and Cassiopeia point sources by following them with steerable aerials. These observations usually took the form of a 24-hour run on each source once or twice per week throughout the year. Daytime observations were limited during some months by strong radio emissions from active areas on the Sun (of the order of 10^3 intensity of the galactic source radiation), by atmospherics from thunderstorms during the summer months, and occasionally by strong local interference.

The results of this series of observations may be summarized as follows :—

(i.) For a source at high angles of elevation the fluctuations are very closely related with the presence of spread F, and as this latter is essentially a night time phenomenon, fluctuations at high angles of elevation are usually confined to the hours of darkness. Thus, near upper culmination fluctuations were observed on 35 per cent occasions when transit occurred during the hours 1800–0600, but on less than 5 per cent for transit during the daylight hours 0600–1800.

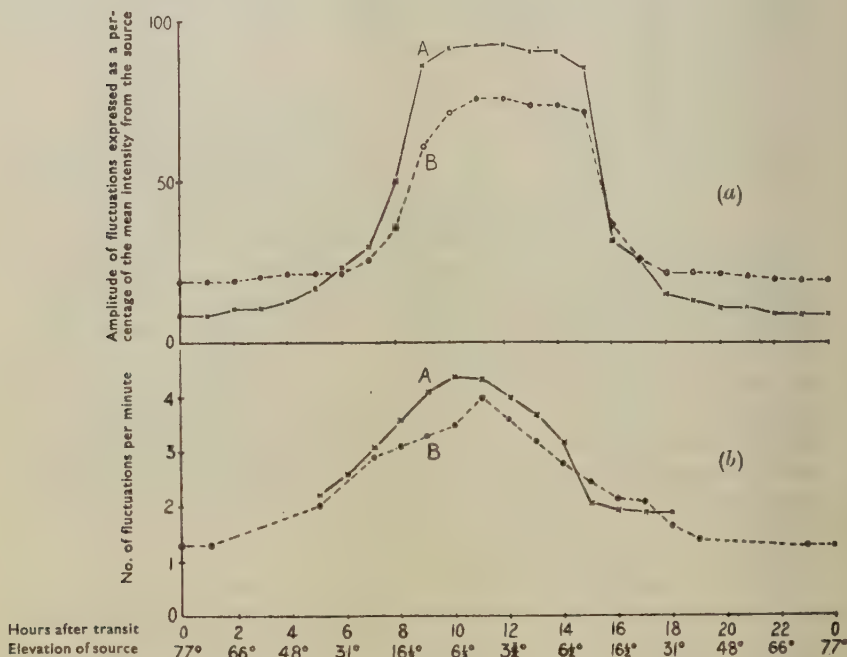
(ii.) At low angles of elevation when the line of sight crosses the ionosphere at high magnetic latitudes, fluctuations were always observed, independent of the hour of day. These fluctuations were in general less marked in the case of Cassiopeia (minimum elevation 21°) than for Cygnus (minimum elevation 4°).

(iii.) The amplitude of the fluctuations of the Cygnus source (corrected for aerial ground lobes) plotted against the elevation of the source is shown in fig. 2 (a). It is seen that for angles below 20° the average amplitude of the fluctuations, expressed as a fraction of the mean intensity of the radiation from the source, increases rapidly, reaching a maximum

of about 90 per cent at lower culmination. It will also be seen that for lower culmination in daylight the maximum amplitude of the fluctuations is significantly less than for lower culmination at night.

(iv.) The marked elevation effect associated with fluctuations from the Cygnus source is further illustrated in fig. 3. In this diagram the "onset" and "cessation" of the fluctuations (taken here as the time at which the fluctuations respectively increase or decrease to an amplitude of 25 per

Fig. 2.



(Upper diagram). Average amplitude of Cygnus fluctuations plotted against elevation of the source.

(Lower diagram). Average number of Cygnus fluctuations per minute plotted against elevation of the source.

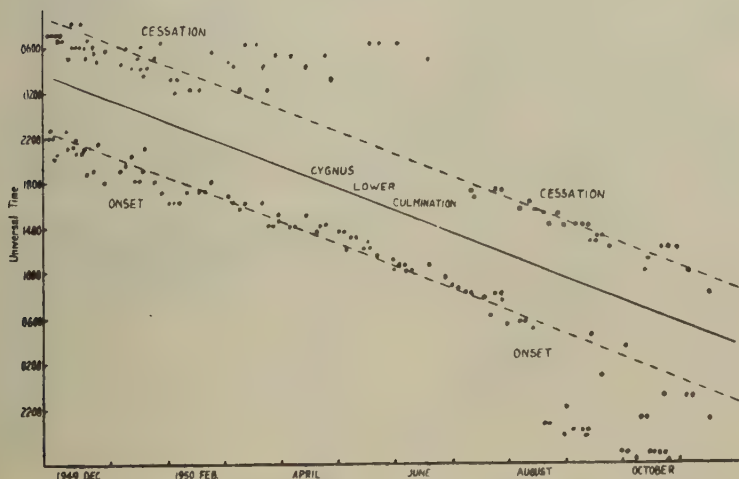
In each case curve A represents the average values during the six winter months (October–March), and curve B the average values during the six summer months (April–September). Cygnus lower culmination occurs in daylight during the summer, and in darkness during the winter.

cent) is plotted throughout the year. It is seen that the onset of the fluctuations occurs at approximately the same *sidereal* time each day, about 5 hours before lower culmination, corresponding to an elevation of 23° , and that the fluctuations cease approximately 5 hours after lower culmination. The spread of points during the August–November period

on the onset curve, and during March–June on the cessation curve, correspond to fluctuations at high angles of elevation during the hours of darkness.

(v.) The duration of individual fluctuations at any given angle of elevation and azimuth varies considerably from night to night. For example, individual fluctuations at transit of the sources may last for 2 or 3 minutes on some nights, whilst on other nights for only 20 seconds. Typical durations, however, range from about 1 minute at high angles of elevation to about 15 seconds at low angles of elevation. The number of fluctuations of the Cygnus source per minute plotted as a

Fig. 3.



Times of "onset" and "cessation" of Cygnus fluctuations. The two dotted lines correspond to a source elevation of 23° (i. e. 5 hours before and after lower culmination respectively).

function of the angle of elevation is shown in fig. 2 (b); it will be seen that the number of fluctuations per minute for lower culmination in daylight is somewhat less than for lower culmination at night.

§ 7. DISCUSSION.

(i.) *The Mechanism of Fluctuations: Diffraction in the Ionosphere.*

It was suggested by Little and Lovell that the galactic noise fluctuations could be caused by diffraction of the incident radiation by localized irregularities in the refractive index of an ionospheric layer. These irregularities would cause a distortion of the incident wavefront due to the different optical path lengths in the ionosphere, and the resultant diffraction pattern would be observed as an irregular distribution of amplitude across the ground. This distribution would not be constant with time,—due to

the presence of winds and turbulence in the ionosphere, and to the apparent change in position of the star as the Earth rotates,—and hence a fixed receiver would observe fluctuations in the intensity of the incident radiation.

The detailed implications of these ideas have been discussed by Little (1951) on the basis of a theorem by Booker, Ratcliffe and Shinn (1950), in which it is shown that the auto-correlation function of the diffraction pattern across the ground is the same as that of the distortions of the wavefront emerging from the ionosphere; that is, the scale of the pattern at ground level is the same as that of the distortions in the emergent wavefront. On the assumption that the scale of the distortions in the wavefront is the same as that of the irregularities in the 3-dimensional ionospheric screen, then the experimental results described in this paper will give some indication of the lateral dimensions of the irregularities.

(ii.) *Correlation between records from spaced receivers.*

In §5 it is shown that the correlation between fluctuation records begins to fall off at spacings of approximately 4 km., and it would appear, therefore, that the ionospheric irregularities causing the fluctuations have lateral dimensions of the order of 4 km.

If we now compare the observations made at the transit and the lower culmination of, say, Cassiopeia by two receivers 11.2 km. apart on a North-South base line, then allowance must be made for the changes in the "effective" base line (§5 (iv.)). Thus at transit, when the source is at an elevation of 85° and the effective base line is nearly 11.2 km., we should expect poor correlation if the F region irregularities are of diameter approximately 4 km. Towards lower culmination, however, when the source is at an elevation of 21° , and the effective base line tends toward a minimum of 4.1 km., the correlation would be expected to be good. This is in agreement with the experimental observations.

The above correlation results indicate that the scale of the diffraction pattern, in a plane normal to the incident radiation, is independent of the elevation of the source for elevations greater than 20° . In the case of Cygnus lower culmination (elevation 4°), the sight line crosses the ionosphere at high magnetic latitudes, and the correlation only becomes significant when the effective base line is 1 km. or less. This suggests that the ionospheric irregularities at these high magnetic latitudes are appreciably smaller than those at medium latitudes.

(iii.) *Fluctuations at low angles of elevation.*

There are clearly two important differences between transit observations and those taken near lower culmination: (a) as shown in fig. 4, the sight line from Jodrell Bank to the Cassiopeia and Cygnus sources at lower culmination crosses the F region of the ionosphere at latitudes of 62° N. and 71° N. respectively,—the latter well within the auroral zone. At these high latitudes the ionospheric structure is not well defined and fluctuates rapidly with time; sporadic F is much more intense and occurs during the day as well as at

night; sporadic E densities are also greatly in excess of the densities at lower magnetic latitudes. (b) When the sources are low in elevation the depth of ionosphere along the line of sight is increased. The variation of the amplitude of the Cygnus fluctuations with the change in the effective thickness of the ionosphere is shown in fig. 5. (This latter has been plotted for a disturbing region of two assumed heights and thicknesses: viz., between 300 and 500 km. and between 250 and 1000 km.; owing to the curvature of the earth the thickness factor does not follow a simple cosecant law.) It is seen that the effective thickness and

Fig. 4.

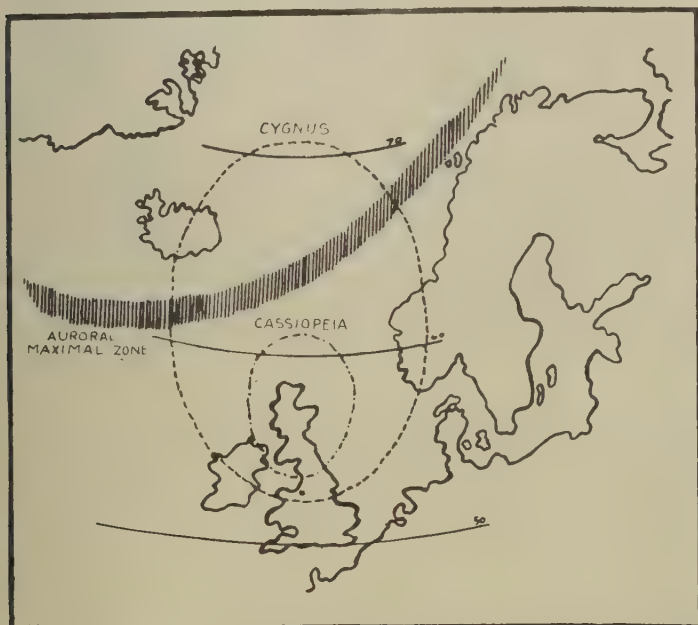
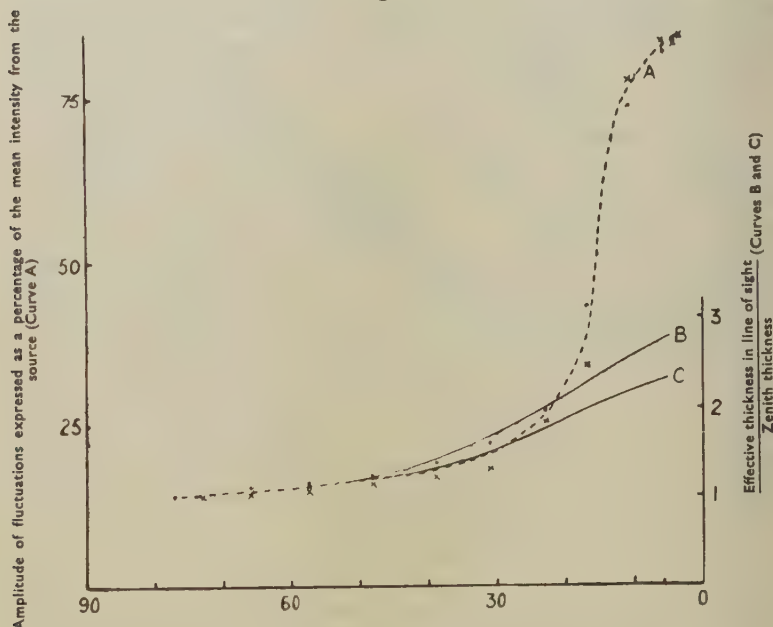


Diagram showing positions at which radiation from the Cygnus and Cassiopeia sources incident at Jodrell Bank crosses the F region of the ionosphere (assumed at a height of 400 km.). At low angles of elevation the sight lines cross the F region near the auroral zone.

amplitude curves follow each other closely for elevations greater than 20°, and it would therefore appear that down to an amplitude of about 20° the increase in fluctuation amplitude could be accounted for in terms of increased thickness of the disturbing region. Below 20°, however, where the rate of increase in the amplitude of the fluctuations is much greater than the corresponding rate of increase in effective thickness, it would seem that the disturbed nature of the ionosphere at high magnetic latitudes is the main contributing factor.

The effect of the troposphere at these low angles of elevation is not readily determinable. However, on metre wavelengths, and for a minimum elevation of 4° , it is unlikely that fluctuations of the type observed could be introduced by the troposphere, because (a) the variations in the refractive index of the troposphere are too small: of the order of 10^{-6} (cf. Booker and Gordon 1950), compared with 10^{-4} – 10^{-3} for the ionosphere, and (b) the effective thickness of the troposphere traversed at 4° elevation is about 100 km., compared with 1000 km. for the effective thickness of the F region of the ionosphere.

Fig. 5.



Curve A: Amplitude of Cygnus fluctuations with elevation. × source setting, ● source rising (averages over 12 months).

Curves B and C: Ratio of effective thickness of disturbing region in line of sight to zenith thickness—(Curve B for a disturbing region of assumed minimum height 300 km. and maximum height 500 km.; curve C for assumed minimum height 250 km. and maximum height 1000 km.).

(iv.) *The duration of individual fluctuations.*

Time variations in the intensity of the galactic radiation could be brought about in several ways: (a) a random growth and decay of the irregularities, (b) a turbulent motion of the irregularities, (c) the movement of the ionospheric irregularities as a whole under the influence of an ionospheric wind, (d) the apparent motion of the star relative to the ionospheric irregularities due to the rotation of the earth.

Ionospheric observations have shown that changes in the electron density of the F region are of periods very much longer than 30 seconds, the average duration of an individual fluctuation. This, together with the observation that correlation between fluctuation records is high over base lines of 4 km., suggests that fluctuations are not introduced to any great extent by turbulence, or by random growth and decay.

The duration of individual fluctuations should therefore be determined by the ratio of the size of phase irregularities in the ionosphere to the components of wind and star velocity in their plane. Wind velocities of approximately 7 km./min. have been found by Munro (1948), and for 4 km. irregularities would lead to fluctuations with a period of the order of 30 seconds. In the absence of winds, the apparent motion of the star due to the rotation of the earth would lead to fluctuations with a period of approximately 3 minutes. These figures agree fairly well with the observed limits of from about 20 seconds to 5 minutes for the fluctuations at transit.

The results described in § 6 (v.) and illustrated in fig. 2 (b) show that the period of the fluctuations is significantly less near lower culmination (decreasing steadily for elevations less than about 20°) than at transit. This effect is to be expected for three reasons: (a) the radiation then traverses the ionosphere near the disturbed auroral regions, (b) the depth of the ionosphere along the line of sight is considerably increased, and (c) ionospheric winds of 20 km./min. are reported to exist at high latitudes (Meek 1949).

§ 8. CONCLUSION.

The main conclusion to be drawn from the experiments described above is that the fluctuations in intensity of the radio emission from the galactic sources are introduced when the radio waves pass through an inhomogeneous ionospheric region, and spaced receiver experiments suggest that these inhomogeneities are of the order of 4 km. in size. Correlation with ionospheric phenomena indicates that the F region is mainly responsible, but it is not possible to exclude other ionospheric effects in cases where the radiation passes through disturbed auroral regions.

Further investigation of galactic noise fluctuations on various frequencies, and over varying base lines, should yield valuable information on the structure of the upper regions of the ionosphere.

ACKNOWLEDGMENTS.

The work described in this paper forms part of the research programme of the Jodrell Bank Experimental Station. The authors wish to express their thanks to Dr. A. C. B. Lovell, Director of the station, for his helpful advice and criticism, to Dr. A. F. Wilkins and the Director of the Radio Research Station, Slough, for the ionospheric information, to the Air Ministry for permission to locate a mobile equipment at the Mobberley Direction Finding Station of Ringway Airport and to Mr. C. Hazard for

assistance in making the radio observations. A considerable portion of this work has been made possible by the grant from the Department of Scientific and Industrial Research for the development of the experimental work at Jodrell Bank. The authors are personally indebted to the Department of Scientific and Industrial Research for the award of a maintenance grant (C.G.L.) and a research grant (A.M.).

REFERENCES.

- BOLTON, J. G., and STANLEY, G. J., 1948, *Nature*, **161**, 312.
BOOKER, H. G., and GORDON, W. E., 1950, *Proc. I.R.E.*, **38**, 401.
BOOKER, H. G., RATCLIFFE, J. A., and SHINN, D. H., 1950, *Phil. Trans. Roy. Soc. A*, **262**, 579.
HEY, J. S., PARSONS, S. J., and PHILLIPS, J. W., 1946, *Nature*, **158**, 234.
LITTLE, C. G., 1951 (in publication).
LITTLE, C. G., and LOVELL, A. C. B., 1950, *Nature*, **165**, 423.
MEEK, J. H., 1949, *J. Geophys. Res.*, **54**, 339.
MUNRO, G. H., 1948, *Nature*, **162**, 886.
SMITH, F. G. 1950, *Nature*, **165**, 422.

XXXI. *The Electric Quadrupole Moment and the Magnetic Moment of the Bromine Nucleus.*

By J. D. RANADE*,
Royal Holloway College†.

[Received January 9, 1951.]

ABSTRACT.

Deviations from the interval rule have been observed in the hyperfine structure of the bromine arc spectrum. These are attributable to an electrical quadrupole moment of the bromine nucleus. Coupling constants are determined for the term involved. The nuclear quadrupole moment is calculated to be 0.28×10^{-24} cm.², and the magnetic moment 1.8 nuclear magnetons.

§ 1. INTRODUCTION.

DEVIATIONS from the interval rule in the BrI spectrum were first observed in the term $5s^4P_{5/2}$ by Tolansky and Trivedi (1940). These can be attributed to the nuclear electrical quadrupole moment. The separations in this term were measured accurately from lines in the red and the infra-red regions where the resolving power of the Fabry-Perot interferometer is high. There is no evidence of any possible perturbation from another configuration. Table I. shows the observed positions of the hyperfine structure levels as compared with those calculated from the interval rule.

TABLE I.

F value	4	3	2	1
Observed.....	417	218	83	0
Calculated.....	417	232	93	0
(Interval rule)				

At the time the quadrupole moment was not evaluated for want of the coupling constants of the term. Hence, here, following a method similar to that used by Schmidt (1939) for iodine, coupling constants of the term involved and thus the quadrupole moment are determined.

§ 2. QUADRUPOLE MOMENT.

The interaction between the angular momentum J of a non-spherically symmetrical configuration and the spin I of a non-spherically symmetrical nucleus takes the form

$$E = a_0 + \frac{a_1}{2}c + bc(c+1),$$

where

$$c = F(F+1) - I(I+1) - J(J+1).$$

* At present, at the Institute of Science, Bombay, India.

† Communicated by Professor S. Tolansky.

In this interaction law a_0 , a_1 and b are constants, a_0 being the displacement of the centre of gravity of the hyperfine structure pattern from the position the term would have occupied if the spin had been zero, a_1 is the hyperfine structure interval factor which is a function of the nature of the electron configuration and is also proportional to the nuclear magnetic moment, b is a measure of the deviation from the interval rule. The quantity b is a function of the nuclear electrical quadrupole moment of the nucleus.

The values of the interaction constants given by the observed intervals are (units $\text{cm.}^{-1} \times 10^{-3}$)

$$a_0 = 223,$$

$$a_1 = 47.1,$$

$$b = 0.17.$$

For the calculation of the quadrupole and the magnetic moments, it is necessary to know the coupling constants for the configuration electrons. For these, first, the coupling constants of the $4p^4$ electron group in the singly ionized bromine atom is calculated, then the attachment of a $5s$ electron to this group, giving rise to the $4p^4.5s$ configuration of the neutral atom is considered. It is assumed that the attachment of a $5s$ electron to the $4p^4$ group does not alter the coupling constants in the group. The p^4 electron group can be treated as equivalent to the p^2 group. Hence for calculation $p^4.s$ can be treated as $p^2.s$. The effect of this on the quadrupole moment formula is a change of sign since the spin-orbit interaction changes sign. The eigenfunctions for the p^2s configuration are written in terms of the single electron functions. The term $^4P_{5/2}$ arises from the term 3P_2 of BrII. Thus for $J=2$ and $m=2$ the eigenfunctions for the configuration p^2 are, as given by Breit and Wills (1933)

$$\left[\begin{smallmatrix} 3 & 1 \\ 2 & 2 \end{smallmatrix} \right]_2^2 = \frac{1}{\sqrt{2}} (p_{3/2}^{3/2} p_{1/2}^{1/2} - p_{1/2}^{1/2} p_{3/2}^{3/2}),$$

$$\left[\begin{smallmatrix} 3 & 3 \\ 2 & 2 \end{smallmatrix} \right]_2^2 = \frac{1}{\sqrt{2}} (p_{3/2}^{3/2} p_{3/2}^{1/2} - p_{3/2}^{1/2} p_{3/2}^{3/2}).$$

Here $p_{3/2}^{3/2}$ etc. signify the single electron eigenfunctions, the magnetic quantum number being given by the superscript to the right. The eigenfunction of the 3P_2 term is a linear combination of the above functions and is given by

$$\psi(^3P_2) = c_1 \left[\begin{smallmatrix} 3 & 1 \\ 2 & 2 \end{smallmatrix} \right]_2^2 + c_2 \left[\begin{smallmatrix} 3 & 3 \\ 2 & 2 \end{smallmatrix} \right]_2^2.$$

The coefficients c_1 and c_2 are to be determined from the multiplet structure and from the value of the spin-orbit interaction. The values of the spin-orbit interaction (δ) and the electrostatic energy integral (F_2) are given by Robinson and Shortley (1937). Using the values

$$\delta = 2958 \text{ cm.}^{-1} \quad \text{and} \quad F_2 = 1750 \text{ cm.}^{-1}$$

and the term values for BrII, leads to

$$c_1 = 0.434 \quad \text{and} \quad c_2 = 0.901.$$

The eigenfunctions of the ${}^4P_{5/2}$ term arising from the attachment of the s-electron to the p^2 group are given by

$$\psi({}^4P_{5/2}^{5/2}) = s_{1/2}^{1/2} \cdot \psi({}^3P_2^2).$$

The formula for the electrical quadrupole moment q as given by Casimir (1935) for a p-electron is

$$q = -\frac{b \cdot Z_i \cdot H}{\delta(3 \cos^2 \bar{d} - 1)} \cdot 2i(2i-1)j(2j-1) \times 0.986 \times 10^{-24},$$

where H is a relativity correction. The average value of $(3 \cos^2 \bar{d} - 1)$ is determined by using the above eigenfunction in conjunction with formulæ given by Schüller and Schmidt (1936). For ${}^4P_{5/2}$ we have

$$(3 \cos^2 \bar{d} - 1) = -\frac{2}{5}(2\sqrt{2}c_1c_2S_1 - c_1^2R_1'),$$

where S_1 and R_1 are the relativity corrections and c_1 and c_2 are the constants already computed. Thus finally

$$q = -\frac{bZ_iH2i(2i-1)j(2j-1) \times 0.986 \times 10^{-24}}{\delta, -\frac{2}{5}(2\sqrt{2}c_1c_2S_1 - c_1^2R_1')}.$$

With $c_1 = 0.434$, $c_2 = 0.901$, $S = 1.07$, $R_1' = 1.045$, $H = 1.024$, $i = \frac{3}{2}$, $j = \frac{5}{2}$, $Z_i = 31$ [($Z-4$) for a p-electron] and $\delta = 2958 \text{ cm.}^{-1}$ giving

$$q = b \times 1.612 \times 10^{-24} \text{ cm.}^2$$

and with $b = 0.17$,

$$q = +0.28 \times 10^{-24} \text{ cm.}^2.$$

No separation of the isotopes is revealed by hyperfine structure. The value obtained here compares well with the values found by the micro-wave technique and reported by Townes, Holden and Merrit (1948), as

$${}^{81}\text{Br}_{81} \cdot q = +0.28 \times 10^{-24} \text{ cm.}^2,$$

$${}^{79}\text{Br}_{79} \cdot q = +0.23 \times 10^{-24} \text{ cm.}^2.$$

§ 3. MAGNETIC MOMENT.

Using the earlier data of Tolansky (1932) for the separations of the terms ${}^4P_{5/2}$, ${}^4P_{3/2}$ and ${}^2P_{3/2}$ of BrI, Schmidt (1938) calculated the nuclear magnetic moment of bromine as 2.6 nuclear magnetons. Since then Tolansky and Trivedi (1940) have remeasured and redetermined the separations more accurately. The interval factor for the term ${}^4P_{3/2}$ is now given to be $20 \text{ cm.}^{-1} \times 10^{-3}$ instead of the value $42 \text{ cm.}^{-1} \times 10^{-3}$ first given and used by Schmidt (1936). Therefore the nuclear magnetic moment has been re-determined using the improved data now available. The total splittings for the terms ${}^4P_{5/2}$ and ${}^4P_{3/2}$ which are now being used are

$$({}^4P_{5/2}) = 417 \text{ cm.}^{-1} \times 10^{-3},$$

and

$$({}^4P_{3/2}) = 120 \text{ cm.}^{-1} \times 10^{-3}.$$

Breit and Wills (1933) have calculated the interval coupling factors for the $4P_{5/2}$ and $4P_{3/2}$ terms, in intermediate coupling, giving

$$A(4P_{5/2}) = \frac{1}{5}a(s) + \frac{1}{5}[(3c_1^2 + 4c_2^2)a' + c_1^2a'' + 4\sqrt{2}c_1c_2a'''],$$

$$A(4P_{3/2}) = -\frac{1}{5}a(s) + \frac{3}{10}[(3c_1^2 + 4c_2^2)a' + c_1^2a'' + 4\sqrt{2}c_1c_2a'''].$$

Here $a(s)$ is the interval constant for the s-electron and a' , a'' and a''' are the interval constants for the p-electrons, c_1 and c_2 are the coupling constants as computed above. The constants a' , a'' and a''' are related as follows.

$$a'' = a' \cdot 5F''/F'$$

and

$$a''' = -a' \cdot 5/16 \cdot G/F'.$$

Here F' , F'' and G are the relativity corrections.

Using the values $c_1 = 0.434$, $c_2 = 0.901$, $F'' = 1.09$ and $F' = G = 1.02$ leads to the interval factors

$$A(4P_{5/2}) = 0.2a(s) + 0.823a',$$

$$A(4P_{3/2}) = -0.2a(s) + 1.235a'.$$

From these relations and the known values of

$$A(4P_{5/2}) = 47.1 \text{ cm.}^{-1} \times 10^{-3} \quad \text{and} \quad A(4P_{3/2}) = 20 \text{ cm.}^{-1} \times 10^{-3}$$

given by Tolansky and Trivedi, it follows that

$$a(s) = 101.3 \text{ cm.}^{-1} \times 10^{-3},$$

$$a' = 32.6 \text{ cm.}^{-1} \times 10^{-3}.$$

For $a(s)$, Goudsmit's formula leads to

$$\mu = \frac{a(s) \cdot i \cdot n_{\text{eff}}^3 \cdot 0.1185}{ZZ_0^2 F'' (1 - ds/dn)} \quad \dots \quad (1)$$

For a' ,

$$\mu = \frac{a' \cdot i \cdot Z_i H \cdot 3.446}{\delta \cdot F'} \quad \dots \quad (2)$$

In equation (1), n_{eff} is the effective quantum number for the s-electron when it is the only valence electron present. This happens in BrV. The corresponding configuration is $4s^2 \cdot 5s$. In neutral bromine the configuration is $4s^2 \cdot 4p^4 \cdot 5s$. The absolute value of this term of BrV is not experimentally known. It is, however, here determined by extrapolation using the known term values for the $5s^2 \cdot 5s$, $5s^2 \cdot 6s$ etc. terms of the iso-electronic sequence gallium I, germanium II and arsenic III. The term values for these are taken from Goudsmit and Bacher (1932). From this $n_{\text{eff}} = 3.95$ and $(1 - ds/dn) = 0.65$. With $i = \frac{3}{2}$, $Z = 35$, $Z_i = 31$, $H = 1.024$, $F' = 1.02$, $F'' = 1.09$, $n_{\text{eff}} = 3.95$, $(1 - ds/dn) = 0.65$, and $Z_0 = 5$ (Br V), giving

$$\text{from } a(s): \mu = 1.79,$$

$$\text{and from } a': \mu = 1.77,$$

The agreement between these values is perhaps fortuitous and much better than can be expected. One can take closely enough

$$\mu = 1.8 \text{ nuclear magnetons.}$$

The determination of the nuclear magnetic moment of bromine has been carried out by the nuclear paramagnetic resonance absorption method and the magnetic beam resonance in CsBr and LiBr. The values given by Pound (1947) are

$$(\text{Br}^{81}) = 2.2 \text{ nuclear magnetons,}$$

$$(\text{Br}^{79}) = 2.1 \text{ nuclear magnetons.}$$

When the approximations used here are taken into account the difference is not significant and indeed the two methods give reasonably concordant results.

ACKNOWLEDGMENTS.

My thanks are due to Professor S. Tolansky for his constant interest and kind continual encouragement during the progress of this work.

REFERENCES.

- BREIT and WILLS, 1933, *Phys. Rev.*, **44**, 270.
GOUDSMIT and BACHER, 1932, *Atomic Energy States*.
POUND, 1947, *Phys. Rev.*, **72**, 1273.
ROBINSON and SHORTLEY, 1937, *Phys. Rev.*, **52**, 715.
TOLANSKY, 1932, *Proc. Roy. Soc. A.*, **136**, 585.
TOLANSKY and TRIVEDI, 1940, *Proc. Roy. Soc. A.*, **175**, 366.
TOWNES, HOLDEN and MERRIT, 1948, *Phys. Rev.*, **74**, 370.
SCHMIDT, 1938, *Zeits. f. Physik*, **108**, 408.
SCHMIDT, 1939, *Zeits. f. Physik*, **112**, 199.
SCHULER and SCHMIDT, 1936, *Zeits. f. Physik*, **99**, 717.

XXXII. *Hyperfine Structure in the Spectrum of Bromine.*—II.

By J. D. RANADE*,
Royal Holloway College†.

[Received January 9, 1951.]

ABSTRACT.

Measurements for the hyperfine structures of 18 classified and 21 unclassified lines of the first spark spectrum of bromine are reported. The spectrum was excited by a high-frequency electrodeless discharge in pure bromine vapour. The patterns are analysed and interval factors for fourteen terms are given.

§1. INTRODUCTION.

MEASUREMENTS for the hyperfine structures of several lines of the arc spectrum of bromine have been reported earlier by Tolansky (1932) and Tolansky and Trivedi (1940), who proved that both the bromine isotopes 79 and 81 have the same nuclear spin, $3/2$, and have practically identical nuclear magnetic moments. Tolansky and Trivedi also reported measurements of the hyperfine structure for four lines of the first spark spectrum of bromine.

The measurements reported here consist of a study of the classified and the unclassified lines of the spark spectrum of bromine. The first spark spectrum of bromine was partially classified by Lacroute (1935), who studied the Zeeman effect but could not exploit them fully due to lack of hyperfine structure data.

§2. EXPERIMENTAL.

The spark spectrum was excited in bromine vapour with an electrodeless high-frequency discharge which is gentle and can be considered essentially as a low voltage excitation in which arc lines tend to predominate. A brilliant arc spectrum can be excited in bromine vapour at a pressure of about 1 mm. As the gas pressure is lowered, the increase in the mean free path enables the ions to acquire higher energies between collisions and spark lines appear. Sharper spark lines result than those excited in a Geissler discharge tube. By reducing the bromine vapour pressure below 1 mm. and by using a capillary more constricted than that necessary for an arc spectrum, strong spark lines were excited.

Oscillations were generated by a 500 watt thermionic valve, the wavelength being of the order of 20 m. The field was applied by means of an external electrode of copper foil to a pyrex discharge tube which

*Communicated by Professor. S. Tolansky.

† At present at the Institute of Science, Bombay, India,

was incorporated in a vacuum circulating system having charcoal and liquid oxygen traps in the circuit. A continuous stream of pure bromine vapour was circulated through the discharge tube from a side limb cooled by immersion in a flask containing liquid oxygen. By adjusting the height of the bottom of the limb above the liquid oxygen surface, the bromine could be cooled to a temperature of -80°C . at which a good excitation of the spark spectrum resulted. Cooling to -45°C . is necessary for the arc spectrum. No carrier gas was used. The portion of the discharge tube emitting the spectrum was cooled by directing on to it a strong blast of air.

The high resolving power instruments used were a variable gap Fabry-Perot interferometer coated either with silver, aluminium or an aluminium-magnesium alloy, and a quartz Lummer plate by Hilger, (20 cm. long and 3.42 mm. thick). The interferometer was used in an external beam mounting crossed with a large Hilger glass-quartz Littrow spectrograph.

§ 3. OBSERVATIONS.

Table I. contains hyperfine structures measured for classified lines of BrII spectrum. The wavelengths and allocations are taken from Lacroute. The units used are $\text{cm.}^{-1} \times 10^{-3}$ and beneath each component is indicated a visual estimate of its intensity. The lines are classed A, B, C according to whether the resolution in the pattern is good (A), moderate (B) or poor (C). The factors affecting the class are the complexity and the narrowness of the patterns and the widths of the lines. For lines classed as A, the errors are some 1 or 2 $\text{cm.}^{-1} \times 10^{-3}$. Whenever two components are not completely resolved, the blend is indicated by binding of components with a hyphen. Measurements for a number of unclassified lines are given in Table II.

§ 4. ANALYSIS.

For the singly ionized bromine atom Hund's theory predicts three families of terms arising from the basic terms 4S, 2D and 2P of BrIII. All the lines classified by Lacroute (1935) belong to the 4S system. The analysis of lines involving common terms will now be considered.

Of the three lines $\lambda 5164.4$, 5238.2 and 5182.4 one has a term with a zero J value and hence no structure. The three lines have a common lower term $5s^3S_1$, the upper terms being $5p^3P_0$, 3P_1 , 3P_2 respectively. The structure of the line $\lambda 5164.4$ $5s^3S_1 - 5p^3P_0$ gives that of the term $5s^3S_1$. From this, the structures of the upper $5p^3P_1$ and $5p^3P_2$ terms follow as shown by fig. 1. The agreement between the predicted and the observed patterns is reasonably good and $5s^3S_1$ is not fully resolved.

The term $5s^5S_2$ will give rise to regular quartets in lines for which the upper terms have narrow structure. The two lines $\lambda 4193.5$ and 4230.0 have a common lower term $5s^5S_2$. Since the structures of the upper terms $5p^3P_1$ and $5p^3P_2$ have been derived above, these lines give the structure of the term $5s^5S_2$. The two central components of $\lambda 4230$ are not properly resolved.

The lines λ 4816.7, 4785.5 and 4704.9 have well resolved quartet patterns. The structures in these lines are essentially those of the term $5s^5S_2$ and the number of components directly gives the spin. The analysis is

TABLE I.
Hyperfine structures, of classified Br II lines.
Units $\text{cm.}^{-1} \times 10^{-3}$.

Wavelength	Allocation	Structure		Class
		Red	Violet	
5238.2	$5s^3S_1-5p^3P_1$	0	95	C
		(1)	(2)	
5182.4	$5s^3S_1-5p^3P_2$	0	38 93	B
		(1)	(2) (3)	
5164.4	$5s^3S_1-5p^3P_0$	0	48	C
		(1)	(2)	
4848.8	$5p^5P_3-6s^5S_2$	Borad single-width		
			50	
4816.7	$5s^5S_2-5p^5P_1$	0	154 264 323	A
		(5)	(3) (2) (1)	
4785.5	$5s^5S_2-5p^5P_2$	0	125 213 270	B
		(4)	(3) (2) (2)	
4766.0	$5s^5P_2-6s^5S_2$	0	65	C
		(2)	(1)	
4735.4	$5p^5P_1-6s^5S_2$	0	76	B
		(2)	(3)	
4704.9	$5s^5S_2-5p^5P_3$	0	130 219 274	A
		(5)	(3) (2) (1)	
4396.4	$5p^3P_2-4d^5D_2$	0	— 75	C
		(1)	(1)	
4356.9	$5p^3P_1-4d^5D_2$	Single		
4230.0	$5s^5S_2-5p^3P_1$	0	188 270	B
		(3)	(2) (1)	
4193.7	$5s^5S_2-5p^3P_2$	0	130 219 280	B
		(4)	(3) (2) (1)	
3980.4	$5p^5P_3-4d^5D_4$	0	— 49	C
		(2)	(1)	
3980.0	$5p^5P_3-4d^5D_3$	Single		
3935.2	$5p^5P_2-4d^5D_1$	Width 50		
3914.5	$5p^5P_1-4d^5D_1$	Single		
3914.1	$5p^5P_1-4d^5D_0$	Single		

illustrated in fig. 2 giving the structures of the upper terms $5p^5P_1$, 5P_2 and 5P_3 . The agreement between the predicted and the observed values is good.

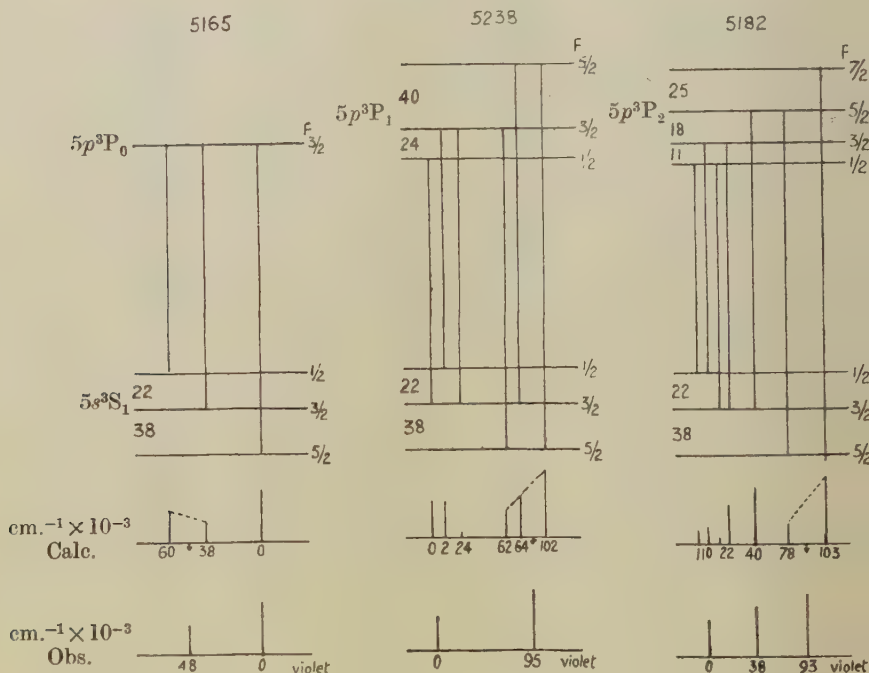
TABLE II.
Hyperfine structures of unclassified BrII lines.
Units $\text{cm.}^{-1} \times 10^{-3}$.

Wavelength	Structure			
	Red	Violet		
4921.3	0 (1)	112 (3)		
4802.3	434 (1)	337 (2)	188 (3)	0 (5)
4742.7	0 (5)	122 (3)	198 (1)	237 (1)
4728.2	Single			
4719.8	0 (2)	59 (2)	119 (5)	
4693.3	0 (6)	144 (3)	218 (1)	384 (1)
4678.7	Single			
4542.9	0 (1)	121 (2)	254 (5)	362 (9)
4365.6	0 (2)	67 (2)	156 (3)	
4351.2	0 (5)	176 (3)	344 (1)	
4297.8	0 (3)	156 (1)	246 (1)	
4291.4	0 (9)	158 (6)	266 (4)	364 (3)
4223.9	118 (3)	0 (10)	215 (5)	341 (2)
4179.6	0 (7)	146 (2)	232 (5)	
4140.4	Single			
4135.9	Single			
3986.3	132 (1)	0 (10)	205 (3)	338 (5)
3970.6	Single			
3968.3	0 (9)	129 (6)	224 (4)	
3955.4	Single			
3950.6	Single			

The lines λ 4766.0, 4735.4 and 4848.8 have complex structures. Except for λ 4735.4, the components are closely packed so that resolution is poor. λ 4848, appears as a broad single line pattern of width $50 \text{ cm.}^{-1} \times 10^{-3}$. The structure of the $6s^5S_2$ term is obtained from these lines.

The group of $4d^5D$ terms combines with the $5p^3P_{012}$ and $5p^5P_{123}$ multiplets which have narrow structures. Most of the lines from these transitions appear single but $\lambda 3980.9$ shows two blended components. Therefore the 5D terms have all narrow structures. The width of $\lambda 4396.4$ enables an estimate to be made of the structure of $5d^5D_1$ while from $\lambda 3980$, the total width of $4d^5D_4$ can be estimated. The line $\lambda 3935$ gives an approximate structure of the term $4d^5D_1$. There is no check available.

Fig. 1.



§ 5. DISCUSSION.

Table III. shows the term hyperfine structures derived. A minus sign before the first interval implies that the whole structure is inverted, the highest F value lying deepest.

The term interval factors derived from these structures are given in the last column of the same table.

The $5s^5S_2$, $6s^5S_2$ and $5s^3S_1$ terms are spherically symmetrical and are not therefore affected by any nuclear electric quadrupole moment which leads to deviation from the interval rule in the arc spectrum of bromine for some lines. For these terms, the interval rule should be strictly obeyed unless perturbations are caused by configuration interaction. The structures of these terms as determined here show that the interval rule is obeyed within the limits of measurement.

Fig. 2.

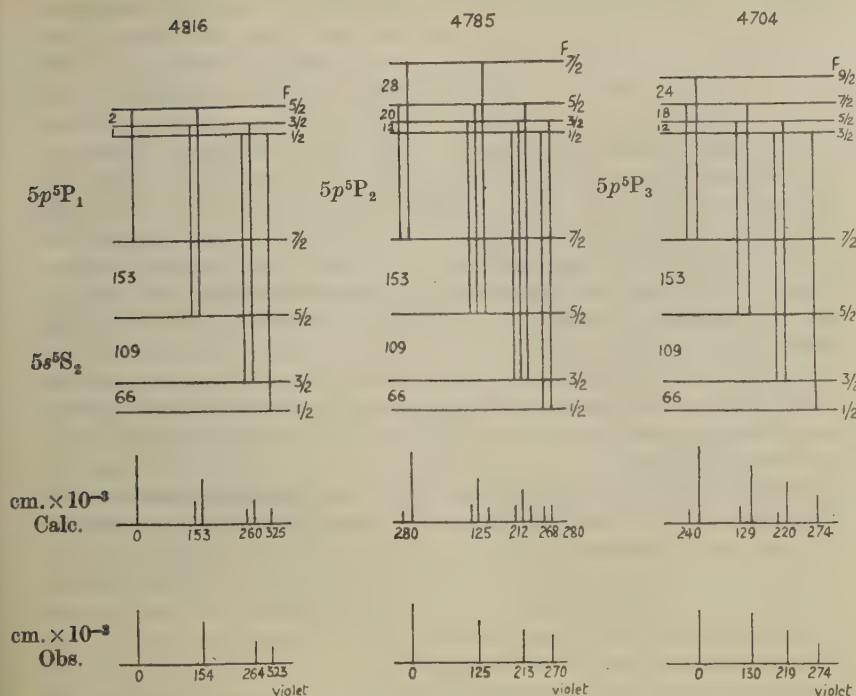


TABLE III.

Hyperfine Structures in the terms of BrII—Intervals.

Configuration	Term	Structure cm. ⁻¹ × 10 ⁻³			Interval factors cm. ⁻¹ × 10 ⁻³
4s ² .4p ³ .5s	⁵ S ₂	153	109	66	44
	³ S ₁	-38	22		-14
4s ² .4p ³ .5p	⁵ P ₃	24	18	12	5
	⁵ P ₂	28	20	12	8
	⁵ P ₁	2	1		1
	³ P ₂	25	18	11	6
	³ P ₁	40	24		16
	³ P ₀				0
	⁵ S ₂	36	27	15	10
4s ² .4p ³ .6s	⁵ D ₄	Very small.			
4s ² .4p ³ .4d	⁵ D ₃	Very small.			
	⁵ D ₂	-21	15	9	-6
	⁵ D ₁	10	6		4
	⁵ D ₀				0

The interval factor for the term 5s⁵S₂ is about four times that of the term 6s⁵S₂. This is similar to what was found by Tolansky and Forester (1938) for the first spark spectrum of iodine. These terms arise from the

addition in parallel of an s -electron to the electron core of the basic ion term $4p^3.4S_{3/2}$ of the doubly ionized bromine atom, according to the coupling theory of White (1930). Thus from the smallness of the interval factor of the $6s^5S_2$ term, it follows that the coupling of the $4p^3$ group is small. The term 3S_1 is formed by the addition of an s -electron, anti-parallel to the $4p^3$ group of BrIII. The interaction energy is proportional to $\cos JS$ which is equal to -1 in this case. Thus the interval factor for the 3S_1 term should be negative and numerically smaller than the positive interval factor of the term 5S_2 . The value of the interval factor for 3S_1 as found here ($-14 \text{ cm.}^{-1} \times 10^{-3}$) fits in the above theory. The magnitude, however, suggests that the coupling constant of the $4p^3$ electrons is about $4/7$ ths that of the $5s$ -electron. This is not as small as one would expect from the interval factor of the $6s^5S_2$ term. The interval factors of the $4d^5D$ terms are small and this suggests that the coupling of the $4p^3$ group is not strong since a $4d$ electron is not expected to possess penetrating properties. In contrast to singly ionized iodine, the coupling of the $4p^3$ electron group in BrII is weak and the interval factor of the $5s^3S_1$ term rather larger than would be expected under these circumstances. In BrI, the group $4p^5$ has a large coupling constant. This may mean that there is a change in the nature of the electron coupling, in moving from the $4s^2.4p^3$ to $4s^2.4p^4$ configuration. This can also be inferred from the fact that contrary to expectations the singly ionized bromine atom shows structures which are no wider than those of the neutral bromine atom.

No anomalies appear except for $\lambda 4356.9$. It is a transition from the $4d^5D_2$ to the $5p^3P_1$ term. The structure of this line, which appears as a sharp single, does not fit in with the observed structures of the two terms involved. It is possible that the line is wrongly classified.

Regarding the unclassified lines these can be arranged in groups showing similar structures. The two lines $\lambda 4223.9$ and $\lambda 3986.3$ have similar structure suggesting that they involve the same common term. This is substantiated by the Zeeman splittings given by Lacroute. The lines $\lambda 4719$ and $\lambda 4365$ both show a triplet structure roughly of the same order while the three lines $\lambda 4297$, 4179 and 3968 have similar patterns. From the data on Zeeman effect given by Lacroute, it seems that none of these lines can belong to the classified levels of the $4S$ system.

ACKNOWLEDGMENTS.

My thanks are due to Professor S. Tolansky for his constant interest and kind continual encouragement during the progress of this work.

REFERENCES.

- LACROUTE, 1935, *Ann. Phys. Paris*, **3**, 5.
 TOLANSKY, 1932, *Proc. Roy. Soc. A.*, **136**, 585.
 TOLANSKY and FORESTER, 1938, *Proc. Roy. Soc. A.*, **168**, 78.
 TOLANSKY and TRIVEDI, 1940, *Proc. Roy. Soc. A.*, **175**, 366.
 WHITE, 1930, *Proc. Nat. Acad. Sci.*, **16**, 68.

XXXIII. *The Electrical Resistance of Gold, Silver and Copper at Low Temperatures.*

By E. MENDOZA and J. G. THOMAS,
H. H. Wills Physical Laboratory, University of Bristol*.

[Received January 19, 1951.]

ABSTRACT.

A brief review of published papers on the subject of electrical resistance at very low temperatures shows that several metals exhibit a feature which has not yet been explained theoretically, namely that the resistance goes through a minimum value as the temperature decreases, whereas present theories indicate that it should remain constant. An apparatus is described for measuring electrical resistance below 1°K. ; by means of its use, the effect was confirmed in gold and silver and also found in copper. There was no tendency for the curves to flatten off even at the lowest temperatures. The gold behaved in magneto-resistance experiments as if it contained less than 1 part in 10^6 of ferromagnetic impurity. Slight anomalies in the shapes of some of the curves seem also to exist.

§ 1. INTRODUCTION.

AT very low temperatures it is regarded as usual behaviour for the electrical resistance of a non-superconducting metal specimen to fall to a value which is constant, independent of temperature. The accepted explanation is that when the thermal vibrations of the lattice are negligible, the mean free path for electron scattering, which determines the electrical resistance, is constant with temperature, being in turn limited only by the imperfections in the crystal lattice. The imperfections include foreign impurity atoms and "physical" impurities such as dislocations, a mosaic crystal structure or other departures from perfect regularity, which do not change with temperature.

A considerable number of exceptions to this rule have however been noted. Among metals whose resistance begins to increase again as the temperature is decreased, the best known is gold which has been the subject of several investigations at liquid helium temperatures (Meissner and Voigt 1930, de Haas, de Boer and van den Berg 1934, de Haas and van den Berg 1936, 1937, Giaque, Stout and Clark 1937, de Haas, Casimir and van den Berg 1938, Stout and Barieau 1939, Nakhimovich 1941, Garfunkel, Dunnington and Serin 1950). Of a number of specimens of silver which have been investigated, one was found to exhibit the same phenomenon (de Haas and van den Berg 1936). Similar behaviour was

* Communicated by Dr. L. C. Jackson.

noted in gallium by Keesom (1933), and in sodium, magnesium, aluminium, molybdenum, cobalt, and cerium by Meissner and Voigt (1930). Sodium had been previously found to exhibit an increase with decreasing temperature by Woltjer and Kamerlingh Onnes (1924); the specimen measured by Justi (1948) exhibited a decrease at low temperatures while MacDonald and Mendelssohn (1950) found "normal" behaviour for a purer specimen. Keesom (1934) and more recently Garfunkel, Dunnington and Serin (1950) and MacDonald and Mendelssohn (1950) have confirmed the effect in magnesium. Keesom (1933) apparently observed a minimum for aluminium, but Boorse and Niewodniczanski (1936) and Garfunkel, Dunnington and Serin (1950) found no minima for their specimens of aluminium, while Steiner and Fünfer (1936) found none for molybdenum.

The phenomenon in gold is regarded as one not merely due to spurious causes; the effects of varying the measuring current, of attaching the electrical leads to the specimens differently, and of varying the heat treatment of the metal were all eliminated by de Haas and van den Berg (1937). The phenomenon still occurred in specimens for which no trace of ferromagnetic impurity was quoted, but the possible effect of such impurities may nevertheless be important and is dealt with later in the present paper.

Among suggestions as to the cause of the phenomenon there are those due to Justi (1942) that it is a size effect and Gorter (1938) that it may be a thermodynamic necessity—both of which have been criticized by MacDonald and Mendelssohn (1950)—while Lane (1949) has suggested that scattering at grain boundaries may play a part, though this mechanism would not seem to lead to a variation of resistance with temperature. The theory of Vonsovsky (1940) apparently refers to electric fields which are many orders of magnitude greater than those encountered experimentally. Sondheimer and Wilson (1947) have treated the problem of electrical resistance using a model more complicated than the free-electron model and have shown that at intermediate temperatures the resistance cannot be split up into two additive components (temperature-variable and temperature-independent). They assume from the outset, however, the existence of a temperature-independent residual resistance at very low temperatures. The interactions introduced by Fröhlich (1950) into the free electron model to account for the phenomena of superconductivity seem to have no bearing on the present problem.

It is an open question whether the rise in resistance continues as the temperature is decreased, particularly below 1° K. The only experiment so far performed in this region is that of Casimir, de Haas and van den Berg (1938) on gold. They showed that the rise did continue but the accuracy of their results was apparently impaired by poor thermal contact between the gold wire and the paramagnetic salt used to attain the low temperature. The present experiments are an attempt to repeat

this work—measurements being also taken throughout the liquid helium range, 4.2° K. to 1° K.—and to extend it to other metals; this report presents preliminary results.

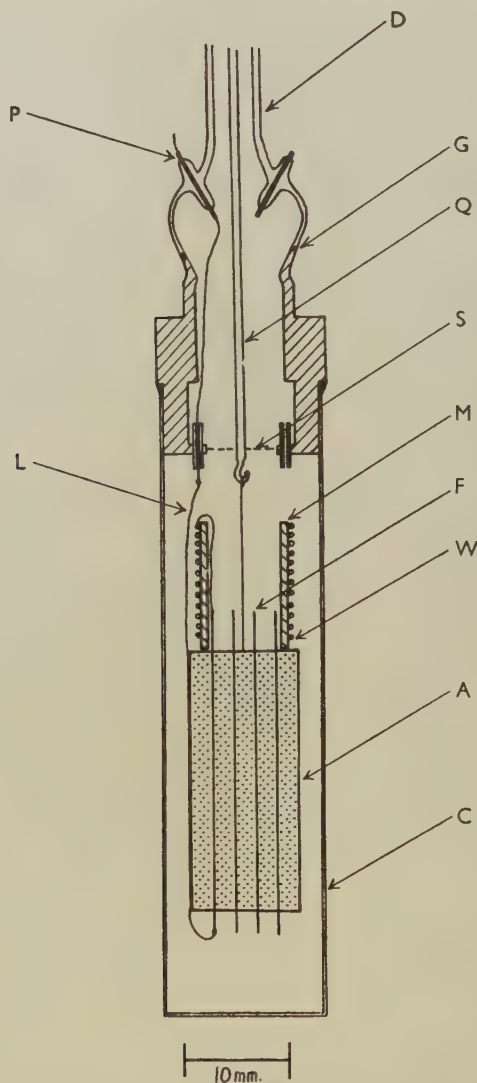
§ 2. APPARATUS.

A method has been described (Mendoza 1948) for establishing thermal contact between a metal specimen and a paramagnetic salt cooled by adiabatic demagnetization below 1° K. The metal specimen is joined to copper fins of comparatively large surface area embedded inside the pill of compressed powdered salt. When the salt is demagnetized, the metal cools. If power is then generated in the metal specimen—for instance, by the passage of a measuring current—a temperature difference is set up between the metal and the salt. Other things being fixed, this temperature difference increases rapidly with decreasing temperature; its order of magnitude may be estimated, and it can be made small if the dissipating area of the fins is made large enough. At the same time, the provision inside the salt of layers of metal of comparatively high thermal conductivity is advantageous, reducing the inhomogeneities of temperature which might otherwise persist inside the salt and lead to errors of measurement.

An apparatus embodying these data was constructed for resistance measurements; the low-temperature part, which was immersed in a liquid helium bath, is shown in fig. 1. The salt A—iron or chrome alum—was cylindrical in external form, 12.5 mm. in diameter and about 30 mm. long, and contained four or more copper fins F, 5 mm. wide, 0.1 mm. thick, placed parallel to one another, running the whole length of the salt and projecting from the ends. The fins had a number of small holes cut in them to increase the mechanical strength of the block of salt; their total surface area was approximately 12 cm.^2 . The assembly was made in one operation by pressing in a suitable die. M was a former, a hollow cylinder of copper, 10 mm. external diameter, 0.5 mm. thick and 16 mm. long. It had a spiral groove on its outside, deep enough to hold, without strain, the wire W whose resistance was to be measured, and the surface was insulated with a thin covering of a bakelite varnish. M was connected by a wire to one of the fins. With this construction consistent results were obtained. The ends of the specimen W were joined to short potential and current leads connected separately to the fins. The other ends of the fins were soldered to superconducting leads (of which one is shown at L), made most conveniently from 0.03 mm. diameter constantan wire, tin plated electrolytically then covered with a thin layer of soft solder. Such leads were found to be robust, flexible and easy to solder and to have a high thermal resistance. They passed from the fins, along the outside of the salt and joined on to platinum wires which passed through platinum seals such as P into the helium bath, the length of lead between the salt and the platinum wire being about 5 cm. The magnetic susceptibility of the salt was measured by a static (Gouy) method, since

this ensured freedom from the eddy current heating in the fins and wire which might have occurred had dynamic methods been used. A was suspended by a nylon thread from a quartz rod Q, attached in turn to

Fig. 1.



a Sucksmith balance (Sucksmith 1929, Jackson 1933) at the top of the cryostat. A number of flat spiral springs retained the quartz rod centrally inside the glass down-tube D; the lowest of these springs, S, also served

to maintain the top of the nylon thread at the temperature of the helium bath. The assembly was housed in a thin-walled calorimeter C, G being a copper-glass seal. Contact gas could be introduced into the calorimeter and pumped away again.

The dimensions of the wire specimen W were chosen as follows. The smallest voltage that could be measured with the given potentiometer to the required degree of accuracy ($50\text{ }\mu\text{V.}$ to 0.2 per cent in our case) was one datum, the other was the need to limit the power dissipation in the wire to a value determined by the area of the fins and the maximum tolerable uncertainty of temperature (in our case, the order of 10^{-1} erg/sec. giving a difference of less than 10^{-3} deg. at 10^{-1} °K. and 3×10^{-3} deg. at 6×10^{-2} °K.; the heat conducted down the leads L also had to be dissipated but this was calculated to be less than 10^{-2} erg/sec. and was negligible). These conditions defined the resistance of W and the measuring current (0.25 ohm and 0.2 ma.), and, when using good conductors like gold, compelled the use of long thin wires. It was then necessary however to check that two further conditions were satisfied. The first was that the diameter so determined was sufficiently great, compared with the mean free path for electron scattering, for the effect on the electrical resistance of scattering by the surface of the wire to be negligible (in our case the diameter was usually at least 10 times the mean free path). The second condition concerned the temperature distribution along the length of the wire; had the wire been thermally isolated from its surroundings, except for ends maintained at the temperature of the fins, its temperature would have varied approximately parabolically along its length because of the generation of Joule heat at all points. In practice, an imperfect thermal contact probably existed with the former M, and the value of the temperature inhomogeneity calculated from estimates of the thermal conductivity of the wire represented an upper limit. Nevertheless the precaution was sometimes taken of connecting one or two points along W to separate fins. (With sections 20 cm. long, the maximum inhomogeneity of temperature was calculated to be of the order of 3×10^{-3} deg. at 10^{-1} °K. and 5×10^{-3} deg. at 6×10^{-2} °K. for most of our specimens.) A final restriction on the experimental conditions was to note that the warming time of the salt after demagnetization was sufficiently long compared with the thermal time-constant of the salt calculated from its known thermal diffusivity (Garrett 1950) and the linear dimension between fins. (This was easily satisfied, even for warming times as low as two hours.)

The above conditions allowed measurements of known maximum uncertainty to be made below 1° K. For measurements on the same specimens at liquid helium temperatures, contact gas was introduced into the calorimeter and the same measuring power introduced negligible errors of temperature. Those specimens which were measured only in the helium range were immersed directly in liquid helium; they were wound on a wax-coated mica cruciform, the wax being later dissolved away to leave the wire hanging freely. Again, during measurement the

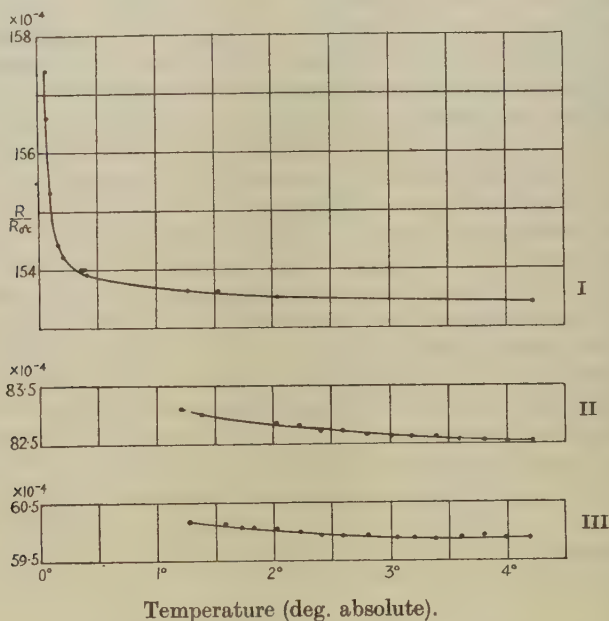
rise of temperature of the specimen above that of the bath, due to the Kapitza sub-surface layer of poor thermal conductivity (Kapitza 1941) was kept to a low value with the small power dissipation. (In some measurements done in the past on short, fat specimens of high electrical conductivity, this condition may not always have been satisfied.)

§ 3. RESULTS AND DISCUSSION FOR GOLD.

Measurements in Zero Magnetic Field.

The variations of resistance with temperature for three specimens are shown in fig. 2. All were from the same batch of material, the wires being

Fig. 2.



drawn by Johnson Matthey from their Lab. No. 3459 "by methods where there was virtually no likelihood that they should pick up ferromagnetic impurities", the spectroscopic analysis of the wire when 0.5 mm. diameter showing the presence of Fe and Ni (all sensitive lines) with Ag, Cu and Mg lines faintly visible and Sn and Na very faintly visible. The specimens were as follows: Curve I., diameter 0.025 mm. not annealed, measuring current 0.18 ma.; curve II. 0.025 mm. diameter, annealed *in vacuo* for two hours at 500°C., measuring current 5.1 ma.; curve III., 0.10 mm. diameter, same heat treatment as II., measuring current 20 ma.

It is seen that the resistance still continues to rise at the lowest temperatures reached. van der Leeden (1940) found a term proportional to the concentration of chemical impurity and varying as $T^{-\frac{1}{2}}$ to fit the Leiden results; our results do not fit any simple power law but vary more strongly with temperature than $T^{-\frac{1}{2}}$. Our curves tend to rise more steeply with increasing minimum resistance, in agreement with the observations of previous workers.

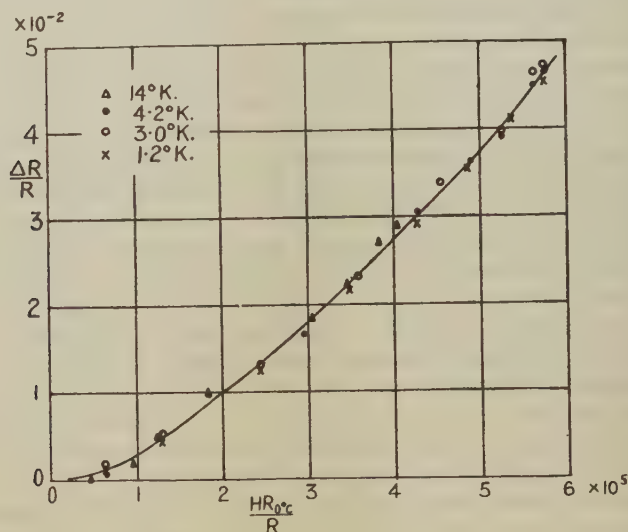
Magnetoresistance Experiments.

Magnetoresistive effects are conveniently shown on Kohler diagrams, where the fractional increase in resistance $\Delta R/R$ is plotted as a function of $H \cdot R_{0^\circ C}/R$, where H is the applied field; curves for different temperatures are then usually superposable (see for example Blom (1950), where however the curve for gold is wrongly drawn). However, Stout and Barieau (1939) found that for a gold wire of high minimum resistance ($R/R_{0^\circ C} \sim 650 \times 10^{-4}$), which exhibited a marked rise of resistance in the helium range, the magnetoresistance curve for transverse fields at 1.5°K. lay well below that at 4.2°K. The indication was that the effect would have been zero at approximately 1°K. ; below this temperature it would presumably have changed sign and a negative magnetoresistance effect was in fact found at 1.5°K. in another specimen by Giauque and Stout (1938). Previously Meissner and Scheffers (1929) noted a negative effect at one temperature, 4.2°K. , with a gold wire in small fields. The anomaly was attributed to ferromagnetic impurity in the wire and this was confirmed by Nakhimovich (1941) who made a careful study of the effect of adding iron impurity to the gold. He found that the deviations from Kohler's rule, including a negative magnetoresistance effect, could be observed with gold wires in which of the order of 10^{-2} per cent of iron was dissolved; the presence of the iron made the metal paramagnetic at low temperatures, and of high minimum resistance. The magnetoresistive change could be considered as consisting of two approximately additive components: a "normal" positive component, and an "anomalous" negative component, which was due to the presence of the iron; the positive component could be increased with respect to the other by annealing.

We have measured the transverse magnetoresistance effect in fields up to 10 kilogauss with gold wires from the same batch as those used for measurements in zero field. No anomalous effects were noted, curves from 14°K. down to 1.2°K. being shown in fig. 3; the facts that these are closely superposable and that plotted on a reduced Kohler diagram (Blom 1950) they join on to high-temperature curves for gold and silver seem, in view of the results of Nakhimovich, to indicate that the specimens were free from ferromagnetic impurity—even more free than Nakhimovich's purest specimens. It is possible to make a rough estimate of an upper limit of the concentration of iron in our specimens, by assuming first that Kohler's rule holds for iron-free specimens, and secondly that the

percentage difference between the magnetoresistance effects at approximately 4.2°K. and 1.3°K. for specimens containing iron is proportional to the concentration. On the basis of the trend of the points in fig. 3, compared with the data for Nakhimovich's specimen 13 and Stout and Barieau's specimen, 10^{-4} per cent is set as this upper limit. Though this does not demonstrate that the rise of resistances in zero field takes place in the absence of all ferromagnetic impurity, it would nevertheless seem surprising if 1 part in 10^6 of dissolved iron impurity were the cause of increases plotted in fig. 2.

Fig. 3.

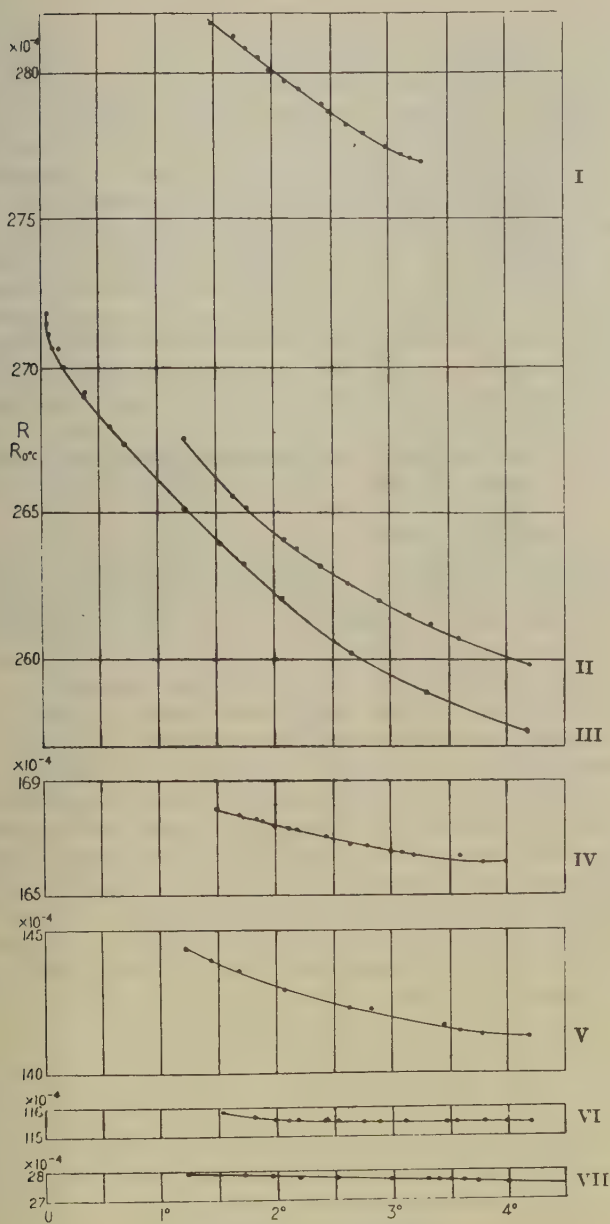


§ 4. RESULTS AND DISCUSSION FOR SILVER.

Measurements in Zero Magnetic Field.

The silver specimens were all 0.05 mm. diameter, drawn by Johnson Matthey from their Lab. No. 3406. Spectrographic analysis of the original silver showed the presence of Fe, Mg, Mn, Pb, Si, Cd (faintly visible) and Sn, Na, Cu (very faintly visible). Some resistance-temperature curves are shown in fig. 4. Details of the specimens are as follows: Curves I., II. and III., specimens not annealed; measuring currents 14.5, 2.5, and 0.18 ma. respectively. Another specimen Ag3 gave a curve which coincided within very small limits with curve III. between 4.2 and 1.23°K. , (12 ma. measuring current.) It was then annealed for two hours at 450°C. in a vacuum of better than 10^{-5} mm.; curve IV. was then obtained with 14.5 ma. measuring current. It was then given three further heatings to 600°C. in helium gas; curve VI. was later observed using 14.7 ma. measuring current. This specimen was also used for magnetoresistance

Fig. 4.



Temperature (deg. absolute).

experiments. Curve V. was for a specimen given the same heat treatment as that for curve IV., with 21 ma. measuring current. Curve VII. is taken for comparison from de Haas and van den Berg (1936) and is for a specimen of Hilger silver drawn down to 0.06 mm. diameter, annealed *in vacuo* at 450–500° C. for three hours; measuring current not stated.

The increase of resistance with decreasing temperature occurs with all specimens, implying minima in the curves above the helium range. The curves do not fit any simple power law. There is a general tendency for them to rise more sharply as the minimum value of the resistance increases, but this is not observed exactly. As remarked by de Haas and van den Berg (1937) concerning their work on gold, variations in the shape of the curves for unannealed specimens are not unexpected but there exists also a lack of homogeneity between the curves for the annealed specimens, which one might have expected all to have belonged to the same family. The anomalies observed by MacDonald and Mendelssohn (1950) in the resistance-temperature curves of potassium and caesium may be in some way analogous to these variations. It is also possible that the effects of dissolved gases, undetected spectroscopically, but capable of varying in amount and distribution on annealing, may be important.

Magnetoresistance Experiments.

The specimen measured by Stout and Barieau (1939) (which in zero field gave $R/R_{0^\circ\text{C.}} = 194.2 \times 10^{-4}$, constant throughout the helium range) followed Kohler's rule in its transverse magnetoresistive behaviour, their curves for temperatures from 20.3° K. down to 1.54° K. being closely superposable; the dotted line in fig. 5 is for this specimen.

Our specimen Ag3 however gave different results, similar in some but not all respects to the results for gold contaminated with iron. In fig. 5 are shown the curves in transverse fields at 4.2° K. and 1.23° K. for the specimen before annealing. After the first annealing however the effect plotted in this way was quite unchanged, though the resistance at any temperature had been greatly reduced. As mentioned above Nakhimovich noted a different result for gold, namely a tendency to reduce the departures from Kohler's rule after annealing. It is conceivable that this difference of behaviour is in some way connected with the fact that iron, though it can dissolve in gold, is insoluble in silver (Constant 1945) so that the effects of annealing on the impurity are likely to be very different.

§ 5. RESULTS AND DISCUSSION—COPPER.

Three samples of enamel-covered commercial copper wire were investigated, and the results are shown in fig. 6. All samples showed traces of Ca, Cd, Mg, Si, Pb, Mn and Zn on spectroscopic analysis, the total impurity content being estimated at less than 10^{-2} per cent. The wire for Curve I. was 0.035 mm. diameter, and the measuring current 0.2 ma.; for Curve II. 0.05 mm., 0.18 ma.; for Curve III. 0.10 mm., 4.5 ma. None was annealed. The comparative lowness of the residual

Fig. 5.

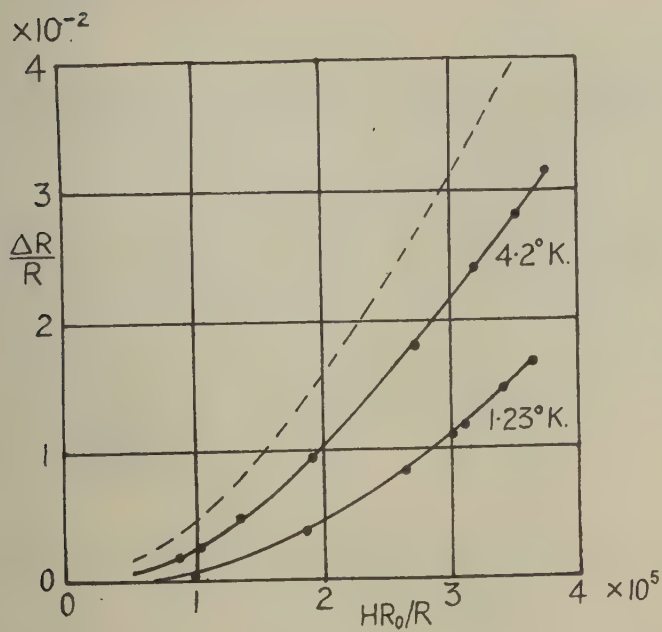
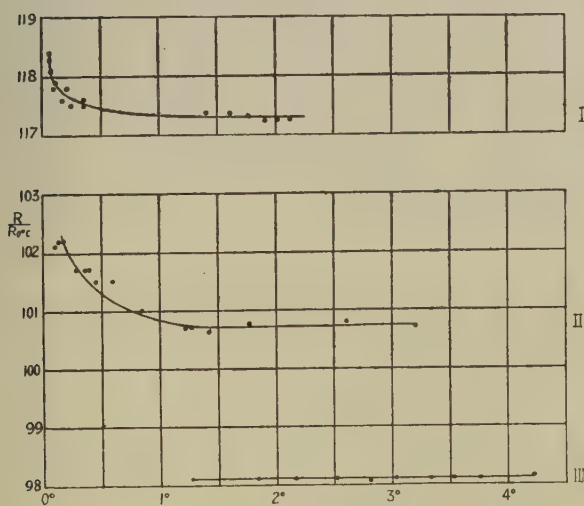


Fig. 6.



Temperature (deg. absolute).

resistances was unexpected when Curves I. and II. were measured, with the result that the measuring accuracy for both these curves was not high. The rise of resistance at the lowest temperatures is nevertheless outside experimental error.

One further sample from a reel of copper wire, 0.035 mm. in diameter, of curious composition was also investigated. It contained 0.94 per cent of Sn, and also showed traces of Mn. It had a very high resistance at helium temperatures (Allen 1933), and the following values of R/R_0 at 0°C . were noted: 4.19°K ., 0.4322; 2.50°K ., 0.4324; 1.46°K ., 0.4325; 0.418°K ., 0.4326; 0.067°K ., 0.4327.

Previous investigations of copper have given the following results. The readings of Meissner and Voigt (1930) show variations at liquid helium temperatures which are probably due to experimental error. de Haas and van den Berg (1934) found that the curves for several samples of pure copper were not parallel at liquid hydrogen temperatures; van den Berg (1948) found that unannealed technical copper wires gave constant residual resistances at liquid helium temperatures.

No magnetoresistance measurements have so far been taken on copper.

§ 6. CONCLUSION.

It appears from previously published work and from our own experiments that the rise of resistance at very low temperatures is a phenomenon occurring in a fairly large number of metals. It has only been noted so far in specimens which were far from being ideally pure, but in any case theory gives no indication as to the cause of the rise in connection either with pure or impure metals. It remains undecided, however, whether the rise is to be associated with the presence of small amounts (less than 1 part in 10^6 in our gold specimens) of ferromagnetic impurity. It also appears to be a fairly common occurrence that resistance-temperature curves for different specimens of a given metal do not always vary from one to another in a simple manner as the impurity is varied (see for example the curves for copper given by de Haas and van den Berg (1934) and our own curves for silver (above)). Presumably this means that different impurities may produce curves of the same minimum value of resistance but of different shapes.

ACKNOWLEDGMENTS.

The thanks of the authors are due to Dr. L. C. Jackson for much help and advice at all stages of the work, to the other members of the low temperature Group for assistance during experiments, and to Professor N. F. Mott for discussions.

The analyses of the copper wires were kindly carried out by the Research Department of the National Smelting Co., Avonmouth, and by the City Analyst, Bristol.

One of us (J. G. T.) is in receipt of a grant from the Department of Scientific and Industrial Research.

REFERENCES.

- ALLEN, J. F., 1933, *Phil. Mag.* [7], **16**, 1005.
 BLOM, J. W., 1950, *Physica*, **16**, 152.
 BOORSE, H. A., and NIEWODNICZANSKI, H., 1936, *Proc. Roy. Soc. A*, **153**, 463.
 CONSTANT, F. W., 1945, *Revs. Mod. Phys.*, **17**, 81.
 DE HAAS, W. J., DE BOER, J., and VAN DEN BERG, G. J., 1934, *Physica*, **1**, 1115.
 DE HAAS, W. J., CASIMIR, H. B. G., and VAN DEN BERG, G. J., 1938, *Physica*, **5**, 225.
 DE HAAS, W. J., and VAN DEN BERG, G. J., 1936, *Physica*, **3**, 440 ; 1937, *Ibid.*, **4**, 683.
 FRÖHLICH, H., 1950, *Phys. Rev.*, **79**, 845.
 GARFUNKEL, M. P., DUNNINGTON, F. G., and SERIN, B., 1950, *Phys. Rev.*, **79**, 211.
 GARRETT, C. G. B., 1950, *Phil. Mag.* [7], **41**, 321.
 GIAUQUE, W. F., and STOUT, J. W., 1938, *J. Amer. Chem. Soc.*, **60**, 388.
 GIAUQUE, W. F., STOUT, J. W., and CLARK, C. W., 1937, *Phys. Rev.*, **51**, 1108.
 GORTER, C. J., 1938, *Physica*, **5**, 483.
 JACKSON, L. C., 1933, *Proc. Roy. Soc. A*, **140**, 695.
 JUSTI, E., 1942, *Forschungen u. Fortschritte*, Berlin, **18**, 7 ; 1948, *Ann. Phys., Lpz.*, **3**, 183.
 KAPITZA, P. L., 1941, *J. Phys., U.S.S.R.*, **4**, 181.
 KEESOM, W. H., 1933, *Commun. Phys. Lab. Univ. Leiden*, No. 224c ; 1934, *J. Phys. Radium*, **5**, 373.
 LANE, C. T., 1949, *Phys. Rev.*, **76**, 304.
 MACDONALD, D. K. C., and MENDELSSOHN, K., 1950, *Proc. Roy. Soc. A*, **202**, 103, 523.
 MEISSNER, W., and SCHEFFERS, H., 1929, *Phys. Z.*, **30**, 827.
 MEISSNER, W., and VOIGT, B., 1930, *Ann. Phys., Lpz.*, **7**, 761, 892.
 MENDOZA, E., 1948, *Cérémonies Langevin-Perrin, Paris*, 53.
 NAKHIMOVICH, N. M., 1941, *J. Phys., U.S.S.R.*, **5**, 141.
 SONDHEIMER, E. H., and WILSON, A. H., 1947, *Proc. Roy. Soc. A*, **190**, 435.
 STEINER, K., and FÜNFER, E., 1936, *Congrès Int. du Froid, s'-Grav.*, **1**, 388.
 STOUT, J. W., and BARIEAU, R. E., 1939, *J. Amer. Chem. Soc.*, **61**, 238.
 SUCKSMITH, W. 1929, *Phil. Mag.* [7], **8**, 158.
 VAN DEN BERG, G. J., 1948, *Physica*, **14**, 111.
 VAN DER LEEDEN, P., 1940, *Thesis*, Leiden.
 VONSOVSKY, S. V., 1940, *J. Phys., U.S.S.R.*, **2**, 113.
 WOLTJER, H. R., and KAMERLINGH ONNES, H., 1924, *Commun. Phys. Lab. Univ. Leiden*, No. 173 a.

XXXIV. *On Pair Production by Fast Electrons.*

By J. E. HOOPER, D. T. KING and A. H. MORRISH,
The H. H. Wills Physical Laboratory, University of Bristol *.

[Received January 18, 1951.]

[Plate XIII.]

SUMMARY.

A study has been made of electron "pairs" directly produced by fast electrons in photographic emulsions. Evidence is presented to show that this process is of importance in the development of electromagnetic cascades present in the "soft" component of the cosmic radiation. It is found that the variation with energy of the cross-section for the interaction agrees with that predicted by theory.

§ 1. INTRODUCTION.

OBSERVATIONS on the creation of electron "pairs" by fast electrons in photographic emulsions have been reported by Occhialini (1949) and by Bradt, Kaplon and Peters (1950). In this laboratory we have now searched, with immersion objectives, 2.8 cm.³ of electron-sensitive emulsion exposed to the cosmic radiation at an altitude of 22 km.; and we have found 80 examples of these so-called "trident" or "giraffe" events. Of these, the path-length in the emulsion, either of the "primary" or of the three "secondaries", is in 50 cases of sufficient length to permit a determination of the energy of the primary electron by the scattering method.

In favourable examples it is possible to make measurements of the energy of all the particles associated with a given "trident". In almost all such cases, we have found that the energy of the primary particle is equal to the sum of the energies of the out-going particles, within the limits of experimental error. Such a conservation of energy is confirmed by the work of Dilworth *et al.* (1950), who have, in addition, found strong evidence that charge is also conserved in the interaction. In those events in which the energy of the primary particle cannot be directly measured we can, in favourable cases, infer it from the total energy of the three secondaries. In determining the energies of particles we have adopted scattering constants and procedures recently developed by our colleagues in this laboratory and shortly to be published.

The formation of secondary electrons as a result of interactions between fast charged particles and the Coulomb field of nuclei was suggested by Oppenheimer. Studies of theoretical aspects of such processes have been made by Furry and Carlson (1933) and many other authors. Bhabha (1935) has extended the treatment to include the effects of screening and gives an extensive bibliography to the earlier work.

* Communicated by Professor C. F. Powell, F.R.S.

§ 2. IDENTITY OF THE TRIDENT PARTICLES.

Two examples of tridents are shown in Pl. XIII. In A, two of the secondary particles originating at P are of relatively low energy and cannot have a rest-mass greater than $100m_e$. We may, therefore, with confidence, assume them to be electrons. Event B is typical of those in which the energy of the primary is shared almost equally among the three secondary particles. In such tridents, the origin is indicated by an apparent sudden increase in the grain density of the primary track, clearly seen at P. The collimation of the three tracks is so close that they are only just resolvable under high magnification at a point 300 microns from P; and they are not separated to the extent shown by event A until a point several millimetres from their origin has been reached.

A number of observations give strong support for the view that at least most of the primary charged particles which produce pairs are electrons. It is well known that there are difficulties, in principle, in distinguishing between the tracks of particles, of charge $|e|$ but of different rest-mass, when they are moving with great kinetic energy. Recent evidence from this laboratory strongly suggests, however, that the fast "shower" particles emerging from nuclear interactions are exclusively or almost exclusively, π -mesons or protons (Camerini *et al.* 1950). We have never observed pair-production by such a particle.

Further, the tracks of electrons of great energy can commonly be identified, if the length in the emulsion is greater than 2 cm., as a result of the reduction in energy of the particles through the creation of *bremssstrahlung*; and we have frequently observed such effects in dealing with the primary particles of tridents.

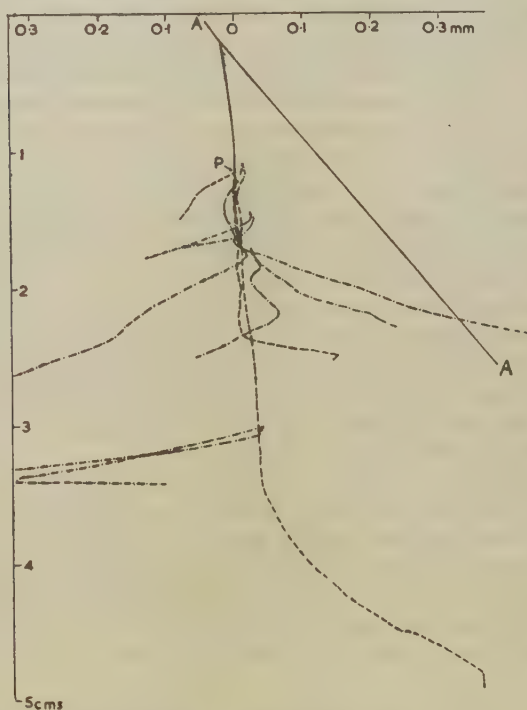
Finally, tridents are occasionally found to be produced by one of the components of an electron pair created by a photon; and in favourable cases, when there is a considerable length of path in the emulsion, they may be observed to be associated with electron cascade phenomena. An example of such an event is shown in the line drawing reproduced in fig. 1. In this case the primary particle of the trident is a fast recoil particle, almost certainly an electron, produced by an energetic heavy particle of charge $|e|$. The lateral scale in this diagram has been extended by a factor of 50, relative to the longitudinal, so that the characteristics of the different tracks may be displayed. The evidence for the electronic nature of the secondary particles is easier to obtain. They are frequently of such low energy that their rest-mass can be shown, as a result of scattering measurements, to be less than $100m_e$. We therefore regard the evidence as very strong that both the primary and secondary particles of the trident events are electrons.

§ 3. TRIDENTS AS A DISTINCT PHYSICAL PROCESS.

It has been suggested to us by Professor Peierls that the trident events might be due, not to the direct production of a pair of electrons by the charged primary particle, but to *bremssstrahlung* γ -rays, which by chance,

have converted to electron pairs at points very close to the track of the parent electron (Hooper and King 1950). In order to examine this point we have made the following observations:—In the searched area of the plates we have found 150 pairs which evidently occur as a result of the cascade process in the emulsion-glass assembly. Events of this type may be seen in fig. 1. The perpendicular distance R , from the point of origin of the pair to the nearest parallel track, has been measured in each of these examples, and the distribution in R is shown in fig. 2.

Fig. 1.



A reproduction of the tracks of a cascade shower plotted on a scale greatly extended laterally. AA represents the track of the heavy particle, and a trident is formed at P on the recoil electron track. The dashed lines indicate trident secondaries and the dot-dash lines the tracks of electrons from pairs.

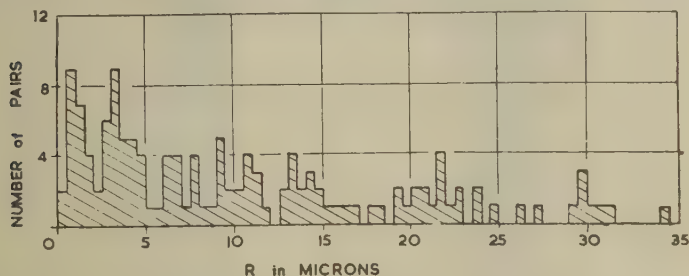
The magnitude and shape of this distribution at small values of R appears to be inconsistent with the view that the 80 tridents ($R < 0.25 \mu$), are due to the same process. In such a case the distribution in the values of R would include those for the tridents ($R < 0.25 \mu$) and would show a very sharp peak for very low values of R , followed by a slowly decreasing frequency from $R = 0.5 \mu$ to 20μ . We have not calculated the distribution in the values of R to be expected from cascade theory, for it involves

extensive integrations, but it appears certain that it could not yield a distribution such as is obtained if the tridents are attributed to the conversion of photons. We therefore regard the observations as providing very strong evidence that most of the tridents are due to the direct production of pairs of electrons in the interactions of fast electrons with atomic nuclei.

§ 4. THE CROSS-SECTION FOR TRIDENT PRODUCTION.

It appears to be possible, in principle, to determine the cross-section for the interaction leading to production of tridents, and its variation with energy, by measuring the total length in the searched area of the plates of electrons in different energy intervals: and by comparing the results thus obtained with the corresponding numbers of observed tridents. Such an experiment demands, however, a very extensive investigation, for it depends on an identification of the electrons by the methods to which we have already referred. For this purpose only particles of great range in the emulsion can be employed and they are rarely observed.

Fig. 2.



Distribution in the values of the perpendicular distance, R , from the pair origin to the nearest parallel track. There are 14 events with $R > 35$ microns. The 80 tridents ($R < 0.25 \mu$), found in the same volume, would contribute a peak in the first interval.

In these circumstances, we have determined the relative values of the cross-section as a function of the energy of the primary electrons. This can be done since the distribution in energy of the electrons in the plates employed has already been determined (Carlson *et al.* 1950). We assume the track length L —in the total volume of emulsion examined—due to electrons with energy between E and $E+dE$ to be represented by the equation

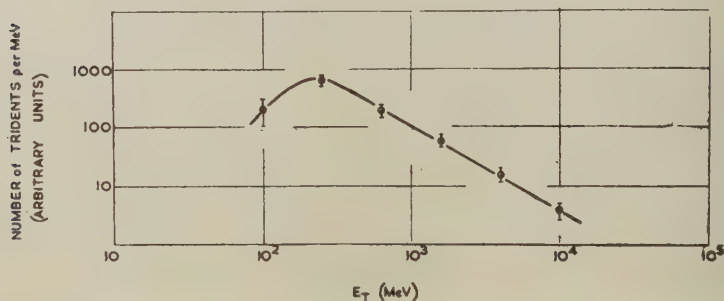
$$L(E) dE = aE^\gamma dE, \quad \dots \dots \dots (1)$$

where a is a constant, and $\gamma = -1.7$.

The distribution in the values of the energy of the primary particles of the 50 tridents on which it has been possible to make measurements, are shown in fig. 3. Fig. 4 shows the corresponding relative values of the cross-section for six energy intervals between 60 and 16,000 MeV.

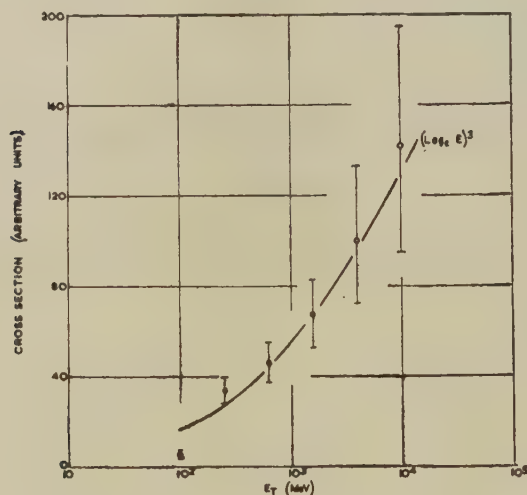
It is possible to determine a mean, absolute, value of σ over a very large energy interval, by considering those tridents which occur on one of the tracks of an electron pair created in the emulsion. These are then compared with the total track length of electrons, in the same energy interval, which originate in pair events in the emulsion.

Fig. 3.



The distribution, per unit energy interval, of the frequency of occurrence of tridents observed in Ilford G5 emulsions.

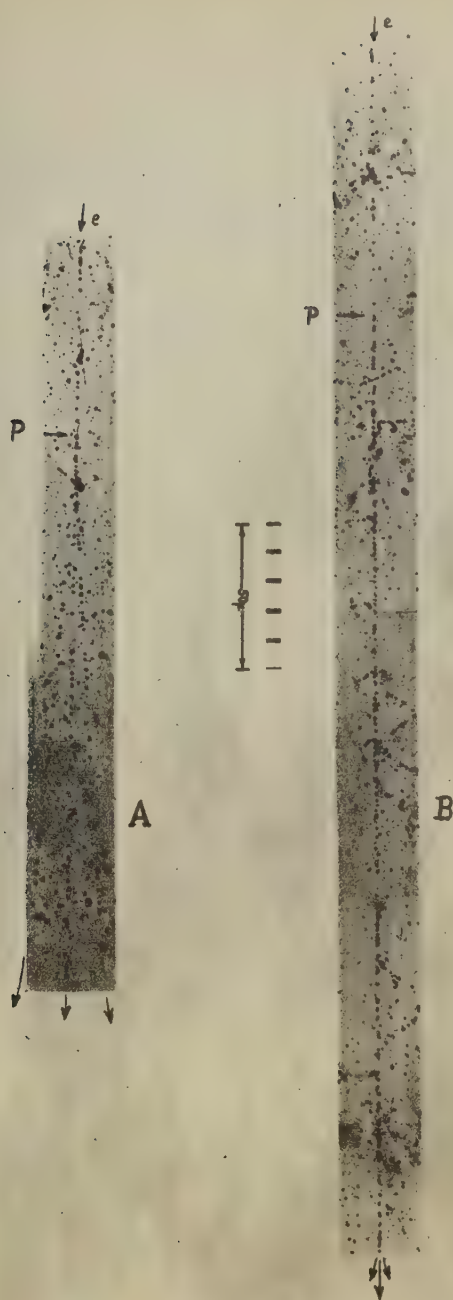
Fig. 4.



The observed variation with energy of the trident cross-section. The curve represents the theoretical variation normalized to the point at 1600 MeV.

It may be shown that the expected number of tridents in the energy interval from E_1 to E_2 is given by the relation

$$N_{E_1}^{E_2} = aK \int_{E_1}^{E_2} E^\gamma \left\{ \log \frac{E}{mc^2} \right\}^3 \cdot dE, \quad \dots \quad (2)$$



Examples of two tridents. The creation by a fast electron of a pair (A) of low energy and wide divergence may be contrasted with one (B) of high energy and marked collimation. In both events the primary energy is about 1.3×10^4 MeV.

where a is defined in (1) and K is a constant depending on the absolute cross-section. Since we have observed only four tridents to originate on an arm of a pair, the value of 80 cm. obtained for the trident "mean free path" at $E=10^3$ MeV. is subject to a large statistical error, of the order of 70 per cent. The observed value is, however, consistent with that calculated by Ravenhall; viz. 99 cm. It will presumably be possible, for values of E up to 300 MeV., to determine an accurate absolute value for the trident cross-section in experiments with electrons from high energy accelerators.

ACKNOWLEDGMENTS.

We are indebted to Professor C. F. Powell, F.R.S., for extending to us the hospitality and facilities of this laboratory. We also wish to thank Mrs. J. Cowie, Mrs. D. M. Ford, Miss J. Jones, Miss M. Jones and Miss J. Witchell for their assistance in collecting the data. The authors were supported by grants from the Department of Scientific and Industrial Research, the Medical Research Council and the National Research Council of Canada, respectively. This work has been carried out as part of a research programme supported by the Department of Scientific and Industrial Research.

REFERENCES.

- BHABHA, 1935, *Proc. Roy. Soc. A*, **152**, 559.
BRADT, KAPLON, and PETERS, 1950, *Helv. Phys. Acta.*, **24**, 23.
CAMERINI, FOWLER, LOCK, and MUIRHEAD, 1950, *Phil. Mag.*, **41**, 413.
CARLSON, HOOPER, and KING, 1950, *Phil. Mag.*, **41**, 701.
DILWORTH, GOLDSACK, GOLDSCHMIDT-CLERMONT, and LEVY, 1950, *Phil. Mag.*, **41**, 1032.
FURRY, and CARLSON, 1933, *Phys. Rev.*, **44**, 237.
HEITLER, 1944, *Quantum Theory of Radiation*, 2nd. Ed. (Oxford: University Press).
HOOPER, and KING, 1950, *Phil. Mag.*, **41**, 1194.
OCCHIALINI, 1949, *Nuovo. Cim. Supp.*, **6**, 3, 413.
RAVENHALL, 1950, *Proc. Phys. Soc. A*, **63**, 1177.

XXXV. CORRESPONDENCE.

Intrinsic Crystalline Structure and the Strength of Metals.

By W. A. WOOD,

The Baillieu Laboratory, University of Melbourne*.

[Received January 1, 1951.]

IN his paper "On the Strength of Quasi-Isotropic Solids", Fürth (1949) makes use of the idea that a solid contains an intrinsic block structure and derives a relation, similar to one obtained by Bragg, in which the strength varies inversely as the size of the blocks. Discussing the source of the structure, he suggests that the blocks might be accounted for by a recent theory due to Born, and goes on to imply that this theory would also explain the block structure in metals proposed by my colleagues and myself on the basis of X-ray diffraction work. This paper has been followed by a note by Paterson (1950) who queries these suggestions on the grounds that Born's theory predicts a decrease in size of the blocks with increase of temperature. According to Paterson it ought then to follow from Fürth's hypotheses that a metal is stronger at higher temperatures, and that the X-ray diffraction lines from a deformed metal show greater broadening at higher temperatures of deformation. But, in practice, both these effects usually go the other way.

It would be unfortunate, however, if the matter were allowed to rest at that, for the block theory of strength is the only one of any promise, being the only one that can be substantiated by direct observation. It might be worthwhile pointing out therefore that the arguments advanced by Paterson are less conclusive than they might seem at first sight. The essential point of the block theory should be that the strength, and the X-ray pattern, depend on the production in the structure of elements that are "dislocated" or "disoriented"; for only when they are dislocated or disoriented sufficiently can they provide sub-boundaries that are effective barriers to slip, or become incoherent X-ray reflectors. But there is no reason why these disoriented elements should always coincide with the ultimate blocks in any and every type of mechanical test; they could be multiples of ultimate blocks; and this aspect, as indicated below, is especially relevant in tests at higher temperatures.

We think it is so important to distinguish between the actual "disoriented elements" and the intrinsic ultimate blocks that it might be useful to illustrate the point by referring to the X-ray results. In

* Communicated by the Author.

these, the fundamental observation is that the process of deformation reduces the grains of a metal to disoriented elements. If the deformation is drastic enough the elements become very small, but for a given metal they do not become smaller than a characteristic minimum size. Now it is evident that the breakdown could not be produced at all unless the grains in the first place contained enough lines of planes of weakness. Whether these faults form a static or dynamic pattern in the grain it is impossible to say. Nor, so far as the strength is concerned, does it matter; for the only way of measuring the strength is by deforming the metal and as soon as the metal is deformed an observable disoriented substructure is produced at once. Therefore, for all practical purposes, we may speak of an intrinsic sub-structure, and this sub-structure has a lower limiting size.

The next observation is that the size of the actual disoriented elements into which the grain breaks up is determined by the conditions of deformation, and in particular by the temperature and rate of strain. Thus, to quote from actual experiment: if aluminium of grain size 10^{-2} cm. is strained at 300°C . at a rate of 0.1 per cent per hour, the resulting sub-structure is coarse; the size of the elements is about 10^{-3} cm., as against an ultimate crystallite or block size of less than 10^{-4} cm. for deformation at room temperature. At first sight it might appear that at the higher temperature the pattern of faults in the grain before deformation is spaced more widely, so that the grains could break down to correspondingly coarse elements only. But this is not so; for we can break the grains down to a finer sub-structure merely by increasing the rate of strain at the same temperature, and there is no doubt that by a sufficiently fast rate of strain we could break them down to the characteristic lower limiting size.

Further, direct observations show clearly that the strength exhibited by the metal under given conditions of deformation is primarily determined by the size of the actual disoriented elements produced by that deformation. Using the aluminium again as example, we find that during deformation at 300°C . at an extremely slow rate the grains do not break down at all; this is because the deformation presumably occurs mainly by viscous flow at the grain boundaries, but this aspect here is immaterial. The relevant point is the parallel observation that in the absence of breakdown the metal exhibits little or no resistance to the applied strain; its strength is negligible. This is one extreme. But if we increase the rate of strain at the same temperature we break down the grains and the sub-structure becomes increasingly finer as the rate of strain is greater; and at the same time we find that the resistance or strength of the metal increases in proportion. Conversely, we can change the fine sub-structure back into a coarse sub-structure, still at the same temperature, by reducing the rate of strain again; then we find the strength exhibited by the metal is again reduced. Because of this interdependence of sub-structure, temperature and strain-rate, it can be shown that a

specimen strained rapidly at an elevated temperature may be stronger than one strained slowly at a lower temperature. By experiments such as these it is not difficult to demonstrate that the strength follows the size of the sub-structure.

These illustrations will therefore serve to indicate that the block theory of strength is on the right lines. It is true that in the form usually advanced by theoretical workers it is often open to criticism, of which the remarks by Paterson on the Fürth theory are an example. But the weakness of this theory as it stands (and of the corresponding Bragg theory) is not in the assumption of an intrinsic block structure, but in failing to take into account the experimental observation that the operative elements are not always the ultimate blocks; they may contain a group of blocks. It is also clear, however, that the block theory can easily be brought into line with experiment if so desired.

Quadruple Moments and the Nuclear Shell Model.

By B. TOUSCHEK,

Department of Natural Philosophy, The University, Glasgow*.

[Received January 22, 1951.]

It has been pointed out by Hill (1949) that the quadrupole moments of atomic nuclei are in reasonable qualitative agreement with the nuclear shell model recently suggested by Haxel, Jensen and Süss (1949, 1950) and M. G. Mayer (1949, 1950). We want to show that this model makes quite definite predictions about the quadrupole moments of a certain category of odd nuclei and that on the whole these predictions are in good agreement with experiment. One should expect that the quadrupole moments of nuclei of the form $(A-Z, Z)=(M, M\pm 1)$, where M is one of the magic numbers 8, 20, (28, 40), 50, 82, 126 should be determined by the odd proton alone, since the contribution to the quadrupole moment of the closed shells is zero. The periodic table shows two nuclei of this type: ${}_{19}\text{K}_{20}^{41}$ and ${}_{83}\text{Bi}_{126}^{909}$. The quadrupole moment from a proton in a state with spin j should be

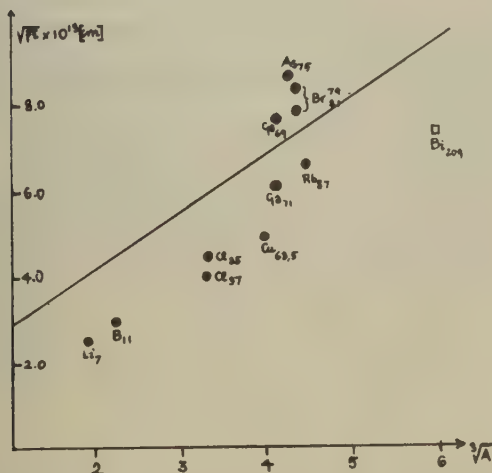
$$Q = \pm C \frac{2j-1}{2j+2} \bar{r}^2,$$

where the $-$ sign corresponds to a nucleus $(M, M+1)$ as ${}_{82+1}\text{Bi}$ the $+$ sign to a nucleus $(M, M-1)$ as ${}_{20-1}\text{K}$. $C = (1 - (2A-Z)/A^2)$ is a factor correcting for the motion of the mass centre and \bar{r}^2 is the average square distance of the odd (or missing) proton. It is obvious that the sign of the quadrupole moment predicted for K^{41} is wrong (as noticed by Hill), but the present experimental value is hardly more than an estimate.

* Communicated by the Author.

Determining $(\overline{r^2})^\dagger$ for Bi one finds a value 7.4×10^{-13} cm. which is fairly near to the fast neutron radius ($\sim 9 \cdot 10^{-13}$ cm.). A further category of nuclei for which simple predictions can be made are odd proton nuclei with spin 3/2. Since the neutrons can only contribute very little to the quadrupole moment (via the centre of gravity motion, their contribution being $Z/A^2 \times$ smaller than that of a free proton) the quadrupole moment must stem from the protons. According to the shell theory the spin 3/2 should only occur in connection with a shell of spin 3/2, so that an odd proton can only mean one or three protons in a 3/2 shell. The prediction of the shell theory is therefore

$$Q = \pm \frac{2}{5} C \overline{r^2}$$



the + sign holding for the case of three odd protons. In the figure $\sqrt{(\overline{r^2})}$ for such nuclei is plotted against $A^{1/3}$ and it is seen that the general trend of the curve is in good agreement with the curve (drawn out) representing the nuclear radii as measured by fast neutron experiments (Gamow and Critchfield 1949). It is worth noting that the positions of isotopes are according to their neutron numbers. Thus Cl³⁷ with a magic neutron number (20) lies lower than Cl³⁵, Ga⁷¹ (40) lower than Ga⁶⁹ (38), and the positions of the Bromine isotopes may be due to the approach of the magic number 50. Bi with 126 neutrons lies comparatively low, and the high quadrupole moment of As may be due to the small no. (2) of neutrons in the $g_{9/2}$ shell. That the fluctuations in the case of quadrupole moments tend to be greater than those for the fast neutron radii seems to be a confirmation of a one particle picture, which will naturally lead to larger fluctuations than the statistical picture applicable to the determination of neutron radii.

That the odd neutron nuclei should have quadrupole moments comparable in size with the odd proton nuclei need not be a contradiction to the shell model, since the cancellation of the proton spins in pairs does not imply a simultaneous cancellation of the quadrupole moments. The check of these moments would require the determination of the contribution to the quadrupole moment of an arbitrary number of particles in an unfinished shell. A few quadrupole moments (as those of Eu) are very large (about three times the size of the moments shown in the figure), and it is quite plausible to assume that they are the result of collaboration between three or more protons. This is further enhanced by the fact that none of the nuclei with "abnormal" quadrupole moments has a spin $<5/2$.

REFERENCES.

- GAMOW, W., and CRITCHFIELD, 1949, *Atomic Nuclei and Nuclear Energy Sources* (Oxford), p. 10.
 HAXEL, O., JENSEN, J., and SÜSS, H., 1949, *Phys. Rev.*, **75**, 1766; 1950, *Zeits. f. Phys.*, **128**, 294.
 HILL, R. D., 1949, *Phys. Rev.*, **76**, 998.
 MAYER, M. G., 1949, *Phys. Rev.*, **75**, 1969; 1950, *Ibid.*, **78**, 16, 22.

The Velocity of Second Sound in Liquid Helium near the Absolute Zero.

By J. C. WARD and J. WILKS,
 The Clarendon Laboratory, Oxford*.

[Received January 25, 1951.]

RECENT measurements by Atkins and Osborne (1950) indicate that the velocity of second sound in liquid helium approaches the value 150 m./sec. at absolute zero, which is in agreement with Landau's prediction of $C/\sqrt{3}$ where C is the velocity of ordinary sound. Landau (1941) obtained this expression from the usual two fluid formula for second sound $C_2 = (TS^2/C)(\rho_s/\rho_n)$ where (ρ_s/ρ_n) was calculated in a rather obscure way from a model in which liquid helium at sufficiently low temperatures is represented by a phonon gas. However it is possible to derive the expression $C/\sqrt{3}$ directly from the phonon gas model without having recourse to the two fluid theory at all.

We follow Landau in representing liquid helium near the absolute zero by a phonon gas consisting of the elementary (Debye) excitations, for which $E = pC$ where C is the velocity of ordinary sound and may be taken as constant. We also assume that at these temperatures interactions in the helium are very small so that the collisions between phonons are elastic and conserve momentum. Actually Landau makes all these

* Communicated by the Authors,

assumptions in calculating (ρ_s/ρ_n) . Suppose now that a compressional "sound" wave is propagated through this phonon gas, then there will be periodic variations of the phonon density. These periodic variations in the model will correspond to temperature variations in liquid helium, that is to second sound.

Hence the velocity of second sound is the velocity of a sound wave in a phonon gas where the conservation laws of energy and momentum hold and also the relation $E=pc$. The expression for this velocity will be similar to that for the velocity of a sound wave in a photon gas for that too depends only on the two conservation laws and the relation $E=pc$.

The velocity of sound in a relativistic gas has been given by Hoffmann and Teller (1950) for the general case when a magnetic field is present. We may derive the same answer for the velocity in a phonon gas more directly by using a result due to Curtis (1950) that the velocity of sound in general relativity is $\sqrt{(\partial P/\partial \eta)}$ where η is the energy density. In a photon gas η is defined by $\Sigma E=\eta C^2$ so by analogy in a phonon gas

$$\eta C^2 = \Sigma E = v \int_0^\infty A \{ \exp (pc/kT) - 1 \}^{-1} \cdot pc \cdot dp. \quad (1)$$

Now the pressure of the gas is given by

$$\begin{aligned} P &= \iint \left(\frac{1}{2} vc \sin \theta \cos \theta d\theta \right) (2p \cos \theta \cdot A \{ \exp (pc/kT) - 1 \}^{-1} dp) \\ &= \frac{1}{2} vc \int_0^\infty A p \{ \exp (pc/kT) - 1 \}^{-1} dp. \end{aligned} \quad (2)$$

Comparing (1) and (2)

$$\begin{aligned} P &= \frac{1}{3} \eta C^2, \\ C_2 &= \sqrt{\left(\frac{\partial P}{\partial \eta} \right)} = C/\sqrt{3}. \end{aligned}$$

This derivation gives no indication of the region in which we may expect this expression to be valid. Clearly it will fail if (a) the collisions between phonons do not satisfy the conservation laws of energy and momentum and (b) if the excitations of the liquid cannot be adequately represented by phonons. All we can say is that if at a sufficiently low temperature the specific heat of the liquid varies as T^3 then we should expect the velocity of second sound to be $C/\sqrt{3}$. It seems possible that this method could be used to predict the velocity at higher temperatures provided we knew a satisfactory expression for the other types of excitation which may occur. Landau in his theory covers the region above 0.6° by introducing excitations called rotons but we can see no theoretical basis for his expression for them.

As this model could also be used to represent a crystalline solid at low temperatures, it emphasizes a suggestion by Peshkov (1947) that second sound might be observed in crystals*. As he points out it will be necessary

* It is interesting to note that Nernst (1917) suggested that in good thermal conductors at low temperatures heat might have sufficient inertia to give rise to an oscillatory discharge.

to experiment with a crystal in which the scattering of phonons by inhomogeneities and irregularities is a minimum. In a pure crystal however the essential criteria for second sound are probably that the number of elastic collisions between the phonons should be sufficient to ensure that the phonon gas is not in the Knudsen region while at the same time very few collisions of the umklapp type should occur. (This is important because in this kind of collision it is inadmissible to apply the momentum conservation law (Peierls 1929)). Measurements of thermal conductivity by Berman *et al.* (1950) and Wilkinson and Wilks (1951) have shown that the number of umklapp type collisions rapidly decreases as the temperature falls and should be negligible in the region where the conductivity is limited by size effect. Therefore we intend to look for second sound in a corundum crystal at helium temperatures where umklapp collisions should be rare.

REFERENCES.

- ATKINS, K. R., and OSBORNE, D. V., 1950, *Phil. Mag.*, **41**, 1078.
 BERMAN, R., KLEMENS, P. G., SIMON, F. E., and FRV, T. M., 1950, *Nature, Lond.*, **166**, 864.
 CURTIS, A. R., 1950, *Proc. Roy. Soc. A*, **200**, 248.
 HOFFMANN, F. DE, and TELLER, E., 1950, *Phys. Rev.*, **80**, 692.
 LANDAU, L., 1941, *J. Phys. U.S.S.R.*, **5**, 71.
 NERNST, W., 1917, "Die theoretischen . . . Grundlagen des n. Wärmesatzes" (Halle: Knapp).
 PEIERLS, R. E., 1929, *Ann. Phys. Lpz.*, **3**, 1055.
 PESHKOV, V., 1947, *Report on Cambridge Low Temperature Conference* (London: Physical Society), p. 19.
 WILKINSON, K. R., and WILKS, J., 1951 *Proc. Phys. Soc. A*, **64**, 89.

[The Editors do not hold themselves responsible for the views expressed by their correspondents.]

XXXVI. *A New Method of Determining the Charge and Energy of Heavy Nuclei in the Cosmic Radiation.*

By A. D. DANTON, P. H. FOWLER and D. W. KENT,
H. H. Wills Physical Laboratory, University of Bristol*.

[Received February 5, 1951.]

SUMMARY.

The charge and energy of a heavy particle in cosmic radiation may be determined from the frequency of the accompanying delta rays and the multiple scattering in its path through an emulsion. The method is illustrated by the charge spectrum of 220 tracks in emulsions exposed at 95,000 feet.

§1. INTRODUCTION.

SINCE the discovery of the presence of heavy nuclei in the cosmic radiation (Freier *et. al.* 1948), several experimenters have employed the photographic method to determine the magnitude of the charges of the individual particles. The problem is of great importance because a knowledge of the "charge spectrum" of the primary radiation is essential for any discussion of its origin (Bradt and Peters 1950 a and b).

The method employed hitherto has been based on the measurement of, (a), the frequency of occurrence, N_s , per unit length of the track, of δ -rays with energies in excess of a certain minimum value; together with, (b), the ranges of the particles in the assembly of glass and emulsion constituting the photographic plates employed to record the tracks. At geomagnetic latitudes less than 30° , most of the primary particles are moving at relativistic velocities. For such particles, N_s varies as Z^2 and this relation is independent of the precise value of the energy. The charge can therefore be deduced from the observed value of N_s without an exact knowledge of the range, except in the few cases where an observable change of N_s with range indicates that a particle is of lower energy.

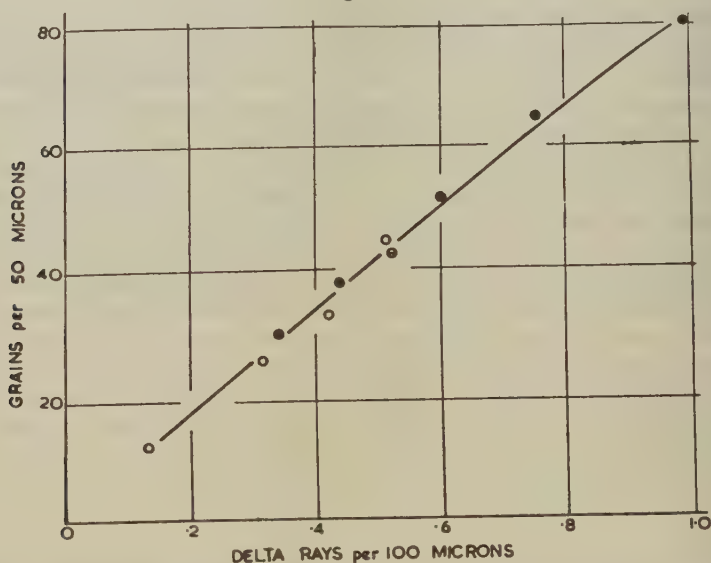
Bradt and Peters (1950 b) have recently refined this method by using insensitive emulsions. The grain-density in the tracks of multiply charged particles is then so reduced that it can be determined by grain counts. Such observations give a measure of the ionization of the particle with a much greater statistical weight than a determination of N_s deduced from an equal length of track.

For particles of lower energy, which occur frequently in the primary radiation at geomagnetic latitudes greater than 45° , the above methods suffer from the fact that, in general, the charge and the energy can be accurately determined only if the particle happens to reach the end of its range in one of the emulsions of the assembly. It is therefore important to develop other modes of attack, and for this purpose we have found it possible to modify the methods employed in this laboratory in determining the energy of fast protons and other particles of charge $|e|$.

* Communicated by Prof. C. F. Powell, F.R.S.

In the observation on the tracks of fast protons, the energy of a particle can be determined, and its identity established in favourable cases, by measuring, (a), the grain density, g , in the track; and, (b), the average angular deviation in the direction of motion, $\bar{\alpha}$, per unit length of the track, due to multiple coulomb scattering. In extending this method to the heavy particles, we have made similar observations on the scattering, but instead of the grain-density in the track, we determine N_δ , the frequency of occurrence of δ -rays. By these observations it is possible to determine the charge and energy of a particle if its track in a single emulsion is long enough to allow measurement of $\bar{\alpha}$ and N_δ to be made with sufficient statistical weight. A knowledge of the range of the particle is unnecessary. Further, the method appears to be sufficiently precise to allow elements of low atomic number to be identified with little ambiguity, so that the charge spectrum shows clearly resolved peaks due to the different elements.

Fig. 1.



Relation between grain-density, g , and delta-ray density, N_δ , in the trajectory of particles of charge $|e|$. Measurements on π -mesons are shown thus : ● ; on protons and deuterons, thus : ○ ; and on fast α -particles, thus : ⊗ .

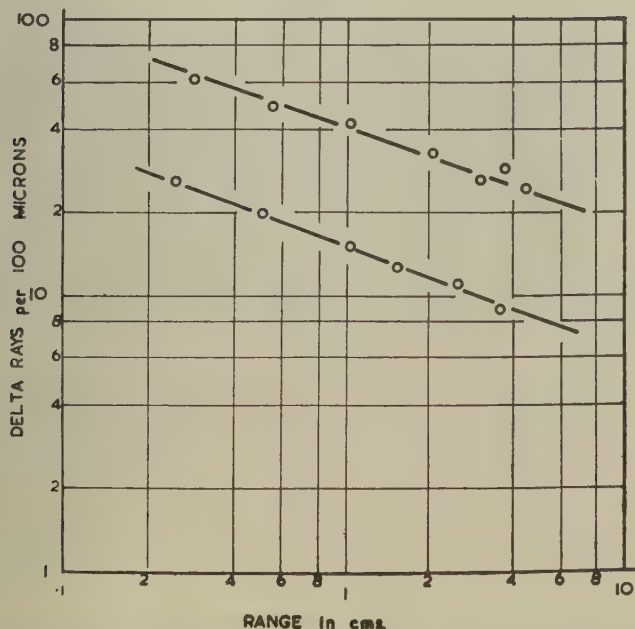
§2. RELATION BETWEEN N_δ AND VELOCITY FOR PARTICLES OF DIFFERENT CHARGE.

In order to determine the relationship between the δ -ray density in the track of a particle of known charge and its velocity, we have made observations on particles of charge $|e|$. For these particles, the relationship between residual range and velocity, and between grain-density and velocity, is now well established, for the type of emulsion in which the present tracks are recorded.

In the first instance, we made measurements on the tracks of π^+ or π^- particles of which the range in the emulsion was about 8 mm., and which were identified by the secondary effects observed at the end of their range; viz., either μ -decay, or the nuclear absorption of the particle and the formation of a "star" with two or more branches. The observed values of N_δ were plotted against the corresponding values of grain-density in the track, for various values of the residual range, and the results are shown in fig. 1. In making the observations, only δ -rays giving rise to a track containing four or more grains were accepted.

Similar observations of greater statistical weight were made on the tracks of fifty protons and deuterons emitted from nuclear explosions occurring in the emulsion, particles of which the identity had been established by the

Fig. 2.



Variation of delta-ray density with range for tracks of a carbon and of a magnesium nucleus which reach the end of their range in the emulsion. The nuclei were identified by observations of N_δ and range.

methods previously described (Fowler 1950). It will be seen from fig. 1, that for particles of charge $|e|$, moving at velocities for which the grain density is less than five times the minimum value ($g < 5g_{\min}$), the values of N_δ are proportional to the grain-density. On the basis of these observations, curves can be drawn showing the relation between N_δ and the scattering parameter $\bar{\alpha}$ —for particles with any value of the charge Ze , and mass, A —using the relation between $\bar{\alpha}$ and g established for π -particles (Camerini *et al.* 1950).

As a check on equation (1), values of N_0 were determined by observations on long tracks of magnesium and carbon nuclei which came to rest in the emulsion, and which could be identified by the original method based on determinations of N_0 and range. The observations showed that

$$N_0 \propto R^{0.42}, \quad \dots \dots \dots (1)$$

where R is the residual range; see fig. 2. Using this result and the established relation between range and energy for particles moving in a photographic emulsion,

$$E \propto R^{5.78}, \quad \dots \dots \dots (2)$$

the relation between N_0 and β was computed*. The result thus obtained was found to be consistent, within the limits of experimental error, with the calculated family of curves.

§3. OBSERVATIONS ON THE SCATTERING OF HEAVY NUCLEI.

The measurements of the deviations in the tracks of heavy nuclei due to multiple coulomb scattering present no particular difficulties and have been carried out in the manner described by Fowler (1950). The thickness of the track gives rise to larger reading errors than in the case of similar observations with fast protons or α -particles, but these are not important. In order to evaluate the mean angle of scattering from the readings taken on the microscope, we have corrected for reading errors, stage "noise" and distortion, by the procedures to be described in a later communication. If A is the mass number and Z the charge number of the nucleus, its energy, corresponding to a given value of $\bar{\alpha}$, can be calculated from the relation:—

$$\bar{\alpha} = Zk/APv, \quad \dots \dots \dots (3)$$

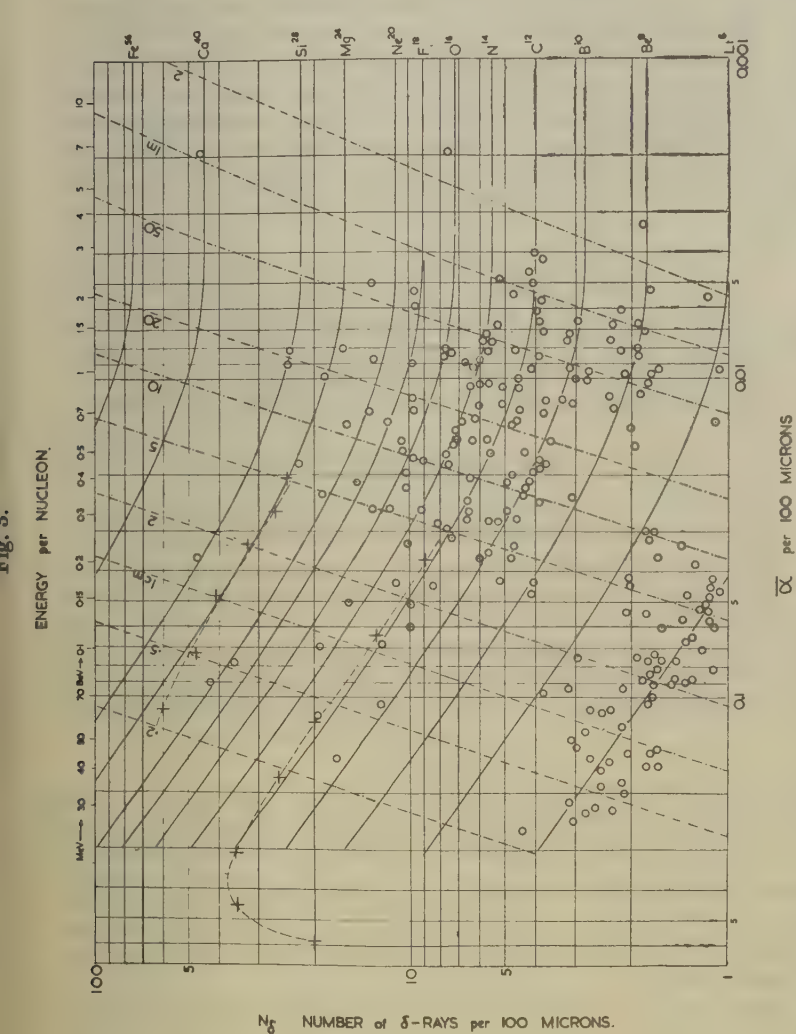
where p is the momentum of the nucleus per nucleon. With the units commonly employed, the scattering constant k is taken as 26, a value indicated by a preliminary determination made in this laboratory. With the present exposures, "noise" and distortion prevent any accurate measurement of energies greater than 3 BeV./nucleon. It may, however, be possible to refine the processing technique in order to diminish the distortion errors and thus to improve the precision of the measurements.

§4. CHARGE SPECTRUM OF HEAVY NUCLEI.

The present methods were employed in a study of the charge distribution of the heavy nuclei recorded in an assembly of Ilford G5 plates exposed by means of free balloons at an altitude of 95,000 ft., 40 c.c. of the emulsion of these plates were searched for tracks of which the length in any one emulsion was greater than 6 mm., and in which the value of N_0 was greater than 1.0 per 100 μ . For each of these tracks the values of $\bar{\alpha}$ and N_0 were determined. The results thus obtained are represented in fig. 3.

* Equation (3) is not seriously invalidated, for particles with values of the energy with which we are here dealing, by the processes of "capture and loss" of electrons occurring at the end of the range of the heavy particles.

The family of full lines in fig. 3 represent the expected relation between N_δ and $\bar{\alpha}$ for different values of the charge number Z . They have been calculated on the assumption that the mass number of a nucleus, A , is equal to $2Z$. This assumption is approximately justified for stable nuclei



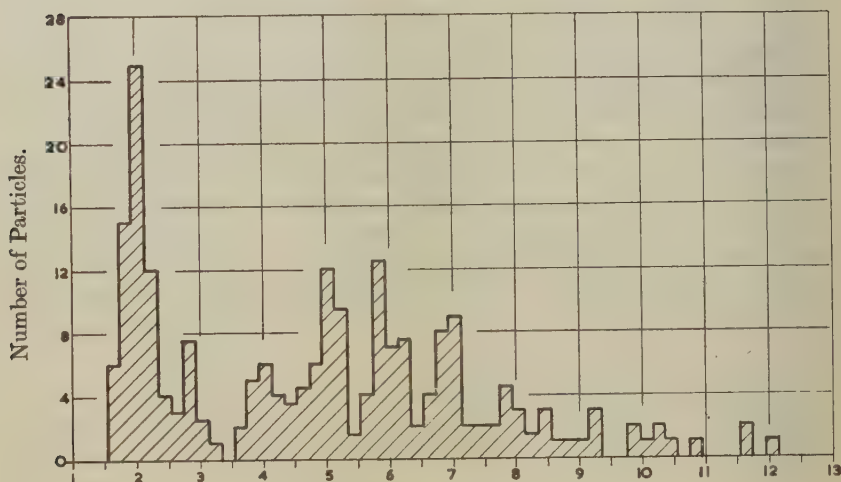
Relation between N_δ and $\bar{\alpha}$ (100μ) for the tracks of 230 particles. Observations on tracks found in a systematic survey of 40 c.c. of emulsion are shown thus:—O. Measurements on two tracks which terminate in the emulsion after travelling over 4 cm. in a single plate (see fig. 2), are shown thus:—+—+—+. The full lines represent lines of constant charge, whilst the dashed lines: lines of constant range. An energy scale is included at the top of the figure.

up to $Z \sim 20$; any nuclei of greater charge seldom occur in the primary radiation. Further, it seems very unlikely that any but stable or very long-lived isotopes will have survived the long periods believed to be involved in the acceleration process which produces the primary particles.

The approximation is therefore adequate, with the present state of precision of the mass measurements, in the case of the primary particles. The greatest errors are likely to occur in the case of nuclei of lithium and beryllium, but they can hardly be serious.

From the results, the value of the charge for each individual particle can be determined and the resulting charge "spectrum" is shown in fig. 4. The spectrum includes results due to slow α -particles, many of which are products of the fragmentation of heavier nuclei as a result of nuclear collisions. Lithium nuclei are also present with energies as low as 60 MeV./nucleon. Energetic lithium nuclei are sometimes emitted from nuclear explosions caused by protons, neutrons, or α -particles

Fig. 4.



Charge Number Z.

Charge spectrum of 226 of the tracks represented in fig. 3. The four other tracks observed in the systematic survey were of charge Z greater than 12; three of them were identified as due to silicon, and the fourth due to calcium nucleus.

(Sørensen 1951), but they occur very infrequently. Most of the particles of charge $Z=3$ observed in the present experiment must therefore have been either produced by the fragmentation of heavier nuclei, or they are true primary particles.

The charge spectrum shown in fig. 4 has not been corrected for loss of particles by ionization—an effect which would tend to reduce the numbers of more massive nuclei observed—or for the general degradation in charge due to nuclear collisions in the atmosphere above the plates. Even after making allowance for these factors, however, it is difficult to account for the observed numbers of beryllium and boron nuclei if these elements are absent from the primary radiation at this latitude. Such a result, if

it can be maintained by observations of greater statistical weight, would appear to be at variance with those of other observers working at a geomagnetic latitude of 30° N. (Bradt and Peters 1950 b).

§5. APPRAISAL OF THE METHOD.

The most important advantage of the present method of determining the charge of fast atomic nuclei over those previously employed is that, at high geomagnetic latitudes, if the track of a particle is of sufficient length, the observations on it can be confined to a single emulsion. Further, for values of Z between three and six inclusive, the accuracy of the measurements appears to be greater than that previously attained (Bradt and Peters 1950 a, Hoang 1950, Dainton and Kent 1950). It is difficult, for example, to evaluate the charge of such particles, even when they are of low velocity, from the changes in the values of N_0 as the particle passes from one emulsion to another in traversing the stack.

In addition to the determination of the charge, the method gives the energy of the particles as a result of the same limited observations and a scale of energy per nucleon is included in fig. 3. It would be premature to discuss the detailed features of the observations at this stage of the investigation.

ACKNOWLEDGMENTS.

In conclusion, we wish to thank Professor C. F. Powell, F.R.S., for his continued encouragement; Dr. M. M. Shapiro for assistance in obtaining the exposure; Mr. U. Camerini for helpful discussions, and Dr. H. Heitler for technical assistance. We also extend our thanks to Miss Margaret Stott, who made the scattering measurements, and to Miss Eleanor James, who scanned the plates. The investigation was carried out as part of a programme of research supported by the Department of Scientific and Industrial Research, to whom one of us (A.D.D.) is also indebted for a maintenance grant.

REFERENCES.

- BRADT and PETERS, 1950 a, *Phys. Rev.*, **77**, 54; 1950 b, *Ibid.*, **80**, 943.
 CAMERINI *et al.*, 1951, *Phil. Mag.* (in course of publication).
 CAMERINI, FOWLER, LOCK and MUIRHEAD, 1950, *Phil. Mag.*, **41**, 413.
 DANTON and KENT, 1950, *Phil. Mag.*, **41**, 963
 FOWLER, 1950, *Phil. Mag.*, **41**, 169.
 FREIER, LOFGREN, NEY, OPPENHEIMER, BRADT and PETERS, 1948, *Phys. Rev.*, **74**, 213.
 HOANG TCHANG-FONG, 1950, *Thesis*, Paris.
 SÖRENSEN, 1951, *Phil. Mag.*, **42**, 188.

XXXVII. *An Interferometric Study of Cleavage Surfaces of Artificially Grown Crystals of Sodium Chloride.*

By S. AMELINCKX,
University of Ghent, Belgium*.

[Received January 30, 1951.]

[Plate XIV.]

ABSTRACT.

Cleavage surfaces of an artificially grown crystal of sodium chloride are examined by multiple-beam interferometry. Two main features are noted, namely long narrow, more or less parallel strips, and superposed on this is a secondary fine grain structure. Silver films on sodium chloride are found to be unstable and apparently photosensitive. The cleavage mechanism is discussed.

CLEAVAGE faces of an artificially grown crystal of NaCl have been examined by means of optical interference methods, using both multiple-beam Fizeau fringes and fringes of equal chromatic order (Tolansky 1948). The silvered specimen was matched against a high-grade silvered optical flat accurate to within $\lambda/40$.

Cleavage was induced in a large clear crystal (grown by Hilger) by striking perpendicular to a face with a razor blade. Rocksalt shows three cleavage directions parallel to (001), (010) and (100), which are considered as crystallographically equivalent. This was confirmed since no specific difference could be detected between them.

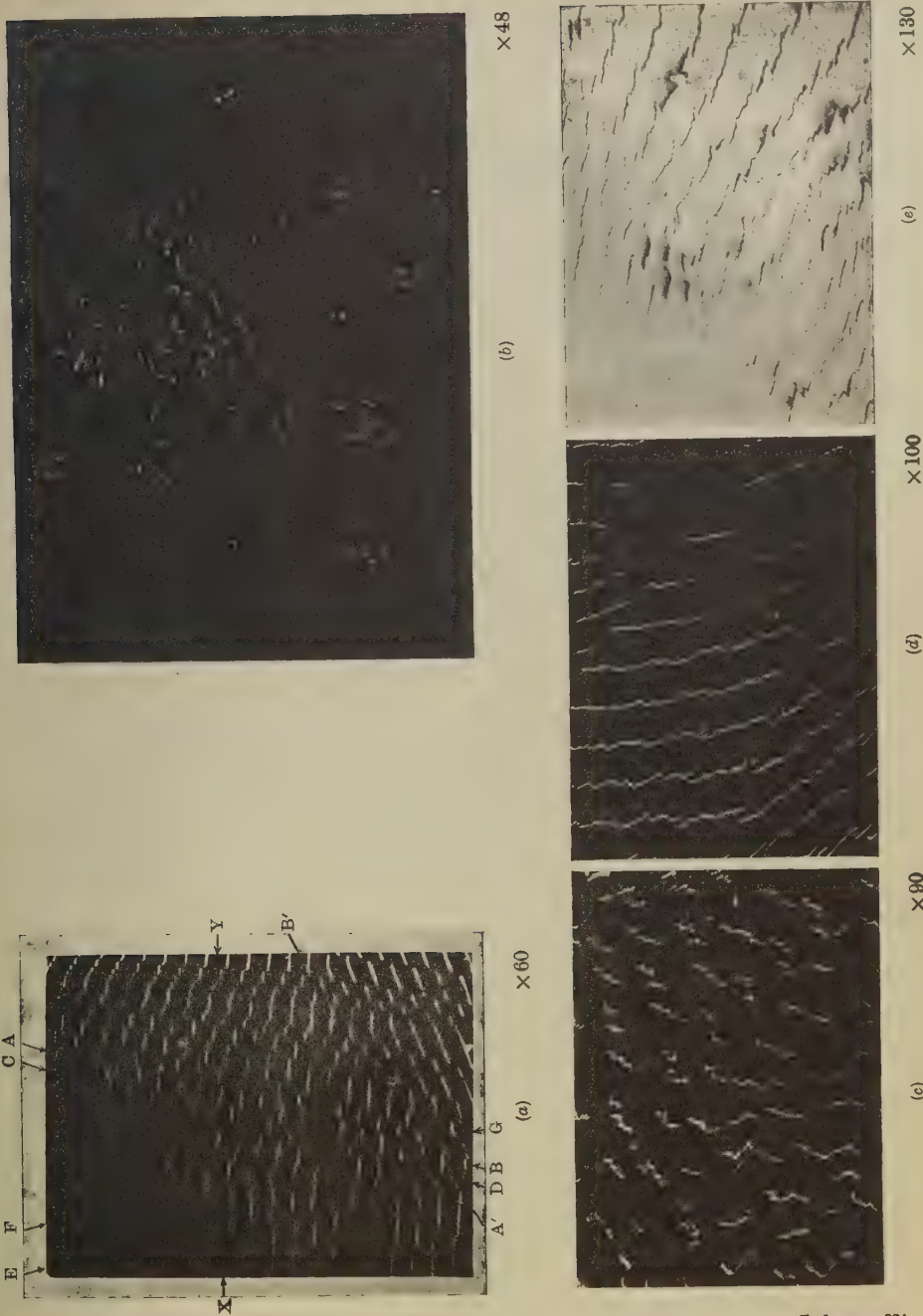
Although the cleavage is generally described as "perfect", interferometric examination revealed a rather complex structure on these faces. The Fizeau fringes (λ 5461) for a typical low magnification of a well-cleaved specimen is shown on fig. 1*a*. This shows the presence of narrow strips, generally more or less parallel to each other and radiating out from the point where the cleavage was induced. There is a close resemblance between this picture and that of the calcite cleavage plane reported by Tolansky and Khamsavi (1946).

The strip widths vary from $1/100$ to $1/10$ mm. and their lengths are of the order of 1 mm. The planes of the strips are not always parallel but are sometimes inclined one to another as in the case of selenite (Tolansky 1945). In fig. 1*a* the strip AB is inclined to the strip CD at an angle of 1.33×10^{-4} radians.

Another fact of interest is clearly visible. The part of the cleavage face in the right bottom corner (below the line A'B') is inclined to the adjacent

* Communicated by Professor Tolansky.

Fig. 1.



region above A'B' at an angle of 2.11×10^{-3} radians. The part of the crystal face to the left of the strip CD consists of strips all very nearly parallel to the strip CD; whereas the part to the right of AB consists of strips all very nearly parallel to AB.

The strips CD and AB themselves are inclined one to another. The part of the crystal face shown here consists consequently of three main regions which are inclined one to another over very small angles.

Fig. 2

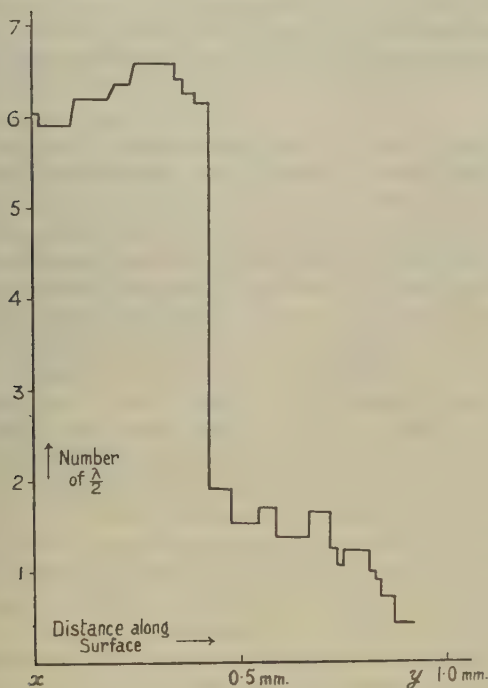


Fig. 1 (Pl. XIV.) shows some other characteristics of the rock salt cleavage structure rarely seen on other cleavage structures investigated such as mica (Tolansky 1945, Tolansky and Morris 1947), selenite and calcite (*loc. cit.*). Besides well defined steps the change in level sometimes takes place gradually as can be seen along the lines ED and FG on fig. 1a. Fig. 2 represents a cross-section along a line XY, overlapping order allocations being ascertained by using several wavelengths of light. The gradual changes in level are probably due to the non-resolution of very small steps. The elementary distance, perpendicular to the face as given by X-ray diffraction, is $d_{100} = 5.63 \text{ \AA}$. which is beyond the resolving power of the method.

Although in general within a narrow strip cleavage must probably proceed along a lattice plane, in some cases curved strips were seen (fig. 1 *b*). Some radii of curvature calculated by using the approximation: $R = 1/2\lambda[d_1d_2(d_1+d_2)]/[d_1-d_2]$, where d_1 and d_2 are the distances between three adjacent fringes, are for example, $R=1.58$, 2.02 and 3.29 metres respectively.

Uniform areas are rare and very small and in general high dispersion gives ragged fringes, indicating a complicated fine structure as in figs. 1 *c* and 1 *d*. This fine structure, probably also due to non-resolved steps, corresponds to level changes up to 200 Å.

Fig. 1 *b* shows another striking feature of the rocksalt cleavage. The surface is striated in two directions: one parallel to (100) and the other parallel to the cleavage lines. The striations lead to the dotting of the fringes.

The following proposed cleavage mechanism is suggested by the fringe patterns. When a knock is applied to a crystal face, cleavage starts in the plane under the razor blade's edge containing the largest number of dislocations or defects. Cleavage will proceed along this plane until reaching the immediate neighbourhood of some other plane which contains a higher concentration of dislocations. Cleavage then jumps and continues along that new plane. The result is a repeated change of level and the production of steps. This mechanism would probably account for the smaller steps only. The higher steps could be associated with inner cracks existing previously in the crystal or with the boundaries of the separate blocks which build up a coarse mosaic structure of the crystal. Evidence in favour of this last argument may be found in the fact that the large step of fig. 2 occurs in the immediate neighbourhood of the border between two inclined crystal-blocks.

According to this view the quality of a cleavage would depend on the concentration of lattice defects and on their distribution in the crystal and consequently on growth conditions. This view is supported by fig. 2 of Tolansky and Khamsavi's paper on calcite (1946).

This investigation of the rocksalt cleavage involved certain difficulties. As rocksalt is hygroscopic it was necessary to silver the specimens immediately after cleavage. Keeping the silvered specimens in a desiccator filled with P_2O_5 was not sufficient to prevent the immediate attack on the rocksalt. One hour only is needed to make this effect visible. It results in a decrease of reflectivity and an increase of the absorption of the silver layer. A specimen is completely spoiled and unusable for examination some twelve hours after silvering.

The break-up of the film is much more visible with reflection fringes than with transmission, as the local loss of reflectivity is then seen as a dark region on a bright background. In transmission on the contrary the effect is seen only as an interruption in the bright fringes. The disintegration could therefore be studied much easier in reflection. There is some indication that it starts in regions of maximum illumination

which, as Holden (1949) has shown is asymmetrically on one side of the dark reflection fringe. It appears to spread out in the direction of the illuminated region and stops abruptly when a cleavage line is reached (fig. 1e).

Although the silver break-up is undoubtedly partly due to the hygroscopic character of rocksalt, it may be that a photosensitive effect contributes if it be supposed that the silver in contact with the sodium chloride forms a certain amount of silver chloride, which is photosensitive.

Further evidence in favour of this hypothesis is this: the rocksalt specimens when subjected to a glow discharge turned yellow, in accordance with known expectations. It is found that yellowish specimens were spoiled much more quickly than the others. Fig. 1e referring to such a specimen, the picture being taken approximately half an hour after the exposure to the glow discharge followed by silvering.

In terms of Mott's explanation (1940) of Pohl's experiments the formation of silver chloride can be explained in the following way. The glow discharge results in a stoichiometric excess of the metal. As a consequence a certain amount of chlorine becomes available. When afterwards the silver is deposited some silver chloride will be formed, which has a low photosensitivity. If exposed only to low intensity daylight, the darkening takes place slowly, but under the influence of the very intense Hg source of illumination, used in interferometry, the silver chloride shows the "print-out" effect which causes the dark stains in the picture. This picture was taken a very short time after the specimen was silvered, it was completely clean when putting it in the light beam. Once in the interferometer the fringe system was kept fixed. As a result one can see the preferential darkening on one side of the dark fringes, *i. e.* on the side at which the light has a reflection maximum. If this is indeed the correct explanation then the effect is highly critical since the maximum on the side of the fringe is but a few per cent above that of the intensity between fringes.

This work has been carried out whilst holding a Fellowship from the "Centre National Belge de Chimie Physique Moleculaire", and a visit to the laboratory at Royal Holloway College, London, was made possible with aid from the "Fonds pour les relations culturelles Anglo-Belges". I am very much indebted to Professor S. Tolansky; without his constant advice and encouragement this work would have been impossible.

REFERENCES.

- HOLDEN, J., 1949, *Proc. Phys. Soc. B.*, **62**, 405.
 MOTT, N. F., 1940, *Electronic processes in Ionic Crystals*, (Oxford University Press), p. 111.
 TOLANSKY, S., 1945, *Proc. Roy. Soc. A*, **184**, 51; 1948, *Multiple-beam Interferometry of Surfaces and Films*, Clarendon Press, Oxford, p. 96.
 TOLANSKY, S., and KHAMSAVI, A., 1946, *Nature*, **157**, 661.
 TOLANSKY, S., and MORRIS, P. G., 1947, *Min. Mag.* XXVIII, **198**, 137.

XXXVIII. *The Hydrogen and Carbon Total Cross-Sections for Neutron Energies between 39 MeV. and 156 MeV.*

By A. E. TAYLOR, T. G. PICKAVANCE, J. M. CASSELS and T. C. RANDLE,
Atomic Energy Research Establishment, Harwell*.

[Received January 30, 1951.]

ABSTRACT.

The total cross-sections of carbon and hydrogen have been measured at neutron energies of 39, 64.5 and 97 MeV., using a recoil proton telescope as a neutron detector. At these three energies the hydrogen cross-sections are 223 ± 7.6 , 126 ± 3 and $73.9 \pm 3.0 \times 10^{-27}$ cm.² respectively. The corresponding carbon cross-sections are 1100 ± 20 , 784 ± 5 and $508 \pm 5 \times 10^{-27}$ cm.².

INTRODUCTION.

NEUTRON beams, produced by proton bombardment of internal beryllium targets at various radii in the 110-inch Harwell cyclotron, have been used to measure the n-p total cross-section at 39 MeV., 64.5 MeV., and 97 MeV. The method employed was similar to that used at 156 MeV. (Taylor, Pickavance, Cassels, and Randle 1950, 1951).

The collimation of the neutron beam and geometrical layout of the apparatus differed little from the previous arrangements, but at each new energy a change was needed in the polythene radiator and carbon absorber of the triple coincidence telescope. The thicknesses of these are included in the summary of the results.

EFFECTIVE ENERGY.

As before, only the high energy end of the neutron spectrum was used (see Table), and the limits of detection were now such that not less than 98 per cent of the recoiling protons counted came from the hydrogen content of the polythene radiator. The effective energy was determined in a subsidiary experiment at each energy by counting the number of recoiling protons as a function of absorber thickness in the telescope and hence as a function of energy. The maximum neutron energy determined this way was compared with the value expected knowing the energy of the internal proton beam and the geometrical arrangement. These results were used to check the range energy relation, and so an estimate of the error in the effective energy was obtained.

To test for "hardening" of the neutron beam in the attenuator, the effective energy after passing through the carbon was determined in the course of the 64.5 MeV. experiment. Since this differed from the effective

* Communicated by the Authors.

energy of the unattenuated beam by less than 1 MeV., no appreciable hardening was taking place. The mean of the two values was taken as the effective energy.

ATTENUATORS.

The carbon and polythene $2\frac{1}{2}$ -inch diameter bars were of such lengths that the polythene attenuator contained the same number of carbon atoms as the carbon attenuator and the attenuation produced by the hydrogen content varied between $\exp(0.5)$ and $\exp(0.8)$. Details of the attenuators are given in the Table.

RESULTS.

The results, including those at 156 MeV., are presented in the Table. The hydrogen total cross-section, σ_H , is plotted as a function of energy in the figure (p. 330).

TABLE.

Effective energy (MeV.)	39	64.5	97	156
Estimated error in effective energy (MeV.)	± 1	± 1.6	± 1.5	± 3
Upper energy limit of neutrons in the beam (MeV.)	45.7	74	107	169
Lower energy limit of detection (MeV.)	34.5	59	91	149
Absorber in telescope (gm.cm. ⁻² of carbon equivalent)	1.14	3.01	6.49	15.8
Radiator thickness (gm.cm. ⁻² of polythene)	0.29	0.63	0.87	1.7
Carbon attenuator (gm.cm. ⁻²)	23.51	70.76	70.76	120.23
Polythene attenuator (gm.cm. ⁻²)	27.50	82.41	82.41	136.93
Hydrogen total cross-section $\times 10^{27}$ (cm. ²)	223	126	73.9	46.4
	± 7.6	± 3.0	± 3.0	± 1.2
Carbon total cross-section $\times 10^{27}$ (cm. ²)	1100	784	508	330
	± 20	± 5	± 5	± 3

DISCUSSION.

The value obtained for the hydrogen total cross-section at 97 MeV. is in good agreement with the most accurate experiment at Berkeley, in which the effective energy was 95 MeV. (DeJuren and Knable 1950). However, the result at 39 MeV. is greater than that expected from earlier Berkeley measurements at 40 MeV. (Hadley, Kelly, Leith, Segrè, Wiegand, and York 1949), but in good accord with the more recent determination at 42 MeV. (Hildebrand and Leith 1950).

It may be of interest that a simple empirical relation can be used to fit the results within the experimental errors quoted, namely,

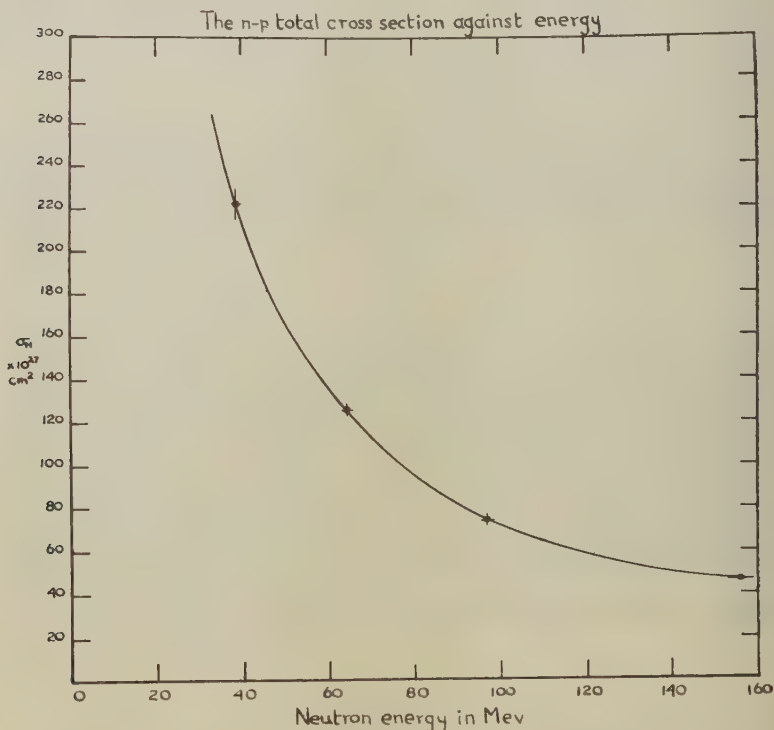
$$\sigma_H = \frac{10,342}{E} - 45.7 + 0.157E,$$

where σ_H is in units of 10^{-27} cm.² and E in MeV. This relation also gives agreement with the results at 14 MeV. (Salent and Ramsey 1940), 25 MeV. (Sherr 1945), and 280 MeV. (Fox, Leith, Wouters, and MacKenzie 1950).

ACKNOWLEDGMENTS.

Thanks must be expressed to Mr. E. Wood for help in carrying out the measurements and to the cyclotron crew for their cooperation.

This paper is published by the permission of the Director, Atomic Energy Research Establishment, Harwell.



REFERENCES.

- DEJUREN, J., and KNABLE, N., 1950, *Phys. Rev.*, **77**, 606.
 FOX, R., LEITH, C., WOUTERS, L., and MACKENZIE, K. R., 1950, *Phys. Rev.*, **80**, 23.
 HADLEY, J., KELLY, E., LEITH, C., SEGRÈ, E., WIEGAND, C., and YORK, H., 1949, *Phys. Rev.*, **75**, 351.
 HILDEBRAND, R. H., and LEITH, C. E., 1950, *Phys. Rev.*, **80**, 842.
 SALENT, E. O., and RAMSEY, N. F., 1940, *Phys. Rev.*, **57**, 1075.
 SHEER, R., 1945, *Phys. Rev.*, **68**, 240.
 TAYLOR, A. E., PICKAVANCE, T. G., CASSELS, J. M., and RANDLE, T. C., 1950, *Nature Lond.*, **165**, 967; 1951, *Phil. Mag.*, **42**, 20.

XXXIX. *Rate of Production of Neutrons in Ice by Cosmic Rays.*

By S. LATTIMORE,
Imperial College, London*.

[Received January 30, 1951.]

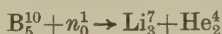
ABSTRACT.

The rate of production in ice of fast neutrons is given. It is shown that the number of fast neutrons produced at any point in the ice is approximately proportional to the number of cosmic ray stars at that point. The results are compared with those of other investigations, and it is pointed out that many previous results are too low due to the misuse of a formula given by Bethe *et al.* (1940).

INTRODUCTION.

DURING recent years there have been many experiments to find the absolute rate of production of neutrons by cosmic rays, and the variation of this rate with the height of production. In general the results of these experiments have been in agreement only as far as the height variation is concerned, the values found for the rates of production varying by a factor as large as five. It has been found that the variation with height over the lower part of the atmosphere is exponential, the rate of production at a depth x gm./cm.² below the top of the atmosphere being proportional to $\exp(-x/\lambda)$ where λ is 140–150 gm./cm.². This height variation is the same as that found for stars observed in photographic emulsions.

For measurements on slow neutrons, the use of boron loaded nuclear emulsion has a great advantage over counter or ionization chamber technique, in that the boron disintegrations



can actually be observed and there is therefore no doubt as to what is being measured. In the electronic devices, on the other hand, elaborate precautions must be taken to eliminate background counts, and one can never be certain that no spurious events are counted, or that all true counts are recorded. The photographic plate, however, requires long exposures, of the order of 50 days, and cannot, therefore, be used to examine short term fluctuations, such as have recently been observed by Adams (1950) and others, using electronic devices, after intense solar activity.

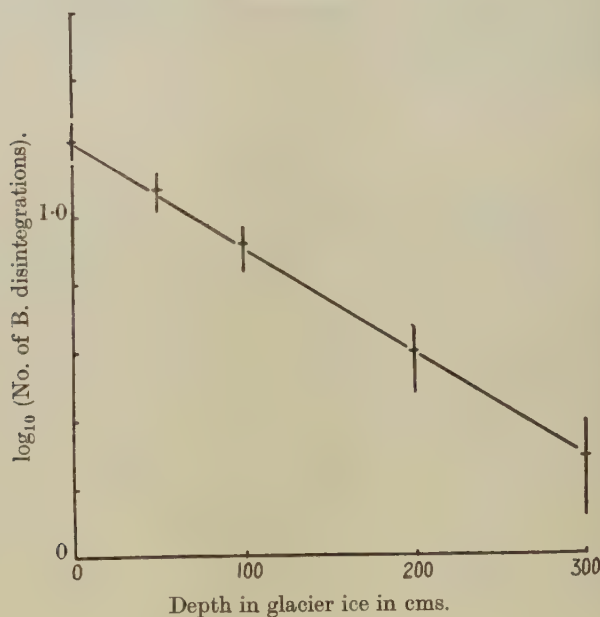
* Communicated by Sir George Thomson.

EXPERIMENTAL.

The plates used were Ilford 100 μ C.2 boron loaded emulsion and were exposed vertically, at depths of 0, 0.5, 1, 2 and 3 metres below the surface of the glacier ice at 3600 m. elevation at the Jungfrauoch. The geometry was excellent, the plates being contained in an iron pipe, internal diameter 2 $\frac{1}{8}$ inch., wall thickness $\frac{1}{8}$ inch., which had been sunk into the ice. The glacier ice was covered with approximately 15 gm./cm.² of snow.

The results are shown in fig. 1, where the numbers of boron disintegrations observed (in arbitrary units) are plotted logarithmically against the depth below the glacier ice. As can be seen, the results are consistent

Fig. 1.



with an exponential absorption. The best values for the range in ice and the number of disintegrations at the surface of the ice were calculated by the method of least squares, and were found to be :

Range in ice = 126 gm./cm.².

No. of boron disintegrations at the surface of the ice = 893/c.c. of emulsion/day.

INTERPRETATION OF RESULTS.

In the following paragraphs we shall show how the number of neutrons captured at any point, which is the quantity we measure, is related to the number of neutrons produced at that point.

The boron disintegrations are produced by thermal and near-thermal neutrons only, since it is only in this region that the cross section is large. The neutrons will be slowed down to thermal energies by elastic collisions with the hydrogen in the ice. It seems probable that the neutrons will be produced in cosmic ray stars in the ice. We shall assume that (1) the neutrons are produced in stars, and that the mean number of neutrons/star is independent of the depth in the ice. In this case, the neutron production will decrease exponentially with depth in the ice, with a range of 130 gm./cm.² (Harding 1950). (2) the neutrons can be divided into two groups, one group consisting of those neutrons that are evaporated from stars, the second of those neutrons that correspond to the high energy tail (Perkins 1947) observed in the proton spectrum. The evaporated neutrons will have an energy spectrum given by the formula

$$P(E) dE = A \frac{E}{T^2} \exp(-E/T) dE, \quad (1)$$

where $P(E)$ is the number of neutrons emitted with energies between E and $E+dE$, A is the total number of neutrons emitted, and T is a constant, with the dimensions of an energy. From a study of the protons it has been found that for stars of three or more visible tracks, T is equal to 4 MeV. It has further been found that the evaporated protons are emitted isotropically, (Harding *et al.* 1949), and we shall suppose that this is also true for the evaporated neutrons. Now, from formula (1), we can calculate that 96 per cent of the evaporated neutrons will have energies less than 20 MeV. We shall therefore assume that all those neutrons with energies below 20 MeV. are evaporated, and have an isotropic angular distribution, while none of those with energies greater than 20 MeV. are evaporated, but they are all strongly collimated downwards. We shall deal with these two groups separately.

EVAPORATED NEUTRONS.

Bethe *et al.* (1940) have shown that the mean square distance \bar{r}^2 travelled by a neutron in losing energy from E_1 to E_2 is given by

$$\bar{r}^2 = M \int_{E_2}^{E_1} l^2(E) \frac{dE}{E}, \quad (2)$$

where M is the atomic weight of the moderating material and $l(E)$ is the mean free path at an energy E . If we put E_1 and E_2 equal to 20 Mev. and 1eV. (thermal energies) and neglect the scattering with the oxygen, we find

$$\bar{r}^2 = 120 \text{ (gm./cm.}^2\text{)}^2.$$

This value will be greater than the true value because of the neglect of the oxygen scattering. We should note that the value of \bar{r}^2 decreases as E_1 decreases.

Bethe *et al.* have also shown that the distribution, after the slowing down process of neutrons produced at a depth x_0 , is given by

$$N(x) dx = \pi^{-1} L^{-1} \exp [-(x-x_0)^2/L^2] dx, \quad \dots \quad (3)$$

where $N(x) dx$ is the fraction of the neutrons that will be found between x and $x+dx$ as thermal neutrons and L is given by

$$L = \left(\frac{\bar{r}^2}{3}\right)^{\frac{1}{2}} = 7 \text{ gm./cm.}^2 \text{ for 20 MeV. neutrons.}$$

It must be emphasized that formula (3) holds only if the neutrons are emitted isotropically.

Now, the number $n'(x)$ of evaporated neutrons produced at a depth x in the ice can be written

$$n'(x) = n'(0) \exp (-x/\lambda) / \text{gm./sec.} \quad \dots \quad (4)$$

where $\lambda = 130 \text{ gm./cm.}^2$.

Using equations (3) and (4), we find that $B'(x)dx$, the number of neutrons of the first group, assumed all to have energies of 20 MeV., reaching thermal energies/sec. between depths x and $x+dx$ is given by

$$\begin{aligned} B'(x) dx &= dx \frac{n'(0) \exp (-x/\lambda)}{\pi^{\frac{1}{2}} L} \int_{-\infty}^x \exp (y/\lambda) \exp (-y^2/L^2) dy \\ &= dx \frac{n'(0) \exp (-x/\lambda)}{\pi^{\frac{1}{2}} L} \exp (L^2/4\lambda^2) \int_{-\infty}^x \exp (-y^2/L^2) dy. \end{aligned} \quad \dots \quad (5)$$

Now, for $L = 7 \text{ gm./cm.}^2$, we find that the upper limit of the integral in equation (5) can be replaced by ∞ with less than 3 per cent error for all values of $x > 10 \text{ gm./cm.}^2$.

Then we find

$$B'(x) = n'(0) \exp (-x/\lambda) \exp (L^2/4\lambda^2),$$

and for $L = 7 \text{ gm./cm.}^2$, $\lambda = 130 \text{ gm./cm.}^2$, $\exp (L^2/4\lambda^2)$ is very nearly unity (0.999), so therefore we can write

$$B'(x) = n'(0) \exp (-x/\lambda) = n'(x) \quad \dots \quad (6)$$

We have derived equation (6) by considering all the evaporated neutrons to be emitted with an energy of 20 MeV. In fact, the majority of the neutrons will have energies of only three or four MeV. For these lower energy neutrons, \bar{r}^2 , and therefore L , will be reduced. This will make the contribution between $y = \pm 10 \text{ gm./cm.}^2$ to the integral in equation (5) even larger than 97 per cent, and will make $\exp (L^2/4\lambda^2)$ nearer unity, therefore equation (6) will still hold.

HIGH ENERGY NEUTRONS.

The scattering mean free path in ice for neutrons of energy greater than 20 MeV. is largely governed by the oxygen cross section, and further, varies only slowly with the energy. For a 50 MeV. neutron the mean free path is of the order of 20 gm./cm.^2 . Now, since the oxygen nucleus

is massive compared to the neutron the scattering is very large, and therefore, after one collision the neutrons will have an isotropic angular distribution. We will take the mean energy of the fast neutrons as 50 MeV. and suppose that all the neutrons have this energy. Let the number of fast neutrons produced at a depth x be given by

$$n''(x) = n''(0) \exp(-x/\lambda) \quad . \quad . \quad . \quad (7)$$

where λ is again equal to 130 gm./cm.².

Then the number of fast neutrons produced *isotropically* at a depth x will be approximately equal to the number of fast neutrons produced from stars a distance 20 gm./cm.² above x , since these fast isotropic neutrons are produced after one collision from the fast collimated neutrons.

We can now apply equations (2), (3) and (5) to these isotropic neutrons, and we then find that

$$\bar{r}^2 = 6,500 \text{ (gm./cm.}^2\text{)}^2,$$

$$L = 30 \text{ gm./cm.}^2$$

and that

$$B''(x) = n''(x-20), \quad . \quad . \quad . \quad (8)$$

provided x is greater than 50 gm./cm.².

$B''(x) dx$ is the number of neutrons, which were originally fast collimated neutrons, that reach thermal energies between x and $x+dx$. For values of x less than 50 gm./cm.², $B''(x)$ will not have the full contribution from the neutrons produced in the ice, but this will be compensated for by the entry of fast neutrons from the air.

From this analysis, we can say that, for depths of more than 50 gm./cm.² of ice, the total number of neutrons reaching thermal energies/sec. at a depth x is given by

$$B'(x) + B''(x) = n'(x) + n''(x-20),$$

and that for values of x between 15 and 50 gm./cm.², we will have the full contribution to $B'(x)$, but a reduced contribution to $B''(x)$ from neutrons produced in the ice, which will be compensated to some extent by neutrons produced in the air. This view is strengthened by a study of fig. 1, which shows that all the experimental points lie on a straight line, with a slope corresponding very closely to that expected for a value of $\lambda = 130$ gm./cm.².

We can now find $B'(x) + B''(x)$ for $x = 15$ gm./cm.². Bethe *et al.* show that if $\rho(x)$ is the number of boron disintegrations/c.e./day at a depth x gm./cm.², then

$$\rho(x) = \frac{D'}{D} \frac{\sigma_0^1}{\sigma_0} (B'(x) + B''(x)) \rho,$$

where D' and D are the number of boron atoms/c.e. of emulsion and the number of hydrogen atoms/c.e. of ice respectively, ρ_0^1 and ρ_0 the atomic

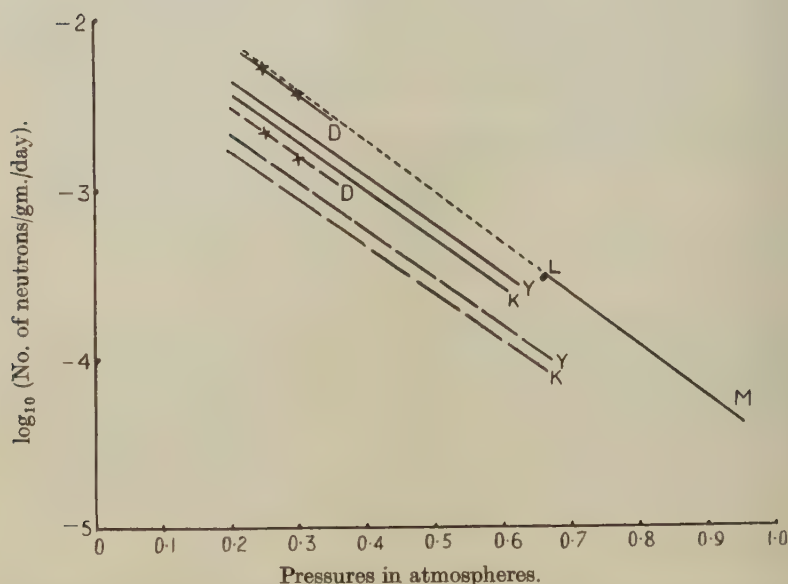
capture cross sections of boron and hydrogen respectively, and ρ the density of ice. It is assumed that no capture occurs in the oxygen. Putting

$$\left. \begin{aligned} \sigma_0^1 &= 115 \text{ borons,} \\ \sigma_0 &= 0.049 \text{ borons,} \end{aligned} \right\} \text{R. K. Adair (1950)}$$

we find

$$B'(15) + B''(15) = 20/\text{gm./day in ice.}$$

Fig. 2.



This figure shows some results obtained for the rate of neutron production as a function of the atmosphere depth, both before (dashed lines) and after (full lines) the corrections given in this paper have been applied.

D—Davis (1950).

K—Korff and Hamermesh 1946.

L—Lattimore (present results).

M—Montgomery and Tobey 1949 (no corrections required).

Y—Yuan 1946.

If we assume that only the oxygen in the ice produces neutrons, and also correct for the absorption in the 15 gm./cm.² of snow by multiplying by $\exp(15/130)$, we find

$$B'(0) + B''(0) = 25/\text{gm. of oxygen/day}$$

at an elevation of 3600 m. Now,

$$\begin{aligned} B'(x) + B''(x) &= n'(x) + n''(x-20) \\ &= n'(x) + 1.15n''(x), \end{aligned}$$

since $n''(x-20) = \exp(20/130) n''(x)$. (See equation (7).)

If we assume that the neutron and proton spectra are similar, $n''(x)/n'(x)$ is of the order of $\frac{1}{3}$, and we can therefore write

$$n'(x) + 1.15n''(x) = 1.04(n'(x) + n''(x)),$$

$$B'(0) + B''(0) = 1.04(n'(0) + n''(0)),$$

and therefore the rate of production of fast neutrons in oxygen at 3600 m. is given by 25 divided by 1.04 which is equal to 24/gm./day.

Rate of production of fast neutrons = 24/gm. of oxygen/day at 3600 m.

DISCUSSIONS OF RESULTS.

The value obtained for the absorption of the neutron producing primaries, namely 126 gm./cm.² of ice, is in excellent agreement with that found by Harding (1950) for the star producing radiation. The rate of production also agrees well with that found in carbon at the same elevation by Montgomery and Tobey (1949), who used a similar method to that used here, that is to say, they surrounded an ionization chamber with large masses of paraffin wax. These two values are, however, greater by a factor of about two than those given for air by several other investigators. As had been pointed out in another paper (Lattimore 1951), this is probably due to the misuse of a formula given by Bethe *et al.* (1940) which involves the nitrogen cross section/molecule. In many cases the cross section/atom has been used, which gives a rate of production of only half the true value. In fig. 2 is shown some corrected values, and it can be seen that the agreement between these and the results presented here is much improved.

ACKNOWLEDGMENT.

I must express my thanks to Professor Sir George Thomson for much helpful advice during the course of this work.

REFERENCES.

- ADAIR, 1950, *Rev. Mod. Phys.*, **22**, 3, 249.
 ADAMS, N., 1950, *Phil. Mag.*, **41**, 503-5.
 BETHE, H. A., KORFF, S. A., and PLACZEK, G., 1940, *Phys. Rev.*, **57**, 573.
 DAVIS, W. D., 1950, *Phys. Rev.*, **80**, 150.
 HARDING, J. B., 1950, (unpublished).
 HARDING, J. B., LATTIMORE, S., and PERKINS, D. H., 1949, *Proc. Roy. Soc. A*, **196**, 325-43.
 KORFF, S. A., and HAMERMESH, B., 1946, *Phys. Rev.*, **69**, 155.
 LATTIMORE, S., 1951, *Phys. Rev.* (in the press).
 MONTGOMERY, G. G., and TOBEY, A. R., 1949, *Phys. Rev.*, **76**, 1478-81.
 PERKINS, D. H., 1947, *Nature*, **160**, 299.
 YUAN, L. C. L., 1946, *Phys. Rev.*, **74**, 504.

XL. *The Binding Energies of Three- and Four-particle Nuclei.*

By J. IRVING,

Department of Natural Philosophy, The University of Glasgow*

[Received January 30, 1951.]

ABSTRACT.

The binding energies of the nuclei H^3 , He^3 and He^4 are calculated, using the standard variation method with a simple two-parameter wave-function of a new form. Purely central interactions of the Yukawa and exponential types are considered. It is found that, when the nuclear parameters are chosen to fit the low-energy scattering and deuteron data, reasonable values are obtained for the three-particle nuclei, but the α -particle binding energy is too high. This result is in agreement with the calculations of Rarita and Present for the exponential potential, and those of Svartholm for the Yukawa potential. In contrast with Svartholm's method of calculation, the potential and kinetic energies of the nuclei are obtained explicitly. In the case of the α -particle, the Yukawa potential yields exceptionally high values for these quantities, and results also in a very concentrated nucleus. The exponential potential, on the other hand, does not give rise to such high values for the potential and kinetic energies nor does it concentrate the nucleus to the same extent as the former potential †.

§ 1. INTRODUCTION.

NUMEROUS investigations have been made on the binding energies of the three- and four-particle nuclei, using a central two-body interaction with various forms of potential well. The methods of calculation adopted in these investigations and the conclusions arising therefrom have been summarized by Rosenfeld (1948). The so-called consistency problem may be stated as follows :—

(1) A set of parameters compatible with the deuteron and low-energy scattering data, and with the binding energy of the triton, yields too large a binding energy of the α -particle.

(2) A set of parameters yielding the correct binding energy of H^2 , He^3 and He^4 involves a longer range than allowed by the $p-p$ data and gives rise to a bound 1S state of the deuteron.

In this paper the problem is approached from the point of view of the first statement.

The standard variation method is used with a new two-parameter wave-function of simple form for both the Yukawa and exponential central interactions. The wave-functions chosen give rise to relatively simple

* Communicated by the Author.

† See note added in proof.

mathematical analysis, no approximations being necessary in the evaluation of the integrals involved. This is to be contrasted with the more laborious calculations of Rarita and Present (1937) for the exponential potential, using the variation and equivalent two-body problem techniques; and the work of Svartholm (1945), using the much more tedious, but admittedly very accurate variation-iteration method. The conclusion reached from the calculations carried out here is given in statement (1), and is thus in agreement with that of Rarita and Present, and Svartholm. It might be remarked, however, that the Yukawa potential yields results for the α -particle, which, though agreeing with the latter's conclusion, differ from those of Fröhlich *et al.* (1947) for the longer range of the forces—corresponding to a meson mass of $210\text{--}220\ m_e$ —which they use. The value obtained here for the binding energy for this particular range is approximately twice as large as that of Fröhlich.

The total kinetic and potential energies for each nucleus are given explicitly in contrast with Svartholm's calculations, where the nuclear parameters are evaluated to fit the experimentally known binding energies. It is found in the case of the α -particle that the kinetic energy for the Yukawa potential is exceptionally high; the excess binding energy is large; and, moreover, the nucleus is very concentrated. The exponential potential, on the other hand, gives rise to a much smaller excess binding energy, more reasonable values of the kinetic energy and a not so concentrated nucleus*.

The calculations of Gerjuoy and Schwinger (1942) have indicated, of course, that the introduction of a non-central interaction of the tensor type would considerably reduce the excess binding energy of the α particle. In fact, their investigations with a square well potential have yielded too small binding energies for the triton and the α -particle. However, if one considers the exceptionally large binding energy obtained for the Yukawa potential with purely central forces, it is feasible that the introduction of tensor forces might reduce it sufficiently so that the experimental value might be obtained when the normal ranges of the forces used to fit the two-body data are considered. This problem is now being investigated with the wave-functions used in the present calculations.

The wave-functions introduced in this paper are of a form which might be extended for systems of more than four particles, provided the space-part is so modified as to have the correct symmetry properties for the particles in p -states.

§ 2. BINDING ENERGY FORMULAE AND WAVE-FUNCTIONS.

The two-particle central interaction with a mixture of Wigner, Bartlett, Heisenberg and Majorana forces may be written in the form (Rosenfeld, 1948)

$$V_{\text{nuc}} = V(r_{12}) \{ a_0 + a_\sigma \hat{\sigma}^{(1)} \hat{\sigma}^{(2)} + a_\tau \tau^{(1)} \tau^{(2)} + a_{\sigma\tau} \sigma^{(1)} \hat{\sigma}^{(2)} \tau^{(1)} \tau^{(2)} \}$$

or

$$V_{\text{nuc}} = V(r_{12}) \{ W + BP_\sigma - HP_\tau - MP_\sigma P_\tau \},$$

* See note added in proof.

where $V(r_{12})$ is the two-particle triplet potential, r_{12} being the distance between the particles, and the other quantities have their usual meanings. Now the ground states of the nuclei H^3 , He^3 and He^4 are S-states, so that an interaction consisting of a mixture of Majorana and Heisenberg forces—so-called exchange forces—yields the same binding energy as an equivalent mixture of Wigner and Bartlett forces. For a wave-function symmetrical in space coordinates the formula for the total energy of the nucleus has the well-known form (Rosenfeld 1948),

$$E^{(3)} = -(\hbar^2/2M) \int \psi \Delta^{(3)} \psi dv^{(3)} + (3/2)(1+q) \int V(r_{12}) \psi^2 dv^{(3)} + E_{\text{Coul}} \quad (1)$$

for the three-particle system, and

$$E^{(4)} = -(\hbar^2/2M) \int \phi \Delta^{(4)} \phi dv^{(4)} + 3(1+q) \int V(r_{12}) \phi^2 dv^{(4)} + E_{\text{Coul}} \quad (2)$$

for the four-particle system. Here q is the ratio of singlet to triplet well depth, $\Delta^{(3)} = \sum_{i=1}^3 \Delta_i$ and $\Delta^{(4)} = \sum_{i=1}^4 \Delta_i$, where Δ_i is the Laplace operator acting on the coordinates of particle whose position vector is \mathbf{r}_i ; ψ and ϕ are the space parts of the wave-functions for the three- and four-particle systems respectively; M is the mass of the nucleon. E_{Coul} denotes the Coulomb energy of the protons in the nucleus and will be treated in the usual way as a perturbation.

The problem of the calculation of the binding energy involves the choice of a good trial wave-function with one or more parameters, subsequent evaluation of the integrals, and minimization with respect to the variation parameters. The Gaussian wave-function has been frequently used in calculations in nuclear problems, because of the great simplification it usually gives in the mathematical analysis. It has, however, an incorrect asymptotic behaviour, and is a very poor approximation to the correct wave-function for a three- or four-particle system, when a Yukawa potential is used. The following new wave-functions with an exponential type of asymptotic behaviour are introduced in the subsequent calculations and result in fairly simple mathematical analysis.

(a) *Three-particle system.*

Let

$$\psi = B^{1/2} \exp \{ -\alpha(r_{12}^2 + r_{13}^2 + r_{23}^2)^{1/2} \} / \{ r_{12}^2 + r_{13}^2 + r_{23}^2 \}^n \quad (3)$$

be the wave-function for the three-particle system, where $B^{1/2}$ is the normalization coefficient; α and n are parameters; r_{12} , r_{13} and r_{23} are the distances between the particles 1 and 2, 1 and 3, 2 and 3 respectively.

The wave-function is of course a function of the relative coordinates of the particles and it may be simplified by a transformation.

Let

$$\rho = -\mathbf{r}_1 + (\mathbf{r}_2 + \mathbf{r}_3)/2, \quad \mathbf{r} = (\sqrt{3}/2)(\mathbf{r}_2 - \mathbf{r}_3), \quad \mathbf{R} = (\mathbf{r}_1 + \mathbf{r}_2 + \mathbf{r}_3)/3, \quad (4)$$

\mathbf{r}_1 , \mathbf{r}_2 and \mathbf{r}_3 being the position vectors of the particles 1, 2 and 3 respectively. Relation (3) then assumes the form

$$\psi' = N_1^{1/2} \exp \{ -\sqrt{2\alpha(\rho^2 + r^2)^{1/2}} / (\rho^2 + r^2)^n \}, \quad (5)$$

$N_1^{1/2}$ being the normalization coefficient in the new coordinate system and $\rho = |\mathbf{p}|$, $r = |\mathbf{r}|$.

In this system of coordinates it is easily shown that the operator $-(\hbar^2/2M)\Delta^{(3)}$ becomes $-(\hbar^2/2m)(\Delta_{\mathbf{r}} + \Delta_{\mathbf{p}}) - (\hbar^2/6M)\Delta_{\mathbf{R}}$, where $\Delta_{\mathbf{r}}$, $\Delta_{\mathbf{p}}$ and $\Delta_{\mathbf{R}}$ act on the coordinates \mathbf{r} , \mathbf{p} and \mathbf{R} respectively; and $m = 2M/3$. Now \mathbf{R} is the position vector of the centre of mass of the three particles, so that, since ψ or ψ' is a function of the relative coordinates, the expectation value of the kinetic energy of the mass-centre is zero.

Equation (1) may then be written in the form

$$E^{(3)} = -(\hbar^2/2m) \int \psi' (\Delta_{\mathbf{r}} + \Delta_{\mathbf{p}}) \psi' d\mathbf{r} d\mathbf{p} + (3/2)(1+q) \int V(r_{12}) \psi'^2 d\mathbf{r} d\mathbf{p} + E_{\text{Coul}}. \quad (6)$$

The Coulomb energy for two protons, that is, the He^3 nucleus, may be written in the form

$$E_{\text{Coul}} = e^2 \int (1/r_{12}) \psi'^2 d\mathbf{r} d\mathbf{p}, \quad (7)$$

e being the electronic charge.

(b) Four-particle system.

The form of the wave-function taken for this case is similar to that of ψ in equation (3).

Let

$$\phi = C^{1/2} \exp \{ -\alpha(r_{12}^2 + r_{13}^2 + r_{14}^2 + r_{23}^2 + r_{24}^2 + r_{34}^2)^{1/2} / \{ r_{12}^2 + r_{13}^2 + r_{14}^2 + r_{23}^2 + r_{24}^2 + r_{34}^2 \}^n \}, \quad (8)$$

where $C^{1/2}$ is the normalization coefficient; α and n are parameters: r_{12} , etc. are the distances between the particles 1 and 2, etc. The transformation

$$\left. \begin{aligned} \mathbf{u} &= (\mathbf{r}_1 + \mathbf{r}_2)/2 - (\mathbf{r}_3 + \mathbf{r}_4)/2, & \mathbf{R} &= (\mathbf{r}_1 + \mathbf{r}_2 + \mathbf{r}_3 + \mathbf{r}_4)/4, \\ \mathbf{v} &= (\mathbf{r}_1 - \mathbf{r}_2)/\sqrt{2}, & \mathbf{w} &= (\mathbf{r}_3 - \mathbf{r}_4)/\sqrt{2}, \end{aligned} \right\} \quad (9)$$

where \mathbf{r}_1 , \mathbf{r}_2 , \mathbf{r}_3 and \mathbf{r}_4 are the position vectors of the particles 1, 2, 3 and 4 respectively, applied to (8) gives

$$\phi' = N_2^{1/2} \exp \{ -2\alpha(u^2 + v^2 + w^2)^{1/2} / \{ u^2 + v^2 + w^2 \}^n \}, \quad (10)$$

$N_2^{1/2}$ being the normalization coefficient in the new coordinate system, and $u = |\mathbf{u}|$, $v = |\mathbf{v}|$, $w = |\mathbf{w}|$. It is easily shown that equation (2) becomes

$$E^{(4)} = -(\hbar^2/2M) \int \phi' (\Delta_{\mathbf{u}} + \Delta_{\mathbf{v}} + \Delta_{\mathbf{w}}) \phi' d\mathbf{u} d\mathbf{v} d\mathbf{w} + 3(1+q) \int V(r_{12}) \phi'^2 d\mathbf{u} d\mathbf{v} d\mathbf{w} + E_{\text{Coul}}. \quad (11)$$

in the new coordinate system, the expectation value of the kinetic energy of the mass-centre vanishing as in the case of the three-particle system.

$\Delta_{\mathbf{u}}$, $\Delta_{\mathbf{v}}$ and $\Delta_{\mathbf{w}}$ are the Laplace operators acting on the coordinates \mathbf{u} , \mathbf{v} and \mathbf{w} respectively.

The Coulomb energy for the two protons may be written in the form

$$E_{\text{Coul}} = e^2 \int (1/r_{12}) \phi'^2 d\mathbf{u} d\mathbf{v} d\mathbf{w}, \quad (12)$$

e being the electronic charge.

§ 3. EVALUATION OF BINDING ENERGY OF H^3 and He^3 .

The normalization coefficient $N^{1/2}$ for the wave function (5) is easily determined.

$$\int \psi^2 d\mathbf{p} d\mathbf{r} = N_1 (4\pi)^2 \int_0^\infty [\exp \{-\beta(\rho^2 + r^2)^{1/2}\} / (\rho^2 + r^2)^{2n}] \rho^2 r^2 d\rho dr = 1,$$

where $\beta = 2\sqrt{2}\alpha$.

Using the transformation $\rho = R \cos \psi$, $r = R \sin \psi$ it is found that

$$N_1 = (\alpha^{6-4n} \cdot 2^{9-6n}) / \{\pi^3 (5-4n)!\}. \quad (13)$$

For the above-mentioned wave-function, the kinetic energy of the nucleons, corresponding to the first term on the right-hand side of equation (6), is given by

$$-(\hbar^2/2m) N_1 \int [\exp \{-\beta(\rho^2 + r^2)^{1/2}\} / (\rho^2 + r^2)^{2n+1}] \\ \times [2\alpha^2(\rho^2 + r^2) - \sqrt{2}\alpha(5-4n)(\rho^2 + r^2)^{1/2} - n(8-4n)] d\mathbf{p} d\mathbf{r}.$$

This is simply evaluated, using the transformation $\rho = R \cos \psi$, $r = R \sin \psi$, so that the kinetic energy is

$$\frac{3}{2} \cdot \frac{(5-n)}{(1-n)(5-4n)} \cdot \frac{\hbar^2}{M} \alpha'^2$$

or

$$\frac{(5-n)}{4(1-n)(5-4n)} \cdot \frac{\hbar^2}{M} \kappa'^2 c'^2, \quad (14)$$

where $c' = \sqrt{6}\alpha/\kappa$, $(1/\kappa)$ being the range of the nuclear forces.

When the wave-function (5) is substituted in the expression (7) for the Coulomb energy, then, since from symmetry considerations r_{12} may be replaced by r_{23} ,

$$E_{\text{Coul}} = \frac{16\sqrt{6}e^2\alpha}{3(5-4n)\pi} = \frac{16e^2\kappa}{3(5-4n)\pi c}, \quad (15)$$

where $c = \kappa/\sqrt{6}\alpha$.

(a) *Yukawa potential well*: $V(r_{12}) = -A \exp(-\kappa r_{12})/(\kappa r_{12})$.

The second term on the right-hand side of equation (6) represents the potential energy of the three-particle system apart from the Coulomb energy. Now, when the wave-function given by (5) is used,

$$\int V(r_{12}) \psi'^2 d\mathbf{r} d\mathbf{p} = -AN_1 \int \exp \{-\beta(\rho^2 + r^2)^{1/2} - \kappa r_{12}\} / \{\kappa r_{12}(\rho^2 + r^2)^{2n}\} d\mathbf{r} d\mathbf{p}.$$

Since from symmetry considerations r_{12} may be replaced by r_{23} , that is, $2r/\sqrt{3}$, the integral may be written in the form

$$-(AN_1/\kappa') \int_0^{\pi/2} \cos^2 \psi \sin \psi d\psi \int_0^\infty R^{4-4n} \exp(-\gamma R) dR,$$

where $\gamma = \beta + \kappa' \sin \psi$, $\kappa' = 2\kappa/\sqrt{3}$ and the transformation $\rho = R \cos \psi$, $r = R \sin \psi$ has been applied. Hence, by elementary integration, the potential energy has the form

$$-\{(24/\pi)(1+q)Ac'/(5-4n)\} \int_0^{\pi/2} \frac{\cos^2 \psi \sin \psi}{(1+c \sin \psi)^{5-4n}} d\psi, \quad (16)$$

where $c' = 1/c = \sqrt{6}\alpha/\kappa$.

Thus, for the H^3 nucleus, the total energy is given by

$$E = \frac{(5-n)}{4(1-n)(5-4n)} \cdot \frac{\hbar^2}{M} \kappa^2 c'^2 - \frac{24(1+q)Ac'}{\pi(5-4n)} \int_0^{\pi/2} \frac{\cos^2 \psi \sin \psi}{(1+c \sin \psi)^{5-4n}} d\psi. \quad (17)$$

The total energy for the He^3 nucleus is obtained by the addition of the Coulomb energy term given in equation (15).

The expression (17) is now minimized with respect to the parameters c and n for different values of the range $(1/\kappa)$, with the corresponding values of A and q fixed by the low-energy $n-p$ scattering and deuteron data. The integral appearing in the expression is easily evaluated for the values $n=0$, $1/4$, $1/2$ and $3/4$. These are given in § 1 of the Appendix. Minimization with respect to c is carried out for each of the values of n mentioned. It should be noted that n must be less than or equal to $3/4$ for convergence of the integral representing the kinetic energy.

TABLE I.

Minima of E for H^3 and He^3 with respect to c for each value of n .

n	c	K. E. (MeV.)	P. E. (MeV.)	H^3/E_{\min} (MeV.)	E_{Coul} (MeV.)	He^3/E_{\min} (MeV.)
0	0.38	52.3	-60.2	-7.9	1.10	-6.8
1/4	0.46	56.5	-65.0	-8.5	1.13	-7.4
1/2	0.70	46.3	-53.3	-7.0	0.99	-6.0
3/4	1.60	25.1	-27.2	-2.2	0.65	-1.5

Table I. gives the minimum values of E for H^3 for each value of n considered, for the range $(1/\kappa) = 1.17 \times 10^{-13}$ cm., which corresponds to a meson mass of $326 m_e$, A and q having the values 67.3 MeV. and 0.69 respectively. The corresponding values of the kinetic and potential energies, the Coulomb energies for the He^3 nucleus and the resultant values of the binding energy for the latter nucleus are also tabulated.

The values given in Table I. indicate that the maximum value of $|E|$ of approximately 8.5 MeV. arises for $n \sim 1/4$, and $c = 0.46$, that is, $1/\alpha = 1.318 \times 10^{-13}$ cm. The value of $(1/\alpha)$ gives an indication of the "size" of the nucleus. The maximum value of $|E|$ for He^3 is 7.4 MeV.

The experimental value of the mass-difference of the nuclei H^3 and He^3 , that is, the Coulomb energy of the protons, is accurately known, being 771 ± 6 keV. (Tollestrup *et al.* 1949). Comparison of the theoretical value with this gives a check on the accuracy of the binding energy calculations. From Table I., it is seen that the theoretical values of the Coulomb energy are rather high, though the actual values of the binding energies of H^3 and He^3 are in good agreement with the experimental values of (8.51 ± 0.091) MeV. and (7.739 ± 0.1) MeV. respectively.

Svartholm, using the variation-iteration method, has calculated the value of the parameter A to fit a triton binding energy of 8.33 MeV. for the ranges 1.185×10^{-13} cm. and 1.835×10^{-13} cm. Brown (1939) has also fitted the binding energy of the triton for the latter range, using the variation method with a large number of parameters. Table II. gives the binding energies for these ranges with the new wave-functions, using the values of q and A corresponding to Brown and Svartholm's calculations. Considering the simplicity of the present calculations the results obtained are reasonable.

TABLE II.

Values of the binding energy of H^3 with new wave-functions corresponding to different sets of nuclear parameters.

	$1/\kappa$ (10^{-13} cm.)	A (MeV.)	q	Binding-energy of H^3 (MeV.)
(Svartholm)	$\begin{cases} 1.185 \\ 1.835 \end{cases}$	$\begin{matrix} 61.01 \\ 33.80 \end{matrix}$	$\begin{matrix} 0.75 \\ 0.58 \end{matrix}$	$\begin{matrix} 6.1 \\ 8.4 \end{matrix}$
(Brown)	1.835	32.06	0.58	6.3
(Assumed)	1.17	67.3	0.69	8.5

(b) *Exponential well*: $V(r_{12}) = -A \exp(-\kappa r_{12})$.

The analysis for this potential is of the same form as that for the Yukawa case. The potential energy reduces to the expression

$$-(24/\pi)(1+q)A \int_0^{\pi/2} \frac{\cos^2 \psi \sin^2 \psi}{(1+c \sin \psi)^{6-4n}} d\psi. \quad \dots \quad (18)$$

The integral in (18) may be evaluated by elementary methods for $n=0$, $1/4$, $1/2$, $3/4$. [The values for $n=0$ and $n=1/4$ are given in § 2 of the Appendix.] Thus, for the H^3 nucleus, the total energy is given by

$$E = \frac{(5-n)}{4(1-n)(5-4n)} \cdot \frac{\hbar^2}{M} \kappa^2 c'^2 - (24/\pi)(1+q)A \int_0^{\pi/2} \frac{\cos^2 \psi \sin^2 \psi}{(1+c \sin \psi)^{6-4n}} d\psi. \quad \dots \quad (19)$$

The values taken for the nuclear parameters are: $(1/\kappa) = 0.865 \times 10^{-13}$ cm., $A = 123.3$ MeV., $q = 0.6$. The minimum value of E in this case occurs at approximately $n=0$, $c=0.69$, the kinetic and potential energies having the

values 29.1 MeV. and -36.7 MeV. respectively. Thus the minimum value for E of -7.6 MeV. for H^3 is reasonably good. The Coulomb term given in the relation (15) has the value 1.02 MeV. at this minimum, so that the binding energy of the He^3 nucleus is approximately 6.5 MeV. The value of $(1/\alpha)$, corresponding to $c=0.69$, is 1.462×10^{-13} cm., indicating the "size" of the nucleus. It is to be noted that there is a considerable difference in the values of the kinetic energies for the Yukawa and exponential potentials at the minimum of E^* .

Rarita and Present (1937) have fitted the value of the binding energy of the triton, using the exponential potential and the same values of the nuclear parameters as above, but a much more complicated trial wave-function than that used here has to be introduced.

§ 4. EVALUATION OF THE BINDING ENERGY OF He^4 .

The normalization coefficient $N_2^{1/2}$ for the wave-function ϕ' , given by equation (10), is easily determined

$$\int \phi'^2 d\mathbf{u} d\mathbf{v} d\mathbf{w} = N_2 (4\pi)^3 \int_0^\infty [\exp \{-\beta(u^2 + v^2 + w^2)^{1/2}\} / (u^2 + v^2 + w^2)^{2n}] \\ \times u^2 v^2 w^2 du dv dw = 1,$$

where $\beta = 4\alpha$.

Using the transformation

$$u = R \sin \theta \cos \phi, \quad v = R \sin \theta \sin \phi, \quad w = R \cos \theta, \quad (20)$$

it is found that

$$N_2 = (105 \cdot 2^{13-8n} \cdot \alpha^{9-4n}) / \{\pi^4 (8-4n)!\}. \quad (21)$$

For the above mentioned wave-function, the kinetic energy of the nucleons, corresponding to the first term on the right-hand side of equation (11), is given by

$$-(\hbar^2/2M) \int [\exp \{-\beta(u^2 + v^2 + w^2)^{1/2}\} / (u^2 + v^2 + w^2)^{2n+1}] \\ \times [4\alpha^2(u^2 + v^2 + w^2) - 2\alpha(8-4n)(u^2 + v^2 + w^2)^{1/2} - n(14-4n)] d\mathbf{u} d\mathbf{v} d\mathbf{w}.$$

This is simply evaluated, using the transformation (20), so that the kinetic energy is

$$\frac{(28-2n)}{4(4-2n)(7-4n)} \cdot \frac{\hbar^2}{M} \kappa^2 c^2, \quad (22)$$

where $c = 2\sqrt{2}\alpha/\kappa$.

When the wave-function (10) is substituted in the expression (12) for the Coulomb energy, this may be evaluated, using (20), to give

$$E_{\text{Coul}} = \frac{35\sqrt{2}e^2\alpha}{32(2-n)} = \frac{35e^2c\kappa}{64(2-n)}. \quad (23)$$

* See note added in proof.

(a) *Yukawa potential well*: $V(r_{12}) = -A \exp(-\kappa r_{12})/(\kappa r_{12})$.

The second term on the right-hand side of equation (11) represents the potential energy of the four-particle system apart from the Coulomb energy. Now when the wave-function ϕ' given by (10) is used,

$$\int V(r_{12}) \phi'^2 d\mathbf{u} d\mathbf{v} d\mathbf{w} \\ = -AN_2 \int \exp\{-\beta(u^2+v^2+w^2)^{1/2} - \kappa r_{12}\} / \{\kappa r_{12}(u^2+v^2+w^2)^{2n}\} d\mathbf{u} d\mathbf{v} d\mathbf{w}.$$

Since from symmetry considerations r_{12} may be replaced by r_{34} , that is, $\sqrt{2}w$, the integral may, with the help of the transformation (20), be written in the form

$$-(AN_2/\kappa')(4\pi)^3 \int_0^{\pi/2} \sin^2 \phi \cos^2 \phi d\phi \int_0^{\pi/2} \sin^5 \theta \cos \theta d\theta \int_0^\infty R^{7-4n} \exp(-\gamma R) dR,$$

where $\kappa' = \sqrt{2}\kappa$ and $\gamma = \beta + \kappa' \cos \theta$. Hence, by elementary integration, the potential energy has the form

$$-\frac{315(1+q)A\kappa^{9-4n}}{32(2-n)} \int_0^1 \frac{u(1-u^2)^2}{(u+c)^{8-4n}} du, \quad \dots \quad (24)$$

where $u = \cos \theta$ and $c = \beta/\kappa' = (2\sqrt{2}\alpha/\kappa)$.

Thus for the He^4 nucleus the total energy is given by

$$E = \frac{(28-2n)}{4(4-2n)(7-4n)} \cdot \frac{\hbar^2}{M} \kappa^2 c^2 \\ - \frac{315(1+q)A\kappa^{9-4n}}{32(2-n)} \int_0^1 \frac{u(1-u^2)^2}{(u+c)^{8-4n}} du + E_{\text{Coul}}, \quad \dots \quad (25)$$

E_{Coul} being given by (23).

The minimization is carried out in the same way as in § 3 (a) for the H^3 nucleus, the Coulomb term being omitted in this stage, and then added later as a perturbation. The values of $n=0, 1/4, 1/2, 1, 5/4, 3/2$ are considered; convergence of the integral for the kinetic energy imposes the condition that $n \leq 3/2$. The values of the integral appearing in the potential energy term in equation (25) are given in § 3 of the Appendix. The results for the values $(1/\kappa) = 1.17 \times 10^{-13} \text{ cm.}$, $A = 67.3 \text{ MeV.}$, $q = 0.69$ are given in Table III.

TABLE III.

Minima of E for He^4 with respect to c for each value of n .

n	c	K. E. (MeV.)	P. E. (MeV.)	E_{min} (MeV.)	E_{Coul} (MeV.)	Binding energy (MeV.)
0	5.0	188.9	-243.5	-54.6	1.97	52.6
1/4	4.5	200.4	-255.4	-55.0	1.73	53.3
1/2	3.7	176.6	-230.8	-54.2	1.66	52.5
1	2.3	173.5	-220.0	-46.5	1.55	44.9
5/4	1.5	139.0	-174.0	-35.0	1.33	33.7
3/2	0.63	75.0	-88.4	-13.4	0.85	12.5

The values given in Table III. show that the parameter n for values from 0 to $1/2$ does not influence the value of $|E|$ very much. The maximum value of the binding energy is approximately 53.3 MeV. for $n=1/4$, $c=4.5$, that is $(1/\alpha)=0.735 \times 10^{-13}$ cm. Thus a very large excess binding energy is obtained, proving the inadequacy of the central Yukawa interaction. The kinetic energy of the nucleons is exceptionally high and the nucleus itself is very concentrated. The Coulomb energy too is rather large.

The minimum values obtained for the binding energy, for the nuclear parameters of Svartholm and Brown, are given in Table IV. In addition, the binding energy is calculated for the parameter $(1/\kappa)=1.185 \times 10^{13}$ cm., $q=0.75$, $A=56.0$, assuming this to be the approximate convergence limit for A for the iteration method. Svartholm gives only the value obtained by the first iteration. It is also shown that the very long range of 1.9×10^{-13} cm. has to be taken to obtain a value, which is fairly near the experimental binding energy of 28.2 MeV. It might be mentioned that the value obtained by Fröhlich *et al.* (1947) for a comparable range is only half of the experimental value.

TABLE IV.

Values of the binding energy of He^4 with new wave-functions corresponding to different sets of nuclear parameters.

	$1/\kappa$ (10^{-13} cm.)	q	A	Binding energy (MeV.)
(Svartholm)	1.185	0.75	61.01 *	43
"	1.185	0.75	60.034 †	40
"	1.835	0.58	56 (assumed)	27
"	1.835	0.58	33.80 *	39
(Brown)	1.835	0.58	29.69 ‡	23
(Assumed)	1.9	0.57	32.06 *	32
(Assumed)	1.17	0.69	29.3 §	27
			67.3 §	53

* Depth of well obtained by variation-iteration method to fit binding energy of H^3 .

† Depth of well obtained in one iteration to fit binding energy of He^4 .

‡ Depth of well obtained by two iterations to fit binding energy of He^4 .

§ Depth of well to fit deuteron and low-energy scattering data.

Thus the simple wave-functions introduced in this investigation yield results in close agreement with the calculations of Svartholm for the Yukawa potential.

(b) *Exponential potential well*: $V(r_{12}) = -A \exp(-\kappa r_{12})$.

The analysis for this potential is of the same form as that for the Yukawa case. The potential energy reduces to the expression

$$-(315/8)(1+q)Ac^{9-4n} \int_0^1 \{u^2(1-u^2)^2/(u+c)^{9-4n}\} du. \quad (26)$$

The integral in (26) is of a similar form to that in (25). Its values for $n=0, 1/4, 1/2$ are given in § 4 of the Appendix. The total energy of the He^4 nucleus is then given by

$$E = \frac{(28-2n)}{4(4-2n)(7-4n)} \cdot \frac{\hbar^2}{M} \kappa^2 c^2 \\ - (315/8)(1+g)Ac^{9-4n} \int_0^1 \frac{u^2(1-u^2)^2}{(u+c)^{9-4n}} du + E_{\text{Coul}}, \quad (27)$$

E_{Coul} being given by (23).

The values taken for the nuclear parameters are: $(1/\kappa) = 0.865 \times 10^{-13}$ cm., $A = 123.3$ MeV., $g = 0.6$. The maximum value of the binding energy occurs at approximately $n=0$, $c=2.25$, the kinetic, potential, and Coulomb energies having the values 70 MeV., -102.9 MeV. and 1 MeV. respectively. Thus the maximum binding energy is approximately 31.9 MeV., an excess of 3.7 MeV. over the experimental value of 28.2 MeV. The value of $(1/\alpha)$ corresponding to $c=2.25$ is 1.087×10^{-13} cm. Thus there is a considerable difference in the effect of the Yukawa and exponential central interactions on the binding energy of the α -particle. The latter potential gives a much smaller excess binding energy, a much lower kinetic energy, and does not concentrate the nucleus so much as the former potential*.

The conclusion that the exponential potential leads to too much binding energy for the α -particle is in agreement with the calculations of Rarita and Present, though their method results in a slightly larger value for the excess binding energy.

Since the above calculations confirm that central Yukawa and exponential interactions are inadequate for a description of the binding energy of the α -particle, consistent with the binding energy of the three-particle system, the deuteron and the low-energy scattering data—the same conclusions have been reached by Svartholm, and Rarita and Present for the Gaussian interaction—the question of non-central forces should be considered. A tensor force is of course necessary to explain the quadrupole moment of the deuteron. Gerjuoy and Schwinger, using a square-well potential with a mixture of central and tensor forces, have come to the conclusion that tensor forces are not very effective in binding the triton and α -particle. More recent calculations on the binding energy of the triton (Rarita and Feshbach, 1949, Clapp, 1949, Hu and Hsu, 1950) have shown that it is possible to obtain fairly good agreement with the experimental binding energy with a mixture of central and tensor forces when a Yukawa potential is used. It is still an open question whether such a mixture can account for the binding energy of the α -particle when the parameters are chosen to fit the deuteron and low-energy scattering data.

ACKNOWLEDGMENTS.

The author is indebted to Professor J. C. Gunn for the interest he has shown in these calculations and for useful discussions. He also wishes to thank the Nuffield Foundation for the award of a Fellowship during the tenure of which the work was carried out.

* See note added in proof.

APPENDIX.

The values of the integrals listed in the following sections are used in the text :—

$$\S 1. \quad \int_0^{\pi/2} \frac{\cos^2 \psi \sin \psi}{(1+c \sin \psi)^{5-4n}} d\psi.$$

$$n=0 : \quad (1/24)\{8+9c^2-2c^4\}/(1-c^2)^3-15c \cos^{-1} c/(1-c^2)^{7/2}, \quad c \leq 1.$$

$$n=1/4 : \quad (1/6)\{(2+c^2)/(1-c^2)^2-3c \cos^{-1} c/(1-c^2)^{5/2}\}, \quad c \leq 1.$$

$$n=1/2 : \quad -(1/2c^3)\{\pi-c/(1-c^2)-(2-3c^2) \cos^{-1} c/(1-c^2)^{3/2}\}, \quad c \leq 1.$$

$$n=3/4 : \quad (1/c^3)\{\pi-2c-(2-c^2) \cos^{-1} c/(1-c^2)^{1/2}\}, \quad c \leq 1.$$

$$(1/c^3)\{\pi-2c-(2-c^2) \log \{c+(c^2-1)^{1/2}\}/(c^2-1)^{1/2}\}, \quad c \geq 1.$$

$$\S 2. \quad \int_0^{\pi/2} \frac{\cos^2 \psi \sin^2 \psi}{(1+c \sin \psi)^{6-4n}} d\psi.$$

$$n=0 : \quad (1/120)\{15(1+6c^2) \cos^{-1} c/(1-c^2)^{3/2}-c(81+28c^2-4c^4)/(1-c^2)^4\}, \quad c \leq 1.$$

$$n=1/4 : \quad (1/24)\{3(1+4c^2) \cos^{-1} c/(1-c^2)^{7/2}-c(13+2c^2)/(1-c^2)^3\}, \quad c \leq 1.$$

$$\S 3. \quad \int_0^1 \frac{u(1-u^2)^2/(u+c)^{3-4n}}{du}.$$

$$n=0 : \quad (35c^3+47c^2+25c+5)/\{210c^6(1+c)^5\}.$$

$$n=1/4 : \quad (5c^2+4c+1)/\{30c^5(1+c)^4\}.$$

$$n=1/2 : \quad \log \{(1+c)/c\}-(15c^2+36c+23)/\{15(1+c)^3\}-(2c^2-1)/(20c^4).$$

$$n=1 : \quad (10c^2-2) \log \{(1+c)/c\}+5+1/6c^2-10c-4/\{3(1+c)\}.$$

$$n=5/4 : \quad 10c^2+1/2c-5c-8/3-(10c^3-6c) \log \{(1+c)/c\}.$$

$$n=3/2 : \quad (5c^4-6c^2+1) \log \{(1+c)/c\}+5c^2/2+13c/3-5c^3-7/4.$$

$$\S 4. \quad \int_0^1 \frac{u^2(1-u^2)^2/(u+c)^{5-4n}}{du}.$$

$$n=0 : \quad (64c^3+69c^2+30c+5)/\{840c^6(1+c)^6\},$$

$$n=1/4 : \quad (8c^2+5c+1)/\{105c^5(1+c)^5\},$$

$$n=1/2 : \quad \log \{(1+c)/c\}-(4c^2-1)/(60c^4) \\ -(30c^3+103c^2+122c+51)/\{30(1+c)^4\}.$$

Note added in proof.—Since this paper was written, the author has investigated the effect of changing the range in the case of the exponential potential to the value given by a recent analysis of the low-energy $p-p$ scattering data by Jackson and Blatt (1950). The values for the nuclear parameters are then :

$$(1/\kappa)=0.709 \times 10^{-13} \text{ cm.}, \quad A=173.0 \text{ MeV.}, \quad q=0.64.$$

The method of calculation of the triplet well depth is given by Blatt and Jackson (1949).

For H^3 the maximum value of $|E|$ is approximately 9.5 MeV., corresponding to $n \sim 0$ and $c = 0.72$, that is, $1/\alpha = 1.25 \times 10^{-13}$ cm. The binding energy of He^3 is then 8.5 MeV. Thus an excess binding energy is obtained in this case for the three-particle nuclei. The kinetic energy of H^3 is 39.7 MeV. For He^4 a binding energy of 47 MeV. is obtained, corresponding to $n \sim 0$, $c = 2.32$, that is, $1/\alpha = 0.864 \times 10^{-13}$ cm., the Coulomb energy of 1.3 MeV. being taken into account. Thus the shorter range exponential potential of Jackson and Blatt yields a much greater excess binding energy for the α -particle than the range used by Rarita and Present. The excess is in fact comparable to that obtained for the Yukawa potential. The kinetic energy of 106.2 MeV. obtained for the α -particle for this case is much more reasonable than the value given by the Yukawa potential.

REFERENCES.

- BLATT, J. M., and JACKSON, J. D., 1949, *Phys. Rev.*, **76**, 18.
 BROWN, F., 1939, *Phys. Rev.*, **56**, 1107.
 CLAPP, R. E., 1949, *Phys. Rev.*, **76**, 873.
 FESHBACH, H., and RARITA, W., 1949, *Phys. Rev.*, **75**, 1384.
 FRÖHLICH, H., HUANG, K., and SNEDDON, I. N., 1947, *Proc. Roy. Soc. A*, **191**, 61.
 GERJUOY, E., and SCHWINGER, J., 1942, *Phys. Rev.*, **61**, 138.
 HU, T., and HSU, K., 1950, *Phys. Rev.*, **78**, 633.
 JACKSON, J. D., and BLATT, J. M., 1950, *Rev. Mod. Phys.*, **22**, 77.
 RARITA, W., and PRESENT, R., 1937, *Phys. Rev.*, **51**, 788.
 ROSENFELD, L., 1948, *Nuclear Forces*. North-Holland Publishing Company (Amsterdam).
 SVARTHOLM, N., 1945, *The Binding Energies of the Lightest Atomic Nuclei*. Thesis (Lund).
 TOLLESTRUP, A. V., *et al.*, 1949, *Phys. Rev.*, **75**, 1947.

XLI. *The Equilibrium of Linear Arrays of Dislocations.*

By J. D. ESHELBY, F. C. FRANK,

H. H. Wills Physical Laboratory, University of Bristol,

and F. R. N. NABARRO,

Department of Metallurgy, University of Birmingham*.

[Received February 1, 1951.]

ABSTRACT.

A method is given for finding the equilibrium positions of a set of like dislocations in a common slip-plane under the influence of a given applied stress. Their positions are given by the roots of a certain set of orthogonal polynomials. The case of a set of free dislocations piled up against a fixed dislocation by a constant applied stress is discussed in detail and the resulting stress-distribution is compared with that produced by a crack with freely slipping surfaces.

§1. INTRODUCTION.

THE following problem (Frank 1951, Kuhlmann 1951, Nabarro 1951) arises in interpreting the plastic behaviour of solids in terms of dislocations. A set of identical dislocations lie in the same slip-plane. What positions will they take up under the combined action of their mutual repulsions and the force exerted on them by a given applied shear stress, in general a function of position along the plane?

Since the dislocations (assumed to be of infinite length and parallel to one another) repel each other inversely as the distance between them the problem is unchanged if they are replaced by a set of line-charges and the applied stress is replaced by an electric field. This electrostatic problem was used by Stieltjes (1885) (*cf.* also Szegő 1939) to illustrate the properties of the zeros of orthogonal polynomials. In the present paper we show how the properties of the classical orthogonal polynomials may be used to discuss the dislocation problem.

Stieltjes solved the problem by minimizing the potential energy of the charges. We start from the idea of the force acting on a dislocation. The two methods are equivalent.

§2.

Suppose that there is an infinite straight dislocation parallel to the z -axis, having the plane $y=0$ as slip plane, and passing through the point $x=x_i$. Consider the shear stresses p_{xy} , p_{yz} in the slip-plane. If the

* Communicated by the Authors.

dislocation is of pure screw type $p_{xy}=0, p_{yz} \neq 0$. If it is of pure edge type $p_{xy} \neq 0, p_{yz}=0$. In either case the non-vanishing stress component which it produces at the point x in the slip-plane is

$$p = \frac{A}{x-x_i} \quad \dots \quad (1)$$

For a screw dislocation $A=A_s=\mu b/2\pi$ and for an edge dislocation

$$A=A_e=\mu b/2\pi(1-\sigma)$$

(Burgers 1939). Here μ is the shear modulus, σ is Poisson's ratio and b is the magnitude of the Burgers vector \mathbf{b} which gives the change of the displacement vector on passing once round the dislocation line. For an edge dislocation in an anisotropic material $A=Kb/2\pi$ where K is a certain function of the elastic constants (Eshelby 1949).

A screw dislocation is acted on by a force bp_{yz} per unit length, where p_{yz} is the total stress acting at its centre, excluding that produced by itself. Similarly an edge dislocation is acted on by a force bp_{xy} . If there are n dislocations at the points $x_1, x_2 \dots x_n$, all of the same type and each one is in equilibrium, the equations

$$\sum_{\substack{i=1 \\ i \neq j}}^n \frac{A}{x_j-x_i} + P(x_j) = 0, \quad j=1, 2, \dots, n \quad \dots \quad (2)$$

must hold. $P(x)$ is the appropriate component of the applied stress at the point x , i. e. the xy component for edge and the yz component for screw dislocations.

Equations (1) and (2) apply, more generally, to any set of parallel like dislocations lying in their common slip plane. If ψ is the angle between the line and Burgers vector of each dislocation, we then have

$$A=A_s \cos \psi + A_e \sin \psi,$$

$$P(x)=P_{yz}(x) \cos \psi + P_{xy}(x) \sin \psi,$$

since the screw and edge components interact independently with one another.

In all cases, therefore, the following condition must be satisfied at each dislocation: the component in the direction of \mathbf{b} of the traction on the plane $y=0$ due to the other dislocations and to the applied stress must vanish.

It will be convenient to choose the unit of stress so that $A=1$. The condition of equilibrium is then

$$\sum_{i \neq j} \frac{1}{x_j-x_i} + P(x_j) = 0, \quad j=1, 2 \dots n. \quad \dots \quad (3)$$

We may regard the x_i as the zeros of the polynomial

$$f = \prod_{i=1}^n (x-x_i). \quad \dots \quad (4)$$

f has the convenient property that its logarithmic derivative is equal to the stress due to all the dislocations :

$$\frac{f'}{f} = \sum_{i=1}^n \frac{1}{x-x_i}.$$

The stress when the j th dislocation is missing is

$$\frac{f'}{f} - \frac{1}{x-x_j}. \quad . \quad . \quad . \quad . \quad . \quad . \quad . \quad (5)$$

The value of this expression when $x=x_j$ is

$$\lim_{x \rightarrow x_j} \frac{(x-x_j)f'(x)-f(x)}{(x-x_j)f(x)} = \frac{1}{2} \frac{f''(x_j)}{f'(x_j)}, \quad . \quad . \quad . \quad . \quad . \quad (6)$$

by double differentiation of numerator and denominator.

The conditions (2) can thus be written

$$\left. \begin{aligned} f(x_j) &= 0 \\ \frac{1}{2} \frac{f''(x_j)}{f'(x_j)} + P(x_j) &= 0 \end{aligned} \right\} j=1, 2 \dots n. \quad . \quad . \quad . \quad . \quad . \quad (7)$$

Consider the differential equation

$$f''(x) + 2P(x)f'(x) + q(n, x)f(x) = 0. \quad . \quad . \quad . \quad . \quad . \quad (8)$$

Suppose that we can choose q so that this equation has a polynomial solution of the n th degree all of whose roots are real and distinct. Then if q does not have a pole at any of the roots the conditions (7) are satisfied and the problem is solved.

In the physical problem we may be interested in cases where certain of the dislocations are "locked" in fixed positions (Cottrell 1948). If a dislocation is locked at $x=x_\alpha$ we imply that it lies in a stress field $p(x) = \text{const.} \delta'(x-x_\alpha)$ where δ' is the derivative of Dirac's δ -function. The dislocation is in equilibrium at $x=x_\alpha$ where $p(x)=0$. Also, since $p'(x_\alpha)$ is negatively infinite, the equilibrium is stable and an added stress will shift the position of equilibrium only infinitesimally. The other dislocations are unaffected by $p(x)$. It is then convenient to omit $p(x)$ from the expression for the applied stress and to regard one of the dislocations as "locked" at the point x_α .

Suppose, then, that in addition to the n "free" dislocations there are locked dislocations at $x_{n+1}, x_{n+2} \dots x_v$. The equilibrium positions of the free dislocations are found by regarding the stresses produced by the locked dislocations as forming part of the applied stress, so that (8) becomes

$$f'' + 2 \left\{ P(x) + \sum_{\alpha=n+1}^v \frac{1}{x-x_\alpha} \right\} f' + q(n, x)f = 0. \quad . \quad . \quad . \quad (9)$$

In this case we expect q to have a pole at each x_α in order that f'/f shall not vanish there.

The solution will be of the form (4) and f'/f will give the stress due to the free dislocations alone. If we make the substitution

$$F(x) = f(x) \prod_{\alpha=n+1}^{\nu} (x-x_{\alpha})$$

(9) becomes

$$F'' + 2PF' + \frac{Q(n, x)}{\prod_{\alpha} (x-x_{\alpha})} F = 0, \quad \dots \dots \dots (10)$$

where

$$\frac{Q(n, x)}{\prod_{\alpha} (x-x_{\alpha})} = q(n, x) - 2P(x) \sum_{\alpha} \frac{1}{x-x_{\alpha}} - \sum_{\substack{\alpha, \beta \\ \alpha \neq \beta}} \frac{1}{(x-x_{\alpha})(x-x_{\beta})}$$

and α, β take the values $n+1, n+2 \dots \nu$. At the zeros $x_1, x_2 \dots x_n$ the conditions (7) are satisfied (free dislocations) whilst at the zeros $x_{n+1}, x_{n+2}, \dots x_{\nu}$ the last term in (10) has a finite value owing to the vanishing of a factor in the denominator, and the second of the conditions (7) (with F replacing f) is not satisfied (locked dislocations). F'/F is the stress produced by locked and free dislocations.

If a particular problem has been solved in this way it remains to verify that the arrangement of dislocations is stable. The condition for this is that the x -derivative of the total stress at the position of a free dislocation (excluding its own stress) shall be negative, i. e. that

$$\lim_{x \rightarrow x_j} \frac{d}{dx} \left\{ \frac{F'(x)}{F(x)} - \frac{1}{x-x_j} + P(x) \right\} < 0.$$

After some calculation this reduces to the condition that

$$I(x) \equiv Q - P^2 - P' > 0 \quad \dots \dots \dots (11)$$

for $x = x_1, x_2 \dots x_n$. $I(x)$ is the "invariant" of equation (10) which can be reduced to the form

$$v'' + I(x)v = 0 \quad \dots \dots \dots (12)$$

by the substitution

$$v = F \exp \left(\int P dx \right). \quad \dots \dots \dots (13)$$

v has the same zeros as F with possibly additional ones. A region in which $I < 0$ can usually be dealt with by the following argument. Suppose that v has a zero (which may be at infinity) in the region. Since v'' has the same sign as v the curve $v = v(x)$ is convex to the x -axis and there can be no other zero in the region. In particular, if $I < 0$ for $x > x'$ and $v \rightarrow 0$ as $x \rightarrow \infty$ then F can have no zero for $x > x'$.

It is easily seen that v'/v gives the total stress due to free and locked dislocations and the applied stress.

§ 3.

The general method will be illustrated by some cases of physical interest.

(i.) A row of n dislocations under zero applied stress, the outer two being locked at $x = \pm L$. If $L=1$, (9) becomes

$$f'' + 2 \left\{ \frac{1}{x-1} + \frac{1}{x+1} \right\} f' + q(n, x) f = 0,$$

or if we take

$$q = \frac{n(n-1)-2}{1-x^2},$$

$$(1-x^2)f'' - 4xf' + \{n(n-1)-2\}f = 0$$

which is satisfied by $f = P'_{n-1}(x)$, the first derivative of the $(n-1)$ th Legendre polynomial. Hence

$$f = P'_{n-1}(x/L), \quad F = (L^2 - x^2)f = P'_{n-1}(x/L)\sqrt{(L^2 - x^2)}.$$

In ordinary stress units the stress on one of the locked dislocations is

$$\pm AF''(1)/F'(1) = \pm \frac{1}{2}n(n-1)A/L.$$

The roots of f up to $n-1=8$ have been given by Kopal (1946).

(ii.) A row of n free dislocations with an applied stress proportional to x . Such a uniformly varying stress exists near the centre of a beam supported at the ends and uniformly loaded. We have $P = x(dP/dx)$ with dP/dx constant. The resulting force on a dislocation can be regarded as arising from a potential energy $V = -\frac{1}{2}bx^2(dP/dx)$. "Potential troughs" of this type may exist in real crystals owing to the presence of various defects (Mott and Nabarro 1948). If we choose $1/\sqrt{(dP/dx)}$ as the unit of length the equation for $F(=f)$ is

$$F'' - 2xF' + QF = 0.$$

If $Q=2n$, (10) is satisfied by the n th Hermite polynomial, $H_n(x)$. The invariant $I = 2n+1-x^2$ is positive if $|x| < \sqrt{(2n+1)}$ and negative otherwise. The reduced equation is satisfied by $v = H_n(x) \exp(-\frac{1}{2}x^2)$, so that by the argument following equation (13) all dislocations lie in the region $|x| < \sqrt{(2n+1)}$. (cf. also Appendix, § A2).

In ordinary units of length and stress

$$F = H_n \left\{ x \sqrt{\left(\frac{dP/dx}{A} \right)} \right\}$$

and all dislocations lie in the region

$$|x| < \sqrt{\left\{ \frac{(2n+1)A}{dP/dx} \right\}}.$$

(iii.) A set of $n-1$ free dislocations along the positive x -axis in equilibrium under the combined effect of a locked dislocation at the origin and a uniform stress tending to move them in the negative direction. This case is discussed in detail in § 4.

(iv.) Two locked dislocations as in (i.) with an applied stress as in (iii.). This leads to an equation occurring in the theory of the hydrogen molecular ion. There is an extensive literature (Wilson 1928, Teller 1930, Hylleraas 1937) but no general discussion of the polynomial solutions. As we should expect there are n polynomial solutions of order n , since we can put $0, 1, 2 \dots n$ dislocations in the interval $-L < x < L$ and the remainder in the interval $L < x$.

§ 4.

For case (iii.) above we have $P(x)$ constant and equal to say $-\tau_0$. Equation (8) becomes

$$f'' + 2(x^{-1} - \tau_0)f' + qf = 0,$$

If we take $1/2\tau_0$ as the unit of length and put $q = (n-1)/x$ this becomes

$$xf'' + (2-x)f' + (n-1)f = 0 \quad . \quad . \quad . \quad (14)$$

which is satisfied by the first derivative of the n th Laguerre polynomial, $L'_n(x)$. Thus in ordinary units of length and stress

$$f = L'_n(2\tau_0 x/A), \quad F = (2\tau_0 x/A) L'_n(2\tau_0 x/A).$$

The spacing of the dislocations is the same as that of the radial nodes of a hydrogen atom in the ns state.

The invariant of (14), $I = nx^{-1} - \frac{1}{4}$ is positive if $x < 4n$. The reduced equation is satisfied by $v = xL'_n(x) \exp(-\frac{1}{2}x)$ so that all zeros of f must occur for $x < 4n$. A lower bound for the greatest root is obtained in the Appendix, § A.1. Since

$$L'_n(x) = - \sum_{k=0}^{n-1} \frac{n! (-x)^k}{k! (k+1)! (n-k-1)!} \quad . \quad . \quad . \quad (15)$$

there are no negative roots.

When x is small compared with n we may neglect $\frac{1}{4}$ in comparison with n/x and the reduced equation $v'' + Iv = 0$ becomes

$$v'' + (n/x)v = 0$$

with the solution

$$v = \sqrt{x} \cdot J_1\{\sqrt{(4nx)}\} \quad . \quad . \quad . \quad (16)$$

so that near the origin the position of the i th dislocation is given by $x \cong j_i^2/4n$ where j_i is the i th zero of the Bessel function J_1 . The position of the free dislocation nearest to the locked dislocation is $x_1 \cong 3.67/n$. Since $j_i \cong \pi i$ for large i the number, i , of dislocations between the origin and the point x is

$$i \cong (2/\pi)\sqrt{(nx)}, \quad 1 \ll i \ll n.$$

Returning to ordinary units of stress and length in which x becomes $2\tau_0 x/A$ we have the following approximate results for large n :

L , the length of the slip plane occupied by dislocations

$$= 2nA/\tau_0 \quad . \quad . \quad . \quad (17)$$

the number of dislocations lying between 0 and x

$$= \frac{2}{\pi} \sqrt{\left(\frac{2n\tau_0 x}{A}\right)} \quad . \quad . \quad . \quad (18)$$

d , the distance between the locked and nearest free dislocation

$$= 1.84 A/n\tau_0 \quad . \quad . \quad . \quad (19)$$

The difference between the L of equation (17) and the true distance between the locked and furthest free dislocation, L' say, can be estimated from the inequality

$$1.47n^{-2/3} - 0.55n^{-5/3} < \frac{L-L'}{L} < 2.56n^{-2/3},$$

obtained by combining the result of § A.1 with an inequality given by Szegő (1939, equation 6.32.6). In what follows we shall refer to L (and not the accurate L') as the length of the row of dislocations. Equation (18) is true in the sense that if $1 \ll i \ll n$ the ratio of the right-hand side of (18) to the correct i approaches unity as n tends to infinity. Actually (18) is in error by a factor of only $4/\pi$ even if $i=n$ and in error by only one or two units for small i provided n is large. d must be larger than a few atomic distances if our results are to be valid, since the expression (1) is inaccurate very close to a dislocation. (Nabarro 1940).

If we move along the x -axis the discontinuity Δ in the displacement on crossing the slip plane changes by b each time a dislocation is passed. The curve $\Delta = \Delta(x)$ is thus stepped, but according to (17) and (18) it will approximate to the smooth curve

$$\Delta = \frac{2b\tau_0}{\pi A} \sqrt{(Lx)}, \quad (20)$$

provided n is large and we do not go too far from the origin.

From the coefficients of x^{n-1} and x^{n-2} in (16) we find $(2\tau_0/A)\Sigma x_i = n(n-1)$ so that the centre of gravity of the free dislocations is at the point $x = nA/2\tau_0 = \frac{1}{2}L$ whilst the centre of gravity of the n dislocations is at $x = (n-1)A/2\tau_0$. The coefficients of x and x^0 give $A\Sigma x_i^{-1} = (n-1)\tau_0$. According to (1) this is the stress at the locked dislocation produced by the free dislocations. The total stress on the locked dislocation is thus $n\tau_0$. This also follows from (14) which gives $f'(0)/f(0) = \frac{1}{2}(n-1)$ which must be multiplied by $2\tau_0$ to convert to ordinary units. Cottrell (1949) has already obtained this result by a virtual work argument.

The behaviour of the stress, τ , beyond the locked dislocation ($x < 0$) is also of physical interest (Frank 1951). To discuss it, it is convenient to reverse the sign of x so that the dislocations lie on the negative x -axis. The most important region is that in which x is of the order of L , or, in the reduced units in which $2\tau_0/A = 1$, $x \sim n$. In these units the solution (16) with the sign of x changed is

$$v = \text{const. } y I_1(y), \quad y = \sqrt{(4nx)}$$

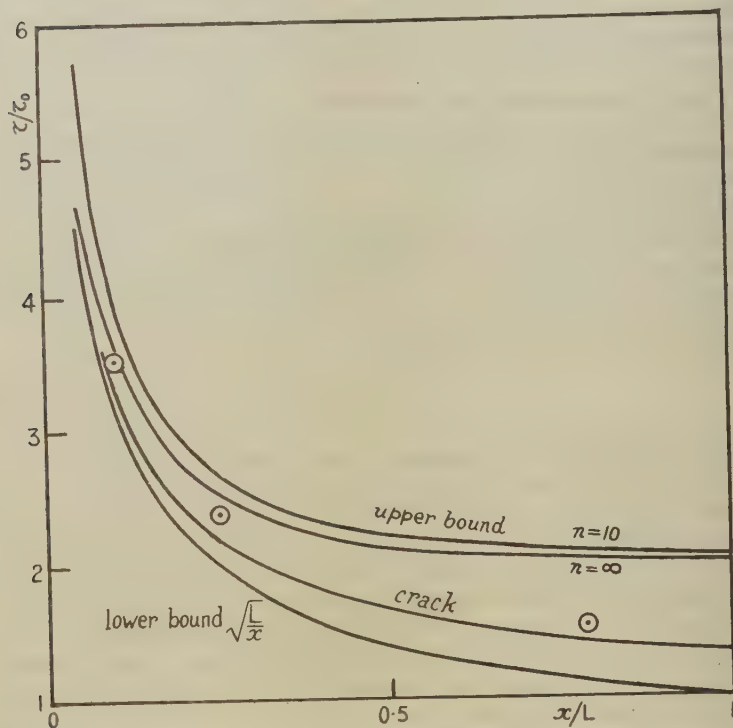
and this is a good approximation when $x \ll 4n$. The total stress is given by v'/v , for which we find

$$\frac{v'}{v} = \sqrt{\left(\frac{n}{x}\right)} \cdot \frac{I_0(y)}{I_1(y)}, \quad x \ll 4n.$$

From known properties of Bessel functions $I_0/I_1 \rightarrow 1$ as $y \rightarrow \infty$ and $I_0/I_1 \rightarrow 2/y$ as $y \rightarrow 0$ so that $v'/v = \sqrt{(n/x)}$ if $1/4n \ll x \ll 4n$ and $v'/v = 1/x$ if $x \ll 1/4n$ or in ordinary units

$$\begin{aligned} \tau/\tau_0 &= \sqrt{(L/x)}, \quad \frac{1}{15}d \ll x \ll L & \dots \dots \dots (21) \\ \tau &= A/x, \quad \frac{1}{15}d \ll x. \end{aligned}$$

Fig. 1.



Shear stress in front of a row of held-up dislocations. Upper and lower bounds from equations (22). ○ exact values calculated from the polynomial (15) for $n=10$. For comparison the stress due to a crack of length $4L$ is given, according to equation (24).

The last equation implies that the effect of the locked dislocation is dominant at points much closer to it than is the nearest free dislocation. It is shown in the Appendix, (§ A3) that

$$\left. \begin{aligned} \frac{\tau}{\tau_0} &= \sqrt{\left(\frac{L}{x}\right)} \cdot \left[1 + \theta \left\{ \frac{x}{L} + \frac{1}{2n} \sqrt{\left(\frac{L}{x}\right)} \right\} \right], \quad 0 < \theta < 1 \\ \text{and also} \quad \tau &> A/x, \quad \tau > \tau_0. \end{aligned} \right\} \dots \dots (22)$$

These relations enable us to set bounds to the departure of τ/τ_0 from the simple expression $\sqrt{(L/x)}$ for a given x ; see figs. 1 and 2.

For large x we have

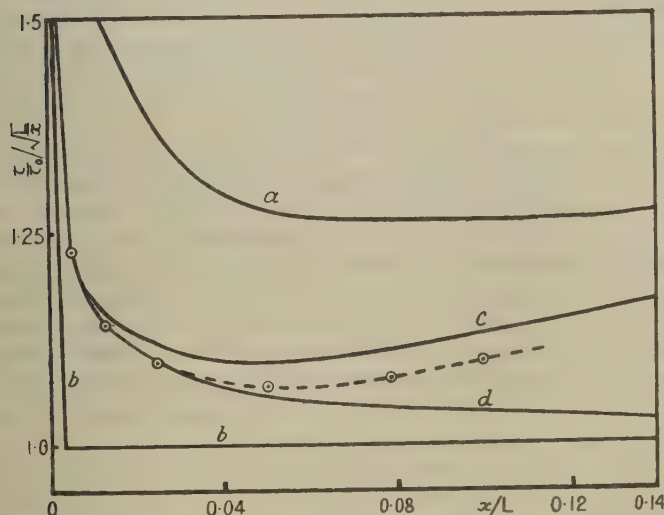
$$\tau = \tau_0 + nA/x \quad \text{or} \quad \tau/\tau_0 = 1 + \frac{1}{2}L/x, \quad x \ll L, \quad \dots \quad (23)$$

as can be seen from the inequality

$$\frac{nA}{x+L} < \frac{A}{x} + \sum_i \frac{A}{x+|x_i|} < \frac{nA}{x}$$

which follows from the facts that $0 < |x_i| < L$. Equation (23) shows that at large distances the stress is the sum of the applied stress and that due to all the dislocations regarded as congregated at the origin.

Fig. 2.



Shear stress in front of a row of ten held-up dislocations. a, b upper and lower bounds from equations (22). c, d upper and lower bounds from equation (a9) (Appendix, §A.3). \odot , accurate values calculated from the polynomial (15). The stress falls off monotonically with x : the convexity arises from plotting $\tau/\tau_0\sqrt{(L/x)}$ instead of τ/τ_0 .

Zener (1948) has compared a slip-band both to a crack and to an array of dislocations and it is interesting to compare the results of this section with those of Starr (1928) for a crack. He finds the following expressions for an infinitely narrow two-dimensional crack of length l extending along the x -axis from $x=0$ to $x=-l$ when the body containing it is subjected to a uniform applied shear stress $p_{xy} = \tau_0$. The stress in the plane $y=0$ beyond the tip of the crack is given by the exact formula

$$\frac{\tau}{\tau_0} = \frac{x + \frac{1}{2}l}{\sqrt{\{x(x+l)\}}} = \sqrt{\left(\frac{l}{4x}\right)} \cdot \left(1 + \frac{x}{l} - \frac{1}{2}\frac{x^2}{l^2} + \dots\right). \quad \dots \quad (24)$$

If the crack is not infinitely narrow but has a radius of curvature ρ at the end (24) is only correct if $x \gg \rho$. τ/τ_0 then reaches a maximum in the neighbourhood of $x = \rho$ and falls to zero at $x = 0$. We have

$$\tau/\tau_0 = 1 + \frac{1}{2}(l/2x)^2, \quad x \gg l \quad . \quad . \quad . \quad . \quad . \quad (25)$$

far from the crack.

The discontinuity in the displacement in crossing the x -axis, *i. e.* the relative displacement of the two faces of the crack, is given by the exact expression

$$\Delta = \frac{b\tau_0}{\pi A} \sqrt{\{l - |x|\} |x|}, \quad -l < x < 0$$

reducing to

$$\Delta = \frac{b\tau_0}{\pi A} \sqrt{l |x|}, \quad x < 0, \quad |x| \ll l \quad . \quad . \quad . \quad . \quad . \quad (26)$$

if we do not go too far from the tip of the crack.

The elastic constants have been expressed in terms of b and A (*cf.* equation (1)) to aid comparison, though of course the problem of the crack does not involve the Burgers vector. A is to be given its value for edge dislocations, $b\mu/2\pi(1-\sigma)$. It can be shown that the last four equations also apply to a crack in an anisotropic medium if we give A the value $bK/2\pi$. They also cover the case of a crack in an isotropic body in a state of anti-plane strain with τ_0 and τ representing the yz stress component provided we put $A = b\mu/2\pi$, the value appropriate to screw dislocations. Consequently these equations can be used to compare a crack under plane strain or anti-plane strain with an array of edge or screw dislocations respectively.

Comparison of (22) and (24) or of (20) and (26) shows that over a certain range of x the row of dislocations of length L simulates a crack of length $4L$ (*cf.* fig. 1).

It will be noted that near the origin the stress produced by the dislocations and the crack with a finite curvature at the tip diverge in opposite directions from the value $\tau_0\sqrt{(L/x)}$.

From (23) and (25) it will be seen that for the dislocations $\tau - \tau_0$ falls off as x^{-1} at large distances, but for the crack as x^{-2} , that is, in the same way as for a group of positive dislocations near a group of an equal number of negative ones. It is also clear that the array of dislocations simulates only one end of the crack. These facts suggest that a better imitation of a crack would be given by the following sequence of dislocations: a locked positive dislocation, n free positive dislocations, n free negative dislocations, a locked negative dislocation. The free dislocations are prevented from coalescing by the applied stress and the locked dislocations prevent them from spreading and define the length of the equivalent crack (*cf.* Zener 1948, fig. 4). The method of the present paper is not capable of finding their equilibrium positions.

§ 5.

The polynomial F also has a physical interpretation for complex values of its argument. Let $Z=x+iy$. Then for a set of screw dislocations the displacement w and stresses at the point (x, y) are given in the isotropic case by

$$\phi + iw = \frac{b}{2\pi} \log F(Z),$$

$$p_{yy} + ip_{xx} = \frac{\mu b}{2\pi} \frac{F'(Z)}{F(Z)}.$$

ϕ is the electrostatic potential in the corresponding Stieltjes line-charge problem. These results follow from the fact that for a single screw dislocation at the origin $w = (b/2\pi) \tan^{-1}(y/x)$.

For an array of edge dislocations the results are less simple since problems in plane stress or strain cannot be solved in terms of a single complex variable. We find for the isotropic case

$$(p_{xx} + p_{yy}) + 2i\mu\varpi/(1-\sigma) = -2iG'$$

$$p_{xy} + \frac{1}{2}i(p_{xx} - p_{yy}) = G' + iyG''$$

where

$$G(Z) = A \log F(Z), \quad A = \mu b/2\pi(1-\sigma)$$

and ϖ is the rotation. The results follow from the value $\chi = -Ay \log r$ of the Airy function for an edge dislocation at the origin (Koehler 1941).

ACKNOWLEDGMENTS.

Our thanks are especially due to Professor H. Heilbronn, who first indicated to us the connection between a set of algebraic equations of the form (2) and a differential equation of the form (8) upon which the whole analysis is based. He also obtained the important inequality of § A.1. We wish to thank Dr. C. S. Davis for much assistance and Mr. K. M. Baird for stimulating discussion.

APPENDIX.

§ A.1.

The reduced equation for the problem of § 4 is

$$v'' + \left(\frac{n}{x} - \frac{1}{4}\right)v = 0. \quad \dots \dots \dots (a1)$$

Let $X = x_{n-1}$ be the greatest root of v . We can arrange that $v > 0$ for $x > X$. Choose a constant $\xi > X$. We can write (a1) in the form

$$v'' + \lambda^2 v = g(x) \quad \dots \dots \dots (a2)$$

where

$$\lambda^2 = \left(\frac{n}{\xi} - \frac{1}{4}\right), \quad g(x) = n \left(\frac{1}{\xi} - \frac{1}{x}\right)v(x).$$

It is easily verified that v and v_1 agree in value and first derivative at the origin. Solving (a5) as an inhomogeneous equation in the usual way, making use of the relation

$$I_0 K_1 + K_0 I_1 = 1/y, \quad . \quad . \quad . \quad . \quad . \quad . \quad (a7)$$

we have

$$v = y I_1(y) + y \{ I_1(y) \mathcal{K} - K_1(y) \mathcal{J} \} / 8n \quad . \quad . \quad . \quad . \quad . \quad (a8)$$

with the abbreviations

$$\mathcal{J} = \int_0^x y' I_1(y') v(x') dx', \quad \mathcal{K} = \int_0^x y' K_1(y') v(x') dx', \quad y' = \sqrt{(4nx')}.$$

The term $y \{ \} / 8n$ vanishes with its first derivative at the origin so that solving the integral equation (a8) would give the exact solution (a6). Differentiating (a8) we have

$$v' = 2n I_0 + \frac{1}{4} (I_0 \mathcal{K} + K_0 \mathcal{J}).$$

If we write (a8) in the form

$$v = y I_1 / [1 - y (I_1 \mathcal{K} + K_0 \mathcal{J}) / 8nv]$$

we find, using (a7) again,

$$\frac{v'}{v} = \frac{2n I_0}{y I_1} \left(1 + \frac{\mathcal{J}}{v} \frac{1}{8n I_0} \right).$$

By finding upper and lower limits for \mathcal{J}/v we can give upper and lower limits for v'/v . The simplest approximation is the following. Since $v(x)$ is a monotonically increasing function of x

$$0 < \mathcal{J}/v < \int_0^x y' I_1(y') dx' = y^2 I_2(y) / 2n$$

and so, using the relation $y I_2 = y I_0 - 2 I_1$,

$$\frac{I_0}{I_1} < \frac{y}{2n} \frac{v'}{v} < \frac{I_0}{I_1} \left(1 + \frac{y^2}{16n^2} \right) - \frac{y}{8n^2}. \quad . \quad . \quad . \quad . \quad . \quad (a9)$$

This estimate could, of course, be improved. Using the recurrence relations for Bessel functions and the fact that, if $m < n$, I_m/I_n decreases monotonically to unity as y increases we find the following inequalities:

$$\frac{I_0}{I_1} > 1, \quad \frac{2}{y} < \frac{I_0}{I_1} < \frac{2}{y} + 1.$$

With the help of these we can derive from (a9) this weaker relation free from Bessel functions:

$$\max \left(\frac{2}{y}, 1 \right) < \frac{y}{2n} \frac{v'}{v} < 1 + \frac{2}{y} + \frac{y^2}{16n^2}.$$

The notation on the left implies that we are to choose the greater of $2/y$ and 1. Equation (22) in the text follows from the fact that

$$y = 4n\sqrt{(x/L)}, \quad yv'/2nv = \tau\sqrt{x}/\tau_0\sqrt{L}$$

in ordinary units.

REFERENCES.

- BURGERS, J. M., 1939, *Proc. Kon. Ned. Akad. v. Wet.*, **42**, 293.
- COTTRELL, A. H., 1948, *Report of a Conference on the Strength of Solids* (London : Physical Society), p. 30 ; 1949, *Progress in Metal Physics* (London : Butterworths Scientific Publications), p. 105.
- ESHELBY, J. D., 1949, *Phil. Mag.*, **40**, [7], 903.
- FRANK, F. C., 1951, Symposium on Plastic Deformation of Crystalline Solids, May 1950, Carnegie Institute of Technology, Pittsburgh (in the press).
- HYLLERAAS, E. A., 1937, *Ann. Inst. Henri Poincaré*, **7**, 121.
- KOEHLER, J. S., 1941, *Phys. Rev.*, **60**, 397.
- KOPAL, Z., 1946, *Astrophys. J.*, **104**, 61.
- KULHMANN, D., 1951, *Proc. Phys. Soc.*, **64**, 140.
- MOTT, N. F., and NABARRO, F. R. N., 1948, *Report of a Conference on the Strength of Solids* (London : Physical Society), p. 1.
- NABARRO, F. R. N., 1940, *Proc. Phys. Soc.*, **52**, 34 ; 1951, *Some Recent Developments in Rheology* (London : United Trade Press Ltd., for the British Rheologists' Club), p. 38.
- STARR, A. T., 1928, *Proc. Camb. Phil. Soc.*, **24**, 489.
- STIELTJES, T. J., 1885, *Acta Math.*, **6**, 321.
- SZEGÖ, G., 1939, *Orthogonal Polynomials* (Amer. Math. Soc. Colloquium Publications, **23**), p. 136.
- TELLER, E., 1930, *Z. Phys.*, **61**, 458.
- WILSON, A. H., 1928, *Proc. Roy. Soc. A*, **118**, 617, 635.
- ZENER, C., 1948, *Fracturing of Metals* (Symposium, American Society for Metals, Cleveland, Ohio), p. 3.

XLII. *The Use of Plasticine Models to Simulate the Plastic Flow of Metals.*

By A. P. GREEN, B.A.,

British Iron and Steel Research Association, Sheffield,
Mechanical Working Division*.

[Received January 11, 1951.]

[Plates XV. & XVI.]

SUMMARY.

The behaviour of plasticine when permanently deformed is compared with that of an ideal metal, and the necessary conditions for similarity between their flow patterns are examined for flow in two and three dimensions. A brief account of the mechanical properties of plasticine includes a description of stress-strain curves obtained by compressing cylinders between lubricated plates at constant rates of loading. Plane strain experiments, using a plasticine model marked with a grid on a cross-section parallel to the plane of flow, are described, and photographs of the deformed grids are compared with theory. The processes thus examined were: extrusion through square and wedge-shaped dies; indentation of a plane surface by a single wedge and by a row of wedges; and compression of a narrow wedge by a flat die. The profile of a deep narrow block after a small indentation by a flat punch is also compared with theory. All these plane strain plasticine experiments agree well with theory. One experiment using a metal was performed—the compression of a narrow copper wedge by a smooth flat die. This copper wedge deformed in a similar way to the plasticine wedge.

§1. INTRODUCTION.

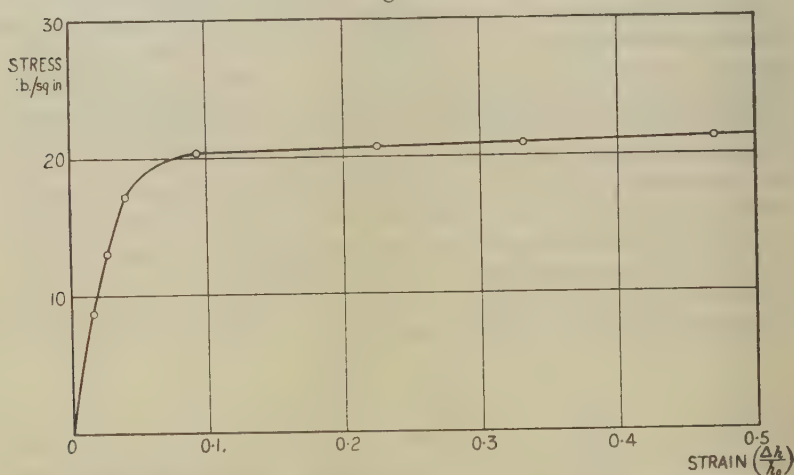
MANY metal working processes can be simulated by plasticine model experiments. The models are cheap and easy to make, and only a small amount of apparatus is needed. In the present paper an attempt is made to examine the mechanical properties that plasticine (or, indeed, any substance) should possess, in order that its manner of deformation should approximate to that of an ideal metal, for flow in two and three dimensions. That plasticine does in fact deform in a similar manner to an ideal metal, under conditions of plane strain, is shown by the close agreement between the model experiments described below and calculations made on the basis of existing theory for an ideal plastic-rigid non-hardening metal. There is no evidence, as yet, that this agreement will extend to flow in three dimensions. However, a model experiment should give a qualitative idea of the flow, provided the hydrostatic component of stress is compressive.

* Communicated by R. Hill.

§2. PROPERTIES OF PLASTICINE.

Plasticine is a mixture of an inert mineral oil, probably petroleum jelly, and a mineral filler, mainly calcite. Sometimes an organic dye is added. Its compressive stress-strain curves at three different rates of loading were found by compressing cylindrical specimens, $\frac{1}{2}$ -in high and 1-in. diameter, between the parallel plates of a beam test apparatus. During the course of compression the sides of the specimens became slightly concave. This effect was probably due to extrusion of the grease lubricant between the ends of the specimens and the compression plates. In all the stress-strain curves there is a sharp bend, after which the material deforms at an approximately constant stress. Unfortunately, the curves cannot be directly compared, because the temperatures at which the tests were carried out differed by 1–2° C. and the yield stress is very temperature dependent. A rise in temperature from 17° C. to

Fig. 1.



Stress-strain curve for plasticine under uniaxial compression.
Rate of loading 21.15 lbs.min.⁻¹. Temp. 21° C.

21° C. caused a decrease in yield stress of about 30 per cent. The curve for the rate of loading 21.15 lb./min.⁻¹ at 21° C. is shown in fig. 1. The curves for the two lower rates are similar, except that for strains greater than about 0.1, the small constant slope of the curve is greater. For the rates 21.15, 15.66, and 11.93 lb./min.⁻¹, the slopes are, approximately, 3.0, 4.0 and 4.5 lb./sq. in.⁻¹ respectively. The rates of loading were chosen to produce rates of strain comparable to those which occurred in the model experiments. If, at any stage of a compression test, loading is stopped and the load is kept constant, deformation continues at a rapidly decreasing rate becoming negligible after a few minutes. For example, at the end of a test where the rate of loading was 21.15 lb.min.⁻¹,

the load was kept constant, and after one minute the strain had increased from 0.51 to 0.53; after a further ten minutes it was 0.54 and over the next sixteen hours it increased to 0.55. Provided air bubbles are removed by working the material, its permanent compressibility is negligible. This was checked by weighing cylindrical specimens in water before and after 50 per cent compression. The change in volume was always less than 0.2 per cent.

There appears to be no generally accepted explanation of the stress-strain properties of plasticine. It is possible that friction between the mineral particles embedded in the petroleum jelly prevents continuous flow until a critical shear stress is reached. There may be, in addition, electrostatic forces between the particles, as has been suggested for clay and paints (Houwink 1937).

§3. COMPARISON OF PLASTICINE AND METAL.

It might appear surprising that close comparison is possible between the deformation of plasticine and that of a metal. It will now be shown why this comparison is possible under conditions of plane strain. Consider plastic flow in plane strain, where plastic strains are large, and the freedom of movement of the material in plastic flow is not constrained completely by material still elastic. Under these conditions of pure shear, plasticine behaves like a non-hardening isotropic metal, provided the flow is slow, so that it can be treated as quasi-static. This is because any element of either material deforms in shear under an approximately constant stress; both are virtually incompressible; and their principal axes of stress and strain-increment coincide. The last property must be true of any isotropic body for which the ratios of the plastic strain-increment components depend only on the ratios of the current stress components, and not on the previous stress or strain history. This can be expected on physical grounds, if, after deformation, the new random arrangement of the mineral particles is indistinguishable from the original one, so that there is no "memory" of past deformations. This appears to be true for plasticine judging by the agreement between theory and experiment. The precise degree of similarity between the plasticine and the metal flow patterns depends, of course, on how closely the shapes of the respective shear stress-strain curves correspond.

The equations governing the plane plastic strain of an ideal non-hardening metal were originally derived by Hencky (1923), (stress equations), and Geiringer (1930), (velocity equations). The theoretical flow patterns given in this paper were calculated on the basis of this theory. The flow patterns for plasticine can be expected to differ in the region of small strains from the calculated patterns, because its yield point is not quite sharp, nor, of course, is it rigid before yielding.

It is not known how closely plasticine will correspond to a non-hardening metal in three-dimensional plastic flow, since no experiments have yet been made. If good agreement is to be obtained, the yield criterion for

plasticine must approximate closely to that of the metal; for many metals, the Mises criterion is a good approximation. In addition, the relation between Lode's variables for stress and strain-rate must be the same for the two materials. For a Newtonian viscous fluid Lode's variables are equal; this is also a good approximation for many metals (Hill 1950).

§4. EXPERIMENTAL DETAILS.

Stone-coloured plasticine, containing no dye, was used for most of the experiments. After carefully working the plasticine by hand to eliminate air bubbles, the specimens were cut to shape with a fine wire. Each specimen was made in two halves, $\frac{1}{4}$ -in. thick. On the inner face of one half a $\frac{1}{10}$ -in. square grid was lightly stamped in ink. French chalk was used to prevent the two halves sticking when placed together. After deformation between parallel lubricated constraints, the two halves could be easily separated and the deformed grid photographed. If it is inconvenient to have the specimen in two halves, either the grid must be ruled on an outer face, or the model may be built up in layers, using two different colours of plasticine (see expt. 5 below). Unfortunately it is difficult to find different colours with exactly the same mechanical properties. Medium grease was used for the lubrication of external surfaces.

§5. COMPARISON OF THEORY AND EXPERIMENT.

With one exception, the following experiments were carried out under conditions of plane strain, using plasticine models. The exception is the compression of a narrow wedge of annealed copper by a smooth flat die (see expt. 6).

(1) Direct extrusion through a square die with 66.7 per cent reduction (figs. 2a and b, Pl. XV.).

(a) Full friction at the container walls.

The container was lined with emery paper to ensure that the friction was sufficiently high to cause local yielding of the plasticine at the walls. The distortion of a square grid was calculated, using the slip line field given by Hill (1948 a) for direct extrusion. It is particularly interesting that the observed region of dead plasticine agrees well with that *assumed* in the theory.

(b) Smooth container walls and die face.

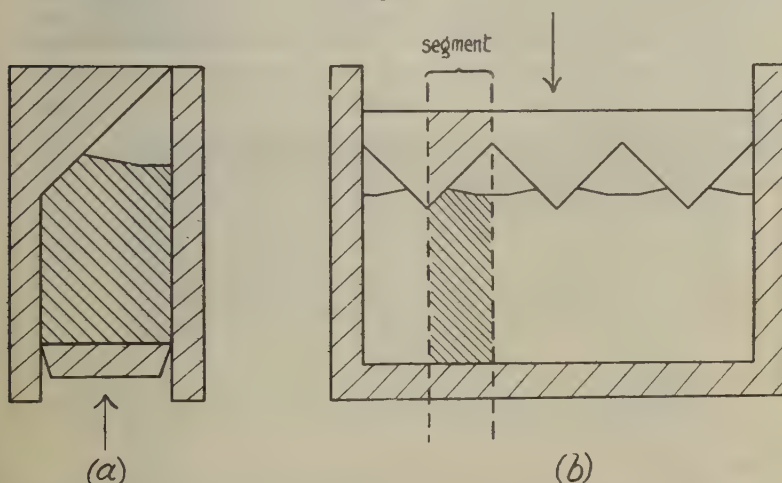
The slip-line field is an extreme case of the one given by Hill (1948 a) for extrusion through a smooth wedge-shaped die (the die-angle here being 90°). In the theory it is assumed that there is no dead region, but in practice lubrication was not quite perfect, and it was impossible to avoid a small dead region in the corner, which modified the flow pattern. The cusps on the centre line in the theoretical pattern are a result of the tangential velocity discontinuities across the entry and exit slip lines. In practice, since the yield point of plasticine is not sharp, there is a region of rapid shear instead of a velocity discontinuity, and the cusps and sharp

corners in the flow lines are rounded off. The experimental and theoretical grids are out of step, because the actual moment of comparison was not the same.

(2) Direct extrusion through a smooth wedge-shaped die ; semi-angle of die 15° ; 34 per cent reduction (fig. 3, Pl. XV.).

The slip-line field for this problem (Hill 1948 a) is the same as that found for the plane strain problem of sheet drawing. The latter problem is dealt with in a paper by Hill and Tupper (1948), and the theoretical distortion of a square grid is taken from that paper. The theoretical region of uniform motion is well demonstrated in the experimental pattern. The squares become parallelograms, in this special configuration, due to a single line of shear at entry ; the preservation of the parallelograms indicates uniform flow. The boundary of the region of large plastic

Fig. 8.



(a) Diagram of the experimental arrangement for wedge indentation and coining.
(b) Segment of the coining process.

strains, defined by the sharp bends in the longitudinal flow lines, agrees well with theory. There is again a rounding off of cusps and sharp corners. The slope of the straight sections of the deformed transverse lines is greater than in theory, probably due to friction at the die face.

(3) Indentation of a plane surface by a smooth wedge of semi-angle 50° (fig. 4, Pl. XV.).

The distortion of a square grid was calculated according to the theory given by Hill, Lee and Tupper (1947), who computed one for a wedge of semi-angle 30° . The wider semi-angle of 50° was chosen for this experiment because the region of non-uniform motion is larger, and a clearer comparison can be made with the theory. It is difficult in practice to obtain good lubrication using a full wedge. Instead, therefore, a rectangular block,

constrained between two parallel lubricated guides was compressed against an oblique face (fig. 8 *a*). This face represented half a wedge, and one of the guides replaced the line of symmetry through the apex of the wedge. It is assumed that the slip-line field and velocity solution are the same as for one half of the field of a full wedge, so long as there still remains a part of the original surface undeformed. The stresses in the plastically deforming region differ only by the addition of a hydrostatic pressure due to the lateral constraint of the guides. The oblique face was removed and re-lubricated intermittently, but there still remained an appreciable amount of friction due to newly sheared plasticine being continually presented to the face, both at the tip of the half wedges and the apex of the plasticine lip. Calculations by Hill (1950, unpublished) show that the effect of friction is to lessen the slope of the lip which, however, remains straight if the friction is uniform. By comparing measurements on the experimental block with the theory, the mean coefficient of friction was deduced to be approximately 0.3. This high value appears reasonable in view of the breakdown of lubrication which occurs for the reason already explained. The curvature of the surface near the apex of the lip is, no doubt, partly due to uneven friction, and partly to strain hardening.

(4) Indentation of a plane surface by a row of smooth wedges of semi-angle 45° (fig. 5, Pl. XVI.).

EXPLANATION OF THE PLATES.

PLATE XV.

Fig. 2.

Direct extrusion of plasticine through a square die with 66.7 per cent reduction. (*a*) Perfect friction; (*b*) Smooth.

Fig. 3.

Direct extrusion of plasticine through a smooth wedge-shaped die with 34 per cent reduction; total die angle 30° .

Fig. 4.

Indentation of a plane plasticine surface by a smooth 100° wedge.

PLATE XVI.

Fig. 5.

Three stages in a plasticine coining process using smooth 90° wedges: Ratios of depths of indentation to width of specimen. (*a*) 0.3, (*b*) 0.42, (*c*) 0.5.

Fig. 6.

Compression of a 40° plasticine wedge by a smooth flat die.

Fig. 7.

Compression of a 34° annealed copper wedge by a smooth flat die.

(*a*) Vertical section.

(*b*) View from above showing compressed surface.

Fig. 2.

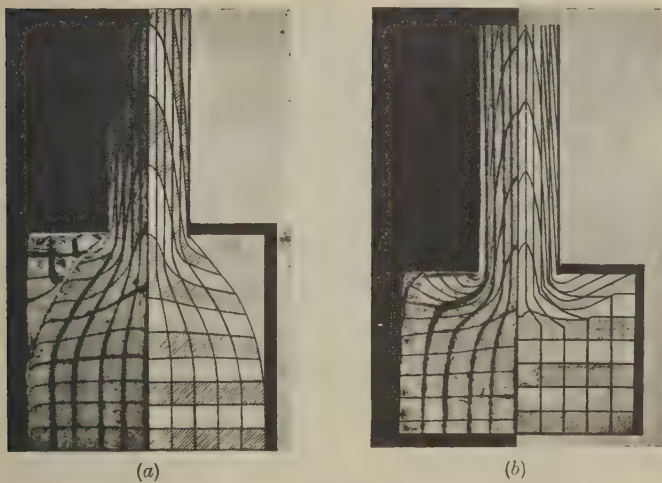


Fig. 3.

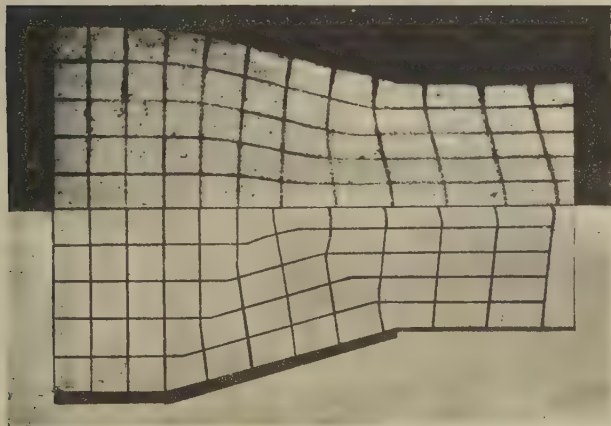
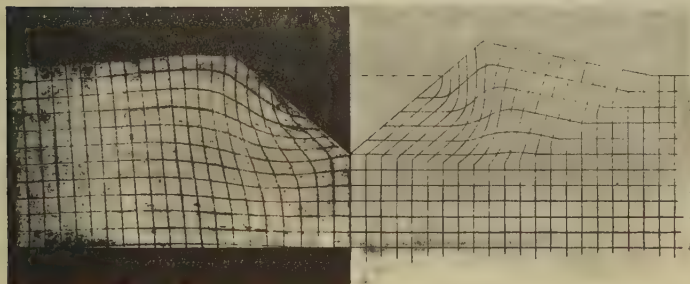


Fig. 4.



To face page 370

Fig. 5.



Fig. 6.

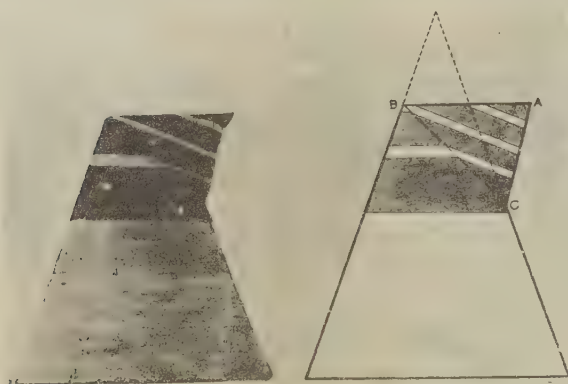
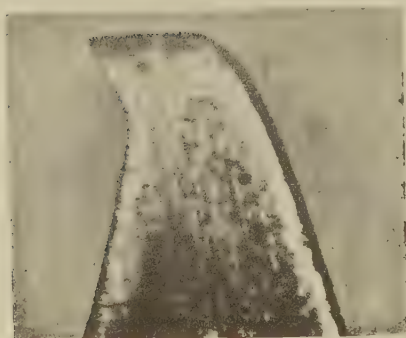


Fig. 7.



(a)



(b)

This may be regarded as a process of coining. A block is constrained on all faces, except the surface which is to be indented. The flow pattern can be split up into exactly similar segments between the planes of symmetry through the angles of the wedges (fig. 8 b). Each of these segments is identical with that for half-wedge indentation, described in the previous section, and the experiment can, therefore, be carried out in a similar manner. In this case, however, compression was continued, until the specimen was completely "coined". After the region of deformation has reached the line of symmetry between adjacent wedges, (*i. e.* the outer guide), the configuration is no longer geometrically similar. The slip-line field is then continually changing and no theoretical solution has yet been found. It is interesting to see that there is little deformation below the tip of the wedge.

(5) Compression of a 40° wedge by a smooth flat die (fig. 6, Pl. XVI.).

The model was made of layers of two different colours. The mode of deformation shown in fig. 6 (Pl. XVI.) is one of the ways in which a narrow wedge can deform. The observed deformation suggested the following theory. It appears that a simple shear takes place along a single moving slip-line, BC, which makes an angle of 45° with the smooth die. Any element of the wedge remains stationary until reached by the moving slip-line. It then shears instantaneously, and continues to move as part of the rigid body ABC, parallel to BC. If angle ACB were less than 45° , the material in ABC would be unable to support the calculated forces on BC. This restricts the range of validity of the solution to wedge angles less than 45° . The experimental pattern agrees well with this theory. The bends in the deformed layers are sharp and lie on a straight line which makes an angle of 43° with the die face.

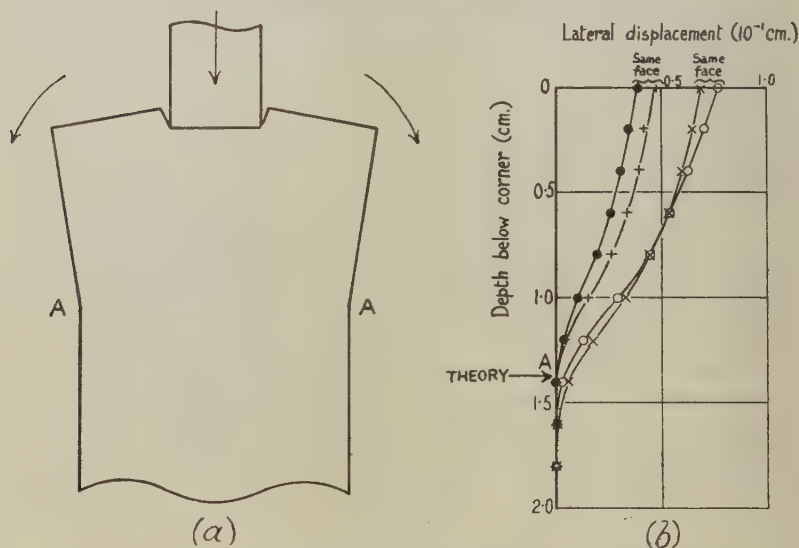
Other experiments were attempted with wider angle wedges but it was difficult to obtain consistent results because of varying friction conditions at the die face. Two possible symmetrical solutions have been suggested by Hill (1948 b). In one of these a steadily increasing wedge-shaped region of material is carried down with the die. This type of solution tends to occur when lubrication is poor, since it involves no relative motion between the die and the plasticine surface in contact with it. It is valid for wedge angles greater than $28^\circ 4'$. When lubrication is good the other type of solution, which is valid for wedge-angles greater than $53^\circ 12'$, is sometimes observed. The wedge gradually divides down the centre; newly sheared plasticine is continually presented to the die face from the centre and is then displaced outwards towards the sides. Sometimes a wedge will change its mode of deformation as frictional conditions alter.

(6) Compression of a 34° annealed copper wedge by a smooth flat die (figs. 7 a and b, Pl. XVI.).

The wedge was not constrained at its ends, but towards the centre conditions approximated to plane strain, since the ratios of depth of compression to the dimensions of the wedge were small. Initially, the

wedge was 0.75 in. high and 1.36 in. long. It was compressed through 0.1 in., in six stages, between polished plates made of sintered hard metal, which were lubricated intermittently with calcium oleate. There was no deformation at the base, but the length of the top of the wedge increased by 0.06 in. After compression the wedge was sectioned vertically (*i. e.* along a plane perpendicular to its length), 0.35 in. from one end (fig. 7 *a*, Pl. XVI.). It can be seen that its mode of deformation was similar to that shown in fig. 6. Although work-hardening broadened the single slip line, BC, into a region of rapid shear, the final shape of the section, except for the rounded corners, agrees well with the theory for an ideal metal. Initially, some vertical sections of the wedge commenced to shear to one side and some to the other, while some sections even

Fig. 9.



Indentation of a narrow plasticine block by a smooth flat punch.

- (a) Diagram showing nature of initial deformation (exaggerated);
 (b) Profile of block after indentation.

deformed symmetrically. Viewed from above, the compressed surface zig-zagged along its length. As compression continued, the longer unsymmetrical sections began to carry the other sections with them. Finally, half the wedge was shearing to one side and half to the other (fig. 7 *b*, Pl. XVI.).

(7) Indentation of a deep narrow block by a smooth flat punch*.

* The theory has been worked out by R. Hill (1950) and I quote, by kind permission, from his as yet unpublished results.

With a sufficiently narrow block, the plastic region spreads out to the sides as the load is increased, and the initial deformation of the corners is a rotation outwards (fig. 9 *a*). The rotation on each side takes place along a curved slip line which meets the side of the block at a point, A, whose position can be calculated. A plasticine block, $\frac{3}{4}$ -in. wide, was indented to a depth of $\frac{1}{25}$ -in. by a flat lubricated punch $\frac{1}{4}$ -in. wide. After indentation the shapes of the lateral faces of the block were plotted with a travelling microscope. The occurrence of a rigid-body rotation and the position of A agreed well with theory (fig. 9 *b*).

§ 6. CONCLUSION.

Under conditions of plane strain, agreement with theory has been shown to be encouragingly good. It is planned to extend these experiments to other processes, and also to measure the applied loads. This should provide an additional test of the similarity between plasticine and an ideal metal. Similar experiments using a metal such as pre-strained copper are desirable for further comparison with theory and with plasticine. An experiment in which lead blocks were indented by steel wedges coated with vaseline is described in the paper on wedge indentation (Hill, Lee and Tupper 1947). When the theory is not known, a plasticine experiment may assist in finding a solution (for example, see expt. 5).

ACKNOWLEDGMENTS.

The author is greatly indebted to Dr. R. Hill for his help and counsel during this work. He would also like to thank his colleagues Mr. F. Carr for the photography and Mr. G. Douglass for the calculation of the theoretical flow patterns shown in figs. 2 *a* and 4. He thanks the Director of the British Iron and Steel Research Association for permission to publish this paper.

REFERENCES.

- GEIRINGER, H., 1930, *Proceedings of the Third International Congress for Applied Mechanics* (Stockholm), 2.
HENCKY, H., 1923, *Zeits. f. Math. Mech.*, **3**, 241.
HILL, R., 1948 *a*, *J. Iron & Steel Inst.*, **158**, 182; 1948 *b*, *Proceedings of the Seventh International Congress for Applied Mechanics* (London).
HILL, R., LEE, E. H., and TUPPER, S. J., 1947, *Proc. Roy. Soc. A*, **188**, 273.
HILL, R., and TUPPER, S. J., 1948, *J. Iron & Steel Inst.*, **159**, 359.
HILL, R., 1950, *The Mathematical Theory of Plasticity*, pp. 44-5. (Oxford : Clarendon Press.)
HOUWINK, R., 1937, *Elasticity, Plasticity and Structure of Matter*. (Cambridge : Cambridge University Press.)

XLIII. *Collective Electron Ferromagnetism: Rectangular Energy Bands.*

By E. P. WOHLFARTH, Ph.D.,

Department of Mathematics, Imperial College, London*.

[Received January 18, 1951.]

SUMMARY.

Calculations similar to those of Stoner (1938, 1939) are carried out for an energy band for which the energy density of states is constant. These have a bearing on calculations of the actual band form for nickel (Fletcher and Wohlfarth 1951). After brief reference to previous work and a statement of the basic assumptions of the treatment, relations are derived giving the dependence on temperature and the interchange interaction energy of the spontaneous magnetization below and the susceptibility above the Curie point. Various explicit limiting relations are deduced. The numerical results of the calculations are given in Table I. and fig. 1 (§2). Formulæ are also derived which give the internal energy and specific heat over the whole temperature range. Relations are given for the most important experimentally observable thermal characteristics, such as the specific heat discontinuity at the Curie point. The results are shown in figs. 2 and 3 (§3). Experimental results which are briefly discussed (§4) include those on the magnetic properties of nickel and its alloys and the thermal properties of nickel, including the energy and specific heat characteristics, the temperature variation of specific heat and the magneto-caloric effect. The high temperature specific heat of paramagnetics is also discussed. In an Appendix certain results for an energy band of more general form are given.

§1. INTRODUCTION.

THE collective electron treatment of ferromagnetism was originally developed by Stoner (1938 a, 1939, 1948, 1951) for an energy band of standard form, for which the energy density of states is proportional to the square root of the energy. In the present paper similar calculations are carried out for an energy band for which the density of states is constant. Consideration of this problem arose mainly as a result of calculations, which are still proceeding, aiming at a determination of the actual band form for nickel. Preliminary results of these calculations (Fletcher and Wohlfarth 1951) indicate that the actual band form near the top of the band is almost certainly intermediate between that assumed by Stoner and that considered here. A comparison of the two sets of theoretical results serves to show to what extent discrepancies between theory and experiment are due to the assumption of a particular band form and to what extent

* Communicated by the Author.

Fundamental relations. With the above assumptions a development of the statistical treatment (Stoner 1938a) leads to the following expressions for ζ as a function of temperature, T , and applied field, H :

$$\left. \begin{aligned} \zeta &= \frac{1}{2} \frac{kT}{\epsilon_0} \{F_0(\eta + \beta + \beta') - F_0(\eta - \beta - \beta')\}, \\ 1 &= \frac{1}{2} \frac{kT}{\epsilon_0} \{F_0(\eta + \beta + \beta') + F_0(\eta - \beta - \beta')\}. \end{aligned} \right\} \dots (2.3)$$

Here η is related to the chemical potential, ξ , by $\eta = \xi/kT$ and $\beta = k\theta'\zeta/kT$, $\beta' = \mu H/kT$. The function F_0 is the Fermi-Dirac integral of zero order which may be evaluated exactly,

$$F_0(\eta) = \int_0^\infty \frac{dx}{\exp(x - \eta) + 1} = \ln(1 + e^\eta). \dots (2.4)$$

In the absence of an applied field manipulation of (2.3) and (2.4) gives an implicit relation for spontaneous magnetization in the form

$$\frac{k\theta'}{\epsilon_0} = \frac{\tau}{2\zeta} \ln \left\{ \frac{\exp[(1 + \zeta)/\tau] - 1}{\exp[(1 - \zeta)/\tau] - 1} \right\}, \dots (2.5)$$

where $\tau = kT/\epsilon_0$. Two useful alternative relations may be obtained:

$$\frac{k\theta'}{\epsilon_0} - \frac{1}{2} = \frac{\tau}{\zeta} \tanh^{-1} \{ \tanh(\zeta/2\tau) / \tanh(1/2\tau) \}, \dots (2.6)$$

$$\frac{k\theta'}{\epsilon_0} - 1 = \frac{\tau}{\zeta} \sinh^{-1} \{ \exp(-1/\tau) \sinh \beta \}, \dots (2.7)$$

where $\beta = (k\theta'/\epsilon_0) \zeta/\tau$. The Curie temperature, θ , is given by

$$\left. \begin{aligned} \frac{\epsilon_0}{k\theta} &= -\ln \left(1 - \frac{\epsilon_0}{k\theta'} \right), \\ \text{or inversely} \quad \frac{\epsilon_0}{k\theta'} &= [1 - \exp(-\epsilon_0/k\theta)]. \end{aligned} \right\} \dots (2.8)$$

The inverse of the susceptibility above the Curie point, χ , is given by (2.3) and (2.4) as

$$\frac{1}{\zeta} \frac{\mu H}{\epsilon_0} = \frac{1}{\chi} \frac{N\mu^2}{\epsilon_0} = [1 - \exp(-1/\tau)]^{-1} - k\theta'/\epsilon_0, \dots (2.9)$$

if $\mu H/kT$ and ζ are small compared with 1.

Limiting relations. (i.) The limit $k\theta'/\epsilon_0 \rightarrow \infty$. Relation (2.8) shows that in this limit $\theta' \rightarrow \theta$ and hence, from (2.6), $\zeta = \tanh(\zeta\theta'/T)$, the classical Weiss relation for spontaneous magnetization. Relation (2.9) shows that in the same limit $\chi = N\mu^2/k(T - \theta)$, the Curie-Weiss law.

(ii.) *Condition for ferromagnetism.* *Relative magnetization at absolute zero.* Relation (2.8) shows the condition for ferromagnetism (finite spontaneous magnetization at absolute zero) to be $k\theta'/\epsilon_0 > 1$ and (2.5) shows that as soon as ferromagnetism occurs at all the relative magnetization at absolute zero,

ζ_0 , is unity. As shown in the Appendix (relation (A.8)), however, in a band of general form there is usually a range of values of $k\theta'/\epsilon_0$ over which, although ζ_0 is finite, it may be less than 1. For parabolic bands, for example, this range was shown by Stoner (1938 a, relation (5.10)) to be $\frac{2}{3} < k\theta'/\epsilon_0 < 2^{-1/3}$, the lower limit giving the condition for ferromagnetism in that case. In this respect, therefore, the rectangular band form with strictly constant density of states is a very special case.

(iii.) *Approach to saturation*, $kT/\epsilon_0 \rightarrow 0$. In this limit $\zeta \rightarrow \zeta_0 = 1$ and relation (2.5) gives the law of approach to saturation as

$$\zeta = 1 - \frac{kT}{\epsilon_0} \exp \left\{ -\frac{2\epsilon_0}{kT} \left(\frac{k\theta'}{\epsilon_0} - 1 \right) \right\}, \quad \quad (2.10)$$

analogous to Stoner's relation (1938 a, relation (5.21)) for parabolic bands in the range of values of $k\theta'/\epsilon_0$ for which $\zeta_0 = 1$. For parabolic bands, however, the law of approach takes the form $(\zeta/\zeta_0)^2 = 1 - \alpha(\zeta_0)(T/\theta)^2$ when $\zeta_0 < 1$, where α is in general close to 1 (Stoner 1938 a, relation (5.26))

(iv.) *Magnetization near the Curie point*, $T/\theta \rightarrow 1$. Relation (2.6) may be used to show that in the neighbourhood of the Curie point

$$\zeta^2 = 6k\theta/\epsilon_0 \tanh(\epsilon_0/2k\theta)(1 - T/\theta),$$

which, on transforming (2.8) into $\coth(\epsilon_0/2k\theta') = 2k\theta'/\epsilon_0 - 1$, gives

$$\zeta^2 = \frac{6k\theta/\epsilon_0}{2k\theta'/\epsilon_0 - 1} (1 - T/\theta). \quad \quad (2.11)$$

Relation (2.11) gives correctly the classical dependence of magnetization on temperature near the Curie point, $\zeta^2 = 3(1 - T/\theta)$ for $k\theta/\epsilon_0 \rightarrow \infty$, but shows that the slope of the ζ^2 , T/θ curve decreases as $k\theta/\epsilon_0$ decreases. In the limit $k\theta/\epsilon_0 \rightarrow 0$, $k\theta'/\epsilon_0 \rightarrow 1$, (2.11) becomes $\zeta^2 = 6k\theta/\epsilon_0 (1 - T/\theta)$.

Computations. Relation (2.5) was used to compute values of ζ for $T/\theta = 0.0$ (0.1) 0.9 (0.05) 1.0 and for $k\theta'/\epsilon_0 = 1.01$, 1.04, and 1.10, using a balancing method of solution. Since $\zeta_0 = 1$, ζ equals the usual reduced specific magnetization, σ/σ_0 . The range of values of $k\theta'/\epsilon_0$ covered is indicated by the susceptibility results to include practically all ferromagnetic metals and alloys. The susceptibility above the Curie point was calculated using relation (2.9) for $T/\theta = 1.0$ (0.2) 3.0 and the above 3 values of $k\theta'/\epsilon_0$, in the form

$$\frac{1}{\zeta} \frac{\mu H}{\epsilon_0} \frac{\epsilon_0}{k\theta} = \frac{1}{\zeta} \frac{\mu H}{k\theta} = \frac{\mu\sigma_0}{k\theta} \frac{1}{\chi},$$

which gives the classical curve as the straight line $(\mu\sigma_0/k\theta) 1/\chi = T/\theta - 1$. The final results are given in Table I. and fig. 1.

Fig. 1 also includes the values calculated by Stoner (1938 a) for parabolic bands with $k\theta'/\epsilon_0 = 2^{-1/3}$. The most marked difference between the results for ζ calculated for rectangular and for parabolic bands is that for the former the ζ , T/θ curves move downwards as $k\theta'/\epsilon_0$ decreases. For the latter (cf. Stoner 1938 a, fig. 5) the curves giving ζ/ζ_0 move downwards as

$k\theta'/\epsilon_0$ decreases to the lower limiting value ($2^{-1/3}$) for $\zeta_0=1$, but they actually move very slightly upwards as $k\theta'/\epsilon_0$ decreases further to the lower critical value $\frac{2}{3}$, mainly as a result of the simultaneous decrease of ζ_0 .

The susceptibility curves, on the other hand, have similar characteristics for both types of band form. The reduced curves move downwards as $k\theta/\epsilon_0$ decreases, coinciding with the T/θ axis as $k\theta/\epsilon_0 \rightarrow 0$ (cf. also Wohlfarth 1949a, fig. 9).

TABLE I. Spontaneous magnetization and susceptibility.

$k\theta'/\epsilon_0$	1.01	1.04	1.10	∞
$k\theta/\epsilon_0$	0.2167	0.3069	0.4170	∞
T/θ	Relative magnetization.			
0.0	1.0000	1.0000	1.0000	1.0000
0.1	0.9889	0.9976	0.9996	1.0000
0.2	0.9553	0.9799	0.9919	0.9999
0.3	0.9083	0.9468	0.9702	0.9974
0.4	0.8505	0.9003	0.9341	0.9856
0.5	0.7826	0.8410	0.8834	0.9575
0.6	0.7041	0.7679	0.8161	0.9073
0.7	0.6122	0.6780	0.7286	0.8286
0.8	0.5015	0.5638	0.6123	0.7104
0.9	0.3556	0.4058	0.4448	0.5254
0.95	0.2517	0.2897	0.3189	0.3795
1.0	0.0000	0.0000	0.0000	0.0000
Reduced inverse susceptibility.				
1.2	0.0546	0.1006	0.1363	0.2000
1.4	0.1312	0.2219	0.2879	0.4000
1.6	0.2271	0.3587	0.4501	0.6000
1.8	0.3388	0.5071	0.6199	0.8000
2.0	0.4638	0.6646	0.7952	1.0000
2.2	0.5995	0.8287	0.9748	1.2000
2.4	0.7439	0.9983	1.1577	1.4000
2.6	0.8955	1.1560	1.3429	1.6000
2.8	1.0533	1.3496	1.5303	1.8000
3.0	1.2157	1.5299	1.7193	2.0000

T/θ , reduced temperature. For $T/\theta < 1$ the figures give ζ , the relative magnetization. For $T/\theta > 1$ they give $(\mu\sigma_0/k\theta)(1/\chi)$, the reduced inverse mass susceptibility. The ζ values for $k\theta/\epsilon_0 = \infty$ are taken from Stoner (1938a, Table I.); the susceptibility values in this limit are given by

$$(\mu\sigma_0/k\theta)(1/\chi) = T/\theta - 1.$$

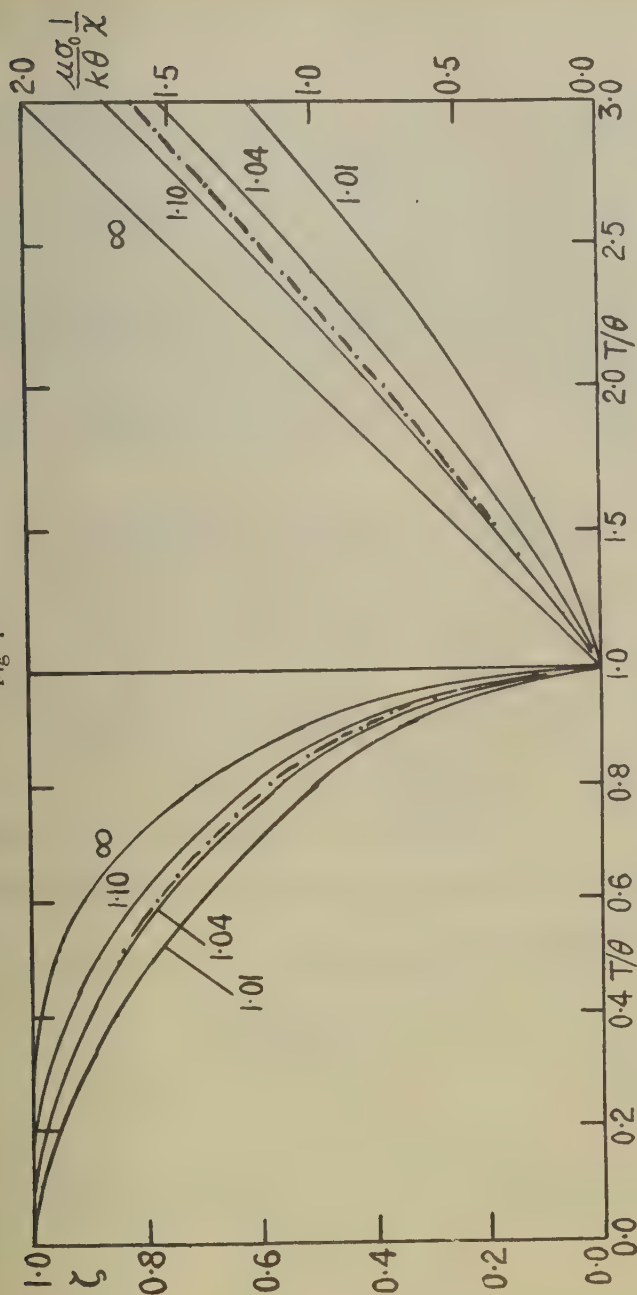
§3. THERMAL PROPERTIES.

Fundamental relations. With the basic assumptions as in §2 and Stoner's nomenclature (1939) the expressions for the reduced electronic and "molecular field" energies in the absence of an external field become

$$\frac{E_E}{N\epsilon_0} = \frac{1}{2} \left(\frac{kT}{\epsilon_0} \right)^2 \{F_1(\eta + \beta) + F_1(\eta - \beta)\}, \quad (3.1)$$

$$\frac{E_M}{N\epsilon_0} = -\frac{1}{2} \frac{k\theta'}{\epsilon_0} \zeta^2, \quad (3.2)$$

Fig. 1



Spontaneous magnetization and susceptibility.

ζ , relative magnetization; $(\mu_0/k\theta)(1/\chi)$, reduced inverse susceptibility; T/θ , reduced temperature. Values of $k\theta'/\epsilon_0$ as shown. The broken curves are for parabolic bands with $k\theta'/\epsilon_0 = 2^{-1/3}$ (Stoner 1938a, fig. 5). The curves marked ∞ are given by the classical relations.

and the total internal energy is given by the sum $E = E_E + E_M$. Here

$$F_1(\eta) = \int_0^\infty x dx / [\exp(x - \eta) + 1],$$

the Fermi-Dirac function of order 1 (Rhodes 1950), and η and β were defined in §2. The reduced specific heat, C/Nk , may be calculated, with Stoner, as the sum of three contributory terms

$$\begin{aligned} C_1/Nk &= \{\partial(E_E/N\epsilon_0)/\partial\tau\}_\zeta, \\ C_2/Nk &= \{\partial(E_E/N\epsilon_0)/\partial\zeta\}_\tau d\zeta/d\tau, \\ C_M/Nk &= \{d(E_M/N\epsilon_0)/d\zeta\} d\zeta/d\tau, \end{aligned}$$

where $\tau = kT/\epsilon_0$. These may be calculated directly from (3.1) and (3.2) if use is made of the following auxiliary relations, derived from (2.3), (2.4) and the general relation $F'_s(\eta) = sF_{s-1}(\eta)$ (Rhodes 1950),

$$\frac{dF_1(\eta \pm \beta)}{d(\eta \pm \beta)} = F_0(\eta \pm \beta) = \ln[1 + \exp(\eta \pm \beta)] = (1 \pm \zeta)/\tau. \quad (3.3)$$

It is found that

$$\left. \begin{aligned} \frac{C_1}{Nk} &= \frac{2}{\tau} \frac{E_E}{N\epsilon_0} - \frac{1}{2\tau} \{(1 + \zeta)^2 X_+ + (1 - \zeta)^2 X_-\}, \\ \frac{C_2}{Nk} &= \frac{1}{2} \{(1 + \zeta) X_+ - (1 - \zeta) X_-\} \frac{d\zeta}{d\tau}, \\ \frac{C_M}{Nk} &= -\frac{k\theta'}{\epsilon_0} \zeta \frac{d\zeta}{d\tau}, \end{aligned} \right\} \dots (3.4)$$

where $X_\pm = \{1 - \exp[-(1 \pm \zeta)/\tau]\}^{-1}$.

The functions X_\pm may be expressed in more convenient form using (2.5) and (2.7), giving

$$X_\pm = \frac{\sinh n\zeta/\tau}{\sinh \zeta/\tau} \exp[\mp(n-1)\zeta/\tau], \quad (3.5)$$

where $n = k\theta'/\epsilon_0$. The relations for the contributory specific heat terms then become

$$\left. \begin{aligned} \frac{C_1}{Nk} &= \frac{1}{\tau} \left[\frac{2E_E}{N\epsilon_0} - \frac{\sinh n\zeta/\tau}{\sinh \zeta/\tau} \{(1 + \zeta^2) \cosh(n-1)\zeta/\tau - 2\zeta \sinh(n-1)\zeta/\tau\} \right], \\ \frac{C_2}{Nk} &= \{\zeta \cosh(n-1)\zeta/\tau - \sinh(n-1)\zeta/\tau\} \frac{\sinh n\zeta/\tau}{\sinh \zeta/\tau} \frac{d\zeta}{d\tau}, \\ \frac{C_M}{Nk} &= -n\zeta \frac{d\zeta}{d\tau}. \end{aligned} \right\} \dots (3.6)$$

The value of η , required for the evaluation of $E_E/N\epsilon_0$ and C_1/Nk , may be calculated from the relation, derived from (3.3) and (3.5),

$$\eta = \frac{1}{\tau} - \ln \frac{\sinh n\zeta/\tau}{\sinh \zeta/\tau}, \quad (3.7)$$

and the temperature derivative $d\zeta/d\tau$ from (2.7), giving

$$\frac{d\zeta}{d\tau} = \frac{\zeta}{\tau} + \frac{1}{\tau} \left\{ (n-1) \coth \frac{(n-1)\zeta}{\tau} - n \coth \frac{n\zeta}{\tau} \right\}^{-1} \quad (3.8)$$

Energy and specific heat characteristics. Limiting values. Relations giving the internal energy and specific heat at low temperatures and at the Curie point as functions of the specifying parameter $k\theta/\epsilon_0$ are useful in briefly summarizing the thermal properties of a wide range of ferromagnetics. The relations may be used immediately in an analysis of experimental results (§ 4). With Stoner (1939) calculations are made of the internal energy change between absolute zero and the Curie point and the specific heat at low temperatures and just below and just above the Curie point. The relations are obtainable in algebraical form by direct manipulation of the expressions derived above. In the derivation use is made of the limiting relations for $F_1(\eta)$, viz.

$$\begin{aligned} F_1(\eta) &= \frac{1}{2}\eta^2 + \frac{1}{6}\pi^2 - O(e^{-\eta}), & \eta \rightarrow \infty, \\ F_1(\eta) &= e^\eta - O(e^{2\eta}), & \eta \rightarrow -\infty. \end{aligned}$$

(i.) *Internal energy change between 0°K and the Curie point.*

It follows from (3.1), (3.2) and (3.7) that

$$\frac{E_\theta - E_0}{Nk\theta} = \frac{k\theta}{\epsilon_0} F_1 \left(\frac{\epsilon_0}{k\theta} - \ln \frac{k\theta'}{\epsilon_0} \right) - \frac{\epsilon_0}{k\theta} \left(1 - \frac{1}{2} \frac{k\theta'}{\epsilon_0} \right) \quad (3.9)$$

(ii.) *Specific heat in the limit $kT/\epsilon_0 \rightarrow 0$.*

In this limit C_2 and C_M tend to zero since $d\zeta/d\tau \rightarrow 0$ (cf. (2.10)), so that $C = C_1$. Also from (2.10), (3.3) and (3.7)

$$\eta + \beta = \frac{2}{\tau}, \quad \eta - \beta = -\frac{2}{\tau} \left(\frac{k\theta'}{\epsilon_0} - 1 \right),$$

where $\tau = kT/\epsilon_0$. Hence from (3.1)

$$\frac{E_E}{N\epsilon_0} = 1 + \frac{1}{12}\pi^2\tau^2,$$

so that

$$\frac{C}{Nk} = \frac{1}{6}\pi^2\tau,$$

i. e.

$$\left(\frac{C/Nk}{T/\theta} \right)_{T/\theta \rightarrow 0} = \frac{1}{6}\pi^2 \frac{k\theta}{\epsilon_0} \quad (3.10)$$

(iii.) *Specific heat just below Curie point.*

The three contributory terms become from (2.11), (3.1), (3.6) and (3.7)

$$\left. \begin{aligned} \left(\frac{C_1}{Nk} \right)_{\theta \rightarrow 0} &= 2 \left(\frac{k\theta}{\epsilon_0} \right) F_1 \left(\frac{\epsilon_0}{k\theta} - \ln \frac{k\theta'}{\epsilon_0} \right) - \frac{\theta'}{\theta}, \\ \left(\frac{C_2}{Nk} \right)_{\theta \rightarrow 0} &= 3 \frac{\theta'}{\theta} \frac{k\theta'/\epsilon_0 - 1}{2k\theta'/\epsilon_0 - 1} - 3 \frac{k\theta'/\epsilon_0}{2k\theta'/\epsilon_0 - 1}, \\ \left(\frac{C_M}{Nk} \right)_{\theta \rightarrow 0} &= 3 \frac{k\theta'/\epsilon_0}{2k\theta'/\epsilon_0 - 1}. \end{aligned} \right\} \quad (3.11)$$

(iv.) *Specific heat just above Curie point. Specific heat discontinuity.*

It is easily seen that $(C/Nk)_{\theta+0} = (C_1/Nk)_{\theta-0}$, given in (3.11), and hence the specific heat discontinuity at the Curie point becomes

$$\Delta C/Nk = (C/Nk)_{\theta-0} - (C/Nk)_{\theta+0} = \frac{3\theta'}{\theta} \frac{k\theta'/\epsilon_0 - 1}{2k\theta'/\epsilon_0 - 1} \cdot \cdot \cdot \quad (3.12)$$

(v.) *Temperature variation of specific heat of paramagnetics.*

An immediate application of the relation for $(C_1/Nk)_{\theta-0}$ in (3.11) is to the calculation of the electronic specific heat of paramagnetics. This may be derived from (3.11) by replacing $k\theta/\epsilon_0$ by $\tau = kT/\epsilon_0$ and consequently $k\theta'/\epsilon_0$ by $\{1 - \exp(-1/\tau)\}^{-1}$ (cf. (2.8)). The resulting expression is

$$\left(\frac{C}{Nk}\right)_p = 2\tau F_1 \{ \ln [\exp(1/\tau) - 1] \} - \{ \tau [1 - \exp(-1/\tau)] \}^{-1} \cdot \cdot \cdot \quad (3.13)$$

An alternative derivation of (3.13) is by direct differentiation of the expression for the internal energy of paramagnetics

$$\left(\frac{E}{N\epsilon_0}\right)_p = \tau^2 F_1 \{ \ln [\exp(1/\tau) - 1] \},$$

which may be derived from (3.1) and (3.3) by putting $\beta = 0$.

Relation (3.13) shows that in the limit $\tau \rightarrow 0$

$$\left(\frac{C}{Nk}\right)_p = \frac{1}{3}\pi^2\tau, \quad \cdot \cdot \cdot \cdot \cdot \cdot \cdot \quad (3.14)$$

twice as large as the low temperature specific heat of ferromagnetics (cf. (3.10)). This change arises from the fact that in a paramagnetic the states near the top of the Fermi distribution are doubly occupied at low temperatures, while in a ferromagnetic, with saturation always complete in the case of rectangular bands, they are singly occupied. For parabolic bands saturation may not be complete at 0°K. if $k\theta'/\epsilon_0$ is small enough and the corresponding increase of specific heat as $k\theta'/\epsilon_0$ decreases is more gradual (cf. Stoner 1939, relation (3.15); also Appendix).

(vi.) *The limit $k\theta/\epsilon_0 \rightarrow \infty$.*

The expression for internal energy in this limit may be derived from (3.1), (3.2) and (3.3), giving

$$\left. \begin{aligned} E/N &= kT - \frac{1}{2}k\theta\zeta^2, \\ C/Nk &= 1 - \frac{1}{2}d\zeta^2/d(T/\theta), \end{aligned} \right\} \cdot \cdot \cdot \cdot \cdot \quad (3.15)$$

so that since here $\theta' \rightarrow \theta$. Relations (3.15) for rectangular bands may be compared with the corresponding limiting relations for parabolic bands (Stoner 1939, relations (3.1), (3.2))

$$\left. \begin{aligned} E/N &= \frac{3}{2}kT - \frac{1}{2}k\theta\zeta^2, \\ C/Nk &= \frac{3}{2} - \frac{1}{2}d\zeta^2/d(T/\theta). \end{aligned} \right\}$$

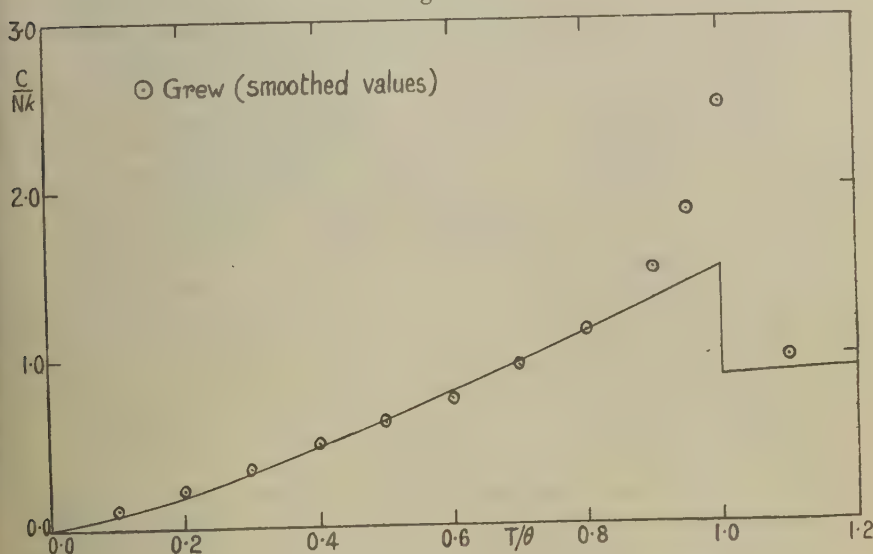
The second term in the expression for C/Nk , the classical "magnetic" specific heat, is the same for both types of band form. The first term, however, the electronic specific heat, is different in the two cases. This dependence on band form also appears in the limiting values of the various energy and specific heat characteristics derived above. For rectangular bands, in the limit $k\theta/\epsilon_0 \rightarrow \infty$,

$$(E_0 - E_0)/Nk\theta = 1.5, \quad (C_1/Nk)_{\theta=0} = (C/Nk)_{\theta=\infty} = (C/Nk)_p = 1,$$

$$(C_2/Nk)_{\theta=0} = 0, \quad (C_M/Nk)_{\theta=0} = 1.5, \quad (C/Nk)_{\theta=0} = 2.5, \quad (\Delta C/Nk) = 1.5;$$

the corresponding limiting values for parabolic bands are 2, 1.5, 0, 1.5, 3, 1.5. A similar dependence on band form is immediately apparent in the respective expressions for the electronic specific heat at low temperatures (*cf.* (3.10), (3.14) and Stoner 1939, relation (4.15); also Appendix).

Fig. 2.



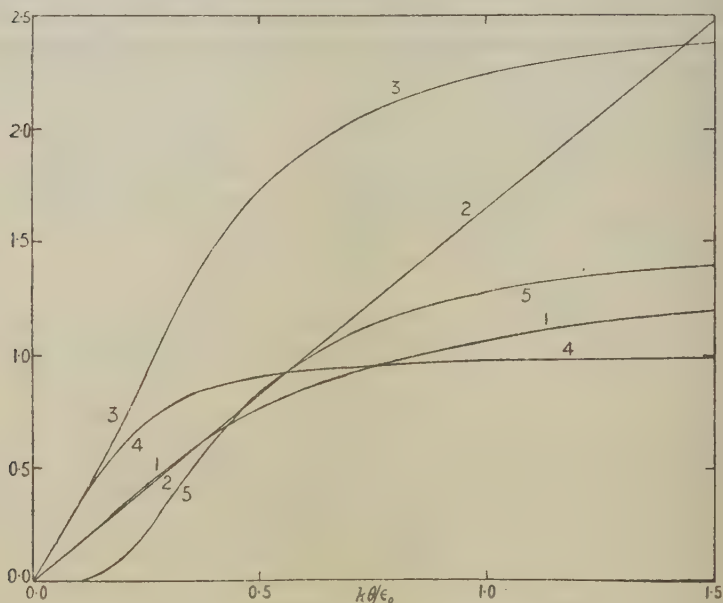
Temperature variation of specific heat.

C/Nk , reduced specific heat, T/θ , reduced temperature. Calculated values are for $k\theta'/\epsilon_0 = 1.10$. Experimental values are for nickel, due to Grew (1934; *cf.* also Stoner 1936, and § 4).

Computations. The internal energy and specific heat expressions derived above were evaluated numerically for $T/\theta = 0.0$ (0.1) 0.9 (0.05) 1.0 and for $k\theta'/\epsilon_0 = 1.10$, using the corresponding values of ζ given in Table I. The particular value of $k\theta'/\epsilon_0$ chosen is indicated by the susceptibility results to be close to the actual value for nickel (*cf.* § 4). The calculated variation of C/Nk with T/θ is shown in fig. 2, together with experimental values for nickel discussed in § 4.

The curve may be compared with Stoner's (1939, fig. 2), from which it differs only slightly in shape. Watanabe (1948) also gives a calculated specific heat curve for nickel, using a value of $k\theta'/\epsilon_0$ larger than the one of fig. 2 owing to an incorrect analysis of the susceptibility results (*cf.* §4). He gives, moreover, no indication in his paper that values of ζ as dependent on T/θ , which are clearly necessary, have been calculated. Watanabe's final curve, however obtained, agrees quite closely in shape with Stoner's and the present curve.

Fig. 3.



Energy and specific heat characteristics.

- 1, $(E_\theta - E_0)/Nk\theta$, reduced internal energy change between absolute zero and the Curie point, θ ; 2, $\{(C/Nk)/(T/\theta)\}_{T \rightarrow 0}$, ratio of reduced specific heat to reduced temperature in the limit $T/\theta \rightarrow 0$; 3, $(C/Nk)_{\theta=0}$, reduced specific heat just below the Curie point; 4, $(C/Nk)_{\theta=0+}$, reduced specific heat just above the Curie point; 5, $\Delta C/Nk$, reduced specific heat discontinuity at the Curie point. For limiting values as $k\theta/\epsilon_0 \rightarrow \infty$, see text.

Computations have also been made of the various energy and specific heat characteristics given by the relations (3.9), (3.10), (3.11), (3.12) which were evaluated numerically for $k\theta/\epsilon_0 = 0.0 \ (0.05) \ 0.5 \ (0.1) \ 1.5$. The results are shown in fig. 3.

The curves may be compared with those derived by Stoner (1939, figs. 3, 4 and 5) for parabolic bands. The most marked differences appear in the limiting values as $k\theta/\epsilon_0 \rightarrow \infty$, already noted, and in the low temperature specific heat curve (*i.e.* fig. 5, curve 2).

§4. DISCUSSION OF SOME EXPERIMENTAL RESULTS.

In previous papers (for summaries see Stoner 1948, 1951) results of experimental investigations into the magnetic and thermal behaviour of ferromagnetic metals and alloys were fully discussed on the basis of the collective electron treatment with the assumption of a particular, parabolic, band form. In this section it will suffice, therefore, to consider very briefly certain of the experimental data in the light of the theoretical results obtained above with the assumption of a rectangular band form. As before, it is mainly nickel and its alloys which are to be considered.

(i.) *Susceptibility above the Curie point.* It has been shown (Wohlfarth 1949 a) that for nickel the experimental reduced susceptibility curve lies very close to the curve of fig. 1 for a parabolic band with $k\theta'/\epsilon_0 = 2^{-1/3}$ if this is corrected for band overlap effects. Inspection of fig. 1 thus indicates that with rectangular bands the appropriate value of $k\theta'/\epsilon_0$ for nickel is about 1.10, and hence from (2.8) $k\theta/\epsilon_0 = 0.42$. For iron and cobalt the analysis is, for several reasons, less conclusive, but Stoner's discussion (1938 b) shows that the reduced susceptibility curves for these metals lie very close to that for nickel. Although it is questionable whether for these two metals the assumption of either a parabolic or a rectangular band form over the whole of the relevant energy range is justified, an estimate for $k\theta/\epsilon_0$ of about 0.4 may be accepted provisionally for all three metals. It may be noted, incidentally, that the value of $k\theta/\epsilon_0$ corresponding to $k\theta'/\epsilon_0 = 2^{-1/3}$ for parabolic bands is also close to 0.4. Watanabe (1948), on the other hand, gives the following as estimates for iron, cobalt and nickel respectively: $k\theta/\epsilon_0 = 0.45, 0.37, 0.50$, basing his estimates on a Curie-Weiss representation of the susceptibility results. With $k\theta/\epsilon_0 = 0.4$ the values of ϵ_0/k are 2.6, 3.5 and 1.6×10^3 °K. for iron, cobalt and nickel respectively, the nickel value being close to that estimated previously.

The analysis of the susceptibility results given previously for nickel alloys shows that in general alloying is accompanied by a shift of the reduced $1/\chi, T$ curves towards the T axis as the alloying content increases. For both types of band form (cf. fig. 1) this decrease indicates primarily a decrease of $k\theta/\epsilon_0$ on alloying, not, as Watanabe believes, an increase in importance of band overlap effects (cf. also Wohlfarth 1949 a).

It may be concluded that the analysis of the susceptibility results is essentially similar for both types of band form.

(ii.) *Spontaneous magnetization.* It has already been shown (Wohlfarth 1949 b) that the experimental curve relating σ/σ_0 and T/θ for nickel lies considerably above that calculated for parabolic bands (with $k\theta'/\epsilon_0 = 2^{-1/3}$, as given by the susceptibility results). The observed curve lies in fact, very close to the classical curve ($k\theta'/\epsilon_0 \rightarrow \infty$). Inspection of fig. 1 shows a similar discrepancy although slightly less serious, between the observed curve (close to the classical curve) and that calculated for a rectangular band (with $k\theta'/\epsilon_0 = 1.10$). The main reason for the discrepancy is believed to be the temperature variation of the effective θ' below the Curie point,

owing to the fundamental relation (2.2) being an oversimplified representation of the interchange interaction energy. This effect, called for brevity the " θ' effect " below, is apparently of greater importance in determining the shape of magnetization, temperature curves than is the band form.

Only two complete sets of curves for ferromagnetic alloys are available, for Ni-Cu and Ni-Co. These have been analyzed by Wohlfarth (1949 c). For Ni-Co the reduced curves were shown to coincide over the whole concentration range (*l.c.* fig. 6), in agreement with the coincidence of the reduced susceptibility curves (*l.c.* fig. 3). For Ni-Cu the reduced experimental magnetization curves shift towards the temperature axis as the copper concentration increases (*l.c.* fig. 7). For parabolic bands, as already noted, the reduced theoretical curves for different ζ_0 values coincide very nearly if $k\theta'/\epsilon_0 \leq 2^{-1/3}$. The interpretation of the observed shift for Ni-Cu was here based on the decrease of ζ_0 with increasing copper concentration and the consequent increasing accuracy of (2.2) in representing the interchange interaction energy. For rectangular bands the theoretical curves themselves shift as $k\theta'/\epsilon_0$ decreases (*cf.* fig. 1), but ζ_0 remains equal to unity. The interpretation of the experimental shift is thus more straightforward, but it is perhaps easy to see that fundamentally it is similar to that already put forward for parabolic bands.

(iii.) *Energy and specific heat characteristics.* The values of the five characteristics given in fig. 3, with $k\theta/\epsilon_0 = 0.42$, the estimated value for nickel, Stoner's values for parabolic bands ($k\theta'/\epsilon_0 = 2^{-1/3}$) and experimental values for nickel due to Grew (1934) and Keesom and Clark (1935), analysed by Stoner (1936), are shown in Table II.

TABLE II. Calculated and observed energy and specific heat characteristics for nickel. For symbolism see caption to fig. 3.

	$\frac{E_\theta - E_0}{Nk\theta} \left(\frac{C/Nk}{T/\theta} \right)_{T/\theta \rightarrow 0}$	$\left(\frac{C}{Nk} \right)_{\theta \rightarrow 0}$	$\left(\frac{C}{Nk} \right)_{\theta \rightarrow 0}$	$\frac{\Delta C}{Nk}$	
Rectangular band ($k\theta/\epsilon_0=0.42$)	0.67	0.69	1.52	0.87	0.65
Parabolic band ($k\theta'/\epsilon_0=2^{-1/3}$)	0.86	1.26	1.76	1.19	0.57
Experimental (nickel)	0.8	0.91	2.5	1.0	1.5

It is seen (a) that the theoretical values, for the two types of band form, for $(E_0 - E_\theta)/Nk\theta$ and $(C/Nk)_{\theta \rightarrow 0}$ agree quite closely with each other and bracket the experimental value in either case, (b) that the theoretical values for $\{(C/Nk)/(T/\theta)\}_{T/\theta \rightarrow 0}$ differ by nearly 100 per cent but that they again bracket the experimental value, (c) that the theoretical values for $(C/Nk)_{\theta \rightarrow 0}$ and $\Delta C/Nk$ are quite close to each other, but are considerably smaller than the observed values. The discrepancies in (c) are doubtless due to the " θ' effect " mentioned above, which brings about discrepancies between observed and calculated magnetization, temperature curves. The effect of assuming a particular band form is shown in Table II. to be important only

in the case of low temperature specific heat. Here, as in (a), the experimental results for nickel seem to show that close agreement between theory and observation should be obtainable if the assumed band form is intermediate between parabolic and rectangular form, bearing out the conclusion of Fletcher and Wohlfarth's calculation for the metal (1951). It may be noted, on the other hand, that the values of $\{(C/Nk)/(T/\theta)\}_{T \rightarrow 0}$ for cobalt and iron are much smaller than that for nickel, 0.49 and 0.28 respectively, so that these metals must have a much more complicated band form than that considered satisfactory for nickel.

(iv.) *Temperature variation of specific heat.* Grew's results for nickel (1934; cf. Stoner 1936) are shown in fig. 2 together with calculated values for a rectangular band form ($k\theta'/\epsilon_0=1.10$). It is seen that the agreement between the two curves is very close up to $T/\theta=0.8$, but that for $0.8 < T/\theta < 1$ the observed values lie markedly above the theoretical curve. The disagreement close to the Curie point is, as already stated, believed to be due to the " θ' effect". Although this has been shown to introduce discrepancies between observed and calculated magnetization, temperature curves over the whole T/θ range, the magnetization and its temperature derivative enter in the expressions for specific heat in such a complicated way (cf. relations (3.6)) that here the discrepancies seem to cancel over most of the lower temperature range.

(v.) *Magneto-caloric effect.* As stated by Stoner (1951) calculations on the magneto-caloric effect on the basis of the collective electron treatment are now in progress at Leeds. It will suffice, therefore, to indicate by an example how such calculations could be carried out in a particularly simple way for a rectangular energy band. The example chosen concerns the magneto-caloric effect in the temperature range below the Curie point where the applied field is negligible compared with the "molecular field". The relevant experimental results for nickel have been considered by Stoner (1936).

If classical statistics were applicable the effective molecular field coefficient, ν , could be derived immediately from the observed adiabatic change of temperature with magnetization, since in negligible fields ($H \ll \nu I$)

$$\nu = -\frac{1}{I} \left(\frac{\partial E}{\partial I} \right)_T = \frac{\rho C_1}{I} \left(\frac{\partial T}{\partial I} \right)_S, \quad \dots \quad (4.1)$$

where C_1 is the specific heat at constant magnetization I and ρ the density. The classical relation for internal energy, E , is just that derived above (relation (3.15)), giving the well known relation between ν and the Curie temperature θ ,

$$\nu = \frac{Nk\theta}{I_0^2}, \quad \dots \quad (4.2)$$

where $\zeta = I/I_0$. With Fermi-Dirac statistics applicable, however, the correct relation for internal energy is $E = E_E + E_M$, given by (3.1) and (3.2).

Hence the *apparent* molecular field coefficient, derivable from the magneto-caloric data, becomes

$$\nu' = \frac{Nk\theta'}{I_0^2} - \frac{1}{I_0^2} \frac{1}{\zeta} \left(\frac{\partial E_E}{\partial \zeta} \right)_T$$

The second term is closely related to the specific heat term C_2 given in (3.6) and it is readily found that

$$\left. \begin{aligned} \nu' &= \frac{Nk\theta'}{I_0^2} \phi(T/\theta, k\theta'/\epsilon_0), \\ \text{where } \phi &= 1 - \left\{ \zeta \cosh(n-1)\zeta/\tau - \sinh(n-1)\zeta/\tau \right\} \frac{\sinh n\zeta/\tau}{n\zeta \sinh \zeta/\tau}, \end{aligned} \right\} \quad (4.3)$$

and where $n = k\theta'/\epsilon_0$, $\tau = kT/\epsilon_0 = (k\theta/\epsilon_0)(T/\theta)$ and ζ is a function of $k\theta'/\epsilon_0$ and T/θ (cf. relation (2.5)). It follows from (4.2) and (4.3) that the ratio r of the apparent molecular field coefficient, ν' , to that derived from classical statistics, ν , is given by

$$r = \nu'/\nu = (\theta'/\theta) \phi(T/\theta, k\theta'/\epsilon_0), \quad . \quad . \quad . \quad (4.4)$$

a function of temperature. If the approximate value of $k\theta'/\epsilon_0$ for nickel, 1.10, is inserted into (4.3) and (4.4) it is found that r increases very nearly linearly with T/θ from

$$\begin{aligned} r_0 &= (\theta'/\theta) \phi(0, k\theta'/\epsilon_0) = (\epsilon_0/k\theta)(k\theta'/\epsilon_0 - 1) = 0.24 \text{ to} \\ r_1 &= (\theta'/\theta) \phi(1, k\theta'/\epsilon_0) = (\theta'/\theta)(\epsilon_0/k\theta)(k\theta'/\epsilon_0 - 1) = 0.63 \end{aligned}$$

as the temperature increases from 0°K to θ . Stoner's analysis (1936) of the results for nickel indicates a temperature increase of the apparent molecular field coefficient below the Curie point of this order of magnitude, although close to the Curie point ν' is strongly field dependent (*l.c.* p. 180).

(vi.) *High temperature specific heat of paramagnetics.* Relation (3.13) shows that for rectangular bands the electronic specific heat of paramagnetics tends to the value Nk at high temperatures ($kT/\epsilon_0 > 1$). The corresponding limiting value for parabolic bands is $1.5Nk$. This dependence on band form has a bearing on the experimental finding that the high temperature electronic specific heat of palladium is considerably smaller than that of nickel above the Curie point. The observed values are about 1 and 2 cal. mol.⁻¹ deg.⁻¹ respectively, whereas the number of holes per atom, proportional to N , is roughly the same for both metals, about 0.6. This anomaly has been variously mentioned (*e.g.* by Mott 1949), but does not seem to have been interpreted by an explicit consideration of differences in the band form for the two metals. It must be pointed out, however, that other effects, such as the anharmonicity of the lattice vibrations and band overlap effects, make a quantitative discussion of high temperature electronic specific heats of much less direct significance than discussions of thermal and magnetic properties at lower temperatures.

APPENDIX.

Results for a more general band form.

The discussion of the preceding sections indicates that some of the results of the treatment do not depend very markedly on the band form, parabolic or rectangular, but that others are, in fact, quite sensitive to it. In this Appendix a very brief discussion is given of such results as are easily obtainable for energy bands of more general form.

If the energy dependence of the density of states, $\nu(\epsilon)$, were only available in numerical form, all but a very few results would have to be derived by a long process of numerical integration. It is easily seen, however, that in the limit $k\theta/\epsilon_0 \rightarrow \infty$ the magnetic properties, spontaneous magnetization and susceptibility, are independent of the band form and are given by the relations based on classical statistics. The thermal properties, however, depend on the band form even in the classical limit, as shown in § 3, and it does not seem possible to derive any general results in this case. For a band for which the density of states is given by the simple relation

$$\nu(\epsilon) = a\epsilon^m, \quad \dots \dots \dots (A.1)$$

the expressions for internal energy and specific heat in the limit $k\theta/\epsilon_0 \rightarrow \infty$, corresponding to (3.15), are

$$\left. \begin{aligned} E/N &= (m+1)kT - \frac{1}{2}k\theta\zeta^2, \\ C/Nk &= (m+1) - \frac{1}{2}d\zeta^2/d(T/\theta). \end{aligned} \right\} \dots \dots \dots (A.2)$$

In the low temperature limit the internal energy and specific heat are easily calculable for an energy band of general form, such as that which has been obtained for nickel. If ϵ_{01} and ϵ_{02} denote the energy widths of the unoccupied states for the two spin directions at 0° K. and ϵ_0 the corresponding width for zero spontaneous magnetization, then

$$\frac{N}{2} = (1 + \zeta_0)^{-1} \int_0^{\epsilon_{01}} \nu(\epsilon) d\epsilon = (1 - \zeta_0)^{-1} \int_0^{\epsilon_{02}} \nu(\epsilon) d\epsilon = \int_0^{\epsilon_0} \nu(\epsilon) d\epsilon, \quad (A.3)$$

giving ϵ_{01} , ϵ_{02} as functions of ζ_0 , the relative magnetization. The internal energy is therefore an implicit function of ζ_0 ,

$$E = E(\zeta_0) = \int_0^{\epsilon_{01}} \epsilon \nu(\epsilon) d\epsilon + \int_0^{\epsilon_{02}} \epsilon \nu(\epsilon) d\epsilon - \frac{1}{2} N k \theta^2 \zeta_0^2, \quad \dots \dots (A.4)$$

and the condition for E to be a minimum gives the relation between ζ_0 and $k\theta'/\epsilon_0$, as well as the values of ϵ_{01} and ϵ_{02} . The low temperature specific heat is then given by

$$C = \frac{1}{3} \pi^2 k^2 T \{ \nu(\epsilon_{01}) + \nu(\epsilon_{02}) \}. \quad \dots \dots \dots (A.5)$$

If $\nu(\epsilon)$ is given by (A.1) it is easily found that

$$\frac{E}{N\epsilon_0} = \frac{1}{2} \left(\frac{m+1}{m+2} \right) \{ (1+\zeta_0)^{m+2/m+1} + (1-\zeta_0)^{m+2/m+1} \} - \frac{1}{2} \frac{k\theta'}{\epsilon_0} \zeta_0^2, \quad (\text{A.6})$$

and

$$\frac{C}{Nk} = \frac{m+1}{6} \pi^2 \frac{kT}{\epsilon_0} \{ (1+\zeta_0)^{m/m+1} + (1-\zeta_0)^{m/m+1} \}. \quad (\text{A.7})$$

The relative magnetization at absolute zero is found from (A.6) and is given by

$$\frac{k\theta'}{\epsilon_0} = \frac{1}{2\zeta_0} \{ (1+\zeta_0)^{1/m+1} - (1-\zeta_0)^{1/m+1} \}; \quad (\text{A.8})$$

hence the condition for ferromagnetism is $k\theta'/\epsilon_0 > 1/(m+1)$ and the range of incomplete saturation at absolute zero ($0 < \zeta_0 < 1$) is given by

$$\frac{1}{m+1} < \frac{k\theta'}{\epsilon_0} < 2^{-m/(m+1)}. \quad (\text{A.9})$$

The relations given above for rectangular and parabolic bands may be derived at once by putting $m=0, \frac{1}{2}$.

REFERENCES.

- FLETCHER, G. C., and WOHLFARTH, E. P., 1951, *Phil. Mag.*, **42**, 106.
 GREW, K. E., 1934, *Proc. Roy. Soc. A*, **145**, 509.
 KEESOM, W. H., and CLARK, C. W., 1935, *Physica*, **2**, 513.
 MOTT, N. F., 1949, *Proc. Phys. Soc. A*, **62**, 416.
 NÉEL, L., 1938, *C.R. Acad. Sci., Paris*, **206**, 1471.
 RHODES, P., 1950, *Proc. Roy. Soc. A*, **204**, 396.
 STONER, E. C., 1936, *Phil. Trans. Roy. Soc. A*, **235**, 165; 1938 a, *Proc. Roy. Soc. A*, **165**, 372; 1938 b, *Proc. Leeds Phil. Soc.*, **3**, 457; 1939, *Proc. Roy. Soc. A*, **169**, 339; 1948, *Phys. Soc. Rep. Progr. Phys.*, **11**, 43; 1951, *Proc. Grenoble Conference, J. Phys. Radium* (in the press).
 WATANABE, H., 1948, *J. Phys. Soc., Japan*, **3**, 12, 317.
 WOHLFARTH, E. P., 1949 a, *Proc. Roy. Soc. A*, **195**, 434; 1949 b, *Phil. Mag.*, **40**, 703; 1949 c, *Ibid.*, **40**, 1095.

XLIV. *The Virial Theorem in Quantum Mechanics.*

By T. L. COTTRELL and S. PATERSON,

I.C.I. Ltd., Nobel Division, Research Department, Stevenston, Ayrshire †.

[Received January 16, 1951.]

SUMMARY.

A derivation is given of a form of the virial theorem in quantum mechanics suitable for the discussion of a system of particles in a box.

IF T and V are the kinetic and potential energies of a system, and \mathbf{r}_i is the position vector of the i th particle, the virial theorem in classical mechanics states that

$$-2\bar{T} = -\overline{\sum_i \mathbf{r}_i \cdot \nabla_i V}, \quad \dots \dots \dots (1)$$

where the bars denote time averages, and the R.H.S. is known as the virial. This result has been used in the discussion of equations of state (*cf.* Jeans 1925). In the discussion of the thermal equation of state derived from quantum dynamical principles, de Boer (1949) has used the virial theorem, a procedure which is only justifiable if it can be shown that it holds in quantum mechanics. In view of the recent controversy concerning quantum mechanical equations of state (*cf.* Green 1949, Uhlenbeck and Riddell 1950) it seemed particularly desirable to examine the validity of this assumption.

de Boer justifies the use of the theorem in quantum mechanics by referring to Slater (1933), who concluded that it is valid if the time averages of classical theory are replaced by quantum mechanical averages. A similar conclusion had been reached by Finkelstein (1928). It appears, however, that these proofs apply only to systems where there are no infinite discontinuities of potential, and are thus not applicable to a system in an enclosure where the potential is infinite at the walls. As it is under just these conditions that the theorem is applied in the discussion of equations of state, a further proof is required. The subject has been touched upon again in more recent publications, though only incidentally, and these contributions will be discussed in relation to our treatment.

After some manipulation of the Schrödinger equation, Slater obtains the result

$$\sum_i -\frac{\hbar^2}{2m_i} \sum_j x_j \left(\psi^* \frac{\partial^3 \psi}{\partial x_i^2 \partial x_j} - \frac{\partial \psi}{\partial x_j} \frac{\partial^2 \psi^*}{\partial x_i^2} \right) + \psi^* \left(\sum_j x_j \frac{\partial V}{\partial x_j} \right) \psi = 0, \quad \dots (2)$$

† Communicated by James Taylor.

where the symbols have their obvious significance. To integrate this, use is made of the identity

$$\sum_j x_j \left(\psi^* \frac{\partial^2 \psi}{\partial x_i^2 \partial x_j} - \frac{\partial \psi}{\partial x_j} \frac{\partial^2 \psi^*}{\partial x_i^2} \right) = -2\psi^* \frac{\partial^2 \psi}{\partial x_i^2} + \frac{\partial}{\partial x_i} \left[\psi^* \frac{\partial}{\partial x_i} \frac{\sum_j x_j \frac{\partial \psi}{\partial x_j}}{\psi^*} \right]. \quad (3)$$

The second term on the R.H.S. is set equal to zero after integration with respect to x_i , because ψ^{*2} is zero at the limits. It may be seen on performing the differentiation inside the brackets, however, that the term

$$\left[-\sum_j x_j \frac{\partial \psi}{\partial x_j} \cdot \frac{\partial \psi^*}{\partial x_i} \right]_{l_1}^{l_2}, \quad \dots \quad (4)$$

where l_1 to l_2 is the range of integration, remains, and that this is zero only if $\partial \psi^* / \partial x_i$ vanishes. In free space where the range of integration is $-\infty$ to $+\infty$, the derivative of the wave function vanishes at the limits, but this does not happen when we are concerned with a system inside a box. Here ψ is typically a sine function with a non-vanishing derivative at the limits. This term must be concerned with the virial of the external forces acting on the system by virtue of the walls, and we shall now show that, if a is a parameter defining the scale of the box, the neglected term is equal to $a(\partial E / \partial a)$, giving the final result

$$2\bar{T} = -a \frac{\partial E}{\partial a} + \overline{\sum_i \mathbf{r}_i \cdot \nabla_i V}, \quad \dots \quad (5)$$

which is the form in which the theorem has, in fact, generally been used.

If
$$H = T + V = -\sum_i \frac{\hbar^2}{2m_i} \nabla_i^2 + V(\mathbf{r}_i), \quad \dots \quad (6)$$

and the wave equation $H\psi = E\psi$ and its complex conjugate hold, it is easy to show, by differentiating with respect to a , keeping \mathbf{r}_i constant, that

$$\frac{\partial E}{\partial a} = -\sum_i \frac{\hbar^2}{2m_i} \int \left(\psi^* \nabla_i^2 \frac{\partial \psi}{\partial a} - \frac{\partial \psi}{\partial a} \nabla_i^2 \psi^* \right) d\tau. \quad \dots \quad (7)$$

In the above, as in all following equations, the volume integral is over the volume of the box for each particle. This volume integral may be transformed into a surface integral using Green's theorem, the surface being that corresponding to the volume through which the \mathbf{r}_i integration is carried. This allows one of the terms to be dropped because ψ^* is zero when any position-vector \mathbf{r}_i terminates on the surface S_i . We obtain

$$\frac{\partial E}{\partial a} = \sum_i \frac{\hbar^2}{2m_i} \iint \left[\frac{\partial \psi}{\partial a} (\nabla_i \psi^*) \cdot d\mathbf{S}_i \right] d\tau_i, \quad \dots \quad (8)$$

where $d\tau$ has been replaced by $d\mathbf{r}_i \cdot d\tau'_i$ in the usual convention.

Similarly, starting with the wave equation and proceeding in the same manner as Slater, we obtain

$$-\psi^* \mathbf{r}_j \cdot \nabla_j V = \psi^* \mathbf{r}_j \cdot \nabla_j \left(\sum_i \left(\nabla_i^2 \psi \right) - \left(\sum_i \left(\nabla_i^2 \psi^* \right) \right) \mathbf{r}_j \cdot \nabla_j \psi \right) \quad (9)$$

which is equation (2) expressed in vector notation. It can easily be shown by expansion that

$$\sum_j \mathbf{r}_j \cdot \nabla_j \left(\sum_i \left(\nabla_i^2 \psi \right) \right) \equiv \sum_i \left(\nabla_i^2 \right) \left(\sum_j \mathbf{r}_j \cdot \nabla_j \psi \right) - 2 \sum_i \left(\nabla_i^2 \psi \right) \quad (10)$$

On substituting in (9) we obtain, after integration throughout the available configuration space,

$$\begin{aligned} -2\bar{T} + \overline{\sum_j \mathbf{r}_j \cdot \nabla_j V} \\ = - \sum_i \left(\nabla_i^2 \right) \int [\psi^* \nabla_i^2 (\sum_j \mathbf{r}_j \cdot \nabla_j \psi) - (\sum_j \mathbf{r}_j \cdot \nabla_j \psi) \nabla_i^2 \psi^*] d\tau \\ = \sum_i \left(\nabla_i^2 \right) \int [(\sum_j \mathbf{r}_j \cdot \nabla_j \psi) \nabla_i^2 \psi^* \cdot d\mathbf{S}_i] d\tau'_i \quad (11) \end{aligned}$$

If a defines the scale of the box then it may be shown (see Appendix) that $\sum_j \mathbf{r}_j \cdot \nabla_j \psi = -a(\partial\psi/\partial a)$. Comparing this result with equation (8) we conclude that

$$2\bar{T} - \overline{\sum_j \mathbf{r}_j \cdot \nabla_j V} + a \frac{\partial E}{\partial a} = 0, \quad (12)$$

which is the form in which the virial theorem is usually used.

Since this work was carried out, it has come to our notice that Price (1950) has derived an expression for the stress tensor at the boundary in a fluid using a similar transformation to a surface integral. By applying Fröhlich's method of boundary perturbations, he obtained a result which can, by combining his equations (25) and (39), be put into the usual form of the virial theorem.

It is true that if the virial in Slater's discussion is regarded as the sum of the virial of the external and internal forces, the result is formally correct, but because of the infinite discontinuity at the walls, the integration of equation (2) throughout infinite space cannot properly be carried out, as has been pointed out by Uhlenbeck and Riddell (1950). These authors attempted to get round this difficulty by considering a smooth though nearly step-like potential at the wall of the box. This does not define the box properly, as pointed out by Green (1950), but it is possible to use Uhlenbeck and Riddell's analytical method together with an infinite

potential wall, to give the correct result. Their method, which has also been applied by Zwanzig (1950) in a similar connection, used a device due to Green (1949) to differentiate the Hamiltonian, but as there seems to be some confusion about the Hermitian character of one of the terms involved, and also because this seems to be a more elegant, if less superficially convincing method, we apply it here.

In Cartesian coordinates the Hamiltonian is

$$H=T+V=-\sum_i \frac{\hbar^2}{2m_i} \left(\frac{\partial^2}{\partial x_i^2} + \frac{\partial^2}{\partial y_i^2} + \frac{\partial^2}{\partial z_i^2} \right) + V(x_1 \dots z_n). \quad (13)$$

We introduce new variables ξ_i, η_i, ζ_i defined by $x_i=a\xi_i, y_i=a\eta_i, z_i=a\zeta_i$, and differentiate the Hamiltonian with respect to a , keeping ξ, η, ζ constant. Thus

$$\frac{\partial H}{\partial a} = -\sum_i 2 \frac{\hbar^2}{2m_i a^3} \left(\frac{\partial^2}{\partial \xi_i^2} + \frac{\partial^2}{\partial \eta_i^2} + \frac{\partial^2}{\partial \zeta_i^2} \right) + \frac{\partial V}{\partial a}, \quad (14)$$

and so

$$a \frac{\partial H}{\partial a} = -2T + \sum_i \mathbf{r}_i \cdot \nabla_i V, \quad (15)$$

$$\therefore a \int \psi^* \frac{\partial H}{\partial a} \psi d\tau = -2\bar{T} + \overline{\sum_i \mathbf{r}_i \cdot \nabla_i V}. \quad (16)$$

By differentiating the Schrödinger equation, and integrating the result, we have

$$\frac{\partial E}{\partial a} = \int \psi^* \frac{\partial H}{\partial a} \psi d\tau + \int \psi^* (H-E) \frac{\partial \psi}{\partial a} d\tau. \quad (17)$$

Since $(\partial\psi/\partial a)_{\xi, \eta, \zeta} = 0$ at the wall (see Appendix), the second term on the R.H.S. is Hermitian, and so disappears, giving a result which may be combined with (16) to give the virial theorem (12). Green (1950) has stated that when the potential at the wall is infinite, this term is not Hermitian because $\partial\psi/\partial a$ is not zero at the surface. This seems to be due to a confusion about what is kept constant in the partial differentiations. In the present treatment we are concerned with $(\partial\psi/\partial a)_{\xi, \eta, \zeta}$, which is zero at the wall. $(\partial\psi/\partial a)_{x, y, z}$, on the other hand, which we used in the previous treatment, is finite at the wall.

APPENDIX.

Let the equation of the box in rectangular Cartesian be

$$S(\xi, \eta, \zeta) = 0, \quad (18)$$

where $\xi = x/a$, etc. We can also write

$$\psi(x_i, y_i, z_i, a) \equiv \Psi(\xi_i, \eta_i, \zeta_i, a), \text{ say.} \quad (19)$$

Then provided ξ_i, η_i, ζ_i satisfy (18) for any single i , i. e. provided the i th particle is on the surface, Ψ is identically zero.

$$\therefore \left(\frac{\partial \Psi}{\partial a} \right)_{\xi, \eta, \zeta} \equiv 0 \quad \text{when} \quad S(\xi_i, \eta_i, \zeta_i) = 0. \quad (20)$$

But

$$a \frac{\partial \Psi}{\partial a} = \sum_i \left(x_i \frac{\partial \psi}{\partial x_i} + y_i \frac{\partial \psi}{\partial y_i} + z_i \frac{\partial \psi}{\partial z_i} \right) + a \frac{\partial \psi}{\partial a} \equiv \sum_i \mathbf{r}_i \cdot \nabla_i \psi + a \left(\frac{\partial \psi}{\partial a} \right)_{x, y, z}. \quad (21)$$

The R.H.S. of (21) is, therefore, also zero.

REFERENCES.

- DE BOER, J., 1949, *Physica*, **15**, 843.
 FINKELSTEIN, B. N., 1928, *Z. f. Physik*, **50**, 293.
 GREEN, H. S., 1949, *Physica*, **15**, 882; 1950, *J. Chem. Physics*, **18**, 1123.
 JEANS, J. H., 1925, *The Dynamical Theory of Gases*, Cambridge, 4th Edition, Ch. VI.
 PRICE, P. J., 1950, *Phil. Mag.*, **41**, 948.
 SLATER, J., 1933, *J. Chem. Physics*, **1**, 687.
 UHLENBECK, G. E., and RIDDELL, R. J., 1950, *J. Chem. Physics*, **18**, 1066.
 ZWANZIG, R. W., 1950, *J. Chem. Physics*, **18**, 1412.

XLV. *The Processing of Thick Photographic Emulsions.*

By A. D. DAINTON, A. R. GATTIKER, and W. O. LOCK,
H. H. Wills Physical Laboratory, University of Bristol*.

[Received February 27, 1951.]

[Plate XVII.]

SUMMARY.

An attempt has been made to determine satisfactory processing conditions for Ilford G5 electron-sensitive emulsions up to 600μ in thickness. The penetration and temperature characteristics of metol-hydroquinone, para-aminophenol, and p-diaminophenol developers have been investigated. The observations show that a p-diaminophenol developer gives satisfactory results and a suitable procedure for processing is described. In addition the problems of fixing, washing and drying, have been studied.

INTRODUCTION.

PHOTOGRAPHIC emulsions have been used as detectors of charged particles ever since Reinganum, in 1911, discovered that an alpha-particle was capable of producing tracks which were observable under a microscope. The early emulsions did not possess great sensitivity; consequently accurate measurements of the properties of nuclear particles could not be made. In 1946, however, Ilford Ltd. in Great Britain produced "Nuclear Research" emulsions containing about eight times the normal amount of silver bromide per unit volume (Powell *et al.* 1946). These emulsions were capable of recording the tracks of particles with a specific ionization of five or more times the minimum value. Their thickness was usually $50\text{--}100\mu$ and no particular difficulties were encountered during processing. Owing to the high concentration of silver bromide, however, it was found advantageous to agitate the fixing solution and to change it fairly frequently (Powell and Occhialini 1947).

When emulsions of 150μ thickness or greater were produced, the application of the processing methods previously employed resulted in a large variation of development with depth. This was found to be due to the fact that the developer took a considerable time to penetrate the emulsion. This difficulty was overcome by Dilworth, Occhialini and Payne (1948) by the method of "temperature development" in which the developer is allowed to penetrate the emulsion at a low temperature, and is subsequently warmed to allow the main development to occur. Details have been given by Wilson and Vaneslow (1949), while the results of an extensive investigation have been published by Dilworth, Occhialini and Vermaesen (1950).

An alternative approach has been suggested by Blau and De Felice (1948). They first soak the emulsion in a developing solution made up

* Communicated by Professor C. F. Powell, F.R.S.

without alkali. When permeation is complete the plate is transferred to developer containing excess alkali. This is known as the "two bath" method. For the successful application of this method to thick emulsions, it is necessary that the speed of travel of a pH change through gelatin from the surface should be much greater than the rate of diffusion of the developer as a whole. This condition is not satisfied (Waller 1951). The "temperature development" method has therefore come into general use, and forms the subject of the work to be described in this paper.

In 1948 Kodak Ltd. produced an emulsion, 200 μ in thickness, capable of recording the tracks of particles at minimum ionization (Berriman 1948). Similar emulsions are now manufactured by Ilford Ltd. The production of such emulsions represented an important technical advance and has made possible a considerable extension of the field of research in nuclear physics. The analysis of the tracks of charged particles by a study of their multiple scattering and grain density requires tracks of great length in the emulsion. With the early thin emulsions, the number of tracks of sufficient length was, for simple reasons of geometry, relatively small, and it became desirable to employ emulsions of greater thickness. The first successful steps in this direction were taken by Dilworth *et al.* (1948).

For the successful application of the scattering method, distortion of the emulsion must be reduced to a minimum, for at the present time errors due to this cause commonly determine the maximum energy of a particle of given track length which can be measured, and contribute to the errors of any given measurement. These considerations emphasize the importance of processing emulsions of relatively great thickness with a minimum of distortion.

In this paper we give an account of the processing methods which have been found satisfactory for Ilford G5 emulsions up to 600 μ in thickness. These methods are not necessarily the best or the only ones available but they may be employed in dealing with large numbers of plates. It must be emphasized that each batch of plates is slightly different from any other, and the optimum processing conditions must be found by trial and error.

§ 1. THE DEVELOPING AGENT.

General Considerations.

Following Dilworth *et al.* (1950) we may specify several conditions which an ideal developer should satisfy. For the "temperature development" method a satisfactory developer should:—

- (i.) be capable of penetrating the emulsion reasonably quickly.
- (ii.) possess a moderate or high-temperature coefficient.
- (iii.) produce negligible background fog and stain in the emulsion.
- (iv.) be stable at temperatures up to 30° C.
- (v.) have a pH as close as possible to that of the emulsion.

Each of these factors will be considered in turn. The developers chosen for investigation were: D19b (metol-hydroquinone), Azol (para-aminophenol), Amidol (p-diaminophenol) and Amidol-bisulphite. Details of the constitution of the solutions are given in Table I.

The Characteristics of the Developers.

(i.) *Penetration characteristics.*

There has been little published work on the penetration times of various developers in "electron-sensitive" emulsions. Payne (1949) has shown that for thin emulsions the rate of diffusion of any developing agent

TABLE I.
The Developing Solutions Investigated

Name	D19b	Azol	Normal amidol	Amidol bisulphite
Developing agent	Metol-hydroquinone	Para-amino-phenol	p-diamino-phenol	p-diamino-phenol
Formula used	Metol 2.2 g. Hydroquinone 8.8 g. Anhydrous sodium sulphite 72.0 g. Sodium carbonate 48.0 g. Potassium bromide 4.0 g. Distilled water to 2000 mls. The above stock solution diluted 1 : 1 with distilled water	Johnson's Azol solution 16 mls. 1 per cent potassium bromide 88 mls. Distilled water (add) 384 mls.	Amidol 3.0 g. Anhydrous sodium sulphite 12.0 g. Distilled water (add) 1000 mls.	Amidol 3.0 g. Anhydrous sodium sulphite 6.7 g. Sodium bisulphite liquor (S.G. 1.34)* 1.4 mls. Distilled water (add) 930 mls.
pH	10.0	11.5	7.2	6.7

* The sodium bisulphite liquor is a commercial preparation supplied by British Drug Houses Ltd.

increases with decreasing pH of the solution; and that pre-soaking the emulsion in water reduces the developer penetration time by as much as 40 per cent; see also Dilworth *et al.* (1948).

The method adopted for the determination of the penetration times of various developers in Ilford G5 emulsions was the following. Plates coated with emulsion of different thicknesses up to 1000μ were cut into pieces of dimensions $\frac{3}{4}$ in. \times $\frac{3}{4}$ in. The back of each plate was exposed to the image of a characteristic pattern, produced by a photographic

enlarger. As the light impinged on the emulsion from the back of the plate, a latent image was produced in the emulsion at the glass-emulsion interface. The exposure time was such that a clearly defined image was produced at the bottom surface of an emulsion 5μ thick, when developed in the D19b developer at 20°C . for one to two seconds. Even at 5°C . the corresponding period is only about 70 seconds. The same exposure was given to all the emulsions, of various thickness, by means of an accurate photographic timer, the voltage supply to the light source and "timer" being accurately controlled.

To ensure that the photographic latent image was confined to the glass-emulsion interface, the light from the enlarger was passed through a Wratten No. 35 filter before striking the plate. Such a filter transmits red and blue light but not the intermediate wavelengths. The silver halide is sensitive only to the blue light which is strongly absorbed, and the latent image formed is confined to a layer approximately 3μ thick at the glass-emulsion interface. Thus, no trace of the geometrical pattern appeared on the surface of the emulsion 5μ thick exposed in this way. The first appearance of the pattern at the bottom of an emulsion is therefore a good indication of the time the developer has taken to penetrate the full thickness of the emulsion in sufficient strength to develop the exposed grains of silver halide. For the purpose of the present experiment, we may define the penetration time as the period the developer takes to penetrate to the bottom of the emulsion and develop the image of the geometric pattern. It may be emphasized that the penetration time so defined is not appreciably affected by the variation with temperature of the time taken to develop the image once the developer is present at a given concentration: for all temperatures this time is relatively very short.

Details of the emulsion thicknesses used are given in Table II.

TABLE II.

Emulsion Thicknesses Used.

Nominal Thickness	Actual Thickness
50 μ	45 μ
100 μ	105 μ
200 μ	230 μ
300 μ	260 μ
400 μ	400 μ
600 μ	675 μ
800 μ	720 μ
1000 μ	1050 μ

The measurements were first carried out at 20°C . with the different developing solutions. One complete set of plates was first pre-soaked in distilled water for three hours, whilst a second set was not pre-soaked. The results obtained are given in Table III. and in fig. 1.

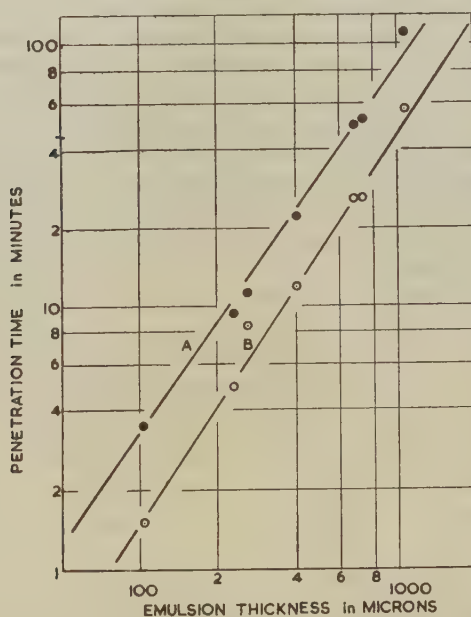
TABLE III.

Penetration Times of the Different Developing Solutions at 20° C., in Pre-soaked and non Pre-soaked Emulsions.

Developer	Soaking	Penetration Time in Minutes for Different Thicknesses						
		105 μ	230 μ	260 μ	400 μ	675 μ	720 μ	1050 μ
Azol	Pre-soaked	4½	17	22	38	96	96	210
	Non Pre-soaked	6	21	27	50	138	123	330
D19b	Pre-soaked	3½	9½	14½	21	50	64	140
	Non Pre-soaked	5	12	20	37	110	125	270
Normal amidol	Pre-soaked	1½	6	8½	12	26	26	58
	Non Pre-soaked	3½	9½	11½	22	49	52	120
Amidol bisulphite	Pre-soaked	2	6½	8	12	25	25	55
	Non Pre-soaked	2	8½	10	20½	53	46	110

All pre-soaked emulsions soaked in distilled water for three hours irrespective of thickness.

Fig. 1.



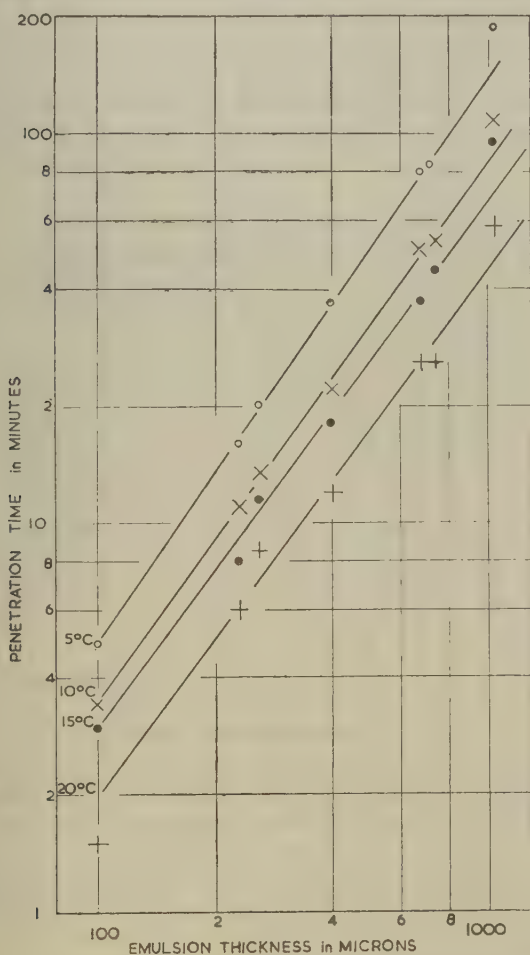
Penetration time of the developer as a function of emulsion thickness for normal amidol at 20° C.; curve A for emulsion without pre-soaking; curve B emulsion pre-soaked in distilled water at 20° C. for three hours.

These show that pre-soaking the emulsion in water considerably reduces the penetration time of the developer. The ratio of average penetration times, without and with pre-soaking, for the various developers is :—

Azol	1.34 ± 0.05
D19b	1.70 ± 0.13
Normal amidol	1.86 ± 0.12
Amidol bisulphite	1.65 ± 0.14

It will be seen that the amidol and amidol bisulphite developers are equivalent in penetrating power, and they penetrate the emulsion more rapidly than D19b or Azol.

Fig. 2.



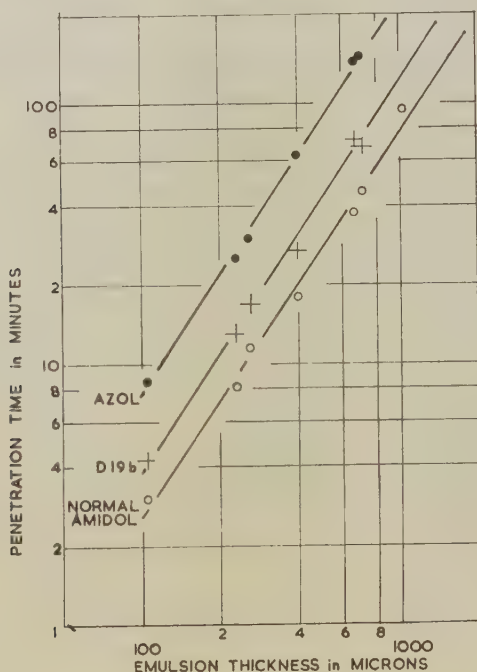
Penetration time of the developer as a function of emulsion thickness for normal amidol at 5° C., 10° C., 15° C., and 20° C. All emulsions pre-soaked in distilled water for three hours at the appropriate temperature.

In view of these results, the penetration measurements at 15° C., 10° C., and 5° C. were carried out, using only the first three developing solutions specified in Table I., and always pre-soaking the emulsions in distilled water for three hours at the appropriate temperature, whatever the thickness of the emulsion. The results obtained are displayed in Table IV. and plotted graphically in figs. 2 and 3. The penetration time, T , may be expressed in terms of the thickness of the emulsion, t , by a relation of the form

$$T = k \cdot t^x,$$

where x is of the order of 1.4, and k is a constant for a given developer at a given temperature.

Fig. 3.



Penetration time of the developer as a function of emulsion thickness for normal amidol, D19b and Azol developing solutions at 15° C. All emulsions pre-soaked in distilled water for three hours at 15° C.

It must be emphasized that T is the penetration time as defined above and not necessarily the time required for satisfactory processing. The latter periods are given in Table VIII.

(ii.) *Temperature characteristics.*

It was also desirable to determine the temperature characteristics of the different developers in the G5 emulsion. Strips of dimensions

$\frac{3}{8}$ in. \times $\frac{3}{4}$ in. were cut from 2 in. \times 2 in. plates with emulsion 5μ thick. These were exposed to light passed through a step wedge (15 steps of density range 0-2) held in a photographic enlarger, the image of this step wedge being formed on the glass-emulsion interface of the plate. The exposure was accurately controlled as in the previous experiment and was such that the image of the middle portion of the wedge was satisfactorily developed using the D19b developer at 20°C . for 10 minutes.

For any one developer at any one temperature, five emulsion strips were used. These were immersed in the developer in question for various times, depending on the normal time used for that developer. For example, the D19b developer is usually used for 20 minutes at 20°C .; thus strip no. 1 was removed from the developer and put to fix after $1\frac{1}{2}$ minutes, no. 2 after 3 minutes, no. 3 after 7 minutes, no. 4 after 15 minutes, and no. 5 after 30 minutes. At a lower temperature, these times were increased, *e. g.* at 5°C . using the same developer the times were twice those used at 20°C .

TABLE IV.

Penetration Times, in Pre-soaked Emulsions, of the Various Developing Agents at 5°C ., 10°C ., 15°C ., and 20°C .

Developer		Penetration Time in Minutes						
		105μ	230μ	260μ	400μ	675μ	720μ	1050μ
Azol	5°C .	11	45	50	100	270	300	300
	10°C .	$8\frac{1}{2}$	27	34	70	185	208	210
	15°C .	$8\frac{1}{2}$	25	30	63	145	150	210
	20°C .	$4\frac{1}{2}$	17	22	38	96	96	210
D19b	5°C .	6	21	27	58	165	172	270
	10°C .	5	$16\frac{1}{2}$	19	37	108	114	210
	15°C .	4	13	17	27	72	68	220
	20°C .	$3\frac{1}{2}$	$9\frac{1}{2}$	$14\frac{1}{2}$	21	50	64	140
Normal amidol	5°C .	5	16	20	37	80	84	190
	10°C .	$3\frac{1}{2}$	11	$13\frac{1}{2}$	22	51	$53\frac{1}{2}$	110
	15°C .	3	8	$11\frac{1}{2}$	18	$37\frac{1}{2}$	45	95
	20°C .	$1\frac{1}{2}$	6	$8\frac{1}{2}$	12	26	26	58

The figures for 20°C . are given again for comparison purposes.

The above procedure was carried out at 5°C ., 10°C ., and 20°C . for each of the four developers under consideration. When all the plates had been processed and dried the density of each step in each wedge was determined using an Ilford densitometer and recorder.

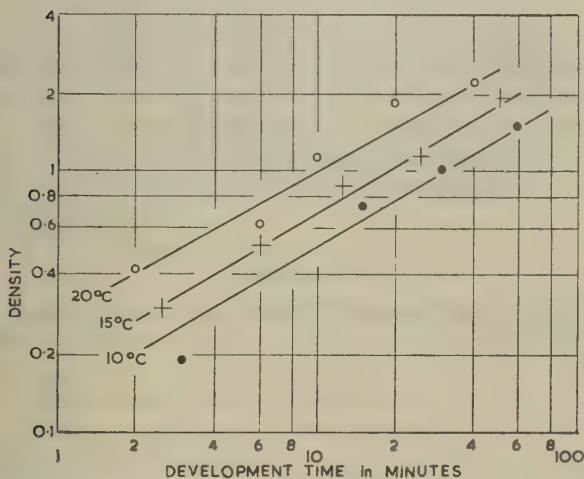
The usual method of determining temperature coefficients was found to be inapplicable in this experiment owing to the extreme contrast of the plates. Instead, the times to produce equal densities on the same step (no. 6 in this case) of each wedge were used as a basis of comparison between developers. Equivalent readings were not available in the case of Azol, which was found to be incapable of giving images of sufficiently high density. The results are given in Tables V. and VI. and are presented

TABLE VI.

Development Time for Unit Density as a Function of Temperature.

Developer		Time for Density 1 in Minutes	Figures Normalized to Density $3\frac{1}{2}$ at 20° C.
D19b	5° C.	—	—
	10° C.	30	30
	15° C.	8	8
	20° C.	$3\frac{1}{2}$	$3\frac{1}{2}$
Normal amidol	5° C.	45	45
	10° C.	18	18
	15° C.	—	—
	20° C.	$3\frac{1}{2}$	$3\frac{1}{2}$
Amidol bisulphite	5° C.	—	—
	10° C.	30	$10\frac{1}{2}$
	15° C.	18	6
	20° C.	10	$3\frac{1}{2}$
Azol	15° C.	400	$3\frac{1}{2}$
	20° C.	1200	$10\frac{1}{2}$

Fig. 4.



Density of step 6 of the step wedge as a function of development time for amidol bisulphite developer at various temperatures.

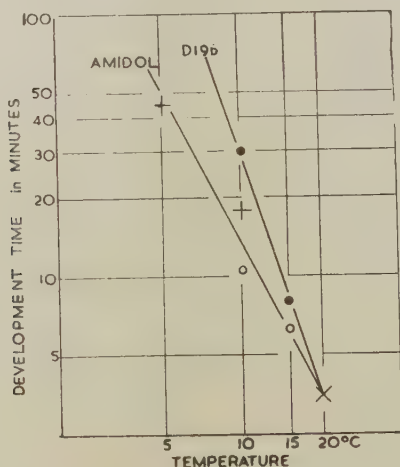
graphically in figs. 4 and 5. It may be seen that the rate of action of all the developers changes rapidly with temperature. The measurements suggest that D19b is more sensitive than the amidol developers. Azol, although very sensitive to temperature, has very low activity.

(iii.) *Background formation and staining properties of developers.*

Background grains not associated with recognizable tracks are due, in part, to particles traversing the emulsion at a large angle of dip, and to fog grains arising from (a) chemical action during the preparation of the emulsion, and (b) the action of the developing agent.

A measure of the number of background grains per unit area was obtained by counting the number of such grains in focus under specified optical conditions. The microscope used was a Cooke M4000 with $\times 95$ objective and $\times 15$ eyepieces. Some results for emulsions exposed and processed under different conditions are given in Table VII. A background of as much as 80 grains per $10,000 \mu^2$ can be tolerated in emulsions in which the grain density in the track of a particle with minimum specific ionization is of the order of 15 grains per 50μ .

Fig. 5.



Time for unit density of step 6 against temperature, for amidol type and D19 b developing solutions. The figures are normalized at 20°C .

TABLE VII.

Exposure	Developer	Stop Bath	Background Grains/ $10,000 \mu^2$		Percentage of Light Transmitted
			5μ from surface	5μ from glass	
1. G5 400μ $1\frac{1}{2}$ hrs. at 68,000 ft.	Azol	5 per cent sodium bisulphite	35 ± 2	Too misty	27
2. G5 400μ $5\frac{1}{2}$ hrs. at 64,000 ft.	Normal amidol	pH3 HCl	95 ± 5	74 ± 3	17
3. G5 400μ $5\frac{1}{2}$ hrs. at 64,000 ft.	Amidol bisulphite	2 per cent acetic acid	34 ± 2	33 ± 2	40
4. G5 500μ Glass 2 mm. 6 hrs. at 75,000 ft.	Amidol bisulphite	$\frac{1}{2}$ per cent acetic acid	59 ± 3	61 ± 3	25

The degree of stain in an emulsion is difficult to define quantitatively. We may estimate the combined effect of background and stain by means of an Ilford densitometer which measures the percentage of light transmitted by the photographic plate. The figures given in Table VII. show that the stain is not necessarily related to the background grain density. It may also be seen that the use of amidol bisulphite developer results in plates of good optical quality.

(iv.) *Stability of the developer as a function of temperature.*

Following Dilworth *et al.* (1950), who drew attention to the possibility of employing developing solutions at higher temperatures than those commonly used, we have found that very satisfactory results are obtained when a temperature of the order of 27° C. is used in the hot stage of the temperature cycle. For such work it is necessary that the developer should remain stable at these temperatures, and all the developers given in Table I. are satisfactory in this respect.

(v.) *pH considerations.*

It has been shown that when Ilford Nuclear Research emulsions are immersed in a solution the swelling of the emulsion decreases as the pH of the solution is reduced. In fact, the emulsion will even shrink when placed in dilute acid (Waller 1951). These considerations make it desirable that the developer employed should be slightly acid, for the less the swelling of the emulsion, the smaller the distortion introduced at this stage of the processing.

CONCLUSIONS.

From a consideration of the factors discussed above, it appeared to us that amidol promised to give the most satisfactory results. It was therefore adopted as a standard developer for emulsions up to 300 μ in thickness. For thicker emulsions it was found that normal amidol produced a slight variation of development with depth. We have succeeded in reducing this variation by adding sodium bisulphite to the developing solution (Balagny 1912). Balagny employed normal photographic emulsions and his recommended value for the pH of the developer was not found to be suitable for thick electron sensitive emulsions. Using the amidol bisulphite developing solution given earlier, with a pH of about 4, we have found it possible to develop the lower regions of an emulsion without developing the surface layers. The pH of the solution which gives satisfactory development throughout the entire thickness of the emulsion is 6.7.

Experiments were also carried out in an attempt to reduce the formation of fog in the emulsion by reducing the concentration of amidol, but tracks of particles of minimum ionization were not recorded for concentrations less than 3 gm./litre.

§ 2. THE DEVELOPMENT PROCESS.

We may now consider the details of the development procedure. The results given in the previous section suggest that: (a) the emulsion should be pre-soaked in water before being placed in the developing solution; and (b) that the developer used should be amidol in some form.

In our procedure the plate is therefore first immersed in distilled water at room temperature. The water is then cooled to 5° C. and maintained at this temperature for a time which depends on the thickness of the emulsion. It is then transferred to the developing solution, which is also at 5° C., and remains in this solution until the developer has completely permeated the emulsion. During this time little development will have taken place.

For the main development process two alternative methods may be employed. The developer and plate together may be warmed to about 18° C., and the temperature maintained at this value for the time required to give satisfactory development. Alternatively, following Dilworth *et al.* (1950), the plate may be separated from the developing solution, any excess solution being removed by means of filter paper, and the plate then placed glass downwards on a dry surface. This surface is then brought to a temperature between 25 and 30° C., and maintained at a constant value for the requisite time. In this method one thus relies upon the developer already present in the body of the emulsion and avoids over-development at the top of the emulsion due to the entry of fresh developer. This is known as the "hot-plate" method.

In our experience the second method gives the more satisfactory results. To obtain tracks of particles with minimum ionization, the actual value of the temperature of the "hot plate" does not appear to be critical. If, however, it is important to preserve uniformity of development among plates from different batches it is necessary to introduce an accurate system of temperature control. Care must also be taken to ensure good thermal contact between the plates and the "hot plate".

If amidol is used as the developing solution, the surface of the emulsion, after processing, is usually covered with a deposit of silver. This may sometimes, although not always, be swabbed off with cotton wool soaked in methylated spirits, when the emulsion is thoroughly dry. For some experiments, such as those with artificially accelerated particles, it is important to know the exact point where a particle entered the surface. Any surface silver deposit is therefore to be avoided if possible. It has been suggested by Dilworth *et al.* (1950) that developing the plates in an inert atmosphere may lead to a diminution in the amount of the surface deposit. Alternatively, for emulsions less than 400 μ in thickness, azol may be employed, using the first of the development methods described above, since it commonly leaves little or no surface deposit.

The next problem is to stop the development at the correct moment. The general procedure is to transfer the plates to a "stop bath" which is at a temperature near to that of the "hot plate"; the temperature of the solution is then lowered to about 5° C. and kept at that value until all

development has ceased. The solution and plates may then be warmed to the temperature of the fixing solution, and after a short wash in water, transferred to it. Thus development is stopped both by the application of a stopping agent and by the use of low temperature. We have tried several stopping agents including distilled water, a 1 per cent potassium bromide solution, a 5 per cent sodium bisulphite solution, $\frac{1}{2}$ per cent solution of hydrochloric acid and solutions of acetic acid. The best results were obtained with the acetic acid. The concentration did not appear to be critical, and we find that a $\frac{1}{2}$ per cent solution is satisfactory.

In all the processes mentioned above, the plates are kept horizontal. This is especially important when dealing with very thick emulsions.

§ 3. FIXATION.

The critical importance of avoiding distortion has already been stressed. The main causes of distortion are the stresses introduced when the emulsion suffers volume changes including those during manufacture. These changes may be caused by mechanical agitation, temperature variations, pH changes, and the removal of the unsensitized silver halide from the emulsion. Since most of the silver halide, which constitutes a large fraction of the unprocessed emulsion, is removed during processing, it is probable that most of the distortion is introduced during fixation, washing and drying. After the fixing solution has been washed out and the plate allowed to dry, the emulsion has less than half its original thickness.

The plate is fixed with sodium thiosulphate—'hypo'. Camerini and Franzinetti (1947), working with thin emulsions, found that a concentration of 40 grams of hypo to 100 mls. of water gives the most satisfactory results. We have confirmed this result for emulsions $400\ \mu$ thick.

Owing to the large amount of silver halide in electron-sensitive emulsions the fixing process takes a relatively long time. It is well known that ammonium thiosulphate acts rapidly as a fixing agent. The addition of a small amount of ammonium chloride to the hypo solution also shortens the total fixing time. We have found, however, that a fixing solution of this nature tends to remove some of the developed grains near the surface of the emulsion, especially in the case of thick emulsions where the total fixing time may be of the order of two or three days. This has also been observed by Wilson and Vaneslow (1949). Because of this effect we do not favour the use of ammonium chloride.

On the other hand, we have found it advantageous to add sodium bisulphite to the hypo solution; this leads to a reduction of the stain in the finally processed emulsion (Mees 1942). The fixing solution which has been adopted as standard in this laboratory is:—

Sodium thiosulphate	400 grams.
Sodium bisulphite	30 grams.
Water to add	1,000 mls.

The pH of this solution is 5.0,

Agitation.

It has been found by several workers that gentle agitation of the fixing solution leads to a reduction in the total fixing time (Powell and Occhialini 1947; Wilson and Vaneslow 1949). It is essential that the plates are kept horizontal and that the agitation, if any, is very gentle. This is especially important for emulsions thicker than $400\ \mu$. If, for example, a $500\ \mu$ emulsion is held vertically during the fixing process, the emulsion tends to "creep", and it is frequently observed that tracks near to the bottom are discontinuous. An example of this nature which we call 'chopping' is shown in Pl. XVII. *a*. Similar effects sometimes occur in emulsions processed horizontally (Herz 1950) and have been seen in emulsions $200\ \mu$ thick.

We have found that suitable agitation is provided by a slow steady flow of the fixing solution over the surface of the plates. Satisfactory results may also be obtained by placing the plates in a static fixing bath, provided the bath is changed fairly frequently. A fixing bath is considered to be exhausted when the concentration of silver in it rises above between five and seven grams per litre.

Fixation time.

The period for complete fixation is usually taken as one and a half times that for the emulsion to clear, that is, when the last trace of opaque silver halide has disappeared from the bottom of the emulsion. For a $400\ \mu$ emulsion, the total fixation time is of the order of 24 hours, while for a $1,000\ \mu$ emulsion it may be as long as 100 hours.

§ 4. WASHING AND DRYING.

Washing.

When all the surplus silver halide has been removed from the emulsion, the fixing solution must be washed out. Thin emulsions may be washed in a stream of tap water. When this method is employed with emulsions $600\ \mu$ thick, however, the emulsion frequently distorts, and "bubbles" may be formed on the surface.

We have therefore found it necessary to commence washing with water at a low temperature ($5-10^\circ\text{C}$). The plates are placed in a large dish of fixing solution and the cold water is allowed to trickle in slowly at first. As the concentration of the fixing solution is reduced, the rate of flow of the water and its temperature may be increased. The washing process may take as long as two or three days, and it is only considered complete when the washing solution gives no indication of the presence of hypo as judged by the potassium permanganate test.

Drying.

Following a suggestion of Mr. C. Waller, we next soak the plates in a solution of glycerine for approximately an hour. This prevents the emulsion from stripping off the glass after it has dried. A 1 per cent solution has been found to be satisfactory for this purpose. We have

found some indication that the use of a 5 per cent solution tends to reduce the distortion, although the processed emulsion is then rather soft.

After removal from the glycerine solution, the plates are placed side by side in the form of a square or a rectangle in an enclosed box. If they are of a small size it is of some advantage to place a "guard ring" of wet emulsion around the plates to be dried (Dilworth 1950). It is more convenient, however, to use large plates, say 8 in. \times 8 in. and then cut them to 6 in. \times 6 in. after they have dried. The distortion effects at the edges are thus almost completely eliminated.

A preliminary investigation has shown that distortion is reduced if the drying of the plates is not unduly prolonged. A batch of plates was allowed to dry for seven days at a relative humidity of 90 per cent, and then for a further seven days during which the relative humidity was gradually lowered to about 55 per cent. The distortion in these plates was a little greater than that in emulsions of equal thickness which had been dried over a period of three days. Drying by gently blowing air over the plates is undesirable and introduces severe C-shaped distortion. Warming the plates by means of a 25 watt electric light bulb at a distance of a few feet appears to give satisfactory results.

§ 5. CONCLUSIONS.

Distortion.

The effect of distortion on the measurement of the scattering of a track has been briefly discussed by Fowler (1950), while Cosyns and Vanderhaeghe (1950) have described a method of estimating its magnitude. It is, of course, most severe at the edges of a plate; examples of both C- and S-shaped distortion at the edge of a 400 μ plate are shown in Pl. I. *b* and *c*. The elimination of these edge effects has been discussed in the previous section.

The distortion in the centre of a large emulsion is usually of the C-type and its effect on the scattering of a track may then be estimated. On the other hand, it may occasionally take the form of irregular and local "chopping" for which no correction can be made.

General considerations.

The results given above have been summarised in Tables VIII. and IX. which detail satisfactory processing methods for G5 emulsions of various thicknesses.

The methods given in Table VIII. have been used in the processing of Ilford C2, D1, and E1 emulsions 200 μ thick (Danyasz 1950; Muirhead 1950), Ilford C2 emulsions 600 μ thick (Smith 1950) and Kodak NT4 emulsion 200 μ thick (King 1950). Satisfactory results were obtained in all cases.

In collaboration with Mr. M. G. K. Menon, and Mr. G. T. Zorn, the investigations described are being extended to still greater emulsion thicknesses, and to the diluted emulsions recently produced by Ilford Ltd. (Dodd and Waller 1950).

TABLE VIII.

Amidol Type Developer.

	Emulsion Thickness.				
	100 μ	200 μ	400 μ	600 μ	1000 μ
Soak in distilled water	15 mins.	25 mins.	90 mins.	120 mins.	240 mins.
Developer at 5° C.	15 "	25 "	90 "	120 "	300 "
" Hot plate " 27° C.	25 "	25 "	30 "	30 "	35 "
Stop bath	10 "	20 "	90 "	120 "	180 "
Fixing	2 hours	5 hours	24 hours	70 hours	100 hours
Washing	4 "	12 "	60 "	72 "	120 "
Drying	6 "	12 "	60 "	100 "	120 "

TABLE IX.

Azol Developer.

	Emulsion Thickness		
	100 μ	200 μ	400 μ
Soak in distilled water	15 mins.	25 mins.	90 mins.
Developer at 5° C.	30 "	90 "	120 "
Warm stage 18° C.	105 "	105 "	105 "
Stop bath	30 "	45 "	90 "
Fixing	2 hours	5 hours	24 hours
Washing	4 "	12 "	60 "
Drying	6 "	12 "	60 "

The stop bath may be 5 per cent sodium bisulphite or $\frac{1}{2}$ per cent acetic acid.

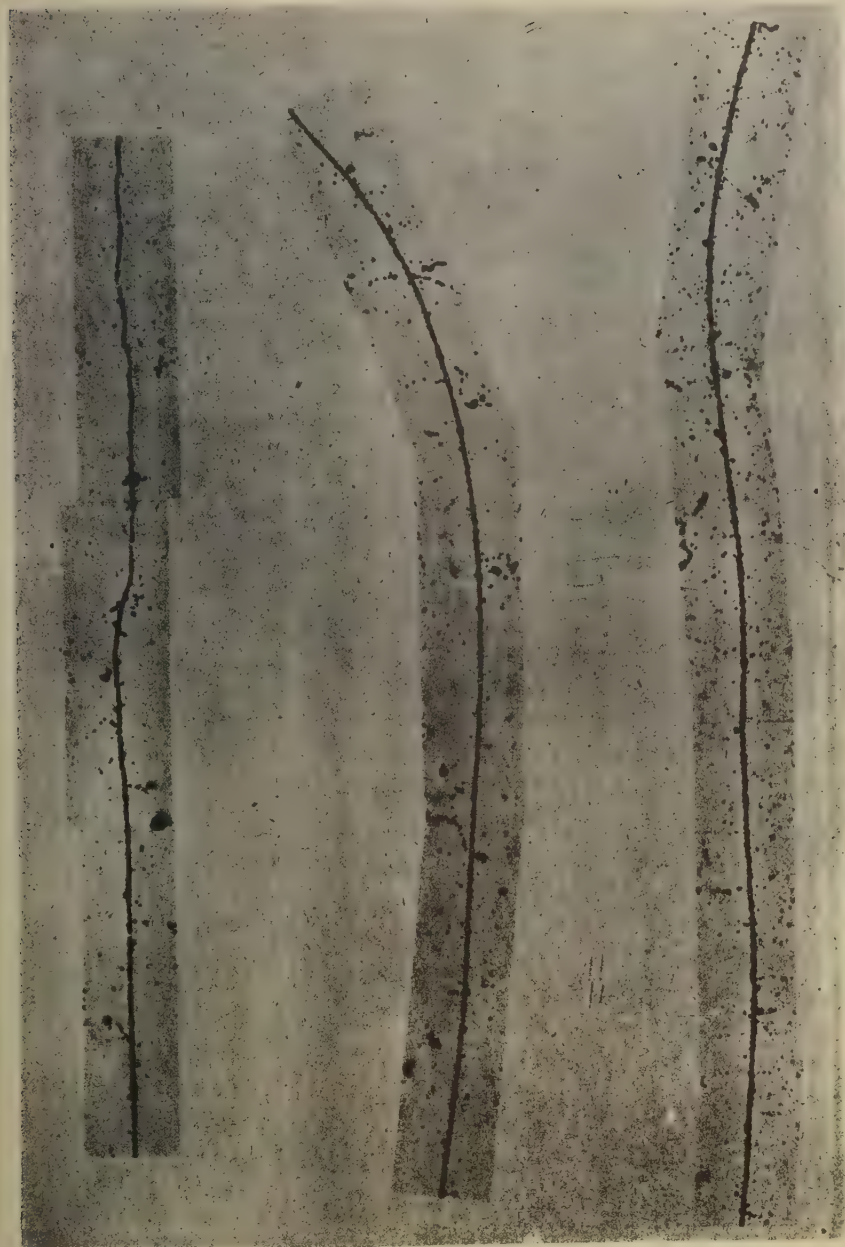
ACKNOWLEDGMENTS.

This work was originally undertaken in collaboration with Mr. H. Muirhead, now at the University of Glasgow, and we are indebted to him for introducing us to the problem and for his advice and criticism.

We have pleasure in thanking Professor C. F. Powell, F.R.S., for his continued interest and encouragement; Mr. C. Waller and Mr. M. A. Vincent of Ilford Ltd., who have supplied us with the emulsions of many different sizes and thicknesses, and who have given us the benefit of their experience with electron-sensitive emulsions; Dr. R. H. Herz of Kodak Ltd., who has supplied us with test samples of NT4 emulsions; Miss C. C. Dilworth and Professor G. P. S. Occhialini of the University of Brussels for helpful advice; Miss Mary Blundell of the University of Manchester, who kindly gave us the formula for the Azol developer; and Mr. A. J. Herz of Imperial College, London, for discussions.

Finally we would like to express our appreciation to those members of the laboratory research team who have helped in various ways at all hours, particularly Mr. J. H. Davies, Mr. D. W. Kent, Mr. D. T. King, Mr. M. G. K. Menon and Mr. G. T. Zorn; and to Dr. H. K. Heitler, Mr. H. Ellacott and Mr. M. A. Roberts, for considerable technical assistance.

This work has been carried out as part of a programme of research supported by the D.S.I.R., and two of us (A.D.D. and W.D.L.) are indebted to this body for maintenance grants.



(a) (b) (c)
Examples of (a) "chopping", (b) C-shaped distortion, and (c) S-shaped distortion in 400μ G5 emulsions.

To face page 412

REFERENCES.

- BALAGNY, G., 1912, *Bull. Soc. Franc. Photogr.* (3) **3**, 198.
BERRIMAN, R. W., 1948, *Nature, Lond.*, **162**, 992.
BLAU, M., and DE FELICE, J. A., 1948, *Phys. Rev.*, **74**, 1198.
CAMERINI, U., and FRANZINETTI, C., 1948, Private Communication.
COSYNS, M., and VANDERHAEGHE, E., 1950, *Bulletin du Centre de Physique Nucleaire de L'Universite Libre de Bruxelles*, No. 15, February.
DANYSZ, M., 1950 Private Communication.
DILWORTH, C. C., 1950, *Bristol Photographic Conference*.
DILWORTH, C. C., OCCHIALINI, G. P. S., and PAYNE, R. M., 1948, *Nature, Lond.*, **163**, 102.
DILWORTH, C. C., OCCHIALINI, G. P. S., and VERMAESEN, L., 1950, *Bulletin du Centre de physique Nucleaire de L'Universite Libre de Bruxelles*. No. 13 a, February.
DODD, E. C., and WALLER, C., 1950, *Bristol Photographic Conference*.
FOWLER, P. H., 1950, *Phil. Mag.*, **41**, 169.
HERZ, A. J., 1950, Private Communication.
MEES, C. E. K., 1942, *The Theory of the Photographic Process* (New York : Macmillan), p. 528.
MUIRHEAD, H., 1950, Private Communication.
PAYNE, R. M., 1949, Private Communication.
POWELL, C. F., and OCCHIALINI, G. P. S., 1947, *Nuclear Physics in Photographs*. (Oxford : Clarendon Press), p. 110.
POWELL, C. F., OCCHIALINI, G. P. S., LIVESEY, D. L., and CHILTON, L. V., 1946, *J. Sci. Instrum.*, **23**, 102.
SMITH, C. L., 1950, Private communication.
WALLER, C., 1951, Private communication.
WILSON, M. J., and VANESLOW, S., 1949, *Phys. Rev.*, **75**, 1144.

XLVI. *A Theory of the Plastic Distortion of a Polycrystalline Aggregate under Combined Stresses.*

By J. F. W. BISHOP and R. HILL,
Wills Physical Laboratory, University of Bristol.*

[Received February 8, 1951.]

SUMMARY.

A general relationship between stress and plastic strain in a polycrystalline aggregate is derived for any metal in which individual crystals deform by slipping over preferred planes under a critical shear stress. Full account is taken of the non-uniform distortion due to mutual constraints between the grains of an aggregate. It is shown that a plastic potential exists which is identical with the yield function. Upper and lower bounds are obtained for an approximate calculation of this function for any applied system of combined stresses.

§1. INTRODUCTION.

THE macroscopic theory of plastic deformation in a polycrystalline metal is based on observations of the behaviour of the metal in bulk. It rests also on the simplifying hypothesis that the material is locally homogeneous (though not necessarily isotropic). The theory so constructed is found to be adequate as a first approximation when applied to many problems in engineering science and metal technology. There remains, however, the task of relating the macroscopic observations to ones more fundamental, for example, the mechanisms by which a single crystal deforms under load. Such an investigation might hope to attain two main objectives: first, to show which of the several microscopic modes of distortion are chiefly responsible for the behaviour of the aggregate as a whole; and second, to indicate, more precisely than experiment at present can, what refinements should be added to the macroscopic theory and what these might be for any particular metal. Several previous writers have dealt with related problems, and the most important papers will be discussed briefly.

In single crystals of many metals it is known that the main mechanism of plastic distortion on a microscopic (though not atomic) scale is simple shear parallel to preferred planes and directions. At ordinary temperatures both the planes and directions are generally those of closest atomic packing. It is observed that pronounced slip (or glide) is initiated along the particular plane and direction for which the corresponding component of shearing stress first reaches a certain critical value under increasing external load. This critical value depends on the temperature and rate

* Communicated by the Authors.

of straining, but not on the crystal orientation or the type of load (provided the loading-path is not such as to induce hysteresis effects). This has been established for metals such as copper, aluminium, nickel, magnesium, zinc and cadmium by the experiments of Mark, Polanyi and Schmid (1922), Taylor and Elam (1923), Polanyi and Schmid (1923) and Schmid (1924), among others. Double slipping is observed if the critical shear stress is reached simultaneously on two of the possible planes and directions.

The problem of predicting the tensile yield stress of a polycrystalline face-centred cubic metal was considered by Sachs (1928) and by Cox and Sopwith (1937) on the assumptions that (i) each grain is subjected to a uniaxial stress parallel to the specimen axis sufficient to initiate slipping in the most highly stressed direction; (ii) all orientations are equally likely; (iii) each grain is in the same state of work hardening. The resultant axial load on the specimen was calculated as the sum of the individual loads in the constituent grains. The value obtained for the macroscopic uniaxial yield stress was 2.2τ (approximately), where τ is the shear yield stress of a single crystal. This treatment is open to the objections that the grains could not form a coherent whole if only a single homogeneous glide occurred in each, and that the necessary conditions of equilibrium could not be satisfied across grain boundaries if the stress in each were a simple tension of varying amount.

Kochendörfer (1941) added the further hypothesis that the grains extend by the same amounts in the direction of the specimen axis. This enabled him to calculate the stress-strain curve of the aggregate. For in each grain

$$\sigma/\tau = d\gamma/d\epsilon = m$$

where σ is the axial stress in a grain, $d\epsilon$ is the common axial strain-increment, $d\gamma$ is the increment of shear strain in the slip direction, and m is a dimensionless factor depending only on orientation. (In passing, it may be noted that the virtual work equation $\sigma d\epsilon = \tau d\gamma$ is naturally satisfied). We now interpret the various symbols as mean values over all orientations, so that $m \simeq 2.2$ from Sachs' calculations. It follows that the stress-strain curve of the aggregate is

$$\sigma = m\tau(\gamma) = m\tau(m\epsilon)$$

where $\tau(\gamma)$ is the shear-hardening curve (the transition from $d\gamma = m d\epsilon$ to $\gamma = m\epsilon$ is legitimate since m is independent of the amount of strain on the assumption of continuing isotropy). However, the best fit of this $\sigma(\epsilon)$ relation to Taylor's experimental curve for aluminium gives a value of about 3.1 for m .

In a recent paper (1950) Calnan and Clews considered the particular directions in which a pure tension would need to be applied to operate simultaneously either 4, 6, or 8 shears in a face-centred cubic lattice. They assumed the stress state in each grain to be a uniaxial tension of this kind and of the requisite amount. Each grain is assumed to undergo

the specimen extension (and not the strain as a whole). Thus, the objections raised against previous work with regard to the independent action of the grains apply here, also. Despite this Calnan and Clews' computations led to a stress-strain curve in fair agreement with that measured for polycrystalline aluminium.

A more realistic calculation of the tensile yield stress of a face-centred cubic aggregate is due to Taylor (1938), who assumed that each grain undergoes the same uniform strain (so maintaining cohesion). This requires, in general, the operation of at least 5 independent shears out of the 12 operable at ordinary temperatures. Hence, if only geometry is considered, many choices are possible for a given strain. Taylor introduced the hypothesis that the actual active set of shears is that for which the sum of their separate magnitudes is least. The hypothesis has no obvious *a priori* justification, but Taylor based it on observations of single crystals under uniaxial stress and on a postulated analogy with the dynamics of a non-conservative mechanical system. By adding the further assumption that the shear hardening of a crystal during simultaneous glide depends only on the sum of the absolute shears, Taylor was able to compute a stress-strain curve for an aluminium aggregate in fairly close agreement with the measured curve. There are two main criticisms of this approach: first, it is not proved that a combined stress could always be found to operate any geometrically possible set of shears (without exceeding the critical shear stress in non-active directions); and, second, no account is taken of stress-continuity conditions across grain boundaries.

All these previous investigations have been confined to an aggregate under simple tension or compression. In the present paper no such restriction is placed on the applied load.

§ 2. THE MACROSCOPIC THEORY OF PLASTICITY.

In order to appreciate the aim of the present work it is necessary to be familiar with the premises of the macroscopic theory of plasticity. These will be summarized here; a full discussion has been given by Hill (1950).

The theory assumes a locally homogeneous material (possibly anisotropic) having a sharp yield point after work-hardening. The yield criterion for a metal in a given state of hardening is assumed not to depend on the hydrostatic component σ of the applied stress σ_{ij} , and is usually taken to have the form

$$f(\sigma'_{ij}) = c; \quad \sigma'_{ij} = \sigma_{ij} - \sigma \delta_{ij}. \quad \dots \dots \dots (1)$$

This equation may be regarded as defining a surface in stress hyperspace; the surface is "cylindrical", with generators parallel to the direction δ_{ij} . An assumption adequate for many applications, though not necessary in principle, is that the function f does not involve parameters depending on the previous strain-history. The dependence of the shape and size

(iii) *Complementary Minimum Principle.*

Consider a mass in an equilibrium plastic state $(\sigma_{ij}, d\epsilon_{ij})$ and let $d\epsilon_{ij}^*$ be any strain-increment; $d\epsilon_{ij}$ and $d\epsilon_{ij}^*$ are derived from continuous displacement increments du_i and du_i^* taking the same values on the surface and having zero divergence everywhere. It may be proved (Hill, *op. cit.*, p. 67) that

$$\int (|\sigma'_{ij}| |d\epsilon_{ij}|) dV \leq \int (|\sigma'_{ij}| |d\epsilon_{ij}^*|) dV, \quad \dots \quad (7)$$

where

$$|\sigma'_{ij}| = \sqrt{(\sigma'_{ij}\sigma'_{ij})}, \text{ etc.,}$$

provided the material is isotropic and the plastic potential is a *circular* cylinder in principal-stress space; i.e. $f = \sigma'_{ij}\sigma'_{ij}$ in (3). If the state of hardening is uniform, (7) reduces to Markov's result

$$\int |d\epsilon_{ij}| dV \leq \int |d\epsilon_{ij}^*| dV. \quad \dots \quad (8)$$

The analogue of (7) for any plastic potential is

$$\int (\sigma_{ij} d\epsilon_{ij}) dV = \int (\sigma_{ij} d\epsilon_{ij}^*) dV \leq \int (\sigma_{ij}^* d\epsilon_{ij}^*) dV,$$

where (4) is used to derive the inequality, σ_{ij}^* being the plastic stress-state corresponding to $d\epsilon_{ij}^*$.

§ 3. PLASTICITY OF A SINGLE CRYSTAL.

We assume that the only mechanism of plastic distortion in a single crystal is by glide parallel to preferred planes and directions, and we examine the consequences of such an assumption. Let there be n possible slip directions a_1, \dots, a_n (on associated glide planes), for a certain crystal lattice. The displacement of any point of the crystal, due to simultaneous infinitesimal shears $d\gamma_1, \dots, d\gamma_n$ (positive or negative), in the respective directions may be found by simple geometry. The corresponding tensor representing the homogeneous strain has five independent components (its hydrostatic part being necessarily zero), each of which is found as a certain linear combination of $d\gamma_1, \dots, d\gamma_n$. For given $d\gamma_k$ ($k=1, \dots, n$) the strain tensor is thereby uniquely determined.

On the other hand, when the components of the strain tensor are given (the hydrostatic part being zero), we have n unknown $d\gamma_k$ and 5 equations between them. If n is less than 5 (as in a hexagonal metal) a combination of shears cannot be found to produce an *arbitrary* strain. If n is equal to 5 there is a unique set of the $d\gamma_k$ if the determinant of the coefficients is non-zero. If n exceeds 5, a set of 5 slip directions can be selected in any one of nC_5 ways, but the corresponding set of shears can only be found when the associated determinant is non-zero, i.e. when the slip directions form an *independent* set. It may also be possible to find combinations of 6 or more shears to produce the prescribed strain.

any one of a number of stresses (not differing merely by a hydrostatic component), but these stresses all do the same work. For if σ_{ij}^* is also a physically possible stress,

$$(\sigma_{ij}^* - \sigma_{ij}) d\epsilon_{ij} \geq 0,$$

in addition to (9), and therefore $\sigma_{ij}^* d\epsilon_{ij} = \sigma_{ij} d\epsilon_{ij}$.

It is also to be remarked that many sets of shears (even associated with the same stress) may produce, in certain cases, the same strain. That is, more than one set of shears may be physically, as well as geometrically, possible. However, since there are only 5 disposable stress components it is clear that only for certain sets of 5 slip-directions is it possible to find a stress to activate them in *prescribed senses*, since the critical shear stress must also not be exceeded in the non-active directions.

(ii) Minimum Shear Principle for a Single Crystal.

Let $d\epsilon_{ij}$ be a prescribed increment of strain and let σ_{ij} be a stress which will produce this strain by activating a set of shears $d\gamma$. Let $d\gamma^*$ be any set of shears which are geometrically equivalent to the prescribed strain, but which are not necessarily operable by any stress satisfying the yield conditions. The virtual work equation can be written in two ways:

$$\sigma_{ij} d\epsilon_{ij} = \Sigma \tau d\gamma = \Sigma \tau d\gamma^*.$$

If $\tau_k = \tau'_k$ for each direction (no Bauschinger effect),

$$\Sigma \tau d\gamma = \Sigma \tau_k |d\gamma|, \text{ and } \Sigma \tau d\gamma^* \leq \Sigma \tau_k |d\gamma^*|.$$

$$\text{Hence} \quad \Sigma \tau_k |d\gamma| \leq \Sigma \tau_k |d\gamma^*|. \quad (10)$$

In particular, when all directions are equally hardened,

$$\Sigma |d\gamma| \leq \Sigma |d\gamma^*|. \quad (11)$$

This states that the sum of the absolute values of a physically possible set of shears producing a given strain is less than that for a set which is only geometrically possible. If more than one set is physically possible the sums of their absolute values are equal.

We have thereby proved the hypothesis (11) suggested by Taylor (1938), and extended it (10) to the case when the hardening is unequal.

§ 4. POLYCRYSTALLINE AGGREGATE.

The experimental laws of plastic deformation in an aggregate (as a whole) express relations between macroscopic measures of stress and strain. An ideal experiment is designed so that the measuring device gives an average value of stress or strain over a large number of crystal grains. In the interpretation of such measurements the following two assumptions are involved.

(a) The measuring device extends over a volume of such size that the distribution of orientations and hardnesses of crystals (or perhaps fragmented "crystallites") does not vary significantly from one part to another. That is, the specimen is regarded as homogeneous in the macroscopic sense. This does not preclude a macroscopic state of anisotropy, since the actual orientations are not necessarily randomly distributed over all possible ones.

It is convenient to refer to the smallest cubical volume possessing this property as a "unit" cube.

(b) No correlation exists between microscopic stress and position over any plane section of "unit" area. This is the necessary and sufficient condition for the stress resultant over such a unit section to be a single force through the centroid of the section. The Cartesian components of the resultant force per unit area are, of course, the conventional measures of the corresponding components of macroscopic stress. These form a tensor (as a direct consequence of the conditions for linear equilibrium) and the tensor is symmetric if the stress resultant on a plane is a force, and not a force and irreducible couple. If a correlation did exist between microscopic stress and position (and this appears possible in principle), the macroscopic stress tensor would not necessarily be symmetric, and the conditions for angular equilibrium would take another form. These remarks are equally pertinent, of course, to the concept of *microscopic* stress in a single crystal and its dependence on the distribution of interatomic forces.

The definition of a normal component of an infinitesimal *homogeneous* strain is the increment of distance between two points initially unit distance apart in the direction under consideration. The definition of a component of shearing strain is based on the total relative tangential displacements of two pairs of perpendicular planes at unit distance apart. The analogous definition of the macroscopic strain-increment components for a "unit cube" of an aggregate is

$$dE_{ij} = \frac{1}{2} \int (l_i du_j + l_j du_i) dS, \quad \dots \dots \dots (12)$$

where the integral is taken over the surface of the unit cube, l_i being the unit outward normal, and du_i the incremental microscopic displacement (the coordinate axes are taken parallel to the cube edges). When the microscopic displacement is a continuous function of position (no opening of cavities or sliding of one grain over another), Green's theorem gives

$$\begin{aligned} dE_{ij} &= \frac{1}{2} \int \left\{ \frac{\partial}{\partial x_i} (du_j) + \frac{\partial}{\partial x_j} (du_i) \right\} dV, \\ &= \int (d\epsilon_{ij}) dV, \end{aligned}$$

taken through the volume of the unit cube, where $d\epsilon_{ij}$ is the microscopic strain-increment. Since the latter is a symmetric tensor with zero hydrostatic part so also is dE_{ij} .

Consider the work of deformation within a unit cube. It is

$$dW = \int (\sigma_{ij} d\epsilon_{ij}) dV = \int (\sigma_{ij} du_i l_j) dS, \quad (13)$$

provided the displacement function is continuous and the equilibrium equations are satisfied. At grain boundaries, or elsewhere, the microscopic stress is not necessarily continuous in all its components, and only the stress resultants acting on opposite sides of such a surface must be the same for equilibrium.

We now postulate that the grains are distributed in the unit cube in such a way that there is no correlation between any component of the microscopic stress and any component of the displacement over any plane section of unit area. This is so provided that

$$\int \sigma_{ij} dA \times \int du_k dA = \int (\sigma_{ij} du_k) dA (i, j, k = 1, 2, 3), \quad . . (14)$$

where the integration extends over the unit section. In particular, this is satisfied when the stress is uniform or when the strain is uniform (the stress being distributed according to (b) above). Applying (14) to each face of the unit cube, we find from (13) that

$$dW = \int (\sigma_{ij} d\epsilon_{ij}) dV = S_{ij} dE_{ij}, \quad (15)$$

where S_{ij} is the macroscopic stress tensor defined in (b).

(i) *Maximum Work Principle for an Aggregate.*

Let S_{ij}^* be any macroscopic stress corresponding to an equilibrium microscopic distribution σ_{ij}^* not violating the yield conditions at any point of a unit cube. Then, from (15),

$$(S_{ij} - S_{ij}^*) dE_{ij} = \int \{(\sigma_{ij} - \sigma_{ij}^*) d\epsilon_{ij}\} dV \geq 0, \quad (16)$$

since (9) holds at every point. We have thereby derived (4) from assumed properties of a single crystal. It is worth noting that (16) is still true even if du_i is tangentially discontinuous across certain surfaces provided the corresponding frictional stress vanishes. This is approximately true in high-temperature creep where relative slip occurs between grains.

(ii) *Minimum Shear Principle for an Aggregate.*

Let du_i and du_i^* be two continuous displacement distributions, with zero divergence, taking the same values on the surface of a unit cube. du_i is associated with an equilibrium distribution of stress σ_{ij} satisfying the yield conditions. Then

$$\int (\sigma_{ij} d\epsilon_{ij}) dV = \int (\sigma_{ij} d\epsilon_{ij}^*) dV \quad \text{or} \quad S_{ij} dE_{ij} = S_{ij}^* dE_{ij}^*,$$

and so

$$\int (\Sigma \tau d\gamma) dV = \int (\Sigma \tau d\gamma^*) dV.$$

If $\tau_k = \tau'_k$ for each direction at any point (no Bauschinger effect),

$$\Sigma \tau d\gamma = \Sigma \tau_k |d\gamma|, \quad \Sigma \tau d\gamma^* \leq \Sigma \tau_k |d\gamma^*|.$$

Hence

$$S_{ij} dE_{ij} = \int (\Sigma \tau_k |d\gamma|) dV \leq \int (\Sigma \tau_k |d\gamma^*|) dV. \quad . . . (17)$$

When the critical shear stress is uniform throughout the aggregate :

$$\int (\Sigma |d\gamma|) dV \leq \int (\Sigma |d\gamma^*|) dV. \quad (18)$$

This is true whether or not the aggregate has the properties ascribed to the unit cube. There is a close formal analogy between (17) and (7), and between (18) and (8).

On combining (16) and (17) we have for a unit cube, when $\tau_k = \tau'_k$

$$S_{ij} dE_{ij} \leq S_{ij} dE_{ij} \leq \int (\Sigma \tau_k |d\gamma^*|) dV. \quad (19)$$

Another inequality that will be used later is

$$S_{ij} dE_{ij}^* \leq \int (\Sigma \tau_k |d\gamma^*|) dV, \quad (20)$$

where du_i^* is any continuous distribution.

It is to be noticed carefully that in establishing these extremum principles for an aggregate there is an implicit assumption, not merely that slip is the only mechanism of distortion, but that it is also a *sufficient* mechanism. In other words, it is assumed that the equations of equilibrium (5) can be satisfied throughout an aggregate by a stress distribution which, at the same time, will everywhere operate sufficient shears to produce a continuous displacement. For this to be mathematically possible, it may well be that the microscopic stress and strain must be allowed to vary *continuously*, and not be restricted to take constant values within each of a finite number of regions (which may be grains or parts of grains). If a continuous variation is envisaged, the relations between microscopic stress and strain, established for a crystal of a certain finite size, must be assumed to apply *at a point*. This, of course, is a procedure that is adopted in every branch of mechanics.

§ 5. CALCULATION OF THE YIELD SURFACE.

In § 4 (i) a maximum work principle for an aggregate has been shown to hold when slipping under a critical shear stress is the only microscopic mechanism of distortion. It follows from § 2 (ii) that a plastic potential governs the relation between macroscopic stress and strain-increment, and that the plastic potential is identical with the yield function. If, therefore, the yield function can be calculated for any particular metal the relationships between the ratios of the stress components and the ratios of the strain-increment components follow immediately from (3).

We consider first what general properties of the yield function follow from the assumption of deformation by slip. It is evident that the hydrostatic part of the applied stress has no influence on yielding ; that is, the yield surface is cylindrical (though not, of course, necessarily circular). This follows since the superposition of a uniform hydrostatic stress throughout a plastic aggregate does not disturb the equilibrium of the microscopic stresses, nor does it alter the active slip-directions at any point, when the influence of elasticity is disregarded. In reality, however, a certain effect of hydrostatic stress would be expected in an aggregate of elastically anisotropic grains.

If the critical shear stress does not depend on the sense of slip, and if the aggregate is free from internal stress when the applied loads are removed after cold-work, the yield surface for that state is symmetrical about the origin. That is, if S_{ij} produces yielding when the aggregate is reloaded under constant stress-ratios so also will $-S_{ij}$. For the elastic compatibility equations are linear in the stresses, and hence if a microscopic distribution σ_{ij} corresponding to S_{ij} can be established by monotonic loading from a stress-free state so also can a distribution $-\sigma_{ij}$ corresponding to $-S_{ij}$. Furthermore, if σ_{ij} satisfies the yield conditions at any point so does $-\sigma_{ij}$, and if $d\epsilon_{ij}$ is the increment of strain associated with σ_{ij} , $-d\epsilon_{ij}$ is the increment associated with $-\sigma_{ij}$. Plastic deformation would therefore be initiated under the stress $-S_{ij}$.

When the aggregate is macroscopically isotropic the yield surface can be shown to possess a six-fold symmetry in principal-stress space (Hill 1950, p. 18). Since this symmetry does not depend on any particular mechanism of plastic distortion, we do not need to discuss it here.

The exact calculation of the yield surface appears to be a matter of some difficulty. In the present paper we shall merely show that it is possible to calculate, with comparative ease, two cylindrical surfaces between which the yield surface must certainly lie when there is no Bauschinger effect. For this purpose we use the inequalities established in the last section. In one case we consider an aggregate in which the stress is uniform but displacement continuity is violated, and in the other case we consider an aggregate in which the strain is uniform but equilibrium is violated.

Take first the uniform stress distribution

$$\sigma_{ij}^* = \lambda^* r_{ij}, \quad r_{ij} = S_{ij} / (S_{ij} S_{ij})^{1/2}, \quad \dots \dots (21)$$

where, for given stress-ratios r_{ij} , λ^* is to be chosen so that the critical shear stress corresponding to σ_{ij}^* is just attained in one slip-direction at the "weakest" point of the aggregate. It is then certain that σ_{ij}^* does not violate the yield conditions anywhere in the aggregate. σ_{ij}^* is therefore an equilibrium distribution such as is envisaged in (16) (the displacement function being continuous) which leads to

$$(S_{ij} S_{ij})^{1/2} = |S_{ij}| \geq \lambda^*. \quad \dots \dots (22)$$

Hence, for each direction r_{ij} in stress hyperspace, (22) supplies a lower limit to the length of the corresponding "radius" to the yield surface. Since we know that the surface is cylindrical we need only take stresses S_{ij} with zero hydrostatic part in (21).

Next take any *uniform* strain distribution $d\epsilon_{ij}^* = dE_{ij}^*$ with zero hydrostatic part, and such that $r_{ij} dE_{ij}^* > 0$. Let $d\gamma^*$ be any of the sets of shears which are equivalent to the strain dE_{ij}^* . $d\gamma^*$ is a function of position since the lattice orientation varies through the aggregate. Let a quantity μ^* be defined such that

$$\mu^* = \int (\Sigma \tau_k |d\gamma^*|) dV / r_{ij} dE_{ij}^*, \quad \dots \dots (23)$$

where r_{ij} is defined in (21) and the integration extends through the unit cube. Then, by (20),

$$|S_{ij}| \leq \mu^* \quad \dots \quad (24)$$

According to (10) the least possible value of μ^* for any choice of dE_{ij}^* is to be obtained by taking $d\gamma^*$ to be a *physically* possible set of shears for each orientation, the "crystallites" being supposed completely independent. Then

$$\mu^* = (dE_{ij}^* \int \sigma_{ij}^* dV) / (r_{ij} dE_{ij}^*), \quad \dots \quad (25)$$

where σ_{ij}^* is a stress which would produce the strain dE_{ij}^* in a free crystal. An advantageous choice of dE_{ij}^* appears to be $dE_{ij}^* = r_{ij}$ (an arbitrary scale factor can obviously be omitted for convenience). Then, since $r_{ij}r_{ij}=1$,

$$\mu^* = r_{ij} \int \sigma_{ij}^* dV. \quad \dots \quad (26)$$

This value of μ^* is equal to the work which would be done if a unit cube of aggregate were split into its constituent regions of uniform orientation and each were separately given the strain r_{ij} .

§ 6. DEPENDENCE OF YIELD SURFACE ON STRAIN-HISTORY.

We have not yet considered how the shape and size of the yield surface depend on the previous strain-history. For simplicity let us disregard possible Bauschinger effects both in a crystal grain and in the aggregate as a whole, and suppose also that the critical shear stress is the same in all slip directions. If there were no work-hardening it is evident that the shape and size of the yield surface would be preserved during continued deformation, provided the distribution of orientations did not vary. (This last condition will not be satisfied whenever a preferred orientation is developed during cold-working). When work-hardening occurs the grains harden by different amounts, due partly to the non-uniform distortion and partly to their different orientations. However, to a first approximation, it seems reasonable to expect that the yield surface will simply increase in size without changing shape. The size will be proportional to some mean value of the critical shear stress.

There is some evidence (Taylor 1927) that the shear yield stress of a crystal is, very roughly, a function only of the total shear. That is,

$$\tau = F(\Sigma\gamma),$$

where the function F is the hardening curve in simple slip. Now we have seen that the work done on the aggregate unit cube during an increment of strain is

$$\begin{aligned} dW &= \int (\tau \Sigma |d\gamma|) dV, \\ &= \tau \Sigma |d\gamma|, \end{aligned}$$

say, where τ and γ now denote mean values over the aggregate. Hence, approximately

$$dW = \tau d\tau / F'$$

where F' is the slope of the shear-hardening curve. Since F' is a function of τ only, so also is W . Conversely, the mean critical shear stress is a function only of the total plastic work.

These qualitative considerations lead, therefore, to the conclusion that the size of the yield surface is mainly a function of the total plastic work, and that other factors are secondary (in the absence of Bauschinger effects). This, indeed, is observed for face-centred cubic metals (see Hill 1950, pp. 27-32).

ACKNOWLEDGMENT.

We wish to thank the Director of the Mechanical Engineering Research Organization, D.S.I.R., for permission to publish this paper, one of us (J. F. W. B.) being seconded by D.S.I.R. to the Wills Physical Laboratory.

REFERENCES.

- CALNAN, E. A., and CLEWS, C. J. B., 1950, *Phil. Mag.*, **41**, 1085.
 COX, H. L., and SOPWITH, D. G., 1937, *Proc. Phys. Soc.*, **49** (ii), 134.
 HILL, R., 1950, *The Mathematical Theory of Plasticity* (Oxford: Clarendon Press).
 KOCHENDÖRFER, A., 1941, *Reine und angewandte Metallkunde* (Berlin: Springer).
 MARK, H., POLANYI, M., and SCHMID, E., 1922, *Z. f. Phys.*, **12**, 58.
 POLANYI, M., and SCHMID, E., 1923, *Z. f. Phys.*, **16**, 336.
 SACHS, G., 1928, *Z. d. Ver. deut. Ing.*, **72**, 734.
 SACHS, G., and SHOJI, H., 1927, *Z. f. Phys.*, **45**, 776.
 SCHMID, E., 1924, *Proc. Int. Congr. App. Mech. (Delft)*, 342.
 TAYLOR, G. I., 1927, *Proc. Roy. Soc. A*, **116**, 39; 1938, *Journ. Inst. Met.*, **62**, (i), 307; 1938, *S. Timoshenko Anniversary Volume*, 218 (New York: Macmillan).
 TAYLOR, G. I., and ELAM, C. F., 1923, *Proc. Roy. Soc. A*, **102**, 643; 1925, *Ibid.*, **108**, 28.

XLVII. ABSTRACT.

The Capacitance of a Parallel-Plate Condenser with an Anisotropic Dielectric Cylinder in Torsion between its Plates.

By C. MACK,

The British Cotton Industry Research Association,
Shirley Institute, Manchester*.

[Received February 1, 1951.]

An abstract of the above paper is given here.

[The full paper will be published in the Shirley Institute Memoirs and copies may be obtained from the Director, Shirley Institute, Manchester, 20.]

1. PROBLEMS SOLVED.

THE solution to this problem is important in estimating the accuracy of the capacitance method of measuring the irregularity of cotton yarn (Boyd 1949 and Walker 1950). The dielectric properties of cotton fibres are such that (Balls 1946) a single cotton yarn may be represented by a uniformly twisted cylinder which, in the untwisted state, has one dielectric constant value along its length but a different, though axially symmetric, transverse value.

We first find the field when the cylinder is placed in a general type of field $F(R)$ $[\cos n\phi - \sin n\phi]$ (see equation (1)). This calculation is carried out by using a molecular model and mathematical process akin to that of Lorentz's molecular dielectric theory, thus obtaining a pair of simple simultaneous integral equations (see (3)). If the twist is not too great a series solution is obtained when $F(R) = R^n$. With this series the field when the cylinder is placed parallel to and between two infinite conducting planes at different potentials is found by means of multipliers which can be determined to any required accuracy. By assuming that finite plates do not alter the field, the charge on the plates is calculated and finally the capacity. For non-midway positions the calculated capacity is not quite exact but is a good approximation if the plates are wide compared with their distance apart. An approximate solution valid for most midway cases is given (see (10)).

Acknowledgments are due to Mr. C. Illingworth of Manchester University for many helpful discussions and to Miss M. Castle of the Shirley Institute who has checked much of the mathematics and carried out the numerical work.

* Communicated by the Author.

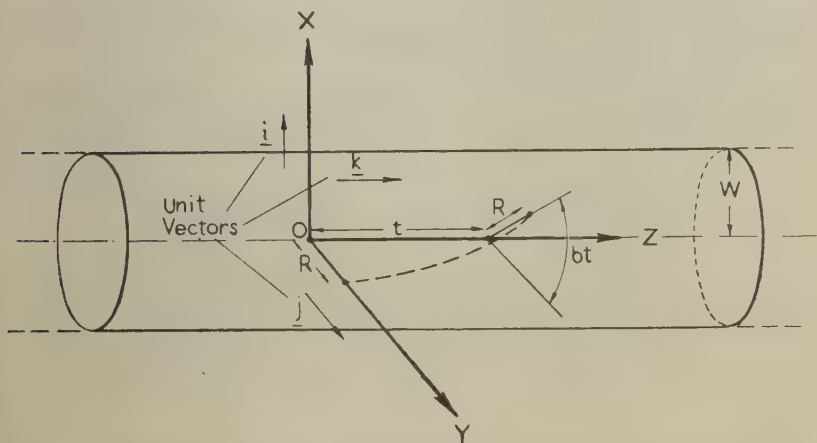
2. RESULTS.

We consider an infinitely long circular cylinder of radius W which has a dielectric constant K_2 parallel to its axis but an axially symmetric transverse value K_1 . It is then twisted so that a line of molecules originally parallel to OZ , the axis, lies along the helix $x=R \cos bt$, $y=R \sin bt$, $z=t$, where b is a constant, $0 \leq R < W$ and $-\infty \leq t < +\infty$ (fig. 1).

We then prove that an externally applied field

$$F(R) [\cos N\phi i - \sin N\phi j] \quad . \quad . \quad . \quad (1)$$

Fig. 1.



where $N=0, 1, 2, \dots$, $x=R \cos \phi$ and $y=R \sin \phi$, produces a distribution of molecular dipoles of density

$$[A' \cos N\phi + B' \cos (N+2)\phi] i + [-A' \sin N\phi + B' \sin (N+2)\phi] j + C' \sin (N+1)\phi k \quad . \quad . \quad (2)$$

where $A'=k_1 A + bR J$, $B'=k_1 B - bR J$, $C'=k_1 C - 2J$

$$4\pi k_2 (K_2 + 2) = 3(K_2 - 1), \quad 4\pi k_1 (K_1 + 2) = 3(K_1 - 1)$$

$$2J(1 + b^2 R^2) = (k_2 - k_1) [bR(A - B) - C], \quad 3C = 4\pi C'$$

$$A - F(R) = -2\pi \left[A'(R)/3 + B'(R) - \frac{2}{3}(N+1)R^N \int_R^W \left\{ B'(S)/S^{N+1} \right\} dS \right]$$

$$B = -2\pi \left[B'(R)/3 + A'(R) - 2(N+1)R^{-(N+2)} \int_0^R A'(S)S^{N+1} dS \right] \quad . \quad . \quad (3)$$

Outside the cylinder the field resulting from (2) is

$$D'[\cos(N+2)\phi i - \sin(N+2)\phi j]/R^{N+2}, \quad D' = 4(N+1)\pi \int_0^W A'(S)S^{N+1} dS \quad . \quad . \quad (4)$$

Straightforward expansions solve the simultaneous integral equations (3) when $F(R)=2\pi(bR)^N$. Writing $bR=u$, $bW=U$

$$A'=u^N \sum_0^\infty a_m u^{2m}=A'_N, \text{ say; } B'=u^N \sum_1^\infty b_m u^{2m}=B'_N, \text{ say;}$$

$$C'=u^{N-1} \sum_1^\infty c_m u^{2m}=C'_N, \text{ say; } D'=2\pi(N+1)W^{2N+2} \sum_0^\infty a_m U^{2m}/(N+m+1) \\ =D'_N, \text{ say}$$

$$6K_1 a_m = J_{m-1}(K_1+2) [2K_1 + (N+1)(K_1-1)/m], \quad 3c_m = -2J_{m-1}(K_1+2),$$

$$6K_1 b_m = -J_{m-1}(K_1+2) [2K_1 - (N+1)(K_1-1)/(m+N+1)],$$

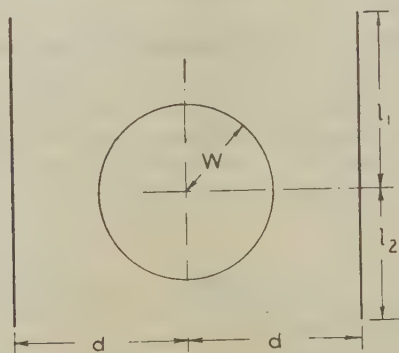
$$m=1, 2, 3 \dots, |U| \leq 1,$$

$$J_m/J_{m-1} = -1 + (K_2 - K_1)(N+1)^2/[4K_1 m(m+N+1)],$$

$$3(K_1-1)J_0 = 2(K_2+2)a_0$$

$$a_0(K_1+1) - (N+1)(K_1-1)[b_1 U^2 + b_2 U^4/2 + b_3 U^6/3 + \dots] = K_1 - 1 \dots \quad (5)$$

Fig. 2.



All quantities are first expressed in terms of a_0 then from the last equation the value of a_0 is found.

When the cylinder is placed between two infinite parallel conducting planes kept at different potentials we assume the dipole density to be

$$\sum_{N=0}^{\infty} \mu_N R^N [\{A'_N \cos N\phi + B'_N \cos (N+2)\phi\}i + \{-A'_N \sin N\phi \\ + B'_N \sin (N+2)\phi\}j + C'_N \sin (N+1)\phi k] \dots \quad (6)$$

At each image of the cylinder we imagine a cylinder with the same distribution (6) except that, for odd N , the μ_N change sign. At the images of these images we assume (6) with unchanged sign. At the images of these, odd μ_N change sign and so on. We then calculate the field at the original cylinder due to the original field and these images and we expand it thus

$$\sum_{N=0}^{\infty} F_N R^N [\cos N\phi i - \sin N\phi j] \dots \quad (7)$$

where the F_N are infinite linear combinations of the μ_N . From (5) the dipole density (7) would generate is calculated and must equal (6). By neglecting μ_N for $N \geq M$ we obtain a finite number of linear equations for the μ_N . Numerical results indicate that by taking M large enough any desired accuracy can be achieved.

The case of the cylinder midway between the plates is considered in detail (Fig. 2). Provided the potential difference between the plates is $2d$, we have, writing

$$\sum_1^{\infty} (1/s)^r = S_r$$

$$\pi\mu_0 = \frac{1}{2} + \sum_0^{\infty} \mu_{2m} D'_{2m} S_{2m+2} (2d)^{-(2m+2)}, \quad \pi b^2 \mu = \sum_0^{\infty} \mu_{2m+3} C_{2\mu_{2m}} D'_{2m} S_{2m+4} (2d)^{-2m-4}$$

$$\pi b^4 \mu_4 = \sum_0^{\infty} \mu_{2m+5} C_{4\mu_{2m}} D'_{2m} S_{2m+6} (2d)^{-2m-6} \text{ etc.}; \quad \mu_1 = \mu_3 = \mu_5 = \dots = 0. \quad (8)$$

The charge per unit length induced on the width AB (fig. 2) is

$$\frac{1}{2} \sum_{m=0}^{\infty} (-1)^m \frac{\mu_{2m} D'_{2m} W_{4m+2}}{(2m+1)!} \left(\frac{\pi}{2d} \right)^{2m+1} \left[\frac{d^{2m} \tanh \beta}{d\beta^{2m}} \right]_{\beta=\pi l_1/(2d)}. \quad (9)$$

The charge induced on AB' is the same with l_1 replaced by l_2 . In the case of finite plates we assume that the charge induced is not materially altered. Dividing by the potential difference we obtain the increase in capacity per unit length δC . For fig. 2 a good approximation is

$$\delta C \doteq \frac{3D'_0 \{ \tanh[\pi l_1/(2d)] + \tanh[\pi l_2/(2d)] \}}{4(24\pi d^2 - \pi^2 D'_0)}. \quad (10)$$

A method of successive approximations is also given which may be applicable to other problems.

The solution, in the form of an expansion, to an applied field

$$R^M [\cos N\phi i - \sin N\phi j], \quad M \neq N$$

is also found (hence the more general case $\sum f_M R^M [\cos N\phi i - \sin N\phi j]$ can be solved).

REFERENCES.

- BALLS 1946, *Dielectric Properties of Raw Cotton*, *Nature*, 1946, **158**, 9-11.
 BOYD 1949, *An Electronic Instrument for Measuring Weight Variations in Silvers, Rovings and Yarn*, *Journal of the Textile Institute (Transactions)*, July, 1949.
 WALKER 1950, *The Electronic Measurement of Sliver, Roving and Yarn Irregularity*, Annual Conference of the Textile Institute, 1950.

XLVIII. CORRESPONDENCE.

The Resistance-Minimum in Gold.

By D. K. C. MACDONALD and I. M. TEMPLETON,
The Clarendon Laboratory, Oxford*.

[Received February 1, 1951.]

THE definite observation of a minimum in the electrical resistance of gold at low temperatures was first made by de Haas, de Boer and van den Berg (1933) and has so far received no satisfactory theoretical explanation. Later measurements by de Haas and van den Berg (1936, 1937) and Giaque, Stout, Clark (1937); Stout and Barieau (1939) have given evidence that the temperature of the minimum was a unique function of the relative resistance at the minimum (usually measured as $(R_{\min}/R_{0^\circ \text{C.}})$) for annealed specimens and that for an ideally pure specimen the minimum would occur at absolute zero. It has been suggested (*cf.* Gorter 1938) that the resistance of any specimen would rise towards infinity if the temperature were lowered sufficiently far, but this suggestion hardly seems feasible particularly in view of the remarkable behaviour then to be expected at extremely low temperatures in a specimen of vanishingly small impurity.

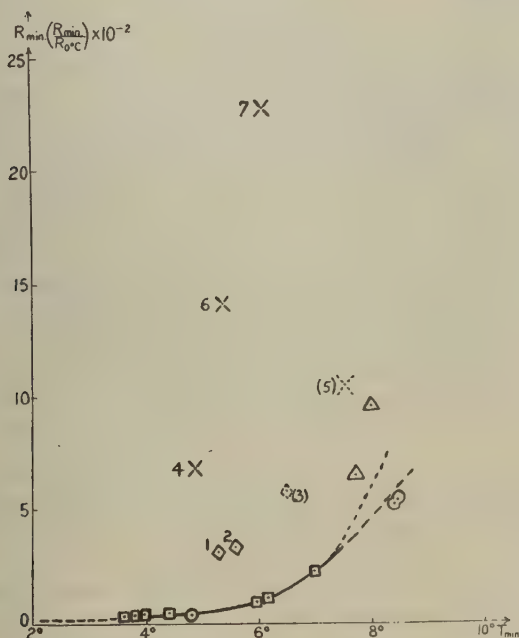
Two very tentative theories by one of us (D. K. C. McD.) suggest that the resistance would pass through a point of inflexion below the minimum and then flatten off ultimately on approach to absolute zero at a higher value than the minimum. Both theories suggest, however, that the nature of the particular impurity atoms present would affect the situation of the minimum. Since it appears likely that the major impurity present in the specimens available to the Dutch and American workers would generally be silver (the latter workers in fact worked specifically in one case with a range of Au-Ag alloys and report silver as the major impurity in the later work) it seemed profitable to investigate some prepared alloys containing other specific impurities. At the same time specimens with *no* intentionally inserted impurity were examined by us.

Alloys containing respectively 0.05 per cent (by weight) of Cu and Ni and 0.2 per cent of Ni were made for us by Messrs. Johnson, Matthey and Co. Ltd., and we also experimented with a sample of fine gold which we drew down to a suitable diameter and a sample of "spectrographically pure" gold. As may be seen from the accompanying graph which also displays the data obtained elsewhere, the latter two specimens agree rather well with the curve of R_{\min} against T_{\min} suggested by the other workers. (It should be noted that the minima derived in America are only

* Communicated by the Authors

approximate since they do not have experimental results above $\sim 4^\circ \text{K.}$ or below $\sim 10^\circ \text{K.}$). However the results for our "alloys" do not agree at all and this suggests very strongly that the presumption of a simple variation with residual resistance alone cannot be accepted. In fact, it seems tempting to assume that there is a characteristic curve for each type of impurity atom.

Fig. 1.



□ : Data of : de Haas and v. d. Berg. △ : Data of Giaque, Stout *et al.*
 ○ : Data of : Present work—“Specpure” and “fine” gold.

◇ : Data of : Present work—0.05% Cu/Au { 1. “Hot” annealed.
 2. “Cold” annealed.
 3. Unannealed.

× : Data of : Present work—Ni/Au { 4. 0.05% “Hot” annealed.
 5. 0.05% Unannealed.
 6. 0.2% “Hot” annealed.
 7. 0.2% “Cold” annealed.

Since it was thought that the precise method of annealing might be critical (*e. g.* Stout and Barieau annealed their wire for three hours at 450°C.) we have annealed specimens at $\sim 400^\circ \text{C.}$ for 2–3 hours and also at $\sim 850^\circ \text{C.}$ (onset of bright red heat) for about the same period. There appears to be little difference in the cases of the “pure” gold specimens and Cu/Au alloy but in the 0.2 per cent Ni/Au alloy a considerable

improvement in residual resistance occurred with the "hot" annealing over the "cold" process with a slight shift of the minimum to a lower temperature. We may also mention that in the 0.05 per cent Ni and Cu alloys annealing by either method produced a considerable minimum shift to a lower temperature—the points for the unannealed specimens are shown by dotted characters on the graph.

Further experiments are in progress and it is hoped to publish the work in more detail later.

REFERENCES.

- GIAUQUE, STOUT and CLARK, 1937, *Phys. Rev.*, **51**, 1108.
GORTER, 1938, *Physica*, **5**, 483.
* DE HAAS, DE BOER, and V. D. BERG, 1933, *Physica*, **1**, 1115.
* DE HAAS and V. D. BERG, 1936, *Physica*, **3**, 440; 1937, *Ibid.*, **4**, 683.
STOUT and BARRIEAU, 1939, *Journ. Amer. Chem. Soc.*, **61**, 238.

The Range-Energy Relation for Slow Alpha-Particles in Air.

By JOAN M. FREEMAN and W. E. BURCHAM,
Cavendish Laboratory, Cambridge†.

[Received February 13, 1951.]

DURING some recent work on (α) reactions (Burcham and Freeman 1949 a, b) the ranges in air of a number of groups of alpha-particles with energies between 1 and 2.5 MeV. were compared. The measured range differences were used to obtain the energy differences for the corresponding groups of alpha-particles, with the aid of the range-energy relation given by Holloway and Livingston (1938). This range-energy relation was constructed on the assumption that the number of ions formed by an alpha-particle stopping in air was strictly proportional to its energy; this assumption has recently been shown to be incorrect (Jesse and Sadauskis 1950), and a new range-energy relation has been given by these authors and also by Bethe (1950). The difference between the new and old range-energy curves is most significant for energies below about 2.5 MeV., and the new relation is in good agreement with observations on the ${}^6\text{Li}(\alpha x)$ and ${}^{10}\text{B}(\alpha x)$ reactions, for which the alpha-particle ranges have been measured, and the energy releases are also accurately known as a result of magnetic deflection experiments (see Bethe 1950). The number of points on the range-energy curve for energies less than 2.5 MeV., for which direct measurements of range and energy have been made is however small. It was therefore thought

* Or see: V. D. BERG, 1938, *Thesis*, Leiden, "De Electriche Weerstand van zuivere Metalen bij lage . . . Temperaturen".

† Communicated by the Authors.

to be of some interest to use the range measurements made during the work on ($p\alpha$) reactions to check the slope of the range-energy curve in the region from 2.5 down to 1.0 MeV.

The measurements were made by a method previously described (Burcham and Freeman 1949 a, § 3 (a)). The reactions studied, together with the energy releases deduced from recent magnetic deflection measurements are shown below (Table I.).

TABLE I.
Energy Releases in ($p\alpha$) reactions.

Reaction	Q (MeV.)	Reference
${}^9\text{Be}(p\alpha){}^8\text{Li}$	2.121 ± 0.012 2.142 ± 0.006	Tollestrup, Fowler and Lauritsen (1949) Strait <i>et al.</i> , quoted by Hornyak, Lauritsen, Morrison and Fowler (1950)
${}^{10}\text{B}(p\alpha){}^7\text{Be}$	1.148 ± 0.006 1.152 ± 0.004 1.147 ± 0.010	Brown, Chao, Fowler and Lauritsen (1950) Van Patter, Sperduto, Strait and Buechner (1950) Burcham and Freeman (1950)
${}^{19}\text{F}(p\alpha_1){}^{16}\text{O}^*$	1.977 ± 0.008 1.979 ± 0.009	Chao, Tollestrup, Fowler and Lauritsen (1950) Freeman (1950)
${}^{19}\text{F}(p\alpha_2){}^{16}\text{O}^*$	1.204 ± 0.008 1.200 ± 0.010	Chao, Tollestrup, Fowler and Lauritsen (1950) Freeman (1950)
${}^{19}\text{F}(p\alpha_3){}^{16}\text{O}^*$	1.002 ± 0.008 0.996 ± 0.010	Chao, Tollestrup, Fowler and Lauritsen (1950) Freeman (1950)

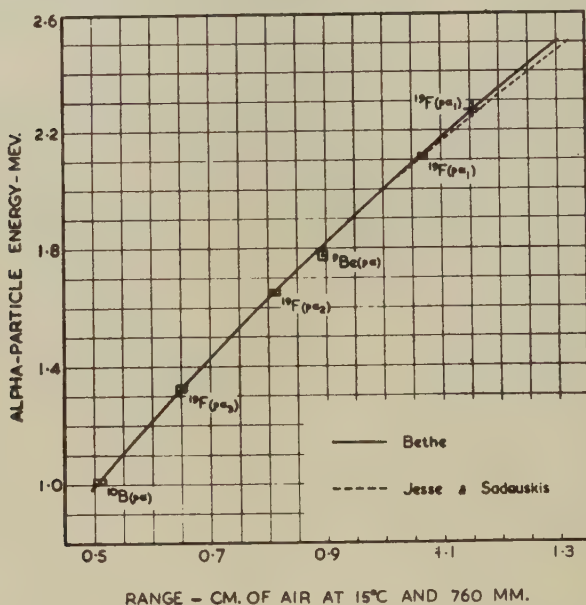
At the time at which the measurements were made the Q-value for ${}^9\text{Be}(p\alpha)$ seemed the best known, and all range comparisons were made with the alpha-particles from this reaction taken as standard. We have now chosen the ${}^{19}\text{F}(p\alpha_1)$ reaction with $E_p = 873.5$ keV. and angle of observation 83° , as the standard, giving alpha-particles of energy 2.272 ± 0.010 MeV.; the corresponding mean range, from the curve given by Bethe (1950), is 1.157 cm. The observed range differences then lead, after small corrections for differences of straggling and target thickness, to the mean ranges given in Table II. The energies shown in this Table were calculated, for the given conditions of bombardment, from the Q-values listed in Table I.; for the ${}^{19}\text{F}(p\alpha)$ reactions the Q-values given by Chao, Tollestrup, Fowler and Lauritsen were used, since the values obtained by Freeman, although in good agreement, were based on a spectrometer calibration which involved the Q-value of the ${}^9\text{Be}(p\alpha)$

reaction. This was assumed at the time to be 2.121 MeV., but the more recent measurement gives an appreciably higher value (see Table I.). The weighted mean of the two Q-values was used to calculate the energy given in Table II. for the alpha-particles from the ${}^9\text{Be}(p\alpha)$ reaction.

TABLE II.
Range Energy Relation.

Reaction	E_p (keV.)	E_α (MeV.) (Angle of observation 83°)	Mean range cm. of air at 15°C ., 760 mm.
${}^{19}\text{F}(p\alpha_1){}^{16}\text{O}^*$	669	2.113 ± 0.010	1.068 ± 0.008
${}^9\text{Be}(p\alpha){}^6\text{Li}$	860	1.774 ± 0.015	0.895 ± 0.008
${}^{19}\text{F}(p\alpha_2){}^{16}\text{O}^*$	873.5	1.649 ± 0.010	0.812 ± 0.008
${}^{19}\text{F}(p\alpha_3){}^{16}\text{O}^*$	669	1.326 ± 0.010	0.651 ± 0.008
${}^{10}\text{B}(p\alpha){}^7\text{Li}$	630	1.113 ± 0.007	0.559 ± 0.011

Fig. 1.



These results are plotted in fig. 1, together with the curves proposed by Bethe (1950) and Jesse and Sadauskis (1950). The standard point for ${}^{19}\text{F}(p\alpha_1)$ at $E_p = 873.5$ keV. has been placed on the former curve, and

all the other points, except that for ${}^9\text{Be}(p\alpha)$, lie within 10 keV. of the curve. The position of the point for ${}^9\text{Be}(p\alpha)$ suggests that the higher Q-value of the two given in Table I. is the more nearly correct.

The results confirm the slope of the new range-energy curves over the energy range 1.0–2.3 MeV. ; they are in slightly better agreement with the curve given by Bethe (1950) than with the figures given by Jesse and Sadauskis in the region where these differ. .

REFERENCES.

- BETHE, H. A., 1950, *Rev. Mod. Phys.*, **22**, 213.
BURCHAM, W. E., and FREEMAN, J. M., 1949 a, *Phil. Mag.*, **40**, 807 ; 1949 b, *Phys. Rev.*, **75**, 1756 ; 1950, *Phil. Mag.*, **41**, 337.
BROWN, A. B., CHAO, C. Y., FOWLER, W. A., and LAURITSEN, C. C., 1950, *Phys. Rev.*, **78**, 88.
CHAO, C. Y., TOLLESTRUP, A., FOWLER, W. A., and LAURITSEN, C. C., 1950, *Phys. Rev.*, **79**, 108.
FREEMAN, J. M., 1950, *Phil. Mag.*, **41**, 1225.
HOLLOWAY, M. G., and LIVINGSTON, M. S., 1938, *Phys. Rev.*, **54**, 18.
HORNIAK, W. F., LAURITSEN, T., MORRISON, P., and FOWLER, W. A., 1950, *Rev. Mod. Phys.*, **22**, 291.
JESSE, W. P., and SADAUSKIS, J., 1950, *Phys. Rev.*, **78**, 1.
TOLLESTRUP, A., FOWLER, W. A., and LAURITSEN, C. C., 1949, *Phys. Rev.*, **76**, 428.
VAN PATTTER, D. M., SPERDUTO, A., STRAIT, E. N., and BUECHNER, W. W., 1950, *Phys. Rev.*, **79**, 900.

XLIX. *Notices of New Books and Periodicals received.*

Weltsystem, Weltather, und die Relativitaetstheorie. By K. JELLINCK. Pp. 450. (Verlag, Basel : Wepf and Co., 1949.) Price 45 S.Fr.

Verstandliche Elemente der Wellenmechanik. By K. JELLINCK. 1 Teil. Pp. 304. (Verlag, Basel : Wepf and Co., 1950.) Price 34 S.Fr.

PROFESSOR JELLINCK may be known to many readers as the author of an extensive work on Physical Chemistry. In the preface to the book on the Theory of Relativity he confides that he has always wanted to understand this theory, but not finding a suitable textbook, he decided to write one both for himself and for the great number of experimental physicists and chemists.

As the title suggests the author believes that the Theory of Relativity can be understood only by postulating an absolute frame of reference with respect to which all galaxies are, on the average, at rest (*Weltbezugs system*). The General Theory of Relativity states that even if it could be found, it must in no way be distinguishable from any other inertial frame of reference. It therefore seems unnecessary to introduce the *Weltbezugs system* in the first place. But this concept has, apparently, helped Professor Jellinck to a better understanding of the theory, and it may likewise help many others. Apart from this special attitude the book is easy to read and abounds in detailed discussions of particular problems. The tensor calculus is made familiar by working out many examples. This is probably the best way of becoming used to a new method. A discussion of the electro-magnetic equations, which should appeal strongly to experimentalists by showing at once the power and simplicity of the Special Theory of Relativity is unfortunately not included.

The other book by Professor Jellinck is the first of two volumes on the principles and methods of wave mechanics. The demands on the reader with regard to mathematical knowledge are very small, as all necessary concepts are developed in the book. An attractive feature of the book is the discussion of various examples, such as harmonic oscillator, spinning top, and Kepler problem, from the points of view of Classical Mechanics, of the old Quantum Theory, and of Wave Mechanics. The final section is devoted to the problem of potential barriers and its applications.

The text is amply illustrated and very readable.

One unsatisfactory feature of the book must, however, be mentioned. It concerns the interpretation of some results of Wave Mechanics. For instance, in the case of the harmonic oscillator, Professor Jellinck asks : How is it possible for a particle with a definite energy to be found with a finite probability outside the classically allowed range ? The answer is, of course, that as long as the energy is known exactly the position of the particle is completely unknown, but as soon as the position of the particle has been determined by experiment its energy is no longer known precisely.

Professor Jellinck, however, argues as follows : The particle apparently can get to a place where its potential energy is greater than its total energy ; but its kinetic energy cannot be negative. Therefore the total energy as calculated by Wave Mechanics is only the constant average of the rapidly fluctuating actual energy of the particle. This fluctuating energy comes from the ether, which Professor Jellinck introduces very early in the book, together with the absolute frame of reference (*Weltbezugs system*). The ether has the property not only to propagate the wave function but also to interact energetically with the dynamical system.

This way of explaining the " paradoxes " of Wave Mechanics is contrary to the logical scheme of Wave Mechanics, and misleading for the student.

Ultrasonics. By P. VIGOUREUX. Pp. 163. (Chapman and Hall, 1950.) Price 25s.

THE author has dealt with the technique and with the theory of ultrasonics in simple terms which brings the work within the scope of a wide circle of readers including undergraduates.

Readers may remember the standard of work of Bergmann to which the author refers and which appeared in 1937. The author gives a good account of the progress which has been made since then in the study of attenuation, and in the effects associated with the vibrational states of molecules both in gases and in liquids.

The Mathematical Theory of Plasticity. By R. HILL. [Pp. 354.] (Oxford: University Press.) Price 35s.

THE mathematical theory of plasticity has undergone great development in the past dozen years or so, not only in its extension to more complex problems of industrial interest, but in its fundamental concepts and techniques. Much has been done to remove the reproach that it was one of the unrealistic branches of applied mathematics. This book is principally concerned with the behaviour of a model substance with the following properties: (i.) it is and remains isotropic; (ii.) it has a yield point; (iii.) this depends on the kind of stress in accordance with von Mises' hypothesis (the yield surface in "principal stress space" is a right circular cylinder) or, as an occasional alternative, with Tresca's hypothesis of critical shear stress; (iv.) work hardening occurs as a function of the irrecoverable work done, or of Odquist's integral plastic strain, or not at all; (v.) the principal axes of the plastic strain increment are parallel to the principal axes of the stress, frequently with the simplification that the principal strain increments are proportional to the deviatoric principal stresses; (vi.) the superimposed effects of elasticity are consistently regarded throughout.

Considerable care is given to showing that these are the best assumptions, within the range of those capable of mathematical treatment, for conformity with the requirements of metal physics: and they lead to results in very satisfactory conformity with experimental measurements. The weakest of the assumptions is clearly (i.), and a final chapter on plastic anisotropy develops the attack against this weakness. The author, who has been intimately concerned with the modern developments of the subject, has been in the fortunate position of being able to write what is simultaneously a complete text-book and a report of recent advancements.

F. C. F.

Mathematical Snapshots. By Prof. HUGO STEINHAUS, Oxford University Press. [Pp. 265, with 295 illustrations.] (London: Geoffrey Cumberlege.) Price 27s. 6d. net.

THIS book attempts with notable success to present mathematical ideas and theorems attractively to the layman with the help principally of illustrations. These are many and imaginative, while the text is always clear and to the point, if occasionally perhaps too brief. The author ranges widely, without evident design, from pursuit paths to polyhedra, from longimeters to loxodromes, from tessellations to topology, from counterfeit coins to cartography. Really difficult theorems are included, for example ones due to Minkowski and Lebesgue. A few results are proved; most are stated with a challenge to the reader, but a bibliography of original papers is thoughtfully provided. Even a mathematical specialist, whatever his field, will surely find much in this book to divert him.

R. H.

Electromagnetic Theory. By OLIVER HEAVISIDE. [Pp. xxx+386.] (New York, Dover Publications Inc. British Agents: Interscience Publishers, Ltd.). Price 60s.

THIS is a photographic reproduction in one volume (12 in. by 9 in.) of the three volumes which appeared in 1883, 1899 and 1912. Four pages of the original appear on one page of the reproduction. Despite the reduction in size the print is quite as readable as in the reprint of 1925. Besides the original text there are a portrait of the author, a biographical sketch and an appraisal of Heaviside's contribution to vector analysis, electromagnetism and communication theory.

J.D.E.

[The Editors do not hold themselves responsible for the views
expressed by their correspondents.]

L. Hyperfine Structure in Paramagnetic Salts and Nuclear Alignment.

By B. BLEANEY, F.R.S.,
Clarendon Laboratory, Oxford*.

[Received February 14, 1951.]

ABSTRACT.

Abragam and Pryce (1951) have shown that the hyperfine structure in paramagnetic salts can be interpreted using a simple Hamiltonian involving components of the electron and nuclear spins. On the basis of this Hamiltonian, general formulæ are given for the allowed transitions in strong magnetic fields, assuming that the paramagnetic ions have axial symmetry and that interactions with the electric quadrupole moment of the nucleus are small compared with those involving the magnetic dipole moment.

As far as possible, general formulæ are also given for the energy levels in zero magnetic field, and the allowed transitions are indicated. The use of hyperfine structure in paramagnetic salts for the production of nuclear alignment is discussed, with some quantitative data.

§1. INTRODUCTION.

IN a general survey of the theory of paramagnetic resonance and hyperfine structure, Abragam and Pryce (1951) have shown that it is possible to represent the behaviour of the energy levels by the following Hamiltonian, if the anisotropy has axial symmetry about the z -axis:

$$\mathcal{H} = \beta \{ g_x H_z S_z + g_1 (H_x S_x + H_y S_y) \} + D \{ S_z^2 - \frac{1}{3} S(S+1) \} \\ + A S_z I_z + B (S_x I_x + S_y I_y) + Q \{ I_z^2 - \frac{1}{3} I(I+1) \} - \gamma \beta_N \mathbf{H} \cdot \mathbf{I}, \quad (1)$$

β = Bohr magneton,

β_N = Nuclear magneton.

Here the effective electron spin S is defined by setting the multiplicity of the electronic energy levels equal to $2S+1$, and I is the nuclear spin. g is a tensor, with principal values $g_{||}$ and g_{\perp} . The term in D represents the presence of initial splittings of the electronic levels due to second order effects of the crystalline electric field. The terms in A , B correspond to the interaction between the nuclear magnetic moment and the magnetic field of the unfilled electron shell. The term in Q † is due to the interaction of the nuclear electric quadrupole moment with the gradient of the electric field at the nucleus, while the last term takes account of the direct effect of the external magnetic field on the nuclear magnetic moment.

* Communicated by the Author.

† Unfortunately this nomenclature differs from that customary where Q is used for the actual quadrupole moment of the nucleus. The relation between them is that Q (this paper) = $3eQ \partial^2 V / \partial z^2 / 4I(2I-1)$ (usual nomenclature).

This Hamiltonian is very convenient for the interpretation of paramagnetic resonance spectra, since it involves only the electronic and nuclear spins, together with a set of parameters representing the strength of the various interactions. These can be regarded as a set of unknowns to be determined experimentally by a comparison of the observed spectrum with that calculated from the Hamiltonian given above. This spectrum is normally relatively simple, but the anisotropy introduces a complicated variation with the direction of the external magnetic field. The computed variation has already been compared with experiments in a number of specific cases and good agreement found.

The purpose of this paper is threefold. First, to give general formulæ for the allowed transitions in strong magnetic field, using perturbation theory carried to the second order. This is only possible with two limitations: (a) the axial symmetry presumed in equation (1); (b) the magnitude of the quadrupole parameter Q must be small compared with A , B . Second, to give, as far as possible, formulæ for the energy levels in zero magnetic field, together with the allowed transitions. These transitions are important because they can give more accurate values of the parameters (in particular, the quadrupole parameter Q) than the strong field case. The energy levels of zero fields are important also because of their effects in experiments on adiabatic demagnetization. Third, to consider the use of hyperfine structure in producing alignment of the nuclear spin, as suggested by Gorter (1948) and Bleaney (1951a).

§ 2. THE STRONG FIELD SPECTRUM.

In strong fields it is convenient to choose the axes so that elements in S_x , S_y do not occur in the major term $g\beta H \cdot S$ in the Hamiltonian. When g is anisotropic this is equivalent to taking the axis about which the spin precesses as the new z -axis. Then, if the external field is applied at an angle θ to the axis of crystalline symmetry, the usual rules for rotation of the axes may be applied to the Hamiltonian if allowance is made for the non-commuting properties of the spin components. We will consider first the fine structure which arises in the absence of nuclear spin from the presence of a crystalline splitting of the electronic levels.

2.1. The Fine Structure.

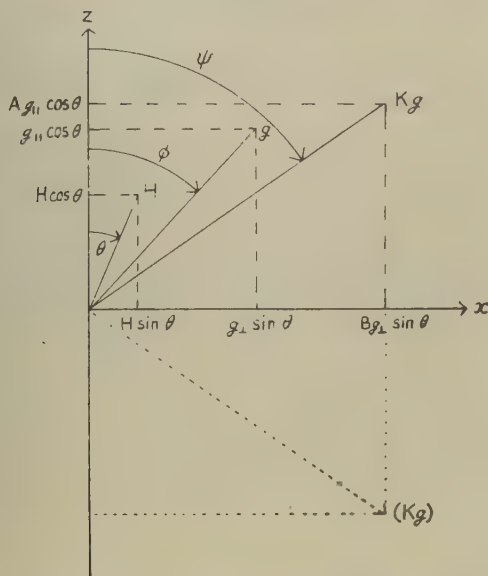
In strong fields the allowed transitions are of the type $\Delta M = \pm 1$. For the transition $M \rightarrow M-1$, we have

$$\begin{aligned} h\nu = & g\beta H + D(M - \tfrac{1}{2}) \left\{ 3 \frac{g_{\parallel}^2}{g^2} \cos^2 \theta - 1 \right\} \\ & - \left(\frac{Dg_{\perp}g_{\parallel} \cos \theta \sin \theta}{g^2} \right)^2 \left(\frac{1}{2g\beta H_0} \right) \{ 4S(S+1) - 24M(M-1) - 9 \} \\ & + \left(\frac{Dg_{\perp}^2 \sin^2 \theta}{g^2} \right)^2 \left(\frac{1}{8g\beta H_0} \right) \{ 2S(S+1) - 6M(M-1) - 3 \}, \quad \dots \quad (2) \end{aligned}$$

$$\text{where} \quad g^2 = g_{\parallel}^2 \cos^2 \theta + g_{\perp}^2 \sin^2 \theta. \quad \dots \quad (3)$$

The physical basis of (3) can be seen from fig. 1. The magnetic field H has components $H \cos \theta$ and $H \sin \theta$ respectively along and normal to the symmetry axis. The components of the magnetic moment are therefore proportional to $g_{\parallel} H \cos \theta$ and $g_{\perp} H \sin \theta$, and g is proportional to the length of the vector making an angle ϕ with the z -axis which is formed by compounding these two. This vector is parallel to the resultant magnetic moment of the electrons, but is not parallel to H . This is responsible for the factors (g_{\parallel}/g) and (g_{\perp}/g) which appear as coefficients multiplying $\cos \theta$ and $\sin \theta$ respectively everywhere in equation (2); for $\cos \phi = (g_{\parallel}/g) \cos \theta$; $\sin \phi = (g_{\perp}/g) \sin \theta$.

Fig. 1.



Orientation of magnetic field (H), electron spin (g), and nuclear spin (Kg) when anisotropy is present. The figure is drawn for $g_{\parallel} > g_{\perp}$, and $B > A$. The dotted vector (Kg) refers to the case where A is negative.

The fine structure results in a splitting into 2S lines, which are equally spaced in the first approximation. The spacing varies with angle, falling to zero where $(g_{\parallel}/g) \cos \theta = 1/\sqrt{3}$. This equal spacing is disturbed by the second order terms which vanish in strong fields, or along the axis of symmetry ($\theta = 0$). The perturbation denominator in these second order terms is taken as $(g\beta H_0)$, the average spacing of successive levels. The significance of H_0 is that in the absence of the fine structure all the lines would coincide and occur at this field. Writing $h\nu = g\beta H_0$, the formula (2) can be re-arranged in the form

$$H = H_0 - \frac{D}{g\beta} (M - \frac{1}{2}) f_1(\theta) - \left(\frac{D}{g\beta} \right)^2 \frac{1}{H_1} f_2(\theta) \dots \quad (2a)$$

This formula shows that when the spectrum is displayed at constant frequency as a function of field, as is normally the case in paramagnetic resonance, its appearance is fundamentally the same (but reversed) as if it were displayed at constant field as a function of frequency. The value of the parameter D can be found from the separations (in field) between the lines.

The intensity of these strong transitions is given by the formula

$$\text{Power absorbed by crystal} = Z\{S(S+1) - M(M-1)\}, \quad . \quad . \quad (4)$$

where

$$Z = \frac{\pi \nu^2 (g\beta' H')^2}{4kT} \frac{N}{2S+1} F(\nu, \nu_0, \Delta\nu),$$

N = no. of paramagnetic ions in crystal.

$F(\nu, \nu_0, \Delta\nu)$ is a "shape factor" depending on the line width. At the centre of the line where $\nu = \nu_1$, $F \approx 1/\Delta\nu$, where $\Delta\nu$ is the half-width at half-intensity.

The formula for Z is only approximate because it has been assumed that the radio-frequency field $H' \cos(2\pi\nu t)$ inducing the transitions is normal to the axis about which the spin precesses, and g' is the value of the spectroscopic splitting factor along this normal. In practice H' is usually normal to H , and therefore makes an angle $(\theta - \phi)$ with the assumed direction. The absolute intensities will therefore differ slightly from (4), but the relative intensities given here and later will be correct. A minor consequence of the anisotropy is that the intensities will not be quite zero if the r.f. field H' is parallel to H ; and this can occur also through second order effects of the splitting in weak fields, even when g is isotropic.

In finite fields transitions corresponding to changes in M of greater than unity can be observed. These are smaller in intensity than the main transitions by a factor of the order $(D/H)^2$, and vanish only if the external field is parallel to the symmetry axis. The actual intensity formulæ are rather complicated, and show that the intensity does not vary greatly with the angle between the external and r.f. fields. We shall content ourselves with giving the formula for the positions of the lines corresponding to the transition $M \rightarrow M-2$ in the strong field quantum numbers. This is

$$\begin{aligned} h\nu = & 2g\beta H + 2D(M-1) \left\{ 3 \frac{g_{\parallel}^2}{g^2} \cos^2 \theta - 1 \right\} \\ & - \left(\frac{Dg_{\parallel}g_{\perp} \cos \theta \sin \theta}{g^2} \right)^2 \left(\frac{2}{g\beta H_0} \right) \{ 4S(S+1) - 24M(M-2) - 33 \} \\ & + \left(\frac{Dg_{\perp}^2 \sin^2 \theta}{g^2} \right)^2 \left(\frac{1}{2g\beta H_0} \right) \{ 2S(S+1) - 6M(M-2) - 9 \} \quad . \quad . \quad . \quad (5) \end{aligned}$$

(note that H_0 in the perturbation denominators refers again to the mean field at which the $\Delta M = \pm 1$ transitions occur).

2.2. The Hyperfine Structure.

In the presence of hyperfine structure the strong allowed transitions are those in which $\Delta m = 0$, where m is the nuclear magnetic quantum number. The position of the transition $(M, m) \rightarrow (M-1, m)$ is found by adding to the right-hand side of equation (2) the quantity

$$\begin{aligned} Km + \frac{B^2}{4g\beta H_0} \left(\frac{A^2 + K^2}{K^2} \right) \{I(I+1) - m^2\} \\ + \frac{B^2}{2g\beta H_0} \frac{A}{K} m(2M-1) \\ + \frac{1}{2g\beta H_0} \left(\frac{A^2 - B^2}{K} \right)^2 \left(\frac{g_{\parallel} g_{\perp}}{g^2} \right)^2 \sin^2 \theta \cos^2 \theta m^2 \\ + \frac{Q^2 \cos^2 \theta \sin^2 \theta}{2KM(M-1)} \left(\frac{ABg_{\parallel} g_{\perp}}{K^2 g^2} \right)^2 m \{4I(I+1) - 8m^2 - 1\} \\ - \frac{Q^2 \sin^4 \theta}{8KM(M-1)} \left(\frac{Bg_{\perp}}{Kg} \right)^4 m \{2I(I+1) - 2m^2 - 1\}, \quad \dots \dots \dots (6) \end{aligned}$$

where

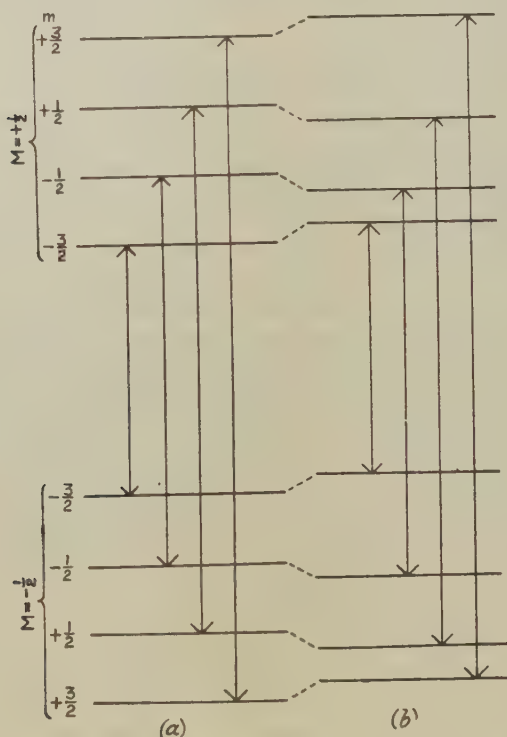
$$K^2 g^2 = A^2 g_{\parallel}^2 \cos^2 \theta + B^2 g_{\perp}^2 \sin^2 \theta \quad \dots \dots \dots (7)$$

The physical significance of the relation (7), which is due to Pryce (1949), is similar to that of (3). The magnetic moment of the electrons has projections proportional to $g_{\parallel} \cos \theta$ and $g_{\perp} \sin \theta$ parallel and normal to the symmetry axis respectively. The components of the magnetic field acting on the nucleus are therefore proportional to $Ag_{\parallel} \cos \theta$ and $Bg_{\perp} \sin \theta$, respectively, and the nucleus is aligned parallel to their resultant (see fig. 1). It may be noted that in deducing these formulæ the axes of quantization of electron and nucleus are taken parallel to their respective magnetic moments. This is responsible for the introduction of factors such as (Ag_{\parallel}/Kg) multiplying $\cos \theta$, etc.

In the first approximation, the result of the nuclear interaction is to split each electronic transition into $2I+1$ equally spaced components, with separation K between successive lines. Each component has the intensity given by (4), divided by $2I+1$. Where there is considerable anisotropy the splitting which, measured in field, equals $(K/g\beta)$, may go through a maximum value at an angle to the axis, as in cobalt (Bleaney and Ingram 1951a); this is due to the different angular variation of K and g . It should be noted that there is no first order effect due to the quadrupole interaction so long as $Q \ll B$. The quadrupole interaction produces a first order shift of the energy levels (see fig. 2), but this is the same for all levels with the same value of m , and does not affect transitions where $\Delta m = 0$. This is true for all values of Q if the external magnetic field is parallel to the axis of symmetry, for the quadrupole term then contains only diagonal elements. If H is at an angle with this axis the quadrupole interaction will break down the ordinary selection rule when $Q \approx K$, because of the competition between the magnetic and electrostatic

interactions which are each trying to align the nucleus along its own preferred axis. Perturbation theory can then only be applied if $Q \ll K$, that is, $Q \ll A, B$. This is reflected in the fact that K appears in the denominator in the second order terms in Q^2 , which do not therefore vanish in strong fields. The remaining second order terms do.

Fig. 2.



Hyperfine structure and allowed transitions in strong magnetic fields for $S=\frac{1}{2}$, $I=3/2$. (a) Magnetic interaction only, (b) electric quadrupole interaction added.

It is convenient to consider these two types of second order terms independently. From those which vanish in strong fields, one can separate terms in zero, first and second powers of m . The first of these produces a constant shift of all lines to higher frequencies (lower magnetic fields) which is unimportant except in accurate determinations of the g -value. The second produces a change in the separation of the hyperfine lines, which is different for different electronic transitions. This is important, for it can be used (except when $S=\frac{1}{2}$) to determine the relative signs of

the parameters D , A and B , which cannot be found from any of the first order terms. This point is considered more fully by Bleaney and Ingram (1951b), with reference to the manganese spectrum. The third terms, in m^2 , produce a linear change in the separation of the hyperfine lines within a given electronic transition. For $\theta=0$ or 90° , the separation increases always towards higher fields, but in intermediate directions it may reverse. For example, in cobalt ammonium sulphate (Bleaney and Ingram 1951a), where there is great anisotropy, the reversal takes place only $1\frac{1}{2}^\circ$ from the perpendicular direction. Note that none of the terms is really independent of θ , owing to the variation in g and K with angle, unless both g and the hyperfine structure are isotropic.

The second order terms in Q^2 are of importance because they form one method of detecting the presence of a small quadrupole interaction. They contain terms in m , which produce a constant change in the spacing of a group of hyperfine lines, and terms in m^3 which cause the spacing to be greater at the ends of a group than in the middle, when $\theta=90^\circ$. This effect is reversed as θ decreases, owing to the opposite sign of the two terms in Q^2 , and both terms become zero at $\theta=0^\circ$. The effects are greatest for the transition $M=\frac{1}{2}\rightarrow-\frac{1}{2}$. If $A>B$, and $g_{\parallel}>g_{\perp}$, the unequal spacing is greatest at some intermediate value of θ between 0° and 90° , but if the inequalities are the other way, it may be greatest at $\theta=90^\circ$. The quadrupole terms may be differentiated from the other second order shifts in two ways: (a) they do not vanish in strong fields; (b) the separation of successive hyperfine lines is greatest in the middle or at the ends, instead of showing a progressive increase or decrease.

A second method of discovering a small quadrupole interaction depends on the weak lines corresponding to changes of ± 1 and ± 2 in the nuclear quantum number m , which have intensities of the order of $(Q/K)^2$ compared with the main hyperfine lines. The positions of these lines involve the first power of Q instead of (Q^2/K) , and we shall neglect small shifts of the order Q^2/K , and $(A, B)^2/(g\beta H_0)$. In the intensities we shall neglect contributions of the order $(A, B)^2/(g\beta H_0)^2$ which vanish in strong fields, unlike the quadrupole effects. We have then lines $(M, k\pm\frac{1}{2})\rightarrow(M-1, k\mp\frac{1}{2})$,

$$\text{Energy} = Kk \pm \{K(M-\frac{1}{2}) + Q'k - \gamma'\}, \quad (8)$$

$$\text{Intensity} = 4k^2 \{(I+\frac{1}{2})^2 - k^2\} X, \quad (9)$$

where k takes on the values $(I-\frac{1}{2}), (I-\frac{3}{2}), \dots, -(I-\frac{1}{2})$, and for the lines $(M, m\pm 1)\rightarrow(M-1, m\mp 1)$

$$\text{Energy} = Km \pm \{K(2M-1) + 2Q'm - 2\gamma'\}, \quad (10)$$

$$\text{Intensity} = \{(I+1)^2 - m^2\} \{I^2 - m^2\} Y, \quad (11)$$

where m takes on the values $(I-1), (I-2), \dots, -(I-1)$.

In these equations

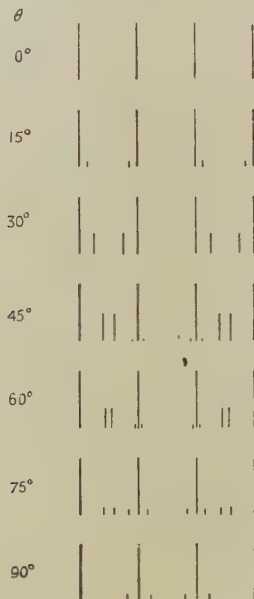
$$X = \frac{Z}{(2I+1)} \left\{ \frac{Q}{2KM(M-1)} \right\}^2 \left(\frac{ABg_{\parallel}g_{\perp}}{K^2g^2} \right)^2 \cos^2 \theta \sin^2 \theta, \quad . \quad . \quad . \quad (12a)$$

$$Y = \frac{Z}{(2I+1)} \left\{ \frac{Q}{8KM(M-1)} \right\}^2 \left(\frac{Bg_{\perp}}{Kg} \right)^4 \sin^4 \theta, \quad . \quad . \quad . \quad . \quad . \quad (12b)$$

$$Q' = Q \left(\frac{3A^2g_{\parallel}^2}{K^2g^2} \cos^2 \theta - 1 \right), \quad . \quad . \quad . \quad . \quad . \quad . \quad (13a)$$

$$\gamma' = \gamma\beta_N H (Ag_{\parallel} \cos^2 \theta + Bg_{\perp} \sin^2 \theta) / Kg. \quad . \quad . \quad . \quad . \quad . \quad (13b)$$

Fig. 3.



Quadrupole effects in spectrum for $S=\frac{1}{2}$, $I=3/2$, with no anisotropy and $A=B=5Q$.

The significance of these formulæ can best be appreciated by reference to a simple case. Fig. 3 shows the spectrum at various angles for a hypothetical ion where $S=\frac{1}{2}$, $I=3/2$, with no anisotropy ($A=B$ and $g_{\parallel}=g_{\perp}$), and $Q=0.2B$. The term $\gamma\beta_N H$ is neglected. As θ increases from zero, four lines corresponding to $\Delta m = \pm 1$ increase in intensity and appear at symmetrical points between the two outer pairs of main lines. They collapse to two lines at $\cos \theta = 1/\sqrt{3}$, then separate out again and disappear. The lines $\Delta m = \pm 2$ are strongest at $\theta=90^\circ$, and are symmetrically disposed about the two inner main lines, coinciding with them at $\cos \theta = 1/\sqrt{3}$. It will be seen that the spectrum is always symmetrical, and no information can be obtained about the relative signs of Q , A and B .

At fields of the order of 10,000 gauss, the direct effect of the external field on the nucleus is no longer negligible, and important information about the signs of the constants A , B , and Q can be obtained. The term $\gamma\beta_N H$ acts with the quadrupole interaction in increasing the separation of satellite doublets on one side of the spectrum, and against it to decrease the separation on the other side. If A , B , Q and $\gamma\beta_N H$ are all positive, the separation is smaller at the high frequency (low field) end of the spectrum when $\cos\theta < 1/\sqrt{3}$, and greater for values of $\cos\theta$ greater than this. (The separation is no longer zero exactly at $\cos\theta = 1/\sqrt{3}$ but goes through zero at a smaller angle for the satellites on the high frequency side, and at a greater angle for those on the other side.) If the sign of Q or $\gamma\beta_N H$ is reversed, the asymmetry is also reversed.

When anisotropy is present the nature of the spectrum is not altered in principle, but the angular dependence and relative intensities are changed. The positions of the satellite lines are the same as in fig. 3, if we plot them against the angle ψ between the nucleus and the symmetry axis, for Q' is simply $Q(3\cos^2\psi - 1)$.

The term γ' in $\gamma\beta_N H$ now contains a multiplying factor which is just the cosine of the angle $(\psi - \theta)$ which the nuclear axis makes with the external field. If A and B are of opposite sign this factor passes through zero, since at some angle the nuclear axis will be perpendicular to the external field, as can be seen from fig. 1.

The considerable intensity of the satellite lines $\Delta m = \pm 1$ at intermediate angles makes these generally the most sensitive method of detecting a small quadrupole interaction, if there is adequate intensity in the observed spectrum. If not, accurate measurement of the line separation, as described previously, is the best, but no information concerning the signs can be obtained.

The question of what nuclear information can be obtained from the relative signs needs careful analysis. The experiments give the relative signs of $(A\gamma)$, $(B\gamma)$ and Q ; but the signs of A , B themselves depend on that of γ , since they involve the product of the nuclear magnetic moment and the field of the electrons. Essentially, therefore, the sign of the latter is compared with Q , which is itself the product of $(\partial^2 V / \partial z^2)$ and the nuclear quadrupole moment. The sign of the nuclear quadrupole moment can therefore be established if crystalline field theory gives the signs of the electronic magnetic field and electric field gradient. The sign of the nuclear magnetic moment cannot be found; this difference arises because use is made of an external magnetic field.

§ 3. ENERGY LEVELS AND SUSCEPTIBILITY AT ZERO MAGNETIC FIELD.

3.1. Levels for $S = \frac{1}{2}$.

In zero magnetic field, evaluation of the energy levels is somewhat more complicated than in the strong field case because in general we cannot apply perturbation theory. Thus in the case $S = \frac{1}{2}$ the two electronic levels $M = +\frac{1}{2}$ and $M = -\frac{1}{2}$ are degenerate in the absence of hyperfine structure, and the perturbation denominators arising from the

term $B(S_x I_x + S_y I_y)$ in the Hamiltonian would be zero. The energy matrix splits up into a number of doublets in this case, however, so that we can give an explicit formula (14) for the levels by solving the quadratic secular equations

$$W = -\frac{A}{4} + Q\{k^2 + \frac{1}{4} - \frac{1}{3}I(I+1)\} \\ \pm \frac{1}{2}\sqrt{[k(A-2Q)+G]^2 + B^2\{(I+\frac{1}{2})^2 - k^2\}}, \quad . \quad . \quad (14)$$

where $k=M+m$ takes the values $(I+\frac{1}{2}), (I-\frac{1}{2}), \dots, -(I+\frac{1}{2})$; with the restriction that only the positive sign is to be taken before the square root when $k=+(I+\frac{1}{2})$, and only the negative sign when $k=-(I+\frac{1}{2})$. Here $G=g_{\parallel}\beta H$, and the effect of a magnetic field along the symmetry axis has been included, since to do so causes no great complication. The significance of k is that, except for $|k|=I+\frac{1}{2}$, the levels are linear combinations of the states (M, m) and $(M-1, m+1)$. In zero magnetic field they are all doublets, the states k and $-k$ being degenerate, except for the case $k=0$, which gives two singlets of separation $B(I+\frac{1}{2})$. The levels given by $k=\pm(I+\frac{1}{2})$ form a doublet in zero field also, with nuclear magnetic quantum numbers $m=I$ and $-I$ respectively.

The allowed transitions in zero magnetic field are rather complicated when $B \neq 0$, owing to the admixture of wavefunctions in the different levels. A simple case arises when a radio-frequency field is applied parallel to the symmetry axis, which is the axis about which electron and nuclear spin precess. The levels which are found by taking the alternative signs outside the square root in (14) each consist of admixtures of the same states and transitions are allowed between them except in the special cases when either both A and Q are zero, or $B=0$. These transitions, which are all doublets, occur at

$$h\nu = \sqrt{[k^2(A-2Q)^2 + B^2\{(I+\frac{1}{2})^2 - k^2\}]}. \quad . \quad . \quad (15)$$

This formula shows that an accurate value of the quadrupole parameter Q may be obtained from the spectrum in zero field in cases where no effect can be observed in the strong field spectrum.

When an r.f. field is applied normal to the symmetry axis the allowed transitions are rather complicated. We shall content ourselves with pointing out that they can arise between any of the levels found by assigning values to k differing by one unit in (14). Here again the frequencies of the transitions may be used to find Q : in particular, a number of transitions fall into doublets where the separation of the components is $2Q(2k-1)$. This splitting gives Q directly, independent of A, B .

3.2. Levels for $S > \frac{1}{2}$.

No simple formulæ can be given for this case except when the electronic splitting parameter D is large compared with the hyperfine structure parameters. In the first approximation we have, then, for levels where $M \neq \pm \frac{1}{2}$,

$$W = D\{M^2 - \frac{1}{3}S(S+1)\} + AMm + Q\{m^2 - \frac{1}{3}I(I+1)\}. \quad . \quad . \quad (16)$$

These are all doublets in this approximation (except when M or $m=0$), the states (M, m) and $(-M, -m)$ are degenerate.

For $M=\pm\frac{1}{2}$, the formulæ given in the last section still apply, in the first approximation, if the parameter B is replaced by $B(S+\frac{1}{2})$. All the levels will have shifts of the order B^2/D , due to the off-diagonal elements.

The allowed transitions in zero field may be outlined as follows. If the r.f. magnetic field is parallel to the symmetry axis, only transitions internal to the levels $M=\pm\frac{1}{2}$ are allowed, and in the first approximation, these are given by our modified equation (15). When the r.f. field is perpendicular to the symmetry axis, the allowed transitions are of the same type as in strong fields, viz. $\Delta M=\pm 1$, $\Delta m=0$, except where the levels $M=\pm\frac{1}{2}$ are involved. Here again the remarks of §3.1 apply for transitions internal to these levels. Transitions are also allowed between the level $(3/2, m)$ and either of the levels given by $k=(m+\frac{1}{2})$, and between $(-3/2, m)$ and either given by $k=(m-\frac{1}{2})$, in (14); these alternative levels are those corresponding to taking the alternative signs before the square root.

These transition rules only apply when $D \gg A, B$. When they are of the same order the spectrum will be much more complicated.

3.3. Susceptibility at Zero Magnetic Field.

At high temperatures ($kT \gg A, B, Q, D$) the presence of a hyperfine structure produces almost no effect on the susceptibility of a paramagnetic salt. Bleaney (1950) has pointed out that if the susceptibility is expressed as a power series in $1/T$, the hyperfine structure leaves the term in $1/T$ unaltered, and introduces no term in $1/T^2$, even for a single crystal. The presence of an electronic splitting gives an anisotropic term in $1/T^2$ (equation (4) of Bleaney 1950) which averages to zero for a powder.

At temperatures where kT is of the same order as the splitting parameters A, B, Q, D , the susceptibility varies in a complicated manner and no general formula can be given. One or two special cases are worthy of mention, however, being limiting cases where simple formulæ can be given. These illustrate the general behaviour of the susceptibility.

The cases of $S=\frac{1}{2}$, $B=Q=0$ has been evaluated previously (Bleaney 1951 b) since it approximates closely to several salts of cobalt. Reference to equation (14) shows that when $B=0$ the energy levels show a first order Zeeman effect when a small field is applied along the axis. The magnitude of the Zeeman splitting is the same for all the levels, and the susceptibility therefore follows Curie's law, irrespective of the changing population of the hyperfine doublets. If a small field is applied perpendicular to the axis, only a second order Zeeman effect is produced, and the susceptibility is given by the formula

$$\chi_1 = \frac{Ng_A^2 \beta^2}{kA} \left\{ \frac{\sum_m \frac{1}{2m} \sinh \frac{mA}{2kT}}{\sum_m \cosh \frac{mA}{2kT}} \right\}, \quad \dots \dots (17)$$

where m takes the positive values $1, (1-1), \dots \frac{1}{2}$ or 0 . (In the latter case the terms for which $m=0$ must be weighted by a factor $\frac{1}{2}$ in the summation.) At very low temperatures χ_1 passes through a maximum and then falls to a limiting constant value as $T \rightarrow 0$.

For substances where $S > \frac{1}{2}$, the susceptibility will not differ, in the first approximation, from the case of no nuclear interaction, except for the levels $M = \pm \frac{1}{2}$. If these lie at the bottom (D positive) the remarks of the previous paragraph apply at temperatures where only these levels are occupied, and formula (17) holds if $D \gg A$. If D is negative, these levels lie uppermost, and they will not be populated at temperatures where the deviations due to nuclear interaction would show up. In this case we have simply when $kT \ll D(2S-1)$ (*i. e.* only lowest levels occupied),

$$\chi_{||} = \frac{NS^2 g_{||}^2 \beta^2}{kT},$$

$$\chi_{\perp} = - \frac{8S^2 g_{\perp}^2 \beta^2}{(2S-1)D}.$$

Note that χ_{\perp} is not really negative because this formula applies only when D is negative.

Paramagnetic ions which do not have Kramers degeneracy in their electronic levels (*i. e.* where S is not half-integral), are not often used in adiabatic demagnetization work, and the levels in zero field are not of great interest. The remarks of this section apply equally to them, however, except when D is positive. The lowest level is then $M=0$, which has no temperature dependent susceptibility contribution in the first approximation. The hyperfine splitting of this level is also zero, except for second order and quadrupole effects.

§ 4. NUCLEAR ALIGNMENT.

Three methods of producing nuclear alignment at low temperatures by means of hyperfine structure have been proposed. The first of these (Gorter 1948, Rose 1949) utilizes the hyperfine structure due to magnetic interaction in a paramagnetic salt. The method proposed is to demagnetize a paramagnetic salt to a small field, around which the electronic spin will precess. The nuclei are then aligned also parallel to this field by the much more powerful field (10^5 – 10^6 gauss) of the electrons. The splitting of the nuclear levels produced by this latter field is of the order of 0.01 to 0.1°K. , and at such temperatures an appreciable degree of nuclear polarization will be set up.

The second method, due to Pound (1949), utilizes the electric quadrupole interaction to split the nuclear levels. This causes, not a polarization, but only an alignment of the nuclei, since the levels $\pm m$ remain degenerate. This is, however, sufficient for experiments involving radioactive emission, which depends only on even multiples of the angle with the axis of alignment (Spiers 1948, 1949). The latter is, of course, determined by

the crystallographic symmetry, and ideally a substance with one ion in unit cell is required. Since this method does not require the use of paramagnetic salts, it will not be further considered here.

The third method, suggested by Bleaney (1951a), is similar to that of Gorter in that the magnetic interaction between the nucleus and the electrons of a paramagnetic ion is used, but differs in that no residual magnetic field is applied. As in Pound's method, an alignment, not a polarization, of the nuclei is set up. The nuclei precess about an axis determined by the crystalline field, and again, a substance with one ion in unit cell is required. This method has the advantage over Gorter's that lower temperatures will be reached, since there is no external magnetic field.

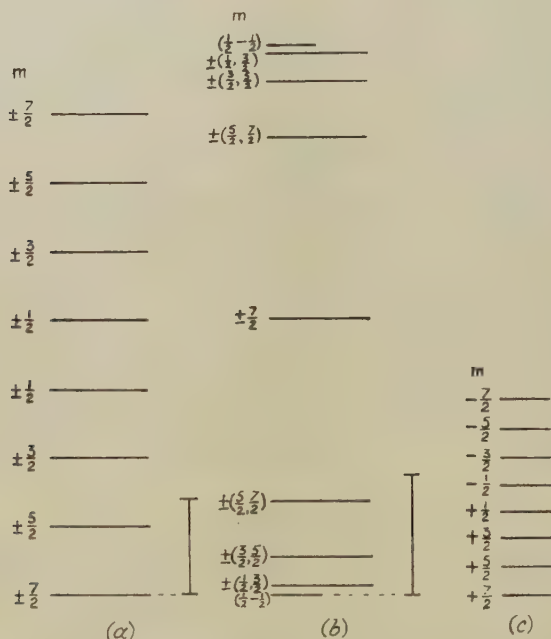
At first sight, on the other hand, Gorter's method seems to be simpler in that single crystals are not required, and the method can be used with any paramagnetic salt. Closer examination of the effects of the crystalline electric field shows that this is not the case for small residual magnetic fields and almost the same conditions are required in the two methods. The reason for this is that, in general, a small magnetic field applied normal to the crystalline symmetry axis produces only a second order Zeeman effect, and the spins remain aligned along the crystal axis until fields large enough to overcome the crystalline splitting (if present) or hyperfine splitting are applied. Thus a powder, or a single crystal with many ions in unit cell, such as iron alum, will be unsuitable, and a crystal with only a single ion per unit cell is required, as in the other methods. The magnetic field must then be applied parallel to the axis of this ion. In the following paragraphs some attempt is made to calculate the degree of polarization and of alignment in zero field that can be achieved in limiting cases.

4.1. Nuclear Alignment and Polarization with $B=Q=0$.

For both methods the ideal case arises when the energy matrix of the lowest electronic level (assumed a doublet) has vanishing elements off the diagonal. This can occur in two ways: (a) if the lowest levels are $M = \pm \frac{1}{2}$, and there is considerable anisotropy so that $A \gg B$; (b) if the lowest levels are $M \neq \pm \frac{1}{2}$, in a salt with considerable splitting of the electronic levels in zero magnetic field ($D \gg A, B$). Examples of salts approximating to these two extremes are cobalt fluosilicate and manganese fluosilicate, both of which have only a single ion in unit cell. Then, if the off-diagonal elements are neglected, the lowest energy levels consist simply of a set of $2I+1$ doublets, equally spaced by $A \times |M|$ (cf. Bleaney 1951a,b). Each doublet contains levels in which the electronic spins are opposed and the nuclear magnetic quantum numbers are m and $-m$ respectively. The top and bottom levels have $m = \pm I$, and the intermediate levels are in order of m changing by one unit (see fig. 4a). At a temperature T , the combined population of the two states with a given value of m is proportional to $\cosh (AMm/kT)$.

Fig. 4 *a* has been drawn for the case of $S=\frac{1}{2}$, $I=7/2$, which is appropriate to the stable isotope, cobalt 59. The lowest temperature which could be reached by adiabatic demagnetization of such a cobalt salt is equivalent to $kT=0.7A$, and is represented by a vertical line. The populations of the nuclear levels $\pm 7/2 : \pm 5/2 : \pm 3/2 : \pm 1/2$ would then be $1 : 0.53 : 0.32 : 0.21$, showing a considerable preponderance in the states of high m . The radioactive isotope, cobalt 60, is thought to have a spin of approximately 4, and if its magnetic moment is about the same as that of the stable isotope, there would be a similar preponderance.

Fig. 4.



Energy levels in zero magnetic field for $S=\frac{1}{2}$, $I=7/2$, for the extremes
(a) $B=Q=0$, (b) $A=Q=0$.

Cobalt ammonium sulphate approximates to (a), and, for comparison, the nuclear levels of a diamagnetic cobalt compound in a field of 100,000 gauss are shown to scale in (c). The vertical lines in (a) and (b) represent kT for the lowest temperatures which could be reached by demagnetization from 1°K .

If a magnetic field is applied parallel to the axis, a first order Zeeman effect splits each doublet by an amount $2g_{\parallel}\beta |M|H$. In each case the two levels originating from the same doublet have opposite signs of m ; for the upper doublets the lower component is that with negative m (assuming A positive), but for the lower doublets this is reversed. If it be assumed that the degree of nuclear polarization produced is measured by the ratio

of the total nuclear magnetic moment σ along the axis to the saturation nuclear magnetic moment $\sigma_{\text{sat.}}$ (cf. Rose 1949), a simple expression for this ratio can be found. It is

$$(\sigma/\sigma_{\text{sat.}}) = \tanh \frac{M [g_{\parallel} \beta H]}{kT} \frac{\sum_m m \sinh \frac{m |M| A}{kT}}{\sum_m \cosh \frac{m |M| A}{kT}}, \quad \dots (19)$$

where m takes the values $I, I-1, \dots, \frac{1}{2}$ or 0 . (In the summation, the terms for which $m=0$ should be weighted by a factor $\frac{1}{2}$.)

As an illustration, we will suppose that a field is applied which would split each doublet by an amount equal to A . In cobalt this would require a field of about 100 gauss, and the temperature would rise so that approximately $kT=A$ instead of $0.7A$. Then (19) gives $(\sigma/\sigma_{\text{sat.}})=0.3$ under these conditions. This calculation is, of course, based on the assumption that the cooling of the salt is due entirely to the paramagnetism of the cobalt ions. If the temperature could be lowered, for the same residual field, by the use of another paramagnetic salt in contact with the cobalt salt, the degree of nuclear polarization could be improved.

4.2. Nuclear Alignment with $A=Q=0$.

It is of some interest to examine the other extreme case which can occur for $S=\frac{1}{2}$, namely, when both A and Q are negligible compared with B . The energy levels in this case are given by the equation

$$W = \pm B \sqrt{(I + \frac{1}{2})^2 - k^2},$$

where k takes all values $(I + \frac{1}{2}), (I - \frac{1}{2}), \dots, (-I + \frac{1}{2})$. Each of these levels is a singlet composed of equal admixtures of the nuclear states $m = k \pm \frac{1}{2}$, but (except when $k=0$), the levels $\pm k$ coincide to give doublets. The energy levels for $I=7/2$ are shown in fig. 4 *b*, the scale being such that B in fig. 4 *b* is assumed equal to A in fig. 4 *a*. The vertical line again represents the value of kT at the lowest temperature which could be reached by adiabatic demagnetization of such a salt. At this temperature the populations of the nuclear states $\pm 7/2 : \pm 5/2 : \pm 3/2 : \pm 1/2$ would be $0.34 : 0.62 : 0.86 : 1.0$. The predominance lies with the states $\pm \frac{1}{2}$, corresponding to the fact that in this case we have a "plane magnet", *i.e.* a magnet precessing in the plane normal to the symmetry axis. The nuclear alignment is a good deal less favourable than in the preceding case of $B=0$ because of the concentration of energy levels near the bottom.

As already pointed out, a small magnetic field applied in any direction produces only a second order Zeeman splitting, so that this is not a favourable case for Gorter's method.

From these extreme cases of $B=Q=0$ and $A=Q=0$ it is easy to see what happens in intermediate cases, which are obviously less favourable.

If A is large but B is not entirely negligible and $|M| = \frac{1}{2}$, the energy levels in fig. 4 *a* are displaced by amounts of the order B^2/A , and each level m has admixed with it the state $(m-1)$ or $(m+1)$ to an extent $(B/A)^2$. This is not serious until B becomes comparable with A . The case $B=A$ corresponds to no anisotropy, and the energy levels fall into the usual two groups for $S = \frac{1}{2}$, corresponding to a new quantum number F with values $I + \frac{1}{2}$ and $I - \frac{1}{2}$. The splitting of this doublet (for $I = 7/2$) is $4A = 4B$ and each level contains an equal admixture of all the nuclear states m , so that no nuclear alignment in zero field is achieved at any temperature. This corresponds to the fact that with no anisotropy there is no preferred axis of alignment. As the value of B increases further relative to A the situation gradually changes to the extreme case $A=0$ which has already been considered.

The remarks of this section can be applied when $S > \frac{1}{2}$, if the levels $M = \pm \frac{1}{2}$ are lowest and $D \gg A, B$, if the parameter B is everywhere replaced by $B(S + \frac{1}{2})$. Thus a substance of this kind will approximate to the case of A negligible, even if $A=B$, when S is large, since the essential criterion is $A \ll B(S + \frac{1}{2})$.

§ 5. DISCUSSION.

From the point of view of entropy, the use of the same paramagnetic salt for cooling and alignment can be summarized as follows. When the salt is magnetized in a very strong field at 1°K. , the electronic entropy is completely removed. On demagnetizing to zero field, the entropy remains constant, but is divided between the electron and nuclear spins. In the simple cases considered in §4, each level is a doublet, and in the two levels of every doublet the electron spins are oppositely oriented. Thus at all temperatures the "electronic entropy" will be $R \log 2$ in zero field, with a corresponding decrease in the nuclear entropy, giving a degree of alignment. When a magnetic field is applied, the electronic entropy decreases, and the nuclear entropy increases, until at fields large enough to separate the electronic levels so that their hyperfine patterns do not overlap, the electronic entropy is again zero, and the nuclear entropy $R \log_e (2I+1)$, with no polarization or alignment[†].

For this reason the discussion of the merits of the Gorter-Rose method has primarily been limited to the case of small magnetic fields. The formulæ given by Rose correspond, however, to the case of an applied field so large that the hyperfine structures of the different electronic levels no longer overlap (*cf.* fig. 2). Rose assumes that only the lower electronic level is occupied, and further, that the temperature is so low that the nuclear levels corresponding to the splitting of this electronic level are not all equally populated. This can only be achieved by the use of a second paramagnetic salt to produce the cooling, but it would be necessary to adopt an experimental arrangement whereby the external magnetic field used to produce the nuclear polarization is not applied to the second paramagnetic salt.

The requirement of a "dilute" paramagnetic salt for these experiments has already been pointed out (Bleaney 1951a). The reason for this is that the random magnetic fields of neighbouring ions broaden the energy levels, and if these overlap considerably, the alignment will be largely destroyed. The criterion for the degree of dilution required is that the hyperfine structure shall be reasonably well resolved in the paramagnetic resonance spectrum. Thus salts of the iron group will require "dilution" with isomorphous diamagnetic compounds, but in the rare earth group this will probably not be necessary if the ethyl sulphates are used. These have only one ion in unit cell, and hyperfine structure lines can be resolved in the neodymium salt without dilution (Bleaney and Ingram 1949). The use of such dilute salts is also advantageous in cooling, since lower temperatures can be obtained; a disadvantage is that the rate of warming is larger owing to the smaller heat capacity.

§ 6. CONCLUSION.

In the first section of this paper general formulæ are given for the allowed transitions in the paramagnetic resonance spectrum. These are used to determine the magnitude of the parameters in the Hamiltonian (1). When a hyperfine structure is present, a certain amount of nuclear data may be obtained from the spectrum, the simplest datum being the value of the nuclear spin I from the multiplicity. From the experiments, values of the hyperfine structure constants A and B , and Q , if it is comparable in magnitude with A and B , can be found with fair accuracy. The relative signs of the parameters A , B , Q and D are much more difficult to elucidate from the spectrum, since they can only be found from second order effects. Where a crystalline splitting of the electronic levels is present ($D \neq 0$), second order effects in the overall size of the hyperfine structure in intermediate fields can be used for this purpose. An example of this is manganese (Bleaney and Ingram 1951b), where, in addition, a subsidiary experiment on the anisotropy of the susceptibility gave the sign of D , and so determined all the signs.

For a salt where $S = \frac{1}{2}$, relative signs can only be found when weak transitions involving changes in the nuclear magnetic quantum number are observable. In strong fields such transitions arise from the electric quadrupole interaction, but, of the salts so far investigated, only those of copper have shown such an effect (Ingram 1949). In other cases the relative signs of A and B can in principle be found from the second order transitions $\Delta m = \pm 1$, which occur in weak fields, using the small displacement of these transitions due to the direct effect of the external field on the nuclear moment. This method is not generally feasible, since this effect is too small to detect except in strong fields, and there the transitions vanish in intensity, if the quadrupole interaction is negligible.

In cases where no weak transitions $\Delta m = \pm 1$ are visible, or no anomalous spacing of the hyperfine structure is detectable, the formulæ given in § 2.2

can be used to obtain upper limits for the magnitude of Q . A more sensitive method is observation of the allowed transitions in zero magnetic field, as emphasized in §3. This necessitates covering a wide wavelength range, generally in the decimetre wavelength region, where the sensitivity of the method, using a small single crystal to obtain the greatest accuracy, is rather low. Such experiments are under way in this laboratory.

In this paper the author has not attempted to consider the relation of the parameters D , A , B , and Q to the electronic state of the ion and the crystalline field. The intricate theory required for this purpose has been the subject of a general review by Abragam and Pryce (1951a). It seems that the theory is now sufficiently accurate to enable quantitative data concerning the nuclear moments to be deduced from the paramagnetic spectra in many cases (see, for example, Elliott and Stevens 1951). Relative values of the moments of different isotopes of the same element can be obtained, of course, directly from the spectra.

ACKNOWLEDGMENT.

The author wishes to acknowledge the many contributions made by Professor M. H. L. Pryce in discussion, particularly in the evaluation of the transitions in strong fields, and the use of the direct effect of the external field on the nucleus to obtain the relative signs of the parameters in the Hamiltonian. He is also indebted to Dr. K. W. H. Stevens for much helpful discussion and criticism.

REFERENCES

- ABRAGAM, A., and PRYCE, M. H. L., 1951, *Proc. Roy. Soc. A*, **205**, 135.
 BLEANEY, B., 1950, *Phys. Rev.*, **78**, 214; 1951a, *Proc. Phys. Soc. A*, **64**, 315; 1951b, *Proc. Phys. Soc. A*, **64**, 316.
 BLEANEY, B., and INGRAM, D. J. E., 1949, *Nature, Lond.*, **164**, 116; 1951a, *Proc. Roy. Soc. A* (in publication); 1951b, *Proc. Roy. Soc. A*, **205**, 336.
 ELLIOTT, R. J., and STEVENS, K. W. H., 1951, *Proc. Phys. Soc. A*, **64**, 205.
 INGRAM, D. J. E., 1949, *Proc. Phys. Soc. A*, **62**, 664.
 GORTER, C. J., 1948, *Physica*, **14**, 504.
 POUND, R. V., 1949, *Phys. Rev.*, **76**, 1410.
 PRYCE, M. H. L., 1949, *Nature, Lond.*, **164**, 116.
 ROSE, M. E., 1949, *Phys. Rev.*, **75**, 213.
 SPIERS, J. A., 1948, *Nature, Lond.*, **161**, 807; 1949, *Directional Effects in Radioactivity* (Chalk River, Ontario: National Research Council of Canada).

LI. *The Communal Entropy of Dense Systems.*

By J. A. POPLE,

Department of Theoretical Chemistry, University of Cambridge*.

[Received February 16, 1951].

SUMMARY.

This paper contains an approximate method of calculating the communal entropy of an assembly of monatomic particles. The method of dealing with dense systems may be regarded as an extension of that used by Lennard-Jones and Devonshire in their theory of liquids and dense gases. The available volume is divided into cells and the communal free energy expressed in terms of a set of parameters related to the probability of two, three or more particles occupying a given cell simultaneously. Application to an assembly of rigid spheres leads to the conclusion that the communal entropy does not become appreciable until the available volume is over five times that of a close-packed assembly. This suggests that, for more accurate intermolecular potentials, the communal entropy is practically zero in the solid and liquid states, but that the extra terms in the free energy may have an appreciable effect on the calculated critical constants and vapour pressures.

§1. INTRODUCTION.

ACCORDING to classical statistical mechanics, the thermodynamic functions of a system of N particles confined to a volume v can be derived from the free energy A given by

$$\exp(-A/kT) = \frac{1}{N!} \left(\frac{2\pi mkT}{h^2} \right)^{3N/2} \int^v \dots \int^v \exp(-V/kT) dv_1 \dots dv_N, \quad (1.01)$$

where V is the potential energy of any configuration and $\int^v dv_i$ indicates integration of the coordinates of particle i over the whole volume v .

The only exact method of calculating the integral in (1.01) is that of Mayer (1937). However, this only applies to a limited range of densities and is exceedingly difficult to handle mathematically. Of the approximate methods used many (Eyring and Hirschfelder 1937, Lennard-Jones and Devonshire 1937) have been based on a model in which each particle is confined to a cell by its neighbours. Lennard-Jones and Devonshire calculate the field in such a cell on the assumption that the neighbours are in their equilibrium positions. An improved form for the cell field has recently been suggested by Kirkwood (1950).

Although these cell models may give a reasonable picture of molecular environment at high densities, they will become increasingly inaccurate as the cell size increases. At low densities restriction to cells will prevent

* Communicated by Prof. Sir John Lennard-Jones.

collisions occurring and the method gives no second virial coefficient. An attempt to remedy this situation and to extend the cell method to low densities has recently been made by Buehler, Wentorf, Hirschfelder and Curtiss (1951). In addition to the model used by Lennard-Jones and Devonshire, which they call the "empty centre model", they consider another in which the wandering particle moves in the field of particles fixed at the centres of neighbouring cells and one fixed at the centre of the cell in question. This is called the "occupied centre model"*. The arithmetic mean of the two free volumes is then used to construct the partition function. This method reduces to that of Lennard-Jones and Devonshire at high densities and gives the correct second virial coefficient at low densities. No theoretical justification is given for this averaging process, however; in the intermediate region the arithmetic mean formula is no more than a convenient method of interpolation.

When the cell method was originally developed, it was pointed out by Hirschfelder, Stevenson and Eyring (1937) and also by Lennard-Jones and Devonshire (1937) that the approximation of placing one particle in each cell, from which all others were excluded, constitutes an artificial restriction on the region of phase space over which integration is to be performed. It can be shown that, in the limit of low density, this corresponds to the omission of a factor e^N in the partition function and leads to an error of k per particle in the calculated entropy. This extra term is usually referred to as the communal entropy; it has been discussed in some detail by Lennard-Jones (1940). The chief purpose of this paper is to examine this term and show how it is connected with the work of Buehler *et al.*

Although we know that the communal entropy increases from zero to k per particle as the volume increases to infinity, no satisfactory theory of the point at which it becomes effective has been advanced. Originally, it was suggested by Hirschfelder, Stevenson and Eyring (1937) that it becomes available at the melting point. This hypothesis has been examined by O. K. Rice (1938) who concludes that it is without sufficient justification and that the communal entropy is unlikely to play a major part in the fusion process. We shall see that the theory of this paper confirms Rice's conclusions.

In this and subsequent work (1944) Rice has discussed the communal entropy of an aggregate of hard spheres in some detail. In the later paper he claims to show that for a gas of hard elastic spheres the communal entropy is fully excited for each direction of space, and amounts in all to $3R$ per mole. As these results are at variance with those obtained in this paper, it is well to find the cause of the discrepancy before proceeding further. The difference lies in the meaning attached to the phrase "restriction to a cell". Rice interprets this as meaning that the whole of the molecule must lie within the cell. Although this has a precise meaning in the case of hard elastic spheres, it leads to difficulties when we deal with

* In the published version of their work, Buehler *et al.* have used the terms "soft-centre model" and "hard-centre model".

actual molecules which have no fixed boundaries. Here we shall say that a given particle occupies a certain cell if its centre (or some fixed point of the molecule if it is non-central) lies in that cell.

In this paper we shall discuss the way we should set about calculating the communal entropy and free energy in a general manner. These are expressed in terms of a set of quantities $\omega_2, \omega_3, \dots$ which are related to the probability of two, three or more particles occupying a given cell simultaneously. It is shown that ω_2 is the most important of these and that a good approximation to the extra terms in the thermodynamic functions can be obtained if we neglect the others. This is followed by a simple model for the calculation of ω_2 . With some further approximations, it is found that ω_2 can be expressed in terms of the free volumes of the empty and occupied centre models used by Buehler *et al.* In this way we have obtained a formula for the communal free energy which is, in effect, a theoretical foundation for the use of these models. The most important result of the investigation is the modification of the arithmetic mean formula. If v_{fe} and v_{fo} are the free volumes of the empty and occupied centre models respectively, it is suggested that the true free volume should be calculated from

$$v_f = v_{fe} + \sqrt{(2v_{fe} v_{fo})}. \quad (1.02)$$

At the end of the paper, this formula is applied to estimate the communal free energy of a system of rigid spheres, using the values of v_{fe} and v_{fo} calculated by Buehler *et al.*

§ 2. A GENERAL METHOD FOR CALCULATING THE COMMUNAL ENTROPY.

We shall base our work on the recent analysis of the cell method given by Kirkwood (1950), using a similar notation. If we write

$$Z = \int^v \dots \int^v \exp(-V/kT) dv_1 \dots dv_N, \quad (2.01)$$

the free energy is given by

$$\frac{A}{NkT} = -\frac{3}{2} \log \frac{2\pi mkT}{h^2} - \frac{1}{N} \log Z + \frac{1}{N} \log N! \quad (2.02)$$

Kirkwood now supposes the volume v to be divided up into a lattice of N equal cells and writes $Z^{(m_1 \dots m_N)}$ for the restricted phase integral in which the cells are occupied by $m_1 \dots m_N$ particles respectively. $Z/N!$ can then be divided up as follows:

$$\frac{Z}{N!} = \sum_{\substack{m_1 \dots m_N \\ \sum m_i = N}}^N \frac{1}{\prod m_s!} Z^{(m_1 \dots m_N)}. \quad (2.03)$$

The usual cell method is concerned with an approximate evaluation of $Z^{(1 \dots 1)}$. If we write

$$\frac{Z}{N!} = \sigma^N Z^{(1 \dots 1)}, \quad (2.04)$$

the communal free energy may be defined as $-NkT \log \sigma$ and the communal entropy as

$$Nk \left\{ \log \sigma + \frac{T}{\sigma} \left(\frac{\partial \sigma}{\partial T} \right) \right\}.$$

From (2.03) and (2.04) we see that the value of σ will depend on the ratio of the phase integral with multiple occupation $Z^{(m_1 \dots m_N)}$ to $Z^{(1 \dots 1)}$. We shall suppose that this ratio can be expressed as a product of the form

$$\frac{Z^{(m_1 \dots m_N)}}{Z^{(1 \dots 1)}} = \prod_{s=1}^N \omega_{m_s}, \quad \dots \quad (2.05)$$

where there is an ω -factor for each type of occupation (vacancy, single occupation, double occupation, etc.). Clearly we must have $\omega_1 = 1$. Also we may take $\omega_0 = 1$ without loss of generality, for if $\omega_0 \neq 1$ we may replace it by 1 and at the same time replace $\omega_i (i \neq 0)$ by $\omega_0^{i-1} \omega_i$ without altering $\prod \omega_{m_s}$.

The approximation (2.05) is equivalent to assuming that multiply occupied cells do not interfere with one another. It will be accurate at high densities when there are very few multiply-occupied cells and at low densities when the cells are large and effectively independent. It therefore seems reasonable to use it throughout the full range of volume. ω_2 may be described as the ratio in which the restricted phase integral is altered if we remove a particle from a singly occupied cell and move it to another also singly occupied, leaving a doubly occupied cell and a hole. $\omega_3, \omega_4, \dots$ may be defined in similar ways.

We next have to solve the problem of finding σ when we are given the values of the ω 's. The full expression,

$$\sigma^N = \sum_{\substack{m_1 \dots m_N \\ \sum m_i = N}} \prod_{s=1}^N \left(\frac{\omega_{m_s}}{m_s!} \right), \quad \dots \quad (2.06)$$

obtained from (2.03), (2.04) and (2.05) has to be converted into a less unwieldy form.

Suppose that a given partition $m_1 \dots m_N$ contains $n_i (m_1 \dots m_N)$ cells with i and not more than i particles. Then, since we are dealing with N particles and N cells, we must have

$$\left. \begin{aligned} \sum_{i=0}^N i n_i &= N, \\ \sum_{i=0}^N n_i &= N. \end{aligned} \right\} \dots \quad (2.07)$$

The number of partitions $m_1 \dots m_N$ with n_0 empty cells, n_1 singly occupied cells, etc., is

$$\frac{N!}{n_0! (N-n_0)!} \frac{(N-n_0)!}{n_1! (N-n_0-n_1)!} \dots = \frac{N!}{n_0! n_1! \dots n_N!} \quad (2.08)$$

Equation (2.06) can therefore be written

$$\sigma^N = \sum_{n_0, n_1, \dots, n_N}^* \frac{N!}{n_0! n_1! \dots n_N!} \prod_{s=0}^N \left(\frac{\omega_s}{s!} \right)^{n_s}, \quad (2.09)$$

where Σ^* indicates summation over those values of n_0, n_1, \dots, n_N which satisfy (2.07). As we shall only be concerned with the logarithm of σ we may follow the usual procedure and replace the series in (2.09) by its largest term. We therefore seek the unconditional maximum of

$$G = \log \left\{ \frac{N!}{n_0! n_1! \dots n_N!} \prod_{s=0}^N \left(\frac{\omega_s}{s!} \right)^{n_s} \right\} + \left(\log \frac{\lambda}{N} \right) \sum_{i=0}^N n_i + (\log \mu) \sum_{i=0}^N i n_i, \quad (2.10)$$

$\log(\lambda/N)$ and $\log \mu$ are Lagrange multipliers taken in this form for convenience in the subsequent analysis.

Using Stirling's formula we find that the maximum term occurs when

$$n_i = N \lambda \mu^i \omega_i / i! \quad (i=0, \dots, N), \quad (2.11)$$

where the parameters λ and μ are determined from the conditions

$$\left. \begin{aligned} \sum_{i=0}^N N \lambda \mu^i \frac{\omega_i}{i!} &= N, \\ \sum_{i=0}^N N \lambda \mu^i \frac{\omega_i}{(i-1)!} &= N. \end{aligned} \right\} \quad (2.12)$$

If we define

$$f(x) = \sum_{i=0}^N (\omega_i / i!) x^i, \quad (2.13)$$

(2.12) may be written

$$\lambda^{-1} = f(\mu) = \mu f'(\mu). \quad (2.14)$$

Finally we have

$$\sigma = \left[\left\{ \frac{N!}{n_0! \dots n_N!} \prod_{s=0}^N \left(\frac{\omega_s}{s!} \right)^{n_s} \right\}_{\max} \right]^{1/N} = \frac{1}{\lambda \mu} = f'(\mu). \quad (2.15)$$

The complete solution may therefore be written in implicit form

$$\sigma = f(\mu) / \mu = f'(\mu). \quad (2.16)$$

§ 3. THE CONTRIBUTION OF DOUBLE OCCUPATION.

If all the ω 's except ω_2 vanish, equation (2.16) can be solved explicitly. In this case

$$f(x) = 1 + x + \frac{1}{2} \omega_2 x^2, \quad (3.01)$$

whence

$$\mu = \sqrt{(2/\omega_2)}, \quad \sigma = 1 + \sqrt{(2\omega_2)}. \quad (3.02)$$

This leads to a free energy

$$\frac{A}{NkT} = -\frac{3}{2} \log \frac{2\pi mkT}{h^2} - \log Z^{(1\dots 1)} - \log \{1 + \sqrt{(2\omega_2)}\}. \quad (3.03)$$

This is the solution we get if we replace the limitation of single occupation by a condition which prevents more than two particles occupying a cell simultaneously. We know that ω_2 varies for 0 to 1 as the volume increases, so (3.03) shows at once that at low densities $\log \{1 + \sqrt{2}\}$ or 88 per cent of the communal entropy is due to double occupation of cells. It is also possible to get the equation of state from (3.03) by the usual formula

$$\frac{pv}{RT} = v \frac{\partial}{\partial v} \left(-\frac{A}{NkT} \right). \quad (3.04)$$

To find ω_2 at low densities we may neglect the effect of particles in other cells and write

$$\begin{aligned} \omega_2 &= \frac{N^2}{v^2} \int^\Delta \int^\Delta \exp [-E(r_{12})/kT] dv_1 dv_2 \\ &= 1 - \frac{N^2}{v^2} \int^\Delta dv_1 \int^\Delta \{1 - \exp [-E(r_{12})/kT]\} dv_2, \end{aligned} \quad (3.05)$$

where $E(r_{12})$ is the intermolecular energy of the pair of particles 1 and 2. As far as terms of order v^{-1} are concerned, we can replace integration over Δ with respect to v_2 by integration to infinity, so that we get

$$\omega_2 = 1 - \frac{4\pi N}{v} \int_0^\infty r^2 \{1 - \exp [-E(r)/kT]\} dr. \quad (3.06)$$

From (3.03) and (3.06) we now get the equation of state

$$\frac{pv}{RT} = 1 + \frac{1}{1 + 1/\sqrt{2}} \frac{2\pi N}{v} \int_0^\infty r^2 \{1 - \exp [-E(r)/kT]\} dr + O\left(\frac{1}{v^2}\right). \quad (3.07)$$

From this equation we see that the theory allowing for double occupation gives a second virial coefficient equal to $\sqrt{(2)}/[\sqrt{(2)+1}]$ or 58.6 per cent of the correct value. Thus, even in the limiting case, (3.03) corrects the major part of the deficiency of the original cell method. At higher densities, the value of ω_3 , ω_4 , etc. will be smaller relative to ω_2 and (3.03) will become even more accurate. It seems very probable that, in the critical region, the terms ω_3 , $\omega_4 \dots$ will, in fact, be quite unimportant, so we shall not discuss them further.

§ 4. MODELS FOR EVALUATING ω_2 .

The next step in the theory is to set up simple models for the calculation of the multiple occupation factor ω_2 . To find this we shall use a modification of the method of Lennard-Jones and Devonshire, in which each particle is treated as moving independently in a cell field $\psi(\mathbf{r})$. We shall make the further approximation of supposing that this field is unaltered when a neighbouring cell becomes vacant or doubly occupied. The errors in the two cases to some extent cancel. ω_2 can then be expressed in terms of the phase integral for two particles moving in the ordinary cell field $\psi(\mathbf{r})$. If we write

$$\psi_1(\mathbf{r}) = \psi(\mathbf{r}) - \psi(0), \quad (4.01)$$

this expression for ω_2 is, from the definition in § 2.

$$\omega_2 = \frac{\int^{\Delta} \int^{\Delta} \exp \{ -[\psi_1(\mathbf{r}_1) + \psi_1(\mathbf{r}_2) + E(r_{12})]/kT \} dv_1 dv_2}{\left\{ \int^{\Delta} \exp [-\psi_1(\mathbf{r})/kT] dv \right\}^2} \quad (4.02)$$

where \int^{Δ} indicates integration over the cell. Similar formulæ could be given for ω_3, ω_4 , etc.

If the integral in the numerator of (4.02) is written as I_2 , we have

$$I_2 = \int^{\Delta} Q(\mathbf{r}_1) \exp [-\psi(\mathbf{r}_1)/kT] dv_1, \quad (4.03)$$

where $Q(\mathbf{r}_1) = \int^{\Delta} \exp \{ -[\psi_1(\mathbf{r}_2) + E(r_{12})]/kT \} dv_2, \quad (4.04)$

$Q(\mathbf{r}_1)$ may be described as the free volume of particle 2 in the cell, given that particle 1 is the point \mathbf{r}_1 .

In the case of a spherically symmetric cell, $Q(\mathbf{r})$ can be expanded about the origin as follows:

$$Q(r_1) = \sum_{i=0}^{\infty} \frac{r_1^{2i}}{(2i)!} \left(\frac{\partial^{2i} Q}{\partial r^{2i}} \right)_0. \quad (4.05)$$

The integral I_2 then becomes

$$I_2 = \sum_{i=0}^{\infty} \left(\frac{\partial^{2i} Q}{\partial r^{2i}} \right)_0 \frac{1}{(2i)!} \int^{\Delta} r^{2i} \exp [-\psi(r)/kT] dv. \quad (4.06)$$

The coefficients $\left(\frac{\partial^{2i} Q}{\partial r^{2i}} \right)_0$ can be written

$$\left(\frac{\partial^{2i} Q}{\partial r^{2i}} \right)_0 = \int^{\Delta} \left\{ \frac{\partial^{2i}}{\partial r^{2i}} \exp [-E(r_{12})/kT] \right\}_0 \exp [-\psi_1(r_2)/kT] dv_2, \quad (4.07)$$

leading to

$$\begin{aligned} (Q)_0 &= \int^{\Delta} \exp \{ -[\psi_1(r) + E(r)]/kT \} dv, \\ \left(\frac{\partial^2 Q}{\partial r^2} \right)_0 &= -\frac{1}{kT} \int^{\Delta} \left[\frac{2}{3r} E' + \frac{1}{3} \left(E'' - \frac{E'^2}{kT} \right) \right] \exp \{ -[\psi_1(r) + E(r)]/kT \} dv. \end{aligned} \quad (4.08)$$

A simple first approximation would be to neglect all but the first term in (4.05) and write $Q = (Q)_0$. Examination of equation (4.08) shows that this is just the free volume of the occupied-centre model used by Buehler, Wentorf, Hirschfelder and Curtiss (1951). In their notation v_{fe} is the free volume in an empty cell and v_{fo} is the free volume when there is a particle at the centre*. Thus to this approximation

$$Q = v_{fo}, \quad I_2 = v_{fe} v_{fo}, \quad \omega_2 = v_{fo}/v_{fe}. \quad (4.09)$$

If we neglect ω_i for $i > 2$ the free energy is given by

$$\frac{A}{NkT} = -\frac{3}{2} \log \frac{2\pi mkT}{h^2} - \log v_{fe} - \frac{\Phi_0}{NkT} - \log \{ 1 + \sqrt{(2v_{fo}/v_{fe})} \}, \quad (4.10)$$

* Buehler *et al.* use v_{fe} and v_{fh} in the published version of their paper.

Lennard-Jones and Devonshire (1938) included the additional factor e^N in the liquid partition function. At the end of their paper, however, they stated that if this factor was omitted, the calculated vapour pressures would be reduced by a factor of e and the calculated boiling points by about 9 per cent. The present work shows that these corrections should be applied.

The author is indebted to Professor Sir J. Lennard Jones for the loan of an advance copy of a paper by Buehler, Wentorf, Curtiss and Hirschfelder, sent to him by Professor Hirschfelder.

REFERENCES.

- BEUHLER, R. J., WENTORF, R. H., HIRSCHFELDER, J. O., and CURTISS, C. F., 1951, *J. Chem. Phys.*, **19**, 61.
EYRING, H., and HIRSCHFELDER, J. O., 1937, *J. Phys. Chem.* **41**, 249.
HIRSCHFELDER, J. O., STEVENSON, D., and EYRING, H., 1937, *J. Chem. Phys.*, **5**, 896.
KIRKWOOD, J. G., 1950, *J. Chem. Phys.*, **18**, 380.
LENNARD-JONES, J. E., 1940, *Proc. Phys. Soc.*, **52**, 729.
LENNARD-JONES, J. E., and DEVONSHIRE, A. F., 1937, *Proc. Roy. Soc. A*, **163**, 53; 1938, *Ibid.*, **165**, 1.
MAYER, J. E., 1937, *J. Chem. Phys.*, **5**, 67.
RICE, O. K., 1938, *J. Chem. Phys.*, **6**, 476; 1944, *Ibid.*, **12**, 1.

LII. *Grain Boundary Diffusion in Metals.*

By A. D. LE CLAIRE,

Atomic Energy Research Establishment, Harwell*.

[Received February 16, 1951.]

ABSTRACT.

By an extension of a recent analysis of the problem of grain boundary diffusion in metals, the expression

$$\frac{D'}{D} = \frac{1}{\delta} \cdot 2 (\pi Dt)^{1/2} \cot^2 \alpha$$

has been derived relating the diffusion coefficients D' and D for grain boundary and for volume diffusion, δ the effective "width" of the grain boundary and α the angle at time t between a line of constant concentration and the grain boundary at the point where it meets the grain boundary. Some remarks are made on the use of the equation and when it is applied to a recent experimental observation on grain boundary diffusion of copper in nickel, the result is deduced that $D' = 8 \text{ cm.}^2/\text{day}$ at 1000°C .

A discussion follows on some aspects of the relation of other work on grain boundaries to grain boundary diffusion. Evidence is presented, based on models of the grain boundary, which suggests that the activation energies for grain boundary and for volume diffusion may not differ appreciably.

§1. INTRODUCTION.

WORK on preferential grain boundary diffusion in metals has in the past been hampered by the lack both of a quantitative treatment of the process and of reliable experimental methods for studying it. It is the purpose of this note to extend a recent analysis (Fisher 1950) of the problem in such a way that the simple qualitative method of study reported from this laboratory (Barnes 1950) can be made to yield quantitative results with very little extra work. A discussion is then given of the importance of such quantitative studies insofar as they may give information on the nature of the grain boundaries themselves.

§2. QUANTITATIVE METHODS FOR GRAIN BOUNDARY DIFFUSION STUDIES.

(a) *Fisher's Analysis.*

Fisher (1950) has recently obtained, with certain assumptions, an expression for the concentration of diffusing material in the neighbourhood of a grain boundary in terms of the time t during which diffusion has been

* Communicated by the Author.

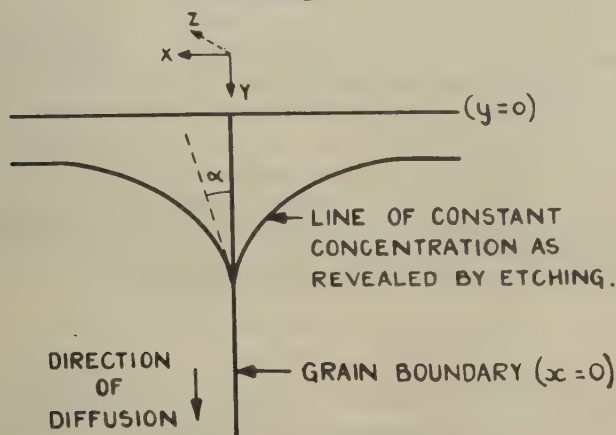
taking place down the grain boundary, the coordinates x, y , (see fig. 1) and the coefficients D' and D for grain boundary and for volume diffusion respectively.

$$C = \text{Exp} \left(\frac{-y_1 \sqrt{(2)}}{(\pi t_1)^{1/4}} \right) \cdot \text{Erfc} \left(\frac{x_1}{2t_1^{1/2}} \right)^* \quad \dots \quad (1)$$

where $t_1 = \frac{Dt}{\delta^2}$; $x_1 = \frac{x}{\delta}$; $y_1 = \frac{y}{\delta} \left(\frac{D'}{D} \right)$.

The grain boundary commences at the point $x=0, y=0$ and δ is its effective "width".

Fig. 1.



Diffusion down a grain boundary.

As a confirmation of the validity of equation (1), Fisher has successfully applied it to an interpretation of the results of an experiment on the grain boundary diffusion of radioactive silver in polycrystalline silver, by the standard technique of measuring the activity of layers of silver perpendicular to the diffusion direction, machined from the diffusion zone. He obtains with the assumption $\delta = 5 \times 10^{-8}$, i. e. about two atomic spacings,

$$D'/D = 9.4 \times 10^5.$$

(b) Author's Extension.

More recently a publication from this laboratory (Barnes 1950) has described how the contours of concentration in the neighbourhood of a grain boundary, down which preferential diffusion (in this case of copper in the grain boundaries of nickel) is taking place, can be revealed by etching. It was suggested therein that the angle α between the grain boundary and a

* $\text{Erfc } x = 1 - \frac{2}{\sqrt{(\pi)}} \int_0^x e^{-t^2} dt,$

concentration contour at the point where it meets the grain boundary could be used as a measure of the ratio of the rates of diffusion down the grain boundary and into the grain. This ratio of course is only of secondary importance but by development of equation (1) measurements of the angle α can be used to calculate the ratio of the actual diffusion coefficients for grain boundary and for volume diffusion.

Simple differentiation of equation (1) gives the slope at any point (x, y) of a line of constant concentration c at time t . From this is readily deduced the equation

$$\frac{D'}{D} = \frac{1}{\delta} 2(\pi Dt)^{1/2} \cot^2 \alpha. \quad (2)$$

connecting the ratio of D' and D with the angle α . When this equation is applied to the previously published work on copper-nickel, taking $\alpha=30^\circ$ (see fig. 1, Barnes 1950) $D \sim 10^{-5}$ cm.²/day and assuming again $\delta=5 \cdot 10^{-8}$, we find

$$D'/D = 8 \cdot 10^5 \text{ at } 1000^\circ \text{C.},$$

a ratio the order of magnitude of which is the same as that obtained for self diffusion in silver.

Inserting the known value of D into this equation gives

$$D' = 8 \text{ cm.}^2/\text{day}.$$

Fisher's analysis provides the first real attempt to study grain boundary diffusion in metals in a quantitative way and it is suggested that the extension of his relation to give equation (2), together with the experimental method for providing values of α , constitute a simpler and quicker means of obtaining grain boundary diffusion coefficients in metals than a sectioning technique such as used by Fisher. Possibly many micro-photographs showing diffusion in metals may already exist in which a preferential grain boundary penetration is apparent and to which the relation (2) could be usefully applied.

A calculation of D'/D from equation (2) requires some assumption as to the magnitude of δ , the width of the grain boundary. This is usually stated as being a "few atomic diameters", this estimate being based on the assumption of the transitional lattice theory of the grain boundary and the assertion of very short range forces between atoms. A precise evaluation of δ , and so of D' , is not possible at present, but for practical purposes we may use $D'\delta$ in place of D' to characterize grain boundary diffusion rates, for $D'\delta$ clearly represents the amount of material diffusing in unit time under unit concentration gradient per unit length of the grain boundary in the "z" direction (fig. 1) and perpendicular to that length. $D'\delta$ can be obtained by measurement of only α , D and t , and requires no assumptions about the structure of the grain boundary. The results for copper in nickel give

$$D'\delta/D = 0.04 \text{ cms.}$$

There are two points that need bearing in mind in any use of equation (2). The first is to ensure that the grain boundary is normal to the plane in which α is being measured, and that the grain boundary has not migrated during the diffusion anneal. The second point is to remember that the equation (1) is derived on the assumption that D and D' are independent of concentration, so that the value of D'/D obtained will only be a mean value for the concentration range covered in the experiment. It should be noted that any variation of α with the position of the point on the grain boundary at which it is measured will indicate a variation not of D'/D but of $D'/D^{3/2}$ with concentration. (Such a variation was in fact found in the experiment on copper and nickel.) It can probably be assumed that each value of D'/D corresponds, although probably only roughly when D'/D is strongly dependent on concentration, with the concentration at the point where the corresponding value of α was measured.

§3. GRAIN BOUNDARY MODELS AND DIFFUSION.

It is interesting to consider how other work on the properties of grain boundaries might be related to grain boundary diffusion studies.

In view of the difference between D' and D it is important to know whether it is due to a decrease in the activation energy " Q " for grain boundary diffusion over volume diffusion, or to an increase in the constant term D_0 in the expression usually used to express the temperature dependence of diffusion rates.

$$D = D_0 \exp(-Q/RT). \quad . \quad . \quad . \quad . \quad . \quad (3)$$

We may perhaps draw some conclusions by considering some of the grain boundary models that have been proposed.

To explain his result that the activation energy for grain boundary slip in several metals is the same as that for their volume diffusion and for the constant rate creep of single crystals, Kê (1949) has suggested the concept of "disordered groups" of atoms as the units responsible for all three processes. These exist in certain concentration in the body of the crystal, but in much higher concentration at the grain boundary which therefore consists of regions of good fit separated by regions of disorder, the "disordered groups". The rearrangement of atoms within a group normally constitutes a diffusion process, but in the presence of a shear stress leads to slip. The equality of the activation energies for the three processes considered by Kê is thus satisfactorily explained. But the same rearrangement of the atoms of a disordered group at the grain boundary will lead to grain boundary diffusion, so that on Kê's model, the activation energies for volume and grain boundary diffusion will also be the same.

A study of the temperature dependence of D' and comparison with that of D would both settle the relative values of the corresponding activation energies Q' and Q and provide useful confirmation or otherwise of such grain boundary models as this one of Kê. In such studies one must remember that any impurities which segregate in the grain boundary will most likely

have an effect on Q' out of all proportion to their total concentration. As an example of the great importance of impurities in grain boundary studies, we may quote Kê (1949) who found that even very small quantities of impurity may completely block grain boundary slip.

Dislocation models of the grain boundary have been proposed in the past (Burgers 1940, Bragg 1940) and recently studied by Read and Shockley (1950), some of whose conclusions have been verified by Aust and Chalmers (1950). On this model the grain boundary is made up of a suitable array of dislocations. With certain assumptions it can be shown that the measured value of $D'\delta/D$ can be explained on the further assumption that $Q' \doteq Q$.

Dislocations exist also, of course, within the crystal, and we will suppose that for our present purpose the grain boundary differs from the crystal only in that it contains a much higher concentration of dislocations. Seitz (1950) has suggested that it is dislocations which provide the very high density of vacancies in crystals required to explain certain phenomena, particularly the Kirkendall Effect. We will assume then that the main sources of vacancies are the dislocations, and further, that the density of vacancies in any region is proportional to the density of dislocations. The vacancies provided by the dislocations will then lead to diffusion by the normal vacancy mechanism, so that we can write

$$D = \text{const. } \rho \exp(-Q/RT), \quad (4)$$

where D is the diffusion coefficient in a region where the density of dislocations is ρ . Q is the activation energy for the diffusion process and does not include the energy of formation of a vacancy, as it does when it is supposed that the vacancies exist in thermal equilibrium with the lattice. In the present case the energy required to form a vacancy, from a dislocation, is negligible. If we suppose first that Q and Q' are not equal, we can write for $D'\delta/D$, from equation (4),

$$\frac{D'\delta}{D} = \frac{\rho_{gb}}{\rho_e} \frac{\exp(-Q'/RT)}{\exp(-Q/RT)}, \quad (5)$$

where ρ_{gb} and ρ_e are the densities of dislocations per unit length of the grain boundary and per unit area of the crystal respectively. We should expect the excess density of dislocations at the grain boundaries to provide an excess density of vacancies for some distance from the grain boundary, so that for diffusion the effective width δ of the grain boundary will be greater than the distance over which the normal lattice structure is disturbed. We avoid having to make an estimate of δ by considering in equation (5) the ratio $D'\delta/D$ instead of D'/D .

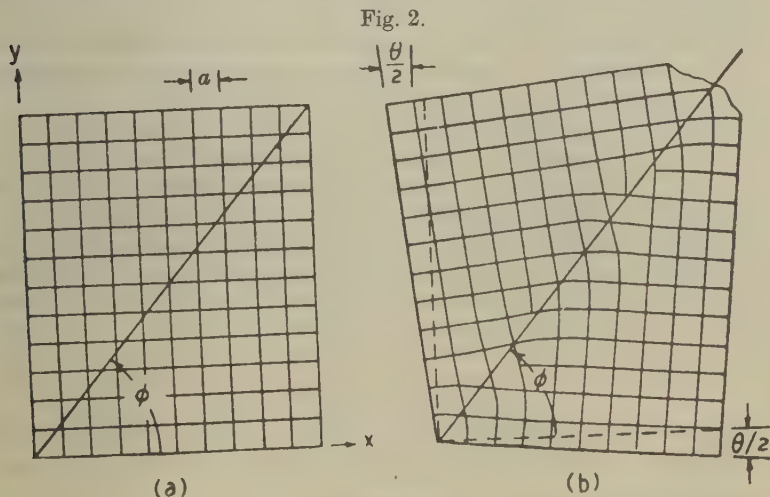
With estimates of ρ_{gb} and ρ_e we can calculate the difference between Q' and Q that would be necessary to account for the measured ratio of $D'\delta/D$. We may take for ρ_e the value of 10^8 , an estimate for fully annealed metals based upon the dislocation theory of their strength (see Cottrell 1949). The value of ρ_{gb} will vary considerably with the orientation difference between

the two grains adjoining the grain boundary. As a maximum value of ρ_{gb} we may take $1/2a$ (a =lattice constant), for we should not expect the number of dislocations in the grain boundary to exceed about one every two lattice planes. With $a=3 \times 10^8$ cm. this gives $\rho_{gb}(\text{max.})=1.5 \times 10^7/\text{cm}$.

A minimum value for ρ_{gb} can be estimated from the expression given by Read and Shockley for the density of dislocations in a grain boundary defined by the angles θ and ϕ (see fig. 2),

$$\rho_{gb}=2 \cdot \frac{\sin \frac{1}{2} \theta}{a} \{\cos \phi + \sin \phi\}.$$

Taking $\phi=0$ (ρ_{gb} is not very sensitive to the value of ϕ) and $\theta \sim 2^\circ$ we find $\rho_{gb}(\text{min.})=1.3 \times 10^6$.



Characterization of a grain boundary in terms of the angles θ and ϕ .
(Read and Shockley 1950.)

Inserting these values of ρ_{gb} and of ρ_e into equation (3) and using the value of $D'\delta/D=0.04$ (Cu/Ni) we find, when

$$\left. \begin{array}{ll} \rho_{gb}(\text{max.})=1.5 \times 10^7 & Q-Q'=-2.7 \text{ K.cals/mole,} \\ \rho_{gb}(\text{min.})=1.3 \times 10^6 & Q-Q'=+2.2 \text{ K.cals/mole.} \end{array} \right\} \text{ for } T=1000^\circ \text{ K.}$$

It is also readily shown that Q and Q' would be equal if we supposed the grain boundary to have characteristic angles $\theta=6^\circ$, $\phi=0$, which are not unlikely values.

We see then that the measured ratio of $D'\delta$ to D can be well accounted for on the assumption that Q and Q' are equal, and therefore from equation (3) that the whole of the difference in the diffusion rates for grain boundary and for volume diffusion arises from a difference in the D_0 term in equation (3). But if the activation energies do differ, they will not do so by more than about 2.5 K. cal/mole.

Similar calculations based on Kê's model of the grain boundary are impossible in the absence of estimates of the grain boundary and volume densities of disordered groups.

The experimental results at present available in the literature on the relative values of Q and Q' are very few and conflicting. Measurements of the diffusion coefficient of molybdenum in tungsten by Van Liempt (1932) and of thorium in tungsten by Fonda *et al.* (Fonda, Young and Walker 1933) show that D_0 increases with decreasing grain size, but that the activation energy is independent of the grain size of the tungsten, indicating the $Q=Q'$. On the other hand (Langmuir 1934) finds that $Q-Q'$ for the diffusion of thorium in tungsten is about 25 K. cal/mole and that D_0 for grain boundary diffusion is less than for volume diffusion. (See Barrer 1941.)

On the other hand, we have seen that theoretical considerations lead us to expect that Q and Q' might be equal and experimental work to confirm or disprove this would be very interesting.

Another important line of work would be a study of the dependence of D'/D upon the relative orientations of the crystal faces forming the boundary. Any marked dependence would provide further evidence in favour of the "transitional lattice" theory of the grain boundary.

A study of grain boundary diffusion rates is then of importance, not only as a diffusion study but also in investigating other properties of grain boundaries. It is hoped that this new method of investigation, requiring only micrographical techniques, will facilitate such studies.

ACKNOWLEDGMENT.

The author is indebted to the Director, Atomic energy Research Establishment, Harwell, for permission to publish this note.

REFERENCES.

- AUST, K. T., and CHALMERS, B., 1950, *Proc. Roy. Soc. A*, **204**, 359.
 BARNES, R. S., 1950, *Nature, Lond.*, **166**, 1032.
 BARRER, R. M., 1941, *Diffusion in and through solids* (Cambridge: University Press).
 BRAGG, W. L., 1940, *Proc. Phys. Soc.*, **52**, 54.
 BURGERS, J. M., 1940, *Proc. Phys. Soc.*, **52**, 23.
 COTTRELL, A. H., 1949, *Progress in Metal Physics*, Vol. 1, p. 104.
 FISHER, J. C., 1950, *General Electric Research Lab. Report GEPM 18*.
 FONDA, G., YOUNG, A., and WALKER, A., 1933, *Physics*, **4**, 1.
 KÊ T'ING SUI, 1949, *J. Appl. Phys.*, **20** (3), 274-80.
 LANGMUIR, I., 1934, *J. Franklin Inst.*, **217**, 543.
 READ, W. T., and SHOCKLEY, W., 1950, *Phys. Rev.*, **78** (3), 275-89.
 SEITZ, F., 1950, *Phys. Rev.* **79** (6), 1002.
 VAN LIEMPT, J. A. M., 1932, *Rec. Trav. Chim. Pays Bas*, **51**, 117.

LIII. *The Rectification and Observation of Signals in the Presence of Noise.*

By R. E. BURGESS, B.Sc.,
National Physical Laboratories*.

[Received January 10, 1951.]

SUMMARY.

The rectification of random narrow-band noise in the presence of a C.W. or modulated signal is analysed. The detector considered is of the type providing a rectified voltage which is a function of the instantaneous amplitude of the input wave. The smoothing present in the detector circuit is such that the high-frequency components of the applied wave are removed but the low-frequency variations of its envelope are faithfully transmitted.

The mean (or D.C.) component of the rectified voltage and its r.m.s. fluctuation about that mean (or L.F. noise output) are calculated as a function of the input signal/noise ratio and particular attention is paid to linear and square-law detectors.

The output signal/noise ratio for an amplitude-modulated signal input and for the audible beat reception of a C.W. signal are calculated.

The spectrum of the L.F. noise output from a detector supplied with random noise is shown to be closely similar for linear and square-law detectors.

The discrimination of a weak signal in noise is shown to be not critically dependent upon the law of the detector, and in particular the difference for a linear and a square-law detector is negligible.

The effect of receiver bandwidth, meter time-constant and integration time in improving the discernment of a weak signal is considered.

MORE IMPORTANT SYMBOLS.

A=instantaneous amplitude of the wave applied to the detector.

B=bandwidth of input noise.

E=r.m.s. input noise voltage.

$F(\omega)$ =input noise spectrum.

$G(\omega_n)$ =output noise spectrum.

H=amplitude of heterodyne voltage.

M=r.m.s. improvement due to meter time-constant.

N=number of observations.

Q=detector discrimination.

$R(\tau)$ =an autocorrelation coefficient of the input noise.

S=amplitude of C.W. signal.

T=time constant of meter.

* Communication from the National Physical Laboratory.

T_0 =duration of period of integration.

X, Y="in phase" and "quadrature" amplitudes of noise voltage.

$f_p(\omega_a)$ =normalized component spectra of the L.F. output noise.

m =depth of signal modulation.

n =exponent of detector law.

u =instantaneous rectified voltage.

v =instantaneous input noise voltage.

$x=S/\sqrt{(2)}E$ =r.m.s. signal/noise ratio.

$y=A/\sqrt{(2)}E$.

$\beta=2\pi B$ =angular bandwidth.

θ =instantaneous meter indication.

τ =time interval in autocorrelation.

ω_a =angular frequency in L.F. output.

ω_0 =central angular frequency of input noise.

§1. INTRODUCTION.

THE calculation of the transmission of signal and noise voltages by a linear amplifier is a familiar and simple process for it is known that the output from an amplifier supplied with a mixture of signal and noise is the sum of the outputs if each were applied separately. However, this principle of superposition cannot be applied when the signal and noise pass through a non-linear circuit such as a rectifier or a limiter.

The rectification of noise and of a mixture of noise and signal is of practical importance in relation to

- (i.) its effect on the signal/noise ratio in reception,
- (ii.) the measurement of noise,
- (iii.) the measurement of a signal in the presence of noise, and
- (iv.) the measurement of receiver sensitivity.

The analysis of the rectification of noise presents difficulties which arise partly from the non-linear characteristics of the circuit and partly from the inherent characteristics of the noise which can only be specified statistically. (It should be stated at this stage that only fluctuation noise is considered in the present paper.)

Fränz (1940) considered the case of a detector whose current/voltage characteristic could be represented by a power series. The results of the analysis were not applicable to the case of the discontinuous characteristic of the linear detector nor did they refer to the practical condition in which the detector output follows the envelope of the applied wave rather than the instantaneous voltage.

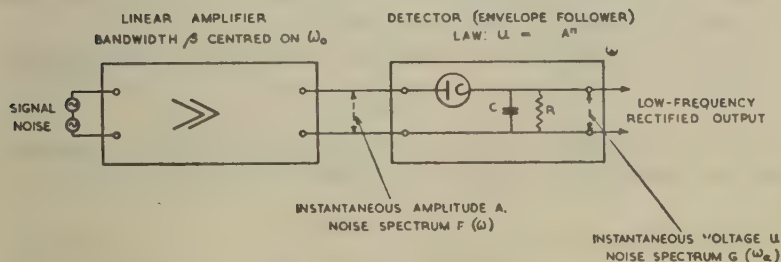
Fränz (1941) later published an analysis of the rectification of noise by a detector with a discontinuous linear characteristic. In this paper the method of using a singular integral to represent the characteristic was successfully applied to derive the mean rectified voltage, and the spectrum of the low frequency output.

Ragazzini (1942) considered the rectification of a mixture of a modulated signal and noise by an ideal linear detector in which the output voltage accurately follows the envelope of the applied wave. In order to make the analysis tractable it was found necessary to approximate in the evaluation of the components of the envelope and for this reason some of the equations are not exact.

In the present paper it is proposed to analyse by elementary methods the rectification of a mixture of signal and noise by linear and square-law detectors and to compare the results so obtained with those appearing in the papers mentioned above. The practical application of the formulæ to the evaluation of the sensitivity of reception of modulated signals and of C.W. signals using a heterodyning oscillator is also discussed.

It is convenient to draw attention at this point to the significance of the time constant of the detector circuit. Fig. 1 shows a typical

Fig. 1.



Schematic circuit of a typical receiver.

arrangement of a receiver; the amplifier having a central frequency ω_0 and bandwidth β passes the signal and noise to a detector having a load circuit RC across which the rectified voltage is developed. There are three possible cases of the time constant RC to be considered:

$$(a) \quad RC \ll \frac{1}{\omega_0}.$$

In this case there is practically no smoothing of the rectified voltage so that the latter consists of the positive half-waves of the applied voltage with the result that a considerable high-frequency component is present in the output and rectification is inefficient. This is the case considered by Fränz, but it does not conform with the usual circuital practice.

$$(b) \quad \frac{1}{\omega_0} \ll RC \ll \frac{1}{\beta}.$$

In this case the high frequency components are filtered from the output and yet the time constant is small enough for the output to follow accurately the envelope of the input voltage. This is the case of practical importance in receiving technique.

Now v , X and Y have a normal or Gaussian distribution about zero ; thus for v ,

$$P(v) \cdot dv = \frac{1}{\sqrt{(2\pi) \cdot E}} \exp\left(-\frac{v^2}{2E^2}\right) \cdot dv. \quad . \quad . \quad . \quad (4)$$

From this distribution the following averages may be formed :

$$\begin{aligned} \overline{v^2} &= \overline{X^2} = \overline{Y^2} = E^2, \\ \overline{XY} &= 0, \\ |\overline{v}| &= |\overline{X}| = |\overline{Y}| = \sqrt{(2/\pi)E}. \end{aligned}$$

The amplitude or envelope of the fluctuation noise voltage is given by the positive value of

$$r = \sqrt{(X^2 + Y^2)}$$

and its distribution function is of the Rayleigh type

$$P(r) \cdot dr = \frac{r}{E^2} \exp\left(-\frac{r^2}{2E^2}\right) \cdot dr, \quad . \quad . \quad . \quad (5)$$

from which

$$\overline{r^2} = 2E^2 \text{ and } \bar{r} = \sqrt{(\pi/2)E}.$$

If now a sinusoidal signal $S \cos \omega_0 t$ is added to the noise the r.m.s. signal/noise voltage ratio is given by

$$x = \frac{S}{\sqrt{(2)E}}$$

or $20 \log_{10} x$ in decibels.

The instantaneous amplitude A of the mixture is given by

$$A = \sqrt{(X+S)^2 + Y^2} \quad . \quad . \quad . \quad . \quad . \quad (6)$$

whose distribution is readily shown (Appendix I.) to be given by

$$P(A) \cdot dA = \frac{A}{E^2} \exp\left(-\frac{A^2 + S^2}{2E^2}\right) I_0\left(\frac{AS}{E^2}\right) \cdot dA, \quad . \quad . \quad . \quad (7)$$

I_0 being the modified Bessel Function of the first kind, zero order. If the parameter

$$y = \frac{A}{\sqrt{(2)E}}$$

is introduced we may write (7) in the form

$$P(y) \cdot dy = 2y \exp(-y^2 - x^2) \cdot I_0(2yx) \cdot dy. \quad . \quad . \quad . \quad (8)$$

For weak signals ($x \ll 1$) the amplitude distribution of the mixture is still of the Rayleigh type

$$P(y) \cdot dy = \frac{2y}{1+x^2} \exp\left(-\frac{y^2}{1+x^2}\right) dy, \quad . \quad . \quad . \quad (9)$$

which shows that the addition of the weak signal effectively increases the r.m.s. noise voltage from E to $E(1+x^2)^{\frac{1}{2}}$, which is equal to $(E^2 + \frac{1}{2}S^2)^{\frac{1}{2}}$ the r.m.s. voltage of the mixture. This property will be found useful later in considering signals below noise level.

In the case of large signals ($x \gg 1$) we have from the asymptotic expansion of I_0

$$P(y) \cdot dy \sim \sqrt{(y/\pi x)} \exp [-(y-x)^2] \cdot dy \quad . \quad . \quad . \quad (10)$$

which shows that the amplitude distribution of the mixture is centred on the signal amplitude and is approximately Gaussian with r.m.s. fluctuation equal to the r.m.s. noise voltage E .

§3. THE MEAN RECTIFIED VOLTAGE.

If the voltage output V from the rectifier is related to the amplitude A of the applied voltage by the n th-power law, the d.c. or mean rectified voltage which would be indicated by a voltmeter of long time constant is

$$\begin{aligned} \bar{u} = \overline{A^n} &= \int_0^\infty A^n P(A) \cdot dA \\ &= 2(\sqrt{(2)E})^n \int_0^\infty y^{n+1} \exp(-y^2 - x^2) I_0(2yx) \cdot du, \end{aligned}$$

where, as above, the signal/noise ratio is denoted by x . This integral can be evaluated by a general relation due to Hankel which leads to

$$\bar{u} = \overline{A^n} = (\sqrt{(2)E})^n \left(\frac{n}{2}\right)! {}_1F_1\left(-\frac{n}{2}, 1, -x^2\right), \quad . \quad . \quad (11)$$

in which ${}_1F_1$ is the hypergeometric function expressible by the Kummer series

$${}_1F_1\left(-\frac{n}{2}, 1, -x^2\right) = 1 + \frac{(-n/2)}{1} \frac{(-x^2)}{1!} + \frac{(-n/2)(1-n/2)}{1 \cdot 2} \frac{(-x^2)^2}{2!} +$$

(This function is denoted by M in Jahnke-Emde's Tables.)

It is clear that if n is a positive even integer the series terminates and the average of A^n can be simply expressed. Thus for a square law rectifier $n=2$ for which

$$\bar{A^2} = 2E^2(1+x^2), \quad . \quad . \quad . \quad . \quad . \quad (12)$$

showing that the mean rectified voltage is accurately proportional to the mean square value of the applied voltage, as in the case of the thermocouple for measurement of coexistent signal and noise. The anode-bend and the diode rectifier approximate to this condition for small input voltages.

The mean square output voltage is obtained in the general case by replacing n by $2n$ in equation (11):

$$\overline{u^2} = \overline{A^{2n}} = (2E^2)^n n! {}_1F_1(-n, 1, -x^2). \quad . \quad . \quad . \quad (13)$$

A case of practical importance is the linear rectifier ($n=1$) for which

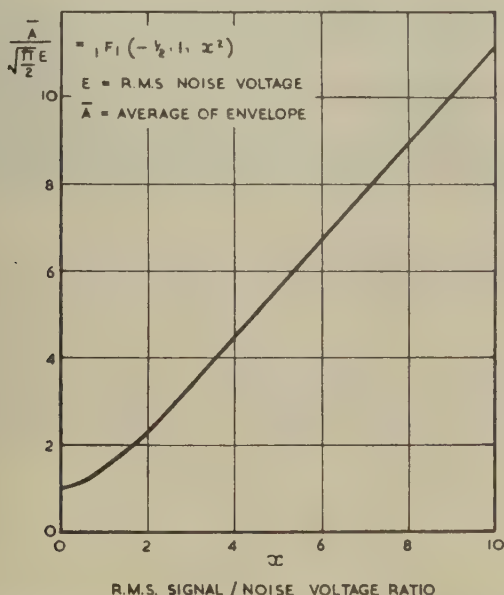
$$\bar{u} = \bar{A} = \sqrt{(\pi/2)} E {}_1F_1(-\tfrac{1}{2}, 1, -x^2). \quad (14)$$

Fig. 2 shows $\bar{A}/\sqrt{(\pi/2)}E$ as a function of the signal/noise ratio x . For a small signal/noise ratio ($x \ll 1$) the Kummer series gives

$$\begin{aligned} \bar{A} &= \sqrt{(\pi/2)} E \left(1 + \tfrac{1}{2}x^2 - \tfrac{x^4}{16} + \tfrac{x^6}{96} \dots \right) \\ &= \sqrt{[(\pi/2)E^2(1+x^2)]} \text{ approx.} \quad (15) \end{aligned}$$

showing that the linear rectifier tends to give an indication proportional to the r.m.s. value of the mixture of signal and noise when the latter predominates.

Fig 2



Average amplitude of the envelope of a mixture of signal and noise
(as would be indicated by a linear rectifier).

For a large signal/noise ratio ($x \gg 1$) the asymptotic expansion of the hypergeometric function

$${}_1F_1\left(-\frac{n}{2}, 1, -x^2\right) \sim \frac{x^n}{(n/2)!} \left(1 + \frac{n^2}{4x^2} + \dots \right) \quad . . (16)$$

gives

$$\bar{A} = \sqrt{(2)} E x \left(1 + \frac{1}{4x^2} \right). \quad (17)$$

In the above it has been assumed that the time constant of the rectifier circuit is such that the R.F. or I.F. is removed from the output, but sufficiently small for the envelope to be accurately followed, the long time constant of the meter providing the averaging. In Fränz's analysis (1941) of the linear rectifier, however, it was assumed that no smoothing was present, so that the rectified output consisted of the positive half-waves of the applied voltage. Since the average positive voltage is related to the average amplitude by

$$\bar{v}_+ = \frac{1}{2\pi} \int_0^\pi \bar{A} \sin \theta \cdot d\theta = \frac{\bar{A}}{\pi}, \quad \dots \dots \dots (18)$$

it is seen that Fränz's rectified output should be $1/\pi$ of the value calculated above, *i. e.*

$$\bar{v}_+ = \frac{E}{\sqrt{(2)\pi}} {}_1F_1(-\tfrac{1}{2}, 1, -x^2). \quad \dots \dots \dots (19)$$

Fränz (1941) obtained the average in the form

$$\bar{v}_+ = \frac{E}{\sqrt{(2)\pi}} \left[x^2 {}_1F_1(\tfrac{1}{2}, 2, -x^2) + \exp\left(-\frac{x^2}{2}\right) I_0\left(\frac{x^2}{2}\right) \right]. \quad \dots (20)$$

It may be shown that equations (20) and (19) are identical by using Kummer's relation for the Bessel function and the recurrence formulæ for F . For :

$$\left. \begin{aligned} e^{-\frac{1}{2}x^2} I_0(\tfrac{1}{2}x^2) &= {}_1F_1(\tfrac{1}{2}, 1, -x^2), \\ e^{-\frac{1}{2}x^2} [I_0(\tfrac{1}{2}x^2) + I_1(\tfrac{1}{2}x^2)] &= {}_1F_1(\tfrac{1}{2}, 2, -x^2), \\ x^2 {}_1F_1(\tfrac{1}{2}, 2, -x^2) + {}_1F_1(\tfrac{1}{2}, 1, -x^2) &= {}_1F_1(-\tfrac{1}{2}, 1, -x^2). \end{aligned} \right\} \dots (21)$$

§ 4. MEAN SQUARE VOLTAGE OF THE OUTPUT NOISE.

The noise output from a linear rectifier which accurately follows the envelope of the applied voltage can be expressed in terms of the fluctuation of the envelope about its average value. Thus the mean square noise output is given by

$$u_n^2 = \bar{A}^2 - (\bar{A})^2 = E^2 \left[2(1+x^2) - \frac{\pi}{2} F^2 \right], \quad \dots \dots (22)$$

where F denotes the hypergeometric function in equation (14).

If the signal/noise ratio is small ($x \ll 1$) the noise output is

$$u_n^2 = \left(2 - \frac{\pi}{2}\right) E^2 (1+x^2) = 0.43(1+x^2) E^2, \quad \dots \dots (23)$$

which shows that the mean square noise output is proportional to the total mean square value of the applied signal and noise.

For large signal/noise ratios ($x \gg 1$) the output noise tends to the limit given by

$$u_n^2 = E^2, \quad \dots \dots \dots (24)$$

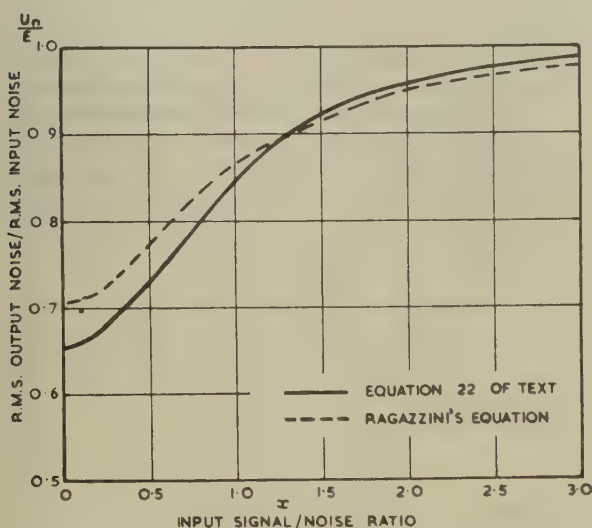
which shows that in the presence of a large C.W. signal the r.m.s. values of the input and output noise are equal.

To illustrate equation (22) the ratio u_n/E has been plotted as a function of x in fig. 3. It is of interest to compare this evaluation with the approximate analysis by Ragazzini (1942) who finds the simpler but less accurate value

$$u_n^2 = E^2 \left[\frac{x^2 + \frac{1}{2}}{x^2 + 1} \right], \quad \dots \quad (25)$$

which gives $\frac{1}{2}E^2$ instead of $0.43E^2$ for the output in the absence of a signal, but tends to the same upper limit of E^2 as above. For comparison Ragazzini's equation is plotted as a dashed curve in fig. 3, and it is seen to give a very good approximation to the exact value of $x > 1$.

Fig 3



Response of a linear rectifier to a mixture of noise and C.W. signal.

For the linear rectification of noise in the absence of a signal and with no smoothing Fränz (1941) found for the mean square output noise voltage

$$u_n^2 = \frac{E^2}{8\pi} \sum_{r=1}^{\infty} 16^{1-r} \frac{(2r-2)!^2}{r!^2(r-1)!^2}.$$

Now in this series the ratio of the $(r+1)$ th term to the r th term is $(r-\frac{1}{2})^2/(r+1)^2$ showing that the series is hypergeometric and is in fact equal to $4[F(-\frac{1}{2}, -\frac{1}{2}, 1, 1) - 1]$ which by Gauss's theorem $= 4[(4/\pi) - 1]$ (Fränz gave 25/2816 instead of the correct value 25/4096 for the fourth term). Thus Fränz's expression becomes

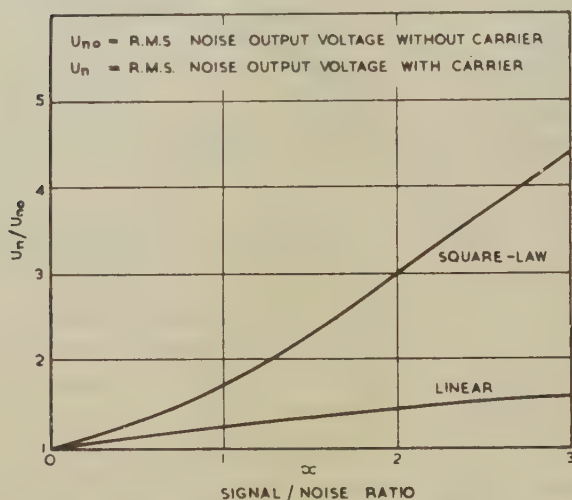
$$u_n^2 = \frac{1}{\pi^2} \left(2 - \frac{\pi}{2} \right) E^2,$$

which is $1/\pi^2$ of the value given by equation (23) for the output from an envelope follower with no signal. This reduction factor occurs since in Fränz's case of no smoothing the noise output arises from fluctuations in the average of the positive voltage (\bar{v}_+) which was seen in the last section to be $1/\pi$ times the corresponding average of the envelope \bar{A} .

The square law detector can be considered in a manner similar to that used for a linear detector. In this case the mean square noise output is given by

$$\begin{aligned} u_n^2 &= \overline{u^2} - \bar{u}^2 = [\overline{A^4} - (\bar{A}^2)^2] \\ &= E^4 \left[8 \left(1 + 2x^2 + \frac{x^4}{2} \right) - 4(1+x^2)^2 \right] \\ &= 4E^4(1+2x^2) = 4E^2(E^2+S^2), \quad (26) \end{aligned}$$

Fig 4



Increase of noise output from a linear and from a square-law rectifier on the introduction of a C.W. signal.

which shows that the noise output rises uniformly as the signal is increased instead of tending to a limit as in the case of the linear rectifier. The ratio of the r.m.s. output noise voltage with signal present to that with signal absent is shown in fig. 4 as a function of the signal/noise x .

§5. FREQUENCY SPECTRUM OF THE OUTPUT NOISE.

The formulæ given in the last section for u_n^2 are for the total mean square output noise voltage; in point of fact the noise is spread out in a continuous spectrum whose integral is equal to u_n^2 . The form of this spectrum is of importance in determining the effect which post-detector selectivity will have on the noise voltage and on its ratio to a signal.

The frequency distribution of the output noise can be conveniently expressed in terms of the spectrum $G(\omega_a)$ where ω_a is the audio frequency. This spectrum is such that the mean square noise voltage in a frequency interval $d\omega_a$ is given by $G(\omega_a)d\omega_a$ with

$$\int_0^\infty G(\omega_a) \cdot d\omega_a = u_n^2 \quad (27)$$

Clearly the spectrum of the output noise is a function of the spectrum applied to the input of the rectifier; since the noise impulses at their origin are extremely short, the input spectrum is determined by the frequency characteristics of the amplifier between the noise source and the rectifier. The rate at which the envelope of the noise varies from moment to moment is inversely dependent upon the bandwidth of the amplifier since the narrower the bandwidth the greater the lengthening of the impulses and hence the closer the correlation at successive instants of time. The correlation function of a random disturbance and its power spectrum are connected by the Fourier cosine transform.

The frequency spectrum of the input noise to the detector denoted by $F(\omega)$ is defined in a manner similar to that used above for the output noise, namely, that the mean square voltage in a frequency interval $d\omega$ is $F(\omega) \cdot d\omega$. Then

$$\int_0^\infty F(\omega) \cdot d\omega = E^2, \quad (28)$$

where E^2 is the mean square noise voltage.

If ω_0 is the mid-band frequency, it is possible to specify an effective bandwidth β for the noise at the input of the rectifier:

$$\beta = \frac{\int_0^\infty F(\omega) \cdot d\omega}{F(\omega_0)} = \frac{E^2}{F(\omega_0)} \quad (29)$$

Consider first the response of the square-law rectifier to a mixture of noise and signal. If the rectifier characteristic is given by

$$u = A^2$$

it is seen that when two sinusoidal voltages $A_1 \sin \omega_1 t$ and $A_2 \sin \omega_2 t$ are applied, the rectified voltage can be written

$$u = [A_1^2 + A_2^2 + 2A_1A_2 \cos (\omega_1 - \omega_2)t],$$

which has a pure modulation product of amplitude $2A_1A_2$. Hence, if any number of sinusoidal voltages are applied to the square-law rectifier, the low frequency products will be *linearly superposed*, so that the components of u have the general form

$$u = 2 \sum_r \sum_s A_r A_s \cos (\omega_r - \omega_s)t. \quad (30)$$

The mean square output voltage thus has the form

$$\overline{u^2} = 2 \sum_r \sum_s A_r^2 A_s^2 \dots \dots \dots (31)$$

In these summations the products are only to occur once so that $A_s A_r$ is taken as being included in $A_r A_s$.

If now fluctuation noise of spectrum $F(\omega)$ and a sinusoidal signal of amplitude S and frequency ω_0 are applied to the rectifier the mean square noise output in an interval ω_a to $\omega_a + d\omega_a$ has two components—that arising from the cross-products of the noise terms and given by

$$2 \int_0^\infty 2F(\omega) \cdot 2F(\omega + \omega_a) \cdot d\omega \cdot d\omega_a$$

and that arising from the product of the signal and the noise :

$$2S^2[2F(\omega_0 + \omega_a) + 2F(\omega_0 - \omega_a)]d\omega_a.$$

Thus the output noise spectrum is given by

$$G(\omega_a) = 4 \left[2 \int_0^\infty F(\omega)F(\omega + \omega_a) \cdot d\omega + S^2\{F(\omega_0 + \omega_a) + F(\omega_0 - \omega_a)\} \right].$$

For simplicity it will be assumed that the input noise spectrum is symmetrical about ω_0 and thus

$$G(\omega_a) = 8 \left[\int_0^\infty F(\omega)F(\omega + \omega_a) \cdot d\omega + S^2F(\omega_0 + \omega_a) \right] \dots \dots (32)$$

This formula will be applied to a rectangular input noise spectrum corresponding to an ideal band-pass characteristic.

If the pass band is β it is seen from equation (29) that within this band the input spectrum is given by

$$F(\omega) = E^2/\beta \dots \dots \dots (33)$$

and is zero outside it.

Hence equation (32) gives for the output spectrum

$$\left. \begin{aligned} G(\omega_a) &= 8E^4 \left[\frac{\beta - \omega_a}{\beta^2} + \frac{2x^2}{\beta} \right] \text{ for } \omega_a < \frac{\beta}{2}, \\ G(\omega_a) &= 8E^4 \frac{\beta - \omega_a}{\beta^2} \text{ for } \frac{\beta}{2} < \omega_a < \beta, \\ G(\omega_a) &= 0 \text{ for } \beta < \omega_a. \end{aligned} \right\} \dots \dots \dots (34)$$

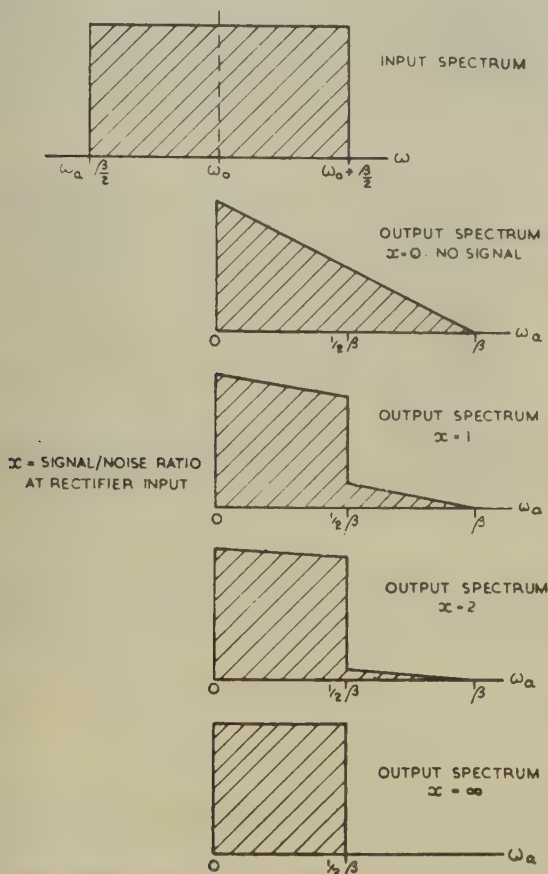
The integration of $G(\omega_a)$ gives

$$u_n^2 = \int_0^\infty G(\omega_a) \cdot d\omega_a = \int_0^\beta G(\omega_a) \cdot d\omega_a = 4E^4(1 + 2x^2)$$

in accordance with equation (26) for the mean square noise output from a square-law rectifier.

Fig. 5 shows the output spectrum for a number of values of signal/noise ratio. It is seen that in the absence of a signal the spectrum is triangular and of width β at the base which is twice as wide as the input spectrum about its central frequency ω_0 . As the signal increases the output spectrum progressively tends to coincide with the bisected input spectrum. These results can be easily understood from a physical point of view by

Fig 5'



Output noise spectrum from a square-law rectifier when the input spectrum is rectangular.

consideration of the relative contribution to the output by the various cross-products of the noise components with each other and with the signal.

The results derived above apply to the square-law detector and are of practical application, since for small values of applied voltage detectors

tend to behave as square-law rather than linear devices. It is of interest, however, to know how the output spectrum from the linear detector differs from that from the square-law detector; the difference between the output noise spectra of the two detectors is least when a large sinusoidal signal is present, since the input spectrum is faithfully reproduced. On the other hand, if the detector is supplied with noise having a rectangular spectrum and no signal is present, then, as is shown in § 8, the output spectrum of the linear detector is very little different from the triangular spectrum given by the square-law detector. Therefore, a good approximation to the frequency distribution is obtained if equation (22) is used for the total output noise instead of equation (26) and the output spectrum shape is assumed to be the same as for the square-law detector.

§ 6. SIGNAL/NOISE RATIO FOR RECEPTION OF MODULATED WAVES.

If the signal of carrier frequency ω_0 and amplitude S_0 is modulated at frequency ω_m to a depth m , the wave can be written

$$S_0(1+m \cos \omega_m t) \cos \omega_0 t \\ = S_0 \left[\cos \omega_0 t + \frac{m}{2} \cos (\omega_0 - \omega_m)t + \frac{m}{2} \cos (\omega_0 + \omega_m)t \right],$$

whose r.m.s. value is $\frac{1}{2}S_0(1+\frac{1}{2}m^2)$.

It will be assumed that the input spectrum is rectangular and of width β and the detector is square-law, and furthermore, that

$$\omega_m < \frac{\beta}{2},$$

since otherwise the sidebands would not be passed to the detector.

The fundamental component of the rectified output at frequency ω_m has the form

$$2mS_0^2 \cos \omega_m t$$

the mean square value of which is

$$u_s^2 = 2m^2S_0^4 = 8m^2x_0^4E^4$$

taking $x_0 = S_0/\sqrt{(2)E}$, the r.m.s. carrier/noise ratio. The ratio of the r.m.s. values of the modulated signal to the noise is then $x = x_0(1+\frac{1}{2}m^2)^{\frac{1}{2}}$.

Now the mean square noise output due to the components of the noise mixing with each other and with the carrier is given by the value already found :

$$4E^4(1+2x_0^2).$$

The mean square noise output due to the components of the noise mixing with the two sidebands is easily shown to be

$$4E^4m^2x_0^2.$$

The total mean square noise output is therefore

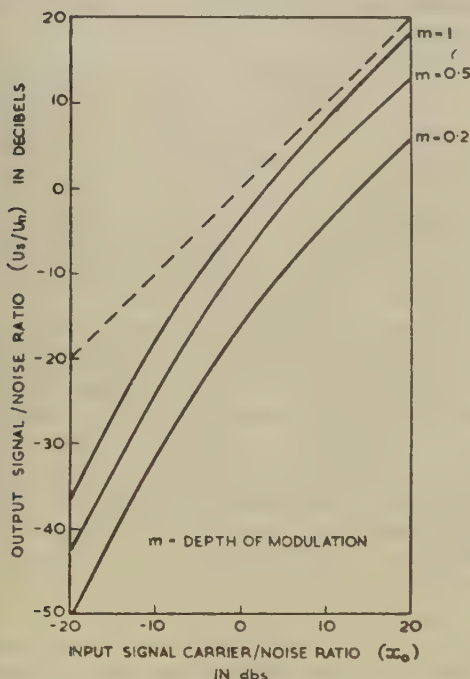
$$u_n^2 = 4E^4(1 + m^2x_0^2 + 2x_0^2). \quad (35)$$

Thus the output signal/noise ratio is given by

$$\frac{u_s}{u_n} = \frac{mx_0^2}{\sqrt{[\frac{1}{2} + x_0^2(1 + \frac{1}{2}m^2)]}}, \quad (36)$$

which is the ratio of the r.m.s. audio output voltage of frequency ω_m to the total r.m.s. output noise voltage. Fig. 6 shows the variation of u_s/u_n with the carrier/noise ratio x_0 at the input for $m=1, 0.5$ and 0.2 .

Fig. 6.



Relation between the signal/noise ratio at the output and input of a square-law detector for an amplitude modulated signal.

Even the best case ($m=1$, x_0 large) the loss in signal/noise ratio is 1.8 db., but it can be much greater than this in conditions of small input signal/noise ratio x , since then u_s/u_n is proportional to x_0^2 . This suppression of the signal by the noise when the latter preponderates is clearly seen in fig. 6 as a change of slope as x_0 decreases through unity (0 db).

In this analysis any contribution of the second harmonic $2\omega_m$ to the useful signal output has been ignored, since its inclusion would only increase u_s by a factor of $(1+m^2/16)^{1/2}$ which is always negligible.

§ 7. SIGNAL/NOISE RATIO FOR HETERODYNE RECEPTION OF C.W. SIGNAL.

A commonly used method of reception of a C.W. signal consists in producing an audible beat tone by heterodyning the signal at the detector by means of a local oscillator. Let the local oscillation be of amplitude H and the signal of amplitude S and let their frequencies lie within the rectangular pass-band $(\omega_0 - \beta/2)$ to $(\omega_0 + \beta/2)$ of the amplifier preceding the detector.

The amplitude of the beat note produced by a square-law detector is $2 HS$ and so the mean square signal output voltage is

$$u_s^2 = 2H^2S^2. \quad \dots \dots \dots (37)$$

The mean square noise output voltage can easily be derived from the results of the earlier sections :

$$u_n^2 = 4E^2(E^2 + H^2 + S^2). \quad \dots \dots \dots (38)$$

Thus putting

$$h = \frac{H}{\sqrt{(2)E}},$$

the output signal/noise ratio is found to be

$$\frac{u_s}{u_n} = \frac{hx}{\sqrt{(h^2 + x^2 + \frac{1}{2})}}. \quad \dots \dots \dots (39)$$

Fig. 7 shows the signal/noise ratios at the input and at the output of the square-law detector as a function of the heterodyning voltage. If this voltage is large compared with both the noise and signal voltages, the signal/noise ratio is seen to be unimpaired by the detector; in fact the detector behaves as a linear frequency changer and leaves the spectra and the relative magnitudes of the signal and noise components unaffected apart from a common translation in frequency.

This equality of signal/noise ratio before and after detection for large values of heterodyning voltage also applies to the linear detector; in fact for any type of detector the transfer ratio will tend to unity if the heterodyning voltage is made sufficiently large.

These remarks apply to the frequency-changing stage of a super-heterodyne as well as to the audible beat method of C.W. reception. However, it should be remembered that the present analysis is not concerned with the effect of any noise introduced by the heterodyning detector itself.

§ 8 THE RESPONSE OF A DETECTOR TO NOISE OR TO NOISE WITH A WEAK SIGNAL.

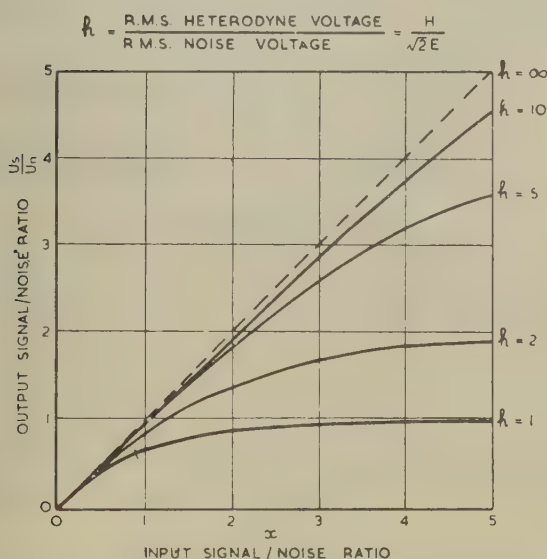
The preceding sections have dealt with the detection of a mixture of signal and noise with particular emphasis on square-law detectors and a general ratio of signal to noise. However, when the signal is weak compared with the noise as is the practical case in many problems of

marginal reception we have seen (equation (9)) that the amplitude of the mixture is statistically similar to that of random noise having a mean square value equal to the sum of the mean square values of the signal and the noise. Thus results may be derived for the output from an n th power envelope detector which are reasonably accurate and indicate the behaviour of such a detector in the observation of signals below noise level.

In order to derive the output spectrum of a detector to which random noise has been applied it is quickest to calculate the autocorrelation function of the output voltage and then form its cosine transform. Now in the n th power detector the output voltage is given by

$$u = A^n$$

Fig 7.



Relation between the signal/noise ratio at the input and at the output of a square-law detector for heterodyne reception of a C.W. signal.

and hence the autocorrelation function

$$\overline{u_1 u_2} = \overline{A_1^n A_2^n}$$

where the suffices 1 and 2 refer to instants of time separated by an interval τ . Then it is shown in Appendix 2 that

$$\overline{u_1 u_2} = 2^n E^{2n} (\frac{1}{2}n)!^2 F\left(-\frac{n}{2}, -\frac{n}{2}, 1, R^2\right), \quad \dots \quad (40)$$

where F is the hypergeometric function and R is a function of τ having the form

$$R(\tau) = \frac{\sin \frac{1}{2}\beta\tau}{\frac{1}{2}\beta\tau}, \quad \dots \quad (41)$$

in the case of a rectangular input noise spectrum of width β .

The audio output spectrum then has the form

$$G(\omega_a) = \frac{2}{\pi} \int_0^\infty (\overline{u_1 u_2} - \overline{u}^2) \cos \omega_a \tau \cdot d\tau. \quad \dots \quad (42)$$

Now since $\overline{u_1 u_2}$ is a series in R^2 it may be written

$$\overline{u_1 u_2} = a_0 + a_1 R^2 + a_2 R^4 + \dots \quad \dots \quad (43)$$

which will terminate if n is an even integer and be an infinite series otherwise. Each term in this series can be regarded as producing its own component spectrum

$$\begin{aligned} G(\omega_a) &= \frac{2}{\pi} \int_0^\infty \sum_1^\infty a_m \left(\frac{\sin \frac{1}{2}\beta\tau}{\frac{1}{2}\beta\tau} \right)^{2m} \cos \omega_a \tau \cdot d\tau \\ &= \sum_1^\infty a_m f_{2m}(\omega_a), \quad \dots \quad (44) \end{aligned}$$

where

$$f_p(\omega_a) = \frac{2}{\pi} \int_0^\infty \left(\frac{\sin \frac{1}{2}\beta\tau}{\frac{1}{2}\beta\tau} \right)^p \cos \omega_a \tau \cdot d\tau \quad \dots \quad (45)$$

is the p th normalized component spectrum each of which is a function of ω_a/β alone and has unit content, *i. e.*

$$\int_0^\infty f_p(\omega_a) \cdot d\omega_a = 1.$$

The properties of these spectra have been investigated by Fränz (1940) and some of these are given in Appendix III.

From equation (43) the d.c. component of the output voltage is

$$\overline{u} = u_0 = \sqrt{a_0}, \quad \dots \quad (46)$$

while the mean square output voltage is

$$\overline{u^2} = a_0 + a_1 + a_2 + \dots \quad \dots \quad (47)$$

and the mean square L.F. output voltage is therefore

$$\overline{u^2} - u_0^2 = a_1 + a_2 + \dots = \int_0^\infty G(\omega_a) \cdot d\omega_a. \quad \dots \quad (48)$$

For an n th law detector

$$u_0 = [\sqrt{(2)E}]^n (\frac{1}{2}n)! \quad \dots \quad (49)$$

$$\overline{u^2} = (2E^2)^n (\frac{1}{2}n)!^2 F\left(-\frac{n}{2}, -\frac{n}{2}, 1, 1\right) = n! (2E^2)^n \quad \dots \quad (50)$$

and the mean square noise output is hence

$$\overline{u^2} - u_0^2 = [n! - (\frac{1}{2}n)!^2](2E^2)^n. \quad (51)$$

The last three relations are consistent with equations (11) and (13) derived earlier and can in fact be obtained directly from the Rayleigh distribution. The spectral composition of u will now be considered in more detail. The low frequency limit of the L.F. spectrum is given by

$$G(0) = \sum_1^{\infty} a_m f_{2m}(0).$$

This must not be confused with the d.c. component of the detector output which corresponds to a spectral "line" at zero frequency of infinitesimal width but finite content.

The square-law detector will be discussed briefly first, since it has already been dealt with in an elementary fashion in §5. For this case

$$\overline{u_1 u_2} = 4E^4(1 + R^2), \quad (52)$$

whence the mean square L.F. noise voltage output is

$$\overline{u^2} - u_0^2 = 4E^4 \quad (53)$$

and the spectrum therefore has only one component:

$$G(\omega_a) = 4E^4 f_2(\omega_a) = \frac{8E^4}{\beta} \left(1 - \frac{\omega_a}{\beta}\right), \quad (54)$$

which agrees with the earlier equation (34) when the signal is put equal to zero ($x=0$).

The effect of varying the bandwidth β of the predetector circuits on the detector output spectrum is seen to be to increase both the height and the width of spectrum proportionally to β since $E^2/\beta = F$ (the input noise spectral density) is assumed to be constant.

It is noted from equations (52) and (53) that the autocorrelation coefficient of the output of a square-law detector (*i.e.* of the square of amplitude of a noise voltage) is given simply by

$$\rho_2(\tau) = \frac{\overline{u_1 u_2} - u_0^2}{\overline{u^2} - u_0^2} = R^2. \quad (55)$$

In the linear envelope detector ($n=1$) the output voltage is equal to the envelope of the noise current and its autocorrelation function is

$$\begin{aligned} \overline{u_1 u_2} &= \frac{\pi}{2} E^2 F(-\tfrac{1}{2}, -\tfrac{1}{2}, 1, R^2) \\ &= \frac{\pi}{2} E^2 \left(1 + \frac{R^2}{4} + \frac{R^4}{64} + \frac{R^6}{256} + \dots\right). \end{aligned} \quad (56)$$

The mean square L.F. noise output voltage is

$$\overline{u^2} - u_0^2 = \frac{\pi}{2} E^2 [F(-\tfrac{1}{2}, -\tfrac{1}{2}, 1, 1) - 1] = \left(2 - \frac{\pi}{2}\right) E^2, \quad (57)$$

which is consistent with the results of § 4.

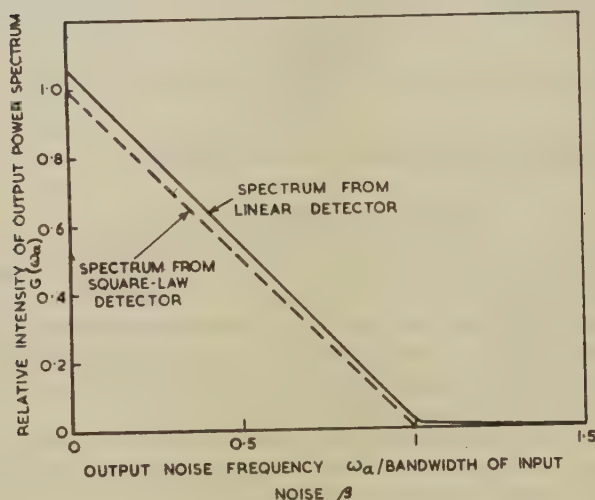
Now the spectrum of the L.F. noise output is obtained from equations (45) and (56)

$$G(\omega_a) = \sum_1^{\infty} a_m f_{2m} = \frac{\pi}{2} E^2 \sum_1^{\infty} \frac{(m-3/2)!^2}{4\pi m!^2} f_{2m}(\omega_a). \quad (58)$$

Since the content of the first spectral component $a_1 f_2$ is 16 times that of the following component $a_2 f_4$ (for $a_2 = a_1/16$ and all the f_n have unit content) it is seen that this component provides a close approximation to the noise output spectrum

$$G(\omega_a) \approx \frac{\pi}{8} E^2 f_2(\omega_a) = \frac{\pi}{8} E^2 \frac{2}{\beta} \left(1 - \frac{\omega_a}{\beta}\right) \quad (59)$$

Fig. 8.



Spectral distribution of noise output from linear and square-law detectors when input noise has rectangular spectrum of width β .

up to β , and zero beyond. This is in fact of just the triangular form which is realized exactly with a square-law detector. The higher order component spectra represent the small departure from the triangular shape but their combined content is under 8 per cent of the total L.F. noise given by (57).

One point of difference from the square-law detector is that in the linear detector, when the bandwidth β of the input noise is increased (leaving its spectral density E^2/β constant), the height of the spectrum does not change although its width increases proportionately with β . Fig. 8 illustrates the very close similarity in form of the output noise spectra from the linear and square-law detector.

From equation (56) it is seen that the autocorrelation coefficient of the envelope of a noise voltage is given by

$$\rho_1(\tau) = \frac{\overline{u_1 u_2} - u_0^2}{u^2 - u_0^2} = \frac{\pi}{4(4-\pi)} \left(R^2 + \frac{R^4}{16} + \frac{R^6}{64} + \dots \right). \quad (60)$$

The numerical factor $\pi/4(4-\pi) = 0.91$ and it is seen that the autocorrelation coefficient of the amplitude will always lie between $0.91 R^2$ (for R small, τ large) and R^2 (R nearly unity, τ small), and is therefore only slightly different from that of the square of the amplitude.

§ 9. SIGNAL/NOISE DISCRIMINATION OF A DETECTOR.

In a receiver used for the observation or measurement of weak signals the law of the detector plays a part in determining the discrimination against noise since upon it depends both the incremental output for a small applied signal and the fluctuations of output due to the applied noise.

In the case of meter indication a weak signal would be observed by first noting the reading in the absence, and then in the presence of the signal, the difference of reading providing a measure of the signal intensity. The initial reading due to the noise can be "backed off" (*i.e.* compensated electrically or mechanically) and the sensitivity of measurement so increased since a more sensitive meter may now be used. The limit to this process is set by the fluctuations of the meter readings about their average positions arising from the noise. These fluctuations may be reduced by the use of a meter of long time constant but correspondingly the duration of a measurement is prolonged; the effect of the meter time constant is discussed in the next section.

The signal/noise discrimination of a detector can be objectively expressed in terms of the ratio of the increase of the average (or d.c.) output on applying a certain signal to the r.m.s. fluctuation of the output (*i.e.* the L.F. output) about the average. The effect of long-term observation and averaging on the discrimination is considered in the next section.

Usually in the condition of limiting sensitivity the signal/noise ratio at the detector is small and this enables a simpler parameter to be obtained to express the discrimination of a detector in terms of its law. If the noise of r.m.s. voltage E is accompanied by a signal $S \cos \omega_0 t$ and is applied to an n th power-law detector the d.c. output voltage is given by

$$u_0 = [\sqrt{(2)}E]^n \left(\frac{n}{2}\right)! {}_1F_1\left(-\frac{n}{2}, 1, -x^2\right), \quad \dots \quad (11)$$

where

$$x = \frac{S}{\sqrt{(2)}E}$$

is the signal/noise ratio as before.

The total mean-square output voltage from the detector is given by

$$u^2 = 2^n E^{2n} n! {}_1F_1(-n, 1, -x^2).$$

For the signal/noise ratio x small the mean-square fluctuation of the output will be given approximately by

$$u_n^2 = (2E^2)^n \left[n! - \left(\frac{n}{2} \right)!^2 \right]$$

as already given by equation (51).

The increase of d.c. output voltage due to the signal is found from equation (11) to be

$$u_0(x) - u_0(0) = [\sqrt{(2)E}]^n \left(\frac{1}{2}n \right)! \frac{n}{2} x^2 \quad . \quad . \quad . \quad . \quad (61)$$

for x small. It is noted that the detector behaves as a square-law device as regards the increase of output due to a weak signal owing to the suppression effect of the stronger noise.

A convenient parameter for expressing the detector discrimination for very small signals is thus :

$$Q = \frac{u_0(x) - u_0(0)}{u_n x^2} = \frac{\frac{1}{2}n}{\left[\frac{n!}{\left(\frac{n}{2} \right)!^2} - 1 \right]^{\frac{1}{2}}} \quad . \quad . \quad . \quad . \quad (62)$$

It is found that Q has a maximum of unity at $n=2$ but this maximum is very flat, so that, in practice, superiority of a square-law detector in this respect is of no significance. For example :

$$n = \frac{1}{2}, \quad Q = 0.90,$$

$$n = 1, \quad Q = 0.96,$$

$$n = 2, \quad Q = 1,$$

$$n = 4, \quad Q = 0.89.$$

A greater practical advantage of the square-law detector is that the d.c. output for a signal and noise input is given by

$$u_0 = 2E^2(1 + x^2) = 2(E^2 + \frac{1}{2}S^2),$$

showing that whatever the signal/noise ratio x , a change of indication can be directly interpreted as a change of mean-square input voltage.

§10. INFLUENCE OF THE METER TIME CONSTANT AND INTEGRATION TIME ON SENSITIVITY.

If the time constant of the indicating instrument connected to the detector output be increased the disturbing effect of the fluctuation of indication is reduced, so giving enhanced sensitivity at the expense of speed of measurement, or in statistical language, we would say that the random variations of the measured quantity are smoothed out by sampling over a longer time.

If the time constant of the meter is T the mean-square fluctuation of the output voltage is reduced in the ratio

$$\frac{1}{M^2} = \frac{\int_0^\infty \frac{G(\omega_a) \cdot d\omega_a}{1 + \omega_a^2 T^2}}{u_n^2} = \frac{\pi G(0)}{2T u_n^2} \quad \text{very nearly,}$$

if the receiver bandwidth is large compared with the reciprocal of the meter time constant. It is assumed that the signal is small compared with the noise so that the output spectrum is substantially the same as that found earlier for a noise input only.

The improvement factor due to the meter time constant is thus

$$M = \sqrt{\left[\frac{2T u_n^2}{\pi G(0)} \right]}, \quad (63)$$

which for a square-law detector is found from equations (53) and (54) to be

$$M_2 = \sqrt{(\beta T / \pi)} = \sqrt{(2BT)}. \quad (64)$$

While for a linear detector from equations (57) and (58)

$$M_1 = 1.03 \sqrt{(2BT)}, \quad (65)$$

which is negligibly different from the value for the square-law detector.

Thus combining these results with those of the previous section the ratio of the increase of indication to the r.m.s. fluctuation is

$$\frac{u_0(x) - u_0(0)}{u_n / M} = x^2 Q M = x^2 \sqrt{(2BT)} \quad (66)$$

to a close approximation for both square-law and linear detectors.

Since the signal/noise power ratio x^2 is inversely proportional to the receiver bandwidth B , the discrimination y is seen to be proportional to $\sqrt{(T/B)}$. Hence, halving the receiver bandwidth or doubling the meter time constant is equivalent to a 1.5 db increase of signal voltage.

Another method of improving the sensitivity of measurement of a weak signal in noise is by taking the average of meter readings over a time T_0 long compared with the meter time constant T and so extending the period of integration. Clearly it is pointless to take readings too frequently in a given period since the closeness of correlation between successive values will prevent any further improvement in accuracy being obtained.

Consider the case in which N readings of the meter indication θ are taken. Their average is

$$\bar{\theta} = \frac{1}{N} \sum_{v=1}^N \theta_v$$

and the standard deviation σ of this average due to the random fluctuations in θ about its true average θ_0 is given by

$$\begin{aligned} \sigma_N^2 &= \left[\frac{1}{N} \sum_1^N (\theta_v - \theta_0) \right]^2 \\ &= \frac{1}{N^2} \left[N \sigma_1^2 + 2 \sigma_1^2 \sum_1^{N-1} (N - \mu) r_\mu \right], \quad (67) \end{aligned}$$

where σ_1 is the standard deviation of a single reading and r_μ is the correlation coefficient between readings spaced μ apart. In the case of readings evenly spaced by a time s and a meter time constant T

$$r_\mu = \exp(-\mu s/T)$$

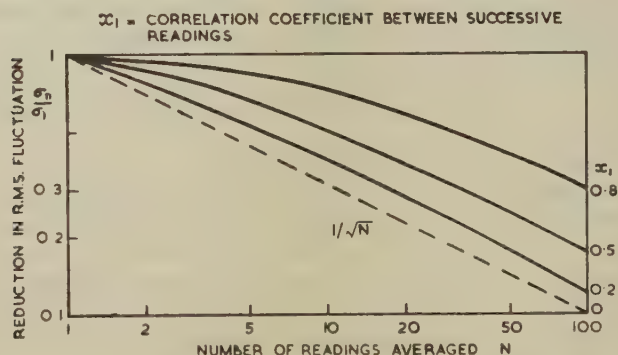
and

$$\frac{\sigma_N}{\sigma_1} = \frac{\sqrt{[N(1-r_1^2) - 2r_1(1-r_1^N)]}}{N(1-r_1)}, \quad \dots \dots \dots (68)$$

where $r_1 = \exp(-s/T)$ is the correlation coefficient between successive readings. Naturally when this tends to unity corresponding to readings taken in very close succession $\sigma_N = \sigma_1$ and there is no improvement due to averaging.

At the other limit σ_N tends to σ_1/\sqrt{N} as the correlation tends to zero and this factor \sqrt{N} represents the maximum improvement obtainable. Fig. 9 shows the smoothing factor as a function of N for various degrees

Fig. 9.



Reduction of fluctuation by averaging N regularly spaced readings.

of correlation. However, it is more useful to know what improvement can be obtained in a given observing time T_0 than with a given number of observations.

Imagine an integrating circuit which at any moment continuously provides the average value of the indications over the previous period of length T_0 , that is, it forms the quantity

$$z = \frac{1}{T_0} \int_{t_0 - T_0}^{t_0} \theta \cdot dt$$

at the time t_0 of observation. The fluctuations in z can be calculated directly or as a limit to the summation given by equation (67) when discrete observations are made at infinitesimal spacings. It is found that the mean square deviation in z is given by

$$\sigma_{T_0}^2 = \frac{2\sigma_1^2}{T^2} \int_0^T (T-t)r(t) \cdot dt, \quad \dots \dots \dots (69)$$

which for an exponential correlation $r(t) = \exp(-t/T)$ of indications gives

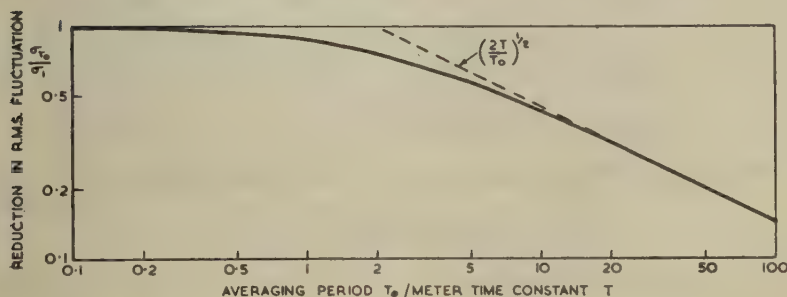
$$\frac{\sigma_{T_2}}{\sigma_1} = \sqrt{\left[\frac{2T}{T_0} \left(1 + \frac{T}{T_0} \exp(-T_0/T) - \frac{T}{T_0} \right) \right]}, \quad (70)$$

which is shown in fig. 10.

Now from equations (63), (64) and (65), $\sigma_1 = u_n/M$, and thus the overall improvement due to the meter time constant T and continuous averaging over T_0 which is assumed large compared with T is given by

$$\frac{u_n}{\sigma_{T_n}} = M \sqrt{\left(\frac{T_0}{2T} \right)} = \sqrt{BT_0}. \quad (71)$$

Fig. 10.



Reduction of fluctuation by continuous averaging over time T_0 .

ACKNOWLEDGMENTS.

The work described was carried out as part of the programme of the Radio Research Board to whom it was communicated in confidential reports in 1944 and 1945. It is published by permission of the Director of the National Physical Laboratory and of the Director of Radio Research of the Department of Scientific and Industrial Research.

REFERENCES.

- FRÄNZ, K., 1940, *Elekt. Nachr.-tech.*, **17**, 215-230; 1941, *Hochfreq. tech. u. Elektroak.*, **57**, 146-151.
 RAGAZZINI, J. R., 1942, *Proc. Instn. Radio Engrs.*, N.Y., **30**, 277-288.

APPENDIX I.

PROBABILITY DISTRIBUTION OF C.W. SIGNAL PLUS NARROW-BAND NOISE.

The instantaneous amplitude A of the mixture of signal and noise is given by

$$A^2 = (X+S)^2 + Y^2.$$

Now $(X+S)$ and Y have independent normal distributions each of standard deviation E and centred on S and zero respectively. Putting $\xi=(X+S)^2$, $\eta=Y^2$ and $\alpha=A^2=\xi+\eta$, we see that

$$\begin{aligned} P(\xi) &= \frac{1}{2E\sqrt{(2\pi\xi)}} \left\{ \exp \left[-\frac{[\sqrt{(\xi)}-S]^2}{2E^2} \right] + \exp \left[-\frac{[-\sqrt{(\xi)}-S]^2}{2E^2} \right] \right\} \\ &= \frac{1}{E\sqrt{(2\pi\xi)}} \exp \left(-\frac{\xi+S^2}{2E^2} \right) \cosh \left[\frac{S\sqrt{(\xi)}}{E^2} \right], \\ P(\eta) &= \frac{1}{E\sqrt{(2\pi\eta)}} \exp \left(-\frac{\eta}{2E^2} \right), \end{aligned}$$

whence

$$\begin{aligned} P(\alpha) &= \frac{1}{2\pi E^2} \int_0^\alpha \frac{1}{\sqrt{[\xi(\alpha-\xi)]}} \exp \left(-\frac{\eta+\xi+S^2}{2E^2} \right) \cosh \frac{S\sqrt{\xi}}{E^2} \cdot d\xi \\ &= \frac{1}{2\pi E^2} \exp \left(-\frac{\alpha+S^2}{2E^2} \right) \int_0^{\pi/2} 2 \cosh \left[\frac{S\sqrt{(\alpha)} \sin \theta}{E^2} \right] \cdot d\theta \\ &= \frac{1}{2E^2} \exp \left(-\frac{\alpha+S^2}{2E^2} \right) I_0 \left[\frac{S\sqrt{(\alpha)}}{E^2} \right]. \end{aligned}$$

Thus the probability distribution for the amplitude $A=\alpha^{\frac{1}{2}}$ is

$$P(A) = \frac{A}{E^2} \exp \left(-\frac{A^2+S^2}{2E^2} \right) I_0 \left(\frac{SA}{E^2} \right),$$

which is equation (7) of the text.

APPENDIX II.

AUTOCORRELATION FUNCTION FOR THE NTH POWER OF THE NOISE AMPLITUDE.

If

$$\begin{aligned} v_1 &= X_1 \cos \omega_0 t_1 + Y_1 \sin \omega_0 t_1, \\ v_2 &= X_2 \cos \omega_0 t_2 + Y_2 \sin \omega_0 t_2 \end{aligned}$$

are the noise voltages at times spaced by $(t_2-t_1)=\tau$, their autocorrelation is

$$E^2 r(\tau) = \overline{v_1 v_2} = \frac{1}{2} (\overline{X_1 X_2} + \overline{Y_1 Y_2}) \cos \omega_0 \tau$$

when the spectrum is symmetrical, *i.e.* $\overline{X_1 Y_2} = \overline{X_2 Y_1} = 0$. In the case of a rectangular spectrum $F(\omega) = E^2/\beta$ and

$$r(\tau) = \frac{1}{\beta} \int_{\omega_0 - \frac{1}{2}\beta}^{\omega_0 + \frac{1}{2}\beta} \cos \omega \tau \cdot d\omega = \frac{\sin \frac{1}{2}\beta\tau}{\frac{1}{2}\beta\tau} \cos \omega_0 \tau.$$

Thus

$$\overline{X_1 X_2} = \overline{Y_1 Y_2} = E^2 \frac{\sin \frac{1}{2}\beta\tau}{\frac{1}{2}\beta\tau} = E^2 R(\tau),$$

where

$$R(\tau) = \frac{\sin \frac{1}{2}\beta\tau}{\frac{1}{2}\beta\tau}$$

is the "envelope" of the correlation function $r(\tau)$.

The joint distribution of $X_1 Y_1 X_2 Y_2$ is thus the product of two bivariate normal distributions

$$P(X_1, Y_1, X_2, Y_2) = \frac{1}{4\pi^2 E^4 (1-R^2)} \exp \left[-\frac{X_1^2 + X_2^2 - 2R X_1 X_2 + Y_1^2 + Y_2^2 - 2R Y_1 Y_2}{2E^2 (1-R^2)} \right].$$

Now we require the autocorrelation of

$$A^n = (X^2 + Y^2)^{n/2}$$

which is given by

$$\overline{A_1^n A_2^n} = \iiint \int_{-\infty}^{+\infty} (X_1^2 + Y_1^2)^{n/2} (X_2^2 + Y_2^2)^{n/2} P(X_1, Y_1, X_2, Y_2) dX_1 dY_1 dX_2 dY_2.$$

In order to evaluate this, a convenient substitution is

$$\begin{aligned} X_1^2 &= q e^p E^2 (1-R^2) \cos^2 \phi_1, & Y_1^2 &= q e^p E^2 (1-R^2) \sin^2 \phi_1, \\ X_2^2 &= q e^{-p} E^2 (1-R^2) \cos^2 \phi_2, & Y_2^2 &= q e^{-p} E^2 (1-R^2) \sin^2 \phi_2, \end{aligned}$$

which for the transformation to the variables p, q, ϕ_1 and ϕ_2 has the Jacobian

$$|J| = q E^4 (1-R^2)^2,$$

whence

$$\begin{aligned} \overline{A_1^n A_2^n} &= \frac{E^{2n} (1-R^2)^{n+1}}{4\pi^2} \int_0^\infty dq \int_0^\infty dp \int_0^{2\pi} d\phi_1 \int_0^{2\pi} d\phi_2 \cdot q^{n+1} \\ &\quad \times \exp [-q \cosh p - q R \cos (\phi_2 - \phi_1)] \\ &= E^{2n} (1-R^2)^{n+1} \int_0^\infty q^{n+1} K_0(q) I_0(qR) dq \\ &= (2E^2)^n (1-R^2)^{n+1} \left(\frac{n}{2}\right)!^2 F\left(\frac{n+1}{2}; \frac{n+1}{2}; 1; -R^2\right) \\ &= (2E^2)^n \left(\frac{n}{2}\right)!^2 F\left(-\frac{n}{2}, -\frac{n}{2}, 1, -R^2\right), \end{aligned}$$

which is equation (40) of the text.

APPENDIX III.

THE COMPONENTS OF THE OUTPUT SPECTRUM DUE TO A RECTANGULAR INPUT SPECTRUM.

The component spectra of the detector output voltage are defined by

$$f_p(\omega_a) = \frac{2}{\pi} \int_0^\infty \left(\frac{\sin \frac{1}{2} \beta \tau}{\frac{1}{2} \beta \tau} \right)^p \cos \omega_a \tau \cdot d\tau.$$

They have the normalizing property

$$\int_0^\infty f_p(\omega_a) \cdot d\omega_a = 1.$$

Each f_p is represented by a polynomial in ω_a/β with coefficients changing at each integral value of this variable. Furthermore, each f_{2m} cuts off at $m\beta$ beyond which it is identically zero. The first three even spectra are as follows :

$$f_2(\omega_a) = \frac{2}{\beta} \left(1 - \frac{\omega_a}{\beta} \right),$$

$$f_4(\omega_a) = \frac{1}{3\beta} \left[\left(2 - \frac{\omega_a}{\beta} \right)^3 - 4 \left(1 - \frac{\omega_a}{\beta} \right)^3 \right] \quad 0 < \omega_a < \beta$$

$$= \frac{1}{3\beta} \left(2 - \frac{\omega_a}{\beta} \right)^3, \quad \beta < \omega_a < 2\beta$$

$$f_6(\omega_a) = \frac{1}{60\beta} \left[\left(3 - \frac{\omega_a}{\beta} \right)^5 - 6 \left(2 - \frac{\omega_a}{\beta} \right)^5 + 15 \left(1 - \frac{\omega_a}{\beta} \right)^5 \right] \quad 0 < \omega_a < \beta$$

$$= \frac{1}{60\beta} \left[\left(3 - \frac{\omega_a}{\beta} \right)^5 - 6 \left(2 - \frac{\omega_a}{\beta} \right)^5 \right] \quad \beta < \omega_a < 2\beta$$

$$= \frac{1}{60\beta} \left(3 - \frac{\omega_a}{\beta} \right)^5, \quad 2\beta < \omega_a < 3\beta$$

The higher order normal spectra tend rapidly to the Gaussian form since

$$\left(\frac{\sin z}{z} \right)^p \sim \exp(-pz^2/6) \text{ for } p \text{ large,}$$

whence

$$f_p(\omega_a) \sim \frac{2}{\beta} \sqrt{\left(\frac{6}{\pi p} \right)} \exp \left(-\frac{6\omega_a^2}{p\beta^2} \right).$$

APPENDIX IV.

RECTIFICATION EFFICIENCY OF A DIODE DETECTOR.

For small applied voltages (*i. e.* such that the anode is not more positive than +0.2 V. with respect to the cathode) the current *vs* voltage characteristic of typical diodes is of the exponential form appropriate to the retarding-field region with negligible space charge :

$$i = c \exp(KV),$$

where

$$K = (\epsilon/kT_c) \text{ is usually about } 10 \text{ volt}^{-1},$$

ϵ = electronic charge,

k = Boltzmann's constant,

T_c = cathode temperature.

If now a sinusoidal voltage $A \sin \omega t$ is applied to the detector and \bar{i} is the mean current over one cycle

$$V = A \sin \omega t - \bar{i}R,$$

$$\bar{i} = \frac{c}{2\pi} \int_0^{2\pi} \exp [K(A \sin \omega t - \bar{i}R)] d(\omega t) = c \exp (-K\bar{i}R) I_0(KA).$$

In the absence of an applied voltage there is an initial diode current i_0 given by

$$i_0 = c \exp (-Ki_0R).$$

The rectified voltage is thus given implicitly by

$$u = (\bar{i} - i_0)R = i_0R [\exp (-Ku) I_0(KA) - 1].$$

$$\text{If } KA \ll 1, I_0(KA) \approx 1 + \frac{1}{2}K^2A^2, \exp (-Ku) \approx 1 - Ku,$$

whence

$$u \approx \frac{K^2 i_0 R}{4(1 + Ki_0 R)} A^2,$$

demonstrating the square-law behaviour of the detector.

At large amplitude $KA \gg 1$,

$$I_0(KA) \approx \frac{\exp (KA)}{(2\pi KA)^{\frac{1}{2}}}$$

and thus

$$1 - \frac{u}{A} = \frac{1}{KA} \log_e \left(1 + \frac{u}{i_0 R} \right) + \frac{\log_e 2\pi KA}{KA},$$

showing that the rectification efficiency u/A approaches unity as KA becomes large. When A becomes very large the exponential law no longer holds for the diode and the current tends to be more nearly proportional to the voltage. It is easy to show that in this condition the rectified voltage approaches more and more closely to proportionality with the amplitude of the applied wave.

LIV. *A Radio Echo Apparatus for the Delineation of Meteor Radiants.*

By A. ASPINALL, J. A. CLEGG, Ph.D., and G. S. HAWKINS,
Jodrell Bank Experimental Station, University of Manchester*.

[Received February 13, 1951.]

[Plates XVIII. & XIX.]

ABSTRACT.

This paper describes a radio echo apparatus for the continuous recording of meteor activity, and the determination of the coordinates of active meteor radiants. It has been in operation since September 1949, and the occurrence of well known night time showers during this period have provided an opportunity to estimate its performance. The results obtained during the Geminid shower of 1949 and 1950 are described as an example, and its accuracy and resolving power are discussed.

§1. INTRODUCTION.

THE radio echo technique has been used extensively during the past five years to detect meteor ionization in the atmosphere, and with the development of methods of radiant determination (Hey and Stewart 1947, Clegg 1948, McKinley and Millman 1949) and velocity measurement Hey and Stewart 1947, Ellyett and Davies 1948, Manning, Villard and Peterson 1949), has proved valuable in the observation of meteors under conditions which render visual watching impossible. The earlier radio investigations were concerned primarily with the well-known night time meteor showers, but the experiments of Hey and Stewart (1947) and Prentice, Lovell and Banwell (1947) revealed a high level of daytime activity during the summer months of 1945 and 1946, and more comprehensive surveys in 1947 (Clegg, Hughes and Lovell 1947) and 1948 (Aspinall, Clegg and Lovell 1949) confirmed the existence of a number of rich meteor streams incident on the sunlit side of the earth between May and July. This work has now been extended, and an apparatus has been developed to record meteor activity continuously throughout the whole year. It is designed to determine the radiants of the major daytime and night time showers occurring in the Northern hemisphere, to detect the minor streams, and to measure the hourly rate of sporadic meteors.

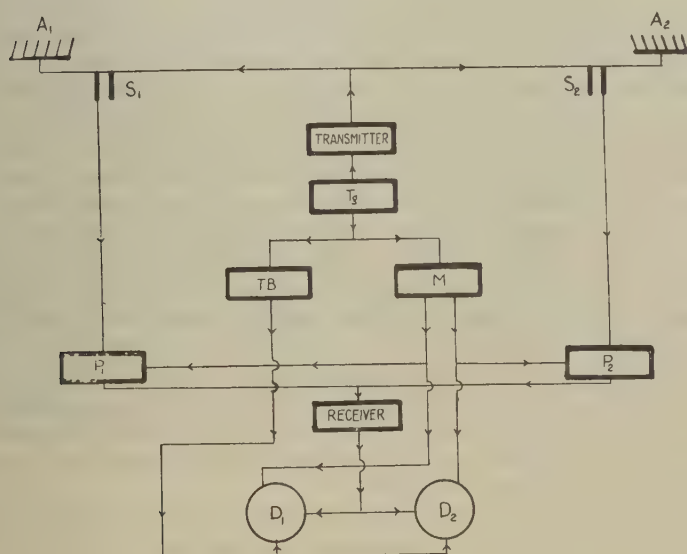
The method of radiant determination is similar to that described by Clegg (1948); but in order to obtain a more complete record the single rotatable aerial used in earlier experiments (Lovell, Banwell and Clegg 1947)

* Communicated by Dr. A. C. B. Lovell.

has been replaced by two fixed arrays which operate independently, producing low elevation beams, one directed towards the North of West and the other towards the South of West. The radiant coordinates are calculated from the times at which echoes appear at maximum range on the two systems.

The equipment has been fully operational since September 1949, and the results of the continuous survey and of the work on the summer daytime streams which has been carried out since that date will be discussed in detail elsewhere (Aspinall and Hawkins 1951). The purpose of the present paper is to describe the apparatus and to discuss the accuracy and limitations of the method of radiant determination employed.

Fig. 1.



A brief account of the observations made during the Geminid meteor shower is included, however, in order to illustrate its performance.

§2. APPARATUS.

A schematic diagram of the apparatus is shown in fig. 1. It operates on a frequency of 72 Mc./s., and comprises two independent beamed aeriels A_1 and A_2 , which are directed at low elevation, on azimuthal bearings of 242° and 292° respectively *. These arrays are common to the transmitter and receiver, and the pulses from the transmitter are radiated simultaneously by both. The received signals are fed through

* The azimuthal directions being measured in degrees East of North.

the transmitter-receiver switches, $S_1 S_2$, into the preamplifying stages, P_1, P_2 , and after further amplification and detection are applied to the grids of the intensity modulated display tubes, D_1 and D_2 . The sequence of operations is initiated from a master control unit by the unit T_g , which provides pulses to trigger the transmitter, the multivibrator M , and the common time base TB of the two display tubes. The square waves from the multivibrator are used to suppress the preamplifying stages P_1 and P_2 alternately, and are also applied to the grids of the cathode ray tubes D_1 and D_2 , so that the signals from each aerial are displayed separately side by side, and are photographed on a film which moves continuously in a direction perpendicular to that of the time bases.

The unit T_g is capable of providing pulses with a number of different recurrence frequencies, and the apparatus can be triggered in a variety of ways. For normal observations the transmitter is usually operated at a pulse recurrence frequency of 150 c./s. and the time base unit at a frequency of 75 c./s. Under these circumstances the transmitter pulses appear twice on each display, at the beginning of each time base and at a range of 1000 Kms. This serves as a useful check on the range calibration, although subsidiary range markers can be supplied from the triggering system at intervals of 200 or 250 Kms. along the time base. One of the most serious difficulties encountered during the early experiments was that of differentiating between short duration echoes and the random noise impulses which present a similar appearance on the photographic record. This form of interference was considerably reduced by inserting a discriminator unit, similar to that used by Davies and Ellyett (1949), in the output of the receiver, but it has also been found advisable to trigger the transmitter with a pair of pulses separated by approximately 300 μ sec., so that a true echo appears as a double. A portion of a record, taken with a film speed of 12 cms. per hour, is shown in fig. 2 (Pl. XVIII). The continuous lines A, B, A', B' correspond to the double transmitter pulses, and a number of echoes are visible as at C, D and E.

The photograph in fig. 3 (Pl. XIX.) shows the general arrangement of the two aerial systems, which are situated at longitude $2^\circ 18' W.$, latitude $53^\circ 14' N.$, and are placed symmetrically on either side of the building housing the transmitter and receiver. Each array consists of 6 Yagi aerials mounted at horizontal distances of 1.2λ apart and at a height of 1.57λ above the ground. They produce identical beams of elevation 8.5° and of half amplitude width $\pm 5^\circ$ and have a power gain of 165 over a half wave dipole. The horizontal and vertical radiation patterns are shown in figs. 4a and 4b.

The minimum detectable signal at the receiver is 7×10^{-14} w., and in normal operation the peak power of the transmitter is 5 Kw., with a pulse length of 8 μ s. Simultaneous visual and radio observations have shown that under these conditions the echo rate produced by an active shower, when the radiant is at 90° elongation to either of the aerial beams, corresponds closely to the rate of occurrence of visual meteors.

§ 3. THE DETERMINATION OF METEOR RADIANTS.

The method of radiant determination has been described previously (Clegg 1948) and only a brief description of its application to the present apparatus will be given.

Fig. 4a.

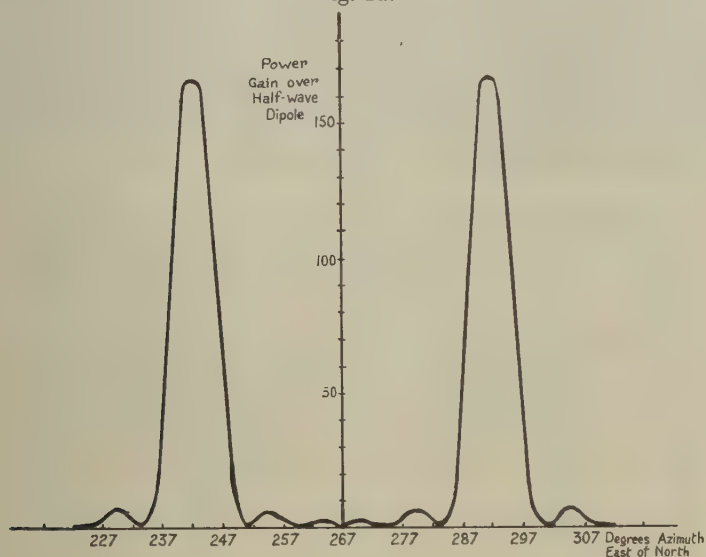
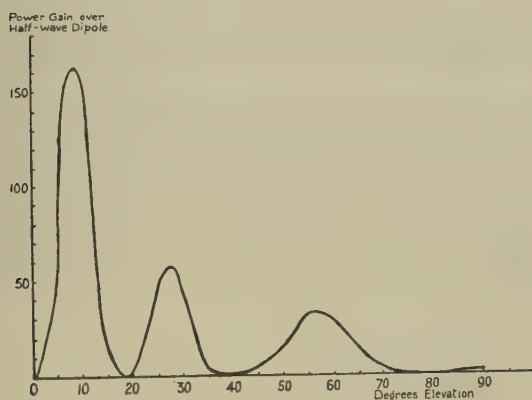


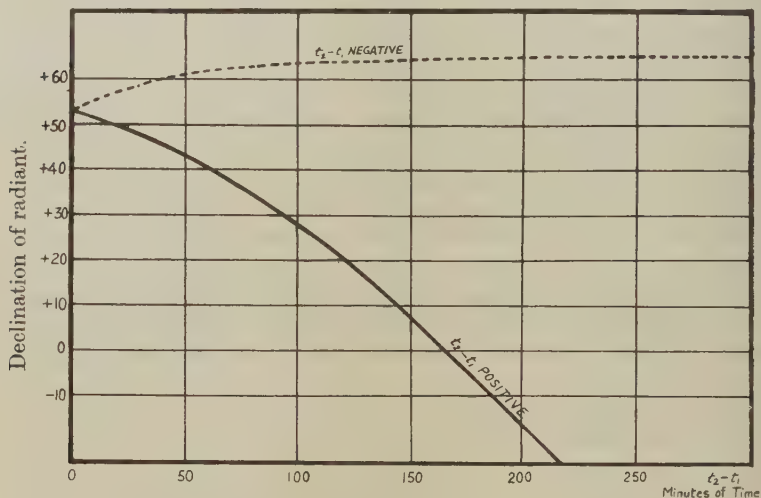
Fig. 4b.



It follows from the condition of specular reflection (Hey and Stewart 1947, Lovell, Banwell and Clegg 1947), that when the earth passes through an active meteor stream, the radio echoes observed on frequencies of the

order of 72 Mc./s. are returned from a narrow zone of the atmosphere, of limited depth, which lies in a plane passing through the observing station and perpendicular to the direction of the radiant. The rate of occurrence and ranges of the echoes depend on the position and orientation of this plane relative to the aerial coverage, and vary with time as the radiant moves across the sky. It can be shown that with an aerial directed at low elevation on an azimuthal bearing of 270° , echoes attain a maximum range when the radiant is close to the central meridian. For a radiant close to upper culmination, the passage of the echo zone through the beam is accompanied by the initial appearance of echoes at short ranges, followed by a gradual increase in range to a maximum value R_{\max} , and a final sudden decay in the echo rate.

Fig. 5.

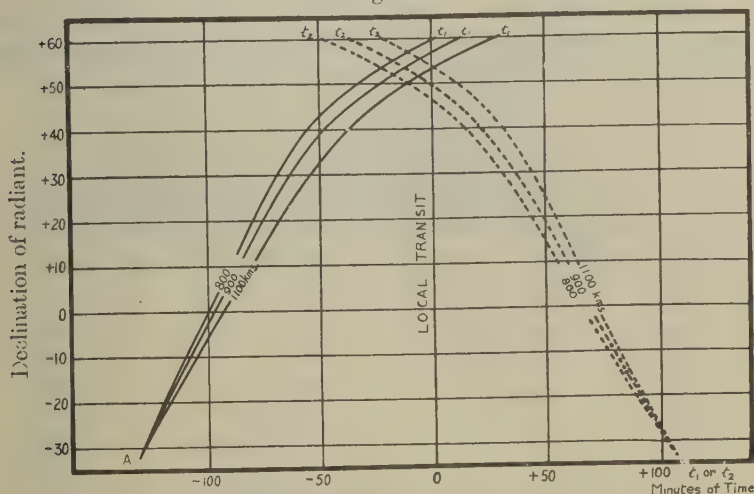


If the aerial characteristics are such that echoes can be detected down to the horizon, R_{\max} is equal to the distance at which the meteor zone cuts the horizon circle of the station, and for a typical shower of medium velocity, for which the mean height of the zone can be taken as approximately 95 Kms., $R_{\max} = 1100$ Kms. Under these circumstances the time of maximum range, T , is the time at which the azimuth of the radiant differs from that of the beam by 90° and corresponds to the transit of the radiant. For aerals directed along azimuths $270^\circ + \theta_1$ and $270^\circ + \theta_2$, the echoes reach a maximum range at times $T + t_1$ and $T + t_2$. The time difference $t_2 - t_1$ is a function of the declination, δ , of the radiant, θ_1 , θ_2 , and the latitude of the station. This function is plotted in fig. 5 for the case of $\theta_1 = -28^\circ$, $\theta_2 = +22^\circ$ and lat. $= 53^\circ \text{N.}$, and from this curve the declination of the radiant may be found. From the curve labelled 1100 Kms. in fig. 6, t_1 and t_2 may be determined separately and the time of transit then found from the observed values of $T + t_1$ and $T + t_2$.

It may be noted that t_1 is negative for radiants which transit south of the zenith and echoes appear first in aerial 1 and then in aerial 2. For radiants which transit north of the zenith (dec. $> 53^\circ$) this order is reversed, and $t_2 - t_1$ becomes negative. If the declination is greater than 76° the echo zone never enters the coverage of aerial 2, but remains for many hours in the beam of aerial 1. A radiant position can still be determined however by fitting theoretical range curves to the range/time plots.

In practice, owing to the conditions governing the reflection of radio waves from the surface of the earth, the aerial sensitivity falls off rapidly in directions close to the horizontal, and echoes are never observed out to ranges exceeding 1000 Kms. Under these circumstances the times of occurrence of echoes of maximum range are advanced by an amount

Fig. 6.



depending on the declination of the radiant and the observed value of R_{\max} . This has been taken into account in the curves labelled 900 and 800 Kms. in fig. 6, from which the time of transit is found, but since the displacement is to a close approximation the same for both aerials, the curve of fig. 5 and determination of declination is not affected. Finally, a small correction has to be applied if the mean height of the meteors in a stream is not 95 Kms. This correction, which affects only the time of transit, is given in Table I.

§4. RESULTS OBTAINED DURING THE GEMINID METEOR SHOWER.

The range-time plots obtained during the Geminid shower of 1949 and 1950, which are shown in fig. 7, provide a typical example of the results obtained with the apparatus. Times are shown as abscissæ, and the ranges of individual echoes are indicated by the lengths of the vertical lines. The results obtained on each aerial, between 0000 and 0400 U.T. on Dec. 13, 1949 and Dec. 13, 1950 are shown separately.

These plots indicate clearly the general variation in echo rate and range which occur as the echo zone sweeps through each beam in turn. The occurrence of echoes at maximum range, and the subsequent sharp fall in rate, appear at approximately 0110 U.T. on the first arial, and at approximately 0240 U.T. on the second arial. The radiant positions obtained from these plots are as follows :—

	<i>Time of local transit.</i>	<i>Radiant coordinates.</i>
Dec. 13, 1949	0214 U.T.	R.A. 111.5°, Dec. 32.5° U.T.
Dec. 13, 1950	0218 U.T.	R.A. 112.2°, Dec. 32.5° U.T.

When the radiant position has been determined, theoretical range-time curves can be constructed. These are shown as dotted lines in fig. 7. In the case of an ideal point radiant, in the absence of sporadic meteor activity, these envelopes should contain all the echoes, and they provide a useful indication of the diffuseness of the radiant.

TABLE I.

Correction in minutes of time to be applied to time of transit.

Height kms.	δ	-20°	-10°	0°	10°	20°	30°	40°	50°	60°
115		2	3	4	5	6	7	8	10	12
110		1	2	3	3	4	4	5	7	8
105		0	1	1	1	1	1	2	2	3
95		0	0	0	0	0	0	0	0	0
85		-0	-1	-1	-1	-1	-1	-2	-2	-3
80		-1	-2	-3	-3	-4	-4	-5	-7	-8
75		-2	-3	-4	-5	-6	-7	-8	-10	-12

§5. ACCURACY OF RADIANT DETERMINATION.

The results obtained with this apparatus during the major daytime and night time showers have shown that when the echo rate, during the passage of the echo zone through the beam, exceeds 30 per hour, times t_1 and t_2 can be measured to within ± 5 minutes. This corresponds to an error of $\pm 1^\circ$ in right ascension and $\pm 1.5^\circ$ in declination. In the exceptional case of a major stream with a radiant lying within 20° of the celestial pole, the position must be determined by the curve fitting method, and the accuracy is necessarily reduced.

For weaker streams the accuracy of radiant determination falls off markedly with decreasing echo rate, particularly if the shower rate does not exceed that of the sporadic background by a sufficiently high factor. Indeed, in the case of minor streams occurring during times of high sporadic activity, it is often difficult to distinguish between true and spurious

Fig. 7a.

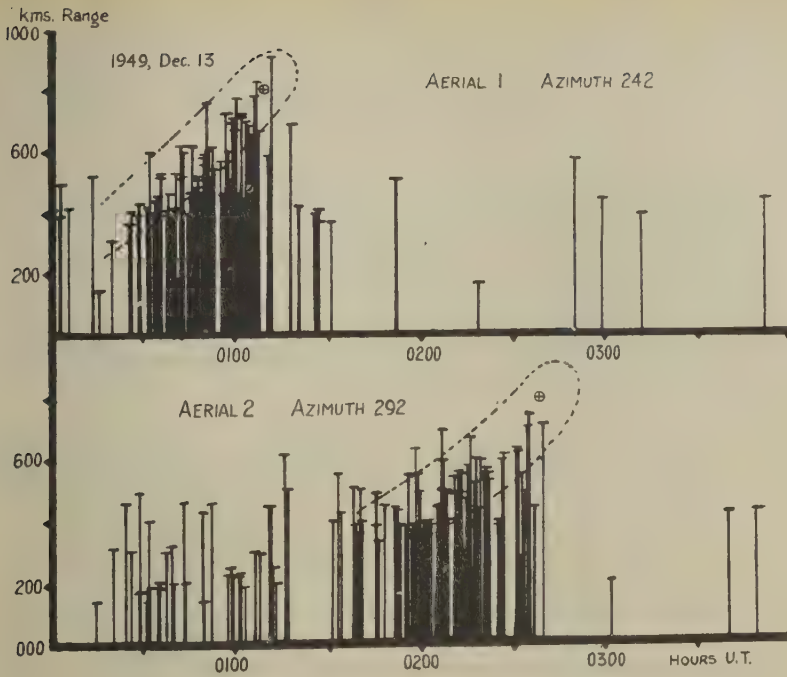
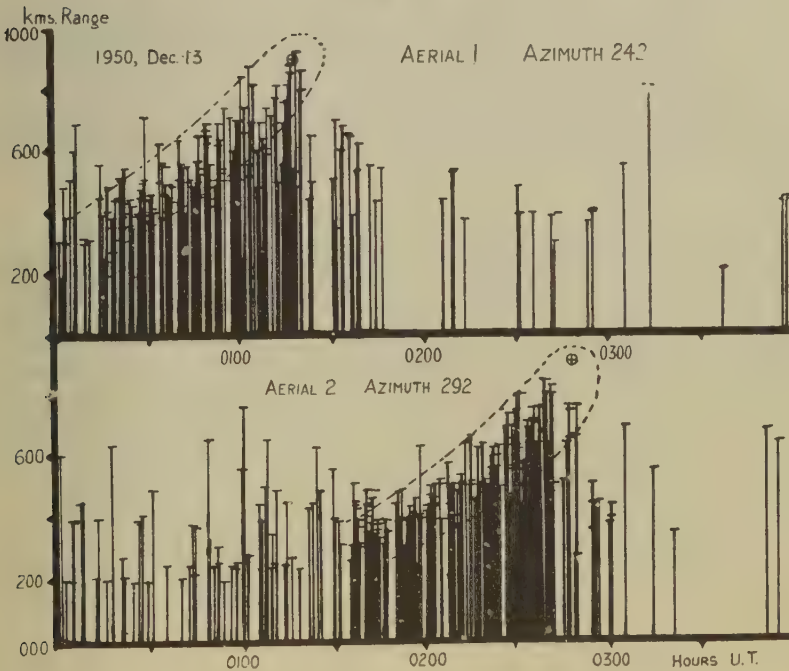


Fig. 7b.



radiants, and for this reason it has been found necessary to classify showers for the purposes of radiant determination in the following way :

CLASS A, which comprises the most active and prominent showers, and which is defined by the following criteria :

- (1) During the passage of the echo zones through the two beams there must be at least 3 echoes of range greater than 700 Kms. appearing on each aerial.
- (2) Two-thirds of the total number of echoes observed must fall within the theoretical range envelopes.

A statistical analysis shows that the probability of a radiant of this class being spurious is less than $1/100$, so that all showers which fulfil the foregoing conditions may be taken to be real.

CLASS B. This is defined as follows :—

- (1) During the passage of the echo zone through the two beams there must be at least 3 echoes of range greater than 600 Kms. appearing on each aerial.
- (2) One-half of the total number of echoes observed must fall within the theoretical range envelope.

A range-time plot fulfilling these criteria is not by itself considered to afford definite proof of the existence of a shower, but only to provide confirmatory evidence in cases where a Class A radiant appears on the previous or the following day.

CLASS C. This Class is used to monitor the meteor activity from a region of the sky containing a suspected radiant for which the plots do not fulfil the conditions required by A and B.

In estimating the radiant position of a shower which is active for several days, a mean of individual radiant positions is taken, weighting the plots of Class A, B and C in order of importance in the ratio 2 : 1 : 0.

§6. RESOLVING POWER.

It occasionally happens, particularly during the summer daytime streams, that two radiants are simultaneously active ; and if the apparatus is to resolve between two such centres, their range-time plots on at least one of the two aerials must be separated by approximately 30 minutes. This time separation depends on the relative positions of the two radiants, and is most conveniently expressed in terms of their angular separation, s , and their relative position angle, ϕ , as indicated in fig. 8. This figure represents a small portion of the celestial sphere, viewed internally, with two radiants situated at R_1 and R_2 . If ABC is the meridian bisecting the great circle arc $R_1 R_2$ at B, then the position angle ϕ is defined as the angle ABR_2 .

Fig. 9 shows the angular separation s required for resolution on each of the two aerials, plotted as a function of ϕ for different values of the declination of the radiant R_1 . It is evident from these curves that any

pair of radiants whose angular separation is greater than 20° can be resolved by at least one of the two aerials, while for more favourable cases the degree of resolution is considerably higher than this.

Fig. 8.

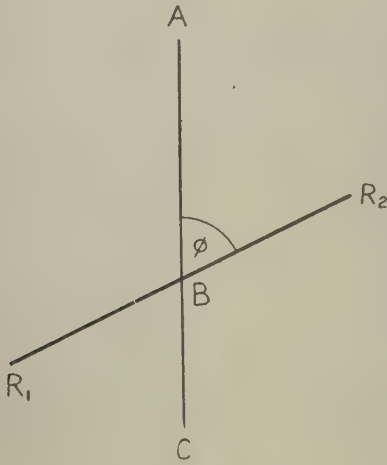
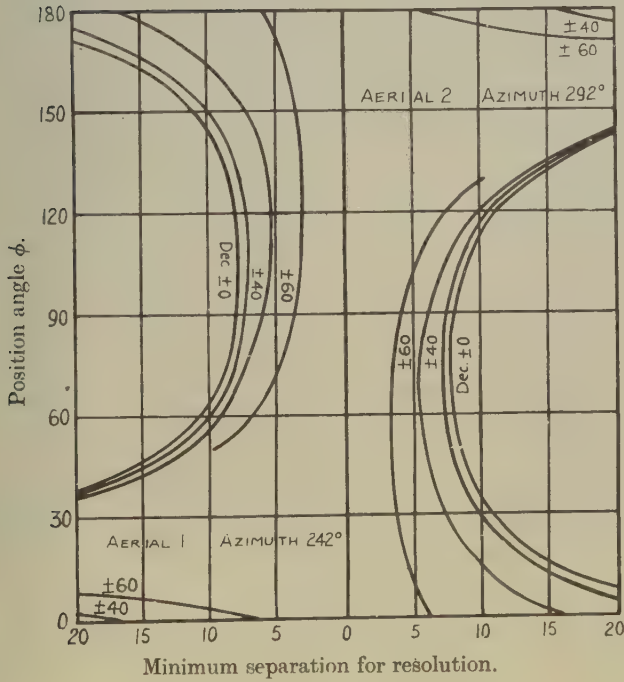


Fig. 9.



ACKNOWLEDGMENTS.

This apparatus has been built at the Jodrell Bank Experimental Station of the University of Manchester under the auspices of Dr. A. C. B. Lovell, whose advice and encouragement has been appreciated. Much of the capital expenditure has been borne by the Department of Scientific and Industrial Research, and two of the authors (A.A., G.S.H.) are indebted to the Department individually for the award of maintenance grants.

REFERENCES.

- ASPINALL, A., CLEGG, J. A., and LOVELL, A. C. B., 1949, *Mon. Not. Roy. Astr. Soc.*, **109**, 352.
 ASPINALL, A., and HAWKINS, G. S., 1951, *Mon. Not. Roy. Astr. Soc.*, in publication.
 CLEGG, J. A., 1948, *Phil. Mag.*, **39**, 577.
 CLEGG, J. A., HUGHES, V. A., and LOVELL, A. C. B., 1947, *Mon. Not. Roy. Astr. Soc.*, **107**, 369.
 DAVIES, J. G., and ELLYETT, C. D., 1949, *Phil. Mag.*, **40**, 614.
 ELLYETT, C. D., and DAVIES, J. G., 1948, *Nature, Lond.*, **161**, 596.
 HAWKINS, G. S., and MARY ALMOND, 1950, *J. Brit. Astr. Ass.*, **60**, 251.
 HAWKINS, G. S., and ASPINALL, A., 1951, in preparation.
 HEY, J. S., and STEWART, G. S., 1947, *Proc. Phys. Soc.*, **59**, 858.
 LOVELL, A. C. B., BANWELL, C. J., and CLEGG, J. A., 1947, *Mon. Not. Roy. Astr. Soc.*, **107**, 164.
 MANNING, L. A., VILLARD, O. G., and PETERSON, A. M., 1949, *J. Appl. Phys.*, **20**, 475.
 MCKINLEY, D. W. R., and MILLMAN, P. M., 1949 a, *Canad. J. Res.*, **27A**, 53 ; 1949 b, *Proc. Inst. Radio Engrs.*, **37**, 364.
 PRENTICE, J. P. M., LOVELL, A. C. B., and BANWELL, C. J., 1947, *Mon. Not. Roy. Astr. Soc.*, **107**, 155.

FIG. 2.

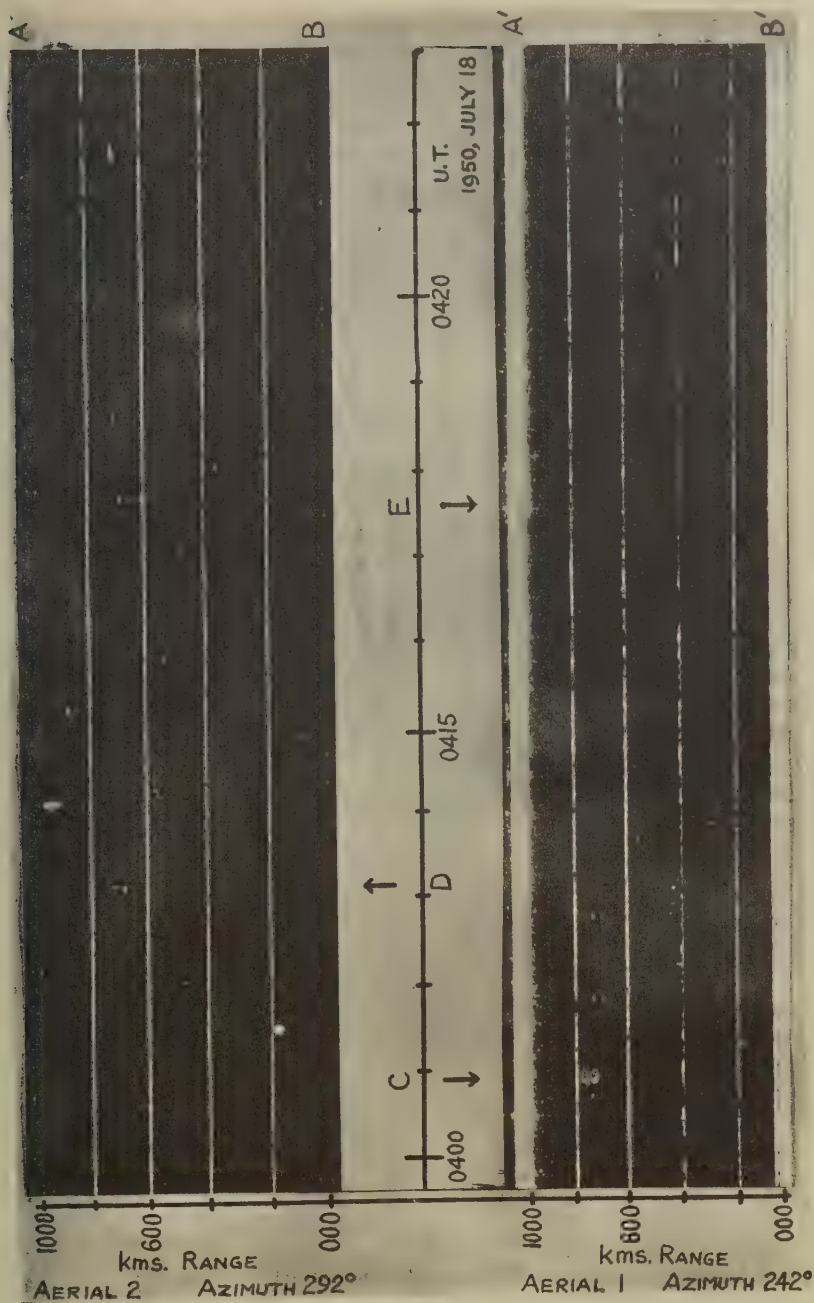
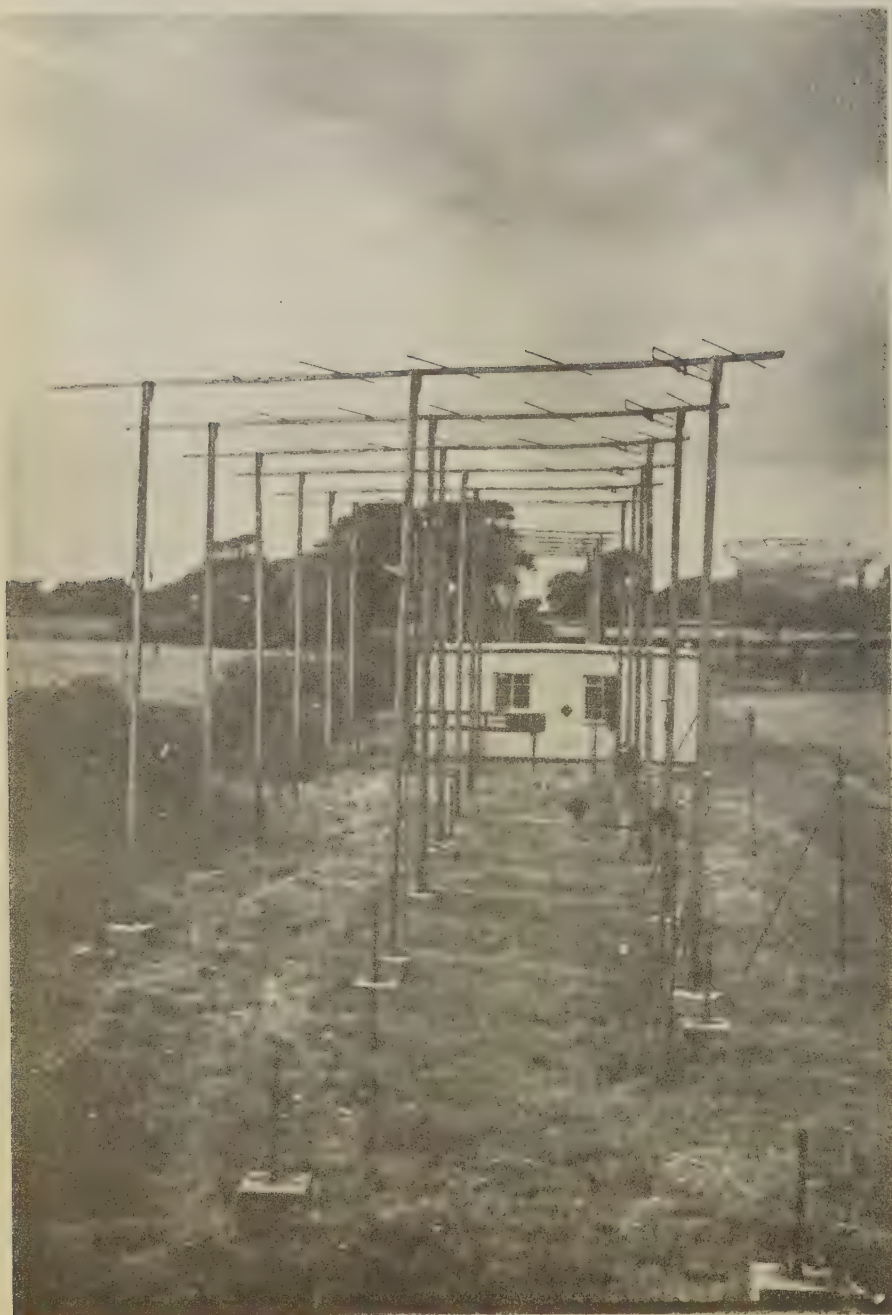


FIG. 3.



LV. *Transit-time Phenomena in Electron Streams.—III.*
The Electron-Ion Plasma and Beam Fluctuations.

By D. K. C. MACDONALD,
 Clarendon Laboratory, Oxford*.

[Received February 13, 1951.]

ABSTRACT.

Continuing the investigation started in earlier papers, we analyse here the equilibrium (isothermal) fluctuations ("noise") in a travelling electron beam taking into account full space-charge interaction. The results are then considered in relation to a number of practical electron valve problems. Because of its relevance to the general problem we also present first a short discussion of the characteristics of electron-ion and electron plasmas based on a "lattice" model.

§1. INTRODUCTION.

IN two previous papers in this Journal (MacDonald 1949, 1950) we have studied systematically the problem of fluctuations ("noise") in a travelling electron beam and their growth. In the first paper we neglected interaction entirely while in the second an average, or "smoothed", potential-variation due to space-charge (*e.g.* Child's law) was taken into account. In the present paper we derive the equilibrium shot noise in a travelling beam where the complete fluctuating interaction is included insofar as this is expressed by Poisson's law at any instant. A general expression emerges which enables a number of very suggestive comparisons to be made with a range of valve problems.

When undertaking this work we were naturally led to consider models for an electron-plasma and in particular found a "lattice" model illuminating in several respects. We have therefore thought it relevant at this time to present first a brief discussion of such a model although it should be emphasized that the fluctuations analysis which follows is essentially independent of this model, being in fact based on quite general premisses.

§2. PLASMA MODELS.

In the past it has been customary (*e.g.* Tonks and Langmuir 1929, Bohm and Gross 1949, Twiss 1950, Gabor 1950) to consider an electron plasma or electron-ion plasma as a quasi-continuum of essentially gas-like (*cf.* also v. Laue 1918) properties. If we assume the average inter-charge distance to be d then the potential energy per charge will be in the order of e^2/d , while at temperature T the random kinetic energy $\sim kT$. Since generally in electron-tube problems $kT \gg e^2/d (= (\rho e^5)^{1/3})$ the gas (or rather

* Communicated by the Author.

perhaps fluid) approximation is essentially justified. However, it appears useful, as has often been done in the corresponding metallic "electron-gas" problem, to consider the properties—particularly as regards the frequency spectrum—of a "rigid" charge lattice of inter-atomic distance d . The well known difficulties associated with three-dimensional lattices restrict us to a linear lattice, following closely Brillouin (1946).

2.1. *Electron-Ion Lattice.*

Consider then a linear chain of ions (mass M , charge $+e$) and electrons (mass m , charge $-e$). In order to maintain this chain in a stable state it will be necessary to assume some repulsive force in addition to the Coulomb attraction*. Born assumed a potential law of the form A/r^n when dealing with the alkali-halide solid and we shall follow him here.

Let d be the distance between electrons, and let U be the potential energy between an adjacent electron-ion pair. Then it may readily be shown (cf. Brillouin, *loc. cit.*, Cap 3) that two separate modes of vibration of the lattice can occur. In the lower-frequency branch, generally known as the "acoustical" branch, neighbouring electrons and ions will essentially be oscillating in phase with one another while, after a "forbidden-zone" of frequencies, we arrive at an upper branch—the "optical" branch—where electrons and ions will effectively be in anti-phase.

If, as a first approximation, we consider only "nearest-neighbour" interaction then the frequency/wavelength relations for the two branches are given by

$$\omega_a^2 = \left(\frac{\partial^2 U}{\partial r^2} \right)_0 \left\{ \frac{1}{m} + \frac{1}{M} - \left[\left(\frac{1}{m} + \frac{1}{M} \right)^2 - \frac{4 \sin^2 \frac{\pi d}{\lambda}}{mM} \right]^{1/2} \right\}, \quad (1)$$

$$\omega_0^2 = \left(\frac{\partial^2 U}{\partial r^2} \right)_0 \left\{ \frac{1}{m} + \frac{1}{M} + \left[\left(\frac{1}{m} + \frac{1}{M} \right)^2 - \frac{4 \sin^2 \frac{\pi d}{\lambda}}{mM} \right]^{1/2} \right\}, \quad (2)$$

where r is the distance between an electron-ion pair, ω_a and ω_0 are the (angular) acoustical and optical frequencies and the differentials are to be evaluated at $r=d/2$.

Since $m/M \ll 1$, these reduce to

$$\omega_a = \sqrt{\left[\frac{2}{M} \left(\frac{\partial^2 U}{\partial r^2} \right)_0 \right]} \cdot \sin \frac{\pi d}{\lambda} \quad \dots \quad (3)$$

and

$$\omega_0 = \sqrt{\left[\frac{2}{m} \left(\frac{\partial^2 U}{\partial r^2} \right)_0 \right]} \cdot \dots \quad (4)$$

Now with the foregoing assumptions we may set

$$\left(\frac{\partial^2 U}{\partial r^2} \right)_0 = 8(n-1)e^2/d^3 = 8(n-1)e\rho,$$

* It should be emphasized that this is merely a convenient *ad hoc* assumption to enable us to treat the problem effectively as a lattice. In fact, the thermal energy of the plasma could be regarded for our purpose as playing in part the rôle of this repulsive potential. If T is too small, then electron-ion recombination will simply occur.

where ρ is the density of electrons (or ions) in the corresponding three-dimensional "lattice". For $\lambda \gg d$, (3) may then be written

$$\omega_a = \sqrt{\left[\frac{16(n-1)e\rho}{M} \right]} \cdot \frac{\pi d}{\lambda} \quad \dots \quad (3a)$$

corresponding to travelling waves with a phase—(and group)—velocity

$$v = \frac{d}{2} \sqrt{\left(\frac{16\gamma e\rho}{M} \right)}, \quad \dots \quad (5)$$

where $\gamma = n - 1$.

For $\lambda \sim d$, dispersion becomes evident and a limiting frequency, $\hat{\omega}_a$, occurs for $\lambda = 2d$ where the group-velocity becomes zero (standing waves):

$$\hat{\omega}_a = \sqrt{\left(\frac{16\gamma e\rho}{M} \right)} \quad \dots \quad (3b)$$

This may be compared with the "plasma-ion (angular) frequency" (cf. Tonks and Langmuir, *loc. cit*) given by

$$\Omega p = \sqrt{\left(\frac{4\pi e\rho}{M} \right)} \quad \dots \quad (3c)$$

From (4) above it is clear that the "optical" frequency branch has degenerated into a single standing-wave vibration with

$$\omega_0 = \sqrt{\left(\frac{16\gamma e\rho}{m} \right)}, \quad \dots \quad (4a)$$

which then corresponds directly to the "plasma-electron frequency". To our approximation the wavelength may then assume any value greater than $2d$ which is the common limit for both classes of oscillation.

2.2. Electron Lattice.

With a linear lattice consisting purely of electrons, only the acoustical branch can exist and we have now, to the "nearest-neighbour" approximation,

$$\omega = \sqrt{\left[\frac{4}{m} \left(\frac{\partial^2 U}{\partial r^2} \right)_0 \right]} \sin \frac{\pi d}{\lambda} \quad \dots \quad (6)$$

Taking now U , the potential energy between two adjacent electrons, as simply e^2/d in this case we see that for $\lambda \gg d$ we have *travelling* waves with phase —, and group —, velocity

$$v = \frac{d}{2} \sqrt{\left(\frac{8e\rho}{m} \right)}, \quad \dots \quad (7a)$$

(7a) may also be written :

$$\frac{1}{2}mv^2 = \frac{e^2}{d} \quad \dots \quad (7b)$$

Again a maximum frequency (*standing* waves) occurs for

$$\hat{\omega} = \sqrt{\left(\frac{8e\rho}{m} \right)} \quad \dots \quad (6a)$$

and

$$\lambda_{\min} = 2d, \quad \dots \quad (6b)$$

which may again be compared with the familiar plasma-electron frequency.

2.3. Effect of Thermal Energy.

So long as kT is less than, or the order of e^2/d —the electrostatic energy—we shall not expect in our model appreciable deviation from these results within their degree of approximation. When, however, kT exceeds e^2/d significantly we should expect the velocity in (7) to be given now rather by

$$\frac{1}{2}mv_i^2 \sim \frac{kT}{2}, \quad \text{i. e.} \quad v_i \sim \sqrt{\left(\frac{kT}{m}\right)}, \quad \dots \quad (8)$$

$$\text{while} \quad \lambda_{\min} \sim \frac{v_i}{f} \sim \sqrt{\left(\frac{kT}{m}\right)} \left[2\pi \sqrt{\left(\frac{m}{8e\rho}\right)} \right], \quad \sim 2\pi \sqrt{\left(\frac{kT}{8e\rho}\right)}. \quad (9a)$$

$$\text{If in fact we set} \quad \hat{\omega} = \sqrt{\left(\frac{4\pi e\rho}{m}\right)},$$

the plasma electron frequency, we have

$$\lambda_{\min} = \sqrt{\left(\frac{kT}{m}\right)} \left[2\pi \sqrt{\left(\frac{m}{4\pi e\rho}\right)} \right] = 2\pi \sqrt{\left(\frac{kT}{4\pi e\rho}\right)}, \quad \dots \quad (9b)$$

which is essentially just the Debye characteristic length (*cf. e. g.* Bohm and Gross, *loc. cit.*)

3. Noise in Travelling Electron Beams.

We turn now to a beam travelling as a whole with velocity v_0 such that $\frac{1}{2}mv_0^2 = \Phi$, say. We wish to determine the *equilibrium* observable current fluctuations in such a beam due to thermal agitation. The "atomicity" of electricity (*cf.* the "shot effect") will introduce itself naturally as a consequence of the frequency characteristics of the discrete lattice discussed above.

Consider then an electron beam of mean density, ρ_0 , velocity v_0 , which has been travelling "for a sufficiently long time", to be regarded as being in thermal equilibrium at a temperature*, T . Let us also take a length, L , of the beam of "sufficient" extent for the end conditions to be neglected and let us assume an arbitrary disturbance of electron density, ρ , and of velocity, v , which has been analysed into Fourier components over this interval. Let the component at (angular) frequency, ω , say, of electron-density be

$$\tilde{\rho}_\omega = \rho_\omega \sin \left(\omega \left(t - \frac{x}{v_0} \right) + \theta \right), \quad \dots \quad (10a)$$

and of velocity be

$$\tilde{v}_\omega = v_\omega \sin \left(\omega \left(t - \frac{x}{v_0} \right) + \phi \right). \quad \dots \quad (10b)$$

The corresponding component of current is given by

$$\left. \begin{aligned} \tilde{I}_\omega &= A(\tilde{\rho}_\omega v_0 + \rho_0 \tilde{v}_\omega) \\ \text{(where this is essentially a vector addition)} \end{aligned} \right\} \dots \quad (11)$$

$$= \tilde{I}_{1\omega} + \tilde{I}_{2\omega}, \quad \text{say}$$

where A is cross sectional area of the beam.

* The question of the actual temperature appropriate to a beam is returned to briefly later.

From (10a) using Poisson's equation we derive the corresponding potential variation, and hence that the perturbation energy corresponding to (11) is *

$$E = \frac{\pi v_0^2 \rho_0^2 AL}{\omega^2} + \frac{\rho_0 v_0^2 AL}{4} \frac{m}{e} \quad (12)$$

We can then write down immediately the probability distribution function for the beam current components and phases

$$f(I_1, I_2; \theta, \phi) dI_1 dI_2 d\theta d\phi \\ = \left(\frac{L}{A\omega^2 kT} \right) \left(\frac{Lm}{4\pi e \rho_0 A kT} \right) I_1 \epsilon^{-\frac{\pi L I_1^2}{A\omega^2 kT}} \cdot I_2 \epsilon^{-\frac{m L I_2^2}{4e \rho_0 A kT}} dI_1 dI_2 d\theta d\phi. \quad (13)^\dagger$$

And, in particular,

$$\bar{I}_1^2 = \frac{\omega^2 kTA}{\pi L}; \quad \bar{I}_2^2 = \frac{4e \rho_0 A kT}{mL} \quad (14)$$

Since, further, in a bandwidth B there will be BL/v_0 components, we may write

$$\overline{\delta I_f^2} \left[\equiv \frac{BL}{v_0} \left(\frac{\bar{I}_1^2 + \bar{I}_2^2}{2} \right) \right] = \left(\frac{\omega^2 kTA}{2\pi v_0} + \frac{2e \rho_0 A kT}{m v_0} \right) B, \quad (15)$$

which may finally be arranged as

$$\overline{\delta I_f^2} = \frac{kT}{2\Phi} \left[1 + \left(\frac{\omega}{\omega_p} \right)^2 \right] 2e I_0 B, \quad (16)$$

noting that I_0 (the d.c. current) $= \rho_0 v_0 A$, and that ω_p , the electron plasma frequency, is given by $\omega_p^2 = 4\pi e \rho_0 / m$.

3.1. Discussion of Derived Formula ‡ .

In an actual thermionic valve one may expect that the above expression for $\overline{\delta I_f^2}$ should lead to a lower limit for the average value of current noise which will be observed. Let us consider first a parallel-plane diode at low frequencies (thus $\omega \ll \omega_p$); in the strongly space-charge limited condition let us assume Child's Law to hold as a sufficient approximation

$$I_0 = CV_a^{3/2},$$

therefore

$$\frac{1}{V_a} = \frac{2}{3} g_a / I_0, \quad \left(g_a = \frac{\partial I_0}{\partial V_a} \right).$$

* The omission in the first integration of a term linear in x corresponds of course to the "removal" of a d.c. potential variation which is irrelevant.

† We are using here the well-known result that for a system in thermal equilibrium characterized by canonical coordinates p_i, q_i , say, the distribution function for these coordinates is given by

$$f(p_i, q_i) dp_i dq_i \sim e^{-E(p_i, q_i)/kT} dp_i dq_i.$$

‡ This comparison of our derived formula with particular valve problems is to be considered as essentially heuristic in nature rather than in any way rigorous; we mention below some aspects which require further careful consideration.

Now eV_a represents the *final* anode energy and it might seem therefore rather more appropriate to insert in (16) some effective average value for Φ . A direct time-average, for example, for Φ yields in fact $\Phi_{\text{eff}} = \frac{1}{5} \Phi$ whence, substituting, we find

$$\overline{\delta I_f^2} = 4kTg_a \left(\frac{5}{6} \right) B. \quad . \quad . \quad . \quad . \quad . \quad (17)$$

This may be compared with the classical detailed analysis of North *et al.* (1940) and Schottky and Spenke (1937) of the noise in a diode at low frequencies which under extreme space-charge limitation yields

$$\overline{\delta I_f^2} = 4kTg_a \left[3 \left(1 - \frac{\pi}{4} \right) \right] B. \quad . \quad . \quad . \quad . \quad . \quad (18)$$

We might therefore suggest that the diode *under strong space-charge limitation* behaves very much as a current stream in thermal equilibrium. That is, we may consider that the available accelerating energy is used efficiently in a quasi-reversible manner through the medium of the space-charge barrier to maintain the noise at practically its lower thermal level.

Again, the electron-current in a diode under purely retarding-field conditions has its x -component of velocity given everywhere by $\frac{1}{2}m\overline{v_x^2} = kT$, and it seems not unreasonable in this case to define Φ , the effective transport energy, by $\frac{1}{2}m\overline{v_x^2} = kT/2$, $= kT/2$, whence from (16) we have

$$\overline{\delta I_f^2} = 2eI_0B \quad . \quad . \quad . \quad . \quad . \quad (19)$$

in agreement with other approaches to the problem and with experiment (MacDonald and Fürth 1947).

On the other hand, in the case of a *saturated* diode (*i. e.* having a high enough anode voltage to prevent the formation of any potential minimum) where experiment and theory show that $\overline{\delta I_f^2} = 2eI_0B$ it is clear from comparison with (16) that the system is then *very far from thermal equilibrium*, as is otherwise quite evident.

The discussion above of the space-charge limited diode suggests that a cylindrical, or, *a fortiori*, a spherical-structure would exhibit lower noise since in that case the final energy is effectively achieved in transit more quickly than in the parallel-plane valve. A detailed analysis by Wainstein (1947) of the cylindrical diode based on the concept of a single-valued velocity-equivalent of the random thermal energy as first introduced by Rack (1938) proposed this and his analysis indicates that for $r_a/r_c \approx 20$, the reduction factor over the parallel-plane diode would be as low as $\sim (0.4)^2 = 0.16$. On the other hand, a direct application of our equations (16) and (17) suggests that one might expect a lower limit to be given by

$$\overline{\delta I_f^2} \approx 4kTg_a \left(\frac{1}{6} \right) B. \quad . \quad . \quad . \quad . \quad . \quad (20)$$

Turning to the general travelling beam problem without restriction on frequency, it is clear from the first part of this paper that (16) will only be valid up to an (externally "observed") frequency $\hat{f} = v_0/\lambda_{\min}$, where λ_{\min} is

defined by (9b). v_0 is given by $\frac{1}{2}mv_0^2 = \Phi$ or—more strictly it appears—for a beam originally emitted from a cathode at temp. T , by $\frac{1}{2}mv_0^2 = \Phi - kT/2$.

$$\text{Thus} \quad \frac{\bar{\omega}^2}{\omega_p^2} = \frac{mv_0^2}{kT},$$

$$\text{therefore} \quad 1 + \frac{\bar{\omega}^2}{\omega_p^2} = 2\Phi,$$

and thus at this frequency limit we have

$$\bar{\delta I_f^2} = 2eI_0B, \quad (21)$$

characteristic of a purely random electron flow (pure "shot effect").

Thus, generally,

$$\bar{\delta I_f^2} = \frac{kT}{2\Phi} \left(1 + \frac{\omega^2}{\omega_p^2} \right) 2eI_0B \quad (16a)$$

$$\left. \begin{aligned} \text{for} \quad & \left[\omega < \sim \sqrt{\left(\frac{4\pi e\rho v_0^2}{kT} \right)} \right] \\ & = 2eI_0B \left[\omega > \sim \sqrt{\left(\frac{4\pi e\rho v_0^2}{kT} \right)} \right]. \quad . . . (16b) \end{aligned} \right\}$$

The introduction of the limiting frequency and the approximation of spectral variation in (16a, b) are closely analogous to the limiting frequency involved in the Debye treatment of the specific heat of a crystalline solid.

It is very interesting to notice here also that Pierce, Smullin (1949) and Robinson (1950) have recently derived an expression for the noise current at high frequencies *emerging from an electron gun*, again on the basis of Rack's approximation in combination with a detailed analysis of the gun as a diode at high frequencies (*cf.* Llewellyn and Peterson : 1944).

They find

$$\bar{\delta I_f^2} = (4 - \pi) \left(\frac{\omega^2}{\omega_p^2} \right) \left(\frac{kT}{2\Phi} \right) 2eI_0B, \quad (22)$$

which may again be compared with our (16).

The analysis and experiment (Cutler and Quate 1949) also indicate that if the beam then drifts freely the noise magnitude will show an oscillatory variation along the drift-space about this value. Ultimately, however, this variation must decay with transit time, τ , due to the thermal velocity spread; the decay time will be given approximately by $\tau \sim 1/2\pi f (kT/2\Phi)$ (*cf.* MacDonald 1949).

3.2 : Outstanding Considerations.

A more precise application of our results to valve structures would require a rather careful consideration of the influence of the boundary conditions at the cathode in terms of the effective degrees of freedom of the system. The situation then is of course very similar to that encountered in a discussion of the thermal energy and specific heat of a crystal,

but in the *latter* cases we are not indeed interested in the actual behaviour in the neighbourhood of the physical boundaries but only in so far as it may affect our specification of the normal modes of vibration. Consequently, an idealized artifice such as Born's "Cyclic crystal" is adequate in that situation. It appears in fact to the writer that if one specifies the current emerging from a thermionic cathode by $I = A\rho v$ then only v may be regarded as an independent degree of freedom, "near" the cathode.

Since also electron beams in practice presumably correspond more nearly to adiabatic than isothermal systems care would also be necessary in ascribing an equilibrium temperature in a particular situation and more work remains to be done on both these aspects of the problem.

ACKNOWLEDGMENTS.

I should like to thank Dr. R. Kompfner and Mr. F. N. H. Robinson very sincerely for their continued interest and for stimulating discussions in this work.

REFERENCES.

- BRILLOUIN, L., 1946, *Wave Propagation in Periodic Structures* (New York: McGraw-Hill).
 BOHM, D., and GROSS, E. P., 1949, *Phys. Rev.*, **75**, 1851.
 CUTLER, C. C., and QUATE, C. F., 1949, *Bell Lab. Memo. MM-49-160-36* (20/12/49).
 GABOR, D., 1950, *A Survey of the Present State of Plasma Oscillations and Electron Interaction* (Imperial College of Science and Technology).
 LAUE, M., 1918, *Jahrb. d. Radioakt. u. Elek.*, **15**, 205.
 LLEWELLYN, F. B., and PETERSON, 1944, *Proc. Inst. Rad. Eng.*, **32**, 144.
 MACDONALD, D. K. C., and FÜRTH, R., 1947, *Proc. Phys. Soc.*, **59**, 375.
 MACDONALD, D. K. C., 1949, *Phil. Mag.*, **40**, 561; 1950, *Ibid.*, **41**, 863.
 NORTH, D. O., *et al.*, 1940, *R.C.A. Rev.*, **4**, 5.
 RACK, A. J., 1938, *Bell Syst. Tech. Journ.*, **17**, 592.
 ROBINSON, F. N. H., 1950, *S.E.R.L. Memo* 23/5/50.
 SCHOTTKY, W., and SPENKE, E., 1937, *Wiss. Veroff a. d. Siemens. Werk.*, **16**, 127.
 SMULLIN, L. D., 1949, *M.I.T. Tech. Report* 142 (24/10/49).
 TONKS, L., and LANGMUIR, I., 1929, *Phys. Rev.*, **33**, 195.
 TWISS, R. Q., 1950, *Extract Quart. Journ. S.E.R.L.*
 WAINSTEIN, L. A., 1947, *Journ. Tech. Phys. (U.S.S.R.)*, **17**, 1035.

LVI. *The Production of Mesons in Proton-Proton Collisions.*

By J. C. GUNN, E. A. POWER and B. F. TOUSCHEK,
Department of Natural Philosophy, University of Glasgow*.

[Received February 14, 1951.]

SUMMARY.

A method of estimating the cross-sections for meson production in proton-proton collisions near the threshold is outlined, together with detailed calculations for spin zero meson fields under certain simplifying assumptions concerning the nuclear forces. It is found that, for the final continuous neutron-proton system, a low energy for the neutron-proton relative motion is favoured; this, together with a large contribution from transitions to a final bound deuteron, leads to a meson spectrum well peaked at the highest allowed energies in agreement with recent experiments. While the total cross-section is dependent more on the shape and size of the inter-nucleon potential than on the meson type, the spectrum at a given angle and, more particularly, the angular distribution are critically dependent on the parity of the produced meson. Comparison with experiment favours scalar mesons.

§1. INTRODUCTION.

THE problem of the production of mesons in nucleon-nucleon collisions has previously received treatment by Heitler (1943-5) and his collaborators, and more recently by Morette (1949) and by Foldy and Marshak (1949). The emphasis of earlier work is on the effect of strong radiation damping of the meson field in reducing the otherwise divergent cross-sections calculated by perturbation theory. In the present paper we do not intend to deal with the case where the nucleon kinetic energies become greater than their rest mass, so that some approximate non-relativistic treatment should be applicable to the nucleon motion. The mesons, however, are given relativistic treatment. Recent measurements by Cartwright *et al.* (1950) and Peterson *et al.* (1950) at 345 MeV. are such as to come within our treatment. It is natural to make the further step of replacing the inter-nucleon interaction by a phenomenological one. In doing so we ignore the fact that nuclear forces are, at least in part, due to π -meson exchange. This approach has already been adopted by Foldy and Marshak, who discuss briefly the errors likely to be introduced as compared with a full field theoretic treatment, such as that of Morette. (These questions have been more fully investigated by one of us (E.A.P.) and will be reported elsewhere.) The advantage of the phenomenological approach is that the internucleon wave functions can then be described with an accuracy

* Communicated by the Authors.

limited only by the inadequacy of existing data on scattering to provide nuclear potentials. These scattering experiments have been very much studied recently, and the analysis of the experimental results by various authors, see for example Jackson and Blatt (1950), has led to several at least qualitative conclusions regarding the internucleon potential.

In the present paper we take as a working assumption that :—

1. The interaction in states of odd parity is so small that it may be neglected. This assumption has been introduced by Serber and is based on the approximate symmetry about 90° of the angular distributions in n - p scattering.

2. The interaction in states of even parity is charge independent and may be best represented by a singular form of potential with a long tail.

No account is taken of tensor forces, or of possible spin orbit forces. Some such addition is clearly necessary to account for the observed p - p scattering and will be considered in later calculations. We further confine attention to the production of positive mesons in proton-proton collisions, limiting ourselves to scalar and pseudo-scalar meson fields.

§2. GENERAL FORMALISM.

The Hamiltonian of the interaction between the nucleon and meson fields will generally be represented by

$$H' = \int \psi^\dagger(x) Q \phi(x) \psi(x) dx + \text{adjoint}, \quad (1)$$

where ψ is the field operator of the nucleons and ϕ the field operator of the mesons. The operator Q differs according to charge and spin dependence of the meson theory. The matrix-elements of the Hamiltonian (1) may be evaluated following a method discussed by Becker and Leibfried (1946), the term appropriate to a transition from an initial state o to a final state f each with A nucleons being

$$H' = \int dx_1 \dots \int dx_A \psi_0^\dagger(x_1 \dots x_A) \left\{ \sum_{i=1}^A (Q_i \phi(x_i) + Q_i^\dagger \phi^\dagger(x_i)) \right\} \psi_f(x_1 \dots x_A). \\ . . . (2)$$

Here ψ_0 and ψ_f are the properly antisymmetrized and normalized wave-functions of the initial and final states of the nucleon system, expressed as functions of the space, spin and charge variables. The term with ϕ^\dagger corresponds to the annihilation, the term with ϕ to the creation of a π^+ meson.

Calculations have been carried out in detail for scalar and pseudo-scalar meson fields, using a scalar coupling in the first case and a pseudo-vector coupling in the second. The equivalence theorem shows that, in the approximation used here, pseudo-scalar and pseudo-vector coupling should give identical results in the pseudo-scalar meson theory. With the usual Fourier expansion of the meson field we then find for the matrix-element

describing the emission of a positive π -meson with momentum k and energy ω from a two nucleon system :

$$H'_{0f} = g \sqrt{\frac{2\pi}{\omega}} \iint d\mathbf{r}_1 d\mathbf{r}_2 \psi_0^\dagger(\mathbf{r}_i, \tau_i, s_i) \left\{ \sum_{i=1}^2 \Pi^{(i)} \beta^{(i)} \exp(i\mathbf{k} \cdot \mathbf{r}_i) \right\} \psi_f(\mathbf{r}_i, \tau_i, s_i),$$

. . . (3 S)

for scalar mesons and

$$H'_{0f} = \frac{if}{\mu} \sqrt{\frac{2\pi}{\omega}} \iint d\mathbf{r}_1 d\mathbf{r}_2 \psi_0^\dagger \left\{ \sum_{i=1}^2 \Pi^{(i)} (\boldsymbol{\sigma}^{(i)} \cdot \mathbf{k} - \rho_1^{(i)} \omega) \exp(i\mathbf{k} \cdot \mathbf{r}_i) \right\} \psi_f.$$

. . . (3 P)

Here and in the following S denotes scalar mesons, P pseudo-scalar ones ; $\beta^{(i)}$, $\boldsymbol{\sigma}^{(i)}$, $\rho_1^{(i)}$, are the usual Dirac matrices applicable to the i th nucleon, $\Pi^{(i)}$ is the charge operator changing nucleon i from a neutron into a proton, τ_i and s_i are the isotopic and spin variables of the i th nucleon, μ is the rest energy of the meson and we work in natural units with $\hbar=c=1$.

The frame of reference will be chosen so that in the initial state the total momentum is zero, i. e. if \mathbf{p}_1 , \mathbf{p}_2 denote the momenta of the two nucleons

$$(\mathbf{p}_1)_0 = -(\mathbf{p}_2)_0 = \mathbf{p}_0.$$

In the final state it follows from the conservation of energy and momentum that

$$(\mathbf{p}_1 + \mathbf{p}_2)_f = \mathbf{P} = -\mathbf{k}.$$

The motion of the nucleon mass centre corresponding to \mathbf{P} is fairly slow (i. e. non relativistic), so that we may suppose an approximate separation

$$\psi_f(\mathbf{r}_1, \mathbf{r}_2; s_i, \tau_i) = \exp(i\mathbf{P} \cdot \mathbf{R}) u_f(\mathbf{r}, s_i, \tau_i), \quad (4)$$

where \mathbf{R} is the position of the mass-centre and \mathbf{r} the relative position vector of the two nucleons. The isotopic factor in u_0 and u_f may also be separated out. In the problem considered the initial state contains two protons so that $\psi_0 = u_0(\mathbf{r}, s_i) {}^3(\tau)_1$; the final state may be either the charge singlet ${}^1(\tau)_0$ or charge triplet ${}^3(\tau)_0$ state. Using the properties

$$\Pi^{(1)} {}^1(\tau)_0 = -\Pi^{(2)} {}^1(\tau)_0 = -\frac{1}{\sqrt{2}} {}^3(\tau)_1,$$

$$\Pi^{(1)} {}^3(\tau)_0 = \Pi^{(2)} {}^3(\tau)_0 = \frac{1}{\sqrt{2}} {}^3(\tau)_1$$

of the change of charge operator Π , one may write for the matrix elements (3)

$$H'_{0f} = g \sqrt{(\pi/\omega)} \int d\mathbf{r} u_0^\dagger(\mathbf{r}, s_i) \left\{ \mp \beta^{(1)} \exp(\tfrac{1}{2}i\mathbf{k} \cdot \mathbf{r}) + \beta^{(2)} \exp(-\tfrac{1}{2}i\mathbf{k} \cdot \mathbf{r}) \right\} u_f(\mathbf{r}, s_i)$$

. . . (5 S)

$$H'_{0f} = if/\mu \sqrt{(\pi/\omega)} \int d\mathbf{r} u_0^\dagger \left\{ \mp (\boldsymbol{\sigma}^{(1)} \cdot \mathbf{k} - \omega \rho_1^{(1)}) \exp(\tfrac{1}{2}i\mathbf{k} \cdot \mathbf{r}) \right. \\ \left. + (\boldsymbol{\sigma}^{(2)} \cdot \mathbf{k} - \omega \rho_1^{(2)}) \exp(-\tfrac{1}{2}i\mathbf{k} \cdot \mathbf{r}) \right\} u_f. \quad . . (5 P)$$

In these expressions the alternative $-$ and $+$ signs hold for the final charge singlet and charge triplet states respectively. In accordance with approximate non-relativistic treatment of the nuclear motion the wave-function u_0 and u_f may be reduced to their large components. To the first order in the velocity this corresponds to replacing β and σ (which do not mix large and small components) by 1 and the 2×2 σ -matrices respectively. On the other hand

$$u_0^\dagger \rho_1^{(1)} u_f \simeq i/2M v_0^\dagger \sigma^{(1)} \cdot (\overleftarrow{\nabla} - \overrightarrow{\nabla}) v_f, \quad M = \text{nucleon mass},$$

where v_0 and v_f denote the large components of u_0 and u_f and ∇ is the gradient with respect to the relative coordinate \mathbf{r} . Introducing these expressions into (5S) and (5P) we arrive at the final approximate form for the matrix elements

$$H'_{0f} = g\sqrt{(\pi/\omega)} \int d\mathbf{r} v_0^\dagger \{ \mp \exp(\frac{1}{2}i\mathbf{k} \cdot \mathbf{r}) + \exp(-\frac{1}{2}i\mathbf{k} \cdot \mathbf{r}) \} v_f, \quad (6S)$$

$$H'_{0f} = if/\mu\sqrt{(\pi/\omega)} \int d\mathbf{r} v_0^\dagger \{ \mp \sigma^{(1)} \cdot [\mathbf{k} - (i\omega/M)\overleftarrow{\nabla}] \exp(\frac{1}{2}i\mathbf{k} \cdot \mathbf{r}) \\ + \sigma^{(2)} \cdot [\mathbf{k} + (i\omega/M)\overleftarrow{\nabla}] \exp(-\frac{1}{2}i\mathbf{k} \cdot \mathbf{r}) \} v_f \quad (6P)$$

for scalar and pseudo-scalar meson theories. The $-$ and $+$ signs hold for the final charge singlet and triplet states respectively.

The cross-sections for the various processes by which a pair of protons may produce a positive meson must now be evaluated by using equations (6). The chief problem that remains is the selection of suitable wave-functions to describe the motion of the nucleons. In this we shall be guided by the information acquired in the fitting of the deuteron and two body scattering data by internuclear potentials. We shall find that the cross-sections are in fact rather sensitive to the choice of potential.

§3. TRANSITIONS TO THE DISCRETE STATE.

We first consider the production of a meson when the transition of the nucleons leads to the ground state of the deuteron. Separate consideration must be given to the two possibilities that the protons are initially in the spin triplet or spin singlet states. In the case of an initial spin triplet the wave function v_0 will be of the form

$$v_0 = {}^3(\sigma)_{m_s} v_0(\mathbf{r})$$

so that the matrix element in the pseudo-scalar case becomes

$$H'_{0f} = if/\mu\sqrt{(\pi/\omega)} \int d\mathbf{r} {}^3(\sigma)_{m_s} v_0^* \{ -\mathbf{k} \cdot [\sigma^{(1)} \exp(\frac{1}{2}i\mathbf{k} \cdot \mathbf{r}) - \sigma^{(2)} \exp(-\frac{1}{2}i\mathbf{k} \cdot \mathbf{r})] \\ + i\omega/M [\sigma^{(1)} \cdot \overleftarrow{\nabla} \exp(\frac{1}{2}i\mathbf{k} \cdot \mathbf{r}) + \sigma^{(2)} \cdot \overleftarrow{\nabla} \exp(-\frac{1}{2}i\mathbf{k} \cdot \mathbf{r})] \} {}^3(\sigma)_{m_s} v_f.$$

The evaluation of this matrix element will in general require the consideration of integrals such as

$$\int v_0^* \exp(\frac{1}{2}i\mathbf{k} \cdot \mathbf{r}) v_f d\mathbf{r}, \quad \int \nabla v_0^* \exp(\frac{1}{2}i\mathbf{k} \cdot \mathbf{r}) v_f d\mathbf{r}, \quad \dots \quad (8)$$

where v_0 and v_f are solutions of Schrödinger-equations, say,

$$\left. \begin{aligned} \nabla^2 v_0 + (p_0^2 + MU_0)v_0 &= 0, \\ \nabla^2 v_f + (p_f^2 + MU_f)v_f &= 0, \end{aligned} \right\} M = \text{nucleon-mass.} \quad . \quad . \quad . \quad (9)$$

The potential functions U_0 and U_f will in general be different on account of the spin and charge dependence of nuclear forces. We shall, however, always restrict ourselves to central forces of the same range and shape, so that

$$U_0 = J_0 w(r) \quad \text{and} \quad U_f = J_f w(r),$$

where the J 's are constants of the dimension of an energy and $w(r)$ is a dimensionless function of r depending only on one parameter — the range of the forces.

It can immediately be shown from equation (9) that

$$(p_0^2 - p_f^2) \int v_0^* v_f d\mathbf{r} = M \int (U_f - U_0) v_0^* v_f d\mathbf{r} \quad . \quad . \quad . \quad (10)$$

and this identity allows one to restrict the space integration to an interval of the order of the range of the nuclear forces. There is, however, no transformation directly available for the integrals (8). It is here that the assumption of "no interaction" in odd parity states leads to some simplification, for according to this assumption, $U_0 = 0$ in the initial spin triplet states, and we may write

$$v_0 = [\exp(i\mathbf{p}_0 \cdot \mathbf{r}) - \exp(-i\mathbf{p}_0 \cdot \mathbf{r})] / \sqrt{2}.$$

The matrix element (7P) can now be written

$$\begin{aligned} H'_{0f} = & -if/\mu \sqrt{(\pi/\omega)} \langle {}^3\sigma_{m_s} | \sigma^{(1)} + \sigma^{(2)} | {}^3\sigma_{m_s'} \rangle \cdot [\mathbf{k} \{ I(\mathbf{p}_0 + \tfrac{1}{2}\mathbf{k}) - I(\mathbf{p}_0 - \tfrac{1}{2}\mathbf{k}) \} \\ & + (\omega/M) \mathbf{p}_0 \{ I(\mathbf{p}_0 + \tfrac{1}{2}\mathbf{k}) + I(\mathbf{p}_0 - \tfrac{1}{2}\mathbf{k}) \}], \quad . \quad . \quad . \quad (11P) \end{aligned}$$

where as an abbreviation we have put

$$I(\mathbf{p}_0) = \int \exp(i\mathbf{p}_0 \cdot \mathbf{r}) v_f d\mathbf{r}. \quad . \quad . \quad . \quad (12)$$

If the initial state is a singlet state its parity will be even, so that $U_0 \neq 0$ and no simple approximation will be possible to the integrals (8). However, as an estimate of the order of magnitude of the even parity contribution we shall make use of the approximation

$$H'_{0f} = -\frac{if}{\mu} \sqrt{\left(\frac{2\pi}{\omega}\right)} \frac{(J_f - J_0)}{J_f} \langle {}^1(\sigma)_0 | \sigma^{(1)} - \sigma^{(2)} | {}^3(\sigma)_{m_s'} \rangle \cdot I(\mathbf{p}_0) \mathbf{k}, \quad . \quad . \quad (13)$$

which is equivalent to assuming that of all states with even parity only the 2 proton S-state contributes, and that the momentum of the meson in the integrals (8) can be neglected. The expression (13) can then be expected to give the right order of magnitude and to represent an upper limit in the sense that consideration of the meson momentum will tend to decrease the value of the integrals (8).

For the calculation of the cross-section we need $\Sigma |H'_{0f}|^2$ summed over the final spin states of the deuteron and averaged over the orientations of the original spin. This is now given by

$$\Sigma |H'_{0f}|^2 = \frac{\pi f^2}{\mu^2 \omega} \left[\left\{ \mathbf{k} (I(\mathbf{p}_0 + \frac{1}{2}\mathbf{k}) - I(\mathbf{p}_0 - \frac{1}{2}\mathbf{k})) + \frac{\omega}{M} \mathbf{p}_0 (I(\mathbf{p}_0 + \frac{1}{2}\mathbf{k}) + I(\mathbf{p}_0 - \frac{1}{2}\mathbf{k})) \right\}^2 + 2k^2 I(\mathbf{p}_0)^2 \left(\frac{\Delta J}{J} \right)^2 \right],$$

where $\Delta J = J_f - J_0$, and we have written J for J_f .

The differential cross-section can be determined from

$$\frac{d\sigma}{d\Omega} = \frac{k\omega}{4\pi^2 V_f} \Sigma |H'_{0f}|^2, \quad \dots \quad (14)$$

where V is the initial relative velocity of the nucleons and $d\Omega$ is the element of solid angle for the meson.

For the evaluation of I some assumption has to be made about the inter-nucleon potential. Present scattering evidence on the whole favours a fairly singular, long tailed potential for which we may use as a simple analytical expression the potential suggested by Hulthén (1942):

$$U(r) = J \exp(-\kappa r) / [1 - \exp(-\kappa r)], \quad \dots \quad (15)$$

The normalized wave function of the ground state of the deuteron is then

$$v_f(r) = \sqrt{\left\{ \frac{\kappa b(b^2 - 1)}{8\pi} \right\}} \frac{1}{r} \exp[-\frac{1}{2}(b-1)\kappa r] [1 - \exp(-\kappa r)]$$

with

$$b = MJ/\kappa^2. \quad \dots \quad (16)$$

The depth and range of the potential well must be adjusted so as to fit the deuteron data. We shall use the values

$$1/\kappa = 1.17 \times 10^{-13} \text{ cm.}, \quad ({}^3J) = 46.6 \text{ MeV.}, \quad ({}^1J) = 27.2 \text{ MeV.},$$

where $({}^3J)$ and $({}^1J)$ refer to the spin triplet and singlet states respectively. The integral I from equation (12) may now be easily evaluated yielding

$$I(\mathbf{p}_0) = \frac{\sqrt{\{2\pi b^3(b^2 + 1)\kappa^5\}}}{(p_0^2 + MW_D)(p_0^2 + \left(\frac{b+1}{2}\right)^2 \kappa^2)}.$$

In the energy region which we can compare with experiment we find $p_0 \simeq 400 \text{ MeV.}$ and $k \simeq 90 \text{ MeV.}$, and, therefore, in good approximation

$$I(\mathbf{p}_0 + \frac{1}{2}\mathbf{k}) + I(\mathbf{p}_0 - \frac{1}{2}\mathbf{k}) \simeq 2I(\mathbf{p}_0),$$

$$I(\mathbf{p}_0 + \frac{1}{2}\mathbf{k}) - I(\mathbf{p}_0 - \frac{1}{2}\mathbf{k}) \simeq -(4k/p_0) \cos \theta I(\mathbf{p}_0),$$

where θ is the angle between \mathbf{k} and \mathbf{p}_0 . This gives finally an approximate expression for the cross-section describing the formation of a deuteron under meson emission

$$\frac{d\sigma}{d\Omega} = \frac{f^2}{V\mu^2} \left\{ 1 + \frac{b^3(b^2 - 1)}{(b+1)^2 \kappa^2} \right\}^2 \frac{k^3 \kappa^5}{p_0^8} \left\{ \left(\frac{\Delta J}{J} \right)^2 + 2 \left(\frac{\omega p_0}{kM} \right)^2 - \frac{8\omega}{M} \cos^2 \theta \right\}, \quad \dots \quad (17 P)$$

where f^2 denotes the square of the coupling constant in "ordinary" units. A numerical discussion of this result will be given in § 5.

The corresponding result for scalar meson theory is

$$\frac{d\sigma}{d\Omega} = \frac{12g^2}{V} \frac{b^3(b^2-1)}{\left\{1 + \frac{(b+1)^2\kappa^2}{4p_0^2}\right\}^2} \frac{k^3\kappa^5}{p_0^{10}} \cos^2\theta. \quad (17 S)$$

In this case no nuclear spin changes are allowed owing to the assumed central character of the forces. The only effective initial states, therefore, are triplet states. For the transition to be allowed the mesons must be emitted in states of odd parity. The approximate formula (17 S) represents the emission of a p -wave meson, though some contributions from interference with higher angular momentum waves are included. The cross-section for scalar mesons increases more slowly just above the threshold than that for pseudo-scalar mesons which may be emitted in s -waves. However, with 345 MeV. protons (in the laboratory system) the two cross-sections have become comparable. If $g^2=f^2$ the pseudo-scalar total cross-section is about twice the scalar at this energy. In the forward direction, however, the differential scalar cross-section is larger than the pseudo-scalar one. The angular variation $\cos^2\theta$ of the cross-section for scalar mesons is more in accord with present experimental evidence than that for pseudo-scalar mesons, where interference between s - and d -waves leads to an approximate cancellation in the forward direction.

§ 4. TRANSITIONS TO CONTINUOUS STATES.

The transitions to the continuous final states of the proton-neutron system can be treated in a manner very similar to that applied in the discrete case. In the energy region considered the relative motion of neutron and proton in the final state is very slow, so that it will be sufficient to deal only with final S-states of the neutron-proton system. For pseudo-scalar mesons the final S-states of the n - p system can be reached either from the odd initial triplet states under emission of an even parity meson, or from the even initial singlet states with emission of an odd parity meson. The 1S final states can only be reached from initial triplet states, the transition $^1S \rightarrow ^1S$ being totally forbidden. The contribution to the total cross-section from transitions to the final nucleon 1S -states will be found to be negligible. For scalar mesons the only allowed transitions are triplet-triplet and singlet-singlet transitions, the latter giving a negligible contribution.

Turning to the detailed treatment of the case of pseudo-scalar mesons we deal first with transitions to the final triplet states. The matrix elements may be calculated as in the previous section. The integrals can be taken over, provided that v_f is normalized so that

$$v_f \sim (1/pr) \sin(pr + \delta) \quad (18)$$

asymptotically, where p denotes the momentum of relative motion of the nucleons in the final state. In the evaluation of I a transformation of the

type (10) is always made so that only the behaviour of v_f near the origin is important. In this region v_f can be adequately represented by the form of the ground-state solution

$$v_f = (N/r) \exp \left[-\frac{1}{2}(b-1)\kappa r \right] [1 - \exp(-\kappa r)].$$

The normalization factor N has to be derived from the asymptotic behaviour of the true continuous s -waves in a Hulthen potential. It is then found that

$$N = \frac{1}{\kappa} \left[\frac{b\pi \sinh 2\pi\alpha}{\alpha \{ \cosh 2\pi\alpha - \cos 2\pi\sqrt{(b-\alpha^2)} \}} \right]^{\frac{1}{2}}, \quad \dots \quad (19)$$

where $\alpha = p/\kappa$ and b has been defined in equation (16). In the region of interest we may simply put

$$N = (b\pi/\kappa p)^{\frac{1}{2}}, \quad \dots \quad (19^1)$$

and it is then found that

$$I(\mathbf{q}) = \frac{4}{p_0^4} \left(\frac{\pi^2 b^3 \kappa^3}{p} \right)^{\frac{1}{2}} F(\mathbf{q}), \quad \dots \quad (20)$$

where

$$F(\mathbf{q}) = \frac{p_0^{\frac{1}{2}}}{(p_0^2 - q^2) \left(p_0^2 + \frac{(b+1)^2 \kappa^2}{4} \right)}. \quad \dots \quad (20^1)$$

The differential cross-section for a transition to a final 3S state with the production of a meson in the energy interval ω to $\omega + d\omega$ is then given by

$$\begin{aligned} \frac{d\sigma}{d\omega d\Omega} = & \frac{f^2 b^3 k M \kappa^3}{V \mu^2 p_0^8} \left[\{ \mathbf{k}(F(\mathbf{p}_0 - \tfrac{1}{2}\mathbf{k}) - F(\mathbf{p}_0 - \tfrac{1}{2}\mathbf{k})) \right. \\ & \left. + \frac{\omega}{M} \mathbf{p}_0(F(\mathbf{p}_0 + \tfrac{1}{2}\mathbf{k}) + F(\mathbf{p}_0 - \tfrac{1}{2}\mathbf{k})) \}^2 + 2k^2 \left(\frac{\Delta J}{J} \right)^2 F(\mathbf{p}_0)^2 \right]. \quad (21 P) \end{aligned}$$

Using the same approximation as in the treatment of the discrete state one obtains

$$\frac{d\sigma}{d\omega d\Omega} = \frac{4f^2}{V} \frac{b^3}{\left\{ 1 + \frac{(b+1)^2 \kappa^2}{4p_0^2} \right\}^2} \frac{k\kappa^3 \omega}{\mu^2 p_0^6} \left\{ \frac{\omega}{M} - 4 \frac{k^2}{p_0^2} \cos^2 \theta + \frac{2k^2 M}{p_0^2 \omega} \left(\frac{\Delta J}{J} \right)^2 \right\}. \quad (22 P)$$

The result exhibits the same tendency towards cancellation in the forward direction as was found for the cross-section in the discrete case.

Transitions to the final 1S states can be similarly treated. The resulting cross-section, however, as is evident from equation (22 P), is proportional to the cube of the well depth of the final state. This reduces the contributions from singlet transitions by a factor of at least 8 and as a result they may be neglected in calculations of the present approximate character.

In the case of scalar mesons the same method leads to a cross-section

$$\frac{d\sigma}{d\omega d\Omega} = \frac{3g^2 b^3 k \kappa^3 M}{2V p_0^8} \{ F(\mathbf{p}_0 + \tfrac{1}{2}\mathbf{k}) - F(\mathbf{p}_0 - \tfrac{1}{2}\mathbf{k}) \}^2, \quad \dots \quad (21 S)$$

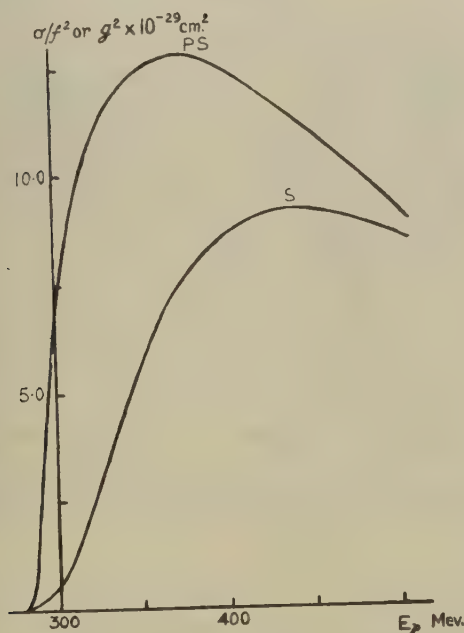
which can be approximated by

$$\frac{d\sigma}{d\omega d\Omega} = 24 \frac{g^2}{V} \frac{b^3}{\left\{1 + \frac{(b+1)^2 \kappa^2}{4p_0^2}\right\}^2} \frac{k^3 \kappa^3 M}{p_0^{10}} \cos^2 \theta. \quad (22S)$$

§5. NUMERICAL RESULTS.

We have first calculated the variation of the total cross-section for the production of scalar and pseudo-scalar mesons in a transition to the ground-state of the deuteron as a function of the energy of the incident proton in

Fig. 1.



The cross-sections for meson production, scalar and pseudo-scalar, in proton-proton collisions against energies of incident proton, in cases where final nucleons form a bound system.

the laboratory system. The results are shown in fig. 1. Corresponding to the possibility of production of the mesons in an s -state the cross-section for pseudo-scalar mesons is considerably higher near the threshold ($E_p=290$ MeV.). A maximum is reached at $E_p=370$ MeV. At $E_p=350$ MeV., $\sigma_{sc} \simeq 5g^2 \times 10^{-29} \text{ cm}^2$, $\sigma_{ps} \simeq 12f^2 \times 10^{-29} \text{ cm}^2$. It has already been noted that the results are rather dependent on the internucleon

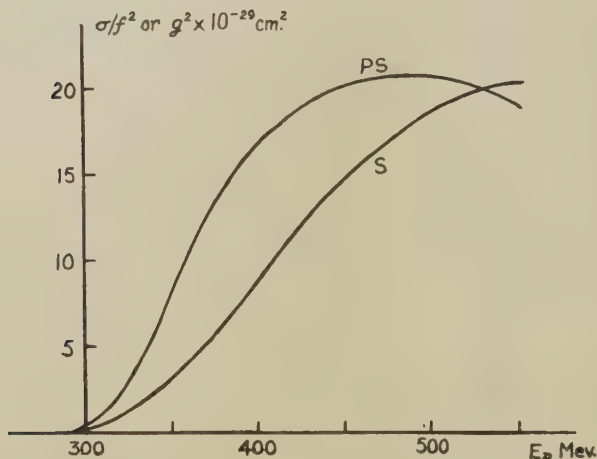
well shape. For comparison these cross-sections have also been evaluated for a square well potential

$$^{(3)}J=41 \text{ MeV.}; \quad a=1.85 \times 10^{-13} \text{ cm.}$$

and yield results smaller by a factor 1/25.

Fig. 2 represents the energy dependence of the integrated total cross-section for transitions to the continuous part of the deuteron spectrum. The result in each case naturally increases more slowly above the threshold than in the discrete case. At $E_p=350 \text{ MeV. approx.}$ —the energy of the Berkeley experiments— σ_{cont} is about half of σ_{disc} for scalar mesons and about $\frac{2}{3}$ for pseudo-scalar mesons. The fall in the continuous cross-section

Fig. 2.



The integrated cross-sections for meson production in proton-proton collisions against energies of incident proton, in cases where final neutron-proton system is in a continuous state.

indicated in fig. 1 should not be taken too seriously. At these energies higher angular momentum contributions as well as higher order corrections to the meson field must be considered. The ratio of the continuous to the discrete cross-section is consistent with experiment for both types of meson.

The transformation to the laboratory system has the effect of throwing more mesons into the forward direction. We shall now denote by k' , ω' , θ' , the momentum, energy and the angle at which the meson is emitted in the centre of mass system and by k , ω and θ , the corresponding quantities in the laboratory system. Taking, for example, the differential cross-section for the production of scalar discrete mesons to be

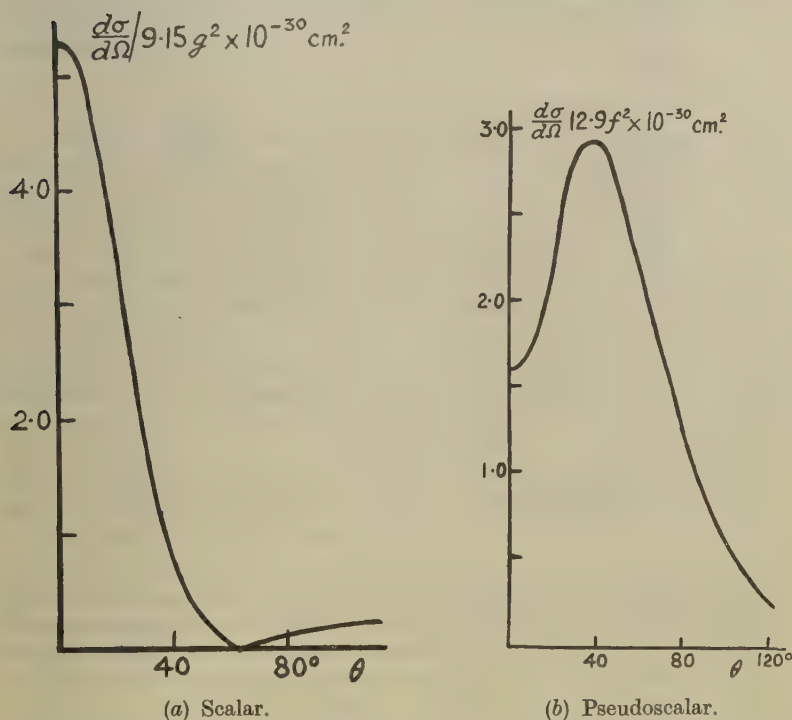
$$d\sigma/d\Omega' = A \cos^2 \theta'$$

in the centre of mass system, the corresponding cross-section in the laboratory system is

$$d\sigma/d\Omega = A\gamma \frac{k^2}{k'^3} \frac{(k \cos \theta - v\omega)^2}{(k - v\omega \cos \theta)^2},$$

where v is the relative velocity of the two frames of reference and $\gamma = (1 - v^2)^{-1/2}$. The results have been evaluated for incident 350 MeV. protons for the production of both types of mesons. They are shown in fig. 3. The cross-section for scalar mesons is strongly peaked in the forward

Fig. 3.



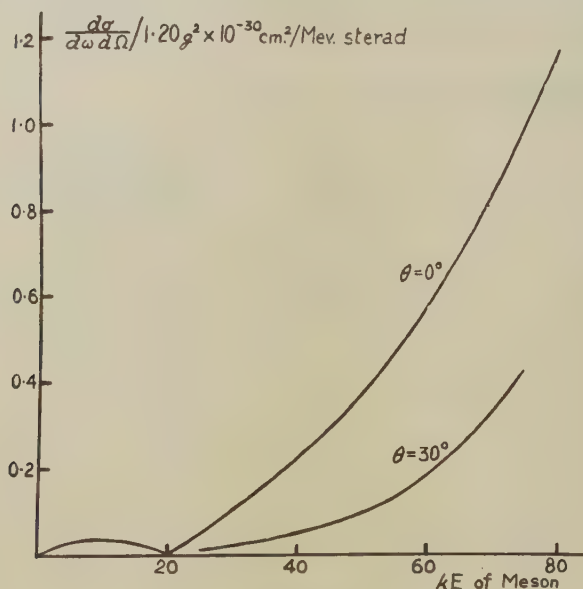
Variation of the differential cross-section for meson production with the angle of emission of the meson, in laboratory system, is shown for incident 350 MeV. protons and mesons of maximum energy.

direction where it obtains its maximum value of $49g^2 \times 10^{-30} \text{ cm.}^2/\text{sterad.}$ The cancellation in the forward direction for pseudo-scalar mesons is still apparent in the laboratory system. The maximum of the angular distribution of $39f^2 \times 10^{-30} \text{ cm.}^2/\text{sterad.}$ is reached at an angle of between 30° and 40° .

The determination of the continuous contributions in the laboratory system is more laborious. In fig. 4 $d\sigma/d\omega d\Omega$ is plotted against the kinetic energy for scalar mesons—assuming a proton energy of 350 MeV. for observations at 0° and 30° . The differential cross-sections are both peaked towards the upper end favouring high meson energies. Integrating over all energies we find at 0° ,

$$\frac{d\sigma}{d\Omega} = 32g^2 \times 10^{-30} \text{ cm.}^2/\text{sterad. and at } 30^\circ, \frac{d\sigma}{d\Omega} = 3.4g^2 \times 10^{-30} \text{ cm.}^2/\text{sterad.}$$

Fig. 4.



The cross-section per sterad. per unit energy is shown against the kinetic energy of the emitted scalar meson in the forward direction and at 30° to the beam of incident 350 MeV. protons. The differential cross-section in angle falls off rapidly from the forward direction as the results show, *e.g.*

$$\left(\frac{d\sigma}{d\Omega}\right)_{30^\circ} \sim \frac{1}{10} \left(\frac{d\sigma}{d\Omega}\right)_{0^\circ}$$

The cross-section falls away very rapidly from the forward direction. Pseudo-scalar mesons show a very differently shaped differential cross-section, approximately proportional to $(\omega - \mu)^{\frac{1}{2}}$ so that there is not the same favouring of high meson energies. The approximate integrated contributions to the differential cross-section are for pseudo-scalar mesons

$$\text{at } \theta = 0, \quad \frac{d\sigma}{d\Omega} = 30f^2 \times 10^{-30} \text{ cm.}^2/\text{sterad,}$$

$$\theta = 30^\circ, \quad \frac{d\sigma}{d\Omega} = 20f^2 \times 10^{-30} \text{ cm.}^2/\text{sterad.}$$

Recent experiments have all been carried out with 345 MeV. protons and so the correct dependence of the cross-sections on energy cannot yet be discussed. The angular distributions at this energy can, however, be compared with experiment as cross-sections have been reported at angles 0° , 18° and 30° to the beam. Agreement appears possible only with a $\cos^2\theta$ type of distribution at these angles, and so favours scalar rather than pseudo-scalar type mesons. Also the marked peak in the continuous spectrum at high meson energies is predicted by scalar theory.

The forward cross-sections appear to require rather a large coupling constant ($g^2 \simeq 3$, $f^2 \simeq 5$). However these cross-sections are rather susceptible to fine changes in shape and size of the nuclear well. It is perhaps also of interest to note that Brueckner (1950) found $f^2 \simeq 0.2$ to fit the observed meson production by photons (assuming the mesons to be pseudo-scalar).

§6. CONCLUSIONS.

It has not been the purpose of this paper to give the most complete description possible of meson production with the use of all the available data on the n - p and p - p interactions. Rather, by means of relatively simple analytical approximations for the potentials, and by using approximate methods, we have shown how important it is, in the low energy region (say up to 500 MeV.), to take accurate account of the nucleon wave functions. In this region indeed allowance for the detailed behaviour of the nucleons is likely to be more important than the inclusion of any field theoretical refinements. Increasingly at higher energies the neglect of higher order reactive terms from the meson field will affect the results and simultaneously the concept of internucleon potential will lose its validity. At the same time multiple meson production will begin affecting the results. We believe, however, that in the low energy region the methods applied in this paper should be expected to give at least qualitatively correct results.

If the use of Serber forces can be regarded as satisfactory then a considerable difference has been established between the behaviour of pseudo-scalar and scalar mesons. The angular distributions are quite different: for scalar mesons the distribution goes with $\cos^2\theta$ in the centre of mass system; for pseudo-scalar mesons the angular distribution though isotropic near the threshold has come nearer to a $\sin^2\theta$ law at the maximum of the total cross-sections. These results can only be fitted to present experimental evidence with the assumption of scalar mesons. It is interesting to compare this conclusion with that suggested by other meson processes. In making this comparison we disregard the information about the meson character which can be obtained from processes in which they are only involved as virtual particles—magnetic moments, nuclear forces, etc. This leaves the evidence from the production of mesons by photons, and from the various capture processes in hydrogen and deuterium. The first of these has recently been considered by Brueckner (1950), and his conclusions are decidedly against scalar mesons. The evidence from the capture processes is perhaps less certain. On the other

hand, we have made no exhaustive effort to discover how, by alteration of the internucleon potential—say by addition of spin orbit forces—the results for the pseudo-scalar meson theory in the present investigation might be affected.

One of us (E.A.P.) is indebted to the Department of Scientific and Industrial Research for a Maintenance Allowance during the tenure of which this work was carried out.

REFERENCES.

- BECKER, R., and LIEBFRIED, G., 1946, *Phys. Rev.*, **69**, 34.
BRUECKNER, K. A., 1950, *Phys. Rev.*, **79**, 641.
CARTWRIGHT, W. F., RICHMAN, C., WHITEHEAD, M. N., and WILCOX, H. A.,
1950 a, *Phys. Rev.*, **78**, 823 ; 1950 b, *Bull. Amer. Phys. Soc.*, **25**, 6, 9.
FOLDY, L. L., and MARSHAK, R. E., 1949, *Phys. Rev.*, **75**, 1493.
HEITLER, W., and PENG, H. W., 1943, *Proc. Roy. Irish Acad.*, **49** A, 101.
HEITLER, W., 1945, *Proc. Roy. Irish Acad.*, **50** A, 155.
HULTHÉN, L., 1942, *Arkiv. f. Mat. Ast. och Fysik*, **28** A, 5 ; **29** B, 1.
JACKSON, J. D., and BLATT, J. M., 1950, *Rev. Mod. Phys.*, **22**, 77.
MORETTE, C., 1949, *Phys. Rev.*, **76**, 1432.
PETERSON, V., ILOFF, E., and SHERMAN, D., 1950, *Bull. Amer. Phys. Soc.*, **25**,
6, 4.

LVII. *The Energy Loss of Slow Deuterons in Heavy Ice.*

By A. P. FRENCH,

Cavendish Laboratory, Cambridge

and

F. G. P. SEIDL,

Brookhaven National Laboratory, Upton, Long Island, U.S.A*.

[Received January 16, 1951.]

ABSTRACT.

A review is made of experimental evidence on the energy losses of protons and deuterons in materials of low atomic number, at energies below about 350 keV. The discrepancies between results of different experiments are discussed, and an attempt is made to arrive at a plausible curve of energy loss as a function of energy for deuterons in heavy ice at energies below 700 keV. The region 0–100 keV., which is of considerable interest in the study of the D–D reaction, is given special attention.

§1. INTRODUCTION.

In this paper we shall attempt to deduce, from existing experimental evidence, the rate of energy loss of deuterons in a D_2O (heavy ice) target, for the special case of very low bombarding energies (10 to 100 keV.). The determination of this quantity is of obvious importance in obtaining D+D reaction cross-sections from measured values of thick target yields.

There are not, in fact, any published data on energy losses in ice. The nearest approach to what we need is contained in a paper by Crenshaw (1942), who studied the energy loss of deuterons in water vapour. Unfortunately, however, the lowest energy at which he worked was 60 keV.; for information on the rather critical region of lower energies we have to look elsewhere. We propose to review the low-energy data first, obtaining from them a tentative energy-loss curve which can then be compared with Crenshaw's results over the region common to both.

Setting aside Crenshaw's work for the moment, the data most pertinent to our problem are contained in several papers by Gerthsen (1930 a & b) and his collaborators (Eckardt 1930, and Reusse 1932), concerning the energy loss of slow protons in various media (air, hydrogen and celluloid). Their results may be applied in the present case, provided that one makes the following assumptions:—

(a) That the rates of energy loss of a proton and a deuteron having the same velocity are identical in any medium.

(b) That the atomic stopping powers of H and D are identical.

(c) That the molecular stopping power of D_2O can be found by suitably combining the atomic stopping powers of two atoms of D and one atom of O

* Communicated by the Authors.

(d) That the stopping power of D_2O is independent of its physical state.

Although there has been no experimental verification of assumption (a) for the very lowest energies, Crenshaw (1942) found it to hold good between 60 keV. and 300 keV. deuteron energy ($\equiv 30$ keV. and 150 keV. proton energy) for energy losses in hydrogen. Moreover, it is a general principle that a proton and a deuteron having the same velocity will lose energy through electronic interactions at equal rates, whatever the exact nature of the energy loss process*. We shall therefore take it that this assumption is rigorously justified. In general we shall speak in terms of proton energies; any relation arrived at will then be true for deuterons of twice the energy.

With regard to (b), measurements have been made by Crenshaw (1942) and others (Joos 1942, Jussuf 1942, and Koops 1938) of the relative total amounts of ionization produced by protons and deuterons in hydrogen and deuterium gas. The sum total of the evidence is that a difference of ionizing effects, if it exists at all, is very slight, and becomes noticeable only at very low incident-particle velocities ($\sim 6 \cdot 10^7$ cm./sec.) corresponding to 2 keV. protons or 4 keV. deuterons. Thus, for proton or deuteron velocities greater than $6 \cdot 10^7$ cm./sec., one may consider the atomic stopping powers of H and D to be equal.

Assumption (c) has purposely been written in a rather vague form. At high energies the suitable combination appears to be simple addition. The molecular stopping power of a chemical compound is equal (to about 2 per cent) to the sum of the atomic stopping powers of its constituent atoms. This result, however, is based upon measurements with alpha particles, and for such energies the difference in stopping power due to differences of chemical binding is expected on theoretical grounds to be less than 1 per cent. (The problem is more fully discussed in a review article by Gray (1944).) The situation is markedly changed at the energies in which we are here interested, and according to Crenshaw's measurements the stopping power of D_2O is significantly less than one would obtain by adding the component atomic stopping powers. We shall defer a full discussion of this matter until later in the paper.

The evidence to support assumption (d) is practically non-existent. There are some grounds for believing that the stopping powers of a substance in solid and gaseous forms are equal, but this result again is for alpha particles, for which no significant difference is expected theoretically. (References and discussion may be found in Gray's paper†.) By assuming that the stopping power of heavy ice is equal to that of water vapour we therefore subject ourselves to some uncertainty.

After this general introduction to the problem we will proceed to a survey and analysis of the experiments of Gerthsen, Eckardt and Reusse.

* See, for example, Livingston and Bethe (1937), *Rev. Mod. Phys.*, **9**, 271.

† See also Wilkinson, 1948, *Proc. Camb. Phil. Soc.*, **44**, 114; Appleyard, 1949, 1949, *Nature, Lond.*, **163**, 526.

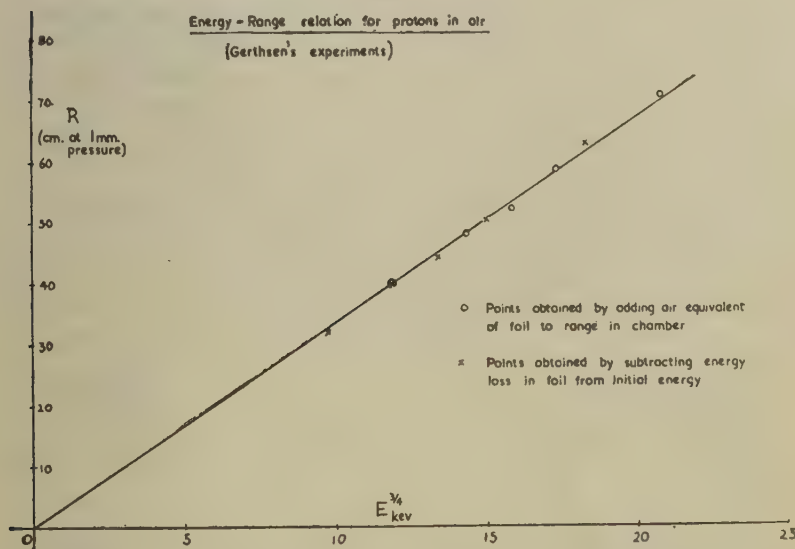
§2. THE ENERGY LOSS OF SLOW PROTONS IN MATTER.

The experiments on the loss of energy of protons in matter can be classed into two types, *integral* and *differential*. In the first type of experiment the total range in a gas of a proton of given initial energy is measured. This is the experiment described by Gerthsen (1930 a & b). His results are shown in fig. 1 for the case of protons in air. The ranges R are expressed in cms. of air at 1 mm. pressure Hg, and the proton energies E in keV. Gerthsen found (*cf.* fig. 1) that R as a function of E could be very closely represented by the formula

$$R = \alpha E^{3/4}. \quad (1)$$

We have applied a least-squares analysis to his data and have found that the results are better fitted if the power of E is 0.773; this difference,

Fig. 1.



however, is scarcely significant. Now the quantity of interest in determining the cross-section for a nuclear reaction is $-dE/dx$, the energy loss per unit distance in the target at a given energy. If we accept Gerthsen's formula, we have

$$-\frac{dE}{dx} = \frac{4}{3\alpha} E^{1/4} = \text{const. } v^{1/2}, \quad (2)$$

dE/dx as a function of velocity is plotted in fig. 2.

In the differential experiments the loss of velocity of protons in traversing a very small quantity of matter is directly observed. This is the type of experiment described by Eckardt (1930) and Reusse (1932). A proton beam was passed through celluloid films of various thicknesses Δx . For a given film the energy loss ΔE in passing through it was

measured as a function of the initial energy E . The results are shown in fig. 3. By considering the results for the various films one can find

Fig. 2.

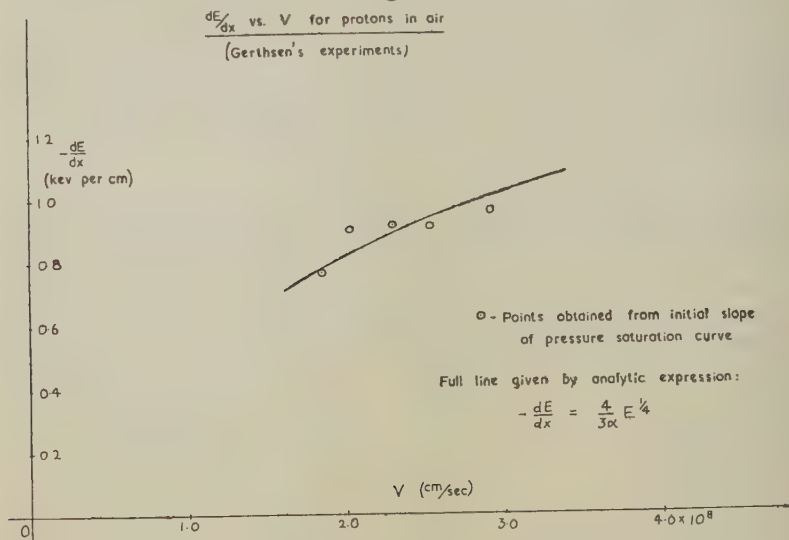
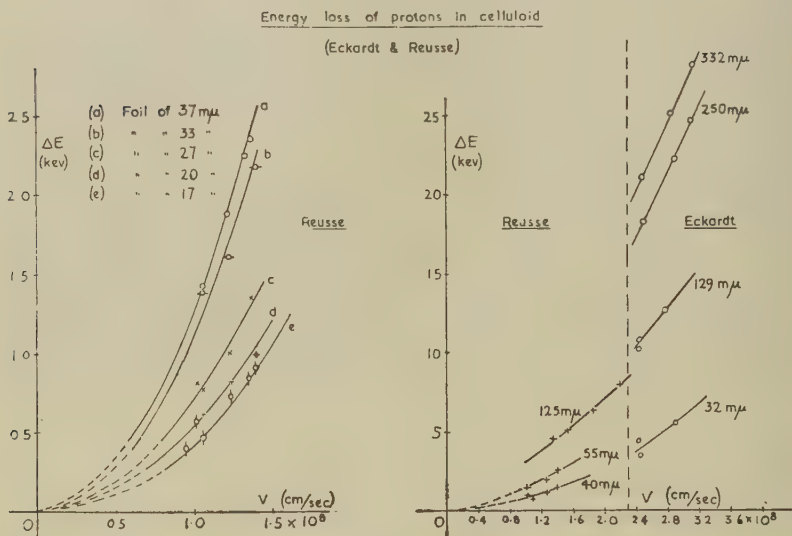


Fig. 3.



the magnitude of $\Delta E/\Delta x$ as a function of Δx for a given E . The relation between them is found to be linear, of the form

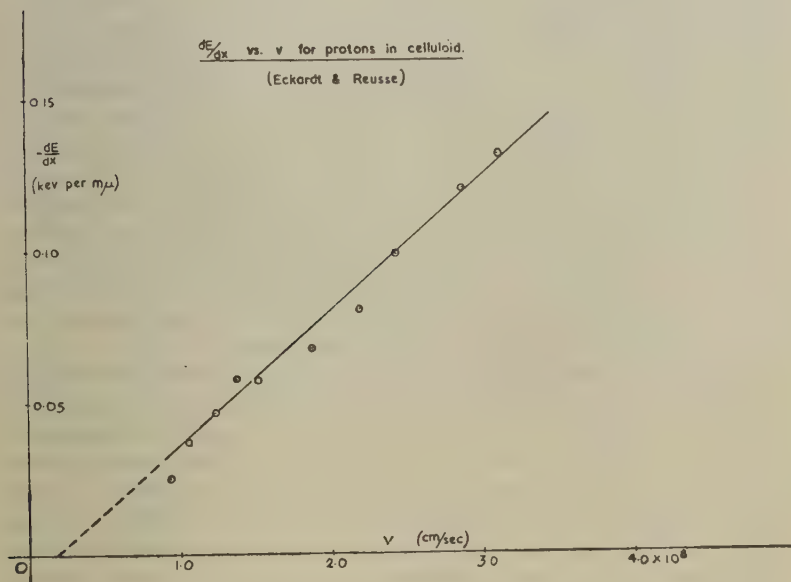
$$-\frac{\Delta E}{\Delta x} = a' - b' \Delta x. \quad \dots \dots \dots (3)$$

By extrapolating the line to zero film thickness one finds the value of dE/dx at the initial energy E . By performing this analysis for a series of values of E one can obtain dE/dx as a function of velocity. We have treated all of the data of Eckardt and Reusse in this way, using least-squares solutions throughout, and find that they are consistent with a relation

$$-\frac{dE}{dx} = \beta(v - v_0). \quad (4)$$

This is plotted in fig. 4.

Fig. 4.



The discrepancy between the results of Gerthsen (equation (2)) and of Eckardt and Reusse (equation (4)) is very striking. From the one experiment one finds that dE/dx is proportional to the velocity, from the other to its square root. It is true that the values of $\Delta E/\Delta x$, obtainable from the measurements of Eckardt and Reusse, lead more directly to a value for dE/dx than do Gerthsen's measurements of total range, but both experiments are open to criticism and merit more detailed consideration.

§3. THE EXPERIMENT OF GERTHSEN.

A proton beam generated in a canal-ray tube was magnetically analysed and passed through a thin celluloid window situated at the centre of curvature of a hemispherical ionization chamber. The thickness of the window was $80\ m\mu$ ($1\ m\mu = 10^{-6}\ \text{mm.} = 10\ \text{A.U.}$). The ionization chamber could be filled to any desired pressure (up to a few cms. Hg) with air or H_2 . The positive ions produced by the protons in traversing the

chamber were collected on an electrode which was made negative with respect to the walls of the chamber. The charge collected in a given time was registered on an electrometer; a second electrometer recorded the charge carried by the primary beam entering the chamber. The ionization current was found to increase steadily with increasing gas pressure up to a certain critical pressure p_c and thereafter remained constant. At the pressure p_c the protons are just failing to reach the walls of the chamber, so that for this and higher pressures they lose their whole energy in the gas. If the radius of the chamber is ρ the proton range r at unit gas pressure is ρp_c .

Gerthsen's experiment consisted in measuring p_c for air and H_2 for several values of E between 27 and 57 keV. He found that the range in H_2 at all energies was 2.50 times the corresponding range in air, so that the same form of the energy-range relation must hold for protons in air and in H_2 . It is necessary to point out that the value of E was measured before the protons passed through the celluloid window. Gerthsen assumed that the window was equivalent to the same thickness δ of air at all energies, and calculated δ by considering the celluloid to be composed of hydrogen and "air-like" atoms. In this latter category he placed the C, N and O atoms which comprised 94.4 per cent by weight of the celluloid. δ was then added to each observed value of r to give the total range R . δ was about 10 per cent to 20 per cent of R , so that any error in its value could materially affect the final results.

There exists an additional way of evaluating dE/dx from Gerthsen's experiment, which he himself describes (1930 a). When the pressure in the ionization chamber was very low the ionization current was found to be a linear function of pressure. The slope of the current vs. pressure curve in this region gives directly the number of ion pairs, per mm. pressure of gas in the chamber, produced by the whole proton beam. Since the primary proton beam was simultaneously recorded, it is possible to state the number, n , of ion pairs per cm. of path, in gas at 1 mm. pressure, produced by one proton of energy E' , where E' is the energy of a proton after it has lost energy ΔE in traversing the celluloid foil. With the assumed value of δ , ΔE and thence E' could be calculated for various values of E .

To translate n into a rate of energy loss it is necessary to know the mean energy, W , required to produce an ion pair in the gas at the energy E' . Gerthsen could not determine W at a single energy, but by dividing the saturation current in the ion chamber by the current of primary protons, he could determine the total number N of ion pairs produced by a single proton of energy E' . The quotient E'/N then gave the average value of W over the energy range zero to E' . This ratio was found to be independent of the value of E' ; it was therefore assumed that W itself was independent of energy and equal to the constant quotient E'/N . (From our evaluation of the data we find $W=38$ eV. Gerthsen gives $W=35$ eV., but we have cause to suspect the values of E on which this is based—see below.)

The rate of energy loss, $-dE'/dx$, of a proton of energy E' is then given by the product nW (keV. per cm. of path at 1 mm. pressure).

Support for the assumed constancy of W is to be found in a paper of Joos (1942). He quotes an experiment in which the ratio E'/N for protons in H_2 is found constant for energies from 4 to 14 keV.

As Gerthsen has published his results, the values of dE/dx derived by this second method from his one experiment are very different from its values as derived from the first method mentioned earlier (dE/dx appears to be proportional to v , not to $v^{\frac{1}{2}}$ as required by equation (2)). Upon careful re-evaluation of the results we found that his values of ΔE , and hence of E' , were at variance with the integral energy-range relation (equation (1)). That is to say, the curve obtained by plotting $(r+\delta)$ against E does not coincide with the plot of r against $(E-\Delta E)$ if one uses the values of δ and ΔE postulated by Gerthsen. It would appear that the discrepancy may have arisen through numerical errors; in our own treatment of the data we have found that the values for dE/dx are essentially the same by either method of evaluation and satisfy the relation expressed by equation (2). (See fig. 2.) In determining ΔE we took the mean of values obtained by three different methods:—

(1) The method used by Gerthsen (1930 a.) (although our results differ from his and satisfy the integral energy-range relation).

(2) We assume that the loss of velocity, Δv , in the celluloid foil was independent of the energy of incidence E (a result found by Eckardt and Reusse, *v. inf.*) and accept Gerthsen's value for the air equivalent δ of the foil.

(3) We find directly from the data of Eckardt and Reusse the loss of energy suffered by a proton of various energies, E , in passing through a celluloid foil of 80μ thickness.

We consider that this point is sufficiently important to merit setting out the values obtained by the three methods, and this is done in Table I. below. One can see that the degree of concordance is quite satisfactory and gives some meaning to the average values of ΔE given in the last column:

TABLE I.

 ΔE keV.

E keV.	Method 1	Method 2	Method 3	Average
27.1	6.8	5.9	6.6	6.4
34.6	7.9	6.7	7.7	7.4
39.6	8.1	7.2	8.4	7.9
45	8.0	7.8	8.9	8.2
57	8.3	8.6	10.2	9.0

The outcome of Gerthsen's experiment would from this analysis appear to be that over the range 20 to 60 keV. the rate of energy loss of

protons in air or hydrogen is proportional to the square root of the velocity. The actual magnitude of this loss, in keV. per cm. of path in either gas at 1 mm. pressure, follows directly from the experimental results, and for air is given by

$$-\left(\frac{dE}{dx}\right)_{\text{air}} = (5.90 \pm 0.10) \times 10^{-5} v^{1/2} \text{ keV. per cm., with } v \text{ in cm./sec.}$$

§4. THE EXPERIMENTS OF ECKARDT AND REUSSE.

A proton beam generated in a canal-ray tube was accelerated through an additional potential drop and was then magnetically analysed. Protons or H_2^+ ions of a specified velocity were thus selected. The range of proton energies covered was from 4 to 50 keV. After passing through a thin celluloid film the protons were subjected to a further magnetic analysis in order to determine their velocity upon emergence. There was of course a spread of energy in the emergent beam, but the velocity at the peak of the distribution was measured as the significant one. The experiment was repeated for celluloid films of various thicknesses (from 20 to 330 μ).

It may be noted that the celluloid films were extremely thin, the thickest being only about 3000 A.U. Thus it was impossible to measure the thickness directly through the use of interference fringes. The method employed was (a) to note the change of interference colour when one of the thin films was placed over a relatively thick film of celluloid, or (b) to superpose portions cut from a single large foil until an interference colour was obtained. Unfortunately the account of the procedure as given by Eckardt (1930) is not very detailed, and its accuracy must remain open to question.

The conclusions reached by Eckardt and Reusse are (a) that for a given incident velocity, the loss of velocity in passing through a foil is proportional to its thickness, and (b) that in passing through a given foil the energy loss is a linear function of the incident velocity v . These results may be expressed by the following equations:

$$-\Delta v = a \Delta x, \quad \dots \dots \dots (5a)$$

$$-\Delta E = bv - c, \quad \dots \dots \dots (5b)$$

It will be noted that equations (5) are not the same as the equations (3) and (4) which we have used in evaluating dE/dx as a function of velocity. The two sets of equations may, however, be readily related. Suppose that the rate of energy loss is given by

$$-\frac{dE}{dx} = f(v), \quad \dots \dots \dots (6)$$

i. e. $-m v dv = f(v) dx$, where m = mass of proton.

$$\left. \begin{aligned} \text{Then } \Delta x &= -m \int_v^{v+\Delta v} \frac{v dv}{f(v)} = -m \int_v^{v+\Delta v} \phi'(v) dv, \quad \text{say,} \\ &= +m[\phi(v) - \phi(v + \Delta v)]. \end{aligned} \right\} \dots \dots (7)$$

If we accept equation (5a), we have

$$\Delta x = -\frac{1}{a} \Delta v, \text{ and hence the identity:}$$

$$-\frac{1}{a} \Delta v \equiv m[\phi(v) - \phi(v + \Delta v)] \\ = -m\phi'(v)\Delta v + \dots$$

Consequently $\phi(v) = +\frac{1}{am} = +\frac{v}{f(v)}$ (from (7))

so that $-\frac{dE}{dx} = amv$, from (6). (8)

Differentiating (8),

$$-\frac{d^2E}{dx^2} = am \frac{dv}{dx} = -a^2m, \text{ from (5a). (9)}$$

Now we may write $\Delta E \sim \frac{dE}{dx} \Delta x + \frac{1}{2} \frac{d^2E}{dx^2} (\Delta x)^2$, which by (8) and (9) becomes

$$-\frac{\Delta E}{\Delta x} \sim amv - \frac{1}{2}a^2m\Delta x$$

or $-\frac{\Delta E}{\Delta x} = \alpha_1 v - \alpha_2 \Delta x$, (10)

where $\alpha_1 v = -\frac{dE}{dx}$, and α_1 and α_2 are constants.

Equation (10) may be seen at once to express the results of both equation (3) and equation (5b)—to the former when v is fixed and Δx varies, to the latter when Δx is fixed and v varies.

The following table sets out some values of $\alpha_1 v (= -dE/dx)$, $\alpha_1 v/E^{1/2}$ and α_2 as we have calculated them by a least-squares analysis of the experimental data of Eckardt and Reusse:

TABLE II.

E keV.	$\alpha_1 v$ keV/ $m\mu$ of celluloid	$\alpha_1 v/E^{1/2}$	α_2
5.8	0.0395 ± 0.0062	0.0164 ± 0.0026	0.00018 ± 0.00008
10.2	0.0621 ± 0.0040	0.0195 ± 0.0013	0.00019 ± 0.00003
31	0.0890 ± 0.0059	0.0160 ± 0.0011	0.00009 ± 0.00001
44	0.1313 ± 0.0061	0.0198 ± 0.0009	0.00017 ± 0.00001

The fact that α_1 and α_2 are essentially independent of velocity may readily be seen. However, the value of $(\alpha_1^2 v^2)/(\alpha_2 E)$, which should be 4 (cf. equations (10)), is found from Table II. to be 2.4 ± 0.6 (approx.).

In comparing equation (8) with equation (4) we see that they are in agreement only if v_0 is set equal to zero. The discrepancy probably arises because we have made a more careful analysis of the data, using least-squares solutions throughout, than did Eckardt and Reusse. In this analysis the parameter v_0 appeared, but it is doubtful that the experiments in themselves are accurate enough to give v_0 any significance. In any case it is clear that the energy loss cannot cease at and below v_0 , as equation (4) would demand (v_0 corresponds to about 0.2 keV. proton energy).

The result of the experiments of Eckardt and Reusse is, therefore, that for protons traversing celluloid the rate of energy loss, $-dE/dx$, is a linear function of velocity. The quantitative expression of this relation is

$$-\left(\frac{dE}{dx}\right)_{\text{celluloid}} = (4.45 \pm 0.11) \times 10^{-2} (v \times 10^{-8} - 0.18) \text{ keV. per } m\mu \text{ with } v \text{ in cm./sec.}$$

The result is of use to our problem only if we can derive from it the absolute value of the rate of energy loss in air or in hydrogen, and thus, using our initial assumptions, find the energy loss in a layer of ice. It is important to attempt this conversion, since the celluloid measurements extend to much lower energies (4 keV.) than do the measurements on air and H_2 . We will therefore consider this matter in the next section.

§ 5. CONVERSION OF CELLULOID DATA TO AIR.

To convert $(dE/dx)_{\text{celluloid}}$ into $(dE/dx)_{\text{air}}$ two alternative methods are possible. The first method is briefly as follows: over the small range of velocities covered by Gerthsen, the plot of (dE/dx) vs. v (fig. 2) does not depart by more than about ± 10 per cent from the linear relation expressed by equation (4). If, therefore, one draws a straight line through these points, with an intercept at v_0 on the v axis, its slope is not likely to be in error by more than about ± 10 per cent. By comparing this slope with the slope of the corresponding line for the energy loss in celluloid (*cf.* fig. 4), one finds the number of cms. of air at 1 mm. pressure which are equivalent to 1 $m\mu$ of celluloid. The result of this comparison is

$$-\left(\frac{dE}{dx}\right)_{\text{air}} = (0.40 \pm 0.04)(v \times 10^{-8} - 0.18), \quad . . . \quad (11)$$

where v is in cm./sec. and $(dE/dx)_{\text{air}}$ is in keV. per cm. of air at 1 mm. pressure.

The second method is to assume, with Gerthsen, that celluloid may be considered as a combination of air and hydrogen. That is

$$\begin{aligned} \left(\frac{dE}{dx}\right)_{\text{celluloid}} &= A \left(\frac{dE}{dx}\right)_{\text{air}} + B \left(\frac{dE}{dx}\right)_{\text{H}_2} \\ &= (A + 0.4B) \cdot \left(\frac{dE}{dx}\right)_{\text{air}} \end{aligned}$$

The constants A and B may be evaluated from the composition and density of celluloid. For the density, which is not stated by Eckardt and Reusse, we have assumed a value of 1.48 gm./cm.³, which lies midway between the accepted limits of 1.35 and 1.60. We thus subject ourselves to a possible error of ± 10 per cent. Our estimate of $(dE/dx)_{\text{air}}$ by this means is

$$-\left(\frac{dE}{dx}\right)_{\text{air}} = (0.37 \pm 0.04)(v \times 10^{-8} - 0.18). \quad . \quad . \quad (12)$$

The striking agreement between (11) and (12) is heartening but probably fortuitous. We shall average them and so obtain, as the final outcome of the experiments of Eckardt and Reusse, the following relation for energy losses of protons in air between 4 and 50 keV.:

$$-\left(\frac{dE}{dx}\right)_{\text{air}} = (0.385 \pm 0.04)(v \times 10^{-8} - 0.18) \text{ keV. per cm. at 1 mm.}$$

We have now arrived at two expressions for the energy loss of protons in air, one from Gerthsen's experiments (formula in § 3) and the other from Eckardt and Reusse, above. Before converting these into energy losses in D₂O, we will discuss Crenshaw's work, on which the conversion will largely depend.

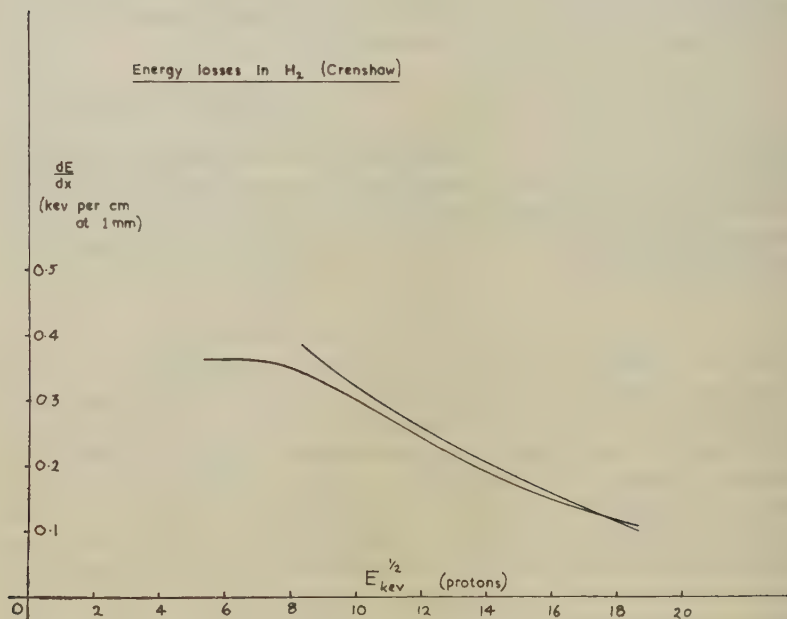
§ 6. THE EXPERIMENTS OF CRENSHAW.

We have already made several references to Crenshaw's paper, which describes a very useful study of the energy losses of hydrogen ions in air, H₂ and D₂, He and water vapour.

A resolved beam from a Cockcroft-Walton accelerator was passed through a series of small diaphragms into a chamber which could be filled to a few mm. pressure with a gas without impairing the vacuum in the acceleration tube. After traversing the chamber the beam passed once more into high vacuum through a second series of diaphragms. It was then bent by a magnet, and fell upon a fluorescent screen. The shift of the beam spot caused by the admission of gas to the retarding chamber was compensated by altering the magnetic field. Pairs of values of magnetic field with and without gas in the chamber were obtained for numerous values of initial beam energy, mostly between 60 and 340 keV. The initial energy was measured with a carefully calibrated resistance voltmeter. The energy loss was found from the change of magnetic field, this latter being itself calibrated in terms of the resistance voltmeter. The experiment was performed for several values of pressure in the retarding chamber, and was thus precisely analogous to the differential measurements on celluloid. The initial slope of a curve of ΔE vs. Δp led to the value of (dE/dx) . End effects in the retarding chamber, due to pressure gradients in the diaphragm systems, were eliminated by changing the distance between the entrance and exit systems.

The point most carefully studied in these experiments was the identity of energy losses by protons and deuterons in H_2 and D_2 . Some earlier work by Crenshaw and others (1942) had indicated a difference of energy losses in H_2 and D_2 , but this was not substantiated. Within the spread of the measurements (about ± 10 per cent at the highest energies and ± 5 per cent at the lowest) all four rates of energy loss were found to be equal for a given proton or deuteron velocity. After this had been established, further measurements on the energy losses of protons in

Fig. 5.



H_2 and D_2 were carried out. The results of these two investigations are shown graphically in fig. 5. For convenience, \sqrt{E} is used as abscissa, and (dE/dx) is in keV. per cm. at 1 mm. pressure.

The other aspect of Crenshaw's work which interests us here is his study of the stopping powers of hydrogen and water vapour relative to air. In fig. 6 we have plotted the stopping power of hydrogen relative to air over the range 40 keV. to 5 MeV. proton energy. In this graph the results of Gerthsen, Crenshaw and Bethe* are combined. It may be seen that a good smooth curve can be drawn through them, so that the ratio $S.P.(H_2)/S.P.(air)$ is well defined at all energies. We propose to

* Livingston and Bethe, 1937, *Rev. Mod. Phys.*, 9, 272.

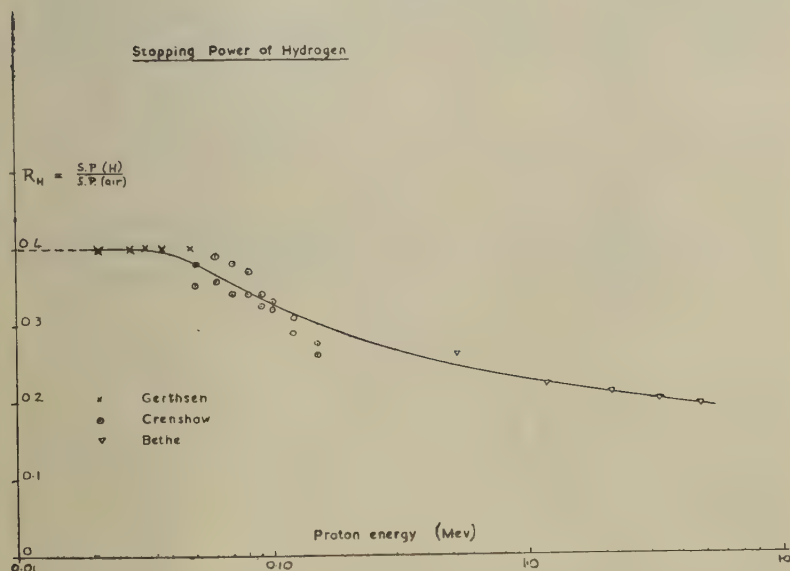
use this curve to obtain $S.P.(D_2O)/S.P.(H_2)$, and hence the energy loss in ice, in the following manner :

(1) We read off values of $S.P.(H_2)/S.P. (air)$ for various energies.

(2) We compute $S.P.(H_2O)/S.P. (air)$ from the relation

$$\begin{aligned}\frac{S.P.(H_2O)}{S.P. (air)} &= \frac{S.P. (H_2)}{S.P. (air)} + \frac{1}{2} \frac{S.P. (O_2)}{S.P. (air)} \\ &= \frac{S.P. (H_2)}{S.P. (air)} + 0.535.\end{aligned}$$

Fig. 6.



The figure 0.535 for oxygen is valid for alpha-particles near the end of their range*, and cannot be very seriously in error at lower energies. The smooth curve resulting from this is shown as A in fig. 7.

(3) We plot Crenshaw's own values of $S.P.(H_2O)/S.P.(air)$ also in fig. 7, and draw through them a line (B) parallel to the curve A of (2) above. This we take to be the true representation of $S.P.(D_2O)/S.P.(air)$. We consider this procedure is preferable to using Crenshaw's individual values of $S.P.(H_2O)/S.P.(air)$ as they stand, because it takes into account the probable trend of the stopping power with energy. With this curve we can now convert the results of Gerthsen, Eckardt and Reusse into energy losses in D_2O . (We may comment, parenthetically, that Crenshaw's

* Rutherford, Chadwick and Ellis, 1930, *Radiations from Radioactive Substances* (Cambridge: University Press), p. 97.

Fig. 7.

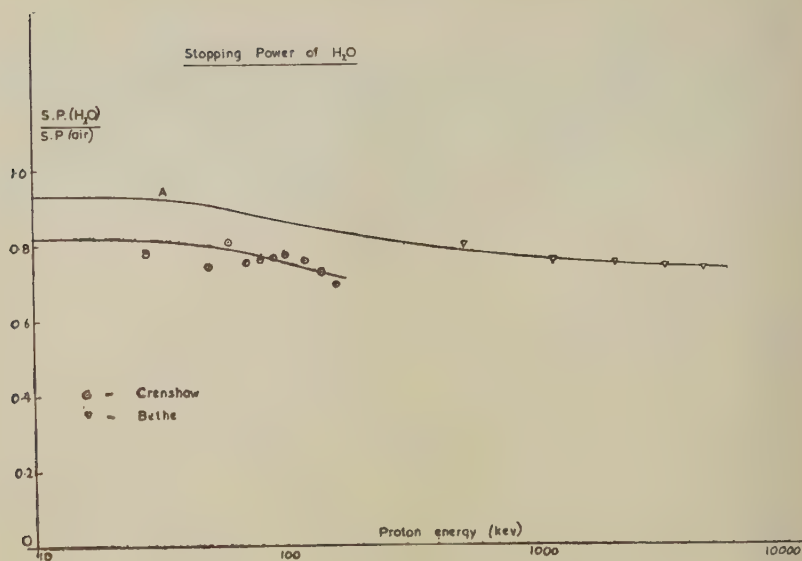
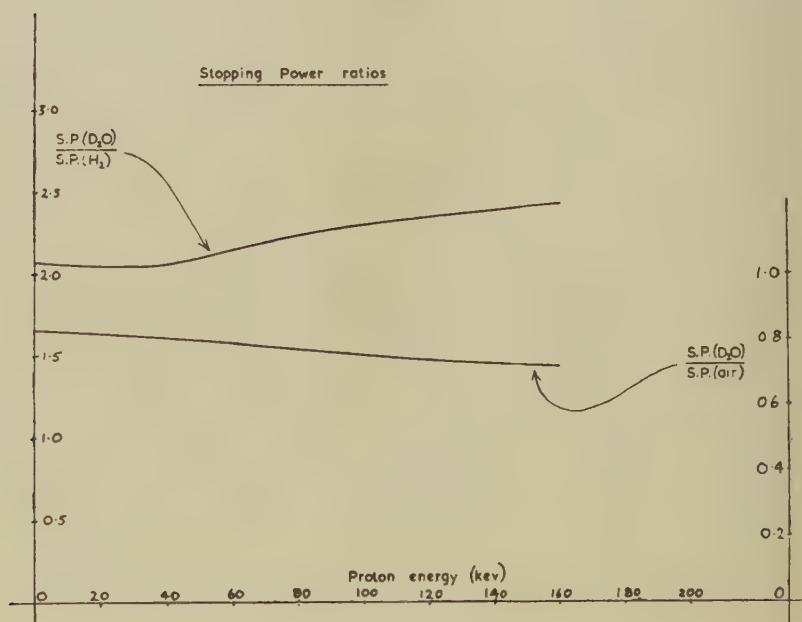


Fig. 8.



values of the stopping power of D_2O do seem surprisingly low, and cannot readily be joined to the computed curve at high energies. This, however, does not entitle us to ignore his results.)

(4) Using the curve of fig. 6 and curve B of fig. 7, we find the ratio

$$\frac{S.P.(D_2O)/S.P.(air)}{S.P.(H_2)/S.P.(air)} = S.P.(D_2O)/S.P.(H_2).$$

The resulting curve is shown in fig. 8. For completeness our final curve of $S.P.(D_2O)/S.P.(air)$ is also shown on this same graph.

(5) With the aid of our curve from (4), we can now convert Crenshaw's values (fig. 5) of energy losses in hydrogen into energy losses in D_2O .

The above procedure may seem unduly elaborate, but we consider that it extracts a maximum of significant data from Crenshaw's results. To use the measurements on water vapour alone would be to discard the largest and most carefully conducted section of his work.

§7. THE ENERGY LOSS IN ICE.

We now have five sets of measurements which we can adapt to our needs in obtaining a final version of the energy loss curve. They are :

- | | |
|-----------------------|---|
| 1. Gerthsen | Protons in air. 20 to 60 keV. |
| 2. Eckardt and Reusse | Protons in celluloid. 4 to 50 keV. |
| 3. Crenshaw | Protons and deuterons in H_2 and D_2 .
(Equivalent proton energy : 30 to 340 keV.) |
| 4. Crenshaw | Protons in H_2 and D_2 . 60 to 340 keV. |
| 5. Crenshaw. | Deuterons in H_2O .
(Equivalent proton energy : 50 to 170 keV.) |

Using the results of the previous section, we have converted the first four into energy losses in D_2O vapour. The fifth is brought into line by plotting the points as though they were obtained for protons of half the energy. Fig. 9 shows the collected values, as usual in keV. per cm. path at 1 mm. pressure. The broken line is our attempt to integrate the various data into a single curve for the energy loss of protons from zero energy up to 340 keV. The maximum deviation from any of the parent curves may be seen to be about 10 per cent, which we regard as tolerably satisfactory in view of the numerous assumptions that have gone into the analysis.

It remains only to make the final conversion into energy losses in ice, on the basis of our initial assumption (d) (§1). This we have done, with the supposition that both Gerthsen and Crenshaw conducted their experiments at a laboratory temperature of about $15^\circ C$. Under these conditions, one $cm.^3$ of D_2O vapour weighs 1.11 micrograms. Table III. below lists the values of (dE/dm) in keV. per microgram at representative points over the whole range of energies covered in this review. Fig. 10 presents the results as a smooth curve over the limited range 10–120 keV. deuteron energy. (Note that Table III. goes up to 700 keV. equivalent deuteron energy.)

Fig. 9.

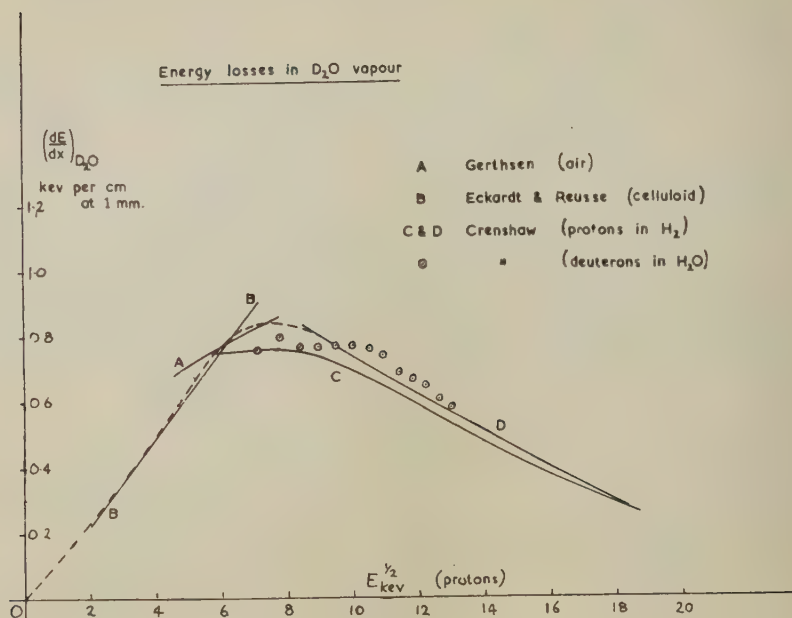
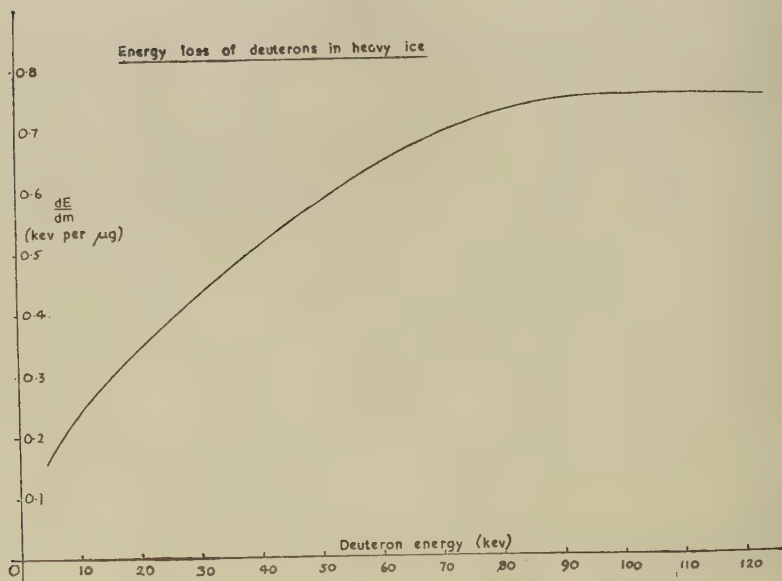


Fig. 10.



§ 8. CONCLUDING REMARKS.

Of the probable accuracy of the results given in Table III. we can say little. One might hope, taking an optimistic view, that they were good to ± 10 per cent, but we are after all confronted with complete uncertainty concerning the relative stopping powers of water vapour and ice. It is therefore of interest to mention a somewhat different approach to the problem.

The analysis presented in this paper was undertaken in order to deduce the cross-section of the $D(d, p)$ reaction, as a function of deuteron energy E , from measured values of thick target yields $N(E)$. In the original account (Bretscher and the authors 1948) of the experiments, values of both yields and cross-sections are given. The former are considered to be fairly accurate, but the latter were, by an oversight, obtained without reference to Crenshaw's work on energy losses, and the present analysis should lead to more significant values of cross-sections.

TABLE III.

$\sqrt{E_p}$	E_p keV.	(dE/dm) keV. μg	$\sqrt{E_p}$	E_p keV.	(dE/dm) keV. μg
2	4	0.211	11	121	0.608
3	9	0.325	12	144	0.556
4	16	0.451	13	169	0.506
5	25	0.580	14	196	0.455
6	36	0.700	15	225	0.407
7	49	0.753	16	256	0.356
8	64	0.748	17	289	0.300
9	81	0.712	18	324	0.262
10	100	0.660	18.7	350	0.230

This view has recently acquired support through the publication of results by Sanders, Moffatt and Roaf (1950). These workers obtained the $D+D$ cross-section at a given energy directly by employing thin targets. Thus one can in fact use their values of cross-section, combined with values of dN/dE from Bretscher, French and Seidl (1948) to deduce values of dE/dx . If we do this, we find almost perfect agreement with the curve of fig. 10 at the lowest energy, and a maximum divergence of about 15–20 per cent at the highest energy for which a comparison is possible. (The values of Table III. rise more steeply than they should in this region). Unfortunately the measurements of Sanders *et al.* do not go to a high enough energy to permit a comparison over the whole range of Table III., but the extent of agreement where the comparison is possible conforms rather well to the estimated accuracy of our values of dE/dx .

When more complete data on thin target yields are available, these can clearly be used to establish a more reliable energy-loss curve than that of fig. 10. In the meantime, however, it is hoped that our present range-energy relation may be of value. It should also be applicable to tritons in D_2O , subject to our initial assumption (a) that hydrogen nuclei with equal velocities lose energy at equal rates.

REFERENCES.

- BRETSCHER, FRENCH and SEIDL, 1948, *Phys. Rev.*, **73**, 815.
CRENSHAW, 1942, *Phys. Rev.*, **62**, 54.
CRENSHAW, YOUNG and MANNING, 1942, *Phys. Rev.*, **61**, 388.
ECKARDT, 1930, *Ann. d. Phys., Lpz.*, **5**, 401.
GERTHSEN, 1930 a, *Ann. d. Phys. (Lpz.)*, **5**, 657 ; 1930 b, *Phys. Zeits.*, **31**, 948.
GRAY, 1944, *Proc. Camb. Phil. Soc.*, **40**, 72.
JOOS, 1942, *Ann. d. Phys. (Lpz.)*, **41**, 426.
JUSSUF, 1942, *Ann. d. Phys. (Lpz.)*, **41**, 435.
KOOPS, 1938, *Ann. d. Phys. (Lpz.)*, **33**, 57.
REUSSE, 1932, *Ann. d. Phys. (Lpz.)*, **15**, 256.
SANDERS, MOFFATT and ROAF, 1950 a, *Bull. Am. Phys. Soc.* ; 1950 b, *Phys. Rev.*, **77**, 754.

LVIII. *The Photodisintegration of the Deuteron.*

By W. M. GIBSON,

H. H. Wills Physical Laboratory, University of Bristol
andT. GROTDAL, J. J. ORLIN and B. TRUMPY,
Fysisk Institutt, University of Bergen*.

[Received March 16, 1951.]

SUMMARY.

The photodisintegration of the deuteron has been observed in photographic plates exposed, while wet with heavy water, to the γ -rays arising from the bombardment of fluorine with 1.4 MeV. protons. Two groups of protons, produced by the known γ -ray lines at 6.15 MeV. and 7.01 MeV., have been clearly resolved. It is shown that γ -ray energies of this order of magnitude can be measured with a probable error of 0.05 MeV., and γ -ray lines with an energy difference of 0.6 MeV. can be resolved. Suggestions are made for a further improvement of the technique which should increase the resolving power of the method.

The angular distribution of the protons produced by each of the two γ -ray lines has been measured, but statistical uncertainties must be further reduced before any useful comparison with theory can be made.

§1. INTRODUCTION.

THE photo-disintegration of the deuteron into a neutron and a proton, one of the simplest of nuclear processes, has been the subject of many experimental and theoretical investigations. The importance of the study lies, first, in the fact that any theory must be able to give a detailed account of the cross section and angular distribution of the products of the interaction for photons of different quantum energy, and accurate observations of these characteristics should provide a stringent test of the validity of different theories; and, second, because the process makes it possible to determine γ -ray energies and thus provides a method for the investigation of γ -ray spectra.

At first sight it would appear that the reaction is particularly susceptible to detailed and accurate investigation. The absorption of the γ -ray leads to the production of only two product particles, a neutron and proton, which recoil from one another. Suppose the quantum energy and the direction of motion of the γ -ray to be known: its momentum is then defined, and the observation of the velocity of the recoiling proton is sufficient for the complete solution of the dynamics of the disintegration.

* Communicated by Professor C. F. Powell, F.R.S.

In practice, however, it has proved to be very difficult to make observations of sufficient precision. This is largely due to the very low cross section for the reaction, which is of the order of 10^{-27} cm.² for γ -rays of energy less than 20 MeV. As a result, competing nuclear processes can give rise, in some of the experimental conditions employed, to large numbers of protons which may be confused with those due to the disintegration of the deuteron; and in other experiments the proton tracks have to be distinguished against a dense background of electrons produced by Compton recoil or pair production.

In spite of these difficulties, the cross-section has been recently measured with a sufficient accuracy to provide a test of the validity of the various theories. Measurements have been made at quantum energies up to 2.76 MeV. by Bishop, Collie *et al.* (1950), and at a series of energies, ranging from 4.45 MeV. to 17.6 MeV. (2.2 MeV. to 15.4 MeV. above the threshold), by Wilkinson (1950). Theoretical calculations for these and higher energies have been made by Hansson and Hulthen (1949) and by Marshall and Guth (1949).

Information about the angular distribution of the emitted protons is, however, very limited. Rough determinations, at a number of energies, have shown that there are no serious divergences from the predictions of the various theories, but the observations are not sufficiently precise to provide a crucial test. For such experiments Phillips, Lawson and Kruger (1950) have employed a Wilson chamber containing heavy methane, CD₄, whilst other observers have detected the disintegration protons, emitted from solid or gaseous targets containing deuterium, by observing their tracks in neighbouring photographic plates. Most observations, however, have been made with the "target" deuterium atoms incorporated in sensitive photographic emulsions, a method first suggested by Powell (1940).

The use of emulsions "loaded" with deuterium has the advantage that, as in similar experiments with a Wilson chamber, the point of origin of a proton track can usually be accurately determined. Its length can therefore be measured with precision, and the inaccuracies which arise in experiments where the protons originate in a separate target of finite thickness can be eliminated. Further, the photographic method has an advantage over the expansion chamber, for these particular experiments, in being continuously sensitive. Whilst there are difficulties in applying the method to determinations of the absolute values of the cross-section for the reaction, it is well suited for making studies of the angular distributions.

In applying the photographic method to the present problem, the most important technical difficulty to be overcome is that of incorporating the deuterium in the plates in sufficient concentration and in the form of a suitable chemical compound. The maximum γ -ray flux which can be allowed to pass through the plate is limited by the maximum background fog, due to secondary electrons, which can be tolerated if the proton

tracks are to be distinguished. With this flux, and if the deuterium content of the plate is low, the number of disintegration protons per unit area is small and the work of searching the plate arduous. On the other hand, if the amount of loading material is large, there is a reduction in the quality of the proton tracks which leads to a reduction in the precision of the measurements of range; and the inaccuracies are accentuated by the increase in the shrinkage factor of the emulsion, which leads to larger errors in the determination of the angles of dip of tracks.

Several methods of "loading" an emulsion with deuterium have been employed: Gibson, Green and Livesey (1947) described experiments in which calcium nitrate, with about 6 per cent by weight of heavy water of crystallization, was incorporated in the emulsion, but this method has various disadvantages; the most important of these are that the calcium nitrate adversely affects the recording properties of the emulsion, and that the plates must be kept in hermetically sealed boxes to prevent water from the atmosphere taking the place of the heavy water in the emulsion.

Tests have been made with emulsions containing about 50 per cent by volume of hexa-deutero-diacetin, but although these appeared promising, their properties do not yet appear to have been described in the literature.

The method of loading most frequently employed has been to soak the emulsions in heavy water and to expose them to the γ -radiation while wet (Goldhaber 1948, Waffler and Younis 1949, Hough 1950). The most important advantage of this procedure is that it gives a plate containing a large and reproducible concentration of deuterium, so that the number of proton tracks per unit area is relatively large for a given amount of γ -ray blackening; but there are the corresponding disadvantages, mentioned above, associated with the greatly increased volume of the emulsion during exposure and its large shrinkage when processed. The effect on the quality of the tracks can now be overcome, at least in part, by the use of more sensitive emulsions, but the difficulty of the inaccuracies introduced in the measurements of the angles of dip remains.

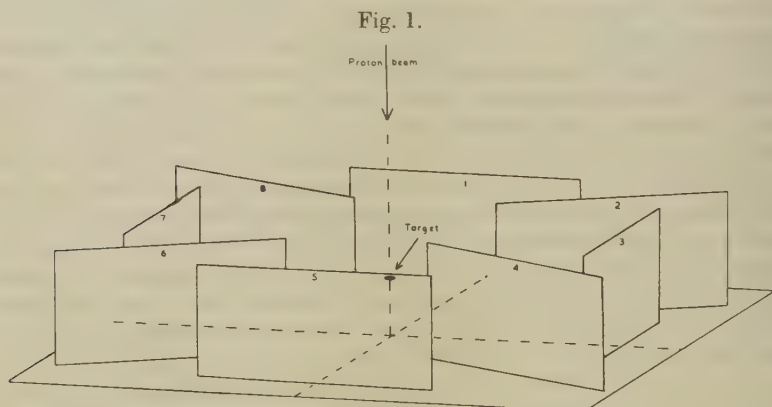
In the present paper it is shown that modern emulsions soaked in heavy water can be successfully employed for the measurement of γ -ray energies in the region of 6 MeV. with an accuracy of 0.05 MeV., and allow γ -ray lines with a separation of ~ 0.5 MeV. to be resolved. Secondly, results are described of experiments on the angular distribution of the protons produced in the disintegration of deuterons by 6.15 MeV. and 7.01 MeV. γ -rays, and methods for the further improvement of the measurements are discussed.

§ 2. IRRADIATION OF PLATES.

The γ -rays employed for the irradiation of the plates were produced by bombarding a thick target of calcium fluoride with 1.4 MeV. protons. The latter were accelerated by the 1.7 MeV. Van der Graaf generator, built for the University of Bergen from designs by O. Dahl and B. Trumpy, which came into operation in March 1950. The target was 5 mm. in

diameter, and eight plates were located with their centres 10 cm. from it and in a plane perpendicular to the proton beam. Four plates were orientated (see fig. 1) so that the γ -rays entered their surfaces at, or near, normal incidence, and the other four so that the mean angle of incidence was 15° . This disposition of the plates was based on the following considerations:—

The most accurate measurements of range are those made on tracks with small angles of dip. Further, for determining γ -ray energies, the most accurate results are obtained from the measurements on protons ejected at nearly 90° to the line of motion of the parent photon: for in such cases the momentum of the photon has little influence on the calculated energy of the neutron, which is nearly equal to that of the proton. For a given exposure the plates placed with their surfaces normal to the γ -ray flux yield the greatest number of tracks fulfilling these conditions, and they are therefore most suitable for the determination of the energy of the γ -radiation.



Arrangement of plates around target: plates 1, 3, 5, 7 received γ -rays approximately perpendicularly, plates 2, 4, 6, 8 obliquely; plates 1, 2, 3, 4, were soaked in D_2O , 5, 6, 7, 8 in H_2O .

On the other hand, the best conditions for the investigation of the angular distribution of the protons are provided by plates in which all angles of emission are observed with equal probability. If observations are confined to tracks with small angles of dip, these conditions are provided by allowing the γ -rays to pass nearly tangentially through the emulsion. For such experiments an angle of approach of 15° has been chosen to avoid appreciable reduction of the intensity of the radiation in passing obliquely through the walls of the containers and through the emulsions.

The plates were contained in boxes of thin brass securely bolted to a base-plate which was attached to the target-holder, so that the geometry

was well defined; there were no unnecessarily large masses of metal present, and the γ -rays before reaching the emulsion had to traverse not more than a few millimetres of brass.

An hour before the exposure, an Ilford C2 plate, 4 in. \times 2 in., with emulsion $200\ \mu$ thick, was placed in each box, and half the boxes were filled with D_2O and half with H_2O . After exposure, during which the total flux of protons to the target corresponded to the passage of 18 millicoulombs, the plates were dried to prevent fading of the latent image, and later processed by the "temperature development" method. This procedure was found to be more convenient than one in which processing commenced immediately after exposure.

Direct measurements with a micrometer showed that the ratio of the thicknesses of the emulsion during exposure and after processing and drying was 8.5 ± 0.5 .

§ 3. EXAMINATION OF PLATES.

A total of 943 tracks has been measured in one of the plates soaked in D_2O and exposed with the γ -rays entering at 15° . With some tracks it was impossible to be certain of the direction of motion of the proton, and these were rejected. It was confirmed that these tracks constituted a random sample, exceptional only because they were nearly rectilinear, the increased scattering commonly observed at the end of the range being not apparent. Their rejection therefore produced no effect on the measured distributions in energy or angle of the protons. For each of the 943 tracks the following quantities were measured:—

- (i.) the coordinates, x and y , of the point of origin of the proton in the plate;
- (ii.) the length, a , of its projection on a plane parallel to the surface of the emulsion, in units of length $0.85\ \mu$;
- (iii.) the difference in depth, h , in microns, of the beginning and end points of the track: this quantity, multiplied by 10, gives, in units of $0.85\ \mu$, the original difference in depth of these points at the time the track was formed, since the shrinkage factor is equal to 8.5;
- (iv.) the angle α (see fig. 2) between the direction of the projection of the track on the surface of the emulsion and a standard direction OX , usually chosen to correspond to one of the edges of the plate.

From these observations it is possible to calculate

- (v.) the angle of dip, δ , at the time of formation of the track: this angle is the mean inclination of the track, at the time of its formation, to the surface of the emulsion;
- (vi.) the true range of the proton in the wet emulsion, in units of $0.85\ \mu$;
- (vii.) two angles η and ϵ (see fig. 2) defining the direction of motion of the parent γ -ray and analogous to α and δ : η and ϵ are functions of x and y ;

(viii.) the angle θ between the direction of motion of the incident γ -ray and the projected proton. θ was directly determined from α , δ , η , and ϵ by a method of stereographic projection.

Fig. 2.

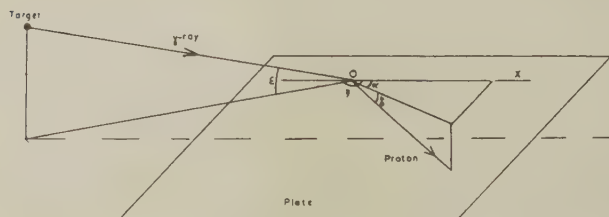
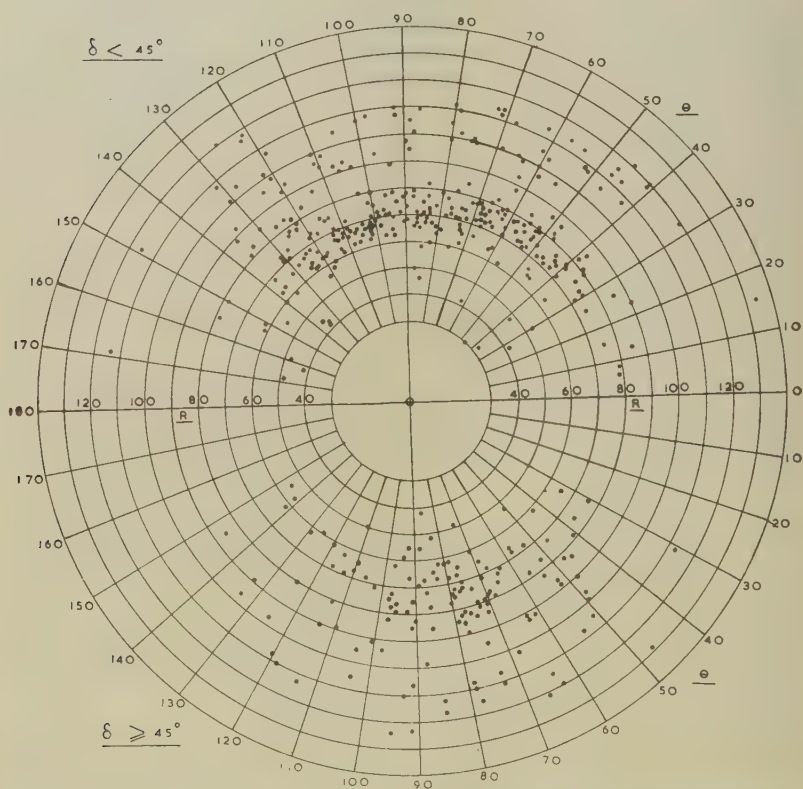


Diagram to show how α , δ , η , ϵ define the proton and γ -ray directions.

Fig. 3.



Plot of range R (one div. = 0.85μ) against laboratory angle θ . 425 tracks.

The results of the measurements for each track were plotted in a polar diagram showing R as a function of θ , those for which $\delta \geq 45^\circ$ being plotted separately from those for $\delta < 45^\circ$. In the most unfavourable conditions, corresponding to large values of δ , the errors in θ were sometimes as great as 5° , and in R five divisions. For $\delta < 45^\circ$ the probable errors in θ and R were 1.5° and one division respectively. A typical result for 425 tracks is shown in fig. 3.

§ 4. CALCULATIONS.

The distribution in energy of the γ -rays, and the angular distribution of the disintegration protons in a coordinate system—the C-system or centre of mass system—moving with the deuteron after the absorption of the γ -ray, were determined from the observed values of R and θ by the following method:

(a) Calculations of the stopping power to be expected for an emulsion saturated with D_2O , based on the range-energy relation for a normal emulsion (Rotblat 1951), and the data of Livingston and Bethe (1937), give, for the range-energy relation between 1.5 MeV. and 3 MeV.,

$$\left. \begin{aligned} R &= 19.3 E^{1.65} \text{ (in microns),} \\ \text{or} \quad R &= 22.7 E^{1.65} \text{ (in units of } 0.85 \mu\text{),} \end{aligned} \right\} \dots \dots (1)$$

where the energy E is measured in MeV.

(b) The dynamics of the photodisintegration of the deuteron give, for the energy, E_c , of the proton in the centre of mass system—to a very close approximation—the relation

$$E_c = E_L (1 - 0.102 \cos \theta) \dots \dots \dots (2)$$

where E_L is the observed energy of a proton emitted at an angle θ in the laboratory system of coordinates, the L-system.

Equations (1) and (2) together give for the range R_c , of a proton of energy E_c

$$R_c = R (1 - 0.168 \cos \theta),$$

where R is the observed range. R_c is also the expected observed range of a proton emitted at right angles to the direction of motion of the parent photon.

Now, to a close approximation, E_c is related to the γ -ray energy E_γ by the relation

$$E_c = \frac{1}{2} (E_\gamma - 2.202), \dots \dots \dots (4)$$

all energies being measured in MeV. It follows that, for any particular γ -ray energy, E_c and the corresponding range R_c may be calculated.

By means of the above relations a map was constructed on tracing paper showing lines corresponding to given values of E_γ on the polar diagram R, θ . These lines are defined by the relation

$$R (1 - 0.168 \cos \theta) = \text{constant},$$

and with a very small (calculable) error they are circles, of radius R_c , with centre at a distance of $0.168 R_c$ from the origin. They were drawn at intervals of 0.2 MeV. in the values of E_γ .

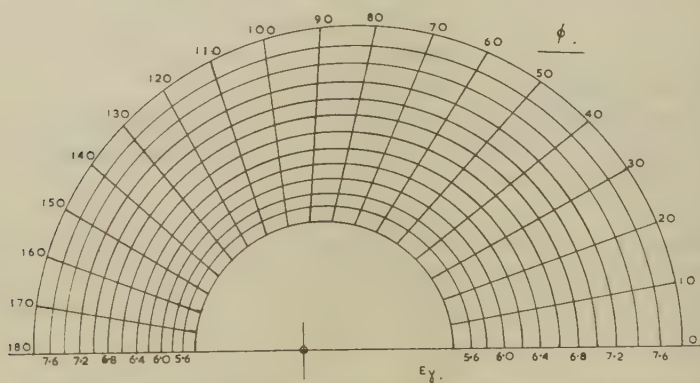
The mechanics of the reaction give, to an adequate approximation, $\tan \theta = \sin \phi / (\cos \phi + 0.051)$, where ϕ is the angle of emission of the proton in the C-system. From this relation lines of constant ϕ were drawn on the map at 10° intervals.

It may be noted that this map, reproduced in fig. 4, is completely independent of the measurements; it is based on theoretical calculation and well-established experimental facts, and no arbitrary parameters are involved.

§ 5. ENERGY DISTRIBUTIONS.

When the map was superimposed on the plots of the results, it was seen that the points were distributed in two clearly marked bands, corresponding to two photon energies very close to the accepted values for the γ -rays arising from the bombardment of fluorine with protons. The fact that in each plot the mean line through the points forming the more abundant band is so nearly parallel to the line for $E_\gamma = 6.15$ MeV. gives a

Fig. 4.



Map for obtaining γ -ray energy E_γ and centre of mass angle ϕ from R and θ .

very satisfactory check of the correctness of the calculations. The marked departure of the distribution of the experimental points in fig. 3 from circular symmetry is a direct demonstration of the momentum of the photon, and the agreement of the experimental distribution with that anticipated is a confirmation of the generally accepted relationship between momentum and energy for a particle of zero rest-mass.

Fig. 5 shows three plots of the distribution of the values of the energy of the γ -rays as deduced from the observations. They were obtained, for 0.2 MeV. intervals in the value of E_γ , by counting the numbers of experimental points between successive lines of constant E_γ . Fig. 5(a) is based on tracks with $\delta \geq 45^\circ$, and shows poor resolution because of the inaccuracies, resulting from the large shrinkage factor, in the determinations of the range of these tracks. Fig. 5(b) is based on tracks with $\delta < 45^\circ$, and gives clear evidence for the presence of two unresolved groups of different intensity. Fig. 5(c), which shows two completely separated

groups with mean energies 6.15 ± 0.05 MeV. and 7.06 ± 0.07 MeV., has been deduced from the tracks for which $\delta < 45^\circ$ and $60^\circ < \phi < 120^\circ$. Curves (b) and (c) presumably differ because the direction of motion of a small

Fig. 5.

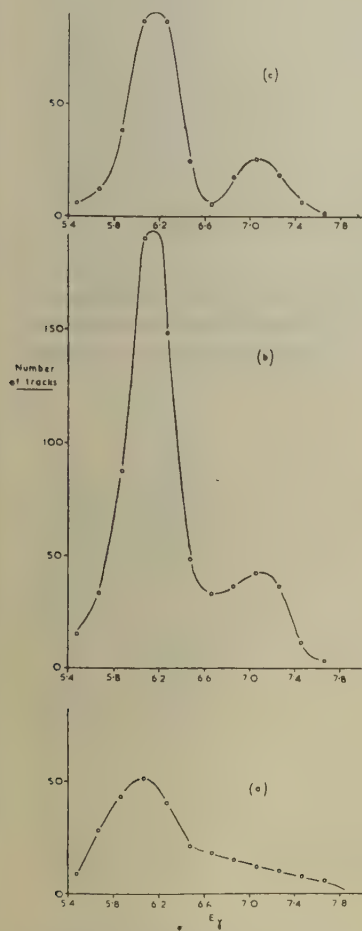
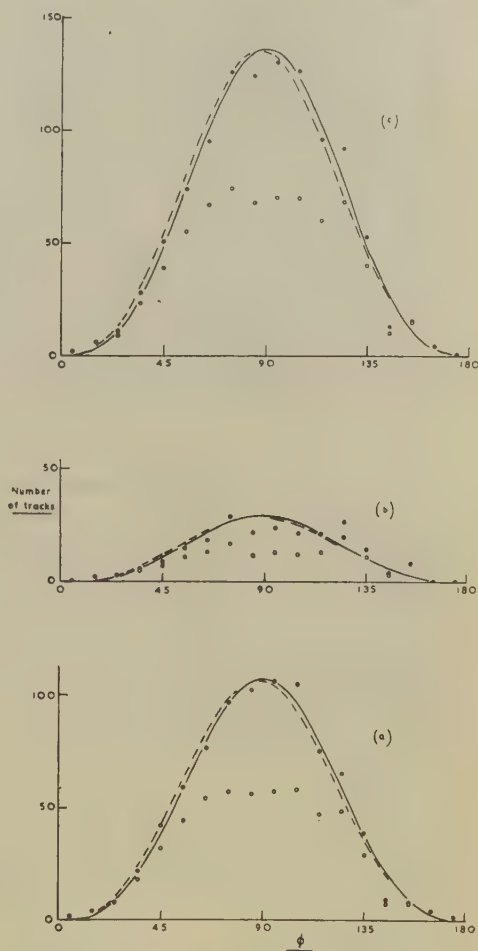


Fig. 6.



Numbers of tracks within 0.2 MeV. intervals of E_γ , plotted against E_γ ; (a) is based on tracks with angle of dip $\delta \geq 45^\circ$, (b) on tracks with $\delta < 45^\circ$, and (c) on tracks with $\delta < 45^\circ$ and $60^\circ < \phi < 120^\circ$.

Centre of mass angular distributions: circles represent observed numbers of tracks with $\delta < 45^\circ$, dots the numbers corrected for the effect of the limitation on the dip, full lines the distributions predicted by the simple theory, and broken lines the distributions predicted by the theory of Marshall and Guth. (a) is for the 6.15 MeV. group, (b) for the 7.01 MeV. group, and (c) for the two groups together.

proportion of the protons has been wrongly identified; for values of ϕ near to 90° such an error makes little difference to the calculated value of E_γ , but the resulting error is much greater if the value of ϕ is near 0° or 180° .

The γ -ray energies 6.15 ± 0.05 MeV. and 7.06 ± 0.07 MeV. are in good agreement with the values 6.15 MeV. and 7.01 MeV. which the energies measured by Rasmussen, Hornyak and Lauritsen (1950), together with the relative yields obtained by Bennett, Bonner, Mandeville and Watt (1946) for the various resonances in the disintegration of fluorine by protons, give for the mean energies of the γ -rays produced when 1.4 MeV. protons fall on a thick target containing fluorine. The close agreement for the 6.15 MeV. line shows that systematic errors are slight, and that the uncertainty arising from "straggling" of the proton ranges, and from inaccuracies of measurement and geometry, is not greater than our estimate of 0.05 MeV. Less accuracy is claimed for the figure 7.06 MeV., since it is based on relatively few tracks.

The degree of resolution of the two groups shown in fig. 5(c) indicates that it would be possible to observe as separate peaks two γ -ray lines of which the energies differed by as little as 0.6 MeV., and to infer the existence of a doublet even if the separation were considerably less than this value.

§ 6. ANGULAR DISTRIBUTIONS.

The lines of constant ϕ in the map shown in fig. 4 are used to obtain distributions of the observed tracks, corresponding to each of the two γ -ray lines, according to the angle of emission of the proton in the centre of mass system. The observed distribution with $\delta < 45^\circ$ is shown in fig. 6, together with the corrected results when account is taken of geometrical factors involved in limiting the tracks to those with angles of dip less than 45° . The total number after correction is slightly greater than the total number of tracks observed with all values of δ , a result which is to be expected in view of the difficulty of observing very steeply dipping tracks, and of their greater chance of escaping from the emulsion. It was calculated that the effect of escape on the angular distribution obtained from tracks with $\delta < 45^\circ$ would be negligible in comparison with the statistical uncertainties, so no correction has been applied for it.

Fig. 6 shows the expected angular distributions in the centre of mass system if the number of protons emitted per unit solid angle, at angle ϕ , were proportional to

(a) $\sin^2 \phi$;

(b) $a + \sin^2 \phi (1 + 2\beta \cos \phi)$, where β is the ratio of the velocity of the proton to that of light. (a) would result from a simple electric dipole interaction of the photon with the deuteron, and (b) if there were interference between electric dipole and quadrupole terms (Marshall and Guth 1949). The constant 'a' is related to the nature of the neutron-proton interaction, but it has a magnitude of only about 0.02 at this γ -ray energy, and makes very little difference to the shape of the curve.

It will be seen that our observed angular distributions are consistent with both (a) and (b); detailed examination of the results suggests that an increase of about a factor 4 in the number of measured tracks might reduce the statistical errors sufficiently to allow it to be shown whether or not this interference effect takes place.

CONCLUSION.

The results given above show that photographic plates soaked in heavy water are capable of giving useful information when used for measuring both γ -rays energies and the angular distributions of protons from the photodisintegration of deuterons. It would therefore be valuable to increase the ease and accuracy with which the measurements can be made, and to this end we are studying the use of plates exposed at right angles to the incident γ -rays and of more sensitive emulsions; the former would make it possible to observe a given number of tracks suitable for the accurate determination of γ -ray energy with less effort and calculation, and the latter would make the tracks themselves easier to find and would give more reliable measurements. This would probably more than offset any increase in the background due to electrons. Meanwhile, the statistical accuracy of the determinations of the angular distributions is being increased by the measurement of more tracks in plates exposed with the γ -rays entering obliquely.

ACKNOWLEDGMENTS.

Finally, we should like to express our thanks to all those who helped to make the exposures successful, to Miss J. A. Burnell and Miss M. J. Chapple for their valuable work at the microscope, to Dr. E. J. Burge for assistance with some of the calculations, and to Prof. C. F. Powell for his advice and encouragement.

We also wish to acknowledge the financial support of Norges Teknisk-Naturvitenskapelig Forskningsråd in the construction of the 1.7 MV. generator, and one of us (W. M. G.) is glad of this opportunity to record his sincere thanks for the hospitality which he received in Bergen.

REFERENCES.

- BENNETT, BONNER, MANDEVILLE and WATT, 1946, *Phys. Rev.*, **70**, 882.
BISHOP, COLLIE, HALBAN *et al.*, 1950, *Phys. Rev.*, **80**, 211.
FULLER, 1950, *Phys. Rev.*, **79**, 303.
GIBSON, GREEN, and LIVESEY, 1947, *Nature, Lond.*, **160**, 534.
GOLDHABER, 1948, *Phys. Rev.*, **74**, 1725.
HANSSON, and HULTHEN, 1949, *Phys. Rev.*, **76**, 1163.
HOUGH, 1950, *Phys. Rev.*, **80**, 1069.
LIVINGSTON and BETHE, 1937, *Rev. Mod. Phys.*, **9**, 245.
MARSHALL, and GUTH, 1949, *Phys. Rev.*, **76**, 1879, 1880; 1950, *Ibid.*, **78**, 738.
PHILLIPS, LAWSON, and KRUGER, 1950, *Phys. Rev.*, **80**, 326.
POWELL, 1940, *Nature, Lond.*, **145**, 155.
RASMUSSEN, HORNYAK, and LAURITSEN, 1950, *Phys. Rev.*, **77**, 617.
ROTLAT, 1951, *Nature, Lond.*, **167**, 550.
WAFFLER, and YOUNIS, 1949, *Helv. Phys. Acta*, **22**, 414.
WILKINSON, 1950, *Harwell Conference Report*.

LIX. CORRESPONDENCE.

Alpha-particles from the Proton Bombardment of Oxygen-18.

By J. SEED,

Cavendish Laboratory, Cambridge*.

[Received February 28, 1951.]

THE yield of alpha-particles from the reaction $^{18}\text{O}(p\alpha)^{15}\text{N}$ has been studied using protons of energies 490 to 960 keV. having an energy homogeneity of 0.5 per cent.

The alpha-particles emitted at an angle of 120° with the incident proton beam were analysed magnetically, and were detected by a thin zinc sulphide screen and E.M.I. photomultiplier.

The oxygen targets were in the form of thin layers of oxide on copper discs, and were prepared as follows: a polished copper target button was heated to redness *in vacuo* by means of an induction heater, and about 0.2 c.c. (at N.T.P.) of oxygen gas enriched about 30 times in ^{18}O was allowed to enter, so that the surface of the disc was thinly oxidized. The oxide film was hardly visible, and from the observed width of the $(p\alpha)$ group and known analyser resolution (4 per cent in energy), the target thickness was estimated to be about 5 keV. for 600 keV. protons.

The yield of alpha-particles from these copper oxide targets was studied as a function of incident proton energy by observing the maximum intensity of the alpha-particle group obtained in the analyser: this is justified because the resolution width of the analyser was greater than the natural width of the alpha-particle group, calculated from target thickness and beam homogeneity.

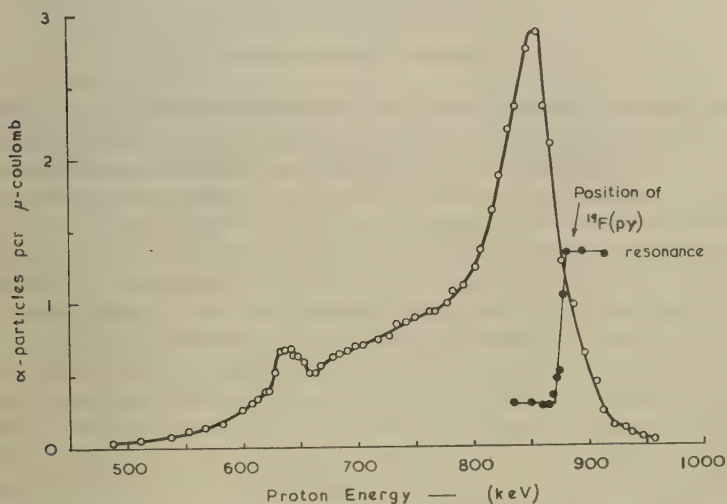
The excitation function, given in the figure, shows resonances at 640 and 850 keV. The former resonance is close to that found at 680 keV. by Mileikowsky and Pauli (1950), who studied the alpha-particles from the $^{18}\text{O}(p\alpha)$ reaction at an angle of 90° with the incident protons. The difference is larger than can be accounted for by error in the proton energy in the present experiment, for which the voltage scale of the high tension equipment was calibrated directly at 441.4 and 873.5 keV. by observation of the thick target γ -ray excitation functions of the reactions $^7\text{Li}(p\gamma)^8\text{Be}$ (Fowler and Lauritsen 1949), and $^{19}\text{F}(p, \alpha\gamma)^{16}\text{O}$ (Chao *et al.* 1950).

The magnetic analyser used in the present experiment was calibrated by observations on the alpha-particle and proton groups from the reactions $^9\text{Be}(d\alpha)^7\text{Li}$, $^9\text{Be}(d\alpha)^7\text{Li}^*$ ($Q=7.150 \pm 0.008$ MeV. and $Q=6.668 \pm 0.009$ MeV. respectively, Buechner and Strait 1949 and 1950 a) and $^{12}\text{C}(dp)^{13}\text{C}$

* Communicated by the Author.

($Q=2.716 \pm 0.005$), Buechner and Strait 1950 b). From measurement of the energy of the alpha-particle group from $^{18}\text{O}(p\alpha)$ at the 850 keV. resonance, a Q value of 3.96 ± 0.04 MeV. was obtained for the transition to the ^{15}N ground state, in confirmation of the values reported in the literature (Burcham and Smith 1939, Freeman 1950).

Taking this value for the energy release, the resonances at proton energies of 640 and 850 keV. would correspond to levels at 8.59 and 8.80 MeV. in the ^{19}F nucleus. No other reaction has yet given evidence of levels in ^{19}F in this region, though the reaction $^{18}\text{O}(pn)$ shows closely spaced levels at about 10 MeV. excitation: by analogy with similar nuclei (^{11}B , ^{15}N) having one particle less than an alpha-particle core, one would expect the ^{19}F nucleus to have a fairly large number of low-lying excited states.



Excitation function for the reaction $^{18}\text{O}(p\alpha)^{15}\text{N}$ taken at 120° , and showing the position of the 873.5 keV. resonance in the reaction $^{19}\text{F}(p\gamma)$.

A search for an alpha-particle group corresponding to transitions to excited states of ^{15}N was made using protons of energy 685, 837, and 957 keV. and of homogeneity 30 keV. No group of intensity greater than one-tenth of the main group at alpha-energies greater than 1.2 MeV. was found.

I wish to express my thanks to Dr. A. S. Baxter and Dr. A. P. French for help and advice during the experiment, and to Sir John Cockroft and his staff at the Atomic Energy Research Establishment, Harwell, for the gift of the enriched oxygen used in this work, also to the Department of Scientific and Industrial Research for a grant.

REFERENCES.

- BUECHNER, W. W., and STRAIT, E. N., 1949, *Phys. Rev.*, **76**, 1547; 1950 a, *Rev. Mod. Phys.*, **22**, 306; 1950 b, *Ibid.*, **22**, 331.
 BURCHAM, W. E., and SMITH, C. L., 1939, *Nature, Lond.*, **143**, 795.
 CHAO, C. V., TOLLESTRUP, A. V., FOWLER, W. A., and LAURITSEN, C. C., 1950, *Phys. Rev.*, **79**, 108.
 FOWLER, W. A., and LAURITSEN, C. C., 1949, *Phys. Rev.*, **76**, 314.
 FREEMAN, J. M., 1950, *Proc. Phys. Soc. A*, **63**, 668.
 MILEIKOWSKY, C., and PAULI, R. T., 1950, *Nature, Lond.*, **166**, 602.

The Isomeric State of RaE.

By N. FEATHER, F.R.S.,
 The University, Edinburgh†.

[Received March 16, 1951.]

THE published results of Neumann, Howland and Perlman (1950) already make it very probable that $^{210}_{83}\text{RaE}$ possesses an isomeric state which decays predominantly by α -disintegration, with disintegration energy 5.12 ± 0.05 MeV., to produce $^{206}_{81}\text{Tl}$ (4.2 m.). These authors concluded that the lifetime for α -emission from the isomeric state is greater than 25 years. They also indicated some of the difficulties in accounting for the facts, which they established, that RaF is not produced to the extent of more than 1 in 2000 disintegrations of RaE* (either directly by β -disintegration or indirectly through isomeric transition to RaE followed by β -disintegration), and that RaD is not produced to the extent of more than about 1 in 200 disintegrations (by electron capture). On the assumption that the α -disintegration of RaE* is to the ground state of $^{206}_{81}\text{Tl}$ —which leads to the smallest permissible value for the excitation energy of the isomeric state—they suggested that the chief difficulty lies in explaining the slowness of the isomeric transition $\text{RaE}^* \rightarrow \text{RaE}$. Even if this transition is of the fifth order they concluded that the excitation energy must lie very close to the lower limit of the experimentally deduced value of 0.18 ± 0.11 MeV. Moreover, in this connection it should not be forgotten that the nucleus $^{210}_{83}\text{RaE}$ is already known to possess at least three non-isomeric states in the range of excitation energies from 0 to 0.05 MeV. (Feather 1949).

Accepting a lifetime of the order of 100 years for α -emission, it is clear that the difficulty in explaining the slowness of the isomeric transition $\text{RaE}^* \rightarrow \text{RaE}$ is more acute than that regarding the competing β -disintegration $\text{RaE}^* \rightarrow \text{RaF}$. It being generally accepted that the normal β -disintegration of RaE is characterized by the spin change $2 \rightarrow 0$, reference to the revised Sargent diagram of Feather and Richardson (1948) indicates

† Communicated by the Author.

that β -disintegration from the isomeric state need not be characterized by a spin change of more than $5 \rightarrow 0$ in order to explain its non-observation. This would only require the change $5 \rightarrow 2$ (with or without change of parity) for the isomeric transition.

There are, however, some difficulties regarding the important assumption that the α -disintegration of RaE^* is to the ground state of $^{206}_{81}\text{Tl}$. The spin of this β -active state is likely to be 0 or 1, for the β -disintegration of $^{206}_{81}\text{Tl}$ is clearly allowed (Feather and Richardson 1948) and $^{206}_{82}\text{Pb}$ is generally regarded as having spin 0. On the above assumption, then, and accepting the conclusions which follow from it, we should expect the α -disintegration $^{210}_{83}\text{RaE}^* \rightarrow ^{206}_{81}\text{Tl}$ to be considerably less favoured than the parallel disintegration from the ground state RaE . The latter disintegration would be characterized by the spin change $2 \rightarrow 0(1)$, the former by the change $\geq 6 \rightarrow 0(1)$. Plainly contrary to this conclusion is the evidence from the Geiger-Nuttall diagram for $Z=83$ (Broda and Feather 1947). On the basis of this diagram the α -disintegration of RaE^* ($\tau \sim 100$ y.) appears more favoured, by a factor possibly as great as 10 (rather than less favoured by a factor of the order of 10^3) than the α -disintegration of RaE , due allowance being made for the difference in energy. It would appear that there are three possibilities of resolving this seeming contradiction:

- (i) the lifetime of RaE^* for α -emission may in fact be of the order of 10^5 to 10^6 y.;
- (ii) the β -disintegration of RaE^* may be to an isomeric state of $^{206}_{81}\text{Tl}$;
- (iii) the α -disintegration of RaE^* may be abnormal in the sense that it violates the general regularities exhibited in the Geiger-Nuttall diagram.

No doubt direct evidence concerning (i) will not long continue lacking, but, judging the present position it would appear surprising that the activity of RaE^* has been detected at all, if its lifetime is really as long as 10^5 y. Also, the longer the lifetime for α -emission, the smaller the experimental upper limit to the transition probability for the isomeric transition $\text{RaE}^* \rightarrow \text{RaE}$ and the larger the spin which has to be assigned to the isomeric state in order to explain its properties. Possibility (i), in fact, does not alone provide a satisfactory basis of resolution.

Possibility (ii) introduces similar difficulties. Since its acceptance leads inevitably to the conclusion that the excitation energy of the isomeric state RaE^* is greater than previously supposed, it likewise makes more difficult the problem of explaining the relative slowness of all processes, except α -disintegration, which lead to the de-excitation of this state. Again, an isomeric state of $^{206}_{81}\text{Tl}$ is hardly likely to have escaped detection in the experiments of Fajans and Voigt (1940) and Neumann *et al.* (1950).

Concerning possibility (iii), this would be realized formally if the effective nuclear radius of the isomeric state RaE^* were greater than that of the ground state RaE . Physically, however, the smallness of the

α -disintegration constants which characterize all ground-state nuclei having $Z=83$ (when these are compared with the α -disintegration constants of nuclei for which $Z \geq 84$) is most probably connected not so much with a real decrease in nuclear radius as Z decreases from 84 to 83 as with the difficulty of formation of the nascent α -particle when only one of its constituent protons is available in a loosely bound state ("outside" the closed shell of 82 protons). If possibility (iii) were to be interpreted in this way it would obviously imply that one of the properties of RaE^* , the isomeric state of the nucleus containing $(126+1)$ neutrons and $(82+1)$ protons, is that the intranuclear formation of an α -particle is less difficult in this state than it is in the ground state of the same system—or in any of the known non-isomeric states of any nucleus of proton number 83 and neutron number 128 or greater. This is a possibility of a type not hitherto considered in theories of α -disintegration.

REFERENCES.

- BRODA, E., and FEATHER, N., 1947, *Proc. Roy. Soc. A*, **190**, 20.
 FAJANS, K., and VOIGT, A. F., 1940, *Phys. Rev.*, **58**, 177.
 FEATHER, N., 1949, *Nucleonics*, **5**, 22.
 FEATHER, N., and RICHARDSON, H. O. W., 1948, *Proc. Phys. Soc.*, **61**, 452.
 NEUMANN, H. M., *et al.*, 1950, *Phys. Rev.*, **77**, 720.

An Example of the $(n, p; \pi^-)$ Reaction in the Photographic Emulsion.

By S. J. GOLDSACK and N. PAGE,
 University, Manchester*.

[Received March 9, 1951.]

[Plate XX.]

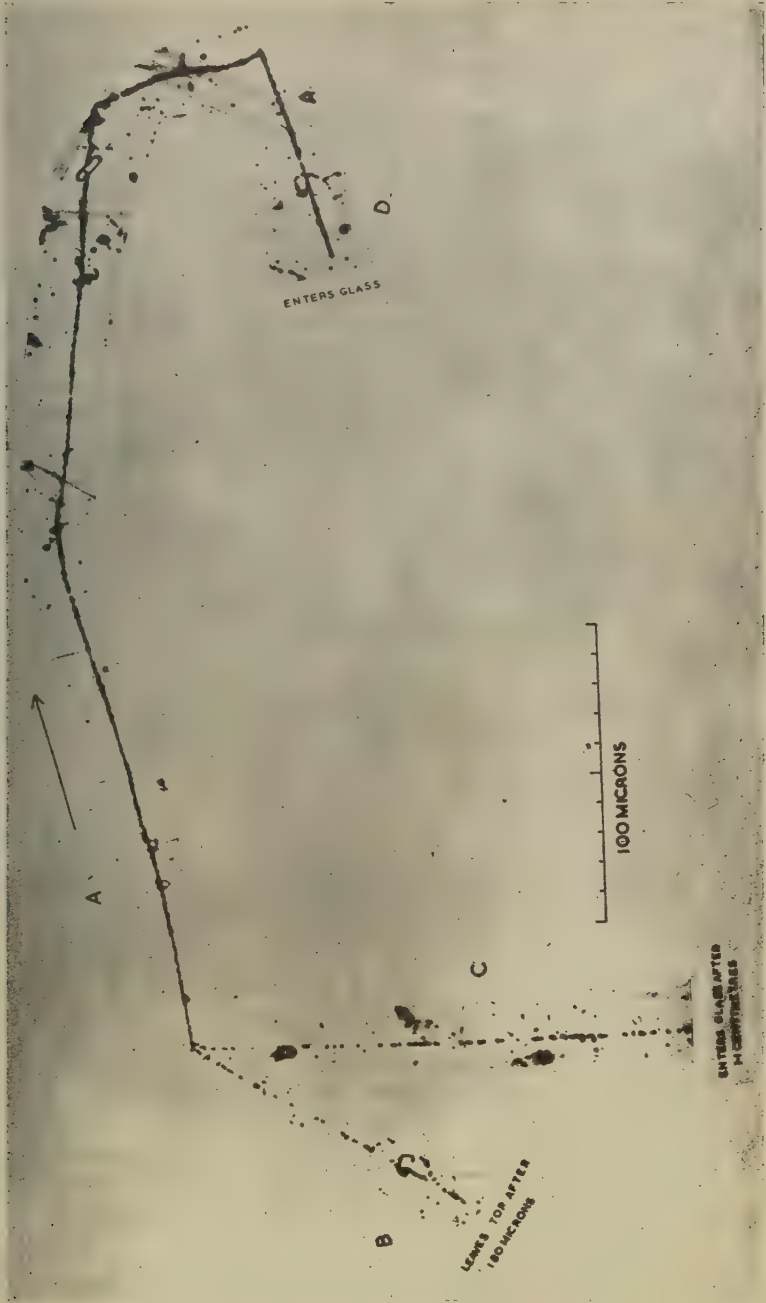
WE have recently found the event shown in Pl. XX. in a 400 micron thick Ilford G5 Nuclear Research Emulsion, exposed vertically for 21 days at an altitude of 2860 m. in a magnetic field of 34,000 gauss (Dilworth *et al.* 1950). The event is interpreted as the production of a π^- -meson (track A) in the collision of a high-energy, cosmic-ray neutron with a proton in the emulsion, according to the following scheme :



The technical details of the event are as follows. Track A is almost continuous throughout its length and shows marked scattering especially towards the right-hand end of the track where there are two sharp deflections. The grain density of the track increases noticeably from the

* Communicated by G. D. Rochester.

↑ Vertical
Fig. 1.



Observer: Mrs. J. Cunliffe.

centre of the star up to the second sharp deflection, but at this point there is a decrease in grain density and the track becomes quite straight (D). The grain density and scattering of track A are consistent with its having been produced by a slow meson (presumably a π^- -meson) moving to the right and producing a single-prong star (D) at the end of its range. The small scattering and high grain density of track D exclude the possibility of its being a μ^+ -meson arising from the decay of a positive π -meson. The range of the meson is 370μ corresponding to a kinetic energy of 3.6 MeV.

The meson is created in a star which has two lightly-ionizing particles (B and C) but no evaporation or recoil particles. The track B is only 180μ long and is therefore too short to be identified, but its grain density is near minimum. Minimum ionization in this plate corresponds to 34.2 ± 0.8 grains/ 100μ : track B has 37.0 ± 6.0 grains/ 100μ . Track C, which is 1.1 cm. long, has a grain density of 46.8 ± 0.7 grains/ 100μ and is therefore slightly above minimum. The small angle multiple scattering of this track has been measured by the method of Fowler (1950), and the arithmetic mean angle of scattering is $0.048 \pm 0.006^\circ/100\mu$ corresponding to a value of $p\beta = 700 \pm 85$ MeV./c.

The grain density of a proton showing this scattering should be 1.5 ± 0.15 times minimum. The particle is therefore identified as a proton, the kinetic energy being 400 ± 50 MeV., and the momentum 990 ± 120 MeV./c. This identification is confirmed by the sign of the magnetic deflection. The total deviation between the ends of the track is 1.23° . To this must be added a small correction for the distortion of the emulsion: measured by the method of Cosyns and Vanderhaeghe (1950), this proves to be $+0.05^\circ$. Assuming that the particle is moving downwards from the star, it is positive with a probability of 97 per cent.

It is clear that the equation (1) is the simplest interpretation of the event which is consistent with conservation of charge, the third particle being a knock-on proton, initially at rest in the emulsion.

If the particle B is a proton, its energy must be at least 650 MeV. and hence the kinetic energy of the incident neutron which produced the star must have been at least 1200 MeV.

Finally it is of interest to review the evidence for possible simple schemes for single meson production in nucleon-nucleon interactions. These are collected in Table I.

It is seen from the Table that at least six such reactions are possible all of which might be observed in the Ilford G5 emulsion. Events 1 and 2 can occur in collisions with hydrogen nuclei in the emulsion which, it is estimated, account for 4 per cent of the total geometrical cross section of the emulsion. All six events could occur in collisions with nucleons in the nuclei of heavier atoms in the emulsion, but in such cases an evaporation star or a nuclear recoil fragment would usually be observed. It is possible, however, that the two interacting nucleons might leave the nucleus without imparting an appreciable amount of energy to it.

Event 2 has been observed in the cloud chamber (Armenteros *et al.* 1951 a); two examples of type 3 occurring in Ilford G5 emulsion have been reported by Cosyns *et al.* (1949), and a similar event was produced in Ilford C2 emulsion using artificially produced neutrons from the Berkeley cyclotron (Smith *et al.* 1950). Armenteros *et al.* (1951 b) have pointed out that the event described by Hopper and Biswas (1950) and interpreted by them as an example of the decay of a neutral V particle similar to those found by Rochester and Butler (1947) and by Seriff *et al.* (1950) may be another example of this process.

At present it appears impossible to distinguish, in the emulsion, between high energy events of the types 3 and 4 b and the decay of V particles.

TABLE I.

Types of simple star involving the production of one meson.

Type	Incident Particle	Target Particle	Products	No. of prongs per star	References
1 (a)	Neutron	Proton	$p + p + \pi^-$	3	Present letter Armenteros <i>et al.</i> 1951 a Cosyns, <i>et al.</i> 1949 Smith, <i>et al.</i> 1950
(b)	Neutron	Proton	$n + n + \pi^+$	1	
2	Proton	Proton	$n + p + \pi^+$	3	
3	Neutron	Neutron	$n + p + \pi^-$	2	
4 (a)	Proton	Neutron	$p + p + \pi^-$	4	
(b)	Proton	Neutron	$n + n + \pi^+$	2	

REFERENCES.

- ARMENTEROS, R., BARKER, K. H., BUTLER, C. C., CACHON, A., and CHAPMAN, A. H., 1951 a, (private communication); 1951 b, *Nature, Lond.*, **167**, 501.
 COSYNS, M., DILWORTH, C. C., OCCHIALINI, G. P. S., and SCHÖNBERG, M., 1949, *Nature, Lond.*, **164**, 129.
 COSYNS, M., and VANDERHAEGHE, G., 1950, Note No. 15. *Bull. Cen. Phys. Nuc. de L'Université Libre de Bruxelles*.
 DILWORTH, C. C., GOLDSACK, S. J., GOLDSMIDT-CLERMONT, Y., and LEVY, F., 1950, *Phil. Mag.*, **41**, 1032.
 FOWLER, P. H., 1950, *Phil. Mag.*, **41**, 169.
 HOPPER, V. D., and BISWAS, S., 1950, *Phys. Rev.*, **80**, 1099.
 ROCHESTER, G. D., and BUTLER, C. C., 1947, *Nature, Lond.*, **160**, 855.
 SERIFF, A. J., LEIGHTON, R. B., HSIO, C., COWAN, E. W., and ANDERSON, C. D., 1950, *Phys. Rev.*, **78**, 290.
 SMITH, F. M., GARDNER, E., and BRADNER, H., 1950, *Phys. Rev.*, **77**, 562.

[The Editors do not hold themselves responsible for the views expressed by their correspondents.]

LX. *A Mechanism for the Growth of Deformation Twins in Crystals.*

By A. H. COTTRELL and B. A. BILBY,
Department of Metallurgy, University of Birmingham *.

[Received February 24, 1951.]

SUMMARY.

The principal difficulty in developing a dislocation theory of mechanical twinning has been to explain how a twin grows through a finite thickness of crystal. By extending the recent theory of slip bands, proposed by Frank and Read, it is possible to show that a dislocation can move steadily from plane to plane in a crystal. A theory of mechanical twinning, which is formally analogous to Frank's theory of crystal growth, can then be developed. The theory is applied to the body-centred and face-centred cubic lattices.

§ 1. INTRODUCTION.

THE idea that mechanical twinning takes place in crystals by the continuous growth on an atomic scale of twinned material, and not by the simultaneous movement of all the atoms involved, has often been suggested; for example, by Frenkel and Kontorova (1939), Seitz and Read (1941), and Frank and van der Merwe (1949). The general arguments for a dislocation mechanism of mechanical twinning are the same as those for the dislocation theory of slip. First, it is scarcely believable that the atoms concerned should all move simultaneously, and second, twinning takes place at stresses far below the theoretical shear strength of a perfect lattice.

In some examples of mechanical twinning the atomic movements required to produce the twinned lattice from the original one are more complicated than those that produce slip. The movements can usually be described in terms of a homogeneous shear of all the atoms involved, together with localized rearrangements in which neighbouring atoms move in different directions from one another. The twinning shear of one plane of atoms over another can be produced by the movement in the twinning plane of a dislocation of the usual type, but with a Burgers vector that is not a lattice vector (an "imperfect dislocation"). On the other hand, the localized rearrangements cannot be described formally in terms of a dislocation. In practice, of course, these rearrangements will usually be produced automatically by the passage of the dislocation, because the arrangement of atoms is almost certainly mechanically unstable until the transformation is completed. In this paper a dislocation mechanism is suggested for the shear component of the twinning movements, and the extension of the theory to those cases where localized rearrangements also

* Communicated by the Authors.

If dislocation 3 is perfect it can move in any plane ν where $\mathbf{b}_3 \cdot \nu = 0$, and if neither \mathbf{s}_1 nor \mathbf{s}_2 lie in the plane ν then \mathbf{s}_3 can spiral in this plane, producing repeated increments of slip on it. It is essential, if this process is to produce a simple multiplication of slip on this plane, that the vectors \mathbf{b}_1 and \mathbf{b}_2 should also lie in the plane. However, relation (1) requires only that

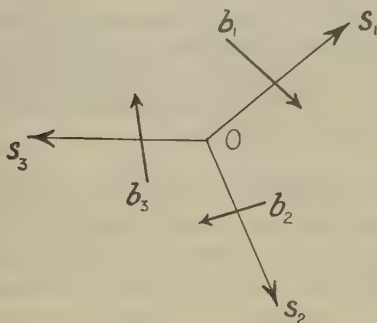
$$\nu \cdot (\mathbf{b}_1 + \mathbf{b}_2) = 0, \quad \dots \dots \dots (2)$$

and interesting topological consequences follow if we extend Frank and Read's mechanism to the case where \mathbf{b}_1 and \mathbf{b}_2 do not lie in the plane ν . There is then a component

$$\mathbf{t} = (\mathbf{b}_1 \cdot \nu)\nu = (-\mathbf{b}_2 \cdot \nu)\nu, \quad \dots \dots \dots (3)$$

perpendicular to the plane, and the dislocation line \mathbf{s}_3 is displaced by \mathbf{t} for every complete revolution that it makes about \mathbf{s}_1 . Hence, instead of repeated slip on the original plane ν , a slip \mathbf{b}_3 takes place on each of a

Fig. 1.



series of planes parallel to ν and spaced \mathbf{t} apart. The sweeping dislocation climbs, as it were, round the helical surface that is formed because the Burgers vector of the pole dislocation has a component perpendicular to the sweeping plane. The shear deformation which results is thus of the homogeneous type that occurs in twinning and shear transformations.

A mechanical twin or transformed structure generated by this process will build up conically in a way similar to the pyramids suggested by Frank (1949) in his theory of crystal growth, and the sweeping dislocation will rapidly assume the form of a helix, since the parts near the pole will have the highest angular velocity. The formation of twins from sweeping dislocations connecting two poles is also to be expected. There is thus a close formal correspondence with the theory of crystal growth, the terraced steps of the latter being replaced in the present case by imperfect dislocations separating the transformed and untransformed material.

The usual elastic interactions will occur between the sweeping dislocations and other singularities in the crystal, while the final shape and size of the twinned piece of the crystal will be determined by its strain energy and by the positions of large obstacles in the material.

If mechanical twinning in a given crystal is to occur by this process, several conditions must be satisfied :

1. The sweeping dislocation must produce the right shear displacement to generate the transformed structure on the sweeping plane.
2. The Burgers vector of the pole dislocation must have a component perpendicular to the sweeping planes that is equal to the spacing of these planes.
3. The pole dislocation must be anchored strongly enough to prevent it from moving under the stress causing the sweeping dislocation to move. Strong anchoring is ensured if the pole dislocation is of the sessile type.
4. The sweeping and pole dislocations, together perhaps with other associated dislocation lines, must form a node and in this node the sweeping dislocation must be free to move in a sweeping plane which is intersected by the pole.

In the following sections it will be shown that these conditions can be satisfied for $\{112\}$ mechanical twinning in the body-centred cubic lattice, while in the case of $\{111\}$ twinning in the face-centred cubic lattice the second part of the last condition is not satisfied, with the result that only monolayer twins can be formed.

§ 3. THE BODY-CENTRED CUBIC LATTICE.

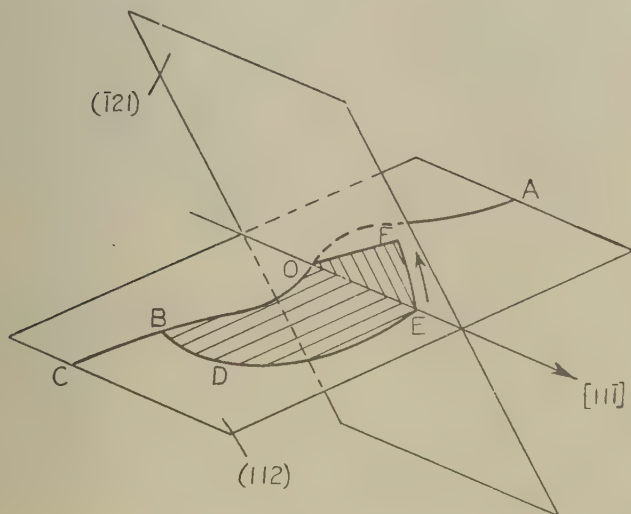
A twinned structure can be formed in this lattice by a shear of $1/\sqrt{2}$ or $\sqrt{2}$ in a $\langle 111 \rangle$ direction on a $\{112\}$ plane, and reliable evidence exists to show that the Neumann bands in α -iron are mechanical twins of this type (*e. g.* Smith, Dee and Young 1928). Consider a portion of a line of perfect dislocation of $\frac{a}{2}[111]$ type which lies in (112) but not along $[11\bar{1}]$. Then (fig. 2), if sufficient energy is available from external sources, a dissociation of the type :

$$\frac{a}{2}[111] \rightarrow \frac{a}{3}[112] + \frac{a}{6}[11\bar{1}] \quad . \quad . \quad . \quad . \quad . \quad (4)$$

can occur along a length BO of the line, forming nodes at B and O. Suppose for definiteness that the Burgers vectors of the lines OA, OB and OFEDB are, using the nodal convention of §2, $\frac{a}{2}[111]$, $-\frac{a}{3}[112]$ and $-\frac{a}{6}[11\bar{1}]$. Then the line OB is pure edge and sessile, while the line BDEO, in moving away from OB, has formed a sheet of stacking fault in (112) . This stacking fault is, in fact, the simplest possible on the (112) planes if the planes are to retain the original packing of nearest neighbours,

and corresponds to the insertion of two fault planes in the (112) stacking sequence; this sequence is a congruence to modulus 6 and the stacking fault is of the type 12345616123456. Since the line BDEO is glissile it may in its motion become pure screw; a length OE can then move into either $(\bar{1}21)$ or $(2\bar{1}1)$, since it is a twinning dislocation for these planes. On account of the unidirectional character of the twinning movement the line OE must move so that the new stacking faults generated on $(\bar{1}21)$ or $(2\bar{1}1)$ make acute angles with the original fault in (112). The node at O can now produce twinning if OF sweeps about AOB as pole, since the components of the Burgers vector of OA perpendicular to $(\bar{1}21)$ and $(2\bar{1}1)$ are $\frac{a}{6}[\bar{1}21]$ and $\frac{a}{6}[2\bar{1}1]$, respectively. The sweeping dislocation thus

Fig. 2.



Dissociation in the body-centred cubic lattice of a unit dislocation. AO=unit dislocation $\frac{a}{2}[\bar{1}11]$; OB=sessile dislocation $-\frac{a}{3}[\bar{1}12]$; OFEDB=twinning dislocation $-\frac{a}{6}[\bar{1}1\bar{1}]$.

climbs along OB into the stacking fault as it rotates; it can pass through the latter since this is identical with a mono-layer twin on (112) and the twins on the three planes (112), $(\bar{1}21)$ and $(2\bar{1}1)$ have the same direction of twinning movement. The movements possible at the node O have been described explicitly but complementary movements can also occur at B, again causing a macroscopic twin on $(\bar{1}21)$ or $(2\bar{1}1)$ to grow into the stacking fault.

§ 4. THE FACE-CENTRED CUBIC LATTICE.

The analogous dissociation in this case is

$$\frac{a}{2}[110] \rightarrow \frac{a}{3}[111] + \frac{a}{6}[11\bar{2}]. \quad . \quad . \quad . \quad . \quad . \quad (5)$$

Here, $\frac{a}{2}[110]$ represents a unit, perfect dislocation; the line of this dislocation could lie in any direction and the two $\{111\}$ type slip planes on which it could glide are (111) and (111). When the line lies in the (111) plane the above dissociation is possible because $\frac{a}{3}[111]$ represents a sessile dislocation in this plane. It forms the boundary of a fault, such as 1231231312312, in the stacking of successive (111) layers on one another. This fault has low energy because it preserves the close-packed arrangement of nearest neighbours; the frequent occurrence of annealing twins on $\{111\}$ planes in recrystallized face-centred cubic metals, across which the stacking arrangement is of the type 12312321321, also shows that this type of fault is energetically preferred in this lattice. The other dislocation, $\frac{a}{6}[11\bar{2}]$, formed by the dissociation can glide in (111) and in so doing produces a twinning shear of the layers between which it passes.

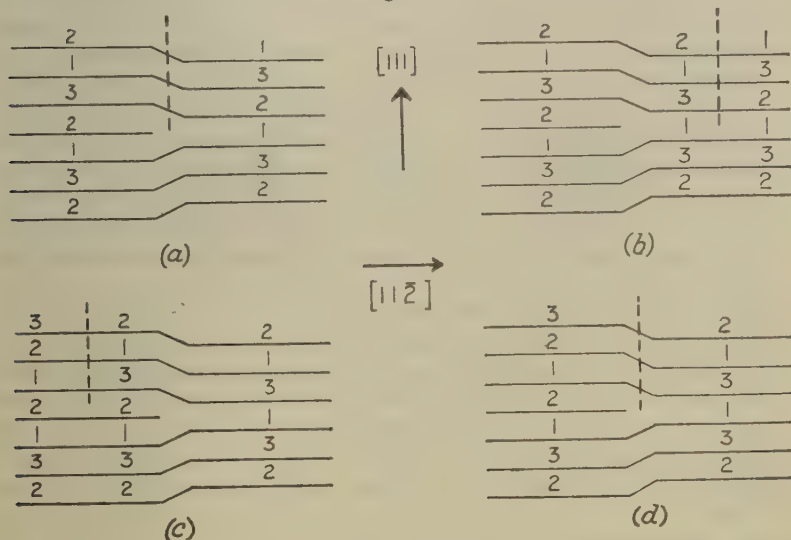
The strength of the component of the Burgers vector perpendicular to (111) is, for both the $\frac{a}{2}[110]$ and $\frac{a}{3}[111]$ dislocations, the same as the spacing $a/\sqrt{3}$ of successive (111) layers, so that these dislocations form a suitable pole for twinning on (111) when this is the sweeping plane. However, the $\frac{a}{3}[111]$ dislocation lies in (111) so that the sweeping $\frac{a}{6}[11\bar{2}]$ dislocation must meet it as it rotates in this plane. Because of this, only one revolution of the sweeping dislocation can occur, even in the case where the undissociated part of the unit dislocation does not lie in (111) and the nodal point can then act as a point of emergence from the plane. Thus only a monolayer stacking fault can be formed.

That repeated rotation of the sweeping dislocation is impossible may be seen by considering fig. 3. These diagrams show a set of (111) planes viewed from the side, perpendicularly to $[11\bar{2}]$. Diagram (a) shows the unit $\frac{a}{2}[110]$ dislocation before it dissociates; here the numbers refer to the stacking positions of the (111) layers and the broken vertical line is a boundary across which the stacking numbers are changed. By crossing this line from left to right the number of a layer is increased by 2; since the sequence 123123 forms a congruence to modulus 3, then $4 \equiv 1$ and $5 \equiv 2$, etc. The dissociation occurs when the broken line is moved to the right, as in diagram (b). The sessile $\frac{a}{3}[111]$ dislocation remains in the site

of the original dislocation, while the sweeping $\frac{a}{6} [11\bar{2}]$ dislocation is situated at the lower end of the broken line. In the region between these dislocations the stacking sequence contains the fault 12313123.

As the sweeping dislocation moves away it extends this stacking fault between the central (111) layers. By rotating about the point of emergence it eventually approaches the sessile dislocation again, and from the left-hand side. It reappears here between either the central 2 and 3, or 1 and 2, layers, respectively, according as the undissociated section of the dislocation line emerges from the (111) plane on its lower or upper side. Diagram (c) illustrates the first of these possibilities. The final diagram

Fig. 3.



Stages in the formation of a stacking fault on (111) by the dissociation of an $\frac{a}{2} [110]$ unit dislocation in the face-centred cubic lattice.

shows the arrangement when the sweeping dislocation has rejoined the sessile one, after forming a stacking fault over the entire plane. The sweeping dislocation cannot continue the same movement further because if it did, it would then be making a second circuit between the same layers, and would create a fault of the type 1231123 in which nearest neighbours are not packed correctly.

The single rotation just described is the only possible motion for the sweeping dislocation. The dislocation cannot move towards the left, starting from its position in diagram (a), because this would create a fault of the forbidden type (either 2311231 or 2312231) between the central (111) half-layer and one of its neighbours. Furthermore, it cannot move in any

other type of $\{111\}$ plane because it can only glide into a different plane from (111) when it is of pure screw type, *i. e.* when its line lies along $[11\bar{2}]$, and $\{111\}$ planes do not intersect one another along this direction.

It follows that this pole mechanism produces only monolayer stacking faults in the face-centred cubic lattice, and cannot cause the growth of mechanical twins. It is interesting that, while stacking faults are known to be formed by cold working metal crystals with this lattice, no-one so far has demonstrated unambiguously that mechanical twins can also be formed in them (Barrett 1950).

§5. DISCUSSION OF THE PROPOSED TWINNING MECHANISM.

The question of the energy involved in the dissociation of the unit dislocation at the node deserves attention. In both of the dissociations proposed in §3 and §4, the Burgers vectors of the resultant dislocations are perpendicular to each other, which means that these dislocations exert no forces on each other from their stress fields and that the elastic energy of the field of the dislocations is unchanged by the dissociation. However, as the sweeping dislocation moves away from the other one, it trails in its path a layer of stacking fault, and the extra energy of this fault must cause a force on the sweeping dislocation. When the distance between the dislocations exceeds a few atomic spacings the energy of the stacking fault is directly proportional to its area. Thus if the energy per unit area of the fault is ϵ then the force per unit length on the dislocation is also ϵ . This force is equivalent to a shear stress $\sigma_s = \epsilon/b$, where b is the strength of the sweeping dislocation, acting on the sweeping plane against the direction of the shear displacement caused by the dislocation. Little is known of the magnitude of ϵ , except that it is much smaller than typical grain boundary energies; the energy of $\{111\}$ boundaries of annealing twins in copper has recently been determined by Fullman (1950), who obtains the value 17 erg. cm.^{-2} . Taking $\epsilon \simeq 10 \text{ erg. cm.}^{-2}$ and $b \simeq 10^{-8} \text{ cm.}$, then $\sigma_s \simeq 10^9 \text{ dyne. cm.}^{-2}$. This value, which is much smaller than the theoretical shear strength, is not unreasonable.

The formation of the first layer of a twin will be more difficult than the subsequent growth of successive layers, because the addition of more twinned layers to an existing twin crystal does not increase appreciably the area of misfit between the twin and matrix. It follows that, if the stress needed to drive a twinning dislocation through the fields of various obstacles (other dislocations, faults, precipitates, etc.) in the crystal is σ_i , then the applied stress needed to start twinning is $\sigma_i + \sigma_s$, while that needed to continue the growth of a twin is only σ_i . Twinning resembles the yield phenomenon in this respect and it may be useful to define upper and lower twinning stresses for the start and propagation of the process. The characteristically rapid formation of twinned crystals, accompanied by discontinuities in the stress-strain relation, is almost certainly due to this effect.

It is well-known that twins can form extremely quickly and the work of Mason, McSkimin and Shockley (1948) on tin, and Millard (private communication 1950) on zinc, shows that they can form in times of the order of a few microseconds. It is important to consider how quickly a twin could form by the pole mechanism. Here we may take advantage of the analogy between the pole mechanism and the theory of crystal growth proposed by Frank (1949). When a steady spiral has built up the process of growth continues by a rotation of this spiral. The spiral makes $v/\pi l$ turns per second, where, in the present case, v refers to the velocity of the dislocation normal to itself and l is twice the limiting radius of curvature about which a section of the line can be bent by the applied stress. One layer is added to the twinned crystal for each rotation of the spiral. Following Mott and Nabarro (1948) we take $l=2(\mu/\sigma)b$, where μ is the shear modulus and σ is the applied stress; a reasonable value is $l=10^{-5}$ cm. The velocity v cannot exceed that of sound and we shall assume a limiting value $v=10^4$ cm. sec.⁻¹. Then the time needed for the twin to grow by one atom layer is of the order 3×10^{-3} microseconds. The time required to build up the steady spiral is determined by the size of the crystal and the applied stress. In the case of a 1 mm. crystal, and using the above value for l , about 1000 turns would be required. Thus the twinned crystal can be formed by the pole mechanism in a time of the order of a few microseconds.

ACKNOWLEDGMENTS.

We wish to thank Professor D. Hanson, Director of the Department of Metallurgy, for his interest and support.

REFERENCES.

- BARRETT, C. S., 1950, *Trans. Amer. Inst. Min. Met. Eng.*, **188**, 123.
FRANK, F. C., 1949, *Report of Conference on Crystal Growth* (London: The Faraday Society), p. 48.
FRANK, F. C., and READ, W. T., 1950, *Phys. Rev.*, **79**, 722.
FRANK, F. C., and VAN DER MERWE, J. H., 1949, *Proc. Roy. Soc. A*, **198**, 205.
FRENKEL, J., and KONTOROVA, T., 1939, *Journal Phys. U.S.S.R.*, **1**, (2), 137.
FULLMAN, R. L., 1950, *U.S. Atomic Energy Commission, Unclassified Report*, RL-351.
MASON, W. P., MCSKIMIN, H. J., and SHOCKLEY, W., 1948, *Phys. Rev.*, **73**, 1213.
MOTT, N. F., and NABARRO, F. R. N., 1948, 1947 *Bristol Conference Report* (London: The Physical Society), p. 1.
SEITZ, F., and READ, T. A., 1941, *J. App. Phys.*, **12**, 470.
SMITH, S. W. J., DEE, A. A., and YOUNG, J., 1928, *Proc. Roy. Soc. A*, **121**, 477.

LXI. *On Virial Coefficients and the Born-Green Theory of Fluids.*

By G. S. RUSHBROOKE and H. I. SCOINS,
Clarendon Laboratory, Oxford*.

[Received January 31, 1951.]

SUMMARY.

The validity of the superposition approximation used in the Born-Green theory of classical fluids is examined by obtaining a virial expansion of the pressure in powers of the density. It is found that the second and third virial coefficients are given correctly, but that the fourth is not. The discrepancy is illustrated numerically by considering explicitly the case of a gas of rigid spheres.

The corresponding equations for a two-component mixture are also considered and it is shown that the equations are mutually consistent only when linearized.

§ 1. INTRODUCTION.

As is well known, the Born-Green theory of classical fluids embodies a so-called "superposition approximation", first introduced by Kirkwood and Boggs (1942, 1949). In the notation of Born and Green, this is expressed by the equation

$$n_3^{(123)} = n_2^{(12)} n_2^{(23)} n_2^{(31)} / n_1^3, \quad \dots \quad (1)$$

where the n 's denote appropriately normalized configurational distribution functions. And it has been asserted (see, for instance, Rodriguez 1949) that this approximation is valid at sufficiently low and sufficiently high temperatures: *i. e.* for almost perfect crystals and near-perfect gases. It is our present purpose to examine in some detail the validity of equation (1) at high temperatures or, more precisely, at low values of the density of the assembly. We shall, in fact, examine how far the Born-Green theory predicts expressions for the successive virial coefficients of an imperfect gas in agreement with the exact expressions for these coefficients that have been given by Mayer (1937-8).

We shall find that, if the pressure is written in the form

$$p = \rho kT(1 + B\rho + C\rho^2 + D\rho^3 + \dots), \quad \dots \quad (2)$$

where ρ denotes the number of systems (atoms) per unit volume in the assembly, then B and C are given correctly by the Born-Green theory

* Communicated by the Authors.

but D is not. The discrepancy will be illustrated numerically by considering explicitly the case of a gas of rigid spheres, for which the calculations can be performed very simply.

Finally, we shall consider the corresponding equations for a two-component mixture, and shall see that in this case a consistent formalism can be obtained only by subsequently linearizing the equations.

§ 2. BORN-GREEN EQUATIONS AND VIRIAL COEFFICIENTS.

Using a slightly different notation from that of (1), we denote $n_2(r), n_1^2$ by $g(r)$ or, more precisely, $g(r, \rho, T)$. The radial distribution function, $g(r)$, is then so normalized that $g(r) \rightarrow 1$ as $r \rightarrow \infty$. Also, of course, $n_1 = \rho$.

Then the equation for the pressure, p , is

$$p = \rho kT - \frac{\rho^2}{6} \int_0^\infty g(r, \rho, T) \phi'(r) 4\pi r^3 dr, \quad \dots \quad (3)$$

where $\phi(r)$ is the interaction energy between two systems distance r apart. This equation is exact, and does not depend on any of the subsequent approximations of the Born-Green theory. This theory, which makes use of equation (1), is essentially epitomized in a non-linear integral equation for $g(r)$, namely

$$\log g(r) + \frac{\phi(r)}{kT} = \pi \rho \int_0^\infty \int_{-s}^s (s^2 - t^2) \frac{t+r}{r} [g(t+r) - 1] dt g(s) \frac{\phi'(s)}{kT} ds. \quad \dots \quad (4)$$

In order to obtain from (3) and (4) a virial expansion of the form (2), we must expand $g(r, \rho, T)$ as a power series in ρ . Following de Boer (1949), we write

$$g(r, \rho, T) = \left[\exp [-\phi(r)/kT] \right] \left[1 + a_1 \rho + a_2 \frac{\rho^2}{2} + \dots + a_n \frac{\rho^n}{n!} + \dots \right] \quad \dots \quad (5)$$

and then (4) gives a set of equations for the $a_n(r, T)$. Substitution in (3) then yields the requisite virial expansion.

Writing $\exp [-\phi(r)/kT] - 1 = \alpha(r)$, it is easily verified that the equations for a_1 and a_2 are

$$a_1(r) = -\pi \int_0^\infty \int_{-s}^s (s^2 - t^2) \frac{t+r}{r} \alpha(t+r) dt \alpha'(s) ds \quad \dots \quad (6)$$

and

$$\begin{aligned} a_2(r) - a_1^2(r) = & -2\pi \int_0^\infty \int_{-s}^s (s^2 - t^2) \frac{t+r}{r} \alpha(t+r) dt a_1(s) \alpha'(s) ds \\ & - 2\pi \int_0^\infty \int_{-s}^s (s^2 - t^2) \frac{t+r}{r} a_1(t+r) [\alpha(t+r) + 1] dt \alpha'(s) ds. \end{aligned} \quad \dots \quad (7)$$

Consequently, if we denote the result of substituting these expressions in (3) by

$$p = \rho kT(1 + B_1\rho + C_1\rho^2 + D_1\rho^3 + \dots),$$

then

$$B_1 = \frac{1}{6} \int_0^\infty 4\pi r^3 \alpha'(r) dr, \quad \dots \dots \dots (8)$$

$$C_1 = \frac{1}{6} \int_0^\infty 4\pi r^3 \alpha'(r) a_1(r) dr, \quad \dots \dots \dots (9)$$

$$D_1 = \frac{1}{12} \int_0^\infty 4\pi r^3 \alpha'(r) a_2(r) dr. \quad \dots \dots \dots (10)$$

These formulæ, which give the successive virial coefficients on the basis of the Born-Green theory, embodying the Kirkwood-Boggs superposition approximation, have now to be compared with the exact formulæ for these virial coefficients which we know from Mayer's work are

$$B = -2\pi \int_0^\infty r^2 \alpha(r) dr, \quad \dots \dots \dots (11)$$

$$C = -\frac{1}{3} \iint \alpha_{12} \alpha_{23} \alpha_{31} d\tau_2 d\tau_3 \quad \dots \dots \dots (12)$$

and

$$D = -\frac{1}{8} \iiint [\alpha_{12} \alpha_{23} \alpha_{31} \alpha_{41} \alpha_{42} \alpha_{43} + 6\alpha_{12} \alpha_{23} \alpha_{31} \alpha_{41} \alpha_{42} + 3\alpha_{12} \alpha_{23} \alpha_{34} \alpha_{41}] d\tau_2 d\tau_3 d\tau_4, \quad \dots \dots (13)$$

where $\alpha_{ij} = \alpha(|\mathbf{r}_i - \mathbf{r}_j|)$, and $d\tau_i$ denotes a volume element at the point \mathbf{r}_i .

It is obvious at once, by partial integration, that $B_1 = B$. Before proceeding further with the comparison, however, it is convenient to derive some useful mathematical formulæ involving Fourier transforms.

§ 3. SOME MATHEMATICAL LEMMAS.

I. With the notation illustrated by fig. 1

$$\begin{aligned} & \int \dots \int_{(n)} f_1(r_1) f_2(r_2) \dots f_n(r_n) f_{n+1}(r_{n+1}) d\tau_1 d\tau_2 \dots d\tau_n \\ &= (2\pi)^{\frac{3n-1}{2}} \int_{-\infty}^{\infty} u \mathcal{F}_1(u) \mathcal{F}_2(u) \dots \mathcal{F}_{n+1}(u) \frac{\sin ux}{x} du \end{aligned}$$

where $u \mathcal{F}_i(u) = \frac{1}{\sqrt{(2\pi)}} \int_{-\infty}^{\infty} r f_i(r) \sin ur dr$

and the f_i are even functions of r .

This result is easily obtained by induction. We start by considering the case illustrated in fig. 2. Since

$$d\tau = r_1 r_2 dr_1 dr_2 d\chi/s,$$

where χ denotes an angle of rotation about AB, we have

$$\int f_1(r_1)f_2(r_2) d\tau = 2\pi \int_0^\infty \int_{s-r_2}^{s+r_2} \frac{r_1 f_1(r_1) r_2 f_2(r_2)}{s} dr_1 dr_2.$$

Writing $r_1 f_1(r_1) = \frac{1}{\sqrt{(2\pi)}} \int_{-\infty}^\infty u \mathcal{F}_1(u) \sin r_1 u du$, and interchanging the

Fig. 1.

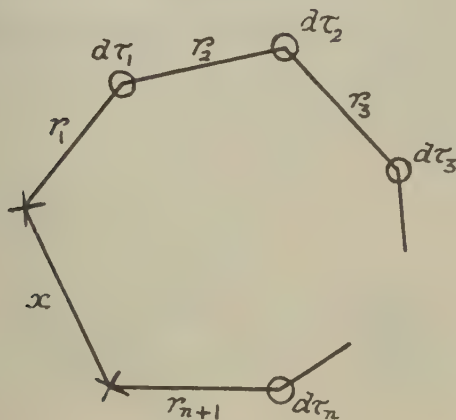
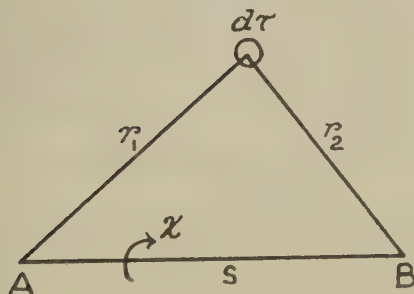


Fig. 2.



order of integration, we find

$$\begin{aligned} \int f_1(r_1)f_2(r_2) d\tau &= 2\pi \frac{2}{\sqrt{(2\pi)}} \int_0^\infty dr_2 \int_{-\infty}^\infty \frac{\sin su}{su} u \mathcal{F}_1(u) r_2 f_2(r_2) \sin r_2 u du \\ &= 2\pi \int_{-\infty}^\infty u \mathcal{F}_1(u) \mathcal{F}_2(u) \frac{\sin su}{s} du. \end{aligned}$$

Considering next the integral (see fig. 3)

$$I \equiv \iint f_1(r_1)f_2(r_2)f_3(r_3) d\tau d\tau',$$

we have

$$\begin{aligned} I &= (2\pi)^2 \int \dots \int dr_1 dr_2 \frac{r_1 f_1(r_1) r_2 f_2(r_2)}{s} \frac{s r_3 f_3(r_3)}{t} ds dr_3 \\ &= (2\pi)^2 \int_{-\infty}^{\infty} \int_0^{\infty} \int_{t-r_3}^{t+r_3} u \mathcal{F}_1(u) \mathcal{F}_2(u) \frac{\sin su}{t} r_3 f_3(r_3) ds dr_3 du \\ &= (2\pi)^{5/2} \int_{-\infty}^{\infty} u \mathcal{F}_1(u) \mathcal{F}_2(u) \mathcal{F}_3(u) \frac{\sin tu}{t} du. \end{aligned}$$

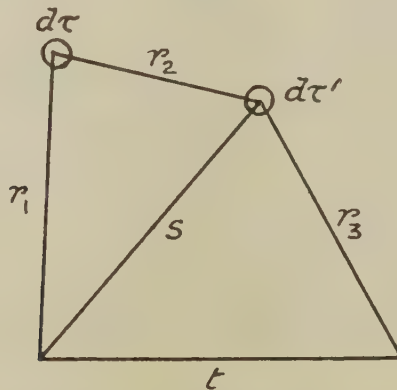
The general result stated in I. follows by simply repeating the argument.

Letting $x \rightarrow 0$, we have

II. With the notation illustrated by fig. 4

$$\begin{aligned} \int \dots \int_{(n)} f_1(r_1) f_2(r_2) \dots f_{n+1}(r_{n+1}) d\tau_1 d\tau_2 \dots d\tau_n \\ = (2\pi)^{\frac{3n-1}{2}} \int_{-\infty}^{\infty} u^n \mathcal{F}_1(u) \mathcal{F}_2(u) \dots \mathcal{F}_{n+1}(u) du. \end{aligned}$$

Fig. 3.



These results are also proved in a paper by Montroll and Mayer (1941), but their method of derivation is considerably longer than ours. For the formulæ to be valid the interatomic potential must decrease more rapidly than for purely ionic interactions, which is certainly so for the van der Waal's forces normally responsible for gaseous imperfections.

§ 4. DISCUSSION OF C AND C_1 .

On account of II. above, equation (12) gives at once

$$C = -\frac{1}{3}(2\pi)^{5/2} \int_{-\infty}^{\infty} u^2 [\beta(u)]^3 du, \quad \dots \dots \dots (14)$$

where

$$u\beta(u) = \frac{1}{\sqrt{(2\pi)}} \int_{-\infty}^{\infty} r\alpha(r) \sin ur dr, \quad \dots \dots \dots (15)$$

$\alpha(r)$ being regarded as an even function of r .

To obtain from (9) an analogous equation for C_1 we must first consider $a_1(r)$. On replacing $(t+r)\alpha(t+r)$ in (6) by its Fourier transform according to (15), namely

$$\frac{1}{\sqrt{(2\pi)}} \int_{-\infty}^{\infty} u\beta(u) \sin u(t+r) du$$

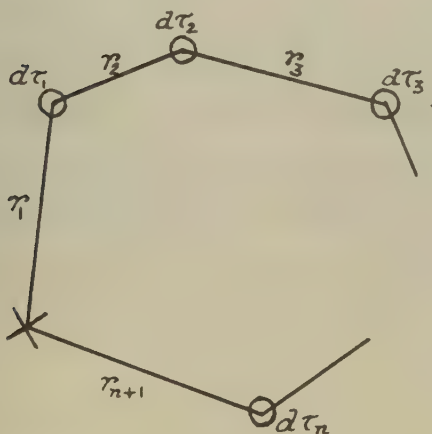
and integrating first with respect to t and then with respect to s , we find that

$$ra_1(r) = 2\pi \int_{-\infty}^{\infty} u[\beta(u)]^2 \sin ur du. \quad (16)$$

Consequently, by (9),

$$C_1 = \frac{4\pi^2}{3} \int_0^{\infty} r^2 \alpha'(r) \int_{-\infty}^{\infty} u[\beta(u)]^2 \sin ur du dr.$$

Fig. 4.



Integrating partially with respect to r we have, since $\alpha(r)$ vanishes at infinity,

$$C_1 = -\frac{4\pi^2}{3} \int_{-\infty}^{\infty} \left\{ \sqrt{(2\pi)} u^2 [\beta(u)]^3 + \frac{\sqrt{(2\pi)}}{2} u^2 [\beta(u)]^2 \frac{d}{du} (u\beta(u)) \right\} du$$

and the second term on the right vanishes since for interaction potentials of the type under consideration $u\beta(u)$ vanishes at infinity. Thus

$$C_1 = -\frac{1}{3} (2\pi)^{5/2} \int_{-\infty}^{\infty} u^2 [\beta(u)]^3 du = C$$

and the third virial coefficient is given correctly by the non-linear integral equation of the Born-Green theory.

§ 5. DISCUSSION OF D AND D₁.

On account of II., and by applying Parseval's theorem to equation (16), we have for the last term on the right hand side of (13),

$$-\frac{3}{8} \iint \alpha_{12} \alpha_{23} \alpha_{34} \alpha_{41} d\tau_2 d\tau_3 d\tau_4 = -\frac{3}{8} (2\pi)^4 \int_{-\infty}^{\infty} u^2 [\beta(u)]^4 du \\ = -\frac{3\pi}{2} \int_0^{\infty} r^2 a_1^2(r) dr. \quad (17)$$

For the second term on the right hand side of (13), application of I. and II. leads to

$$-\frac{3}{4} \iint \alpha_{12} \alpha_{23} \alpha_{34} \alpha_{41} \alpha_{42} d\tau_1 d\tau_2 d\tau_3 = -\frac{3}{4} (2\pi)^{2/5} \int_{-\infty}^{\infty} u^2 \mathcal{F}(u) [\beta(u)]^2 du,$$

where

$$u \mathcal{F}(u) = \frac{1}{\sqrt{(2\pi)}} \int_{-\infty}^{\infty} tf(t) \sin ut dt \text{ and } tf(t) = 2\pi \alpha(t) \int_{-\infty}^{\infty} u [\beta(u)]^2 \sin ut du.$$

Using Parseval's theorem, and (16), we thus obtain

$$-\frac{3}{4} \iint \alpha_{12} \alpha_{23} \alpha_{31} \alpha_{41} \alpha_{42} d\tau_2 d\tau_3 d\tau_4 = -3\pi \int_0^{\infty} r^2 \alpha(r) a_1^2(r) dr. \quad (18)$$

We have not been able to obtain any such simple formula for the first term on the right hand side of (13), but we shall find that the expressions involving $a_1(r)$ in (17) and (18) arise naturally in the evaluation of D₁, to which we now turn.

From equations (7) and (10) we obtain, after partial integrations of (7),

$$\left. \begin{aligned} D_1 &= \frac{\pi}{3} \int_0^{\infty} r^3 \alpha'(r) a_1^2(r) dr & (i.) \\ &+ \frac{2\pi^2}{3} \int_0^{\infty} r^2 \alpha'(r) \int_0^{\infty} \int_{-s}^s (s^2 - t^2) (t+r) \alpha(t+r) dt \cdot a_1(s) \alpha(s) ds dr & (ii.) \\ &+ \frac{4\pi^2}{3} \int_0^{\infty} r^2 \alpha'(r) \int_0^{\infty} \int_{-s}^s (t+r) \alpha(t+r) dt \cdot s a_1(s) \alpha(s) ds dr & (iii.) \\ &+ \frac{4\pi^2}{3} \int_0^{\infty} r^2 \alpha'(r) \int_0^{\infty} \int_{-s}^s (t+r) \alpha(t+r) a_1(t+r) dt \cdot s \alpha(s) ds dr & (iv.) \\ &+ \frac{4\pi^2}{3} \int_0^{\infty} r^2 \alpha'(r) \int_0^{\infty} \int_{-s}^s (t+r) a_1(t+r) dt \cdot s \alpha(s) ds dr. & (v.) \end{aligned} \right\} \quad (19)$$

It is convenient to number the successive terms on the right hand side of (19), (i.), (ii.), . . . (v.).

Then using the techniques already illustrated above, we can show without difficulty that

$$(v.) = -\frac{3\pi}{2} \int_0^{\infty} r^2 a_1^2(r) dr = (17)$$

and

$$(iii.) = (iv.) = -\pi \int_0^{\infty} r^2 \alpha(r) a_1^2(r) dr + \frac{\pi}{3} \int_0^{\infty} r^3 \alpha(r) a_1(r) a_1(r) dr$$

so that

$$(i.) + (iii.) + (iv.) = -3\pi \int_0^{\infty} r^2 \alpha(r) a_1^2(r) dr = (18).$$

Thus the second and third terms on the right hand side of (13) are accounted for by the terms (i.), (iii.), (iv.) and (v.) of (19). But the remaining part of D_1 , namely term (ii.) in (19), is *not* equal to the remaining part of D , i. e. to the first term on the right hand side of (13). This is clear from dimensional arguments and, as we shall see, is confirmed when we make explicit calculations for the case of hard spheres in §7 below. For the purposes of calculation it is convenient to write (ii.) in the form

$$(ii.) = -\frac{2\pi^2}{3} \int_0^{\infty} r^2 a_1'(r) \alpha(r) \frac{d}{dr} \left[r^6 \frac{d}{dr} \left\{ \frac{1}{r^6} \int_{-\infty}^{\infty} \frac{[\beta(u)]^2}{u} \sin ur du \right\} \right] dr. \quad (20)$$

We thus see that the Born-Green non-linear integral equation, (4), for $g(r)$, deriving from the superposition approximation, fails to give correctly the fourth virial coefficient, D , of an imperfect gas: and that the reason for this failure is that it does not do justice to the term involving $\iiint \alpha_{12} \alpha_{23} \alpha_{34} \alpha_{41} \alpha_{42} \alpha_{43} d\tau_2 d\tau_3 d\tau_4$ in the correct expression for this virial coefficient.

Before giving the results of explicit calculations for the simple case of a gas of hard spheres it will be well to consider how these results are affected, if at all, if we base discussion not on (4) but on a linear approximation to this non-linear equation. Most of the attempts made so far to determine explicit distribution functions for a given intermolecular potential have been based on such a linearization technique. We confine our discussion to the particular method of linearization used by Rodriguez (1949).

§ 6. EFFECT OF LINEARIZING THE EQUATION FOR $g(r)$.

Rodriguez has shown that if, in (4), we write

$$g(r) = \exp [f(r) - \phi(r)/kT], \quad . \quad . \quad . \quad . \quad . \quad . \quad (21)$$

keep only terms linear in $f(r)$ and replace certain products $f(r)\alpha(r)$ and $f(r)\alpha'(r)$ by $(\epsilon-1)\alpha(r)$ and $(\epsilon-1)\alpha'(r)$, respectively, where

$$\epsilon - 1 = \frac{\int_0^{\infty} r^2 f(r) \alpha(r) dr}{\int_0^{\infty} r^2 \alpha(r) dr}, \quad . \quad . \quad . \quad . \quad . \quad . \quad (22)$$

then the resulting linear equation can be solved, the solution being given by

$$rf(r) = \frac{1}{\sqrt{(2\pi)}} \int_{-\infty}^{\infty} \frac{\epsilon^2 s [\beta(s)]^2 \sin rs}{\lambda - \epsilon \beta(s)} ds, \quad . \quad . \quad . \quad . \quad . \quad . \quad (23)$$

where $\lambda^{-1} = (2\pi)^{3/2}\rho$. The precise nature of these approximations is not at all clear, but our final paragraph will suggest that when dealing with binary mixtures some such technique is not only convenient but necessary, and it will be well therefore to discuss briefly the virial coefficient problem on the basis of equations (23), (22), (21) and (3).

The procedure is exactly as before, except that now we must also expand ϵ as

$$\epsilon = 1 + c_1\rho + c_2\rho^2 + \dots \quad (24)$$

There is no need to enter into the details of the calculation. It is sufficient to state that if we express the pressure p as

$$p = \rho kT[1 + B_2\rho + C_2\rho^2 + D_2\rho^3 + \dots].$$

Then we find

$$B_2 = B_1 = B,$$

$$C_2 = C_1 = C,$$

but

$$\left. \begin{aligned} D_2 &= \frac{8\pi^2}{3} c_1 \int_0^\infty r^2 \alpha'(r) \int_{-\infty}^\infty s[\beta(s)]^2 \sin rs \, ds \, dr & (a) \\ &+ \frac{2\pi}{3} (2\pi)^{5/2} \int_0^\infty r^2 \alpha'(r) \int_{-\infty}^\infty s[\beta(s)]^3 \sin rs \, ds \, dr & (b) \\ &+ \frac{4\pi^3}{3} \int_0^\infty r \alpha'(r) \left[\int_{-\infty}^\infty s[\beta(s)]^2 \sin rs \, ds \right]^2 dr, & (c) \end{aligned} \right\} \quad (25)$$

where

$$c_1 = (2\pi)^{3/2} \int_0^\infty u^2 [\beta(u)]^3 du / \int_0^\infty r^2 \alpha(r) \, dr = 3C/2B. \quad (26)$$

It is then not difficult to show that, comparing the terms of (25) and (19),

$$(b) = (v.),$$

$$(c) = (i.)$$

but

$$(a) \neq (ii.) + (iii.) + (iv.).$$

In fact

$$(a) = 3C^2/B. \quad (27)$$

Thus linearization does not affect the second and third virial coefficients B and C , but does affect the fourth virial coefficient.

We shall now illustrate these results by using the above formulæ to calculate B , C , D_1 and D_2 for a gas of hard spheres. The value of D (as also B and C) for such a hypothetical gas has already been calculated by Happel and by Majumdar: see Fowler and Guggenheim (1939).

§ 7. CALCULATIONS FOR A GAS OF HARD SPHERES.

We consider hard spheres of diameter a . Then $\phi(r) = \infty$, $r < a$ and $\phi(r) = 0$, $r > a$. Whence

$$\alpha(r) = -1, \quad 0 < r < a; \quad \alpha(r) = 0, \quad a < r.$$

Then

$$u\beta(u) = \sqrt{\left(\frac{2}{\pi}\right)} \frac{d}{du} \left(\frac{\sin ua}{u} \right)$$

and, by (16),

$$\begin{aligned} ra_1(r) &= 0, \quad |r| > 2a \\ &= \frac{\pi}{12} r(r-2a)^2(r+4a), \quad |r| < 2a. \end{aligned}$$

From (11),

$$B = \frac{2\pi a^3}{3} = 4v = b \text{ say,}$$

where v is the volume of one of the spheres.

From (14),

$$C = \frac{5\pi^2 a^6}{18} = \frac{5}{8} b^2.$$

We now consider the various contributions to D_1 and D_2 . They are given in Table I. below :

TABLE I.

D_1	Value	D_2	Value
(i.)+(iii.)+(iv.) from (18)	$\frac{6347}{4480} b^3$	(a) from (27)	$\frac{75}{64} b^3$
(v.) from (17)	$-\frac{34}{35} b^3$	(b) from (17)	$-\frac{34}{35} b^3$
(ii.) from (20)	$-\frac{493}{2240} b^3$	(c) from (i.)	$\frac{25}{128} b^3$
Total D_1	$\frac{1009}{4480} b^3$	Total D_2	$\frac{1773}{4480} b^3$
=	$0.2252 b^3$	=	$0.3958 b^3$

These values have to be compared with the value $D=0.2869b^3$ calculated by Happel and by Majumdar. We see that the non-linear integral equation leads to rather too small a value for D , while Rodriguez's method of linearization yields too large a value.

Finally we would observe that (26) shows that for hard spheres ϵ should increase with the density ρ . If, however, we adopt the crudest form of linearization and take $\epsilon=1$ throughout, then B_2 and C_2 are unchanged, but D_2 loses the contribution (a) and becomes $D_2 = -\frac{3477}{4480} b^3$, which has the wrong sign. Here we have not ignored f^2 in finding p ; if we do so we get $D_2' = -\frac{34}{35} b^3$, which is also negative.

§ 8. BINARY MIXTURES.

In this discussion we shall try to keep the mathematical exposition as short as possible since the calculations though essentially straightforward are necessarily cumbersome if presented at all fully. To obtain the

equations we have simply to follow Born and Green's procedure. We derive first an infinite set of equations for the equilibrium distribution functions, and then cut these off by means of the superposition approximation. We now need, however, four equations of type (1), namely (with a self-explanatory notation)

$$\left. \begin{aligned} n_{AAA}(123) &= n_{AA}(12)n_{AA}(23)n_{AA}(31)/n_A^3, \\ n_{AAB}(123) &= n_{AA}(12)n_{AB}(23)n_{AB}(13)/n_A^2n_B, \end{aligned} \right\} \quad (28)$$

and the two equations which result from interchanging A and B.

We then obtain, in place of (4), four non-linear integral equations which may be written

$$\begin{aligned} \log g_{ij}(r) + \frac{\phi_{ij}(r)}{kT} &= \pi \rho_A \int_0^\infty \int_{-s}^s (s^2 - t^2) \frac{t+r}{r} [g_{iA}(t+r) - 1] dt g_{jA}(s) \frac{\phi'_{jA}(s)}{kT} ds \\ &+ \pi \rho_B \int_0^\infty \int_{-s}^s (s^2 - t^2) \frac{t+r}{r} [g_{iB}(t+r) - 1] dt g_{jB}(s) \\ &\quad \times \frac{\phi'_{jB}(s)}{kT} ds, \quad \dots \quad (29) \end{aligned}$$

where $i=A$ or B , $j=A$ or B , and the order of the suffices is immaterial. In terms of the n 's, $g_{ij}(r) = n_{ij}(r)/n_i n_j$ and $\rightarrow 1$ as $r \rightarrow \infty$. Moreover

$$n_A = N_A/V = \rho_A \quad \text{and} \quad n_B = N_B/V = \rho_B.$$

The equation for the pressure is

$$\begin{aligned} \frac{p}{kT} &= \rho - \frac{\rho^2}{6kT} \int_0^\infty [x_A^2 g_{AA}(r) \phi'_{AA}(r) + 2x_A x_B g_{AB}(r) \phi'_{AB}(r) \\ &\quad + x_B^2 g_{BB}(r) \phi'_{BB}(r)] 4\pi r^3 dr, \quad \dots \quad (30) \end{aligned}$$

where $\rho = (N_A + N_B)/V$, $x_A = N_A/(N_A + N_B)$ and $x_B = N_B/(N_A + N_B)$.

To obtain a virial expansion we proceed exactly as before except that now we have to use double power series in the two variables ρ_A and ρ_B instead of simply power series in ρ . If we write

$$p = \rho kT [1 + B\rho + C\rho^2 + D\rho^3 + \dots]$$

then we find

$$B = -2\pi \left[x_A^2 \int_0^\infty \alpha_{AA}(r) r^2 dr + 2x_A x_B \int_0^\infty \alpha_{AB}(r) r^2 dr + x_B^2 \int_0^\infty \alpha_{BB}(r) r^2 dr \right] \quad \dots \quad (31)$$

and

$$\begin{aligned} C &= -\frac{1}{3} \left[x_A^3 \iint \alpha_{AA}(r_{12}) \alpha_{AA}(r_{23}) \alpha_{AA}(r_{13}) d\tau_2 d\tau_3 \right. \\ &\quad + 3x_A^2 x_B \iint \alpha_{AA}(r_{12}) \alpha_{AB}(r_{23}) \alpha_{AB}(r_{13}) d\tau_2 d\tau_3 \\ &\quad + 3x_A x_B^2 \iint \alpha_{BB}(r_{12}) \alpha_{AB}(r_{23}) \alpha_{AB}(r_{13}) d\tau_2 d\tau_3 \\ &\quad \left. + x_B^3 \iint \alpha_{BB}(r_{12}) \alpha_{BB}(r_{23}) \alpha_{BB}(r_{13}) d\tau_2 d\tau_3 \right]. \quad \dots \quad (32) \end{aligned}$$

And these are the correct expressions for the second and third virial coefficients of a binary mixture (Mayer 1939).

To this stage the calculations, though laborious, are essentially straightforward. The only mathematical tool required, apart from algebraic manipulation, is the result

$$\int_0^\infty \int_{-s}^s (s^2 - t^2)(t+r)f(t+r)g'(s) dt ds \\ = \int_0^\infty \int_{-s}^s (s^2 - t^2)(t+r)g(t+r)f'(s) dt ds, \quad \dots \quad (33)$$

which is easily proved by introducing the Fourier transforms of $rf(r)$ and $rg(r)$. We need (33) in order to show that the two equations of type (29) for $g_{AB}(r)$, obtained by taking $i=A, j=B$ and $i=B, j=A$ respectively, are mutually consistent as far as terms linear in ρ are concerned.

When however, we proceed to calculate D we meet an entirely new difficulty. For we now find that these two equations for $g_{AB}(r)$ are *not* mutually consistent when we include terms quadratic in ρ . Indeed, it can be shown that the reason for the inconsistency can be traced to precisely the same defect in the superposition principle that led to $D_1 \neq D$ for a one-component assembly.

We thus find that when the Born-Green formalism is extended to binary mixtures the superposition approximation leads to four non-linear equations for the three equilibrium radial distribution functions, and that these four equations are not mutually consistent. If, however, we linearize the equations in the manner due to Rodriguez, then in place of (29) we have the four equations

$$rf_{ij}(r) = 2\pi\rho_A \int_0^\infty \int_{-s}^s (t+r)[f_{iA}(t+r) + \epsilon_{iA}\alpha_{iA}(t+r)] dt \epsilon_{jA}s\alpha_{jA}(s) ds \\ + 2\pi\rho_B \int_0^\infty \int_{-s}^s (t+r)[f_{iB}(t+r) + \epsilon_{iB}\alpha_{iB}(t+r)] dt \epsilon_{jB}s\alpha_{jB}(s) ds, \quad (34)$$

$i=A, B$ and $j=A, B$; and it is easy to show that these equations are entirely mutually consistent. Their solution, by the method of Fourier transforms, can be found without difficulty: we shall not, however, give it here as the expressions are rather unwieldy and we do not wish to discuss them further at present.

REFERENCES.

- DE BOER, J., 1949, *Reports on Progress in Physics*, **12**, (London: The Physical Society), p. 305.
 BORN, M., and GREEN, H. S., 1949, *A General Kinetic Theory of Liquids*, (Cambridge: University Press), Ch. I. and II.
 FOWLER, R. H., and GUGGENHEIM, E. A., 1939, *Statistical Thermodynamics*, (Cambridge: University Press), § 717.
 KIRKWOOD, J. G., and BOGGS, E. M., 1942, *J. Chem. Phys.*, **10**, 394.
 MAYER, J. E. *et al.*, 1937-8, *J. Chem. Phys.*, **5**, 67, 74; **6**, 87; 1939, *Ibid.*, **43**, 71.
 MONTROLL, E. W., and MAYER, J. E., 1941, *J. Chem. Phys.*, **9**, 626.
 RODRIGUEZ, A. E., 1949, *Proc. Roy. Soc. A*, **196**, 73.

LXII. *The Critical Magnetic Fields of Aluminium, Cadmium, Gallium and Zinc.*

By B. B. GOODMAN and E. MENDOZA *,
Royal Society Mond Laboratory, Cambridge †.

[Received March 7, 1951.]

ABSTRACT.

The low temperatures produced by the adiabatic demagnetization of a paramagnetic salt have been used to cool specimens of aluminium, cadmium, gallium and zinc, and their critical fields have been measured down to 0.1° K. The magnetic measurements on the metal and the salt were made independently and the experimental arrangement had the further advantage that the quality of the thermal contact between the metal and the salt could be studied. The results could be accurately expressed by relations of the form $H_c = H_0(1 - (T/T_c)^2)$; values of H_0 and T_c for each metal are tabulated.

§ 1. INTRODUCTION.

COMPARATIVELY little information is at present available on the critical fields of superconductors with low transition temperatures. In this paper measurements of the critical fields of aluminium, cadmium, gallium and zinc are described. The low temperatures were produced by the adiabatic demagnetization of a paramagnetic salt, using a technique already described briefly by one of us (Mendoza 1948), in which the metal specimen and the salt were separated but were in thermal contact through a long copper rod. This arrangement has the advantage that it is possible to make magnetic observations on the metal specimen and the salt independently. Moreover the condition of the specimen can be more easily controlled than in the method used by Kurti and Simon (1935 b) and more recently by Daunt and Heer (1949 a, b), where the salt and chips of the metal were pressed together into a pill. The superconducting transitions in various steady magnetic fields were studied by measuring the effective susceptibility of the metal in a low-frequency alternating field; the specific resistance of the normal metal could also be deduced from these measurements.

§ 2. THE EXPERIMENTAL ARRANGEMENT.

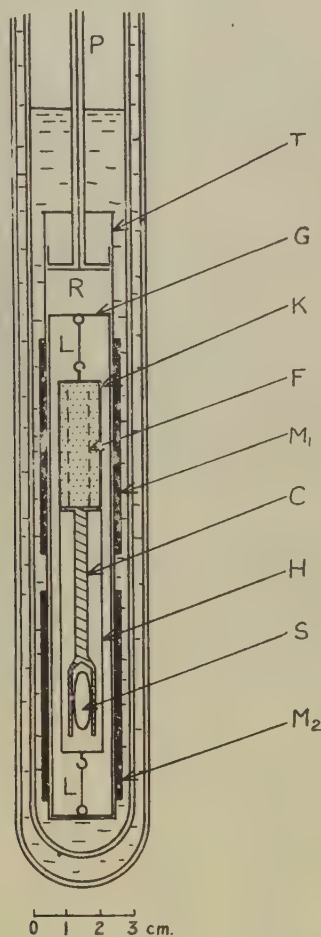
A diagram of the low temperature part of the apparatus is shown in fig. 1. The salt-tube T stood in a Dewar flask of liquid helium, itself surrounded by a Dewar of liquid air. The metal specimen S was gripped in the cup at the lower end of the copper rod C. Strips of copper foil F with a total area of about 6 cm.² were hard soldered to the top of C;

* Now at the H. H. Wills Physical Laboratory, Bristol.

† Communicated by Dr. D. Shoenberg.

there was no evidence that the magnetic observations were affected by the hard solder. A paste of powdered paramagnetic salt (either ferric ammonium alum or chromium potassium alum) mixed with a solution of a plastic cement in acetone was pressed around the foil in a cylindrical

Fig. 1.



The low temperature part of the apparatus.

die under a pressure of 2000 atm.; the resulting pill K was 1.6 cm. in diameter and about 4 cm. long. It was found that this arrangement gave adequate thermal contact between the salt and the superconductor, and that within five minutes of demagnetizing the salt to 0.1°K . good thermal equilibrium had been reached. The amount of heat reaching

S and C from stray sources was reduced by a cylindrical shield of copper foil H in good thermal contact with the salt K. Vertical slots were cut in H and in the cup holding S in order to reduce the effect of eddy currents; the slots in the cup also made it easier to grip S. The whole system was suspended by cotton threads L from the framework G which stood inside the salt-tube T. Hot gas molecules coming down the pumping tube P were prevented from impinging on the cold salt K by the radiation shutter R.

The longitudinal magnetic field needed for the critical field determinations was provided by a solenoid which could be suspended around the liquid air Dewar. This solenoid gave a field which was uniform within $\frac{1}{2}$ per cent over a length of 3.0 cm., and the effect of its field on the temperature of the salt was always negligible.

M_1 and M_2 are mutual inductances surrounding the salt and the superconductor respectively. Since the value of the empty mutual inductance was not known very accurately, only changes in susceptibility of K or S could be deduced from measurements of the mutual inductance. Owing partly to losses in the circuit and partly to losses in the specimen (particularly for the metal in the normal state) each mutual inductance can be regarded as complex and will be denoted by $M' - jM''$. Values of M' and M'' for both mutual inductances were measured by a Hartshorn A.C. bridge. The measuring current was supplied by a 40 c./s. frequency-stabilized alternator and detection was by means of an amplifier and a vibration galvanometer.

The contribution to M'_1 was of order $(400/T) \mu\text{H}$ from the salt and the change of M'_2 corresponding to the transition of the metal from the normal to the superconducting state was of order $40 \mu\text{H}$. By using a measuring field of amplitude 1 gauss the bridge could be set to an accuracy of $0.05 \mu\text{H}$ in the absence of a steady magnetic field, but only to $0.3 \mu\text{H}$ in a field owing to the effect on the galvanometer of fluctuations in the field.

TABLE I.
Characteristics of the Metal Specimens.

	Source	Estimated % purity	Length (mm.)	Diam. (mm.)	n	$(\rho/\rho_{273}) \times 10^4$
Aluminium	J 1011	99.995	26.2	6.5	0.074	18
Cadmium	N	99.996	28.5	7.1	0.074	3.1
Gallium	J 3419	~99.99	26.8	3.00	0.023	1.0
Zinc	J 1790	99.999	27.5	6.8	0.074	14

J=Johnson, Matthey & Co.

N=New Jersey Zinc Co.

The quantities n and ρ/ρ_{273} are referred to later in the paper.

§ 3. THE SPECIMENS.

The characteristics of the metal specimens are given in Table I. The aluminium and zinc specimens were both turned to an accurately ellipsoidal shape. The cadmium and gallium specimens were cast in

thin-walled glass tubes which were approximately ellipsoidal in internal shape, and the glass was afterwards cracked away. Each specimen was annealed in a helium atmosphere to remove internal strains, and then lightly etched in acid to remove surface impurities.

§ 4. EXPERIMENTAL PROCEDURE.

(a) *The temperature of the specimen.*

The demagnetizations were made from magnetic fields of up to 20 kilogauss provided by a water-cooled solenoid which could be raised into position around the liquid air Dewar. It was found that unless demagnetizations were carried out from a helium bath temperature of about 1.5°K . or more the rate of warming of the cold salt was rapid above about 0.7°K . It seems probable that at lower initial temperatures the out-gassing of the salt tube was much less complete, and after demagnetization helium from the salt-tube wall condensed on the cold salt, only to evaporate and destroy the thermal vacuum when the salt warmed to about 0.7°K . Under the best conditions the natural heat input into the cold system was about 3 ergs sec.^{-1} .

The temperature of the salt after demagnetization was determined by standard procedure (Kurti and Simon 1935 b). The mutual inductance of M_1 was first measured at three or four temperatures in the helium range, while helium gas in the salt-tube at a pressure of about 0.1 mm. of mercury maintained the salt in thermal equilibrium with the helium bath. The helium bath temperature was deduced from the pressure in the cryostat using the 1949 scale of temperature (van Dijk and Shoenberg 1949). A graph was plotted of M'_1 against $1/(T-\Delta)$, where $\Delta = \lambda f(4\pi/3 - N)$; f is the filling factor, λ the Curie constant per c.c. and N is the demagnetizing factor of the external shape of the pill; the parameter Δ which was usually about 0.02°K . was introduced in order to allow for the non-spherical shape of the specimen. The graph was a straight line as was to be expected for a salt obeying a Curie law. After demagnetization the value of M' was again measured and a magnetic temperature T^* was deduced from the value of $1/(T-\Delta)$ given by linear extrapolation of the graph. The values of T^* obtained at low temperatures differed slightly from thermodynamic temperatures T owing to departures from Curie's law and were corrected on the basis of various published data (Casimir, de Haas and de Klerk 1939, Cooke 1949). The reliability of this procedure for deducing T is indicated by the agreement between estimates of T for a given critical field of a zinc specimen using ferric ammonium alum and chromium potassium alum respectively. At 0.2°K . the two sets of measurements were in agreement to better than 10^{-2} deg. although the values of $T^* - T$ were of order $3 \times 10^{-2}\text{ deg.}$

(b) *Measurement of the critical field.*

After the demagnetization the specimen was superconducting and measurements of M'_2 and M'_2 were made as the magnetic field of the

solenoid B was steadily increased. The real part M_2' was constant as long as the specimen was wholly superconducting, but owing to coupling with the solenoid there was a small increase in M_2'' as the resistance of the solenoid circuit was lowered. At the entry to the intermediate state a sharp rise of both M_2' and M_2'' was observed, and the steady field corresponding to this was assumed to be $(1-n)$ times the critical field H_c of the superconductor, where $4\pi n$ was the demagnetizing coefficient of the specimen. The cadmium and gallium specimens were not accurately ellipsoidal but the resulting uncertainty in allowing for the demagnetizing effect was only of order $\frac{1}{2}$ per cent. Immediately after the sharp rise in M_2' and M_2'' had been observed the value of M_1' was measured, thus giving the temperature at which H_c had been measured. Owing to the gradual warming of the salt a small correction was necessary to allow for the rise in temperature between the measurement of H_c and the measurement of M_1' . By repeating the whole procedure as the salt warmed up to bath temperature a series of values of H_c at various temperatures between 0.1°K. and the transition temperature was obtained.

The transitions in the absence of an applied magnetic field were studied by following M_2' and M_2'' as the metal warmed through the transition temperature. Values of T_c deduced in this way agreed well with those obtained by extrapolation of the critical field curves. From the change of M_2' and M_2'' between the superconducting and normal state the value of the specific resistance of the normal metal could be calculated using standard eddy current theory. For this purpose the specimens were treated as if they were long cylinders; the error due to this assumption is probably not more than a few per cent. Values of the ratio ρ/ρ_{273} of this resistivity to the resistivity at 273°K. which are a guide to the quality of the specimens, are given in Table I.

§ 5. CORRECTIONS AND SOURCES OF ERROR.

The measurements of the specimen temperature and the corresponding critical field were subject to a number of corrections and sources of error which need discussion.

(a) Temperature.

In preliminary measurements by one of us (Mendoza 1948) it was found that the thermal contact between the copper rod and the salt was inadequate for the amount of heat being developed in the rod by eddy currents (no heat of course was developed in the superconductor). This was revealed by the fact that the values of T recorded for a given H_c increased when a g.e. measuring currents were used. In the present arrangement the thermal contact between the copper rod and the salt was improved; a correction was applied for the temperature difference between the rod and the salt produced by eddy current heating but this was only of order 10^{-2} deg. for the measuring currents actually used.

There remains the possibility that the temperatures of the specimen and the salt may differ owing to a thermal gradient set up by the natural warming of the whole system. Estimates of the probable value of the temperature difference between the salt and the specimen due to this cause showed that under the actual experimental conditions and at temperatures above 0.1°K . it was unlikely to exceed 10^{-3} deg. and no correction was therefore applied.

Taking into account these possible sources of error and possible inaccuracies in the 1949 scale of temperature, the final values of the temperature of the specimens can probably be considered reliable to within 10^{-2} deg.

(b) *Critical field.*

The effect on the earth's field was allowed for by making the measurements with the solenoid field alternately with and against the vertical component of the earth's field. In order to allow for the finite amplitude of the measuring field the peak value was added as a correction to the applied field. Measuring fields of between 0.5 and 5 gauss r.m.s. were used in the experiments and after the application of this correction results were obtained with an internal consistency of better than 0.5 gauss.

The main uncertainty of interpreting the critical field measurements lies in assessing the effect of strains and impurities in the specimen. Since the value of M_2 was determined by the currents flowing in the specimen and not by its magnetic moment it follows that the present method studies the electrical resistance of the specimen rather than its magnetization, and the effect of strains or impurities in the specimens is to give values of H_c which are larger than the true values. An estimate of the magnitude of this effect is provided by the behaviour of the zinc specimen. The effect of annealing was to reduce H_c at 0.2°K . by only 4 per cent while the breadth of the zero field transition was reduced from about 4×10^{-2} deg. to not more than 5×10^{-3} deg. If a single mechanism is responsible in a superconductor for the broadening of the zero field transition and for raising the critical field above its true value then it seems probable that systematic errors in the values of H_c for the annealed specimen of zinc due to this uncertainty do not amount to more than about 2 per cent. All the other specimens had zero field transitions at least as sharp as the zinc specimen, and it seems plausible to assume that errors in H_c values for those metals due to strains and impurities are of the same order of magnitude as for zinc.

§ 6. RESULTS.

It was found that the temperature variation of the critical fields could be represented by the formula $H_c = H_0(1 - (T/T_c)^2)$; this is illustrated in figs. 2 and 3 where H_c has been plotted against T^2 , and it can be seen that the points lie well on straight lines. Values of H_0 and T_c deduced from these graphs are given in Table II.

Measurements on aluminium and gallium have previously been made by Shoenberg (1940) and appear to differ appreciably from the present results. The discrepancies are much reduced however when due account is taken of the differences between the 1932 and 1949 scales of temperature,

Fig. 2.

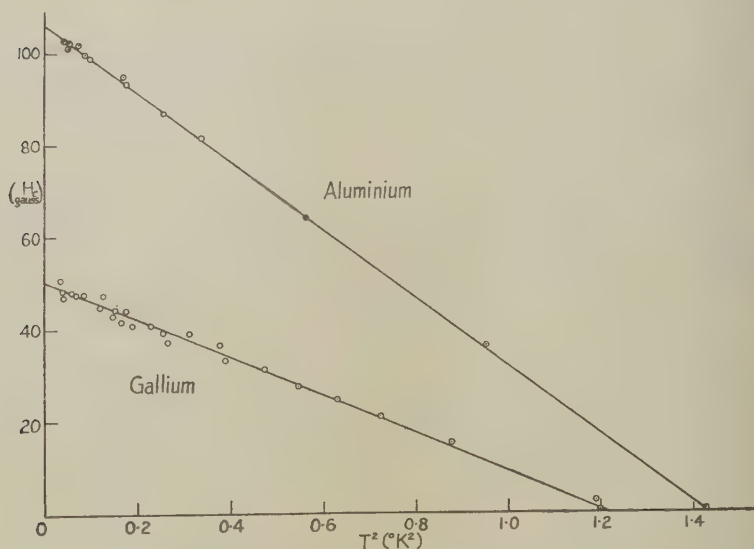
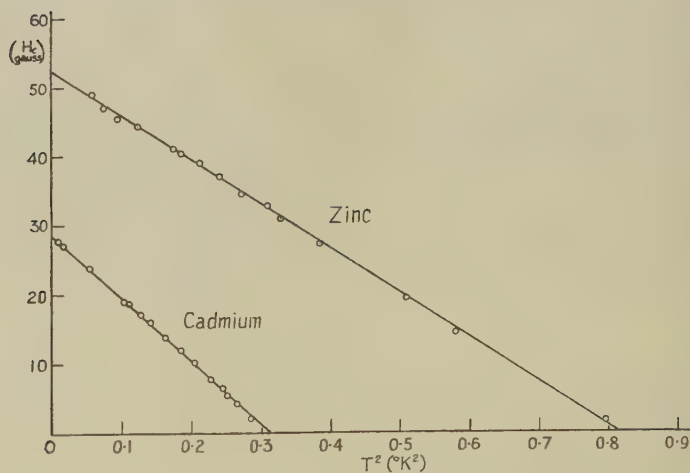
Variation of H_c with T^2 for aluminium and gallium.

Fig. 3.

Variation of H_c with T^2 for cadmium and zinc.

and of the fact that no allowance was made in Shoenberg's measurements for the pressure drop between the liquid helium level and the top of the Dewar flask*. In fact, the diameter of his flask was only 9 mm. and a pressure drop of order 0.07 mm. of mercury could have been expected at the lowest temperatures, corresponding to an error in temperature determination of order 3×10^{-2} deg. Thus Shoenberg's measurements may be regarded as supporting the present results. Kurti and Simon (1935 b) obtained in measurements on cadmium $T_c = 0.54 \pm 0.02^\circ \text{K.}$ and an initial slope of the critical field curve of order 100 gauss deg. $^{-1}$; the present values of $T_c = 0.560^\circ \text{K.}$ and 103 gauss deg. $^{-1}$ respectively are in good agreement.

TABLE II.
Summary of the Results.

	T_c ($^\circ \text{K.}$)	H_0 (gauss)	$\gamma \times 10^4$ cal. mole. $^{-1}$ deg. $^{-2}$		$\frac{\gamma}{VT_c} \times 10^6$ cal. cm. $^{-3}$ deg. $^{-3}$
			(a)	(b)	(a)
Aluminium	1.197	106.0	2.95	3.48*	24.9
Cadmium	0.560	28.8	1.28	—	17.9
Gallium	1.103	50.3	0.91	—	7.2
Zinc	0.905	52.5	1.16	1.25† 1.5‡	14.1

γ is the coefficient of T in the expression for the specific heat of the normal metal, and V is the atomic volume.

(a) Calculated from the present results.

(b) Calorimetric measurement: * Kok and Keesom (1937); † Keesom and van den Ende (1932) recalculated by Silvini and Daunt (1950); ‡ Silvini and Daunt (1950).

The values of H_c obtained by Daunt and Heer (1949 b) using Kurti and Simon's method are of order 4 gauss lower than the present results for aluminium and are of order 8 gauss higher than the present results for zinc. It therefore seems improbable that a single factor is responsible for these discrepancies. It is possible that the stresses the metal is subjected to when pressed into a pill with the salt may be responsible for the high values of H_c recorded for zinc. Furthermore, the difficulty of interpreting the complex magnetic behaviour of the mixed pills of salt and metal used may possibly be responsible for unsuspected errors in measuring both H_c and T .

The critical field measurements may also be compared with various calorimetric data. The difference in entropy per unit volume between the normal and superconducting states is given by the thermodynamical relation

$$s_s + s_n = \frac{H_c}{4\pi} \left(\frac{dH_c}{dT} \right).$$

* This possibility was pointed out to us by Dr. Shoenberg.

The experiments of Keesom and Kok (1934) on thallium and of Keesom and van Laer (1938) on tin suggest there is no linear term in the specific heat of a metal in the superconducting state. Therefore for those metals for which a relation of the type $H_c = H_0(1 + (T/T_c)^2)$ holds the linear term in the specific heat of the normal metal must be of the form $(VH_0^2/2\pi T_c^2)T$ erg mole.⁻¹ deg.⁻¹, where V is the molecular volume. Values of γ , the coefficient of T in this expression, calculated from the present results are in fair agreement with calorimetric data as can be seen from Table II.

Evidence for an empirical correlation among superconductors has recently been put forward by Daunt (1950). He observes from a plot of γ/V and T_c that the elements for which reliable information is available fall on one of two straight lines through the origin. In other words he suggests that $\gamma/V = KT_c$ where $K = 30 \times 10^{-6}$ cal. cm.⁻³ deg.⁻³ for the hard group of superconductors and $K = 6.7 \times 10^{-6}$ cal. cm.⁻³ deg.⁻³ for the soft superconductors. The values of γ/VT_c in Table II. calculated from the measurements on the four soft superconductors studied in this paper suggest that the correlation is at best only approximate.

ACKNOWLEDGMENTS.

We should like to thank Dr. J. Ashmead and Dr. D. Shoenberg for many valuable discussions, and Dr. C. G. B. Garrett for his practical assistance and advice. We have also to thank the Department of Scientific and Industrial Research for maintenance grants received while carrying out this work.

REFERENCES.

- CASIMIR, H. B. G., DE HAAS, W. J., and DE KLERK, D., 1939, *Physica*, **6**, 365.
 COOKE, A. H., 1949, *Proc. Phys. Soc. A*, **62**, 269.
 DAUNT, J. G., 1950, *Phys. Rev.*, **80**, 911.
 DAUNT, J. G., and HEER, C. V., 1949 a, *Phys. Rev.*, **76**, 715; 1949 b, *Ibid.*, **76**, 1324.
 VAN DIJK, H., and SHOENBERG, D., 1949, *Nature, Lond.*, **164**, 151.
 KEESOM, W. H., and VAN DEN ENDE, J. N., 1932, *Commun. Phys. Lab. Univ. Leiden*, No. 219 b; *Proc. Roy. Acad., Amsterdam*, **35**, 143.
 KEESOM, W. H., and VAN LAER, P. H., 1938, *Physica*, **5**, 193.
 KEESOM, W. H., and KOK, J. A., 1934, *Physica*, **1**, 175.
 KOK, J. A., and KEESOM, W. H., 1937, *Physica*, **6**, 835.
 KURTI, N., and SIMON, F. E., 1935 a, *Proc. Roy. Soc. A*, **149**, 152; 1935 b, *Ibid.*, **151**, 610.
 MENDOZA, E., 1948, *Cérémonies Langevin-Perrin, Paris*, 53.
 SHOENBERG, D., 1940, *Proc. Camb. Phil. Soc.*, **36**, 85.
 SILVIDI, A. A., and DAUNT, J. G., 1950, *Phys. Rev.*, **77**, 125.

LXIII. *A Mechanical Kick-sorter (Pulse Size Analyser).*

By S. G. F. FRANK, O. R. FRISCH and G. G. SCARROTT.

Cavendish Laboratory, Cambridge*.

[Received March 15, 1951.]

SUMMARY.

This instrument serves to obtain the size distribution of electric pulses coming, for example, from an ion chamber or counter. Each pulse causes a small steel ball to be propelled along an inclined board; the ball describes a parabolic path and lands in one of 30 parallel grooves. As balls accumulate in the grooves a histogram of the pulse size distribution is built up.

The paper describes the mechanical construction and the associated electronic circuits. The latter serve, among other things, to eliminate pulses which are either too large or too small to be recorded, or which follow too close upon the last recorded pulse.

INTRODUCTION.

A KICK-SORTER (or pulse size analyser, also pulse spectrograph) serves to obtain the amplitude distribution of electric pulses, *e.g.* from an ion chamber or proportional counter. The pulses must first be amplified by a standard pulse amplifier (see Sands and Elmore 1949); the kick-sorter then sorts them into a number of channels (size groups), recording the number in each channel separately.

It occurred to one of us (O. R. F.) in 1947 that a mechanical system might be cheaper and more reliable than the usual electronic gear which involves a great many valves (usually several per channel). In the meantime electronic kick-sorters have been much improved (see in particular Wilkinson 1950, Hutchinson and Scarrott 1951), but the instrument described here (in use since 1949) has still some advantages, chiefly cheapness and the fact that the information it contains is displayed as a histogram all the time. Its main disadvantage is low storage capacity (about 100 per channel) and slowness: pulses are sorted at most at the rate of about 6 a second.* However, in many cases that is enough.

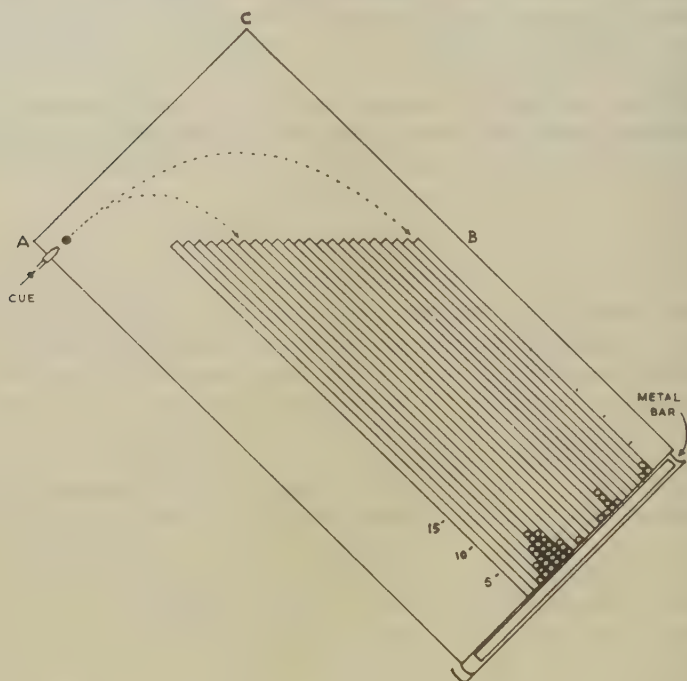
GENERAL DESCRIPTION.

Each pulse suitable for recording (see later) causes a steel ball ($\frac{1}{8}$ in. diameter) to be propelled along an inclined board (1) with 30 parallel grooves (fig. 1). The ball describes a parabolic path and lands in one groove, depending on its initial speed which in turn depends on the

* Communicated by the Authors.

amplitude of the pulse. As balls accumulate in the grooves a histogram of the pulse size distribution is built. Immediately after one ball has been fired a new one is deposited by an electrically operated "feeder" (2). The balls are projected by a little "billiard cue" (3) mounted on a coil which is driven like the coil in a dynamic loudspeaker. The current pulse which makes the coil move, and the one which actuates the feeder, come from the electronic pre-sorter (4) which contains some twenty valves. Here the pulses issuing from the standard amplifier are first lengthened (4.1) to $100\text{ }\mu\text{sec.}$; if they are bigger than an adjustable

Fig. 1.

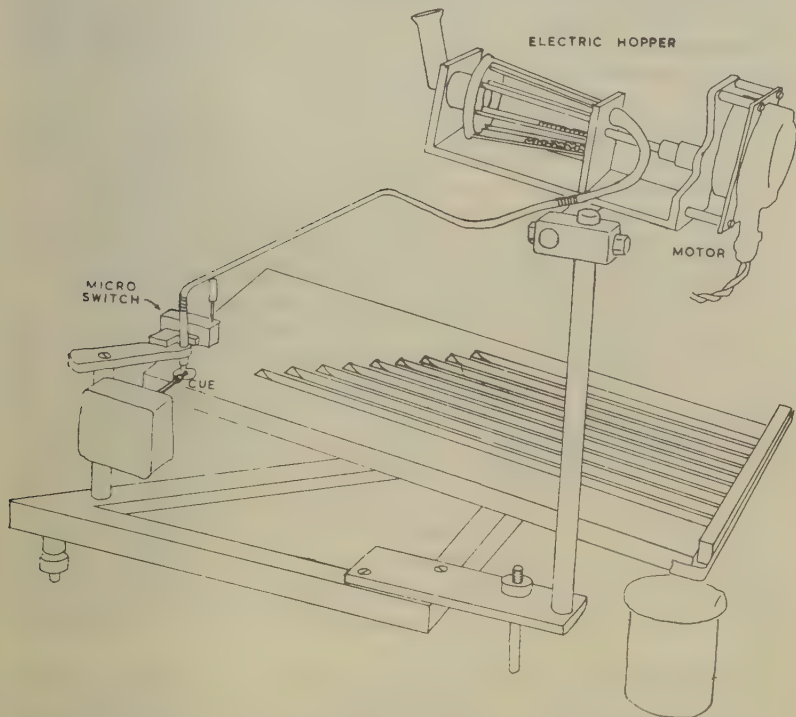


bias B their excess over B is then further amplified (4.2). The next section (4.3) selects pulses whose amplitudes lie within a certain range; the limits of this range can be adjusted so that they correspond to the first and the last groove on the board. The waiting-time unit (4.4) closes a gate after each pulse, for a time T (0.1 to 0.2 seconds) which is adjusted to make sure that the next pulse does not arrive before the next ball is in position to be fired. The output unit (4.5) lengthens the pulse further and gives it enough power to drive the billiard cue; it also produces a suitable pulse to actuate the "feeder".

DETAILED DESCRIPTION.

1. *The Board* (see figs. 1 and 2) was made of polystyrene, 23 cm. by 48 cm., $\frac{1}{2}$ in. thick. Thirty grooves just over $\frac{1}{8}$ in. wide and $\frac{1}{8}$ in. deep were cut in with a miller; this tapers the upper end of the groove and allows the ball to enter without bouncing. The board is mounted on three adjustable legs and is tilted by about 10 degrees in such a way that the line AB remains horizontal. The balls are propelled parallel to AC and hence describe parabolas each of which enters the appropriate

Fig. 2.



groove without a break. If a ball describes a parabola which leads to the ridge between two grooves, then it will be caught in the lower groove a little lower down.

At the lower end the grooves are closed by a removable metal bar. As more and more balls accumulate in the grooves, they build up a histogram of the pulse size distribution. Lines corresponding to 5, 10, 15 etc. ball diameters are drawn on the board so that the number of balls in each groove can be quickly read off after a run. This done, the metal bar is removed, and the balls run out into a gutter and from there into a beaker, ready to be used again.

On dry days the top ball in a groove often comes to rest several millimetres above the remainder, presumably due to electric charge acquired by friction. Such a charge may slightly influence the path of the ball though we have no evidence that it does. A board made of metal rather than polystyrene would eliminate this.

2. *The feeder* is a simple escape mechanism, connected to the armature of a small electromagnet (a commercial relay). When the armature is attracted the lowest ball is released; on the return motion the whole line of balls in the feeding tube is allowed to advance one unit, making a fresh ball ready for release. On being released, the ball drops by about $1\frac{1}{2}$ diameters, on the spot from which its predecessor has just been fired.

To prevent bouncing, the platform on which the ball drops is a mica membrane cemented over a metal ring and smeared thickly with grease from below. This has proved very durable and is remarkably bounce-free; balls are stopped dead even if dropped from a height of several inches. There is some slight bouncing from the two locating posts which prevent the balls from rolling off. This could probably be improved by suitable design of the posts, and then a waiting time of 0.05 seconds between balls should suffice. As it is, we find operation getting erratic if the waiting time is made shorter than 0.15 second.

The feeding tube can only hold a few dozen balls, otherwise the pressure on the release mechanism gets too heavy. The electrically operated hopper shown can store many hundred balls and is very reliable. It consists of a hollow cone (its walls transparent for convenience) with a number of scoopers on its inside. The cone is slowly turned by a small motor and gear (4 revs./min.). Each scooper picks up some twenty balls, carries them to the top where it becomes suitably inclined because of the conical arrangement, and feeds them into the feeding tube. The latter has a crooked section which is hinged to the remainder by two short lengths of spiral spring (or soft rubber tube). When this section contains enough balls it presses upon a microswitch and turns off the motor which drives the hopper; when it is partly emptied the motor starts again.

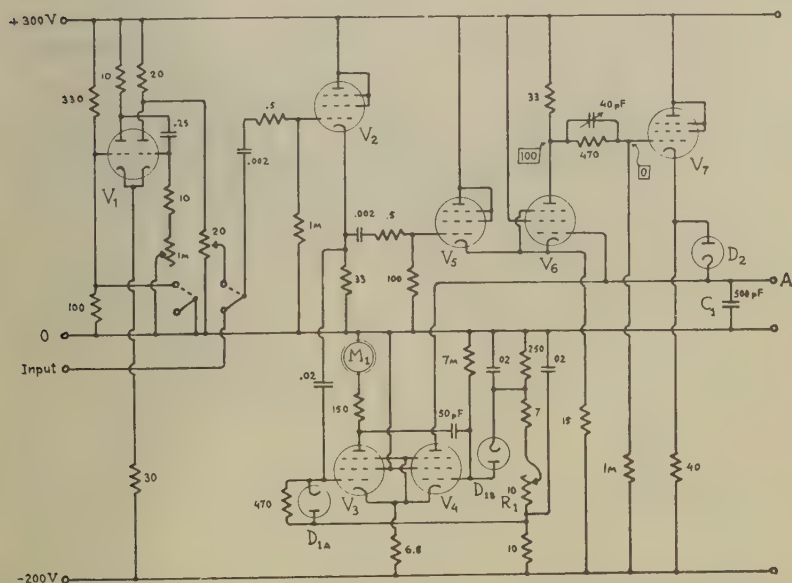
3. The propelling mechanism is a little billiard cue, driven electro-dynamically. The tip of the cue was made of polystyrene and seems quite satisfactory. The shaft is an aluminium rod, 2 mm. thick, threaded over its whole length (of about 7 cm.). It is clamped, with the help of four nuts, onto two V-shaped supports of beryllium copper foil so that it can move lengthwise only. Its other end is screwed on the driving coil (22 mm. diameter, 800 turns of 48 S.W.G. enamelled wire) which moves in the annular gap of a commercial loudspeaker magnet.

When the cue strikes it gives the ball a velocity which is in a fixed proportion to its own (twice if the cue were much heavier than the ball, and perfectly elastic). The distance the ball will travel is proportional to the square of its speed (neglecting friction). In order to make that distance proportional to the pulse amplitude the speed of the ball (and

hence that of the cue as it strikes) must be proportional to the square root of the pulse amplitude. This will be so if the cue is uniformly accelerated from rest until it touches the ball, by a force proportional to the pulse amplitude. To achieve uniform acceleration, one has to avoid all damping and friction; yet the return motion ought to be damped to avoid bouncing. This damping was produced by a 5 Kohm resistor parallel to the coil, the resistor being in series with a diode which becomes conducting during the return motion only.

4. The valves of the electronic presorter are contained in one standard chassis; a second chassis contains a power supply of standard design, supplying +300 volts (up to 300 mA.) and -200 volts (up to 150 mA.), both stabilized.

Fig. 3.

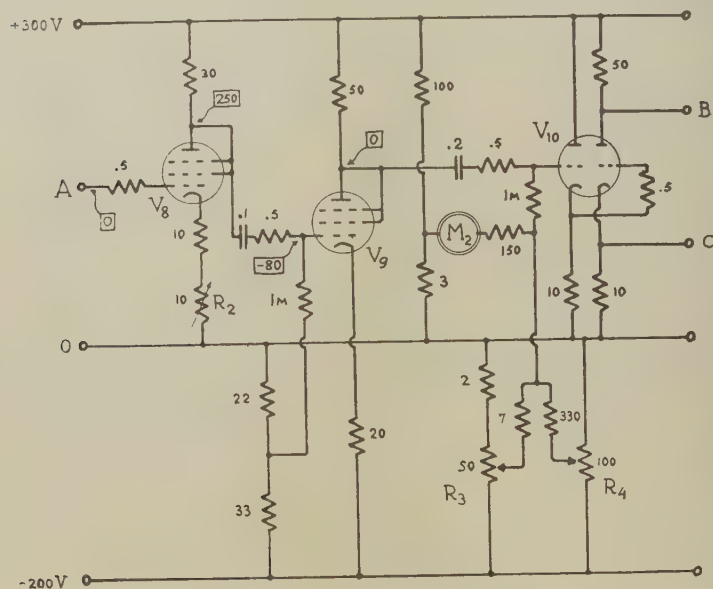


Standard pulse generator and pulse lengthener. All resistances are in kilohm and capacities in μF except where otherwise stated. M means megohms pF means $\mu\mu\text{F}$; numbers given thus $\overline{20}$ indicate steady state voltages.

4.1. (See fig. 3.) The input pulses must be positive and between 7 and 50 volts in size. They come either from the input terminal or else from a multivibrator (valve V_1) which produces standard pulses of adjustable amplitude and recurrence frequency, for testing. After being fortified by a cathode follower (valve V_2) those which are larger than a certain preset value (adjustable through R_1) trigger the valve pair 3-4 whereby valve 4 is rendered non-conducting for about 100 μ sec. At the

same time, as the potential of the control grid of V_5 rises with the pulse, the difference between it and the potential at A is amplified by V_6 and causes V_7 to produce current which tends to abolish this potential difference. Thus A follows the pulse until it reaches its maximum; thereafter D_2 ceases to conduct, and C_1 remains charged to the amplitude of the input pulse until valve V_4 becomes again conducting. In this way each input pulse (provided it is large enough) produces at the point A a voltage equal to its own peak voltage, remaining constant for about $100 \mu\text{secs.}$ and then returning to zero. R_1 is adjusted so as to exclude noise pulses, yet to include all pulses which we want to analyse. The

Fig. 4.



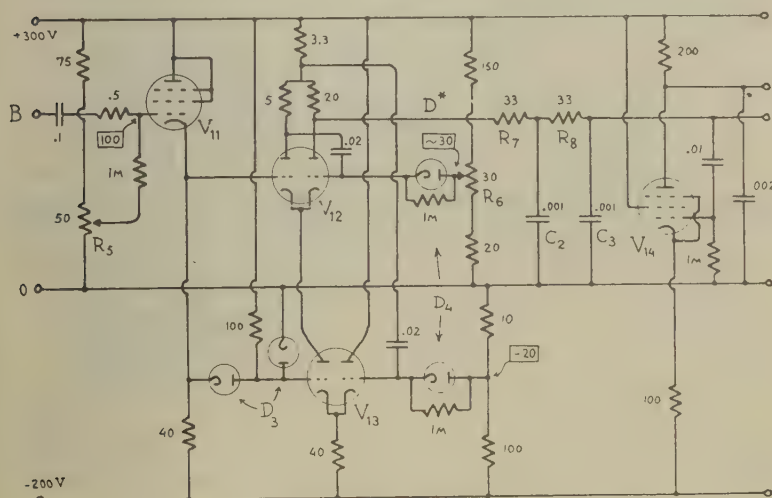
Amplifier and biased amplifier.

meter M_1 averages the current through V_3 and thus indicates the rate at which pulses pass this hurdle: this rate should not exceed about 200 pulses per second or else some bias levels will shift.

4.2. (See fig. 4.) Valves V_8 and V_9 form an amplifier with a gain of about 4 (adjustable through R_2). The first half of valve V_{10} is a biased cathode follower (which will not draw grid current, even for large pulses), feeding the second half, a triode amplifier of gain 5. The (negative) bias has coarse and fine adjustment (R_3 and R_4) and is indicated on the meter M_2 . Pulses below a certain minimum size (which depends on the bias) are not amplified by this arrangement; of larger pulses, the portion exceeding the minimum size is linearly amplified and appears at the point B, now as negative pulses.

4.3. (See fig. 5.) After passing through valve V_{11} which serves to adjust (through R_5) the D.C. level, the pulses are supplied, in parallel, to the double triodes V_{12} and V_{13} . V_{12} forms a trigger circuit which will produce a certain negative potential on point D* if the potential on its left-hand grid drops below a certain level v_1 , adjustable through R_6 . However, if the pulse is so large that it drops below v_2 , then V_{13} is triggered as well; the current in V_{12} is thereby turned off and point D* becomes positive again. In this case only a very brief negative pulse is produced, which is filtered out by the low-pass network $R_7C_2R_8C_3$. Thus a negative pulse of standard size, somewhat delayed and rounded off by the low-pass network, is produced at point D every time the input pulse has an amplitude between v_1 and v_2 . These "control pulses"

Fig. 5.



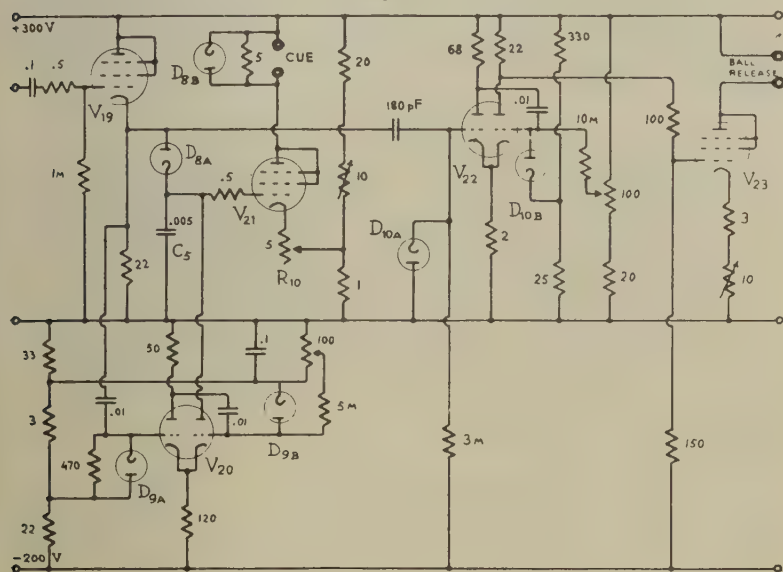
Discriminator.

can be counted by an external scaler connected to the terminal E. They serve, furthermore, to open a gate (see 4.5) which admits the pulse proper to the output valve.

4.4. (See fig. 6.) The waiting time T is determined by the time constant (adjustable through R_9) of the trigger circuit formed essentially by valve V_{17} . When triggered, this circuit renders conducting the right-hand half of valve V_{15} , thus preventing further control pulses from getting through until the waiting time is over. If the control pulse does get through it is sharpened and reversed by the trigger circuit V_{16} . Its leading edge places positive charge on the left-hand grid of valve V_{17} : its trailing edge triggers it and "shuts the door behind itself", for a time sufficient to allow another ball to be placed in position to be fired.

A number of electronic adjustments have to be made before the kick-sorter can be used. R_2 is first adjusted so that an amplification factor of 4 is obtained between the input pulse and the pulse appearing at the input to the biased amplifier (V_{10}). M_2 will then indicate how much voltage the bias removes from the original pulse height. Next R_6 (section 4.3) is adjusted so that the range of pulses admitted corresponds to 5 volts at the input terminals. When these adjustments have been made it is necessary to arrange for the smallest pulse to fire its balls into groove 1 and the largest one into groove 30. This requires a combination of adjustments of R_5 and R_{10} . R_5 adjusts the ratio of the smallest to

Fig. 7.



Final pulse lengthener and output valves.

largest pulse passed, R_{10} just varies the absolute magnitude of the output pulse. R_5 and R_{10} have to be adjusted alternately by successive approximations.

When clean the kick-sorter will remain stable to one channel after the initial warming up period and will fire between 80 per cent and 90 per cent of the balls into one groove with a standard pulse, the remaining balls being distributed over the two adjacent grooves.

One of us (S. G. F. F.) wishes to thank the Department of Scientific and Industrial Research for a maintenance grant.

REFERENCES.

- HUTCHINSON, G. W., and SCARROTT, G. G., 1951, *Phil. Mag.*, **42** (in the press).
 WILKINSON, D. H., 1950, *Proc. Camb. Phil. Soc.*, **46**, 508.

LXIV. *A Localizing Geiger Counter.*

By S. G. F. FRANK,
Cavendish Laboratory, Cambridge*.

[Received March 15, 1951.]

SUMMARY.

The constant speed with which the discharge spreads along the wire in a Geiger counter is used to localize ionizing particles. Signals are obtained from the wire and also from two electrodes near its ends; from these signals a pulse is derived whose amplitude indicates the position of the initial ionizing event. Provision is made for stabilizing the speed of spread.

THIS instrument determines the position of the initial ionizing event along the length of a Geiger counter, with an error of less than 1 cm. Its operation is based on the fact that the discharge in a Geiger counter spreads along the central wire in both directions with a constant velocity of about 10 cm. per micro-second. The time which elapses between the start of the discharge and its arrival at one end of the counter is therefore proportional to the distance of the original ionizing event from that end of the counter. Furthermore the sum of the times taken by the discharge to reach both ends of the counter should be independent of the position of the ionizing event, and this serves as a check on the correct operation of the counter.

To obtain all the required information about the discharge, two small auxiliary cathodes of about 1 cm. length and 2 mm. diameter are placed at the two ends of the anode. Their potential is adjusted to that of the equipotential which they occupy in the counter. At the start of the discharge a sharp negative pulse is obtained from the anode by differentiation, using a 1000 ohm resistance earthed through a $0.25 \mu\text{F}$. condenser. Two positive pulses are obtained directly from the two auxiliary cathodes when the discharge reaches the two ends of the counter. All three pulses are fed into head amplifiers, which produce positive output pulses. These are then amplified by identical wide-band amplifiers which operate three fast trigger circuits (see fig. 1). The trigger circuit (*b*) actuated by the anode produces a *negative* square wave lasting about 20 microseconds. The trigger circuits (*a*) and (*c*) actuated by the auxiliary cathodes produce similar *positive* pulses lasting about twice as long. Pulses from the triggers (*a*) and (*b*) pass through an "interval converter" which generates a signal p_1 whose amplitude is proportional to the time interval between the onset of the pulses from

* Communicated by Professor O. R. Frisch, F.R.S.

Fig. 2 shows the electronics in the blocks (a) and (1). The first pentode (head amplifier) is placed close to the counter; the next three pentodes

Amplifier and Trigger

Interval Converter

[illegible]

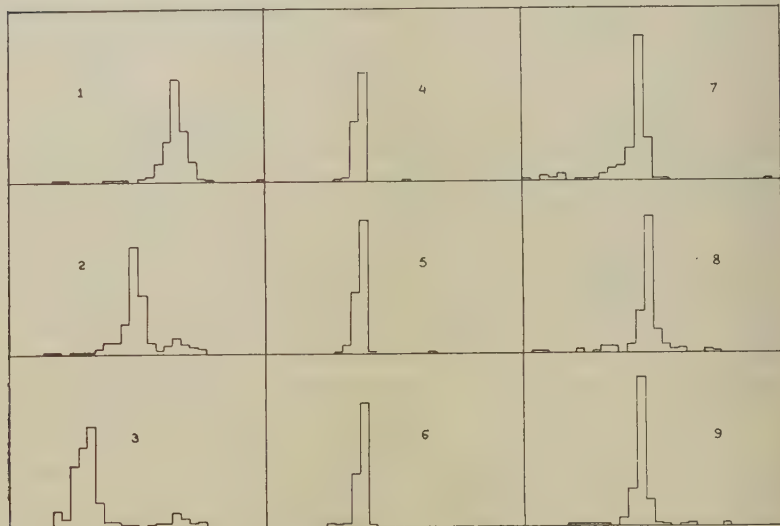
form a fast amplifier which is coupled through a diode to the trigger circuit, comprising the next two pentodes. The last two pentodes and the last diode form the interval converter (1), which works as follows. The pulse from trigger (b) cuts off the valve (8); this allows the condenser C_1 to charge up through a diode and a 125 k ω resistor until the positive pulse from (a) brings valve (7) into conduction. The voltage

in C_1 is kept small compared to 240 volts, and therefore rises linearly in the time between pulse (a) and pulse (b). Thereafter C_1 is discharged (much more slowly) through a 1 megohm resistor to the bias line.

The electronics in block (c) is entirely similar; in block (b) it differs in that the first pentode is used not as a cathode follower but as a phase inverter, with an anode resistor of $1.6\text{ k}\Omega$, and that the required positive signal for both interval converters comes from point A, not B, as shown in fig. 1.

The propagation velocity of the discharge increases with increasing over-voltage. It is thus possible to control the over-voltage of the counter in such a way as to keep $p_1 + p_2$ constant. This stabilizes the

Fig. 3.



Pulse size distributions obtained from localizing counter. Diagrams 1, 2, 3: pulse p_1 , with β -source at 5 cm., 12 cm. and 19 cm. respectively, from "lower" end of counter.

Diagrams 4, 5, 6: pulse $\frac{1}{2}(p_1 + p_2)$ for the same source positions as in diagrams 1, 2 and 3 respectively.

Diagrams 7, 8, 9: pulse p_1 with α -source at 2, 12 and 22 cm. from end of counter. A bias of 6.9, 4.9 and 2.9 V. respectively was used to keep the group near the centre; 1 volt bias means a shift of six channels.

constant of proportionality relating both p_1 and p_2 to the position of the ionizing event, and also serves to keep the counter in the correct operating condition. To get the sum of the two pulses they are applied to the two ends of a resistor, from the centre of which a pulse equal to $\frac{1}{2}(p_1 + p_2)$ is then obtained. The circuit used to control the over-voltage is similar to that designed by D. H. Wilkinson (1950) for the stabilization of proportional counters.

The counter used had brass walls with an internal diameter of about 3.8 cm., and an active length of about 25 cm. ; it was fitted with a narrow mica window extending over the whole of its active length, had a tungsten anode of 0.1 mm. diameter, and was filled with 10 cm. pressure of argon and 1.5 cm. of alcohol vapour. To test it a beam of β -particles about 2 mm. wide was directed at the counter window at various points along the counter. The pulses were analyzed with a 30-channel kick-sorter (Frank, Frisch and Scarrott 1951) and the results are shown in fig. 3. The small subsidiary group shown on diagrams 2 and 3 is thought to be due to spurious counts originating at that point of the counter.

The spread of the individual pulse groups is much greater than that of the groups due to $p_1 + p_2$ (see diagrams 4, 5 and 6) ; hence it could not have been due to any shortcomings of the instrument, but perhaps to scattering of the incoming β -particles at the window. To test this another similar counter was made with a thin enough window to admit α -particles which would be scattered very much less. Indeed the groups were very much sharper, as shown on diagrams 7, 8 and 9. In this case one channel width on the kick-sorter corresponds to about 8 mm. along the Geiger counter, and it is seen that localization is possible with a standard error of less than 1 cm.

My thanks are due to Professor Frisch who suggested this work, to Mr. G. G. Scarrott for his advice about the electronics, and to the Department of Scientific and Industrial Research for a grant.

REFERENCES.

- FRANK, S. G. F., FRISCH, O. R., and SCARROTT, G. G., 1951, *Phil. Mag.*, **42**, 603.
WILKINSON, D. H., 1950, *J. Sci. I.*, **27**, 36.

LXV. *The Development of Deformation Textures in Metals.*—Part II. *Body-Centred Cubic Metals.*

By E. A. CALNAN and C. J. B. CLEWS,
National Physical Laboratory *.

[Received February 19, 1951.]

§1. INTRODUCTION.

THE aim of the present treatment is to explain the development of deformation textures in polycrystalline aggregates from the behaviour of their single crystals, while at the same time attempting to overcome certain difficulties and limitations of previous methods. Its application to face-centred cubic metals led to the prediction of the polycrystalline stress-elongation curve, and, in a qualitative fashion, to the preferred orientations resulting from tension, compression, rolling, and wire drawing operations, (Calnan and Clews 1950, subsequently referred to as Part I.). It was shown that these predictions are in reasonable accord with experimental observations, although the latter are by no means comprehensive.

It has been shown (Mises 1928, Taylor 1938) that, in the idealized case of homogeneous deformation, multiple slip, *i. e.* slip on three or more systems, must take place in order to preserve the external form of the specimen and to maintain cohesion at the grain boundaries. It is now postulated that for this multiple slip to occur the stress system within a grain or part of a grain must be such as to give equal resolved shear stresses on all the operative slip systems. The simplest stress system satisfying this condition is a single tensile stress, previously referred to in Part I. as the effective stress, T_e , lying, in the case of a face-centred cubic metal, in a [100], [110] or [111] direction. In the initial condition with perfectly annealed material, at the instant of application of a small applied tensile stress, T_a , the effective stress direction is coincident with the direction of this applied stress. As soon as elastic deformation takes place intergranular stresses generally come into play. If the applied stress is then increased and slip does not occur when the applied stress resolved on the most favourable slip system reaches the critical value for slip, then T_e must have moved away from T_a in such a direction as to reduce the resolved shear stress on this system. With further increase in the applied stress, provided no slip has occurred, T_e continues to move until it reaches one of the minimum positions of resolved shear stress, which are, of course, the points of multiple slip already referred to above. Having arrived at such a position, no further movement of T_e is possible and there must be slip on all the symmetrically disposed equivalent systems when the critical stress is reached. Slip will frequently occur, however, before this condition is attained; there will be single slip if T_e is within the reference

* Communicated by the Authors.

stereographic unit triangle, or duplex slip if T_c is on a boundary between two equivalent slip systems. The operation of slip relieves the intergranular stresses and the whole sequence above recommences. Thus the deformation of a single grain or part of a grain within the polycrystalline mass is visualized as a discontinuous process made up of elements of multiple, duplex, and single slip. It is clear that inhomogeneous deformation is implicit in this treatment.

Due to the symmetrical disposition of the equivalent slip systems at the positions of multiple slip there is no grain rotation and the development of preferred orientation thus depends on the rotations resulting from single and duplex slip. Consequently, in order to produce the high degree of preferred orientation observed after extensive deformation, there must be a considerable amount of single and duplex slip, although some multiple slip is necessary to retain both cohesion at the boundaries and specimen shape.

These concepts, described in greater detail in Part I., have now been applied to the more complex case of the deformation of a body-centred cubic metal where slip can occur on systems of the types $\{110\}\langle 111 \rangle$, $\{112\}\langle 111 \rangle$, or $\{123\}\langle 111 \rangle$. Andrade and his co-workers (1940), who have made an extensive study of the slip systems in body-centred cubic metals, find that the slip direction $\langle 111 \rangle$ is invariable but that the slip plane depends on the temperature in such a way that it is the same for many metals for the same ratio of test temperature, T , to melting temperature, T_m (Table I.).

TABLE I.
Slip Planes in Body-Centred Cubic Metals.

Metal	Slip plane	T/T_m
Mo, W, Na	112	0.08 to 0.24
β -brass, Mo, Na	110	0.26 to 0.50
Na, K	123	0.80 to 0.87

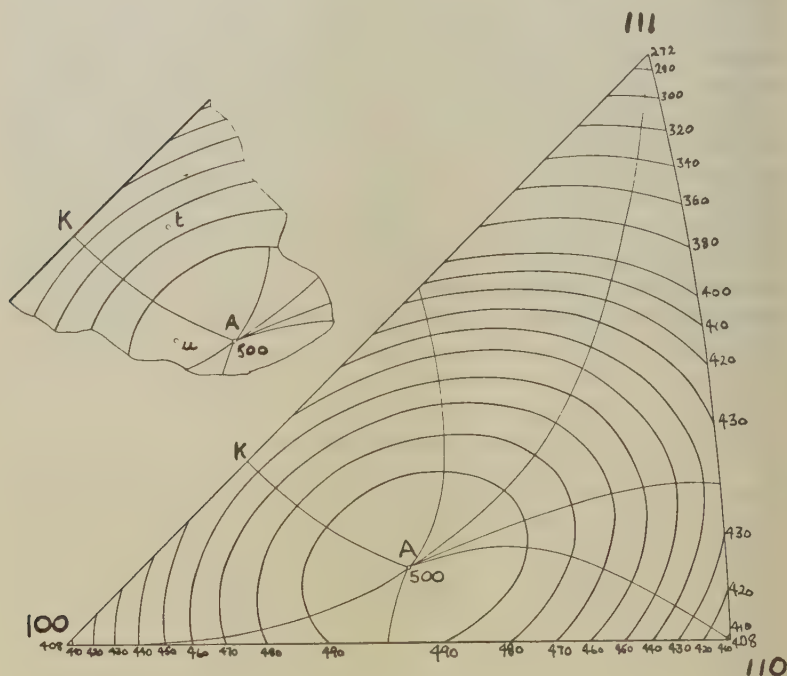
The systems operative in α -iron have been studied by Barrett, Ansel and Mehl (1937 a), who find that slip takes place on all three planes at temperatures between 20°C . and -195°C . Silicon ferrite, deformed at low temperatures or containing more than 4 per cent silicon, slips only on $\{110\}$ planes. In conditions where all three planes are operative, however, the ratio of the critical shear stresses for $\{110\}$, $\{112\}$, and $\{123\}$ slip, determined by Smoluchowski and Opinsky (1950), is 100 to 103 to 105.

Deformation textures have been derived for each of the three slip planes operating independently, for the three systems simultaneously operative with equal critical shear stresses, and for the three systems with critical shear stresses in the ratios referred to above.

§ 2. MAXIMUM RESOLVED SHEAR STRESS DIAGRAMS.

Values of the function $\cos \chi \cos \lambda$, where χ and λ are respectively the angles which the slip direction and the slip plane normal make with any particular direction of applied stress, have been tabulated at 1° intervals over ranges of α and β from 0° to 90° ; α is the angle of co-latitude and β the angle of longitude of the pole of the stress direction on a standard stereographic projection. They have been calculated to three figures on Hollerith machines by the Mathematics Division of the National Physical Laboratory.

Fig. 1.



Maximum resolved shear stress contours, to three decimal places, plotted on a standard stereographic unit triangle for the systems $\{110\}\langle 111 \rangle$ and $\{111\}\langle 110 \rangle$. Some lines of quickest descent from the maximum at A are also shown.

Contour diagrams of these functions for $\{110\}$, $\{112\}$ and $\{123\}$ systems have been published previously by Fahrenhorst and Schmid (1932). The justification for reproducing the diagrams based on these new tables lies not only in their greater accuracy but also in that they reveal some features overlooked in these earlier diagrams.

$\{110\}\langle 111 \rangle$ and $\{111\}\langle 110 \rangle$ Systems.

From the point of view of the evaluation of the function $\cos \chi \cos \lambda$ these two systems are of course identical, although they are different

crystallographically. The system $\{111\}\langle 110 \rangle$, i. e. slip on $\{111\}$ planes in $\langle 110 \rangle$ directions, has been considered in Part I. The related system $\{110\}\langle 111 \rangle$, slip on $\{110\}$ planes in $\langle 111 \rangle$ directions, is required in the present discussion. The maximum resolved shear stress contours are shown in fig. 1. The most favourable system, that corresponding to these maximum resolved shear stress values, is the $(101)[11\bar{1}]$ throughout the unit triangle. Along the edges of the unit triangle the maximum resolved shear stress is found on two symmetrically placed systems, while at the corners of the triangle the maximum value is on four, six or eight equivalent systems (Table II.).

TABLE II.
Most Favourable $\{110\}\langle 111 \rangle$ Slip Systems.

	Slip systems	Number
Unit triangle	$(101)[11\bar{1}]$.	1
Boundary $[100][110]$	$(101)[11\bar{1}]$, $(10\bar{1})[111]$.	2
Boundary $[100][111]$	$(101)[11\bar{1}]$, $(110)[1\bar{1}1]$.	2
Boundary $[110][111]$	$(101)[11\bar{1}]$, $(011)[1\bar{1}1]$.	2
Point $[110]$	$(101)[11\bar{1}]$, $(10\bar{1})[111]$, $(011)[1\bar{1}1]$, $(01\bar{1})[111]$.	4
Point $[111]$	$(101)[11\bar{1}]$, $(101)[1\bar{1}1]$, $(011)[1\bar{1}1]$, $(011)[111]$, $(110)[1\bar{1}1]$, $(110)[111]$.	6
Point $[100]$	$(101)[11\bar{1}]$, $(101)[1\bar{1}1]$, $(110)[1\bar{1}1]$, $(110)[111]$, $(10\bar{1})[111]$, $(10\bar{1})[1\bar{1}1]$, $(1\bar{1}0)[111]$, $(1\bar{1}0)[1\bar{1}1]$.	8

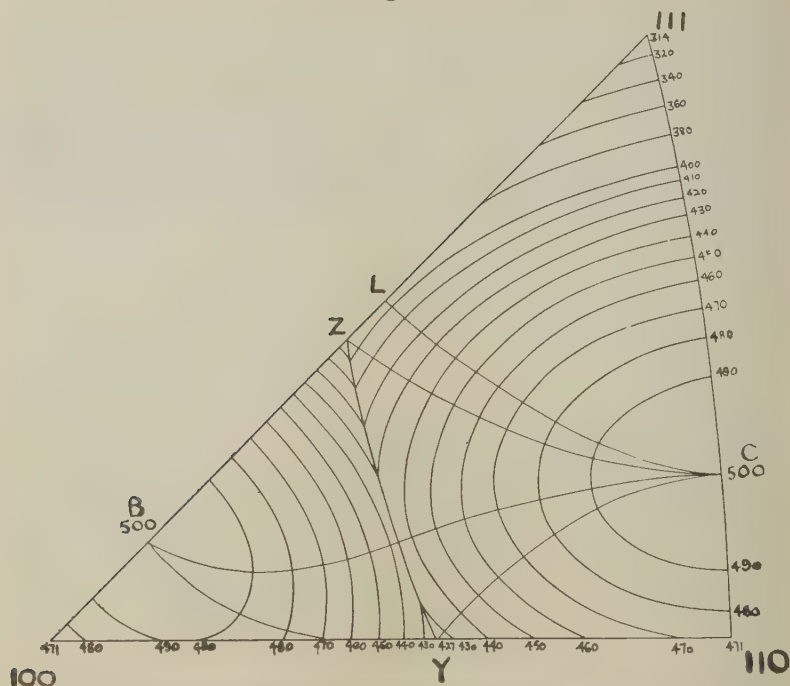
$\{112\}\langle 111 \rangle$ System.

The maximum resolved shear stress contours for the $\{112\}\langle 111 \rangle$ system are shown in fig. 2. This case is not as simple as the previous one, in that the same slip plane and direction are not the most favourable throughout the unit triangle. In the area $[100]YZ$ the operative plane and direction are $(2\bar{1}1)$ and $[111]$ respectively, while in the area $[111][110]YZ$ they are (112) and $[11\bar{1}]$. Along the line YZ the resolved shear stresses for these two systems are equal. The most favourable slip planes and directions at triangle edges and corners are listed in Table III. It should be noted that the maximum number of most favourable equivalent systems is four, occurring at $[100]$ and Y .

The position of the boundary YZ between the two systems may be determined geometrically as follows. Consider the general case of two slip systems $(p_1q_1r_1)[p_2q_2r_2]$ and $(p_3q_3r_3)[p_4q_4r_4]$. At any point of indices h, k, l the resolved shear stress on the system $(p_1q_1r_1)[p_2q_2r_2]$ is equal to $\cos \chi \cos \lambda$, where χ and λ are respectively the angles which the slip direction $[p_2q_2r_2]$ and the slip plane normal $[p_1q_1r_1]$ make with the direction $[hkl]$. $\cos \chi \cos \lambda$ is therefore equal to

$$\frac{hp_1 + kq_1 + lr_1}{\sqrt{(p_1^2 + q_1^2 + r_1^2)}\sqrt{(h^2 + k^2 + l^2)}} \cdot \frac{hp_2 + kq_2 + lr_2}{\sqrt{(p_2^2 + q_2^2 + r_2^2)}\sqrt{(h^2 + k^2 + l^2)}} = P. \quad \dots (1)$$

Fig. 2.



Maximum resolved shear stress contours for the system $\{112\}\langle 111 \rangle$, showing some lines of quickest descent from the maxima at B and C, and the boundary YZ between regions of different operative slip planes and directions.

TABLE III.

Most Favourable $\{112\}\langle 111 \rangle$ Slip Systems.

	Slip systems	Number
Area $[100]YZ$	$(2\bar{1}\bar{1})[111]$.	1
Area $[111][110]YZ$	$(112)[1\bar{1}\bar{1}]$.	1
Boundary $[110]Z$	$(2\bar{1}\bar{1})[111]$.	1
Boundary $[110][111]$	$(112)[111]$.	1
Boundary $[100]Y$	$(2\bar{1}\bar{1})[111]$, $(2\bar{1}\bar{1})[1\bar{1}\bar{1}]$.	2
Boundary $[110]Y$	$(112)[111]$, $(112)[1\bar{1}\bar{1}]$.	2
Boundary $[111]Z$	$(112)[111]$, $(121)[1\bar{1}\bar{1}]$.	2
Boundary YZ	$(2\bar{1}\bar{1})[111]$, $(112)[1\bar{1}\bar{1}]$.	2
Point $[110]$	$(112)[111]$, $(112)[1\bar{1}\bar{1}]$.	2
Point Z	$(112)[111]$, $(121)[1\bar{1}\bar{1}]$, $(2\bar{1}\bar{1})[111]$.	3
Point $[111]$	$(112)[111]$, $(121)[1\bar{1}\bar{1}]$, $(211)[1\bar{1}\bar{1}]$.	3
Point $[100]$	$(2\bar{1}\bar{1})[111]$, $(2\bar{1}\bar{1})[1\bar{1}\bar{1}]$, $(211)[1\bar{1}\bar{1}]$, $(2\bar{1}\bar{1})[1\bar{1}\bar{1}]$.	4
Point Y	$(2\bar{1}\bar{1})[111]$, $(2\bar{1}\bar{1})[1\bar{1}\bar{1}]$, $(112)[1\bar{1}\bar{1}]$, $(112)[111]$.	4

There is a similar expression, Q , for the resolved shear stress on the other system, and the boundary is given by $P=Q$, *i. e.* the equation

$$\begin{aligned} &h^2(Rp_1p_2 - p_3p_4) + k^2(Rq_1q_2 - q_3q_4) + l^2(Rr_1r_2 - r_3r_4) \\ &+ hk(Rp_1q_2 + Rp_2q_1 - p_3q_4 - p_4q_3) \\ &+ hl(Rp_1r_2 + Rp_2r_1 - p_3r_4 - p_4r_3) \\ &+ kl(Rq_1r_2 + Rq_2r_1 - q_3r_4 - q_4r_3) = 0, \end{aligned} \quad (2)$$

where

$$R = \left\{ \frac{(p_3^2 + q_3^2 + r_3^2)(p_4^2 + q_4^2 + r_4^2)}{(p_1^2 + q_1^2 + r_1^2)(p_2^2 + q_2^2 + r_2^2)} \right\}^{\frac{1}{2}}.$$

This equation is homogeneous in the second degree and therefore is the equation of a cone. In the special case where the determinant

$$\Delta = \begin{vmatrix} (Rp_1p_2 - p_3p_4) & \frac{1}{2}(Rp_1q_2 + Rp_2q_1 - p_3q_4 - p_4q_3) & \frac{1}{2}(Rp_1r_2 + Rp_2r_1 - p_3r_4 - p_4r_3) \\ \frac{1}{2}(Rp_1q_2 + Rp_2q_1 - p_3q_4 - p_4q_3) & (Rq_1q_2 - q_3q_4) & \frac{1}{2}(Rq_1r_2 + Rq_2r_1 - q_3r_4 - q_4r_3) \\ \frac{1}{2}(Rp_1r_2 + Rp_2r_1 - p_3r_4 - p_4r_3) & \frac{1}{2}(Rq_1r_2 + Rq_2r_1 - q_3r_4 - q_4r_3) & (Rr_1r_2 - r_3r_4) \end{vmatrix} \quad (3)$$

vanishes the equation corresponds to a pair of planes.

There is a further boundary corresponding to the equation

$$P = -Q, \quad (4)$$

which is also homogeneous in the second degree. The physical significance of this second boundary is that here the resolved shear stresses on the two systems are numerically equal but of opposite sign. The full expansion of (4) and its determinant differ from (2) and (3) only in that product terms with suffixes 3 and 4 are reversed in sign. The intersections of the cones, or pairs of planes, with the edges $[100][111]$, $[100][110]$, and $[110][111]$ of the reference unit triangle may be determined by substituting $l=k$, $l=0$, and $h=k$ respectively in (2) and (4). In the case of pairs of planes these intersections are sufficient to define the planes and hence the boundaries in the triangle. The form of the boundaries within the unit triangle in the case of the cones may be determined by numerical solution in this region, and confirmed by the resolved shear stress tables.

Applying these general results to the determination of the boundary YZ in the $\{112\}\langle 111 \rangle$ system, equation (2) takes the form

$$h^2 - hk - 2k^2 - 3lk + l^2 = 0, \quad (5)$$

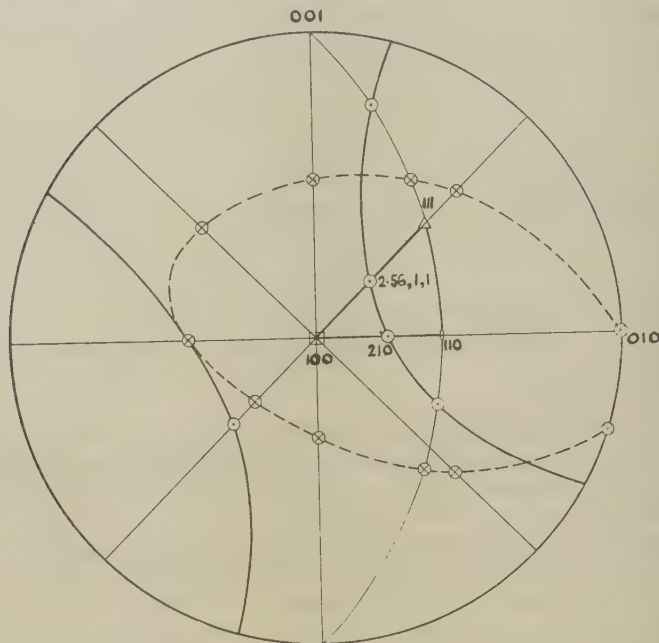
which, since the determinant (3) does not vanish, represents a cone. The solutions of (5) for the conditions $l=k$, $l=0$, and $h=k$ are respectively, $h=2.56k$ or $h=-1.56k$, $h=2k$ or $h=-k$, and $h=-1.78l$ or $h=0.28l$. A similar procedure for equation (4) shows that this boundary cone intersects $l=k$ at $h=0.59k$ and $h=-2.26k$, $l=0$ at $h=0$ and $h=-k$, and $h=k$ at $h=0.63l$ and $h=-0.80l$. These points of intersection are shown on

a standard stereographic projection in fig. 3. Thus the point Y is $[210]$ and Z is $[2\cdot56, 1, 1]$. Fig. 2 has been drawn to be consistent with this information.

$\{123\}\langle 111 \rangle$ System.

The $\{123\}\langle 111 \rangle$ system is more complex than either of those already discussed, since it involves three different most favourable slip systems within the unit triangle. The maximum resolved shear stress contours are shown in fig. 4 and the most favourable systems are listed in Table IV.

Fig. 3.



Standard stereographic projection showing the traces of the boundary cones corresponding to equation (2) for the systems $(2\bar{1}1)[111]$ and $(1\bar{1}2)[11\bar{1}]$ equal in magnitude and sign (full line), and equation (4) for these systems equal in magnitude and opposite in sign (broken line).

It is interesting to note that the corner points have the same number of equivalent systems as the $\{110\}\langle 111 \rangle$ case, and in addition there are six equivalent systems at X and four at Y.

Consider now the boundary XY between the systems $(3\bar{1}2)[11\bar{1}]$ and $(213)[11\bar{1}]$. Equation (2) reduces to a pair of planes

$$h+k-l=0, \quad \dots \dots \dots (6a)$$

$$h-2k-l=0, \quad \dots \dots \dots (6b)$$

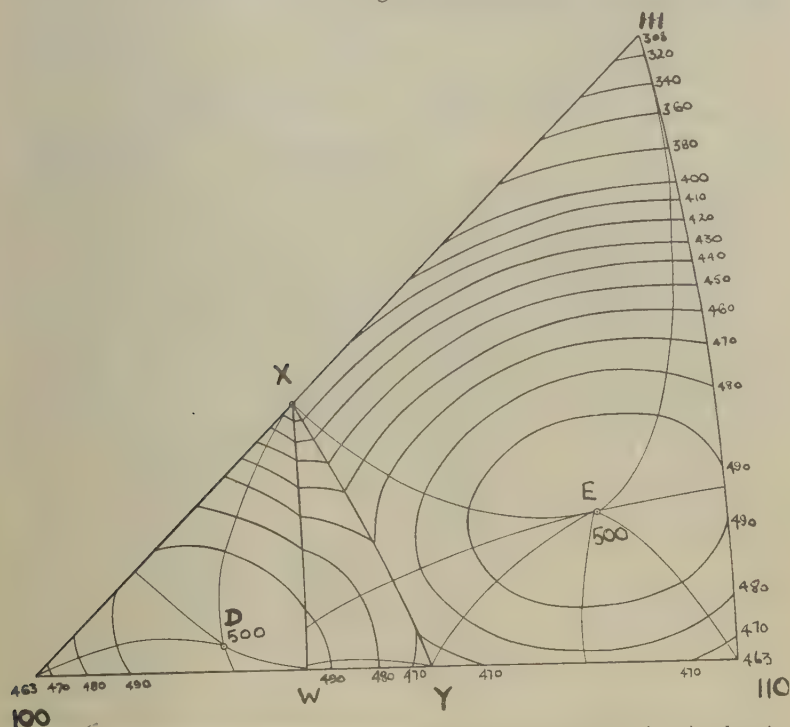
while equation (4) also reduces to two planes

$$h+k-l=0, \quad . \quad . \quad . \quad . \quad . \quad . \quad (7a)$$

$$h+l=0. \quad . \quad . \quad . \quad . \quad . \quad . \quad (7b)$$

It will be seen that the two cones degenerate into *three* distinct planes. Moreover, this degeneracy will always occur when the two slip systems under consideration have a common pole. The only plane which intersects the edges of the unit triangle is (6*b*), from which it may be deduced

Fig. 4.



Maximum resolved shear stress contours for the system $\{123\}\{111\}$, showing some lines of quickest descent from maxima at D and E.

that X is $[311]$ and Y is $[210]$, and further that the boundary is the great circle from $[101]$ through these points to $[11\bar{1}]$. For the other pair of slip systems, $(3\bar{1}2)[111]$ and $(3\bar{1}2)[11\bar{1}]$, (2) and (4) become respectively

$$3kl-hl=0, \quad . \quad . \quad . \quad . \quad . \quad . \quad (8)$$

and

$$3h^2+2hk-k^2-2l^2=0. \quad . \quad . \quad . \quad . \quad . \quad . \quad (9)$$

The cone (9) does not intersect the reference triangle edges and may be neglected. (8) obviously represents a pair of planes $l=0$ and $h=3k$, the traces of which are $[100]Y$ and XW , where X is $[311]$, Y is $[210]$, and W is $[310]$. These boundaries are the parts of great circles.

Three Active Systems.

(a) *Equal Critical Shear Stresses.* The simplest case to consider when the systems $\{110\}\langle 111 \rangle$, $\{112\}\langle 111 \rangle$, and $\{123\}\langle 111 \rangle$ are all possible slip systems is when the critical resolved shear stresses for the activation of these systems are equal. An indication of the most favourable systems may be obtained by the superposition of the shear stress contour diagrams for the individual systems, figs. 1, 2, and 4. The exact positions of the boundaries between the systems may be found by the method of the preceding sections. As may be expected, the system of boundaries within the unit triangle is relatively complicated (fig. 9).

TABLE IV.
Most Favourable $\{123\}\langle 111 \rangle$ Slip Systems

	Slip systems	Number
Area [100]WX	$(3\bar{1}2)[111]$.	1
Area WXY	$(3\bar{1}2)[\bar{1}\bar{1}\bar{1}]$.	1
Area [110][111]XY	$(213)[11\bar{1}]$.	1
Boundary [100]Y	$(3\bar{1}2)[111]$, $(3\bar{1}2)[\bar{1}\bar{1}\bar{1}]$.	2
Boundary Y[110]	$(213)[11\bar{1}]$, $(213)[\bar{1}\bar{1}\bar{1}]$.	2
Boundary [110][111]	$(213)[11\bar{1}]$, $(123)[11\bar{1}]$.	2
Boundary [111]X	$(213)[11\bar{1}]$, $(231)[\bar{1}\bar{1}\bar{1}]$.	2
Boundary X[100]	$(3\bar{1}2)[111]$, $(3\bar{2}1)[111]$.	2
Boundary WX	$(3\bar{1}2)[111]$, $(3\bar{1}2)[\bar{1}\bar{1}\bar{1}]$.	2
Boundary XY	$(213)[11\bar{1}]$, $(3\bar{1}2)[\bar{1}\bar{1}\bar{1}]$.	2
Point Y	$(213)[11\bar{1}]$, $(21\bar{3})[111]$, $(3\bar{1}2)[111]$, $(3\bar{1}2)[\bar{1}\bar{1}\bar{1}]$.	4
Point [110]	$(213)[11\bar{1}]$, $(21\bar{3})[111]$, $(12\bar{3})[111]$, $(123)[\bar{1}\bar{1}\bar{1}]$.	4
Point X	$(3\bar{1}2)[111]$, $(3\bar{2}1)[111]$, $(213)[11\bar{1}]$, $(3\bar{1}2)[\bar{1}\bar{1}\bar{1}]$, $(3\bar{2}1)[\bar{1}\bar{1}\bar{1}]$, $(231)[\bar{1}\bar{1}\bar{1}]$.	6
Point [111]	$(213)[11\bar{1}]$, $(123)[11\bar{1}]$, $(312)[11\bar{1}]$, $(321)[\bar{1}\bar{1}\bar{1}]$, $(132)[\bar{1}\bar{1}\bar{1}]$, $(231)[\bar{1}\bar{1}\bar{1}]$.	6
Point [100]	$(3\bar{1}2)[111]$, $(3\bar{2}1)[111]$, $(3\bar{1}2)[\bar{1}\bar{1}\bar{1}]$, $(3\bar{2}1)[\bar{1}\bar{1}\bar{1}]$, $(312)[\bar{1}\bar{1}\bar{1}]$, $(321)[\bar{1}\bar{1}\bar{1}]$, $(312)[11\bar{1}]$, $(321)[11\bar{1}]$.	8

(b) *Unequal Critical Shear Stresses.* The preliminary results of Smoluchowski and Opinsky (1950) suggest that the critical shear stresses of the three systems are not equal. This case may be dealt with in the same straightforward manner with (2) and (4) modified to

$$P = \pm \frac{C_P}{C_Q} Q, \quad \dots \dots \dots (10)$$

where C_P and C_Q are respectively the critical resolved shear stresses on the systems corresponding to the terms P and Q. The changes in the positions of the boundaries for the observed critical shear stress ratios may be seen by comparison of figs. 9 and 11.

§ 3. TENSION AND COMPRESSION TEXTURES.

Slip on $\{110\}\langle 111 \rangle$ System.

Although the resolved shear stress contours are the same for the $\{110\}\langle 111 \rangle$ system and for the $\{111\}\langle 110 \rangle$ system discussed in Part I., the textures developed under tension and compression are interchanged. This is because under tension the stress direction tends to move towards the operative slip direction, the $\langle 111 \rangle$ in the $\{110\}\langle 111 \rangle$ case, and the $\langle 110 \rangle$ in the $\{111\}\langle 110 \rangle$ case, while under compression the stress direction moves towards the pole of the operative slip plane, the $\langle 110 \rangle$ and the $\langle 111 \rangle$ respectively. The directions of the rotations corresponding to single and duplex slip on the $\{110\}\langle 111 \rangle$ system in various parts of the unit triangle may be derived from a consideration of the operative slip systems listed in Table II. These are shown diagrammatically in figs. 3 and 6 of Part I. which now refer to *compression* and *tension* respectively. From these components, bearing in mind the relative probability of single and duplex slip, the general trends of rotation throughout the unit triangle are obtained. For example, at a point t (fig. 1) it will be seen from the contours that the path of the effective stress, T_e , is first for a short distance to an adjacent point on the $[100][111]$ boundary and thence for a much greater distance along the boundary to $[111]$. Thus it is reasonable to suppose that, in general, slip will occur more frequently when T_e is situated on the boundary than when it is between the point t and the boundary; that is to say, duplex rotation is the more probable. For a point u in the area $[100]AK$ near to A it will be deduced from similar considerations that single crystal rotation occurs more frequently. This leads to a *tension* texture as shown in fig. 8, Part I., and a *compression* texture as shown in fig. 5, Part I. Although minor components are predicted in these textures as a result of the sluggishness of rotations in the neighbourhood of the points of multiple slip, such components may well be absent after extremely severe deformation.

The tension texture is principally a $[110]$ texture with a spread between $[311]$ and $[110]$, which decreases with increasing deformation. There are no experimental data available for textures resulting from pure tension and discussion of this texture will be deferred.

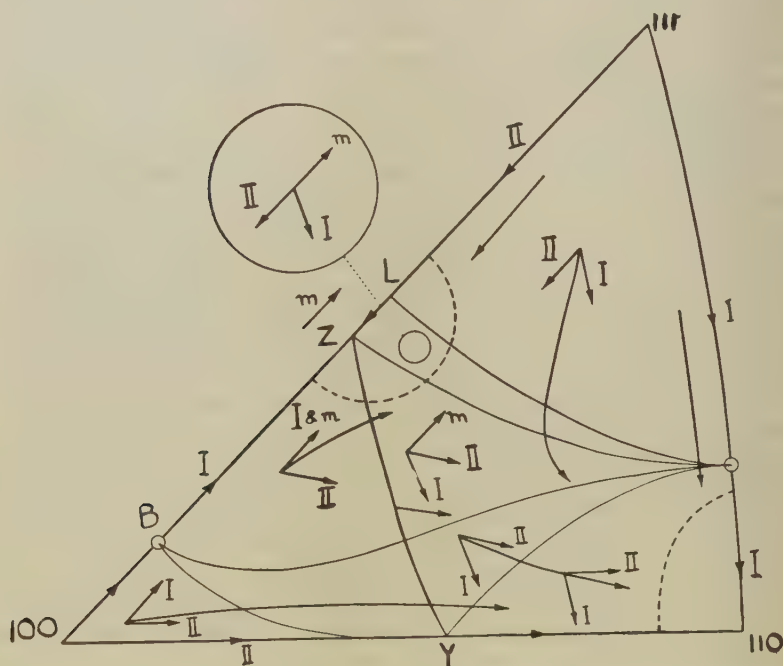
The compression texture is $[111]$, $[211]$ and $[100]$, the last being the weakest component. Again it is probable that the $[100]$ and $[111]$ components decrease in importance with increasing deformation.

Slip on the $\{112\}\langle 111 \rangle$ System.

The single, duplex and multiple slip systems operative for the $\{112\}\langle 111 \rangle$ system are listed in Table III., and with the aid of these the general trend of crystal rotations in a specimen under tension may be derived (fig. 5). It is clear from this diagram that the texture will be mainly $[110]$. An interesting situation arises, however, in the region near to the minimum point, Z , in the resolved shear stress diagram. When the effective stress, T_e , reaches Z slip occurs on three equivalent systems which are

not symmetrically disposed, resulting in rotation in the direction $Z \rightarrow [111]$. The part of this region lying in the triangle LCZ shows a complex behaviour, since the multiple and duplex rotations are in opposite directions quite distinct from the single crystal direction. Considering a single grain, or part of a grain, undergoing deformation, at some stages of the process it may suffer rotations corresponding to multiple slip and at other stages the reverse rotations corresponding to duplex slip. This clearly leads to a subsidiary texture which may persist until a very late stage in the deformation. Superimposed on these conflicting rotations

Fig. 5.

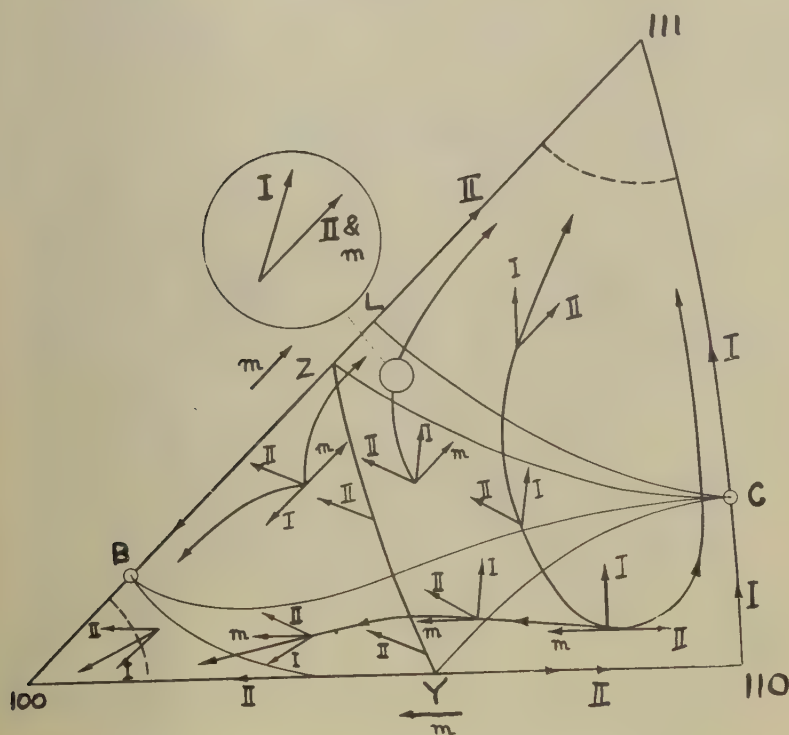


$\{112\}\langle 111 \rangle$ system. Tension rotations and texture. Regions of preferred orientation bounded by broken line. I, direction of single crystal rotation; II, direction of duplex rotation; m , direction of rotation due to multiple slip on unsymmetrically disposed systems.

there is a general drift towards $[11\bar{1}]$, the operative single crystal slip direction, which augments the $[110]$ texture at the expense of this subsidiary texture. The point Y is also a minimum of resolved shear stress and a point at which multiple but unsymmetrically disposed slip occurs. Here, however, the multiple and duplex slip directions are the same, and the general trend of rotations towards the $[110]$ as deduced from the duplex rotations is unaltered. The deformation texture is not modified therefore by the presence of this point of multiple slip.

The behaviour under compression is illustrated in fig. 6, and it may be seen that there is a double $[111]$, $[100]$ texture. In the main, orientations within the area $[111][110]YZ$ rotate towards $[111]$ while those in the area $[110]YZ$ move towards $[100]$, so that the former texture predominates. The unsymmetrically disposed multiple slip systems at Y and Z modify this to a small extent, but do not give rise to subsidiary textures as in the case of tension. This is because, under compression, in the regions where the multiple and duplex rotations are opposed,

Fig. 6.



$\{112\}\langle 111 \rangle$ system. Compression rotations and texture.

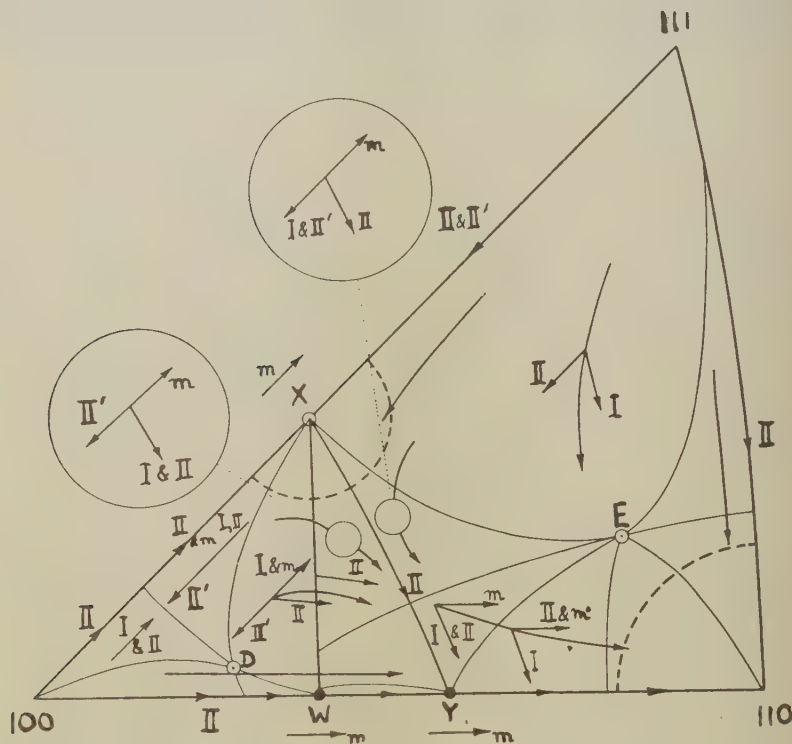
operation of a given rotation leads to a new orientation which favours further rotation of the same kind, whereas under tension operation of a given type of rotation leads to a new orientation which favours rotation in the reverse direction.

Slip on the $\{123\}\langle 111 \rangle$ System.

From an examination of fig. 7 showing the grain rotations to be expected when slip takes place on the $\{123\}\langle 111 \rangle$ system under tension it is evident that the principal texture is $[110]$. The rotations near to X, $[311]$,

are complicated by the multiple slip at X, and they give rise to a subsidiary [311] texture which may be expected to persist until a late stage in the deformation process. The compression case is illustrated in fig. 8. Here there is a double [111], [100] texture, with [111] as the main component, and a subsidiary transitional texture around [311].

Fig. 7.



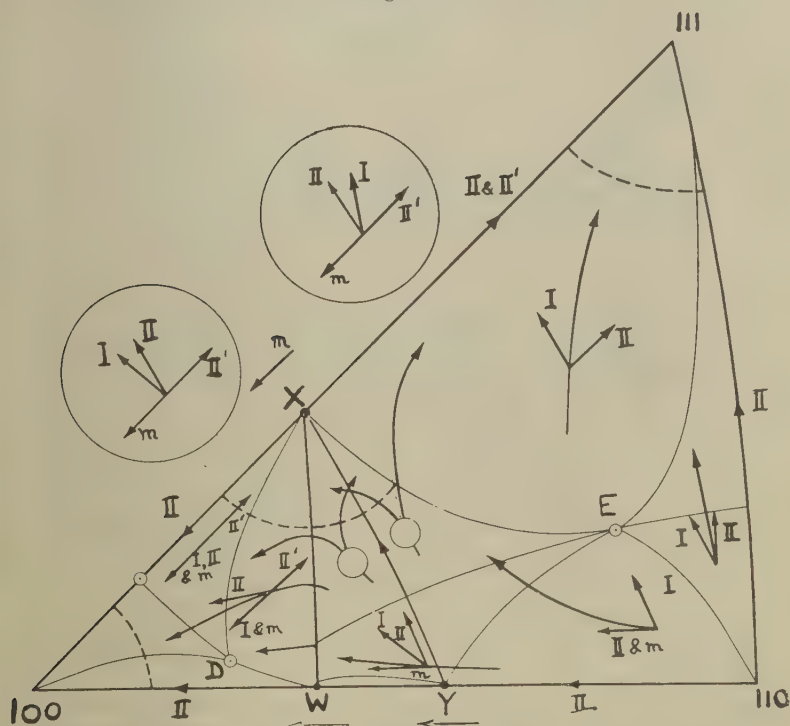
{123}<111> system. Tension rotations and texture. I, II, and m have the same significance as in previous figures. II' indicates a further possible duplex rotation.

Slip on Three Systems.

(a) *Equal Critical Shear Stresses.* The rotations leading to the development of the principal tension texture, [110], and the subsidiary texture around [411] are shown in fig. 9. The subsidiary texture is due to the opposing influence of multiple and duplex rotations in this region. Since unsymmetrical multiple slip occurs at both the points U and V the subsidiary texture is rather more extensive than in previous cases. The compression texture is shown in fig. 10, with [111] as the main component, [100] as a minor component, and [411] as a transitional subsidiary component.

(b) *Unequal Critical Shear Stresses.* Comparison of figs. 9 and 11 shows that the differences in rotations and the textures developed are relatively small despite the considerable changes in magnitude of the areas over which the individual slip systems operate. It appears that both the tension subsidiary texture and the compression [100] minor component are slightly reduced.

Fig. 8.



{123}<111> system. Compression rotations and texture.

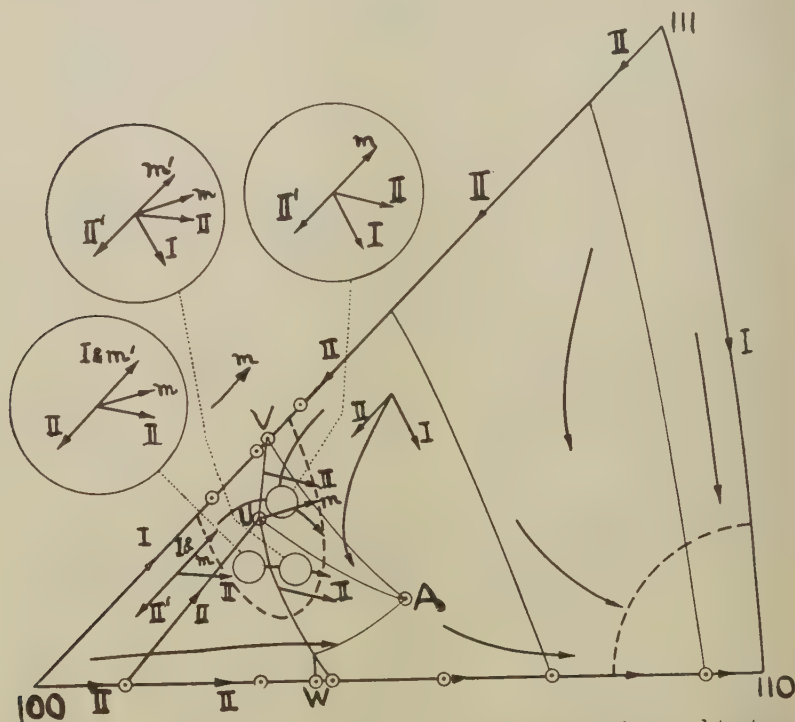
§ 4. ROLLING AND DRAWING TEXTURES.

The rolling and drawing textures resulting from slip on any one or combination of the systems discussed may be derived in the manner described briefly in Part I. For example, with slip on three systems giving compression textures [111], [100], and [411], and tension textures [110] and [411], the [111] and [110] compression end points and the [110] tension end point may be simultaneously satisfied. The [411] transitional texture in compression satisfies both the tension end point [110] and, to a close approximation, the tension transitional texture at [411] as well as any spread from this point towards the [110]. It is therefore reasonable

to suppose that, although the $[411]$ components are transitional both in tension and compression, they persist in the rolling texture which therefore includes, in order of decreasing magnitude, $(411)[110 \leftarrow 411]$, $(111)[110]$, and $(100)[110]$.

The rolling textures to be expected from slip on the various systems are listed in Table V.

Fig. 9.



Three systems; equal critical shear stresses. Tension rotations and textures. I, II, II' and m have the same significance as in previous figures. m' is a further possible direction of rotation due to multiple slip on unsymmetrically disposed systems.

TABLE V.
Rolling Textures.

System	Textures in order of decreasing magnitude
$\{110\}\langle 111 \rangle$	$(211)[110 \leftarrow 311]$, $(111)[110]$, $(100)[110]$.
$\{112\}\langle 111 \rangle$	$(111)[110 \leftarrow 211]$, $(100)[110]$.
$\{123\}\langle 111 \rangle$	$(311)[110 \leftarrow 311]$, $(111)[110]$, $(100)[110]$.
Three systems	$(411)[110 \leftarrow 411^*]$, $(111)[110]$, $(100)[110]$.

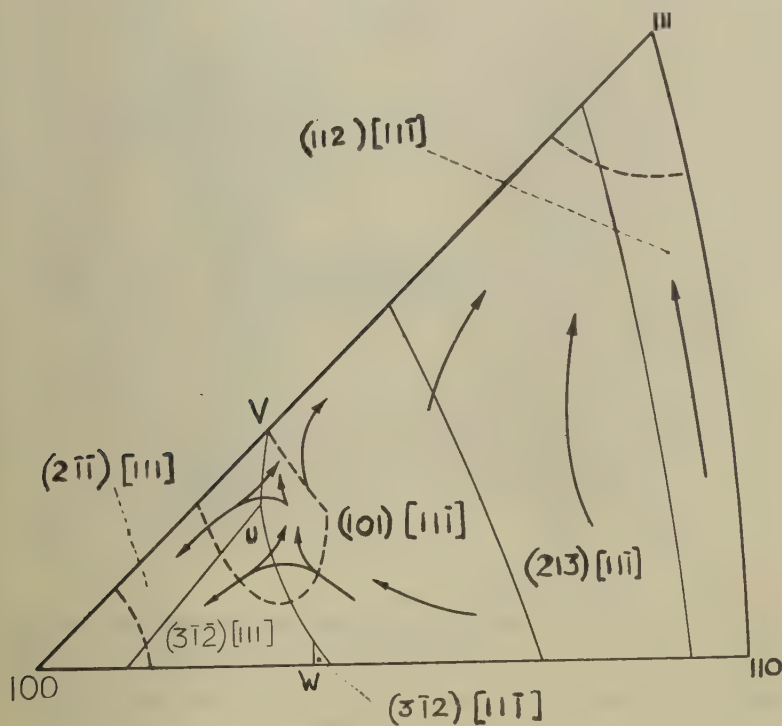
* $(411)[411]$ is not strictly a texture but $(411)[511]$ is and the angular difference between the two is a matter of only about 3° .

The methods of Part I. may also be applied to wire drawing textures. These lead in all cases, after severe deformation, to a simple $[110]$ fibre texture.

§ 5. DISCUSSION.

The most striking feature of the tension and compression textures derived above is their similarity for all the slip systems considered: it is only in the transitional components that they differ.

Fig. 10.



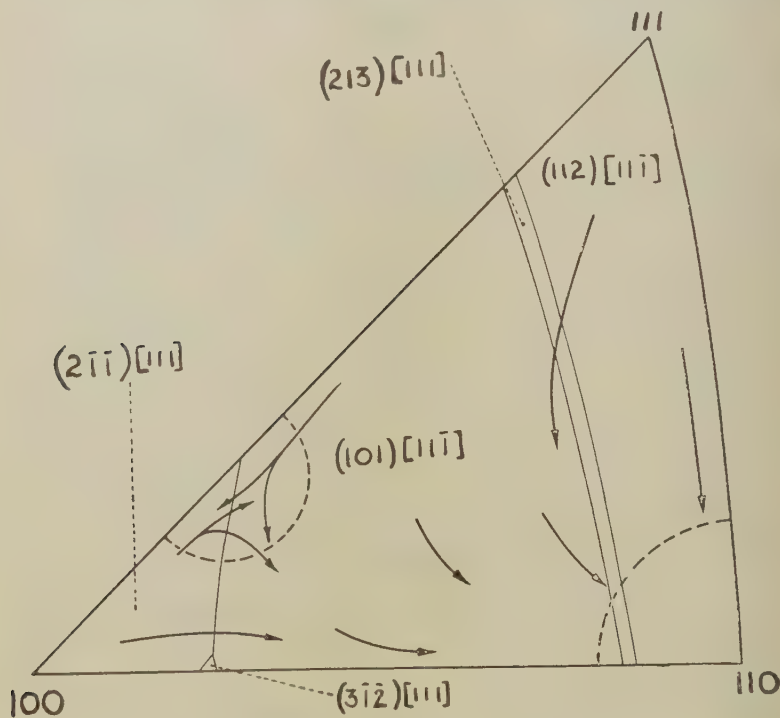
Three systems; equal critical shear stresses. Compression texture and operative slip systems.

As for the face-centred cubic metals there are no data on pure tension textures. For compression, the experimental observations by Heger (1941) on an iron alloy containing 4.6 per cent silicon, which deforms on $\{110\}\langle 111 \rangle$, showed a double fibre texture with $[111]$ and $[100]$ parallel to the axis of compression. The only other compression data available are for α -iron, where all three systems are active. Here again a double $[111]$, $[100]$ fibre texture was found with the $[100]$ component the weaker (Barrett 1939). This double texture, with $[100]$ the weaker, is predicted by the present treatment in all cases. It is expected, however, that

with only the $\{110\}\langle 111 \rangle$ system operative a $[211]$ texture develops at the expense of the double texture after severe deformation. This has not yet been confirmed by experiment.

In view of its industrial importance there is a considerable amount of experimental information on rolling textures in iron and steel, and a large measure of agreement from observer to observer. The most careful studies would appear to be those carried out in the Carnegie Institute of

Fig. 11.

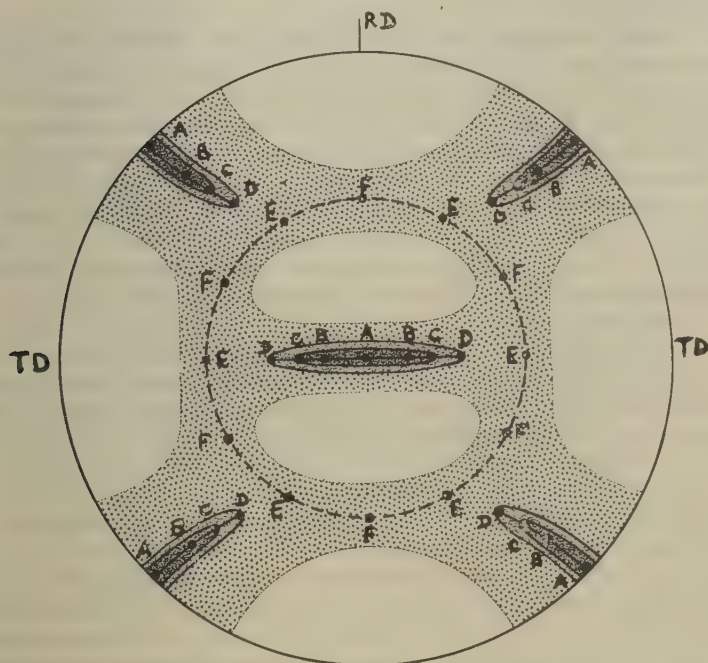


Three systems; unequal critical shear stresses. Tension texture and operative slip systems.

Technology (Gensamer and Mehl 1936; Barrett, Ansel and Mehl 1937 b; Barrett and Levenson 1941). They have examined the textures of rolled silicon iron alloy which deforms on $\{110\}\langle 111 \rangle$, and α -iron which deforms on the three systems. A typical (100) pole figure is reproduced in fig. 12. They concluded that there are two continuous sets of end points: (1) a set including the textures (100)[110], (511)[110], (311)[110], and (211)[110] indicated by the points A, B, C and D respectively, which have the $[110]$ direction parallel to the rolling direction and the (100) plane at any angle up to 45° or 55° from the rolling plane; and (2) a set of orientations including the textures (111)[110], E, and (111)[211], F, which have the (111) plane in the plane of the sheet and all possible positions of the rolling

direction in this plane. It was further found that, with $\{110\}\langle 111 \rangle$ slip or slip on all three systems, the only difference in the pole figures was that in the former case the scatter of (100) planes about the rolling axis was 55° to 60° compared with 40° to 45° for the three systems. It is obvious that no one of the predicted textures listed in Table V. can account for these continuous ranges of orientation.

Fig. 12.



(100) pole figure for rolled iron showing various ideal orientations: A, (100)[110]; B, (511)[110]; C, (311)[110]; D, (211)[110]; E, (111)[110]; F, (111)[211]. Heavy full lines represent a continuous set containing A to D. Circle in broken line is a second continuous set containing E and F. (Barrett and Levenson.)

The introduction of a further simple assumption not only overcomes this difficulty but also explains the characteristically wavy slip lines in α -iron. It is that the ratio of critical shear stresses for the three slip systems varies from one part of a grain to another such that the polycrystalline aggregate may be considered as composed of units, some deforming on each one of the three systems and some on all three systems. From the considerable movement of the boundaries in figs. 9 and 11 it is evident that the variations of the ratios of critical shear stress from one region to another in a grain need not be large. The rolling texture of iron will thus include all those orientations listed in Table V., that is, those orientations illustrated by Barrett and Levenson (1941), with the trifling exception

that (411)[110] replaces (511)[110]. Moreover, the major textures of Table V. give the stronger set of components A to D, referred to in the preceding paragraph, with the exception of (100)[110] which is predicted as a weaker texture. This is probably a small point as the spread from the (411)[110] on either side of the centre of the pole figure may well maintain this orientation. On the other hand it may be pointed out that Kurdjumow and Sachs (1930) did indeed find a saddle at the centre of their (100) pole figure.

The careful experimental work of Gough (1928) showed that at low deformations the wavy slip bands in single crystals of iron can be resolved into short separate traces of slip planes of the now accepted forms. This he interpreted as duplex slip on the two planes nearest to the plane of highest resolved shear stress, but he was unable to explain why the deformation takes place by small elements of slip alternating from one plane to another rather than the production of two interlacing sets of straight slip bands. On the present assumption, however, the small segments of a wavy slip band correspond to parts of the crystal in which the different ratios of critical resolved shear stress produce different most favourable systems.

The compression and tension textures predicted here now need reconsideration when applied to α -iron. The main textures are unaltered, but there are additional transitional subsidiary textures corresponding to slip on each of the three individual systems, *i. e.* main tension texture [110] with subsidiary textures [211], [311] and [411], and main compression textures [111], [100] and subsidiary textures [211], [311], and [411]. These subsidiary textures are likely to coalesce into a general spread of orientation between [100] and [111].

The objection may be raised that in an iron alloy containing 4.6 per cent silicon the slip lines are usually very much straighter than in α -iron. Consequently this material must deform on a single system shown to be the $\{110\}\langle 111 \rangle$, and so could not attain the full rolling texture observed. However, Barrett, Ansel and Mehl (1937) have suggested that after severe deformation the same slip mechanism may operate in this alloy as in α -iron, which presumably implies that the effect of the silicon in solid solution in raising the critical shear stresses on the $\{112\}\langle 111 \rangle$ and the $\{123\}\langle 111 \rangle$ systems, although appreciable in the early stages, may be comparatively small after severe work-hardening with these as latent systems. The straight slip lines, of course, relate to observations on material after deformation slight in comparison with the rolling reductions under consideration. Furthermore, the predominance of the $\{110\}\langle 111 \rangle$ system may be expected to increase the component corresponding to this system in the final texture, the (211)[110 \leftarrow 311] causing a greater spread of orientation along the equator of the (100) pole figure which has been confirmed experimentally. Thus it appears that the $\{110\}\langle 111 \rangle$ system plays a greater part in the deformation of this alloy especially in the earlier stages, and even in the later stages of deformation when the other systems are active in producing the full rolling texture.

Finally, it may be remarked that the predicted simple [110] fibre texture in cold-drawn wires is amply confirmed by experiments on all body-centred cubic metals so far examined.

§ 6. CONCLUSIONS.

The qualitative treatment of the development of deformation textures in face-centred cubic metals described in Part I. has been extended to those of body-centred cubic structure. The main features of tension, compression, rolling and drawing textures have been satisfactorily predicted. The detailed examination of the rolling textures of iron alloys presents some difficulty and necessitates the introduction of the further assumption that in adjacent regions within a single metallic grain there are differences in the ratios of the critical shear stresses. This is justified in that it leads to the explanation of wavy slip lines in α -iron, a well established fact, and permits the prediction not only of the complete rolling textures of iron alloys but also some of the minor variations among them.

It seems likely that the general concepts of this theory may be applicable to other aspects of the deformation of both single crystals and polycrystalline aggregates. For example, there appears to be a close connection between the alternative directions of rotation discussed here and the development of deformation bands.

Further accurate experimental work on deformation textures is necessary before the details of the theoretical predictions may be fully tested.

ACKNOWLEDGMENTS.

The authors acknowledge the considerable assistance given by members of the staff of Mathematics Division of the National Physical Laboratory who calculated the Resolved Shear Stress Tables.

The work described above has been carried out as part of the research programme of the National Physical Laboratory, and this paper is published by permission of the Director of the Laboratory.

REFERENCES.

- ANDRADE, E. N. DA C., 1940, *Proc. Phys. Soc.*, **52**, 1.
 BARRETT, C. S., ANSEL, G., and MEHL, R. F., 1937 a, *Trans. A.S.M.*, **25**, 702;
 1937 b, *Trans. A.I.M.E.*, **125**, 516.
 BARRETT, C. S., 1939, *Trans. A.I.M.E.*, **135**, 296.
 BARRETT, C. S., and LEVENSON, L. H., 1941, *Trans. A.I.M.E.*, **145**, 281.
 CALNAN, E. A., and CLEWS, C. J. B., 1950, *Phil. Mag.*, **41**, 1085.
 FAHRENHORST, W., and SCHMID, E., 1932, *Z. Physik*, **78**, 383.
 GENSAMER, M., and MEHL, R. F., 1936, *Trans. A.I.M.E.*, **120**, 277.
 GOUGH, H., 1928, *Proc. Roy. Soc. A*, **118**, 498.
 HEGER, J. J., 1941, Unpublished Senior Thesis, Carnegie Inst. of Tech.; cited by
 Barrett, C. S., 1943, *Structure of Metals* (New York: McGraw-Hill),
 p. 387-388.
 KURDJUMOW, G., and SACHS, G., 1930, *Z. Physik*, **62**, 592.
 MISES, R. V., 1928, *Z. angew. Math. Mech.*, **8**, 161.
 SMOLUCHOWSKI, R., and OPINSKY, A. J., 1950, *Carnegie Inst. of Tech. Conference
 on Plastic Deformation of Crystalline Solids* (in press).
 TAYLOR, G. I., 1938, *J. Inst. Metals*, **62**, 307.

LXVI. *Highly Forbidden Transitions in the Decay of Na^{24}*

By J. F. TURNER and P. E. CAVANAGH *.
Atomic Energy Research Establishment, Harwell.

[Received March 29, 1951.]

ABSTRACT.

A description is given of the use of an organic scintillation counter in conjunction with a thin lens β -spectrometer to detect low intensity, high energy electron groups in the presence of a high background. Evidence for a 4.17 MeV. β -group in the radiations from Na^{24} has been found, and a value of branching-ratio obtained. Measurements made on the secondary electron spectrum from Na^{24} show the presence of a high energy γ -ray, possibly from the cross-over γ -transition in Mg^{24} .

§ 1. INTRODUCTION.

THE angular correlation measurements of Brady and Deutsch (1950) suggest that the spins to be associated with the 4.14 MeV., 1.38 MeV., and ground states of Mg^{24} are 4, 2, 0, respectively, and that both the 2.76 and 1.38 MeV. γ -rays correspond to quadrupole transitions. This assignment, in the case of the 2.76 MeV. γ -ray, is in disagreement with the results of Rae (1949) who, from a measurement of the internal pair production coefficient, deduced that this was a dipole transition. Later measurements by Mims, Halban and Wilson (1950) on annihilation quanta arising from internally produced pairs gave results which were more compatible with a quadrupole transition. Another line of attack on this problem is the investigation of the cross-over γ -transition by Bishop, Wilson and Halban (1950), who measured the energy spectrum of photo-protons in a deuterium filled ionization chamber counter. The crossover γ -ray was not observed, and an upper limit of 3×10^{-7} has been placed on its occurrence. A further investigation is that of Grant (1950) who attempted to measure higher energy β -rays corresponding to highly forbidden transitions to the ground and intermediate states using a thin lens spectrometer, with a coincidence counter pair for recording the focused β -particles. No high energy β -particles were observed and the upper limit placed on the intensity of the 4.14 MeV. β -transition was 1 in 10^4 .

§ 2. THE TECHNIQUE USED.

The present work was pursued independently of that of Grant whose results only came to hand when the investigation was completed. Essentially, it was the same type of investigation as Grant's except that an organic crystal scintillator was used to record the focused β -particles. We

* Communicated by the Authors.

have already given a very brief description of the technique (1950). The spectrum of pulses resulting from the irradiation of the crystal by the almost monokinetic electrons focused by the spectrometer is in the form of a symmetrical peak, with half width determined by the energy of the electrons and the crystal-photo-multiplier combination. In general this will be superimposed on a background due to cosmic radiation, and direct and scattered γ -radiation. Scattered quanta and electrons will cause an increase in the pulse height distribution at small amplitudes. The pulse amplitude corresponding to the peak and the focused momentum will be related in the same way as energy and momentum of an electron. The use of the technique does enable one to pick out those pulses corresponding to electrons of the focused momentum from, in some instances, the much larger number of pulses arising from other causes, but recorded at the same value of coil current.

§ 3. THE EXPERIMENTAL ARRANGEMENT.

The thin lens spectrometer, adapted for ring focusing, gave a resolution of 5 per cent and transmission of 0.4 per cent when used with a 1 cm. diameter source. The sources were compressed blocks of sodium fluoride inside a thin aluminium covering, and with thicknesses ranging from 10 to 40 mg./cm.². The scintillator used was in the form of a clear block of naphthalene +1 per cent anthracene 5 cm. in diameter and 3.8 cm. thick, grown by Mr. R. F. Jackson, Junior of A.E.R.E. and located outside the spectrometer behind a vacuum tight window of 7 mg./cm.² aluminium. The resolution obtained with this crystal was about 20 per cent for electrons of 1 MeV. The magnetic field due to the main coil was neutralized over the region of the photomultiplier by means of a set of coils carrying the main current, so that the gain was substantially independent of the focused energy. The response from the multiplier was amplified and analysed by means of a five channel Pulse Analyser Type 1074A.

§ 4. THE HIGH ENERGY β -SPECTRUM.

Fig. 1 shows the pulse distribution obtained at values of momentum above that of photoelectrons from the 2.76 MeV. γ -rays, and peaks due to the high energy β -group are clearly visible, superimposed on a background due largely to direct and narrow angle scattered γ -radiation. It was found that the pulse amplitude at the peak was directly proportional to the focused energy, as expected. Moreover a Fermi analysis of the results gave a straight line plot with an end point at 4.17 MeV. (fig. 2) in excellent agreement with the maximum energy of the β -transition to the intermediate state. Measurements extending over several half periods showed that the decay of the high energy β -transitions must be quite close to that of the main transition. An estimate of the relative intensities was made by comparing the slopes of the two Fermi distributions. This gave a value of 3×10^{-5} for the intensity of the 4.14 relative to the 1.38 MeV. β -rays, a result compatible with Grant's.

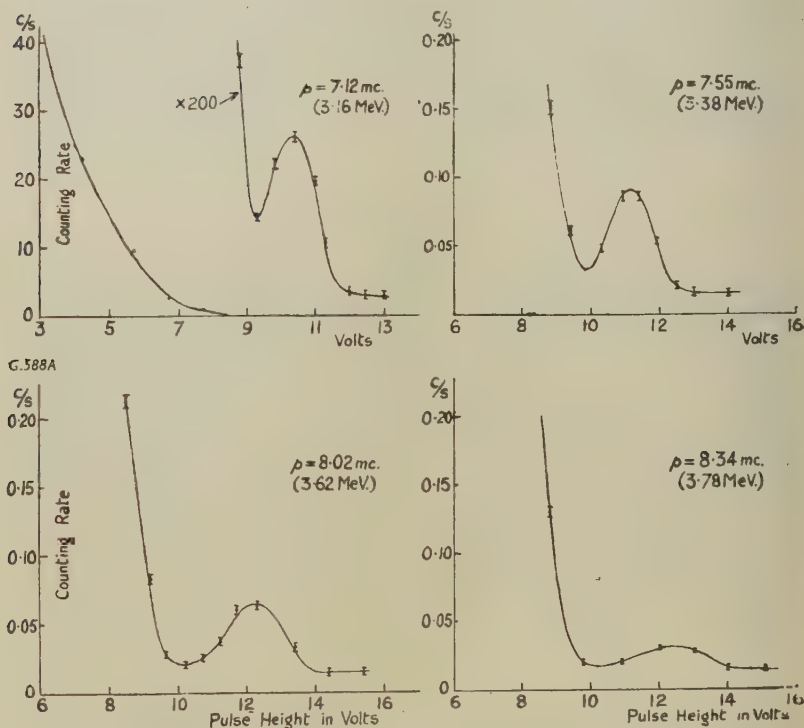
The region beyond the end-point of the 4.14 MeV. β -ray was carefully investigated but no trace of the 5.53 MeV. β -transition to the ground state was found. $f\tau$ values derived for the three transitions are

$$f\tau(1.38 \text{ MeV.}) = 1.22 \times 10^6,$$

$$f\tau(4.14 \text{ MeV.}) = 5.0 \times 10^{12},$$

$$f\tau(5.53 \text{ MeV.}) > 1.2 \times 10^{15}.$$

Fig. 1.



Variation of pulse analyser curves with focused momentum.

The last two may be small by a factor of about two arising out of the assumption of a straight line Fermi plot for the forbidden transitions. The energy of the intermediate transition is in agreement with the order of emission of the two γ -rays, as indicated by the results of inelastic scattering experiments by Beghian, Grace, Preston and Halban (1950) and by Rhoderick (1949).

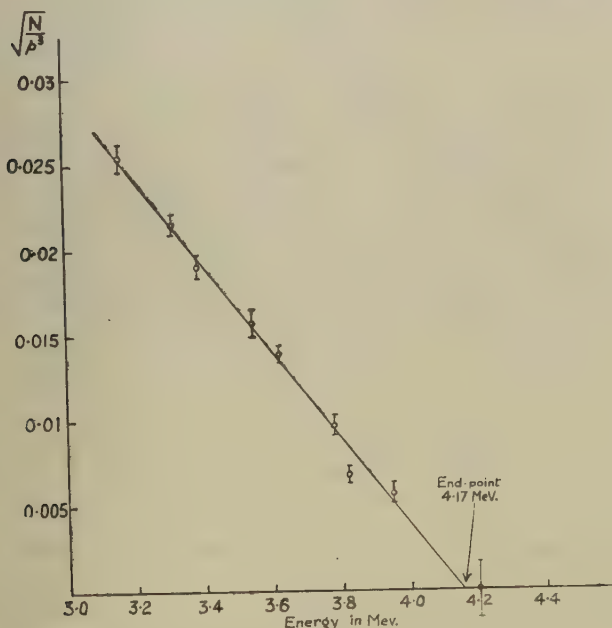
§ 5. THE HIGH ENERGY γ -RADIATION.

It was while performing a further check on the nature of the particles observed that it was noticed that the placing of a thick absorber over the source, so far from eliminating the peak in the pulse distribution due to

high energy β -particles, actually increased its height considerably. There can, we believe, be only one explanation to this phenomenon, and that is that the source emits high energy γ -rays. A later check, however, using as a reference the Compton electrons due to the 2.76 MeV. γ -ray ejected from the bare source, enabled us to show that in this latter case, at any value of the momentum, less than 10 per cent of the counting rate of high energy electrons could be ascribed to a high energy γ -ray, and that the great majority were in fact due to the high energy β -transition.

Measurements were continued with more intense sources, up to 10 mC., better resolution ~ 3.5 per cent and with saturation thicknesses of both lead and copper radiators. The shapes of the secondary electron spectra

Fig. 2.

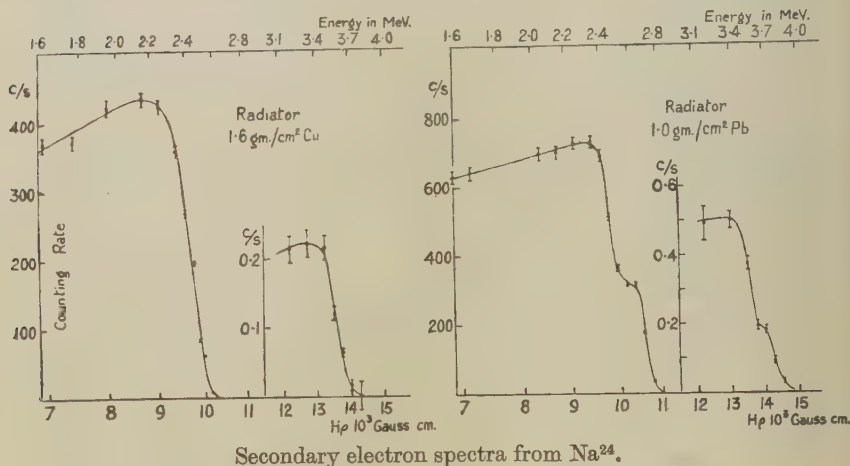
Fermi plot of high energy β -rays of Na^{24} .

obtained (fig. 3) were quite different from the β -ray distribution, and had maxima in about the expected place. Some evidence of a photoline was obtained in the case of a lead radiator, but the value obtained for the energy of the γ -ray from the photoline position, no correction being made for the finite thickness of the radiator, was some 8 per cent lower than the energy expected for the cross-over γ -ray of 4.14 MeV. The value obtained from an extrapolation of the Compton distribution was 4 per cent lower than 4.14 MeV. The values obtained for the energy of the 2.76 MeV. γ -ray

from the Compton distribution and photoline, however, were correct within 1 per cent after applying the 1 per cent correction in the energy of the photoline due to the saturation thickness of radiator, found to be appropriate at lower energies. It is felt, however, that the results are not necessarily incompatible with a γ -ray of energy equal to the cross-over γ -ray, since at 4 MeV., in lead, energy loss of fast electrons by bremsstrahlung, is becoming important, and may effect the shape of both Compton and photoelectric distributions with a thick radiator. However, the possibility remains that the γ -ray is some 4–7 per cent lower in energy than the cross-over, though this does not appear to be likely theoretically.

By comparing the two Compton distributions the relative intensities of the high energy and the 2.76 MeV. γ -rays was determined as 5×10^{-4} , a result completely incompatible with that of the Oxford group. The results

Fig. 3.



of chemical analysis of both the sodium fluoride and a later source of anhydrous sodium carbonate, however, leave little doubt that the γ -ray arises from the neutron irradiation of sodium, and measurements made with sources irradiated under cadmium, and in a lower neutron flux, exclude the possibility of a fast neutron reaction or neutron capture by Na^{24} giving rise to the radiation. This, together with an approximate measurement of half-period makes it reasonably certain that the γ -ray is associated with the decay of Na^{24} .

§ 6. DISCUSSION.

If the high energy γ -ray and the 2.76 MeV. γ -ray do in fact arise from the same level, the use of the Segre-Helmholtz formula, and the relative intensities, indicates that they differ by one order of multipolarity, and that consequently, the parities of the ground and intermediate states of Mg^{24} differ. This demands that the 1.38 MeV. γ -ray be of odd multipole

order, almost certainly dipole, and is incompatible with the angular correlation measurements. In the case, however, where the 2.76 MeV. γ -ray is dipole, since it is known that the probabilities of emission of dipole and quadrupole radiation are about equal, it is possible that the cross-over γ -ray could be octupole. This would require that the β -transition to the intermediate state, with a spin change of 2 and no parity change, should be second forbidden, and does not appear to be at all likely. The interpretation of the $f\tau$ values of the various β -transitions is difficult because of uncertainty in the magnitude of the nuclear matrix elements. However, if the main β -transition is first forbidden, it is probable that the 4.14 MeV. β -ray is at least third forbidden, and the 5.53 MeV. β -ray at least fourth forbidden.

ACKNOWLEDGMENT.

Acknowledgment is made to the Director, A.E.R.E., for permission to publish.

REFERENCES.

- BEGHIAN, L. E., GRACE, M. A., PRESTON, G., and HALBAN, H., 1950, *Phys. Rev.*, **77**, 286.
BISHOP, G. R., WILSON, R., and HALBAN, H., 1950, *Phys. Rev.*, **77**, 416.
BRADY, E. L., and DEUTSCH, M., 1950, *Phys. Rev.*, **78**, 558.
CAVANAGH, P. E., 1950, *Proc. Harwell Nuclear Physics Conference*, p. 98.
GRANT, P. J., 1950, *Proc. Phys. Soc. A*, **63**, 1298.
MIMS, W., HALBAN, H.; and WILSON, R., 1950, *Nature, Lond.*, **166**, 1027.
RAE, E. R., 1949, *Phil. Mag.*, **40**, 1155.
RHODERICK, E. H., 1949, *Nature, Lond.*, **163**, 898.

LXVII. *The Thermal Conductivity of Some Alloys at Low Temperatures.*

By R. BERMAN,
Clarendon Laboratory, Oxford*.

[Received March, 29, 1951.]

ABSTRACT.

The thermal conductivities of German silver, stainless steel and constantan have been determined between 2 and 90° K. and the electronic and lattice components of the conductivity have been calculated.

The electronic conductivity is limited by scattering by "impurities". The lattice conductivity is limited by scattering of the lattice waves by electrons at the lower temperatures and by "impurities" at higher temperatures.

A table is given showing the heat flow along specimens of each alloy resulting from temperature differences commonly met with in practice in low-temperature work.

§1. INTRODUCTION.

OF the various sets of experiments which have been made on the thermal conductivity of alloys at low temperatures the most detailed have been concerned with superconducting alloys. Measurements have been made on other alloys by Karweil and Schäfer (1939), Allen and Mendoza (1948), Wilkinson and Wilks (1949), Schmeissner and Meissner (1950) and by Hulm (1951).

The present experiments, on German silver, constantan and a stainless steel, were made originally because of their practical value and cover a wider temperature range than do any of the previous experiments. The thermal conductivity was measured between 2 and 90° K. and the electrical conductivity at a few temperatures in this interval.

The electronic contribution to the heat conductivity has been estimated and, by subtracting this from the total conductivity, the lattice heat conductivity has been deduced. This is an appreciable fraction of the total conductivity over the temperature range of these measurements. It is shown that up to about 25° K. the lattice conductivity is limited mainly by scattering of the lattice waves by electrons, but that above this temperature "impurity" scattering predominates.

§2. THE EXPERIMENTS.

The apparatus used was the same as that described elsewhere (Berman 1951), in which the temperature drop along the specimens is measured by two gas thermometers. The thermometers were fixed with Wood's metal

* Communicated by Professor F. E. Simon, F.R.S.

to copper bands soldered to the specimens. The measurements of electrical conductivity were made in the same apparatus.

The German silver was in the form of a $\frac{1}{4}$ -inch rod, obtained from Messrs. Rollets, with composition Cu 47 per cent, Pb 2 per cent, Zn 41 per cent, Ni 9 per cent, and was measured as received. The grain size was estimated from a photomicrograph, using a grain contrast etch. The mean diameter was in the region of 0.02 mm.

For the main experiments the length used was 5 cm., but two measurements were also made with a length of 2.5 cm. This was to verify (1) that the length to be assumed for calculating the conductivity is equal to the distance between the centres of the bands soldered to the specimen, and (2) that the corrections for heat losses are as small as had been calculated ($2\frac{1}{2}$ per cent at 95° but less than $\frac{1}{2}$ per cent below 60° K.). The agreement between the two sets of experiments is very close (\bigcirc and \bigcirc in fig. 1) and it was not considered necessary to repeat this check for the other alloys.

As the ratio of the room temperature electrical resistance to the residual resistance was very small (1.1) compared with the value found by Allen and Mendoza for a rod of similar composition, the specimen was given a similar heat treatment and heated to a dull red heat for a few minutes and allowed to cool slowly. The resistance ratio was, however, unaltered.

The constantan specimen (Cu 60 per cent, Ni 40 per cent) consisted of 317 enamelled wires of 36 gauge, in parallel. These measurements were made because constantan leads of about this gauge are frequently used in various low-temperature apparatus in which it is necessary to estimate the heat flow down them. The wires were soldered together at their ends and two copper collars were soldered round them at a distance apart of 3.5 cm.

The stainless steel specimen consisted of three rods, of 2 mm. diameter, in parallel. This was an austenitic 18/8 titanium stabilized material of composition Ni 7.9 per cent, Cr 18.9 per cent, Si 0.7 per cent, Ti 1 per cent, C about 0.1 per cent. The austenite grains were estimated to be about 0.01 mm. with some ferrite grains of about 0.002 mm. precipitated in the grain boundaries of the austenite.

§ 3. RESULTS.

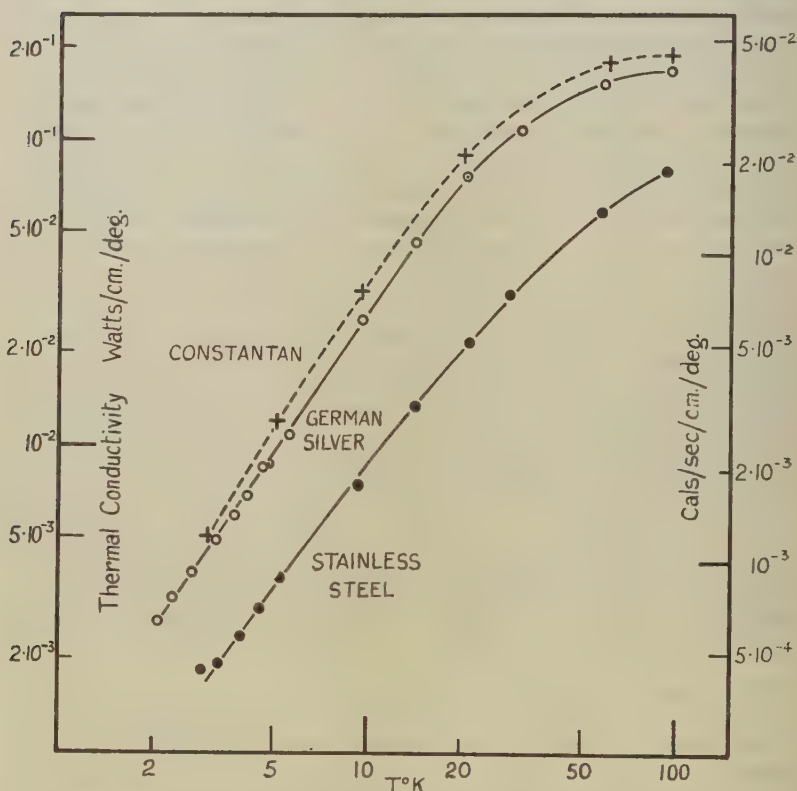
The thermal conductivity and electrical resistivity of these alloys are shown in figs. 1 and 2. For the three alloys the thermal conductivity at the lowest temperatures varies as a power of the absolute temperature slightly greater than 1. At higher temperatures the conductivity becomes less temperature dependent.

These results can be compared with those of other authors. The German silver specimen had a similar composition to both the German silver measured by Allen and Mendoza and the "Silver bronze" measured by Karweil and Schäfer. Allen and Mendoza found, for a specimen with much lower electrical resistivity, that the thermal conductivity, measured between 1.3 and 4° K., was proportional to the cube of the absolute temperature. Hulm has raised some doubts as to the validity of the values

found by these authors. The present results agree well, however, with those of Karweil and Schäfer who measured between 5 and 24° K. The extrapolated value at 113° K. is in good agreement with the value determined by Lees (1908) on a specimen of somewhat different composition which had a similar electrical resistivity.

The values obtained on stainless steel are slightly higher than those of Wilkinson and Wilks between 10 and 20° K. on a specimen of similar

Fig. 1.



Thermal conductivities of German silver, stainless steel and constantan.

composition. They are, as would be expected, considerably lower than those of Karweil and Schäfer who measured a steel with only 1 per cent of "foreign" atoms.

It is of interest to note that below about 20° K. the thermal conductivity of this stainless steel is very similar to that of "contracid", measured by Karweil and Schäfer, and of "chroman B2Mo", measured by Schmeissner and Meissner. The apparent rapid rise of conductivity above 70° K. found by the latter authors for chroman B2Mo has not been found for stainless steel.

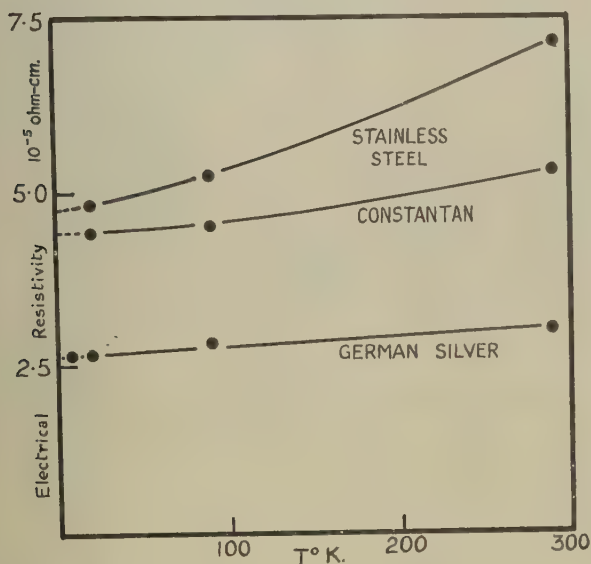
There seem to be no previous measurements on constantan in the temperature range of the present experiments, but the values are similar to those found for another Cu-Ni alloy by Hulm, below 20° K.

§ 4. DISCUSSION OF RESULTS.

The heat conducted by a metal or alloy is the sum of the heat conducted by the electrons and by the lattice. The heat conductivity, K , can therefore be written

$$K = K_e + K_g,$$

Fig. 2.



Electrical resistivities of German silver, stainless steel and constantan.

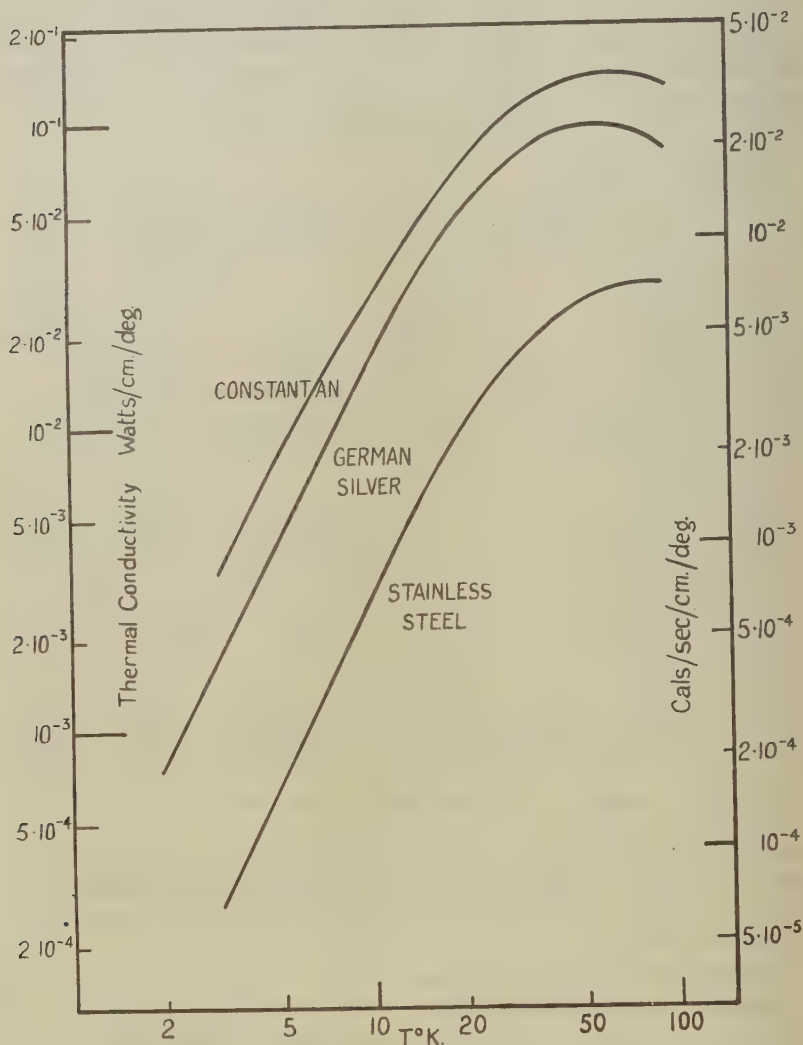
where K_e is the electronic heat conductivity and K_g the lattice conductivity. These two components are determined by the processes which scatter electrons and phonons (lattice waves) respectively and give rise to heat resistance.

Heat conducted by the electrons.

The electronic thermal resistivity, $W_e (= 1/K_e)$, is, to a first approximation, the sum of the "ideal" resistance W_i , due to the thermal vibrations of the atoms, and the resistance due to the aperiodicity of the lattice field produced by the presence of "impurities". According to Makinson (1938) the ideal resistance of a metal at low temperatures should be proportional to the square of the absolute temperature. Although this ideal thermal resistance is not simply related to the ideal electrical resistivity, the thermal resistance which is due to impurities should be directly related to

the residual electrical resistance, ρ_0 , by the Wiedemann-Franz-Lorenz law and is therefore equal to ρ_0/L_0T , where L_0 is the Lorentz constant ($\frac{1}{3}(\pi k/e)^2 \equiv 2.45 \times 10^{-8}$ Watt-ohm/deg.²). From measurements by

Fig. 3.



Calculated lattice thermal conductivities in German silver, stainless steel and constantan.

Grüneisen and Goens (1927) of the thermal conductivity of copper and iron it is possible to estimate the order of magnitude of W_i for the alloys measured. Using the extrapolated values of ρ_0 from fig 2, W_i is about

1 per cent of ρ_0/L_0T for German silver and constantan at 90° K. and about 2 per cent for stainless steel.

As W_i decreases with decreasing temperature while ρ_0/L_0T increases, the electronic resistance can be ascribed to impurity scattering over the range of the present experiments. The electronic conductivity is therefore L_0T/ρ_0 , and the lattice conductivity, K_g , must be $K - L_0T/\rho_0$.

Heat conducted by the lattice.

The lattice conductivity for the three alloys is shown in fig. 3. Up to about 20° K. it is proportional to T^2 , but above this temperature it increases more slowly and reaches a maximum value. In the case of German silver, the lattice conductivity decreases with increasing temperature at the highest temperatures at which measurements were made.

In the same way as the electronic thermal resistance can be considered as the sum of the resistances due to different scattering processes, so the thermal resistivity of the lattice, W_g , is due to several processes which scatter the momentum of the phonons. The resistances due to these causes are not strictly additive but there are temperature regions in which one process is dominant and may be identified by the temperature variation of the resistance.

W_U is the resistance due to "Umklapp" processes by which the phonons mutually interact. At low temperatures $W_U \propto T^\nu e^{-\theta/2T}$, where ν is a constant and θ is the Debye characteristic temperature (Peierls 1929).

W_D is the resistance due to small scale lattice defects and impurities. At low temperatures $W_D \propto T$ but is less temperature dependent at high temperatures.

W_B is the resistance due to scattering of phonons at the grain boundaries and is proportional to T^{-3} (Casimir 1938).

These three scattering processes are also present in dielectric crystals, and the temperature dependence of the resistances due to them have been verified in other experiments (Berman 1951). In metals and alloys there is an additional resistance due to scattering of phonons by electrons; this resistance may be written as W_E and should be proportional to T^{-2} at low temperatures according to Makinson.

For German silver the lattice resistivity, $1/K_g$, has been analysed into these various components, as shown in fig. 4.

W_U is estimated roughly from measurements on dielectrics having a similar value for θ ($\sim 300^\circ$ K.). W_U is of the order of 10 per cent of the total lattice resistance at 95° K. and this ratio falls off very rapidly with decreasing temperature.

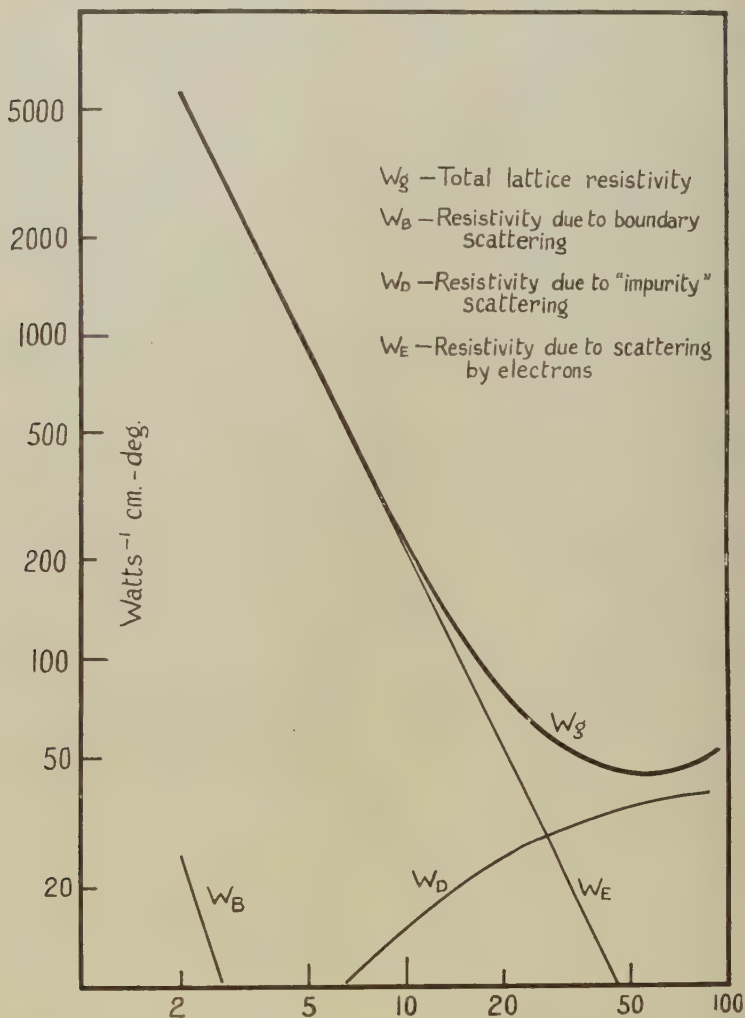
W_B is calculated from Casimir's formula

$$W_B \simeq 4.5 \times 10^{-6} \theta^2 / r T^3 \text{ Watts}^{-1} \text{ cm. deg.},$$

where r is the linear dimension of the grains. Taking θ as 300° K. and r as 0.02 mm., W_B is about 25 Watt⁻¹ cm. deg. at 2° K., which is only $\frac{1}{2}$ per cent of the total resistance at this temperature. At higher temperatures this ratio falls off very rapidly.

In the temperature range of the experiments the lattice resistance can therefore be attributed mainly to W_D and W_E . At the lowest temperatures W_θ is seen to be proportional to T^{-2} ; this is the temperature dependence of the lattice resistance, W_E , due to scattering of phonons by electrons.

Fig. 4.



Estimated contributions to the lattice thermal resistivity in German silver from scattering of phonons by electrons, "impurities" and grain boundaries.

Assuming that W_E follows the same relation to higher temperatures, W_D can be deduced, since $W_\theta = W_U + W_E + W_D$. In agreement with theory, W_D is found to be proportional to T at the lowest temperatures but to become less temperature dependent at higher temperatures.

§ 5. CONCLUSIONS.

In the alloys measured the heat conducted by the electrons and by the lattice are of the same order of magnitude. The electronic conductivity is limited by scattering due to the aperiodicity of the lattice, and the "ideal" resistance due to thermal vibrations is negligible below 100° K. The lattice conductivity appears to be limited mainly by scattering of the lattice waves by the electrons at the lower temperatures, and by the "impurities" at higher temperatures.

In the case of German silver if the effect of the electrons were removed the heat conducted by the lattice would increase to a value which, below 4° K., would be determined by the boundary scattering and not by the percentage of "impurity" in the alloy.

Mendelssohn and Olsen (1950) have found that, in contrast to the behaviour of most metals, for some alloys of lead and for columbium the heat conductivity is greater in the superconducting state than in the normal state. To explain this they postulate a circulation heat flow analogous to that which has been used to account for the high heat conductivity of liquid helium II. Hulm (1950) has suggested that for these specimens the lattice conduction is appreciable and increases when the specimen becomes superconducting owing to the reduction in the number of electrons capable of scattering the lattice waves. If this is so, then, although the electronic conductivity decreases, the total conductivity in the superconducting state may be higher than in the normal state.

For the metals and alloys on which such experiments have been made, the impurity concentrations are much smaller than in German silver, so that the thermal resistance due to them will also be smaller. For relatively large grains (1/10 to 1 mm.) therefore, the lattice resistance due to even 1 per cent of impurity would be less than the resistance due to boundary scattering at 2° K. If at this temperature the electrons no longer take part in both heat conduction and in scattering of lattice waves, then the total conductivity would increase by a large factor.

It would therefore be of interest to determine the electronic and lattice conductivities, in the normal state, and the grain sizes of specimens which show the behaviour found by Mendelssohn and Olsen. It might then be possible to decide whether it is necessary to postulate a new heat transport mechanism to explain their results.

APPENDIX.

In the design of low temperature apparatus it is often necessary to calculate the heat flow, along tubes or wires, between parts which are at very different temperatures. If the temperatures at the end of a specimen 1 cm. long are T_1 and T_2 , the heat flow per unit area per second is equal to $\int_{T_1}^{T_2} K dT$ and may be considered as $(T_2 - T_1)\bar{K}$, where \bar{K} is the "mean" conductivity in the temperature interval T_1 to T_2 .

For convenience, the following table gives the heat flowing along specimens of German silver and stainless steel, 10 cm. long and 1 sq. mm. cross sectional area, and along a constantan wire of 36 gauge (2.9×10^{-2} mm.²), also 10 cm. long, when the temperatures at the ends vary from 80° to 0° K.

Rate of Heat Flow along Specimen—in watts.

Temperatures at ends of Specimen °K. T_2 T_1		German Silver 10 cm. long 1 mm. ² cross-section	Stainless Steel 10 cm. long 1 mm. ² cross-section	Constantan 36 gauge (2.9×10^{-2} mm. ²) 10 cm. long
80	20	8.0×10^{-3}	3.0×10^{-3}	2.7×10^{-4}
60	20	4.8×10^{-3}	1.7×10^{-3}	1.6×10^{-4}
20	4	5.8×10^{-4}	1.7×10^{-4}	2.1×10^{-5}
10	4	9.3×10^{-5}	3.1×10^{-5}	3.5×10^{-6}
4	1	1.0×10^{-5}	4.2×10^{-6}	3.5×10^{-7}
1	0	4.0×10^{-7}	1.8×10^{-7}	1.0×10^{-8}

As these heat flows are often of interest in the determination of the volumes of liquid hydrogen and liquid helium which they cause to be evaporated, it should be noted that 1 watt evaporates about 100 c.c. of liquid hydrogen per hour and about 1 litre of liquid helium per hour.

ACKNOWLEDGMENTS.

I should like to thank Professor F. E. Simon, F.R.S., for his continued interest in the work, also Dr. J. W. Christian for the grain size determinations.

REFERENCES.

- ALLEN, J. F., and MENDOZA, E., 1948, *Proc. Camb. Phil. Soc.*, **44**, 280.
 BERMAN, R., 1951, To be published in *Proc. Roy. Soc. A*.
 CASIMIR, H. G. B., 1938, *Physica*, **5**, 495.
 GRÜNEISEN, E., and GOENS, E., 1927, *Z. Phys.*, **44**, 615.
 HULM, J. K., 1950, *Proc. Roy. Soc. A*, **204**, 98; 1951, *Proc. Phys. Soc. B*, **64**, 207.
 KARWEIL, J., and SCHÄFER, K., 1939, *Ann. Phys., Lpz.*, **36**, 567.
 LEES, C. H., 1908, *Phil. Trans. Roy. Soc. A*, **208**, 381.
 MAKINSON, R. E. B., 1938, *Proc. Camb. Phil. Soc.*, **34**, 474.
 MENDELSSOHN, K., and OLSEN, J. L., 1950, *Proc. Phys. Soc. A*, **63**, 2, 1182.
 PEIERLS, R., 1929, *Ann. Phys. Lpz.*, **3**, 1055.
 SCHMEISSNER, F., and MEISSNER, H., 1950, *Z. angew. Phys.*, **2**, 423.
 WILKINSON, K. R., and WILKS, J., 1949, *J. Sci. Instrum.*, **26**, 19.

LXVIII. *Observation of Cosmic Ray Events in Nuclear Emulsions
Exposed in a Glacier at 3550 m.*

By J. B. HARDING*,
Imperial College, London †.

[Received March 7, 1951.]

ABSTRACT.

Photographic emulsions have been exposed at various depths under ice at 3550 m. The variation in the numbers of slow μ -mesons with depth is in fair agreement with a predicted variation.

From the variation of the numbers of "stars" with depth, the best estimate for the absorption mean free path of the star producing radiation is 170 ± 10 gm./cm.².

The variation of the numbers of π^+ -mesons with depth is consistent with an absorption path length for nuclear interaction corresponding to a few times the geometric value. A large upward stream of π -mesons has been observed and possible interpretations are discussed.

§1. INTRODUCTION.

IN previous notes (Harding *et al.* 1949 a and b) we have reported results on the absorption of the star producing radiation and on the variation of the number of π -mesons with depth in ice. In order to improve the statistics and the geometry, the experiment at the Jungfraujoch 3550 m. has been repeated. Experimental results for stars and mesons will be given.

§2. EXPERIMENTAL DETAILS.

In order to obtain good geometry a steel pipe ($2\frac{1}{8}$ -in. internal diameter, $\frac{3}{16}$ -in. wall thickness) closed at the lower end was sunk vertically to a depth of 9 m. into a glacier. Boxes of plates coated with Ilford G.5 "Nuclear Research" emulsion 200μ thick were exposed vertically at depths down to 5 m. for 89 days. The pre- and post-exposure amounted to about four days spent mainly at sea level. Plates were also exposed at depths of $6\frac{1}{2}$ and $8\frac{1}{2}$ m., but these emulsions were poured at the Jungfraujoch under a large thickness of rock. The pre- and post-exposure of these plates amounted to 2 hours at 3550 m. The spaces between the boxes in the top 3 m. of pipe were filled with cylinders of paraffin wax, density 0.9 gm./c.c., which should produce nearly the same effects on cosmic ray particles as ice itself.

* Present address, Atomic Energy Research Establishment, Harwell.

† Communicated by Sir George Thomson, F.R.S.

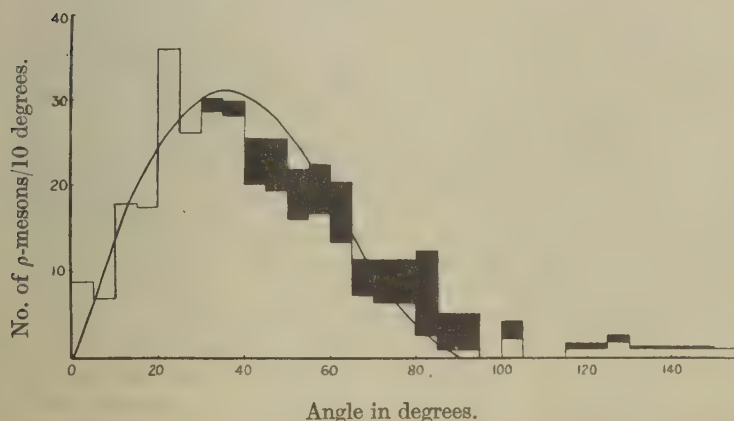
TABLE I.

1.	Depth in gm./cm. ² ice	0	45	90	135	180	225	270	360	450	585	765
2.	Stars observed	905	455	470	530	543	238	262	114	108	32	16
3.	Stars/c.c./day	{ 16.2 ± 0.5	10.6 ± 0.5	6.6 ± 0.3	5.3 ± 0.2	3.8 ± 0.16	2.8 ± 0.15	1.8 ± 0.11	1.07 ± 0.1	0.52 ± 0.05	0.19 ± 0.03	0.08 ± 0.02
4.	Star rate corrected for pre-exposure	{	{	16.2 ± 0.5	10.6 ± 0.5	6.6 ± 0.3	5.3 ± 0.2	3.8 ± 0.16	2.8 ± 0.15	1.8 ± 0.11	1.02 ± 0.1	0.48 ± 0.05	0.18 ± 0.03	0.07 ± 0.02
5.	No. of π^+ -mesons	0-60°	..	1	10	16	20	16	10	9	3	4	1	1
6.		60-90°	..	2	4	10	10	7	3	5	3	1	1	1
7.		90-120°	..	10	9	4	10	4	2	7	1	0	1	1
8.		120-180°	..	9	3	3	8	2	1	3	2	1	0	0
9.	No. of π^+ -mesons	0-60°	..	1	12	18	27	16	12	12	8	5	2	1
10.		60-90°	..	8	7	11	15	9	5	9	6	3	1	1
11.		90-120°	..	14	5	6	9	4	4	6	1	3	1	0
12.		120-180°	..	10	7	6	9	6	4	7	2	2	2	1
13.	$[\pi^+$ -mesons (0-60°)/stars] 100	..	{ 0.022 ± 0.016	0.48 ± 0.11	0.68 ± 0.12	0.89 ± 0.13	0.92 ± 0.21	0.59 ± 0.10	0.92 ± 0.21	0.80 ± 0.17	0.96 ± 0.30	0.84 ± 0.28	0.94 ± 0.53	1.25 ± 0.89
14.	ρ -mesons/c.c./day	0-90°	..	{ 2.56 ± 0.21	2.70 ± 0.25	2.35 ± 0.18	2.50 ± 0.16	2.03 ± 0.12	2.08 ± 0.14	2.03 ± 0.12	1.41 ± 0.12	1.30 ± 0.08	1.17 ± 0.09	1.04 ± 0.09
15.		90-180°	..	{ 0.26 ± 0.06	0.23 ± 0.07	0.23 ± 0.06	0.19 ± 0.04	0.16 ± 0.04	0.16 ± 0.14	0.16 ± 0.13	0.09 ± 0.03	0.07 ± 0.02	0.04 ± 0.01	0.01
16.	μ -mesons/c.c./day	0-90°	..	{ 2.50 ± 0.23	2.48 ± 0.28	2.09 ± 0.20	2.28 ± 0.16	1.94 ± 0.13	1.99 ± 0.15	1.95 ± 0.13	1.37 ± 0.13	1.28 ± 0.08	1.16 ± 0.09	1.04 ± 0.07
17.		90-180°	..	{ 0.04 ± 0.08	0.08 ± 0.08	0.09 ± 0.07	0.07 ± 0.05	0.12 ± 0.04	0.08 ± 0.04	0.12 ± 0.03	0.06 ± 0.03	0.06 ± 0.02	0.03 ± 0.03	—

§ 3. EXPERIMENTAL RESULTS.

In Table I. the frequency of occurrence of the various events are shown. We have assumed that the density of ice was uniform and equal to 0.9 gm./c.c. Only ρ -mesons of projected lengths greater than $130\ \mu$ have been recorded; a ρ -meson being defined as one that does not produce a visible star nor that gives rise to a secondary meson. The numbers of π^+ -mesons which stop in the emulsions and are travelling at angles $0-60^\circ$, $60-90^\circ$, $90-120^\circ$, $120-180^\circ$ with the downward vertical at their points of entry, are given. All errors given represent standard deviation, based on the numbers of events recorded. Non-uniformity of the emulsion thickness may introduce additional errors of about 5 per cent. A random sample of plates were searched twice and by this means the overall efficiency for recording stars was estimated as 97 per cent, while for ρ -mesons the efficiency was about 80 per cent.

Fig. 1.



Angular distribution of ρ -mesons. The shaded areas must be added to the observed distribution (unshaded histogram) in order to correct for loss of tracks at large zenith angles caused by the thinness of the emulsion.

The angular distribution of ρ -mesons arriving at the plate is shown in fig. 1. This distribution has been obtained by measuring 100 mesons at each of the following depths:—0, 180 and 585 gm./cm.². Since mesons making large zenith angles have a smaller chance than those of small zenith angles of producing a track of at least $130\ \mu$ (and therefore of being recorded), this distribution is weighted to small angles. By considering the distribution in the angle of dip for various zenith angles approximate correction factors have been obtained and the corrected distribution is shown by the addition of shaded areas. The curve in this figure represents a $\cos^2 \theta$ distribution per unit solid angle.

The ρ -mesons that we observe represent three types of events :—

(a) 28 per cent of π^- -mesons leave no visible star on coming to rest in the emulsion (Bradner 1949) and these will be recorded as ρ -mesons.

(b) Some will be μ^+ -mesons produced from decay at rest of π^+ -mesons in the immediate neighbourhood of the emulsion, the π^+ -mesons having been locally created.

(c) The majority are the μ^+ -mesons which form the hard component of cosmic rays.

We shall now estimate the quantities (a) and (b) and obtain by subtraction those mesons which form the hard component.

For every 100 π^- -mesons which produce stars,

$$28 \left(\frac{100}{100-28} \right) = 39 \pi^- \text{ mesons}$$

stop in the emulsion and fail to produce stars. Only 80 per cent of the π^- -mesons which produce stars have ranges exceeding 130μ and there is no reason to suppose that this ratio will be different for those π^- -mesons which produce no visible star. Because of searching inefficiency only 80 per cent of ρ -mesons of lengths greater than 130μ are recorded. Therefore for every 100 π^- -mesons which produce stars $39 \times 0.8 \times 0.8 = 25 \pi^-$ -mesons will be recorded as ρ -mesons.

It is estimated that for every 100 π^+ -mesons stopping in the emulsion, $37 \mu^+$ -mesons (of length greater than 130μ) will also stop in the emulsion due to the decay at rest of π^+ -mesons in the surrounding material which is assumed to have the same stopping power as the emulsion itself. The slightly (~ 20 per cent) lower stopping power of glass, which, with the emulsion of the neighbouring plates, forms the bulk of the surrounding material, will only produce a second order correction. From range measurements on the μ^+ of π - μ events, it is estimated that we recorded only about 80 per cent of the π^+ -mesons which stopped in the emulsion and as stated above, the searching efficiency for ρ -mesons of length greater than 130μ was also about 80 per cent. Thus for every 80 π^+ -mesons observed to stop in the emulsion approximately $37 \times 0.8 = 30 \mu^+$ -mesons are observed as ρ -mesons.

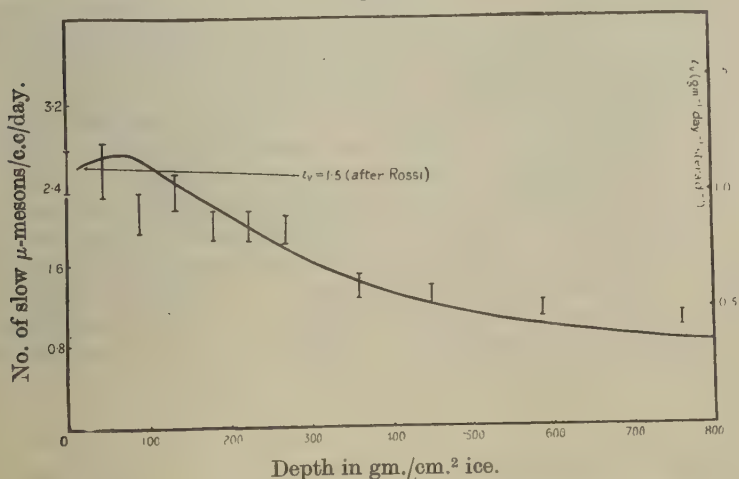
Therefore, for every 180 π -mesons (80 π^+ - and 100 π^- -mesons) observed to stop, $30 + 25 = 55$ mesons are recorded as ρ -mesons, and must be associated with the π -mesons rather than with the μ^+ -meson of the hard component. By subtracting $55/180 \sim 30$ per cent of the numbers of π -mesons at any depth from the numbers of ρ -mesons observed, we are left with the numbers of μ -mesons of the hard component. The values are shown in rows 16 and 17 of Table I. It is seen that only about 4 per cent of the μ -mesons travel upwards, and this upward stream can reasonably be attributed to Coulomb scattering.

Working from the energy spectrum of μ -mesons at sea level, and the variation of the μ -meson intensity with altitude, Sands (1950) has derived the expected form of the differential range distribution of μ -mesons in

air at mountain altitudes. The experimental results for the numbers of μ -mesons (Table I. row 16) travelling downwards and coming to rest in the emulsion, are plotted against depth of ice in fig. 2. Sands' curve, in arbitrary units, has been corrected for the different medium (ice instead of air) and is shown in this figure. Thus assuming no μ -mesons are produced in the ice, other than by the decay of π -mesons, the variation with depth in ice of the number of slow mesons, is in fair agreement with the predicted variation.

As regards the absolute flux of μ -mesons, Rossi (1948) has given the absolute value i_v of the differential range spectrum at 10 gm./cm.^2 at various atmospheric depths, *i. e.* the number of μ -mesons/day/steradian in the vertical direction, which stop in one gram of air at various depths in

Fig. 2.



the atmosphere. At 3550 m. $i_v = 1.5 \text{ gm.}^{-1} \text{ diem.}^{-1} \text{ sterad}^{-1}$. This fixes the ordinate of Sands' curve. In order to compare our intensity with Rossi's value we have to correct for

- (a) the angular distribution of the mesons ($\cos^2 \theta$ per sterad),
- (b) loss due to thin emulsions. We have recorded only mesons of length $\geq 130 \mu$ whereas we require the numbers of mesons of length greater than zero,
- (c) relative stopping powers per gram of air and emulsion ($1 \text{ gm. air} \equiv 1.7 \text{ gm. emulsion} \equiv 0.43 \text{ c.c. emulsion}$),
- (d) correction factor for searching efficiency is $1/0.8$.

We have recorded μ -mesons arriving at the plate and coming from the upper hemisphere. It is to be expected that a photographic emulsion records the "integrated intensity" of slow mesons, *i. e.* the number of

from which a value of $\alpha=200$ gm./cm.² was obtained. The difference can only be explained by poor geometry, *e. g.* large holes in the ice in the first experiment.

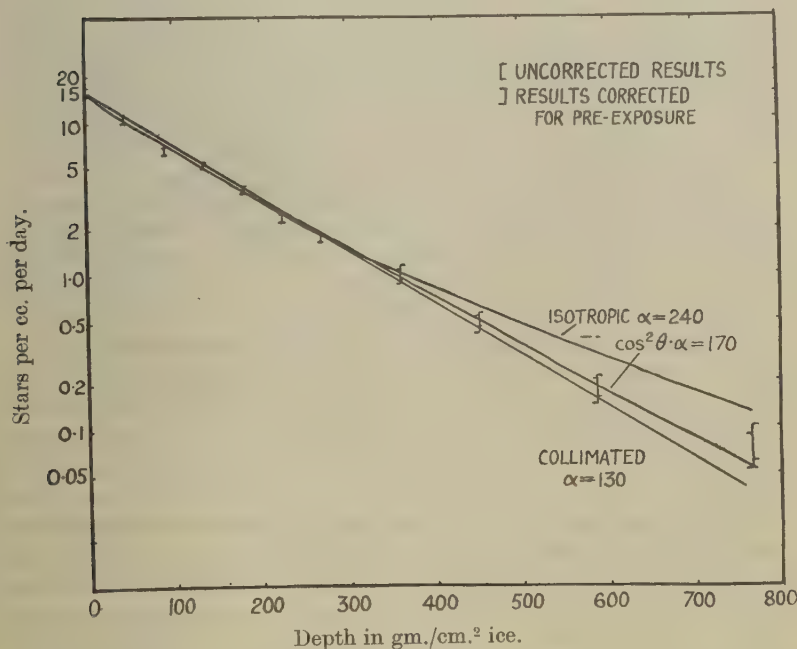
It may be argued that, because of an angular distribution of the star producing radiation, we should not expect exponential absorption. For an isotropic distribution at the ice surface of primaries, which are assumed to travel in straight lines, we would expect (see Rossi 1948)

$$I/I_0 = e^{-x/\alpha} - (x/\alpha) \text{Ei}(-x/\alpha) \quad . \quad . \quad . \quad (2)$$

or for a $\cos^2 \theta$ distribution per unit solid angle

$$I/I_0 = e^{-x/\alpha} (1 - \frac{1}{2}(x/\alpha) + \frac{1}{2}(x/\alpha)^2) - \frac{1}{2}(x/\alpha)^3 \text{Ei}(-x/\alpha). \quad . \quad . \quad . \quad (3)$$

Fig. 3.



In order to obtain agreement between the experimental results and a theoretical curve over the first 300 gm./cm.² in the case of equation (2). There is then poor agreement for depths beyond 450 gm./cm.². In the case of equation (3), if we take $160 < \alpha < 180$ gm./cm.² good agreement is obtained between the theoretical curve and the experimental points even down to 765 gm./cm.² of ice.

So far we have taken an exceptionally simple picture of the star production process inasmuch as we have assumed that all stars are produced by one component which is incident on the ice surface with

a certain ($\cos^2 \theta$) angular distribution. It seems likely that the star producing particles are not absorbed in a single nuclear encounter, or, what probably comes to the same thing, that in producing a star, the primary also produces one or more particles which can then act as primary particles for further stars, *i.e.* a cascade process. Provided these secondary particles have the same mean free path for star production and are produced at any depth with an angular distribution similar to that of the primary particles at that depth, then the above equations should equally apply for such a cascade process, but α no longer represents the absorption path length of the star producing radiations.

It is thought that the nucleonic component is mainly responsible for the production of stars. However George *et al.* (1950) have suggested a cross-section, σ , per nucleon for star production by μ -mesons of approximately 10^{-29} cm.². They have therefore shown ~ 0.1 stars/c.c./day should be produced in emulsion at 3550 m. This of course is negligible compared with the 16 stars c.c./day observed at the ice surface. Production of fast μ -mesons in the ice is negligible and hence at 760 gm./cm.² of ice there are ~ 1000 fast μ -mesons crossing a square centimetre/day (see above). Thus the expected number of stars per c.c. per day produced by μ -mesons is $1000N\rho\sigma$ where N =Avagadro's number and ρ =density of emulsion. This comes to 0.024 stars/c.c./day which is approximately one-third of the observed number at the lowest point. About 15 per cent of the stars at 585 gm./cm.² of ice could be formed by μ -mesons. Thus even making allowance for stars formed by mesons, the experimental points still lie on a curve given by equation (3) with $\alpha = 170 \pm 10$ gm./cm.².

It is concluded that the experimental results are consistent with the assumption that the majority of stars are produced by primaries (nucleons) having an incident distribution $\cos^2 \theta$ per steradian and an apparent absorption mean free path of 170 ± 10 gm./cm.².

π -Mesons.

In a previous note (Harding and Perkins 1949 b) we obtained the variation in the number of π -mesons with depth in ice, and concluded that they were produced with a mean range ~ 100 gm./cm.² ice. Since then, an energy spectrum for the production of π -mesons in photographic emulsion has been obtained by Camerini *et al.* (1950). If we assume that this spectrum can be used to represent the production spectrum *in ice* we can obtain certain limits for λ , the absorption mean free path in nuclear interactions for fast π -mesons in ice.

It is assumed :—

(a) the rate of production of mesons at a given depth is proportional to the star intensity at that depth,

(b) mesons travel in straight lines,

(c) the energy, or range distribution of mesons at production is independent of angle. Thus $q(R) dR \cdot f(\theta) d\theta$ is the probability that

a meson is produced with a range R to $R+dR$ at θ to $\theta+d\theta$ with the downward vertical. The spectrum $q(R) dR$ is obtained from Camerini's spectrum using a theoretical range-energy relation.

Let $P(x, \theta) d\theta$

$$= \frac{\text{No. of mesons stopping at depth } (x, dx) \text{ travelling at angle } (\theta, d\theta)}{\text{No. of stars at depth } (x, dx)},$$

where the star intensity (see above) can be approximated by

$$I/I_0 = e^{-x/\alpha}.$$

Let $g(R) dR$ be the probability that a meson of range R gm./cm.² ice will not decay in flight, i. e.

$$g(R) = \exp \left[- \int_0^R \frac{E_0 dR'}{c\beta\tau_0(E+E_0)} \right]$$

E being the kinetic, and E_0 the rest energy of a meson. The lifetime τ_0 is taken as $7 \cdot 10^{-9}$ secs.

It can then be shown that

$$P(x, \theta) d\theta \propto \int f(\theta)/\cos \theta \int_{R=0}^{x/\cos \theta} e^{\frac{R/\cos \theta}{\alpha}} e^{-R/\lambda} g(R) q(R) dR d\theta.$$

Considering mesons in the angular range $0-60^\circ$, we can write as a sufficient approximation

$$P(x) \bar{\theta} \propto \int_{R=0}^{x/\overline{\cos \theta}} e^{\frac{R \overline{\cos \theta}}{\alpha}} e^{-R/\lambda} g(R) q(R) dR,$$

where we take $\overline{\cos \theta}$ as the average value of $\cos \theta$ for mesons arriving at the plate (fig. 5). $\overline{\cos \theta} = 0.77$. We take $\alpha = 130$ gm./cm.². The form of $P(x)$ can be obtained for various values of λ , and these are plotted in fig. 4 together with the experimental results. We have fitted theoretical curves to obtain the best agreement with the experimental points by a method somewhat analogous to least squares. We choose the ordinate scale for the theoretical curves such that $\sum_i e_i^2/\sigma_i^2$ is a minimum, where e_i is the difference between the experimental i th point and the curve, and σ_i is the uncertainty of the i th point.

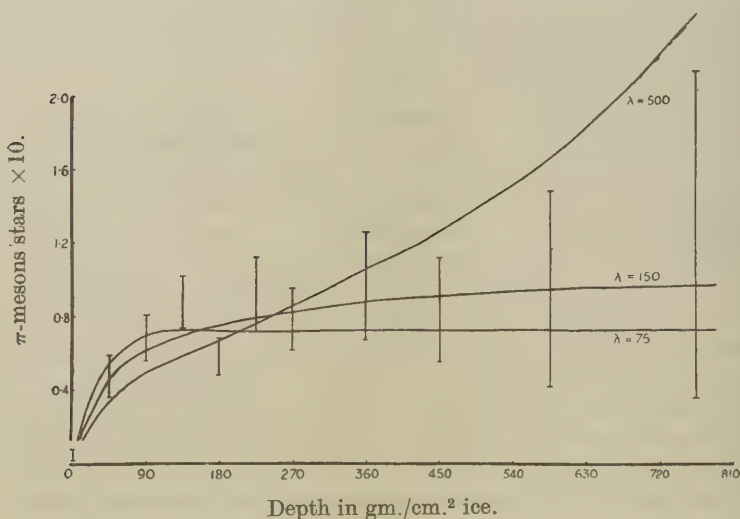
On this criterion, the experimental points best fit the curve for $\lambda = 150$ gm./cm.². The fit is about three times better than for $\lambda = 75$ and 90 times better than for $\lambda = 500$ gm./cm.². We conclude that the variation with depth of the number of π -mesons is consistent with an absorption path length for nuclear interaction corresponding to the geometric, or to a few times the geometric value of 70 gm./cm.² (neglecting the effect of hydrogen). If the proper lifetime of π -mesons is larger than we have assumed, say 10^{-8} instead of $7 \cdot 10^{-9}$ seconds, then small values of λ are still further favoured.

Assuming :—

- (a) mesons are produced only in oxygen in the ice ;
- (b) on the average the same number of mesons are produced in oxygen disintegrations, as in disintegrations of nuclei in photographic emulsion ;
- (c) the rate of nuclear disintegrations (and hence meson production) is proportional to the total geometrical cross-section of the nuclei, then we observe about $1\frac{1}{2}$ times as many mesons stopping as we would expect from a calculation in which a value of $\lambda=75$ gm./cm.² was used. This shows that the numbers of mesons observed is of the magnitude expected : no particular significance is attached to the ratio of $1\frac{1}{2}$.

Since equilibrium between mesons and stars seems to be established for depths below 225 gm./cm.² ice, we should expect the angular distribution of π -mesons to be constant at these depths. We are therefore justified

Fig. 4.



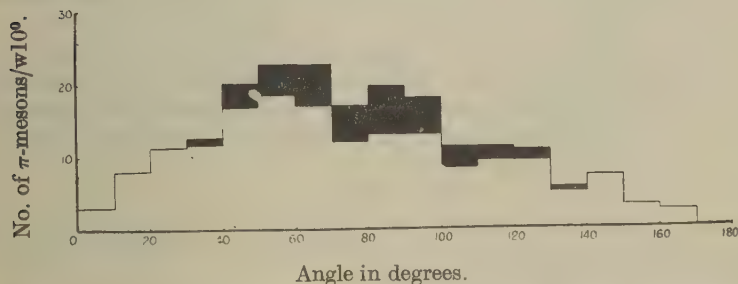
in classing together mesons at all these depths when considering the angular distribution of mesons arriving at the plate. This distribution is shown in fig. 5 in which a correction has been applied (shaded histogram) for loss of steeply dipping tracks. It is seen that approximately one-third of all π -mesons were travelling in an upward direction when coming to rest in the emulsion. Unfortunately, complete data on the angular distribution at production of mesons have not been published. Brown *et al.* (1949) have shown that at 3550 m. in showers of more than five particles 93 per cent of the shower particles (the majority of which are mesons with energies above 60 MeV.) are directed downwards and nearly obey a $\cos \theta \sin \theta d\theta$ distribution. We may assume the lower

energy mesons to be isotropic. From an analysis of stars formed at 70,000 ft. Perkins (private communication) concludes that in light elements about 10 per cent of shower particles travel backwards with respect to the incident star producing radiation. Due to the angular distribution about the zenith of the meson producing radiation (which is likely to be more collimated than the total star producing radiation since higher energy events are involved), the percentage of upward travelling shower particles at production will exceed 10 per cent. A liberal estimate of this percentage would be 20 per cent. We make the following assumption about the angular distribution of mesons at production and will then calculate the expected ratio of the numbers of mesons coming to rest after travelling in an upward cone of 60° to the number of those coming to rest after travelling in a downward cone of 60° .

Assume :—

(a) Mesons of energy below 60 MeV. are produced isotropically in the laboratory system. These form 12 per cent of the total number of mesons.

Fig. 5.



Angular distribution of π -mesons. Shaded areas represent corrections for loss of steeply dipping tracks.

(b) Twenty per cent of mesons of energy greater than 60 MeV. are produced isotropically in the upper hemisphere.

(c) The remainder of the mesons are produced downward with a $\cos \theta$ distribution per unit solid angle.

Consider one meson produced in the upward 60° cone and one in the downward 60° cone due to group (a) mesons. Then it can be shown that there will be three mesons produced in the upward cone due to class (b) mesons and 18 in the downward cone due to class (c) mesons. With these assumptions we find that four mesons are produced in an upward cone to 19 in the downward cone. However, the downward moving mesons, being produced with higher average energies have longer ranges (electronic stopping) than the upward moving mesons. Therefore they should stand more chance of being lost through nuclear interactions

(for $\lambda = 75 \text{ gm./cm.}^2$). Taking this into account, in a calculation somewhat similar to the above, it is deduced that one slow meson should be observed in the upward cone for every 3.6 in the downward cone. The experimental figure is $1 : 2.7 \pm 0.6$.

The calculations have been carried through on the assumption that mesons travel in straight lines. We have seen that the Coulomb scattering of μ -mesons is small (~ 4 per cent are back-scattered) and the scattering of π -mesons is expected to be of the same order. We therefore conclude that for the given assumptions concerning the angular distribution at production of π -mesons, the observed ratio of the upward to downward flux of π -mesons is not significantly different from the expected ratio. If, however, the results of further experiments should show that π -mesons are more strongly collimated than has been assumed above, then the observed upward flux would suggest that nuclear scattering of π -mesons is an important process. Indeed, preliminary results of Bernadini *et al.* 1950, suggest that π -mesons are scattered in flight through angles of greater than 30° with a cross-section of about one-quarter of the geometrical value. Scattering of this magnitude would lead to almost perfect agreement between the observed and calculated upward flux of π -mesons.

ACKNOWLEDGMENTS.

I should like to express my thanks to Professor Sir George Thomson for guidance during the course of this work and to Dr. E. P. George for an interesting discussion concerning the upward stream of π -mesons.

REFERENCES.

- BRADNER, H., 1949, *Review of Work on Artificially produced mesons* (Berkeley).
 BERNALINI, *et al.*, 1950, *Phys. Rev.*, **80**, 924.
 BROWN, *et al.*, 1949, *Phil. Mag.*, **40**, 862.
 CAMERINI, *et al.*, 1950, *Phil. Mag.*, **41**, 413.
 GEORGE, and EVANS, 1950, *Proc. Phys. Soc. A*, **63**, 1248.
 HARDING, LATTIMORE, LI, and PERKINS, 1949 a, *Nature, Lond.*, **163**, 319.
 HARDING, and PERKINS, 1949 b, *Nature, Lond.*, **164**, 285.
 KRAUSHAAR, W. L., 1949, *Phys. Rev.*, **76**, 1045.
 LATTES, OCHIALINI and POWELL, 1947, *Nature, Lond.*, **169**, 486.
 ROSSI, B., 1948, *Rev. Mod. Phys.*, **20**, 537.
 SANDS, M., 1950, *Phys. Rev.*, **77**, 180.

LXIX. CORRESPONDENCE.

Meson Production in the Atmosphere.

By J. D. PULLAR and E. G. DYMOND,

Department of Natural Philosophy, University of Edinburgh*.

[Received March 12, 1951.]

THE variation with altitude of the vertical intensity of the penetrating component of cosmic radiation has been measured in a series of balloon flights from Edinburgh, geomagnetic latitude 59° N. A telescope, ABC, of three counters with 8 cm. of lead absorber was used, giving a ground rate of 57.4 ± 0.7 counts per hour. Radio transmission of the counts during flights and of the air pressure record, gave the necessary data. Particular attention has been paid to accuracy of pressure measurement, since the important information is obtained at the lowest pressures. A minimum pressure of 4 mb. (maximum altitude of 124,000 ft.) was reached during these flights.

Curve 1 shows the mean result of seven flights with identical equipments. The intensity, extrapolated to zero pressure, is 23 times the ground value. Pomerantz (1949) has published a similar curve, deduced from a single flight at $\lambda 52^\circ$ N. and with 7.5 cm. Pb. His curve, when normalized to ours at the ground, agrees within statistical error at the top of the atmosphere, but is some 25 per cent lower between 200 and 50 mb. At 27 mb. Schein, Jesse and Wollan (1941) found an increase of 16 times over ground rate, which is considerably lower than our result. Lack of published detail, however, prevents accurate comparison with our work.

The counter arrangement ABC measures not only the flux of mesons and primary particles able to penetrate 8 cm. Pb., but also electron showers coming in from the side. The influence of these was measured in two further flights, by counting the fourfold coincidences between counters ABCD. The results are shown in Curve 2. At the lowest pressure of 12 mb. the number of showers is rising very steeply and amounts to 20 per cent of the threefold rate ABC.

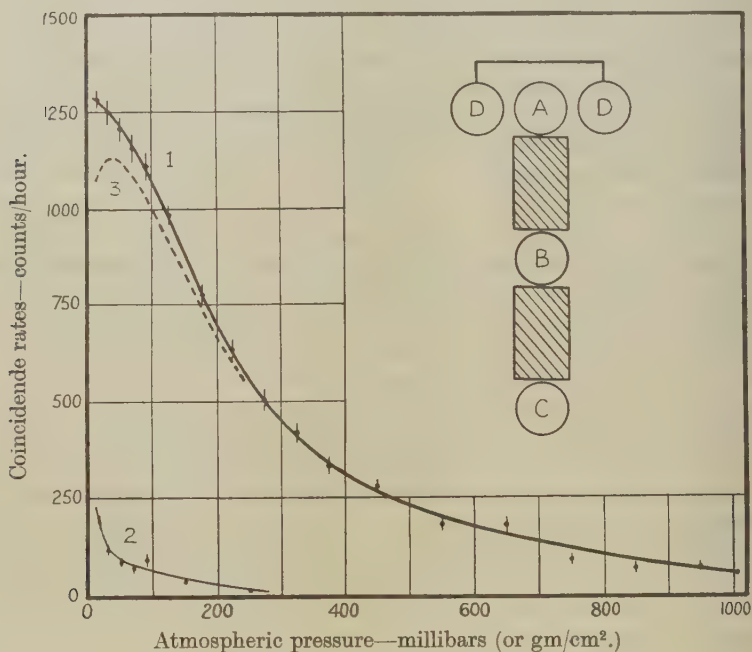
Electronic showers arriving at large angles to the zenith are to be expected at very low pressures. Such showers reach maximum development after traversing 100 gm./cm.^2 of the atmosphere. Measured horizontally the atmosphere has this thickness at a point where the pressure is 2.5 mb., thus the horizontal showers will increase in importance until this value of the pressure is reached. It is of course possible for the fourfold coincidence system ABCD to respond also to vertical showers containing at least one penetrating particle. However, the interaction length of protons is about 70 gm./cm.^2 , so that a sharp rise in counting rate in the uppermost 20 gm./cm.^2 is not to be expected from this cause.

* Communicated by Professor N. Feather, F.R.S.

We are therefore justified in regarding Curve 2 as due to side showers only, and by subtraction from Curve 1 we get the true vertical penetrating flux in Curve 3. This shows a maximum at 35 mb., representing the production of mesons by particles of the primary beam. The agreement of our uncorrected curve with that of Pomerantz (who gave reasons for ignoring the shower correction) appears to be fortuitous.

Extrapolation of Curve 3 back to zero pressure in order to determine the flux of primary penetrating particles remains doubtful until more accurate values of the lateral shower correction are available in the pressure range below 10 mb. Further work is in progress in this direction.

Fig. 1.



Curve 1 : Coincidence rate of ABC.

Curve 2 : Coincidence rate of ABCD (lateral showers).

Curve 3 : Difference of 1 and 2, giving true vertical rate.

REFERENCES.

- POMERANTZ, M.A., 1949, *Phys. Rev.*, **75**, 69.
 SCHEIN, M., JESSE, W. P., and WOLLAN, E. O., 1941, *Phys. Rev.*, **59**, 615.

Cross-section for the Reaction ${}^9\text{Be}(p, p2n){}^7\text{Be}$ at 156 MeV.

By T. C. RANDLE, J. M. DICKSON and J. M. CASSELS,
Atomic Energy Research Establishment, Harwell*.

[Received March 22, 1951.]

IN the course of some experiments to measure neutron production cross-sections a "sandwich" target containing two thick sheets of beryllium and three thin sheets of carbon was bombarded with 171 MeV. protons. The γ -ray activities induced in both the target elements have since been followed for 104 days, using a Geiger counter and a standard geometrical arrangement.

As usual (Dickson and Randle 1950, 1951), the radiation from the carbon part of the target quickly become characteristic of ${}^7\text{Be}$. The cross-section for the formation of this nucleus from carbon is $11.0 \pm 1.0 \times 10^{-27} \text{ cm}^2$. at the effective proton energy of 156 MeV.

The activity of the beryllium part of the target could be analysed into two components, with half-lives of 10 days and 53 days respectively. The first component, which was much the weaker of the two, must have been due to an unidentified impurity. The second component was identified as ${}^7\text{Be}$, which has a half-life of 52.9 days. This assignment was confirmed by investigating the γ -ray energy spectrum 57 days after bombardment, using a scintillation γ -ray spectrometer (Hofstadter and McIntyre 1950). Mr. R. B. Owen, to whom we are indebted for this measurement, reported a single γ -ray energy of 0.48 MeV. The γ -rays emitted in the decay of ${}^7\text{Be}$ have an energy of 0.485 MeV.

A comparison of the activities of the two parts of the target showed that the ratio of the ${}^9\text{Be}(p, 2n){}^7\text{Be}$ cross-section to the ${}^{12}\text{C}(p, 3p3n){}^7\text{Be}$ cross-section is 0.84 ± 0.04 at the effective proton energy of 156 MeV. The ${}^9\text{Be}(p, p2n){}^7\text{Be}$ cross-section is therefore $9.2 \pm 0.9 \times 10^{-27} \text{ cm}^2$.

One of us (J.M.D.) intends to investigate the excitation curve for this reaction, which should prove useful for monitoring high energy proton bombardments of beryllium targets.

We should like to thank Dr. A. Blainey for providing us with the beryllium targets.

REFERENCES.

- DICKSON, J. M., and RANDLE, T. C., 1950, *Nature, Lond.*, **166**, 235.
DICKSON, J. M., and RANDLE, T. C., 1951, Submitted to *Proc. Phys. Soc. A*.
HOFSTADTER, R., and MCINTYRE, J. A., 1950, *Phys. Rev.*, **80**, 631.

* Communicated by the Authors.

The Reactions $^{11}\text{B}(\gamma\alpha)^7\text{Li}$ and $^{11}\text{B}(\gamma\text{T})^8\text{Be}$.

By MARGARET E. CALCRAFT and E. W. TITTERTON,
Atomic Energy Research Establishment, Harwell †.

[Received March 16, 1951.]

As a result of experiments with the A.E.R.E. synchrotron, Goward, Titterton and Wilkins (1950) gave evidence for the reaction

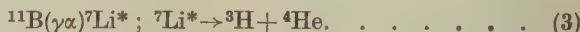


and found that at least some of the events observed involved a two-stage process



the intermediate nucleus ^8Be being formed in the well known 3 MeV. state.

Recent observation of the photodisintegration of Lithium-7 into a triton and an alpha-particle (Titterton 1950) suggests the alternative disintegration scheme



In the case where the ^7Li is left in its ground state a two-particle event would result according to the reaction



instead of the three-particle stars of equations (1), (2) and (3). The reaction (4) has not been previously observed.

To obtain information about these possible modes of disintegration Boron loaded E_1 emulsions have been exposed to Lithium gamma-rays from the 440 KeV. ($p\gamma$) resonance. Controlled under-development by the temperature method was employed to achieve discrimination between the disintegration products of reaction (4) if present.

Although the experiment is still in progress and the statistics are poor certain conclusions emerge which are worth reporting at this stage.

First, there is definite evidence for reaction (4) which is identified by the techniques discussed by Titterton (1950). A photomicrograph of one event is given in fig. 1 and the cross-section at 17.6 MeV. is estimated to be $2 \times 10^{-28} \text{ cm}^2$. Twelve events have been observed, one of which is due to the 14.8 MeV. γ -rays.

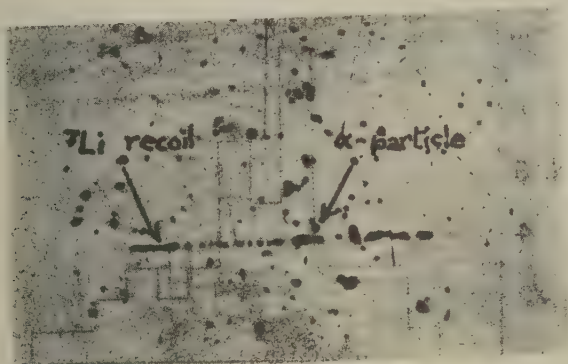
Second, among the 750 three-particle stars which have been observed 50 have been identified as resulting from reaction (1). The usual methods of the momentum and energy balance not only settle the assignment but enable a decision to be made as to which of the three particles is the triton. This is important in attempting to decide between reaction mechanisms indicated by (2) and (3).

† Communicated by the Authors.

Of the 50 events six result from the 14.8 MeV. and 44 from the 17.6 MeV. γ -ray. The cross-section for the reaction at 17.6 MeV. calculated in terms of the $^{12}\text{C}\gamma^3\alpha$ cross-section given by Wäffler and Younis (1949) is $(0.6 \pm 0.3) \times 10^{-28} \text{ cm}^2$.

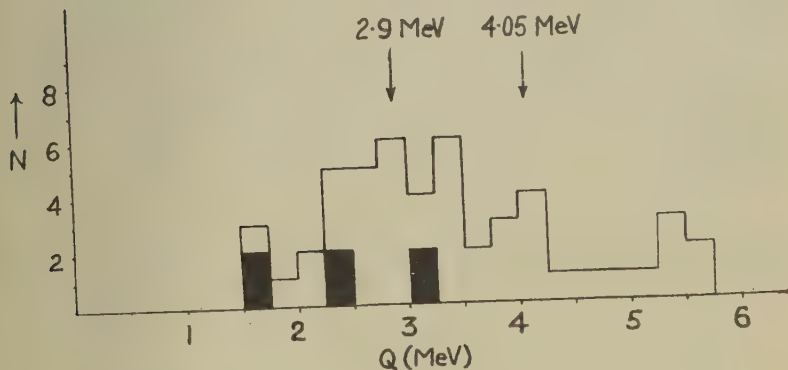
Assuming all events to result according to the mechanism of equation (2) the Q of the break up of the recoiling ^8Be nucleus is calculated in each case and the result plotted in fig. 2. The histogram suggests two broad

Fig. 1.

Photomicrograph of event due to reaction $^{11}\text{B}(\gamma)^7\text{Li}$.

Observer: Miss M. Hart.

Fig. 2.

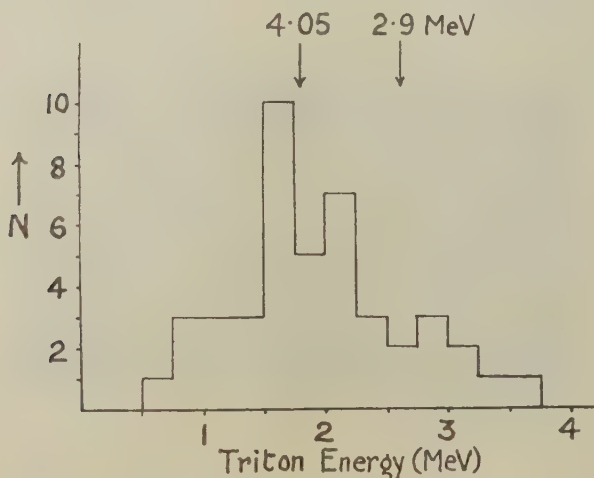


Q Value histogram. 6 blacked-out events due to 14.8 MeV. γ -ray as distinct from the others.

unresolved ^8Be levels which can be identified as the well known 2.9 MeV. level and a level at about 4 MeV., evidence for which has been given by Green and Gibson (1949). There is no known level of ^8Be corresponding

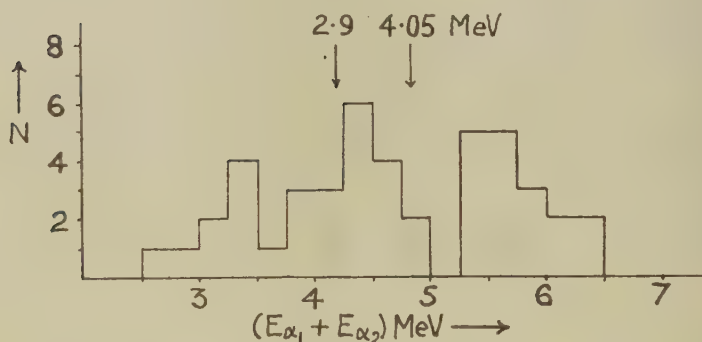
to the small group at 5.5 MeV. In the case of the 2.9 and 4 MeV. levels the appropriate energy of a triton emitted at 90° to the incoming γ -ray and the energy of the corresponding α -particle pair can be calculated from the conservation conditions for the 17.6 MeV. γ -ray. The values obtained are indicated on the histograms given in figs. 3 and 4 which

Fig. 3.



Energy spectrum of emitted tritons.

Fig. 4.

Energy spectrum of α -particle pairs following triton emission.

show the triton energy distribution and the energy distribution of the corresponding pairs of alpha-particles for events due to the 17.6 MeV. γ -ray. In each case the observed distribution is consistent with the presence of events arising from the 2.9 and 4.05 MeV. levels. The groups

are not resolved but the distributions are consistent with the known resolution of the emulsion for low energy particles (Titterton and Brinkley 1949) and the spread due to the angular distribution of the triton relative to the incoming γ -ray, provided this is not markedly anisotropic.

The 2.9 MeV. level of ^8Be is well known and has been much discussed; the 4 MeV. level was observed by Green and Gibson in experiments on the neutrons from the reaction $^7\text{Li}(dn)^8\text{Be}$ but they were unable to estimate the width of the state. However, as the only γ -ray observed in the experiments of Bennett *et al.* (1941 and 1947) had an energy of 4.9 MeV. and the corresponding neutron group was observed by Green and Gibson it is reasonable to suppose that the 4 MeV. level leads to a pair of α -particles as indicated by the present experiment and has a width similar to the 2.9 MeV. level. The 4 MeV. level would then have even angular momentum or even parity or both.

The mechanism indicated by equation (3) has been considered in a similar fashion. The known ^7Li level at 7.38 MeV. which breaks up into a triton and an α -particle can be excluded immediately since none of the events show a low energy α -particle as would be necessary from the energetics of the reaction. The question then arises whether there is a lower level of ^7Li which disintegrates by triton emission. The analysis is complicated by the fact that the first α -particle to be emitted is not known and each α -particle must be considered in turn. Two Q values relating to the break-up of ^7Li into a triton and an α -particle (second stage of reaction (3)) are found for each event one of which is correct and the other incorrect. A histogram similar to fig. 2 plotted with the results should show a peak superimposed on a background if a level of ^7Li is involved. In fact, no such peak is observed and the experiment indicates that at least 85 per cent of the events proceed through the mechanism of equation (2).

This result is consistent with recently published level schemes (Hornyak, Lauritsen, Morrison and Fowler 1950) for the mirror pair ^7Li and ^7Be neither of which has a level between the low lying γ -ray emitting states and the states at 7.38 and 7.02 MeV. respectively which are known to be unstable to α -emission.

Our thanks are due to Miss E. M. Chellingworth and Miss M. Hart for microscope work and to Professor O. R. Frisch and Dr. D. H. Wilkinson for permission to use the Cavendish Laboratory H.T. set.

REFERENCES.

- BENNETT, BONNER, RICHARDS, and WATT, 1941, *Phys. Rev.*, **59**, 904; 1947, *Ibid.*, **71**, 11.
GOWARD, TITTERTON, and WILKINS, 1950, *Proc. Phys. Soc. A*, **63**, 172.
GREEN, and GIBSON, 1949, *Proc. Phys. Soc. A*, **62**, 407.
HORNYAK, LAURITSEN, MORRISON, and FOWLER, 1950, *Rev. Mod. Phys.*, **22**, 291.
TITTERTON, 1950, *Proc. Phys. Soc. A*, **63**, 915.
TITTERTON, and BRINKLEY, 1949, *A.E.R.E. Report G/R 326*.
WAFFLER, and YOUNIS, 1949, *Helv. Phys. Act.*, **22**, 614.

Observation of Growth of Cadmium Iodine from Aqueous Solution.

By A. J. FORTY,

H. H. Wills Physics Laboratory, University of Bristol*.

[Received April 23, 1951.]

[Plate XXI.]

ACCORDING to the ideas of F. C. Frank (1949, 1950; see also N. F. Mott 1949), the growth of crystals from vapour or solution can occur by two mechanisms. At high degrees of supersaturation (greater than about 50 per cent), successive growth layers can be added to a perfect flat surface; but for lower values, the free energy of surface nucleation is too high to permit this. At low supersaturation growth can only occur on surfaces where one of more screw dislocations terminate; and the step-lines between growth layers should form spirals ending on the dislocations. Such patterns of monolayer step-lines have been observed by Griffin (1950) on prism faces of natural beryl crystals, using an optical microscope, and on paraffin crystals grown from solution by Dawson and Vand (1951), using the electron microscope.

The appearance of certain faces of cadmium iodide crystals shown in the I.C.I. film on "Crystal Growth" (Bunn and Emmett 1949) suggests that, in addition to these monomolecular steps, steps of much greater height are formed. At present unpublished work by Verma and the author independently, suggests the same thing for carborundum; these steps also form spirals. The spirals must end on a *group* of dislocations all of the same sign, the total strength or Burger's vector of the groups being considerable.

This letter records a series of photographs (Pl. XXI.) (taken with an optical metallurgical microscope) of the actual growth of a cadmium iodide crystal from aqueous solution, and shows the successive stages in the formation of the growth patterns of this type.

Flakes of cadmium iodide were added to a drop of distilled water on a heated microscope slide until the solution was just under-saturated at 60° C. Rapid crystallization around the edges of a cover slip placed over the drop formed a closed cell. The solution became slightly supersaturated as it cooled, and the growing crystal faces were examined in reflection with an ordinary metallurgical microscope. Step visibility was considerably improved by using a narrow illuminating pencil of light.

A large number of small tabular crystals (about 100 microns across) were observed to grow quickly from the supersaturated solution, usually with the (0001) face parallel to the cover slip. Most of the faces exhibited patterns of diffuse concentric steps and the growth centres could not be

* Communicated by the Author.

Fig. 1.



Fig. 2.



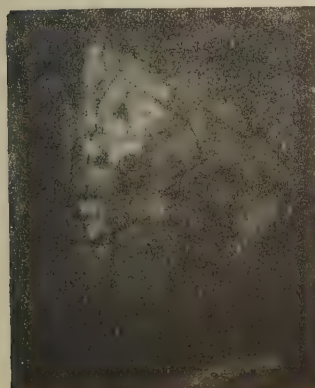
Fig. 3.



Fig. 4.



Fig. 5.



Figs. 1-5. ($600\times$) taken at 60 min. intervals, showing the upward growth of (0001) face of cadmium iodide crystal.

resolved clearly. In some regions of the solution, however, where the supersaturation was probably lower, giving a slower uniform growth, polyhedral layers were observed. The step-lines between these were sharp and sufficiently spaced for resolution of the growth centres, all of which showed patterns based on dislocation systems. A single screw dislocation dominating the growth of a crystal face produced the familiar rotation spiral of step-line attached to it. A pair of screw dislocations of opposite hand, sufficiently close together to form a growing terrace, cooperated to produce a closed-loop pattern. Growth from two dislocations of the same hand gave a pattern of two parallel spirals, while growth from a system of three dislocations (two of one hand and one of the other) was indicated by a closed-loop pattern dominated by a single spiral. More complicated growth patterns have been observed from centres of many dislocations. On some very thin crystal plates, spirals have been observed on both surfaces with their origins one vertically above the other. This shows how a screw dislocation persists through the crystal layer lattice, producing a self-perpetuating step on both faces of the plate as it emerges.

This "spiral growth" of the crystals is observed both for unpurified cadmium iodide and recrystallized cadmium iodide. In all cases, thin hexagonal or triangular plates grow rapidly from the supersaturated solution, and then a number of growth centres appear suddenly, to commence growth in thickness. Usually the growing face is dominated by one or two of the centres.

It is likely that the lateral growth of the plates takes place by two-dimensional nucleation, from a high supersaturation, on the less closely packed (10 $\bar{1}0$) of the hexagonal structure. This quickly lowers the effective supersaturation and further growth can only occur by the dislocation mechanism. F. C. Frank (1951) has suggested that the non-uniform distribution of impurities is sufficient to self-stress the thin plates beyond the theoretical yield stress. Buckling, followed by slip, produces the dislocation groups which have large screw components terminating in the (0001) face; the crystal plate now grows in thickness from a low supersaturation.

Photographs 1-5 are part of a sequence taken during the development of a particular crystal face. The step-lines have high visibility and show the trigonal character of the growth layers. The photographs illustrate the outward growth of the natural terrace between a pair of screw dislocations dominating the face, until a closed-loop and a new terrace are generated. The cycle is repeated indefinitely, and the step-lines move outwards in closed-loops as the face develops upwards at the rate of one layer thickness per cycle. The growth of faces dominated by other dislocation systems has been recorded similarly.

By illuminating the microscope with parallel monochromatic light, Fizeau fringes have been produced across this crystal face due to reflections from the glass-solution and solution-crystal surfaces. The thickness of

the growth layers has been calculated to be $750 \text{ \AA} \pm 100 \text{ \AA}$. from the fringe displacement across the step-lines ; the steps are big and this accounts for their high visibility.

As already indicated, this is not the growth of a crystal face from a pair of simple screw dislocations having unit Burger's vector, generating unimolecular layers (these would have thickness 6.84 \AA . according to the X-ray data of Bozorth (1922)) as in the case of monolayer growth on beryl. The growth must be initiated from a pair of "dislocation groups", each having a total Burger's vector with a component normal to the face of about 110 thicknesses of the minimum layer. The two groups cooperate to send out single growth layers $750 \text{ \AA} \pm 100 \text{ \AA}$. thick. Theoretically a dislocation group can exist of any total strength (*i. e.* any Burger's vector normal to the face) and promote growth in layers of corresponding thickness.

The two dislocation groups are not quite equal in strength and a small step corresponding to their difference extends outwards from the centre, crossing the main loops. At each crossing, the height of the main steps and consequently their rate of advance, changes abruptly, producing a characteristic sequence of pronounced kinks in the loops. Similar rows of kinks are observed in spirals on carborundum which grows in a like manner; cadmium iodide can be used as a model for this type of growth.

A further paper will give a more detailed account of these observations, with evidence that cadmium iodide crystals, like carborundum, can be polytypic.

ACKNOWLEDGMENTS.

I should like to thank Dr. F. C. Frank for his interest in this work and for invaluable discussion. I am grateful for a grant from the Department of Scientific and Industrial Research.

REFERENCES.

- BOZORTH, P. M., 1922, *J. Amer. Chem. Soc.*, **44**, 2232.
 BUNN, C. W., and EMMETT, H., 1949, *Discussion of Faraday Soc.*, **5**, 119 ; and "Crystal Growth", film, shown by I.C.I.
 DAWSON, I. M., and VAND, V., 1951, *Nature, Lond.*, **167**, 476.
 FRANK, F. C., 1949 a, *Discussion of Faraday Soc.*, **5**, 48 ; 1949 b, *Ibid.*, **67** ; 1950, *Phil. Mag.*, **41**, 200 ; 1951, to be published in *Phil. Mag.*
 GRIFFIN, L. J., 1950, *Phil. Mag.*, **41**, 196.
 MOTT, N. F., 1950, *Nature, Lond.*, **165**, 295.
 VERMA, A. R., 1951, to be published in *Phil. Mag.*

[The Editors do not hold themselves responsible for the views expressed by their correspondents.]

LXX. *Anelastic Measurements of Diffusion Coefficients in F.C.C. Substitutional Solid Solutions.*

By A. D. LE CLAIRE,

Atomic Energy Research Establishment, Harwell*.

[Received April 3, 1951.]

SUMMARY.

It is shown in this paper how in face-centred cubic substitutional solid solutions of metals, measurements upon that form of anelasticity which is associated with the preferential reorientation of pairs of solute atoms in the presence of a tensile stress, may be used to obtain the diffusion coefficient of the solute atoms. The method is closely analogous to the one employed recently by Zener and by Wert to measure diffusion coefficients in interstitial solid solutions.

The theory is applied to some previously reported anelastic measurements on (70/30) α -brass by Zener and by Kê to give the diffusion coefficient of zinc in the brass. The results show good agreement with directly measured and suitably corrected diffusion coefficients when these are extrapolated to the lower temperatures at which the anelastic measurements were made.

There follows a discussion of the advantages and disadvantages of this method of measuring diffusion coefficients and of some possible further developments of the theory.

§1. INTRODUCTION.

SEVERAL recent papers (Wert 1950 a, b, Wert and Zener 1949) have made use of the possibility of calculating the diffusion coefficient of solute atoms in interstitial solid solutions from measurements on the anelasticity of such solutions associated with the siting of solute atoms on preferred positions in the presence of an applied stress. Such calculations provide values of the diffusion coefficient at much lower temperatures than those at which direct measurements are possible. It is the purpose of this paper to show that the same can be done for substitutional solid solutions, by measurements on the anelasticity of such solutions associated with the preferential orientation of pairs of solute atoms induced by an applied stress.

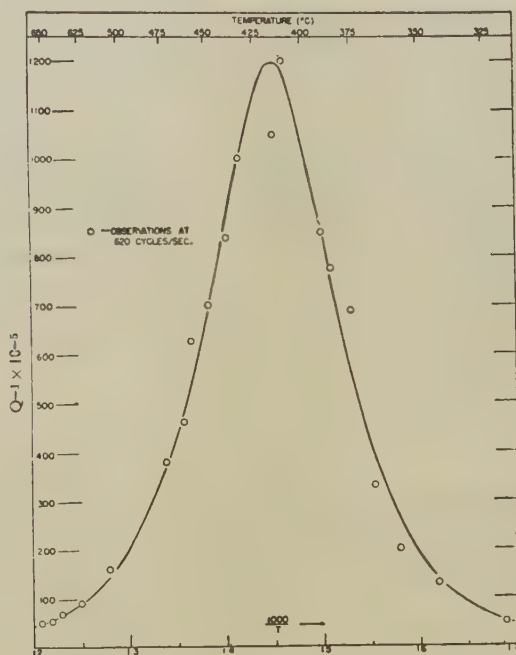
§2. THE ANELASTICITY ARISING FROM THE PREFERENTIAL ORIENTATION OF SOLUTE ATOM PAIRS.

In a face-centred cubic solid solution such as α -brass, the zinc and copper atoms are arranged at random on a face-centred cubic lattice. Since the zinc atoms are larger than the copper atoms, each zinc atom will be the

* Communicated by the Author.

centre of an elastic distortion in the lattice, which for lone zone atoms will have a cubic symmetry. But the distortion around a pair of zinc atoms will no longer have cubic symmetry and the lattice will be extended more along the axis of the pair than in any other direction. In the absence of any stress the pair axes will be distributed at random over all the crystallographically permissible directions; but if, say, a tensile stress is applied to the lattice the axes of the pairs of atoms will tend to orient themselves along those allowed crystallographic directions which make the least angle with the stress direction. A certain time will be required for the establishment of this new equilibrium, in which the pair axes are no

Fig. 1.



Internal friction plotted against $1/T$ for the transverse oscillations of a single crystal α -brass bar (Zener 1947).

longer distributed at random among all the permissible directions, so that the strain will lag behind the stress. This hysteresis will give rise to relaxation and other anelastic effects in the specimen, such as internal friction.

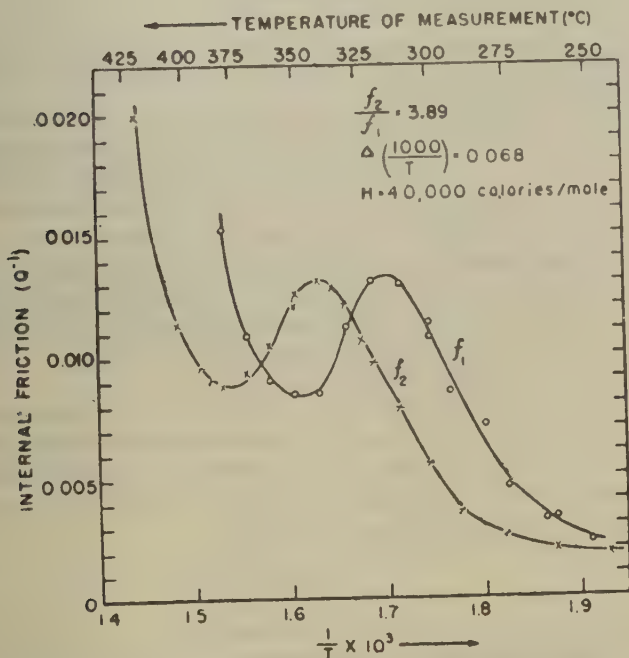
Zener (1943) was the first to observe an anelastic effect in α -brass which he was later able to attribute to this relaxation mechanism (Zener 1947). Further measurements, also on α -brass, were later made by Kê (1948 a). Zener measured, as a function of the temperature T , the internal friction, Q^{-1} , of the transverse oscillations of constant frequency of a single crystal

bar of α -brass; Kê made similar measurements on the torsional oscillations of a coarsely crystalline α -brass wire. Their results are reproduced in figs. 1 and 2. (The rapid rise in Q^{-1} above about 350°C . in fig. 2 is associated with relaxation of the stress by grain boundary slip, and does not concern us here.)

Assuming that the relaxation time τ_R , for the atomic process we have described depends upon the temperature through the equation

$$\tau_R = \tau_{R_0} \exp(H/RT), \quad \dots \dots \dots (1)$$

Fig. 2.



Internal friction plotted against $1/T$ for the torsional oscillations of a coarsely polycrystalline α -brass wire. f_2 , oscillations at 2.3 c.p.s.; f_1 , oscillations at 0.6 c.p.s. (Kê 1948 a).

where τ_{R_0} is a constant and H the activation energy for the relaxation process, Zener showed that his results were well represented by the equation

$$Q^{-1} = \Delta E \frac{\tau \omega}{1 + (\tau \omega)^2}, \quad \dots \dots \dots (2)$$

ω is the angular frequency at which the measurements of Q^{-1} were made and ΔE is the relaxation strength for the process, defined as

$$\Delta E = \frac{E_U - E_R}{E_U},$$

Here, E_U is the unrelaxed Young's modulus, *i. e.* the modulus measured in a time $t \ll \tau_R$ by dynamic methods and E_R the relaxed modulus measured after a time $t \gg \tau_R$.

Since equation (2) represents well the experimental results, we can infer from formal anelasticity theory (Zener 1948) that the relaxation process is characterized by a single relaxation time and that the rate at which the distribution of solute atom pair axes approaches equilibrium is given by the simple logarithmic relation

$$\frac{d\Delta N}{dt} = -\frac{\Delta N}{\tau_R}, \quad (3)$$

where ΔN is the number of solute atom pairs whose axes must still reorient for equilibrium to be attained.

Since the atomic process involved in the relaxation is clearly the migration of one member of a pair of zinc atoms from one lattice position to another, that is a diffusion process, the assumption expressed by equation (1) is a very reasonable one for diffusion rates are always found to vary exponentially with $1/T$. For the same reason τ_R will be closely related to and of the same order of magnitude as τ , the mean time of a stay of an atom of zinc on one lattice position. We shall make use of equation (3) in deriving the exact relation between τ and τ_R and then, having obtained a relation between τ and the diffusion coefficient D , we shall be in a position to calculate D from measured values of τ_R .

The curves in figs. 1 and 2 show a maximum at a well defined temperature, as always occurs when the extent of the relaxation is limited (Zener 1943). From equation (2) we see that provided ΔE is independent of T , the internal friction is a maximum for that temperature at which the corresponding relaxation time τ_R is given by

$$\tau_R \varpi = 1. \quad (4)$$

From the maxima of the three curves in figs. 1 and 2 we can obtain three values of τ_R , and therefore of D , corresponding to the temperatures at which the maxima occur. The heights of the maxima of the two curves in fig. 2 are sufficiently equal for us to assume that over the temperature range covered by each peak ΔE is sufficiently independent of temperature for the relaxation time at the temperature of the maxima to be given by equation (4). Further, the position of the maximum is not affected by the superposition (in fig. 2) of the internal friction due to relaxation by grain boundary slip. Equation (2) represents a function symmetrical with respect to its maximum at $\tau_R \varpi = 1$, so that we can separate out the high temperature portions of the full line curves in fig. 2 into the contributions from grain boundary slip and from the preferential reorientation of solute atom pairs. When this is done it is found that at the temperatures of the maxima, the variation with temperature of the contribution from grain boundary relaxation is negligible.

§ 3. THE RELATION BETWEEN D AND τ .

Consider diffusion taking place in the face-centred cubic lattice along the [100] direction. If " a " is the lattice parameter, then there are successive planes of atoms, the (200) planes, at distances of $a/2$. Each atom in any one of these planes may jump into any one of the twelve nearest neighbour positions. Four of these twelve possible jumps take the atom into the next (200) plane a distance $+a/2$ measured along the x direction, another four into the next (200) plane a distance $-a/2$ along the x direction, while the remaining four jumps lead to *no* movement along the x direction. Suppose now that a concentration gradient exists in the lattice so that there are $(\alpha + \Delta\alpha)$ atoms of one type per unit area on one (200) plane and $(\alpha - \Delta\alpha)$ atoms per unit area on the next adjacent (200) plane, a distance $a/2$ away. If τ is the average time of stay of an atom on a lattice site, so that each atom jumps $1/\tau$ times per second, the nett flow of atoms down the concentration gradient will be

$$(\alpha + \Delta\alpha) \frac{1}{3\tau} - (\alpha - \Delta\alpha) \frac{1}{3\tau} = \frac{2}{3} \frac{\Delta\alpha}{\tau},$$

since of the $1/\tau$ jumps per second, only $1/3$ carry the atom forward and $1/3$ carry it backward along the x direction.

But the concentration gradient is given by

$$\left(\frac{\alpha + \Delta\alpha}{a/2} - \frac{\alpha - \Delta\alpha}{a/2} \right) / \frac{a}{2} = \frac{8\Delta\alpha}{a^2},$$

so that the diffusion coefficient D will be given by

$$D = \frac{a^2}{12\tau} \quad \dots \quad (5)$$

The same result is of course obtained along whichever axis one considers the diffusion to be taking place.

Equation (5) can be more readily obtained by making use of a general result of random walk theory (Chandrasekhar 1943). If the probability of a migration, by diffusion, of amount and direction \mathbf{r} is given by $R(\mathbf{r})$, then the diffusion coefficient for diffusion say along the x axis is given by

$$D = \frac{1}{2\tau} \langle x^2 \rangle,$$

where $\langle x^2 \rangle$ is the second moment of R about x . In a face-centred cubic lattice R is zero in all but 12 directions and for all values of r except $r = a\sqrt{2}$. Its second moment about x is then readily seen to be $a^2/6$, so that we arrive again at the expression for D given in equation (5).

§ 4. THE RELATION BETWEEN τ AND τ_R .

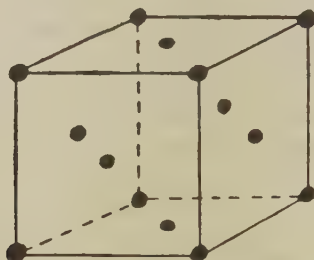
The relation between τ and τ_R depends to some extent upon the direction of the stress applied to the crystal. We shall derive in detail the relation for one principal direction of applied tensile stress and then more briefly the relation for two other principle directions.

(a) *Tensile stress applied along [111] direction.*

The pair axes of the solute atoms may be along any of the six $\langle 110 \rangle$ directions. Of these six directions, three, namely $[011]$ $[101]$ and $[110]$ have a direction cosine of $(2/3)^{1/2}$ with respect to the $[111]$ axis, and we shall refer to these as the "*p* class" of pair axes. The remaining three, $[0\bar{1}1]$ $[\bar{1}01]$ and $[\bar{1}10]$ are normal to the $[111]$ direction and will be referred to as the "*n* class" of pair axes. A tensile stress along the $[111]$ direction will then tend to reorient pair axis from the *n* class into the *p* class, *i. e.* tend to bring pair axes more nearly parallel to the stress axis.

Now if we assume a vacancy mechanism for the diffusion, a solute atom pair can only reorient itself, remaining a pair, when a vacancy occupies a position which is adjacent to the positions of each of the members of the pair. It is readily shown that if in this circumstance one member of the pair changes places with the vacancy, *i. e.* diffuses, then the probability is one half that the concomitant reorientation of the pair leads to a change of the pair from one class (*p* or *n*) to another. That is to say, only one half

Fig. 3.



Face-centred cubic lattice.

of those diffusion processes which lead only to a change of orientation of the pair (and not a break up of the pair) will lead to a relaxation of a stress along the $[111]$ direction. This can easily be seen by considering all possible initial positions of pairs of atoms and of vacancies. Take for example the case of the possible reorientations of an $[011]$ pair, a member of the *p* class, composed of atoms at (000) and $(0\frac{1}{2}\frac{1}{2})$. There are four possible positions for a vacancy which is to be a common nearest neighbour of the pair of atoms, and with which either of the atoms may change places so as to reorient the pair. These are given in the first column of Table I.; the second and third column show the class of the pair after it has been reoriented by a migration of the (000) and $(0\frac{1}{2}\frac{1}{2})$ atoms respectively.

As can be seen, only one half of the reorientation processes lead to a change in the class of the pair. The same result will be true for the other members of the *p* class, for the axes of all members of this class are symmetrically disposed with respect to the $[111]$ axis. A similar study of the possible

reorientations of a member of the n class leads to the same conclusion, that only half the reorientations lead to a change in the class of the pair considered.

Consider again the possible migration paths of the members of any pair of solute atoms. Each solute atom has four neighbours in common with the other and seven neighbours not in common. Each solute atom may migrate into any of the 11 positions available to it and we assume that vacancies occur on the 11 positions with equal probability.

The probability per unit time that one atom moves $= 1/\tau$. The probability that when it moves it occupies one of the four common sites so that the pair remains a pair but is reoriented—i. e. probability of reorientation by migration of one atom $= 4/11\tau$.

Similarly, the probability of reorientation by migration of the other atom $= 4/11\tau$.

Thus the probability per unit time of a reorientation of the pair while remaining a pair $= 8/11\tau$. Therefore the probability per unit time of a reorientation leading to a change in class of the pair $= 4/11\tau$.

TABLE I.

 Reorientations of a [011] (p -class) of Solute Atom Pair.

Position of common neighbour vacancy	Pair axis originally [011]. Class of pair axis after	
	(1) Migration of atom at (000)	(2) Migration of atom at ($0\frac{1}{2}\frac{1}{2}$)
$(\frac{1}{2}\frac{1}{2}0)$	n $[\bar{1}01]$	p $[110]$
$(-\frac{1}{2}\frac{1}{2}0)$	p $[101]$	n $[\bar{1}10]$
$(\frac{1}{2}0-\frac{1}{2})$	n $[\bar{1}10]$	p $[101]$
$(-\frac{1}{2}0\frac{1}{2})$	p $[110]$	n $[\bar{1}01]$

Similarly, it can be seen that the probability per unit time of the pair breaking up, by movement of either atom into one of the seven positions allowed to each atom $= 14/11\tau$.

We shall assume that for each pair that breaks up in this way, another is formed of the same class at some other point in the lattice by diffusion of lone solute atoms toward one another, i. e. the number of pairs of each class is only changed by a reorientation process, and the break-up of a pair leads to no nett change in the total number of its class.

In stress free equilibrium let there be N_p^0 p pairs of solute atoms and N_n^0 n pairs. Since there are equal numbers of possible p and n directions we shall have $N_p^0 = N_n^0$. Let us suppose that at any time after the application of a tensile stress along the [111] direction, ΔN pairs of solute atoms have changed from the n class to the p class. If N_p and N_n then represents the numbers of p and n pairs respectively

$$N_p = N_p^0 + \Delta N,$$

$$N_n = N_n^0 - \Delta N.$$

We assume also that the total number of pairs remains constant so that

$$N_n + N_p = N_n^0 + N_p^0.$$

If the tensile stress is now removed N_p will change back to its equilibrium value of N_p^0 . With all the above assumptions the rate of this change is given by

$$\frac{dN_p}{dt} = \frac{d\Delta N}{dt} = -(N_p^0 + \Delta N) \frac{4}{11\tau} + (N_n^0 - \Delta N) \frac{4}{11\tau}, \quad \dots \quad (6)$$

where the first term on the right hand side represents the decrease in N_p due to p pairs changing to n pairs and the second term the increase in N_p due to n pairs changing to p pairs. Equation (6) reduces to the form

$$\frac{d\Delta N}{dt} = -\frac{8\Delta N}{11\tau}, \quad \dots \quad (7)$$

and by comparison with equation (3) we see that the measured relaxation time is related to the mean time of stay τ by the equation

$$\tau = \frac{8}{11} \tau_R, \quad \dots \quad (8)$$

We have dealt so far with the relations for the changes towards a stress free equilibrium, but the same result can be deduced for the opposite case where the system is changing towards an equilibrium in the presence of a tensile stress. In this case, the probability per second of an atomic migration which reorients a solute atom pair from the n class to the p class is greater than the probability of a migration which leads to a change from the p to the n class. If the probability of any migration in the absence of a stress is given as a function of temperature by

$$\frac{1}{\tau} = \frac{1}{\tau_0} \exp(-H/RT),$$

then the unequal probabilities $1/\tau_{np}$ and $1/\tau_{pn}$ for atomic migrations in the presence of a tensile stress which lead to class changes of n to p and of p to n respectively may be written

$$\left. \begin{aligned} \frac{1}{\tau_{np}} &= \frac{1}{\tau_0} \exp(-(H-U)/RT), \\ \frac{1}{\tau_{pn}} &= \frac{1}{\tau_0} \exp(-(H+U)/RT), \end{aligned} \right\} \dots \quad (9)$$

where $2U$ is the change in energy arising from the change in class of a solute atom pair in the presence of the tensile stress. At equilibrium the ratio of the numbers of p and of n pairs is given by $\exp(2U/RT)$ from which we deduce that ΔN_p^0 , the number of p pairs in excess of those existing in the absence of a stress, N_p^0 , is given by

$$\Delta N_p^0 = \frac{UN_p^0}{RT}, \quad \dots \quad (10)$$

since U is small compared to RT .

§ 5. CALCULATION OF D AND COMPARISON WITH DIRECTLY MEASURED VALUES.

We have calculated the relation between τ and τ_R for three representative directions of stress. Since Kê used only a polycrystalline wire in his experiments it is reasonable to suppose that the appropriate value of τ to use in the calculation would be some mean value of $8\tau_R/11$ and $12\tau_R/11$. Zener used a single crystal bar but does not report its orientation so that the best we can assume again is that the appropriate value of τ to use will be near to the range $8\tau_R/11$ to $12\tau_R/11$. We shall then calculate from the data given by Kê and by Zener the values of D corresponding to these two values of τ , for which the relations are from equations (4), (5), (8) and (11).

$$D = \frac{22\pi\nu a^3}{96} \text{ cm.}^2 \text{ sec.}^{-1} \text{ for } \tau = 8\tau_R/11,$$

$$D = \frac{22\pi\nu a^2}{144} \text{ cm.}^2 \text{ sec.}^{-1} \text{ for } \tau = 12\tau_R/11,$$

ν is the frequency in cycles per second at which the anelastic measurements were made and a is the lattice constant. Both Kê and Zener used approximately 70/30 brass for which we take $a = 3.675 \text{ \AA}$. The appropriate data and results are set out in Table II.

TABLE II.

Calculation of Diffusion Coefficient from Anelastic Measurements.

Temperature at which maximum occurs in $Q^{-1} \sim 1/T$ curve °K. ..	689	614	588
1000/T	1.450	1.628	1.700
Frequency of measurement <i>v.c.p.s.</i> ..	620	2.3	0.6
D cm. ² sec. ⁻¹ for $\tau = 8\tau_R/11$..	6.04×10^{-13}	2.24×10^{-15}	5.84×10^{-16}
Log D	13.781	15.350	16.766
D cm. ² sec. ⁻¹ for $\tau = 12\tau_R/11$..	4.02×10^{-13}	1.49×10^{-15}	3.89×10^{-16}
Log D	13.604	15.173	16.590
Reference	Zener 1947	Kê 1948	Kê 1948

It remains to compare these results with the directly measured coefficients of diffusion in α -brass. A large number of investigators have studied this system and their work has recently been reviewed and assessed by Kubaschewski (1950). The only useful results for our purpose are those of Kirkendall (1942) and of Kirkendall, Thomassen and Upthegrove (1939), for these only were obtained for well defined zinc concentrations, close to those used by Kê and Zener. Their values of D are given in Table III., but they cannot be compared with our calculated values of D until certain corrections have been made. These are, in order of importance,

- A thermodynamic correction,
- A correction arising from the Kirkendall Effect in α -brass (Darken 1948),
- A concentration correction.

(a) *Thermodynamic correction*

In a conventional diffusion coefficient measurement the driving force for the diffusion flow is derived not only from the concentration gradient, in terms of which alone the diffusion coefficient is defined, but also since the solution is never ideal, from an internal energy gradient. The partial molar internal energy of each species present varies with concentration so that whatever the direction of the concentration gradient, there is also a tendency for atoms to flow in the direction of their decreasing partial molar internal energy. In extreme cases this latter tendency is stronger than the tendency to equalize the concentrations (*i. e.* increase entropy of mixing) and the phenomenon of "uphill" diffusion against the concentration gradient occurs. The author has discussed this at length elsewhere (Le Claire 1949) and the result is that the diffusion coefficient D_M measured in the presence of a concentration gradient, is related to the true diffusion coefficient D_T that would be obtained in the absence of a chemical concentration gradient, say by the use of tracers or of the anelastic method we are now discussing, by the relation

$$D_M = D_T \left(1 + \frac{\partial \log \gamma}{\partial \log c} \right), \quad \dots \dots \dots (11)$$

where γ is the activity coefficient of the diffusing species is c and the concentration at which D_M was measured.

The activity data of Hargreaves (1949) as smoothed by Fisher, Holloman and Turnbull (1948) have been used in computing the values, shown in Table III., of the thermodynamic factor in equation (11).

TABLE III.

Directly Measured Diffusion Coefficients in α -brass with Corrections.

T °K	873	928	993	1053
1000/T	1.146	1.078	1.007	0.949
c per cent Zn	28.3	26.8	25.3	26.0
" True " c per cent	29.9	28.4	26.9	26.0
D_M cm. ² sec. ⁻¹	$8.6.10^{-11}$	$3.54.10^{-10}$	$1.31.10^{-9}$	$3.8.10^{-9}$
$\left(1 + \frac{\partial \log \gamma}{\partial \log c} \right)$	2.46	2.33	2.19	2.09
D_T cm. ² sec. ⁻¹	$3.49.10^{-11}$	$1.52.10^{-10}$	$5.98.10^{-10}$	$1.82.10^{-9}$
m	-0.02	+0.01	+0.10	+0.04
D_c cm. ² sec. ⁻¹	$3.99.10^{-11}$	$1.76.10^{-10}$	$6.99.10^{-10}$	$2.4.10^{-9}$
Log. D_c	II.601	IO.245	IO.844	9.330

(b) *Kirkendall Effect correction.*

A second but smaller correction is necessary because the anelastic measurements give the separate diffusion coefficient of zinc in α -brass whereas it can be shown (Darken 1948, Le Claire 1949) that D_T is composite in the sense that

$$D_T = c_{Zn} D_{Cu} + c_{Cu} D_{Zn},$$

where D_{Zn} and D_{Cu} are the separate true diffusion coefficients of zinc and copper and c_{Zn} and c_{Cu} are the fractional concentrations of zinc and copper at which the measurement of D_{M} was made. In view of a Kirkendall effect in α -brass, D_{Zn} and D_{Cu} are not equal and from Darken's calculations, based on the observed magnitude of the Kirkendall effect, we find

$$\frac{D_{\text{Zn}}}{D_{\text{T}}} = 1.15.$$

We shall assume that this relatively small correction is the same at the higher concentrations ($c_{\text{Zn}} = 0.29$) and lower temperatures ($\sim 300^\circ \text{C.}$) employed in the anelastic measurements.

(c) *Concentration correction.*

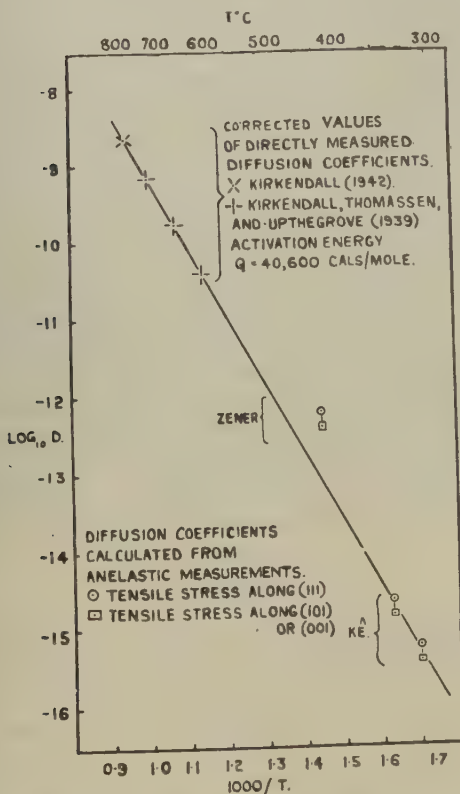
There is a third correction m for the difference in concentration between the samples used by Kê and Zener (~ 29 per cent Zn) and those of Table III. This difference is not quite as great as appears at first sight. The content of zinc as given in the papers of Kirkendall and of Kirkendall *et al.* was measured by determination of the lattice parameter, but the relations between composition and lattice parameter used in the two papers do not appear to be the same. Using the precision lattice parameter determinations of Owen and Roberts (1939) to obtain the correct zinc concentrations corresponding to the lattice constants reported, we find that the first three values in Table III. must be increased by approximately 1.6 to give the true weight per cent of zinc, but that the fourth is correct. The corrected values are given in the fourth column of Table III.

Using the data of Sieth and Kraus (1938) for the variation of D_{M} with concentration, we find that D_{T} as calculated from D_{M} increases by about 4 per cent for a rise of 5 per cent in the concentration of zinc in the range 25–30 per cent zinc. This correction, though very small, has been applied to the data in Table III. in order to convert all values of D_{T} to the values corresponding to the concentration of 29 per cent zinc used by Kê. But if we use the data of Rhines and Mehl (1938) the correction is very much larger and we find that a 2 per cent increase in zinc concentration leads to a 30 per cent increase in D_{T} . The data of Sieth and Kraus are preferred because only they measured D_{M} as a mean value over a relatively small range of concentration. Also, we should expect their accuracy to be the same for all concentrations, whereas the Matano method of analysis used by Rhines and Mehl falls off in accuracy towards the limits of the much wider concentration ranges (0–30 per cent zinc) that they used. This is clearly seen by the way in which their D_{M} increases rapidly towards the high zinc end of the concentration range used, irrespective of the actual concentration of zinc at this end of the concentration range. (Compare samples 30 and 32 of their fig. 9.) The much more rapid increase in D_{M} with increasing and high zinc concentration found by Rhines and Mehl is then very suspect.

Our values of D calculated from the anelastic measurements are then to be compared with the corrected values D_c of directly measured diffusion coefficients, given by

$$D_c = \left[\frac{D_M}{\left(1 + \frac{\partial \log \gamma}{\partial \log c}\right)} + m \right] \times 1.15.$$

Fig. 4.



Comparison of directly measured and calculated diffusion coefficients.

These values, with their logarithms, are given in rows 9 and 10 of Table III. On the assumption, which was justified in the analogous case of interstitial diffusion (Wert 1950 a), that the well known relation between D and T

$$D = D_0 \exp(-H/RT)$$

holds true with constant H and D_0 down to the temperatures at which the anelastic measurements were made, $\log D_c$ is plotted against $1/T$ in fig. 4, and the straight line through the points extrapolated down to these temperatures. The values of $\log D$ calculated from the anelastic measurements

are plotted on the same figure, and show an excellent agreement between the measured D_c and the values of D calculated from Kê's results. By measurement of the displacement of the two curves in fig. 2, Kê calculated directly from his results an activation energy for the relaxation process of about 40,000 cal./gm. mole which agrees excellently with the activation energy of 40,600 cal./gm. mole calculated for the slope of the line in fig. 4. This agreement may also, of course, be appreciated from fig. 4 alone.

The diffusion coefficient calculated from Zener's result shows less good agreement with the directly measured values, and it is difficult to see how such a discrepancy could arise. No likely error in the measurement of ν could account for it, and it is hardly possible that a direction for the stress axis could be found for which the relation between τ and τ_R would differ so much from those already found as to give a value for D very much closer to the line of fig. 4. However, if we suppose there to have been an error in temperature measurement of $22^\circ\text{C}.$, the value of D calculated for the case $=12\tau_R/11$ would lie on the straight line in fig. 4. Zener (1943) does mention that for the purposes of this particular experiment the internal friction apparatus was heated "as hot as it was thought capable of standing" and that "the apparatus, in fact, was damaged by the experiment". It is then conceivable that under such severe conditions of usage an error in temperature measurement of about $20^\circ\text{C}.$ (at $420^\circ\text{C}.$) may have occurred. There is the further point against accepting Zener's result as being as reliable as Kê's, that the activation energy of 33,600 cal./gm. mole which Zener calculated from the slope of the curve in fig. 1 is much less than the values of Kê and of fig. 4. Kê's measurements were in fact made primarily to give a more accurate value of this activation energy.

§ 6. DISCUSSION.

The good agreement obtained between the directly measured and properly corrected diffusion coefficients, and those calculated from anelastic measurements both confirm Zener's original identification of a relaxation peak as due to the mechanism of preferential orientation of solute atom pairs, and warrants the use of this method in the study of diffusion in substitutional solid solutions of metals. There are many advantages to be gained from such a use. Measurements can be made at much lower temperatures than are necessary for the conventional methods and in a very much shorter time, for we are here concerned with diffusional motion over a distance of only one atomic spacing. This means that D can be studied over a much wider range of temperature than previously so that a more precise knowledge of activation energies and of their possible dependence on temperature becomes possible. Also for the first time we have the possibility of studying the dependence of D on such variables as cold work, and an excess number of vacancies introduced by quenching from high temperatures, both of which are greatly changed during the long times required for conventional measurements of D . Studies of the variation

of D over considerable ranges of concentration could also be made in a very much shorter time than by the old methods and would have the added advantage that D would be measured at a fixed concentration rather than over the range of concentrations that is necessary in the conventional methods. In view of the great need in diffusion theory for accurate experimental data with which to compare the theoretical predictions, the advantages of the anelastic method are that it is rapid, that the concentration is well defined and also that it provides the theoretically more significant true or ideal diffusion coefficient (Le Claire 1949); thermodynamic data from which to calculate the true from the measured diffusion coefficient are then not required.

The anelastic method has also of course certain limitations. The solute and solvent atoms must differ appreciably in size and the concentration must not be so low that the number of solute atoms pairs is inappreciable. For too low a concentration and too small a difference in size, the relaxation strength, which measures the height of the peak in the curve of Q^{-1} against $1/T$, may become too small for any peak to be observed. The extent of these limitations is probably best determined by experiment. However, as we might expect, and as Zener shows (1947,) ΔE , which is twice the maximum value of Q^{-1} (see equation (2)) is proportional to the total number of solute atom pairs. If this number was proportional to the actual solute concentration we might expect to be able to observe a peak for a concentration as low as say 3 per cent zinc, for then the curve in fig. 1 would have an observable maximum as about $Q^{-1} = 120 \cdot 10^{-5}$. The number of solute atom pairs will, however, fall more rapidly than the concentration, so that 3 per cent will probably be below the lowest concentration at which anelastic measurements of D can be made on α -brass. Zener (1947) has shown that the relaxation strength is roughly proportional to the square of the rate of change of lattice parameter with composition so that the larger the difference in size between solute and solvent atoms, the lower will be the concentration at which a measurable anelastic peak will be obtained. Zener also shows that ΔE , and therefore also the minimum concentration at which an anelastic peak can be observed, will vary with the direction of the applied stress, but that it never becomes zero, as it does in the case of body-centred cubic solid solutions.

Another limitation is that the method only measures the diffusion coefficient of one of the atomic species present, although this may not always be a disadvantage.

Further attention to some of the assumptions made in the development of a relation between τ and τ_R might be necessary. We have assumed that the total number of solute atom pairs is always constant and that the number of pairs in a particular class only changes as the result of a reorientation process; a pair which breaks up is always replaced by another of the same class as a result of lone solute atoms diffusing towards one another to form a pair. However, it is unlikely that attention to such refinements would change appreciably the values of the diffusion coefficients

obtained above. More important may be the possible cooperative effects arising from interactions between pairs of solute atoms and altering the rate of change towards equilibrium. This could be studied, as was the interaction between interstitial solute atoms in tantalum (Kê 1948 b), by measurements of ΔE over a considerable range of temperature and the plotting of $1/\Delta E$ against T . Zener showed (Zener 1948) that ΔE varies with the absolute temperature T in the manner

$$\Delta E = \frac{T_0}{T - \beta T_0},$$

where T_0 is a temperature independent factor and β a numerical coefficient which takes account of solute atom interaction. The intersection with the T axis of a plot of $1/\Delta E$ against T will then give a measure of β .

Finally, it will be necessary to study the relation between τ and τ_R for any arbitrary direction of stress. This is important because it is not always easy to grow large single crystals with precisely the required orientation and because from it we can derive an accurate mean relation applicable to polycrystalline material.

It is hoped shortly to publish a further paper dealing with the extensions and refinements of the theory.

ACKNOWLEDGMENTS

The author wishes to thank Dr. H. M. Finnieston, Messrs. B. G. Childs and R. S. Barnes for useful discussions and is indebted to Sir John Cockcroft, Director, A.E.R.E., for permission to publish this paper.

REFERENCES.

- CHANDRASEKHAR, S., 1943, *Rev. Mod. Phys.*, **15**, 1.
 DARKEN, L. S., 1948, *Trans. Amer. Inst. Min. Met. Engrs.*, **175**, 184.
 FISHER, J. C., HOLLOMAN, J. H., and TURNBULL, D., 1948, *Trans. Amer. Inst. Min. Met. Engrs.*, **175**, 202.
 HARGREAVES, R., 1939, *J. Inst. Metals*, **64**, 115.
 KÊ T'ING SUI, 1948 a, *J. App. Phys.*, **19**, (3), 285 ; 1948 b, *Phys. Rev.*, **74** (1), 16.
 KIRKENDALL, E. O., THOMASSEN, L., and UPTHEGROVE, C., 1939, *Trans. Amer. Inst. Min. Met. Engrs.*, **133**, 186.
 KIRKENDALL, E. O., 1942, *Trans. Amer. Inst. Min. Met. Engrs.*, **147**, 104.
 KUBASCHOWSKI, O., 1950, *Trans. Far. Soc.*, **46**, 713.
 LE CLAIRE, A. D., 1949, *Progress in Metal Physics*, **1**, (Ed. B. Chalmers ; London : Butterworths) Chap. 7.
 OWEN, E. A., and ROBERTS, E. W., 1939, *Phil. Mag.*, **27**, 294.
 RHINES, F. N., and MEHL, R. F., 1938, *Trans. Amer. Inst. Min. Met. Engrs.*, **128**, 185.
 SEITH, W., and KRAUS, W., 1938, *Zeit. f. Electrochem.*, **44**, 98.
 WERT, C. A., and ZENER, C., 1949, *Phys. Rev.*, **76** (8), 1169.
 WERT, C. A., 1950 a, *Phys. Rev.*, **79** (4), 601 ; 1950 b, *J. App. Physics*, **21** (11), 1196.
 ZENER, C., 1943, *Trans. Amer. Inst. Min. Met. Engrs.*, **152**, 122 ; 1947, *Phys. Rev.*, **71** (1), 34 ; 1948, *Elasticity and anelasticity of metals* (Chicago : University Press).

LXXI. *The Distribution of Energy in Randomly Modulated Waves**.

By DAVID MIDDLETON,
 Cruft Laboratory, Harvard University, U.S.A.†.

[Received March 30, 1951.]

ABSTRACT.

The distribution of energy in high-frequency oscillations which are modulated by stationary, random disturbances such as shot and thermal noise is here examined in a number of important practical situations. In (a) the theory for frequency- and phase-modulation by normal random noise is developed in particular, as a model for speech-modulated carriers. The effect of spectral shape of the modulating noise on the intensity distribution of the modulated carrier is considered, and it is found that the lowest-frequency components of the modulation are most significant in this respect. For example, in frequency-modulation the carrier term is entirely absent when the modulating noise has a finite spectral density at and near zero-frequency, while in phase-modulation by the same disturbance the carrier component may contain a noticeable fraction of the modulated wave's energy. Particular attention is also given to the limiting cases of very slow frequency deviation, and it is found that such adiabatic sweeps spread the original spectrum. Part (b) contains a parallel discussion for the amplitude-modulation by normal random noise, including the effects of possible over-modulation.

1. INTRODUCTION.

BECAUSE noise is the unfailing and undesirable companion of intelligence transmitted or received by electronic and acoustical systems, it is essential for any proper theory of communication to provide suitable methods for studying the physical properties of a noise wave and its interaction with a desired signal. On the one hand a successful technique of measurement is required to control or minimize the noise, and on the other an adequate theory is necessary to guide experiment and interpret the data. Accordingly, the purpose of this paper is to present a number of new results, obtained by the analytical methods developed in recent years (Wiener 1926, 1930, Khintchine 1934, Cramér 1940, Chandrasekhar 1943, Bennett 1944, Rice 1944, 1945, Blanc-Lapierre 1945, Wang and Uhlenbeck 1945, Boonimovich 1946, Middleton 1946, 1948 a, b, 1949, van der Pol

* The research reported in this document was made possible through support extended Cruft Laboratory, Harvard University, jointly by the Navy Department (Office of Naval Research), the Signal Corps of the U.S. Army, and the U.S. Air Force, under ONR Contract N5ori-76, T.O.1.

† Communicated by Sir Edward Appleton, F.R.S.

1946, Van Vleck and Middleton 1946) for the following important problems*. (In all the cases considered here the noise is assumed to belong to the fluctuation type, characteristic of shot and thermal noise which belongs to a normal random process (Wang and Uhlenbeck 1945, Middleton 1948 a, 1949). Impulsive noise, such as atmospheric and solar static, is not treated, although the general methods are, the same.) Our treatment in the present paper is limited to a discussion of noise only; analysis of the case of signal and noise is considered elsewhere. We discuss specifically:—

(i.) *Carrier phase- or frequency-modulated by noise*: this problem is of particular interest when normal random noise is used as an approximate model of speech†.

(ii.) *Carrier amplitude-modulated by noise*: this situation is similar to (i.), except that now amplitude- rather than frequency-distortion of the carrier wave is the mechanism producing the modulation. The important case of over-modulation is discussed.

We remark further that, apart from the specific applications to problems (i.) and (ii.), the results are needed in the general theory of noise measurement, for here the central objective is to be able to determine by measurements on the output wave following various linear and non-linear operations (such as amplification, rectification, clipping, mixing, modulation, discrimination, etc.), the “structure” of the original input disturbance, *i. e.* whether or not it is an amplitude- or frequency-modulated wave, how the noise and carrier occur together, and other qualitative and quantitative data.

The quantities of chief physical interest are (a), the *mean* or steady component of the disturbance, (b), the mean intensity of the wave, and (c), the spectral distribution $W(f)$ of the mean intensity. The latter quantity is in fact sufficient to give us the other two; the mean intensity is obtained as the area under the spectral density curve $W(f)$, while the

* The details of the analysis, including a discussion of the case of signal and noise, are given in a series of papers, “On the Distribution of Energy in Noise- and Signal-Modulated Waves” (D. Middleton), scheduled to appear in the *Quarterly J. of Applied Mathematics* (U.S.A.). For the complete and detailed discussion see D. Middleton, *On the Distribution of Energy and Noise- and Signal-Modulated Waves*, Cruft Laboratory Technical Report No. 99, March 1, 1950.

† Recent experiments of W. B. Davenport, Jr. (*A Study of Speech Probability Distributions*, M.I.T. Report No. 148, August 25, 1950) indicate that speech is more satisfactorily described statistically in terms of an impulsive or “static” noise model, where overlapping among individual (and independent) pulses is assumed to be small, of the order of 30–50 per cent of the time. This is different from the usual model of fluctuation or normal random noise, which assumes complete and highly multiple overlapping between the elementary transients. However, such normal random noise has the great advantage of mathematical simplicity, and its use as a speech model is therefore justified on these and physical grounds, at least as a first approximation.

(square of the) steady component is given by the constant (or frequency-independent) term in the expression for the spectrum. It is assumed that we are dealing with a stationary (and ergodic) random process, namely, a process for which the underlying mechanism does not change with time. Then time averages and ensemble or statistical averages are equivalent (James, Nichols and Philips 1946) to within a set of random functions of probability zero, so that if we represent our stochastic, time-dependent disturbance by $y(t)$ we may write the steady component (a) as*

$$\langle y(t_0) \rangle_{av} \equiv \lim_{T \rightarrow \infty} \int_0^T \frac{1}{T} y(t_0) dt_0 = \overline{y(t_0)} = \int_{-\infty}^{\infty} y W_1(y) dy. \quad (1.1)$$

and the mean intensity (b)

$$\langle y(t_0)^2 \rangle_{av} \equiv \lim_{T \rightarrow \infty} \int_0^T \frac{1}{T} y(t_0)^2 dt_0 = \overline{y(t_0)^2} = \int_{-\infty}^{\infty} y^2 W_1(y) dy; \quad (1.2)$$

$W_1(y) dy$ is the probability that (at any initial time t_0) y lies in the range $y, y+dy$. The moment of greatest interest, however, is given by

$$R(t) \equiv \langle y(t_0)y(t_0+t) \rangle_{av} = \lim_{T \rightarrow \infty} \frac{1}{T} \int_0^T y(t_0)y(t_0+t) dt. \quad (1.3)$$

The quantity $R(t)$ is the auto-correlation function of y and may be found statistically when the second-order probability density $W_2(y_1, y_2; t)$ is known; W_2 has the following interpretation:

$W_2(y_1, y_2; t) dy_1 dy_2$ = the joint probability that at some (initial) time t_0 , $y (=y_1)$ lies in the range (y_1, y_1+dy_1) and at a later time t_0+t , $y (=y_2)$ falls in the interval (y_2, y_2+dy_2) (1.4)

Because time and ensemble averages are equivalent here, equation (1.3) becomes

$$R(t) = \overline{y_1 y_2} = \int_{-\infty}^{\infty} \int_{-\infty}^{\infty} y_1 y_2 W_2(y_1, y_2; t) dy_1 dy_2, \quad (1.5)$$

and since the process is stationary, the initial times t_0 do not enter: one is concerned only with the time intervals (t) between observations.

Knowledge of the correlation function $R(t)$ is important, for by the theorem of Wiener (1930) and Khintchine (1934) the mean intensity spectrum follows at once as the cosine Fourier transform of $R(t)$, namely

$$W(f) = 4 \int_0^{\infty} R(t) \cos \omega t dt, \quad (\omega = 2\pi f) \quad (1.6 a)$$

with the inverse relation

$$R(t) = \int_0^{\infty} W(f) \cos \omega t df. \quad (1.6 b)$$

* We distinguish here between time and statistical averages by $\langle \rangle_{av}$ and the superscript bar ($\overline{}$), respectively. The equivalence of these averages follows from the ergodic theorem (Chandrasekhar 1943, James, Nichols and Phillips 1946).

To determine the desired energy spectrum $W(f)$ the simplest procedure is first to obtain the correlation function and then apply (1.6 a). Note from (1.6 b) that setting $t=0$ in $R(t)$ gives the mean total intensity of the random wave, namely

$$R(0) = \int_0^\infty W(f) df \lim_{t \rightarrow 0} \int_{-\infty}^{+\infty} y_1 y_2 W_2(y_1, y_2; t) dy_1 dy_2 = \bar{y}^2, \quad (1.7)$$

which is the area under the spectral distribution curve $W(f)$, as expected. On the other hand, allowing t to become infinite in $R(t)$ yields the steady component \bar{y} , since $\lim_{t \rightarrow \infty} W_2(y_1, y_2; t) = W_1(y_1)W_1(y_2)$, so that (1.4) becomes

$$\lim_{t \rightarrow \infty} R(t) = \iint_{-\infty}^{+\infty} y_1 y_2 W_1(y_1) W_1(y_2) dy_1 dy_2 = \bar{y}_1 \cdot \bar{y}_2 = \bar{y}^2, \quad (1.8)$$

from (1.1). For a pure noise wave \bar{y} vanishes, as there are no steady components. However, when y does not represent a purely stochastic variable, but contains steady and periodic terms as well, $\lim_{t \rightarrow \infty} R(t)$ will not die down in time, but will oscillate indefinitely. If $R(t)$ is then expanded in a Fourier series, the coefficient of each periodic component represents the mean power (or energy, as the case may be) associated with that component; setting $t=0$ in $R(t)$ still gives the mean total power in the wave.

In a similar way we may find the correlation function for a general function $g(y)$ of the random variable y . By definition (Rice 1944, 1945 Middleton 1948a, 1949) we have

$$\begin{aligned} R(t) &\equiv \langle g[y(t_0)]g[y(t_0+t)] \rangle_{av} = \overline{g(y_1)g(y_2)} \\ &= \iint_{-\infty}^{+\infty} g(y_1)g(y_2)W_2(y_1, y_2; t) dy_1 dy_2. \quad (1.9) \end{aligned}$$

The spectrum follows from (1.6 a). For the problems (i.)–(iii.) of the present paper the modulated wave $V(t)$ is expressed as a function of a statistical variable y , and the choice of $g(y)$ is based on the pertinent physical model which describes the problem. In general, $g(y)$ is not a linear function of y , and so the evaluation of the auto-correlation function becomes difficult.

2. RESULTS AND CONCLUSIONS.

We consider first

(a) Frequency- or Phase-Modulation of a Carrier by Noise.

We start here with the following narrow-band wave :

$$g(y) = V(t) = A_0 \exp \{i[\omega_0 t + \Psi(t)]\}, \quad (y = \Psi(t)). \quad (2.1)$$

In (2.1) A_0 is the peak amplitude of the modulated carrier $\exp [i\omega_0 t + i\Psi(t)]$, $\omega_0 (=2\pi f_0)$ is the central or resonant (angular) frequency of the intermediate (IF) or radio frequency (RF) band of the apparatus in which $V(t)$ is generated*, and $\Psi(t)$ is a varying phase, which has the form

$$\Psi(t)=D(t), \quad \text{or} \quad \Psi(t)=\int^t D(t') dt', \quad . \quad . \quad . \quad (2.2)$$

respectively, for phase- or frequency-modulation. The amplitude A_0 and modulation Ψ are real quantities, so that the instantaneous voltage or current wave is given either by the real or imaginary part of the complex disturbance $V(t)$. For a moment we leave open the precise nature of $\Psi(t)$, and hence of $D(t)$, except to note that $\Psi(t)_{\max}$ must be much less than $\omega_0 t$, and $\Psi(t)_{\max} = [(d\Psi/dt)(t)]_{\max}$ considerably smaller than ω_0 for $\Psi(t)$ to represent a true phase- or frequency-modulation (van der Pol 1946).

By a slight modification of (1.3) to account for the complex character of $V(t)$, the auto-correlation function $R(t)$ is here

$$R(t) = \frac{1}{2} \operatorname{Re} [\overline{V(t_0)} V(t_0+t)^*] \\ = \frac{A_0^2}{2} \operatorname{Re} \{ \exp (-i\omega_0 t) \{ \exp [i\Psi(t_0) - i\Psi(t_0+t)] \}_{\text{stat av}} \}. \quad . \quad . \quad . \quad (2.3)$$

For the present discussion $D(t)$, and therefore $\Psi(t)$, belong to a normal random process, since the modulation $D(t)$ is fluctuation noise (Rice 1944, 1945, Wang and Uhlenbeck 1945, Middleton 1946, 1948 a, b, 1949), and may be written explicitly as

$$D(t) = D_0 V(t)_N, \quad \text{with } D_0 = \text{r.m.s. phase (or angular frequency)} \\ \text{deviation/r.m.s. modulating voltage}, \quad (2.4 a)$$

since one has $\overline{D(t)^2} = D_0^2 \overline{V(t)_N^2}$. Consequently, for frequency-modulation and phase-modulation an r.m.s. (angular) deviation and an r.m.s. phase deviation can be defined respectively by

$$\omega_d^2 = \overline{D(t)^2} = D_0^2 \overline{V(t)_N^2} \quad \text{and} \quad \theta_d^2 = D_0^2 \overline{V(t)_N^2},$$

where, in the former, D_0 is measured as frequency/volt, while in the latter instance D_0 has the units (volt⁻¹), so that θ_d is a pure number. Expressing the auto-correlation function (2.3) now in terms of the statistical average, we use the joint second-order probability density [cf. (1.4)] for the pair of normal random variables $\Psi_1 = \Psi(t_0)$ and $\Psi_2 = \Psi(t_0+t)$, which is well known to be (Rice 1944, 1945, Middleton 1948 a, 1949)

$$W_2(\Psi_1, \Psi_2; t) = (2\pi \overline{\Psi^2} \sqrt{[1-\rho^2]})^{-1} \\ \exp [-(\Psi_1^2 + \Psi_2^2 - 2\rho(t)\Psi_1\Psi_2)/2\overline{\Psi^2}(1-\rho^2)], \quad . \quad . \quad . \quad (2.4 a)$$

* It is assumed that any local oscillator noise, generated in the process of mixing the modulation and carrier, or background noise, accompanying the carrier or signal, is heavily suppressed relative to the principal modulation product $V(t)$, (2.1).

where $\overline{\Psi^2} = \overline{\Psi_1^2} = \overline{\Psi_2^2}$, and $\rho = \rho(t) = \overline{\Psi_1 \Psi_2} / \overline{\Psi^2}$. The correlation function (2.3) is finally

$$R(t) = \frac{A_0^2}{2} \operatorname{Re} \{ \exp(-i\omega_0 t + \overline{\Psi_1 \Psi_2} - \overline{\Psi^2}) \} = \frac{A_0^2}{2} \exp[-D_0^2 \Omega(t)] \cos \omega_0 t, \quad (2.5)$$

with $\Omega(t) = (\overline{\Psi^2} - \overline{\Psi_1 \Psi_2}) / D_0^2$.

For phase modulation by noise $\Omega(t)$ is found, on applying familiar Fourier integral methods (Madelung 1936), to be specifically

$$\Omega_{\varphi M}(t) = \int_0^\infty W_{\varphi M}(f)(1 - \cos \omega t) df. \quad . \quad . \quad . \quad (2.6 a)$$

The spectral intensity $W_{\varphi M}(f)$ of the phase-modulating noise $V_N(t)$ may be obtained directly from (1.3) and (1.6 a) on application of the Wiener-Khinchine theorem. In a similar manner we find for the more common case of frequency-modulation equation (2.2) that now

$$\Omega_{FM}(t) = \int_0^\infty W_{FM}(f)(1 - \cos \omega t) df / \omega^2. \quad . \quad . \quad . \quad (2.6 b)$$

From (1.6 a) and (2.5) the corresponding mean power spectrum for the modulated carrier is

$$W(f) = A_0^2 \int_0^\infty dt [\cos(\omega_0 + \omega)t + \cos(\omega_0 - \omega)t] \exp(-D_0^2 \Omega(t)), \quad (\omega = 2\pi f), \quad . \quad . \quad . \quad (2.7)$$

showing that the original carrier is either wholly or in part "smeared out" into a continuum, which is symmetrical about the central frequency f_0 .

The mean total power W_τ in the wave is $A_0^2/2$ and the mean power (W_{per}) remaining in the discrete components after modulation is given by the oscillating portions of the correlation function in the limit $t \rightarrow \infty$ (Wang and Uhlenbeck 1945, Middleton 1948 a, 1949), and of this the coefficient of $\cos \omega_0 t$ yields the power W_{f_0} remaining in the carrier. Consequently, the mean power W_c in the continuous part of the spectrum is $W_c = W_\tau - W_{\text{per}}$. Since we are assuming here modulation by a pure noise, then $\lim_{t \rightarrow \infty} \Omega(t)$ does not oscillate indefinitely but approaches a steady value, which may be zero, finite (>0), or even infinite, and the only discrete component is the carrier itself. We may write, therefore,

$$W_{\text{per}} = W_{f_0} = \frac{A_0^2}{2} \exp[-D_0^2 \Omega(\infty)], \quad \text{and} \\ W_c = W_\tau - W_{f_0} = \frac{A_0^2}{2} (1 - \exp[-D_0^2 \Omega(\infty)]) \quad . \quad . \quad . \quad (2.8)$$

for the mean power in the continuum.* For phase-modulation by a purely random noise $V_N(t)$, $\Omega_{FM}(\infty)$ is a finite constant. The case of frequency-modulation is less simple. We investigate the behaviour of $\Omega_{FM}(\infty)$ by expanding $W_{FM}(\omega)$ in a power series about $\omega=0$, viz. $W_{FM}(\omega)=C_0+C_1\omega+C_2\omega^2+\dots$, and substituting the resulting series into (2.6 b) to obtain finally, on integration by parts,

$$\Omega_{MF}(\infty)=0\left(\frac{C_0}{\omega}-C_1\log\omega-C_1+C_2\omega+\dots\right)_{\omega\rightarrow 0+}. \quad (2.9)$$

We distinguish three cases :

$$\text{I. } C_0>0: \quad \Omega_{FM}(\infty)\rightarrow +\infty, \quad 0\left(\frac{1}{\omega}\right)\Big|_{\omega\rightarrow 0} \text{ or } 0(t)_{t\rightarrow\infty},$$

$$\text{II. } C_0=0, C_1>0: \quad \Omega_{FM}(\infty)\rightarrow +\infty, \quad 0(-\log\omega)_{\omega\rightarrow 0}, \text{ or } 0(\log t)_{t\rightarrow\infty},$$

$$\text{III. } C_0=C_1=0, C_2\neq 0: \quad \Omega_{FM}(\infty)\rightarrow a \text{ constant } (>0). \quad (2.10)$$

Thus, if $W_{FM}(0)$ be finite, i. e. $C_0>0$, or if $W_{FM}(0)$ vanishes no more rapidly than $0(\omega)$ (i. e. $C_0=0, C_1>0$), $\Omega_{FM}(\infty)$ is positively infinite and, therefore by equation (2.8) all the unmodulated carrier power is distributed among the components of the continuum, and no energy remains in the carrier. On the other hand, if the modulating noise contains no harmonics at or near $f=0$, so that $W_{FM}(0)$ vanishes sufficiently rapidly as $f\rightarrow 0$, i. e. $C_0=C_1=0, C_2\neq 0$ at least, then $\Omega_{FM}(\infty)$ may be a finite constant, and we have effectively an example of the phase-modulation type discussed above, where some power remains in the original carrier.

The different spectral distributions obtained in phase- and frequency-modulation are explained by the fundamental observation that the mean power associated with any frequency interval is directly proportional to the time the wave spends on the average in that interval. Therefore, in the instance of frequency-modulation, when the carrier is deviated at a very slow rate (with a fixed maximum or r.m.s. swing) corresponding on the average to frequencies at and very close to $\omega=0$ [i. e. $W_{FM}(0)>0$], it spends an infinitely longer time at the limits of each swing than near the central, or unperturbed, frequency, namely, near $f_0\pm D_0/2\pi$ rather than about f_0 . Since the power in the wave is finite, the ratio of the energy distributed about $f_0\pm D_0/2\pi$ to the energy in the spectral vicinity of the carrier is infinite: there is consequently no contribution to the carrier from these modulating components. Similar remarks apply for the higher modulating frequencies, except that now the energy (or power) ratio is finite, since the slowest possible rate of excursion through the

* However, when $\lim_{t\rightarrow\infty}\Omega(t)$ oscillates indefinitely, because of periodic components in the modulating wave, we may obtain the discrete portions of the spectrum (2.7) by expanding $\exp[-D_0^2\Omega(t)]$ and collecting the periodic terms which appear in $\Omega(t)$, $\Omega(t)^2$, etc. Combining these with $\cos(\omega_0\pm\omega)t$ according to (2.7) then gives an (infinite) set of discrete harmonics, which are located in frequency at $f_0\pm nf_a$ (where f_a represents a typical harmonic of the periodic part of the disturbance) and whose intensities are the coefficients of $\cos(\omega_0\pm n\omega_a)t$.

allowed frequency range cannot be less than the lowest modulation component. Furthermore, it is always the lowest modulating frequency which effectively determines the ratio of power at the limits of the swing relative to the power distributed about the centre of the band. The contributions of the higher frequencies are of secondary importance, since the time spent in any spectral region in the course of the frequency modulation is essentially infinitely longer for the very slow and zero, or "adiabatic" shifts than for the displacements occurring at greater ratio. Accordingly, when the modulating noise contains (nearly) zero-frequency components (*i. e.* $W_{FM}(0) > 0$), the mean power in the carrier and in the continuum is completely specified by the behaviour of $W_{FM}(f)$ at and in the immediate vicinity of $f=0$. Similarly, when the modulating noise contains a band of frequencies, for which there are no zero- or very low-frequency terms, a finite amount of power remains in the carrier.

The same argument applies for phase-modulation. We have only to observe that the phase modulation can be replaced by an equivalent frequency-modulation, *cf.* (2.6 *a*), where the spectra of the two disturbances are related by $W_{FM}(f) = \omega^2 W_{\varphi M}(f)$. Since $W_{\varphi M}(0)$ may exceed zero, it follows that the corresponding spectrum $W_{FM}(f)$ is $O(f^2)$ as $f \rightarrow 0$, at least, and consequently $W_{FM}(f)$ represents a *band* of noise. This is sufficient to give a finite ratio of mean side-band to mean carrier power, which by (2.8) is explicitly $\exp(D_0^2 \psi_N) - 1$.

A number of general observations concerning the spectrum of the modulated wave can now be made. For all ratios (ω_d/ω_b) of the r.m.s. (angular) frequency deviation to the r.m.s. (angular) rate of deviation (or ω_b), or for all magnitudes of the r.m.s. phase change θ_d , it is possible to develop a series expansion for the mean spectrum. This is obtained from (2.7) once the explicit form of $\Omega(t)$ has been determined. However, it is sometimes possible to develop in series directly, without first determining $\Omega(t)$. In the case of frequency-modulation we find that (2.7) becomes*

$$W(f)_{FM} = A_0^2 \exp[-D_0^2 \Omega_{FM}(\infty)] \sum_{n=0}^{\infty} \frac{(-D_0^2)^n}{n!} \times \int_0^{\infty} [\Omega_{FM}(t) - \Omega_{FM}(\infty)]^n \cos(\omega_0 - \omega)t \, dt, \quad . \quad (2.11)$$

provided $\Omega_{FM}(\infty)$ exists, which by (2.10) will occur only if the modulating noise is a band with a lower cut-off frequency which vanishes, as $f \rightarrow 0$, sufficiently rapidly. On the other hand, for phase-modulation we find at once from (2.6 *a*) that a general expansion in powers of θ_d , the r.m.s.

* Only when $f \sim f_0$ is there any appreciable contribution to the integrals in (2.11), since the modulation is a narrow band about $f=f_0$. Accordingly, the terms in $\cos(\omega_0 + \omega)t$ are quite ignorable, as they oscillate far too rapidly (when $f \sim f_0$) to make a noticeable addition to the resulting spectrum, distributed about $f=f_0$.

phase deviation, can be effected. Again from (2.7) the spectrum of the modulated carrier becomes

$$W(f)_{\varphi M} = A_0^2 \exp(-\theta_d^2) \sum_{n=0}^{\infty} \frac{\theta_d^{2n}}{n!} \int_0^{\infty} r_0(t)^n \cos(\omega_0 - \omega)t dt, \quad (2.12)$$

where $r_0(t)$ is the normalized auto-correlation function of the modulating noise $V_N(t)$, namely $V_N(t_0)V_N(t_0+t)/\overline{V_N(t_0)^2}$, which by equation (1.6 b) is, in terms of the spectrum of the modulation $V_N(t)$,

$$r_0(t) = \int_0^{\infty} W(f)_{\varphi M} \cos \omega t df / \int_0^{\infty} W(f)_{\varphi M} df.$$

When the r.m.s. deviation is large compared to the r.m.s. rate of deviation, or equivalently, when the r.m.s. phase variation is great, the series (2.11) and (2.12) above do not converge rapidly enough to be useful, and so an (asymptotic) expansion in inverse powers of ω_d/ω_b or θ_d is required. Such an expansion is easily obtained, provided now that $\Omega(t)$ possesses all derivatives at $t=0$, for then we can develop $\Omega(t)$ in a MacLaurin series about $t=0$, retain terms in t and t^2 only in $\exp[-\Omega(t)]$, and expand the rest in a series. We obtain finally the mean intensity spectrum of the modulated carrier

$$\begin{aligned} W(f) = & \frac{A_0^2}{D_0(\Omega^{(2)})^{1/2}} \left\{ \phi^{(0)}(\beta) - \frac{\Omega^{(4)}}{D_0^2 4! \Omega^{(2)2}} \phi^{(4)}(\beta) \right. \\ & + \frac{1}{D_0^4} \left[\frac{\Omega^{(6)}}{6! \Omega^{(2)3}} \phi^{(6)}(\beta) + \frac{\Omega^{(4)2}}{2! 4! \Omega^{(2)4}} \phi^{(8)}(\beta) \right] \\ & - \frac{1}{D_0^6} \left[\frac{\Omega^{(8)}}{8! \Omega^{(2)4}} \phi^{(8)}(\beta) + \frac{\Omega^{(4)} \Omega^{(6)}}{4! 6! \Omega^{(2)5}} \phi^{(10)}(\beta) + \frac{\Omega^{(4)3}}{3! 4!^3 \Omega^{(2)6}} \phi^{(12)}(\beta) \right] \\ & + \frac{1}{D_0^8} \left[\frac{\Omega^{(10)}}{10! \Omega^{(2)5}} \phi^{(10)}(\beta) + \frac{1}{2! \Omega^{(2)6}} \left(\frac{\Omega^{(6)2}}{6!^2} + \frac{2 \Omega^{(4)} \Omega^{(8)}}{4! 8!} \right) \phi^{(12)}(\beta) \right. \\ & \left. + \frac{\Omega^{(4)2} \Omega^{(6)}}{2! 4!^2 6! \Omega^{(2)7}} \phi^{(14)}(\beta) + \frac{\Omega^{(4)4}}{4! 5 \Omega^{(2)8}} \phi^{(16)}(\beta) \right] + \dots \Big\}, \\ & (\omega_b/\omega_d)^2 < 1, \quad \text{or} \quad \theta_d^2 < 1. \quad \dots \quad (2.13) \end{aligned}$$

where

$$\phi^{(n)}(x) = \frac{d^n \exp(-x^2/2)}{dx^n} \Big|_{x=x},$$

and in which specifically

$$\Omega_{FM}^{(0)} = 0; \quad \Omega_{FM}^{(2)} = \int_0^{\infty} W_{FM}(f) df = b_0, \quad (\sim \omega_b); \quad D_0(\Omega^{(2)})^{\frac{1}{2}} = D_0 \sqrt{(b_0)} = \omega_d; \\ \beta = \beta_{FM} = (\omega_0 - \omega)/\omega_d; \quad \dots \quad (2.14 a)$$

$$\Omega_{\varphi M}^{(0)} = b_0; \quad \Omega_{\varphi M}^{(2)} = \int_0^{\infty} W_{\varphi M}(f) \omega^2 df = b_2, \quad (\sim \omega_b^3); \\ D_0(\Omega^{(2)})^{\frac{1}{2}} = D_0 \sqrt{b_2} = \theta_d \sqrt{(b_2/b_0)}; \quad \beta = \beta_{\varphi M} = (\omega_0 - \omega)/\gamma \theta_d; \quad \gamma \equiv \sqrt{(b_2/b_0)}; \\ \dots \quad (2.14 b)$$

$$b_n \equiv \int_0^{\infty} \omega^n W(f) df; \quad \dots \quad (2.14 c)$$

$$\therefore \Omega_{FM}^{(2n)} = (-1)^{n-1} b_{2n-2}, \quad (n \geq 1); \quad \Omega_{\varphi M}^{(2n)} = (-1)^{n-1} b_{2n}, \quad (n \geq 0). \quad \dots \quad (2.14 d)$$

Note that as the mean intensity of the modulating noise ($\sim \omega_b$) becomes very small, or as the r.m.s. deviation ($\sim \omega_d$, or θ_d) becomes very great, the other parameters of the system remain constant, *one always approaches a gaussian modulation spectrum, quite independent of the precise power distribution of the modulating wave* (in all cases for which $\Omega^{(2)}(0)$ exists). As can be seen from (2.1), (2.3)–(2.5), (2.7), and (2.13), the gaussian limiting form is a direct consequence of the *normal* statistics of the modulating wave and the fact that $V(t)$, equation (2.1), is a true frequency- or phase-modulated carrier, *i. e.* there is no amplitude distortion of the carrier in the final output after modulation. For non-normal random noise such as precipitation or impulsive static, W_2 will not be a normal frequency-function and consequently the limiting spectrum will no longer be gaussian.

We are ready now to summarize the results for specific examples of the gaussian modulation spectrum :

(i.) *Frequency-modulation.*

In this case the gaussian spectral distribution of $V_N(t)$ is given by

$$W_{FM}(f) = W_0 \exp(-\omega^2/\omega_b^2), \quad . \quad . \quad . \quad (2.15)$$

and therefore, according to (2.6 b) and (2.7), we have finally the spectrum

$$W(f)_{FM} = \frac{A_0^2}{\omega_b} \int_0^\infty dx \cos \beta x \exp \left[-\sqrt{(\pi)} \frac{\omega_d^2}{\omega_b^2} \left\{ x \Theta(x/2) - \frac{2}{\sqrt{(\pi)}} [1 - \exp(-x^2/4)] \right\} \right],$$

$$\beta \equiv \frac{\omega_d - \omega}{\omega_b}. \quad . \quad . \quad . \quad (2.16)$$

To evaluate the integral we approximate the exponent, $f_1(x)$, by a suitable function $f_2(x)$ which fits the true function $f_1(x)$ closely ; in this instance we require that $f_2(x)$ have the same values as $f_1(x)$ at and near $x=0$ and as $x \rightarrow \infty$. Since $\lim_{x \rightarrow \infty} f_1(x) = x - 2/\sqrt{(\pi)}$ we seek a form of $f_2(x)$ which facilitates the integration of (2.16) and which consequently does not contain an exponential of argument other than x . Our choice is $f_2(x) = x - 2/\pi + (ax+b) \exp(-cx)$. The above conditions on $f_2(x)$ give us finally $a - bc = -1$; $b = 2/\sqrt{(\pi)}$; $bc^2/2 - ac = 1/2\sqrt{(\pi)}$, which yield

$$a_{\pm} = \frac{2c_{\pm}}{\sqrt{(\pi)}} - 1 = \frac{0.672}{-0.672} \Bigg\} ; \quad b = 2/\sqrt{(\pi)} = 1.129 ;$$

$$c_{\pm} = \frac{\sqrt{(\pi)} \pm \sqrt{(\pi-2)}}{2} = \frac{1.481}{0.291} \Bigg\} . \quad . \quad . \quad (2.17)$$

It is found that c_+ , and accordingly a_+ , give the best fit, being at the worst about 7 per cent too great for $x \sim 1$ and proportionately better for smaller

and larger x . Substituting these results into (2.16) and expanding the exponential containing $\exp(-cx)$ gives finally the mean spectrum

$$W(f)_{\text{FM}} = \frac{A_0^2}{\omega_b} \exp(2\omega_d^2/\omega_b^2) \sum_{n=0}^{\infty} \frac{[-2\omega_d^2/\omega_b^2]^n}{n!} \sum_{k=0}^n {}_n C_k \left(\frac{\pi-2}{2}\right)^k \\ \times \text{Re}[i^{-k} \Phi^{(k)}(\beta_n^+)] / [\sqrt{(\pi)\omega_d^2/\omega_b^2 + c + n}]^{k+1}, \quad \dots \quad (2.18)$$

$$\beta_n^+ = (\omega_0 - \omega) / \omega_b [\sqrt{(\pi)\omega_d^2/\omega_b^2 + c + n}],$$

where $\Phi^{(m)}(\alpha) = m! i^m / (1 - i\alpha)^{m+1}$; $\text{Im}(\alpha) > -1$.

When ω_d^2/ω_b^2 is larger than unity we may use the asymptotic development (2.13); in this instance we observe from (2.14) and (2.15) that

$$\Omega_{\text{FM}}^{(2m)} = \frac{(-1)^{m-1} (2m-2)!}{\sqrt{(\pi)} 2^{2m} (m-1)!} W_0 \omega_b^{2m-1},$$

and so, after some reduction, (2.13) becomes explicitly

$$W(f)_{\text{FM}} \simeq \frac{A_0^2 \pi}{\omega_d} \left\{ \phi^{(0)}(\beta') + \frac{1}{48} \left(\frac{\omega_b}{\omega_d}\right)^2 \phi^{(4)}(\beta') \right. \\ + \frac{1}{2^{56}!} \left(\frac{\omega_b}{\omega_d}\right)^4 [24\phi^{(6)}(\beta') + 5\phi^{(8)}(\beta')] + \frac{1}{2^{69}!} \left(\frac{\omega_b}{\omega_d}\right)^6 [1080\phi^{(8)}(\beta') \\ + 504\phi^{(10)}(\beta') + 35\phi^{(12)}(\beta')] + \frac{1}{3 \cdot 2^{1010}!} \left(\frac{\omega_b}{\omega_d}\right)^8 [20160\phi^{(10)}(\beta') \\ + 16848\phi^{(12)}(\beta') + 2520\phi^{(14)}(\beta') + 175\phi^{(16)}(\beta')] + \dots \left. \right\}, \quad \dots \\ \omega_b/\omega_d < 1; \beta' = \frac{\omega_0 - \omega}{\omega_d}. \quad \dots \quad (2.19)$$

Fig. 1 illustrates a typical frequency-modulation spectrum for a number of values of the ratio ω_d/ω_b for spectra normalized to unity (at $\beta=0$). We remark that the asymptotic expression (2.19) can be used with fair accuracy for values of $\omega_b/\omega_d \cong 1$; the spectral intensities for $\beta > 2$, however, become progressively too low as β increases.

(ii.) Phase-modulation.

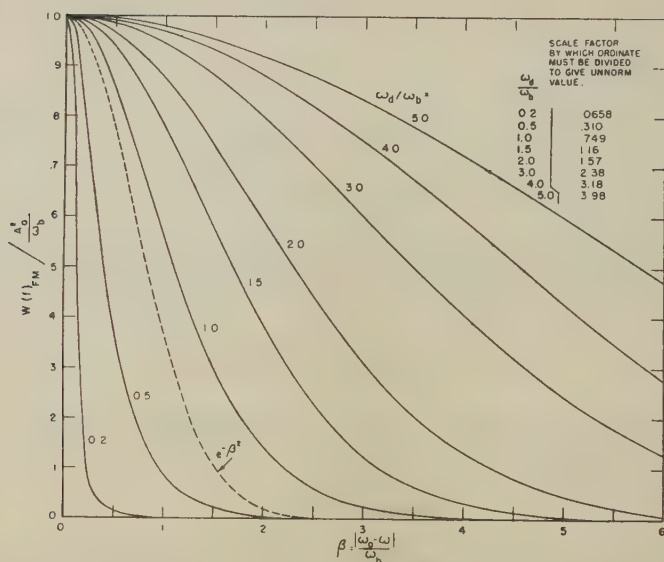
If we substitute the expression (2.15) for the mean intensity distribution of the modulating noise into (2.6 a) we find at once that

$$\Omega_{\text{PM}}(t) = \theta_d^2 [1 - r_0(t)], \text{ with } r_0(t) = \exp(-\omega_b^2 t^2/4),$$

and therefore the mean spectrum of the modulated carrier becomes

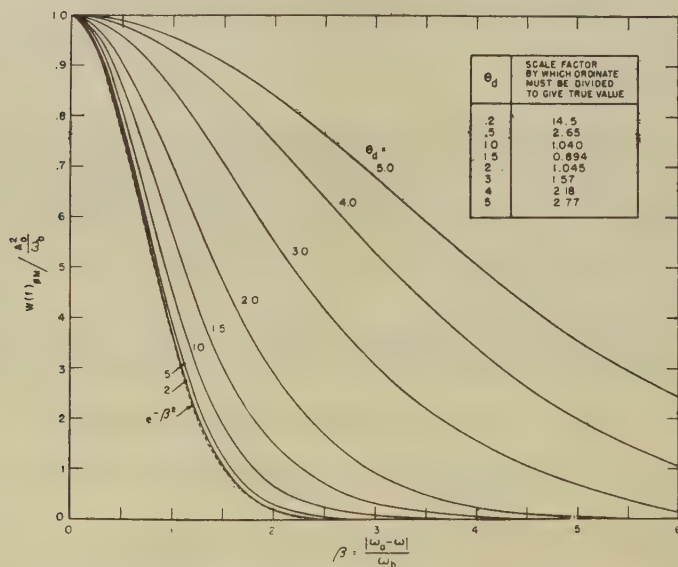
$$W(f)_{\text{PM}} = \frac{A_0^2 \exp(-\theta_d^2)}{2} \left\{ \delta(f - f_0) + \frac{2\sqrt{(\pi)}}{\omega_b} \sum_{n=1}^{\infty} \frac{\theta_d^{2n}}{n! \sqrt{(n)}} \right. \\ \left. \exp[-(\omega - \omega_0)^2/n\omega_b^2] \right\}. \quad \dots \quad (2.20)$$

Fig. 1.



Normalized spectral distributions of a carrier frequency-modulated by normal random noise.

Fig. 2.



Normalized spectral distributions of a carrier phase modulated by normal random noise.

As explained in (a) above, a finite amount of power, $(A_0^2/2) \exp(-\theta_d^2)$, remains in the carrier. Again, when θ_d is much larger than unit it is convenient to use the asymptotic development (2.13), for which now

$$\Omega_{\varphi M}^{(2m)} = \frac{(-1)^{m-1} (2m)!}{\sqrt{\pi} 2^{2m+2} m!} W_0 \omega_b^{2m+1}.$$

One has finally

$$\begin{aligned} W(f)_{\varphi M} \simeq & \frac{A_0^2 \pi \sqrt{(2)}}{\omega_b \theta_d} \left\{ \phi^{(0)}(\beta'') + \frac{\theta_d^{-2}}{8} \phi^{(14)}(\beta'') + \frac{15}{2 \cdot 6!} \theta_d^{-4} [2\phi^{(6)}(\beta'') + 3\phi^{(8)}(\beta'') \right. \\ & + \frac{105\theta_d^{-6}}{2^3 \cdot 8!} [8\phi^{(8)}(\beta'') + 8\phi^{(10)}(\beta'') + \phi^{(12)}(\beta'')] \\ & + \frac{315}{2^5 \cdot 10!} \theta_d^{-8} [96\phi^{(10)}(\beta'') + 200\phi^{(12)}(\beta'') + 60\phi^{(14)}(\beta'') \\ & \left. + 15\phi^{(16)}(\beta'')] + \dots \right\}, \quad \beta'' = \frac{(\omega_0 - \omega) \sqrt{(2)}}{\omega_b \theta_d}. \quad (2.21) \end{aligned}$$

The carrier term $A_0^2/2 \exp(-\theta_d^2) \delta(f-f_0)$ is concealed in (2.21); when $\omega \rightarrow \omega_0$ the asymptotic series changes in the proper way to give the correct carrier power, for note that from (2.21) $\int_0^\infty W(f)_{\varphi M} df \approx A_0^2/2$; only the leading term makes a contribution. Compare with (2.20), which is valid for all θ_d . Fig. 2 illustrates a number of representative spectra and, like fig. 1, here shows spectra normalized to a maximum value of unity.

As expected, large modulation indices yield correspondingly large spectral spreads. In the case of frequency-modulation (fig. 1) one gets in the limit of very small deviations or very rapid swings (*i. e.* $(\omega_d/\omega_b)^2 \ll 1$) a very narrow spectrum, which becomes essentially a discrete component at the carrier frequency (f_0) when $\omega_d/\omega_b \rightarrow 0$. This is explained by observing that, since the (r.m.s.) rate of deviation ($\sim \omega_b$) is now so rapid relative to the (r.m.s.) interval ($\sim \omega_d$) over which the frequency excursion takes place, a vanishingly small fraction of the wave's energy in any spectral region (proportional to the time the wave spends in that region) is distributed outside the immediate neighbourhood of the carrier f_0 . The case of phase-modulation (fig. 2) exhibits a similar behaviour, but with a number of important differences. There is now effectively a finite lower bound to the width of the equivalent frequency-modulating noise which has a spectrum $W(f) \sim \omega^2 \exp(-\omega^2/\omega_b^2)$, as compared with the usual frequency-modulation case above, where $W(f) \sim \exp(-\omega^2/\omega_b^2)$, as a consequence of the fact that by definition the wave-form of the modulations for the same noise disturbances are related as integrand and integral (*cf.* equation (2.2)). This in turn sets a lower limit to the spectral width for phase-modulation by noise, which approaches in shape the spectral distribution of the modulating wave, here $\sim \exp(-\omega^2/\omega_b^2)$. However, since this limiting spectral intensity is

proportional to θ_d^2 ($\theta_d^2 \ll 1$), the spectrum vanishes when θ_d goes to zero, and we are left with the original, undistorted carrier. Frequency-modulation yields a greater spectral spread than phase-modulation (for the same deviation and identical noise waves) whenever the (r.m.s.) modulation index (θ_d or ω_d/ω_b) is of the order unity or greater, as comparison of figs. 1 and 2 shows. The reverse is true for indices less than about unity. The phenomenon is explained by the fact that the modulating frequencies of maximum intensity in the FM case lie near ($\omega=0$), while for ϕM they fall in the neighbourhood of ($\omega \sim \omega_b$) (since the spectrum of the equivalent frequency-modulating wave is proportional to $\omega^2 \exp(-\omega^2/\omega_b^2)$). Accordingly, the phase-modulation cannot sweep the carrier through a given deviation more slowly than a frequency of order ω_b , and this sets an *upper* limit on the amount of power available in any spectral region. We therefore expect less spectral spread in phase-modulation (for sufficiently large indices) because of the effectively greater rate of sweep. For small indices the reverse is true.

(b) *Carrier Amplitude-modulated by Noise.*

As in the preceding examples of frequency-modulation (*cf.* § (a)), we represent the IF (or RF) wave by a complex disturbance

$$g(y) = V(t) = A_0(t) \exp(i\omega_0 t), \quad (\omega_0 = 2\pi f_0), \quad . \quad . \quad (2.22 a)$$

where $A_0(t)$ is a real quantity. The amplitude modulation is specifically

$$\left. \begin{aligned} A_0(t) &= A_0(1 + kV_N(t)), & y &= kV_N(t) \geq -1 \\ &= 0, & y &= kV_N(t) \leq -1 \end{aligned} \right\}, \quad . \quad . \quad (2.22 b)$$

in which $V_N(t)$ is a normal random noise voltage (or current) and k is a modulation index, with dimensions (volts)⁻¹. When the instantaneous amplitude $V_N(t)$ is less than $-1/k$, *over-modulation* occurs, and the signal generator does not oscillate until $V_N(t)$ is once more greater than $-1/k$. Since we assume a purely normal random noise, large, and even infinite, amplitudes are possible, and consequently we may expect over-modulation for a noticeable part of the time, unless the modulating noise is weak. The analysis of this and succeeding sections assumes the common type of modulation in which the instantaneous amplitude of an oscillator's output is modified according to some signal or other low-frequency disturbance applied to a suitable control grid. Frequently, however, a modulated output is produced by applying the *sum* of the separately generated oscillations and the modulation to the input of a (half-wave linear) rectifier. The tube acts now as a mixing device, which yields a suitably modulated output carrier wave *only if the original carrier oscillations are very intense relative to the modulation*. Otherwise one obtains serious distortion due to the significant additional harmonics generated in the non-linear mixing of the carrier and the background noise. Thus, if a mixer is used, equations (2.22 a) and (2.22 b) apply here

approximately, provided the modulation is weak, while (2.22 *a*) and (2.22 *b*) are valid models for all degrees of carrier and modulation strengths when the alternative system of a modulated oscillator is employed.

We consider now the general case (2.22 *b*), which includes over-modulation. To represent the discontinuities in $A_0(t)$, cf. (2.22 *b*), we express $A_0(t)$ in terms of its Fourier transform

$$A_0(t) = \frac{-A_0}{2\pi} \int_C z^{-2} dz \exp \{ +iz[1 + kV_N(t)] \}, \quad (2.23)$$

where C is a contour extending along the real axis from $-\infty$ to $+\infty$ and is indented downward in an infinitesimal semicircle about the singularity at $z=0$. The correlation function (2.3) is now

$$R(t) = \frac{A_0^2}{2} \operatorname{Re} \left\{ \frac{\exp(-i\omega_0 t)}{4\pi^2} \int_C \frac{dz}{z^2} \exp \{ iz[1 + kV_N(t_0)] \} \right. \\ \left. \int_{C^*} \frac{d\xi}{\xi^2} \exp \{ -i\xi[1 + kV_N(t_0 + t)] \} \right\}_{\text{stat av}} \quad (2.24)$$

since no coherence between carrier and modulation is assumed. Here C^* is the contour conjugate to C , extending from $+\infty$ to $-\infty$, and is indented *upward* in an infinitesimal semi-circle about the point $\xi=0$. The ensemble average in (2.24) may be effected in a straightforward way if we note that since $V_N(t_0)$ ($=V_1$) and $V_N(t_0+t)$ ($=V_2$) are normal random variables, their joint distribution is given by a relation similar to (2.4 *a*). Observing that the statistical average yields the characteristic function (cf. equation (2.16) of Chandrasekhar (1943)) for the noise :

$$F_2(z, \xi; t)_N = \exp \left[-\frac{1}{2} k^2 \psi(0)(z^2 + \xi^2) - z\xi \psi(t) \right],$$

we have finally

$$R(t) = \frac{A_0^2}{2} \operatorname{Re} \left\{ \frac{\exp(i\omega_0 t)}{4\pi^2} \int_C \frac{dz \exp(iz - k^2 \psi z^2/2)}{z^2} \right. \\ \left. \int_C \frac{d\xi}{\xi^2} \exp \left[i\xi - k^2 \psi \xi^2/2 - k^2 \psi(t) z\xi \right] \right\} \\ = \frac{A_0^2 h_{0,0}^2}{2} \cos \omega_0 t + \frac{A_0^2}{2} \sum_{n=1}^{\infty} \frac{[-k^2 \psi r_0(t)]^n}{n!} h_{0,n}^2 \cos \omega_0 t, \quad (2.25)$$

where

$$h_{0,n} = \frac{1}{2\pi} \int_C z^{n-2} \exp(iz - k^2 \psi z^2/2) dz = -i^{-n} (k^2 \psi)^{(1-n)/2} 2^{(n-3)/2} \\ \times \left\{ {}_1F_1 \left(\frac{n-1}{2}; \frac{1}{2}; -\frac{1}{2k^2 \psi} \right) / \Gamma \left(\frac{3-n}{2} \right) \right. \\ \left. + \frac{2}{\sqrt{2k^2 \psi}} {}_1F_1 \left(\frac{n}{2}; \frac{3}{2}; -\frac{1}{2k^2 \psi} \right) / \Gamma \left(\frac{2-n}{2} \right) \right\}, \quad (2.26)$$

from equation (A 3.17) of Chandrasekhar (1943); ${}_1F_1$ is a confluent hypergeometric function. Specifically (*cf.* (A 3.9) of Chandrasekhar (1943)) we have for the amplitude functions h_0, n :

$$h_{0,0} = \frac{1}{2} \{ [1 + \Theta(1/\sqrt{(2k^2\psi)})] + \sqrt{(k^2\psi/2\pi)} \exp(-1/2k^2\psi) \}, \quad . \quad . \quad (2.27 a)$$

$$h_{0,1} = \frac{1}{2} \{ 1 + \Theta[1/(2k^2\psi)] \}, \quad . \quad . \quad . \quad . \quad (2.27 b)$$

$$h_{0,n} = (-1)^{-n/2} (k^2\psi)^{(1-n)/2} \phi^{(n-2)} [1/\sqrt{(k^2\psi)}], \quad (n=2, 3, 4, 5, \dots); \quad . \quad . \quad . \quad (2.27 c)$$

where $\Theta(x) \equiv 2/\sqrt{(\pi)} \int_0^x \exp(-y^2) dy$; $\phi^{(n)}(x) = \frac{d^n}{dx^n} \exp(-x^2/2)/\sqrt{(2\pi)}$, $n \geq 0$.

(See also Appendix II. of Chandrasekhar (1943).) By equation (1.6 *a*) the mean intensity spectrum is the Fourier transform of (2.25), which becomes explicitly, when the modulating noise has a gaussian spectrum, *cf.* (2.15),

$$W(f) = \frac{A_0^2}{2} h_{0,0}^2 \delta(f-f_0) + \frac{\sqrt{(\pi A_0^2 k^2 \psi)}}{\omega_b} \left\{ h_{0,1}^2 \exp\left(-\frac{(\omega_0 - \omega)^2}{\omega_b^2}\right) + \sum_{n=2}^{\infty} \frac{\phi^{(n-2)}[1/\sqrt{(k^2\psi)}]^2}{n! \sqrt{(n)}} \exp\left[-\frac{(\omega_0 - \omega)^2}{n\omega_b^2}\right] \right\}. \quad (2.28)$$

Fig. 3 shows typical intensity spectra for a number of values of $\sqrt{(2k^2\psi)}$ between 0 and ∞ .

When essentially no over-modulation takes place the correlation function reduces to

$$[\sqrt{(2k^2\psi)} \rightarrow 0]: R(t) = \frac{A_0^2}{2} \cos \omega_0 t \cdot \{1 + k^2\psi r_0(t)\}, \quad (k^2\psi < 0.18 \text{ for less than } 1 \text{ per cent over-modulation}) \quad . \quad . \quad . \quad (2.29)$$

Additional correction terms may be found in straightforward but tedious fashion. We note in fig. 3 that the mean intensity spectrum is here more widely distributed about f_0 than for the case of ignorable over-modulation. The additional harmonics are (carrier \times noise) noise products, stemming from the clipping process inherent in over-modulation. However, unlike the examples of frequency- or phase-modulation discussed earlier in section (*a*), there is a limit to the spread of the spectrum, determined by the fact that over-modulation can occur at the maximum but 50 per cent of the time. On the other hand, since the amount of clipping inherent in the weak modulation cases is ignorable, no significant spectral spread is obtained there, *vide* fig. 3. In any case the spectral spread is relatively small.

Whereas the spectrum requires a series development, the total mean power W_r and the total intensity W_c of the continuous part of the disturbance are easily obtained in precise, closed form from equation (2.22 *b*) if we remember that $kV_N(t) = y$ is normally distributed with the first-order probability density $W_1(y)$:

$$W_1(y) = \frac{1}{\sqrt{(2\pi k^2\psi)}} \exp(-y^2/2k^2\psi). \quad . \quad . \quad . \quad (2.30)$$

The power in the carrier after modulation is (cf. (1.1) and (1.2)),

$$W_f = \frac{A_0^2}{2} \left| \int_{-1}^{\infty} (1+y) W_1(y) dy \right|^2 = \frac{A_0^2}{2} h_{0,0}^2$$

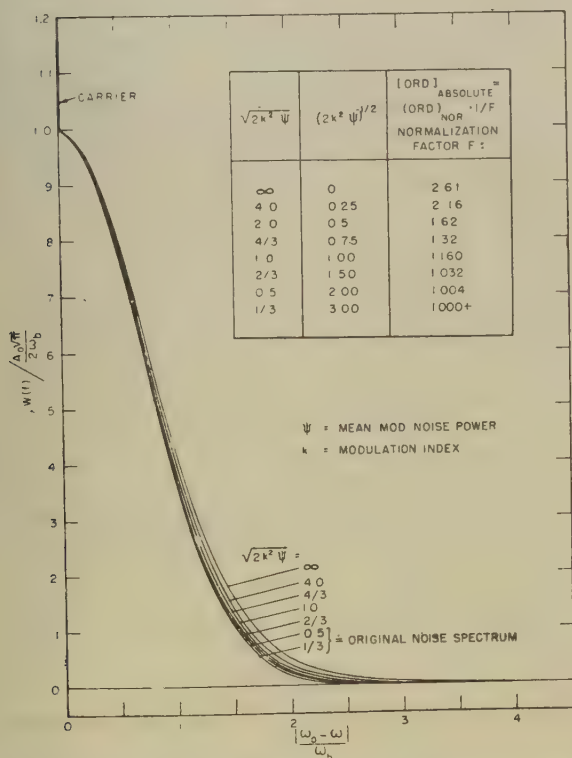
$$= \frac{A_0^2}{2} \left\{ \frac{1 + \Theta[1/\sqrt{(2k^2\psi)}]}{2} - k^2\psi\phi^{(1)}(1/\sqrt{(k^2\psi)})^2 \right\}. \quad (2.31)$$

and

$$W_r = R(0) = \frac{A_0^2}{2} \int_{-1}^{\infty} (1+y)^2 W_1(y) dy \quad (2.32)$$

$$= \frac{A_0^2}{2} \left[\left(\frac{1+k^2\psi}{2} \right) \{ \Theta[1/\sqrt{(2k^2\psi)} + 1] - k^2\psi\phi^{(1)}[1/\sqrt{(k^2\psi)}] \} \right], \quad (2.32)$$

Fig. 3.



Mean intensity spectrum of carrier amplitude-modulated by noise.

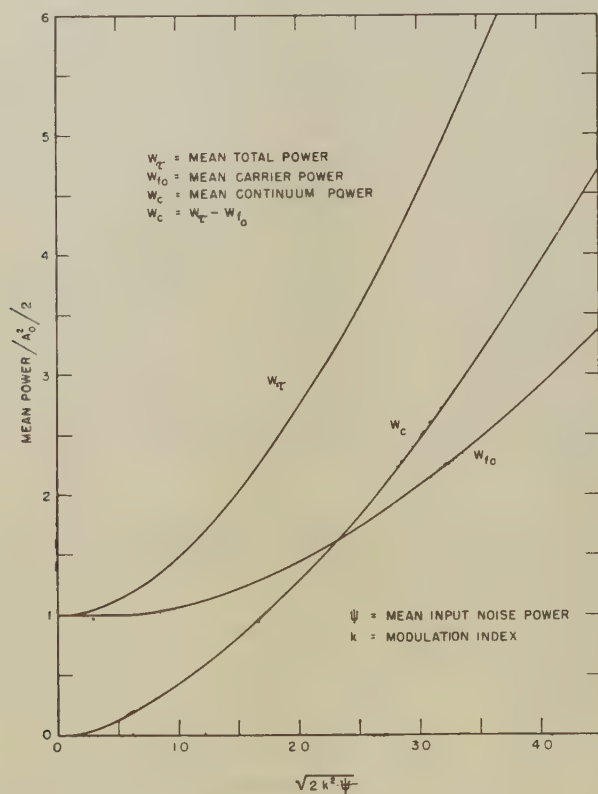
and so,

$$W_e = W_r - W_f = \frac{A_0^2}{2} \left[\frac{1}{4} + \frac{k^2\psi}{2} \{ \Theta[1/\sqrt{(2k^2\psi)}] + 1 \} \right.$$

$$\left. - \left\{ \frac{\Theta[1/\sqrt{(2k^2\psi)}]}{2} - k^2\psi\phi^{(1)}[1/\sqrt{(k^2\psi)}] \right\}^2 \right]. \quad (2.33)$$

Fig. 4 illustrates the behaviour of the mean intensities W_T , W_{f_0} , W_c for different degrees of over-modulation. As the intensity of the modulating noise is increased, a correspondingly greater proportion of the modulated wave's power is distributed in the (noise \times noise) noise sidebands generated in the process of modulation and the clipping due to possible over-modulation, as shown in fig. 4. We remark that the amount of power in the carrier component and in the continuum is quite independent of the

Fig. 4.



Mean power in carrier amplitude-modulated by noise.

particular spectral distribution of the original (normal random) noise, and depends only on the clipping level at which over-modulation occurs, since power in a given band of frequencies is proportional to the integrated intensity of the band. One can consider also more complicated modulations, such as square-law modulation, viz., $A_0(t) = [1 + kV_N(t)]^2$: the treatment is identical with that of the linear case examined here, following an appropriate modification of the transform relation (2.23).

REFERENCES.

- BENNETT, W. R., 1944, *J. Amer. Acoust. Soc.*, **15**, 165.
 BOONIMOVICH, V., 1946, *J. Physics, U.S.S.R.*, **10**, 35.
 CHANDRASEKHAR, S., 1943, *Rev. Mod. Phys.*, **15**, 1.
 MIDDLETON, D., 1946, *J. Appl. Phys.*, **17**, 778; 1948 a, *Quart. J. Appl. Math.*, **5**, 445; 1948 b, *Proc. Inst. Radio Engrs.*, **36**, 1467; 1949, *Quart. J. Appl. Math.*, **7**, 129.
 VAN DER POL, B., 1946, *J. Instn. Elect. Engrs.*, **93**, III, 153.
 RICE, S. O., 1944, *Bell Syst. Tech. J.*, **23**, 282; 1945, *Ibid.*, **24**, 46.
 VAN VLECK, J. H., and MIDDLETON, D., 1946, *J. Appl. Phys.*, **17**, 940.
 WANG, M. C., and UHLENBECK, G. E., 1945, *Rev. Mod. Phys.*, **17**, 323.
- For primarily mathematical references, see
- BLANC-LAPIERRE, A., 1945, *Dissertation*, University of Paris.
 CRAMÉR, H., 1940, *Ann. Math. Ser.*, **2**, **44**, 215; 1946, *Mathematical Methods of Statistics* (Princeton University Press).
 JAMES, H. M., NICHOLS, N. B., and PHILLIPS, R. S., 1946, *Theory of Servomechanisms* (M.I.T.) (Radiation Laboratory Series), **25**, (New York: McGraw-Hill), Chap. 6.
 KHINTCHINE, A., 1934, *Math. Annalen*, **109**, 604.
 MADELUNG, E., 1936, *Die Mathematischen Hilfsmittel des Physikers* (Berlin: J. Springer).
 WIENER, N., 1926, *J. Math. and Phys. (M.I.T.)*, **5**, 99; 1930, *Acta Math.*, **55**, 117.

LXXII. *Observations on the Multiple Scattering of Ionizing Particles in Photographic Emulsions.*—Part I. *The Value of the Scattering Constant.*

By K. GOTTSTEIN*, M. G. K. MENON, J. H. MULVEY,
C. O'CEALLAIGH† and O. ROCHAT,
H. H. Wills Physical Laboratory, University of Bristol ‡.

[Received May 10, 1951.]

SUMMARY.

The theories of multiple scattering of Williams, Molière, Snyder and Scott are briefly surveyed. The results of five independent determinations of the scattering constant for G.5 nuclear research emulsions, details of which are to be presented in the following papers, are compared and discussed. The constant has been found to vary with cell-size and β in a manner which is in agreement with theory. The effect of rejecting large angles due to plural scattering is considered, and also those errors which arise from the presence of spurious scattering.

§1. STATEMENT OF THE PROBLEM.

THE method of estimating the energy of fast ionizing particles in photographic emulsions by measuring the deviations in their tracks produced by multiple scattering was first suggested by Bose and Choudhuri (1941), and is now one of the standard techniques of applied nuclear physics. Its most fruitful application has been to the study of cosmic radiation. The analogous method has also been applied with success to the tracks of electrons in the Wilson cloud-chamber (Groetzinger *et al.* 1950).

During the past two years several papers have appeared dealing both with the theory and with the experimental applications of the method (see References). In particular, following an important advance in the technique described by Fowler (1950), a series of publications has appeared from this laboratory. Certain of these papers describe how the scattering method has been used to establish the mass of those particles of great energy which form the charged component of the penetrating showers (Camerini *et al.* 1950).

The scattering method has also been used in experiments which demonstrate the presence in these showers, of neutral mesons of short life (Carlson, Hooper, King 1950), and again, in a general study of the properties of the soft component of cosmic radiation (Hooper and King

* On leave of absence from the Max Planck Institut für Physik, Göttingen.

† On leave of absence from University College, Cork.

‡ Communicated by Professor Powell.

1950, Hooper, King and Morrish 1951). The somewhat different technique developed by the Brussels group (1950) has also been used successfully to study a wide range of similar problems.

The mean deviation of a charged particle which passes through a given layer of matter will later be shown to be directly proportional to the charge, and inversely proportional to the product momentum \times velocity. The constant of proportionality depends chiefly on the composition of the scattering medium. Thus, to calculate the energy and momentum of a particle from the observed mean angle of scattering in a given emulsion, we must know the value of the "scattering constant" appropriate to the experimental conditions.

Values of this constant which show fair agreement with each other may be calculated by using various theories. On the other hand, there appears to be definite disagreement between previous experimental determinations. Since the chief use of the method is to estimate the energies of ionizing

TABLE I.

Particle	Energy in MeV. (corrected for loss)	β^2	Origin
1. Positrons	105	1	Cornell Synchrotron
2. Positrons	185	1	Cornell Synchrotron
3. Protons	336	0.46	184 in. Berkeley Cyclotron
4. Protons and mesons	5-50 MeV.	0.07	Cosmic ray particles ending in emulsion
5. Protons	9-35 MeV.	0.02	Protons ejected from cosmic ray stars

particles, it has been felt desirable to obtain an experimental value for the constant applicable to the conditions of the work in progress in this laboratory. At the same time, because of its intrinsic interest, it was hoped to compare the experimental value of the constant with that predicted by theory.

§2. SCOPE OF PRESENT EXPERIMENTS.

The calibration of Ilford G.5 emulsions has been carried out in two independent ways. In one approach, the measurements of scattering were made on the tracks of artificially produced monoenergetic particles. In the other, particles were used which had their origin in cosmic-ray events. Those selected came to rest in the emulsion having travelled such distance that their mass and energy could be determined accurately.

The above Table lists the particles on which scattering measurements have been carried out, and shows the corresponding values of their energy and of the parameter $\beta^2 = v^2/c^2$.

As will be seen later, the value of the scattering constant is dependent to some extent on the velocity of the particle. Since the measurements above include the complete range of velocities from the classical to the extreme relativistic, they may be used to test experimentally whether the velocity dependence predicted by theory is correct.

This programme of work has been carried out as three separate investigations. In the present paper, however, it has been thought best to discuss the results taken as a whole. In this way we avoid repeating definitions, and the argument will be the clearer for the absence of distracting experimental details. In the four succeeding papers of this series the experimental procedure will be fully described.

§3. RESUMÉ OF THEORIES OF MULTIPLE SCATTERING.

We deal briefly with the theoretical treatment of the problem of multiple scattering in thin foils given by Williams, Molière and Snyder and Scott, although we shall make most use of that of Molière since it has the widest range of application and has been presented in a convenient form.

Following is a list of the most important symbols used in the present and in the succeeding papers of this series.

Φ = projected angle of scattering on a plane at right angles to the line of observation.

α = deflections due to all scattering in thin sheets of matter as found by the theory of Williams. $\bar{\alpha}$ = mean absolute values of these angles.

$\langle \Phi \rangle$ = mean absolute value of the resultant of individual deflections.

N, Z, t = number of scattering centres per c.c., atomic number and thickness in cm. of the scattering medium.

ze, p, v, M_0 = charge, momentum, velocity and rest-mass of scattered particle.

m = electronic rest-mass. $\gamma = Zz/137\beta$.

$\sigma = T/M_0c^2$ = kinetic/rest energy of scattered particle.

$\delta = \frac{2e^2(NZ^2)^{1/2}zt^{1/2}}{pv}$ an angular unit common to all theories.

s = cell-size in units of 100 microns.

(a) *Theory of Williams.*

The earliest simple theory of multiple scattering in a form which could conveniently be applied to the direct measurement of momentum is that of E. J. Williams (1935, 1939, 1940). He assumed that a charged particle passing through a thin layer of matter suffers a deviation which is the resultant of a very large number of individual deflections, the probability of any one of which is given by the Rutherford scattering law. He

conjectured, moreover, that the angle Φ between the direction of incidence and the projected direction of emergence is distributed about zero in accordance with the normal law.

The mean square value of all such projected deflections was found using Rutherford's expression for the probability of single scattering, and integrating between limits Φ_{\min} and Φ_{\max} . This is taken to be the variance of the assumed normal distribution of Φ . The result may equally well be expressed in terms of $\langle \Phi \rangle$ the mean absolute deviation of the distribution, and this is given by (1).

$$\langle \Phi \rangle = \frac{2e^2(NZ^2)^{\frac{1}{2}}t^{\frac{1}{2}}}{pv} \left(\ln \frac{\Phi_{\max}^2}{\Phi_{\min}^2} \right)^{\frac{1}{2}} = \delta \cdot L. \quad (1)$$

The angle Φ_{\max} is the greatest single-scattering angle which can contribute to the observed deflection. Physically, it is determined by the finite size of the nucleus. As a first approximation to Φ_{\max} , Williams takes the angle Φ_1 which is such that in traversing a thickness " t " of absorber, the particle will suffer on the average just one deflection greater than Φ_1 . It follows that $\Phi_1 = \delta \sqrt{\pi/2}$.

Φ_{\min} is an effective minimum angle. Its magnitude is determined by the "screening". In deriving the basic single-scattering formulæ, using the Fermi-Thomas statistical model of the atom to allow for the effect of screening, Williams considers separately the cases $\gamma = Zz/137\beta \ll 1$ (Born approximation valid), and $\gamma \gg 1$ (classical case). For $\gamma \ll 1$ this calculation yields

$$\Phi_{\min} = \frac{1.75mcZ^{1.3}}{137p}. \quad (2)$$

With these assumptions he finds a mean deviation

$$\bar{\alpha}_1 = \delta \sqrt{\ln \left(\frac{2\pi Z^{4/3} N t \hbar^2 z^2}{5.1 m^2 c^2 \beta^2} \right)} = \delta \cdot (\ln M)^{\frac{1}{2}}. \quad (3)$$

M is a measure of the average number of collisions suffered by the particle in traversing the foil.

Further calculations designed to take into account the contribution of deflections $> \Phi_1$, yield the following expression for the mean deviation due to all Φ

$$\bar{\alpha} = (1.45\delta + 0.80\bar{\alpha}_1). \quad (4)$$

(b) *Theory of Molière.*

To avoid the dichotomy $\gamma \gg 1$, $\gamma \ll 1$, Molière (1947, 1948) first solves the problem of obtaining an expression for Φ_{\min} by making an exact quantum-mechanical calculation of the cross-section for single scattering. Using the Fermi-Thomas model he obtains an expression (5) valid at both limits $\gamma \gg 1$ and $\gamma \ll 1$, and which also holds with sufficient approximation in the intermediate region.

$$\Phi_{\min} = \frac{Z^{1.3} \hbar}{0.4865 \times 10^{-8} p} [1.13 + 3.76\gamma^2]^{\frac{1}{2}}. \quad (5)$$

The problem of the composition of individual acts of scattering to yield the observed resultant deflection is solved by the method of Wentzel (1922). This leads to the definition of the parameter B which is the greater solution of the equation

$$B - \ln B = \ln \Omega_b - 0.115, \quad (6)$$

where $\Omega_b = \pi \delta^2 / \Phi_{\min}^2$.

Ω_b is a measure of the average number of collisions suffered by the particle in traversing a distance t in the scattering medium. For the approximations to be valid, $1/B^n$ must be negligible for $n > 2$. This will be the case for $B \gtrsim 4.5$, a condition satisfied by most materials for $t \gtrsim 10^{-3}$ cm. The *standardized* distribution of the projected angles of emergence will then be

$$P(\phi) d\phi = [(2/\pi^{\frac{1}{2}}) \epsilon^{-\phi^2} + f^{(1)}(\phi)/B + f^{(2)}(\phi)/B^2] d\phi, \quad . . . (7)$$

where $f^{(1)}(\phi)$, $f^{(2)}(\phi)$ are functions tabulated by Molière. The expression $P(\phi) d\phi = (2/\pi^{\frac{1}{2}}) \epsilon^{-\phi^2}$ is called by Molière the normal approximation to the scattering distribution, whence we may see that $\pi^{\frac{1}{2}} B^{\frac{1}{2}} \delta = \sigma_N \sqrt{2}$, where σ_N is the standard deviation of this approximation.

The mean deviation of Φ is

$$\langle \Phi \rangle = \delta \cdot B^{\frac{1}{2}} [1 + 0.982/B - 0.117/B^2] = \delta \cdot L_m \quad . . . (8)$$

and may thus be expressed in a form similar to that of Williams (1), but may be expected to hold for all γ . Its derivation, moreover, is less dependent on artificial assumptions. We may note that as the thickness t of the absorber increases, so also does " B ", and hence that the distribution of Φ will tend slowly towards the normal as t increases. Physically, this is easily understood in terms of a decreasing probability that the observed deflection is the result of single or plural scattering.

Goldschmidt-Clermont (1950) has published an instructive family of curves giving L_m (above) as a function of $\sigma = T/M_0 c^2$ for various cell-sizes in photographic emulsions. It will be seen that L_m increases slowly both with the thickness of the absorber traversed and with decreasing velocity of the scattered particle.

(c) *Theory of Snyder and Scott.*

The treatment given by these authors (1949) of the problem of the multiple scattering of charged particles is based on a solution of the fundamental diffusion equation due to Fermi (Rossi and Greisen 1941). The theory assumes the existence of conditions which justify the use of the Born approximation. Because of this, and the method of treatment of the screening, its validity is restricted to scattering of fast particles in thin foils.

The results are expressed in terms of two dimensionless parameters η/η_0 and t/λ . η/η_0 is the angle of deflection in terms of an angular unit η_0 determined by the screening radius and defined as follows:

$$\eta_0 = \frac{\hbar Z^{1/3}}{a_0 p}, \quad (9)$$

where a_0 is the radius of the first Bohr orbit of the hydrogen atom. This is analogous to the Φ_{\min} of Williams and Molière. λ is a unit path-length in the absorber. In terms of constants already defined, the expression becomes

$$1/\lambda = \pi \delta^2 / t \eta_0^2. \quad (10)$$

$1/\lambda$ is thus closely related to the Ω_b/t of Molière, and is a measure of the number of collisions which take place in unit path-length of the absorber.

Although tables of the distribution function are given, the values of mean deviation must be computed by quadrature methods. For this reason, and because the theory of Snyder and Scott is restricted to the region of validity of the Born approximation, the present experiments have been compared with Molière's theory only.

The work of the other authors (Goldschmidt-Clermont 1950, Groetinger *et al.* 1950, and Corson, private communication) indicates that the agreement between the theories of Snyder-Scott and Molière is satisfactory for fast particles ($\beta^2 \sim 1$).

§4. DEFINITION OF SCATTERING CONSTANT.

We have seen that the above theoretical investigations agree that the mean deviation of the distribution of the projection of Φ may be expressed in the form $\delta \cdot L$, but they differ slightly as to the calculated magnitude of L .

Since the principal use of the theory is the estimation of the momenta of particles by measurement of $\langle \Phi \rangle$, we may conveniently recast the formula as follows:

$$\langle \Phi \rangle = \frac{K_1 z t^{\frac{1}{2}}}{pv}, \quad (11)$$

where $K_1 = 2e^2(NZ^2)^{\frac{1}{2}}L$.

We call K_1 the scattering constant. Because of the nature of the factor L , it will be seen to depend chiefly on the properties of the scattering medium, and only slightly upon the values of t and velocity.

In a mixed medium such as the photographic emulsion, the appropriate value of $(NZ^2)^{\frac{1}{2}}$ is $[\sum_j N_j Z_j^2]^{\frac{1}{2}}$, where N_j is the number of atoms per unit volume, and Z_j the atomic number of the j th atomic species. Similar, but more complicated averaging is needed to compute the effective value of L (Molière 1948, equations (6.9') and (6.10')).

§5. EXPERIMENTAL METHODS.

There are two well-established techniques of measuring the multiple scattering of tracks in cloud chambers and in photographic emulsions. In both, the tracks are divided into equal cells of length $=s$, and changes in direction which take place from cell to cell are then measured.

(1) The angular method in which a direct measurement of the angles is made (Goldschmidt-Clermont *et al.* (1948), Davies, Lock and Muirhead (1949)). In principle their method determines the mean absolute value

of the angle between successive tangents. In practice, however, angles are measured between "best lines" fitted to the track. It has recently been much improved by the Brussels Group (Goldschmidt-Clermont (1950), Levi Setti (1950)).

Lattimore (1948), on the other hand, in his measurements on the mass of the σ -mesons, used the angular method to determine the angles between successive chords.

(2) The coordinate method of Fowler (1950).

In this very rapid and convenient method, the coordinates of the track at intervals of one cell-length are measured and are used to determine the mean absolute value of the angles between successive chords.

The values of $\langle\Phi\rangle$ as determined for the same track by the methods of tangents and chords are not equal. It may be shown, however, that in a sufficiently extended series of measurements, the value of the ratio $\langle\Phi\rangle_{\text{tan}}$ to $\langle\Phi\rangle_{\text{chord}}$ tends to $(3/2)^{\frac{1}{2}}$. Reducing the value of $\langle\Phi\rangle$ to degrees per cell-length of 100μ and using the results of Molière, we may express the scattering constant applicable to the coordinate method as

$$K_{\text{chord}} = 8.203B^{\frac{1}{2}}(1 + 0.982/B - 0.117/B^2) \frac{\text{degrees} \times \text{MeV.}}{(100\mu)^{\frac{1}{2}}} \quad (12)$$

For the limiting case $\beta^2 \rightarrow 1$ we have

$$K_{\text{chord}} = 24.45 \frac{\text{degrees} \times \text{MeV.}}{(100\mu)^{\frac{1}{2}}} \quad \text{for } s=1. \quad (13)$$

In general we have, for singly-charged particles,

$$\langle\Phi\rangle_{\text{chord}} = \frac{8.203L_{(s,\beta)}s^{\frac{1}{2}}}{T\left(\frac{2+\sigma}{1+\sigma}\right)} \quad (14)$$

As so defined, the scattering constant depends slightly on s and σ , but the value appropriate to the conditions may be found from the curves of Goldschmidt-Clermont (1950), already referred to.

We find that the variation of L with cell-size is very well represented by the formula for the case $\beta^2 = 1$

$$L_{(s)} = 1.45 + a(\log s)^{\frac{1}{2}}, \quad (15)$$

where the factor a has been determined empirically to be 1.19.

§ 6. EXPERIMENTAL RESULTS.

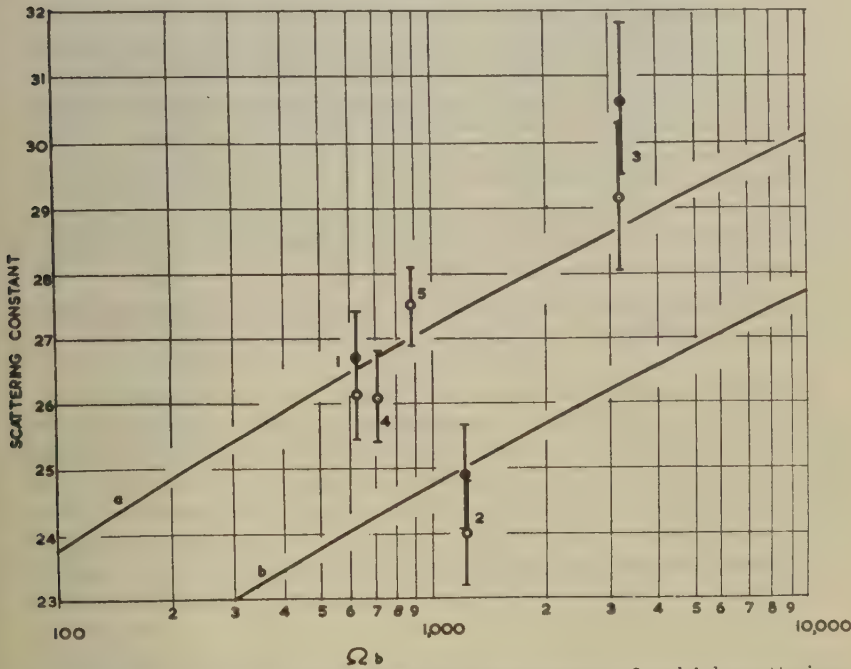
The results of the present series of determinations of the scattering constant are shown in fig. 1 and Table II. Experimental values obtained are plotted as a function of the parameter Ω_b of Molière's theory (6), which defines the number of collisions per cell. The numerals shown in fig. 1 are those identifying the experiments given in Table II. The number of collisions per 100μ , Ω_b/s , is a function of β only. It is given in the graph of fig. 2 for particles of charge $|e|$ in G.5 emulsion.

The upper curve in fig. 1 represents the theoretical variation of the scattering constant as a function of Ω_b , (12). The second line has been calculated for the cases where all angles larger than four times the mean

TABLE II.

Experiment	β^2	Cell-size	Ω_b/s	Ω_b	K without cut-off experimental	K with cut-off experimental
1. Positrons 105 MeV.	1	200 μ	310	620	26.7 \pm 0.6	26.2 \pm 0.6
2. Positrons 185 MeV.	1	400 μ	310	1240	24.9 \pm 0.8	24.0 \pm 0.8
3. Protons 336 MeV.	0.46	600 μ	515	3150	30.7 \pm 1.0	29.2 \pm 1.0
4. Protons and mesons 5-50 MeV.	0.07	80 μ	900	710	—	26.1 \pm 0.7
5. Protons 9-35 MeV.	0.02 $\langle \alpha v \rangle$	72 μ	1320	850	—	27.5 \pm 0.5

Fig. 1.

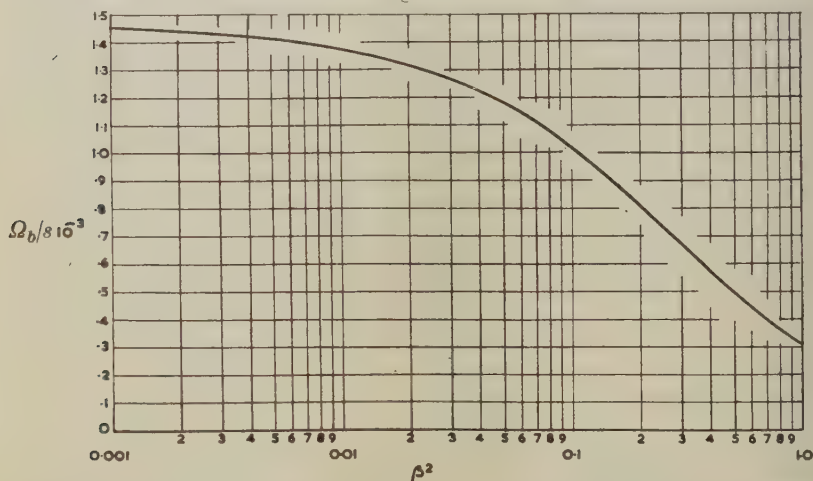


Comparison of experimental results with Molière's theory of multiple scattering. Curve (a) and points marked ●, without cut-off; curve (b) and points marked ○, with cut-off. The numbers refer to the experiments listed in Table I.

are eliminated from the statistics. It shows a scattering constant about 10 per cent smaller than the upper curve. (Numerical integration of $\int_0^{4\langle\sigma\rangle} \phi P(\phi) d\phi$ with $P(\phi)$ as given in (7)). We shall deal with this point in greater detail in Part II. of the present series.

The experimental values indicated by black dots have been obtained without elimination of large angles. They should be compared with the upper curve. Those shown by open circles correspond to results obtained after elimination of large angles, and are to be compared with the lower curve. The uncertainties indicated are standard deviations calculated from the number of angles observed. If the uncertainty in energy is taken into account the limits of error will be somewhat greater.

Fig. 2.



Calculated value of the parameter Ω_b/s for Ilford G.5 emulsion as a function of β^2 for particles of unit charge. s = cell-size in units of 100μ , $\beta = v/c$.

The experimental results show a satisfactory agreement with theory. As will be observed, however, the difference between the experimental results without and with "cut-off" appears to be less than that calculated from theory and shown by the difference between curves *a* and *b*. The statistical weight is such that the discrepancy in the individual cases cannot be regarded as significant. However, the fact that in all cases the difference observed is smaller than that calculated, seems to indicate the operation of some genuine effect. In Part II. of this series this discrepancy will be discussed at greater length. It is shown that because there we are dealing with an emulsion only 100μ thick, rejecting a large signal is likely to have less effect than that calculated by quadrature of Molière's expression (7). It is probable that the energy of the electrons is less accurately known than that of the 336 MeV. protons. In the

case of 196 MeV. electrons corrections amounting to 6 per cent must be applied to the nominal energy to correct for energy loss by Bremsstrahlung and by ionization. We must remark, however, that our statistics do not include the tracks of electrons which were suspected of having suffered large losses through Bremsstrahlung while passing through the emulsion. The scattering constant has been determined by using cell-sizes so chosen that the results are little affected by the presence of spurious scattering.

The results of experiments 4 and 5 (Table II.), using tracks ending in the emulsion, are in good agreement with each other. They correspond, however, more closely to the theoretical value without cut-off, even though angles $>4\langle\Phi\rangle$ had been eliminated.

Influence of Spurious Scattering.

The influence of spurious scattering on the results obtained for 336 MeV. protons, 105 and 185 MeV. electrons is illustrated by the graph of fig. 3, in which the mean angles of multiple scattering measured for these three groups of particles are plotted as a function of cell-size. In the case of electrons, two types of points are plotted. The points represented with black symbols (squares or circles) correspond to values obtained after cut-off. Those represented with open symbols correspond to values which include large angles. The full line (a) and dotted line (b) refer to the theoretical value of the mean angle calculated from Molière's theory. (a) shows the value without, and (b) with a cut-off at four times the mean.

Three different microscopes have been used for these determinations. To test the "noise" of these instruments, the same persons who measured the tracks of particles of lower energy have also measured the scattering of a fast primary. Using a cell-size of $4000\ \mu$ the mean angle of scattering per $100\ \mu$ of this track was found to be of the order of 0.0007 degrees corresponding to a mean sagitta of $0.046\ \mu$ in $1000\ \mu$. Evidently the results obtained with cells smaller than $1000\ \mu$ were entirely due to spurious scattering. Thus for each microscope we could determine the level of the noise for different cell-sizes and they are represented in fig. 3 by the points located on the lines marked noise.

For the pair of microscopes used for the electrons, the results of the measurements made on the fast primary were sufficiently close to each other for us to draw a single noise line valid for both. The noise line of the third microscope is significantly lower. It may be observed that none of these lines have been found to be inclined at 45° to the x -axis, as would be expected if the magnitude of the spurious second differences were independent of cell-size. Thus, the observations are consistent with the hypothesis of an increase of the spurious second difference with cell-size (Part II. to follow).

Taking the theoretical value of the angle of scattering of our mono-energetic particles and the observed value of the "noise" of the microscope used, we have calculated curves representing the apparent scattering as a function of cell-size. This calculation depends on the

§7. CONCLUSIONS.

Within the limits of the statistical errors, the results obtained are in agreement with theory. The trend of the variation of the scattering constant with cell-size and β follows that predicted. In principle, this variation should be taken into account when estimating energy from measurements of multiple scattering. In practice, however, its effect is lessened because of the experimental procedure generally adopted. For a particle of given momentum, the cell-size is chosen so that the ratio signal/noise has the minimum acceptable value (about 2). In this way a compromise is struck between the conflicting requirements:

- (1) small correction for noise,
- (2) a sufficient number of independent readings of angle of scattering, the track being of limited length.

Thus, fast tracks will be measured in large cell-sizes, but the value of constant appropriate to them will differ little from that for slower tracks which will be measured in smaller cells. This is because an increase with cell-size in the value of the constant will be offset by a decrease due to high velocity. This compensation will not hold in the extreme relativistic region where the value of $\beta^2 \rightarrow 1$.

Thus, in routine measurements on tracks of particles other than electrons, it is reasonable to use a constant independent of cell-size and β . The value of $26.0 \text{ MeV. degree}/(100 \mu)^{\frac{1}{2}}$ may be used for this purpose.

The use of this constant over the whole range of measurement of practical importance cannot introduce a systematic error greater than ± 8 per cent. In most cases, the estimate of the energy of a single track is subject to a much greater uncertainty due to the small number of angles available. The nomogram of fig. 4 has been calculated in order to give within 1 per cent accuracy the quantity $p\beta$ for protons as a function of the angle of scattering per 100μ . For particles of other masses the value $M\bar{\alpha}_{100\mu}$ (M =mass of the particle in protonic units) must be used; it corresponds to the quantity $p\beta/M$ in MeV.

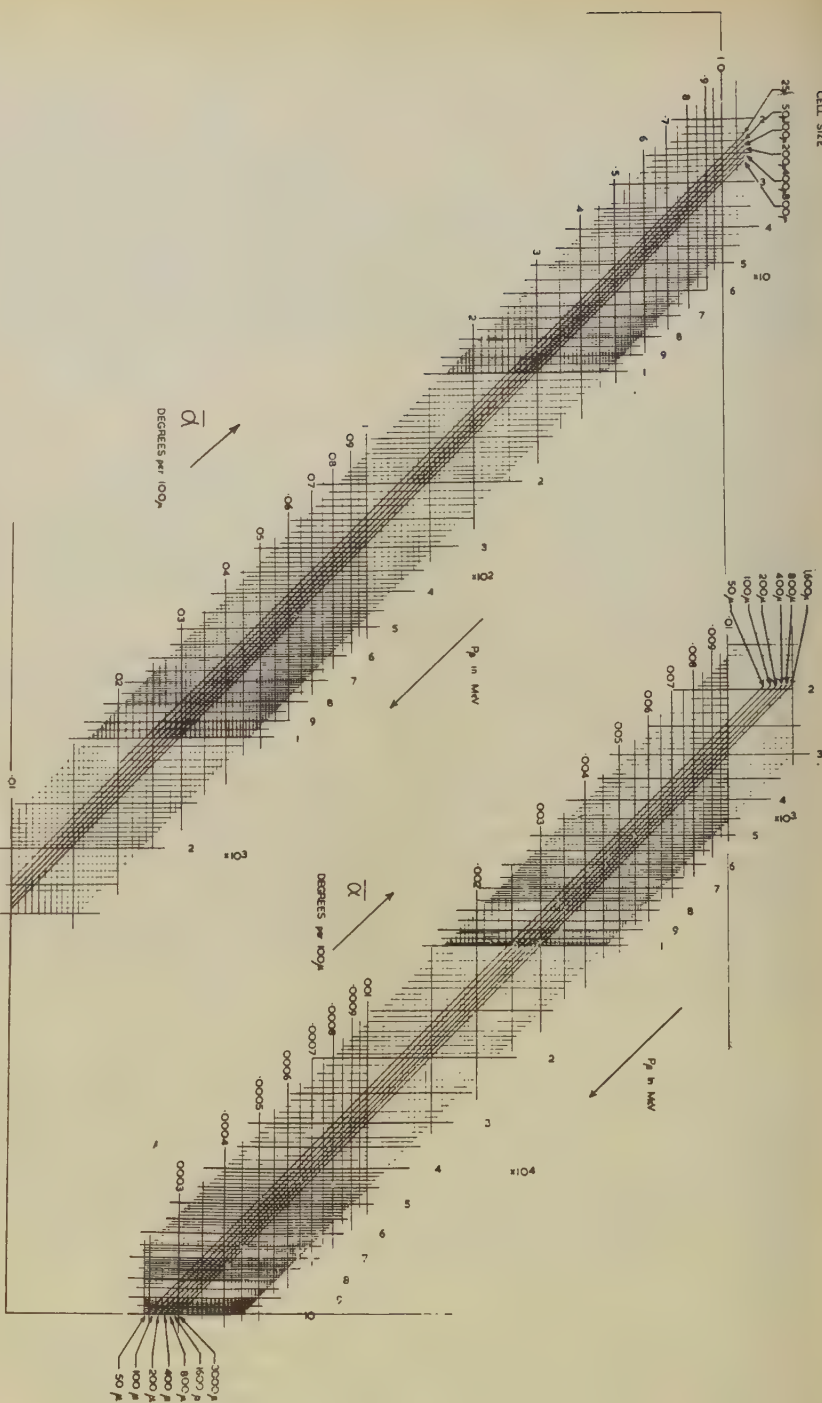
ACKNOWLEDGMENTS.

We wish to express our gratitude to Professor C. F. Powell, F.R.S., for extending to us the facilities of his laboratory, and for criticism and suggestions from which we have derived much benefit. Our best thanks are due to Professor Dale R. Corson who has very kindly put at our disposal plates exposed to a beam of electrons selected from the Cornell synchrotron, and to Dr. W. H. Barkas for his kind cooperation in arranging the exposure of plates to 336 MeV. protons in the Berkeley cyclotron.

It is a pleasure to thank Dr. H. Heitler and Miss J. Burnell for drawing the diagrams and Mr. A. R. Gattiker for the photographic reproduction.

We are much indebted to Dr. G. Molière of the Max Planck Gesellschaft, Hechingen, for communicating to us in manuscript form the results of

Fig. 4.



Nomogram giving the relationship between $M_p c^2 \beta^2 \sqrt{1-\beta^2}$ expressed in MeV, $\bar{\alpha}_{100\mu}$ expressed in degrees and cell-size in microns, for protons, calculated using Molière's theory without cut-off. For singly charged particles of mass " M_0 ", the values of $\bar{\alpha}_{100\mu}$ must be multiplied by M_0/M_p and the values obtained for $\gamma\beta$ multiplied by the same ratio. M_p is the mass of the proton.

work not yet published. Certain of us wish to render thanks to the following bodies for maintenance grants : D.S.I.R. (J. H. M.), University College, Cork (C. O'C.), British Council (O.R.). Two of us have been granted leave of absence. One of us (K. G.) wishes to thank Professor W. Heisenberg, and the other (C. O'C.), the Governing Body of University College, Cork.

REFERENCES.

- BOSE and CHOUDHURI, 1941, *Nature, Lond.*, **147**, 240.
 CAMERINI, FOWLER, LOCK and MUIRHEAD, 1950, *Phil. Mag.*, **41**, 413.
 CARLSON, HOOPER and KING, 1950, *Phil. Mag.*, **41**, 701.
 DAVIES, LOCK and MUIRHEAD, 1949, *Phil. Mag.*, **40**, 1250.
 FOWLER, 1950, *Phil. Mag.*, **41**, 169.
 GOLDSCHMIDT-CLERMONT, KING, MUIRHEAD and RITSON, 1948, *Proc. Phys. Soc.*, **61**, 183.
 GOLDSCHMIDT-CLERMONT, 1950, *Nuovo. Cimento*, **7**, 331.
 GROETZINGER, BERGER and RIBE, 1950, *Phys. Rev.*, **77**, 584.
 HOOPER and KING, 1950, *Phil. Mag.*, **41**, 1194.
 HOOPER, KING and MORRISH, 1951, *Phil. Mag.*, **42**, 304.
 LATTIMORE, 1948, *Nature, Lond.*, **161**, 518.
 LEVI SETTI, 1950, Note No. 22, *Bull du Cen. de Phys. Nuc de l'Univ. Libre de Bruxelles*.
 MOLIÈRE. 1947, *Z. fur Naturforschung*, **2a**, 133 ; 1948, *Ibid.*, **3a**, 78 ; 1951, private communication.
 ROSSI and GREISEN, 1941, *Rev. Mod. Phys.*, **13**, 240.
 SNYDER and SCOTT, 1949, *Phys. Rev.*, **76**, 220.
 WENTZEL, 1922, *Ann. Physik.*, **69**, 335.
 WILLIAMS, 1935, *Phys. Rev.*, **47**, 568 ; 1939, *Proc. Roy. Soc. A*, **169**, 531 ; 1940, *Phys. Rev.*, **58**, 292.

LXXIII. *On Combined Bending and Twisting of Thin Tubes in the Plastic Range.*

By R. HILL * and M. P. L. SIEBEL †,
University of Bristol ‡.

[Received March 7, 1951.]

SUMMARY.

Equations for the determination of the stresses and warping in a partly plastic thin tube of arbitrary section are obtained for any monotonic loading by bending and twisting couples. The analysis is based on the von Mises yield criterion and the Reuss stress-strain relations. The equations are solved numerically for a circular tube for various loading programmes.

§1. FORMULATION OF THE PROBLEM.

THERE appears to be no published calculation of the stresses and distortion in a tube which is partly overstrained by the simultaneous action of bending and twisting couples §. This problem is relevant to the design of tubular structures where permanent deformation might be advantageously permitted in some members. Its solution would be a matter of some difficulty when the tube is thick-walled, but is straightforward in principle when the variations of stresses through the thickness can be disregarded. This is assumed here; the error should be insignificant when the thickness-diameter ratio is less than one tenth. Buckling appears improbable when this ratio is greater than one fiftieth, so long as a substantial fraction of the tube is not overstrained (Donnell 1934). A further simplification in treating a thin-walled tube with this approximation is that we avoid, without inconsistency, the need to take account of a triaxial state of stress such as that in a bent beam when Poisson's ratio differs from one half (Hill 1950, p. 82).

We shall consider a monotonic process of distortion defined by an otherwise arbitrary loading programme. The aim of the analysis is to calculate the angles of bend and twist, the warping of the cross-section, and the distribution of stress at any moment.

* Wills Physical Laboratory, Royal Fort.

† Mechanical Engineering Laboratory.

‡ Communicated by the Author.

§ In unpublished work (1950) R. M. Haythornthwaite (Department of Civil Engineering, Sheffield University) has examined the problem by an approximate method which differs in principle from the analysis of the present paper (private communication).

and vanishes identically only if $A_s \propto s$, i. e. if the section is such that the perpendicular from the centre to any tangent is of constant length. This is true, in particular, when the section is circular or rhombic. The bending and twisting couples are

$$B = EI\psi, \quad T = 2At\tau, \quad \dots \dots \dots (5)$$

where $I = \oint y^2 ds$ is the second moment of the contour about the axis of bending. The relation between the ratio of the angles of bend and twist to the ratio of the couples is therefore

$$r = \frac{\psi}{\theta} = \frac{2A^2}{pI} \cdot \frac{B}{(1+\nu)T}, \quad \dots \dots \dots (6)$$

where ν is Poisson's ratio.

We shall suppose that work-hardening is negligible and take the yield criterion to be that of von Mises:

$$\frac{1}{3}\sigma^2 + \tau^2 = k^2, \quad \dots \dots \dots (7)$$

where k is the shear yield stress. It is evident from (5) that plastic yielding first occurs where y is greatest: that is, at the extremities of the y axis (supposing the section to be convex outwards at all points). Let the y diameter of the tube be $2a$. Then, if a suffix zero denotes the value of any quantity when yielding first occurs,

$$\frac{Ga\psi_0}{k} = r \left(\frac{4A^2}{a^2p^2} + \mu r^2 \right)^{-\frac{1}{2}}, \quad \frac{\tau_0}{k} = \left(\frac{4A^2}{a^2p^2} + \mu r^2 \right)^{-\frac{1}{2}}, \quad \dots \dots (8)$$

where

$$\mu = \frac{4}{3}(1+\nu)^2.$$

If the ratio of the couples is given, their separate values at the yield-point are found from

$$\frac{1}{3} \left(\frac{B_0 a}{tI} \right)^2 + \left(\frac{T_0}{2tA} \right)^2 = k^2. \quad \dots \dots \dots (9)$$

In terms of the strain-ratio r the yield-point couples are

$$\frac{B_0}{2ktA} = (1+\nu) \frac{Ir}{Aa} \left(\frac{4A^2}{a^2p^2} + \mu r^2 \right)^{-\frac{1}{2}}, \quad \frac{T_0}{2ktA} = \frac{2A}{ap} \left(\frac{4A^2}{a^2p^2} + \mu r^2 \right)^{-\frac{1}{2}}. \quad \dots \dots (10)$$

§ 3. PARTLY PLASTIC TUBE.

During continued deformation two plastic zones spread towards the axis of bending. Since the section has two axes of symmetry, and since from (7) σ has equal and opposite values in the two plastic zones, the latter must cover a region $|y| \geq c$, say, at any moment. The plastic boundaries $|y| = c$ are such that elements just on the elastic side are on the point of yielding; σ must therefore be continuous across the boundary. In the elastic zone σ is still equal to $Ey\psi$ and hence, by (7),

$$\mu \left(\frac{Gc\psi}{k} \right)^2 = 1 - \frac{\tau^2}{k^2}. \quad \dots \dots \dots (11)$$

In the plastic zones σ has the uniform values

$$\sigma = \pm \sqrt{\{3(k^2 - \tau^2)\}} = \pm 2(1 + \nu)Gc\psi. \quad (12)$$

The couples are now given by

$$\frac{B}{2kAt} = (1 + \nu) \frac{G\psi}{kA} \left(\int_E y^2 ds + c \int_P |y| ds \right), \quad \frac{T}{2kAt} = \frac{\tau}{k}, \quad (13)$$

where the suffixes P and E denote integration over the plastic and elastic zones respectively.

If B and T are given, the equations (11), (12) and (13) suffice to determine τ , σ , c and ψ uniquely (the loading having been monotonic). The problem is thus statically determined. The angle of twist and the warping, however, can only be found by following the entire loading history, the relations between stress and plastic strain being incremental. When, on the other hand, the strain-path is prescribed (and not the loads) the problem is not statically determined and the stresses themselves can only be found by following the strain-history.

The Reuss stress-strain relations (see, for instance, Hill 1950, p. 39) imply that the shear stress does not affect the through-thickness and peripheral strains, which are therefore equal. Denoting them by ϵ' , we have

$$\epsilon + 2\epsilon' = (1 - 2\nu) \frac{\sigma}{E},$$

since the volume change is entirely elastic. Hence, from (1), (3) and (12),

$$\epsilon' = \begin{cases} (\frac{1}{2} - \nu)c\psi - \frac{1}{2}y\psi, & c \leq y \leq a; \\ -\nu y\psi, & -c \leq y \leq c; \\ -(\frac{1}{2} - \nu)c\psi - \frac{1}{2}y\psi, & -a \leq y \leq -c. \end{cases} \quad (14)$$

When $\nu \neq \frac{1}{2}$, the rate of variation in thickness as we travel round the tube changes discontinuously at the plastic boundaries. We observe also that ϵ' has equal and opposite values at the ends of a diameter.

The Reuss equations give, further, a relation between the incremental changes of stress and strain in each element:

$$\frac{d\gamma - d\tau/G}{d\epsilon - d\sigma/E} = \frac{3\tau}{\sigma}, \quad |y| \geq c. \quad (15)$$

With the help of (1), (2), (11) and (12), this may be reduced to

$$\frac{\partial}{\partial s} \left(\frac{\partial w}{\partial \psi} \right) + 2 \frac{dA_s}{ds} \cdot \frac{d\theta}{d\psi} = \left[1 + \frac{3\tau^2}{2(1 + \nu)(k^2 - \tau^2)} \right] \frac{1}{G} \frac{d\tau}{d\psi} + \frac{3}{2(1 + \nu)} \cdot \frac{\tau |y|}{Gc\psi};$$

$|y| \geq c.$

In the elastic zone, $d\tau = Gd\gamma$ or

$$\frac{\partial}{\partial s} \left(\frac{\partial w}{\partial \psi} \right) + 2 \frac{dA_s}{ds} \cdot \frac{d\theta}{d\psi} = \frac{1}{G} \frac{d\tau}{d\psi}; \quad |y| \leq c.$$

The condition that $\partial w/\partial \psi$ should be a continuous function of position round the periphery is

$$\oint \frac{\partial}{\partial s} \left(\frac{\partial w}{\partial \psi} \right) ds = 0.$$

Since this holds at each moment, w itself is then automatically continuous (being continuous when the tube was completely elastic). The last three equations lead to

$$\begin{aligned} & \left[1 - \left\{ 1 - \frac{3}{2(1+\nu)p} \int_p ds \right\} \frac{\tau^2}{k^2} \right] \frac{1}{G} \frac{d\tau}{d\psi} \\ &= \left(1 - \frac{\tau^2}{k^2} \right) \left[\frac{2A}{p} \frac{d\theta}{d\psi} - \frac{3}{2(1+\nu)} \frac{\tau}{Gpc\psi} \int_p |y| ds \right]. \quad \dots \quad (16) \end{aligned}$$

If the loading path is given, τ , c , and the integrals can be calculated as functions of ψ as already explained. (16) then gives the quantity $d\theta/d\psi$ explicitly as a function of ψ , and hence θ after integration, using the yield-point values from (6) and (8). In particular, if the tube is rendered partly plastic by bending alone and then twisted as well, the initial torsional rigidity is equal to its value in a purely elastic tube; for, when $\tau=0$ in (16), $d\tau/d\theta=2GA/p$ as in (3). If, on the other hand, the strain-path is given, θ is a prescribed function of ψ . (16) is then a differential equation which, with (11), must be integrated numerically to obtain the unknowns τ and c . The corresponding values of the couples are finally found from (13).

It is essential to find the limitation on the loading-path such that no plastic element ceases to deform plastically. The previous analysis is valid so long as the rate of performance of plastic work is not negative in any element. In view of (15) the condition for this is

$$\sigma(d\epsilon - d\sigma/E) \geq 0,$$

or, from (1) and (12),

$$(|y|-c)d\psi - \psi dc \geq 0 \quad \text{when } |y| \geq c.$$

This is certainly satisfied when the bending is monotonic ($d\psi \geq 0$) and the plastic zone increases steadily ($dc < 0$); the numerical solutions presented later fulfil these conditions.

§ 4. LIMITING VALUES OF THE COUPLES.

If either B/T or ψ/θ is held constant, calculations show that B and T approach certain limiting values (work-hardening being neglected). The approach is very close even after a deformation which is only a few times that at the yield point and so still small enough for the tube to be treated as approximately cylindrical. These limiting values of the couples have, therefore, a practical significance (especially in regard to buckling and collapse), even though they are deduced on the assumption that the tube can be treated as cylindrical after unlimited strain.

Since the stresses approach constant values the limiting conditions are to be found by setting $d\tau/d\psi=0$ in (16). This gives

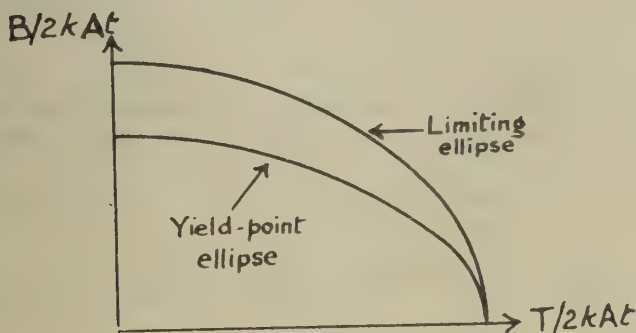
$$\frac{|\sigma|}{\tau} = - \frac{3 \oint |y| ds}{2A} \cdot \frac{d\psi}{d\theta}, \quad \dots \quad (17)$$

after using (12) to eliminate $c\psi$ (which remains finite). When B/T is held constant, ψ/θ varies and $d\psi/d\theta$ in (17) is the limiting value of the derivative. From (6), (11) and (13) the limiting value of the couples satisfy

$$\frac{B_{\infty}}{T_{\infty}} = 3 \left[\frac{\oint |y| ds}{2A} \right]^2 \frac{d\psi}{d\theta}, \quad \frac{1}{3} \left[\frac{B_{\infty}}{t \oint |y| ds} \right]^2 + \left(\frac{T_{\infty}}{2tA} \right)^2 = k^2. \quad (18)$$

B_{∞} and T_{∞} may be regarded as the couples that would be needed to initiate deformation in a tube of plastic-rigid material (in which the rigidity modulus has an infinitely great value). They may thus be alternatively obtained by an application of the maximum work principle for a plastic-rigid material (Hill 1948). The work done per unit length of tube in the

Fig. 2.



first increment of strain is $B_{\infty} d\psi + T_{\infty} d\theta$ (the work done in the warping having equal and opposite amounts at the ends of the tube). For given $d\psi$ and $d\theta$, the work is a maximum for couples satisfying the second of (18): that is, when

$$\Delta B_{\infty} d\psi + \Delta T_{\infty} d\theta = 0,$$

where

$$\frac{B_{\infty} \Delta B_{\infty}}{3 \left(\oint |y| ds \right)^2} + \frac{T_{\infty} \Delta T_{\infty}}{(2tA)^2} = 0.$$

On combining these we regain the first of (18).

It is instructive to compare the yield point couples with their limiting values. Equations (9) and the second of (18) define two ellipses if $B/2kAt$ and $T/2kAt$ are taken as rectangular coordinates (fig. 2). When a pure torque is applied, its value remains constant after the yield-point. When a pure bending moment is applied, its limiting value exceeds the yield-point value by the factor

$$a \oint |y| ds / \oint y^2 ds.$$

This is greater than unity since $|y| \leq a$. The yield-point ellipse therefore lies within the limiting ellipse, but their distance apart is comparatively small for normal sections. When the section is circular, for instance, the above factor is $4/\pi \sim 1.28$.

On comparing (6) and (18) we see that if ψ/θ is held constant the limiting value of B/T is less than the yield-point value when

$$\frac{2}{3}(1+\nu)p_1 > \left(\oint |y| ds \right)^2$$

For a circular section this is true when $1+\nu > 12/\pi^2$ or $\nu > 0.216$. From (10) and (18) it may be shown that $T_\infty \geq T_0$ if

$$\frac{2}{3}(1+\nu)pa \geq \oint |y| ds \quad (B \neq 0).$$

This is certainly so for $\nu = \frac{1}{2}$, whatever the section, and it is true for a circular section for normal values of ν . On the other hand, we shall see later that, when the deformation is predominantly twisting, $B_\infty < B_0$.

§ 5. WARPING.

On integrating the previous equations for the warping round the tube at a given moment, and choosing $\partial w/\partial \psi = 0$ on the axis of bending, we find that

$$\left. \begin{aligned} \frac{\partial w}{\partial \psi} &= \frac{s}{G} \frac{d\tau}{d\psi} - 2A_s \frac{d\theta}{d\psi}, & 0 \leq y \leq c; \\ \frac{\partial w}{\partial \psi} &= \frac{s}{G} \frac{d\tau}{d\psi} - 2A_s \frac{d\theta}{d\psi} + (s-s_c) \frac{3\tau^2}{2(1+\nu)(k^2-\tau^2)} \cdot \frac{1}{G} \frac{d\tau}{d\psi} \\ &\quad + \frac{3\tau}{2(1+\nu)Gc\psi} \int_{s_c}^s |y| ds; & c \leq y \leq a; \end{aligned} \right\} \dots (19)$$

where s_c is the value of s when $y=c$. The tube being symmetrical about the (x, y) axes, $\partial w/\partial \psi$ vanishes also on the y axis, in view of (16). It is found, further, that $\partial w/\partial \psi$ is antisymmetric with respect to the (x, y) axes; that is, it takes the same value at opposite ends of a diameter while the values on a pair of symmetrically disposed diameters are equal and opposite.

The warping in any element is obtained by integrating the above equations with respect to ψ , using the first while the element is elastic and the second while it is plastic.

§ 6. NUMERICAL RESULTS.

When the section is circular the bending moment is given by

$$\frac{B}{ka^2t} = 2(1+\nu)(\pi + \sin 2\alpha - 2\alpha) \frac{Ga\psi}{k}, \quad \dots (20)$$

where $c = a \cos \alpha$. The calculated variation of the bending moment with the angle of bend is shown in fig. 3 for loading under the constant ratios $B/T = \frac{1}{2}, 1, 2$, and ∞ ($\nu = 0.3$). The variation of both T and τ with the

angle of bend is, of course, exactly similar. The yield-point and limiting ellipses are

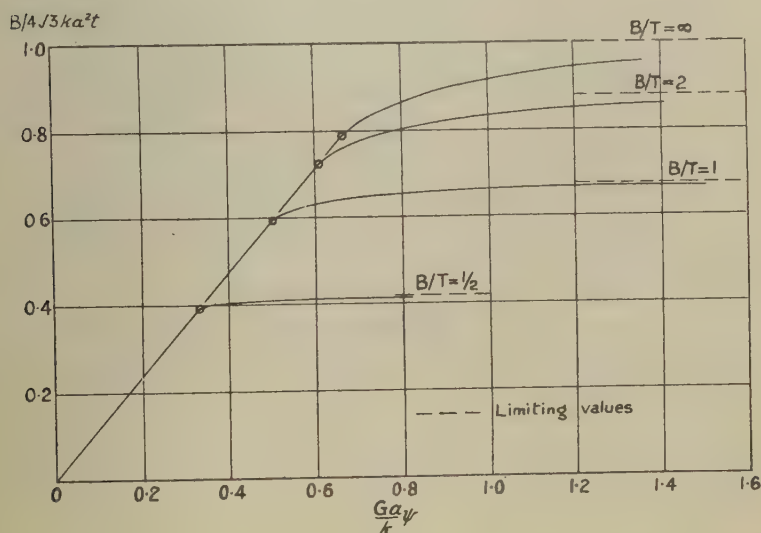
$$\frac{4}{3}B_0^2 + T_0^2 = (2\pi ka^2t)^2 = \frac{\pi^2}{12}B_\infty^2 + T_\infty^2,$$

since $I = \pi a^3$, $\oint |y| ds = 4a^2$, for a circular section. Hence, when B/T is constant,

$$\frac{B_\infty}{B_0} = \left(\frac{4B^2/3T^2 + 1}{\pi^2 B^2/12T^2 + 1} \right)^{1/2}.$$

These limiting values are indicated by broken lines in fig. 3. It will be observed that when $B/T = \frac{1}{2}$, or 1, B is within 2 per cent of the limiting value when the angle of bend is only twice its yield-point value; when no torque is applied, B is within 5 per cent of its limiting value at this

Fig. 3.



stage. The extent of the plastic zone can be judged from fig. 4, which shows the relation between the angle of bend and the fraction of the tube which is plastic.

The relative rate $d\theta/d\psi$ of twisting to bending, calculated from (16), is given in fig. 5, and the relation between the angles of bend and twist in fig. 6. From (18) the limiting value of $d\theta/d\psi$ is equal to $12T/\pi^2B$, and this is indicated by the broken lines in fig. 5. The relation between torque and twist is shown in fig. 7.

The warping, calculated by integrating (19), is shown in fig. 8 for $B/T = 1$ at an angle of bend such that $G\alpha\psi/k = 1.077$; α is then equal to 65° , so that just over two-thirds of the tube is plastic.

The solution for deformation under constant strain-ratios $\theta/\psi = 1$ and 2 has also been computed for Poisson's ratio $\frac{1}{2}$. The variation of the couples

Fig. 4.

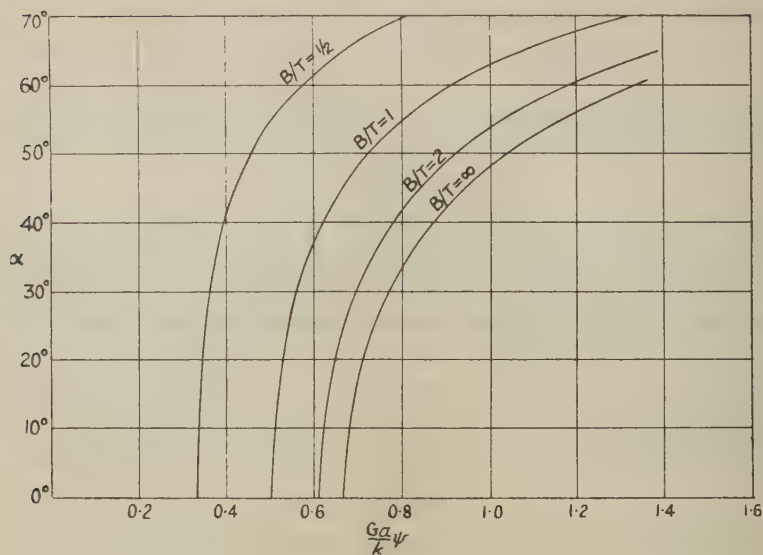
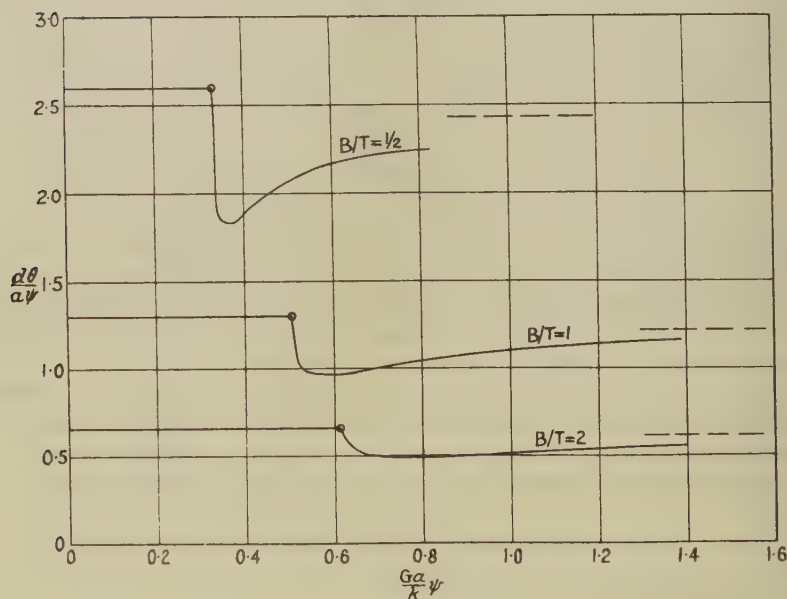


Fig. 5.



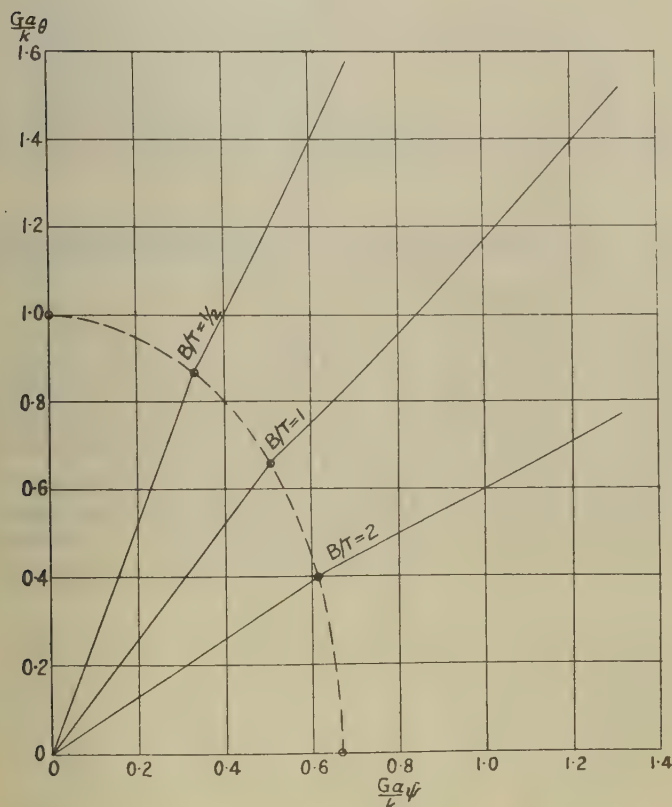
with the angle of bend is shown in fig. 9. It will be noticed that the approach to the limiting value is oscillatory. Despite the fact that one or other of the couples (but not both together) temporarily decreases, the plastic zone continues to expand steadily (fig. 10) and no plastic element of the tube unloads.

§ 7. SOLUTION BASED ON HENCKY RELATIONS.

In view of the labour involved in solving the equations based on the Reuss incremental-strain relations, it is worth examining whether the simpler solution based on the Hencky total-strain relation is in this problem sufficiently accurate (though admittedly not acceptable physically; see Hill 1950, pp. 45-8). When Poisson's ratio is $\frac{1}{2}$, the Hencky relations lead to

$$\tau = \frac{2GA\theta}{p + \int_P \left(\frac{|y|}{c} - 1 \right) ds}$$

Fig. 6.

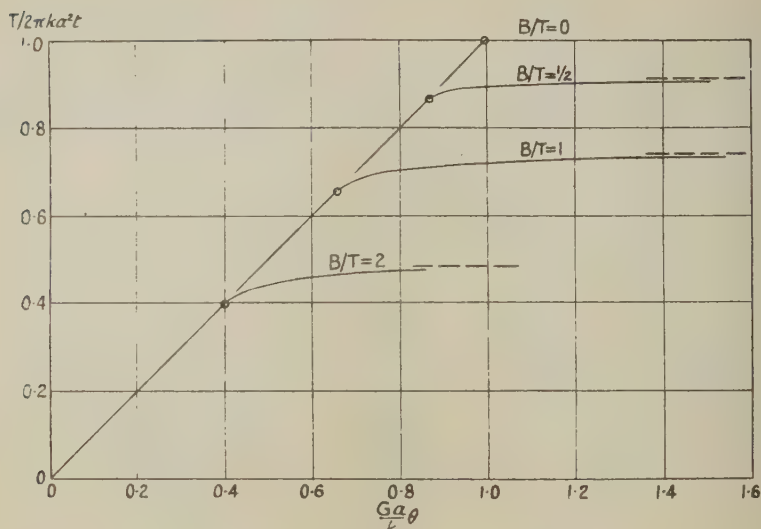


in place of (16), and

$$w = s \cdot \frac{\tau}{G} - 2\theta A_s, \quad 0 \leq y \leq c;$$

$$w = s_c \cdot \frac{\tau}{G} - 2\theta A_s + \frac{\tau}{Gc} \cdot \int_{s_c}^s |y| ds, \quad c \leq y \leq a;$$

Fig. 7.



in place of (19). The equations (17) and (18) retain the same form, but ψ/θ replaces $d\psi/d\theta$.

For a circular section,

$$\frac{T}{2\pi a^2 t} = \tau = \frac{\pi G a \theta}{\pi + 2 \tan \alpha - 2\alpha}, \quad \sqrt{3} \left(\frac{G a \psi}{k} \right) \cos \alpha = \sqrt{\left(1 - \frac{\tau^2}{k^2} \right)}, \quad (21)$$

where $c = a \cos \alpha$. The solution of (20) and (21) when $\theta/\psi = 1$ and 2 is shown in fig. 9 for comparison with the solution for the Reuss theory. The limiting values of the couples are the same and the approach is again oscillatory. As was to be expected, the difference between the values of the couples predicted by the two theories is comparatively small when the ratio of the angles of bend and twist is held constant.

Fig. 8.

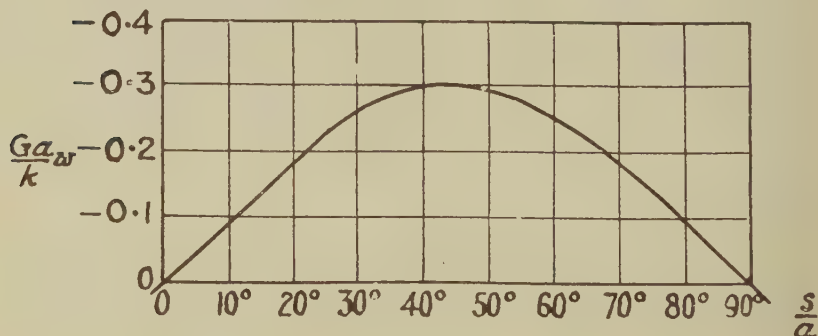


Fig. 9.

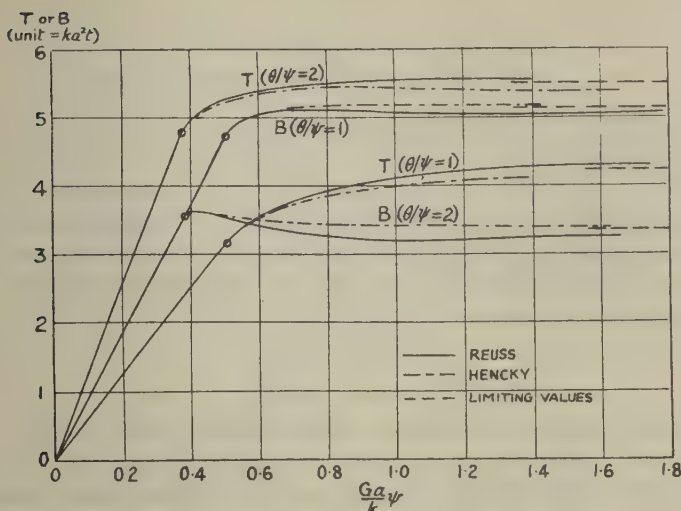
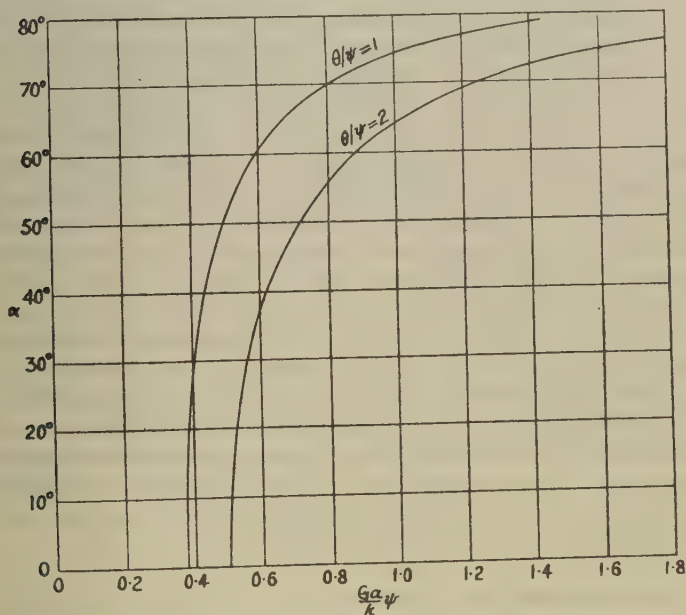


Fig. 10.



REFERENCES.

- DONNELL, L. H., 1934, *Trans. Amer. Soc. Mech. Eng.*, **56**.
 HILL, R., 1948, *Quart. Journ. Mech. Appl. Math.*, **1**, (18); 1950, *The Mathematical Theory of Plasticity* (Oxford: Clarendon Press).

LXXIV. *Internal Barriers in Semi-Conductors.*

By H. K. HENISCH, Ph.D., A.Inst.P.
Department of Physics, The University, Reading*.

[Received March 14, 1951.]

ABSTRACT.

The temperature dependence of conductivity is calculated for a semi-conducting specimen containing internal barriers of various heights. This leads to a new interpretation of activation energies as deduced from conduction measurements.

§ 1. INTRODUCTION.

THE results obtained by various workers (Verwey 1950) (Volger 1950) (Miller 1950) (Chasmar 1948) (Henisch 1950) during recent years show that a good deal of importance must be attached to the presence of inter-granular barriers in many types of semi conducting materials. Such barriers are expected to constitute a source of high resistance, and the *effective* constants of a bulk specimen may be controlled by them. In particular, the frequency dependence of the effective resistivity is usually ascribed to capacitive short-circuiting of inter-granular barriers. The unexpectedly large dielectric constants observed on some materials can also be interpreted on the basis of this model. The barriers in question may arise from the discontinuity of the lattice itself or, more probably, from adsorbed impurities. (Mott 1950.)

The temperature dependence of conductivity in micro-crystalline specimens containing inter-granular barriers would be controlled by the barrier height. If all barriers are of equal height ϕ , the conductivity would be approximately proportional to $\exp(-\phi/kT)$. In general, however, it is more probable that barriers of different height are represented, *e. g.* due to a varying density of surface states at grain boundaries. It is shown in this paper how the temperature dependence of conductivity can be calculated for this more complicated system. The present treatment can also be generalized to apply to internal barriers which may arise in single crystals. The conclusions are of general importance in connection with the interpretation of activation energies derived from conductivity measurements over a range of temperatures.

§ 2. TEMPERATURE DEPENDENCE OF EFFECTIVE BULK CONDUCTIVITY.

The calculations in this section are restricted to direct or low frequency currents, and it is assumed that the various barrier heights are *normally* distributed about some mean value with a certain standard deviation.

* Communicated by the Author.

The voltage across any particular barrier is taken to be small compared with kT/e , so that the barrier resistance can be treated as independent of voltage. Deviations from Ohm's law would normally be expected only if measurements are carried out with high-voltage pulses.

Given a cross-section through the material perpendicular to the direction of current flow, it will be clear that most of the current will cross this section in places where the barrier height ϕ is small, since the current is very sensitive to changes of ϕ . This applies to *any* section. The current will thus flow along filaments of low ϕ value, and the experimental observations will therefore relate mainly to the properties of these filaments. Let the number of barriers per filament be \mathcal{N} . Among these barriers, various values of ϕ will be represented, and the number of barriers $d\mathcal{N}_\phi$ whose height is between ϕ and $\phi+d\phi$ will be given by

$$d\mathcal{N}_\phi = \frac{\mathcal{N}}{s\sqrt{(2\pi)}} \exp\left[-\frac{1}{2}\left(\frac{\phi-\bar{\phi}}{s}\right)^2\right] d\phi, \quad \dots \quad (1)$$

if $\bar{\phi} \gg s$, where $\bar{\phi}$ and s are the mean ϕ and its standard deviation for the particular filament. We shall assume, for the sake of simplicity, that all the filaments are of equal cross-section and that they contain equal numbers of barriers. The barriers connected in series in this way will carry a common current Δj , so that

$$\alpha \Delta j = U_{\phi_1} \exp(-\phi_1/kT) = U_{\phi_2} \exp(-\phi_2/kT) = \dots U_\phi \exp(-\phi/kT), \quad \dots \quad (2)$$

where α is some constant and U_ϕ is the barrier voltage. The voltage across the $d\mathcal{N}_\phi$ barriers of height ϕ will be $U_\phi d\mathcal{N}_\phi$. Using the continuous frequency distribution, the total voltage applied to the ends of the filament becomes

$$U = \frac{\mathcal{N}}{s\sqrt{(2\pi)}} \int_0^\infty U_\phi \exp\left[-\frac{1}{2}\left(\frac{\phi-\bar{\phi}}{s}\right)^2\right] d\phi. \quad \dots \quad (3)$$

Substituting from (2) this gives

$$U = \Delta j \frac{\alpha \mathcal{N}}{s\sqrt{(2\pi)}} \int_{-\infty}^\infty \exp\left[-\frac{1}{2s^2}\left(\phi^2 - 2\phi\bar{\phi} + \bar{\phi}^2 - \frac{2\phi s^2}{kT}\right)\right] d\phi. \quad \dots \quad (4)$$

It is now convenient to put $\chi = \phi - (\bar{\phi} + s^2/kT)$. Substitution and rearrangement then leads to

$$U = \Delta j \frac{2\alpha \mathcal{N}}{s\sqrt{(2\pi)}} \exp\left[\frac{-\bar{\phi}^2 + (\bar{\phi} + s^2/kT)^2}{2s^2}\right] \int_0^\infty \exp(-\chi^2/2s^2) d\chi, \quad \dots \quad (5)$$

and hence

$$U = \Delta j \alpha \mathcal{N} \exp[(\bar{\phi} + s^2/2kT)/kT]. \quad \dots \quad (6)$$

This shows that the principal term which controls the temperature dependence of the filamentary current is still approximately exponential,

provided s is not too large and the considerations are applied to a restricted temperature range. The *effective* barrier height is then given by

$$\phi_{\text{eff}} = \bar{\phi} + s^2/2kT. \quad (7)$$

The above considerations apply to a single filament. It is then necessary to sum the contributions Δj towards the total current over all the filaments which are now connected to parallel and which are characterized by somewhat different values of $\bar{\phi}$ and s . If it is assumed that the various values of $\bar{\phi}$ are themselves normally distributed, this second summation leads to a new effective barrier height, characteristic for the parallel assembly all the filaments. Thus, the resistivity would still be an approximately exponential function of temperature. It can be shown that this new effective barrier height will be given by an expression of the same form as (7), though the terms involved will have somewhat more complicated definitions.

Consider now a practical example in which a quantity ϵ_{obs} is deduced from conductive measurements within the temperature range 200° K. to 500° K. using the expression

$$\sigma = \sigma_0 \exp(-\epsilon_{\text{obs}}/2kT). \quad (8)$$

We shall take $\bar{\phi}$ as 0.1 eV and s as 0.01 eV. For an impurity content of 10^{17} centres/cm.³ and a dielectric constant equal to 10, the establishment of a barrier of this height would require less than 10^{12} trapped electrons per unit area. Taking into account the temperature dependence of α which would be controlled by the activation energy ϵ in the interior of the semiconductor, we obtain for the average value of the exponent

$$\epsilon_{\text{obs}} = \epsilon + [(\phi_{\text{eff}})_1 + (\phi_{\text{eff}})_2], \quad (9)$$

where the suffixes refer to the two temperatures. Substitution into (7) shows that

$$(\phi_{\text{eff}})_1 = 0.103 \text{ eV.} \quad (200^\circ \text{ K}) \quad \text{and}$$

$$(\phi_{\text{eff}})_2 = 0.101 \text{ eV.} \quad (500^\circ \text{ K})$$

$$\text{Hence} \quad \epsilon_{\text{obs}} = 0.204 + \epsilon \text{ eV.} \quad (200^\circ \text{ K to } 500^\circ \text{ K}).$$

The evaluation of ϵ_{obs} thus involves an uncertainty of

$$2[(\phi_{\text{eff}})_1 - (\phi_{\text{eff}})_2]/\epsilon_{\text{obs}},$$

which is less than 2 per cent, the exact value depending on ϵ . This is quite comparable with normal experimental accuracy for measurements of this kind. Hence a standard deviation of as much as 10 per cent in the value of ϕ would not normally result in any detectable departure from the exponential form of the temperature dependence.

§ 3. DISCUSSION.

It is a common observation that the activation energies measured on different specimens of the same substance can vary between relatively wide limits. Considering equations (7) and (9), it is plausible that the value of ϕ_{eff} and its mean over a temperature range could vary from specimen to specimen, depending on the precise conditions prevailing at inter-granular contacts. On the other hand, the true activation energy ϵ is expected to be a constant for a given substance, unless the impurity content is very high. Variations of ϵ_{obs} in micro-crystalline semi-conductors of low impurity content must, therefore, be ascribed to the existence of inter-granular barriers. If the impurity content is very high, an alternative interpretation may be available, based on the interaction between neighbouring impurity centres. However, no satisfactory quantitative theory on impurity interaction has so far been established (Seitz 1950). In any case, such interaction would be expected to produce a whole spectrum of activation energies, corresponding to random variation of the distance between neighbouring centres. An averaging process similar to that described in the previous section would thus be again required to account for the observed exponential temperature dependence of conductivity.

The above refers to activation energies deduced from conduction measurements. Activation energies deduced from thermo-electric measurements which do not involve current flow should be almost independent of inter-granular barriers. In micro-crystalline specimens, thermo-electric activation energies should thus be generally smaller than ϵ_{obs} . The exact consequences of grain structure and inter-granular barriers on the temperature dependence of the Hall coefficient still remain to be ascertained.

If variations of ϵ_{obs} from specimen to specimen arise in *single* crystals of low impurity content, an additional hypothesis would be required, though it is one which is thought to be readily acceptable. It would be necessary to assume that the concentration of impurity centres is subject to local variations. This would produce localized space charges and fields in the manner already described (Henisch 1948), no matter whether we are dealing with a single crystal or with a granular medium. Any electron traps occurring within the crystal would have similar consequences, particularly if they occur in clusters. The barriers which impede the passage of current carriers are then no longer "inter-granular", but a treatment similar to that used above could again be applied in principle. As in the previous case, we would be concerned with a whole spectrum of barrier heights, and the value ϵ_{obs} resulting from their summation could vary from specimen to specimen. The activation energy ϵ could then be taken as a constant for the material. This treatment is also applicable to deficit semi-conductors for which no satisfactory theory of inter-granular barriers is at present available.

ACKNOWLEDGMENT.

Grateful acknowledgment is made to Professor R. W. Ditchburn for his support of this research, and to him, Dr. C. A. Hogarth and Dr. T. B. Rymer for the help received during many stimulating discussions.

REFERENCES.

- CHASMAR, R. P., 1948, *Nature, Lond.*, **161**, 281.
HENISCH, H. K., 1948, *Electrical Communication*, **25**, 163 ; 1950, *Proceedings of the Conference on the Properties of Semi-Conducting Materials*, University of Reading (Butterworths 1951), p. 234.
MILLER, P. H., 1950, *Proceedings of the Conference on the Properties of Semi-Conducting Materials*, University of Reading (Butterworths 1951), p. 172.
MOTT, N. F., 1950, *Proceedings of the Conference on the Properties of Semi-Conducting Materials*, University of Reading (Butterworths 1951), p. 1.
SEITZ, F., 1950, *Proceedings of the Conference on the Properties of Semi-Conducting Materials*, University of Reading (Butterworths 1951), p. 8.
VERWEY, E. J. W., 1950, *Proceedings of the Conference on the Properties of Semi-Conducting Materials*, University of Reading (Butterworths 1951), p. 151.
VOLGER, J., 1950, *Proceedings of the Conference on the Properties of Semi-Conducting Materials*, University of Reading (Butterworths 1951), p. 162.

LXXV. *The Moving Griffith Crack.*

By ELIZABETH H. YOFFE, Ph.D. *

[Received February 28, 1951.]

SUMMARY.

The stress field is calculated about a straight crack moving through an elastic medium. The stresses depend on the velocity and reduce to Inglis' solution when the velocity is zero. The results may be applied to the spicular fracture of glass.

INTRODUCTION.

THIS problem was proposed by Dr. Orowan in connection with the spicular fracture of glass and other materials. It is hoped that he will shortly publish a full account of its applications both to brittle fracture and to the multiplication of dislocations in a strained crystal. In the meantime the mathematical solution is given here for the stress field around a crack propagating with a finite velocity, and the stresses near the head of the crack are compared with those of the static case. The known stresses about a stationary crack show that fracture may be expected to occur in the line of the crack, but Dr. Orowan anticipated that at high velocities there might be a tendency to turn out of this line, giving a curved or branching crack. It was assumed that fracture would occur normal to the maximum tensile stress, and the stresses are therefore calculated at points on a circle of small radius about the head of the crack.

§ 1.

The problem is to find the stresses near the head of a rapidly propagating crack in a plate of isotropic elastic material. The crack has the form of a straight narrow slit, and may be regarded as the limit of an ellipse of semi-axes a , b where b approaches zero. If a sufficiently large transverse tension T is applied to the plate, the crack may be expected to spread in both directions along its length. In this treatment it has been assumed for simplicity that the crack propagates to the right only, remaining of constant length $2a$. This is justified by the fact that the stress distribution close to one end of the crack is not influenced by its distance from the other end, as is shown later.

By keeping the crack of constant length the problem becomes that of a plate in uniform tension, across which a disturbance passes at a constant speed and without change of form. This disturbance is represented by a system of elastic waves, from which the solution is obtained.

The method used is very similar to that of Eshelby (1949) in his investigation of a moving dislocation. The same form of solution is

* Communicated by Sir Lawrence Bragg.

obtained by representing the moving disturbance by two sets of surface waves, but there are some differences in the treatment of the boundary conditions.

§ 2.

The boundary conditions for a crack extending along the x -axis from $x=-a$ to $x=a$ across an otherwise uniform tension field are

$$\left. \begin{aligned} \widehat{xx} &= 0, \\ \widehat{yy} &= T, \\ \widehat{xy} &= 0, \end{aligned} \right\} \text{at infinity}$$

$$\widehat{yy} = 0 = \widehat{xy} \text{ on } y=0, \quad -a < x < a.$$

The uniform tension is removed in order to consider separately the moving part of the system. This has the boundary conditions

$$\left. \begin{aligned} \widehat{yy} &= -T, \\ \widehat{xy} &= 0, \end{aligned} \right\} \text{on } y=0, \quad -a < x < a$$

and all stresses zero at infinity.

The solution must be symmetrical with respect to the x -axis, and it is therefore sufficient to consider only the upper half-plane $y > 0$, provided continuity is maintained at the axis, outside the crack. Let u, v be components of displacement in the x, y directions, and let

$$x' = x - ct,$$

where c is the velocity of propagation and t the time. Then a dynamic elastic system is to be determined throughout $y > 0$, satisfying the boundary conditions

$$\left. \begin{aligned} \widehat{yy} &= -T & \text{on } y=0, & \quad -a < x' < a \\ \widehat{xy} &= 0 & \text{on } y=0, & \quad \text{all } x' \\ v &= 0 & \text{on } y=0, & \quad |x'| > a \end{aligned} \right\} \dots \dots (1)$$

and all stresses zero at infinity.

§ 3.

In accordance with the general theory given by Love (1920), elastic waves may travel with velocity c in the x direction at the surface of the half space $y > 0$, without displacement in a direction normal to the x, y plane, provided they are composed of displacements of the two types

$$\left. \begin{aligned} u_1 &= A_s \exp(-\gamma sy) \sin sx', \\ v_1 &= A_s \gamma \exp(-\gamma sy) \cos sx', \\ u_2 &= B_s \beta \exp(-\beta sy) \sin sx', \\ v_2 &= B_s \exp(-\beta sy) \cos sx', \end{aligned} \right\} \dots \dots (2)$$

Differentiating equations (5) gives

$$\begin{aligned} f'(z_1) &= \frac{\partial V_1}{\partial x} + i\gamma \frac{\partial U_1}{\partial x} \\ &= \frac{\partial U_1}{\partial y} - \frac{i}{\gamma} \frac{\partial V_1}{\partial y} \\ &= P + iQ, \\ g'(z_2) &= \beta \frac{\partial V_2}{\partial x} + i \frac{\partial U_2}{\partial x} \\ &= \frac{1}{\beta} \frac{\partial U_2}{\partial y} - i \frac{\partial V_2}{\partial y} \\ &= R + iS, \end{aligned}$$

where P, Q, R, S , are real functions. The stresses may then be expressed as

$$\left. \begin{aligned} \widehat{xx} &= \left(\frac{\lambda + 2\mu}{\gamma} - \lambda\gamma \right) Q + 2\mu S, \\ \widehat{yy} &= \left(\frac{\lambda}{\gamma} - (\lambda + 2\mu)\gamma \right) Q - 2\mu S, \\ \widehat{xy} &= 2\mu P + \mu \left(\beta + \frac{1}{\beta} \right) R. \end{aligned} \right\} \dots \dots \dots (6)$$

By (4) the functions f, g in this problem differ only by a constant factor when referred to the same argument,

$$g(z) = -\frac{2\beta}{1+\beta^2} f(z). \quad \dots \dots \dots (7)$$

§ 4.

The problem is now to determine the unknown function $A(s)$ in (4) so as to satisfy the boundary conditions (1). Direct substitution in the conditions

$$\begin{aligned} \widehat{yy} &= -T & (-a < x' < a), \\ v &= 0 & (|x'| > a) \end{aligned}$$

would give equations of the form

$$\begin{aligned} \int_0^\infty s A(s) \cos sx' ds &= \text{constant} & (-a < x' < a), \\ \int_0^\infty A(s) \cos sx' ds &= 0 & (|x'| > a). \end{aligned}$$

It is clear that more convenient equations would be obtained if the boundary conditions determined either \widehat{yy} or v for all x' , instead of part one and part the other. Such equations are obtained by reasoning from the static case.

The static stress field due to an elliptical hole in a body under uniform tension was calculated by Inglis (1913) with the straight narrow crack as a particular case. Removing the uniform tension field and changing from elliptic to cartesian coordinates, his solution gives the following displacements and stresses on the x -axis :

$$\begin{aligned} u &= -\frac{T}{2(\lambda+\mu)} \left\{ \begin{array}{ll} x & (|x| < a) \\ x - \sqrt{(x^2 - a^2)} & (x > a) \\ x + \sqrt{(x^2 - a^2)} & (x < -a), \end{array} \right\} \\ v &= \frac{T(\lambda+2\mu)}{2\mu(\lambda+\mu)} \left\{ \begin{array}{ll} \sqrt{(a^2 - x^2)} & (|x| < a) \\ 0 & (|x| > a), \end{array} \right\} \quad \dots \quad (8) \\ \widehat{xx} = \widehat{yy} &= \left\{ \begin{array}{ll} -T & (|x| < a) \\ T \left(\frac{x}{\sqrt{(x^2 - a^2)}} - 1 \right) & (|x| > a), \end{array} \right\} \\ \widehat{xy} &= 0 \end{aligned}$$

where in each case the positive square root is to be taken.

Westergaard (1939) has given this solution in a more convenient form

$$\left. \begin{aligned} \widehat{xx} &= RlZ - y\mathcal{I}_m Z', \\ \widehat{yy} &= RlZ + y\mathcal{I}_m Z', \\ \widehat{xy} &= -yRlZ'. \end{aligned} \right\} \quad \dots \quad (9)$$

where

$$\begin{aligned} Z &= T \left(\frac{z}{\sqrt{(z^2 - a^2)}} - 1 \right), \\ Z' &= \frac{dZ}{dz} = \frac{T}{\sqrt{(z^2 - a^2)}} \left(1 - \frac{z^2}{z^2 - a^2} \right), \\ z &= x + iy. \end{aligned}$$

When the crack moves some of these boundary values must change. For, from (5) and (7)

$$\left. \begin{aligned} V_1 + i\gamma U_1 &= f(x'), \\ \beta V_2 + iU_2 &= -\frac{2\beta}{1+\beta^2} f(x'), \end{aligned} \right\} \text{ on } y=0$$

and therefore

$$\begin{aligned} u &= \mathcal{I}_m f(x') \left(\frac{1}{\gamma} - \frac{2\beta}{1+\beta^2} \right), \\ v &= -Rl f(x') \left(\frac{2}{1+\beta^2} - 1 \right), \end{aligned}$$

and from (6)

$$\begin{aligned}\widehat{yy} &= \left(\frac{\lambda}{\gamma} - (\lambda + 2\mu)\gamma \right) Q - 2\mu S \\ &= \left(\frac{\lambda}{\gamma} - (\lambda + 2\mu)\gamma + \frac{4\mu\beta}{1+\beta^2} \right) \frac{\partial}{\partial x} [\mathcal{J}_m f(x')] \\ &= H \frac{\partial}{\partial x} [\mathcal{J}_m f(x')],\end{aligned}$$

where

$$H = \frac{\lambda}{\gamma} - (\lambda + 2\mu)\gamma + \frac{4\mu\beta}{1+\beta^2}.$$

So if

$$f(x') = -\frac{iT}{2(\lambda + \mu)} \frac{(x' - \sqrt{(x'^2 - a^2)})}{[(1/\gamma) - 2\beta/(1 + \beta^2)]},$$

(the real square root being taken with the sign of x') then u has the same value as in the static case, but v and \widehat{yy} are multiplied by new factors:

$$\begin{aligned}v &= \frac{T}{2(\lambda + \mu)} \frac{[2/(1 + \beta^2) - 1]}{[1/\gamma - 2\beta/(1 + \beta^2)]} \begin{cases} \sqrt{a^2 - x'^2} & (|x'| < a) \\ 0 & (|x'| > a), \end{cases} \\ \widehat{yy} &= \frac{HT}{2(\lambda + \mu)} \frac{1}{[1/\gamma - 2\beta/(1 + \beta^2)]} \begin{cases} -1 & (|x'| < a) \\ \frac{x'}{\sqrt{(x'^2 - a^2)}} - 1 & (|x'| > a). \end{cases}\end{aligned}$$

Alternatively $f(x')$ may be so chosen that v , or \widehat{yy} , keeps its static value, when u and yy , or u and v must be multiplied by factors of a similar nature. Therefore since v remains zero for $|x'| > a$ whatever the factor, it appears that the boundary conditions (1) may be satisfied by choosing \widehat{yy} to have its static value along all the x' -axis. That is, on $y=0$,

$$\left. \begin{aligned}f(x') &= -\frac{iT}{H} (x' - \sqrt{(x'^2 - a^2)}) \\ \widehat{yy} &= \begin{cases} -T & |x'| < a \\ T \left(\frac{x'}{\sqrt{(x'^2 - a^2)}} - 1 \right) & |x'| > a \end{cases} \\ u &= -\frac{T}{H} \left(\frac{1}{\gamma} - \frac{2\beta}{1 + \beta^2} \right) \begin{cases} x' & (|x'| < a) \\ x' - \sqrt{(x'^2 - a^2)} & (|x'| > a) \end{cases} \\ v &= \frac{T}{H} \left(\frac{2}{1 + \beta^2} - 1 \right) \begin{cases} \sqrt{a^2 - x'^2} & (|x'| < a) \\ 0 & (|x'| > a) \end{cases} \end{aligned} \right\} \quad \dots \quad (10)$$

With any one of equations (10) in place of the boundary conditions (1) the problem is readily soluble.

§ 5.

On $y=0$, from (4) and (10),

$$\begin{aligned} v &= - \int_0^\infty \gamma A(s) \left(\frac{2}{1+\beta^2} - 1 \right) \cos sx' ds \\ &= \frac{T}{H} \left(\frac{2}{1+\beta^2} - 1 \right) \begin{cases} \sqrt{(a^2 - x'^2)} & (|x'| < a) \\ 0 & (|x'| > a). \end{cases} \end{aligned}$$

The cosine transform of this function is given by Titchmarsh (1937) as a particular case of the functions

$$\left. \begin{aligned} (1-x^2)^{\nu-1/2} & \quad (0 < x < 1) \\ 0 & \quad (x > 1) \end{aligned} \right\} \quad . \quad . \quad . \quad 2^{\nu-1/2} \Gamma(\nu + \tfrac{1}{2}) x^{-\nu} J_\nu(x)$$

where J_ν is the Bessel function of order ν . This gives

$$A(s) = - \frac{Ta}{H\gamma} \cdot \frac{J_1(as)}{s} \quad . \quad . \quad . \quad (11)$$

With $A(s)$ determined, the values of u and v may be calculated from (4) for all points in the upper half plane. For it is known (Watson 1922) that

$$\int_0^\infty \frac{\exp(-pt) J_1(qt)}{t} dt = \frac{\sqrt{(p^2 + q^2)} - p}{q}$$

for $\Re l(p+iq) > 0$ and $\Re l(p-iq) > 0$, so that

$$\begin{aligned} V_1 + i\gamma U_1 &= \int_0^\infty \gamma A(s) \exp(-\gamma sy + isx') ds, \\ &= - \frac{Ta}{H} \int_0^\infty \frac{\exp(iz_1 s) J_1(as)}{s} ds, \\ &= \frac{T_i}{H} (z_1 - \sqrt{(z_1^2 - a^2)}) \\ &= f(z_1) \quad \text{for } \gamma y > 0, \quad . \quad . \quad . \quad (12) \end{aligned}$$

and similarly

$$\begin{aligned} \beta V_2 + iU_2 &= \frac{2\beta T_i}{(1+\beta^2)H} (z_2 - \sqrt{(z_2^2 - a^2)}), \\ &= g(z_2). \end{aligned}$$

Then

$$\left. \begin{aligned} f'(z_1) &= - \frac{T_i}{H} \left(1 - \frac{z_1}{\sqrt{(z_1^2 - a^2)}} \right) \\ &= P + iQ, \\ g'(z_2) &= \frac{2\beta T_i}{(1+\beta^2)H} \left(1 - \frac{z_2}{\sqrt{(z_2^2 - a^2)}} \right) \\ &= R + iS, \end{aligned} \right\} \quad . \quad . \quad . \quad (13)$$

and the stresses are given by (6).

The problem is now solved since a system of surface waves has been found which satisfies the boundary conditions (1). It is easily verified that each stress component tends to zero at infinity.

§ 6.

To show that the solution remains correct at zero velocity it is necessary to take the limit as $c \rightarrow 0$.

For c small

$$\gamma \div 1 - \frac{c^2}{2c_1^2},$$

$$\beta \div 1 - \frac{c^2}{2c_2^2},$$

$$\frac{4\beta}{1+\beta^2} \div 2,$$

$$H \div (\lambda + \mu) \frac{c^2}{c_1^2}.$$

Then

$$f(z) \div \frac{-ic_1^2 \Gamma}{(\lambda + \mu)c^2} (z - \sqrt{z^2 - a^2}),$$

$$f'(z_1) \div f'(z) - \frac{ic^2}{2c_1^2} y f''(z)$$

$$= P + iQ,$$

$$g'(z_2) \div -f'(z) + \frac{ic^2}{2c_2^2} y f''(z)$$

$$= R + iS$$

and the stresses are given approximately by

$$\widehat{xx} \div \left(2\mu - (\lambda + \mu) \frac{c^2}{c_1^2} \right) Q + 2\mu S,$$

$$\widehat{yy} \div - \left(2\mu - (\lambda + \mu) \frac{c^2}{c_1^2} \right) Q - 2\mu S,$$

$$\widehat{xy} \div 2\mu(P + R).$$

On substituting, and retaining only the terms of zero order in c^2 , the stresses at zero velocity become :

$$\widehat{xx} = -\mu y \frac{c^2}{c_1^2} \left(1 - \frac{c_1^2}{c_2^2} \right) \Re f''(z) + (\lambda + \mu) \frac{c^2}{c_2^2} \Im_m f'(z),$$

$$\widehat{yy} = \mu y \frac{c^2}{c_1^2} \left(1 - \frac{c_1^2}{c_2^2} \right) \Re f''(z) + (\lambda + \mu) \frac{c^2}{c_1^2} \Im_m f'(z),$$

$$\widehat{xy} = -\mu y \frac{c^2}{c_1^2} \left(1 - \frac{c_1^2}{c_2^2} \right) \Im_m f''(z).$$

Since $1 - c_1^2/c_2^2 = -(\lambda + \mu)/\mu$, and $f'(z) = ic_1^2 Z/(\lambda + \mu)c^2$, these expressions are in agreement with (9) and the solution is therefore correct at zero velocity.

To show that the solution is unique, assume two different solutions satisfying the same equations and boundary conditions, and specified by functions $f_1(z)$, $f_2(z)$, say. Let the difference of these be $h(z)$. Then since the equations are linear the difference in stress of the two solutions is obtained by replacing f by h in the above equations. But at zero velocity these stresses are specified, so the differences must be zero, giving

$$\mathcal{G}_m(h''(z)) = 0 = \mathcal{R}l(h''(z)),$$

$$\mathcal{G}_m(h'(z)) = 0$$

at all points. Also, from the boundary conditions,

$$h'(z) = 0 \text{ at infinity}$$

and

$$\mathcal{R}l(h(z)) = 0 \text{ on } y=0, |x| > a.$$

So $h(z)$ is at most a pure imaginary constant, which can only add a uniform u -displacement without affecting the stresses. The solution is therefore unique.

§ 7.

The next step is to calculate the direct stress acting across a radius from the point $z=a$, at points very close to this centre but at various positions about it. If polar coordinates (r, θ) are taken with centre $x=a, y=0$, such that

$$x-a = r \cos \theta,$$

$$y = r \sin \theta$$

then the stress $\widehat{\theta\theta}$ is to be calculated for a small constant value of r , and θ varying from 0 to $\pi/2$.

Let

$$\begin{aligned} z &= a + re^{i\theta} \\ &= a(1 + ke^{i\theta}), \end{aligned}$$

where k is a small constant. Then

$$\begin{aligned} z_1 &= a(1 + k_1 e^{i\theta_1}), \\ z_2 &= a(1 + k_2 e^{i\theta_2}), \end{aligned}$$

where

$$\left. \begin{aligned} k_1 &= k(\cos^2 \theta + \gamma^2 \sin^2 \theta)^{\frac{1}{2}}, \\ \tan \theta_1 &= \gamma \tan \theta, \\ k_2 &= k(\cos^2 \theta + \beta^2 \sin^2 \theta)^{\frac{1}{2}}, \\ \tan \theta_2 &= \beta \tan \theta. \end{aligned} \right\} \dots \dots \dots (14)$$

As k approaches zero, higher powers of k may be neglected in comparison with the first, and the following approximations are valid:

$$\begin{aligned} P+iQ &= -\frac{Ti}{H} \left(1 - \frac{z_1}{\sqrt{z_1^2 - a^2}} \right) \\ &\doteq -\frac{Ti}{H} \left(1 - \frac{\exp(-i\theta/2)}{\sqrt{(2k_1)}} \right) \\ &\doteq \frac{T}{H\sqrt{(2k_1)}} \left(\sin \frac{\theta_1}{2} + i \cos \frac{\theta_1}{2} \right), \\ R+iS &\doteq -\frac{2\beta}{(1+\beta^2)} \frac{T}{H\sqrt{(2k_2)}} \left(\sin \frac{\theta_2}{2} + i \cos \frac{\theta_2}{2} \right). \end{aligned}$$

The stress is given by

$$\begin{aligned} \widehat{\theta\theta} &= \widehat{xx} \sin^2 \theta + \widehat{yy} \cos^2 \theta - 2\widehat{xy} \sin \theta \cos \theta \\ &= (\lambda + \mu) \left(\frac{1}{\gamma} - \gamma \right) Q - \mu \left(\frac{1}{\gamma} + \gamma \right) Q \cos 2\theta - 2\mu S \cos 2\theta \\ &\quad - 2\mu P \sin 2\theta - \mu \left(\frac{1}{\beta} + \beta \right) R \sin 2\theta, \\ &= \frac{T}{H\sqrt{(2k)}} \left\{ \left[\left((\lambda + \mu) \left(\frac{1}{\gamma} - \gamma \right) - \mu \left(\frac{1}{\gamma} + \gamma \cos 2\theta \right) \cos \frac{\theta_1}{2} \right. \right. \right. \\ &\quad \left. \left. - 2\mu \sin 2\theta \sin \frac{\theta_1}{2} \right) \right] / (\cos^2 \theta + \gamma^2 \sin^2 \theta)^{\frac{1}{2}} \right. \\ &\quad \left. + \frac{2\beta}{1+\beta^2} \left[2\mu \cos 2\theta \cos \frac{\theta_2}{2} \right. \right. \\ &\quad \left. \left. + \mu \left(\frac{1}{\beta} + \beta \right) \sin 2\theta \sin \frac{\theta_2}{2} \right] / (\cos^2 \theta + \beta^2 \sin^2 \theta)^{\frac{1}{2}} \right\}, \end{aligned} \quad \dots (15)$$

with k appearing only in the constant factor. Since a , the half length of the crack, appears nowhere else in (15) it cannot affect the distribution with θ of the stress $\widehat{\theta\theta}$, but only its absolute magnitude. Therefore for the purpose of this calculation the actual length of the crack is irrelevant, as mentioned earlier.

The equation (15) has been used to calculate $\widehat{\theta\theta}$ at various velocities and positions, as shown in Table I. It was assumed that $\lambda = \mu$ giving Poisson's Ratio $\frac{1}{4}$. The limiting form of (15) when the velocity approaches zero is

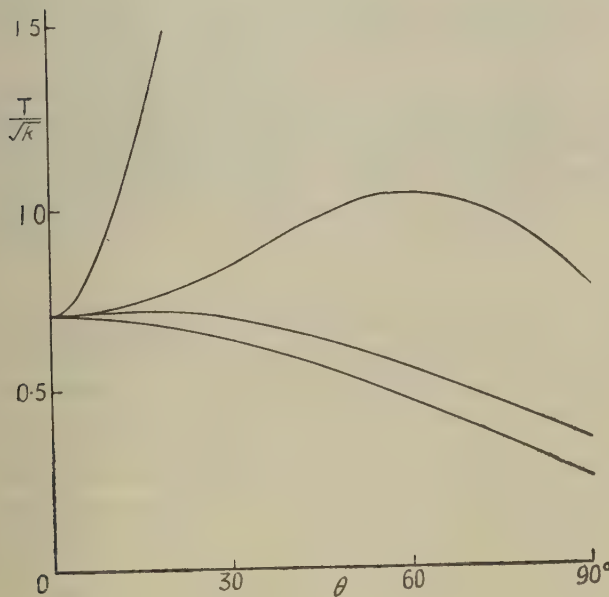
$$\widehat{\theta\theta} = \frac{T}{\sqrt{(2k)}} \cos^3 \frac{\theta}{2},$$

which is in agreement with Inglis and Westergaard. As the velocity increases the curve for $\widehat{\theta\theta}$ as a function of θ first flattens and finally shows a definite maximum at a considerable angle from the x -axis.

TABLE I.

	0°	30°	60°	90°	
$c=0$.707	.64	.46	.25	T/\sqrt{k}
$0.5C_2$.707	.70	.55	.35	T/\sqrt{k}
$0.8C_2$.707	.85	1.04	.78	T/\sqrt{k}
$0.9C_2$.707	2.3	5.0	4.6	T/\sqrt{k}

Fig. 1.



§ 8. CONCLUSION.

From these results it is to be expected that, if the material is such that a crack propagates in a direction normal to the maximum tensile stress, there is a critical velocity of about $0.6 c_2$ at which the crack tends to become curved. At a lower velocity the crack extends in a straight line, but as the speed increases the $\widehat{\theta\theta}$ curve becomes flat and the crack may form branches, since nearly equal stresses exist over a wide arc about the head of the crack. At higher velocities the $\widehat{\theta\theta}$ curve has a

definite maximum again, and each branch tends to curve, as is often seen in cracked glass. These effects have been elegantly demonstrated by Dr. Orowan in sheets of cellophane, and he is expected to discuss them more fully elsewhere.

ACKNOWLEDGMENT.

My thanks are due to Dr. Orowan for many helpful discussions and to the British Iron and Steel Research Association for a grant.

REFERENCES.

- ESHELBY, J. D., 1949, *Proc. Phys. Soc. A*, **62**, 307.
INGLIS, C. E., 1913, *Trans. Inst. Naval Arch.*, 219.
LOVE, A. E. H., 1920, *Elasticity* (Cambridge: University Press), p. 312.
TITCHMARSH, E. C., 1937, *Fourier Series and Integrals* (Oxford: University Press), p. 178.
WATSON, G. N., 1922, *Bessel Functions* (Cambridge: University Press), p. 386.
WESTERGAARD, H. M., 1939, *J. App. Mech.*, **6A**, 49.

LXXVI. *Total Cross-Sections of the Elements for 156 MeV. Neutrons.*

By A. E. TAYLOR, T. G. PICKAVANCE, J. M. CASSELS and T. C. RANDLE.

Atomic Energy Research Establishment, Harwell*.

[Received April 9, 1951.]

ABSTRACT.

Measurements have been made of the total cross-sections of 10 elements for neutrons of effective energy 156 ± 3 MeV. The results are discussed in the light of the theory of Fernbach, Serber and Taylor (1949).

§1. INTRODUCTION.

MEASUREMENTS of the total cross-sections of hydrogen and carbon for neutrons of 156 ± 3 MeV. have already been reported (Taylor, Pickavance, Cassels, and Randle 1951). A wider range of elements has since been investigated using the same apparatus and geometrical arrangement as before. Only the details of the attenuators themselves need to be described here.

§2. ATTENUATORS.

Attenuators of metallic elements were machined to $2\frac{1}{2}$ inches diameter, while attenuators in powder or liquid form were contained in tubes of $2\frac{1}{2}$ inches internal diameter fitted with thin copper end windows. Corrections were applied to the results for these copper windows, and in one case (lead) for a small amount of impurity.

Using the previously determined value of the hydrogen cross-section, the deuterium cross-section was obtained from the difference between the attenuation produced by a heavy water sample and a sample of distilled water containing the same number of oxygen atoms. The same measurements were also used to determine the oxygen cross-section. For the beryllium cross-section, the attenuation of the neutron beam by anhydrous powdered beryllia was measured, and allowance made for the oxygen atoms. In a similar way anhydrous barium carbonate was used to determine the barium cross-section.

The lengths of the attenuators and the geometrical arrangement were such that only small corrections had to be applied for elastically scattered neutrons which reached the detector (Placzek and Bethe 1940). These corrections were 0.6 per cent of the cross-sections of lead and barium

* Communicated by the Authors.

carbonate, and less than 0.3 per cent for all the other attenuators. The attenuators varied in length from one to three times the mean free path of the 156 MeV. neutrons in the attenuator material.

§ 3. RESULTS.

The results of the measurements are contained in the Table, the last column of which records the length of attenuators employed.

TABLE
Neutron total cross-sections at 156 ± 3 MeV.

Element	Total cross-section $\sigma_t \times 10^{24} \text{ (cm.}^2\text{)}$	Collision radius $r = (\sigma_t 2\pi)^{\frac{1}{2}} \times 10^{13} \text{ (cm.)}$	Attenuator length $\text{(gm. cm.}^{-2}\text{)}$
Hydrogen	0.0464 ± 0.0012	0.859	as $(\text{CH}_2)_n$ 136.93
Deuterium	0.0707 ± 0.002	1.061	as D_2O 185.1
Beryllium	0.258 ± 0.014	2.026	as BeO 43.66
Carbon	0.330 ± 0.003	2.291	120.23
Oxygen	0.430 ± 0.004	2.616	as H_2O 166.3
Aluminium	0.677 ± 0.011	3.282	155.5
Iron	1.238 ± 0.016	4.438	225.4
Copper	1.376 ± 0.018	4.697	256.7
Barium	2.476 ± 0.088	6.279	as Ba CO_3 62.52
Lead	3.499 ± 0.026	7.462	156.62

§ 4. DISCUSSION.

Fernbach, Serber, and Taylor (1949) have investigated theoretically the total cross-sections of the elements for high energy neutrons. The various nuclei are regarded as spheres of refractive and absorbent material which distort the wave functions representing the high energy neutrons. There are three parameters entering into the problem :—

- (i.) the nuclear radius R , which is here taken equal to $1.37 A^{1/3} \times 10^{-13}$ cm., A being the atomic weight of a nucleus whose charge is Ze .

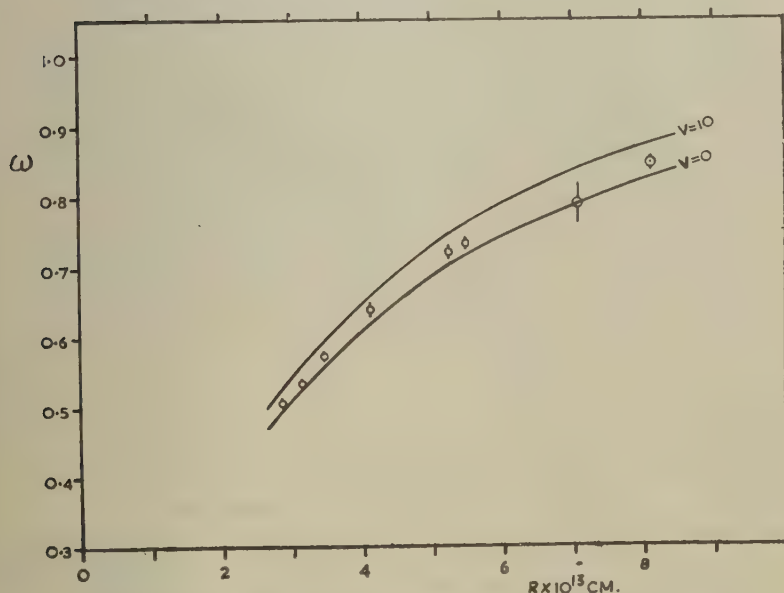
- (ii.) the absorption coefficient K for high energy neutrons inside the nucleus. The value of K is calculated from σ_{np} and σ_{nn} , the free neutron-proton and neutron-neutron cross-sections.

$$K = \frac{3}{4\pi R^3} [Z\alpha_{np}\sigma_{np} + (A-Z)\alpha_{nn}\sigma_{nn}]$$

where α_{np} and α_{nn} are numbers smaller than unity which take into account the fact that some collisions inside the nucleus are forbidden by the Exclusion Principle (Goldberger 1948). Because neutron-proton scattering is large in both forward and backward directions, α_{np} is expected to be smaller than α_{nn} .

- (iii.) the average potential energy V of the neutron inside the nucleus. For the moment V will be regarded as an adjustable parameter.

Fig. 1.



Experimental and theoretical values of ω as a function of R ,
for 156 MeV. neutrons

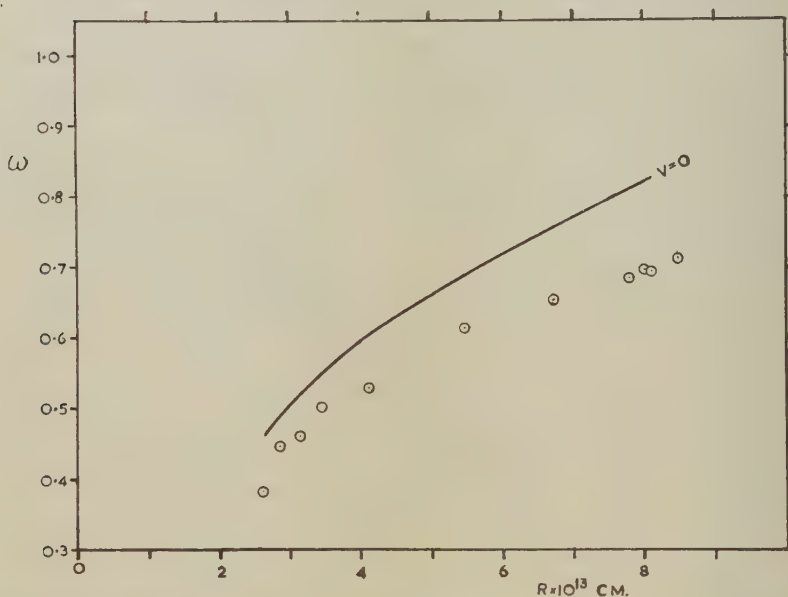
$$\omega = \sigma_t / 2\pi R^2, \quad R = 1.37 A^{1/3} \times 10^{-13} \text{ cm.}$$

In fig. 1 are plotted the experimental "specific total cross-sections" $\omega = \sigma_t / 2\pi R^2$, of the elements at 156 MeV. neutron energy. Theoretical values are also shown for $V=0$ and 10 MeV., the other constants being taken as $\alpha_{np}=0.72$, $\alpha_{nn}=0.85$, $\sigma_{np}=46 \times 10^{-27} \text{ cm.}^2$, and $\sigma_{nn}=57 \times 10^{-27} \text{ cm.}^2$. The figures for α_{nn} and σ_{nn} have been obtained by supposing the neutron-neutron and proton-proton interactions to be equal.

Since changes in ω are proportional to V^2 in the neighbourhood of $V=0$, a very good fit to the data could obviously be obtained by taking $V \sim 6$ MeV. This is smaller than the normal Hartree potential of 30 MeV. which is required to confine the nucleons inside a nucleus. The difference is not altogether surprising. The Hartree potential is an average over both near and distant encounters between nucleons, and in the total cross-section calculations near collisions have already been taken into account through K .

The overall situation at high neutron energies is not, however, so satisfactory as the discussion so far might seem to indicate. The results at 275 MeV. (Fox, Leith, Wouters and MacKenzie 1950, DeJuren 1950)

Fig. 2.



Experimental and theoretical values of ω as a function of R , for 275 MeV. neutrons. The experimental errors quoted for σ_t (Fox, Leith, Wouters and MacKenzie 1950, De Juren 1950) are in most cases smaller than the diameters of the circles.

are compared in fig. 2 with theoretical values of ω for $V=0$, $\alpha_{np}=0.83$, $\alpha_{nn}=0.92$, $\sigma_{np}=35 \times 10^{-27} \text{ cm.}^2$, $\sigma_{nn}=50 \times 10^{-27} \text{ cm.}^2$. There is a considerable discrepancy, and this cannot be resolved by adjustment of V since ω is a minimum for $V=0$.

The most obvious means of escape is to reduce σ_{nn} to about $27 \times 10^{-27} \text{ cm.}^2$, although even then the fit is not perfect. The situation here hardly provides strong evidence that the proton-proton and neutron-neutron interactions are not equal at high energies, but there is certainly a hint in that direction.

ACKNOWLEDGMENTS.

We wish to thank Mr. E. Wood for his valuable assistance in carrying out the measurements, and the cyclotron crew for their cooperation at all times.

This paper is published by permission of the Director of the Atomic Energy Research Establishment, Harwell.

REFERENCES..

- DEJUREN, J., 1950, *Phys. Rev.*, **80**, 27.
 FERNBACH, S., SERBER, R., and TAYLOR, T. B., 1949, *Phys. Rev.*, **75**, 1352.
 FOX, LEITH, WOUTERS and MACKENZIE, 1950, *Phys. Rev.*, **80**, 23.
 GOLDBERGER, M. L., 1948, *Phys. Rev.*, **74**, 1269.
 PLACZEK, G., and BETHE, H. A., 1940, *Phys. Rev.*, **57**, 1075A.
 TAYLOR, A. E., PICKAVANCE, T. G., CASSELS, J. M., and RANDLE, T. C., 1951.
Phil. Mag., **42**, 20.

LXXVII. *Metallic Conduction—The “ Internal Size-Effect ”.*

By D. K. C. MACDONALD,
Clarendon Laboratory, Oxford*.

[Received April 12, 1951.]

ABSTRACT.

The conception as an “ internal size-effect ” of internal boundaries in a metal is proposed and discussed in relation to a number of problems. The behaviour of the electrical resistance under a magnetic field is of particular interest and it is suggested that this may be relevant to the anomalous effects observed in gold (and other metals) at low temperatures and to the peculiar magneto-resistive characteristics of ferromagnetics.

§ 1. INTRODUCTION.

THE limitation of electron mean free path in metals due to the physical size of the specimen is now well-known. A first approximate treatment for a thin “ film ” or plate was made by J. J. Thomson (1901) and more recently the analysis on the modern statistical theory of metals was given by Fuchs (1938) and for wires by Dingle (1950), Chambers (1950) and MacDonald and Sarginson (1950).

It is however clear to-day that the *internal* physical structure of a metal is not entirely uniform and that grain, “ mosaic ” or dislocation boundaries will add to the electrical resistance as well as lattice vibrations and chemical impurity centres. It has been customary to regard such physical “ defects ” as simply contributing more or less uniformly to the electron-scattering without requiring any very specialized treatment. Recently, however, it has been found experimentally (MacDonald 1949) and shown theoretically (MacDonald and Sarginson (*loc. cit.*), Sondheimer (1950)) that the resistance-behaviour of a specimen limited by its external geometrical size is “ anomalous ” in that the resistance may be *decreased* by the application of a magnetic field. This occurs essentially when the size of the intrinsic electron orbit becomes comparable with the physical dimensions of the specimen. This then suggests that it may be valuable to consider the influence of *internal* boundaries in an analogous manner. Specifically, we propose that this may lead to an explanation for the peculiar behaviour of the resistance and magneto-resistance of gold and other metals at low temperatures and also for the anomalous magneto-resistance of ferro-magnetic metals. It also appears of possible importance in the interpretation of deviations from Matthiessen’s Rule which postulates the independent additivity of electrical resistivity components due to thermal and impurity scattering (in the general sense).

* Communicated by the Author.

§ 2. INTERNAL SIZE-EFFECT WITHOUT A MAGNETIC FIELD.

Let us consider a “large” specimen of metal which has internal boundaries in the plane of current flow, partially effective in scattering electrons, which form layers of separation d and let l_0 be the mean free path of electrons due to scattering in the “body” of the metal.

Let the x -axis be in the direction of the applied electric field, E , and the z -axis perpendicular to the plane of the “layers”. Let α be the fraction of electrons penetrating a layer without scattering, and β the fraction which are elastically scattered, the remainder being diffusely scattered.

The appropriate Boltzmann (transport) equation for the perturbation, n , to the electron distribution function is then :

$$v_z \frac{\partial n}{\partial z} + \frac{n}{\tau} = \frac{eE}{m} \frac{\partial N_0}{\partial v_x}, \quad (1)$$

where τ is the relaxation time corresponding to l_0 , and N_0 is the unperturbed distribution. By the nature of the problem it is evident that the solution will be periodic in z , of period d , and we need only consider any one particular layer taking $z=0$ at the lower plane.

The general solution of (1) (cf. Fuchs *loc cit.**) may be taken as :

$$n = \frac{eE\tau}{m} \frac{\partial N_0}{\partial v_x} [1 + \phi(v_z) \exp(-z/\tau v_z)]$$

where ϕ is an arbitrary function.

From symmetry it is then evident that n can be expressed :

$$\begin{aligned} n &= \frac{eE\tau}{m} \frac{\partial N_0}{\partial v_x} [1 + \phi(v_z) \exp(-z/\tau v_z)], & v_z > 0, \\ &= \frac{eE\tau}{m} \frac{\partial N_0}{\partial v_x} [1 + \phi(-v_z) \exp((d-z)/\tau v_z)], & v_z < 0. \end{aligned}$$

If we now consider the electrons leaving $z=0$ with $v_z > 0$ it is clear from our boundary conditions that we may write :

$$\begin{aligned} \frac{eE\tau}{m} \frac{\partial N_0}{\partial v_x} (1 + \phi(v_z)) &= \alpha \left[\frac{eE\tau}{m} \frac{\partial N_0}{\partial v_x} [1 + \phi(v_z) \exp(-d/\tau v_z)] \right. \\ &\quad \left. + \beta \left[\frac{eE\tau}{m} \frac{\partial N_0}{\partial v_x} (1 + \phi(v_z) \exp(-d/\tau v_z)) \right] \right], \end{aligned}$$

the first term on the right corresponding to electrons which have been transmitted “upwards” from the layer beneath and the second term to those which have been reflected at $z=0$ with reversal of the z component of velocity.

* In fact Fuchs writes, more generally, $\phi(\mathbf{v})$ but this is unnecessary in this type of problem.

Thus, setting $p = \alpha + \beta$ we have, solving for $\phi(v_z)$:

$$n = \frac{eE\tau}{m} \frac{\partial N_0}{\partial v_x} \left[1 - \left(\frac{1-p}{1-p \exp(-d/\tau v_z)} \right) \exp(-z/\tau v_z) \right], \quad v_z > 0, \\ = \frac{eE\tau}{m} \frac{\partial N_0}{\partial v_x} \left[1 - \left(\frac{1-p}{1-p \exp(d/\tau v_z)} \right) \exp((d-z)/\tau v_z) \right], \quad v_z < 0. \quad (2)$$

This is then just Fuchs' solution for a thin film if we replace his probability of elastic scattering at the surface (ϵ) by p , the sum of the probabilities of penetration and elastic scattering, as is then evident physically. Consequently the relative conductivity σ/σ_0 , where σ_0 is the conductivity of the metal in the absence of such striation layers, is given by the curves computed by Fuchs (fig. 2, *loc. cit.*) setting $\epsilon = p$.

It is of interest to note that we have then here a case where it is *not* possible to determine universally the effective resistivity of the specimen by a simple addition of inverse "mean free paths". Thus for $d \gg l_0$ we find :

$$\frac{\sigma}{\sigma_0} \sim 1 - \frac{3(1-p)}{8d} \cdot l_0, \quad (3)$$

indicative of an effective mean free path, $\frac{8d}{3(1-p)}$, due to the layer structure; while for $d \ll l_0$:

$$\frac{\sigma}{\sigma_0} \sim \frac{3}{4} \cdot \frac{1+p}{1-p} \cdot \frac{d}{l_0} \log \left(\frac{l_0}{d} \right), \quad (4)^*$$

from which one would deduce an "apparent" mean free path for the layer structure : $\frac{3}{4} \frac{d}{1-p} \left((1+p) \cdot \log \left(\frac{l_0}{d} \right) \right)$, which in addition varies with $\frac{l_0}{d}$.

It may therefore be useful to bear this point in mind when considering the significance of deviations from Matthiessen's Rule in metals, or the combination of resistance due to impurity scattering and physical defects.

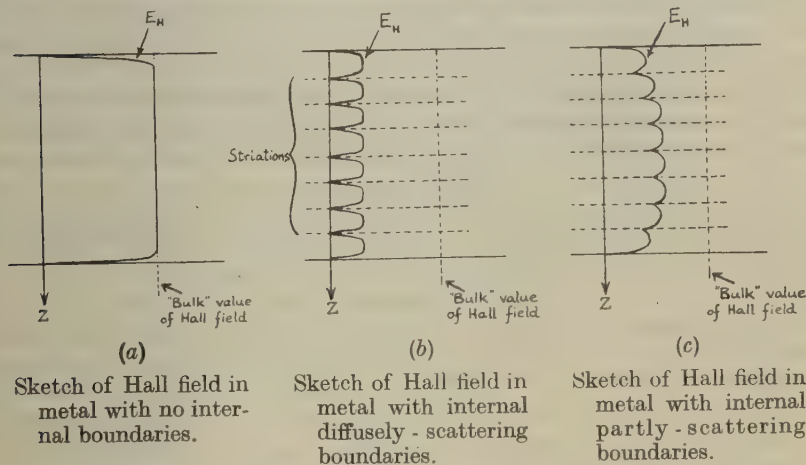
§ 3. APPLICATION OF A MAGNETIC FIELD.

If a magnetic field be now applied perpendicularly to the layers the Hall field will be in the *plane* of the striations and therefore uniform. Consequently, we may take over immediately the expressions derived by Sondheimer (*loc. cit.*) for the variation of conductivity in a "thin film" under a perpendicular magnetic field with the appropriate boundary equations. Initially an increase of resistance is then predicted as the magnetic field is applied but subsequently the resistance falls again and, under suitable conditions, may go below the initial value although the reduction is never great. This phenomenon can occur because the electron-paths are now less often disturbed by the physical boundaries than in the absence of the field.

* See Sondheimer's (*loc. cit.*) correction to Fuchs' quoted formula.

If the magnetic field is applied instead in the plane of the striations (but still perpendicular to E) we must turn to the work of MacDonald and Sarginson (*loc. cit.*) on the influence of a magnetic field applied in the plane of a thin film. The Hall field is now generated perpendicular to the layers and will now be periodic as we traverse them. In the case of purely diffuse scattering the field will fall to zero at each boundary layer as in fig. 1 (b) and the behaviour of the metal will simply be that of a set of separate thin films of thickness d . In this case theory shows that the magnetic field can produce a large decrease of resistance tending ultimately towards the value characteristic of a metal without boundaries and this is confirmed experimentally (MacDonald *loc. cit.*). Partially diffuse scattering will evidently provide an intermediate character and the internal behaviour of the Hall field is sketched in fig. 1 (c), although detailed theory for thin films with partially diffuse scattering in this case has not yet been worked out.

Fig. 1.



(Magnetic field perpendicular to plane of paper; applied electric field along: \longrightarrow : the paper.)

Finally a magnetic field applied *parallel* to the electric field (and therefore in the plane of the striations) produces no Hall field; again the resistance diminishes (due, crudely speaking, to the "focusing" action of the magnetic field) *without initial increase* as has also been confirmed experimentally (*cf.* MacDonald *loc. cit.* and Chambers *loc. cit.*).

It should perhaps be emphasized that these discussions assume an ideal isotropic "electron-gas". The deviations from ideality in a real metal will produce a component of intrinsic "bulk" magneto-resistance which is essentially positive and may be considered very approximately as superimposed on the "size-effect". If of course the intrinsic magneto-resistance is very large then the size-effects will be of small significance.

In all these cases, then, the application of a magnetic field—no matter what its direction—may produce an anomalous *decrease* in the resistance of a metal if the intrinsic magneto-resistance is not too large.

§ 4. THE LOW-TEMPERATURE RESISTANCE OF GOLD AND THE MAGNETO-RESISTANCE OF FERROMAGNETICS.

The electrical resistance of gold exhibits a definite minimum at low temperatures (*e. g.* de Haas, de Boer and van den Berg 1933, van den Berg 1938) as also does magnesium (MacDonald and Mendelssohn 1950) although as yet much less thoroughly investigated (see also the recent work by Mendoza and Thomas (1951) on silver and copper as well). It is established that the location of the minimum in temperature is a function of the impurity present as measured by the residual resistance tending almost certainly to zero for an "ideally pure" specimen; recently (MacDonald and Templeton 1951) it has been shown that for a given location in temperature of the minimum the associated residual resistance is lowest for silver as major impurity and progressively greater for copper and nickel. No theoretical explanation yet exists for this general behaviour.

A remarkable feature is the anomalous magneto-resistive effect which has been noted by Giaque, Stout and Clark (1937) and has also been confirmed recently by the writer. Thus we find that for a gold specimen having a minimum at $\sim 8^\circ \text{K.}$, the magneto-resistive increase at $\sim 4.2^\circ \text{K.}$ is $+1.66$ per cent for a field ~ 8 k gauss, while as the temperature is lowered the magneto-resistance diminishes relatively rapidly, becoming *negative* actually (~ -0.19 per cent at ~ 8 k gauss) at $\sim 1.5^\circ \text{K.}$ A related effect was first noted by Meissner and Scheffers (1929), and it was then suggested that this might have its origin in very small ferromagnetic impurities. The later experiments appear to us to render this hypothesis unlikely.

We are thus led to suggest that in these metals an internal size-effect exists which under appropriate conditions can then account for the observed results. We conceive in this case of some kind of internal layer- or "block-" structure whose size is related essentially to the number (and kind) of impurity atoms present. A crude estimate suggests that the linear dimensions would be at least 10 times that of the dominant mean free path due to direct impurity scattering. Thus the specimen referred to above has a mean free path (at $\sim 4^\circ \text{K.}$) of $\sim 10^{-4} \text{ cm.}$, while the diameter of an electron orbit is a field of 10 k gauss is about 10^{-3} cm.

In order to explain the existence of the minimum of resistance in temperature in zero magnetic field it would be necessary to assume that the relative probability of diffuse scattering at the layer boundaries is still increasing slightly at low temperatures where the ("residual") component of resistance due to impurity scattering is dominant and constant. No obvious mechanism accounts for *this* postulate but we recall the variation of (external) boundary scattering in narrow capillaries of sodium reported by MacDonald and Sarginson (1950) which suggests

that this form of scattering may not yet be fully understood*. If, however, the source of the minimum is to be found in this form of internal boundary scattering then since copper and nickel are progressively more effective impurity-centres for scattering in gold than is silver it appears quite natural that for a given location of minimum the residual resistances should in fact increase in the order observed.

Finally, it is well known that the magneto-resistance of pure ferro-magnetic metals in bulk is anomalous. Thus at room temperature (e.g. Heaps 1911) the transverse magneto-resistance of iron first increases with magnetic field and then decreases, becoming *negative* for fields above ~ 8 k gauss. Since ferro-magnetics are of course characterized by a domain structure it seems quite reasonable to suggest that internal size-effect may here also be directly responsible, in part at least, for this behaviour. Since domain sizes are generally $\sim 10^{-8}$ to 10^{-9} cm.³ (e.g. Bates 1948) and therefore of linear dimensions $\sim 10^{-3}$ cm. this again agrees with the magnitude of a free electron orbit in a field ~ 10 k gauss†.

We should point out, however, that Mott (1936) has interpreted the characteristics of the transition metals in terms of a two band (*s-d*) model and treated in particular the magneto-resistance of nickel. He ascribes the negative magneto-resistance in that metal to the distribution of spin-directions in the unoccupied *d*-states to which *s*-electrons may be scattered.

ACKNOWLEDGMENT.

I am grateful to Professor N. F. Mott, F.R.S., and Dr. E. Mendoza for comments.

REFERENCES.

- BATES, L. F., 1948, *Modern Magnetism*, p. 249, Cambridge (University Press).
 BERG, G. J. van den, 1938, *Thesis*, Leiden.
 CHAMBERS, R. G., 1950, *Proc. Roy. Soc. A*, **202**, 378.
 DINGLE, R. B., 1950, *Proc. Roy. Soc. A*, **201**, 545.
 FUCHS, K., 1938, *Proc. Camb. Phil. Soc.*, **34**, 100.
 GLAUQUE, STOUT and CLARK, 1937, *Phys. Rev.*, **51**, 1108. (See also STOUT and BARIEAU, 1939, *Jour. Amer. Chem. Soc.*, **61**, 238.)
 DE HAAS, DE BOER and v. D. BERG, 1933, *Physica*, **1**, 1115.
 HEAPS, 1911, *Phil. Mag.*, **22**, 900.
 MACDONALD, D. K. C., 1949, *Nature, Lond.*, **163**, 637.
 MACDONALD, D. K. C., and MENDELSSOHN, K., 1950, *Proc. Roy. Soc. A*, **202**, 523.
 MACDONALD, D. K. C., and SARGINSON, K., 1950, *Proc. Roy. Soc. A*, **203**, 223.
 MACDONALD, D. K. C., and TEMPLETON, I. M., 1951, *Phil. Mag.*, **42**, 432.
 MEISSNER and SCHEFFERS, 1929, *Phys. Zs.*, **30**, 827.
 MENDOZA, E., and THOMAS, J. G., 1951, *Phil. Mag.*, **42**, 291.
 MOTT, N. F., 1936, *Proc. Roy. Soc. A*, **153**, 713.
 THOMSON, J. J., 1901, *Proc. Camb. Phil. Soc.*, **11**, 120.

* The recent experiments of Mendoza and Thomas (*loc. cit.*) which show that the resistance-increase below say 1° K. can become rather rapid cast doubt on the likelihood of such a mechanism.

† This discussion is of course rather crude since we have not considered the effect of the "internal" field.

LXXVIII. *The Radiations of ^{203}Hg as Observed by a New Method.*

By H. W. WILSON and S. C. CURRAN,
Department of Natural Philosophy, The University, Glasgow*.

[Received April 30, 1951.]

SUMMARY.

The radioactivity of mercury has been investigated in a new way which makes use of the integrating properties of a proportional counter with an internal source. These allow us to show that the β spectrum is of allowed shape from 20 KeV. to the end point which was found to be $210 \text{ KeV.} \pm 5 \text{ KeV.}$ The energy and internal conversion coefficients of the γ ray which follows the β -emission have been evaluated. Also the half life has been determined as 45.9 ± 0.5 days. A discussion of the decay scheme and further possible use of the technique including its extension to scintillation counters concludes the paper.

§ 1. INTRODUCTION.

THE radiations emitted by the isotope ^{203}Hg have been studied by a number of investigators (Friedlander and Wu 1943, Miller and Curtiss 1945), and in some detail by Saxon (1948) and Slätis and Siegbahn (1949). The essential features of the decay scheme are well established and fig. 1 exhibits these diagrammatically. A negative β -particle of limiting energy close to 208 KeV. is emitted leaving the residual nucleus ^{203}Tl excited to an energy of approximately 280 KeV. The gamma ray transition is strongly internally converted in both K (~ 20 per cent) and L, M, N . . . shells (~ 6 per cent). No direct β -transitions between the ground states of the nuclei have been observed. Both Saxon and Slätis and Siegbahn have studied the form of parts of the spectrum by means of the magnetic β -spectrograph. Saxon concluded it was of allowed form over the range from ~ 40 to ~ 140 KeV. (the rest of the spectrum being masked by a strong conversion line near the end-point) and with the help of a β - γ coincidence technique Slätis and Siegbahn largely eliminated the difficulties due to the presence of the conversion line. They were thus able to show that the form of the spectrum was allowed in the region of 200 KeV.

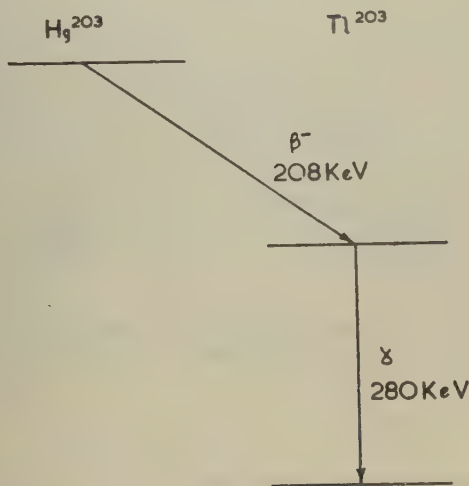
In the present work a new method of attack has been adopted. The integrating features of the proportional counter are such that three distinct possibilities arise. Thus, with a source situated within a proportional counter we see that (1) the unconverted γ -rays largely escape from the detector since the efficiency for such radiations is < 1 per cent and the β -rays of the primary spectrum are recorded;

* Communicated by the Authors.

(2) the γ -rays converted in the K shell give rise to a photo electron of energy approximately 200 KeV. and the counter detects both the photoelectron and time coincident β -particle each with 100 per cent efficiency so giving rise to a second spectrum, displaced on the energy scale by about 200 KeV. ; (3) the γ -rays converted in the L, M, N . . . shells give rise to photoelectrons of energy $\sim 270\text{--}280\text{ KeV.}$, time coincident with the primary β -rays and so producing a third spectrum displaced by about 270–280 KeV.

There are refinements to the above picture. For example, the efficiency of the detector to the K-radiations of Tl was ~ 2 per cent and, hence, occasionally processes of group (2) above will be displaced into group (3).

Fig. 1.



Decay scheme of ^{203}Hg .

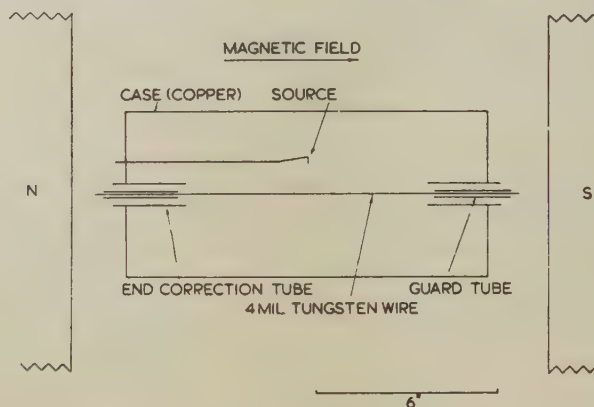
The L, M, N . . . radiations normally emitted together with the K-radiations are almost completely detected and so groups (1) and (2) are usually expected to show a relative displacement of $h\nu_\gamma - h\nu_{K\alpha}$, *i.e.* 208 KeV. Regarding group (3) the L, M, N . . . radiations are likewise captured within the tube and, hence, the whole group is displaced relative to group (1) by almost exactly $h\nu_\gamma$, *i.e.* 280 KeV. The three groups are marked, I, II. and III. in fig. 3. This phenomenon of the successive appearance of the primary spectrum affords some very considerable advantages. Thus, the beginning of the second spectrum, group (2), shows the detailed shape of the spectrum at low energies (see AB of fig. 3). The final end point of group (3), shows the detail of the spectrum near the limiting energy, free from confusion due to the superposition of the K conversion line (Inset curve, fig. 3). The whole spectrum can thus be examined in detail and compared with theory.

Lastly, the relative intensities of the three groups can be estimated by comparing areas and so the K and L, M . . . conversion factors determined rather exactly.

§ 2. EXPERIMENTAL ARRANGEMENTS.

The experimental system for examination of the spectrum was as shown in fig. 2. A large counter with the field adjusting tubes described elsewhere (Cockroft and Curran 1951) was placed within a uniform magnetic field (intensity 1400 gauss) parallel to the wire (Curran 1950). The working length of the counter was 8 in. and the diameter $5\frac{1}{2}$ in. The source was mounted on a separate probe terminating in a circular wire loop $\frac{1}{4}$ in. in diameter. The plane of the loop was parallel to the end

Fig. 2.

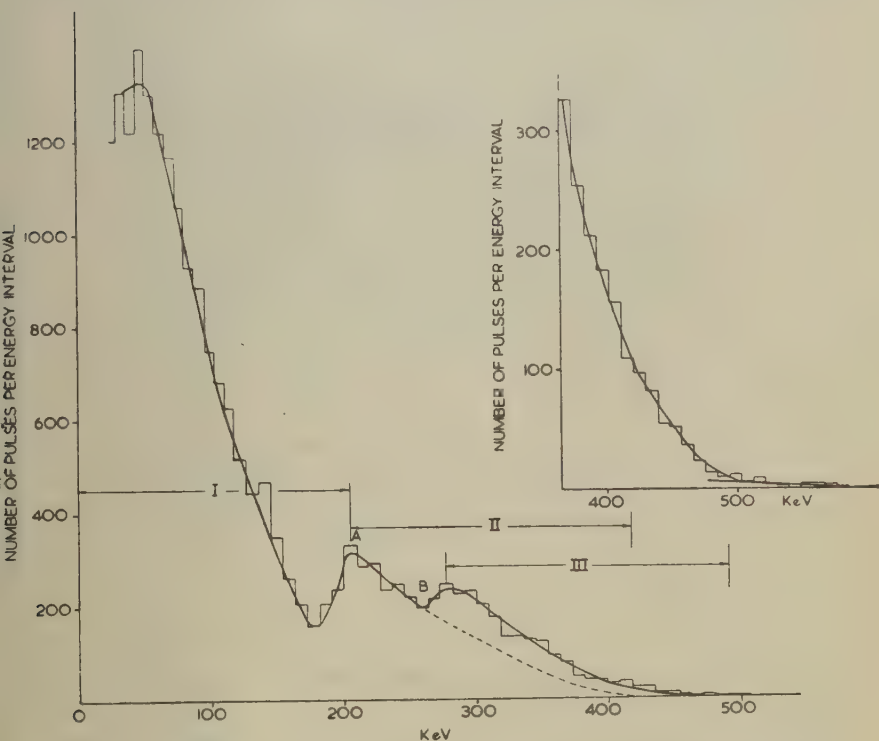


Experimental arrangement of proportional counter in magnetic field.

faces of the counter. The loop was used to support a thin foil of aluminium of mass 0.16 mg./cm.^2 and the radioactive material consisted of HgS which had been sublimed on to the foil from a heated surface *in vacuo*. The mass of the radioactive material was about $3 \mu \text{ gm./cm.}^2$ and almost invisible. The total activity of the source was 12,000 counts per minute. The source was confined to the central portion of the foil and the recorded rays were emitted into 4π solid angle, half of the total number passing, of course, through the thin supporting film. The probe was parallel to the central wire of the tube and the voltage on the probe was adjusted to the correct value appropriate to its position in the counter (1.1 in. from the central wire). The central wire was 4 mil. in diameter and the argon gas was at a pressure of $3\frac{3}{4}$ atmospheres (containing methane to a partial pressure of 20 cm. of mercury). The pressure and the magnetic field were such that no particles from the source could reach the cylindrical wall or escape into the non-counting volume at the ends of the tube.

Calibration of the counter_a was effected with a beam of X-rays, consisting mainly of the characteristic K radiations of tungsten, directed at the wall. The pulses from the counter were amplified linearly and displayed on a cathode ray oscillograph. For the spectrum analysis two methods were used: (1) the pulses were recorded photographically on moving film and analysed by reprojecting on a measuring screen; (2) the pulses from the amplifier were passed into a single channel electronic kick sorter. The results obtained by both methods were in good agreement and the curves given below are representative of those obtained by both techniques.

Fig. 3.



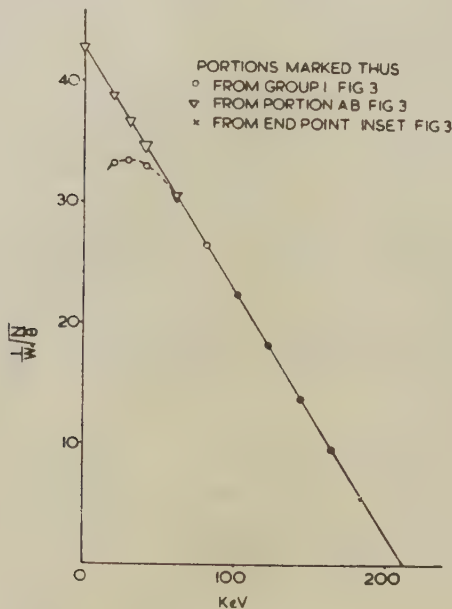
Complete spectrum of pulses observed in pressurized proportional counter.
Detail near end-point shown in inset figure.

The form of the spectra obtained is as shown in fig. 3. It is obvious that the primary spectrum is repeated as expected. The spectrum includes the spectrum of background particles (~ 700 counts/min. total). This, however, was deducted in making the calculations for the Fermi plot and the internal conversion coefficients. No serious effort was made to carry the analysis of the group (1) particles to very low energies since

the beginning of group (2) gives the shape in the very low energy region. Nevertheless the spectrum was looked at with higher gain to give the shape of the low energy region more exactly and the number of counts per energy interval below 130 KeV. in fig. 3 are taken from these results. The ultimate end-point of the distribution is shown in more detail in the inset figure.

Fermi plots, fig. 4, were made as follows: (I.) for the middle range, from group (1); (II.) for the end-point region from group (3); (III.) for the low energy region from the start of group (2), *i. e.* the portion AB of the spectrum. The intensities read from the spectrum were corrected for the

Fig. 4.

Composite Fermi Plot for ^{203}Hg .

background spectrum in making the calculations. The θ term in the ordinate function is taken from a paper by Bleuler and Zünti (1946). The fitting of these three regions together results in a good straight line from ~ 20 KeV. to the end-point which we estimate to be 210 ± 5 KeV. The final end-point of the histogram gives a more precise value of the limiting energy of the β -rays provided the energy of the γ -radiation is known. This was separately determined (278 KeV.) as discussed below, and the β -ray end-point again found to be 210 ± 5 KeV. This agrees with the value given by Slätis and Siegbahn. The Fermi plot is shown

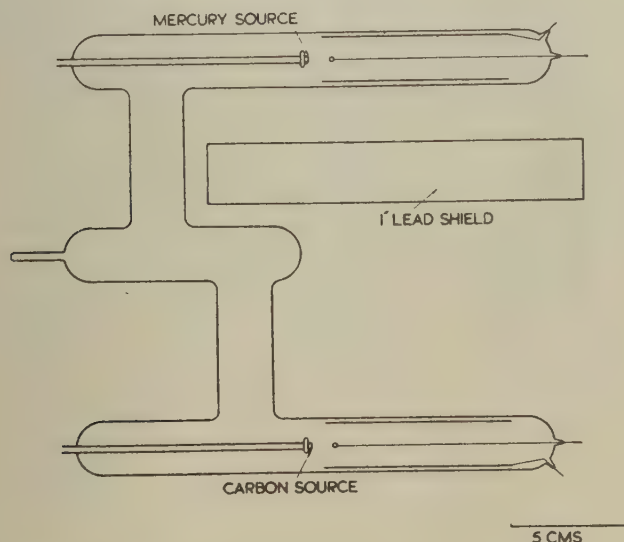
as linear to zero energy, the point at 0 KeV. being calculated from the corresponding point on the curve AB, fig. 3. In view of the aluminium leaf source support, this linearity to such a low energy must be regarded as accidental.

§ 3. ADDITIONAL DATA.

Half Life.

There appeared to be some considerable variation in the value of the half life of ^{203}Hg as determined by different authors (Friedlander and Wu 1943, Saxon 1948) and a careful measurement was made. Two similar Geiger counters were enclosed in a single envelope constructed in such a fashion that each could be individually irradiated. One was exposed to a

Fig. 5.

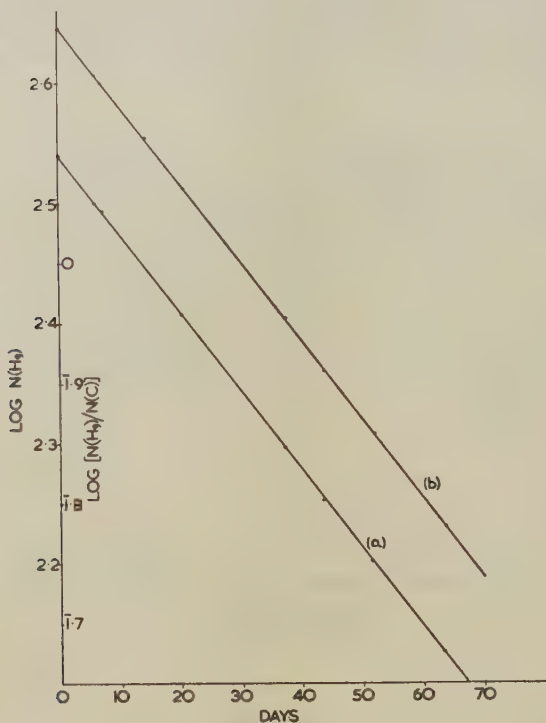


Controlled Geiger tube apparatus used for half-life determination.

source of ^{203}Hg (as mercuric oxide) and the other to a source of ^{14}C (as barium carbonate). The latter was intended as a constant control. Actually, slight temperature-dependent variations appeared in the effectively constant counting rate observed for ^{14}C . These did not show in the curve of decay observed for ^{203}Hg . These variations were allowed for by finding experimentally the law relating the ^{14}C counting rate to temperature and reducing all ^{14}C readings to a standard temperature of 17°C . The apparatus is sketched diagrammatically in fig. 5. It was designed so that the chance of a particle from one source being scattered into the other counter was extremely small. The two counters shared a common gas filling. The lead shield was used to keep mercury γ -rays from affecting the standard ^{14}C counter.

The half-life, after correction for counting losses due to dead time, etc., was found to be 45.9 ± 0.5 day. This lies within the range of previously carefully measured values and ensured us that the isotope was effectively pure. It was prepared for us at A.E.R.E. by bombarding liquid mercury with slow neutrons. The half-life graphs are shown in fig. 6. Graph (a) is the logarithm of the mercury counting rate (after correction for dead

Fig. 6.



Graph of half-life results.

time losses) plotted with respect to time as abscissa, while (b) is the logarithm of the ratio of the mercury counting rate to the standard carbon counting rate. (a) gave a value of 45.84 day and (b) a value of 45.95 day for the half life.

Energy of Gamma Radiation.

A semi-circular magnetic spectrograph (resolution 2 per cent) was employed. A thin platinum radiator (4 mgm./cm.²) was wrapped round the source. A histogram (fig. 7) gave strong K and L peaks and the value of the γ -ray energy was found to be 278 ± 3 KeV.

Absorption Curves for β -rays and Electrons.

Fig. 8 shows the result of some measurements on the β -rays and conversion electrons. The absorber mass scale has been corrected for counter window thickness and air gap (total ~ 6 mgm.). A good end-point is apparent and, according to a graph of Glendenin (1948), the range in the absorber corresponds to an energy of 280 KeV. This

Fig. 7.

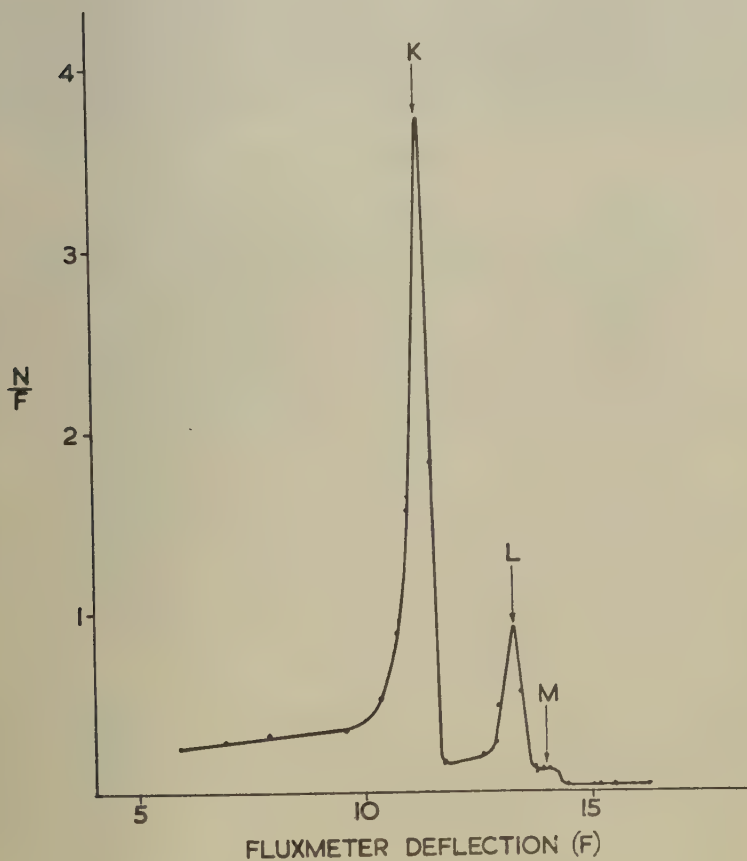


Photo-electric spectrum of the γ -ray of ^{203}Hg ,
with 4 mgm./cm.² Pt radiator.

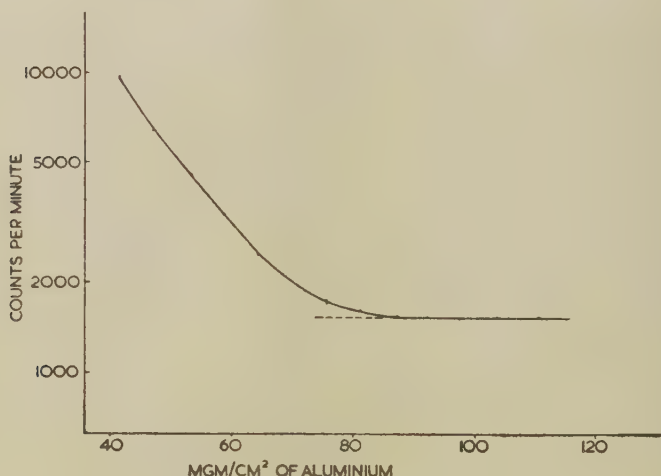
confirms the γ -ray measurement, as there must be photo-electrons released with practically the whole quantum energy. A slight break is apparent on the absorption curve at about 210 keV., the limiting energy of the β -rays. This portion of the graph is not included in the figure.

We were anxious to observe possible evidence of the emission of β -rays in the ground state to ground state transition, but no such evidence appears. From examination of the absorption curve and other data, we believe that the transition to the excited state is more probable than the ground to ground state transition by a factor >100 .

§ 4. DISCUSSION.

The study of the disintegration of ^{203}Hg was considered interesting primarily because of the possibility of determining the shape of the β -spectrum at very low energies with the help of the new integrating feature of the proportional counter. Relatively soft β -emitters of high Z value such as ^{203}Hg have not been examined in detail at low energies in the past and possibly they could exhibit rather unusual features

Fig. 8.



Absorption of beta rays in aluminium.

in this region. Thus, we might expect relatively large effects from the extra-nuclear electrons or again radiative transitions of the type recently discussed by Ivanenko and Lebedev (1950) might be prominent. It is, therefore, particularly notable that the allowed form of the spectrum is rather closely preserved down to ~ 20 keV. as shown above. Still more refined examination of the spectrum at low energy values will be possible when the source is mounted on still thinner supporting films and when the resolution of the instrument is improved. It is thought that traces of electronegative gases impaired the resolving power and a continuously active purifier is being fitted to the counter.

The ft value of ^{203}Hg , assuming $t=46$ day and $f=0.6$ (from the curves of Feenberg and Trigg (1950)) is 2.4×10^6 giving $\log ft=6.38$. It is not completely obvious from this value whether ^{203}Hg is allowed or

forbidden although Feenberg and Trigg remark with regard to fig. 10 of their paper, that the peak at $\log ft=6.2$ is "predominately first forbidden". If we fit the data to the Sargent diagrams (for $80 \leq Z \leq 84$) due to Feather and Richardson (1948) we find that a first forbidden transition with $\Delta I = -1$ and a change of parity is suggested. In either case the allowed form shown by the spectrum is to be expected theoretically.

Internal Conversion Coefficients.

By comparing areas under the three spectra (knowing the Fermi plot is straight allows accurate separation of pulses in group (2) from those in group (3)), we estimate the conversion factors (defined as the number of conversion electrons divided by the total number of γ -ray disintegrations), to be

$$\alpha_K = 15.6 \text{ per cent}; \quad \alpha_{L, M \dots} = 4.2 \text{ per cent}; \quad \alpha = 19.8 \text{ per cent}$$

and the ratio $\alpha_K/\alpha_{L, M \dots} = 3.71$.

We note that Saxon gave the α value as 0.24. If we define α in the more usual manner as the ratio of the number of conversion electrons to the number of γ -rays emitted, our value of α rises to 0.247, in good agreement with Saxon. The work of Slätis and Siegbahn gives the ratio 3.0 for α_K/α_L .

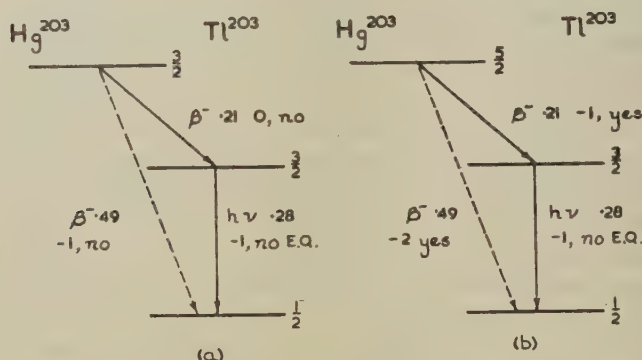
The value of α_K predicted theoretically by Taylor and Mott (1932) for $(mc^2/h\nu) = 1.83$ is close to 14 per cent for electric quadrupole radiation at $Z = 83$. Here we have $Z = 81$. The results suggest strongly that the γ -ray transition in the Tl nucleus is electric quadrupole in type.

Shell Model.

The shell model predictions do not seem to be sufficiently precise in the region of atomic number > 80 to assist materially in the assignment of spin values. It is reasonable, however, according to present views, to suppose that ^{203}Hg has a spin of $\frac{1}{2}$ or $\frac{3}{2}$ and it is much less likely to have a still greater spin value. Moreover, and rather more significantly, the spin values of almost all nuclei in the neighbourhood of mercury and thallium are in the range $0 \leq I \leq \frac{3}{2}$. The ground state spin value of ^{203}Tl has been measured and has the value $\frac{1}{2}$. The spin value of ^{201}Hg in the ground state is $\frac{3}{2}$. It is very reasonable to suppose that the addition of two neutrons to form ^{203}Hg should leave the spin unchanged at the value $\frac{3}{2}$. If we assign this value to ^{203}Hg and $\frac{1}{2}$ to ^{203}Tl we can tentatively construct the decay scheme shown in fig. 9 (a). Here the γ -ray transition is obviously in line with the experimental facts among which has to be noted the conclusion that the life time of the state at 0.28 MeV. is $< 0.3 \times 10^{-8}$ sec. (Deutsch and Wright 1950), or $< 2 \times 10^{-8}$ sec. by an independent experiment of Binder (1950). The β -ray transitions are both allowed according to Gamow-Teller rules but experimentally the $(-1, \text{no})$ transition is apparently forbidden relative to the $(0, \text{no})$. This is clearly the weak link in the scheme and it may be that here the application of the shell model is misleading. It seems to us that the

decay might be more correctly represented by the scheme shown in fig. 9 (b). The spin value $5/2$ is assigned to ^{203}Hg and it is now possible to assign a spin change of -1 and a parity change to the observed β -transition, bringing it into agreement with the conclusions of Feather and Richardson. The ground state to ground state β -transition is $(-2, \text{yes})$. There is evidence that transitions of the type $(\Delta I=2, \text{yes})$ have peculiarly large $(E_0^2-1)ft$ values, of the order of 10^{10} (Shull and Feenberg 1949, Wu 1950). Now, according to our observations, the β -transition of energy 0.49 MeV. is less probable than the observed transition of energy 0.21 MeV. by a factor $\gtrsim 100$. The energy releases favour the higher energy transition by a factor of about 17, according to calculations of Feenberg and Trigg in the paper referred to previously. Hence, the ft value for $(\Delta I=-2, \text{yes})$ has to exceed the ft value for $(\Delta I=-1, \text{yes})$ by a factor $\gtrsim 1700$. This is clearly possible if the respective values are $\sim 10^{10}$ and 2.4×10^6 respectively. On the whole,

Fig. 9.

Possible spin and parity changes in decay of ^{203}Hg .

therefore, the scheme of fig. 9 (b) is perhaps the most satisfactory from the point of view of both experiment and theory. The main point of difficulty which it introduces is its inconsistency with the shell model.

The method of classification of β -emitters due to Dr. K. M. Guggenheimer of this department suggests that the 0.21 MeV. transition is in the allowed class. His work indicates that the 0.49 MeV. transition will be less probable than the low energy transition by a factor of ~ 224 if the first is second forbidden and the second allowed.

A scheme satisfying these conclusions is that of fig. 2 (b) with the β -transitions changed from $(\Delta I=-2, \text{yes})$ and $(\Delta I=-1, \text{yes})$ to $(\Delta I=-2, \text{no})$ and $(\Delta I=-1, \text{no})$. This introduces, of course, disagreement with the classification due to Feather and Richardson. Much of the uncertainty as to the decay scheme would be removed by the experimental measurement of the spin of ^{203}Hg .

§ 5. GENERAL REMARKS.

The method offers to be one of considerable value in those cases of decay in which conversion electrons are of greater energy than the primary β -rays. Under such conditions the separate spectra observed give details of the low energy region of the primary spectrum and conversion coefficients can be readily evaluated. Work is in progress with RaD, which probably satisfies the required condition.

Similar considerations apply to decay schemes in which the γ -radiation following the β -emission is not appreciably converted but can be detected with high efficiency. Obviously, the most suitable detector in this case is the scintillation counter. Thus, if a very thin radioactive source is placed between two crystals of, say, sodium iodide (thorium-activated) the arrangement constitutes a solid proportional counter identical in principle with the gas filled proportional counter arrangement discussed above. The near 100 per cent efficiency for soft γ -rays of the scintillation detector permits its successful application to cases in which appreciable internal conversion does not take place. We are thus enabled to make use of the integrating effect of a proportional counter (with 4π solid angle) in this case also. As examples of the possibilities of the scintillation technique, we note that it is easy to detect almost 100 per cent of the K X-rays of Tl and not very difficult to approach the same complete detection of γ -rays of energy 0.28 MeV. In such circumstances, the group (1) and group (2) pulses, as shown in fig. 3, are displaced towards the right and both coincide with group (3) giving a single spectrum with starting point at 278 KeV. and end-point at 488 KeV. approximately. Preliminary work on mercury with a scintillation counter arrangement, as described above, has resulted in the removal of group (2) leaving a distribution consisting only of group (1) and a strong group (3). Further work with larger crystals will allow us to concentrate all the radiations into a single spectrum. This work will be published separately. Obviously in this case the examination of the β -spectrum is considerably facilitated. Indeed deliberate variation of the sensitivity of the arrangement to the different types of radiation can be used to assist in the analysis of decay schemes. Examples of such sources can be instanced, for example, ^{137}Cs . Another example occurs in the case of RaD where we can detect with nearly 100 per cent efficiency the hardest γ -rays, of energy 46.7 KeV., and so obtain a true picture of the primary β -spectrum displaced along the energy axis by the same amount. This displacement would enable us to observe the complete soft spectrum in some detail. Clearly, both the gas filled and solid type (scintillation) proportional counters offer very interesting possibilities if their integrating action is turned deliberately to good account.

We wish to thank Dr. K. M. Guggenheimer and Mr. D. L. Pursey of this department for helpful discussions on the theoretical side of this work.

REFERENCES.

- FRIEDLANDER, G., and WU, C. S., 1943, *Phys. Rev.*, **63**, 227.
MILLER, L. C., and CURTISS, L. F., 1945, *Pu. Proj. Rep.* CP-3102 (August).
SAXON, D., 1948, *Phys. Rev.*, **74**, 849.
SLÁTIS, H., and SIEGBAHN, K., 1949, *Phys. Rev.*, **75**, 318.
COCKROFT, A. L., and CURRAN, S. C., 1951, *Rev. Sci. Inst.*, **22**, 37.
CURRAN, S. C., 1950, *Atomics*, **1**, 221.
BLEULER, E., and ZÜNTI, W., 1946, *Helv. Phys. Acta*, **19**, 375.
GLEDENIN, L. E., 1948, *Nucleonics*, **2**, 12.
IVANENKO, D., and LEBEDEV, V., 1950, *Jour. Exp. Theor. Phys. U.S.S.R.* **20**, 91-2. (Jan.),
FEENBERG, E., and TRIGG, G., 1950, *Rev. Mod. Phys.*, **22**, 399.
FEATHER, N., and RICHARDSON, H. O. W., 1948, *Proc. Phys. Soc.*, **61**, 452.
TAYLOR, H. M., and MOTT, N. F., 1932, *Proc. Roy. Soc.*, **138**, 665.
DEUTSCH, M., and WRIGHT, W. E., 1950, *Phys. Rev.*, **77**, 139.
BINDER, D., 1950, *Phys. Rev.*, **78**, 325.
SHULL, F. B., and FEENBERG, E., 1949, *Phys. Rev.*, **75**, 1768.
WU, C. S., 1950, *Rev. Mod. Phys.*, **22**, 386.

LXXIX. *Microscopic Studies on Beryl Crystals.—I.*
Observation of Uni-Molecular Steps.

By L. J. GRIFFIN,
 H. H. Wills Physical Laboratory, Bristol*.

[Received May 1, 1951.]

[Plates XXII. & XXIII.]

SUMMARY.

Microscopic methods for observing uni-molecular steps on beryl crystals are described and discussed. Possible causes of the visibility of the steps are considered.

§ 1. GENERAL.

IN the course of topographical studies of prism $\{10\bar{1}0\}$ faces of beryl, it was observed that steps which interferometric measurements proved to be only a few hundred angstroms in height could be detected by the naked eye. This led to the development of a simple microscopic technique for the observation of such steps and it was then found that prism faces of beryl crystals often showed an extensive line structure which behaved in every way as if it corresponded to a step structure.

Individual lines of this structure could not be detected by multiple beam interferometric methods, but within the limits of error of this method the lines were observed to follow contour lines of the surface, being widely spaced when the surface was relatively flat and crowding together on gradients. In particular there were characteristic surface features, the contours of which followed roughly circular arcs; the line structure on such features also followed circular arcs.

Faces of beryl were examined in their natural untouched state and after the deposition of a highly reflecting thin film of silver on the surface. In all cases the appearance and behaviour of the line structure was the same, the sole difference being that the visibility of the lines increased considerably when the surface was silvered. These lines must therefore be genuine geometric surface details and can only represent surface steps.

§ 2. HEIGHT OF THE OBSERVED STEPS.

It was obviously desirable to determine the height of these steps, but even when very sensitive multiple beam interferometric methods were used this did not prove to be easy. However it was easily possible to

* Communicated by Professor N. F. Mott, F.R.S.

fix an upper limit to their height, for when a fringe crossed a line no kink in the fringe was visible. This meant that the steps could not be higher than 20 Å.

In principle any area of a face containing two sections, one of which showed many steps, and the other few steps could be used to determine the average height of the steps. This is possible by determining the angle between the two sections by means of fringes of equal chromatic order and then counting the number of steps in equal lengths of the two sections from a photomicrograph. In practice there were two serious difficulties. Firstly it was normally necessary to work at high magnifications on areas of this kind, and this could result in considerable experimental difficulties in the interferometric observations and measurements. Secondly it is essential for the accuracy of the interferometric measurements that the position of the image of the spectrograph slit on the crystal surface should be known accurately. In this case it was not possible to make reference marks on the surface of the crystal.

One area was discovered when these difficulties could be avoided. In this case a large number of steps suddenly turned through approximately 60°, thus producing the two different gradients, while the area lay between two obvious topographical features which could act as reference marks. The actual angle measurements was made by a method using both multiple beam Fizeau fringes and fringes of equal chromatic order (Barakat 1949) and the dihedral angle between the two sections was found to be $\tan^{-1} 0.57 \times 10^{-3}$. The position of the image of the slit of the spectrograph having been determined, a high magnification photomicrograph showed that in one section the slit had crossed some 110 steps in 1.04×10^{-2} cm. (in approximately the direction of greatest slope). In the other section 40 steps were crossed by the slit in an equal distance. Therefore for 70 steps the average step height is $8.5 \text{ Å} \pm 1 \text{ Å}$. The main error in this measurement was due to the uncertainty in the number of steps crossed by the slit. In some cases steps which were apparently single could be resolved into two steps after turning through 60°, and in several instances it was not possible to decide whether steps were truly single, or unresolved double, steps.

The building unit of beryl appears to be the Si_6O_{18} ring with the attached two Al and three Be ions which make half the unit cell as determined by Bragg and West (1926). These building units are packed side by side in the basal plane of the crystal and are stacked one on top of the other in the direction of the hexad (*c*-) axis, the orientation of alternate Si_6O_{18} rings along this axis differing by 25°. The height of these units is 4.6 Å. and their diameter 7.9 Å. The latter is the dimension which will appear as a step height on the {1010} faces examined. Comparing this value of 7.9 Å. with the experimentally determined value of the step height it is obvious that the steps observed are uni-molecular.

Although this determination was made only on one small area there appears to be no reason to doubt that the result is generally true. The

upper limit which is generally applicable fixes the maximum height at 2 molecules and a considerable amount of crystallographic evidence strongly supports the conclusion that the steps on the prism faces observed are almost always uni-molecular (Griffin 1950, 1951). There are exceptions to this rule, but they can normally be recognized and some cases are discussed below.

§ 3. TECHNIQUES OF OBSERVATION.

All three of the simple microscopic methods used for step observation were used in reflection because

(i.) any difficulties due to imperfections and flaws in the body of the crystal were thereby avoided ;

(ii.) the optical height of the step was thereby increased. For a specimen in air the optical step height in transmission is $(\mu-1)t$ and in reflection $2t$ and in the case of beryl this is equivalent to an increase in optical height of 3.5 times.

For the best results the crystal face to be examined is first coated with a thin film of silver. The reflectivity of this film is not critical and values of 80 per cent–90 per cent are convenient. The silver is deposited under conditions normal for multiple beam interferometry, *i.e.* the surface is carefully cleaned and the silver deposited by thermal evaporation in a vacuum of pressure about 10^{-5} mm. Hg. The presence of the silver layer results in

(i.) a considerable increase in the visibility of the diffraction pattern marking the edges ;

(ii.) a large reduction of the relative intensity of parasitic illumination produced at interfaces in the optical train.

1. *Bright field narrow pencil illumination.*

With this method a normal type of metallurgical microscope was used with the field iris stopped down to give a fairly narrow illuminating beam, the steps being visible immediately the crystal surface came into focus. The optimum aperture of the field iris, which varies a little according to the step height, can be very easily determined by closing down the iris as far as possible and then slowly opening it again. At some point a sudden decrease in visibility of the steps will be noticed and it is advisable to keep the aperture stopped down well below this value.

This method was used throughout the whole of the early part of the work and the effect of the focal setting of the microscope objective was investigated. It was found that

(i.) this diffraction phenomenon is an “in-focus” effect. When the surface of the crystal was truly in focus the diffraction pattern took its simplest form, had the least lateral extension and maximum peak intensities—the criteria usually applied to judge whether an image is “in” or “out of” focus ;

(ii.) that the intensity distributions are not complementary about the in-focus position. By analogy with the usual method for observing small path differences in a transparent body with a transmission microscope the contrary would be expected. An asymmetry of this kind might result from tilt of the specimen or deviations from axiality in components of the microscope. However the variation of focus about the centre, as observed on a photographic plate, appeared to be radially symmetric and with the objective used (focal length, 4 mm., N.A. 0.95) this should constitute a fairly sensitive test for any kind of deviation from axiality;

(iii.) that because of the non-complementary intensity distribution and its lateral asymmetry, it is possible in principle to determine the direction of a step by simple inspection of the diffraction pattern.

In practice, as discussed below, the visibility of the pattern for different steps can vary considerably, and with low visibility patterns it is often difficult to determine the step direction.

(iv.) that the relation between the phase and amplitude of the direct and diffracted waves is complex and varies with the focal setting. In the in-focus position a step is imaged by a narrow minimum with a broader maximum on the low side of the step; when the focal surface of the objective was a few microns from the plane of the face, up to nine maxima and minima could be observed. Major changes in the intensity distribution of the pattern took place for changes in focal setting of less than half a micron.

The type of in-focus imaging mentioned above required that a narrow and not very deep minimum be observed, as the maximum had a very poor visibility against the general bright field. This was necessarily fatiguing and it was found more convenient to work slightly off focus, as this resulted in the minimum becoming broader and more obvious, and therefore easier to see against the bright field.

2. Oblique dark field illumination.

Uni-molecular steps were also found to be visible using a normal type of reflection dark-field illumination. Although the visibility of the steps theoretically has a maximum value in dark field, it was in fact found to be much more convenient and satisfactory to use either of the other methods of observation. This was because foreign material was invisibly found to be deposited on the crystal faces and was visible as a random surface marking. Consequently not only did the step edges scatter light into the objective but the deposits of foreign material, whether point or large-scale, also did so, and as the intensity of light scattered by the steps was very low this randomly scattered light tended to mark the step images.

3. Phase contrast.

This method has been found to be the most sensitive and generally most satisfactory. A commercial type of reflection phase-contrast equipment with a very slightly absorbing phase ring has been used.

This results in the steps being marked by a very deep and narrow minimum and a lesser maximum. This minimum is much deeper than in the narrow pencil method (*i.e.* the visibility is much higher) and the width of the whole pattern is much less. Because of the increased contrast of the "image" it is possible to work with the crystal surface in sharp focus, thus resulting in much crisper definition and higher resolving power. The phase contrast equipment is, in this case, not working in the way for which it was designed for there is no question of any general difference in intensity on either side of the uni-molecular steps. It is, however, understandable that the visibility of the diffraction effect should be greater in phase contrast conditions than with the narrow illuminating pencil method.

§ 4. EFFECT OF NUMERICAL APERTURE OF OBJECTIVES.

The visibility of the diffraction patterns varies with the value of the N.A. of the objective. Comparisons of visibility were made visually and are therefore necessarily very approximate.

One of the main complicating factors was that a change of numerical aperture normally necessitated a change in focal length of the objective. This is almost invariably the case in microscopy and in the discussion below a correspondence will be assumed between increasing N.A. and decreasing focal length. Thus a relationship existed between the lateral extent of the diffraction pattern and the value of the N.A. This probably resulted in a decrease of visibility with increasing N.A., but against this one must balance the tendency of the eye to prefer an easily resolved pattern. These limitations must result in an estimate of the optimum observing N.A. which is very tentative.

Steps of 7.9 \AA . were observed with objectives having an upper limit of N.A. of 1.3 and a lower limit of 0.08. The maximum visibility was obtained with N.A.'s lying between 0.45 and 0.15.

Steps were also observed on terminal faces of beryl (0001), the diffraction patterns in this case always being of much lower visibility than in the case of 7.9 \AA . steps. It was not possible to make any measurement of step height in this case but from crystallographic evidence it appears possible that these steps may only be 4.6 \AA . high. Two additional factors may be considered in this case:

(i.) As the visibility of the pattern has decreased considerably the eye may be able to estimate more easily the onset of "empty magnification" due to the use of an objective of unnecessarily high N.A.

(ii.) The angular spread of the diffracted wave fronts may be dependent upon the height of the step. The difference between simple steps of 7.9 \AA . and 4.6 \AA . however, is not likely to be great.

In this case an observing N.A. of 0.28 definitely resulted in a higher visibility than N.A.'s of 0.45 or greater. The experimental conditions did not permit of the determination of a lower limit to the observing N.A.

The same range of N.A.'s was not available with the phase contrast equipment, but the same conclusions as to the observing N.A. apply at least qualitatively.

Thus maximum visibility is obtained by using objectives of medium or low N.A. In practice, however, it is often necessary to choose the objective primarily for satisfactory lateral resolution of the different diffraction patterns and surface detail, medium to high N.A.'s being necessary. The best working rule is therefore to compromise by using the lowest possible N.A. (*i. e.* longest possible focal length) consistent with satisfactory resolution. Assuming the steps observed on basal faces to be only 4.6 Å. high, then for steps of this, or lesser, height, it may often be necessary to sacrifice resolution for the sake of satisfactory visibility.

§ 5. COMPARATIVE SENSITIVITIES AND ADVANTAGES OF THE PHASE CONTRAST AND NARROW PENCIL METHODS.

With the narrow illuminating pencil method a 7.9 Å. step is visible when the surface is unsilvered, but the contrast is very poor indeed. When the surface is silvered the visibility of such a step increases very considerably. Fig. 1*a* (Pl. XXII.) shows a typical step under these conditions (the visibility of this step when the surface is unsilvered is too small for reproduction). When phase contrast equipment is used a 7.9 Å. step on an unsilvered surface is found to have a greater visibility than when the surface is silvered and the same step observed under narrow pencil illumination (see fig. 1*b*). When the surface is silvered and viewed under phase contrast conditions a further increase in visibility results (fig. 1*c*).

If it could be assumed that the steps on prism faces of beryl were visible merely because of being simple steps, then it would appear that the main advantage of phase contrast methods would lie in the observation of steps of height less than 7.9 Å. For reasons discussed in § 7 and § 8 such a deduction would not seem to be justified.

While the limit of observable step height is under discussion it is worthy of mention that for a step of metrical height t the optical height in reflection is $2\mu t$ where μ is the refractive index of the medium. By using a medium of high refractive index (such as cedar wood oil) in contact with the silver film it is possible to increase the optical height of a step considerably. As it is normally desirable to use a small observing N.A. for steps of low visibility a dry objective must be used. The conditions for an increase in the optical path can be easily satisfied by allowing a thin film of cedar wood oil to spread over the surface and then backing the film of oil with a cover glass. This results in an increase of visibility of the step. As metallurgical objectives are normally corrected for use with uncovered specimens some loss of definition must result, but as the paramount requirement is the observation of small steps this slight loss of definition can be tolerated.

In addition to the greatly increased contrast in the image the two other main practical advantages consequent upon the use of phase contrast are :

(i.) that in many cases it is convenient to work with an unsilvered surface. For example hydrated crystals are likely to decompose when placed in a vacuum for the purpose of silvering. Moreover with a new specimen it is usually necessary to scan the faces for areas of interest and a considerable saving in time results if the different faces of each crystal do not need to be silvered for such a preliminary survey ;

(ii.) that the narrower patterns enable closely spaced steps to be resolved much more easily. Close series of steps which are not resolved with the narrow pencil method can be resolved comfortably in phase contrast conditions.

A truly specularly reflecting surface is necessary if phase contrast equipment is to function most efficiently. Crystal faces which approach this condition are not unduly rare, but very often features of interest lie on faces or areas, which have been much roughened by the deposition of considerable amounts of foreign material. In such cases the increased visibility due to phase contrast may decrease markedly and in extreme cases it can become little, if any, better than when the same area is viewed using narrow pencil illumination.

§ 6. CAUSE OF VISIBILITY OF THE STEPS.

It is surprising that a step of 7.9 \AA . should produce a diffraction effect of relatively high visibility, and we shall therefore consider possible causes.

First it is necessary to note that the measurement of step height only gives the difference in height between two adjacent planes. This does not mean that the *effective* step riser is of this height, for it is conceivable that the original step edge of 7.9 \AA . height has been modified, by the deposit of impurity or other causes, to a much higher ridge. However such a ridge, if present, would have to be of lateral extent less than the resolving limit of an objective of N.A. 1.32, for no trace of continuous structure at the step edge can be observed. This could mean that the "ridge" could only be visible by scattering and one would expect the intensity of the scattered light to be low. The diffraction pattern has, however, a high visibility although superimposed on a bright field.

This line of reasoning appeared to be supported by dark field observations. In this case only scattering can be operative, but the intensities of the maxima making the positions of the steps are very low. For example, a step which required an exposure time of very few seconds with one of the bright field methods required about 15 minutes in dark field conditions, even although in the latter case the actual intensity of illumination was much greater.

The possibility of diffraction at a simple step was therefore considered. It was first shown by Rubinowicz (1917), starting from the ordinary Kirchhoff diffraction integral, that there are two alternative ways of considering diffraction by a plane screen. One can either (a) consider the contribution to the amplitude from every point on the screen, or (b) consider only the edge of the screen as effective, so that the resultant amplitude consists of the sum of the contributions predicted by geometric optics, plus the effect of "boundary waves". The latter are spherical waves which behave as if they emanate from a source at the edge of the screen.

The very fact that the 7.9 Å. steps are uni-molecular means that the planes between risers are true planes and that the riser is a true discontinuity. Even allowing for a good deal of smoothing out of the riser by the deposited silver it must still act as a true discontinuity to the incident light. The conditions are therefore ideal and any diffraction effect should produce the maximum possible intensities. This does not however necessarily account for the observed high visibilities.

§ 7. VARIATIONS IN VISIBILITY OF STEPS OF THE SAME HEIGHT.

Considerable variations in the visibility of 7.9 Å. steps occur and it should be possible to explain these variations in terms of the mechanism which renders the steps visible.

(a) *Effect of visible deposits of foreign material.*

The deposits may consist of (a) a general point speckling of the surface (see, e.g. Pl. XXII., fig. 1). The visibility of steps is normally high in such regions; (b) larger scale markings which often take various distinctive forms. One such type of marking results in the underlying steps being only faintly visible or invisible, while the continuation of the step outside of this area has a high visibility.

From the viewpoint presented above this could be due to poor contouring of the step, resulting in a decreased effective step height, or a non-plane deposit of the material, so that the diffraction conditions are altered, or possibly both effects might be operative together. Complete invisibility might be due to these causes carried to extremes.

The other types of large scale marking, when densely distributed, are associated with a considerable decrease in visibility and the step structure of large areas, or even whole faces, may not be seen. These large scale markings are associated with less obvious "blotchy" deposits which cover most of the available area. An explanation can therefore be offered in terms of a marked decrease in the plane diffracting areas.

(b) *Sudden increases in visibility.*

A very marked effect of this kind is shown in the triangular area in Pl. XXII., fig. 2. Neighbouring areas without well defined limits also show an increased visibility, and other triangular areas of greatly increased

visibility also exist elsewhere on this face. It appears that such behaviour could only be due to a greatly increased step height in this area. This view is supported by dark field observations in which the intensity scattered by the "super-visible" steps is much greater than that scattered by the steps in adjacent areas.

If this increase of visibility is attributed to an increase of height of simple steps, we have the problem of explaining how steps of great height come to be continuous in line with steps of smaller height. It has not been found possible to explain satisfactorily how such steps could be produced. For example, it appears that none of the normal processes of crystal growth would produce such a structure (Frank 1949, Burton, Cabrera and Frank 1951), and it is difficult to consider this as a crystalline overgrowth.

If, however, the increased visibility is considered to be due to the presence of a high "ridge", the formation of such a "ridge" can be satisfactorily accounted for, but one must accept that the mechanism operating in this small area, must also be operative in the adjacent areas, the sole difference presumably being a difference in dimension of the "ridge". It is to be noted that the same type of relationship between the intensities in dark and bright field holds for the triangular area as for other areas.

(c) *Slow variations in visibility.*

In many cases a slow decrease of the visibility of steps takes place over comparatively large areas, the visibility eventually becoming very low. These variations are observed whether the silver film is present or not. All the evidence is in favour of the steps being of uniform height, so that changes in the state of the crystal surface must be responsible for these changes.

It is probably a significant observation that in the low visibility areas there are very few deposits of foreign material to be seen, sometimes none, whereas they are present in all areas of high visibility.

§ 8. VISIBILITY OF STEPS ON OTHER TYPES OF CRYSTALS.

Investigation of the step structure on cleavage faces of mica by A. J. Forty (1950), using phase contrast illumination revealed steps which were probably 20 Å. high, corresponding to the height of the unit cell. The visibility of these steps was very low despite the large step height, but it appeared that these observations might be reconciled with those on beryl, because of the different surface structure in the two cases. As is well known cleavage slips of mica crumple, because of lattice stresses, so that the area between steps is usually by no means plane, and there is often a total variation in height of several wavelengths.

Later work on crystals of silicon carbide by A. R. Verma (1951) showed that steps of 15 Å. (corresponding to the height of the *c*-axis of the unit cell of type 6H) had a consistently very low visibility when viewed under

phase contrast illumination. In this case the area between steps is perfectly plane and it does not appear that any kind of anomalous behaviour can be taking place.

This evidence, and the observation of "super-visibility" areas on beryl, appear to be sufficient to discredit the hypothesis of simple edge diffraction for the areas of high visibility.

§ 9. PRESENCE OF "CLUMPS" OF MATERIAL AT STEP EDGES ON BERYL.

That steps should only have high visibility in areas where deposited impurities can be seen on the surface supports the conclusion that there must be deposited material along the step edge. Moreover the edge pattern always appears spotty, and not truly continuous, when narrow pencil illumination is used. Dark field observations usually show an edge as defined by a line of discrete dots, sometimes with considerable gaps. It therefore appears that the irregular edge patterns are not caused by impurity overlying a "ridge" and therefore blocking out sections of the pattern, but rather that discrete "clumps" of material are present. A puzzling feature was that the spottiness of the edges was considerably reduced when phase contrast illumination was used and photographs were taken in the usual way. The resolving power in such conditions should be considerably higher than with the narrow pencil method. However, by appropriate choice of exposure time it was found that the spottiness of the edge pattern under phase contrast conditions could be very obvious, and that instead of a continuous minimum some edges could be observed as lines of discrete, barely resolved spots.

The low intensities of the dark field images can be ascribed to the "clumps" being shallow, but of sufficient lateral extension to be resolved, or almost so. Moreover if the clumps are some 200–300 Å. high, then this height difference alone could account for a good deal of the deepening of the minimum in phase contrast conditions.

It is of interest to note that high visibility step patterns have been observed on several crystals of beryl which came from very different sources, so that a deposition of clumps of material along step edges is probably quite a common phenomenon. Their chemical nature might be investigated by chemical attack, but this is not permissible with the specimens at present available.

The non-complementary intensity distribution on either side of the true focus is rather puzzling in the light of this explanation. It might have been caused by a deviation from axiality which was not detected: it may be due to combination of a weak simple step-diffraction pattern with the scattering from clumps: or it may be that the clumps differ in structure on the sides against and away from the steps.

In terms of the "clump" explanation the areas of very low visibility may be made visible entirely by a simple step diffraction effect. The spottiness of the patterns in such areas is much reduced and no deposited impurity is normally to be seen on the surface.

The precise form of the "clumps" at step edges should be revealed very easily by an electron microscope, and it is intended to make such observations.

§ 10. EFFECT OF STEP HEIGHT AND NATURE.

On faces of some crystals it is found that the visibility of multi-molecular steps is less than that of small steps. This apparently paradoxical situation is due to the nature of the multi-molecular steps. The growth layers on a crystal face are commonly uni-molecular when first formed and it is necessary for the formation of multi-molecular layers that the unit layers draw together for some reason. This behaviour can take various forms and may apparently be due to various causes; the phenomena is described by the generic term "bunching".

We are concerned here with bunching only as it affects experimental observations. An example is shown in Pl. XXII., fig. 3 in which the unit steps, although drawn together, remain quite widely spaced on a molecular scale. This is an area of major rhombohedral face (1011) of a quartz crystal. The steps are approximately 200 Å. high and yet their visibility is poor when examined with narrow pencil illumination as in this figure. Interferometric measurements showed that the risers of these steps make an angle with the planes of approximately 0.5° . This angle of inclination and step height was roughly maintained over almost the whole of the face, so that it is understandable that risers some 3 microns in lateral extent should produce a diffraction effect of low visibility.

A case where bunching greatly increases the visibility is shown in Pl. XXIII., fig. 4. This is part of a terminal face (0001) of beryl and it appears that the multi-molecular steps make a steep angle with the plane of the face. Consequently the step edge still acts as a true discontinuity and the greater step height therefore results in increased visibility. (The general difference in intensity between neighbouring areas in fig. 4 is, of course, because the step height is great enough for phase differences to be shown as intensity differences.)

It appears possible that all gradations of bunching may exist, from bunches making very small angles with the face to bunches perpendicular to the face. The main experimental significance to be attached to the observation of low angle bunching of the quartz type is that if any one good crystal shows this kind of behaviour consistently it may well be that the great majority of all crystals of this substance will behave in this way. As the most detailed information about growth processes can only be obtained by observation of uni-molecular steps it is therefore advisable to avoid such substances when possible. For example examination of some 50 faces of various forms on quartz crystals by B.T.M. Willis (private communication) has shown that in every case when steps were visible a considerable degree of bunching had taken place, the bunching normally being of the low angle type.

Ionic crystals appear to be particularly susceptible to the onset of bunching, but from a limited amount of work on diamond crystals, for example, it appears that steps on other types of crystals may normally be multi-molecular.

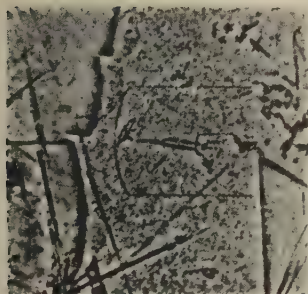
ACKNOWLEDGMENTS.

I am grateful to Dr. F. C. Frank and B. T. M. Willis for much helpful discussion on the visibility of the steps, and to Professor S. Tolansky in whose laboratory the early part of this work was carried out. I am glad to express my thanks to the Department of Scientific and Industrial Research, for financial support during all phases of this work and to the Keeper and staff of the Mineralogical Department, British Museum for the loan of specimens.

REFERENCES.

- BARAKAT, N., 1949, *Nature, Lond.*, **16**, 603.
BRAGG, W. L., and WEST, J., 1926, *Proc. Roy. Soc. A*, **111**, 691.
BURTON, K., CABRERA, N., and FRANK, F. C., 1951, *Phil. Trans. Roy. Soc.*, in press.
FORTY, A. J., 1950, private communication.
FRANK, F. C., 1949, *Discussions Farad. Soc.*, **5**, 48.
GRIFFIN, L. J., 1950, *Phil. Mag.*, **41**, 196 ; 1951, *Ibid.*, in press.
RUBINOWICZ, A., 1917, *Ann. Phys. Lpz.*, **53**, 257.
VERMA, A. R., 1951, *Phil. Mag.*, in press.

(c)



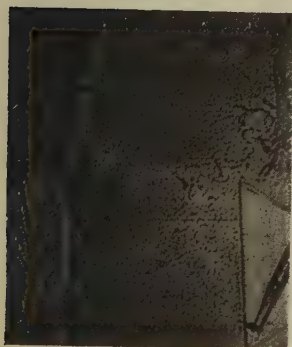
× 270

(b)



× 270

(a)



× 270

Fig. 3.



× 12

Fig. 2.



× 500

Fig. 4.



$\times 120$

LXXX. *A Design of an Ultrasonic Delay-Line.*

By T. GOLD,
Cavendish Laboratory, Cambridge*.

[Received March 29, 1951.]

SUMMARY.

A simple design of a vertical folded mercury delay-line is described. The device is used as a memory unit for electronic apparatus, where it introduces a delay of 1.2 millisecond with a band-width of several megacycles per second.

Design considerations and essential details of construction are given, and the operating conditions are mentioned.

§ 1. INTRODUCTION.

THE device described here is an ultrasonic delay-line, designed for delay or storage of electric pulses. Its present application is in the Pulse Analyser described in another paper (Hutchinson and Scarrott 1951).

The present design is in many respects similar to that which was suggested by the author and adopted for the EDSAC (the high-speed digital computing machine at the Mathematical Laboratory, Cambridge). As usual it employs mercury to propagate the soundwaves, and X-cut quartz plates as electro-mechanical transducers. The delay is approximately 1.2 milliseconds, and the necessary path length of five feet is accommodated in an object of roughly half that length. The necessary reflection is made by means of a perspex corner reflector, possessing three mutually perpendicular surfaces.

This design of a "folded line" reduces the overall length, allows one to mount the device vertically without prejudicing the reliability, and obviates the necessity of precise alignment of the structures at the two ends.

§ 2. DESIGN CONSIDERATIONS.

(1) *Transmission medium.*

The acoustic properties required of the transmission liquid (solids are less suitable) are a low velocity of sound, a low attenuation per unit time, and an acoustic impedance similar to the electro-mechanical transducers used. X-cut quartz is the most suitable material for transducers, and its acoustic impedance (density \times velocity of sound) is 1.52×10^6 in c.g.s. units. Clearly a very dense liquid will be required; and mercury with an acoustic impedance of 1.93×10^6 is satisfactory in all respects.

*Communicated by Professor O. R. Frisch, F.R.S.

(2) *Quartz mounting.*

A mounting in which only one side of the quartz plate is acoustically loaded appears to be the most satisfactory. A slight increase in the transducer bandwidth could be obtained by a double sided loading; but as this bandwidth in the present case is approximately 8 Mc./sec. (about a frequency of 13 Mc./sec.), no such increase is required for most purposes.

The acoustic mismatch from quartz to air is so great, that an airgap of as little as 10^{-5} cm. is practically a complete barrier at frequencies of the order of 10 Mc./sec. Consequently a thin quartz plate can be robustly supported by being pressed firmly onto a smooth, flat, dry backing plate; the very thin air gap which remains when normal engineering methods are employed, will still prevent any appreciable acoustic transmission to the back.

In the present design the thin quartz plates ($\frac{1}{4}$ mm. thick) (see fig. 1 (*k*)) are pressed onto the flat backing plate (*l*, *m*, *n*) by rubber rings which act as mercury seals (*j*). Under these conditions the quartz plates will withstand several atmospheres of hydrostatic pressure, and the line can hence be mounted vertically with the quartz at the bottom.

(3) *The acoustic channel.*

The tube should be wide enough so that (*a*) the sound waves reflected from the walls form a negligible contribution, (*b*) no waves travelling in the wall material are set up. The dimensions chosen here, of an internal tube diameter of one inch and a diameter of the active area of the quartz of $\frac{5}{8}$ of an inch (brass electrode *n*) have been found empirically to avoid such disturbances: but it is known that a considerable departure from these dimensions can be tolerated. In particular, smaller dimensions may be desirable to economize mercury.

(4) *The corner reflector.*

The reflector consists of three mutually perpendicular reflecting surfaces, arranged like the corner of a cube, viewed from the inside. The surfaces must possess a high sonic reflection coefficient in mercury; perspex is suitable for this, and is also easy to shape.

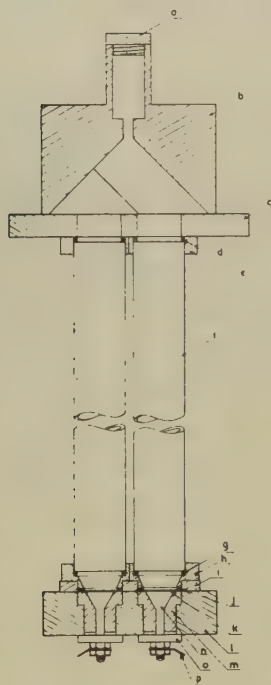
Such a corner reflector has the convenient property that incident and reflected rays are parallel to each other and symmetrically placed on either side of a line parallel to the rays and passing through the point of the corner. The reflection is hence unaffected by a rotation about that point, so long as the ray is reflected by each of the three surfaces.

It is required that the wavefront arriving at the receiving quartz shall be parallel to it to a precision of a fraction of a wavelength over the active area. For the highest frequency components which may be utilized, say 17 Mc./sec., and using the criterion of a quarter wavelength permissible error, this would imply an angular precision of 1.3×10^{-3} radian. It is not easy to construct a line so that the two ends are parallel to such a precision, and structures of great rigidity are then required. The consequence of a

greater angular error would initially be merely to decrease the high frequency response; but errors of more than 5×10^{-3} radian would seriously impede the function over the entire frequency band.

In the present design, these requirements are much easier to satisfy, for it is only necessary that the two quartz mountings, which are side by side, shall be parallel to this precision, and that the corner reflector shall be accurate. But owing to the fortunate property of a corner reflector, no great angular precision need be carried from one end of the object to the other.

Fig. 1.



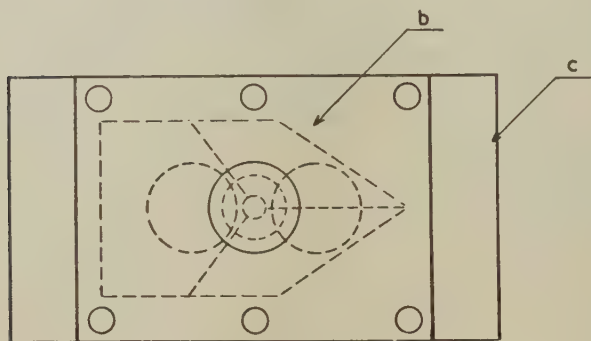
Elevation of delay line. (a) Filling plug with "breathing" hole: Perspex; (b) Corner reflector: made of Perspex in several pieces, glued with perspex solvent; (c) Steel plate; (d) Rubber rings, making the seal between the tubes and the reflector assembly; (e) Steel rings, attached to (c) with four screws each; (f) Steel tubes, 1 inch internal diameter; (g) Rubber rings, as (d); (h) Steel rings, attached by four screws each to plate (l), through clearance holes in plate (i); (i) Steel plate, attached with screws to (l); (j) Rubber rings, making the seal between (h) and the quartz plates (k); (k) Quartz plates, x-cut, 13 Mc./sec. resonant frequency, one inch diameter; (l) Steel backing plate; (m) Tufnol insets; (n) Brass electrodes: (l, m, n, o, p) are assembled before surface grinding; (o) Tufnol washer; (p) soldering tag. The girder linking plates (c) and (l) is not shown.

The less stringent precision requirements of the positioning of the point of the corner (which should be half way between the normals to the centres of the quartz plates) and of the tubes can be met easily, and do not warrant discussion.

§ 3. DETAILS OF CONSTRUCTION AND FILLING.

It has been found convenient not to rely upon the tubes themselves for rigidity, but to mount them in a U-section steel girder. The mercury seals between the tubes and the end assemblies may then be made by rubber rings (*d* and *g*) which are compressed by about 20 per cent as the endplates are tightened onto the ends of the girder. (This girder is not shown in fig. 1; it connects plates *l* and *c*.)

Fig. 2.



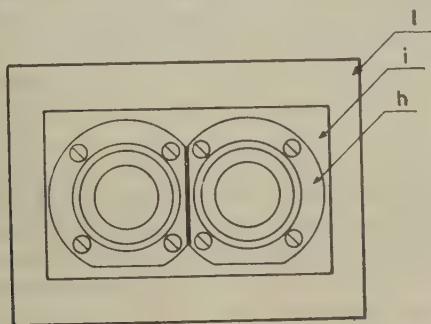
Plan view of the corner reflector and top assembly.

The insets in the backing plate (*m* and *n*) are glued and screwed into position before the entire surface is ground flat. The plate (*i*) and the rings (*h*) will allow the quartz plates to be fitted independently of the rest of the assembly. The rubber rings which bear on the quartz surface (*j*) are compressed by 15 to 20 per cent when the clamping rings are screwed down tight onto the plate (*i*).

The only known causes of subsequent failure of a mercury delay-line are leakage, fracture of quartz plates, or the adhesion of gas to the quartz surface. Leakage is avoided by using high grade rubber or neoprene gaskets cut out of sheet to assure flatness, and by care in adjusting dimensions to give the correct compression. Fracture of the quartz after assembly may result from insufficiently flat or subsequently distorted backing plates; one has to use a sufficiently thick plate and carefully grind the surface after the insets have been fully tightened and allowed to "settle down".

To avoid the adhesion of very small quantities of gas to the quartz surface, which may be sufficient to impede the acoustic transmission, it is advisable to have all internal surfaces very clean before filling, and to use mercury free from impurities which cause scum. For the same reason it is essential to fill the line first with a liquid which wets all surfaces well and thus excludes air, and to replace this liquid directly with the mercury. Alcohol is suitable for this. The present design, with the quartz at the bottom, avoids the risk that small quantities of gas migrate there later: a risk which exists for horizontal lines, and which would presumably be severe in any design where a quartz plate faces downwards.

Fig. 3.



Plan view of quartz mountings.

§ 4. OPERATING CONDITIONS.

The mercury itself acts as the earthed electrode. The input and output are hence applied to the brass electrodes, whose frontal area determines the active area of the quartz, and also the input and output capacity. In the present case, with 13 Mc./sec. *x*-cut quartz plates this capacity is approximately 30 pf. Owing to the small value of the piezo-electric coefficient and the good acoustic match, other terms in the input impedance can usually be ignored for the purpose of circuit design, and the problem is then simply to apply the desired waveform across this capacity. At the output an increase of voltage can be obtained, at the expense of bandwidth, by tuning with an inductance; or alternatively a connection may be made simply to the grid and gridleak of a valve.

The output voltage, when feeding into the small capacity of the grid of a valve, is approximately one thousandth of the voltage applied at the input. As the system cannot in any case pass low frequencies, the output is usually taken to a tuned amplifier.

REFERENCES.

- HUTCHINSON, G. W., and SCARROTT, G. G., 1951, *Phil. Mag.*, **42**, 792.
 WILKES, M. V., and RENWICK, W., 1948, *El. Engin.*, **20**, 208.

LXXXI. *A High Precision Pulse Height Analyser of Moderately High Speed.*

By G. W. HUTCHINSON, M.A., and G. G. SCARROTT,
Cavendish Laboratory, Cambridge*.

[Received February 26, 1951.]

SUMMARY.

A pulse height analyser is described suited particularly to the requirements of nuclear physics. Information is stored in a supersonic delay line and displayed on a cathode ray tube. The accuracy of channel width and the linearity of response are both one part in a thousand. The number of channels and storage capacity per channel may be varied at will to give 60 channels of up to 10^6 pulses, 80 channels of up to 3×10^4 pulses, or 120 channels of up to 1023 pulses. The maximum counting rate is 1600 per second.

A PULSE analyser serves to sort electrical pulses according to their peak voltage. The present analyser, in common with most of the other types which have been described, does this by displaying the number of pulses which have been received during an experiment within each of a series of size ranges; the boundaries between the ranges, or channels, are equally spaced in voltage.

The optimum number of channels is often determined by the experimental scatter of pulse size or by the need to present the information in an easily digestible form, that is, as a number of separate data which is not too large to be readily analysed. Apart from such limitations an analyser should lose as little information as possible in the presentation of a result. This would be achieved by a kicksorter with a large number of channels—about equal to the total number of pulses to be analysed—and a small capacity per channel. In the extreme case with an infinite number of channels and a capacity of one in each channel, none of the information would be lost.

These ideal requirements are modified when we consider the effects of channel boundary drifts. One must distinguish two kinds of drift—common drift which causes an uncertain zero error, and relative drift which causes uncertainty in the channel width. The common drift then places a lower limit to the useful width of each channel, *i. e.* if the common drift is, say, 0.2 V., then no advantage can be gained by making channels much narrower than 0.2 V.

The effect of relative drift is much more serious. Suppose the channel width is v and the counting capacity per channel is n , then unless the probable error in channel width is less than v/\sqrt{n} the full statistical

* Communicated by Professor O. R. Frisch, F.R.S.

significance of the channel counting capacity cannot be realized. This means that if the channel width be made 0.2 V. and n has the modest value of 10^4 , then the channel boundaries must be fixed relative to one another with a precision of 2 mV.

§1.

Several authors (see References) have described electrical pulse height analysers for use in nuclear physics research. Most of these either are slow because they employ a mechanical system to record each pulse, or they use very large numbers of components to provide a scaling circuit before each of many mechanical recorders. In addition, many, but not all of them divide the spectrum of pulses into discrete channels whose boundaries are determined separately by voltages applied to electrodes of different valves. The relative channel boundary drift is therefore as large as the common boundary drift, so that comparatively few large channels can be usefully employed.

The pulse spectrograph (Maeder *et al.* 1947) suffers from neither of these disadvantages, but since it presents its information only as a diagram it is not very suitable for work in which precise knowledge of the number of pulses in a given spectral interval is required. It has also been found liable to serious error due to irregularities in the fluorescent screen of cathode ray tubes.

The analyser designed by D. H. Wilkinson (1949), while limited in speed by mechanical recorders, avoided relative boundary drift by gating an oscillator for a time proportional to the height of the pulse and then determining the appropriate channel by counting the oscillations during this time. This meant that, in effect, beginning from the random instant of arrival of the pulse the various channels were presented in turn using a common mechanism for determining all the channel boundaries.

In the present analyser the channels are presented in turn in a regular cycle, irrespective of the random time of arrival of pulses, the comparison mechanism being again common to all the channel boundaries. Again the definition of the relative channel widths depends on a time measurement which can be very accurate, and on the linearity of a saw-tooth waveform. This comparison with a regularly recurring waveform allows the use of a supersonic delay line memory system to store the information, and hence the combination of high precision with a much higher speed and considerable economy in components.

§2. FUNCTIONAL ARRANGEMENT.

The desirable functions of a pulse analyser may be divided up as shown in fig. 1.

The memory and display are often the same, but functionally they are distinct. The gate is needed unless the rate of presentation of pulses to the machine is very slow compared with the time taken to record a

pulse. It must be shut as soon as a pulse has been accepted for recording and reopened only after the sorting system has been cleared, otherwise more than one pulse may be presented at the same time to the sorter and the spectrum will be distorted in a way determined by the nature of the sorter (*e. g.* the smaller pulses may be masked by the larger). In order to reduce the loss while the gate is shut, the time taken to record a pulse should be as small as possible.

It is not in general required to study a complete spectrum of pulse size. The lower end of the required spectrum may be limited by noise or may be arbitrarily set at a higher value. The ratio of the lower and upper end is also arbitrary. The function of the selector is to allow only those pulses to operate the sorting and gate mechanism which, after passing through the biased amplifier, lie within a specified voltage range. The limits of this range, when referred to the input of the analyser, may be made to agree with those of the required spectrum by the bias and gain controls of the biased amplifier. If a linear scale is required, the selector lower limit must be set at such a level that pulses within the range of the finite non-linearity of the biased amplifier are rejected. The presence of the defined upper limit means that the analyser does not waste time by trying to sort pulses which are larger than the required range.

Fig. 1.



To increase the accuracy of the machine the voltage level of the pulses during the passage through the biased amplifier and sorter should be as high as possible (up to 200 volts in the present case). The pulses enter the machine usually from a standard pulse amplifier producing pulses only up to 50 volts, so it is also desirable to insert a "preamplifier" before the biased amplifier.

Finally, it is useful to have a source of standard and variable pulses available for calibration either by insertion at a 50 volt level directly into the analyser, or at a level of millivolts into a standard condenser connected to the input of the external amplifying system.

All these functions are incorporated in the present analyser, and will be described separately.

§3. ACCURACY AND STABILITY.

The standard voltages with which the voltage levels of the pulses are compared are derived ultimately from a stabilized power supply of conventional series-parallel design. This in turn derives its standard of voltage from a neon stabilizer, type 85A1, whose stability is stated by its makers to be one part in 1000. The circuits of the analyser have been designed to have this same accuracy both in channel width and in linearity of amplifiers and sorting circuits.

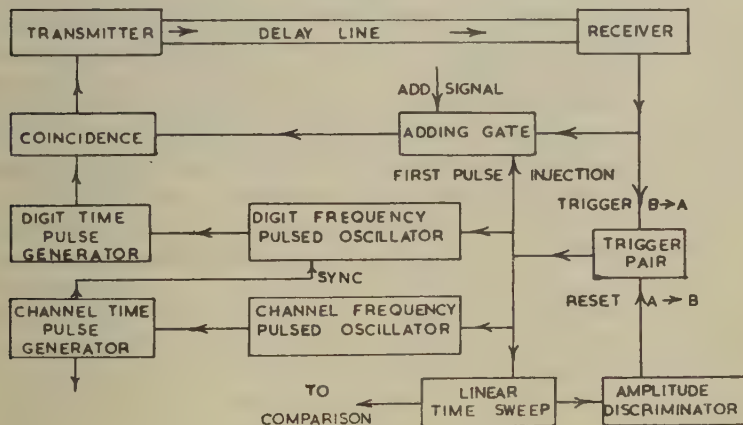
The variations in the effective cathode potentials of valves are known (Gray 1948) to be of the order of fractions of a volt. If drifts were not to exceed 0.1 per cent of 200 V., the voltage level throughout the analyser, it was necessary to arrange that variations within the valves should cancel to the first order. Whenever possible the two halves of one double triode have been used in this cancellation.

As an independent check, the calibration of the test pulses is made to depend in the first instance only on a wire-wound resistance and a sub-standard milli-ammeter, and their stability on that of a dry battery.

§4. MEMORY.

A mercury supersonic delay line (Harvard Annals) is used to store information. To save space, a folded vertical line designed by Mr. T. Gold was used. Impulses are fed to one end of the line by a quartz crystal and are detected after a time T_1 , which is about 1.2 milliseconds, by a similar quartz crystal at the other end. The electrical impulses from the detector crystal are amplified, reshaped, altered if required,

Fig. 2.



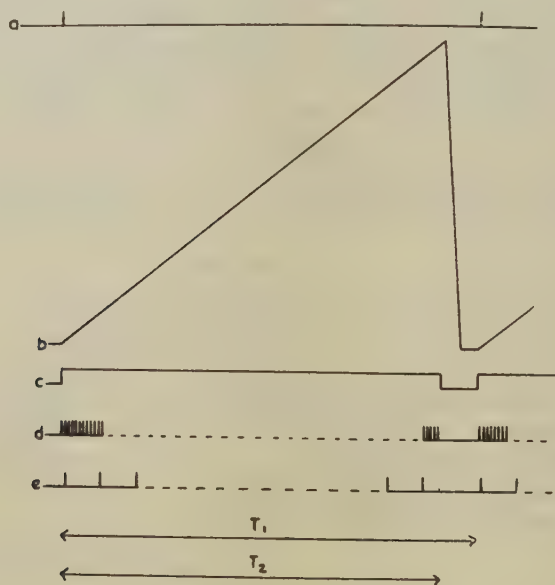
and fed again to the transmitting end of the line. Once a particular time sequence of impulses has been set up in the system it will therefore circulate indefinitely unless it is deliberately altered by an adding gate.

The cycle is synchronized with the comparison system in the following way. While the trigger pair of fig. 2 is in one state A the two pulsed oscillators and the linear time base are free. While it is in the other state B, they are held fixed. The change from B to A injects a pulse into the delay line through the adding gate. The discriminator is arranged at such a level and the linear time base at such a speed that the trigger pair is allowed to remain in the state A only for a time T_2 , which is a little less than T_1 . The trigger pair is A.C. coupled with such time constants that, if running free, it would remain in the state B for a time T_3 , where $T_3 > T_1 - T_2$.

When the instrument is switched on there are no pulses in the delay line. The first transit from B to A produces a pulse (waveform *a* of fig. 3) which reappears from the amplifier after a time T_1 . At this time the trigger pair is in the state B, and it is therefore forcibly triggered into the state A. The cycle is then repeated with the period T_1 so long as the condition $T_3 > T_1 - T_2 > 0$ is fulfilled. Since T_3 can be large, this means that small drifts in T_2 or in T_1 , which varies slightly with temperature, may be tolerated without destroying the synchronism.

The waveforms from the linear time base, the trigger pair and the two pulse generators are as shown at *b*, *c*, *d* and *e* in fig. 3.

Fig. 3.



Any signal occurring during the interval T_2 after the initiating signal, arrives when the trigger pair is already in state A and therefore has no effect on the cycle. This period is divided into about 1200 equally spaced possible signal positions by the waveform *d* (short pulses spaced 1μ sec. apart). Signals occurring during the period $(T_1 - T_2)$ before an initiating signal, would upset the synchronism, but there is no mechanism by which they are ever produced.

Waveform *e* divides the signal positions into equal groups of n . With each group is associated a range of voltage, *i. e.* that traversed by the waveform *b* during the passage of the preceding group through the adding gate. The groups therefore define the channels of the pulse analyser and the pattern of signals present in each group represents the

number of pulses received whose heights lay within the associated voltage range. By using the presence and absence of signals to represent the digits 1 and 0 of the number written in the binary system, any number up to $(2n-1)$ can be recorded.

§ 5. PULSE LENGTHENER.

A pulse to be analysed will in general arrive at random with respect to the cycle of the memory. It can be recorded only at a time when the group of digits appropriate to the height is passing through the adding gate. This will occur at any time up to T_1 after its arrival. Each pulse which is accepted by the selector is therefore made to charge a condenser through a diode to a potential equal to its height. The condenser retains its charge until the pulse has been recorded and is then discharged; a well-known principle of pulse lengthening. But the requirements on the present circuit are unusually stringent. The potential must be held for a random time up to 1.2 milliseconds with a precision of 0.2 V. The capacity, c , of the storage condenser is limited to about $300 \mu\text{F}$. by the minimum length of the incoming pulses and the total source impedance of the charging circuit. Hence the leakage current must not exceed $0.06 \mu\text{A}$. This is easily realized in the condenser itself, and as it is charged by negative pulses and controls only a cathode follower, the anode and grid thus connected to the circuit do not give rise to an appreciable leakage current. In order to discharge the condenser, however, electrons must be removed from it, and if this were done by connecting a heated cathode to the system, the heater-cathode leakage resistance would be much too low. The method used is to heat the discharging cathode from an insulated source of A.C. power whose D.C. potential could follow that of the charged system. Two other alternative methods have been used with success. One is to use the secondary cathode of an electron multiplier valve, and the other is to discharge the system through a neon tube which is held in a non-conducting condition during the duration of the lengthened pulse. Of these, the first is less stable because a secondary cathode is capable of being triggered into a stable condition in which its potential relative to the primary cathode is too low to give a secondary emission ratio greater than unity; it then ceases to act as a discharging cathode until it is reset externally into the operating range. This can be avoided or overcome, but with the secondary emission valves at present available, the stable limits appear to be inconveniently near to the operating range in this circuit.

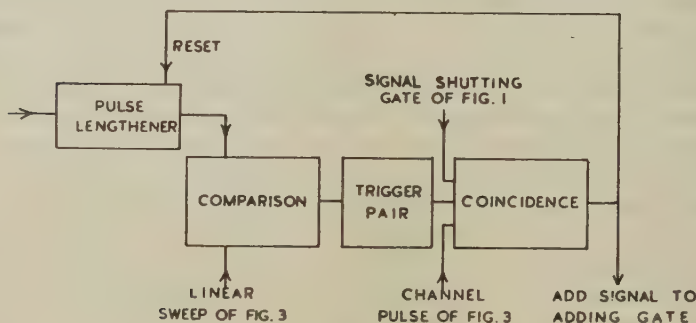
§ 6. SORTER.

The general functional arrangement is shown in fig. 4.

The potential of the cathode follower driven by the pulse lengthener is compared with that of the output of the linear time base of fig. 2 by applying them to the grids of a double triode as shown in fig. 5.

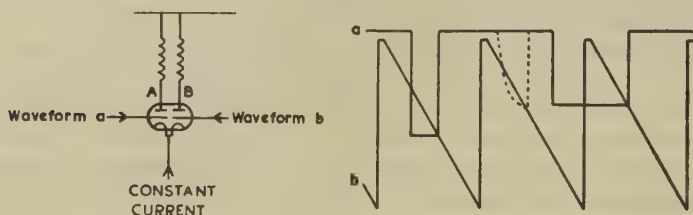
It is arranged that when the potentials of the two anodes become equal and B is becoming more positive, a trigger pair is caused to change its state and transmit an extended negative signal to the negative going coincidence circuit. The coincidence of this signal with the next signal from the channel pulse generator (waveform *e* on fig. 3) indicates the start of the group of digits forming the appropriate channel for recording the pulse.

Fig. 4.



Although this sorting process is carried out by an elaborate combination of valves, many of which can contribute to channel boundary drift, it is clear that the same process is used to define all the channel boundaries so that common drift and not relative drift is the resultant effect.

Fig. 5.



If the rise time of the pulses being analysed is long, a pulse might be recorded before it had reached its full height through an intersection of waveforms in the comparison circuit of the form shown dotted in fig. 5. To prevent this, a third coincidence signal is introduced, which allows a pulse to be recorded only while the gate of fig. 1 is shut.

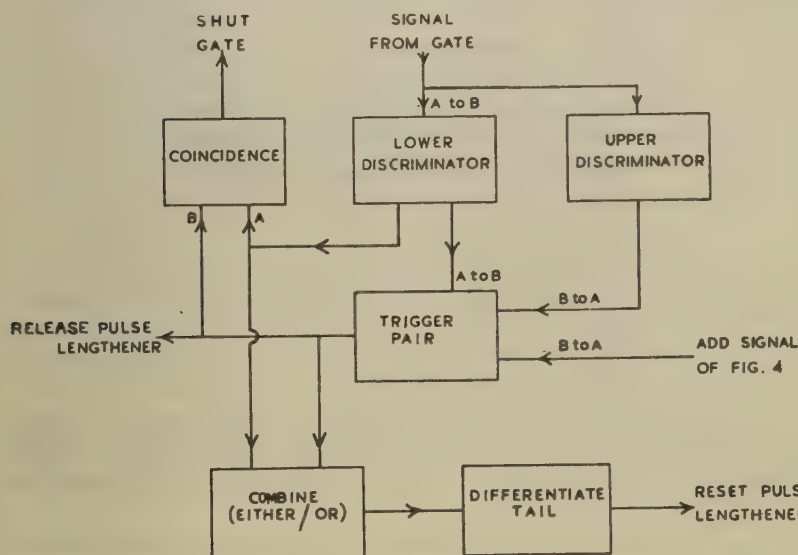
Of the n position in any one group passing through the adding gate, the first, if occupied, has the significance of 2^0 pulses, and the last 2^{n-1} . The process of adding "1" to a number already present in this form

may be stated in two equivalent ways. (a) Change the first digit. If the result is 0, carry 1, *i. e.* change the next digit, and so on. (b) Change all digits as they are presented until a 1 has been written, and then leave the remainder unchanged. The first is the process normally used in electronic calculating machines, and is at present employed. The second involves an equally simple circuit, and has also been used. There is little to choose in the relative merits of the two systems.

§7. PREAMPLIFIER, BIASED AMPLIFIER, GATE AND SELECTOR.

The two amplifiers are negative feed-back rings of three valves having a high loop gain so as to ensure linearity and stability. Their gain is determined by the ratio of high stability carbon resistances. The bias

Fig. 6.



is external to the amplifiers, and is determined by two similar pentodes forming a long-tailed pair. The pulses are negative when passing through the gate, which has the form of a double cathode follower. The functional arrangement of the selector is shown in fig. 6.

A pulse falling within the height range between the lower and upper limits will change the lower discriminator from its quiescent state A to its state B. This in turn changes the state of the trigger pair from state A to B, and thus removes the standing discharging current from the pulse lengthener. When the pulse dies away to a level below the lower limit, the discriminator returns to state A and a coincidence is formed which closes the gate. The gate is reopened and the pulse lengthener is reset by a signal from the sorter that the pulse has been recorded.

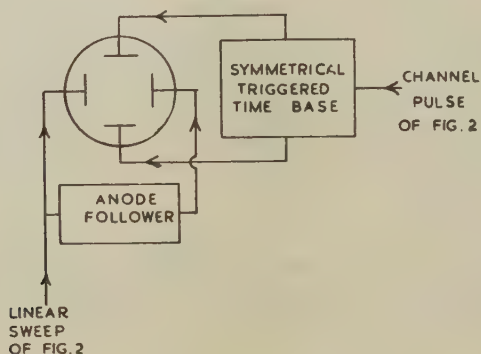
A pulse which passes above both limits resets the trigger pair before the lower limit has returned to state A. The gate is therefore not shut and no pulse is recorded. The act of resetting the trigger pair or resetting the lower limit, whichever occurs the later, resets the pulse lengthener.

§ 8. DISPLAY.

The functional diagram is shown in fig. 7.

A raster of faint vertical lines is produced on a cathode ray tube, each vertical sweep occurring during the passage of the group of positions corresponding to one channel through the adding gate. Pulses from the coincidence unit of fig. 2 are used to brighten the trace, so that each vertical line contains a series of bright dots and faint spaces respectively for the digits 1 and 0. The digits 2° are arranged to occur at the bottom

Fig. 7.



of each line. It is a convenience to allow the 1μ sec. pulses to make a slight modulation of the brightness even in the absence of a "1", since the power of 2 corresponding to any one digit can then more easily be read at a glance.

It would be possible to arrange also for a linear display of the spectrum of pulses, but this has not so far been included. The present display gives a very clear picture of what is going on during the course of an experiment. The height of the uppermost dot in each column gives a rough visual indication of the number of pulses on a logarithmic scale, and with a little practice it soon becomes possible to detect more detailed aspects of the spectrum by regular patterns in the lower dots of the columns. The information can either be decoded directly from the screen or may be traced or photographed. With the aid of a slide rule designed for the purpose by Professor Frisch, the time taken to decode a complete spectrum is about ten minutes.

§ 9. CALIBRATION PULSE GENERATOR.

The principle of the generator is that a standard current is switched from one anode to the other of a long-tailed pair of triodes. The size of the voltage pulses produced is determined by a variable resistance

network in the anode circuit of one of the valves. Provision is made for producing either short pulses for calibration of the analyser directly, or a square waveform of unit mark-space ratio intended for attenuation and injection into the input of an external amplifying system. Pulse repetition rates of 50 and 500 per sec. are provided and individual pulses can also be produced by a press button.

The maximum pulse size is 50 volts adjusted by switches in steps of 10 volts and 1 volt, and by a potentiometer, continuously up to 1 volt. There is an independent attenuator giving multiplying factors of 1, 10^{-1} , 10^{-2} , 10^{-3} and 10^{-4} .

§ 10. SPEED.

The average time taken to record a pulse is $\frac{1}{2}T_1$. Hence the maximum possible counting rate in the present machine is about 1600 per sec. If pulses are presented with a frequency comparable to this, the analyser selects a random sample for recording, but since the sampling is not dependent on pulse height, the spectrum of pulses is not distorted.

The minimum acceptable pulse length is limited by two factors:—

- (a) the charging impedance of the pulse lengthener;
- (b) the short-period overshoot occurring in the negative feed-back amplifiers.

If the pulse length is reduced to $\approx 1 \mu\text{sec.}$, the error from these causes is already of the order of 0.1 per cent. But if the input pulses are made longer than $1 \mu\text{sec.}$ and the counting rate is made more than 1000/sec., an error of more than 0.1 per cent will arise from the absence of D.C. restoration, which would be difficult to introduce before the biased amplifier in the presence of noise. The combination of these effects, therefore, sets an upper limit to the speed which is independent of the time taken to record a pulse.

§ 11. STORAGE CAPACITY AND NUMBER OF CHANNELS.

The number, n , of positions of binary digits in each channel can be varied at will by changing the frequency of the channel Frequency Pulses Oscillator of fig. 2. Three settings are provided: 120 channels each capable of recording 1023 pulses; 80 channels of up to more than 30,000 pulses or 60 channels of up to more than 10^6 pulses each.

If a channel becomes full, the analyser clears it, and incidentally adds one pulse into the next higher channel. By noting the number of times that a given channel is cleared during a run, it is therefore possible to use the analyser, if necessary, for much longer runs than would be indicated by its storage capacity.

§ 12. ALTERNATIVE MEMORY SYSTEMS.

Other types of short-term memory (see References 20–23) such as a cathode-ray tube memory, a magnetic disc or tape, or an electrostatic disc could have been used instead of a supersonic delay line. The delay

line was used because of its great convenience, simplicity and reliability, together with the fact that its most convenient range of delay times gives a suitable compromise between storage capacity and mean recording time.

ACKNOWLEDGMENT.

We wish to express our thanks to Mr. T. Gold for designing for us the very simple and efficient supersonic delay line used in the analyser.

One of us (G. W. H.) wishes to thank the administrators of the University of Cambridge Clerk Maxwell Scholarship Fund for financial support during the course of the work.

REFERENCES.

- Annals of the Computation Laboratory of Harvard University, Vol. 16, pp. 103, 125, 133.
 BALDINGER, E., and CASALE, R., 1949, *Helv. Phys. Acta*, **21**, 172.
 BOOTH, 1949, *Electronic Engineering*.
 COOKE-YARBOROUGH, E. H., BRADWELL, J., FLORIDA, C. D., and HOWELLS, C. A., 1950, *Proc. Inst. Electr. Eng.*, Pt. III, **46**, 108.
 EPPSTEIN, J. S., 1951, *J. Sci. Instrum.*, **28**, 41.
 FREUNDLICH, H. F., 1943, *Brit. Atomic Energy Project*.
 FREUNDLICH, H. F., HINCKS, E. P., and OZEROFF, W. J., 1947, *Rev. Sci. Instrum.*, **18**, 90.
 FRISCH, O. R., 1943, *Brit. Atomic Energy Project*.
 FRISCH, O. R., in course of publication; see also 1948, *Discovery*, **9**, 236.
 FRISCH, O. R., 1951, *Phil. Mag.*, **42**, in course of publication.
 GLENN, W. E., 1949, *Nucleonics*, **4**, 6, 50.
 GOLD, T., 1951, *Phil. Mag.*, **42**, 787.
 GRAY, W. J., 1948, Appendix C to "Vacuum Tube Amplifiers" by G. E. Valley and H. Wallman.
 KAHAN, T., and KWARTIROFF, A., 1946, *J. Phys. Radium*, **7**, 300; *Ibid.*, **7**, 357.
 MAEDER, D., 1947, *Helv. Phys. Acta*, **20**, 139.
 MAEDER, D., HUBER, P., and STEBLER, 1947, *Helv. Phys. Acta*, **20**, 230.
 POOLE, M. J., 1944, *Brit. Atomic Energy Report* (May).
 ROBERTS, A., 1940, *Rev. Sci. Instrum.*, **11**, 44.
 SAYLE, E. A., 1944, *Brit. Atomic Energy Report* (Jan.).
 SELENYI, P., 1935, *Zeits. f. Tech. Physik*, **16**, 607; 1936, *Ibid.*, **17**, 477.
 THIRION, J., 1948, *C.R. Acad. Sci., Paris*, **226**, 706.
 WATKINS, D. A., 1949, *Rev. Sci. Instrum.*, **20**, 495.
 WESTCOTT, C. H., and HANNA, G. C., 1949, *Rev. Sci. Instrum.*, **20**, 181.
 WILKINSON, D. H., 1949, *Proc. Camb. Phil. Soc.*, **46**, 508.
 WILLIAMS, F. C., and KILBURN, T., 1949, *Proc. Inst. Electr. Eng.*, Pt. III, **96**, 81.

APPENDIX.

The following diagrams show the circuit details of the first model. This was designed to work with existing power supplies giving +300 V. and -200 V. stabilized lines. The power supplies for subsequent models have been designed to give three stabilized lines, and this has made possible some simplifications and improvements in the design.

The switch defining potential C is ganged with the gain control of the post-bias amplifier.

Fig. 5.

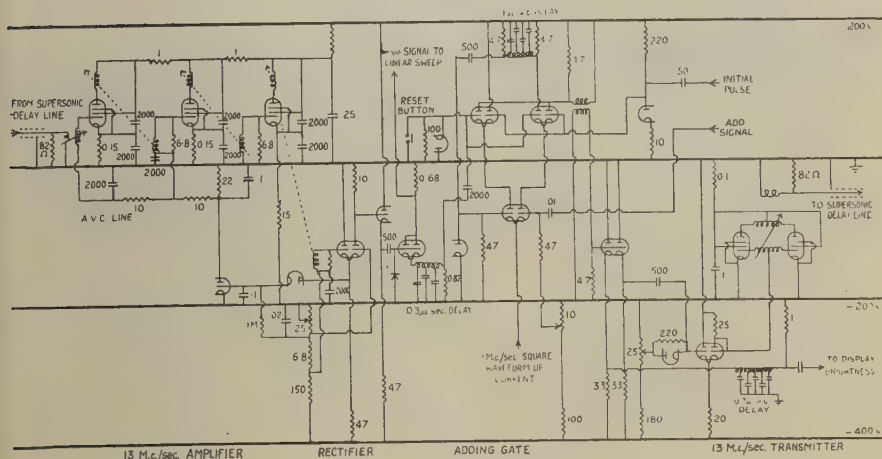


Fig. 6.

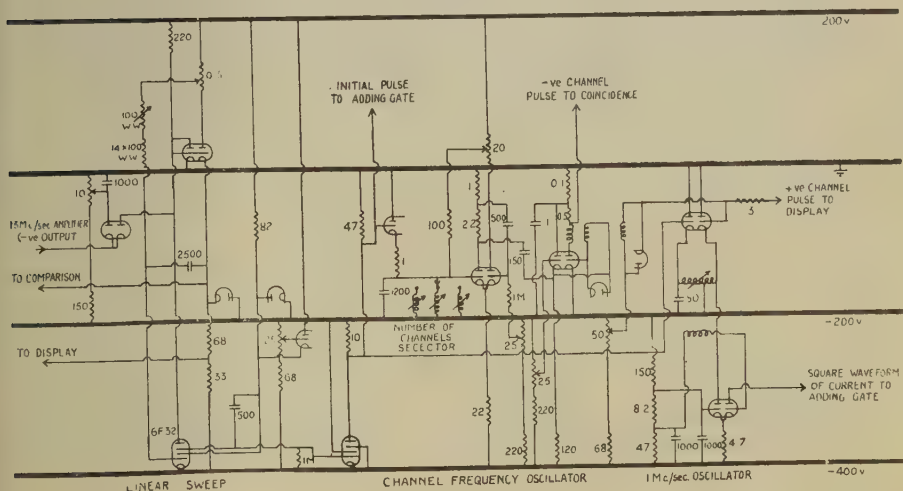
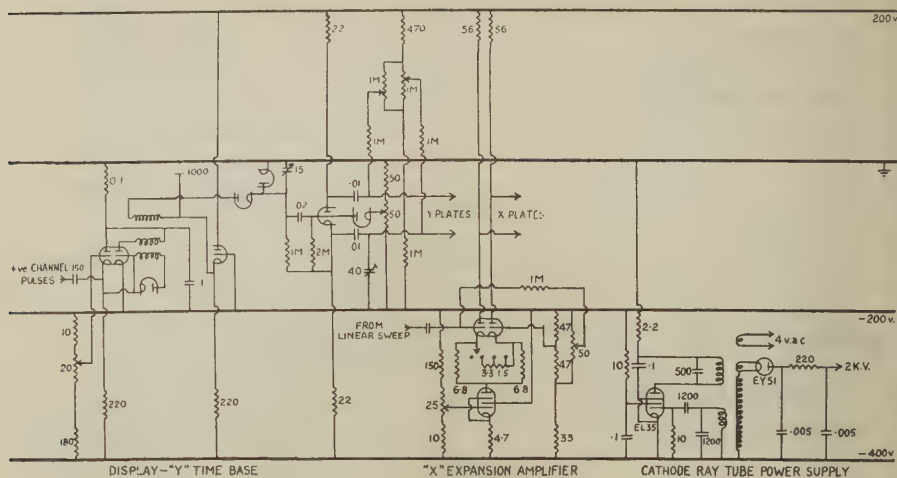


Fig. 7.



LXXXII. CORRESPONDENCE.

On a Generalization of Wilson's Hypothesis.

By GEORGE LUCHAK,

Defence Research Board Experimental Station, Ralston, Alberta*.

[Received April 9, 1951.]

IN his paper "A 4-dimensional Generalization of Wilson's Hypothesis", Dr. A. Papapetrou (1950) postulates that to every mass element at the point x^i with 4-velocity u^i there corresponds another mass element called its "gravitational centre" at X^i with 4-velocity U^i . An observer A measures u^i at x^i and, since, according to Papapetrou, he can find X^i by solving the equations of the gravitational field, he can find U^i . Now he is asked to form $u^i - U^i$. It is not clear how Papapetrou can possibly avoid violating the Special Theory of Relativity by such a procedure. At what times are u^i and U^i to be measured? If they are to be measured simultaneously by A, then a Lorentz transformation indicates that another observer A' would measure $u^{i'}$ at $x^{i'}$, and $U^{i'}$ at $X^{i'}$. However, it is obvious that in general $x^{4'} \neq X^{4'}$; i. e. the measurements by the new observer are not made simultaneously for the two particles. Thus, the concept of simultaneously timed measurements of the two 4-vectors is not permissible if relativistic covariance is required. However, if these measurements are not to be made simultaneously, how are they to be made? How can Papapetrou avoid giving one particular inertial frame preference over the rest in specifying any possible scheme in place of simultaneity? In essence, the postulate which Papapetrou introduces to displace the Wilson Hypothesis appears to be a retrograde step to the Newtonian idea of action at a distance.

Papapetrou introduces a "quantity" ω satisfying the equation

$$\square \omega = \frac{\partial p^i}{\partial x^i}, \quad (1)$$

where

$$p^i = \rho \sqrt{G}(u^i - U^i), \quad (2)$$

and then writes

$$s_i = \frac{\partial \omega}{\partial x^i} - p_i, \quad (p_i = \eta_{ik} p^k), \quad (3)$$

where ρ is the mass density, G is the gravitational constant, η_{ik} is the metric tensor for flat space, s_i is the postulated current to replace the Wilson current and u^i and U^i are defined as above. Since no boundary conditions are stipulated to restrict the generality of solutions of

* Communicated by the Author.

equation (1), it is evident that even if p^i be obtainable in principle, $\partial\omega_i/\partial x^i$ will not be uniquely determined for any prescribed physical conditions by solving equation (1). In Papapetrou's first example of the use of his postulate, he concludes that $\omega=0$ from

$$\square\omega=0, \quad (4)$$

and thus appears to demonstrate that equation (3) reduces to the Wilson expression. It is obvious, however, that equation (4) has an infinity of solutions any one of which might have been used. Papapetrou's other examples all suffer from the same arbitrary use of particular solutions with no justification for his choice.

Finally it is worth noting that, according to Papapetrou's postulate, finite displacements of the "gravitational centre" may occur for infinitesimal displacements of the mass element and consequently, a discontinuity in the current density s_i may take place while the gravitational field, presumably responsible for the current, is zero in value and changing in a continuous fashion. This does not seem physically plausible to the writer. Thus Papapetrou's generalization

- (a) violates the Special Theory of Relativity,
- (b) gives an infinity of solutions for any prescribed physical situation, and
- (c) in particular, does not reduce uniquely to Wilson's Hypothesis.

Any attempt to patch up the theory to eliminate (b) will probably require some specification of the physical significance of ω but such an attempt seems pointless in view of (a).

REFERENCE.

PAPAPETROU, A., 1950, *Phil. Mag.* [7] **42**, 399.

[The Editors do not hold themselves responsible for the views expressed by their correspondents.]

LXXXIII. *Crystal Dislocations.—Elementary Concepts and Definitions.*

By F. C. FRANK,

H. H. Wills Physical Laboratory, University of Bristol*.

[Received April 23, 1951.]

SUMMARY.

The elementary concepts of crystal dislocation theory—in particular the Burgers vector, perfect and imperfect dislocations, sessile dislocations, extended dislocations, twin and twinning dislocations—are defined in a manner independent of particular crystal lattices or models or special orientations of the dislocation: and it is shown how their essential properties arise, in so far as they are independent of the particular crystal in which they occur.

§ 1. INTRODUCTION.

DURING the past three or four years, those accustomed to deal with the theory of crystal dislocations have to some extent developed a private language and a number of special concepts, each simple enough in itself but together forming a substantial self-contained body of theory. The definitions of these concepts are to be found scattered in various papers and have been propagated in conferences and summer schools. A formal collection seems desirable. The concepts and definitions have largely originated in discussions at Bristol, in which, among others, F. R. N. Nabarro, G. Wyllie and the writer have been involved. We attribute the basis of our approach to a paper by J. M. Burgers (1939). We have also made use of important contributions by W. Shockley.

§ 2. THE IDEAL CRYSTAL.

The ideal crystal is built on a mathematical lattice, such that ions of the p th kind are to be found at the points

$$\mathbf{r}_p = l\mathbf{a} + m\mathbf{b} + n\mathbf{c} + \mathbf{r}_{p,q},$$

where l, m, n , are all positive or negative integers, including zero; p takes the values 1, 2, . . . up to u which is the number of kinds of ion in the ideal chemical formula of the substance; and q takes the values 1, 2 . . . up to v_p , which is the number of ions of the p th kind per unit cell. The unit cell is the parallelipiped whose three contiguous edges

* Communicated by the Author.

are the lattice vectors **a**, **b**, **c**. Any three independent linear combinations of **a**, **b** and **c** make alternative lattice vectors. When **a**, **b** and **c** are so chosen that the v_p are as small as possible, they are said to be primitive lattice vectors, and the lattice ($l\mathbf{a} + m\mathbf{b} + n\mathbf{c}$) is called the Bravais lattice of the crystal. The choice is not unique, and all vectors which are members of a set of three satisfying this condition will be called primitive vectors of the lattice. It is these which determine the perfect dislocations (to be defined below) of which the lattice is capable. Classified according to symmetry, there are fourteen different Bravais lattices. For example, if **a**, **b** and **c** are equal in length and make equal angles with each other, the lattice is in general rhombohedral: if the angles are 60° , 90° or $109\frac{1}{2}^\circ$ the lattice has cubic symmetry, these three being the face-centred cubic (f.c.c.), simple cubic (s.c.) and the body-centred cubic (b.c.c.) lattices. Sodium chloride and aluminium have the same (f.c.c.) Bravais lattice and are equivalent in respect of their perfect dislocations.

The further classifications by symmetry which depend on the vectors $\mathbf{r}_{p,q}$, and which give 32 crystal classes and 230 space-groups, do not appear to be useful in classifying the further possibilities for dislocations: the latter are associated more with the twinning possibilities of the lattices, which have never been brought into a formal framework in an entirely successful way.

The conventional unit cell of a crystal is one displaying the symmetry properties, which is not necessarily the primitive cell. Thus, for the three members of the cubic system mentioned above, one uses cubic cells containing respectively 4, 1 and 2 lattice points of the Bravais lattice.

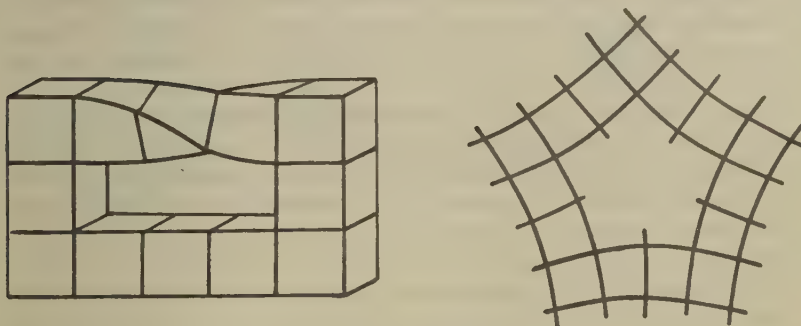
§ 3. ACTUAL CRYSTALS: GOOD AND BAD REGIONS.

The ions in actual crystals have thermal vibrations, and quantum-mechanical uncertainty of position which may be described as "zero-point vibrations". Both of these may be eliminated by taking a time average. There may also be vacant lattice points, interstitial ions, and wrong ions substituted for the right ones at lattice points: all these atomic defects may be notionally rectified, unless present to an excessive extent (*e. g.*, when there are so many interstitial ions that it becomes impossible to recognize which is the principal lattice and which the interstitial one). Finally, the crystal may be continuously deformed, *e. g.* elastically, and yet retain an unmistakable *local* correspondence to the ideal lattice, provided the strains are not too large. Following an admirably simple use of words suggested by Slater at the request of Shockley (private communication), we call all regions in which the strains, and density of atomic defects, are small enough to allow this unmistakable correspondence, regions of good crystal: otherwise, regions of bad crystal. We shall sharpen the definition of good and bad crystal regions presently.

§ 4. ASSOCIATED PATHS.

Consider a good region of real crystal, with its vibrations and atomic defects notionally eliminated, and let a tetrahedron of four neighbouring ions ABCD in this region be associated, one for one, with four corresponding ions $A'B'C'D'$ of an ideal "reference lattice", forming an almost congruent tetrahedron. A fifth neighbouring ion, E, in the real crystal can then be associated unambiguously with one, E' , in the reference lattice, the angles AEB and $A'E'B'$, BEC and $B'E'C'$, etc., taken in corresponding pairs, being almost equal or, at the worst, more nearly equal (say, in the sense of least squares) than if any alternative ion of the reference lattice is taken for the associated ion E' . Continuing this process, using angles made with BCD and E to fix a sixth ion F, and so on, we may extend a path from ion to ion through any region of good crystal, with an unambiguously associated path in the reference lattice. Moreover, a path may be displaced to a neighbouring path

Fig. 1.



"Moebius Crystals"

between the same end points, with an unambiguous corresponding displacement of the associated path. The whole region within which such displacements can be made will now be called "good".

§ 5. THE BURGERS CIRCUIT.

A path which closes on itself in the real crystal will be called a Burgers circuit. A Burgers circuit which lies in a simply connected region of good crystal may be formed by expansion from the initial tetrahedron: hence its associated path is also a closed circuit. The associated path of a Burgers circuit which links a topological torus (or infinite rod) of bad crystal does not necessarily close on itself. In this case the continuity of good crystal round the Burgers circuit ensures only that the associated path closes within a lattice vector.

§ 6. EXCLUDED CASES.

We shall extend the definition of bad crystal so as to avoid certain topological oddities, exemplified by fig. (1), which may be termed "Moebius crystals" by analogy with "Moebius strips". Such geometrical situations may possibly occur in pathological crystals like chrysotile. If unlimited strains are impossible, they necessarily have relatively large cores of emptiness, or of bad crystal in the sense already defined, and are of limited extension in at least one direction. A region extending from the core to a boundary is declared "bad" so that the core cannot be encircled by a Burgers circuit. We do this wherever, otherwise, we should fail to have a single-valued correspondence between *directions* in the real crystal and the reference lattice.

§ 7. CRYSTAL DISLOCATIONS.

If the closed Burgers circuit in the real crystal has an associated path which fails to close on itself, the circuit is said to encircle one or more lines of crystal dislocation (or, briefly, dislocations). We shall call the vector required to complete the associated circuit in the reference lattice the resultant Burgers vector of the dislocations enclosed. Burgers (1939) gave the name "dislocation strength" to the modulus of this vector.

When the Burgers circuit passes continuously through good crystal we shall say we have perfect dislocations. (Other cases will be considered later). Then the Burgers vector (regarded as a free vector) is independent of the starting point on the circuit, and invariant against displacements of the circuit through good crystal regions. It is necessarily a lattice vector of the Bravais lattice.

If two Burgers circuits are separated only by good crystal, they may be united into one circuit, whose Burgers vector is the vector sum of the Burgers vectors of its component circuits. Conversely, one circuit may be dissected into two, the sum of whose Burgers vectors is that of the one, by making a path through good crystal connecting two points on its circumference. When the circuit cannot be further dissected in this way, it may be shrunk on to its central core of bad crystal, which contains a single dislocation.

Since the Burgers circuit can be continuously displaced along the dislocation line, without change in its Burgers vector, a dislocation cannot terminate within the crystal.

§ 8. DISLOCATION NODES.

A dislocation line may branch. The Burgers circuit enclosing the one line may be displaced so that it encloses the two (or more) dislocation lines into which it divides: hence the sum of their Burgers vectors must equal that of the first line. A more symmetrical statement of the situation is that if the Burgers vectors of all dislocation lines meeting

at a node are defined by right-handed circuits, when looking outwards from the node, the sum of these Burgers vectors is zero. This corresponds to a vectorial version of Kirchhoff's law.

§9. THE KINEMATIC PROPERTIES OF PERFECT DISLOCATIONS.

Dislocations can move in many types of crystal. Indeed, the principal role of the dislocation concept in the theory of plastic deformation is to describe briefly the main essentials of the collective atomic motions involved in crystal slip. The possible motions of dislocations include those which do and those which do not involve the production or disappearance of lattice vacancies or interstitial atoms. Consider a Burgers circuit described anywhere in the crystal and let a dislocation line move from outside the circuit to inside it, passing between two adjacent ions P and Q on the circuit. The closure residue of the associated path is thereby changed by the Burgers vector, \mathbf{b} , of the dislocation. Hence the ion P is moved relative to Q by a distance, and in a direction, which locally corresponds to \mathbf{b} in the reference lattice. If the real crystal is, locally, nearly perfect apart from the dislocation considered, we may make the orientation and spacing of the reference lattice correspond to the local region and say that the displacement of P relative to Q is \mathbf{b} , to an approximation of the same order as is usually involved in small-strain elastic theory. In order that our statements may remain valid in severely distorted crystals, however, let us denote by \mathbf{b}' the local vector in the real crystal which corresponds to \mathbf{b} which is an invariant vector associated with the reference lattice. We may call \mathbf{b}' the local Burgers vector when we need a name which distinguishes it from \mathbf{b} . If the line element $d\sigma$ of the dislocation moves so as to sweep a planar element of area, the unit vector normal to which is \mathbf{n} , and there is an elastic stress represented by the stress tensor \mathbf{P} so that the traction on the element of area is \mathbf{nP} , the work done by the elastic field in this motion of the dislocation, per unit area swept, is $(\mathbf{nP}) \cdot \mathbf{b}'$. By virtue of the symmetry of the stress tensor this may also be written $(\mathbf{b}'\mathbf{P}) \cdot \mathbf{n}$. Either of these expressions therefore gives the magnitude of the force, due to an elastic field, per unit length of dislocation line, tending to move the dislocation in the specified plane. This corresponds simply to the existence of a force $(\mathbf{b}'\mathbf{P}) \times d\sigma$ on each element of the dislocation line. Fuller derivations of these formulae have been given by Peach and Koehler (1950) and Nabarro (1951) (though \mathbf{n} has a less general significance in Nabarro's derivation).

There is a change of volume $(\mathbf{b}' \cdot \mathbf{n})$ per unit area when the dislocation moves in the plane specified by \mathbf{n} . When this is positive, it must occur by production of lattice vacancies, or transfer of ions from interstitial sites to lattice sites: when it is negative it must occur by removal of lattice vacancies, or transfer of ions to interstitial sites.

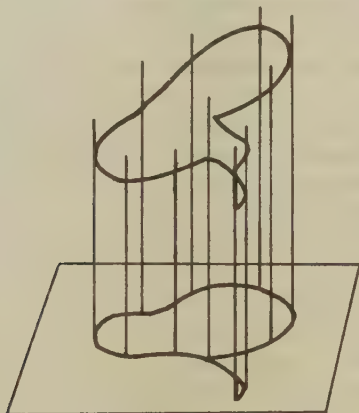
Such motions are accompanied by a change in free energy if the local concentration of atomic defects differs from its equilibrium value. In

the case, probably appropriate to metals in a suitable temperature range, that the only diffusing atomic defects we need consider are vacancies, of one kind of ion only, each occupying a lattice volume v' , and their concentration exceeds the equilibrium value by a factor α , this change in free energy per unit area swept in the plane whose normal is \mathbf{n} is equal to $(\mathbf{b}' \cdot \mathbf{n}/v')kT \ln \alpha$. This may be expressed by saying that there is an osmotic force $(\mathbf{b}' \times d\boldsymbol{\sigma}/v')kT \ln \alpha$ on the dislocation.

The change of volume is zero if, and only if $(\mathbf{b}' \cdot \mathbf{n})$ is zero : *i. e.* if the dislocation line moves in a surface containing itself and its Burgers vector. This is called the glide surface of the dislocation. The only motions (if any) of a dislocation which can occur rapidly under small stresses are glide motions.

In the special case that the dislocation line is parallel to its Burgers vector, all motions are glide motions. A dislocation in this orientation is called a screw dislocation.

Fig. 2.



The glide surface of a dislocation.

Disregarding local changes of \mathbf{b}' we may say that a dislocation is free to glide on the cylinder generated by lines parallel to its Burgers vector, passing through all points along an instantaneous position of the dislocation line, and also, whenever it becomes coincident with one of these generators, on any surface formed by moving the generator parallel to itself : so that its projection, along the direction of the Burgers vector, on to a fixed plane, is invariant in area and in shape, but may acquire any line extensions enclosing no area (fig. 2).

Motion of a dislocation (other than a screw dislocation) normal to its glide surface, by removal or generation of vacancies (alternatively, by generation or removal of interstitialcies) will be called positive or negative climb.

A node of three or more dislocation lines cannot move by glide alone unless their glide surfaces have at least a line in common. In general, they have only a common point. For example, at a triple node the Burgers vectors necessarily have a common plane: unless all three dislocation lines also lie in this plane the node cannot move without climb.

The motion of a dislocation node, changing the lengths of the dislocation lines which meet at it, can effect the progressive union of two or more dislocations into one, or the dissociation of one into a larger number.

§ 10. EDGE AND SCREW DISLOCATIONS.

The screw dislocation is one parallel to its Burgers vector, and is so called because lattice planes normal to this vector are transformed by the presence of the dislocation into one or more helicoidal surfaces. A dislocation lying normal to its Burgers vector is called an edge dislocation, since it may be thought of as lying at the edge of an extra plane inserted into the lattice. It provides a second case whose elastic field is relatively easy to calculate (Burgers 1939), and the elastic field of any straight dislocation may be found by superposing the fields of screw and edge dislocation, in proportion to the cosine and sine of the angle between the Burgers vector and the dislocation line.

§ 11. TRANSLATION TWINS.

It occurs commonly that two like or mirror-image crystals differing in orientation by a particular rotation or reflection will fit on to each other on a particular plane, crystallographically the same for each, with an energy very little greater than the continuing single crystal. This is ordinary twinning*. When two crystal lattices which are parallel, and differ only by a translation, will fit together on a particular plane with low energy, we shall call the situation "translation-twinning". It is not recognized in classical crystallography because it cannot be detected with a goniometer; nor is it visible by X-ray diffraction unless it repeats at short intervals in the specimen. The best-known examples of translation twinning are "stacking faults" in the sphere-packing lattices, *i. e.* breaches of the stacking rules which lead to face-centred cubic or hexagonal close-packing. But other examples should exist. For example, in the crystal of a long-chain paraffin it is probable that a displacement of one-half crystal parallel to the long axis of the molecules will lead to a number of positions at which the energy shows subsidiary minima, not much higher than the absolute minimum characteristic of the perfect crystal.

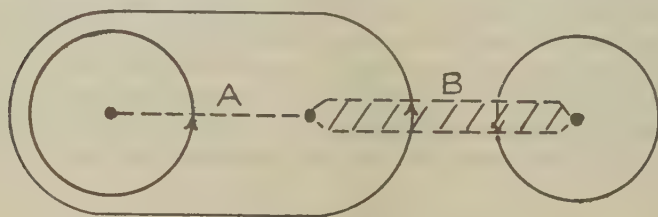
* The converse of this statement is not necessarily true. It probably is true for growth-twins and solid recrystallization twins: but the composition plane of some deformation twins may not be a surface of particularly low energy.

We may distinguish two types of translation twin : type I., or intrinsic, in which the two different lattice patterns are followed right up to the twinning surface (irrespective of whether this occurs on a plane of atoms or no) ; and type II., or extrinsic, in which a layer is sandwiched in between, not belonging to the continuing patterns of either.

§ 12. IMPERFECT DISLOCATIONS.

Unlike an ordinary twin-boundary, a translation-twin-boundary need not go right through the crystal. When it does not, its edge in the interior of the crystal is a dislocation. Assuming that there is no appreciable singularity of elastic properties at the translation-twin surface, it has the same stress-field as an ordinary dislocation. It will be called an imperfect dislocation (alternatively, a partial dislocation) in contrast with perfect dislocations which are surrounded entirely by good crystal.

Fig. 3.



Burgers circuits for imperfect dislocations.

The Burgers vector of the imperfect dislocation bounding a translation twinning surface of type I may be defined in just the same way as that of a perfect dislocation, except that the Burgers circuit must start and finish on the twinning surface instead of at a completely arbitrary point.

The same prescription must be followed when the translation-twinning surface is of type II., with the additional rule that the interpolated layer must be crossed normally, taking an equal distance normal to the corresponding plane when repeating the circuit in the reference lattice.

If the lattice allows translation-twin surfaces of more than one kind ; *e. g.* two kinds, A and B, we may have an imperfect dislocation at the line where an A surface joins a B surface. In this case we make one Burgers circuit round the edge of the A surface, and a second one enclosing both this and the AB junction (fig. 3) : the difference of the residues of the associated paths is the Burgers vector of the AB junction.

The Burgers vector of an imperfect dislocation is not a lattice vector. The Burgers vectors of the various different dislocations which may bound a given translation-twin surface (or provide the junction between two) all differ by lattice vectors.

§ 13. KINEMATICS OF IMPERFECT DISLOCATIONS.

Compared with perfect dislocations, imperfect dislocations are subject to an additional kinematic restraint. As the imperfect dislocation moves

it extends or contracts the bounding surface between crystal regions in translation-twin relationship. This boundary has low energy only when it is parallel to a particular crystallographic plane—the conformity plane. In any other orientation the boundary will have high energy, like an ordinary intercrystalline boundary. Estimates for the metals indicate that the stress required to make the dislocation move into a non-conformity plane will always exceed the practical ultimate breakage stress of the work-hardened metal. This motion might therefore occur on the microscopic scale in regions where stress amplifications due to other dislocations raise the stress to values near to the theoretical yield stress of the perfect crystal. For ordinary stresses, however, we may consider such motions forbidden. Motion which extends or contracts the translation twin surface in the conformity plane is resisted or assisted by a force per unit length equal to the surface energy of the translation-twin surface. The estimates which can be made indicate that this is a force of the same order of magnitude as that exerted by the highest ordinarily applicable stress, higher in some metals and lower in others.

Briefly, under ordinary stresses an imperfect dislocation is confined to its conformity plane. If its Burgers vector does not lie in that plane, it cannot glide: if its Burgers vector does lie in that plane, it cannot climb. Frank (1949) proposed that imperfect dislocations for which glide is forbidden should be called “sessile”.

§ 14. EXTENDED DISLOCATIONS.

Two imperfect dislocations forming the right and left boundaries of a strip of translation-twin surface may be the opposites of each other. In this case (except in a highly inhomogeneous stress field, or in a concentration of vacancies or interstitial atoms far from its equilibrium value) free energy will be released when they move together, annihilating the translation-twin surface and the dislocation pair. If they are not the opposites of each other they cannot annihilate, and if the scalar product of their Burgers vectors is positive (expressing the condition approximately) they repel each other with a force inversely proportional to their separation. This force is balanced against a constant force arising from the surface energy of the translation-twin surface. Hence they assume an equilibrium separation, forming an extended dislocation, as described for the face-centred cubic or close-packed hexagonal lattices by Heidenreich and Shockley (1947). The combination, being surrounded by good crystal, is necessarily a perfect dislocation. Conversely, a perfect dislocation, when brought into the conformity plane of a possible translation-twin, should spontaneously dissociate into a pair of imperfect dislocations with a ribbon of translation-twin surface between them, so lowering its energy.

If the Burgers vectors of both imperfect dislocations lie in the conformity plane, the combination is free to glide in that plane; but in no other, even when it or one of its components becomes a screw dislocation

And it cannot climb. Both statements apply for ordinary stresses, not exceeding the practical ultimate strength.

We shall use the term extended dislocation, in general, for any stable set of imperfect dislocations, connected together by translation-twin surfaces. An extended dislocation is free to glide only if these surfaces, and the Burgers vectors of its components, are coplanar.

§ 15. DISLOCATIONS IN INTERCRYSTALLINE BOUNDARIES.

Intercrystalline boundaries in general constitute continuous "bad" regions separating the "good" regions on either side. It is then impossible to make a Burgers circuit, running continuously in good crystal, and encircling a portion of the boundary. When this is the case, we may prescribe that the boundary region should be crossed to the nearest ion in the good region on the other side, while in the associated path we make an equivalent displacement, and a further displacement to the nearest equivalent ion. This introduces an uncertainty of the order of magnitude of one lattice spacing into the resultant Burgers vector, at each crossing. These are generally negligible errors. However, to continue the path in the second good region we must re-establish the cardinal directions by choosing a further three ions; making a tetrahedron with the first, to associate with a tetrahedron of ions in the reference lattice. The number of ways in which this can be done depends on lattice symmetry—for example, in the cubic system it may be done in twenty-four different ways. For each of these choices we shall find a different value for the resultant Burgers vector of dislocations enclosed in the circuit. We can show (Frank 1950) that if \mathbf{r} is the vector connecting the two points at which the circuit crosses the boundary, and the one crystal is brought parallel to the other by a rotation α about an axis \mathbf{l} (a unit vector), this resultant Burgers vector is $\mathbf{r} \times \mathbf{l} \cdot 2 \sin \frac{1}{2} \alpha$. We have the same multiplicity as before in the choice of \mathbf{l} and α , and can adopt the convention that we choose the \mathbf{l} which makes α least.

When α is small (say, less than 10° to 20° , according to the orientation of the boundary) the structure of the boundary which has lowest energy will probably be one consisting of discrete dislocation lines, a distance of the order of magnitude $|\mathbf{b}|/\alpha$ apart, separated by "good" regions (cf. Burgers (1939, 1940), van der Merwe (1950), Shockley and Read (1950)). A portion of the boundary can then be encircled by a Burgers circuit made entirely in good crystal, and its dislocation content can be unambiguously defined.

When α is large (it may take values up to $63\frac{1}{2}^\circ$ for a cubic crystal), the analysis of a grain boundary into line dislocations is of formal value only.

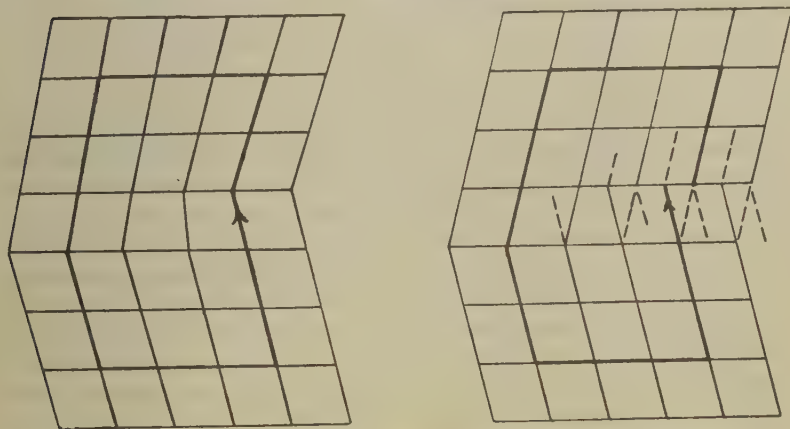
§ 16. TWIN AND TWINNING DISLOCATIONS.

When the real crystal approximates to a perfect twin, the perfect twin may be taken as reference lattice; the whole twinned real crystal, including the twin-boundary, being considered good. Ordinary perfect

and imperfect dislocations may be present, but there are additional possibilities. For, since the twin boundary may be on any one of an infinite succession of parallel equivalent lattice planes called composition planes, the reference lattice is multivalued. The possible Burgers vectors include all the vectors joining a point of the lattice to the points of its twin lattice interpenetrating it. Such dislocations correspond to steps in the twinning boundary, and are therefore confined to the boundary. They may be called twin dislocations.

If the twinning law is one which can be represented by a shearing deformation, with all displacements parallel to the composition plane, the Burgers vector of the dislocation may be parallel to the composition plane (being then equal to the height of the step in the boundary, multiplied by the shear in twinning). If this is so the dislocation may glide under mechanical stress. This motion is the growth of a mechanical twin, and the dislocation involved will be called a twinning dislocation. Fig. (4) illustrates one (*cf.* Frank and van der Merwe, 1949).

Fig. 4.



Burgers circuit and its associated path for a twinning dislocation.

REFERENCES.

- BURGERS, J. M., 1939, *Proc. Kon. Ned. Akad. v. Wet.*, **42**, 293; *Proc. Phys. Soc.*, **52**, 23.
 FRANK, F. C., 1949, *Proc. Phys. Soc. A*, **62**, 202; 1950, *Report of the Pittsburgh Symposium on Plastic Deformation*, May 1950 (Pittsburgh: Carnegie Institute of Technology) (to be published).
 FRANK, F. C., and VAN DER MERWE, J. H., 1949, *Proc. Roy. Soc. A*, **198**, 205.
 HEIDENREICH, R. D., and SHOCKLEY, W., 1947, *Report of the Bristol Conference on the Strength of Solids* (London: The Physical Society), p. 71.
 VAN DER MERWE, J. H., 1950, *Proc. Phys. Soc. A*, **63**, 616.
 NABARRO, F. R. N., 1951, *Phil. Mag.* [7], **42**, 213.
 PEACH, M., and KOEHLER, J. S., 1950, *Phys. Rev.* [2], **80**, 436.
 READ, W. T., and SHOCKLEY, W., 1950, *Phys. Rev.*, **78**, 275.

LXXXIV. *The Axis of Distortion of a Twisted Elastic Prism*

By D. G. ASHWELL,
Engineering Laboratory, Cambridge*.

[Received April 11, 1951.]

SUMMARY.

Duncan, Ellis and Scruton (1933) have shown that if an elastic cantilever is twisted, the displacement of its tip relative to its support consists of a rotation about the flexural centre of its cross-section. In this paper is considered the distortion of a twisted prism without reference to its support, and it is found that the axis of *distortion* of such a prism is in general quite different from the axis of *displacement* found by Duncan, Ellis and Scruton—an effect that has been previously noticed by Cullimore (1949). General expressions are derived for the determination of the axis of distortion, and its effect on practical cantilevers subjected to finite twisting is estimated. Experiments designed to test the analysis are described, and their results are found to confirm it satisfactorily.

§ 1. INTRODUCTION.

THE stresses and strains given by the St. Venant theory for the torsion of a prismatic elastic cantilever, held at one end and twisted at the other, are independent of the axis about which the prism is assumed to twist. Duncan, Ellis and Scruton (1933), discussing this fact, remark that it would appear as though the position of the axis of twist were actually indeterminate—"a conclusion quite at variance with physical intuition"—and go on to show that there can, in fact, be obtained from the St. Venant theory a position of the axis of twist for any specified relationship between the system of coordinate axes chosen and the root cross-section of the cantilever. This is because the root cross-section, like all other cross-sections, suffers warping out of its plane, and in order to specify the relationship between the cantilever and the frame of reference defined by the coordinate axes, three points in this cross-section must be regarded as fixed. The choice of these points determines the direction of the plane at the root of the cantilever relative to which its displacement is measured, and this determines the position of the axis of twist relative to the cantilever. In practical cases the direction of this plane will depend on the local stress distribution at the root—that is, on the system of local stresses which must be added to the St. Venant stresses in order to produce continuity between the cantilever root and its support.

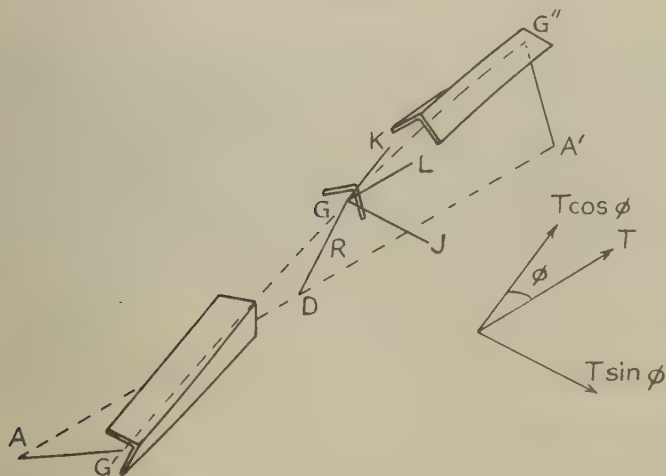
Thus the axis of twist is essentially a means of specifying the *displacement* of the cantilever as opposed to its *distortion*; for while the displacement may be expected to depend on the frame of reference chosen, the distortion

* Communicated by Professor J. F. Baker.

—that is, the displacements of various parts of the cantilever relative to each other—will be quite independent of the external frame of reference—local distortion at the root being, for the moment, ignored. Now physical intuition, while accepting the validity of the axis of twist as an axis of displacement, suggests that there must also be an axis of twist defining the distortion of the prism, and it is with the determination of this axis that the following four sections are concerned. The effect has been previously noticed by Cullimore (1949), who has given a tentative solution based on energy considerations. (See § 4, below.)

The distinction between the axes of twist and distortion is made clear in § 6, where is considered the effect of each of them on practical cantilevers.

Fig. 1.



§ 2. DETERMINATION OF THE DISTORTION AXIS.

First will be considered an elastic prism twisted uniformly in such a way that its distortion is the same everywhere along its length, and that there is no constraint against warping of its cross-sections anywhere. In general, longitudinal filaments that were straight before the prism was strained will become distorted into helices, and since the twisting is uniform, these helices may be expected to have a common axis. The filament lying along this axis will be the only one to remain straight, and its position in any cross-section will be called the distortion centre of the cross-section, and the axis itself will be called the distortion axis of the prism.

Fig. 1 shows a prism being twisted. The centroidal axis has become distorted into the helix $G'GG''$, which has a radius R and makes an angle ϕ with the generators of the cylinder containing it. The torque necessary to maintain the twisting is T , and since its effect at all cross-sections is the

same, it must act about an axis parallel to the axis AA' of the cylinder containing $G'GG''$ —that is, about the distortion axis of the prism. GL is the generator passing through G of the cylinder containing $G'GG''$, GD is a radius of the cylinder, and GJ is a line perpendicular to GD and to the tangent GK to $G'GG''$.

The torque T may be resolved into components $T \cos \phi$ twisting the prism about its centroidal axis, and $T \sin \phi$ bending the prism about GJ .

It can be shown from the geometry of the helix that the twist τ per unit length of the prism about its centroidal axis and its curvature $1/\rho$ about GJ are given by

$$\left. \begin{aligned} \tau &= \frac{1}{R} \sin \phi \cos \phi \\ \text{and} \quad \frac{1}{\rho} &= \frac{1}{R} \sin^2 \phi. \end{aligned} \right\} \dots \dots \dots (1)$$

Consider an elastic prism constrained to twist in such a way that its centroidal axis remains straight, and let its twist per unit length be constant and equal to τ . Let r be the distance of a longitudinal filament from the axis. Then the radius of the helix into which the filament distorts will be r , and its angle $\phi_r = \tan^{-1}(r\tau)$. Further, if e_0 is the strain of the filament lying along the axis, the filament distant r from the axis will suffer an additional strain of $1 - \cos \phi_r$, due to its distortion into a helix, giving a total strain of $e_0 + 1 - \cos \phi_r$. Here it must be mentioned that the warping of cross-sections of the prism out of their planes, due to the twisting, will cause axial displacements of points on the filament, but that since τ is constant and warping unrestricted, this displacement will also be constant along the length of any filament, and hence will produce no additional strain.

The strain of the filament considered, then, is $e_0 + 1 - \cos \phi_r$, and if it may be assumed that lateral stresses acting upon it may be neglected (see § 3, below), the stress in it will be $E(e_0 + 1 - \cos \phi_r)$, where E is Young's Modulus for the material of the prism. The component of this stress in the direction of the centroidal axis will be $E(e_0 + 1 - \cos \phi_r) \cos \phi_r$, and since $\phi_r = \tan^{-1}(r\tau)$, this may be expanded in terms of $r\tau$ to give

$$E[e_0 + \frac{1}{2}(r\tau)^2 - \frac{1}{2}e_0(r\tau)^2 - \frac{5}{8}(r\tau)^4 \dots].$$

If, now, e_0 and $(r\tau)^2$ may be limited to the usual small order of elastic strains, the axial stress at a distance r from the centroidal axis may be taken as $E[e_0 + \frac{1}{2}(r\tau)^2]$, terms containing higher powers of e_0 and $(r\tau)^2$ being neglected. The implications of this limitation are discussed in the next section.

Since there is no resultant axial force in the prism, the value of e_0 may be found by integrating these stresses over the cross-section and equating their sum to zero. This gives

$$Ee_0 = p_0 = -\frac{1}{2}Ek^2\tau^2, \quad \dots \dots \dots (2)$$

where p_0 is the stress corresponding to e_0 and k is the polar radius of gyration of the cross-section about its centroid.

Let Gx and Gy be the principal axes of the cross-section (see fig. 2). Then if (x, y) is the position of an element of area δA referred to these axes, and r is the distance of δA from G , the axial stresses will have resultant moments M_x and M_y about Gx and Gy given by

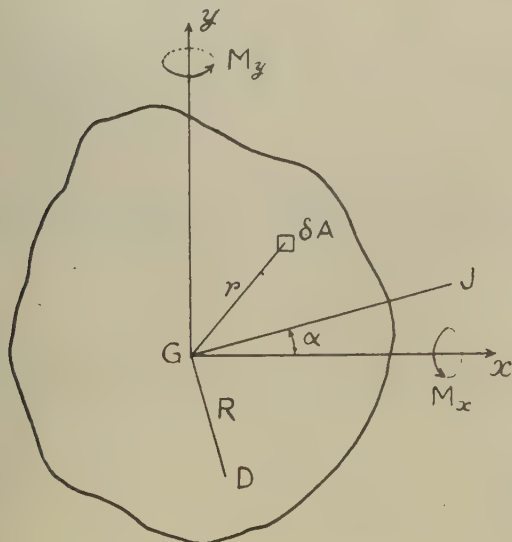
$$M_x = \frac{1}{2} E \tau^2 \int r^2 y \, dA$$

and

$$M_y = -\frac{1}{2} E \tau^2 \int r^2 x \, dA,$$

where the integrals are taken over the whole cross-section.

Fig. 2.



For convenience, let $\int f dA$ be written (f) , so that, for example, $\int r^2 y \, dA = (r^2 y)$. Then

$$\left. \begin{aligned} M_x &= \frac{1}{2} E \tau^2 (r^2 y) \\ M_y &= -\frac{1}{2} E \tau^2 (r^2 x). \end{aligned} \right\} \dots \dots \dots (3)$$

and

M_x and M_y have the sense shown in fig. 2.

Thus if the prism is to twist about its centroidal axis, in addition to the couple required to produce the twist, moments M_x and M_y must be applied. In the absence of such moments the prism will tend to take up curvatures $-M_x/EI_x$ and $-M_y/EI_y$, where I_x and I_y are the moments of inertia of the cross-section about Gx and Gy . These curvatures will combine to produce a curvature about some other axis through G , and this, together with the twist τ , will cause the centroidal axis of the prism to distort into a helix,

Consider again the prism constrained to twist with its centroidal axis straight. The moments about Gx and Gy will be given by (3). Let it now be caused to distort so that its centroidal axis becomes a helix of radius R and angle ϕ . Let D be the position of the distortion centre in fig. 2 and GJ be parallel to the axis about which the resulting curvature $1/\rho$ of the centroidal axis takes place; $D\hat{G}J$ will be a right angle. Let $J\hat{G}x$ be α . Then the curvatures of the centroidal axis about Gx and Gy will be $(1/\rho) \cos \alpha$ and $(1/\rho) \sin \alpha$ and these will require moments about these axes of $(EI_x \cos \alpha)/\rho$ and $(EI_y \sin \alpha)/\rho$. Thus the total moments to be provided about Gx and Gy are

$$\frac{EI_x \cos \alpha}{\rho} + M_x$$

and

$$\frac{EI_y \sin \alpha}{\rho} + M_y.$$

If this distortion is to be that actually suffered by the prism when subjected to a pure torque T applied about the distortion axis, the components of T about Gx and Gy must equal these required moments. Now it was shown above that the component of T tending to bend the prism is $T \sin \phi$ acting about GJ , and so its components about Gx and Gy are $T \sin \phi \cos \alpha$ and $T \sin \phi \sin \alpha$. Thus the equations of equilibrium for the bending of the prism about Gx and Gy are

$$\left. \begin{aligned} T \sin \phi \cos \alpha &= (EI_x/\rho) \cos \alpha + M_x \\ T \sin \phi \sin \alpha &= (EI_y/\rho) \sin \alpha + M_y. \end{aligned} \right\} \quad \dots \quad (4)$$

Furthermore, the component of T twisting the prism about its centroidal axis is $T \cos \phi$, and thus, if CJ is the torsional rigidity of the prism,

$$T \cos \phi = \tau CJ. \quad \dots \quad (5)$$

Finally, τ and ρ are related to R and ϕ by (1) above, and M_x and M_y are given by (3). Eliminating T , τ , ρ , M_x and M_y from (1), (3), (4) and (5), it is found that

$$\left. \begin{aligned} \cos \alpha &= -\frac{E(r^2 y) \cos^2 \phi}{2R(EI_x - CJ)} \\ \sin \alpha &= \frac{E(r^2 x) \cos^2 \phi}{2R(EI_y - CJ)}, \end{aligned} \right\} \quad \dots \quad (6)$$

Squaring and adding these equations, the following equation relating R and ϕ is obtained:

$$\frac{4R^2}{E^2 \cos^4 \phi} = \frac{(r^2 y)^2}{(EI_x - CJ)^2} + \frac{(r^2 x)^2}{(EI_y - CJ)^2} \quad \dots \quad (7)$$

An alternative form of this equation relates R and the angle of twist of the prism per unit length measured along the distortion axis. If θ is this angle of twist, from the geometry of the helix

$$\cos \phi = (1 + R^2 \theta^2)^{-\frac{1}{2}}; \quad \dots \quad (8)$$

and thus

$$\frac{4R^2(1+R^2\theta^2)^2}{E^2} = \frac{(r^2y)^2}{(EI_x - CJ)^2} + \frac{(r^2x)^2}{(EI_y - CJ)^2}, \dots \dots (9)$$

where

$$\left. \begin{aligned} (r^2y) &= \int r^2y dA \\ (r^2x) &= \int r^2x dA, \end{aligned} \right\} \dots \dots \dots (10)$$

and

the integrations being performed over the whole cross-section.

If Gx is an axis of symmetry of the cross-section, (r^2y) will be zero, and the equation relating R and θ becomes

$$2R(1+R^2\theta^2)(EI_y - CJ) = E(r^2x). \dots \dots (11)$$

It is worth pointing out that although equations (9) and (11) are cubic in R , they each have only one real root. If θ is given, and $R^2\theta^2$ is not immoderately large, R can be found quickly to any desired degree of accuracy by the usual iterative method for such equations. The position of D can then be found using equations (6) and (8). If Gx is an axis of symmetry, D is the point $(R, 0)$.

§ 3. ASSUMPTIONS INVOLVED.

In deriving these expressions two assumptions have been made.

The first is that the stresses in longitudinal filaments are E times their strains. Now since the sum of the axial stresses must be zero, and since $\frac{1}{2}(r\tau)^2$ is always positive, e_0 , the strain of the filament lying along the centroidal axis, will be negative—see equation (2). Thus, in general, the assumption is not valid, for if the cross-section has a compact shape with no internal boundaries, the tension in filaments near the external boundary will cause lateral contractions tending to squeeze the centre of the prism, which experiences longitudinal compression; and so the ratio between stress and strain will depend on Poisson's ratio as well as on Young's Modulus. However, prisms with such cross-sections may be expected to have distortion centres closely coinciding with their centroids, and their behaviour in this field is not of much interest. In other types of cross-sections, such as open and closed hollow sections, there will be little or no resistance to lateral contraction, and the ratio between stress and strain may safely be taken as Young's Modulus.

The second assumption is that e_0 and $(r\tau)^2$ may be restricted to the order of magnitude of small elastic strains. This also need not always be true, for if the material of the prism is at a fairly constant distance from the centroidal axis, and if $r\tau$ could be at all large, e_0 and $(r\tau)^2$ might have large numerical magnitudes of opposite sign without overstraining the material. But this could happen only in the case of a circular, or nearly circular, thin-walled hollow tube with a longitudinal slit—a special case in which, again, the distortion centre would very nearly coincide with the centroid.

In all cases which are likely to be of interest, therefore, these two assumptions may be taken as valid.

§ 4. TYPICAL POSITIONS OF THE DISTORTION CENTRE—AN APPROXIMATE EXPRESSION.

In the case of most thin-walled open sections CJ may be neglected in comparison with EI and $R\theta$ will be small compared with unity. Equation (11) then becomes

$$R \simeq (r^2 x) / 2I_y \quad . \quad . \quad . \quad . \quad . \quad . \quad (12)$$

This approximation will be true enough for many practical cases, and typical results obtained from it for thin-walled symmetrical sections are given in the Table. It should be noticed that the Δ given in the Table is not equal to R since it is not measured to the centroids of the sections.

Equation (12) can be obtained very quickly if two modifications are made in the above analysis. Firstly, the bending component $T \sin \phi$ must be ignored; this has the effect of omitting the term CJ from (9) and (11). Secondly, the expression for the longitudinal stresses obtained in § 2 must be referred directly to the distortion axis instead of to the centroidal axis; the effect of this is to invalidate the argument of the second part of § 3, and to cause the omission of the factor $(1 + R^2 \theta^2)$ from (9) and (11). These effects cannot be ignored in the case of flexible sections twisted considerably, or if it is desired to extend the analysis to include the effects of axial forces. A tentative solution due to Cullimore (1949) uses an energy method which yields results for channel and angle sections identical with those obtained from (12) above. The approximate nature of this solution seems to arise because an exact solution cannot be obtained by treating the problem as a small-deflection problem.

§ 5. GENERAL COMMENTS ON THE DISTORTION AXIS.


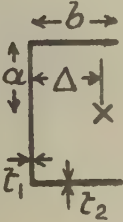
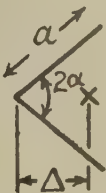
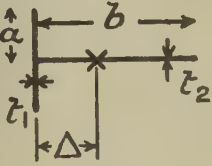
Previous writers on this subject have ignored the effect of the longitudinal stresses here considered, and the curvature they produce, on the ground that they are second-order effects (see Duncan, Ellis and Scruton 1933). But they seem to have overlooked the fact that from (1) and (8) it can be shown that the twist τ of the distorted centroidal axis is $\theta(1 + R^2 \theta^2)^{-1}$ and its curvature $1/\rho$ is $R\theta^2(1 + R^2 \theta^2)^{-1}$. Thus the distortion of the centroidal axis into a helix does in fact require that its curvature should be of the second order in τ even if R is large, and so in determining the position of the axis of distortion second-order effects cannot be ignored.

It must be emphasized that all the analysis in this paper so far is true only if all the cross-sections of the prism are allowed to warp out of their planes in the manner required by the St. Venant stress distribution. If one section is restrained against warping, the torque will be resisted near that section partly by the twisting of the prism and partly by the differential bending of its various parts. In this case the second-order longitudinal stresses due to twisting will certainly be negligible compared with the first-order stresses due to the differential bending near the constrained cross-section, and the usual methods for estimating the additional stiffness of the prism due to the constraint will be unaffected by the work contained in this paper.

§ 6. FINITE DISPLACEMENTS OF PRACTICAL CANTILEVERS.

It remains to distinguish between the axes of twist and distortion by considering their effects on the behaviour of practical cantilevers.

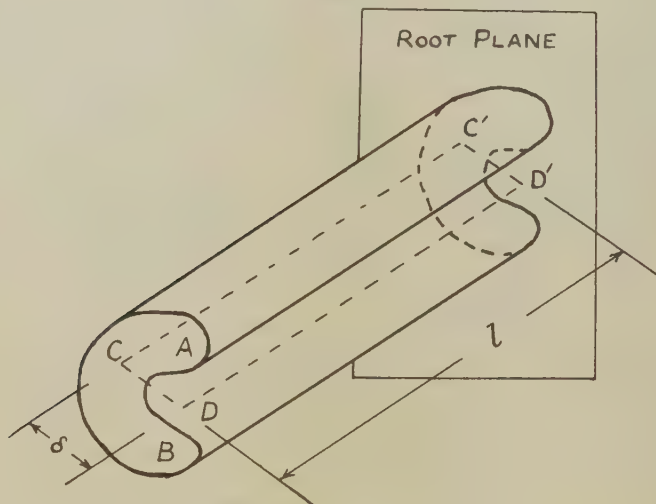
TABLE.

Section.	Δ (measured to mid-line) defines the position of the distortion centre.
	$\Delta = r$
	$\Delta = \frac{4a^3t_1 + 3ab^2t_1 + b^3t_2}{8abt_1 + 2b^2t_2}$
	$\Delta = \frac{a}{2 \cos \alpha}$
	$\Delta = \frac{-4a^3t_1 + 6ab^2t_1 + b^3t_2}{16abt_1 + 2b^2t_2}$

Consider a prismatic cantilever as shown in fig. 3. At the root its cross-section is everywhere attached to a rigid plane support. Its length is l , and

C is the flexural or shear centre at its tip, while D is the distortion centre there. The corresponding points at its root are C' and D' . Let it be twisted by a torque about an axis perpendicular to the supporting plane. The stress distribution along the greater part of its length will be that predicted by St. Venant, and its cross-sections will tend to warp out of their original planes. This they will be able to do except near the root, where an additional stress-system must be applied to produce continuity between the prism and the plane support. These continuity stresses applied at the root will have no resultant force or moment, and their effect may be expected to die out fairly quickly along the prism, so that at no great distance from the root they will have become negligible. Nevertheless, although they are confined to a short length of the cantilever, they may

Fig. 3.



affect its displacement significantly by producing a rotation of it about some axis in the fixed plane. Their precise nature is not known in general, and so it is not possible to determine exactly their effect except in special cases. Duncan, Ellis and Scruton, however, have shown that if the cantilever is twisted slightly, the tip ABC will rotate about C , the centre of flexure. In other words, the continuity stresses are such that the flexural axis of the cantilever remains perpendicular to the root plane.

If the rotation of the tip becomes large, CC' will not remain straight but, according to the analysis given earlier in this paper, will distort into a helix with DD' as axis. This will be true for the greater length of the cantilever, except near the root, where the continuity stresses will determine the distortion. It will still be true, however, that near the root the filament lying along CC' will be perpendicular to the root plane. Thus, since the length affected by the continuity stresses is small compared

with l , it can be said that the distortion of the cantilever will be that discussed in previous sections, while its displacement will be such that the tangent to the flexural axis at the root will remain perpendicular to the root plane. This statement is not strictly accurate owing to the short length affected by the continuity stresses, but if l is sufficiently large for the rotation of the tip to be appreciable, the error involved may be expected to be small.

It is now possible to estimate the displacement of the tip for large deflections. If the twist of the cantilever per unit length is θ , and the distance $C'D'$ is δ , it can be shown from the geometry of the helix that the rotation of DD' relative to the tangent to CC' at C' takes place about $C'D'$ and is of magnitude $\tan^{-1}(\theta\delta)$. In most cases likely to arise in practice this rotation will be small and may be safely approximated to $\theta\delta$. This means that since DD' remains straight, D suffers a linear displacement at right angles to $C'D'$ of magnitude $\theta l\delta$. Now the rotation of ABC , ψ , say, will equal $l\theta$, and so the linear displacement of D will be $\psi\delta$.

If DD' becomes inclined to the root plane, the applied torque, T , assumed above to be about an axis perpendicular to that plane, will have a component tending to bend the cantilever as a beam, but this component, $T\theta\delta$, will be small, and as prisms of types likely to be met with are stiff in bending, the distortion caused by this component will be ignored. It would not be a difficult matter to take account of it in any particular case.

Thus if the quantity $\theta\delta$ is small, and l is large compared with the length near the root affected by the continuity stresses, the displacement of the tip ABC consists of (i) a rotation ψ about D together with (ii) a linear displacement of D equal to $\psi\delta$ perpendicular to $C'D'$. The usually accepted centre of displacement, C , is now seen to be rather the instantaneous centre of rotation of the tip for the position $\psi=0$.

To determine the finite displacement of the tip of a twisted cantilever it is thus necessary first to determine the positions of the flexural and distortion centres for the value of θ concerned, and then to superimpose the linear and rotational displacements stated above.

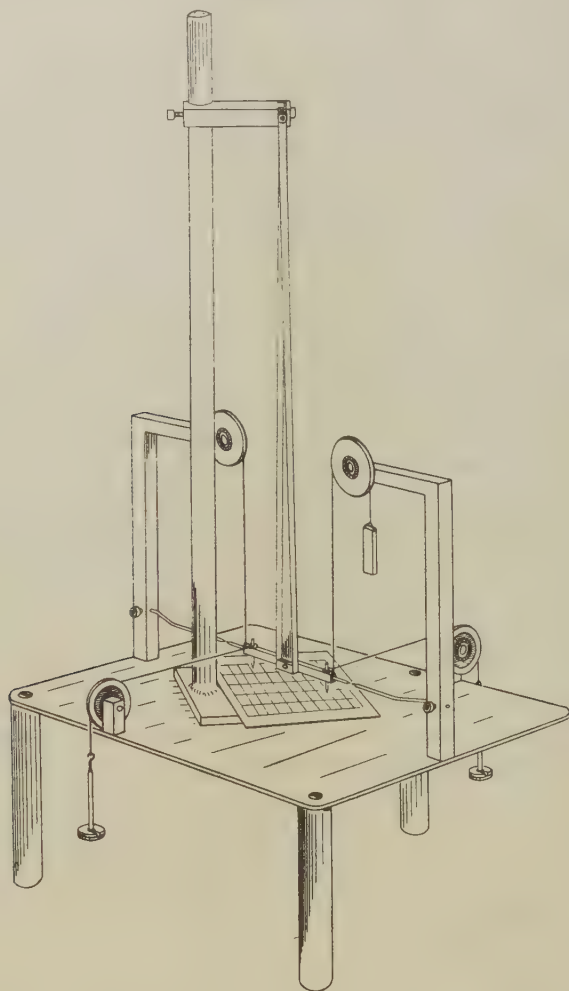
§ 7. EXPERIMENTAL RESULTS.

A series of experiments was carried out to test the analysis given in this paper. They consisted of applying a pure torque to cantilevers with different cross-sections and determining the displacements of their tips for different angles of rotation.

Three specimens were used. Specimens I. and II. were made from beryllium-copper strip of thickness 0.0125 in. Specimen I was formed by bending this strip into a symmetrical angle of side 0.576 in. and length 10 in., the two legs of the angle being at right angles to each other. Specimen II. was a symmetrical channel of dimensions 0.633 in. web, 0.242 in. flanges and length 16.5 in. Specimen III. was a commercial steel pocket tape-measure of the type having a transverse curvature for stiffness. It was especially chosen from a number of such tapes for its

initial straightness, and its dimensions were : thickness 0.0065 in., width 0.596 in., radius of transverse curvature 0.615 in., and length 17 in. Each specimen was provided with a specially made steel clamp which firmly held it at its root along the whole of its cross-section.

Fig. 4.



The testing apparatus is shown in fig. 4. The specimen was held vertically by its clamp, which was supported from the movable base-plate by means of the vertical rod. This base-plate could be moved about on the horizontal table, and carried on its upper surface a piece of graph paper. Attached to the bottom, free, end of the cantiliver was a horizontal cross-piece that had a vertical pointer at some distance on each side of its centre

and a horizontal one projecting from each end. By sliding the base-plate about on the table the tips of these two horizontal pointers could be made to correspond with the tips of two other horizontal pointers that were fixed relative to the table. The apparatus was so arranged that when this was done the forces applied to the cross-piece—and

Fig. 5.

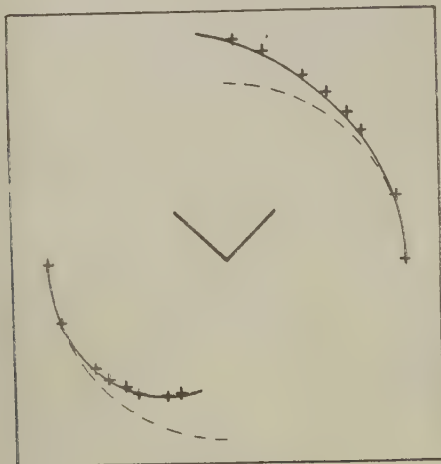
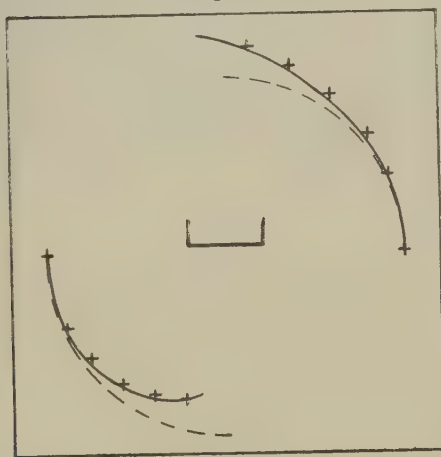


Fig. 6.

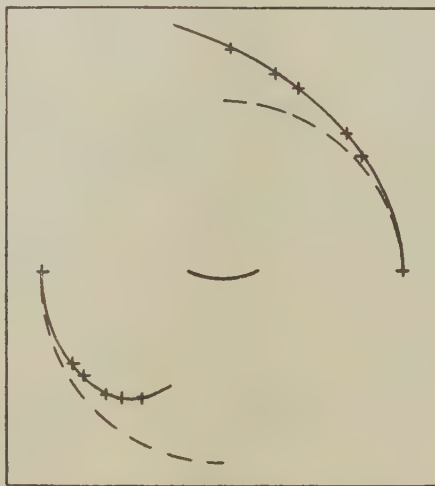


hence to the specimen—by the pair of horizontal strings, resulted in a pure couple about a vertical axis, while the tensions in the vertical strings exactly balanced the weight of the cross-piece. In this way, by varying the equal weights on the two hangers, the displacements of the two vertical pointers relative to the graph paper, and hence to the support of the cantilever, could be measured for various angles of twist. It was hoped that these displacements could be read directly from the lower

ends of the vertical pointers, but the cross-piece tilted slightly as the specimen distorted, and this introduced an appreciable error due to the length of the pointers. So, instead, a small set square was used, with which, by sighting along the lines on the graph paper the coordinates of the centres of the pointers at the level of the end of the specimen could be determined. This method was found to give consistent and satisfactory results.

In figs. 5, 6, and 7 are shown typical results for each specimen. As the tip of the cantilever rotated in an anti-clockwise direction the two vertical pointers traced out paths on the graph paper. In each case the cross-section is shown in its initial position. The full lines show the paths predicted by the analysis of this paper, while the broken lines show the paths that would be traced out if the tips of the cantilevers experienced only rotations about their centres of twist. The crosses are experimental points.

Fig. 7.



It is seen that in each case the agreement between experiment and the analysis given in this paper is satisfactory, while the distinction between this theory and the assumption that the sections rotate about their centres of displacement is most marked.

ACKNOWLEDGMENTS.

The author wishes to express his gratitude to Professor C. Gurney and Dr. E. N. Fox for many helpful discussions during the course of this work, and also to the members of the workshops staff at the Engineering Laboratory, Cambridge, who made the apparatus and specimens.

REFERENCES.

- CULLIMORE, M. S. G., 1949, *Research, Engineering Structures Supplement*, 153.
DUNCAN, W. J., ELLIS, D. L., and SCRUTON, C., 1933, *Phil. Mag.* [7], 16, 201.

LXXXV. *The Reflection of very Low Frequency Radio Waves at the Surface of a Sharply Bounded Ionosphere with Superimposed Magnetic field.*

By K. G. BUDDEN,
Cavendish Laboratory, Cambridge*.

[Received April 10, 1951.]

CONTENTS.

	Page
Summary	833
§ 1. Introduction	834
1.1. Previous work on the theory of the reflection of very low frequency waves	834
1.2. Scope of the present paper.	835
§ 2. The formulæ of the magneto-ionic theory	836
§ 3. The reflection and transmission coefficients for the iono- sphere	838
§ 4. Numerical results	839
4.1. The parameters p_r/p and τ	839
4.2. The reflection coefficients ${}_H R_{ }$ and ${}_H R_{\perp}$	841
4.3. Comparison with experimental results	841
4.4. Comparison with Bremmer's results	845
4.5. The transmitted waves	845
4.6. The thickness of the ionosphere	846
§ 5. Validity of the approximations	847
5.1. The quasi-longitudinal approximation	847
5.2. Variation of parameters with angle of incidence ..	848
5.3. The longitudinal component of the electric field ..	849
Acknowledgments	850
References.....	850

SUMMARY.

The paper discusses the theory of the reflection of very low frequency electromagnetic waves at the boundary of an ionized medium. The medium is assumed to be sharply bounded and homogeneous, and to have a steady magnetic field superimposed. The quasi-longitudinal approximation to the magneto-ionic theory is used (Booker 1935), and the reflection coefficients are then independent of the horizontal direction of the transmission path. The results of the theory are compared with the experimental observations of the propagation of very low

* Communicated by J. A. Ratcliffe, F.R.S.

frequency radio waves (Bracewell *et al.* 1951). It is concluded that the theory will account for the general form of some of the experimental results for frequencies of 10 kc./s. and above. It is likely to be most useful for extending the theory of the propagation of very low frequencies (10 kc./s. and lower) such as are used in the study of the propagation of radio-atmospherics (Gardner 1950, Bowe 1951, Budden 1951).

§ 1. INTRODUCTION.

1.1. *Previous Work on the Theory of the Reflection of Very Low Frequency Waves.*

A CONSIDERABLE amount of information now exists on the nature of the reflection of very low frequency radio waves from the ionosphere (Budden, Ratcliffe and Wilkes 1936, Bracewell *et al.* 1951). By "very low" we mean frequencies from about 10 kc./s. to 100 kc./s. It is of interest to consider what structure of the ionosphere would account for the observed phenomena. Several attempts at this have been made. A number of authors assumed that the ionosphere was a sharply bounded homogeneous medium containing electrons subject to collision damping, and neglected the effect of the earth's magnetic field. Thus Yokoyama and Namba (1932) showed that for such a medium there is an angle of incidence, the quasi-Brewster angle, for which the reflection coefficient is a minimum. They attempted to explain the minimum which is often observed near sunset in the signal from a distant long wave station, by a change in the quasi-Brewster angle during the passage from day to night conditions. Bremmer (1949) and Rydbeck (1949), using similar assumptions about the ionosphere, were able to account for many of the observed facts relating to the propagation of very low frequency waves to great distances. However, it is known that when a plane polarized wave is incident nearly vertically on the ionosphere, the polarization of the reflected wave is different from that of the incident wave. This cannot be accounted for if the reflecting medium is isotropic, that is—if the earth's magnetic field is neglected.

Another group of authors has treated the ionosphere as a horizontally stratified medium, in which the constants vary with height in a distance small compared with one wavelength. The differential equations for the case where the earth's magnetic field is not neglected were first given by Hartree (1929). Solutions for particular models of the ionosphere have been given by Wilkes (1940 and 1947) and Stanley (1950).

It is the purpose of the present paper to give some numerical solutions for the case where the ionosphere is a sharply bounded homogeneous medium with a superimposed magnetic field, and to discuss their applicability to the experimental results. A problem very similar to this was discussed by Lorentz (1909) and Voigt (1915), who were concerned with the theory of the magneto-optical Kerr effect. This effect concerns

the change of polarization which occurs when light is reflected from the metal pole piece of a magnet. Lorentz and Voigt both derived a set of four reflection coefficients similar to equations (22) to (25) of this paper, but they discussed a reflecting medium with properties very different from those of the ionosphere. Bremmer (1949) has given expressions for the various reflection coefficients, but points out that their use in numerical computations is extremely complex. The few numerical results which he gives are discussed in § 4.4. They are based on values of the parameters which are probably different from those which would be expected to apply at the level of reflection of very low frequency waves.

1.2. *Scope of the Present Paper.*

The experimental results on the propagation of very low frequency waves refer mainly to frequencies of 16 kc./s. and higher. We shall show that for these frequencies some—but not all—of the experimental results can be explained by assuming the ionosphere to be homogeneous and sharply bounded. We conclude that at the level of reflection of these waves the variation of the characteristics of the ionosphere, in a vertical distance of one wavelength, is too small for the assumption of a sharp boundary to be valid. It would be necessary to adopt a full wave solution, of the type given by Wilkes (1940, 1947) and Stanley (1950), allowing for the finite rate of variation of the electron density and collision frequency with height. At still lower frequencies, however, such as those used in the study of radio atmospherics (Bureau 1930, 1932, Gardner 1950, Bowe 1951), the wavelength is very long (30 km. or more), and we may expect the theory of the sharply bounded ionosphere to be of some value.

In § 2 of this paper we discuss the application of the Appleton-Hartree magneto-ionic formula to the region of the upper atmosphere, at about 70 to 90 kms. where very low frequency waves are reflected. The quasi-longitudinal approximation (Booker 1935) is used. In § 3 we use the boundary conditions at the surface of the medium to deduce expressions for the various reflection and transmission coefficients. It is convenient to describe the incident and reflected waves in terms of their component electric fields parallel to, and perpendicular to, the plane of propagation, and to consider four coefficients denoted by ${}_{\parallel}R_{\parallel}$, ${}_{\perp}R_{\parallel}$, ${}_{\parallel}R_{\perp}$, ${}_{\perp}R_{\perp}$, to indicate the complex ratio of a specified electric field in the wave after reflection to a specified electric field in the wave before reflection. The first subscript denotes whether the electric field specified in the incident wave is parallel (\parallel) or perpendicular (\perp) to the plane of incidence and the second subscript refers in the same way to the electric field in the reflected wave. In § 4 the results of some numerical calculations are given and their relation to the experimental results are discussed. In § 5 we discuss the validity of the various approximations used.

§ 2. THE FORMULÆ OF THE MAGNETO-IONIC THEORY.

The complete Appleton-Hartree magneto-ionic formula may be written (Appleton 1932) :—

$$x/(\mu^2 - 1) = 1 - jz - \frac{1}{2}y_T^2/(1 - x - jz) \pm \frac{1}{2}\{y_T^4 + 4y_L^2(1 - x - jz)^2\}^{1/2}/(1 - x - jz) \quad (1)$$

where μ = complex refractive index of the medium.

$$x = p_0^2/p^2.$$

$$y = p_H/p.$$

$$z = v/p.$$

$$p = 2\pi \times \text{frequency of the wave.}$$

$$p_0^2 = 4\pi N e^2 / \epsilon_0 m.$$

$$p_H = \mu_0 H e / m = \text{gyro frequency of electrons in the earth's magnetic field.}$$

$$y_T = \text{component of } y \text{ perpendicular to direction of wave propagation.}$$

$$y_L = \text{component of } y \text{ in direction of wave propagation.}$$

$$p_T = y_T/p.$$

$$p_L = y_L/p.$$

$$e, m = \text{charge and mass of the electron.}$$

$$N = \text{number of electrons per c.c.}$$

$$v = \text{collision frequency.}$$

$$H = \text{strength of earth's magnetic field.}$$

$$\epsilon_0, \mu_0 = \text{electric and magnetic permittivities of free space. (This is the only place in this paper where } \mu_0 \text{ is used for the magnetic permittivity of free space. The same symbol is later used for the refractive index of the ordinary wave, but there should be no confusion.)}$$

In this paper we consider the ionosphere to be a homogeneous medium governed by equation (1), with a sharp lower boundary. For this medium there are two characteristic waves, the ordinary and extraordinary waves, corresponding to the two values of μ given by (1). For each of these waves the value of μ and the state of polarization depend on the direction of propagation. This would make the calculation of reflection coefficients very involved for the most general case.

Equation (1) becomes much simpler if it is permissible to make the "Quasi-longitudinal" approximation (Booker 1935). This approximation is valid if

$$|y_T^4/4y_L^2| \ll |1 - x - jz|^2. \quad (2)$$

Then (1) reduces to

$$\mu^2 = 1 - x/(1 - jz \pm y_L) \quad (3)$$

and it can be shown that the ordinary and extraordinary waves are circularly polarized with opposite senses (Booker 1935). Both waves also have a component of the electric vector in the direction of propagation, but it will be shown in § 5.3 that this component is usually small. The quasi-longitudinal approximation is used in obtaining all the numerical results given in this paper. Its applicability is discussed in § 5.1.

The value of μ given by (3) still depends upon the direction of propagation, on account of the term y_L . We shall at first, however, assume that y_L is a constant, and the validity of this assumption will be discussed in § 5.2. Moreover, at the low frequencies considered here, $y_L \gg 1$ and we may write (3)

$$\mu^2 = 1 - jx/(z \pm jy_L) = 1 - j(p_r/p) \exp(\pm j\tau) \quad . \quad . \quad . \quad (4)$$

If y_L is purely real, then

$$p_r/p = x/\sqrt{(z^2 + y_L^2)} = p_0^2/p \sqrt{(v^2 + p_L^2)} \quad . \quad . \quad . \quad . \quad . \quad (5)$$

$$\tan \tau = y_L/z = p_L/v \quad . \quad . \quad . \quad . \quad . \quad . \quad (6)$$

Later, in § 5.2, we shall consider the possibility that y_L may be complex, and the expressions for p_r and τ are then more complicated.

We now take coordinate axes, x_1, x_2, x_3 , where x_3 is measured vertically upwards. We consider a wave with its wave normal in the (x_1, x_3) plane, inclined at an angle, θ , to the x_3 axis and travelling in the direction of both x_1 and x_3 increasing. Let the variation with time, t , be given by a factor $e^{j\omega t}$. We denote by E_{\parallel} the component of the electric vector of the wave in the (x_1, x_3) plane, and by E_{\perp} the component in the direction of x_2 . For such a wave in the northern hemisphere it can be shown that $E_{\perp}/E_{\parallel} = -j$, or $+j$, for the ordinary and extraordinary waves, respectively.

When a plane wave is incident on the ionosphere from below, the disturbance in the ionosphere consists of two waves, the ordinary and the extraordinary, for which the values of θ are different. We shall therefore write

For the ordinary wave :

$$\text{Complex refractive index} = \mu_o = 1 - j(p_r/p)e^{j\tau} \quad . \quad . \quad . \quad . \quad . \quad (7)$$

$$\text{Direction of wave normal} = \theta_o$$

$$\text{Polarization } E_{\perp o}/E_{\parallel o} = -j \quad . \quad . \quad . \quad . \quad . \quad . \quad (8)$$

For the extraordinary wave :

$$\text{Complex refractive index} = \mu_e = 1 - j(p_r/p)e^{-j\tau} \quad . \quad . \quad . \quad . \quad . \quad (9)$$

$$\text{Direction of wave normal} = \theta_e$$

$$\text{Polarization } E_{\perp e}/E_{\parallel e} = +j \quad . \quad . \quad . \quad . \quad . \quad . \quad (10)$$

§ 3. THE REFLECTION AND TRANSMISSION COEFFICIENTS FOR THE IONOSPHERE.

Now consider a plane wave incident from below on the boundary of the ionosphere, with its wave normal at an angle i to the vertical, and with its electric field components given by :

$$\left. \begin{matrix} E_{\parallel i} \\ E_{\perp i} \end{matrix} \right\} \exp [jp\{t - (x_1 \sin i + x_3 \cos i)/c\}]. \quad (11)$$

The reflected wave may similarly be denoted by the expression

$$\left. \begin{matrix} E_{\parallel r} \\ E_{\perp r} \end{matrix} \right\} \exp [jp\{t - (x_1 \sin i - x_3 \cos i)/c\}]. \quad (12)$$

In the ionosphere, the two transmitted waves are described by the expressions

$$E_{\parallel 0} \exp [jp\{t - (x_1 \sin \theta_0 + x_3 \cos \theta_0)\mu_0/c\}] \quad (13)$$

$$\text{and} \quad E_{\parallel e} \exp [jp\{t - (x_1 \sin \theta_e + x_3 \cos \theta_e)\mu_e/c\}] \quad (14)$$

together with equations (8) and (10).

The variation of all these waves in the x_1 direction at the boundary must be the same, and hence we have Snell's law

$$\sin i = \mu_0 \sin \theta_0 = \mu_e \sin \theta_e \quad (15)$$

It should be noted that because μ_0 and μ_e are, in general, complex, the angles θ_0 and θ_e are complex. Consequently y_L is complex. We shall investigate the consequences of this in § 5.2, where we show that, for practical purposes, it is sufficient to ignore the imaginary part of y_L .

Let E_1 , H_1 and E_2 , H_2 , be the components of the electric and magnetic fields E and H parallel to the x_1 and x_2 axes respectively, in either medium. Then the boundary conditions that must be satisfied are :—

$$E_1 \text{ and } E_2 \text{ continuous} \quad (16)$$

$$H_1 \text{ and } H_2 \text{ continuous} \quad (17)$$

Application of these to the wave expressions gives the following four equations :—

$$E_{\parallel i} \cos i - E_{\parallel r} \cos i = E_{\parallel 0} \cos \theta_0 + E_{\parallel e} \cos \theta_e \quad (18)$$

$$E_{\perp i} + E_{\perp r} = -j E_{\perp 0} + j E_{\perp e} \quad (19)$$

$$E_{\parallel i} + E_{\parallel r} = \mu_0 E_{\parallel 0} + \mu_e E_{\parallel e} \quad (20)$$

$$E_{\perp i} \cos i - E_{\perp r} \cos i = -j\mu_0 E_{\perp 0} \cos \theta_0 + j\mu_e E_{\perp e} \cos \theta_e \quad (21)$$

From these we can evaluate the reflection and transmission coefficients. For example, to find ${}_{\parallel}R_1$, we put $E_{\perp i} = 0$, and eliminate $E_{\parallel r}$, $E_{\parallel 0}$ and

$E_{\parallel e}$ from the equations. The result is an equation for $E_{1r}/E_{\parallel i}$, which is ${}_{\parallel}R_{\perp}$. The results are as follows :—

$${}_{\parallel}R_{\parallel} = \{(\mu_0 + \mu_e)(\cos^2 i - \cos \theta_0 \cos \theta_e) + (\mu_0 \mu_e - 1)(\cos \theta_0 + \cos \theta_e) \cos i\} / D \quad (22)$$

$${}_{\perp}R_{\parallel} = 2j \cos i (\mu_0 \cos \theta_0 - \mu_e \cos \theta_e) / D \quad (23)$$

$${}_{\perp}R_{\perp} = 2j \cos i (\mu_0 \cos \theta_e - \mu_e \cos \theta_0) / D \quad (24)$$

$${}_{\perp}R_{\perp} = \{(\mu_0 + \mu_e)(\cos^2 i - \cos \theta_0 \cos \theta_e) - (\mu_0 \mu_e - 1)(\cos \theta_0 + \cos \theta_e) \cos i\} / D \quad (25)$$

where

$$D = (\mu_0 + \mu_e)(\cos^2 i + \cos \theta_0 \cos \theta_e) + (\mu_0 \mu_e + 1)(\cos \theta_0 + \cos \theta_e) \cos i. \quad (26)$$

We may similarly evaluate transmission coefficients at the surface of the ionosphere. These will be denoted by ${}_{\parallel}T_0$, ${}_{\parallel}T_e$, ${}_{\perp}T_0$, ${}_{\perp}T_e$. Here the first subscript indicates whether the incident wave has its electric vector parallel (\parallel) or perpendicular (\perp) to the plane of incidence, and the second subscript indicates whether the transmitted wave is the ordinary (0) or extraordinary (e) component. The transmitted wave is assumed always to be described by that component of its electric vector which is parallel to the plane of incidence, so that

$$\begin{aligned} {}_{\parallel}T_0 &= E_{\parallel 0}/E_{\parallel i} = jE_{10}/E_{\parallel i} & {}_{\perp}T_0 &= E_{\parallel 0}/E_{1i} = jE_{10}/E_{1i} \\ {}_{\parallel}T_e &= E_{\parallel e}/E_{\parallel i} = -jE_{1e}/E_{\parallel i} & {}_{\perp}T_e &= E_{\parallel e}/E_{1i} = -jE_{1e}/E_{1i} \end{aligned}$$

The values of the transmission coefficients are given below :—

$${}_{\parallel}T_0 = 2\mu_0 \cos i (\cos i + \mu_e \cos \theta_e) / D \quad (27)$$

$${}_{\parallel}T_e = 2\mu_e \cos i (\cos i + \mu_0 \cos \theta_0) / D \quad (28)$$

$${}_{\perp}T_0 = -2j\mu_0 \cos i (\mu_e \cos i + \cos \theta_e) / D \quad (29)$$

$${}_{\perp}T_e = -2j\mu_e \cos i (\mu_0 \cos i + \cos \theta_0) / D \quad (30)$$

where D is given by (26).

As a partial check of the formulæ (22) to (30), it is readily verified that they reduce to the Fresnel formulæ for a homogeneous medium, when we put $\mu_0 = \mu_e$, and $\theta_0 = \theta_e$.

§ 4. NUMERICAL RESULTS.

4.1. The parameters p_r/p and τ .

The preceding formulæ have been used to calculate values of ${}_{\parallel}R_{\parallel}$ and ${}_{\parallel}R_{\perp}$ as functions of the angle of incidence, for various values of the parameters p_r/p and τ . The values of these parameters are given approximately by equations (5) and (6), although, as we have already mentioned, some slight modification may be necessary when account is taken of the fact that y_L may be complex. This modification will be

discussed in § 5.2, and will be shown to be small. Equation (6) shows that $\tan \tau$ is proportional to the magnetic gyro frequency for electrons, and inversely proportional to the collision frequency, ν . Equation (5) shows that p_r is equal to $p_0^2/\sqrt{(\nu^2 + p_L^2)}$ where p_0 is the critical frequency that the medium would have in the absence of collisions and magnetic field p_r is therefore directly proportional to the electron density N .

If the earth's magnetic field is zero, τ is zero. Some results for this case are shown in figs. (1) and (9).

If the collision frequency ν is zero, then $\tau = 90^\circ$, and $p_r = p_0^2/p_L$. Some curves for this case, for two different values of p_r/p are shown in figs. 7, 8, 15 and 16.

TABLE I.

Figure No.	p_r/p	τ	Frequency $p/2\pi$ kc./s.	Collision frequency ν sec. ⁻¹	Electron Density N cm. ⁻³
1, 9	1	0°	16	$(\nu/N = 3.17 \times 10^4)$	
1, 9	1	0°	100	$(\nu/N = 5.08 \times 10^3)$	
2, 10	$\frac{1}{2}$	15°	16	2.7×10^7	0.44×10^3
2, 10	$\frac{1}{2}$	15°	100	2.7×10^7	2.75×10^3
3, 11	2	15°	16	2.7×10^7	1.76×10^3
3, 11	2	15°	100	2.7×10^7	11.00×10^3
4, 12	2	60°	16	4.2×10^6	0.53×10^3
4, 12	2	60°	100	4.2×10^6	3.30×10^3
5, 13	4	60°	16	4.2×10^6	1.06×10^3
5, 13	4	60°	100	4.2×10^6	6.62×10^3
6, 14	8	75°	16	1.9×10^6	1.85×10^3
6, 14	8	75°	100	1.9×10^6	11.60×10^3
7, 15	2	90°	16	0	0.46×10^3
7, 15	2	90°	100	0	2.88×10^3
8, 16	8	90°	16	0	1.83×10^3
8, 16	8	90°	100	0	11.40×10^3

We should expect the ionosphere to have characteristics somewhere between the extreme cases just mentioned. To consider the behaviour of a particular medium, we first decide what values to assume for ν and p_L , and derive the corresponding value of τ from equation (6). We can then fix p_r if we know the critical frequency of the medium p_0 . Any pair of values of p_r and τ therefore refers to fixed values of ν and N . The complex refractive indices can then be found from equations (7) and (9), using the known values of p_r , τ , and the wave frequency $p/2\pi$. p_r and p enter these expressions only as a ratio. Since it is convenient to discuss the results in terms of particular wave frequencies, the values of N and ν appropriate to the curves of figs. 1 to 16 for selected wave frequencies are listed in Table I. The frequency 16 kc./s. has been included because many of the experimental results apply to it. The values of ν and N in Table I refer to vertical incidence when the angle of

magnetic dip is 60° . It will be shown in § 5.2 that only small modifications are needed at other angles of incidence, and that the form of the results is independent of the relative directions of the transmission path and the magnetic meridian.

4.2. The Reflection Coefficients ${}_R R_{||}$ and ${}_R R_{\perp}$.

Figs. 1 to 8 show some typical numerical values for the amplitudes of ${}_R R_{||}$ and ${}_R R_{\perp}$, plotted as functions of the angle of incidence i . Figs. 9 to 16 show the corresponding curves for the phases of ${}_R R_{||}$ and ${}_R R_{\perp}/{}_R R_{||}$. This last quantity gives the relative phases of the normal and abnormal components of the reflected wave, and thus determines its state of polarization.

Figs. 1 to 8 show clearly that there is an angle of incidence for which $|{}_R R_{||}|$ is a minimum. This is the quasi-Brewster angle, which exists also when the superimposed magnetic field is zero. Figs. 9 to 16 show that there is a change in the phase of ${}_R R_{||}$ as the angle of incidence varies. The change is most rapid near the quasi-Brewster angle.

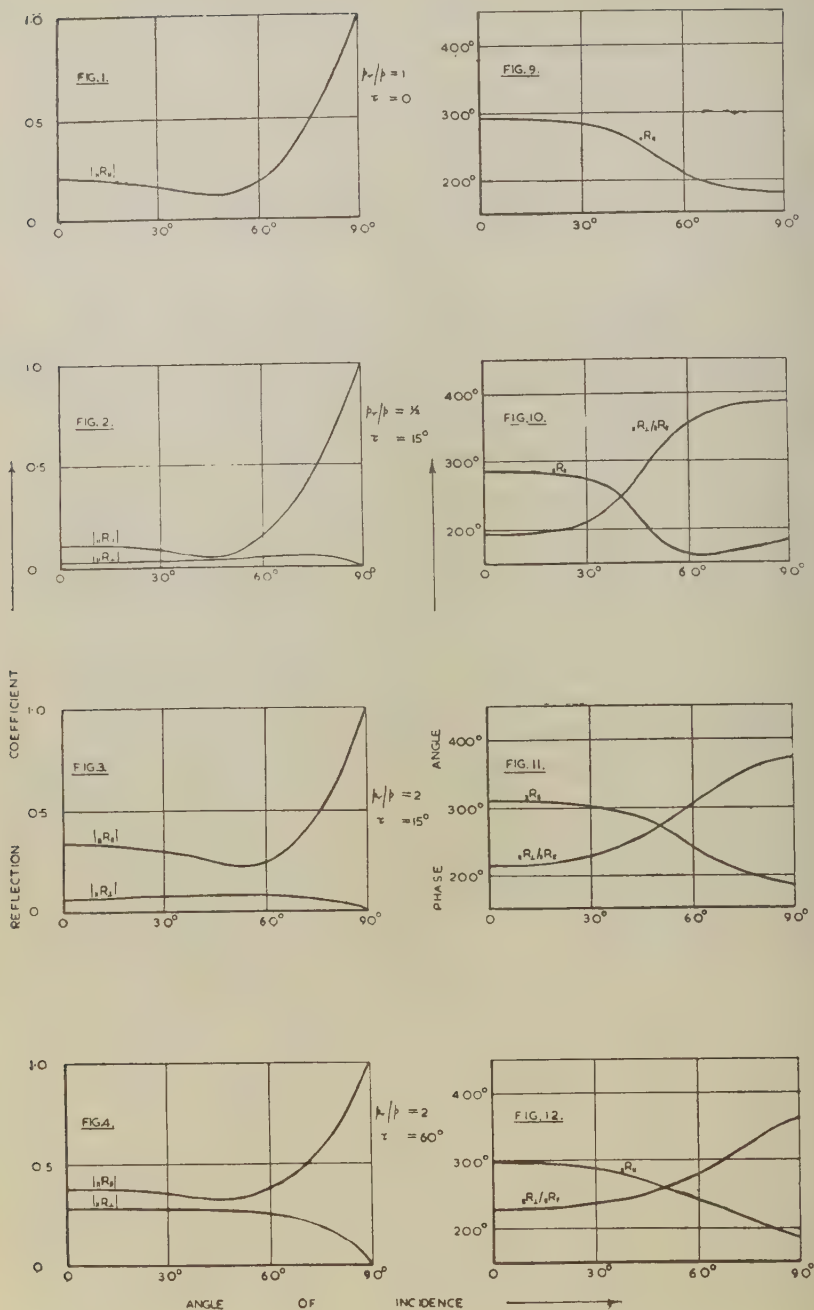
4.3. Comparison with Experimental Results.

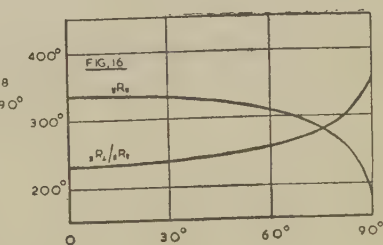
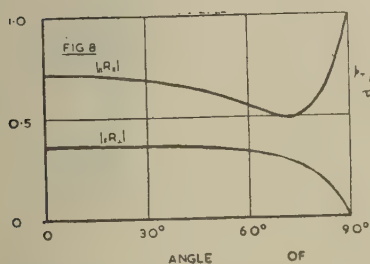
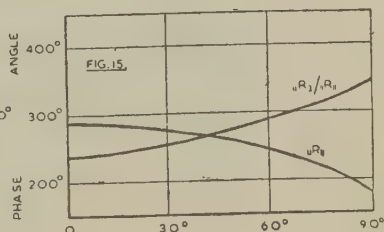
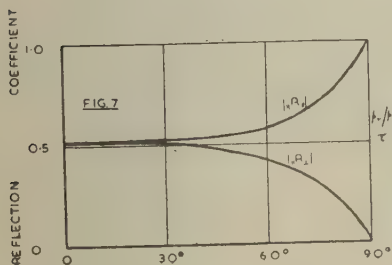
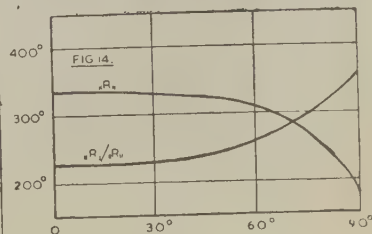
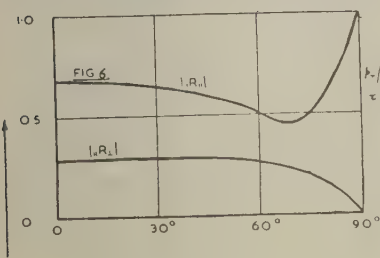
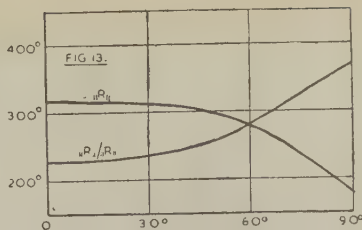
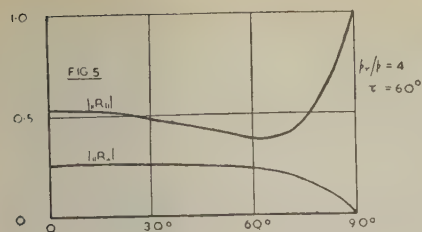
The experimental results for a frequency of 16 kc./s. may be summarized as follows :—(Bracewell *et al.* 1951). For an angle of incidence of about 30° the wave reflected from the ionosphere is roughly circularly polarized with a left-handed sense. The reflection coefficient $|{}_R R_{||}|$ at night is 0.4 to 0.5. In the daytime it is about 0.25 for winter and 0.1 for summer, and increases as the angle of incidence is increased.

The theoretical curves of figs. 10 to 16 show that the polarization of the reflected waves would be elliptical with a left-handed sense. The theoretical curves for which the polarization, at $i=30^\circ$, would be most nearly circular are those of figs. 4 and 12. Here the phase difference between ${}_R R_{||}$ and ${}_R R_{\perp}$ is about 240° , whereas for circular polarization it should be 270° . The corresponding value of $|{}_R R_{||}|$ is about 0.34, so that for this particular angle of incidence the curves of figs. 4 and 12 represent the experimental results fairly well for a winter day. The appropriate values of the parameters are: $p_r/p=2$, and $\tau=60^\circ$. Table I. shows that these correspond to the values: $\nu=4.2 \times 10^6 \text{ sec.}^{-1}$ and $N=530 \text{ cm.}^{-3}$. There are no values of the parameters which will fit the experimental results much better than these.

The curves of figs. 10 to 16 show that as the angle of incidence increases, the polarization of the reflected wave changes, and for very oblique incidence becomes nearly linear. An effect of this sort has been reported by Weekes (1950), whose experiments show that for very oblique incidence the reflected wave is roughly linearly polarized with its plane of polarization at about 45° to the vertical. Weekes' experiments do not give any information about the direction of tilt of the plane of polarization, but it would appear from the results of some experiments made by Mr. Bain in Aberdeen, that the observed direction of tilt is opposite to that given by figs. 10 to 16.

Figs. 1 to 16.



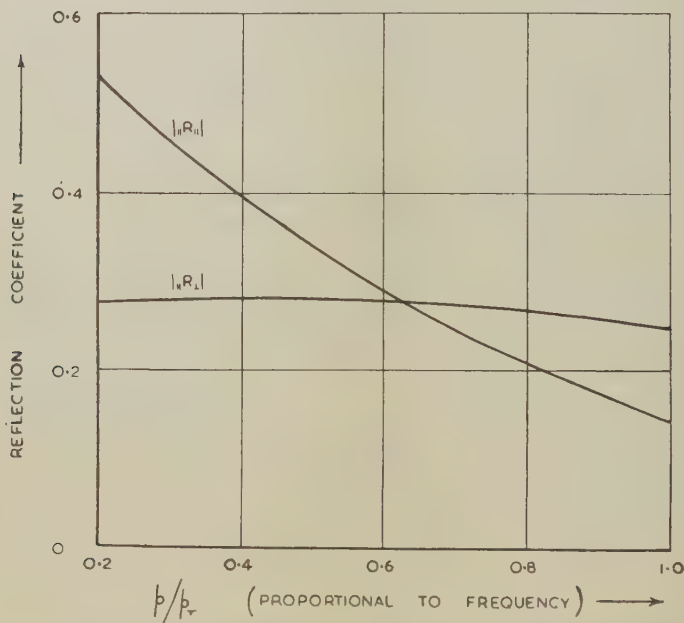


Curves showing reflection coefficients $|R_{||}|$ and $|R_{\perp}|$ and phases of $R_{||}$ and $R_{\perp}/R_{||}$ as functions of angle of incidence. Quasi-longitudinal approximation used. Results are independent of horizontal direction of transmission path.

In fig. 17 we show the values of the reflection coefficients $|_{\parallel}R_{\parallel}|$ and $|_{\parallel}R_{\perp}|$ plotted as functions of frequency for an angle of incidence 30° . It is seen that $|_{\parallel}R_{\parallel}|$ decreases as the frequency increases, and this is in qualitative agreement with the observations. The theoretical decrease of $|_{\parallel}R_{\perp}|$ with frequency is very slight, and the observed decrease is much more rapid.

We conclude that, if we assume the ionosphere to be a sharply bounded homogeneous medium to which the quasi-longitudinal approximation

Fig. 17.



Variation of reflection coefficients $|_{\parallel}R_{\parallel}|$ and $|_{\parallel}R_{\perp}|$ with frequency.

Angle of incidence $i=30^\circ$. $\tau=60^\circ$.

is applicable, we cannot account for the observed phase difference of 90° between the normal and abnormal components of the reflected wave. For an exact theory a more complete treatment is necessary. For example, we might investigate the properties of an ionosphere with values of N and ν for which the quasi-longitudinal approximation is not valid, but Bremmer (1949) has shown that the analysis of this case is extremely complex. Alternative treatments taking account of the finite rate of variation of N and ν with height have been made (Wilkes 1940 and 1947, Stanley 1950), and, for reasons given in § 4.6, these are probably preferable to any extension of the theory of the sharply bounded ionosphere,

However, the sharply bounded model discussed in this paper gives a good rough approximation to the behaviour of the ionosphere for very low frequency waves*.

4.4. Comparison with Bremmer's Results.

Bremmer (1949: *Terrestrial Radio Waves*, pp. 286 to 301) has discussed the reflection of waves at a sharply bounded, homogeneous non-isotropic ionosphere using the full magneto-ionic formula, without making the quasi-longitudinal approximation. He gives numerical results for two cases only. He assumes the earth's magnetic field to be vertical, with $p_H = 9.4 \times 10^6 \text{ sec.}^{-1}$. His results are given in Table II., together with the corresponding values of τ , p_r/p and N . (Bremmer assumes the waves to have a time factor e^{-jpt} . The signs of $\arg ({}_{\parallel}R_{\parallel})$ and $\arg ({}_{\parallel}R_{\perp}/{}_{\parallel}R_{\parallel})$ have been adjusted to agree with the time factor e^{jpt} and the system of axes used in the present paper.)

TABLE II.

Angle of Incidence	76°	76°
Frequency (kc./s.)	300	30
τ	84°	84°
$\nu \text{ (sec.}^{-1}\text{)}$	10^6	10^6
p_r/p	13	29
$N \text{ (cm.}^{-3}\text{)}$	7.2×10^4	1.6×10^4
$ {}_{\parallel}R_{\parallel} $	0.231	0.427
$\arg ({}_{\parallel}R_{\parallel})$	-138°	-55°
$ {}_{\parallel}R_{\perp} $	0.214	0.166
$\arg ({}_{\parallel}R_{\perp}/{}_{\parallel}R_{\parallel})$	312°	256°

It should be noted that the values assumed for the electron density N are very large, and correspond to critical frequencies of 2.4 Mc./s. and 1.1 Mc./s. respectively. These might apply somewhere near the maximum of the E-region, but are much too large for the levels, usually between 65 and 95 km., where very low frequency waves are reflected. The values of $|y^2/(1-x-jz)^2|$ are of the order of .0004 and .007 respectively for the two cases discussed, so that the quasi-longitudinal approximation might have been applied with fair accuracy.

4.5. The Transmitted Waves.

It may be of interest to know the ratio of the amplitudes of the ordinary and extraordinary waves transmitted into the ionosphere. The values of this ratio for various values of the parameters have been calculated from (27) and (28) and are shown in the following Table III.

* It is hoped to use this model to discuss the effects of the earth's magnetic field on the propagation of a radio atmospheric, and it was originally developed for this purpose. For a discussion of the propagation of atmospherics which neglects the earth's magnetic field, see Budden 1951.

It is found that the ratio is always fairly close to unity. It is also of interest to know the direction of propagation of the two waves in the ionosphere. Let ϕ_0 and ϕ_e be the inclination to the vertical of the normals to the planes of constant phase for the ordinary and extraordinary wave, respectively. Then

$$\tan \phi_0 = \mathcal{R}(\sin \theta_0) / \mathcal{R}(\cos \theta_0); \quad \tan \phi_e = \mathcal{R}(\sin \theta_e) / \mathcal{R}(\cos \theta_e)$$

The values of ϕ_0 and ϕ_e are also shown in Table III.

TABLE III.

Angle of incidence	10°	80°	10°	80°	10°	80°	
p_r/p	$\frac{1}{2}$	$\frac{1}{2}$	2	2	8	8	
τ	15°	15°	60°	60°	75°	75°	
Ratio of amplitudes, ordinary wave to extraordinary wave	1.04	1.05	1.09	1.40	0.84	1.06	
Inclination of wave normal	ordinary	8° 20'	56° 12'	4° 50'	39° 20'	4° 4'	19° 10'
	extraordinary	9° 46'	59° 18'	3° 40'	17° 52'	1° 22'	3° 4'

4.6. *The Thickness of the Ionosphere.*

It is of interest to ask how thick the ionosphere must be for the assumption of homogeneity to be justified. The two transmitted waves are both attenuated as the height increases in the ionosphere, and it is found that the ordinary wave is the least attenuated component. The height at which the amplitude of the ordinary wave is reduced to one-half of its value at the boundary has been calculated for some selected values of the parameters. The results are shown in Table IV.

TABLE IV.

Angle of incidence	0°	80°	0°	80°	0°	80°
p_r/p	8	8	4	4	1	1
τ	75°	75°	60°	60°	15°	15°
Thickness of medium in wavelengths for reduction to half amplitude	0.32	0.30	0.24	0.22	0.27	0.19

The above results perhaps provide the strongest reason for rejecting the sharply bounded ionosphere when an accurate theory of the reflection of very long waves is required. Thus, for a frequency of 16 kc./s. (wavelength 18.75 km.), the last row of Table IV. shows thicknesses of the order of 6 km., and there is little doubt that there are large variations of N and ν in distances of this order at the level of reflection of very low frequency waves.

§ 5. VALIDITY OF THE APPROXIMATIONS.

5.1. The Quasi-longitudinal Approximation.

We see from equation (2) that the quasi-longitudinal approximation is valid if

$$|y_T^4/\{4y_L^2(1-x-jz)^2\}| \ll 1. \quad (31)$$

The values of this quantity for some selected values of p_r/p , τ and i , are shown in Table V.

TABLE V.

p_r/p	τ	Angle of incidence i	$ y_T^4/\{4y_L^2(1-x-jz)^2\} $
$\frac{1}{2}$	15°	90°	0.21
2	60°	0°	0.0044
2	60°	30°	0.031
2	60°	60°	0.12
2	60°	90°	0.19
4	60°	30°	0.0055
1	75°	30°	0.79
8	75°	90°	0.0039
2	90°	90°	0.24
8	90°	90°	0.0031

These values all refer to propagation from south to north in the magnetic meridian, since it is for this case that the quasi-longitudinal approximation would be least accurate. It is found that the quantity (31) is greatest for large angles of incidence, for large values of τ , and for small values of p_r/p . It is clear that the quasi-longitudinal approximation may be treated as valid for most of the range covered by the curves of figs. 1 to 16. It begins to be inaccurate at high angles of incidence in figs. 2, 10, 4, 12, 7 and 15.

It might be suggested that further curves of the type of figs. 1 to 16 could be calculated using the quasi-transverse approximation, which is valid if

$$|y_T^4/\{4y_L^2(1-x-jz)^2\}| \gg 1.$$

However, this condition requires values of ν rather lower than 2×10^6 sec.⁻¹, and this is less than would be expected to apply at the level of reflection of very low frequency waves. Moreover, for propagation

in the direction of the magnetic meridian the quasi-transverse approximation would show that the reflected wave should always be linearly polarized in the plane of incidence, whereas the experiments (Bracewell *et al.* 1951) show that it is roughly circularly polarized for small or moderate angles of incidence.

We conclude that as long as p_r/p is large enough, the quasi-longitudinal approximation represents fairly well the behaviour of a sharply bounded ionosphere. It would therefore be the best approximation to use in discussing the propagation of waves of very low frequency (10 kc./s. or less) such as are used in the study of the propagation of atmospherics (Gardner 1950, Bowe 1951).

5.2. Variation of Parameters with Angle of Incidence.

If d is the angle of magnetic dip, and we consider transmission in a horizontal direction ϕ , measured east from magnetic north, then y_L is given by

$$y_L = y(\sin \theta \cos d \cos \phi + \cos \theta \sin d), \quad (32)$$

where θ may be either θ_0 or θ_e . We shall assume in what follows that $d=60^\circ$.

TABLE VI.

Angle of incidence	Ordinary wave			Extraordinary wave		
	0°	30°	90°	0°	30°	90°
τ	$61^\circ 4'$	60°	$56^\circ 23'$	$58^\circ 18'$	60°	$64^\circ 40'$
p_r/p	3.95	4	4.18	4.05	4	3.89

It was mentioned in § 3 that when Snell's Law (equation (15)) was used to derive the directions θ_0 and θ_e of the two waves in the medium, these angles proved to be complex, because the refractive indices μ_0 and μ_e are complex. As a result y_L is complex. We now investigate the consequences of this.

If y_L is a complex number, the denominator of equation (4) must be written

$$z \mp \mathcal{I}(y_L) \pm j \mathcal{R}(y_L) \quad (33)$$

(\mathcal{R} means "real part of" and \mathcal{I} means "imaginary part of"). Both $\mathcal{R}(y_L)$ and $\mathcal{I}(y_L)$ vary with angle of incidence and the result is a change in the values of p_r/p and τ . The modification is most serious at very oblique incidence, but even then the associated changes in the parameters p_r/p and τ are small. If we assume that $\tau=60^\circ$ and $p_r/p=4$ are correct for an angle of incidence 30° , then for west to east transmission in the northern hemisphere, and for a frequency of 16 kc./s. the correct values of τ and p_r/p for other angles of incidence are as shown in Table VI.

The above variations of τ and p_r/p with angle of incidence are not sufficient to affect the general form of the results. It is sufficiently accurate to regard fixed values of p_r/p and τ as referring to fixed values of N and ν for all angles of incidence. This is equivalent to treating y_L as a constant. An important consequence of this is that the reflection coefficients are independent of the horizontal direction of the transmission path.

5.3. The Longitudinal Component of the Electric Field.

The whole of the preceding theory has been worked out on the assumption that the waves in the ionosphere had only transverse electric fields. It is known, however, that the electric fields also have components in the direction of the wave normal. We shall call these the longitudinal fields and denote them by E_{L0} and E_{Le} , respectively, for the ordinary and extraordinary waves, or simply by E_L when the formulæ apply to either wave. It can be shown that if the quasi-longitudinal approximation is valid, then for either ordinary or extraordinary wave

$$|E_L/E_{\parallel}| = |\mu^2 - 1| \cdot |y_T/(1 - x - jz)|. \quad . \quad . \quad . \quad (34)$$

TABLE VII.

p_r/p	τ	Angle of incidence	$ E_L/E_{\parallel} $	$ E_L/E_{\parallel} \cdot \tan \theta $	Component
$\frac{1}{2}$	15°	90°	0.15	0.21	ext.
$\frac{2}{2}$	60°	0°	0.48	0	ext.
2	60°	30°	0.74	0.14	ext.
2	60°	60°	0.99	0.50	ext.
2	60°	90°	1.08	0.66	ext.
4	60°	30°	0.67	0.036	ord.
1	75°	30°	1.32	1.11	ext.
8	75°	90°	4.2	0.53	ext.
2	90°	90°	2.2	2.7	ord.
8	90°	90°	1.2	0.18	ord.

The longitudinal electric fields will in general have components parallel to the boundary of the ionosphere. This would mean that additional terms should appear in the boundary condition equation (18). The ratio of the magnitude of the additional terms to those already on the right hand side of (18) is proportional to the expression (34) and to $\tan \theta$, where θ is either θ_0 or θ_e .

The ratio is therefore small for nearly vertical incidence, for then θ is small and the longitudinal electric field is nearly perpendicular to the boundary. The values of $|E_L/E_{\parallel}|$ and of $|E_L/E_{\parallel}| \cdot |\tan \theta|$ for some other cases are shown in Table VII. These all refer to propagation from south to north in the magnetic meridian, and the figures apply to that wave, ordinary or extraordinary, for which the value is the larger.

A comparison of Tables V. and VII. shows that the errors which arise by neglecting the longitudinal electric field become serious for about the same values of the parameters as those for which the quasi-longitudinal approximation becomes inaccurate. It is found that for very large values of p_r/p the errors are small, which provides further encouragement for using the theory in discussing the behaviour of the lowest frequencies (10 kc./s. and lower).

ACKNOWLEDGMENTS.

This work was carried out at the Cavendish Laboratory as part of a programme of Radio Research supported by the Department of Scientific and Industrial Research.

REFERENCES.

- APPLETON, E. V., 1932, *Journ. Inst. Elec. Eng.*, **71**, 642.
 BOOKER, H. G., 1935, *Proc. Roy. Soc. A*, **150**, 267.
 BOWE, P. W. A., 1951, *Phil. Mag.*, **42**, 121.
 BRACEWELL, R. N., BUDDEN, K. G., RATCLIFFE, J. A., STRAKER, T. W., and WEEKES, K., 1951, *Proc. Inst. Elec. Eng.*, **98**, III, 221.
 BREMMER, H., 1949, *Terrestrial Radio Waves* (Elsevier Pbl. Co.).
 BUDDEN, K. G., 1951, *Phil. Mag.*, **42**, 1.
 BUDDEN, K. G., RATCLIFFE, J. A., and WILKES, M. V., 1939, *Proc. Roy. Soc. A*, **171**, 188.
 BUREAU, R., 1930, *Comptes rendus, Acad. Sci. Paris*, **191**, 64; 1932, *Ibid.*, **195**, 69.
 GARDNER, F. F., 1950, *Phil. Mag.*, **41**, 1259.
 HARTREE, D. R., 1929, *Proc. Camb. Phil. Soc.*, **25**, 97.
 LORENTZ, H. A., 1909, *Encyk. der Math. Wiss.*, **3**, 199.
 RYDBECK, O. E. H., 1944, *On the Propagation of Radio Waves*. Trans. Chalmers Univ., Gothenburg, Sweden, 34.
 STANLEY, J. P., 1950, *Journ. Atm. & Terr. Phys.*, **4**, 65.
 VOIGT, P., 1915, *Graetz, Handbuch d. Elektr. und des Magn.* IV. 2, 667 and 710.
 WEEKES, K., 1950, *Proc. Inst. Elec. Eng.*, **97**, III, 100.
 WILKES, M. V., 1940, *Proc. Roy. Soc. A*, **175**, 143; 1947, *Ibid.*, **189**, 130.
 YOKOYAMA, E., and NAMBA, S., 1932, *Reports, Radio Research in Japan*, **2**, 131.

LXXXVI. *Note on the Analytic Continuation of the S-matrix.*

By N. G. VAN KAMPEN,

Institute for Theoretical Physics, Copenhagen, Denmark*.

[Received April 23, 1951.]

SUMMARY.

It is shown that methods which try to avoid the redundant poles are not likely to be successful. On the other hand, the analytic continuation of the S-matrix is an ill-defined procedure, which cannot be applied until more properties of the S-matrix are known. The redundant poles are caused by the use of the asymptotic expression of the wave function instead of its actual value and have no physical meaning.

§ 1. PRELIMINARIES.

THE scattering of a non-relativistic particle by a fixed central field of force may be described by the equation

$$u''(r) + \{E - V(r)\}u(r) = 0 \quad . \quad . \quad . \quad (1)$$

with the boundary condition $u(0) = 0$. Let $u(E, r)$ be the solution, the arbitrary constant factor being determined by $u'(E, 0) = 1$. For each r the function $u(E, r)$ is an integral function in the complex E -plane. For real positive E we shall write $E = k^2$ with $k > 0$. Then the asymptotic expression of $u(E, r)$ for $r \rightarrow \infty$ is

$$u(E, r) \sim C(k) \sin \{kr - \eta(k)\} \quad \text{for } E = k^2 > 0. \quad . \quad . \quad (2)$$

The problem at issue is to find the discrete eigenvalues E_n of (1) from the phase function $\eta(k)$ only.

Let Γ denote the complex E -plane with the exception of the positive real axis. For each value of E in Γ there is (apart from a constant factor) one solution of the equation (1) which goes to zero for $r \rightarrow \infty$. It can be defined uniquely as the solution $f(E, r)$ of (1) which is asymptotically $\exp[i(\sqrt{E}r)]$, where \sqrt{E} is made unique in Γ by the condition $\text{Im} \sqrt{E} > 0$. For each r , $f(E, r)$ is a one-valued function of E in Γ . When E approaches the cut along the positive real axis from above, $f(E, r)$ tends to that solution for $E = k^2 > 0$ which is asymptotically $f(E+, r) \sim \exp[ikr]$; when E approaches from below $f(E, r)$ becomes $f(E-, r) \sim \exp[-ikr]$.

As shown below (see also Jost 1947), the function $f(E, 0) = f(E)$ is analytic in Γ without singularities. Its zeros are the energies of the bound states; they are necessarily on the negative real axis:

$$f(E_n) = 0, \quad E_n < 0. \quad . \quad . \quad . \quad (3)$$

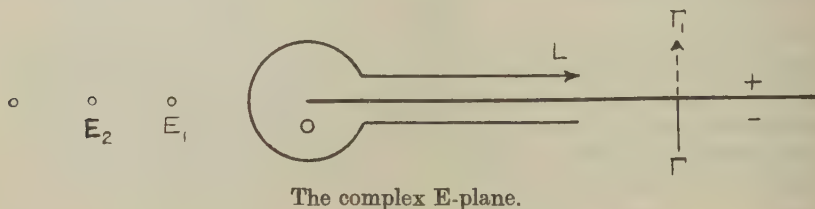
* Communicated by Prof. C. Møller.

The discontinuity of $f(E)$ on the cut is connected with the S-matrix by the relation (Jost 1947)

$$S(E) \equiv \exp [-2i\eta(k)] = f(E-)/f(E+). \quad (4)$$

It should be noted that as yet no appeal has been made to analytic continuation, with the consequence that $S(E)$ has a meaning only for real positive E . Now consider a second sheet Γ_1 of the complex E -plane, connected with Γ along the positive real axis in such a way that one enters Γ_1 on crossing this axis upwards. If $f(E)$ can be continued analytically in Γ_1 , taking the values $f_1(E)$ say, then $S(E) = f_1(E)/f(E)$ is an analytic continuation of (4) in Γ . From (3) it follows that $S(E)$ has poles (in general) for $E = E_n$, which suggests that the discrete spectrum can be found from the analytic continuation of the S-matrix (4).

It is clear, however, that $S(E)$ may have "redundant poles" (Ma 1946), namely, if $f_1(E)$ has poles. Also, if $f_1(E_n) = 0$ for any E_n , then this eigenvalue is not exhibited as a pole of $S(E)$. Because of these difficulties it is tempting to seek a method of determining the discrete spectrum from (4) without an analytic continuation of $f(E)$. This was tried by Wildermuth (1950) without conclusive result. We shall now show why it is not possible.



§ 2. NO ANALYTIC CONTINUATION OF $S(E)$.

Levinson (1949) in a different connection introduced the function

$$F(E) \equiv 1 + \int_0^\infty \exp [i(\sqrt{E}r)] V(r) u(E, r) dr, \quad (5)$$

and proved the following properties. (i) $F(E)$ is analytic in Γ and tends to 1 at infinity. (ii) $F(E)$ tends to a limit when E tends to a point $E = k^2$ on the positive real axis, namely

$$F(E+) = kC(k) \exp [i\eta(k)], \quad F(E-) = kC(k) \exp [-i\eta(k)]$$

(k chosen positive). (iii) The zeros of $F(E)$ are simple and lie on the negative real axis; they determine the discrete spectrum. This last property suggests that $F(E)$ is identical with $f(E)$, which can be shown as follows.

From the constancy of the Wronskian determinant follows

$$u'(\bar{E}, r) f(E, r) - u(E, r) f'(\bar{E}, r) = f(E, 0) \equiv f(E). \quad (6)$$

For large r the left-hand side becomes (if E is in I')

$$\{u'(E, r) - i(\sqrt{E})u(E, r)\} \exp \{i(\sqrt{E})r\}.$$

On the other hand, it can be seen that the latter expression is equal to

$$1 + \int_0^r \exp \{i(\sqrt{E})r\} V(r) u(E, r) dr, \quad . \quad . \quad . \quad (7)$$

because it has the same value for $r=0$ and the same derivative for $r>0$. Hence, by taking $r=\infty$, one finds that (6) is equal to the limit of (7), which is (5). Thus it is proved that $F(E)=f(E)$ and, consequently, $f(E)$ is analytic in I' and tends to 1 at infinity.

Now Levinson showed that $F(E)$ can be expressed in terms of the function $\eta(k)$, when $F(E)$ has no zeros, *i. e.* when there are no bound states. We shall now derive a similar relation for the case that there is a finite number of bound states. In that case, the function

$$g(E) \equiv \log \frac{f(E)}{\prod (1 - E_n/E)} = \log f(E) - \sum \log \left(1 - \frac{E_n}{E}\right) \quad . \quad . \quad (8)$$

is one-valued analytic in I' (because the zeros of $f(E)$ are simple) and vanishes at infinity (when the appropriate branch of the logarithm is chosen). It has a discontinuity along the cut :

$$g(E+) - g(E-) = \log f(E+) - \log f(E-) = \log S(E). \quad . \quad . \quad (9)$$

By means of the Cauchy integral $g(E)$ can be expressed as an integral along the path L in the figure, with the result (for E in I')

$$g(E) = \frac{1}{2\pi i} \int_L \frac{g(E')}{E' - E} dE' = \frac{1}{2\pi i} \int_0^\infty \frac{g(E'+) - g(E'-)}{E' - E} dE'.$$

Inserting (8) and (9) one obtains

$$\log f(E) = \frac{1}{2\pi i} \int_0^\infty \frac{\log S(E')}{E' - E} dE' + \sum \log \left(1 - \frac{E_n}{E}\right), \quad . \quad . \quad (10)$$

where all logarithms are chosen in such a way that they vanish when E (or E') tends to infinity.

From (10) it is clear that the values of S on the positive real axis together with those of E_n , determine the function $f(E)$.* On the other hand, when only S is given, the values of E_n may still be chosen arbitrarily, because for each choice an $f(E)$ results from (10), which has the zeros E_n and the required discontinuity (4) along the cut. Hence it appears that the discrete spectrum cannot be determined by using the function $f(E)$ inside I' only, so that the analytic continuation of $f(E)$ beyond the cut becomes inevitable.

* The same conclusion was reached by Jost (1947).

It may be that $f(E)$ must satisfy some further requirements, which reduce the arbitrariness of the choice of the E_n in (10). For instance, it follows from (10) that for small E

$$\log f(E) = - \left\{ \frac{1}{2\pi i} \log S(0) + N \right\} \log E + \text{finite function},$$

where N is the number of zeros E_n . Now, according to its definition, $f(0)$ is finite when $rV(r)$ is finite for $r=0$. In that case, therefore, the choice of E_n is restricted by the condition

$$N \leq -(1/2\pi i) \log S(0) = \eta(0)/\pi.$$

(If $N < \eta(0)/\pi$, then $f(0) = 0$ and there is a bound state with energy 0 (Bargmann 1949).) However, it is unlikely that the choice of the E_n can be made unique by such general conditions. Consequently, our conclusion can still be maintained.

Wildermuth's method (1950) consists of defining an auxiliary function with a parameter $\alpha > 0$

$$S(E, \alpha) = f(E - i\alpha)/f(E + i\alpha).$$

This function is analytic in the E -plane with the two cuts $i\alpha + \lambda$ and $-i\alpha + \lambda$ ($0 < \lambda < \infty$). Hence it is determined by its values on the positive real axis. For E on the negative real axis one has

$$\lim S(E, \alpha) = 1 \quad \text{for } \alpha \rightarrow 0,$$

except if $f(E) = 0$. In that case one finds, by taking the derivatives of numerator and denominator, $\lim S(E_n, \alpha) = -1$ (since $f'(E_n) \neq 0$). Consequently, the discrete spectrum can be determined if $S(E, \alpha)$ is known for all $E > 0$ and for α in a certain interval $0 < \alpha < \alpha_0$. All the same this is not a solution of the problem, for $S(E, \alpha)$ itself is not determined by the phase function $\eta(k)$. It seems, however, premature to conclude from this (Wildermuth 1950, Heisenberg 1950) that the knowledge of $\eta(k)$ alone is insufficient for the determination of the E_n , because there is still the alternative possibility of analytic continuation of $S(E)$ (as in Kramers' original idea).

§ 3. THE USE OF ANALYTIC CONTINUATION.

The problem of finding the analytic continuation of a function given on the real axis is equivalent to the problem of solving the potential equation in two dimensions, with given values of the potential and the charge density on an open boundary. It is the initial-value problem for a partial differential equation of elliptic type, and can be solved only if the boundary function is given by means of some analytic expression (see for example Courant-Hilbert 1937). That is indeed the case when the function $S(E)$ is obtained by solving equation (1) rigorously. However, in case the S -matrix is found experimentally, or from some approximate calculation, it is known only with a certain error. Then the analytic continuation is undetermined and the poles E_n cannot be found.

In order that the concept of analytic continuation be applicable to that case, it is necessary that $S(E)$ is known on the whole boundary of the domain Γ . Now it appears from Ning Hu's work (1948) that the behaviour of $S(E)$ at infinity can indeed be found from general considerations. However, the values on the lower side of the positive real axis (*i. e.* $S(E-) = f_1(E-)/f(E-)$ for $E > 0$) do not seem to follow from *a priori* arguments. Usually it is postulated (Heisenberg 1946, Ning Hu 1948) that $S(E-) = S(E)^*$, but there is no guarantee that this is the value which follows from analytic continuation through Γ . Until this difficulty has been cleared it is impossible to find the bound states from the *S*-matrix in practical calculations.

In the same way, when $S(E)$ is given for $E > 0$ with a finite precision, it is impossible to find the poles that do not correspond to bound states. Indeed, we know that they can always be introduced or suppressed by an arbitrarily small alteration of $S(E)$ obtained by changing the potential at some large distance (Jost 1947). This change in the potential has no physical meaning, since any actual measurement is performed at a finite distance. Hence it is seen that the redundant poles are caused by using the asymptotic expression of the wave function instead of the actual value at the point of observation. One might ask whether this means that the *S*-matrix theory is based on an unjustified separation of physical systems or only that the equation (1) is too much simplified. At any rate, an uncertainty is involved of the same order as the error made in cutting off the potential (ter Haar 1946) at a distance comparable to the distance of the measuring instruments. Therefore it is legitimate to discard the redundant poles by this device.

I am indebted to Prof. C. Møller for his interest and advice, to Prof. Niels Bohr for the opportunity to work at the Copenhagen Institute, and to the Rask-Ørsted Foundation for a grant which enabled me to stay in Denmark.

Note added in proof.—Recently P. Jauho (Ann. Acad. Scient. Fennicae, A1, nr. 80, 1950) has extended Levinson's work so as to include a Coulomb potential. In the present article that case has been excluded because of eq. (2), but it can be checked that our conclusions remain valid. In particular, it is not possible to build an *S*-matrix theory on Jauho's function χ (the counterpart of Levinson's F), as he suggested (p. 29).

REFERENCES

- BARGMANN, V., 1949, *Rev. Mod. Phys.*, **21**, 488.
 COURANT-HILBERT, 1937, *Meth. Math. Phys.*, **2**, 177 (Berlin).
 TER HAAR, D., 1946, *Physica*, **12**, 501.
 HEISENBERG, W., 1946, *Zs. f. Naturf.*, **1**, 608; 1950, *Ibid.*, **5a**, 368.
 JOST, R., 1947, *Helv. Phys. Acta*, **20**, 256.
 LEVINSON, N., 1949, *Kgl. Danske Vid. Selsk.*, **25**, nr. 9.
 MA, S. T., 1946, *Phys. Rev.*, **69**, 668.
 NING HU, 1948, *Phys. Rev.*, **74**, 131.
 WILDERMUTH, K., 1950, *Zs. f. Phys.*, **127**, 85.

LXXXVII. *The Attenuation of Nucleon Cascades in Lead.*

By W. G. V. ROSSER and M. W. SWIFT,
The University, Manchester*.

[Received May 1, 1951.]

ABSTRACT.

The frequency variation of nuclear interactions under lead has been studied by comparing the rates of stars in Ilford G5 emulsions exposed above and below 30 cms. of lead. The size frequency distribution is the same for stars in both sets of plates.

The attenuation lengths in lead are :--

(305 ± 7) gm./cm.² for all stars,

(380 ± 65) gm./cm.² for penetrating showers ($n_s \geq 2$),

(405 ± 31) gm./cm.² for events with charged relativistic primaries,

(260 ± 34) gm./cm.² for events with uncharged primaries (excluding simple evaporation stars).

The ratio of the attenuation length to the interaction meanfree path for penetrating showers is (1.8 ± 0.3) .

The percentage of all stars produced by charged relativistic primaries increases from $(13.1 \pm .9)$ per cent for the unshielded plates to (17.0 ± 1.0) per cent for the plates under lead due to the formation of stars by π mesons generated in lead. The ratio of charged to uncharged penetrating-shower primaries increases from (0.86 ± 0.21) for the air plates to (1.94 ± 0.32) for the plates exposed under 30 cms. of lead. It is suggested tentatively that the increase is due to the production of penetrating showers by fast π mesons created in the lead.

§1. INTRODUCTION.

THE main properties of cosmic rays in the atmosphere can be accounted for in terms of nucleon cascades initiated by the primary cosmic rays in the upper atmosphere. The primary protons, α -particles and heavier nuclei collide with air nuclei and fast nucleons and mesons are emitted. Following Rossi (1948) the interacting particles will be called N-rays.

It is important to define the interaction mean-free-path λ_i and the attenuation length λ_A of the interacting particles. The interaction mean-free-path is defined as the average distance an N-ray goes before giving rise to a nuclear interaction. The attenuation length is defined as the thickness of absorber in which the intensity of N-rays is reduced by a factor $1 : e$. It is found experimentally that in the lower atmosphere the variation of N-rays with altitude is roughly exponential so that

$$I = I_0 (\exp -x/\lambda_A)$$

* Communicated by Professor P. M. S. Blackett, F.R.S.

where x is the thickness of the absorber. In each nuclear interaction the primary particle loses energy so that in general the next nuclear interaction will be a less energetic event. The attenuation length is defined for the frequency variation of a particular type of event. It is not confined to the absorption of particles in a given energy range which produce these events, because after the first collision these particles will have left the energy range. The attenuation length therefore represents the decrease in intensity of a spectrum of particles which undergo collisions with energy loss, the attenuation being due mainly to the fact that there are fewer high energy particles to take the place of lower energy particles as the N-rays traverse matter.

Following Fujimoto and Hayakawa (1949), we shall call the primaries of penetrating showers the A-rays and the primaries of evaporation stars the B-rays. The division is not complete but is useful in discussing the nature of nucleon cascades. The average energy of B-rays is about 1 BeV. and these rays are, in the main, secondary to the A-rays.

The present experiment had the following main objectives:—

1. To investigate the effect of lead on the A and B components separately.
2. To compare the value of λ_A obtained for penetrating shower primaries under lead with the value of λ_I determined by counter experiments.
3. To ascertain what fraction of stars under lead can be ascribed to fast π mesons whose mean-free-path for star production in lead is shorter than the mean-free-path for decay into μ mesons.

§2. EXPERIMENTAL PROCEDURE.

Ilford G5 plates with emulsion 300μ in thickness were exposed for 21 days at the Pic du Midi, altitude 2860 m., one group of the plates (the "lead" plates) being placed under 30 cm. of lead built in the form of a hemisphere, and the other plates (the "air" plates) 1.5 m. from the lead. Both groups of plates stood on the concrete floor of a hut with a thin aluminium roof, which was covered with about 1 inch of snow during the exposure, making a total thickness of less than 2 gm./cm.². It is estimated that this reduced the star rates by about 0.1 stars/c.c./day and, since both sets of plates were equally affected, no correction was applied. The plates were collected as soon as dry at Messrs. Ilfords, taken at sea level to Bagnères-de-Bigorre and then transported as quickly as possible to the summit of the Pic du Midi. The plates were brought back to sea level immediately after exposure. Since the times at various altitudes were known accurately, the background rate could be calculated. It amounted to 3.3 per cent of the total number of stars observed on the air plates.

The plates were developed in acidified Amidol, using the temperature-cycle method of Dilworth, Occhialini and Payne (1948). They were shown to be sensitive to minimum ionization by observation of $\mu \rightarrow e$ decays

TABLE I.

Types of Stars in Air Plates at 2860 m.

 $N_H \longrightarrow$

	3	4	5	6	7	8	9	10	11	12	13	14	15	16	17	18	19	20	21	22	23	24	25	Total
0n	572	380	193	91	56	51	28	11	8	4	2	1	5	1	1		1							1402
0p	31	28	26	18	8	11	6	3	3	1	1	1		1	1	1		1		1				142
1n	37	19	21	15	8	7	6	3	2	1	2		1		1	1								124
1p	18	13	16	5	3	4	2	2			1							1						65
2n	1	2	5	3	4		3	1	2	1	2	1					1	1						27
2p	3	5	1		1	3	2			1		1		1										18
3n				1		1	1		1	1														5
3p	2			1	1	1			1												1			7
4n													1											2
4p	1				1																			2
5n			1	1																				2
5p				1																				1
>5n																					1(11n)			1
>5p		1(6p)												1(7p)										2

To get the rate/c.c./day after correcting for the background multiply by $\sim 5.0 \times 10^{-3}$.

TABLE II.
Types of Stars under 30 cms. of Lead at 2860 m.

$N_H \longrightarrow$

	3	4	5	6	7	8	9	10	11	12	13	14	15	16	17	18	19	20	21	22	23	24	25	Total
0n	554	356	202	88	45	25	20	5	4	6	2	1		1	2			1						1312
0p	35	31	32	21	18	8	10	4	2	4	2	1		2			1							171
1n	24	22	14	10	4	8	7	3	1	1		2	1			1				1				99
1p	17	16	9	13	8	2	1	1	4	2		2				2								77
2n		2	2	2		1	2			1						1		1				1		13
2p	5	7	1	2	1	1	1		2	1		2		2	1						1			27
3n	1	1			2			1				1			1									7
3p	1	3	1		1				1	1				1		1					1	1		12
4n				1	1				1						1									4
4p													1									1		2
5n				1							1					1								1
5p																								2
>5n														1(6n)						1(14n)				2
>5p														1(9p)		1(6p)								2

To get the rate c.c. day after correcting for the background rate multiply by $\sim 1.74 \times 10^{-3}$.

in the emulsion. The efficiency of detection of minimum ionization tracks was probably only about 90 per cent (Cosyns *et al.* 1949) because of the loss of tracks dipping steeply into the emulsion. Since, however, the main conclusions deduced from the present experiment depend on the relative rates of events above and below lead, if the same percentage loss of minimum ionization tracks occurs in both sets of plates the effect is not important. There is also a possibility of non-associated tracks passing so close to a star that they are accepted as being associated with the star. A strict criterion was adopted, namely, two minimum ionization tracks were not accepted as belonging to a star unless there was an observable deflection between the tracks at the star. In this way spurious events were cut to a minimum.

The choice of thickness of emulsion was dictated by the need for fast and accurate scanning. The rate of accumulation of data increases with increasing thickness of emulsion, but the percentage of events missed also increases. After some test scanning on plates of different thickness it was decided that a thickness of about $300\ \mu$ was the optimum value for our experiment.

The results obtained, when the same area of plate was scanned using first a $10\times$ objective, then a $20\times$ objective, then a $45\times$ objective, were compared. It was found that with the $10\times$ objective 20–30 per cent of all stars were lost, but with the $20\times$ objective less than 2 per cent of all stars were missed. This was less than the statistical accuracy aimed at and, furthermore, the losses affected both sets of plates equally. The scanning was therefore carried out using $20\times$ Cooke objectives and $10\times$ eyepieces. The stars were examined in detail with $45\times$ oil immersion objectives and grain counts were made on the tracks. To be accepted in the analysis a star had to have at least three prongs or two prongs and a short nuclear fragment. No two-pronged stars were accepted, as it was difficult in a large number of cases to distinguish between a two-prong star and a scattering of a heavy particle. Stars which had all tracks less than $65\ \mu$ long were excluded on the grounds that they were probably of radioactive origin. No separation of σ meson stars was made, and thus stars of two or more prongs produced by π mesons at rest were included in the analysis.

The stars were classified in the same way as was used by Brown *et al.* (1949), and the results are shown in Tables I. and II. The number of tracks with a grain density less than 1.5 times minimum is denoted by n_s , and the number with grain density greater than 1.5 times minimum by N_H .

§3. EXPERIMENTAL RESULTS.

The results obtained with the air and lead plates are shown in Tables I. and II. respectively. The total rate of stars observed in the air plates was 9.0 ± 0.3 stars/c.c./day, after correcting for the background rate. This rate can be compared with rates obtained by Brown *et al.* (1949) and Bernardini *et al.* (1950) at 3500 m. Assuming the attenuation

length for all stars in the atmosphere to be 135 gm./cm.^2 , the rate observed at the Pic du Midi is equivalent to a rate of 14.1 ± 0.4 stars/c.c./day at 3500 m. The rate obtained by Brown *et al.* was 10.8 stars/c.c./day. This value is significantly lower than the present result, but the difference is confined to 3- and 4-prong stars. The present result is, however, consistent with the rate of 14.2 ± 0.5 stars/c.c./day observed by Bernardini *et al.*

The rate observed under 30 cms. of lead was 2.96 ± 0.09 stars/c.c./day after correcting for the background rate.

Assuming that the absorption is exponential, the attenuation length of all stars in lead is $305 \pm 7 \text{ gm./cm.}^2$. This value compares favourably with the values of $310 \pm 20 \text{ gm./cm.}^2$ and $300 \pm 20 \text{ gm./cm.}^2$ obtained by George and Jason (1949) and Bernardini *et al.* (1949 a) respectively.

The attenuation lengths for the various types of events are shown in Table III.

TABLE III.
Attenuation Lengths in Lead.

Type of event	Attenuation length gm./cm.^2
All stars	305 ± 7
$0p+1p+2p+\dots$	405 ± 31
$1n+2n+3n+\dots$	260 ± 34
$2n+2p+3n+3p+\dots$ (Penetrating showers)	380 ± 65

The significance of these results will be discussed in the next section.

§4. DISCUSSION OF EXPERIMENTAL RESULTS.

4.1 Constancy of the Size Frequency Distribution.

The experiments of Bernardini, Cortini and Mantredini (1949 a) showed that the size frequency distribution of the stars observed in Ilford C2 emulsions varied little between sea level and 20,000 m., which suggests that the energy spectrum of N-rays has the same shape at all depths in the lower atmosphere. To compare these results with those from the present experiment, the numbers of stars with different numbers of heavy tracks are collected in Table IV. for both sets of plates. The numbers are normalized to 100 for $N_H=5$.

Comparing row (i.) with row (ii.), it will be seen that the frequency distribution for different values of N_H is the same above and below 30 cms. of lead. The results of Bernardini *et al.* (1950) show, however, that there is a much larger proportion of 3- and 4-prong stars under 2 cms. of lead; under 30 cms. of lead this transition effect vanishes.

The results of Malaspina *et al.* (1950) showed a higher rate of stars in plates placed on top of a lead absorber than in plates not placed on lead, suggesting that there is a larger backward emission of secondary neutrons capable of producing 3- and 4-prong stars than in an equivalent thickness of air. The difference is probably connected with the larger size of stars in lead than in air. Under large thicknesses of lead the excess backward flux of star primaries will combine with the secondary N-rays emitted in the forward direction in the lead above the plates, giving the same form for the spectrum of N-rays as in air. In the present experiment the plates were placed on concrete, so that there is a deficiency of star primaries incident on the plates from the concrete. Comparison with the results of Bernardini *et al.* (1950) under 2 cms. of lead shows that the decrease should be equivalent to about 6 per cent of all stars. There is, however, a compensating effect which increases the proportion of 3- and 4-prong stars, namely, an increase in σ meson stars due to the

TABLE IV.
Size Frequency Distribution of Stars.

Absorber \ N_H	Numbers of stars (normalized to 100 for $N_H=5$)								
	3	4	5	6	7	8	9	≥ 10	≥ 6
(i.) light roof	251 ± 10	163 ± 8	100 ± 6	52 ± 4	31 ± 4	30 ± 4	18 ± 5	32 ± 3	162 ± 9
(ii.) 30 cm. lead	245 ± 10	168 ± 7	100 ± 6	53 ± 5	31 ± 4	17 ± 3	16 ± 3	35 ± 3	152 ± 8
(iii.) 2 cm. lead. (After Bernardini <i>et al.</i> 1950)	360 ± 20	244 ± 20	100 ± 6						150 ± 5

fact that in lead π mesons have a greater probability of stopping before decaying into μ mesons than in air. Two-prong stars produced by σ mesons are included in the present analysis. The number of such stars in the air plates depends on the proximity of dense absorbers. Various estimates place the proportion of σ meson stars with two or more evaporation prongs to be about 3 per cent of all stars. According to Bernardini *et al.* (1949 b), the proportion of such stars increases by a factor (2.6 ± 0.7) , under large thicknesses of lead, making an overall increase of about 5 per cent in all stars. The increase occurs mainly in stars of 3 and 4 prongs. This effect tends to compensate the transition effect and accounts for the constancy of the size frequency distribution.

4.2 The Attenuation Length for all Stars.

The attenuation length in lead for all stars is :

$$\lambda_A = 305 \pm 7 \text{ gm./cm.}^2.$$

It is interesting to compare this value with that obtained under other absorbers by various workers.

It has been suggested that the values are proportional to $A^{1/3}$, suggesting that the cross-section for star production is proportional to the geometrical cross-section. As pointed out by Ritson (1950), however, the values given in Table V. are not very consistent with an $A^{1/3}$ law.

The picture of nucleon cascades allows us to interpret the results in a different way. Since the B-component is to a large extent secondary to the A-component the attenuation length of the primaries of evaporation stars depends on the attenuation length of the parent penetrating-shower primaries. This dependence is not complete under 30 cm. of lead since a large number of the N-rays present are due to the B-component incident from the atmosphere. Moreover, since the nuclear interactions of the A-component are included in the analysis, λ_A for all stars depends to a large extent on λ_A for penetrating showers ($n_s \geq 2$). The interaction

TABLE V.
Attenuation Length in Different Materials (in gm./cm.²).

Authors	Material				
	Carbon	Ice	Aluminium	Lead	Air
Barton, George and Jason (1951)	166 \pm 7				
George and Jason (1949)				310 \pm 20	150
Bernardini <i>et al.</i> (1949 a)			220	300 \pm 20	135
Harding, Lattimore, Li and Perkins (1949)	200 \pm 10				

mean-free-paths of the primaries of penetrating showers have been determined for lead and carbon by Cocconi (1949 a, b) and by Walker *et al.* (1950) using counter arrangements. The value for lead is 160 gm./cm.² and is consistent with a cross-section equal to the geometrical cross-section. For carbon Walker *et al.* find (81 \pm 5) gm./cm.² which is longer than the interaction mean-free-path corresponding to the geometrical cross-section, suggesting that there is some transparency of the carbon nucleus.

We see that

$$\frac{\lambda_{I(C)}}{\lambda_{I(Pb)}} \simeq \frac{81}{160} \sim \frac{1}{2}$$

$$\sim \frac{\lambda_{A(C)}}{\lambda_{A(Pb)}}$$

for penetrating showers. This is the same ratio as the attenuation length for all stars. Thus the ratio of the values of λ_A for all stars under lead and carbon can be understood in terms of the absorption of penetrating-shower primaries, with the B-rays keeping in equilibrium with the A-rays.

This is not completely true since some B-rays are incident from the atmosphere but due to the transparency for penetrating showers λ_I need not necessarily be proportional to $A^{1/3}$. Furthermore, approximately one-quarter of all stars are due to B-rays emitted in the backward direction. The number of these depends on the nature of the absorber beneath the plate so that the value for the attenuation length of all stars varies with experimental conditions.

Another interesting fact, pointed out by Barton, George and Jason (1951) is that for all stars λ_A (carbon) is greater than λ_A (air) even though the atomic weight of carbon is less than the atomic weight of air. Barton *et al.* suggested that the difference was due to the production of stars by π mesons since for carbon the mean-free-path for star production is smaller than the mean-free-path for $\pi \rightarrow \mu$ decay whereas in air the mean-free-path for $\pi \rightarrow \mu$ decay is shorter. Therefore the attenuation length for all stars in dense absorbers depends on the local production of π mesons.

4.3. Comparison of λ_A and λ_I for the Primaries of Penetrating Showers.

The interaction mean-free-paths of the primaries of penetrating showers in lead has been determined by Cocconi (1949 a, b), Walker (1950) and Sitte (1950) from experiments with counters. These workers found $\lambda_I \sim 160$ gm./cm.², which is consistent with a cross-section equal to the geometrical cross-section of the lead nucleus. Walker (1950) found that λ_I increased with decreasing number of relativistic secondaries required to trigger his penetrating shower set, for example, λ_I was (150 ± 8) gm./cm.² for $n_s > 5$ and 208 gm./cm.² for $n_s = 3$.

Penetrating showers in the photographic emulsion will be defined as events with $n_s \geq 2$, that is events of the types $2n + 2p + 3n + 3p + \dots$. The attenuation length is determined by observations made with the photographic emulsion and the value obtained is $\lambda_A = (380 \pm 65)$ gm./cm.². The comparable value from Walker's experiment for λ_I is probably ~ 208 gm./cm.². It is seen that the attenuation length is longer than the interaction mean-free-path. The probability that λ_A is less than or equal to 208 gm./cm.² is less than 0.5 per cent so that the increase can be taken as significant, which means that on the average penetrating-shower primaries give rise to more than one penetrating shower in lead. The experimental value of λ_A/λ_I is (1.85 ± 0.3) for events with $n_s \geq 2$.

The value of the interaction mean-free-path in carbon is rather uncertain, because of the inconsistency in the experimental results, so that λ_I for carbon cannot be compared with the attenuation length for penetrating-shower primaries in air. It must be borne in mind that the value of λ_A/λ_I for lead may be larger than the corresponding ratio for air because of the contribution from π mesons produced locally in the lead. On the other hand the ratio may be reduced because of the larger probability for successive nucleon collisions within the same nucleus, with a consequent larger energy loss per interaction.

4.4. Stars Produced by Fast π Mesons under Lead.

In the present experiment it is possible to observe stars produced directly by fast π mesons as they should lead to an increase under lead in the proportion of stars with charged relativistic primaries. The attenuation length in lead for events of the type $0p+1p+2p+\dots$ is (405 ± 31) gm./cm.², and for events of the type $1n+2n+3n+\dots$ is (260 ± 34) gm./cm.². In the lower atmosphere these lengths should be approximately equal. The value of λ_A for events of the type $0p+1p+2p$ is larger than the value for events of the type $1n+2n+\dots$ by almost exactly three times the standard deviation of their difference so that it is safe to conclude that some stars under lead are due to fast π mesons generated locally in lead. From Tables I. and II. it can be seen that the ratio of $0p+1p+2p+\dots$ events to all stars increases from (13.1 ± 0.9) per cent for the air plates to (17.0 ± 1.0) per cent for the plates under 30 cm. of lead, giving an increase equivalent to (3.9 ± 1.3) per cent of all stars.

Twenty-six of the fast charged primaries in the lead plates were suitable for identification from measurements of their multiple Coulomb scattering and grain density (*cf.* Fowler 1950), and of these eight were shown to be less massive than protons. This result is consistent with the estimated proportion of such events which are due to fast π mesons.

The number of stars due to fast π mesons under 30 cm. lead is approximately equal to the number of σ meson stars produced by π mesons at rest. The two are comparable because the probability of a π meson stopping in the emulsion is of the same order as the probability of a fast π meson passing through the emulsion giving rise to a nuclear interaction (*cf.* Bernardini, Cortini and Manfredini (1949 b)).

It is possible that some of the events of the type $1p, 2p, 3p$, etc., in the lead plates are the same as the events observed by George and Evans (1950) at 60 m. water equivalent underground. According to these authors the rate of such events at the altitude of the Pic du Midi should be about 0.03 stars/c.e./day, that is, about 1 per cent of all stars in the lead plates or 12 per cent of $1p+2p+3p+\dots$ events. It is not possible to confirm the presence of such events due to μ mesons because of poor statistics and because such events may be produced by π mesons generated locally.

Since the observed proportion of stars due to π mesons in the lead plates is (3.9 ± 1.3) per cent of all stars probably less than 6 per cent of all stars are produced directly by π mesons generated locally. This proportion in itself is not sufficient to account for the difference between λ_A (air) and λ_A (carbon) observed by Barton *et al.* (1951). However, the π mesons generated locally may give rise to energetic secondary nucleons in nuclear interactions in the absorber above the plates thus increasing the proportion of stars associated with the π mesons generated locally.

From Tables I. and II. the ratio of charged to uncharged primaries of penetrating showers (*i. e.* events of the types $n_s \geq 2$) is (0.86 ± 0.21) for the air plates and (1.67 ± 0.37) for the plates exposed under 30 cm. of lead.

For nucleon cascades in air the ratio should remain constant and close to unity at all depths in the lower atmosphere. However, under lead the ratio increases to 1.67 ± 0.37). Our statistics alone are not good enough to establish the increase with certainty, but a similar experiment carried out at Bristol leads to a similar result. During a preliminary analysis the Bristol workers observed 84 penetrating showers under 30 cm. of lead and of these showers 58 appeared to have charged primaries and 26 neutral. Combining the two sets of results the ratio of charged to uncharged penetrating shower primaries under 30 cm. of lead is (1.94 ± 0.32) . This figure is greater than one with a probability of more than 99 per cent.

It is possible that part of the increase may be due to events of the type observed by George and Evans (1950) who found that four of the ten stars produced at 60 m. water equivalent underground by relativistic primaries had more than one relativistic secondary. This would correspond to an increase of about 15 per cent in the ratio of charged to uncharged penetrating showers but is not sufficient to double the ratio.

A more likely explanation is the production of events of the type $2p + 3p + \dots$ by π mesons generated locally in the lead. One possible scheme for the production of events of the type $2p$ is the elastic collision of a π meson with a proton in a nucleus, both the π meson and proton emerging from the nucleus with relativistic velocities. Such a process is energetically possible for a primary π meson of energy about 2×10^9 eV. The probability for the process depends on the cross-section for the elastic collision of π mesons with protons, and since this cross section is not yet known the contribution cannot be estimated. Two further possible theoretical schemes for the production of penetrating showers by π mesons have been suggested by Heitler and Janossy (1950). In the first scheme it is suggested that a π meson might give a large fraction of its energy to a nucleon inside a nucleus and the nucleon then give rise to a penetrating shower. According to Camerini *et al.* (1950 b) a nucleon needs on the average an energy of 4×10^9 eV. to give rise to an event of the type $n_s \geq 2$, so that the π meson would need more than this energy. Now it has already been shown that approximately 4 per cent of the stars under 30 cm. of lead are due to fast π mesons. Less than 10 per cent of these π mesons would, however, have energies greater than 4×10^9 eV. These π mesons could contribute to a small increase in the ratio of the charged to uncharged penetrating-shower primaries; the maximum increase due to this effect is estimated to be 20 per cent, which is hardly sufficient to account for the observed ratio of (1.94 ± 0.32) . In the second scheme suggested by Heitler and Janossy π mesons may give rise to penetrating showers by a multiple process in which the primary π meson splits up into several mesons. These authors suggest that if the energy of a π meson is about 10^9 eV. it might split into two or three secondary mesons which would be observed as events of the type $2p$ and $3p$ in electron sensitive emulsions. Approximately 30 per cent of the π mesons under 30 cm. of lead have energies greater than 10^9 eV. so that if the probability for such a process were

high it could lead to an appreciable increase in the ratio of charged to uncharged penetrating-shower primaries.

At present no definite conclusions can be drawn about the nature of these events, but it is suggested tentatively that they are mainly produced by fast π mesons generated locally in the lead.

ACKNOWLEDGMENTS.

This experiment was started with the co-operation of Miss C. Dilworth of Brussels University and Dr. Bonetti of Genoa, and we wish to record our thanks for their assistance in the initial stages of the work.

We are greatly indebted to Professor P. M. S. Blackett, F.R.S. for facilities to carry out this work and to Dr. G. D. Rochester who has given us continual help both during the experiment and in the discussion of the results.

We also wish to thank Professor Powell, F.R.S. and Dr. Camerini for sending us the preliminary results obtained at Bristol on the ratio of charged to uncharged primaries of penetrating showers, Professor J. Röscher for facilities to expose the plates on the Pic du Midi, Mr. C. Waller of Ilford Ltd. for supplying the plates, Mr. S. J. Goldsack for exposing them, and Mrs. E. Birchall and Mrs. V. Bouch for carrying out the tedious work of scanning them.

REFERENCES.

- BARTON, J. C., GEORGE, E. P., and JASON, A. C., 1951, *Proc. Phys. Soc. A*, **64**, 175.
 BERNARDINI, G., CORTINI, G., and MANFREDINI, A., 1949 a, *Phys. Rev.*, **76**, 1792; 1949 b, *Nuovo Cimento*, **6**, *Supplemento*, **3**, 431; 1950, *Phys. Rev.*, **79**, 952.
 BROWN, R. H., CAMERINI, U., FOWLER, P. H., HEITLER, H., KING, D. T., and POWELL, C. F., 1949, *Phil. Mag.*, **40**, 812.
 CAMERINI, U., FOWLER, P. H., LOCK, W. O., MUIRHEAD, H., 1950 a, *Phil. Mag.*, **41**, 413.
 CAMERINI, U., FOWLER, P. H., LOCK, W. O., MUIRHEAD, H., and YEKUTELI, 1950 b, private communication.
 COCCONI, G., 1949 a, *Phys. Rev.*, **75**, 1074; 1949 b, *Ibid.*, **76**, 948.
 COSYNS, M. G. E., DILWORTH, C. C., OCCHIALINI, G., SCHOENBERG, M., and PAGE, N., 1949, *Proc. Phys. Soc. A*, **62**, 801.
 DILWORTH, C., OCCHIALINI, G., and PAYNE, R. N., 1948, *Nature, Lond.*, **162**, 102.
 FOWLER, P. H., 1950, *Phil. Mag.*, **40**, 169.
 FUJIMOTO, Y., and HAYAKAWA, S., 1949, *Prog. Theor. Phys.*, **4**, 502.
 GEORGE, E. P., and EVANS, J., 1950, *Proc. Phys. Soc. A*, **63**, 1248.
 GEORGE, E. P., and JASON, A. C., 1949, *Proc. Phys. Soc.*, **62**, 243.
 HARDING, J. B., LATTIMORE, S., LI, T. T., and PERKINS, D. H., 1949, *Nature, Lond.*, **163**, 320.
 HEITLER, W., and JANOSSY, L., 1950, *Helv. Phys. Acta*, **23**, 417.
 MALASPINA, L., MERLIN, M., PROVACCI, D., and ROSTAGNI, A., 1950, *Nuovo Cimento*, **7**, 145.
 RITSON, D. M., 1950, private communication.
 ROSSI, B., 1948, *Rev. Mod. Phys.*, **20**, 537.
 SITTE, K., 1950, *Phys. Rev.*, **78**, 714.
 WALKER, W. D., 1950, *Phys. Rev.*, **77**, 686.
 WALKER, W. D., WALKER, S. P., and GREISEN, K., 1950, *Phys. Rev.*, **80**, 546.

LXXXVIII. *On the State of Stress in a Plastic-Rigid Body at the Yield Point.*

By R. HILL,

H. H. Wills Physical Laboratory, University of Bristol†.

[Received May 9, 1951.]

SUMMARY

The yield point of a plastic-rigid body is defined as the moment when deformation first becomes possible as the load is increased. The practical significance of the yield-point load for an actual plastic-elastic body is discussed. It is then shown that part of the plastic zone at the yield point, namely the part where deformation occurs, depends only on the current surface tractions and not on the previous loading programme. By means of the principle of maximum plastic work and its complimentary minimum principle (Hill 1950) approximations from above and below to the yield-point load can be obtained; some examples are given. Recent American work on the plastic limit design of structures is critically reviewed and shown, when properly regarded, to be a particular application of the principle of maximum plastic work.

§ 1. THE DEFINITION AND SIGNIFICANCE OF THE YIELD POINT.

THE following considerations relate to an ideal work-hardening plastic-rigid material in which Young's modulus is indefinitely large. Consider a mass of such material subjected to some loading sequence. The moment when it first becomes locally plastic is usually known as the *elastic limit*, while the moment when it begins to deform will here be called the *yield point* (the term *collapse*, which has also been suggested, is suitable only when the subsequent deformation would render the body useless). When the elastic limit and the yield point are not coincident, the body remains entirely rigid in the corresponding loading interval, even though partly plastic. The calculation of the stress state and development of the plastic zone while the whole body is rigid have already been discussed by the writer (1950 a, pp. 237-245). Here, it is proposed to examine certain properties of the stress state at the yield point itself which depend only on the current surface tractions and not on the previous loading history.

In the absence of passive constraints the rate at which the loads need to be increased to enforce further distortion following the yield point is governed mainly by the rate of strain-hardening—though also by the changes of shape (so that even if the hardening is zero the load does not

† Communicated by the Author.

generally remain constant during a finite distortion†). When the rate of hardening is of the order of the yield stress, only a slight increase in load is sufficient to produce strains of a magnitude which would, in an actual structure, be regarded as amounting to collapse.

Correspondingly, in a slowly hardening *plastic-elastic* body such strains generally occur under loads differing little from the plastic-rigid yield-point loads. The previous permanent deformation, occurring since the elastic limit, is of an elastic order of magnitude, due to the constraint of the non-plastic material; an overall load-displacement curve has therefore a pronounced bend in a small loading interval in the neighbourhood of the plastic-rigid collapse load. (An obvious exception is when the plastic zone is entirely contained within an elastic zone which accommodates the severe local distortions, as when pressure is applied to a small cavity). In this sense, the plastic-rigid yield-point loads have a significance for an actual (plastic-elastic) body in which the definition of a precise moment of collapse, or yielding, must be somewhat arbitrary. More exactly, if a non-hardening plastic-elastic body is monotonically strained, the requisite loads approach asymptotically (though not necessarily steadily) to the plastic-rigid yield-point loads when changes of shape are ignored in the analysis. The asymptotic values are generally not reached in any finite strain (the contrary is often wrongly stated), but the actual loads differ from them only by an insignificant amount after a permanent strain which is still of an elastic order of magnitude.

The main purpose of the present paper is to examine the factors governing the distribution of stress in a plastic-rigid body at the yield point, and to draw attention to some rather surprising properties which have not been observed before.

These properties are intimately related to certain extremum theorems for a plastic-rigid body, namely the principle of maximum plastic work and its complementary minimum principle established by the writer (1948 and 1950 b). These principles refer to the rate of working of forces on the surface of a plastic zone, at all points of which deformation is occurring (the zone does not necessarily extend over the whole body). Since any equilibrium system of forces acting on a rigid zone does no work, the extremum principles apply also to the work of the forces on a body which is only partly plastic. These theorems supply a means of obtaining approximations, from above and below, to the actual rate of work, and also, in certain situations, to the yield-point loads themselves. However, by contrast to the analogous methods for a perfectly elastic body, they do not furnish approximations to the whole *internal* state of stress in a partly plastic body at the yield point since this depends, *in part*, on the previous loading programme. It is only for particular surface tractions, such that deformation can occur under them at all points, that the whole internal

† For this reason the term "flow limit", suggested in a recent paper by Pell and Prager, is unsatisfactory, as "flow" signifies deformation under constant stress,

Consider, now, the yield point of a body under given forces F_i per unit area over a part S_F of the surface S , and given velocities u_i over the remainder S_U (more generally, certain components of F_i and the complementary components of u_i may be given over the same part of the surface). Consider the set of equilibrium states of stress, and associated velocity distributions, corresponding to the same distribution of hardening and the same given surface conditions. The stress must satisfy (1) and (2) wherever the respective strain-rates do not vanish, and must not violate the yield condition elsewhere. Included among this set are, of course, actual yield-point stress states and their associated distortion modes; such actual states may be considered to be reached from different initial states of residual stress or by different loading programmes. Let (σ_{ij}, u_i) and (σ_{ij}^*, u_i^*) be any two members of the set. Across certain internal surfaces some of the components of stress may be discontinuous; for equilibrium, only the stress resultants need be continuous. Across other internal surfaces the velocity may be tangentially discontinuous; such a surface of discontinuity has to be regarded as the limit of a narrow layer through which the velocity component parallel to the surface changes rapidly. The state of stress at each point of a discontinuity is therefore that corresponding to a simple shear strain-rate in the direction of the relative velocity vector. The material being assumed isotropic, the stress is thus a pure shear, k say, along the discontinuity, together with some hydrostatic component; since f is concave to the origin and is assumed not to involve the hydrostatic component of stress, no shearing stress component can exceed k in a given state of hardening. Let τ^* be the shear component of σ_{ij}^* along a discontinuity of u_i , and τ be the shear component of σ_{ij} along a discontinuity of u_i^* . Then, by virtual work,

$$\int (F_i - F_i^*)(u_i - u_i^*) dS = \int (\sigma_{ij} - \sigma_{ij}^*)(\dot{\epsilon}_{ij} - \dot{\epsilon}_{ij}^*) dV + \int (k - \tau^*)[u] dS_D + \int (k - \tau)[u^*] dS_D^*, \quad (4)$$

where the square brackets denote the absolute amount of the discontinuities across the respective surfaces S_D and S_D^* . The left-hand side vanishes identically since one or other of the factors is zero at each point of the surface of the body. According to (3) and the fact that τ and τ^* cannot exceed k numerically, all terms on the right-hand side are non-negative. Hence they must each be zero. This requires that the deviatoric parts of σ_{ij} and σ_{ij}^* are equal on S_D and S_D^* and wherever $\dot{\epsilon}_{ij}$ or $\dot{\epsilon}_{ij}^*$ is not zero.

In other words, stress states of the set considered, and in particular actual yield-point states, are identical wherever deformation is occurring and can differ only in the common rigid zone. In particular, in plane strain, the slip-line field in the plastically-deforming zone is uniquely determined by the given surface conditions and internal hardening at the yield point. On the other hand, the present analysis says nothing about the possible modes of distortion (except in so far as they must be compatible with the stress). This theorem justifies the procedure adopted in the past

for calculating yield-point loads : namely, to ignore the development of the plastic zone and to find some stress and velocity distribution satisfying boundary conditions at the yield point only. It is necessary also to show that there is an associated stress distribution in the rigid zone, not violating the yield condition ; in so far as this is left unexamined, previous solutions are not completely rigorous, as the writer has frequently emphasized. If the yield condition is in fact locally exceeded in the rigid zone by a certain amount, such a solution is valid for a material which is at least that much harder there than the one under consideration. It is intuitively obvious, and an immediate consequence of the maximum work principle (5) below, that the yield-point load will then tend to be overestimated.

An example of the use of this theorem may be instanced. Consider the slip-line field and associated velocity solution proposed by Prandtl to satisfy the surface conditions at the yield point of a semi-infinite block indented by a flat die. If it could be proved (as seems probable) that there exists an associated stress distribution in the rigid zone, not violating the yield condition, then it would follow that the actual plastic zone certainly extends at least as far as Prandtl's slip-line field. Similar conclusions hold for the notched bar problem (Hill 1950 a, pp. 249-251). It would not necessarily follow, however, that the mode of distortion suggested by Prandtl is the actual one for an initially stress-free and uniformly hardened block. To prove that an assumed mode is correct, it is essential, as remarked by the writer (1950 c), to examine the stress increment occurring during an increment of distortion and to show that all elements assumed to deform have in fact remained plastically stressed. (There is no possibility of overlooking this point when dealing with a plastic-elastic material since the stress increment in any case enters the relations between the ratios of the components of stress and total strain-rate). This applies equally to the alternative mode suggested by the writer for this problem (*op. cit.*). To what extent a yield-point mode is independent of loading history is a matter for future research.

§ 3. EXTREMUM PRINCIPLES.

Let σ_{ij}^* now refer to any equilibrium state that does not violate the yield condition at any point where $\dot{\epsilon}_{ij} \neq 0$ (σ_{ij}^* is not necessarily any actual yield-point state). Then, as in (4),

$$\int (F_i - F_i^*) u_i dS_D = \int (\sigma_{ij} - \sigma_{ij}^*) \dot{\epsilon}_{ij} dV + \int (k - \tau^*) [u] dS_D \geq 0 \quad \dots \quad (5)$$

if $F_i^* = F_i$ on S_F . This is the maximum work principle for a finite body (Hill 1948).

In particular, if $F_i^* = F_i$ all over the surface the left-hand side of (5) vanishes. Since each term on the right-hand side is non-negative, both must be zero and σ_{ij}^* must equal σ_{ij} wherever deformation is occurring (including, of course, velocity discontinuities.) Thus, if given forces act on the surface of a body in a given state of hardening and if it is possible to find some corresponding internal equilibrium distribution of stress σ_{ij} and

velocity u_i , satisfying (1) and (2) where $\epsilon_{ij} \neq 0$ (with positive λ), then, wherever $\epsilon_{ij} \neq 0$, the body must certainly be plastic and this σ_{ij} must be the actual stress.

For the complementary minimum principle consider any velocity distribution u_i^* having zero divergence and such that $u_i^* = u_i$ on S_U . Then, by virtual work,

$$\int F_i u_i^* dS = \int \sigma_{ij} \epsilon_{ij}^* dV + \int \tau [u^*] dS_D^*.$$

Let σ_{ij}^* be the stress that would be needed to produce a strain-rate ϵ_{ij}^* in the given state of hardening; the distribution σ_{ij}^* is not necessarily in equilibrium and is undefined where $\epsilon_{ij}^* = 0$. Then, by the maximum work inequality (3) and the fact that $|\tau| \leq k$,

$$\int F_i u_i dS_U \leq \int \sigma_{ij}^* \epsilon_{ij}^* dV + \int k [u^*] dS_D^* - \int F_i u_i^* dS_F, \quad . \quad . \quad . \quad (6)$$

which is complementary to (5). This result is more general than one obtained previously by the writer (1950 b), which was valid only for the yield criterion of von Mises. For the latter, $|\sigma'_{ij}| = \sqrt{(\sigma'_{ij} \sigma'_{ij})} = \text{const.}$, where σ'_{ij} is the stress deviator, and $\sigma_{ij}^* \epsilon_{ij}^* = |\sigma'_{ij}| |\epsilon'_{ij}|$. In plane strain, $\sigma_{ij}^* \epsilon_{ij}^* = k \dot{\gamma}^*$ whatever the function f , where $\dot{\gamma}^*$ is the maximum shear strain-rate (twice the tensor component).

§ 4. APPROXIMATE ESTIMATION OF YIELD POINT LOADS.

According to (5) a lower bound to the rate of work by the forces over S_U is to be obtained by selecting any equilibrium distribution of stress not violating the yield condition. An upper bound, on the other hand, is to be obtained from (6) by means of any distribution of velocity. With a well-judged choice these bounds can be brought close enough to give a useful approximation to the actual rate of work on S_U .

When the prescribed velocity on S_U is uniform in magnitude and direction, a knowledge of the rate of work is equivalent to a knowledge of the load on S_U in that direction (and similarly when a component of velocity and the complementary component of force are given). This situation arises, for example, when a single load is applied to the body through a rigid plane die (as in indentation) or through a rigid part of the body itself (as in a notched-bar test). Similarly, when the velocity distribution on S_U amounts to a rigid-body rotation or twist, the bending or twisting couple is immediately calculable from the rate of work.

A slightly different problem presents itself when several loads are applied, their ratios at the yield point being given; this includes proportional loading, to which writers on limit design have restricted their attention. The single parameter specifying the absolute magnitudes of the loads is derivable from the extremum principles. To see this, let S_R now denote the part of the surface where the load-ratios r_i are given, S_F standing as before for the part where absolute values of certain loads are prescribed. In addition there may be fixed frictionless constraints, but specified non-zero velocities can no longer be admitted since the

corresponding forces would appear as further unknowns. If $F_i = F r_i$ on S_R at the yield point, then, as in (5),

$$F \geq F^*, \quad (7)$$

on cancelling the factor $\int r_i u_i dS_R$, where σ_{ij}^* is such that $F_i^* = F^* r_i$ on S_R and $F_i^* = F_i$ on S_F . It follows from (7), as remarked by Greenberg and Prager (1951), that the value of F is unique. When the deformation zone develops from a single point a limiting argument appears sufficient to establish the same result. Also, as in (6),

$$F \int r_i u_i^* dS_R \leq \int \sigma_{ij}^* \epsilon_{ij}^* dV + \int k[u^*] dS_D - \int F_i u_i^* dS_F. \quad (8)$$

§ 5. SOME APPLICATIONS.

It is to be noted that the entire discussion and the approximation methods are equally relevant for those problems of steady motion where there is no hardening and where the external contour of the body is known *a priori*. Steady motion can, in fact, be regarded as the integrated result of incremental distortions due to a succession of yield points. So, for that matter, can any plastic problem, but since the external configuration is continually changing, or is not known beforehand, the present methods cannot be applied directly.

As an example of the estimation of a steady-state load, consider the drawing of a sheet in plane strain through a smooth wedge-shaped die (without bulging). An intuitively obvious lower bound is provided by the stress distribution corresponding to radial flow towards the virtual apex of the die: r being the fractional reduction, (5) gives $2k \ln\{1/(1-r)\}$ for a lower bound to the drawing stress, as in elementary theories of drawing. An upper bound is provided by a velocity distribution in which the reduction is effected by block-sliding over a criss-cross of lines, of which the extreme pairs pass respectively through the points of entry and exit. If the lines make equal angles θ with the axis, there is a constant velocity discontinuity across each pair. This is $\sin \alpha / \sin (\theta - \alpha)$ at the first, where 2α is the die angle, and is multiplied at each successive pair by a factor $\sin (\theta + \alpha) / \sin (\theta - \alpha)$. Since the dimensions of successive pairs are multiplied by the inverse factor the work of shearing for each line is the same. If there are n pairs (6) gives an upper bound of

$$\frac{2kn \sin \alpha \cos \alpha}{\sin (\theta - \alpha) \sin (\theta + \alpha)}$$

where

$$(1-r)^{1/n} = \frac{\sin (\theta - \alpha)}{\sin (\theta + \alpha)}.$$

The best approximation, with the corresponding value of θ , is to be obtained from the integral value of n making this upper bound least. In the practical range of reductions only the values $n=1$ and 2 need be considered. For those reductions not so far covered by an exact theory (see Hill 1950 a,

p. 167), the greatest difference between these upper and lower bounds is of order 5 per cent. In this range, then, the elementary theory (which assumes homogeneous distortion) is a fairly good approximation. However, contrary to general belief, there are reasons for thinking that the relative amount of redundant work does not tend to zero *steadily* as the reduction increases, but *oscillates* with a steadily decreasing amplitude.

Consider, finally, the yield point of a symmetrically-notched bar extended in plane strain. Let the width of the bar be w times the smallest section. An upper bound is obtained from a deformation consisting of block-sliding across a pair of lines from the notch roots, intersecting the longitudinal axis in an angle θ , say, and a pair passing from this point to the sides of the bar and making $\frac{1}{2}\pi - \theta$ with the axis. For the stress at the ends of the bar equation (6) gives an upper bound $k(\cot \theta + w \tan \theta)$. The smallest value of this is $2k\sqrt{w}$, when $\cot \theta = \sqrt{w}$. This is valid for any shape of notch geometrically compatible with this fictitious mode of yielding, but is obviously likely to be best for a parallel-sided notch with zero root radius (since this should have the highest constraint factor). An exact solution (Hill 1950, unpublished) gives a yield-point stress of $2.05 \times 2k$ for $w=4.7$, compared with the upper bound of $2.17 \times 2k$. For $w \geq 8.6$ exact calculation gives $2.57 \times 2k$ (Hill 1950 c), while the upper bound exceeds this value when $w \geq 6.6$. We may infer that the constraint factor is not more than a few per cent less than \sqrt{w} when w is less than about 3.

REFERENCES.

- BISHOP, J. F. W., and HILL, R., 1951, *Phil. Mag.*, (April), **42**, 414.
 DRUCKER, D. C., GREENBERG, H. J., and PRAGER, W., 1951, *J. App. Mech.* (in press). Paper No. 51-A3.
 GREEN, A. P., 1951, B.I.S.R.A. Report MW/B/10/51. *Phil. Mag.* **42**, 900.
 GREENBERG, H. J., and PRAGER, W., 1951, *Proc. Am. Soc. Civ. Eng.*, **77**.
 HILL, R., 1948, *Quart. J. Mech. App. Math.*, **1**, 18; 1949, *idem*, **2**, 40; 1950 a, "The Mathematical Theory of Plasticity" (Clarendon Press); 1950 b, *J. App. Mech.*, **17**, 64; 1950 c, *Phil. Mag.*, **41**, 745.
 PELL, W. H., and PRAGER, W., 1951, *Brown University Technical Report* 57.

LXXXIX. *A Theory of the α, α' Phases in the Al-Zn System.*

By R. S. LEIGH,

Mathematics Department, Imperial College, London*.

[Received April 26, 1951.]

SUMMARY.

In the binary alloys of Al-Zn there exists, above a certain temperature, a mixed crystal region in which the two phases α and α' both have the same face-centred cubic structure but with different compositions and lattice spacings. It is shown that an explanation for the formation of these phase boundaries is provided by the electronic theory of the elastic properties of single crystals of aluminium. A maximum in one of the shear constants at an electron concentration corresponding to the $\alpha + \alpha'$ region gives rise to a subsidiary maximum in the temperature-dependent part of the free energy, which leads, according to the usual construction, to a mixed phase region.

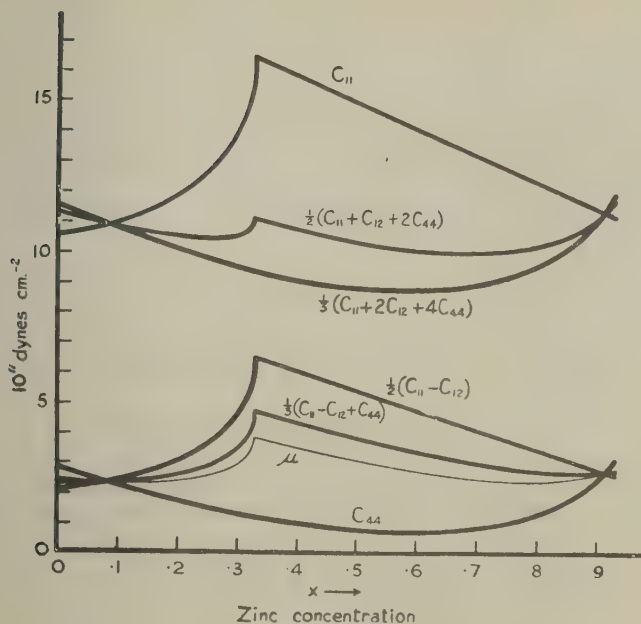
§ 1. INTRODUCTION.

IN a recent paper (Leigh 1951) it has been shown that in aluminium solid solutions a maximum is to be expected in the shear constant $\frac{1}{2}(C_{11} - C_{12})$ at an electron concentration in the neighbourhood of 2.67 per atom. The elastic constants $\frac{1}{2}(C_{11} - C_{12})$ and C_{44} are shown in fig. 1 as functions of the concentration of a divalent solute. In the theory of the elastic properties of pure aluminium it was found necessary, in order to explain the observed values of the shear constants, to assume that there are a small number of electrons overlapping the square faces of the Brillouin zone. The sharp peak in $\frac{1}{2}(C_{11} - C_{12})$ occurs at the point at which this overlap disappears.

It is now shown that the maximum in $\frac{1}{2}(C_{11} - C_{12})$ provides an explanation for the existence of a mixed crystal region which, below 355° C., interrupts the range of stability of the primary solid solution of zinc in aluminium. The aluminium-rich end of the phase diagram of the Al-Zn system (Raynor 1944) is shown in fig. 2, with zinc concentration given in atomic per cent. The mixed crystal region in question is shown as $\alpha + \alpha'$. The phases α and α' both have the face-centred cubic structure, and only differ in composition and lattice spacing, the gap in the solubility disappearing above 355° C. The β phase is the primary solid solution of aluminium in zinc, and has the hexagonal close-packed structure.

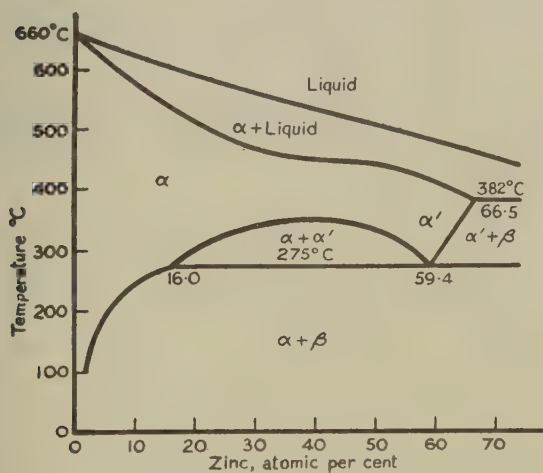
* Communicated by Professor H. Jones,

Fig. 1.



The elastic constants which give the wave velocities in certain special directions, shown as functions of zinc concentration. Also shown is μ , the mean of $\frac{1}{2}(C_{11} - C_{12})$ and C_{44} .

Fig. 2.



The aluminium-zinc phase diagram.

The existence of the solubility gap must be due to a subsidiary maximum in the free energy of the solution regarded as a function of zinc concentration. The positions of the phase boundaries are then given by the points of contact of the common tangent to the parts of the free energy curve on either side of the maximum. The present theory shows that the calculated maximum in $\frac{1}{2}(C_{11}-C_{12})$ leads to a subsidiary maximum of the required form in the contribution to the free energy from the thermal vibrations of the lattice. This provides some confirmation of the hypothesis of overlap over the square faces in pure aluminium.

§ 2. THE FREE ENERGY.

The free energy of a solid solution can be expressed as a sum of contributions from the electronic energy, the mixing entropy and the thermal vibrations.

The elastic constants of the solution, as shown in fig. 1, have been obtained by neglecting changes in the density of states curve as zinc is taken into solution. To this approximation the first derivative of the Fermi energy with respect to electron concentration cannot have a discontinuity anywhere; and the second derivative, given by $1/N(\zeta)$, where $N(\zeta)$ is the density of states at the Fermi surface, cannot be anywhere negative. In the present theory, therefore, no subsidiary maximum in the free energy can arise directly from the Fermi energy. (Compare the discussion by Hume-Rothery (1944), who also postulated overlap over the square faces in aluminium.) It will be assumed that the whole electronic energy varies smoothly and approximately linearly with zinc concentration. It can then be neglected, as it will not affect the positions of the phase boundaries.

The contribution to the free energy per atom from the mixing entropy is given, assuming complete disordering, by the expression

$$kT[x \log x + (1-x) \log (1-x)],$$

where T is the absolute temperature and x is the solute concentration.

The contribution to the free energy per atom from the thermal vibrations is given by the expression

$$\int_0^{\infty} \left\{ \frac{1}{2} h\nu + kT \log [1 - \exp(-h\nu/kT)] \right\} f(\nu) d\nu,$$

where $f(\nu) d\nu$ is the number per atom of normal modes of vibration of the lattice having frequencies lying in the interval ν to $\nu+d\nu$. We are here concerned primarily with the effect on the frequency spectrum $f(\nu)$ of changes in the elastic constants, rather than with the actual form of the spectrum. It is therefore reasonable to neglect the effect on the spectrum of the dependence of the wave-velocities on wavelength, since this effect may be assumed to remain constant or change smoothly with zinc concentration. As a first approximation we use the Debye spectrum

for an isotropic crystal, taking for the value of the rigidity modulus the mean of $\frac{1}{2}(C_{11}-C_{12})$ and C_{44} . The contribution to the free energy per atom is then given by the expression

$$\frac{9}{8}k\Theta_D + 9kT\left(\frac{T}{\Theta_D}\right)^3 \int_0^{\Theta_D/T} \log(1-e^{-\xi})\xi^2 d\xi, \quad . \quad . \quad . \quad (1)$$

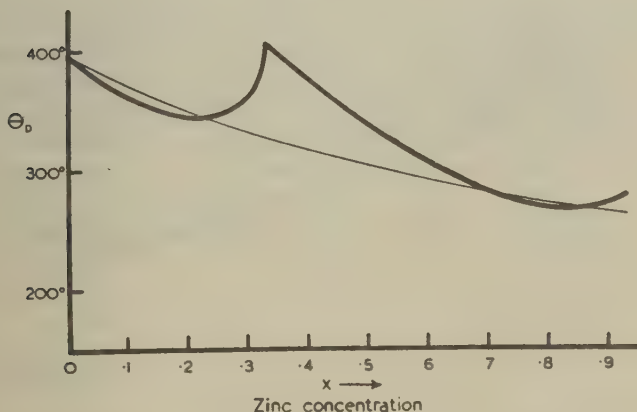
where Θ_D is the Debye characteristic temperature, given by the relation

$$\Theta_D = \frac{h}{k} \left(\frac{3}{4\pi\Omega} \right)^{\frac{1}{3}} c.$$

Ω is the atomic volume, and c is a mean wave velocity given in terms of the density ρ , the bulk modulus K , and the rigidity modulus μ , by the equation

$$\frac{3}{c^3} = \left(\frac{\rho}{K + \frac{4}{3}\mu} \right)^{3/2} + 2 \left(\frac{\rho}{\mu} \right)^{3/2}$$

Fig. 3.



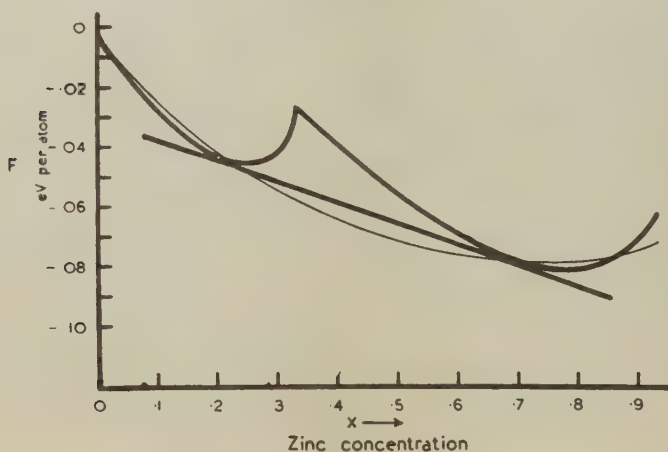
The Debye characteristic temperature as a function of zinc concentration. The thin curve shows how Θ_D would vary if the elastic constants remained constant.

In calculating Θ_D as a function of zinc concentration from the above formulæ, we can neglect the variation of Ω and K . The change in Ω is small, and it is easy to see that the effect on c of any change in K is small. Moreover, there is no reason to suppose that they do not vary smoothly with zinc concentration, and the effect on the positions of the phase boundaries would therefore be very small. In calculating c , K has been taken constant and equal to its value for pure aluminium, which is 7.78×10^{11} dynes cm.⁻² (Lazarus 1949). The large variation of ρ with zinc concentration, arising from the differing atomic weights of zinc and aluminium, has been taken into account.

Figs. 3 and 4 show the variation with zinc concentration of the Debye

temperature Θ_D , and the sum of the mixing entropy and Debye contributions to the free energy. The zero of F has been fixed arbitrarily at the value for pure aluminium. In each case the thin curves show the variation due to ρ alone, with μ constant at its value for pure aluminium. In calculating the free energy, T has been taken equal to 548°K. , the lowest temperature at which the $\alpha + \alpha'$ region exists, though, in fact, the choice of the value of T has practically no effect on the calculated phase boundaries. The common tangent to the two parts of the curve is shown, the points of contact being at approximately 20 and 70 atomic per cent of zinc. The observed phase boundaries at 275°C. are at 16.0 and 59.4 atomic per cent. The positions of the calculated phase boundaries obviously depend almost entirely on the position of the peak in $\frac{1}{2}(C_{11} - C_{12})$, and, in view of the approximations involved in the calculation of the elastic constants, the agreement is surprisingly good.

Fig. 4.



The free energy (Debye and mixing entropy contributions) as a function of zinc concentration. The thin curve shows how the free energy would vary if the elastic constants remained constant.

It is perhaps worth noticing that the qualitative result of this calculation, namely that the maximum in $\frac{1}{2}(C_{11} - C_{12})$ leads to a subsidiary maximum in the free energy, does not depend on the use of the Debye approximation to the frequency spectrum. Apart from neglecting the dependence of the wave velocities on wavelength, this approximation involves (i.) neglecting the dependence of the velocities on direction, and (ii.) allowing for the fact that the number of degrees of freedom of the crystal is limited, by the simple device of cutting off the total spectrum of the continuum (*i.e.* the sum of the contributions from the three frequency branches) at a single maximum frequency. A more general

form for the contribution to the free energy per atom, in which only the dependence of the wave velocities on wavelength is neglected, is given by the expression

$$\frac{1}{3} \left(\frac{4\pi\Omega}{3} \right) \sum_{i=1}^3 (\sigma^*)^3 \left[\frac{9}{8} k\Theta_i^* + 9kT \left(\frac{T}{\Theta_i^*} \right)^3 \int_0^{\Theta_i^*/T} \log(1 - e^{-\xi}) \xi^2 d\xi \right] \frac{d\omega}{4\pi}, \quad (2)$$

in which the free energy is expressed as a sum of contributions from the three frequency branches, each contribution involving an integration over direction. $d\omega$ is an element of solid angle, and σ^* is the magnitude of the maximum wave vector in the direction of $d\omega$. In general the wave vector is restricted to lie within a polyhedron. (If the polyhedron is replaced by a sphere of equal volume, σ^* is constant and equal to $(3/4\pi\Omega)^{1/3}$). Θ_i^* is a temperature corresponding to the maximum frequency in the direction of $d\omega$ in the i th branch, and is given by the relation

$$\Theta_i^* = \frac{h}{k} \sigma^* c_i,$$

where c_i is the corresponding continuum wave velocity in that direction. The dependence of the c_i on direction is very complicated, but the extreme values of the velocity in each branch are simple functions of the elastic constants. The following table gives the values of the c_i in the principal sets of crystallographic directions (see, for example, Blackman 1938).

	(100)	(110)	(111)
ρc_1^2	C_{44}	C_{44}	$\frac{1}{3}(C_{11} - C_{12} + C_{44})$
ρc_2^2	C_{44}	$\frac{1}{2}(C_{11} - C_{12})$	$\frac{1}{3}(C_{11} - C_{12} + C_{44})$
ρc_3^2	C_{11}	$\frac{1}{2}(C_{11} + C_{12} + 2C_{44})$	$\frac{1}{3}(C_{11} + 2C_{12} + 4C_{44})$

These values include the extreme values in each branch. In fig. 1 these values of ρc_i^2 are shown as functions of zinc concentration. The bulk modulus K , which is equal to $\frac{1}{3}(C_{11} + 2C_{12})$, has been taken constant at its value for pure aluminium as before. The effect of an increase in $\frac{1}{2}(C_{11} - C_{12})$ on a value of c_i corresponding to a given direction is to increase it or leave it unchanged, but never to decrease it. The peak in $\frac{1}{2}(C_{11} - C_{12})$, regarded as a function of zinc concentration, therefore gives rise to similar peaks in the c_i in every direction, the size of the peak being very large in the neighbourhood of some directions, *e.g.* the (100) directions in the third branch, and vanishing in the neighbourhood of some others, *e.g.* the (100) directions in the second branch. The same is therefore true of the Θ_i^* , and, since the expression in square brackets in (2) is an increasing function of Θ_i^* , it follows that there must be a subsidiary maximum in the free energy.

The present theory does not account for the disappearance of the solubility gap at higher temperatures. This is not surprising, as the theory of the elastic constants only refers to absolute zero. It might be thought that the explanation lies simply in the direct effect on the Fermi energy contributions to the elastic constants of the finite temperature form of the Fermi distribution, this leading to a smoothing off of the sharp peak in $\frac{1}{2}(C_{11}-C_{12})$. Calculation shows, however, that this is not so, the effect on $\frac{1}{2}(C_{11}-C_{12})$ being only to shift the peak a little in the direction of lower electron concentration.

ACKNOWLEDGMENTS.

The author is indebted to Professor H. Jones for several helpful discussions, and to the Senate of the University of London for a Postgraduate Studentship.

REFERENCES.

- BLACKMAN, M., 1938, *Proc. Roy. Soc. A*, **164**, 62.
HUME-ROTHERY, W., 1944, *Jour. Inst. Metals*, **70**, 229.
LAZARUS, D., 1949, *Phys. Rev.* [2], **76**, 544.
LEIGH, R. S., 1951, *Phil. Mag.* [7], **42**, 139.
RAYNOR, G. V., 1944, *Institute of Metals*, Annotated Equilibrium Diagram Series, No. 1.

XC. *Time and Frequency Uncertainty in Waveform Analysis**.

By P. M. WOODWARD, B.A.,
T.R.E., Ministry of Supply†.

[Received May 21, 1951.]

SUMMARY.

The concept of a structural time-constant is introduced by considering the time auto-correlation function of any waveform, and a structural frequency-constant is similarly defined in terms of the spectral auto-correlation function. By setting up a combined time and frequency auto-correlation function χ , an absolute time-frequency constant is obtained. Its value is always unity, and it is suggested that this expresses time and frequency uncertainty more precisely than the relation $\delta t \cdot \delta f \geq 1/4\pi$. To illustrate the function χ , two special waveforms are considered, namely, the complex Gaussian pulse and the real Gaussian pulse-train.

§1. INTRODUCTION.

No waveform $\psi(t)$ can be confined within a very short time interval and yet have a frequency spectrum $s(f)$ which occupies only a very narrow band of frequencies. A limit is set by the well-known relation

$$\delta t \cdot \delta f \geq \frac{1}{4\pi}, \quad \dots \dots \dots (1)$$

which in its wave mechanical form is of course the Heisenberg inequality. This is a property of any pair of Fourier transforms $\psi(t)$ and $s(f)$; the quantities δt and δf are the standard deviations of t and f in $|\psi|^2$ and $|s|^2$ respectively. Unfortunately, the relation (1) is an equality only when ψ and s are Gaussian in form. It is therefore tempting to seek some stronger expression which, while reducing to the equality (1) for Gaussian waveforms, would yet remain as an equality for waveforms in general. It might be, for instance, that the weakness of inequality arises from using the standard deviation as a measure of spread. This line of attack, however, is quickly ruled out by considering frequency modulated waveforms.

It is suggested in this paper that the elusive feature in terms of which the uncertainty principle can be exactly formulated, is contained in the idea of joint time and frequency auto-correlation. The statement of uncertainty which results from this approach becomes a statement, not

* Original version received April 12, 1951.

† Communicated by the Author.

about spreads, but about the lack of orthogonality between the waveform itself and the same waveform displaced both in time and frequency. Such a time and frequency domain was first discussed by Gabor (1946) and has also been treated by Ville (1948), though not perhaps in precisely the same way as is done here.

§ 2. GENERALIZED TIME AND FREQUENCY CONSTANTS.

The notion of a "time constant" is familiar to every physicist and engineer, but it is not usually defined precisely except for a simple exponential transient. One of the simplest linear electric circuits, for example, is the one whose impulsive response is given by

$$\psi(t) = \begin{cases} 0, & t < 0, \\ A \exp(-t/t_0) & t > 0, \end{cases} \quad \dots \quad (2)$$

and t_0 is known as the time constant of the circuit, or of the waveform ψ . When the input is not a simple impulse the output can be deduced from the impulsive response by the principle of superposition: the output is simply the convolution or resultant of the input and the impulsive response. Rather loosely, it is a degraded form of the input in the sense that any time-structure which is fine compared with t_0 is smoothed out. To formulate *without explicit recourse to a frequency description* what is meant by the "time-structure" of any waveform is a problem which has received considerable attention in the field of random noise fluctuations. Here time-structure may for many purposes be adequately described in terms of a temporal auto-correlation function, though the formalism of auto-correlation is by no means restricted to the study of random functions. For a non-random (and in general complex) waveform $\psi(t)$, the temporal auto-correlation function is given by

$$g(\tau) = \int_{-\infty}^{\infty} \psi(t) \psi^*(t+\tau) dt. \quad \dots \quad (3)$$

If $\psi(t)$ be normalized as in wave mechanics, the function g has the value unity at the origin, and it can be shown that $|g|$ never exceeds unity. It therefore seems reasonable to define the *amount* of temporal auto-correlation, whether it be positive, negative or complex, by the integral

$$T = \int_{-\infty}^{\infty} |g(\tau)|^2 d\tau, \quad \dots \quad (4)$$

since the vanishing of g implies no correlation, or more simply, the orthogonality of $\psi(t)$ and $\psi(t+\tau)$. The constant T may be called the *structural time-constant* of the waveform ψ without conflicting with established use of the unqualified term, since it is readily shown that when ψ is given by equation (2), T is equal to t_0 . Using the proposed definition, the structural time-constant of a Gaussian waveform is given by

$$T = \delta t \sqrt{4\pi}, \quad \dots \quad (5)$$

where δt is the measure of spread which occurs in the Heisenberg inequality.

In a similar manner, we may define a *structural frequency-constant* for any spectrum $s(f)$ by the equation

$$F = \int |G(\phi)|^2 d\phi, \quad (6)$$

where $G(\phi)$ is a frequency auto-correlation function given by

$$G(\phi) = \int_{-\infty}^{\infty} s^*(f)s(f+\phi) df. \quad (7)$$

The relation between $\psi(t)$ and $s(f)$ being the Fourier transformation

$$\psi(t) = \int_{-\infty}^{\infty} s(f) \exp(2\pi i f t) df, \quad (8)$$

$$s(f) = \int_{-\infty}^{\infty} \psi(t) \exp(-2\pi i f t) dt, \quad (9)$$

it is easy to show that $g(\tau)$ and $G(\phi)$ may be expressed in forms alternative to (3) and (7), thus

$$g(\tau) = \int_{-\infty}^{\infty} |s(f)|^2 \exp(-2\pi i f \tau) df, \quad (10)$$

$$G(\phi) = \int_{-\infty}^{\infty} |\psi(t)|^2 \exp(-2\pi i \phi t) dt. \quad (11)$$

By applying Parseval's theorem to equations (10) and (11), we may now express the structural constants in the forms

$$T = \int_{-\infty}^{\infty} |s(f)|^4 df, \quad (12)$$

$$F = \int_{-\infty}^{\infty} |\psi(t)|^4 dt. \quad (13)$$

By comparing equation (5) with the Heisenberg *equality*, we see that for real Gaussian waveforms TF is equal to unity, but this product is certainly not invariant for all waveforms, nor should we expect it to be. Since $|s|^2$ encloses unit area—its normalization resulting from that of $|\psi|^2$ —it can be seen from equation (12) that $1/T$ measures, in a peculiar way, the frequency spread of $|s|^2$. Similarly, $1/F$ is a measure of the extent to which $|\psi|^2$ is spread out in time. We might therefore expect that when we have $\delta t \cdot \delta f \gg 1/4\pi$, we could also have $TF \ll 1$, and it will be shown in §4 that certain very simple frequency modulated waveforms do satisfy both these conditions.

§3. JOINT TIME-FREQUENCY AUTO-CORRELATION.

So far, we have considered auto-correlation independently in time and frequency, but although there may be no correlation between $\psi(t)$ and $\psi(t+\tau)$, nor between $s(f)$ and $s(f+\phi)$ for particular values of τ and ϕ ,

it can happen that a *combined* time and frequency displacement (τ, ϕ) will restore correlation. Let us therefore investigate the joint time-frequency auto-correlation function

$$\chi(\tau, \phi) = \int_{-\infty}^{\infty} \psi(t) \psi^*(t+\tau) \exp(-2\pi i \phi t) dt, \quad \dots \quad (14)$$

suggested by comparison of equations (3) and (11). A little manipulation reveals the alternative form

$$\chi(\tau, \phi) = \int_{-\infty}^{\infty} s^*(f) s(f+\phi) \exp(-2\pi i f \tau) df, \quad \dots \quad (15)$$

which is suggested by comparing equations (7) and (10). This function is not entirely a new one. Ville (1948) has considered it in a very similar form, and Gabor (1946) has considered it in discrete form, except that in his theory, the two ψ functions within the integral are different: one of them is a Gaussian analysis function, the other is the waveform under consideration. His treatment corresponds to cross-correlation rather than auto-correlation.

The main purpose of the present paper is to point out that the amount of auto-correlation in time and frequency combined, may be measured by the value of

$$C = \int_{-\infty}^{\infty} \int_{-\infty}^{\infty} |\chi|^2 d\tau d\phi. \quad \dots \quad (16)$$

This is merely a generalization into two dimensions of the one-dimensional structural constants T and F . It is an *absolute structural constant*, because it turns out to be invariant for all waveforms. Thus, applying Parseval's theorem to equation (14), we have

$$\int_{-\infty}^{\infty} |\chi|^2 d\phi = \int_{-\infty}^{\infty} |\psi(t)|^2 |\psi^*(t+\tau)|^2 dt, \quad \dots \quad (17)$$

and integration with respect to τ gives

$$C = \int_{-\infty}^{\infty} \int_{-\infty}^{\infty} |\chi|^2 d\phi d\tau = \int_{-\infty}^{\infty} |\psi(t)|^2 dt = 1, \quad \dots \quad (18)$$

since $|\psi|^2$ is assumed normalized. This expresses the "uncertainty principle" of waveform analysis in an exact form. One may verify that in wave mechanics, C would equal Planck's constant. Whether or not it proves to be an interesting or useful expression of the uncertainty principle depends solely on whether the concept of time-frequency auto-correlation is found to have any genuine physical significance. It has already arisen in the theory of radar; upon its relevance, if any, to wave mechanics, the writer is not qualified to judge.

It seems worth remarking that, while the functions

$$g(\tau) = \chi(\tau, 0), \quad \dots \quad (19)$$

$$G(\phi) = \chi(0, \phi), \quad \dots \quad (20)$$

do not provide a complete description of the waveform ψ which generates them, there is no loss of information in passing from ψ to χ , a fact which may be proved by considering the two-dimensional Fourier transform of $\chi(\tau, \phi)$.

§4. THE COMPLEX GAUSSIAN WAVEFORM.

It has been remarked that certain "frequency modulated" waveforms are such that $TF \ll 1$. Thus, apparently, there is a lack of auto-correlation in time and frequency when considered separately, but not in a joint time-frequency domain, in view of equation (18). The simplest waveform which illustrates this is given by

$$\psi(t) = A \exp(-\alpha t^2), \quad (21)$$

where α is complex with positive real part. This waveform has a Gaussian modulus, and its instantaneous frequency, or rate of change of phase, is a linear function of time. If a large constant frequency shift were included, the real part would represent a high-frequency pulse enveloping a frequency modulated carrier. Since, however, neither a frequency shift nor a time shift affects the function χ , it will be sufficient to consider the simplest form of ψ —as given by equation (21)—in which the instantaneous frequency is zero at $t=0$, where the modulus is a maximum.

When α is purely real, there is of course no frequency modulation, and figs. 1 and 2 illustrate typical forms of $|\psi|^2$, $|s|^2$, and $|\chi|^2$. In representing $|\chi|^2$, a shaded area has been given, its boundary representing a single contour. Since all the functions considered here have a Gaussian modulus, this representation by means of an ellipse should be adequate. In these two examples, it will be understood that

$$\delta t \cdot \delta f = 1/4\pi, \quad (22)$$

$$TF = 1, \quad (23)$$

and as always $|\chi|^2$ is unity at the origin and encloses unit volume.

Suppose now, that α is complex. It is then possible to obtain both a wide $|\psi|^2$ and also a wide $|s|^2$ as in fig. 3, such that

$$\delta t \cdot \delta f \gg 1/4\pi. \quad (24)$$

The "bandwidth" δf is large because of the spread in frequency occurring in $\psi(t)$, which does not show up in $|\psi|^2$, and therefore does not influence δt . The structural time and frequency constants, however, are each small, such that

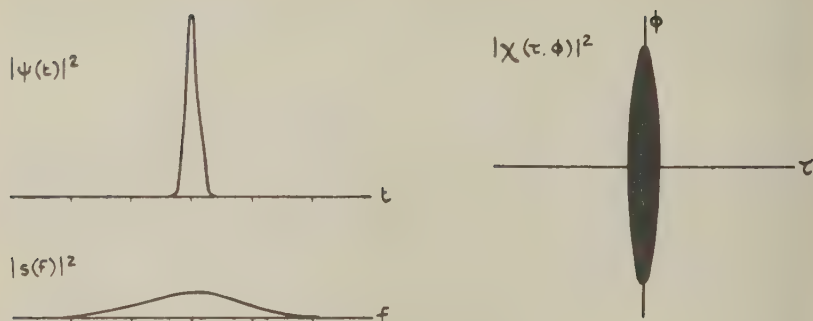
$$TF \ll 1, \quad (25)$$

because of the phase-structure which is masked both in $|\psi|^2$ and in $|s|^2$. The form of $|\chi|^2$ shows that auto-correlation is distributed in a manner which makes mere time and frequency cross-sections quite deceptive.

It can be shown that if we write

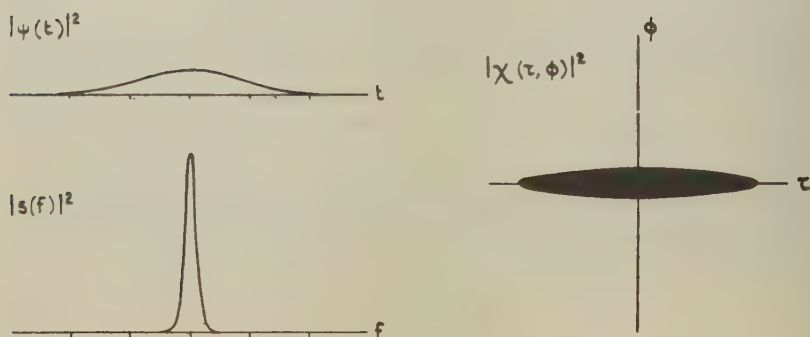
$$\alpha = a + ib, \quad (26)$$

Fig. 1.



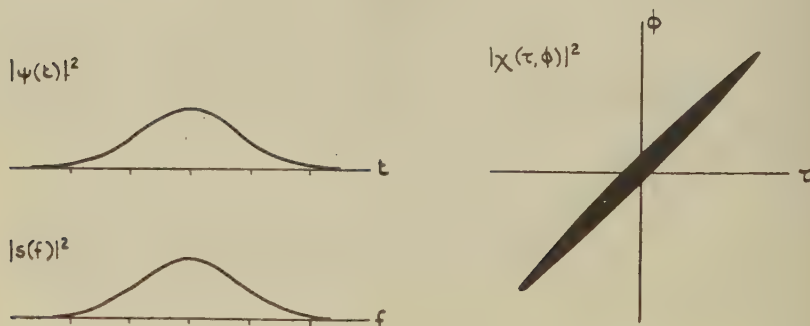
Short Gaussian pulse.

Fig. 2.



Long Gaussian pulse.

Fig. 3.



Complex Gaussian pulse.

the inclination θ of the major axis of $|\chi|^2$ to the τ -axis is given by

$$\tan 2\theta = \frac{2\pi b}{\pi^2 - |\alpha|^2}. \quad (27)$$

The major axis is thus at 45° when $|\alpha| = \pi$. Pure frequency modulation is obtained by allowing the real part of α to tend to zero. The $|\chi|^2$ function then becomes drawn out into a "knife-edge" of unit amplitude and infinite length along a line through the origin which has a slope given by

$$\tan \theta = b/\pi. \quad (28)$$

Apart from sign, this slope is simply the rate of change of the instantaneous frequency, given by

$$2\pi f_i = \frac{d}{dt}(-bt^2). \quad (29)$$

The reason for the difference of sign is that $|\chi(\tau, \phi)|^2$ is unity when a time-advance of τ_0 combined with a frequency advance of ϕ_0 leaves ψ unchanged. If τ_0 and ϕ_0 have the same sign, then the instantaneous frequency must decrease with time.

Knife-edge distributions of $|\chi|^2$ can be obtained mathematically only as the result of a limiting process. A knife-edge along the ϕ -axis arises from a waveform consisting of a single impulse occurring at any time, a knife-edge along the τ -axis arises from a purely sinusoidal waveform or monochromatic spectrum. Pure linear frequency modulation gives a knife-edge at some other angle and is associated with infinite values of both the δf and the δt in the Heisenberg relation.

§5. THE REAL GAUSSIAN PULSE-TRAIN.

As a final illustration, we may consider a train of real positive Gaussian pulses, varying in amplitude according to a wider Gaussian envelope, as indicated in fig. 4. It is assumed that the pulses do not overlap appreciably and that there are a large number having comparable amplitudes. All the following results apply to this approximation.

The forms of $|\psi|^2$ and $|s|^2$ are the same: they differ only in their parameters. Denoting as previously the standard deviations of t and f in $|\psi|^2$ and $|s|^2$ by δt and δf respectively, it is easily shown that

$$\delta t \cdot \delta f \gg 1/4\pi. \quad (30)$$

Further, let us denote the standard deviation of each individual pulse by Δt and that of each broadened spectral line by Δf . Then it can also be shown, as is well known, that

$$\delta t \cdot \Delta f = \Delta t \cdot \delta f = 1/4\pi, \quad (31)$$

so that the Heisenberg relation is an equality for the wrong measurements! One may further show that the structural time constant is

$$T = \frac{4\pi}{a} \delta t \cdot \Delta t, \quad (32)$$

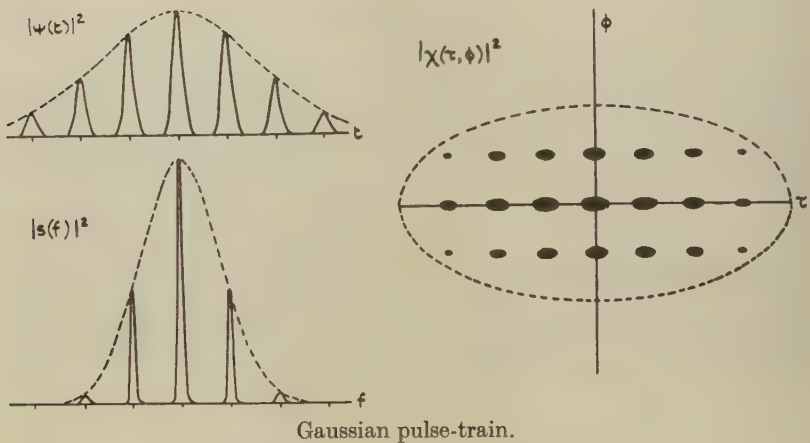
where a is the time separation of the pulses, and that the frequency constant is

$$F = 4\pi a \delta f \cdot \Delta f, \quad (33)$$

where $1/a$ is the separation of the spectral "lines". Consequently, as will be seen by comparing equations (31), (32) and (33), we have

$$TF = 1. \quad (34)$$

Fig. 4.



The reason for this is that the time-frequency auto-correlation function χ is separable as a product

$$\chi(\tau, \phi) = g(\tau)G(\phi), \quad (35)$$

as also in the case of a single real Gaussian pulse. The special characteristic of frequency modulation is that χ is not separable without a rotation of axes.

Shaded areas for $|\chi|^2$ are shown in fig. 4: the function is made up of a lattice of elliptical Gaussian peaks having amplitudes which vary according to a Gaussian envelope indicated by the dotted contour. The enveloping distribution has the same eccentricity as the cellular peaks, since from equation (31) we have

$$\frac{\delta t}{\delta f} = \frac{\Delta t}{\Delta f}, \quad (36)$$

and the area of each unit lattice cell is unity.

It should be clear from these examples that it is an easy matter to make the product of δt and δf , which occur in the Heisenberg relation, greatly exceed $1/4\pi$. Provided, however, that the time-frequency auto-correlation function remains separable, the product of the structural time and frequency constants remains equal to unity. Whether TF can ever exceed unity is not yet known, but the absolute structural constant defined by equation (16) remains equal to unity invariably.

§6. ACKNOWLEDGMENT.

Acknowledgment is made to the Chief Scientist, Ministry of Supply for permission to publish this paper, which is reproduced by permission of the Controller, H.M. Stationery Office (Crown copyright reserved).

§7. REFERENCES.

- GABOR, D., 1946, *Jour. Inst. Elect. Eng.*, **93**, Pt. III, 429.
VILLE, J., 1948, *Câbles et Transmission*, No. 1, p. 61.

XCI. *The Beta Spectrum of Tritium.*

By G. M. INSCH and S. C. CURRAN,

Department of Natural Philosophy, Glasgow University*.

[Received May 21, 1951.]

ABSTRACT.

The beta-spectrum of tritium, H^3 , has been carefully examined by the proportional counter method down to energies ~ 1 KeV. In the present work it has been more thoroughly explored using improved techniques designed to permit accurate measurements of the spectrum shape down to a lower energy limit ~ 200 eV. The improvements consisted chiefly in employing a counter which was made "end-free" by means of field-adjusting tubes and the use of an electronic method of measuring the pulse distribution in addition to the moving film technique. The intensity of the spectrum below 1 KeV. was found to be definitely less than theoretically predicted.

§ 1. INTRODUCTION.

THE beta-decay of tritium is an allowed transition. The recent work of Curran *et al.* (1949 a) has shown that between ~ 1 KeV. and the upper energy limit, the spectrum is in good agreement with Fermi theory. A tentative suggestion of some deficiency in the number of beta-particles in the low energy region was made by these authors. Theoretically, the intensity of the spectrum (particles per unit energy interval) at zero energy should be about 86 per cent of the intensity at the maximum of the distribution. Cooper and Rogers (1950) have constructed a composite of the various published spectra and have concluded that all work on the spectrum indicates an excellent agreement with Fermi theory from 2.5 KeV. to 18 KeV. The introduction of the improvements to the technique makes it possible to examine the spectrum shape to lower energy limits than in the past without appreciable uncertainties arising from spuriously small pulses. These small pulses are those which have their origin in the part of the counter near the ends of the wire, since in this region the gas multiplication is reduced below the normal value unless field-adjusting tubes (Cockroft and Curran 1951) are employed.

§ 2. APPARATUS.

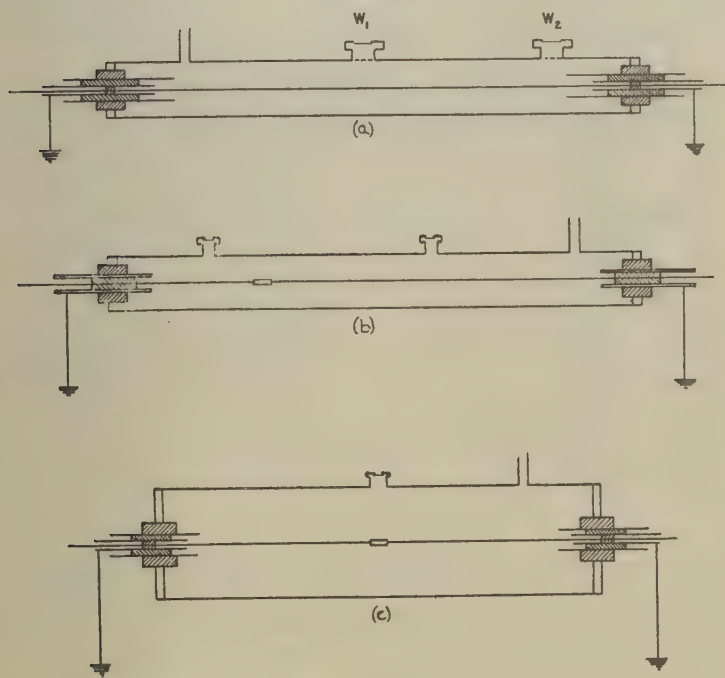
A diagram of the counter normally used in this work is seen in fig. 1 (a). The field-adjusting tubes were held at the potential appropriate to their diameter, thus ensuring a minimum of "end-effect". The value

* Communicated by the Authors.

of this potential was checked by ensuring that pulses from a homogeneous beam of X-radiation, fired through both windows W_1 and W_2 , were of equal size at the centre and end of the counter. The counter was lined with a thin sheet of aluminium to minimize secondary effects at the cathode. The lining was perforated at the window positions to prevent any ionization in the window "neck" from being recorded at the central wire.

The pulses from the counter after amplification, were recorded on a 35 mm. film. Using this technique, it was found difficult to examine the spectrum shape accurately below ~ 300 eV. The thick stems of the

Fig. 1.

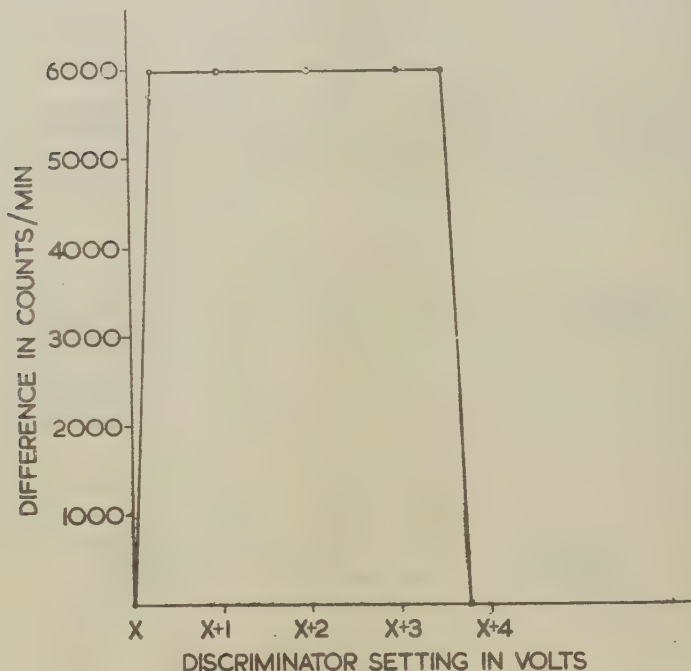


higher energy pulses and the brightness of the baseline itself caused a fogging of the film in the very low energy region. To overcome this limitation, the pulses were measured using a single-stage pulse analyser. This consisted essentially of two scaling units type 1009A. The discriminator of one unit was used to control the first stage of both units. The insertion of a steady source of potential difference (V volts) between the grids of the first stages in each scaling unit supplied a channel width of V volts \pm the small difference in the triggering potentials of each unit. To measure the shape and width of the channel, homogeneous pulses were fed into the analyser. Graphs of the difference in the counting

rate between the two scalers against the discriminator setting were plotted (fig. 2) at various points throughout the range of the discriminator, and it was found that the channel width was constant and that the channel had "rectangular" shape.

The tritium source had argon associated with it to act as a carrier. Before the gas was introduced into the counter its temperature was reduced to about -40°C . to remove tritiated water vapour. Measurements proved that no tritium stuck to the walls of the counter after this treatment.

Fig. 2.



§3. PULSE DISTRIBUTION AT LOW ENERGIES.

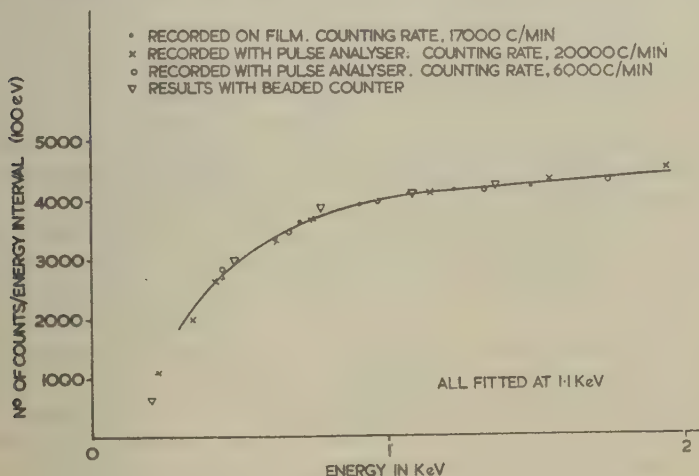
It will be noted that all the above precautions, both in counter design and handling of the source, were introduced to eliminate the possibility of affecting the true spectrum shape, particularly in the direction of moving higher energy particles towards the lower energy region.

Three separate measurements were made on the spectrum with the counter already described. In the first a small quantity of H^3 , giving a counting rate of $\sim 17,000$ c./m. (the background counting rate was ~ 300 c./min.), together with a mixture of methane at a pressure of 16 cm. Hg. and argon at slightly more than 3 atmospheres, was introduced into the counter, fig. 1 (a). The spectrum shape between ~ 200 eV. and

2 KeV. was examined, the pulses being recorded on 35 mm film. The energy scale was calibrated by superimposing on the spectrum the fluorescence $K\alpha$ X-rays of Gallium (energy 9.2 KeV.) arising from the K-capture of Ge^{71} . The amplifier gain was reduced by a factor of 4 to achieve this calibration. The pulse distribution from this measurement on the spectrum is seen in fig. 3, and the intensity below about 1 KeV. appears to be much less than expected on theoretical grounds. We have already mentioned the uncertainty of the curve below ~ 300 eV.

The experiment was repeated under almost identical conditions, using the pulse analyser to record the spectrum shape. Two measurements were made, one with a counting rate ~ 6000 c./min. and the other with a counting rate $\sim 20,000$ c./min. (fig. 3). It was found that the various

Fig. 3.



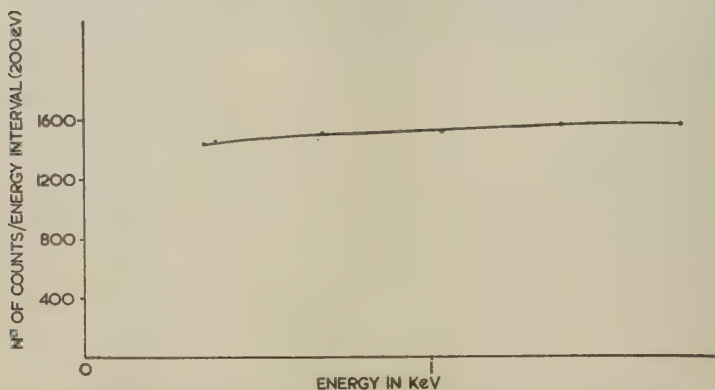
points repeated satisfactorily after several hours. In the case of the low counting rate, it was not possible to obtain readings below about 300 eV. because of poor statistics. The channel width was kept at 100 eV. throughout the experiments, and the energy scale was calibrated in the same manner as before. Since the results obtained from these determinations with different counting rates agree, it seems unlikely that the apparent lack of low energy pulses is due to any limitation of the amplifier. The particular limitation in mind was the possibility of affecting pulse amplitudes when the pulses occurred within too short an average interval.

In all the above measurements, the field-adjusting tubes were held at the potential appropriate to their diameters, thus ensuring a counting tube free from "end-effect". Curran *et al.* (1949 a) have published a result obtained using a counter which was not "end-free" and their experimental curve did not demonstrate any tendency to fall steeply

at low energies. To achieve a result comparable with theirs, the field-adjusting tubes were earthed and the spectrum shape examined (fig. 4) in a manner similar to the two previous measurements. The counting mixture giving a counting rate of 20,000 c./min. was used. The result obtained is in fairly good agreement with that of Curran *et al.*

A "beaded" counter was built for further examination of the spectrum. This additional step was deemed advisable in view of the somewhat surprising result obtained. This counter consisted of a tube $2\frac{1}{4}$ in. in diameter and 24 in. in length (fig. 1 b). The central wire was divided into two sections, one 6 in. long and the other 14 in. long, insulated electrically from each other by a glass bead, 1 cm. long and 1 mm. in diameter. This provided two independent counting volumes having similar "end-effects", and the difference between the spectrum in the long and short ends represents the distribution which would be obtained

Fig. 4.



from a counter of length 8 in. free from "end-effect". Tritium was introduced into the counter, together with a mixture of methane at a pressure of 16 cm. Hg. and argon at 2 atmospheres. The counting rates were about 20,000 c./min. in the long end and 8000 c./min. in the short end, compared with background counting rates of 600 c./min. and 200 c./min. respectively. The spectrum shape obtained from this examination is also seen in fig. 3. The pulse analyser was again used, and the calibration was carried out in the same manner as previously.

§4. DISCUSSION.

The very good agreement between the results achieved by the differing methods employed is striking. We believe that the curves shown are accurate to within 10 per cent down to an energy value of 400 eV. and that even below this energy the shape of the curve is significant. The results obtained are in disagreement with Fermi theory in the low energy region, since the theory predicts that the curve should meet the ordinate at an intensity value about 86 per cent that of the maximum.

There are two possible explanations of the experimental results which remove disagreement with Fermi theory. (1) If the counter were not 100 per cent efficient for detection of very low energy electrons or if the energy lost by the particles per ion pair produced varied with the energy of the ionizing particles, the true shape of the spectrum could possibly be distorted into a shape similar to that obtained. (2) If there were present, in coincidence with the β -particles, quanta or particles of low energy, the results could again be explained.

Fortunately, sufficient data is at hand to discuss the first possibility. The work of Kirkwood *et al.* (1948) together with that of Curran *et al.* (1949 b) seems to establish that in argon, the energy expended on the production of an ion pair is constant down to very low energies. Additional work carried out in these laboratories with the counter shown in fig. 1 (a) has confirmed this result. The K and L X-rays of chlorine (energy 2.6 KeV. and 200 eV., respectively) resulting from K- and L-capture in A^{37} are largely converted by Auger effect. It is found, by using a source of A^{37} that the energy expended per ion pair by slow electrons in argon is constant down to 200 eV. It has also been found that the relative intensities of the two peaks are in agreement with the results of Pontecorvo *et al.* (1949). The low energy peak consists of two unresolved peaks, one due to the K-quantum escaping from the counter, involving the L_{II} or L_{III} shell (200 eV.) and due to nuclear L capture involving L_I electrons (280 eV.). From these results, it seems most unlikely that the counter used is failing to act proportionally down to the lowest energy values.

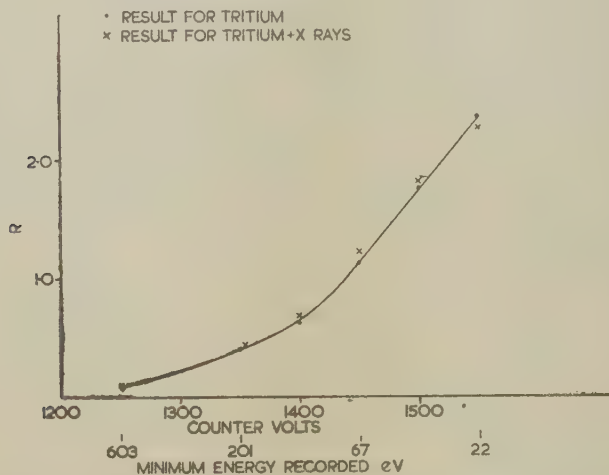
In connection with the second possibility, a homogeneous quantum radiation of energy ~ 400 eV. in coincidence with the β -particles would explain the spectrum shape. Such a radiation would give a peak (Curran, Cockcroft and Angus 1949) of shape approximately represented by $x^{20} \exp(-x)$, and this radiation, together with the β -rays, would give a distribution similar to that observed. The origin of such radiation, however, is difficult to explain theoretically. We know that quanta of total energy about 60 eV. will be released in the de-excitation of the He^3 ion following β -emission from H^3 . These quanta could give rise to about 3 ion-pairs per disintegration, but we require about 13 ion-pairs on the supposition that radiation is responsible for the shape of the spectrum observed. It is extremely improbable that the radiation has its origin in nuclear excitation of He^3 in the normal sense of the term. It is also possible that a number of low energy quanta (energy ~ 50 eV.) released in coincidence with each other and the β -particles could account for the results.

§5. COINCIDENCE MEASUREMENTS.

The presence of quanta of energy ≤ 400 eV. is extremely difficult to establish in a coincidence measurement due to the extreme absorbability of the radiations. However, the following method was adopted in an

endeavour to ascertain whether or not such radiations were present. A counter of $5\frac{1}{2}$ in. diameter and 16 in. in effective length (fig. 1 (c)) was divided into two similar but independently operating volumes by a very thin glass bead ($\sim\frac{1}{2}$ mm. in diameter and 1.5 cm. long). The counting tube was lined with aluminium sheet. Tritium was introduced into the counter with a trace of He to act as carrier and methane was added to give a total pressure of 1 cm. Hg. The counting rate was $\sim 10,000$ c. min. in each volume, and the counter operated satisfactorily at this low pressure with about 1.5 KV. on the case, giving a high gas gain sufficient to detect pulses due to radiation of energy as low as 40 eV. The value for the mass absorption coefficient of methane for low energy quantum radiations does not appear to be accurately known, but from the data available it seemed likely that if quanta of energy 400 eV. were present, coincidences would be obtained. On the other hand,

Fig. 5.



if the quanta had an energy value much less than 400 eV. no coincidences would be recorded. The counter was placed with its axis perpendicular to a magnetic field of sufficient strength to ensure that there were no β - β coincidences due to an electron travelling from one counting volume to the other. The results obtained from this investigation were indecisive. As the counting tube volts were increased the two counting volumes lost their independence and coincidences due to "mutual firing" were recorded. This phenomenon increased in frequency as the gas gain was increased. A curve giving the ratio R of the coincidence counting rate to the total counting rate in terms of the case voltage was plotted (fig. 5). This curve rose steeply at high gas gain. K α fluorescence X-rays of copper were fired through the central window, resulting in an approximate doubling of the counting rate in each volume. An exactly

similar coincidence curve was again plotted (also fig. 5), and it was found that the points on this curve overlapped the points of the previous curve to within the accuracy of the experiment. The X-rays of copper gave pulses of average size roughly the same as those produced by the tritium β -rays. The close similarity of the two sets of observations shows that very few, if any, of the coincidences, observed with tritium alone, can be ascribed to the hypothetical β -quantum decay process. It is unfortunate that this coincidence technique fails to give definite results in the region of 400 eV. Clearly, it makes the technique quite inadequate for testing the hypothesis of much softer quanta ($\ll 400$ eV.).

We are, thus, forced to conclude that the spectrum of H^3 , as observed in a proportional counter, is not in accordance with Fermi theory at energies below about 1 KeV. We are unable to establish experimentally the reason for the discrepancy, although it seems possible that it might have its origin in the simultaneous emission of a quantum or quanta of total energy about 400 eV. This value is considerably higher than the expected energy release (~ 60 eV.) in the de-excitation of the He^3 ion.

REFERENCES.

- COCKROFT, A. L., and CURRAN, S. C., 1951, *Rev. Sci. Instrum.*, **22**, 37.
COOPER, E. P., and ROGERS, F. T., 1950, *Phys. Rev.*, **77**, 402.
CURRAN, S. C., ANGUS, J., and COCKROFT, A. L., 1949 a, *Phil. Mag.*, **40**, 53;
1949 b, *Ibid.*, **40**, 36.
CURRAN, S. C., COCKROFT, A. L., and ANGUS, J., 1949, *Phil. Mag.*, **40**, 929.
KIRKWOOD, D. H. W., PONTECORVO, B., and HANNA, G. C., 1948, *Phys. Rev.*,
74, 497.
PONTECORVO, B., KIRKWOOD, D. H. W., and HANNA, G. C., 1949, *Phys. Rev.*,
75, 982.

XCII. *A Theoretical Investigation of the Compression of a Ductile Material between Smooth Flat Dies.*

By A. P. GREEN,

British Iron and Steel Research Association, Sheffield,
Mechanical Working Division*.

[Received May 18, 1951.]

[Plate XXIV.]

SUMMARY.

A theory is suggested to describe the distribution of stress and velocity in a block of ductile material symmetrically indented on opposite sides by two smooth flat dies. The theory is two-dimensional and an ideal plastic-rigid material is assumed. Slip-line fields are proposed for all ratios of width of dies to height of block greater than one. It is found that the velocity field transforms into its corresponding slip-line field. Other plane plastic problems where this correspondence occurs are cited. Since the velocities are known along only one slip-line boundary, the usual numerical procedure for calculating the field has to be modified and the use of influence coefficients is introduced. Solutions are computed for width/height ratios between one and two, and it is observed that simple analytical relations hold between these ratios and the corresponding velocity discontinuities in the field. The calculated mean pressures on the dies are compared with upper and lower bound curves derived by Hill on the basis of extremum principles. The deformation after different finite indentations is illustrated by photographs of experiments using (a) plasticine models, and (b) aluminium alloy strip.

Similar fields are proposed for extrusion or drawing through a wedge-shaped die with large reductions, but no solutions have been computed.

§1. INTRODUCTION.

THE plane stress-strain curve of a strip, before or after rolling, can conveniently be obtained by symmetrically indenting the strip on opposite sides by two flat dies completely spanning its width. The test was suggested by Orowan and is described by Ford (1948). Provided that the indented area is sufficiently long and narrow, the constraint of the non-plastic material on both sides of the dies inhibits lateral spread, and the deformation of the strip is essentially plane-strain, with the exception of narrow regions near the edges (Hill 1950 a). In this paper the theory of plane plastic strain due to Hencky and Geiringer is applied to analysing the stress and velocity distribution during the course of the indentation when the dies are smooth and their width, $2w$, is greater than the thickness, $2h$, of the material (fig. 2).

* Communicated by the Author.

When the dies are smooth and $w/h < 1$, a complete solution has already been found and the pressure on the dies for different values of w/h has been calculated (Hill 1950 b, p. 256). For perfectly rough dies and $w/h > 3.64$, a complete solution was first obtained by Hill, Lee and Tupper (1945 or 1951; for a shorter account see Hill and Lee 1946). When $3.64 > w/h > 1$ a solution has been suggested by Hill (1950 b, p. 230) which is only valid when there is friction on the dies; but it is uncertain for what range of frictional conditions the solution is appropriate.

In all these theoretical solutions the material under test is supposed to be rigid up to the yield-point; after which the maximum shear stress retains a constant value during plane plastic strain. Such a plastic-rigid body cannot deform until the plastic region attains a certain critical size (depending on the problem); the load-indentation curve has a discontinuity in slope at the yield-point and the load when distortion begins is called the yield-point load. When a real material is indented by rigid dies the bend in the load-indentation curve is well defined if the work-hardening is small. The bend marks the initiation of large plastic strains; at lower loads the amount of indentation is restricted by the elastic resistance of the non-plastic material and all plastic strains are of an elastic order of magnitude. The mean load in the interval corresponding to the bend should approximate closely to the yield-point load of the plastic-rigid material. If the material is annealed, it is not possible to define a load which may be compared with that calculated by the theory. The solution presented here can therefore be applied to the *initial* yielding of a material with a fairly well defined yield-point and to the continued indentation of a non-hardening material.

§2. BASIC EQUATION OF PLANE-STRAIN PLASTIC FLOW.

The theory of plane plastic strain and the slip-line field is set out most clearly by Hill (1950 b) who has considerably simplified and improved the original presentation by Hencky and Geiringer. Only a brief résumé of the basic theory will be given here.

Since the volume of an element of plastic-rigid material does not alter, each incremental distortion in a state of plane strain consists of a pure shear. Hence, for the ideal isotropic material, the state of stress at each point is a pure shear stress k , assumed constant, together with a hydrostatic pressure p . If Tresca's yield criterion is used, k is equal to $Y/2$, while for von Mises' criterion it is equal to $Y/\sqrt{3}$, where Y is the yield stress in uniaxial tension. It is assumed that inertial stresses are negligible compared with k and that the problem can therefore be treated as quasi-static. The plastic stress equations in the plane of flow, consisting of the yield criterion and the two equations of equilibrium, prove to be hyperbolic. The velocity equations in the plastic region express the condition for zero volume change and the fact that for an isotropic material the principal axes of stress and plastic strain-increment must

coincide. These equations are also hyperbolic and their characteristics coincide with those of the stress equations. There are two orthogonal characteristic directions at any point in the plastic field; they are the directions of maximum shear stress or shear strain-rate. The two orthogonal families of curves whose directions at every point coincide with those of the maximum shear stress are known as slip-lines and will be labelled α - and β -lines. By convention, if the α - and β -lines are regarded as a pair of right-handed curvilinear axes, the line of action of the algebraically greatest principal stress falls in the first and third quadrants. The equations governing the variation of p along a slip-line, which were first derived by Hencky (1923), are

$$\left. \begin{aligned} p+2k\phi &= \text{constant, along an } \alpha\text{-line,} \\ p-2k\phi &= \text{constant, along a } \beta\text{-line,} \end{aligned} \right\} \dots \dots (1)$$

where ϕ is the anticlockwise angular orientation of a slip-line with respect to some fixed direction. These relations are completely equivalent to the equilibrium equations.

The equations of Geiringer (1930) for the components of velocity u , v , along the α and β slip-lines, are

$$\left. \begin{aligned} du - v d\phi &= 0 \text{ along an } \alpha\text{-line,} \\ dv + u d\phi &= 0 \text{ along a } \beta\text{-line.} \end{aligned} \right\} \dots \dots (2)$$

They state that the rate of extension along any slip-line is zero.

It can be shown that the normal components of velocity may be arbitrarily prescribed without inconsistency along two intersecting slip-lines. It follows that it is possible to have a discontinuity in the tangential component of velocity across a slip-line. This implies a momentarily infinite rate of shear; but this is permissible since work-hardening is neglected and a slip-line is a direction of maximum shear strain-rate. The discontinuities correspond to what in a real material would be a narrow transition region, where the shear strain-rate is large. It is evident that such transition regions will tend to be less sharp in a metal with a high rate of work-hardening, which emphasizes the fact that this theory is not applicable to such a material.

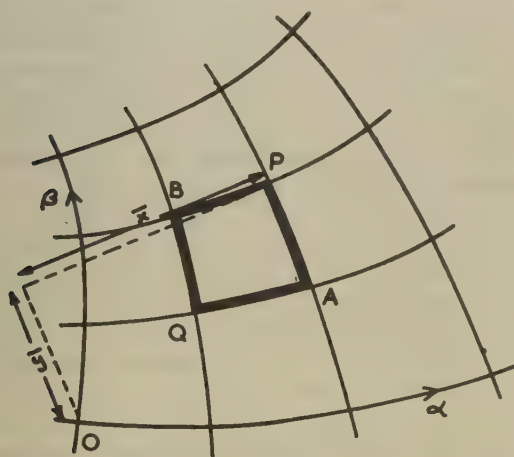
Hencky's first theorem, which is a direct consequence of equations (1), is the geometrical expression of the fact that the pressure difference between two points, calculated by proceeding along either of the two slip-line paths between the points, is the same. If we consider a curvilinear quadrilateral APBQ (fig. 1) bounded by two α -lines, QA and BP, and two β -lines, QB and AP, we deduce from (1) that

$$\phi_A - \phi_P = \phi_Q - \phi_B \dots \dots (3)$$

Any two families of orthogonal curves satisfying this condition constitute a possible slip-line field for a plastically deforming mass under certain boundary conditions. In general the plastic region is divided

into two parts by one or more slip-lines: a part where deformation is occurring, and a part which is rigid. The plastically deforming part consists of a number of subsidiary domains bounded by slip-lines across which the curvature of the slip-lines and/or the tangential components of velocity change discontinuously. The plastic material in the rigid part is prevented from deforming by the constraint of surrounding non-plastic material. In order to solve any problem the slip-line field must be found in the plastically deforming zone. The probable approximate location of this zone is first suggested by physical intuition, aided when possible by experiment. The slip-line field is then constructed to satisfy all the stress and velocity conditions that directly concern the zone, as well as the condition that the rate of plastic work should be everywhere positive. Finally, the solution is valid if the associated stress distribution in the rigid material is such that the yield limit is nowhere exceeded.

Fig. 1.



Slip-line field network showing (\bar{x}, \bar{y}) coordinates.

The most convenient coordinates for defining a point in a slip-line field are the quantities (\bar{x}, \bar{y}) . They are the coordinates of the point P under consideration, referred to axes passing through some fixed origin O, and parallel to the respective slip directions at P (fig. 1). It is easy to show that for any two orthogonal families of curves

$$\left. \begin{aligned} d\bar{y} + \bar{x}d\phi &= 0 \text{ along an } \alpha\text{-line,} \\ d\bar{x} - \bar{y}d\phi &= 0 \text{ along a } \beta\text{-line.} \end{aligned} \right\} \dots \dots \dots (4)$$

In applying these conditions to a slip-line field the geometrical property (3) is introduced which determines ϕ at all points of a network of slip-lines.

The stress and velocity boundary conditions are particularly easy to deal with when the material is in contact with either a smooth or a perfectly rough rigid surface. The slip-lines meet a smooth surface

at 45° , whereas a perfectly rough surface is cut orthogonally by one family of slip-lines since the frictional stress is equal to k . These conditions are independent of the normal pressure and we can therefore proceed with the solution of the slip-line field without specifying beforehand the value of p at any point. The only other simple frictional condition is that the shear stress on the surface has some constant value less than k . Each slip-line then intersects the surface at the same angle. This condition implies, however, that the coefficient of friction decreases with increasing normal pressure on the surface, which is an artificial condition not likely to occur in practice. If the coefficient of friction is constant, the angle of intersection varies with normal pressure along the surface of contact. This is a difficulty inherent in the solution of problems involving intermediate frictional conditions.

§3. FINDING THE SLIP-LINE FIELDS.

In this indentation problem geometric similarity is not maintained, and therefore we have to follow, from the very beginning, the progressive changes in the configuration. At each stage of the indentation there will be a different slip-line field, with its corresponding stress and velocity solution. The initial shape of the overhang does not affect the plastic problem, but for convenience we shall discuss the symmetrical indentation of a rectangular block.

The development of the plastic zones and the momentary boundary between the rigid and the plastically deforming material has been discussed in general terms for indentation by rough dies (Hill and Lee 1946). The present problem is similar in many respects. It may be expected that plastic zones will be initiated at the sharp edges of the dies and will spread inwards until they meet in the geometric centre of the block. Since, however, in this problem there are no frictional stresses, it does not seem possible that there should be a non-plastic area left in contact with the dies at the centre. For the solution presented here, no deformation consistent with Geiringer's equations is possible until the plastic zone has spread completely through the block. Plastic deformation is also restricted by the overhang, part of which must be non-plastic since its surfaces are stress free. It will be assumed that the overhang, even if partly plastic, moves out as a rigid whole. This was the assumption made by Hill and Lee, and it is confirmed by experiment (Nye 1947; see also the plasticine experiments described in this paper). It follows that the external plastic-rigid boundary must pass through the edges of the dies.

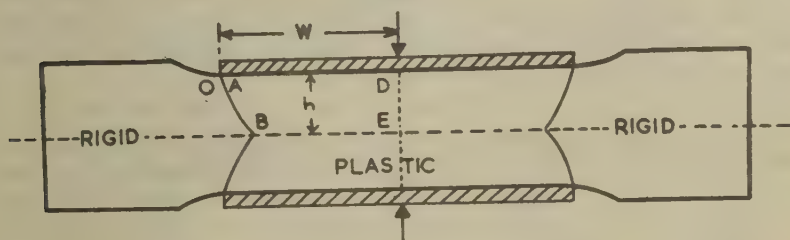
For integral width-height ratios the solution, suggested by Hill (1950 b, p. 232), is very simple. The block deforms momentarily, as a number of independent rigid units, which slide along a criss-cross of straight slip-lines, which meet the smooth dies at 45° . If the dies move with unit speed, there is a constant tangential velocity discontinuity of $\sqrt{2}$ initiated at the block centre and propagated by successive reflection from the dies along the whole length of the block. The solution is only

valid for integral values of w/h because for all other dimensions the discontinuity terminates on the exist slip-lines, which is incompatible with the rigid body motion of the overhang. The solution for intermediate values of w/h must be such that it passes continuously into the simple straight line criss-cross as w/h approaches an integral value.

Consider first the general form of the field in the upper left-hand quadrant of the block, as determined by the boundary conditions (fig. 2). Velocity conditions at the plastic-rigid boundary, OB, determine that this boundary must be a slip-line, and the sense of the relative straining on either side of OB requires that it should be an α -line. Once the position of OB is chosen, the slip-line configuration is uniquely determined by equation (3) and the stress boundary conditions. These are that the slip-lines cut the axes of symmetry, DE and EB, at 45° , and that along OD they meet the smooth surface at 45° .

Assume for the moment that there is a stress singularity at O, and that the radius of curvature of OB does not change sign along its length. OB must then be convex towards the overhang, and the α -lines within a certain angular span pass through O. The field defined by OB and the

Fig. 2.



Rectangular block during indentation.

singularity at O can be continued round O until the α -line that meets the surface of the die at 45° is reached. To avoid ambiguity, the point singularity will in future be denoted by O, or A, according to whether the point is considered to lie on the plastic-rigid boundary or on the surface of the die. Let the difference in ϕ be equal to ψ between O and A. The geometry of the boundary conditions on AD and BE determines that the angle turned through by OB is also ψ . These boundary conditions also make it possible to build up successive domains of the field, the boundaries of which meet the surface of the die at D_1, D_2 , etc., and the horizontal axis of symmetry at E_1, E_2 , etc. (fig. 3). The angle turned through by each domain boundary is equal to ψ . The vertical axis of symmetry must, clearly, be one of the domain diagonals D_1E_1, D_2E_2 , etc. The number of domains through which the field must be extended depends on the value of w/h . For reasons of symmetry, velocity discontinuities can only take place along either $AE_1D_2E_3 \dots$ or $OBD_1E_2D_3 \dots$. This distinguishes two types of field, I. and II., with their velocity discontinuities, V_1 and V_2 , ending at A and O respectively.

Fortunately, it is not necessary to obtain a complete solution of the velocity field in order to verify that the form of the slip-line field developed above is compatible with the velocity boundary conditions. The verification depends on the fact that, in this instance, the velocity field can be transformed into its corresponding slip-line field by means of the relations

$$u=\bar{x}, \quad v=\bar{y}; \quad \alpha \rightarrow \beta. \quad . \quad . \quad . \quad . \quad . \quad . \quad (5a)$$

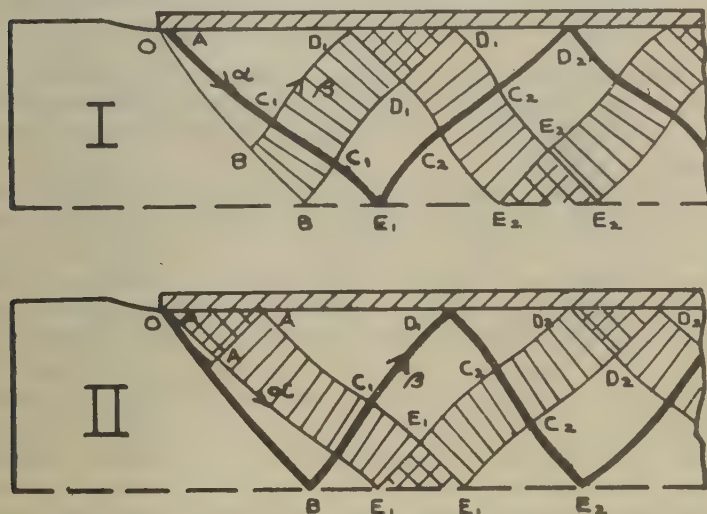
It can be seen, by comparing equations (2) and (4), that the variation of u along an α -line corresponds to the variation of \bar{x} along a β -line, provided that the direction of change of ϕ is the same; v and \bar{y} correspond in a similar manner. The normal boundary velocities u along a β -line transform into the x values along an α -line boundary. Now consider a tangential velocity discontinuity Δu across an α -line, which means that along any β -line as it crosses the discontinuity v and ϕ remain constant, and u increases by Δu . Upon transformation, this becomes a straight α -line region in the (\bar{x}, \bar{y}) field of length Δu . Similarly as we travel along any straight α -line through the region, \bar{y} and ϕ remain constant and \bar{x} increases by Δu . The velocities along a plastic-rigid boundary transform into a singularity in the slip-line field provided that the rigid part is not rotating; in addition, if there is a velocity discontinuity along the boundary, it becomes a circular arc with the singularity as its centre of curvature.

To make the correspondence exact in the present problem, the scales and origins of the two fields must first be adjusted. Let the outward speed of the rigid overhangs be U , corresponding to unit speed of the dies. The upper left hand quadrant is given a velocity U parallel to the dies towards the centre of the specimen so that the speed of the overhang is reduced to zero. The scale of the slip-line field is adjusted so that the half thickness, h , is always unity. The width of the dies will then be equal to $2U$. We choose O as the (\bar{x}, \bar{y}) origin. The boundary conditions for the velocity and slip-line fields can then be written as follows:—

Boundary condition	Slip-line field	Velocity field
OA, β -line, (\bar{x}, \bar{y}) origin.	$\bar{x}=\bar{y}=0$	—
OB, α -line, velocity of rigid overhang is zero.	—	$u=v=0$
AD, slip-lines meet die at 45° ; vertical velocity is unity.	$\bar{x}=\bar{y}$	$u-v=\sqrt{2}$
BE, axis of symmetry; vertical velocity is zero.	$\bar{x}-\bar{y}=\sqrt{2}$	$u=v$
DE, axis of symmetry ($AD=U$); horizontal velocity is U .	$\bar{x}+\bar{y}=U\sqrt{2}$	$u+v=U\sqrt{2}$

It is clear that if the relations (5 *a*) are applied, the velocity boundary conditions transform into those of the (\bar{x}, \bar{y}) field, except that certain boundaries are interchanged. The zero boundary velocities v and u on OB, which is an α -line, correspond to the (\bar{x}, \bar{y}) origin OA, a β -line. The points O, A, B, D₁, E₁, . . . D_n, E_n, in the velocity field correspond to the points O, B, A, E₁, D₁, . . . E_n, D_n, respectively, in the (\bar{x}, \bar{y}) field. The directions of change of ϕ are the same at all corresponding points. It is reasonable to expect, therefore, that the solutions of both fields are identical. This implies that there are straight line regions in the (\bar{x}, \bar{y}) field corresponding to the velocity discontinuity. The two types of slip-line obtained by transforming the two types of velocity field, I. and II., are shown in fig. 3. Although it has not been proved that the rate of work is positive everywhere in the field, it is reasonable to

Fig. 3.



Two types of slip-line field (not to scale).

assume that this is so since the directions of shearing across all the velocity discontinuities imply positive work. An examination of the already existing solution for $w/h < 1$ shows that here also the two fields are equivalent. Discussion of the transformation of fields is continued later in the paper; for the moment, we confine our attention to the indentation problem.

§4. NUMERICAL CALCULATION OF THE FIELDS.

The basis of the usual numerical method of solution is the replacing of the differential form of equations (2) by linear difference relations across a network of slip-lines. In the present problem we are able to

choose the network so that the increments of slope $\Delta\phi$, between consecutive points, is the same throughout the field. This is possible because the angles turned through by the boundaries of all domains are equal to ψ . The field is thus split into an assembly of equal unit cells of which a typical one is shown in fig. 1. In order to calculate the velocities at P in terms of those at A and B, equations (3) are replaced by

$$\left. \begin{aligned} u_P - u_B &= \frac{1}{2}\lambda\Delta\phi(v_P + v_B), \\ v_P - v_A &= -\frac{1}{2}\mu\Delta\phi(u_P + u_A), \end{aligned} \right\} \dots \dots \dots (6)$$

where $\Delta\phi$ denotes the numerical value of the change in angle, and λ and μ must be assigned the values of 1 or -1, according to whether ϕ increases or decreases in travelling towards the point P along the respective slip-lines from A and B. Solving for u_P and v_P , and retaining powers of $\Delta\phi$ only up to the third, there results

$$\left. \begin{aligned} u_P &= (1 - \frac{1}{4}\lambda\mu\Delta\phi^2)u_B + \frac{1}{2}\lambda\Delta\phi(1 - \frac{1}{4}\lambda\mu\Delta\phi^2)(v_A + v_B) - \frac{1}{4}\lambda\mu\Delta\phi^2u_A, \\ v_P &= (1 - \frac{1}{4}\lambda\mu\Delta\phi^2)v_A - \frac{1}{2}\mu\Delta\phi(1 - \frac{1}{4}\lambda\mu\Delta\phi^2)(u_A + u_B) - \frac{1}{4}\lambda\mu\Delta\phi^2v_B. \end{aligned} \right\} \dots (7)$$

If the normal components of velocity are known at net points along two intersecting slip-lines, the velocities at all net points within the domain defined by these slip-lines can be calculated by repeated application of equations (7).

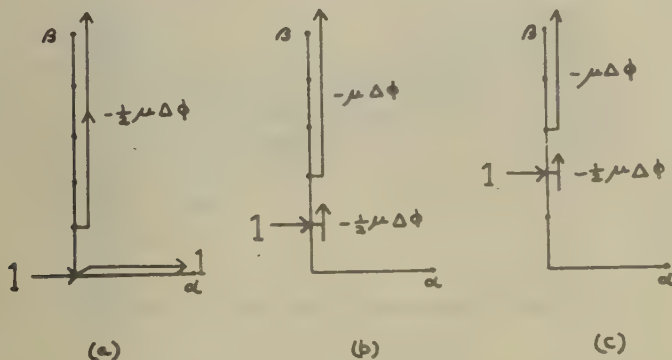
We shall now consider how these equations can be used to obtain numerical solutions of the velocity field for width/height ratios between one and two. The boundary velocities are known initially only on OB, the outer slip-line on the rigid side of which u and v are zero. Neither ψ , nor the velocity discontinuities that correspond to different values of U , are known in advance; and before solutions over the whole range of U have been completed, even the range of ψ can be guessed only approximately. There is, clearly, not sufficient information to calculate the velocities *directly* through the field, in the same way that the velocity solution was calculated, for example, in the rough die indentation problem. It is necessary first to try normal components of velocities on a slip-line adjacent to OB. OA was chosen because the velocities along this slip-line correspond to the (\bar{x}, \bar{y}) coordinates along OB, which are needed when calculating the stress distribution. OA and OB were divided into five equal arcs so that $\Delta\phi$ throughout the field was equal to $\psi/5$.

The normal component of velocity on OA at O, within the plastic region, is either zero, or V_2 , according to whether a solution of type I. or II. is being considered. At the five successive net points on OA after O, the normal components of velocity, u , were taken as a, b, c, d and e . Using the second of equations (6) and the condition that $v=0$ at O, a step integration along OA gives the values of v at the net points on this boundary. Since the equations (7) are linear in u and v , the calculated velocities at all net points are linear functions of the normal boundary velocities on the starting slip-lines OA and OB.

Therefore, groups of boundary velocities containing the different unknowns can be integrated through the field *separately* and the results superposed at each net point. We require a number of solutions in the selected range in order to be able to draw a graph of the mean pressure on the dies against $1/U$. Therefore, instead of repeating the computation several times for chosen values of $\Delta\phi$, it is more convenient to compute in terms of $\Delta\phi$, using equations (7), and neglecting powers of $\Delta\phi$ higher than the third. This can be done fairly rapidly provided an efficient method of tabulating the results is used.

The velocities on AC_1 and BC_1 are first calculated by integrating through the domain OAE_1B . The boundary conditions on the diagonals \hat{AD}_1 and BE_1 enable the calculation to be continued through AC_1D_1 and BC_1E_1 . It should be noticed that the boundary condition on AD_1 introduces a numerical term which must be integrated separately from the terms involving the various unknown velocities. The field in the domain $C_1D_1E_1C_2$ is defined by the calculated velocities on C_1D_1 and C_1E_1 and

Fig. 4.



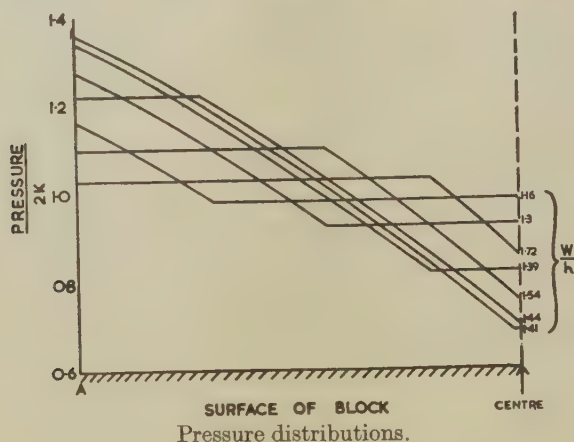
is computed as far as the six diagonal points on D_1E_1 . The velocities on this diagonal must satisfy the condition, $u+v=U\sqrt{2}$, and the velocities at A, in contact with the die, must satisfy the condition, $u-v=\sqrt{2}$. We thus have seven equations for seven unknowns, a, b, c, d, e, U and either V_1 or V_2 , which are solved numerically, substituting a definite value for $\Delta\phi$.

The process of integrating through the different domains of the field is considerably shortened by the use of "influence coefficients". These coefficients are the calculated velocities at net points of a domain, due to a unit normal velocity at a single net point on the initial boundary. The tangential velocities on the initial boundary are found in the usual manner by applying one of the equations (6). Three typical groups of initial boundary velocities are shown in fig. 4. The integrations of grounds (b) and (c) of this figure are clearly similar. The field of (c) is

the same as that of (b) shifted one step along the network. All the influence coefficients for the network can therefore be obtained by integrating groups (a) and (b). As we have already observed, the linearity of the velocity equations enables any group of velocity boundary values to be "integrated" through the domain by simple super-position of their individual effects. We can, if we wish, proceed directly from the initial to any final boundary chosen in the domain, without having to calculate the velocities at any intermediate net points; all we need to know are the influence coefficients on the final boundary, corresponding to each net point on the initial boundary.

For the solution of the present problem influence coefficients were worked out in terms of $\Delta\phi$ (retaining powers of $\Delta\phi$ only up to the third), for integration between the following boundaries:—OA to AC_1 , and BC_1 ; BC_1 to BE_1 , and C_1E_1 ; AC_1 to C_1D_1 ; C_1D_1 to D_1E_1 ; C_1E_1 to D_1E_1 . The reason for calculating the velocities on the diagonal BE_1 ,

Fig. 5.



where $u=v$, is that this corresponds to the surface of the die AD_1 in the slip-line field, along which $\bar{x}=\bar{y}$. The coordinates are required along AD_1 in order to calculate the mean pressure on that surface. The use of influence coefficients reduced the labour of computing the field by about a half. For a problem in which one fixed value of $\Delta\phi$ is sufficient, it would probably be more convenient to calculate the influence coefficients numerically, and the proportion of time saved would probably be greater than in this problem.

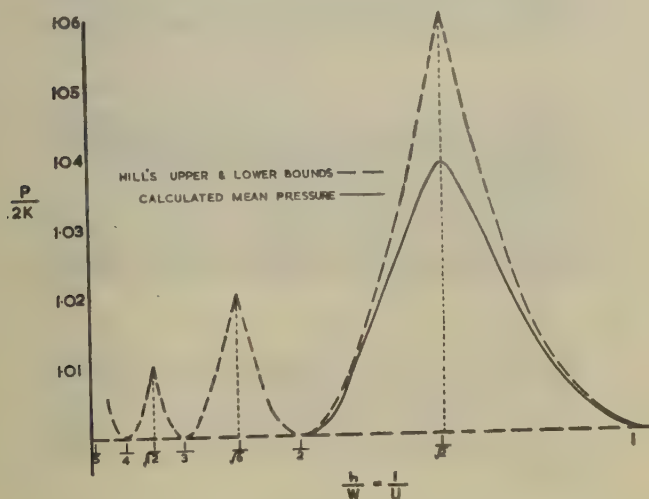
When the slip-line configuration has been completed the values of the mean compressive stress p at all net points can be found from Hencky's equations (1), provided that the value p_0 at one point of the field, say, B is known. This value is provided by the condition that the horizontal component of the total force acting over OB is zero. Fig. 5 shows the distributions of pressure on the die at different stages of the indentation.

The relation between the mean pressure on the die and the ratio $h_0 w = 1/U$, is shown by the full curve in fig. 6.

§ 5. DISCUSSION OF RESULTS.

The velocity fields, and hence the slip-line fields, of types I. and II., have been determined for values of ψ equal to 5° , 10° , 15° and $19^\circ 30'$. In fig. 7, the slip-line fields of both types, for ψ equal to 15° , are shown to scale. In order to plot these fields in detail the shapes of the initial slip-lines, OB, were found by the methods described above. The fields were then re-calculated numerically, using an equiangular network with $\Delta\phi$ equal to 5° . This was quicker than working out the coordinates of net points by substituting known values of $\Delta\phi$ and the initial boundary values in the original calculations.

Fig. 6.



Calculated mean pressures and the two bounds.

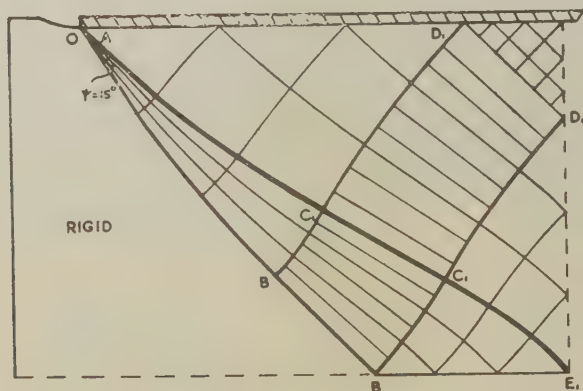
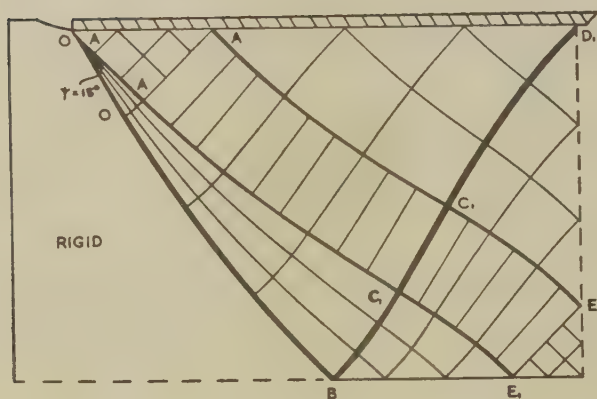
The following simple relations are found empirically from an examination of the numerical results :—

$$\begin{aligned}
 U_1^2 + \frac{1}{2}V_1^2 &= U_2^2 - V_2^2 = 2; \\
 \left. \begin{aligned} U_1 U_2 &= 2 \\ \text{and } P_1 &= P_2 \end{aligned} \right\} &\text{ if } \psi_1 = \psi_2 \quad \dots \quad (8)
 \end{aligned}$$

The suffixes 1 and 2 refer to the two types of solution, I. and II., respectively. The accuracy with which these relations are satisfied by the calculated values is shown in Table I. It can be seen that the discrepancy is nowhere greater than 0.02 per cent. This is a useful

check on the accuracy of the calculations. It seems likely that fairly accurate results would have been obtained even if the cube powers of $\Delta\phi$ had been neglected throughout the solution. The change over from the solution of type I. to that of type II. takes place smoothly when

Fig. 7.

I. $\frac{W}{h} = 1.386$.II. $\frac{W}{h} = 1.443$.

Slip-line fields to scale.

$U_1 - U_2 = \sqrt{2}$ and $V_1 = V_2 = 0$. Since the last two equations of (8) express U_2 and P_2 separately in terms of U_1 and P_1 , it appears that only one type of field need be solved to obtain the variation of P over the whole range considered.

PLASTICINE EXPERIMENTS.

Fig. 8.

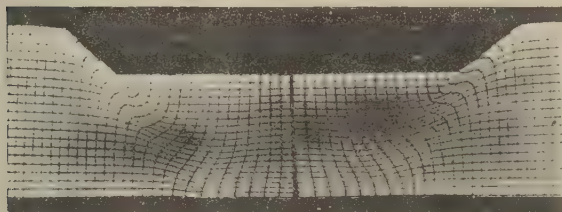
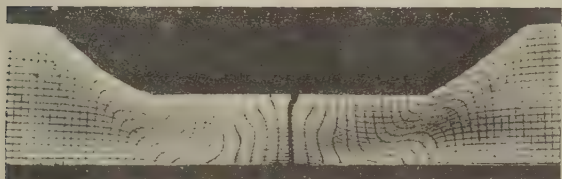
(a)
 $w/h = 1 \rightarrow \sqrt{2}$ (b) $w/h = 1 \rightarrow 2$.

Fig. 9.

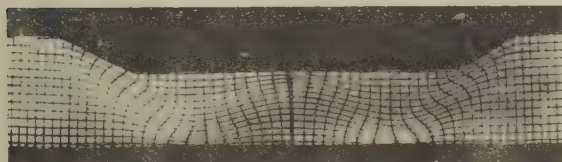
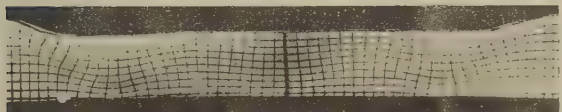
 $w/h = \sqrt{2} \rightarrow 2$.

Fig. 10.

 $w/h = \sqrt{6} \rightarrow \sqrt{12}$.

METAL EXPERIMENTS (Al 7% Mg).

Fig. 11.

 $w/h = 1 \rightarrow 1.34$.

Fig. 12.

 $w/h = \sqrt{2} \rightarrow 1.86$.

A theoretical explanation of equations (8) is not yet known. It seems probable that the general forms of these relations, valid for all U greater than unity, are

$$\left. \begin{aligned} U_1^2 + \frac{m}{2} V_1^2 &= m(m+1), \text{ where } m \leq U_1 \leq \sqrt{m(m+1)}, \\ U_2^2 - \left(\frac{m+1}{2}\right) V_2^2 &= m(m+1), \text{ where } \sqrt{m(m+1)} \leq U_2 \leq m+1; \\ U_1 U_2 &= m(m+1), \\ P_1 &= P_2, \end{aligned} \right\} \begin{aligned} &\text{for the same } m, \text{ if } \psi_1 = \psi_2 \\ &m = 1, 2, \dots \end{aligned} \quad (9)$$

It should also be noted that when U is less than unity but greater than $1/8.74$

$$U^2 - \frac{1}{2} V^2 = 0,$$

which is in agreement with the second of equations (9) when $m=0$.

TABLE I.

ψ	U_1	V_1	U_2	V_2	$U_1^2 + \frac{1}{2} V_1^2$	$U_2^2 - V_2^2$	$U_1 U_2$	$P_1/2k$	$P_2/2k$
0	1	2	2	2	2	2	2	1	1
5°	1.1646	1.1348	1.7174	0.9744	2.0002	2.0000	2.0001	1.0106	1.0108
10°	1.2985	0.7922	1.5400	0.6098	1.9999	1.9993	1.9997	1.0277	1.0279
15°	1.3859	0.3977	1.4429	0.2858	1.9998	2.0003	1.9997	1.0376	1.0377
19° 30'	1.4140	0.0118	—	—	1.9997	—	—	1.0389	—

§ 6. UPPER AND LOWER BOUNDS FOR THE MEAN PRESSURE.

It is interesting to compare the calculated mean pressure on the block with upper and lower bounds derived by Hill†; they were obtained by the application of two extremum principles for a plastic-rigid body (Hill 1950 c), extended to the case where part of the body is non-plastic by Drucker, Greenberg and Prager (1950).

The lower bound is

$$P \geq 2k, \quad (10)$$

which expresses the otherwise obvious fact that it is not possible for the mean pressure to be less than it is in uniform compression. The upper bound is obtained by applying the inequality

$$\int F_i u_i^* dS \leq k \{ \int \gamma^* dV + \int [u^*] ds \}. \quad (11)$$

† Private communication.

F_i is the actual distribution of external stresses on the surface S . The asterisks denote a fictitious velocity distribution, u_i^* , which satisfies the boundary conditions and the conditions of no volume change; γ^* denotes the corresponding maximum shear strain-rate in a volume element dV ; $[u^*]$ is the absolute value of the velocity discontinuity, and the corresponding integral is taken along it. The fictitious velocity solution used to obtain the upper bound of P is as follows:—the block is divided symmetrically into a number of independent rigid units, which slide along a criss-cross of lines inclined at the same angle θ to the faces of the dies. For integral values of U this is, of course, the actual manner of deformation with $\theta=45^\circ$. The integral involving γ^* is now zero, and $[u^*]$ is equal to $1/\sin \theta$ between the rigid units. Assuming that there are m units in contact with each die, it follows from (10) that

$$\int F_i u_i^* dS = PU \leq k \int \frac{ds}{\sin \theta} = \frac{km}{\sin^2 \theta}, \text{ where } \cot \theta = \frac{U}{m}.$$

Hence the least upper bound is defined by

$$\frac{P}{2k} \leq \frac{1}{2} \left(\frac{m}{U} + \frac{U}{m} \right), \quad \dots \dots \dots (12)$$

where $[m(m-1)] \leq U \leq [m(m+1)]$; $m=1, 2, \dots$

The two bounds (10) and (12) are shown as dashed lines in fig. 7. The closer the similarity between the fictitious and the real velocity fields, the nearer the upper bound approaches to the actual mean pressure. Peak values of both the upper bound and the calculated mean pressure occur when $U=\sqrt{2}$, and here the discrepancy between the two curves is greatest. This might be expected since the actual velocity field for this value of U involves no velocity discontinuity and is therefore very different from the fictitious field. The peaks of the upper bound are closely approximated by the expression

$$\frac{P}{2k} \sim 1 + \frac{1}{8U^2}$$

which rapidly approaches unity as U increases. There is no need, therefore, to extend the accurate solution of this problem beyond $U=2$, since for all U greater than 2, $P/2k$ differs from unity by less than 2 per cent.

§7. INDENTATION EXPERIMENTS.

(a) *Plasticine*.

The instantaneous velocities can be found at net points of the slip-line field for any chosen value of w/h , but it would clearly be a very laborious process to calculate the distortion of a square grid after a finite indentation. It is comparatively easy, however, to obtain an approximate picture of the deformation by the use of plasticine models: for it has been shown, by comparing plasticine model experiments with calculations made on the basis of the theory for a non-hardening plastic-rigid material, that in plane strain plasticine deforms in a similar manner to such an ideal material (Green 1951).

Rectangular plasticine blocks were made in two halves, $\frac{1}{4}$ in. thick. On the inner face of one-half a $1/10$ in. square grid was lightly stamped in ink. The two halves were clamped between parallel glass plates lubricated with vaseline to ensure plane strain conditions, and French chalk was used to prevent the two halves sticking together. The blocks were indented from one side only, the horizontal plane of symmetry BE being replaced by a plane lubricated base. The photographs of the deformed grids after indentation between different initial and final values of w/h are shown in figs. 8, 9 and 10 (Pl. XXIV.). For $1 < w/h < \sqrt{2}$ the deformation is mainly confined to regions of intense shear radiating from the edges of the die (fig. 8a). As indentation continues, the mode of deformation clearly changes from type I. to type II., as shown by three relatively undeformed triangular regions in fig. 8b, where w/h has reached the value 2. This is also illustrated in fig. 9 where the formation has been of type II. throughout. Fig. 10 shows a block which has been compressed from $w/h \sim \sqrt{6}$ to $w/h \sim \sqrt{12}$; there are five triangular regions in which the deformation has been small, which is what we should expect from the theory.

(b) *Metal*†.

The deformation of metal strips symmetrically indented on opposite sides by two flat dies is illustrated in figs. 11 and 12 (Pl. XXIV.). Aluminium 7 per cent magnesium alloy was used because the deformation can be clearly demonstrated with this metal. When it is rolled the segregated impurities in the metal are strung out in straight lines along the length of the strip. The distortion of such lines by indentation was shown up by polishing the central longitudinal section of the strip, and etching it with acid ferric chloride. The width of the strip was five times the width of the dies, which were made of tungsten carbide and lubricated with calcium oleate. Since the metal had been cold worked by rolling it to the required thickness, the rate of work-hardening during indentation was small. If the non-dimensional quantity H is defined as the mean slope of the stress-strain curve over the range of strain during indentation, divided by the mean stress in uniaxial compression over the same range of strain, then H was equal to approximately 0.4 and 0.25 for the indentations shown in figs. 11 and 12 respectively. The flow patterns are in qualitative agreement with the theory and are similar to those shown in figs. 8a and 9, the corresponding plasticine experiments, though in the metal the regions of intense shear are more sharply defined.

It will be noticed that experiment confirms the assumption made in the theory, that the overhang moves out as a rigid whole: the material outside the initial area of deformation remains undisturbed and the general shape of this region agrees with the theory. All the photographs demonstrate the inhomogeneous nature of the deformation. It is clear,

† Metal experiments carried out by the Metallurgy Section of the Metal Flow Research Laboratory, Sheffield, under the supervision of Mr. L. Bourne.

therefore, that severe work-hardening will modify the nature of the flow. For example, in similar experiments with annealed metal strip the regions of large shear were much more diffuse, though the type of deformation was similar.

§ 8. TRANSFORMATION OF FIELDS—DISCUSSION AND APPLICATION.

In addition to equation (5a) alternative relations for transforming the velocity field are :

$$\left. \begin{aligned} u &= \bar{y}', & v &= -\bar{x}', & \alpha &\rightarrow \alpha', & \phi &= \phi' (b), \\ u &= \bar{x}', & v &= -\bar{x}', & \alpha &\rightarrow \beta', & \phi &= -\phi' (c), \\ u &= \bar{y}', & v &= \bar{y}', & \alpha &\rightarrow \alpha', & \phi &= -\phi' (d). \end{aligned} \right\} \quad . \quad . \quad . \quad (5)$$

Starting with the velocity field of any quadrant in the present problem, these transformations all result in an (\bar{x}, \bar{y}) field of the same shape as that of the original quadrant. However, either the α - and β -lines are interchanged, in effect reversing the directions of the maximum shear stress throughout the field so that the work of distortion would be negative (*b* and *c*); and/or the field is the mirror image in an axis of symmetry of the field in the original quadrant (*c* and *d*).

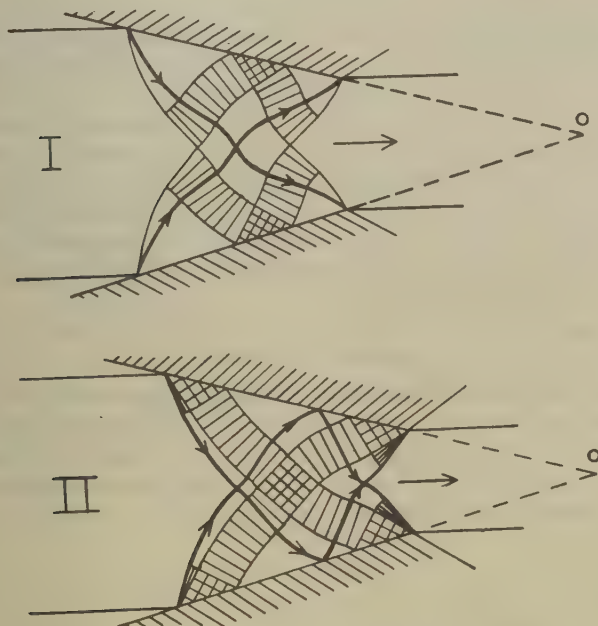
The relations (5) can be used to transform any velocity or slip-line field. In general, the velocity field cannot be expected to transform into its own slip-line field; but it may transform into a slip-line field which has already been computed, thus saving a considerable amount of labour. For example, the transformed velocity fields for symmetrical steady motion problems, such as drawing or extrusion, sometimes involve the field defined by equal circular arcs; this is a standard field that has already been computed and which can also be found analytically. In certain problems with particularly simple stress and velocity boundary conditions the two fields will be equivalent. This occurs, for example, in the following plane strain problems:—symmetrical indentation of a block on opposite sides by two rough flat dies for w/h greater than unity; extrusion or drawing through a smooth square or wedge-shaped die (Hill 1948 a, Hill and Tupper 1948); indentation by a smooth wedge of the plane surface of a semi-infinite block (Hill, Lee and Tupper 1947); expansion of a semi-cylindrical cavity in the surface of a semi-infinite block (Hill 1948 b). The last two are rather trivial examples of this equivalence.

An interesting example is the problem of sheet-drawing through a smooth wedge-shaped die. The solution which is valid for lower reductions fails for certain higher reductions, when the velocity discontinuity terminates on the exit slip-line (Hill and Tupper 1948). The situation is analogous to that encountered in the smooth die indentation problem when w/h has non-integral values greater than unity; the slip-line configuration which overcomes the difficulty is similar in form (fig. 13). The (\bar{x}, \bar{y}) and velocity solutions are again identical if the origin of the (\bar{x}, \bar{y}) field, O, is taken on the axis of symmetry

at the point of intersection of the tangent to the die faces. No numerical calculations of the field or of the corresponding upper bound have yet been made.

The importance of considering the velocity field associated with a slip-line field is emphasized by the solutions presented in this paper. The transformation of fields, and the existence of equivalent fields do not appear to have been discussed in the same manner previously. Geiringer (1937) speaks of "conjugate" solutions, but these involve the

Fig. 13.



Slip-line fields for wedge-shaped die (not to scale).

correspondence between one complete solution (velocity and slip-line field) and another. The transformation equations of the two kinds of conjugate solution which she discusses can be written

$$\left. \begin{aligned} \bar{x}' &= -v ; u' = \bar{y}, \\ \bar{y}' &= -v ; u' = \bar{x}, \end{aligned} \right\} \text{1st kind,}$$

$$\left. \begin{aligned} R' &= -v ; u' = S, \\ S' &= u ; v' = -R, \end{aligned} \right\} \text{2nd kind,}$$

(she actually uses cartesian coordinates for both position and velocity). R and S are the radii of curvature of the α - and β -lines at a point. They satisfy the relations

$$\begin{aligned} dS + R d\phi &= 0 \text{ along an } \alpha\text{-line,} \\ dR - S d\phi &= 0 \text{ along a } \beta\text{-line.} \end{aligned}$$

The particular conjugate solutions which she derives are mainly of academic interest. Transformation relations exist, similar to those expressed by equations (5), but involving (R, S) coordinates. These, however, are not likely to prove so useful in practice, since the stress boundary conditions can usually be expressed more easily in terms of (\bar{x}, \bar{y}) coordinates.

§9. CONCLUSIONS.

The value of the investigation presented in this paper, apart from the interest of the new solutions presented, lies in the formulation of new methods for solving plane plastic problems. The transformation of velocity fields and the use of influence coefficients will often save considerable computational labour. Provided that initially the form of the field can be tentatively built up, the possibility of integrating unknown boundary values from an initial to a final boundary overcomes the difficulty which arises when insufficient boundary values are known for a direct solution. The element of trial and error is thus reduced though not eliminated. The method due to Hill for obtaining upper and lower bounds for mean applied loads is likely to prove most useful in some of the many problems of which the exact solution cannot be found or would be extremely laborious to calculate.

ACKNOWLEDGMENTS.

I am grateful to the Director of the British Iron and Steel Research Association for permission to publish the paper; to Dr. R. Hill for helpful advice and criticism; and to Mr. G. Douglass of the Solid Mechanics Section of B.I.S.R.A. for his valuable assistance in the numerical computations and the photography.

REFERENCES.

- FORD, H., 1948, *Proc. Inst. Mech. Eng.*, **159** 115.
 GEIRINGER, H., 1930, *Proc. 3rd Int. Cong. App. Mech.*, Stockholm, **2**, 185;
 1937, *Mem. Sci. Math.*, **86**.
 GREEN, A. P., 1951, *Phil. Mag.*, **42**, 365.
 HENCKY, H., 1923, *Zeits. ang. Math. Mech.*, **3**, 241.
 HILL, R., 1948 a, *Journ. Iron & Steel Inst.*, **158**, 177; 1948 b, *Proc. 7th Int. Cong. Appl. Mech.*, London; 1950 a, *Phil. Mag.*, **41**, 733; 1950 b, *The Mathematical Theory of Plasticity* (Oxford: Clarendon Press); 1950 c, *J. App. Mech.*, **17**, 64.
 HILL, R., and LEE, E. H., 1946, *Proc. 6th Int. Cong. App. Mech.*, Paris.
 HILL, R., LEE, E. H., and TUPPER, S. J., 1945, *Ministry of Supply, Armament Research Dept., Theoretical Research Rep.* 28/45; 1947, *Proc. Roy. Soc. A*, **188**, 273; 1951, *Journ. App. Mech.*, **18**, 46.
 HILL, R., and TUPPER, S. J., 1948, *Journ. Iron & Steel Inst.*, **159**, 353.
 NYE, J. F., 1947, *Ministry of Supply, Armament Research Dept., Rep.* 39/47.

XCIH. *The Development of Deformation Textures in Metals.*—
Part III. *Hexagonal Structures.*

By E. A. CALNAN, B.Sc., and C. J. B. CLEWS, Ph.D.,
National Physical Laboratory*.

[Received May 11, 1951.]

§ 1. INTRODUCTION.

HEXAGONAL close-packed metals slip on a single crystallographic plane and not on a system of equivalent planes as is the case for cubic metals. Due in part to this simple slip mechanism, considerable attention was devoted to the deformation of the hexagonal metals, notably zinc and magnesium, by the German school during the decade 1925–1935 (Schmid and Boas 1950). There is, however, an additional factor important in the deformation of these metals, namely, the frequent occurrence of deformation twins. The crystallography of the slip and twinning processes has been well established, and the main features of the deformation textures observed have been explained in general terms, but there appears to have been no completely systematic treatment on the basis of slip rotations and twinning re-orientations. Mathewson and his co-workers have attempted to rationalize deformation textures as a whole, but their method is not applicable to hexagonal metals (see for example, Hibbard and Yen 1948).

The purpose of the present paper is to show how the effect of twinning may be introduced into the treatment already developed for face-centred and body-centred cubic metals (Calnan and Clews 1950, 1951, subsequently referred to as Parts I. and II.), and how this treatment may be applied to the prediction of the deformation textures in hexagonal metals.

§ 2. DEFORMATION MECHANISMS.

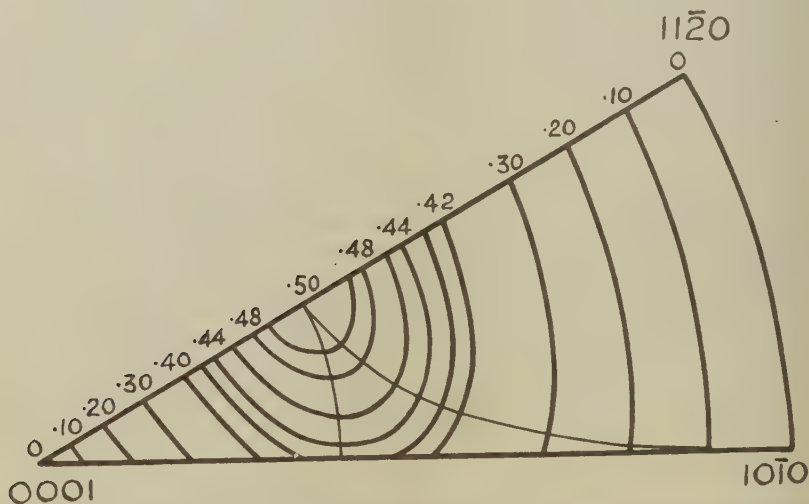
Slip. All hexagonal close-packed metals deformed at room temperature slip on basal planes, (0001), in the $\langle 11\bar{2}0 \rangle$ directions. Approximate resolved shear stress contours are shown in fig. 1. It will be noted that the shear stress varies from the maximum possible value, 0.50 of the applied stress, at 45° from the pole of the slip plane and the slip direction, to zero at 0° and 90° from the pole of the slip plane. The calculation of accurate values of the $\cos \chi \cos \lambda$ function, where χ and λ are the angles which the slip plane normal and the slip direction make with the applied stress direction, was not necessary owing to the simplicity of the system. The rotations under stress are of the usual kind leading under tension towards the slip direction and under compression towards the pole of the slip plane. Tension rotations are shown in fig. 4. Most of

* Communicated by the Authors.

the rotations are those associated with single crystal slip, but at those orientations for which the effective stress, T_e , as defined in Parts I. and II., may reach the boundary $[0001]$ to $[10\bar{1}0]$ duplex slip can occur. There is no position corresponding to multiple slip.

Twinning. The orientation of a twin relative to the matrix may be considered as the result of rotation through 180° about a specific axis, the twinning plane normal. This does not, of course, imply a bodily rotation of the lattice, for the atomic movements correspond to a shear of each atom layer parallel to the twinning plane together with, in many cases, atomic movements perpendicular to this plane. The macroscopic effect of these movements is one of simple shear in the twinning direction. The twinning planes in hexagonal close-packed metals are of the form $\{10\bar{1}2\}$, and for the $(10\bar{1}2)$ plane the twinning direction is the intersection of this plane with the $(\bar{1}210)$.

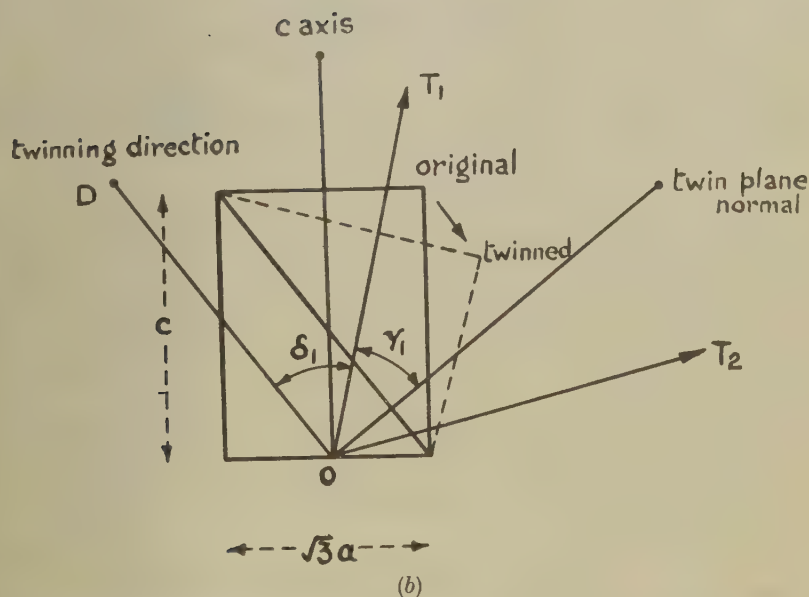
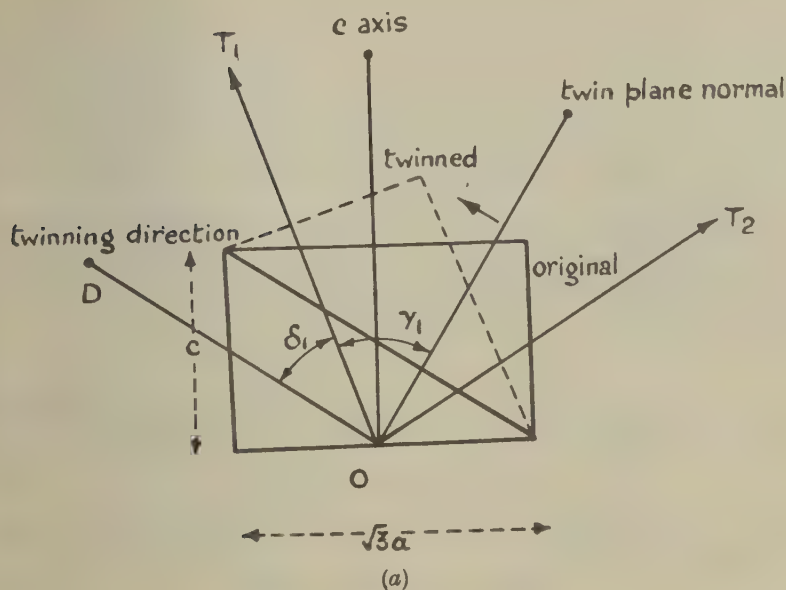
Fig. 1.



Unit triangle of standard hexagonal stereographic projection showing resolved shear stress contours and some lines of quickest descent for slip on (0001) planes in the $[11\bar{2}0]$ direction.

In establishing the conditions under which twinning occurs, it is necessary to take account of the fact that some metals have axial ratios, c/a , less than the ideal close-packed value of $\sqrt{3}$, *e. g.* magnesium, beryllium and titanium, while for others c/a exceeds this value, *e. g.* zinc and cadmium. Figs. 2 (a) and 2 (b) show the geometry of twinning for these two cases. For convenience, the positive sense of the twinning direction is taken as that lying on the opposite side of the c -axis from the twin plane normal. For $c < \sqrt{3}a$, fig. 2 (a), it is obvious that twinning will occur under tension only when the stress is so oriented as to give a component in the positive sense of the twinning direction, OD. The

Fig. 2.



Diagrams illustrating the geometrical conditions for twinning, (a) for $c < \sqrt{3}a$, and (b) for $c > \sqrt{3}a$. The twinning direction, the twin plane normal, and the c -axis are all in the plane of the diagram.

resolved shear stress for twinning is $T \cos \gamma \cos \delta$ where γ and δ are respectively the angles which the stress makes with the twin plane normal and the positive sense of the twinning direction. Thus for twinning $T \cos \gamma \cos \delta$ must be positive. A tension of sufficient magnitude in the direction T_1 will produce twinning, but one in the direction T_2 can never do so. Consideration of fig. 2*b* for $c > \sqrt{3}a$ shows that the condition for twinning under tension is that $T \cos \gamma \cos \delta$ shall be negative. Conversely, under compressive stresses these two conditions are interchanged.

Boundaries between regions of slip and twinning. The boundaries between regions of slip and twinning are the loci of points at which the ratio of the resolved shear stress to the critical stress for slip is equal to the corresponding ratio for twinning, *i. e.*

$$T \cos \chi \cos \lambda / C_s = T \cos \gamma \cos \delta / C_t,$$

where T is the applied stress and C_s and C_t are the critical stresses for slip and twinning. The equation to the boundary is thus

$$\cos \gamma \cos \delta = n \cos \chi \cos \lambda, \quad \dots \dots \dots (1)$$

where $n = C_t / C_s$. Inserting now the sign conditions for twinning, (1) becomes

$$\cos \gamma \cos \delta = +n \cos \chi \cos \lambda \quad \dots \dots \dots (1a)$$

for $c < \sqrt{3}a$ under tension,

and $c > \sqrt{3}a$ under compression,

and

$$\cos \gamma \cos \delta = -n \cos \chi \cos \lambda \quad \dots \dots \dots (1b)$$

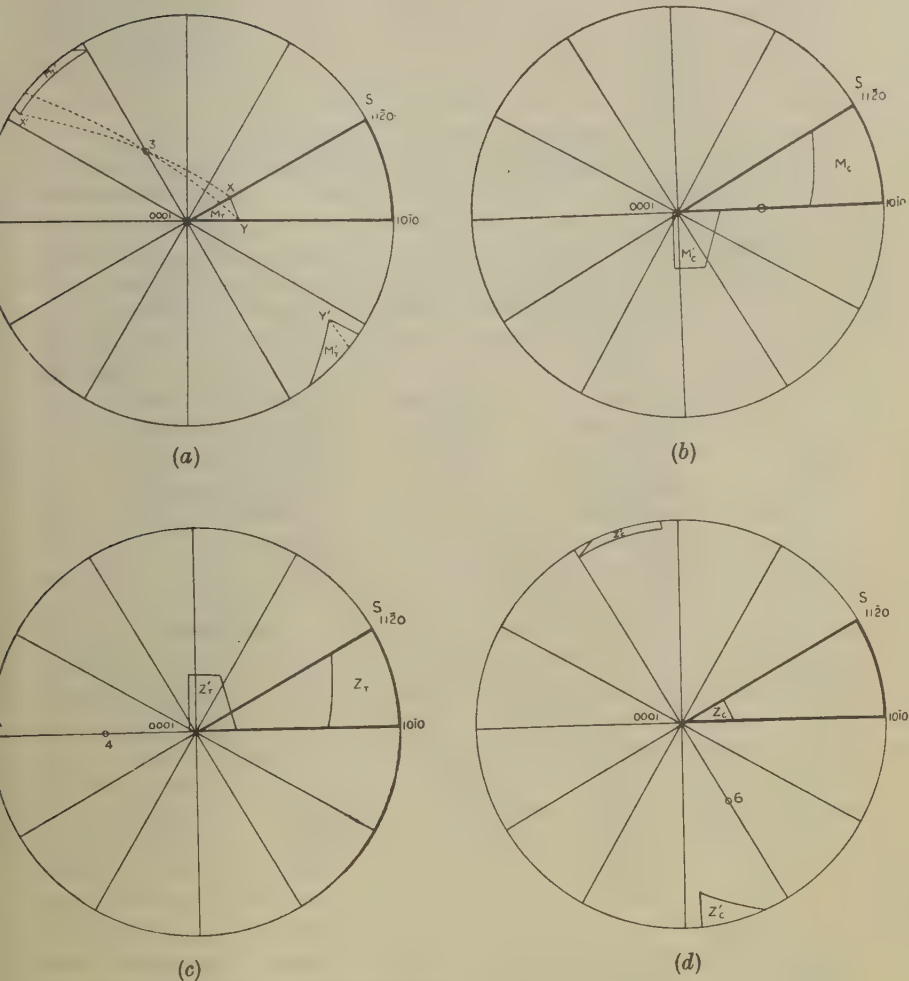
for $c < \sqrt{3}a$ under compression,

and $c > \sqrt{3}a$ under tension.

In the calculations n has been chosen to be unity, the reason for which will be considered later. This choice was not made merely to simplify calculation. The intersections of the boundaries with the sides of the 30° unit triangle were determined for each of the six twinning systems with the most favourable slip system by appropriate substitution in equations (1*a*) and (1*b*). The angular distances of these intersections from the [0001] direction for the tension and compression cases of both zinc and magnesium are listed in Table I. The most favourable twinning system is that which has its boundary nearest to the maximum of the resolved shear stress contours for slip; these are marked with an asterisk in the Table and shown in fig. 3.

Reorientation due to twinning. The new orientation resulting from twinning may be found easily on a stereographic projection. For magnesium under tension twinning takes place from the area M_T on the twinning system 3 (Table I. and fig. 3*a*). The original and twinned orientations are equidistant from the operative twin plane normal on the

Fig. 3.



Hexagonal standard stereographic projection, S is the most favourable slip direction for the reference unit triangle in heavy outline.

(a) Magnesium under tension. Showing the re-orientation from the twinning area M_T to the twinned area M'_T . The operative twin plane normal is the point 3.

(b) Magnesium under compression. Twinning area, M_C , re-orient to the twinned area, M'_C . Operative twin plane normal, 1.

(c) Zinc under tension. Twinning area, Z_T ; twinned area, Z'_T ; twin plane normal, 4.

(d) Zinc under compression. Twinning area, Z_C ; twinned area, Z'_C ; twin plane normal, 6.

great circle, through these three points. Thus, to obtain the twinned orientation X' corresponding to the point X a great circle is drawn through X and the twin plane normal 3 ; the angular distance between X and 3 along this great circle is measured, and an equal angular distance

TABLE I.
Intersections of Twin-Slip Boundaries.

Magnesium : $c/a=1.624$; $n=1$.

Twinning system	Tension		Compression	
	Angles from $[0001]$ along $[0001]$ - $[10\bar{1}0]$ side	Angles from $[0001]$ along $[0001]$ - $[11\bar{2}0]$ side	Angles from $[0001]$ along $[0001]$ - $[10\bar{1}0]$ side	Angles from $[0001]$ along $[0001]$ - $[11\bar{2}0]$ side
1	23.4°	22.4°	64.4°	71.3°*
2	28.4°	22.4°	82.1°	71.3°
3	28.9°*	26.5°*	82.5°	90°
4	25.4°	24.2°	65.5°	72.8°
5	28.9°	24.2°	82.5°	72.8°
6	28.4°	26.5°	82.1°	90°

Zinc : $c/a=1.858$; $n=1$.

Twinning system	Tension		Compression	
	Angles from $[0001]$ along $[0001]$ - $[10\bar{1}0]$ side	Angles from $[0001]$ along $[0001]$ - $[11\bar{2}0]$ side	Angles from $[0001]$ along $[0001]$ - $[10\bar{1}0]$ side	Angles from $[0001]$ along $[0001]$ - $[11\bar{2}0]$ side
1	66.5°	72.9°	25.7°	24.1°
2	82.7°	72.9°	29.0°	24.1°
3	82.1°	90°	27.4°	26.5°
4	64.4°*	71.3°*	23.5°	22.2°
5	82.1°	71.3°	27.4°	22.2°
6	82.7°	90°	29.0°*	26.5°*

* Most favourable twinning system. That the values for magnesium under tension and compression are equal respectively to those for zinc under compression and tension is fortuitous.

beyond 3 is marked off to give the point X' . Similarly the points Y' and $0001'$ may be obtained. The twinning areas and the regions into which they twin are shown in fig. 3 for magnesium and zinc under tension and compression.

§ 3. TENSION AND COMPRESSION TEXTURES.

Magnesium under Tension. In the region $AK[10\bar{1}0][11\bar{2}0]$ of fig. 4 the only deformation mechanism is slip, which causes rotation leading to the $[11\bar{2}0]$ direction. It is now necessary to consider what happens in

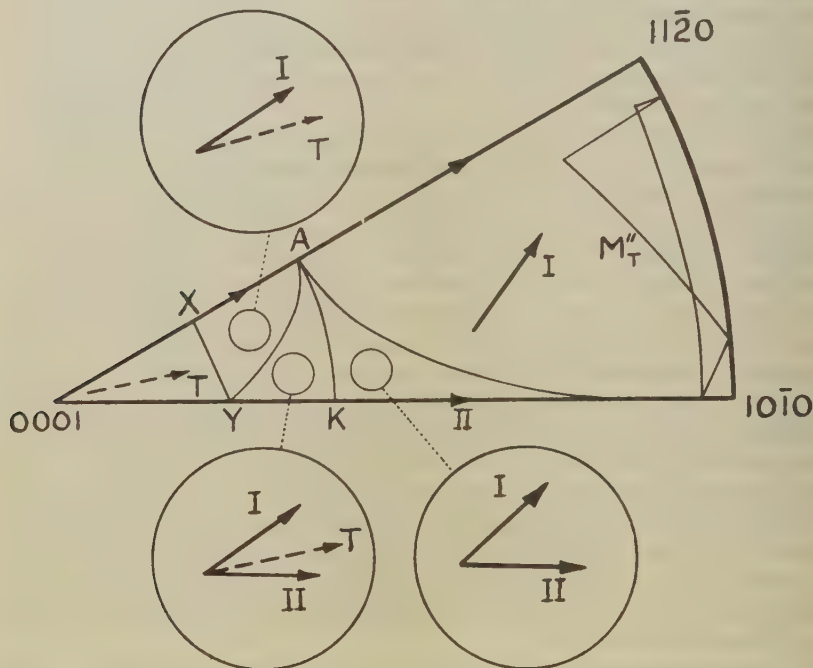
the neighbourhood of the twin-slip boundary XY. In accordance with the general concepts developed in Parts I. and II., it is visualized that if deformation occurs when the effective stress is at a boundary such as XY, then both slip and twinning will occur simultaneously in the small part of a grain under discussion. Since, however, the slip and twinning mechanisms are not necessarily initiated at the same point in this region both may begin. Whether one or both processes are halted by mutual interference is not important here, for the effect may be stated in general terms as producing some material which has slipped and some which has twinned. In a like manner, deformation occurring when the effective stress has reached a point such as Y, where two twin and two slip systems are equally favourable, will produce material of both twinned orientations and some of the orientation resulting from duplex slip rotation. For all the orientations in the area AXY the path of the effective stress leads to the slip-twin boundary XY and thence to Y. Thus, corresponding to the first part of the path of T_e , single slip rotation towards $[11\bar{2}0]$ results; to the second part along XY, the same single slip rotation together with twinning on twin plane 3; and lastly, to deformation at Y, twinning on planes 3 and 5 and duplex slip rotation towards $[10\bar{1}0]$. For the adjacent region AKY also, T_e may reach Y and the same twinning and slip may occur. The further the original orientation from the boundary XY, the greater the path length of T_e during which there may be single or duplex slip, and consequently the more probable are these modes of deformation. As every element of slip rotation moves the original orientation away from the boundary the probability of twinning decreases fairly rapidly across the regions AXY and AKY until it is zero at the boundary AK. Similarly, there is some probability of slip for orientations within the twinning area $[0001]XY$. It will be seen, therefore, that in a polycrystalline aggregate, even assuming a unique value of the ratio of critical shear stresses for slip and twinning, there is no sharply defined boundary between orientations which twin and those which slip, but that the boundary XY defines the regions in which these processes predominate.

In specifying the fibre textures it is sufficient to consider only a single unit triangle of the standard projection, and the orientation after twinning, M'_T of fig. 3, is equivalent to the area M''_T in fig. 4. That is to say, material from the area $[0001]XY$ twins to M''_T . Thus, after considerable deformation, all the orientations will have moved by slip and twinning to the edge of the unit triangle near to the $[11\bar{2}0]$ - $[10\bar{1}0]$ boundary. This corresponds to a texture with all directions in the basal planes parallel to the tension axis. As further deformation can occur only by slip, giving rotation towards the $[11\bar{2}0]$ direction, in final texture with this direction parallel to the stress axis might be expected. However, on the $[11\bar{2}0]$ - $[10\bar{1}0]$ edge the resolved shear stress on the slip system is zero, and the result of T_e reaching here can only be fracture of the grain or part of a grain under consideration. When this occurs

early in the deformation process, fracture of the whole specimen may or may not follow, but in the later stages when it has occurred at a number of places, failure of the whole specimen is practically certain. The probability of fracture is highest for orientations near the $[11\bar{2}0]$ - $[10\bar{1}0]$ edge, and so the development of a very strongly marked $[11\bar{2}0]$ tension texture is unlikely.

Magnesium under Compression. The magnesium compression texture is equally simple. The slip rotations lead towards the pole of the operative

Fig. 4.



Stereographic Unit triangle showing the slip rotations and twinning re-orientations for magnesium under tension. I and II indicate directions of single and duplex slip rotations; T is the general direction of twinning re-orientation.

slip plane, namely the basal plane, and the twinning takes place from a region near the $[11\bar{2}0]$ - $[10\bar{1}0]$ edge to new orientations also near the pole of the basal plane, M'_C in fig. 3. The texture is thus specified as $[0001]$ parallel to the direction of compression.

Zinc under Tension. In zinc the different geometry of the twinning, typical of axial ratios $c/a > \sqrt{3}$, gives an interesting dynamical equilibrium of texture instead of the usual end points. Under tension the slip rotations lead towards the $[11\bar{2}0]$ direction, but orientations

within the twinning area Z_T of fig. 3 and all those which rotate by slip to this area twin back to a region near the pole of the basal plane, Z_T . The ensuing cycle of slip and twinning is not, however, endless, for local fracture occurs whenever T_e reaches the $[0001]$ position where the resolved shear stress on the slip system is zero. Thus, there will be a concentration of orientations in the neighbourhood of the slip-twin boundary, more marked near its intersection with the $[0001]$ - $[11\bar{2}0]$ edge. In the case of $n=1$, this corresponds to $[11\bar{2}0]$ directions at not less than 20° from the tension axis. For higher values of n this angle decreases. Due to the twinning of material back to Z'_T , there will be a continuous spread of orientation from the $[0001]$ pole towards the slip-twin boundary.

Zinc under Compression. Here the twinning region is near the pole of the basal plane, which is also the end point of the slip rotations. Again there may be a cycle of slip and twinning, and the resulting texture, defined by the slip-twin boundary, is, with $n=1$, that of $[0001]$ directions not less than 25° from the direction of compression. In addition, there is a spread of orientation across the unit triangle.

§ 4. ROLLING TEXTURES FOR MAGNESIUM AND ZINC.

The stresses associated with sheet rolling may be simulated by compression parallel to the rolling plane normal and subsidiary tension parallel to the rolling direction. The development of the rolling texture in terms of the basal plane pole figure will now be considered.

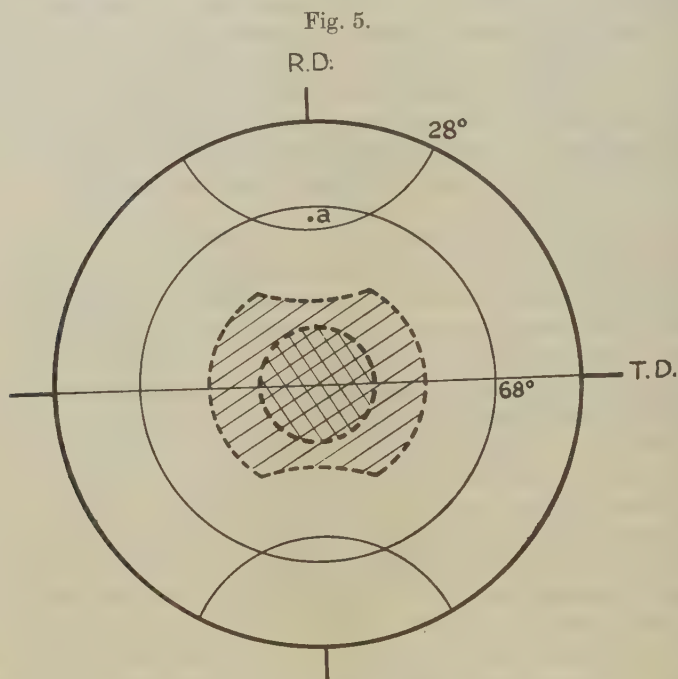
For magnesium, the compression twins all grains having orientations with (0001) poles more than about 68° from the compression axis the centre of the pole figure in fig. 5. This twinning brings the (0001) poles to the centre of the figure to which point also the slip rotations lead. This corresponds to a texture in which the basal planes lie in or near the rolling plane. At the same time, the tension tends, somewhat weakly, to line up $[11\bar{2}0]$ with the rolling direction. These orientations are mutually consistent, but there is some departure from circular symmetry in the pole figure due to further twinning effects. In the region less than 28° from the rolling direction characterized by the point a , only tension twinning occurs to new orientations in the vicinity of the transverse direction. These then twin under compression to the centre of the pole figure. This twinning of the region around a leaves less material to rotate by slip to the centre and gives a corresponding contraction in the intermediate contours of the texture, fig. 5.

In the rolling of zinc the compression gives slip rotations bringing basal plane poles to within 25° of the centre of the pole figure, fig. 6. Inside this circle twinning occurs to orientations near the circumference of the pole figure. The tension causes twinning of all material with basal plane poles more than 70° from the rolling direction, the new orientations being around the rolling direction. Since the tension removes the material from the central band the compression twinning is principally that from orientations such as C . These twin to positions near the transverse

direction and thence under tension to near the rolling direction. Thus, the twinning gives some concentration of orientations in the neighbourhood of the rolling direction rather than at other points around the circumference. From these considerations the semi-quantitative pole figure in fig. 6 was drawn.

§ 5. DISCUSSION.

In magnesium and zinc it can be shown that the texture for cold-drawn wires predicted from a consideration of basal plane slip and twinning on the $\{10\bar{1}2\}$ planes is the same as that for pure tension. This is because



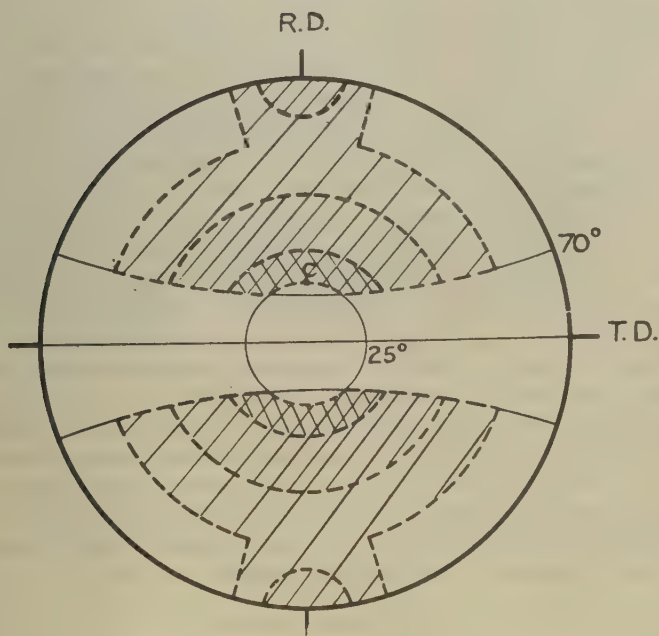
(0001) pole figure for rolled magnesium sheet.

the textures produced by longitudinal tension and radial compression are mutually consistent. Schmid and Wassermann (1929) have shown that in magnesium wire all directions in the (0001) planes are parallel to the wire axis in complete accord with the texture predicted here. It is found, however, with cold-drawn magnesium alloy, Dowmetal, that only the $\langle 10\bar{1}0 \rangle$ directions lie parallel to the wire axis (Morell and Hanawalt 1932). This texture is not predicted by the present treatment but it is consistent with the incidence of pyramidal slip, *i. e.* slip on the $\{10\bar{1}1\}$ planes in the close-packed direction, $\langle 11\bar{2}0 \rangle$. Since this deformation mode is not accepted as playing a principal role in

hexagonal metals at room temperatures it has not been considered here, but it may be profitably introduced at some future time. Zinc wires in the early stages of deformation show [0001] directions parallel to the wire axis, while at later stages the hexagonal axis lies at about 70° from the wire axis, Barrett (1943). This latter texture is predicted and the early [0001] texture is no doubt due to the augmentation of this orientation by the initial twinning.

The simple compression texture derived for magnesium in the previous section is confirmed by the experiments of Tsuboi (1928) who found [0001] directions parallel to the axis of compression. There appear to be no experimental data on the pure compression texture of zinc or other hexagonal metals.

Fig. 6.



(0001) pole figure for rolled zinc sheet.

The general features of the rolling texture of magnesium, basal planes in or near the rolling plane and $\langle 11\bar{2}0 \rangle$ tending towards the rolling direction, are in agreement with the experimental pole figures of Schmid and Wassermann (1930), Caglioti and Sachs (1932) and Bakarian (1942). There are, however, some minor differences in the results of these investigations. It has been shown that some of these differences may be due to changes in composition of rolling technique, Hanawalt (1936), or to inhomogeneity of texture through the sheet, Fuller and Edmunds (1934) and Hargreaves (1945). The other metals titanium, beryllium

and zirconium which have axial ratios less than $\sqrt{3}$ have the same general texture of basal planes lying in or near the rolling plane, but there is definite evidence of a spread of basal plane normals towards the transverse direction (Clark 1950, Smigelskas and Barrett 1949, Burgers and Jacobs 1935). There is also a tendency for the $[10\bar{1}0]$ directions rather than the $[11\bar{2}0]$ directions to lie parallel to the rolling direction. These observations appear to be consistent with the operation of pyramidal slip. It is felt that a detailed consideration of this deformation mode will be justified when the textures have been determined more accurately with the aid of X-ray Geiger counter methods.

The pole figure for zinc, fig. 6, is in good agreement with the pole figures of Caglioti and Sachs (1932) and Valouch (1932). In addition, the increase in density of $[0001]$ directions around the rolling direction found by Fuller and Edmunds (1934) is explained.

All the textures have been derived on the assumption that $n=1$, i.e. that the ratio of critical shear stresses for slip and twinning is unity. This assumption must be examined in the light of the experimental observations on these stresses and the agreement obtained between the observed and the predicted textures. There are few experimental determinations of the critical shear stress associated with the twinning process, and even these are not conclusive. They indicate, however, that in the earliest stages of deformation the critical stress for twinning is several times that for slip, although the twinning stress appears to decrease after slip has taken place (Miller 1936). The ratio of the stresses therefore may well approach unity after the severe deformations required to produce the degree of preferred orientation considered in the foregoing sections. The textures themselves provide further evidence that the effective value of the ratio is near to unity. Cold-drawn zinc wires have the hexagonal axis at about 70° from the wire axis, the predicted angle with $n=1$ being about 69° . Again, in the sheet rolling texture of zinc the hexagonal axes lie at 20 – 25° from the rolling plane normal towards the rolling direction, compared with the predicted value of about 27° . These results suggest that n is slightly greater than unity.

§ 6. CONCLUSIONS.

The manner in which the process of twinning may be incorporated into the treatment of the development of deformation textures described in Parts I. and II. has been demonstrated. Good agreement with the observed textures has been obtained for both magnesium and zinc, hexagonal metals characteristic of those having axial ratios respectively less and greater than the ideal close-packed value.

The method is capable of refinement in the prediction of details of the hexagonal textures by the introduction of the effects of pyramidal slip, and of a more careful consideration of twinning re-orientations should a particular problem arise or more accurate experimental observations become available to justify this course.

ACKNOWLEDGMENTS.

The work described above has been carried out as part of the general research programme of the National Physical Laboratory, and this paper is published by permission of the Director of the Laboratory.

REFERENCES.

- BAKARIAN, P. W., 1942, *Trans. A.I.M.E.*, **147**, 267.
BARRETT, C. S., 1943, *Structure of Metals*, 1st Ed., p. 383 (New York : McGraw-Hill).
BURGERS, W. G., and JACOBS, F. M., 1935, *Metallwirt*, **14**, 285.
CAGLIOTI, V., and SACHS, G., 1932, *Metallwirt*, **11**, 1.
CALNAN, E. A., and CLEWS, C. J. B., 1950, *Phil. Mag.* [7], **41**, 1085 ; 1951, *Ibid.*, **42**, 616.
CLARK, H. T., 1950, *Trans. A.I.M.E.*, **188**, 1154.
FULLER, M. L., and EDMUNDS, G., 1934, *Trans. A.I.M.E.*, **111**, 146.
HANAWALT, J. D., 1936, *Symposium on Radiography and X-ray Diffraction*, (Philadelphia : A.S.T.M.).
HARGREAVES, A., 1945, *J. Inst. Metals*, **71**, 73.
HIBBARD, W. R., and YEN, M. K., 1948, *A.I.M.E.*, T.P. 2334.
MILLER, R. F., 1936, *Trans. A.I.M.E.*, **122**, 176.
MORRELL, L. G., and HANAWALT, J. D., 1932, *J. Appl. Phys.*, **3**, 161.
SCHMID, E., and WASSERMANN, G., 1929, *Naturwiss.*, **17**, 312 ; 1930, *Metallwirt*, **9**, 698.
SCHMID, E., and BOAS, W., 1950, *Plasticity of Crystals*, (English Translation of *Kristallplastizität*), (London : F. A. Hughes & Co.).
SMIGELSKAS, A., and BARRETT, C. S., 1949, *Trans. A.I.M.E.*, **185**, 145.
TSUBOI, S., 1928, *Mem. Coll. Sci. Kyoto Imp. Univ.*, **A11**, 375.
VALOUCH, M. A., 1932, *Metallwirt*, **11**, 165.

XCIV. *Observations on the Multiple Scattering of Ionizing Particles in Photographic Emulsions.*—Part II. *The Scattering of Positrons at 105 and 185 MeV.*

By M. G. K. MENON, C. O'CEALLAIGH*, and O. ROCHAT,
H. H. Wills Physical Laboratory, University of Bristol.†

SUMMARY.

The coordinate method has been used to measure the multiple scattering in Ilford G5 emulsions of positrons of nominal energy 113 and 196 MeV. The energies of the positrons corrected for loss by ionization and radiation are calculated to be 105 and 185 MeV. respectively. The experimental distributions of second differences have been compared with those predicted by the theory of Molière (1947, 1948) and the agreement found to be very satisfactory. Methods of minimizing the effects of spurious scattering and of taking into account the influence of distortion are discussed. Values are found for the scattering constant which are in good agreement with those calculated from the theory of Molière. A discussion of these results has been given in a previous paper of this series (Gottstein *et al.* 1951). A mathematical treatment is given in the Appendices: (I.) the correlation existing between successive second differences, (II.) the distribution of second differences when measured in the presence of spurious scattering, and (III.) a possible method for correcting second differences which have been affected by a large angle scattering.

§ 1. INTRODUCTION.

THE multiple scattering of positive electrons has been measured for two energies in Ilford G5 nuclear research plates. They had been exposed in the Cornell Synchrotron to a beam of positrons selected by a magnetic spectrometer, and have been made available to us through the courtesy and cooperation of Professor Dale R. Corson. He has also supplied us with the following information. Deducting 1 MeV. to allow for loss in the 2.4 mm. of aluminium which the particles traversed before entering the plates, the nominal energies of the positrons were 113 ± 4 MeV. and 196 ± 5 MeV. The uncertainties quoted represent, not probable errors, but limits of uncertainty. It will be shown later that these nominal figures must be corrected for ionization and radiation loss. The final energy values adopted for the purposes of this experiment are 105 ± 4 and 185 ± 5 MeV. respectively.

* On leave of absence from the University College, Cork.

† Communicated by Prof. C. F. Powell, F.R.S.

§ 2. EXPERIMENTAL METHOD.

The scattering has been measured by the coordinate method of Fowler (1950). Two Cooke, Troughton and Simms M4000 nuclear research microscopes were employed. The plates 1 in. \times 3 in. with emulsions 100 μ thick, were mounted so that the paths of the electrons appeared approximately parallel to the x -axis of motion of the stage. The particles entered the plates near one of the shorter edges and followed a path approximately parallel to the longer edges. In order to minimize the effect of errors due to possible distortion of the emulsion, no measurement of scattering was made on any portion of track which was less than 2 mm. from an edge of the plate. This distance has been found adequate, having regard to the magnitude of the multiple scattering and the thickness of the emulsion.

A line 2 mm. from the edge through which the electrons entered the emulsion, and approximately parallel to the y -axis of motion of the stage, was traversed, and particles which crossed this line were selected for measurement if they satisfied the following criteria:

- (1) The angles between the trajectory of the particle and the stage x -axis must be less than 0.04 radians.
- (2) The path length visible in the emulsion must exceed a minimum of 1500 μ for the 105 MeV., and 3000 μ for the 185 MeV. positrons.

By imposing these conditions, it was hoped to exclude both stray particles and such cases of radiation loss as were accompanied by scattering of appreciable magnitude. Each selected track was then traced back to the point at which it entered the emulsion, so that due allowance could be made for such energy loss by ionization and radiation as occurred between the magnetic spectrometer and the point from which measurement of the multiple scattering was carried out.

The measurements were made using oil-immersion objectives $\times 95$ with eyepieces $\times 15$, one of which was furnished with a scale of 120 divisions. This was set perpendicular to the direction of motion of the stage.

The stage was advanced in equal steps by a micrometer screw. These steps will be referred to as the primary cell size. The position of the track was read on the eyepiece scale as shown in fig. 1. We draw in imagination, a mean line passing through the mass centres of such grains as lie within a suitable distance, on either side of the scale. The position of the track is then defined as the point of intersection of this line with the scale axis. In fig. 1 this distance is shown as 10 μ , since the tracks are of minimum grain density and the grains rather widely spaced; in the case of tracks of higher grain densities, the distance used will be smaller.

This procedure results in a smoothing; and we may no longer set the "smoothing factor" $(\langle \Phi \rangle_{\text{chord}} / \langle \Phi \rangle_{\text{tan}})^2 = 2/3$ as would be valid if dealing with chords measured between two points on a continuous curve.

The smoothing factor applicable to our case was calculated to be $(2/3)(1-\gamma^2+3r^3/5)$ (following Molière 1951) where $\gamma=0.1/s$ and s =cell size in units of 100μ . For cells of 50μ or greater this correction will be negligible.

For each track the second differences of the coordinate readings D_j were evaluated for the primary cell-size in the way described by Fowler (1950), and also for other cell-sizes using varying degrees of overlap. A definition of "degree of overlap", and a detailed discussion of

Fig. 1.

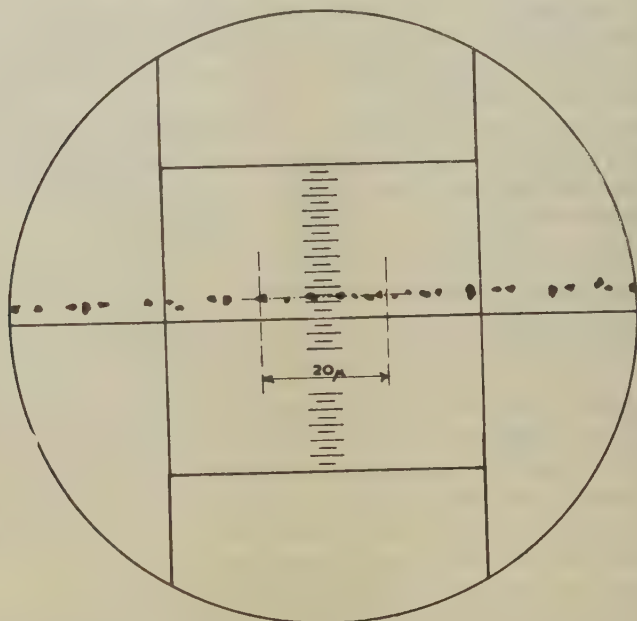


Diagram showing the method of reading the position of the track on the eyepiece scale. For clarity, only 40 divisions are shown on the scale in the diagram. A mean line is drawn in imagination passing through the mass centres of the grains lying about 10μ on either side of the scale axis. The intersection of this line with the scale axis is read off.

its influence on the measurements, is given in the following paper (III.) of this series (O'Ceallaigh and Rochat 1951). The mean of these values of second difference taken without regard to sign we denote by the symbol \bar{D}

We have $\bar{D} = (1/n) \sum_{j=1}^n |D_j|$ where n is the number of individual values of second difference in the track. Physically, this statistic is a measure of the mean value of the angle between successive chords of track segments defined by the cell-size. The symbol " s " will be used to denote the cell-size in units of 100μ and \bar{D}_s the value of the corresponding statistic. The following Table summarizes the relevant information,

TABLE I.

Energy	185 MeV.	105 MeV.
Total number of tracks	56	57
Total length (cm.)	24.0	15.2
Average length per sample (mm.)	4.30	2.67
Prime cell-size (s)	0.5	0.25
Other cell-sizes employed (s)	1, 2, 4, 6, 8	0.5, 1, 2, 3

§ 3. SELECTION OF TRACKS SUITABLE FOR MEASUREMENT.

Among the tracks selected, and included in Table I., there may still be some which have lost energy or which may be unrepresentative. Such tracks have been rejected in accordance with the following systematic procedure.

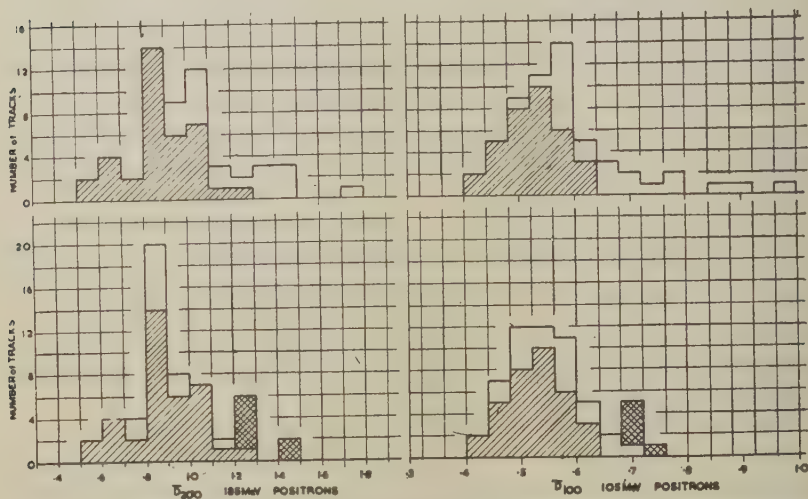
The value of \bar{D} was evaluated for each track using cell-size 100μ for the 105 MeV. and 200μ for the 185 MeV. positrons. A value $\bar{\Delta} = \frac{1}{n} \sum_{j=1}^n \bar{D}_j$ was also obtained by adding together the results for all the individual tracks to obtain a single composite track. $\bar{\Delta}$ will be an unbiased estimate of the \bar{D} of the tracks provided that no track had suffered large energy loss.

The distributions of \bar{D} obtained from the individual tracks are shown in the upper quadrants of fig. 2. Because the tracks are of finite length, the occasional large deviations due to plural or single scattering will be reflected in the sampling histogram by the occurrence of a few unrepresentative tracks with large values of \bar{D} . In order to avoid this inconvenience, it has been usual, before evaluating \bar{D} for any track, to remove from it all values of $D_j \geq 4\bar{D}$. The distributions indicated by single hatching are those of the tracks which contained no signals $D_j \geq 4\bar{D}$. They are exhibited in both upper and lower quadrants, and are thus distinguished from those tracks which contained such excessive values. The unshaded portions show the latter. In the upper quadrants they refer to the tracks before removal of all $D_j \geq 4\bar{D}$ and, in the lower quadrants, to the distribution of \bar{D} after these had been excluded.

Certain tracks remain which exhibit values of \bar{D} so high that it is improbable that they have been observed merely as a matter of chance, but rather, that they are those of electrons, the energy of which has become degraded below that of the beam. Let us assume that $\bar{\Delta}$, the value of \bar{D} obtained from the composite track is that of the universe from which the sample has been drawn, and that this universe is normal. Both assumptions are sufficient approximations. We evaluate for each suspect track in turn, starting with that of greatest \bar{D} , the quantity $\chi^2 = n\bar{D}^2 / \bar{\Delta}^2$ where n is the number of statistically independent cells in the chosen track. The probability of chance occurrence of χ^2 may be found from the well-known tables. In the present case, rejection was fixed at $2\frac{1}{2}$ per cent level. After rejection of each track which failed to satisfy the test, the amended value of $\bar{\Delta}$ was calculated before applying

the test to the next suspect. The probability of chance occurrence of the low values of \bar{D} was examined in a similar way. In all, twelve tracks were excluded, seven for the 185 MeV., and five for the 105 MeV. series. They are represented by cross-hatching in the lower pair of histograms.

Fig. 2.



Distribution of \bar{D} obtained from individual tracks. The effect of removing values of $D_j \geq 4\bar{D}$ and of eliminating tracks of certain unrepresentative electrons is shown as follows.

Upper quadrants: Before elimination of large angles.

Single-hatching-tracks containing no signals $\geq 4\bar{D}$. Unshaded-tracks containing one or more signals $\geq 4\bar{D}$.

Lower quadrants: After elimination of large angles.

Single-hatching-tracks unaffected by the elimination procedure. Unshaded + cross-hatching-tracks to which the elimination procedure had been applied.

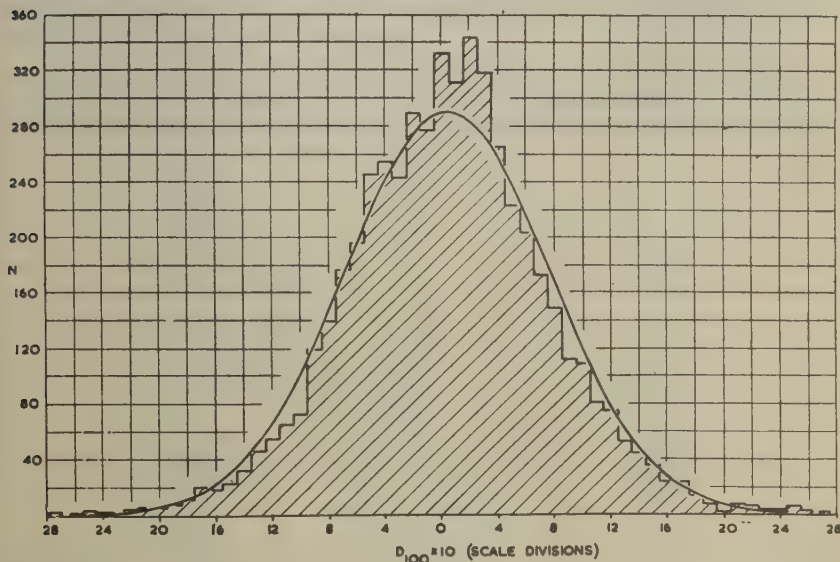
Tracks represented by cross-hatchings in the lower quadrants are those which have been excluded since they are suspected of having suffered Bremsstrahlung loss.

§ 4. INFLUENCE OF DISTORTION.

The precautions taken to exclude distorted tracks have already been touched upon. Since the emulsion was only 100μ thick, distortion is likely to be inappreciable, except in the immediate neighbourhood of corners and edges. Nevertheless, certain further precautions were taken. Histograms were drawn for the composite track, showing the distribution of the individual D_j 's for different cell-sizes. One such histogram is reproduced in fig. 3. The value of the true (algebraic) mean, computed for the 100μ and 200μ cell-sizes, did not differ significantly from zero at any statistical level less than 10 per cent. Further, the distribution of D_j was examined for each individual track. The calculated value of

the algebraic mean was checked by Student's t -Test in order to ascertain the probability that the sample could have been drawn from a universe of mean equal to zero. No track yielded a value which was significant at the 5 per cent level. The observed distributions of the algebraic means for $200\ \mu$ cells, both for the 105 and 185 MeV. positrons, are

Fig. 3.



Distribution of 5249 individual values of D_j in overlapping $100\ \mu$ cells for the 105 MeV. positrons. The curve in full is the normal error curve, the algebraic mean, and standard deviation of which have been chosen to agree with that of the sample.

plotted in fig. 4. The histogram shown in fig. 4(a) is found to compare satisfactorily with the normal distribution of means for samples of track of average length. The histogram of fig. 4(b), on the other hand, shows some evidence of representing a bimodal distribution. It would appear reasonable to suppose that it is due to the superposition on a normal distribution, of values of algebraic mean derived from a few tracks affected by slight positive or negative distortion. Even though the tracks have been selected from a region 2 mm. away from any edge, it is not unlikely that such slight distortion exists in the fringing regions. It may be seen from the histogram, however, that such distortion as may exist in individual tracks cannot have any significant influence on the experimentally determined value of \bar{D} .

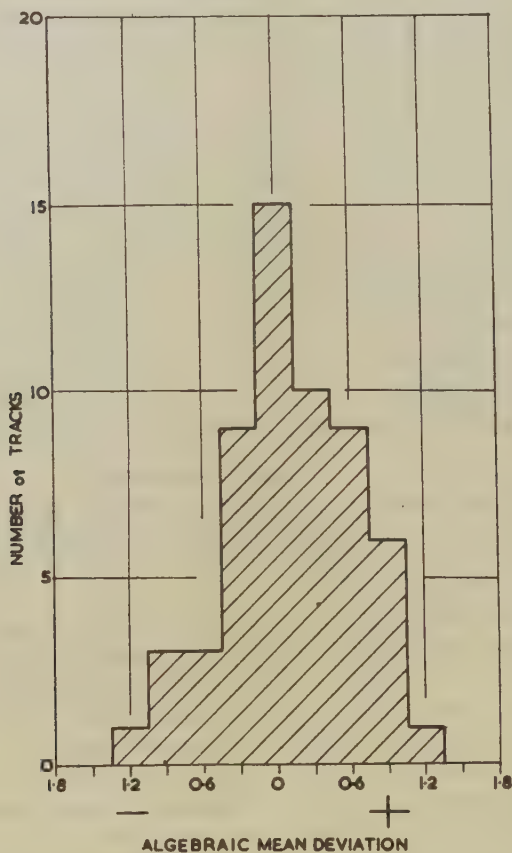
§ 5. CORRECTIONS TO THE NOMINAL ENERGY OF THE TRACKS.

The energy of the electrons, known on emergence from the magnetic spectrometer, must be corrected for loss by ionization and radiation,

first in an aluminium sheet of 2.4 mm. thickness, and then in passing through the glass and emulsion of the plates. It was found that the average electron travelled 1 mm. through glass and 1 mm. through emulsion before reaching the point from which the scattering was measured.

The correction for energy loss by ionization and radiation has been computed for the various absorbers, taking into consideration the

Fig. 4 (a).



Distribution of the algebraic means in 200μ cells for individual tracks.
105 MeV. positrons.

following facts. Particles which had suffered large radiation losses (≥ 50 per cent) up to the point from which the measurements started, have been excluded by the systematic procedure of selection; those in which such losses occurred along the measured path could be recognized from the trend of scattering along the course of each track.

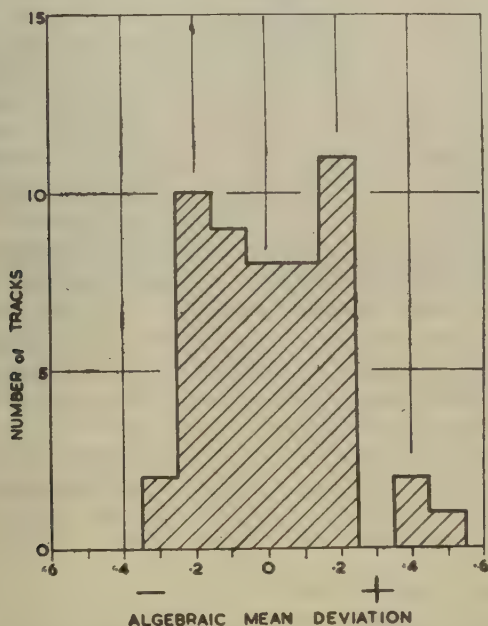
Energy loss along the measured portion of the tracks was allowed for. The energy chosen as appropriate was that corrected to the mid-point of the track of average length. The energies adopted were 105 MeV. and 185 MeV. for the electrons of nominal energy 113 and 196 MeV., and were used both for the purpose of comparison with theory, and for obtaining a value of the scattering constant.

§ 6. EXPERIMENTAL RESULTS.

The value of \bar{D} for the 105 MeV. electrons was determined for cell-sizes 25, 50, 100, 200 and 300 microns.

As each track was being scattered the readings were plotted on squared paper. This proved a useful method of avoiding gross errors. A smooth curve drawn through the readings was assumed to be a good representation

Fig. 4 (b).



Distribution of the algebraic means in 200μ cells for individual tracks.
185 MeV. positrons.

of the course of the track. There is less likelihood of a background grain being mistaken for one belonging to the track when this technique is used, and uncertainties arising from the random distribution of developed grains about the true trajectory of the particle are to some extent smoothed out.

The experimental results are summarized in Table II. In column 2 are listed the experimental values of \bar{D} for the various cell-sizes. The third column gives the value of $\bar{D}_{c.o.}$ which is the mean value of \bar{D} when all

values of $D_j \geq 4\bar{D}$ are excluded and corresponds to the truncated distributions discussed previously (Gottstein *et al.* 1951, henceforth referred to as I.).

TABLE II.

105 MeV. Electrons.		
Cell-size (μ)	\bar{D} Scale Divisions	\bar{D} cut-off
25	—	0.1425
50	0.243	0.234
100	0.556	0.537
200	1.50	1.47
300	2.59	2.55

Corresponding figures for the 185 MeV. electrons are given in Table III.

TABLE III.

185 MeV. Electrons		
Cell-size (μ)	\bar{D} Scale Divisions	\bar{D} cut-off
50	0.220	0.210
100	0.410	0.400
200	0.910	0.870
400	2.24	2.16
600	3.81	3.73
800	5.90	5.76

Since the magnifying power of the instruments is slightly dependent on the interocular distance, the factor for converting scale divisions to microns will vary with different observers. The magnification was found by using a standard object engraved in 10μ divisions, and by means of the stage micrometer. An extreme variation between observers was $2\frac{1}{2}$ per cent and a weighted mean factor of 0.48 was calculated for conversion of scale divisions to degrees/100 μ .

The values of the scattering constant given in Table II. and fig. 1 of Gottstein *et al.* (1951), have been calculated from the results shown in Tables II. and III. The values obtained for the scattering constant (K) are :—

- (1) 105 MeV. positrons, 200μ cells :

$$K_{\text{without cut-off}} 26.7 \pm 0.6, \quad K_{\text{with cut-off}} 26.2 \pm 0.6.$$

- (2) 185 MeV. positrons, 400μ cells :

$$K_{\text{without cut-off}} 24.9 \pm 0.8, \quad K_{\text{with cut-off}} 24.0 \pm 0.8.$$

The influence of noise on these results is very small for these cell-sizes, as will be shown later on in this paper, and has therefore been neglected.

§ 7. DISTRIBUTION OF SECOND DIFFERENCES AND COMPARISON WITH THEORY.

Histograms of the distribution of the individual values of the second difference (D_j) have been studied for different cell-sizes. Fig. 3 gives the results of plotting 5249 values of D_j obtained from overlapping

100 μ cells for the 105 MeV. positrons. The curve in full line is the normal error curve, of which the algebraic mean and standard deviation have been chosen to agree with those of the sample.

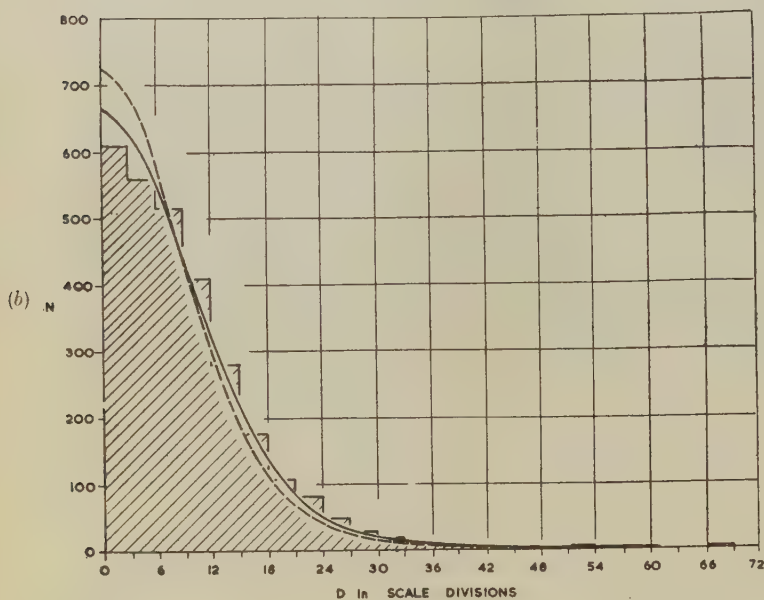
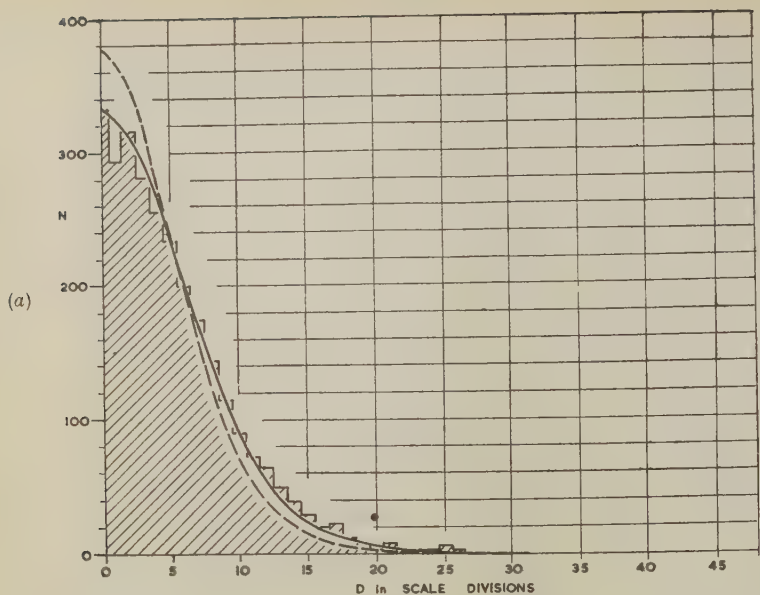
Judged by the χ^2 test, the fit is satisfactory. The appearance of the histogram, however, suggests that the universe from which the values of D_j have been drawn is more peaked than normal. This accords with theory, and receives further support from the fact that the "noise" present in the measurements on 100 μ cells will tend to flatten the experimental distribution. Hence, if the central region is fitted to a normal curve of smaller dispersion, the distribution of the larger values of D_j will appear as a "tail" to this normal curve in the manner envisaged by Williams.

The experimental distributions compared with the theory of Molière are shown in fig. 5(a) (105 MeV. 100 μ cells), and fig. 5(b) (185 MeV. 200 μ cells). All the curves have been drawn for the energies stated above, using figures for the composition of the emulsions supplied by the manufacturers. The curves drawn in dotted lines represent the "normal approximations" defined in I., p. 712. Since the experimental results contain "noise" they may be expected to present a less peaked appearance than the theoretical distributions. We have found it possible, however, to calculate an expected distribution which takes account of the effect of noise. The detailed working is given in Appendix II., and yields the modified theoretical distribution shown by the curves in full line. The agreement with experiment appears to be very satisfactory.

In the experimental distribution of D_j for cell-sizes in excess of 300 μ the "tail" is less in evidence than for the smaller cell sizes, and the distributions tend towards the normal more rapidly than might be expected from the change of L with cell-size (I., p. 714). Since the emulsions used were only 100 μ in thickness, it seems reasonable to suppose that this effect is due to what has been termed by Molière the "Flache Kammer" effect (Molière 1948). Briefly, in evaluating functions $P(\phi)$ it was tacitly assumed that no restriction need be placed on the magnitude of the projected deflection on a plane at right angles to that of the emulsion. For thin emulsions, however, this assumption becomes invalid, especially when measurements are made on large cell-sizes. In these circumstances the tracks selected as being of length sufficient for measurement will tend to be those deficient in large signals.

The distribution functions must be modified so as to take account of this bias. Molière has considered the limiting case of vanishing thickness, and obtains a distribution which differs little from the "normal approximation". Calculations have already been published which apply to cloud chamber measurements where a similar restriction exists because of the finite depth of the illuminated region (O'Ceallaigh and MacCarthaigh 1944, Barker 1948, O'Ceallaigh 1950). It is intended to examine the general case for the photographic emulsion using similar methods.

Fig. 5.



Comparison of the experimental distribution of the absolute values of second difference with the distribution functions of Molière's theory :

dotted lines : " normal approximations " considering only genuine scattering (Molière 1948).

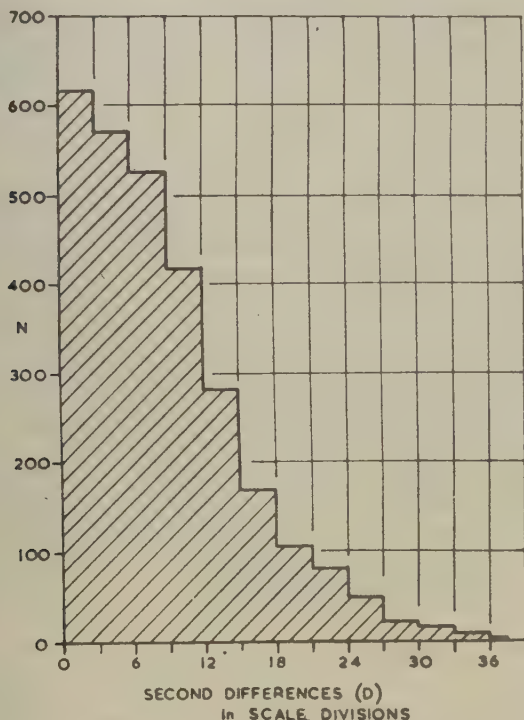
full lines : distribution function of genuine + spurious scattering calculated in the manner shown in Appendix II.

(a) 105 MeV. positrons, 100 μ cells (1 scale division = 0.048°).

(b) 185 MeV. positrons, 200 μ cells (1 scale division = 0.024°).

The distribution of second differences D_j shown in fig. 5(b) for the 185 MeV. positrons (200μ cells) may be compared with that of fig. 6 obtained after applying the procedure shown in Appendix III. This correction results in a cut-off of the "tail" of the distribution at a value corresponding to $4\bar{D}$ without altering the shape of the distribution to any appreciable extent.

Fig. 6.



Histogram showing the distribution of the absolute values of second difference in 200μ cells for 185 MeV. positrons after correcting "single" scattering in the manner shown in Appendix III.

§ 8. ELIMINATION OF "NOISE".

Because of the presence of various sources of uncertainty all the values of \bar{D} listed in Tables II. and III. will be greater than the true value. The chief causes of this excess are (a) reading errors (ϵ_1), (b) errors (ϵ_2) due to the grains being distributed at random about the true path of the particle, (c) errors (ϵ_3) caused by random departures from linearity in the motion of the microscope stage. The resultant effect of such errors is usually termed "noise". Recently, they have been most carefully studied by members of the Brussels group (Goldschmidt-Clermont 1950, Levi Setti 1950), as well as by members of this laboratory. Various

methods of eliminating such errors or neutralizing their effect have been suggested.

An approximate method suggested by Fowler (unpublished) assumes that the various sources of error are statistically independent, and that the resultant quadratic mean noise level is given by

$$\epsilon = (\epsilon_1^2 + \epsilon_2^2 + \epsilon_3^2)^{1/2}. \quad (1)$$

Since we shall have to deal with mean absolute deviation, we denote by $\langle \epsilon \rangle$ the mean absolute value of the resultant noise level. Using equation (16) of (I.) and assuming that L remains independent of cell-size, we may show

$$\bar{D}^2 = K_2^2 s^3 + \langle \epsilon \rangle^2. \quad (2)$$

This implies that the graph of \bar{D}^2 as a function of s^3 is a straight line having slope K_2^2 . Taking the experimental figures \bar{D}_1 and \bar{D}_2 found for cell-sizes s_1 and s_2 , we may eliminate $\langle \epsilon \rangle^2$ and obtain the value of $\langle \Phi \rangle_{100\mu}$ by substitution in the expression

$$\langle \Phi \rangle_{100\mu} = R \sqrt{\left(\frac{\bar{D}_2^2 - \bar{D}_1^2}{s_2^3 - s_1^3} \right)}. \quad (3)$$

R is the constant which reduces the readings of \bar{D} expressed in scale-divisions to degrees/100 μ .

Setting $K_2 = GL_{(s)}$ where G now depends only on the properties of the emulsion, and $L_{(s)}$ is given by I(8), we may correct this formula to take account of the variation of L with cell-size. This correction is particularly important for small cell-sizes where the rate of change is most rapid. We find the more accurate expression

$$\langle \Phi \rangle_{100\mu} = RL_{100\mu} \sqrt{\left(\frac{\bar{D}_2^2 - \bar{D}_1^2}{L_2^2 s_2^3 - L_1^2 s_1^3} \right)}. \quad (4)$$

There is, however, ample evidence that $\langle \epsilon \rangle$ does not remain constant but, on the contrary, that it tends to increase markedly with cell-size due to the increase of the stage noise component $\langle \epsilon_3 \rangle$ (Camerini and Fowler unpublished, Levi-Setti 1950).

Its order of magnitude may be found by measuring in different cell-sizes the scattering of the tracks of relativistic particles, which are the primaries of large cosmic ray showers. The results of such measurements for our microscopes are incorporated in I, fig. 3. Great variations are found in the performances of individual instruments.

The presence of stage noise in the present experiments is shown by a departure of the plot \bar{D}^2 vs s^3 from the form predicted by theory. Since the scattering constant increases as the square root of the logarithm of the cell-size (I. (15)), this plot should appear slightly concave when viewed from above. Experimentally, however, it appears convex when so viewed,

especially for cell-sizes less than $100\ \mu$. This behaviour may be explained if we assume that the noise increases directly as the cell-size, in such manner that we must replace equation (2) by

$$\bar{D}^2 = K_2^2 s^3 + \eta_0^2 (1 + Qs) \quad . \quad . \quad . \quad . \quad . \quad (5)$$

where η_0^2 represents the square of the mean absolute noise level due to ϵ_1 and ϵ_2 , and Q is a pure number of the order of unity.

The assumption that stage noise varies linearly with s agrees with the experimental results of Levi Setti (1950) to which we have already referred.

Q varies widely from instrument to instrument, and also, unfortunately, with the position and the condition of the stage. For this reason it is desirable, as far as is practicable, to confine the measurements to the same region of the stage coordinates, and also to maintain the guides in a clean condition. The magnitude of the stage-noise should be checked at intervals by measurements on a long straight primary track.

Direct evidence for increase of stage-noise with cell-size will be given by noise elimination, on cell-sizes less than $100\ \mu$ using Fowler's formula, or its modified form (4). It will then be found that the highest value of $\langle \Phi \rangle_{100\mu}$ is obtained by elimination between the pair of smallest cells, because, as we have seen, the plot of \bar{D}^2 as a function of s^3 will be convex when viewed from above.

Taking account of the variation of stage-noise with cell-size, we may obtain from (5) the elimination formula

$$\langle \Phi \rangle_{100\mu} = RL \sqrt{\left(\frac{\bar{D}_2^2(1 + Qs_1) - \bar{D}_1^2(1 + Qs_2)}{L_2^2 s_2^3(1 + Qs_1) - L_1^2 s_1^3(1 + Qs_2)} \right)} \quad . \quad . \quad (6)$$

By suitable choice of Q , noise elimination between the various pairs of cell-sizes may be made to yield the same value of $\langle \Phi \rangle_{100\mu}$. These points are illustrated in Table IV, which gives for 105 MeV. electrons, the values for $\langle \Phi \rangle_{100\mu}$ found by using the various methods of elimination.

TABLE IV.

Method	Cell-size (μ)					
	50-25	100-25	100-50	200-25	200-50	200-100
Fowler (3)	0.266	0.250	0.248	0.248	0.248	0.248
Fowler (4)	0.279	0.250	0.246	0.238	0.238	0.236
Present work $Q=5$	0.236	0.235	0.236	0.234	0.234	0.234

The adopted value of $Q=5$ was found to be consistent with the magnitude and variation with cell-size of the stage-noise found directly by using the track of a heavy primary particle of great energy (I, fig. 3).

From the results given in the third row of Table IV., we deduce values of the scattering constant for 100μ cells based essentially on the experimental results for the following cell-sizes:—

$$50\mu = 24.9 \pm 0.4,$$

$$100\mu = 24.9 \pm 0.6,$$

$$200\mu = 24.7 \pm 0.7.$$

The uncertainties are standard deviations and are calculated from the theoretical sampling distribution of mean deviation (III., Eqn. 10). These results are to be compared with that predicted by Molière's theory for particles for which $\beta^2 \sim 1$, I(13), diminished by 10 per cent to take into account the truncation of the distribution caused by excluding all signals $\geq 4\bar{D}$, namely,

$$K_{\text{chord}, \beta^2 \sim 1} = 23.0 \text{ degrees} \times \text{MeV.} / (100\mu)^{1/2}.$$

The agreement would appear to be satisfactory, taking into consideration possible uncertainties in the value of the energy.

The influence of noise on the values of $\langle \Phi \rangle$ will be seen by comparing the second and third rows of Table IV. For 200μ cells the difference of about 1.5 per cent justifies the neglect of noise in the comparison of theory with experiment described in I and illustrated in fig. 1 of that paper.

ACKNOWLEDGMENTS.

We are indebted to Professor C. F. Powell, F.R.S., for his continued interest and encouragement during the course of this work. Our best thanks are due to Professor Dale R. Corson, who has very kindly put at our disposal plates exposed to a beam of positrons in the Cornell Synchrotron, without which this investigation could not have been carried out. We also wish to thank Mrs. M. O'Ceallaigh and Miss R. Mitchell for their valuable assistance with the measurements.

APPENDIX I.

CORRELATION COEFFICIENTS.

In a recent paper Molière (Part IV., 1951) has shown that when the scattering parameter observed (Merkmal) is composed of two parts, genuine and spurious, the correlation coefficient of two successive parameters x_i and x_{i+1} (two successive second differences in the present case), is a quantity which depends upon the ratio of signal to noise *e.g.* the ratio of the mean absolute values (or standard deviations) of the genuine and spurious scattering.

By definition the correlation coefficient is

$$\frac{\overline{x_i x_{i+1}}}{\overline{x_i^2}} = \frac{1 - \frac{2}{3}\mu}{1 + \mu}, \dots \dots \dots (1)$$

where

$$\mu = \left(\frac{\text{noise}}{\text{signal}} \right)^2 = \left(\frac{\bar{\Delta}_n}{\bar{\Delta}_s} \right)^2; \quad \Delta_{n,s} = \text{mean value of } \begin{cases} \text{noise} \\ \text{signal} \end{cases}$$

One way of finding μ and then $\bar{\Delta}_n$ or $\bar{\Delta}_s$ (which is *not* the solution of the variational problem of maximum likelihood, but involves a much simpler calculation) consists in equating the right hand side of the relation (1) to the experimental quantity (2)

$$\frac{(1/(n-1))\Sigma \Delta_i \Delta_{i+1}}{(1/n)\Sigma \Delta_i^2}. \quad . \quad . \quad . \quad . \quad . \quad . \quad (2)$$

Then

$$\bar{\Delta}_s = \sqrt{\left(\frac{2}{\pi}\right)} \sqrt{\left(\frac{1}{\frac{1}{4} + \frac{2}{3}}\right)} \sqrt{\left(\frac{2}{3}\bar{\Delta}^2 - \overline{\Delta_i \Delta_{i+1}}\right)}. \quad . \quad . \quad . \quad (3)$$

$$\bar{\Delta}_n = \sqrt{\left(\frac{2}{\pi}\right)} \sqrt{\left(\frac{1}{\frac{1}{4} + \frac{2}{3}}\right)} \sqrt{\left(\frac{1}{4}\bar{\Delta}^2 + \overline{\Delta_i \Delta_{i+1}}\right)}. \quad . \quad . \quad . \quad (4)$$

The variance of these two quantities is also calculated. A preliminary attempt to apply this method has been made using the tracks of 185 MeV. electrons.

Two hundred and sixty-six angles measured between successive chords (cell-size 200μ) gave the following results expressed in divisions of the eyepiece scale:

$$\begin{aligned} \bar{\Delta}_i^2 &= 1.115, \\ \overline{\Delta_i \Delta_{i+1}} &= +0.0673. \end{aligned}$$

Using formulae (3) and (4) this yields:

$$\begin{aligned} \bar{\Delta}_s &= 0.736, \\ \bar{\Delta}_n &= 0.383. \end{aligned}$$

Transforming into degrees, we obtain:

$$\begin{aligned} |\bar{\alpha}| &= 0.177 \pm 0.0054 \text{ in } 200 \mu \text{ cells,} \\ |\bar{\alpha}|_{\text{noise}} &= 0.092 \pm 0.0011. \end{aligned}$$

The value of the scattering constant then obtained is 23.1 ± 1.1 in close agreement with the theoretical value after cut-off (24.05).

APPENDIX II.

The distribution function of the second differences measured in the presence of spurious scattering is derived from Molière's theory as follows:

We may write

$$x = x_{\text{sp}} + x_{\text{gen}}, \quad . \quad . \quad . \quad . \quad . \quad . \quad (1)$$

where x is the value of the quantity observed, x_{sp} the contribution due to spurious scattering and x_{gen} the contribution due to genuine scattering. We assume the normality of the distribution of x_{sp} and the statistical independence of x_{sp} of x_{gen} .

The exponent of the Fourier transform of the distribution function of x_{gen} is then

$$\frac{x_c^2 \xi^2}{4} \log \left(\frac{\gamma^2 x_a^2 \xi^2}{4e} \right), \quad (2) \text{ (Molière)}$$

whereas the corresponding quantity for the distribution function of x_{sp} is

$$-\frac{(x_0^{\text{sp}})^2}{4} \xi^2, \quad (3)$$

(where $x_0^{\text{sp}} = \sqrt{2}$ standard deviation of x_{sp}).

The sum of (2) and (3) gives the exponent of the Fourier transform of the distribution function of x .

Introducing

$$\left(\frac{x_0^{\text{sp}}}{x_c} \right)^2 = \mu', \quad (4)$$

and

$$\Omega_{b,x}^* = \left(\frac{x_c^2}{x_a^2} \right) e^{\mu'} \quad (5)$$

together with

$$B_x^* - \log B_x^* = \log (e \Omega^* / \gamma^2) \quad (6)$$

as well as the new variable $\eta = x_c \sqrt{(B^*)} \xi$ in place of ξ , the d.f. of x takes the form

$$f(|x|) d|x| = \frac{d|x|}{x_c \sqrt{(B^*)}} \cdot \frac{2}{\pi} \int d\eta \cos \left(\frac{|x|}{x_c \sqrt{(B^*)}} \eta \right) \exp \left(-\frac{\eta^2}{4} + \frac{\eta^2}{4B_x^*} \log \frac{\eta^2}{4} \right) \quad . . . (8)$$

which, after development in powers of $1/B^*$ yields the well known formula

$$f(\phi) d\phi = d\phi \left[\frac{2}{\sqrt{\pi}} e^{-\phi^2} + \frac{1}{B_x^*} f^{(1)}(\phi) + \frac{1}{B_x^{*2}} f^{(2)}(\phi) + \dots \right], \quad . . (9)$$

where now

$$\phi = |x| / x_c \sqrt{(B_x^*)}.$$

When the values of B and Ω for the case of pure scattering are known, the new values B^* and Ω^* are obtained from the relation (6) together with

$$\Omega^* = \Omega e^{B\mu}, \quad (10)$$

where $\mu = \frac{\mu'}{B} = \left(\frac{\text{noise}}{\text{signal}} \right)^2$.

APPENDIX III.

CORRECTION OF "SINGLE" SCATTERING.

The following has been found a convenient procedure for correcting a group of second differences obtained by the method of overlapping cells in a region where the particle has suffered a sharp deflection. It consists in subtracting from each second difference involved a certain quantity which represents the contribution to it due to the "single scattering".

Let

$$\dots y_{p-4}, y_{p-3}, y_{p-2}, y_{p-1}, y_p, y_{p+1}, y_{p+2}, y_{p+3}, y_{p+4}, \dots y_j \dots$$

be the measured coordinates of points of the track, namely, their distance from an arbitrary line of reference. The intervals between two points are s_1/λ where λ =coefficient of overlap, s_1 =cell-size in microns.

Suppose that the "single scattering" of Φ radians occurs between the points of which the coordinates are y_{p-1} and y_p at a distance x from the latter. The second difference D_j in cell-size s_1 will be

$$D_j = y_j - 2y_{j-1} + y_{j-2} \dots \dots \dots (1)$$

Let

$$D_j = a_j + s_j \dots \dots \dots (2)$$

where S_j =contribution due to the single scattering,

a_j =contribution due to the multiple scattering.

Simple geometrical considerations show that a "block" of 2λ such second differences are influenced by the single scattering, corresponding to values of j ranging from $j=p$ to $j=p-1+2\lambda$ and we find readily

$$\left. \begin{aligned} s_p &= x\Phi, \\ s_{p+1} &= \left(\frac{s_1}{\lambda} + x\right)\Phi, \\ s_{p+2} &= \left(2\frac{s_1}{\lambda} + x\right)\Phi, \\ s_{p+3} &= \left(3\frac{s_1}{\lambda} + x\right)\Phi, \\ &\vdots \\ s_{p-1} &= \left(\frac{\lambda-1}{\lambda}s_1 + x\right)\Phi, \\ s_{p+\lambda} &= (s_1 - x)\Phi, \\ s_{p+1+\lambda} &= \left(\frac{\lambda-1}{\lambda}s_1 - x\right)\Phi, \\ &\vdots \\ s_{p-1+2\lambda} &= \left(\frac{s_1}{\lambda} - x\right)\Phi. \end{aligned} \right\} \dots \dots \dots (4)$$

A knowledge of Φ and x , which can often be measured, allows us to correct the second differences, by subtracting from them the quantity S_j

$$a_j = D_j^* = D_j - S_j \dots \dots \dots (5)$$

Approximation.

It can be seen that the quantities $x\Phi$ and $(s_1/\lambda - x)\Phi$ may be obtained approximately in the following manner:—

Let us write

$$\left. \begin{aligned} \delta_1 &= y_p - 2y_{p-1} + y_{p-2}, \\ \delta_2 &= y_{p+1} - 2y_p + y_{p-1}. \end{aligned} \right\} \dots \dots \dots (6)$$

These quantities are the pair of second differences in the prime cell-size of length s_1/λ microns which have been influenced by the single scattering. We have thus

$$\left. \begin{aligned} \delta_1 &= a'_1 + s'_1, \\ \delta_2 &= a'_2 + s'_2, \end{aligned} \right\} \dots \dots \dots (7)$$

with

$$s'_1 = x\Phi, \quad s'_2 = \left(\frac{s_1}{\lambda} - x\right)\Phi.$$

The quantities a'_1 and a'_2 are $\lambda^{3/2}$ times smaller than $a_1 \dots a_2 \dots$ in (2). In many cases these contributions due to multiple scattering in the small cell-size may be neglected. We then have

$$\delta_1 = x\Phi \text{ and } \delta_2 = \left(\frac{s_1}{\lambda} - x\right)\Phi. \dots \dots \dots (8)$$

Thus

$$\left. \begin{aligned} s_p &= \delta_1, \\ s_{p+1} &= 2\delta_1 + \delta_2, \\ s_{p+2} &= 3\delta_1 + 2\delta_2, \\ &\vdots \\ s_{p+1-\lambda} &= \lambda\delta_1 + (\lambda-1)\delta_2, \\ s_{p+\lambda} &= (\lambda-1)\delta_1 + \lambda\delta_2, \\ s_{p+1+\lambda} &= (\lambda-2)\delta_1 + (\lambda-1)\delta_2, \\ &\vdots \\ s_{p-1+2\lambda} &= \delta_2. \end{aligned} \right\} \dots \dots (9)$$

The following table shows an example of the application of this correction on the track of a 185 MeV. electron, for $\lambda=4$ and $s_1=200 \mu$.

j	y_j	$y_j - y_{j-1}$	$y_j - 2y_{j-1} + y_{j-2}$	$y_j - y_{j-4}$	$D_j =$ $y_j - 2y_{j-4} + y_{j-8}$	$S_j =$ Correction	D_j Corrected 2nd dif.
$p-8$	27.4	-0.3	—	—	(+0.6)		
$p-7$	27.1	-0.3	0.0	—	(+0.6)		
$p-6$	26.3	-0.8	-0.5	—	(-0.5)		
$p-5$	25.7	-0.6	+0.2	—	(-0.8)		
$p-4$	25.3	-0.4	+0.2	-2.1	(-0.8)		
$p-3$	24.6	-0.7	-0.3	-2.5	(+1.3)		
$p-2$	24.7	+0.1	+0.8	-1.6	(+0.2)		
$p-1$	23.9	-0.8	-0.9	-1.8	(+0.2)		
p	25.0	+1.1	+1.9 = δ_1	-0.3	+1.8*	-1.9	-0.1
$p+1$	26.2	+1.2	+0.1 = δ_2	+1.6	+4.1*	-3.9	+0.2
$p+2$	27.4	+1.2	0.0	+2.7	+4.3*	-5.9	-1.6
$p+3$	28.7	+1.3	+0.1	+4.8	+6.6*	-7.9	-1.3
$p+4$	29.9	+1.2	-0.1	+4.9	+5.2*	-6.1	-0.9
$p+5$	31.7	+1.8	+0.6	+5.5	+3.9*	-4.1	-0.2
$p+6$	33.3	+1.6	-0.2	+5.9	+3.2*	-2.1	+1.1
$p+7$	34.8	+1.5	-0.1	+6.1	+1.3*	-0.1	+1.2
$p+8$	36.2	+1.4	-0.1	+6.3	+1.4		

The values of D_j in brackets in the sixth column of the Table have been computed using values of y_j corresponding to $j < p-8$ (which are not given in the first column). These values of D_j are listed here in order to show the magnitude of the value of D_j in the region prior to the "single" scattering.

Here the "single" scattering has a visible influence on the sign of the first differences between successive y 's. They are all positive for $j < p$ and become positive afterwards. Thus the point where the deviation occurs can be detected at once.

Also, it can be seen that $\delta_1 = y_p - 2y_{p-1} + y_{p-2}$ is equal to 1.9 div. of eyepiece scale. The eight second differences influenced by the single scattering are marked with crosses. Their absolute values average 3.8 div. All the second differences of the track (5500 μ long) including these, average 1.09 div.

After the entire block of second differences affected has been removed, this average becomes $\bar{D} = .853$ div.

The average of the corrected block is .82 div., and the average of the track, after including the corrected values, becomes $\bar{D} = .851$ div.

REFERENCES.

- BARKER, 1948, *J. Sci. Instrum.*, **25**, 65.
 CAMERINI and FOWLER, 1951, (private communication).
 FOWLER, 1950, *Phil. Mag.*, **41**, 169; 1951 (private communication).
 GOLDSCHMIDT-CLERMONT, 1950, *Nuovo Cimento*, **7**, 331.
 LEVI SETTI, 1950, Note No. 22, *Bull. Du. Cen. de Phys. Nuc. de L'Univ. Libre de Bruxelles*.
 MOLLIERE, 1947, *Z. f. Naturforschung.*, **2A**, 133; 1948, *Ibid.*, **3A**, 78; 1951, unpublished.
 O'CEALLAIGH and MACCARTHAIGH, 1944, *Proc. Roy. Irish Acad. A*, **50**, 13.
 O'CEALLAIGH, 1950, *Proc. Roy. Irish Acad. A*, **53**, 133.

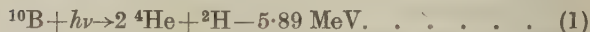
XCV. CORRESPONDENCE.

The reaction $^{10}\text{B}(\gamma, d) 2\ ^4\text{He}$.

By M. J. BRINKWORTH and E. W. TITTERTON,
A.E.R.E., Harwell, Didcot, Berks.*

[Received May 23, 1951.]

THE reaction

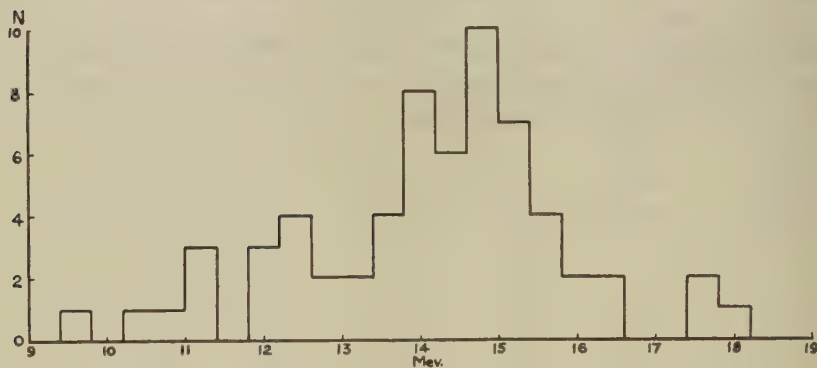


first reported by Goward, Titterton and Wilkins (1950) has been investigated with the γ -rays from the ${}^7\text{Li}(p, \gamma) 440\text{ KeV.}$ resonance. Ilford E_1 emulsions, some of which were loaded with boron of normal isotopic constitution and others with separated ^{10}B , were used.

The boron loading has an intensifying action at development, and as a result it is difficult to distinguish the deuteron from the α -particles by inspection, and the tracks are too short for scattering measurements. A momentum balance is carried out on each event to distinguish the ^{10}B from the ^{11}B and ^{12}C stars, and to identify the deuteron in the ^{10}B stars.

65 events due to reaction (1) have been observed, and a histogram of the γ -ray energies is given in fig. 1. The ${}^7\text{Li}(p, \gamma)$ radiations consist of

Fig. 1.



γ -ray energy distribution.

a narrow peak at 17.6 MeV., and a second peak, about 2 MeV. wide of half the intensity of the first, at 14.8 MeV. (Walker and McDaniel 1948). Only three events fall in the 17.6 MeV. peak, indicating a much smaller value of the cross-section at this energy than at 14.8 MeV. The events

* Communicated by the Authors,

with $E_\gamma < 12$ MeV. are due to γ -rays which are either in the tail of the 14.8 MeV. peak or have suffered Compton scattering in the wall of the target chamber. A quantitative estimate has been made of the relative γ -ray intensity to be expected at energies less than 12 MeV. due to these causes (Brinkworth 1951) and the number of ^{10}B events obtained is approximately twice that which would be given by a uniform cross-section. This suggests that the $^{10}\text{B}(\gamma, d)$ cross-section passes through a maximum at 13 ± 2 MeV.

By normalization against the ^{12}C stars, using the cross-section measured by Wäffler and Younis (1949), the $^{10}\text{B}(\gamma, d)$ cross-section at 14.8 MeV. is estimated to be $(2.9 \pm 1.4) \times 10^{-28} \text{ cm}^2$.

On the assumption that a three-body reaction is not occurring, the course of the ^{10}B photodisintegration is either $^{10}\text{B}(\gamma, d) {}^8\text{Be}^*$; ${}^8\text{Be}^* \rightarrow 2 {}^4\text{He}$ or $^{10}\text{B}(\gamma, \alpha) {}^6\text{Li}^*$; ${}^6\text{Li}^* \rightarrow {}^4\text{He} + {}^2\text{H}$.

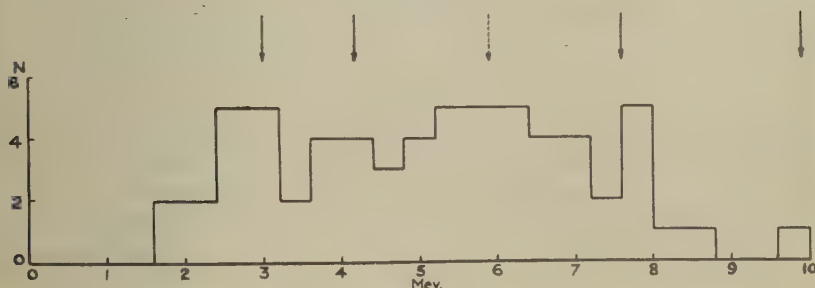
If ${}^8\text{Be}$ is the intermediate nucleus, the energy release Q when it disintegrates is given by

$$Q = E_1/2 + E_2/2 - (E_1 E_2)^{1/2} \cos \theta, \quad \dots \quad (2)$$

where E_1 and E_2 are the energies of the α -particles, and θ is the angle between them. Q is also given by the formula

$$Q = E_1 + E_2 - E_D/4 - p_\gamma^2/8 + (p_\gamma/4) (2 E_D)^{1/2} \cos \phi, \quad \dots \quad (3)$$

Fig. 2.



Q value histogram.

where E_D is the deuteron energy, p_γ the momentum of the γ -ray, and ϕ is the angle between the direction of emission of the deuteron and the incident γ -ray. The terms involving p_γ may be neglected with a maximum error in most of the present calculations of 6 per cent, and 9 per cent in the worst case.

The Q values calculated from the two formulæ are in approximate agreement when the tracks have been correctly identified. About 10 events which had been provisionally identified as $^{10}\text{B}(\gamma, d) 2\alpha$ failed to give concordant Q values, indicating that these events were really $^{10}\text{B}(\gamma, np) 2\alpha$, a reaction which will be discussed in a later communication.

Fig. 2 shows the histogram of the Q values. It appears that if the

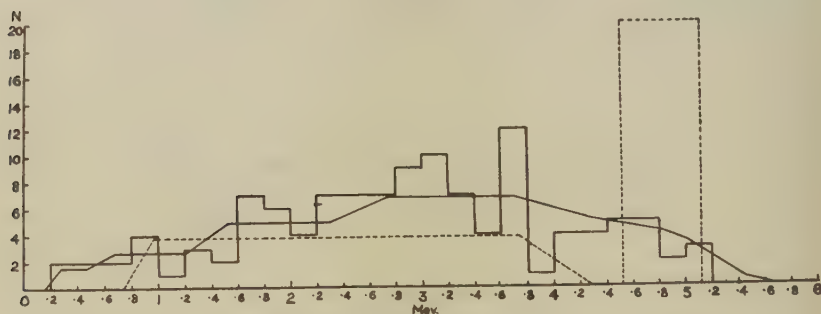
reaction does proceed through ${}^8\text{Be}$ then the known excited levels of this nucleus at 2.9, 4.05, 7.5 and 9.8 MeV. may all be involved (Hornyak, Lauritsen, Morrison and Fowler 1950), the corresponding Q values being indicated by arrows in fig. 2. The resolution of the present experiment is not sufficient to establish whether the level at 4.9 MeV. decays by α -particle emission. Bennett *et al.* have reported a γ -ray from this level (Bennett, Bonner, Richards and Watt 1947).

The Q value histogram in fig. 2 suggests that there may be a broad level in ${}^8\text{Be}$ at about 5.8 MeV., as indicated by the broken arrow. Some indication of a level in this position has been found from the ${}^{11}\text{B}(\gamma, t) 2\alpha$ reaction (Titterton and Calcraft 1951).

A plot of the deuteron energies cannot be used to give the ${}^8\text{Be}$ level scheme in this case owing to the width of the 14.8 MeV. γ -ray peak, the presence of scattered γ -rays, and the variation of cross-section with energy.

The alternative mode of disintegration to be considered is through ${}^6\text{Li}$. Experiments with lithium-loaded plates have shown that the reaction ${}^6\text{Li} + h\nu \rightarrow {}^4\text{He} + {}^2\text{H}$ does not occur (Titterton 1950) but this does not necessarily preclude the ${}^{10}\text{B}$ disintegration from passing through an excited state of ${}^6\text{Li}$. Use of the Q formula to determine these levels is unsatisfactory, because it is not known which of the two α -particles should be taken as resulting from the break-up of the ${}^6\text{Li}^*$.

Fig. 3.



α -particle energy distribution (excluding events due to 17.6 MeV. γ -ray).

A histogram of all the α -particle energies, excluding events due to the 17.6 MeV. γ -ray, is given in fig. 3. If the reaction passes through the 2.4 MeV. level of ${}^6\text{Li}$ (Hornyak *et al.* 1950), half the α -particle energies should fall in a narrow peak, and the other half yield a broad, approximately uniform distribution, as shown by the broken line in fig. 3, level width and γ -ray width having been neglected. It is evident that the reaction cannot proceed exclusively through the 2.4 MeV. level, but it is possible that it proceeds partly through this and other undetermined levels of the nucleus. The α -particle energy distribution is of necessity consistent with the disintegration of ${}^{10}\text{B}$ by way of ${}^8\text{Be}$, if it is assumed that the relative probabilities of the occurrence of the different ${}^8\text{Be}$ levels is

given by the Q histogram in fig. 2. The full line in fig. 3 shows the approximate distribution to be expected on this assumption, the γ -ray and level widths again being neglected.

The experiments suggest that the probable mode of disintegration is through ^8Be , but more events are awaited to confirm this, and to provide more accurate information on the energy levels involved.

Members of the nuclear emulsions group at A. E. R. E. are thanked for microscope work.

REFERENCES.

- BENNETT, BONNER, RICHARDS, and WATT, 1947, *Phys. Rev.*, **71**, 11.
BRINKWORTH, 1951, *A.E.R.E. G/M* 81.
GOWARD, TITTERTON and WILKINS, 1950, *Proc. Phys. Soc. A*, **63**, 172.
HORNYAK, LAURITSEN, MORRISON and FOWLER, 1950 *Rev. Mod. Phys.*, **22**, 291.
TITTERTON, 1950, *Proc. Phys. Soc. A.*, **63**, 915.
TITTERTON and CALCRAFT, 1951, *Phil. Mag.* [7], **42**, 666.
WÄFFLER and YOUNIS, 1949, *Helv. Phys. Acta*, **22**, 614.
WALKER and McDANIEL, 1948, *Phys. Rev.* **74**, 315.

The Disintegration of Light Nuclei by Cosmic Rays.

By P. E. HODGSON,

Imperial College of Science and Technology, London*.

[Received June 5, 1951.]

USING sandwich emulsion composed of alternate layers of C2 emulsion and pure gelatin, Harding (1949, 1951) has analysed the cosmic ray induced disintegrations of the carbon, nitrogen and oxygen nuclei constituting the gelatin. He found that the average charge emitted from the disintegrations in the gelatin was $4.7e$. The average charge on the elements (excluding hydrogen) which constitute the gelatin at normal humidity is $6.63e$. In order to obtain the average expected charge per star, a small correction of ~ 0.2 must be added to this to allow for the proton initiated stars. A charge of about $2.1e$ therefore remained to be accounted for.

As Harding pointed out, this loss of charge may be due to three causes : (1) The ejection of fast singly charged particles which are not recorded in C2 emulsion. (2) The ejection of a group of charged particles of short range, the majority of which remain in the gelatin layer. (3) The ejection of particles of charge greater than two which have been mistaken for alpha-particles.

* Communicated by Sir George Thomson, F.R.S.

Perkins (1950) has since shown that the number of visible particles of charge greater than two is very small for stars of the size found in gelatin layers.

In order to resolve the remaining ambiguity between (1) and (2), sandwich emulsions composed of alternate layers of G5 emulsion and pure gelatin have been exposed to cosmic rays on the Jungfrauoch.

From the thirty-six disintegrations of gelatin nuclei examined in this type of emulsion, there were emitted 140 particles making black or grey tracks and six at or near minimum ionization. Allowing for those particles which were missed because they remained wholly in the gelatin layer or emerged from it too far from the star centre to be observed, these figures become 158 ± 9 and about ten respectively.

In his analysis of gelatin stars in C2 sandwich plates, Harding found 1.50 alpha particles per star, after correcting for loss. This number of the black tracks found in G5 emulsion must therefore be due to alpha particles. Camerini *et al.* (1950) have shown that 17 per cent of shower particles are protons, and so this fraction of the minimum ionization tracks was included in the charge per star. The emitted mesons were assumed to be as often positively as negatively charged and were omitted. Owing to the small number of minimum ionization tracks, any error in estimation of the charge emitted in this way will not critically effect the final result.

The corrected value of the average charge per star emitted as singly or doubly charged particles is therefore $5.96 \pm 0.25 e$.

An average charge per star of $0.87 \pm 0.25 e$ is therefore emitted as short range particles which mostly remain in the gelatin layer and escape detection. On the average, emitted particles have an energy such that, if singly or doubly charged, they would have sufficient range to be observed. These short range particles must therefore have a charge greater than two. Assuming they have an average charge of $4e$, the number of such fragments becomes 0.22 ± 0.006 per star, or 7.9 in the group of stars examined. One such particle was observed, which is of the correct order of magnitude in view of the unfavourable conditions of observation.

Bradt and Peters (1950) have used Harding's result to calculate a value of 0.7 for $p_H(B)$, the probability that a stable lithium, beryllium or boron nucleus will be produced when a relativistic carbon, nitrogen or oxygen nucleus collides with an interstellar hydrogen nucleus, which is the same physical event as that examined here, but with target and projectile interchanged. The present work shows that this value should be modified to 0.22 ± 0.06 , which is close to the 0.23 actually used by Bradt and Peters in their calculations.

Since the stars analysed are mainly produced by neutrons of energies of the order of hundreds of MeV., whereas $p_H(B)$ refers to relativistic collisions, this method depends on the assumption that $p_H(B)$ is the same for the two types of disintegration. This uncertainty could be avoided if only those stars initiated in gelatin by a relativistic proton were

analysed. Unfortunately, however, such stars constitute only a small fraction of all the stars, and in order to find a sufficient number for analysis a prohibitively large plate area would have to be scanned.

Small styles are more likely to be missed during examination of the plates than large ones. Since these have the heavier recoils, this effect will reduce the value found for $\rho_H(b)$, which is consequently only a lower limit.

I should like to express my gratitude to Professor Sir George Thomson and Dr. J. B. Harding for valuable discussions, to Mr. A. J. Herz for developing the plates and to Mr. L. Mandel for assisting with their exposure.

REFERENCES.

- BRADT, H. L., and PETERS, B., 1950, *Phys. Rev.*, **80**, 943.
 CAMERINI, U., FOWLER, P. H., LOCK, W. O., and MUIRHEAD, H., 1950, *Phil. Mag.*, **41**, 413.
 HARDING, J. B., 1949, *Nature. Lond.*, **163**, 440; 1951, *Phil. Mag.*, **42**, 63.
 PERKINS, D. H., 1950, *Proc. Roy. Soc.*, **203**, 399.

ERRATUM

A High Precision Pulse Height Analyser of Moderately High Speed.

By G. W. HUTCHINSON, M.A., and G. G. SCARROTT (*Phil. Mag.*, **42**, 792).

The appendix of this paper was altered in proof to show the latest model of the analyser. By a printer's oversight the paper appeared with the altered diagrams but with the unaltered script of the appendix, which is no longer appropriate.

The circuit details are shown in the following diagrams. Resistances are given in kilo-ohms except where otherwise stated. The capacities of all condensers lie between $5\mu\mu\text{F.}$ and $1\mu\text{F.}$ and are stated in either $\mu\mu\text{F.}$ or $\mu\text{F.}$ since no ambiguity can arise. To avoid confusing the diagrams, many decoupling condensers have been omitted from circuit points which carry only D.C. reference potentials.

The following valves are used except where otherwise stated:—

Single diodes	EA50
Double diodes.....	EB91
Double triodes (cathodes connected)	ECC91
Double triodes (separate cathodes)	12 AT 7
Pentodes	EF91
Selenium rectifiers	M1

The terminal links in the resistance networks of the bias and calibration pulse circuits are provided for the insertion of an external milliammeter.

The four-position switches of figs. 2 and 3 are ganged.

The couplings to the crystals of the supersonic delay line are through matching transformers.

XCVI. *Notices of New Books and Periodicals received.*

Theory of the Interior Ballistics of Guns. By J. CORNER. [Pp. 443.] (New York: John Wiley and Sons; London: Chapman and Hall, 1950.) Price 64s.

THE theoretical study of the motion of a shot in a gun involves at least three distinct, though interrelated, aspects: (i.) the manner of burning of the propellant and its dependence on the surroundings; (ii.) the physical chemistry of the propellant gases; (iii.) the dynamics of the products of burning, the shot, and the gun. The author, who is in a Ministry of Supply establishment, specialized in interior ballistics during and after the war, and has contributed largely to recent research. He has written a clear and carefully ordered account in which the three aspects are thoroughly treated.

Interior ballistics is nowadays a distinctly applied science. The improvement of experimental techniques has shown the great complexity of the subject. The elegant theories constructed by eminent mathematicians of the past have to be augmented by numerous semi-empirical corrections. Much of the book deals with the minutiae of these corrections, which are of concern only to the specialist. However, interior ballistics also raises problems of wider interest, for example in the hydrodynamics of the gases in the chamber of the gun before and after shot-ejection, and in the thermochemistry of propellants. The author has presented a balanced picture of his subject, both close-up and in perspective.

R. H.

Selected Topics in X-ray Crystallography, edited by J. BOUMAN. (Amsterdam: North Holland Publishing Company.)

THIS is the third volume of the series of Monographs on Theoretical and Applied Physics edited by Professors de Boer and Brinkman and Dr. Casimir. The topics dealt with comprise General Methods for Structure Analysis, Distortions in Crystals, Crystal Growth, Quantitative Determinations, and special applications of X-ray methods to the study of photographic emulsions, the amorphous state, natural rubber and some problems in the biological field. The topics discussed are brought well up to date and adequately documented, the articles provide excellent summaries of present practice and it will be seen that the scope of the articles includes features that are of interest to most laboratories dealing with pure or applied crystallographic work. The book can confidently be recommended as likely to prove a valuable addition to the more general treatises to be found in the library of any such laboratory, and will appeal particularly to workers who are commencing research work on any of the applied problems discussed.

S. H. P.

Superfluids—Macroscopic Theory of Superconductivity, Vol. I. [Pp. 161.] By FRITZ LONDON. (Chapman and Hall.) Price 40s.

THIS volume consists of a careful survey of the macroscopic electrodynamics of superconductors and its consequences. It is divided into five sections. The first deals with the thermodynamical correlations between the variables. The second is concerned with the electrodynamics of the pure superconducting state, and is based on the equations first introduced by the Londons in 1935. A section on the intermediate state is followed by one on the various effects due to

surface energies. In the final section Dr. London attempts to isolate the microscopical problem, and concludes that to explain superconductivity it might suffice to prove the existence of a long range order in the momentum.

It might have been helpful to include in such a survey a discussion of the two-fluid thermodynamical model of superconductors suggested by Gorter and Casimir in *Zeit. f. Tech. Phys.*, **15**, 539, 1934. This correlates such data as the specific heat law, the parabolic relation between critical field and temperature, and the temperature dependence of the penetration depth. It would have been of special interest to compare this model of a superconductor with the somewhat similar two-fluid models of Helium II which will presumably play a considerable part in volume II. of Dr. London's work.

This is, however, but a small criticism of a book which is generally excellent alike in choice of material and mode of presentation. R.B.D.

The Identification of Molecular Spectra. By R. W. B. PEARSE and A. C. TAYLOR. Second Revised Edition. (Chapman and Hall, London, 1950.) 50s. net.

THIS book which has become a quite indispensable work of reference in all spectroscopic laboratories has been thoroughly revised and brought up-to-date in this new edition. The valuable table of persistent band heads which allows the emitters responsible for many diffuse "lines" to be identified has been considerably extended. This is of interest to those engaged in both analytical and astrophysical work. The identifications can usually be confirmed by reference to the more detailed data on the band systems and re-examination of the spectra. In addition to such analytical applications, the volume provides (for research workers) a most useful source-book of references to molecular spectra, particularly to spectra which have not yet been analysed in detail and which are therefore often not recorded in the standard works on the subject. This feature of the book has been fully appreciated by the authors who have included many new references in this edition.

Chemical Thermodynamics. By F. D. ROSSINI. (Chapman and Hall, London.) [Pp. 48.] Price 48s

IN this book, the subject of thermodynamics is developed along the general lines of Lewis and Randall's *Thermodynamics and the Free Energy of Chemical Substances* which has played such an important part in the training of physical chemists in the United States of America. Apart from a few minor modifications, their nomenclature is followed.

Professor Rossini has, however, given a much broader treatment of modern chemical thermodynamics and has introduced the methods of statistical mechanics whenever appropriate. In a number of modern textbooks, the fundamentals of thermodynamics are developed by elegant mathematical methods with little or no reference to practical problems, and after reading such books students are often left with an uncertain grasp of the subject. As might be anticipated from his extensive experience in this field and from his previous publications, Professor Rossini blends theoretical deduction and practical application in a thoroughly satisfactory way into an outstandingly clear presentation of the subject. The chapters are followed by well selected references for further reading and by a sound collection of numerical problems. For practical thermodynamics calculation little reference need be made to outside sources, fundamental constants and conversion factors being tabulated in an appendix.

Advanced Dynamics. Vols. I. and II. By E. HOWARD SMART. (Macmillan and Co., Ltd., 1951.) Each volume 40s.

THESE two volumes by the late Professor Smart cover the syllabus of a university degree course. Volume I. is primarily concerned with the dynamics of the particle: for example orbital motion under a central force, motion in a resisting medium, and constrained motion in two or three dimensions. Volume II. proceeds, after an unusually full discussion of plane kinematics, to the dynamics of a solid body and carries the fundamental theory as far as the Hamilton-Jacobi equations and Jacobi's complete integral.

The main feature of the book is the exceptional large number of worked examples, illustrating every type of examination problem. Many points which are glossed over in most textbooks, and which frequently trouble students, are carefully explained; an instance is the dynamics of a system with varying mass. The author has chosen not to follow the modern tendency to use vector notation indiscriminately; indeed, he has gone to the opposite extreme and used Cartesian coordinates throughout.

In many ways the presentation of Newton's laws is quite admirable, and certainly much better than in most books, particularly in regard to the concept of an unaccelerated frame of reference. On the other hand, a discussion of mass is scarcely entered upon, while the real significance of D'Alembert's principle is not mentioned. Apart from this, the development of the theoretical basis could hardly be bettered for clarity and thoroughness. R.H.

Notice.—Electromagnetic Theory. By OLIVER HEAVISIDE. The English re-issues of this book is to be published by E. & F. N. Spon, Ltd., London. Price 63s.

NOTICE TO CONTRIBUTORS

The Symbols Committee of the Royal Society, including representatives of the Chemical, Faraday and Physical Societies, has recently issued a report giving a full list of symbols, signs and abbreviations recommended for British scientific publications.

In the interests of uniformity the Editors of *The Philosophical Magazine* hope that authors will as far as possible conform to these recommendations in the preparation of papers. Copies of the report may be obtained from the Royal Society, Burlington House, W.1, price 9d. per copy.

[*The Editors do not hold themselves responsible for the views expressed by their correspondents.*]

XCVII. An Unbranched Laminar Model of the Intermediate State of Superconductors.

By C. G. KUPER,
Royal Society Mond Laboratory, Cambridge*.

[Received March 20, 1951.]

ABSTRACT.

The experiments of Meshkovsky and Shalnikov on the domain structure of a sphere in the intermediate state give no support to the "branching" model described by Landau. The present theory assumes an unbranched laminar structure, and does not involve any precise assumptions about the shape of superconducting regions near the surface of the specimen. Assuming only that demagnetizing coefficients for the superconducting domains can be defined, the Landau thermodynamical potential $L = F - (HB + hB - hH)/8\pi$ is found. By minimizing this function, the spacing and size of the superconducting domains can be calculated. The magnetization curve for ellipsoidal specimens is calculated, and is in moderate agreement with experiment.

§ 1. INTRODUCTION.

WHEN a superconducting body with non-zero demagnetizing coefficient n is placed in a magnetic field $h \geq (1-n)H_C$ (where H_C is the critical field for a long rod) the body must split up in some way into normal and superconducting regions. For a body of macroscopic dimensions these regions must be small in comparison with the body, as no large-scale equilibrium configuration exists. However, the structure is not indefinitely fine, as there may be a free energy α per unit area associated with an interface between normal (N) and superconducting (S) regions (London 1937, Peierls 1936). It is convenient to work in terms of a quantity of the dimensions of a length $\Delta = 8\pi\alpha/H_C^2$, rather than in terms of α itself.

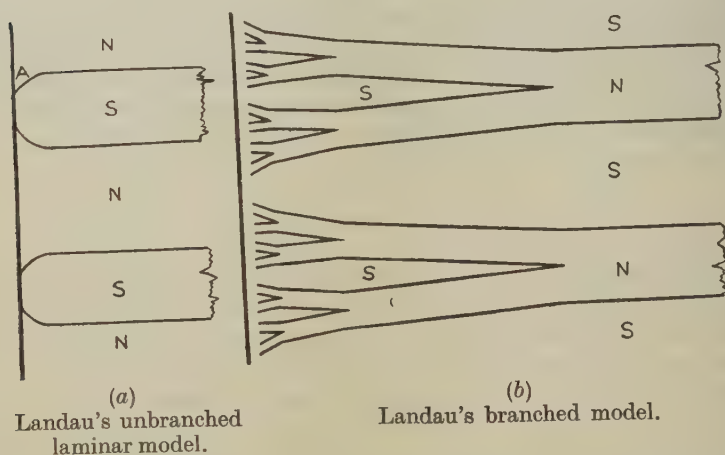
In 1937, Landau put forward the first detailed theory of the structure: a laminar model with the S-layers rounded at the free surface of the specimen (fig. 1*a*). On the interface between any N- and S-laminæ he assumed $H = H_C$. But later he showed that difficulties arise from the curvature of an interface and, to avoid these, proposed a new model (Landau 1938, 1943), in which the N-regions progressively subdivide as they approach the surface, so that the domain pattern does not appear at the surface (fig. 1*b*). Recent experiments (in which the actual magnetic field in a diametral plane and at the surface of a sphere was plotted by traversing it

* Communicated by the Author.

with a small bismuth probe) show, however, that an elaborate domain pattern *does* appear at the surface (Shalnikov 1945, Meshkovsky and Shalnikov 1947 a, b, Meshkovsky 1949). Meshkovsky does find occasional branching, but it is so rare that it is probably of little quantitative importance.

Andrew (1948 b) gave a theoretical calculation of the magnetization curves of superconducting ellipsoids in the intermediate state, both on the basis of Landau's branched laminar model and on a similar branched thread structure. Comparison with the experiments of Désirant and Shoenberg (1948) on thin cylinders and of Andrew and Lock (1950) on thin plates, in transverse fields, gave moderate agreement but with some noteworthy divergencies. Owing to difficulties in interpretation, the resistance measurements of Andrew (1948 a) give rather less

Fig. 1.



information than the magnetization curves, but appear to accord reasonably well with the magnetization measurements of Désirant and Shoenberg for the same specimens. In view of the above experimental evidence that branching does not occur, similar calculations using an unbranched model, more like Landau's original (1937) structure, have been carried out.

The objections raised by Landau (1943) to his unbranched model (1937) appear less serious than when first raised. For if the interface moves into the region (A, fig. 1 (a)) where the field is less than H_C , while it is true that the free energy in the specimen is lowered, the field energy is raised, and so we should expect to find an equilibrium configuration.

In Landau's (1937) theory, despite its mathematical complexity, the simplifying assumption was made that $H = H_C$ on an N-S interface. However, it can readily be shown (as in Kelvin's treatment of vapour

pressure over curved surfaces) that $H'_C/H_C = 1 - \Delta/2r$, where H'_C is the modified critical field and $1/r$ is the Gaussian curvature. A correction on these lines ought also to be made for the sharp corners involved in Landau's branching model, and for the penetration of the field into the thinner regions of the superconducting domains.

The present theory, on the other hand, does not involve a detailed assumption about the shape of the interface near the free surface. It deals instead with the demagnetizing coefficients and the surface/volume ratios of S-domains.

In §2 we begin by writing down the Landau thermodynamic potential (Landau 1943), which is shown in the appendix to be the appropriate one if h , the applied external field, is specified,

$$L = \int d\tau \{ F - (\mathcal{H}\mathcal{B} + h\mathcal{B} - h\mathcal{H})/8\pi \},$$

for an unbranched laminar structure. We then minimize L with respect both to the number of S-domains and their size. The condition for the minimum will be used in §3 to compute the magnetic behaviour of ellipsoidal specimens. The Landau thermodynamic potential for the present model has a lower value than for Landau's "branched" theory over a part of the range of applied magnetic field. Over the remainder of the range the unbranched state may perhaps be metastable, but this question is not investigated here. The above procedure restricts us to an equilibrium theory (as for Landau's 1943 theory). However, the experiments of Andrew and Lock (1950) show that irreversible effects may be of considerable importance. After investigating the equilibrium properties we shall discuss in what circumstances hysteresis is to be expected.

We need not make any explicit allowance for penetration of magnetic flux into the S-regions, for it has been shown that, to the first order in λ/r , the effect of penetration is merely to introduce an additional surface energy $\lambda H_C^2/8\pi$. (λ is here the penetration depth (Ginsburg 1945, Pippard 1951).) If γ is defined as the "true" total surface energy per unit area when allowance is made for penetration, then $\Delta = (8\pi\gamma/H_C^2) - \lambda$. Our Δ corresponds to Ginsburg's $\alpha'_{ns} \cdot 8\pi/H_C^2$, or Désirant and Shoenberg's Δ' .

As in the older theories, we will only consider models in which the N-S interfaces are parallel to the applied field except near the surface of the specimen. The justification for this is that any other configuration would increase the field energy without any compensating reduction in the interfacial surface energy. In the plane perpendicular to the applied field the structure is found experimentally to be complex—both thread-like and warped laminar domains seem to be present (Meshkovsky 1949). This suggests that the Landau function is rather insensitive to details of the structure, a conclusion borne out by Andrew's (1948 b) comparison of branched thread and laminar models. Any model amenable to calculation must be an idealization, and we shall choose a laminar structure for simplicity.

§ 2. THE UNBRANCHED LAMINAR MODEL.

We shall use the following notation :

h = the applied magnetic field.

\mathcal{H} = the local value of the magnetic intensity at any point in the body

\mathcal{B} = the local value of the magnetic induction.

H = the mean magnetic intensity, taken over a region large enough to include several domains.

B = the mean magnetic induction, taken over a similar region.

We use the macroscopic description of a superconductor in which the magnetic fields of the persistent currents are allowed for by assuming a difference between \mathcal{B} and \mathcal{H} in the S-domains, rather than by the London (1937) method of specifying the currents themselves and taking $\mathcal{B} = \mathcal{H}$ everywhere. The two pictures are equivalent provided the S-regions are simply connected.

Temperley (see appendix) has investigated the use of the Landau thermodynamic potential and has shown that it is expressible in the form

$$8\pi L = \text{const.} + h \int_{S\text{-regions}} \mathcal{H} d\tau + \int_{N\text{-regions}} H_c^2 d\tau + \int_{\text{interfaces}} \Delta H_c^2 dS \quad (1)$$

Provided we are dealing with a body fairly large compared with the domain size, it is unnecessary to make detailed assumptions about the form of the interphase surfaces near the edge. The only actual assumption is that the domains are sufficiently nearly ellipsoidal to be described in terms of a demagnetizing coefficient. For this purpose we may regard the regions outside the body where the field is very small (A, fig. 2) as part of the appropriate S-domains, but if the width of the domain is small compared with the thickness of the specimen, this correction will be of little importance.

The method to be used will apply only to ellipsoidal *specimens*, and to them only on the assumption that the density of S-domains is homogeneous throughout the body. If this assumption is true, then H is constant throughout the body and the body can be described in terms of a demagnetizing coefficient n , such that

$$h = nB + (1-n)H \quad (2)$$

If A is the cross-section of an S-domain and p is the number of S-domains per unit area of cross-section of the specimen,

$$B = H(1 - pA) \quad (3)$$

If ν is the demagnetizing coefficient of an S-domain, and \mathcal{H} is the magnetic field within it,

$$H = (1 - \nu)\mathcal{H} \quad (4)$$

\mathcal{B} is zero since we are dealing with an S-domain. Hence

$$\mathcal{H} = h / [(1 - \nu)(1 - npA)] \quad (5)$$

Then the Landau function per unit volume, apart from constant terms, is given by

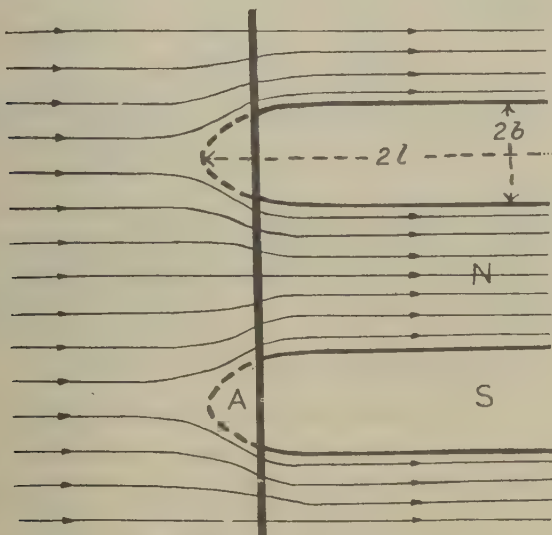
$$8\pi L = \mathcal{L} = \hbar^2 p A / [(1-\nu)(1-npA)] - H_C^2 p A (1 - \Delta s/A) \quad . \quad . \quad . \quad (6)$$

or, defining $\eta = \hbar/H_C$,

$$\mathcal{L} = H_C^2 p A \{ \eta^2 / [(1-\nu)(1-npA)] - (1 - \Delta s/A) \} \quad . \quad . \quad . \quad (6')$$

s is the perimeter of an S-region in the cross-section perpendicular to the applied field h .

Fig. 2.



Field distribution for an unbranched model, showing the external regions (A) where the field is small.

Ginsburg's (1945) surface energies at the free surface of the body have been neglected. According to recent work by Pippard (1951) the difference between the N and S surface energies is in any case zero.

Minimizing \mathcal{L} with respect to p , we find

$$(1-npA)^2 = \eta^2 / [(1-\Delta s/A)(1-\nu)]$$

or

$$npA = 1 - \eta / \sqrt{[(1-\Delta s/A)(1-\nu)]} \quad . \quad . \quad . \quad (7)$$

Substituting (7) in (6) and simplifying gives

$$\mathcal{L} = -(1/n)[\hbar/\sqrt{(1-\nu)} - H_C \sqrt{(1-\Delta s/A)}]^2 \quad . \quad . \quad . \quad (8)$$

For further progress it is necessary to specialize the model. We shall discuss the case of laminae, since the expression for the demagnetizing coefficient for a thread is mathematically more complicated, involving a

logarithmic factor. For a circular lamina of radius l and thickness $2b$ we take the demagnetizing coefficient ν as that of an oblate spheroid with the same major axis and the same volume. The minor axis a of this spheroid is then $4b/\pi$, and $\nu = \pi a/4l = b/l$. We will also require explicit expressions for s and A , which are :

$$s = 4l; \quad A = \pi la = 4lb.$$

The expression for \mathcal{L} than becomes

$$\mathcal{L} = -(1/n)[h/\sqrt{1-b/l} - H_c\sqrt{1-\Delta/b}]^2. \quad (9)$$

Minimizing with respect to b we have

$$\frac{hb/l}{(1-b/l)^{3/2}} = \frac{H_c\Delta/b}{(1-\Delta/b)^{1/2}}. \quad (10)$$

Assuming that $l \gg b \gg \Delta$, and expanding by the binomial theorem, we have

$$b^2 = (\Delta l/\eta) \{1 - \frac{1}{2}\mu[\sqrt{\eta} - 3/\sqrt{\eta}] + O(\mu^2)\} \quad (11)$$

where $\mu = (\Delta/l)^{1/2}$.

Substituting (11) in (9) and simplifying, we have

$$\mathcal{L} = -(1/n)H_c^2[1 - \eta - \mu\sqrt{\eta} - \mu^2(3/\eta - \eta)/8 + O(\mu^3)]^2 \quad (12)$$

or to the first order

$$\mathcal{L} = -(H_c^2/n)\{(1-\eta)^2 - 2\mu(1-\eta)\sqrt{\eta}\}. \quad (13)$$

§ 3. THE MAGNETIZATION CURVE.

We shall now show that our theory gives a curve basically similar to that of Andrew (1948 b), based on the Landau (1943) theory. Initially the magnetization increases linearly with the applied field, and according to the zero order approximation discussed by Peierls (1936) and London (1937), this continues until $\eta = 1 - n$, whereupon the body enters the intermediate state and the magnetization falls linearly with further increase of η , reaching the value zero when $\eta = 1$. We shall see that, just as in Landau's theory, the pure superconducting state actually persists for a short range above $\eta = 1 - n$ to a value ρ , say, where the intermediate state becomes thermodynamically favourable; the magnetization then falls abruptly to the value appropriate to the intermediate state. The condition for the transition is equality of the Landau functions for the superconducting and intermediate states. Since for the pure superconducting phase $\mathcal{L} = H_c^2\eta^2/(1-n)$, this gives

$$\rho^2/(1-n) = 1 - (1/n)\{(1-\rho)^2 - 2\mu(1-\rho)\sqrt{\rho} + O(\mu^2)\}. \quad (14)$$

The zero order result $\rho = 1 - n$ follows at once, and the next two approximations are

$$\rho = (1-n)\{1 + \mu^{1/2}n\sqrt{2}/(1-n)^{1/4}\}$$

$$\text{and} \quad \rho = (1-n)\{1 + \mu^{1/2}n\sqrt{2}/(1-n)^{1/4} - \mu^3/4n^{2/4}(2-n)^{1/2}\}. \quad (15)$$

The magnetization in the intermediate state then falls smoothly with increase of field. The magnetic moment M of the specimen is

$$M = \frac{1}{4\pi} \int_{\text{Specimen}} (\mathcal{B} - \mathcal{H}) d\tau = -\frac{1}{4\pi} \int_{\text{S-domains}} \mathcal{H} d\tau$$

(for in the N-regions $\mathcal{B} = \mathcal{H}$; in the S-regions $\mathcal{B} = 0$).

Thus $-4\pi M = h V p A / \{(1 - \nu)(1 - npA)\}$,

where V is the volume of the specimen.

$$\text{Hence } -4\pi M = \frac{H_C V}{n} \left[\sqrt{\left(\frac{1 - \Delta s/A}{1 - \nu} \right)} - \frac{\eta}{1 - \nu} \right],$$

or, after simplification,

$$-4\pi M = (H_C V/n) [1 - \eta - \frac{1}{2}\mu(3\eta - 1)/\sqrt{(\eta)} + O(\mu^2)] \quad (16)$$

It appears from (16) that the magnetization falls to zero where

$$1 - \eta = \frac{1}{2}\mu(3\eta - 1)/\sqrt{(\eta)} \text{ or, since } \mu \ll 1, \eta = 1 - \mu. \quad (17)$$

But we observe from (11) that when $\eta \rightarrow 1$, b remains finite and tends to $\sqrt{(\Delta l)}$. This means that M cannot approach zero continuously, but has to do so stepwise; for it is p which tends to zero, and the number of domains cannot be fractional. Thus M will fall to zero when the last S-domain is expelled. When there is just one domain

$$-4\pi M = \int_{\text{one S-domain}} \mathcal{H} d\tau = \{h/(1 - \nu)\} \{\pi l^2 \cdot 2b\}$$

or, since h is nearly H_C ,

$$-4\pi M = H_C \cdot 2\pi l^2 b.$$

Using this value in (16), and putting $\eta = 1$ in the terms in μ , we have

$$H_C 2\pi l^2 b = -4\pi M = (V H_C/n) \{1 - \eta - \mu + O(\mu^2)\}.$$

Whence $\eta = 1 - \mu - 2\pi l^2 b n/V$ or, since $b = \sqrt{(\Delta l/\eta)}$ or $b/l = \mu$, for η nearly 1,

$$\eta = 1 - \mu(1 + 2\pi n). \quad (18)$$

Also the field for no domain is $\eta = 1 - \mu$, by (17). Hence a linear interpolation gives the field at which the last domain is expelled as

$$\eta_D = 1 - \mu(1 + \pi n). \quad (19)$$

If the field is reduced, some hysteresis effects should appear, even under ideal conditions. For even apart from the "supercooling" of the normal phase (see the region P in fig. 3) there is the effect arising from the "horn" (region CBG in fig. 3). As there is no mechanism available for expelling the flux at C (fig. 3), the intermediate state will continue metastably to G, the place where (7) gives $pA = 1$. This will occur for

$$\begin{aligned} \eta &= (1 - n)\sqrt{[(1 - \Delta s/A)(1 - \nu)]} \\ &= (1 - n)[1 - \frac{1}{2}\mu(2 - n)/\sqrt{(1 - n)} + O(\mu^2)] \end{aligned} \quad (20)$$

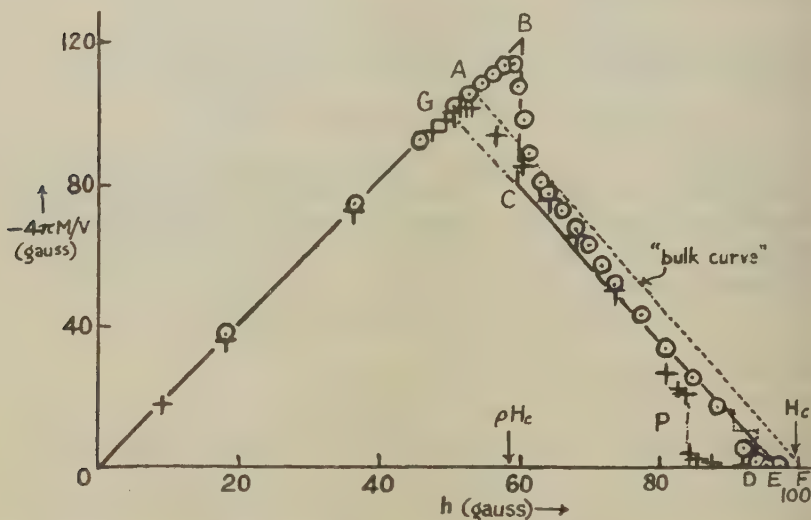
§4. COMPARISON WITH EXPERIMENT.

There are three sets of experiments to be discussed, viz.,

- (a) Désirant and Shoenberg (1948) ; Andrew (1948 a).
- (b) Andrew and Lock (1950).
- (c) Meshkovsky and Shalnikov (1947 a, b) ; Meshkovsky (1949).

(a) Only the experiments of Désirant and Shoenberg, who found the magnetization curves for long cylinders in transverse fields, need be considered, as Andrew's resistance measurements under similar conditions give values of ρ in fair agreement with those of Désirant and Shoenberg.

Fig. 3.



Magnetization curve for cylinder in transverse field. \circ increasing fields; $+$ decreasing fields. The experimental points shown are those for Désirant and Shoenberg's tin specimen S9 at 3.000°K . The theoretical curve is drawn for $\Delta/r = 0.67 \times 10^{-3}$, i. e. $\Delta = 0.5 \times 10^{-5} \text{ cm}$.

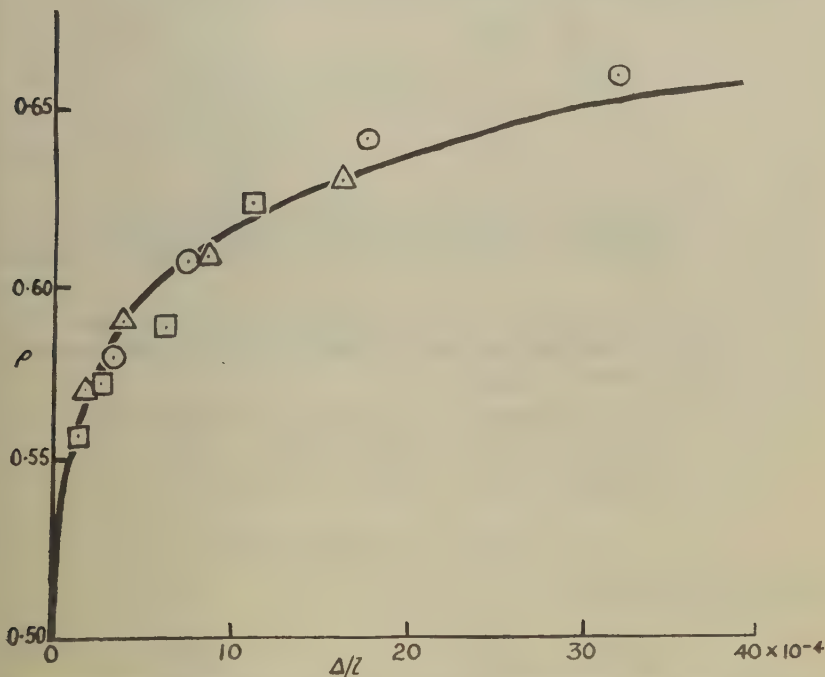
There are several ways of estimating Δ from the observations, but as it is $(\Delta/l)^{1/2}$, or in some cases even $(\Delta/l)^{1/4}$, that appears in the formulæ, the magnetization curve is rather insensitive to the assumed value of Δ . Also the model is a considerable over-simplification, and a more rigorous theory may well involve extra numerical factors of order unity, which will be squared or raised to the fourth power if one attempts to calculate a value of Δ from an experimental result. Thus we may find, for instance, that the value of μ chosen to fit one aspect of the curve differs by a factor of about 3 from the best value for fitting some other aspect, and this would lead to a discrepancy of order 3^2 or 10 in Δ . These difficulties also appear when one attempts to fit the branched model to the experiments.

Four different methods of fitting a value of Δ to the magnetization curve will be discussed. These are based on

- (i.) the value of ρ (fig. 3, BC).
- (ii.) the value of η where M has half the maximum value it attains for the bulk curve.
- (iii.) the value of η at $M=0$.
- (iv.) the slope of the falling part CD of the curve (fig. 3).

We shall see that values of Δ obtained from (i.), (ii.) and (iii.) agree quite well with each other, but not with those from (iv.), which are too large by a factor of 50.

Fig. 4.



Size variation of ρ for tin cylinders. ○ 3.5° K. , assuming $\Delta = 0.55 \times 10^{-5} \text{ cm.}$; △ 3.0° K. , assuming $\Delta = 0.28 \times 10^{-5} \text{ cm.}$; □ 2.1° K. , assuming $\Delta = 0.19 \times 10^{-5} \text{ cm.}$

(i.) Fig. 4 shows the theoretical curve for ρ as a function of Δ/l . Owing to the slow convergence of (15), this curve has been obtained by solving (14) for μ as a function of ρ . The experimental points of Désirant and Shoenberg are indicated, assuming the same temperature-dependence of Δ as they did, but reducing their actual values of Δ by a factor 3.6. This makes $\Delta_1 = 0.55 \times 10^{-5} \text{ cm.}$ at 3.5° K. , $0.28 \times 10^{-5} \text{ cm.}$ at 3.0° K. , and $0.19 \times 10^{-5} \text{ cm.}$ at 2.1° K. The present curve is seen to fit the experimental points rather better than that predicted by Landau's branching theory.

(ii.) For the bulk curve $M = \frac{1}{2}H_c/4\pi$ for $\eta = 3/4$; according to (16) this would occur in the actual specimen for

$$\frac{1}{2} = 2(1 - \eta) - \mu(3\eta - 1)/\sqrt{\eta} + O(\mu^2),$$

since $n = \frac{1}{2}$ for a long cylinder in a transverse field. Inserting the zero approximation $\eta = \frac{3}{4}$ in the second term on the R.H.S., we find the next approximation,

$$\frac{1}{2} = 2(1 - \eta) - \mu \cdot \left(\frac{5}{4}\right)[2/\sqrt{(3)}]$$

or

$$\mu = \sqrt{(3)}(3 - 4\eta)/5.$$

Also from the geometry of the magnetization curve (fig. 3)

$$\frac{\eta - \eta_D}{\eta_G - \eta_D} = \frac{M}{M_G} = \frac{\frac{1}{2}}{2\eta_G}$$

or

$$\eta - \eta_D = (\eta_G - \eta_D)/4\eta_G = -(1/\sigma - 1)/4.$$

Thus

$$\mu = \sqrt{(3)}(4 - 1/\sigma - 4\eta_D)/5, \quad . \quad . \quad . \quad . \quad . \quad (21)$$

where $\sigma = \eta_G/\eta_D$.

The values of μ and of Δ deduced from Désirant and Shoenberg's experimental results by means of (21) are shown in the Table under the headings μ_{II} and Δ_{II} .

(iii.) According to (19), $\eta_D = 1 - 2.6\mu$, for a cylinder. The values of μ and Δ estimated from Désirant and Shoenberg's values of η_D are shown in the Table under the headings μ_{III} and Δ_{III} .

(iv.) The slope of the magnetization curve at $\eta = 3/4$ is given by

$$\begin{aligned} -\frac{4\pi}{H_c V} \frac{dM}{d\eta} &= 2\left\{-1 + \frac{1}{2}\mu(3\eta/2 - \frac{1}{2})\eta^{-3/2} + \dots\right\} \\ &= 2\left\{-1 + 23\mu/6\sqrt{(3)} + O(\mu^2)\right\}. \end{aligned}$$

From the geometry of fig. 3

$$\begin{aligned} -\frac{4\pi}{H_c V} \frac{dM}{d\eta} &= \frac{2\eta_G}{\eta_D - \eta_G} \quad (\text{since } -M_G = 2\eta_G \cdot H_c V/4\pi) \\ &= 2\sigma/(1 - \sigma), \end{aligned}$$

whence

$$\sigma/(1 - \sigma) = 1 + \mu(23/6\sqrt{3}). \quad . \quad . \quad . \quad . \quad . \quad (22)$$

The values of μ and Δ deduced from the experimental values of σ by (22) are shown as μ_{IV} and Δ_{IV} in the Table.

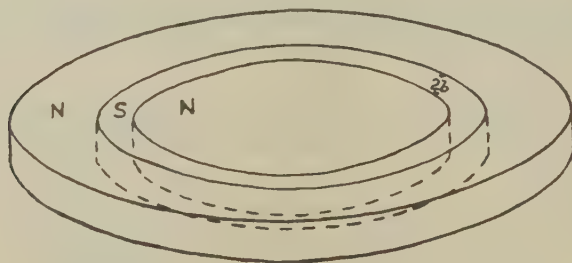
The high values of Δ given by method (iv.) are perhaps due to the sensitiveness of this method to irreversible effects. For if (as in fig. 3) the experimental values of M , for η just above ρ , are above the theoretical curve, the slope is likely to be greatly altered, while method (ii.) will give almost unaltered values of Δ . The values from (ii.) are thus likely to be the most reliable.

Specimen	Temp. °K.	Radius $\times 10^4$ (cm.)	σ	η_0	μ_{II} $\times 10^2$	Δ_{II} $\times 10^5$ (cm.)	μ_{III} $\times 10^2$	Δ_{III} $\times 10^5$ (cm.)	μ_{IV} $\times 10^2$	Δ_{IV} $\times 10^5$ (cm.)
S8	3.5		0.560	0.5441	1.31	0.310	1.3	0.29	12.3	27
	3.0	179	0.556	0.5370	1.84	0.603	1.5	0.37	11.3	23
	2.1		0.534	0.5282	0.485	0.042	0.5	0.052	6.6	7.7
S9	3.5		0.563	0.5211	4.84	1.75	3.1	0.72	12.4	11.6
	3.0	75	0.561	0.5343	2.81	0.582	2.1	0.33	12.6	11.9
	2.1		0.535	0.5197	1.80	0.243	1.4	0.14	6.8	3.4
S7	3.5		0.664	0.5914	4.43	0.620	4.5	0.73	43.7	61
	3.0	31.6	0.617	0.5727	3.04	0.293	3.6	0.42	28.0	25
	2.1		0.586	0.5571	2.25	0.160	2.8	0.25	18.6	10.9
S5	3.5		0.743	0.6242	5.43	0.512	4.2	0.31	85.1	126
	3.0	17.3	0.647	0.5752	5.30	0.485	4.5	0.35	37.6	24
	2.1		0.608	0.5532	4.91	0.416	3.8	0.25	24.8	10.3

Fig. 3 is a typical magnetization curve. Actually it is the curve for $\mu=0.026$. The points are those found by Désirant and Shoenberg for the specimen S9 at 3.000°K . For S9 $l=75\times 10^{-4}\text{ cm.}$, and we have taken $\Delta=0.5\times 10^{-5}$. (This is a typical value, from Δ_{ii}). The curve is in slightly worse general agreement with the experimental points than the curve predicted by Andrew (1948 b) from Landau's branched model. The experiments show a smooth fall of M to zero, rather than the stepwise termination we have suggested. The absence of steps may perhaps be explicable by using a thread model in the region where the ratio of superconducting to normal volumes is small.

(b) The experiments of Andrew and Lock (1950) on the magnetization curves of thin plates may also be compared with the theory in several ways. The consistency proves to be much poorer than in (a), and the general trend is to give very much larger values for Δ . Little weight should, however, be given to the numerical values of Δ , for the reasons given on p. 968 and also because we have assumed a laminar structure in which the laminae are circular, each of radius l (which need not be

Fig. 5.



Flat plate showing one "toroidal" S-domain.

constant for all laminae). While this is a reasonable assumption for the cases of the sphere and the cylinder, the flat disk will probably form "toroidal" laminae (see fig. 5), and if we unfold them into flat laminae they will have the form of long thin rectangles, rather than circles. There is evidence for such toroidal domains in that the magnetization curves for falling field show large amounts of "trapped" flux, suggesting the presence of multiply connected S-domains. It is very difficult to estimate the correction required to take account of this effect, but we might expect the value of Δ calculated on the basis of flat laminae to be too great by a factor of order $\sqrt{(d/l)}$, where d is the mean diameter of such a lamina, *i. e.* of the order of the radius of the disk. This factor, of order 10 to 10^2 , might bring the results into reasonable accord with those deduced from the experiments of Désirant and Shoenberg. However, comparisons which depend on the functional form of our expressions rather than on the actual value of Δ are less likely to depend on such details of the laminar structure and should give a more reliable check.

(i.) As in (a), we compare the values of ρ with the theory. The experimental work does not give the values of ρ directly, but rather I_{max} , the maximum intensity of magnetization. As the initial slope of the magnetization curve is $1/(1-n)$,

$$-4\pi I/h = 1/(1-n)$$

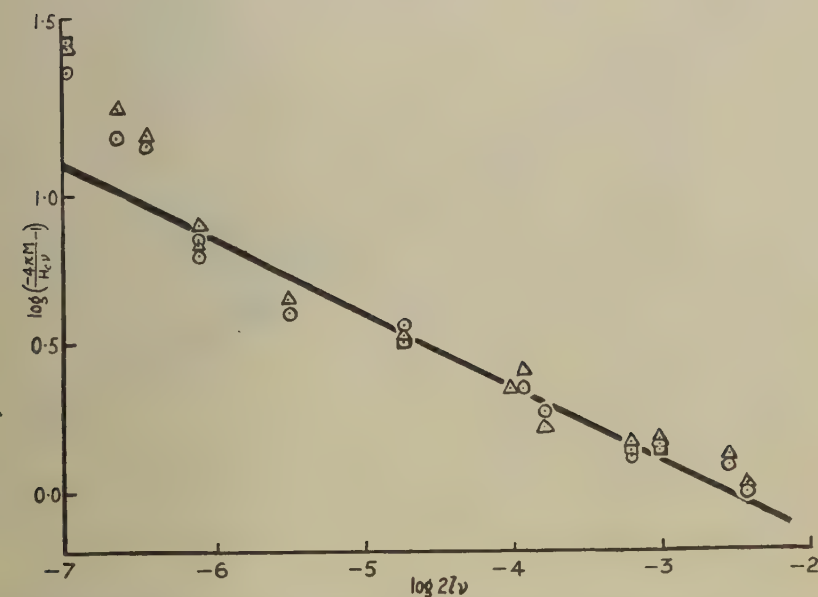
and in particular

$$-4\pi I_{max}/H_C = \rho/(1-n). \quad . \quad . \quad . \quad (23)$$

Also from (15)

$$\rho/(1-n) = 1 + n\sqrt{(2)(1-n)^{-1/4}\mu^{1/2}}.$$

Fig. 6.



Logarithmic graph of $4\pi I_{max}/H_C - 1$ against $2l\nu$. \square 2.5° K.; \triangle 2.99° K.; \circ 3.49° K. Full curve is theoretical.

In these experiments n is nearly unity and, therefore,

$$-4\pi I_{max}/H_C = 1 + \sqrt{(2)\{\Delta/[l(1-n)]\}}^{1/4}. \quad . \quad . \quad . \quad (24)$$

Andrew and Lock have plotted $\log \{(-4\pi I_{max}/H_C) - 1\}$ against $\log 2l(1-n)$ ($2l=L$ in their notation), and if the present theory is correct, the curve (fig. 6) should be a straight line of slope $-\frac{1}{4}$, in marked contrast to the theory of Landau and Andrew, for which the slope ought to be $-\frac{2}{5}$. It is seen that our law fits the experimental points very much better than the $-\frac{2}{5}$ power law. It deviates significantly only for the thinnest specimens, where we might expect our approximations to

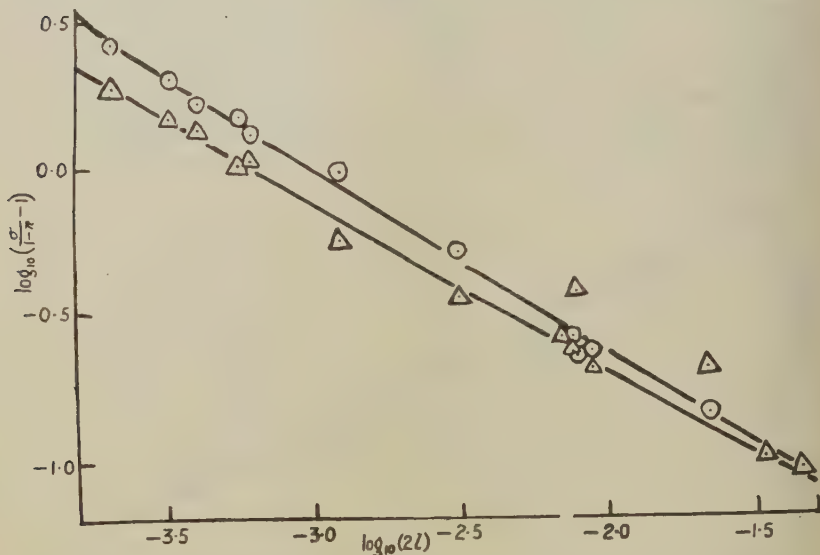
break down; in particular it is no longer likely to be true that we can take the lengths of the domains to be $2l$ (since the regions outside the body from which the field is excluded become important, see fig. 2). The value of Δ deduced from this curve (fig. 6) is, however, very high: thus at $2l(1-n)=10^{-3}$

$$4\pi I_{max}/H_C - 1 = 1,$$

i. e. $4\pi I_{max}/H_C = 2 = \sqrt{2} \cdot \Delta^{1/4} / 10^{-3/4} (\frac{1}{2})^{1/4} + 1,$

giving $\Delta = 3.5 \times 10^{-4}$ cm.

Fig. 7.



Logarithmic graph of $\sigma/(1-n)-1$ against $2l$. Δ 2.99°K., \circ 3.49°K.

(ii.) and (iii.) have not been attempted for these experiments since insufficient data exist. In particular, Andrew and Lock did not record the value of H_C in all of their experiments.

(iv.) Here we have

$$\frac{\sigma}{1-n} = \left\{ \left[\frac{d}{d\eta} \left(\frac{4\pi M}{H_C V} \right)_{\eta=\frac{1}{2}} \right]^{-1} - (1-n) \right\}^{-1}$$

from the geometry of the magnetization curve, where σ has now been computed from the slope of the curve at $\eta=\frac{1}{2}$. Hence, from (16),

$$\sigma/(1-n) = 1 + \mu_5 \sqrt{2}/4. \quad \dots \dots \dots (25)$$

A noteworthy difference appears between the present theory and the branching theory, for where the latter requires $\sigma/(1-n)-1$ proportional to $(2l)^{-2/3}$, our theory requires proportionality to $(2l)^{-1/2}$. In fig. 7 $\log \{\sigma/(1-n)-1\}$ is plotted against $\log(2l)$ for these experiments,

and the slopes of the lines drawn are found to be -0.49 and -0.52 at 3.5 and 3.0°K . respectively. However, the value of Δ deduced from the curve is again rather high: thus where $2l=10^{-3}$, we find $\log\{\sigma/(1-n)-1\}=\bar{1}.883$ for the 3.5°K . curve. Hence $\Delta=9.9\times 10^{-5}\text{cm}$. at 3.5°K .

(c) Shalnikov (1945) and Meshkovsky and Shalnikov (1948 a) proved the inhomogeneity of the intermediate state directly by observing the field distribution along a diameter in the equatorial plane of a split sphere. Later experiments (Meshkovsky and Shalnikov 1948 b) show that the non-uniformity of the field is also found on the surface of the sphere. The most recent work in this series of experiments (Meshkovsky 1949) summarized in the form of a contour map of the field in the slit between their hemispheres, shows the structure to be far from simple, both thread-like and laminar domains being in evidence.

The size of the S-domains is directly measurable, using a case such as (A) or (B), fig. 11, p. 9, of their 1947 a paper ($T=3.16^\circ\text{K}$., $h=72\text{ Oe.}$), where the fraction of superconductor is small, so that our model of S-domains in a matrix of N-metal is as realistic as possible. In their fig. 11 (A), the number of domains is about 15, over a length of 4 cm., suggesting a domain size $b=0.03\text{ cm}$. (since x_n , the fraction of N-metal $=0.81$); while a direct measurement of a typical single domain gave $b=0.015\text{ cm}$.; thus $b=0.02\text{ cm}$. may be regarded as a typical value. Substituting $\Delta=10^{-5}\text{ cm}$. (a rather high estimate) in equation (11), with $l=4\text{ cm}$., we find $b\div 7\times 10^{-3}\text{ cm}$., which is too small by a factor of 3. However, Meshkovsky (1949) comments on the apparent presence of a "fine structure" in the domains which would reduce the observed value of b , thus improving the agreement with the theoretical predictions.

It is of interest to compare the values of b predicted by different models. Landau (1937) found $b=\sqrt{(\pi\Delta l/2)}$ for η near to unity for an unbranched model. This is similar to our form. On the other hand, for a branched model he found $b=8\Delta^{2/3}l^{1/3}$, which with $\Delta=3\times 10^{-5}\text{ cm}$. gives $b=0.01\text{ cm}$. Unfortunately no experiments to test the variation of domain size with specimen size have yet been reported.

Meshkovsky and Shalnikov (1947 a) have reported a difference between the structures observed (A) as h is raised at constant temperature T , and (B) as T is lowered at constant h . The difference is probably not due to the fact that h is varied in (A) and T in (B), but simply to the fact that in (A) x_n , the fraction of N-metal, is decreased, while in (B) it is increased; for two disjoint S-regions will exert very little influence on each other, and if they arise from two different nuclei (as is the case for x_n increasing), there will be less correlation in their positions than if they arise from a single lamina which has broken up.

I wish to express my thanks to Mr. H. N. V. Temperley, my supervisor, and to Dr. D. Shoenberg and other members of the Mond Laboratory for many helpful discussions. I am indebted to Cambridge University for a Research Maintenance Grant, during the tenure of which this work was done.

APPENDIX.

By H. N. V. TEMPERLEY.

Landau's proof (1943) that $L = \int d\tau [F - (\mathcal{H}\mathcal{B} + h\mathcal{B} - h\mathcal{H})/8\pi]$ is the appropriate potential to use in the theory when the field h is specified is incomplete. In particular he has not given a proof that L is the only function satisfying the required conditions. The potential, Ψ per unit volume, is assumed by Landau to satisfy

$$\left(\frac{\partial \Psi}{\partial B}\right)_{T,h} = 0; \quad \left(\frac{\partial \Psi}{\partial h}\right)_{T,B} = (H-B)/4\pi; \quad \dots \quad (26)$$

$$\text{together with} \quad h = nB + (1-n)H. \quad \dots \quad (2)$$

Let $\Psi = F + W$, where F is the Helmholtz free energy per unit volume; $dF = H dB/4\pi - S dT$. Then

$$\left(\frac{\partial F}{\partial B}\right)_{T,h} = \left(\frac{\partial F}{\partial B}\right)_{T,H} + \left(\frac{\partial H}{\partial h}\right)_{T,B} \left(\frac{\partial F}{\partial H}\right)_{T,B} = H/4\pi = (h-B)/4\pi(1-n) \quad \dots \quad (27)$$

$$\text{and} \quad \left(\frac{\partial F}{\partial h}\right)_{T,B} = \left(\frac{\partial F}{\partial H}\right)_{T,B} \left(\frac{\partial H}{\partial h}\right)_{T,B} = 0. \quad \dots \quad (27')$$

$$\text{Therefore} \quad -(nB-h)/4\pi(1-n) + \left(\frac{\partial W}{\partial B}\right)_{T,B} = 0;$$

$$\left(\frac{\partial W}{\partial h}\right)_{T,B} = (H-B)/4\pi = (h-B)/4\pi(1-n),$$

and on integration

$$W = (nB^2/2 - hB + h^2/2)/4\pi(1-n).$$

From (2)

$$1/(1-n) = (H-B)/(h-B); \quad n/(1-n) = -(h-H)/(h-B).$$

Whence

$$W = (-HB - hB + hH)/8\pi,$$

and

$$\Psi = F - (HB + hB - hH)/8\pi \quad \dots \quad (28)$$

apart from an additive constant.

As we require $L = \int \Psi d\tau$ for the whole body, we may replace H, B by \mathcal{H}, \mathcal{B} , since the volume integration will average these variables, provided that the dimensions of the body are large compared with the domain size. We therefore have finally

$$L = \int [F - (\mathcal{H}\mathcal{B} + h\mathcal{B} - h\mathcal{H})/8\pi] d\tau. \quad \dots \quad (29)$$

For a body in the intermediate state L takes the form

$$L = \int_{S\text{-regions}} \Psi_S d\tau + \int_{N\text{-regions}} \Psi_N d\tau + \int_{\text{interfaces}} \gamma \cdot dS, \quad \dots \quad (30)$$

where Ψ_S and Ψ_N are the Landau functions per unit volume in the S- and N-regions respectively and γ is the surface energy per unit N-S surface, introduced on p. 963. If F_S and F_N are the corresponding Helmholtz free energies per unit volume, then

$$\Psi_S = F_S + (h\mathcal{H} - \mathcal{H}\mathcal{B} - h\mathcal{B})/8\pi$$

and $\Psi_N = F_N - \mathcal{H}^2/8\pi$ (since in N-regions $\mathcal{B} = \mathcal{H}$.) Also if F_N^0 is the Helmholtz free energy for the N-metal in zero field,

$$\begin{aligned} F_N &= F_N^0 + \mathcal{H}^2/8\pi \\ &= F_S + (H_C^2 + \mathcal{H}^2)/8\pi. \end{aligned}$$

Thus

$$\begin{aligned} L &= \int_{N+S\text{-regions}} F_S d\tau + \int_{N\text{-regions}} H_C^2 d\tau/8\pi - \int_{S\text{-regions}} h(\mathcal{B} - \mathcal{H}) d\tau/8\pi \\ &\quad + \int_{\text{interfaces}} \gamma \cdot dS. \\ &= \text{const} + \int_{N\text{-regions}} H_C^2 d\tau/8\pi - h \int_{S\text{-regions}} (\mathcal{B} - \mathcal{H}) d\tau/8\pi + \int_{\text{interfaces}} \gamma \cdot dS. \end{aligned}$$

This result involves no approximations in the penetration law. If, however, the S-domains are thick compared with the penetration layer, we may, as Ginsburg (1945) has shown, replace γ by $\gamma - \lambda H_C^2/8\pi = \Delta H_C^2/8\pi$ and omit explicit reference to the field penetration. Then

$$L = \text{const.} + \int_{N\text{-regions}} H_C^2 d\tau/8\pi + \int_{S\text{-regions}} h\mathcal{H} d\tau/8\pi + \int_{\text{interfaces}} (\Delta H_C^2/8\pi) dS. \quad \dots (1)$$

REFERENCES.

- ANDREW, E. R., 1948 a, *Proc. Roy. Soc. A*, **194**, 80; 1948 b, *Proc. Roy. Soc. A*, **194**, 98.
 ANDREW, E. R., and LOCK, J. M., 1950, *Proc. Phys. Soc. A*, **63**, 13.
 DÉXIRANT, M., and SHOENBERG, D., 1948, *Proc. Roy. Soc. A*, **194**, 63.
 GINSBURG, V. L., 1945, *J. Phys. U.S.S.R.*, **9**, 305.
 LANDAU, L., 1937, *Phys. Z. Sowjet.*, **11**, 129; 1938, *Nature*, **147**, 688; 1943, *J. Phys. U.S.S.R.*, **7**, 99.
 LONDON, F., 1937, *Une Conception Nouvelle de la Supra-Conductibilité* Actualités Scientifiques et Industrielles, 458 (Paris: Hermann).
 MESHKOVSKY, A., 1949, *Zh. Eksp. Teor. Fiz. U.S.S.R.*, **19**, 1.
 MESHKOVSKY, A., and SHALNIKOV, A., 1947 a, *J. Phys. U.S.S.R.*, **11**, 1
 1947 b, *Zh. Eksp. Teor. Fiz. U.S.S.R.*, **17**, 851.
 PEIERLS, R., 1936, *Proc. Roy. Soc. A*, **155**, 613.
 PIPPARD, A. B., 1951, *Proc. Camb. Phil. Soc.*, **47**, 617.
 SHALNIKOV, A., 1945, *J. Phys. U.S.S.R.*, **9**, 202.

XCVIII. *The Cascade Production of Cosmic Ray Stars and the Relative Number of Charged and Uncharged Particles.*

By Sir GEORGE THOMSON, F.R.S., and P. E. HODGSON,
Imperial College of Science and Technology, London*.

[Received April 25, 1951.]

SUMMARY.

A calculation has been made of the consequences of assuming that stars are produced in a cascade process by charged and uncharged particles according to a very simple law. The constants in this law can be chosen to give agreement with experiment to the extent to which the quantities are known and also fall within the ranges that are *a priori* permissible. It does not appear possible to determine them with much accuracy from existing data, but it seems that a fair proportion of the stars with less than five prongs are due to primaries of fairly high energy.

§1. INTRODUCTION.

THE opinion has been growing for some time that the particles responsible for the production of the stars seen in photographic plates exposed to cosmic rays can and do make more than one star before coming to rest (Thomson 1949, Harding 1949, 1951 a). Also it is known (Camerini *et al.* 1949) that, in the larger stars at least, secondaries of large energy are possible which can themselves make stars. This opens up the possibility that the production of stars is a "cascade" process, and this view has been developed in some detail by Messel and Ritson (1950) following a suggestion in a note to a paper by Heitler and Jánossy (1949). Messel and Ritson did not, however, distinguish between the production of stars by charged and by neutral particles†. This has been studied by the Bristol school (Brown *et al.* 1949, Camerini *et al.* 1949). They find that the proportion of charged primaries is greater for the larger stars and is greater high up in the atmosphere. It seemed of interest to see if the cascade theory can account for this effect and what, if anything, can be deduced as to the production and energy of the secondaries.

In order to do so we made the simplest assumptions which seemed to offer any chance of representing the main facts, since the mathematics of cascades readily becomes complicated and makes it difficult to see the physics behind the calculations.

* Communicated by the Authors.

† Messel has since done so (1951 and private communication).

Leaving aside the question of obliquity, to which we return in §7, we suppose particles moving vertically downwards through the atmosphere. These are of two classes—charged and uncharged. The latter will probably mostly be neutrons since the lifetime of the neutral mesons is too small for them to play any large part, and photons are usually excluded as an important factor because little or no correlation has so far been observed between stars and the “showers” of the soft component. Since photons of sufficient energy can cause stars in the laboratory, this conclusion may prove too sweeping, but we shall accept it here. The charged particles will be mostly protons and π -mesons except right at the top of the atmosphere, where the true primaries still survive in appreciable numbers and α -particles, not to say heavier nuclei, become important. Because of this difference, our calculations will not apply to the top of the atmosphere. We shall assume that protons and π -mesons have the same cross-section for star production (Camerini *et al.* 1950) and the same chance of producing secondaries. Most of the π -mesons will decay before they make a nuclear collision; this simply means that the number effective for our purpose is less than the total actually produced. We take the cross-section for star-production, both by neutral and charged particles, to be the same, and denote the corresponding free path in gm./cm.² by λ . In each act of star production we suppose that ϕ charged and ϕ' neutral particles, capable themselves of producing stars, are formed, each of which goes forward with the fraction q of the energy E of the primary. Thus $E[1 - \phi + \phi'q]$ is the energy used in those particles of the stars which have too little energy to produce further stars, and in producing π -mesons which decay in the air. The lower limit for star production is written E_0 . We assume an energy spectrum of the form $N(E) dE \propto E^{-n}$ to be valid at some point of the atmosphere which we take as origin, $x=0$. Though the form of our solution is such that this law will not hold strictly elsewhere, our results show (see §8) that the divergence is not great, so that it is not a matter of critical importance where the origin is taken.

We suppose that the only way in which the neutrals lose energy is by making stars, but that the positives lose energy by ionization at the rate p per g./cm.² of path corresponding to minimum ionization.

In §2 we give the mathematical solution of the cascade problem, in §3 we discuss the most suitable values of the quantities λ , p , E_0 , q , ϕ , ϕ' and n , in §§4, 5 and 6 numerical values are given, in §§7 and 8 the effects of obliquity and of variations of the initial constants are considered, and in §§9 and 10 we set out the comparison between our theory and the experiments.

§2. CASCADE EQUATION.

Let $N(E, x)dE$ be the number of charged particles/cm.²/sec. at depth x gm./cm.² in the energy range E to $E+dE$ capable of making stars, and let $N'(E, x)dE$ be the same for uncharged particles.

Then the rates of change of these numbers of particles are given by

$$\left. \begin{aligned} \frac{\partial N(E, x)}{\partial x} &= -\frac{N(E, x)}{\lambda} + \frac{\phi}{\lambda q} \left[N\left(\frac{E}{q}, x\right) + N'\left(\frac{E}{q}, x\right) \right] + p \frac{\partial N(E, x)}{\partial E} \\ \text{and} \\ \frac{\partial N'(E, x)}{\partial x} &= -\frac{N'(E, x)}{\lambda} + \frac{\phi'}{\lambda q} \left[N\left(\frac{E}{q}, x\right) + N'\left(\frac{E}{q}, x\right) \right]. \end{aligned} \right\} \quad (1)$$

The first term on the right-hand side of these equations represents the particles lost by star production and the second the particles produced in more energetic stars of energy E/q . The last term in the first equation represents the reduction in the number of charged particles due to ionization losses.

We solve these equations by assuming a solution in the form of a power series :

$$\left. \begin{aligned} N(E, x) &= \exp(-x/\lambda) E^{-n} \{a_0 + a_1(x/\lambda) + a_2(x/\lambda)^2 + \dots\}, \\ N'(E, x) &= \exp(-x/\lambda) E^{-n} \{b_0 + b_1(x/\lambda) + b_2(x/\lambda)^2 + \dots\}, \end{aligned} \right\} \quad (2)$$

where $a_1, a_2, \dots, b_1, b_2, \dots$ depend on E but not on x , and a_0 and b_0 are constants. The $\exp(-x/\lambda)$ factor is suggested by the exponential decrease in the number of particles with depth and the E^{-n} factor by the power form of the energy spectrum.

By substituting the equations (2) in the equations (1) one obtains, after some reduction, the relations

$$\left. \begin{aligned} \left\{ \frac{a_1}{\lambda} + \frac{2a_2x}{\lambda^2} + \frac{3a_3x^2}{\lambda^3} + \dots \right\}_E &= \frac{\phi q^{n-1}}{\lambda} \left\{ a_0 + b_0 + (a_1 + b_1) \frac{x}{\lambda} + \dots \right\}_{E/q} \\ &+ p \left\{ \frac{da_1}{dE} \cdot \frac{x}{\lambda} + \frac{da_2}{dE} \cdot \left(\frac{x}{\lambda}\right)^2 + \dots \right\}_E - \frac{pn}{E} \left\{ a_0 + a_1 \left(\frac{x}{\lambda}\right) + \dots \right\}_E \\ \left\{ \frac{b_1}{\lambda} + \frac{2b_2x}{\lambda^2} + \frac{3b_3x^2}{\lambda^3} + \dots \right\}_E &= \frac{\phi' q^{n-1}}{\lambda} \left\{ a_0 + b_0 + (a_1 + b_1) \frac{x}{\lambda} + \dots \right\}_{E/q}, \end{aligned} \right\} \quad (3)$$

where the suffixes outside the brackets show the energy at which the a 's and the b 's are to be evaluated. For convenience of calculation we write $E = p\lambda/\alpha$, $v = \phi q^{n-1}$, $v' = \phi' q^{n-1}$.

By equating coefficients in the equations (3) recurrence relations may be derived :

$$\left. \begin{aligned} ra_r &= \bar{a}_{r-1}v - a_{r-1}n\alpha - \alpha^2 \frac{da_{r-1}}{d\alpha} + \bar{b}_{r-1}v, \\ rb_r &= v'(\bar{a}_{r-1} + \bar{b}_{r-1}), \end{aligned} \right\} \quad (4)$$

where \bar{a}_r, \bar{b}_r mean that a_r, b_r are reckoned at E/q instead of E . These relations enable the a 's and the b 's to be calculated as power series in α .

§ 3. CHOICE OF VALUES OF THE CONSTANTS OF THE THEORY.

In this section the most suitable values of the constants λ , p , E_0 , q , ϕ , ϕ' and n are discussed.

If the cross-section for star production is geometrical, then the interaction mean free path λ will be about 60 gm./cm.². But Bernardini *et al.* (1950) found a value of only 45 per cent of geometrical for the production of stars by 350–400 MeV. protons. For shower particles, which are mostly π -mesons, Camerini *et al.* (1950) found a cross-section of 95 ± 39 per cent of geometrical for production of secondary stars in emulsion. Although Bernardini's results refer to much lower energies than we are considering, we choose a value of λ nearer to his than to Camerini's for two reasons. First, we are mainly concerned with the effects of protons as he was, and not of π -mesons, which produced most of Camerini's stars; secondly, we propose to consider only stars of five and more tracks, since the smaller stars can be produced by particles of less energy than we can consider, but *some* of the smaller stars are likely to be produced by high energy particles, making grazing impacts, and hence the cross-section for the larger stars can hardly have the full geometrical value. We take a value for the cross-section of one-half the geometrical, which corresponds to $\lambda \sim 120$ gm./cm.².

The rate of energy loss for a relativistic proton is about 1.5 MeV./gm./cm.² (Braddick 1939). The lowest proton energy of which account is taken in this theory is 450 MeV. (see below), and these have a rate of energy loss only 30 per cent above the minimum. It is therefore a good approximation to take the ionization energy loss of the charged particles as constant.

The series (2) converge only if $\alpha x/\lambda < 1$, and since the atmosphere, when obliquity is taken into account, is about 12 mean free paths, $|x/\lambda|$ may reach the value 6 and we must have $\alpha < \frac{1}{6}$. In practice, for reasonably rapid convergence, we take $\alpha \leq \frac{1}{10}$. Since $E = \frac{p\lambda}{\alpha} = \frac{1.5 \times 120}{\alpha}$ this means that $E > 1800$ MeV. Particles of greater than the limiting energy $E_1 = 1800$ MeV. are referred to as of high energy.

In addition, it is possible to calculate the number of particles in the energy range from $E_1 q$ to E_1 MeV. (see § 5). Particles in this range are referred to as of medium energy. Particles of energy less than $E_1 q$, the slow particles, are not covered by this theory.

The value of q , the fraction of the energy of the primary given to the average secondary, is taken as $\frac{1}{4}$.

The lowest energy of particles considered here, $E_1 q = E_0$, is, therefore 450 MeV., which corresponds on the average to stars with five or more heavy tracks (Barton, George and Jason 1951).

The stars produced by high energy particles are mainly of more than ten tracks, for which Brown *et al.* (1949) found about one shower particle per star at 11,000 ft., while Camerini *et al.* (1949) found 2.0 per star at 70,000 ft. Many of the stars of ten or more tracks but no shower particles

will in fact have been produced by medium energy particles, and, if all these stars are omitted, the corresponding numbers of shower particles per star at the two altitudes are 2.3 and 3.2. Also, Fowler has shown that 75 per cent of the shower particles are π -mesons, which mostly decay in flight before producing a star. These particles must be excluded by dividing the above figures by four. The value of ϕ is consequently rather uncertain, and we take $\phi = \frac{2}{3}$. This is probably a slight over-estimate.

Harding (1949, 1951a) has shown that in most cases the primary particle when neutral retains a large fraction of its energy. It will count as a secondary for our purposes, and there may of course be others. Allowing these to compensate the cases where the primary does not retain enough energy to make another star, we take $\phi' = 1$.

Probably ϕ and ϕ' vary rather considerably with energy, whereas here we take them independent of it. This is unfortunate, but for the higher energy particles the theory only depends on ϕ and ϕ' through ν and ν' . Now while ϕ and ϕ' probably increase with energy, q falls. Thus ν and ν' vary more slowly with E than ϕ and ϕ' .

The exponent n in the energy spectrum, both for primary particles (Hoang 1951) and for stars (Barton *et al.* 1951), has been shown to be about 2.5, and we took this value for convenience of calculation, though some recent experiments indicate that it may be a little high.

§ 4. HIGH ENERGY PARTICLES.

From (2) the number of high energy charged particles at depth x is

$$\begin{aligned} \int_{E_1}^{\infty} \exp(-x/\lambda) E^{-2.5} \left\{ a_0 + a_1 \left(\frac{x}{\lambda} \right) + \dots \right\} dE \\ = \frac{\exp(-x/\lambda)}{(p\lambda)^{1.5}} \int_0^1 \frac{1}{\alpha^{\frac{5}{2}}} \left(a_0 + a_1 \frac{x}{\lambda} + \dots \right) d\alpha. \end{aligned}$$

The coefficients $a_1, a_2, \dots, b_1, b_2, \dots$ were calculated as power series in z multiplied by a_0 or b_0 and the integral evaluated for various x/λ .

A similar calculation was made for the high energy neutral particles.

§ 5. MEDIUM ENERGY PARTICLES.

The medium energy particles at any depth x are produced in nuclear interactions above x . It is therefore necessary to evaluate the number produced at any height z that reach x and integrate from the top of the atmosphere down to x .

The rate of production of neutral particles of energy E to $E+dE$ produced at a height z is

$$\frac{\phi'}{\lambda} [N(E/q, z) + N'(E/q, z)] \frac{dE}{q}.$$

The fraction that reaches a depth x is $\exp [-(x-z)/\lambda]$. Therefore the total number of medium energy uncharged particles at x is

$$\int_{-H}^x \int_{E_0}^{E_1} \frac{\phi'}{\lambda q} \exp \{-(x-z)/\lambda\} [N(E/q, z) + N'(E/q, z)] dE dz,$$

where H is the height of the top of the atmosphere from the origin of x . This was taken at -7λ .

This expression can be integrated exactly, and was evaluated as a function of x/λ . The corresponding calculation for medium energy charged particles has to take into account the energy $p(x-z)$ lost as the particle goes from z to x . The expression for the total number of medium energy charged particles is

$$\int_{-H}^x \int_{E_0+p(x-z)}^{E_1+p(x-z)} \frac{\phi}{\lambda q} \exp \{-(x-z)/\lambda\} [N(E/q, z) + N'(E/q, z)] dE dz.$$

This cannot be integrated exactly, and so graphical methods were used.

§ 6. RESULTS OF CALCULATION.

In this section the results of the calculations of the last two sections are presented. These results for each class of particles consist of a part in a_0 added to a part in b_0 , where a_0 and b_0 are adjustable constants. The relative numbers of the various types of particles depend on the ratio a_0/b_0 .

The variation of the neutral and charged particles and of the high energy and medium energy particles with atmospheric depth x/λ is plotted in figs. 1 and 2 in arbitrary units for various a_0/b_0 . The factor $\exp (-x/\lambda)$ is omitted from the curves shown as its inclusion would make it harder to see the run of the curves.

The variation of the ratio of charged to uncharged particles with atmospheric depth is plotted in fig. 3 for various values of a_0/b_0 .

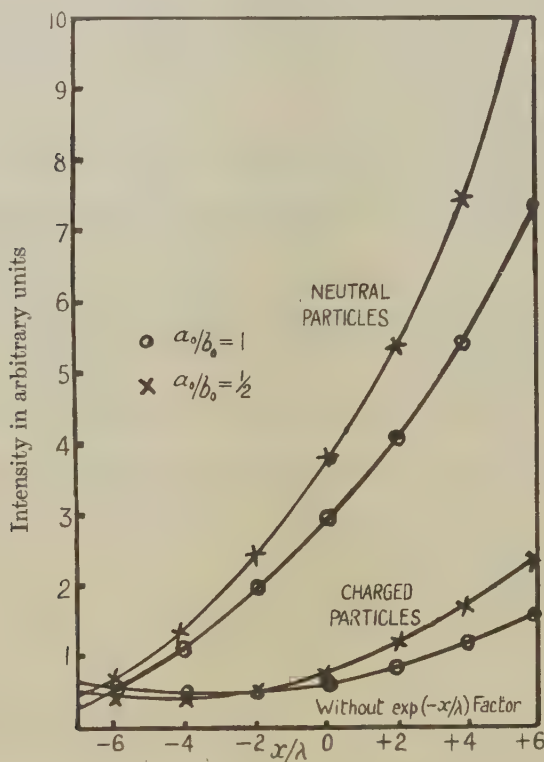
§ 7. THE ANGULAR DISTRIBUTION OF THE STAR-PRODUCING RADIATION.

The theory as developed so far is one-dimensional, and takes no account of the angular spread of the cosmic radiation.

If it is assumed that the secondaries all continue in the same direction as their primary, then it is possible in principle, though rather laborious in practice, to extend the theory to three dimensions. Instead, we take the angular spread of the cosmic rays into account by altering the scale of the curves by a factor equal to the average ratio of the vertical distance between two atmospheric depths and the distance covered by a particle in going from one depth to the other. This is only an approximate method since the scale factor alters with atmospheric depth. Its use is equivalent to assuming that the angular distribution of the cosmic radiation does not vary with depth.

The radiation at the top of the earth's atmosphere is roughly isotropic, but, as it proceeds through the atmosphere, the particles whose directions make a large angle with the vertical are preferentially absorbed, with the result that the radiation becomes *more* collimated as it penetrates the atmosphere. But the secondaries do not continue in the direction of their primaries, having an angular distribution about them. This tends to make the radiation *less* collimated.

Fig. 1.



Variation of intensities of charged and neutral particles with depth.

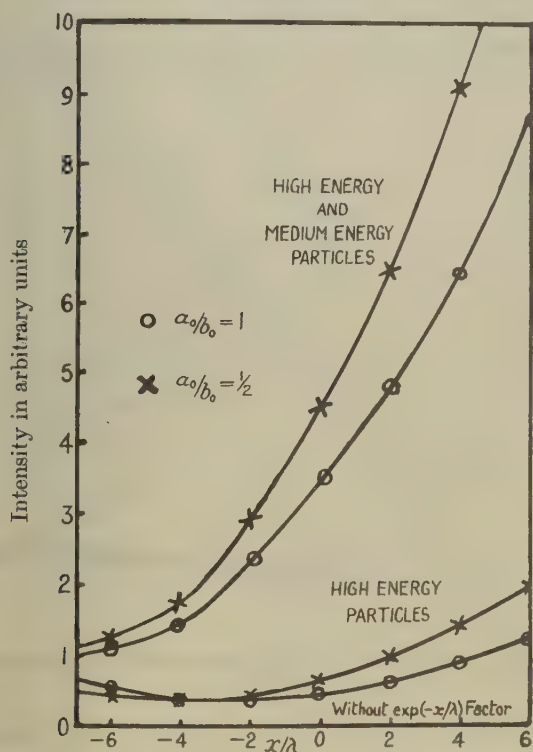
These two effects oppose one another, with the result that over the middle and lower regions of the atmosphere the angular distribution does not vary much. This conclusion is supported by the work of the Bristol group (Brown *et al.* 1949) and of Lord and Schein, whose results on the angular distribution of the star-producing radiation at 11,000 ft. and at 53,000 ft. show little difference.

These results give an average obliquity factor of 0.8. The assumption of constancy of angular distribution, while probably approximately correct for the middle and lower regions of the atmosphere, is certainly

quite incorrect near the top. The results of this theory are not therefore applicable to the first one or two collision mean free paths of the atmosphere. This would have been the case even if the complication due to obliquity was absent, owing to the presence of the heavy primaries.

This method of allowing for obliquity is undoubtedly crude, but a more refined treatment would have to take into account not only the angular distribution of the star-producing radiation but also the angular

Fig. 2.



Variation of intensities of medium and high-energy particles with depth.

distribution of the secondaries about the direction of motion of the primaries, which introduces great mathematical complexity. It is preferable to using the Gross transformation and neglecting the latter effect, since this predicts a considerable increase in collimation.

§ 8. EFFECT OF VARIATIONS OF THE INITIAL CONSTANTS.

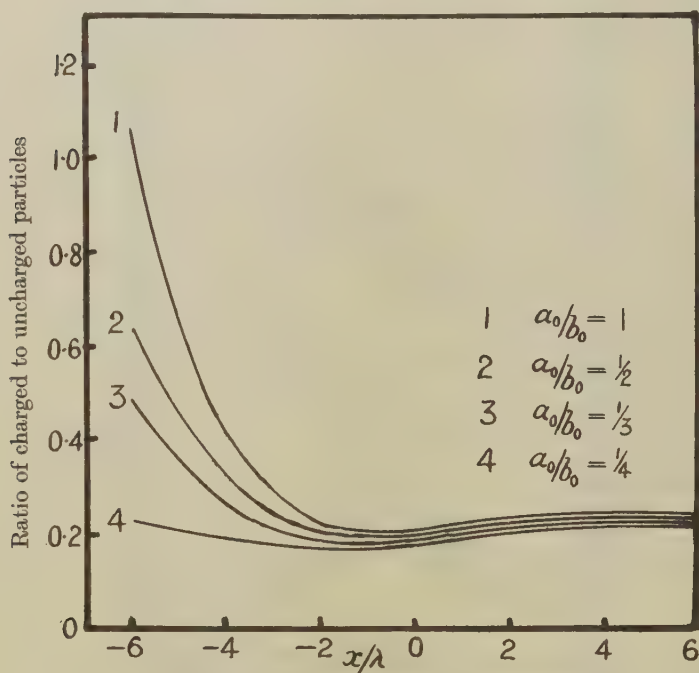
The constants whose values are the most uncertain are ϕ , ϕ' , q and λ .

If there were no cascade or obliquity effect, the absorption mean free path as observed should equal the interaction mean free path, which we

have assumed to be 120 gm./cm.^2 . The effect of the cascade is to increase the expected absorption mean free path to 150 gm./cm.^2 . Correction for obliquity brings it back to about 120 gm./cm.^2 , which is close to the observed value.

The absorption mean free path of 150 gm./cm.^2 is thus composed of a part depending on λ and a part depending on ϕ , ϕ' and q . The same absorption mean free path can be obtained for a smaller value of λ by increasing the latter constants. But a limit is set to this process by the

Fig. 3.



Variation with depth of the ratio of charged to uncharged particles.

approximate experimental values of ϕ and ϕ' , and by the inequality $(\phi + \phi')q < 1$, where the inequality must allow both for the slow particles and the stars and most of the π -mesons. It is not therefore possible to vary very much the value of λ we have taken.

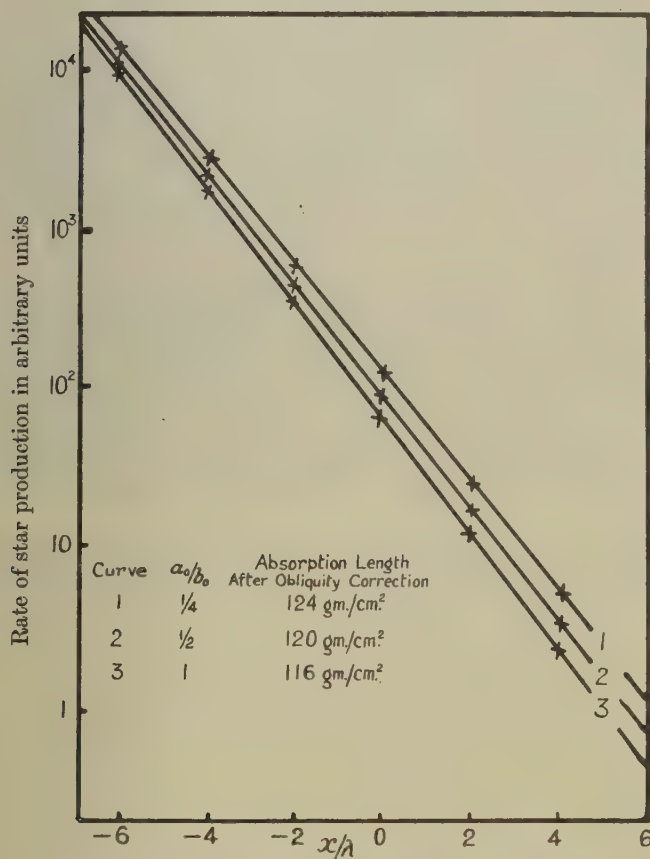
Increasing both ϕ and ϕ' increases the ratio of charged to uncharged particles, since it makes the relative effect of the ionization loss less important. The ratio of charged to uncharged particles is also increased by increasing ϕ/ϕ' .

When ϕ and ϕ' have been chosen, the above inequality and the known characteristics of stars sets limits on the value of q . The main features of the theory do not depend critically on the choice of q .

§ 9. VARIATION OF THE RATE OF STAR PRODUCTION AND OF THE ENERGY DISTRIBUTION OF THE STAR-PRODUCING RADIATION WITH HEIGHT.

The variation of the rate of star production with height is shown in fig. 4 for various a_0/b_0 . It is closely exponential, giving absorption mean free paths of 145, 150 and 155 gm./cm.² for $a_0/b_0=1, \frac{1}{2}$ and $\frac{1}{4}$

Fig. 4.



Variation of the rate of star production with depth.

respectively. The corresponding mean free paths when the angular distribution of the star-producing radiation is taken into account are 116, 120 and 124 gm./cm.².

The energy distribution of the star-producing radiation was calculated at three heights, and it was found to be still closely a power spectrum,

but with slightly different index. The index of the power law increases with altitude from 2.2 at sea level to 3.0 three-quarters of the way up the atmosphere.

§ 10. COMPARISON OF THE RESULTS OF THE THEORY WITH EXPERIMENT.

The calculated ratio of charged to uncharged particles decreases with atmospheric depth, in accord with experiment, for Camerini *et al.* (1949) found a ratio of 0.58 for stars of five or more tracks and 0.47 for stars of four or more tracks at 70,000 ft., while Brown *et al.* (1949) found corresponding ratios of 0.36 and 0.26 at 11,000 ft. (The slight minimum in the calculated curve is not considered significant.) The value at the higher altitude can be fitted by suitable choice of a_0/b_0 , but that at the lower altitude is higher than predicted by the theory. However, Brown *et al.* (1949) find only 10.8 stars per c.c. per day at the Jungfrau, while Harding (1951 b) finds 16.2. Assuming, as is likely, that the missing stars are mostly small, for which the ratio is very low, the values 0.36 and 0.26 will be too high.

In making these comparisons it should be remembered that the theory refers to a cascade in air, whereas the stars investigated by the Bristol group occurred in photographic emulsion. In the latter medium, unlike air, charged π -mesons frequently produce stars, thus increasing the apparent ratio of stars with charged to stars with uncharged primaries. This effect cannot be evaluated, since the π -meson flux depends on the amount of matter surrounding the plates, which is not known, but taking it into account would improve the agreement between theory and experiment.

The calculated ratio of medium to high energy star-producing particles at 11,000 ft. is 6.1, and on our scheme only the high energy particles will be able to produce shower particles. Since $\phi = \frac{2}{3}$, and only one in four of the shower particles are protons, this gives 0.37 shower particles per star, in good agreement with the values 0.38 and 0.29 found by Brown *et al.* for stars of five or more and four or more tracks respectively.

Our calculated exponential variation of the rate of star production has been found by many investigators (see Messel and Ritson 1950). The observed absorption length varies with energy and, therefore, with star size (Addario and Tamburino 1949) and falls from about 145 gm./cm.² for star sizes 3, 4, 5 to about 113 gm./cm.² for star sizes greater than 6, which agrees sufficiently with the calculated range of 116–124 gm./cm.².

Laboratory observations show that particles of a given energy do not all produce stars of the same size, but give quite a broad distribution of star sizes. This makes a comparison between theory and experiment difficult.

Our theory does not take account of the small stars. These may be due either to particles of low energy or to particles of any energy which make glancing collisions with the nucleus. For the present it seems

difficult to disentangle the two classes, but the small value we are led to assume for the cross section for star production is an indication that the second class is important.

ACKNOWLEDGMENTS.

We should like to express our gratitude to Mr. S. Lattimore for valuable discussions, to Dr. H. Messel for communicating the results of his work before publication, and to Mrs. H. Goldring for assistance in the numerical calculations.

REFERENCES.

- ADDARIO and TAMBURINO, 1949, *Phys. Rev.*, **76**, 983.
BARTON, GEORGE and JASON, 1951, *Proc. Phys. Soc. A*, **64**, 175.
BERNARDINI, BOOTH and LINDENBAUM, 1950, *Phys. Rev.*, **80**, 905.
BRADDICK, 1939, *Cosmic Rays and Mesotrons* (Cambridge Physical Tract).
BROWN, CAMERINI, FOWLER, HEITLER, KING and POWELL, 1949, *Phil. Mag.*, **40**, 862.
CAMERINI, COOR, DAVIES, FOWLER, LOCK, MUIRHEAD and TOBIN, 1949, *Phil. Mag.*, **40**, 1073.
CAMERINI, FOWLER, LOCK, and MUIRHEAD, 1950, *Phil. Mag.*, **41**, 413.
HARDING, 1949, *Phil. Mag.*, **40**, 530 ; 1951 a, *Ibid.*, **42**, 63 ; 1951 b (in the press).
HEITLER and JÁNOSSY, 1949, *Proc. Phys. Soc. A*, **62**, 374.
HOANG TCHANG FONG, 1950, *Thesis*, Paris.
LORD and SCHEIN, 1950, *Phys. Rev.*, **77**, 19.
MESSEL, 1951, *On the Theory of a Nucleon Cascade* (Dublin) ; 1951, *Proc. Phys. Soc.* (in the press).
MESSEL and RITSON, 1950, *Proc. Phys. Soc. A*, **63**, 1359.
THOMSON, 1949, *Phil. Mag.*, **40**, 589.

XCIX. *The Deflection of a Cable due to a Single Point Load.*

By E. MARKLAND,
The University of Nottingham*.

[Received May 28, 1951.]

SUMMARY.

A method is given for calculating the deflected shape of a uniform inextensible cable supported with each end at the same level, when a small point load is placed anywhere along the cable.

The analytical treatment is straightforward and a method of successive approximations for the numerical solution of the equations is suggested. Results have been computed for the case of span to sag ratio of 10 and ratio of point load to cable weight of 0.1, and are compared with experimental values.

THE method of flexibility coefficients has recently been introduced (Pugsley 1949 a and b) for analysing a stiffened suspension bridge. To obtain a numerical solution it is necessary to know the behaviour of a suspended cable when a single load is placed anywhere along it. Professor Pugsley emphasized that the deflection of any point of the cable is not a linear function of the applied load, and the required deflections for an arbitrary magnitude of applied load were obtained experimentally.

The calculation of the deflected shape of the cable, although presenting no theoretical difficulty, is arithmetically troublesome. It has been found, however, that the problem may be solved reasonably quickly by the method given below.

Consider the uniform, heavy, flexible cable of weight W shown in fig. 1, in which the ends A and B are supported at the same level. It is assumed that the initial dip at the centre, D_0 , is small compared with the span, $2L$, so that the initial shape ACB is very nearly parabolic and the load per unit horizontal length is constant.

When a vertical load w is applied to the point G_0 , the cable deflects to the shape AGB, AG and BG being parabolic arcs.

The horizontal distance of the loaded point from the mid-point of AB increases from a_0L to aL and the vertical distance below AB from D_0 to D . The horizontal movement is taken to be small so that the loads per unit horizontal length of the arcs AG and BG are equal.

$$\text{Let} \quad c = \frac{2HL}{W}, \quad (1)$$

* Communicated by the Author.

where H is the horizontal component of cable tension. Then the equations of AG and BG referred to the rectangular axes shown on the figure are

$$\text{for AG :—} \quad y = A_1 x + \frac{x^2}{2c}, \quad (2)$$

$$\text{for BG :—} \quad y = A_2 x + \frac{x^2}{2c}, \quad (3)$$

where A_1 and A_2 are the slopes of the arcs AG and BG at G. Resolving forces vertically at G, we obtain

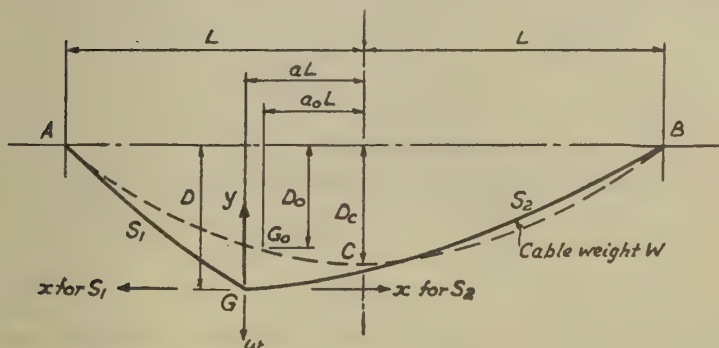
$$A_1 + A_2 = \frac{2L}{c} \cdot \frac{w}{W}. \quad (4)$$

Substituting $x = L(1-a)$ in equation (2) and $x = L(1+a)$ in equation (3) and solving for A_1 and A_2 , we obtain

$$\text{for AG :—} \quad y = \frac{L}{c} \left[(1+q) \frac{w}{W} + a \right] x + \frac{x^2}{2c}. \quad (5)$$

$$\text{for BG :—} \quad y = \frac{L}{c} \left[(1-a) \frac{w}{W} - a \right] x + \frac{x^2}{2c}. \quad (6)$$

Fig. 1.



For a specified value of a_0 , the lengths of arcs AG_0 and BG_0 of a given cable may be computed. Let these be S_1 and S_2 respectively. Then, since the cable is inextensible, $S_1 = \text{arc length AG}$, $S_2 = \text{arc length BG}$. Hence

$$\frac{S_1}{L} = \frac{1}{2} \left| u \left(1 + \frac{L^2 u^2}{c^2} \right)^{1/2} + \frac{c}{L} \log \left\{ \frac{Lu}{c} + \left(1 + \frac{L^2 u^2}{c^2} \right)^{1/2} \right\} \right|_{u=(1+a)\frac{w}{W}+1}^{u=(1+a)\frac{w}{W}+a} \quad (7)$$

and

$$\frac{S_2}{L} = \frac{1}{2} \left| u \left(1 + \frac{L^2 u^2}{c^2} \right)^{1/2} + \frac{c}{L} \log \left\{ \frac{Lu}{c} + \left(1 + \frac{L^2 u^2}{c^2} \right)^{1/2} \right\} \right|_{u=(1-a)\frac{w}{W}-a}^{u=(1-a)\frac{w}{W}+1} \quad (8)$$

By inserting the known initial values of S_1/L , and S_2/L into these equations, we have two simultaneous equations in a and c/L which may be solved by trial for a given value of w/W . The numerical work is helped by forming approximate values for S_1 and S_2 as follows :

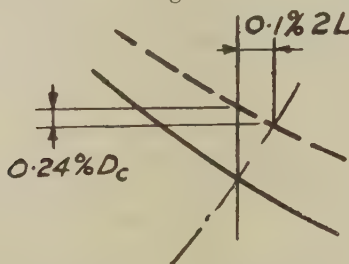
$$S_1 = \int_0^{L(1-a)} \left\{ 1 + \frac{1}{2} \left[\frac{L}{c} \left(\overline{1+a} \frac{w}{W} + a \right) + \frac{x}{c} \right]^2 + \dots \right\} dx,$$

$$S_2 = \int_0^{L(1+a)} \left\{ 1 + \frac{1}{2} \left[\frac{L}{c} \left(\overline{1-a} \frac{w}{W} - a \right) + \frac{x}{c} \right]^2 + \dots \right\} dx.$$

Upon integration, and subsequent partial differentiation with respect to a and c/L respectively, the following results are obtained :

$$\left. \begin{aligned} \alpha_1 &\equiv \frac{\partial(S_1/L)}{\partial a} = -1 + \frac{L^2}{2c^2} \left[\frac{w}{W} \left(\overline{1+a} \frac{w}{W} + 1 \right)^2 - \left(1 + \frac{w}{W} \right) \left(\overline{1+a} \frac{w}{W} + a \right)^2 \right], \\ \alpha_2 &\equiv \frac{\partial(S_2/L)}{\partial a} = +1 - \frac{L^2}{2c^2} \left[\frac{w}{W} \left(\overline{1-a} \frac{w}{W} + 1 \right)^2 - \left(1 + \frac{w}{W} \right) \left(\overline{1-a} \frac{w}{W} - a \right)^2 \right], \\ \beta_1 &\equiv \frac{\partial(S_1/L)}{\partial(c/L)} = -\frac{1}{3} \left(\frac{L}{c} \right)^3 \left[\left(\overline{1+a} \frac{w}{W} + 1 \right)^3 - \left(\overline{1+a} \frac{w}{W} + a \right)^3 \right], \\ \beta_2 &\equiv \frac{\partial(S_2/L)}{\partial(c/L)} = -\frac{1}{3} \left(\frac{L}{c} \right)^3 \left[\left(\overline{1-a} \frac{w}{W} + 1 \right)^3 - \left(\overline{1-a} \frac{w}{W} - a \right)^3 \right]. \end{aligned} \right\} \quad \dots (9)$$

Fig. 2.



Approximate values of these partial differential coefficients may be computed by inserting trial values of a and c/L , then the total differentials

$$d(S_1/L) = \alpha_1 da + \beta_1 d(c/L),$$

$$d(S_2/L) = \alpha_2 da + \beta_2 d(c/L)$$

are known approximately.

If trial values of a and c/L yield discrepancies $\Delta(S_1/L)$ and $\Delta(S_2/L)$ in equations (7) and (8), the required corrections Δa and $\Delta(c/L)$ are given approximately by

$$\left. \begin{aligned} \Delta a &= \frac{\beta_2 \Delta(S_1/L) - \beta_1 \Delta(S_2/L)}{\alpha_1 \beta_2 - \alpha_2 \beta_1} \\ \Delta(c/L) &= - \left(\frac{\alpha_2 \Delta(S_1/L) - \alpha_1 \Delta(S_2/L)}{\alpha_1 \beta_2 - \alpha_2 \beta_1} \right). \end{aligned} \right\} \quad (10)$$

and

By making corrections in this way it is found that equations (7) and (8) may be solved after a few attempts.

The equations of AG and BG are therefore known and the difference in ordinates between them and the original curve AG_0CB may be computed. Strictly, the vertical component of displacement of a point on the cable is not the difference in ordinates since each point of the cable has, in general, a horizontal displacement as well. However, tests on a cable in which horizontal deflections were measured at each of nine points in turn, show that the maximum horizontal deflection at an unloaded point was 0.10 per cent of the span for $2L/D_c=10$ and $w/W=0.1$, and was measured at a point one-fifth of the span from one end. The maximum error in the calculated vertical deflection is, as indicated on fig. 2, about one-quarter of one per cent of the central dip. Both horizontal and vertical components of the displacement of the loaded point are of course obtained correctly from the calculations.

Calculated results for the nine stations defined on fig. 3 are given below :

Fig. 3.

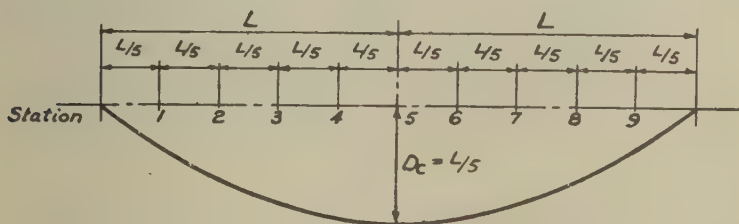


TABLE.

Vertical deflections expressed as percentage of central dip.

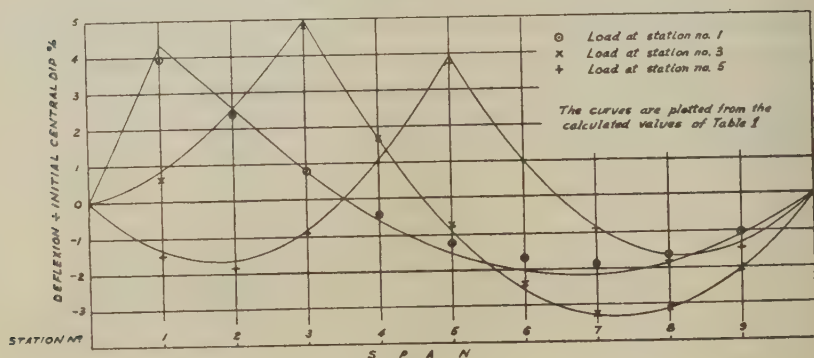
Span : dip ratio = 10 : 1.

$w/W=0.1$.

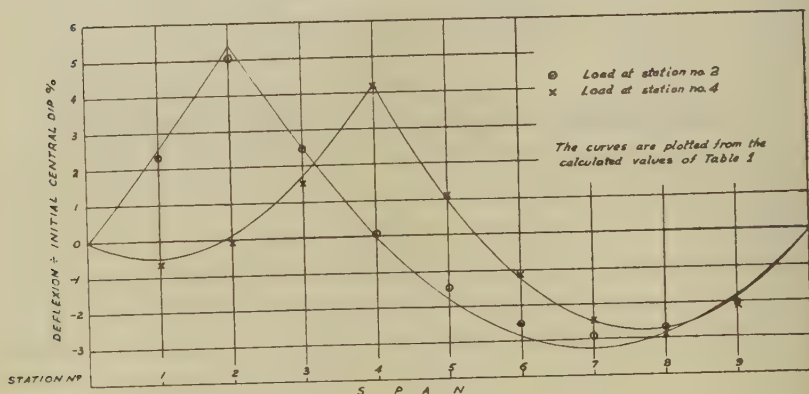
Deflection at station no.	Load at station no.				
	1	2	3	4	5
1	+4.32	+2.59	+0.82	-0.47	-1.35
2	+2.59	+5.41	+2.57	+0.09	-1.63
3	+0.79	+2.52	+4.99	+1.68	-0.85
4	-0.59	-0.01	+1.65	+4.24	+1.02
5	-1.54	-1.81	-0.93	+0.97	+3.95
6	-2.08	-2.89	-2.59	-1.29	+1.02
7	-2.19	-3.25	-3.32	-2.52	-0.85
8	-1.88	-2.89	-3.13	-2.72	-1.63
9	-1.15	-1.81	-2.03	-1.88	-1.35

Tests were made on a chain of about 5 feet length and 0.93 lb. weight and deflections were measured at each of nine stations along the chain with a travelling microscope. Some trouble was experienced, especially towards the ends, with friction between the links, but the results shown on fig. 4 agree reasonably well with calculated values. Experimental values previously published appear to be somewhat at variance with the present results.

Fig. 4.



(a)



(b)

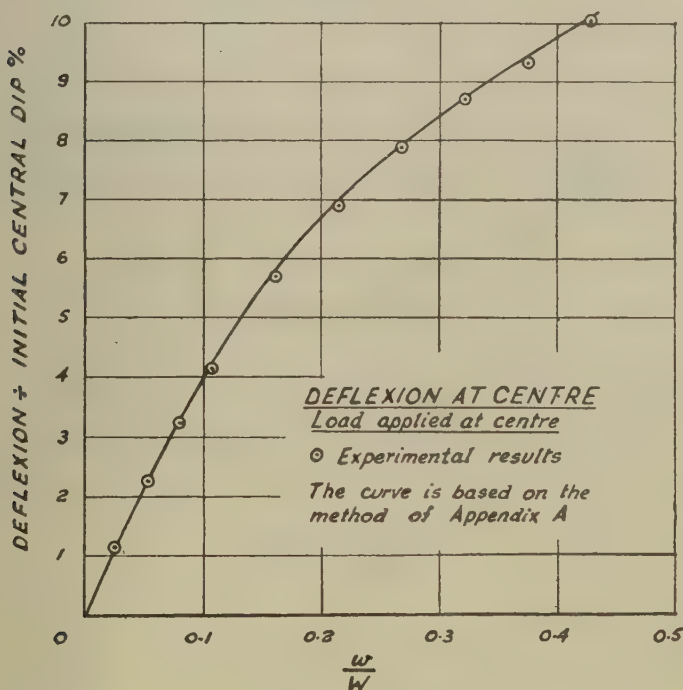
As a check on the accuracy of the apparatus, the deflection of the central point has been measured over a wide range of loads applied at this point, and a comparison with calculations in which the simplifying assumption of a parabolic initial shape is not made, is shown on fig. 5. The method of this straightforward calculation is given in the Appendix.

The span to sag ratio of the experimental chain was varied between 5 and 10, and it is interesting to note that deflections expressed as a fraction of the central dip varied little over this range. It appears,

therefore, that the values given in the Table would not vary greatly for the different ratios of span to dip likely to be encountered in suspension bridge practice.

Acknowledgment is due to Mr. R. A. Dorton for his help with the experimental work and to Mr. R. C. Coates for many valuable suggestions. The author is indebted to Professor J. A. Pope for placing the facilities of the Engineering Department and Workshop of Nottingham University at his disposal.

Fig. 5.



REFERENCES.

PUGSLEY, A. G., 1949 a, *Journ. Inst. Civ. Eng.*, 32, 226; 1949 b, *The Structural Engineer*, 27, 327.

APPENDIX.

Referring to the centrally loaded cable of fig. 6, the equations relating the coordinates of any point of the cable AG to the intrinsic angle at that point are

$$y/c = \sec \psi, \quad \dots \dots \dots (1)$$

$$x/c = \log (\sec \psi + \tan \psi), \quad \dots \dots \dots (2)$$

and the distance along the curve from P is given by

$$s/c = \tan \psi. \quad \dots \dots \dots (3)$$

Hence

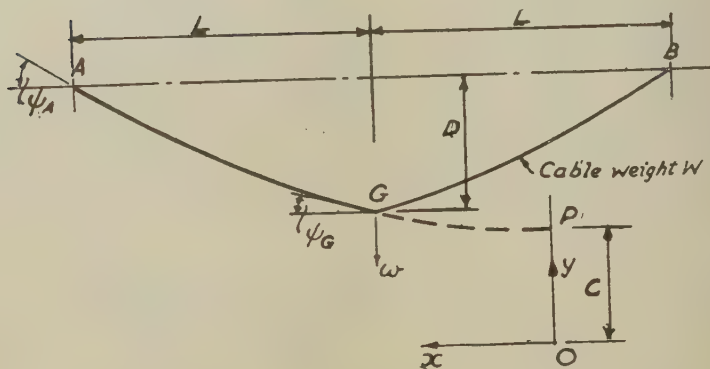
$$D/c = \sec \psi_A - \sec \psi_G, \quad \dots \dots \dots (4)$$

$$L/c = \log \left(\frac{\sec \psi_A + \tan \psi_A}{\sec \psi_G + \tan \psi_G} \right) \quad \dots \dots \dots (5)$$

and

$$\frac{S}{L} = \frac{\tan \psi_A - \tan \psi_G}{\log \left(\frac{\sec \psi_A + \tan \psi_A}{\sec \psi_G + \tan \psi_G} \right)} \quad \dots \dots \dots (6)$$

Fig. 6.



Now

$$\frac{\tan \psi_A}{\tan \psi_G} = \frac{w + W}{w}$$

or

$$\frac{w}{W} = \frac{\tan \psi_G}{\tan \psi_A - \tan \psi_G} \quad \dots \dots \dots (7)$$

The computing procedure adopted was to assign a value to ψ_G and to calculate ψ_A from equation (6) above knowing the value of S/L . D/C and L/C follow from equations (4) and (5). The corresponding value of w/W is obtained from equation (7).

C. *The State of Ionization in Lithium Hydride.*

By M. S. AHMED,
University College, London*.

[Received May 7, 1951.]

SUMMARY.

Single crystal photographs of LiH have shown that the structure is of the NaCl-type, $a=4.09$ A., $Z=4$. The intensities of reflection from planes having all even and all odd indices give atomic form factors for Li^{+X} and H^{-X} respectively which, when extrapolated to $(\sin\theta)/\lambda=0$, lead to the value $X=0.25\pm0.25$. This result is not modified by taking into consideration the thermal vibrations of the atoms. It follows therefore that in the solid state LiH has only 25 per cent ionic character, with limiting values (much less probable) of 50 per cent ionic character or complete covalency.

§1. INTRODUCTION.

IN the NaCl-like structures, it is well known that the percentage of ionic character may vary according to the polarizability of the component ions.

The state of ionization is particularly interesting in the case of lithium hydride, since it might at first be thought that when Li and H combine chemically to form LiH, a complete transference of an electron from the outermost L shell of Li to the innermost shell of H would occur; thus both Li^+ and H^- ions would have the helium stable configuration. In this paper it is shown by X-ray methods that this is not the case for LiH in the solid crystallized state.

The structure of lithium hydride has been determined by different workers, using the powder method. Many discrepancies appear in some of the work that has already been done. Some research workers have, by extrapolation of their results, concluded that LiH possesses 100 per cent ionic character. Other assume without proof, that in LiH both Li and H ions possess two electrons.

§2. REPORTED WORK ON THE STRUCTURE AND STATE OF IONIZATION IN LiH.

(A) Bijvoet and Karssen (1922) prepared powder photographs for LiH using Cu and Cr radiations. Because of the chemical reactivity of the substance, photographs of LiO and LiOH were also taken in order to eliminate lines due to them arising from the possible decomposition of LiH. Their results were as follows :

* Communicated by Professor Kathleen Lonsdale, F.R.S.

1. The observed lines were in the positions which would be expected from a NaCl or ZnS arrangements, with a unit cell edge of 4.10 kX; four molecules per cell.

2. They then made a comparison between observed and calculated intensities (see following Table). The first column gives the indices of the reflections, columns 2 and 3 the observed intensities using Cu and Cr radiation respectively, columns 4 and 5 the calculated intensities assuming a zincblende and NaCl arrangement respectively. If LiH has the NaCl grouping, then, they argued, it would be anticipated that +ve Li ions and -ve H ions would be present in its crystals.

Indices	$I_{\text{obs}}(\text{CuK}\alpha)$	$I_{\text{obs}}(\text{CrK}\alpha)$	$I_{\text{calc}}(\text{ZnS-type})$	$I_{\text{calc}}(\text{NaCl-type})$
111	medium weak	weak	10	0
200	strong	medium strong	0	10
220	medium strong	medium strong	9.5	8.8
113	medium	very strong	6.5	0
222	very weak	strong	0	3.6

From the above Table they concluded that there is a better fit with the NaCl arrangement, than with the zincblende arrangement.

3. The poor agreement obtained they explained by saying that it is not to be expected that with such simple atoms there would be good agreement with calculations which neglected the electronic distribution.

(B) Bijvoet (1923) published a further paper on the structure of Li and LiH but with no improvement in the observed intensities of powder lines for LiH. He mentions that after the exposures in most cases the lithium hydride had been reduced 15–20 per cent by weight. The time of exposure varied from 2 to 12 hours. In some of the long exposures the sample was renewed after a few hours.

Now it is clear that the intensity values given cannot be reliable in these circumstances. The relative intensities, using Cu and Cr radiations, do not seem to be consistent among themselves or to agree particularly well either with the NaCl-like or with the zincblende-like arrangement.

(C). In 1929, Bijvoet and Frederikse published a paper called "The Scattering power for X-rays and the electron distribution of the H^- ion", in which curves were given for $(f_{\text{Li}} + f_{\text{H}})$ and $(f_{\text{Li}} - f_{\text{H}})$ (but without any experimental intensity measurements to support them). From these curves it was argued that complete ionization is almost certain, but it was admitted that the photometrically measured values of the intensities (not given) showed considerable fluctuations amongst themselves. Observations of intensities of reflections appearing on single crystal rotation photographs do not agree with the data given by these workers. It is probable that decomposition of their LiH powder occurred during the exposures.

(D). Zintl and Harder (1931) also determined the structure of LiH using the powder method. The unit cell constant was given as 4.084 kX (± 0.001). These workers obtained reproducible values for

the intensities. $\text{CuK}\alpha$ radiation was used and the intensities were measured by a photometer. The intensity formula used, neglecting absorption and temperatures factors, is

$$I \propto \frac{1 + \cos^2 2\theta}{\sin^2 \theta \cos \theta} \cdot p' \cdot F^2$$

$$\propto z \cdot p' \cdot F^2 \quad (p' = \text{multiplicity}).$$

The intensities given by Zintl and Harder are :—

hkl	I_{phot}	$p'z$	$F^2 \propto \frac{I_{\text{phot}}}{p'z}$
111	11.0	64.8	.17
200	20.5	34.5	.60
220	10.5	29.5	.36
311	7.0	41.3	.17
222	3.5	12.7	.28
400	1.5	8.2	.18
331	3.0	35.0	.09
420	4.0	37.1	.11

From the above Table they concluded that $(F_{\Sigma h=2n})^2 > (F_{\Sigma h=2n+1})^2$ always, and that therefore LiH has the NaCl-like structure. If the structure were of the zincblende type the observed structure factors would have to satisfy the relations

$$(F_{\Sigma h=4n})^2 > (F_{\Sigma h=4n+1})^2 > (F_{\Sigma h=4n+2})^2.$$

In their discussion on LiH, Zintl and Harder pointed out that if Li^+ and H^- ions existed, each with two electrons, then all the "odd" reflections should disappear.

They claimed that the appearance of all the odd reflections can be explained as being the same effect found by Debye and Scherrer (1918) in NaF, by Gerlach and Pauli (1921) in MgO, and by Mark and Tolksdorf (1925) in SrCl_2 : namely a differential decrease of scattering power f of different sorts of atomic particle, with increasing θ .

They pointed to a reported change in the conductivity of LiH near the melting point, which although smaller than, is similar to that for alkali halides, and they concluded that the conductivity of LiH is cationic. This does not necessitate, however, that Li and H are *completely* ionized in the solid state of LiH.

Assuming complete ionization in LiH, Zintl and Harder calculated the radius of the H^- ion to be equal to 1.26 kX units (using $r_{\text{Li}^+} = 0.78$ as given by Goldschmidt).

(E). In 1932, two short notes, one by Bijvoet and Karssen and a reply to it by Zintl and Harder were published: but these did not clarify the position further. Had Zintl and Harder drawn the graphs $(f_{\text{Li}} + f_{\text{H}})$ and $(f_{\text{Li}} - f_{\text{H}})$ for the "all even" and "all odd" reflections respectively, thus deducing the graphs for f_{Li} and f_{H} , they could have seen that Li and H are by no means completely ionized, as they assumed them to be.

Since that time it seems to have been taken for granted that LiH is completely ionized. The following work will show that this cannot be the case.

§3. SINGLE CRYSTAL ROTATION PHOTOGRAPHS.

By careful cleavage from a rather big crystal of LiH it was possible to obtain small crystals without distortion on any of the crystal faces. These were quickly sealed into Lindemann glass tubes, and no unwanted powder lines were found on the short-exposure rotation photographs required for intensity measurements. Powder lines showing orientation were, however, observed on rotation photographs of larger crystals used for "diffuse spot" measurements.

The crystal was set with $[1\bar{1}0]$ vertical, and Cu radiation was used from Victor and Machlett tubes run under similar conditions. Intensity measurements were made using spots appearing on the zero layer line only.

The crystal dimensions were roughly 0.25~0.30 mm. along $[100]$, 0.35 mm. along $[010]$, and 0.35~0.40 mm. along $[001]$. The crystal, while rotating, was completely bathed in the incident filtered X-ray beam.

Cylindrical rotation photographs were taken, with times of exposure of one, two, four, five and ten minutes, and the multiple film technique was used.

With such short exposures the intensity of the incident X-ray beam was fairly constant, and white radiation radial streaks could not be observed on the rotation photographs, which showed small undistorted Bragg spots on a clear background.

With the Weissenberg camera, an intensity scale was made for eye estimation of intensities, using the 004 reflection from the same crystal.

The unit cell dimension from rotation photographs is $a=4.086$ Å. The value given by Zintl and Harder (formerly expressed in kX units) is $a=4.092$ Å.

Observed structure factors.

In the following Table, the observed mean relative intensities from different rotation photographs are given for comparison with those of previous observers. The observed structure factors are obtained after allowing for the multiplicity, polarization and Lorentz factors only;

z denotes $\frac{1+\cos^2 2\theta}{\sin 2\theta}$, p the multiplicity on the rotation photograph.

The single crystal rotation photographs of LiH, therefore, confirm that the structure is of a NaCl type.

In Table I. the observed structure factors F_s obtained from the single crystal method, and those given by Zintl and Harder, using the powder method, F_p , are compared.

It may be seen that the ratio F_s/F_p is nearly constant, within the experimental errors of both methods.

Atomic scattering factors.

Atomic scattering curves for the Li^{-X} ion and for the H^{-X} ion (uncorrected for temperature vibration) may be deduced from the observed structure factors curves for "all even" reflections ($f_{\text{Li}}+f_{\text{H}}$) and "all odd" reflections ($f_{\text{Li}}-f_{\text{H}}$). For any given value of $(\sin \theta)/\lambda$

$$f_{\text{Li}} = \frac{1}{2} \{ (f_{\text{Li}} + f_{\text{H}}) + (f_{\text{Li}} - f_{\text{H}}) \},$$

$$f_{\text{H}} = \frac{1}{2} \{ (f_{\text{Li}} + f_{\text{H}}) - (f_{\text{Li}} - f_{\text{H}}) \}.$$

The extrapolation of the graphs for f_{Li} and f_{H} to $\sin \theta/\lambda = 0$ is difficult because of the wide gap involved, but taking the intercepts on the $\sin \theta/\lambda = 0$ ordinate as OY, OY' for Li and H respectively, it is found that possible limits of the ratio OY/OY' are 3 : 1 and 2.5 : 1.5.

Now this intercept is proportional to the number of electrons in the atom. Hence OY/OY' = $3 - X/1 + X$ with $0.5 > X > 0$. The most probable value is $X = 0.25$.

This means that the Li-H bond has 25 per cent ionic character. The limiting values would be 50 per cent ionic character or complete covalency.

TABLE I.

hkl	$\frac{\sin \theta}{\lambda}$	$p \cdot z$	I_{phot}	$\left(\frac{I_{\text{phot}}}{p \cdot z} \propto F_s^2 \right)$	$F_s = f_{\text{Li}} \pm f_{\text{H}}$	F_p	F_s, F_p	e^{-B}	$\left(\frac{\sin \theta}{\lambda} \right)^2$	F_0^2
111	.212	5.22	35	6.7	2.6	.41	6.3	.93		2.8
002	.245	2.16	60	27.8	5.3	.77 ₅	6.8	.91		5.8
220	.346	1.31	25	19.1	4.4	.60	7.3	.83		5.3
113	.406	2.12	14	6.6	2.6	.41	6.2	.775		3.3
222	.424	2.04	20	9.8	3.1	.53	5.9	.765		4.1
004	.490	1.03	8	7.8	2.8	.42	6.6	.69		4.0
331	.534	2.4	8	3.3	1.8	.30	6.1	.465		2.8
224	.600	4.2	15	3.6	1.9			.571		3.3
115-333	.636	18.04	30	1.66	1.3			.535		2.4

for any value of $\frac{\sin \theta}{\lambda}$, $F_{\Sigma h=2n}$ is always $> F_{\Sigma h=2n+1}$.

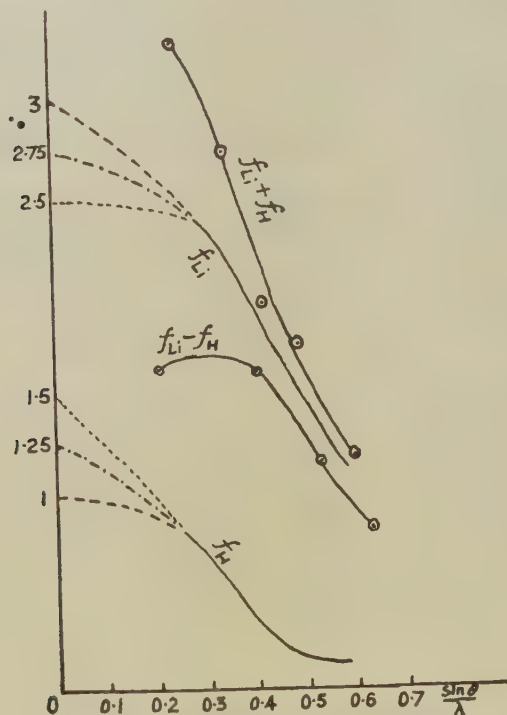
§ 4. THERMAL VIBRATION IN LiH.

The thermal scattering of LiH and LiF has been studied by means of "diffuse" Laue photographs and compared with that of KCl and other alkali halides (Ahmed : Thesis, London, 1950). The results suggest that the elastic behaviour of LiH is similar to that of LiF, but that the values of the elastic constants are higher for LiH than for LiF. The elastic behaviour of LiH is different from that of KCl.

From the results of Günther (1920), Ubbelohde (1936) calculated the Debye characteristic temperature for LiH and found $\Theta_D = 815^\circ \text{K}$. at 293°K . But Θ_D is a measure of the restoring force on the displaced lattice points and so is larger the greater this force; in other words, the harder the crystal. For simple crystals the characteristic temperature is a convenient measure of hardness in this sense (James and Brindley 1931).

Θ_D for LiF is 648°K. at 273°K. , which means that LiH is harder than LiF. This is in accordance with the evidence of the diffuse spots themselves that the elastic constants for LiH are greater than those for LiF. The mean square amplitude of atomic vibrations in LiH at 293°K. , using for Θ_D the value of 815°K. , is given by Lonsdale (1948) as $\bar{u}^2 = 0.0585 \text{ \AA}^2$. The Debye-Waller formula, $I = I_0 e^{-2M}$, which applies to cubic crystals composed of one kind of atom only, at temperatures not near to the

Fig. 1.



Atomic scattering curves uncorrected for thermal vibration.

melting point, gives $F = F_0 e^{-2M}$ where F_0 is the structure factor for the ideal crystal at rest, F is the observed structure amplitude and

$$2M = \frac{8\pi^2}{3} \left(\frac{\sin \theta}{\lambda} \right)^2 \cdot \bar{u}^2 \quad \text{or} \quad F = F_0 e^{-B \left(\frac{\sin \theta}{\lambda} \right)^2} \quad \text{where} \quad B = \frac{8\pi^2}{3} \cdot \bar{u}^2.$$

In the case of LiH, a different value of B ought to be applied to each atom, since using the same value of B implies that Li and H should vibrate with equal amplitudes. The amplitude of vibration of the lighter H atom is probably greater than that of the Li atom, and in general, thermal vibrations must be different for every crystallographically different atom

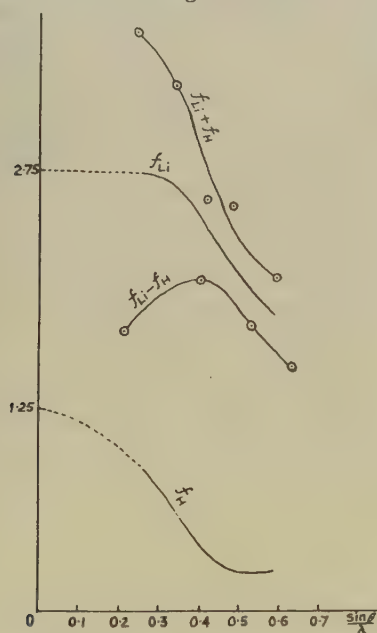
in a unit cell, since they depend on the surroundings of the atom as well as on its inertia. Due to the uncertainty in the value of B however, to a first approximation B may be taken to be the same for Li and H in LiH.

$$B = \frac{8\pi^2}{3} \overline{u^2} = 1.54 \text{ \AA}^2.$$

In Table I. the structure amplitudes F_0^s corrected for the temperature factor $e^{-B \left(\frac{\sin \theta}{\lambda}\right)^2}$ are tabulated in the last column.

Thus the curves representing $(f_{\text{Li}} + f_{\text{H}})$, and $(f_{\text{Li}} - f_{\text{H}})$ (corrected for the temperature factor) for the "all even" and for the "all odd" reflections are obtained. From these, the separate atomic scattering curves for Li^{+X} ion and H^{-X} ion, (corrected for temperature scattering), are deduced,

Fig. 2.



Atomic scattering curves corrected for thermal vibration.

and are shown in fig. 2. These give the same value of X as before. A relative variation in the temperature corrections for Li and H respectively would appear mainly in the high orders and would not affect the conclusions drawn concerning the state of ionization in LiH.

ACKNOWLEDGMENTS.

The author wishes to thank the Egyptian Government for a scholarship which made possible a period of research in England.

He is greatly indebted to Professor Kathleen Lonsdale who has been unsparing of help and advice throughout the work.

REFERENCES.

- AHMED, M. S., 1950, *Nature, Lond.*, **165**, 246.
BIJVOET, J. M., 1923, *Rec. Trav. Chem.*, **42**, 859.
BIJVOET, J. M., and FREDERIKSE, W. A., 1929, *Rec. Trav. Chem.*, **48**, 1041.
BIJVOET, J. M., and KARSSSEN, A., 1922, *Proc. Acad. Sci., Amsterdam*, **25**, 27.
BIJVOET, J. M., and KARSSSEN, A., 1932, *Z. Phys. Chemie. B*, **15**, 415.
DEBYE, P., and SCHERRER, P., 1918, *Physikal. Z.*, **19**, 474.
GERLACH, W., and PAULI, O., 1921, *Z. Physik.*, **7**, 116.
GÜNTHER, 1920, *Ann. Phys.*, **63**, 476.
JAMES, R. W., and BRINDLEY, G. W., 1931, *Phil. Mag.*, **12**, 81.
LONSDALE, K., 1948, *Acta Cryst.*, **1**, 142.
MARK, H., and TOLKSDORF, 1925, *Z. Physik.*, **33**, 681.
ÜBBELOHDE, A. R., 1936, *Trans. Faraday Soc.*, **32**, 525.
ZINTL, E., and HARDER, A., 1931, *Z. Phys. Chemie. B*, **14**, 265; 1932, *Ibid.*, **B, 15**, 416.

CI. *Observations on Carborundum of Growth Spirals Originating from Screw Dislocations.*

By AJIT RAM VERMA,

Royal Holloway College, University of London*.

[Received April 25, 1951—Revised May 26, 1951.]

[Plates XXV.–XXVIII.]

ABSTRACT.

Numerous growth spirals with shapes ranging from circular to regular hexagonal have been observed on carborundum crystals of types I. and II., by coating the crystal faces with a thin film of silver of reflectivity nearly 90 per cent and then working in reflection, using phase contrast illumination. The shapes of these spirals, in relation to the crystal structure, are shown to be in accordance with the predictions of Frank's theory. On a type II. crystal, hexagonal interlaced spirals have been observed. The annihilation of growth fronts where they meet, and other properties of growth fronts are illustrated and hence the observed patterns for two or more screw dislocations are explained. The observed density of dislocations ranges from small values up to a maximum of 10^4 per sq. cm. For a typical circular spiral the calculated values of the radius of the critical nucleus is 2μ and supersaturation is 0.2 per cent. By the application of multiple-beam interference, using both Fizeau fringes and fringes of equal chromatic order, the step heights in spirals have been measured accurately for type II. crystal and found to be 15 Å. This is equal to the height of the unit cell, proving that these are growth spirals originating from screw dislocations, in exact accordance with theoretical prediction.

§1. INTRODUCTION.

ACCORDING to Burton, Cabrera and Frank (1949) growth of crystals at low supersaturations can take place only in the presence of dislocations. A crystal should, therefore, have a number of dislocations with a screw component terminating on the crystal face. Frank (1949) showed that when growth takes place on the molecular terraces so exposed, the edges of monomolecular layers develop as "growth spirals" centred on the dislocation. Experimental evidence supporting this was found on beryl by Griffin (1950). The present paper deals with dislocations and "growth spirals" found on the faces of carborundum crystals.

* Communicated by Professor S. Tolansky.

§ 2. THE CRYSTAL STRUCTURE AND TYPES OF CARBORUNDUM.

Carborundum, a strongly homopolar crystal, occurs in at least eight known types. One of these is cubic, sometimes called β -SiC. All other types (α -SiC) are based on either hexagonal or rhombohedral unit cells. All types have identical layers, but differ in their arrangements. Each type is distinguished by the number of layers in the unit cell. The basal pinacoid is predominantly developed, and it is on this that these growth spirals have been observed.

The crystals studied were either pale green, dark green or black. Some, which have a few well developed faces, have had their structural types determined by a goniometric method (Thibault 1944). X-ray diffraction methods will be required for the others.

No cubic crystal has been studied. Most of the crystals examined were of the commonest type, carborundum II. Its unit cell is hexagonal with six layers, and in Ramsdell's notation is 6 H (Ramsdell 1947). The lattice parameters are

$$a=3.073 \text{ \AA}, \quad c=15.079 \text{ \AA}.$$

In this work the only other type available was carborundum I. This has a rhombohedral unit cell and referred to the hexagonal axes consists of fifteen layers. In Ramsdell's notation it is 15 R with

$$a=3.073 \text{ \AA}, \quad c=37.70 \text{ \AA}.$$

§ 3. VISIBILITY OF GROWTH SPIRALS.

Numerous "growth spirals" have been observed on the faces of carborundum (SiC) crystals. These spirals are well developed; over thirty turns of the spiral can be traced in some cases. The spirals are centred on a dot which must mark the point of emergence of a screw dislocation on the crystal face.

The clean surface of the crystal when examined by a metallurgical microscope, using bright field illumination, does not show up these features, the surface appearing smooth. A little amount of impurity makes these features slightly visible (fig. 8, Pl. XXVI. has been taken by this method). Breathing lightly on the crystal face, while it is under observation, increases the visibility and the "lines" flash out, but soon disappear when the water re-evaporates. The "lines" seen by breathing are dotted and slightly diffuse, but the visibility obtained by this method is high. Though convenient for visual observations, the procedure is not suitable for photography.

Following Griffin's technique, contrast was increased by deposition of a thin film of silver on the crystal face using thermal evaporation. This was improved by the use of phase contrast illumination. The photographs have been taken using positive phase contrast, the absorption of the phase plate being 80 per cent and phase retardation equal to $\frac{1}{2}\pi$. With this equipment many features are often still faint and only

just visible. Usual photographic methods for increasing the contrast have been employed in some of the photographs given.

In fig. 13 (Pl. XXVIII.), it is seen that the visibility and contrast is high compared with other photographs. The surface of this crystal was not very clean when it was silvered. The silver deposit was not uniform, the surface appearing mottled. Examination with phase contrast illumination gave high visibility. This suggests that impurity can make the steps more visible.

§ 4. SHAPE OF THE SPIRAL FOR A SINGLE SCREW DISLOCATION.

The growth spiral will have a shape depending upon the rate of advance of a growth front in different crystallographic directions.

For growth taking place in accordance with Frank's ideas two cases arise :—

- (a) when the Frenkel kinks on the step (exchange sites) are close together and the distance moved by an adsorbed molecule before it hits a step is large ;
- (b) when the kinks are few or the distance moved by the adsorbed molecule is small.

When the former conditions exist, which are more likely to occur in growth from vapour, the molecule will have a high probability of adhering to the step if adsorbed near it, irrespective of the crystallographic orientation of the step. Thus for growth from the vapour, taking the rate of advance of the ledge to be independent of direction, the ledge will form a simple spiral under steady uniform supersaturation. The form of the spiral can be represented by the Archimedian equation

$$r=2\rho_c\theta,$$

and the constant spacing between turns is

$$\delta r=4\pi\rho_c,$$

where ρ_c is the radius of critical nucleus, equal to $a\phi/2kT\ln\alpha$, and where α is the supersaturation ratio, a is the interatomic distance and ϕ is the neighbour-neighbour binding energy of the crystal.

These predictions are confirmed by the circular spirals shown in figs. 1, 2, 3 and 8 (Pls. XXV., XXVI.). It is to be noted, however, that the spiral turns are more closely spaced at the centre, and the spacing gradually increases on going away from the centre until it becomes nearly constant. This is in accordance with the prediction of theory (Burton, Cabrera and Frank 1951).

Any dependence of the rate of advance of a growth front on the orientation of the step-line could impose a distortion of the growth spirals, so that they exhibit the symmetry of the crystal face. Such an effect has been found in fig. 4 (Pl. XXVI.), where the spiral is nearly circular at the centre, and gradually takes on the hexagonal symmetry of the

crystal face (carborundum type II.). In fig. 7 (Pl. XXVI.) is a hexagonal spiral observed on a crystal identified to be of type II. This is a regular hexagonal spiral, showing clearly the dependence of the growth rate on the crystallographic orientation. The step-lines very near the centre show a curvature, which, as predicted by theory, decreases with distance from the centre. However, soon the straight step-lines start rounding off at the corners and become gradually curved on moving away from the centre. These step-lines do not meet the line of discontinuity sharply, but tend to curve away from it, as shown in fig. 7, for the outer five or six step-lines.

The straight edges show that under certain conditions there is a sharp minimum in the growth rate as a function of orientation.

In figs. 10 and 11 (Pl. XXVII.) further spirals are shown. Fig. 10 has been observed on a rhombohedral crystal type I.

§5. PROPERTIES AND BEHAVIOUR OF GROWTH FRONTS.

The growth pattern for two or more screw dislocations ending on a face is complex and depends on the properties of the growth fronts. The growth fronts starting from a single screw dislocation will spread on the surface of the crystal face in regular shapes, but the presence of a boundary or an obstruction will distort its regular shape. When the advancing growth fronts meet an obstruction they can propagate round corners, as shown at the upper end of the obstruction in fig. 4; this point behaves almost as a source of secondary growth fronts.

The growth fronts emitted by two sources of opposite sign annihilate each other where they meet. Numerous examples of this can be seen in figs. 2 and 3 (Pl. XXV.). When there are several screw dislocations actively emitting growth fronts, a point on the crystal face will be in the dominant field of only one of these, and this alone determines the number of growth fronts passing through it. This is exemplified in fig. 2 where there are five screw dislocations. By choosing the point of observation, say, near the bottom screw dislocation, the number of growth fronts passing through it is solely determined as if this alone were active.

§6. GROWTH SPIRALS FOR TWO OR MORE SCREW DISLOCATIONS.

In fig. 17 is drawn schematically the growth pattern for two screw dislocations A and B of the same hand. The ledge starting from A goes on rotating and generating the spiral until it meets at p_1 the ledge originating from B where it terminates. At p_1 the two ledges fuse with one another. As the spirals unfold themselves the ledges meet at $p_1, p_3, p_5 \dots$ in the upper half and at $p_2, p_4, p_6 \dots$ in the lower half of the figure. The locus of points of intersection for two equal spirals has been shown to be a cartesian oval (Burton, Cabrera and Frank 1951). Between p_1 and p_2 (p_3, p_4), etc., the missing parts of the two spirals are shown by the dotted lines. The resultant figure is the solid line curve.

Starting from A and going round the spiral we descend by one step in each complete turn till we come to the point p_1 . From p_1 we go round the spiral B to the point p_4 and then again on the spiral A to the point p_5 . Thus in going round the resultant curve once, we descend by two steps from p_1 to p_5 to p_9 and so on. Similarly, starting from B and going round we will descend by two steps, from p_2 to p_6 , etc. . . . As the curves gradually smooth out at the points of contact, the figure will appear to be two spirals alternately spaced. Fig. 17 has been drawn for circular spirals, and the case for spirals with straight edges can similarly be drawn where the behaviour will be the same. In fig. 3 (Pl. XXV) the case for circular spirals is illustrated.

Fig. 17.

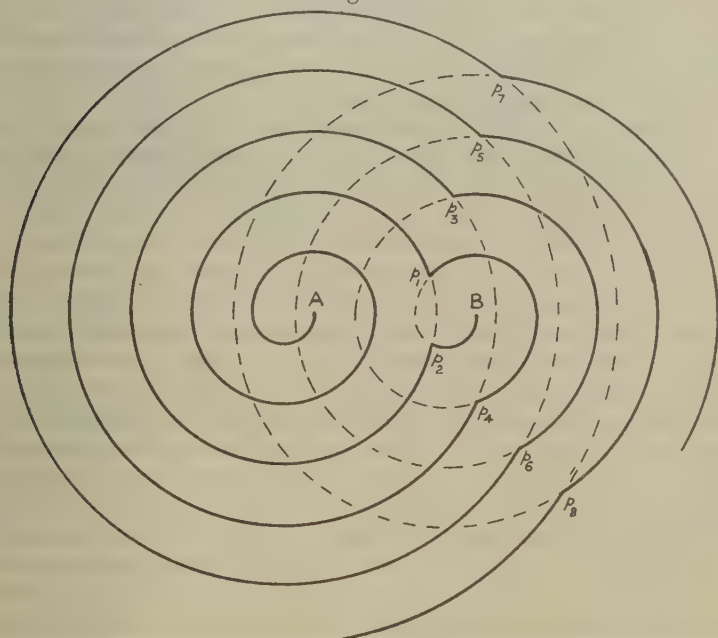


Fig. 8 (Pl. XXVI.) illustrates a unique example in which the spiral is doubled with the members strictly "parallel". It may be that the twin form arises from two close-by dislocations of the same sign, cooperating closely.

In fig. 9 (Pl. XXVII.) is illustrated the case of two screw dislocations of the same sign close to each other. The spirals are circular and developed for two or three turns after which the ledges from other neighbouring dislocations interact with them.

In fig. 10 (Pl. XXVII.) is shown another case of two similar screw dislocations close to each other, so that growth starts from both of them. The spirals are circular at the centre for one or two turns after which they settle down as spirals with straight edges. The meeting of the growth fronts

§ 9. RESULT OF MEASUREMENT OF STEP HEIGHT.

It is seen below that the step height measured in the cases so far is equal to just one unit cell.

Fizeau fringes	Fringes of equal chromatic order	Method by counting No. of steps	Crystals
15.2 Å 14.1 Å	17.1 Å	14.8 Å	Spiral in fig. 4, Type II.
14.5 Å 15.5 Å 15.0 Å 15.3 Å			Circular spiral, right of fig. 2.

§ 10. DISCUSSION OF RESULTS.

From fig. 2 (Pl. XXV), which is at magnification $\times 90$, the spacing between the successive arms of the circular spiral when it is nearly constant is approximately 2.5 mm. Using $\delta r = 4\pi\rho_c$ we have

$$\rho_c = \frac{2.5}{90 \times 4\pi} \text{ mm.} \approx 2\mu.$$

From $\rho_c = a\phi/2kT \ln \alpha$ and using Trouton's rule to estimate ϕ/kT according to which $\phi/kT = 3.5T_b/T = 6$ at an absolute temperature of 0.6 of the boiling point of the material we get

$$\alpha \approx 0.2 \text{ per cent.}$$

§ 11. DENSITY OF DISLOCATIONS.

The density of dislocations varies widely on different specimens of carborundum. In fig. 4 (Pl. XXVI.) there is only one which dominates the growth of the face. In figs. 1, 2, 3, 11 and 12 (Pls. XXV., XXVII.) there are several. The largest density of dislocations observed is shown in fig. 16 (Pl. XXVIII.). Here there are nearly 10^4 screw dislocations per square centimetre.

Another noteworthy point is that in fig. 16 (Pl. XXVIII.) there are nearly twenty screw dislocations, most of which are of the right-handed type. It is characteristic that in any one region there is a large predominance either of right-handed or of left-handed screw dislocations.

§ 12. SUMMARY.

Numerous growth spirals starting from points of emergence of screw dislocations have been photographed on the surfaces of carborundum crystals. These spirals have characteristic shapes. The shape is discussed in relation to the crystal structure. The behaviour and properties of

Fig. 2.

Fig. 1.

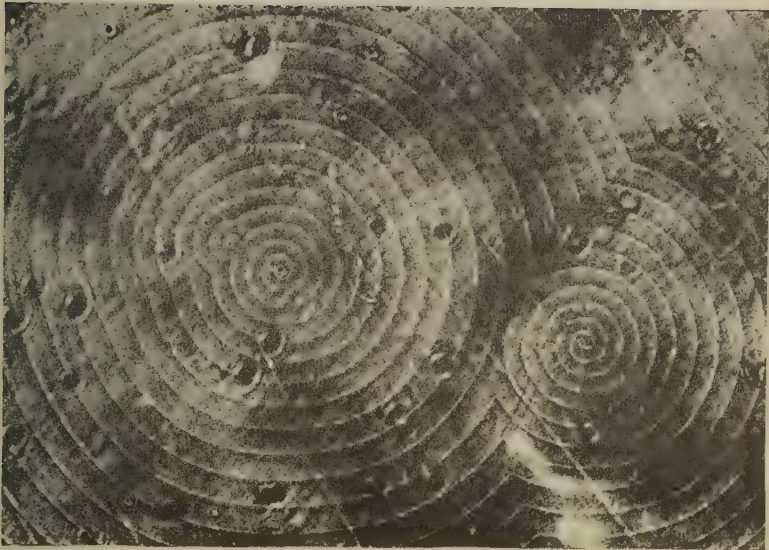


×72



×72

Fig. 3.



×200

Fig. 4.



×72

Fig. 5

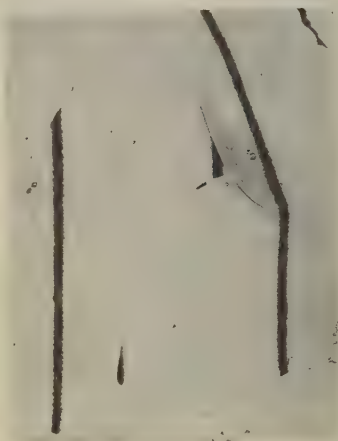
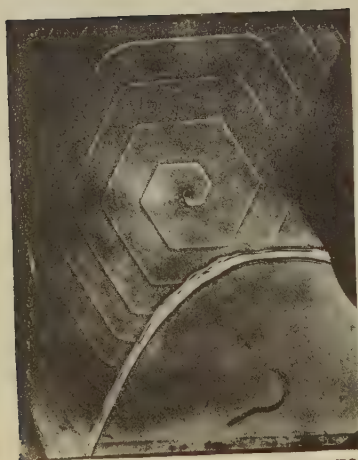


Fig. 6.

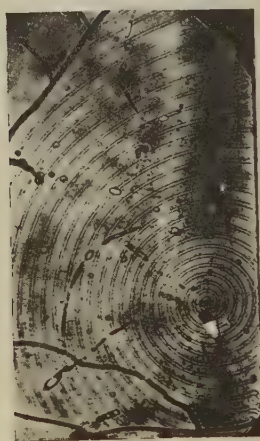


Fig. 7.



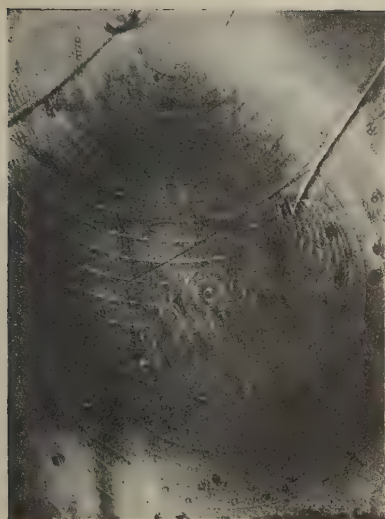
×72

Fig. 8



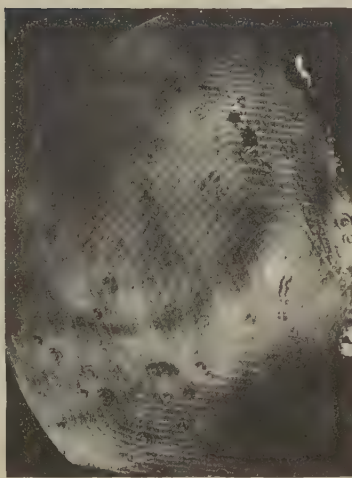
×120

Fig. 9.



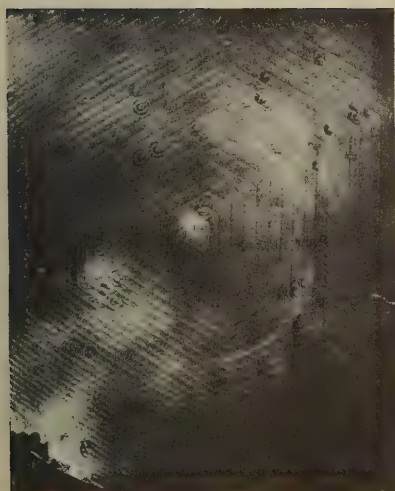
$\times 112$

Fig. 10.



$\times 72$

Fig. 11.



$\times 72$

Fig. 12.



$\times 280$

Fig. 13.



Fig. 14.



Fig. 15.

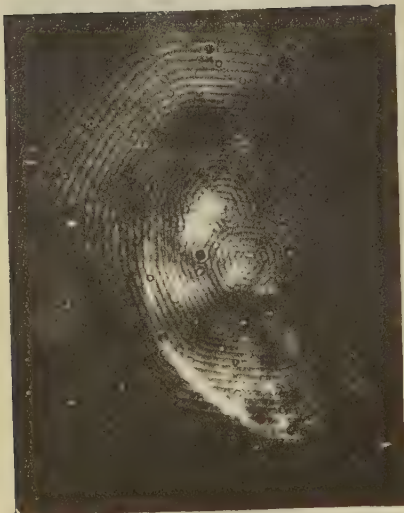


Fig. 16.



growth fronts and the growth patterns for two and more screw dislocations are illustrated. From the observations on the photographs it is shown that the type of information that can be derived is the determination of the radius of the critical nucleus, the supersaturation and density of dislocations.

The step height has been measured accurately by multiple-beam interference fringes. The step height at the edges of these growth spirals is found to be one unit cell.

ACKNOWLEDGMENTS.

I am grateful to Professor S. Tolansky for his kind interest and encouragement in the course of this work. Thanks are due to Dr. F. C. Frank for his valuable suggestions on the subject, and also to B. T. M. Willis and H. E. Rahbek for useful discussion. I am indebted to Sir K. S. Krishnan, F.R.S., and Dr. J. T. Kendall for the supply of the crystals, to the British Council, for the award of a scholarship, and to the University of Delhi for granting the study leave. This work has been carried out with instruments made available by grants by the Royal Society and the D.S.I.R.

REFERENCES.

- BURTON, W. K., CABRERA, N., and FRANK, F. C., 1949, *Nature, Lond.*, **163**, 398; 1951, *Phil. Trans. Roy. Soc.* (in press).
FRANK, F. C., 1949, *Discussions of the Faraday Society*, 5, "Crystal Growth"; 1951, this journal, page
GRIFFIN, L. J., 1950, *Phil. Mag.*, **41**, 196.
RAMSDELL, L. S., 1947, *Amer. Min.*, **32**, 64.
THIBAUT, N. W., 1944, *Amer. Min.*, **29**, 249.
TOLANSKY, S., 1948, *Multiple-beam Interferometry of Surfaces and Films* (Oxford: University Press).

CII. *The Growth of Carborundum : Dislocations and Polytypism.*

By F. C. FRANK,

H. H. Wills Physical Laboratory, University of Bristol*.

[Received June 5, 1951.]

ABSTRACT.

A discussion is given of certain features of the growth of carborundum, as illustrated in Verma's paper. It is shown that polytypism may occur as a result of growth through the rotation of a spiral growth step.

§1. INTRODUCTION.

IN the preceding paper, A. R. Verma describes growth markings that he has observed on carborundum, and shows that they are in accord with the theory of crystal growth developed by Burton, Cabrera and Frank (1949, 1951). This note deals with certain features, mainly peculiar to carborundum, which were not predicted in the paper quoted. I would like to thank Mr. Verma for showing me his photographs before publication.

§2. SHAPE OF SPIRALS.

According to our theory, growth of a crystal from the vapour should usually produce round growth spirals rather than polygonal ones. This conclusion follows from the supposition that similar forces bind a building unit into the crystal and into an adsorption position on a close-packed face: whence calculations show that on the closest-packed edge of a crystal monolayer the distance between "Frenkel kinks" is likely to be small compared with the average distance which an adsorbed molecule diffuses on the surface. The edge can only advance by the adhesion of building units to these kinks; thus the rate of advance of a step is independent of its orientation and round spirals result. If, on the other hand, the distance between kinks is large, the spirals become polygonal, tending to be straight in the orientations of slow advance, which are those in which this distance is greatest.

Carborundum, however, does not grow from *its* vapour. The most likely presumption is that the transport of C and Si from carbon and silica to the growing carborundum crystal proceeds by gas molecules of CO and SiO; the oxygen being removed as CO₂ (or perhaps O₂) which regenerates CO on the hot carbon, while CO also reduces SiO₂ to the relatively volatile SiO. Most probably the surface of the SiC crystal has a layer of combined oxygen, during growth, on which adsorbed SiO and CO molecules undergo surface diffusion. The state of the surface would then vary with temperature and with the CO-CO₂ balance

* Communicated by the Author.

in the atmosphere. Thus the surface conditions would be much more complex than those we assumed. The appearance of both round and polygonal spirals, while still unexplained in detail, does not, therefore, constitute a failure of theoretical prediction. There is indication, *e. g.* in fig. 12, that the rounded form of spiral belongs to the final stage of growth, at which it might be connected either with a lower temperature or a less strongly reducing atmosphere.

§3. VARIABILITY OF SPACING.

In nearly every case the turns of the spirals are more closely spaced near the centre than further out. This must be attributed to increased supersaturation shortly before growth ceased, which would be the natural accompaniment of a fall in temperature, but which could again be complicated by changes in composition of the atmosphere. The variations are in some cases gradual, in others, *e. g.* figs. 11 and 12, abrupt. In fig. 11 the result is that previously dominated dislocations have begun to develop their own little growth pyramids of two or three spiral turns in extent. Before the increase of supersaturation the growth steps attached to these would never have developed a full turn before the arrival of another step from the dominating centre.

Spacing is also liable to be non-uniform across a crystal face, as well as radially on each hill, as, for example, in fig. 11, where the widest spacing, indicating the fastest advance of steps, occurs in the right hand central region. The most probable cause is screening of the crystal surface by other crystals, though internal strain could also be responsible. The same cause must explain the dominance of the central dislocation over similar ones below it.

§4. HOLLOW DISLOCATIONS.

In most of Verma's pictures there is a plainly visible dot at the site of the dislocation, suggesting that its core is a hollow tube with a diameter of the order of magnitude 1 or 2 microns. This is generally to be expected from theory (Frank 1951) with dislocations of Burgers vector exceeding about 10 Å, because the large strain energy near the dislocation is then insufficient to overcome the surface energy, which tends to close the tube up.

§5. CRYSTAL STRUCTURES OF CARBORUNDUM : STACKING OPERATORS AND ZHDANOV SYMBOLS.

Before proceeding further with the discussion of Verma's photographs; it is necessary to consider the crystal structures of carborundum. In each of the known structures there is a silicon lattice, and an identical interpenetrating carbon lattice, which is one of the infinity of structures resulting from the layered close-packing of spheres. (The word layered is inserted here, because no mathematical proof appears yet to have been given for the strong presumption that every close-packing of spheres

can be dissected into close-packed layers.) As is well known, in all such structures the layers projected normally on to a plane parallel to one of them fall into three possible positions, by which they may be labelled a , b or c . The possible close-packings correspond to any sequence of these letters in which no two successive letters are alike. Taking any such sequence, for example, $abcacab \dots$, and letting these letters represent Si layers and the corresponding Greek letters represent C layers (or conversely), we obtain from it a carborundum structure $\alpha x \beta y \gamma z \alpha x \gamma \beta y \dots$. This places each atom of one kind at the centre of a tetrahedron formed by four of the other kind.

We obtain a simpler notation by introducing a pair of "stacking operators", as suggested by Nabarro (private communication). We shall use Δ and ∇ , where he proposed $+$ and $-$. These describe the relationship between a pair of layers. b after a , c after b , a after c (or, in carborundum, βy after αx , etc.) is denoted by Δ ; c after a , b after c or a after b is denoted by ∇ . With suitable choice of coordinates, Δ or ∇ represents the orientation of a triangle of spheres providing a crevice into which a sphere of the next layer fits: and the notation has mnemonic value for the fact that a rotation of 60° converts the operation Δ into ∇ .

In the special case of carborundum, Δ and ∇ have an alternative interpretation. Atoms of the crystal have strong lateral bonding in double layers (αb), (βc), etc. Instead of calling Δ and ∇ stacking operators, in this case they may be considered to denote such layers directly, Δ signifying (αb), (βc) or (γa) and ∇ signifying (γb), (βa) or (αc). It would not be a certain inference, however, that the surface layers during growth are necessarily of (αb), etc., rather than (αx), etc., type: *i. e.* whether the outer layer of atoms belonging to the crystal are triply or singly bonded to it. In the presence of gases containing oxygen this remains an open question.

In this notation the structure $\alpha x \beta y \gamma z \alpha x \gamma \beta y$ becomes $\Delta \Delta \Delta \nabla \nabla$. If the latter sequence is continuously repeated we have the structure of carborundum I. In abc notation the sequence only repeats after 15 layers. The notation can be further contracted in Zhdanov's symbol (Zhdanov 1945), which consists of pairs of numbers in each of which the first is a number of consecutive Δ s and the second the following number of consecutive ∇ s. We shall write it $Z(p_1 p_2 p_3 p_4 \dots p_{2q-1} p_{2q})$. Carborundum I. corresponds to $Z(32)$. The commonest carborundum is carborundum II., $Z(33)$, but there are many rare forms such as Ramsdell's 87 R, $Z(33 \ 33 \ 33 \ 33 \ 32)$. Cubic carborundum, $Z(10)$, which is also rare, is the only one whose conditions of formation appear to be distinctive with any certainty. It has long been recognized that the relationship between the various forms of carborundum is so close as to deserve a special name "polytypism" (Baumhauer 1915, Thibault 1943).

Ramsdell (1947) made an important generalization concerning the types of carborundum, from the eight types of ascertained structure at that date, $Z(10)$, $Z(22)$, $Z(32)$, $Z(33)$, $Z(34)$, $Z(33 \ 32)$, $Z(33 \ 33 \ 32)$,

Z(33 33 33 32): namely, that the number pair 33, which applies to the commonest type of carborundum, also occurs within the Zhdanov symbol of most of the others. He also noted the non-occurrence of the number 1. (Since Z(10) can also be written Z(nO) it does not make a necessary exception.)

It seems probable that the Z(33) structure is one either of real thermodynamic stability, or of particularly favourable growth rate, and certain that some other cause than thermodynamic stability must be responsible for structures differing from this by a change in the packing at large regular intervals. This is clear enough with the last two structures listed above, without needing to refer to such extreme cases as one which repeats its layer sequence at intervals of 198 layers (Honjo *et al.* 1950).

All the layered sphere-packings, and hence all the carborundum types have trigonal symmetry by simple rotation. One layer has 2-, 3- and 6-fold axes normal to its plane. When another layer, or more, is placed on it, the 2-fold axes fail to coincide and vanish, while 6-fold axes coincide with 3-fold axes, so that 3-fold axes remain. If the Zhdanov symbol is divisible into two similar parts, each of an odd number of terms, *e.g.* Z(11), Z(33) or Z(31 13 11), the structure becomes hexagonal by virtue of a 6_3 screw-axis. The crystal then has macroscopic hexagonal symmetry; but the force field of any close-packed layer still only has trigonal symmetry.

Apart from these hexagonal structures, the single cubic structure, and aperiodic structures, all remaining structures can be described as rhombohedral. When the difference between the number of Δ and ∇ operators is zero or divisible by 3, however, there is an alternative trigonal cell containing one-third as many atoms: there is no known example in carborundum*. The rhombohedral unit cell extends through three times as many layers as the true stacking sequence: so that the structure Z(33 33 33 32) which repeats its pattern after 29 layers is called 87 R by Ramsdell.

§6. DISLOCATIONS AND POLYTYPISM.

Polytypism as observed in carborundum is readily comprehensible in terms of the dislocation theory of crystal growth. A crystal only increases in thickness (save in the large supersaturations generally absent after nucleation of a sufficient number of crystals) by reason of the dislocations it contains. The crystal that grows hereafter is not composed of an indefinite number of layers stacked upon each other, as ideally considered, but of a finite number of interleaved helicoids (or other, more complex, expanded Riemann surfaces). Each helicoid axis is a dislocation. The structure necessarily repeats with a period corresponding to the pitch of the screw.

* Note added in proof.—One such, Z(32 23), has now been discovered: Ramsdell, L. S. and Kohn, J. A. (1951), *Acta. Cryst.*, **4**, 111.

When one observes under the microscope the growth from aqueous solution of CdI_2 or of PbI_2 to which some CdI_2 has been added (Forty 1951) one may see very thin crystal plates increasing to a considerable lateral extension (say, 1 mm.) with perfectly uniform and constant interference tint, *i. e.* not increasing in thickness at all. Quite suddenly a group of growth pyramids will appear, followed perhaps by a second and third group, each appearing suddenly. After the growth of these pyramids has proceeded for a while the observer can begin to resolve spiral growth terraces on these pyramids. Ultimately one or two will dominate the growth and the crystal will continue to increase in thickness in a steady way by the slow spreading of turns of these spirals. It is thought that the initial plate-like growth, for high degrees of supersaturation, may occur by surface nucleation, without dislocations: and that the crystal then probably becomes self-stressed through the non-uniform distribution of impurities, ultimately up to its theoretical yield stress, when the thin plate buckles and shears, so raising terminated steps in its surface. Similar phenomena may well occur in initial thin tabular crystals of carborundum, though in this case there will be alternative sources of stress, for example, due to crystals in contact, and thermal stresses due to partially screened intense radiation, etc. When this happens, if the shear is by a uniform amount with a fairly abrupt termination, the structure which grows thereafter will be that of the exposed edge at the step. If the original crystal has some simple initial structure, say, $Z(33)$, and slip is by an integral multiple of the repetition period of this structure, the same structure then grows in thickness. But if slip is by a non-integral multiple of this period the result is a polytype whose period equals the step height. Such slip leaves a misfit on the slipped surface, so should be less common than the integral slip. This would account for $Z((33)_n, 32)$ structures. It can also generate the cubic structure. It seems improbable that this always arises secondarily in this way from hexagonal $Z(33)$, but it is of interest that Thibault (1943) reports that isotropic carborundum generally contains lamellæ of $\alpha\text{-SiC}$. It requires something more to explain the absence of $Z((33)_n, 31)$, $Z((33)_n, 36)$, $Z((33)_n, 35)$ and of $Z((33)_n, 34)$ apart from the one example $n=0$. The explanation may be connected with growth rate as mentioned below, or may be connected with the severity of misfit at the slipped surface. It is alternatively possible that the initial structure contains a stacking fault in the region whose edge becomes exposed: this also gives rise to a polytype with period equal to the step height.

Before the observations of Forty and Verma were available, the author sought for an explanation of dislocations predominantly of $(33)_n$ type in the commencement of SiC growth on a quartz crystal (which has Si atoms at almost exactly the same separation). The attempt to explain the large screw pitches in this way was not successful.

Whatever the origin of the dislocations, their nature determines the crystal structure which can grow on each particular crystal seed. These

structures will differ in thermodynamic potential and in growth rate under particular conditions of supersaturation. Unstable structures will not grow if the supersaturation is small: but probably most of the observed polytypes of carborundum differ in thermodynamic potential by an amount negligible compared with the supersaturation actually occurring. On the other hand, the non-occurrence of structures with a 1 in the Zhdanov symbol can well be due to thermodynamic selection. The same may apply to those with 5 or 6 in the symbol.

It remains possible that the cubic structure is actually the thermodynamically stable one. Since its close-packed faces will form a closed body (an octahedron) it will not normally develop a thin platelet but will grow slowly in all directions. Hence, even though stable, it is at a disadvantage in growth rate when the medium is also supersaturated with respect to the alternative structures. All of these are bounded by a parallel pair of close-packed faces only, so that they can grow into large thin plates without benefit of dislocations. Their growth rates in this direction will be correlated with thermodynamic stability, and the evidence suggests that Z(33) is the preferred one of those structures.

§7. SEPARATED DISLOCATIONS.

The step generated by slip will usually not terminate abruptly, but macroscopically speaking, taper away: on the atomic scale, however, the tapering will proceed by discrete dislocations of a whole number of SiC layers, and usually a whole period of the initial lattice—six SiC layers if this is Z(33). Then the end of the slipped zone consists of a number of dislocations, all right-handed or all left-handed and usually all of the same kind. Since like dislocations repel each other, they will tend to spread apart, out of the line in which they are formed, as growth proceeds. This will account for Verma's observation that in any one area the dislocations are commonly all of the same kind. Since this is observed both on Z(33) (type II.) and Z(32) (type I.) carborundum crystals, we must infer that Z(32), as well as Z(33), is sometimes the initial structure. It could, however, be formed secondarily: *i. e.* a first buckling and slip in Z(33) could generate Z(32) and a second buckling and slip in this material generate a number of Z(32) dislocations.

There is a critical separation of dislocations, of the same order of magnitude as the diameter of the critical nucleus of the Gibbs-Volmer-Becker-Döring surface nucleation theory, and the spacing of turns of a single-branched growth spiral, such that dislocations closer than this cooperate in crystal growth, dislocations further apart do not. When they cooperate, the growth layers emanating from each of them interleave*.

*Verma's fig. 12 illustrates the phenomenon of cooperation. The three central dislocations are at such a distance apart that they do not cooperate under the high supersaturation of the final stage of growth. In the earlier phase, with wider spacing of the spirals, the two above cooperated, dominating the one below, as can be seen from the shape of the first widely spaced spiral turns.

Three cooperating dislocations, Z(33), Z(33) and Z(32), will generate a crystal of structure Z(33 33 32). It will, however, have a misfit surface on the line joining the dislocations. The surface energy of this surface will oppose their mutual repulsions and, as growth proceeds, gather them together. Finally, probably, they will unite in a single hollow core.

On the other hand, if one of the three dislocations is too far away to cooperate, and is dominated by the other two, it will constitute an imperfect dislocation of the resulting structure, attached to a fault surface extending outwards and tending to draw it away. For example, if a Z(33) and a Z(32) dislocation cooperate, the structure will be Z(33 32) and the other Z(33) dislocation will bound a fault surface extending more or less radially away from the centre of the growth hill. If the two Z(33) dislocations cooperate, the structure will be Z(33) and the Z(32) dislocation will mark the edge of a fault surface extending outwards in the same way. Changes in supersaturation can then lead to a change in the structure of the crystal which grows on a given dislocation system. But with the progress of growth the dislocations will tend to rearrange themselves in a way which reduces the sensitivity to such changes.

The fault surfaces mentioned may act as barriers to the progress of growth layers. It is possible that the discontinuity lines seen on Verma's photographs, or some of them, are of this nature.

The commonly observed coalescence or "syntaxis" (Baumhauer (1915), Ungemach (1935), Thibault (1943), Honjo (1950)) of various types of carborundum is now entirely comprehensible.

§8. CROSS-LACED GROWTH PATTERNS.

The striking cross-laced growth patterns shown in Verma's figs. 13, 14 and 15 have a simple interpretation. In all these crystals, hexagonal or otherwise, the symmetry for any growth layer advancing over another is trigonal. For each successive monolayer in the repetition sequence of the crystal the force field is slightly different. In a given orientation of the step, one monolayer in the repetition sequence will have the slowest rate of growth: the rest should therefore overtake it and pile up behind it, forming a step of height corresponding to the whole repetition period. Now, if the structure is Z(33), *i. e.*,

$$\dots \Delta \Delta \Delta \nabla \nabla \nabla \Delta \Delta \Delta \dots$$

whichever layer is the slowest growing one in a particular orientation—say, the first Δ after a series of ∇ s—then the third layer after it is necessarily the slowest growing one in an orientation inclined at 60° to the first. Hence on alternate sides of the hexagon the growth layers form alternate groupings—say ($\nabla \nabla \nabla \Delta \Delta \Delta$) and ($\Delta \Delta \Delta \nabla \nabla \nabla$). The growth steps are six layers high (15 A) on the sides of the hexagons and three layers high on the zig-zags at the edges of the hexagonal pyramids. Fig. 14, showing alternate trigonal spirals, assists the

interpretation of figs. 13 and 15, but its explanation is slightly more complicated : probably slight surface oxidation has caused the layers to retract, separating them into groups only three layers high.

The conditions necessary for this phenomenon could in principle occur on non-hexagonal structures, *e.g.* Z(32), but are not necessarily present as they are for the hexagonal structures.

Fig. 7, an apparently perfect hexagonal spiral on the hexagonal crystal, is actually more difficult to understand. We normally expect the rate of advance of a multiple step to be controlled by the deposition rate at the bottom of the step : and the symmetry here is trigonal. However, the rather high visibility of the phase-contrast image and the large central hollow at the dislocation suggests that we probably have a dislocation whose strength is a multiple of the repetition period. If so, the edge of the step will not be a close-packed surface, but will contain re-entrant angles for all orientations. The bottom of the step is then not a privileged position and hexagonal symmetry of the growth spiral is comprehensible. Indeed, it is slightly under-privileged, with respect to diffusion of molecules from the gas. It is this fact which can make the step stable against dissociation into steps of height corresponding to one repetition period, in a spiral of more than one branch.

REFERENCES.

- BAUMHAUER, H., 1915, *Zeits. Krist.*, **55**, 249.
BURTON, W. K., CABRERA, N., and FRANK, F. C., 1949, *Nature, Lond.*, **163**, 398;
1951, *Phil. Trans. Roy. Soc.* (in press).
FORTY, A. R., 1951, to be published.
FRANK, F. C., 1951, *Acta Crys.* (submitted for publication).
HONJO, G., MIYAKE, S., and TOMITA, T., 1950, *Acta Crys.*, **3**, 396.
RAMSDELL, J. S., 1947, *Amer. Mineralogist*, **32**, 64.
THIBAUT, N. W., 1944, *Amer. Mineralogist*, **29**, 249, 327.
UNGEMACH, H., 1935, *Zeits. Krist.*, **91**, 1.
VERMA, A. R., 1951, *Phil. Mag.*, **42**, 1005.
ZHDANOV, G. S., 1945, *C.R. Acad. Sci., U.R.S.S.*, **48**, 39.

CIII. *The Correlation Function in the Analysis of Directive Wave Propagation.*

By HENRIK NODTVEDT,
Cavendish Laboratory*.

[Received June 5, 1951.]

SUMMARY.

It is shown that the auto-correlation function might be applied when investigating the directive properties of waves which cover a wide frequency spectrum. Examples are given which clearly show that the subsidiary maxima in the calculated polar diagrams are reduced when widening the frequency band of the received signals. These subsidiary maxima are, further, smaller than those obtained when using ordinary phase comparison methods under the same conditions.

Some possible implications in the field of audio-acoustics are mentioned, dealing with the sense of directivity of the human ears.

§ 1. INTRODUCTION.

DURING the last decade a considerable amount of literature dealing with directive wave-propagation has appeared. Ramsay (1946, 1947, 1948), Schelkunoff (1943), Silver (1949) and Stenzel (1939) might be taken as representative of the methods used and of the results obtained. In far the most cases the waves considered are of a single frequency, and the direction of propagation is determined by comparing the phase of the wave at two or more points in space. The received waves are added and, due to the interference, the receiving system will have a definite angular discrimination determined by the position of the receiving points in addition to whatever amplitude or phase modifications are added afterwards. The resulting so-called polar diagrams might be of varying shapes and sharpness. Commonly, however, one is interested in getting a maximum sensitivity in one particular direction, and in reducing the sensitivity in other directions, particularly the so-called secondary lobes or subsidiary maxima.

The single frequency approach is largely due to the importance attached to the directive properties of aerials in high frequency and radar work. Since all the energy transmitted in these cases is contained in a very narrow frequency band, a receiving equipment with the same narrow bandwidth is essential in order to achieve optimum signal to noise performance.

If, however, one is dealing with electro-magnetic fields of the type caused by radio stars, or with an audio-acoustic field, the energy in the field is distributed over a wide frequency spectrum. If it is required to

* Communicated by Sir Lawrence Bragg, F.R.S.

determine the direction of such fields, it is, of course, possible by suitable filtering to suppress all but a narrow frequency band, and then treat the problem with single frequency methods. In this case, however, the energy contained in the rest of the spectrum is wasted, and the sensitivity of the system is consequently reduced.

It is possible in certain cases to adapt the additive phase comparison method to directivity calculations of wideband frequency fields (Stenzel 1939, p. 27), but it seems natural when dealing with such fields to explore the possibilities of the correlation methods.

§2. PRINCIPLE.

If a function of time $f(t)$ is multiplied by the value of the function τ seconds later, the product integrated with respect to time and averaged one obtains the so-called auto-correlation function

$$\phi_{11}(\tau) = \lim_{T \rightarrow \infty} \frac{1}{T} \int_0^T f(t) f(t+\tau) dt. \quad (1)$$

This function has achieved great importance in communication theory, and its characteristics have been studied for various time functions. The parameter in the integrand, indicating the delay between the two factors in the product, is in communication analysis altered by suitable delay networks, and the measurement of the correlation function is then carried out by electronic multiplication in connection with an integrating circuit.

Dealing with functions representing the propagation of waves in a field, the parameter can be given a special significance. Considering two non-directional receivers in a field (electro-magnetic or acoustic), the difference between the times of arrival of the waves at the two receivers is given by:—

$$\tau = \frac{2a \sin \gamma}{c},$$

where $2a$ = distance between receivers, c = velocity of propagation.

Realizing the simple connection between the auto-correlation parameter and the angle of approach of the incoming waves, it is obvious that the correlation function of the received signals at the two receivers is a measure of the directivity of the system. By correlating the two signals according to equation (1), a multiplicative comparison is substituted for the additive comparison used in ordinary single frequency phase methods. Using the correlation method the phase composition of the incoming waves is of no importance. This will be seen more easily if equation (1) is transformed according to Wiener's theorem (Wiener 1930). According to this the correlation function can be written as:—

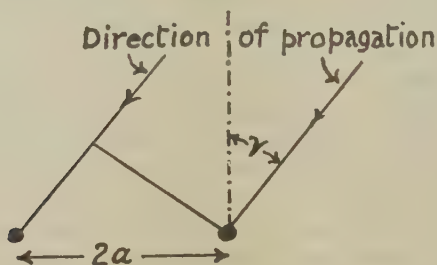
$$\phi_{11}(\tau) = \int_{-\infty}^{\infty} \phi(\omega) \cos \omega \tau d\omega, \quad (2)$$

where $\phi(\omega)$ is the frequency power spectrum of the incoming wave.

Since the angle of approach γ is contained in the parameter τ , a calculation of $\phi_{11}(\tau)$ will give a polar diagram of the receiving system, depending upon the frequency characteristic of the incoming waves and upon the frequency response of the receiving system. For the sake of simplicity, it will be assumed in the following that the sensitivity of the receivers is constant over the frequency band in question and zero outside. Likewise, it will be assumed that the energy distribution of the incoming waves will be constant over this band. This condition might be approached by suitable filtering.

If, as was assumed earlier, the two receivers are non-directional, $\phi(\omega)$ will be constant over the region of integration, and the calculation can easily be carried out. However, if receivers with finite linear dimensions are introduced, they will have a directivity of their own depending upon the frequency of the waves received. The frequency

Fig. 1.



response of the receiving system for a certain angle of approach γ will then be determined by the directive properties of the individual receivers. $\phi(\omega)$ will consequently express these directive properties as the frequency is varied, and the variation of $\phi(\omega)$ will, of course, depend on the angle of approach γ . This angle will, therefore, appear as a parameter in $\phi(\omega)$ as it appears in the other term in the integrand.

As will be known, calculation of the directive properties of electromagnetic and acoustic radiators or receivers leads to integrals of the following type (Silver 1949, chap. III. etc., Rayleigh 1896):

$$N = \int_F \eta(xy) \frac{\exp(-ikr)}{r} dF. \quad (3)$$

In the electromagnetic case N expresses one of the field components at a point in space, $\eta(xy)$ the value of the component at the surface. In the acoustic case N is the value of the velocity potential, while $\eta(xy)$ expresses the normal velocity amplitude distribution on the vibrating surface.

Further :

$$k = \frac{2\pi}{\lambda} = \text{wave constant.}$$

r = distance from integrating element to point in space.

F = radiating or receiving surface. Multiplicative constants have been ignored.

Since, however, $\phi(\omega)$ in equation (2) involves the power spectrum of the incoming signals, the expression in equation (3) has to be squared before inserting. The expression for the correlation function then takes the following form :

$$\phi_{||}(\tau) = \int_{\omega_1}^{\omega_2} N^2 \cos \omega \tau d\omega. \quad . \quad . \quad . \quad . \quad (4)$$

It will be assumed that the distance between the receivers and the source of the radiation is great compared with the linear dimensions of the receivers, and also great compared with the distance between the receivers, such that the incoming waves might be considered as plane. This is closely approximated in most practical cases. The solution of the integral in equation (3) has with these limitations been obtained for a variety of surfaces, and the solution of equation (4) is consequently simplified. Before dealing with directive receivers, however, the non-directive case will be considered.

§3. APPLICATIONS.

Case 1. Two non-directional receivers.

In this case the integration of equation (4) gives

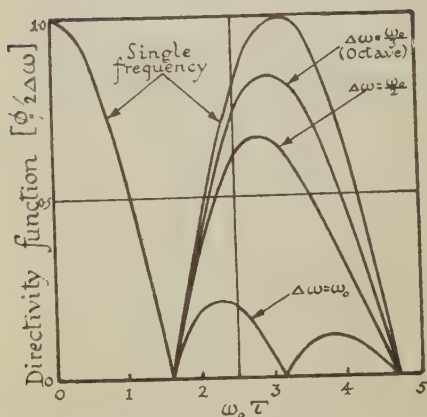
$$\phi_{||}(\tau) = 2\Delta\omega \frac{\sin \Delta\omega\tau}{\Delta\omega\tau} \cos \omega_0\tau, \quad . \quad . \quad . \quad . \quad (5)$$

where ω_0 = centre frequency of received bandwidth and $2\Delta\omega$ = received bandwidth.

It will be seen from equation (5) that the directivity of the system, apart from being determined by the distance between the receivers, is also influenced by the bandwidth. As was to be expected, the strength of the received signal is proportional to the bandwidth, but in addition, the shape of the polar diagram is modified. On fig. 2 the value of $(\sin \Delta\omega\tau / \Delta\omega\tau) \cos \omega_0\tau$ is plotted against $\omega_0\tau$ for various values of $\Delta\omega$. The first subsidiary maximum in the polar diagram is clearly reduced by increasing the bandwidth, and will for the limiting case of $\Delta\omega = \omega_0$ take the value 21.6 per cent. It is also seen that a considerable bandwidth is necessary to get a noticeable reduction. The first subsidiary maximum in per cent of the main lobe sensitivity is plotted in fig. 3. Even for a reception of an octave of the spectrum, the subsidiary maximum is only reduced to 84 per cent of the single frequency

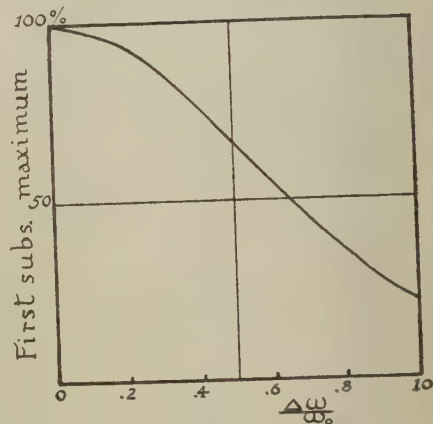
value. Since the curves for the primary maxima do not vary appreciably with varying bandwidth, this part of the function is plotted for the single frequency case only.

Fig. 2.



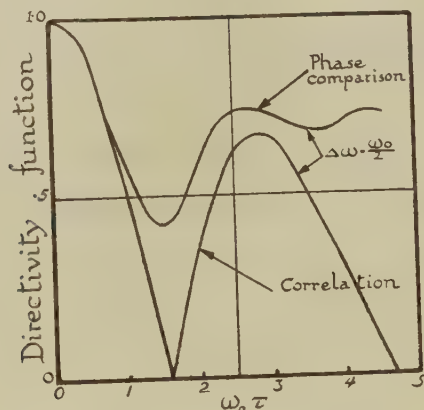
Directivity functions for two non-directional receivers.

Fig. 3.



Reduction of secondary lobes with increasing bandwidth.

Fig. 4.



Comparison of phase and correlation methods.

As a matter of interest, the directivity curve for the two non-directional receivers, calculated by Stenzel (1939, p. 28) is plotted in fig. 4. The curve is given by the equation

$$R = \sqrt{\left(\frac{1}{2} + \frac{1}{2} \frac{\sin \omega_0 \tau}{\omega_0 \tau} \cos \omega_0 \tau\right)}, \quad \dots \dots (6)$$

for $\Delta\omega = \frac{1}{2}\omega_0$. The directivity curve based on correlation is also plotted for the same bandwidth for comparison. While the correlation curve obviously approaches zero for increasing $\omega_0\tau$ the curve given by equation (6) approaches $\frac{1}{2}\sqrt{2}$. This limiting value will be independent of the bandwidth as long as two receivers are used.

Case 2. Two directional receivers.

As was mentioned, the sensitivity at a certain angle of approach of a directive receiver will vary with frequency according to equation (3). The function $\eta(xy)$ expresses how the sensitivity of the receiving surface itself varies with space coordinates independent of frequency.

In evaluating the integral in equation (4) a particular case will be taken in which the receiving surfaces are identical and rectangular, and the sensitivity function $\eta(xy)$ constant over the surfaces. Considering points at great distances from the receivers in the plane containing the surface normal and one of the sides of the rectangle, the directivity in this plane is given as

$$R = \frac{\sin x}{x},$$

where

$$x = \frac{\omega}{c} 2b \sin \gamma = \omega\tau',$$

$2b$ = side of rectangle,

γ = angle between surface normal and direction of approach.

Squaring this expression and inserting in equation (4) the following integral has to be solved:

$$\phi_{11}(\tau) = \int_{\omega_1}^{\omega_2} \left(\frac{\sin \omega\tau'}{\omega\tau'} \right)^2 \cos \omega\tau d\omega. \quad . \quad . \quad . \quad (7)$$

The solution of this is straightforward but somewhat tedious. Integrating by parts one obtains

$$\begin{aligned} \phi_{11}(\tau) = \omega \left\{ 2 \cos \alpha\omega\tau \left(\frac{\sin \omega\tau'}{\omega\tau'} \right)^2 + \frac{\alpha}{\omega\tau} \int_0^{\alpha\omega\tau} \frac{\sin x}{x} dx - \frac{2-\alpha}{2\omega\tau} \int_0^{(2-\alpha)\omega\tau} \frac{\sin x}{x} dx \right. \\ \left. - \frac{2+\alpha}{2\omega\tau} \int_0^{(2+\alpha)\omega\tau} \frac{\sin x}{x} dx \right\} \Bigg|_{\omega_1}^{\omega_2}. \quad . \quad . \quad (8) \end{aligned}$$

Here is

ω_2 = upper frequency of received bandwidth.

ω_1 = lower frequency of received bandwidth.

$\alpha = \tau/\tau'$ = ratio of distance between the centre lines of the receivers to the linear dimensions of the individual receiver.

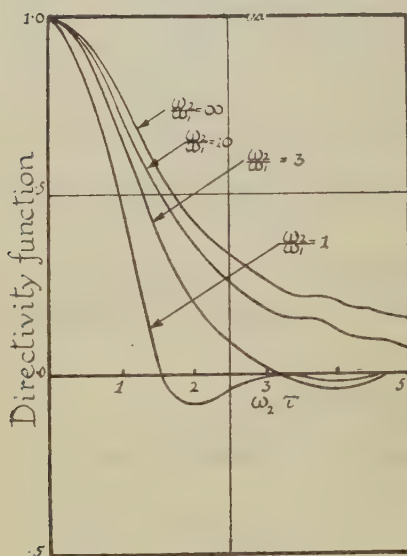
The integral might also be solved by using the convolution theorem. A rectangular gating function of width $(\omega_2 - \omega_1)$ is introduced in the integrand, and the limits are increased to infinity. The Fourier transform

of the function $(\sin x/x)^2$ is a triangle, while the transform of the gating function will be an expression of the form $\sin x/x$. Convolution of these transforms in the time domain leads to the solution.

Choosing various values for α the polar diagrams (directivity functions) for the receiving system are plotted on figs. 5, 6, 7, using the tabulated values for the Sine Integral and reducing the maximum amplitudes to unity. The ratios between the upper and lower frequencies of the band are in all cases given the values 1, 3, 10, ∞ , corresponding to bandwidths of 0, 50, 91 and 100 per cent.

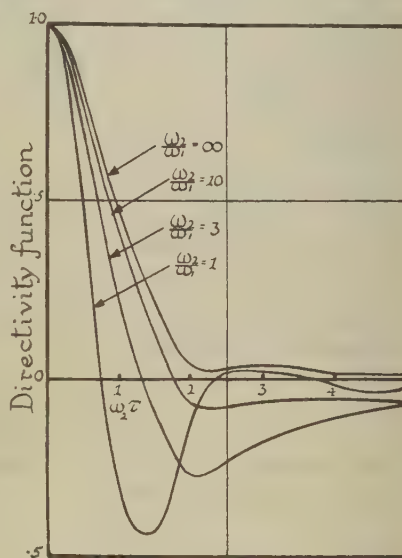
The reduction of the subsidiary maxima is most predominant when the two receivers are close together, *i. e.* when α is small. As will be seen, the secondary lobes might almost be brought to disappear when $\alpha=1$

Fig. 5.



Directivity functions when
 $\frac{\text{Distance between receivers}}{\text{Dimensions of receivers}} = \alpha = 1.$

Fig. 6.



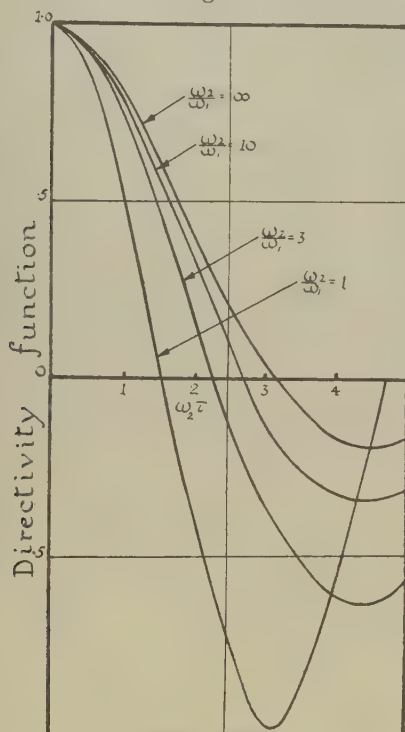
Directivity function when
 $\frac{\text{Distance between receivers}}{\text{Dimensions of receivers}} = \alpha = 2.$

or $\alpha=2$, by a sufficient widening of the spectrum. For big values of α , although the relative reduction is quite considerable, the value of the secondary lobe is still a high percentage of the primary maximum, as is shown on fig. 7 for $\alpha=10$. In fact, for increasing distance between the receivers, the secondary lobe is approaching 21.6 per cent of the primary when widening the bandwidth to the maximum possible extent, as in the earlier described case. This is of course due to the fact that the

fairly slow variation of the directivity of the individual receivers is negligible compared with the rapidly varying term caused by the separation of the receivers.

A plotting of polar diagrams for the receiving system for values of α greater than 10 is therefore not considered necessary, unless the other subsidiary maxima, where the individual directivity makes itself felt, have to be investigated.

Fig. 7.



Directivity functions when

$$\frac{\text{Distance between receivers}}{\text{Dimensions of receivers}} = \alpha = 10.$$

It ought to be noticed that even in single frequency fields the polar diagram based on correlation has smaller secondary lobes than that based on phase comparison. In the case of $\alpha=1$, the first subsidiary maximum would in the latter case be 21.6 per cent. From fig. 5 it is realised that this is considerably more than the value reached by the curve for $\omega_2/\omega_1=1$. The reason for the reduced secondary lobe by using correlation in this case, is due to the multiplicative comparison resulting in a squaring of the original directivity curve.

The preceding calculation may be carried out for receivers of various shapes. For two receivers with circular surfaces, the individual directivity curve is given by

$$R = \frac{J_1(kr)}{kr},$$

where $J_1(kr)$ = Bessel Function of first order,
 r = radius of receiving surface.

This curve differs from $\sin x/x$ in being slightly blunter for the same argument, and in having smaller subsidiary maxima. It will, however, not give radically differing results when introduced in the calculations. The calculations get increasingly difficult when receivers with varying sensitivity over the surfaces are introduced. Likewise, a correlation of more than two received signals will in most cases be too complex to be analysed.

§ 4. CONCLUSIONS.

It has been shown that correlation methods can be applied to directivity calculations, especially dealing with waves covering a wide frequency spectrum. The secondary lobes are reduced by increasing the bandwidth and might in certain cases take negligible values. To get a substantial reduction of these lobes, however, bandwidths of 50 per cent or more must be used. It is therefore doubtful if the method will be of practical importance in high frequency problems, even if a reduction of secondary lobes is also obtained in single frequency cases.

In audio-acoustics, however, bandwidths of several octaves are frequently encountered. In fact, single frequency fields seldom occur. The sensitivity of the human ear to sound waves stretches from 16 c./sec. to 16,000 c./sec., for a person with a normal sense of hearing. Over this frequency range a pair of human ears has a surprisingly accurate sense of direction (Kock 1950). Experiments with single frequency sound sources have led to the belief that the sense of direction is based on phase comparison, since in this case the determination of direction coincides with the direction of phase equality. It is known, however, that the direction of pulses, transient waves and complex noises generally is more easily determined than is that of continuous single frequency sound. In the case of those complex wide-band frequency noises, phase equality will exist for several frequency components for various angles, apart from the ahead direction, and one ought to expect that the sense of direction would be impaired. Attempts to explain the sense of direction at higher frequencies have taken diffraction phenomena around the head into account, and this might be the reason for the experienced results.

On the other hand, if the sensitivity of direction of the human ears is based on a sort of correlation mechanism, the phase composition of the incoming sounds would be of no importance and the sense of direction

would automatically be improved by an increasing bandwidth. For single frequency sounds the correlation would lead to the same results as experienced in the experiments carried out.

One further argument for the correlation point of view is the fact that a sound is detected more easily against a "white noise" background if the sound and noise sources are angularly displaced, *i. e.* the masking effect of the noise source is gradually decreasing if it is moved away from the ahead direction. It is difficult to see how this can be explained on a pure phase basis, while according to the preceding treatment the influence of the auto-correlation function of the noise received at the two ears will be reduced when the noise source is angularly displaced from the sound source.

ACKNOWLEDGMENTS.

This work was done during the tenure of a fellowship from Norges Teknisk Naturvidenskapelige Forskningsråd, to which institution acknowledgment is paid. Thanks are also due to Mr. J. A. Ratcliffe, Cavendish Laboratory for helpful suggestions and discussions.

REFERENCES.

- KOCK, W. E., 1950, *J. Acoust. Soc. Amer.*, **22**, 801-804.
RAMSAY, J. F., 1946, *Marconi Review*, **9**, No. 4; 1947, *Ibid.*, **10**, Nos. 1, 2, 3, 4; 1948, *Ibid.*, **11**, Nos. 1 and 2.
RAYLEIGH, 1896, *Theory of Sound*, Vol. II., p. 107.
SCHELKUNOFF, S. A., 1943, *Bell. Syst. Tech. J.*, **22**, 80-107.
SILVERS, 1949, *Microwave Antenna Theory and Design* (M.I.T. Radiation Laboratory Series), Vol. 12.
STENZEL, H., 1939, *Leitfaden zur Berechnung von Schallrörgängen* (Berlin: Springer).
WIENER, N., 1930, *Acta Mathematica*, **55**, 117-258.

CIIV. *Masses and Modes of Decay of Heavy Mesons**.—
Part I. κ -Particles.

By C. O'CEALLAIGH †,
H. H. Wills Physical Laboratory, University of Bristol ‡.

[Received July 15, 1951.]

[Plates XXIX. & XXX.]

SUMMARY.

Observations by the photographic method are described which establish the existence of heavy charged mesons, of mass about $1200 m_e$, which decay with the emission of a single charged particle. In one case, it is shown that the secondary charged particle is a μ -meson of energy 5.9 MeV. In another, it is a particle of charge $|e|$ and of energy about 200 MeV. If the two particles are of the same type with similar modes of decay, then the charged secondary particle must be accompanied by at least two neutral particles. The question whether the κ -particles are identical with the τ -mesons which decay into three charged particles, is discussed.

§1. INTRODUCTION.

FOUR events have recently been found in this laboratory, recorded in photographic plates exposed to the cosmic radiation, which represent the decay of charged particles of mass $\sim 1200 m_e$. The particles were at, or very close to, the end of their range when they transformed into a single particle of charge $|e|$ and one or more neutral particles. It will be convenient to refer to such unstable heavy particles with this mode of decay, as κ -mesons.

The four examples found hitherto have all occurred in plates of type Ilford G5, with emulsion thickness 400μ , exposed on the Jungfrauoch high altitude station under a lead plate 30 cm. thick. Two of them, which we shall refer to as κ_1 and κ_2 , respectively, give particularly favourable conditions for measuring the mass and energy of the particles, and it is with a study of these two particles that this paper is chiefly concerned.

The first example of these heavy mesons was found while studying the distribution in energy of the electrons emitted in the decay of μ -mesons. Superficially the event appeared to be of this type, but scattering observations showed that the energy of the secondary particle, if an

* The main features of this and the following paper were given at the Copenhagen Conference on Quantum Physics on July 5th, 1951.

† On leave of absence from University College, Cork.

‡ Communicated by Professor C. F. Powell, F.R.S.

electron, was ~ 240 MeV. This is more than four times the maximum energy of the decay electrons from μ -mesons, and the characteristics of the primary particle were therefore examined. Its track was then found to provide unambiguous evidence that the primary particle was several times more massive than a μ -meson, but less massive than a proton.

§ 2. CHARACTERISTICS OF THE PRIMARY PARTICLE κ_1 .

A photo-micrograph of the event is shown in Pl. XXIX. The primary particle decayed near the glass of the plate. It had entered the emulsion through the surface, and its path could be traced in the emulsion of another plate facing it. The track of the secondary particle also passed out of the surface of the emulsion, but near one of the cut-edges of the plate so that it was lost to further observation.

The point of decay of the primary particle is at P in Pl. XXIX. That its direction of motion was towards P is proved by the trend in the values of both multiple scattering and grain density. The appearance of the end of the track is that of a particle which had come to rest before decaying, and in what follows, it will be assumed to have done so.

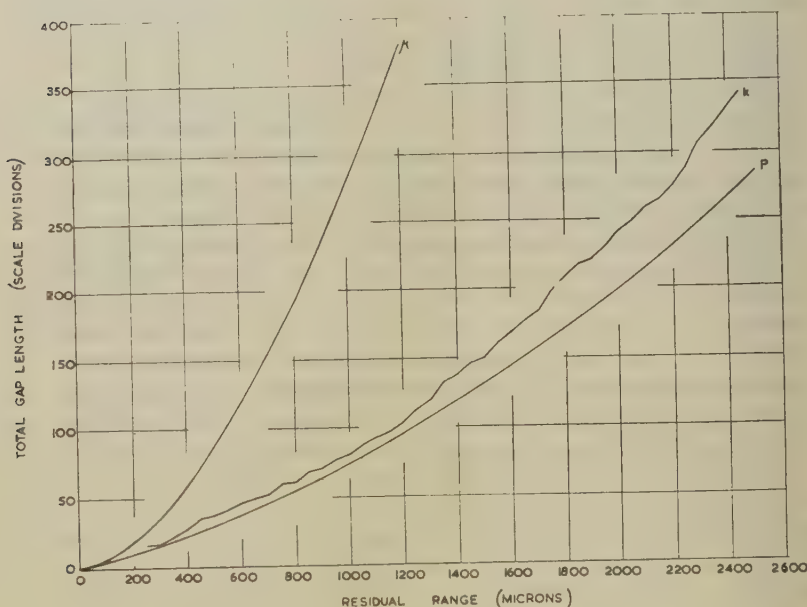
Since the length of the track exceeded 4000μ , it was possible to obtain a good estimate of the particles' mass by measuring the multiple scattering as a function of residual range. In determining the mass, allowance was made for the variation of energy along the track by a method developed in this laboratory by Menon and Rochat (1951). The track was long enough to allow four independent estimates of the mass of the primary particle to be made. The measurements were repeated by three different observers, and gave a mean value of $1260 \pm 290 m_e$.

An independent estimate of the mass of the primary particle was made by measuring the "gap-length" in the track as a function of residual range (Hodgson 1950), and for this purpose the emulsion was calibrated by making gap-counts on the tracks of four identified μ -mesons and six protons. These particles all travelled from the direction of the surface and, following a similar path, came to rest in the emulsion at about the same depth as the primary particle κ_1 . This precaution was taken to make the comparison as exact as possible. It was necessary because overfixing had produced some "etching" of the tracks in the surface layers of emulsion down to a depth of about 50μ .

The measurements of gap-length were confined to regions $>50\mu$ from the surface, and the results are shown in fig. 1. Mean curves are given for the total gap-count (in eye-piece scale divisions) as a function of residual range, for μ -mesons (μ) and protons (P). The curve of total gap-length for the primary particle is denoted by κ . This evidence alone proves that the decaying particle is more massive than a π - or a μ -meson. The estimate of its mass was derived from the results shown in fig. 1 by a procedure due to Perkins (1948). Further, an empirical relation, deduced from the experimental results for the μ -mesons, allowed the mass of any particle of unit charge to be expressed in terms of the total gap-count

in its track—as measured between any selected pair of values of the residual range. This gave a second estimate of the mass. A number of independent values were obtained by both procedures and showed satisfactory agreement. The mean value was $1385 \pm 200 m_e$, and this is in accord with the value $1260 \pm 290 m_e$ obtained by the independent method based on observations of scattering and residual range. Giving equal weight to the two results, we adopt a value $1320 \pm 170 m_e$ for the mass of particle κ_1 .

Fig. 1.



§ 3. THE SECONDARY PARTICLE.

The visible length of track of the secondary particle was 2200μ , and its grain-density 18.5 ± 0.9 per 50μ , a value not significantly different from the minimum value observed in the same plate; namely, $g_{\min} = 17 \pm 0.8$. The mean deviation $\langle \phi \rangle$, due to multiple scattering, was very carefully determined by several observers using different microscopes. The results, which were consistent, were analysed using several cell-sizes. The mean value, reduced to the standard cell-size of 100μ , was $\langle \phi \rangle_{100} = 0.10 \pm 0.014^\circ$. This allows an estimate of the value of the quantity $p\beta$ for the particle. We have $p\beta c = K_{100} / \langle \phi \rangle_{100}$, where K_{100} is the so-called "scattering constant" for 100μ cells. We set $K_{100} = 25$ giving $p\beta c = 250$ MeV. (Gottstein *et al.* 1951).

The above values of $\langle\phi\rangle_{100}$ and grain-density are such that the probability that the mass exceeds $400m_e$ is negligible. The scattering measurements therefore show that the momentum of the particle was within the interval from 250–300 MeV./c.

§ 4. NATURE OF THE NEUTRAL PARTICLES.

The conservation laws of momentum and energy demand that one or more neutral particles be emitted in the decay of the parent particle. If a single neutral particle is produced, an approximate value of its mass may be determined if the nature of the charged secondary particle is assumed. The results are summarized in Table I. It will be seen that the uncertainties in the mass of the primary particle, and of the momentum of the secondary, result in large limits of error for the estimated mass of the neutral particle.

TABLE I.

Assumed nature of charged particle	π	μ
Mass of neutral particle (m_e)	$430 \begin{smallmatrix} +370 \\ -430 \end{smallmatrix}$	$540 \begin{smallmatrix} +330 \\ -540 \end{smallmatrix}$

The limits of uncertainty given in Table I. have been estimated by assuming that the experimental measurements of m_κ and $\langle\phi\rangle_{100}$ are each in error by one standard deviation, and then choosing the combinations of these which yield extreme values. Thus, we see that if a two-body decay is assumed, the experimental results do not exclude any of the following modes of decay :

$$\kappa_1 \rightarrow \pi \text{ or } \mu \quad +\nu \quad . \quad . \quad . \quad . \quad . \quad . \quad (1)$$

$$+\pi_0 \quad . \quad . \quad . \quad . \quad . \quad . \quad (2)$$

$$V_0 (800m_e) \quad . \quad . \quad . \quad . \quad . \quad . \quad (3)$$

$$\rightarrow e \quad +\nu, \quad . \quad . \quad . \quad . \quad . \quad . \quad (4)$$

where ν , π_0 and V_0 represent, respectively, the neutrino, the neutral π -meson and the lighter neutral V-particle, evidence for the existence of which has been put forward by Rochester and Butler (1947) and by Armenteros *et al.* (1951).

§ 5. PARTICLE κ_2 .

Photo-micrographs of the second example of the decay of a heavy meson, κ_2 , are shown in Pl. XXX. Superficially the event appears to represent the successive decay of a π -particle, $\pi \rightarrow \mu \rightarrow e$, but the μ -meson has the exceptional range of 1098μ .

The range of a μ -meson emitted in the decay of a π -meson is very sensitive to any small residual velocity of the parent particle, and further, it is well known that the departures from the mean of the values of the range commonly observed, can be attributed to straggling (Powell 1948). The residual range of the π -meson at its point of decay in a solid material must commonly be less than a fraction of a micron. It must be anticipated, however, that decay in flight will sometimes be observed in the emulsions of a second plate facing it, and at first sight it appears reasonable to attribute the present observation to such a process. It is, however, very difficult to maintain this view.

The observed range of the μ -meson in the present event is 1098μ . Since its range is much greater than that resulting from the decay of a π -meson at rest it must, if due to such a process, have been thrown forward, and not backward, with respect to the line of motion of the parent particle. It will be seen, however, that the μ -meson was apparently ejected backward. To overcome this difficulty it is necessary to make the unlikely assumption that immediately before its instant of decay the parent particle was scattered backwards through a large angle, subsequently decaying before the change in its direction of motion had been made manifest on its track.

In view of these considerations, the track of the parent particle was studied in detail. The track κ_2 is only 350μ long, but the particle entered at the surface and its path can be traced in the facing plate, its length in this emulsion being $\sim 5800\mu$. Determinations of the mass of the particle by methods similar to those described for κ_1 , give a mean value of $1125 \pm 140 m_e$. Hence, in this case also, we are dealing with the decay of a particle several times more massive than a π -meson.

§ 6. NATURE OF THE CHARGED SECONDARY PARTICLE.

It has been assumed that the secondary particle is a μ -meson and the evidence for this view is very strong. Its track is sufficiently long to allow estimates of its mass to be made, and the value thus obtained is between 200 and $300m_e$. If it is a particle of which the existence is already established, it must therefore be either a π^- or a μ -meson. The particle emitted at the end of its range has a specific ionization not significantly different from the minimum value. The direct β -decay of π -mesons has never been observed, and in an extended study, by Menon, Muirhead and Rochat (1951), of more than 3000 π^- -stars of all types, only two cases have been found where relativistic particles were emitted (electrons ~ 5 MeV.). These reasons seem sufficient to reject the possibility that the parent meson is a π -particle. On the other hand, the observations are completely consistent with the view that the secondary particle is a μ -meson which decays into an electron. The track of this final particle is too short, $\sim 150\mu$, to allow further support for this view

to be obtained by a measurement of its energy, but the straightness of the track suggests that this was greater than ~ 10 MeV.

§ 7. NATURE OF THE NEUTRAL PARTICLES.

If a single neutral particle is assumed to provide the momentum and energy balance in the transmutation, its mass can be determined with much greater precision than in the case of κ_1 . In the present event the momentum and mass of the charged secondary particle are accurately known, and the errors arise almost entirely from the uncertainties in the mass of κ_1 . Further, the momentum of the charged particle is so small that most of the residual energy must appear as the rest-mass of the secondary neutral particle. The result obtained for the mass of the neutral particle is $900 \pm 130 m_e$, and the "Q" value of reaction is ~ 7 MeV. Thus decay of κ_2 to μ accompanied by either ν or π_0 is excluded, but it is possible to identify the neutral particle with the neutral V particle of mass $800\text{--}900 m_e$. Armenteros *et al.* (1951) describe a remarkable case of the decay in flight of a charged V-particle which was apparently associated with the decay in flight of a V^0 -particle. At first sight it would seem reasonable to identify the postulated two-body decay of κ_2 with this process. However, calculations show that the Q-value of the cloud-chamber event must be several times greater than that of the decay of κ_2 . It seems very unlikely, therefore, that both events are examples of a similar two-body decay of the same type of particle.

In addition to the events κ_1 and κ_2 , two other examples of decay of a heavy meson have been observed, in which the secondary particle produces a track of minimum grain-density, but the geometry of the events is such that the mass of the decaying particles cannot be accurately measured. It is, however, possible to show that they have a mass several times that of the π -meson, and it is reasonable to suppose that we are dealing with events similar in character to κ_1 and κ_2 . In both cases the grain-density of the track of the secondary particle was indistinguishable from the minimum.

Hitherto, no consideration has been given to the possibility that the two events κ_1 and κ_2 represent similar modes of decay of particles of the same type. Since the estimates of the masses of the two particles do not differ significantly, this possibility cannot be excluded. If it is correct, both particles must decay with the emission of a μ -meson and two or more neutral particles.

If the two particles κ_1 and κ_2 are indeed of the same type, it is at first sight surprising that in the first two examples observed to decay at rest, there is such a wide disparity in the energy of the charged μ -meson. This difficulty largely disappears when it is considered that an event of the type κ_2 is much less likely to escape observation than one of type κ_1 . It is clearly essential to observe other examples of similar

particles which provide tracks suitable for measurement, both of the primary and secondary particles, before any final decision on these questions can be reached.

§ 8. RELATION OF THE κ - AND τ -PARTICLES.

The determinations of the mass of the κ -particles and the results of similar measurements on the τ -particles are summarized in Table IV. of the following paper. The results suggest that the κ -particles are about 1.3 times more massive than the τ -particles, but the inaccuracies in the experimental values are such that the possibility cannot be excluded that they represent alternative modes of decay of particles of the same type. Further, they may also be of the same type as the unstable charged particles of Rochester and Butler which are observed to decay in flight. It has been pointed out by Bethe (1951) that this is the most economical assumption, in the sense that it calls for the smallest number of different types of heavy mesons. We believe, however, that the experimental evidence, while not decisive, is against such a view. The most cogent reasons are the following :

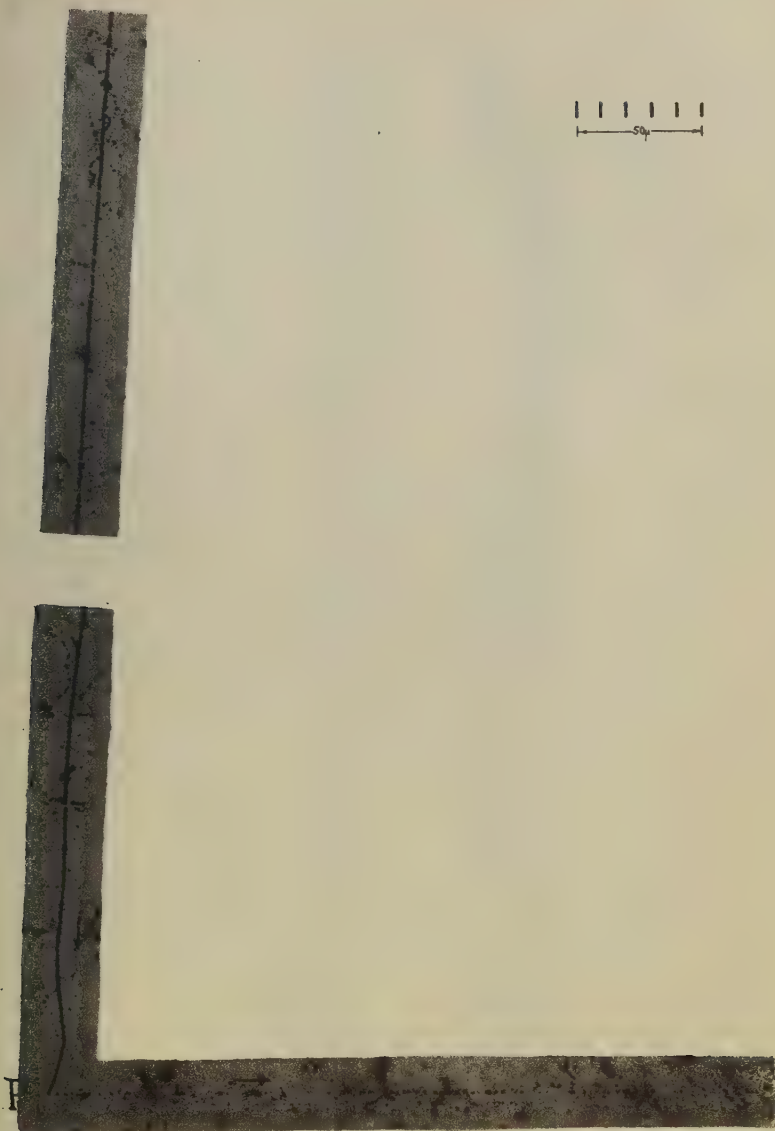
Assuming that $\kappa_1 \equiv \kappa_2 = \kappa$; and that $\kappa = \tau$, it follows that the spins of τ and κ are equal. Further, since τ is believed to decay into three π -particles, it follows that its spin is integral.

Suppose that κ decays with the emission of a μ -meson of half-integral spin and two neutral particles. Since κ is assumed to be of integral spin the two neutral particles cannot be similar. One must be half integral and the other integral. The simplest mode of decay of κ , involving known particles only, is then represented :—

$\kappa \rightarrow \mu + \nu + \pi_0$, (i.) where ν and π_0 represent a neutrino and a neutral π -particle respectively.

The most accurate determination of the mass of a heavy meson appears to be that of the τ -particle, viz., $966m_e$, and assuming the identity of τ and κ , this is also the mass of κ . In the event κ_1 , however, the scattering $\langle \phi \rangle_{100}$ of the secondary particle corresponds to a value of the quantity $p\beta$ equal to $250 \text{ MeV./}c$; if this secondary particle is a μ -meson, its energy is therefore 182 MeV. Applying the conservation principles to the mode of decay (1), and assuming the neutrino to have negligible energy, the mass m_e is found to be $1160m_e$. The uncertainties in the value of $\langle \phi \rangle_{100}$ for the secondary particle are such that we cannot exclude this mode of decay for a particle of mass $966m_e$. Since, however, we have assumed little energy to be taken by the neutrino, it appears improbable that the mass of the parent meson κ_1 is as low as $966m_e$.

These considerations do not exclude the possibility that the various charged V and κ particles, which emit a single charged secondary particle, represent a variety of modes of decay of particles of the same type. But it would be surprising to find several different modes, occurring with approximately equal probability, such as the limited experimental material suggests.



A heavy meson, κ_1 , reaches the end of its range and decays with the emission of a single particle of charge $|e|$. The track of κ_1 was longer than 4000 microns and measurements of scattering and grain-density give a value for the mass of the particle $1320 \pm 170 m_e$. The energy of the secondary particle, if a μ -meson, is 180 MeV.; if an electron, 250 MeV.

Observer : Miss A. Stradling ; Photograph by : A. R. Gattiker and Miss P. Dyer.

To face page 1038

CV. *Masses and Modes of Decay of Heavy Mesons**.—
Part II. τ -Particles.

By P. H. FOWLER, M. G. K. MENON, C. F. POWELL and O. ROCHAT,
H. H. Wills Physical Laboratory, University of Bristol†.

[Received July 15, 1951.]

(Plates XXXI. & XXXII.)

SUMMARY.

Further evidence which establishes the existence of heavy charged mesons which decay into three charged particles is presented. It is shown that the three secondary particles are probably π -particles, and that the mass of the parent mesons, called τ -particles, is $966 \pm 8m_e$. The frequency of occurrence of κ - and τ -particles at the Jungfraujoch, in comparison with the number of π -particles, is discussed, and it is shown that in the nuclear collisions involving protons of energy greater than 10 BeV., a large fraction of the energy lost in the creation of mesons, must appear as κ - and τ -particles. The evidence suggests that the life-time of the heavy mesons is about 10^{-9} sec. The most favourable conditions for the detection of the particles by the photographic method are discussed.

§1. INTRODUCTION.

MORE than two years ago a description was given (Brown *et al.* 1949) of an "event", recorded in a photographic emulsion, which appeared to represent the spontaneous decay of a charged particle with mass $\sim 1000m_e$ into three mesons, probably π -particles. Photo-micrographs of the tracks are reproduced in Pl. XXXI. Although the evidence for the interpretation was very strong, it was necessary to observe similar events before the existence of heavy mesons with this particular mode of decay could be taken as established.

Support was long in coming, but about a year ago, Harding (1950) published a description of two observations similar to the first. In each, three particles appeared to diverge from a point at the end of the range of another particle, and the directions of motion of the three emergent particles were co-planar. Further, one of the two new events allowed the mass of the parent particle to be estimated, and the value obtained was again of the order of $1000m_e$.

Another example with similar characteristics, which gives exceptionally favourable conditions for measuring the mass of the primary particle, has recently been found in this laboratory. The mass of the particle is $969 \pm 10m_e$, assuming that of the π -meson to be $274m_e$ (Alvarez 1950). The observations on the two previous events have been reinterpreted,

* A letter to the Editor on the same subject by P. E. Hodgson is also published in this issue, *see* p. 1060.—*Editor.*

† Communicated by Professor C. F. Powell, F.R.S.

and they are shown to be consistent with this value. We therefore believe that the existence of these particles with their distinctive mode of decay can now be taken as established. It will be convenient to refer to them as τ -mesons.

In this paper, the main features of the new observations are first outlined and compared with the earlier results; the original evidence on the nature of the secondary particles is supported and an improved value for the mass of the τ -particles deduced. The frequency of occurrence of the heavy mesons and the best experimental conditions for their detection by the photographic method are then discussed.

§ 2. NEW OBSERVATIONS.

A mosaic of photo-micrographs of the new event which was found in an Ilford G5 emulsion, 400μ thick, exposed for five weeks at the Jungfraujoeh under 30 cm. of lead, is shown in Pl. XXXII. The direction of motion of the particle which produced the track τ is unambiguous, and the particle was at, or very close to, the end of its range at the point P. The total length of the track in the emulsion is 2070μ . The measurements of the scattering of the particle as a function of the residual range gave a value of $1015 \pm 280m_e$ for its mass. Using, in addition, the information given by gap-counting, the best value obtained was $1000 \pm 180m_e$.

From the point P, three particles with charge $|e|$ diverged, and they all left the emulsion before coming to rest. One particle, however, track a , moved nearly parallel to the plane of the emulsion, and it entered the glass 6.4 mm. from P. It was then moving relatively slowly, as shown by the scattering of the track, and its residual range at the point of exit from the emulsion was only about 400μ . Tracks (b) and (c) dip much more steeply and, in the emulsion, they are only 120μ and 490μ long, respectively. These values represent the true lengths after correction for dip.

The tracks, a , b and c are sufficiently long, and sufficiently straight, to allow their orientations to be measured accurately. The observations show that the initial directions of motion of the particles were co-planar to within the limits of error of the measurements: in the emulsion, before processing, the direction of any one particle was inclined to the plane containing those of the other two at an angle of $2^\circ \pm 2^\circ$. This feature—also observed in the three events previously described—makes it reasonable to assume that the charged particles are the only products of the decay of the parent meson.

The great length of the track (a) makes it possible to determine the mass of the particle—by observations on the grain-density and the scattering parameter, $\bar{\alpha}$ —over a succession of segments of the track, and the mean of the values thus obtained was $285 \pm 20m_e$. It is therefore almost certain that the particle was not a μ -meson, and the result strongly suggests that it was either a π -meson or an unknown particle of nearly equal mass. We shall assume the former.

Results obtained for the mean angle of scattering, $\bar{\alpha}$, and grain-density for different intervals along the track are given in Table I. The measurements show conclusively that the particle had lost almost all its initial energy before it entered the glass. By comparing the results of Table I. with similar data obtained on tracks of μ -mesons and protons which stopped in the emulsion, we have deduced a value for the residual range, r , of the particle as it left the emulsion of $400 \pm 200 \mu$. The best value for the initial energy of the particle is then determined from its range in the emulsion, which is $R = 6.8 \pm 0.2$ mm. The value of the initial energy thus determined is insensitive to the errors in the estimate of r ; the uncertainty in the energy of the particle at P, introduced by these errors, is of the same order of magnitude as that due to straggling. Using the range-energy relation for protons (Lattes *et al.* 1947, Bradner *et al.* 1950), the energy of a particle of mass $274m_e$ and range 6.80 mm. can be shown to be 19.0 ± 0.4 MeV.; and its momentum 75.4 MeV./c.

TABLE I.

Variation of the grain-density and the scattering parameter, $\bar{\alpha}$, along the track of particle *a*, see Pl. XXIX. The ranges referred to are the distances measured along the track from the point at which the particle entered the glass.

Interval in range	Mean range	$\bar{\alpha}_{100\mu}^\circ$	grain-density ./50 μ
6375 μ —2575 μ	4500 μ	0.85 ± 0.076	51
2615 μ —1335 μ	2000 μ	1.26 ± 0.189	63
500 μ — 0	250 μ	3.0 ± 0.45	black

The relative directions of motion of the three secondary particles in their common plane at the time of their formation can be easily determined. Knowing the momentum of particle *a*, and assuming the vector sum of the momenta of the three particles to be zero, the momenta of particles (*b*) and (*c*) can be calculated. The values thus obtained are 85.8 ± 1 MeV./c and 98.3 ± 1 MeV./c, respectively. These observations, together with the grain-density in the tracks, allow estimates of the masses of the particles to be made. It is thus found that the mass of particle (*b*) is $240 \pm 30m_e$, and of particle (*c*), $280 \pm 15m_e$, the limits of error corresponding to the standard deviations in the number of grains counted. We believe that for particle (*b*), the observed mass-value is too low owing to a tendency to underestimate the grain-density in steeply dipping tracks.

These observations give strong support for the original assumption that the secondary particles are all π -mesons. If this is so, the energy of the particles can be deduced from their momenta and the values thus

obtained are:—particle (a), 19.0 ± 0.4 MeV.; (b), 24.2 ± 2.0 MeV.; and (c), 32.0 ± 2.0 MeV. The total kinetic energy of the three particles is therefore 75.2 ± 5.0 MeV.

§3. THE ENERGY RELEASE IN THE DECAY OF THE τ -PARTICLE.

In order to compare the present determination of the release of kinetic energy with that in the two previous events on which measurements were possible, the old observations have been re-examined using the latest values for the mass of the π -meson, $m_\pi = 274 \pm 2 m_e$ (Alvarez 1950). The results are summarized in Table II.

TABLE II.
Total Kinetic Energy of the Decay Particles.

Event	Assumed to be π -particles			
	Particle (a)	Particle (b)	Particle (c)	Total
1	1.04 ± 0.10 MeV.	31 ± 4 MeV.	33 ± 4 MeV.	65 ± 8 MeV.
2	50 ± 7.5 MeV.	13 ± 2 MeV.	22 ± 3 MeV.	85 ± 15 MeV.
3	19 ± 0.4 MeV.	24.2 ± 2 MeV.	32 ± 2 MeV.	75 ± 5 MeV.
Weighted Mean 73.5 ± 4 MeV.				

The corresponding value of m_τ is $966 \pm 8 m_e$, assuming $m_\pi = 274 m_e$.

The method employed for the analysis of event No. 1 was similar to that used above, and depended upon the knowledge of the energy of particle (a). In event (1) this particle—almost certainly a π^- -particle—is of short range, and the estimated value of its energy is subject to errors of ± 6 per cent owing to straggling. Further, tracks b and c are inclined to one another at an angle of only $\sim 10^\circ$, and the values of the momenta of the corresponding particles, deduced from that of (a) by assuming a conservation of momentum, are sensitive to errors in the precise value of this angle.

In event number (2), the determination of the energy depended on measuring the scattering parameter for one of the tracks, of length 1300μ , and the values thus obtained were subject to greater statistical fluctuations than those based on range measurements.

The weighted mean of the three determinations is 73.5 ± 4 MeV. Assuming all the product particles are π -mesons the mass of the parent particle, m_τ , is $966 \pm 8 m_e$. Events (2) and (3) were isolated for detailed study because of their resemblance to event number (1); and only after a detailed analysis was it established that, in each case, the directions of motion of the three secondary particles were co-planar, and that the magnitude of the energy release was closely similar to that in the first

event. No other event has been found in this laboratory with even superficially similar characteristics. It can hardly be doubted, therefore, that the events represent similar modes of decay of particles of the same type. Otherwise very improbable and arbitrary assumptions have to be introduced in order to account for the events in any other way.

§4. THE NATURE OF THE SECONDARY PARTICLES.

The above value of m_τ depends on the correctness of the assumptions, (1), that the three charged particles produced by the decay of the τ -particle are not accompanied by any form of neutral radiation; and, (2), that they are all π -mesons. The evidence for the nature of the secondary particles derived from a study of all three events can be presented in the following alternative manner:—

We have seen that, for any one event, it is generally possible to measure the angles between the directions of motion of the three secondary particles in their common plane, and the grain-density of their tracks. This makes it possible to determine the relative values of the masses for the three secondary particles in each event. Thus, if the assumption of a momentum balance is correct, the momentum of one particle is proportional to the sine of the angle between the directions of motion of the other two. In addition, the grain density in a track gives a measure of the quantity $\beta/\sqrt{1-\beta^2} = \frac{\text{momentum}}{\text{rest mass}} = f(g)$. It follows that the ratio of the rest masses can be written:

$$m_a : m_b : m_c :: \frac{\sin \phi_{bc}}{f(g_a)} : \frac{\sin \phi_{ac}}{f(g_b)} : \frac{\sin \phi_{ab}}{f(g_c)},$$

where $\phi_{b,c}$ represents the angle between the directions of motion of particles b and c , etc., and g_a is the grain density of track a , etc.

In event No. 1, only two tracks can be compared in this way, but the other, track (a) is due to a π^- -particle of very short range. For tracks b and c it is found that $m_b : m_c :: 1 : 1.02 \pm 0.10$.

In event No. 2 (Harding 1950), using data given by the author, we find:

$$m_a : m_b : m_c :: 1 : 1.1 \pm 0.15 : 1 \pm 0.1;$$

and for the present event, the corresponding results are:

$$m_a : m_b : m_c :: 1 : 0.88 \pm 0.10 : 1.03 \pm 0.05.$$

The results are shown in Table III. which summarizes information about the masses of all the nine secondary particles on which measurements have been made.

From Table III. it will be seen that all the particles on which measurements have been made give results which are consistent with a unique mass, and in three cases the evidence is in fact very strong that these particles are π -mesons. Whilst the possibility cannot be excluded that one of the three product particles produced in this mode of decay of a τ -particle is a μ -meson, the evidence strongly favours the assumption that they are all π -particles.

The co-planarity of the three secondary particles appears to be an invariable feature of the transmutation. We cannot, however, exclude the possibility that neutrinos, or γ -radiation, of relatively low energy and momentum, are emitted in the transmutation. Thus, a neutrino of

TABLE III.

Absolute or Relative Values of Mass of Secondary Particles.

Event	Particle (a)	Particle (b)	Particle (c)
1	$\pi = 274m_e$	280 ± 30	$1.02 \pm 12\%$
2	1	$1.10 \pm 15\%$	$1.0 \pm 10\%$
3	$285 \pm 20m_e$	$0.88 \pm 11\%$	$1.03 \pm 5\%$

energy ~ 10 MeV. would produce an average departure from co-planarity of the tracks of the three charged particles of only $\sim 3^\circ$, and the precision of the angular measurements does not yet allow us to exclude it as a possibility. If such unobserved particles are emitted, the mass m_τ might be too low by about $20m_e$. It appears very improbable, however, that in the three observed events which correspond to the decay of the τ -meson, the assumed fourth particle of a four-body decay should in every case have been of exceptionally low energy and momentum.

The results obtained for the mass of the τ - and κ -mesons, using the various methods, are summarized in Table IV.

TABLE IV.

Mass of Primary Particle in m_π

Particle	Authors	Length of track	$\bar{\alpha} v R$	g.d. $v R$	Conservation of momentum	Mode of decay
τ	Brown <i>et al</i>	3100μ	990 ± 270	1080 ± 160	949 ± 16	$\tau \rightarrow \pi + \pi + \pi$
τ	Harding	740μ	—	—	989 ± 30	„
τ	Fowler <i>et al</i>	2070μ	1015 ± 280	910 ± 220	969 ± 10	„
κ_1	O'Ceallaigh	4100μ	1260 ± 290	1350 ± 180		
κ_2	O'Ceallaigh	5670μ	1125 ± 260	1125 ± 150		$\kappa \rightarrow \mu +$

§5. FREQUENCY OF OCCURRENCE OF τ - AND κ -PARTICLES.

Although the statistical weight of the observations is at present very low, they suggest that in energetic nuclear collisions a considerable part of the available energy appears in the form of heavy mesons. In plates exposed under 30 cm. of lead on the Jungfrauoch, five τ - or κ -particles

(O'Ceallaigh 1951) have been found in a volume of emulsion in which 750 π -particles are recorded. We may therefore write $N_{\kappa,\tau}/N_{\pi}=1/150$, where $N_{\kappa,\tau}$ is the sum of the number of τ - and κ -particles. For the following reasons, the order of magnitude of this ratio is very suggestive.

Recent experiments in this laboratory (Camerini *et al.* 1951) show that in the disintegrations produced by protons of energy, E , in the range from 2 to 10 BeV., the total energy appearing in the form of emitted π -mesons is approximately proportional to E . Let us assume, first, that in the nuclear collisions involving protons of energy above 10 BeV., the same fraction of the energy appears as mesons; secondly, that this energy is equally divided among π -particles on the one hand, and τ - or κ -particles on the other; and thirdly, that the τ - or κ -mesons are produced in the centre-of-mass system of the interacting nucleons with a distribution in velocity and angle similar to that determined for the π -particles. With these assumptions, and knowing the distribution in energy of the fast protons and neutrons in the cosmic radiation at the Jungfraujoch, the expected ratio of the numbers of π -particles produced to that of heavy mesons can be calculated. The result is $N_{\kappa,\tau}/N_{\pi}\sim 1/75$, which is of the same order of magnitude as that observed.

The above result is particularly striking because no account has been taken of the difficulties of recognizing the tracks of κ -mesons. These particles have to be distinguished from μ -mesons which are about a thousand times more numerous, and they can only be identified with confidence if the track of the primary particle is longer than 2 or 3 mm., so that the mass can be determined; or if the secondary particle is of energy greater than 100 MeV. and produces a track longer than 3 mm. These requirements are so stringent that we can be certain that we fail to recognize at least twice as many κ -particles in our emulsions as we identify. On the other hand, like the π -mesons, a τ -particle should be recognized with a high degree of efficiency.

The above considerations take no account of the possibility that the κ - and τ -particles may be the products of decay of heavier mesons; or that the κ - and τ -mesons are short-lived so that they have an appreciable chance of decaying in flight even when moving in solid substances. Both these features would tend to reduce the expected value of the ratio $N_{\kappa,\tau}/N_{\pi}$, and this would make the number actually observed even more surprising. The observations therefore give strong support for the view that in the nuclear transmutations produced by nucleons of energy above 10 BeV., a considerable fraction of the energy available in the collision is transformed into κ - or τ -particles.

In the preceding paragraphs we have made no distinction between κ - and τ -particles because we have no precise knowledge of their relative frequencies of occurrence. There are, however, reasons for believing that the κ -particles are more numerous than the τ 's.

In the Plates, in which the present events are recorded, four κ - and one τ -particle have been found. We have seen that the mode of decay of the

τ -meson makes it easily recognized. On the other hand, the κ -particles can be distinguished from μ -mesons only with difficulty and in favourable cases. It is therefore possible that there is a large preponderance of κ -particles, and if this is so the remarks in the following paragraphs on the life-time of the particles and the best conditions for their detection, would largely apply to the κ -particles.

§6. LIFE-TIME OF THE HEAVY MESONS.

The total time taken by a τ - or κ -particle to traverse its observed track in the emulsion before coming to rest can easily be calculated, and these time intervals, for all the κ - and τ -particles identified in this laboratory, are of the order of 5×10^{-11} sec. We cannot, however, draw any conclusions from this observation because we do not know how many similar particles decayed in flight.

The considerations of the preceding section give strong support, however, for the view that the heavy mesons have a mean life-time not less than 10^{-9} sec. Thus, assume a life-time of 5×10^{-10} sec., and a distribution in velocity of the τ - or κ -particles postulated in the previous section. It is then found that, if moving in copper, only about 5 per cent of the particles would be brought to rest before decaying. For a life-time of 10^{-9} sec., the corresponding result is about 25 per cent. The actual number expected might be considerably less than this if the particles can also be removed through collisions with nuclei. Since we have already accounted for the observed number of κ, τ -particles without assuming any loss by these processes, it is reasonable to suppose that the life-time is not less than 10^{-9} sec.

§7. SIGN OF THE CHARGE OF THE κ - AND τ -PARTICLES.

There is no direct evidence, provided by the present experiments, for the sign of the charge of the κ - and τ -particles. We may assume tentatively, however, that they are produced in nucleon-nucleon collisions and have a strong interaction with nuclei. It is then reasonable to consider the possibility that negative heavy mesons, if absorbed by nuclei, will produce σ -stars similar to those resulting from the nuclear capture of π -particles. Because of the greater mass of heavy mesons, such disintegrations might be correspondingly more energetic, and lead to the emission of more charged particles than are commonly found in the σ -stars. No such examples which could be attributed to the nuclear capture of a heavy meson have been found in this laboratory, but for the following reasons, this result is not decisive:—

There is, first, the possibility that following capture by nuclei, most of the rest-energy of the heavy mesons may escape in the form of neutral particles or γ -radiation. Such is the case in the nuclear disintegrations produced by μ^- -particles. If this is so, the σ -stars produced by heavy mesons might easily be confused with those due to the capture of negative

π -particles. A search was therefore made for such events, in plates exposed to the cosmic radiation, by measuring the masses of the particles producing the σ -stars. In 100 examples examined hitherto none has been found in which the parent particle could be identified as a heavy meson.

It must also be borne in mind that since the κ - and τ -particles are much more massive than π -mesons the scattering of the particles and the variation of grain-density with range are much less than for the π -mesons. This makes it more difficult for an observer to recognize the parent track of such an event. Particularly if it is short, he may mistake it for the track of an outgoing particle, and regard the event as an ordinary cosmic-ray star.

In addition to these considerations, it is not certain that negative τ - and κ -particles, even if directly produced in nucleon-nucleon collisions, will, when captured by an atom, lead to the disintegration of its nucleus. The observed events may therefore represent the spontaneous decay of both positive and negative heavy mesons. Since the total energy of the three π -particles is not extremely great, and since their directions of emission are co-planar, it may be possible, in favourable cases and in thick emulsions, to identify all the product π -mesons, and thus the sign of the charge of the parent particle.

§8. DESIGN OF EXPERIMENTS FOR DETECTION OF κ - and τ -PARTICLES.

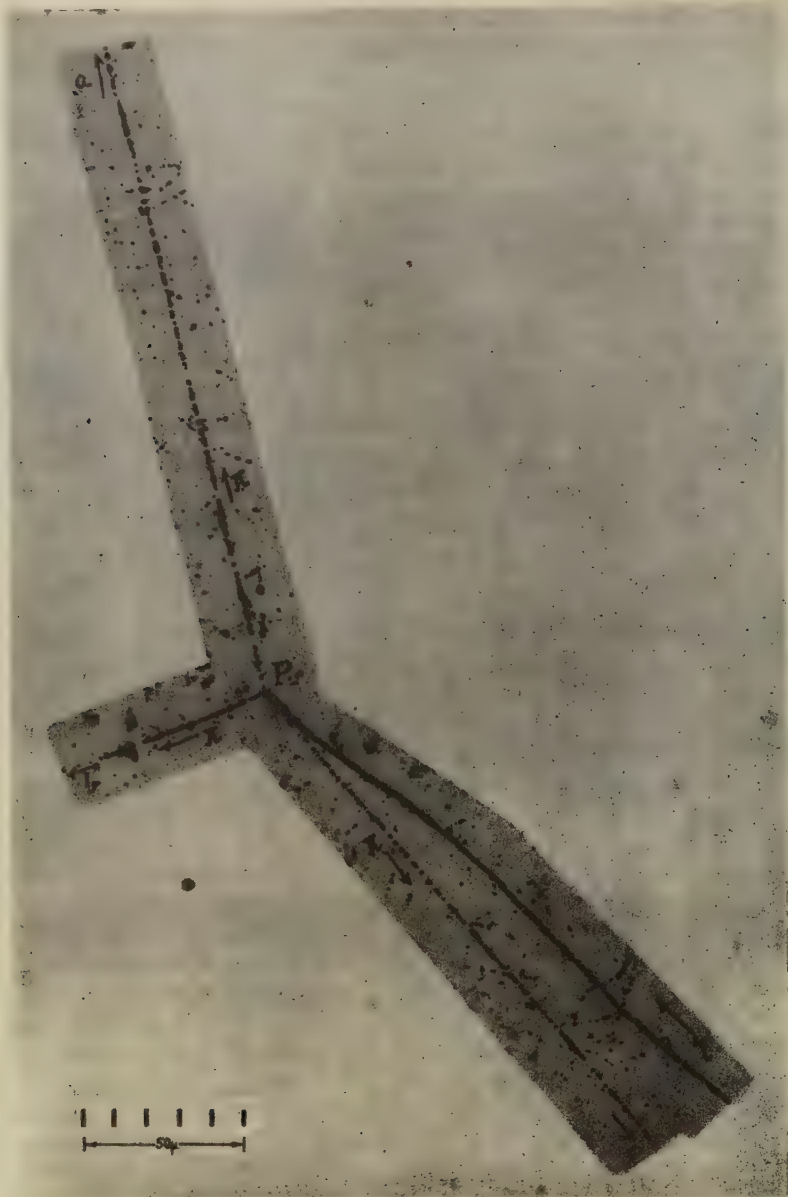
The frequency of occurrence of heavy mesons in nuclear disintegrations of great energy, and their significance for the development of meson theory, make it a matter of great importance to observe many of the particles so that their properties may be established. They occur so rarely that such a programme would seem to demand, for its successful completion, the joint efforts of experimenters all over the world using all available technical devices. It is therefore appropriate to consider the most suitable design of experiments for the recording of the particles by the photographic method.

The principal difficulty which has to be met in studying the κ - and τ -particles is that they must be detected amongst a much greater number of particles of different types. Thus in searching for κ -particles it is desirable to examine the tracks of all protons and μ -mesons which stop in the emulsion. This work would be more fruitful if the proportion of κ -particles could be increased. Since the heavy mesons can only be produced by particles of great energy, and since disintegrations by particles of energy below ~ 5 BeV. only contribute to an undesirable "background" of tracks, the most favourable experimental conditions would be provided by experiments at great altitudes at geomagnetic latitudes less than 40° . At such latitudes, the "cut-off" ensures that the minimum energy of the protons reaching the top of the atmosphere is about 5 BeV.; and by going to great altitudes we ensure that nuclear collisions in the atmosphere have not produced a large flux of particles of lower energy.



A heavy meson, τ , comes to the end of its range in the emulsion and decays into 3 charged particles, one of which is a π^- -particle of short range which produces a nuclear disintegration. There is strong evidence that the tracks *b* and *c* were also produced by π -mesons. The direction of motion of the three secondary particles are co-planar.

Observer Mrs. Van der Merwe. Photograph by A. R. Gattiker and Miss P. Dyer.



A heavy meson, τ , reaches the end of its range at the point P and decays with the emission of three charged particles, probably π -particles. The grain-density and scattering in the track of the particle, τ , gives a measure of its mass and the value thus found is about $1000m_e$. The tracks of the secondary particles are co-planar.

Observer Mrs. I. Powell. Photograph by A. R. Gattiker and Miss P. Dyer.

In such experiments on heavy mesons it is necessary to surround the photographic plates by local matter in which the particles can be generated. The best design for this assembly depends on the lifetime of the particles and this, it has been suggested, is greater than 5×10^{-10} sec. Further, the experiments with expansion chambers on the charged V-particles, in which they are observed to decay in flight, suggests that the lifetime is not much greater than 10^{-9} sec. Taking this as the best value at present available, it may be shown that the most favourable conditions for observing the heavy mesons are given by surrounding the photographic plates by material of medium atomic weight, such as copper, to a thickness of about 10 cm. Such an assembly would weigh about 80 lb., and it could be carried to great altitudes by balloons. There would be some advantage in increasing the thickness of the surrounding material, but it would be offset by the great increase in the load, and the reduction in the altitudes which could then be reached.

§ 10. CONCLUSIONS.

The most important conclusions which follow from the present experiments may be summarized in the following terms:—

- (a) Taken in conjunction with those of Harding, the observations confirm the existence of charged mesons of mass $\sim 1000m_e$, called τ -particles, which decay into three particles of charge $|e|$.
- (b) Most of the secondary particles are π -mesons and the evidence is very strong, but not finally decisive, that they are all of this type.
- (c) If the τ -meson decays into three π -particles its mass is $966 \pm 8m_e$.
- (d) The lifetime of the heavy mesons (κ, τ) is of the order of 10^{-9} sec., and good conditions for their detection, using the photographic method, can be obtained by making high altitude balloon flights at geomagnetic latitudes less than 40° .

ACKNOWLEDGMENTS.

We are indebted to Mr. A. R. Gattiker and Miss P. Dyer for their work in making the mosaics of photo-micrographs and to Mrs. Isobel Powell, Miss A. Stradling and other observers for scanning the plates. One of us (O. R.) is indebted to the British Council for a scholarship.

These experiments were carried out as part of a programme of research supported by the Department of Scientific and Industrial Research

REFERENCES.

- BROWN, CAMERINI, FOWLER, MUIRHEAD, POWELL and RITSON, *Nature. Lond.*, **163**, 82.
 HARDING, 1950, *Phil. Mag.* **41**, 405.
 ALVAREZ, 1950, *Proc. Harwell Nuclear Physics Conference*, p. 1.
 LATTES, FOWLER and CUER, 1947, *Proc. Phys. Soc.* **59**, 883.
 O'CEALLAIGH, 1951, *Phil. Mag.*, **42**, 1032.
 BRADNER, SMITH, BARKAS and BISHOP, 1950, *Phys. Rev.* **77**, 462.

CVI. *Observations on the Multiple Scattering of Ionizing Particles in Photographic Emulsions.*—Part III. *Statistics of the Sampling Distributions of Second Differences and the Technique of Overlapping Cells.*

By C. O'CEALLAIGH* and O. ROCHAT,
H. H. Wills Physical Laboratory, University of Bristol†.

[Received May 30, 1951.]

SUMMARY.

Predictions based on a theoretical treatment (Molière 1951) of the problem of overlapping cells, are in satisfactory agreement with the results of experiment. They would indicate that the dispersions of the sampling distributions of certain statistics commonly used to estimate the scattering of particles, are almost independent of λ , the coefficient of overlap. The dispersions are found to differ but little from those of measurements based on a smaller number of non-overlapping cells which are shown to be independent in the sense of ordinary statistical theory of small samples. It is concluded that the advantage of employing the technique of overlap is inappreciable.

§1. DEFINITION OF OVERLAP.

To obtain the best value for $\bar{D}_{(c)}$ the mean absolute value of second difference for cell-size c microns, it has been common practice to make use of measurements on overlapping cells. This is done by measuring the coordinates of the track at intervals c' , a submultiple of c , such that $c' = c/\lambda$. We refer to c' as the prime cell-size. The overlapping values of second difference are then obtained by using all those pairs of prime cell coordinate readings which are separated by an interval c .

Overlap is defined to exist for $\lambda > 2$, so we term λ the coefficient of overlap, and use it as a convenient measure of the degree of overlap. Suppose that $y_0, y_1, y_2 \dots y_j \dots y_r$ are the track coordinates at prime-cell interval c' . The following will be the expressions for the j th second difference.

Without overlap, $D_j = y_{j-1} - 2y_j + y_{j+1}$ (cell-size = c'). (1)

With overlap, $D_{j(\lambda)} = y_{j-\lambda} - 2y_j + y_{j+\lambda}$ (cell-size = $\lambda c'$). (2)

Consider now, a track of length = L and any chosen cell-size c_1 . Sequences of second difference corresponding to various degrees of overlap may be obtained by suitably reducing c_1/λ , the interval between readings. The

* On leave of absence from University College, Cork.

† Communicated by Professor C. F. Powell, F.R.S.

number of readings of second difference thus obtained will be $N_\lambda = \frac{\lambda L}{c_1} - (2\lambda - 1)$. These, however, will not be statistically independent.

Since the labour of computing the differences is increased by a factor of order λ , it is important to enquire whether the use of overlap will result in any commensurate decrease in the dispersion of the experimental results.

§2. STATISTICS OF SAMPLING DISTRIBUTIONS.

Consider a universe of monoergic particles, and suppose that we may select from it tracks all of length= L measured in cell-size= c_1 . Each track regarded as a sample from this universe, will contain n values of second difference D_j . Let conditions be such that these n values are statistically independent.

As shown in (I.), any measure of the dispersion of the above universe may also be used to measure the energy of the tracks. We choose any parameter " p " characteristic of the universe which is a convenient measure of the energy. The estimate of p derived from the individual samples is called a statistic, and will be distributed about this universal value. The sampling distribution of the chosen statistic is known in certain cases. To determine satisfactorily the energy of any individual track, the standard deviation σ_p of the sampling distribution must be small. For the present purposes we consider only the following measures of dispersion. For these, except for very small samples, theory shows that σ_p will depend sensibly on $n^{-1/2}$ where n is the number of independent readings in each sample.

(1) The mean deviation of D_j , from assumed universal mean= 0 . This is the statistic commonly used, and has already been termed \bar{D} . It is defined as

$$m_0 = \bar{D} = \frac{1}{n} \sum_{j=1}^n |D_j|. \quad (3)$$

(2) The mean deviation m of D_j from the sample mean

$$m = \frac{1}{n} \sum_{j=1}^n \left| D_j - \frac{1}{n} \sum_{j=1}^n D_j \right|. \quad (4)$$

(3) The standard deviation

$$s = \left[\frac{1}{n} \sum_{j=1}^n D_j^2 - \left(\frac{1}{n} \sum_{j=1}^n D_j \right)^2 \right]^{1/2}. \quad (5)$$

We distinguish the universal parameters by Greek letters, setting the standard deviation= σ and the mean deviation= μ . The distributions of the statistics (4) and (5) are known. That of (1) however, although of greatest interest, appears not to have been studied. In cases where slight C-shaped distortion of the emulsion is suspected, it seems best to use (4) or (5). In essence this has already been suggested by Fowler (1950).

§3. STANDARD DEVIATION OF SAMPLING DISTRIBUTION FOR OVERLAPPING CELLS.

Molière (1951) has examined the problem of determining the standard deviation of the sampling distribution, when the individual values, of which each sample is composed, are not statistically independent. Adapting his method to the present case, we find that the second differences obtained with overlap are strongly correlated. Table I. gives as a function of increasing λ , the values of the elements a_{jk} in the j th row of the coupling matrix.

TABLE I.
Correlation Coefficients a_{jk} .

λ	1	2	3	4
\cdot	\cdot	\cdot	\cdot	\cdot
$k=j-7$	0	0	0	1/256
$j-6$	0	0	0	8/256
$j-5$	0	0	1/108	27/256
$j-4$	0	0	8/108	1/4
$j-3$	0	1/32	1/4	121/256
$j-2$	0	1/4	60/108	174/256
$j-1$	1/4	23/32	93/108	235/156
j	1	1	1	1
$j+1$	1/4	23/32	93/108	235/256
$j+2$	0	1/4	60/108	174/256
$j+3$	0	1/32	1/4	121/256
\cdot	\cdot	\cdot	\cdot	\cdot

For the degree of overlap λ , the general term a_{jk} , $k=j-\nu$ will be

$$a_{jk} = \frac{(2\lambda - \nu)^3 - 4(\lambda - \nu)^3}{4\lambda^3}, \quad \nu < \lambda$$

and

$$= \lambda(2\lambda - \nu)^3 / 4\lambda^3, \quad \nu > \lambda. \quad (6)$$

In each sample there will be N_λ values of second difference. We seek to determine the number of these which may be regarded as independent from the viewpoint of the theory of sampling.

Using the methods of large-sample statistics, and assuming that the universe is normal, we may deduce from (6) the following expression for $\sigma_{s(\lambda)}/\sigma$; $\sigma_{s(\lambda)}$ is the S.D. of the sampling distribution of $s(\lambda)$; $s(\lambda)$ is the statistic "standard deviation of D_j defined by (2)".

$$\frac{\sigma_{s(\lambda)}}{\sigma} = \left[\frac{\psi(\lambda)}{2N_\lambda/\lambda} \right]^{1/2} \quad \dots \quad (7)$$

$\psi(\lambda)$ is a numerical factor which is found to have the following values.

$N_2/\lambda = L/C_1 - 2 + 1/\lambda$, will not differ appreciably from $L/C_1 - 1$, the number of second differences obtained without overlap, and the factor $\psi(\lambda)$ decreases very slowly with λ . It follows that sharpening of the sampling distributions obtained by increasing λ is quite negligible. We conclude therefore that the advantage of using overlapping cells, is not commensurate with the increased labour involved.

The ratio σ_s/σ for samples of N independent readings from a normal universe is known to be (Kenney, (a) Mathematics of Statistics II.).

$$\sigma_s/\sigma = \left(\frac{1}{2N} - \frac{2}{8N^2} - \frac{3}{16N^3} \dots \right)^{1/2} \sim (1/2N)^{1/2} \dots \quad (8)$$

Comparing (7) with (8) we infer that for an overlap λ a fraction $g(\lambda) = 1/\lambda\psi(\lambda)$ of the second differences may be regarded as independent from the viewpoint of the statistical theory of sampling, as the quantity $N_2g(\lambda)$ plays the same rôle in formula (7) as the quantity N in formula (8). For the case $\lambda=1$ this fraction is $1/1.125$ or 89 per cent. For values of $\lambda > 1$ the rate of variation of $g(\lambda)$ and N_2 with λ is such that their product remains practically constant. Thus the standard deviation of the sampling distribution will be sensibly independent of λ .

TABLE II.

λ	1	2	3	4
$\psi(\lambda)$	1.125	1.10	1.076	1.045

These conclusions depend on two assumptions which in fact are not rigorously satisfied. (a) that the universe is normal, and (b) that the methods of large sample statistics may be applied to samples of the size commonly used, viz. 10-30 independent cells per sample. Nevertheless, we conclude that they are not seriously in error, as will appear from the results of the experimental investigation to be described.

§ 4. EXPERIMENTAL STUDY OF SAMPLING DISTRIBUTIONS WITH AND WITHOUT OVERLAP.

The electrons of energy 105 MeV. have been used for the experimental investigation. The scattering measurements were carried out as described in (II.) on a prime cell-size of 25μ . The readings which were studied were those on 100μ cells with maximum degree of overlap corresponding to $\lambda=4$.

The tracks were divided into segments of 1400μ . Eighty-five segments were thus obtained, each containing 49 values of $D_j(\lambda)$ for $\lambda=4$. Each segment was regarded as being an independent sample from a universe of electron tracks of energy 105 MeV. From each segment two further sub-samples were obtained. One consisted of the 13 values of D_j corresponding to $\lambda=1$. The other was made up of 7 values of D_j obtained by choosing from the samples of 49, ($\lambda=4$), every 8th reading

starting with the first. Since the correlation between the individual values of D_j in the samples of 7 was negligible, it was expected that the standard deviation of their sampling distribution would agree with that predicted by the statistical theory of small samples. It is shown later that this was indeed the case.

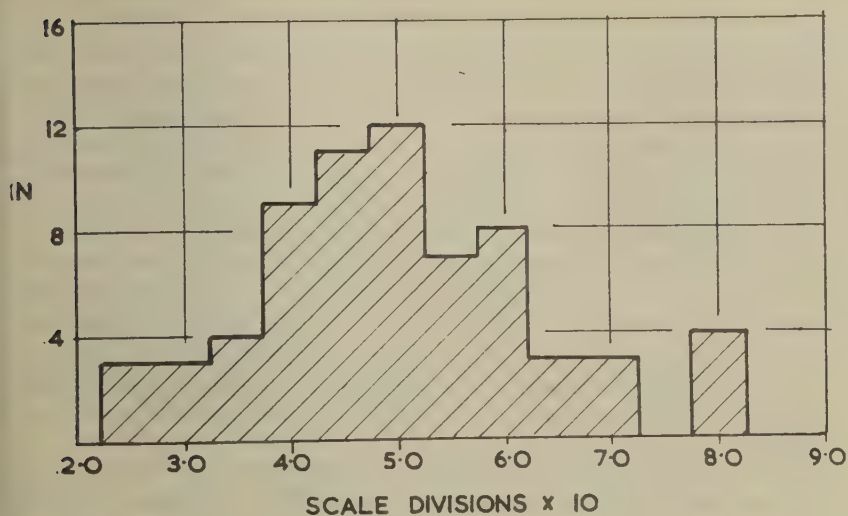
To examine the effect of increasing λ on the spread of the sampling distribution, the statistic chosen was m_0 ((3), above). Because of the small number of signals in the samples, inclusion of the occasional large value of D_j would have a serious influence on the measured spread. To reduce this, all tracks which contained as components of the samples of 49, one or more values of D_j greater than $4\bar{D}$, were temporarily excluded from the statistics. It was felt that this procedure rendered more exact the comparison between the standard deviations of the different samples. The results are summarized in Table II. The symbol $E(m_0)$ represents the expectation of m_0 , and is the mean value of the sample values of m_0 . It is the best estimate of μ , the mean deviation of the universe. σ_{m_0} is the experimental standard deviation. The uncertainties quoted are the estimated S.D. of σ_{m_0} . The upper histogram in fig. 1 shows the experimental distribution for the samples of 7 (virtual independence), and the lower, that for the samples of 49, ($\lambda=4$).

TABLE III.
Fifty-seven Samples of Electron Track $L=1400\mu$.

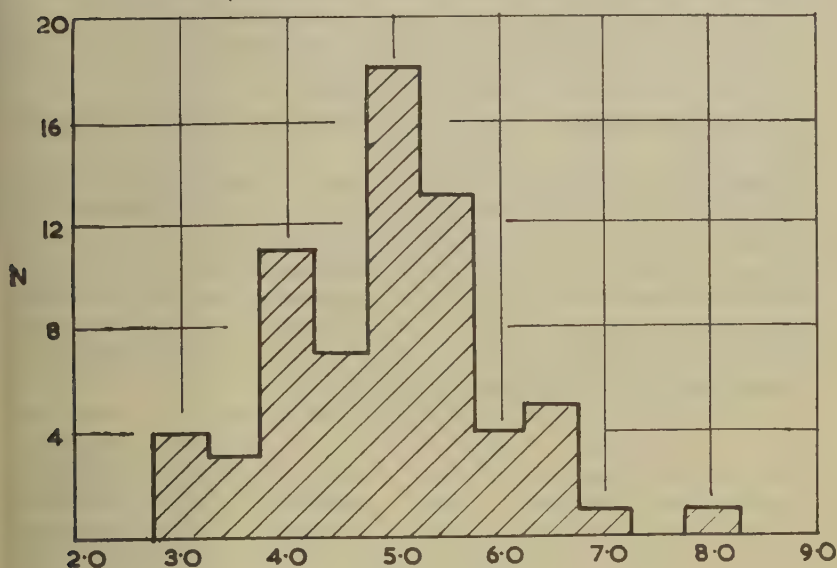
λ	N	$E(m_0)$	σ_{m_0}
4	49	0.516	0.099 ± 0.009
1	13	0.531	0.114 ± 0.010
—	7	0.525	0.130 ± 0.012

These results appear quite consistent with those predicted by the theory of Molière, when the statistical weight of the experiment is taken into consideration. Though the theoretical argument has been based on a different statistic, viz., s , it seems reasonable to suppose that the validity of the conclusions will be little affected, even for samples as small as 7. The results given in Table V. lend support to this supposition. The difference between the results for σ_{m_0} was tested for significance by the F-test. (Hoel, *Introduction to Mathematical Statistics*, p. 152.) Considering the results for the independent samples of 7, it was found that they differed significantly (at a level of ~ 3 per cent) from those for the samples of 49, ($\lambda=4$), but not from those obtained for the samples of 13, ($\lambda=1$). Bearing in mind the trend of the results and the appearance of the histograms, we conclude that a small but definite sharpening of the sampling distribution occurs as λ is increased, but that the degree of improvement which results, is quite out of proportion to the increased labour. These experimental conclusions agree with those to be drawn from the theoretical treatment of Molière.

Fig. 1.



Upper histogram.



Lower histogram.

Experimental distribution of the statistic m_0 (mean deviation from assumed universal mean=0) for 105 MeV. positrons, 100μ cells. Lower histogram for samples of 49, ($\lambda=4$). Upper histogram for samples of 7 (independent).

§5. SAMPLING DISTRIBUTION OF SAMPLES OF 7.—COMPARISON
WITH THEORY OF SMALL SAMPLES.

Our samples of 7 were so chosen that they were composed of independent values of D_j . The sampling distributions of the statistics should agree with those predicted by the theory of small samples. An experiment on the decay spectrum of μ -mesons at present in progress, depends for its interpretation on a knowledge of the form of the sampling distributions. (O'Ceallaigh 1951). It is of interest, therefore, to test experimentally the correctness of the above assumptions.

Eighty samples of 7 were chosen. They differed in one respect only, from the 57 samples already discussed. As before the signals $D_j \geq 4\bar{D}$ were rejected, but the loss was now made up by including the value of D_j next following. The values of all three statistics defined in (3), (4) and (5) were computed for each sample and their distributions were plotted as histograms. The standard deviation of each was calculated.

The observed distributions are reproduced in fig. 2. The upper histogram which gives the distribution of the standard deviation s , (5), is compared with the theoretical distribution of the S.D. of samples of 7 drawn from a normal universe. This is given by the well known expression of (Kenney 1940, *Mathematics of Statistics*.—II.):

$$h(s) = \frac{2(n/2\sigma^2)^{\frac{1}{2}(n-1)}}{\Gamma_{\frac{1}{2}}(n-1)} \exp(-\frac{1}{2}ns^2/\sigma^2)s^{n-2}, \quad \dots \quad (9)$$

where σ is the standard deviation of the universe, and s that of the sample of size n .

Experimental values of mean and standard deviation for 100μ cells are derived from the distribution of (I.) fig. 3. These values, respectively 0.537 and 0.690 scale divisions, are used throughout the present paper as the best estimates of μ and σ the universal parameters.

The lower histograms represent the experimental distribution of the mean deviations of m , (4) full line, and m_0 , (3) broken line. The theoretical distribution for m for samples of 7 from a normal universe has been calculated from the tables of Godwin (1945).

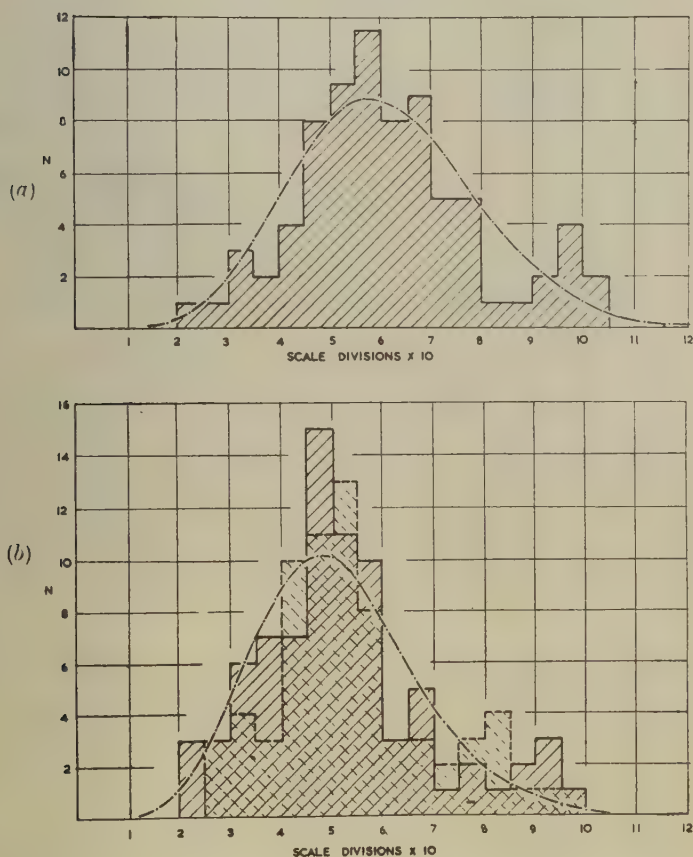
Agreement between the experimental results and the theoretical curves is satisfactory. There is some evidence that the histograms represent distributions more peaked than would be obtained from a normal universe. This does not seem unreasonable when we remember that the universe from which the samples were drawn is, in fact, somewhat more peaked than the normal. While the position of the mode of the distribution of m (full line) agrees well with theory, that for the distribution of m_0 seems to have a higher value which appears to coincide with the mathematical expectation of the statistic (*cf.* Table IV.).

The values of the standard deviations of the experimental distributions are given in Table IV. where they are compared with the theoretical

values. That of the distribution of s was obtained by substituting $N=7$ in (9). That for m was found from the expression (Kendall 1947).

$$\sigma_m = \mu \frac{\sqrt{(n-1)}}{n} \left[\pi/2 + \sqrt{[n(n-2)]} - n + \arcsin \left(\frac{1}{n-1} \right) \right]^{1/2} \sim \mu \left(\frac{\pi-2}{2n} \right)^{1/2} . \quad (10)$$

Fig. 2.



Sampling distribution of the various statistics for 80 samples of 7 (independent)—for 105 MeV. positrons, 100μ cells.

- (a) Comparison of the experimental distribution of the standard deviation with the theoretical distribution obtained for samples of 7 drawn from a normal universe.
- (b) Histograms giving the experimental distribution of: the mean deviation, m , from sample mean (full line), and m_0 , from assumed universal mean=0 (broken line). Curve gives the theoretical distribution as calculated from the tables of Godwin (1945), for m , for samples of 7 drawn from a normal universe.

The theoretical expected values of the statistics, namely those the mean of the individual values of m , m_0 and s are also given, and compared with experiment.

TABLE IV.
 $\sigma=0.690$; $\mu=0.537$.

Statistic	S.D. Sampling Distribution		Mathematical Expectation	
	Experiment	Theory	Experiment	Theory
m_0	0.153		0.541	0.537
m	0.154	0.156	0.504	0.509
s	0.178	0.177	0.612	0.613

Agreement between experiment and theory is better than might be expected. We may conclude that when the individual values of D_j are chosen, as in these samples of 7, they are effectively independent. We may safely use the customary theory of small samples to estimate the spread of the sampling distributions of statistics derived from them.

§6. EXPERIMENTAL DISTRIBUTION OF SAMPLES FOR $\lambda=1$.

To obtain results of greater statistical weight than those given for $\lambda=1$ in Table III., samples of 7 were selected instead of the samples of 13 already discussed. They were chosen exactly as were the samples of 7 independent readings, except that every fourth instead of every eighth signal in each track was used. There resulted 157 samples of 7 for which $\lambda=1$. The distributions of m_0 and s were plotted, and their standard deviations were calculated. The results are given in Table V.

TABLE V.
S.D. of Sampling Distributions of Mean and S.D. for Samples of 7.

Condition of Sampling	m_0	s	Number of Samples
Independent	0.154	0.178	80
$\lambda=1$	0.162	0.189	157

If we apply to the results for s the argument given on p. 1053, we find that 89 per cent of the total number of second differences obtained with $\lambda=1$, may be regarded as being independent when computing the S.D. of the sampling distribution by means of (9) or (10). This figure of 89 per cent is in exact agreement with that deduced from the theory of Molière. The percentage change in the S.D. of the sampling distribution of m_0 appears to be about the same as that of s .

We note, however, that the difference between the experimentally determined standard deviations is not significant at the 5 per cent level.

Comparison between the histograms of the experimental distributions for independent cells with those for $\lambda=1$, seems to indicate that the experimental distribution for $\lambda=1$ is less peaked than that for the independent samples, and thus are more in agreement with the theoretical distributions for samples of 7 for a normal universe.

REFERENCES.

- FISHER, 1920, *Mon. Not. Roy. Ast. Soc.*, **80**, 758.
FOWLER, 1950, *Phil. Mag.*, **41**, 169.
GODWIN, 1945, *Biometrika*, **33**, 254.
HOEL, 1946, *Introduction to Mathematical Statistics*, p. 152.
KENDALL, 1947, *The Advanced Theory of Statistics* (Griffin), 3rd. Ed.
KENNEY, 1940, *Mathematics of Statistics*.—II. (London: Chapman and Hall),
(a) p. 136, (b) p. 135.
MOLIÈRE, 1951, to be published.
O'CEALLAIGH, 1951, in preparation.

CVII. CORRESPONDENCE.

The τ -Meson.

By P. E. HODGSON,

Imperial College of Science and Technology, London*.

[Received July 27, 1951.]

IN 1949, Brown, Camerini, Fowler, Muirhead, Powell and Ritson reported the discovery in a photographic emulsion exposed to the cosmic radiation of a particle having a mass about a thousand times that of the electron. On coming to rest, it decayed into three singly charged particles, one of which was certainly a π -meson, and the others probably π -mesons also. A year later, Harding reported two more of these events, which are generally known as τ -mesons. They were found in plates exposed in a pipe sunk in a glacier on the Jungfrauoch. Recently, Powell (1951)† has given details of a fourth τ -meson.

The fact that two τ -mesons were observed by Harding in plates surrounded by ice, while only a comparable number was observed in the vastly greater volume of emulsion examined by the Bristol group and others suggested that perhaps τ -mesons are more likely to be emitted from hydrogen. Those produced in nucleon-nucleon collisions inside larger nuclei may have a high probability of absorption before escape.

A further batch of 400 μ Ilford G5 plates was therefore exposed in the glacier and one further τ -meson has been observed. A facsimile projection drawing of the event is shown in the figure.

The track of the τ -meson dips too steeply in the emulsion for any measurements to be made on it. The tracks of the three secondary particles, none of which ends in the emulsion, are coplanar within 2°. They have ranges in the emulsion of 445 μ , 720 μ and 990 μ , respectively. The multiple scattering of the longest track was $1.25 \pm 0.5^\circ/100\mu$. The values expected for protons, π -mesons and μ -mesons of the same rate of energy loss are $0.2^\circ/100\mu$, $1.4^\circ/100\mu$ and $1.9^\circ/100\mu$ respectively. It is therefore almost certain that the particle which made this track was a π -meson or a μ -meson. The energies of the particles producing the other two tracks were too great for reliable scattering measurement to be made on the length of track available. Assuming all the secondary particles to be π -mesons, their energies were found to be 33.5 ± 5 , 31 ± 4 and 9 ± 1.5 MeV. from grain counting. Assuming the π -meson mass to be $274 \pm 2m_e$, this gives the mass of the τ -meson as $969 \pm 15m_e$. This result is in good agreement with those of the Bristol group and Harding.

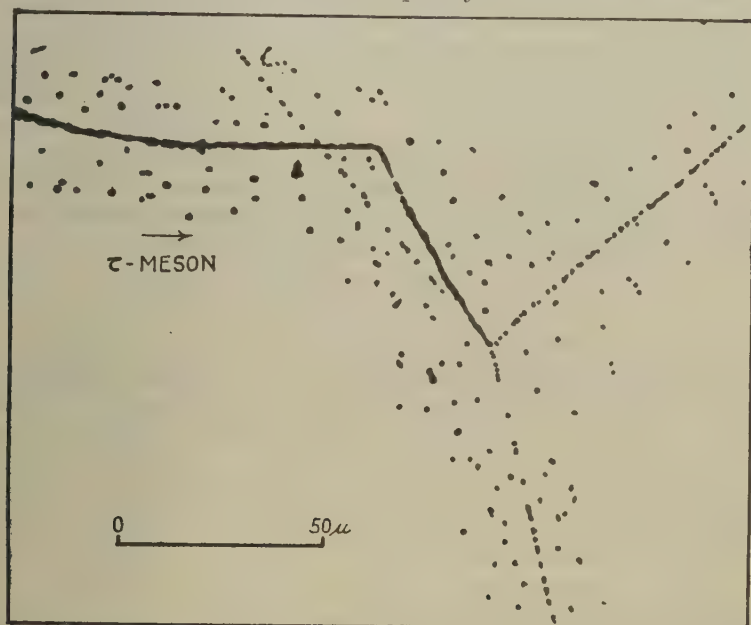
If momentum was conserved in the decay process, it was calculated from the angles between the directions of emission of the secondary particles that their energies were in the ratio 1 : 0.78 : 0.29. The observed values are in the ratio $1 : 0.93 \pm 0.18 : 0.27 \pm 0.06$. This

*Communicated by Sir George Thomson.

† A report of this work appears in this issue (page 1040).—Editor.

agreement, together with the fact that the tracks are coplanar, shows that there are no more than three particles emitted in the decay process. The total energy released is 73.5 ± 7 MeV.

It is a curious fact that of the τ -mesons reported by Harding, one came upwards and the other sideways. The new τ -meson was also coming upwards when it entered the emulsion at an angle of 47° with the vertical. This can be understood if the τ -mesons emitted downwards are more energetic than those emitted upwards. They will then take longer to come to rest and are more likely to decay in flight than those emitted upwards, which come to rest quickly.



Facsimile projection drawing of an event interpreted as the decay of a τ -meson. (Observer: P. E. Hodgson).

The event described in this letter provides further confirmation of the existence of τ -mesons, and also gives some support to the view that these particles have a larger probability of being produced in hydrogen than in the other elements. Further examination of the plates is in progress.

I should like to express my thanks to Professor Sir George Thomson for a valuable discussion of this event, to Mr. R. M. Tennent for making the multiple scattering measurement on the track of one of the secondary particles, and to Mr. A. J. Herz for developing the plates.

REFERENCES.

- BROWN, R., CAMERINI, U., FOWLER, P. H., MUIRHEAD, H., POWELL, C. F., and RITSON, D. M., 1949, *Nature* **163**, 82.
 HARDING, J. B., 1950, *Phil. Mag.* **41**, 405.
 POWELL, C. F., 1951, *Copenhagen Conference on Nuclear Physics, Phil. Mag.* **42**, 1040.

Paramagnetic Resonance in Gadolinium Ethylsulphate.

By B. BLEANEY, F.R.S., R. J. ELLIOTT, H. E. D. SCOVIL and
R. S. TRENAM.

The Clarendon Laboratory, Oxford*.

[Received July 11th, 1951.]

KETELAAR'S (1937) determination of the crystal structure of the rare earth ethyl sulphates indicates that the rare earth ion is in a electric field of D_{3h} symmetry. On this basis Elliott and Stevens (1951) have succeeded in explaining a number of paramagnetic resonance results. In the case of Gd^{+++} the ion is in an 8S state, which is affected by the crystal field only through high-order interactions which are difficult to evaluate. We may assume, however, that the energy levels should fit a spin Hamiltonian of the form

$$\mathcal{H} = g\beta H.S + A_2^0 P_2^0(S) + A_4^0 P_4^0(S) + A_6^0 P_6^0(S) + A_6^6 P_6^6(S) \quad (1)$$

which reflects hexagonal symmetry about the z -axis. Here $P_l^m(S)$ is a form of operator which has the same transformation properties as the corresponding real surface harmonic Y_l^m ; typical forms are

$$P_2^0 = 3S_z^2 - S(S+1),$$

$$P_6^0 = \frac{1}{2}(S_+^6 + S_-^6).$$

The coefficients A_l^m are related to the crystal field but not in any simple way.

Previous work on gadolinium salts has always been interpreted in terms of a crystal field of predominantly cubic symmetry. We have therefore carried out a number of measurements on gadolinium ethylsulphate diluted with lanthanum ethyl sulphate to verify the correctness of the Hamiltonian (1). Experiments at 1.3 cm. wavelength showed that the spectrum consists of seven roughly equally spaced lines, whose splitting varies approximately as $(3 \cos^2 \theta - 1)$ with the angle θ between the external magnetic field and the crystalline hexagonal axis. This shows that in the Hamiltonian the predominant term is P_2^0 , with axial symmetry, not cubic symmetry. Thus gadolinium is comparable with manganese, where the splitting of the 6S state, previously interpreted by a cubic field, is known to be mainly axial in symmetry (Bleaney and Ingram 1951).

To determine the values of the higher terms in (1), measurements were made at 3 cm. wavelength in an apparatus incorporating a proton resonance system for determining the magnetic field accurately. From measurements at 20° K. with $\theta = 0$ (magnetic field parallel to hexagonal axis), the constants are determined as (in units of 10^{-4} cm.^{-1})

$$3A_2^0 = +200.3; \quad 60A_4^0 = -3.93; \quad 1260A_6^0 = +0.52.$$

The lines are symmetrically placed about the central line within $2 \times 10^{-4} \text{ cm.}^{-1}$ showing that off-diagonal elements of the Hamiltonian (such as P_6^6) are small.

* Communicated by B. Bleaney, F.R.S.

The spectrum observed perpendicular to the axis ($\theta=90^\circ$) is markedly asymmetrical. This is due to second order effects which agree within a few units of 10^{-4} cm.^{-1} with those calculated from (1) transformed to take the new direction of the field as the axis of quantization. These second order effects can be eliminated by taking the mean of the corresponding intervals on the low and high field-sides of the spectrum, and a set of constants can be determined independently of the previous measurement except for a small third order correction. These are (in 10^{-4} cm.^{-1})

$$3A_2^0 = +201.3; \quad 60A_4^0 = -3.77; \quad 1260(\frac{5}{16}A_6^0 - \frac{1}{16}A_6^0) = +0.41.$$

Comparison with the previous set shows good agreement for A_2^0 and A_4^0 , and we are justified in using the previous result for A_6^0 to obtain $1260 A_6^0 = -4.0$. The value of g has been determined in two ways: (a) comparison of the $\frac{1}{2} \longleftrightarrow -\frac{1}{2}$ transition with the resonance line of diphenyl tri-nitro-phenyl-hydrazil (f. Bleaney and Ingram (1951)) at 1.3 cm. wavelength, which gives $g = 1.992 \pm 0.002$ both parallel and perpendicular to the axis; (b) comparison with the proton resonance at 3 cm. wavelength which gives g (parallel) $= 1.994 \pm 0.001$, g (perpendicular) $= 1.994 \pm 0.002$. The error is greater in the latter case owing to the second order effects which are more important at 3 cm. and which may be due in part to small off-diagonal terms omitted in (1).

In an effort to elucidate such terms the lines have been plotted into zero magnetic field at long wavelengths. Owing to the Kramers-degeneracy they reduce to three, at 0.1127, 0.0834 and 0.0489 cm.^{-1} ; the values calculated from the proton measurements using (1) are 0.1130, 0.0833 and 0.0455 cm.^{-1} respectively. The discrepancy in the last is well outside the experimental error, but so far it seems impossible to account for it by adding terms to (1) (such as P_4^3 , P_6^3 , which reflect trigonal symmetry) without upsetting the agreement with the spectrum observed at the shorter wavelengths.

The reduced population of the upper levels at 20° K. in the strong fields necessary to observe resonance at 1.3 cm. wavelength enables us to determine the signs of the coefficients as given above from the asymmetry in the intensities of the lines. Hence at zero field the levels lie at 0, 0.049, 0.132 and 0.245 cm.^{-1} , the $\pm 7/2$ levels being uppermost.

Measurements at higher temperatures show that the overall splitting is about 11 per cent less at room temperature than at 20° K. At 90° K., the gadolinium resonance has been observed as an impurity in crystals of the ethyl sulphates of cerium, neodymium and samarium. The splitting decreases as the atomic number of the predominant ion increases, the change being equivalent roughly to a decrease of 3 per cent in the coefficients A_2^0 , A_4^0 per unit increase in atomic number.

Preliminary measurements on gadolinium bromate, nitrate and sulphate show that the spectrum is of the same nature as in the ethyl sulphate. The splitting is rather smaller in the bromate, and larger in the nitrate and sulphate than in the ethylsulphate.

As previously reported (Bleaney and Scovil 1950) no hyperfine structure due to the odd isotopes of Gd could be observed, and it must therefore be obscured by the tails of the strong lines due to the even isotopes. In view of the large hyperfine structure found in Nd and Er, this indicates that the 8S state of Gd must be substantially a pure $4f^7$ state.

REFERENCES.

- BLEANEY, B., and INGRAM, D. J. E., 1951, *Proc. Roy. Soc. A*, **205**, 336.
 BLEANEY, B., and SCOVIL, H. E. D., 1950, *Proc. Phys. Soc. A*, **63**, 1369.
 ELLIOTT, R. J., and STEVENS, K. W. H., 1951, *Proc. Phys. Soc. A*, **64**, 205.
 KETELAAR, J. A. A., 1937, *Physica*, **4**, 619.

CVIII. *Notices of New Books and Periodicals received.*

Reports on Progress in Physics, Vol. XIV, 1951. £2 10s. 0d. Postage 1s.

IN this period when physics is advancing so rapidly, and when so many contributions to original research appear in the scientific journals, there is a very great need for summarizing articles which will allow scientists, without too great an expenditure of labour, to find out what is going on in subjects akin to their own. Physicists are therefore indebted to the Physical Society for continuing to maintain the high standards of *Reports on Progress in Physics*, which is at present the only journal in this country which contains such summarizing reports.

The present volume contains eleven contributions; these deal with spectroscopy, including optics, with the physics of the atmosphere, and with nuclear physics and cosmic rays. The volume ends with an article by Professor Mayneord on applications of nuclear physics to medicine.

N. F. M.

[The Editors do not hold themselves responsible for the views expressed by their correspondents.]

CIX. *Theory of Barium Titanate.*—Part II.

By A. F. DEVONSHIRE,

H. H. Wills Physical Laboratory, University of Bristol*.

[Received June 7, 1951.]

SUMMARY.

The phenomenological theory of barium titanate given in an earlier paper has been extended, and expressions obtained for the piezoelectric constants, elastic coefficients for constant field and dielectric constants for constant strain in terms of other physical constants of the material. Curves are drawn showing these quantities as functions of temperature, and some comparison made with experiment. The relations of the constants of the ceramic to those of the single crystal are then briefly discussed.

§ 1. INTRODUCTION.

In an earlier paper we discussed the properties of single domains of BaTiO_3 in a phenomenological way, that is we used some of the known physical quantities to predict the values of others. We were able to account for the existence of three transition temperatures, and to correlate the observed dielectric constants, spontaneous polarization and spontaneous strains. In this paper we extend the calculations to other physical constants: first we calculate the piezoelectric constants; then we use these to calculate the clamped dielectric constants, which are very different from the free ones; finally we calculate the elastic constants for constant field, which are very different from those for constant polarization. These calculations are on similar lines to those made by Mason (1948) for the ceramic. Finally, we discuss tentatively the relations between the constants of the single domain and the ceramic.

§ 2. THEORY.

The method we used in Part I. (Devonshire 1949) was to expand the free energy as a function of strain and polarization, taking it to be zero when the crystal was in equilibrium and had cubic symmetry; the tetrahedral, orthorhombic and rhombohedral states were treated as strained forms of the cubic state. The expression for the free energy given in I., 9.21 was

$$\begin{aligned}
 A = & \frac{1}{2}c_{11}^P(x_x^2 + y_y^2 + z_z^2) + c_{12}^P(y_y z_z + z_z x_x + x_x y_y) + \frac{1}{2}c_{44}^P(x_x^2 + y_y^2 + z_z^2) \\
 & + g_{11}(x_x P_x^2 + y_y P_y^2 + z_z P_z^2) + g_{12}\{x_x(P_y^2 + P_z^2) + y_y(P_z^2 + P_x^2) + z_z(P_x^2 + P_y^2)\} \\
 & + g_{44}\{y_z P_y P_z + z_x P_z P_x + x_y P_x P_y\} + \frac{1}{2}\chi''(P_x^2 + P_y^2 + P_z^2) \\
 & + \frac{1}{4}\xi_{11}''(P_x^4 + P_y^4 + P_z^4) + \frac{1}{2}\xi_{12}''(P_y^2 P_z^2 + P_z^2 P_x^2 + P_x^2 P_y^2) + \frac{1}{6}\zeta''(P_x^6 + P_y^6 + P_z^6). \quad (2.1)
 \end{aligned}$$

* Communicated by the Author.

The c^P 's are the elastic constants of the cubic crystal and χ'' its reciprocal susceptibility. If we regard the strains as of order P^2 equation (2.1) includes all terms of order P^4 or lower and some of order P^6 (the latter are omitted in Part I.). Equations for the stresses and the electric field can be derived from (2.1) by the usual thermodynamic formulæ :

$$\left. \begin{aligned} X_x &= -\frac{\partial A}{\partial x_x} = -c_{11}^P x_x - c_{12}^P y_y - c_{12}^P z_z - g_{11} P_x^2 - g_{12} P_y^2 - g_{12} P_z^2, \\ &\dots\dots\dots \\ Y_z &= -\frac{\partial A}{\partial y_z} = -c_{44}^P y_z - g_{44} P_y P_z, \\ &\dots\dots\dots \\ E_x &= \frac{\partial A}{\partial P_x} = P_x(\chi'' + \xi_{11}' P_x^2 + \xi_{12}' P_y^2 + \xi_{12}' P_z^2 + \zeta' P_x^4) \\ &\quad + 2P_x(g_{11} x_x + g_{12} y_y + g_{12} z_z) + P_y g_{44} x_y + P_z g_{44} z_x, \\ &\dots\dots\dots \end{aligned} \right\} \quad (2.2)$$

If we solve these for x_x etc., then we have

$$\left. \begin{aligned} x_x &= -s_{11}^P X_x - s_{12}^P Y_y - s_{12}^P Z_z + Q_{11} P_x^2 + Q_{12} P_y^2 + Q_{12} P_z^2, \\ &\dots\dots\dots \\ y_z &= -s_{44}^P Y_z + Q_{44} P_y P_z, \\ &\dots\dots\dots \\ E_x &= P_x(\chi'' + \xi_{11}' P_x^2 + \xi_{12}' P_y^2 + \xi_{12}' P_z^2 + \zeta' P_x^4) \\ &\quad + 2P_x(Q_{11} X_x + Q_{12} Y_y + Q_{12} Z_z) + P_y Q_{44} X_y + P_z Q_{44} Z_x, \\ &\dots\dots\dots \end{aligned} \right\} \quad (2.3)$$

where

$$\left. \begin{aligned} (s_{11}^P - s_{12}^P)(c_{11}^P - c_{12}^P) &= 1, \quad (s_{11}^P + 2s_{12}^P)(c_{11}^P + 2c_{12}^P) = 1, \quad s_{44}^P c_{44}^P = 1, \\ Q_{11} - Q_{12} &= -(s_{11}^P - s_{12}^P)(g_{11} - g_{12}), \\ Q_{11} + 2Q_{12} &= -(s_{11}^P + 2s_{12}^P)(g_{11} + 2g_{12}), \quad Q_{44} = -s_{44}^P g_{44}, \\ \xi_{11}' &= \xi_{11}'' + 2g_{11} Q_{11} + 4g_{12} Q_{12}, \\ \xi_{12}' &= \xi_{12}'' + 2(g_{11} Q_{12} + g_{12} Q_{11} + g_{12} Q_{12}) + g_{44} Q_{44}. \end{aligned} \right\} \quad (2.4)$$

These equations are now in a similar form to those given by Mason (1948) for the ceramic; but in that case the substance when unstrained and unpolarized is isotropic instead of cubic, so that

$$\left. \begin{aligned} s_{44}^P &= 2(s_{11}^P - s_{12}^P), \\ Q_{44} &= 2(Q_{11} - Q_{12}). \end{aligned} \right\} \dots\dots\dots (2.5)$$

Mason also uses as a variable $D/4\pi$ (where D is the displacement) instead of P ; this, however, makes little difference, since P is always large compared with E .

Now as barium titanate is cooled it passes successively through cubic, tetragonal, orthorhombic and rhombohedral phases; and in the last three it has permanent polarization along an edge, face diagonal and body diagonal, respectively, of the original cube. We shall, therefore, consider in turn the physical constants for each of these phases.

In the tetragonal phase let the permanent polarization P_s be along the z -axis. Therefore in equations (2.3) let us replace P_z by $P_z + P_s$ (so that P_z is now the difference of the polarization from its saturation value), and neglect all terms in P_x^2 , P_y^2 and P_z^2 . The equations then become

$$\left. \begin{aligned} x_x &= Q_{12}P_s^2 - s_{11}^P X_x - s_{12}^P Y_y - s_{12}^P Z_z + 2Q_{12}P_s P_z, \\ y_y &= Q_{12}P_s^2 - s_{12}^P X_x - s_{11}^P Y_y - s_{12}^P Z_z + 2Q_{12}P_s P_z, \\ z_z &= Q_{11}P_s^2 - s_{12}^P X_x - s_{12}^P Y_y - s_{11}^P Z_z + 2Q_{11}P_s P_z, \\ y_z &= -s_{44}^P Y_z + Q_{44}P_s P_y, \\ z_x &= -s_{44}^P Z_x + Q_{44}P_s P_x, \\ x_y &= -s_{44}^P X_y, \\ E_x &= \chi'_{11}P_x + Q_{44}P_s Z_x, \\ E_y &= \chi'_{11}P_y + Q_{44}P_s Y_z, \\ E_z &= \chi'_{33}P_z + 2Q_{12}P_s(X_x + Y_y) + 2Q_{11}P_s Z_z, \end{aligned} \right\} \dots (2.6)$$

where

$$\left. \begin{aligned} \chi'_{11} &= \chi'' + \xi'_{12}P_s^2, \\ \chi'_{33} &= \chi'' + 3\xi'_{11}P_s^2 + 5\xi'P_s^4. \end{aligned} \right\} \dots (2.7)$$

Now the linear relations between stress, strain, polarization and field for any crystal can be written in the Voigt tensor notation:

$$\left. \begin{aligned} X_h &= -c_{hi}^P x_i + a_{mh} P_m, & (a) \\ E_m &= -a_{mh} x_h + \chi'_{km} P_k, & (b) \\ X_h &= -c_{hi}^E x_i + e_{mh} E_m, & (c) \\ P_m &= e_{mh} x_h + \eta'_{km} E_k, & (d) \\ x_h &= -s_{hi}^P X_i + b_{mh} P_m, & (e) \\ E_m &= b_{mh} X_h + \chi'_{km} P_k, & (f) \\ x_h &= -s_{hi}^E X_i + d_{mh} E_m, & (g) \\ P_m &= -d_{mh} X_h + \eta'_{km} E_k, & (h) \end{aligned} \right\} \dots (2.8)$$

where the summation convention has been used, that is each product is summed over all values of any suffix occurring twice in it. In the Voigt notation

$$\left. \begin{aligned} x_1 &= x_x, \quad x_2 = y_y, \quad x_3 = z_z, \\ x_4 &= y_z = z_y, \quad x_5 = z_x = x_z, \quad x_6 = x_y = y_x, \end{aligned} \right\} \dots (2.9)$$

with a similar notation for the X 's, so that the suffixes h and i run from 1 to 6, and k and m from 1 to 3. The physical meanings of the various constants are implicit in the equations; thus the d 's are clearly the

piezoelectric coefficients as normally defined. Between the constants there are numerous relations, which can easily be derived from the equations: if, for example, we eliminate P between (e) and (h) and compare the resulting equation with (g) we find that

$$\left. \begin{aligned} s_{hi}^E &= s_{hi}^P + b_{mh} d_{mi}, \\ d_{kh} &= b_{mh} \gamma'_{km}. \end{aligned} \right\} \dots \dots (2.10)$$

Other relations that we shall need are:

$$\left. \begin{aligned} a_{ki} &= b_{kh} c_{hi}^P, \\ \chi_{km} &= \chi'_{km} + a_{kh} b_{mh} \\ &= \chi'_{km} + b_{ki} b_{mh} c_{hi}^P, \\ c_{hi} s_{ij} &= \delta_{hj}, \\ \chi_{ki} \eta_{lm} &= \delta_{km}, \end{aligned} \right\} \dots \dots (2.11)$$

where δ is the tensor defined so that it is zero if the suffixes are different and 1 if they are the same.

By comparing (2.8 e) with (2.6), we see that in the tetragonal phase

$$\left. \begin{aligned} b_{11} &= b_{12} = b_{13} = b_{14} = b_{16} = 0, \quad b_{15} = Q_{44} P_s, \\ b_{21} &= b_{22} = b_{23} = b_{25} = b_{26} = 0, \quad b_{24} = Q_{44} P_s, \\ b_{31} &= b_{32} = 2Q_{12} P_s, \quad b_{33} = Q_{11} P_s, \quad b_{34} = b_{35} = b_{36} = 0. \end{aligned} \right\} \dots (2.12)$$

We also have

$$\left. \begin{aligned} \eta'_{11} &= \eta'_{22} = 1/\chi'_{11}, \quad \eta'_{33} = 1/\chi'_{33}, \\ \eta'_{12} &= \eta'_{31} = \eta'_{23} = 0, \end{aligned} \right\} \dots \dots (2.13)$$

and

$$\left. \begin{aligned} c_{11}^P &= c_{22}^P = c_{33}^P, \quad c_{12}^P = c_{31}^P = c_{23}^P, \quad c_{44}^P = c_{55}^P = c_{66}^P, \\ (c_{11}^P + 2c_{12}^P)(s_{11}^P + 2s_{12}^P) &= 1, \\ (c_{11}^P - c_{12}^P)(s_{11}^P - s_{12}^P) &= 1, \\ c_{44}^P s_{44}^P &= 1, \end{aligned} \right\} \dots (2.14)$$

while all the other c 's vanish. Hence from (2.10) and (2.11) it follows that

$$\left. \begin{aligned} d_{11} &= d_{12} = d_{13} = d_{14} = d_{16} = 0, \quad d_{15} = Q_{44} P_s \eta'_{11}, \\ d_{21} &= d_{22} = d_{23} = d_{25} = d_{26} = 0, \quad d_{24} = Q_{44} P_s \eta'_{11}, \\ d_{31} &= d_{32} = 2Q_{12} P_s \eta'_{33}, \quad d_{33} = 2Q_{11} P_s \eta'_{33}, \quad d_{34} = d_{35} = d_{36} = 0, \end{aligned} \right\} (2.15)$$

and

$$\left. \begin{aligned} s_{11}^E &= s_{22}^E = s_{11}^P + 4Q_{12}^2 P_s^2 \eta'_{33}, \quad s_{33}^E = s_{11}^P + 4Q_{11}^2 P_s^2 \eta'_{33}, \\ s_{12}^E &= s_{12}^P + 4Q_{12}^2 P_s^2 \eta'_{33}, \quad s_{13}^E = s_{23}^E = s_{12}^P + 4Q_{11} Q_{12} P_s^2 \eta'_{33}, \\ s_{44}^E &= s_{55}^E = s_{44}^P + Q_{44}^2 P_s^2 \eta'_{11}, \quad s_{66}^E = s_{44}^P, \end{aligned} \right\} \dots (2.16)$$

and

$$\left. \begin{aligned} \chi''_{11} &= \chi''_{22} = \chi'_{11} + c_{44}^P Q_{44}^2 P_s^2, \\ \chi''_{33} &= \chi'_{33} + 4\{c_{11}^P Q_{11}^2 + 4c_{12}^P Q_{11} Q_{12} + 2(c_{11}^P + c_{12}^P) Q_{12}^2\} P_s^2. \end{aligned} \right\} \quad (2.17)$$

In the orthorhombic phase let the permanent polarization have components P_s along the y and z -axes of the crystal. In equations (2.3) let us replace P_z and P_y by $P_z + P_s$ and $P_y + P_s$, and neglect all terms in P_x^2 , P_y^2 and P_z^2 . The equations then become

$$\left. \begin{aligned} x_x &= 2Q_{12}P_s^2 - s_{11}^P X_x - s_{12}^P Y_y - s_{12}^P Z_z + 2Q_{12}P_s P_y + 2Q_{12}P_s P_z, \\ y_y &= (Q_{11} + Q_{12})P_s^2 - s_{12}^P X_x - s_{11}^P Y_y - s_{12}^P Z_z + 2Q_{11}P_s P_y + 2Q_{12}P_s P_z, \\ z_z &= (Q_{11} + Q_{12})P_s^2 - s_{12}^P X_x - s_{12}^P Y_y - s_{11}^P Z_z + 2Q_{12}P_s P_y + 2Q_{11}P_s P_z, \\ y_z &= Q_{44}P_s^2 - s_{44}^P Y_z + Q_{44}P_s P_y + Q_{44}P_s P_z, \\ z_x &= -s_{44}^P Z_x + Q_{44}P_s P_x, \\ x_y &= -s_{44}^P X_y + Q_{44}P_s P_x, \\ E_x &= \chi'_{11}P_x + Q_{44}P_s Z_x + Q_{44}P_s X_y, \\ E_y &= \chi'_{33}P_y + \chi'_{23}P_z + 2Q_{12}P_s X_x + 2Q_{11}P_s Y_y + 2Q_{12}P_s Z_z + Q_{44}P_s Y_z, \\ E_z &= \chi'_{23}P_y + \chi'_{33}P_z + 2Q_{12}P_s X_x + 2Q_{12}P_s Y_y + 2Q_{11}P_s Z_z + Q_{44}P_s Y_z, \end{aligned} \right\} \quad (2.18)$$

where

$$\left. \begin{aligned} \chi'_{11} &= \chi'' + 2\xi'_{12}P_s^2, \\ \chi'_{33} &= \chi'' + (3\xi'_{11} + \xi'_{12})P_s^2 + 5\xi'P_s^4, \\ \chi'_{23} &= 2\xi'_{12}P_s^2. \end{aligned} \right\} \quad (2.19)$$

By comparing these equations with (2.8) e or f we see that

$$\left. \begin{aligned} b_{11} &= b_{12} = b_{13} = b_{14} = 0, \quad b_{15} = b_{16} = Q_{44}P_s, \\ b_{21} &= b_{31} = b_{23} = b_{32} = 2Q_{12}P_s, \quad b_{22} = b_{33} = Q_{11}P_s, \\ b_{24} &= b_{34} = Q_{44}P_s, \quad b_{25} = b_{26} = b_{35} = b_{36} = 0. \end{aligned} \right\} \quad (2.20)$$

We also have

$$\left. \begin{aligned} \eta'_{11} &= 1/\chi'_{11}, \quad \eta'_{12} = \eta'_{13} = 0, \quad \eta'_{22} = \eta'_{33}, \\ (\eta'_{33} + \eta'_{23})(\chi'_{33} + \chi'_{23}) &= 1, \quad (\eta'_{33} - \eta'_{23})(\chi'_{33} - \chi'_{23}) = 1, \end{aligned} \right\} \quad (2.21)$$

and the c^P 's are given by (2.14), so that by substituting in (2.10) and (2.11) we have

$$\left. \begin{aligned} d_{11} &= d_{12} = d_{13} = d_{14} = 0, \quad d_{15} = d_{16} = Q_{44}P_s \eta_{11}, \\ d_{21} &= d_{31} = 2Q_{12}P_s(\eta'_{33} + \eta'_{23}), \\ d_{23} &= d_{32} = 2P_s(Q_{12}\eta'_{33} + Q_{11}\eta'_{23}), \\ d_{22} &= d_{33} = 2P_s(Q_{11}\eta'_{33} + Q_{12}\eta'_{23}), \\ d_{24} &= d_{34} = Q_{44}P_s(\eta'_{33} + \eta'_{23}), \\ d_{25} &= d_{26} = d_{35} = d_{36} = 0, \end{aligned} \right\} \quad (2.22)$$

and

$$\left. \begin{aligned}
 s_{11}^E &= s_{11}^P + 8Q_{12}^2 P_s^2 (\eta'_{33} + \eta'_{23}), \quad s_{22}^E = s_{33}^E = s_{11}^P \\
 &\quad + \{8Q_{11}Q_{12}\eta'_{23} + 4(Q_{11}^2 + Q_{12}^2)\eta'_{33}\}P_s^2, \\
 s_{12}^E &= s_{13}^E = s_{12}^P + 4Q_{12}(Q_{11} + Q_{12})P_s^2(\eta'_{33} + \eta'_{23}), \\
 s_{23}^E &= s_{12}^P + \{8Q_{11}Q_{12}\eta'_{33} + 4(Q_{11}^2 + Q_{12}^2)\eta'_{23}\}P_s^2, \\
 s_{14}^E &= 4Q_{12}Q_{44}P_s^2(\eta'_{33} + \eta'_{23}), \quad s_{24}^E = s_{34}^E = 2(Q_{11} + Q_{12})Q_{44}P_s^2(\eta'_{33} + \eta'_{23}), \\
 s_{15}^E &= s_{25}^E = s_{35}^E = s_{16}^E = s_{26}^E = s_{36}^E = 0, \\
 s_{44}^E &= s_{44}^P + 2Q_{44}^2 P_s^2(\eta'_{33} + \eta'_{23}), \quad s_{55}^E = s_{66}^E = s_{44}^P + Q_{44}^2 P_s^2 \eta'_{11}, \\
 s_{56}^E &= Q_{44}^2 P_s^2 \eta'_{11}, \quad s_{46}^E = s_{45}^E = 0,
 \end{aligned} \right\} \quad (2.23)$$

and

$$\left. \begin{aligned}
 \chi''_{11} &= \chi'_{11} + 2c_{44}^P Q_{44}^2 P_s^2, \\
 \chi''_{22} &= \chi''_{33} = \chi'_{33} \\
 &\quad + [4\{Q_{11}^2 c_{11}^P + 4Q_{11}Q_{12}c_{12}^P + 2Q_{12}^2(c_{11}^P + c_{12}^P)\} + c_{44}^P Q_{44}^2]P_s^2, \\
 \chi''_{31} &= \chi''_{12} = 0, \\
 \chi''_{23} &= \chi'_{23} \\
 &\quad + [4\{Q_{11}^2 c_{12}^P + 2Q_{11}Q_{12}(c_{11}^P + c_{12}^P) + Q_{12}^2(c_{11}^P + 3c_{12}^P)\} + Q_{44}^2 c_{44}^P]P_s^2.
 \end{aligned} \right\} \quad (2.24)$$

In all these equations for the orthorhombic phase it must be remembered that the resultant saturation polarization is $P_s\sqrt{2}$.

In the rhombohedral phase the permanent polarization will have the same component P_s along each axis of the crystal. Hence in equations (2.3) we replace P_x , P_y and P_z by $P_x + P_s$, $P_y + P_s$ and $P_z + P_s$, and neglect terms in P_x^2 , P_y^2 and P_z^2 . The equations then become

$$\left. \begin{aligned}
 x_x &= (Q_{11} + 2Q_{12})P_s^2 - s_{11}^P X_x - s_{12}^P Y_y - s_{12}^P Z_z + 2Q_{11}P_s P_x \\
 &\quad + 2Q_{12}P_s P_y + 2Q_{12}P_s P_z, \\
 \dots \dots \dots \\
 y_z &= Q_{44}P_s^2 - s_{44}^P Y_z + Q_{44}P_s P_y + Q_{44}P_s P_z, \\
 \dots \dots \dots \\
 E_x &= \chi'_{11}P_x + \chi'_{12}P_y + \chi'_{12}P_z + 2Q_{11}P_s X_x + 2Q_{12}P_s Y_y \\
 &\quad + 2Q_{12}P_s Z_z + Q_{44}P_s Z_x + Q_{44}P_s X_y, \\
 \dots \dots \dots
 \end{aligned} \right\} \quad (2.25)$$

where

$$\left. \begin{aligned}
 \chi'_{11} &= \chi'' + (3\xi'_{11} + 2\xi'_{12})P_s^2 + 5\xi'P_s^4, \\
 \chi'_{12} &= 2\xi'_{12}P_s^2.
 \end{aligned} \right\} \quad (2.26)$$

By comparing these equations with (2.8) *e* or *f* we see that

$$\left. \begin{aligned}
 b_{11} &= b_{22} = b_{33} = 2Q_{11}P_s, \\
 b_{12} &= b_{13} = b_{21} = b_{23} = b_{31} = b_{32} = 2Q_{12}P_s, \\
 b_{14} &= b_{25} = b_{36} = 0, \\
 b_{24} &= b_{34} = b_{15} = b_{35} = b_{16} = b_{26} = Q_{44}P_s.
 \end{aligned} \right\} \quad (2.27)$$

We also have

$$\left. \begin{aligned} \eta'_{11} &= \eta'_{22} = \eta'_{33}, \quad \eta'_{23} = \eta'_{31} = \eta'_{12}, \\ (\eta'_{11} + 2\eta'_{12})(\chi'_{11} + 2\chi'_{12}) &= 1, \quad (\chi'_{11} - \chi'_{12})(\eta'_{11} - \eta'_{12}) = 1, \end{aligned} \right\} \quad (2.28)$$

and the c^P 's are given by (2.14), so that by substituting in (2.10) and (2.11) we have

$$\left. \begin{aligned} d_{11} &= d_{22} = d_{33} = (2Q_{11}\eta'_{11} + 4Q_{12}\eta'_{12})P_s, \\ d_{12} &= d_{13} = d_{21} = d_{23} = d_{31} = d_{32} = \{2Q_{12}\eta'_{11} + 2(Q_{11} + Q_{12})\eta'_{12}\}P_s, \\ d_{14} &= d_{25} = d_{36} = 2Q_{44}\eta'_{12}P_s, \\ d_{15} &= d_{16} = d_{24} = d_{26} = d_{34} = d_{35} = Q_{44}(\eta'_{11} + \eta'_{12})P_s, \end{aligned} \right\} \quad (2.29)$$

and

$$\left. \begin{aligned} s_{11}^E &= s_{22}^E = s_{33}^E = s_{11}^P + 4\{(Q_{11}^2 + 2Q_{12}^2)\eta'_{11} + (4Q_{11}Q_{12} + 2Q_{12}^2)\eta'_{12}\}P_s^2, \\ s_{23}^E &= s_{31}^E = s_{12}^E = s_{12}^P \\ &\quad + 4\{(2Q_{11}Q_{12} + Q_{12}^2)\eta'_{11} + (Q_{11}^2 + 2Q_{11}Q_{12} + 3Q_{12}^2)\eta'_{12}\}P_s^2, \\ s_{14}^E &= s_{25}^E = s_{36}^E = 4\{Q_{12}Q_{44}\eta'_{11} + (Q_{11} + Q_{12})Q_{44}\eta'_{12}\}P_s^2, \\ s_{15}^E &= s_{16}^E = s_{24}^E = s_{26}^E = s_{35}^E = s_{36}^E \\ &\quad = 2\{(Q_{11} + Q_{12})Q_{44}\eta'_{11} + (Q_{11} + 3Q_{12})Q_{44}\eta'_{12}\}P_s^2, \\ s_{44}^E &= s_{55}^E = s_{66}^E = s_{44}^P + 2Q_{44}^2(\eta'_{11} + \eta'_{12})P_s^2, \\ s_{56}^E &= s_{64}^E = s_{45}^E = Q_{44}^2(\eta'_{11} + 3\eta'_{12})P_s^2, \end{aligned} \right\} \quad (2.30)$$

and

$$\left. \begin{aligned} \chi''_{11} &= \chi''_{22} = \chi''_{33} = \chi'_{11} \\ &\quad + [4\{c_{11}^P Q_{11}^2 + 4c_{12}^P Q_{11}Q_{12} + 2(c_{11}^P + c_{12}^P)Q_{12}^2\} + 2c_{44}^P Q_{44}^2]P_s^2, \\ \chi''_{23} &= \chi''_{31} = \chi''_{12} = \chi'_{12} \\ &\quad + [4\{c_{12}^P Q_{11}^2 + 2(c_{11}^P + c_{12}^P)Q_{11}Q_{12} + (c_{11}^P + 3c_{12}^P)Q_{12}^2\} + c_{44}^P Q_{44}^2]P_s^2. \end{aligned} \right\} \quad (2.31)$$

In all these equations for the rhombohedral phase it must be remembered that the resultant saturation polarization is $P_s\sqrt{3}$.

§ 3. NUMERICAL RESULTS.

In the previous sections we have found formulæ for the piezoelectric coefficients (d), the elastic compliance coefficients for constant field (s^E), and the reciprocal susceptibilities for constant strain (χ''). To evaluate these formulæ we must know the permanent polarization P_s , the compliances and elastic constants for constant polarization (s^P and c^P), the susceptibilities for constant stress (η') and the electrostrictive coefficients for the cubic form (Q). In Part I. we showed how to calculate P_s and χ' (and hence η') as functions of temperature by using a limited number of experimental results, and we shall use these calculated values here. The electrostrictive constants Q can be determined

by comparing the measured spontaneous strains (Kay and Vousden 1949) with the measured spontaneous polarization (Merz 1949 a); in this way we find that

$$\left. \begin{aligned} Q_{11} &= 2.9 \times 10^{-12}, \\ Q_{12} &= -1.1 \times 10^{-12}, \\ \text{and } Q_{44} &= 2.7 \times 10^{-12} \end{aligned} \right\} \dots \dots \dots (3.1)$$

in c.g.s. units. These values can be checked by using Merz measurements of the shift of transition temperature with hydrostatic pressure; for it can be shown that if T_c is the transition temperature

$$\frac{\partial T_c}{\partial p} \frac{\partial \chi''}{\partial T} = Q_{11} + 2Q_{12}. \dots \dots (3.2)$$

Now, according to Merz, the upper transition temperature is lowered by about 1°C. per 170 atmospheres, and measurements on the dielectric constant in the cubic phase show that $\partial \chi'' / \partial T$ is about 10^{-4} , so that

$$Q_{11} + 2Q_{12} = 0.6 \times 10^{-12},$$

which agrees reasonably well with (3.1). Elastic constants for the single crystal have been measured by Bond, Mason and McSkimin, who found that

$$\left. \begin{aligned} c_{11}^P &= 2.07 \times 10^{12}, \\ c_{44}^P &= 1.27 \times 10^{12}. \end{aligned} \right\} \dots \dots \dots (3.3)$$

There are no measurements of c_{12}^P , so we have assumed it equal to c_{44}^P ; we then find that

$$\left. \begin{aligned} s_{11}^P &= 0.90 \times 10^{-12}, \\ s_{12}^P &= 0.34 \times 10^{-12}, \\ s_{44}^P &= 0.79 \times 10^{-12}. \end{aligned} \right\} \dots \dots \dots (3.4)$$

Both the Q 's and the s^P 's must be functions of temperature, but the temperature dependence has not been measured, so we have treated them as constants, which is probably not far wrong.

It is interesting to compute the quantities g and ξ'' , since they are directly related to the forces between the ions. We gave values for these in Part I. (Devonshire 1949), but these now need revision as more experimental data are available. From (2.4), (3.1) and (3.4) we find that

$$\begin{aligned} g_{11} &= -3.2, \\ g_{12} &= 0, \\ g_{44} &= -3.4, \end{aligned}$$

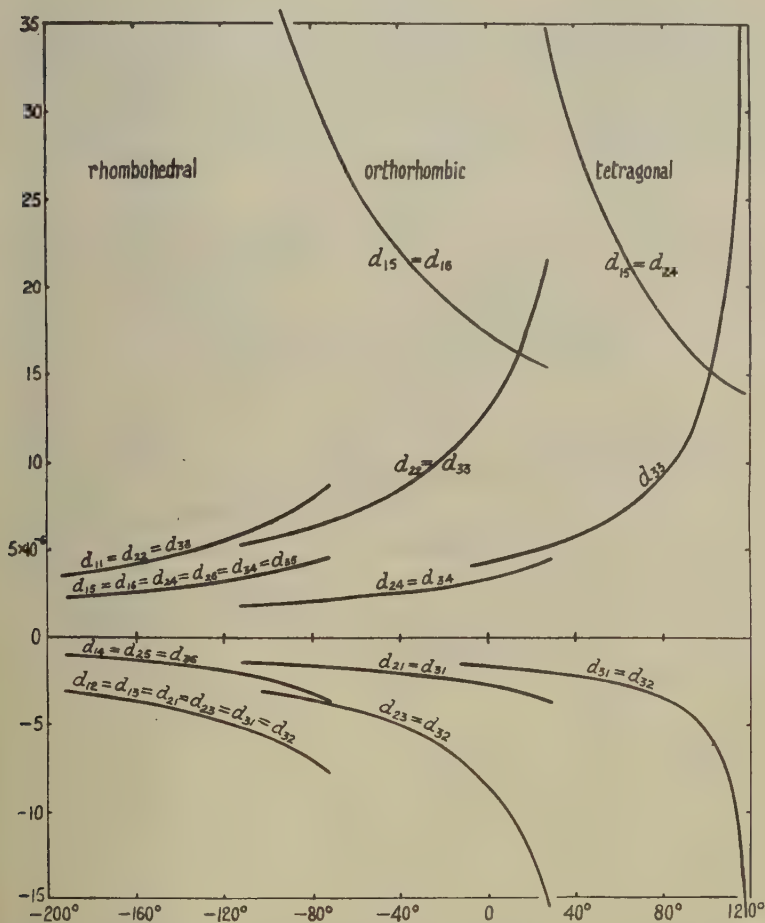
and using the values for ξ'_{11} and ξ'_{12} given in Part I. equations (7.14) and (7.15) we have

$$\begin{aligned} \xi''_{11} &= 14.1 \times 10^{-12}, \\ \xi''_{12} &= 7.4 \times 10^{-12}. \end{aligned}$$

We can now calculate the components of d , s^E and η'' as functions of temperature, and the results are shown graphically in figs. 1, 2 and 3.

The piezoelectric constants are seen to be very large and to vary rapidly with temperature. Piezoelectric constants are usually of the

Fig. 1.



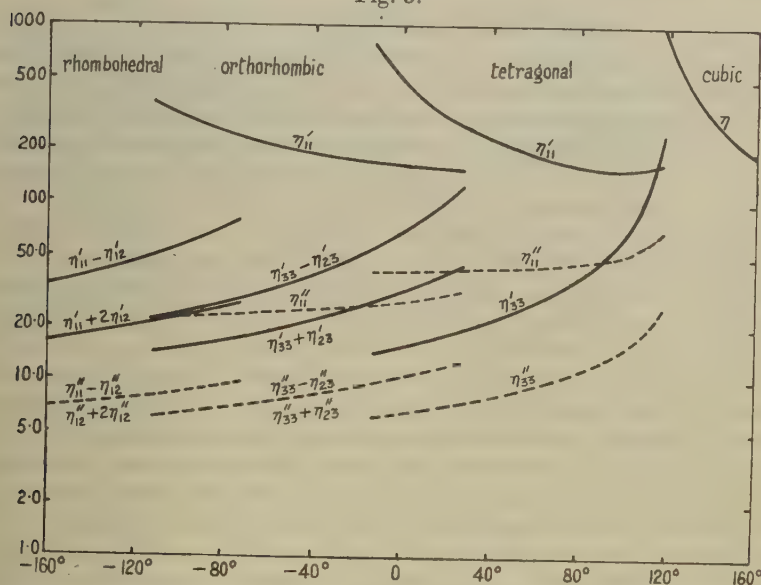
Piezoelectric coefficients d of BaTiO_3 calculated as functions of temperature.

The suffixes in all cases refer to the principal axes of the cubic or tetragonal phase; these are not, of course, principal axes in the orthorhombic and rhombohedral phases. The directions of polarization are (001), (011) and (111). Values in c.g.s. units.

order of 10^{-7} , so these are about a hundred times larger; these large values are also found in other ferroelectrics such as Rochelle salt or KH_2PO_4 .

There are not many measurements of the d 's and they are confined to the tetragonal phase. The coefficient d_{31} has been determined by Merz and Caspari by measuring the extension produced by a known electric field; they found that d_{31} is about -10^{-6} at room temperatures with a very sharp rise to -7×10^{-6} at the upper transition temperature. These values are less than the calculated ones; this is probably partly, but not entirely, due to the fact that they were measured with a strong biasing field in order to keep the crystal as a single domain. The piezoelectric coefficients can also be measured by a dynamic method; by measuring the resonance and antiresonance frequencies of a crystal oscillator both the piezoelectric constants and the elastic compliances can be determined; the theory of this method has been given by Mason

Fig. 3.



Dielectric susceptibilities for constant stress (η') and for constant strain (η'') of BaTiO_3 calculated as functions of temperature. The suffixes refer to the same axes as in fig. 1, so that $\eta_{33}-\eta_{23}$, etc., are the values for the principal axes of the orthorhombic or rhombohedral phase. The susceptibilities are related to the dielectric constants (ϵ) by the equation $\epsilon = 1 + 4\pi\eta$. The vertical scale is logarithmic.

(1950). Dynamic measurements of d_{31} have been made by Caspari and Merz (1950), who found a sharp increase near the upper transition temperature as in their static measurements, but they did not measure absolute values. Dynamic measurements at room temperature have been made by Bond, Mason and McSkimin (1951) who found that

$$d_{31} = -3.1 \times 10^{-6},$$

$$d_{33} = 10.4 \times 10^{-6}.$$

These values are higher than the theoretical ones; the crystals were not, however, strictly single domains. Measurements of s^E were also made, and these agree fairly well with the theoretical values.

Fig. 3 shows that the "clamped" susceptibilities (η'') are smaller than the free susceptibilities η' by a factor that varies from 2 to 10; this is a very large effect. The "clamped" susceptibilities can be determined by making measurements at frequencies greater than the resonance frequencies. Measurements made by Bond, Mason and McSkimin (1951) show that at room temperatures η_{33} is halved when measurements are made at frequencies higher than the resonance frequency. Similar measurements have been made on ceramics, but we shall consider these in the next section.

§ 4. PHYSICAL CONSTANTS OF CERAMICS.

As most of the experimental work on BaTiO_3 , and all the earlier work, has been done on the ceramic, it is desirable to consider its properties. It must in principle be possible to derive the constants of the ceramics from the constants of the single domain—one would expect the ceramic constants to be some kind of directional average of the single domain constants. The average may, however, be made in many ways; for example we can average either the susceptibilities (η) or the reciprocal susceptibilities (χ); again we can average either the compliances (s) or the elastic constants (c), and since s^E is the same as s^P for the unpolarized ceramic we can average over s^E , s^P , c^E or c^P . For a nearly isotropic substance it matters little how we take the average, but for a substance so very anisotropic as BaTiO_3 it matters much. Now the method of averaging depends on the boundary conditions; if the boundary condition were that stress is continuous then it would be correct to average over the s 's and not the c 's. Boundary conditions are not, however, so simple; if there is no slip then three components of stress and three of strain are continuous; if the boundary is perpendicular to the z -axis then the continuous stress-components are T_{zz} , T_{xx} , and T_{yy} , and the continuous strain-components are S_{xx} , S_{yy} , and S_{zz} . Again the electrical conditions at a boundary are that the normal components of polarization* and the tangential components of field are continuous. Thus we cannot take a simple average for any of the physical constants, and the correct way of taking the average is not apparently known.

The directional average of a symmetrical tensor of the second order is given by

$$A_{11} = \frac{1}{3}(A_{11} + A_{22} + A_{33}). \quad \dots \quad (4.1)$$

For a fourth order tensor having the symmetry of the elastic constants there are two independent averaged quantities, namely

* More precisely of displacement, but the distinction is of little importance for BaTiO_3 .

$$\bar{B}_{1111} = \frac{1}{5}(B_{1111} + B_{2222} + B_{3333}) + \frac{2}{15}(B_{2233} + B_{3311} + B_{1122}) + \frac{4}{15}(B_{2323} + B_{3131} + B_{1212}), \quad (4.2)$$

and

$$\bar{B}_{1122} = \frac{1}{15}(B_{1111} + B_{2222} + B_{3333}) + \frac{4}{15}(B_{1122} + B_{2233} + B_{3311}) - \frac{2}{15}(B_{1212} + B_{2323} + B_{3131}),$$

while

$$B_{1212} = \frac{1}{2}(B_{1111} - B_{1122}).$$

When translating these into Voigt notation we must remember that

$$s_{44} = 4s_{1212},$$

but that

$$c_{44} = c_{1212}.$$

As an example of the effect of different methods of averaging we shall calculate s_{11} and s_{12} in four different ways. We pointed out in the last section that we could average over s^E or s^P , or alternatively average over c^E or c^P and then calculate s by using the usual relations between the s 's and the c 's. We give the results below, where we have used the theoretical values for s^E and s^P at 20° C. The experimental values are those of Mason (1948), obtained by resonance methods.

	Average over s^P	Average over s^E	Average over c^P	Average over c^E	Experi- mental
$\bar{s}_{11} \times 10^{12}$	0.56	1.50	0.41	0.83	0.88
$\bar{s}_{12} \times 10^{12}$	-0.17	-0.61	-0.13	-0.29	-0.236

The problem of averaging the electro-restrictive constants is even more difficult, since the strain corresponding to a given polarization is not necessarily always the same. The polarization of the ceramic may be produced by altering the direction of some of the domains or by changing the magnitude of their polarization, and the corresponding strain will be different in the two cases. Mason (1950 b) found that for the ceramic

$$Q_{11} = 3.6 \times 10^{-12},$$

$$Q_{12} = -1.35 \times 10^{-12}.$$

The values obtained by averaging the constants for the cubic crystal are

$$Q_{11} = 1.8 \times 10^{-12},$$

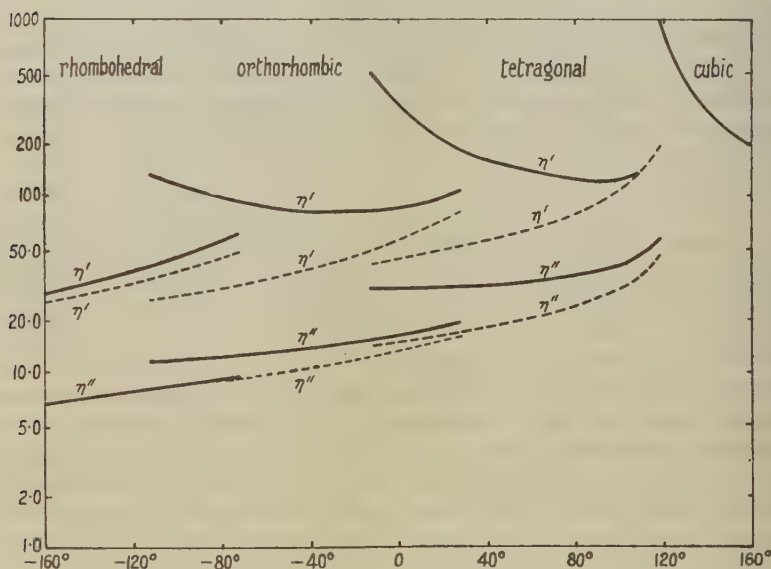
$$Q_{12} = -0.6 \times 10^{-12}.$$

Fig. 4 shows the susceptibilities for both the free (η') and the clamped (η'') material averaged in two different ways—directly and over the reciprocal susceptibilities. The differences are sometimes large; and for η' the discontinuities at the lower transition temperatures are reversed. Measurements of the free susceptibilities for the ceramic have been given by many authors. In particular an extensive series of measurements have been made by Von Hippel, Breckenridge, Chesley and Tisza (1946)

and measurements for temperatures down to a few degrees absolute by Blunt and Love (1949). The measured values follow a curve which, for the most part, lies in between the two mean curves for η' .

The clamped constant η'' would presumably be obtained if measurements were made at such high frequencies that the strain could not follow the polarization. Powles (1948) found that at a frequency of 9.45×10^9 cycles the dielectric constant had dropped considerably (by a factor of about 5). A further drop occurred at a frequency of 24.5×10^9 cycles. These frequencies are extremely high for piezoelectric resonance frequencies (*e. g.* those found by Mason for his single crystals and polarized ceramics were about 10^6 cycles). However, in an unpolarized

Fig. 4.



Dielectric susceptibilities of BaTiO_3 for constant stress (η') and for constant strain (η'') averaged over all directions. The full lines represent direct averages, and the dotted lines averages made over the reciprocal susceptibility.

ceramic, which consists of polarized domains pointing in various directions, there will be no vibration of the material as a whole in an alternating field, and the effective resonance frequency will be approximately that of a single domain; since resonance frequencies are inversely proportional to linear dimensions it is possible to have high values if the domains are small enough; Powles results suggest that the domain size is of the order of 10^{-3} mm.; this agrees with measurements of the "Barkhausen" effect by Newton, Ahearn and McKay (1949).

A different explanation of Powles' results has been put forward by Mason and Matthias (1948). In their model of barium titanate the titanium ion alternates between a number of positions of equilibrium; there is naturally a relaxation frequency associated with the movement of the titanium ion, and if we make the right assumption about the size of the potential hill separating the equilibrium positions it will correspond to the frequency at which the dielectric constant falls. This explanation is supported by the fact that Powles found a drop in dielectric constant even above the Curie point; here the crystal is not piezoelectric, so that there should be no difference between the free and the clamped dielectric constants. The fall in dielectric constant is, however, much less above the Curie point, and in a ceramic there will probably be internal strains, so that there may exist tetragonal regions even above the Curie point, as has been suggested by Caspari and Merz (1950). Moreover the difference between the "free" and "clamped" constants certainly exists and is about the right amount to account for Powles' results; its existence does not depend on any particular model, and it must be observed if we go to sufficiently high frequencies. This does not mean of course that there may not be other relaxation effects associated with a particular model such as Mason's.

ACKNOWLEDGMENT.

The author wishes to thank the Electrical Research Association for financial assistance in aid of this work, and for permitting its publication.

REFERENCES.

- BLUNT and LOVE, 1949, *Phys. Rev.*, **76**, 1202.
BOND, MASON and McSKIMIN, H. J., 1951, *Phys. Rev.*, **82**, 442.
CASPARI and MERZ, 1950, *Phys. Rev.*, **80**, 1082.
DEVONSHIRE, 1949, *Phil. Mag.*, **40**, 1040.
KAY and VOUSDEN, 1949, *Phil. Mag.*, **40**, 1019.
MASON, 1948, *Phys. Rev.*, **74**, 1134; 1950 a, *Piezoelectric Crystals* (D. Van Nostrand), Chap. 5; 1950 b, *Ibid.*, Chap. 12.
MASON and MATTHIAS, 1948, *Phys. Rev.*, **74**, 1622.
MERZ, 1949 a, *Phys. Rev.*, **76**, 1221; 1949 b, *Phys. Rev.*, **78**, 52.
NEWTON, AHEARN and MCKAY, 1949, *Phys. Rev.*, **76**, 459.
POWLES, 1948, *Nature*, **161**, 25; **162**, 614 and 655.
POWLES and JACKSON, 1949, *Proc. Inst. Elect. Eng.*, **96**, 383.
VON HIPPEL, BRECKENRIDGE, CHESLEY and TISZA, 1946, *Ind. and Eng. Chem.* **38**, 1097.

CX. *Remarks on the Two-Fluid Model of Helium II.*

By R. B. DINGLE,

Royal Society Mond Laboratory, Cambridge*.

[Received June 5, 1951.]

ABSTRACT.

In §1 it is shown that Gorter's assumption that the forces acting on the normal and superfluid are equal and opposite is true only if there is no entropy of mixing: §2 shows that his derivation of the fountain effect pressure assumes also that entropy is proportional to concentration. In §3 we point out an additional assumption implicitly made by Gorter, Tisza, and by Nakajima and co-workers—that effective mass is proportional to concentration. §4 is devoted to a proof that whatever the energy spectrum the entire entropy and internal energy and all the excited atoms (or excitations) follow the motion of the tube in which they are contained; this is not in agreement with Temperley's suggestion that other states besides the very lowest one contribute to the superfluid density. In §5 we calculate the extra terms arising from the creation of new phonons during the motion of the normal fluid. The status of the relation $\rho_n \propto S$ in the two-fluid theory is discussed in §6. The next section is concerned with the theoretical condition determining the lambda-point, and §8 with the expected differences in behaviour of He^4 and He^3 .

§1. THE FORCES ACTING ON THE NORMAL AND SUPERFLUID.

GORTER (1949) has recently attempted to generalize the equations of the two-fluid model by discarding the usual assumption that there is no entropy of mixing. In his derivation he assumes that when there is only a temperature gradient in Helium II, the normal and superfluid components diffuse into each other, and that the effect may be described by a diffusion force equal in magnitude but opposite in sign for the two fluids: this means that $K_s(T) = -K_n(T)$ in his notation. From this assumption the values of K_n and K_s are found by an argument analogous to the standard derivation of Kelvin's equations for thermo-electricity.

Let us now examine the possible bases of the assumption that $K_s = -K_n$. First, we note that it does not follow from Newton's third law—that action and reaction are equal and opposite—since each force vanishes under equilibrium conditions, *i. e.* when there is no temperature gradient. Secondly, we observe that it implies that the rate of change of momenta of the two fluids are equal and opposite, so that $\partial(\rho_s v_s)/\partial t = -\partial(\rho_n v_n)/\partial t$, whence $\rho_s v_s + \rho_n v_n = 0$ and $\rho_s x_s + \rho_n x_n = 0$. Thus Gorter's assumption

* Communicated by the Author.

implies that the centre of gravity of the two fluids remains fixed if a temperature gradient is imposed. Although irrelevant to our argument, we may note that there seems to be no reason why this should be generally true; even in ordinary gaseous systems thermal diffusion may lead to its violation.

In a previous paper (Dingle 1949 b) we showed how the forces K_s and K_n may be calculated separately. Generalizing the model discussed in that paper, we now determine the conditions under which $K_s = -K_n$. In the notation of that paper, the force acting on the superfluid per unit volume of Helium II is, for any two-fluid model (*loc. cit.* §4 (i)),

$$\rho \nabla \left(\frac{\partial \delta W}{\partial \nabla \cdot x_s} \right)_{x_n} = \rho \left(\frac{\partial \delta S}{\partial \nabla \cdot x_s} \right)_{x_n} \nabla \left(\frac{\partial \delta W}{\partial \delta S} \right)_s + \rho \left(\frac{\partial \delta \rho}{\partial \nabla \cdot x_s} \right)_{x_n} \nabla \left(\frac{\partial \delta W}{\partial \delta \rho} \right)_s, \quad (1.1)$$

where δW is the change in potential energy. Since the total mass of the fluid is conserved,

$$\delta \rho / \rho + \nabla \cdot x = 0, \quad (1.2)$$

where x is the coordinate representing the centre of gravity of the two fluids. As we have seen, this is stationary on Gorter's assumptions provided there is no pressure gradient, so that $\delta \rho = 0$, and the second term in (1.1) vanishes. Repeating the argument for the force on the normal fluid (*loc. cit.* §4 (ii)), we see that $K_s = -K_n$ only if

$$\left(\frac{\partial \delta S}{\partial \nabla \cdot x_s} \right)_{x_n} = - \left(\frac{\partial \delta S}{\partial \nabla \cdot x_s} \right)_{x_s}. \quad (1.3)$$

Let us suppose that when the normal fluid moves a distance x_n a certain quantity of entropy $\rho_n S_n$ moves with it, and similarly for the superfluid. No assumption has been made as yet that there is no entropy of mixing, or that these entropies borne along by the fluids bear any relation to the entropy of the fluid considered as a whole, ρS say. If no entropy is destroyed by irreversible processes,

$$0 = \frac{\partial(\rho S)}{\partial t} + \rho_n S_n \nabla \cdot \dot{x}_n + \rho_s S_s \nabla \cdot \dot{x}_s. \quad (1.4)$$

Any entropy of mixing is here expressed by the fact that ρS is not necessarily the simple sum of $\rho_n S_n$ and $\rho_s S_s$, but may be a more complicated function. Now (1.4) may be written

$$0 = S \left\{ \frac{\partial \rho}{\partial t} + \rho_n \nabla \cdot \dot{x}_n + \rho_s \nabla \cdot \dot{x}_s \right\} + \left\{ \rho \frac{\partial S}{\partial t} - (S - S_n) \rho_n \nabla \cdot \dot{x}_n - (S - S_s) \rho_s \nabla \cdot \dot{x}_s \right\}. \quad (1.5)$$

The terms in the first bracket together vanish, since the total mass $\rho = \rho_n + \rho_s$ is conserved*. Hence

$$\rho \delta S = \rho_n (S - S_n) \nabla \cdot x_n + \rho_s (S - S_s) \nabla \cdot x_s. \quad (1.6)$$

* See the final paragraph of §4 of the present paper.

and (1.3) is satisfied only if

$$\rho S = \rho_n S_n + \rho_s S_s. \quad (1.7)$$

The condition for the validity of Gorter's assumption is therefore simply that entropies are additive. Gorter's results do not therefore appear to constitute any valid generalization of the theory, since they can only be correct when there is no entropy of mixing, the assumption made by previous workers.

§ 2. THE FOUNTAIN EFFECT.

Assuming that $K_s = -K_n$, Gorter finds that the force per unit volume is given by

$$K_n = X(1-X)\rho \frac{\partial S}{\partial X} \nabla T, \quad (2.1)$$

where X is the relative concentration of normal fluid present. This force leads to a fountain effect of magnitude

$$\nabla p = \rho X \frac{\partial S}{\partial X} \nabla T. \quad (2.2)$$

This reduces to the customary expression (London 1939)

$$\nabla p = \rho S \nabla T \quad (2.3)$$

only if $X(\partial S/\partial X) = S$, *i. e.* if $S \propto X$. We shall show in § 6 that for this to be so the normal fluid must retain its identity when the entropy of the fluid as a whole changes, which is true only for an ideal gas. Gorter has indeed apparently assumed this in his derivation of the magnitude of the forces, for it corresponds in his thermo-electrical analogy to the fact that the same charge travels right round the circuit. We shall return to this point in § 6, merely noting here that no such assumption is necessary to obtain (2.3), since the concentration of normal fluid does not enter London's argument.

§ 3. CONCENTRATION AND EFFECTIVE MASS.

In writing down the equations of motion resulting from the forces K_n and K_s , Gorter makes the further implicit assumption that the effective masses of normal and superfluid are ρX and $\rho(1-X)$ respectively; *i. e.* that their effective masses are proportional to their respective concentrations. In other words, it is assumed that the effective mass—defined as the quantity by which the velocity must be multiplied to obtain the momentum, and hence capable of measurement (or calculation) only by an essentially dynamic method such as sound propagation or the Andronikashvili experiment—is equal to the actual material mass of the component present, a quantity which could only be measured when the system is essentially static. These two masses are identical for a perfect gas, but not otherwise. This point is well illustrated by the model treated by Temperley (1951 a) in which the energy spectrum is assumed to be

of the form* $E=Ap^n$. The concentration of excited atoms is then found to be proportional to $T^{3/n}$, and the effective mass to be proportional to $T^{5/n-1}$. For a perfect gas $n=2$ and the fraction by effective mass is equal to the concentration.

The work of Landau (1941), Ward and Wilks (1951), and the author (1948, 1949), is free from the implicit assumption that the effective mass is identical with the actual mass. On the other hand, Gorter (1949) has implicitly made such an assumption by ascribing the same symbol X to each, whilst Tisza (1947) and Nakajima and co-workers (1950 b) have done so by first attempting to prove that entropy is proportional to the concentration of normal fluid† and then replacing this concentration by ρ_n/ρ (the fractional effective mass) without giving any reason.

§4. THE FLUX OF ENTROPY AND EXCITATIONS.

Assuming an energy spectrum of the form $E=Ap^n$, Temperley (1951 a) compares the value of ρ_n/ρ calculated as the fraction of the number of excited atoms with the value given by Landau's method. Finding that when $n \neq 2$ (*i. e.* for systems other than a perfect gas) the methods give different results, with the experimental evidence in favour of Landau's treatment, Temperley concludes that this is "tantamount to saying that if liquid Helium II can be represented as a condensed Bose-Einstein assembly, other states of the material particles besides the very lowest one contribute to ρ_s ". We shall now show that this suggestion is unsound. Let F be the Helmholtz free energy, S the entropy, U the internal energy, and N_{exc} the number of excited atoms (or excitations), all measured per unit volume. Now

$$F = \pm \frac{4\pi kT}{h^3} \int_0^\infty \ln(1 \mp \lambda \exp\{-E(p)/kT\}) p^2 dp \quad . \quad . \quad (4.1)$$

the upper signs being taken for the case of Bose-Einstein statistics, the lower for Fermi-Dirac. S , U and N_{exc} may then be determined at once from the relations $S = -\partial F/\partial T$, $U = -T^2 \partial(F/T)/\partial T$ and $kTN_{\text{exc}} = -\lambda \partial F/\partial \lambda$. If we now suppose the liquid to be contained within an infinitely long tube, and move the tube with velocity v along its own length, we may calculate the amount per unit volume of free energy, entropy, internal energy, and the number of excitations carried along with the tube. Let the flux of these quantities be $F'v$, $S'v$, $U'v$, and $N'_{\text{exc}}v$, respectively. To allow for the motion of the tube, E must be replaced by $E - pv \cos \theta$, θ being the

* The usual statistical formulae involving the energy levels of individual atoms can then be used only if the interatomic forces are adequately described by a self-consistent field.

† Which is itself unsound, as we shall see in §6.

‡ We are taking into account only the free energy contributed by the excitations, the lowest state $p=0$ being automatically excluded from (4.1) by the presence of the statistical weight factor p^2 .

angle between p and v . Since an excitation moves in the direction of its momentum p with a (group) velocity given by Hamilton's equation as $\partial \mathcal{H} / \partial p = \partial E(p) / \partial p$, the flux of free energy is

$$F'v = \pm \frac{4\pi kT}{\hbar^3} \frac{1}{4\pi} \int_{p=0}^{\infty} \int_{\theta=0}^{\pi} \int_{\phi=0}^{2\pi} \ln \{1 \mp \lambda \exp(pv \cos \theta - E)/kT\} \\ \times \left(\frac{\partial E}{\partial p} \cos \theta \right) p^2 \sin \theta \cdot dp \cdot d\theta \cdot d\phi \quad \dots \quad (4.2)$$

$$= \mp \frac{4\pi kT}{\hbar^3} \frac{v}{4\pi} \int_0^{\pi} \cos^2 \theta \cdot \sin \theta \cdot d\theta \int_0^{2\pi} d\phi \int_0^{\infty} \frac{\partial}{\partial E} \ln(1 \mp \lambda e^{-E/kT}) \frac{\partial E}{\partial p} p^3 dp \\ \dots \quad (4.3)$$

to the first order in v . On integration by parts we see that

$$F'v = \pm \frac{4\pi kT}{\hbar^3} \frac{1}{4\pi} \frac{2}{3} 2\pi \int_0^{\infty} \ln(1 \mp \lambda \exp\{-E/kT\}) 3p^2 dp = F, \quad (4.4)$$

the integrated term vanishing provided that $E(p) \rightarrow \infty$ as $p \rightarrow \infty$. By differentiation with respect to T and λ , we deduce that $S' = S$, $U' = U$, and $N'_{\text{exc}} = N_{\text{exc}}$ also. We have therefore proved that for any energy spectrum the entire entropy and internal energy and all the excited atoms (or excitations) follow the motion of the tube in which they are contained; *i. e.* none of them contribute to the superfluid.

The lack of proportionality between the effective mass and concentration is therefore not due, as Temperley suggests, to the fact that other states besides the very lowest one contribute to ρ_s . Instead, it appears to be a consequence of the fact that if there are interactions each energy level has associated with it its own effective mass. For if we take $E = Ap^n = \frac{1}{2}p^2/(p^{2-n}/2A)$, it is plausible to suppose that the effective mass per state $m(p)$ is proportional to p^{2-n} ; averaging over all momenta then gives

$$\rho_n \propto \int \frac{p^{2-n} p^2 dp}{\lambda^{-1} \exp(Ap^n/kT) \mp 1} \propto T^{5/n-1} \quad \dots \quad (4.5)$$

which is to be compared with

$$N_{\text{exc}} \propto \int \frac{p^2 dp}{\lambda^{-1} \exp(Ap^n/kT) \mp 1} \propto T^{3/n}. \quad \dots \quad (4.6)$$

This result for ρ_n is just that found rigorously by Landau's method.

In the notation used above, the effective mass, defined as the quantity by which the velocity must be multiplied to find the momentum, is, for small velocities,

$$\rho_n = - \frac{4\pi}{\hbar^3} \frac{1}{3} \int_0^{\infty} p^4 dp \frac{\partial}{\partial E} \left\{ \frac{1}{\lambda^{-1} \exp(E/kT) \mp 1} \right\} \quad \dots \quad (4.7)$$

per unit volume. The effective mass cannot therefore be obtained from the free energy simply by a process of differentiation, as can the other variables.

Landau's method of determining the value of ρ_n involves a steady flow of normal fluid moving forward with the tube at a velocity v , the superfluid remaining stationary. If the centre of gravity of the two fluids is required to remain at rest, as in second sound, we must imagine that a piston is introduced into the tube and moved with a velocity $u = -\rho_n v / \rho$ relative to the tube. Such a piston will move the liquid as a whole, giving it a momentum ρu , which must be considered as the sum of the extra momentum $\rho_n u$ imparted to the normal fluid, and a momentum $\rho_s u$ transferred to the superfluid. Thus we have $\rho = \rho_n + \rho_s$. The sum of the effective masses of normal and superfluid is therefore equal to the actual material mass of the fluid considered as a whole.

§ 5. THE CREATION OF PHONONS.

In the particular case of phonon excitations, $E = pc$, it is possible to determine F' , S' , U' , N'_{exc} and ρ_n without approximation. The results are

$$\frac{F'}{F} = \frac{S'}{S} = \frac{U'}{U} = \frac{N'_{\text{exc}}}{N_{\text{exc}}} = \left(1 - \frac{v_n^2}{c^2}\right)^{-2} \quad \dots \quad (5.1)$$

and
$$\rho_n = \frac{4U}{3c^2} \left(1 - \frac{v_n^2}{c^2}\right)^{-3}, \quad \dots \quad (5.2)$$

where v_n is the velocity of the normal fluid. The terms in v_n^2 are due to the creation of new phonons during the motion. Such terms need not be considered in second sound propagation, as they are of higher degree in v_n than those leading to shock waves: (cf. Temperley 1951 b, Osborne 1951). On the other hand (5.2) gives a critical velocity above which there can be no superfluidity; this critical velocity,

$$v_{\text{crit}} = c \left\{ 1 - \left(\frac{4U}{3\rho c^2} \right)^{1/3} \right\}^{1/2}, \quad \dots \quad (5.3)$$

might be a determining factor close to the lambda-point.

§ 6. THE STATUS OF THE RELATION $\rho_n \propto S$ IN THE TWO-FLUID THEORY.

Apparently not accepting Landau's method of calculating ρ_n , Tisza (1947) attempted to prove that $\rho_n \propto S$. He imagines a cell fitted with a piston impermeable to normal fluid. On moving this piston inwards, a certain quantity of superfluid leaves the cell through the pores of the piston, but no normal fluid can leave. The total entropy in the cell remains unchanged since the process is supposed adiabatic. According to Tisza the concentration of entropy will therefore change in the same proportion as the concentration of normal fluid, so that $\rho_n \propto S$.

This argument appears to be in error on three counts:—

(1) It is implicitly assumed in the derivation that since no normal fluid leaves the cell, the total amount in the cell does not change. This is not generally true, since the density of normal fluid is fixed by the temperature of the contents of the cell; this is decided by the entropy concentration, which in its turn is determined by the essential condition

that the total entropy within the cell remains constant. (If the normal density is not the same as that given by Tisza's relation, a relaxation effect will probably take place, its value assuming at once the value given by the relation, and then tending towards its equilibrium value determined by the entropy concentration.)

(2) The process is assumed to be an adiabatic one, and any relation derived merely provides us with a method of calculating the change in temperature within the cell. Without further assumptions (such as that the normal density is independent of pressure) we cannot use the relations obtained to determine equilibrium values for given temperatures (*cf.* Dingle 1948, §12).

(3) It is implicitly assumed that the effective mass-density ρ_n is proportional to the concentration of normal fluid. We have shown in §3 that this is true only for an ideal gas.

Nakajima and Shimizu (1950 b) also make these assumptions. They attempt to justify the supposition that normal fluid mass is conserved by remarking that "the two-fluid theory is formulated self-consistently with respect to this assumption, for we can derive the following equation from this theory :

$$\int \Gamma \cdot d\tau = \frac{1}{S_\lambda} \left[\int \left(\frac{dS}{dt} \right)_{\text{irreversible}} d\tau + \int \frac{q \cdot d\sigma}{T} \right],$$

where Γ is the rate of transformation from the superfluid to the normal fluid per unit volume . . .". On referring to the proof of this expression (1950 a), one finds that the Tisza relation has been used in its derivation, so that the argument given by Nakajima and Shimizu is merely a circular one. The particular two-fluid theory with $\Gamma=0$ and $\rho_n \propto S$ presented by these authors (1950 a) is certainly self-consistent ; but so also is a general theory with $\Gamma \neq 0$ and ρ_n not proportional to S .

Nakajima and Shimizu (1950 b) point out that it is curious that the normal fluid should be conserved in an adiabatic change, but show that this is indeed the case for a condensed perfect Bose-Einstein gas. We remark only that if a general energy spectrum is introduced to allow for interactions, the normal fluid is no longer conserved.

§ 7. THE LAMBDA-POINT.

All authors have tacitly assumed that on the two-fluid model the lambda-point is given by

$$\rho_n(T_\lambda) = \rho ; \quad \text{i. e.} \quad \rho_s(T_\lambda) = 0. \quad . \quad . \quad . \quad . \quad (7.1)$$

This is in agreement with the experimental fact that the velocity of second sound $u_2 = (TS^2\rho_s/C\rho_n)^{1/2}$ tends to zero at the lambda-point.

At first sight it appears that (7.1) has no theoretical justification. As we have seen, ρ_n is an effective mass which can only be relevant when there is relative motion of the normal and superfluids. How then can it be involved in any relation determining the lambda-point in the specific heat, a phenomenon observed when the liquid is stationary? The

lambda-point must be due to the breakdown of the two-fluid model, and should therefore occur at the temperature for which $N_{\text{exc}} \simeq N$ rather than that for which $\rho_n = \rho$. In the general theory these two conditions lead to quite different values for the lambda-temperature.

The experimental fact that the velocity of second sound tends to zero at just the same temperature as that of the thermodynamical lambda-point provides strong circumstantial evidence in favour of the author's theory that the high entropy and specific heat of Helium II are due to supersonic waves of second sound (Dingle 1949 a, 1949 c). Such a theory leads to a critical point when the velocity of second sound tends to zero, and provides an immediate explanation for the appearance of the effective mass in the theoretical expression for T_λ .

§ 8. EXPECTED DIFFERENCES IN BEHAVIOUR OF He^4 AND He^3 .

Under some conditions a system of fermions (such as He^3) may be described in terms of an equivalent assembly of bosons (Tomonaga 1950). It seems plausible to suppose that this will be the case if the interaction energy between the particles is much greater than the thermal energy, for then the actual statistics obeyed by the particles should be of little importance. If this is true, the behaviour of He^3 at sufficiently low temperatures should be similar to that of He^4 . For instance, second sound propagation should be possible, with its velocity u_2 tending to $u_1/\sqrt{3}$ at absolute zero, just as for He^4 .

At higher temperatures the difference in statistics should become more marked as the thermal agitation of the atoms overcomes their mutual interactions. He^4 will continue to obey a two-fluid model because the normal and superfluid densities are comparable in a Bose-Einstein condensation, but He^3 will cease to obey such a model because there is no condensation on Fermi-Dirac statistics and the superfluid density therefore becomes negligible much more rapidly as the temperature is raised. He^3 may therefore have some sort of lambda-point at an extremely low temperature—perhaps at about 0.2°K ., the temperature at which the phonon model for He^4 probably breaks down (Atkins and Osborne 1950)—as compared to that of He^4 at 2.19°K .—the temperature of the Bose-Einstein condensation phenomenon.

The velocity of second sound in a mixture of He^3 and He^4 will also tend to $u_1/\sqrt{3}$ at very low temperatures, where u_1 is the velocity of first sound in the mixture. This disagrees with Pomeranchuk's (1949) prediction that the value of u_2 in mixtures should be very small near absolute zero. To obtain his result, Pomeranchuk has used the relation $(\rho_n/\rho)_{T=0} = \epsilon\mu/m$, where ϵ is the fraction of He^3 atoms, μ the effective mass of a roton, and m the actual mass of an He^4 atom. This amounts to just the same thing as assuming that all the He^3 atoms contribute to the normal fluid (their effective mass being μ), which could hardly remain a valid approximation at the very low temperatures for which any description in terms of normal and superfluid atoms becomes quite inadequate.

ACKNOWLEDGMENT.

I am grateful to Mr. H. N. V. Temperley for a number of criticisms of this work.

REFERENCES.

- ATKINS, K. R., and OSBORNE, D. V., 1950, *Phil. Mag.*, **41**, 1078.
DINGLE, R. B., 1948, *Proc. Phys. Soc.*, **61**, 9; 1949 a, *Ibid.*, A, **62**, 154; 1949 b, *Ibid.*, A, **62**, 648; 1949 c, *Proceedings of the International Conference on the Physics of very low temperatures*, M.I.T., Cambridge, Massachusetts, p. 7.
GORTER, C. J., 1949, *Physica*, **15**, 523.
LANDAU, L., 1941, *J. Phys., U.S.S.R.*, **5**, 71.
LONDON, H., 1939, *Proc. Roy. Soc. A*, **171**, 484.
NAKAJIMA, S., TOMITA, K., and USUI, T., 1950 a, *Phys. Rev.*, **78**, 768.
NAKAJIMA, S., and SHIMIZU, M., 1950 b, *Prog. Theor. Phys. Japan*, **5**, 1010.
OSBORNE, D. V., 1951, *Proc. Phys. Soc. A*, **64**, 114.
POMERANCHUK, I., 1949, *J. Exp. Theor. Phys. U.S.S.R.*, **19**, 42.
TEMPERLEY, H. N. V., 1951 a, *Phil. Mag.*, **42**, 74; 1951 b, *Proc. Phys. Soc.*, A, **64**, 105.
TISZA, L., 1947, *Phys. Rev.*, **72**, 838.
TOMONAGA, S., 1950, *Prog. Theor. Phys.*, **5**, 544.
WARD, J. C., and WILKS, J., 1951, *Phil. Mag.*, **42**, 314.

CXI. *Observations on the Multiple Scattering of Ionizing Particles in Photographic Emulsions.*—Part IV. *Protons of 336 MeV. from the Berkeley Cyclotron. Cosmic Ray Protons and Mesons of 5 to 50 MeV.*

By K. GOTTSTEIN* and J. H. MULVEY,
H. H. Wills Physical Laboratory, University of Bristol†.

[Received May 30, 1951.]

SUMMARY.

The first section describes a determination of the scattering constant by measuring the multiple scattering of 336 MeV. protons in Ilford G5 nuclear research emulsions which had been exposed in the 184" Berkeley cyclotron.

Then follows an account of an experimental determination of the relation between the scattering parameter and residual range for protons and mesons of the cosmic radiation. A second value of the scattering constant was found, using the range and energy of μ -mesons from the decay of π -mesons stopping in the emulsion. The result was used to obtain a range energy relation for protons of energy up to 200 MeV.

§ A. PROTONS OF 336 MeV.

ILFORD G5 emulsions $400\ \mu$ thick were dropped through the proton beam of the 184" Berkeley cyclotron. This method was chosen because it reduced the density of tracks in the emulsion and so made easier the identification of individual tracks. The beam was highly collimated and its energy was given as 340 ± 1 MeV. No tracks were employed which differed noticeably in direction from that of the main flux. The tracks were inclined at an angle of 0.5° to the plane of the emulsion and entered at the surface.

Experimental Procedure.

Scattering measurements were made with a Cooke, Troughton and Simms M4000 type microscope, using $\times 95$ objective and $\times 15$ eyepieces. The "coordinate method" as described by Fowler (1950) was applied. Details of the technique have been discussed by Menon *et al.* (1951). To minimize the effects of emulsion distortion, the measurements were confined to regions of the plate at least 1 cm. away from any edge. The total length of track measured was 20 cm., and no individual track was less than 8 mm. in length.

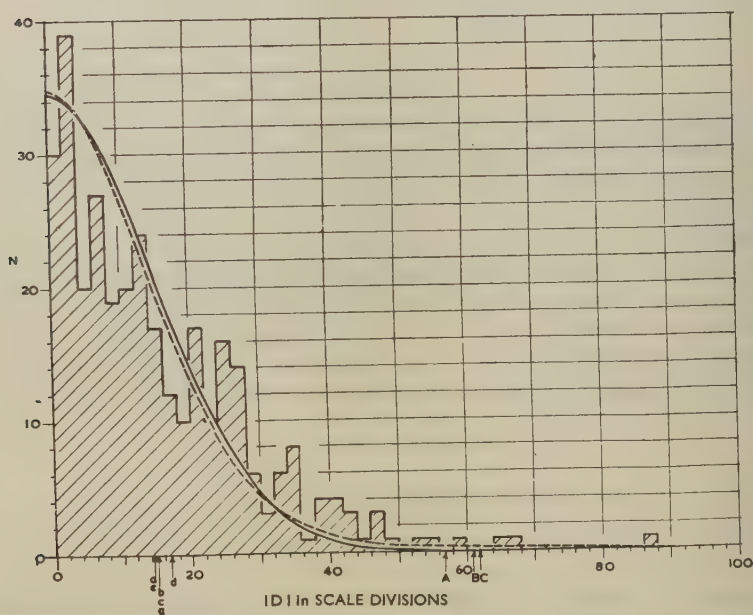
* On leave of absence from the Max-Planck Institut für Physik, Göttingen.

† Communicated by Professor C. F. Powell, F.R.S.

Results and Discussion.

Second differences D were obtained for cell-sizes of 200, 400, 600, 800 and 1000 microns. Fig. 1 shows the distribution of $|D|$ s from 330 non-overlapping cells for a cell-size of 600μ . The distribution function, according to Molière's theory (Gottstein *et al.* 1951, referred to as I.), and a normal curve are drawn for comparison. Both have been

Fig. 1.



Distribution of second difference, from 330 non-overlapping cells. A normal curve — and Molière-distribution curve --- are given for comparison.

$d: \overline{D}_1$ (no cut-off),

$c: \overline{D}_2$ (corresponding cut-off: C),

$a: \overline{D}_3$ (corresponding cut-off: A),

$b: \overline{D}$ for overlapping cells applying "single value cut-off" (B),

$g:$ standard deviation of normal curve.

normalized to the same number of $|D|$ s; the standard deviation of the normal curve is indicated by arrow "g". The mean value was determined in three different ways:

(1) the mean value of all $|D|$ s was taken.

Result: $\overline{D}_1 = 1.70$.

This includes a number of rather large values (see fig. 1) of $|D|$ which, if included in a sample of limited size, would yield too large a value for the mean, thus giving rise to a systematic error in the

estimation of the energy. It has been found convenient in previous work (Goldschmidt-Clermont *et al.* 1948, Fowler 1950) to apply a " $4\bar{D}$ cut-off". Although in the present case the sample is fairly large, we have applied the same "cut-off" in the following two ways, in order to study its influence on the scattering-constant K_1 .

(2) The mean was taken of all $|D|$ s remaining after removal of those values, $|D| > 4\bar{D}_2$. This was done by successive approximation.

Result : $\bar{D}_2 = 1.55$.

(3) A value of $|D| > 4\bar{D}$ occurring in a cell of the smallest size employed ($200\ \mu$) indicates the position of a large angle scattering. In the larger cells all the values of $|D|$ related to this "single scattering" were removed. This is equivalent to "cutting" a track at a position of a single scattering and measuring the scattering of each side independently. In the case of overlapping cells the effect is to remove a block of D s from the column of values as recorded, and so we refer to it as a "block" cut-off.

The method yielding \bar{D}_2 is called "single-value cut-off".

Result (for overlapping cells) : $\bar{D}_3 = 1.45$.

These values, \bar{D}_1 , \bar{D}_2 , \bar{D}_3 are shown in fig. 1 with the corresponding "cut-offs".

The "block cut-off" gives a smaller \bar{D} than the "single value cut-off". This is because the former tends to exclude from the statistics the values of $|D|$ which, being just below $4 \times \bar{D}$, would therefore not have been eliminated by a "single value cut-off". In the case of a small sample (short track) a "block cut-off" seems to be preferable to a "single value cut-off", since it eliminates more rigorously such values of $|D|$ as are well above the average and so might falsify the result if included.

A mean has also been calculated for the distribution of 990 $|D|$ s from overlapping $600\ \mu$ cells. This was obtained using a single value cut-off. The mean is indicated in fig. 1 by the arrow "b".

For $600\ \mu$ cells the "noise" was found to be negligible compared with the "true scattering", so noise elimination was not needed (fig. 3, I.). (The microscope used here was M40135.)

In fig. 2, \bar{D}_3^2 is shown plotted as a function of s^3 . Within experimental error it is a straight line. This indicates that distortion of the emulsion is negligible, since the presence of distortion would have given this curve a pronounced upwardly concave shape (unpublished observations).

The energy lost by the protons as they passed through the emulsion was taken into account, and the mean energy corresponding to the multiple scattering measured was calculated to be 336 MeV. The values of the scattering constant (as defined by I., eqn. (12)) obtained from the total distribution for $600\ \mu$ cells are

(a) with single value cut-off 29.2 ± 1 ,

(b) without cut off..... 30.7 ± 1 .

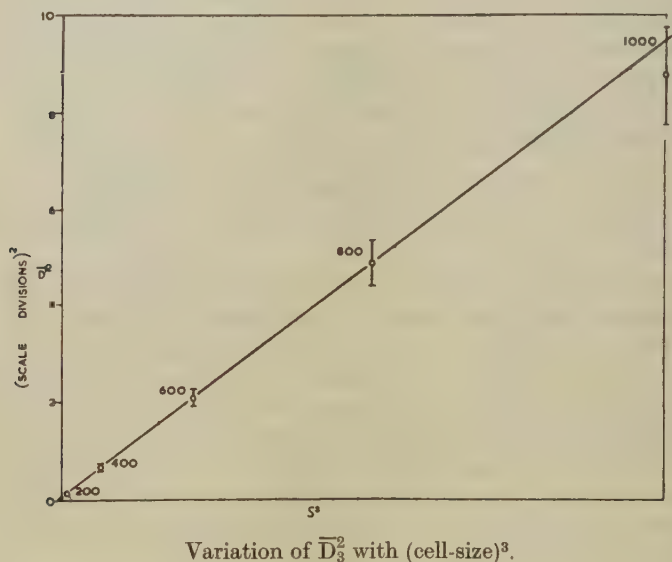
Energies were measured in MeV. and cell-sizes in units of 100μ . The comparison of these results with Molière's theory has been discussed in I.

§ B. PROTONS AND MESONS OF FROM 5 TO 50 MeV.

Experimental Procedure.

Ilford G5 nuclear research emulsions were exposed to the cosmic radiation during a high-altitude balloon flight. We selected for investigation nineteen tracks with total length of 20 cm. ending in the emulsion; each track was at least 8 mm. long.

Fig. 2.



Tracks produced by protons were identified by measuring their grain density and scattering (Fowler 1950). Tracks of particles giving rise to typical σ -stars, or suffering μ -decay were accepted as those of π -mesons; μ -mesons were identified by the characteristic electron decay at the end of their range.

Of the 19 tracks selected, 11 were protons, 4 were π -mesons and 4 μ -mesons. Scattering measurements were made as described in § A with a primary cell-size of 40μ . As before, no tracks lying near the edges of the plates were used.

Results.

Second differences D were obtained for cell-sizes of 40 and 80 microns. Protons π - and μ -mesons were considered as three distinct groups and $|\bar{D}|$ was calculated for both cell-sizes as a function of range. This was

done by dividing each track into sections of 1.4 mm. length, starting from the point at which the particle came to rest. Then, adopting a single value cut-off, the mean of all $|D|$ s belonging to sections of equal residual range was found.

All emulsions used in this investigation were processed together. Measurements of the curvature of steeply dipping tracks indicated that the contribution of distortion to the scattering observed was negligible. However, with these small cell-sizes, the contribution of "noise" cannot be neglected. We have applied a method of noise elimination assuming noise to be independent of cell-size, and neglecting the variation of the L-term (see I.) with cell-size. If noise be taken as proportional to $S^{1/4}$ (Fowler, private communication), any error in $\bar{\alpha}$ due to these two approximations is, in this case, less than 2 per cent.

Thus the equation used for obtaining the "true" value of \bar{D} for each residual range was

$$\bar{D}_{(100\mu)} = \sqrt{\frac{(\bar{D}_2^2 - \bar{D}_1^2)}{s_2^3 - s_1^3}}, \quad \dots \dots \dots (1)$$

(comp. eqn. (3))
(Menon *et al.* 1951.)

From this α was calculated.

In fig. 3, $\log \bar{\alpha}$ is shown as a function of $\log R$. Here R is the effective residual range obtained when the energy loss by the particle along the track is taken into account. In our case it differs very slightly from the range at the centre of each section, and is given by

$$R = \left[\frac{0.15 \cdot (R_2 - R_1)}{R_1^{0.15} - R_2^{0.15}} \right]^{0.87}, \quad \dots \dots \dots (2)$$

where R_1 and R_2 are the ranges of the extreme points of the section considered. This is obtained from the range energy relation for protons

$$E = C \cdot R^{1.578}, \quad \dots \dots \dots (3)$$

where C is a constant, the numerical value of which is not required here, and the equation

$$\bar{\alpha}_{\text{eff}}^2 = \int_{R_1}^{R_2} \frac{\bar{\alpha}^2 dR}{(R_2 - R_1)}, \quad \dots \dots \dots (4)$$

where $\bar{\alpha}_{\text{eff}}$ is the mean multiple scattering parameter observed for the section, and $\bar{\alpha}$ is taken to be inversely proportional to the kinetic energy.

The values of $\bar{\alpha}$ and R obtained from the π - and μ -meson tracks have been replaced in fig. 3 by their equivalents for a proton of the same velocity, assuming the masses of the mesons to be

$$\begin{aligned} m_\mu &= 210 \pm 4, & (\text{Smith } et al. 1950, \\ m_\pi &= 276 \pm 6, & \text{Lederman } et al. 1951.) \end{aligned}$$

in units of the electron rest mass.

The theoretical formula relating $\log \bar{\alpha}$ with $\log R$ is that of a curve which deviates from a straight line by less than 2 per cent in the energy interval considered, as follows from eqn. (12) (I.) and the range-energy relation. This deviation is smaller than the statistical spread of the experimental points and so a straight line was fitted as a convenient approximation.

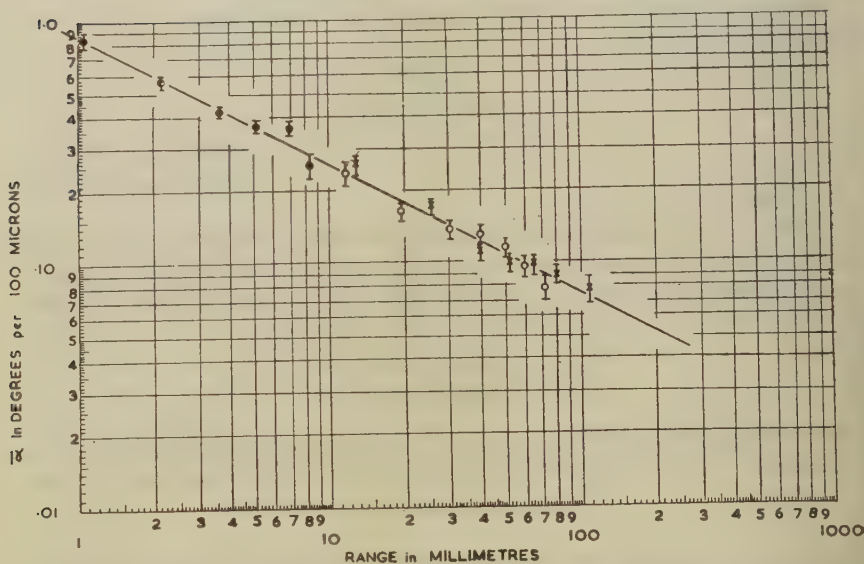
Determination of the Scattering Constant.

Using the decay scheme

$$\pi \rightarrow \mu + \text{neutrino}$$

(Lattes *et al.* 1947, Marshak and Bethe 1947, O'Ceallaigh 1950.)

Fig. 3.



$\bar{\alpha}$ as a function of range for protons. The measurements were made on protons (...), π -mesons and μ -mesons. Instead of the values obtained for the mesons their equivalents for a proton of equal velocity have been plotted (ooo for π -mesons, x for μ -mesons).

and the above values of the meson masses, the kinetic energy of a μ -meson arising from the decay of a π -meson at rest can be shown to be 4.1 MeV. The corresponding range of a μ -meson in the plates used for this investigation we found to be 595 ± 5 microns. These values of energy and range were transformed to their equivalents for a proton of the same velocity, and the $\bar{\alpha}$ corresponding to the transformed range was obtained from fig. 3. Then (with $z=1$ and s in units of 100μ)

$$K_1 = \bar{\alpha}(100 \mu)pv = 26.1 \pm 0.7$$

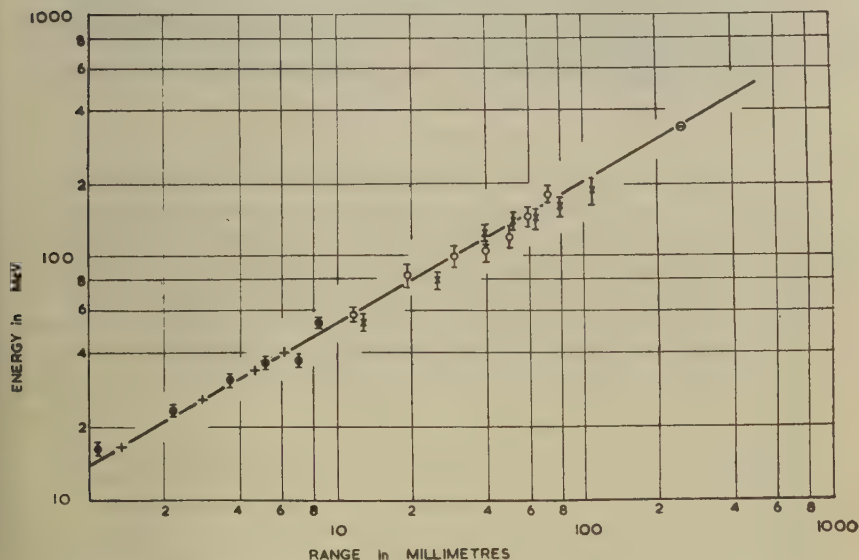
for cell-size of 80μ and $\beta=0.26$. This value of K_1 is included in fig. 1 (I.).

Range Energy Relation.

K_1 , as determined in this manner, is very insensitive to variations in the value of the exponent in eqn. (3), which was used only for the application of a very small correction to the range R . From fig. 3 an independent range-energy relation for protons may be derived in regions which have not yet been covered by range-energy measurements in the photographic emulsion. Fig. 4 shows the extrapolated curve of Bradner *et al.* (1950), together with our experimental points. The uppermost point (at 336 MeV.) was obtained from the measurements described in § A, making use of fig. 3.

The agreement between the curve of Bradner *et al.* and our experimental points is within the limits of our statistical errors.

Fig. 4.



Range-energy relation as derived from fig. 3. Notation is the same as in fig. 3. The divided circle denotes the point obtained from the experiment described in § A (protons of 336 MeV.). The full line gives the extrapolated range-energy relation of Bradner *et al.* (1950), the upright crosses denoting experimental points of these authors.

ACKNOWLEDGMENTS.

We should like to thank Professor C. F. Powell, F.R.S., for the hospitality extended to us in this laboratory, and for his encouragement in this work. We are also indebted to Mr. P. H. Fowler for helpful discussions and advice. It is a pleasure to thank Professor L. W. Alvarez and Dr. W. H. Barkas for their kind cooperation in exposing plates for us in the Berkeley cyclotron.

One of us (K. G.) wishes to thank Professor W. Heisenberg for leave of absence granted to enable him to carry out this work at Bristol. The other (J. H. M.) is maintained by a grant from the Department of Scientific and Industrial Research.

REFERENCES.

- BRADNER, SMITH, BARKAS and BISHOP, 1950, *Phys. Rev.*, **77**, 462.
FOWLER, 1950, *Phil. Mag.*, **41**, 169.
GOLDSCHMIDT-CLERMONT, KING, MUIRHEAD, and RITSON, 1948, *Proc. Phys. Soc.*, **61**, 183.
GOTTSTEIN, MENON, MULVEY, O'CEALLAIGH, and ROCHAT, 1951, *Phil. Mag.*, **42**, 708.
LATTES, FOWLER, and CUER, 1947, *Proc. Phys. Soc.*, **59**, 883.
LATTES, OCCHIALINI, and POWELL, 1947, *Nature, Lond.*, **160**, 453.
LEDERMAN, TINLOT, and BOOTH, 1951, *Phys. Rev.*, **81**, 281.
MARSHAK, and BETHE, 1947, *Phys. Rev.*, **72**, 506.
MENON, O'CEALLAIGH, and ROCHAT, 1951, *Phil. Mag.*, **42**, in course of publication.
O'CEALLAIGH, 1950, *Phil. Mag.*, **41**, 838.
SMITH, BARKAS, BISHOP, BRADNER, and GARDNER, 1950, *Phys. Rev.*, **78**, 86.

CXII. *Electron and Gamma Ray Spectroscopy with Scintillation Detectors.*

By R. C. BANNERMAN, G. M. LEWIS and S. C. CURRAN,
Department of Natural Philosophy, The University of Glasgow*.

[Received June 11, 1951.]

ABSTRACT.

An account is given of β - and γ -ray energy measurements. Various coincidence techniques appropriate to scintillation detectors are examined experimentally, and an investigation is made of the application of a single crystal, with source buried inside, to the elucidation and closer examination of decay schemes. Work is described on standard sources, on Hg^{203} , and in some detail on La^{140} . • New information is given for La^{140} concerning the 0.093 γ -ray, the high energy γ -ray and the decay scheme.

§ 1. INTRODUCTION.

THE detection of individual particles, or quanta, by means of the combination of phosphor and photo-sensitive electron multiplier has been the subject of considerable research and development since it was first used by Curran and Baker (1944) for α -particles. As in the case of other instruments of fundamental importance much of this early research has been of a rather tentative and exploratory nature. The instrument lends itself to studies of this type since it contains at least three major elements which may be varied over wide ranges of performance. Thus we have :—

- (1) The fluorescent crystal ; obviously several criteria of performance can be exhaustively studied such as the conversion efficiency of the kinetic energy of the particle, or particles, to light of suitable frequency, the transparency of the crystal to such light, together with many other factors such as excitation and decay times, ease of growth, etc.
- (2) The photo-sensitive layer ; clearly the efficiency of conversion of the quanta excited in the chosen fluorescent substances to useful photo-electrons is the most important consideration, but this has to be regarded closely in relation to the emission of thermal electrons from the cathode, since such emission determines, to a considerable extent the ultimate sensitivity of the device, particularly for particles of low energy.
- (3) The multiplier ; the chief objective here is to secure uniformly high and stable gain per stage.

* Communicated by the Authors.

The extensive researches made in recent years with the scintillation detector show that the best commercial photo-multipliers satisfy largely the requirements (2) and (3) and gradually the data acquired on (1) is clarifying the situation. Thus, at present, many workers with solid crystals have chosen to regard naphthalene, anthracene and stilbene as standards among the organic materials, while sodium iodide, thallium activated, is preferred among the inorganic substances. In the present work we report results obtained with crystals of anthracene and activated sodium iodide, particularly in the field of γ -ray spectroscopy. It is in this application that the detector perhaps acquires its greatest significance, owing to the fact that its high absorption gives it a very high efficiency. We discuss our results in the light of the possibility of using large volumes of certain liquids containing phosphors as the fluorescent substances. It is shown that, in certain circumstances, new methods of studying the decay schemes of radioactive substances are practicable.

§ 2. GAMMA RAY SPECTROSCOPY.

γ -rays passing through substances are absorbed or scattered mainly in the following processes:—

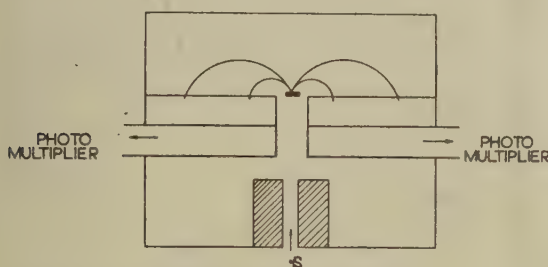
(i) *Photoelectric Effect*.—The quantum ejects an electron from one of the K, L, M, . . . shells. There is a high probability of conversion of the energy of the X-ray quantum excited in this process to kinetic energy of electrons, and a single peak may be observed corresponding to the full energy of the γ -quantum. To secure maximum sensitivity it is obviously useful to employ crystals containing elements of high Z value such as iodine in NaI (Tl). If then the photo-electric process greatly predominates, as in the region below $h\nu \sim 25$ MeV., say, we can use a single crystal (~ 1 cm.³) as a spectrometer. For greater $h\nu$ values the second process becomes evident:—

(ii) *The Compton Process*.—The scattered quantum and the recoil electron share the energy of the incident quantum, and a large range of energy values of the recoil electron results. However, the electrons projected in a definite direction relative to the direction of incidence are homogeneous. This principle has been made the basis of a method of measuring the quantum energy by Hofstadter and McIntyre (1950). We shall consider some of the features of this method in detail below.

(iii) *The Production of Pairs*.—The process of creation of pairs has a threshold at an energy $h\nu = 2m_0c^2$, and it is not appreciably evident in light materials up to $h\nu \sim 2$ MeV. It offers an attractive method of measuring quantum energies at high $h\nu$ values, since the pair of electrons have constant total energy $h\nu - 2m_0c^2$. Using the fact that the annihilation of a positron leads to the emission of two oppositely directed quanta of energy $h\nu = m_0c^2$, Johansson (1950) selected pulses due to electron pairs from a background of pulses, and so secured good resolution. However, the straightforward exploitation of the process of pair formation requires crystals containing a high Z value element, large

enough to confine a high percentage of electrons entirely within the volume and to trap the bremsstrahlung emitted in flight. This is a formidable requirement. At present it would appear useful to explore the possibility of replacing the two arrays of Geiger Müller counters in the method of magnetic spectrography due to Walker and McDaniel (1947) with two large crystals, or liquid counters, from which the separate light signals due to the positrons and negatrons could be piped to a pair of multipliers, adjusted to give equal output pulses for equal input signals. This is indicated in fig. 1. The two output voltages would be fed to a fast coincidence circuit and then simply added in amplitude. In this way the rather elaborate circuitry required to correlate all the pair distributions would be avoided. The magnetic field would be set at a suitably high fixed value. It need not be uniform or regulated since it is a mere particle separator. A pulse analyser would directly give the spectrum of the added pulses and hence of the γ -radiation. The crystal or liquid counters need to be thick enough to stop the incident electrons and wide enough to satisfy the solid angle requirements of the pair spectrometer.

Fig. 1.



Pair spectrograph with scintillation detectors.

Anthracene has been shown by Hopkins (1950) to give a light output to the multiplier proportional to the energy of incident electron in the region 100 KeV. to 1 MeV., but deviating slightly from linearity at lower energies. Activated sodium iodide has been investigated by West, Meyerhof and Hofstadter (1951) and has shown a linear response in the range 2 KeV.-500 KeV. We can corroborate the linear response of activated sodium iodide in the range 20 KeV.-2½ MeV., from experiments listed below, and other experiments.

§ 3. EXPERIMENTAL RESULTS AND DISCUSSION OF WORK WITH SINGLE CRYSTALS.

I. γ -ray and β -ray Energy Measurements (In¹¹⁴ and La¹⁴⁰).

Spectroscopy with single crystals offers many outstanding advantages, provided that the resolution can be made sufficiently good. This is particularly true if collimation of the γ -ray beam is not required. In

this event the crystal can be used as a spectrometer of very large solid angle, and γ - γ and β - γ experiments can be performed, with two scintillation detectors, in which particular γ -rays can be related to specific β -particles and γ -rays. This is, however, not readily achieved with complex sources and higher energy γ -rays.

The results which are shown in figs. 2 and 3 refer to work with crystals of anthracene (2 mm. \times 4 mm.²) and NaI (Tl) (1 cm.³) with the radiations of In¹¹⁴ and La¹⁴⁰. The crystals were coated with paraffin and mounted on an E.M.I. tube 5311. The crystal of NaI (Tl) was covered with an aluminium reflector. Thus, in fig. 2 we have the peak, due to photo-absorption, superimposed on a Compton background, as observed in

Fig. 2.

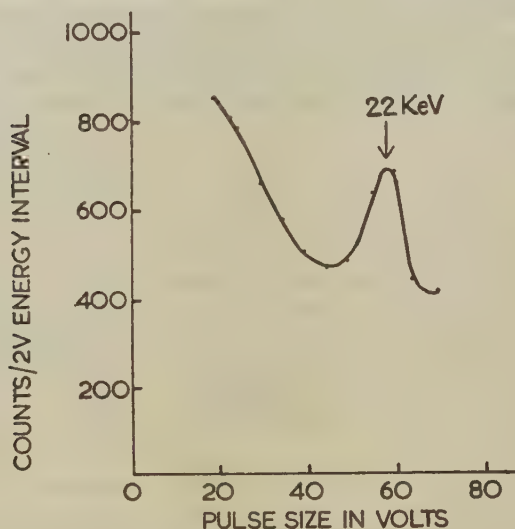


Photo-peak due to ~ 22 KeV. X-rays as observed in thin anthracene exposed to radiations of In¹¹⁴.

anthracene with an uncollimated In¹¹⁴ source. The X-rays emitted after the internal conversion of the γ -ray of energy 190 KeV. show as a photo-electric peak in the range 22 to 25 KeV. as expected.

In fig. 3 we show the results obtained with a single crystal of NaI (Tl) and a source of La¹⁴⁰. More will be said of the γ -rays from this source below, but the figure shows in some detail the results for the rays of energy 0.335 MeV. The Compton edge and photo peak are both evident. Actually, a Compton edge due to a hard γ -ray (0.49 MeV.) is noticeable, though obscured by the 0.335 MeV. photo-peak. For this complex source of radiation the resolution achieved is fairly satisfactory for some purposes. The last peak of fig. 3 is due to hard γ -rays saturating the amplifier.

It has been shown by Beach, Peacock and Wilkinson (1949) that La^{140} should emit γ -rays of energy 0.093, 0.335, 0.49, 0.82, 1.62, 2.5 MeV., but they did not directly observe, by means of a photo peak, the γ -ray of energy 2.5 MeV. and the evidence for the 93 KeV. radiation is not well founded. The decay scheme proposed by them is sketched in fig. 4.

Fig. 3.

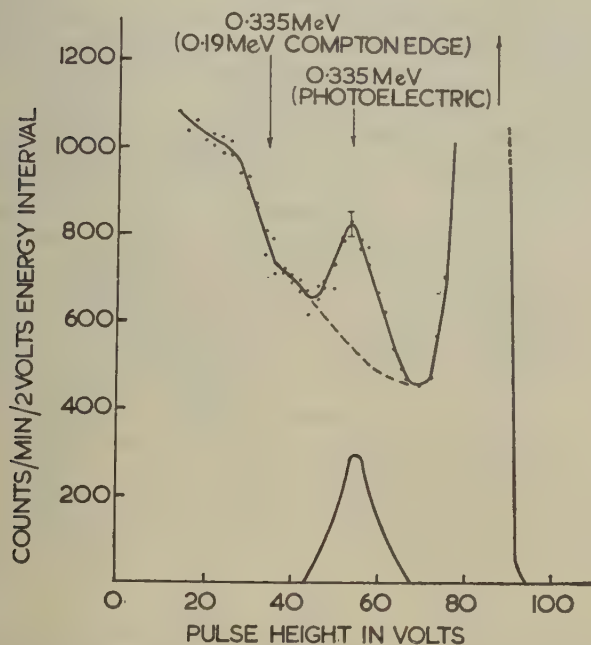
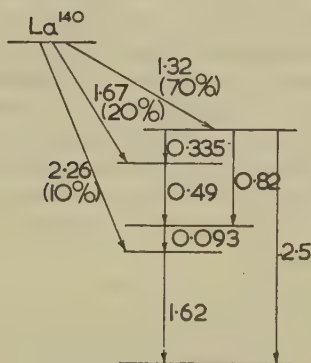
Part of response curve of 1 cm.³ crystal of NaI (Tl) to radiation of La^{140}

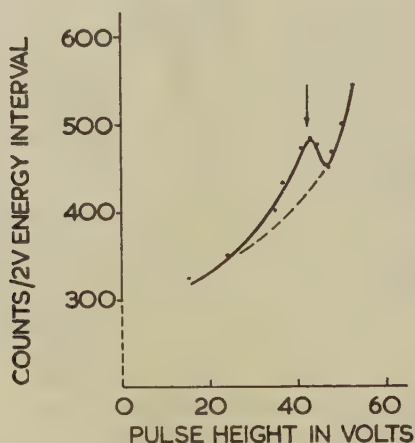
Fig. 4.

Decay scheme of La^{140} .

Here we discuss the radiation of low energy. A number of separate investigations were made, and the extension of the curve of fig. 3 shows a rather smooth variation over the range below and above 90 KeV.

From the nearly 100 per cent efficiency of the detector for such radiation we estimate that γ -radiation of energy ~ 90 KeV. cannot be emitted in more than 15 per cent of the disintegrations. This matter is discussed further in the double crystal method below. Since, according to the proposed decay scheme, the majority of the disintegrations result in transitions of this energy, a thin crystal (1 mm.) of anthracene was used to detect the conversion electrons from a very thin source of La^{140} (several $\mu\text{gm./cm.}^2$). The results of the analysis are shown in fig. 5. A peak of very low intensity was observed of energy 55 ± 5 KeV.; presumably corresponding to internal conversion in the K shell of a γ -ray of energy

Fig. 5.



Conversion electrons, energy ~ 55 KeV., due to weak γ -ray, energy 90–95 KeV., as observed in thin anthracene exposed to electrons from La^{140} .

about 90–95 KeV. The intensity is found to correspond to about 1 per 100 disintegrations and seems to establish the necessity of modifying the decay scheme. Using a 1 cm.³ crystal of anthracene the β -spectrum was found to extend up to the region of 2.26 MeV. A weak counting rate in excess of background was found up to ~ 2.4 MeV., but this could be due to accidental pile up of lower energy pulses which are relatively very numerous. The K conversion peak was detected for the 0.335 MeV. γ -line, but that from the 0.49 MeV. γ -ray was not strong enough to appear, in this particular run.

II. Coincidence Measurements (using La^{140}).

It is frequently necessary in the investigation of decay schemes to determine which γ -rays are in cascade with one another. By placing a source (with the β -particles screened off) between two scintillation

counters, the simultaneous arrival of γ -rays in the counters can be recorded in a coincidence unit. The pulses arriving at either counter can, after amplification, be displayed on a cathode ray tube and the brightness of the display can be made negligibly weak unless a coincidence occurs. In such circumstances determination of the pulse height distribution from either counter on the cathode ray tube gives information concerning the γ -rays which are in coincidence with one another. For instance, if only two γ -rays appear in the distribution, the two γ -rays are evidently in cascade. If several γ -rays appear, it is desirable to determine specifically how they are associated. The output pulse distribution of one of the counters can be passed through a single-channel "kicksorter" so that only pulses associated with one particular γ -ray are passed on to the coincidence unit from that counter. The γ -rays in coincidence with this one γ -ray can then have their pulse heights displayed. In this method care has to be taken to keep random coincidences low. This latter technique can be employed advantageously for β - γ processes also, if the decay scheme is not too complex.

β - γ and γ - γ coincidences with La^{140} have been reported by Osborne and Peacock (1946), Mitchell, Langer and Brown (1947), Mandeville and Scherb (1948), but without any direct evidence being obtained for the energies of the γ -rays in coincidence.

γ - γ coincidences have been investigated for La^{140} , using anthracene as the material of the crystal in the counter connected to the display unit. In the first case no attempt was made to select specific γ -rays in the other counter. The pulse height distribution curve in the anthracene crystal at coincidence is shown at (a) in fig. 6. The response of the crystal (where all γ -ray pulses are recorded whether in coincidence or not) is shown for comparison at (b). The 1.62, 0.82, 0.49 MeV. lines appear strongly in the coincidence curve.

In the next case the second counter was connected to a discriminator, and only pulses greater than 0.8 MeV. were allowed to pass on to the coincidence unit. The curve so obtained is shown at (a) in fig. 7, the Compton type curve giving the normal single crystal response to γ -rays from the source (whether in coincidence or not) is shown for comparison. No counts were observed above 0.8 MeV. now, while below this energy the coincidence curve follows the same trend as the Compton type curve. The coincidence rate was too low for any detail in the curve to be seen.

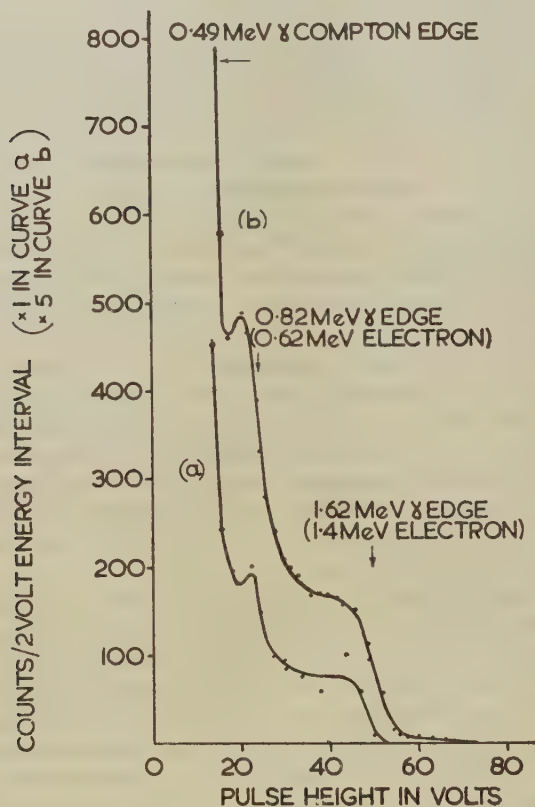
The 0.49 and 0.82 MeV. γ -rays are, therefore, in coincidence with the higher energy 1.62 MeV. line. It was similarly shown that the 0.335 MeV. γ -line was in coincidence with the 1.62 MeV. line.

III. Integrating Method (using Hg^{203}).

As already indicated, one of the great advantages of single crystal spectrometry is to be found in the analysis of decay schemes, by means of coincidence experiments. The use of crystals makes it possible to introduce new methods of observing the inter-relationships of the particles

and quanta. Thus, suppose we first consider the type of de-excitation process indicated in fig. 8, where two γ -quanta occur in cascade. With a source at some distance from the crystal we can observe the relative intensities of the γ -radiations by taking a histogram. Thus, if the transition of energy $h\nu_3$ be of negligible intensity no corresponding peak is observed. However, if the source be placed very near the crystal the number of coincidences of the cascade quanta will increase, and a peak

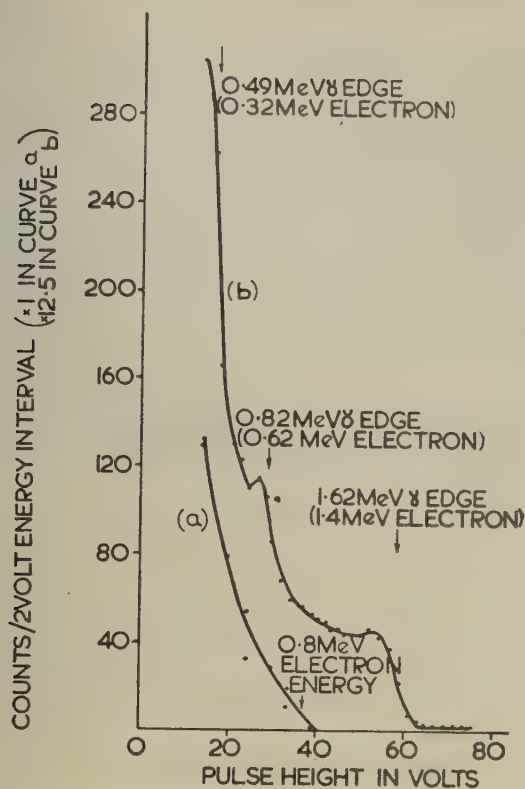
Fig. 6.



- (a) Part of spectrum of La^{140} for γ -rays in coincidence with some other γ -ray.
 (b) Same part of spectrum of γ -rays of La^{140} as observed without any coincidence control.

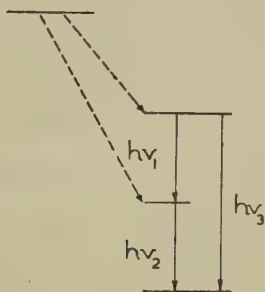
corresponding to the sum of the energies $h\nu_1 + h\nu_2$, or $h\nu_3$, will be observed. This will establish that $h\nu_1$ and $h\nu_2$ are in coincidence and if the source be placed within the crystal (between two flat-faced blocks, say) the relative intensities of the peaks due to $h\nu_1$, $h\nu_2$ and $h\nu_1 + h\nu_2$ can be used to determine the number of decay processes that are in coincidence.

Fig. 7.



- (a) Spectrum observed in anthracene for γ -rays of La^{140} in coincidence with the γ -ray of energy 1.62 MeV .
 (b) Some part of spectrum as observed without any coincidence control.

Fig. 8.

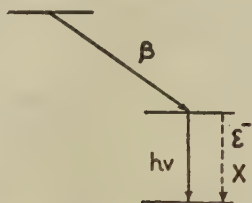


De-excitation process from two excited states.

Thus, if the γ -rays are detected with 100 per cent efficiency a single peak due to $h\nu_3$ and $h\nu_1 + h\nu_2$ is obtained. If, on the other hand, the number of quanta of energy $h\nu_2$ exceeds those of energy $h\nu_1$ (for example in complex β -decay) then two peaks, one corresponding to $h\nu_2$ quanta (not in coincidence with $h\nu_1$) and one to $h\nu_3$ and $h\nu_1 + h\nu_2$ will be obtained. In this way complex schemes may be readily investigated. Variation of the resolving time of the coincidence circuit can be introduced to see whether any of the states have measurable life-times.

Above we considered γ -rays only, foil shielding the source when β -rays were emitted. Fig. 9 serves as an example of a decay giving rise to β - γ coincidences. Since it is typical of many disintegration schemes, we will indicate the possibilities of the method by applying it to Hg^{203} . Saxon (1948) and Slätis and Siegbahn (1949) have shown that Hg^{203} decays with the emission of a β -ray of energy 208 KeV. and a γ -ray of energy 278 KeV. This γ -ray is internally converted in the K and L shells (~ 20 per cent and 5 per cent respectively), giving rise to photo-electrons of energy ~ 200 KeV. and ~ 270 KeV. respectively.

Fig. 9.

De-excitation following β -emission.

A thin source ($\sim 1 \mu\text{gm./cm.}^2$) of HgS was evaporated on to an aluminium foil of thickness 1.8 mg./cm.^2 , and this was placed between two blocks of NaI (Tl) each $1 \text{ cm.} \times 1 \text{ cm.} \times \frac{1}{2} \text{ cm.}$ A single multiplier, type 5311, was arranged symmetrically with respect to this assembly. The efficiency of each of the two halves of the crystal was more than 99 per cent for all X-radiations following internal conversion of the γ -radiation. Thus, conversion in the K, L, M, . . . shell, giving rise to photo-electrons of different energies, resulted in the same amount of electron energy release in the crystal.

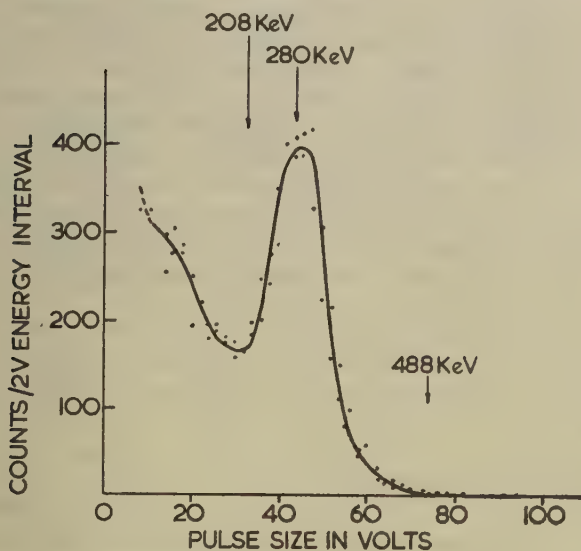
Hence the integrating effect of the crystal is such that we expect mainly two types of pulses:—

- (1) β -rays—those accompanied by γ -rays which are not counted and which escape from the counter.
- (2) β -rays—those accompanied by photo-electrons. These photo-electrons can arise in several ways, so that this group can contain:—
 - (i.) β -particle + L conversion electron + photo-electrons released in the crystal by capture of X-radiation.

- (ii.) β -particle + K conversion electron + photo-electrons released by the capture of X-rays.
- (iii.) β -particle + photo-electrons arising from photo-absorption of γ -rays in the crystal.

These two main groups should thus result in two spectra, one due to particles of the normal β -spectrum ending at 208 KeV. and another due to particles of the β -spectrum carried forward by photo-electrons, so that the group starts at 278 KeV. These two groups are clearly separated. The second displays clearly the form from zero energy of the particle right up to the end point, lying on the energy scale between 278 KeV. and 486 KeV., where its form can be examined readily over the whole range. In the main, the group (2) particles of fig. 10 show the advantage

Fig. 10.



Spectrum of Hg^{203} as observed for source clamped between two blocks of NaI (Tl).

of the crystal in stopping all electrons or hard X-rays within the volume of the detectors. Furthermore, the method can be applied very widely when high efficiency of detection of high energy quanta can be achieved. Even with the fairly small crystal used in the above work with Hg^{203} , the γ -ray quanta are detected with an efficiency of ~ 50 per cent. With still larger crystals almost 100 per cent absorption of the radiation could be expected. We see from fig. 10 that the Compton process is appreciable and it results, unfortunately, in a filling-in of the gap between group (1) and group (2) particles. It would, therefore, be very advantageous if the Compton process could be made to contribute

usefully; this can be done only if scattered quanta are not allowed to escape, so that a pulse of definite amplitude corresponding to the full energy of the incident γ -radiation arises from the multiple Compton scattering process.

Clearly, it is not at all easy to satisfy the last requirement except with very large crystals of good optical quality. Liquid phosphors would appear to offer greater promise. With a sufficiently large flask of liquid the escape of scattered quanta could be made negligible for incident γ -rays of several MeV. energy. However, the efficient collection of light from a volume of some litres introduces considerable difficulties, and a possible method of overcoming this obstacle is being explored. In this method a large bath of the phosphor is placed in close proximity to an efficient large high voltage photo-cell. The anode of the photo-cell is covered with an efficient phosphor such as ZnS(Ag), so that the energy of the photo-electrons accelerated to this anode is converted again to light quanta, which are then piped efficiently to the cathode of an orthodox commercial photomultiplier. The device is actually a type of head amplifier. With an acceleration voltage of 10 kV. across the unit, which is in effect a simplified image tube, a stage gain yield of quanta of about 4 can be expected. It has been shown by Krisek and Vand (1946) that at 20 kV. a unit similar in principle to the above has achieved a gain of 20 in light flux. A system like this seems to offer many advantages, but has one disadvantage, *e. g.* that efficient phosphors such as ZnS(Ag) are relatively slow, and the major advantage of rapid response is lost.

§ 4. DOUBLE CRYSTAL METHOD OF MEASURING ENERGY (USING La^{140} , Co^{60} , ThC'').

This method was tested with several sources of gamma radiation, among them La^{140} , Co^{60} , ThC'' and some new information was obtained concerning La^{140} .

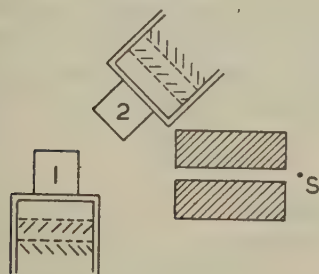
This experimental method, based on the Compton effect, is made possible by the fact that backward scattered quanta do not differ much in energy. The energies of electrons corresponding to quanta scattered at angles of 90° , 120° , 150° and 180° for various values of incident quantum energy are tabulated:—

	0.5 MeV.	1 MeV.	2 MeV.
90°	.25	.67	1.59
120°	.30	.75	1.71
150°	.32	.78	1.76
180°	.33	.80	1.78

It is seen that there is a good degree of homogeneity, and within the range 120° to 150° , which applies to most of the work described here, the theoretical resolving power is ~ 3 per cent. This is the main component

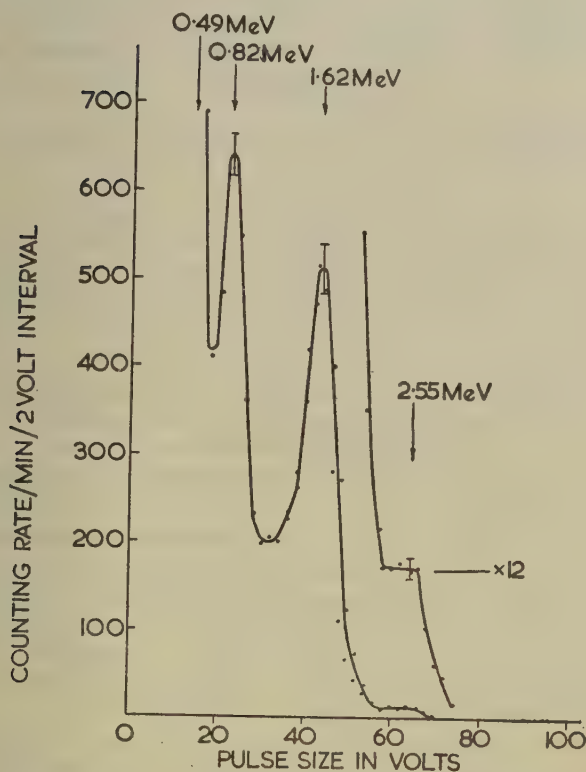
of the total width of the lines as determined by this method. Obviously the ideal geometry would be with the source placed between two crystals, utilizing an angle of scatter $\sim 180^\circ$, where the uncertainty in energy is

Fig. 11.



Two-crystal Compton method of γ -ray analysis.

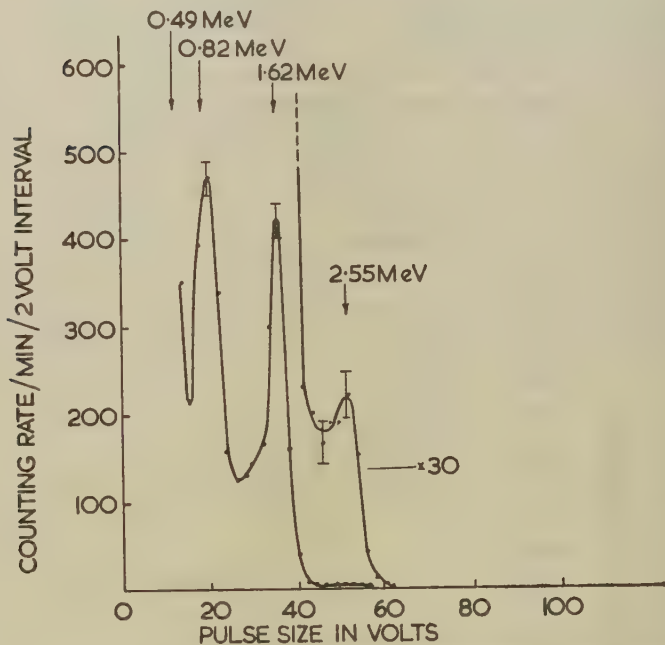
Fig. 12.



Gamma ray spectrum for La^{140} with 1 cm.^3 of anthracene as scattering crystal.

least and the intensity greatest. This arrangement is generally not practicable for complex sources because of the γ - γ coincidences due to the emission of time-related quanta. The arrangement shown in fig. 11, using collimation, works extremely well. For maximum sensitivity the crystal 2 should be toroid shaped since this does not interfere with resolving power. However, in practice, crystal 2 consisted of a $\frac{3}{4}$ -inch diameter crystal of NaI (Tl), crystal 1 was a 1-cm. cube of anthracene or of NaI (Tl). The lead collimator was 4 inches in length and such that the γ -rays incident on crystal 1 lay in a cone of semi-angle 3° .

Fig. 13.



Gamma ray spectrum for La^{140} with 1 cm.³ of NaI (Tl) as scattering crystal.

It is proposed to replace crystal 2 with a specially formed vessel filled with terphenyl in xylene. Results for the different sources are shown in figs. 12, 13. Figs. 12 and 13 were obtained with a source of La^{140} , using crystals of anthracene and sodium iodide (Tl) as scattering crystals and using Co^{60} and ThC'' as calibration sources. Peaks were obtained corresponding to γ -rays of energy 1.62, 0.82, 0.49 and 0.335 MeV., two of which are shown in these figures.

The weak high energy γ -line was also found, which by comparison with the ThC'' line (2.62 MeV.) had an energy of 2.55 MeV. ± 2 per cent. We have to note that this radiation has been detected by Wattenberg

Provided that K is nearly constant over the range V , say, the relationship (1) can be utilized in many investigations. Thus, calibration with radiation of known V , say, V' gives us

$$N_0' V' \phi = I_0'$$

where $\phi = \alpha \epsilon M / K = \text{constant}$.

For an unknown radiation, we have

$$N_0'' V'' \phi = I_0''$$

so that :

$$V'' = V' N_0' I_0'' / N_0'' I_0' \quad . \quad . \quad . \quad . \quad . \quad . \quad (2)$$

This direct procedure can be of considerable value in preliminary investigation of sources, since the total energy release per disintegration can be deduced. This information can be of considerable value in setting up a decay scheme, although it is limited, of course, by virtue of the escape of neutrinos.

In conclusion, we wish to thank Professor P. I. Dee, F.R.S., for encouraging the prosecution of the work, and Mr. J. G. Balfour for his work in connection with the kicksorter.

REFERENCES.

- BEACH, L. A., PEACOCK, C. L., and WILKINSON, R. G., 1949, *Phys. Rev.*, **76**, 1624.
 BISHOP, G. R., WILSON, R., and HALBAN, H., 1950, *Phys. Rev.*, **77**, 416.
 CURRAN, S. C., and BAKER, W., 1944, *Rad. Lab. Report* 7.6.16.
 HANSON, A. O., 1949, *Phys. Rev.*, **75**, 1794.
 HOFSTADTER, R., and MCINTYRE, J. A., 1950, *Phys. Rev.*, **78**, 619.
 HOPKINS, J. I., 1950, *Phys. Rev.*, **77**, 406.
 JOHANSSON, S. A. E., 1950, *Nature, Lond.*, **166**, 794.
 KRIZEK, V., and VAND, V., 1946, *Electronic Eng.*, **18**, 316.
 MANDEVILLE, C. E., and SCHERB, M. V., 1948, *Phys. Rev.*, **73**, 1434.
 MITCHELL, A. C. G., LANGER, L. M., and BROWN, L. J., 1947, *Phys. Rev.*, **71**, 140.
 OSBORNE, R. K., and PEACOCK, W. C., 1946, *Phys. Rev.*, **69**, 679.
 RALL, W., and WILKINSON, R. G., 1947, *Phys. Rev.*, **71**, 321.
 SAXON, D., 1948, *Phys. Rev.*, **74**, 849.
 SLÄTIS, H., and SIEGBAHN, K., 1949, *Phys. Rev.*, **75**, 318.
 WALKER, R. L., and McDANIEL, B. D., 1948, *Phys. Rev.*, **74**, 315.
 WATTENBERG, A., 1947, *Phys. Rev.*, **71**, 497.
 WEST, H. J., MEYERHOF, W. E., and HOFSTADTER, R., 1951, *Phys. Rev.*, **81**, 141.

CXIII. *The Properties of Neutral V-Particles.*

By R. ARMENTEROS, K. H. BARKER, C. C. BUTLER and A. CACHON,
The Physical Laboratories, University of Manchester*.

[Received August 15, 1951.]

[Plates XXXIII.-XL.]

ABSTRACT.

In a cloud-chamber investigation at 2867 m. altitude 70 V-tracks due to the decay of neutral V-particles have been observed. An analysis has been made on the basis of the two-body decay processes: $V_1^0 \rightarrow P^+ + \pi^-$ and $V_2^0 \rightarrow \pi^+ + \pi^-$ and it is concluded that the present limited data are consistent with these two processes. The ratio of the numbers of the two types of V-particles is found to be $N_{V_1}/N_{V_2} = 1.6 \pm 0.5$ and accurate mass estimates have been obtained for 12 examples of the first type of decay and for eight examples of the second type. The results are consistent with the unique mass values $(2203 \pm 12)m_e$ and $(796 \pm 27)m_e$ respectively. The possibility that there are neutral secondary particles among the decay products cannot be excluded. However, some evidence is presented that seems to exclude an explanation of the observations in terms of two modes of decay of a heavy particle each giving a nucleon and two mesons. Finally, it is concluded that there are probably two different types of neutral V-particles.

CONTENTS.

	Page
§1. Introduction	1114
§2. The experimental arrangement	1114
(i.) Some important features of the arrangement	1114
(ii.) The counter selection system	1114
(iii.) Measurements of the curvature of cloud-chamber tracks ...	1115
(iv.) Estimates of momenta and the measurement of angles ...	1116
§3. An analysis of events occurring in the gas of the cloud chamber ...	1116
(i.) Nuclear interactions in the gas	1116
(ii.) V-tracks observed in the gas of the cloud chamber	1117
§4. The properties of the decay products of neutral V-particles	1118
(i.) Measurement of heavily-ionizing secondary particles	1118
(ii.) The momentum spectra of the secondary particles	1120
(iii.) The penetrating properties of the secondary particles	1121
(iv.) Neutral secondary particles	1122
§5. The masses of neutral V-particles	1123
(i.) The classification of V-tracks	1124
(ii.) The decay process: $V_1^0 \rightarrow \rho^+ + \pi^-$	1128
(iii.) The decay process: $V_2^0 \rightarrow \pi^+ + \pi^-$	1130
§6. Momenta spectra and relative frequencies of neutral V-particles ...	1130
§7. Discussion	1131
§8. Conclusion	1133
§9. Acknowledgments	1133

* Communicated by Professor P. M. S. Blackett, F.R.S.

§ 1. INTRODUCTION.

V-SHAPED tracks, usually associated with energetic nuclear interactions, have been found in many cloud-chamber investigations. Seriff *et al.* (1951), Bridge and Annis (1951), Astbury *et al.* (1951) and the authors have found these tracks at mountain altitudes and Rochester and Butler (1947), McCusker and Millar (1951), Fretter (1951), Thompson *et al.* (1951) and Leighton *et al.* (1951) have observed them at sea-level. The majority of these tracks are due to the decay of hitherto unknown particles, which have been provisionally called V-particles. The present paper contains a detailed analysis of 70 V-tracks, due to the decay of neutral V-particles, obtained at an altitude of 2867 m. on the Pic-du-Midi in the French Pyrenees. In a preliminary publication (Armenteros *et al.* 1951) it was established that the neutral V-particles are not homogeneous and that at least two separate decay processes are involved. In one process the charged decay products are a proton and a negative π -meson while in the other both charged secondaries are probably π^- or μ^- -mesons. These conclusions have been confirmed by Thompson *et al.* and by Leighton *et al.* The latter authors have considered the possibility that a nucleon and two mesons may be emitted in each decay process and have concluded that their results can be interpreted in this way. The significance of this interpretation is discussed in § 7 of this paper.

§ 2. THE EXPERIMENTAL ARRANGEMENT.

The cloud chamber, 28 cm. in diameter, has been used in a field of about 7500 gauss, produced by an 11-ton electro-magnet. The equipment is basically the same as that used in previous investigations of penetrating showers at sea-level by Barker and Butler (1951) and by earlier workers. Since accurate momentum- and angle-measurements are required, special precautions have been taken to avoid distortions in the chamber and in order to measure the angles accurately the events are carefully reconstructed in three dimensions.

(i.) *Some important features of the arrangement.*

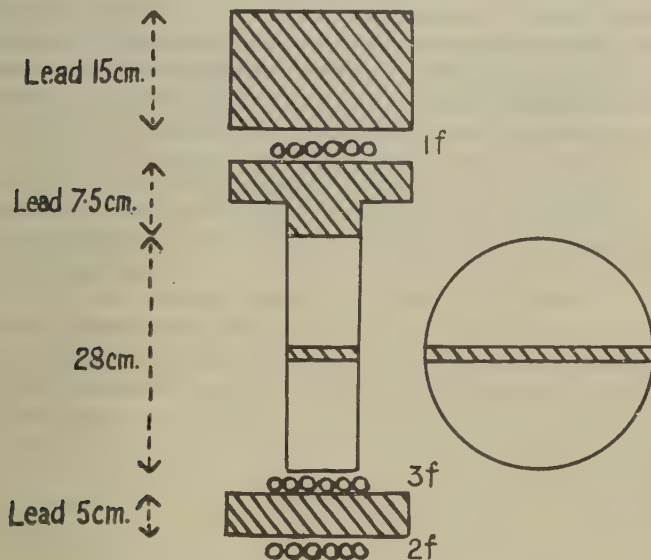
The apparatus was operated in a permanent stone-built laboratory, the air temperature being regulated to within 1°C . The cloud chamber was isolated thermally from the core of the electro-magnet and its temperature maintained constant at about 15°C ., to within $\frac{1}{4}^\circ\text{C}$., by a water-jacket fed from a thermostated supply. This close control of temperature is essential in order to reduce convection currents in the chamber to a minimum. The time interval between expansion and photography was 0.07 sec., as short as possible consistent with adequate intensity of the photographic images.

(ii.) *The counter selection system.*

The first V-tracks to be discovered were associated with energetic nuclear interactions or penetrating showers and therefore counter systems which detect such interactions efficiently have since been used. Further-

more, owing to the discovery that the majority of the V-tracks are due to the decay of particles with short lifetimes, the material in which the interactions occur should be very dense and as near to the cloud chamber as possible. The six-fold counter system used on the Pic-du-Midi (fig. 1) can be operated by only one ionizing particle above the chamber. This ensures that energetic interactions, produced by protons in the lead absorbers immediately above, or inside, the cloud chamber, will be recorded. The average energy of a shower required to operate the counter system is greater than 10^{10} eV. The counting rate was (7.2 ± 0.1) per hour at 2867 m. altitude and it is estimated that more than half of this rate was due to nuclear interactions. With a resetting time of 6 minutes after each expansion, the rate of photography was 4.2 per hour.

Fig. 1.



Side view of cloud chamber on Pic-du-Midi.

(iii.) *Measurements of the curvature of cloud-chamber tracks.*

The cloud-chamber tracks were photographed by a pair of Leitz Hektor lenses (focal length 2.8 cm. ; aperture f/6.3) on 35 mm. Ilford 5G91 film, at a mean magnification of 0.1. Several methods have been used for measuring the curvatures of the track images, the choice of method depending upon the magnitude of the curvatures. For curvatures smaller than 1 m.^{-1} on the film the prism compensator, devised by Blackett (1937), was used. For greater curvatures, the track images have been measured with a travelling microscope or have been projected on to a screen and compared with a set of standard circular arcs.

The minimum-detectable curvature on a counter-controlled track is a function of the length of the track, for given condensation conditions, chamber illumination and specific ionization of the particle giving rise to the track. It has been found that for good track images of particles at minimum ionization, longer than about 1 cm., the limit is set by the curvature due to gaseous distortions. The curvature produced by chamber distortions has been determined from an examination of μ -meson tracks, 10 cm. long in the chamber, which were photographed in zero magnetic field. The probable curvature due to distortion derived from these measurements was 0.2 m.^{-1} and corresponds to a maximum-detectable momentum of 10^{10} eV./c. , for a mean magnification of 0.1 and an average magnetic field of 7500 gauss. For track images shorter than 1 cm., the random deviations of the drop images from the true trajectory become important. Thus, for example, the maximum-detectable momentum for track images 0.5 cm. long is reduced to about $7 \times 10^9 \text{ eV./c.}$ A lead plate across the centre of the chamber was used during part of the running time and slight distortions sometimes occurred close to the plate. Sections of a track that are slightly distorted in this way can be rejected when making curvature measurements with the prism compensator.

(iv.) *Estimates of momenta and the measurement of angles.*

In order to derive the momentum of a particle from the curvature of its track image, average values are found for the magnetic field over the trajectory and for the magnification of the track on the film. These values are obtained from calibration measurements, the position of the track being determined by reprojecting the stereoscopic photographs through a pair of Leitz Hektor lenses, nearly identical optically with those used to photograph the chamber. A correction is made for the uniform dilation of the track due to the expansion of the cloud-chamber gas.

The angle between the branches of a V-track is also obtained from reprojection measurements, the accuracy of the results depending on the magnitude of the angle and the track curvatures. The accuracy obtained in the present series of measurements was usually better than 5 per cent but, in some cases for which the angle is small and the plane of the fork is inclined appreciably to the plane of the chamber, the error may be as high as 10 per cent.

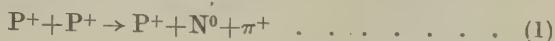
§ 3. AN ANALYSIS OF EVENTS OCCURRING IN THE GAS OF THE CLOUD CHAMBER.

About 105 V-shaped tracks and six events in which more than two tracks diverge from a point in the gas have been found among 13,500 photographs obtained on the Pic-du-Midi.

(i.) *Nuclear interactions in the gas.*

Of the six events in the gas involving more than two ionizing particles, three are typical of nuclear interactions produced by neutrons of moderate

energies and one is an energetic penetrating shower produced in the gas just below the top wall of the cloud chamber. The remaining two events, each consisting of three energetic ionizing particles, seem to be examples of specially simple types of interactions. The simplest interpretations are that they represent the following interactions :



and



It is extremely unlikely that both of these interactions, due to charged particles, involved collisions with free hydrogen nuclei in the gas of the cloud chamber, the geometric cross-section of which is less than 5 per cent of that of the argon nuclei present. If heavy nuclei took part in the collisions the emission of evaporation particles would be expected, whereas none are observed. It is possible, however, that both of the events were associated with recoil tracks less than 1 mm. in length. The Y-shaped event, which can be interpreted by scheme (1), is reproduced in Pl. XXXIII.

An estimate of the number of interactions in the gas of the chamber can be made in a variety of different ways and is of the same order of magnitude as the observed number. Hence, it is concluded that not more than one or two of the V-tracks discussed in (ii.) below can be due to nuclear interactions. A detailed discussion has been given by Armenteros *et al.* (1951).

(ii.) *V-tracks observed in the gas of the cloud chamber.*

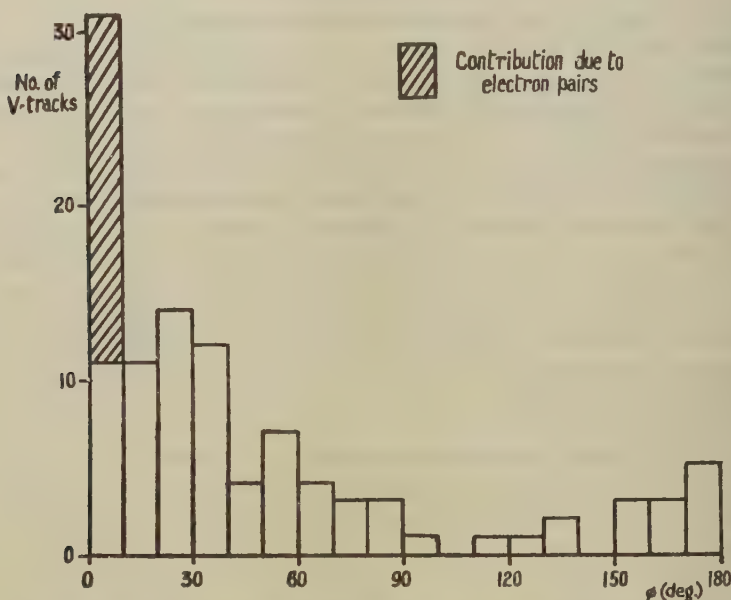
The stereoscopic pairs of photographs of the V-tracks have been carefully reprojected to ensure that, in each case, the apex of the event is within the illuminated region of the chamber. This procedure is essential because V-tracks are quite frequently simulated by two tracks crossing very close to the edge of the light beam. The angle of each V-track, namely the angle between the two ionizing tracks, has been measured and the distribution of the angles is shown in fig. 2. The majority of the events have angles smaller than 90°, while the remainder have angles close to 180°. In general, their orientation with respect to accompanying tracks suggests that the V-tracks in the first group are due to neutral particles and that those in the second group are due to charged particles.

There are about 20 V-tracks, with angles smaller than 1°, which are characteristic of electron pairs produced by photons and most of them contain identifiable electron tracks. It is probable that a few electron pairs have been missed during the examination of the photographs; the smallness of the observed number, however, is sufficient to exclude the possibility that any of the V-events were due to nuclear interactions of photons. The ratio of the cross-sections for nuclear interaction and for pair production by energetic photons is less than 10⁻³.

The distribution of the observed angles cannot be explained by the scattering of charged particles. Furthermore, only one V-track has a recoil track at the apex, although an argon recoil track would be 1 mm. long and just visible even if its momentum were as low as 5×10^7 eV./c.

The majority of the V-tracks must be due to the spontaneous decay of unstable particles, provisionally called V-particles, and the remainder of this paper is concerned with an analysis of the 70 V-tracks produced by neutral V-particles.

Fig. 2.



The distribution of the angle between the two tracks forming a V-track.

§ 4. THE PROPERTIES OF THE DECAY PRODUCTS OF NEUTRAL V-PARTICLES.

The properties, such as ionizing- and penetrating-power, of the decay products of neutral V-particles must be determined before the nature of the decay processes and of the unstable particles can be elucidated.

(i.) *Measurement of heavily-ionizing secondary particles.*

Sixteen secondary particles produced heavily-ionizing tracks in the cloud chamber, eight of which were positively charged and eight negatively charged. Estimates of the specific ionization and of the momentum can be obtained for nine of these tracks; the data enable good estimates to be made of the masses of the particles. The ionizations were found by a procedure which has been discussed in detail by Butler *et al.* (1950). Five of the slow positive particles have estimated masses close to that of the proton; the tracks of two of these particles are

reproduced in Pls. XXXIV. and XXXV. and the data for all five are given in Table I. Probably the remaining three slow positive particles were also protons. No identifiable negative protons have been found. No evidence has been found for the existence of slow secondary particles of mass about $1200 m_e$. It is probable that the heavy particles found by Leighton *et al.* (1951) were protons, despite the rather low mass estimates in several cases.

TABLE I.

Momentum and estimated ionization for five proton secondaries.

Event no.	33	43	47	56	92
Momentum (10^8 eV./c.)	2.42 ± 0.2	4.8 ± 0.5	3.5 ± 0.35	4.50 ± 0.45	6.0 ± 0.6
Estimated ionization (I_{\min})	8-15	3-4	4-6	3-4	2-3
Mass range (m_e)	1550-2400	1700-2400	1450-2300	1600-2250	1450-2500
Calculated ionization for proton (I_{\min})	9.3	3.1	5.0	3.3	2.3

The four negative particles that have been measured have masses close to those of the π^- and μ^- mesons, the data are given in Table II. The measurements are not sufficiently accurate to permit discrimination between π^- and μ^- mesons. A study of the dynamics (*cf.* §5) of the four events shows that the positive secondary particles, which accompany the four slow these negative particles, were probably protons. The remaining four negative particles, on which accurate measurements could not be made, were all less massive than a proton. It may be noticed that no slow positive mesons have been observed among the secondary particles.

TABLE II.

Momentum and estimated ionization for four meson secondaries.

Event no.	3	7	65	86
Momentum (10^8 eV./c.)	1.05 ± 0.05	0.80 ± 0.04	0.78 ± 0.14	0.74 ± 0.04
Estimated ionization (I_{\min})	2-3	2-4	3-4	2.5-3.5
Mass range (m_e)	270-430	210-380	290-370	230-330
Calculated ionization for π^- -meson (I_{\min})	2.0	2.7	2.8	3.0

Seriff *et al.* (1950) have identified one slow secondary particle as a meson. Hopper and Biswas (1951) found that one of the tracks forming a V-track in a photographic emulsion was due to a proton, and Thompson *et al.* (1950) have identified two protons among the secondaries of a sample of neutral V-particles.

The behaviour of one of the slow negative secondaries observed on the Pic-du-Midi is of particular interest. A neutral V-track, shown in Pl. XXXVI., was produced just above the thin lead plate and the negative secondary particle was just heavily ionizing above the plate and much more heavily ionizing below the 7 mm. plate. Five centimetres below the plate the track of this particle is apparently deflected through 23° in the gas, without any marked change in ionization.

TABLE III.

Momentum and estimated ionization for the decay
of a negative secondary particle.

Track No. on Pl. XXXVI.	Track (2)	Track (3)
Momentum (10^8 eV./c.)	7.8 ± 0.4	6.1 ± 0.3
Estimated ionization (I_{\min})	3-4	3-4
Calculated ionization for π -meson	2.8	4.0
Calculated ionization for μ -meson	2.0	2.8

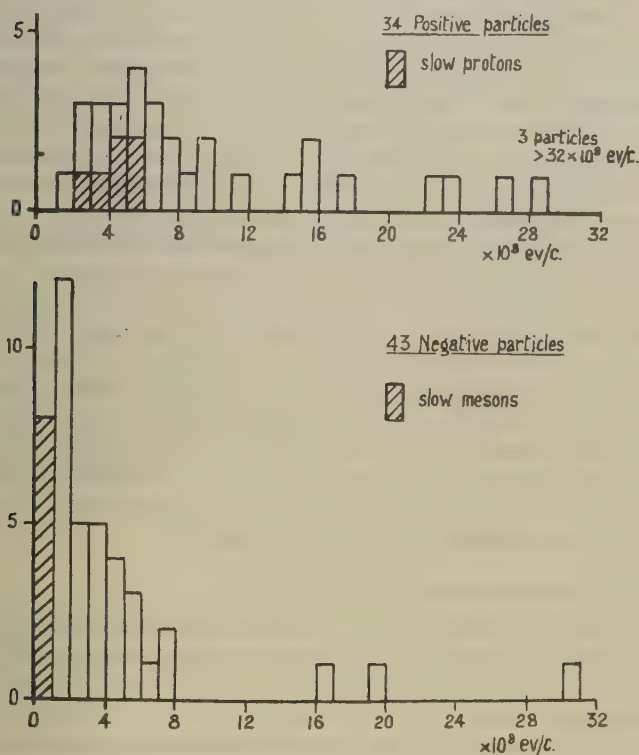
From the measurements on the track, summarized in Table III., it is concluded that the change of direction of the track is most probably due to the decay-in-flight of a negative π -meson. The angle of deflection is close to the most probable value for the disintegration of a π -meson having the measured momentum. Furthermore, it is estimated that, if all the observed low-momentum negative secondaries of neutral V-particles were π -mesons, the probability of having observed one decay is about 25 per cent. Since the probability of a large-angle single scattering in the gas is extremely small, this event is regarded as convincing evidence for the existence of negative π -mesons among the decay products of neutral V-particles.

(ii). *The momentum spectra of the secondary particles.*

Momentum measurements have been made on 43 negative secondary particles and on 34 positive particles; the frequency distributions are shown in fig. 3. A striking feature of these spectra is that the average momentum of the negative particles is markedly lower than that of the positive particles; this disparity indicates that a considerable fraction of the neutral V-events has positive secondaries which are much heavier than

the negative secondaries (cf. §5). The contributions of heavily-ionizing particles are indicated on the histograms by shaded areas. Although no heavily-ionizing positive mesons have been found, there are positive particles at approximately minimum ionization in the momentum range below 7×10^8 eV/c. where protons would appear heavily-ionizing. This indicates that positive mesons are present, since it is unlikely that there are any electrons among the secondary particles (cf. section (iii.) below).

Fig. 3.



Frequency distribution of measured momenta of secondary particles.

Some of these mesons which produced tracks at minimum ionization could have been of $1000m_e$ type, but for the present this possibility is excluded and they are assumed to have been either π - or μ -mesons.

(iii.) The penetrating properties of the secondary particles.

During part of the experiment a lead plate was placed across the centre of the chamber in order to examine the penetrating properties of the constituents of the V-tracks. In all, the secondary particles traversed

20 cm. of lead without any evidence of radiative energy loss ; on the other hand two probable interactions occurred. This is in good agreement with the results of Seriff *et al.* (1950) and suggests that electrons do not occur among the secondary particles.

Pl. XXXVII. shows an interaction by a negative secondary particle, of measured momentum 3.5×10^8 eV./c., in the 2 cm. plate with the production of a slow proton. The angle of the fork is 3° and the possibility that the V-track was due to an electron pair can be excluded. It is probable that the particle responsible for the interaction was a negative π -meson. The positive secondary had a considerably higher momentum and was probably a proton. The second interaction, produced by a positive secondary, is reproduced in Pl. XXXVIII. ; this secondary particle was deflected through 15° in traversing the 2 cm. lead plate. Unfortunately the momentum of the particle cannot be measured accurately, but it is probable that it was greater than 5×10^8 eV./c. The momentum of the negative secondary was $(3.3 \pm 0.3) \times 10^8$ eV./c. ; it was probably a meson. Since the momentum of the secondary particles transverse to the direction of the decaying particle was greater than 1.6×10^8 eV./c. and using the arguments outlined in § 5, section (i.), it is probable that both secondaries were mesons (*cf.* fig. (6b)).

A tentative value of the cross-section for the nuclear interactions of the secondaries of V-particles, on the basis of the four interactions found in the present work and in the work of Seriff *et al.*, is about 10 cm. of lead, whereas the geometrical cross-section of the lead nucleus corresponds to 15 cm. of lead. This supports the conclusion that at least a considerable fraction of the secondary particles, produced by the decay of neutral V-particles, have strong nuclear interactions. The observations, however, are not yet sufficiently extensive to exclude the presence of an appreciable number of μ -mesons among the secondary particles.

(iv.) *Neutral secondary particles.*

No conclusive evidence has yet been reported for the existence of neutral particles among the decay products. The most direct way of testing for their presence would be to find a discrepancy between the direction of the V-particle, as deduced from its point of origin, and the direction of the vector sum of the momenta of the two secondary particles. Thus, the conservation of momentum, transverse to the plane of the V-track, may be examined by a coplanarity test and that in the plane of the V-track, by testing whether the transverse momentum components of the secondary particles are equal.

In the present experiment, the majority of the V-particles originated in thick lead absorbers above the cloud chamber and it has not been possible, in any of these examples, to locate the origin accurately. Nine V-particles originated in nuclear interactions in a lead plate placed across the middle of the chamber, and, for two of these examples, reasonably accurate measurements have been made ; one is reproduced in Pl. XXXIX. The

angles between the branches of these V-tracks were 46° and 77° respectively and coplanarity was established to within the experimental error, estimated at about 5° . The distances traversed before decay were 4.1 cm. and 1.9 cm. respectively. The momentum balance in the plane of the V-particle, perpendicular to the line of flight, was also examined. The differences in the transverse momentum components, for the two examples, were $(0.1 \pm 0.3) \times 10^8$ eV./c. and $(0.4 \pm 0.2) \times 10^8$ eV./c. respectively, and thus there is no evidence for the existence of a third neutral particle. In each of these cases the secondary particles were both mesons.

Another method of testing for the presence of a third particle is to look for experimental evidence of interactions in the lead plate, due to neutral decay products. Photons or neutral π -mesons, which decay extremely rapidly into two photons, can initiate electromagnetic cascades, and neutrons can give rise to nuclear interactions. Four photographs, in each of which a V-particle decayed immediately above a 0.5 cm. lead plate across the centre of the chamber and both the ionizing secondary particles penetrated the plate, have been carefully examined. Two of these events contained low-momentum negative secondaries, and, in the other two, the secondary particles were of comparable momentum. No evidence has been found of clearly associated electromagnetic radiation (*cf.* Pl. XXXVI.).

§ 5. THE MASSES OF NEUTRAL V-PARTICLES.

Since protons and both positive- and negative-mesons have been found among the decay products of neutral V-particles, it must be concluded that there are at least two decay processes involved. Assuming that no third neutral particle is produced, the most likely two-body processes are :

$$V_1^0 \rightarrow P^+ + \pi^- \quad . \quad . \quad . \quad . \quad . \quad . \quad . \quad . \quad (3)$$

and

$$V_2^0 \rightarrow \pi^+ + \pi^- (4)$$

Some evidence has been found for π -mesons accompanied by protons but the nature of the mesons in scheme (4) is uncertain; they may be μ -mesons. Schemes (3) and (4) may be modified by the presence of neutral particles, but no direct evidence of their existence has yet been discovered. In the present analysis the consistency of the experimental data with the assumed two-body processes (3) and (4) will be examined.

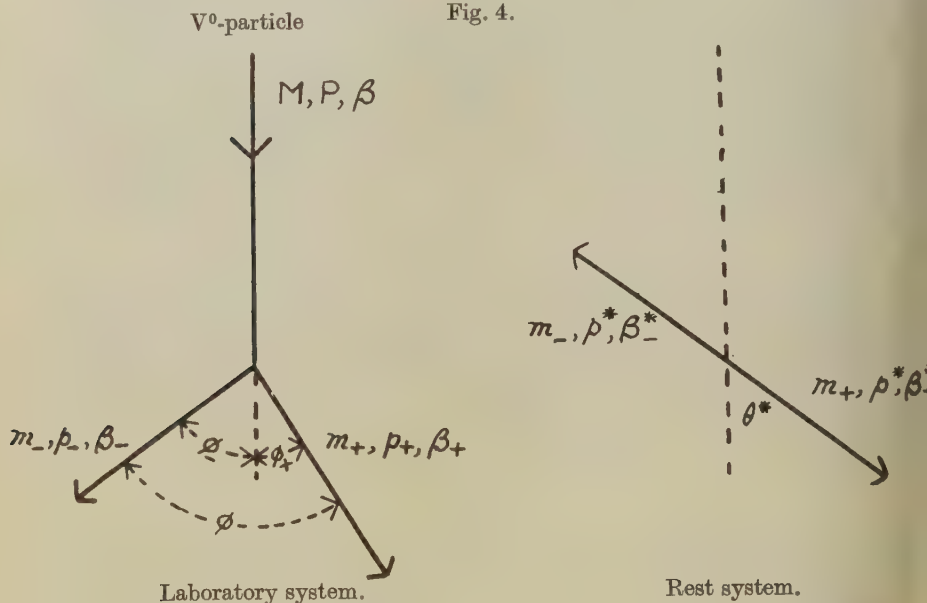
The analysis of the data is complicated because many of the measured V-tracks have both secondary tracks at minimum ionization and therefore they cannot be directly assigned to one or other of the two schemes. Some events, however, can be directly assigned to either scheme (3) or to scheme (4) and, using the measurements on these events, a procedure has been devised for separating statistically the remaining data between the assumed schemes. This classification procedure is outlined in section (i.) below and the data for each decay process are examined in detail in sections (ii.) and (iii.).

(i.) *The classification of V-tracks.*

The decay-in-flight of a V^0 -particle, mass M , into two secondary particles with masses m_+ and m_- is shown schematically in fig. 4. If the momentum of each secondary particle in the rest system of the unstable particle is denoted by p^* and if the secondary particles are emitted in the rest system at an angle θ^* to the direction of the V^0 -particle, then the transverse momentum component is invariant and equal to $p^* \sin \theta^*$. Further, it can be shown that, for random emission of the secondary particles in the rest system, the probability that the transverse component lies between p_T and $p_T + dp_T$ is

$$\mathfrak{P}(p_T) dp_T = \frac{p_T}{p^*(p^{*2} - p_T^2)^{1/2}} dp_T.$$

Fig. 4.



Thus, for a given decay process, the probability that the secondary particles have transverse momentum components close to p^* is very high. The experimental distribution of p_T for a number of V-tracks can be used to check that the directions of emission in the rest system are at random.

It is useful to define a quantity α given by :

$$\alpha = \frac{p_+ \cos \phi_+ - p_- \cos \phi_-}{p_+ \cos \phi_+ + p_- \cos \phi_-},$$

where $p_+ \cos \phi_+$ and $p_- \cos \phi_-$ are the longitudinal momentum components of the positive- and negative-secondary particles (cf. fig. 4). It can be shown that

$$\alpha = \frac{p_+^2 - p_-^2}{P^2} = \frac{m_+^2 - m_-^2}{M^2} + 2p^* \cos \theta^* \left\{ \frac{1}{M^2} + \frac{1}{P^2} \right\}^{1/2},$$

where M and P are respectively the mass and momentum of the V-particle. For simplicity, the last equation may be written in the form

$$\alpha = \alpha_0 + f(P, \cos \theta^*)$$

and thus the longitudinal momentum components of the secondary particles can be related simply to the invariant quantity α_0 , where $\alpha_0 = (m_+^2 - m_-^2)/M^2$, because the mean value of $f(P, \cos \theta^*)$, for a number of decay events randomly oriented in their rest systems, is zero, *i. e.* the mean value of α equals α_0 .

Values of α and p_T are used when deciding by which of the two likely decay schemes a particular V-track can be interpreted. These values can be calculated for the 29 measured V-tracks; the quantities p_+ , p_- and ϕ are known for each of these events and the value of p_T can be obtained conveniently from the relation $p_T = p_+ p_- \sin \phi / P$.

Five of the 29 V-tracks have slow proton secondaries, which have been identified with considerable certainty. These five events can only be interpreted by scheme (3); the average of four of the values of α is $+0.60$. The fifth value is very small and is neglected in the preliminary determination of α ; it can be shown that the latter event (Catalogue no. 33) is an improbable one although consistent with scheme (3). The average value of p^* is $(1.10 \pm 0.10) \times 10^8$ eV./c.

The secondaries of three of the other neutral V-particles were all lighter than the proton; they cannot be identified, however, because the ionization of their tracks is close to the minimum value, but the evidence, given in §4, suggests that they were probably π - or μ -mesons. Thus these three V-tracks can only be explained by decay scheme (4) and are due to the decay of V_2^0 -particles. The average value of α for the three V-tracks is $+0.08$; this value is not significantly different from zero, the value expected if the assumed decay scheme is the correct one. The average value of p^* is $(1.40 \pm 0.15) \times 10^8$ eV./c.

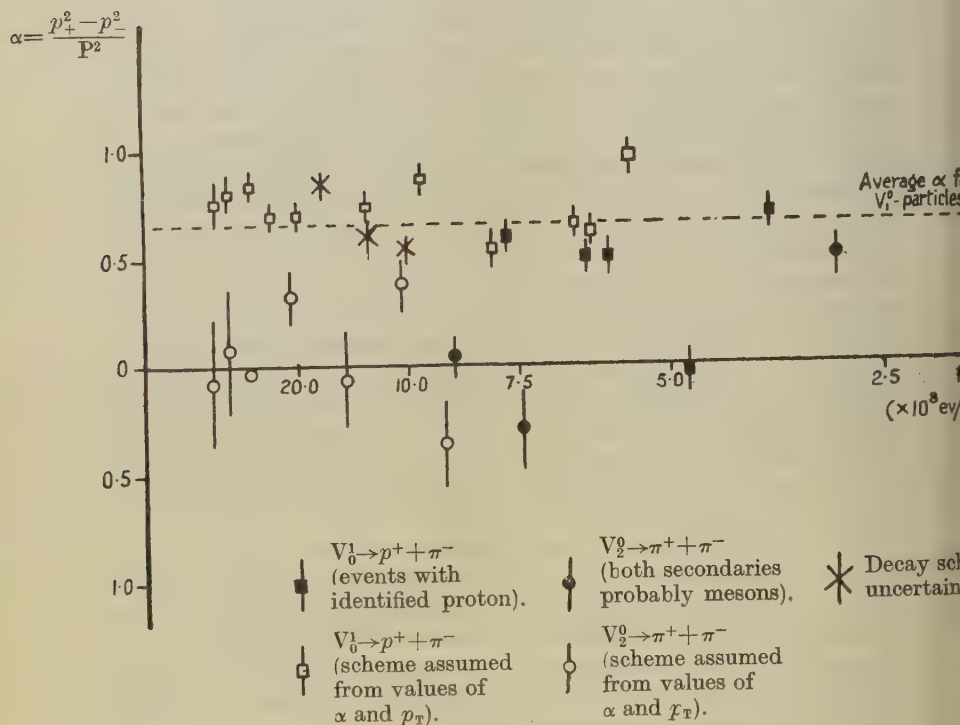
It will be noticed that the average values of α , namely α_0 , for the two schemes are different and the experimental value of p^* derived from only three cases, for scheme (4) is probably greater than the value of p^* for scheme (3). These experimental values of α and p^* , for the two schemes, can be used to decide on the interpretation of the remaining 21 V-tracks. The positive-secondary tracks of these events are substantially at minimum ionization and, with one exception, may have been produced by either protons or mesons. One of the positive particles cannot have been a proton and was probably a meson. The majority of the negative-secondary tracks must have been produced by mesons.

Values of α and p_T can be calculated for the 21 V-tracks, because they are independent of the constants of the decay scheme. A preliminary classification of the events can be effected by deciding with which of the two values of α_0 these values of α are most consistent. The 29 values of α and their probable errors are shown in fig. 5, where they are plotted against $1/P$. A number cluster around the line $\alpha = 0.65$, which is close to the value of α_0 found for four of the tracks which probably decayed

according to scheme (3). In addition, a number of the values cluster around zero, the expected value for scheme (4).

The preliminary classification may be checked by considering the value of p_T , in addition to the value of α , for each event. If $\alpha \approx \alpha_0$, then $\theta^* \approx \pi/2$ and therefore $p_T \approx p^*$. Now it has already been shown that, for a given scheme, the majority of the values of p_T are close to p^* ; this result may be used to advantage when assigning data to one or other of the two schemes. For example, if $\alpha = 0.7$ and $p_T = 0.2 \times 10^8$ eV./c., the event cannot be interpreted by scheme (3) but can probably be interpreted by scheme (4).

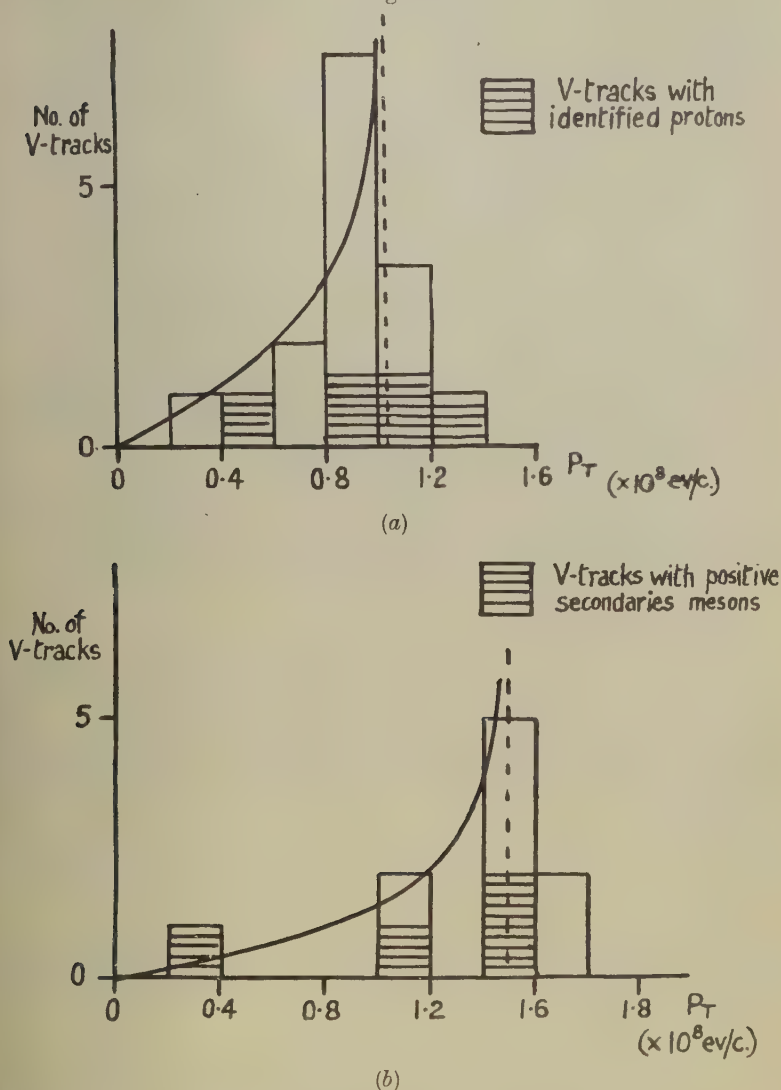
Fig. 5.



A detailed examination of the 29 sets of α and p_T reveals that 16 of the V-tracks can be explained by scheme (3) and ten by scheme (4); the interpretation of the remaining three events is uncertain. For example, for one of the latter events $\alpha = 0.84$ and $p_T = 0.46 \times 10^8$ eV./c. The value of p_T is small for the value of α , if the event decayed according to scheme (3); alternatively, the value of α is large for scheme (4). For the latter scheme $p_T = 0$ when $\alpha = 0.7$, since P , the momentum of the particular V_0 -particle, is 1.7×10^9 eV./c.

The average value of α for the 16 V -tracks due to the decay of V_1^0 -particles is 0.65 ± 0.02 and is shown by a dotted line in fig. 5; the corresponding value of the mass of the V_1^0 -particle is $(2250 \pm 35)m_e$. The distribution

Fig. 6.



The transverse momentum distributions.

of the transverse momentum components, p_T , is shown in fig. 6 (a) and is consistent with the theoretical distribution, indicated by the curve, for a V -particle of mass $2200m_e$ decaying into a proton and a π -meson.

Considerably more data are required before the theoretical distribution can be checked in detail.

The average value of α for the decay of V_2^0 -particles is $+(0.05 \pm 0.06)$ and the distribution of the values of p_T is shown in fig. 6 (b), where the curve has been calculated for a value of $p_T = 1.5 \times 10^8$ eV./c., corresponding to about $800m_e$ mass.

The sample of 29 V-tracks is very small and therefore it is difficult to assess the efficiency with which their classification has been made. If P, the momentum of the V^0 -particle, is less than about 6×10^8 eV./c., the proton, if present, will be heavily ionizing and therefore the classification of these V-tracks can be effected directly. For V-particles with momenta above 6×10^8 eV./c., it can be shown in the case of V_1^0 particles with $\alpha_0 = 0.65$ and $p^* = 1.1 \times 10^8$ eV./c. that their α values cannot be negative. Thus the total number of V_2^0 -particles, with momenta greater than 6×10^8 eV./c. can be assessed, within statistical fluctuation, by doubling the observed number of events with negative values of α . Finally, while there may be doubt about the interpretation of individual V-tracks with P greater than 6×10^8 eV./c., it can be shown that the overall separation of the data is at least 85 per cent efficient, provided that the individual values of α and p_T are known to an accuracy of about 15 per cent.

When a larger number of accurately measured V-tracks are available, a detailed examination could be made of the two distributions of the transverse momentum components obtained for the two schemes, which would provide a check on the classification procedure outlined above.

(ii.) *The decay process $V_1^0 \rightarrow P^+ + \pi^-$.*

It has been shown that 16 of the measured V-tracks were probably due to the decay of V_1^0 -particles. The secondary tracks of 12 of these have been measured accurately and the mass values calculated, using the laws of conservation of energy and momentum. An explicit formula for M, the mass of the V-particle, in terms of measurable quantities may be written :

$$M^2 = m_+^2 + m_-^2 + 2p_+p_- \left[\left\{ 1 + \left(\frac{m_+}{p_+} \right)^2 \right\}^{1/2} \left\{ 1 + \left(\frac{m_-}{p_-} \right)^2 \right\}^{1/2} - \cos \phi \right],$$

where m_+ and m_- are the masses, in energy units, of the proton and π -meson respectively. The energy of disintegration, or Q-value, can be calculated using the value of M since

$$Q = M - (m_+ + m_-).$$

The values of M, Q, α and p_T for the 12 V_1^0 -particles are given in Table IV.

The average mass value of the V_1^0 -particles is $2203m_e$ and the corresponding average Q-value is 46 MeV. The errors quoted in columns (4) and (5) of Table IV. are probable errors, which were obtained by combining

the known distortion errors in the chamber and the various measurement errors. The possibility that sources of systematic error may have affected individual mass values cannot be excluded. For example, unexpectedly large gas distortion, which escaped detection, may have occurred on one or more photographs, since it is not possible to measure the magnitude of the gas distortion on an individual photograph. It is considered that the errors quoted must be regarded as minimum values.

TABLE IV.

Mass values of 12 V_1^0 -particles.

(Mass of proton = $1836m_e$; mass of π -meson = $276m_e$.)

Catalogue no.	α	p_T (10^8 eV./c.)	Mass value (m_e)	Q-value (MeV.)
33*	-0.03	0.78	2277 ± 40	82 ± 20
37	+0.84	0.94	2228 ± 40	58 ± 20
42	+0.74	1.00	2186 ± 20	37 ± 10
43*	+0.50	1.15	2218 ± 10	53 ± 5
47*	+0.70	1.31	2228 ± 10	58 ± 5
49	+0.70	0.82	2160 ± 20	24 ± 10
50	+0.70	0.92	2183 ± 20	36 ± 10
56*	+0.53	0.88	2181 ± 10	40 ± 5
85	+0.67	1.02	2188 ± 10	38 ± 5
88	+0.76	0.72	2157 ± 30	23 ± 15
92*	+0.60	0.81	2169 ± 10	29 ± 5
96	+0.79	0.97	2256 ± 50	72 ± 25

* Events containing an identified proton secondary.

The probable error of the mean mass value is $11.6m_e$, calculated from the scatter of the 12 mass values, and $8.0m_e$ calculated from the individual probable errors. Thus the average mass is $(2203 \pm 12)m_e$ and the average Q-value (46 ± 6) MeV. With such a small number of events and with individual probable errors of the order of $20m_e$, it is not possible to decide whether the events give a unique mass value, or whether there is a significant distribution of values. For example, photograph 88 apparently gives a low Q-value, namely (23 ± 15) MeV., but the difference (23 ± 16) between this value and the average is not significant, particularly as the error quoted is a probable error. Similarly, photograph 33 apparently gives a high Q-value of 74 MeV., but again the difference between this value and the average is hardly significant. Leighton *et al.* (1951) have obtained seven Q-values from events which probably decayed according to scheme (3); their average value is 49 MeV. and the individual values range from 32 to 65 MeV. These values are consistent with those given in Table IV. and, as their errors are also comparable, it is hardly possible to reach their conclusion that the Q-values are distributed over

a range of values. Thompson *et al.* (1951) have reported two Q-values of (31 ± 5) MeV. and (28 ± 10) MeV. for events which, if they were two-body decays, probably followed scheme (3).

(iii.) *The decay process* $V_2^0 \rightarrow \pi^+ + \pi^-$.

Eight of the ten events, which are due to the decay of V_2^0 particles, have been measured reasonably accurately and their masses and Q-values are given in Table V. These events are less satisfactory than those described in section (ii.) above, since the majority involve measurements on high-momentum secondary particles. Most of the values in columns (4)

TABLE V.
Mass values of eight V_2^0 particles.

$$V_2^0 \rightarrow \pi^+ + \pi^-.$$

Catalogue no.	α	p_T (10^8 eV./c.)	Mass (m_e)	Q-value (MeV.)
5	-0.07	1.46	796 ± 130	122 ± 65
35	+0.38	1.56	883 ± 50	165 ± 25
38	+0.33	1.60	872 ± 50	160 ± 25
53	-0.03	1.66	841 ± 60	144 ± 30
63*	-0.29	1.46	820 ± 50	134 ± 25
66*	+0.51	1.03	700 ± 30	74 ± 15
69	+0.07	0.98	673 ± 100	61 ± 50
			- 50	-25
90*	+0.05	1.41	785 ± 30	116 ± 15

* Events in which both secondary particles must have been less massive than the proton.

and (5) of Table V. are compatible with the average mass value of $(796 \pm 27)m_e$ and average Q-value of (122 ± 13) MeV., if the secondary particles are π -mesons. If the secondaries are μ -mesons, then the corresponding average values are $(705 \pm 32)m_e$ and (142 ± 16) MeV. respectively, the errors being probable errors of the means.

Pls. XXXIX. and XL. show examples of the decay of a V_2^0 -particle into two mesons. In the first event, both secondaries were less massive than the proton and were probably mesons. In the second case, both secondaries could be of protonic mass, but the dynamics of the decay show that the event can only be interpreted by the decay of a V_2^0 -particle.

§ 6. MOMENTUM SPECTRA AND RELATIVE FREQUENCIES OF NEUTRAL V-PARTICLES.

An estimate has been made of the relative numbers of the two types of neutral V-particles that decayed in the chamber; the result obtained is $N_{V_1^0}/N_{V_2^0} = 1.6 \pm 0.5$. There are insufficient data to decide whether

this ratio varies significantly with distance from the lead absorbers; such a variation would, in general, be expected if there are two types of V-particle with different lifetimes.

The differential momentum spectra of the V_1^0 - and V_2^0 -particles are given in Table VI. (a) and (b); the data for the V_2^0 -particles has been normalized to the observed number of V_1^0 -particles. These results can only be regarded as preliminary, but it appears that the average momentum of the V_1^0 -particles is about the same as that of the V_2^0 -particles. A possible interpretation of this result is discussed in the next paragraph.

TABLE VI.

Differential momentum spectra of V^0 -particles.

Momentum range (10^8 eV./c.)	0-8	8-16	16-24	24-32	32-40	>40
(a) Observed spectrum of V_1^0 -particles	6	3	2	2	1	2
(b) Observed spectrum of V_2^0 -particles	3.2	6.4	1.6	1.6	—	3.2
(c) Calculated spectrum of V^0 -particles	13	3	—	—	—	—

§ 7. DISCUSSION.

The preliminary data that have been presented in § 5 are consistent with the existence of two types of neutral V-particle, each with a unique mass. This interpretation suggests that there are two entirely different neutral V-particles which must possess similar mean lifetimes, since comparable numbers of the two types decay in the cloud chamber. The evidence for the existence of neutral V-particles with mass greater than the proton is conclusive but the existence of neutral mesons of mass about $800m_e$ is less certain. It may be noted that the latter particles could be the neutral counterparts of the charged particles with masses of the same order of magnitude. The evidence in favour of the heavy charged particles is already very strong and it is probable that the majority of the charged V-particles observed in the cloud chamber are of this type.

It is possible to explain the observed neutral V-tracks as different modes of decay of the same type of particle if these modes involve three secondary particles; for example, the following symmetrical schemes may be possible:

$$V_1^0 \rightarrow P^+ + \pi^- + \pi^0, \quad . \quad . \quad . \quad . \quad . \quad . \quad (5)$$

$$V_2^0 \rightarrow N^0 + \pi^+ + \pi^-, \quad . \quad . \quad . \quad . \quad . \quad . \quad (6)$$

Leighton *et al.* (1951) have pointed out that the apparent Q -value of process (5) (calculated from data on the two charged secondaries only) is probably about half the apparent Q -value of process (6) and that the latter value should be roughly equal to the real Q of the three-body disintegration. This follows, since in the rest system of a V^0 -particle all three secondary particles will, on the average, have the same momenta, but the two lighter particles will take nearly all of the available kinetic energy. Therefore the apparent Q of process (6) is about double that of process (5). In fact, the measured Q of scheme (4) is (122 ± 13) MeV. while that of scheme (3) is (46 ± 6) MeV.; thus the observed ratio is 2.6. Thus the present data are not in contradiction with the prediction made by Leighton *et al.* and would be consistent with a neutral V -particle mass of approximately $2600m_e$. No evidence has, however, been found for the existence of either neutrons or neutral π -mesons among the secondaries of neutral V -particles.

However, the momentum spectra shown in Table VI. (a) and (b) provide some evidence against the explanation of the neutral V -tracks by the two symmetrical three-body decay schemes (5) and (6). The spectrum of the particles giving proton and meson secondaries, namely that of V_1^0 -particles, appears to include a few more low momentum examples than does the spectrum of the V_2^0 -particles, which decay into two mesons. This is just the reverse of the expected behaviour if the decays really followed the three-body schemes (5) and (6) because it can be shown that, in the great majority of cases, the nucleon has a considerably higher momentum in the laboratory frame of reference than that of either of the mesons. The momentum of the nucleon is the largest component of the momentum of the V -particle; this is true for schemes (3), (5) and (6). Thus the spectrum of the V_2^0 -particles of scheme (6), omitting the contribution of the neutrons, should include many more low momentum cases than does the spectrum of V_1^0 -particles of scheme (3), or of scheme (5) omitting the contribution of the neutral π -meson.

On the average, the two mesons in the symmetrical schemes (5) and (6) will have about the same momenta. The spectrum of the negative π -mesons can be obtained from the data on the V_1^0 -particles and if this spectrum is doubled an approximate spectrum for the V_2^0 -particles is obtained, of course, without the contribution of the neutrons. This calculated spectrum is given in Table VI. (c) and may be compared with the observed spectrum in Table VI. (b). If the two symmetrical schemes (5) and (6) are the correct ones, then it appears that most of the V_2^0 -particles should be of much lower momentum than those observed. There seems to be no obvious explanation of the absence of low momentum V -tracks of the type interpreted as due to the decay of V_2^0 -particles; their apparent absence can hardly be explained as being due to instrumental or selection bias. It is concluded that the observed spectra of the V^0 -particles are not in agreement with the consequences of the symmetrical schemes (5) and (6).

The above argument, based on the difference between the spectra of the V_1^0 - and V_2^0 -particles, assuming only two secondary bodies, may, of course, be invalidated if there is more than one type of neutral V-particle giving two charged mesons as decay products.

§ 8. CONCLUSIONS.

The main conclusions reached from the analysis of a small sample of 70 V^0 -tracks are as follows :

(i.) Slow protons and slow negative mesons have been identified among the secondary particles. These negative mesons were probably π -mesons and the corresponding positive secondaries were probably protons.

(ii.) Several positive secondary particles, less massive than the proton, have been observed. In three of these cases the corresponding negative particles were much lighter than the proton and were probably mesons.

(iii.) The neutral V-tracks can be interpreted by two different schemes, each involving two particles, namely

$$V_1^0 \rightarrow P^+ + \pi^-$$

and

$$V_2^0 \rightarrow \pi^+ + \pi^- \quad (\text{or } V_2^0 \rightarrow \mu^+ + \mu^-).$$

(iv.) No evidence has been found that suggests the presence of neutral secondary particles.

(v.) Unique mass values for the two decay processes have been found ; they are $(2203 \pm 12)m_e$ for the V_1^0 -particles and $(796 \pm 27)m_e$ or $(705 \pm 32)m_e$ for the V_2^0 -particles.

(vi.) Rather more of the first type of decay than of the second type have been found, but the mean lifetimes appear to be comparable.

(vii.) An alternative explanation of the above results can be made by assuming two symmetrical three-body processes each involving a nucleon and two mesons, but as yet there is no direct evidence in favour of this hypothesis. Preliminary investigations have been made on the differential momentum spectra of the V_1^0 - and V_2^0 -particles and the results do not appear to be in agreement with the symmetrical three-body schemes.

§ 9. ACKNOWLEDGMENTS.

The authors wish to thank Professor P. M. S. Blackett for his interest and help with the analysis of the results. They are very much indebted to Professor J. Rösch, director of the Observatoire du Pic-du-Midi de Bagnères-de-Bigorre, for his help during the experimental work, and also to Mr. A. H. Chapman who gave valuable assistance both during the experiments on the Pic-du-Midi and with the measurement of the tracks. They wish to thank Dr. J. Podolanski, Dr. G. D. Rochester and Dr. J. G. Wilson for many helpful discussions. Financial assistance, which is much appreciated, has been received from the Nuffield Trustees and the Department of Scientific and Industrial Research. One of the authors (A.C.) wishes to thank the Centre National de la Recherche Scientifique for a grant.

REFERENCES.

- ARMENTEROS, R., BARKER, K. H., BUTLER, C. C., CACHON, A., and CHAPMAN, A. H., 1951, *Nature, Lond.*, **167**, 501.
 ASTBURY, P., CHIPPINDALE, P., NEWTH, J. A., and SAHAR, A. B., 1951 (private communication).
 BARKER, K. H., and BUTLER, C. C., 1951, *Proc. Phys. Soc. A*, **64**, 4.
 BLACKETT, P. M. S., 1937, *Proc. Roy. Soc. A*, **159**, 1.
 BRIDGE, H. S., and ANNIS, M., 1951, *Phys. Rev.*, **81**, 445.
 BUTLER, C. C., ROSSER, W. G. V., and BARKER, K. H., 1950, *Proc. Phys. Soc. A*, **63**, 145.
 FRETTER, W. B., 1951 (private communication).
 HOPPER, V. D., and BISWAS, S., 1950, *Phys. Rev.*, **80**, 1099.
 LEIGHTON, R. B., WANLASS, S. D., and ALFORD, W. L., 1951 (private communication).
 MCCUSKER, G. B. A., and MILLAR, D. D., 1951, *Nuovo Cimento*, **8**, 289.
 ROCHESTER, G. D., and BUTLER, C. C., 1947, *Nature, Lond.*, **160**, 855.
 SERIFF, A. J., LEIGHTON, R. B., HSIAO, C., COWAN, E. W., and ANDERSON, C. D., 1950, *Phys. Rev.*, **78**, 290.
 THOMPSON, R. W., COHN, H. O., and FLUM, R. S., 1951, *Phys. Rev.*, **83**, 175.

DESCRIPTION OF THE PLATES.

PLATE XXXIII.

A nuclear interaction in the gas.

The interaction was produced below the plate by particle (1); tracks (3) and (4) were produced, along with a heavy blob of ionization, which was probably due to a nuclear recoil. Track (1) cannot be measured because it is partially obscured by a low-energy δ -ray. The positive track (2) has a measured momentum of 3.5×10^8 eV. c., and an ionization of (4-5) times minimum; it was probably a proton. The positive track (3) has a measured momentum of 6.5×10^8 eV. c. and is inclined at an angle of about 7° to the plane defined by tracks (1) and (2). Momentum is apparently not conserved in a direction at right angles to the incident particle; thus the event is not an elastic scattering. The simplest scheme appears to be:

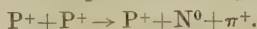


PLATE XXXIV.

An identified proton secondary from a V_1^0 -particle (Catalogue no. 47).

The data for the positive track (1) are given in Table I.; the positive particle was probably a proton. The momentum of the negative particle was $(1.42 \pm 0.10) \times 10^8$ eV. c. and the angle of the fork was 87.5° . The mass of the V_1^0 -particle was $(2228 \pm 10)m_e$ (cf. Table VI.).

PLATE XXXV.

An identified proton from a V_1^0 -particle (Catalogue no. 56).

The data for the positive track (1) are given in Table I.; the positive particle was probably a proton. The momentum of the negative particle was $(1.62 \pm 0.10) \times 10^8$ eV. c. and the angle of the fork was 44° . The mass of the V_1^0 -particle was $(2181 \pm 10)m_e$ (cf. Table IV.).

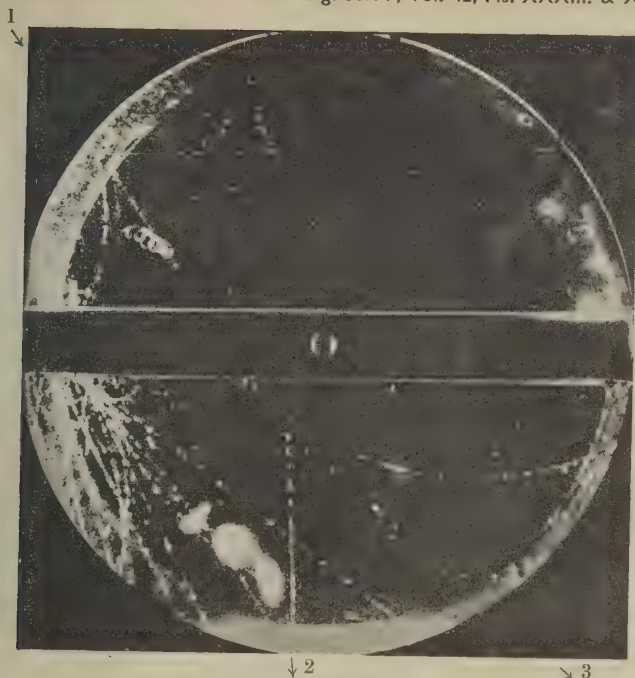
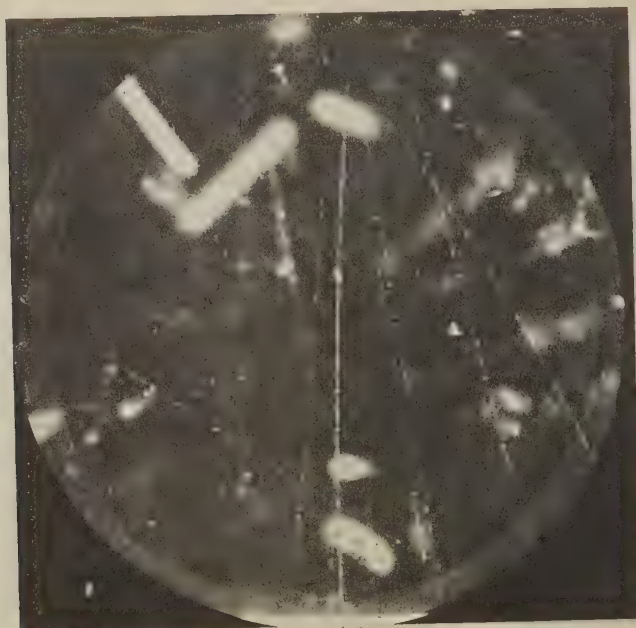


PLATE XXXIII.



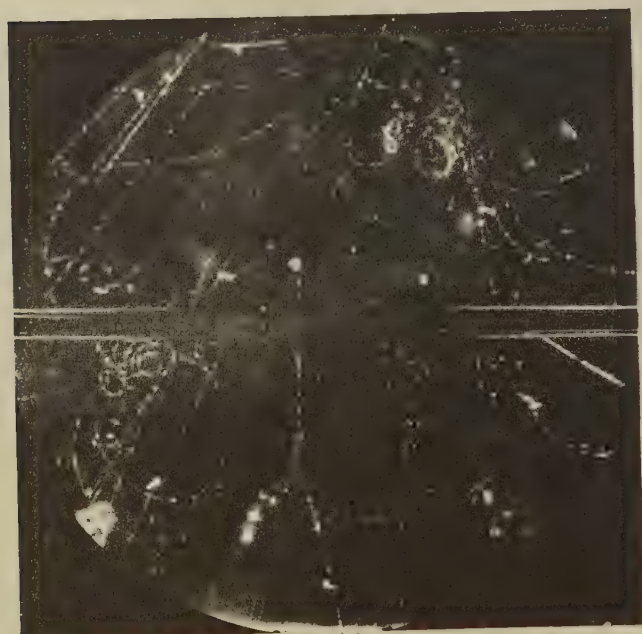
PLATE XXXIV.



↙ 2

↓ 1

PLATE XXXV.



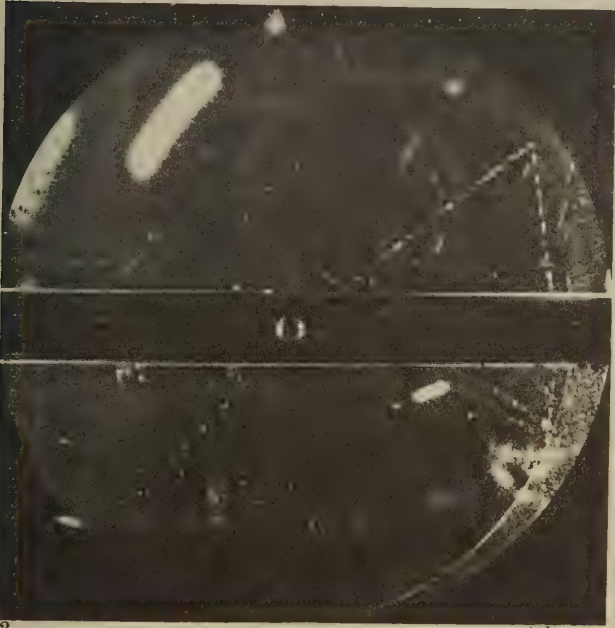
↙ 4 ↙ 5 ↙ 1

↓ 2 ↓ 3

PLATE XXXVI.



2 1
PLATE XXXVII.



2 1
PLATE XXXVIII.

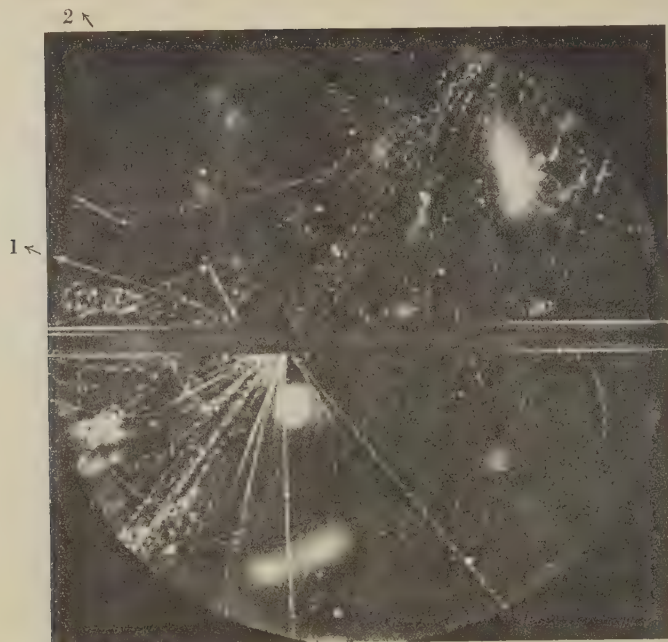


PLATE XXXIX.



PLATE XL.

PLATE XXXVI.

The decay-in-flight of the negative secondary of a V_1^0 -particle.

This photograph is described in § 4, section (i.); the data for the negative secondary particle are given in Table III. Tracks (4) and (5) form a second V -track; the measured momenta are approximately $+3 \times 10^8$ and -7×10^8 eV./c. and the angle of the fork is about 10° . This fork was probably produced by a V_2^0 -particle.

PLATE XXXVII.

A nuclear interaction produced by the negative secondary of a V^0 -particle.

This photograph is described in § 4, section (iii.). The negative secondary particle (2) had a momentum of about 3.5×10^8 eV./c. and interacted in the plate with the production of a slow proton. It is probable that the particle responsible for the interaction was a negative π -meson.

PLATE XXXVIII.

Two penetrating secondary particles.

This photograph is described in § 4, section (iii.). The positive particle (1) was scattered through 15° in the plate and the negative particle (2) has a momentum of 3.3×10^8 eV./c. It can be shown that both secondaries were probably π -mesons.

PLATE XXXIX.

The decay of a V_2^0 -particle (Catalogue no. 66).

The V^0 -particle was produced in a secondary nuclear interaction in the 7 mm. lead plate. The momentum of the positive secondary particle (1) was measured as 2.6×10^8 eV./c. and that of the negative secondary (2) as 1.3×10^8 eV./c. Both secondary tracks are approximately at minimum ionization and must have been due to mesons. The mass of the V_2^0 -particle is $(700 \pm 30)m_e$, assuming that the secondaries were π -mesons (cf. Table V.).

PLATE XL.

The decay of a high-energy V_2^0 -particle (Catalogue no. 53).

The fork consists of two high-energy tracks (1) and (2) at an angle of 12° . The measured momentum of the positive track is 1.5×10^9 eV./c. and that of the negative track (2) is 1.6×10^9 eV./c. For this event $\alpha = -0.03$ and $p_T = 1.66$ and it is concluded that the V^0 -particle probably decayed into two π -mesons (scheme (4)); the mass value of the V_2^0 -particle is $(841 \pm 60)m_e$ (cf. Table V.).

CXIV. *The Nuclear Scattering of Electrons and Positrons in Argon.*

By A. F. HOWATSON* and J. R. ATKINSON,
Natural Philosophy Department, Glasgow University†.

[Received June 14, 1951.]

ABSTRACT.

An automatic Wilson cloud chamber with specially constructed cameras was used to obtain data on the nuclear scattering in argon of electrons from indium 114 and positrons from copper 62. The tracks were analysed by the method of projected angles. The experimental angular scattering distribution was compared with calculated values based on Dirac's relativistic electron theory, the ratio expt/theory over the angular range 20° – 90° being 1.02 for electrons and 0.92 for positrons. Similar calculations based on the semi-classical Rutherford scattering formula gave for the positron case a ratio expt/theory of 0.79. This is regarded as evidence in favour of the Dirac theory which gives a smaller scattering cross-section for positrons than for electrons.

§ 1. INTRODUCTION.

NUMEROUS investigations have been made with the purpose of testing the theory of scattering of fast electrons by atomic nuclei. The experiments fall, in general, into two classes; in the first the scattering material is in the form of a thin foil and the scattered electrons are detected by ionization chambers or counters, and in the second the electrons are scattered in the gas of a Wilson cloud chamber.

Both experimental techniques present considerable difficulties, and much of the earlier work was inconclusive and inconsistent. However, recent investigations of the first type by Van de Graaff *et al.* (1946, 1947) and by Buechner *et al.* (1947) gave good agreement with the relativistic theory of electron scattering for the particular energies, angular range and scattering elements selected.

Randels, Chao and Crane (1940, 1945) have summarized the results obtained by the cloud chamber method prior to 1945, and reported an extensive investigation covering a number of gases and a wide range of energy. They found no evidence for the large discrepancies from the theoretical predictions reported by some earlier investigators.

The theoretical cross-section for the nuclear scattering of high energy electrons has been derived by Mott (1929) in the form of a conditionally convergent infinite series. The first approximation yields the "Mott formula" which is applicable only to elements of low atomic number.

* Now at the Glasgow Royal Cancer Hospital Research Department.

† Communicated by the Authors.

Bartlett and Watson (1940) have summed the series for the case of mercury ($Z=80$), and McKinley and Feshbach (1948) have extended the calculation to obtain the cross-section for scattering of fast electrons by all elements to an accuracy of 1 per cent. The results are given in terms of the ratio of the calculated scattering cross-section to the Rutherford cross-section (modified for the variation of mass with energy), namely :—

$$\sigma = \left(\frac{Ze^2}{2m_0c^2} \right)^2 \frac{1-\beta^2}{\beta^4} \operatorname{cosec}^4 \frac{\theta}{2} \dots \dots \dots (1)$$

The calculation shows that for elements of high atomic number a large departure from the Rutherford scattering cross-section is predicted.

The scattering of fast positrons by nuclei is also of considerable interest since the theoretical angular distribution is modified appreciably by the change in sign of the Coulomb force, through the medium of the spin-orbital interaction. This results again in a departure from the Rutherford value which is quite different from that obtained for electrons. Following the procedure of Bartlett and Watson, Massey (1942) has calculated the cross-section for positron scattering by mercury nuclei for various energies. The calculated cross-section is lower than the Rutherford value over the whole angular range. The difference is still appreciable, even for elements of low atomic number and should be experimentally demonstrable. It may be noted that the method used by Van de Graaff *et al.* is not applicable to the positron case, since it involved the use of an artificially accelerated beam of electrons.

No experiments on the single nuclear scattering of positrons appear to have been reported at the time of writing, though Fowler and Oppenheimer (1938) and also Lasich (1948) obtained evidence for an excess of electron over positron scattering in lead and gold respectively, under conditions in which the scattering was multiple, merging into a single scattering "tail" at large angles.

The present paper reports the results of the analysis of 198 metres of electron and 163 metres of positron track obtained with a Wilson cloud chamber containing argon as the scattering element.

§ 2. EXPERIMENTAL PROCEDURE.

The cloud chamber method is particularly suitable for studying scattering phenomena in that a record is obtained of each individual event, and no difficulties occur such as ensuring conditions of single scattering and eliminating stray electrons which may arise from X-rays or by reflection from the walls of the vessel. Moreover, electron-nuclear and electron-electron collisions can easily be distinguished, and the energy before and after collision can be determined by measuring the curvature of the track in a known magnetic field. The main disadvantage lies in the difficulty of accumulating sufficient data to provide results of statistical reliability.

In undertaking the present investigation, it was decided (a) to design a cloud chamber and camera system which would be capable of automatically recording a large track length without sacrificing the high quality of track photography which is necessary for accurate work, and (b) to employ a method of analysis which would ensure an accurate comparison with theory without entailing a prohibitive amount of labour.

The cloud chamber was of the moving rubber diaphragm type, 30 cm. in diameter by 6.5 cm. deep. It was illuminated by a single Philips, xenon-filled discharge lamp which dissipated in each flash about 500 joules. The illuminated region of the chamber was restricted to a depth of 2.5 cm. by means of masks placed between the lamp and chamber.

The cameras, which were specially designed and constructed for use in this type of work, were entirely automatic. The shutter was operated by a solenoid and plunger, and the film was wound on one frame after each exposure by an electric motor activated by a cam and microswitch incorporated in the camera. The cameras were mounted on a brass framework which fitted on to the upper ring of the cloud chamber; the axis of one was vertical and the other had its axis inclined at 20° to the vertical. The lenses were a matched pair of 80 mm. focal length, f/4.5 Taylor-Taylor-Hobson "Ental" enlarging lenses. Each camera could carry in a special cassette 100 feet of 60 mm. recording film. The film was, however, supplied in 25-foot lengths, covering about 150 exposures, a convenient number for a normal run of the apparatus. The film was held flat in the position of exposure by a spring-loaded glass pressure plate. A circular hole in the back plate, covered during photography by a light-tight metal disc, allowed the insertion of a condensing lens system for use in the reprojection of tracks, described in a later section. The cloud chamber was mounted between a pair of large Helmholtz coils, each consisting of six flat coils of $\frac{1}{2}$ in. wide copper strip insulated by "Armite" paper and energized from the D.C. mains. The whole assembly comprising cloud chamber, cameras, magnet coils, vacuum reservoir and associated electrical circuits for operating the chamber release valve, lamp delay, camera shutter, etc., was mounted on a trolley. A second trolley carried the vacuum pump, and the condensers and charging unit for the discharge lamp.

The source of electrons was indium 114 prepared by neutron bombardment of a strip of indium metal in the Harwell pile. This isotope, which has an effective half-life of 48 days, proved a convenient and prolific source of electrons of energy up to 2 MeV. In order to achieve good collimation and some energy resolution of the electrons, and to avoid the presence in the chamber of clumps of ionization due to the low energy γ -rays emitted by the source, the latter was mounted on a brass block and placed between the poles of a resolving magnet. The magnet current and the position of the source were adjusted until a suitable number of

tracks appeared in the chamber per expansion. Lead blocks placed at suitable points between the source and the chamber provided any further screening required. A shutter operated by a solenoid via a relay which was "slugged" by a variable resistance to introduce a short time delay, prevented electrons from entering the chamber until the expansion was nearly complete, thus reducing the number of diffuse tracks in the photographs. The electrons entered the chamber through five portholes consisting of thin mica discs attached to brass rings which were waxed into holes drilled in the glass cylinder of the chamber.

The taking of photographs was entirely automatic, the whole process being initiated by pressing a button on the control panel. The sequence of events, with approximate times, was as follows :

1. Zero time : button pressed ; camera shutter opens.
2. 1/50 sec. : expansion completed ; source shutter opens.
3. 1/5 sec. : lamp flashes.
4. 1 sec. : camera shutter closes ; source shutter closes ; slow expansions start ; film winds on one frame.
5. 60 secs. : slow expansions completed.

After an interval of 40 seconds to allow temperature equilibrium to be reached, the cycle is repeated.

The selection of a suitable positron source presented some difficulty. Inspection of the table of radioactive isotopes shows that all those of suitable energy have such short half lives that irradiation in atomic piles is not practicable. It was decided therefore to use copper 62 which may be obtained by a γ - n reaction with the stable isotope copper 63, the threshold energy being about 10 MeV. The maximum energy of the positron is 2.6 MeV., but the half life is only 10.5 minutes. The source was prepared by irradiating five $\frac{1}{2}$ in. side, 1/16 in. thick copper squares for 20 minutes in the beam of the Glasgow University synchrotron. After irradiation, the squares were attached to an aluminium support and placed one in front of each of the chamber portholes. As the activity weakened the squares were brought nearer the chamber, and in this way a useful working life of 30-40 minutes was obtained per radiation.

§ 3. ANALYSIS OF TRACKS.

Since stereographic pairs of photographs were taken, it would have been possible to make measurements in three dimensions. It was decided, however, to employ the method of projected angles used by Randels, Chao and Crane, and further developed by O'Ceallaigh and MacCarthaigh (1944) and by Barker (1948). In this method the projections of the scattering angles and the curvatures in the plane of the chamber are measured, and the scattering formula is expressed in terms of the projections.

The projected form of the general scattering law has been derived by O'Ceallaigh and MacCarthaigh in the form of a double integral. This involves a parameter $\rho = \lambda_c/2a$, where $2a$ is the depth of the

illuminated part of the chamber and λ_c is the "critical" length. Deflected tracks shorter than λ_c are rejected since such tracks would not allow accurate measurement of scattering angles and curvatures. Barker, and O'Ceallaigh and MacCarthaigh show that if the minimum track length condition is applied, the ratio of the number of scattering events in a given angular range in the projected system to the three-dimensional value is lowest at small angles, projection having little effect at large angles. As interest usually centres on large angle scattering statistics, this is a distinct advantage as it effectively reduces the number of small angle scattering events. In addition, there is the enormous increase in the speed and accuracy of the measurement of angles and curvatures when only a single plane is involved. The second, oblique photograph is, nevertheless, most invaluable in clarifying cases where the association of crossing tracks is in doubt.

Barker (1948) and O'Ceallaigh (1950) have drawn up tables for various values of ρ from which may be calculated the number of scattering events predicted by theory in successive intervals of scattering angle. In the present work the illuminated depth was 2.5 cm. The minimum track length was taken to be 2.5 cm. also, so that the value of ρ was 1.

§ 4. MEASUREMENT OF TRACKS.

To make measurements on the tracks the developed films were returned to the cameras, which, together with the supporting framework, were removed from the cloud chamber and placed above a table. A full-size image of the vertical photograph was projected on to a sheet of paper on which was drawn a circle 23 cm. in diameter, the latter being adjusted to be concentric with the image of the chamber. Tracks which emerged from the windows and were of good quality were traced on the paper with a sharp pencil. The oblique image was also examined but the tracks were not traced, its function being, as previously mentioned, to clear up doubtful cases where tracks crossed.

Each track was numbered and the following information entered in a Table at the upper right-hand corner of the sheet.

1. The length l within the limits of the circle, determined by means of a map measurer.
2. The radius of curvature, obtained by finding the best fit of a series of curves consisting of arcs of concentric circles engraved on a celluloid sheet.
3. Nuclear deflections were noted and the angle of scattering measured where this exceeded a certain minimum value.

Deflections occurring outside the circle were ignored, though parts of tracks outside the circle were often used in measuring angles and curvatures relating to events occurring inside. The drawing of the circle serves the same purpose as the fixing of a minimum track length; viz., it ensures that no scattering events are recorded of which it is impossible by reason of the shortness of the scattered track to measure accurately

the curvature and the angle of scattering. The mean radius of curvature and hence the mean energy of the particles was obtained by forming the sum $\Sigma\{l/(H\rho)^2\}$ and equating it to $\Sigma l/(H\rho_{AV})^2$.

§ 5. DISCUSSION OF RESULTS.

The calculation of the scattering angle distribution in the projected system is based on the fact that the usual scattering formulæ can be expressed in the form :—

$$P(\theta) d\theta = Nf(Z, \beta)F(\theta)2\pi \sin \theta d\theta,$$

where $P(\theta)d\theta$ is the probability that a particle moving at speed βc through a medium containing N nuclei of atomic number Z per unit volume will be scattered once through an angle lying between θ and $\theta+d\theta$ in a path-length of 1 cm., and where $F(\theta)$ is of the form :—

$$\text{cosec}^4 \theta/2 + A \text{cosec}^3 \theta/2 + B \text{cosec}^2 \theta/2 + C \text{cosec} \theta/2$$

e. g. in Mott's formula :—

$$F(\theta) = \text{cosec}^4 \theta/2 - \beta^2 \text{cosec}^2 \theta/2 + \pi Z\alpha\beta(\text{cosec}^3 \theta/2 - \text{cosec} \theta/2) \quad .(2)$$

or, in the formula derived by McKinley and Feshbach :—

$$F(\theta) = \text{cosec}^4 \theta/2 - \beta^2 \text{cosec}^2 \theta/2 + \pi Z\alpha\beta(\text{cosec}^3 \theta/2 - \text{cosec}^2 \theta/2) \quad .(3)$$

The probability of scattering into the angular range ϕ to $\phi+d\phi$ where ϕ is the projection of θ in a plane perpendicular to the axis of the camera (y -axis) is (O'Ceallaigh and MacCarthaigh, 1944) :—

$$P(\phi)d\phi = \frac{2Nf(Z, \beta)}{a} \sec^2 \phi \int_{-a}^a dy \int_{\phi}^{\theta_M} \frac{F(\theta) \sin \theta}{\sqrt{(\sec^2 \theta - \sec^2 \phi)}} d\theta d\phi,$$

where
$$\cos \theta_M = \frac{\lambda_c \cos \phi}{\{\lambda_c^2 + (a \pm y)^2\}^{1/2}}.$$

Barker gives values of $P_n(\phi)/Nf(Z, \beta)$ corresponding to $\phi = 10^\circ, 20^\circ \dots 90^\circ$, for $F(\theta) = \text{cosec}^n \theta/2$ where $n = 1, 2, 3$ and 4 , and for values of $\rho = 0, 0.5, 1.0$ and 2.0 . From these figures, by graphical integration or otherwise, the integrated values over suitable angular ranges may be calculated. O'Ceallaigh (1950) presents similar Tables containing the integrated values calculated for the angular ranges 20° – 30° , 30° – 40° , etc., for a number of different values of ρ .

The number of scattering events observed, together with the number predicted from theory, in angular intervals of 10° in the range 20° – 90° are shown in Table I. The theoretical values are based on formula (3). The half integers occur because angles of $20^\circ, 30^\circ, 40^\circ$, etc., were assigned half to the lower and half to the upper interval.

The agreement with theory is excellent over the range 20° – 90° . The total number of scattering events predicted is 69.4, the observed number 70.5, giving a ratio of experiment/theory of 1.02. This is well within the

range of statistical fluctuations and experimental error. The distribution of number of events with scattering angle also agrees very well with theory. In particular, there is no indication of the excessive scattering between 25° and 55° , of which Randels, Chao and Crane claimed to have

TABLE I.

Scattering of electrons and positrons in argon ; comparison of experimental and theoretical results.

ELECTRONS			POSITRONS		
Energy Range (MeV.) 0.2—2.0			Energy Range (MeV.) 0.2—2.4		
Effective Energy (MeV.) 0.83			Effective Energy (MeV.) 0.7		
Angular Range	Expt.	Theory	Expt.	Theory (1)	Theory (2)
20° — 30°	49.5	44.9	41.5	52.8	47.1
30° — 40°	13.5	13.6	15.5	16.4	13.8
40° — 50°	3.0	5.6	3.5	6.7	5.3
50° — 60°	2.5	2.6	3.0	3.4	2.5
60° — 70°	1.0	1.4	1.0	2.0	1.3
70° — 80°	1.0	0.8	1.0	1.3	0.8
80° — 90°	0	0.5	0	0.7	0.4
20° — 90°	70.5	69.4	65.5	83.3	71.2

TABLE II.

Scattering of electrons in argon ; Randels, Chao and Crane (1945).

Angular Range	Energy Range 0.8—3.3 MeV.		Energy Range 3.3—9.3 MeV.	
	Effective Energy 2.4 MeV.		Effective Energy 4.6 MeV.	
	Expt.	Theory	Expt.	Theory
15° — 25°	30.0	30.3	52.0	32.2
25° — 35°	10.5	7.2	10.5	7.6
35° — 45°	5.0	2.7	4.5	2.8
45° — 55°	2.5	1.3	5.0	1.4
55° — 65°	1.0	0.7	1.0	0.7
65° — 75°	0	0.4	0	0.4
75° — 85°	1.0	0.2	0	0.2
85° — 90°	0	0.1	0	0.1
15° — 90°	50.0	42.9	73.0	45.4

obtained strong, though not conclusive, evidence from their observations over several gases. The results obtained for argon by Randels, Chao and Crane are shown for comparison in Table II. Table III. gives a summary of earlier results of Zuber (1938), Stepanowa (1937, 1939) and Bleuler (1942).

The assessment of experimental error is difficult, since the observer's judgment is necessarily involved to some extent in the selection and measurement of tracks. It cannot be too strongly emphasized that unless the quality of the tracks and of the track photography is of a high standard serious errors in interpretation are likely to occur. The standard appropriate to this type of work is such that individual background drops should be clearly distinguishable over the whole of the illuminated part of the cloud chamber. Since it is only within recent years that rare gas discharge lamps have been developed of sufficient output to allow the vertical photography of individual drops and thinly ionizing tracks over a large cloud chamber volume, it seems probable that the large discrepancies observed by some earlier workers are attributable to experimental difficulties in the photography, and consequent inaccuracies in the analysis of the tracks.

TABLE III.

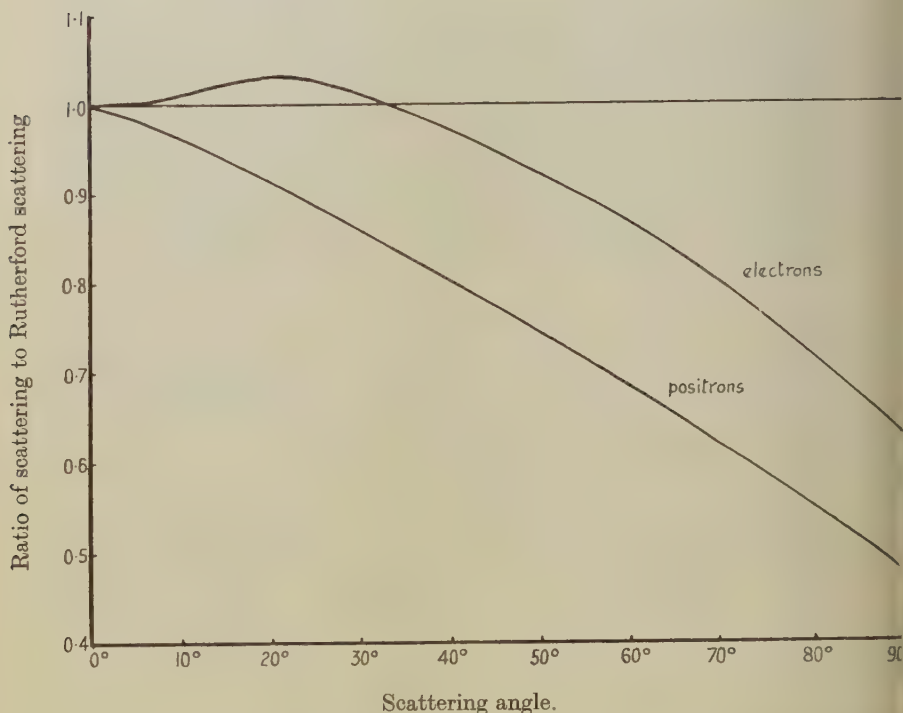
Scattering of electrons in argon ; summary of earlier measurements.

Energy Range (MeV.)	Angular Range	Track Length (metres)	Number of Deflections	<i>Expt.</i> Theory	Author	Date
1.7-2.4	30°-180°	350	48	0.75	Zuber	1938
0.2-1.1	20°-150°	103	308	1.0	Stepanowa	1939
1.5-3.0	20°-150°	130	84	2.5	Stepanowa	1939
0.2-3.0	20°-180°	708	153	1.5	Bleuler, Scherrer & Zunti.	1942

In the present experiments it was found that the agreement between theory and experiment did not extend below 20°. Scattering angles were measured down to 15°, but for a calculated value of 82.1 in the range 15°-20° the observed number was 49 : for positrons the corresponding figures were 97.8 and 55. This discrepancy is attributed to small angle scattering which is always present to some extent, and which makes the detection of clear-cut scattering events difficult at angles as small as 15° or so. The effect becomes rapidly less important as the scattering angle increases.

An important objective in scattering experiments is to distinguish between the relativistic scattering formula which is based on the Dirac electron theory and the semi-classical Rutherford formula. A comparison

of the two for the case of scattering of 1 MeV. electrons in argon (calculated for projected angles with $\rho=1$) is shown in the fig. The graph shows that for electrons the difference is too small in the significant angular range 20° – 60° to be detected by the present method. The corresponding curve for positrons shows, however, that the difference is much larger, being of the order of 20 per cent in the range 20° – 60° . It is feasible therefore to attempt to distinguish experimentally between the two theoretical predictions, even with a scattering element of low atomic number such as argon.



1 MeV. electrons and positrons: calculated ratio of scattering to Rutherford scattering (projected angles, $\rho=1$) in Argon.

The experimental angular distribution for positron scattering was compared with the calculated values based on (1) the Rutherford formula with relativistic mass (R), and (2) the formula derived on the assumption that the positron is a positively charged Dirac particle. This may be written:—

$$R\{1 - \beta^2 \sin^2 \theta/2 - \pi\alpha\beta Z(\sin \theta/2 - \sin^2 \theta/2)\},$$

and differs from the corresponding formula for electrons only in the change in sign of the third term. These results are also shown in Table I. The ratio experiment/theory in the angular range 20° – 90° is for case (1) 0.79; for case (2) 0.92.

The results obtained under similar experimental conditions for electron scattering in argon provide a good basis for assessing the significance of the above figures. The authors consider that the first value is outside and the second inside the limits of error appropriate to the conditions of measurement, which are estimated to be about ± 10 per cent and that the experiments therefore provide evidence in favour of the relativistic theory of scattering of positrons.

CONCLUSIONS.

The cross-section for the nuclear scattering in argon of high energy electrons over the whole of the angular range 20° – 90° agrees with theoretical predictions, but the experiments are not sufficiently sensitive to distinguish between different formulae. The corresponding formulae for positron scattering are such that it is possible to distinguish experimentally between predictions based on semi-classical theory which gives the same scattering cross-section as for electrons, and on the relativistic theory of Dirac which gives a smaller cross-section. The experimental results are in agreement with the latter theory. It follows that the cross-section for positron scattering is in these experiments shown to be significantly smaller than the cross-section for electron scattering.

ACKNOWLEDGMENTS.

The authors wish to thank Professor P. I. Dee and Professor J. C. Gunn for many helpful discussions, and acknowledge their indebtedness to Mr. P. R. Price for his part in the design and construction of the equipment, and for assistance in the analysis of the tracks.

REFERENCES.

- BARKER, F. C., 1948, *J. Sci. Inst.*, **25**, 65.
 BARTLETT, J. H., and WATSON, R. E., 1940, *Proc. Amer. Acad. Arts and Sci.*, **74**, 53.
 BLEULER, E., SCHERRER, P., and ZUNTI, W., 1942, *Phys. Rev.*, **61**, 95.
 BUECHNER, W. W., GRAAFF, R. J. VAN DE, SPERDUTO, A., BURRHILL, E. A., Jr., and FESHBACH, H., 1947, *Phys. Rev.*, **72**, 678.
 FOWLER, W. A., and OPPENHEIMER, J., 1938, *Phys. Rev.*, **54**, 320.
 GRAAFF, R. J. VAN DE, BUECHNER, W. W., and FESHBACH, H., 1946, *Phys. Rev.*, **69**, 452; 1947, *Ibid.*, **71**, 142A.
 LASICH, W. B., 1948, *Aus. J. Sci. Res. A.*, **1**, 249.
 MCKINLEY, W. A., and FESHBACH, H., 1948, *Phys. Rev.*, **74**, 1759.
 MASSEY, H. S. W., 1942, *Proc. Roy. Soc. A.*, **181**, 4.
 MOTT, N. F., 1929, *Proc. Roy. Soc. A.*, **124**, 426; *Ibid.*, **126**, 259.
 O'CEALLAIGH, C., 1950, *Proc. Roy. Irish Acad. A.*, **53**, 133.
 O'CEALLAIGH, C., and MACCARTHAIGH, M. D., 1944, *Proc. Roy. Irish Acad. A.*, **50**, 13.
 RANDELS, R. B., CHAO, K. T., and CRANE, H. R., 1940, *Phys. Rev.*, **58**, 201; 1945, *Ibid.*, **68**, 64.
 STEPANOWA, E. G., 1937, *Phys. Z. Sowjet.*, **12**, 550; 1939, *J.P., U.S.S.R.*, **1**, 204.
 ZUBER, K., 1938, *Helv. Physica Acta*, **11**, 370.

CXV. *Micro-slip in Metal Crystals.*

By A. F. BROWN and R. W. K. HONEYCOMBE,
Cavendish Laboratory, Cambridge*.

[Received June 14, 1951.]

[Plate XLI.]

SUMMARY.

Aluminium crystals, the surfaces of which have been prepared for examination solely by electropolishing, show extremely fine slip bands (displacements of 150 Å. or less) after small plastic deformations of about 0.5–2 per cent. The more familiar coarse bands involving displacements of the order of 5000 Å. appear subsequently. However, if the metal surface is mechanically polished prior to electrolytic polishing, the coarse bands occur in the earliest stages of deformation.

Two possibilities are considered: firstly that the micro-slip is a phenomenon restricted to the vicinity of the surface and is highly dependent on the nature of it. Secondly it is suggested that the fine slip is typical of initial slip processes within the metal, but becomes almost entirely suppressed as the deformation proceeds.

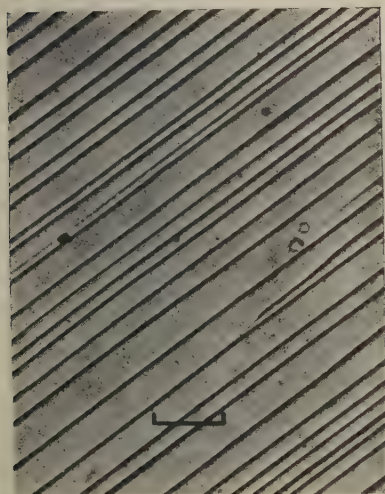
It has become accepted that the appearance of slip bands on the surface of a plastically deformed metal is evidence that the deformation is not homogeneous, but is concentrated on relatively few atomic planes. At small strains and at room temperature slip band spacings are usually of the order of several microns.

During some recent work on the deformation of aluminium single crystals it was noticed that, on specimens which had been polished purely electrolytically, with no preliminary mechanical preparation, the slip band spacing after small strains was much less than usual. Most of the bands were diffuse and the finer ones could not be resolved by the light microscope. Specimens which had been mechanically polished, however, showed the usual sharp, widely spaced slip bands. This suggested that the condition of the metal surface was responsible for the difference, so a detailed study has been made of the effect of surface treatment on the appearance of slip bands produced by subsequent deformation.

In a typical experiment, one face of a large, flat single crystal of 99.99 per cent aluminium was rubbed along its length and for half its width with coarse 150 carborundum paper and then smoothed off with successively finer papers. The other half of the crystal was not abraded and the surface remained the same as when the crystal was formed. The whole

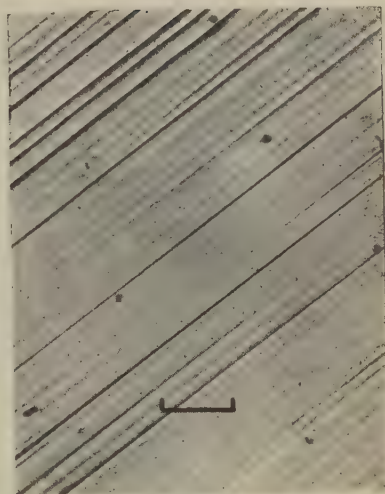
* Communicated by Sir Lawrence Bragg, F.R.S.

Fig. 1.



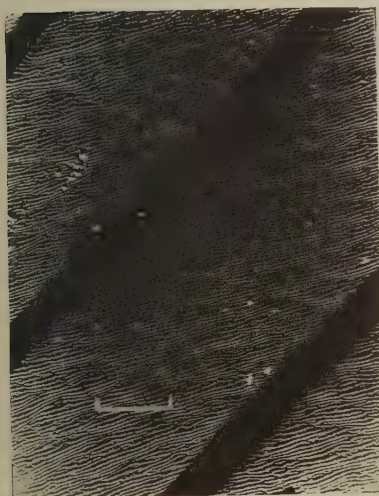
Slip bands in the abraded zone of a crystal after 5% extension. Optical micrograph $\times 500$.

Fig. 2.



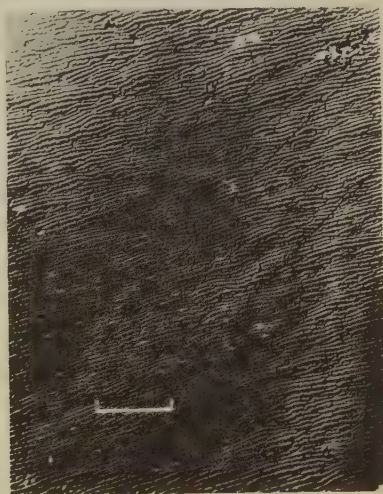
Slip bands in the un-abraded zone of a crystal after 5% extension. Optical micrograph $\times 500$.

Fig. 3.



Electron micrograph corresponding to fig. 1. $\times 10,000$.

Fig. 4.



Electron micrograph corresponding to fig. 2. $\times 10,000$.



crystal was then electrolytically polished in the De Sy-Haemers bath (20 per cent by volume perchloric acid and 80 per cent absolute ethyl alcohol) until about 60μ of metal had been removed. At this stage polishing scratches were no longer visible. The crystal was then deformed 0.7 per cent in tension and examined microscopically. In the zone which had been mechanically polished the slip bands were sharp and widely spaced (20μ apart). There were no fine bands. On the other hand, the zone which had been polished purely electrolytically showed a very large number of closely spaced diffuse markings parallel to the coarse bands in the other zone. The spacing was not measurable in the light microscope. After further deformation to 3.3 per cent extension, the mechanically polished zone showed sharp slip bands about 10μ apart, while in the zone which had not been mechanically worked there was a high density of small, diffuse slip markings together with a few more sharply defined bands parallel to them. On further deformation the number of slip bands in the mechanically polished zone continually increased. In the other zone, the fine markings predominated, but as the deformation proceeded the more sharply defined bands increased in number. The appearance of the two zones after 5 per cent extension is shown in figs. 1 and 2 (Pl. XLI.).

After 6.8 per cent extension the crystal was repolished electrolytically to remove all traces of slip bands. When the straining was resumed the new slip bands appearing were mainly of the coarse, sharp type in both zones. Thus, tensile deformation of the crystal produces eventually the same effect as prior mechanical polishing: the very small diffuse slip bands are suppressed and the more familiar widely spaced bands alone appear. Throughout the experiment, the appearance of the underside of the mechanically polished zone of the crystal, which had been electropolished only, was the same as that of the non-mechanically polished zone of the upper surface. Thus the effect of mechanical polishing did not penetrate to the underside of the crystal. The depth of penetration depended on the severity of the mechanical polishing. This was investigated by removal or known thicknesses of metal by electropolishing, followed by re-straining and examination of the new slip bands, the total strain throughout remaining small. The effects of the rubbing with 150 carborundum paper were still very marked after 70μ had been removed and X-ray micrographs taken at this stage showed that the fresh surface was considerably distorted. After 100μ had been removed the effects of the 150 carborundum still persisted but were less obvious. The coarse slip lines could be produced by rubbing the surface with the finest polishing alumina but then the effects did not penetrate more than a few microns into the crystal. Annealing crystals for an hour at 600°C . completely removed the effects of any surface polishing treatment.

Examination of the abraded and un-abraded zones by means of the electron microscope gave the results shown in figs. 3 and 4 (Pl. XLI.) respectively. These are from the same specimen and at the same strain as the light micrographs in figs 1 and 2. The replica technique used was

as follows: methyl-methacrylate monomer was polymerized on the surface of the specimen and, when hard, stripped off to form an intermediate replica. This was then shadowed with gold palladium alloy at a low angle to the surface and in the direction *down* the slip steps. By this means each slip step on the surface is revealed by its shadow, and from measurements of this the height of the step and the slip distance can be calculated. For the abraded zone the slip distance is about 5000 Å. per band, a figure in good agreement with that calculated from the measured strain and the observed density of slip bands. In the case of the un-abraded zone, slip bands can be clearly measured with slip distances less than 200 Å. However, in this case it appears that the bands large enough to be observed cannot account for the whole strain: there must therefore be some still smaller bands, perhaps with slip distances down to atomic dimensions.

Figs. 3 and 4 are crossed by a furrow-like structure with a mean spacing of about 650 Å. This structure is developed in the electrolytic polishing bath and it has been suggested that it is the traces of planes making up a surface of minimum energy.

Preliminary experiments have shown that micro-slip is also observed on un-abraded surfaces of copper, lead and gold.

The problem set by the above results is: which type of slip band is initially operating in the interior of the metal? If, as has hitherto been assumed, slip takes place by large amounts on isolated planes, then the micro-slip must be a purely surface phenomenon. In order to be visible on the surface, a slip process approaching from below must either create a new piece of surface by breaking through, or it must stretch the existing surface. In either case energy is required corresponding to the increase of surface energy, so any condition which reduces surface energy makes it easier for slip to appear on the surface. Severe working of the surface produces a high concentration of dislocations there. Thus the surface energy is reduced (since less work is required to remove atoms from a disordered surface than from a perfect one) and coarse slip results. At an undisturbed surface, where the surface energy has its full normal value, a slip process on one slip plane and involving several hundred atoms, may gain energy by dissociating near the surface into a number of micro-slips covering a relatively wide area. Some support for this view is given by the observation that the fine slip bands, as seen in the electron microscope, usually form clusters separated by regions apparently free from slip.

On the other hand, it is possible that the fine slip bands, which are always observed on the surface of specimens free from previous mechanical distortion, are typical of initial slip processes within the metal. Since these fine bands have spacings much closer to atomic dimensions than the slip bands observed by previous workers, the difficulty of explaining why slip should be nucleated in very large amounts on isolated planes is partly removed. Instead, it is necessary to consider how this micro-slip is blocked, for it has been shown above that blocking occurs immediately, as a result

of deformation of the surface, or gradually, as a result of overall tensile deformation of the specimen. The most probable cause of the latter is that dislocations on planes as closely spaced as the micro-slip interact strongly, preventing further movement except on a relatively small number of slip planes. This mechanism can also account for the high rate of strain hardening in the early stages of plastic deformation when the coarse slip bands which are usually observed, are too far apart to interact. Abrasion of the surface also results in the high concentration of dislocations required to stop micro-slip. Annealing the specimen at a high temperature causes the dislocations to migrate and results in the re-appearance of micro-slip.

An alternative source of the blocking of micro-slip is the oxide film which is known to be particularly coherent in aluminium. Very small slip processes could appear on the surface as diffuse bulges without breaking the film, but, as the deformation increased the resistance of the film would be overcome occasionally, thus giving the opportunity for a coarse slip band to develop and appear as a sharp step on the surface. With a mechanically worked surface, the oxide is probably less coherent and the slip processes would then have less difficulty in penetrating it. If this mechanism exists, then the appearance of micro-slip should be strongly dependent on crystal orientation: a small slip process approaching a surface normally is much more likely to break a surface film than one approaching obliquely. Thus, when the slip planes are almost normal to the surface, coarse slip should be observed at an earlier stage of deformation than when the slip planes are obliquely inclined to the surface. Some support for this is given by the study of deformed polycrystals. However, while an oxide film may assist in blocking the micro-slip in aluminium, it cannot do so in gold.

Examination of the surface alone will not decide whether initially metals deform entirely by micro-slip or not. A sensitive technique is needed which is capable of revealing very fine slip bands in the interior of deformed crystals.

This work is being carried out during the tenure of an I.C.I. Fellowship (A.F.B.) and the Armourers and Brasiers' Research Fellowship (R.H.), which we gratefully acknowledge.

CXVI. *Some General Theorems for Non-Linear Systems Possessing Resistance.*

By WILLIAM MILLAR,
Atomic Energy Research Establishment, Harwell*.

[Revised MS. received June 8, 1951.]

SUMMARY.

This paper introduces some ideas and general theorems pertaining to non-linear or mechanical systems. Thus in the case of a resistive network, the dissipation is divided into two parts—the “content” and “co-content”—which are duals of each other. The dissipation itself has stationary properties in *linear* but not (in general) in *non-linear* networks, but it can be shown that the “content” and “co-content” have stationary and additive properties in the non-linear case. The idea of “content” is extended to reactive systems, and it is shown that the total content of any system in motion is an invariant.

This paper is intended as a companion to the paper by E. C. Cherry.

§ 1. INTRODUCTION.

THE mathematical analysis of non-linear systems is difficult, and often tends to obscure essential behaviour. An attempt is made in this and a companion paper to present some new concepts and general theorems which might assist in forming a more physical approach to the analysis and synthesis of systems possessing either incidental or intentional non-linearities. The arguments are presented in terms of electrical networks, but the concepts are equally applicable to mechanical and electro-mechanical systems. The approach here is based upon the methods of generalized dynamics, which in essence is a way of obtaining the differential equations pertaining to a dynamical system. Much work has already been done on the solution of non-linear differential equations; here, however, attention is concentrated, not on mathematical methods of solution, but rather on examining the fundamental aspects of the subject and trying to extract useful physical concepts from them.

One of the first theorems relating to *linear* networks was due to Maxwell (1873), the “Minimum Heat Theorem”. (See § 2.) It can be shown that the theorem is not applicable, as it stands, to non-linear networks; the heat generated is not in general stationary, but a related quantity called the “content”, which is proportional to the heat in the linear case, is shown in § 4 to have a stationary property. A summation theorem is also given, on the “content” of two-terminal networks. In § 6 the idea of “content” is extended to reactive networks, where it is shown to be an invariant of the motion of such systems.

* Communicated by the Author.

Maxwell's theorem applies only to linear networks, and it can in fact be shown, by the methods of § 4, that $(W - 2P_v)$ is *not* in general stationary if any of the elements are non-linear. The search for some other quantity which does have the stationary property forms the starting-point here.

§ 3. DEFINITIONS RELATING TO NON-LINEAR NETWORKS.

3.1. *Elements*.—A very general type of 2-terminal element may be specified by a relation of the form

$$f\left(i, \frac{di}{dt}, \frac{d^2i}{dt^2}, \dots, v, \frac{dv}{dt}, \frac{d^2v}{dt^2}, \dots, t\right) = 0, \quad \dots \quad (7)$$

where i and v are the current and voltage at the terminals. If the time-derivatives are absent the element is said to be *non-reactive*, and is then specified by a relation of the form $f(i, v, t) = 0$. Problems in which all the elements are non-reactive can be solved *at any instant* in terms of *time-invariant* non-reactive elements specified by a relation of the form $f(i, v) = 0$. Discussion of non-reactive elements is therefore confined to this latter case, in which elements are specified at all times by the single characteristic, $f(i, v) = 0$. Such an element is said to be "*passive*" if the characteristic cuts the i - v axes nowhere except at the origin; otherwise it is said to be "*active*". It is sometimes desirable to distinguish between "*simple*" and "*non-simple*" elements, according as to whether or not the current and voltage are everywhere single-valued functions of each other.

3.2. *Generators*.—A "*generator*" is a particular form of active non-reactive element in which *either* the current *or* the voltage is absent from the defining function $f(i, v)$. Thus generators are either of the "constant voltage" or "constant current" type. In what follows, expressions such as "all the elements of the network" will include the generators unless stated otherwise.

3.3. *Networks*.—A "*passive non-reactive network*" is defined to be one which contains only passive non-reactive elements. It is assumed that if two vertices of such a network are chosen as terminals, the whole network between the terminals may be regarded as an element with its own passive non-reactive characteristic.

3.3.1. Although Thévenin's network theorem is well known, certain points which have a bearing on this discussion are worth clarifying. This useful theorem really consists of two parts; as usually proved they are (for non-reactive networks):

(i.) A 2-terminal linear active resistive network can always be replaced by a new 2-terminal network consisting only of a constant-voltage generator E_1 , in series with a linear resistor R_1 , so far as any *linear* element outside the terminals is concerned.

(ii.) Further, E_1 is given by the open-circuit voltage at the terminals of the original network, and R_1 is given by the resistance at the terminals of the original network when the voltage generators are short-circuited and the current generators removed.

If the *load* is non-linear, the theorem may be shown still to apply, although the usual proof for the linear case is no longer valid. If the *network* is non-linear the theorem of course does not apply; all that can now be said in place of part (i.) of the theorem is that, for external purposes, the 2-terminal network may be replaced by a single active non-linear element (the "equivalent" element).

3.4. "Content" and "co-content".—Suppose that a current i_1 is passing through an element specified by the characteristic $f(i, v)=0$, such as that shown in fig. 1 (a). The voltage across it will then be v_1 , where $f(i_1, v_1)=0$. We now define a quantity G , which we shall call the "content" of the element when it is in the particular state (i_1, v_1) , by the integral

$$G = \int_0^{i_1} v \, di.$$

The content has the dimensions of power. The dual quantity, obtained by interchanging current and voltage everywhere, we shall call the "co-content", denoted by J . Thus

$$J = \int_0^{v_1} i \, dv.$$

The integrals G and J are shown as areas on fig. 1 (a). If the element is passive (fig. 1 b), G and J are respectively the areas below and above the characteristic curve. If the total dissipation in the passive element is W , it can be seen from fig. 1 (b) that

$$W = i_1 v_1 = G + J. \quad (8)$$

A *linear passive* element is a special kind of passive element in which $f(i, v) \equiv Ri - v$, where R is a property (the "resistance") of the element. In this case, $G = J = W/2$ for all values of current and voltage. Fig. 1 (c) shows the characteristic of an element which is a *constant-voltage* generator. In this case, $G = -P_v$, where P_v is the power supplied by the generator; no meaning can be attached to J . Similarly, fig. 1 (d) shows a *constant-current* characteristic. Here $J = -P_i$, while no meaning can be attached to G . If the elements are *non-simple*, G and J must be interpreted with care.

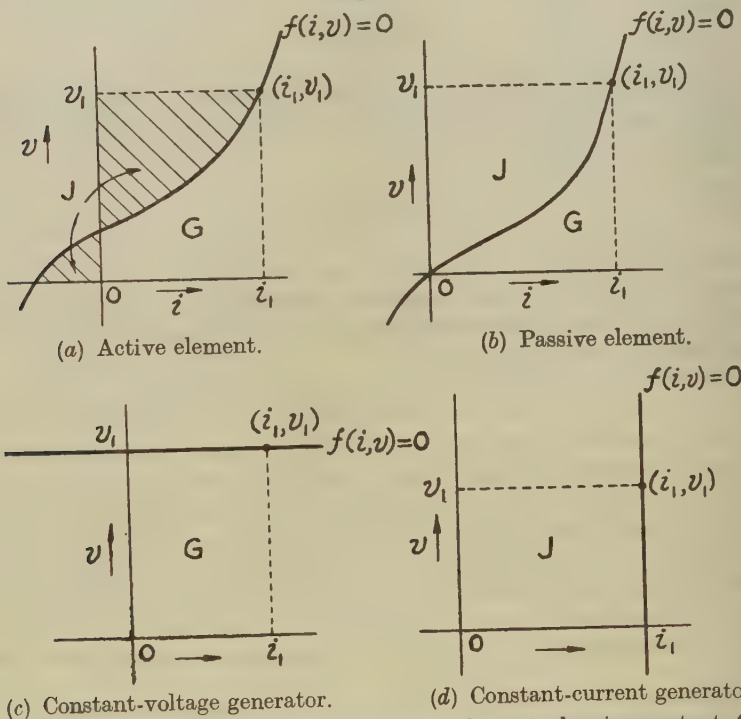
§ 4. THEOREMS OF "CONTENT" AND "CO-CONTENT".

4.1. In this section four network theorems are given. Theorems III. and IV. are the duals of I. and II., and will be stated without proof since they follow from the Principle of Duality. These theorems apply at every instant of time.

Theorem I. } The co-content } of a two-terminal network, regarded as
 III. } content } an element between the terminals, is the sum of the co-contents } of the
 constituent elements.

Theorem II. } If in an active non-reactive network the sum $\frac{G}{J}$ } of the
 IV. } contents } of all the constituent elements is expressed in terms of the
 defining number of generalized current } coordinates in the network, subject
 only to the restrictions of Kirchhoff's current } law, then $\frac{G}{J}$ } is stationary for
 the actual distribution of currents } voltages }.

Fig. 1.



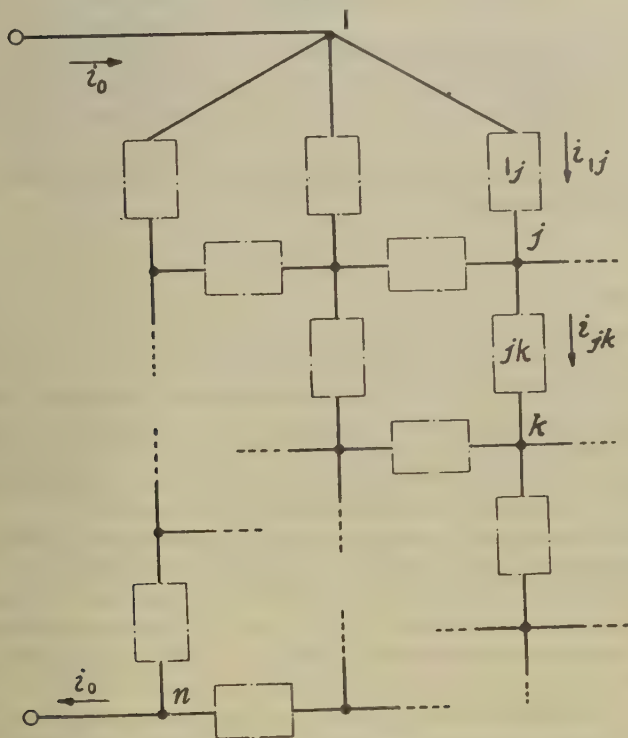
Typical characteristics of various kinds of element, showing content, G , and co-content, J , as areas.

4.2. To prove these theorems, Kirchhoff's two laws are used. For Theorem I., consider a network such as that shown in fig. 2, in which each branch is a non-reactive element. These branches meet in $(n+1)$ vertices,

numbered $0, 1, 2, \dots, j, k, \dots, n$. Take the vertices 0 and n as terminals, and let a current i_0 be flowing in at vertex 0 and out at vertex n . Let the resulting voltage at vertex j be v_j . (This use of "vertex voltages" automatically incorporates Kirchhoff's voltage law in the proof.) Without loss of generality, we may put $v_n=0$. Also let the resulting current in branch jk , measured from vertex j to vertex k , be i_{jk} . Now suppose that i_0 is increased slightly by an amount Δi_0 . All the branch currents will then change by an amount Δi_{jk} , and the vertex voltages by an amount Δv_j . It follows from Kirchhoff's current law that

$$\sum_{k=0}^n \Delta i_{jk} = \begin{cases} 0, & j \neq 0, j \neq n, \\ \Delta i_0, & j=0, \\ -\Delta i_0, & j=n. \end{cases} \dots \dots (9)$$

Fig. 2.

A typical network, showing vertices j, k and branch jk .

The change ΔG_{jk} in the content of each element is given, from Taylor's theorem, by

$$\begin{aligned} \Delta G_{jk} &= (v_j - v_k) \Delta i_{jk} + \frac{1}{2} \Delta i_{jk} (\Delta v_j - \Delta v_k) + \dots \\ &= (v_j - v_k) \Delta i_{jk}, \text{ to first order.} \end{aligned}$$

(The adjacent current values can only obtain if Kirchhoff's voltage law is violated, and hence cannot themselves be also actual values.) Let the variation in the content of each element be ΔG_{jk} , and in the sum of all the contents be ΔG .

We have

$$2\Delta G = \sum_j \sum_k \Delta G_{jk} \\ = \sum_j \sum_k (v_j - v_k) \Delta i_{jk}, \text{ to the first order, and hence, by the}$$

same reasoning as used in the proof of Theorem I,

$$G = \sum_j \left[v_j \sum_k \Delta i_{jk} \right];$$

whence

$$\Delta G = 0, \text{ from (13).}$$

This proves the theorem.

4.4. It should be noted that *either* Theorem II. or Theorem IV. is sufficient to determine all the currents and voltages in a network. This is done by using the equations corresponding to (5) and (6) in § 2. They are

$$\frac{\partial G}{\partial i_r} = 0 \quad (14)$$

and

$$\frac{\partial J}{\partial v_j} = 0, \quad (15)$$

where $r=1, 2, \dots, m$ and $j=1, 2, \dots, n$, for a network of m meshes and ($n=1$) vertices. The expressions in (14) and (15) are written as *partial derivatives* with respect to *independent generalized coordinates*, such as, for example, mesh currents or vertex voltages. (In computing the number $\left. \begin{smallmatrix} m \\ n \end{smallmatrix} \right\}$

of generalized $\left. \begin{smallmatrix} \text{current} \\ \text{voltage} \end{smallmatrix} \right\}$ coordinates, constant $\left. \begin{smallmatrix} \text{current} \\ \text{voltage} \end{smallmatrix} \right\}$ generators, if any, are not counted as branches, but they appear as making contributions of the branch $\left. \begin{smallmatrix} \text{currents} \\ \text{voltages} \end{smallmatrix} \right\}$ when the latter are expressed in terms of the generalized coordinates.)

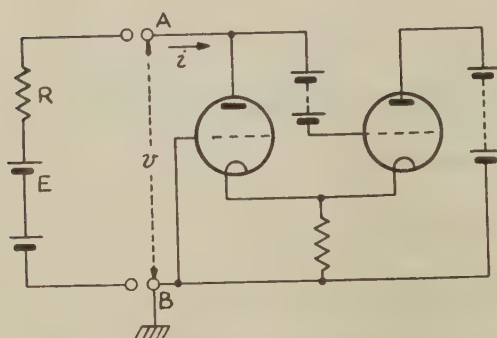
An example of the case $n=1$ is given in the next section.

§ 5. A SIMPLE PRACTICAL EXAMPLE OF THEOREM IV.

This section illustrates the rather trivial one-variable case of Theorem IV. Consider the "scale-of-two" circuit, whose essentials are shown in fig. 3 (a). The right-hand portion of this circuit can be treated as a passive element, which may be shown to have the characteristic given by the full line in the *upper* part of fig. 4. If now the two halves of the circuit are connected together, the voltage across the right-hand

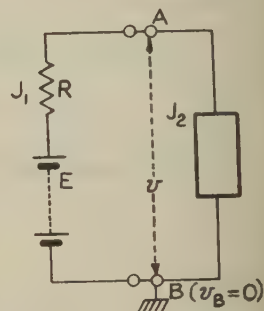
element will take up one of the "actual values" consistent with Kirchhoff's two laws. There are three such values, as may be seen by drawing the "load-line" for R , shown dotted in fig. 4. (The question

Fig. 3.



(a)

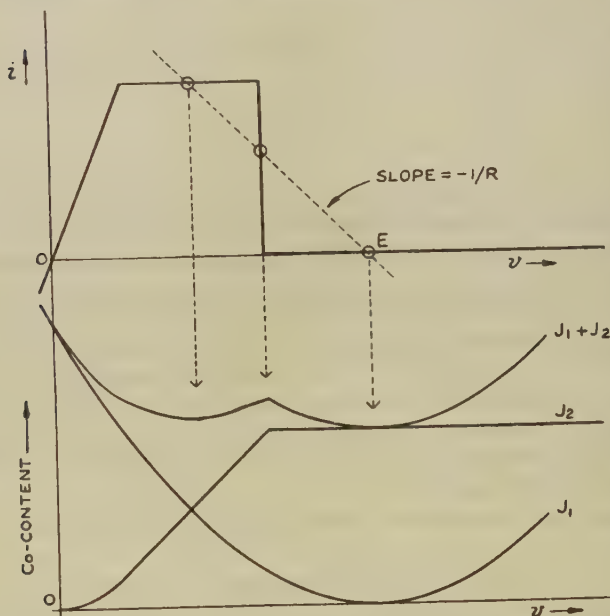
Essentials of "scale-of-two" circuit.



(b)

Schematic of fig. 3 (a).

Fig. 4.



Co-contents J_1 and J_2 of the elements in fig. 3 (b), plotted as a function of the voltage variable v . The sum $(J_1 + J_2)$ is also shown.

of stability is not discussed here since it involves times; in a physical circuit, the stability of each of these three positions depends upon reactive elements inevitably present.) Now consider the network to be

drawn schematically as in fig. 3 (b). This is a two-element passive network fed by a voltage generator; it has only one degree of freedom for voltages, and so, taking the voltage at B as zero, the voltage v at A may be chosen as variable. If, without using Kirchhoff's current law, the co-contents J_1 and J_2 are plotted as functions of v , the curves shown in the lower half of fig. 4 are obtained. Also shown on the same figure is J , which is the sum of J_1 and J_2 . It will be seen that J has stationary values at, and only at, the "actual values" of v .

§ 6. INVARIANTS OF THE MOTION FOR GENERAL CIRCUITS INCLUDING REACTANCE.

Consider now a network consisting of general elements of the type defined by equation (7), but with t not appearing explicitly in the defining function f . Suppose that a complete solution has been obtained for all the currents and voltages in the network. Then, for each element, an i - v diagram may be drawn; this diagram is not in general a characteristic of the element, but represents a trajectory in a type of so-called "phase space". The *change in content* of the element in going from the position (i_1, v_1) to the position (i_2, v_2) may be defined by the integral

$$G_2 - G_1 = \int_{i_1}^{i_2} v di \quad . \quad . \quad . \quad . \quad . \quad (16)$$

and similarly

$$J_2 - J_1 = \int_{v_1}^{v_2} i dv \quad . \quad . \quad . \quad . \quad . \quad (17)$$

We are interested here in studying only the *change* in content as the currents alter with time, so we may simply talk of the "content", G , without concerning ourselves with the original state to which it is referred. Now Theorem II. as stated applies only to non-reactive elements, but there is nothing in the argument to exclude reactive elements, since the theorem depends only upon Kirchhoff's laws. If then we write G or J for the *total* content or co-content of the network (*i. e.* the sum of all the G_{jk} 's or J_{jk} 's), including that of any generators, we have from (14) and (15)

$$\frac{\partial G}{\partial i_r} = 0 \quad . \quad . \quad . \quad . \quad . \quad (18)$$

and

$$\frac{\partial J}{\partial v_j} = 0, \quad . \quad . \quad . \quad . \quad . \quad (19)$$

where $r=1, 2, \dots, m$, and $j=1, 2, \dots, n$. The *total* time-derivatives of G and J are given by

$$\frac{dG}{dt} = \frac{\partial G}{\partial t} + \frac{\partial G}{\partial i_1} \cdot \frac{di_1}{dt} + \frac{\partial G}{\partial i_2} \cdot \frac{di_2}{dt} + \dots + \frac{\partial G}{\partial i_m} \cdot \frac{di_m}{dt} \quad . \quad (20)$$

and

$$\frac{dJ}{dt} = \frac{\partial J}{\partial t} + \frac{\partial J}{\partial v_1} \cdot \frac{dv_1}{dt} + \frac{\partial J}{\partial v_2} \cdot \frac{dv_2}{dt} + \dots + \frac{\partial J}{\partial v_n} \cdot \frac{dv_n}{dt} \quad . \quad (21)$$

Consider now any period of time during which all the voltage and current generators, if any, have steady voltages and currents respectively. During this time, t does not appear explicitly in the defining functions of any of the elements, and so $\frac{\partial G}{\partial t} = \frac{\partial J}{\partial t} = 0$. Hence from equations (18), (19), (20) and (21),

$$\frac{dG}{dt} = 0$$

and

$$\frac{dJ}{dt} = 0.$$

We can state this result as follows :—

Theorem V. *In any network of time-invariant elements (possibly including generators), the total content and the total co-content are invariants of the motion.* This theorem could, for instance, be applied to any circuit for all time following an impulsive change in a current or voltage generator, or in, say, a capacitor element. Note that it is very general, and applies even to dissipative systems in which the total energy is not invariant. The content and co-content, used in the above sense, are akin to *integral invariants*; information on these is given by Whittaker (1904).

ACKNOWLEDGMENTS.

The author is indebted to Mr. E. C. Cherry, of the Imperial College of Science, London, for much stimulating discussion and valuable help; and to the Director of the Atomic Energy Research Establishment, Harwell, for permission to publish this paper.

REFERENCES.

- MAXWELL, JAMES CLERK, 1873, *A Treatise on Electricity and Magnetism*, Vol. I. Third Edition, p. 407. (See also footnote by J. J. Thomson on p. 408.)
WHITTAKER, EDMUND, 1904, *Analytical Methods in Dynamics*, Chapter X.

CXVII. *Some General Theorems for Non-Linear Systems possessing Reactance.*

By COLIN CHERRY, M.Sc., A.M.I.E.E.,
Imperial College, London*.

[Received in revised form May 30, 1951.]

SUMMARY.

The theorems and concepts presented here are generally applicable to circuits of electrical or mechanical elements with non-linear characteristics. The quantity called the *co-energy* (the dual of energy) is shown to possess stationary properties (maximum or minimum) and superposition properties; this is sufficient to establish the concept of an "equivalent element" for any 2-terminal system of like elements (all-inductor, all-capacitor, all-springs, etc.). The unfamiliar "rectangle representation" of a circuit of linear resistors is explained and extended to the non-linear case, including reactive elements.

It is shown that the equations of motion of a non-linear system, possessing reactance, may be expressed in Lagrangian form, thus emphasizing the importance of co-energy and also showing that the Principle of Duality is applicable.

Finally, systems are considered possessing mutual inductance and moving magnetic circuits (as in rotating machines).

This paper is intended as a companion paper to the accompanying one by W. Millar.

§ 1. INTRODUCTION.

THIS paper is concerned not with the solution of non-linear differential equations, but rather with certain general properties of a non-linear physical system. In order to develop some simple, but fundamental, concepts and theorems, a return is made to the methods employed by Maxwell, J. J. Thomson and others when first deriving the basic properties of linear lumped networks, namely the methods of general dynamics and the use of simple variational principles (Jeans 1948). Although specific reference is made here to *electric* circuits, it will be apparent that the results apply generally to other systems, also to mixed systems such as "Servo" systems.

§ 2. TYPES OF NON-LINEAR CHARACTERISTICS.

It is important to distinguish between circuit element characteristics (the relation between the mutually dependent quantities x , y , which defines the element operation), which are (a) non-linear but bilateral and

* Communicated by the Author.

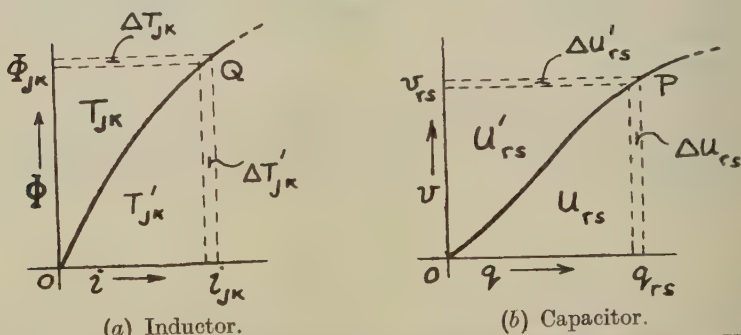
(b) *unilateral*. Elements of the latter type can transmit energy one way only and are essentially *control* elements (for example, relays, triode valves).

Bilateral characteristics of elements, which are the only type that are considered here, again divide into two classes. The first contains *simple* characteristics which here imply a single-valued relationship between the two variables x, y ; the second contains *non-simple* characteristics which imply a multi-valued relationship (for example a dynatron valve, an inductor with hysteresis loss, or gears with backlash). The theorems which follow will refer directly also to the non-simple class in an obvious manner.

§ 3. ENERGY AND "CO-ENERGY" STORAGE.

The power dissipated in any resistor at any instant is $W=vi$, the area of the rectangle (inst. volts \times current), independently of the shape of the v/i characteristic. In a companion paper Millar has divided this area into two parts, lying respectively below and above the curved characteristic of the element, called the *content*, $G=\int v di$, and the *co-content*, $J=\int i dv$.

Fig. 1.



(a) Inductor. (b) Capacitor.
Characteristics ("simple") of non-linear elements, showing energies T, U and Co-energies T', U' .

In non-linear resistive circuits G and J possess certain properties. It may be shown that similar analogous, yet physically quite distinct, notions arise in connection with inductor and capacitor elements; with reactance elements *time* is involved. Thus with reference to fig. 1(a), the rectangle $\Phi_{jk}i_{jk}$ is divided into two parts T and T' by the characteristic; Q is the instantaneous working point.

$$T = \int_0^{\Phi} i d\Phi, \text{ the inductive energy (area above curve),} \quad \dots \quad (1)$$

$$T' = \int_0^i \Phi di, \text{ called the inductive co-energy* (area below curve),} \quad \dots \quad (2)$$

* An invented term; it is, in a sense, dual to energy, and is a quantity of sufficient fundamental interest to justify the allocation of a special term.

where $\Phi = N\phi$, the flux-linkage. Note that T , in a non-linear inductor, may be derived from the work expression $vi \, dt$:

$$T = \int_0^t vi \, dt = \int_0^t i \frac{d\Phi}{dt} \cdot dt = \int_0^\Phi i \, d\Phi. \quad \dots \quad (3)$$

Similarly with non-linear capacitor elements (fig. 1 (b)):

$$\left. \begin{aligned} U' &= \int_0^v q \, dv, \text{ called the capacitive co-energy (area above curve),} \\ U &= \int_0^q v \, dq, \text{ the capacitive energy (area below curve).} \end{aligned} \right\} \quad \dots \quad (4)$$

Again U is derivable from the work done:

$$U = \int_0^t vi \, dt = \int_0^t v \frac{dq}{dt} \, dt = \int_0^q v \, dq. \quad \dots \quad (5)$$

Observe that in *linear* cases $T = T'$ and $U = U'$ and energy = co-energy. It will be shown later that this equality obscures the importance of the co-energy.

The characteristics in fig. 1 have, for simplicity, been taken as *simple* (unique, time invariant and single-valued; hysteresis is excluded).

§ 4. THEOREMS CONCERNING MULTI-MESH NON-LINEAR REACTIVE CIRCUITS.

4.1. The Energy Rectangle Theorem (fig. 2).

A linear or a non-linear circuit of resistor elements may be represented by a set of contiguous rectangles fitting inside a bounding rectangle; each component rectangle has sides of length v_{jk} and i_{jk} , representing the instantaneous voltage and current on any one branch of the circuit, while the area $(v_{jk}i_{jk})$ represents the instantaneous power in the branch. The bounding rectangle represents v_0, i_0 , the source voltage and current (and power).

This is a valuable concept* which, although first put forward for linear resistive circuits many years ago, is not well known (Hering 1927). It is valid also for all-inductor and all-capacitor circuits, linear or non-linear, though it applies only *instantaneously*. Fig. 2 shows an example; by whatever path is chosen between the external terminals AB, the total P.D. is v_0 , while at the same time, if a dividing line XY be imagined to cut the circuit anywhere between the terminals AB, it always intersects the same total current i_0 . That the set of rectangles $v_{jk}i_{jk}$ always forms contiguous areas inside the rectangle v_0i_0 merely illustrates the truth of (a) Kirchhoff's equations and (b) the conservation of energy. In those cases in which an internal branch contains a generator the component rectangle may have a side $-v_{jk}$ or $-i_{jk}$, and the construction may require overlapping rectangles.

* Brooks, Smith, Stone, and Tutte: "The Dissection of Rectangles into Squares", *Duke Math. Journ.*, vol. 7, Dec. 1940. For explanation see Cherry (1949).

If the diagram in fig. 2 (b) is imagined as being turned on its side, so that everywhere v and i are interchanged, the diagram is relevant to the dual circuit, dual in the sense of Cauer's construction (Cauer 1934), everywhere voltage and current are interchanged, as are also meshes and nodes.

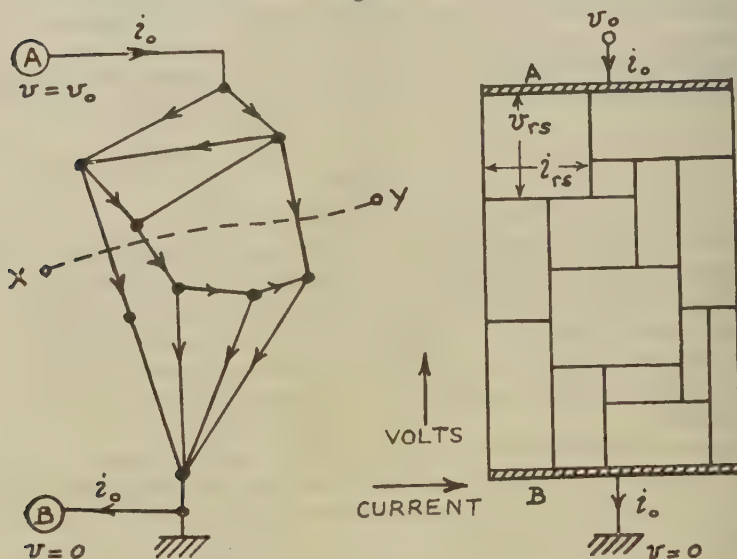
4.2. The Superposition of Energies and Co-energies.

4.2.1.—*Theorem.* At any instant the power supplied by various sources to any linear or non-linear circuit equals the rate of change of the energy stored in the inductor and capacitor elements plus the power dissipated in the resistors.

This follows of course from the Conservation of Energy, and is illustrated by the rectangle theorem referred to above. We may write

$$P = F + \frac{d}{dt}(T + U), \quad \dots \dots \dots (6)$$

Fig. 2.



(a) A circuit configuration, and (b) its energy rectangle representation.

where P is the power supplied and F is the total dissipation. It will now be shown that the co-energies T' and U' possess certain properties when the circuits consist of any network of like-elements, i. e. all-inductor or all-capacitor.

4.2.2.—*Theorem.* At any instant the co-energy in any "simple" 2-terminal non-linear all-inductor circuit regarded as a single element between the terminals is equal to the linear sum of the co-energies in the constituent inductors.

For the moment we exclude hysteresis and mutual inductance and also assume that the cores of the inductors are immovable. A simple circuit of

this type is illustrated by fig. 3 (a). Let v_0, v_1, \dots, v_n be the potentials of the various nodes of the circuit, assuming, without loss of generality, that $v_n = 0$. Let i_{jk} be the current in the branch jk and i_0 be the current fed to the external terminals. Consider the growth of the branch currents from zero at $t = 0$. Due to an increment Δi_{jk} the co-energy in the branch jk will change by an increment $\Delta T'_{jk}$; the total co-energy in the whole circuit will then change by $\Delta T'$, where, to a first approximation,

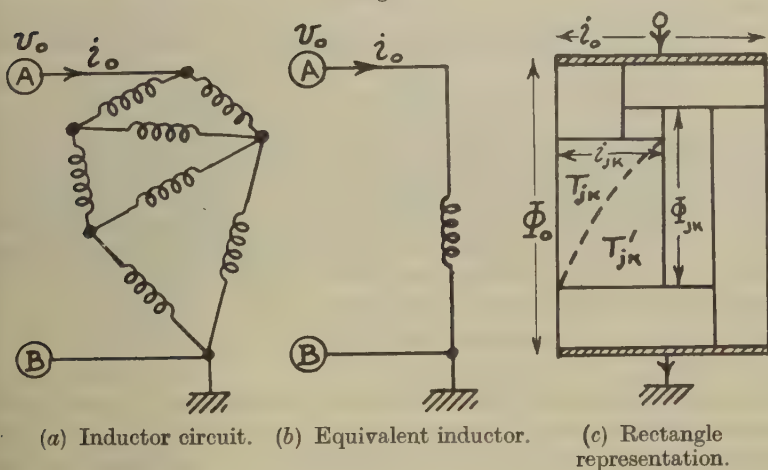
$$\Delta T' = \frac{1}{2} \sum_j \sum_k \Delta T'_{jk} = \frac{1}{2} \sum_j \sum_k [\Phi_{jk} \Delta i_{jk}] \quad \dots \quad (7)$$

(see fig. 1 (a)), the $\frac{1}{2}$ appearing by virtue of the double-suffix notation.

But

$$\Phi_{jk} = \int_0^t (v_j - v_k) dt, \quad \dots \quad (8)$$

Fig. 3.



A non-linear 2-terminal inductor circuit and the "equivalent" inductor.

which is independent of the voltage wave form, and dependent only upon its integral. The integration constant is zero if we assume $\Phi = 0$ at $t = 0$. Then

$$\Delta T' = \frac{1}{2} \sum_j \sum_k \left[\int_0^t (v_j - v_k) dt \right] \Delta i_{jk} = \sum_j \int_0^t v_j dt \left[\sum_k \Delta i_{jk} \right], \quad \dots \quad (9)$$

since $i_{jk} = -i_{kj}$. But from Kirchhoff's current law $\sum_k \Delta i_{jk} = 0$ at every node except at the external terminals, where it is Δi_0 . At this point $v_j = v_0$. Therefore

$$\Delta T' = \Delta i_0 \cdot \int_0^t v_0 dt.$$

This we may write as

$$\Delta T' = \Delta i_0 \cdot \Phi_0, \quad \dots \quad (10)$$

where Φ_0 is a hypothetical flux associated with the integral of the applied voltage v_0 . Integrating these increments of co-energy,

$$T' = \int_0^{i_0} \Phi_0 di_0, \quad \dots \quad (11)$$

which itself represents a co-energy expressed entirely as a function of the input quantities Φ_0, i_0 .

This theorem suggests that it may be possible to construct the characteristic of the "equivalent" inductor point-by-point. Before so doing it is necessary to establish a law governing the distribution of currents amongst branches, in order to define the instantaneous working points v_{jk}, i_{jk} (see sub-section 4.3, below).

Since both the energies T_{jk} and co-energies T'_{jk} add linearly in this way to give the overall energy T and co-energy T' of the inductor circuit, as measured at the external terminals, then so also do their sums add linearly:

$$\left. \begin{aligned} T + T' &= \frac{1}{2} \sum_j \sum_k [T_{jk} + T'_{jk}] \\ \Phi_0 i_0 &= \frac{1}{2} \sum_j \sum_k [\Phi_{jk} i_{jk}] \end{aligned} \right\} \dots \quad (12)$$

This conservation of flux-current is of considerable importance. It suggests that a rectangle construction, similar to that in Theorem (4.1) (fig. 2) is applicable to an all-inductor circuit. Thus fig. 3 (c) illustrates the rectangle diagram appropriate to the inductor circuit (a) at some given instant; by whatever path we trace between the external terminals we shall encounter the same total flux Φ_0 since

$$v_0 = v_1 + v_2 + v_3 \dots$$

and integrating gives $\Phi_0 = \Phi_1 + \Phi_2 + \Phi_3 \dots$

Note that each rectangle may be divided into two areas T_{jk} and T'_{jk} by the element characteristic, corresponding to the diagram fig. 1 (a); one such rectangle division is illustrated in fig. 3 (c). From Theorems 4.2.1 and 4.2.2 these areas superimpose separately, giving the corresponding areas for the *composite* characteristic.

Duality is now interpreted in quite a new way; turning the diagram, fig. 3 (c), on its side interchanges flux-linkages Φ and currents i everywhere, and converts nodes to meshes. This provides completely general rules for finding the "equivalent circuit" of any loaded transformer; alternatively it shows that a circuit containing only electrical constraints, as that in fig. 3 (a), may be assembled upon a transformer and so be given only magnetic constraints. This has been made the subject of a previous study (Cherry 1949): it is here shown to be an equally useful theory when the magnetic circuits have *non-linear* characteristics.

4.2.3. These theoretical points concerning all-inductor circuits may be shown to have their equivalents in relation to *all-capacitor* circuits. Fig. 1 (b) illustrates a typical "simple" non-linear characteristic, with P an instantaneous working-point and U'_{rs} and U_{rs} the co-energy and energy at that instant.

4.2.4.—*Theorem.* At any instant the co-energy in any "simple" 2-terminal non-linear all-capacitor circuit, regarded as a single element between the terminals, is equal to the linear sum of the co-energies in the constituent capacitors.

This theorem is exactly dual to Theorem 4.2.2. For proof, it is simplest to work on a *mesh* basis, using i_0, i_1, \dots, i_n as mesh currents and to consider the co-energy increment $\Delta U'_{rs}$ due to a branch voltage increment Δv_{rs} . Again, flux Φ in the above theorem is replaced by charge q (the dual). The proofs are then analogous.

Again, since both energies U_{rs} and co-energies U'_{rs} superimpose linearly, so also must their sum,

$$U + U' = \frac{1}{2} \sum_r \sum_s [U_{rs} + U'_{rs}]$$

$$\text{or} \quad v_0 q_0 = \frac{1}{2} \sum_r \sum_s v_{rs} q_{rs},$$

and a rectangle theorem similar to that illustrated by fig. 3 (c) is applicable.

4.3. Stationary Value Theorems for Non-linear Systems.

The following theorems establish variational principles which govern the distribution of currents in the branches of non-linear "simple" all-inductor or all-capacitor circuits. These theorems are later extended (§§ 5 and 6) to circuits including mutual inductance and rotating (or sliding) cores, such as those of rotating machines.

4.3.1.—*Theorem.* In a circuit of voltage-driven non-linear inductor elements the total energy T has a stationary value* with respect to voltage variations.

Working on a mesh basis, let i_0, i_1, \dots, i_n be the Maxwell mesh circulating currents. These currents will take up their *natural* values; however, imagine the voltages across elements v_{rs} to be artificially varied by Δv_{rs} to *unnatural* values such that around every mesh Kirchhoff's voltage law still applies:

$$\sum_s \Delta v_{rs} = 0 \quad . \quad . \quad . \quad . \quad . \quad . \quad . \quad (13)$$

(where these variations Δv_{rs} are zero across all voltage-generator terminals) while the current law is violated, at the various nodes

$$\sum i \neq 0 \quad . \quad . \quad . \quad . \quad . \quad . \quad . \quad (14)$$

(the circulating currents no longer have "natural" values). The energy stored in any element rs is thus varied by $(i_r - i_s) \Delta \Phi_{rs}$ to a first approximation; the total energy of the circuit is then varied by ΔT :

$$\Delta T = \frac{1}{2} \sum_r \sum_s (i_r - i_s) \Delta \Phi_{rs}, \quad . \quad . \quad . \quad . \quad . \quad . \quad . \quad (15)$$

* i, e , maximum, minimum, or inflected.

But $\Delta\Phi_{rs} = \int_0^t \Delta v_{rs} dt$, assuming that $\Phi_{rs} = 0$ at $t=0$. Then

$$\begin{aligned} \Delta T &= \frac{1}{2} \sum_r \sum_s (i_r - i_s) \int_0^t \Delta v_{rs} dt \\ &= \sum_r i_r \left[\sum_s \int_0^t \Delta v_{rs} dt \right], \quad (16) \end{aligned}$$

since $v_{rs} = -v_{sr}$. But the integrands here sum to zero, from equation (13).

Hence $\Delta T = 0$, (17)

or the energy T has a stationary value, at every instant.

4.3.2.—*Theorem. In a circuit of current-driven non-linear inductor elements the total co-energy T' has a stationary value with respect to mesh-current variations.*

Working on a node basis, let v_0, v_1, \dots, v_n be the node potentials. Imagine the current i_{jk} in any branch to be artificially varied by Δi_{jk} to some unnatural value such that at every node Kirchhoff's current law holds, while the voltage law is necessarily violated :

$$\sum_k \Delta i_{jk} = 0; \quad \sum v \neq 0. \quad (18)$$

The co-energy increment in the branch jk is $\Delta T'_{jk}$; summing in all the branches,

$$\Delta T' = \frac{1}{2} \sum_j \sum_k \int_0^t (v_j - v_k) dt \cdot \Delta i_{jk}, \quad (19)$$

which may be written

$$\Delta T' = \sum_j \int_0^t v_j dt \left[\sum_k \Delta i_{jk} \right],$$

since $i_{jk} = -i_{kj}$. But from equation (18) this is zero, or

$$\Delta T' = 0 \text{ at every instant,} \quad (20)$$

meaning the co-energy T' has always a stationary value.

4.3.3.—*Theorem. In a circuit of non-linear capacitor elements driven by any number of voltage (current) sources the currents will distribute so as to give the total co-energy U' (energy U) a stationary value at any instant with respect to voltage (current) variations.*

The proofs of this theorem are exactly dual to the proofs given above; for node we substitute mesh, voltage for current, charge for flux.

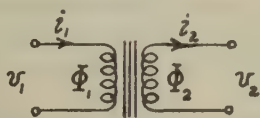
The properties of all-inductor or all-capacitor circuits may be summarized as in Table I. :—

TABLE I.

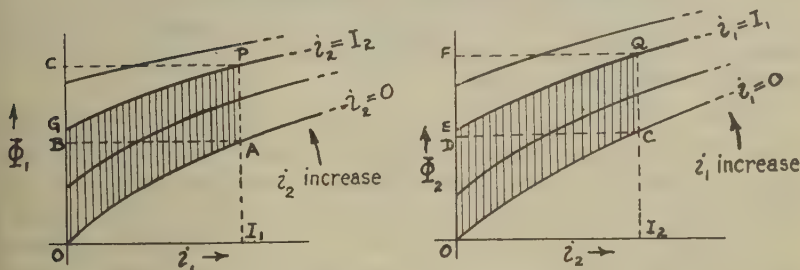
	All-inductor	All-capacitor	Mixed circuit
Voltage drive	$\Delta T=0$ (voltages varied)	$\Delta U'=0$ (voltages varied)	$\Delta \int_0^t (T-U') dt=0$
Current drive	$\Delta T'=0$ (currents varied)	$\Delta U=0$ (currents varied)	$\Delta \int_0^t (T'-U) dt=0$

The properties shown here for the "mixed circuit" will be demonstrated later in sub-section 7.3.

Fig. 4.



(a) Transformer with non-linear core.



(b) Transformer characteristics.

Energy stored in a non-linear transformer.

§ 5. INCLUSION OF MUTUAL INDUCTANCE.

If circuits contain mutual inductances they nevertheless satisfy Kirchhoff's laws, and the instantaneous power acting on any branch jk is $v_{jk} i_{jk}$ where, however, v_{jk} may be a function of more than one current. Consequently the Theorem 4.2.2 relating to the superposition of co-energies applies equally well to circuits containing transformers, with linear or non-linear iron cores.

However, the quantity "co-energy" needs careful definition. Consider any two branches of a circuit which are coupled by mutual inductance possessing non-linear properties (fig. 4 (a)); the energy stored at any instant is

$$T_M = \int_0^t v_1 i_1 dt + \int_0^t v_2 i_2 dt, \quad \dots \quad (21)$$

where, if Φ_1 and Φ_2 are the total fluxes linking the primary and secondary coils respectively,

$$v_1 = \frac{d}{dt} \Phi_1(i_1, i_2) \quad \text{and} \quad v_2 = \frac{d}{dt} \Phi_2(i_1, i_2), \quad \dots \quad (22)$$

Assume that families of characteristics have been plotted, as in fig. 4 (b), giving relations between Φ_1 and i_1 for different settings of i_2 and also between Φ_2 and i_2 for different settings of i_1 . Assume also that the Φ values are unique functions of i_1 and i_2 and that T_M depends only on the final values of i_1 and i_2 and not upon the manner in which they reach these values; that is, hysteresis is excluded.

Substitution from (22) into (21) gives T_M four components :

$$T_M = \int_0^{I_1} i_1 \frac{\partial \Phi_1}{\partial i_1} \cdot di_1 + \int_0^{I_1} i_1 \frac{\partial \Phi_1}{\partial i_2} di_2 + \int_0^{I_2} i_2 \frac{\partial \Phi_2}{\partial i_2} di_2 + \int_0^{I_1} i_2 \frac{\partial \Phi_2}{\partial i_1} \cdot di_1, \quad (23)$$

If the point P, Q is the working-point (currents I_1 and I_2) in fig. 4 (b), it may be reached in two particularly simple ways : (a) With $i_2=0$ raise i_1 to I_1 (points A and E on the characteristics); the stored energy is represented by the area OAB corresponding to the first integral in (23). Next raise i_2 to I_2 , keeping $i_1=I_1$ constant (points P, Q); the energy has two components, represented by ABCP and EQF, corresponding to the 2nd and 3rd integrals above; the 4th integral is zero. (b) Alternatively, with $i_1=0$ raise i_2 to I_2 (points C, G); then raise i_1 to I_1 (points P, Q). The energies are respectively given by the areas OCD, DCQF and GPC. Equating these stored energies,

$$OAB + ABCP + EQF = OCD + DCQF + GPC, \text{ or } OAPG = OCQE, \quad (24)$$

so that the shaded areas in fig. 4 must be equal. Similarly the areas enclosed between any corresponding pairs of characteristics, at every instantaneous pair of working currents, must be equal.

Consider sets of characteristics to be plotted, as in fig. 5, at small current intervals Δi_1 and Δi_2 . The actual loci of the currents i_1 and i_2 starting from zero may be plotted on these characteristics, as illustrated by the dotted lines. These loci may then be approximated by repeating the process, described above, of increasing i_1 and i_2 alternately, but now in small steps Δi_1 , Δi_2 . If this is done the sum of the two areas T_1 and T_2 lying above the working loci is the total stored energy in the transformer at the working point P, Q. Then we may define the total co-energy as the sum of the areas T'_1 and T'_2 lying *under* the working loci.

To see how the various theorems, described previously, may be applied to circuits containing mutual inductance, consider *one* current i_1 to be increased by Δi_1 . The *total* increase in co-energy is $\Delta T'_1 = \Phi_1 \cdot \Delta i_1$ since $\Delta T'_2$ will be zero. Similarly, if i_2 is increased by Δi_2 , then the *total* co-energy increases by $\Delta T'_2$, while $\Delta T'_1 = 0$. Thus Theorems 4.2.2, 4.3.2, relating to superposition and stationary values of co-energy, are still directly applicable since they depend only on Kirchhoff's current law and upon expressing the *total* circuit co-energy increment as $\Delta T'$ (see equation (7)).

Similarly, with reference to fig. 5, if the flux Φ_1 is given an increment $\Delta\Phi_1$, the total energy changes only by $i_1 \Delta\Phi_1$; in a similar manner, then, Theorems 4.2.1, 4.3.1, relating to superposition and stationary values of energy, are also applicable since they depend only on Kirchhoff's voltage law and upon expressing the total circuit energy as ΔT (see equation (15)).

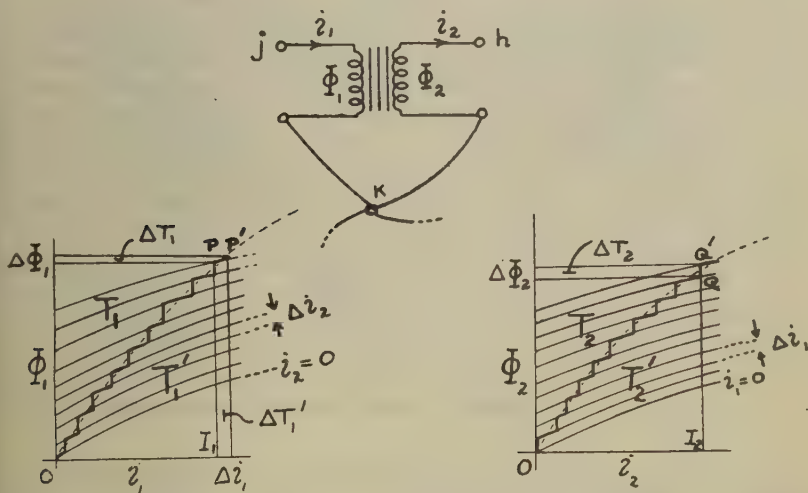
5.1. Equivalent Inductor Theorem.

From Theorems 4.2.1, 4.2.2 and 4.3.1 or 4.3.2, above, it is clear that the following theorem is also valid:

5.1.1.—*Theorem. For any circuit of non-linear "simple" inductors, with two external terminals A, B, the concept of a unique "equivalent" inductor, connected between A, B, is a valid one.*

The total energy T and total co-energy T' at any instant equal the sums of the instantaneous energies and co-energies, respectively, of the constituent inductors, while T (or T') has a stationary value with respect to voltage

Fig. 5.



Energy and co-energy in a non-linear transformer.

(or current) variations, if a constant voltage (or current) generator be connected to the terminals A, B. The theorem is valid also when mutual inductors are present, which may have non-linear characteristics, of the "simple" (non-hysteresis) class.

This theorem suggests that point-by-point methods may be evolved, at least in principle, whereby the equivalent-inductor flux/current characteristics may be computed. Finally, an analogous theorem is applicable to any circuit of "simple" non-linear capacitors.

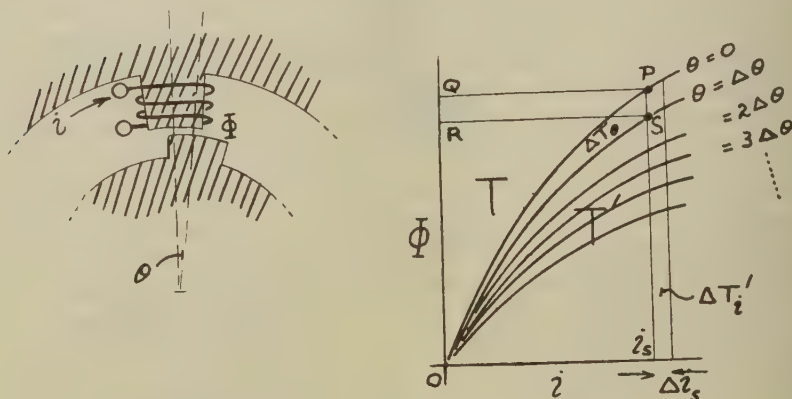
§ 6. SYSTEMS WITH MOVABLE CIRCUITS—ROTATING ELECTRICAL MACHINES.

Consider any one coil of a rotating (or a linear stroke) machine, the reluctance of the magnetic path depending upon θ , the position of some moving magnetic member (fig. 6). Then $\Phi = \Phi(i, \theta)$. Let the coil current be held constant at $i = i_s$ while the rotor is moved $\Delta\theta$; if F is the rotor force, $F = F(i, \theta)$, and the mechanical work done $= F \cdot \Delta\theta$. The working points move from P to S , and the electro-magnetic work done on the circuit connected to the coil terminals is proportional to the area $PQRS$. Further, the stored inductive energy falls by an amount proportional to the difference of the areas OPQ and OSR . Thus

$$F \cdot \Delta\theta = PQRS - (OPQ - OSR) = POS, \quad \dots (25)$$

being the area $\Delta T'_\theta$ between the adjacent characteristics. Note that in the linear case $POS = \frac{1}{2} (PQRS)$.

Fig. 6.



The characteristics of a coil on a rotating machine.

Again, if we regard the co-energy of the coil as the area lying under the working characteristic, T' , this mechanical work $F \cdot \Delta\theta$ (the area POS) represents a loss in co-energy which may be called $\Delta T'_\theta$. However, if θ be held constant and i increased by Δi , this co-energy increases by $\Delta T'_i = \Phi \cdot \Delta i$. Thus the total co-energy increment in a short interval of time, of the coil jk for example, is $\Delta T'_{jk}$:

$$\Delta T'_{jk} = [\Delta T'_i - \Delta T'_\theta]_{jk} = \Phi_{jk} \Delta i_{jk} - F_{jk} \Delta \theta_{jk}. \quad \dots (26)$$

The total co-energy of this coil is then found by integrating from zero:

$$T'_{jk} = \int_0^{i_{jk}} \Phi_{jk}(i, \theta) \cdot di - \int_0^{\theta_{jk}} F_{jk}(i, \theta) \cdot d\theta. \quad \dots (27)$$

If the machine has a number of such coils, coupled together in some complex circuits, with two external terminals, the total co-energy increment of the entire machine is then :

$$\Delta T' = \frac{1}{2} \left[\sum_j \sum_k \{ \Phi_{jk} \Delta i_{jk} - F_{jk}(i, \theta) \cdot \Delta \theta_{jk} \} \right] \quad (28)$$

But $\Phi_{jk} = \int_0^t (v_j - v_k) dt$. Using an argument similar to that used in the proof of Theorem 4.2.2, we may write

$$\Delta T' = \sum_j \int_0^t v_j dt \left[\sum_k \Delta i_{jk} \right] - \frac{1}{2} \sum_j \sum_k F_{jk} \cdot \Delta \theta_{jk}$$

and again, at every node $\sum \Delta i_{jk} = 0$ except at the external terminals, where it equals Δi_0 , and where $v_{jk} = v_0$. Then

$$\Delta T' = \Phi_0 \Delta i_0 - \frac{1}{2} \sum_j \sum_k F_{jk} \cdot \Delta \theta_{jk} \quad (29)$$

where $\Phi_0 = \int_0^t v_0 dt$: this equals the increment in electrical co-energy $\Phi_0 \Delta i_0$ at the external terminals less the total mechanical work done. This is then a modified version of the co-energy theorem 4.2.2 for rotating machines ; note that in simple machines, with a single rotating core, all the $\Delta \theta_{jk}$ are identical. Again, mutual inductance is usually present but, as deduced in the last section, makes no difference to this Theorem. However, note that the concept of a unique Φ_0, i_0 characteristic, as measured at the external terminals, is not now valid since Φ_0 is a function of both i_0 and θ , which are independent variables. Nevertheless, if all θ values are equal, as in most rotating machines, (29) expresses $\Delta T'$ entirely in terms of external quantities Φ_0, i_0, θ , and so suggests that a family of equivalent characteristics is a valid concept.

The stationary value Theorems, 4.3.1 and 4.3.2, may also be interpreted for this case of a rotating machine, or other electro-magnetic-mechanical system, because the proofs of these theorems were not in any way restricted to time-invariant inductor elements.

§ 7. THE GENERAL NON-LINEAR CIRCUIT OF INDUCTORS, CAPACITOR, RESISTORS AND GENERATORS.

It appears difficult to find general theorems relating to circuits containing a mixture of elements. However, certain properties emerge from expressing the circuit equations in Lagrangian form.

7.1. Non-Linear Circuit Equations in Lagrangian Form.

Fig. 7 (a) represents part of some circuit of non-linear R, L, C elements and voltage generators. Let the coordinates $\dot{q}_1 \dot{q}_2 \dots \dot{q}_n$ be the Maxwell mesh currents. Then around, say, the r th mesh

$$L^r v_r + C^r v_r + R^r v_r = e_r, \quad (30)$$

where L^v, C^v, R^v, e are the total inductive, capacitive, resistive P.D.'s and generated voltages around a mesh. Consider these voltages separately; firstly $L^v v_r$. Write $\dot{q}_r = i_r$:

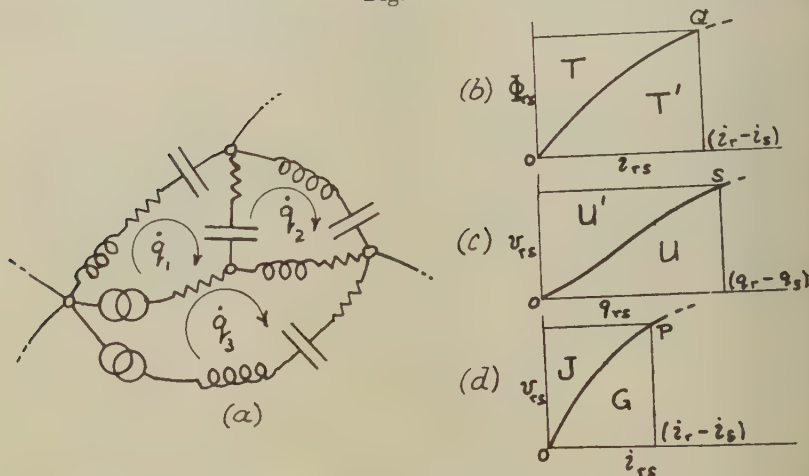
The flux in any inductor, rs , in the r th mesh is a function only of the total current $(i_r - i_s)$, where s denotes the adjacent mesh. The co-energy T'_{rs} is then

$$T'_{rs} = \int_0^{(i_r - i_s)} \Phi_{rs} di \quad (31)$$

(see fig. 7 *b*). The total inductor co-energy in the entire circuit is then T' :

$$T' = \frac{1}{2} \sum_r \sum_s \int_0^{(i_r - i_s)} \Phi_{rs} . di, \quad (32)$$

Fig. 7.



A general non-linear circuit; L, R, C elements and voltage generators.

Differentiating the total circuit co-energy T' with respect to i_r (or i_s) from (32) gives

$$\frac{\partial T'}{\partial i_r} = \sum_{s=0}^n \Phi_{rs}, \quad (33)$$

since only those inductors around mesh r carry the current i_r . In this summation $s=0$ relates to the external mesh; the current i_0 is assumed zero, without loss of generality. From (33) the total mesh r inductive voltage is

$$L^v v_r = \frac{d}{dt} \sum_{s=0}^n \Phi_{rs} = \frac{d}{dt} \left(\frac{\partial T'}{\partial i_r} \right). \quad (34)$$

Similarly for the capacitor voltage around the r th mesh; the capacitor in the branch rs supports a charge $(q_r - q_s)$ and the voltage across this element

is $v_{rs}=v(q_r-q_s)$. The total energy (not co-energy) of all the circuit capacitors is then U (see fig. 7 (c)) :

$$U=\frac{1}{2} \sum_r \sum_s \int_0^{(q_r-q_s)} v_{rs} dq. \quad (35)$$

Then

$$\frac{\partial U}{\partial q_r} = \sum_{s=0}^n v_{rs} = {}_C v_r, \quad (36)$$

the total capacitive voltage round mesh r .

Finally the resistor voltages. These may be expressed in terms of the resistor content and co-content (see § 3). The resistor content of the entire circuit is G :

$$G=\frac{1}{2} \sum_r \sum_s \int_0^{(i_r-i_s)} v_{rs} di, \quad (37)$$

so that, differentiating,

$$\frac{\partial G}{\partial i_r} = \sum_{s=0}^n v_{rs} = {}_R v_r. \quad (38)$$

Then substituting in (30) from (34) (36) and (38), the equation of the r th mesh of the circuit is

$$\frac{d}{dt} \left(\frac{\partial T'}{\partial \dot{q}_r} \right) + \frac{\partial u}{\partial q_r} = e_r - \frac{\partial G}{\partial \dot{q}_r}, \quad (39)$$

which is recognized to be Lagrange's equation of a dissipative system. If we define the *Lagrangian function* of the circuit as $\mathcal{L}=T'(\dot{q})-U(q)$, the equation (39) may be re-written

$$\frac{d}{dt} \left(\frac{\partial \mathcal{L}}{\partial \dot{q}_r} \right) - \frac{\partial \mathcal{L}}{\partial q_r} = e_r - \frac{\partial G}{\partial \dot{q}_r}, \quad (40)$$

and a similar equation applies to every mesh $r=1, 2, \dots, n$. If required, this form of the equation serves also for circuits containing movable-core inductors, as with rotating machines. Thus, as seen from equation (27), the co-energy T' then includes the mechanical energy and becomes a function of both i and θ .

7.2. The Dual of a Non-Linear Circuit.

The concept of a pair of *dual* or inverse circuits (A. Russell 1904) is, in the linear field, a most important one. In this present paper it has been noted that certain theorems may be derived from others directly, merely by the substitution of capacitors for inductors, of voltages for currents, of nodes for meshes, and vice-versa. This may now be generalized formally, as applying to non-linear systems.

The Lagrangian equations (40), above, were derived from the mesh equations (30) of a given circuit. Imagine a topologically dual circuit pattern which, if drawn superposed on the original ("parent") circuit has one of its n nodes lying inside one of the n meshes of the parent circuit (Cauer 1934). Then the *node* equations of the circuit will be

$${}_L i_j + {}_C i_j + {}_R i_j = i_j, \quad (41)$$

The capacitive co-energy U'_{jk} , the inductive energy T_{jk} and the resistive co-content J_{jk} in the elements connected to the node j are

$$U'_{jk} = \int_0^{(v_j - v_k)} c_{jk} \cdot dv; \quad T_{jk} = \int_0^{(\Phi_j - \Phi_k)} L_{jk} d\Phi; \quad J_{jk} = \int_0^{(v_j - v_k)} R_{jk} \cdot dv,$$

if $v_1 v_2 \dots v_j \dots v_n$ are the nodes potentials and if $v_j = \dot{\Phi}_j$. By differentiation

$$\frac{d}{dt} \left(\frac{\partial U'_{jk}}{\partial v_j} \right) = c_{jk} \dot{v}_j; \quad \left(\frac{\partial T_{jk}}{\partial \Phi_j} \right) = L_{jk} \dot{\Phi}_j; \quad \left(\frac{\partial J_{jk}}{\partial v_j} \right) = R_{jk} \dot{v}_j.$$

But note that, for example, $\partial U'_{jk} / \partial v_j = \partial U' / \partial v_j$. Thus the suffixes may be dropped and the expressions U' , T , J adopted, which refer to the *entire* circuit. Adding these current components, as in (41),

$$\frac{d}{dt} \left(\frac{\partial U'}{\partial v_j} \right) + \frac{\partial T_j}{\partial \Phi_j} = \dot{v}_j - \frac{\partial J}{\partial v_j}, \quad \dots \dots \dots (42)$$

which again is a form of Lagrange's equation (40); however, in this current-driven case the Lagrangian function \mathcal{L} is

$$\mathcal{L} = U'(v) - T(\Phi). \quad \dots \dots \dots (43)$$

A comparison of equations (42) with the mesh equations (39) establishes the duality concept. Thus, using the symbol \rightarrow , meaning "replaced by", we have that, given the set of equations (39) referring to the meshes of a parent circuit,

$$\left. \begin{array}{l} \dot{q}_r \rightarrow v_j \\ q_r \rightarrow \Phi_j \end{array} \right\} \left. \begin{array}{l} \partial T' / \partial \dot{q}_r \rightarrow \partial U' / \partial v_j \\ \partial U / \partial q_r \rightarrow \partial T / \partial \Phi_j \\ \partial G / \partial \dot{q}_r \rightarrow \partial J / \partial v_j \end{array} \right\} \quad \dots \dots \dots (44)$$

leads directly to the node equations of the dual circuit.

In practice this may be of limited interest since it may not be possible to construct physical elements having the required curvature of characteristics. Nevertheless, the transformations (44) define the theoretical relation required between the element characteristics. For example, if the three characteristics (b) (c) (d) in fig. 7 refer to elements of the parent circuit, then exchange of the ordinates and abscissæ gives the characteristics of the corresponding elements in the dual circuit.

7.3. *Dissipationless Circuits—Force-free Oscillations.*

If a dynamical system can be expressed in the form of Lagrange's equation (40) it is a matter of simple algebra to show that, if the dissipation is zero ($G=0$) and if the generators are removed ($e_r=0$), the force-free oscillations which may occur in what is now a non-linear but purely reactive circuit are governed by Hamilton's Principle,

$$\Delta \int_0^t \mathcal{L} \cdot dt = 0, \quad \dots \dots \dots (45)$$

a variational principle (Whittaker 1904), meaning that the natural wave-forms of the currents are such as to keep the integral of \mathcal{L} ($=T' - U$ or $U' - T$), in the dual, stationary at every instant. (Note that in the linear case $T' \equiv T$ and the more familiar form of $\mathcal{L} = (T - U)$ appears.)

This variational principle has been added to the list in Table I. (sub-section 4.3.3). This principle tells us nothing new about the non-linear circuit; it is to be emphasized that it is merely the most fundamental statement of its behaviour, being in the form of a single equation. In a given example, if the equations of the non-linear characteristics of the various elements are known, it may be possible to express the Lagrangian as a function thus:

$$T' = \frac{1}{2} \sum_j \sum_k T'_{jk}, \text{ where } T'_{jk} = T'(q_j \dot{q}_k t),$$

$$U = \frac{1}{2} \sum_j \sum_k U_{jk}, \text{ where } U_{jk} = U(q_j q_k t),$$

and substitution into \mathcal{L} and calculation of the result of arbitrary variation of the q, \dot{q} variables leads to a set of n simultaneous equations of the Lagrangian form (40) (with $G=0$) which are the non-linear equations of the n -mesh circuit.

In the linear field Hamilton's principle (45) leads to a general formulation of the conditions for the natural modes of oscillations, as expressed by Foster's Reactance Theorem. It is possible that in the non-linear field there may be some corresponding set of energy relations which defines the various characteristic types of stability or conditional stability that can occur; this possibility will not be pursued here.

REFERENCES.

- CHERRY, E. C., 1949, *Proc. Phys. Soc. B*, **62**, 101.
 GUILLEMIN, E., 1933, *Communication Networks*, Vol. II. (John Wiley).
 JEANS, JAMES, 1948, *Electricity and Magnetism*, 5th Ed. (Cambridge : University Press).
 SPARLING, S. G., 1912, *Electricity and Magnetism*, 1st Ed. (Bell).
 WHITTAKER, E. T., 1904, *Analytical Dynamics* (Chap. XX.) (Cambridge : University Press).

CXVIII. *A Perturbation Treatment of Closed States in Quantized Field Theories.*

By B. TOUSCHKE,

Department of Natural Philosophy, The University Glasgow*.

[Received May 30, 1951.]

ABSTRACT.

The paper discusses an iteration method by means of which it is possible to obtain approximate solutions for field theoretical problems involving bound states.

§ 1.

THE treatment of bound states in quantized field theories has recently received much attention. After the elimination of divergences by the work of Tomonaga, Schwinger, Feynman, Dyson (1949) and others this problem which is related to the convergence of the whole series of approximations progressing in powers of the coupling constant, has become the central problem of field theory. Dyson (1951) attributes the difficulty of the problem to two facts, (i.) the free particle nature of the initial and final states in the customary S-matrix formalism and (ii.) the impossibility of representing the wavefunction of a bound state in terms of a convergent power series in the coupling constant. A failure of the formalism which apart from the renormalization procedure is essentially Born's approximation method may also be expected in those cases in which bound states manifest themselves in their virtual form as in the theory of nuclear resonances.

Recently Ferretti (1951) and Dyson (1951) have attempted to overcome the difficulties associated with the occurrence of bound states; Ferretti by considering adiabatic changes of the coupling constant, and Dyson by considering changes of the coupling constant in a fictitious world coincident with the real world at time t . At $t = \infty$ Ferretti thus enforces the justification for using free particle expansions and Dyson succeeds in doing the same at least in the fictitious world. In this note an alternative method is suggested which, though its convergence has yet to be demonstrated and its relativistic properties have to be investigated, allows one to treat stationary states and is capable of leading to quite definite predictions. Considerations to a similar end have been recently investigated by Power (1951), who could show† that after minor modifications the two methods of approach are essentially equivalent. The method used here consists in adding a suitable operator representing an interaction energy to the Hamiltonian of the free particles (nucleons and mesons)

* Communicated by the Author.

† Private communication.

the states to which the indices of the S-matrix refer. To see this more clearly it is useful to fix the formal meaning of the quantities occurring in equations (1) to (6). The Schrödinger-vector $\chi = \chi(q, t)$ is a function of the physical variables q of the system and the time t . The solutions of equation (4) are of the form $\phi_N(q, t) = \Psi_N(q) \exp(-iE_N t)$, where the E_N are the energy values of the free particles in the interaction field V . There may be a discrete spectrum superimposed on the continuous spectrum of the centre of mass motion. (5) reads explicitly $\chi = \sum_N \Psi_N(q) \exp(-iE_N t) S_N(t)$. If the states represented by the solutions of (2) are labelled by an index κ —distinguishing the true states of the system— $\chi(q, t)$ will be of the form $\Psi_\kappa(q) \exp(-iE_\kappa t)$ and S turns into a matrix $S_N^\kappa(t)$ which thus represents the coefficients in an expansion of the true solutions in terms of the solutions of the model system (4). (In the customary interaction representation the true states and the free particle states are usually labelled by the same index so that the mixed nature of the S matrix is masked.) Our equation (6) therefore differs from the corresponding equation of the interaction representation in that in (6) the “rows” of S refer to the (possibly closed) states N of the model system and therefore do not differ qualitatively, *i.e.* in their asymptotic behaviour from the true states as in the interaction representation.

The typical matrix-elements of K are of the form

$$K_{MN} \exp[i(E_M - E_N)t]. \quad . \quad . \quad . \quad . \quad . \quad . \quad (7)$$

If it is assumed that V can be chosen $\propto g^2$ one may write

$$K = K^{(1)} + K^{(2)} \quad \text{with} \quad K^{(1)} = \phi^{-1} H' \phi, \quad K^{(2)} = -\phi^{-1} V \phi, \quad . \quad . \quad (8)$$

where the upper indices indicate the lowest power of g , *i.e.* the way in which an operator vanishes if $g \rightarrow 0$. Thus in general $F^{(n)} = g^n F(g)$ with $F(0) \neq 0$, because of the implicit dependence of ϕ on g . The successive approximations of S become:

$$S^{(0)} = I,$$

$$S^{(1)} = -i \int_0^t K^{(1)}(t_1) dt_1,$$

$$S^{(2)} = -i \int_0^t K^{(2)}(t_1) dt_1 + (-i)^2 \int_0^t dt_1 K^{(1)}(t_1) \int_0^{t_1} dt_2 K^{(1)}(t_2). \quad . \quad . \quad . \quad (9)$$

The first equation establishes a 1-1 correspondence $N \leftrightarrow \kappa$ between the true states of the system and the states of the model system.

We now make use of our freedom to choose V . Clearly the ideal choice of V should ensure that the perturbation method when applied to equation (6) yields most rapidly converging results. However this aim can hardly be formulated in a mathematical fashion. For definiteness we therefore try to determine V in such a way that the pure interaction terms arising in the second approximation in equation (9) vanish. For this we remember that H' will only contain terms corresponding to the emission and absorption of a meson. The same will hold for $K^{(1)}$ since V

leaves the number of mesons unaltered. It will therefore be possible to split the second term on the right-hand side of the last equation (9) into two terms

$$\int^t dt_1 K^{(1)}(t_1) \int^{t_1} dt_2 K^{(1)}(t_2) = \int^t dt_1 (I + II), \quad . . . \quad (10)$$

where I represents all those matrix elements for which the number of mesons does not change and II those matrix elements for which the number of mesons changes by 2. If therefore

$$K^{(2)} = iI \quad \quad (11)$$

all the interaction terms will vanish in the second approximation and the interaction potential is "adapted to the second order of perturbation theory".

Equation (11) is an implicit relation from which V has to be determined. It appears that this can be done in rapidly converging steps, for the interaction energy I draws most of its strength from the highly excited states of the system—owing to the short range of nuclear forces—so that the deformation of the particle wavefunctions caused by the presence of the interaction energy I should be small. The self-consistent "potential" V can thus be determined in the following manner. Let n, \dots denote free particle states. As a first step in the process leading to the self-consistent V satisfying (11) one chooses $V'_{mn} = iI_{mn}$. Inserting this V into equation (4) one obtains a new set of states n', \dots with energies $E_{n'}, \dots$. I is now determined in terms of the new eigenstates n' . A new V'' is determined from (11), viz.: $V''_{m'n'} = iI_{m'n'}$ and the process is repeated. If this procedure converges it will lead to a limiting set of states $N = \lim (n', \dots; n'', \dots, \dots)$ and to a limiting potential $V = \lim (V', V'', \dots)$, which when inserted into equation (8) will satisfy the condition (11). A rough estimate of the convergence of the procedure shows that, for example, in the case of the nucleon-nucleon interaction, successive steps of the approximation will add a correction of the order E_D/μ where E_D is the binding energy of the "deuteron" and μ the rest energy of the meson. This rapid convergence stems from the fact that the energy denominators of the customary second approximation formalism are of the order μ and is in this way related to the short range $1/\mu$ of nuclear forces. This seems to indicate that the present method may not be applicable to quantum electrodynamics where the range of forces is ∞ .

In second approximation V will—in addition to self energy-terms—contain only two terms corresponding to the interaction between two nucleons and between a nucleon and a meson respectively. These interactions can be represented by the two 2-vertex Feynman graphs



$$\quad \quad (12)$$

The internucleon term represents the two-body contribution to nuclear forces. The second graph will cause a distortion of the mesonic waves in the neighbourhood of a nucleon. It represents the perturbation energy in terms of which the scattering of mesons by nucleons may be described. In the case of scalar charged mesons it will correspond to an attractive force between protons and π^+ -mesons and neutrons and π^- -mesons respectively. The forces between protons and π^- -mesons and neutrons and π^+ -mesons are of opposite character. It should be noted that these forces cannot be described in terms of a simple potential function $V(\mathbf{r})$, in which \mathbf{r} is the distance between the meson and the nucleon. It will rather be of the character $V(\mathbf{r}, \mathbf{r}')$ attributing a certain energy to the annihilation of a meson at \mathbf{r}' and its re-emergence at \mathbf{r} . In \mathbf{k} -space the first "Hartree-approximation" for infinite mass nucleons will be

$$V'(\mathbf{k}\mathbf{k}') = \frac{g^2}{2L^3} (\mu^2 + k^2)^{-\frac{1}{2}} (\mu^2 + k'^2)^{-\frac{1}{2}}, \quad \dots \quad (13)$$

where L^3 is the volume of the normalization cube. The states containing one positive meson may be expressed in terms of the one meson Hilbert-vector :

$$\chi^{(1)} = \sum_{\mathbf{k}} u(\mathbf{k}) a^+(\mathbf{k}) \chi_0. \quad \dots \quad (14)$$

Here χ_0 is the Hilbert-vector of the vacuum, a^+ the operator representing the creation of a positive meson of momentum \mathbf{k} and $u(\mathbf{k})$, the one meson Schrödinger function normalized to $\sum_{\mathbf{k}} |u(\mathbf{k})|^2 = 1$. In our approximation energies and wavefunctions of the meson in the presence of an ∞ -mass nucleon are the eigenvalues E and solutions $u(\mathbf{k})$ of the time independent Schrödinger-equation :

$$\sum_{\mathbf{k}'} (\delta_{\mathbf{k}\mathbf{k}'} (\omega_{\mathbf{k}} - E) + V'_{(\mathbf{k}\mathbf{k}')}) u(\mathbf{k}') = 0. \quad \dots \quad (15)$$

For large energies $V(\mathbf{k}, \mathbf{k}')$ will represent a small perturbation and Born's approximation will give approximate expressions for the distortion of the wavefunctions near the nucleon. The distortions may become considerable for low meson energies. The possibility of bound states can be investigated by using Hyleraas' variational method. It turns out that at least for $g^2 > \pi^2$ the system becomes unstable, giving bound states of infinite negative energy. This can be shown by using the trial function $u(\mathbf{k}) = N e^{-\alpha k}/k$ (where N is a normalization factor, and α is the parameter which is to be varied). The energy E comes out smaller than $-\text{const}/\alpha$. For values of g less than a certain critical value—of which π is a rough estimate—no bound states will occur. This can be made plausible by the following consideration. The energy of the perturbation will be of the order $g^2\mu$ and will be $\neq 0$ only in a neighbourhood of dimensions $1/\mu$ of the nucleon. This energy has to be balanced against the energy required for the localization of a meson in this neighbourhood. This energy is μ . It thus appears that the possibility of obtaining energy-values less than μ only depends on the magnitude of g . The critical value of g represents the limit between weak and strong coupling theories. Restricting ourselves to weak coupling theories, we will expect no bound states

between mesons and nucleons and equation (15) will only be used to account for the distortion of (low energy) meson waves.

This distortion may contribute to some of the well-known asymmetries observed in meson-production processes.

When the self-consistent potential V has been determined up to the second approximation one arrives at a definite set of states N , . . . which one may call the set of states adapted to the 2nd order of perturbation theory. Each state will represent a definite pattern of motion—including that typical of scattering experiments—of bare particles interacting via the “phenomenological” potential V . Some of the states N may have the asymptotic behaviour of closed states. The first-order matrix-elements in (9) will describe the absorption or emission of one meson coupled to a nuclear transition $M \rightarrow N$. A special case of such a process has been treated by Gunn, Power and Tauschek (1951). Their results show that the deformations caused by the assumed phenomenological internucleon potential may greatly affect the cross section for meson production. The high energy region of this process has received exhaustive treatment by C. Morette, whose results, however, cannot be extrapolated into the threshold region where—owing to the possibility of the formation of closed states between the nucleons—Born’s approximation is bound to break down. From the point of view of the present investigation the G.P.T.-treatment of the problem is still incomplete owing to the neglect of a possible distortion of the meson waves.

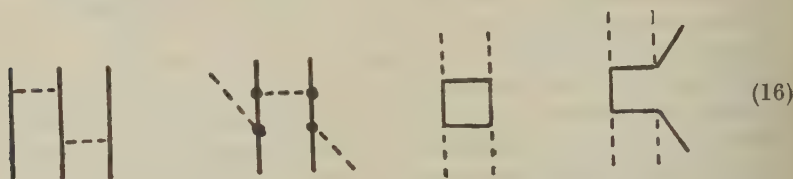
The remaining terms of the second approximation to equation (6) will describe processes involving the emission and absorption of two mesons.

The third approximation will give further terms to the matrix-elements for the emission and absorption of one meson, in addition to three meson terms. It is clear that the terms of the first approximation together with those 1-meson terms arising from the third approximation should add up to C. Morette’s results in the range of validity of Born’s approximation. The terms arising in the third order will therefore describe the transition from the strong interaction low energy region treated in G.P.T. to the region of validity of Born’s approximation. The energy at which this transition is expected to occur will be of the order of the average well depth above the threshold. Recent experiments lie just in that region and therefore cannot be directly compared with any of the present calculations on the subject of meson production in proton-proton collisions.

§ 3.

So far we have only adapted the phenomenological potential V to the second approximation of perturbation theory. A possible method for the continuation of the process would be to leave V unaltered and continue the solution of equation (8) by orthodox methods and with a fixed potential and in terms of the stationary states determined in the second approximation. This treatment will be successful only if the higher even approximations do not lead to new forces sufficiently strong to produce bound states which have not already been accounted for in

the second approximation. The fourth-order formalism will introduce interaction terms of the form



in addition to interaction (and self-energy) terms already treated in the second approximation. The first graph represents three nucleon forces, the second the interaction between a meson and two nucleons, the third the interaction between two mesons and the fourth the interaction between two mesons and a nucleon. The order of magnitude of the forces arising from the graphs (16) could be estimated by computing the matrix-elements corresponding to the graphs (16) in terms of the second-order states N . If any of these graphs gives a contribution sufficient to lead to the formation of bound states a new supplementary potential V has to be introduced, capable of producing such states and fitted in such a manner that it compensates for all the even interaction terms including those of the fourth order. This means that the whole process described in § 2 has to be repeated. As we have seen, this retracing of the steps need not be compulsory, and it will indeed be unnecessary if the potential V adapted to the second approximation exhausts all the possible closed states of the system. The possibility of this situation is related to the short range of nuclear forces resulting from the non-vanishing mass of the meson. It is more likely in meson-theory than in quantum electrodynamics where the infinite range of nuclear forces entails an accumulation of bound states (level-density = infinite) at the boundary between the discrete and continuous spectrum.

A possible objection to the suggestions outlined in this paper may be raised against its lack of relativistic invariance. Though, of course, the total results obtained in the case of a convergent procedure should be relativistically invariant this is not true for the individual contributions $S^{(1)}$, $S^{(2)}$, . . . to the S -matrix. The reason for this is the obviously non-relativistic character of bound states between bare particles. It appears, however, that this lack of invariance is due to the physical interpretation of scattering experiments in terms of such bound states, which with the introduction of V is imposed upon the formalism. An investigation of the relativistic properties of the method will be attempted elsewhere.

REFERENCES.

- DYSON, F. J., 1949, *Phys. Rev.*, **75**, 486 and 1736; 1951, in press.
 FERRETTI, B., 1951, *Nuovo Cimento*, **8**, 108.
 GUNN, J. C., POWER, E. A., and TOUSCHER, B., 1951, *Phil. Mag.*, **43**, 523.
 POWER, E. A., 1951, in press.
 MORETTE, C., 1949, *Phys. Rev.*, **76**, 143.

CXIX. CORRESPONDENCE.

On Loading Nuclear Emulsions with Wires.

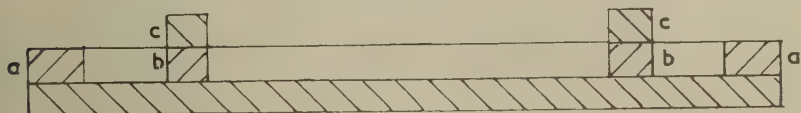
By M. DANYSZ and G. YEKUTIELI,
H. H. Wills Physical Laboratory, University of Bristol*.

[Received July 17, 1951.]

A METHOD of loading nuclear emulsion with wires, similar to that recently published by Meulmans, Occhialini and Vincent (1951), has been developed independently in this laboratory. Nylon threads and copper wires of thickness 25, 40 and 60 microns have been used. In general, for substances which do not react with the emulsion, there is no difficulty in developing the plates. For substances which do react, such as copper, we have found that satisfactory protection of the emulsion can be given by coating the wires with a thin layer of enamel.

The most important technical problem met in processing such plates is the elimination of the distortion introduced by the presence of the wires. This arises from volume changes of the emulsion, and movements

Fig. 1.



of the wires relative to it, during processing. The degree of distortion increases rapidly with the thickness of the wires employed, and it arises from two principal causes :—

(1) "Longitudinal" distortion is introduced by a lengthwise displacement of the wires with respect to the emulsion. The wires, when first placed in the emulsion, are under a slight tension, and it is important that this should be released in the early drying stage, so that it is not "frozen in". Should any tension remain when the plates are dry, it will be released during processing, and thus cause a displacement both of the emulsion and of the tracks in the immediate vicinity of the wires.

(2) "Volume" distortion is caused by the shrinkage of the emulsion round the wires after processing, and is the more serious.

To eliminate both longitudinal and volume distortion, the following methods of loading and threading the emulsion were adopted. The wire or thread is first evenly wound on a lathe, round a prepared frame (aa), fig. 1, to which it is stuck with shellac. The frame itself is made of glass 1 mm. thick and 1 cm. wide, and half the threads are cut away, only those attached to one face of the frame being retained.

* Communicated by Professor C. F. Powell, F.R.S.

The plates upon which the emulsion is poured are of specially treated glass supplied by Messrs. Ilford Ltd. On such a plate is placed, first, another glass frame (bb), with inside area equal to that of the desired emulsion surface, the upper and lower surfaces of (bb) having been first smeared with vaseline. The larger frame (aa) is now placed over (bb) so that the wires rest on its upper surface without bending or extra tension. A third frame, (cc), exactly similar to (bb), and of which the surfaces have also been smeared with vaseline, is placed over the top of (bb).

The emulsion is now poured on the glass plate—within the area defined by the frames (bb) and (cc)—until its upper surface is just level with the top surface of (cc). When the emulsion gels, usually after $1\frac{1}{2}$ hours, the wires are cut away from the frame with a sharp razor blade, and the frames removed. The exact stage at which this is done is critical, for the emulsion must be sufficiently solidified to be able to support the wires, but not yet so rigid that it "freezes in" the tensions. If the emulsion is now left to dry it shrinks to a thickness of approximately 300 microns.

The most serious distortion, volume distortion, arises because the gelatine shrinks as the result of the removal of the large quantities of silver halide during processing, whereas the wires are unaffected. The only way to avoid it is to prevent the shrinkage of the emulsion, and we have succeeded in doing so by the following method:—

In effect, we replace the silver salt by a suitable transparent substance, and for this purpose we introduce resin into the emulsion, a method which has been developed in collaboration with Mr. J. E. Hooper. After washing, the water in the emulsion is replaced by alcohol by immersion in a succession of baths of gradually increasing concentration of alcohol. The plates are then soaked in a solution of resin in alcohol for a time of the order of two days, and then allowed to dry.

The final thickness of the resulting emulsion appears to depend on the strength of the resin solution used and the period of soaking. Concentrations of 30 gm. of resin in 100 c.c. of alcohol, and soaking for two days give a final emulsion thickness close to that before processing; but even greater thickness can be achieved, so that the emulsion is expanded instead of contracted.

Nylon loaded plates exposed to cosmic radiation and treated by these methods have been examined, and the results show that both types of distortion had been almost completely eliminated. We believe that, apart from its particular applications to the present problem, the impregnation of emulsions with resins and other substances has other more general advantages and applications. These will be described in a later communication.

REFERENCE.

- MEULEMANS, G., OCCHIALINI, G. P. S., and VINCENT, A. M., 1951, *Nuovo Cimento*, **8**, no. 5,

Neutron Emission from Nuclei Excited by High Energy Protons.

By D. M. SKYRME,

Atomic Energy Research Establishment, Harwell,

and

W. S. C. WILLIAMS,

University College, London*.

[Received August 1, 1951.]

NUCLEAR reactions induced by high energy protons are thought to take place in two stages (Serber 1947). In the first stage the incoming particle makes collisions with individual nucleons in the target nucleus, and some of the products of these collisions pass directly out of the nuclear field. These "prompt" particles have high kinetic energy and they are emitted predominantly in the direction of motion of the incoming particle. After their departure the residual nucleus is left highly excited, and in the second stage of the reaction the excitation energy is dissipated by the emission of neutrons, charged particles and eventually γ -rays. These "evaporation" particles have relatively low energies, and they are emitted isotropically because of the comparatively long lifetime of the intermediate nuclei. Evaporation protons have often been studied before (*e.g.* Harding, Lattimore and Perkins 1949), but there has been little investigation of the neutrons following high energy reactions. This letter reports preliminary results of an investigation of evaporation neutrons from carbon and tungsten targets bombarded in the Harwell cyclotron. Values have been obtained for the differential cross-section for neutron evaporation as a function of the kinetic energy of the emitted neutron. If some assumptions are made as to the value of the proton inelastic cross-section of the target nuclei, the average number of neutrons emitted per excited nucleus can be determined also.

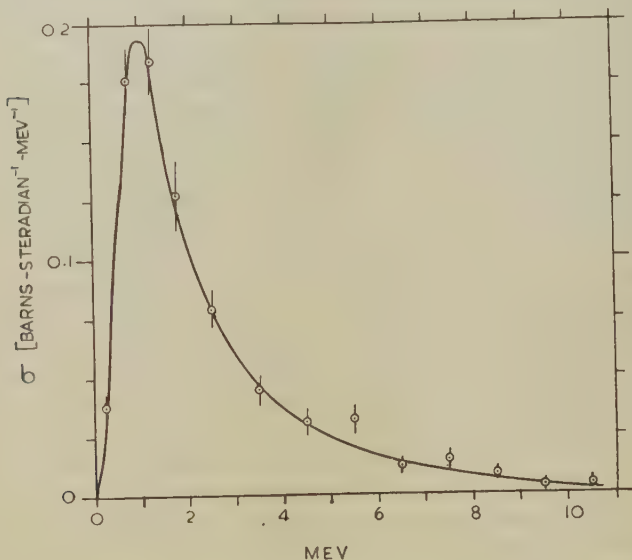
The two targets were exposed in turn to the internal proton beam, whose maximum energy was calculated to be 171 MeV. Slowing down in the targets reduces the effective primary proton energy to about 157 MeV. in both cases. Neutrons emitted backwards (*i.e.* at 180° to the direction of the ingoing proton beam) were collimated by 2 in. diameter holes in concrete blocks and entered photographic plates 18.9 metres from the target. The distributions in energy of these neutrons were determined by means of the tracks of recoil protons produced in the photographic emulsions (Champion and Powell 1944). The numbers of primary protons striking the targets in the two runs were determined measuring the amount of ^7Be produced by the $^{12}\text{C}(p, 3p3n)^7\text{Be}$ reaction, whose cross-section is known with an accuracy of 10 per cent (Dickson and Randle 1951). Several thin plates of carbon were incorporated in the tungsten target for this purpose. Two subsidiary experiments were carried out to check that the neutrons did, in fact, come directly from the target. Negligible numbers of recoil proton tracks were observed

* Communicated by the Authors.

in the plates (*a*) when the target was out of line with the collimating holes, (*b*) when the target was realigned and the collimating holes were blocked with copper rods.

The differential cross-section, σ , for neutron evaporation from the tungsten target is shown in fig. 1. The value given for neutrons with energy less than 0.5 MeV. may be as much as 30 per cent low (Nereson and Reines 1950). A change of this magnitude will not, however, significantly affect the integrated cross-section. The total cross-section, for neutron energies up to 11 MeV. is found to be (6.0 ± 0.9) barns (1 barn = 10^{-24} cm.²), and the mean energy of an evaporation neutron is 2.6 MeV. There are 675 tracks in the spectrum below 11 MeV.; only

Fig. 1.



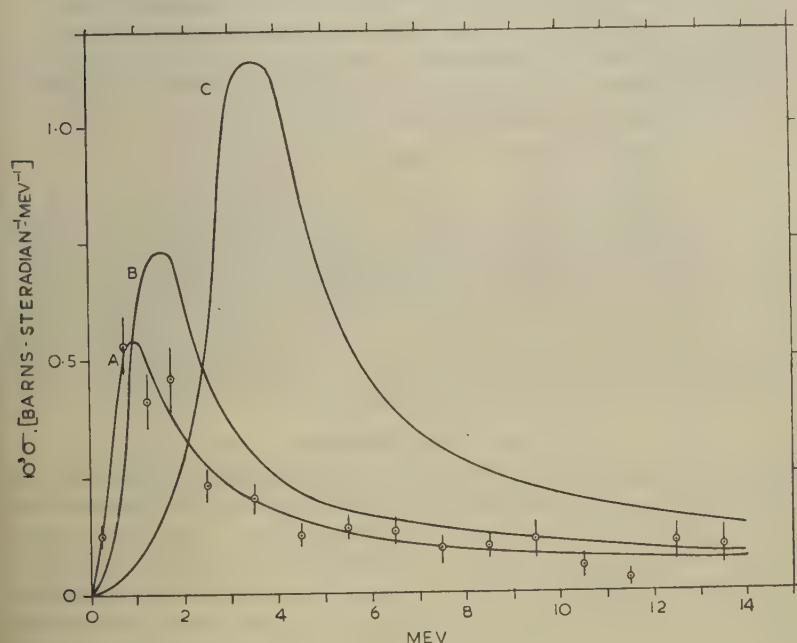
Neutron spectrum from tungsten target.

two tracks corresponding to neutron energies greater than this were observed. The shape of this spectrum agrees fairly well with that to be expected from evaporation theory (Weisskopf 1937), if account is taken of the fact that more than one neutron can be evaporated from each excited nucleus.

In order to calculate the average number of neutrons evaporated from an excited nucleus, it is necessary to know the cross-section for inelastic collisions of protons with the target nuclei. Such values are not available, but it is known that the total cross-section of carbon for 156 MeV. neutrons is (0.330 ± 0.003) barns (Taylor, Pickavance, Cassels and Randle 1951 a), and that of tungsten for neutrons of the same energy is 3.1 barns (Taylor, Pickavance, Cassels and Randle 1951 b). If it is assumed that one-half the neutron total cross-section is inelastic, and that at these energies the inelastic neutron and proton cross-sections are equal,

the number of neutrons evaporated per excited nucleus in the tungsten target is equal to 4.0. If the binding energy of the most loosely bound neutron in a nucleus in the neighbourhood of tungsten is taken to be 6 MeV., the average energy lost in neutron evaporation by a nucleus in the tungsten target is 34.4 MeV. An estimate of the mean excitation energy of the evaporating nucleus may be obtained if it is assumed that one proton with an average kinetic energy of 10 MeV. is evaporated per nucleus, and that 7 MeV. are lost in other processes, including γ -emission (Le Couteur 1950). If the binding energy of the evaporated proton is taken as 7 MeV., the value $(34+17+7)=58$ MeV. is obtained

Fig. 2.



Neutron spectrum from carbon target.

for initial excitation energy—*i.e.* 0.37 of the energy of the primary protons. Goldberger (1948) calculates that the average excitation energy of a heavy nucleus when bombarded with 90 MeV. neutrons is 42.5 MeV. It is hoped to investigate, by a method similar to that described here, the energy spectrum of the evaporated protons, and the cross-section for this process, in order to obtain more precise information on the average energy of the excited nucleus.

Results obtained with the carbon target are shown in fig. 2. Curve A shows the differential cross-section for neutron emission, assuming that the evaporating nucleus was at rest in laboratory space. In fact, on account of its small mass, it may have been recoiling with sufficient velocity to affect the observed spectrum. It is difficult to estimate an

average value for the recoil velocity, but this will certainly be much less than that corresponding to the full transfer of momentum from the incident proton to the nucleus as a whole. Curve C, in fig. 2, is derived on the basis of full momentum transfer, and is therefore greatly over-corrected for recoil. Curve B, calculated on the assumption of 30 per cent momentum transfer, probably represents a more reasonable corrected spectrum. The presence of a relatively large number of high energy neutrons makes it difficult to give unambiguous values for the total "evaporation" cross-section and for the mean neutron energy. The figures given below were obtained by cutting off the spectra at 14 MeV.

	Curve A	Curve B	Curve C
Total cross-section for "evaporation" of neutrons (barns)	0.027	0.038	0.068
Mean kinetic energy of neutrons (MeV.)	4.5	4.6	5.4
Average number of neutrons per excited nucleus	0.16	0.23	0.41

The general conclusions to be drawn from these data are fortunately not affected by the considerable uncertainties in the corrections which have been applied to the observed spectrum. The average number of neutrons "evaporated" is less than one per excited nucleus, and there are relatively more high energy neutrons than would be expected from a nucleus in thermodynamic equilibrium.

ACKNOWLEDGMENTS.

We wish to thank Dr. J. M. Cassels for suggesting this problem, and Dr. T. G. Pickavance for helpful discussions during the course of the work. We wish also to express our thanks to the cyclotron operating crew for their co-operation. One of us (W.S.C.W.) would like to thank the Director of the Atomic Energy Research Establishment for allowing him to use the facilities at Harwell, and the Department of Scientific and Industrial Research for a maintenance grant.

REFERENCES.

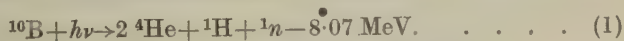
- CHAMPION, F. C., and POWELL, C. F., 1944, *Proc. Roy. Soc. A*, **183**, 64.
 DICKSON, J. M., and RANDLE, T. C., 1951, *Proc. Phys. Soc.* In the press.
 GOLDBERGER, M. L., 1948, *Phys. Rev.*, **74**, 1269.
 HARDING, J. B., LATTIMORE, S., and PERKINS, D. D., 1949, *Proc. Roy. Soc. A*, **196**, 325.
 LE COUTEUR, K. J., 1950, *Proc. Phys. Soc. A*, **63**, 259.
 NERESON, N., and REINES, F., 1950, *Rev. Sci. Ins.*, **21**, 534.
 SERBER, R., 1947, *Phys. Rev.*, **72**, 1114.
 TAYLOR, A. E., PICKAVANCE, T. G., CASSELS, J. M., and RANDLE, T. C., 1951 a, *Phil. Mag.*, **42**, 20.
 TAYLOR, A. E., PICKAVANCE, T. G., CASSELS, J. M., and RANDLE, T. C., 1951 b, *Phil. Mag.* In the press.
 WEISSKOPF, V., 1937, *Phys. Rev.*, **52**, 295.

The Photodisintegration of ^{10}B into Neutron, Proton and two α -Particles.

By M. J. BRINKWORTH and E. W. TITTERTON*,
Atomic Energy Research Establishment, Harwell†.

[Received July 27, 1951.]

IN the investigation of the reactions $^{11}\text{B}(\gamma, t)2\ ^4\text{He}$ (Titterton and Calcraft 1951) and $^{10}\text{B}(\gamma, d)2\ ^4\text{He}$ (Brinkworth and Titterton 1951) with the $^7\text{Li}(p, \gamma)$ radiation of 14.8 and 17.6 MeV. energy, three-pronged stars have been observed in Ilford E_1 boron loaded emulsions, which fail to give a momentum balance for either of these reactions, or for the reaction $^{12}\text{C}(\gamma, 3\alpha)$. The impossibility of a momentum balance is immediately obvious in some cases, when all three tracks fall within an angle less than 180° . It appears that at least one neutron is emitted in each of these events. The disintegrations are consistent with the reaction



which was reported by Goward, Titterton and Wilkins (1950).

Sometimes the proton track may be distinguished from the α -particle tracks by its lower grain density, but in many cases this is impossible, due to the intensifying action at development of the boron loading. In such cases, it is only when one track is too long to be an α -particle, from energy considerations, that the proton can be identified. Consequently, the proton energy distribution is known only for energies greater than about 2 MeV.

Of the 182 observed events which have been ascribed to reaction (1), 101 are such that the proton can be identified. In these cases the neutron energy can be deduced by application of the conservation of momentum, but the probable errors in the observed energies of the proton and α -particles are too great for this to be a satisfactory method. In consequence, only those events with $E_\gamma - E_n > 15\text{ MeV.}$ can definitely be assigned to the 17.6 MeV. γ -ray; those with $E_\gamma - E_n < 15\text{ MeV.}$ may be due to either the 14.8 or 17.6 MeV. γ -rays. It is therefore difficult to obtain the variation of cross-section with energy, but the experiment indicates that it does not fall off rapidly from 14.8 to 17.6 MeV. as does the $^{10}\text{B}(\gamma, d)2\ ^4\text{He}$ cross-section (Brinkworth and Titterton 1951). This rapid fall of the (γ, d) cross-section may be due to the competition of reaction (1) with increasing energy. The mean cross-section of reaction (1) for the $^7\text{Li}(p, \gamma)$ radiation is estimated to be $(3.2 \pm 1.3) \times 10^{-28}\text{ cm.}^2$.

The selection of events consequent on the inability to identify low energy protons in the present experiments renders it difficult to decide on the course of the reaction.

* Communicated by the Authors.

† Now at Research School of Physical Sciences, Australian National University, Canberra.

Neglecting a three-body reaction, the possible modes of disintegration which need to be considered are :—

(i.) Initial (γ, n) reaction, the residual excited ${}^9\text{Be}$ decaying through either ${}^8\text{Be}^*$ or ${}^5\text{Li}^*$. If the reaction proceeded through the ground state of ${}^9\text{Be}$, the event would be too small to be observed.

(ii.) Initial (γ, p) reaction, the residual ${}^9\text{Be}^*$ decaying through either ${}^8\text{Be}^*$ or ${}^5\text{He}^*$. The level of ${}^9\text{Be}$ at 2.42 MeV. (Hornyak, Lauritsen, Morrison and Fowler 1950) would result in a proton energy of 5.3 or 7.8 MeV. for the 14.8 and 17.6 MeV. γ -rays respectively. Two events have been obtained with protons of the latter energy. The only three events with proton energy of approximately 5.3 MeV. have each too great a total energy to be caused by the 14.8 MeV. γ -ray.

(iii.) Initial (γ, α) reaction, leaving ${}^6\text{Li}^*$. Although the reaction ${}^{10}\text{B}(\gamma, d)2\,{}^4\text{He}$ does not appear to proceed through ${}^6\text{Li}$ (Brinkworth and Titterton 1951) the reaction (1) may well do so, since it is known that the reaction $\text{Li}^6 + h\nu \rightarrow {}^4\text{He} + {}^1\text{H} + {}^1\text{n}$ does occur (Titterton and Brinkley 1951).

(iv.) Emission of a deuteron in the singlet state, dissociating into neutron and proton, since neutron scattering in ortho- and para-hydrogen shows that the singlet state is virtual. The residual ${}^8\text{Be}^*$ would yield two α -particles.

An attempt to decide between these alternatives can be made only when it is possible to identify the protons in all events so that complete distributions of particle energies or Q values may be examined.

Members of the nuclear emulsions group at the Atomic Energy Research Establishment are thanked for microscope work.

REFERENCES.

- BRINKWORTH and TITTERTON, 1951, *Phil. Mag.*, [7], **42**, 952.
 GOWARD, TITTERTON, and WILKINS, 1950, *Proc. Phys. Soc. A*, **63**, 172.
 HORNYAK, LAURITSEN, MORRISON, and FOWLER, 1950, *Rev. Mod. Phys.*, **22**, 291.
 TITTERTON and BRINKLEY, 1951, *Proc. Phys. Soc. A*, **64**, 212.
 TITTERTON and CALCRAFT, 1951, *Phil. Mag.*, [7], **42**, 666.

[The Editors do not hold themselves responsible for the views expressed by their correspondents.]

CXX. *The Interaction in the Theory of Beta Decay.*

By D. L. PURSEY*,

Department of Natural Philosophy, Glasgow University†.

[Received July 5, 1951.]

ABSTRACT.

The cross terms occurring in the expression for the theoretical n th forbidden beta spectrum are given for an arbitrary mixture of interactions. Relations are derived between the n th first forbidden vector nuclear matrix elements. Comparison with experiment is made for first forbidden transitions with allowed shape beta spectra. The results are discussed in relation to other recent work in the theory of beta decay. It is concluded that the interaction is most probably tensor with little or no admixture of other interactions.

§ 1. INTRODUCTION.

THE Fermi type theory of beta decay postulates an interaction between heavy and light particle fields proportional to a linear combination of the five Lorentz invariant expressions:

$$\left. \begin{aligned} S &= (\Psi^* \beta \Phi)(\psi^* \beta \phi), \\ V &= (\Psi^* \Phi)(\psi^* \phi) - (\Psi^* \alpha \Phi)(\psi^* \alpha \phi), \\ T &= (\Psi^* \beta \sigma \Phi)(\psi^* \beta \sigma \phi) + (\Psi^* \beta \alpha \Phi)(\psi^* \beta \alpha \phi), \\ A &= (\Psi^* \sigma \Phi)(\psi^* \sigma \phi) - (\Psi^* \gamma_5 \Phi)(\psi^* \gamma_5 \phi), \\ P &= (\Psi^* \beta \gamma_5 \Phi)(\phi^* \beta \gamma_5 \phi), \end{aligned} \right\} \quad (1)$$

where Ψ , Φ , ψ and ϕ are the proton, neutron, electron and neutrino fields respectively, and α , σ , β and γ_5 are the usual Dirac matrices. There is no good theoretical reason for preferring any particular linear combination of these interactions over any other, and consequently the interaction is free to be fitted with experiment. The large amount of accurate experimental information which has become available during the past few years not only has firmly established this type of theory for allowed and certain forbidden transitions, but helps considerably towards the experimental determination of the interaction.

Because of the arguments favouring the Gamow-Teller selection rules (summarized by Konopinski 1943), the interaction has long been thought to contain at least a proportion of either T or A. The most

* Now at Physics Department, King's College, London.

† Communicated by Professor J. C. Gunn.

convincing evidence for this now available, however, is the experimental discovery of several beta spectra having the characteristic shape, predicted only by T and A, for first forbidden transitions with an angular momentum change of two units and parity change. An excellent survey of recent experimental work, including the results just mentioned, has been given by Wu (1950).

With a mixture of interactions, cross terms may occur which affect the predicted spectrum shape. For allowed transitions, such cross terms occur only for mixtures of S with V or of A with T, and have the effect of multiplying the allowed spectrum by a factor $(1+a/W)$, where W is the beta particle energy in units of mc^2 . These cross terms have been calculated by Fierz (1937), who neglected the Coulomb field of the nucleus, and more recently by De Groot and Tolhoek (1950). The latter authors give an upper limit of $\frac{1}{10}$ for a , and conclude that mixing of S with V or of A with T, if it occurs at all, must be very slight.

It is clear from the foregoing that to be consistent with recent experimental evidence on forbidden transitions the interaction must contain either T or A, while evidence on allowed spectra forbids interactions containing both T and A, or both S and V. There remain unconsidered, however, a fair number of transitions which, although forbidden according to the semi-empirical *ft* classification, nevertheless have allowed shape beta spectra. Some of these transitions may be interpreted as first forbidden with an angular momentum change of 0 or 1 unit and change of parity, and they will be used here to gain further information about the beta decay interaction.

§ 2. CORRECTION FACTORS.

Greuling (1942, equations (11)–(16)) has given the correction factors by which the allowed spectrum must be multiplied to give the theoretical n th forbidden spectrum for each of the five interactions. For this paper, however, the correction factors associated with cross terms are also required. To obtain these, the n th forbidden correction factor for an arbitrary mixture of interactions was calculated by the method given by Konopinski and Uhlenbeck (1941). The correction factors for the cross terms are rather cumbersome, and to avoid interrupting the argument, they are given in an appendix. These cross terms when used in conjunction with Greuling's formulæ give the complete n th forbidden correction factor for an arbitrary mixture of interactions, except for a few terms unimportant except for $J=0$ to $J=0$ transitions, and a few terms which can be regarded as small corrections to the $(n-1)$ th forbidden correction factor. As an example, the n th forbidden correction factor for the mixture $A+yS$ is $C_{nA}+y^2C_{nS}+yC_n(S, A)$, where C_{nA} and C_{nS} are the correction factors given by Greuling for the pure axial vector and pure scalar interactions respectively, and $C_n(S, A)$ is the cross term given in the appendix.

§ 3. THE PSEUDOSCALAR INTERACTION.

By convention, P in this paper is regarded as having no allowed transitions. It is then seen from Greuling's formulæ, and from the cross terms given in the appendix, that the selection rules for an n th forbidden transition according to the interaction P are the same as those for an $(n-2)$ th forbidden transition according to the interactions T and A . Hence the correction factors will be almost independent of the amount of P in the interaction unless this is great enough to overcome the extra forbiddenness. If this were the case, one would expect the first forbidden pseudoscalar matrix element of P to give apparently superallowed transitions; all the observed superallowed transitions, however, with the exception of B^{12} , are already well explained by Wigner's theory of supermultiplets (see, for example, Konopinski 1943), and for none of them does a parity change seem reasonable. Furthermore, if the third forbidden P matrix element were strong enough to affect first forbidden transitions with unit angular momentum change, it would certainly dominate the much weaker transitions with angular momentum change of two units, and this does not appear to be the case. For these reasons, it is concluded that, while the amount of P in the interaction may be quite large, it is not sufficient to affect the correction factors for first forbidden transitions with unit angular momentum change. The correction factor for first forbidden transitions with no angular momentum change, however, may well be modified or even dominated by the presence of P in the interaction.

§ 4. NUCLEAR MATRIX ELEMENTS.

In the first forbidden correction factor, terms occur involving twelve different matrix elements. Of these, two are the second order tensors responsible for the transitions with angular momentum change of two units; their contribution to other first forbidden transitions is small, and will be ignored. Four of the matrix elements are pseudoscalars, and therefore cannot contribute to transitions involving an angular momentum change. In this section, relations will be found between the remaining six matrix elements, all of which are vectors.

The notation $(f|\mathbf{a}|i)$ will be used for these matrix elements, instead of the notation $[\mathbf{a}]$ used by Konopinski and Uhlenbeck (1941); by this is to be understood (for electron emission)

$$(f|\mathbf{a}|i) = \int d\mathbf{r}^1 \dots \int d\mathbf{r}^A \Psi_f^* \sum_{j=1}^A \frac{1}{2}(\tau_1^j - i\tau_2^j) \mathbf{a}^j \Psi_i, \quad \dots \quad (2)$$

where Ψ_i and Ψ_f are respectively the nuclear wave functions for the initial and final states, \mathbf{a} is a charge independent vector operator, τ_1 and τ_2 are the usual isotopic operators, the superscripts refer to the particles in the nucleus, and the integration includes summation over spin and isotopic spin states. As is usual in the theory of beta decay,

that representation of the Dirac matrices is chosen in which β and α become in non-relativistic approximation -1 and $-\mathbf{v}/c$ respectively, while the units of action, velocity and mass are chosen to be \hbar , c and m_e .

In the absence of any relativistic model of the nucleus the results of this section must be regarded as essentially non-relativistic, although relativistic notation will be used for the sake of convenience. It is therefore permissible to replace β by its non-relativistic approximation -1 , provided it commutes with the other operators appearing in the matrix element, and hence

$$(f|\beta\mathbf{r}|i) = -(f|\mathbf{r}|i); \quad (f|\beta\boldsymbol{\sigma}\wedge\mathbf{r}|i) = -(f|\boldsymbol{\sigma}\wedge\mathbf{r}|i). \quad \dots \quad (3)$$

Further relations can be derived using the Hartree type of single particle model. A sufficient condition that the single particle states should be eigenstates of the operator $k = \beta[(\boldsymbol{\sigma} \cdot \mathbf{m}) + 1]$, where \mathbf{m} is the orbital angular momentum, is that the magnitudes l and j of the orbital and total angular momentum of the states should both be good quantum numbers. This condition is certainly satisfied by the shell model of Mayer (1949, 1950) and of Haxel, Jensen and Süss (1949, 1950). The operator k is the well-known angular momentum operator of relativistic theory (see, for example, Dirac 1947), and has eigenvalues

$$k = \begin{cases} -(j + \frac{1}{2}), & j = l + \frac{1}{2} \\ + (j + \frac{1}{2}), & j = l - \frac{1}{2} \end{cases} \quad \dots \quad (4)$$

The following relations, in which $[\]$ and $\{ \}$ denote commutators and anti-commutators respectively, are easily verified :

$$\left. \begin{aligned} [k, \mathbf{r}] &= -i\beta\boldsymbol{\sigma}\wedge\mathbf{r}, \\ [k^2, \boldsymbol{\alpha}] &= \{k, \beta\boldsymbol{\alpha}\}, \end{aligned} \right\} \quad \dots \quad (5)$$

$$\left. \begin{aligned} [k, [k^2, \mathbf{r}]] &= \{k, \mathbf{r}\}, \\ [k, [k^2, \boldsymbol{\alpha}]] &= \{k, \boldsymbol{\alpha}\}, \end{aligned} \right\} \quad \dots \quad (6)$$

(6) expresses the selection rules $k_i + k_f = 0$ or $k_i - k_f = \pm 1$ for the matrix elements of \mathbf{r} and $\boldsymbol{\alpha}$; from (4) they are seen to be equivalent to $\Delta j = 0, \pm 1$, yes. (5) gives the relations

$$(f|\beta\boldsymbol{\sigma}\wedge\mathbf{r}|i) = -i\epsilon(f|\mathbf{r}|i); \quad (f|\beta\boldsymbol{\alpha}|i) = -\epsilon(f|\boldsymbol{\alpha}|i), \quad \dots \quad (7)$$

where $\epsilon = k_i - k_f$. If $k_i + k_f = 0$, the second of these relations is true only in non-relativistic approximation. These relations, together with (3), enable the six vector matrix elements to be reduced to two, namely $(f|\mathbf{r}|i)$ and $(f|\boldsymbol{\alpha}|i)$.

The selection rules for $(f|\boldsymbol{\sigma}|i)$ are found similarly to be $k_i = k_f$ or $k_i + k_f = \pm 1$, while, provided $k_i \neq k_f$,

$$(f|\beta\boldsymbol{\sigma}|i) = (k_i + k_f)(f|\boldsymbol{\alpha}|i). \quad \dots \quad (8)$$

Since β commutes with σ , it may be replaced in non-relativistic approximation by -1 . Consequently the matrix element for transitions with $k_i + k_f = +1$ must vanish in non-relativistic approximation, and must therefore be of order $(v/c)^2$; indeed, it is clear that (8) is self-consistent for such transitions only if the large components of the wave functions do not contribute to the matrix element. Obviously, transitions of this type will appear to be forbidden, and they must not be confused with genuinely first forbidden transitions, all of which involve a parity change. From (4) it is seen that the selection rule $k_i + k_f = +1$ is equivalent to $\Delta j = \pm 1$, $\Delta l = \pm 2$; for the allowed transitions with $k_i + k_f = -1$ or $k_i = k_f$, $\Delta l = 0$.

To obtain a relation between $(f|\alpha|i)$ and $(f|\mathbf{r}|i)$, the nuclear Hamiltonian is assumed to be

$$\begin{aligned} H = & - \sum_{j=1}^A \{(\boldsymbol{\alpha}^j \cdot \mathbf{p}^j) + \frac{1}{2}\beta^j[(1+\tau_3^j)M_n + (1-\tau_3^j)M_p]\} \\ & + \frac{1}{2} \sum_{j=1}^A \sum_{k \neq j}^A \{V_0(jk) + (\boldsymbol{\tau}^j \cdot \boldsymbol{\tau}^k)V_c(jk) - (\boldsymbol{\sigma}^j + \boldsymbol{\sigma}^k) \cdot (\mathbf{r}^j - \mathbf{r}^k) \wedge (\mathbf{p}^j - \mathbf{p}^k)V_s(jk) \\ & + \frac{1}{4}(1-\tau_3^j)(1-\tau_3^k)V_c(jk)\}, \quad \dots \quad (9) \end{aligned}$$

where V_0 , V_c , V_s and V_e are the ordinary, charge exchange, spin-orbit and Coulomb potentials between two nucleons respectively, and M_n and M_p are the neutron and proton masses. As before, the use of relativistic notation is for convenience only, and this Hamiltonian is to be considered valid only in non-relativistic approximation. For the sake of simplicity, and in the absence of any evidence to the contrary, the spin-orbit coupling is supposed not to be of charge exchange type.

By calculating the commutator of $\frac{1}{2} \sum_{j=1}^A (\tau_1^j - i\tau_2^j)\mathbf{r}^j$ with H , it is found that

$$\begin{aligned} (f|\alpha|i) = & i(W_i - W_f)(f|\mathbf{r}|i) + i(M_n - M_p)(f|\beta\mathbf{r}|i) \\ & - \frac{1}{2}i \sum_{j=1}^A \sum_{k \neq j}^A \int d\mathbf{r}^1 \dots \int d\mathbf{r}^A \Psi_f^*(\tau_1^j - i\tau_2^j) \{ \tau_3^k(\mathbf{r}^j - \mathbf{r}^k)V_c(jk) \\ & - i(\boldsymbol{\sigma}^j + \boldsymbol{\sigma}^k) \wedge (\mathbf{r}^j - \mathbf{r}^k)V_s(jk) - \frac{1}{2}(1-\tau_3^k)\mathbf{r}^j V_e(jk) \} \Psi_i. \quad (10) \end{aligned}$$

The last term in this expression will be averaged over the particles k , assuming they form a spin saturated spherical core of uniform density and radius ρ equal to the nuclear radius.

For both the exchange force and spin-orbit coupling contributions to (10), the problem is essentially that of averaging $(\mathbf{r}^j - \mathbf{r}^k)V(r)$, where $r = |\mathbf{r}^j - \mathbf{r}^k|$, over the core formed by the particles k . If $V(r)$ is expanded in a series of Legendre polynomials of the cosine of the angle between \mathbf{r}^j and \mathbf{r}^k and the spherical symmetry of the core is used, this averaging becomes elementary, and gives

$$\overline{(\mathbf{r}^j - \mathbf{r}^k)V(r)} = \mathbf{r}^j (3/16r_j^3\rho^3) \int_{|\rho-r_j|}^{\rho+r_j} V(r)[(\rho+r_j)^2 - r^2]^{1/2} [(\rho-r_j)^2 + r^2]^{1/2} r dr, \quad (11)$$

where $r_j = |\mathbf{r}^j|$. Since the transforming particle is presumably in an outer shell, r_j may be taken approximately equal to ρ . For a Yukawa well of depth v and range $1/k$, the averaging then gives

$$\mathbf{r}^j v (3A/2k^3 \rho^3) \{ (k\rho)^{-1} - 3(k\rho)^{-3} + \exp(-2k\rho)[2 + 5(k\rho)^{-1} + 6(k\rho)^{-2} + 3(k\rho)^{-3}] \} \quad (12a)$$

(Hughes and Le Couteur (1950) have also found this result, using a rather different method), while for a square well of depth v and range $1/k$, one obtains

$$\mathbf{r}^j v (3A/16k^4 \rho^4) [1 - \frac{1}{8}(k\rho)^{-2}]. \quad (12b)$$

In the charge exchange contribution to $(f|\boldsymbol{\alpha}|i)$, the factor τ_3^k gives on averaging a factor $(N-Z)/A$ where N is the neutron number of the initial nucleus and Z the proton number of the product nucleus. V_c is assumed to be of the form $[a_1 + a_2(\boldsymbol{\sigma}^j \cdot \boldsymbol{\sigma}^k)]V(jk)$ but because of the spin saturation of the core, only the term with coefficient a_1 will contribute; for the same reason, any tensor forces of the usual type will vanish. Using the value given by Rosenfeld (1948) for a_1 , based on the ratio of the triplet and singlet s potentials and the requirement of saturation for heavy nuclei, the effective V_c is found to be $-(1/10)V(^3s)$ where $V(^3s)$ is the triplet s potential. Taking the nuclear radius ρ to be $r_0 A^{1/3}$, and using both a Yukawa well of depth 100mc^2 and range r_0 and a square well of depth 40mc^2 and range $2r_0$ for $V(^3s)$, the exchange force contribution to $(f|\boldsymbol{\alpha}|i)$ is found to be

$$\text{Yukawa well:} \quad -15iA^{-4/3}(N-Z)(1-3A^{-2/3})(f|\mathbf{r}|i). \quad (13a)$$

$$\text{Square well:} \quad -12iA^{-4/3}(N-Z)(1-\frac{2}{3}A^{-2/3})(f|\mathbf{r}|i). \quad (13b)$$

The two wells give results in fair agreement. This exchange contribution is so small in any case that the use of more accurate well parameters is unnecessary.

Hughes and Le Couteur (1950) estimate that for V_s a Yukawa well of range r_0 and depth 1 MeV. is consistent both with the probable spin-orbit separation in He^5 and with the separation necessary according to the spin-orbit coupling shell model to account for the apparent level order in heavy nuclei. (The factor 2 difference in the depth given above from that given by Hughes and Le Couteur is due to a different definition of $\boldsymbol{\sigma}$; in this paper the spin angular momentum is $\frac{1}{2}\boldsymbol{\sigma}$). On averaging, the contribution to $(f|\boldsymbol{\alpha}|i)$ from the spin-orbit coupling is found to be

$$-3A^{-1/3}(1-3A^{-2/3})(f|\boldsymbol{\sigma} \wedge \mathbf{r}|i) = -3i\epsilon A^{-1/3}(1-3A^{-2/3})(f|\mathbf{r}|i) \quad (14)$$

on using (7).

The Coulomb contribution to $(f|\boldsymbol{\alpha}|i)$ can be estimated by a similar averaging procedure, and is found to be $i(Z\alpha/\rho)(f|\mathbf{r}|i)$. Collecting these results, one obtains

$$(f|\boldsymbol{\alpha}|i) = ix(f|\mathbf{r}|i)$$

where

$$x = (W_i - W_f) - (M_n - M_p) + (Z\alpha/\rho) - 15A^{-4/3}(N-Z)(1-3A^{-2/3}) - 3\epsilon A^{-1/3}(1-3A^{-2/3}). \quad (15)$$

For most first forbidden transitions, the first two terms in x approximately cancel, while the exchange force and spin-orbit terms are small compared to the Coulomb term. For positron emitters, the second, third and fourth terms in x change sign.

§ 5. COMPARISON WITH EXPERIMENT.

It was pointed out in the introduction that the interaction cannot contain both S and V, or both T and A, while the pseudoscalar interaction P was discussed in § 3 and found not to contribute to first forbidden transitions involving an angular momentum change. To avoid consideration of P, attention will be confined to transitions in which an angular momentum change of one unit for the transforming single particle state seems plausible according to the shell model of Mayer and of Haxel, Jensen and Süss. Consequently the only mixtures that need be discussed are those of S with T, A with V, V with T and S with A. The first two of these have almost identical correction factors, and therefore only the first of them will be considered. The correction factors for these mixtures and the type of transition under consideration may be found from the general formulæ of Greuling together with the cross terms given in the appendix, and may be further simplified using the relations between matrix elements found in the last section. In low Z approximation, they are

$$\begin{aligned} T+yS: C = & \{ \xi^2 + (2\xi/3W) + (\eta/18) + \frac{1}{9} \} \\ & - 2y\epsilon \{ \xi[(Z\alpha/2\rho) + (\zeta/3)] + (W_0\zeta/9) + (Z\alpha/\rho)/(6W) \} \\ & + y^2 \{ (Z\alpha/2\rho)^2 + (Z\alpha/\rho)(\zeta/3) + (\eta/3) - \frac{2}{9}(W_0 - W)(W - 1/W) \}. \\ & \dots \quad (16a) \end{aligned}$$

$$\begin{aligned} T+yV: C = & (1+y^2) \{ \xi^2 + (2\xi/3W) + (\eta/18) + \frac{1}{9} \} + y^2(\eta/6) \\ & - 2y\epsilon \{ (\xi^2/W) + (2\xi/3) + (W_0/9)(2 - W_0/W) \}. \quad \dots \quad (16b) \end{aligned}$$

$$\begin{aligned} A+yS: C = & (1+y^2) \{ (Z\alpha/2\rho)^2 + (Z\alpha/\rho)(\zeta/3) + (\eta/6) - \frac{2}{9}(W_0 - W)(W - 1/W) \} \\ & + y^2(\eta/6) - 2y\epsilon \{ [(Z\alpha/2\rho)^2 - (Z\alpha/\rho)(W_0/3)](1/W) + (Z\alpha/3\rho) \}, \\ & \dots \quad (16c) \end{aligned}$$

$$\text{where} \quad \left. \begin{aligned} \xi &= x - (Z\alpha/2\rho) - W_0/3, \\ \eta &= W_0^2 - 1 - 2W_0W + 2W^2, \\ \zeta &= 2W - W_0 - 1/W, \end{aligned} \right\} \quad \dots \quad (17)$$

x is the ratio of $(f|\alpha|i)$ to $i(f|\mathbf{r}|i)$, and $\epsilon = k_i - k_f = \pm 1$, depending on the transition. A factor $|f|\mathbf{r}|i|^2$ has been omitted from all of these correction factors. For positron emitters, the sign of Z must be changed throughout, and the sign of the cross term (proportional to y) changed in the mixture $T+yS$.

Only transitions with an ft value greater than 10^6 and whose experimental Kurie plot is straight to within 5 per cent for a reasonable energy range will be regarded as sufficiently forbidden and sufficiently accurately investigated to warrant detailed comparison with theory.

A search in the literature for such transitions has yielded the following : Na²² (Good, Peaslee and Deutsch 1946), Na²⁴ (Siegbahn 1946), Sc⁴⁶ (Peacock and Wilkinson 1948), V⁴⁸ (Peacock and Deutsch 1946), Pr¹⁴⁶ (Feldman, Lidofsky, Macklin and Wu 1949), Pm¹⁴⁷ (Agnew 1950, Langer, Motz and Price 1950, Lidofsky, Macklin and Wu 1949), Hf¹⁸¹ (Chu and Wiedenbeck 1949), Re¹⁸⁶ (Beach, Peacock and Wilkinson 1949, Langer and Price 1949), W¹⁸⁷ (Peacock and Wilkinson 1948), Au¹⁹⁸ (Langer and Price 1949, Saxon 1948, Steffen, Huber and Humbel 1949). P³², Ga⁶⁶ and Cs¹³⁴ are more probably of the $\Delta j=1$, $\Delta l=2$ type of transition mentioned in the last section, while Mo⁹⁹ and I¹³¹ are not easily interpreted on the shell model picture ; these five interactions are therefore not considered.

The sign of ϵ is obtained from the shell model interpretation of the transition. The level scheme given by Haxel, Jensen and Süß (1950) is used in conjunction with the measured spins of neighbouring odd nuclei to suggest the initial state, and, if the transition is between ground states, also the final state, of the transforming nucleon. If the transition is to an excited level of the product nucleus, a reasonable transition involving parity change must be postulated. In this case, for heavy nuclei with a large neutron excess the transforming neutron need not belong to the outermost occupied neutron shell, and several interpretations may be possible.

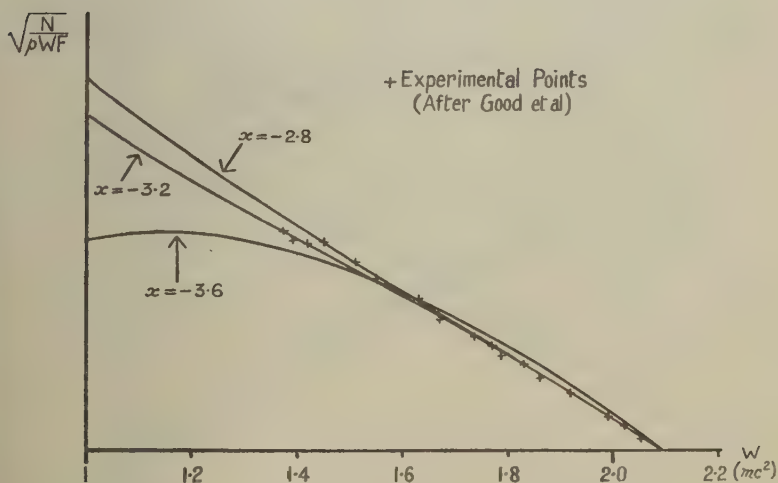
For Na²² and Na²⁴, the shell model interpretation is complicated by the anomalous filling of the $d_{5/2}$ shell ; however, for Na²² the most probable transition seems to be $p_{3/2} \rightarrow s_{1/2}$, for which $\epsilon = -1$, while for Na²⁴ the transition is probably $d_{5/2} \rightarrow f_{7/2}$ with $\epsilon = +1$. For both Sc⁴⁶ and V⁴⁸, the only reasonable transition is $f_{7/2} \rightarrow d_{5/2}$, with $\epsilon = -1$. Pr¹⁴³ and Pm¹⁴⁷ undergo ground state to ground state transitions, and are almost certainly of the type $h_{9/2} \rightarrow g_{7/2}$ with $\epsilon = +1$. For Hf¹⁸¹, Re¹⁸⁶ and W¹⁸⁷ the transition may be any of $i_{13/2} \rightarrow h_{11/2}$, $f_{5/2} \rightarrow g_{7/2}$, $p_{1/2} \rightarrow d_{3/2}$, $f_{7/2} \rightarrow d_{5/2}$, all with $\epsilon = -1$, or $h_{9/2} \rightarrow g_{7/2}$ with $\epsilon = +1$, or $f_{7/2} \rightarrow g_{7/2}$ in which case the transition is not of the required type ; for these transitions ϵ was assumed to be -1 . For Au¹⁹⁸, the transition is probably $f_{5/2} \rightarrow d_{3/2}$ with $\epsilon = +1$.

The correction factors (16 *a*) and (16 *b*) are not very sensitive to the value of x unless ξ is small. This is the case for Na²², and fig. 1 shows theoretical Kurie plots for this transition according to the tensor interaction for different values of x . (15) gives for x the value -2.5 , and this gives an almost straight Kurie plot in fair agreement with experiment. The possibility of error, however, cannot be denied, and in particular if ϵ is $+1$ instead of -1 as assumed, (15) gives $x = -3.9$ and a Kurie plot far from straight. It seems unlikely, therefore, that any reliance can be put on conclusions about mixtures involving T or V based on this transition. It is also found that for the positron emitters Na²² and V⁴⁸ the Kurie plots for all mixtures of the type $A+yS$ are reasonably straight in the experimentally measured region. Consequently, no

reliable information about any mixtures of interactions can be obtained from the available evidence on Na^{22} ; and this transition will no longer be considered. For all the other transitions, the theoretical spectrum shapes are not very sensitive to the value of x , and the estimate of § 4 should give fairly reliable results.

For heavy nuclei with fairly low end points, the spectrum shapes predicted by all the pure interactions are indistinguishable from the allowed shape. For mixtures, however, if the cross term is negative there may be a large cancellation causing the theoretical spectrum to deviate strongly from the allowed shape. This is illustrated for

Fig. 1.



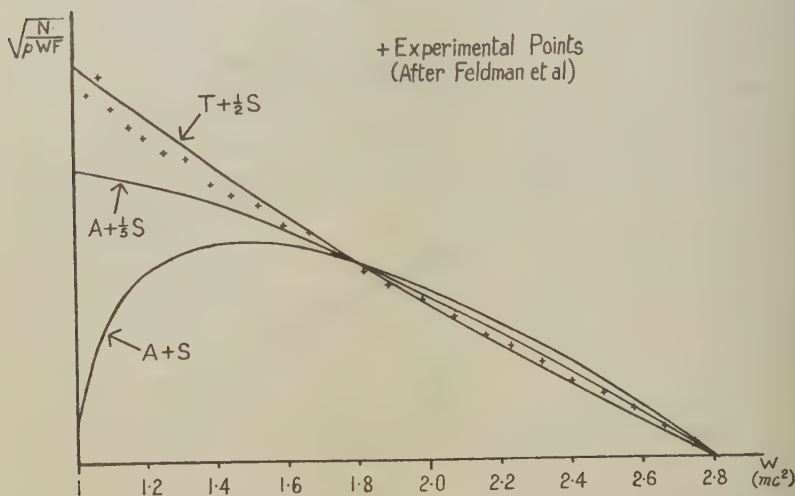
Theoretical Kurie plots for Na^{22} according to the tensor interaction, with different values for the ratio x of $-i(f|\alpha|i)$ to $(f|\mathbf{r}|i)$. The estimate of § 4 gives $x = -2.5$.

Pr^{143} in fig. 2. For all mixtures, if $y = -1$ the theoretical Kurie plot is similar to that shown for the mixture $A+S$, while if y increases or decreases, the Kurie plot approaches a straight line. The mixtures $T+yS$ and $V+yA$ are remarkable in that the theoretical Kurie plot changes from "concave down" through an S-shape to "concave up" before becoming straight; this change is very rapid, and for Pr^{143} it is complete when $y = 0.8$. Frequently the experimental Kurie plot shows an excess of low energy electrons which may be due to experimental difficulties such as source thickness effects, or to a second low energy transition, or it may be genuine. As a precaution which should be more than adequate to prevent false conclusions being drawn, only that part of the Kurie plot which is experimentally straight is compared with

theory. Theoretical and experimental Kurie plots are regarded as consistent with each other if the discrepancy between them is not more than 5 per cent at the low energy end and 10 per cent at the high energy end of the straight portion. For Pr^{143} , only that part of the Kurie plot above 1.4 mc^2 is used, and the Kurie plots for the mixtures $A + \frac{1}{2}S$ and $T + \frac{1}{2}S$ both show the maximum allowed discrepancy. Since the sign of the cross term depends on ϵ and therefore on the transition, it is clear that by considering different transitions both lower and upper limits can be obtained for the ratio γ of the interaction constants in any mixture.

For lighter nuclei such as Na^{24} , the picture is very similar, except that the predicted spectrum shapes for pure A and S are no longer

Fig. 2.



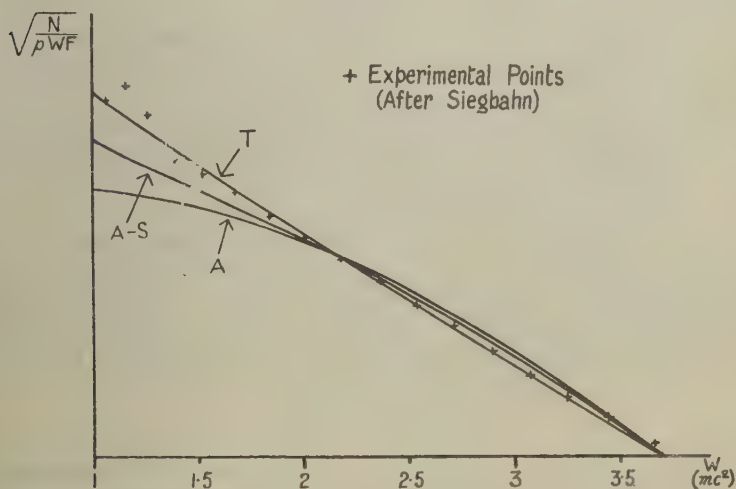
Theoretical Kurie plots for Pr^{143} for various mixtures of interactions.

allowed, and indeed for Na^{24} no mixture whatsoever of S with A gives an allowed shape spectrum. Fig. 3 gives theoretical Kurie plots for Na^{24} for the interactions A, A-S and T, of which only the last is consistent with experiment. It was pointed out in the introduction that the interaction must contain either T or A, but not both; the spectrum of Na^{24} seems to favour T, but A with a large admixture of V cannot be ruled out. Of the nine transitions under consideration, Na^{24} is the only one capable of distinguishing between T and A in this way, and it should be kept in mind that the Na^{24} result is valid only if the transition is genuinely first forbidden and not a highly unfavoured allowed transition, and if the first forbidden pseudoscalar matrix elements do not contribute. This will be the case whatever the angular momentum change of the nucleus as a whole, provided, as was assumed

above, the single particle transition is of the type $d_{5/2} \rightarrow f_{7/2}$; if, however, the transition is, for example, $d_{5/2} \rightarrow f_{5/2}$, the result will be valid only if the nucleus as a whole changes its angular momentum.

The limits to the amount of mixing found from each of the nine transitions considered are given in Table I. The first-named interaction in each mixture is assumed to predominate, so that y is numerically less than one; since, however, the mixtures $S+yA$ and $V+yT$ are almost identical with the mixtures $A+yS$ and $T+yV$ respectively, and since the limits are given for both $T+yS$ and $S+yT$, this means no loss of generality. The mixtures $V+yA$ and $A+yV$ are almost identical to the mixtures $T+yS$ and $S+yT$ respectively.

Fig. 3.



Theoretical Kurie plots for Na^{24} for various interactions. No mixture of the type $A+yS$ is consistent with experiment.

From Table I. it is seen that very little admixture of S with A , and little admixture of V with T is permissible. Mixtures of T and S , or of V and A , are possible, but one or other of the two interactions must predominate. If the evidence of Na^{24} is accepted, then the only permissible interactions are T with perhaps a small admixture of either V or S , and a mixture of A and V with V predominating. The tensor interaction T is the only pure interaction consistent both with the interpretation given for Na^{24} and with all the other experimental data on beta spectrum shapes.

The validity of these results, of course, depends on the accuracy of the estimates used for the ratios of the nuclear matrix elements, and on the correctness of the shell model interpretations of the transitions. An error in the relations between the matrix elements will cause a proportionate error in some or all of the limits given in Table I.; such an

error, however, would have to be very large before it would alter the main features of the table. An error in the shell model interpretation may cause the adoption of the wrong sign for ϵ ; in this case, the limits given will be true for $-y$ instead of for y .

TABLE I.
Upper and Lower Limits for the Mixture Parameter y .

Mixture	Na ²⁴	Sc ⁴⁶	V ⁴⁸	Pr ¹⁴³	Pm ¹⁴⁷	Hf ¹⁸¹	Re ^{186*}	W ¹⁸⁷	Au ¹⁹⁸
A+yS	X	-0.5		0.2	0.2	-0.33	-0.1	-0.7	0.1
T+yV	0.2	-0.5	-0.5	0.33	0.33	-0.5	-0.33		0.33
T+yS	0.35 -0.7	-0.65	0.25	0.5	0.7	-0.7	-0.5	-0.65	0.5
S+yT	X	-0.75	0.7	0.5	0.9		-0.5	-0.75	0.6

The first-named interaction is assumed to predominate. The upper and lower rows of figures for each mixture are respectively upper and lower limits for y , while the columns indicate the transitions from which the limits are derived. X denotes that no values of y are consistent with experiment.

* See note added in proof.

§ 6. CONCLUSION.

In the introduction, it was pointed out that because of the arguments in favour of the Gamow-Teller selection rules, and because of the discovery of spectra having the characteristic first forbidden spin change of two shape, the interaction must contain either T or A. From the allowed spectrum shapes, it was seen that the interaction cannot contain both S and V, or both T and A. Taken in conjunction with these results, the work of this paper shows that the interaction must either be mainly T with possibly a small admixture of S or V, or mainly V with an admixture of A. If the evidence of Na²⁴ is not accepted a predominantly axial vector interaction is also possible. The decays of RaE of Cs¹³⁷ are almost certainly second forbidden, and their spectrum shapes appear to demand an interaction in which either T or V predominates (Konopinski and Uhlenbeck 1941, Langer and Moffat 1951), though not all possible mixtures have been considered. By considering the lifetimes of superallowed transitions, and assuming Wigner's theory of supermultiplets, Moszkowski (1951) has concluded that the interaction is either almost entirely T or almost entirely A. Marshak (1942) and Greubig (1942) have calculated theoretical half-lives for various forbidden

transitions using the tensor interaction, and found reasonable agreement with experiment. It appears therefore that the experimental evidence strongly favours the pure tensor interaction, although none of the above evidence precludes an admixture of P.

Tiomno Wheeler and Rau (1949) and Tiomno and Wheeler (1949) have shown that the beta decay and the capture by protons of μ -mesons can both be explained by quadrilinear interactions with the same interaction constant as in nuclear beta decay, and this has led to the idea of a universal quadrilinear interaction. For such an interaction, symmetry properties with respect to the interchange of fields having similar physical properties may have physical significance. The best known interaction having such properties is the Critchfield interaction S-A-P (Critchfield 1943), which, if the fields are quantized so that any two anti-commute, is symmetric with respect to the interchange of any pair of fields. Apart from the pure interactions, all of which are either symmetrical or anti-symmetrical with respect to the interchange of the light particle or the heavy particle fields, the only two other interactions having special symmetry properties which are consistent with allowed beta spectra are S-T+P and 3S+T+3P, which are respectively symmetrical and antisymmetrical with respect to the interchange of the two neutral or the two charged fields. Of these three interactions, only the last is consistent with the results of Table I., and it is inconsistent with Moszkowski's results, and probably also with the RaE and Cs¹³⁷ spectra. On changing the order of the charged and neutral fields in the interaction to that used by Michel (1950) in calculating the theoretical beta spectrum from μ -meson decay, 3S+T+3P becomes pure tensor, which predicts a spectrum in complete disagreement with experiment. Consequently a universal interaction, if one exists, can have no special symmetry properties, and the ordering of the fields in the interaction must therefore be uniquely determined by their physical properties such as charge, or sign of magnetic moment of a neutral particle. This need not preclude the hypothesis of a Majorana neutrino, provided there are some neutral particles which are not of Majorana type; this is, however, the case, since, both because of its magnetic moment and because of the stability of nuclei, the neutron cannot be a Majorana particle. By comparing either with Michel's results or with the figures given by Tiomno, Wheeler and Rau, it is seen that the tensor interaction with the ordering of the fields usual in the theory of nuclear beta decay is consistent with the beta spectrum from μ -meson decay, whether the neutrino is a Dirac or a Majorana neutral particle.

ACKNOWLEDGMENTS

The author is indebted to Professor J. C. Gunn and Dr. B. F. X. Tauschek for suggesting this problem and for many stimulating discussions, and to the Department of Scientific and Industrial Research for a maintenance grant during the tenure of which this work was performed.

APPENDIX.

The correction factors for the cross terms occurring in the expression for the theoretical n th forbidden beta spectrum for an arbitrary mixture of interactions are given below, using Greuling's (1942) notation except that $Q_n(\mathbf{a})$ is written for Greuling's $Q_n(\mathbf{a}, \mathbf{r})/(n!)$. The units of action, velocity and mass are chosen to be \hbar , \mathbf{c} and \mathbf{m}_e respectively. The method of using these correction factors was explained in § 2.

$$\begin{aligned}
 C_n(S, V) = & -[Q_n(\beta \mathbf{r})Q_n^*(\mathbf{r}) + \text{c.c.}] \sum_{\nu=0}^n \{A_{n\nu}Q_\nu q^{2(n-\nu)-2} + D_{n\nu}P_\nu q^{2(n-\nu)}\} \\
 & + i[Q_n(\beta \mathbf{r})Q_n^*(\boldsymbol{\alpha}) - \text{c.c.}] \sum_{\nu=0}^n \{A_{n\nu}R_\nu q^{2(n-\nu)-2} + C_{n\nu}P_\nu q^{2(n-\nu)-1}\}, \\
 C_n(S, T) = & i[Q_n(\beta \mathbf{r})Q_n^*(\beta \boldsymbol{\alpha}) - \text{c.c.}] \sum_{\nu=0}^n \{A_{n\nu}N_\nu q^{2(n-\nu)-2} + C_{n\nu}L_\nu q^{2(n-\nu)-1}\} \\
 & + i[Q_n(\beta \mathbf{r})Q_n^*(\beta \boldsymbol{\sigma} \wedge \mathbf{r}) - \text{c.c.}] \sum_{\nu=0}^n \{A_{n\nu}M_\nu q^{2(n-\nu)-2} \\
 & + (D_{n\nu} - B_{n\nu})L_\nu q^{2(n-\nu)}\}, \\
 C_n(S, A) = & -i[Q_n(\beta \mathbf{r})Q_n^*(\boldsymbol{\sigma} \wedge \mathbf{r}) - \text{c.c.}] \sum_{\nu=0}^n \{A_{n\nu}Q_\nu q^{2(n-\nu)-2} - 2C_{n\nu}R_\nu q^{2(n-\nu)-1} \\
 & + (D_{n\nu} - B_{n\nu})P_\nu q^{2(n-\nu)}\}, \\
 C_n(V, T) = & [Q_n(\boldsymbol{\alpha})Q_n^*(\beta \boldsymbol{\alpha}) + \text{c.c.}] \sum_{\nu=0}^n A_{n\nu}P_\nu q^{2(n-\nu)-2} \\
 & - i[Q_n(\mathbf{r})Q_n^*(\beta \boldsymbol{\alpha}) - \text{c.c.}] \sum_{\nu=0}^n \{-A_{n\nu}R_\nu q^{2(n-\nu)-2} + C_{n\nu}P_\nu q^{2(n-\nu)-1}\} \\
 & - i[Q_n(\mathbf{r})Q_n^*(\beta \boldsymbol{\sigma} \wedge \mathbf{r}) - \text{c.c.}] \sum_{\nu=0}^n \{A_{n\nu}Q_\nu q^{2(n-\nu)-2} + 2C_{n\nu}R_\nu q^{2(n-\nu)-1} \\
 & + (D_{n\nu} - B_{n\nu})P_\nu q^{2(n-\nu)}\} \\
 & - [Q_n(\boldsymbol{\alpha})Q_n^*(\beta \boldsymbol{\sigma} \wedge \mathbf{r}) + \text{c.c.}] \sum_{\nu=0}^n \{-A_{n\nu}R_\nu q^{2(n-\nu)-2} + C_{n\nu}P_\nu q^{2(n-\nu)-1}\}, \\
 C_n(V, A) = & [Q_n(\boldsymbol{\alpha})Q_n^*(\boldsymbol{\sigma} \wedge \mathbf{r}) + \text{c.c.}] \sum_{\nu=0}^n \{A_{n\nu}N_\nu q^{2(n-\nu)-2} + C_{n\nu}L_\nu q^{2(n-\nu)-1}\} \\
 & + i[Q_n(\mathbf{r})Q_n^*(\boldsymbol{\sigma} \wedge \mathbf{r}) - \text{c.c.}] \sum_{\nu=0}^n \{A_{n\nu}M_\nu q^{2(n-\nu)-2} \\
 & + (D_{n\nu} - B_{n\nu})L_\nu q^{2(n-\nu)}\}, \\
 C_n(V, P) = & -i[Q_{n-1}(\boldsymbol{\alpha} \wedge \mathbf{r})Q_{n-1}^*(\beta \gamma_5 \mathbf{r}) - \text{c.c.}] \sum_{\nu=0}^{n-1} \{A_{n-1,\nu}Q_\nu q^{2(n-\nu-1)-2} \\
 & - 2C_{n-1,\nu}R_\nu q^{2(n-\nu-1)-1} + (D_{n-1,\nu} - B_{n-1,\nu})P_\nu q^{2(n-\nu-1)}\},
 \end{aligned}$$

$$\begin{aligned}
C_n(T, A) = & -[Q_{n+1}(\beta\sigma)Q_{n+1}^*(\sigma) + \text{c.c.}] \sum_{\nu=0}^n B_{n\nu} P_\nu q^{2(n-\nu)} \\
& -[Q_n(\beta\sigma \wedge \mathbf{r})Q_n^*(\sigma \wedge \mathbf{r}) + \text{c.c.}] \sum_{\nu=0}^n \{A_{n\nu} Q_\nu q^{2(n-\nu)-2} \\
& + \left(D_{n\nu} - \frac{1}{n+1} B_{n\nu}\right) P_\nu q^{2(n-\nu)}\} \\
& + [Q_n(\beta\alpha)Q_n^*(\sigma \wedge \mathbf{r}) + \text{c.c.}] \sum_{\nu=0}^n \{A_{n\nu} R_\nu q^{2(n-\nu)-2} + C_{n\nu} P_\nu q^{2(n-\nu)-1}\}, \\
C_n(T, P) = & -i[Q_n(\beta\sigma)Q_n^*(\beta\gamma_5 \mathbf{r}) - \text{c.c.}] \sum_{\nu=0}^n \{A_{n\nu} N_\nu q^{2(n-\nu)-2} + C_{n\nu} L_\nu q^{2(n-\nu)-1}\}, \\
C_n(A, P) = & i[Q_n(\sigma)Q_n^*(\beta\gamma_5 \mathbf{r}) - \text{c.c.}] \sum_{\nu=0}^n \{A_{n\nu} R_\nu q^{2(n-\nu)-2} + C_{n\nu} P_\nu q^{2(n-\nu)-1}\}.
\end{aligned}$$

These last two correction factors represent a mixing of the $(n+1)$ th forbidden P spectrum with the $(n-1)$ th forbidden T and A spectra respectively.

The quantities P_ν , Q_ν , and R_ν are defined analogously to L_ν , M_ν and N_ν by

$$\begin{aligned}
P_\nu &= (2p^2 F_0)^{-1} [g_\nu^2 - f_{-(\nu+2)}^2] \rho^{-2\nu}, \\
Q_\nu &= (2p^2 F_0)^{-1} [g_{-(\nu+2)}^2 - f_\nu^2] \rho^{-2(\nu+1)}, \\
R_\nu &= (2p^2 F_0)^{-1} [f_\nu g_\nu + f_{-(\nu+2)} g_{-(\nu+2)}] \rho^{-2\nu-1}.
\end{aligned}$$

By expanding the radial functions g and f in powers of ρ and neglecting the first and higher powers, one obtains

$$\begin{aligned}
P_\nu &= (F_\nu/F_0) \left(\frac{2^\nu \nu!}{(2\nu+1)!} p^\nu \right)^2 \left(\frac{s_\nu(\nu+1+s_\nu)}{2(\nu+1)^2} \right) \frac{1}{W}, \\
Q_\nu &= (F_\nu/F_0) \left(\frac{2^{\nu+1} \nu!}{(2\nu+2)!} p^\nu \right)^2 \left\{ -\frac{2s_\nu}{\nu+1+s_\nu} \left(\frac{Z\alpha}{2\rho} \right)^2 \frac{1}{W} + \frac{(Z\alpha)^2}{\nu+1+s_\nu} \left(\frac{Z\alpha}{\rho} \right) \right. \\
&\quad + \frac{s_\nu(\nu+1)}{(2s_\nu+1)^2} \left[1 + \frac{s_\nu(Z\alpha)^2}{(\nu+1)(\nu+1+s_\nu)} \right] \frac{p^2}{W^2} \\
&\quad \left. + \left[1 - \frac{(4s+3)(Z\alpha)^2}{\nu+1+s_\nu} \right] \left(\frac{Z\alpha}{2s_\nu+1} \right)^2 W \right\}, \\
R_\nu &= (F_\nu/F_0) \left(\frac{2^{\nu+1} \nu!}{(2\nu+2)!} p^\nu \right)^2 \left\{ -\frac{s_\nu}{W} \left(\frac{Z\alpha}{2\rho} \right) + (Z\alpha)^2 \right\}.
\end{aligned}$$

For low Z , s_ν may be put equal to $\nu+1$, $F_\nu = F_0$, and $(Z\alpha)^2 = 0$ to give the simpler expressions

$$\begin{aligned}
P_\nu &= \left(\frac{2^\nu \nu!}{(2\nu+1)!} p^\nu \right)^2 \frac{1}{W}; \quad Q_\nu = \left(\frac{2^{\nu+1} \nu!}{(2\nu+2)!} p^\nu \right)^2 \left\{ -\frac{1}{W} \left(\frac{Z\alpha}{2\rho} \right)^2 + \left(\frac{\nu+1}{2\nu+3} \right)^2 \frac{p^2}{W} \right\}, \\
R_\nu &= -\left(\frac{2^\nu \nu!}{(2\nu+1)!} p^\nu \right)^2 \frac{1}{\nu+1} \left(\frac{Z\alpha}{2\rho} \right) \frac{1}{W}.
\end{aligned}$$

For positron emitters, the sign of Z and, as De Groot and Tolhoek (1950) have shown, the signs of $C_n(S, V)$, $C_n(S, T)$, $C_n(V, A)$, $C_n(T, A)$, $C_n(V, P)$ and $C_n(T, P)$ should be changed.

Note added in proof.—Since this paper was written, papers by Metzger and Hill (1951) and Steffen (1951) have been received confirming the result of Grant and Richmond (1949) that the spectrum of Re^{186} is complex. In calculating Table I., this spectrum was assumed to be simple: consequently the limits in Table I. derived from the Re^{186} transition are narrower than experiment now warrants.

REFERENCES.

- AGNEW, H. M., 1950, *Phys. Rev.* [2], **77**, 655.
 BEACH, L. A., PEACOCK, C. L., and WILKINSON, R. G., 1949, *Phys. Rev.* [2], **76**, 1585.
 CHU, K. Y., and WIEDENBECK, M. L., 1949, *Phys. Rev.* [2], **75**, 226.
 CRITCHFIELD, C. L., 1943, *Phys. Rev.* [2], **63**, 417.
 DE GROOT, S. R., and TOLHOEK, H. A., 1950, *Physica*, **16**, 456.
 DIRAC, P. A. M., 1947, *Quantum Mechanics*, 3rd. Ed., p. 266 (Oxford: The University Press).
 FELDMAN, L., LIDOFKY, L., MACKLIN, P., and WU, C. S., 1949, *Phys. Rev.* [2], **75**, 1888.
 FIERZ, M., 1937, *Zeits. f. Phys.*, **104**, 553.
 GOOD, W. M., PEASLEE, D., and DEUTSCH, M., 1946, *Phys. Rev.* [2], **69**, 313.
 GRANT, P. J., and RICHMOND, R., 1949, *Proc. Phys. Soc., A*, **62**, 573.
 GREULING, E., 1942, *Phys. Rev.* [2], **61**, 568.
 HAXEL, O., JENSEN, J. H. D., and SUSS, H. E., 1949, *Phys. Rev.* [2], **75**, 1766; 1950, *Zeits. f. Phys.*, **128**, 294.
 HUGHES, J., and LE COUTEUR, K. J., 1950, *Proc. Phys. Soc. A*, **63**, 1219.
 KONOPINSKI, E. J., 1943, *Rev. Mod. Phys.*, **15**, 209.
 KONOPINSKI, E. J., and UHLENBECK, G. E., 1941, *Phys. Rev.* [2], **77**, 798.
 LANGER, L. M., and MOFFAT, R. J. D., 1951, *Phys. Rev.* [2], **82**, 635.
 LANGER, L. M., MOTZ, J. W., and PRICE, H. C. Jr., 1950, *Phys. Rev.* [2], **77**, 798.
 LANGER, L. M., and PRICE, H. C. Jr., 1949, *Phys. Rev.* [2], **76**, 641.
 LIDOFKY, L., MACKLIN, P., and WU, C. S., 1949, *Phys. Rev.* [2], **76**, 1888.
 MARSHAK, R. E., 1942, *Phys. Rev.* [2], **61**, 431.
 MAYER, M. G., 1949, *Phys. Rev.* [2], **75**, 1969; 1950, *Phys. Rev.* [2], **78**, 16, 22.
 METZGER, F. R., and HILL, R. D., 1951, *Phys. Rev.* [2], **82**, 646.
 MICHEL, L., 1950, *Proc. Phys. Soc. A*, **63**, 514, 1371.
 MOSZKOWSKI, S. A., 1951, *Phys. Rev.* [2], **82**, 118.
 PEACOCK, W. C., and DEUTSCH, M., 1946, *Phys. Rev.* [2], **69**, 306.
 PEACOCK, C. L., and WILKINSON, R. G., 1948, *Phys. Rev.* [2], **74**, 297.
 ROSENFELD, L., 1948, *Nuclear Forces*, Chap. XI. (Amsterdam: North-Holland Publishing Company).
 SAXON, D., 1948, *Phys. Rev.* [2], **70**, 127.
 STEFFEN, R. M., 1951, *Phys. Rev.* [2], **82**, 827.
 STEFFEN, R. M., HUBER, O., and HUMBEL, F., 1949, *Helvetica physica Acta*, **22**, 167.
 TIOMNO, J., and WHEELER, J. A., 1949, *Rev. Mod. Phys.*, **21**, 153.
 TIOMNO, J., WHEELER, J. A., and RAU, R. R., 1949, *Rev. Mod. Phys.*, **21**, 144.
 WU, C. S., 1950, *Rev. Mod. Phys.*, **22**, 386.

CXXI. *Ultrasonic Propagation in Liquid Helium near the Lambda-Point.*

By A. B. PIPARD,

The Royal Society Mond Laboratory, Cambridge*.

[Received June 27, 1951.]

ABSTRACT.

It is suggested that the sharp minimum in velocity and maximum in attenuation of ultrasonic waves in liquid helium in the region of the λ -point is a consequence of fluctuations which lead to the production of inclusions of He II in He I above the λ -point, and of He I in He II below the λ -point. Expressions are derived for the velocity and attenuation in an inhomogeneous fluid, and are applied, with some modifications, to liquid helium. It is found that the shape of the velocity curve may be accounted for satisfactorily, and that the observed attenuation just above the λ -point requires the inclusions of He II to consist of about 850 atoms. It is shown that fluctuation theory predicts the presence of inclusions of this size in the concentration required to explain the experimental results.

§ 1. INTRODUCTION.

EXPERIMENTS on the propagation of ultrasonic waves in liquid helium have revealed peculiarities of behaviour at temperatures near the λ -point (2.18°K.): the velocity drops to a sharp minimum at the λ -point, and at the same time the attenuation rises rapidly to a peak. The effect which culminates at the λ -point begins to be apparent not far below 3°K. , at which temperature the specific heat also displays the first symptoms of its rise to a sharp maximum, so that it is probable the two effects are intimately related. Naturally the specific heat variation is reflected in a corresponding variation of γ , the ratio of the principal specific heats, which drops to a value near unity at the λ -point, and this provides a satisfactory phenomenological explanation of the shape of the velocity curve. It does not, however, in itself suggest a mechanism for the rapid increase in attenuation, for which a number of tentative proposals have been made, none of which has been worked out fully enough to carry conviction. The present paper is intended as a crude analysis of a model of liquid helium above the λ -point which provides a qualitative explanation of the observed attenuation. A complete theoretical investigation would be of far too great a complexity to be practicable at present.

It has been suggested by Lennard-Jones and Keesom (1935) that the increase in the specific heat of He I between 3.0°K. and 2.18°K. is to be attributed to thermodynamical fluctuations of sufficient magnitude to

* Communicated by the Author.

lead to the formation of inclusions of He II in the liquid, and, although their analysis is not sufficiently refined to give more than a rough estimate of the importance of this effect, there can be little doubt of its essential correctness. As a starting-point, therefore, we shall assume that in this temperature range the liquid is inhomogeneous in the sense that it contains small inclusions whose thermodynamical properties, if not exactly the same as those of He II in bulk, are at least markedly different from those of He I. Their influence on γ may be readily understood by considering the reduction which they bring about in the temperature rise during adiabatic compression. For the present purpose it is convenient to think of the effect of adiabatic compression as equivalent, so far as temperature changes are concerned, to the injection of heat at constant pressure. The inclusions are now seen to exert a two-fold influence. In the first place they reduce the temperature rise by increasing the mean specific heat of the liquid, and in the second place they actually reduce the equivalent heat input; for while in order to simulate the temperature changes accompanying adiabatic compression heat must be injected into He I, it must be removed from He II on account of the negative expansion coefficient of the latter. The net result is that the temperature rise of the liquid is less than it would be in the absence of inclusions, and correspondingly γ and the velocity of sound are reduced.

As mentioned above, a detailed analysis of the processes taking place in a real liquid subject to fluctuations during passage of a sound wave would be a very difficult matter to treat rigorously, and we shall therefore in the next section consider a model of an inhomogeneous liquid from which the major theoretical obstacles have been eliminated. We shall then be enabled to discuss qualitatively the extent to which the behaviour of this model parallels that of liquid helium, and hence to demonstrate that the fluctuation theory is capable of accounting for the general features observed experimentally.

§2. PROPAGATION OF SOUND IN AN INHOMOGENEOUS MEDIUM.

Consider a medium consisting of a number of spherical inclusions of uniform size embedded at random in a matrix of different properties, and initially at the same temperature. In order to determine the propagation characteristics for a compressional wave of angular frequency ω in this medium it is necessary to calculate the adiabatic compressibility. It is clear from the previous section that if the temperature rise of the inclusions during compression is less than that of the matrix, and if there is thermal equilibrium between the two, the compressibility of the medium as a whole will be affected by the presence of the inclusions. Moreover, if ω is so high that thermal equilibrium is not perfect, the volume oscillations of the medium will lag behind the pressure oscillations, and there will be a continuous conversion of the mechanical energy of the wave into heat.

If a fraction x of the medium is in the form of inclusions, whose compressibility under the conditions of the experiment is k_2 , while the compressibility of the matrix is k_1 , the mean compressibility will be given by the expression :

$$\bar{k} = (1-x)k_1 + xk_2. \quad . \quad . \quad . \quad . \quad . \quad . \quad (1)$$

The actual compressibility of the matrix, k_1 , is related to its adiabatic compressibility, k_{1a} , by the expression :

$$k_1 = \gamma_1 k_{1a} - \beta_1 \frac{dT_1}{dp}, \quad . \quad . \quad . \quad . \quad . \quad . \quad (2)$$

where β_1 is the expansion coefficient, $1/V (\partial V / \partial T)_p$, of the matrix, and dT_1/dp is the rise of temperature of the matrix as a result of compression under the conditions of the experiment. Since for adiabatic compression of the matrix,

$$\left(\frac{\partial T_1}{\partial p} \right)_s = \frac{\gamma_1 - 1}{\beta_1} k_{1a},$$

we may rewrite (2) in the form,

$$k_1/k_{1a} = \gamma_1 - (\gamma_1 - 1)h_1, \quad . \quad . \quad . \quad . \quad . \quad . \quad (3)$$

where $h_1 = \{dT_1/dp\} / (\partial T_1 / \partial p)_s$. Similarly for the inclusions

$$k_2/k_{2a} = \gamma_2 - (\gamma_2 - 1)h_2. \quad . \quad . \quad . \quad . \quad . \quad . \quad (4)$$

If h_1 and h_2 vary from point to point they must be replaced by their average values \bar{h}_1 and \bar{h}_2 . Thus the determination of \bar{k} is resolved into the problem of determining \bar{h}_1 and \bar{h}_2 .

As explained earlier, we may simulate the effects of adiabatic compression by injecting heat; for a given rate of change of pressure let the appropriate rate of injection of heat be q_1 per unit volume of matrix and q_2 per unit volume of inclusions. It is a simple matter to show thermodynamically that

$$q_2/q_1 = \beta_2/\beta_1 = \lambda \text{ (say).}$$

If the heat is injected and withdrawn periodically with frequency ω , the resulting temperature oscillations of the matrix and inclusions would be represented, in the absence of thermal contact, by the equations

$$i\omega C_1 T_1 = q_1 \quad \text{and} \quad i\omega C_2 T_2 = q_2,$$

in which T_1 and T_2 are the departures from the mean of the temperatures of matrix and inclusions respectively, and C_1 and C_2 are specific heats per unit volume. As is common in the solution of periodic problems, $\partial/\partial t$ is replaced by $i\omega$.

In order to calculate the effects of thermal transfer it is convenient to divide the heat sources into two parts, which may be superposed to give the complete solution. Let us first supply heat at a rate q_1 per unit volume of matrix and μq_1 per unit volume of inclusion, where $\mu = C_2/C_1$.

This we shall refer to as the standard state, in which the temperature oscillation is the same, $q_1/i\omega C_1$, for both matrix and inclusions, without the necessity of heat exchange between the two. To represent the actual state of affairs we must in addition supply heat to the inclusions at a rate $q_1(\lambda-\mu)$ per unit volume. We may first consider one inclusion only to be supplied with this additional heat, the rest being in the standard state, and solve the resulting conduction problem. Afterwards the result may be summed over all inclusions, since all the effects are additive.

If the material outside the one inclusion considered be smoothed out into a uniform material of specific heat $C (= (1-x)C_1 + xC_2)$, the conduction problem is straightforward. The equation of heat conduction in the material surrounding the inclusion takes the form, for spherical symmetry,

$$\frac{d^2T}{dr^2} + \frac{2}{r} \frac{dT}{dr} - \frac{i\omega C}{\kappa} T = 0,$$

where κ is the thermal conductivity; and the appropriate solution, in which T tends to zero as r tends to infinity, may be written:

$$T = \frac{u}{r} \exp(-\zeta r), \quad \text{where} \quad \zeta = \sqrt{(i\omega C/\kappa)}.$$

The integration constant, u , is determined by the boundary condition at the surface of the inclusion, where $r=a$. For simplicity we shall suppose the inclusion to be at a uniform temperature at all times, the same as that of the matrix immediately surrounding it, that is $[T]_a$. Then since heat is supplied to the inclusion at a rate $\frac{4}{3}\pi a^3 q_1(\lambda-\mu)$ from the exterior source, and at a rate $4\pi a^2 \kappa [dT/dr]_a$ by conduction from the matrix, the rate of rise of temperature of the inclusion, $i\omega [T]_a$, is governed by the equation

$$\frac{3\kappa}{a} [dT/dr]_a - i\omega C_2 [T]_a + q_1(\lambda-\mu) = 0.$$

From this equation u may be determined, and the amplitude of the temperature oscillation of the inclusion is found to be given by the expression

$$[T]_a = \frac{a^2}{3\kappa} \cdot \frac{q_1(\lambda-\mu)}{1+a\zeta+i\omega\tau}, \quad \text{where} \quad \tau = C_2 a^2/3\kappa. \quad \dots (5)$$

Thus of the heat $q_1(\lambda-\mu)$ supplied to unit volume of the inclusion, the amount which remains within it is given by $i\omega C_2 [T]_a$, *i. e.*

$$i\omega\tau \cdot \frac{q_1(\lambda-\mu)}{1+a\zeta-i\omega\tau}, \quad \dots (6)$$

and the rest, which is conducted to the surrounding material is given by $q_1(\lambda-\mu) - i\omega C_2 [T]_a$, *i. e.*

$$(1+a\zeta) \cdot \frac{q_1(\lambda-\mu)}{1+a\zeta+i\omega\tau}. \quad \dots (7)$$

Now the surrounding material is made up of matrix and inclusions in the standard state, and the heat (7) will be divided among them in the proportions :

$$\frac{1-x}{1+(\mu-1)x} \text{ to the matrix, } \frac{\mu x}{1+(\mu-1)x} \text{ to the inclusions.*} \quad (8)$$

Let us now add together the effects of all the inclusions, acting in the same way. In unit volume of material there will be a volume x occupied by inclusions, so that, combining (7) and (8), we see that the heat supplied to the matrix by all the inclusions amounts to

$$(1+a\zeta) \frac{q_1(\lambda-\mu)}{1+a\zeta+i\omega\tau} \frac{x(1-x)}{1+(\mu-1)x},$$

or, since the total volume of matrix is $(1-x)$,

$$(1+a\zeta) \frac{q_1(\lambda-\mu)}{1+a\zeta+i\omega\tau} \frac{x}{1+(\mu-1)x}$$

per unit volume of matrix. To this we must add the heat supplied to unit volume of matrix in the standard state, which is just q_1 , to give for the resultant total rate of heat supplied per unit volume to the matrix

$$q'_1 = q_1 \left\{ 1 - \frac{x(1+a\zeta)(\mu-\lambda)}{(1+a\zeta+i\omega\tau)[1+(\mu-1)x]} \right\}.$$

Similarly we may calculate the resultant total rate of heat supply per unit volume to the inclusions

$$q'_2 = q_2 \left\{ 1 + \frac{1}{\lambda} \cdot \frac{(1-x)(1+a\zeta)(\mu-\lambda)}{(1+a\zeta+i\omega\tau)[1+(\mu-1)x]} \right\}.$$

Now $q'_1/q_1 = \bar{h}_1$ and $q'_2/q_2 = \bar{h}_2$; hence from (1), (3) and (4),

$$\begin{aligned} \bar{k} &= (1-x)k_{1a} + xk_{2a} \\ &+ \frac{x(1-x)(\mu-\lambda)(1+a\zeta)}{(1+a\zeta+i\omega\tau)[1+(\mu-1)x]} [k_{1a}(\gamma_1-1) - k_{2a}(\gamma_2-1)/\lambda], \\ &= (1-x)k_{1a} + xk_{2a} + \frac{x(1-x)(\mu-\lambda)^2(1+a\zeta)(\gamma_1-1)k_{1a}}{\mu(1+a\zeta+i\omega\tau)[1+(\mu-1)x]}, \end{aligned} \quad (9)$$

since, by a well-known thermodynamical formula, $\gamma-1 = \beta^2 T/Ck$.

From this expression for the mean compressibility it will be seen that at sufficiently high frequencies only the first two terms are important, and this clearly corresponds to such rapid oscillations of pressure that no heat is exchanged between the inclusions and the matrix. The last term expresses the modification brought about by heat exchange at

* This is true only if there is thermal equilibrium between the matrix and inclusions, *i. e.* at low frequencies, but the error involved at higher frequencies should not be great, provided that x is not too large.

lower frequencies. When $\omega=0$, $a\zeta$ and $\omega\tau$ vanish, and for frequencies low enough for $a\zeta$ and $\omega\tau$ to be much smaller than unity, (9) may be rewritten in a slightly simpler, approximate form:

$$\bar{k} \doteq (1-x)k_{1a} + xk_{2a} + \frac{x(1-x)(\mu-\lambda)^2(\gamma_1-1)k_{1a}}{\mu[1+(\mu-1)x]}(1-i\omega\tau). \quad (10)$$

Since the velocity of sound, $v=1/\sqrt{(k\rho)}$, where ρ is the density, the velocity and attenuation of a sound wave may be immediately deduced from (9) or (10). If v_0 is the limiting velocity at high frequencies, corresponding to a compressibility given by the first two terms of (10), and Δv is written for v_0-v , then from (10),

$$\frac{\Delta v}{v_0} \doteq \frac{x(1-x)(\mu-\lambda)^2(\gamma_1-1)k_{1a}}{2\mu[1+(\mu-1)x][(1-x)k_{1a}+xk_{2a}]}, \quad (11)$$

and the attenuation per unit distance,

$$\alpha \doteq \frac{x(1-x)(\mu-\lambda)^2(\gamma_1-1)\omega^2\tau}{2\mu v_0[1+(\mu-1)x]}. \quad (12)$$

This expression for α is, of course, valid only when $\omega\tau \ll 1$; as the frequency is increased α rises as ω^2 at first, but more slowly as $\omega\tau$ approaches unity, and finally, when $\omega\tau \gg 1$, it increases only as $\sqrt{\omega}$ so that the attenuation per wavelength actually decreases. If k_{1a} and k_{2a} are not greatly different, equations (11) and (12) may be combined to yield a simple expression for α at frequencies for which $\omega\tau \ll 1$,

$$\alpha \doteq \frac{\omega^2\tau\Delta v}{v_0^2} = \frac{\omega^2 C_2 a^2 \Delta v}{3\kappa v_0^2}. \quad (13)$$

Before discussing the relation between the model we have analysed and the actual state of affairs in liquid helium, we may take the argument one stage further. Up to now we have assumed that the medium contains permanent inclusions, but it would more nearly approximate to a fluctuating liquid if we considered the inclusions as transient, appearing and disappearing in a random manner at all points in the medium. As will appear below, this transience of the inclusions does not modify equation (11) for the velocity, but it may reduce the attenuation. In order to understand the effect let us return to an early stage in the previous calculation, and consider one inclusion surrounded by the material in the standard state. The inclusion oscillates in temperature with an amplitude $[T]_a$ given by (5), in addition to the oscillation of the standard state. Thus the actual amplitude under these conditions is

$$\frac{q_1}{i\omega C_1}(1-i\omega\tau'), \text{ if } \omega\tau' \ll 1, \text{ where } \tau' = \tau(1-\lambda/\mu).$$

The oscillation of the inclusion is thus of very nearly the same amplitude as that of the rest of the material, but with a time-lag of τ' .

Now consider a small region of the material, which, if the inclusions are transient, will spend a fraction x of the time as part of an inclusion, and the rest $(1-x)$, as part of the matrix. So long as it is part of the matrix its temperature will stay in phase with that of the standard state, but as soon as it becomes part of an inclusion it will tend to lag behind the standard state, and if it remains part of an inclusion for a time long compared with τ' it will assume the time-lag τ' corresponding to dynamical equilibrium. When, with the disappearance of the inclusion, it becomes once more part of the matrix, the time-lag will revert to zero with a time constant approximately equal to τ' . Thus if the time of persistence of the inclusions is much greater than τ' , the mean time-lag of the inclusions will be the same as if they were permanent, and the results of the previous calculation will apply. On the other hand, if the inclusions persist only for a time shorter than τ' they will not take up the full time-lag before they disappear, their mean time-lag will be less than τ' and the attenuation will be correspondingly reduced. For any given time of persistence of the inclusions, their mean time-lag, $f\tau'$ (say), where $f < 1$, may in principle be calculated, and the previous arguments may be carried through exactly as before, with τ everywhere replaced by $f\tau$. Clearly equation (11) for the velocity will be unaltered, since it does not involve τ , but (12) and (13), expressing the attenuation, will be modified, and a new approximation to the attenuation coefficient may be written :

$$\alpha \doteq \frac{\omega^2 f C_2 a^2 \Delta v}{3\kappa v_0^2} . \quad . \quad . \quad . \quad . \quad . \quad (14)$$

We shall return later to a discussion of the value to be assigned to f .

§ 3. APPLICATION TO LIQUID HELIUM.

The model which we have analysed in some detail resembles the actual state of affairs in liquid helium only superficially, and the analysis has been given mainly in order to make clear the nature of the processes which may affect the velocity and attenuation in an inhomogeneous fluid. The major difference between a fluctuating liquid and the model lies in the fact that in the former the inclusions exist essentially as a result of temperature fluctuations, so that it is not possible to consider the initial state of the material, before the passage of a sound wave, as one of uniform temperature. In spite of this difference, however, a close analogy may be drawn between the two systems, and to a large extent the fluctuations may be disregarded except in so far as they are the mechanism responsible for the appearance of inclusions. This may be understood by reference to a new model which more closely resembles a real fluctuating liquid. Let us suppose that the liquid is initially entirely free from spontaneous fluctuations and is uniform in temperature and in all other properties ; now let heat be injected into and withdrawn from the liquid from point to point in a random manner, in such a way that the total internal energy remains constant. The temperature of the

liquid will now fluctuate randomly, and the energy flow resulting from its thermal conductivity will be similar to that which occurs spontaneously in a real liquid. If the mean temperature is not too much higher than the λ -point the local withdrawals of heat may be sufficient to produce transient inclusions of He II. Now let us superimpose on this random heat injection an orderly injection which will simulate the effect produced by adiabatic compression; that is, we inject heat at a uniform rate into every region of the matrix (He I), and at a different, but uniform, rate into every inclusion (He II). If the amount of heat injected in this way is very much smaller than the random injections its influence on the distribution of the inclusions will not be very great, though, as we shall see below, it cannot be entirely neglected. Since the equation of heat conduction is linear the energy flow due to each cause is independent, so that the ordered heat flow is the same as if matrix and inclusions were initially at the same temperature. Moreover, the effect of each type of energy flow on the volume of the liquid is independent, so that each contributes independently to the compressibility. The random fluctuations, however, do not affect the volume, so that they may be disregarded. To this degree of approximation, therefore, the real liquid may be treated as exactly analogous to the model which we have studied, and the expressions for the velocity and attenuation of a sound wave may be taken over directly.

There is, however, one assumption in the preceding argument which is not strictly valid, namely that the passage of a sound wave does not affect the distribution of the inclusions. In fact the heating of the material by compression shortens the lifetime of each inclusion in such a way as to decrease appropriately the number of inclusions present at a higher temperature. If this effect were negligible it would be possible, as in the model, to express the specific heat, C , in the form $(1-x)C_1 + xC_2$; but, in fact, there will be an important contribution arising from dx/dT . Any attempt to calculate the specific heat of liquid helium above the λ -point would involve a complete statistical description of the assembly, and would be at least as difficult as an exact calculation of the specific heat arising from an order-disorder transition. Since, therefore, we cannot justify the analogy between the actual liquid and our model so far as the specific heat is concerned, we shall modify the argument so as to incorporate experimental values of the specific heat. The calculation may be simplified without serious error by taking as zero the expansion coefficient, β_2 , of He II. This assumption is equivalent to neglecting λ in comparison with μ in the model already analysed, and is justified by the fact that the relative change in specific heat at the λ -point is much greater than the relative change in expansion coefficient. At the same time we must for consistency put $\gamma_2 = 1$ and hence $k_2 = k_{2a}$. A short calculation now leads to an expression for the real part of the mean compressibility at frequencies such that $\omega\tau \ll 1$, which, as may be seen from equation (10), may be obtained by assuming thermal equilibrium between matrix and

inclusions. The rate of input of heat per unit volume is $q_1(1-x)$, since $q_2=\beta_2q_1/\beta_1=0$, and thus the rate of rise of temperature of the matrix is $q_1(1-x)/C$. Since for the pure matrix the corresponding rate would be q_1/C_1 , we have immediately, that $\bar{h}_1=C_1(1-x)/C$. Hence, from (1) and (3),

$$\bar{k}/k_{1a}=1+x\Delta k/k_{1a}+(\gamma_1-1)(1-x)[1-b(1-x)],$$

where

$$\Delta k=k_{2a}-k_{1a} \text{ and } b=C_1/C.$$

If now we write v_1 for $1/\sqrt{(\rho_1k_{1a})}$, the velocity of a sound wave in an extended volume of the pure matrix (He I), and v_2 for $1/\sqrt{(\rho_2k_{2a})}$, the velocity in an extended volume of the material of the inclusions (He II), and further introduce the definitions :

$$\Delta v_0=v_1-v_2,$$

$$\Delta v'=v_1-v,$$

where v is the velocity in the actual material, we have that

$$\Delta v'=x\Delta v_0+\frac{1}{2}v_1(\gamma_1-1)(1-x)[1-b(1-x)]. \quad . \quad . \quad (15)$$

It is worth emphasizing that γ_1 in (15) is not the experimentally determined value of γ in actual He I, but the value which would be observed if there were no inclusions of He II. This "ideal γ ", as we shall show later when comparing theory and experiment, can be fairly precisely estimated by extrapolation from higher temperatures.

So far as the attenuation coefficient is concerned, it seems likely that the expression (14) derived from the model, for values of $\omega\tau$ much less than unity, needs little modification when applied to the real liquid; the attenuation arises from the lag of the temperature oscillation of the inclusions behind the pressure oscillation, which should not be influenced to any great extent by the variations in the mean lifetime of the inclusions brought about by the temperature oscillation, provided that the amplitude of the temperature oscillation is small. We shall therefore use (14) in comparing theory and experiment, choosing some plausible value for C_2 , the specific heat of the material which composes the inclusions. It is also necessary to ascribe a value to f , which can only be done by guessing the mean life-time of the inclusions. It will be remembered that $f=1$ if this life-time is much greater than τ' and decreases to zero as the life-time becomes much smaller than τ' . Now since τ' is the relaxation time for heat transfer between the matrix and the inclusions it is reasonable to suppose that the life-time of the inclusions will be of the order of τ' , under which conditions f will be approximately $\frac{1}{2}$. Probably at temperatures well above the λ -point, at which inclusions are only rarely formed as a result of an unusually large fluctuation, the life-time of such inclusions will be rather shorter than τ' and f will be correspondingly smaller; conversely, near the λ -point the inclusions will be readily formed, and may persist for times

longer than τ' . In the absence of any detailed theory of the fluctuations the best that can be done is to take $\frac{1}{2}$ as a compromise value of f with reasonable assurance that except very near and very far from the λ -point it will not be wrong by more than a factor 2. We shall therefore write for the attenuation coefficient:

$$\alpha \doteq \frac{\omega^2 C_2 a^2 \Delta v}{9 \kappa v_0^2}, \quad \dots \dots \dots (16)$$

where, as in the model, v_0 is the limiting velocity at high frequencies, corresponding to a compressibility $(1-x)k_{1a} + xk_{2a}$, and $\Delta v = v_0 - v$.

§ 4. COMPARISON OF THEORY AND EXPERIMENT.

In order to compare the predictions of (15) and (16) with experiment it is necessary to choose values for the physical quantities entering into these expressions. The two which particularly need discussion are C_1 and γ_1 the specific heat and ratio of principal specific heats of "ideal He I" containing no inclusions of He II. These must be estimated by extrapolation from higher temperatures, and, since the properties of helium in the range from 2.18° to nearly 3° K. are to varying extents influenced by the presence of inclusions, the required extrapolation is considerable. Fortunately, however, a few plausible assumptions enable the extrapolation to be carried out without too much uncertainty. The data which will be used are to be found most conveniently exhibited in Keesom's (1942) book, and the references in the following paragraphs are to diagrams therein.

We consider first the "ideal specific heat" of helium I, C_1 . It is clear from diagram 4.17 that between 4° and 3° K. the specific heat falls almost linearly, that is, much more slowly than might be expected for a normal liquid, and this trend is exhibited in an even more striking fashion by the entropy diagram 4.40. From the latter diagram it is clear that the entropy of solid He and He II at 0° K. takes a value about -0.85 (the entropy of liquid He I at the normal boiling point is taken as zero), and it is very nearly to this value that the entropy curve of He I above 3° K. extrapolates. It is likely, therefore, that the λ -transition in helium is in this respect analogous to that in superconductors rather than to order-disorder transitions; that is to say, even if the phase-transition did not occur there would be still no excess entropy at 0° K.* In parenthesis it may be remarked that if liquid He_3 is similar to He_4 I, then there need be no cause, on thermodynamical grounds, for surprise that no transition occurs. All that is necessary to eliminate the entropy by the time the liquid has cooled to 0° K. is that the specific heat shall vary roughly as T , as apparently occurs in He I. To return to the immediate problem, we shall assume that the entropy curve 4.40 can be extrapolated almost linearly to a value -0.85 at 0° K., and hence derive an almost linear ideal specific heat curve for He I.

* Note added in proof.—This behaviour has already been noted by Daunt and Mendelssohn (1946).

In fig. 1 are exhibited the experimental curve of C and the assumed curve for C_1 , from which the ratio $b(=C_1/C)$ may be determined as a function of temperature. In this diagram C and C_1 are referred to unit mass rather than unit volume, and are measured at the vapour pressure of the liquid.

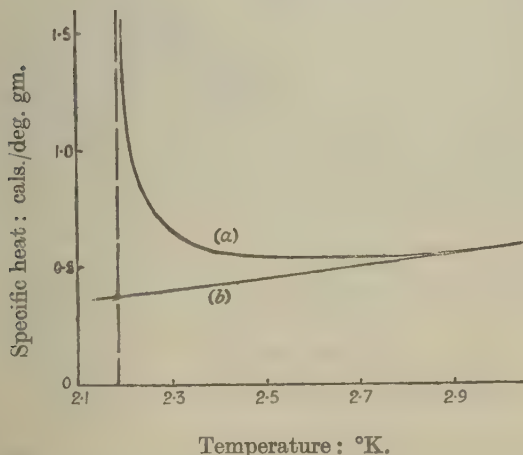
The ideal ratio of the principal specific heats, γ_1 , may be derived from the thermodynamic relation :

$$\frac{\gamma-1}{\gamma} = -\frac{T}{\rho^2 C_p} \left(\frac{\partial p}{\partial T} \right)_e \left(\frac{\partial \rho}{\partial T} \right)_p,$$

where C_p is the specific heat per unit mass at constant pressure.

We have already considered the extrapolated curve for C_1 , which is measured at the vapour pressure, and a small correction for the variation of vapour pressure with temperature must be applied to convert it into

Fig. 1.



Specific heat of HeI : (a) Experimental curve.

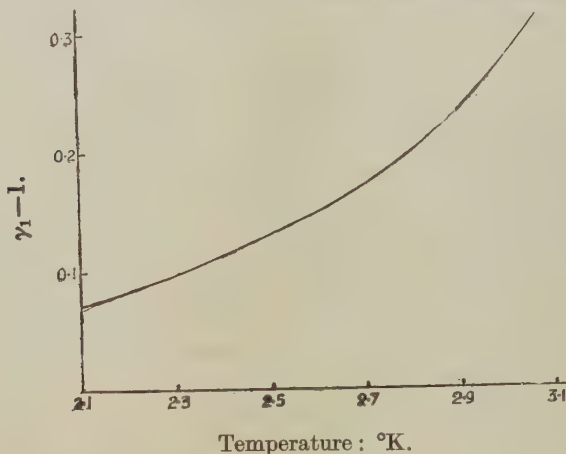
(b) Assumed curve for "ideal HeI".

a curve for C_p . The density, ρ , changes so slowly with temperature that there is no need to correct the measured values, but the two differential coefficients in the expression are affected by the approach to the λ -point and require correction. Keesom's curves 4.38 for $(\partial p / \partial T)_e$ at various densities give a clear indication of how the extrapolation should be made, since they lie close together and run parallel above 2.7° K., only diverging as each approaches its discontinuity at the λ -point. Now the λ -point for helium of density 0.18 gm./cm.³ lies 0.3° K. lower than that of helium under its vapour pressure, so that at 2.2° K. it will hardly be affected by the approaching discontinuity. The ideal curve for $(\partial p / \partial T)_e$ of helium under its vapour pressure may therefore be constructed by

continuing the curve above 3°K. parallel to the curve corresponding to a density of 0.18 gm./cm.^3 . No similar method is available for $(\partial\rho/\partial T)_p$, which is exhibited in 4.39, but the extrapolation presents no difficulties. Values of $(\partial\rho/\partial T)_p$ were plotted against T for temperatures above 3.0°K. and the curve was extrapolated by eye to 2.1°K. , bearing in mind that it must tend to zero, according to Nernst's theorem, as T tends to zero. From these extrapolated curves a curve for $(\gamma_1 - 1)$ was constructed, and the result is shown in fig. 2.

We are now in a position to see whether the expression (15) provides a satisfactory explanation of the variation of the velocity with temperature, of which the experimental curve (Atkins and Chase 1951) is shown in

Fig. 2.



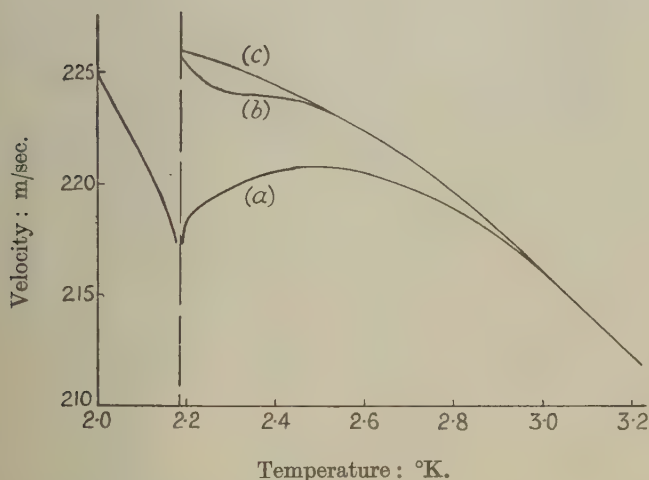
Ratio of principal specific heats of "ideal He I".

fig. 3 (a). One might tackle this problem by guessing a reasonable form of the curve for v_1 (which should join smoothly on to the experimental curve at about 3°K.); the difference between this curve and the experimental curve would give values of $\Delta v'$, which could then be compared with the predictions of equation (15). We prefer, however, to work in the reverse order, estimating $\Delta v'$ from (15) and hence constructing a curve for v_1 . The aim is now to see whether a curve may be thus obtained which behaves in the expected way, becoming steadily flatter as the temperature is lowered, and tending to a zero gradient at 0°K. in accordance with Nernst's theorem. Since the major contribution to $\Delta v'$ arises from b rather than x , especially at the higher temperatures, we may as a first approximation to $\Delta v'$ put $x=0$ in equation (15), obtaining the simpler expression

$$\Delta v' \doteq \frac{1}{2} v_1 (\gamma_1 - 1) (1 - b).$$

Values of $\Delta v'$ calculated in this way for different temperatures and added to the experimental values of v give a first approximation to the curve of v_1 versus T , which is shown as curve (b) in fig. 3. It is encouraging that this curve joins smoothly to the experimental curve above 3°K . Below 2.5°K ., however, it takes a less satisfactory shape, and it is in this region that non-zero values of x must be assumed in order to smooth out the curve. It is now necessary to use values of Δv_0 in (15), and therefore to estimate v_2 , the velocity of sound in the material of the inclusions. Since it is not possible without a detailed theory to determine the extent to which the inclusions resemble small regions of He II, there must obviously be considerable latitude in the choice of v_2 . For the present comparison a value of 217.5 m./sec. has been chosen, corresponding approximately to the velocity just below the λ -point, but other values

Fig. 3.



Velocity of sound in helium :

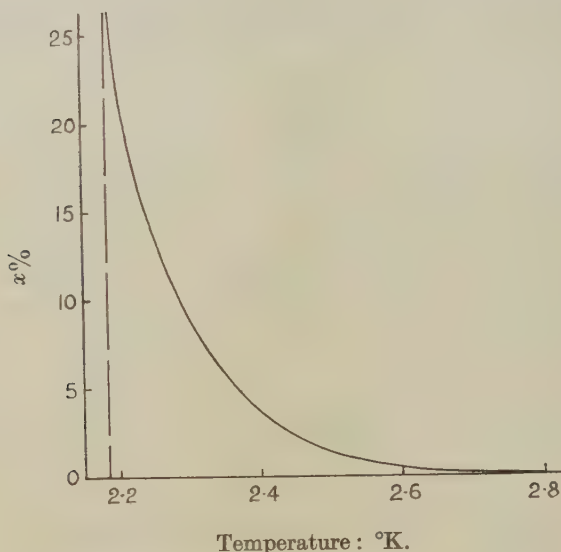
- (a) Experimental curve.
- (b) First approximation to curve for "ideal HeI".
- (c) Final curve for "ideal HeI".

are equally likely, and the calculations which follow could readily be modified to suit them. It is now a matter only of finding such values of x that a smooth curve for v_1 may be drawn, using the complete expression (15) for $\Delta v'$. One possible variation of x with T is shown in fig. 4, and the corresponding curve for v_1 as curve (c) in fig. 3. The values which it is necessary to ascribe to x appear to be fairly reasonable, but, since the velocity is not highly sensitive to variations in x and the parameters occurring in (15) are not very accurately known, it would be unwise to regard the curve for x as having more than qualitative validity.

However, we may conclude from this analysis that the hypothesis of a non-uniform composition of helium above the λ -point is capable of accounting for the observed velocity curve, since the form of curve 3 (c) is very much what one would expect for a uniform liquid, such as "ideal He I" is assumed to be.

Finally we must see whether equation (16) predicts an attenuation of the right order of magnitude. Here the comparison between theory and experiment is even more uncertain than with the velocity, since α depends critically on the size of the inclusions, about which nothing is known. We shall therefore calculate the value of a which will lead to the

Fig. 4.



Temperature variation of concentration of inclusions.

right value of α at a given temperature, and see whether inclusions of this radius are likely, according to simple fluctuation theory, to be present at that temperature in the concentration, x , found above. It will be necessary to choose a value for C_2 , and here again there is very little guidance from theory which will enable a wise choice to be made. According to the measurements of Keesom and Keesom (1935) the specific heat of He II in bulk rises, just below the λ -point, at least to 6 cal./gm. deg., but the rise is very rapid, and it is unlikely that the inclusions on the average take so high a value. We shall here assume C_2 to be 1.5 cal./gm. deg., or 0.22 cal./cm.³ deg. According to the recent data of Atkins and Chase the attenuation constant α , at 2.3° K. and a frequency of 14 Mc./s. is 0.27/cm., of which approximately 0.10/cm. is explicable in terms of viscous damping and thermal conduction in "ideal He I" (Pellam and Squire 1947). The difference, 0.17/cm. we

suppose to result from the presence of the inclusions. Putting $v_0 = 224.3$ m./sec., $\Delta v = 4.5$ m./sec. and $K = 4.4 \times 10^{-5}$ cal./deg. cm. sec.* in equation (16), we find that the observed attenuation may be accounted for if the mean radius of the inclusions is about 2.1×10^{-7} cm., corresponding to a cluster of about 850 atoms.

In order to determine whether inclusions of radius 2.1×10^{-7} cm. might be present in such numbers as to occupy 9 per cent of the total volume, as required by our analysis of the velocity curve, we may carry out a simple calculation which, though based on quite inexact assumptions, should give a qualitatively correct answer. Suppose the liquid at 2.3° K. to be divided into regions whose volumes, V , are equal to the estimated volume of an inclusion, 3.9×10^{-20} cm³. If these regions, having the properties of ideal He I, are regarded as weakly interacting with one another we may immediately calculate the proportion which through fluctuations have temperatures less than 2.18° K. This proportion, by standard fluctuation theory, is given by $\frac{1}{2}[1 - \text{erf}(\Gamma\delta T)]$ where $\delta T = 0.12^\circ$ K. and $\Gamma = \sqrt{(C_1 V / 2kT^2)}$ deg.⁻¹, and substitution of numerical values leads to a value 11 per cent. The agreement with the desired value 9 per cent is probably better than the assumptions warrant, especially in view of the uncertainties in the values to be ascribed to various parameters occurring in the theory. We may, however, conclude that the suggested mechanism of the extra attenuation near the λ -point is capable in principle of explaining the magnitude of the effect.

As the λ -point is approached the attenuation rises very rapidly, and probably increases by a factor greater than 20. This cannot be explained on the assumption that the inclusions stay constant in volume, but, on the other hand, if they increase in size nearer the λ -point, as it is very plausible to assume, there is no difficulty in explaining the rapid rise, since α depends on a^2 . Below the λ -point the attenuation drops again sharply, presumably as the liquid becomes more and more completely homogeneous, but we shall not attempt to calculate the attenuation when the liquid is mainly He II, with inclusions of He I, since in the absence of any adequate microscopic theory of He II the foundations of such a calculation would be even less firmly secure than those of the present work.

ACKNOWLEDGMENT.

I should like to express my thanks to Dr. K. R. Atkins and Mr. C. E. Chase for allowing me to make use of their results before publication.

REFERENCES.

- ATKINS, K. R. and CHASE, C. E., 1951 to be published in *Proc. Phys. Soc.*
 DAUNT, J. G., and MENDELSSOHN, K., 1946, *Proc. Roy. Soc. A*, **185**, 225.
 KEESOM, W. H., 1942 *Helium* (Elsevier).
 KEESOM, W. H., and KEESOM, A. P., 1935, *Physica* **2**, 557.
 PELLAM, J. R. and SQUIRE, C. F., 1947, *Phys. Rev.* **72**, 1245.

* I am indebted to Mr. C. Grenier for information concerning his as yet unpublished measurements of the thermal conductivity of He I.

CXXII. *The Synthesis of Elastic Dislocation Fields.*

By F. R. N. NABARRO,

Department of Metallurgy, The University of Birmingham †.

[Received June 13, 1951.]

SUMMARY.

The static field of an infinitesimal loop of dislocation lying in its glide plane is calculated. The field of any plane loop lying in its glide plane may be obtained by integration of the result. The field produced by the sudden creation of an infinitesimal loop is calculated as a function of time. The field of an arbitrarily moving plane loop may be obtained by integration. The method is illustrated by simple examples.

§1. INTRODUCTION.

THE process of plastic deformation in a crystal may be represented (*cf.* Cottrell 1949) by the following deformation of an isotropic elastic continuum. A cut is made over a finite area of a plane, the *glide plane*, and the opposite faces of the cut are moved relative to one another a distance \mathbf{b} in a direction, the *glide direction*, which lies in the glide plane. The elastic deformation is thus a particular type of *dislocation*, as discussed by Volterra (1907). Burgers (1939) has shown that the static displacements produced by such a dislocation can be expressed by integrals along the line bounding the area which has slipped. We shall here express the same general result as a double integral over the area which has slipped, and extend the method to give the instantaneous displacements produced by a moving dislocation. In §2 we derive the static displacements produced by an infinitesimal loop of dislocation in an infinite body; §3 digresses to give the static displacements produced by such a loop at the centre of a finite sphere. In §4 the method of synthesis is illustrated by the screw dislocation, in which the cut surface is a half plane bounded by a line parallel to \mathbf{b} , and the edge dislocation, in which the cut is made over a half plane bounded by a line perpendicular to \mathbf{b} . The displacements produced if an infinitesimal loop of dislocation is suddenly created are calculated in §5, and, as an example of the method, the displacements produced by a rigid motion of a screw dislocation are calculated in §6.

§2. THE FIELD OF AN INFINITESIMAL LOOP OF DISLOCATION LYING IN ITS GLIDE PLANE.

Consider an infinitesimal loop of dislocation with Burgers vector ‡ $\mathbf{b} = (0, 0, -b)$ lying in the xz plane close to the origin. Let the area of

† Communicated by the Author.

‡ The vector \mathbf{b} used in this paper is identical with the vector \mathbf{f} of Burgers (1939). The current convention (*cf.* Frank 1951) is to take $\mathbf{b} = -\mathbf{f}$.

the loop be δA , while a typical element of its perimeter is $d\xi$. The stress field of this dislocation in an infinite body may be found from the formula of Burgers (1939), which gives at the point \mathbf{x} a displacement \mathbf{u} of the form

$$\mathbf{u} = \mathbf{u}^* + \mathbf{u}^{**} + \text{grad } \psi, \quad (1)$$

where

$$\mathbf{u}^* = \Omega \mathbf{b} / 4\pi, \quad (2)$$

$$\mathbf{u}^{**} = \frac{\mathbf{b}}{4\pi} \wedge \int \frac{d\xi}{r} \quad (3)$$

and

$$\psi = \frac{\lambda + \mu}{4\pi(\lambda + 2\mu)} \int \mathbf{b} \wedge (\mathbf{x} - \xi) \frac{d\xi}{r}. \quad (4)$$

Here Ω is the solid angle subtended by the loop at the point \mathbf{x} , λ and μ are Lamé's elastic constants, and $r = |\mathbf{x} - \xi|$.

In this case,

$$\left. \begin{aligned} 4\pi \mathbf{u}^* &= (0, 0, -b\delta A y / r^3), \\ 4\pi \mathbf{u}^{**} &= (0, -b\delta A z / r^3, 0), \\ 4\pi \psi &= (\lambda + \mu)b\delta A y z / (\lambda + 2\mu)r^3, \\ B^{-1}u_x &= \frac{\lambda + \mu}{\lambda + 2\mu} \frac{3xyz}{r^5}, \\ B^{-1}u_y &= \frac{\lambda + \mu}{\lambda + 2\mu} \left(\frac{3y^2z}{r^5} - \frac{z}{r^3} \right) + \frac{z}{r^3}, \\ B^{-1}u_z &= \frac{\lambda + \mu}{\lambda + 2\mu} \left(\frac{3yz^2}{r^5} - \frac{y}{r^3} \right) + \frac{y}{r^3}, \end{aligned} \right\} \quad (5)$$

and

where

$$B = -b\delta A / 4\pi. \quad (6)$$

This field may be derived from the "first type of simple solutions" of Boussinesq, given by Love (1927) at §§ 131, 132. In Love's notation it is

$$(u_x, u_y, u_z) = \frac{1}{2} \partial(u_2, v_2, w_2) / \partial z + \frac{1}{2} \partial(u_3, v_3, w_3) / \partial y. \quad (7)$$

If u_{ij} is the component in the direction of x_j of the displacement at the point x_k produced by a force in the direction x_i at the origin, this displacement field is of the form

$$u_{kij} = \frac{1}{2} \left(\frac{\partial u_{ij}}{\partial x_k} + \frac{\partial u_{ik}}{\partial x_j} \right), \quad i \neq k. \quad (8)$$

The forces applied at the origin have zero resultant and zero moment.

The corresponding diagonal terms with $i = k$ are "double forces without moment" (Love). The strength of an infinitesimal loop of dislocation is thus a tensor, in which one suffix represents the normal to the plane of the loop and one the Burgers vector. The non-diagonal terms represent elementary acts of slip, while the diagonal terms represent non-conservative motions (Nabarro 1951).

§ 3. A LOOP AT THE CENTRE OF A SPHERE.

If the dislocation exists in a finite body with free surfaces, a complementary field must be added which neutralizes the traction across the boundary. For a sphere of radius R centred on the loop, such a field is given by

$$\left. \begin{aligned} \gamma B^{-1}u_x &= 48(\lambda + \mu)(2\lambda + 7\mu)xyz, \\ \gamma B^{-1}u_y &= 48(\lambda + \mu)(2\lambda + 7\mu)y^2z - 24(\lambda + \mu)(5\lambda + 7\mu)r^2z \\ &\quad + 5(27\lambda^2 + 56\lambda\mu + 28\mu^2)R^2z \\ \text{and } \gamma B^{-1}u_z &= 48(\lambda + \mu)(2\lambda + 7\mu)yz^2 - 24(\lambda + \mu)(5\lambda + 7\mu)r^2y \\ &\quad + 5(27\lambda^2 + 56\lambda\mu + 28\mu^2)R^2y, \end{aligned} \right\} \quad (9)$$

where

$$\gamma = 2(\lambda + 2\mu)(19\lambda + 14\mu)R^5. \quad (10)$$

These displacements may be derived by a superposition of two solutions of the types given by Love at §172, taking $\omega_2 = yz$ and $\phi_2 = yz$.

On the surface $r = R$, the total displacement derived from (5) and (9) is given by

$$\left. \begin{aligned} \gamma B^{-1}u_x &= 210(\lambda + \mu)(\lambda + 2\mu)xyz, \\ \gamma B^{-1}u_y &= 210(\lambda + \mu)(\lambda + 2\mu)y^2z + 15\lambda(\lambda + 2\mu)R^2z, \\ \text{and } \gamma B^{-1}u_z &= 210(\lambda + \mu)(\lambda + 2\mu)yz^2 + 15\lambda(\lambda + 2\mu)R^2y. \end{aligned} \right\} \quad (11)$$

In spherical polar coordinates with Ox as axis, these become

$$\left. \begin{aligned} \gamma B^{-1}u_r &= 15(8\lambda + 7\mu)(\lambda + 2\mu)R^3 \sin^2 \theta \sin 2\phi, \\ \gamma B^{-1}u_\theta &= 15\lambda(\lambda + 2\mu)R^3 \sin \theta \cos \theta \sin 2\phi \\ \text{and } \gamma B^{-1}u_\phi &= 15\lambda(\lambda + 2\mu)R^3 \sin \theta \cos 2\phi. \end{aligned} \right\} \quad (12)$$

Suppose a homogeneous stress p_{ij} is exerted on the sphere before the dislocation is made. The work done by the displacements (12) against this stress is obtained by integrating $u_r p_{rr} + u_\theta p_{r\theta} + u_\phi p_{r\phi}$ over the surface of the sphere. The only components which do not vanish in the integration over ϕ are those arising from p_{yz} and p_{zy} , which are

$$\left. \begin{aligned} p_{rr} &= p_{yz} \sin^2 \theta \sin 2\phi, \\ p_{r\theta} &= p_{yz} \sin \theta \cos \theta \sin 2\phi \\ \text{and } p_{r\phi} &= p_{yz} \sin \theta \cos 2\phi. \end{aligned} \right\} \quad (13)$$

The work done W is given by

$$\left. \begin{aligned} \gamma B^{-1}W &= 8(\lambda + 2\mu)(19\lambda + 14\mu)\pi R^5 p_{yz} \\ \text{or } W &= -b\delta A p_{yz}. \end{aligned} \right\} \quad (14)$$

§ 4. SYNTHESIS OF THE EDGE AND THE SCREW.

Returning now to the infinite body, we may take the loop to be rectangular, with $\delta A = \delta x \delta z$. By replacing z by $z - \zeta$ and integrating (5) over all ζ , we obtain the displacements produced by a pair of screw dislocations of opposite sign lying close to the z axis, and separated by δx . These are

$$u_x = 0, \quad u_y = 0, \quad u_z = -b y \delta x / 2\pi (x^2 + y^2). \quad . . . \quad (15)$$

Replacing x by $x - \xi$ and integrating again from $\xi = -\infty$ to $\xi = 0$, we obtain the displacements produced by a single screw dislocation along the z axis, which, apart from a constant, are

$$u_x = 0, \quad u_y = 0, \quad u_z = -(b/2\pi) \tan^{-1} y/x. \quad . . . \quad (16)$$

Alternatively, we may first integrate over all ξ to obtain a pair of edge dislocations close to the x axis, with displacements

$$\left. \begin{aligned} u_x &= 0, \\ u_y &= -\frac{b \delta z (\lambda + \mu)}{\pi (\lambda + 2\mu)} \frac{y^2 z}{(y^2 + z^2)^2} - \frac{b \delta z \mu}{2\pi (\lambda + 2\mu)} \frac{z}{y^2 + z^2}, \\ u_z &= -\frac{b \delta z (\lambda + \mu)}{\pi (\lambda + 2\mu)} \frac{y z^2}{(y^2 + z^2)^2} - \frac{b \delta z \mu}{2\pi (\lambda + 2\mu)} \frac{y}{y^2 + z^2}. \end{aligned} \right\} . . . \quad (17)$$

To obtain an edge dislocation lying along the x axis, we integrate from $\zeta = -\infty$ to $\zeta = 0$. The resulting displacements are, apart from a constant,

$$\left. \begin{aligned} u_x &= 0, \\ u_y &= -\frac{b (\lambda + \mu)}{2\pi (\lambda + 2\mu)} \frac{y^2}{y^2 + z^2} - \frac{b \mu}{4\pi (\lambda + 2\mu)} \log (y^2 + z^2), \\ u_z &= -\frac{b (\lambda + \mu)}{2\pi (\lambda + 2\mu)} \frac{y z}{y^2 + z^2} + \frac{b}{2\pi} \tan^{-1} \frac{y}{z}. \end{aligned} \right\} . . . \quad (18)$$

§ 5. THE SUDDEN CREATION OF AN INFINITESIMAL LOOP.

The movement of a dislocation in its glide plane may be regarded as the result of the continuous addition of infinitesimal loops to its boundary. If the displacement produced by the sudden creation of such a loop is known as a function of time, the field of a dislocation moving arbitrarily in its glide plane with subsonic speeds may be obtained by superposition. The known solutions for the field of a moving dislocation have each been obtained by some special artifice: the present method gives an explicit solution in the general case, although, as will be seen from § 6, its application in simple cases is rather laborious.

The displacement arising from the sudden creation of a loop of dislocation may be derived from that arising from the sudden application of a single force by the same process of differentiation and combination (7) as can be used to derive (5) from the known expressions for the static

displacements produced by a single force. Love (1904) has given the displacements arising from a single force suddenly applied and then continuously maintained. If the force is applied instantaneously, the results involve discontinuous functions, and the differentiation of these is not straightforward. It is more convenient to start from the formulæ of Stokes (1849) giving the displacement produced by a force which is an arbitrary function of the time, and to carry out the differentiations before passing to the special case of a force suddenly applied. A typical formula is given by Love (1927, § 212). The displacement produced at time t at the point x_k by a force in the x_i direction applied at the origin and proportional to $\chi(t)$ has a component u_{ij} in the direction of x_j given by

$$u_{ij} = \frac{\partial^2 r^{-1}}{\partial x_i \partial x_j} \int_{r/a}^{r/c} t' \chi(t-t') dt' + r^{-3} x_i x_j [a^{-2} \chi(t-r/a) - c^{-2} \chi(t-r/c)] + \delta_{ij} r^{-1} c^{-2} \chi(t-r/c), \quad (19)$$

where a and c are the speeds of dilatational waves and of shear waves. The displacements corresponding to the formation of a loop of dislocation in the orientation already considered are given, in analogy with (7), by

$$u_j = \partial u_{yji} / \partial z + \partial u_{zji} / \partial y. \quad (20)$$

Substituting (19) in (20) leads to the expression

$$u_j = 2 \frac{\partial^3 r^{-1}}{\partial x_j \partial y \partial z} \int_{r/a}^{r/c} t' \chi(t-t') dt' - \frac{x_j y z}{r^5} \left(12 - 2r \frac{d}{dr} \right) [a^{-2} \chi(t-r/a) - c^{-2} \chi(t-r/c)] + \frac{1}{r^3} \frac{\partial(yz)}{\partial x_j} \left[2a^{-2} \chi(t-r/a) - 3c^{-2} \chi(t-r/c) + r \frac{d}{dr} c^{-2} \chi(t-r/c) \right]. \quad (21)$$

If the force is applied suddenly at time $t=0$ and then maintained, $\chi(t)=0$ for $t<0$, $\chi(t)=F$ for $t \geq 0$. The expression (21) then takes different forms in the three regions $t < r/a$, $r/a \leq t \leq r/c$, $t > r/c$. It may be written

$$t < r/a: F^{-1} u_j = 0. \quad (22)$$

$$r/a \leq t \leq r/c: F^{-1} u_j = \frac{x_j y z}{r^7} \left\{ \frac{3r^2}{a^2} - 15t^2 - 2r^3 [a^{-3} \delta(t-r/a) - c^{-3} \delta(t-r/c)] \right\} + \frac{1}{r^5} \frac{\partial(yz)}{\partial x_j} \left\{ 3t^2 - \frac{r^2}{a^2} - r^3 c^{-3} \delta(t-r/c) \right\} \quad (23)$$

and

$$t > r/c: F^{-1} u_j = -\frac{3x_j y z}{r^5} \left(\frac{1}{c^2} - \frac{1}{a^2} \right) - \frac{1}{a^2 r^3} \frac{\partial(yz)}{\partial x_j}. \quad (24)$$

In (23), terms have been omitted which occur only at the end points of the range, and are there finite, so that they contribute nothing to the integral over a distribution of loops. If the density of the medium is ρ_0 , we have

$$a^2 = (\lambda + 2\mu) / \rho_0, \quad c^2 = \mu / \rho_0,$$

and (24) agrees with (5) if

$$F = -c^2 B = bc^2 \delta A / 4\pi. \quad (25)$$

§ 6. RIGID MOTION OF A SCREW DISLOCATION IN A STRAIGHT LINE.

Consider a straight screw dislocation lying parallel to the z axis, and moving so that at time τ it intersects the plane $z=0$ at the point $(\xi(\tau), 0, 0)$, where $|\xi'(\tau)| < c$. The motion of the dislocation is equivalent to the creation of rows of infinitesimal loops of the type already discussed. The displacement corresponding to the creation of a single loop spreads out in a wave of finite thickness, bounded by the waves of dilatation and of shear. The displacement at $(x, y, 0, t)$ corresponding to the creation of a single loop at $(\xi, 0, \zeta, \tau)$ begins as soon as $t-\tau=r/a$, where

$$r^2 = (x-\xi)^2 + y^2 + \zeta^2. \quad (26)$$

The component u_z arising from the point $\zeta=0$ does not vanish, and arrives when $t-\tau=\rho/a$, where

$$\rho^2 = (x-\xi)^2 + y^2. \quad (27)$$

According to (15), the resultant displacement obtained by integrating over all ζ is without dilatation in the final state. It does not follow from this alone that the disturbance spreads from the line of the dislocation with the speed c of a shear wave. For example, (Love 1927, § 213, (iv.)) the displacement around a centre of compression, which in the static case (*ibid.* § 132, (a')) is a pure shear, is propagated entirely with the velocity a of longitudinal waves. However, in the present case the resultant displacement is at all times parallel to the z direction, and independent of z . The dilatation always vanishes, and the disturbance spreads as a shear wave, being first observed when $t-\tau=\rho/c$. Disturbances from different parts of the dislocation line propagated with speeds lying between a and c arrive before this time, but continuously cancel one another.

In synthesizing the displacement, there are three situations to consider.

$t-\tau < \rho/a$: the longitudinal wave from the nearest element of the dislocation has not yet reached $(x, y, 0)$;

$\rho/a \leq t-\tau < \rho/c$: the longitudinal wave from the nearest element has arrived, but the shear wave has not;

$t-\tau \geq \rho/c$: the displacement produced by the nearest element has reached its final value.

The displacements u_x and u_y are odd in ζ , and vanish on integration.

In the case $t-\tau < \rho/a$, the expression $t-\tau-r/a$ is negative for every element of the dislocation. It follows from (22) that u_z vanishes.

In the case $\rho/a \leq t-\tau < \rho/c$, the expression $t-\tau-r/a$ is negative when $\zeta^2 > Z_a^2$ and zero or positive when $\zeta^2 \leq Z_a^2$, where

$$\rho^2 + Z_a^2 = a^2(t-\tau)^2. \quad (28)$$

The expression $t-\tau-r/c$ is always negative. The contribution of elements with $\zeta^2 > Z_a^2$ is zero, and the contribution of the remaining elements is given by (23) and (25) as

$$\frac{4\pi u_z}{bc^2 y \delta \xi} = \int_{-Z_a}^{Z_a} \left\{ \left(\frac{3}{r^5} - \frac{15\zeta^2}{r^7} \right) (t-\tau)^2 + \frac{3\zeta^2}{a^2 r^5} - \frac{1}{a^2 r^3} - 2\zeta^2 r^{-4} a^{-3} \delta(t-\tau-r/a) \right\} d\zeta, \quad (29)$$

where the integral is taken over the closed range. The terms in $\delta(t-\tau-r/c)$ have been omitted, since they vanish in this range. The terms not involving $\delta(t-\tau-r/a)$ are readily integrated, giving $4Z_a/a^5(t-\tau)^3$. The contribution of the δ function from the points $\zeta^2=Z_a^2$ exactly cancels this at all times in the range. There is thus no disturbance until the shear wave arrives.

In the case $t-\tau \geq \rho/c$, there is again no contribution from the points with $\zeta^2 > Z_a^2$. When $Z_a^2 \geq \zeta^2 \geq Z_c^2$, the elements contribute according to (23), and when $\zeta^2 < Z_c^2$ they contribute according to (24), where

$$\rho^2 + Z_c^2 = c^2(t-\tau)^2. \quad (30)$$

The contribution from the second region is given by

$$\frac{4\pi u_z}{bc^2 y \delta \xi} = 2 \int_{Z_c}^{Z_a} \left\{ \left(\frac{3}{r^5} - \frac{15\zeta^2}{r^7} \right) [(t-\tau)^2 - r^2/a^2] - \frac{12\zeta^2}{a^2 r^5} + \frac{2}{a^2 r^3} - 2\zeta^2 r^{-4} [a^{-3} \delta(t-\tau-r/a) - c^{-3} \delta(t-\tau-r/c)] - r^{-2} c^{-3} \delta(t-\tau-r/c) \right\} d\zeta, \quad (31)$$

taken over the closed range. The terms not involving δ functions yield

$$\frac{4Z_a}{a^5(t-\tau)^3} - \frac{4Z_c}{c^5(t-\tau)^3} + \frac{2Z_c}{c^3(t-\tau)^3} \left(\frac{1}{a^2} - \frac{1}{c^2} \right).$$

The δ functions yield

$$-\frac{4Z_a}{a^5(t-\tau)^3} + \frac{4Z_c}{c^5(t-\tau)^3} - \frac{2}{Z_c c^3(t-\tau)},$$

and the total contribution from this region is

$$\frac{4\pi u_z}{bc^2 y \delta \xi} = \frac{2Z_c}{c^3(t-\tau)^3} \left(\frac{1}{a^2} - \frac{1}{c^2} \right) - \frac{2}{Z_c c^3(t-\tau)}. \quad (32)$$

The contribution from the region $\zeta^2 < Z_c^2$ is given by

$$\begin{aligned} \frac{4\pi u_z}{bc^2 y \delta \xi} &= - \int_{-Z_c}^{Z_c} \left\{ \frac{3\zeta^2}{r^5} \left(\frac{1}{c^2} - \frac{1}{a^2} \right) + \frac{1}{a^2 r^3} \right\} d\zeta \\ &= - \frac{2Z_c^3}{\rho^2 c^5(t-\tau)^3} - \frac{2Z_c}{a^2 c^3(t-\tau)^3}. \quad (33) \end{aligned}$$

Adding (32) and (33) gives the total displacement in the region $t-\tau \geq \rho/c$ as

$$u_z = - \frac{by \delta \xi}{2\pi \rho^2} \cdot \frac{c(t-\tau)}{[c^2(t-\tau)^2 - \rho^2]^{\frac{1}{2}}}. \quad (34)$$

As t increases, this tends to the static value given by (15).

In this particular problem the result could be obtained much more easily by noting that the displacement is ultimately equal to (15), and travels as a pure shear wave. This suggests a trial solution of the form

$$u_z = \frac{y}{\rho^2} f\left(\frac{\rho}{ct}\right). \quad (35)$$

The solution must obey the equation

$$\left(\frac{\partial^2}{\partial x^2} + \frac{\partial^2}{\partial y^2} - \frac{1}{c^2} \frac{\partial^2}{\partial t^2}\right) u_z = 0, \quad (36)$$

which is satisfied if

$$w(1-w^2)f''(w) = (2w^2+1)f'(w), \quad (37)$$

where

$$w = \rho/ct. \quad (38)$$

The solution of (37) subject to the boundary conditions at $w=0$ and $w=\infty$ leads at once to (34).

The total displacement is

$$u_z = -\frac{by}{2\pi} \int_{-\infty}^{\tau_0} \frac{\xi'(\tau)c(t-\tau) d\tau}{\rho^2[c^2(t-\tau)^2 - \rho^2]^{\frac{1}{2}}}, \quad (39)$$

where τ_0 is given by

$$[x - \xi(\tau_0)]^2 + y^2 = c^2(t - \tau_0)^2. \quad (40)$$

For the particular case of steady motion, $\xi(\tau) = v\tau$, and (39) may be integrated by introducing the variable η , where

$$\cos \eta = \cos \psi / \cos \alpha,$$

$$\sin \psi = \rho/c(t - \tau)$$

and

$$\sin \alpha = vy/c[(x - vt)^2 + y^2]^{\frac{1}{2}}.$$

This leads to the known result

$$u_z = -\frac{b}{2\pi} \tan^{-1} \frac{(1 - v^2/c^2)^{\frac{1}{2}} y}{x - vt}. \quad (41)$$

I am indebted to Dr. J. D. Eshelby for suggesting improvements in the presentation of this paper:

REFERENCES.

- BURGERS, J. M., 1939, *Proc. K. Ned. Akad. Wet.*, **42**, 293.
- COTTRELL, A. H., 1949, *Progress in Metal Physics*, **1**, (London: Butterworth Scientific Publications), p. 77.
- FRANK, F. C., 1951, *Phil. Mag.*, **42**, 809.
- LOVE, A. E. H., 1904, *Proc. London Math. Soc.* [2] **1**, 291; 1927, *The Mathematical Theory of Elasticity*.
- NABARRO, F. R. N., 1951, *Phil. Mag.*, **42**, 213.
- STOKES, G. G., 1849, *Trans. Camb. Phil. Soc.*, **9**, 1.
- VOLTERRA, V., 1907, *Ann. Ecole. Norm. Supér.* [3] **24**, 400.

CXXXIII. *Observations on the Multiple Scattering of Ionizing Particles in Photographic Emulsions.*—Part V. *Scattering Measurements on Tracks of Slow Protons.*

By M. G. K. MENON and O. ROCHAT,
H. H. Wills Physical Laboratory, University of Bristol*.

[Received May 30, 1951.]

SUMMARY.

The scattering constant has been determined by measurements of the multiple scattering along proton tracks ending in the emulsion. A value of 27.8 ± 0.5 has been obtained (for $\beta^2 \sim 0.03$ and an average cell-size of 72μ).

A simple method involving the combined measurements of multiple scattering and residual range has been used to identify the particles. A parameter $P = 2.37 \log \hat{\alpha}_{100\mu} + 1.37 \log R$ was determined for each track (R being the range in microns and $\hat{\alpha}_{100\mu}$ the mean angle of multiple scattering—per 100μ —measured along the faster half of the trajectory); P is a linear function of the logarithm of the mass of the particle. A scale of values of P has been calibrated experimentally using tracks of protons from artificial sources and those of σ -mesons. Using this method tracks of 83 protons have been identified amongst a group of 136 particles of charge $|e|$ ejected from cosmic ray stars. The mean value of P for the 83 protons was found to be 4.275 ± 0.013 . The resolution between π -mesons, protons, deuterons and tritons was found to be satisfactory. An appendix gives the coupling matrix calculated for the sagitta method, taking into account the loss of energy.

§ 1. INTRODUCTION.

THE scattering constant as defined in a previous paper (Gottstein *et al.* 1951) can be determined by measuring the multiple scattering along tracks which end in the emulsion, and which are produced by particles of known mass.

The main advantage of this method is that the value of the initial energy of the particle can be determined reasonably well by measuring its residual range. The inaccuracy inherent in such a range measurement is of the order of 2 per cent—this being the probable error due to straggling (Rotblat 1950). The calculations are more complicated because, in contrast to the normal case in high energy tracks, the energy here can no longer be considered constant in that part of the track used for scattering measurements. The loss of energy along the track by ionization must be taken into account.

* Communicated by Professor C. F. Powell, F.R.S.

In a previous paper, Goldschmidt-Clermont *et al.* (1948) have used a statistical variable ϵ_i defined as the product of each angle α_i by the energy T_i corresponding to the centre of the cell. The mean $|\bar{\epsilon}|$ is a parameter which depends only on the mass of the particle and the scattering constant. In principle, this method enables one to carry on the measurements to the very end of the track—decreasing the cell size as the end is approached, and so increasing the statistical weight of the result. But such a procedure would make it difficult to determine the scattering constant, as energy is lost rapidly towards the end of the track and it is hard to eliminate effectively the Rutherford single scattering from the measurements.

However, if the scattering be measured in a part of the trajectory where the change of energy is not too large, then a constant cell length could be maintained for all the measurements, thereby introducing a simplification into the determination of the parameter ϵ .

In the present investigation, we have arbitrarily limited the scattering measurements to the faster half of the track. In our calculations, the average $\frac{1}{n_i} \sum |\alpha_i T_i|$ has been replaced by the statistically equivalent quantity $\left(\frac{1}{n_i} \sum |\alpha_i| \right) \times \left(\frac{1}{n_i} \sum T_i^{-2} \right)^{-1/2}$. The identical mathematical expectations and the slightly differing variances of these two parameters are indicated in the Appendix.

For the present investigation, we have employed 83 tracks of slow protons which ended in the emulsion. The experimental procedure adopted for identifying the particles producing these tracks is described below.

§ 2. EXPERIMENTAL PROCEDURE.

1. Selection of Tracks for Measurement.

One hundred and fifty-four tracks ending in the emulsion, of length greater than 500μ , originating from cosmic ray stars, have been systematically investigated. Tracks due to particles of charge greater than one (*i. e.* He, Li, Be, . . . nuclei) were identified by visual examination of the track for delta rays (Sorensen 1949, 1951) and by gap measurements (Hodgson 1950). Eighteen such tracks were found amongst the 154 tracks investigated. The remaining 136 tracks judged to be caused by particles of charge one, were used for the range and scattering measurements.

2. Measurement of Range.

The tracks were divided into segments of 48μ and smaller. Horizontal and vertical projections were measured in each segment. In calculating the vertical projection in the unprocessed emulsion a shrinkage factor of 2.5 was adopted. From repeated measurements on the same track the total probable error in these determinations has been found to be less than 1 per cent. Tracks inclined at angles greater than 15° to the surface of the emulsion were not used.

3. Measurement of Multiple Scattering.

The first half of the range determined above was used to measure the multiple scattering. This distance was divided into " n " cells, each of size " s ". " s " will be referred to as the "primary cell size". The tracks actually measured varied in length from 500μ to about 4000μ , so the numbers " n " and " s " have also varied. " s " was so chosen that " n " was at least equal to 30, the values of " s " being limited to sequence 8, 16, 24, . . . 48μ (8μ being the smallest unit on our eye-piece scale). In one eye-piece we used a scale of 48μ divided into segments of 8μ each, placed parallel to the displacement of the stage. The track was moved in steps of $s\mu$ along this scale. In the other eye-piece and perpendicular to this displacement, we used the scattering scale as described in previous papers. The position of the track was read on this scale at each step.

4. Calculation of the Mean Angle $\hat{\alpha}$.

Second differences were computed in cell-sizes which were integral multiples of the primary cell-size. This enabled us to choose the optimum cell length, defined as that for which the \bar{d} has a value greater than four times the total noise in the cell. The noise of the microscope M4074 was determined for different cell sizes by use of a primary track 2 cm. in length, which had a finally determined mean angle of scattering of $0.0007^\circ/100\mu$ when measured in 4000μ cells. The results of these measurements have been described in a previous paper (Gottstein *et al.* 1951). Noise elimination as described in previous contributions (Menon *et al.* 1951) cannot be used in this case owing to the simplification we have introduced. A signal to noise ratio of at least four must be maintained to keep the influence of noise on the final result to within a few per cent. The absolute values of the second difference thus obtained were transformed into an angle $\hat{\alpha}$ expressed in degrees per 100μ .

§ 3. IDENTIFICATION OF MASS.

Using this angle and the value of the range already measured, we have determined a parameter $P = 1.37 \log R + 2.37 \log \hat{\alpha}$ (R in μ and $\hat{\alpha}$ in degrees/ 100μ). This parameter is a linear function of the logarithm of the mass of the particle. It has been computed from the range energy relation expressed in the form of a power law $R = E^{1.73} \times M$ and from the definition of $\hat{\alpha}$ (see Appendix).

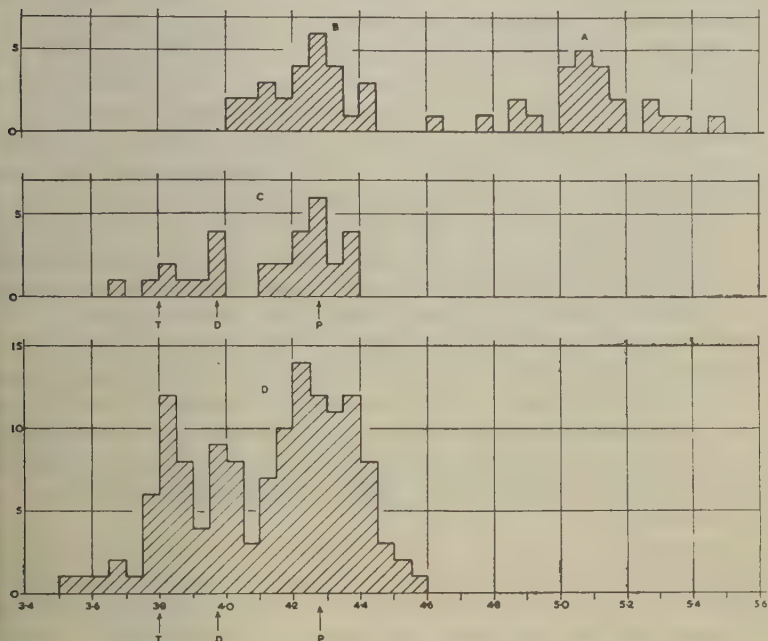
Before P can be employed as a parameter to identify masses of the particles, a scale of values of P must be calibrated for particles of known mass. This calibration has been carried out in the following manner.

We chose twenty-four tracks of σ -mesons which ended in the emulsion and which were longer than 500μ . They have all been attributed to π^- -mesons. The possibility that these σ -mesons are due to μ^- -mesons is extremely small, for these reasons: the tracks were chosen from plates exposed in balloon flights at 65,000 ft. and 75 per cent of the σ -meson tracks

chosen had produced stars with more than two prongs. It is known that σ -stars produced by μ^- -mesons are mostly 1-pronged (George and Evans 1951). The probability of their producing stars with two or more prongs is very small. It is therefore reasonable to assume that almost all the σ -meson tracks are in fact due to π -mesons.

By measuring the range and the scattering in the first half of the trajectory, one may compute a value of P for each of these tracks, and plot them in a histogram as in fig. 1(A). These values are distributed

Fig. 1.



Histogram showing the values of the parameter $P = 1.37 \log_{10} R + 2.37 \log_{10} \hat{\alpha}$ ($\hat{\alpha}$ in $^{\circ}/100\mu$, R =total range in microns), for:

A—24 tracks of σ -mesons.

B—28 tracks of protons from the $N^{14}(d, p)N^{15}$ reaction.

C—30 tracks identified previously by grain density versus multiple scattering.

D—136 tracks due to particles of charge 1 ejected from cosmic ray stars.

The ordinates give the number of tracks per interval of 0.05 of P .

The arrows, P, D, T, refer to the calculated values of the parameter P for protons, deuterons and tritons, assuming $P_{\pi}=5.1$ and mass of proton/mass of π -meson=6.7.

with mean 5.1. Adopting $P=5.1$, for π -mesons, and a value 6.7 for the ratio of the mass of the proton to that of the π -meson, values of P for different particles may be calculated as: $P(\text{proton})=4.27$, $P(\text{deuteron})=3.98$, $P(\text{triton})=3.80$.

The values of $P(\text{proton})$ were calibrated experimentally using tracks of protons ($1200\mu > \text{range} > 1000\mu$ which came to the end of their range in the emulsion) from the reaction $N^{14}(d, p)N^{15}$. The Q value of this reaction is 8.165 MeV. These were obtained in plates exposed to 8 MeV. deuterons in the Liverpool cyclotron. Fig. 1 (B) shows the P values for 28 of these tracks.

To study the overlap of the values $P(\text{proton})$, $P(\text{deuteron})$, $P(\text{triton})$, in a mixed group of particles, the calibration has been extended to include all particles of charge 1, using tracks ending in emulsion of length > 3 mm. originating from cosmic ray stars. The particles producing these tracks had been identified in this laboratory, by measurements of the grain density and multiple scattering by Camerini, Fowler, Lock and Muirhead, who have very kindly given us their results. The P values obtained for this group of 30 tracks are shown as a histogram in fig. 1 (C).

We then determined the P values of 136 tracks (previously identified as being due to particles of charge 1). These were from cosmic ray stars in Ilford G5 plates, 400μ thick, exposed in a high altitude balloon flight. The P values obtained have been plotted as a histogram in fig. 1 (D). The peak for $P(\text{protons})$ is in agreement with those obtained in fig. 1 (B) and (C). It is also consistent with the value of 4.27 obtained using $P\pi = 5.1$ and $m_p/m_\pi = 6.7$. Corson (1951) has made a plot of the parameter $p = \langle \alpha(x) \cdot R^{0.58} / \sqrt{x} \rangle_{av}$, where x and R (the cell-size and range respectively) are expressed in units of 100μ . He obtains a value of $\bar{p} \sim 5.9$ for 76 proton tracks. Our results similarly plotted, give $\bar{p} \sim 5.6$. The agreement may in fact be even better than these figures show, since Corson remarks that since he uses a cell of 20μ for a range of 500μ his values are perhaps a little large, owing to noise introduced into the measurements.

To determine the scattering constant, we have taken the group lying between $4.05 < P < 4.60$ as protons. A certain number of protons which exhibit low multiple scattering would have been lost in the deuteron and triton peaks. On the other hand, the proton group will contain a certain number of deuterons and tritons as impurity. The magnitude of such contamination is less than 10 per cent, and its effect on the determination of the scattering constant will be very small.

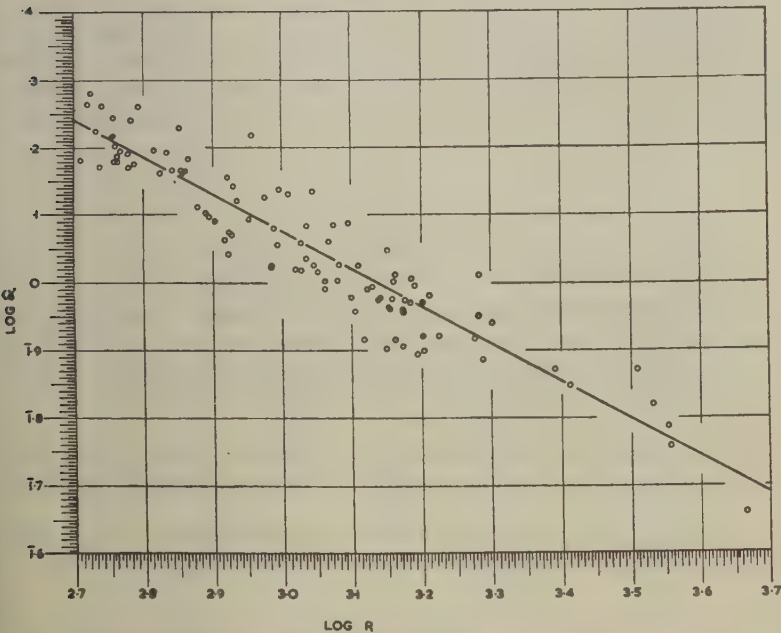
§ 4. DETERMINATION OF THE SCATTERING CONSTANT.

Using the identified group of slow protons, a plot has been made of $\log \hat{\alpha}$ against $\log R$. This is shown in fig. 2. The best line fitted to these points gives a slope of -0.554 ± 0.011 (the error being the probable error). This value is in good agreement with that obtained (0.578) for the range-energy relation by more accurate methods. However, as the linearity of the regression line is not certain in the region considered, the scattering constant has been finally determined as shown in Table I.

The points on the $\log \hat{\alpha}$ - $\log R$ plot (fig. 2) have been divided into groups using equal intervals of 0.1 along the $\log R$ axis. The coordinates of the

centres of gravity of these groups are given in columns 1 and 2 of Table I. Column 3 gives the effective range ($=0.72 R$ —see Appendix) and column 4 the corresponding energy as obtained from the range energy relation (Rotblat 1951, Catala and Gibson 1951, Bradner *et al.* 1950).

Fig. 2.



Plot of $\log_{10} \hat{\alpha}_{100\mu}$ versus $\log_{10} R$ for tracks having values of the parameter P in the interval $4.05 < P < 4.60$. The best line fitted to these points has a slope -0.554 ± 0.011 .

TABLE I.

$\log R$	$\log \hat{\alpha}$	$R_{\text{eff}}=0.72 R$	$T(R_{\text{eff}})$ in MeV.	$T(R_{\text{eff}}) \times \hat{\alpha}$
2.758	0.215	413	8.50	13.99
2.857	0.166	518	9.75	14.29
2.951	0.093	643	11.00	13.63
3.053	0.056	814	12.56	14.29
3.152	1.965	1022	14.25	13.15
3.235	1.944	1237	15.90	13.99
3.333	1.902	1550	18.00	14.36
3.412	1.845	1859	20.00	14.00
3.579	1.765	2731	25.00	14.54
3.665	1.658	3329	28.00	12.74

The product $\hat{\alpha}T(R_{\text{eff}})$ (which is equal to half the scattering constant in the units described previously) is given in column 5—the mean value of which is 13.9 ± 0.25 . The final value of the scattering constant as thus obtained is 27.8 ± 0.5 (the errors given being the standard deviation).

ACKNOWLEDGMENTS.

We are indebted to Professor C. F. Powell, F.R.S., for extending to us the hospitality and facilities of this laboratory. We would like to express our thanks to Miss R. Mitchell and Mrs. S. Rochat for their assistance with the scattering measurements. We are also thankful to Dr. W. M. Gibson for providing us with the proton tracks from plates exposed in the Liverpool cyclotron.

APPENDIX.

APPROXIMATION INVOLVED IN CALCULATING $|\hat{\alpha}|_{100\mu}$.

The n -dimensional distribution function of successive angles measured on the track between the points of residual ranges R_0 and R_n is characterized by a square matrix (A_{ik}) . Its elements A_{ik} are equal to the quantities $\overline{\alpha_i \alpha_k}$ —this being the expectation of the product of the i th angle by the k th.

These elements may be calculated using the range energy relation $T = K_a R^m$ in the case of the coordinate method, following Molière's theory (1951). Making the non-relativistic approximation $T \frac{2+\sigma}{1+\sigma} = 2T$, (σ being the kinetic energy in terms of the rest mass) we obtain (see equation, p. 1239).

In the present experimental investigation none of these terms exceeds 0.01. For the following argument they may be neglected.

The experimental procedure as described consists in calculating the arithmetic mean of " n " successive angles. This quantity being taken as proportional to the r.m.s. value, we may set

$$|\hat{\alpha}|_s = \frac{1}{n} \Sigma |\alpha|_i \sim \sqrt{\left(\frac{1}{n} \Sigma \alpha_i^2\right)}. \quad \dots \dots (2)$$

By definition, the expectation of the last term in (2) is given by

$$\sqrt{\left(\frac{1}{n} \Sigma A_{ik} \delta_i^k\right)} = \frac{K_1}{2K_a} \sqrt{s} \sqrt{\left(\frac{\pi}{2}\right)} \sqrt{\left(\frac{1}{n} \Sigma R_i^{-2m} \dots (1 + \dots)\right)}. \quad (3)$$

If we replace, in the square root, the Σ by the integral we get finally

$$|\hat{\alpha}|_s = \frac{K_1}{2K_a} \sqrt{s} \sqrt{\left(\int_{R_0}^{R_n} \frac{dR}{(R_0 - R_n)} \cdot R^{-2m}\right)}. \quad \dots \dots (4)$$

Introducing

$$|\hat{\alpha}|_{100\mu} = \frac{1}{2} K_1 / T_{(R_{\text{eff}})} = \frac{1}{2} \frac{K_1}{K_a} R_{\text{eff}}^{-2m}, \quad \dots \dots (5)$$

$$A_{ik} = s \left(\frac{K_1}{2K_a} \right)^2 \cdot \frac{\pi}{2} \begin{bmatrix} R_1^{-2m}(1+\delta_1) & 0.25 \left(R_1 - \frac{s}{2} \right)^{-2m} (1+\epsilon_1) & 0 & 0 \\ 0.25 \left(R_2 + \frac{s}{2} \right)^{-2m} (1+\epsilon_2) & R_2^{-2m}(1+\delta_2) & 0.25 \left(R_2 - \frac{s}{2} \right) (1+\epsilon_2) & 0 \\ \vdots & \vdots & \vdots & \vdots \\ 0 & (1+\epsilon_i) \cdot 0.25 \left(R_i + \frac{s}{2} \right)^{-2m} & R_i^{-2m}(1+\delta_i) & (1+\epsilon_i) 0.25 \left(R_i - \frac{s}{2} \right)^{-2m} \\ \vdots & \vdots & \vdots & \vdots \end{bmatrix} \quad (1)$$

R_i = residual range corresponding to the angle α_i ; s = cell length.

K_1 = scattering constant as defined in Gottstein *et al.* (1951); the change of the "logarithmic" term with range has been neglected here.

K_a = constant of the range energy relation.

The values of δ_i and ϵ_i are respectively $\delta_i = \frac{m(2m+1)}{10} \left(\frac{s}{R_i} \right)^2$ and $\epsilon_i = \frac{3m(2m+1)}{10} \left(\frac{s}{R_i} \right)^2 + \text{term in } \frac{s^3}{R^3}$.

we define an effective range

$$R_{\text{eff}} = \left[\frac{1}{R_0 - R_n} \int_{R_n}^{R_0} \frac{dR}{R^{2m}} \right]^{1-2m} \quad (6)$$

For

$$R_0 = 2R_n \quad \text{and} \quad m = 0.578, \quad R_{\text{eff}} = 0.72R_0.$$

The scattering constant will then be obtained from (5)

$$\frac{K_1}{2} = |\hat{\alpha}|_{100\mu} T_{(R_{\text{eff}})} \quad (7a)$$

It is clear that $\frac{K_1}{2}$ is also the expectation of the quantity $\frac{1}{n} \sum_i |\alpha_i| T_{i(R_i)}$

$$\frac{K_1}{2} = \frac{1}{\sqrt{s}} \cdot \frac{1}{n} \sum |\alpha_i| T_{i(R_i)} \quad (7b)$$

Thus this simplified method yields the same results as the more precise one in which each angle is multiplied by the corresponding energy.

The variance $\left(\frac{\delta K_1}{K_1}\right)$ for (7a) is

$$\frac{\delta K_1}{K_1} = \sqrt{\left[\frac{\left(1 + \frac{2}{16}\right) \int_{R_0}^{R_n} R^{-4m} \frac{dR}{R_n - R_0}}{2n \left(\int_{R_0}^{R_n} R^{-2m} \frac{dR}{R_n - R_0} \right)} \right]} = \frac{76.5}{\sqrt{n}} \text{ per cent.} \quad (8a)$$

whereas for the estimate given by (7b) it is

$$\frac{\delta K_1}{K_1} = \sqrt{\left[\frac{\left(1 + \frac{2}{16}\right)}{2n} \right]} = \frac{74}{\sqrt{n}} \text{ per cent.} \quad (8b)$$

The variance given in (8a) would be greatly increased in comparison with that in (8b) if larger portions of the track were used.

REFERENCES.

- BRADNER, SMITH, BARKAS and BISHOP, 1950, *Phys. Rev.*, **77**, 462.
 CATALA and GIBSON, 1951, *Nature, Lond.*, **167**, 553.
 CORSON, 1951 (private communication).
 GEORGE and EVANS, 1951, *Proc. Phys. Soc. A*, **64**, 193.
 GOLDSCHMIDT-CLERMONT, KING, MUIRHEAD and RITSON, 1948, *Proc. Phys. Soc.*, **61**, 183.
 GOTSTEIN, MENON, MULVEY, O'CEALLAIGH and ROCHAT, 1951, *Phil. Mag.*, **42**, 708.
 HODGSON, 1950, *Phil. Mag.*, **41**, 725.
 MENON, O'CEALLAIGH, and ROCHAT, 1951, *Phil. Mag.*, **42**, 932.
 MOLIÈRE, 1951, *Z. Natur.* (in course of publication).
 ROTBLAT, 1950, *Nature, Lond.*, **165**, 387; 1951, *Ibid.*, **167**, 550.
 SORENSSEN, 1949, *Phil. Mag.*, **40**, 947; 1951, *Ibid.*, **42**, 188.

CXXIV. *Nuclear Transmutations Produced by Cosmic-Ray Particles of Great Energy.*—Part VI. *Experimental Results on Meson Production.*

By U. CAMERINI*, J. H. DAVIES, P. H. FOWLER, C. FRANZINETTI†, H. MUIRHEAD‡, W. O. LOCK, D. H. PERKINS and G. YEKUTIELI§,

H. H. Wills Physical Laboratory, University of Bristol.]

[Received July 30, 1951.]

[Plates XLII.–XLIV.]

SUMMARY.

An analysis has been made of the secondary particles ejected from nuclear disintegrations observed in electron sensitive emulsions exposed to the cosmic radiation at 68,000 ft. Scattering and grain density measurements have been carried out on the tracks of 2000 particles associated with these stars. In addition, the grain density and angular distribution of 3070 shower particles and 1508 "grey" tracks have been measured.

For 200 stars, the energy of the primary particle which produced the disintegration was measured. A detailed analysis was made of such events. Single fast π -mesons of kinetic energy less than 1 BeV. are found to interact strongly with nuclear matter.

An estimate of the frequency of occurrence of neutral mesons was made from a consideration of the energy balance in stars of low multiplicity, n_s .

§ 1. INTRODUCTION.

IN Parts I. to V. of the present series of papers a description has been given of the disintegrations produced in photographic emulsions by the high energy protons, neutrons and α -particles of the cosmic radiation. Parts I. and II. contained a phenomenological description of the principal features of the disintegrations observed at an altitude of 11,000 ft. and above 50,000 ft.; in Parts III. and IV. it was shown that a large proportion of the shower particles were π -mesons, which interact strongly with nuclei, and their distribution in energy was determined; and in Part V. evidence was given that neutral π -mesons are emitted, together with the charged π -particles, in the "showers", that they have a lifetime less than 10^{-13} secs., and that their decay into two *quanta* gives rise to most of the soft component of the cosmic radiation.

In this and the final paper which follows, Part VII., an attempt has been made to elucidate the nature of the physical processes which occur within the nucleus under bombardment by energetic protons, processes which

* Now at the University of Rio de Janeiro, Brazil.

† Now at the University of Rome.

‡ Now at the University of Glasgow.

§ On leave from the Hebrew University, Jerusalem.

| Communicated by Professor C. F. Powell, F.R.S.

result in the production of the "showers" of mesons, and nuclear fragments. This first paper contains a description of observations on 15,000 nuclear disintegrations recorded in plates "exposed" at 68,000 ft. In about 200 stars, the observed track of the primary particle which produced the disintegration was long enough to allow the energy to be determined. For such events a much more detailed analysis has been possible.

Part VII. contains an analysis of the new experimental material. In approaching the problem, it is assumed that the disintegrations can be described in terms of a succession of two-body interactions occurring in the nucleus (nucleon-nucleon and meson-nucleon) which can lead, if the interacting particles are sufficiently energetic, to the creation of π -particles. Recent observations, in this and other laboratories (O'Ceallaigh 1951, Fowler *et al.* 1951) strongly suggest that in the nuclear interaction of protons and neutrons of energy ≥ 10 BeV. the production of more massive mesons may become important. But at the rather lower energies, < 10 BeV., with which we have been mainly concerned, any such process, and those involving the creation of pairs of nucleons, if they occur, can hardly play an important role.

§ 2. NOMENCLATURE.

In describing the observations, it will be convenient to adopt the nomenclatures given in Part I. A closer analysis has been found desirable, however, in the case of the more heavily ionizing particles. The tracks produced by the particles emerging from nuclear disintegrations are therefore divided into three classes:—

(i.) *Tracks of "shower" particles.* These are tracks in which the grain-density, g , is less than 16 grains per 50μ ; in the conditions of the experiment, this value corresponds to a particle with the electronic charge and a specific ionization less than 1.4 times the minimum value, i_{\min} . The great majority of such tracks are produced either by π -mesons of energy greater than 80 MeV., or by protons of energy greater than 500 MeV. The total number of such tracks associated with a given "star" is denoted by n_s .

(ii.) *"Grey" tracks.* These are tracks with a grain density in the interval from 16 to 80 grains per 50μ , and their number for any star is represented by N_g . They can be produced by protons with energy in the interval from 25 to 500 MeV. Only a very small proportion of the protons emitted during the "evaporation" of highly excited nuclei have energies as great as 25 MeV. Most of the "grey" tracks are therefore due to protons, recoiling from fast nucleons and produced at an early stage of the disintegration. Some, however, are due to deuterons and tritons, and about 18 per cent to π -mesons of energy less than 80 MeV.

(iii.) *"Black" tracks.* These tracks have a grain density greater than 80 grains per 50μ , and their number is denoted by N_b . They are due to protons of energy less than 25 MeV.; to deuterons and tritons of energy

less than 50 MeV. and 75 MeV., respectively; and to α -particles less than 800 MeV.

The sum $N_a + N_b$ is represented by N_h . A "star" is characterized in terms of $N_h + n_s$ together with a suffix to denote the nature of the particle producing the disintegration; viz., n, p, π, α —for neutron, proton, π -meson or α -particle respectively. Stars with $n_s \geq 2$ are referred to as "showers".

§ 3. SCOPE OF THE OBSERVATIONS.

In an examination of 87 c.c. of emulsion, 15,300 nuclear disintegrations or "stars" were observed. Measurements of scattering and grain density were made on 2000 of the tracks associated with these stars, the only criterion for selection being that the track, in the emulsion, was longer than 3 mm.

Measurements of grain density and of the angular distribution of the ejected particles were also made on the tracks of 3070 shower particles, and 1508 grey tracks including those which were shorter than 3 mm. In addition, all stars in which the track of the primary particle was long enough to allow the energy to be determined, were analysed in detail.

§ 4. COMPOSITION OF STARS.

The distribution of the 15,300 nuclear disintegrations according to the number of shower particles, n_s , and the number of heavily ionizing particles, N_h , is shown in Table I. The results given are those recorded by the observers; but a more detailed study of individual stars, selected at random, indicated that the errors in the observations of both N_h and n_s were small.

It will be convenient to describe first the distributions in the values of the energy, mass and angular distribution of the different types of secondary particles; and where possible, the variation of these quantities with the star parameters N_h and n_s .

4.1. "Shower Particles".

Of the 2000 tracks for which the scattering parameter $\bar{\alpha}$ was determined, 470 were shower particles. These were sub-divided into three groups—according to whether they could be identified as mesons, or protons; or whether their nature was uncertain. We denote particles of the three types by the symbols π_s, p_s and π, p , respectively.

π_s . Mesons with kinetic energy in the interval from 80 to 1100 MeV. The particles in this group constitute about 60 per cent of the total number of shower particles.

p_s . Protons of energy between 500 and 800 MeV. (20 per cent of the total).

π, p . Particles with a mean angle of scattering, $\bar{\alpha}$, less than 0.0226 degrees per 100 μ . For such particles, the grain density in the tracks, both of mesons and protons, is equal to the minimum value, and the two types of particle cannot be distinguished in the conditions of the experiment. (20 per cent of the total.)

The distribution in energy of the π_s particles for stars of different types indicates that there is no significant dependence on either N_h or n_s . In other words, the energy distribution of the mesons is nearly the same for disintegrations in which a heavy nucleus of silver and bromine is completely

TABLE I.
ANALYSIS OF 15,300 STARS OBSERVED IN PLATES FLOWN AT 69,000 FT. N_h = NUMBER OF HEAVILY IONIZING PARTICLES ($g > 1.5g_{\text{min}}$); n_s = NUMBER OF SHOWER PARTICLES ($g < 1.5g_{\text{min}}$).

$N_h \backslash n_s$	3	4	5	6	7	8	9	10	11	12	13	14	15	16	17	18	19	20	21	22	23	24	25	26	27	28	29	30	Totals.		
0 n	2499	2132	1499	938	576	367	238	169	124	100	89	67	47	37	29	24	18	11	7	3	4	1	1	3	2	1	1	1	1	8977	
0 p	225	310	356	305	204	137	116	92	75	45	49	55	52	32	22	12	10	11	9	8	3	2	4	1	2	1	1	1	1	2117	
1 n	133	194	195	199	128	97	88	65	51	53	28	34	23	13	25	15	18	3	8	1	2	1	1	2	1	1	1	1	1	1378	
1 p	91	146	151	135	96	79	52	50	44	36	28	25	24	15	15	18	11	6	10	5	1	8	6	3	2	3	3	3	3	1063	
2 n	33	36	44	51	37	26	26	23	20	17	16	27	17	15	15	9	3	4	2	7	1	2	3	2	1	2	2	2	2	437	
2 p	24	42	28	49	32	24	29	29	22	15	20	23	20	13	7	7	7	3	8	1	2	3	2	1	1	1	1	1	1	424	
3 n	9	5	8	7	6	10	5	4	4	5	2	2	5	2	1	2	4	5	2	1	2	2	2	1	2					83	
3 p	13	15	25	17	14	14	12	12	18	10	11	16	12	7	1	7	4	5	2	1	6	2	2	1	1					229	
4 n	3	6	7	6	7	2	6	2	2	2	1	4	2	5	6	8	3	1	2	1	1	1	2	1	3	1	1	1	1	61	
4 p	3	11	15	11	11	9	9	10	5	4	6	2	5	6	8	1	4	5	4	2	5	4	2	1	3	1	1	1	1	148	
5 n	3	2	1	4	3	1	1	5	1	4	2	1	4	4	3	2	4	1	1	1	2	1	1	3	1	1	1	1	1	37	
5 p	8	5	8	9	7	5	6	6	5	5	2	4	4	3	2	1	4	1	1	2	2	1	1	1	1	1	1	1	1	97	
6 n	5	2	3	7	5	4	1	3	1	5	2	6	2	1	3	4	1	1	1	1	3	1	2	2	1	1	1	1	1	28	
6 p	5	5	3	7	5	2	5	2	2	5	2	6	2	1	3	4	1	1	1	1	3	1	1	1	1	1	1	1	1	68	
7 n	1	2	1	2	1	2	1	3	4	5	2	6	2	1	2	1	1	1	1	1	3	1	1	1	1					6	
7 p	1	2	1	2	1	2	1	3	4	5	2	6	2	1	2	1	1	1	1	2	1	2		2						39	
8 n				2	1	4	2	1	3	3	3	1	1	2	1	2	1	1	1	2	3	2		1						4	
8 p				2	1	4	2	1	3	3	3	1	1	2	1	2	1	1	1	2	3	2		1						34	
9 n	1	1	1	1	2	1	1	1	1	1	1	1	1	1	2	1	1	1	1	1	2			3	1					6	
9 p	1	1	1	1	2	1	1	1	1	1	1	1	1	1	2	1	1	1	1	1	2			3	1					14	
10 n				2	1		2																							4	
10 p				2	1		2																							15	
11 n																														0	
11 p							1																							6	
12 n																														0	
12 p							1																							3	
13 n																														0	
13 p						1		1	1																					9	
14 n																														1	0
14 p																														3	0
>15 n																														11	11
>15 p																															11
Grand Total: 15,300																															

Grand Total :- 15,300

disrupted [as for those in which only a few heavily ionizing particles emerge, many of which are due to the disruption of light elements such as carbon or oxygen; and it is the same for "showers" in which many mesons are created as for those in which there are only a few. This feature

is displayed in Table II., which shows values of the average kinetic energy of the particles for stars with different values of N_h and n_s . It may be emphasized that although we are dealing here with the low-energy end of the energy spectrum of the ejected mesons, it contains more than 60 per cent of all these particles produced in the disintegrations.

TABLE II.

Average kinetic energy of the π -mesons of energy E , where $1100 \text{ MeV} > E > 80 \text{ MeV}$ for stars of different types.

n_s	1	2-4	5- ∞
E	385 ± 40	340 ± 35	395 ± 40
N_h	3-8	9-14	15- ∞
E	385 ± 45	360 ± 40	360 ± 30

A similar analysis of the distributions in energy of the protons, p_s , and unidentified particles, (π, p) , is subject to large statistical errors, but the results are given in Tables III. *a* and III. *b*. These show the proportions of protons and unidentified particles, (π, p) , among the shower particles of all types, for different kinds of stars. The most important fact established by the results is that the proportion of these energetic particles (π, p) is greater for large than for small showers. If we consider all the stars in which a given number of shower particles, n_s , is produced the proportion of fast shower particles (π, p) is greater for the small than for large values of N_h .

TABLE III. *a*.

Number of π - p particles per shower particle.

		N_h 3-8	N_h 9- ∞	N_h 3- ∞
n_s	1	0.15 ± 0.04	0.09 ± 0.05	0.13 ± 0.03
n_s	2-4	0.22 ± 0.05	0.22 ± 0.05	0.22 ± 0.03
n_s	5- ∞	0.41 ± 0.09	0.14 ± 0.04	0.23 ± 0.04
n_s	1- ∞	0.23 ± 0.03	0.16 ± 0.02	0.20 ± 0.02

TABLE III. *b*.

Number of proton shower particles per shower particle.

		N_h 3-8	N_h 9- ∞	N_h 3- ∞
n_s	1	0.21 ± 0.04	0.18 ± 0.06	0.20 ± 0.04
n_s	2-4	0.16 ± 0.04	0.13 ± 0.04	0.14 ± 0.04
n_s	5- ∞	0.05 ± 0.03	0.12 ± 0.03	0.10 ± 0.03
n_s	1- ∞	0.16 ± 0.03	0.13 ± 0.02	0.14 ± 0.02

We shall see later that the first of these facts is a simple consequence of the greater average energy of the primary particles of stars with greater multiplicity; and that the second is due to secondary interactions and loss of energy of the shower particles in escaping from the nucleus in which they are produced.

In order to calculate the average energy required to produce the π, p particles, it is necessary to make assumptions about the proportions of π -mesons and protons among them. This has been done in the following way: the energy spectrum of the μ -mesons in the cosmic radiation, most of which are produced by the decay in flight of π -particles, has been determined by Sands (1950). From this spectrum, the energy distribution of the parent π -particles can be computed: and thence, from the low energy distribution of π -mesons observed in the present experiments, the total number to be expected among the (π, p) particles can be calculated. The result is about two-thirds of all the (π, p) particles, and the rest are therefore attributed to protons. Assuming that this proportion is constant for stars of all types, the average energy of a (π, p) particle is found to be 1930 MeV.

Using this value, and taking into account the rest-energy of the π -particles, the average energy of the shower particles can be found for stars of different types. The results are shown in Table IV.; they reflect the different proportions of fast shower particles (π, p) in different kinds of stars.

TABLE IV.

Average total energy of shower particles $(\pi_s + p_s + \pi, p)$ as a function of N_h and n_s .

n_s	1	2-4	5- ∞
E	750 ± 40 MeV	850 ± 40 MeV	910 ± 45 MeV
N_h	3-8	9-14	15- ∞
E	855 ± 40 MeV	775 ± 55 MeV	730 ± 45 MeV

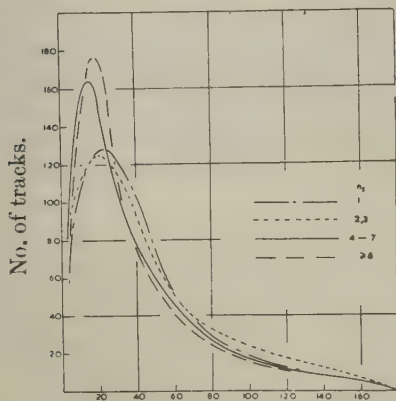
4.2. Angular Distributions.

The angular distribution of the shower particles with respect to the line of motion of the charged primary particles has been determined by observations on more than 1000 "stars". The results have been separated into a number of classes according to the characteristics of the stars and are shown in figs. 1 and 2. Most of the shower particles are emitted in directions making angles, θ , less than 40° with that of the primary particle, but some are ejected backwards, $\theta > 90^\circ$. The angular distribution of the backward-moving particles is nearly isotropic.

Fig. 1 shows that the "width" at half-maximum of the angular distributions decreases—but only very slowly—as n_s , the number of shower particles in a star increases: fig. 3 shows the variation with multiplicity, n_s , of the median angle of the distribution, η , for stars of a given type. The observations can be easily interpreted in terms of the increase of the average energy of the primary particles required to produce stars of increasing multiplicity. This involves an increase in the velocity of the C-system of the interacting nucleons, and therefore an increasing tendency for the mesons to be thrown forward, in the L-system, in directions near that of the primary particle.

The "half-widths" of the angular distributions increase with the value of N_h (fig. 3), an effect which can be interpreted in terms of interactions of the shower particles with the parent nucleus. Such interactions will contribute, first, to excitation energy of the nucleus, and thus to the

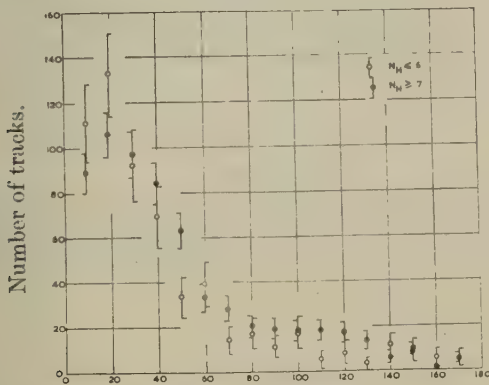
Fig. 1.



Angle to primary.

The angular distributions of shower particles in the laboratory system for different ranges of multiplicity. The ordinate gives the number of tracks per angular interval.

Fig. 2.



Angle to primary.

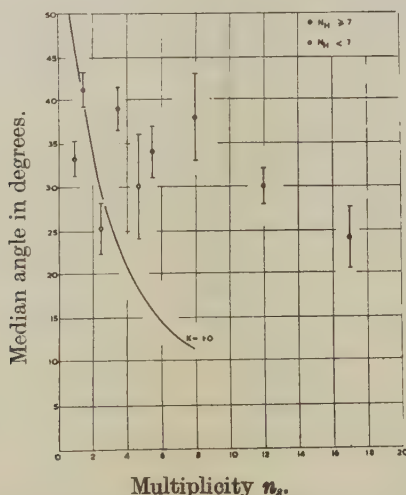
The angular distribution of shower particles for stars of $N_h \leq 6$ and $N_h \geq 7$.

completeness of the disintegration of the nucleus, *i. e.* to an increase in N_h , and, secondly, to a scattering of the emerging mesons, and so to the breadth of the angular distributions.

The fraction of the shower particles projected at angles greater than 90° to the direction of the primary, is denoted by B . Observations on

this quantity also have an important bearing on the question of secondary interactions of the shower particles in escaping from the parent nucleus, and it will be convenient to refer to it as the "backward fraction". As shown in fig. 4, it decreases only slowly with increase in the value of n_s , the multiplicity of the star. There is, however, a strong dependence on N_h . Thus, taking all stars with shower particles, $n_s \geq 1$, the value of B is equal to 0.113 ± 0.016 for $N_h \leq 7$; and to 0.171 ± 0.012 for $N_h > 7$. Almost all stars for which $N_h > 7$ must be due to the disintegration of the heavy elements in the emulsion, silver and bromine; and also some, at least, of those for which $N_h \leq 7$. It follows that the ratio of the backward fraction due to the disintegration of the heavier elements, B_H , to that for the lighter elements, B_L , must be greater than $17.1/11.3$, *i. e.* $B_H/B_L > 1.5 \pm 0.24$.

Fig. 3.



The variation of the median angle of the showers with the multiplicity, for stars of $N_h \geq 7$ and $N_h < 7$. The curve shows the variation expected on the assumption of multiple production in a single nucleon-nucleon collision ($K=1.0$).

4.3. "Grey" Tracks.

The grey tracks are due almost entirely to protons, deuterons and tritons, and the results of a study of the distribution in energy and the relative proportions of the different types of particles have been given in Part IV. These quantities appear to be constant for stars of different types, with the exception of type O_n , and fig. 5 shows their average number per star for different values of n_s .

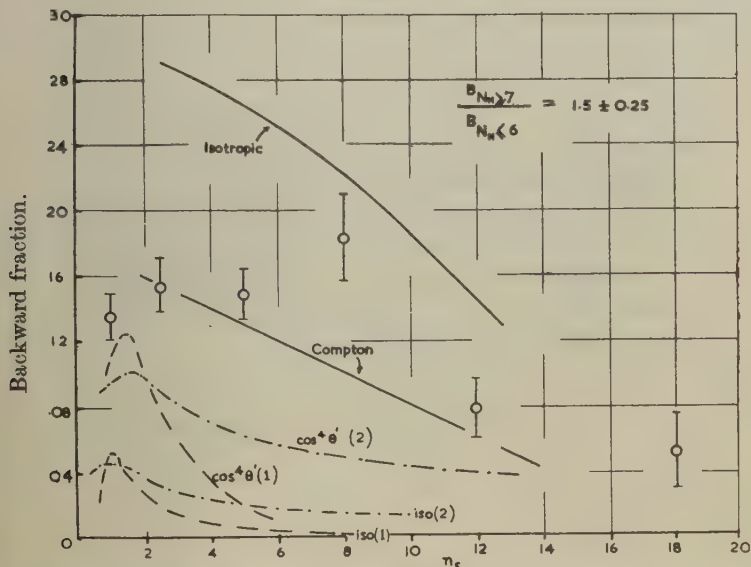
From a knowledge of the number and the average kinetic energy of the particles producing the "grey" tracks the average energy required to produce the heavily ionizing particles which appear as "grey" and

"black" tracks has been calculated. Following the procedure described in Part I. (Brown *et al.* 1949) the total energy E_{N_h} of these particles, including neutrons of the same speeds, may be calculated. The results may be expressed by the relation:—

$$E_{N_h} = f(N_h) = 155 N_h - 100 \text{ MeV. } (N_h > 1).$$

This formula applies for stars of all types with the important exception of type O_n . The formula given in Part I., viz: $E_{N_h} = 37N_h + 4N_h^2$, was obtained using a selection of stars which were predominantly type O_n for low values of N_h .

Fig. 4.



The variation of backward fraction with multiplicity. Experimental points \bar{O} . Curves marked "iso" calculated variation on the assumption of pure multiple production with isotropic angular distribution of the mesons in the C-system of the colliding nucleons for (1) and (2) generations. " $\cos^4 \theta'$ " variation calculated on the assumption of an angular distribution in the C-system of form $\cos^4 \theta' \sin \theta' d\theta'$. The full line curves indicate the fraction projected backward on the assumption that each meson is elastically scattered by a nucleon in its exit through the nucleus, either by Compton-type scattering, or by scattering isotropic in the C-system of meson and nucleon, with cross-section independent of energy.

The angular distributions of the particles which produce the grey tracks, divided into three groups according to the energies of the particles, are shown in fig. 6. The observed tendency for the fast protons to be emitted at only small angles to the direction of motion of the primary particle is in accord with the results of Crussard (1950), Harding (1951) and Osborne (1951).

4.4. "Black" Tracks.

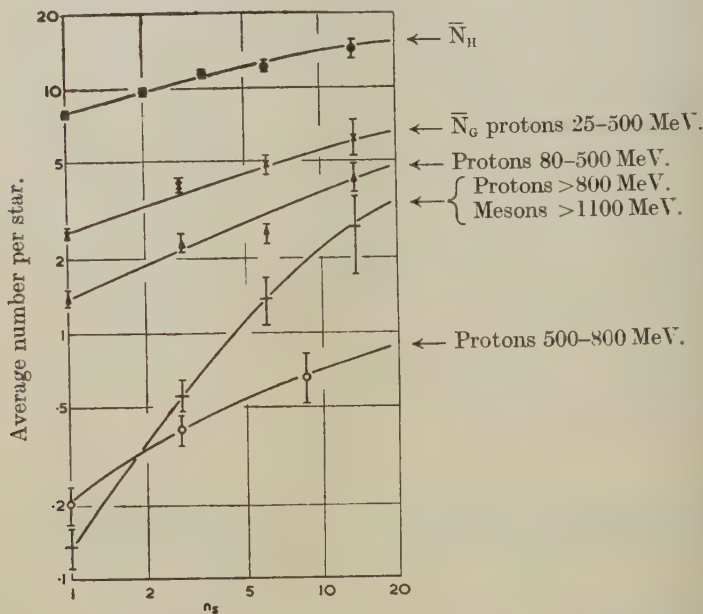
The "black" tracks are emitted almost isotropically, and their observed energy "spectrum" is consistent with the view that they arise as a result of the evaporation of the nucleons from a highly excited nucleus (Harding, Lattimore and Perkins 1949).

§5. STARS PRODUCED BY PRIMARY PARTICLES OF KNOWN ENERGY.

In analysing the experimental material, a track has been identified as due to a singly-charged primary particle producing a star if it satisfies the following conditions:—

- (1) Its grain-density must be less than 16 grains per 50μ .
- (2) The track must be in the upper hemisphere.

Fig. 5.



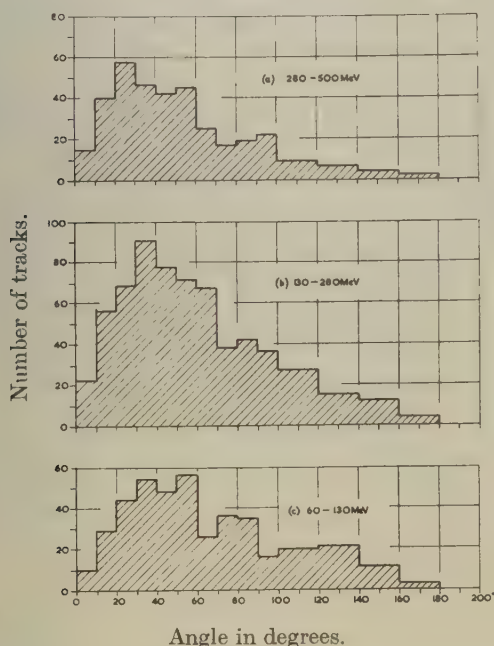
Variation with multiplicity of the number of protons and mesons of different energies and of the number of heavily ionizing particles N_H .

- (3) For stars of higher multiplicity, $n_s > 2$, the track of the particle assumed to be the primary must be not widely inclined to the average direction of the secondary shower particles.
- (4) The energy of the assumed primary particle, if measurable by the scattering method, must be sufficiently great to have produced the star and the shower particles.

Of 2000 tracks on which scattering measurements and grain counts have been made, 200 satisfied these conditions.

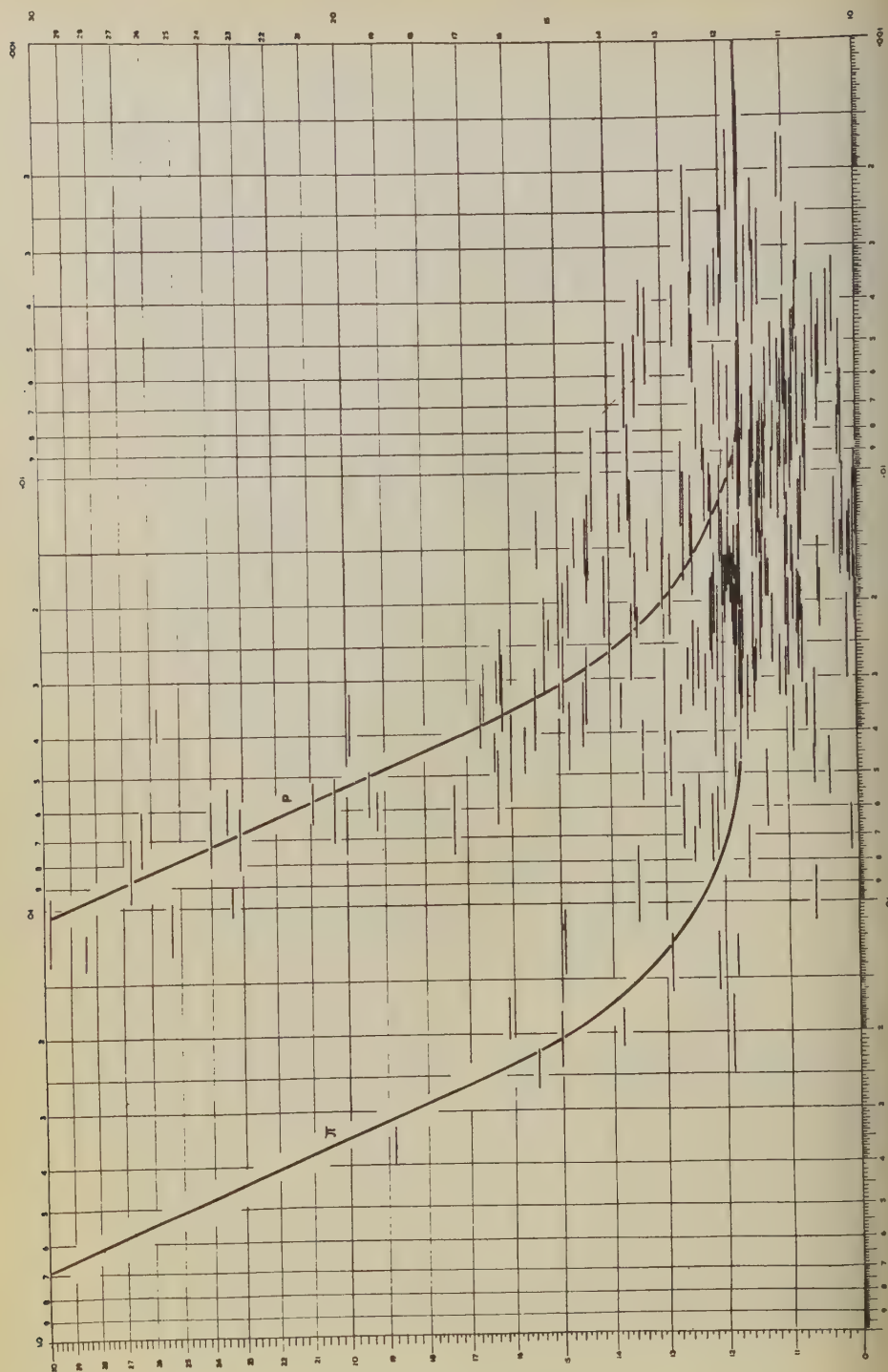
It is well known that mesons produced in nuclear interactions may be emitted backwards, the direction of motion being nearly opposite to that of the parent particle. It is therefore possible to make errors of identification and to attribute a track to a primary particle when it was, in fact, due to an ejected meson—the true primary particle being a neutron. Such errors are most serious in the case of stars of low multiplicity. A star produced by a fast neutron in which a single fast meson is ejected vertically upwards, type 1_n , may be wrongly classed as of type 0_p . The proportion of such errors can be estimated in the following ways :—

Fig. 6.



The angular distribution of the "grey" protons as a function of energy.

The fraction of secondary shower particles from stars of type 1_p which have directions of motion in the upper hemisphere, is found to be 0.15. If it is assumed that the angular distribution of the secondary fast particles produced in stars of type 1_n is similar to that in type 1_p , then it follows that only 10 per cent of the "primary" particles of stars of type 0_p are, in fact, secondary particles. The probability of wrongly identifying a charged primary particle in events from which several shower particles are emitted is small, because the average energy of "backward" moving shower particles is low so that the scattering measurements prove them to be insufficiently energetic to have produced the star.



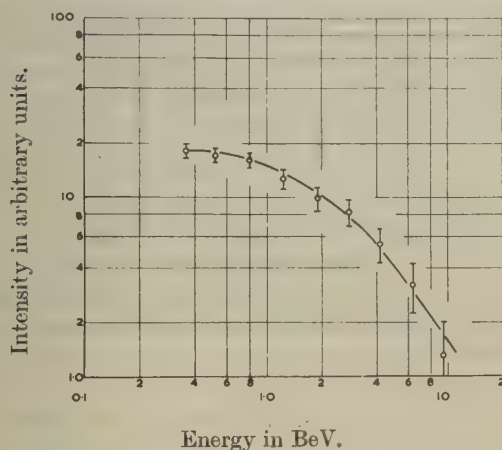
Mean deviation \bar{a} in degrees per 100 microns.

A plot of the values of g and $\bar{\alpha}$ for all the track of "primary" particles identified by these criteria is shown in fig. 7. The distribution in energy of the particles—deduced from the results shown in fig. 7, after correction for geometrical factors and with the assumption that all the fastest particles (π, p) are protons, is represented in fig. 8.

It is possible to determine directly the distribution in energy of the π -mesons among the primary particles in the interval $<10^3$ MeV. Extrapolating the results to greater energies, it was found that only about 15 per cent of the fast primaries (π, p ; $E < 1.2$ BeV.) are due to π -mesons. A second estimate of this ratio was obtained by the following method:—

The energy spectrum of the secondary (π, p) particles is known, and the cross-section for their interaction with nuclei is close to the geometrical value. It is therefore possible to estimate how many of the high energy

Fig. 8.
Integral spectrum of "primary" protons and π -particles.

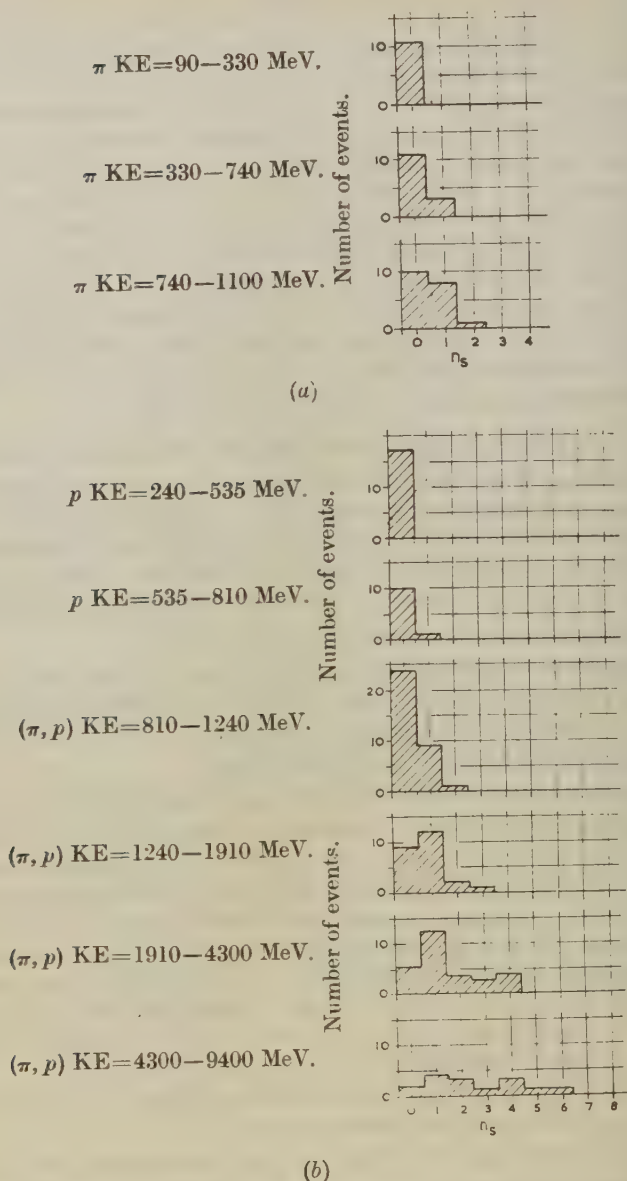


The integral distribution of the "primary" protons and π, p particles.

π, p) particles, produced in nuclear disintegrations in the plate assembly, will interact with another nucleus in the local matter. Such calculations show that only about 10 per cent of the fast primaries (π, p) have been generated in the plate assembly and, because of the short life-time of the π -mesons and the very weak interaction of μ -mesons, most of the others must be protons. Further, some of the fast (π, p) primaries locally generated are protons, thus only about 6 per cent of the fast primary particles of energy $>10^3$ MeV. can be attributed to π -mesons.

Similar calculations allow estimates to be made of the proportion of primary particles of lower energy which it should be possible to identify as π -mesons. The expected number thus obtained, for the particular conditions of the experiment, is 40, a number in good agreement with that observed, viz., 43.

Fig. 11.



Distribution of multiplicity, n_s , in stars produced by (a) π -mesons, (b) protons and " π, p " particles, as a function of energy.

for the shower particles which are protons and for the neutral mesons which are not recorded, we can estimate the proportion of elastic and

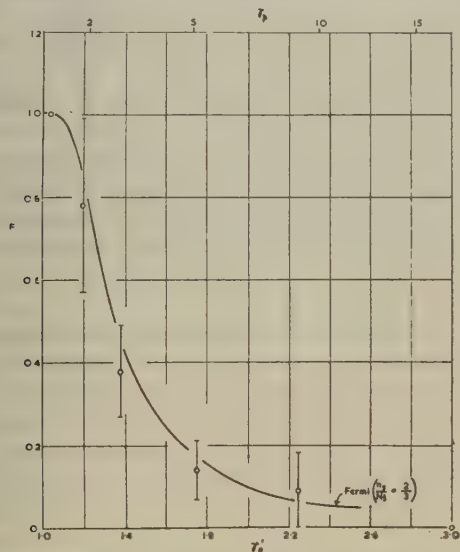
inelastic collisions made by primary particles of different energy. In making the analysis, it has been assumed that the mesons have a probability of $2/3$ of being charged (Carlson *et al.* 1950).

TABLE V.

Star Type	Kinetic energy of incident meson (MeV.)	Kinetic energy of emergent meson (MeV.)	% energy loss
$2+0_\pi$	79 ± 8	67 ± 13	15
$7+1_\pi$	640 ± 100	40 ± 8	94
$6+1_\pi$	755 ± 150	450 ± 90	43
$5+0_\pi$	825 ± 180	17 ± 3	98
$6+0_\pi$	900 ± 190	29 ± 6	97
$3+1_\pi$	1040 ± 210	120 ± 20	88
$3+2_\pi$	1050 ± 200	$\begin{cases} 375 \pm 70 \\ 365 \pm 70 \end{cases}$	70

Fig. 12.

Proportion F of 0_p stars versus primary energy.



Proportion of " 0_p stars" plotted as a function of γ_p , the total energy of the primary proton in terms of its rest energy. The curve represents the values predicted by Fermi's theory. (See text.)

Fig. 12 shows the proportion of primary particles which do *not* produce shower particles, for different values of the primary energy E_p . For $E_p = 1.6$ BeV. (total energy $\gamma_p = 2.7$), half the primary particles do not produce shower particles, and the curve shows the rapid fall of the cross-section for "elastic" scattering as the energy of the primary particle

increases. The theoretical minimum value of E_p for the production of a π -meson of energy 80 MeV., is 360 MeV. The results shown in fig. 12 indicate that for values of $E_p < 1600$ MeV. most of the collisions are not completely inelastic.

The full curve in fig. 12 represents the values deduced from Fermi's theory (Fermi 1950, 1951) (see also Part VII.). These predicted values take into account production of mesons of all energies, including those of less than 80 MeV. which are too slow to appear among the "shower particles". Such particles are few, however, so that their inclusion does not seriously invalidate a comparison between the theoretical curve and the experimental results. The agreement between them is seen to be satisfactory.

5.3. The Production of Neutral Mesons; Missing Energy.

It is now established that neutral as well as charged π -mesons are produced in energetic nuclear encounters. An estimate of their frequency of occurrence has been made by comparing the total energy represented by the secondary particles emitted from stars of a given class with the mean energy of the primary particles producing them. It has thus been shown that there is some missing energy which it is reasonable to attribute to the creation of neutral mesons.

The analysis was restricted to stars, with $n_s \leq 4$, produced by primary particles of velocity βc , where $\beta > 0.7$. The upper limit to n_s was applied in order to avoid the inclusion of large numbers of primary particles of energy greater than 10 BeV. If such particles were included, large errors would have been introduced in this analysis. The limit to the value of β was introduced because primary particles of lower velocity cannot be identified with certainty. The results obtained are summarized in Tabel VI.

Column (1) shows the observed frequency of the different kinds of tracks. Values of the average kinetic energies of the particles in group (a) have been taken from the results of Harding *et al.* (1949); the other values in column (2) have been determined from the present observations. For the groups P, D, T, the energies quoted in columns (2), (3), (4), (5), are for each proton, whether ejected individually or as part of a deuterium or tritium nucleus. It has then been assumed that the total number of neutrons of energy greater than 25 MeV. is equal to 1.25 times the number of these protons. Column (6) gives the total number of nucleons, or mesons, associated with one ejected charged particle (*i. e.* one track) of the type under consideration.

The results show that the mean energy represented by the secondary nucleons, \bar{E}_n , is 1458 ± 60 MeV.; and by the ejected mesons, \bar{E}_π , $\chi(630 \pm 40)$ MeV., where χ is the ratio of the sum of neutral and charged mesons to the charged mesons alone. The total energy associated with the "average" star is then $\bar{E}_p = \bar{E}_n + \chi \bar{E}_\pi$. The average energy of the primary particles of this group, directly observed, was found to be

$\bar{E}_p = 2700 \pm 150$ MeV. It follows that $\chi = E_p - E_{\text{nucleon}}/E_\pi = 2.0 \pm 0.3$, a value which corresponds to a ratio of neutral to charged mesons of 1.0 ± 0.3 . This result does not depend significantly on the assumed proportions of mesons and protons among the (π, p) particles, but only on the correction factor for the "grey" and "shower" particles.

Carlson, Hooper and King (1950) have estimated the ratio of neutral to charged mesons produced in nuclear disintegrations, by observing the materialization of the γ -rays into which the neutral mesons decay. They restricted their observations to showers with $n_s \geq 3$, average value 4.5, and found a value $N_{\pi^0}/N_\pi \pm 0.45 \pm 0.10$. Gregory and Tinlot (1951), using a cloud chamber, obtained a value of ~ 0.3 .

TABLE VI.

Species of track	No. per star	Kinetic energy per track	Binding energy per track	Total energy per track	Energy per star (uncorrected)	Correction factor for neutral particles	Total energy per star
P, D, T,	3.6	10	8	18	65	2.75	179
α	1.8	10	3	13	23	1	23
P, D, T,	2.48	131	8	139	344	2.25	775
π	0.22	47	140	187	41	χ	41 χ
P	0.18	625	8	633	114	2.25	256
π	0.60	395	140	535	321	χ	321 χ
P	0.063	1582	8	1590	100	2.25	225
π	0.127	1960	140	2100	266	χ	266 χ

All energies in MeV.

The discrepancy between the present result for stars with $\bar{n}_s = 1.1$ and that obtained for showers with $\bar{n}_s = 4.5$, may be attributed, at least in part, to the fact that by selecting small values of n_s , we also favour the selection of showers in which the ratio of neutral to charged mesons is large, and *vice versa*. In nuclear encounters which lead to the production of a given number of mesons, it may be assumed that the division between charged and neutral particles in any individual case will be subject to statistical fluctuations. If we therefore impose a restriction $n_s > 4$, we shall include in the sample stars with four charged and no neutral mesons, four charged and one neutral, etc. Because of the rapid fall in the number of stars as n_s increases, such observations will tend to give a lower value of the ratio N_{π^0}/N_π .

ACKNOWLEDGMENTS.

We have pleasure in thanking Professor C. F. Powell, F.R.S., for his constant interest and encouragement; Miss M. Stott, Miss M. Merritt, Mrs. M. L. Andrews, Mrs. M. J. Harris and Mr. M. J. Harris for assistance with the measurements; Miss J. Burnell and Dr. H. K. Heitler for the diagrams; Miss P. Dyer and Mr. A. R. Gattiker for the photographs; and the team of microscope observers of this laboratory for their careful scanning of the plates.

This work has been carried out as part of a programme of research supported by the Department of Scientific and Industrial Research, and two of us (J. H. D. and W. O. L.) are indebted to this body for maintenance grants.

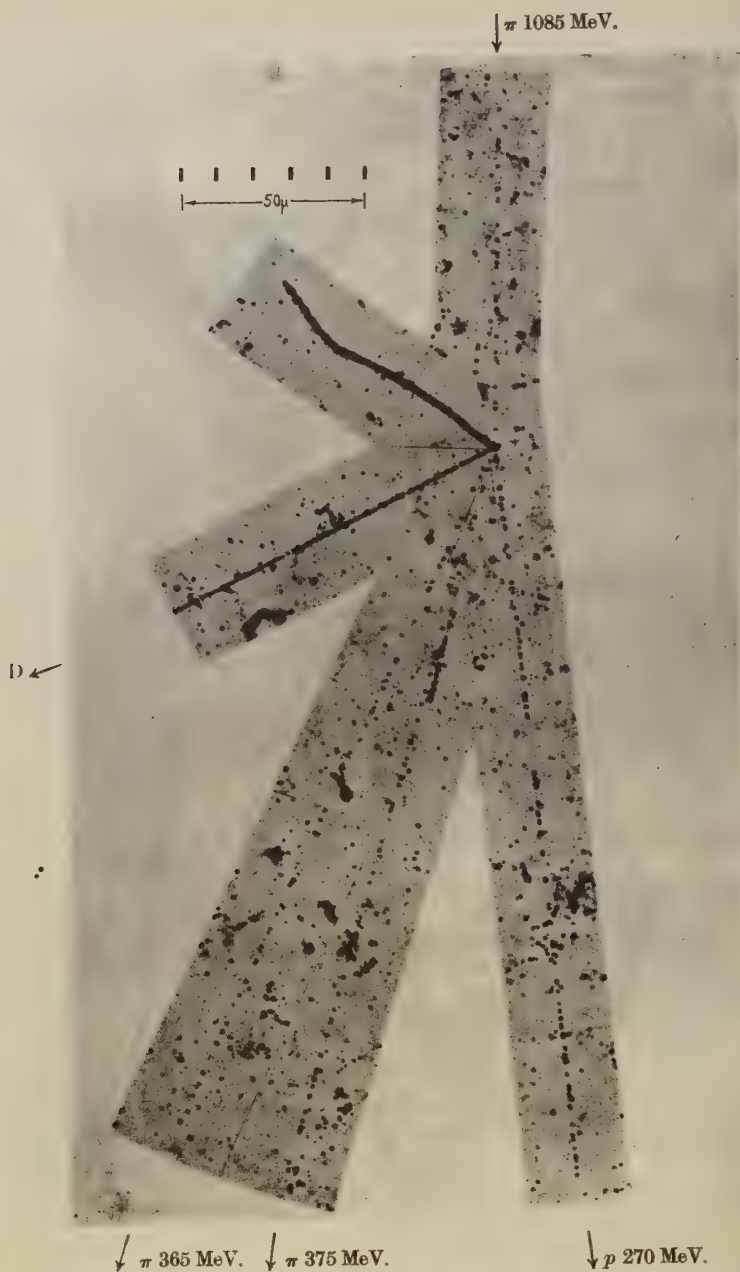
REFERENCES.

- BERNADINI, G., BOOTH, E. T., LEDERMAN, L., and TINLOT, J. H., 1950, *Bombay Conference on Fundamental Particles*, 1951. *Phys. Rev.* **82**, 105.
- BROWN, R. H., CAMERINI, U., FOWLER, P. H., HEITLER, H., KING, D. T., and POWELL, C. F., 1949, *Phil. Mag.*, **40**, 862, (I).
- CAMERINI, U., COOR, T., DAVIES, J. H., FOWLER, P. H., LOCK, W. O., MUIRHEAD, H., TOBIN, N., 1949, *Phil. Mag.*, **40**, 1073 (II).
- CAMERINI, U., FOWLER, P. H., LOCK, W. O., and MUIRHEAD, H., 1950, *Phil. Mag.*, **41**, 413 (IV).
- CARLSON, A. G., HOOPER, J. E., and KING, D. T., 1950, *Phil. Mag.*, **41**, 701 (V).
- CRUSSARD, 1950, *Bombay Conference on Fundamental Particles*.
- FERMI, E., 1950, *Prog. Theor. Phys.*, **5**, 570 ; 1951, *Phys. Rev.*, **81**, 863.
- FOWLER, P. H., 1950, *Phil. Mag.*, **41**, 169. (III).
- FOWLER, P. H., MENON, M. E. K., POWELL, C. F., and ROCHAT, O., 1951, in course of publication.
- GREGORY, B. P., and TINLOT, J. H., 1951, *Phys. Rev.*, **81**, 675.
- HARDING, J. B., 1951, *Phil. Mag.*, **42**, 63.
- HARDING, J. B., LATTIMORE, S., and PERKINS, D. H., 1949, *Proc. Roy. Soc. A*, **196**, 325.
- HEISENBERG, W., 1949, *Z. Phys.*, **126**, 569.
- O'CEALLAIGH, C., 1951, in course of publication.
- OSBORNE, L. S., 1951, *Phys. Rev.*, **81**, 239.
- SANDS, M., 1950, *Phys. Rev.*, **77**, 180.

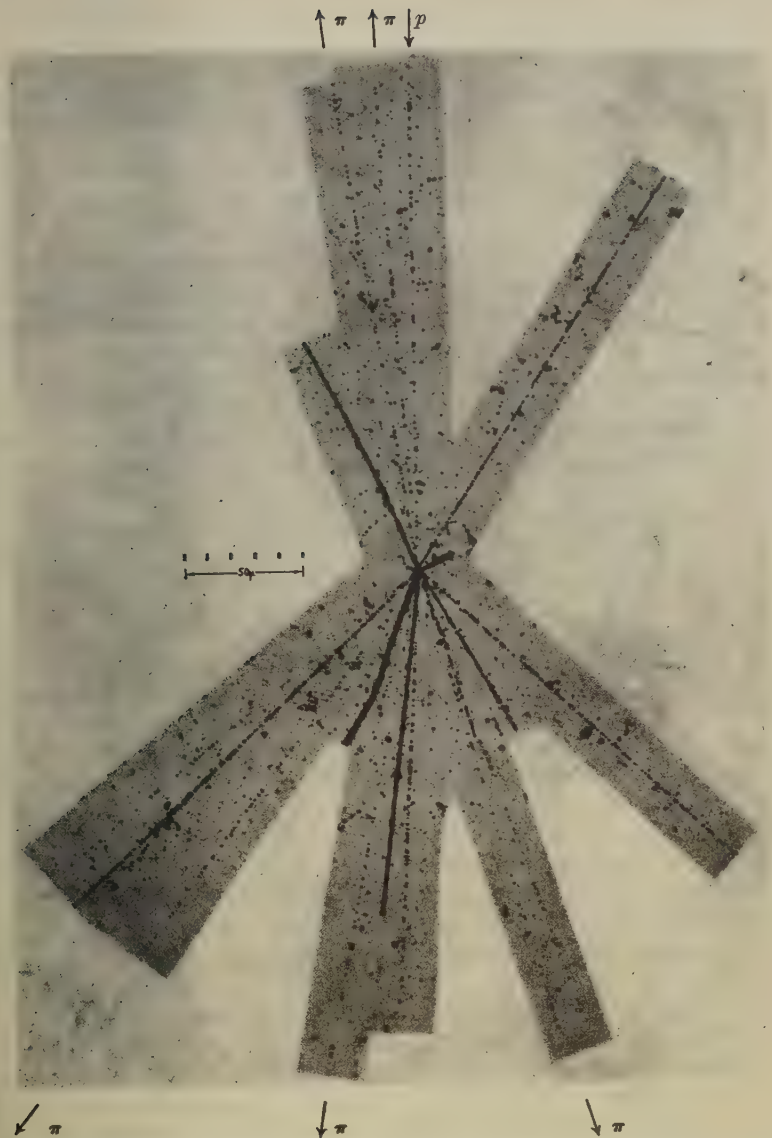


A star of type $2+1p$ in which a meson of 120 MeV. kinetic energy is produced, the primary proton having an energy of 600 MeV.

To face page 1260



Disintegration initiated by a π -meson of kinetic energy 1085 MeV. in which two π -mesons of energy 365 and 375 MeV. are produced, together with a proton of 270 MeV.



A star of type $11+8p$ in which two mesons of energy ~ 80 MeV. are ejected backwards in the laboratory system. Three of the forward shower particles have been identified as π -mesons.

CXXXV. *Nuclear Transmutations Produced by Cosmic Ray Particles of Great Energy.*—PART VII. *Interpretation of the Experimental Results.*

By U. CAMERINI, J. H. DAVIES, C. FRANZINETTI, W. O. LOCK,
D. H. PERKINS and G. YEKUTIELI.

H. H. Wills Physical Laboratory, University of Bristol *.

[Received July 30, 1951.]

SUMMARY.

The observations presented in the preceding paper are analysed and compared with the current theories of meson production. In making the analyses, account is taken of the interaction with the parent nucleus both of the recoil nucleons and the created mesons.

It is found that the observations do not provide decisive evidence in favour of either plural or multiple meson production. The experimental results can be explained in terms of either the multiple theory with secondary generation of mesons, or the plural theory assuming many-body collisions.

Some other conclusions arising from the work are given at the end of this paper.

§ 1. INTRODUCTION TO THE ANALYSIS.

THE simplest conditions for studying the generation of mesons in nucleon-nucleon collisions would be provided by experiments in which fast nucleons collided with protons in a hydrogen target, but such observations have hitherto been impracticable. Although such collisions must occur in a photographic emulsion, they are rare, and we are therefore forced to attempt to infer the nature of the complex physical processes which take place in the nucleus from the results of the collisions of the nucleons with the mixture of nuclei found in the emulsion. In addition to hydrogen, which is the most common element, this mixture contains a variety of nuclei which can conveniently be divided into two groups; the heavier, mostly silver and bromine; and the lighter, carbon, nitrogen and oxygen.

In approaching this problem, the basic assumption is made that the disintegrations can be described in terms of encounters between individual pairs of nucleons. Unfortunately, the experimental data available do not permit a definite proof of the correctness of this assumption. If the physical processes taking place cannot be described in terms of such collisions, the interpretation of the experimental results becomes very difficult, for no theoretical guidance, regarding many-body problems is yet available.

* Communicated by Professor C. F. Powell, F.R.S.

If, however, the disintegrations can always be described in terms of a number of elementary collisions, nucleon-nucleon and meson-nucleon, the problem is reduced to an enquiry into their characteristics, and we have to determine the following quantities :

(i.) The cross-sections for radiative and elastic scattering, and their variation with the energy of the incident particle.

(ii.) The probability of radiating as mesons a fraction, K , of the energy of the two colliding particles which is available in the C-system, and the dependence of K on the primary energy.

(iii.) The distributions in energy, and in angle of emission, of all the secondary particles involved ; for radiative collisions, the number of mesons created ; and the dependence of all these distributions on K , and on the primary energy.

The analysis proceeds as follows :

The experimental results are first compared with predictions based on the pure plural theory of meson production (Heitler-Janossy 1949, 1950) in which it is assumed that the mesons are produced individually in interactions between pairs of nucleons. Secondly, a similar comparison is made for the pure multiple theories (Heisenberg 1949, Fermi 1950, 1951) in which it is assumed that many mesons may be produced in a single collision. An attempt is then made to reduce the observed discrepancies by considering both for the plural and the multiple theories the secondary generation of mesons by recoiling nucleons and, for the multiple theory only, the effect of meson-nucleon interactions.

§ 2. PURE PLURAL THEORY.

The plural theory, as originally stated by Heitler and Janossy (1949) was based upon the following assumptions : (a) in each nucleon-nucleon collision only one meson is produced ; (b) the mean free path for collision of a nucleon in the nucleus is of the order of the inter-nucleon distance ; (c) the nucleus is completely transparent to the created mesons.

(a) *Comparison of observations with the Heitler-Janossy Theory.*

In the pure plural theory, the total number of mesons, charged and neutral is given by the number of encounters, N_s , made by the primary particle in traversing the nucleus, for it is assumed that one meson is created at each collision ; it follows that

$$N_s = \frac{\log(\gamma_p - 1) - \log(\gamma_c - 1)}{-\log(1 - \sigma)} + 1. \quad . \quad . \quad . \quad (1)$$

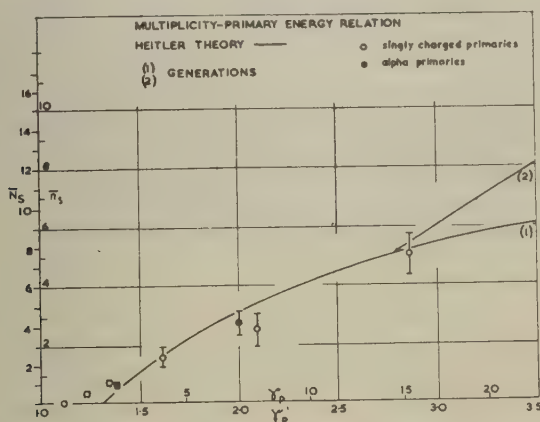
In this formula γ_p is the total energy of the primary particle in terms of its rest-mass energy and γ_c is the "cut-off" energy in the same units, below which the primary cannot generate mesons. σ , assumed to be a constant, is the fraction of the kinetic energy lost by a primary particle

in each collision; Heitler takes $\sigma=0.25$. The recoiling nucleon takes a fraction α of the primary energy, the meson ($\sigma-\alpha$). If we consider only those mesons for which $\gamma_s \geq 1.7$ (shower particles), then the cut-off is given by

$$(\sigma-\alpha)R(\gamma_c-1)=1.7; R=\frac{M_p}{M_\pi}=6.7.$$

The variation of n_s with E_p , taking $n_s=\frac{2}{3}N_s$ is then determined by σ and α only. Heitler assumes further that $\alpha=\sigma-\alpha=\frac{1}{3}$ and γ_c then equals 3.1. The value of N_s given by relation (1), multiplied by a factor $\frac{2}{3}$ is plotted in fig. 1, and shows good agreement with the experimental results for values of $n_s \leq 6$.

Fig. 1.



Variation of average multiplicity with primary energy; comparison of the experimental results with the predictions of the plural theory. γ_p =total energy of the primary proton, in terms of its rest energy. For the α -particles the multiplicity per nucleon is plotted against energy per nucleon.

Messel (1951) suggests a value of $(\sigma-\alpha) \sim 1/3$, and that the remaining energy is divided symmetrically between the two nucleons. The multiplicity using these parameters is somewhat higher than the values shown in fig. 1.

Heitler and Janossy suggest that at high primary energy the recoil nucleons can themselves produce mesons, thus accounting for showers of very high multiplicity. The contribution of the recoils is shown in curve (2), fig. 1.

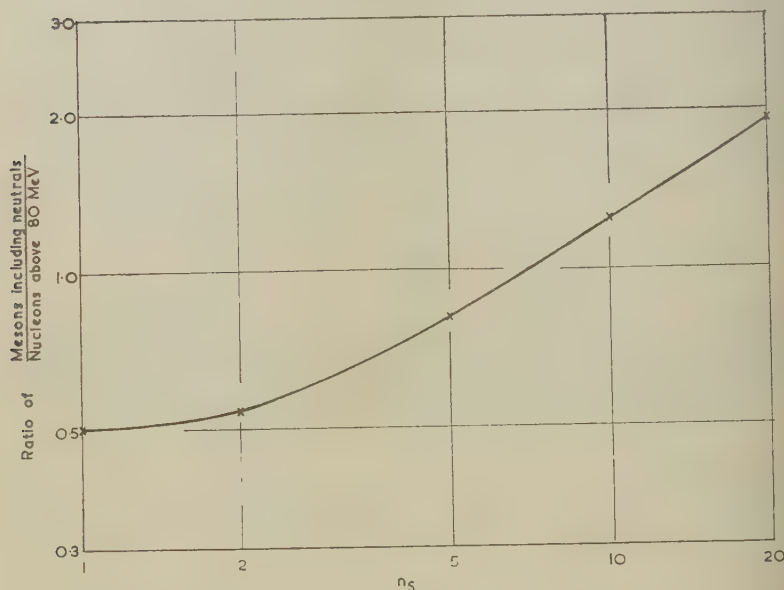
According to the above picture of plural production, the ratio of mesons to recoil nucleons, generated in meson producing collisions will be less than or equal to unity. We cannot of course measure directly the number S_{rad} of recoil nucleons originating exclusively from meson-producing collisions. However, if we consider all nucleons emerging with energies

above 80 MeV. we shall certainly obtain an upper limit for S_{rad} . In Table I. and fig. 2 we have displayed as a function of n_s the ratio of charged plus neutral mesons $\{=3/2 \times (\text{no. of identified mesons} + 0.66 \times \text{no. of } (\pi, p) \text{ particles})\}$, to the number of nucleons above 80 MeV. energy $\{=2 \times (\text{no. of protons between 80 and 800 MeV.} + 0.33 \times \text{no. of } (\pi, p) \text{ particles})\}$. The data are taken from fig. 5 of Part VI.

TABLE I.

n_s	No. of mesons including neutrals	No. of nucleons >80 MeV.	Ratio $\left(\frac{\text{nucleons}}{\text{mesons}}\right)$
1	1.65	3.30	0.50
2	2.4	4.60	0.52
5	6.2	7.60	0.81
10	13.0	10.6	1.23
20	26.8	14.2	1.9

Fig. 2.



Thus at high multiplicity ($n_s > 10$), the ratio exceeds unity, and thus there appears to be more than one meson produced per radiative collision. This conclusion would not be affected by choosing a somewhat lower limit (*i. e.* <80 MeV.) for the energy of nucleons recoiling from radiative collisions. The results in Table I. depends also on the proportions of mesons and protons in the (π, p) particles (see Part VI.). However, any variation in these proportions cannot affect the ratio of mesons to nucleons by more than 30 per cent.

(b) *Modifications of the Plural Theory.*

In an attempt to meet these difficulties, Heitler and Janossy (1950) and Heitler and Therreaux (Heitler 1950, 1951), have modified the plural theory in the following manner. The primary nucleons and the successive recoil nucleons are assumed to be confined within a very narrow cone. It is then visualized that at a certain stage in the disintegration, n moving nucleons may all be interacting with the same nucleon "at rest" giving n further mesons, but only one more recoil nucleon. After m stages of this process, there will be $m(m+1)/2$ mesons, with only $(m+1)$ recoil nucleons. With this assumption Therreaux finds that the percentage of recoil protons amongst the shower particles decreases with increasing n_s , and that the number of "grey" recoil protons is almost constant for $3 < n_s < 20$.

The degradation of energy as such a cascade develops will, however, lead to an increased angular spread of the emitted particles. If so, the true picture lies between the two extremes: that in which the ratio of mesons to recoil nucleons is equal to $m/2$, and that of the original theory, where there are equal numbers of mesons and recoil nucleons.

A ratio of mesons to recoil nucleons lying somewhere between these extreme values is certainly compatible with our observations. On the assumption of a contribution from such many-body collisions therefore, the predictions of the plural theory are in accord with the experimental data.

§ 3. PURE MULTIPLE THEORY.

The multiple theory of meson production, in its simplest form, assumes: (a) that the mesons are created in a single nucleon-nucleon collision; and (b) that the nucleus is transparent to both the recoiling nucleons and the mesons. Heisenberg (1950) has calculated the variation of \bar{N}_s with γ_p . He assumes that the mesons are produced with an energy distribution in the C-system of the colliding nucleons which is independent of γ_p , except that it extends up to a maximum value which varies with the total available energy in the system. This assumed spectrum is of the form $f(\gamma'_s)d\gamma'_s = d\gamma'_s/\gamma'^2_s$, where γ'_s is the total energy of a meson in the C-system in terms of its rest-mass. If the theory gives an adequate picture of meson production, the form of the spectrum can be determined from the present experimental observations, provided certain conditions are satisfied. The method is as follows:

In the case of 23 showers, it was possible to determine the energy both of the primary particle and of one or more secondary shower particles by observations on the scattering parameter $\bar{\alpha}$. Assuming that all the primary particles are protons and that all the shower particles of a particular event are mesons produced in a single nucleon-nucleon collision, a Lorentz transformation enables the energy and direction of motion of the mesons in the C-system to be determined. It is also assumed, tentatively, that any loss of energy and change of direction of a meson in its escape from the nucleus can be neglected.

In making the transformation, it is convenient to measure energy in terms of the rest energy of the particle, and velocity as a ratio to that of light.

Let γ_p = total energy of primary particle in the L-system ;

γ'_p = total energy of primary particle in the C-system.

It follows that :

$$\gamma'_p = \sqrt{[(\gamma_p + 1)/2]}.$$

The total kinetic energy of the two nucleons in the C-system in terms of the meson rest-mass is, before collision,

$$2R(\gamma'_p - 1)$$

and the amount radiated as mesons is

$$\epsilon = 2R(\gamma'_p - 1)K,$$

where K = degree of inelasticity, and R , the ratio of the masses of the proton and meson, equals 6.7.

The maximum energy which a single meson can take is either

$$\epsilon' = \epsilon, \text{ or } \epsilon' = \frac{R(\gamma_p'^2 - 1)}{\gamma'_p} \quad . \quad . \quad . \quad . \quad . \quad (2)$$

whichever is the smaller.

Now γ'_s and θ' , the energy of the meson, and its angle of emission with respect to the line of motion of the primary, in the C-system, are related to the corresponding quantities γ_s and θ in the L-system by the transformations :—

$$\gamma'_s = \gamma_s \gamma'_p - \sqrt{(\gamma_s^2 - 1)} \cdot \sqrt{(\gamma_p'^2 - 1)} \cdot \cos \theta, \quad . \quad . \quad . \quad . \quad (3)$$

$$\tan \theta' = \frac{\sin \theta}{\gamma'_p (\cos \theta - \beta_p / \beta_s)}, \quad . \quad . \quad . \quad . \quad . \quad (4)$$

$$\tan \theta = \frac{\sin \theta'}{\gamma'_p (\cos \theta' + \beta_p / \beta_s)}. \quad . \quad . \quad . \quad . \quad . \quad (5)$$

Each secondary is given a geometrical weighting factor $g(\theta)$, which is introduced to take account of the relative probability of observing long tracks for different values of θ . The analysis is confined to those stars of which the energy of the primary particle has been determined, and this can only be done for long tracks nearly parallel to the surface of the emulsion. Shower particles ejected at angles near $\theta = 0^\circ$ and $\theta = 180^\circ$ with respect to the line of motion of the primary particle will therefore have a much greater chance of remaining in the emulsion than those with $\theta = 90^\circ$. The observations therefore lead to a series of weighted values of θ' and γ'_s , the angle of emission and the energy, respectively, of the meson in the C-system.

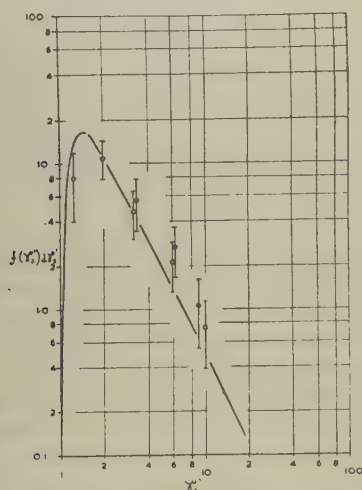
The angular distribution of all such mesons is given in Table II.

TABLE II.

θ' (in degrees)	0—30	30—60	60—90
Number Observed	34 ± 23	70 ± 30	99 ± 35
Isotropic distribution	27	74	102

Within the large statistical errors, it is consistent with an isotropic distribution. The ratio of backward to forward-moving mesons is 0.95 ± 0.44 , a result consistent with the value expected from symmetry considerations.

Fig. 3.



The energy spectrum of the mesons in the C-system derived on the assumption of a single nucleon-nucleon collision. γ'_s is the total energy of the meson in terms of the rest energy.

● $K=0.5$; ○ $K=1.0$. The curve represents the spectrum $p^2 dp \gamma^4$.

Collecting together all values of γ'_s , we obtain a distribution in energy $f(\gamma'_s) d\gamma'_s$. This however cannot be compared directly with Heisenberg's spectrum which corresponds to infinite available energy in the C-system of the interacting nucleons. To make the necessary corrections to the observations, we divide by the factor $p(\gamma'_p)$ representing the observed fraction of showers having primaries such that γ'_p is greater than the value given either by $\gamma'_s = 2RK(\gamma'_p - 1)$

or by
whichever is smaller.

$$R(\gamma'^2_p - 1)/\gamma'_p$$

The corrected distribution $f(\gamma'_s) d\gamma'_s$ is shown in fig. 3, for $K=1$ and for $K=0.5$. The peak at $\gamma'_s \sim 2$ is presumably a consequence of the

conservation of momentum in the C-system. The distribution can be represented analytically by the equation

$$p^2 dp / \gamma_s'^4,$$

where $p = \sqrt{(\gamma_s'^2 - 1)}$, which falls off at high energies as $1/\gamma_s'^2$. This is in satisfactory agreement with the spectrum chosen by Heisenberg.

It may be mentioned that, even if the pure multiple theory is inadequate, valuable information may be obtained by making such transformations in favourable cases.

3.1. Yield Curve on Pure Multiple Theory.

The average number of mesons produced in the collision is

$$\bar{N}'_s = \frac{\epsilon}{(\gamma_s')_{av}},$$

where

$$(\gamma_s')_{av} = \int_1^{\epsilon'} \gamma_s' f(\gamma_s') d\gamma_s' / \int_1^{\epsilon'} f(\gamma_s') d\gamma_s'. \quad \dots \dots (6)$$

The number of mesons classed as shower particles (energy in L-system $\gamma_s > 1.7$) is

$$\bar{N}_s = \chi \bar{N}'_s,$$

where the factor χ is nearly unity, and is easily calculated. In reaching this result, an isotropic angular distribution of the mesons in the C-system has been assumed. If one-third of all the mesons produced are neutral, the average number of mesons which appear as shower-particles is $\bar{n}_s = (2/3)\bar{N}_s$; and n_s is therefore determined as a function of $\epsilon = 2RK(\gamma_p' - 1)$. The results for three values of K , 1.0, 0.7 and 0.3—are shown in fig. 4. It will be seen that with low values of γ_p , the results indicate a small mean value of K , contrary to the Heisenberg assumption, $K=1$. For such values of γ_p , some of the collisions will be completely elastic—see fig. 12, Part VI.—and the remainder correspond to a finite value of K , which must, as shown by energy considerations, be near unity. If only a single meson-producing collision occurs in the nucleus, a mean value of K , near to unity, must be assumed to obtain agreement with the experimental results for large values of γ_p .

The yield curve according to Fermi's theory is included in fig. 4. At high energies, the predicted average multiplicity appears to be too small, though presumably the agreement could be improved by a suitable choice of his fundamental parameter Ω .

Fluctuation of n_s in stars produced by protons of given energy.

The results represented in fig. 11 of Part VI. which show the large fluctuations in the values of n_s for stars produced by primary protons of a given energy may be due to:—

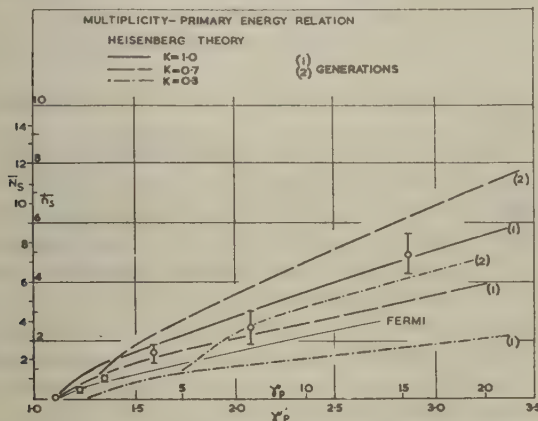
(a) variations in the kinetic energy of individual mesons in the C-system;

- (b) variations in the degree of inelasticity, K , of the collisions; and
 (c) statistical fluctuations in the ratio of charged to neutral mesons.

Assuming on the average, that $2/3$ of the mesons are charged, the effect of (c) is readily calculated. The spread then predicted in Fermi's theory is found to be in good agreement with experiment.

The effect of (a) was computed numerically on the Heisenberg theory, for different values of K . Assuming a spread in K , and mean values of K as deduced from the yield curve (fig. 4), there is again found to be satisfactory agreement with the observations.

Fig. 4.



Variation of average multiplicity with primary energy; comparison of the experimental results with the predictions of the multiple theory.
 $\gamma_p' = \sqrt{(\gamma_p + 1)/2}$ = energy of nucleon in C-system.

3.2. Angular Distribution of mesons in the Laboratory System.

The question may now be asked "How far does the assumption of a single meson-producing collision, without secondary interactions of the mesons in their escape from the nucleus, explain the observed angular distribution?". It has been found by calculation that the form of the observed angular distribution of the mesons in the L-system cannot be uniquely explained in terms of simple assumptions regarding their energy and angular distribution in the C-system. On the other hand, the median angle η , and the backward fraction of the emitted mesons B , as observed in the L-system, do not depend so critically on the assumed features of the distributions in the C-system. Thus assuming only that equal numbers of mesons are projected backwards and forwards in the C-system, the median angle is given by equation (5)

$$\tan \eta = 1/\gamma_p' (\beta_p'/\beta_s') \quad . \quad . \quad . \quad . \quad . \quad . \quad (7)$$

or since $\beta_p'/\beta_s' \sim 1$, $\tan \eta = 1/\gamma_p'$. The value of $\tan \eta$ given by this equation is an upper limit because a small proportion of mesons, emitted backwards

with low velocity in the C-system, will appear in directions $\theta < \eta$ in the L-system.

The variation of η with n_s , as calculated from equations (6) and (7), is shown in fig. 3 of Part VI. The observed median angle decreases much more slowly with increasing n_s than the simple theory predicts, and this is evidence against a pure multiple process. The difference in the observed value of B for $N_h \leq 7$ and $N_h > 7$ also indicates that secondary interactions play a role.

If the angular distribution of mesons in the C-system is of the form $F(\theta')d\theta' = \cos^n \theta' d\theta'$, the fraction of mesons with velocity β'_s which travel backwards in the L-system is given by the equation

$$B = \frac{1}{2} \left[1 - \left(\frac{\beta_p}{\beta'_s} \right)^{n+1} \right]; \beta'_s > \beta_p. \quad . \quad . \quad . \quad . \quad (8)$$

If shower particles only are considered ($\gamma_s > 1.7$), the above formula is slightly modified.

Using the spectrum $f(\gamma'_s)d\gamma'_s$ we can therefore find the value of B as a function of γ'_p or γ_p by numerical integration. Again using the γ'_p versus \bar{n}_s relation, we get a curve relating B with average multiplicity \bar{n}_s .

It is found that the actual slope and peak of the curve does not depend very strongly on the value of n ; the absolute magnitude however, varies almost linearly with $(n+1)$ as can be seen by binomial expansion of (8). The curves (fig. 4, Part VI.), were calculated for $K=1$ and $n=0$ and $n=4$ respectively. The slope of these curves is quite different from the experimental B versus n_s relation. The correct slope can be secured by assuming secondary nucleon-nucleon collisions (see 4.1) and in order to account for the absolute magnitude of B we have to postulate an anisotropic component in the C-system angular distribution. Alternatively, it may be assumed that elastic scattering of the mesons by nucleons can occur, a possibility which is considered in more detail in § 5.

§ 4. MULTIPLE THEORY WITH SECONDARY PROCESSES.

4.1. Secondary nucleon-nucleon collisions.

The agreement between the experimental observations and the predictions of the pure multiple theory may be considerably improved by assuming that a second generation of mesons is created. Such mesons may be produced in collisions involving nucleons recoiling from the primary particle. In considering such effects, we first neglect any secondary interactions of the mesons in escaping from the nucleus.

If such secondary generation occurs, a simple Lorentz transformation is no longer valid, for the mesons are created in several collisions involving nucleons of different energy. If, however, we make a statistical study of a large number of showers, produced by primary particles of similar energy, it is sufficient to assume an effective value of γ'_p , γ_p^* . γ_p^* is a mean value of γ'_{p1} and γ'_{p2} , the values of γ'_p for the first and second

generation, suitably weighted according to the number of mesons arising in each. If it is assumed that the nucleus is so large that all meson-producing collisions which are energetically possible actually occur, then it may be shown that $\gamma_p'^*/\gamma_p'$ is nearly independent of the value of K ; and that it lies within the limits 0.8 and 1.

The above considerations indicate that the average values for γ_s' for the secondary particles $(\gamma_s')_{av}$, as deduced from the spectrum of § 3 in which it is assumed that they are produced in a single collision, are at most, 10 per cent too large. The errors are thus not greater than those due to the poor statistical weight of the observations at present available. It is therefore reasonable to estimate the proportion of mesons due to secondary generation, using the value of $(\gamma_s')_{av}$ and the results are included in fig. 4. The calculations have been made for three values of $K=0.3$, 0.7 and 1.0.

4.2. *Angular distributions including effects due to secondary generation.*

As previously mentioned, the assumption both of secondary generation, and of anisotropy in the angular distribution of the mesons in the C-system, is needed to explain the observations on the backward fraction, B. The calculations have been made assuming $K=1$, and neglecting the spread in multiplicity n_s for a given primary energy γ_p . It is reasonable to suppose however, that these simplifications will not seriously affect the general trend of the theoretical curves. For a given value of γ_p , the average meson energy in the C-system will be greater than $(\gamma_s')_{av}$ if $n_s < \bar{n}_s$; see equation (6). The backward fraction will therefore also be greater. The reverse is true if $n_s > \bar{n}_s$. Thus the general slope of the theoretical curve should remain almost unaffected.

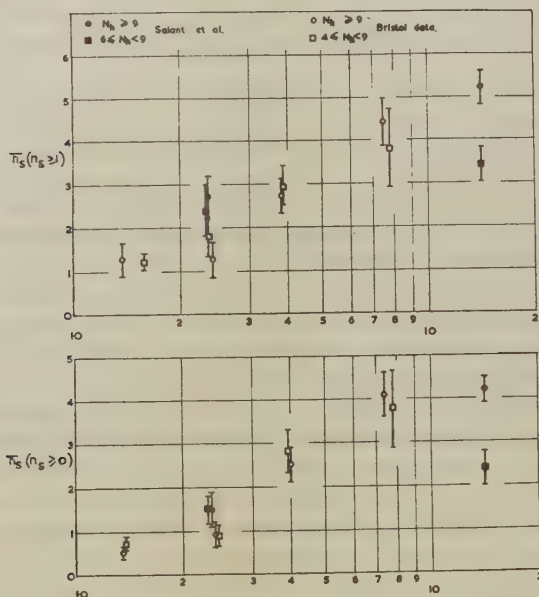
When $K < 1$, calculation of the backward fraction is very complicated, for the nucleons from the first collision recoil at an angle to the direction of motion of the primary particle. This must lead to a broadening of the angular distribution of which it is difficult to estimate the magnitude.

4.3 *Variation of Multiplicity n_s , with star size N_h .*

If the secondary generation of mesons plays an important role at high primary energies, it will be more likely to occur in heavy than in light nuclei. Stars with $N_h > 8$ must almost always be due to the disintegration of silver or bromine nuclei, whilst stars of smaller N_h may be due either to the disintegration of nuclei of the light elements carbon, nitrogen or oxygen, or to those of silver and bromine. If therefore we consider stars produced by primary particles of the same energy, secondary generation, more likely in heavy nuclei, would contribute to making the average multiplicity of stars with $N_h > 8$ greater than those with $N_h < 8$. On the other hand, any reabsorption of mesons in the parent nucleus will tend to reduce the number of mesons and increase the number of recoiling nucleons.

In view of these considerations, we have plotted the average multiplicity n_s , as a function of primary energy, E_p , for the two classes of stars; see fig. 5. Included in the figure are the results of Salant *et al.* (1950) for primary particles of energy between 1 and 8 BeV., and for those of energy greater than 8 BeV. (average energy 14 BeV.). At high energies, there is a significant difference between the average multiplicities of the two types of stars. It is reasonable to infer that secondary processes frequently take place in heavy nuclei bombarded by protons of great energy, and that re-absorption of the mesons is relatively unimportant.

Fig. 5.



Observed variation of average multiplicity with kinetic energy of the primary particle in BeV, for stars of different prong number N_h .

It may be remarked that the results of Salant *et al.* relate to stars of $N_h = 2-8$ and $N_h \geq 9$, while our figures are for stars of $N_h = 4-8$, and $N_h \geq 9$. This may explain the difference between the two sets of observations at 2.4 BeV.

§ 5. MESON-NUCLEON INTERACTIONS.

Hitherto any interaction of the mesons with the parent nucleus has been neglected, and an attempt has been made to explain the experimental results in terms of nucleon-nucleon collisions alone. The results given in 5.2 (b) of Part VI., show, however, that mesons have a strong interaction with nucleons, and we now consider the effects of such interactions.

5.1 Elastic Scattering of Mesons.

In order to estimate the effect of the elastic scattering of mesons during their escape from the parent nucleus, we have considered two possibilities. In the first, the scattering process is regarded as analogous to the Compton effect, the relative probability of different angles of scattering being similar to that in electro-magnetic case. On being scattered, a meson may then be deflected through a large angle and may lose a large fraction of its energy. On the second assumption, the scattering is regarded as "isotropic"; the cross-section for the interaction is assumed to be constant irrespective of the energy of the meson, and after the encounter, all directions of motion of the meson, in the C-system of the interacting particles, are equally probable.

In calculating the effect of such scattering, we have made the simplifying assumption, that the original angular distribution of the mesons can be represented by a δ -function; *i.e.* all mesons are initially projected in the line of motion of the primary nucleon. Assuming each meson to be once scattered in escaping from the nucleus, the fraction B' of the mesons which emerge in the backward hemisphere can be calculated for a given value of the primary energy γ_p . The calculation depends upon the known distribution in the values of γ_s , and the energy "spectrum" $f(\gamma'_s) d\gamma'_s$. These quantities and the relation between \bar{n}_s and γ_p allow the two curves in fig. 4 of Part VI. to be computed. The actual magnitude of B' will be greater than that calculated since the initial angular distribution of the mesons is certainly quite broad. A slight error is introduced when the curves are taken as plots of B' against n_s , instead of $\bar{n}_s(\gamma_p)$, because of the spread of n_s for a given primary energy. This effect has already been considered in 4.2.

It is reasonable to suppose that any backward fraction unaccounted for by the Lorentz transformation is due to large-angle scattering, and this view is supported by the fact that the angular distribution of the mesons in the backward hemisphere is nearly isotropic.

The backward fraction due to single scattering calculated by the above method is certainly an underestimate. Comparison of the observed and calculated values of B therefore allows us to obtain an upper limit (for $n=1$, equation (8)) for the probability of large-angle scattering, and the value thus obtained is 0.3. For the nuclei considered, this value indicates that the cross-section for the scattering process is of the order of 1/10 the geometrical cross-section per nucleon.

In the scattering process, the meson projects a nucleon, and this particle, if a proton, produces a "grey" track. The above value of the cross-section is consistent with the observed slow increase of \bar{N}_g with n_s . The ratio $Q=B(N_h>8)/B(N_h\leq 8)=1.5\pm 0.25$. If Q' represents the ratio $(B \text{ heavy nuclei})/(B \text{ light nuclei})$, then from the effect arising purely from the Lorentz transformation, one expects $Q'\sim 1.0$; from scattering alone a value of $Q'=1.8$. Since the observed value does not represent complete separation of light and heavy nuclei, the observed value of Q' , 1.5, is in reasonable agreement with that predicted from scattering alone.

5.2 Reabsorption of Mesons in the Nucleus.

The evidence presented in section 4.3 of Part VI. precludes the possibility that any substantial fraction of fast mesons created in the primary act, or acts, can be re-absorbed and annihilated by nucleons, in the parent nucleus. The average total energy of such a meson is ~ 860 MeV., and the disappearance of this energy would result in a considerable increase in N_n . Thus if strong absorption takes place N_n should increase rapidly with increasing n_s , which is contrary to the observations.

5.3. Generation of Mesons in Meson-Nucleon Collisions.

In traversing nuclear matter, a very energetic meson may produce further mesons in two ways: (i.) First, it may be elastically scattered by a nucleon; and this nucleon may recoil with sufficient energy to produce one or more mesons in collision with another nucleon. (ii.) Secondly, in the scattering process, the meson may generate further mesons directly.

A meson primary originates, of course, as a shower particle and, to be identified, it must have an energy less than 1100 MeV. Such a particle can have only a small probability of producing further mesons by process (i.) since it cannot transfer more than 880 MeV. in collision with a nucleon, and the average value is only ~ 500 MeV. We should therefore expect to observe only the elastic scattering of such particles, and the result of their collision with a nucleus should commonly be a "star" without shower particles.

As described in Part VI. (see Table V. and Pl. XXXVI.) one star has been observed in which an incident meson of 1050 ± 200 MeV. energy produces two mesons of energy 375 ± 70 MeV. and 365 ± 70 MeV. and a recoil proton of 270 ± 50 MeV. On process (i.) it follows from the conservation laws that one of the mesons should be ejected backwards, which is contrary to observation. Thus the event can only be explained in terms of process (ii.).

By analogy with the nucleon-nucleon collisions which result in the creation of mesons, we may refer to the reproductive process (ii.) as "inelastic scattering". Heitler estimates that for mesons in the range of energy under consideration, the ratio of inelastic to elastic scattering is ~ 10 per cent. This value suggests that among the 37 examples of stars produced by π -mesons which we have observed, there should be one in which the primary particle leads to the emission of two identifiable mesons; and we have seen that one such event has been found.

Although meson production occurs rarely in the nuclear interactions of π -mesons of energy less than 1 BeV., it is reasonable to suppose that it becomes important at higher energies. This view is supported by the experiments of Rosser and Swift (1951) who have exposed photographic emulsions, at an altitude of 2860 m., above and below 30 cm. of lead. They found that the ratio of charged primaries to neutral primaries for disintegrations with $n_s \geq 2$ was 0.86 ± 0.21 above the lead, and 1.76 ± 0.48

below it. For the following reasons they suggest that the difference is due to mesons created in the lead :—

The average energy of a primary nucleon which produces a penetrating shower of $n_s \geq 2$ is of the order of 4 BeV. If the observed showers are attributed to fast nucleons recoiling from the π -mesons, then the incident π -mesons must have an energy greater than this value, *i. e.* > 4 BeV. The number of π -mesons of such great energy is not sufficient, from this point of view, to account for the magnitude of the effect observed. On the other hand, the results are readily explained if it is assumed that π -mesons of energy greater than 1 BeV. can produce showers of π -mesons directly, the cross-section for the process being approximately equal to the geometrical value.

§ 6. PRODUCTION OF MESONS BY ENERGETIC α -PARTICLES.

It is reasonable to suppose that, in producing mesons by collisions with a nucleus, a relativistic α -particle will act as a beam of four nucleons. Included in fig. 1 are the results obtained in studying showers produced by α -particles of known energy. For such showers, the multiplicity per nucleon has been plotted against the energy per nucleon, and the agreement between these results and those for proton primaries gives support for the above view.

§ 7. CONCLUSIONS.

The conclusions which follow from the present experiments may be briefly summarized as follows :—

(i.) At low energies (< 1 BeV.) most of the nucleon-nucleon collisions are completely elastic. The “inelastic” scattering cross-section does not become comparable with that for “elastic” scattering until an energy of about 2 BeV. is reached.

(ii.) For a given value of the primary energy, a wide range in the number of charged mesons emitted is observed in different disintegrations. The multiplicity, n_s , therefore gives an unreliable indication of the primary energy.

(iii.) Assuming pure “multiple” production, the energy and angular distributions of mesons in the C-system of the two colliding nucleons can be calculated. The angular distribution thus found is approximately isotropic; the energy spectrum can be represented by $p^2 dp / \gamma^4$ (p =momentum, γ =energy).

(iv.) The simple theory of multiple production, with no secondary radiative collisions, is inadequate. To obtain agreement with experiment, it must be assumed that mesons are also produced in secondary nucleon-nucleon and meson-nucleon collisions.

(v.) The modified plural theory, which considers meson production in many-body collisions by both the primary nucleon and the recoil nucleons, also gives satisfactory agreement with the experimental data.

(vi.) The observations therefore do not provide a decisive test between the two theories, and there appears to be nothing to choose between them regarding economy of hypothesis. The multiple picture introduces a strong-coupling theory, whereas on the plural picture it seems necessary to postulate many-body collisions.

(vii.) The number of neutral mesons ejected from stars of multiplicity between 0 and 4 is found to be 1.0 ± 0.3 times the number of charged mesons.

(viii.) Re-absorption of fast mesons by the parent nucleus in which they are created is very improbable, although such a process may explain the very large stars (N_n) of small multiplicity, n .

The cross-section for elastic scattering of these mesons by the nucleons (Compton-type scattering) is ~ 10 per cent of the geometrical value.

(ix.) On the contrary, single fast π -mesons of energy less than 1 BeV. interact strongly with nuclear matter; in ~ 50 per cent of the cases they emerge from an encounter with a nucleus having lost a large fraction of their energy. It is not possible, from the present observations, to decide whether in the remaining cases, the mesons are absorbed, or whether they suffer charge exchange, so that the outgoing meson is undetected.

ACKNOWLEDGMENTS.

We have pleasure in thanking Professor C. F. Powell, F.R.S., for his interest and encouragement during the analysis, and Professor W. Heitler for several informative discussions and permission to quote the unpublished calculations of M. Therreaux. We wish especially to express our thanks to Dr. H. Messel, for his very thorough and painstaking reading of a preliminary draft of this work, and for many useful suggestions and criticisms.

This work has been carried out as part of a programme of research supported by the Department of Scientific and Industrial Research, and one of us (W. O. L.) is indebted to this body for a maintenance grant.

REFERENCES.

- FERMI, E., 1950, *Prog. Theor. Phys.*, **5**, 570; 1951, *Phys. Rev.* **81**, 863.
 HEISENBERG, W., 1949, *Z. Phys.*, **126**, 569.
 HEITLER, W., and JANOSSY, L., 1949, *Proc. Phys. Soc.*, A **62**, 364, 669; 1950, *Helv. Phys. Acta.*, **23**, 417.
 HEITLER, W., 1950., *Bombay Conference on Fundamental Particles*: 1951, Private Communication.
 LEWIS, H. W., OPPENHEIMER, J. R., and WOUTHUYSEN, S. A., 1948, *Phys. Rev.*, **73**, 127.
 MESSEL, H., 1951, *Proc. Phys. Soc. A*, **64**, 726.
 ROSSER, W. E. V., and SWIFT, M. W., 1951, Private Communication.
 SALANT, E. O., HORNOSTEL, J., FISK, C. B., and SMITH, J. E., 1950, *Phys. Rev.* **79**, 184.

CXXVI. *Associated Penetrating Particles of Cosmic Rays Underground.*

By H. J. J. BRADDICK, W. F. NASH and A. W. WOLFENDALE,
The Physical Laboratories, University of Manchester*.

[Received July 19, 1951.]

ABSTRACT.

Two cloud chambers have been used at a depth underground equivalent to 26 m. of water in a study of the penetrating cosmic ray particles. Pairs of associated penetrating particles have been observed originating in lead plates in the chamber and also entering it from above. It is considered that the process is one in which a μ -meson produces a penetrating secondary of mean energy $\sim 10^9$ eV., the penetrating secondary being either a μ -meson or a π -meson. The cross-section for the process is estimated to be about 5×10^{-29} cm.² per nucleon for lead and of the same order of magnitude for sandstone.

§ 1. INTRODUCTION.

THE discovery of associated pairs of penetrating particles underground was first reported by Braddick and Hensby (1939) as a result of cloud chamber experiments at a depth of 60 metres water equivalent. It is probable that these events are not identical with penetrating showers as observed at sea level, for it is known that the primaries responsible for penetrating showers are so attenuated as to be negligible at this depth.

Pairs of penetrating particles have also been observed under thick absorbers at sea level by Shutt (1946) who interpreted them as pairs of μ -mesons.

The present work was undertaken to verify and elucidate these results. Cloud chambers have been operated in a cave at 26 m.w.e. depth, using simple counter control and a number of events involving associated penetrating particles (A.P.P.) were photographed stereoscopically. While the work was in progress underground phenomena involving A.P.P. have been reported by George and Evans (1950), using photographic emulsions, and by Greisen *et al.* (1951), using counter arrangements. The relation of these results to ours will be discussed.

It seems likely that the events described are secondary to μ -mesons and that the interaction of μ -mesons with matter is greater than was thought.

* Communicated by Professor P. M. S. Blackett, F.R.S.

§ 2. EXPERIMENTAL ARRANGEMENT.

The apparatus was installed in a cave at Stockport under 2600 gm./cm.² of rock, which was mainly red sandstone of mean density 2 gm./c.c. The vertical cosmic-ray intensity was about $\frac{1}{4}$ of that at sea level. Two cloud chambers were used at different times, they were installed in the same position with their centres 170 cm. below the roof. The whole cave was maintained at a temperature of 18° C.

In the first series of experiments the apparatus consisted of a cloud chamber of normal design 30 cm. in diameter and 13 cm. deep, with a lead plate 2 cm. thick placed across the centre. This plate was used to distinguish between electrons and penetrating particles, electrons usually being recognized by the production of electron showers on passing through the plate.

In order to investigate further the properties of A.P.P. a multiple plate chamber was constructed. The chamber was 40 cm. \times 39.5 cm. \times 36 cm. in size and could contain up to thirteen 1 cm. lead plates. The chamber was illuminated through the back and the expansion was produced by the symmetrical lateral movement of two rubber diaphragms on opposite sides of the chamber.

The selection system usually consisted of a simple 3-fold counter telescope. Only one penetrating particle passing through the central part of the chamber was therefore required to cause an expansion.

§ 3. EXPERIMENTAL RESULTS.

3.1. *Cylindrical cloud chamber. Series I.*

Two thousand two hundred photographs were taken with the arrangement shown in fig. 1 *a*. The counting rate of the 3-fold counter system was 81 ± 2 per hour, being $\frac{1}{4}$ of that at sea level. The total time during which the chamber was available to record incoming particles (sensitive time) was 27.5 hours.

Thirteen photographs of this series each showed two penetrating particles which were considered associated (the criteria for acceptance as associated will be stated later).

3.2. *Cylindrical cloud chamber with 3 cm. lead above. Series II.*

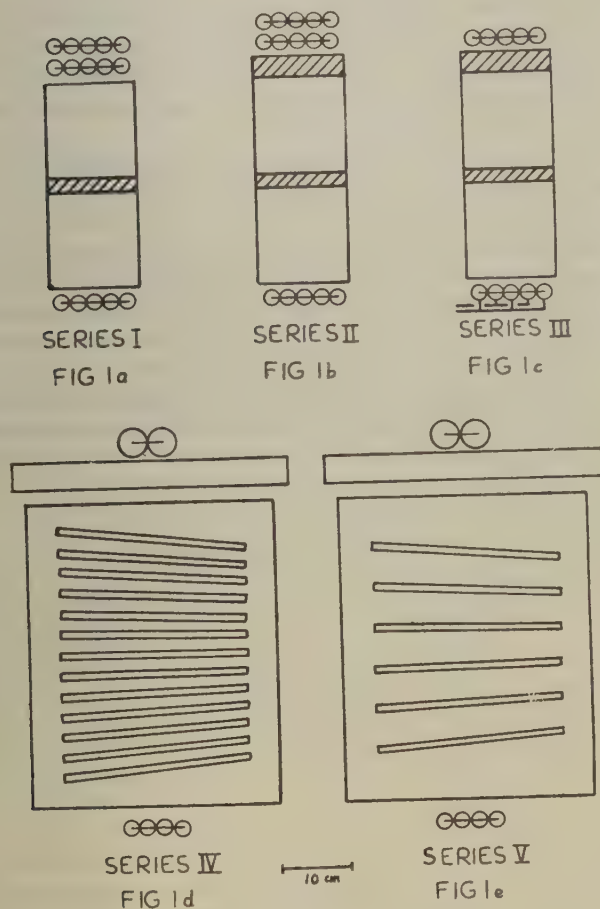
The second series of photographs was taken with the arrangement shown in fig. 1 *b*. The 3 cm. lead absorber above the chamber was used to increase the probability of degrading any electronic component. The position of the counters was not exactly the same as before and the triple coincidence rate was 50 ± 2 per hour.

Two thousand six hundred photographs were taken, the total sensitive time being 52 hours. Twelve apparent A.P.P. were observed, four of which had originated in the lead absorber above the chamber.

3.3. Cylindrical cloud chamber with 3 cm. lead above and a split counter tray below. Series III.

To increase the efficiency of detecting A.P.P. relative to random associations of particles, a split counter tray was placed below the chamber as shown in fig. 1c. This arrangement was sensitive to electron

Fig. 1.



Experimental arrangements.

showers in addition to A.P.P. The counting rate was 8 ± 0.9 per hour at sea level and 5 ± 0.4 per hour underground. The total number of photographs taken was 2400 and the total sensitive time was 480 hours. Thirty photographs showed apparent A.P.P., of which twelve originated in the 3 cm. lead absorber above the chamber.

3.4. Multiple plate cloud chamber containing thirteen 1 cm. lead plates. Series IV.

For all the observations with the multiple plate chamber a simple threefold counter telescope was used. The arrangement is as shown in fig. 1 *d* and the counting rate was 12.5 per hour. In a sensitive time of eighteen hours, 215 photographs were taken, each showing at least one particle penetrating all the plates.

One pair of apparent A.P.P. was observed to originate in one of the lead plates. One small penetrating shower was observed and one pair of A.P.P. originating in the sandstone above the chamber was found.

3.5. Multiple-plate cloud chamber containing six 1 cm. lead plates. Series V.

In order to increase the visibility of the tracks and to make it possible to distinguish possible "heavy" tracks from contamination α -particles, alternate plates were removed.

One thousand two hundred and seventy-six photographs, showing at least one particle penetrating all the plates, were taken with this arrangement. Seven examples of pairs of A.P.P. originating above the chamber and traversing the lead plates were observed. Two cases of pairs of A.P.P. originating in the lead plates in the chamber and one penetrating shower produced in a lead plate in the chamber were found. Two photographs showed three penetrating particles entering and traversing the chamber. For ease of comparison an analysis of all the penetrating events observed is given in the table below.

TABLE I.

Series	Total sensitive time in hrs.	No. of apparent pairs produced		No. of penetrating showers produced	
		In lead	Externally	In lead	Externally
I.	27.5	—	13	—	0
II.	52	4	8	0	0
III.	480	12	18	0	0
IV.	18	1	1	1	0
V.	142	2	8	2	2

§ 4. DISCUSSION OF RESULTS ON PAIRS OF ASSOCIATED PENETRATING PARTICLES.

4.1. Random associations.

It is necessary to consider the possibility that these pairs of A.P.P. are due to random associations. When the pairs are produced in the lead inside the chamber the probability of random association is negligible. When the pairs are produced above the chamber we impose the following criteria:—

- (a) The pairs must be visually contemporary in the chamber and parallel or diverging downwards.

(b) On reprojection the pairs must appear coplanar to within about 2° .

The number of random associations expected on criterion (a) is approximately 1 in 1000 for the cylindrical chamber and approximately 20 in 1000 for the multiple plate chamber. Criterion (b) reduces these figures by a factor of about 20. Many of the pairs rejected due to criterion (b) are probably genuine pairs of associated penetrating particles, for which the lack of coplanarity is due to the effect of scattering in the lead or sandstone.

4.2. *Knock-on electrons.*

Mesons traversing matter are known to give energy to electrons by collision (knock-on process), and it is necessary to consider whether any of the events appearing as cases of pair production are really events of this type. In the arrangements IV. and V., where the particles are observed to penetrate several plates without the production of electron showers, the probability of their being electrons is negligible.

In the arrangements I., II. and III. the particles are observed penetrating only one plate in the chamber and the probability of their being electrons must be calculated.

Consider the arrangement used in series II. and III. A meson accompanied by a knock-on electron produced in the 3 cm. lead above the chamber where both particles penetrate the 2 cm. lead plate inside the chamber, would probably satisfy the criteria for acceptance as a pair. The theoretical energy distribution of electrons knocked-on by the meson spectrum was obtained, and for each energy the probability of the electron emerging from the upper plate and passing without multiplication through the lower plate was calculated. For the final electron distribution, the scattering distribution of fig. 2 was calculated and compared with the observed scattering.

It is seen that very few of the pair particles which show small deflections are likely to be knock-on electrons, although the few particles which are scattered through large angles could be explained in this way.

A further indication that the pair events in general are not knock-on electrons is given by the fact that there is no correlation between the angle between the particles of a pair and the angle of scattering of the more scattered particle. In a knock-on process, a small pair angle would be correlated with high electron energy and small scattering angle. We may conclude that most of the pairs of associated penetrating particles, observed in series II. and III. and originating in the lead above the chamber, are genuine.

In series I. the same argument may be applied to pairs which originate in the sandstone roof, and we conclude that the pairs are genuine.

In series II. and III. any electrons which originate in the roof would have to pass through two lead plates to qualify as components of pairs, and we consider that all the pairs enumerated are genuine. The possibility that electrons secondary to meson bremsstrahlung might simulate A.P.P. has been considered and found to be negligible.

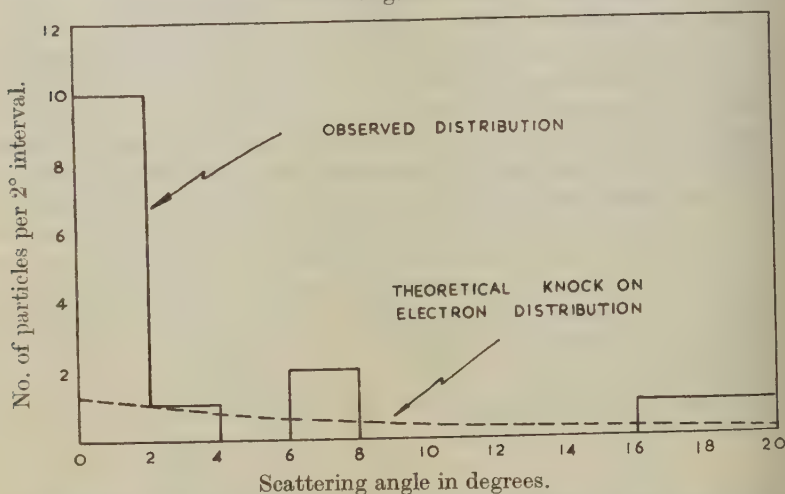
From the above considerations, it is clear that associated penetrating particles do exist. It is now necessary to consider whether the production of these A.P.P. can be explained by known processes.

4.3. Nature of primaries.

The nucleon component which is mainly responsible for the production of penetrating showers at sea level is highly absorbed with an absorption length ~ 100 gm./cm.². Thus the probability that a nucleon arrives at the underground station is $\sim e^{-26}$. This is far too small to account for the observed number of pairs.

The possibility that these events are π -meson induced is excluded if it is assumed that the absorption length for π -mesons is the same as that for nucleons. However, the behaviour of high energy π -mesons (energy $\sim 10^9$ eV.) is not at all clear. It is possible to eliminate π -mesons from sea level as the primaries responsible for pairs observed

Fig. 2.



Differential scattering distribution for the more scattered member of a pair, originating in the lead absorber above the chamber, in Series II. and III.

underground on the following considerations. Let us assume as the most unfavourable case that all mesons with $E > 10^{11}$ eV. at sea level are π -mesons since π -mesons of this energy produced near the top of the atmosphere will not have had time to decay before they reach sea level.

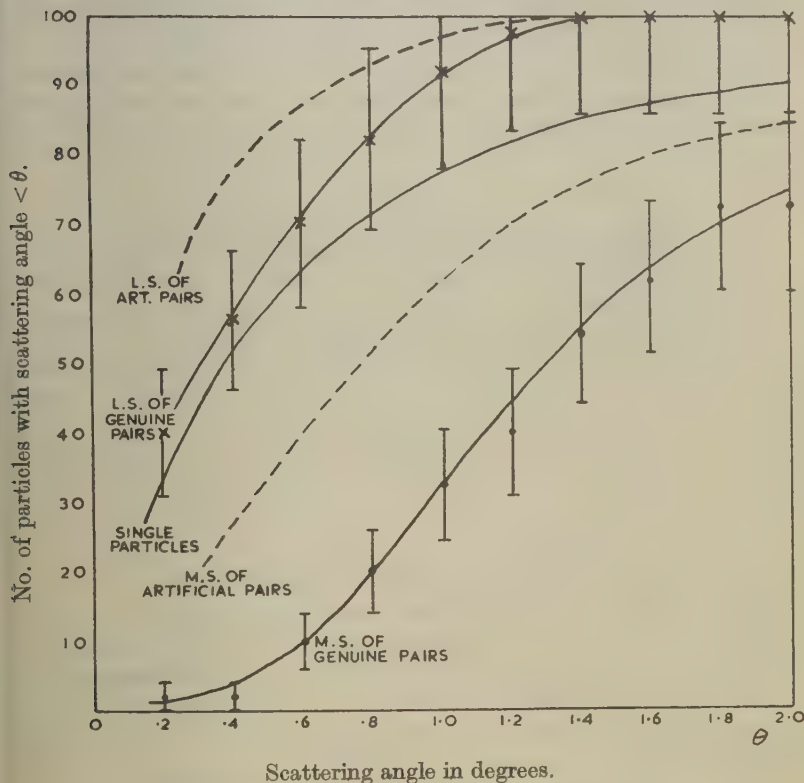
Such π -mesons would be $1/4000$ of the total cosmic ray flux at sea level. In addition there are at sea level a small number of π -mesons produced locally; these have however limited range and decay to form μ -mesons. In order to account for the observed rate of production of pairs of A.P.P. in terms of production by π -mesons, all the high energy π -mesons must reach the underground station and then must all interact in 3 cm. Pb. This is obviously impossible.

The above considerations eliminate nucleons and π -mesons as the source of pairs. Unless we assume that these events are induced by unknown particles the only particles which remain in sufficient numbers are μ -mesons.

4.4. Nature of the pair particles.

In these experiments the main indication of the nature of the pair particles is given by their scattering on traversing the lead plates in the cloud chambers.

Fig. 3.



Comparison of the integral scattering distributions.

In series I., II. and III. accurate scattering measurements were possible to within 0.1° and the scattering of each member of the pair in the 2 cm. lead block was measured using a low power microscope fitted with a goniometer eyepiece. The pair particles were divided into two groups, containing respectively the less and more scattered members (L.S. and M.S.) of each pair. The integral scattering distributions, together with that for single particles, are shown in fig. 3. It is

seen that the less scattered members can be correlated with the single particles, *i. e.* the normal μ -mesons beam present at the station. On the other hand, the more scattered members are obviously not the normal μ mesons. In order to determine whether the difference in the distributions is due to the method of analysis the scattering angles for single penetrating particles were measured, these were taken in pairs and the distributions for the more and less scattered members of these artificial pairs plotted. It can be seen that the difference in the distributions for the genuine pairs cannot be explained in this way. It is concluded that the more scattered member or penetrating secondary, as we will call it, is probably a μ -meson of mean energy $\sim 10^9$ eV., although the possibility of its being a π meson cannot be ruled out.

Observations in series IV. and V. show that as a rule the penetrating secondary has energy greater than 10^9 eV., only one case being observed where it has energy less than this. This result is not consistent with that just given.

TABLE II.

Cross-section for production of pairs of A.P.P. in lead.

Series	Metres of Pb. traversed by s	Observed No. of pairs accepted	Corrected No. of pairs produced	Interaction length in metres of Pb.	Cross-section in cm. ² /nucleon
II.	78	3	3	26	5.7×10^{-29}
III.	1150	9	30	38	4.0×10^{-29}
IV. } V. }	89	3	3	30	5.0×10^{-29}

4.5. Cross-section for the production of pairs in lead.

Assuming that the primary responsible for the production of a pair is a μ -meson, and that the interaction is between the μ -meson and a nucleon, it is possible to calculate a cross-section for the process.

In the results of series III. corrections have been applied for loss of efficiency due to (a) the split tray arrangement, and (b) the narrow angle pairs lost due to the finite size of the counters.

Angular distribution of pair particles.

A histogram of the angular distribution of pair particles originating in the lead absorber in series II. and III. is shown in fig. 4. A correction has been applied for narrow angle pairs lost in the split tray experiments as mentioned previously.

4.6. Pairs entering from outside the chamber.

Quantitative results for these events are difficult to evaluate owing to the effects of scattering in the sandstone. A pair of A.P.P. originating

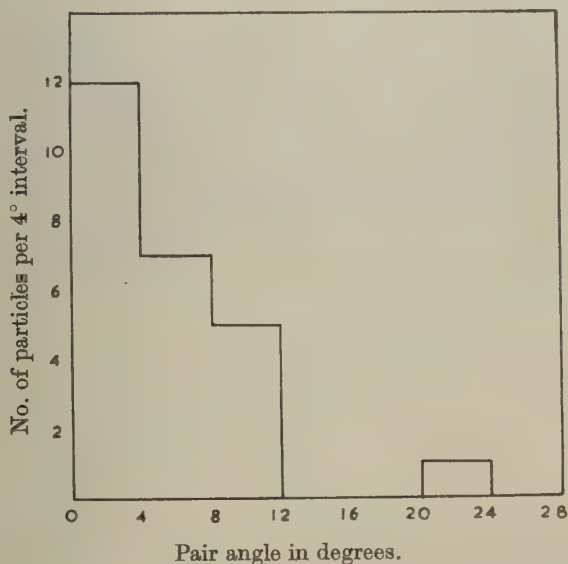
in the sandstone and being scattered through an appreciable angle before entering the cloud chamber will be rejected under the criteria for selection mentioned in § 4.1.

The angular distribution is very similar to that for pairs originating in the lead, indicating that the events are of a similar nature.

Cross-section for production of pairs of A.P.P. in sandstone.

This determination demands a knowledge of the angular distribution and energy of the pair particles since these quantities determine how thick a layer of sandstone is effective. From what has been said previously concerning the nature of the pair particles it seems probable that the penetrating secondary is a meson (μ or π) of mean energy $\sim 10^9$ eV.

Fig. 4.



Corrected angular distribution of pair particles, originating in the lead absorber above the chamber, in Series II. and III.

Assuming a unique energy of formation of 10^9 eV. for the penetrating secondary an estimate of the cross-section for sandstone can be made; this neglects the effects of scattering previously mentioned and so the value obtained for the cross-section is a lower limit.

An estimate of the absolute lower limit to the value of the cross-section or sandstone production can be made by assuming that the penetrating secondary has infinite energy (instead of 10^9 eV.), in this case the whole thickness of sandstone above the equipment contributes to the flux of pairs crossing the cloud chambers. This calculation has been made assuming the Gaussian distribution of pair angles approximating to the histogram in fig. 4.

The cross-sections calculated are $1/3$ of those given in Table II. Thus the cross-section for sandstone production of pairs is in any case greater than 5×10^{-30} cm.² per nucleon.

Apparent pairs produced in air.

Three cases in each of series I. and V. have been found in which pairs of A.P.P. appear to have originated in the air above the cloud chambers. The pair angles and probable angles of scattering in the lead plates inside the cloud chambers are such that the cases cannot be explained in terms of scattering in the roofs of the chambers. The probability that these cases are examples of the random association of two particles is low, but this possibility cannot be entirely ruled out. Further investigations must be carried out before this phenomenon can be established.

TABLE III.

Cross-section for production of pairs of A.P.P.'s in sandstone assuming a unique energy of formation of 10^9 eV.

Series	No. of single mesons traversing chamber	No. of pairs observed	Cross-section in cm. ² /nucleon
I.	2200	9	5×10^{-29}
II.	2600	8	3.5×10^{-29}
III.	24000	18	1.5×10^{-29}
IV. } V. }	1500	5	3×10^{-29}

§5. PENETRATING SHOWERS.

In series IV. and V. two cases have been observed of penetrating showers of low multiplicity produced in the chamber. These showers differ from those observed at sea level in that the penetrating particles are emitted at large angles to the direction of the incident particle.

Two cases have been found where three A.P.P. enter the cloud chamber, and in each case one of the penetrating particles suffers two large angle deflections in the lead plate. It is probable that these deflected particles are π -mesons from a penetrating shower produced in the sandstone. Several cases of three or more parallel A.P.P. incident obliquely in the cloud chamber and penetrating a few lead plates have been observed, these are probably remnants of the penetrating particles present in extensive air showers.

§6. COMPARISON WITH OTHER OBSERVATIONS.

Braddick and Hensby (1939) using an arrangement similar to that for series I.-III. at 60 mwe. found five cases of pairs of A.P.P. out of 2000 photographs taken with a counter selection system requiring one penetrating particle. This rate is similar to that found in this

investigation. George and Trent (1951), using a cloud chamber containing two 3 cm. lead plates, have found two cases of pairs of A.P.P., out of 1500 photographs, originating in the upper lead plate and traversing the lower one without deflection. Both these experiments were carried out at a depth of 60 mwe. These experiments show about the same cross-section as ours, and this result is in provisional agreement with the hypothesis that the pairs are produced by μ -mesons. However, the statistical weight of these experiments is as yet very low. Experiments by Shutt (1946) at sea level using a cloud chamber under 88 cm. lead showed the existence of pairs of A.P.P. The cross-section calculated from Shutt's results is $\sim 10^{-29}$ cm.²/nucleon for pair production in lead and agrees with that found in the present investigations within the statistical errors involved. George and Jason (1947), using a penetrating shower counter set requiring at least three A.P.P. at a depth of 60 mwe., found no coincidences in 45 days continuous recording. George and Trent (1949), however, using a counter set of lower selectivity, found events which could be explained in terms of the production of penetrating groups of mesons of low multiplicity, by mesons. A cross-section of 5×10^{-29} cm.²/nucleon has been calculated for the production of these showers in lead, this value compares well with that found in this investigation for the production of pairs. George and Evans (1950) have found stars and penetrating showers produced by μ -mesons in photographic emulsions exposed underground. The cross-sections found for these events are $\sim 10^{-29}$ cm.²/nucleon for stars and $\sim 4 \cdot 10^{-30}$ cm.²/nucleon for penetrating showers. The shower particles observed by George and Evans are π -mesons and the most probable multiplicity is about three: a multiplicity of shower particles as high as eight has been observed. The two cases in the present investigation in which three penetrating particles are observed are probably events of this type. The majority of the pairs of A.P.P. observed in our experiments cannot be explained in terms of penetrating showers containing two penetrating particles, since the total cross-section for shower production calculated by George and Evans is only $4 \cdot 10^{-30}$ cm.² per nucleon and showers containing only two particles form a small proportion of the showers observed. It is likely that the production of a pair of A.P.P. is an event of a more elementary type than the production of a penetrating shower. If heavy particles are associated with these events it seems certain that they would have been observed in photographic plate experiments, and we are led to infer that the interaction observed is one in which a μ -meson produces only a single penetrating secondary.

CONCLUSIONS.

- (1) μ -mesons produce penetrating secondaries on passing through matter, one penetrating secondary being produced in each event.
- (2) The cross-section for this process is $\sim 5 \times 10^{-29}$ cm.²/nucleon for lead and of the same order of magnitude (certainly greater than 5×10^{-30} cm.²/nucleon) for sandstone.

(3) The penetrating secondary is probably a μ -meson of mean energy $\sim 10^9$ eV., but there is a possibility that it is a π -meson.

ACKNOWLEDGMENTS.

We are glad to record our indebtedness to Professor P. M. S. Blackett for his interest in these experiments, to Dr. J. G. Wilson, Dr. E. P. George and Dr. P. T. Trent for discussion. We thank also Stockport Corporation for permission to work in the cave, and its officers for help in examining the caves and determining their position. W. F. Nash and A. W. Wolfendale are indebted to the D.S.I.R. for maintenance grants.

REFERENCES.

- BRADDICK, H. J. J., and HENSBY, G. S., 1939, *Nature*, **14**, 1012.
GEORGE, E. P., and EVANS, J., 1950, *Proc. Phys. Soc.*, **63**, 1248.
GEORGE, E. P., and JASON, A. C., 1949, *Nature*, **160**, 327.
GEORGE, E. P., and TRENT, P. T., 1949, *Nature*, **164**, 838.
GEORGE, E. P., and TRENT, P. T., 1951, Private communication.
GREISEN, K., COCCONI, G., and BOLLINGER, L. M., 1951, *Phys. Rev.*, **82**, 294.
SHUTT, R. P., 1946, *Phys. Rev.*, **69**, 261.

CXXVII. *On Field Theories with Non-localized Interaction.*

By JERZY RAYSKI,

Nicolas Copernicus University, Torun, Poland*.

[Received June 13, 1951.]

SUMMARY.

It is shown that a method of direct quantization of field equations (completely avoiding the canonical formalism) is applicable to a wide class of fields with a non-local interaction. In §1 the extended source theory of Peierls and McManus is quantized and discussed. The S-matrix is computed by the method of C. N. Yang. A general rule for an immediate transcription of the traditional S-matrix elements into the new form is given. In §2 another type of a non-local interaction is discussed and it is shown that all the usual convergence difficulties may be easily avoided if we give up the strict localizability of charge, energy, etc., and if we abandon the postulate of gauge invariance of the second kind. This is acceptable since it is possible to guarantee the integral conservation laws without the continuity equations and to secure a vanishing photon rest mass by other devices, not necessarily by the formal gauge invariance. In the limit $\lambda \rightarrow 0$ where λ is a fundamental length, the discussed field theory goes over into the traditional quantum electrodynamics.

§1. QUANTIZATION OF THE PEIERLS AND McMANUS FIELD.

LET us discuss first the field described by Peierls and McManus (1948) with the following Lagrangian

$$L = L^{(0)} + L', \quad (1)$$

where $L^{(0)}$ is the usual Lagrangian for the electromagnetic and spinor fields without interaction while the interaction part L' is

$$L' = \frac{1}{2} \int d^4x \{ j_\mu(x), A_\mu^R(x) \}, \quad (2)$$

where

$$\{a, b\} = ab + ba, \quad (3)$$

while

$$a^R(x) = \int d^4x' F(x-x') a(x'), \quad (4)$$

where $F(x)$ is a function of the argument x_μ . In order to get a correspondence with the traditional theory $F(x)$ should be a delta-like function

$$F(x) = \frac{1}{(2\pi)^4} \int d^4k \exp(ik_\mu x_\mu) f(k_\mu^2, \lambda), \quad (5)$$

* Communicated by Professor R. E. Peierls, F.R.S.

where the Fourier transform $f(k_\mu^2, \lambda)$ is a function of $k_\mu k_\mu$ and of a parameter λ with the dimension of length. We may assume, e. g.

$$f(k_\mu^2, \lambda) = 1/1 + (\lambda^2 k_\mu^2)^2 \quad \text{or} \quad f(k_\mu^2, \lambda^2) = \exp \{ -(\lambda^2 k_\mu^2)^2 \}, \quad . \quad . \quad (6)$$

which become unity in the limit $\lambda \rightarrow 0$. We notice the following properties :

$$\int d^4x F(x) = 1, \quad f(0, \lambda) = 1 \quad . \quad . \quad . \quad (7)$$

whence we get the identity

$$A_\mu^{(0)R} \equiv A_\mu^{(0)}, \quad . \quad . \quad . \quad (8)$$

where the index zero means an unperturbed field obeying the Laplace equation

$$\square A_\mu^{(0)} = 0. \quad . \quad . \quad . \quad (9)$$

The interaction part of the Lagrangian may also be written as

$$L' = \frac{1}{2} \int d^4x \{ j_\mu^R(x), A_\mu(x) \}. \quad . \quad . \quad . \quad (10)$$

The Lagrange equations are

$$\square A_\mu = -j_\mu^R, \quad . \quad . \quad . \quad (11')$$

$$\gamma^\mu \frac{\partial \psi}{\partial x_\mu} + m\psi = (ie/2) \{ \gamma^\mu \psi, A_\mu^R \}, \quad . \quad . \quad . \quad (11'')$$

$$\frac{\partial \bar{\psi}}{\partial x_\mu} \gamma^\mu - m\bar{\psi} = -(ie/2) \{ A_\mu^R, \bar{\psi} \gamma^\mu \}. \quad . \quad . \quad . \quad (11''')$$

The above equations are invariant under the usual gauge transformation

$$A_\mu \rightarrow A_\mu - \frac{\partial \Lambda}{\partial x_\mu}, \quad \psi \rightarrow \psi \exp(-ie\Lambda), \quad . \quad . \quad . \quad (12)$$

where

$$\square \Lambda = 0. \quad . \quad . \quad . \quad (12')$$

To prove the invariance we use the fact that A^R is identical with Λ . Equations (11) may be replaced by the equivalent integral equations expressed by means of retarded and advanced potentials (compare C. N. Yang (1950) and G. Källén (1950).

$$A_\mu(x) = A_\mu^{\text{in}}(x) + \int d^4x' D^{\text{ret}}(x-x') j_\mu^R(x'), \quad . \quad . \quad . \quad (13')$$

$$\psi(x) = \psi^{\text{in}}(x) + (e/2i) \int d^4x' S^{\text{ret}}(x-x') \{ \gamma^\mu \psi(x'), A_\mu^R(x') \}, \quad . \quad (13'')$$

$$\bar{\psi}(x) = \bar{\psi}^{\text{out}}(x) + (e/2i) \int d^4x' \{ A_\mu^R(x'), \bar{\psi}(x') \gamma^\mu \} S^{\text{ret}}(x'-x), \quad . \quad (13''')$$

where

$$D^{\text{ret}} = \bar{D} - \frac{1}{2} D, \quad S^{\text{ret}} = \bar{S} - \frac{1}{2} S, \quad . \quad . \quad . \quad (14)$$

$$A_\mu(x) = A_\mu^{\text{out}}(x) + \int d^4x' D^{\text{adv}}(x-x') j_\mu^R(x'), \quad . \quad . \quad . \quad (15')$$

$$\psi(x) = \psi^{\text{out}}(x) + (e/2i) \int d^4x' S^{\text{adv}}(x-x') \{ \gamma^\mu \psi(x'), A_\mu^R(x') \}, \quad (15'')$$

$$\bar{\psi}(x) = \bar{\psi}^{\text{in}}(x) + (e/2i) \int d^4x' \{ A_\mu^R(x'), \bar{\psi}(x') \gamma^\mu \} S^{\text{adv}}(x'-x), \quad . \quad (15''')$$

where

$$D^{\text{adv}} = \bar{D} + \frac{1}{2} D, \quad S^{\text{adv}} = \bar{S} + \frac{1}{2} S. \quad . \quad . \quad . \quad (16)$$

We may write equations (13') and (15') also in the form

$$A_\mu^R(x) = A_\mu^{\text{in (out)}}(x) + \int d^4x' D^{\text{R ret (adv)}}(x-x') j_\mu^R(x').$$

By adding together the equations (13) and (15) we get

$$A_{\mu}^R(x) = A_{\mu}^{(0)R}(x) + \int d^4x' \bar{D}^{RR}(x-x') j_{\mu}(x'), \quad (17')$$

$$\psi(x) = \psi^{(0)}(x) + (e/2i) \int d^4x' \bar{S}(x-x') \{\gamma^{\mu} \psi(x'), A_{\mu}^R(x')\}, \quad (17'')$$

$$\bar{\psi}(x) = \bar{\psi}^{(0)}(x) + (e/2i) \int d^4x' \{A_{\mu}^R(x'), \bar{\psi}(x') \gamma^{\mu}\} \bar{S}(x'-x), \quad (17''')$$

where $A_{\mu}^{(0)}$, $\psi^{(0)}$, $\bar{\psi}^{(0)}$ mean half the sum of the ingoing and outgoing waves, *e. g.*

$$A_{\mu}^{(0)} = \frac{1}{2}(A_{\mu}^{\text{in}} + A_{\mu}^{\text{out}}). \quad (18)$$

By subtracting the equations (13) and (15) we get

$$A_{\mu}^{\text{in}}(x) - A_{\mu}^{\text{out}}(x) = \int d^4x' D^{RR}(x-x') j_{\mu}(x'), \quad (19')$$

$$\psi^{\text{in}}(x) - \psi^{\text{out}}(x) = (e/2i) \int d^4x' S(x-x') \{\gamma^{\mu} \psi(x'), A_{\mu}(x')\}, \quad (19'')$$

$$\bar{\psi}^{\text{in}}(x) - \bar{\psi}^{\text{out}}(x) = -(e/2i) \int d^4x' \{A_{\mu}(x'), \bar{\psi}(x') \gamma^{\mu}\} \bar{S}(x'-x). \quad (19''')$$

The traditional Hamiltonian formalism is not adequate for the quantization of fields with a non-local interaction. On the other hand it is possible to quantize directly the fundamental integral equations (13) and (15) or the equivalent (17) and (19) by assuming the usual (interaction-free) commutation relations for the ingoing and outgoing waves. The same relations hold for $A_{\mu}^{(0)}$, $\psi^{(0)}$ and $\bar{\psi}^{(0)}$:

$$[A_{\mu}^{(0)}(x), A_{\nu}^{(0)}(x')] = i\delta_{\mu\nu} D(x-x'), \quad (20')$$

$$\{\psi^{(0)}(x), \bar{\psi}^{(0)}(x')\} = -iS(x-x'), \quad (20'')$$

$$\begin{aligned} \{\psi^{(0)}(x), \psi^{(0)}(x')\} &= \{\bar{\psi}^{(0)}(x), \bar{\psi}^{(0)}(x')\} \\ &= [A_{\mu}^{(0)}(x), \psi^{(0)}(x')] = [A_{\mu}^{(0)}(x), \bar{\psi}^{(0)}(x')] = 0. \end{aligned} \quad (20''')$$

The commutation relations between the perturbed waves follow automatically from the field equations (13) or (15) or (17) which may be solved successively in a power expansion of the coupling parameter *e*. For the quantization of the field equations it is essential to symmetrize the expression for the product of ψ and A_{μ}^R since these quantities do not commute with each other in case of a non-local interaction. We should also use the symmetrized current

$$j_{\mu} = (ie/2)[\bar{\psi}, \gamma^{\mu} \psi]. \quad (21)$$

Although we do not know the exact form of the commutation relations between the perturbed wave functions (as the exact solution of the field equations is not known), we may surely find some general properties of the commutators or anticommutators, *e. g.*, the anticommutator between two perturbed spinor functions must be a covariant function of the argument $x_{\mu} - x'_{\mu}$:

$$\{\psi_{\alpha}(x), \bar{\psi}_{\beta}(x')\} = -iU_{\alpha\beta}(x-x'), \quad (22)$$

which follows from the invariance of the formalism under space and time translations. Hence, for the perturbed wave functions taken at the same space-time point x_μ we have the same commutations relations as for the unperturbed ones

$$U_{\alpha\beta}(0)=S_{\alpha\beta}(0), \quad . \quad . \quad . \quad . \quad . \quad . \quad (23)$$

since we may translate the common point x_μ to the infinite past (or future) where we have to do with the ingoing (or outgoing) waves only.

This last property enables the proof of the validity of the continuity equation for the perturbed current j_μ . By multiplying (11'') and (11''') to the right or left by $\bar{\psi}$ and ψ we get

$$\frac{\partial}{\partial x_\mu} j_\mu = (1/4) \gamma_{\alpha\beta} [\{\psi_\alpha(x), \bar{\psi}_\beta(x)\}, A_\mu^R(x)] = 0, \quad . \quad . \quad . \quad (24)$$

since the anticommutator between two field functions taken at the same point is (from (23)) a number and, thus, commutes with everything. Also the averaged current obeys the continuity equation

$$\frac{\partial}{\partial x_\mu} j_\mu^R = 0. \quad . \quad . \quad . \quad . \quad . \quad . \quad (24')$$

Due to (24) the problem of auxiliary condition is the same as in the usual quantum electrodynamics

$$\frac{\partial}{\partial x_\mu} A_\mu | \rangle = 0. \quad . \quad . \quad . \quad . \quad . \quad . \quad (25)$$

We may develop the Lorentz condition in a Taylor series and show, as usual, that all terms of the expansion vanish (due to (11') and (24')) if two initial conditions

$$\frac{\partial}{\partial x_\mu} A_\mu(\vec{r}, t) | \rangle_{[t=t_0]} = 0, \quad \frac{\partial}{\partial x_\mu} \dot{A}_\mu(\vec{r}, t) | \rangle_{[t=t_0]} = 0 \quad . \quad . \quad . \quad (26)$$

are satisfied.

By applying the method described by C. N. Yang (1950) we may construct the S-matrix for the extended source theory. Since the ingoing and outgoing waves satisfy the same commutation relations, there should exist a unitary matrix transforming the ingoing into the outgoing waves

$$A^{\text{out}} = S^{-1} A^{\text{in}} S, \quad \psi^{\text{out}} = S^{-1} \psi^{\text{in}} S. \quad . \quad . \quad . \quad . \quad . \quad (27)$$

From (17), (19) and (27) we get

$$[A_\mu^{(0)R} S] = -\frac{1}{2} \{S, [d^4 x' D^{RR}(x-x') j_\mu(x')]\}, \quad . \quad . \quad . \quad (28')$$

$$[\psi^{(0)}, S] = -(e/4i) \{S, [d^4 x' S(x-x') \{\gamma^\mu \psi(x'), A_\mu^R(x')\}]\}, \quad . \quad . \quad (28'')$$

$$[\bar{\psi}^{(0)}, S] = (e/4i) \{S, [d^4 x' \{A_\mu^R(x'), \bar{\psi}(x') \gamma^\mu\} S(x'-x)]\}. \quad . \quad (28''')$$

From (17) and (28) the S-matrix may be computed as a power series in the coupling constant e

$$S = 1 + \sum_{n=1}^{\infty} R^{(n)}. \quad . \quad . \quad . \quad . \quad . \quad (29)$$

The explicit computation of $R^{(1)}$ and $R^{(2)}$ shows that the equations (17) and (28) are compatible in this approximation and yield the result

$$R^{(1)} = i \int d^4x A_\mu^{(0)R} j_\mu^{(0)}, \quad \dots \quad (30')$$

$$R^{(2)} = \frac{1}{2}(R^{(1)})^2 + P + Q, \quad \dots \quad (30'')$$

where

$$P = \frac{i}{2} \iint d^4x' d^4x'' \{ j_\mu^{(0)}(x'), j_\mu^{(0)}(x'') \} \bar{D}^{RR}(x' - x''), \quad \dots \quad (30''')$$

$$Q = (ie^2/8) \iint d^4x' d^4x'' ([\bar{\psi}^{(0)}(x'') \gamma^\mu \bar{S}(x'' - x'), \gamma^\lambda \psi^{(0)}(x')] \\ + [\bar{\psi}^{(0)}(x'), \gamma^\lambda \bar{S}(x' - x'') \gamma^\mu \psi^{(0)}(x'')]) \{ A_\lambda^{(0)R}(x'), A_\mu^{(0)R}(x'') \}. \quad \dots \quad (30^{iv})$$

The S-matrix is obviously unitary in this approximation and differs from the usual one merely by the fact that every A_μ has been replaced by the averaged A_μ^R and every \bar{D} has been replaced by the twice averaged \bar{D}^{RR} . This is exactly the same replacement which converts the traditional equations of a local theory into our new fundamental equations (17) and (28). We may easily guess the form of the S-matrix elements in all higher approximations. They will differ from the traditional ones by the same replacements which convert the usual field equations into the new equations (17) and (28). However, in the S-matrix elements appear only the unperturbed potentials $A_\mu^{(0)}$ whence (taking account of (8)) the general rule for the transcription of the traditional S-matrix elements into the new form is very simple: we have to replace every \bar{D} function by the twice averaged \bar{D}^{RR} while every $A_\mu^{(0)}$ and every $D^{(1)}$ function (which will be obtained by taking a vacuum expectation value) remain unchanged.

The very fact that it has been possible to construct a unitary S-matrix confirms the compatibility of the set of quantized equations (13) and (15).

We have to examine finally whether the extended source theory is able to improve the situation with respect to the convergence problem. The expressions of the vacuum polarization current and the photon self-energy remain unchanged (since the \bar{D} function does not appear in the well-known tensor $K_{\mu\nu}$). On the other hand the expression for the self-mass of the electron derivable from the S-matrix is

$$\delta m = -\frac{e^2}{2} \int d^4x \gamma^\mu (S^{(1)}(x) \bar{D}^{RR}(x) + \bar{S}(x) D^{(1)}(x)) \gamma^\mu \exp(-ip_\mu x_\mu). \quad (31)$$

If we assume a suitable function $F(x)$ the first term will converge while the second term is left unchanged and diverges.*

* A convergent expression for the electron self-energy could be obtained if we used the integrations of the causal function D_C of Stueckelberg and Feynman in the complex plane instead of Schwinger's \bar{D} and $D^{(1)}$ functions integrated as principal values.

§ 2. ANOTHER TYPE OF A NON-LOCAL INTERACTION.

Let us investigate another type of non-local interaction derivable from the following Lagrangian

$$L=L^{(0)}+L', \quad . \quad . \quad . \quad . \quad . \quad . \quad . \quad . \quad . \quad . \quad (1)$$

where

$$L'=s_\mu A_\mu \quad . \quad . \quad . \quad . \quad . \quad . \quad . \quad . \quad . \quad . \quad (1')$$

with

$$s_\mu=(ie/2)[\bar{\psi}^R, \gamma^\mu \psi^R], \quad . \quad . \quad . \quad . \quad . \quad . \quad . \quad . \quad . \quad . \quad (2)$$

where ψ^R and $\bar{\psi}^R$ are the averaged spinor wave functions obtained with the aid of a general rule

$$a^R(x)=\int d^4x' G(x-x')a(x'). \quad . \quad . \quad . \quad . \quad . \quad . \quad . \quad . \quad . \quad . \quad (3)$$

G is again a delta-like function

$$G(x)=\frac{1}{(2\pi)^4} \int d^4k \exp(ik_\mu x_\mu) g(k_\mu^2, \lambda), \quad . \quad . \quad . \quad . \quad . \quad . \quad . \quad . \quad . \quad . \quad (4)$$

where

$$g(k_\mu^2, 0)=1. \quad . \quad . \quad . \quad . \quad . \quad . \quad . \quad . \quad . \quad . \quad (5)$$

For a spinor field *in vacuo* we have

$$\psi^{(0)R}(x)=g(-m^2, \lambda)\psi^{(0)}(x), \quad . \quad . \quad . \quad . \quad . \quad . \quad . \quad . \quad . \quad . \quad (6)$$

where m is the rest mass of the electron so that the current $s_\mu^{(0)}$ *in vacuo* differs from the usual current merely by a charge renormalization

$$e'=eg^2(-m^2, \lambda). \quad . \quad . \quad . \quad . \quad . \quad . \quad . \quad . \quad . \quad . \quad (7)$$

Thus, it will be convenient to use g -functions with the property

$$g(-m^2, \lambda)=1. \quad . \quad . \quad . \quad . \quad . \quad . \quad . \quad . \quad . \quad . \quad (8)$$

For example we may assume

$$g(k_\mu^2, \lambda)=\frac{1}{1+\lambda^4(k_\mu^2+m^2)^2} \quad \text{or} \quad g(k_\mu^2, \lambda)=\exp\{-\lambda^4(k_\mu^2+m^2)^2\}. \quad . \quad (9)$$

With such functions G the current $s_\mu^{(0)}$ will be identical with the usual $j_\mu^{(0)}$. On the other hand the property § 1 (7) is lost :

$$\int d^4x G(x)=g(0, \lambda), \quad . \quad . \quad . \quad . \quad . \quad . \quad . \quad . \quad . \quad . \quad (10)$$

where $g(0, \lambda)$ is different from unity but tends to unity for $\lambda \rightarrow 0$.

The field equations derivable from (1) are

$$\square A_\mu = -s_\mu, \quad . \quad . \quad . \quad . \quad . \quad . \quad . \quad . \quad . \quad . \quad (11)$$

$$\gamma^\mu \frac{\partial \psi(x)}{\partial x_\mu} + m\psi(x) = ie \int d^4x' G(x-x') \gamma^\mu \psi^R(x') A_\mu(x') \quad . \quad (12)$$

with a similar equation for $\bar{\psi}$.

It should be noticed that, with this type of interaction, neither j_μ nor s_μ satisfy the continuity equations. This unusual feature of the field theory seems acceptable since it is possible to guarantee the integral conservation

laws without continuity equations. In particular, the charge conservation is secured simply by the gauge invariance of the first kind.* The non-existence of the continuity equation for the current four-vector should be interpreted as a fundamental uncertainty preventing a strict localizability of charge.

The field equations (11) and (12) violate the postulate of gauge invariance of the second kind.* The resignation of this postulate seems also acceptable since we may replace it by a less stringent requirement that the experimental rest mass of the photon should be zero. This may be achieved either by formal renormalization or by the so-called realistic compensation (Jost and Rayski 1949). In this respect the new formalism by no means constitutes any drawback in comparison with the traditional quantum electrodynamics which was gauge invariant only formally so that we were also obliged to remove the (infinite!) self-mass of the photon by means of a renormalization or compensation.

The equations (11) and (12) may be integrated by means of retarded potentials which yield

$$A_{\mu}(x) = A_{\mu}^{\text{in}}(x) + (ie/2) \int d^4x' D^{\text{ret}}(x-x') [\bar{\psi}^{\text{R}}(x'), \gamma^{\mu} \psi^{\text{R}}(x')], \quad (13)$$

$$\psi(x) = \psi^{\text{in}}(x) + (e/2i) \int d^4x' S^{\text{R ret}}(x-x') \{\gamma^{\mu} \psi^{\text{R}}(x'), A_{\mu}(x')\}, \quad (14)$$

where the products have been written in a symmetrized form. Similar equations hold for the advanced potentials. By adding and subtracting the equations with the retarded and advanced potentials we get

$$A_{\mu}(x) = A_{\mu}^{(0)}(x) + (ie/2) \int d^4x' \bar{D}(x-x') [\bar{\psi}^{\text{R}}(x'), \gamma^{\mu} \psi^{\text{R}}(x')], \quad (15)$$

$$\psi(x) = \psi^{(0)}(x) + (e/2i) \int d^4x' \bar{S}^{\text{R}}(x-x') \{\gamma^{\mu} \psi^{\text{R}}(x'), A_{\mu}(x')\} \quad (16)$$

and

$$A_{\mu}^{\text{in}}(x) - A_{\mu}^{\text{out}}(x) = (ie/2) \int d^4x' D(x-x') [\bar{\psi}^{\text{R}}(x'), \gamma^{\mu} \psi^{\text{R}}(x')], \quad (17)$$

$$\psi^{\text{in}}(x) - \psi^{\text{out}}(x) = (e/2i) \int d^4x' S^{\text{R}}(x-x') \{\gamma^{\mu} \psi^{\text{R}}(x'), A_{\mu}(x')\} \quad (18)$$

where $\psi^{(0)}$ and $A_{\mu}^{(0)}$ mean half the sum of the ingoing and outgoing waves. From (16) and (18) we get analogous formulæ for the averaged ψ^{R}

$$\psi^{\text{R}}(x) = \psi^{(0)\text{R}}(x) + (e/2i) \int d^4x' \bar{S}^{\text{RR}}(x-x') \{\gamma^{\mu} \psi^{\text{R}}(x'), A_{\mu}(x')\}, \quad (16')$$

$$\psi^{\text{R in}}(x) - \psi^{\text{R out}}(x) = (e/2i) \int d^4x' S^{\text{RR}}(x-x') \{\gamma^{\mu} \psi^{\text{R}}(x'), A_{\mu}(x')\}. \quad (18')$$

We quantize directly the field equations by assuming again that the ingoing and outgoing waves satisfy the well-known commutation relations for the separate fields *in vacuo*. The commutation relations for the perturbed wave functions will follow automatically from the field equations.

The S-matrix may be computed from the formulæ

$$[A_{\mu}^{(0)}, \mathbf{S}] = -(ie/4) [\mathbf{S}, \int d^4x' D(x-x') [\bar{\psi}^{\text{R}}(x'), \gamma^{\mu} \psi^{\text{R}}(x')], \quad (19)$$

$$[\psi^{(0)\text{R}}, \mathbf{S}] = -(e/4i) [\mathbf{S}, \int d^4x' S^{\text{RR}}(x-x') \{\gamma^{\mu} \psi^{\text{R}}(x'), A_{\mu}(x')\}] \quad (20)$$

* For a definition of this, see Wentzel (1949), §§4, 11, 16.

with the aid of (15) and (16). There is little doubt in the compatibility of our fundamental formulæ and we may immediately guess the S-matrix elements in any approximation. They will be quite similar to the usual ones with the only difference that every $\psi^{(0)}$, $\bar{\psi}^{(0)}$ and \bar{S} should be replaced by $\psi^{(0)R}$, $\bar{\psi}^{(0)R}$, and \bar{S}^{RR} . Due to (6) and (8) the general rule for an immediate transcription of the usual S-matrix into the new form is simply: *every \bar{S} should be replaced by \bar{S}^{RR} .*

The new S-matrix elements yield non-vanishing probabilities only for processes in which energy, momentum and charge are conserved. Thus, integral conservation laws are secured in spite of the absence of the notion of densities satisfying continuity equations.

As the perturbed current s_μ does not satisfy the continuity equation, the question arises as to the form of the auxiliary condition. In order to answer this question we introduce (15) into (16) and get a new equation

$$\psi(x) = \psi^{(0)}(x) + (e/2i) \int d^4x' \bar{S}^R(x-x') \times \{\gamma^\mu \psi(x'), A_\mu^{(0)}(x') + \int d^4x'' \bar{D}(x'-x'') s_\mu(x'')\} \quad (21)$$

(and a similar equation for $\bar{\psi}$) where only $A_\mu^{(0)}$, but not A_μ , appear explicitly. In the same way, by substituting (15) into (20) we get new formulae for the computation of the S-matrix in which only the unperturbed potentials $A_\mu^{(0)}$ appear explicitly. Now (15) may be treated as a definition and not as one of the equations. Thus, the perturbed potentials A_μ become secondary quantities without influence upon the fundamental equations. Now we may limit ourselves to the unperturbed $A_\mu^{(0)}$ and assume the Lorentz condition as a restriction upon the state vector

$$\frac{\partial}{\partial x_\mu} A_\mu^{(0)} | \rangle = 0, \quad (22)$$

which reduces to two well-known initial conditions, as usual, due to the fact that the unperturbed potentials obey the Laplace equation

$$\square A_\mu^{(0)} = 1. \quad (23)$$

The computation of the vacuum polarization current yields now

$$\langle j_\mu(x) \rangle_{\text{vac}} = -4e^2 \int d^4x' K_{\mu\nu}(x-x') A_\nu(x'), \quad (24)$$

where

$$K_{\mu\nu} = \frac{\partial \bar{\Delta}^R}{\partial x_\mu} \frac{\partial \Delta^{(1)}}{\partial x_\nu} + \frac{\partial \bar{\Delta}^R}{\partial x_\nu} \frac{\partial \Delta^{(1)}}{\partial x_\mu} - \delta_{\mu\nu} \left(\frac{\partial \bar{\Delta}^R}{\partial x_\lambda} \frac{\partial \Delta^{(1)}}{\partial x_\lambda} - m^2 \bar{\Delta}^R \Delta^{(1)} \right) \quad (25)$$

or

$$\langle s_\mu(x) \rangle_{\text{vac}} = -4e^2 \int d^4x' L_{\mu\nu}(x-x') A_\nu(x'), \quad (26)$$

where $L_{\mu\nu}$ differs from $K_{\mu\nu}$ merely by the fact that every $\bar{\Delta}$ is averaged twice, $\bar{\Delta}^{RR}$. The appearance of a $\bar{\Delta}^R$ or $\bar{\Delta}^{RR}$ changes essentially the situation in the problem of the induced current and secures convergence. The condition for the gauge invariance and the continuity equation for the induced current is, of course, violated as

$$\frac{\partial}{\partial x_\mu} K_{\mu\nu} = \delta_\nu^R \cdot \frac{\partial}{\partial x_\nu} \Delta^{(1)} \quad (27)$$

is different from zero. However, the regularized delta function

$$\delta^R(x) = G(x) \quad . \quad . \quad . \quad . \quad . \quad . \quad . \quad . \quad (28)$$

is even and essentially different from zero only in the neighbourhood of zero while $\partial/\partial x_\nu \Delta^{(1)}$ is odd, so that (27) vanishes if integrated over a small region about the origin. Hence, the continuity equation and the gauge invariance are still valid in the mean. The photon self-energy and the self-charge are finite so that the procedures of mass and charge renormalization are now mathematically correct and may be applied consistently.

The electron self-energy derivable from the S-matrix is

$$\delta m = -(e^2/2) \int d^4x \gamma^\mu (S^{(1)}(x) \bar{D}(x) + \bar{S}^{RR}(x) D^{(1)}(x)) \exp(-ip_\mu x_\mu). \quad (29)$$

where the second term is convergent but the first term still diverges. By comparing (29) with §1 (31) we see that a full convergence may be achieved by combining both modifications discussed in this paper. The convergence will be generally secured if we assume the following Lagrangian

$$L' = (ie/4) \{ [\bar{\psi}^R(x), \gamma^\mu \psi^R(x)], A_\mu^R(x) \}, \quad . \quad . \quad . \quad . \quad (30)$$

where ψ and $\bar{\psi}$ are averaged by means of a delta-like function $G(x)$ while A_μ is averaged by means of another delta-like function $F(x)$. The question of the definitive form of the delta-like function lies beyond the scope of the present investigation. We mention here only that other types of non-local field theories (*e.g.* the non-local field of Yukawa) may be quantized by the method of a direct quantization of field equations. An investigation of Yukawa's non-local field will be published by the author elsewhere.

ACKNOWLEDGMENT.

I thank Professor Rzewuski for making his paper on a related subject available to me prior to publication and for stimulating discussions.

REFERENCES.

- OST, R., and RAYSKI, J., 1949, *Helv. Phys. Acta*, **22**, 457.
 FÄLLÉN, G., 1950, *Arkiv för Fysik*, **2**, 371.
 FIERLS, R., and McMANUS, H., 1948, *Proc. Roy. Soc. A*, **195**, 323.
 VENTZEL, G., 1949, *Quantum Theory of Fields* (Interscience Publishers).
 TANG, C. N., and FELDMAN, D., 1950, *Phys. Rev.*, **79**, 972.

CXXXVIII. *A Theoretical Derivation of the Plastic Properties of a Polycrystalline Face-Centred Metal.*

By **J. F. W. BISHOP** and **R. HILL**,
H. H. Wills Physical Laboratory, University of Bristol †.

[Received June 22, 1951.]

SUMMARY

In continuation of a previous paper (Bishop and Hill 1951) it is conjectured that the work done in plastically deforming a polycrystal is approximately equal to that which would be done if the grains were free to deform equally. In conjunction with the principle of maximum plastic work, this enables the yield function of an aggregate to be calculated. This is done for an isotropic aggregate of face-centred cubic crystals, following a determination of the stresses needed to produce multi-slip. The theoretical yield criterion lies between those of Tresca and von Mises, in good agreement with observation for copper and aluminum. It is shown further that the work-hardening of an aggregate would be a function only of the total plastic work if the grains hardened equally; the departure from this functional relation is expressed explicitly in terms of the non-uniform hardening.

§ 1. RÉSUMÉ OF PREVIOUS WORK.

In a recent paper (Bishop and Hill 1951, henceforward referred to as BH) some general theorems were proved for an aggregate in which the crystals individually deform by slip according to the Schmid law. The theorems depend, in essence, on a principle of maximum plastic work for a homogeneously deformed single crystal (BH, equation (9)). This principle states that if a crystal is caused to deform plastically through an increment of strain $d\epsilon_{ij}$, the work done by the required stress σ_{ij} is not less than that done by any other stress σ_{ij}^* not violating the yield condition; thus

$$(\sigma_{ij} - \sigma_{ij}^*) d\epsilon_{ij} \geq 0. \quad \dots \dots \dots (1)$$

The yield condition is that the component shear-stress in any of the possible slip-directions, and over the associated slip-planes, cannot exceed the corresponding critical shear-stress in the current state of hardening. The critical shear-stress may vary from one slip-direction to another, due to differential hardening, or may be different in the two opposite senses of the same slip-direction, due to a microscopic Bauschinger effect. In a statistically homogeneous aggregate, in which cohesion between crystals is maintained by multi-slip, the same principle was proved for the *macroscopic* stress S_{ij} and strain-increment dE_{ij} . (BH, equation (16)).

† Communicated by the Authors.

In words: the actual work done is equal to the work that would be done if the grains all underwent the same (macroscopic) strain.

In particular, when the slip-directions in any one grain all have the same critical shear-stress τ (in both senses), we may define an average value $\bar{\tau}$ for the aggregate, such that

$$\bar{\tau} = \int \tau \, dV.$$

Then, if σ_{ij}^* would produce a strain dE_{ij} in a grain with critical shear stress τ , $\bar{\sigma}_{ij}^* = \bar{\tau} \sigma_{ij}^* / \tau$ would produce the same strain in a grain of the same orientation but with critical shear stress $\bar{\tau}$. Hence

$$\bar{\tau} \int \sigma_{ij}^* \, dV = \int \tau \bar{\sigma}_{ij}^* \, dV = \bar{\tau} \int \bar{\sigma}_{ij}^* \, dV,$$

assuming that there is no correlation between $\bar{\sigma}_{ij}^*$ and τ . Therefore:

$$\int \sigma_{ij}^* \, dV = \int \bar{\sigma}_{ij}^* \, dV,$$

and so, from (6),

$$S_{ij} \, dE_{ij} = dE_{ij} \int \bar{\sigma}_{ij}^* \, dV. \quad \dots \dots \dots (7)$$

We can thus evaluate the work using the average value of the critical shear stress in the aggregate.

But equations (5) and (6) cannot be strictly true since (6) implies that the deviatoric part of σ_{ij} is equal to that of σ_{ij}^* , all components of which are generally discontinuous across grain boundaries or wherever else the lattice orientation changes. (It is shown later that a general strain can only be produced by some one of a *finite* set of stresses.) However, we are inclined to think (though we have not found a rigorous proof) that equation (6) is not much in error, and we assume it as an approximation.

§ 3. METHOD OF CALCULATION OF THE YIELD FUNCTION.

The way in which f can be calculated is conveniently visualized geometrically. A strain increment dE_{ij} can be considered as a free vector in stress hyperspace. According to (6) the scalar product $S_{ij} \, dE_{ij}$ is calculable in terms of the slip properties of a single crystal. The extremity of the stress vector S_{ij} , corresponding to a strain-increment dE_{ij} , is thus known to lie on a plane which is perpendicular to dE_{ij} and whose distance from the origin is

$$\frac{dE_{ij} \int \sigma_{ij}^* \, dV}{(\bar{dE}_{ij} \bar{dE}_{ij})^{1/2}}. \quad \dots \dots \dots (8)$$

(Although the point $\int \sigma_{ij}^* \, dV$ lies on the plane, it does not, of course, necessarily coincide with S_{ij} .) Now according to (3), the normal to the yield surface at the point S_{ij} is parallel to dE_{ij} , and so perpendicular to the plane. The plane is therefore tangential to the yield surface at S_{ij} . The surface is thereby found as the envelope of planes whose distances from the origin are given by (8). Since possible strains have zero hydrostatic part (being the result of simultaneous simple shears), the surface is cylindrical with generators parallel to the direction δ_{ii} .

When the aggregate as a whole is isotropic the principal axes of the stress and strain-increment tensors are coincident, and we only need to consider the relation between their principal values represented in three dimensional space. The aggregate will be statistically isotropic when the orientations of grains in the same state of hardening are randomly distributed; this condition must be satisfied for each of the various states of hardening at any moment in the differentially-hardened aggregate (if not, the aggregate might be anisotropic despite the absence of a preferred orientation).

The numerical calculations in the present paper are restricted to such an isotropic aggregate in which, moreover, the slip-directions in any grain are equally hardened (so that equation (7) is applicable). The development of deformation textures and their effect on the yield surface is left to a later paper.

§ 4. MULTI-SLIP IN A FACE-CENTRED CUBIC CRYSTAL.

At ordinary temperatures and rates of strain, glide occurs in a face-centred cubic crystal on the octahedral planes in the directions of the octahedron edges. Each of the four distinct glide-planes contains three possible slip-directions, making twelve in all, each of which has two opposite senses. The positive senses of the slip-directions are arbitrarily chosen here according to the following Table; letters *a*, *b*, *c*, *d* refer to the four glide-planes, and with suffixes 1, 2, or 3, denote incremental shears in the respective positive senses. The components, referred to the

Plane	(111)			$(\bar{1}\bar{1}1)$			$(\bar{1}1\bar{1})$			$(1\bar{1}\bar{1})$		
near	<i>a</i> ₁	<i>a</i> ₂	<i>a</i> ₃	<i>b</i> ₁	<i>b</i> ₂	<i>b</i> ₃	<i>c</i> ₁	<i>c</i> ₂	<i>c</i> ₃	<i>d</i> ₁	<i>d</i> ₂	<i>d</i> ₃
direction	01 $\bar{1}$	$\bar{1}01$	$\bar{1}\bar{1}0$	0 $\bar{1}\bar{1}$	101	$\bar{1}10$	0 $\bar{1}\bar{1}$	101	$\bar{1}\bar{1}0$	0 $\bar{1}\bar{1}$	101	$\bar{1}10$

principal axes, of the strain tensor $d\epsilon_{ij}$, due to simultaneous shears in the twelve directions are given by the equations (Taylor 1933 a)

$$\left. \begin{aligned} \sqrt{6} d\epsilon_{11} &= -a_2 + a_3 - b_2 + b_3 - c_2 + c_3 - d_2 + d_3, \\ \sqrt{6} d\epsilon_{22} &= a_1 - a_3 + b_1 - b_3 + c_1 - c_3 + d_1 - d_3, \\ \sqrt{6} d\epsilon_{33} &= -a_1 + a_2 - b_1 + b_2 - c_1 + c_2 - d_1 + d_2, \\ 2\sqrt{6} d\epsilon_{23} &= a_2 - a_3 - b_2 + b_3 + c_2 - c_3 - d_2 + d_3, \\ 2\sqrt{6} d\epsilon_{31} &= -a_1 + a_3 + b_1 - b_3 + c_1 - c_3 - d_1 + d_3, \\ 2\sqrt{6} d\epsilon_{12} &= a_1 - a_2 + b_1 - b_2 - c_1 + c_2 - d_1 + d_2. \end{aligned} \right\} \dots (9)$$

any possible strain has five independent components (the hydrostatic part being zero), and therefore in general can only be produced by multi-slip over a group of directions containing an independent set of five.

Of the ${}^{12}C_5 = 792$ sets of five shears, only 384 are independent. The remaining 408 include dependent combinations of type

$$a_1 + a_2 + a_3 = 0 \quad (144),$$

$$a_1 + b_2 + d_3 = 0 \quad (228),$$

$$a_1 - b_1 + c_1 - d_1 = 0 \quad (36),$$

or their equivalents; these equations are to be interpreted as meaning that such combinations of *unit* shears produce zero resultant strain. Of the 384 independent sets of five shears, 216 have two shears on each of two planes, and 168 have two shears on one plane only (the latter were apparently thought by Taylor to be dependent sets).

If the components of a stress applied to the crystal are σ_{ij} referred to the cubic axes, the shear stress components, multiplied by $\sqrt{6}$, are equal to

$$\left. \begin{array}{lll} A - G + H (a_1), & B + F - H (a_2), & C - F + G (a_3), \\ A + G + H (b_1), & B - F - H (b_2), & C + F - G (b_3), \\ A + G - H (c_1), & B + F + H (c_2), & C - F - G (c_3), \\ A - G - H (d_1), & B - F + H (d_2), & C + F + G (d_3), \end{array} \right\} \quad (10)$$

where

$$\begin{array}{lll} A = \sigma_{22} - \sigma_{33}, & B = \sigma_{33} - \sigma_{11}, & C = \sigma_{11} - \sigma_{22}, \\ F = \sigma_{23}, & G = \sigma_{31}, & H = \sigma_{12}. \end{array}$$

It will be observed that the 12×6 matrix of coefficients in the relations (10) between the 12 shear stress components and the 6 applied stress components is just the transpose of the 6×12 matrix of coefficients in (9). This is a simple consequence of the virtual work equation $\sigma_{ij} d\epsilon_{ij} = \Sigma \tau d\gamma$, and does not depend on any particular lattice geometry. It follows that we can always find a stress for which the component shear stresses attain the critical values in prescribed senses in a given set of five independent slip-directions (the respective minors being identical and non-zero). The critical value would usually be exceeded in one or more of the other seven directions, but, for any given strain, it is always possible to find at least one of the independent sets for which there exists a physically possible stress to operate the constituent shears. However, in evaluating the expression (8) there is no need to determine a physically possible combination of shears which are equivalent to the strain. It is necessary merely to calculate the works done in the given strain by stresses not violating the yield condition, and to select from these works the greatest. In fact it is only necessary to make the choice from the works done by 56 particular stresses, which correspond to the "vertices" of the polyhedral surface in stress space representing the yield criterion for the crystal. Proofs of these statements are left to a subsequent paper.

The 56 stresses may be classified in five groups, in which the typical values of (A, B, C, F, G, H)/ $\sqrt{6}\tau$ are as follows when the critical shear stress τ is the same in all the slip-directions:

- (i.) (1, -1, 0, 0, 0, 0). Tension or compression of amount $\sqrt{6}\tau$ along cubic axis.
- (ii.) (0, 0, 0, 1, 0, 0). A pure shear of amount $\sqrt{6}\tau$ in a cubic plane and parallel to a cubic axis.
- (iii.) ($\frac{1}{2}$, $\frac{1}{2}$, -1, 0, 0, $\pm\frac{1}{2}$). A pure shear of amount $\sqrt{3}\tau$ in a cubic plane and at $22\frac{1}{2}^\circ$ to the cubic axes.
- (iv.) ($\frac{1}{2}$, $-\frac{1}{2}$, 0, $\pm\frac{1}{2}$, $\pm\frac{1}{2}$, 0). Principal stresses $\pm\sqrt{6}\tau(1, -\frac{1}{2}, 0)$ with the second normal to an octahedral plane and the third along a slip-direction in that plane.
- (v.) (0, 0, 0, $\frac{1}{2}$, $\pm\frac{1}{2}$, $\pm\frac{1}{2}$). Tension or compression of amount $\frac{2}{3}\sqrt{6}\tau$ normal to an octahedral plane.

The 56 stresses have 6 members in each of (i.) and (ii.), 12 in (iii.), 4 in (iv.), and 8 in (v.). The critical shear-stress is attained in 8 slip-directions for (i.), (ii.), and (iii.), and in 6 slip-directions for (iv.) and (v.).

§ 5. THE NUMERICAL METHOD.

For a calculation of the yield function of an isotropic aggregate in which there is no Bauschinger effect, it is only necessary to consider macroscopic strains dE_{ij} whose principal values are $(1, -\lambda, \lambda-1)dE$ where $\frac{1}{2} \leq \lambda \leq 1$ (Hill 1950, p. 17 *et seq.*). The work done in such a strain of a free crystal has to be computed for each orientation of the strain axes to the cubic axes. If (θ, ϕ, ψ) are the Eulerian angles of the strain axes with respect to the cubic axes, all essentially distinct orientations occur once only in the intervals

$$0 \leq \phi \leq \pi/4, \quad 0 \leq \cot \theta \leq \sin \phi, \quad 0 \leq \psi \leq \pi,$$

in view of the lattice symmetry and the assumption of equally hardened slip-directions. In other words, it is sufficient to restrict the major strain axis to one of the 48 identical spherical triangles in the stereographic projection, and allow the other axes to rotate through half a revolution. If dW is the work done on unit volume of crystal in a strain defined by given values of λ, θ, ϕ and ψ ($\bar{\tau}$ being the average critical shear stress), then, from (7),

$$S_{ij} dE_{ij}(\lambda) = \iiint dW \sin \theta d\theta d\phi d\psi / \iiint \sin \theta d\theta d\phi d\psi.$$

In the computation, net points were taken at 5° intervals of θ and ϕ , and 18° intervals in ψ . Five values of λ were taken in steps of $\frac{1}{8}$ between $\frac{1}{2}$ and 1. It was found convenient to express dW in terms of the principal values of the 56 stresses and the angles between the stress and strain axes. The angles were read from a stereographic net on which were marked the axes of the 56 stresses.

If p denotes the perpendicular (8) from the origin to a tangent plane of the yield surface in principal stress space, the results of the calculations are

λ	$\frac{1}{2}$	$\frac{5}{8}$	$\frac{3}{4}$	$\frac{7}{8}$	1
$\sqrt{(\frac{3}{2})}p/\tau$	3.06	3.04	2.98	2.91	2.86

The error involved in the integration is estimated to be not more than one unit in the second decimal place.

§ 6. DISCUSSION OF RESULTS.

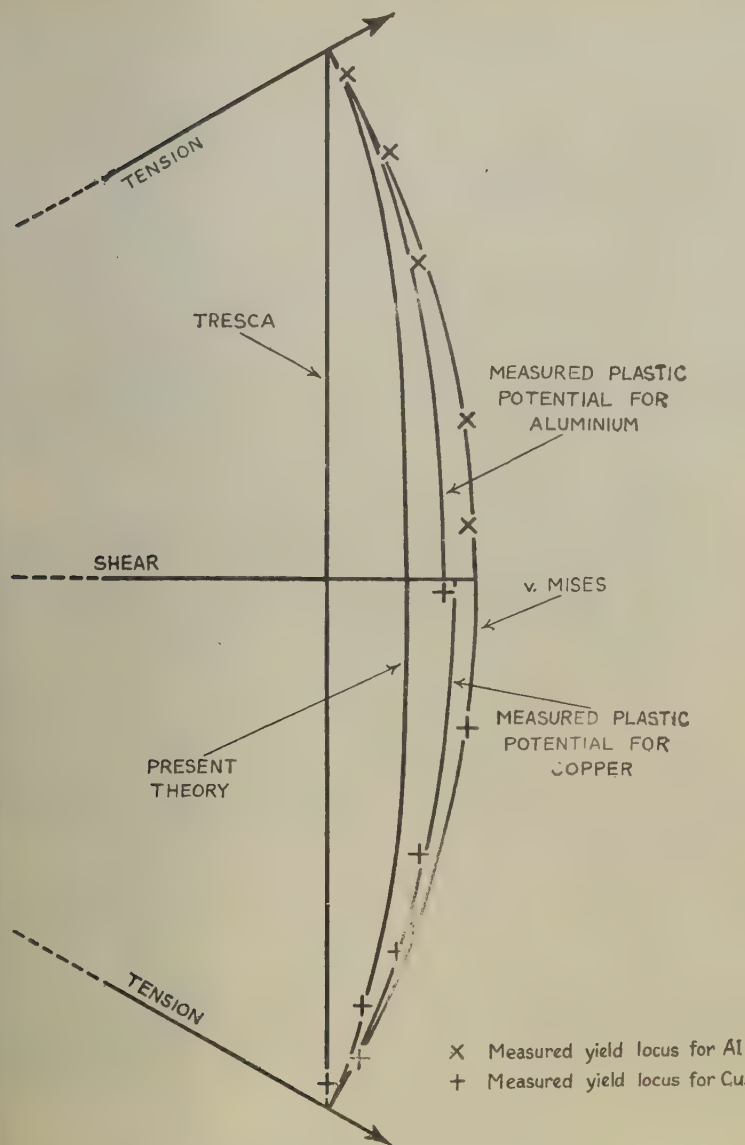
Fig. 1 shows a typical 60° sector of the cross-section of the yield surface, obtained from the values of p as described in § 3. The calculated curve cuts orthogonally the radii corresponding to pure shear and to pure tension, and lies between the Tresca hexagon and the von Mises circle when all are made to coincide for tension. In particular, the ratio of the yield stress in shear to that in tension is $2.86/(\sqrt{3} \times 3.06) = 0.540$, compared with 0.500 and 0.577 for the Tresca and Mises criteria.

The experimental data of Taylor and Quinney (1931) for copper and aluminium are also shown in the figure, and tend to lie between the Mises circle and the theoretical curve. The small discrepancy may be due to defects in the theory such as the approximation involved in equation (6), unequal hardening of slip-directions in individual crystals, or microscopic modes of distortion other than slip in the 12 directions. On the other hand, the experimental data may not be completely reliable, due to anisotropy or to a slight uncertainty in the extrapolation used to circumvent the hysteresis loop.

Also shown in the figure are the plastic potential curves computed from Taylor and Quinney's measured relation between the directions of the stress and strain-increment vectors; Taylor's (1947) calculations for copper have been corrected in some instances. The agreement of the plastic potential curves with the directly measured yield loci suggests the substantial validity of (3), the theoretical derivation of which does not involve the further assumptions made in the present computation of the actual form of f .

The comparison can also be made in terms of Lode's diagram, but in our opinion, this over-magnifies small variations in the stress-strain relations, and is responsible for frequent statements that the Lévy-Mises equations are merely a moderate approximation. Thus, to the uncritical eye, a typical observed pair of Lode variables (0.5, 0.4), compared with the Lévy-Mises prediction (0.5, 0.5) might suggest an error of 20 per cent. However, it can be seen from the figure that the maximum difference in direction between the normals to the Mises circle and the measured plastic potential curves for copper and aluminium is only about 4°; without any theory at all the strain-increment vector could be anywhere in the 360° range.

Fig. 1.



§7. INFLUENCE OF RESIDUAL STRESSES.

When the external loads are removed from a plastically-deformed aggregate, a residual distribution of internal stress remains. According to the maximum work principle for the aggregate (BH, equation (16)),

the yield function for the aggregate does not depend in any way on these internal stresses, but only upon the intrinsic hardening of the grains (as specified by the current values of the critical shear stresses in the slip directions). This conclusion is directly due to the neglect of elasticity in the present theory. In effect, the theory assumes that the elastic moduli are indefinitely large, so that a single crystal remains rigid under increasing load until it yields plastically. Similarly, an aggregate remains rigid until all grains are stressed to their individual yield points, and there is therefore no hysteresis loop. During loading, the weakest grain becomes plastically stressed under a load which may be termed the elastic limit of the aggregate. The elastic limit is generally appreciably lower than the yield-point load of the aggregate and clearly depends directly on the residual stresses. With increasing load other grains in turn are plastically stressed, but are prevented from deforming (or hardening) by the remaining non-plastic, and therefore rigid, grains. Hence, apart from the restricted possibilities of a stress adjustment within the individual yield surfaces of such plastically stressed grains, the greater part of further increments of load is borne by the non-plastic grains.

In an actual aggregate, elasticity permits plastic distortion and hardening of the weakest grains as soon as the elastic limit is reached. The immediate consequence is a hysteresis loop, greatly dependent on residual stresses (and correspondingly removable by a mild annealing), and with a breadth equivalent to a strain of elastic magnitude. When the hardening during the loop is small, it is naturally to be expected (in accord with observation) that the reloading branch of the loop will bend over fairly sharply to rejoin, virtually, the continuation of the previous stress-strain curve. Moreover, the local ordinate of the curve should be effectively identical with the yield-point stress calculated for a plastic-rigid aggregate. Many parallels might be instanced in stress analyses of structural parts on the basis of the macroscopic theory for a plastic-elastic homogeneous solid.

Similar considerations apply to the hysteresis loop during reverse loading, and to the tendency of the residual stresses to act so as to lower the elastic limit (Bauschinger effect). However, a further distinction must be made here. When the sign of dE_{ij} is reversed, the value of S_{ij} calculated from equation (6) would not be merely reversed when there is a *microscopic* Bauschinger effect; that is, when the critical shear stress on a slip-plane depends on the sense of slip. Thus, even for the plastic-rigid model, one would expect in such circumstances a macroscopic Bauschinger effect on the *yield-point*.

§ 8. WORK HARDENING OF AN AGGREGATE.

The calculated value of the tensile yield stress is 3.067. This agrees closely with the value obtained by Taylor (1938 b), who assumed that an aggregate *actually* deforms uniformly (whereas we have conjectured that the work done is *as if* it did). Taylor was able to determine the yield

CXXIX. *Note on the Boundary Layer on a Rotating Sphere* *.

By L. HOWARTH, F.R.S.,

Department of Mathematics, University of Bristol †.

[Received July 6, 1951.]

SUMMARY.

The solution of the boundary layer equations for the flow associated with a rotating sphere is considered and an approximate solution is obtained. The solution on either hemisphere is thought to be valid up to the immediate vicinity of the equator where it is invalidated by the interaction with the flow from the other hemisphere.

A short appendix gives the flow due to a semi-infinite cylinder rotating in a uniform stream.

§ 1. INTRODUCTION.

THE problem of the flow engendered by a sphere rotating about a diameter in otherwise undisturbed fluid has two features which are not without interest. In the first place it provides an example in which the curvature terms in the three-dimensional boundary layer equations are important. In the second place the boundary layers from the two hemispheres impinge on each other in the neighbourhood of the equator and their interaction is, in itself, of interest.

The object of this note is to discuss in some detail the first of these aspects and to place the second on record as a problem still to be solved in detail. In explanation of this second problem, it may be said at once that the boundary layers on the two hemispheres may be regarded as originating at the poles (where the flow approximates to the rotating disk solution) and developing towards the equator where they impinge on each other. The boundary layer equations can deal adequately with most of this development but must fail to represent the region of interaction between the two impinging layers if for no other reason than the parabolic character of the equations.

§ 2. THE BOUNDARY LAYER EQUATIONS.

We shall use spherical polar coordinates r, θ, ϕ with r measured radially outwards from the centre of the sphere, θ measured from the axis of rotation and ϕ the azimuth. In order to preserve w for the velocity normal to the surface (*i. e.* in the direction r increasing) we shall use

* This paper forms a small part of one of the essays to which the Adams Prize was awarded in 1951.

† Communicated by the Author.

u, v for the velocities in the directions θ, ϕ increasing respectively. The boundary layer equations can then be derived directly from the full equations of flow in spherical polar coordinates or from Howarth (1951) by placing $K_1=0, K_2=-(1/a) \cot \theta$, where a is the radius of the sphere. They are :

$$\frac{u}{a} \frac{\partial u}{\partial \theta} + w \frac{\partial u}{\partial r} - \frac{v^2}{a} \cot \theta = \nu \frac{\partial^2 u}{\partial r^2}, \quad (1)$$

$$\frac{u}{a} \frac{\partial v}{\partial \theta} + w \frac{\partial v}{\partial r} + \frac{uv}{a} \cot \theta = \nu \frac{\partial^2 v}{\partial r^2}, \quad (2)$$

$$\frac{1}{a} \frac{\partial u}{\partial \theta} + \frac{\partial w}{\partial r} + \frac{u}{a} \cot \theta = 0, \quad (3)$$

where use has been made of the fact that derivatives with respect to ϕ all vanish and that there is no imposed pressure gradient.

Apart from the curvature terms $(v^2/a) \cot \theta$ and $(uv/a) \cot \theta$, we should have the ordinary kind of two-dimensional boundary layer in u and w , with v determined by a convection equation. We may regard the $(v^2/a) \cot \theta$ term in (1) effectively as an imposed pressure gradient (whose intensity varies across the layer) essentially accelerating in character, since it is positive over the range 0 to $\pi/2$ in θ to which attention is restricted. At the surface, with Ω denoting the angular velocity of the sphere,

$$v = \Omega a \sin \theta,$$

so that

$$\frac{v^2}{a} \cot \theta = \Omega^2 a \sin \theta \cos \theta.$$

The effect of this term is therefore a maximum when $\theta = \pi/4$ and tends to zero as either the pole or the equator is approached. It is to be noted at once, in support of what has been said earlier, that it is most unlikely that forward integration of equations (1)–(3) from $\theta = 0$ to $\pi/2$ will lead to a solution at $\theta = \pi/2$ in which $u = 0$ throughout the layer. In other words the boundary layer equations, which present us with the prospect of the layer from the two hemispheres meeting head-on at the equator, are inadequate to deal with the flow in this vicinity. Nevertheless, it is to be expected that the interaction will be limited to the immediate vicinity of the equator and that it will lead to an outflow in the equatorial plane of the same order as the mass flows through the boundary layers. Since the solution of the rotating disk problem is known to lead to inflow along the axis, we may reasonably expect inflow at the poles, and this combined with the outflow at the equator gives us a picture similar to the one envisaged by Stokes (1845). The arguments used here must however be regarded as essentially different from Stokes's, his being based on pressure which, to the order of the approximation here, has been regarded as uniform.

§ 3. THE SOLUTION NEAR THE POLES.

A solution of equations (1), (2), (3) in series in powers of θ is obtainable, though it is unlikely to converge sufficiently rapidly to make an approach to the equatorial conditions practicable. To obtain it we put

$$\left. \begin{aligned} Z &= \left(\frac{\Omega}{\nu}\right)^{1/2} (r-a), \\ u &= a\Omega[\theta F_1 + \theta^3 F_3 + \dots], \\ v &= a\Omega[\theta G_1 + \theta^3 G_3 + \dots], \\ w &= (\nu\Omega)^{1/2}[H_1 + \theta^2 H_3 + \dots], \end{aligned} \right\} \dots \dots \dots (4)$$

and find the following equations for the first six functions

$$\left. \begin{aligned} F_1^2 + F_1' H_1 - G_1^2 &= F_1'', \\ 2F_1 G_1 + H_1 G_1' &= G_1'', \\ 2F + H_1' &= 0. \end{aligned} \right\} \dots \dots \dots (5)$$

$$4F_1 F_3 + F_1' H_3 + F_3' H_1 + \frac{1}{3} G_1^2 - 2G_1 G_3 = F_3'', \quad \dots \dots \dots (6)$$

$$2F_3 G_1 + 4F_1 G_3 + H_3 G_1' + H_1 G_3' - \frac{1}{3} F_1 G_1 = G_3'', \quad \dots \dots \dots (7)$$

$$4F_3 + H_3' - \frac{1}{3} F_1 = 0. \quad \dots \dots \dots (8)$$

The boundary conditions are $F_1 = F_3 = 0$, $G_1 = 1$, $G_3 = -\frac{1}{6}$, $H_1 = 0$, $H_3 = 0$ at $Z = 0$.

$F_1 \rightarrow 0$, $F_3 \rightarrow 0$, $G_1 \rightarrow 0$, $G_3 \rightarrow 0$ as $Z \rightarrow \infty$.

Equations (5) are, as mentioned earlier, the equations determining the flow due to a rotating disk Kármán (1921). It is to be doubted whether, since the functions defined in equations (6), (7), (8) refer to this specific problem only, the labour involved makes their integration worth while. The significance of the expansion lies in giving the form of that solution near the poles.

§ 4. THE SOLUTION BY THE KÁRMÁN METHOD.

We may look to the momentum integral equation to provide a more rapid though approximate solution. Integrating (1) through the boundary layer and making use of (3) we have, writing $z = r - a$,

$$\int_0^\delta \frac{\partial}{\partial \theta} u^2 dz + a \left[wu \right]_0^\delta + \int_0^\delta (u^2 - v^2) \cot \theta dz = -\nu a \left(\frac{\partial u}{\partial z} \right)_0,$$

that is

$$\frac{d}{d\theta} \int_0^\delta u^2 dz + \int_0^\delta (u^2 - v^2) \cot \theta dz = -\nu a \left(\frac{\partial u}{\partial z} \right)_0, \quad \dots \dots \dots (9)$$

since $u = 0$ when $z = 0$ and $z = \delta$.

Similarly from (2)

$$\int_0^\delta \frac{\partial}{\partial \theta} (uv) dz + a \left[vw \right]_0^\delta + 2 \int_0^\delta uv \cot \theta dz = -\nu a \left(\frac{\partial v}{\partial z} \right)_0,$$

that is

$$\frac{d}{d\theta} \int_0^\delta uv \, dz + 2 \int_0^\delta uv \cot \theta \, dz = -\nu a \left(\frac{\partial v}{\partial z} \right)_0, \quad \dots \quad (10)$$

since $u=v=0$ when $z=\delta$ and $w=0$ when $z=0$.

We may now follow Kármán's approximate method of solution of the rotating-disk problem by putting

$$\left. \begin{aligned} u &= A[Z - 3Z^3 + 2Z^4] - \frac{\delta^2 \Omega^2 a}{\nu} \sin \theta \cos \theta \left[\frac{1}{2} Z^2 - Z^3 + \frac{1}{2} Z^4 \right], \\ v &= \Omega a \sin \theta \left[1 - \frac{3}{2} Z + \frac{1}{2} Z^3 \right], \end{aligned} \right\} \quad \dots \quad (11)$$

where $Z=z/\delta$; these expressions satisfy the conditions

$$\left. \begin{aligned} u=0, \quad \frac{\partial^2 u}{\partial Z^2} &= -\frac{\Omega^2 \delta^2 a}{\nu} \sin \theta \cos \theta \text{ at } Z=0; & u=0, \quad \frac{\partial u}{\partial Z} &= 0 \text{ at } Z=1, \\ v &= \Omega a \sin \theta, \quad \frac{\partial^2 v}{\partial Z^2} = 0 \text{ at } Z=0; & v=0, \quad \frac{\partial v}{\partial Z} &= 0 \text{ at } Z=1, \end{aligned} \right\} \quad \dots \quad (12)$$

the conditions on the second derivatives at $z=0$ being obtained direct from equations (1) and (2). The significance of A is that it is $\delta(\partial u/\partial z)_0$. The quantities A and δ are unknown and are to be determined by (9) and (10). Let us for convenience write $A = (\chi \Omega^2 \delta^2 a/\nu) \sin \theta \cos \theta$, $\delta = (\nu/\Omega)^{1/2} \lambda$, so that χ , λ are the new unknowns.

In the solution of the rotating-disk problem it is certainly true that

$$\int_0^\delta v^2 \, dz \gg \int_0^\delta u^2 \, dz. \quad \dots \quad (13)$$

We may therefore make a tentative approach to the present problem by neglecting the terms containing $\int_0^\delta u^2 \, dz$ on the left-hand side of (9).

It then follows from (9) that

$$\chi = \int_0^1 \left(1 - \frac{3}{2} Z + \frac{1}{2} Z^3 \right)^2 dZ, \quad \dots \quad (14)$$

$$\text{so that} \quad \chi = 0.2357. \quad \dots \quad (15)$$

It then follows from (10) that

$$\left(\frac{d}{d\theta} + 2 \cot \theta \right) (0.00864 \sin^2 \theta \cos \theta \lambda^3) = \frac{3}{2\lambda} \sin \theta, \quad \dots \quad (16)$$

so that

$$\frac{3}{4} \sin \theta \cos \theta \frac{d\lambda^4}{d\theta} + (4 \cos^2 \theta - \sin^2 \theta) \lambda^4 = 173.6, \quad \dots \quad (17)$$

and therefore

$$\frac{d}{d\theta} [\sin^{16/3} \theta \cos^{4/3} \theta \lambda^4] = 231.5 \sin^{13/3} \theta \cos^{1/3} \theta. \quad \dots \quad (18)$$

Hence

$$\lambda^4 = \frac{231.5}{\sin^{16/3} \theta \cos^{4/3} \theta} \int_0^\theta \sin^{13/3} \theta \cos^{1/3} \theta \, d\theta. \quad \dots \quad (19)$$

For small θ this solution should agree with the rotating-disk solution. From (19) we see that $\lambda^4=43.4$ when θ is small, so that

$$\lambda=2.57, \quad \left(\frac{\partial u}{\partial z}\right)_0=0.61 \frac{\Omega^{3/2} a \theta}{\nu^{1/2}}, \quad \left(\frac{\partial v}{\partial z}\right)_0=-0.58 \frac{\Omega^{3/2} a \theta}{\nu^{1/2}}.$$

Cochran (1934), using this type of approximate solution for the rotating disk but retaining the terms in u^2 , gives the corresponding numerical coefficients as 2.79, 0.54 and -0.54 respectively. In the solution he obtained by numerical integration of the full equations the first of these coefficients is infinite, of course, and the other two are 0.51 and -0.62 respectively.

Returning now to the rotating sphere, the solution of (19) for λ is given in Table I. The value $\chi=0.2357$ given in (13) leads to

$$\frac{u\lambda_0^2}{\lambda^2 a \Omega \sin \theta \cos \theta} = \lambda_0^2 [0.2357Z - 0.5Z^2 + 0.2929Z^3 - 0.0286Z^4] \quad (20)$$

$$\text{and} \quad \frac{v}{a \Omega \sin \theta} = 1 - 1.5Z + 0.5Z^3, \quad \dots \dots \dots (21)$$

where λ_0 is the value 2.57 taken by λ when $\theta=0$.

TABLE I.

θ (degrees)	λ	$\frac{u_{\max}}{a\Omega}$	$\frac{v_{\max}}{a\Omega}$	$\frac{u_{\max}}{v_{\max}}$	$\frac{1}{(\Omega\nu)^{1/2}} \int_0^\delta u \, dz$	$\frac{-w_\delta}{(\Omega\nu)^{1/2}}$
0	2.57	0.000	0.000	0.22	0.000	0.62
10	2.58	0.039	0.174	0.22	0.054	0.62
30	2.74	0.110	0.500	0.22	0.164	0.60
50	3.12	0.127	0.766	0.21	0.276	0.56
70	4.06	0.180	0.940	0.19	0.395	0.50
80	5.28	0.161	0.985	0.16	0.459	0.44
90	∞	0	1.000	0.00	0.497	0.00

The right-hand sides of (20) and (21) are both functions of Z only and are given in Table II. It will be seen that the approximation we have obtained is such that u and v retain the same *form* throughout the range 0 to $\pi/2$ for θ , the actual scale and amplitude alone varying with θ .

TABLE II.

Z	$\frac{u\lambda_0^2}{\lambda^2 a \Omega \sin \theta \cos \theta}$	$\frac{v}{a \Omega \sin \theta}$	Z	$\frac{u\lambda_0^2}{\lambda^2 a \Omega \sin \theta \cos \theta}$	$\frac{v}{a \Omega \sin \theta}$
0.0	0.0000	1.0000	0.4	0.2133	0.4320
0.1	0.1246	0.8505	0.6	0.1386	0.2080
0.2	0.1944	0.7040	0.8	0.0450	0.0056
0.3	0.2205	0.5635	1.0	0.0000	0.0000

The maximum values of the right-hand sides of (20) and (21) considered functions of Z are 0.22 and 1 respectively. The variation of the associated values u_{\max} and v_{\max} are included in Table I. The ratio u_{\max}/v_{\max} is also included in Table I.

It follows from (20) that

$$\frac{1}{a(\Omega\nu)^{1/2}} \int_0^\delta u \, dz = 0.0184\lambda^3 \sin \theta \cos \theta. \quad \dots \quad (22)$$

furthermore, from (3)

$$w_\delta = -\frac{1}{a} \left[\frac{d}{d\theta} \int_0^\delta u \, dz + \cot \theta \int_0^\delta u \, dz \right],$$

where w_δ is the value of w at the edge of the boundary layer. Hence, from (22),

$$\left. \begin{aligned} w_\delta &= -0.0184 (\Omega\nu)^{1/2} \left[\frac{d}{d\theta} (\lambda^3 \sin \theta \cos \theta) + \lambda^3 \cos^2 \theta \right] \\ &= 0.0184 (\Omega\nu)^{1/2} \left[(2 \cos^2 \theta - \sin^2 \theta) \lambda^3 + \frac{3}{4\lambda} \sin \theta \cos \theta \frac{d\lambda^4}{d\theta} \right], \end{aligned} \right\} \quad (23)$$

so that by equation (17)

$$w_\delta = -0.0184 (\Omega\nu)^{1/2} \left[\frac{173.6 - 2 \cos^2 \theta \lambda^4}{\lambda} \right]. \quad \dots \quad (24)$$

Values of w_δ are included in Table I. It will be noticed that the solution gives an inflow throughout the whole range.

It follows from (19) that λ (and hence δ) behaves like $c \cos^{-1/3} \theta$ (where c is constant) in the vicinity of $\theta = \pi/2$. In such circumstances, neglect of the first term in (9) is no longer justified and we must expect our solution to break down in this vicinity. However, in view of the nature of the singularity, we should expect the breakdown to be limited to the immediate vicinity of the equator where, anyway, the interaction with the flow from the other hemisphere will be important. Since this interaction is probably largely determined by the flux through the boundary layers, which our solution will give with little error, it is worth while examining our results in this neighbourhood further. It follows from (20) and (21) that, as $\theta \rightarrow \pi/2$,

$$u \rightarrow 0^* \text{ and } \frac{v}{a\Omega} \rightarrow 1$$

throughout the layer. The limiting values of both $(\partial u / \partial z)_0$ and $(\partial v / \partial z)_0$ are zero. It appears therefore that the solution presents us with something akin to separation at the equator.

Although $u \rightarrow 0$, $\int_0^\delta u \, dz$ remains finite and equal to $0.497 (\Omega\nu)^{1/2}$, so that

* This result appears to contradict earlier remarks but it should be remembered that the value of u is unlikely to be correct in this region although the non-zero value of $\int_0^\delta u \, dz$ (see below) may be more reliable.

there is a net flux through the equatorial plane. This is to be expected from our solution, since as we have seen there is an inflow into the boundary layer and it can readily be verified that

$$2\pi a \left[\int_0^\delta u \, dz \right]_{\theta=\pi/2} = -2\pi a^2 \int_0^{\pi/2} w_\delta \sin \theta \, d\theta \quad . \quad . \quad . \quad (25)$$

as continuity requires.

This flux through the equatorial plane cannot of course take place from symmetrical considerations and must be annihilated by the flow from the other hemisphere. As indicated earlier on general grounds, a complete solution must take account of this interaction which one might reasonably expect to be confined to the vicinity of the equatorial plane and to give a mass outflow of the order of the total flux from the two hemispheres.

On the basis of this solution it appears likely therefore that inflow will occur over a large part of the surface, the outflow necessary to maintain continuity being confined to the vicinity of the equatorial plane.

Moreover, the general equations (1) and (2) confirm that inflow probably occurs at the edge of the boundary layer. At the outside of the layer these equations may be written approximately

$$w_\delta \frac{\partial u}{\partial r} = \nu \frac{\partial^2 u}{\partial r^2}, \quad . \quad . \quad . \quad . \quad . \quad (26)$$

$$w_\delta \frac{\partial v}{\partial r} = \nu \frac{\partial^2 v}{\partial r^2}, \quad . \quad . \quad . \quad . \quad . \quad (27)$$

where w_δ is the outflow at the edge of the layer. Now it is most unlikely that $\partial u/\partial r$ and $\partial v/\partial r$ are other than negative and that $\partial^2 u/\partial r^2$ and $\partial^2 v/\partial r^2$ are other than positive in the outer parts of the layer and hence w_δ must be negative—that is there must be inflow.

APPENDIX.

Another example of an essentially three-dimensional boundary layer is provided by the boundary layer along a thin hollow semi-infinite circular cylinder which is made to rotate with constant angular velocity ω about its axis and placed in a uniform stream moving with velocity U parallel to the axis.

It has been shown by Howarth (1951) amongst others that the curvature terms disappear from the equations of flow for the boundary layer along such a cylinder, so that we have the following equations:

$$u \frac{\partial u}{\partial x} + w \frac{\partial u}{\partial z} = \nu \frac{\partial^2 u}{\partial z^2}, \quad . \quad . \quad . \quad . \quad . \quad (28)$$

$$u \frac{\partial v}{\partial x} + w \frac{\partial v}{\partial z} = \nu \frac{\partial^2 v}{\partial z^2}, \quad . \quad . \quad . \quad . \quad . \quad (29)$$

$$\frac{\partial u}{\partial x} + \frac{\partial w}{\partial z} = 0, \quad . \quad . \quad . \quad . \quad . \quad (30)$$

where x is measured parallel to the axis from the leading edge, y around a right section and z normal to the surface.

Equation (28) is the boundary layer equation for flow along a flat plate, so that we have

$$u = \frac{1}{2} U F'(Z),$$

where

$$Z = \frac{1}{2} \left(\frac{U}{\nu x} \right)^{1/2} z$$

and

$$F''' + FF'' = 0,$$

with $F = F' = 0$ at $Z = 0$ and $F' = 2$ as $Z \rightarrow \infty$ *.

It follows from equation (30) that

$$w = \frac{1}{2} \left(\frac{\nu U}{x} \right)^{1/2} (ZF' - F)$$

and then from (21) that

$$v = \frac{1}{2} \omega a (2 - F'),$$

since $v = \omega a$ when $z = 0$.

The surface traction in this case has components

$$\tau_{zx} = 0.332 \rho \left(\frac{\nu U^3}{x} \right)^{1/2},$$

$$\tau_{zy} = -0.332 \rho \omega a \left(\frac{\nu U}{x} \right)^{1/2}.$$

The drag on the cylinder is thus unaffected by its rotation and the frictional moment M which has to be overcome in order to maintain the rotation is $1.3282 \pi \rho \omega a^3 (\nu U)^{1/2}$ for a length l of the cylinder; the moment coefficient C_M is given by

$$C_M = \frac{M}{\pi a^2 l U^2 \rho} = 1.3282 \frac{\omega a}{U} \left(\frac{\nu}{U l} \right)^{1/2}.$$

As a result of this nature can clearly be applied to determine the rate at which the spin would be lost if the rotation were not artificially maintained, provided the rate of loss were sufficiently slow for the aerodynamic problem to be considered steady at all stages. In such guise it is not without interest ballistically.

REFERENCES.

- COCHRAN, 1934, *Proc. Camb. Phil. Soc.*, **30**, 365-375.
 HOWARTH, 1951, *Phil Mag.*, **42**, 239-243.
 KÁRMÁN, 1921, *Z.A.M.M.*, **1**, 244-247.
 STOKES, 1845, *Trans. Camb., Phil., Soc.*, **8**, 287; *Collected Papers*, **1**, 75-129.

* For a table of values of $\frac{1}{2}F'$ see for example *Modern Developments in Fluid Dynamics* Goldstein, Oxford Univ. Press (1938), vol. I., p. 136.

CXXX. *The Melting Curve at High Pressures.*

By C. DOMB,
Clarendon Laboratory, Oxford *.

[Received July 5, 1951.]

ABSTRACT.

An attempt is made to derive theoretically the Simon formula for the variation of the melting point of a solid with pressure. The model used is similar to that of Lennard Jones and Devonshire, but the interpretation of the results is different. A formula of the right type results, but a detailed examination shows that the melting temperatures are much too high, and the reasons for the discrepancy are discussed. The theory predicts the absence of a solid-fluid critical point, and this is in disagreement with recent general work of Münster.

§ 1. INTRODUCTION.

THE form of the solid-fluid transition curve at high pressures has been the subject of considerable discussion for some time. Particular attention has been fixed on the question whether a solid-fluid critical point exists ^{above} which there is continuity of state, as in the liquid-vapour transition. There were quite lively discussions on this matter between those who favoured the existence of such a critical point and those who were convinced that it could not exist. All these discussions were, however, based on very insufficient experimental data, and on the extrapolation of interpolation formulæ. The later and more complete experimental work of Bridgman showed no indication of the existence of such a critical point, and Bridgman considers that the evidence is fairly conclusively against it (see Bridgman 1949, p. 201, for a detailed discussion). On the other hand it has been pointed out by Simon (1937) that thermodynamic reasoning alone cannot suffice to decide either way, and also that there are no obvious reasons which exclude the one or the other possibility.

Some years ago Simon proposed, on semi-empirical grounds, the following formula for the melting curve :

$$\frac{p}{p_i} = \left(\frac{T}{T_0} \right)^c - 1. \quad . \quad . \quad . \quad . \quad . \quad . \quad (1)$$

(Here T_0 is the normal melting temperature, p_i the internal pressure and c is a constant.) This formula is the first one to connect the melting curve with properties of the substance. It fits all the available experimental data with reasonable accuracy, the values of the internal pressure are

* Communicated by Professor F. Simon, F.R.S.

found to be in good agreement with those calculated by van der Waals' equation, and the value of c turns out to be round about 2 for most substances (about 4 for metals). Simon argued that if one wants to penetrate relatively to very high temperatures and pressures one has to carry out experiments on substances with low internal pressures, and he therefore used the substance with the lowest internal pressure, helium, as a model substance. Recent work on helium (Simon *et al.* 1950) has shown that the formula fits the experimental data with values of T/T_0 ranging up to 50° .* It is of interest to examine the possibility of deriving theoretically a formula which fits experimentally over such a wide range.

In 1939 Lennard Jones and Devonshire put forward a theory of melting analogous to the theory of order-disorder transitions in alloys. At sufficiently low temperatures they obtained isothermals of van der Waals shape with two stationary values, which they interpreted in the usual way as a first-order phase transition. At higher temperatures the two stationary values disappeared, thus indicating the existence of a critical point. However, Lennard Jones and Devonshire pointed out that they considered the model too crude to make any reliable predictions. This model was refined slightly by Blaisse (1946) without substantially altering the conclusions. On using an adaptation of the Born theory of melting, Blaisse was able to derive a formula of type (1), but the value of c obtained was less than 1.

In the present paper we shall adopt a model similar to that of Lennard Jones and Devonshire. Our interpretation of the consequences of this model will differ, however, and we shall derive a formula similar to (1) for the melting curve. We shall also indicate the mathematical developments required to improve the theory.

§ 2. FORMULATION OF THE PROBLEM.

We shall throughout assume classical theory, interactions between molecules being given by central forces of limited range. Our results will therefore only be applicable to systems in which the binding forces can be regarded as central, such as the inert gases, and will not be valid for metals in which the bonding is of a different character. The partition function for an assembly of classical particles reduces to a product of two factors, a kinetic energy factor $(2\pi mkT)^{3/2}/h^3$ per particle, and a configurational factor arising from the potential energy terms. The configurational factor can be conveniently specified in the following manner. Let us take an arbitrary lattice structure whose spacing is small compared with the intermolecular distance in the solid state. Suppose that molecules are restricted to occupy positions in the centre of a lattice cell. Between any two molecules in different lattice cells there is an interaction energy ϵ_i . The intermolecular forces can be ignored outside a certain radius, and for

* The normal melting point of helium would correspond to about 1° abs. if quantum effects did not interfere.

any finite lattice spacing the ϵ_i form a finite set r . In any possible configuration of the assembly let n_i be the number of pairs of molecules with interaction energy ϵ_i . The energy of this configuration is

$$\sum_{i=1}^r n_i \epsilon_i.$$

Let $W(n_1, \dots, n_i, \dots, n_r)$ be the number of possible configurations of the assembly in which there are n_1 pairs of energy ϵ_1, \dots, n_r pairs of energy ϵ_r . The configurational partition function is then

$$Z_c = \sum_{n_1 \dots n_r} W(n_1 \dots n_i \dots n_r) \exp \left[- \sum_{i=1}^r n_i \epsilon_i / kT \right]. \quad (2)$$

The expression (2) is only exact in the limiting case of infinitely small lattice spacing. But any finite spacing which contains a sufficient number of points to give a fair description of the intermolecular energy curve should provide a reasonable approximation.

The lattice used above is fixed and artificial and, provided that it is sufficiently fine, any given crystal structure can be fitted in to it. At lowest temperatures the system will choose the configuration of minimum energy, and if the law of force is of Lennard Jones type ($\lambda/r^m - \mu/r^n$), this corresponds to the face-centred cubic structure (Lennard Jones and Ingham 1925). An increase in pressure is represented by an increase in the density of particles, and the formula (2) also embraces the possibility of polymorphic transitions. In fact the description is too general for our purposes, since we are concerned with the disordering of a particular crystal structure, and we shall therefore modify the model.

We consider the number of particles as fixed, but the lattice spacing as variable, an increase in pressure corresponding to a decrease in lattice spacing; we also confine our attention to a particular crystal structure (fig. 1). At constant volume our problem is now formulated as a generalized order-disorder transition in which many neighbour interactions must be taken into account; the ratio of occupied to vacant cells is very much less than $\frac{1}{2}$. It should be observed that thermal vibrations are automatically taken into account in this formulation.

§ 3. APPROXIMATE MODEL

If we could solve the above problem exactly we should find that as the temperature was raised from zero a point would be reached at which the partition function had a singularity. This singularity would correspond to a first-order transition, and would be associated with the disappearance of long-range order; it could thus be interpreted as the melting point. Unfortunately the only reliable information we have concerning order-disorder transitions is in regard to systems containing equal ratios of constituents and in which only nearest neighbour interactions are taken into account. We are therefore forced to use a drastic approximation in our model, and we must then decide whether any information provided by this approximation can be considered reliable. Following Lennard Jones

Fig. 1.

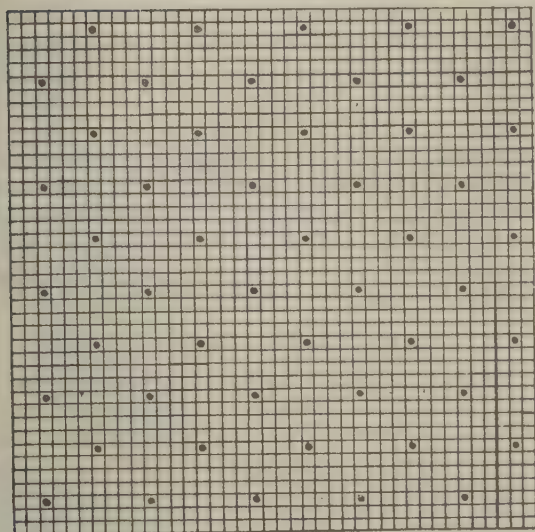


Fig. 2.



and Devonshire, we take account of small displacements from equilibrium by assuming a harmonic vibration spectrum, the kinetic energy terms now being included in the partition function; the gradual disordering of the

crystal structure is allowed for by assuming that the molecules can jump into a single interstitial position, as shown in fig. 2. An essential physical difference between the solid and fluid states is the presence or absence of long-range order, and the model can take this into account. We can thus divide the partition function into two components,

$$F = F_{\text{vib}} + F_{\text{or}}, \quad (3)$$

F_{vib} being vibrational and F_{or} being given by order-disorder theory.

In their discussion of the problem Lennard Jones and Devonshire use a refined calculation for F_{vib} , averaging the inter-molecular energy over a cell to which a molecule is confined by its neighbours. We do not consider that the crudeness of the model warrants any such detailed calculation, and we shall use a simple Debye model, so that

$$F_{\text{vib}} = -3NkT \ln kT/\hbar\bar{\nu}, \quad (4)$$

$\bar{\nu}$ being a mean frequency. In fact we do not consider that the present model is capable of yielding any detailed information on the nature of the singularity, and hence on matters such as the magnitude of the latent heat. Nevertheless, we do believe that it is possible to derive a reasonable idea of the position of the singularity. This assumption is based on the experience of order-disorder transitions for which an exact solution is available in two dimensions (Onsager 1944, Wannier 1945). It is there evident that crude approximations are quite incorrect in regard to the nature of the singularity, but provide a fair approximation to its position. The exact solution shows that the singularity is associated with the disappearance of long-range order, so that we can speak with precision of an ordered and a disordered phase meeting at the singularity. This is essentially different from a liquid and vapour above the critical point, where there is complete continuity, and a single analytic function for the partition function. We shall interpret the above singularity as corresponding to the melting point.

For F_{or} we shall use the Bethe approximation with a coordination number equal to 12 (Rushbrooke 1949, p. 306). Then if ϵ is the repulsive energy between a molecule in equilibrium and an interstitial molecule, the temperature of the singularity is given by

$$kT_c = a\epsilon \left[a = \frac{1}{2 \ln 12/10} = 2.87 \right]. \quad (5)$$

To determine the corresponding pressure we must take account of the variation of ϵ and $\bar{\nu}$ with volume, using the formula $p = -\partial F/\partial v$. For $\bar{\nu}$ we shall use Gruneisen's assumption $\bar{\nu} = K/v^\gamma$, so that for the vibrational term

$$p_{\text{vib}} = -\frac{\partial F_{\text{vib}}}{\partial v} = -\frac{3NkT}{\bar{\nu}} \frac{\partial \bar{\nu}}{\partial v} = \frac{3NkT\gamma}{v}. \quad (6)$$

For the intermolecular energy we shall assume a formula of Lennard Jones type, the attractive part of which can be neglected in the interstitial position. Thus

$$\epsilon = A\epsilon_0 \left(\frac{r}{r_0} \right)^{-n} = A\epsilon_0 \left(\frac{v}{v_0} \right)^{-n/3}, \quad (7)$$

where v_0 is the equilibrium volume of the substance and A is a constant. (If the interstitial position is at a distance from equilibrium equal to $1/\sqrt{2}$ of the spacing between atoms, the value of A is $2^{n/2}$.) Typical values of the constants for various substances are given in Fowler and Guggenheim (1939, p. 285).

Hence we have

$$p_{or} = -\frac{\partial F_{or}}{\partial v} = -Nb \frac{\partial \epsilon}{\partial v} = \frac{Nbn A \epsilon_0}{3} \left(\frac{v}{v_0}\right)^{-(n/3)-1} \quad (8)$$

$$\left(b = \frac{1}{4} \cdot \frac{12 \cdot 10}{11} = 2.73\right).$$

Combining (6) and (8), and substituting from (7) in (5), we find

$$\frac{p_c}{\varpi} = A \left(\frac{v_0}{v_c}\right)^{(n/3)+1} \left[3\gamma a + \frac{nb}{3}\right] \quad \varpi = \frac{N\epsilon_0}{v_0} \quad (9)$$

and

$$\frac{T_c}{\tau} = Aa \left(\frac{v_0}{v_c}\right)^{n/3} \quad \tau = \epsilon_0/k. \quad (10)$$

The pressure ϖ is determined by the lattice energy at the absolute zero and is related to the internal pressure, and τ is related to the ordinary melting temperature. Therefore

$$\frac{p_c}{B\varpi} = \left(\frac{T_c}{\tau}\right)^{(n+3)/n} \quad B = \frac{3\gamma + nb/3a}{(Aa)^{3/n}} \quad (11)$$

At sufficiently high pressures this is a formula similar to (1) with $c = 1 + 3/n$. If $n = 9$, $c = 1.33$, and if $n = 12$, $c = 1.25$.

§ 4. DISCUSSION OF RESULT.

It was pointed out by Simon (1937) that the existence of a universal formula of type (1) implied a law of corresponding states for melting. Lennard Jones and Devonshire (1939) observe that as long as the intermolecular energy curves of various substances can be adequately represented by an expression with two free parameters (such as (7) with fixed n), we will be led to a law of corresponding states. However, Bridgman is opposed to the idea of corresponding states for melting (1931, p. 207), since it is clear experimentally that latent heats and volume changes on melting cannot be fitted into such a law. Nevertheless, a law of corresponding states should only be regarded as a rough approximation; it may well be that a feature such as the melting point depends only in an average way on the shape of the intermolecular energy curve, whereas features such as latent heats and volume changes are much more sensitive to details. In this connection it is worth noting that the formula (11) is not very dependent on the coordination number used in the model.

From the experimental point of view Simon (1951) has shown in a recent article that the data for the melting curve of a number of substances fit a law of corresponding states with considerable accuracy.

When we attempt a detailed comparison between (11) and experiment we find two serious discrepancies. The value of c is too low, and the values of T_0 required to fit formula (1) are about three times too large. If we re-examine our approximate model it is not difficult to trace the source of the discrepancy. The single interstitial position we have taken corresponds to a very high energy; for $n=12$ the repulsive energy in this position is 64 times its value in equilibrium. Clearly a violent degree of thermal agitation and disorder would be required before this position would become occupied with any frequency, and this is far more than is required for melting. Interstitial positions much closer to the equilibrium position are sufficient to provide the disorder required for melting, and these would correspond to much lower temperatures. They are also situated on a flatter region of the intermolecular energy curve, and should therefore give rise to a larger value of c , since (11) indicates that the value of c varies inversely as the steepness of the curve. Confirmation of this interpretation is provided by X-ray diffraction experiments which show no very marked change in the shape of the first maximum between solid and fluid states.

It may also be noted that the Lindemann melting formula, which is well satisfied experimentally, assumes that melting occurs when the average vibration amplitude is about one-tenth of the minimum distance between atoms in the solid lattice (Grüneisen 1926). Our choice of the average interstitial position has been arbitrary, and if we were to take an interstitial position at this distance from equilibrium, our results would be in better agreement with experiment.

Unfortunately, although one can account for the disagreement qualitatively, it is difficult to see how to take adequate account of it theoretically without tackling the more complicated problem of generalized order-disorder transitions. We could start with a problem of the type indicated in fig. 3 in which nearest and second neighbours both have a repulsive energy of interaction, so that the lowest energy state is as indicated. Then we should try to introduce more intervening repulsive interactions. Our resulting critical temperature would only be expected to tend to a non-zero value as the number of interactions increased indefinitely for a three-dimensional model, since Peierls (1936) has shown that thermal vibrations on their own are sufficient to destroy long-range order in two dimensions.

§ 5. THE EXISTENCE OF A CRITICAL POINT.

In a recent paper Münster (1951) attempts to show very generally that all first-order phase transitions disappear at sufficiently high temperatures, and hence that these transitions end in a critical point. This conclusion contradicts the result of the present paper, and we believe it to be incorrect. Münster's argument is rather intricate, but Mr. R. O. Davies has pointed out to the writer that an error arises in the passage from a finite canonical ensemble of N particles to a grand canonical ensemble

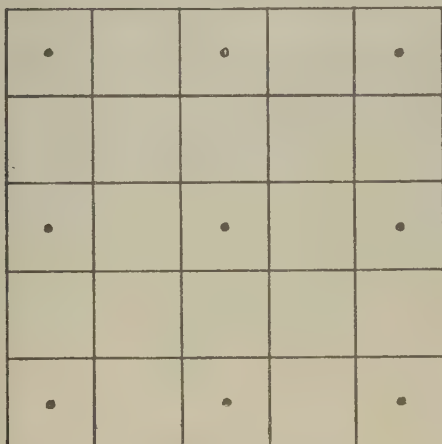
which provides in principle for an indefinitely large N . The finite limit to which $\partial \bar{E}_q / \partial \Theta$ tends as $\Theta \rightarrow \infty$ may well depend on N , and its behaviour for large N must be investigated.

This point may be aptly illustrated by a particular physical example. Consider an order-disorder transition in a two-dimensional quadratic lattice with equal numbers of the two constituents. An exact solution is available (Onsager 1944), and although the transition is not first order, the specific heat is infinite at the Curie point, the fluctuations are large, and Münster's argument should apply. For any given number N the Curie point is given by

$$T_c = 1.14 \epsilon / k, \quad (12)$$

where ϵ depends on the intermolecular spacing, and hence on α/N (α being the area of the assembly). As N increases so does ϵ , and hence T_c . If there is no upper bound to ϵ there is likewise no upper bound to T_c .

Fig. 3.



It seems clear, therefore, that a critical point could only arise in general if there were an upper limit to the intermolecular energy as the intermolecular distance decreases to zero. At the present moment there is no indication, theoretical or experimental, of the existence of such a limit. Theoretically the repulsive energy is of the form

$$R(r) \exp(-r/\rho), \quad (13)$$

where ρ is a constant and $R(r)$ is a polynomial containing small inverse powers of r (Slater 1928). Even if $R(r)$ is replaced by a constant, P , the numerical values of P given in Fowler and Guggenheim, p. 293, would correspond, from equation (5), to melting temperatures 10^6 times the normal melting temperature.

We may sum up by saying that we have indicated the possibility of deriving, for a classical model, a formula of type (1) from the melting curve.

The parameters occurring in this formula can be related to the normal melting temperature and internal pressure. It should be emphasized, however, that the Simon formula (1) is of much greater general validity than the present theory since it applies even when quantum effects are present (Simon 1951).

ACKNOWLEDGEMENTS.

The author is indebted to Professor F. E. Simon, F.R.S., for many valuable discussions. He is also grateful to the University of Oxford for the award of an I.C.I. Fellowship.

REFERENCES

- BLAISSE, B. S., 1946, *Thesis*, Amsterdam.
 BRIDGMAN, P. W., 1949, *The Physics of High Pressure* (London: G. Bell).
 FOWLER, R. H., and GUGGENHEIM, E. A., 1939, *Statistical Thermodynamics* (Cambridge: University Press).
 GRÜNEISEN, E., 1926, *Handbuch der Physik* X (Berlin: Springer), p. 51.
 LENNARD JONES, J. E., and DEVONSHIRE, A. F., 1939, *Proc. Roy. Soc. A*, **170**, 464.
 LENNARD JONES, J. E., and INGHAM, A. E., 1935, *Proc. Roy. Soc. A*, **107**, 636.
 MÜNSTER, A., 1951, *Z. Naturforschg.*, **6a**, 139.
 ONSAGER, L., 1944, *Phys. Rev.*, **65**, 117.
 PEIERLS, R. 1936, *Helv. phys. Acta*, Suppl. (ii), 81.
 RUSHBROOKE, G. S., 1949, *Introduction to Statistical Mechanics*, (Oxford: University Press).
 SIMON, F. E., HOLLAND, F. A., HUGGILL, J. A. W., and JONES, G. O., 1950, *Nature, Lond.*, **165**, 147.
 SIMON, F. E., 1937, *Trans. Farad. Soc.*, **33**, 65.
 SIMON, F. E., 1951, *Farkas Memorial Volume*, in the press.
 SLATER, J. C., 1928, *Phys. Rev.* **32**, 349.
 WANNIER, G. H., 1945, *Rev. Mod. Phys.* **17**, 50.

CXXXI. CORRESPONDENCE.

The Influence of Exchange Energy on the Specific Heat of Free Electrons in Metals.

By A. B. LIDIARD,
King's College, London*.

[Received August 15, 1951.]

IN a recent paper Wohlfarth (1950) has published calculations of the effect of the exchange energy on the thermal properties of free electrons. His starting point is an expression (due to Koppe (1947)) for the free energy, F , in terms of the distribution function $f(k)$. (His equation (2.1) is, in fact, only $\frac{1}{2}F$ and should be multiplied by 2.) The first two terms in this expression are respectively the kinetic energy and the exchange energy of the electrons; together they make up the *internal* energy, E . The third term is the entropy, S , multiplied by $-T$. As an approximation it is assumed that S is the same function of $f(k)$ as it would be in the absence of exchange interactions. We should expect this to be a good approximation when the exchange energy is small compared with the kinetic energy, simply because it is correct when the exchange energy is actually zero. An integral equation for $f(k)$ may be obtained by putting the variation $\delta F=0$, namely

$$\frac{\hbar^2}{8\pi^2m} k_1^2 - \frac{e^2}{\pi k_1} \int_0^\infty k_2 f(k_2) \ln \left| \frac{k_1 + k_2}{k_1 - k_2} \right| dk_2 - \zeta = kT \ln \left(\frac{1 - f(k_1)}{f(k_1)} \right). \quad (1)$$

ζ is a parameter introduced by the condition that the total number of electrons, N , is a constant. It is equal to the chemical potential $\partial F / \partial N$. Owing to the difficulty of solving equation (1) its derivation by putting $\delta F=0$ is made the basis of a variation treatment. As Wohlfarth takes a rather crude variation function $f(k)$ (equation 2.3), it seems desirable to obtain some confirmation that the results of its use are not seriously in error.

Firstly we note the possibility, in principle, of solving (1) by a method of successive approximations, an n th approximation for $f(k)$ being inserted on the L.H.S. to give an $(n+1)$ th approximation on the right. We could therefore consider Wohlfarth's variation function as a starting point in this iterative process. This we have done, and found that for low temperatures the next approximation was, in its variation with k , graphically indistinguishable from a simple Fermi-Dirac function, in which the temperature T is replaced by a parameter τ , say. τ was

* Communicated by Professor C. A. Coulson, F.R.S.

several times smaller than T , in general agreement with Wohlfarth's result that the specific heat was greatly decreased by the exchange energy.

This means that probably a very good *variational* distribution function would be

$$f(k) = \left[\exp \frac{1}{k\tau} \left(\frac{\hbar^2}{8\pi^2 m} k^2 - \zeta \right) + 1 \right]^{-1}. \quad (2)$$

The parameter ζ may be found as usual by the condition that the total number of electrons is a constant, N . The second parameter τ will be determined by putting $\partial F / \partial \tau = 0$: when the exchange energy is not included, this method, of course, yields $\tau = T$, as is necessary. Now Yokota (1949), in the course of a paper on the Thomas-Fermi-Dirac equation, has evaluated the exchange term in the expression for F , using the (incorrect) Fermi-Dirac distribution function. It is thus only necessary to substitute τ for T in his result (6) to obtain $F(\tau)$, since the kinetic energy and entropy expressions are well known. (There is a minor error in Yokota's equation (6) which is corrected here.) In this way we obtain

$$\begin{aligned} \frac{F}{N\epsilon_0} = & \frac{3}{5} \left(1 + \frac{5x^2}{12} \right) - \frac{3}{4} \frac{\epsilon_j}{\epsilon_0} \left[1 + \frac{x^2}{6} \left(\ln x + \frac{\gamma}{2} - \ln \pi - 1 \right) \right] \\ & - \frac{\pi k T}{\epsilon_0} \cdot \frac{x}{2}, \quad x \ll 1, \quad (3) \end{aligned}$$

in which

$$x = \frac{\pi k T}{\epsilon_0}, \quad \epsilon_0 = \frac{\hbar^2}{8m} \left(\frac{3N}{\pi V} \right)^{2/3}, \quad \epsilon_j = e^2 \left(\frac{3N}{\pi V} \right)^{1/3}$$

and γ is a numerical constant. (In terms of γ_1 , γ_2 , and γ_3 , defined in Yokota's paper,

$$\gamma = 3 - 4 \ln 2 + 12\gamma_1/\pi^2 - \gamma_2 + 2\gamma_3 :$$

the 3 appears incorrectly as a 2 in his paper.) We have evaluated γ numerically and found it to be 0.648. The quantity ϵ_0 is just the Fermi energy, and ϵ_j/ϵ_0 gives a convenient measure of the exchange energy. By minimizing F with respect to x (*i. e.* with respect to τ) we obtain as the equation determining x as a function of T

$$\frac{\pi k T}{\epsilon_0} = x - \frac{\epsilon_j}{\epsilon_0} \left[\frac{x}{2} \ln x - \frac{x}{2} \left(-\frac{\gamma}{2} + \ln \pi + \frac{1}{2} \right) \right], \quad x \ll 1. \quad (4)$$

These two equations (3) and (4) are to be compared with Wohlfarth's equations (2.6) and (2.7), namely

$$\begin{aligned} \frac{F}{N\epsilon_0} = & \frac{3}{5} \left(1 + \frac{5x^2}{12} \right) - \frac{3}{4} \frac{\epsilon_j}{\epsilon_0} \left[1 + \frac{x^2}{6} \left(\ln x - \ln 2 - \frac{13}{12} \right) \right] \\ & - \frac{3kT}{\epsilon_0} \cdot \frac{x}{2}, \quad x \ll 1, \quad (5) \end{aligned}$$

$$\frac{3kT}{\epsilon_0} = x - \frac{\epsilon_j}{\epsilon_0} \left[\frac{x}{2} \ln x - \frac{x}{2} \left(\ln 2 + \frac{7}{12} \right) \right], \quad x \ll 1. \quad (6)$$

Apart from the substitution of 3 for π in the entropy terms, these two equations differ from (4) and (5) only in the replacement of $\left(\ln \pi + \frac{1}{2} - \frac{\gamma}{2}\right) = 1.32$ by $\left(\ln 2 + \frac{7}{12}\right) = 1.28$, i. e. a difference of 4 per cent. Finally, Wohlfarth's equation (2.8) for the specific heat, C , is replaced by

$$C/C^0 = \left\{ 1 - \frac{1}{2} \cdot \frac{\epsilon_j}{\epsilon_0} \ln x - \frac{\epsilon_j}{\epsilon_0} \left(\frac{1}{4} + \frac{\gamma}{4} - \frac{1}{2} \ln \pi \right) \right\}^{-1}, \quad (7)$$

where C^0 is the Sommerfeld specific heat $\frac{1}{2}\pi^2 Nk(kT/\epsilon_0)$. This again is equivalent to the replacement of $\ln 2 + 7/12$ by $\ln \pi + \frac{1}{2} - \gamma/2$. This reaffirms the result that the specific heat is greatly *decreased* by the inclusion of the exchange energy. For it is clear from (4) and (6) that as $T \rightarrow 0$, $x \rightarrow 0$ and from (7) that as $x \rightarrow 0$, $C/C^0 \rightarrow 0$.

This close agreement between the results obtained by using the first and second order variation functions is strong evidence for the validity of the variation method. This is confirmed by a comparison of the approximate and exact values of the thermodynamic functions for a perfect Fermi-Dirac gas without exchange interactions (published elsewhere, Lidiard 1951).

In conclusion I should like to thank Isaaki Yokota for supplying the derivation of his equation (6) which has been used here.

REFERENCES.

- KOPPE, H., 1947, *Z. Naturforsch.*, **2A**, 429.
 LIDIARD, A. B., 1951, *Proc. Phys. Soc. A*, **64**, 814.
 WOHLFARTH, E. P., 1950, *Phil. Mag.*, **41**, 534.
 YOKOTA, I., 1949, *J. Phys. Soc. Japan*, **4**, 82.

A Dislocation Reaction in the Face-Centred Cubic Lattice.

By W. M. LOMER,
 Cavendish Laboratory, Cambridge*.

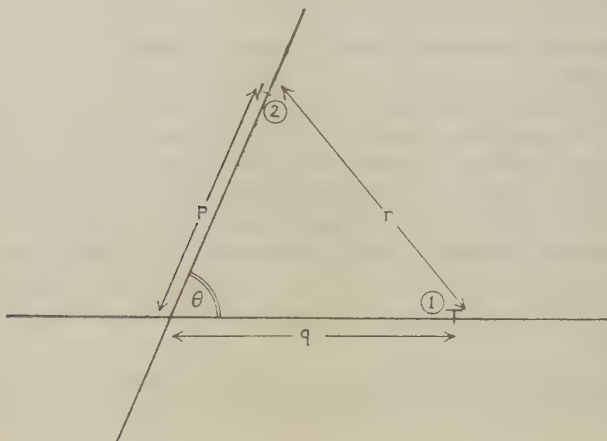
[Received July 15, 1951.]

THE marked difference in the initial rates of strain-hardening of hexagonal and cubic crystals has often been ascribed to some form of interference between slip on non-parallel planes in the cubic material. It is shown in this paper that dislocations on two intersecting slip planes can attract one another and combine to form a "sessile" dislocation (Frank 1949), which may act as a considerable immobile nucleus of internal stress, and so cause the crystal to harden.

* Communicated by the Author.

Consider two dislocations on slip planes inclined at an angle θ as shown in fig. 1. (Only dislocation lines parallel to the line of intersection will interact strongly, so the problem is effectively two dimensional.) The force per unit length exerted on dislocation 2 by dislocation 1 is $b_2\tau$, where b_2 is the Burgers vector of number 2, and τ is the shear stress due

Fig. 1.



Coordinate system used for calculations.

to number 1 resolved first into the slip plane of 2, and then into the slip direction. A full analysis shows that the force can be derived from the following energy functions :—

$$1 \text{ and } 2 \text{ both screw type } E = \frac{\mu b_1 b_2}{2\pi} \log r.$$

$$1 \text{ and } 2 \text{ both edge type } E = \frac{\mu b_1 b_2}{2\pi(1-\nu)} \left\{ \cos \theta \log r + \frac{pq \sin^2 \theta}{r^2} \right\}.$$

$$1; \text{ edge and } 2; \text{ screw, or } \textit{vice versa}, E=0.$$

where μ = modulus of rigidity, = Poisson's ratio,

b_1, b_2 = Burgers vectors,

p, q, r as diagram.

In the close-packed cubic lattice the planes may be for instance (111) and ($\bar{1}\bar{1}\bar{1}$), intersecting in $[1\bar{1}0]$ and making an angle $\cos^{-1} 1/3$ with each other. The only dislocation lines considered are therefore those parallel to $[1\bar{1}0]$. Possible displacement vectors (excluding "half-dislocations" (Heidenreich and Shockley 1948) for reasons explained later) are in the directions $[1\bar{1}0]$; $[10\bar{1}]$; $[01\bar{1}]$, in the first plane, and $[1\bar{1}0]$; $[101]$; $[011]$, in the second. The first one of each of these sets is a pure screw, and of no particular interest. The reaction to be studied in detail is

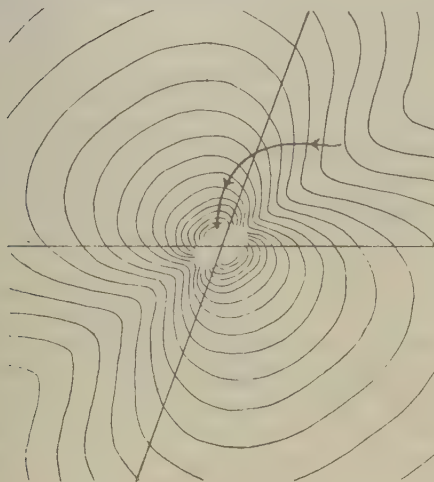
that between $[10\bar{1}]$ and $[011]$ which can add to give $[110]$, a single dislocation of the same strength as each of the two combining ones. This resulting dislocation line is parallel to $[1\bar{1}0]$ and its displacement vector is $[110]$; these two directions are not contained in the same close-packed plane, and so the dislocation is sessile.

The displacement vectors may be resolved into screw and edge components as follows, with a —length of unit cell edge :—

$$\frac{1}{2}^*a[10\bar{1}] = \frac{1}{4}a ([1\bar{1}0] + [11\bar{2}])$$

$$\frac{1}{2}a[011] = \frac{1}{4}a(-[1\bar{1}0] + [11\bar{2}])$$

Fig. 2.



Interaction energy contour map for reaction $[10\bar{1}] + [011] \rightarrow [110]$; energy contour interval— $\frac{\mu a^2}{32\pi}$ ergs per cm. = 0.85 e.V. per atom plane in copper.

giving the screw components a magnitude $a/2\sqrt{2}$ and the edges $\sqrt{3}a/2\sqrt{2}$. With these values, and taking $\nu=1/3$ we get, adding all the energy contributions

$$E = \frac{\mu a^2}{32\pi} \left\{ 5 \log r + \frac{7pq}{r^2} \right\}.$$

It is convenient to represent the energy as a function of the oblique coordinates p and q by the contour map of fig. 2, where the energy value for dislocation 1 at q and dislocation 2 at p is plotted at the point p, q .

* $\frac{a}{2}[10\bar{1}]$ is a vector with components $\frac{a}{2}, 0, -\frac{a}{2}$ and so on.

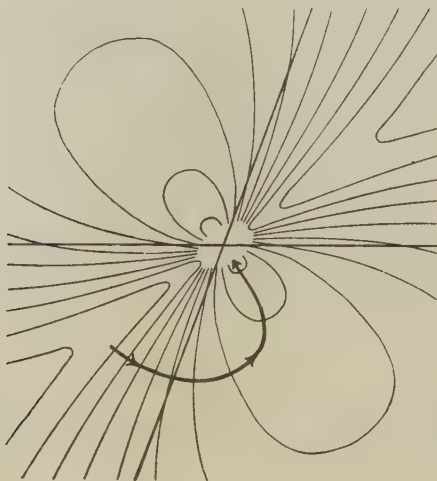
It may be presumed that the representative point of the system will move down the line of greatest slope on the diagram, so that both dislocations will in practice move simultaneously. A typical "trajectory" for the system has been sketched in.

There is also an attractive force between dislocations with Burgers vectors $[10\bar{1}]$ and $[101]$. It is small and depends on the fact that the self-energy of a screw dislocation per unit length is less than that for an edge with the same displacement vector. The energy function for this pair is

$$E = \frac{\mu a^2}{32\pi} \left\{ \log r + \frac{7pq}{r^2} \right\}.$$

This is mapped in fig. 3; the trajectory shows that at first the dislocations adjust their angular relationship, and only when p/q is approximately -1 do they both approach the centre.

Fig. 3.



Interaction energy contour map for reaction $[10\bar{1}] + [101] \rightarrow [200]$; contour interval as fig. 2.

The details of this picture probably depend on the assumptions made, such as the infinitely long, straight dislocations, and on neglecting the effect of the dissociation into half dislocations. Since it is believed that the halves will only separate by some 10 Å, this cannot have a large effect on interactions at a considerable distance, but might play some part in the details of the actual process of coalescence of the dislocations. The production of sessile dislocations by the interaction of mobile ones, and not only by stacking faults in the growth process, should almost certainly have some effect on the rate of hardening, but it is not yet

clear to what extent it will be important, or what the exact mechanism of the interaction of the sessile dislocations with those still mobile would be.

Recent experimental work has shown that hardening is very closely associated with the occurrence of deformation bands (Honeycombe, in the press), and that the latter occur more frequently in crystals with several slip planes. This may imply that the effect dealt with in this paper is not important, although it is perhaps possible that sessile dislocations produced in this way help the formation and stabilization of the deformation bands.

REFERENCES.

- FRANK, F. C., 1949, *Proc. Phys. Soc. A*, **62**, 202.
 HEIDENREICH, R. D., and SHOCKLEY, W., 1948, *The Strength of Solids*, (London : Physical Society), p. 57.
 HONEYCOMBE, R. W. K., *J. Inst. Met.* (in the press).

Lattice Defects in Silver Bromide at Room Temperature.

By H. D. KEITH and J. W. MITCHELL,
 University of Bristol*.

[Received September 7, 1951.]

As a result of the experiments of Tubandt and Eggert (1920), Wagner and Beyer (1936), Berry (1951) and others, it has now been established fairly conclusively that, at temperatures above 200° C., the lattice disorder in silver bromide is predominantly of the Frenkel type. Concerning the nature of the lattice disorder in this material at lower temperatures, however, little direct experimental evidence is available, and an attempt has therefore been made to determine the "soundness" of pure silver bromide at room temperature from newly-measured values of its lattice-parameter and density.

The experiment consisted of comparing the molecular weight of silver bromide as determined by X-rays, that is, as calculated by means of the formula (Straumanis 1949)

$$M_x = k \frac{N_s a^3 d}{n},$$

(where k is a factor introduced to correct for an error in the value of the molecular weight of calcite used by Siegbahn, N_s is the effective Avogadro's number, a is the lattice-parameter in kX , n is the number of molecules in the unit cell of the ideal lattice and d is the density in gm./c.c.), with the value, M , of the molecular weight which is known from accurate

* Communicated by the Authors.

chemical data. If $D=(M_x-M)$ is negative and greater than the experimental error, then it can be concluded that the silver bromide contains vacancies which may be located either at grain or mosaic boundaries or within the lattice (Schottky disorder and/or aggregates of vacant lattice sites); the experiment does not, however, enable the presence of Frenkel disorder to be detected since interstitial ions and vacant lattice sites in *equal* concentrations do not affect the macroscopic soundness of a crystal.

The lattice-parameter of pure silver bromide was measured at 25° C. by means of the X-ray powder method, the results of two determinations carried out with a directly calibrated 19 cm. "Unicam" camera and with a 64 mm. Straumanis camera agreeing to within 1 part in 4×10^4 ($a=5.7633$ kX). The densities of large well-annealed polycrystalline specimens of silver bromide were determined by the displacement of doubly-distilled water using the method of Snoek (1950) and the results obtained with three such specimens agreed to within 1 part in 2×10^4 ($d=6.4799$ gm./c.c. at 18° C.). For the purpose of correcting the value of the lattice-parameter for temperature differences, the value of the thermal expansion coefficient given by Strelkow (1937) was used.

The averaged result of six determinations of D gave the result $(D/M)=+8.6 \times 10^{-5}$ but, due to experimental errors and uncertainties in certain fundamental constants, this may be in error to the extent of $\pm 1.6 \times 10^{-4}$. The maximum possible number of vacant lattice sites in pure silver bromide at room temperature represents, therefore, a fraction $(1.6-0.86) \times 10^{-4}=7.4 \times 10^{-5}$ of the total number of lattice sites in the ideal crystal. This is probably an over-estimate and, as allowance has to be made for the probably not inconsiderable number of vacancies associated with mosaic and grain boundaries, it is therefore unlikely that Schottky defects are present in sufficiently large numbers to contribute significantly either to ionic conductivity or to the mechanisms of latent image formation. The situation may well be different, however, in the sensitized silver bromide grains of photographic emulsions (Mitchell 1951).

REFERENCES.

- BERRY, C. R., 1951, *Phys. Rev.*, **82**, 422.
 MITCHELL, J. W., 1951, *Photographic Sensitivity* (London: Butterworths), p. 242.
 SNOEK, J. L., 1950, *Phil. Mag.*, [7], **41**, 1188.
 STRAUMANIS, M. E., 1949, *Acta Cryst.*, **2**, 82.
 STRELKOW, P. G., 1937, *Phys. Zeits. d. Sowjetunion*, **12**, 73.
 TUBANDT, C., and EGGERT, S., 1920, *Zeits. f. Anorg. Chemie*, **110**, 196.
 WAGNER, C., and BEYER, J., 1936, *Zeits. f. Phys. Chem. B*, **32**, 113.

A Note on the Trace of the Product of Dirac's Matrices.

By L. M. YANG,
The University, Edinburgh*.

[Received September 7, 1951.]

It is well known that the trace of the product of any odd number of Dirac's matrix γ_μ is zero. For a product of any even number of γ_μ 's, the trace can be written down simply in the following manner :

$$\chi\{\underbrace{\gamma_\mu\gamma_\nu\cdots\gamma_\eta\gamma_\zeta}_{2n \text{ factors}}\} = 4\Sigma \pm \delta_{n_\mu n_\nu} \cdots \delta_{n_\eta n_\zeta}, \quad \dots \quad (1)$$

where $\chi\{\dots\}$ denotes taking the trace of the matrices in the bracket, and the summation sign indicates summing over all possible pairings ($[(2n)!]/[n!(2!)^n]$ in number), preceded by a positive or negative sign according to whether an even or odd number of transpositions are required to bring $(n_\mu n_\nu) \dots (n_\eta n_\zeta)$ to $(\mu, \nu) \dots (\eta, \zeta)$, transposition within each pair not counted.

The proof of the relation consists in the repeated application of the relation $\gamma_\mu\gamma_\nu + \gamma_\nu\gamma_\mu = 2\delta_{\mu\nu}$

$$\begin{aligned} \chi\{\gamma_\mu\gamma_\nu\gamma_\lambda\cdots\gamma_\eta\gamma_\zeta\} &= 2\chi\{\gamma_\lambda\cdots\gamma_\eta\gamma_\zeta\}\delta_{\mu\nu} - \chi\{\gamma_\nu\gamma_\mu\gamma_\lambda\cdots\gamma_\eta\gamma_\zeta\} \\ &= 2[\chi\{\gamma_\lambda\cdots\gamma_\eta\gamma_\zeta\}\delta_{\mu\nu} - \chi\{\gamma_\nu\cdots\gamma_\eta\gamma_\zeta\}\delta_{\mu\lambda} + \dots \\ &\quad + \chi\{\gamma_\nu\gamma_\lambda\cdots\gamma_\eta\}\delta_{\mu\zeta}] - \chi\{\gamma_\nu\gamma_\lambda\cdots\gamma_\eta\gamma_\zeta\gamma_\mu\}. \end{aligned}$$

Since any circular permutation of the factors inside the bracket does not alter the value of the trace, one has therefore

$$\begin{aligned} \chi\{\gamma_\mu\gamma_\nu\gamma_\lambda\cdots\gamma_\eta\gamma_\zeta\} &= \chi\{\gamma_\lambda\cdots\gamma_\eta\gamma_\zeta\}\delta_{\mu\nu} - \chi\{\gamma_\nu\cdots\gamma_\eta\gamma_\zeta\}\delta_{\mu\lambda} \\ &\quad + \dots + \chi\{\gamma_\nu\gamma_\lambda\cdots\gamma_\eta\}\delta_{\mu\zeta}. \quad \dots \quad (2) \end{aligned}$$

The sign preceding each term on the right-hand side of (2) is positive or negative according as the number of transpositions required to bring the array of indices to the initial order on the left-hand side of (2). The process can obviously be repeated and the argument holds for each subsequent reduction until finally each term contains $n-1$ Kronecker δ 's multiplied by a factor of the typical form $\chi\{\gamma_\eta\gamma_\zeta\} = 4\delta_{\eta\zeta}$. Thus (1) is proved.

For practical purposes, the possible pairings and their appropriate signs can most easily be obtained by labelling the $2n$ indices $\mu, \nu, \lambda \dots \eta, \zeta$ on the circumference of a circle and connecting the pairs by lines drawn outside the circle. The sign is determined by counting the number of crossings of the lines in a given graph, positive for the even number of crossings and minus for odd ones.

* Communicated by Professor M. Born.

Three-Photon Decay of Positronium.

By J. M. RADCLIFFE,
University of Birmingham*.

[Received August 31, 1951.]

THE two spin states of positronium in its ground state have markedly different life-times against annihilation. Positronium in the singlet state has the shorter life-time ($\tau = 1.25 \times 10^{-10}$ sec.) since it can decay into two photons. Such a decay from the triplet state is forbidden (see e. g. Yang 1950), the simplest decay allowed being one into three photons. Three different results of three calculations of the life-time against the latter process have been published (Lifshits 1948, Ivanenko and Sokolov 1948, Ore and Powell 1949).

As direct experimental determination of the life-time is now possible, it was thought worthwhile to repeat the calculation. Ore and Powell's value for the mean life-time, 1.4×10^{-7} sec., was confirmed.

A covariant approach, using the methods developed recently by Feynman, simplified the work considerably, especially in the sum over the polarizations of the photons. The matrix element was evaluated using zero-velocity free-particle wave functions, normalized so that the density was that of the electron at the positron in the ground state of positronium. (The effect of binding is to multiply this matrix element by a factor $[1 + O(\alpha)]$, $\alpha = e^2/\hbar c$.) Also it has been shown that three-photon decay from the singlet state does not occur, at least in the limit of zero relative velocity of the two particles. This means that the matrix element which occurs can be conveniently summed over all spin states of the particles.

The writer is indebted to Dr. G. E. Brown for helpful advice, and to the Department of Scientific and Industrial Research for the award of a maintenance grant.

REFERENCES.

- IVANENKO, D., and SOKOLOV, A., 1948, *Doklady Akad. Nauk, S.S.S.R.*, **61**, 51.
LIFSHITS, E. M., 1948, *Doklady Akad. Nauk, S.S.S.R.*, **60**, 211. (See also *Science Abstracts*, 1949, 52A, abs. 1006.)
ORE, A., and POWELL, J. L., 1949, *Phys. Rev.*, **75**, 1696.
YANG, C. N., 1950, *Phys. Rev.*, **77**, 242.

* Communicated by Professor R. E. Peierls, F.R.S.

CXXXII. *Notices of New Books and Periodicals received*

Josiah Willard Gibbs. By L. P. WHEELER. (Yale University Press. London : Geoffrey Cumberlege.) [Pp. 264.] Price 25s.

'In the course of the thirty-two years of his teaching somewhat less than one hundred students attended Gibbs' courses.'" "Only a handful of these students still survive." "In the whole period of his teaching there were but a baker's dozen of dissertations which can be said to owe their inspiration to Gibbs."

Lynde Phelps Wheeler, from whose book the above quotations are taken, is one of the few survivors of the lucky dozen. Having received three separate requests to write a biography of Gibbs, he was eventually persuaded reluctantly to undertake the difficult task. Mathematicians, physicists, chemists and all interested in the history of science will be grateful to him for carrying out this labour of love as thoroughly, honestly and conscientiously as humanly possible.

The theme of this book is in the author's own words "Gibbs' scientific work was Gibbs". There is little else, that is live, to tell. In this biography, or any other biography of Gibbs, there is a tragedy for him who can read between the lines. Whereas Gibbs was honoured and recognized as at least an equal by such giants as Maxwell and Rayleigh, and at Yale he was undoubtedly well liked and respected by his immediate colleagues, when he died in 1903 his genius was inadequately appreciated in his own country. No proper care was paid at the time of his death to preserving his correspondence. Not until a score of years had passed was there any active desire to know more about the man and then it was too late. Wheeler is able to tell us something of Gibbs as a lecturer, but scarcely an anecdote of his private life.

An epitaph, similar to Wren's, would seem apposite to Gibbs: "Si momentum requiris, opera lege mea".

E. A. G.

An Introduction to the Theory of Control in Mechanical Engineering. By R. H. MACMILLAN. (Cambridge : University Press, 1951.)

Fundamentals of Automatic Control. By G. H. FARRINGTON. (Chapman and Hall, London, 1951.)

THE present applications of automatic control, or as it has recently been termed "feed-back engineering" are by far too numerous and wide-spread to mention. The study of the theory of control, which is now well formulated, is of major interest in almost all branches of engineering and of more than passing interest in the fields of economics and physiology, since the recent work of Wiener, Tustin, *et al.*, have shown the dependence of many natural phenomena upon the same laws and equations applicable to mechanical systems.

The foundations of the basic control theory can be traced to a classical paper by Clerk Maxwell, "On governors" (*Proc. Roy. Soc.*, 16, 270, 1868), but the modern development dates essentially from the application of the Nyquist method of harmonic response analysis, originally developed for use with electronic circuits. There is now a very considerable literature on the subject, but no British text-book dealing exhaustively with the subject has previously appeared. It is thus gratifying to note the almost simultaneous appearance of the above two books.

The former, by MacMillan, claims only to be an introduction to the subject, but correlates excellently the very diverse fields of application which respond to the same basic theory and to identical methods of analysis, *e.g.* regulation, position control servo-mechanisms, and process control. The early chapters are mainly descriptive, leading to the concept of transfer functions and system

equations. The human operator and non-linear effects are discussed only qualitatively, but a very full account is presented of the methods of transient and harmonic analysis by both analytical (Laplace) and graphical (Nyquist diagram) methods. An extensive bibliography is provided and the book should be intelligible to any engineer or physicist and of particular value to the student in this subject.

MacMillan uses throughout the nomenclature and notation of servo-mechanisms, and it is to be regretted that there are significant differences between this and the corresponding nomenclature of process control as used by Farringdon. This may confuse the general reader who is not aware of the independent lines of development and the consequently different nomenclature used in these allied fields.

Farringdon deals solely with the theory of process control: in general the treatment is basically similar to that of MacMillan, but greater emphasis is naturally placed on the types of control and discontinuities normally encountered in process applications. There is an excellent discussion of analogous transfer stages, and the system equations utilising proportional, integral and derivative controls. Plant characteristics, and the control discontinuities and non-linearities such as are found in process regulating units are also discussed. There is a very interesting analysis of typical pneumatic controlling instruments. The mathematical treatment is generally adequate and not beyond the capabilities of the graduate in physics or engineering.

This book will be of greatest interest to those workers concerned with process control—to the designer rather than the operator or user, but it will amply repay study by those interested in the other related fields, if only to correlate the extremely wide fields of application.

A. P.

ERRATA.

Total Cross-Sections of the Elements for 156 MeV. Neutrons, by A. E. TAYLOR, T. G. PICKAVANCE, J. M. CASSELS, and T. C. RANDLE, 1951, *Phil. Mag.*, **42**, 751.

The experimental results reported in this paper were discussed briefly in the light of the optical model of nuclei. The discussion involved the mean free paths of neutrons in nuclear matter, and these were incorrectly calculated because wrong values had been adopted for the proton-proton cross-section. The error arose from the fact that the total cross-section for proton-proton

scattering is $\int_0^\pi 2\pi\sigma(\theta) \sin \theta d\theta$, and not $\int_0^{2\pi} 2\pi\sigma(\theta) \sin \theta d\theta$, where $\sigma(\theta)$ is the differential cross-section as conventionally defined.

Correction of this point removes most of the difficulties which were thought to follow from the assumption that the neutron-neutron and proton-proton interactions are the same at high energies. Some discrepancy still remains, as the theoretical results of Jastrow (1951) have shown.

R. JASTROW, 1951, *Phys. Rev.*, **82**, 1951.

A Theoretical Investigation of the Compression of a Ductile Material between Smooth Flat Dies, by A. P. GREEN, 1951, *Phil. Mag.*, **42**, 917.

Equation below fig. 13 should read :

$$\left. \begin{array}{l} \bar{x}' = -v; \quad u' = \bar{y}; \\ \bar{y}' = u; \quad v' = -\bar{x}, \end{array} \right\} \text{1st kind.}$$

[The Editors do not hold themselves responsible for the views expressed by their correspondents.]

CXXXIII. *Microscopic Studies on Beryl Crystals.—II. Dislocations and the Growth of $\{10\bar{1}0\}$ Prism Faces.*

By L. J. GRIFFIN,
H. H. Wills Physical Laboratory, Bristol*.

[Received July 20, 1951.]

[Plates XLV.–LII.]

SUMMARY.

It is shown that the type of growth predicted by the dislocation theory of growth takes place on $\{10\bar{1}0\}$ faces of beryl. The growth layers, in general, produce a complex topography. The behaviour of layers at surface obstacles is discussed. Examples are given of the propagation of a dominant layer group past lines of dislocations, and inactive dislocation groups, and the mode of propagation by cross-linking is discussed. Typical examples of lineage boundaries and limited slip zones are shown; these features are observed as lines of dislocations. The dependence of growth rate of the layers on crystallographic orientation is considered. The types of layer structure observed on natural and synthetic crystals are compared. It is shown that the dislocation theory of growth can be applied to give such information as the supersaturation and temperature at which growth took place.

§1. GENERAL.

THE areas between the uni-molecular steps observed on prism faces of beryl (Griffin 1950, 1951) are in general plane. In some cases, however, the uni-molecular steps stop abruptly, and it is possible to describe a path from the low to the high side of a step without at any point crossing a discontinuity in height. The point of termination of the step must therefore mark a point of singularity of the surface corresponding to the point of emergence on the face of a dislocation with a screw component normal to the face. Any dislocation of this kind must necessarily mark one end of a step, which can only run off to the edge of the face or end at another screw dislocation.

§2. SPIRALS AND LOOPS.

A case is shown in fig. 1 (Pl. XLV.) of a step, attached to a single dislocation, which takes a spiral form. Such behaviour has been predicted on purely theoretical grounds for the case of the advance of a layer attached to a single dislocation when the rate of advance of the layer is dependent on the crystallographic orientation (Burton, Cabrera and

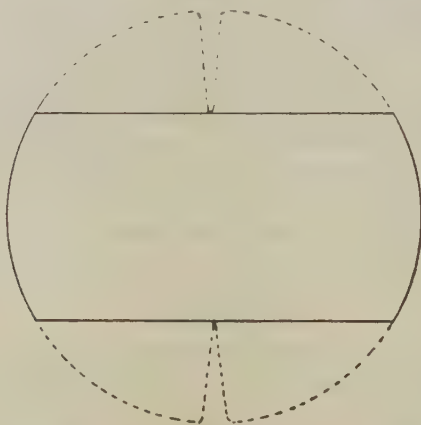
* Communicated by the Author.

Frank 1951). The agreement between theoretical prediction and observation is so close that there can be no doubt but that the layer in fig. 1 (Pl. XLV.) has been winding itself up during growth.

The case of an edge joining two dislocations of opposite hand is shown in fig. 2 (Pl. XLVI.), this edge lying in the centre of the figure. The behaviour predicted by Frank was that the inner unclosed loop would expand during growth so as to generate successive closed loops, typified by the outer loop of fig. 2 (Pl. XLVI.). (The triangular area cutting into the closed loop of fig. 2 (Pl. XLVI.), probably consists of an overgrowth of foreign crystalline material.)

The dependence of growth rate upon crystallographic orientation of a layer can be represented by means of a two-dimensional polar diagram (Frank 1950). A close packed direction (Burton and Cabrera 1949) corresponds to a minimum growth rate and will manifest itself as an

Fig. 3.



almost straight edge. The dislocation pair in fig. 2 (Pl. XLVI.) has been operating unhampered by the presence of other dislocations so that this case is almost ideal for consideration of growth rates. In this case the longitudinal edges must correspond to a close-packed direction. (These almost straight longitudinal edges are parallel to the *c*-axis and are most useful in defining the orientation of any area.)

The two transverse edges of the outer closed loop are very nearly arcs of the same circle, so that the rate of growth must be independent of orientation for the range covered by these edges ($\pm 30^\circ$). It is therefore possible to construct a polar diagram as shown in fig. 3. This diagram coincides with the "razor-blade" outline over the circular arcs at the ends and at the mid points of the longitudinal edges. The dotted sections of the diagram are uncertain, and it is only possible to say, from the present information, that the polar diagram must lie outside these sections.

When two dislocations of the same hand are closer together than a certain distance (equal to 4π times the size of the critical nucleus) the theory predicts that the dislocations will work together cooperatively and produce steps which form two arms of a spiral. Examples of this behaviour have also been observed.

The examples so far quoted are the ideally simple cases and are comparatively seldom observed. More usually a complex layer system is seen on any area of a face, and we shall now consider some characteristic examples.

§3. BEHAVIOUR AT OBSTACLES.

A typical example of the behaviour of a layer system at a surface obstacle is shown in fig. 4 (Pl. XLV.). This layer system is of considerable extent and a small part of it has met with an obstacle to its steady growth, this obstacle being probably a crystal inclusion. The layers are forced to divide into two parts by the obstacle and as they advance towards the right of the figure the obstacle decreases in extent. It is therefore necessary for the layers to "fill in" by inward growth of the straight edges. Due to the fact that growth is more rapid parallel to the *c*-axis than perpendicular to it, the two sections of the system only unite at some distance beyond the obstacle. The points to be noted are:—

(a) The rapid elimination of the re-entrant angle at the junction of the two sections. As the re-entrant is parallel to the direction of rapid growth this would be expected on almost any theory of growth.

(b) The relative rate of growth parallel and perpendicular to the *c*-axis. The ratios of these rates are dependent upon the local conditions, being 1.7 and 2.1 for the two parts of this system, and in other similar cases 2.9 and 2.76, 2.36 and 2.37, 2.1 and 1.9.

(c) Each edge is a contour, with a vertical interval of 7.9 Å. The obstacle thus results in a triangular V-shaped valley with a maximum depth of 38 molecules (300 Å).

An obstacle of this kind appears to result in an increased curvature of the edges close to it, but as the effect on the two sections of the system is asymmetrical it is difficult to determine whether the effect is regular.

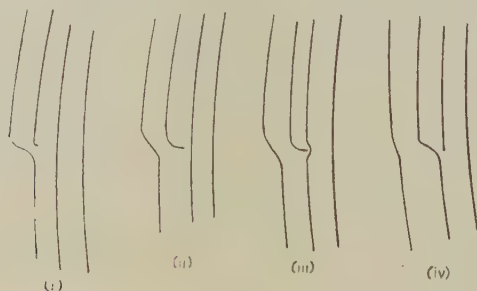
This difficulty can be overcome in the case of fig. 5 (Pl. XLVI.) in which the layers advancing from the right are split into three sections by a succession of crystal inclusions, which again act as obstacles. The central system formed in this way is affected equally on both sides and it can be immediately seen that it behaves as if a "virtual source" was present.

The approximate position of the virtual source can be found by producing back lines drawn through the points of junction of the curved and straight edges; it lies on the upper edge of the narrow neck between the two obstacles. The ratio of the radius of curvature of the transverse edges of this small system to their distance from this "source" is constant and equal to unity. Moreover, this relation is still maintained, after junction with the lower section, for those parts of the first four layers of

the joint system which originated from the central section. The system expanding from the "virtual source" thus behaves in precisely the same way as the closed loop in fig. 2 (Pl. XLVI.).

The behaviour of layer systems at obstacles provides valuable confirmatory evidence that the observed steps are normally uni-molecular. Thus in fig. 5 (Pl. XLVI.) the central and lower sections first combine again to form a single system. Counting from the last edge before division commences on the right, there are 37 edges in both the lower and central sections before a junction takes place. Similarly, considering the junction beyond the third obstacle there are 57 edges in both the upper and lower sections between the first division of the edge and the first joint edge. Similarly in fig. 4 (Pl. XLV.) in both the upper and lower systems there are 70 edges between the first division of the incident layer and the first joint layer. Such behaviour would be very difficult to comprehend for steps of more than one molecule high, for one would expect the steps in such circumstances either to split into smaller units or to combine to form multiple steps.

Fig. 6.



§4. PROPAGATION PAST INACTIVE DISLOCATIONS.

The theory predicted that certain dislocations and dislocation groups on a face could be more active than others, resulting in those active dislocations "dominating" less active dislocations (*i.e.* the layers emanating from active dislocations propagate past "dominated" groups or single dislocations with only a slight delay and a slight change in outline). The mode of propagation in such cases and the type of cross-linking which occurs is shown in fig. 6. The layers are advancing from right to left and in (i) one layer has just passed the dislocation. In (ii) the layer originating from the inactive dislocation has grown in the normal way, while the layer advancing from the right is quite close to it. The kink in the layer on the left is being eliminated as the layer extends. In (iii) the incident layer is being held up at the dislocation, as this layer is now close to the region of deformed lattice around the dislocation, and an effective small repulsion exists between the dislocation and the

incident layer. By stage (iv) sufficient molecules have built on to the requisite section of the incident layer, probably because of a statistical fluctuation, to enable the layer to link across with the layer running from the dislocation. The dislocation is consequently attached to the shorter edge, which originally formed part of the incident layer. Meanwhile the kink in the left-hand layer has been almost eliminated. This type of behaviour can be repeated indefinitely.

Fig. 7 (Pl. XLVII.) and fig. 8 (Pl. XLVII.) show two examples of this kind of behaviour from the large number observed. In fig. 7 (Pl. XLVII.) a dominant layer system is advancing from the left and meets with a line of dislocations which are all of the same hand and all the stages of cross linking drawn in fig. 6 can be seen.

Fig. 8 (Pl. XLVII.) illustrates more clearly the kinking of the layers after the dislocations have been left behind, the dominant layer system moving from right to left in this case. In both figures it can be seen that the layers pass on with only very slightly modified outline, and, that some five layers after the dislocations are encountered, the layer outlines show no trace of the action of the dislocation groups.

Fig. 8 (Pl. XLVII.) is also of interest because of the evidence it provides of varying activities of layer systems, a subject which will be dealt with fully in a later paper. On the left of this figure there is a sudden considerable increase in layer spacing. Now layer spacing can most simply be equated against supersaturation, but in a case like this it is not likely that the supersaturation varied over this area. It would rather appear that the widely spaced layers on the left were produced by a dislocation group of low activity, this low degree of activity being due to a low supersaturation or other causes. At a later date in the history of the growth of this face another system has become active (possibly because of an increase in supersaturation, or the creation of new dislocations), producing more closely spaced layers which have gradually obliterated the old layer system, *i. e.* the new system has become the dominant one in this area. Thus the area in fig. 8 (Pl. XLVII.) shows the farthest point of advance of the new system before growth ceased.

§5. LINEAGE STRUCTURES.

It is generally accepted that most crystals consist of a lineage structure, *i. e.* of crystals blocks, sometimes macroscopic, which are slightly disoriented with respect to one another. The atomic structure of the boundaries between such blocks can be explained most satisfactorily in terms of dislocation systems lying in the boundaries, for dislocations necessarily produce a rotation of the lattice at distances far from the dislocation. Such a picture has proved valuable in investigations on grain boundaries in metals, but the evidence in favour of the presence of dislocations which results from such work, is necessarily indirect. On faces of beryl crystals, however, the structure of such boundaries can be observed directly. An example of a well marked lineage boundary

is shown in fig. 9 (Pl. XLVIII.). There are some 85 dislocations in the boundary, the left-hand part of which is partially obscured by foreign material, all the dislocations being of the same hand. The distance between dislocations, measured in atomic spacings, is equal to the angle of rotation between the two crystal blocks. In this case the angle of rotation across the boundary is approximately 2.8 minutes of arc.

It is certain that these features consist of a line of dislocations. The layers would not curve round in this way if this feature was merely a surface step, for a considerable body of evidence shows that in all such cases the layer configuration would be quite different. For example, the behaviour at obstacles shown in fig. 4 (Pl. XLV.) and fig. 5 (Pl. XLVI.) can be contrasted with fig. 9 (Pl. XLVI.). Moreover, the layers running from lineage boundaries often terminate on neighbouring dislocations.

The step marking this boundary is very obvious under narrow pencil illumination and this is understandable for, because of the dislocation structure, the higher end of the boundary must project 670 Å. above the central region of fig. 9 (Pl. XLVIII.).

There are many tilt boundaries which are much smaller than the above example. One such case is shown in fig. 10 (Pl. XLV.). From each dislocation of the lower line a spiral edge starts, the straight sections being so closely packed that they are barely resolved. An edge also starts from each dislocation of the upper line, which again is marked as a series of dots, the two systems combining to form a large spiral. (The area blocking out part of the spiral is probably composed of foreign material.) The second, lower, set of straight edges forming the spiral is not parallel to the original set, a very unusual feature. These edges end in an irregular boundary which has been formed by the main growth region. From the position and behaviour of the series of edges above the dislocation system it appears probable that these may originally have formed part of the spiral. The angle of rotation at the two parallel boundaries is approximately 8 seconds of arc in each case.

A very heavily lineaged area is shown in fig. 11 (Pl. XLVIII.). Almost every layer in this figure runs from a lineage boundary, these boundaries lying close together in the lower part of the figure. (The obvious black feature which runs diagonally across the figure is a crack.) The layers are so closely spaced that the longitudinal edges are not resolved. On one side of this lineaged area there are some 140 dislocations of one hand, with some 180 dislocations of opposite hand on the other side. The result of these two groups being almost equal is that the difference in orientation of the lattice on either side of the area will be small, and will in fact amount only to approximately 20 seconds of arc. The actual difference in orientation produced by either group is much greater, being about 2.4 minutes of arc.

The position and nature of these lineages make it possible that they originated in the form of limited slip-zones, a type of feature discussed immediately below. The constituent halves of these zones would grow

apart if the dislocation lines were set at a slight angle to each other, so that each half of a zone could eventually act independently as a lineage boundary.

It will be noticed that the examples of lineage boundaries which have been shown are all parallel to the *c*-axis of the crystal. This appears to be true for the majority of such features which have been observed.

§6. LIMITED SLIP-ZONES.

Another type of dislocation distribution very often observed is that corresponding to a limited slip-zone. Such features will be composed of a line of dislocations which is divided about the centre into two equal groups of opposite hand, the line lying along the trace of the appropriate glide plane in the face. A feature of this kind which lies parallel to the *c*-axis is shown in fig. 12 (Pl. XLIX.). This is unusually large and consists of two groups of approximately 90 dislocations each. (Evidence supporting the interpretation of these features as limited slip-zones will be given in a later paper. We are only concerned here with these slip-zones as typical dislocation groups.)

An example of a limited slip-zone perpendicular to the *c*-axis is shown in fig. 13 (Pl. XLIX.). Isolated slip-zones of this orientation are much less common than cases parallel to the *c*-axis. However, a not uncommon feature consists of a number of contiguous small slip-zones which form a long, closely packed line of dislocations perpendicular to the *c*-axis. In fig. 13 (Pl. XLIX.) the dislocation group has been sufficiently active to cause a local variation in the shape of the dominant layer system which is advancing from the left.

§7. PROPAGATION OF LAYERS PAST A DISLOCATION GROUP.

The case of the propagation of layers past dominated dislocations of the same hand has already been discussed. The more general case consists of the propagation of a dominant layer system through an inactive group of dislocations, and there are some significant differences in behaviour in this case.

In fig. 14 (Pl. L.) the dominant system is advancing from the right and meets a group of dislocations which are only sufficiently active to cause local variations in the outline of the layers. Almost all the steps in the bottom part of this figure run between pairs of dislocations and several of the layers tend toward the characteristic razor-blade shape.

Several steps in this group have a reversed S-shape. Such behaviour is not contrary to the theory but, as we shall see, is merely due to the dominant characteristics of the incident system. For example, a very acute elbow runs from a single dislocation in the upper part of the figure. It is obvious that this edge, which originally curved downwards, must form a re-entrant of this type on junction with the incident layers. Moreover, this re-entrant cannot be rapidly eliminated as it lies in the direction corresponding to a minimum growth rate.

In order to illustrate some of the points which arise a part of the dislocation group is isolated and drawn in full line in fig. 15 (i). It is necessary to consider a limited area only in order to simplify the actual

Fig. 15 (i).

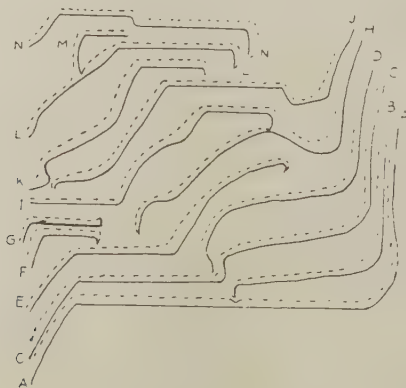


Fig. 15 (ii).

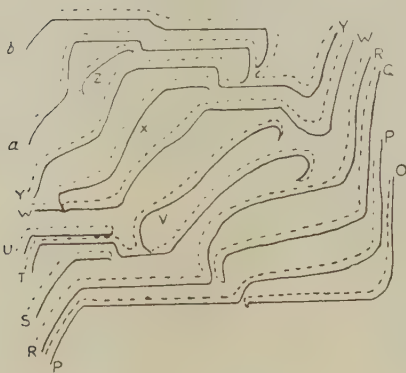
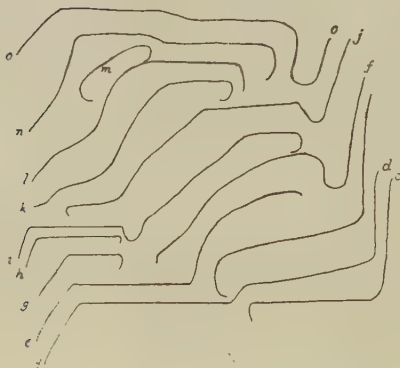


Fig. 15 (iii).



behaviour. Thus, the curved edges running down on the left of fig. 14 (Pl. L.) terminate at dislocations which are all of one hand. These terminations have not been shown in order to keep the diagrams down to a reasonable size, and also because only a simple type of cross linking takes place in this area. Hence, over the area shown in fig. 15, these curved edges can be considered to propagate regularly without any considerable deviation from the true conditions.

In these diagrams the propagation of the layers has not been drawn exactly to scale but only approximately so. This means that deviations from the order of events shown in these diagrams might have occurred had the crystal continued to grow, but the aim is to show the general way in which propagation by cross-linking takes place.

In (i), (ii) and (iii) five successive positions of the layers are shown. The advance of the layers from their original position in any of these diagrams is shown by a dotted line, and the position of layer I, for example, after an advance will be referred to as I'.

Let us consider the position of the layers in fig. 15 (i) after a slight advance has taken place. A' is held up at the parent dislocation of B', and cross-linking will soon take place. Similarly, C' is now very close to the dislocation of D'. E' and F' show no important change (G' is growing normally, but G was initially of an anomalous shape due to causes to be discussed in a later paper). The advance of H has caused cross-linking to take place with I, so that the joint layer I'H' and a new double dislocation loop are formed. J' and K' show little change, but L and M have cross-linked to form the layer L'M' and a double dislocation loop L' has been formed. A further stage of advance of these layers is shown in full line in (ii). The lowest four layers have now cross-linked to give O and P and Q and R, R continuing with a considerable kink because of the cross-linking. E' has cross-linked with F' to give S and the layer T which is held up at the lower dislocation of the loop V. J' has linked with K' to form the double dislocation loop X, and cross-linking of this loop with W is imminent. No marked change has taken place in the other layers.

Another advance immediately causes T to cross-link with the double loop V, so that a dislocation is now attached to the right-hand section of T, and the layer T'U' carries on with an obvious re-entrant. W and X have linked so that the two dislocations of the loop X now function separately. Y and a have linked so that the left-hand part of Y' is attached to a dislocation. Meanwhile the joint layer a'Y' almost immediately links with b' so that a' is again attached to a dislocation, while the joint layer b'Y' passes on with a large re-entrant due to the rapid cross-linkings. The edge b'Y' being nowhere attached to a dislocation (in this figure at least), is thus the first layer to pass through this group.

The position after a final advance is shown in fig. 15 (iii). O', P', Q' have advanced undisturbed to the positions c, d and e. (In fact, of course, another layer would by now have advanced from below to cross-link

with *c*.) R' has linked with the double loop T', leaving the two dislocations attached to the layers *e* and *f*. T' has linked with U' to give the layers L and *i*. Layer L is held up by one of the dislocations of the loop *m* and linking is about to take place. Otherwise there is no considerable change.

This group of dislocations which has been studied is both small and comparatively widely spaced. In the case of many of the larger closely packed groups it is obvious that the general outline of the layers will be complicated and varying very rapidly, so that any one layer in its passage through the group must very soon lose any semblance of composition from its original layer and will undergo a great many changes in outline.

It can be seen from fig. 15 (i) and (iii) that the original and final positions of the layers are similar. This would be more marked if the original position of the layers did not show certain slight anomalies explicable in terms other than growth. A certain periodicity is bound to occur if the conditions remain uniform, and if the incident edges advance in a regular way, a cycle of quite short period should result. Normally the conditions may fluctuate sufficiently to prevent the establishment of such a cycle, although a semi-periodic behaviour should result.

Fig. 15 shows that when dislocations, whatever their hand, are spaced with one or more layers between them, only a considerable kinking of the layer edges is likely to result. However, when successive layers run from dislocations of opposite hand, a succession of double-dislocation loops and single dislocation layers must be formed very rapidly. If a considerable number of such dislocations of opposite hand lie together, then a complicated pattern of looping and linking must ensue as any one layer progresses through the system.

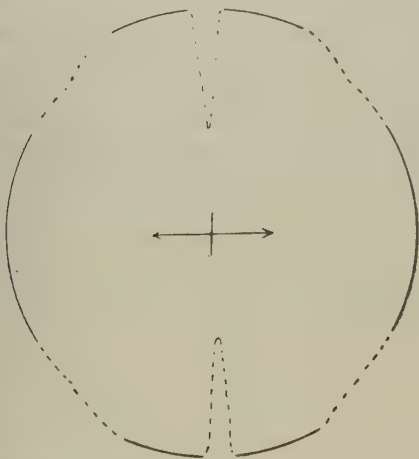
§8. ADDITIONAL EVIDENCE OF THE DEPENDENCE OF GROWTH RATE ON ORIENTATION.

In fig. 16 (Pl. L.) a dominant system is advancing from the left when it meets a barrier formed by a closely spaced line of dislocations. The main system is forced to spread downwards from the upper limit of this barrier, until it meets the independent layer system running from the dislocations. At the junction between the two systems a slightly curving edge results which runs at a slight angle to the *c*-axis and continually encroaches on the curved edges of the upper system. This encroachment continues until the slightly curved edges spread across to make a junction with the straight longitudinal edges (see fig. 17 (Pl. LI.)) and so completely eliminate the curved edges. At this point the edges are slightly concave in curvature and make an angle of approximately 25° with the *c*-axis.

This junction continues for some 5 mms. along the face (*i. e.* some 1,000 layers) and the edges gradually become straighter and progressively less inclined to the *c*-axis. A locally dominant system then altered the conditions, and these edges were replaced by the normal type of curved edges. The general conclusion to be drawn from this behaviour appears to be that edges inclined at small angles to the *c*-axis can grow more

rapidly than the normal curved edges. This conclusion is supported by observations of other similar events which gave a total range of inclinations of these rapidly growing edges of 4° – 25° . It is therefore possible to make additions to the polar diagram shown in fig. 3 to produce the more complete diagram, fig. 18. The dotted lines still indicate the uncertain sections. It should be noted that these polar diagrams are only strictly applicable to other beryl crystals if they have grown in identical conditions. Considerable variations are observed in the proportions of these diagrams, but the shape is usually of the same kind. However, examples have been observed when even the shape is quite different.

Fig. 18.



§9. SYNTHETIC EMERALD.

In addition to naturally occurring beryl crystals originating from various sources, two synthetic emeralds were examined. These crystals had been grown by Nacken by a hydrothermal process (Van Praagh 1948), the details of which have not been revealed. The faces of both crystals were very rough on a microscopic scale and a regular structure could only be detected on some of the faces. In all cases the surfaces were too irregular to allow very fine structure to be observed.

All the faces suitable for observation showed a number of very similar hills standing out above the surface. A typical feature of this kind as seen under oblique illumination is shown in fig. 19 (Pl. LI.). All the steps appear to be multi-molecular and the hill builds up to a definite point, the inference being that one central group of dislocations has been responsible for the growth of the hill.

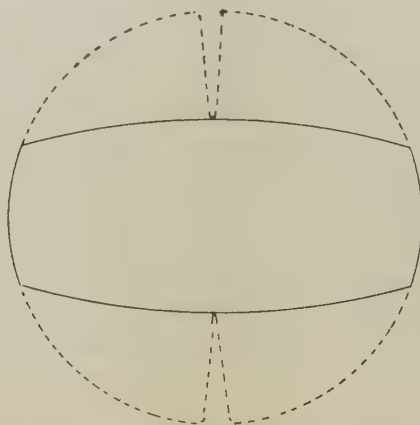
This type of behaviour can be contrasted with the typical plateaus seen on natural crystals, as shown for example, in figs. 20 and 21 (Pl. LII.). These plateaus stand some wavelengths above the general surface level,

but they still retain the typical shape characteristic of a simple uni-molecular layer as shown in fig. 2 (Pl. XLVI.). The main plateaus of these figures are very flat, very few uni-molecular steps being visible. The single spiral shown in fig. 1 (Pl. XLV.) lies on the plateau of fig. 20 (Pl. L.) and its position can be identified by the gross black feature. This appeared to be one of the very few dislocations active on this plateau.

The two other main points of difference between the structures on natural and synthetic crystals are :—

(i.) The differing shapes of the layers. The longitudinal edges on the synthetic crystal have a considerable curvature; the significance of this point is discussed below.

Fig. 22.



(ii.) The presence of a rough structure on the transverse gradients of the natural crystals. This rough structure actually consists of close-packed "rods"—features which will be fully discussed in a later paper. It need only be said that they invariably occur on steep gradients parallel to the *c*-axis on the natural crystals studied. No trace of such features was observed on the synthetic crystals.

It is possible to construct a polar diagram of growth rate for these synthetic crystals. The transverse edges are again almost arcs of the same circle, so that the growth rate must be independent of orientation over a range of $\pm 20^\circ$. The polar diagram is shown in fig. 22 where the dotted lines again indicate uncertain areas.

§10. APPLICATION OF DISLOCATION THEORY OF GROWTH.

The theory predicts that for directions not far removed from a close-packed direction an edge will have a radius of curvature $(1+2B)$ times its distance from the point of origin, where $B = \frac{1}{2} \exp(\phi/kT)$ and ϕ is a neighbour-neighbour interaction energy. The radius of curvature of the almost straight edges of the outer loop of fig. 2 (Pl. XLVI.) is some 120 times the distance from the centre. Therefore ϕ/kT is about 6.2.

The average values of these constants for the two synthetic emeralds examined were :—

	B	ϕ/kT
Specimen 1	3.83	3.42
Specimen 2	3.71	3.39

These values are very similar and it appears probable that both specimens have grown in almost identical conditions. If one assumes that both the natural and synthetic crystals have grown from similar media then the differing values of ϕ/kT can be ascribed to variations in T , and the natural crystal must have grown at an absolute temperature of a little more than half that of the synthetic crystals. The value of Nacken's operating temperature is not known, but it was probably close to the critical temperature of water. The natural crystal must therefore have grown at a temperature of approximately 80°C . This may appear surprisingly low, but it is of interest to note that the temperature of growth of a beryl crystal found in a pegmatite vein was 175°C ., as determined by a liquid inclusion method (Ingersoll 1947). Moreover, the temperature of 80°C . can probably be taken as the lower limit, for the values of B were determined from measurements on multi-molecular steps, and such steps usually give results which are inaccurate unless one concludes that the values of B are greater than would hold for uni-molecular steps.

It is possible to estimate the size of the critical nucleus (ρ_c) by measurement of the distance between two dislocations of opposite hand which are linked by an edge which has been expanding outwards. The distance between the dislocations must be equal to, or greater than, $4\pi\rho_c$ where ρ_c is defined by $\rho_c = a\phi/kT\sigma$, where a is the inter-atomic spacing and σ is the supersaturation. Knowing the value of ϕ/kT we can deduce from fig. 2 (Pl. XLVI.) that the supersaturation in this area was about 0.5 per cent.

The accuracy with which the supersaturation in any area can be determined will always be dependent on the presence of two dislocations with a spacing of just $4\pi\rho_c$. This means that the closest spacing should be taken as giving the most accurate value, but it is sometimes difficult to be sure whether a given edge has been expanding. As an example there are tabulated a number of observations on another face of the crystal on which fig. 2 (Pl. XLVI.) was taken. In this case an asterisk denotes loops which may possibly not have been expanding.

From this table it would seem that the loops corresponding to values of 0.29 and 0.35 microns had not been expanding. Neglecting these two values and the rather high final value, the average value of ρ_c over this region of the face was probably quite close to 0.49 microns. Taking $\phi/kT = 6.2$ this is equivalent to an average supersaturation of about 1 per cent.

Area	ρ_c (microns)
Active group	0.5 0.35*
Groups of fig. 13.....	0.46 0.41*
Centre of very large dominant group	0.55 0.29*
—	0.75

§ 11. CONCLUSIONS.

The observations show that the dislocation theory of growth is not only correct in principle, but also in detail. This is the more surprising when it is recalled that this theory was derived primarily for homopolar crystals, formed from spherical or cubic molecules, growing from the vapour phase. In this case beryl is an ionic crystal with complex molecules and growth has taken place from solution.

The dislocation theory of growth provides, for the first time, a quantitative account of crystal growth, and it is possible to learn a good deal about the conditions under which any crystal has grown from simple measurements on the faces. This theory also marks a considerable advance in the unification of growth phenomena and modern theories of the solid state, two fields which had previously been largely divorced.

Lineage and transition surfaces have been explained for some time in terms of dislocation theory as arrays and grids of dislocations. The observations provide direct visual evidence that this explanation is correct.

ACKNOWLEDGMENTS.

I am indebted to Dr. F. C. Frank for much valuable discussion; to the Mineralogy Department, British Museum, for the loan of specimens; to Dr. G. Van Praagh for the loan of synthetic beryl crystals; and to the Department of Scientific and Industrial Research for grants which have made this work possible.

REFERENCES.

- BURTON, W. K., and CABRERA, N., 1949, Discussions, *Farad. Soc.*, **5**, 33.
 BURTON, W. K., CABRERA, N., and FRANK, F. C., 1951, *Phil. Trans. Roy. Soc.*, **243**, 299.
 FRANK, F. C., 1950, *Phil. Mag.*, **41**, 200.
 GRIFFIN, L. J., 1950, *Phil. Mag.*, **41**, 196.
 GRIFFIN, L. J., 1951, *Ibid.*, **42**, 775.
 INGERSOLL, E., 1947, *Am. Min.*, **32**, 375.
 VAN PRAAGH, G., 1948, Research, **1**, 458.

EXPLANATION OF THE PLATES.

PLATE XLV.

Fig. 1.

The dislocation lies at the origin of the spiral. The kink in the right-hand edge of the spiral has possibly been caused by impurity obstructing steady growth.

Fig. 10.

The black area at the top is a hole in the crystal surface. The two boundaries lie a little down from this. This is a case where resolution has to be sacrificed to visibility.

PLATE XLVI.

Fig. 2.

The inner step-line runs between two dislocations of opposite hand, the points of emergence of these dislocations being imaged as obvious black dots.

PLATE XLVII.

Fig. 7.

The line of inactive dislocations lies close to the centre of the figure, and its presence is made noticeable by the kinking of the edges close to it. The dislocations are shown as black dots. In the top part of the figure the layer edges are running parallel to the *c*-axis, but are too closely spaced to be resolved.

Fig. 8.

The dark band at the bottom marks the edge of the face. The line of dislocations starts near the centre of the edge and from there runs upward and slightly to the right, almost to the top.

PLATE XLVIII.

Fig. 9.

The lineage boundary runs from left to right just below the centre, its left-hand extremity being partially obscured. To the left of the mid-point of the boundary the step-lines become much more closely spaced and less clearly visible, while the corresponding longitudinal sections are too closely packed to be resolved.

Fig. 11.

The position of the different boundaries can be most easily found by following the downward path of the curved edges. There are at least six boundaries, all situated in the lower central part of this area.

PLATE XLIX.

Fig. 12.

The slip-zone is the line running horizontally from which all the curved edges commence.

Fig. 13.

The dislocations are quite widely spaced along this slip-zone which runs vertically upwards to the left of centre. Most of the layers to the right of this line run between pairs of dislocations of opposite hand.

PLATE L.**Fig. 14.**

The black band at the bottom marks the edge of the face. The inactive group lies centrally in the lower two-thirds of this area.

Fig. 16.

The closely spaced line of dislocations runs vertically upwards on the left of this area; individual dislocations cannot be distinguished at this magnification. The edges at an angle to the *c*-axis form at the junction of the two systems a little to the left and down from the centre of the figure.

PLATE LI.**Fig. 17.**

The orientation is, as usual, given by straight edges which are barely resolved in the upper third of this area. The system which is being eliminated lies on the left and the rapidly growing layers are seen on the right.

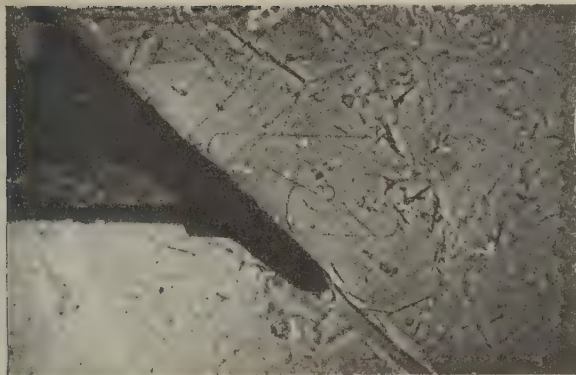


Fig. 1.

×280

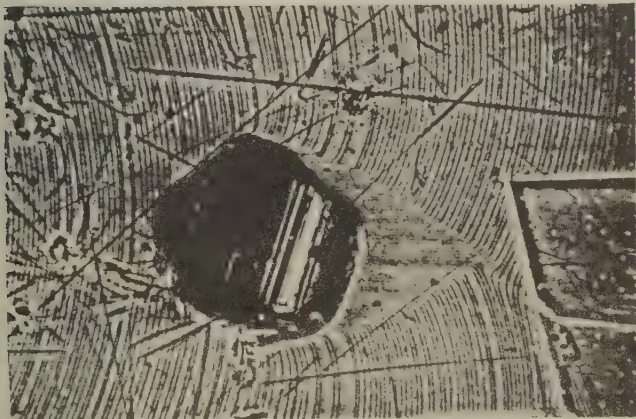


Fig. 4.

×400



Fig. 10.

×400

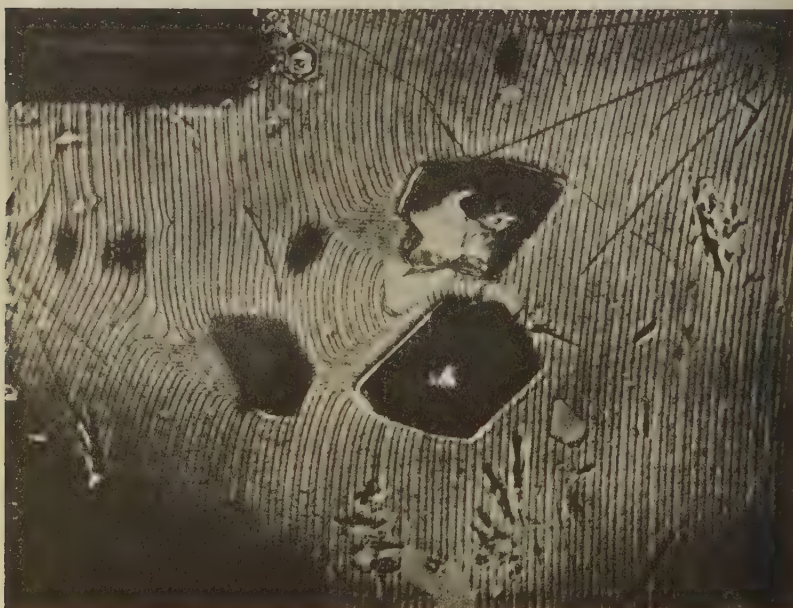
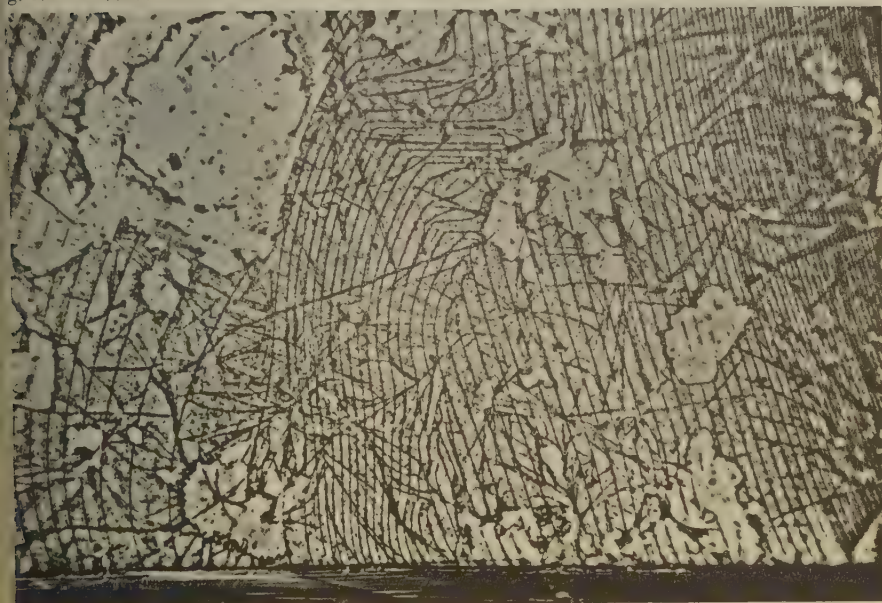
Fig. 2. $\times 1050$ Fig. 5. $\times 650$ 



Fig. 7. $\times 650$

g. 8. $\times 400$



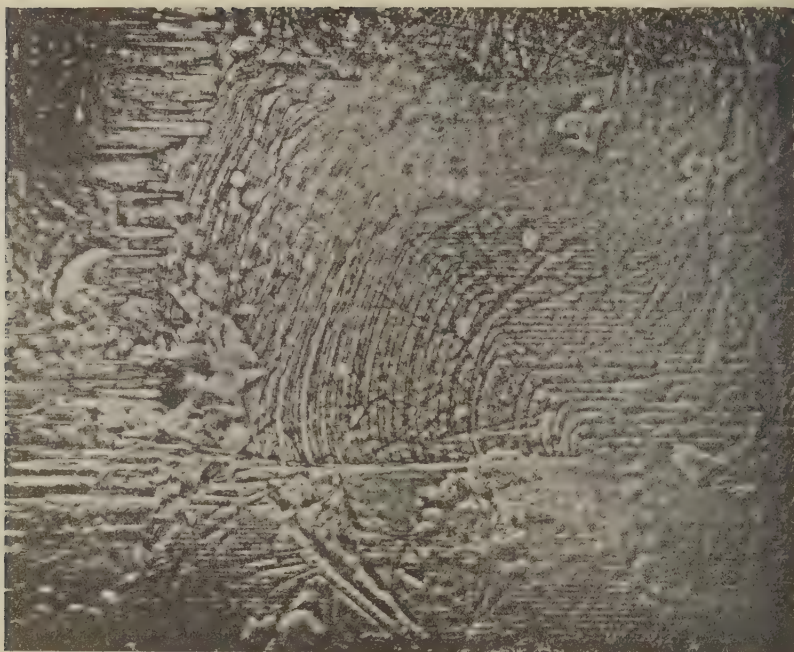


Fig. 11. $\times 250$

Fig. 9. $\times 650$



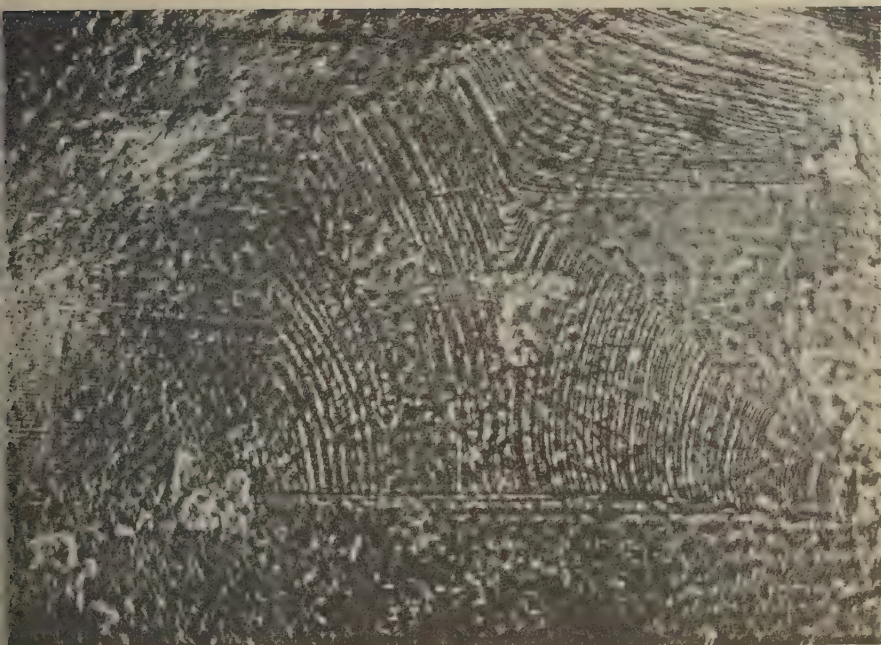


Fig. 12. $\times 650$

Fig. 13. $\times 650$

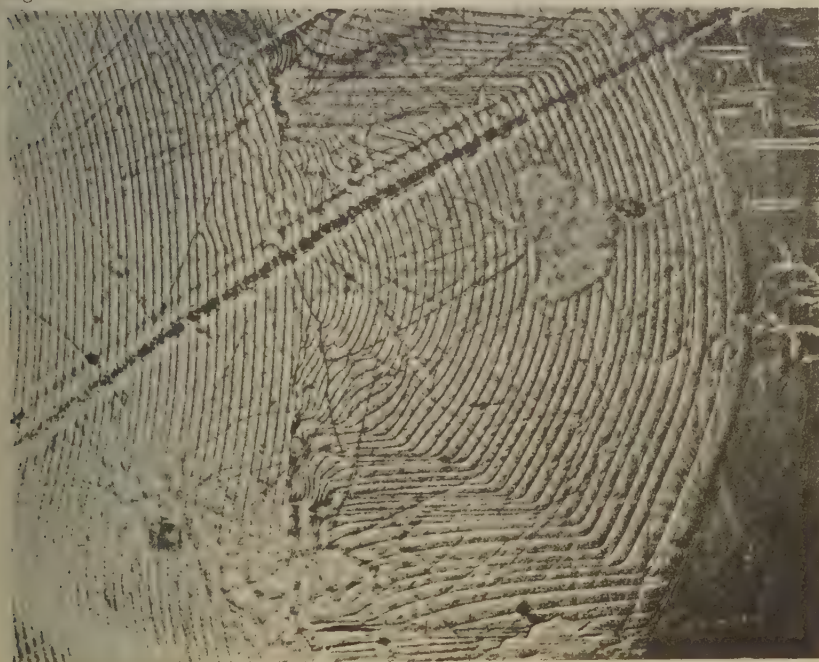




Fig. 14. $\times 312$

Fig. 16. $\times 250$

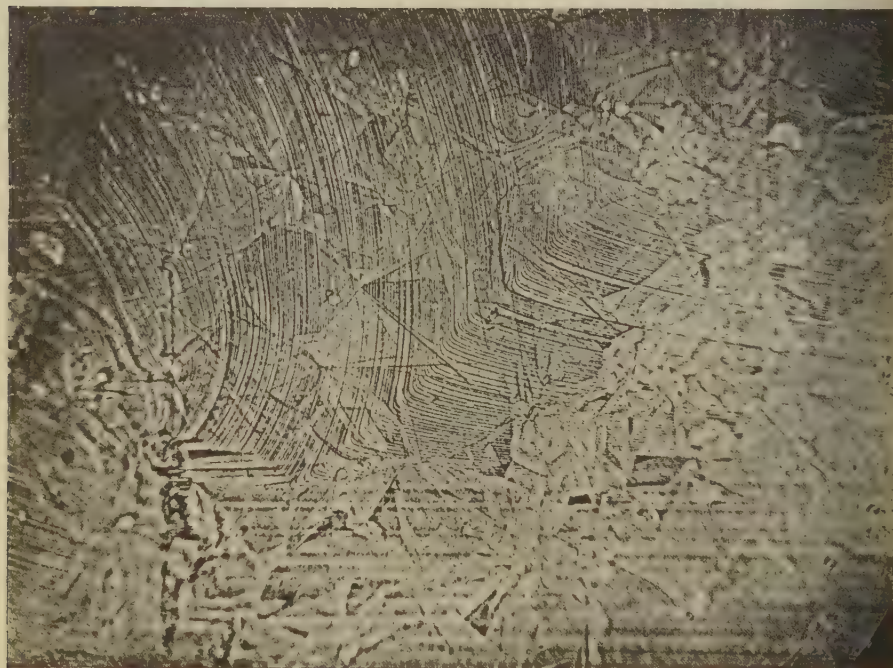
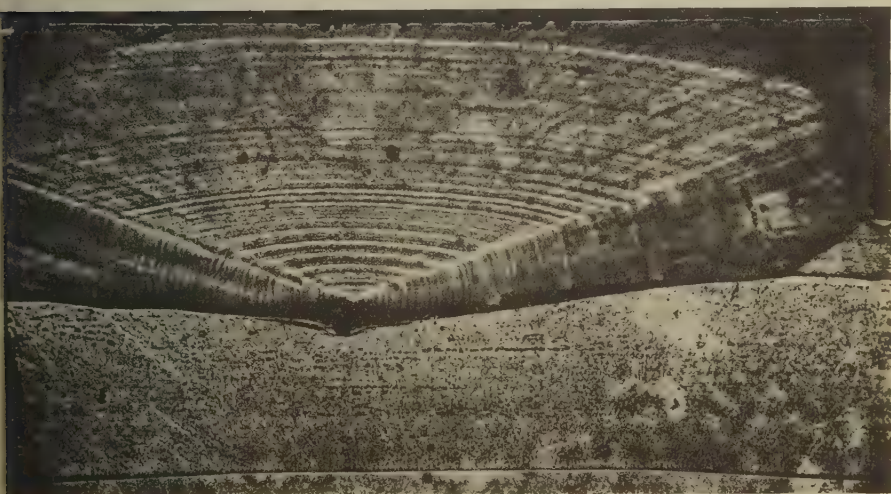


Fig. 17.



$\times 250$

Fig. 19.



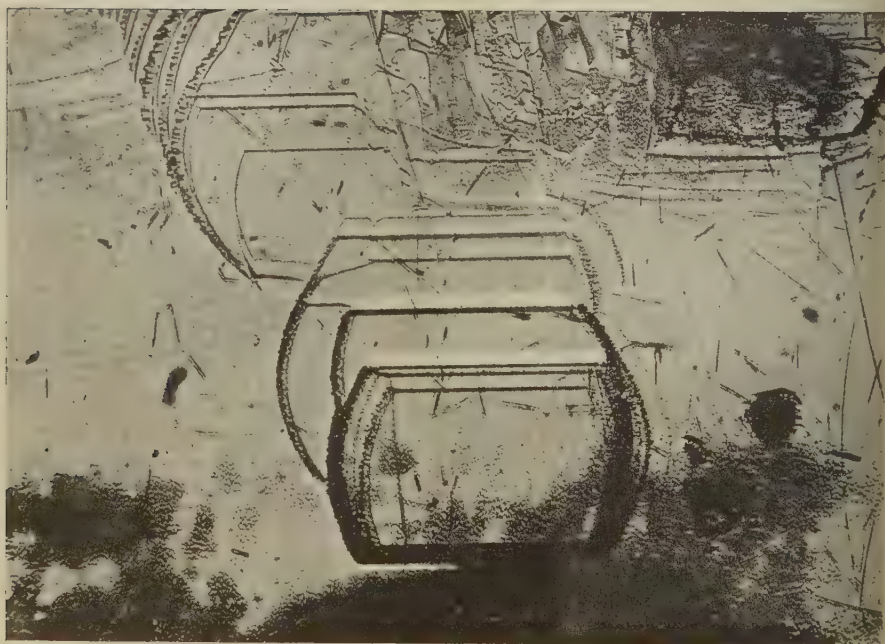
$\times 120$

Fig. 20.



×44

Fig. 21.



×36

CXXXIV. *The Photo-electric Disintegration of Three- and Four-Particle Nuclei.*

By J. C. GUNN and J. IRVING,

Department of Natural Philosophy, University of Glasgow*.

[Received June 12, 1951.]

ABSTRACT.

The two-particle and complete photo-electric disintegration cross-sections for three- and four-particle nuclei are calculated, using Gaussian and new exponential wave-functions. By suitable adjustment of a scale constant photo-disintegration, curves can be found with the maximum cross-section at any chosen energy above the threshold. For a given position of the maximum the Gaussian wave functions require a bigger nucleus than the exponential, and then give a larger maximum cross-section. The theoretical predictions are concerned with the small amount of experimental data available, mainly from the inverse processes of p-D and p-T capture. The exponential wave functions appear to fit more reasonably with this evidence.

§ 1. INTRODUCTION.

SINCE the detailed study of the deuteron and two-nucleon scattering data has not yet yielded a satisfactory nuclear interaction, it is of interest to investigate further nuclear problems involving more than two nucleons so that the adequacy or inadequacy of the proposed two-body interaction for such problems may be demonstrated. The n-D and p-D scattering problems have already been investigated by Buckingham, Burhop and Massey (1941, 1948) with various forms of the two-body interaction, using the resonating group structure method, first introduced by Wheeler. Comparison with experiment should then indicate the best form of the interaction. These authors also deduced the photo-electric disintegration cross-section of tritium into a neutron and deuteron. Their method, however, while neglecting the polarization of the deuteron, involves a great deal of computation. The object of the present investigation was to see how far an account could be given of the three- and four-body photo-disintegration problems with the use of simple analytical wave functions. Verde (1950) has treated the photo-disintegration of the three-particle system with Gaussian wave functions in an elementary manner. While the present work was in progress there has also appeared a discussion of the He^4 photo-disintegration, using Gaussian wave functions, by Flowers and Mandl (1951).

* Communicated by the Authors.

In this paper the photo-electric disintegration of both three- and four-particle systems is considered, attention being limited to electric dipole transitions. The treatment is crude in the sense that the final states of the systems are taken to be plane waves. Equally, for the initial tritium and helium nuclei, only the space symmetric part of the wave function is considered. The calculations, however, indicate the great sensitivity of the cross-sections to the value of the parameters occurring in the wave functions of the initial states. Cross-sections for inverse processes are calculated by the method of detailed balance.

Calculations were first carried out with Gaussian wave functions at about the same time as those of Verde. Since the Gaussian wave function has an incorrect asymptotic behaviour, it seemed worthwhile to investigate the effect of a wave function with a better behaviour in this respect. The wave functions worked out by Svartholm (1945), using the variation-iteration method, were found to be rather complicated to handle in photo-disintegration calculations, as also were wave functions of the form $\exp \{-\alpha(r_{12}+r_{13}+\dots)\}$ which have been used by a number of authors in binding energy calculations, for example, Fröhlich *et al.* (1947). The new wave functions, used by Irving (1951) for calculations of the binding energies of three- and four-particle systems, however, were found to lead to fairly simple analysis in the calculation of photo-electric disintegration cross-sections. Detailed calculations have been carried out for these wave functions and the results compared with those for Gaussian wave functions. The theoretical results are compared with the experimental data from p-D capture by Fowler *et al.* (1949) and p-T capture by Argo *et al.* (1950)*. If the parameters appearing in the wave functions are determined by variational calculations of the binding energies of three- and four-particle systems, very low values for the cross-sections are obtained. One reason for this is that the variational calculations of the binding energies with a central two-body interaction are incorrect and lead to values of the variation parameter which, in the case of the new wave functions, concentrate the nucleus too much. Calculations of the binding energies, when a mixture of central and tensor forces is used, indicate that more reasonable values of the variation parameters are then obtained.

It is to be hoped that when detailed experimental evidence of p-D and p-T capture cross-sections—or, alternatively, the inverse processes—is available, the theoretical formulae arising from the exponential wave functions may be found to give the correct variation of the cross-section with energy. In fact, if the parameter can then be chosen to give the correct magnitude for the cross-section, thus determining the “size”

* Experiments with the Glasgow 30 MeV. Synchrotron have demonstrated the γ - p process with He^4 , but are not yet complete (private communication from J. R. Atkinson). Preliminary measurements with the G.E.C. betatron (Gaertner and Yeater) on the same process indicate an integrated yield of 4×10^{-26} cm.² MeV. with mean quantum energy about 27 MeV. We are very grateful to these authors for a report of their results.

of the nucleus, the value obtained should agree with the value calculated by a variational method which takes into account non-central forces. A characteristic difference between the exponential and Gaussian wave functions may be mentioned here. This is that the exponential wave functions, for a given "size" of nucleus, lead to an earlier maximum cross-section, than the Gaussian. For a given position of the maximum above the threshold the magnitude of the cross-section is smaller with the exponential wave functions.

§ 2. GENERAL FORMALISM.

As we intend to deal in this paper with the photo-disintegration of both three- and four-particle systems, it seems worthwhile first to summarize the general formalism applicable to the photo-disintegration of a system of A particles of equal mass. It is in the first place convenient to separate the motion of the mass-centre by the change to the coordinates

$$\mathbf{R} = \frac{1}{A} \sum_{j=1}^A \mathbf{r}_j, \quad \dots \dots \dots (1)$$

$$\mathbf{r}_{1j} = \mathbf{r}_j - \mathbf{r}_1, \quad j \neq 1$$

where \mathbf{r}_j denotes the coordinates of the A particles. In the problem chiefly considered in this paper one of the particles only is ejected, say, particle 1; a suitable set of coordinates is then

$$\left. \begin{aligned} \mathbf{p}_1 &= \mathbf{r}_1 - \mathbf{R}' = -\frac{1}{(A-1)} \sum_2^A \mathbf{r}_{1j} \\ \mathbf{R}' &= \frac{1}{(A-1)} \sum_{j=2}^A \mathbf{r}_j = \mathbf{R} + \frac{1}{A(A-1)} \sum_2^A \mathbf{r}_{1j} \\ \mathbf{r}_{2m} &= \mathbf{r}_{1m} - \mathbf{r}_{12}, \quad m=3, 4 \dots A. \end{aligned} \right\} \dots \dots (2)$$

It may easily be verified that the Jacobian of each of these transformations has unit modulus. The second set of coordinates corresponds physically with the mass-centre and relative coordinates of the residual nucleus of $(A-1)$ nucleons, together with the coordinates relative to this mass-centre of the ejected nucleon.

The wave function of the initial motion may be taken in the form

$$\Psi_i = u_i(\mathbf{r}_{1j}) \exp i(\mathbf{P}_0 \cdot \mathbf{R})$$

and similarly for the final state

$$\Psi_f = u_f(\mathbf{r}_{2m}) \exp i(\mathbf{p} \cdot \mathbf{r}_1 + \mathbf{P}' \cdot \mathbf{R}').$$

These wave functions will in general have to be given the right spin, isotopic spin and symmetry properties. It is most simple, however, to consider these for individual cases. We shall, in this investigation, limit consideration to electric dipole transitions for which the matrix element reduces to the form

$$\int u_f^*(\mathbf{r}_{2m}) \exp \{-i(\mathbf{p} \cdot \mathbf{p}_1)\} \left\{ \sum_{i=1}^A \tau_i(\mathbf{r}_i - \mathbf{R}) \cdot \mathbf{E}_0 \right\} u_i(r_{1j}) d\mathbf{p}_1 d\mathbf{r}_{2m}.$$

Here τ_i is the usual isotopic variable, \mathbf{E}_0 represents the electric field vector at, say, the mass centre of the system, and the integral corresponding with overall momentum conservation has been removed. The probability per unit time of disintegration into a group of final states F by a quantum of energy k , with its polarization vector along the z -axis, is

$$w = 4\pi^2 k e^2 \left| \int u_f^*(\mathbf{r}_{2m}) \exp(-i\mathbf{p} \cdot \mathbf{p}_1) \left\{ \sum_{i=1}^A \tau_i (\mathbf{r}_i - \mathbf{R})_z \right\} u_i(r_{1j}) d\mathbf{p}_1 d\mathbf{r}_{2m} \right|^2 \rho(E_f). \quad (3)$$

Here $\rho(E_f)$ is the density of the final states per unit energy interval, and the necessary averaging over the initial nucleon spin states, and sum over the final spin states must be carried out. Natural units $\hbar=c=1$ are employed.

§ 3. CHOICE OF WAVE FUNCTIONS.

For analytical simplicity Gaussian wave functions immediately suggest themselves. Their bad asymptotic behaviour, however, seems likely to lead to an underestimate of the photo-disintegration cross-sections. These, however, have been worked out using wave functions of the space symmetric form

$$\psi = N^{\frac{1}{2}} \exp(-\mu^2 \sum_{i>j} r_{ij}^2). \quad (4)$$

In order to obtain an improvement on the Gaussian wave functions it seemed desirable to find functions, which, whilst retaining reasonable analytical simplicity would have a more correct asymptotic behaviour. The wave functions developed by Svartholm were considered for this purpose, but in fact greater analytical simplicity is given by the general form

$$\psi = N^{\frac{1}{2}} \exp \left\{ -\mu \left(\sum_{i>j} r_{ij}^2 \right)^{\frac{1}{2}} \right\} / \left(\sum_{i>j} r_{ij}^2 \right)^n. \quad (5)$$

An extensive series of variational calculations has been carried out for wave functions of this form, and has been separately described by one of us (Irving 1951).

With both types of wave function a choice has to be made of the appropriate value of μ for the deuteron, tritium and helium ground states, denoted subsequently by μ_D , μ_T and μ_α . This choice is discussed later when the photo-disintegration cross-sections are derived.

§ 4. PHOTO-DISINTEGRATION OF H^3 AND He^3 (TWO-PARTICLE).

For electric dipole transitions the probability per unit time of disintegration into a group of final states F is

$$w = 4\pi^2 k e^2 \left| (F | \sum_{i=1}^A \tau_i (\mathbf{r}_i - \mathbf{R})_z | 0) \right|^2 \rho_{E_F}$$

where the initial quantum is regarded as polarized in the z -direction. The initial state O , say, for the tritium case, is the 2S ground state of

H^3 . The final state F contains one neutron moving as a plane wave with momentum \mathbf{p} , the resultant deuteron being in either the ${}^3(\sigma)_{\pm 1}$, or the ${}^3(\sigma)_0$ state. Carrying out the elementary spin summations leads to the result

$$w = \frac{2}{3} \pi^2 k e^2 \left| \int u_f^* \rho_{1z} \exp \{-i(\mathbf{p} \cdot \mathbf{r}_1)\} u_i d\mathbf{r}_1 d\mathbf{r}_{23} \right|^2 \rho(E_F) \quad (6)$$

or, for the differential cross-section for the absorption of a quantum k with the neutron ejected into a solid angle $d\Omega$

$$d\sigma = \frac{e^2}{18\pi} k p M \left| \int u_f^* \rho_{1z} \exp \{-i(\mathbf{p} \cdot \mathbf{r}_1)\} u_i d\mathbf{r}_1 d\mathbf{r}_{23} \right|^2 d\Omega \quad (7)$$

Here u_i , u_f are the initial tritium, and final deuteron wave functions expressed as functions of \mathbf{r}_1 and \mathbf{r}_{23} . For the case of He^3 the result is exactly similar except that allowance must be made for the Coulomb force between the outgoing proton and deuteron.

(a) Photo-disintegration of Tritium.

Using the Gaussian wave functions defined in equation (4) the differential cross-section for disintegration of H^3 with ejection of a neutron of momentum p is

$$d\sigma = \sqrt{\left(\frac{\pi}{6}\right)} e^2 k p^3 M \cos^2 \theta \frac{\mu_D^3}{\mu_T^4 (3\mu_T^2 + 2\mu_D^2)^3} \exp\left(-\frac{ME}{3\mu_T^2}\right) d\Omega \quad (8)$$

where E is the kinetic energy available for the disintegration so that $p^2 = \frac{4}{3}ME$, with M the nucleon mass. The total cross-section σ is then given by

$$\sigma = \frac{16\sqrt{2}}{27} \pi^3 e^2 \frac{M^{5/2} \mu_D^3}{\mu_T^4 (3\mu_T^2 + 2\mu_D^2)^3} k E^{3/2} \exp\left(-\frac{ME}{3\mu_T^2}\right) \quad (9)$$

Suitable values of μ_T are found from variational calculations with different Gaussian wells, $1/\mu_T = 4.2 \times 10^{-13}$ cm. corresponding with the results of Margenau and Warren (1937), and $1/\mu_T = 3.65 \times 10^{-13}$ cm. with the more recent force constants (Rosenfeld 1948)

$$1/\kappa = 1.9 \times 10^{-13} \text{ cm.}, \quad {}^3J^{(0)} = 43.7 \text{ MeV.}, \quad {}^1J^{(0)}/{}^3J^{(0)} = 0.62.$$

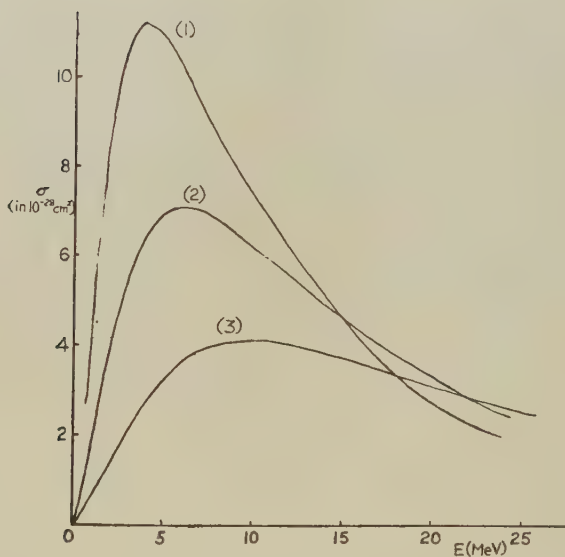
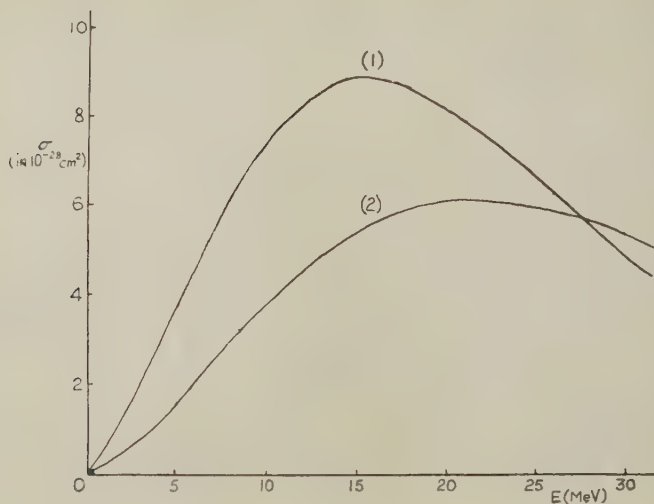
This second value gives a Coulomb energy of about 0.75 MeV. for He^3 . The cross-section is plotted in fig. 1 (a) with those values of μ_T , and with $\mu_D/\mu_T = 1.12$.

The calculations were then repeated with the new form of wave functions. For simplicity in the evaluation of the integral (6) these were taken in the form

$$\psi_T = A \frac{\exp \{-\mu_r(r_{12}^2 + r_{23}^2 + r_{31}^2)^{\frac{1}{2}}\}}{(r_{12}^2 + r_{23}^2 + r_{31}^2)^{\frac{1}{2}}} = \frac{N_1^{\frac{1}{2}} \exp \{-\sqrt{2}\mu_T(\rho^2 + r^2)(\rho^2 + r^2)^{\frac{1}{2}}\}}{(\rho^2 + r^2)^{\frac{1}{2}}} \quad (10)$$

$$\left. \begin{array}{l} \text{with} \\ \text{and} \end{array} \right\} \begin{array}{l} \mathbf{p} = \mathbf{r}_1 - \frac{1}{2}(\mathbf{r}_2 + \mathbf{r}_3) \\ \mathbf{r} = \frac{\sqrt{3}}{2}(\mathbf{r}_3 - \mathbf{r}_2) \end{array} \quad (11)$$

Figs. 1 (a) and 1 (b).



Cross-sections for two particle photo-disintegration of H^3

(a) for Gaussian wave functions with the values

(1) $1/\mu_T = 4.2 \times 10^{-13} \text{ cm.}$, (2) $1/\mu_T = 3.65 \times 10^{-13} \text{ cm.}$

(b) for exponential wave functions with

(1) $1/\mu_T = 3.0 \times 10^{-13} \text{ cm.}$, (2) $1/\mu_T = 2.5 \times 10^{-13} \text{ cm.}$, (3) $1/\mu_T = 2.0 \times 10^{-13} \text{ cm.}$

The variational calculations of binding energy then show that $1/\mu_T = 2.0 \times 10^{-13}$ cm. is a suitable value of the parameter, corresponding to a binding energy of 7.1 MeV. for a standard Yukawa potential

$$1/\kappa = 1.17 \times 10^{-13} \text{ cm.}, \quad {}^3J^{(0)} = 67.3 \text{ MeV.}, \quad q = 0.69 \quad . \quad . \quad (12)$$

(cf. Irving (1951)). If, rather than using the best variational value, μ_T is chosen to fit the Coulomb energy of He^3 , then $1/\mu_T = 2.5 \times 10^{-13}$ cm., corresponding with a Coulomb energy of 0.8 MeV. (binding energy of $\text{H}^3 = 6.3$ MeV.) is suggested. In the curves of fig. 1*b* the rather extreme case of $1/\mu_T = 3.0 \times 10^{-13}$ cm. is also shown. The binding energy with the potential (12) is then 5 MeV.

For the deuteron we take

$$\psi_D = N_D \sqrt{3} e^{-\gamma r} / (2r), \quad . \quad . \quad . \quad . \quad . \quad (13)$$

with r as defined in (11) and γ determined by the deuteron binding energy W_D , $\gamma = 2(MW_D/3)^{1/2}$. The integrals involved are long but quite elementary and lead to the result for the total cross-section

$$\sigma = 2^5 e^2 \frac{k E^{3/2}}{W_D^{5/2}} \frac{\mu_T^4}{M^3 W_D^3} \{f(\lambda)\}^2 \quad . \quad . \quad . \quad . \quad . \quad (14)$$

with
$$f(\lambda) = \frac{7\lambda - 2}{\lambda^2(\lambda - 1)^2} - \frac{15}{(\lambda - 1)^3} + \frac{15}{(\lambda - 1)^{7/2}} \cos^{-1} \left(\frac{1}{\sqrt{\lambda}} \right),$$

and $\lambda = (p^2 + 2\mu_T^2)/\gamma^2$. This cross-section is shown plotted as a function of photon energy in fig. 1*b*.

(b) Photo-disintegration of He^3 .

In this case allowance must be made for the Coulomb interaction between the outgoing proton and deuteron; otherwise the general formulae are as for H^3 . In view of the approximate nature of the calculation, it is felt that this allowance can be adequately made by multiplying the H^3 form of cross-section by a barrier penetration factor (Bethe 1937), at the same time taking note of the different binding energy of He^3 (7.74 MeV.), which brings the threshold to $k = 5.5$ MeV. Detailed curves are not drawn for this case but the p -wave barrier penetration factors for a few energies are shown in Table I.

TABLE I.

E (MeV.)	0.5	1.0	1.5	2.0	2.5
exp $(-P_n)$ ($R = 4.0 \times 10^{-13}$ cm.)	0.02	0.11	0.27	0.49	0.81
exp $(-P_n)$ ($R = 5.0 \times 10^{-13}$ cm.)	0.05	0.25	0.64	1.0	—

E = energy in mass centre system.

R = barrier range.

Reviewing the results, we have found for the two-particle disintegrations it must be admitted that neither the results for the Gaussian nor for the exponential wave functions can be very accurate. Considering for the

moment, for comparison, the case of photo-disintegration of the deuteron, it is known that a fairly good result can be obtained with the use of an asymptotic form for the initial wave functions and plane waves for the final neutron and proton. This possibility arises from the fact that the neutron and proton forming a deuteron exist for the greater part of the time outside the range of the nuclear forces. For the three- and four-particle nuclei this effect becomes successively weaker, and the central portion of the dipole matrix element integral becomes more important. Allowance for distortion of the outgoing waves is difficult to make, but it will probably tend in the direction of increasing the cross-sections at low energies and bringing the maxima nearer to low energies. In favour of the exponential wave functions it can at least be stated that they have a fairly correct asymptotic form, and should give the general shape of the cross-section better than the Gaussian form. (It may be recalled that even for the case of photo-disintegration of the deuteron Gaussian wave functions give a rather poor result.)

Unfortunately, only very little experimental information is available with which to compare the theoretical predictions. It is limited to the p-D capture cross-section reported by Fowler *et al.* (1949). These measurements indicate an approximate cross-section

$$\sigma_c = 0.74 E_p^{0.72} \times 10^{-29} \text{ cm.}^2 \quad . \quad . \quad . \quad . \quad . \quad (15)$$

for the $\text{H}^2(p, \gamma) \text{He}^3$ capture process in the region 0.5—1.5 MeV. The capture cross-section for this process is given in terms of the corresponding inverse photo-disintegration by

$$\sigma_c(E_p) = (k^2/2ME)\sigma_d(k). \quad . \quad . \quad . \quad . \quad . \quad (16)$$

Here E_p is the proton bombarding energy in the laboratory system (deuteron stationary), and related to the earlier E (energy in the mass centre system) by $E_p = \frac{3}{2}E$. The corresponding quantum energy k is given by $k = E + B$, where in this case $B = 5.5$ MeV. From (16) the theoretical capture cross-sections may be derived using the earlier (9) and (14). For the present we merely note that for small energies $\sigma_c \propto E_p^{\frac{1}{2}}$. It has, thus, neglecting Coulomb barrier effects, a very swift rise above threshold, for any type of wave function or choice of parameters. The difference between different theoretical models is only observable when measurements beyond the initial rise are available. This is by no means true in the present case. Indeed, the experimental results given in (15) apply only up to $E_p = 1.5$ MeV., when the Coulomb barrier effects are still appreciable, and can easily be fitted, at least in shape, with either type of wave function using the barrier penetration factors of Table I. The most significant use to make of (15) seems to be to derive the magnitude of the corresponding photo-disintegration cross-section. We find that this should have the value $4 \times 10^{-28} \text{ cm.}^2$, for $E = 1$ MeV. The corresponding cross-section without barrier should be at least $16 \times 10^{-28} \text{ cm.}^2$. This should be approximately equal to the cross-section

for the $H^3(\gamma, n)H^2$ process at 1 MeV. above the threshold. Comparison with figs. 1 (a) and (b) shows that none of the theoretical cross-sections has such a rapid rise above the threshold. Even the exponential wave functions with $1/\mu_T = 3.0 \times 10^{-13}$ cm. gives only a cross-section of 5×10^{-28} cm.² In this energy range the distortion of the outgoing wave may be important and give rise to the discrepancy noted.

§ 5. PHOTO-DISINTEGRATION OF H^3 AND He^3 (THREE-PARTICLE).

As most of the binding energy of H^3 or He^3 is lost when the disintegrations $H^3 \rightarrow n + D$, $He^3 \rightarrow p + D$ are carried out, we might expect, in view of the greater phase space available, that, except just near the threshold, the three-particle disintegrations, of which $H^3 \rightarrow n + n + p$ is typical, should predominate. Calculations along the lines of the preceding ones confirm this belief. They have been carried out both for the Gaussian and for the new exponential form of wave functions, once more using the approximation of plane waves for the outgoing particles. With the same notation as previously the two cross-sections are

Gaussian

$$\sigma = \frac{\pi^2 k e^2}{3^7 \mu_T^{10}} M^4 E^3 \exp\left(-\frac{ME}{3\mu_T^2}\right). \quad (17)$$

Exponential

$$\sigma = \frac{150\pi^2 e^2}{M^2} \left(\frac{\mu_T}{M}\right)^4 \frac{kE^3 M^3}{\left(E + \frac{3\mu_T^2}{2M}\right)}. \quad (18)$$

For the Gaussian wave functions the maximum cross-section comes approximately when

$$E = 500 \text{ MeV.} / \left\{ \frac{1}{\mu_T} \text{ in } 10^{-13} \text{ cm.} \right\}^2$$

and the magnitude of the cross-section varies approximately as $1/\mu_T^2$. In Table II. these maximum cross-sections are shown for various values of $1/\mu_T$, for the disintegration of H^3 .

TABLE II.

Maximum cross-sections for $H^3 \rightarrow n + n + p$
(Gaussian wave functions).

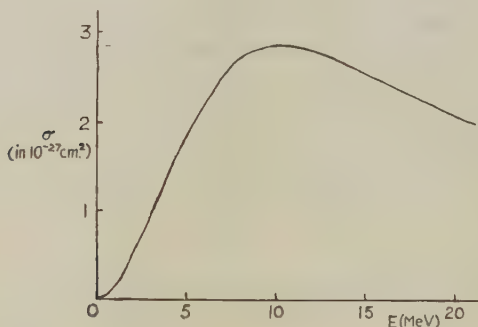
$1/\mu_T$ (units 10^{-13} cm.)	3.65	4.2	5.48
E_{\max} (MeV.)	35	28.4	17
σ_{\max} (units 10^{-27} cm. ²)	2.2	2.9	4.8

For the exponential type wave functions rather similar values of cross-sections are obtained; for reasonable values of $1/\mu_T$, however, the maxima of the cross-sections again occur at lower energies. The maximum cross-section is approximately proportional to $1/\mu_T^2$, and the

corresponding energy to μ_T^2 . In fig. 2 the results are shown with $1/\mu_T = 2.5 \times 10^{-13}$ cm. It will be noted how these values dwarf the two-particle disintegration cross-sections of § 4, except at the threshold where only the two-particle process is possible. This will add to the already considerable experimental difficulties in the way of observation of the $\text{He}^3(\gamma, p)\text{H}^2$, $\text{H}^3(\gamma, n)\text{H}^2$ processes.

We have earlier noted the dangers in the use of the Born approximation, *i. e.* plane waves in the final state, in excitation problems of this sort. The method is to some extent consistent in that, for the initial state also, wave functions are used which have only asymptotic validity.

Fig. 2.



Three particle photo-disintegration cross-section of H^3 , for exponential wave function, $1/\mu_T = 2.5 \times 10^{-13}$ cm.

§ 6. TWO-PARTICLE PHOTO-DISINTEGRATION OF α -PARTICLE.

Here we consider only the transition $\text{He}^4(\gamma, p)\text{H}^3$, neglecting at first the Coulomb interaction between the outgoing proton and triton. This is, in any case, negligible for quanta above about 22 MeV. From the general formulae given in § 2 we have

$$w = \pi^2 k e^2 \left| \int u_f^* \rho_{12} \exp(-i\mathbf{p} \cdot \boldsymbol{\rho}_1) u_i d\boldsymbol{\rho}_1 d\mathbf{r}_{23} d\mathbf{r}_{24} \right|^2 \rho_{\text{EF}} \quad \dots \quad (19)$$

The initial state is the $1S$ ground state of He^4 , and the final state F contains one proton moving as a plane wave with momentum \mathbf{p} , the resultant triton being in a $2S$ state.

Introducing the coordinates

$$\left. \begin{aligned} \mathbf{u} &= -\mathbf{r}_1 + \frac{1}{3}(\mathbf{r}_2 + \mathbf{r}_3 + \mathbf{r}_4) \\ \mathbf{v} &= \frac{1}{2}(\mathbf{r}_3 + \mathbf{r}_4) - \frac{1}{3}(\mathbf{r}_2 + \mathbf{r}_3 + \mathbf{r}_1) \\ \mathbf{w} &= \mathbf{r}_3 - \mathbf{r}_4 \end{aligned} \right\} \dots \dots \dots (20)$$

we have

$$\left. \begin{aligned} \frac{1}{2} \sum_{i,j=1}^4 \mathbf{r}_{ij}^2 &= 3u^2 + 24v^2 + 2w^2 \\ \frac{1}{2} \sum_{i,j=1}^3 \mathbf{r}_{ij}^2 &= \frac{3}{4}(24v^2 + 2w^2). \end{aligned} \right\} \dots \dots \dots (21)$$

Gaussian wave functions: The calculations are elementary leading to

$$\sigma = 3 \times 4^{\frac{1}{2}} \pi^{3/2} e^2 M^{5/2} \frac{\mu_T^6}{\mu_\alpha (3\mu_T^2 + 4\mu_\alpha^2)^6} k E^{3/2} \exp \left\{ -\frac{ME}{4\mu_\alpha^2} \right\} \dots \dots (22)$$

The parameters μ_α and μ_T may be determined by variational calculations of the binding energies of the α -particle and triton, assuming, for example, a Gaussian well. The nuclear parameters

$$1/\kappa = 1.9 \times 10^{-13} \text{ cm.}, \quad {}^3J^{(0)} = 43.7 \text{ MeV.}, \quad q = 0.62$$

then give $1/\mu_T \cong 1/\mu_\alpha = 3.65 \times 10^{-13} \text{ cm.}$ yielding binding energies of approximately 4 MeV. and 23 MeV. for the triton and α -particle respectively. The Coulomb energy of He^3 is then approximately 0.75 MeV. The nuclear parameters $1/\kappa = 2.25 \times 10^{-13} \text{ cm.}$, ${}^3J^{(0)} = 35.6 \text{ MeV.}$, $q = 0.6$ determined by Margenau and Warren (1937) to fit the triton binding and deuteron data give slightly too small a value for the α -particle binding energy. For this case $1/\mu_\alpha \cong 1/\mu_T = 4.2 \times 10^{-13} \text{ cm.}$ In fig. 3 (a) σ is graphed against E for $1/\mu_\alpha = 1/\mu_T$, several values of the parameters being taken to show the dependence on them. $1/\mu_\alpha = 1/\mu_T = 5.25 \times 10^{-13} \text{ cm.}$ has already been considered by Flowers and Mandl (1951).

The calculations were repeated with exponential wave functions of the form

$$\begin{aligned} \psi_\alpha &= N_\alpha^{1/2} \exp \left\{ -\mu_\alpha \left(\sum_{i>j}^2 r_{ij}^2 \right)^{\frac{1}{2}} \right\} / \left\{ \sum_{i>j}^2 r_{ij}^2 \right\}^{\frac{1}{2}} \\ &= \frac{N_\alpha^{1/2} \exp \left\{ -\mu_\alpha (3u^2 + 24v^2 + 2w^2)^{\frac{1}{2}} \right\}}{(3u^2 + 24v^2 + 2w^2)^{\frac{1}{2}}} \dots \dots \dots (23) \end{aligned}$$

$$\begin{aligned} \text{and} \quad \psi_T &= N_T^{1/2} \exp \left\{ -\mu_T (r_{12}^2 + r_{23}^2 + r_{31}^2)^{\frac{1}{2}} \right\} / (r_{12}^2 + r_{23}^2 + r_{31}^2)^{\frac{1}{2}} \\ &= \frac{N_T^{1/2} \exp \left\{ -\frac{1}{2} \sqrt{3} \mu_T (24v^2 + 2u^2)^{\frac{1}{2}} \right\}}{\left\{ \frac{1}{2} \sqrt{3} (24v^2 + 2w^2)^{\frac{1}{2}} \right\}} \dots \dots \dots (24) \end{aligned}$$

The cross-section is then given by

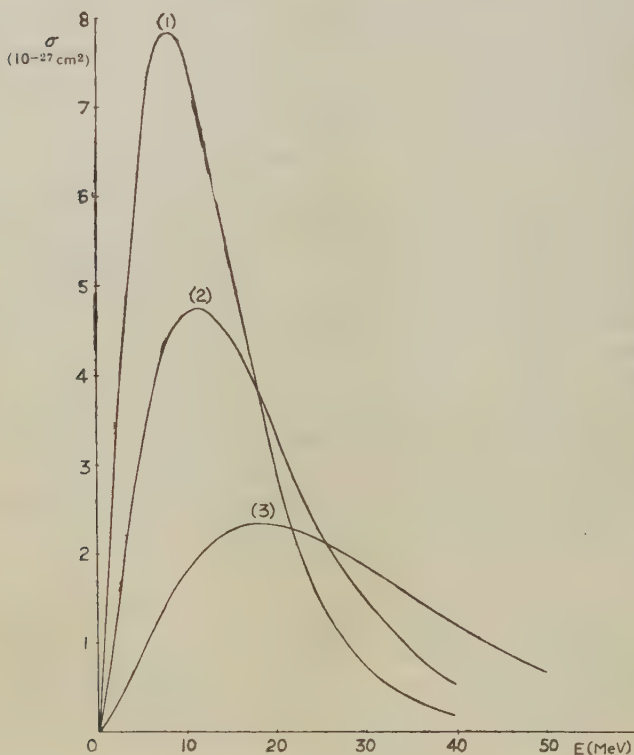
$$\sigma = \frac{7 \times 4^{11} \pi}{3^9 \sqrt{2}} e^2 M^{5/2} \frac{\mu_\alpha^7}{\mu_T^4} k E^{3/2} z^{20} \{f(z)\}^2 \dots \dots \dots (25)$$

$$\text{where} \quad f(z) = \left[(735 + 3465z^2)/8 + 21/(1+z^2) + 2/(1+z^2)^2 \right. \\ \left. - \frac{3 \cot^{-1} z}{8z} (1155z^4 + 630z^2 + 35) \right]$$

$$\text{and} \quad \frac{1}{z^2} = \frac{2ME}{3\mu_T^2} + \frac{4\mu_\alpha^2}{3\mu_T^2} - 1.$$

The graph of σ against E is shown in fig. 3 (b) for different values of the parameters. $1/\mu_T = 2.5 \times 10^{-13}$ cm. gives the correct Coulomb energy of He^3 . $1/\mu_\alpha = 1.7 \times 10^{-13}$ cm. gives a binding energy of 28 MeV. for He^4 ; $1/\mu_\alpha = 2.0 \times 10^{-13}$ cm. a binding energy of 20.5 MeV.; $1/\mu_\alpha = 2.5 \times 10^{-13}$ cm., a binding energy of 12.5 MeV. The rapid rise of the cross-section is evident. The exponential wave functions give earlier maxima than the

Fig. 3 (a).



Cross-sections for two particle photo-disintegration of He^4

(a) Gaussian wave functions with $1/\mu_\alpha = 1/\mu_T$ having values

(1) 6.10×10^{-13} cm., (2) 5.25×10^{-13} cm., (3) 4.20×10^{-13} cm.

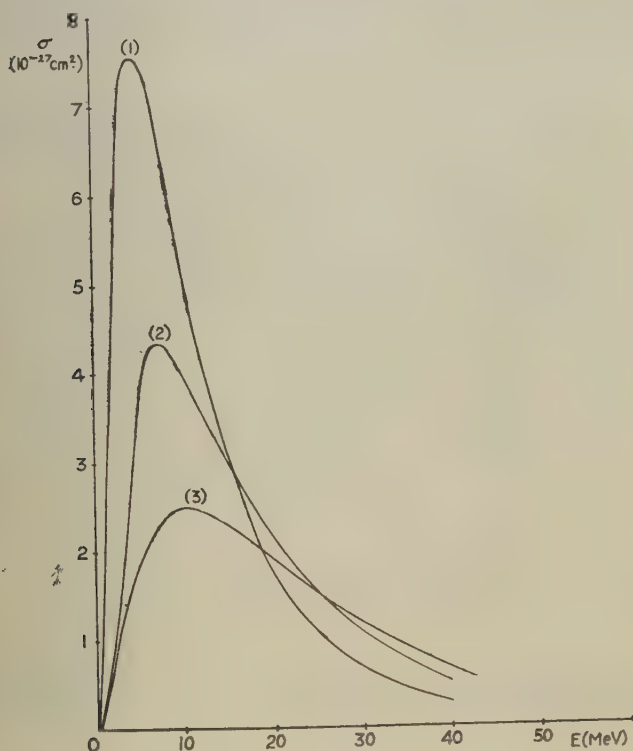
Gaussian, the values of the parameters being smaller as well; that is, a more concentrated nucleus is found for cross-sections of comparable magnitude.

The cross-section for the inverse capture process can again be calculated by the method of detailed balance yielding

$$\sigma_c(E_p) = (k^2/3ME)\sigma_d(k). \quad . \quad . \quad . \quad . \quad . \quad (26)$$

Here, as previously, E_p denotes the proton bombarding energy in the laboratory system, $E(=\frac{3}{4}E_p)$ is the corresponding energy in the centre of mass system, and $\sigma_d(k)$ denotes the photo-disintegration cross-section for quantum energy k . To illustrate the general form of the theoretical capture curves, the capture cross-section is given in fig. 4 for the exponential form of wave function with $1/\mu_T=1/\mu_\alpha=2.5 \times 10^{-13}$ cm., and for the Gaussian form of wave function with $1/\mu_T=1/\mu_\alpha=6.10 \times 10^{-13}$ cm.

Fig. 3 (b).

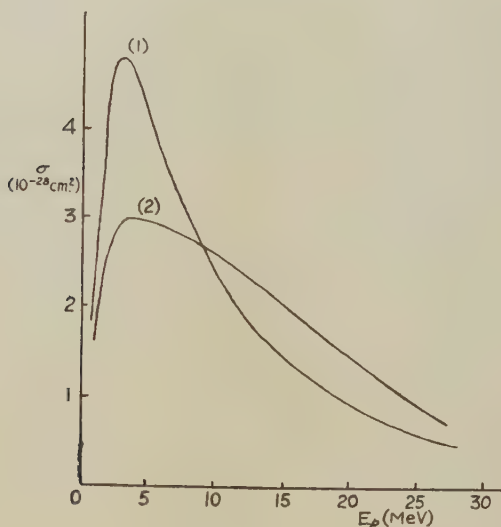
Cross-sections for two particle photo-disintegration of He^4

(b) Exponential wave functions with (1) $1/\mu_\alpha=1/\mu_T=2.5 \times 10^{-13}$ cm.,
 (2) $1/\mu_\alpha=2.0 \times 10^{-13}$ cm., $1/\mu_T=2.5 \times 10^{-13}$ cm., (3) $1/\mu_\alpha=1.7 \times 10^{-13}$ cm.,
 $1/\mu_T=2.5 \times 10^{-13}$ cm.

The experimental evidence available relates mainly to the capture process, coming from the measurements of Argo *et al.* (1950). Experiment has only been carried out up to a bombarding energy $E_p=2.6$ MeV., which is just approaching the top of the barrier for p -wave protons. It is clear that the shape of the experimental curve can, as noted by Flowers

and Mandl (1951), be explained by a combination of the initial shape without barrier $\sigma_p \propto E_p^{\frac{1}{2}}$, and suitable barrier penetration factors, more particularly in view of the rather arbitrary calculations involved in the latter. Once again, however, the magnitude of the capture cross-section is interesting. This is quoted as approximately 10^{-27} cm.² at $E_p = 2.6$ MeV. The corresponding photo-disintegration cross-section is about 10^{-26} cm.² at $k = 2$ MeV. None of the theoretical curves predicts so sharp a rise in the cross-section above the threshold, though once again the exponential wave functions give a better agreement. If the experimental evidence regarding the photo-disintegration process mentioned in a footnote in § 1 is confirmed, then support is provided for a cross-section approximately

Fig. 4.



Cross-section for proton capture by tritium, neglecting Coulomb barrier (1) with exponential wave function, $1/\mu_T = 1/\mu_\alpha = 2.5 \times 10^{-13}$ cm., (2) with Gaussian wave function, $1/\mu_T = 1/\mu_\alpha = 6.0 \times 10^{-13}$ cm.

of the form given by the exponential wave functions with $1/\mu_T = 1/\mu_\alpha = 2.5 \times 10^{-13}$ cm. These measurements give an integrated yield of 4×10^{-26} cm.² MeV. for the cross-section, with about 40 per cent of the events below $k = 24$ MeV., which could not be reconciled with any of the curves based on Gaussian wave functions.

In conclusion then it appears that a reasonably good fit to the photo-disintegration and inverse processes for the three- and four-particle nuclei may be hoped for with the exponential wave functions. They are at least superior to the Gaussian functions in predicting the early rise of the cross-sections above the threshold. There is at present, however,

too much uncertainty regarding the choice to be made of the parameters, μ_T and μ_α . The binding energy calculations with central forces (Irving 1951) are certainly inadequate for this purpose, but the hope is that their extension to include non-central forces may yield a consistent picture. We should then, in the exponential wave functions, have an analytical model of reasonable simplicity for three- and four-particle nuclei, with the possibility of extension to other light nuclei.

Complete disintegration of He⁴.

Using the same approximations as in the case of the three-particle system, the cross-section for the process

$$\text{He}^4 + \gamma \rightarrow n + n + p + p$$

is easily calculated.

For the Gaussian wave functions, we have

$$\sigma = \frac{1}{945} \frac{\pi^{3/2}}{4^4} e^2 \frac{M^{11/2}}{\mu_\alpha^{13}} k E^{9/2} \exp \left\{ -\frac{ME}{4\mu_\alpha^2} \right\} \quad (27)$$

The values of σ_{\max} for several values of the parameter are then as follows :

$1/\mu_\alpha$ (10^{-13} cm.)	E (MeV.)	σ_{\max} (10^{-27} cm. ²)
3.6	66.4	3.04
4.2	48.0	4.58
5.25	30.0	8.66
6.1	22.0	13.7

For the exponential wave function,

$$\sigma = \frac{2^{21} \sqrt{2\pi}}{45} e^2 \frac{1}{M^{9/2}} \frac{\mu_\alpha^7 k E^{9/2}}{(E + 2\mu_\alpha^2/M)^{10}} \quad (28)$$

yielding the following results for σ_{\max} :

$1/\mu_\alpha$ (10^{-13} cm.)	E (MeV.)	σ_{\max} (10^{-27} cm. ²)
1.7	28.7	3.7
2.0	20.0	6.2
2.5	12.2	12.8

The maxima for the exponential wave function again occur at much lower energies than those for the Gaussian wave function. It would be interesting if experimental information could be obtained on this point.

ACKNOWLEDGMENT.

One of us (J. I.) wishes to thank the Nuffield Foundation for the award of a Fellowship, during the tenure of which this work was carried out.

REFERENCES.

- ARGO, A. V., GITTINGS, H. T., HEMMENDINGER, A., JARVIS, G. A., and TASCHEK, R. F., 1950, *Phys. Rev.*, **78**, 691.
- BETHE, H. A., 1937, *Rev. Mod. Phys.*, **9**, 177.
- BUCKINGHAM, R. A., and MASSEY, H. S. W., 1941, *Proc. Roy. Soc. A*, **179**, 123.
- BURHOP, E., and MASSEY, H. S. W., 1948, *Proc. Roy. Soc. A*, **192**, 156.
- FLOWERS, B. H., and MANDL, 1951, *Proc. Roy. Soc. A*, **206**, 131.
- FOWLER, W. A., LAURITSEN, C. C., and TOLLESTRUP, A. V., 1949, *Phys. Rev.*, **76**, 1767.
- FRÖHLICH, H., HUANG, K., and SNEDDON, I. N., 1947, *Proc. Roy. Soc. A*, **191**, 61.
- IRVING, J., 1951, *Phil. Mag.*, **42**, 338.
- MARGENAU, H., and WARREN, D., 1937, *Phys. Rev.*, **52**, 790.
- ROSENFELD, L., 1948, *Nuclear Forces* (Amsterdam : North Holland Publishing Co.), p. 131.
- SVARTHOLM, N., 1945, *The binding energies of the lightest atomic nuclei*, Thesis, Lund.
- VERDE, M., 1950, *Helv. Phys. Acta*, **23**, 453.

CXXXV. *The Recrystallization Texture of Drawn Aluminium Wire.*

By J. SAWKILL and N. THORLEY,

Physics Department, King's College, Newcastle-upon-Tyne*.

[Received June 26, 1951. Revised August 9, 1951.]

[Plate LIII.]

ABSTRACT.

The recrystallization texture of high purity (99.995 per cent) cold drawn aluminium wire has been found to be double, viz., [322], [100]. The [100] component is relatively weak. The scatter in the major [322] component increases, and the amount of the [100] component decreases, the higher the temperature of anneal.

RECENTLY it has been suggested (Hibbard 1950) that the double [111], [100] deformation texture of drawn face-centred cubic metal wires previously described (*e.g.* Schmid and Wassermann 1927) is actually an intermediate texture which changes to a single [111] texture with sufficient deformation. The [111] texture has been predicted on theoretical grounds (Hibbard and Yen 1948, Calnan and Clews 1950). Observations Hibbard made on drawn wires of six metals showed that for a large deformation (98 per cent reduction in diameter) all the wires had essentially a single [111] texture. In the case of aluminium, however, there was a minor [100] component, which Hibbard ascribed to room temperature recrystallization. His reasons for this were that aluminium of the purity used (99.994 per cent) has been known to recrystallize at room temperature; that the [100] component on the X-ray photograph was characteristic of diffraction from large recrystallized strain-free grains (*i.e.* "spotty" rather than diffuse); that the [100] component increased in intensity with increasing deformation above 90 per cent; and that the deformation texture of less pure drawn aluminium wire has been reported previously as single [111].

It is interesting to observe that v. Göler and Sachs (1927) working with less pure aluminium (99.93 per cent) did find evidence of a [100] recrystallization texture. The wire they used had been reduced in diameter by 80.6 per cent and the deformation texture was [111] with

* Communicated by the Authors.

a trace of [100]. An annealing temperature of at least 200° C. was required before recrystallization was evident as faint spots on the Debye-Scherrer rings of the X-ray photographs. After complete recrystallization, requiring temperatures of at least 375° C., the [111] deformation texture was observed to be preserved and an appreciable amount of [100] texture was also present.

Recent experiments in this department have also shown the existence of a minor [100] component in the recrystallization texture of high purity aluminium wire. The actual texture is double, viz., [322], [100]. The majority of grains have the [322] texture, the minor [100] component being relatively weak.

The aluminium, kindly supplied by the British Aluminium Co. Ltd., was of 99.995 per cent purity and had received a 95.2 per cent reduction in diameter. Plate LIII. (a) is a flat film X-ray photograph showing the deformation texture, taken with partially filtered $\text{MoK}\alpha$ radiation with the beam perpendicular to the vertical wire axis. It shows the [111] texture on a background of complete rings from the randomly oriented grains. On the first ring there is a weak reflection at A (Plate LIII. (a)) which can be accounted for if a small percentage of the grains have the [100] direction along the wire axis. In this case a slight intensity maximum would be expected at B on the second ring, and this can be seen on the original negative. A weak [100] component then exists in addition to the strong [111] component and the small percentage of grains of random orientation. The reflections at A due to the [100] component are not spotty, *i. e.* not characteristic of large recrystallized strain-free grains. The wire was annealed at various temperatures and in all cases a new texture appeared. Plate LIII. (b) is a typical photograph. Here the wire had been annealed at 275° C. for two hours and a comparison with Plate LIII. (a) shows the change in texture. At regions A and B (Plate LIII. (b)) on the first and second rings respectively the fairly weak reflections are at the positions predicted by a [100] texture. For these reflections the maximum angular deviation of the [100] direction from the axis of the wire is about 5°. For the remainder of the reflections an analysis has shown that the texture can be accounted for almost exactly with the [322] direction along the wire axis. The randomly oriented grains disappear. Anneals were given from approximately 150° C. to 550° C. and this new texture was always found. It is due to primary recrystallization; subsequent grain growth did not affect the texture. The amount of the [100] component decreased, and the scatter in the [322] component increased, the higher the temperature of anneal. In Plate LIII. (b) the maximum angular deviation of the [322] direction from the axis of the wire is between 2° and 3°.

v. Göler and Sachs (1927) used aluminium of three different purities and found the minor [100] recrystallization component strongest for the purest metal.

Their results were as follows :—

(i.) a preservation of the [111] deformation texture and the appearance of a [100] component with recrystallization of 99.93 per cent aluminium (previously mentioned) ;

(ii.) a partial preservation of the [111] deformation texture and a suggestion of a [100] component with recrystallization of 99.0 per cent aluminium ; and

(iii.) a partial preservation of the [111] deformation texture with recrystallization below 500° C. but increasing randomness with recrystallization above this temperature and no [100] recrystallization component for 98.7 per cent aluminium.

Other observers (Schmid and Wassermann 1928) found no evidence of a [100] recrystallization component for 99.95 per cent aluminium.

Nevertheless, the results of v. Göler and Sachs suggest that the amount of the [100] recrystallization component depends on purity, and it may be significant that with the higher purity material in the present work temperatures lower than the 375° C. of v. Göler and Sachs produced this component. This seems to support Hibbard's suggestion that the room temperature [100] component in his aluminium wire is due to recrystallization. In the particular case observed here, however, the existence of the minor [100] recrystallization component does not definitely establish that the room temperature component is due to recrystallization. Two possibilities exist :—

(i.) that it is due to deformation only and that recrystallization preserves it ; and

(ii.) that it is already present due to recrystallization and higher temperature anneals merely retain it.

The fact that the room temperature [100] component here was not " spotty " and that temperatures of at least 150° C. were required before the X-ray rings did become " spotty " tends to discount (ii.) while some of Hibbard's previously mentioned observations would seem to discount the first possibility. It is evident that further investigations are necessary to determine the true origin of this room temperature [100] component in aluminium wires after large deformations.

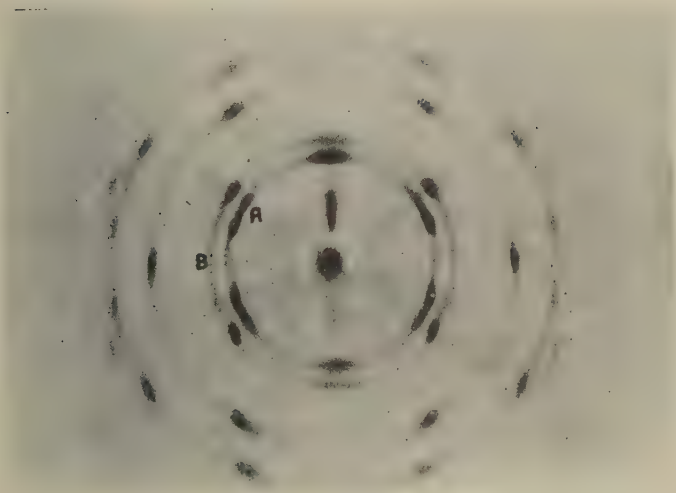
The major [322] recrystallization component has not hitherto been reported. It may be characteristic of this wire only, as purity, prior deformation and mode of recrystallization are determining factors for the resulting texture. In many cases in face-centred cubic metals a certain relative orientation, corresponding to a rotation of 30° to 40° about the [111] axis, has been found between a highly oriented cold worked matrix and strain-free grains growing in this matrix (Beck and Hu 1949). The same relative orientation was found with coarsening or secondary recrystallization. The retention of the [111] drawing texture on annealing, previously observed, would be in keeping with this

orientation relationship, but the production of the [322] texture on annealing from the [111] drawing texture, observed here, does not agree with this relationship.

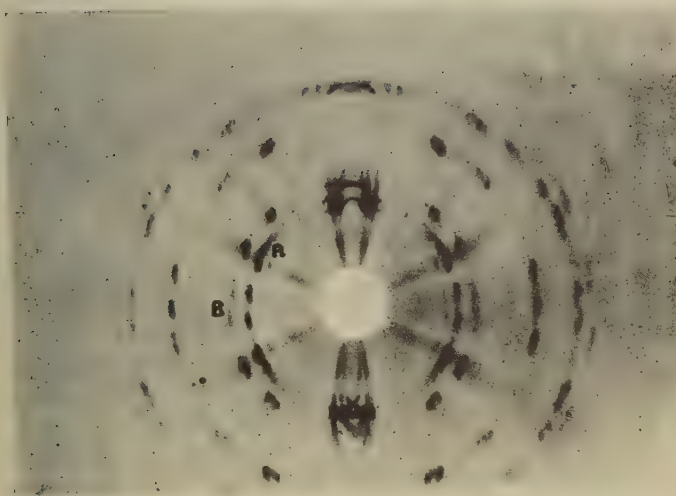
With increasing purity of available metals it is more necessary than ever, when stating recrystallization textures, to quote the purity, temperature of anneal, mode of recrystallization and the magnitude of the previous deformation.

REFERENCES.

- BECK, P. A., and HU, H., 1949, *Trans. Amer. Inst. Min. Met. Eng.*, **185**, 627.
CALNAN, E. A., and CLEWS, C. J. B., 1950, *Phil. Mag.*, **41**, 1085.
VON GÖLER, F., and SACHS, G., 1927, *Z. Metallkunde*, **19**, 90.
HIBBARD, W. R., 1950, *J. Inst. Metals, Lond.*, **77**, 581.
HIBBARD, W. R., and YEN, M.-K., 1948, *Trans. Amer. Inst. Min. Met. Eng.*, **175**, 126.
SCHMID, E., and WASSERMANN, G., 1927, *Z. Physik*, **42**, 779; 1928, *Z. Tech. Physik*, **9**, 106.



(a)



(b)

CXXXVI. *On the Quantum Mechanics of Helium II.*

By O. PENROSE,

Royal Society Mond Laboratory, Cambridge*.

[Received June 2, 1951; revised June 29, 1951.]

ABSTRACT.

The quantum mechanics of a system of identical interacting particles must lead to the classical hydrodynamic equations of motion at high temperatures, because of the correspondence principle. On the other hand, the behaviour of helium II shows that this is not always the case at low temperatures. In this paper it is shown that in certain cases the quantum description requires an extra parameter, which is the potential of a new velocity field superimposed on the classical motion. Expressed in semi-classical terms, the condition for the existence of this new parameter is that the probability, in the equilibrium state, of a particle having a very large de Broglie wavelength (that is, a negligible momentum) is finite. This condition is satisfied in one model of a superfluid system, a condensed Bose-Einstein gas, but not in a crystal. A tentative theoretical interpretation of two basic equations of the empirical two-fluid theory of helium II is given, in which this new parameter determines the velocity of the superfluid.

§ 1. INTRODUCTION.

BORN AND GREEN (1947, 1948) described a method of studying transport processes in a system of identical interacting particles obeying quantum mechanics by using the analogy with the corresponding classical system. Gurov (1948, 1950) carried out a similar calculation. In both cases the conclusion was that the equations of hydrodynamics and heat transfer were identical in form with the classical equations. These treatments assumed that the three quantities describing a "normal" state of the system (Born and Green 1947, Chapman and Cowling 1939) were the same as for a classical system: the density, velocity and temperature fields. In other words, if at one instant the system is in a state described by given fields of these three parameters, its state at a later time is sufficiently described by the new fields of the parameters resulting from the thermohydrodynamical equations of motion. From the correspondence principle it is clear that the three parameters of classical mechanics are sufficient in quantum mechanics at high temperatures, but, as we shall see, this is not always true at low temperatures.

* Communicated by the Author.

§ 2. PROPERTIES OF THE REDUCED DENSITY MATRICES.

Suppose the system consists of N identical particles of mass m interacting by central forces whose potential is U , and let the Schrödinger representative of the density matrix of the corresponding Gibbs ensemble (Dirac 1947) be

$$D(\mathbf{q}_1, \dots, \mathbf{q}_N; \mathbf{q}'_1, \dots, \mathbf{q}'_N),$$

where $\mathbf{q}_1, \dots, \mathbf{q}_N$ are the position vectors of the N particles, and D is Hermitian. The reduced density matrices, which are also Hermitian, are defined by

$$R_k(\mathbf{q}_1, \dots, \mathbf{q}_k; \mathbf{q}'_1, \dots, \mathbf{q}'_k) = [N!/(N-k)!] \times \int \dots \int D(\mathbf{q}_1 \dots \mathbf{q}_N; \mathbf{q}'_1 \dots \mathbf{q}'_k, \mathbf{q}_{k+1} \dots \mathbf{q}_N) d\mathbf{q}_{k+1} \dots d\mathbf{q}_N. \quad (1)$$

The equation of motion for D is

$$i\hbar \partial D / \partial t = HD - DH, \quad (2)$$

where H is the Hamiltonian operator of the system. After setting $\mathbf{q}_2 = \mathbf{q}'_2, \dots, \mathbf{q}_N = \mathbf{q}'_N$, this may be integrated over $\mathbf{q}_2, \dots, \mathbf{q}_N$, giving

$$i\hbar \partial R_1(\mathbf{q}_1; \mathbf{q}'_1) / \partial t = -(\hbar^2/2m)(\nabla_1^2 - \nabla_1'^2)R_1(\mathbf{q}_1; \mathbf{q}'_1) + \int [U(\mathbf{q}_1 - \mathbf{q}_2) - U(\mathbf{q}'_1 - \mathbf{q}_2)]R_2(\mathbf{q}_1, \mathbf{q}_2; \mathbf{q}'_1, \mathbf{q}_2) d\mathbf{q}_2, \quad (3)$$

where $\nabla_j = \partial/\partial \mathbf{q}_j$, etc.

By using Wigner's result (Wigner 1932, Moyal 1949) that a density matrix $R_1(\mathbf{q}_1; \mathbf{q}'_1)$ corresponds to a classical probability density $F(\mathbf{x}, \mathbf{p})$ for the position \mathbf{x} and momentum \mathbf{p} of one particle such that

$$R_1(\mathbf{q}_1; \mathbf{q}'_1) \sim \int d\mathbf{p} F(\frac{1}{2}[\mathbf{q}_1 + \mathbf{q}'_1], \mathbf{p}) \exp[i\mathbf{p} \cdot (\mathbf{q}_1 - \mathbf{q}'_1)/\hbar], \quad (4)$$

combined with the classical result

$$F(\mathbf{x}, \mathbf{p}) \propto \exp[-\mathbf{p}^2/2mkT], \quad (5)$$

or alternatively by approximately solving the Bloch equation $\partial D / \partial (kT)^{-1} = -HD$ (Husimi 1940), we obtain a high temperature approximation

$$R_1(\mathbf{q}_1; \mathbf{q}'_1) \propto \exp[-(\mathbf{q}_1 - \mathbf{q}'_1)^2 mkT / 2\hbar^2], \quad (6)$$

for equilibrium at the temperature T . Therefore

$$\lim_{|\mathbf{q}_1 - \mathbf{q}'_1| \rightarrow \infty} R_1(\mathbf{q}_1; \mathbf{q}'_1) = 0. \quad (7)$$

At low temperatures (7) may not be satisfied for every type of system. To see the physical significance of the failure of (7) let us assume for the moment that $R_1(\mathbf{q}_1; \mathbf{q}'_1)$ depends only on $|\mathbf{q}_1 - \mathbf{q}'_1|$ and approaches a constant value L when $|\mathbf{q}_1 - \mathbf{q}'_1| \rightarrow \infty$. Then the Fourier inverse of (4) yields a divergent integral which may be interpreted as

$$F(\mathbf{x}, \mathbf{p}) = f(\mathbf{p}) + L\delta(\mathbf{p}), \quad (8)$$

where $f(\mathbf{p})$ is a regular function. That is to say, the probability of one particle having zero momentum is the finite fraction $L/R_1(\mathbf{x}; \mathbf{x})$. Since (8) is in fact an expression for the mean occupation numbers of single-particle levels, L must vanish (and (7) therefore be satisfied) in a Fermi-Dirac system, where the exclusion principle limits the occupation numbers.

§ 3. ASYMPTOTIC BEHAVIOUR OF THE REDUCED DENSITY MATRIX FOR ONE PARTICLE.

In the general case when (7) does not hold we shall consider the behaviour of $R_I(\mathbf{q}_I; \mathbf{q}'_I)$ for values of $|\mathbf{q}_I - \mathbf{q}'_I|$ large compared with both $\hbar(mkT)^{-1/2}$ and the range of U . The integral in (3) may be written, using the Hermitian property of R_2 ,

$$\int U(\mathbf{r})[R_2(\mathbf{q}_I, \mathbf{q}_I + \mathbf{r}; \mathbf{q}'_I, \mathbf{q}_I + \mathbf{r}) - R_2^*(\mathbf{q}'_I, \mathbf{q}'_I + \mathbf{r}; \mathbf{q}_I, \mathbf{q}'_I + \mathbf{r})] d\mathbf{r}. \quad (9)$$

Suppose that the asymptotic form of $R_2(\mathbf{q}_I, \mathbf{q}_I + \mathbf{r}; \mathbf{q}'_I, \mathbf{q}_I + \mathbf{r})$ for large $|\mathbf{q}_I - \mathbf{q}'_I|$ is

$$R_2(\mathbf{q}_I, \mathbf{q}_I + \mathbf{r}; \mathbf{q}'_I, \mathbf{q}_I + \mathbf{r}) \sim A(\mathbf{q}_I, \mathbf{r}) R_I(\mathbf{q}_I; \mathbf{q}'_I), \quad (10)$$

just as the neighbour distribution function of a liquid obeys

$$R_2(\mathbf{q}_I, \mathbf{q}_2; \mathbf{q}_I, \mathbf{q}_2) \sim R_I(\mathbf{q}_I; \mathbf{q}_I) R_I(\mathbf{q}_2; \mathbf{q}_2) \quad (11)$$

for large $|\mathbf{q}_I - \mathbf{q}_2|$. For large $|\mathbf{q}_I - \mathbf{q}'_I|$ (3) becomes

$$i\hbar \partial R_I(\mathbf{q}_I; \mathbf{q}'_I) / \partial t \sim -(\hbar^2/2m)(\nabla_I^2 - \nabla_I'^2) R_I(\mathbf{q}_I; \mathbf{q}'_I) + [X(\mathbf{q}_I) - X^*(\mathbf{q}'_I)] R_I(\mathbf{q}_I; \mathbf{q}'_I), \quad (12)$$

where

$$X(\mathbf{q}) = \int A(\mathbf{q}, \mathbf{r}) U(\mathbf{r}) d\mathbf{r} = V(\mathbf{q}) + iW(\mathbf{q}). \quad (13)$$

Since the variables in (12) are separable the general solution is a linear combination of expressions of the form

$$\Psi(\mathbf{q}_I) \Psi^*(\mathbf{q}'_I), \quad (14)$$

where

$$i\hbar \partial \Psi / \partial t = -(\hbar^2/2m) \nabla^2 \Psi + X \Psi. \quad (15)$$

At equilibrium $D = e^{-\beta H}$, and since the Schrödinger representative of H is real, those of D and the R 's are also real. The state of the liquid is uniform, and, therefore, for large enough $|\mathbf{q}_I - \mathbf{q}'_I|$ it may be assumed that

$$R_I(\mathbf{q}_I; \mathbf{q}'_I) \sim \text{const.}$$

This is of the form (14) with $\Psi = \text{const.}$ If the density matrix of a non-equilibrium state is sufficiently similar to $e^{-\beta H}$ the required solution of (12) will still be a single expression of the form (14):

$$R_I(\mathbf{q}_I; \mathbf{q}'_I) \sim \Psi(\mathbf{q}_I) \Psi^*(\mathbf{q}'_I). \quad (16)$$

The example of a condensed Bose gas may clarify the argument of this section. Equation (16) is true, with Ψ the wave-function of the single-particle state into which condensation has taken place. Husimi's formula (1940)

$$R_2(\mathbf{q}_I, \mathbf{q}_2; \mathbf{q}'_I, \mathbf{q}'_2) = R_I(\mathbf{q}_I; \mathbf{q}'_I) R_I(\mathbf{q}_2; \mathbf{q}'_2) + R_I(\mathbf{q}_I; \mathbf{q}'_2) R_I(\mathbf{q}_2; \mathbf{q}'_I)$$

is not valid for a condensed Bose gas; for example, at absolute zero, when all the particles are in the ground state,

$$R_I(\mathbf{q}_I; \mathbf{q}'_I) = \Psi(\mathbf{q}_I) \Psi^*(\mathbf{q}'_I),$$

$$R_2(\mathbf{q}_I, \mathbf{q}_2; \mathbf{q}'_I, \mathbf{q}'_2) = \Psi(\mathbf{q}_I) \Psi(\mathbf{q}_2) \Psi^*(\mathbf{q}'_I) \Psi^*(\mathbf{q}'_2).$$

The correct formula is

$$R_2(\mathbf{q}_I, \mathbf{q}_2; \mathbf{q}'_I, \mathbf{q}'_2) = R_I(\mathbf{q}_I; \mathbf{q}'_I) R_I(\mathbf{q}_2; \mathbf{q}'_2) + R_I(\mathbf{q}_I; \mathbf{q}'_2) R_I(\mathbf{q}_2; \mathbf{q}'_I) - \Psi(\mathbf{q}_I) \Psi(\mathbf{q}_2) \Psi^*(\mathbf{q}'_I) \Psi^*(\mathbf{q}'_2) \quad (17)$$

(compare London 1943). Assuming that this formula holds for non-equilibrium states, (10) and (11) may be verified, with

$$A(\mathbf{q}, \mathbf{r}) = R_I(\mathbf{q} + \mathbf{r}; \mathbf{q} + \mathbf{r}) + R(\mathbf{q}; \mathbf{q} + \mathbf{r})\Psi(\mathbf{q} + \mathbf{r})/\Psi(\mathbf{q}) - \Psi(\mathbf{q} + \mathbf{r})\Psi^*(\mathbf{q} + \mathbf{r}).$$

Madelung's transformation (1927) brings equations (15) and (16) into a form similar to the hydrodynamic equations of motion with velocity potential ϕ , density $|\Psi|^2$, external forces of potential V and a source distribution of strength $2|\Psi|^2 W/\hbar$:

$$R_I(\mathbf{q}_I; \mathbf{q}'_I) \sim Q_\infty(\mathbf{q}_I; \mathbf{q}'_I) \exp \{im[\phi(\mathbf{q}_I) - \phi(\mathbf{q}'_I)]/\hbar\}, \quad \dots (18)$$

where

$$\left. \begin{aligned} Q_\infty(\mathbf{q}_I; \mathbf{q}'_I) &= |\Psi(\mathbf{q}_I)| |\Psi(\mathbf{q}'_I)|, \\ \partial |\Psi|^2 / \partial t + \nabla \cdot (|\Psi|^2 \nabla \phi) &= 2|\Psi|^2 W / \hbar, \\ \partial \phi / \partial t + \frac{1}{2}(\nabla \phi)^2 + V/m &= \hbar^2 \nabla^2 |\Psi| / 2m^2 |\Psi| \simeq 0. \end{aligned} \right\} \quad \dots (19)$$

At equilibrium Q_∞ depends only on the density and temperature, so that even for non-equilibrium states it is a function of the parameters of the classical description. On the other hand, the velocity $\nabla \phi$ corresponds to no quantity in the classical description; it differs from the classical velocity in its laws of change and in being irrotational.

§ 4. THE TWO-FLUID MODEL OF HELIUM II.

The two-fluid model may be interpreted tentatively as follows: Assume that real functions $Q_n(\mathbf{q}_I; \mathbf{q}'_I)$ and $Q_s(\mathbf{q}_I; \mathbf{q}'_I)$ can be chosen, with $Q_n \rightarrow 0$ as $|\mathbf{q}_I - \mathbf{q}'_I| \rightarrow \infty$, such that if at one instant

$$\begin{aligned} R_I(\mathbf{q}_I; \mathbf{q}'_I) &= Q_n(\mathbf{q}_I; \mathbf{q}'_I) \exp \{im(\mathbf{q}_I - \mathbf{q}'_I) \cdot \mathbf{u}(\frac{1}{2}[\mathbf{q}_I + \mathbf{q}'_I])/\hbar\} \\ &\quad + Q_s(\mathbf{q}_I; \mathbf{q}'_I) \exp \{im[\phi(\mathbf{q}_I) - \phi(\mathbf{q}'_I)]/\hbar\} \\ &\quad + O(\nabla \mathbf{u}) + O(\nabla \nabla \phi). \end{aligned} \quad \dots (20)$$

(where the velocities \mathbf{u} and $\nabla \phi$ do not alter appreciably in a distance $\hbar(mkT)^{-1/2}$), then at later instants it is of the same form, with new real functions Q_n , Q_s , \mathbf{u} , and ϕ . If $Q_s = 0$ this would describe a system with classical velocity field \mathbf{u} (Gurov 1948). The density is

$$\begin{aligned} \rho(\mathbf{x}) &= mR(\mathbf{x}; \mathbf{x}) = mQ_n(\mathbf{x}; \mathbf{x}) + mQ_s(\mathbf{x}; \mathbf{x}) \\ &= \rho_n(\mathbf{x}) + \rho_s(\mathbf{x}), \end{aligned} \quad \dots (21)$$

and the current density (Born and Green 1948)

$$\begin{aligned} \mathbf{J}(\mathbf{x}) &= -(i\hbar/2)(\nabla_I - \nabla'_I)R_I(\mathbf{q}_I; \mathbf{q}'_I) \quad [\mathbf{q}_I = \mathbf{q}'_I = \mathbf{x}] \\ &= \rho_n(\mathbf{x})\mathbf{u}(\mathbf{x}) + \rho_s(\mathbf{x})\nabla \phi(\mathbf{x}). \end{aligned} \quad \dots (22)$$

These two equations are the basis of the two-fluid theory (Landau 1941, Tisza 1947); in Landau's version the superfluid velocity is irrotational.

§ 5. EXAMPLES.

Two examples will illustrate the argument. In a crystal the single-molecule wave-functions are confined to small regions, so that (7) is true and classical ideas should explain its mechanical properties. In a condensed

Bose-Einstein gas with negligible repulsive forces and periodic boundary conditions (Bogoliubov 1947)

$$\left. \begin{aligned} R_l(\mathbf{q}_l; \mathbf{q}_l') &= B^{-1} \sum_l n_l \exp i\mathbf{l} \cdot (\mathbf{q}_l - \mathbf{q}_l'), \\ Q_\infty(\mathbf{q}_l; \mathbf{q}_l') &= n_0/B \neq 0, \end{aligned} \right\} \dots \dots (23)$$

where B is the volume of the container and n_l is the mean occupation number of the single-particle state whose wave-number is \mathbf{l} , given by

$$\left. \begin{aligned} n_l &= [\exp(\mathbf{l}^2 \hbar^2 / 2mkT) - 1]^{-1}, \quad [\mathbf{l} \neq 0], \\ \sum_l n_l &= N. \end{aligned} \right\} \dots \dots (24)$$

Bogoliubov claimed that such a system shows superfluidity.

We conclude that (7) is the condition for the classical equations of heat transfer and hydrodynamics to apply, and that when (7) is not satisfied a new quantity enters the equations. This quantity is the potential of a new velocity field superimposed on the classical motion.

ACKNOWLEDGMENTS.

I am very much indebted to Mr. H. N. V. Temperley for supervising this work, to Mr. P. J. Price for discussions, to many of my colleagues for criticizing the manuscript, and to King's College, Cambridge, for awarding me the R. J. Smith Memorial Studentship.

REFERENCES.

- BOGOLIUBOV, N. N., 1947, *J. Phys. U.S.S.R.*, **11**, 23.
 BORN, M., and GREEN, H. S., 1947, *Proc. Roy. Soc. A.*, **190**, 455; 1948, *Ibid.*, **191**, 168.
 CHAPMAN, S., and COWLING, T. G., 1939, *The Mathematical Theory of Non-Uniform Gases*, (Cambridge: University Press) p. 117.
 DIRAC, P. A. M., 1947, *The Principles of Quantum Mechanics*, 3rd edition, (Oxford: University Press) pp. 131-135.
 GUROV, K. P., 1948, *Jour. Exp. and Theor. Phys. U.S.S.R.*, **18**, 110; 1950, *Ibid.*, **20**, 279.
 HUSIMI, K., 1940, *Proc. Physico-Math. Soc. Japan*, [3] **22**, 264.
 LANDAU, L., 1941, *J. Phys. U.S.S.R.*, **5**, 71.
 LONDON, F., 1943, *J. Chem. Phys.*, **11**, 203.
 MADELUNG, E., 1927, *Zeit. für Phys.*, **40**, 322.
 MOYAL, J., 1949, *Proc. Camb. Phil. Soc.*, **45**, 99.
 TISZA, L., 1947, *Phys. Rev.*, **72**, 838.
 WIGNER, E. P., 1932, *Phys. Rev.*, **40**, 749.

CXXXVII. *On the Tomonaga Method for Intermediate Coupling in Meson Field Theory.*

By R. H. DALITZ and D. G. RAVENHALL,

Department of Mathematical Physics, University of Birmingham.*

[Received August 3, 1951.]

ABSTRACT.

The iteration method of Svartholm (1945) is employed to improve the approximate wave function used by Tomonaga (1947) to describe the scalar meson field of an isolated nucleon. It is found that this wave-function of Tomonaga is surprisingly good, even in the region of intermediate coupling, the change in coupling parameter for given energy being at most 3 per cent after the first iteration.

§ 1.

COMPARISON of recent experimental data concerning nucleon-nucleon interactions and meson production with the results of perturbation theory calculations, which depend on the smallness of the meson-nucleon interaction, shows that this interaction may not in fact be regarded as "weak". For the opposite limit of "strong" coupling, Wentzel (1940) has proposed a semi-classical method, and more recently, Tomonaga (1947) has discussed a new approach to the problem, which covers also the intermediate region between these limiting cases. In this work of Wentzel and Tomonaga it was necessary to cut off the high momentum components of the meson field in an arbitrary way in order to obtain finite results. Recently Dyson (1951) has shown how by renormalization of mass and field strength a Hamiltonian can be obtained for which such difficulties do not occur. Accordingly it is of interest to re-examine Tomonaga's method, and it is the purpose of the present work to test the validity of the trial wave-functions proposed by Tomonaga, in the region of intermediate coupling.

§ 2.

Tomonaga investigates the stationary state of a nucleon coupled with a scalar meson field, considering the nucleon as infinitely heavy, so that its recoil and the creation of nucleon pairs are neglected. Here these assumptions are retained.

For charged mesons the Hamiltonian is, in this case,

$$\mathcal{H} = \int \omega(a_k^* a_k + b_k^* b_k) d^3k - l \int G(\mathbf{k}) [(a_k + b_k^*) \tau_+ + (a_k^* + b_k) \tau_-] d^3k, \quad (1)$$

* Communicated by Professor R. E. Peierls, F.R.S.

where a_k, a_k^* are annihilation and creation operators for the Fourier component \mathbf{k} of the positive meson field, b_k, b_k^* the corresponding operators for negative mesons, and $\omega = \sqrt{(\mu^2 + \mathbf{k}^2)}$. With $G(\mathbf{k})$ as used below, the relation of l to g , the usual coupling constant, is $l = g\sqrt{4\pi}$. The divergence difficulties associated with the Hamiltonian (1) are avoided by including in $G(\mathbf{k})$ a cut-off function $F(\mathbf{k})$, and in the work below we shall find it convenient to use the expression

$$G(\mathbf{k}) = F(\mathbf{k})/\sqrt{\omega} = e^{-\omega/M}/\sqrt{\omega},$$

M being of the order of the nucleon mass. (In fact we have chosen $M = 5\mu$.)

Following Fock (1934) we let functions $\chi_{n,m}(\mathbf{k}_1 \dots \mathbf{k}_n; \mathbf{K}_1 \dots \mathbf{K}_m)$ describe the presence of n positive mesons of momenta $\mathbf{k}_1 \dots \mathbf{k}_n$, and m negative mesons of momenta $\mathbf{K}_1 \dots \mathbf{K}_m$. These functions are symmetrical for interchanges within $(\mathbf{k}_1 \dots \mathbf{k}_n)$ and $(\mathbf{K}_1 \dots \mathbf{K}_m)$ separately, and they vanish unless $n=m$, $m+1$ because of the requirement of charge conservation (for the case of a proton). The Schrödinger equation for a stationary state of the system,

$$E\Psi = \mathcal{H}\Psi, \quad (2)$$

becomes

$$\left. \begin{aligned} E\chi_{00} &= -l\int G(\mathbf{k}_1)\chi_{10}(\mathbf{k}_1)d^3k_1, \\ &\dots\dots\dots \\ (E - \Sigma_k\omega - \Sigma_K\omega)\chi_{n,n} \\ &= -l\left\{\frac{1}{\sqrt{n}}\sum_{i=1}^n G(\mathbf{K}_i)\chi_{n,n-1}(\mathbf{k}_1 \dots \mathbf{k}_n; \mathbf{K}_1 \dots \mathbf{K}_{i-1} \mathbf{K}_{i+1} \dots \mathbf{K}_n) \right. \\ &\quad \left. + \sqrt{(n+1)}\int G(\mathbf{k}_{n+1})\chi_{n+1,n}(\mathbf{k}_1 \dots \mathbf{k}_{n+1}; \mathbf{K}_1 \dots \mathbf{K}_n)d^3k_{n+1}\right\}, \\ (E - \Sigma_k\omega - \Sigma_K\omega)\chi_{n+1,n} \\ &= -l\left\{\frac{1}{\sqrt{(n+1)}}\sum_{j=1}^{n+1} G(\mathbf{k}_j)\chi_{n,n}(\mathbf{k}_1 \dots \mathbf{k}_{j-1} \mathbf{k}_{j+1} \dots \mathbf{k}_{n+1}; \mathbf{K}_1 \dots \mathbf{K}_n) \right. \\ &\quad \left. + \sqrt{(n+1)}\int G(\mathbf{K}_{n+1})\chi_{n+1,n+1}(\mathbf{k}_1 \dots \mathbf{k}_{n+1}; \mathbf{K}_1 \dots \mathbf{K}_{n+1})d^3K_{n+1}\right\}, \\ &\dots\dots\dots \end{aligned} \right\} \quad (3)$$

Tomonaga proposed as an approximate solution of (3) the product function

$$\chi_{n,m}(\mathbf{k}_1 \dots \mathbf{k}_n; \mathbf{K}_1 \dots \mathbf{K}_m) = c_{n,m}\phi(\mathbf{k}_1) \dots \phi(\mathbf{k}_n)\psi(\mathbf{K}_1) \dots \psi(\mathbf{K}_m), \quad (4)$$

the functions ϕ, ψ being normalized, and the $c_{n,m}$ being chosen to minimize the expectation value of the energy of the system. For simplicity ϕ and ψ are taken to be of identical form, the most natural choice being

$$\phi(\mathbf{k}) = \psi(\mathbf{k}) = G(\mathbf{k})/(K_2\omega) \quad (5)$$

where $K_2^2 = \int G^2(\mathbf{k}) d^3k / \omega^2$. A perturbation solution of (3) suggests the suitability of the form (5) for ϕ and ψ , and in fact for neutral mesons such a product form is an exact solution with (5) and suitable coefficients c_n .

It is clear that this is an adequate approximation in the limit of "weak" coupling, where the possibility of having more than one meson present is negligible. In the case of strong coupling Tomonaga shows that this wave-function leads to the same energy value as that given by the more rigorous theory of Wentzel. Physically this is clear, since the correlations between positive and negative mesons are unimportant when only $\chi_{n,m}$ involving many mesons contribute appreciably, and further, a wave-function of the form (4) is an exact solution for neutral mesons. Tomonaga also presents numerical calculations covering the region of intermediate coupling between these well-known limiting cases. It is clearly of interest to investigate to what extent the neglect of the correlation between the mesons, implied in (4), is justifiable in this intermediate region.

§ 3.

As in Svartholm's (1945) treatment of the momentum-space integral equation for the deuteron, we use the fact that the Schrödinger equation (3), which has the form

$$(E - T)\Psi = -lV\Psi, \quad \dots \dots \dots (6)$$

may be derived from the variational principle $\delta J = 0$, where

$$J = \langle \Psi^* (E - T) \Psi \rangle / \langle \Psi^* V \Psi \rangle. \quad \dots \dots \dots (7)$$

The minimum value J_{\min} is simply the coupling parameter l for the assumed energy value.

In the present work it has been found convenient to restrict the wave-function (4) by requiring $c_{n,m}$ to be of the form

$$c_{n,m} = \alpha^n \beta^m / (n! m! N^2)^{\frac{1}{2}}, \quad \dots \dots \dots (8)$$

where

$$N^2 = \sum_{n=0}^{\infty} \left(\frac{\alpha^{2n} \beta^{2n}}{(n!)^2} + \frac{\alpha^{2n+2} \beta^{2n}}{n! (n+1)!} \right) = I_0(2\alpha\beta) + \frac{\alpha}{\beta} I_1(2\alpha\beta),$$

I_0 and I_1 , being the Bessel functions of imaginary argument. With the wave-function (4) (referred to as $\chi^{(0)}$) then at once

$$(E - T)_{00} = \langle \chi^{(0)*} (E - T) \chi^{(0)} \rangle = \lambda \left\{ 2\alpha^2 I_0(2\alpha\beta) + \left(2\alpha\beta - \frac{\alpha}{\beta} \right) I_1(2\alpha\beta) \right\}, \quad (9a)$$

$$V_{00} = \langle \chi^{(0)*} V \chi^{(0)} \rangle = -2K_2 \lambda \alpha \{ I_0(2\alpha\beta) + I_1(2\alpha\beta) \}, \quad \dots \dots \dots (9b)$$

where $\lambda = \int \omega \phi^2(\mathbf{k}) d^3k = 2.671 \mu$. The ratio $(E - T)_{00} / V_{00}$ is then minimized by choice of α, β . This may be carried out analytically in the limiting cases of weak and strong coupling. With the notation $\kappa^2 = -E/\lambda$, for weak coupling $\alpha = \kappa + \dots$, $\beta = \frac{1}{2}\kappa + \dots$ and $K_2 l = \kappa(1 + \kappa^2/4 + \dots)$, and for strong coupling $\alpha = \beta = \kappa$ with $K_2 l = \sqrt{2\kappa(1 - 1/(4\kappa^2) + \dots)}$. Clearly the value of l does not depend critically on the choice of α and β , since

l is stationary. The values given here for l agree thus far with the corresponding expressions obtained from the more rigorous theories in these limits. For the several values of E chosen in the intermediate region it was found that the energy value obtained using the approximation (8) differed by less than 0.2 per cent from that obtained from the best possible choice for $c_{n,m}$.

§ 4.

Svartholm (1945) has proposed an iterative method for the solution of eigenvalue problems of the type (6), (7). From an initial function $\Psi^{(0)}$ a sequence of functions $\{\Psi^{(n)}\}$ is defined by the relation

$$(T-E)\Psi^{(n)} = V\Psi^{(n-1)}. \quad (10)$$

Under the conditions that $(T-E)$ and V are positive definite, he has proved that the sequence $l_0, l_{1/2}, l_1, \dots, l_n, l_{n+1/2}, l_{n+1}, \dots$ is monotonic decreasing, where $l_n = (T-E)_{nn}/V_{nn}$ and $l_{n+1/2} = V_{nn}/(T-E)_{n+1, n+1}$.

In the weak coupling limit the first steps of this process may be carried out directly. At once

$$\left. \begin{aligned} \chi_{00}^{(1)} &= K_2 \alpha \chi_{00}^{(0)} / \kappa, \\ \chi_{10}^{(1)} &= K_2 \chi_{10}^{(0)} (1 + \alpha \beta \lambda / \omega) (1 - \lambda \kappa^2 / \omega + \dots), \\ \chi_{11}^{(1)} &= K_2 \chi_{11}^{(0)} \alpha \omega_2 / (\omega_1 + \omega_2). \end{aligned} \right\} \quad (11)$$

whence

$$\left. \begin{aligned} (E-T)_{11} &= 2\lambda K_2^2 (1 + \mathcal{J} \kappa^2 / 2 + \dots), \\ V_{11} &= 2\lambda K_2^3 (1 + (\mathcal{J} - \frac{1}{2}) \kappa^2 + \dots), \end{aligned} \right\} \quad (12)$$

where \mathcal{J} is the definite integral $\iint \omega_2^2 \phi^2(\mathbf{k}_1) \phi^2(\mathbf{k}_2) d^3 k_1 d^3 k_2 / (\lambda(\omega_1 + \omega_2))$. (In fact $\mathcal{J} = 0.568$.) The sequence $\{l_n\}$ is then

$$\left. \begin{aligned} l_0 &= \kappa (1 + \kappa^2 / 4 + \dots) / K_2, \\ l_{1/2} &= l_1 = \kappa (1 + (1 - \mathcal{J}) \kappa^2 / 2 + \dots) / K_2. \end{aligned} \right\} \quad (13)$$

It is apparent from (13) that the important modification of the wave function is that $\chi^{(1)}$ allows to some extent for the correlation between the various mesons. In the same way, $(l_0 - l_{1/2})/l_0$ has been calculated as far as terms of order κ^4 , as shown in curve (A) of the figure.

§ 5.

In the general case, the iterated functions are given by

$$\chi_{n,n}^{(1)}(\mathbf{k}; \mathbf{K}) = K_2 \chi_{n,n}^{(0)}(\mathbf{k}; \mathbf{K}) \{(\Sigma_K \omega) / \beta + \lambda \alpha\} / (E - \Sigma_K \omega - \Sigma_K' \omega), \quad (14a)$$

$$\chi_{n+1,n}^{(1)}(\mathbf{k}; \mathbf{K}) = K_2 \chi_{n+1,n}^{(0)}(\mathbf{k}; \mathbf{K}) \{(\Sigma_K \omega) / \alpha + \lambda \beta\} / (E - \Sigma_K \omega - \Sigma_K' \omega), \quad (14b)$$

from which $(E-T)_{11}$ and V_{11} may be calculated. For this the integral representation

$$\frac{\mu}{-E + \Sigma \omega} = \int_0^\infty e^{(E - \Sigma \omega)t/\mu} dt \quad (15)$$

is found convenient, and the expression finally obtained is

$$(E-T)_{11} = -K_{\frac{1}{2}}^2 \mu \int_0^{\alpha} e^{E t \mu} dt \left[\left(I_0 + \frac{\alpha}{\beta} I_1 \right) (D_2 + 2\lambda \alpha \beta D_1 / \mu) + \lambda^2 \alpha \beta \left(\frac{\alpha}{\beta} I_0 + I_1 \right) / \mu^2 + D_1^2 \alpha \beta \left(I_1 + \frac{\alpha}{\beta} I_2 \right) \right], \quad (16)$$

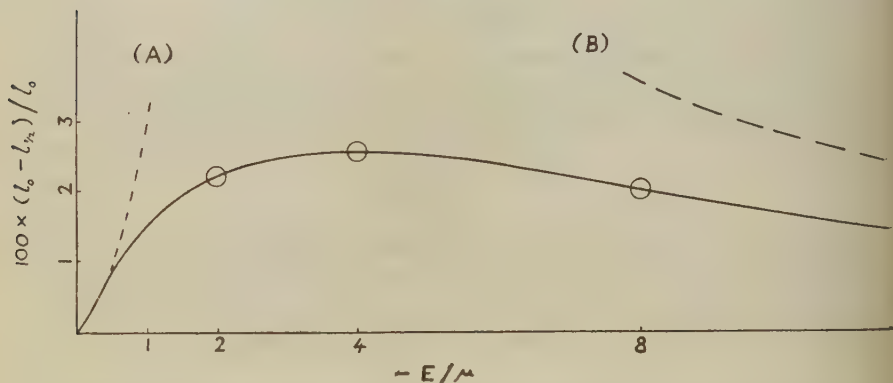
in which $I_0 = I_0(2\alpha\beta D_0)$, $I_1 = I_1(2\alpha\beta D_0)$, $I_2 = I_2(2\alpha\beta D_0)$, D_0 , D_1 , and D_2 being the integrals $D_n(t) = \int \omega^n e^{-\omega t \mu} \phi^2(\mathbf{k}) d^3 k / \mu^n$, expressible in terms of Bessel functions K_n and their integrals. A similar but more complex expression may also be obtained for V_{11} but this will not be required here.

The expression (16) has been obtained numerically for three energy values, and the coupling constants l_0 , l_1 calculated. The results are expressed in the table.

E, μ	α	β	$-(E-T)_{00} \mu$	$-V_{00}/\mu$	$-(E-T)_{11}/\mu$	l_0	l_1
8	1.26	1.04	13.89	16.03	18.88	0.866	0.849
4	0.95	0.675	6.64	11.56	20.65	0.574	0.560
2	0.73	0.455	3.44	8.86	23.86	0.380	0.372

Table of values of α , β , $(E-T)_{00}$, V_{00} , $(E-T)_{11}$, l_0 , and l_1 for some values of E .

Fig. 1.



The proportional change produced in l_0 by the first iteration, as a function of the energy.

In the limit of strong coupling, asymptotic expressions for I_0 , I_1 , I_2 may be used to obtain an analytical expression for $(E-T)_{11}$. With $\alpha = \beta = \kappa$ this leads finally to

$$(E-T)_{11} = \frac{e^{2\kappa^2}}{\sqrt{\pi\kappa}} \lambda (1 + (2\mu^2 D_2(0) - \lambda^2) / (8\lambda^2 \kappa^2) + \dots),$$

whence $l_1 = \sqrt{2\kappa(1 - \mu^2 D_2(0) / (4\lambda^2 \kappa^2) + \dots)}$, in comparison with the value $l_0 = \sqrt{2\kappa(1 - 1/(4\kappa^2))}$. The proportional improvement in the value of l_0 is

sketched in the accompanying graph, together with the curves (A) and (B) obtained in the limiting cases.

It should be noted that because of the arbitrariness in the cut-off used in (1) the physically significant quantities are not l_0, l_1, \dots but α and β , which by (8) give a measure of the average number of mesons present in the system.

§ 6.

The eigenvalue equation (6) will have a series of eigenvalues $l^{(0)}, l^{(1)}, \dots, l^{(n)}, \dots$ with corresponding eigen-functions $\psi_0, \dots, \psi_n, \dots$ satisfying the orthogonality relations $(\psi_n, \psi_m) = 0$ unless $m = n$. If the initial wave function $\Psi^{(0)}$ for the iteration procedure is

$$\Psi^{(0)} = \sum_n a_n \psi_n,$$

then the r th iterated wave function $\Psi^{(r)}$ is

$$\Psi^{(r)} = \sum_n a_n \psi_n / (l^{(n)})^r,$$

so that if $l^{(1)}, \dots$ greatly exceed the lowest eigenvalue $l^{(0)}$, the rate of convergence to the wave function ψ_0 is rapid. The sequence of approximations $\{l_{s/2}^{(0)}\}$ of Svartholm may then be expressed in the form

$$l_{s/2}^{(0)} = \frac{\sum_n |a_n|^2 \mathcal{T}_{nn} / (l^{(n)})^s}{\sum_n |a_n|^2 \mathcal{T}_{nn} / (l^{(n)})^{s+1}},$$

where \mathcal{T}_{nn} is the expectation value of $(T - E)$ in state ψ_n . Accordingly the first step in the sequence $\{l_{s/2}^{(0)}\}$ should provide the major correction to $l_{00}^{(0)}$ provided the ratios $l^{(0)}/l^{(n)}$ are sufficiently small, which will be the case if there do not exist any low-lying excited nucleon states—in fact, with this assumption,

$$(l_{1/2}^{(0)} - l_1^{(0)}) / (l_0^{(0)} - l_{1/2}^{(0)}) \simeq l^{(0)} / l^{(1)}$$

and

$$(l_0 - l_{1/2}) / l_0 \simeq \sum_{n=1}^{\infty} \left| \frac{a_n}{a_0} \right|^2 \mathcal{T}_{nn} / \mathcal{T}_{00},$$

if $\Psi^{(0)}$ is a good approximation to ψ_0 . In the present work we have found that $(l_0 - l_{1/2}) / l_0$ does not exceed 3 per cent so that the wave function of Tomonaga appears to be a surprisingly good approximation to ψ_0 , even in the region of intermediate coupling.

We should like to thank Professor Peierls (who suggested this investigation) and Mr. F. J. Dyson for their stimulating interest. One of us (D. G. R.) acknowledges with thanks financial support from the Department of Scientific and Industrial Research.

REFERENCES.

- DYSON, F. J., 1951, *Proc. Roy. Soc.*, **207**, 395.
 FOCK, V., 1932, *Zeit. f. Phys.*, **75**, 622.
 SVARTHOLM, N., 1945, *Univ. Lund* (Thesis Phys. Inst.).
 TOMONAGA, S., 1947, *Prog. Theor. Phys.*, **2**, 6.
 WENTZEL, G., 1940, *Helv. Phys. Acta*, **13**, (4), 269.

CXXXVIII. *Application of Dislocation Theory to the Polytypism of Silicon Carbide.*

By V. VAND*,

Chemistry Department, The University, Glasgow†.

[Received June 8, 1951. Revised copy received July 14, 1951. Amended copy received August 1, 1951.]

ABSTRACT.

Polytypism of silicon carbide can be understood if the assumption is made that the crystal grows out of the primary nucleus as a single sheet several atomic layers in thickness. The sheet winds itself spirally upwards along a bunch of screw dislocations which are situated at the spiral axis. If there are stacking faults in the original growth layer, they repeat themselves with the periodicity of the pitch of the screw throughout the crystal and thus determine the type and the dimensions of the unit cell. Similar typism occurs in graphite and possibly in diamond and other substances.

AFTER Frank (1951) drew our attention to the existence of spiral growth-steps on carborundum crystals, we examined several hundred well-developed crystals of artificial silicon carbide. The crystal surfaces were not treated in any way and were examined under an optical microscope, using oblique illumination at low magnification. Spiral growth markings, similar to those described by Verma (1951) in the preceding paper, were observed on about 3 per cent of the crystals examined. Some of the steps are obviously many atomic layers in height, whereas some are revealed by preferential deposition or crystal overgrowth of foreign matter, the step acting as a nucleus for overgrowth.

In some cases, preferential etching seemed to take place along the groove of the spiral. In one case a previously invisible spiral has been made plainly visible by smearing and wiping off grease from the crystal face. Some grease deposit remained caught near the spiral step, thus modifying the reflecting power of the crystal surface.

Curved spirals of a type described by Menzies and Sloat (1929) and straight-edged triangular and hexagonal spirals were observed. The outline of the crystal usually bears a close relationship to the shape of the spiral.

We have reached independently similar conclusions regarding the origin of the polytypism of carborundum to those put forward by Frank (1951) in the preceding paper.

* I.C.I. Research Fellow.

† Communicated by the Author.

In carborundum crystals the [0001] face, which shows the spiral growth-steps, is the slowest-growing face. If we limit ourselves to the conditions of growth at low supersaturation, then the presence of a primary nucleus initiating a single screw dislocation line would give rise to a needle with the dislocation line as its axis. The cross-section of the needle would remain constant and equal to that of the primary nucleus. Similarly, two straight screw dislocation lines which are not parallel would give rise to a very thin plate of a thickness equal to that of the primary nucleus.

Assuming straight dislocation lines, a crystal can grow in three dimensions only when three screw dislocations are present, not all in the same plane. This rule does not hold for curved dislocation lines, but in general, three-dimensional growth cannot proceed unless there are points of emergence of dislocation lines on at least three different (non-parallel) faces of the crystal.

One can imagine that the first stages of the crystal growth are very thin needles or plates based on one or two straight dislocation lines. However, when dimensions of these exceed certain critical limits, they become very fragile. Depending on the stresses imposed by the environment, deformation and breakage would ultimately occur. If the broken parts carry with them screw dislocations, as needles must do, they can serve as new nuclei (this probably accounts for the hitherto unexplained multiplication of ice nuclei in the high atmosphere), whereas cracks and slip deformations in thin plates, as suggested by Frank in the preceding paper, would give rise to growth-steps having large Burgers (1939) vectors.

It is likely that in carborundum crystals, small steps grow faster than larger ones. The original short screw dislocations, which initiated the plate growth, would in most cases remain unaltered by cracking, so that the plate sides would remain fast-growing. However, if the large face of the plate acquires a screw dislocation with a large Burgers vector, it begins to grow, but remains the slowest-growing face. Even if further dislocations with the small Burgers vector appear on the same face, the large dislocation would tend to remain dominant; the fast-growing small steps would merge with the large steps when overtaking them.

The crystal can be essentially pictured as a single growth-sheet several atomic layers in thickness, which winds itself upwards spirally using the large Burgers vector as its axis. Provided there is a mistake in the growth-sheet and the dislocation is stable, *i.e.* no new dislocations appear or disappear during growth, the crystal would exhibit periodicity determined by the length of the Burgers vector and the type of the mistake in stacking.

It is most likely that silicon carbide is only one typical example of the occurrence of polytypism by spiral growth from screw dislocations possessing a large Burgers vector. Similar behaviour is to be expected in numerous other substances, the crystals of which grow out by the

screw dislocation mechanism. Silicon carbide shows this type of behaviour to a marked extent because of the great stability of its screw dislocation system. Other softer substances probably do not possess such stability and the phenomenon would occur only on a microscopic scale. Graphite behaves in such a manner, as polytypism similar to that of carborundum has been observed by Lipson and Stokes (1942 a, 1942 b) by X-rays and Hoerni (1949) on individual microcrystals by electron diffraction technique. However, the most interesting case might prove to be that of diamond, which should probably behave in the same manner as silicon carbide. Curved faces and edges appear on diamond. Tolansky and Wilcock (1946) have shown that the curved faces are the result of successive stepped growth-sheets. These almost certainly originate as spirals at growth-points located near the centre of the face. It is well known that at least two modifications of diamond, types I. and II., exist. It is therefore to be expected that if not the whole, then at least substantial parts of each crystal of diamond should be all of the same type, as in silicon carbide crystals. Thibault (1944) also mentions the minerals coquimbite and paracoquimbite, both $\text{Fe}_2\text{O}_3 \cdot 3\text{SO}_3 \cdot 9\text{H}_2\text{O}$ and parisite and synchisite, both $(\text{CeF})_2 \text{Ca}(\text{CO}_3)_3$ as displaying polytypism similar to silicon carbide.

I wish to thank Professor J. Monteath Robertson, F.R.S., for his interest, Dr. I. M. Dawson and Dr. F. C. Frank for valuable discussions on the subject of dislocations and Professor M. J. Buerger for pointing out the necessity of three dislocations and Dr. E. D. Currie and Dr. A. Taylor for the loan of carborundum samples.

REFERENCES.

- BURGERS, J. M., 1939, *Proc. Kon. Akad. Wet.*, **42**, 294, 378.
 FRANK, F. C., 1951, *Phil. Mag.*, **42**, 1014.
 HOERNI, J., 1949, *Nature*, **167**, 1045.
 LIPSON, H., and STOKES, A. R., 1942 a, *Nature*, **149**, 328; 1942 b, *Proc. Roy. Soc.*, **181**, 101.
 MENZIES, A. W. C., and SLOAT, C. A., 1929, *Nature*, **123**, 348.
 THIBAUT, N. W., 1944, *Amer. Mineralogist*, **29**, 249, 327.
 TOLANSKY, S., and WILCOCK, W. L., 1946, *Nature*, **157**, 583.
 VERMA, A. R., 1951, *Phil. Mag.*, **42**, 1005.

(XXXIX. *The Fitting of Polynomials to Unequally-Spaced Data.*

By J. G. HAYES and T. VICKERS,
National Physical Laboratory, Middlesex*.

[Received July 10, 1951.]

SUMMARY.

A technique is given for carrying out rapidly the computations involved in fitting a polynomial by least squares to unequally-spaced data. The technique is obtained by adapting the "triangular resolution" methods of solution of linear equations and inversion of matrices given by Fox (1950) and Fox and Hayes (1951) in a way similar to that in which Guest (1950) has adapted a slower method of Doolittle. The method proposed affords the additional advantage of being able to decide, early in the computation, which degree of polynomial curve is appropriate to the data. The theory is presented to establish the validity of the technique and two numerical examples are carried out to deal with two different sets of requirements.

References are made throughout the text to the appropriate sections of the above three papers, but the present paper is intended to be complete in itself, and does not require a prior knowledge of those papers.

§1. INTRODUCTION.

THE use of orthogonal polynomials in the fitting of regression polynomials to equally-spaced observations is now well-known, accounts of it having been given by several authors, *e.g.* Fisher and Yates (1943). In this case the method has considerable advantages over the straightforward method of solving the normal equations derived from the power terms of the regression polynomial, but these advantages are lost in the case of unequally-spaced observations and it is usual to fall back on the straightforward method as the quickest way to carry out the computation.

Guest (1950) has, however, given a method of computation for this case which, while solving the normal equations of the power terms, adapts the solution to keep in view the technique of orthogonal polynomials and thereby preserves many of the advantages of this technique. No work is saved in the calculation of the regression coefficients, but Guest's method does obtain all curves of degree less than p , and their associated residual sums of squares, in the calculation for the curve of degree p , thus enabling the curve of degree best suited to the data to be selected at the end of the calculation. This process has the further important advantage that the calculation of the standard errors of the coefficients of the power terms and of the standard errors of points on the estimated regression curve is considerably simplified.

*Communication from the National Physical Laboratory.

The method of solving the normal equations which Guest adapts for this purpose is that of Doolittle, but much of the gain due to using such a systematic method of solution is nullified since he writes down the results of all the multiplications in the computation before summing them instead of, as is usual, accumulating the products on a desk calculating machine and writing down only the sums. Consequently, as Guest states, the arithmetic becomes extremely tiresome in the fitting of curves of degree higher than the third. This extension would, however, be quite straightforward if Doolittle's method were followed rather more closely.

There are now available, however, methods of solution of linear equations and inversion of matrices which are far quicker than this method of Doolittle. Some of these, depending on the technique of "triangular resolution", have been recently presented in papers by Fox (1950) and Fox and Hayes (1951) with particular emphasis on arrangement on the computing sheet. We are concerned here only with those methods for symmetric matrices. The present paper adopts these methods, as Guest has done with Doolittle's method, to the fitting of polynomial curves to unequally-spaced data, preserving, at the same time, the above-mentioned advantages of orthogonal representation.

The major gain in the proposed method, beyond that of the use of a quicker method of inversion, is due to the inclusion of a method of obtaining very early in the computation—in fact, in its first stage—the contribution to the total sum of squares of each of the orthogonal polynomials. With this information, we are able to determine which degree of polynomial is best suited to the data and thus carry out the rest of the calculation for a polynomial of this degree, thereby saving the work of computing, for example, an eighth degree polynomial when a fourth degree one proves to be quite adequate.

Moreover, the elementary matrix theory given by Fox (1950) to develop the "triangular resolution" technique can easily be extended to fulfil our present purpose, and enables the theory underlying our method of fitting polynomials by least squares to be presented very concisely.

The theory of our method is presented in the following sections, but its only purpose is to demonstrate the validity of the computational technique given in the examples, which can easily be carried out by computers having no knowledge of the matrix theory.

Two examples are given which involve slightly different forms of the basic method, designed to meet two different sets of requirements. The data used in the examples are those given by Guest (1950), to enable a direct comparison to be made with his method.

§2. THEORY.

(a) *Fitting of Power Terms.*

The usual algebra for the fitting of the power terms of the regression polynomial by least squares is now outlined in matrix notation. Matrices will be denoted by capital letters in Clarendon type, except for those

with only one column, which will be denoted by small letters in Clarendon type.

We have a "dependent" variable y which we take to be related to the "independent" variable x by the equation, of degree q in x ,

$$y = \mathbf{x}'\mathbf{b} + \delta, \quad \dots \quad (1)$$

where $\mathbf{x}' = [1 \ x \ x^2 \ \dots \ x^q]$, $\mathbf{b}' = [b_0 \ b_1 \ \dots \ b_q]$, the row matrix of the coefficients of corresponding powers of x , and δ is the error term, which, as usual, we take to be normally distributed with mean zero and variance σ^2 independent of x .

Our problem is to estimate the b_s , the standard errors of these estimates, and the standard error of any point on the estimated regression curve.

We make n pairs of observations x_s, y_s ($s=1, \dots, n$) of x and y respectively, and our n equations of the form of (1) are represented by

$$\mathbf{y} = \mathbf{X}'\mathbf{b} + \boldsymbol{\delta}, \quad \dots \quad (2)$$

where $\mathbf{y}' = [y_1 \ y_2 \ \dots \ y_n]$, $\mathbf{X} = [\mathbf{x}_1 \ \mathbf{x}_2 \ \dots \ \mathbf{x}_n]$ and $\boldsymbol{\delta}$ is the column matrix of the random errors $\delta_1, \delta_2, \dots, \delta_n$, which are assumed to be statistically independent of each other.

Regression Coefficients.

We then minimize $\Sigma \delta_s^2 \equiv \boldsymbol{\delta}'\boldsymbol{\delta} \equiv [\mathbf{y}' - \mathbf{b}'\mathbf{X}][\mathbf{y} - \mathbf{X}'\mathbf{b}]$ with respect to \mathbf{b} , obtaining the normal equations

$$\mathbf{X}\mathbf{X}'\hat{\mathbf{b}} = \mathbf{X}\mathbf{y},$$

where $\hat{\mathbf{b}}$ is our estimate of \mathbf{b} .

We shall write this as

$$\mathbf{A}\hat{\mathbf{b}} = \mathbf{h}, \quad \dots \quad (3)$$

where

$$\mathbf{A} = \mathbf{X}\mathbf{X}', \quad \dots \quad (4)$$

$$\mathbf{h} = \mathbf{X}\mathbf{y}. \quad \dots \quad (5)$$

Our estimated regression curve is then

$$y = \mathbf{x}'\hat{\mathbf{b}}, \quad \dots \quad (6)$$

where $\hat{\mathbf{b}}$ is the solution of equation (3).

Residual Mean Square.

The sum of squares of residuals is

$$[\mathbf{y}' - \hat{\mathbf{b}}'\mathbf{X}][\mathbf{y} - \mathbf{X}'\hat{\mathbf{b}}]$$

which reduces to

$$\mathbf{y}'\mathbf{y} - \hat{\mathbf{b}}'\mathbf{h}.$$

The mean square of residuals, which estimates σ^2 is then

$$s_R^2 = \frac{1}{n-q-1} (\mathbf{y}'\mathbf{y} - \hat{\mathbf{b}}'\mathbf{h}). \quad \dots \quad (7)$$

Standard Errors of Regression Coefficients.

We have, from equations (2) and (3),

$$\hat{\mathbf{b}} - \mathbf{b} = \mathbf{A}^{-1}\mathbf{X}\boldsymbol{\delta}.$$

(b) *Orthogonal Polynomials.*

We shall now give the algebra for the least squares fitting of the regression curve by means of orthogonal polynomials in order to demonstrate how this approach can be of assistance in the fitting of the power terms of the regression polynomial, dealt with in the previous section, particularly with regard to an early decision on which degree of polynomial is best suited to the data. The methods for the solution of linear equations and the inversion of matrices dealt with by Fox (1950) and Fox and Hayes (1951) lend themselves easily to this approach.

The basis of these methods for the symmetric case, in which we are interested, is the resolution of the matrix \mathbf{A} into the product of a lower triangular matrix \mathbf{L} and its transpose \mathbf{L}' . That is, we obtain \mathbf{L} such that

$$\mathbf{A} = \mathbf{L}\mathbf{L}', \quad \dots \dots \dots (12)$$

where \mathbf{L} has zeros above the principal diagonal.

The orthogonal polynomials, p_r , which we shall consider in fitting our polynomial curve are given by

$$p_r = \sum_{s=0}^r l^{(r,s)} \cdot x^s, \quad r=0, 1, \dots, q,$$

where $l^{(r,s)}$ is the element (r,s) in \mathbf{L}^{-1} , also a lower triangular matrix.

In matrix notation these can be written as

$$\mathbf{p} = \mathbf{L}^{-1}\mathbf{x}, \quad \dots \dots \dots (13)$$

Our n observations, $\mathbf{p}_1, \dots, \mathbf{p}_n$, of \mathbf{p} are then given by

$$\mathbf{P} = \mathbf{L}^{-1}\mathbf{X},$$

where $\mathbf{P} = [\mathbf{p}_1 \mathbf{p}_2 \dots \mathbf{p}_n]$.

That these polynomials are, in fact, orthogonal can be seen at once, since

$$\begin{aligned} \mathbf{P}\mathbf{P}' &= \mathbf{L}^{-1}\mathbf{X}\mathbf{X}'(\mathbf{L}^{-1})', \\ &= \mathbf{L}^{-1}\mathbf{A}(\mathbf{L}^{-1})' \quad \text{from (4),} \\ &= \mathbf{L}^{-1}\mathbf{L}\mathbf{L}'(\mathbf{L}^{-1})' \quad \text{from (12),} \end{aligned}$$

giving

$$\mathbf{P}\mathbf{P}' = \mathbf{I}, \quad \dots \dots \dots (14)$$

where \mathbf{I} is the unit matrix of order $(q+1)$.

These orthogonal polynomials are not the ones used by Guest (1950), but are multiples of them. One coefficient in each of the $(q+1)$ polynomials can be chosen arbitrarily: Guest has made the coefficient of the highest power of x in each polynomial equal to unity, whereas we have chosen the polynomials which produce equation (14).

In fitting to our observations a regression curve in the form of a sum of these orthogonal polynomials, we write the fundamental equation (1) in the form

$$y = \mathbf{p}'\mathbf{c} + \delta, \quad \dots \dots \dots (1')$$

where

$$\mathbf{p}'\mathbf{c} \equiv \mathbf{x}'\mathbf{b}.$$

Similarly, in place of equation (2), we have

$$\mathbf{y} = \mathbf{P}'\mathbf{c} + \boldsymbol{\delta} \quad \dots \quad (2')$$

and we estimate \mathbf{c} by $\hat{\mathbf{c}}$, obtained by minimizing $\boldsymbol{\delta}'\boldsymbol{\delta}$ with respect to \mathbf{c} .

The algebra is then exactly the same as in the previous section with \mathbf{X} replaced by \mathbf{P} and $\hat{\mathbf{b}}$ replaced by $\hat{\mathbf{c}}$.

Also, therefore,

$\mathbf{A} (\equiv \mathbf{X}\mathbf{X}')$ is replaced by $\mathbf{P}\mathbf{P}'$, which is equal to \mathbf{I} ,

and

$\mathbf{h} (\equiv \mathbf{X}\mathbf{y})$ is replaced by $\mathbf{P}\mathbf{y}$, which is equal to $\mathbf{L}^{-1}\mathbf{h}$.

Our estimate $\hat{\mathbf{c}}$ is therefore given by the equation (corresponding to equation (3))

$$\hat{\mathbf{c}} = \mathbf{L}^{-1}\mathbf{h}, \quad \dots \quad (3')$$

and our estimated regression curve is

$$y = \mathbf{p}'\hat{\mathbf{c}}. \quad \dots \quad (6')$$

This curve is, of course, identical with that of the previous section (equation (6)), as can easily be shown algebraically using equations (3'), (13), (12) and (3).

Similarly, equation (7) becomes the equivalent equation

$$s_R^2 = \frac{1}{n-q-1} (\mathbf{y}'\mathbf{y} - \hat{\mathbf{c}}'\mathbf{L}^{-1}\mathbf{h}),$$

or, in a more usual form, from equation (3'),

$$s_R^2 = \frac{1}{n-q-1} (\mathbf{y}'\mathbf{y} - \hat{\mathbf{c}}'\hat{\mathbf{c}}),$$

or

$$s_R^2 = \frac{1}{n-q-1} \left(\sum_{r=1}^n y_r^2 - \sum_{r=0}^q \hat{c}_r^2 \right). \quad \dots \quad (7')$$

Finally, equation (9) becomes,

$$V(\hat{c}_i) = s_R^2, \quad \dots \quad (9')$$

which is not usually of any interest to us, and equation (11), written in the form of equation (10), becomes the equivalent equation

$$V(y_e) = s_R^2 \cdot \mathbf{p}'\mathbf{p}. \quad \dots \quad (11')$$

It is equation (3'), together with equation (7'), which proves to be of value in obtaining the standard errors associated with the regression curve. We know that \hat{c}_r^2 is the reduction in the total sum of squares due to fitting the orthogonal polynomial of degree r , and, therefore, what is equivalent, \hat{c}_r^2 is the extra amount removed from the total sum of squares when a power series of degree r is fitted instead of a power series of degree $(r-1)$. (It may be noted, incidentally, that this latter fact can easily be established as an algebraic identity without reference to orthogonal polynomials, $\hat{\mathbf{c}}$ then being defined by equation (3'). The use of these polynomials, however, allows a better understanding of the computational procedure and of the meaning of the numbers that occur in the calculations.)

The coefficients \hat{c}_r are, in fact, produced as by-products in the first stage of the solution of linear equations for the symmetric case, as given by Fox (1950) in his Example 4: \mathbf{L} is produced a column at a time, and as column r is produced so also is the element r of a row matrix \mathbf{z}' , which is the solution of the equation

$$\mathbf{Lz}=\mathbf{h}.$$

(In Fox's notation this is $\mathbf{Ly}=\mathbf{b}$.) That is,

$$\mathbf{z}=\mathbf{L}^{-1}\mathbf{h}.$$

\mathbf{z} is, therefore, from equation (3'), our column of coefficients \hat{c}_r . By considering the reduction in the total sum of squares due to each \hat{c}_r in turn as it is produced at the end of column r of \mathbf{L} , we can decide which degree of power series is most appropriate to our data, and can complete our computation for this degree. We thus save the waste of labour which is consequent on calculating a regression series which proves to be either too short or too long.

§3. DETAILS OF COMPUTATION.

A decision has to be taken as to what degree of polynomial curve is to be considered at the start, that is, what is the highest power of x we are going to use in calculating the sums of squares and products (the elements of \mathbf{A} and \mathbf{h}). Since, however, we shall know very early in the subsequent calculation which degree of polynomial is, in fact, appropriate to our data, this decision is of only minor importance: if we find that we have used too high a power we merely delete the unnecessary elements of \mathbf{A} , \mathbf{L} , etc.; if we find that we have used too low a power we calculate the further sums of powers and products and elements of \mathbf{L} as required, incurring no unnecessary calculation other than the trivial adjustment of the row and column sums, s_2 and s_3 , referred to below.

To facilitate comparison between the method here presented and that given by Guest (1950), we shall not concern ourselves with this question, but shall carry out the computation exactly corresponding to that of his example, the fitting of a cubic curve to the sixteen pairs of observations he gives. These are

x	y	x	y
-9.0	0.40	0.8	2.30
-7.3	0.53	2.8	2.85
-6.4	1.09	3.5	3.62
-5.5	0.76	4.8	4.50
-4.4	0.80	6.1	6.40
-3.65	1.17	6.25	5.08
-2.2	1.16	7.2	6.85
-1.25	1.45	7.9	8.10

Also following Guest, we shall not concern ourselves with the calculation of the power sums of the x_r , or the sums of products of the y_r with the powers of the x_r , but shall assume these to have been obtained by the method he suggests. In other words, we shall start our computation having already obtained the matrix \mathbf{A} (the element (r, s) of which is given

by $a_{rs} = \sum_{i=1}^n x_i^{r+s}$, $r, s = 0, \dots, q$) and the column \mathbf{h} (the element r of which

is given by $h_r = \sum_{i=1}^n y_i x_i^r$).

We shall, however, work in terms of $x/10$ instead of x , since this makes all the diagonal elements of \mathbf{A} of roughly the same size and order unity, permitting the advantage of keeping a fixed number of decimals throughout the calculation.

Method I.

In outline, this method obtains the regression coefficients, \hat{b}_r , of the power terms from equation (3) by the technique given by Fox (1950) in his Example 4, the first stage of which produces \mathbf{L} and $\hat{\mathbf{c}}$. The latter enables the residual mean square to be calculated from equation (7'), and the decision to be taken as to the degree of polynomial appropriate to the data. The inverse of \mathbf{A} is then computed from \mathbf{L} by Method II. of the paper by Fox and Hayes (1951), and so we are able to obtain the standard errors of the regression coefficients by using equation (9) and of points on the regression curve by using equation (11).

The computation is set out in Example I. below.

\mathbf{A} and \mathbf{h} are placed side by side on the computing sheet. For checking purposes, the column sums of \mathbf{A} and the sum of the elements of \mathbf{h} are entered in the next row as \mathbf{s}'_2 , and the row sums of \mathbf{A} and \mathbf{h} together are entered in the next column as \mathbf{s}_1 .

We then calculate \mathbf{L}' and $\hat{\mathbf{c}}$ (this is a slight variant of Fox's technique, which deals with \mathbf{L} and $\hat{\mathbf{c}}'$) a row at a time from the equations

$$\mathbf{L}\mathbf{L}' = \mathbf{A} \quad . \quad . \quad . \quad . \quad . \quad . \quad . \quad . \quad (12) \text{ bis}$$

and

$$\mathbf{L}\hat{\mathbf{c}} = \mathbf{h}, \quad . \quad . \quad (\text{alternative form of (3')})$$

in the form

$$\text{column } r \text{ of } \mathbf{L}' \times \text{column } s \text{ of } \mathbf{L}' = \text{element } (r, s) \text{ of } \mathbf{A}. \quad . \quad . \quad (15)$$

Here s takes the values r up to $(q+1)$ in turn for each r from 0 up to q in turn, where the column $(q+1)$ of \mathbf{L}' is to be read as $\hat{\mathbf{c}}$ and the element $(r, q+1)$ should be read as the element r of \mathbf{h} , $r = 0, \dots, q$. At each stage, every element in equation (15) is known, except the element (r, s) of \mathbf{L}' , or the element r of $\hat{\mathbf{c}}$, which can therefore be obtained.

When row r of \mathbf{L}' and $\hat{\mathbf{c}}$ has been thus produced, the elements in this row are summed to give element r of \mathbf{s}_3 . The computation of the row is then checked by

$$\text{column } r \text{ of } \mathbf{L}' \times \text{the column } \mathbf{s}_3 = \text{element } r \text{ of } \mathbf{s}_1, \quad . \quad . \quad (16)$$

in which all the elements are known except for those in s_3 which are multiplied by zeros in L' .

It is at this stage that we can decide whether or not a polynomial of degree r is sufficient for fitting our data, and so whether or not we need compute any more rows of L' and \hat{c} . We enter \hat{c}_r^2 in position r of the column "sums of squares due to orthogonal polynomials" and subtract this from the entry $(r-1)$ in the column "residual sum of squares" to obtain the entry r in the latter column. (For $r=0$, we subtract \hat{c}_0^2 from Σy^2 .) In the next column we enter the appropriate number of degrees of freedom ($=n-r-1$, for $r=0, 1, 2, \dots$) and so obtain the residual mean square. These last four columns could be entered beside \hat{c} , but to save computing columns have been entered as a separate table at the end of the main calculation. We can then test the hypothesis \hat{c}_r (and coefficients of all higher degree polynomials) $=0$ by an F test on the ratio of the sum of squares due to the orthogonal polynomial of degree r to the residual sum of squares in the same row, since, under that hypothesis, these are independently distributed as $\chi^2\sigma^2$, on 1 and $(n-r-1)$ degrees of freedom respectively.

We proceed in this way until we obtain a \hat{c}_r , say \hat{c}_k , which does not reduce the sum of squares significantly. We then delete row k of L' , \hat{c} , A and h and column k of L' and A , and all subsequent rows and columns as appropriate, adjust s'_2 and s_3 accordingly, and proceed to the next stage of the calculation using the remainder of L' and \hat{c} .

If, on the other hand, we complete the calculation of L' and \hat{c} without obtaining a \hat{c}_r which does not reduce the sum of squares significantly, we must compute further rows and columns of A and h and, from them, further rows and columns of L' and \hat{c} until we do obtain such a \hat{c}_r , and then we proceed as before. It should be noted that such an increase in the size of A and h , or the final decrease in their size, does not affect the elements of L' and \hat{c} already obtained, the only alteration required being to the row and column sums s'_2 and s_3 .

As stated earlier, however, we shall not concern ourselves in our example with this problem of deciding on the appropriate degree of polynomial to use, but shall carry out the straightforward calculation for fitting the cubic. We are assuming, in effect, that we have carried out our computation so far with five rows and columns ($q=4$) in A etc., found that \hat{c}_4 does not reduce the sum of squares significantly, and consequently deleted row 4 and column 4 of A etc. and adjusted s'_2 and s_3 , leaving ourselves with the elements given in the example.

The next stage is the computation of \hat{b} .

We have, from equations (3) and (12),

$$LL'\hat{b}=h,$$

and, therefore,

$$L'\hat{b}=L^{-1}h,$$

which, by equation (3'), gives

$$L'\hat{b}=\hat{c}. \quad . \quad . \quad . \quad . \quad . \quad . \quad . \quad (17)$$

To obtain $\hat{\mathbf{b}}$ we use equation (17) in the form

$$\text{row } r \text{ of } \mathbf{L}' \times \text{the row } \hat{\mathbf{b}}' = \text{element } r \text{ of } \hat{\mathbf{c}},$$

allowing r to take the values q down to zero in turn, so obtaining $\hat{b}_q, \dots, \hat{b}_0$ in turn.

$\hat{\mathbf{b}}$ is then checked by the equation

$$\text{the row } \mathbf{s}'_2 \times \text{the row } \hat{\mathbf{b}}' = \text{total of column } \mathbf{h}.$$

Finally, we compute \mathbf{A}^{-1} from \mathbf{L}' by Method II. in the paper by Fox and Hayes (1951). From equation (12) we can obtain

$$\mathbf{L}'\mathbf{A}^{-1} = \mathbf{L}^{-1},$$

and use this, to obtain \mathbf{A}^{-1} without needing the unknown part of \mathbf{L}^{-1} , in the form

$$\left. \begin{aligned} \text{row } r \text{ of } \mathbf{L}' \times \text{row } s \text{ of } \mathbf{A}^{-1} &= \text{element } (r, s) \text{ of } \mathbf{L}^{-1} \\ &= 0, \quad \text{when } r < s \\ &= 1/l_{rr}, \quad \text{when } r = s, \end{aligned} \right\} \quad (18)$$

where l_{rr} is the diagonal element r of \mathbf{L}' , $r=0, \dots, q$.

For this purpose the quantities $1/l_{rr}$ are recorded in a row beneath $\hat{\mathbf{b}}$.

By letting s take the values $q, q-1, \dots, r$ in turn for each r from q down to zero, we obtain from equation (18) the elements of \mathbf{A}^{-1} row by row, and in each row from right to left in turn.

When row r has been thus obtained, it is copied into column r and checked by the equation

$$\text{row } r \text{ of } \mathbf{A}^{-1} \times \text{the row } \mathbf{s}'_2 = \text{unity}.$$

Having obtained \mathbf{A}^{-1} , we can calculate the sampling variances of the \hat{b}_r , using equation (9), and of points on the regression curve, using equation (11), in the form

$$V(y_e) = s_R^2(u_0 + u_1x + u_2x^2 + \dots + u_qx^{2q}),$$

where the u_r are the sums of the elements of \mathbf{A}^{-1} in the appropriate backward diagonals. For example, u_2 is the sum of the elements underlined in \mathbf{A}^{-1} of example I. and u_4 is the sum of the elements marked by an asterisk.

EXAMPLE I.

	\mathbf{A}				\mathbf{h}	\mathbf{s}_1
	16.00000	-0.03500	4.78877	-0.17961	47.06000	67.63416
	-0.03500	4.78877	-0.17961	2.28074	19.74100	26.59590
	4.78877	-0.17961	2.28074	-0.26553	16.36283	22.98720
	-0.17961	2.28074	-0.26553	1.29699	8.90970	12.04229
\mathbf{s}'_2	20.57416	6.83490	6.62437	3.13259	92.07353	

\mathbf{L}'

4.00000	-0.00875	1.19719	-0.04490	11.76500	16.90854
	2.18831	-0.07729	1.04206	9.06816	12.22124
		0.91733	-0.14306	3.24722	4.02149
			0.43430	1.04289	1.47719

 $\hat{\mathbf{c}}$ \mathbf{s}_3

$$\hat{\mathbf{b}}' \quad 1.80352 \quad 3.13867 \quad 3.91435 \quad 2.40131$$

$$\mathbf{L}_{rr}^{-1} \quad 0.25000 \quad 0.45697 \quad 1.09012 \quad 2.30256$$

 \mathbf{A}^{-1}

0.17596	0.07893	-0.38575	-0.19341
0.07893	1.38489	-0.34720	-2.49547*
-0.38575	-0.34720	1.31731*	0.82682
-0.19341	-2.49547*	0.82682	5.30177

$$\mathbf{V}(\hat{\delta}_r) \quad 0.0213 \quad 0.1673 \quad 0.1591 \quad 0.6405$$

$$\Sigma y^2 = 233.729$$

r	$\hat{c}_r^2 = \text{sum of squares due to poly. degree } r$	Residual sum of squares	Degrees of freedom	Residual mean square
0	138.415	95.314	15	
1	82.232	13.082	14	0.9344
2	10.544	2.538	13	0.1952
3	1.088	1.450	12	0.1208

$$\mathbf{V}(y_c) = 0.1208 \left[0.1760 + 0.1579 \left(\frac{x}{10} \right) + 0.6134 \left(\frac{x}{10} \right)^2 - 1.0812 \left(\frac{x}{10} \right)^3 - 3.6736 \left(\frac{x}{10} \right)^4 + 1.6536 \left(\frac{x}{10} \right)^5 + 5.3018 \left(\frac{x}{10} \right)^6 \right]$$

$$\begin{aligned} \text{E. g., for } x=10, & \quad \mathbf{V}(y_c) = 0.3803, \\ \text{for } x=5, & \quad \mathbf{V}(y_c) = 0.0215. \end{aligned}$$

Method II.

It often happens that we are not interested in the sampling variances of points on the regression curve, and are required to find only the regression coefficients and their sampling variances. In this case (from equation (9)) we need only the diagonal coefficients of \mathbf{A}^{-1} and it is quicker to compute \mathbf{L}^{-1} instead of \mathbf{A}^{-1} and to obtain the diagonal coefficients of \mathbf{A}^{-1} from this. Our method of computing \mathbf{L}^{-1} is that of Example 2 in the paper by Fox (1950).

The computation for this case is given in our Example II. It proceeds as in our method I. as far as the production of \mathbf{L}' and $\hat{\mathbf{c}}$ and the decision as to the appropriate degree of polynomial except that \mathbf{L} , $\hat{\mathbf{c}}'$ and \mathbf{s}_3' are

recorded, exactly as in Fox's Example 4, instead of their transposes, as in our Example I. That is, equations (15) and (16) are replaced respectively by the equivalent equations

$$\text{row } r \text{ of } \mathbf{L} \times \text{row } s \text{ of } \mathbf{L} = \text{element } (r, s) \text{ of } \mathbf{A},$$

and

$$\text{row } r \text{ of } \mathbf{L} \times \text{the row } \mathbf{s}'_3 = \text{element } r \text{ of } \mathbf{s}_1.$$

\mathbf{L} and $\hat{\mathbf{c}}'$ are thereby obtained column by column.

Having obtained \mathbf{L} , we compute $(\mathbf{L}^{-1})'$ a column at a time by means of the equation

$$\mathbf{L}\mathbf{L}^{-1} = \mathbf{I},$$

in the form

$$\begin{aligned} \text{row } r \text{ of } \mathbf{L} \times \text{row } s \text{ of } (\mathbf{L}^{-1})' &= 1, & \text{when } r=s, \\ &= 0, & \text{when } r \neq s, \end{aligned}$$

where we let s take the values $0, 1, \dots, q$ in turn for each r from 0 to q . In practice, s takes only the values $0, 1, \dots, r$, because of the zeros in \mathbf{L} and $(\mathbf{L}^{-1})'$, the latter having zeros below the principal diagonal. When column r of $(\mathbf{L}^{-1})'$ has been obtained, its elements are summed to give element r of \mathbf{s}'_4 , and the column is checked by means of the equation

$$\text{row } r \text{ of } \mathbf{L} \times \text{the row } \mathbf{s}'_4 = \text{unity}.$$

In passing, it will be remembered from equation (13) that element (r, s) of $(\mathbf{L}^{-1})'$ is the coefficient of x^r in the orthogonal polynomial of degree s .

From equation (17), we have

$$\hat{\mathbf{b}} = (\mathbf{L}^{-1})' \hat{\mathbf{c}},$$

which can be used, to obtain the coefficient \hat{b}_r , in the form

$$\hat{b}_r = \text{row } r \text{ of } (\mathbf{L}^{-1})' \times \text{the row } \hat{\mathbf{c}}'. \quad \dots \quad (19)$$

When all the \hat{b}_r have been obtained, their computation is checked, as in Method I, by

$$\text{the row } \hat{\mathbf{b}}' \times \text{the row } \mathbf{s}'_2 = \text{sum of elements of } \mathbf{h}.$$

To obtain the diagonal coefficients, $a^{(r, r)}$, of \mathbf{A}^{-1} we have from equation (12)

$$(\mathbf{L}^{-1})' \mathbf{L}^{-1} = \mathbf{A}^{-1}, \quad \dots \quad (20)$$

which can be used for this purpose in the form

$$\text{row } r \text{ of } (\mathbf{L}^{-1})' \times \text{row } r \text{ of } (\mathbf{L}^{-1})' = a^{(r, r)}.$$

The $a^{(r, r)}$ yield the sampling variances of the \hat{b}_i by using equation (9).

EXAMPLE II.

	\mathbf{A}				\mathbf{h}	\mathbf{s}_1
	16.00000	-0.03500	4.78877	-0.17961	47.06000	67.63416
	-0.03500	4.78877	-0.17961	2.28074	19.74100	26.59590
	4.78877	-0.17961	2.28074	-0.26553	16.36283	22.98720
	-0.17961	2.28074	-0.26553	1.29699	8.90970	12.04229
\mathbf{s}'_2	20.57416	6.85490	6.62437	3.13259	92.07353	

L

	4.00000			
	-0.00875	2.18831		
	1.19719	-0.07729	0.91733	
	-0.04490	1.04206	-0.14306	0.43430
\hat{c}'	11.76500	9.06816	3.24722	1.04289
s'_3	16.90854	12.22124	4.02149	1.47719
		$(L^{-1})'$		
	0.25000	0.00100	-0.32619	-0.08400
		0.45697	0.03850	-1.08377
			1.09012	0.35909
				2.30256
s'_4	0.25000	0.45797	0.80243	1.49388
\hat{b}'	1.80350	3.13864	3.91435	2.40132
$V(\hat{b}_r)$	0.0213	0.1673	0.1591	0.6405

Table of Sums of Squares, etc. as in Example I.

As has been pointed out, Method II. is suggested for the case where the sampling variances, $V(y_e)$, of points on the regression curve are not required. If, however, after carrying out Method II. we desire to calculate $V(y_e)$, the inverse of \mathbf{A} can be obtained row by row for this purpose from $(L^{-1})'$ by means of equation (20) in the form

$$\text{row } r \text{ of } (L^{-1})' \times \text{row } s \text{ of } (L^{-1})' = \text{element } (r, s) \text{ of } \mathbf{A}^{-1},$$

the check being the same as in Method I.

Method I. is, however, the quicker method if it is intended from the start to obtain \mathbf{A}^{-1} .

It may be seen further that it is possible, in using Method II., to obtain the regression coefficients for a fitted power series of every degree up to q in the process of obtaining those for degree q . This merely requires the writing down of all the sub-totals of the summations involved in calculating the \hat{b}_r from equation (19) since the coefficient, \hat{b}_{rs} , say, of x^r in the regression power series of degree s is given by the equation

$$\hat{b}_{rs} = \sum_{t=0}^s l^{(t,r)} \times \hat{c}_t, \quad . \quad . \quad . \quad . \quad . \quad . \quad (21)$$

where $l^{(t,r)}$ is the element (t, r) of $(L^{-1})'$.

Thus, for example, the coefficient of x (that is, when $r=1$) in the fitted series of degree 1 is $0.45697 \times 9.06816 = 4.14388$; the coefficient of x in the series of degree 2 is this quantity added to 0.03850×3.24722 , giving 4.26890; and that in the series of degree 3, which is \hat{b}_3 in Examples I. and II., is this latter quantity added to -1.08377×1.04289 , giving 3.13864.

All the coefficients obtained from equation (21) are given in the appended table.

TABLE I.

Degree of power series	Coefficient of			
	1	$x/10$	$x^2/100$	$x^3/1000$
0	2.94125			
1	2.95032	4.14388		
2	1.89111	4.26890	3.53986	
3	1.80350	3.13864	3.91435	2.40132

ACKNOWLEDGMENT.

The work described above has been carried out as part of the research programme of the National Physical Laboratory, and this paper is published by permission of the Director of the Laboratory.

REFERENCES.

- FISHER, R. A., and YATES, F., 1943, *Statistical Tables for Biological, Agricultural and Medical Research* (London: Oliver and Boyd Ltd.), 2nd edition.
 FOX, L., 1950, *J. R. Statist. Soc. Ser. B.*, **12**, 120.
 FOX, L., and HAYES, J. G., 1951, *J. R. Statist. Soc. Ser. B* (in press).
 GUEST, P. G., 1950, *Phil. Mag.*, [7] **41**, 124.

CXL. *Dislocations in Thin Plates.*

By J. D. ESHELBY and A. N. STROH,
H. H. Wills Physical Laboratory, University of Bristol*.

[Received August 15, 1951.]

ABSTRACT.

The stress due to a screw dislocation passing normally through an infinite plate or a disc is largely confined to the neighbourhood of the dislocation line, in contrast to the case of a dislocation in an infinite medium. Two screw dislocations in a plate attract or repel one another with a short-range force in place of the inverse first power law for infinite parallel dislocations. The stress due to an edge dislocation is not essentially different in the plate and infinite body so long as the plate remains flat, but in some circumstances the stress may be largely relieved by buckling of the plate.

§ 1. INTRODUCTION.

FORTY (1951) has studied the growth of tabular crystals containing one or more dislocations. Dawson and Vand (1950, 1951) have published photographs of thin crystals with growth spirals terminating on dislocations. It seems worth while, therefore, to contrast the properties of a dislocation in a thin plate and in an infinite body.

We discuss in detail the following configurations of a straight screw dislocation: (i.) meeting normally the surface of a semi-infinite body, (ii.) running normally through an infinite plate and (iii.) along the axis of a disc, with or without a stress-free hole excluding the core of the dislocation. Case (i.) may be of interest in connection with the detailed topography of the surface near the point of emergence of a dislocation (Frank 1951). Fig. 25 of Forty's (1951) paper corresponds almost exactly to case (iii.).

The corresponding problem for an edge dislocation is only briefly touched on.

It is interesting to note that the steps in Forty's growth spirals may be an arbitrary number of lattice spacings (of the order of 100), so that we have to deal with effectively the classical Volterra dislocation with arbitrary Burgers vector, in contrast with the theory of metals where the Burgers vector is assumed to be limited to one of a few simple lattice displacements.

* Communicated by Professor N. F. Mott, F.R.S.

§ 2. A SCREW DISLOCATION NORMAL TO THE SURFACE OF A SEMI-INFINITE BODY.

For a screw dislocation in an infinite body along the z -axis of cylindrical coordinates (r, θ, z) the non-vanishing components of displacement and stress are

$$u_z = \frac{b}{2\pi} \theta, \quad \tau_{\theta z} = \frac{\mu b}{2\pi} \frac{1}{r}. \quad . \quad . \quad . \quad . \quad . \quad (1)$$

The elastic image field which annuls the traction due to the dislocation on the plane $z=0$ is

$$u_\theta = -\frac{b}{2\pi} \frac{r}{R+z}, \quad \tau_{\theta z} = -\frac{\mu b}{2\pi} \frac{r}{R(R+z)}, \quad \tau_{r\theta} = \frac{\mu b}{2\pi} \left(\frac{z^2}{R^3} + \frac{1}{R+z} \right), \quad (2)$$

with $R^2 = r^2 + z^2$ and the other components zero. It is produced by a distribution of couples along the negative z -axis, twisting about the z -axis and with density proportional to distance from the origin. This may be verified by integrating twice with respect to z the expression given by Love (1927, p. 187) for a point-couple. The sum of the states (1) and (2) thus gives the elastic field about a screw dislocation perpendicular to the free surface of the semi-infinite solid $z > 0$.

§ 3. A SCREW DISLOCATION IN A PLATE OR DISC.

To solve the problem of a screw dislocation in an infinite plate we must annul the traction on the planes $z = \pm d$. It is easy to see that this can be done by introducing an infinite series of images of the type (2). A useful expression is, however, more easily found as follows. We take from the image representation the fact that only u_θ , $\tau_{\theta z}$ and $\tau_{r\theta}$ do not vanish. Then

$$\tau_{\theta z} = \mu \partial u_\theta / \partial z, \quad \tau_{r\theta} = \mu (\partial u_\theta / \partial r - u_\theta / r)$$

and the equilibrium condition is

$$\frac{\partial^2 u_\theta}{\partial r^2} + \frac{1}{r} \frac{\partial u_\theta}{\partial r} - \frac{u_\theta}{r^2} + \frac{\partial^2 u_\theta}{\partial z^2} = 0.$$

A simple solution is $u_\theta = \exp(\pm kz) J_1(kr)$. Multiplication by a function of k and integration yields a more general solution. The solution of our problem is easily found to be

$$u_\theta = -\frac{b}{2\pi} \int_0^\infty \frac{\sinh kz}{\cosh kd} J_1(kr) \frac{dk}{k}, \quad . \quad . \quad . \quad . \quad . \quad (3)$$

for then

$$(\tau_{\theta z})_{z=\pm d} = -\frac{\mu b}{2\pi} \int_0^\infty J_1(kr) dk = -\frac{\mu b}{2\pi} \frac{1}{r}.$$

Since

$$\operatorname{sech} x = 2 \sum_{n=0}^{\infty} (-1)^n \exp \{-(2n+1)x\}$$

and

$$\int_0^\infty e^{-kx} J_1(kr) \frac{dk}{k} = \frac{r}{x + \sqrt{x^2 + r^2}}$$

(3) becomes, with $d_n = (2n+1)d$,

$$u_\theta = -\frac{b}{2\pi} \sum_{n=0}^{\infty} (-1)^n \left\{ \frac{r}{d_n - z + \sqrt{[(d_n - z)^2 + r^2]}} - \frac{r}{d_n + z + \sqrt{[(d_n + z)^2 + r^2]}} \right\},$$

exhibiting u_θ as the sum of a set of images of the type (2). Returning to (3), u_θ can be expressed as a series of modified Bessel functions K_1 by contour integration or by following the analysis of Riemann (1855) in a similar problem. In this way the elastic field of a screw dislocation passing perpendicularly through an infinite plate of thickness $2d$ is found to be

$$\left. \begin{aligned} u_z &= \frac{b}{2\pi} \theta, \quad u_\theta = -\frac{b}{2\pi} \frac{z}{r} + \frac{b}{\pi} \sum (\sin \tfrac{1}{2} n\pi) \frac{2}{n\pi} K_1 \left(\frac{n\pi r}{2d} \right) \sin \frac{n\pi z}{2d}, \\ \tau_{\theta z} &= \frac{\mu b}{\pi d} \sum (\sin \tfrac{1}{2} n\pi) K_1 \left(\frac{n\pi r}{2d} \right) \cos \frac{n\pi z}{2d}, \\ \tau_{rz} &= \frac{\mu b}{\pi} \frac{z}{r^2} - \frac{\mu b}{\pi d} \sum (\sin \tfrac{1}{2} n\pi) K_2 \left(\frac{n\pi r}{2d} \right) \sin \frac{n\pi z}{2d}, \\ u_r &= 0, \quad \tau_{rr} = \tau_{\theta\theta} = \tau_{zz} = \tau_{rz} = 0. \end{aligned} \right\} \quad (4)$$

with summation over integral n .

The case of a screw dislocation in the annular disc bounded by the surfaces $z = \pm d$, $r = r_i$, r_o ($r_i < r_o$) can be treated by replacing each K_1 in the u_θ of (4) by a linear combination of K_1 and I_1 and adjusting the constants to annul the traction on the cylindrical surfaces. The result is

$$\left. \begin{aligned} u_z &= \frac{b}{2\pi} \theta, \quad u_\theta = -\frac{b}{2\pi} \frac{z}{r} + \sum \left\{ A_n I_1 \left(\frac{n\pi r}{2d} \right) + B_n K_1 \left(\frac{n\pi r}{2d} \right) \right\} \sin \frac{n\pi z}{2d}, \\ \tau_{\theta z} &= \frac{\mu\pi}{2d} \sum n \left\{ A_n I_1 \left(\frac{n\pi r}{2d} \right) + B_n K_1 \left(\frac{n\pi r}{2d} \right) \right\} \cos \frac{n\pi z}{2d}, \\ \tau_{rz} &= \frac{\mu b}{\pi} \frac{z}{r^2} + \frac{\mu\pi}{2d} \sum n \left\{ A_n I_2 \left(\frac{n\pi r}{2d} \right) - B_n K_2 \left(\frac{n\pi r}{2d} \right) \right\} \sin \frac{n\pi z}{2d}, \\ u_r &= 0, \quad \tau_{rr} = \tau_{\theta\theta} = \tau_{zz} = \tau_{rz} = 0, \end{aligned} \right\} \quad (5)$$

where

$$A_n = \frac{4b}{\pi^2} \frac{1}{n^3} \sin \tfrac{1}{2} n\pi \frac{(2d/n\pi r_i)^2 K_2(n\pi r_o/2d) - (2d/n\pi r_o)^2 K_2(n\pi r_i/2d)}{I_2(n\pi r_o/2d) K_2(n\pi r_i/2d) - I_2(n\pi r_i/2d) K_2(n\pi r_o/2d)}$$

and B_n is obtained from A_n by writing I_2 for K_2 in the numerator.

The energy required to form the dislocation in the annulus is

$$W = \tfrac{1}{2} b \int_{-d}^d dz \int_{r_i}^{r_o} dr \tau_{\theta z}, \quad \dots \dots \dots (6)$$

When the outer radius r_o is infinite

$$\begin{aligned} W &= \frac{8\mu b^2 d}{\pi^3} \sum_{n \text{ odd}} \frac{K_0(n\pi r_i/2d)}{n^2(n\pi r_i/2d)^2 K_2(n\pi r_i/2d)}, \\ &= \frac{\mu b^2}{4\pi} \cdot 2d \cdot \frac{2}{3} \left(\frac{d}{r_i} \right)^2, \quad r_i \gg d, \\ &= \frac{\mu b^2}{4\pi} \cdot 2d \cdot \ln \left(\frac{d}{2 \cdot 24 r_i} \right), \quad r_i \ll d. \quad \dots \dots \dots (7) \end{aligned}$$

When $r_i=0$, $r_o=\infty$ the dislocation at the origin exerts a force

$$F=b' \int_{-d}^d \tau_{\theta z} dz = \frac{4bb'\mu}{\pi^2} \sum_{n \text{ odd}} n^{-1} K_1 \left(\frac{n\pi r}{2d} \right) \quad . \quad . \quad . \quad (8)$$

on another screw dislocation with Burgers vector b' distant r from it.

Since when $x>1$ $I_n(x)$ and $K_n(x)$ respectively increase and decrease exponentially with x the elastic state is given closely by

$$u_z = \frac{b}{2\pi} \theta, \quad u_\theta = -\frac{b}{2\pi} \frac{z}{r}, \quad \tau_{r\theta} = \frac{\mu b}{\pi} \frac{z}{r^2}, \quad \tau_{\theta z} = 0, \quad . \quad (9)$$

if the point r is a few multiples of d away from both the inner and outer edges of the annulus. (9) represents exactly the combined effect of (1) together with (2) and its reflection in the plane $z=0$, with couples of opposite hand. In (4) the terms in K annul the effect of that part of the couple distribution which would lie inside the plate.

§ 4. SCREW DISLOCATION : DISCUSSION.

It will be seen that the elastic state of the plate (equations (4)) is quite different from that of a slab of width $2d$ marked out perpendicular to a screw dislocation in an infinite body (equations (1)). The shear stress $\tau_{\theta z}$ is confined to the neighbourhood of the dislocation. That this must be so is clear: $\tau_{\theta z}$ vanishes at the surface of the plate, and far from the dislocation this state of affairs must persist throughout the thickness of the plate. The energy of a screw dislocation in an infinite plate, with its core excluded by a stress-free hole, is finite, while for a dislocation in an infinite cylinder the integral (6), $(\mu b^2/4\pi) \cdot 2d \cdot \ln(r_o/r_i)$, diverges as $r_o \rightarrow \infty$. Again, in an infinite body two parallel screw dislocations attract like electrostatic line-charges, with a force $(\mu b b'/2\pi) \cdot 2d/r$ per length $2d$, whilst each term in (8) is the force due to a line-charge made up of particles attracting with the Yukawa potential $\text{const. } r^{-1} \exp \{-n\pi r/2d\}$. Because $\tau_{r\theta}$ does not vanish the screw dislocation will also interact with an edge dislocation running parallel to the z -axis. Since $\tau_{r\theta}$ is an odd function of z there will be no net force between them, but only a couple. It is also clear that the image-force attracting the dislocation towards the edge of a lamina will be very small unless the dislocation is only a few multiples of d from the edge. In the simple case where the dislocation is distant D from the edge of a semi-infinite plate this force is given by (8) with $b'=b$, $r=2D$. For comparison the image force on a length $2d$ of a screw dislocation running at a distance D parallel to the free surface of a semi-infinite solid is $\mu b^2 d/D$.

§ 5. EDGE DISLOCATIONS.

The stresses τ_{rr} , $\tau_{\theta\theta}$, $\tau_{r\theta}$ produced by an edge dislocation along the z -axis in an infinite body are derived from the Airy function $\chi = \text{const. } r \ln r \sin \theta$, while $\tau_{zz} = \nu(\tau_{rr} + \tau_{\theta\theta})$ and the remaining components are zero. To solve the problem of an edge dislocation traversing a plate

we must find an image stress system giving $\tau_{rz}=0$ and $\tau_{zz}=\text{const.} \sin \theta/r$ on the planes $z=\pm d$. The necessary analysis would be similar to that of Sneddon (1946). We should have to evaluate integrals like those in his § 5, but with Bessel functions of higher order on account of the angular dependence. The results would not be simple, and the case of an edge dislocation in an annular disc would be quite intractable. The general nature of the result can, however, be made out quite simply. If in the solution (Love, *op. cit.* p. 225) for an infinite hollow cylinder with an edge dislocation we replace λ by $2\lambda\mu/(\lambda+2\mu)$ the resulting expressions give the stresses and displacements averaged across the thickness of a disc cut from the cylinder and having surfaces free of stress (generalized plane stress: Love, *op. cit.*, p. 207). The average stresses will fall off as $1/r$ and the elastic state will not be very different from what it was when the disc formed part of the infinite cylinder.

As long as the plate containing the edge dislocation remains flat there is thus no widespread relaxation of stress, as there is for the screw dislocation. However, the energy may be reduced by buckling of the plate. Take a sheet of paper with a hole in it and make a tuck of constant width b (small compared with the size of the hole) running from the hole to the edge of the sheet. The paper will form a surface given roughly by the equation $z=(b\sqrt{2} \sin \theta)/2\pi$. If the paper is flattened out to form a plane dislocated lamina a large amount of strain-energy will be introduced. On the other hand we should not expect buckling to occur in a thick dislocated disc.

To find out the relations between the Burgers vector and the thickness and inner and outer radii of the annular disc for which buckling is energetically favourable we should have to use the theory of plates with strain in the middle surface (v. Kármán (1910)), modified to take account of initial stress. These equations are non-linear and it is difficult to solve them with the necessary boundary conditions. It seems clear, however, that in certain circumstances an edge dislocation will be able to relieve most of its stress by slight buckling of the plate, except within a few multiples of d from its centre, leading to a state of affairs similar to that discussed for the screw dislocation.

REFERENCES.

- DAWSON, I. M., and VAND, V., 1950, *Nature*, **165**, 295; 1951, *Proc. Roy. Soc.* **206A** 555.
 FORTY, A. J., 1951, *Phil. Mag.*, [7], **42**, 670.
 FRANK, F. C., 1951, *Acta Cryst.* In the press.
 v. KÁRMÁN, TH., 1910, *Ency. der Math. Wiss.* IV, [4], 348, (Leipzig: Teubner).
 LOVE, A. E. H., 1927, *Mathematical Theory of Elasticity*, (Cambridge: University Press).
 RIEMANN, B., 1855, *Ann. der Phys.*, **95**, 130.
 SNEDDON, I. N., 1946, *Proc. Camb. Phil. Soc.*, **42**, 260.

CXLI. *The Influence of Deviations from the Debye Spectrum on the Electrical Conductivity of Metals.*

By F. H. J. CORNISH and D. K. C. MACDONALD,
Clarendon Laboratory, Oxford*.

[Received August 3, 1951.]

IN the modern theory of the electrical resistance of metals, as originally developed by Bloch (1928, 1930) and Wilson (1936), (see also Mott and Jones (1936)), the assumptions made about the thermal vibrations of the crystalline lattice are essentially those which lead to the Debye spectrum familiar in the theory of specific heats. Bloch himself derived rigorous formulæ valid for low ($T \ll \Theta$) and high ($T \gg \Theta$) temperatures, and Grüneisen (1933) suggested a general interpolation formula for all temperatures :

$$\rho \sim \frac{T^5}{\Theta^6} \int_0^{\Theta/T} \frac{z^5 dz}{(e^z - 1)(1 - e^{-z})}, \quad \dots \dots (1)$$

based on Bloch's work, which agrees with the rigorous expressions at both limits of T . More recently Sondheimer (1950) and Rhodes (1950) have extended Bloch's analysis to deal rigorously with the intermediate temperature region and it appears that the Grüneisen formula differs nowhere by more than ~ 10 per cent. Since in our work we have been concerned with trying to interpret experimental deviations from the simple Bloch-Grüneisen theory of several hundreds per cent at low temperatures, we shall accept (1) as an adequate representation of the resistance of an ideal metal with a pure Debye lattice spectrum.

The work of Born and Blackman (1935) on specific heats has shown that the Debye spectrum can only be regarded in general as a rather rough approximation to the actual vibration spectrum of specific crystals. Thus several detailed calculations have been made, based on crystal dynamics, of the actual frequency spectrum (*e.g.* Helen Smith (1948), Kellerman (1940)), and these reveal that the frequency spectrum has several peaks. This has the consequence that experimental specific heat data tend in general at low temperatures to give an apparent fall in the Debye temperature.

It is therefore somewhat surprising that, as far as we are aware, no attempt has yet been made to extend the theory of metallic conduction to allow for a vibrational spectrum of more arbitrary form. This is probably due to the fact that a direct generalization is not immediately obvious as in the case of internal energy and therefore specific heats, and also possibly because it might be expected that the electrical resistance

* Communicated by the Authors.

would depend less critically on the particular vibration spectrum. Thus, for example perhaps, one might look for a crude dependence on lattice entropy (*e. g. cf.* Simon 1924, Mott 1934).

From the fundamental theory of metallic resistance (*e. g.* Wilson, *loc. cit.*) it is quite straightforward to derive the following expression for the resistance as the corresponding generalization of (1) above :

$$\rho \sim \frac{1}{T} \int_0^{\hat{q}} \frac{q^5 dq}{(\exp[\hbar\nu/kT]-1)(1-\exp[-\hbar\nu/kT])}, \quad \dots \quad (2)$$

where q is the lattice wave number, ν is the frequency and $\nu=uq/2\pi$, u being the wave velocity. \hat{q} is the upper limit of wave number determined by the total number of normal modes of the lattice. The Debye temperature is then defined in terms of q by $k\Theta=\hbar u\hat{q}$.

1. If then u is set $=u_0$ (constant for all q), corresponding to the Debye spectrum, then (2) above reduces immediately to (1) as expected.

2. If $\nu=\nu_0$ (constant for all q) corresponding to an "Einstein Model" then we have

$$\rho \sim \frac{1}{T} \cdot \frac{1}{(\exp[\hbar\nu_0/kT]-1)(1-\exp[-\hbar\nu_0/kT])}$$

or, setting $\hbar\nu_0=k\Theta_E$,

$$\rho \sim \frac{1}{T} \cdot \frac{1}{(\exp[\Theta_E/T]-1)(1-\exp[-\Theta_E/T])}, \quad \dots \quad (3)$$

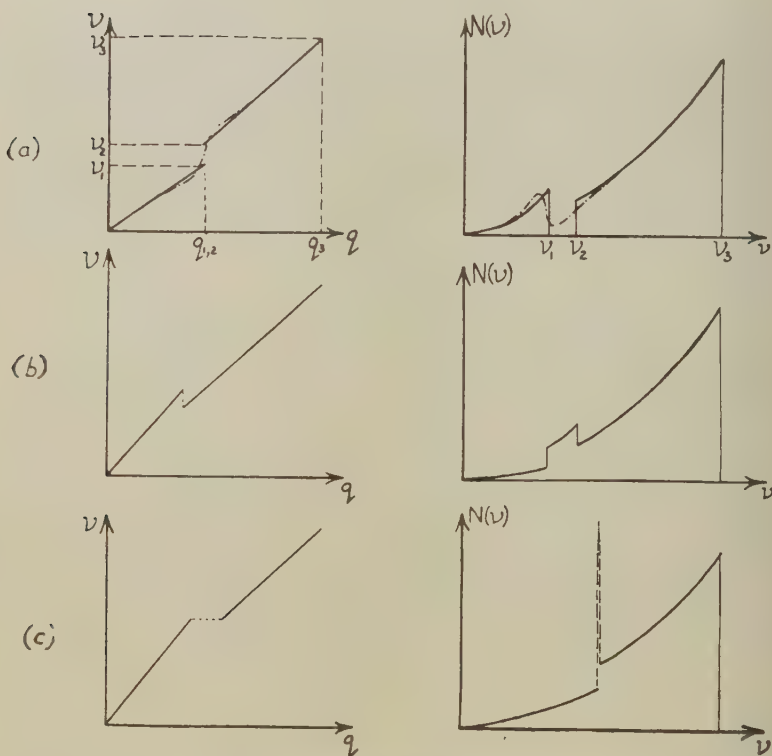
reducing to $\rho \sim T/\Theta_E^2$ for $T \gg \Theta_E$ and $\rho \sim 1/T \exp(-\Theta_E/T)$ for $T \ll \Theta_E$. Since, as Born has pointed out, the highly dispersive optical branches of the lattice spectrum may be approximated closely by Einstein oscillators it is clear from the latter formula that for T appreciably less than Θ_E the contribution to the resistance from these branches is negligible.

We have turned our attention initially to the case of the monovalent alkali metal Lithium which would be expected *a priori* to conform most closely to the ideal free electron model on which the Bloch theory is based. However it is evident from the specific heat measurements of Simon and Swain (1935) that there is considerable deviation from the simple Debye spectrum, and the experimental Θ value drops from $\sim 380^\circ$ K. at 60° K. to $\sim 330^\circ$ K. at 15° K. At the same time electrical resistance measurements (*cf.* Meissner and Voigt 1930, MacDonald and Mendelssohn 1950) have shown that down to $\sim 70^\circ$ K. equation (1) fits the experimental results quite well with $\Theta \doteq 360^\circ$ K., but that at low temperatures there is very strong divergence.

In order to apply equation (2) to a metal with a spectrum departing to some extent from the simple Debye model, we have considered the $\nu-q$ function as made up of linear portions. The three such basic types involving a single discontinuity are sketched in the accompanying figure

together with the resulting $N-\nu$ spectra. In our numerical work thus far we have limited ourselves to Case (a), *i. e.* explicitly :

$$\left. \begin{aligned} \nu &= u_1 \frac{q}{2\pi} & 0 \leq \nu \leq \nu_1 & & 0 \leq q \leq q_1, \\ \nu &= u_2 \frac{q}{2\pi} & \nu_2 \leq \nu \leq \nu_3 & & q_1 = q_2 \leq q \leq q_3. \end{aligned} \right\} \dots (4)$$



$\nu-q$ and $N-\nu$ curves for lattices deviating from simple Debye model.

[Note.—The direct complement to model (c) has been here omitted because a retrogression of wave-number, q , is involved leading to a negative value of $N(\nu)$ at the discontinuity.]

This leads to the following expression for the resistance :

$$\rho \sim T \left[\frac{\alpha^6}{\beta^4} G\left(\frac{\Theta_1}{T}\right) + G\left(\frac{\Theta_3}{T}\right) - \left(\frac{\alpha}{\beta}\right)^4 G\left(\frac{\Theta_2}{T}\right) \right], \dots (5)$$

where $\alpha u_1 = u_2 : \beta \nu_1 = \nu_3 : \nu_1/u_1 = \nu_2/u_2 : k\Theta_r = \hbar \nu_r$

and

$$G\left(\frac{\Theta}{T}\right) = \left(\frac{T}{\Theta}\right)^4 \int_0^{\Theta/T} \frac{z^5 dz}{(e^z - 1)(1 - e^{-z})},$$

i. e. G is the function tabulated by Grüneisen (1933). Two sets of (α, β) values have been used and they lead to the results (normalized at 273° K.) tabulated below. There is clearly improved agreement with experiment

Table of Comparative Results.

T (° K.):	374.5	273	80.1	20.4	11.4	6.0
Observed resistance*	1.443	1.000	0.1252	0.0013	0.00009	0.000007
Grüneisen Eq. (1) ($\Theta=360^\circ$ K.)	1.433	1.000	0.125	0.00042	0.000022	0.000009
New model:						
1. $\alpha=1.3, \beta=2$	1.434	1.000	0.144	0.0015 ₈	0.00009 ₇	0.000004
2. $\alpha=1.3, \beta=3$	1.435	1.000	0.129	0.00118	0.00010 ₃	0.000004 ₃

* With residual resistance subtracted, and normalized to unity at 273° K.

over the Grüneisen formula in the temperature range $T < 70^\circ$ K. This does suggest that a major part of the apparent discrepancy with theory may be attributed to the departure of the lattice spectrum, or rather the ν - q curve, from the simple Debye model. It is, however, quite probable that part is still due to deviation of the electron characteristics from those of an ideal electron gas.

The abrupt gap in the frequency spectrum in the model we have chosen may appear somewhat surprising at first sight. Physically, however, one might rather expect to have ν - q and N - ν curves somewhat as shown by the broken curves in fig. 1(a).

The specific heat for the model chosen is given by

$$C_v = \left(\frac{\alpha}{\beta}\right)^3 (D_1 - D_2) + D_3, \quad \dots \quad (6)$$

where (α, β) are as before in (5) and $D_r = D(\Theta_r/T)$, where D is the specific heat for the simple Debye model. The apparent Θ values for a specific heat based on this model with $\alpha=1.3, \beta=3$ are: at 60° K., $\Theta=354^\circ$ K., and at 15° K., $\Theta=286.5^\circ$ K. This then compares quite favourably with the relative variation of Θ observed by Simon and Swain, although the absolute values are not in agreement. In any case, of course, as Blackman (1951) has emphasized again, the effective spectrum will be different for the specific heat and the electrical resistivity, since in an ideal metal only the longitudinal vibrations produce significant electron scattering.

We intend to extend this work to other metals and to consider also the electronic thermal conductivity and we hope to publish in more detail later.

REFERENCES.

- BLACKMAN, M., 1935, *Proc. Roy. Soc. A*, **148**, 365, 384 ; 1951, *Proc. Phys. Soc. A*, **64**, 681.
- BLOCH, F., 1928, *Z. f. Phys.*, **52**, 555 ; 1930, *Ibid.*, **59**, 208.
- GRÜNEISEN, E., 1933, *Ann. d. Phys.*, **16**, 530.
- KELLERMAN, E. W., 1940, *Phil. Trans. Roy. Soc.*, **238**, 513, 548.
- MACDONALD, D. K. C., and MENDELSSOHN, K., 1950, *Proc. Roy. Soc. A*, **202**, 103.
- MEISSNER, W., and VOIGT, B., 1930, *Ann. d. Phys.*, **7**, 761, 892.
- MOTT, N. F., and JONES, H., 1936, *Theory of the properties of metals and alloys*.
(Oxford : University Press.)
- MOTT, N. F., 1934, *Proc. Roy. Soc. A*, **146**, 465.
- RHODES, P., 1950, *Proc. Roy. Soc. A*, **202**, 466.
- SIMON, F. E., 1924, *Z. Phys.*, **27**, 157.
- SIMON, F. E., and SWAIN, R. C., 1935, *Z. phys. Chem. B*, **28**, 189.
- SMITH, HELEN, 1948, *Phil. Trans. Roy. Soc.*, **241**, 105, 145.
- SONDHEIMER, E. H., 1950, *Proc. Roy. Soc. A*, **203**, 75.
- WILSON, A. H., 1936, *The Theory of Metals*, (Cambridge : University Press).

CXLII. *Effects of the Recoil on Allowed β -Transitions.*

By O. KOFOED-HANSEN,

Institute for Theoretical Physics, University of Copenhagen*.

[Received July 9, 1951.]

SUMMARY.

The recoil corrections to the shape of the Fermi distribution for the β -spectrum are calculated, and it is concluded that they are of the same order of magnitude as other effects, which are usually neglected. Furthermore it is shown that the observed half-life and shape of the β -spectrum of the neutron excludes any coupling in β -decay depending on nuclear $v./c.$ terms only.

§1. INTRODUCTION.

WHEN the shape of the β -spectrum is calculated one considers the β -decaying nucleus as infinitely heavy, and one neglects the kinetic energy of the recoil in the conservation of energy since it is small compared with the energy of the β -particle and the neutrino.

In that approximation, where the neutrino rest mass is neglected, the maximum value of the kinetic energy of the recoil, T_R^{\max} , occurs when the β -particle is emitted with its maximum energy. T_R^{\max} is given by

$$T_R^{\max} = \frac{533}{A} (T_\beta^{\max^2} + 1.022 T_\beta^{\max}) 10^{-6} \quad . \quad . \quad . \quad (1)$$

where T_R^{\max} and T_β^{\max} are given in MeV. A is the mass number of the isobars in question. For the β -decay of the neutron one finds $T_R^{\max} \cong 0.1$ per cent of T_β^{\max} and for He^6 and B^{12} $T_R^{\max} \cong 0.05$ per cent of T_β^{\max} .

The effect on the shape of the β -spectrum is somewhat larger as will be shown in a following section. Although it is not necessary for this calculation to apply so general methods we shall first give an exact relativistic treatment of the phase space calculation for a general three particle process in the next section, and in the following section we shall apply the results of this calculation to the special case of nuclear β -decay.

The effects from the recoil will partly enter in the phase space calculation and partly in the determination of the square of the matrix element for the transition. In the special case of the β -decay of the neutron some particular effects from the recoil appear in the matrix element and give rise to the exclusions of the pseudoscalar coupling case as responsible for the β -decay of the neutron. This special case will be treated in the last section of this paper.

* Communicated by Professor C. Møller.

§ 2. EXACT RELATIVISTIC PHASE SPACE CALCULATION.

The probability of a process where a particle at rest disintegrates into three individual particles is proportional to the integral

$$P = (4\pi)^{-2} \int |\mathcal{M}|^2 d\mathbf{p}_1 d\mathbf{p}_2 d\mathbf{p}_3 \delta(\mathbf{p}_1 + \mathbf{p}_2 + \mathbf{p}_3) \delta(M - E_1 - E_2 - E_3) \quad (2)$$

where \mathcal{M} is the matrix element for the process, p_i is the momentum of the i th particle, and E_i is the corresponding energy including the rest mass m_i . The abbreviation $d\mathbf{p}$ means $dp_x dp_y dp_z$ and the function $\delta(\mathbf{x})$ is the product of the three delta functions in each of the coordinates of the vector \mathbf{x} . M is the mass of the original particle, and $c=1$. The two delta functions express the conservation of momentum and of energy.

If we assume a random orientation in the space of the original particles the process is completely described by two parameters in the momentum triangle, and we can average (2) over all parameters besides such two variables.

Three of the integrations in (2) take away the momentum delta function. This means, however, that we have to take into account the momentum conservation in the form

$$p_3^2 = p_1^2 + p_2^2 + 2p_1 p_2 \cos \theta_{12} \quad (3)$$

in the delta function for the energy. Here θ_{12} is the angle between the vectors \mathbf{p}_1 and \mathbf{p}_2 . By a well-known transformation (see Bethe 1933) we get

$$P = \frac{1}{2} \int E_1 dE_1 E_2 dE_2 E_3 dE_3 |\mathcal{M}|^2 \delta(M - E_1 - E_2 - E_3) \quad (4)$$

One further integration leads to

$$P = \int P(E_1, E_2) dE_1 dE_2 = \frac{1}{2} \int |\mathcal{M}|^2 (M - E_1 - E_2) E_1 dE_1 E_2 dE_2 \quad (5)$$

$P(E_1, E_2)$ is the distribution function for the two variables E_1 and E_2 . These two variables determine the process completely. It must be remembered that for a fixed value of E_1 the variable E_2 cannot assume any value between m_2 and E_2^{max} . It follows from the laws of conservation of energy and momentum that for a fixed value of E_1 the variable E_2 must lie in the interval between the two limits

$$\left. \begin{aligned} E_2' \\ E_2 \end{aligned} \right\} &= [(M - E_1)(M^2 - 2ME_1 + m_1^2 + m_2^2 - m_3^2) \\ &\pm p_1 \{(M^2 - 2ME_1 + m_1^2 - m_2^2 - m_3^2)^2 - 4m_2^2 m_3^2\}^{\frac{1}{2}}] / [2(M^2 - 2ME_1 + m_1^2)]. \end{aligned} \quad (6)$$

This expression can be verified *e. g.* by means of the geometrical picture of the conservation laws of energy and momentum given by Blaton (1950). Fig. 1 shows as an illustration to (6) the area in an $E_1 E_2$ plane inside which these parameters may vary in the special case $m_1 = m_3 = 0.3M$ and $m_2 = 0.2M$.

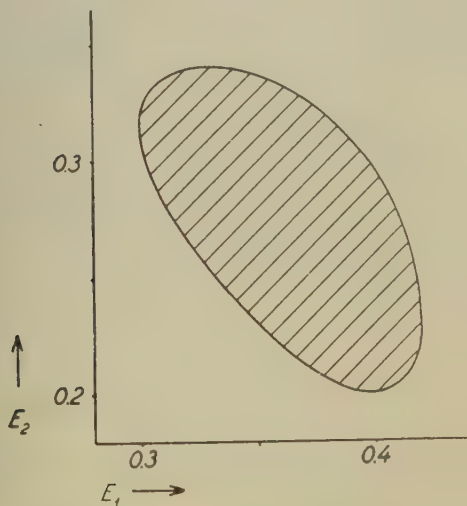
Any one of the particles obtains its maximum energy when the two others travel in the same direction and with the same velocity. This is easily seen by a simple extremum consideration. From this result we find

$$E_1^{\max} = [M^2 + m_1^2 - (m_2 + m_3)^2] / (2M). \quad (7)$$

Let us consider a certain process in which $|\mathcal{M}|^2$ is substantially constant. Then we find the probability distribution of one of the energies simply by an integration of (5) where $|\mathcal{M}|^2$ is taken outside the integral. The integration must be carried out inside the limits given by (6). We find

$$P_{E_1} = \frac{1}{24} p_1 E_1 \{ (M^2 - 2ME_1 + m_1^2 - m_2^2 - m_3^2)^2 - 4m_2^2 m_3^2 \}^{\frac{1}{2}} \{ 3(M - E_1)^2 \cdot [(M^2 - 2ME_1 + m_1^2)^2 - (m_2^2 - m_3^2)^2] - (E_1^2 - m_1^2) [(M^2 - 2ME_1 + m_1^2 - m_2^2 - m_3^2)^2 - 4m_2^2 m_3^2] \} / (M^2 - 2ME_1 + m_1^2)^3 \quad (8)$$

Fig. i.



The hatched area is the area in the $E_1 E_2$ plane inside which E_1 and E_2 may vary in the special case $m_1 = m_3 = 0.3M$ and $m_2 = 0.2M$.

If one wants to determine the total probability for a disintegration one has to carry out one further integration over E_1 , where the integral is taken between the limits m_1 and E_1^{\max} . This integral is the complete relativistic analogue to the Fermi integral in β -decay. The integral can be expressed in terms of complete elliptic integrals of the first, second and third kind in the general case. Only when all three particles may be treated non-relativistically or when one of the particles has zero rest

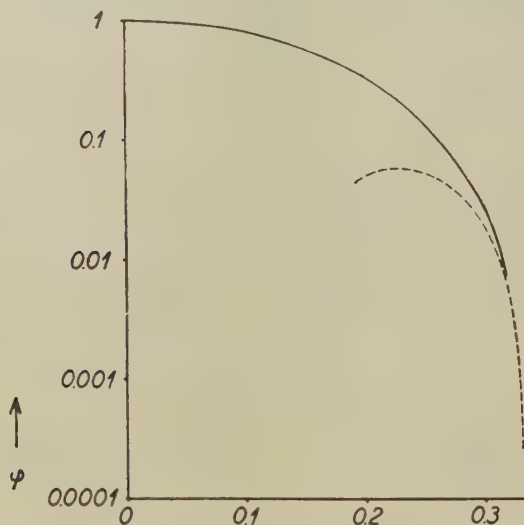
mass can the integral be expressed in terms of simple functions. Fig. 2 shows the value of the integral of (8) in the special case $m_1=m_2=m_3$. The figure gives this integral divided by $7M^5/3840$ and as a function of m/M where m is the common mass for the three particles. The dotted curve is the non-relativistic approximation. The curve illustrates the validity of the non-relativistic approximation.

§ 3. RECOIL EFFECTS ON THE PHASE SPACE CALCULATION IN β -DECAY.

In the β -decay the square of the matrix element for the transition is given by an expression of the type (Hamilton 1947)

$$|\mathcal{M}|^2 = |\mathcal{M}_K|^2 (1 + a(p_\beta/E_\beta) \cos \theta_{\beta\nu}) \dots \dots \dots (9)$$

Fig. 2.



The figure shows the generalized Fermi integral divided by $7M^5/3840$ as a function of m in the special case $|\mathcal{M}| = 1$ and $m_1=m_2=m_3=m$. The dotted curve is the non-relativistic approximation.

where we have neglected the neutrino rest mass. $|\mathcal{M}_K|^2$ is the square of the nuclear matrix element, which we shall consider as a constant in this section. In the derivation of (9) one has neglected all nuclear $v./c$. terms and all higher order terms in the expansion of the lepton wave-functions over the finite extension of the nucleus *i. e.* one has neglected terms of the order R/λ or of higher order where R is the nuclear radius, and where λ is the wavelength of the leptons.

Integrations of the type leading from (5) to (8) are easily performed also when matrix elements such as (9) are taken into account. The

resulting expression is in many respects similar to (8) but of course it is somewhat more involved. If the result is expanded in a series in E_β/M one finds

$$P(E_\beta) = p_\beta E_\beta (E_\beta^{\max} - E_\beta)^2 [1 + 3E_\beta/M - E_\beta^{\max}/M + a(m_\beta^2/(ME_\beta) - 3E_\beta/M)]. \quad (10)$$

This expression is identical with the usual Fermi β -spectrum apart from the extra factor contained in the square bracket.

The deviation is small since the extra factor is very close to unity. The maximum correction amounts to 0.2 per cent for He^6 , 0.5 per cent for the neutron and 0.6 per cent for B^{12} with the choice $a = -1$. The effect is larger for Li^8 , but due to the complicated structure of the Be^8 daughter nucleus this β -spectrum is not directly comparable with the simple Fermi spectrum. In any case higher order effects may influence the shape of the β -spectrum to the same order of magnitude. We shall mention that v./c. terms and R/λ terms may change the allowed shape to the same order of magnitude, namely about 0.1 per cent.

Thus we may conclude that the effects from the neglect of T_R in the energy conservation is of the same order of magnitude as other effects which are usually neglected in the discussion of allowed β -decay.

§ 4. β -DECAY OF THE NEUTRON.

Usually the nuclear matrix element \mathcal{M}_K cannot be calculated since so far no satisfactory theory of nuclei exist. In the case of the β -decay of the neutron, however, one may assume that a satisfactory treatment of the behaviour of the neutron and the recoil proton is obtained when these particles are described by a Dirac equation. In this case it is a simple problem to determine \mathcal{M}_K .

In the scalar coupling case one finds

$$|\mathcal{M}_K|^2 = \frac{1}{2}(E_P M + M m_P)/(E_P M) = 1 \quad (11)$$

where the index P refers to the recoil proton. In the pseudoscalar coupling case one finds

$$|\mathcal{M}_K|^2 = \frac{1}{2}(E_P M - M m_P)/(E_P M) = \frac{1}{4}v_P^2 \quad (12)$$

We remember that we have put $c = 1$.

In case of β -decay of other nuclei than the neutron one would still find in the pseudoscalar coupling case that $|\mathcal{M}_K|^2$ is of the order of v_P^2 but now v_P means the velocity of the nucleon in a bound state, and thus $|\mathcal{M}_K|^2$ would be $\sim 10^4$ as large as for the neutron (see also Marshak 1949) in contradiction to experimental results (Robson 1950, 1951, Snell, Pleasonton and McCord 1950). Thus we may conclude that the

experimental detection of the β -decay of the neutron has ruled out the possibility that the pseudoscalar coupling case can be responsible for the β -decay of the neutron.

Also in case of a pseudoscalar coupling the β -spectrum of the neutron would not be the same as for normal allowed β -spectra, since the variation of (12) with E_β is proportional to

$$|\mathbf{p}_\beta + \mathbf{p}_\nu|^2 \dots \dots \dots (13)$$

In other words the shape of the β -spectrum of the neutron would be of the same type as for first forbidden spectra. This result is also in contradiction with experimental results (Snell 1951).

I wish to thank Professor N. Bohr and Professor C. Møller for their interest in this work.

REFERENCES.

- BETHE, H., 1933, *Handbuch der Physik*, **24**, 1, 354.
 BLATON, J., 1950, *Dan. Mat. Fys. Medd.*, **24**, no. 20.
 HAMILTON, D. R., 1947, *Phys. Rev.*, **71**, 456.
 MARSHAK, R. E., 1949, *Phys. Rev.*, **75**, 513.
 ROBSON, J. M., 1950, *Phys. Rev.*, **78**, 311 ; 1951, *Ibid.*, **81**, 297.
 SNELL, A. H., 1951, *Nucleonics*, **8**, 3.
 SNELL, A. H., PLEASANTON, F., and MCCORD, R. V., 1950, *Phys. Rev.*, **78**, 310.

CXLIII. *Thermal Convection in a Magnetic Field*.*

By W. B. THOMPSON †,
University of Toronto ‡.

[Received August 13, 1951.]

SUMMARY.

The modifications produced in the Rayleigh-Jeffreys theory of slow thermal convection by magneto-hydrodynamic effects in a conducting fluid placed in a magnetic field are examined.

Even for a non-viscous fluid, a critical temperature gradient β_0 must be exceeded in order that convection occur. In this, the place of viscosity η occurring in the Rayleigh-Jeffreys formula is taken by a quantity η_H depending on the conductivity of the fluid, the magnetic field strength H and depth of fluid d , thus $\eta_H = (4/27)(d^2/\pi^2)(\sigma\mu^2 H^2/c^2)$. If the fluid is viscous a multiple of the normal viscosity depending on H must be added to η_H .

An estimate of the critical gradient is made for somewhat artificial boundary conditions and it is found large enough to be experimentally detectable.

The applicability of Jeffreys' method of marginal stability is discussed and the nature of possible oscillations investigated.

INTRODUCTION.

THE interaction between the flow of electrically conducting fluids and magnetic fields has been considered by Alfven (1950) and Walen (1944) in discussing processes in the sun, by Fermi (1949), Richtmeyer and Teller (1949) in a theory of the origin of cosmic rays, and by Elsasser (1946) and Bullard (1949) in an explanation of terrestrial magnetism. Bullard (1949) has proposed a reasonably simple scheme of thermal convection currents and magnetic fields within the core of the earth which might be able to maintain the observed field at the surface by the self-inductive mechanism originally proposed by Larmor. He also showed that the magnetic field is of prime importance in determining the flow.

As a first step toward investigating the hydrodynamical aspects of this process a study has been made of the slow thermal convection currents set up in a plane layer of conducting fluid placed in a homogeneous

* An extract from a thesis submitted in partial fulfilment of the requirements for the degree of Doctor of Philosophy at the University of Toronto.

† Communicated by the Author.

‡ Now at the Atomic Energy Research Establishment, Harwell.

magnetic field and heated from below. The motion occurring when no field is present has been studied experimentally by Bénard (1901) and by Sutton (1951) and examined theoretically by Rayleigh (1917) and Jeffreys (1926).

The stream lines form a system of horizontal vortex rings dividing the plane into cells with fluid flowing up in the centre and down at the edges. Rayleigh's theory described this system, predicted the temperature gradient needed to produce it, and made statements about the shape of the cells. Here the analysis of Rayleigh and Jeffreys will be modified by including the ponderomotive effects of the magnetic field, which involves adding to the hydrodynamic and heat flow equations Maxwell's equations for the electromagnetic fields.

§ 1. MATHEMATICAL FORMULATION OF THE PROBLEM.

We shall consider an infinite horizontal layer of depth d of an incompressible fluid with electrical conductivity σ placed in a homogeneous magnetic field \mathbf{H}_0 and heated from below. At first viscosity will be neglected and Euler's equation for the velocity $\mathbf{V}=(u, v, w)$ written as

$$\rho \left[\frac{\partial \mathbf{V}}{\partial t} + (\mathbf{V} \cdot \nabla) \mathbf{V} \right] = -\nabla p + \rho \mathbf{g} + \frac{\mu}{c} \mathbf{j} \times \mathbf{H}, \quad . \quad . \quad . \quad (1.1)$$

where ρ is the density of the fluid, p the pressure, \mathbf{g} the gravitational acceleration, and $\mathbf{j} \times \mathbf{H}$ the ponderomotive force due to the magnetic field \mathbf{H} , \mathbf{j} being the electric current density.

The motion arises because of the temperature dependence of the density, ρ . This dependence may be taken in a form appropriate to an incompressible fluid with a coefficient of thermal expansion α ,

$$\rho = \rho_0(1 - \alpha T). \quad . \quad . \quad . \quad . \quad . \quad . \quad (1.2)$$

The temperature distribution is determined by Fourier's equation modified by the motion to read

$$\frac{\partial T}{\partial t} + \mathbf{V} \cdot \nabla T = K \nabla^2 T, \quad . \quad . \quad . \quad . \quad . \quad (1.3)$$

where K is the thermal diffusivity.

In addition, the motion is subject to the equation of continuity

$$\text{div } \rho \mathbf{V} = -\frac{\partial \rho}{\partial t}. \quad . \quad . \quad . \quad . \quad . \quad . \quad (1.4)$$

The current \mathbf{j} is given in Gaussian units by

$$\mathbf{j} = \sigma \left(\mathbf{E} + \mu \frac{\mathbf{V}}{c} \times \mathbf{H} \right), \quad . \quad . \quad . \quad . \quad . \quad . \quad (1.5)$$

where σ is the electrical conductivity, and the fields \mathbf{E} and \mathbf{H} satisfy Maxwell's equations with a dielectric constant ϵ , and permeability μ .

$$\left. \begin{aligned} \text{curl } \mathbf{H} &= \frac{4\pi}{c} \mathbf{j} + \frac{\epsilon}{c} \frac{\partial \mathbf{E}}{\partial t}, \\ \text{curl } \mathbf{E} &= -\frac{\mu}{c} \frac{\partial \mathbf{H}}{\partial t}, \\ \text{div } \mathbf{H} &= 0, \\ \text{div } \mathbf{E} &= 4\pi \frac{q}{\epsilon}, \\ \text{div } \mathbf{j} &= -\frac{\partial q}{\partial t}. \end{aligned} \right\} \quad (1.6)$$

Here q is the electric charge density and c is the velocity of light in vacuum.

To render the problem tractable a number of assumptions must be made. First, the equations must be linearized by considering departures from equilibrium so small that their squares can be neglected. By expanding all functions in powers of a constant $\lambda = \bar{v} v_0$ where v represents the mean velocity and v_0 is defined by $\frac{1}{2} \rho v_0^2 = \mu (8\pi) H_0^2$ one can show that the neglect of terms of higher order than the first leads to small errors in the solution provided that λ is small. That is, the linearization can be justified if the kinetic energy per unit volume of fluid is small compared to the magnetic energy density.

A second assumption is that the fractional variation in the density is small and that the continuity equation (1.4) may be replaced by (Hales 1937)

$$\text{div } \mathbf{V} = 0. \quad (1.7)$$

The third assumption is that a physically meaningful result, can be obtained by solving the time independent problem. Jeffreys (1926) gives an argument justifying this procedure derived from the principle of marginal stability. In a later section the modifications produced in this argument by consideration of the magnetic field are discussed and it is shown that Jeffreys' argument remains valid provided $c^2/4\pi\mu K\sigma < 1$.

With these assumptions the zero'th approximation yields the condition of static equilibrium. If a Cartesian coordinate system with the origin in the lower surface of the fluid and the positive Oz axis directed vertically upwards is introduced, the relevant quantities can be written :

$$p_0 = \rho_0 g(z-d) + \rho_0 \alpha g \beta (z^2 - d^2), \quad (1.8)$$

$$T_0 = -\beta z, \quad (1.9)$$

where β is the negative temperature gradient, and ρ_0 is the density at the lower surface of the fluid, where the temperature is considered as zero.

If the static terms are removed, the equations determining the first approximation to the velocity, and the first order corrections p , and T' to the pressure and temperature are

$$0 = -\nabla p - \rho_0 \alpha \mathbf{g} T' + \frac{\mu}{c} (\mathbf{j} \times \mathbf{H}_0) \quad (1.10)$$

$$-\beta w = K \nabla^2 T' \quad (1.11)$$

to which must be added Maxwell's equations for the approximations to the field, and the equation of continuity for velocities.

§ 2. DEDUCTION OF THE FUNDAMENTAL DIFFERENTIAL EQUATION.

From (1.10) and (1.11), the static form of Maxwell's equations, and the continuity equation it is possible to deduce a differential equation for T' . This is done by first applying the operator curl to (1.10) obtaining

$$0 = -\text{curl} (\rho_0 \alpha \mathbf{g} T') + \frac{\mu}{c} \text{curl} (\mathbf{j} \times \mathbf{H}_0) \quad (2.1)$$

The second term may be developed as

$$(\mathbf{H}_0 \cdot \nabla) \mathbf{j} - \mathbf{H}_0 (\nabla \cdot \mathbf{j})$$

which, in view of (1.5) and (1.6) becomes

$$(\mathbf{H}_0 \cdot \nabla) \sigma (\mathbf{E} + \frac{\mu}{c} \mathbf{V} \times \mathbf{H}_0).$$

When this replacement has been made the curl operator may be applied to (2.1) yielding

$$0 = -\text{curl curl} (\rho_0 \alpha \mathbf{g} T') + \frac{\sigma \mu}{c} \mathbf{H}_0 \cdot \nabla \left[\text{curl} \mathbf{E} + \frac{\mu}{c} \text{curl} (\mathbf{V} \times \mathbf{H}_0) \right] \quad (2.2)$$

From this equation curl \mathbf{E} vanishes by (1.6 b), curl $(\mathbf{V} \times \mathbf{H}_0)$ reduces to $(\mathbf{H}_0 \cdot \nabla) \mathbf{V}$ from (1.7) and curl curl $(\rho_0 \alpha \mathbf{g} T')$ can be expanded to leave

$$0 = \nabla^2 (\rho_0 \alpha \mathbf{g} T') - \text{grad} (\rho_0 \alpha \mathbf{g} \cdot \nabla T') + \frac{\sigma \mu^2}{c^2} (\mathbf{H}_0 \cdot \nabla)^2 \mathbf{V} \quad (2.3)$$

Since $\rho_0 \alpha \mathbf{g}$ is a constant vector directed along the negative Oz axis, the Oz component of (2.3) may be written

$$-\rho_0 \alpha g \left(\nabla^2 - \frac{\partial^2}{\partial z^2} \right) T' + \frac{\sigma \mu^2}{c^2} (\mathbf{H}_0 \cdot \nabla)^2 w = 0 \quad (2.4)$$

Finally, w can be eliminated with the help of (1.11) leaving the desired equation

$$\rho_0 \alpha g \left(\nabla^2 - \frac{\partial^2}{\partial z^2} \right) T' + \frac{K}{\beta} \frac{\sigma \mu^2}{c^2} (\mathbf{H}_0 \cdot \nabla) \nabla^2 T' = 0 \quad (2.5)$$

It proves convenient to write this in dimensionless form introducing as a unit of length the depth d of the fluid, and writing the inducing field $\mathbf{H}_0 = H\mathbf{U}$ where \mathbf{U} is a unit vector. Then (2.5) becomes

$$\left[(\mathbf{U} \cdot \nabla)^2 \nabla^2 + A \left(\nabla^2 - \frac{\partial^2}{\partial z^2} \right) \right] T' = 0, \quad \dots \quad (2.6)$$

where

$$A = d^3 \frac{\rho_0 \alpha g}{K} \frac{\beta \cdot c^2}{\sigma \mu^2 H^2}. \quad \dots \quad (2.7)$$

This differential equation with its boundary conditions forms an eigenvalue problem for A and its solution determines the minimum temperature gradient required for the onset of any convective mode, and the form of the temperature perturbation produced. From this, the remaining variables can be determined.

§ 3. SOLUTION TO THE FUNDAMENTAL DIFFERENTIAL EQUATION.

The solution of (2.6) is obtained by the method used by Rayleigh for the analogous problem in the absence of a field. This involves considering, not the close packed hexagonal cells observed experimentally but hypothetical rectangular cells. If the plane layer is infinite we write

$$T' = T'(z) \exp(ikx + imy) + \text{complex conjugate} \quad \dots \quad (3.1)$$

where $\pi d/l$, $\pi d/m$ are the dimensions of the cell considered and x and y are coordinates measured horizontally.

Suitable boundary conditions are those suggested by Rayleigh (1917), the vanishing of the temperature perturbation T' , and of the vertical component of velocity w , corresponding to rigid conducting walls.

(1.11) implies that these boundary conditions are

$$T'(0) = T'(1) = \frac{d^2 T'(0)}{dz^2} = \frac{d^2 T'(1)}{dz^2} = 0.$$

Since (2.6) is homogeneous with constant coefficients we may write

$$T'(z) \sim \exp isz$$

where s is a root of the quartic,

$$(s^2 + l^2 + m^2)(s \sin \phi + l \cos \phi)^2 = A(l^2 + m^2). \quad \dots \quad (3.2)$$

Here, the unit vector $\mathbf{U} = (\cos \phi, 0, \sin \phi)$ making ϕ the inclination of the magnetic field \mathbf{H}_0 to the horizontal. For $\phi = \pi/2$ the field is directed vertically upwards and for $\phi = 0$ along the positive OX axis.

Any solution is a linear combination of four fundamental solutions involving the roots s_1, s_2, s_3 , and s_4 , of (3.2),

$$T'(z) = \sum_{j=1}^4 A_j \exp is_j z.$$

The boundary conditions put four homogeneous conditions on the constants A_j , whose consistency restricts the roots of (3.2) to those satisfying

$$\Delta = \begin{vmatrix} 1 & 1 & 1 & 1 \\ s_1^2 & s_2^2 & s_3^2 & s_4^2 \\ \exp is_1 & \exp is_2 & \exp is_3 & \exp is_4 \\ s_1^2 \exp is_1 & s_2^2 \exp is_2 & s_3^2 \exp is_3 & s_4^2 \exp is_4 \end{vmatrix} = 0. \quad (3.3)$$

Equations (3.3) and (3.2) define Δ as a function of the parameters l, m . The minimum value of $\Delta(l, m)$ determines the temperature gradient needed to start convection, and the corresponding values of l and m determine the nature of the initial motion. The good agreement between Rayleigh's and Jeffreys' results and the measurements of Bénard and Chandra (1938) show that this cell size is preserved for finite values of the velocities.

§ 4. EXISTENCE OF A MINIMUM TEMPERATURE GRADIENT.

It is possible to show that unless the field is horizontal ($\sin \phi = 0$) the negative temperature gradient must exceed a certain critical value before Bénard-Rayleigh convection can occur. With $\Delta = 0$ (3.2) becomes

$$(s^2 + l^2 + m^2)(s \sin \phi + l \cos \phi)^2 = 0 \quad (4.1)$$

which for $\sin \phi \neq 0$ has roots,

$$s_1 = i\sqrt{l^2 + m^2}, \quad s_2 = -i\sqrt{l^2 + m^2}, \quad s_3 = s_4 = -l \cot \phi.$$

Since the characteristic equation has a repeated root the solution can be written

$$T'(z) = A_1 \exp is_1 z + A_2 \exp is_2 z + (A_3 + A_4 z) \exp is_3 z$$

and (3.3) must be replaced by

$$\Delta = \begin{vmatrix} 1 & 1 & 1 & 0 \\ s_1^2 & s_2^2 & s_3^2 & -2is_3 \\ \exp is_1 & \exp is_2 & \exp is_3 & \exp is_3 \\ s_1^2 \exp is_1 & s_2^2 \exp is_2 & s_3^2 \exp is_3 & (s_3^2 - 2is_3) \exp is_3 \end{vmatrix} = 0. \quad (4.2)$$

or

$$(2s^2 y^2 + y^4 + s^4) \sinh y = (y^2 + s^2)^2 \sinh y = 0 \quad (4.3)$$

where $y = \sqrt{l^2 + m^2}$ and $s = l \cot \phi$ are both real. Hence the only possible solution is $l = m = 0$; and unless $\sin \phi = 0$, Δ and consequently β must attain some positive value before convection begins. Physically this means that convection cannot occur until the temperature gradient attains some negative value, as would be expected. However, it is

possible to prove a stronger statement than this, namely: for a non-horizontal field ($\phi \neq 0$) solutions do not exist unless Λ exceeds some definite positive quantity, and hence that convective motions only occur when the negative temperature gradient exceeds a definite critical value β_0 .

In order to do this we must show that not only is there no solution for $\Lambda=0$ but that it is not possible to obtain solutions for arbitrarily small positive values of Λ . To inspect solutions for small values of Λ it is easiest to expand the roots s in a series of powers of Λ and consider only the first terms. For convenience (3.2) is written

$$(s^2 + b^2)(s + a)^2 = c^2 b^2 \quad \dots \quad (4.4)$$

where $a = l \cot \phi$, $b^2 = l^2 + m^2$ and $c^2 = \Lambda \operatorname{cosec}^2 \phi$. For $c=0$ the roots are $s_1 = ib$, $s_2 = -ib$, $s_3 = s_4 = -a$.

We expand s as a Taylor's series in c , thus

$$s = s(0) + c \left(\frac{\partial s}{\partial c} \right)_{c=0} + \dots$$

and from (4.4)

$$\frac{\partial s}{\partial c} = \frac{cb^2}{(s+a)[s(s+a) + s^2 + b^2]},$$

and for $s_1 = -s_2 = ib$, $c=0$; $\partial s / \partial c = 0$, while for $s = -a$

$$\frac{\partial s}{\partial c} = \frac{b^2}{a^2 + b^2} \lim_{c \rightarrow 0} \left(\frac{c}{s+a} \right),$$

$$\left(\frac{\partial s}{\partial c} \right) = \pm \frac{b}{\sqrt{(a^2 + b^2)}}.$$

To first powers of c the four roots may be written

$$s_1 = ib, \quad s_2 = -ib, \quad s_3 = -\left(a + \frac{bc}{\sqrt{(a^2 + b^2)}}\right), \quad s_4 = -\left(a - \frac{bc}{\sqrt{(a^2 + b^2)}}\right). \quad \dots \quad (4.5)$$

The determinant Δ which must vanish if the boundary conditions are to be satisfied may be expanded to read,

$$\Delta = \left[b^4 + \left(a^2 - \frac{b^2 c^2}{a^2 + b^2} \right)^2 + b^2 \left(a^2 + \frac{b^2 c^2}{a^2 + b^2} \right) \right] \sinh b \sin \frac{bc}{\sqrt{(a^2 + b^2)}}. \quad (4.6)$$

The only zeroes of these yielding non-trivial solutions are

$$\frac{bc}{\sqrt{(a^2 + b^2)}} = n\pi;$$

or

$$c = n\pi \sqrt{\left(1 + \frac{a^2}{b^2} \right)};$$

and since a and b are real, $c \geq \pi$ and $\Lambda \geq \pi^2 \sin^2 \phi$.

This establishes that solutions do not exist for arbitrary small values of Λ , but, in view of the approximations used cannot be considered as establishing the actual minimum value for Λ ; however it will be shown below that this value is in fact a good approximation.

§ 5. SOLUTION FOR SPECIAL CASES.

For certain orientations of the inducing field H_0 it is possible to write down exact solutions to the problem.

(a) *Vertical Field.*

(3.2) becomes

$$(s^2 + l^2 + m^2)s^2 = A(l^2 + m^2) \quad \dots \quad (5.1)$$

with roots

$$s = \pm \left[\frac{l^2 + m^2}{2} \left\{ \sqrt{1 + \frac{4A}{l^2 + m^2}} - 1 \right\} \right]^{1/2}$$

$$= \pm i \left[\frac{l^2 + m^2}{2} \left\{ \sqrt{1 + \frac{4A}{l^2 + m^2}} + 1 \right\} \right]^{1/2} \quad \dots \quad (5.2)$$

and (3.3) may be written

$$0 = \sinh \left[\frac{l^2 + m^2}{2} \left\{ \sqrt{1 + \frac{4A}{l^2 + m^2}} + 1 \right\} \right]^{1/2}$$

$$\times \sin \left[\frac{l^2 + m^2}{2} \left\{ \sqrt{1 + \frac{4A}{l^2 + m^2}} - 1 \right\} \right]^{1/2} \quad \dots \quad (5.3)$$

Therefore for a non-trivial solution

$$A = \pi^2 \left(1 + \frac{\pi^2}{l^2 + m^2} \right) \quad \dots \quad (5.4)$$

This has its minimum value π^2 at $l, (l^2 + m^2) = 0$ which implies that in at least one direction the convection cells must be very small; the size in the other direction is indeterminate.

The critical gradient needed for convection is from (2.7)

$$\beta_H = \frac{\pi^2}{d^2} \frac{K}{\rho_0 \alpha g} \frac{\sigma \mu^2 H^2}{c^2} \quad \dots \quad (5.5)$$

For thermal convection in a viscous fluid with the boundary conditions imposed here, Rayleigh (1917) found the critical gradient

$$\beta_\eta = \frac{27}{4} \frac{\pi^4}{d^4} \frac{K}{\rho_0 \alpha g} \eta \quad \dots \quad (5.6)$$

where η = coefficient of viscosity.

This suggests introducing a "magnetic-viscosity"

$$\eta_H = \frac{4}{27} \frac{d^2}{\pi^2} \frac{\sigma \mu^2 H^2}{c^2} \quad \dots \quad (5.7)$$

which depends on the scale of the system. This need not be small; in a one-centimetre layer of mercury a field of 300 gauss produces one centipoise magnetic viscosity. Hence, for conducting fluids magnetic forces should be of considerable importance in the process of thermal convection.

(b) *Horizontal Field, Convection Rolls.*

If the field is horizontal (3.2) becomes

$$(s^2 + l^2 + m^2)l^2 = \Lambda(l^2 + m^2), \quad \dots \quad (5.8)$$

or

$$s = \pm \sqrt{\left(\Lambda \left(\frac{l^2 + m^2}{l^2} \right) - (l^2 + m^2) \right)}.$$

The boundary conditions are satisfied if $s = \pm \pi$, i.e. if

$$\Lambda = l^2 \left(\frac{\pi^2}{l^2 + m^2} + 1 \right), \quad \dots \quad (5.9)$$

which is zero for $l=0$: hence in a horizontal field there is a stable mode of convection for arbitrarily small gradients, in the form of rolls with their axes along the field direction. This type of motion has been observed in the absence of a magnetic field by Chandra (1938) when convection occurs in a gas in non-uniform horizontal motion.

(c) *Convection Rolls in an Arbitrary Field.*

There is an exact solution to the fundamental equation corresponding to Chandra rolls with their axes along the direction of the horizontal component of the field. This is obtained by setting $l=0$ in (3.2) which becomes

$$\sin^2 \phi \cdot s^2(s^2 + m^2) = m^2 \Lambda \quad \dots \quad (5.10)$$

with roots

$$s = \pm \frac{m}{\sqrt{2}} \left[\sqrt{\left(1 + \frac{4\Lambda}{m^2 \sin^2 \phi} - 1 \right)} \right]^{1/2}, \\ \pm \frac{im}{\sqrt{2}} \left[\sqrt{\left(1 + \frac{4\Lambda}{m^2 \sin^2 \phi} \right) + 1} \right]^{1/2}.$$

As in (a) the boundary conditions demand

$$\Lambda = \pi^2 \sin^2 \phi \left(1 + \frac{\pi^2}{m^2} \right) \quad \dots \quad (5.11)$$

which has its minimum $\Lambda = \pi^2 \sin^2 \phi$ at infinite m , yielding two finite values for s . This value of Λ is not, of course, necessarily the minimum possible one as l has been arbitrarily set equal to zero.

§ 6. APPROXIMATE SOLUTIONS FOR ARBITRARY FIELD.

Although the special solutions described above were easily obtained only an approximate solution has been secured for an arbitrary field. One obvious approximation procedure is to use the solution for a vertical field as starting points for an expansion in powers of $l \cot \phi$.

For $\sin \phi \neq 0$, (3.2) can be written again as

$$(s^2 + b^2)(s + a)^2 = c^2 b^2. \quad \dots \quad (6.1)$$

This equation has at least two real roots, the intersections of the curves

$$y = s^2 + b^2 \quad \text{and} \quad y = \frac{c^2 b^2}{(s + a)^2}.$$

The four roots can be written $s_1, s_2, x+iy, x+iy$, where all quantities are real with the exception of y which may be purely imaginary.

The determinant Δ becomes

$$\Delta = 2xy(s_1^2 - s_2^2) \left[\cos(a + s_1 + s_2) - \cosh y \cos \frac{(s_2 - s_1)}{2} \right] \\ + [(x^2 + y^2)^2 + s_1^2 s_2^2 - (s_1^2 + s_2^2)(x^2 - y^2)] \sinh y \sin \frac{(s_2 - s_1)}{2}. \quad (6.2)$$

From (6.1) and (6.2) roots s can be eliminated leaving c as a function of a and b , which can then be minimized to determine the critical gradient and the conditions at the onset of convection. In fact, however, algebraic complexity prohibits this programme, and an expansion in powers of a about $a=0$ must be used, by writing :

$$\left. \begin{aligned} s &= s(0) + a \frac{\partial s}{\partial a}(0) + \frac{a^2}{2} \frac{\partial^2 s}{\partial a^2}(0) + \dots \\ c^2 &= c^2(0) + \frac{a^2}{2} \frac{\partial^2 c^2}{\partial a^2}(0) + \dots \\ \Delta &= \Delta(0) + a \frac{\partial \Delta}{\partial a}(0) + \dots \end{aligned} \right\} \quad (6.3)$$

Since Δ is not an explicit function of a we must use

$$\frac{\partial \Delta}{\partial a} = \sum_i \frac{\partial \Delta}{\partial s_i} \frac{\partial s_i}{\partial a}.$$

It will be noticed that $\partial c^2 / \partial a \sim \partial \Delta / \partial a$ has been equated to zero, the condition for a maximum or minimum of Δ with respect to a .

The values of the partial derivatives of Δ are calculated in terms of b and c with aid of the known values of $s_i(0)$. Requiring that successive terms in the expansion for Δ vanish yields a system of equations for c^2 and its derivatives, and hence to an expression for $\Delta(a, b)$ which to second order in a is

$$\frac{\Delta}{\sin^2 \phi} = \pi^2 \left(1 + \frac{\pi^2}{b^2} \right) + \frac{\pi^2}{b^2} a^2 \left[4 \left(\frac{\pi^2 + b^2}{2\pi^2 + b^2} \right)^2 + 3 \left(\frac{\pi^2 + b^2}{2\pi^2 + b^2} \right) \right]. \quad (6.4)$$

Since a and b are necessarily real, this has its least value at $a=0$, that is, at $l=0$, corresponding to the convection rolls described in § 5. A slight inclination of the field therefore removes the ambiguity encountered in § 5 (a).

The corresponding temperature gradient is

$$\beta_H = \frac{\pi^2}{d^2} \frac{K}{\rho_0 \alpha g} \frac{\sigma \mu^2 H^2}{c^2} \sin^2 \phi. \quad (6.5)$$

This suggests that only the vertical component of the field should be included in the definition of the "magnetic viscosity".

§ 7. THE EFFECT OF VISCOSITY.

It will be noted that in all the solutions discussed the minimum eigenvalue Λ occurs when one of the cell parameters becomes infinite, corresponding to a cell of vanishing dimensions. This obviously arises from neglect of viscosity, which leaves the possible velocity shears unlimited, and in order to obtain physically meaningful flow patterns it is necessary to consider viscous effects. The viscous stress adds to the hydrodynamic equation of motion a force $\mathbf{F}\eta = -\eta \text{curl curl } \mathbf{V}$ which for an incompressible fluid reduces to

$$\mathbf{F}\eta = \eta \nabla^2 \mathbf{V}. \quad (7.1)$$

This addition calls for no change in the procedure used to get the fundamental equation (2.6) which is now modified to read

$$\Lambda \left(\nabla^2 - \frac{\partial^2}{\partial z^2} \right) \mathbf{T}' + (\mathbf{U} \cdot \nabla)^2 \nabla^2 \mathbf{T}' - \Gamma \nabla^2 \mathbf{T}' = 0, \quad (7.2)$$

where

$$\Gamma = \frac{c^2 \eta}{\sigma \mu^2 H^2 d^2} = \frac{27}{4} \pi^2 \frac{\eta}{\eta_H} \sin^2 \phi.$$

This equation may be solved as was (2.6), and if the same boundary conditions are used (although these have admittedly become somewhat artificial) the solution presents no great difficulties for the special cases studied in § 5. In particular, for convection rolls of width $\pi d, m$

$$\frac{\Lambda}{\pi^2 \sin^2 \phi} = 1 + \frac{\pi^2}{m^2} + \Gamma \frac{\pi^4}{m^4} \left(1 + \frac{m^2}{\pi^2} \right)^3. \quad (7.3)$$

Minimizing this yields an equation determining m which is most neatly written by introducing a variable χ such that

$$\pi^2 + m^2 = 3/2 \pi^2 \chi$$

whereupon the condition that Λ be a minimum becomes

$$\chi^2 (\chi - 1) = \frac{\eta_H}{\eta}. \quad (7.4)$$

The corresponding critical temperature gradient is

$$\beta = \frac{27}{4} \frac{K}{\alpha g \rho_0} \frac{\pi^4}{d^4} (\chi^2 \eta + \eta_H) = \chi^2 \beta_\eta + \beta_H. \quad (7.5)$$

For $\eta_H = 0, \chi = 1$ and β reduces to the value given by Rayleigh. Identical results hold in a vertical field with m^2 replaced by $b^2 = l^2 + m^2$.

The width f of the roll is given by

$$f = \frac{\pi d}{m} = \sqrt{\left(\frac{2}{3\chi - 2} \right)} d. \quad (7.6)$$

For square cells occurring in a vertical field this is multiplied by $\sqrt{2}$.

The formula determining the width f of the cell renders (7.5) intelligible. The effect of the magnetic field is to establish a resistance to flow across the lines of force, hence the cell width is reduced, thus diminishing the excursion of any element of fluid across the field lines. This squeezing up

of the cells increases the velocity gradients, hence increasing the viscous stresses. The effect of a field then, is to add a term β_H due to the magnetic viscosity, and a multiple $\chi^2 > 1$ of the normal viscous term β_η .

The effects here described are of sufficient magnitude to be easily detected. For example, for a layer of mercury one centimetre in depth placed in a vertical field of 1000 gauss the relevant quantities are

$$\begin{aligned}\eta &= 0.014 \text{ poise,} & \beta_\eta &= 0.162^\circ \text{ C./cm.,} \\ \eta_H &= 0.152 \text{ poise,} & \beta &= 2.86^\circ \text{ C./cm.,} \\ \chi &= 2.6, & f &= 0.69 \text{ cm.,} \\ & & f_\eta &= 1.41 \text{ cm.}\end{aligned}$$

§ 8. THE NATURE OF THE SOLUTIONS.

Once the cell parameters have been fixed the remaining dynamical quantities can be determined in terms of the temperature perturbation T' . Unfortunately, the theory is linear and homogeneous in the dependent variable, and the solution is only obtained to within a multiplicative factor. This means that in common with existing analytical theories of thermal convection it does not predict the heat transported.

If now, we remove the convention that displacement be measured in units of d , the depth of the layer, the temperature perturbation for the two-dimensional roll solution becomes

$$T' = A \cos \frac{my}{d} \sin \frac{sz}{d} \dots \dots \dots (8.1)$$

From (1.11) the $0z$ component of velocity can be written

$$w = -\frac{K}{\beta} \nabla^2 T' = \frac{K}{\beta d^2} (m^2 + s^2) A \cos \frac{my}{d} \sin \frac{sz}{d} \dots \dots (8.2)$$

The second velocity component v is determined from the equation of continuity as

$$v = -\frac{s}{m} \frac{K}{\beta d^2} (m^2 + s^2) A \sin \frac{my}{d} \cos \frac{sz}{d} \dots \dots \dots (8.3)$$

The electric charge density q is obtained from the continuity equation for the current

$$0 = \text{div } \mathbf{j} = \sigma \left(\text{div } \mathbf{E} + \text{div } \frac{\mu}{c} \mathbf{V} \times \mathbf{H} \right),$$

whence

$$q = \frac{\epsilon}{4\pi} \text{div } \mathbf{E} = -\frac{\epsilon\mu}{4\pi c} \mathbf{H} \cdot \text{curl } \mathbf{V} = -\frac{\epsilon\mu}{4\pi c} H \cos \phi \left(\frac{\partial w}{\partial y} - \frac{\partial v}{\partial z} \right) \dots (8.4)$$

The electric field can be written

$$\mathbf{E} = \left(0, -\frac{\mu H w}{c} \cos \phi, \frac{\mu H v}{c} \cos \phi \right) \dots \dots \dots (8.5)$$

This satisfies $E_{\text{tan}} = 0$ at the boundaries which are assumed perfectly conducting, although the normal component does not vanish but gives a surface charge Σ

$$\Sigma = \frac{\epsilon\mu}{4\pi c} \frac{K}{\beta} \frac{m^2 + s^2}{d^2} \frac{s}{m} H \cos \phi \cdot A \sin my \dots \dots \dots (8.6)$$

The current density \mathbf{j} is given when \mathbf{E} and \mathbf{V} are specified as

$$\mathbf{j} = \left(\frac{\sigma\mu H}{c} \sin \phi \cdot v, 0, 0 \right). \quad (8.7)$$

The induced magnetic field can now be determined since the vector potential within the fluid, a solution of $\nabla^2 \mathbf{A} = (4\pi/c)\mathbf{j}$ can be written

$$\mathbf{A} = \left(-4\pi \frac{\sigma\mu H}{c^2} \frac{K}{\beta} \frac{s}{m} A \sin \frac{my}{d} \cos \frac{sz}{d}, 0, 0 \right),$$

and the field \mathbf{h} within the fluid

$$\mathbf{h} = \left(0, \frac{4\pi\mu\sigma H}{c^2 d} \frac{K}{\beta} \frac{s^2}{m} A \sin \frac{my}{d} \sin \frac{sz}{d}, \frac{4\pi\mu\sigma H}{c^2 d} \frac{K}{\beta} s A \cos \frac{my}{d} \cos \frac{sz}{d} \right). \quad (8.8)$$

Outside the fluid \mathbf{h} is most easily determined by noting that the boundary conditions at the surface are satisfied if $\mathbf{h} = -\nabla\psi$ where ψ is the magnetostatic potential due to a surface pole distribution

$$\frac{\mu\sigma}{c^2} \frac{H}{d} \frac{K}{\beta} s A \cos \frac{my}{d}$$

on the surface $z=0$ and a similar distribution with opposite sign on $z=d$.

The field then has the form

$$\mathbf{h} = \left(0, 4\pi \frac{\mu\sigma}{c^2} \frac{K}{\beta} \frac{H}{d^2} s A \sin \frac{my}{d} \exp \frac{mz}{d}, 4\pi \frac{\mu\sigma}{c^2} \frac{H}{d} \frac{K}{\beta} s A \cos \frac{my}{d} \exp \frac{mz}{d} \right) \quad (8.9)$$

for $z < 0$ and a corresponding quantity varying as $\exp m\left(1 - \frac{z}{d}\right)$ for $z > d$.

Finally, the pressure perturbation is given from the hydrodynamical equations

$$\frac{\partial p}{\partial x} = 0; \quad \frac{\partial p}{\partial y} = -\frac{\sigma\mu^2 H^2}{c^2} \sin^2 \phi \cdot v, \quad \frac{\partial p}{\partial z} = -\rho_0 \alpha g T'.$$

The integrability condition is seen to be equivalent to the equation for T' and the pressure perturbation may be written

$$p' = \rho_0 \alpha g \frac{d}{m} \cdot A \cos \frac{my}{d} \cos \frac{sz}{d}. \quad (8.10)$$

§ 9. STABILITY CONDITIONS.

An important assumption has yet to be considered, the condition for the existence of stable convection currents. The argument used by Jeffreys to justify treating the time independent problem was as follows. Consider a solution with time dependence in the form $\exp \gamma t$, where γ is a function of β the temperature gradient. As β is increased γ moves from negative to positive values, negative values corresponding to static equilibrium and positive ones to instability and the establishing of convection currents. The condition for marginal stability, the case separating these two regions, is that γ vanish. It is however, necessary that γ be real, and Jeffreys appeals to experiment to show that undamped convective oscillations do not occur as they would if γ had a pure imaginary

value at marginal stability. Such an appeal cannot be made for the magneto-hydrodynamic problem, and it has been suggested (Walen 1944) that oscillations do occur, therefore to determine the significance of the solutions for marginal stability it is necessary to examine the time dependent problem. We shall seek a solution to the time dependent problem in the form $f(x, y, z) \exp \gamma t$ where γ will be found to satisfy a cubic equation with coefficients depending on the constants of the material, and flow pattern, and the negative temperature gradient β . For low enough values of β , γ has a negative real part indicating that small motions are damped out, and the conduction of heat through the resting fluid is a stable process. If β is larger the real part of γ is positive and any motion increases with time until limited by non-linear effects. We will find that γ is real if this latter condition holds unless the constants of the material satisfy very stringent conditions, and therefore that steady currents and not oscillations are to be expected.

Again, the linearizing procedure is carried out, but the time independent assumption is not made. The first order equations can be written to determine the significance of the solutions for marginal stability,

$$\frac{\partial \mathbf{V}}{\partial t} = -\frac{1}{\rho_0} \nabla p - \alpha \mathbf{T}' \mathbf{g} + \frac{\mu}{\rho_0 c} \mathbf{j} \times \mathbf{H}_0, \quad . \quad . \quad . \quad (9.1)$$

$$\frac{\partial \mathbf{T}'}{\partial t} - w\beta = K \nabla^2 \mathbf{T}', \quad . \quad . \quad . \quad . \quad . \quad . \quad (9.2)$$

$$\text{div } \mathbf{V} = 0, \quad . \quad . \quad . \quad . \quad . \quad . \quad (9.3)$$

Again, it has been assumed that variations in ρ are small, and moreover that the time variation is slow. Then, the displacement current can be omitted from Maxwell's equations,

$$\text{curl } \mathbf{h} = \frac{4\pi}{c} \mathbf{j}, \quad . \quad . \quad . \quad . \quad . \quad . \quad (9.4)$$

$$\text{curl } \mathbf{E} = -\frac{\mu}{c} \frac{\partial \mathbf{h}}{\partial t}, \quad . \quad . \quad . \quad . \quad . \quad . \quad (9.5)$$

$$\text{div } \mathbf{E} = 4\pi q, \quad . \quad . \quad . \quad . \quad . \quad . \quad (9.6)$$

$$\text{div } \mathbf{h} = 0, \quad . \quad . \quad . \quad . \quad . \quad . \quad (9.7)$$

$$\text{div } \mathbf{j} = \frac{\partial q}{\partial t}, \quad . \quad . \quad . \quad . \quad . \quad . \quad (9.8)$$

$$\mathbf{j} = \sigma \left[\mathbf{E} + \frac{\mu}{c} \mathbf{V} \times \mathbf{H} \right], \quad . \quad . \quad . \quad . \quad . \quad . \quad (9.9)$$

From (9.4), (9.5) and (9.9)

$$\left[\frac{\partial}{\partial t} - \frac{c^2}{4\pi\mu\sigma} \nabla^2 \right] \mathbf{h} = (\mathbf{H} \cdot \nabla) \mathbf{V}, \quad . \quad . \quad . \quad . \quad . \quad (9.10)$$

And from (9.1)

$$\frac{\partial}{\partial t} (-\nabla^2 \mathbf{V}) + \frac{\mu}{4\pi\rho_0} (\mathbf{H}_0 \cdot \nabla) \nabla^2 \mathbf{h} = -\text{curl curl } (\alpha \mathbf{T}' \mathbf{g}), \quad . \quad . \quad (9.11)$$

Using (9.10) to eliminate \mathbf{h} , and (9.2) to eliminate the $0z$ component of velocity leaves the fundamental equations for T' in the form

$$\left(\frac{\partial}{\partial t} - \frac{c^2}{4\pi\mu\sigma} \nabla^2\right) \left(\frac{\partial}{\partial t} - K \nabla^2\right) \frac{\partial}{\partial t} \nabla^2 T' - \frac{\mu}{4\pi\rho_0} (\mathbf{H}_0 \cdot \nabla)^2 \left(\frac{\partial}{\partial t} - K \nabla^2\right) \nabla^2 T' - \alpha g \beta \left(\frac{\partial}{\partial t} - \frac{c^2}{4\pi\mu\sigma} \nabla^2\right) \left(\nabla^2 - \frac{\partial^2}{\partial z^2}\right) T' = 0. \quad (9.12)$$

If we consider a vertical field and use the Rayleigh boundary conditions the appropriate solution can be written as

$$T' \sim \exp(ilx + imy + \gamma t) \sin sz$$

where the parameters satisfy the characteristic equation

$$k^2 \gamma^3 + \left(\frac{c^2}{4\pi\mu\sigma} k^2 + K k^2\right) k^2 \gamma^2 + \left[\frac{\mu}{4\pi\rho_0} H^2 s^2 k^2 - \alpha g \beta (k^2 - s^2) + \frac{K c^2 k^6}{4\pi\mu\sigma}\right] \gamma + \frac{\mu}{4\pi\rho_0} H^2 K s^2 k^4 - \frac{c^2}{4\pi\mu\sigma} \alpha g \beta (k^2 - s^2) k^2 = 0, \quad (9.13)$$

where $k^2 = l^2 + m^2 + s^2$. This equation can be written

$$\gamma^3 + A\gamma^2 + B\gamma + C = 0$$

and in order that steady convection currents appear $C < 0$.

If the equation is to have a complex root with positive real part x , a condition for instability to oscillations, x must satisfy

$$x^3 + 2Ax^2 + (A^2 + B)x + (AB - C) = 0$$

hence the condition that oscillations, not steady motion should occur is

$$C > 0 > AB - C.$$

This in turn, is a condition on the negative temperature gradient

$$\frac{\mu^2 \sigma}{\rho_0 c^2} K H^2 k^2 s^2 > \alpha g \beta (k^2 - s^2) > \frac{c^2}{16\pi^2} \frac{H^2 s^2 k^2}{\rho_0 K \sigma} + \frac{k^6 c^2}{4\pi\mu\sigma} \left[\frac{c^2}{4\pi\mu\sigma} + K \right], \quad (9.14)$$

and the condition for oscillation

$$(\mu K \sigma)^2 > \frac{c^4}{16\pi^2} + \left[\left(\frac{c^2}{4\pi\mu\sigma} \right)^2 + \frac{c^2 K}{4\pi\mu\sigma} \right] \frac{\rho_0 c^2}{H^2} K \sigma \frac{k^4}{s^2}. \quad (9.15)$$

Hence a necessary condition on the material involved is

$$\frac{c^2}{4\pi\mu K \sigma} = \theta < 1. \quad (9.16)$$

The values of μ , K , σ for solid copper give $\theta = 0.7$, hence the condition is not easily satisfied in the laboratory.

A necessary condition on θ for oscillation is obtained by substitution in (9.15)

$$\theta < [\sqrt{5} - 1] \frac{H^2 s^2}{8\pi\rho K^2 k^4}. \quad (9.17)$$

If such oscillations do occur it is possible also to determine the gradient required for the onset of convection, and the frequency of the oscillations at marginal stability,

$$\alpha g \beta_0 = \frac{c^2}{16\pi^2} \frac{H^2 s^2}{\rho K \sigma} + \frac{3}{4} \frac{k^4 c^2}{\pi \mu \sigma} \left[\frac{c^2}{4\pi\mu\sigma} + K \right], \quad (9.18)$$

which with (9.14) gives for the cell parameter $k^2 = 3/2\chi s^2$ and χ a root of

$$\chi^2(\chi-1) = \frac{8}{27} \frac{\mu H^2}{8\pi\rho\kappa^2} \frac{s^2}{\theta+1}. \quad (9.19)$$

The corresponding frequency obtained from (9.13) is

$$\omega = i\gamma = \sqrt{2s} \sqrt{\left(\frac{\mu H^2}{8\pi\rho}\right) \theta} \sqrt{\left(\frac{1-\theta}{\theta^2} - \frac{8\pi\chi^2 s^2}{\mu H^2}\right)}. \quad (9.20)$$

Introducing the magnetic energy per unit mass $\mathcal{E} = (\mu H^2)/(8\pi\rho)$ and $s = \pi/d$ this is

$$\omega = \sqrt{\left(2 - \frac{\pi}{d}\right) \theta} \sqrt{\left(\frac{1-\theta}{\theta^2} \mathcal{E} - \kappa\chi^2 \frac{\pi^2}{d^2}\right)}. \quad (9.21)$$

§ 10. CONCLUSION.

We have examined the modifications produced in the Rayleigh-Jeffreys theory of slow thermal convection by the addition of magnetic forces acting on induced currents. It has been shown that for most materials the flow is steady, although oscillations seem possible in principle. An approximate value for the critical gradient has been found, but as was the case for Rayleigh's analysis this is probably somewhat in error due to improper choice of boundary conditions. A numerical analysis similar to that given by Jeffreys (1926) for ordinary convection would improve the estimate of A . On the other hand, the present analysis is a great deal simplified and the proper dependence of on depth and field strength has probably been deduced. This predicted dependence could be tested experimentally by determining the temperature gradient for which the thermal conductivity law ceases to hold for a thin layer of fluid heated from below as was done by Schmidt and Saunders (1938) for ordinary convection in water.

Finally, the author wishes to express his thanks to Dr. E. C. Bullard who suggested the problem and gave valuable advice and encouragement.

REFERENCES.

- ALFVEN, H., 1950, *Cosmical Electrodynamics* (Oxford: Clarendon Press).
 BÉNARD, H., 1901, *Ann. de Chimie et de Physique*, **23**, 62.
 BULLARD, E. C., 1949 a, *Proc. Roy. Soc. A*, **197**, 433; 1949 b, *Ibid.*, **199**, 413.
 CHANDRA, K., 1938, *Proc. Roy. Soc. A*, **164**, 231.
 ELSASSER, W. M., 1946, *Phys. Rev.*, **67**, 106.
 FERMI, E., 1949, *Phys. Rev.*, **75**, 1169.
 HALES, A. L., 1937, *M.N. R.Ast.Soc. Geo. Sup.*, **4**, 132.
 JEFFREYS, H., 1926, *Phil. Mag.*, **2**, 833.
 RAYLEIGH, 1917, *Phil. Mag.*, **32**, 529.
 RICHTMEYER, R. D., and TELLER, E., 1949, *Phys. Rev.*, **75**, 1729.
 SCHMIDT, R. J., and SAUNDERS, O. A., 1938, *Proc. Roy. Soc. A*, **165**, 216.
 SUTTON, O. G., 1951, *Proc. Roy. Soc. A*, **204**, 297.
 WALÉN, C., 1944, *Ark. f. mat. astr. o. fysik*, **30A**, No. 15.

CXLIV. *The Boundary Layer in Three Dimensional Flow.*—Part II.
The Flow near a Stagnation Point.*

By L. HOWARTH, F.R.S.,

Department of Mathematics, University of Bristol†.

[Received August 16, 1951.]

SUMMARY.

The equations of boundary layer flow in the vicinity of a stagnation point on a general (three dimensional) surface are discussed and shown to be reducible to a pair of simultaneous ordinary third-order differential equations containing a single parameter c which is determined by the mainstream flow. The variation of c can be effectively limited to the range from 0 (corresponding to two dimensional flow) to 1 (corresponding to the axial flow past a body of revolution), and solutions have been computed for the cases $c=0.25, 0.50, 0.75$ and are tabulated below. A series expansion useful for small c is also given.

INTRODUCTION.

IN Part I. (Howarth 1951) the equations of flow in the boundary layer along a general curved surface were derived using an orthogonal coordinate system ξ, η, ζ comprising respectively the surfaces generated by the normals along the lines of curvature and the parallel surfaces. The equations for steady flow were found to be

$$\frac{u}{h_1} \frac{\partial u}{\partial \xi} + \frac{v}{h_2} \frac{\partial u}{\partial \eta} + w \frac{\partial u}{\partial \zeta} - K_2 uv + K_1 v^2 = -\frac{1}{\rho h_1} \frac{\partial p}{\partial \xi} + \nu \frac{\partial^2 u}{\partial \xi^2}, \quad \dots (1)$$

$$\frac{u}{h_1} \frac{\partial v}{\partial \xi} + \frac{v}{h_2} \frac{\partial v}{\partial \eta} + w \frac{\partial v}{\partial \zeta} + K_2 u^2 - K_1 uv = -\frac{1}{\rho h_2} \frac{\partial p}{\partial \eta} + \nu \frac{\partial^2 v}{\partial \eta^2}, \quad \dots (2)$$

$$\frac{1}{h_1} \frac{\partial u}{\partial \xi} + \frac{1}{h_2} \frac{\partial v}{\partial \eta} + \frac{\partial w}{\partial \zeta} - K_1 u - K_2 v = 0, \quad \dots (3)$$

where h_1, h_2, h_3 are the length elements and

$$K_1 = -\frac{1}{h_1 h_2} \frac{\partial h_2}{\partial \xi}, \quad K_2 = -\frac{1}{h_1 h_2} \frac{\partial h_1}{\partial \eta}. \quad \dots (4)$$

The purpose of this paper is to discuss the flow in the neighbourhood of a stagnation point S on the surface. We shall suppose that S is the point $\xi=0, \eta=0, \zeta=0$, that the surface is regular at S and in particular that $\left(\frac{\partial h_1}{\partial \xi}\right)_0, \left(\frac{\partial h_1}{\partial \eta}\right)_0, \left(\frac{\partial h_1}{\partial \zeta}\right)_0, \left(\frac{\partial h_2}{\partial \xi}\right)_0, \left(\frac{\partial h_2}{\partial \eta}\right)_0, \left(\frac{\partial h_2}{\partial \zeta}\right)_0$ are bounded. We

* This paper forms part of one of the essays for which the Adams Prize was awarded in 1951.

† Communicated by the Author.

may, without loss of generality, suppose that ξ and η are so defined in magnitude that at S $h_1=h_2=1$. Then, in the vicinity of S,

$$h_1=1+\left(\frac{\partial h_1}{\partial \xi}\right)_0 \xi+\left(\frac{\partial h_1}{\partial \eta}\right)_0 \eta+\left(\frac{\partial h_1}{\partial \zeta}\right)_0 \zeta, \quad (5)$$

$$h_2=1+\left(\frac{\partial h_2}{\partial \xi}\right)_0 \xi+\left(\frac{\partial h_2}{\partial \eta}\right)_0 \eta+\left(\frac{\partial h_2}{\partial \zeta}\right)_0 \zeta \quad (6)$$

approximately.

The Nature of the Solution.

We shall suppose that the flow in the mainstream outside the boundary layer is irrotational, so that, if we denote by U, V its component velocities in the directions ξ , η increasing respectively,

$$h_2 \frac{\partial V}{\partial \xi} - h_1 \frac{\partial U}{\partial \eta} + V \frac{\partial h_2}{\partial \xi} - U \frac{\partial h_1}{\partial \eta} = 0^*. \quad (7)$$

At S, by definition, U and V vanish and since S is a regular point of the surface, we shall have in its vicinity

$$U = A\xi + B\eta, \quad (8)$$

$$V = D\xi + C\eta, \quad (9)$$

where A, B, C, D are constants. Hence we see from the leading terms in (7) that

$$D = B.$$

Since the velocities in the boundary layer will be dominated by U, V, it is evident that the curvature terms in equations (1), (2), (3) may be neglected and that h_1 and h_2 may each be replaced by unity in determining the leading terms near S†. As we might have anticipated on physical grounds, we see that the equations of flow and the condition of irrotationality of the main flow are to this order exactly the same as if the surface were plane, ζ measured normal to it and ξ and η along two axes at right angles in the surface. We are at this stage, therefore, free to rotate our ξ , η axes about S ζ to any convenient position whilst at the same time maintaining the form of our equations.

Now, by the irrotational condition, the tensor

$$\begin{bmatrix} \left(\frac{\partial U}{\partial \xi}\right)_0 \left(\frac{\partial V}{\partial \xi}\right)_0 \\ \left(\frac{\partial U}{\partial \eta}\right)_0 \left(\frac{\partial V}{\partial \eta}\right)_0 \end{bmatrix}$$

is symmetric and by suitable rotation of the axes S ξ , S η to Sx, Sy, say, we may express it in its principal form. In other words we may take the mainflow outside the boundary layer to have components (ax, by)

* It may perhaps be mentioned here that, just as in the corresponding two dimensional problem, we do not suppose that U, V in themselves satisfy the equation of continuity, but only after due account is taken of the outflow from the boundary layer.

† These assertions may be justified *a posteriori*.

and proceed with the solution as an immediate extension of the standard two dimensional solution. We may assume, without loss of generality, that a is positive.

We find, now using u, v, w for the velocity components referred to our new axes $S(x, y, \xi)$, that

$$\begin{aligned} u &= axf'(z), \\ v &= byg'(z), \end{aligned} \quad (10)$$

$$w = -\frac{v^{1/2}}{a^{1/2}}[af(z) + bg(z)].$$

where

$$z = \frac{a^{1/2}\xi}{v^{1/2}}, \quad (11)$$

and

$$f'^2 - ff'' - cgf'' = 1 + f''', \quad (12)$$

$$g'^2 - gg'' - \frac{1}{c}fg'' = 1 + \frac{1}{c}g''' \quad (13)$$

and

$$c = b/a. \quad (14)$$

The boundary conditions for (12) and (13) are

$$\begin{aligned} f = g = f' = g' &= 0 \quad \text{at } z = 0, \\ f' \rightarrow 1, \quad g' \rightarrow 1 &\quad \text{as } z \rightarrow \infty. \end{aligned}$$

This slightly asymmetric form of the equations is advantageous for discussing conditions when c is small.

The skin friction components $\tau_{\xi x}, \tau_{\xi y}$ are given by

$$\begin{aligned} \tau_{\xi x} &= \rho v^{1/2} a^{3/2} x f''(0), \\ \tau_{\xi y} &= \rho v^{1/2} a^{3/2} c y g''(0). \end{aligned}$$

The following special cases have previously been discussed:—

- (i.) $c=0$, which corresponds to two dimensional flow,
- (ii.) $c=1$, which corresponds to flow round a body of revolution placed symmetrically in a stream. Here we have obviously $g=f$, so that

$$f'^2 - 2ff'' = 1 + f''' \quad (15)$$

and this is Homann's (1936) equation.

We may confine attention to the range $c=0$ to $c=1$ since it can readily be verified that

$$\left. \begin{aligned} f(z, -c) &= f(z, c), & f'(z, -c) &= f'(z, c), \\ g(z, -c) &= -g(z, c), & g'(z, -c) &= -g'(z, c) \end{aligned} \right\} \quad (16)$$

$$\left. \begin{aligned} f\left(z, \frac{1}{c}\right) &= c^{1/2}g\left(\frac{z}{c^{1/2}}, c\right), & f'\left(z, \frac{1}{c}\right) &= g'\left(\frac{z}{c^{1/2}}, c\right), \\ g\left(z, \frac{1}{c}\right) &= c^{1/2}f\left(\frac{z}{c^{1/2}}, c\right), & g'\left(z, \frac{1}{c}\right) &= f'\left(\frac{z}{c^{1/2}}, c\right). \end{aligned} \right\} \quad (17)$$

In any event it is simply a matter of notation to ensure that in any given case $0 \leq c \leq 1$.

Numerical solution.

The solutions of equations (12) and (13) may be obtained by standard numerical methods, but before embarking on them it is convenient to have expansions when c is small, for it is here that conditions change most rapidly with c . To obtain these expansions we write

$$\left. \begin{aligned} f &= f_0 + cf_1 + c^2 f_2 + \dots, \\ g &= g_0 + cg_0 + c^2 g^2 + \dots, \end{aligned} \right\} \dots \dots \dots (18)$$

substitute in equations (12) and (13), equate coefficient of powers of c , and obtain the following equations:—

$$f_0''' + f_0 f_0'' - f_0'^2 = 1, \quad \dots \dots \dots (19)$$

$$f_1''' + f_0 f_1'' - 2f_0' f_1' + f_0'' f_1 = -g_0 f_0'', \quad \dots \dots \dots (20)$$

$$f_2''' + f_0 f_2'' - 2f_0' f_2' + f_0'' f_2 = f_1'^2 - f_1 f_1'' + (g_0 f_1' + g_1 f_0''). \quad \dots \dots (21)$$

$$g_0''' + f_0 g_0'' = 0, \quad \dots \dots \dots (22)$$

$$g_1''' + f_0 g_1'' = -f_1 g_0'' - g_0 g_0'' + g_0'^2 - 1, \quad \dots \dots \dots (23)$$

$$g_2''' + f_0 g_2'' = -f_2 g_0'' - f_1 g_1'' + 2g_0' g_1' - g_0 g_1'' - g_0' g_1. \quad \dots \dots (24)$$

The boundary conditions are $f_r = g_r = f_r' = g_r' = 0$ at $z=0$ ($r=0, 1, 2, \dots$) and

$$f'_0 = g'_0 = 1, \quad f'_r = g'_r = 0 \quad (r=1, 2, 3, \dots) \quad \text{at } z=\infty.$$

Equation (19) is the standard two dimensional equation (see Howarth 1934 for the solution) and equation (22) has previously been integrated by Prandtl (1945) and by Sears (1948). Equations (20), (21), (23), (24) have been integrated numerically and the results for the first derivatives are given in Table I. They enable velocity distributions to be evaluated for small values of c . For completeness, values of f'_0 and g'_0 have been included in the table. The corresponding results for the skin friction components are determined by

$$\begin{aligned} f_0''(0) &= 1.2326, & f_1''(0) &= 0.0478, & f_2''(0) &= 0.059, \\ g_0''(0) &= 0.5705, & g_1''(0) &= 1.0535, & g_2''(0) &= -0.537. \end{aligned}$$

These results, although insufficient for accurate computation as far as $c=1$, were found to give, in conjunction with the known solution when $c=1$, useful starting points for the detailed numerical solution of equations (12) and (13), which has been undertaken for $c=0.25, 0.50, 0.75$ by the Adams method. The results for the first derivatives are shown in Table II. and include the results for $c=1$ computed in the course of an interesting investigation by Miss Hannah (1947) from Homann's equation. (The values of f'_0, g'_0 in Table I. are, of course, the results for $c=0$.) The skin friction is determined by the values in Table III., and a few values of f and g are contained in Table IV.

It may perhaps be remarked that, throughout the range $c=0$ to 1, f varies very slowly—in fact $f''(0)$ only changes from 1.233 to 1.312—whereas in g the changes are much more rapid, the corresponding

TABLE I.

z	f'_0	f'_1	f'_2	g'_0	g'_1	g'_2
0.0	0.000	0.000	0.000	0.000	0.000	0.000
0.1	0.118	0.005	0.006	0.057	0.100	-0.054
0.2	0.227	0.010	0.012	0.114	0.191	-0.107
0.3	0.325	0.014	0.018	0.171	0.271	-0.160
0.4	0.415	0.019	0.023	0.228	0.341	-0.213
0.5	0.495	0.023	0.027	0.284	0.400	-0.264
0.6	0.566	0.027	0.031	0.339	0.450	-0.314
0.7	0.630	0.030	0.035	0.393	0.488	-0.360
0.8	0.686	0.033	0.037	0.446	0.517	-0.404
0.9	0.735	0.035	0.038	0.498	0.536	-0.444
1.0	0.778	0.036	0.039	0.547	0.546	-0.478
1.1	0.815	0.037	0.038	0.594	0.547	-0.507
1.2	0.847	0.037	0.036	0.639	0.540	-0.530
1.3	0.874	0.036	0.034	0.681	0.527	-0.547
1.4	0.897	0.035	0.032	0.720	0.507	-0.557
1.5	0.916	0.033	0.028	0.756	0.481	-0.561
1.6	0.932	0.031	0.025	0.789	0.452	-0.557
1.7	0.946	0.029	0.022	0.819	0.420	-0.548
1.8	0.957	0.026	0.018	0.846	0.385	-0.532
1.9	0.966	0.024	0.015	0.870	0.350	-0.510
2.0	0.973	0.021	0.012	0.891	0.314	-0.484
2.1	0.979	0.019	0.009	0.910	0.279	-0.454
2.2	0.984	0.016	0.007	0.926	0.246	-0.422
2.3	0.988	0.014	0.005	0.939	0.214	-0.387
2.4	0.991	0.012	0.003	0.951	0.184	-0.351
2.5	0.993	0.010	0.002	0.961	0.157	-0.315
2.6	0.995	0.008	0.001	0.969	0.132	-0.279
2.7	0.996	0.007	0.001	0.975	0.111	-0.245
2.8	0.997	0.005	0.000	0.981	0.092	-0.212
2.9	0.998	0.004		0.985	0.075	-0.182
3.0	0.998	0.003		0.988	0.061	-0.154
3.1	0.999	0.003		0.991	0.049	-0.128
3.2	0.999	0.002		0.993	0.039	-0.106
3.3	0.999	0.002		0.995	0.031	-0.086
3.4	1.000	0.001		0.996	0.024	-0.069
3.5		0.001		0.997	0.018	-0.055
3.6		0.001		0.998	0.014	-0.042
3.7		0.000		0.999	0.011	-0.032
3.8				0.999	0.008	-0.024
3.9				0.999	0.006	-0.017
4.0				1.000	0.004	-0.012

variation being from 0.570 to 1.312. These changes are reflected in the series solution in the much larger coefficients, after the first, in the g series as compared with the f .

CONCLUSIONS.

The main conclusions are embodied in Tables I. to IV., but some of the general trends may, however, be worthy of special note.

TABLE II.

	$c=0.25$		$c=0.50$		$c=0.75$		$c=1.0$
z	f'	g'	f'	g'	f'	g'	$f'=g'$
0.0	0.000	0.000	0.000	0.000	0.000	0.000	0.000
0.1	0.120	0.079	0.122	0.097	0.124	0.113	0.126
0.2	0.230	0.156	0.233	0.190	0.238	0.218	0.242
0.3	0.330	0.230	0.335	0.277	0.342	0.315	0.349
0.4	0.420	0.301	0.428	0.359	0.436	0.405	0.445
0.5	0.502	0.369	0.511	0.435	0.521	0.488	0.532
0.6	0.574	0.434	0.585	0.506	0.596	0.562	0.609
0.7	0.639	0.496	0.650	0.572	0.663	0.630	0.677
0.8	0.696	0.554	0.708	0.631	0.722	0.690	0.736
0.9	0.746	0.608	0.758	0.686	0.772	0.742	0.787
1.0	0.789	0.658	0.802	0.734	0.816	0.789	0.830
1.1	0.826	0.704	0.839	0.777	0.852	0.828	0.865
1.2	0.858	0.746	0.870	0.815	0.883	0.862	0.896
1.3	0.884	0.784	0.896	0.848	0.909	0.891	0.920
1.4	0.907	0.817	0.918	0.877	0.929	0.914	0.940
1.5	0.926	0.847	0.936	0.901	0.946	0.934	0.955
1.6	0.941	0.873	0.951	0.921	0.959	0.949	0.967
1.7	0.954	0.896	0.962	0.938	0.970	0.962	0.975
1.8	0.964	0.915	0.971	0.952	0.978	0.971	0.983
1.9	0.972	0.932	0.979	0.963	0.984	0.979	0.988
2.0	0.979	0.946	0.984	0.972	0.988	0.984	0.992
2.1	0.984	0.957	0.988	0.979	0.992	0.989	0.995
2.2	0.988	0.966	0.992	0.984	0.994	0.992	0.997
2.3	0.991	0.974	0.994	0.988	0.996	0.994	0.998
2.4	0.993	0.980	0.996	0.991	0.997	0.996	0.999
2.5	0.995	0.985	0.997	0.994	0.998	0.997	0.999
2.6	0.996	0.988	0.998	0.996	0.998	0.998	
2.7	0.997	0.991	0.998	0.997	0.999	0.998	
2.8	0.998	0.993	0.999	0.998	0.999	0.999	
2.9	0.998	0.995	0.999	0.998	0.999	0.999	
3.0	0.999	0.997	0.999	0.999	1.000	0.999	

TABLE III.

c	0.00	0.25	0.50	0.75	1.00
$f''(0)$	1.233	1.247	1.267	1.288	1.312
$g''(0)$	0.570	0.805	0.998	1.164	1.312

As a matter of notation, since we have restricted attention effectively to $0 \leq c \leq 1$, we may call the axes Sx , Sy respectively, the major and minor principal axes of the mainflow. We may remark first of all that the changes with c in this range are then relatively small for the velocity component in the major direction, though marked in the minor direction.

Secondly, the direction of the velocity vector at a particular station (that is for given x, y) may undergo appreciable changes as we move through the layer. The velocity is zero at the surface, but there is a limiting direction of flow there (which is also the direction of the resultant skin friction), and this direction is inclined to the mainflow direction at an angle

$$\tan^{-1} \left(\frac{g''(0)}{f''(0)} \right) \frac{cy}{x} - \tan^{-1} \frac{cy}{x}.$$

It appears from an examination of Table II. that, as we pass from the mainstream towards the surface, the angular deviation of the velocity vector steadily changes towards this value, the sense of the change being from the mainflow towards the major principal direction. For $c=0.00$, 0.25, 0.50, 0.75, 1.00, $g''(0)/f''(0)$ takes the values 0.463, 0.645, 0.788, 0.903, 1.0, and the maximum values of the corresponding changes in direction are then 21° , 14° , 6° , 3° , 0° respectively; the first four occur respectively when cy/x takes the values 1.47*, 1.25, 1.13, 1.05.

TABLE IV.

	$c=0.00$		$c=0.25$		$c=0.50$		$c=0.75$		$c=1.00$
z	f	g	f	g	f	g	f	g	$f:g$
0.0	0.000	0.000	0.000	0.000	0.000	0.000	0.000	0.000	0.000
0.5	0.134	0.071	0.135	0.095	0.138	0.114	0.140	0.130	0.143
1.0	0.459	0.280	0.466	0.356	0.474	0.412	0.482	0.456	0.492
1.5	0.887	0.609	0.899	0.736	0.913	0.826	0.928	0.892	0.944
2.0	1.362	1.024	1.378	1.188	1.396	1.297	1.413	1.374	1.433
2.5	1.854	1.489	1.872	1.672	1.892	1.789	1.912	1.870	1.932
3.0	2.353	1.978	2.372	2.171	2.392	2.289	2.412	2.370	2.432
3.5	2.852	2.475							
4.0	3.352	2.974							

Thirdly, we may notice that, apart from $c=1$, there is a general tendency for g to approach the mainstream value less rapidly than f , this tendency being most marked at $c=0$. In fact we might artificially speak of two boundary layer thicknesses, one associated with each principal direction, though it must be emphasized that they do not differ vastly. There is a general tendency for both thicknesses to decrease as c increases towards 1, as can be seen from Table II., or from the values of the integrals

$$\int_0^\infty \left(1 - \frac{u}{ax} \right) dz, \quad \int_0^\infty \left(1 - \frac{v}{by} \right) dz$$

which are 0.648, 1.026 when $c=0$; 0.628, 0.829 when $c=0.25$; 0.608, 0.711 when $c=0.50$; 0.588, 0.630 when $c=0.75$; and 0.568, 0.568 when $c=1.0$.

* This is the limiting value as $c \rightarrow 0$, of course.

Finally, it may be remarked that, just as in the corresponding two dimensional solution, the solution given here is in fact a solution of the full equations of viscous motion in Cartesian coordinates.

REFERENCES.

- HANNAH, 1947, *Rep. Aero. Res. Coun.*, No. 10, 482 (not yet published).
HOMANN, 1936, *Zeitschr. f. angew. Math. u. Mech.*, **16**, 153-164.
HOWARTH, 1934, *Rep. Memor. Aero. Res. Coun.*, No. 1632 ; 1951, *Phil. Mag.* [7],
42, 239-243.
PRANDTL, 1945, *Volkenrohde Report and Translation*, No. 64.
SEARS, 1948, *J. Aero. Sci.*, **15**, 49-52.

CXLV. CORRESPONDENCE.

On the Calculation of Characteristic Temperatures from the Elastic Constants.

By M. BLACKMAN,
Physics Department, Imperial College, London *.

[Received September 18, 1951.]

RECENT work (Leigh 1951) on the free energy of alloys has drawn attention to the calculation of θ_D values in cases where the solids are elastically anisotropic. This anisotropy is due to the smallness of the $(C_{11}-C_{12})$ value, where the elastic constants of the (cubic) solid are C_{11} , C_{12} and C_{44} respectively. In such cases no simple method exists for calculating θ_D . One has either to calculate the mean velocity directly, which is a lengthy procedure, or to use the Hopf-Lechner (1914) method, which in these cases is equally lengthy and tedious. While this is immaterial in single cases, the time spent in calculation can become disproportionately large, where a series of alloys has to be considered.

TABLE I.

Substance	Li	Na	K	Cu	Pb	Ag	Au	Al
θ_D^*	354	144	77	342	85	212	158	394
θ_D	(351)	147	82	355	91	203	160	400

The purpose of this note is to communicate a semi-theoretical formula for θ_D designed to cover cases where $(C_{11}-C_{12})$ is relatively small. The method used is to consider the shape of the surfaces of constant frequency (*cf.* Blackman 1935). While this does not lead to a definite formula, it does suggest a reasonable form; a constant which then remains is fixed by fitting close to the value for Lithium calculated by the standard methods.

The resultant form is

$$\nu_D^3 = s \cdot \frac{3 \cdot 15}{8\pi} \cdot \frac{1}{\rho^{3/2} \Delta} (C_{11} - C_{12})^{1/2} (C_{11} + C_{12} + 2C_{44})^{1/2} (C_{44})^{1/2}, \quad (1)$$

where Δ =volume of the unit cell, s =number of particles per cell, ρ =density, and ν =Debye frequency. The Debye θ_D value is equal to $h\nu_D/k$ (h =Planck's constant, k =Boltzmann's constant).

Table I. shows the agreement between (1), and the values of ν_D calculated by standard methods. These, it should be remembered, are not exact calculations and may be several per cent in error. The θ values so obtained are labelled θ_D^* .

* Communicated by the Author.

The validity of (1) is surprisingly wide, but it should be emphasized that it is nevertheless limited. When the above formula is used, the elastic constants should be such that the C_{44}/C_{11} , C_{12}/C_{11} ratios lie inside the region covered by Table I, (*cf.* Blackman 1938, p. 76).

As an example, we take the Ag-Au alloys, the elastic constants for which have been given by Roehl (1933). The θ_D values were calculated by Roehl not from these values, but from averaged elastic constants. The result of direct calculation using (1) is given below.

TABLE II.

Substance	Ag	25 At. % Au	50 At. % Au	75 At. % Au	Au
θ_D	203	195	185	172	160

The conclusion to be drawn from this table is the same as that drawn by Roehl, namely that θ_D is not a linear function of the percentage of gold added to silver.

REFERENCES.

- BLACKMAN, M., 1934, *Proc. Roy. Soc. A*, **149**, 127 ; 1938, *Ibid.*, **164**, 62.
 HOPF, L., and LECHNER, G., 1914, *Verh. Deutsch. Phys. Ges.*, **16**, 643.
 LEIGH, R. S., 1951, *Phil. Mag.*, **42**, 876.
 ROEHL, H., 1933, *Ann. Phys.*, **16**, 887.

Inelastic Scattering of Deuterons.

By R. HUBY and H. C. NEWNS,

Department of Theoretical Physics, The University of Liverpool*.

[Received September 19, 1951.]

THE inelastic scattering of protons has been much studied in experiments, the results of which seem understandable in terms of the formation and decay of a compound nucleus.

Recently, evidence has been obtained showing that deuterons also can be inelastically scattered by nuclei (Greenlees, Kempton and Rhoderick (1949); Holt and Young (1949)). In some cases, *e. g.* the excitation of the 1.38 MeV. level in Mg^{24} , the total cross section seems much larger, at about 10^{-25} cm.², than would be expected for this process on the theory of compound nucleus formation. Further, the angular distribution, which has been measured in the above-mentioned case by Holt and Young, is of a complicated form, with a strong concentration at rather small angles of

* Communicated by the Authors.

scattering, such as would seem unlikely on that theory. The present authors therefore attempted an explanation through electrical interaction of the deuteron with the nucleus, but this was found to yield much too small a cross section to account for the present experiments (Huby and Newns (1951)). In a similar treatment, Mullin and Guth (1951) were able to obtain an angular distribution of approximately the required shape, but to account for the measured total cross section, they would require a dipole moment of the order of three times the nuclear radius, which seems too large to be physically plausible.

The purpose of this letter is to propose a very simple mechanism to account for the main features of the experimental results. The mechanism is suggested by the similarity of the observed angular distributions to those obtained in various (d-p) and (d-n) reactions, and it has something in common with the stripping theory for the latter. We assume that only one of the constituents of the deuteron, say the neutron, interacts with the nucleus, the proton being outside the range of the nuclear forces. The neutron interacts at the surface of the nucleus, exciting it and then "bouncing off", the deuteron emerging as a whole having been inelastically scattered*. A calculation can be made, based on the Born approximation, and following closely a treatment of the (d-p) and (d-n) reactions of Bhatia and Huang (reported by Huby (1950)). Despite its crudity, the latter had considerable success in explaining the observed (d-p) and (d-n) angular distributions, and this seems an encouragement for the present calculation for (d-d*) reactions.

The differential cross section can be written

$$\sigma(\theta) = \frac{2\pi}{\hbar} \left| \int \psi_f^* \chi_f^* \chi_{Df}^* V \psi_i \chi_i \chi_{Di} d\tau d\mathbf{R}_n d\mathbf{R}_p \right|^2,$$

where ψ_i and ψ_f are the initial and final deuteron translational wave functions, χ_i and χ_f the initial and final nuclear wave functions, and χ_{Di} and χ_{Df} the initial and final internal deuteron wave functions. V represents the interaction between the neutron and the nucleus. This can be evaluated if we assume (i.) the interaction V operates only on a sphere of "radius of interaction" a , (ii.) the incident and scattered deuterons waves are plane waves of wave number \mathbf{k}_i and \mathbf{k}_f respectively, (iii.) the ground state of the deuteron is a pure triplet-S state, with radial wave function of the form $\exp\{-\alpha|\mathbf{R}_n - \mathbf{R}_p|\}/|\mathbf{R}_n - \mathbf{R}_p|$.

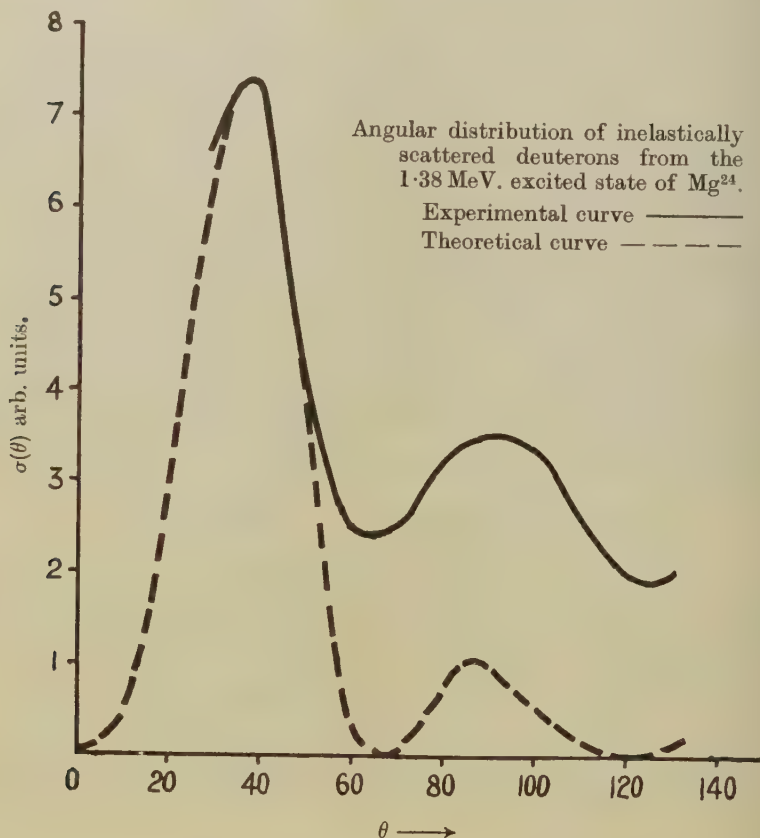
The result obtained is

$$\sigma(\theta) = \sum_l |A_l|^2 \left[\frac{4\alpha}{k} \tan^{-1} \frac{k}{4\alpha} \cdot \left(\frac{\pi}{2ka} \right)^{1/2} J_{l+1/2}(ka) \right]^2,$$

where $k^2 = (\mathbf{k}_i - \mathbf{k}_f)^2 + 4k_i k_f \sin^2 \frac{1}{2}\theta$, and the A_l 's are unknown constants. The formula for σ gives scattering predominantly at small angles. The sum is taken over integers l which are related to the angular momentum

* A rather similar model was in fact proposed by E. Guth (*Phys. Rev.*, **68**, 280 (1945)) in predicting inelastic scattering of deuterons.

change of the nucleus. There are selection rules requiring that if J_i and J_f are the angular momentum of the initial and final states of the nucleus, then $J_f = J_i + 1$ (but when $J_i = 0$, and $l = 0$ then $J_f = 0$ or 1), and l is odd or even according as there is a change of parity or not. The values of l can be determined from the angular distribution. If more than one value of l can contribute, the lowest one usually predominates. Thus the angular distribution of inelastically scattered deuterons can lead to information about the spins and parities of nuclear states.



A particular example is the case of deuterons inelastically scattered from the 1.38 MeV. excited state of Mg^{24} . A theoretical curve for $l=2$ is shown in the figure together with the experimental curve (Holt and Young (1949)). Since the ground state of Mg^{24} has spin zero and even parity, the first excited state has spin 1, 2 or 3 and even parity.

The parameter a is not well defined. One might expect it to be given by the Gamow formula (Gamow and Critchfield (1949)) for the nuclear radius, but as in the (d-p) reaction, the values of a needed are always

larger than this. In the magnesium case discussed above, we used $a=7 \times 10^{-13}$ cm. To make curves for different values of l fit, values of a which seem unreasonable would be required. A spin of 2 for the excited state would be in agreement with the experiments on the angular correlation of successive γ -ray emissions from the nucleus (Brady and Deutsch (1948)).

The angular distribution of deuterons inelastically scattered from the 1.66 MeV. excited state of Ne^{20} has been measured by Middleton and Tai (unpublished). This can be fitted by the theoretical curve for $l=1$. Since the ground state of Ne^{20} has spin zero and even parity, the 1.66 MeV. excited state must have spin 0, 1 or 2 and odd parity.

REFERENCES.

- BRADY, E. L., and DEUTSCH, M., 1948, *Phys. Rev.*, **74**, 1541.
GAMOW, G., and CRITCHFIELD, G. L., 1949, *Atomic nucleus and nuclear energy sources* (Oxford: Clarendon Press).
GREENLESS, G. W., KEMPTON, A. E., and RHODERICK, E. H., 1949, *Nature, Lond.*, **164**, 663.
HOLT, J. R., and YOUNG, C. T., 1949, *Nature, Lond.*, **164**, 1000.
HUBY, R., 1950, *Nature, Lond.*, **166**, 552; also private circulation.
HUBY, R., and NEWNS, H. C., 1951, *Proc. Phys. Soc. A*, **64**, 619.
MULLIN, C. J., and GUTH, E., 1951, *Phys. Rev.*, **82**, 141.

Experiments on the Unsaturated Helium II Film.

By R. BOWERS, D. F. BREWER and K. MENDELSSOHN, F.R.S.,
Clarendon Laboratory, Oxford *.

[Received September 17, 1951.]

THE transfer of the helium II film at pressures lower than the vapour pressure of the liquid has been investigated by a method which consists essentially in measuring the heat conduction of a tube containing He gas under variable percentage saturation.

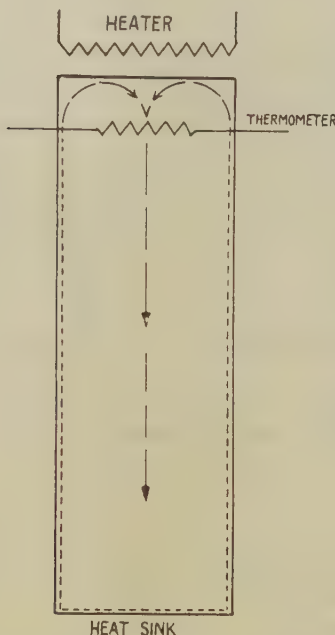
The principle of the apparatus is shown in fig. 1. The bottom of the (thin-walled german silver) tube is connected to a constant-temperature heat sink, while the top contains a heater and a thermometer. When, under fixed conditions of temperature of the sink and of pressure in the tube, heat is supplied at increasing rates \dot{Q} , the thermometer remains constant at its original reading until a certain critical heat input \dot{Q}_c is reached, when it rises sharply. The constancy of temperature is maintained by flow of the film up the inside wall of the tube, the film evaporating at the top, and the helium returning as gas to the bottom of the tube. This circulation provides a powerful means of heat transport, in which the latent heat of the helium is taken up by evaporation at the top, and given

* Communicated by the Authors.

off by condensation at the bottom to the heat sink. Incidentally, the heat of evaporation from the film is slightly larger than that of the bulk liquid (L_B), since it also contains the energy of excitation of the superfluid into the normal state ($T\Delta S$). The circulation process must break down when a film flow rate larger than the critical rate r_c is required to maintain it. The critical heat input \dot{Q}_c thus provides an accurate means of determining the critical rate of mass transport of the He II film since

$$r_c = \frac{\dot{Q}_c}{(L_B + T\Delta S)}.$$

Fig. 1.



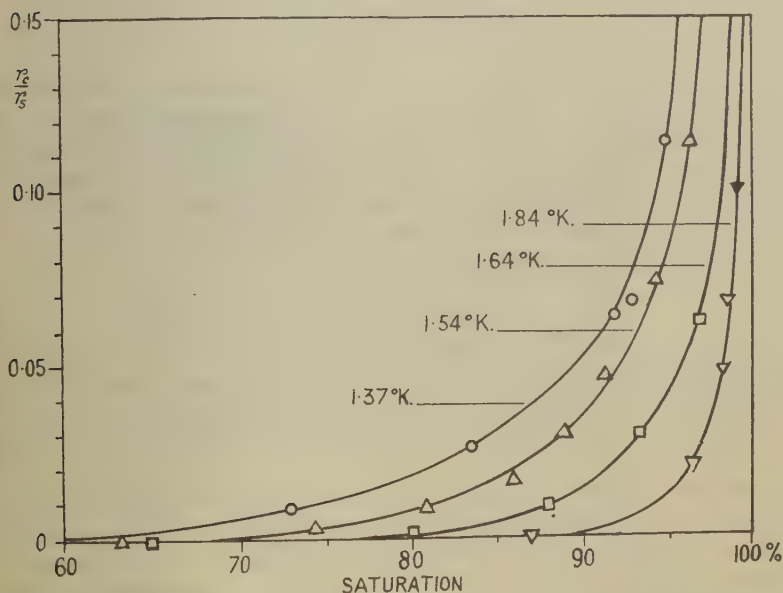
Such factors as might influence the validity of this equation, *e. g.* viscous drag in the returning gas, heat flow by conduction along the metal tube and through the gas, and heat resistance of the partition between the tube and the heat sink, were negligibly small in our case. A check on the validity of the method was provided by plotting the critical flow rates obtained at various temperatures under saturation conditions (r_s) against the absolute temperature. The values derived are in satisfactory agreement with the shape of the curve of transfer rate out of a beaker (Mendelssohn and White 1950).

Transfer rates under various percentage saturations have been obtained for four different temperatures, and the results are given in fig. 2, where the reduced transfer rates r_c/r_s are plotted against the percentage saturation.

The method is sensitive enough to detect mass flow of the order of 0.1 per cent of the saturation flow rates ($r_c/r_s \sim 0.001$).

The results show clearly that any appreciable film transfer will only occur near saturation. In fact, even for the lowest temperature (1.37°K.), the flow rate at 90 per cent saturation is only 5 per cent of the full rate; while nearer the lambda point (1.84°K.), this fraction of the full rate is only reached at 98 per cent saturation. The curves also indicate that for any particular percentage saturation, there exists a temperature above which no film transfer occurs. This "critical" temperature decreases with decreasing percentage saturation.

Fig. 2.



Our values give mass flow rates which can be expressed as a product of the film thickness d , and an average velocity \bar{v} . The only measurements of d close to 100 per cent saturation (Long and Meyer 1949) indeed indicate that this quantity is rising rapidly above 90 per cent saturation. At 80 per cent saturation, where according to Frederikse and Gorter (1950) the film thickness is about 10 per cent of that of the saturated film (Daunt and Mendelssohn 1939, Burge and Jackson 1951), d hardly varies with temperature. On the other hand, it is evident from our measurements that the mobility of the film increases rapidly as the temperature is lowered. It is hoped to obtain better determinations of \bar{v} from improved measurements of the adsorption isotherms near 100 per cent saturation, and from more detailed determinations of the transfer rates which are now in progress. So far, our observations do not suggest that $\bar{v} \times d$ is constant.

REFERENCES.

- BURGE, E. J., and JACKSON, L. C., 1951, *Proc. Roy. Soc. A*, **205**, 270.
 DAUNT, J. G., and MENDELSSOHN, K., 1939, *Proc. Roy. Soc. A*, **170**, 439.
 FREDERIKSE, H. P. R., and GORTER, C. J., 1950, *Physica*, **16**, 402.
 LONG, E. A., and MEYER, L., 1949, *Phys. Rev.*, **76**, 440.
 MENDELSSOHN, K., and WHITE, G. K., 1950, *Proc. Phys. Soc. A*, **63**, 1328.

The Upper Limit for the Neutrino Rest Mass.

By O. KOFOED-HANSEN,

Institute for Theoretical Physics, University of Copenhagen*.

[Received July 9, 1951.]

SINCE the β -spectrum of H^3 has a very low maximum energy it provides us at present with the best possibility for the determination of the rest mass of the neutrino. The following comments on the problem may be of relevance in view of the great experimental progress recently achieved (Curran, Angus and Cockroft 1949, Hanna and Pontecorvo 1949).

For a finite neutrino mass the shape of the β -spectrum is given by

$$P(E) = p \cdot E \cdot (E^{\max} + m_\nu - E) \cdot \{(E^{\max} + m_\nu - E)^2 - m_\nu^2\}^{\frac{1}{2}} \\ \times [1 + bm_\nu m_\beta / (E(E^{\max} + m_\nu - E))] \cdot F(Z, E) \quad \dots \quad (1)$$

where E is the energy of the β -particle including the rest mass m_β , p is the corresponding momentum, E^{\max} is the maximum energy of the β -particle, m_ν is the rest mass of the neutrino in energy units (we put $c=1$), $F(Z, E)$ is the Coulomb factor and b is a constant which we shall discuss in the following.

It has been shown previously (1947) that even if the neutrino mass is not zero the extrapolated maximum β -energy, if sufficiently large, is the same as for vanishing neutrino mass, *i. e.*, it equals the mass difference Δ between the two nuclei involved in the process. Consequently, in this case the maximum β -energy and the mass of the neutrino can only be determined by the original Fermi method, *i. e.* from the shape of the β -spectra in the immediate vicinity of the upper limit.

Pruett (1948) has pointed out that the term in (1) containing b is important for the discussion of the influence of a finite neutrino mass at low energy β -spectra. Pruett adopted the value -1 for b . However, b may also assume the value $+1$, and if linear combinations of the five coupling cases are used also values between ± 1 may occur. Furthermore, no definite sign of b can be attached to a definite coupling case (Yang and Tiomno 1950).

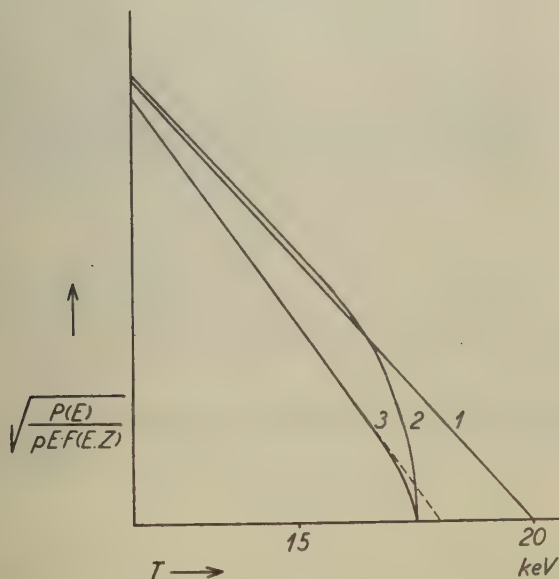
Many authors assume that the result of an extrapolation of the observed β -spectrum when the term containing b in (1) is taken into account and

* Communicated by the Author.

for low maximum energies leads to an extrapolated upper limit of the spectrum which deviates by $m_\nu/2$ from the value obtained for vanishing neutrino mass. Such a result is found when the β -spectrum is expanded in a series in $m_\nu/(E^{\max} + m_\nu - E)$. Unfortunately, however, this series is not adequate for the low energy spectra since the condition for such a series development, viz. $m_\nu \ll E^{\max} + m_\nu - E$, can not be assumed to hold for the major part of the spectrum. A correct procedure is to apply a numerical evaluation of (1). The result is illustrated in fig. 1 where three hypothetical Kurie (or Fermi) plots are given. In this kind of plot one draws

$$\{P(E)/(pE \cdot F(Z, E))\}^{\frac{1}{2}} \quad . \quad . \quad . \quad . \quad . \quad (2)$$

Fig. 1.



The figure shows hypothetical Kurie plots for $(A - m_\beta) = 20$ keV. and for vanishing neutrino mass (curve 1) and for $m_\nu = 2.5$ keV. and $b = +1$ (curve 2) and $b = -1$ (curve 3). The extrapolated curves will cut the abscissa very close to 20 keV. for curve 2 giving no effect of m_ν and at ~ 18 keV. for curve 3 giving an effect of $\sim 4/5 m_\nu \cong m_\nu$. T is the kinetic energy of the β -particle.

as a function of E . If $m_\nu = 0$ the Kurie plot is a straight line cutting the abscissa at $E = E^{\max}$. For $m_\nu \neq 0$ effects of the neutrino mass appear. In the present low energy case the conclusions as regards the mass of the neutrino are that if $b = 1$ one finds a curve which lies rather close to the curve for zero neutrino mass, and in the case $b = -1$ one finds a curve which deviates from the curve for zero neutrino mass by almost the full

amount corresponding to m_ν . This means that if ever a finite neutrino mass is observed then this procedure could be used for a determination of b .

In the case of H^3 one does not know the precise value of the mass difference Δ between the H^3 and He^3 nuclei. The main uncertainty comes from the uncertainty in the n - p mass difference. Nuclear cycles involving β -decay processes are our best tools for the determination of the n - p mass difference (Li, 1951) but obviously they involve the assumption of zero neutrino mass so that we cannot apply the Δ value found in this way. Consequently we cannot compare E_β^{\max} and Δ directly. However, the shape of the spectrum is known very precisely close to the upper limit of the energy, and thus from the shape of the spectrum one has the possibility of a determination of the neutrino rest mass. The experimental result is (Hanna and Pontecorvo 1949) that the Kurie plot deviates from a straight line by less than 1 keV. Since b is not known this deviation may be a measure of $\sim 1/5$ of the neutrino mass only. This represents the lowest curve in fig. 1 corresponding to $b = -1$. Thus we may only conclude that the neutrino mass is smaller than 5 keV. or that the neutrino mass is smaller than $1/100$ of the electron mass. This statement is more conservative than the result given by Hanna and Pontecorvo (1949).

REFERENCES.

- CURRAN, S. C., ANGUS, J., and COCKROFT, A. L., 1949, *Phil. Mag.*, **40**, 36, 53.
 HANNA, G. C., and PONTECORVO, B., 1949, *Phys. Rev.*, **75**, 983.
 KOFOED-HANSEN, O., 1947, *Phys. Rev.*, **71**, 451.
 LI, C. W., WHALING, W., FOWLER, W. A., and LAURITSEN, C. C., 1951, *Phys. Rev.*, **83**, 512.
 PRUETT, J. R., 1948, *Phys. Rev.*, **73**, 1219.
 YANG, C. N., and TIOMNO, J., 1950, *Phys. Rev.*, **79**, 495.

ERRATA

A Theoretical Investigation of the Compression of a Ductile Material between Smooth Flat Dies, by A. P. GREEN, 1951, *Phil. Mag.*, **42**, 900.

On page 916 the transformation equations should read:

$$\left. \begin{aligned} u &= \bar{y}', & v &= -\bar{x}', & \alpha &\rightarrow \alpha', & \phi &= \phi' & (b), \\ u &= \bar{x}', & v &= -\bar{y}', & c &\rightarrow \beta', & \phi &= -\phi' & (c), \\ u &= \bar{y}', & v &= \bar{x}', & \alpha &\rightarrow \alpha', & \phi &= -\phi' & (d). \end{aligned} \right\} \quad . \quad . \quad . \quad (5)$$

Electron and Gamma Ray Spectroscopy with Scintillation Detectors, by R. C. BANNERMAN, G. M. LEWIS and S. C. CURRAN, 1951, *Phil. Mag.*, **42**, 1097.

On page 1102, line 6, the expression "15 per cent" should read "1 per cent".

[The Editors do not hold themselves responsible for the views expressed by their correspondents.]

OBITUARY NOTICE

DR. ALLAN FERGUSON

We regret to announce the death of Dr. ALLAN FERGUSON, for many years an Editor of the Philosophical Magazine, who passed away on Friday, November 9th, 1951.

An appreciation and tribute will be published in a later issue of this publication.

INDEX TO VOL. XLII.

- A**BSORPTION of penetrating shower secondaries (Ritson), 250.
- Ahmed (M. S.), ionization of lithium hydride, 997.
- Allowed β -transitions, effects of recoil (Kofoed-Hansen), 1411.
- Alloys at low temperatures, thermal conductivity (Berman), 642.
- α -particles from O_{18} (Seed), 566.
- α , α' phases in Al-Zn systems (Leigh), 876.
- Amelinekx (S.), interferometric study of cleavage planes of sodium chloride, 324.
- Analastic measurements of diffusion in solid solutions (Le Claire), 673.
- Analytical continuation of the S-matrix (van Kampen), 851.
- Armenteros (R.), Barker (K.), Butler (C. C.) and Cachon (A.), properties of neutral V-particles, 1113.
- Ashwell (D. G.), axis of distortion of twisted elastic prism, 820.
- Aspinall (A.), Clegg (J. A.) and Hawkins (G. S.), radio echo apparatus for delineation of meteor radiants, 504.
- Atkinson (J. R.), *see* Howatson, 1136.
- Atmospherics, waveforms and propagation (Bowe), 121.
- Attenuation of nucleon cascades in lead (Rosser and Swift), 856.
- Bannerman (R. C.), Lewis (G. M.) and Curran (S. C.), electron and γ -ray spectroscopy with scintillation counters, 1097; (erratum), 1450.
- Bardsley (O.), conditions at sharp leading edge in supersonic flow, 255.
- and Mair (W. A.), interaction between an oblique shock-wave and a turbulent boundary layer, 29.
- Barium titanate, theory (Devonshire), 1065.
- Barker (K.), *see* Armenteros, 1113.
- ${}^9\text{Be}(p, p2n){}^7\text{Be}$, cross-section (Randle *et al.*), 665.
- Berman (R.), thermal conductivity of some alloys at low temperatures, 642.
- Beryl crystals, microscopic studies (Griffin).—I., 775.
- , —, —II., 1337.
- Beta decay, interaction in the theory (Pursey), 1193.
- β -spectrum of tritium (Insch and Curran), 892.
- Bilby (A. H.), *see* Cottrell and Bilby, 573.
- Binding energies of 3 and 4 particle nuclei (Irving), 338.
- Bishop (J. F. W.) and Hill (R.), plastic properties of poly-crystalline F.C. metal, theoretical derivation, 1298.
- , theory of plastic distortion of a polycrystalline aggregate under combined stresses, 414.
- Blackman (M.), calculation of characteristic temperatures from elastic constants, 1441.
- Bleaney (B.), hyperfine structure in paramagnetic salts and nuclear alignment, 441.
- , Elliott (R. J.), Scovil (H. E. D.) and Trenam (R. S.), paramagnetic resonance in gadolinium ethylsulphate, 1062.
- Bloch-Nordsieck method, covariant formulation (Thirring and Touschek), 244.
- Books, new :—Alfven, Cosmical electrodynamics, 118; Bouman (J.), Selected topics in X-ray crystallography, 958; Butler and Randall, Progress in Biophysics, 118; Corner (J.), Theory of interior ballistics of guns, 958; Faffingdon (G. H.), Fundamentals of automatic control, 1335; Fisher,

- Mathematical statistics, 119;
 Heavyside (O.), Electromagnetic theory, 440; Hill (R.), Mathematical theory of plasticity, 439;
 Huckel (W.), Structural chemistry of inorganic compounds, 220;
 Jeffreys (H. and B. S.), Methods of mathematical physics, 119;
 Jellinck (K.), Weltsystem etc.; Wellenmechanik, 438; London (F.), Super-fluids, 958; MacMillan (R. H.), Theory of control in mechanical engineering, 1335;
 Pearse and Taylor, Identification of molecular spectra, 959; Progress in physics, Vol. XIV, 1064;
 Rossini (F. D.), Chemical thermodynamics, 959; Smart (E. H.), Advanced dynamics, 960;
 Steinhaus (H.), Mathematical snapshots, 439; Vigoureux (P.), Ultrasonics, 439; Wheeler (L. P.), J. Willard Gibbs, 1335; Wilson (W.), Hundred years of physics, 119.
- Born-green theory of fluids (Rushbrooke and Scovins), 582.
- Bose-Einstein gas, condensation (Fraser).—I., 156.
 —.—II., 165.
- Boundary layer on rotating sphere (Howarth), 1308.
- Boundary layer in three dimensional flow (Howarth).—I., 239,
 —.—II., 1433.
- Bowe (P. W. A.), waveforms of atmospherics and propagation of very low frequency, 121.
- Bowers (R.), Brewer (D. F.) and Mendelssohn (K.), experiments on unsaturated helium film, 1445.
- Braddick (H. J. J.), Nash (W. H.) and Wolfendale (A. W.), associated penetrating particles of cosmic rays underground, 1277.
- Brewer (D. F.), *see* Bowers, 1445.
- Brinkworth (M. J.) and Titterton (E. W.), reaction $^{10}\text{B}(\gamma, d)^2\text{He}$, 952.
 —, Photodisintegration of ^{10}B , 1191.
- Bromine, electric quadrupole and magnetic moment of nucleus, 279.
 —, hyperfine structure, 284.
- Broom (T.), anisotropy of electrical resistance, cold-rolled metals and alloys, 56.
- Brown (A. F.) and Honeycombe (R. W. K.), micro-slip in metal crystals, 1146.
- Brownian movement, velocity (Macdonald), 219.
- Budden (K. G.), propagation of a radio-atmospheric, 1.
 —, reflection of low frequency radio waves, 833.
- Burcham (W. E.), *see* Freeman, 434.
- Burgess (R. E.), rectification and observation of signals in presence of noise, 475.
- Butler (C. C.), *see* Armenteros, 1113.
- Cachon (A.), *see* Armenteros, 1113.
- Calcraft (M. E.) and Titterton (E. W.), reactions $^{11}\text{Be}(\gamma\alpha)^7\text{Li}$ and $^{11}\text{B}(\gamma T)^8\text{Be}$, 666.
- Calnan (E. A.) and Clews (C. J. B.), deformation textures in metals.
 —II., 616.
 —III., 919.
- Camerini (U.), Davies (J. H.), nuclear transmutations of great energy; with Fowler (P. H.) *et al.*—VI., 1241.
 —with Franzinetti (C.) *et al.*—VII., 1261.
- Capacitance of condenser with anisotropic cylinder in torsion (Mack), 428.
- Carborundum growth spirals (Verma), 1005.
 — (Frank), 1014.
- Cassels (J. M.), *see* Taylor, 20, 328, 751.
 —, *see* Randle, 665.
- , Randle (T. C.), Pickavance (T. G.) and Taylor (A. E.), production of neutrons by high energy protons, 215.
- Cavanagh (P. E.), *see* Turner, 636.
- Characteristic temperatures from elastic constants (Blackman), 1441.
- Cherry (C.), non-linear systems possessing reactance, 1161.
- Clegg (J. A.), *see* Aspinall, 504.
- Clews (C. J. B.), *see* Calnan, 616, 919.
- Collision broadening at microwave frequencies (Leslie), 37.
- Combined bending and twisting of thin tubes (Hill and Siebel), 722.

- Communal entropy of dense systems (Pople), 459.
- Compression of ductile material (Green), 900, 1336, 1450.
- Cornish (F. H. J.) and MacDonald (D. K. C.), influence of deviations from Debye spectrum on electrical conductivity of metals, 1406.
- Cosmic radiation, charge and energy of heavy nuclei (Dainton, Fowler and Kent), 317.
- Cosmic rays, origin of stars (Harding), 63.
- — —, disintegration of nuclei (Hodgson), 82, 955.
- — —, emission of Li^8 (Hodgson), 207.
- — —, neutrons in ice (Lattimore), 331.
- — —, events in glacier (Harding), 651.
- — —, stars, cascade production (Thomson and Hodgson), 978.
- — —, associated particles underground (Braddick, Nash and Wolfendale), 1277.
- Cottrell (A. H.) and Bilby (B. A.), mechanism for growth of deformation twins in crystals, 573.
- Cottrell (T. L.) and Paterson (S.), virial theorem in quantum mechanics, 391.
- Critical magnetic fields of Al, Cd, Ga and Zn (Goodman and Mendoza), 594.
- Cross-sections for neutrons (Taylor *et al.*), 20, 328, 751, 1336.
- Crystal dislocations (Frank), 809.
- Crystal plasticity (Nabarro), 213.
- Crystalline structure and strength of metals (Wood), 310.
- Curran (S. C.), *see* Wilson, 762; Insch, 892; Bannerman, 1097.
- Dainton (A. D.), Fowler (P. H.) and Kent (D. W.), new method of determining charge and energy of heavy cosmic nuclei, 317.
- Dainton (A. D.), Gattiker (A. R.) and Lock (W. O.), processing of thick emulsions, 396.
- Dalitz (R. H.) and Ravenhall (D. G.), Tomonaga method in meson field theory, 1378.
- Danyasz (M.) and Yekutieli (G.), loading emulsions with wires, 1185.
- Davies (J. H.), *see* Camerini, 1241, 1261.
- Deflection of cable, single point load (Markland), 990.
- Deformation textures in metals (Calnan and Clews).—II., 616.
- — —, —III., 919.
- — — twins in crystals (Cottrell and Bilby), 573.
- Density of states, $3d$ electrons in nickel (Fletcher and Wohlfarth), 106.
- Devonshire (A. F.), theory of barium titanate.—II., 1065.
- Dickson (J. M.), *see* Randle *et al.*, 665.
- Dingle (R. B.), two-fluid model of helium II., 1080.
- Dirac's matrices, trace of product (Yang), 1333.
- Directive wave propagation (Nodtvedt), 1022.
- Dislocation fieldssynthesis (Nabarro), 1224.
- — — in thin plates (Eshelby and Stroh), 1401.
- — — reaction in F.C. lattice (Lomer), 1327.
- Domb (C.), melting curve at high pressures, 1316.
- Dymond (E. G.), *see* Pullar, 663.
- Elastic constants of aluminium (Leigh), 139.
- Electrical conductivity of metals (Cornish and MacDonald), 1406.
- — — resistance, anisotropy, cold-rolled metals and alloys (Broom), 56.
- — — of gold, silver and copper at low temperatures (Mendoza and Thomas), 291.
- Electron and γ -ray spectroscopy (Bannerman, Lewis and Curran), 1097, 1450.
- Elliott (R. J.), *see* Bleaney, 1062.
- Emulsions, loading with wires (Danyasz and Yekutieli), 1185.
- Energy loss of slow deuterons in D_2O (French and Seidl), 537.
- Equilibrium of linear arrays of dislocations (Eshelby, Frank and Nabarro), 351.
- Eshelby (J. D.), Frank (F. C.) and Nabarro (F. R. N.), equilibrium of linear arrays of dislocations, 351.

- Eshelby (J. D.) and Stroh (A. N.), dislocation in thin plates, 1401.
- Feather (N.), isomeric state of RaE , 568.
- Ferromagnetism, collective electron (Wohlfarth), 374.
- Field theories with non-localized interaction (Rayski), 1289.
- Fletcher (G. C.) and Wohlfarth (E. P.), density of states, $3d$ electrons in nickel, 106.
- Forty (A. J.), growth of cadmium iodine from aqueous solution, 670.
- Fowler (P. H.), Menon (M. G. K.), Powell (C. F.) and Rochat (O.), masses and decay of heavy τ -mesons.—II., 1040.
- Fowler (P. H.), *see* Dainton, Fowler and Kent, 317; Camerini, 1241.
- Frank (F. C.), crystal dislocations, 809.
- , growth of carborundum, 1014.
- , *see* Eshelby, 351.
- Frank (S. G. F.), Frisch (O. R.) and Scarrott (G. G.), mechanical kick-sorter, 603.
- , localizing Geiger counter, 612.
- Franzinetti (C.), *see* Camerini, 1241, 1261.
- Fraser (A. R.), condensation of a perfect Bose-Einstein gas.—I., 156.
- , —II., 165.
- Freeman (J. M.) and Burcham (W. E.), range-energy relation for slow α particles in air, 434.
- French (A. P.) and Seidl (G. F. P.), energy loss of slow deuterons in D_2O , 537.
- , matrix elements for octupole radiative transitions, 263.
- Frisch (O. R.), *see* Frank (S. G. F.), 603.
- Gattiker (A. R.), *see* Dainton, 396.
- Geiger counter, localizing (Frank, S. G. F.), 612.
- Gibson (W. M.), Grotdal (T.), Orlin (J. J.) and Trumpy (B.), photo-disintegration of the deuteron, 555.
- Gold (T.), ultrasonic delay line, design, 787.
- Goldsack (S. J.) and Page (N.), example of n, p ; π^- -reaction in emulsion, 570.
- Goodman (B. B.) and Mendoza (E.), critical magnetic fields of Al, Cd, Ga, and Zn, 594.
- Gottstein (K.), Menon (M. G. K.), Mulvey (J. H.), O'Ceallaigh (C.) and Rochat (O.), multiple scattering of particles in emulsions.—I., 708.
- and Mulvey (J. H.), multiple scattering in emulsions.—IV., 1089.
- Grain boundary diffusion in metals (Le Claire), 468.
- Green (A. P.), flow of metals, plasticine models, 365.
- , compression of ductile material between flat dies, 900; (errata), 1336, 1450.
- Griffin (L. J.), microscopic studies on beryl crystals.—I., 775.
- , —II., 1337.
- Grotdal (T.), *see* Gibson, 555.
- Growth of cadmium iodide from solution (Forty), 670.
- Gunn (J. C.) and Irving (J.), photo-electric disintegration of 3- and 4-particle nuclei, 1353.
- , Power (E. A.) and Touschek (B. K.), production of mesons in proton-proton collisions, 523.
- Hammer tracks in neutron and proton produced stars (Titterton), 113.
- Harding (J. B.), origin of cosmic ray stars, 63.
- , cosmic ray events in a glacier, 651.
- Hawkins (G. S.), *see* Aspinall, 504.
- Hayes (J. G.) and Vickers (T.), fitting of polynomials to unequally-spaced data, 1387.
- Helium II film, unsaturated (Bowers, *et al.*), 1445.
- Helium II, quantum mechanics (Penrose), 1373.
- , two-fluid model (Dingle), 1080.
- Helium, ultrasonic propagation in liquid (Pippard), 1209.
- Henisch (H. K.), internal barriers in semi-conductors, 734.
- Highly forbidden transitions in Na^{24} (Turner and Cavanagh), 636.
- Hill (R.), stress in a plastic-rigid body at yield point, 868.
- and Siebel (M. P. L.), combined bending and twisting of thin tubes in the plastic range, 722.

- Hill (R.), *see* Bishop and Hill, 414, 1298.
- Hodgson (P. E.), disintegration of lead nuclei by cosmic rays, 82.
- Hodgson (P. E.), emission of Li^8 , 207.
- , disintegrations of light nuclei, 955.
- , τ -meson, 1060.
- , *see* Thomson, 978.
- Honeycombe (R. W. K.), *see* Brown, 1146.
- Hooper (J. E.), King (D. T.) and Morrish (A. H.), pair production by fast electrons, 304.
- Howarth (L.), boundary layer on a rotating sphere, 1308.
- , boundary layer in three dimensional flow.—I., 239.
- .—II., 1433.
- Howatson (A. F.) and Atkinson (J. R.), nuclear scattering of electrons and positrons, 1136.
- Huang (K.), thermal pressures in solids, Hildebrand's approximation, 202.
- Huby (R.) and Newns (H. C.), inelastic scattering of deuterons, 1442.
- Hutchinson (G. W.) and Scarrott (G. G.), high precision pulse height analyser of moderately high speed, 792; (Erratum), 957.
- Incompressible viscous fluid, unsteady flow (Sowerby), 176.
- Inelastic scattering of deuterons (Huby and Newns), 1442.
- Insch (G. M.) and Curran (S. C.), β spectrum of tritium, 892.
- Interaction, oblique shock-wave and turbulent boundary-layer (Bardsley and Mair), 29.
- Irving (J.), binding energies of 3- and 4-particle nuclei, 338.
- , *see* Gunn, 1353.
- Keith (H. D.) and Mitchell (J. W.), lattice defects in silver bromide at room temperature, 1331.
- Kent (D. W.), *see* Dainton, 317.
- King (D. T.), *see* Hooper, 304.
- Kofoed-Hansen (O.), allowed β transitions, effects of recoil, 1411.
- , upper limit for neutrino rest mass, 1448.
- Kuper (C. G.), model of intermediate state of superconductors, 961.
- Landau diamagnetism and Meissner effect (Papapetrou), 95.
- Lattimore (S.), rate of production of neutrons in ice by cosmic rays, 331.
- Le Claire (A. D.), grain boundary diffusion in metals, 468.
- , anelastic measurements of diffusion in solid solutions, 673.
- Leigh (R. S.), α , α' phases in Al-Zn systems, 876.
- , elastic constants of aluminium, 139.
- Leslie (D. C. M.), collision broadening at microwave frequencies, 37.
- Lewis (G. M.), *see* Bannerman, 1097.
- Lidiard (A. B.), influence of exchange energy on specific heat of free electrons in metals, 1325.
- Lithium hydride, ionization (Ahmed), 997.
- Liquid helium, ultrasonic propagation (Pippard), 1209.
- Little (C. G.) and Maxwell (A.), radio waves from galactic sources, fluctuations in intensity, 267.
- Lock (W. O.), *see* Dainton, 396; Camerini, 1241, 1261.
- Lomer (W. M.), dislocation reaction in F.C. lattice, 1327.
- Luchak (G.), generalization of Wilson's Hypothesis, 807.
- Macdonald (D. K. C.), velocity in brownian movement, 219.
- , transit-time phenomena in electronstreams.—III., 515.
- , metallic conduction—Internal size-effect, 756.
- , *see* Cornish, 1406.
- and Templeton (I. M.), resistance-minimum in gold, 432.
- Mack (C.), capacitance of parallel-plate condenser with anisotropic dielectric cylinder in torsion between, 428.
- Mair (W. A.), *see* Bardsley, 29.
- Markland (E.), deflection of cable, single point load, 990.
- Masses and modes of decay of heavy mesons.—I., κ particles (O'Ceallaigh), 1032.
- .—II., τ particles (Fowler, *et al.*), 1040.
- Matthews, (P. T.) meson-photon-nucleon interaction, 221.
- Maxwell (A.), *see* Little, 267.

- Mechanical kick-sorter (Frank, *et al.*), 603.
- Melting curve at high pressures (Domb), 1316.
- Mendelssohn (K.), *see* Bowers, 1445.
- Mendoza (E.) and Thomas (J. G.), electrical resistance of gold, silver and copper at low temperatures, 291.
- , *see* Goodman, 594.
- Menon (M. G. K.), O'Ceallaigh (C.) and Rochat (O.), multiple scattering of ionizing particles in emulsions.—II., 932.
- and Rochat (O.), multiple scattering of ionizing particles.—V., 1232.
- , *see* Gottstein, 708; Fowler, 1040.
- Meson field theory, intermediate coupling (Dalitz and Ravenhall), 1378.
- Meson-photon-nucleon interaction, (Matthews), 221.
- Meson production in atmosphere (Pullar and Dymond), 663.
- Mesons, production in proton-proton collisions (Gunn, *et al.*), 523.
- Metallic conduction—Internal size-effect (MacDonald), 756.
- Meteor radiants, radio echo apparatus (Aspinall *et al.*), 504.
- Micro-slip in metal crystals (Brown and Honeycombe), 1146.
- Middleton (D.), distribution of energy in randomly modulated waves, 689.
- Millar (W.), non-linear systems possessing resistance, 1150.
- Mitchell (J. W.), *see* Keith, 1331.
- Morrich (A. H.), *see* Hooper, 304.
- Moving Griffith crack (Yoffe), 739.
- Muirhead (H.), *see* Camerini, 1241.
- Multiple scattering of ionizing particles in emulsions.—I. (Gottstein *et al.*), 708.
- — — — —II. (Menon *et al.*), 919.
- — — — —III. (O'Ceallaigh and Rochat), 1050.
- — — — —IV. (Gottstein and Mulvey), 1089.
- — — — —V. (Menon and Rochat), 1232.
- Mulvey (J. H.), *see* Gottstein, 708, 1089.
- ($n, p; \pi^-$) reaction (Goldsack and Page), 570.
- Nabarro (F. R. N.), law of constant resolved shear stress in crystal plasticity, 213.
- Nabarro (F. R. N.), synthesis of dislocation fields, 1224.
- , *see* Eshelby *et al.*, 351.
- Nash (W. F.), *see* Braddick, 1227.
- Neutral V-particles (Armenteros *et al.*), 1113.
- Neutrino rest mass, upper limit (Kofoed-Hansen), 1448.
- Neutron emission from excited nuclei (Skryme and Williams), 1187.
- Neutrons, production by protons (Cassels *et al.*), 215.
- Newns (H. C.), *see* Huby, 1442.
- Nodtvedt (H.), correlation function in analysis of directive wave propagation, 1022.
- Non-linear systems possessing resistance (Millar), 1150.
- — — — —reactance (Cherry), 1161.
- Nuclear transformations by cosmic ray particles of great energy.—VI. (Camerini, Davies, Fowler *et al.*), 1241.
- — — — —VII. (Camerini, Davies, Franzinetti *et al.*), 1261.
- Nuclear scattering of electrons and positrons (Howatson and Atkinson), 1136.
- Nuclear explosions, helium and lithium emission (Sorensen), 188.
- Octupole transitions (French), 263.
- O'Ceallaigh (C.), masses and decay of heavy (κ) mesons, 1032.
- and Rochat (O.), multiple scattering in emulsions.—III., 1050.
- , *see* Gottstein, 708; Menon, 932.
- Orlin (J. J.), *see* Gibson, 555.
- Page (N.), *see* Goldsack and Page, 570.
- Pair production by fast electrons (Hooper, King and Morrich), 304.
- Papapetrou (A.), Landau diamagnetism and Meissner effect, 95.
- Paramagnetic salts, hyperfine structure and nuclear alignment (Bleaney), 441.
- — — — —resonance (Bleaney *et al.*), 1062.

- Paterson (S.), *see* Cottrell, 391.
- Penrose (O.), quantum mechanics of helium II., 1373.
- Perkins (D. H.), *see* Camerini *et al.*, 1241, 1261.
- Perturbation treatment of closed states in field theories (Touschek), 1178.
- Photodisintegration of ^{10}B (Brinkworth and Titterton), 1191.
- of the deuteron (Gibson *et al.*), 555.
- Pickavance (T. C.), *see* Cassels, 215; Taylor, 20, 328, 751.
- Pippard (A. B.), ultrasonic propagation in liquid helium near the lambda point, 1209.
- Plastic distortion, theory (Bishop and Hill), 414.
- flow of metals (Green), 365.
- properties of F.C. metal (Bishop and Hill), 1298.
- rigid body at yield point (Hill), 868.
- Polytypism of silicon carbide, dislocation theory (Vand), 1384.
- Pople (J. A.), communal entropy of dense systems, 459.
- Positronium, three-photon decay (Radcliffe), 1334.
- Powell (C. F.), *see* Fowler, 1040.
- Power (E. A.), *see* Gunn, 523.
- Processing of thick emulsions (Dainton *et al.*), 391.
- Pullar (J. D.) and Dymond (E. G.), meson production in atmosphere, 663.
- Pulse height analyser (Hutchinson and Scarrott), 792; (Erratum), 957.
- Pursey (D. L.), interaction in β decay, 1193.
- Quadrupole moments and nuclear shell model (Touschek), 312.
- Quantum mechanics of helium II (Penrose), 1373.
- Radcliffe (J. M.), three-photon decay of positronium, 1334.
- Radiations of ^{203}Hg (Wilson and Curran), 762.
- Radio - atmospheric, propagation (Budden), 1.
- Radio waves from galactic sources, intensity fluctuations (Little and Maxwell), 267.
- RaE, isomeric state (Feather), 568.
- Ranade (J. D.), hyperfine structure in bromine spectrum.—II., 284.
- , electric quadrupole and magnetic moment of bromine nucleus, 279.
- Randle (T. C.), Dickson (J. M.) and Cassels (J. M.), cross-section of reaction $^8\text{Be}(p, p2n)^7\text{Be}$ at 156 MeV, 665.
- Randle (T. C.), *see* Taylor, 20, 328, 751.
- , *see* Cassels, 215.
- Range-energy relations, slow alpha particles in air (Freeman and Burcham), 434.
- Randomly modulated waves (Middleton), 689.
- Ravenhall (D. G.), *see* Dalitz, 1378.
- Rayski (J.), field theories with non-localized interaction, 1289.
- Reaction $^{10}\text{B}(\gamma, d)^2\text{He}$ (Brinkworth and Titterton), 952.
- $^{11}\text{Be}(\gamma\alpha)^7\text{Li}$ and $^{11}\text{B}(\gamma T)^8\text{Be}$ (Calcraft and Titterton), 666.
- Recrystallization texture of drawn Al wire (Sawkill and Thornley), 1369.
- Reflection of low frequency waves (Budden), 833.
- Resistance - minimum in gold (MacDonald and Templeton), 432.
- Reversion formulae, application to differential equations (Sim), 228.
- Ritson (D. M.), absorption of penetrating shower secondaries, 250.
- Rochat (O.), *see* Gottstein, 708; Menon, 932, 1232; Fowler, 1040; O'Ceallaigh and Rochat, 1050.
- Rosser (W. G. V.) and Swift (M. W.), attenuation of nucleon cascades in lead, 856.
- Rushbrooke (G. S.) and Scoins (H. I.), virial coefficients and Born-Green theory of fluids, 582.
- Sawkill (J.) and Thornley (N.), recrystallization texture of drawn Al wire, 1369.
- Scarrott (G. G.), *see* Frank (S. G. F.), 603; Hutchinson, 792.
- Scoins (H. I.), *see* Rushbrooke, 582.
- Scovil (H. E. D.), *see* Bleaney, 1062.
- Seed (J.), alpha-particles from proton bombardment of O_{18} , 566.
- Seidl (G. F. P.), *see* French and Seidl, 537.

- Semi-conductors, internal barriers (Henisch), 734.
- Siebel (M. P. L.), *see* Hill and Siebel, 722.
- Signals in presence of noise (Burgess), 475.
- Silver bromide, lattice defects (Keith and Mitchell), 1331.
- Sim (A. C.), reversion formulae with application to non-linear differential equations, 228.
- Skryme (D. M.) and Williams (W. S. C.), neutron emission from nuclei excited by high energy protons, 1187.
- Sodium chloride, study of cleavage planes (Amelinckx), 324.
- Sorensen (S. O. C.), emission of helium and lithium fragments in nuclear explosions, 188.
- Sowerby (L.), unsteady flow of incompressible viscous fluid, 176.
- Specific heat, free electrons, exchange energy (Lidiard), 1325.
- Stars in emulsions by 150 MeV neutrons (Titterton), 109.
- Stroh (A. N.), *see* Eshelby, 1401.
- Superconductors intermediate state (Kuper), 961.
- Supersonic flow, conditions at sharp leading edge (Bardsley), 255.
- Swift (M. W.), *see* Rosser, 856.
- τ meson (Hodgson), 1060.
- Taylor (A. E.), Pickavance (T. G.), Cassels (J. M.) and Randle (T. C.), cross-sections of hydrogen and carbon for neutrons, 20, 328.
- of elements for 156 MeV neutrons, 751; (Erratum), 1336.
- , *see* Cassels, 215.
- Temperley (H. N. V.), velocity of second sound in helium II., 74.
- Templeton (I. M.), *see* Macdonald, 432.
- Thermal convection in a magnetic field (Thompson), 1417.
- pressure in solids (Huang), 202.
- Thirring (W.) and Touschek (B.), covariant formulation of Bloch-Nordsieck method, 244.
- Thomas (J. G.), *see* Mendoza, 291.
- Thompson (W. B.), thermal convection in a magnetic field, 1417.
- Thomson (G. P.) and Hodgson (P. E.), cascade production of cosmic ray showers, 978.
- Thornley (N.), *see* Sawkill, 1369.
- Three and four particle nuclei, disintegration (Gunn and Irving), 1353.
- Titterton (E. W.), *see* Calcraft, 666; Brinkworth, 952, 1191.
- , stars in emulsions by 150 MeV neutrons, 109.
- , hammer tracks in neutron and proton produced stars, 113.
- Touschek (B.), quadrupole moments and nuclear shell model, 312.
- , perturbation treatment of closed states in field theories, 1178.
- , *see* Thirring and Touschek, 244.
- , *see* Gunn *et al.*, 523.
- Transit-time phenomena in electron streams.—III. (MacDonald), 515.
- Trenam (R. S.), *see* Bleaney, 1062.
- Trumpy (B.), *see* Gibson, 555.
- Turner (J. F.) and Cavanagh (P. E.), highly forbidden transitions in Na^{24} , 636.
- Twisted elastic prism, distortion (Ashwell), 820.
- Ultrasonic delay line, design (Gold), 787.
- Unequally-spaced data, polynomials (Hayes and Vickers), 1387.
- Vand (V.), polytypism of silicon carbide, dislocation theory, 1384.
- van Kampen (N. G.), analytical continuation of the S-matrix, 851.
- Velocity of second sound in helium II. (Temperley), 74.
- (Ward and Wilks), 314.
- Verma (A. R.), carborundum growth spirals, 1005.
- Vickers, *see* Hayes, 1387.
- Virial theorem in quantum mechanics (Cottrell and Patterson), 391.
- Ward (J. C.) and Wilks (J.), velocity of second sound in helium near absolute zero, 314.
- Wave-form analysis, uncertainty (Woodward), 883.
- Williams (W. S. C.), *see* Skryme, 1187.
- Wilson (H. W.) and Curran (S. C.), radiations of ^{203}Hg , new method, 762.
- Wilson's hypothesis (Luchak), 807.

- Wohlfarth (E. P.), *see* Fletcher and Wohlfarth, 106.
- , collective electron ferromagnetism; rectangular energy bands, 374.
- Wolfendale (A. W.), *see* Braddick, 1277.
- Wood (W. A.), intrinsic crystalline structure and strength of metals, 310.
- Woodward (P. M.), time and frequency uncertainty in wave-form analysis, 883.
- Yang (L. M.), trace of the product of Dirac's matrices, 1333.
- Yekutieli (G.), *see* Danysz, 1185; Camerini, 1241, 1261.
- Yoffe (E. H.), moving Griffith crack, 739.

END OF THE FORTY-SECOND VOLUME.

